Acc.
18.9.87

eu6-H02924-12- P024442

This issue: ARRS Meeting Section

AJR

12

American Journal of Roentgenology

UNIVERSITY LIBRARY

January 1986

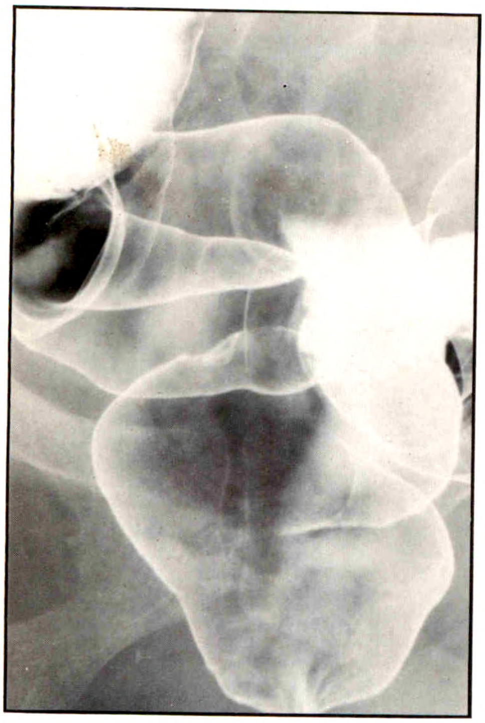

LIQUID POLIBAR™
X-Ray courtesy of Dr. Alec J. Megibow
N.Y.U. Medical Center University Hospital
New York, NY 10016

E-Z-AC™
X-Ray courtesy of Dr. Igor Laufer
Hospital of the University of Pennsylvania
Philadelphia, PA 19104

LIQUID POLIBAR™ PLUS
X-Ray courtesy of Dr. David W. Gelfand
Bowman Gray School of Medicine, Wake Forest Universit
Winston-Salem, NC 27102

Three bariums for superior air-contrast results.

Air Contrast Colon: The procedure of choice with the systems of your choice.

Liquid Polibar™

The original air contrast colon barium with superb coating characteristics. Optimum viscosity assures consistent even coating throughout. Truly the bench mark formulation for air contrast studies.

E-Z-AC™

This fast flowing liquid barium reaches the splenic flexure in only 20 to 30 seconds. Specifically formulated for air contrast procedures where a cleansing enema has not been administered that morning.

Introducing: Liquid Polibar™ Plus

The classic Liquid Polibar formulatio
modified to achieve a faster flow rat
It has the excellent coating characte
tics that you expect from a Polibar f
mula but is more attuned to the spe
necessary in the modern radiology d
partment. Polibar Plus—increased
speed and diagnostic consistency.

For samples and additional information please contact your local E-Z-EM distributor call E-Z-EM directly.

E-Z-EM

E-Z-EM, Inc. 7 Portland Avenue, Westbury, NY 11590 516-333-8230 800-645-3052

© E-Z-EM, Inc. 1

Official Journal
American Roentgen Ray Society

AJR

Diagnostic Imaging and Related Sciences

Editor Robert N. Berk

Associate Editors Alan J. Davidson
Saskia vonWaldenburg Hilton

Associate Editor, Neuroradiology Juan M. Taveras

Consulting Editorial Board Christos A. Athanasoulis
Edward Buonocore • Peter L. Cooperberg • John L. Doppman
Kent Ellis • Robert H. Freiberger • Reginald Greene
N. Thorne Griscom • William R. Hendee • Eugene C. Klatte
John G. McAfee • William B. Seaman • Michel M. Ter-Pogossian
Joseph P. Whalen • David M. Witten

Editorial Staff Gita Braude • Elizabeth Whalen
Barbara Rose • Linda Wood

All business correspondence, including display (not classified) advertising, subscriptions, address changes, reprints, and permission requests should be addressed to Williams & Wilkins, 428 East Preston Street, Baltimore, MD 21202. Correspondence regarding editorial matters and classified advertising should be addressed to the editorial office, AJR, 2223 Avenida de la Playa, Suite 306, La Jolla, CA 92037. For manuscript submission, see Guidelines for Authors, next page. Undelivered or damaged copies replaced within 60 days of publication; 90 days for foreign subscribers. Allow 90 days for address changes.

AJR AMERICAN JOURNAL OF ROENTGENOLOGY (ISSN 0361 803X) is published monthly by American Roentgen Ray Society, 428 E. Preston Street, Baltimore, MD 21202. Annual dues include $50 for journal subscription. Second class postage paid at Baltimore, MD and at additional mailing offices. Postmaster send address changes (Form 3579) to Williams & Wilkins, 428 East Preston St., Baltimore, MD 21202. Subscription rates $90 ($115 foreign); institutions $100 ($125 foreign); in training $25; single copy $16 ($19). Japanese Yen price is available from our sole agent USACO Corporation, 13-12, Shimbashi 1-Chome, Minato-Ku, Tokyo 105, Japan, telephone 03-502-6471. Airmail rates furnished on request. Indexed by *Current Contents* and *Index Medicus*. Copyright © 1986 by American Roentgen Ray Society.

0361-803X/86 $2.00

AJR Guidelines for Authors

Address new and revised manuscripts, correspondence, and classified ads to:

AJR Editorial Office
2223 Avenida de la Playa, Suite 306
La Jolla, CA 92037
telephone: (619) 459-2229

Make inquiries regarding subscriptions, display advertising, reprints, or permission to republish *AJR* material to the publisher:

The Williams & Wilkins Co.
428 E. Preston St.
Baltimore, MD 21202
telephone: (301) 528-4133

Publication Policy

The *AJR* publishes original and timely contributions to the advancement of medical diagnosis and treatment with radiologic methods. Although content is predominantly clinical, laboratory investigations are accepted when their relevance to clinical practice is demonstrable. In prospective clinical investigations, authors should document that informed consent was obtained from patients. The material submitted **must** not have been previously published nor be currently submitted for publication elsewhere (prior publication of simple abstracts without illustrations or tables will not prejudice publication of the complete study). Papers dealing with **neuroradiology** should be addressed to: Editorial Office, American Journal of Neuroradiology, Dept. of Radiology, Massachusetts General Hospital, Boston, MA 02114; telephone: (617) 726-8342. At the discretion of the Editor of *AJR*, *AJNR* articles may be republished in *AJR*.

Decisions on manuscripts are based on peer review. Reviewers receive manuscripts without title pages to protect the identity of authors and to ensure an unbiased review; names of reviewers, in turn, are not revealed to the authors. Accepted manuscripts are subject to editing. Statements within an article, including changes made by the Editor or copy editor, are the responsibility of the author and not *AJR* or its publisher. Authors will receive the edited manuscript, galley proof, and proofs of illustrations usually 6–8 weeks after acceptance. If the corresponding author will not be available, arrangements should be made for a coauthor or colleague to read and return the proof.

Copyright Information

In accordance with *AJR* implementation of the U.S. Copyright Law, authors must release first and subsidiary rights to their manuscript at submission (unless the study was performed as part of their duties as an employee of a U.S. government agency). A dated letter with the signatures of all authors should state: "We, the authors, assign first and subsidiary rights to the American Roentgen Ray Society in the event that our manuscript [insert title] is published by *AJR*. We guarantee that this manuscript contains no matter libelous or otherwise unlawful or which invades individual privacy or which infringes any proprietary right. *AJR*, in turn, grants us the right of republication, subject only to crediting the original source of publication and receiving written permission from the publisher. We understand we will receive no royalty or other compensation from *AJR*. We guarantee that this article and illustrations have not been previously published elsewhere or, if previously published in part or in whole, that permission has been obtained for republication. Copies of these permissions are included and previously published text or illustrations have been identified in the manuscript." (Delete the last sentence if it does not apply.) The covering letter also should state that the manuscript has been seen and approved by all the authors.

Manuscript Form

AJR complies with the Uniform Requirements for Manuscripts Submitted to Biomedical Journals (*Ann Intern Med* 1979;90:95–99). Manuscripts must be ***typed double-space throughout***, including references, tables, and figure legends. Each table, the footnotes, and the figure legend section should begin on separate sheets; a separate title page should be provided. Send the original typescript, one copy, and two sets of illustrations (not photocopies). Authors' names should be on the title page **only** so that author anonymity can be maintained during the review process. Permission to reprint previously published material should accompany the manuscript.

Organization of Major Articles

Title Page

Titles should be brief yet precise, accurately conveying the content of the paper. Limit authors to those who made substantial contributions to the work. Include an address for *each* author, and ZIP or postal code; acknowledgment of grant or other financial support when appropriate; name of meeting, location, and date if the paper was presented; a running head (shortened title); and the name, address, and telephone number of the author to whom correspondence and requests for reprints should be addressed.

Abstract

A description of the purpose, methods, results, and conclusions of the study is required. The factual highlights of each section should be recapitulated.

Introduction

Clearly state the purpose of the investigation, including necessary background facts that indicate its current relevance.

Materials [or Subjects] and Methods

Describe the research plan, the materials or subjects, and the methods, in that order. Proof of disease and control of subjectivity in observations should be detailed. Metric measurements should be used throughout. Put measurements in the International System of Units (SI) in parentheses when appropriate; for example, 400 rad Gy).

Results

Present results in logical sequence. If tables are used, duplicate tabular data but do describe important points and

Case Reports

Individual cases can be described if there are only a few more cases from a large series can be described individu Representative Case Reports. Each report should concentrate the radiologic information and its usefulness.

Discussion

Offer appropriate limitations about the research plan, subjects, and methods to give perspective to their ade purpose of the study. Interpret the results to len importance to the observations. Hypotheses and sp

on the results are encouraged. When results differ from those of previous investigations, an attempt should be made to explain the discrepancy. Conclude with a brief statement regarding clinical significance.

Acknowledgments

Acknowledge only persons who have made *substantive* contributions to the study. Mention grant support on the title page.

References

References should be offered to document major assertions of fact and any opposing evidence and concepts. Discretion in number is requested. References should be cited in the text by number (e.g., [3, 4]). The reference list should be arranged in the numeric order that references are cited in the text and ***typed double-spaced throughout***. References cited *first* or *only* in tables or figure legends should be numbered by the sequence in which the table or figure is first identified in the text. Data for each reference should be arranged according to the style adopted by the U.S. National Library of Medicine and used in *Index Medicus*. ***Accuracy of reference data is the responsibility of the author.*** Provide all authors' (or editors') names when fewer than seven; when seven or more, list the first three and add et al. Provide inclusive page numbers; if an article is only one page, please indicate. Abbreviations for titles of medical periodicals should conform to those published in *Index Medicus*. Articles that appear in both *AJR* and *AJNR* should be a single reference that cites both journals (example 3). Examples

1. Kirks DR, Fram EK, Vock P, Effmann EL. Tracheal compression by mediastinal masses in children: CT evaluation. AJR 1983;141:647–651
2. Khansur T, Yam LT, Tavassoli M. Serum monitors of bone metastasis. In: Stoll BA, Parbhoo S, eds. Bone metastases: monitoring and treatment. New York: Raven, 1983:165–180
3. Sage MR. Review. Kinetics of water-soluble contrast media in the central nervous system. AJNR 1983;4:897–906, AJR 1983; 141:815–824

Unpublished data and personal communications should not be numbered references but should be put in parentheses in the text (e.g., Smith JD, personal communication).

Tables

Tables should be concise and organized to show trends, not merely compilations of raw data. (The Editor may request that tables of backup data too extensive to be published be deposited with the National Auxiliary Publications Service or made available by the author.) Include only data pertinent to the subject. Long itemized case histories are better presented in the text as case reports or summaries. Do not repeat in tabular form material presented in the text. Tables should have titles and headings, but no vertical or horizontal rules.

ustrations

gures should be submitted as 13 × 18 cm (5 × 7 inch) glossy, and-white prints, ***untrimmed and unmounted***. Labels and ar- ust be of professional quality and removable. Number each correspond with the figure legends and indicate the top. Avoid writing directly on the back of the print. Special permission for publication of facial photographs of patients or for previously published pictures is required. Line illustrations or graphs must be professionally drawn in black ink on white background; please send photographic prints (not photocopies), not originals, to avoid damage in handling. Color illustrations will be used at the discretion of the Editor; send color prints. Firm estimates of cost will be sent to the author(s) for approval before publication. Identical anatomic structures in color prints should be the same size to facilitate reproduction and reduce cost.

Legends

Figure legends should carry a title identifying the message of the illustration and the case number if individual cases are described in the text. Legends should be as brief as possible for the informed reader to understand the figure. Detailed clinical data should be avoided. Legends for previously published illustrations should cite the reference number of the source (e.g., Reprinted from [8]).

Organization of Case Reports

Concise case reports will be considered for publication if they present unusual experiences that are medically important and instructive. Clarity and brevity are essential. After preliminary screening by an editor to determine whether the requirement of medical significance has been met, qualifying papers will undergo the same peer review as major papers. To facilitate planning the order and layout of each issue, case reports are limited in length to two journal pages. The introduction should be one short paragraph that gives some general background of the disorder and the specific interest and message of the case presented. Only one case should be described in detail. The case report should concentrate on the radiologic information and its usefulness. The discussion should focus on the specific message of this report and the relevance of radiology in this instance. If the author has encountered other cases, they may be briefly mentioned, and possibly illustrated, but not described in detail. There should be no more than eight references. The figures should be limited to the minimum required to document the case findings, probably not more than four pictures, each a column wide (or the equivalent). Excess illustrations would require severely shortening the text. Figure legends should be as short as possible and should not repeat the text. There can be no tables and no acknowledgments. See previous sections for detailed instructions regarding references and illustrations.

Other Contributions

Technical Notes

Brief descriptions of new techniques or significant modifications of older ones that are directly applicable to the clinical practice will be accepted if review is favorable. Technical notes do not carry abstracts or acknowledgments.

Letters to the Editor

Letters are subject to editing and condensation. Criticism of published articles should be objective and constructive. Letters also may discuss matters of general interest to radiologists.

When all the figuring is done, you can't afford anything less than the quality of Kodak products and services.

© Eastman Kodak Company 1985

Sharpen your pencils. Warm up your calculators and
mputers. It's time to look for ways to cut costs in the
diology department. Prediction: When the figures are
e numbers are crunched and the conclusions are
n, the word will be that quality costs less. The qual-
odak products. Can you afford anything less?

ne example: repeat reduction.

repeats is a great way to cut costs, and Kodak
h quality, because that means consistency.
chnical innovation. Films with wide dynamic
, such as Kodak T-Mat L film, mean fewer
due to exposure variations. And high system
ean fewer repeats due to patient motion. If a
ewhere in the imaging chain is causing
track it down with a computerized pro-
"RRA"—Radiographic Repeat Analysis.

BackUp from Kodak.

st endless list of extras like "RRA," each
utes to cost-effectiveness. There are hands-on, nuts-and-bolts programs like processor seminars. There's a superbly practical Custom Computer Technic Service that provides highly precise charts on a room-by-room basis, as well as a video imaging program to give you the video look you like. And there are also BackUp programs for administrators. Things like Procedural Costing, Room Utilization, Financial Planning.

Your TSR brings it all.

Provider of all these services, and your ally in all things radiographic, is your Kodak technical sales representative. A professional consultant, highly trained and technically experienced in imaging technology and administrative challenges. Troubleshooter, answer person, friend. Whether you call for technical assistance or to arrange a long-term educational program, the response will be immediate and enthusiastic. And a big part of the reason why you can't afford anything less than the quality of Kodak products.

Can you afford anything less?

Kodak

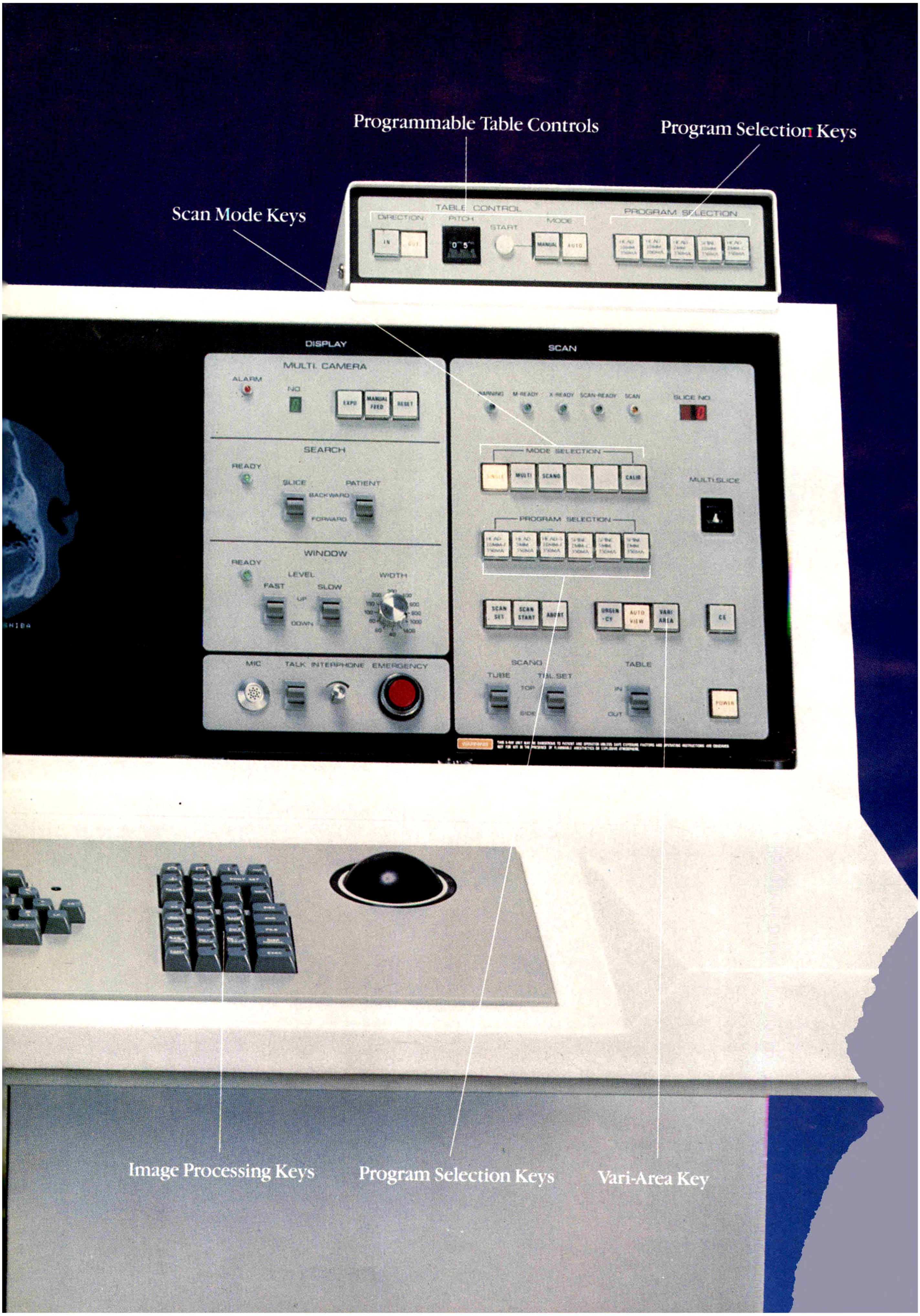
Programmable Table Controls
Program Selection Keys
Scan Mode Keys
Image Processing Keys
Program Selection Keys
Vari-Area Key

Unique Species

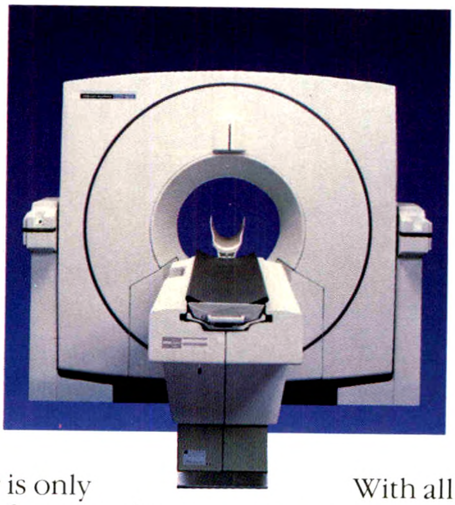

The TCT-20AX is truly one of a kind—a high performance, low-cost CT scanner strictly for neurological examinations of the head, neck and spine. This unique CT neurological scanner is only available from Toshiba, of course, the one company with the CT expertise and sensitivity to customer needs to make it possible.

Optimally designed for neurological applications, the TCT-20AX has a 600mm patient aperture to permit thorough examination of the brain and the entire length of the spine. The TCT-20AX also speeds patient processing with proven third generation rotate/rotate technology, reducing scan speeds to 4.5 and 9 seconds and allowing reconstruction times as short as 5 seconds. Diagnostic capabilities are enhanced with high resolution images and a variety of advanced design features, such as vari-area and multi-slice modes. Various image processing functions, including sagittal/coronal/oblique image conversion, greatly aid diagnostic precision.

With all of its extensive diagnostic capabilities the TCT-20AX is incredibly easy to operate. Outstanding diagnostic and operational performance coupled with high patient throughput make the TCT-20AX a sensible addition to any busy neurological practice. Even with a low volume of patients, affordable pricing makes it a sound investment. And, the TCT-20AX offers outstanding reliability backed by Toshiba's automated quality assurance program, an industry first.

Give us a call. We'll be glad to show you how the TCT-20AX can make both diagnostic and economic sense as a unique addition to your facility. Please call toll-free (800) 421-1968, in California call (714) 730-5000.

In Touch with Tomorrow

TOSHIBA

GLOBAL IMAGING SPECIALISTS

DELTA the Official Airline of the American Roentgen Ray Society

In cooperation with the American Roentgen Ray Society, Delta Air Line's is offering a 35% discount on your round trip Delta Day Coach fare to Washington, D.C.

If you are traveling to Washington, D.C., between April 10-17, 1986, you are eligible for a 35% discount off the regular round-trip, non-discounted Day Coach fares in the Continental U.S. or, if other fares offering greater savings are available, Delta will confirm your reservations at that rate. Either way, special fares have restrictions and/or limited seats, so make your reservations early.

If you normally use the services of a travel agent, have them place your reservations through our toll-free number to obtain the same advantages.

Call 1-800-241-6760 for reservations from 8:30 a.m. to 8:00 p.m. Eastern Time—Daily. **REFER TO FILE NUMBER F0347**. This discount is available only through this number.

ELEMA-SCHONANDER

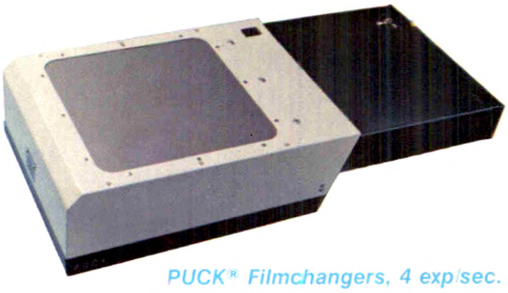

PUCK® Filmchangers, 4 exp/sec.
Model UD4...position-independent, for multi-directional examination units.
Model U4 for a.p. and lateral projections.

Long useful life

is built into every Elema-Schonander angiographic filmchanger system.

The two AOT filmchanger systems shown below were installed in 1967 and are still in frequent use. They are but two of many examples of Elema-Schonander filmchanger systems, working dependably day after day, year after year, for ten...fifteen years or more.

☐ The same quality of engineering, material, workmanship and solid construction demonstrated in these two examples, characterizes also today's generation of AOT and PUCK filmchangers.

☐ The long useful life and dependability of Elema-Schonander filmchanger systems translates directly into lower cost per examination. Together with excellent image quality, these and other Elema-Schonander advantages have been proven again and again over the years.

Elema-Schonander, Inc.
2360 North Palmer Drive
P.O. Box 94517
Schaumburg, IL 60195
Telephone (312) 397-5900

elema-schonander

MG/5810-055

85226

Examples of Elema-Schonander filmchanger systems in frequent use for many years.

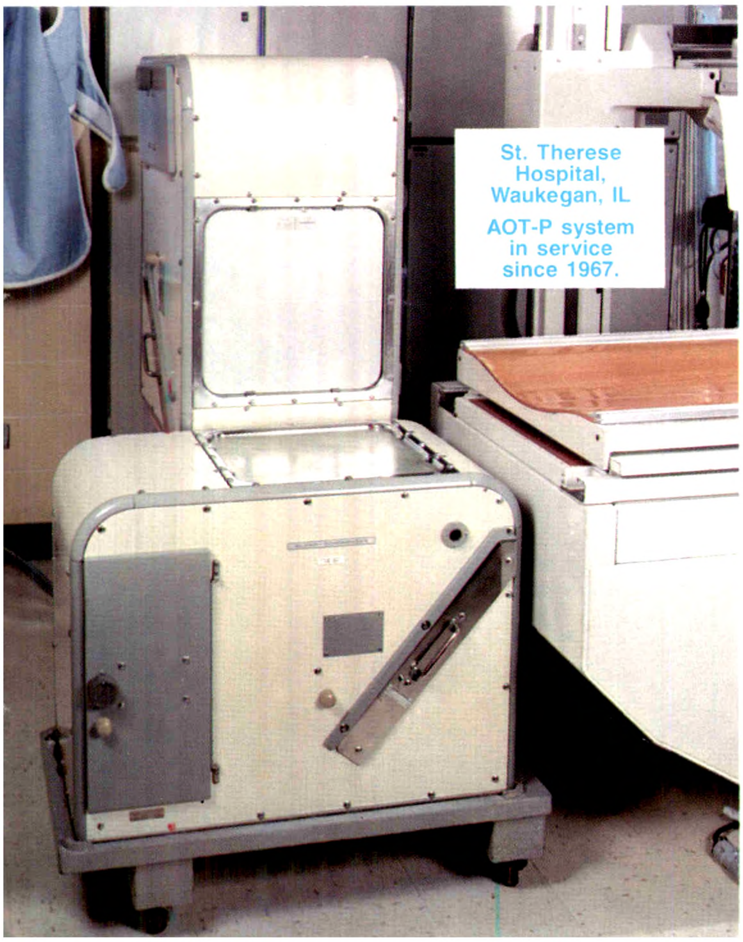

St. Therese Hospital, Waukegan, IL

AOT-P system in service since 1967.

VA Medical Center, North Chicago, IL

AOT-P system in service since 1967.

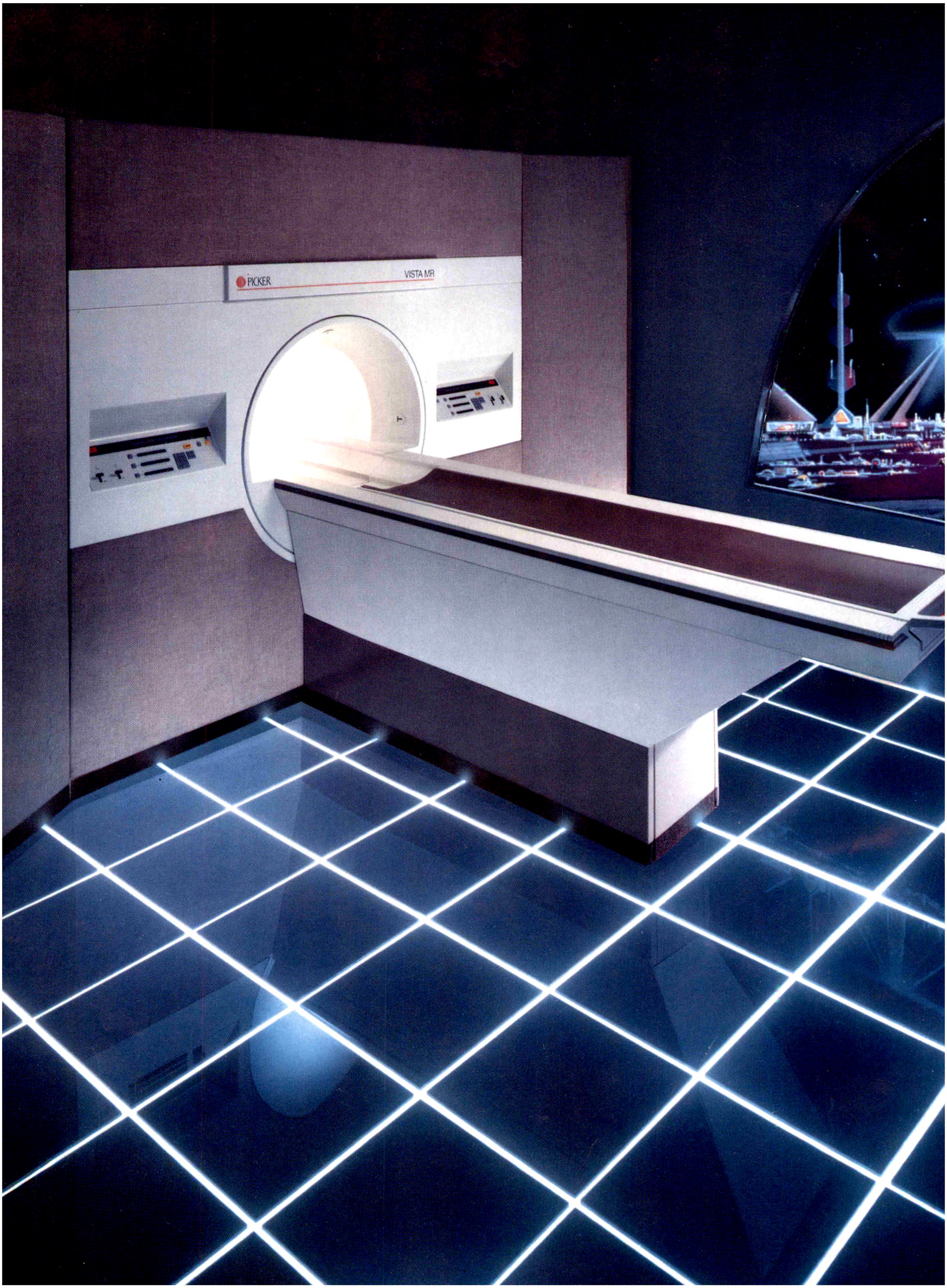
PICKER
VISTA MR

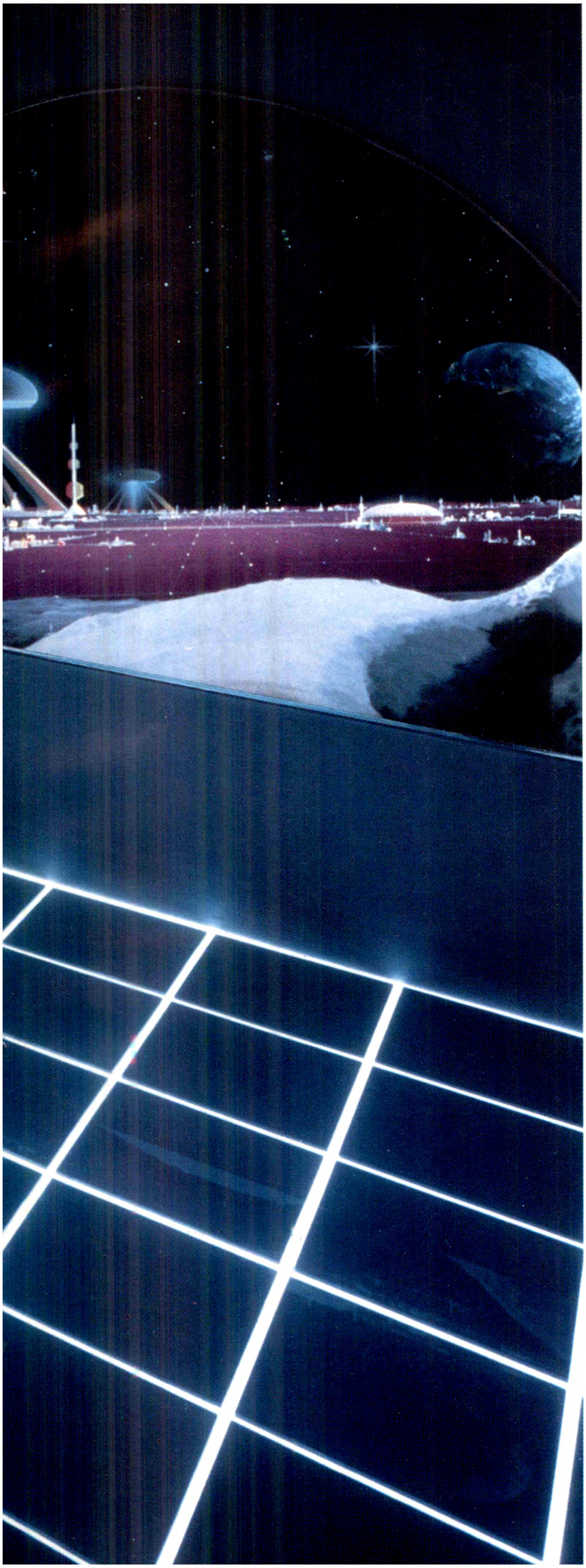

GUARANTEE YOUR MR FUTURE.

Dynamic Blood Flow Analysis, Quantified Cardiac Functions, Time Efficient Volume Studies, Multi-Nuclear Imaging, High Resolution 512^2 Acquisition, 3-D Displays, Ultra-thin Slice Scanning, Real Time Chemical Shift Correction, Variable Field Operation, In Vivo Spectral Analysis, Tumor Differentiation, Thermal Contouring, Therapeutic Application, Stereotaxic Localization, Satellite Data Transmission . . .

Isn't this your vision of MR tomorrow? Our "vista" of MR includes providing for these capabilities in today's product family.

When selecting your high image quality, high throughput system today, make sure you include basic specifications that accommodate tomorrow's applications. The Vista MR 2055 family has been developed with High Performance (HP) architecture including:

- 10-90 MHz Broadband RF Electronics
- 15 kW RF Power
  12 mT/m Maximum Gradient Power
- HYBRID Imaging
- Direct Angle Oblique Acquisition
- 32 bit Array Processor with 18 x 10^6 Floating Point Operations per Second.
- User Selectable — TE Range: 10-240 msec.
  TI Range: 100-900 msec.
- 64 Contiguous Slices Maximum for Total Organ Coverage in a single 4 Echo Multiple Slice Study.

There are many serious questions when considering the right MR system. With Picker, it is easier to be confident in meeting your future MR needs because you know that your system has the intrinsic specifications to get you there.

PICKER

NOTE: NMR systems are classified as investigational devices in the United States under the Medical Device Amendments to the Food, Drug and Cosmetics Act. These devices will become commercially available in the U.S.A.

American Roentgen Ray Society:
Officers, Committees, and Meeting Information

Officers

President: Eugene Gedgaudas
President-elect: Jerome F. Wiot
1st Vice-president: Lee F. Rogers
2d Vice-president: Thomas C. Beneventano
Secretary: Raymond A. Gagliardi
Treasurer: Ronald G. Evens

Executive Council: E. Gedgaudas, J. F. Wiot, L. F. Rogers, T. C. Beneventano, R. A. Gagliardi, R. G. Evens, M. M. Figley, R. N. Berk, F. L. Angell, J. E. Madewell, M. P. Capp, G. W. Hartman, B. G. Brogdon, G. A. Kling, H. C. Carlson, A. K. Poznanski, A. E. James, Jr., J. A. Kirkpatrick, Jr., R. H. Troupin, S. S. Siegelman, chairman

Committees 1984–1985

Editorial Policy: S. S. Sagel, W. J. Casarella, J. T. Ferrucci, Jr., N. C. Whitley, S. Hilton, A. J. Davidson, J. M. Taveras, M. M. Figley, R. N. Berk, M. P. Capp, chairman

Education and Research: C. E. Putman, A. R. Margulis, J. R. Thornbury, R. A. McLeod, G. W. Hartman, ex officio, B. G. Brogdon, chairman

Finance and Budget: B. P. Wood, L. R. James, J. A. Kirkpatrick, Jr., R. H. Troupin F. L. Angell, chairman

Instruction Courses: R. A. McLeod, associate chairman, G. W. Hartman, chairman

Program: H. C. Carlson, R. A. Gagliardi, R. H. Troupin, S. S. Siegelman, M. P. Capp, J. E. Madewell, B. G. Brogdon, G. W. Hartman, G. A. Kling, A. V. Proto, C. E. Bickham, J. F. Wiot, chairman.

Publications: W. J. Casarella, J. T. Ferrucci, Jr., S. S. Sagel, N. C. Whitley, M. P. Capp, chairman

Scientific Exhibits: S. G. Kirchner, E. R. Heitzman, Jr., S. M. Goldman, J. E. Madewell, chairman

Nominating: J. P. Tampas, G. M. Stevens, J. A. Kirkpatrick, chairman

Representatives to Other Organizations

American Board of Radiology: E. C. Klatte, R. W. McConnell, L. F. Rogers

American College of Radiology: J. L. Gwinn, G. A. Kling, G. W. Hartman, J. M. Dennis, E. J. Ferris

American Medical Association House of Delegates: S. F. Ochsner, K. C. Krabbenhoft, alternate

American National Standards Institute: M. Haskin

National Council on Radiation Protection and Measurements: E. L. Saenger, H. L. Friedell

Meetings, Membership, Business Information

Annual Meetings: April 13–18, 1986, Sheraton Washington (DC); April 26–May 2, 1987, Fontainebleau-Hilton, Miami Beach; May 1–6, 1988, Westin Bonaventure, Los Angeles

Scientific Program 1985 Meeting: Jerome F. Wiot, president-elect, Dept. of Radiology, University of Cincinnati Hospital, 234 Goodman St., Cincinnati, OH 45267-0742

Director Annual Meeting: George A. Kling, Harper Hospital, Detroit, MI 48201

ARRS Membership: Stanley S. Siegelman, Dept. of Radiology and Radiological Science, Johns Hopkins Hospital, 601 N. Broadway, Baltimore, MD 21205. The ARRS has two membership categories: active and in-training. For active membership, applicants must practice radiology in the U.S. or Canada. Each must have graduated in good standing from an approved medical school or hold an advanced degree in a physical, chemical, or biological science and be certified by the American Board of Radiology, the Royal College of Physicians and Surgeons of Canada, or otherwise adequately document training and credentials. A member-in-training must be in a radiology residency, a postresidency fellowship program, or a postgraduate student in an allied science. Status must be verified by the program director. For consideration during the 1986 ARRS meeting, completed applications must be received by Dr. Siegelman no later than Feb. 1, 1986.

Business Office: George J. O'Hop, controller, American College of Radiology, Suite 1660, 20 N. Wacker Dr., Chicago, IL 60606

We are the State
OF THE IMAGE

Precise Optics is the World's Largest Manufacturer *specializing only* in the production of Image Intensifier Systems and Components.

With *over thirty years of experience*, Precise has achieved an unsurpassed capability in the design and manufacture of Imaging Systems, suppling major equipment manufacturers throughout the world with our complete Systems and components.

With budgetary constraints and DRGs a current fact of life, Precise Systems offer a *viable high-quality alternative* to more expensively priced equipment.

Precise produces many hundreds of Imaging Systems every year, at an obvious volume cost savings and with *superior tube selection advantage*, while tailoring systems and components to meet your individual, specialized needs.

Our application and production expertise assures that any System requirement can and will be met without compromise, with the performance, reliability and service expected from an industry leader.

All Systems are compatible with new or existing equipment, while satisfying DHHS standards.

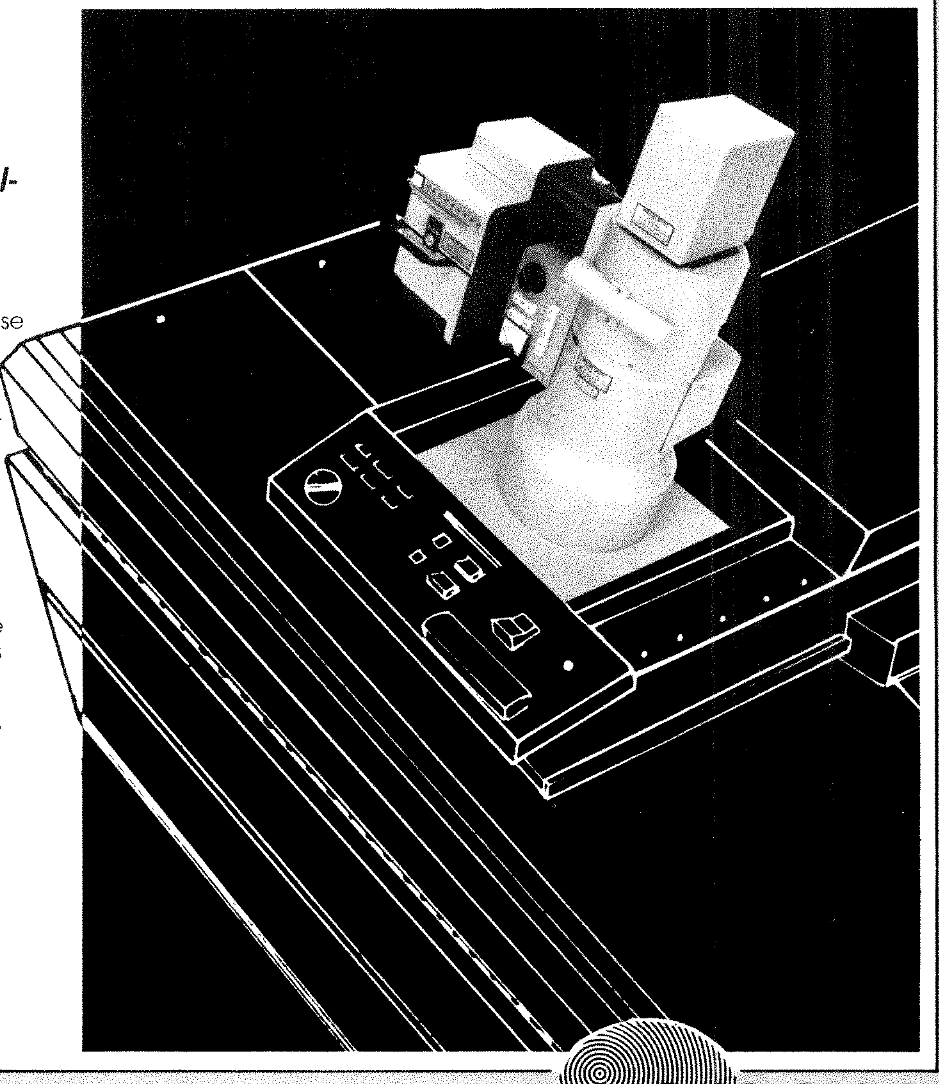

For more information on our line of 6, 9, 12 & 16 inch, Single & Multi-mode Image Intensifier Systems. Write or call . . .

precise optics ®
PHOTO MEDIC
EQUIPMENT, INC.

239 SOUTH FEHR WAY, BAY SHORE N.Y. 11706 **(516) 242-6600 • TWX 510 227-9837**

SIEMENS

The bottom line…

More output in your CT clinically and financially

In CT, accuracy is essential, quality images are a must . . . but *productivity* is the measure by which system efficiency is judged.

SOMATOM CT gives you the highest productivity in the business.

It effectively reduces overall exam time. You can actually scan, reconstruct, image, and archive in less time than it takes other systems just to reconstruct. That's nearly 40% more productivity to measurably improve the overall economics of your CT operation.

SOMATOM productivity increases efficiency.

You can routinely process 30 patients in just 8 hours. The result: more efficient use of resources and, in many cases, the end of second shift staffing. SOMATOM's output enables you to shrink a 12 hour workday to 8 hours and save the reserve capacity for future growth.

SOMATOM productivity improves patient management.

With instant reconstruction, you can verify each scan without the customary wait. Bottlenecks are eliminated and so is batch reconstruction.

OURS…

Department,

You set your caseload and proceed. Images are ready and accessible while the patient is still on the table. Inconvenient retakes are eliminated, too, because you're not forced to scan "blind". And with exam results available sooner, there's no delay in getting the diagnosis to referring physicians.

SOMATOM productivity includes superior image quality.

It's a fact that the SOMATOM is the fastest reconstructing CT scanner, and that its speed costs you *nothing*. No compromising image quality and no costly add-on array processors. You have the best of both worlds – image quality *and* speed.

SOMATOM improves more than the bottom line.

SOMATOM quality and dependability are assured by the Siemens name. No quality has been sacrificed to offer you speed. No corners cut to offer you efficiency.

Contact your Siemens CT representative today. Get the facts that can improve your figures from the company that continues to invest in CT R&D.

Siemens Medical Systems, Inc.
186 Wood Ave. South, Iselin, N.J. 08830 (201) 321-4500

In Canada: Siemens Electric Ltd.
1180 Courtney Park Dr., Mississauga, Ont. L5T 1P1

Conventional wisdom: Fly United to Washington, D.C.

The American Roentgen Ray Society and United Airlines have joined to provide savings on air fares when you fly to Washington, D.C. for the 1986 Annual Meeting, April 14–18, 1986.

United offers you at least 40% off normal Coach fares with no minimum stay restrictions. Or, if you are staying over a Saturday night, a 45% discount can be obtained.

To take advantage of this offer, you or your Travel Agent should call United's toll-free number, 800-521-4041 between 8:00 a.m. and 8:00 p.m. E.S.T. 7 days a week. Just give the Society account number: **602K.**

United's Convention Specialists will provide all information on these fares and any special promotional fares that may be offered from your city. Seats are limited, so call early for the best selection.

You're not just flying, you're flying the friendly skies.

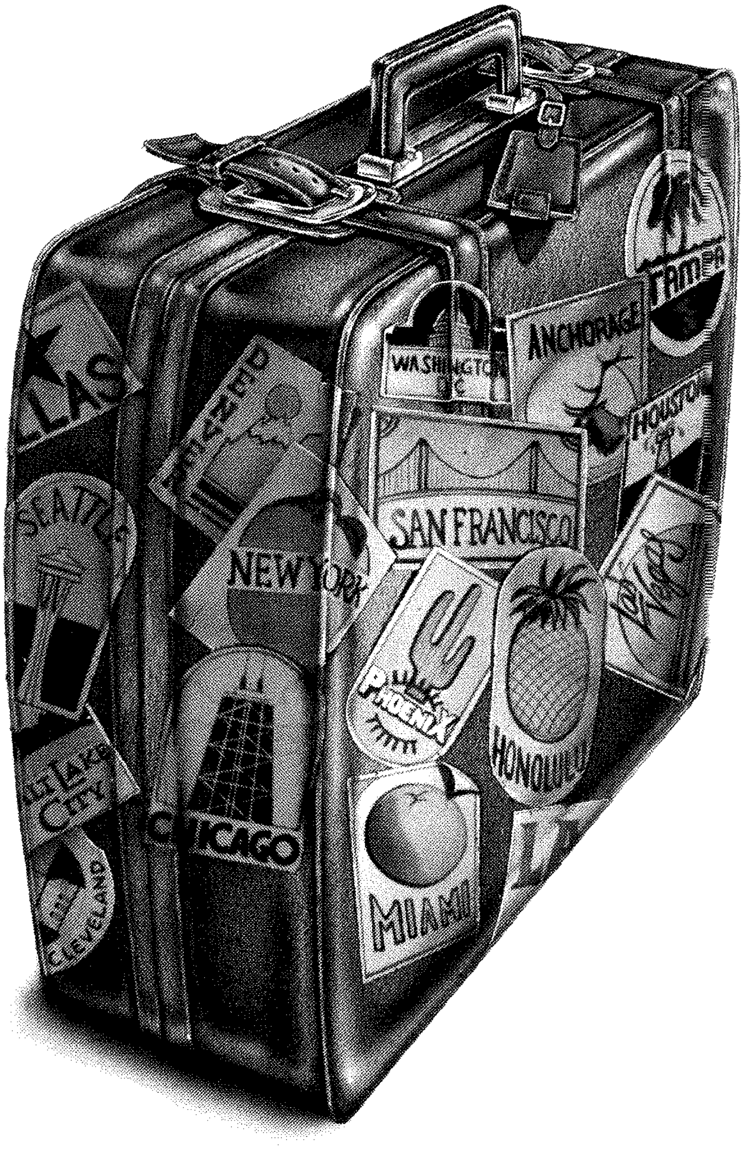

fly the friendly skies®

United

There are reasons

S.&S. X-RAY ACCESSORIES

are preferred...

PROVEN the best in X-Ray Departments throughout the world

UNEQUALLED in design, construction and—quality

REPUTATION unmatched for RELIABILITY and PERFORMANCE

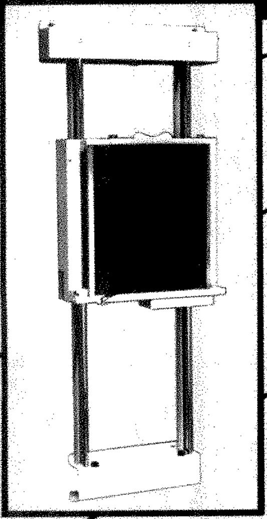

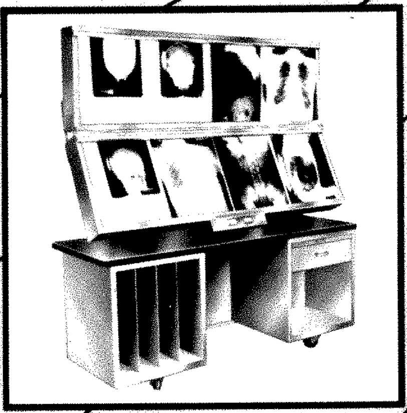

- Motorized Viewers
- Illuminators
- Transfer Cabinets
- File Cabinets
- Protective Panels
- Protective Aprons
- Wall Cassette Holders
- Dryers
- Safelights
- Dark Room Cabinets
- Storage Chests
- Loading Bins
- X-Ray Accessories

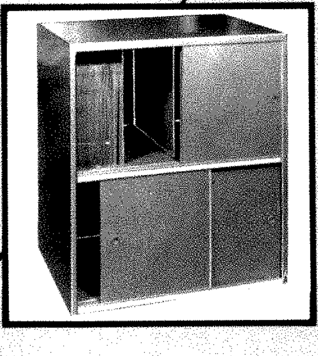

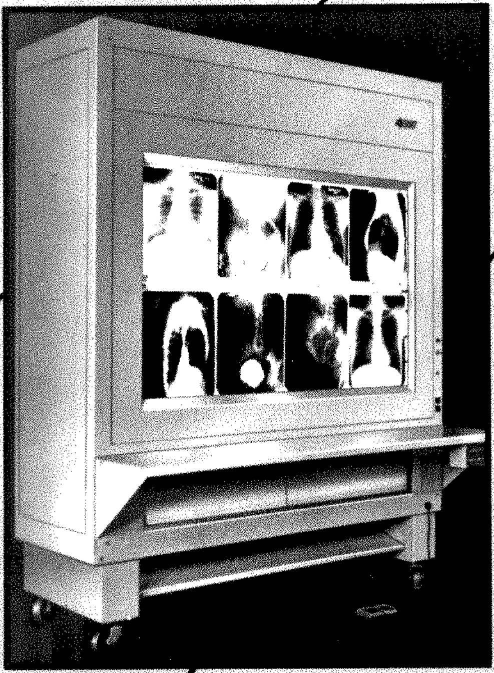

For more than 30 years, S. & S. has been meeting Radiologists' needs with a complete line of illuminators and accessories.

Contact S. & S. or your local x-ray dealer for additional information.

MANUFACTURED BY
S. & S. X-RAY PRODUCTS INC.
The Complete Line of
X-Ray Accessories
(800)221-6634
Telephone: (212) 852-6900
87-93 JAY STREET, BROOKLYN, N.Y. 11201

"See us at RSNA Booth #2323."

Control the future of your practice

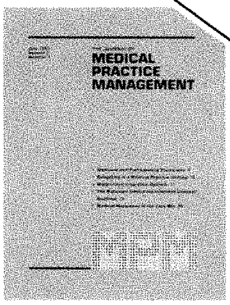

NEW!

The Journal of MEDICAL PRACTICE MANAGEMENT

Editor: **Marcel Frenkel, MD, MBA**

A new journal gives you the management skills you need to pull ahead

Right now you need information on some important topics that weren't covered in medical school. Topics that are having a profound impact on private practice and hospital-based physicians across the country.

Like competition from HMOs. Industrialization of medicine. The sheer number of physicians competing for your patients. Increasing costs.

You know the issues. What you need to know is the best way to face them so your practice will flourish in years to come.

And that's where **The Journal of Medical Practice Management** comes in.

Keep up with the issues that are changing your way of practice forever

The Journal of Medical Practice Management is a new quarterly publication that covers *your* concerns...issues affecting the way you practice now — and the way you'll practice in the future.

Four times a year, an expert editorial board headed by Dr. Marcel Frenkel brings you concise, readable coverage of today's issues and tomorrow's trends.

You'll find departments covering • office procedures and management • malpractice • marketing • manpower • computers • taxation • legal and legislative affairs • and health policy.

You'll also find pertinent features like the **Washington Report,** telling you what's up in the nation's capital and how it affects you...a **Letter from Abroad,** offering perspectives on how physicians are handling health care issues in other countries...and profiles of profit and not-for-profit health care delivery systems.

A multidisciplinary editorial board

Members of the editorial board for **The Journal of Medical Practice Management** have been carefully chosen for their knowledge of the management aspects of practicing medicine. These experts, many with experience in more than one field, give you the perspectives you need from medicine, law, management, government, and education.

You can control the future of your practice

The issues you can't afford to ignore are in **The Journal of Medical Practice Management.** It's a lot of information for a little money. And that's good business for you.

Reserve your charter subscription today!

Just return the attached coupon, or **call our FREE number,** 800-638-6423, from anywhere in the US except Alaska and Hawaii. In Maryland, call 528-4105 collect. **Quarterly**

Williams & Wilkins

428 East Preston Street
Baltimore, Maryland 21202

266 Fulham Road
London SW10 9EL England

YES, I want to control the future of my practice!

Please enter my subscription to **The Journal of Medical Practice Management** (quarterly)

☐ Individuals and Institutions $40

All subscribers: add $10 outside the U.S.

☐ Check enclosed ☐ Bill me
☐ MasterCard ☐ American Express ☐ VISA

Card # Exp. date

Signature

Name

Address

City/State/Zip

Maryland residents add 5% sales tax. Subscriptions outside the US must be prepaid. All subscriptions must be paid in US dollars. Rates valid through April 30, 1987.

Please allow 8 weeks for delivery of your first issue, up to 16 weeks for surface delivery outside the US. Airmail rates available on request.

Williams & Wilkins

P.O. Box 1496
Baltimore, Maryland 21203

266 Fulham Road
London SW10 9EL England

MPMAD 95048 86

PORTA RAY IS PROUD TO INTRODUCE

pixie II

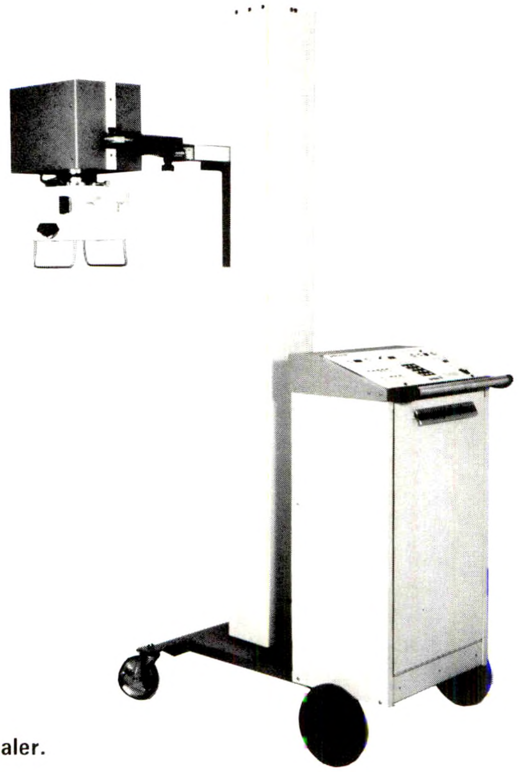

THE BEST OF PIXIE - PLUS

- MICROPROCESSOR CONTROLLED
- SOLID STATE - DIGITALLY PROGRAMMED
- AUTOMATIC EXPOSURE CONTROL - BUILT IN
  Any Size Cassette, Any Examination
- 50mA - 100kVp - 200mas
- AUTOMATIC LINE VOLTAGE REGULATOR
- NO BATTERIES TO CHARGE - AVAILABLE FOR USE 24 HRS. A DAY
- MANUFACTURED IN U.S.A.
- CERTIFIED TO BE IN COMPLIANCE WITH ALL GOVERNMENT REGULATIONS

For more information contact Porta Ray or your local X-Ray dealer.

porta ray inc. 19 Jefryn Blvd. West, Deer Park, N.Y. 11729 U.S.A. (516) 242-0022

Two step film control

Minimize X-ray exposure. Optimize image quality. Stabilize film processor performance, film speed and contrast. Quickly. Easily.

1. The Tobias Model RF Wejex Sensitometer

Produces a precise 11-step wedge exposure on *your* X-ray film. Exposure made just before processing eliminates latent image fade problem.* Features: Precise shutter exposure control. Variable lamp intensity. Provisions for 2″× 2″ ANSI blue, green or other filters, double sided exposures, 8″× 10″ and 35mm test film alignment. And more.

*Lawrence, D.J.: **A Simple Method of Processor Control,** Med. Rad. and Photog. 49, 2-6, 28, 1973 (Reprints available on request)

Wejex Universal Model RF
Also available:
Wejex Standard Model R

For a demonstration, call your Tobias dealer.
Or write for our brochure. Ask about our 30 day free trial.

2. The Tobias Model TBX Digital Densitometer

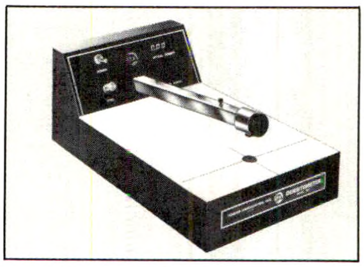

Measures optical transmission density of the Wejex-exposed step wedge over a density range of 0 to 4.50. Accuracy ±0.02. Repeatability ±0.01. State-of-the-art electronics. Lighted digital display. 5 second warm up. Easily portable. Virtually no zero drift.

TOBIAS ASSOCIATES, INC.
50 Industrial Drive, P.O. Box 2699, Ivyland, PA 18974, (215) 322-1500

☐ Send literature on the Wejex Sensitometer and TBX Densitometer.

☐ Please send me a copy of D.J. Lawrence's "A Simple Method of Processor Control."

☐ Tell me more about your 30 day free trial policy.

Name ____________
Title/Organization ____________
____
Address ____________
City ____________ State ____________
Zip ____________ Tel. ____________

The Art of Toshiba

Only Toshiba could brave new worlds.

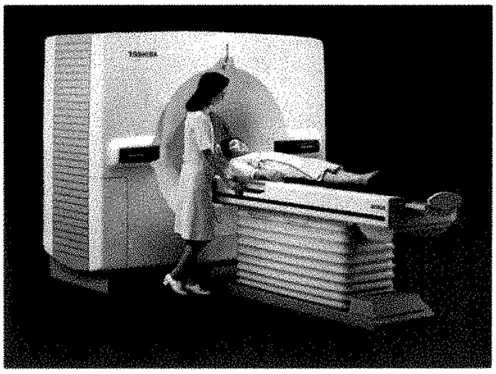

Toshiba challenges you to find sharper, clearer diagnostic imaging from a whole body scanner from any other company in the world.

You won't find it.

Because the new, fourth-generation TCT-900S Whole Body Scanner from Toshiba is diagnostic imaging at the zenith of technology. With spatial and low contrast resolution so unbelievably sharp and clear, you just might not believe what you see.

Believe it. And *explore a previously undetected anatomical world!* Over 2,000 detectors are built into the TCT-900S. The unique nutate/slip ring design provides absolutely incomparable spatial resolution and fantastically detailed low contrast resolution for *unbelievable* imaging. . . but true to life.

Incredibly, this superb diagnostic imaging is delivered in a one-second 360° continuous scan. *True dynamic scan. No interscan delay.*

In fact, no other system can touch the technology built into Toshiba's TCT-900S. With real time MPR in any plane. An ahead-of-our-time optical laser disk system. Diagnostic imaging capability that is, well, out of this world. This technology has catapulted Toshiba to the third largest diagnostic imaging company in the world. The *known* world, that is. We're still discovering new ones.

Call or write: Toshiba Medical Systems, 2441 Michelle Drive, Tustin, CA 92680. In California, call (714) 669-5443. Outside California, call toll-free (800) 421-1968.

In Touch with Tomorrow

TOSHIBA

GLOBAL IMAGING SPECIALISTS

Efficient bowel evacuants for diagnostic procedures

Take one
X-Prep®
for a cleaner, clearer film

Excellent visualization...fewer retakes

- 95% efficacy proven with X-PREP® Liquid in 749 patients prepared for diagnostic procedures such as barium enemas and IVPs*
- Effective for colonoscopy and sigmoidoscopy*

X-PREP® Liquid
2½ fl. oz. (74 ml) (standardized extract of senna fruit)

*Data on file, Medical Department, The Purdue Frederick Company.

Gray Pharmaceutical Co., Affiliate
The Purdue Frederick Company
Norwalk, CT 06856

X-PREP® Bowel Evacuant Kit-1
Contains two SENOKOT-S® Tablets (standardized senna concentrate and docusate sodium), one bottle of X-PREP Liquid 2½ fl. oz. (74 ml), one RECTOLAX® Suppository (bisacodyl 10 mg), plus easy-to-follow instructions.

X-PREP® Bowel Evacuant Kit-2
Contains one pack CITRALAX® Granules 1.06 oz. (effervescent citrate/sulfate of magnesia), one bottle of X-PREP Liquid 2½ fl. oz. (74 ml), one RECTOLAX Suppository, plus easy-to-follow instructions.

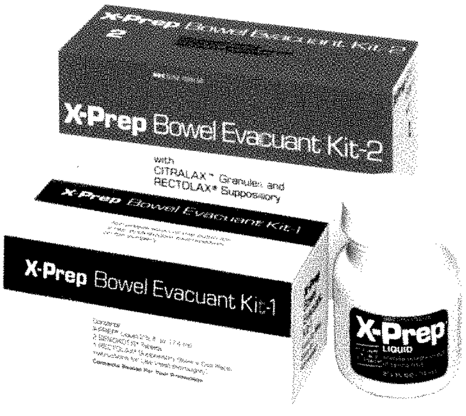
X-Prep Bowel Evacuant Kit-2
with CITRALAX™ Granules and RECTOLAX® Suppository
X-Prep Bowel Evacuant Kit-1
X-Prep LIQUID

© 1984, Gray Pharmaceutical Co. PFR-081/84

Multifocal Abnormalities of the Gastrointestinal Tract in AIDS

Susan D. Wall[1]
Steven Ominsky[1]
David F. Altman[2]
Carol L. Perkins[3]
Richard Sollitto[1]
Henry I. Goldberg[1]
Alexander R. Margulis[1]

On review of 63 barium sulfate examinations in 44 patients with acquired immunodeficiency syndrome (AIDS), 61% of the 23 single-contrast examinations and 98% of the 40 double-contrast examinations were abnormal. Abnormalities involved all areas of the gastrointestinal (GI) tract and covered a wide spectrum of findings including thickened folds, nodularity, increased secretions, superficial erosions, ulcerations, plaque formation, and tumor mass. Abnormalities, when present, were most commonly multifocal (three or more sites) on upper GI study (64%) and barium enema (69%). Thirty-eight patients (86%) had at least one abnormal study; 27 of these patients had multifocal disease in either the upper or lower tract separately or combined. The most common site of abnormality was the duodenum on upper GI study and the sigmoid colon on barium enema. In 27 cases the radiographic abnormalities could be specifically correlated with a malignancy or an opportunistic infection by endoscopy, colonoscopy, culture, biopsy, or autopsy. Multifocal disease of the upper and/or lower GI tract, especially when the duodenum is involved, should suggest AIDS even in patients not thought to be at high risk for the disease.

The gastrointestinal tract is a major target organ of the acquired immunodeficiency syndrome (AIDS) [1]. Kaposi sarcoma and opportunistic infection are the primary forms of involvement. The endoscopic appearance of the gastrointestinal (GI) lesions and the evolution of their clinical course have been described elsewhere [1–7]. However, only limited reports of the radiographic manifestations of the GI lesions are available [8–15]. We describe the frequency and spectrum of radiographic abnormalities of the GI tract in 44 patients with AIDS and report the radiographic findings in 27 patients in whom causative malignancy or infectious organism could be documented.

Materials and Methods

A cross listing of patients with AIDS reported to the San Francisco Public Health Department and of the radiology files of nine hospitals in the San Francisco Bay Area revealed 44 subjects with AIDS who had undergone barium examination of the GI tract. Sixty-three barium examinations of these 44 subjects with AIDS were reviewed retrospectively. The diagnosis of AIDS conformed to the criteria established by the Centers for Disease Control [16]. All subjects were homosexual men with a mean age of 37 years (range, 22–52) and were evaluated at our institution or one of the private hospitals in the San Francisco Bay Area. Fifteen subjects had multiple examinations. There were 42 barium examinations of the upper GI tract; all but two included a small-bowel follow-through. There were 19 barium enemas. One examination was limited to the small bowel and one was limited to the esophagus. Both double-contrast (40 examinations) and single-contrast (23 examinations) techniques were used. A consensus of the abnormal findings was determined by four faculty members in GI radiology. The findings were correlated with the results of endoscopy and colonoscopy, using the Olympus GIF-XQ fiberoptic panendoscope, the Olympus GIF-P2 fiberoptic panendoscope, the Olympus CF-ITS2 fiberoptic sigmoidoscope, and the Olympus CF1TL2 colonoscope, in addition to culture, biopsy, and autopsy when performed. The diagnosis of GI Kaposi sarcoma

Received July 8, 1985; accepted after revision September 30, 1985.

[1] Department of Radiology, University of California School of Medicine, San Francisco, CA 94143. Address reprint requests to S. D. Wall, Dept. of Radiology, Veterans Administration Medical Center (114), 4150 Clement St., San Francisco, CA 94121.

[2] Department of Medicine, University of California School of Medicine, San Francisco, CA 94143.

[3] University of California School of Medicine, San Francisco, CA 94143.

***AJR* 146:1–5, January 1986**
0361–803X/86/1461–0001
© American Roentgen Ray Society

was made by biopsy or by visual inspection on endoscopy/colonoscopy.

Results

The majority (84%) of the 63 examinations were abnormal, with the frequency varying according to the technique used and to the area studied. Abnormalities were noted more often on double-contrast (39/40, 98%) than on single-contrast examinations (14/23, 61%). The frequency of abnormal upper GI examinations (35/42, 83%) was about equal to that of barium enema examinations (16/19, 84%). The one esophagram and the one small-bowel examination were abnormal. Of the 44 patients studied, 38 (86%) had at least one abnormal examination.

The sites of abnormality are summarized in table 1. Twenty-eight patients had at least one abnormal upper GI study, with the duodenum being the most common site of radiographic abnormality (23/28, 82%). Sixteen patients had an abnormal barium enema, with the sigmoid colon being the most common site of radiographic abnormality (12/16, 75%). Abnormalities, when present, were most often multifocal (three or more sites) on both upper GI (18/28, 64%) and barium enema (11/16, 69%). Of the 38 patients with at least one abnormal barium study, 27 (71%) had multifocal disease in either the upper or lower tract separately or combined. The types of abnormality seen and the frequency of each are summarized in table 2. Thick folds, nodularity, aphthous lesions, and mucosal irregularity were the most commonly noted findings. The cause of the radiographic abnormalities, documented in 27 subjects, included malignancy, namely Kaposi sarcoma or a non-Hodgkin Burkitt-like lymphoma, or an opportunistic infection of the GI tract. Twelve subjects had documented GI Kaposi sarcoma (fig. 1). Their radiographic abnormalities, which correlated with endoscopic findings of Kaposi sarcoma, included nodularity, thickened folds, polypoid lesions, plaque formation, central umbilication, and mass effect. One subject had coexistent GI Kaposi sarcoma and lymphoma (fig. 2); the

TABLE 1: **Locations of Abnormalities in AIDS Patients with Abnormal Upper Gastrointestinal or Barium Enema Studies**

Study: Site	No. of Patients (%)
Upper gastrointestinal ($n = 28$):	
Duodenum	23 (82)
Jejunum	18 (64)
Esophagus	17 (61)
Stomach	16 (57)
Bulb	15 (54)
Ileum*	12/26 (46)
Multiple Sites (≥3)	18 (64)
Barium enema ($n = 16$):	
Sigmoid	12 (75)
Rectum	11 (69)
Right Colon	10 (63)
Left Colon	8 (50)
Multiple Sites (≥3)	11 (69)

* 12 (46%) of 26 patients because the ileum was not demonstrated in two subjects.

TABLE 2: **Types of Abnormalities Seen on Barium Examination of the Gastrointestinal Tract in AIDS Patients**

Type of Abnormality	No. of Patients (%)
Thick folds	33 (87)
Nodularity	25 (66)
Aphthous lesions	22 (58)
Mucosal irregularity	18 (47)
Ulceration	10 (26)
Mass	9 (24)
Increased secretions	9 (24)
Narrowing	8 (21)
Rigidity	6 (16)
Dilatation	5 (13)
Plaque	5 (13)
Umbilication	5 (13)
Sessile polyp	4 (11)
Lymphoid nodular hyperplasia	3 (8)

Note.—Data on 38 subjects with at least one abnormal study.

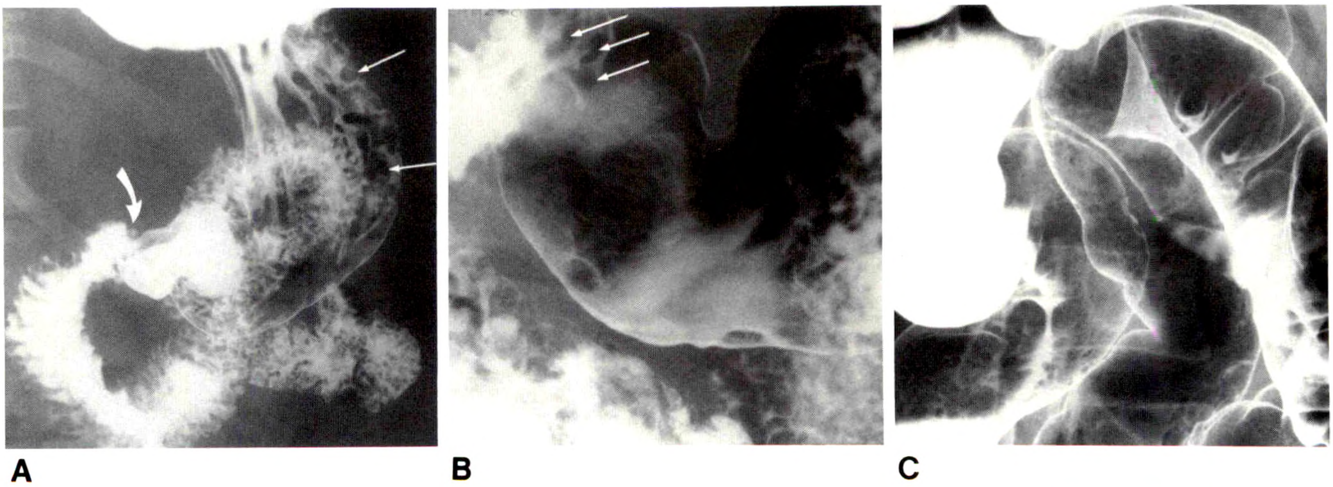

Fig. 1.—All multifocal abnormalities in this 30-year-old homosexual man with AIDS were caused by GI Kaposi sarcoma, which was documented by endoscopy and colonoscopy. **A**, Thickened nodular folds in body of stomach (*straight arrows*) and duodenal bulb (*curved arrow*), and narrowing of lumen of transverse duodenum. **B**, Nodules in gastric antrum and duodenal bulb (*arrows*). **C**, Double-contrast barium enema. Multiple plaques, some with central umbilication.

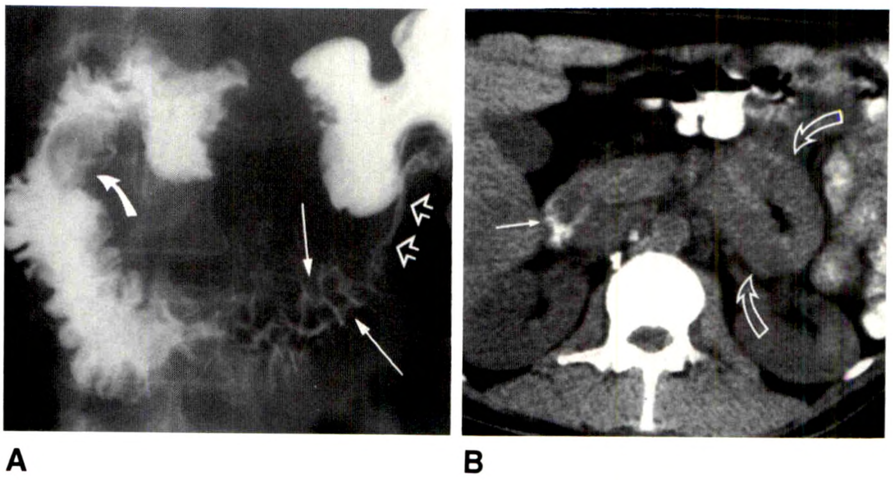

Fig. 2.—Coexistent malignancies demonstrated in duodenum. **A**, Nodular filling defect in descending duodenum (*curved arrow*) was endoscopically diagnosed as Kaposi sarcoma. Nodular tumor infiltration (*straight arrows*) and concentric mass (*open arrows*) narrowing distal transverse duodenum were both shown at surgical exploration and biopsy to be non-Hodgkin Burkitt-like lymphoma. **B**, CT findings of lesions seen on barium study. Small amount of oral contrast in descending duodenum (*straight arrow*) is displaced by mass of Kaposi sarcoma. Distal transverse duodenum (*curved arrows*) has thickened wall and narrowed lumen due to Burkitt-like lymphoma.

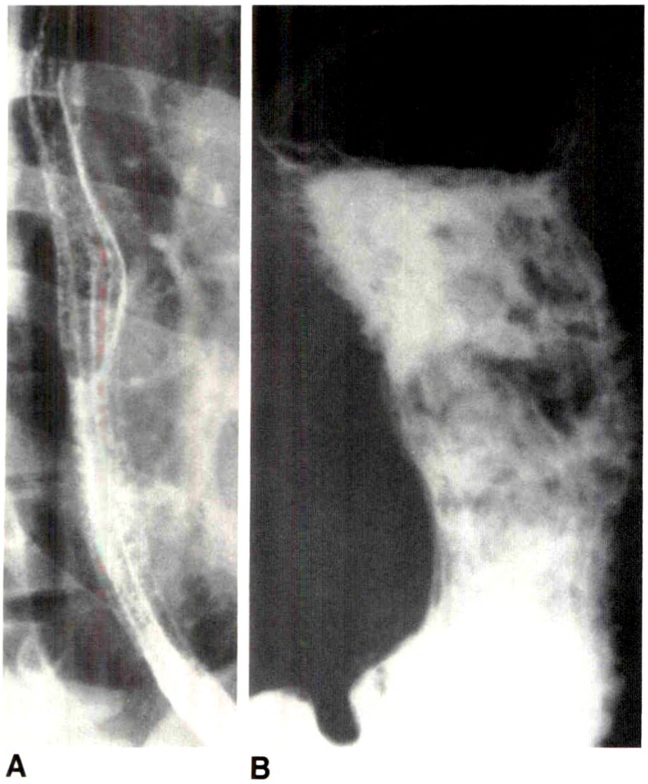

Fig. 3.—Chronic candidiasis caused several sites of abnormality in this 32-year-old homosexual man with AIDS. **A**, Diffuse nodularity throughout esophagus, with collections of barium in interstices of plaque formation. **B**, Gastric bezoar on upper GI study. Large *Candida* fungus ball was found at endoscopy.

latter was demonstrated radiographically by an infiltration of the transverse duodenum and by mass effect with associated narrowing of the lumen near the ligament of Treitz.

Candida albicans (fig. 3A) was the most frequently noted opportunistic organism to infect the GI tract among our group of subjects (15 cases). The radiographic findings of *Monilia* esophagitis ranged from mild mucosal irregularity of the proximal to mid esophagus to diffuse nodularity with extensive plaque formation and occasional deep ulceration. One patient with a long-standing infection had a gastric bezoar noted on upper GI study and a large *Candida* fungus ball on endoscopy (fig. 3B).

The radiographic manifestations of cryptosporidiosis (fig. 4A) in 10 of our patients were nonspecific and varied; they ranged from a diffuse, regular thickening of duodenal and small-bowel folds to a more irregular pattern. Increased secretions were often seen throughout the small bowel and occasionally in the large bowel. A pattern of diffuse colitis was seen in one of our patients (fig. 4B) when parasitic infestation had been documented for a period of more than 6 months.

Cytomegalovirus esophagitis was documented in one patient (fig. 5). Barium swallow demonstrated multiple vertical, linear plaques with occasional central umbilication. Three patients had cytomegalovirus colitis. One had a double-contrast barium enema that showed subtle superficial erosions in the descending colon among the radiographic and endoscopic findings of lymphoid nodular hyperplasia seen throughout the entire colon. The other two had more severe disease of pancolitis with diffuse deep ulcerations. In these two patients, hemorrhagic cytomegalovirus colitis was the cause of death.

Mycobacterium avium-intracellulare was cultured from two foci of esophageal ulceration in one patient (fig. 6) shortly before his death. *M. avium-intracellulare* was not detected elsewhere in this group of patients.

In the remaining subjects there were multiple infections (fig. 7) or the causal factors were not evident. Although all but two subjects with Kaposi sarcoma had coexistent opportunistic infection, only one subject (fig. 7) had infection in the same area as the malignancy.

Discussion

AIDS is characterized by a severe and irreversible acquired defect in cell-mediated immunity, which predisposes the patient to Kaposi sarcoma, *Pneumocystis carinii* pneumonia, or both, or other opportunistic infections [17]. The other oppor-

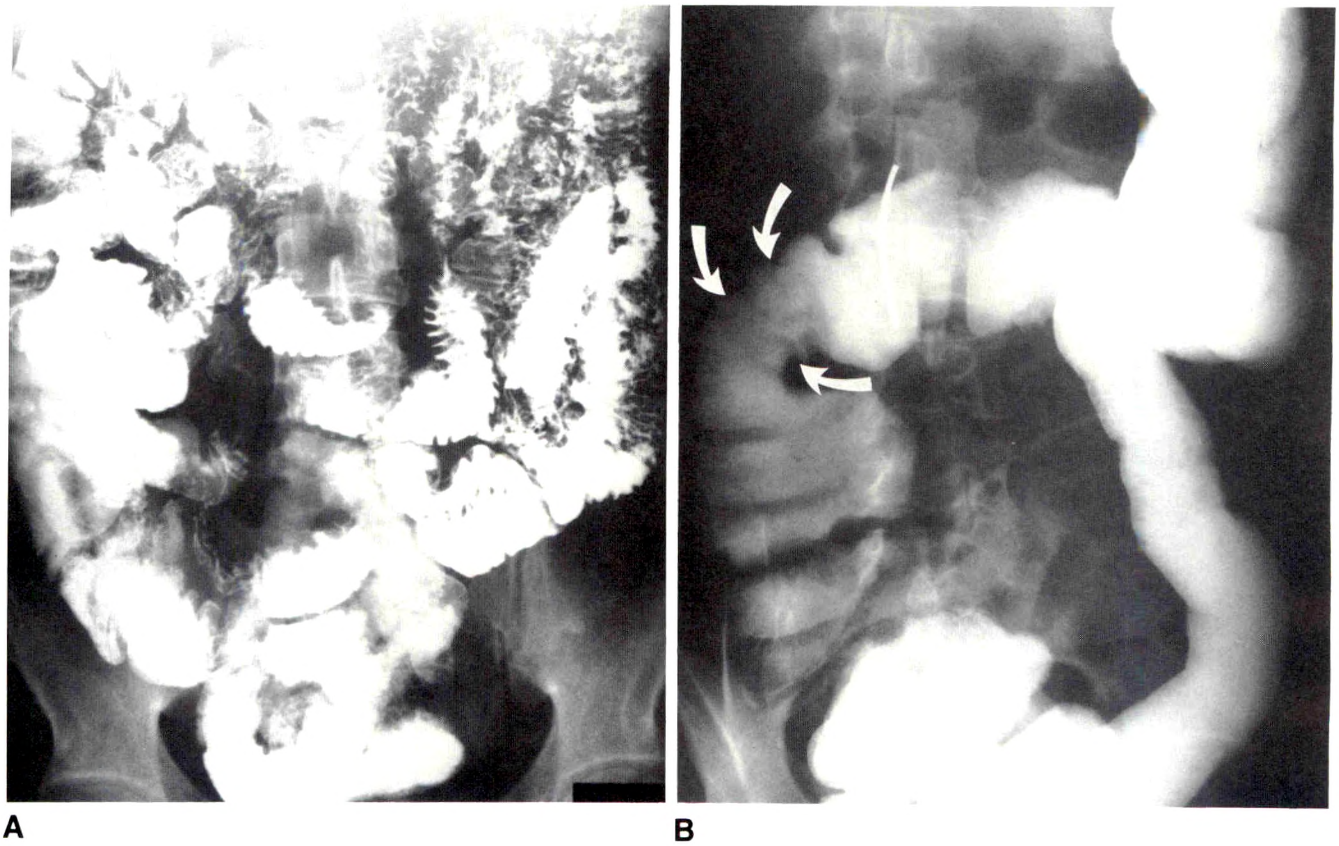

Fig. 4.—33-year-old homosexual man with AIDS who had persistent diarrhea; duodenal aspirate and colonoscopic biopsy both were positive for *Cryptosporidium*. **A**, Small-bowel examination. Thickened mucosal folds, fragmentation of barium column in jejunum, dilution of barium in ileum, and very rapid transit. **B**, Single-contrast barium enema, oblique view. Diffuse nodularity, narrowing and ulceration of hepatic flexure (*arrows*), and loss of haustrations in distal transverse and descending colon.

tunistic infections are caused by a variety of organisms including viruses, protozoa, fungi, and bacteria. The GI tract is the most common target organ for the other opportunistic infections and for Kaposi sarcoma when there is neoplastic involvement beyond the skin and lymph nodes [18].

The results of this study indicate that patients with AIDS who are referred for a radiographic examination of the GI tract have a high incidence and a wide spectrum of abnormal findings. The incidence of abnormality, while generally high, was greater on double-contrast technique than single-contrast studies. Thickening of folds, the single most frequently noted abnormality, was readily detected by both techniques. However, submucosal nodularity and subtle mucosal abnormalities such as ulceration, irregularity, nodularity and aphthous lesions were more frequently noted on double-contrast examinations. Therefore, we conclude that the double-contrast technique is the optimal method of barium examination of the GI tract of patients with AIDS and, when feasible, should be the method of choice.

The radiographic abnormalities noted in this study cover a wide spectrum and are nonspecific. Our results indicate that an abnormality is just as likely to be noted in the upper GI tract as in the colon. Most importantly, multifocal abnormalities will be seen in most patients. In our group of patients, multifocal abnormalities were caused by multiple foci of Kaposi sarcoma, widely distributed opportunistic infection, multiple opportunistic infections, coexistent tumor and infection, and in one case, coexistent Kaposi sarcoma and lymphoma. The high frequency of multiple sites of abnormal radiographic findings has not been reported previously and may be an important indicator of this syndrome when seen in patients at risk for AIDS. The differential diagnosis of abnormalities in multiple sites of the GI tract includes Crohn disease, lymphoma, and isolated infections. However, Crohn disease and lymphoma do not have a high incidence of duodenal involvement as was noted in our patients. Of our 28 patients who had an abnormal upper GI study, 23 (82%) had duodenal disease, most often caused by Kaposi sarcoma or cryptosporidiosis. Consequently, we conclude that when duodenal disease is seen along with disease in other sites of the GI tract, the possibility of AIDS should be considered even in patients not thought to be at high risk for AIDS. Moreover, in patients already diagnosed with AIDS, barium radiography of the GI tract can aid in the selection of patients who might need endoscopy/colonoscopy and can be directive in the selection of site(s) for biopsy.

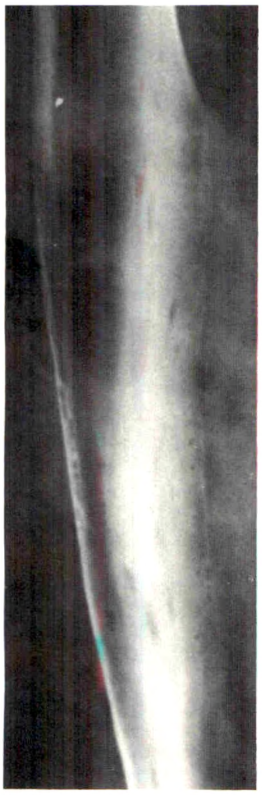

5

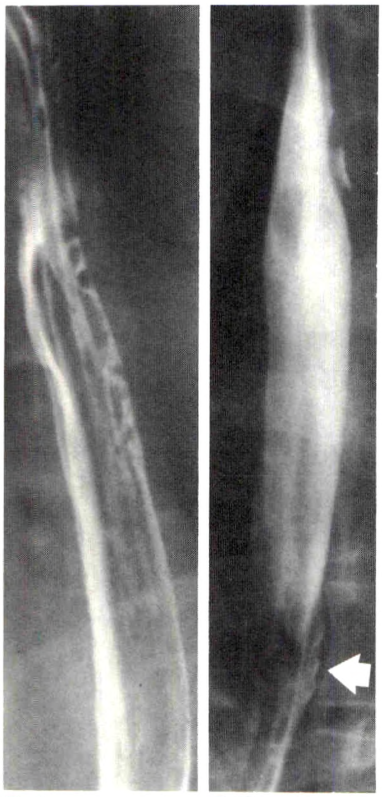

6 A 6 B

Fig. 5.—Multiple vertical, linear plaques with occasional central umbilication were seen throughout esophagus in this patient. Biopsy was culture positive for cytomegalovirus.

Fig. 6.—**A**, Nodularity and irregularity along posterolateral wall of upper-to-mid esophagus in this patient with AIDS. Endoscopy was biopsy positive for *Mycobacterium avium-intracellulare* (MAI). **B**, Study done 17 days later. Discrete ulcer at site corresponds with previous abnormality. In addition, more distal ulceration (*arrow*) was present. Repeat biopsy also was positive for MAI at both sites.

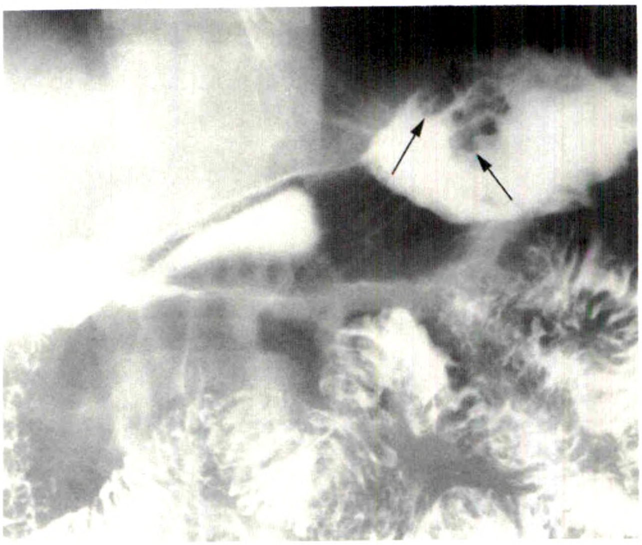

Fig. 7.—Multifocal abnormalities were due to multiple causes in 39-year-old homosexual man with AIDS. Nodular filling defects in gastric fundus (*arrows*) were shown by endoscopy to be Kaposi sarcoma. Cytomegalovirus and *Cryptosporidium* were both present in gastric antrum (nondistensible) and in small bowel (thick folds). (Reprinted from [11].)

REFERENCES

1. Gottlieb MS, Groopman JE, Weinstein WM, Fahey JL, Detels R. The acquired immunodeficiency syndrome. *Ann Intern Med* **1983**;99:208–220
2. Friedman-Kein AE, Laubenstein LJ, Rubinstein P, et al. Disseminated Kaposi's sarcoma in homosexual men. *Ann Intern Med* **1982**;96:693–700
3. Gottlieb GS, Ragaz A, Vogel JV, Friedman-Kien A. A preliminary communication on extensively disseminated Kaposi's sarcoma in young homosexual men. *Am J Dermatol Pathol* **1981**;3:111–114
4. Levine AS. The epidemic of acquired immune dysfunction in homosexual men and its sequelae—opportunistic infections, Kaposi's sarcoma, and other malignancies: an update and interpretation. *Cancer Treat Rep* **1982**;66:1191–1395
5. Port JH, Traube J, Winans CS. The visceral manifestations of Kaposi's sarcoma. *Gastrointest Endosc* **1982**;28:179–181
6. Weprin L, Zollinger R, Clausen K, Thomas FB. Kaposi's sarcoma: endoscopic observations of gastric and colon involvement. *J Clin Gastroenterol* **1982**;4:357–360
7. Friedman SL, Wright TL, Altman DF. Gastrointestinal Kaposi's sarcoma in patients with acquired immunodeficiency syndrome: endoscopic and autopsy findings. *Gastroenterology* **1985**;1:102–108
8. Rose HS, Balthazar EJ, Megibow AJ, Horowitz L, Laubenstein LJ. Alimentary tract involvement in Kaposi sarcoma: radiographic and endoscopic findings in 25 homosexual men. *AJR* **1982**;139:661–666
9. Berk RN, Wall SD, McArdle CB, et al. Cryptosporidiosis of the stomach and small intestine in patients with AIDS. *AJR* **1984**;143:549–554
10. Hill CA, Harle TS, Mansell PWA. The prodrome, Kaposi's sarcoma and infections associated with acquired immunodeficiency syndrome: radiologic findings in 39 patients. *Radiology* **1983**;149:393–399
11. Wall SD, Friedman SL, Margulis AR. Gastrointestinal Kaposi's sarcoma in AIDS: radiographic manifestations. *J Clin Gastroenterol* **1984**;6:165–171
12. Balthazar EJ, Megibow AJ, Hulnick DH. Cytomegalovirus esophagitis and gastritis in AIDS. *AJR* **1985**;144:1201–1204
13. Balthazar EJ, Megibow AJ, Fazzini E, Opulencia JF, Engel I. Cytomegalovirus colitis in AIDS: radiographic findings in 11 patients. *Radiology* **1985**;155:585–589
14. Wall SD. The acquired immune deficiency syndrome: gastrointestinal manifestations. In: Margulis AR, Gooding CA, eds. *Diagnostic radiology: 1984*. San Francisco: University of California, **1984**:191–196
15. Vincent ME, Robbins AH. *Mycobacterium avium-intracellulare* complex enteritis: pseudo-Whipple disease in AIDS. *AJR* **1985**;144:921–922
16. Centers for Disease Control. Update on acquired immune deficiency syndrome (AIDS)—United States. *MMWR* **1982**;31:507–508, 513–514
17. Jaffee HW, Keewhan C, Thomas PA, et al. National case control study of Kaposi's sarcoma and *Pneumocystis carinii* pneumonia in homosexual men: I. Epidemiological results. *Ann Intern Med* **1983**;99:145
18. Weinstein WM. The gastrointestinal tract as a target organ. In: Gottlieb MS, moderator. The acquired immunodeficiency syndrome. *Ann Intern Med* **1983**;99:210–212

AJR Editorial Office Address Change

In January 1986, Robert N. Berk, M.D., will assume the editorship of the *AJR* from Melvin M. Figley, M.D., who will retire. Thus, on Jan. 1, the *AJR* Editorial Office will open in La Jolla, CA. The *AJR* Editorial Office in Seattle will be staffed through Feb. 28.

Please note the addresses of the two offices and the effective dates for the transfer of various editorial operations.

La Jolla Office

AJR Editorial Office
2223 Avenida de la Playa (Suite 306)
La Jolla, CA 92037
(619) 459-2229

Seattle Office

AJR Editorial Office
909 N.E. 43rd Street (Suite 306)
Seattle, WA 98105
(206) 633-2754

Manuscripts and Correspondence

Effective Jan. 1, 1986, send all new and revised manuscripts to the La Jolla office.

Galley Proof

Galley proof for all articles through the March 1986 issue should be returned to the Seattle office. Galleys for the April 1986 and subsequent issues must be mailed to the La Jolla office.

News Items

The Seattle office will compile the news columns through the April 1986 issue of the *AJR*. Mail announcements to the Seattle office until Jan. 15 and to the La Jolla office thereafter.

Classified Advertisements

Send classified advertising copy to the Seattle office through Feb. 1.

	Date La Jolla Address Is Effective
New and revised manuscripts and letters	Jan. 1
Galley proof	Jan. 15
News items	Jan. 15
Classified advertising copy	Feb. 1

Review Abdominal CT in Acquired Immunodeficiency Syndrome

R. Brooke Jeffrey, Jr.[1]
David A. Nyberg[1, 2]
Kent Bottles[3]
Donald I. Abrams[4]
Michael P. Federle[1]
Susan D. Wall[1]
Vivian W. Wing[1]
Faye C. Laing[1]

Acquired immunodeficiency syndrome (AIDS) is a lethal infectious disease that has reached epidemic proportions in urban centers of the United States. Intraabdominal opportunistic infections and malignancies are common features of this syndrome. A prodromal phase or possibly milder form of infection is known as the AIDS-related complex. Abdominal computed tomography (CT) in patients with AIDS-related complex often demonstrates a triad of mild retroperitoneal and mesenteric adenopathy, splenomegaly, and perirectal inflammation. Lymph node enlargement greater than 1.5 cm is unusual in the AIDS-related complex and should prompt CT-guided biopsy. Abdominal adenopathy (>1.5 cm) in AIDS, in our experience, is most commonly related to non-Hodgkin lymphoma, Kaposi sarcoma, or infection with *Mycobacterium avium-intracellulare.* In most instances, CT-guided biopsy with appropriate staining technique can readily distinguish these entities. However, the subtyping of non-Hodgkin lymphoma by fine-needle aspiration biopsy alone remains controversial. Unusual features of abdominal malignancies are common in AIDS. These include a purely lymphadenopathic form of AIDS-related Kaposi sarcoma and a predilection for extranodal sites of lymphoma in AIDS. In general, patients with AIDS-related lymphoma present with advanced stages of disease with highly malignant histologic subtypes. Abdominal CT may be useful clinically for diagnosing intraabdominal complications of AIDS.

Acquired immunodeficiency syndrome (AIDS) is a disorder of cell-mediated immunity resulting in multiple opportunistic infections and certain characteristic malignancies [1–8]. The incidence of AIDS has reached epidemic proportions among patients in high-risk categories in urban centers in the United States. As of April 30, 1985, 10,000 patients in the U.S. were diagnosed as having AIDS, according to surveillance criteria established by the Centers for Disease Control (CDC) [9]. This represents a dramatic increase in the number of reported cases since the initial description of the syndrome in 1981. The dismal prognosis and high mortality associated with AIDS is underscored by the fact that nearly half of all diagnosed cases have already died [9].

The causative agent in AIDS is a retrovirus identified as human T-cell lymphotrophic virus type III (HTLV-III/LAV) [6–8]. It is estimated that at least 400,000 individuals in this country have antibodies to HTLV-III/LAV [6]. In patients without the fullblown syndrome of AIDS, a prodromal phase or possibly milder form of infection by the retrovirus has been designated the AIDS-related complex [10–12]. This entity is characterized by fever, night sweats, generalized lymphadenopathy, malaise, weight loss, diarrhea, and evidence of immune dysfunction. The CDC-established criteria for diagnosis of AIDS are the development of Kaposi sarcoma, multiple opportunistic infections, and/or primary central nervous system lymphoma in patients at high risk for AIDS. These patients include homosexual men, intravenous drug abusers, and recipients of blood products [13, 14].

The intraabdominal manifestations of AIDS are numerous, involving parenchymal, lymph node, and primary gastrointestinal disorders. In patients with suspected gastrointestinal lesions, double-contrast barium studies remain the primary method

Received July 8, 1985; accepted after revision August 28, 1985.

[1] Department of Radiology, University of California School of Medicine, San Francisco General Hospital, 1001 Potrero Ave., San Francisco, CA 94110. Address reprint requests to R. B. Jeffrey, Jr.

[2] Present address: Department of Radiology, University of Washington School of Medicine, Seattle, WA 98195.

[3] Department of Pathology, University of California School of Medicine, San Francisco, CA 94143.

[4] Department of Medicine, University of California School of Medicine, San Francisco, CA 94143.

AJR **146:7–13, January 1986**
0361–803X/86/1461–0007
© American Roentgen Ray Society

for radiologic diagnosis of mucosal abnormalities. However, CT is often helpful in assessing both visceral and nodal abnormalities of AIDS and the AIDS-related complex. Because of the frequent overlap and nonspecificity of findings, CT-guided fine-needle aspiration biopsy (FNAB) is often essential for precise diagnosis. Over the past 4 years, we have performed abdominal CT in over 200 patients with AIDS and AIDS-related complex. This review familiarizes radiologists with the broad CT spectrum of abdominal lesions in AIDS and the AIDS-related complex and emphasizes both the usefulness and limitations of CT-guided FNAB.

Abdominal CT in the AIDS-Related Complex

Patients with the AIDS-related complex exhibit a variety of constitutional symptoms including fever, weight loss, diarrhea, malaise, and night sweats [12–15]. Chronic generalized lymphadenopathy, often noted in the AIDS-related complex, is secondary to reactive lymphoid hyperplasia. This entity is often referred to as the lymphadenopathy syndrome [12, 15]. In general, the diagnostic criteria for the lymphadenopathy syndrome include chronic lymphadenopathy of at least 3 months' duration involving two or more extrainguinal sites. There is no concurrent illness or drug use that may cause lymphadenopathy, and lymph node biopsies demonstrate reactive hyperplasia without evidence of tumor [16].

Initial reports of abdominal CT in patients with the lymphadenopathy syndrome have emphasized a characteristic triad of (1) mild lymphadenopathy (clusters of reactive lymph nodes ranging from 5 mm to 1 cm) involving the retroperitoneal, mesenteric, or pelvic lymph node chains; (2) splenomegaly; and (3) abnormal soft-tissue infiltration of the rectal wall or perirectal fat [17]. The perirectal disease commonly seen in these patients, often asymptomatic, is presumably the result of chronic proctitis from repeated venereal infections (fig. 1). It should be emphasized that abdominal nodal enlargement greater than 1.5 cm, however, is unusual in the lymphadenopathy syndrome and should prompt CT-guided biopsy to exclude neoplastic or infectious nodal disease.

CT of Abdominal Neoplasms in AIDS

The most common abdominal neoplasms associated with AIDS are Kaposi sarcoma and non-Hodgkin lymphoma. Kaposi sarcoma has been recognized for several years as one of the primary manifestations of AIDS. Of the first 1000 patients diagnosed with AIDS in the U.S., 37% had Kaposi sarcoma [4]. Kaposi sarcoma was originally described in 1872 as a rare cutaneous disorder characterized by multiple violaceous macules that may coalesce into nodular lesions [18]. In its classic form, Kaposi sarcoma was described as an indolent cutaneous disorder of elderly European men, with visceral involvement seen only late in its clinical course. Prior to its association with AIDS, a second form of Kaposi sarcoma was recently recognized among African adolescents [19]. This form of the disease is an aggressive systemic disorder that is characterized by a high degree of early lymphatic and visceral involvement and is associated with a poor prognosis.

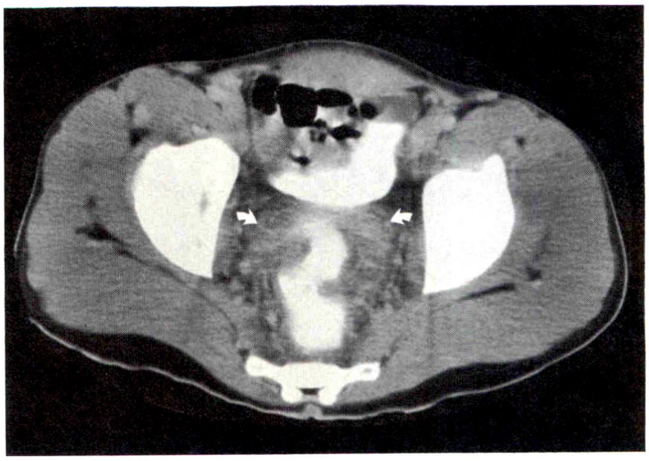

Fig. 1.—Perirectal inflammation in AIDS-related complex. Diffuse soft-tissue infiltration of perirectal space (*arrows*).

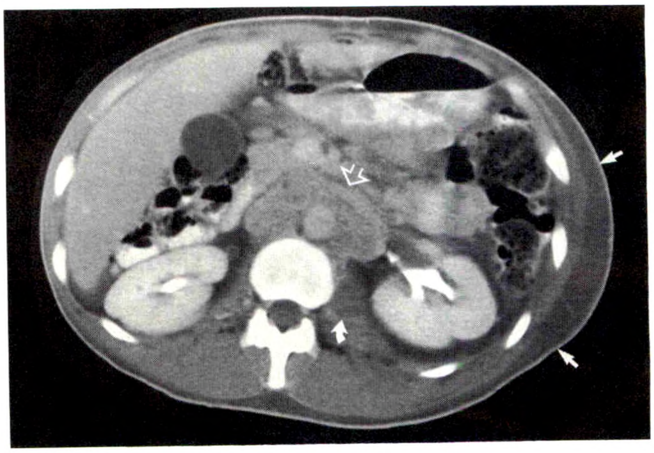

Fig. 2.—Widespread abdominal involvement in AIDS-related Kaposi sarcoma. Paraaortic nodal disease (*open arrow*) and diffuse infiltration of left abdominal wall (*straight arrows*) and left psoas muscle (*curved arrow*). Psoas lesion was confirmed by fine-needle aspiration biopsy.

AIDS-related Kaposi sarcoma is similar in clinical presentation to the aggressive and disseminated form seen in African adolescents. Early lymph node and visceral involvement are the predominant features. Gastrointestinal lesions are quite common, occurring in 50% of patients with AIDS-related Kaposi sarcoma [20]. Late in the course of the disease, widespread lesions may be found involving virtually all organ systems and occasionally unusual sites of involvement (fig. 2).

The radiologic diagnosis of gastrointestinal lesions in Kaposi sarcoma has been described [20]. Initial reports of CT findings in AIDS-related Kaposi sarcoma emphasized the overlap between this entity and the lymphadenopathy syndrome [17]. Splenomegaly and mild retroperitoneal and mesenteric nodal enlargement are common to both, and do not necessarily indicate widespread involvement with Kaposi sarcoma. This is particularly true when the lymph nodes are less than 1.5 cm in greatest diameter. However, bulky nodal

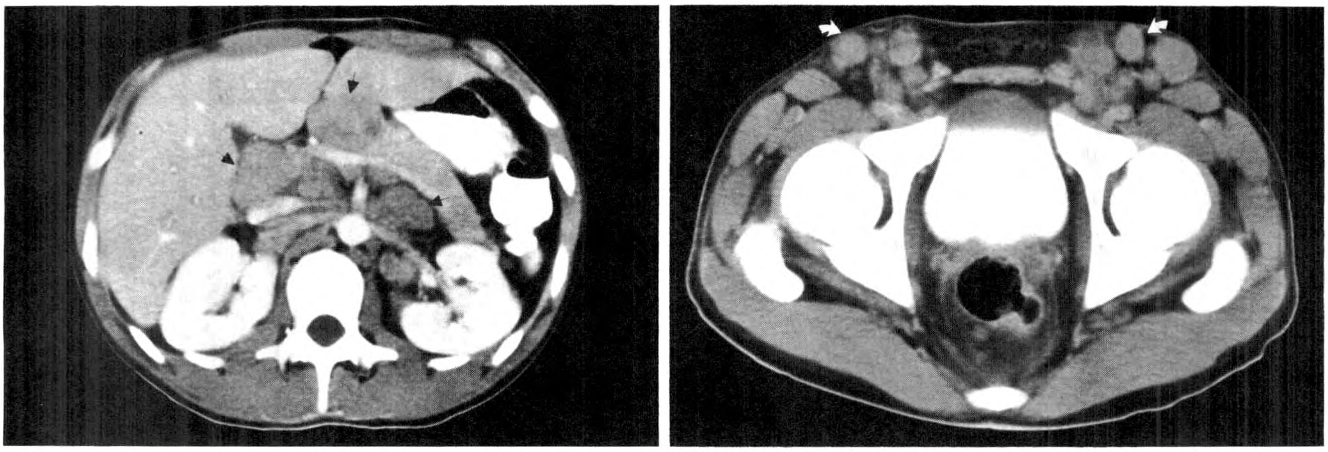

Fig. 3.—Lymphadenopathic form of AIDS-related Kaposi sarcoma. **A**, Bulky peripancreatic, periportal, and retroperitoneal adenopathy (*arrows*). **B**, Extensive inguinal adenopathy proven to be Kaposi sarcoma by fine-needle aspiration biopsy (*arrows*).

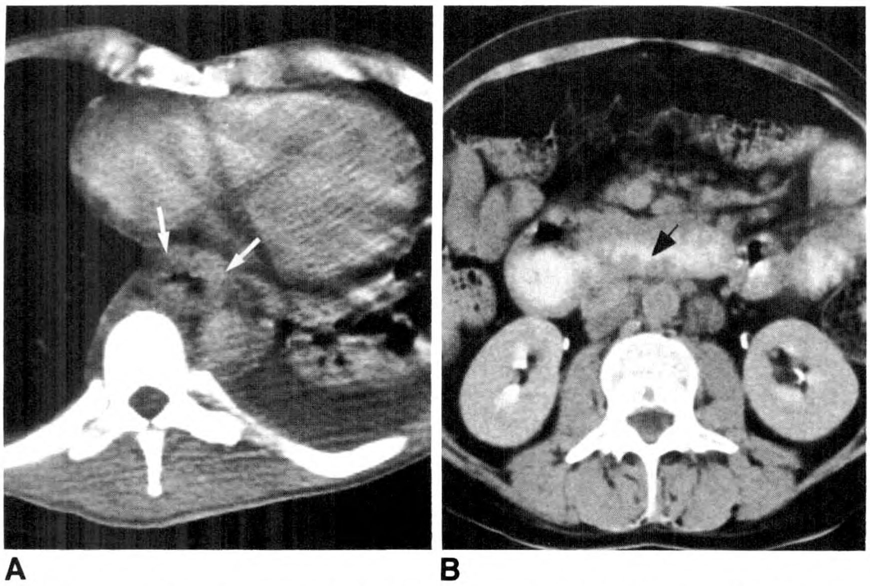

Fig. 4.—Gastrointestinal lesions in AIDS-related Kaposi sarcoma. **A**, Diffuse mural involvement of esophagus (*arrows*). **B**, Nodular infiltration of transverse duodenum (*arrow*).

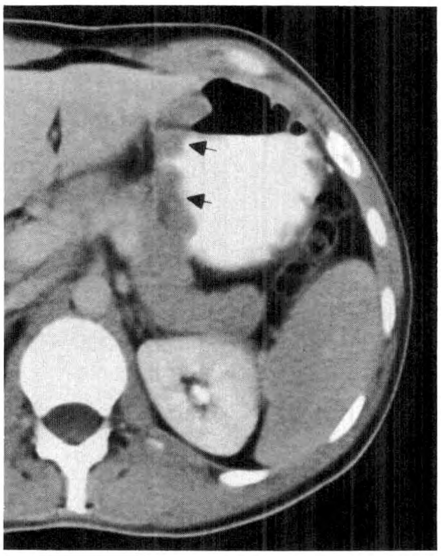

Fig. 5.—Extranodal site of involvement in AIDS-related non-Hodgkin lymphoma. Focal gastric mass along lesser curve (*arrows*).

enlargement may be the only CT evidence of abdominal Kaposi sarcoma. Indeed a purely lymphadenopathic form of AIDS-related Kaposi sarcoma is being recognized with increasing frequency [21, 22] (fig. 3). This is an interesting clinical correlate to the growing histochemical evidence of the origin of Kaposi sarcoma from lymphatic endothelial cells [23]. Without FNAB, it is not possible to distinguish bulky adenopathy in AIDS-related Kaposi sarcoma from lymphoma or infections such as *Mycobacterium avium-intracellulare.*

Although the characteristic "target" Kaposi sarcoma lesions seen on air-contrast studies of the gastrointestinal tract are rarely seen on CT, larger focal masses may be identified by mural thickening (fig. 4). The CT demonstration of focal hepatic or splenic lesions of Kaposi sarcoma in AIDS is uncommon. As with retroperitoneal adenopathy, this sarcoma has a nonspecific CT appearance and cannot be distinguished from other neoplastic or infectious causes without FNAB. In our experience, FNAB has proven quite reliable in diagnosing AIDS-related Kaposi sarcoma [24]. Cohesive clusters of bland spindle cells are arranged in characteristic slitlike spaces [24]. Because Kaposi sarcoma can involve virtually any organ in the body, it may produce unusual intraabdominal lesions

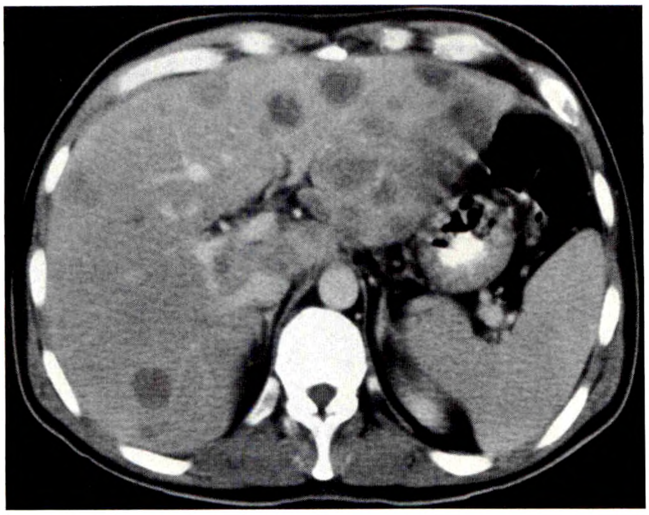

Fig. 6.—Extensive hepatic lesions in non-Hodgkin lymphoma.

that can readily be detected and biopsied under CT guidance.

In addition to Kaposi sarcoma, a variety of aggressive B-cell lymphomas (without primary central nervous system involvement) have been associated with AIDS [25–28]. To date non-Hodgkin lymphoma, including Burkitt type, has been the most common lymphoma in patients with AIDS [27]. However, Hodgkin disease has also been described [25, 26, 28]. In some patients, lymphoma may occur before the onset of fullblown AIDS [27]. In evaluating non-Hodgkin lymphoma in 90 homosexual men, Ziegler et al. [27] emphasized several unique manifestations within this subgroup of patients. There is a dramatic increase in extranodal involvement in AIDS-related lymphoma, including brain, bone marrow, abdominal visceral, and mucocutaneous sites (fig. 5). Of 90 patients reported by Ziegler et al. [27], 88 had extranodal sites of involvement. In addition, patients with AIDS-related lymphoma typically present with highly malignant histologic subtypes of non-Hodgkin lymphoma and advanced stages of disease. In the series of Ziegler et al., 58% of patients presented with stage III or greater lymphoma, and 62% had high-grade malignant histologic cell types. When compared to patients with non-Hodgkin lymphoma without AIDS, the response to treatment has been quite poor with generally an unfavorable prognosis.

As noted, a significant percentage of patients with AIDS-related lymphoma demonstrate focal hepatic and splenic lesions (fig. 6). In our series of 29 AIDS-related lymphomas, 26% of patients with non-Hodgkin lymphoma had biopsy-proven focal hepatic lesions (Nyberg et al., personal communication) compared to an incidence of 4%–6% in non-AIDS patients [29–31]. In patients with relatively diffuse hepatic involvement with lymphoma, smaller microscopic foci (<1 cm) may occasionally be difficult to appreciate on contrast-enhanced CT. We have noted on several occasions that sonography may be useful in depicting disorganized hepatic echogenicity with small hypoechoic foci in patients with hepatomegaly and no obvious focal lesions on CT (fig. 7). The overall sensitivity for CT and sonography in diagnosing hepatic involvement with AIDS-related lymphoma is not known, but it is likely that many cases of microscopic disease will escape detection by current imaging.

The use of FNAB for accurate diagnosis and subtyping of non-Hodgkin lymphoma is controversial. Some authorities emphasize the need for surgical biopsy in all suspected cases of lymphoma. Orell and Skinner [32], on the other hand, noted that FNAB is often quite accurate for tissue subtyping and has correctly established the histologic subtype in 48 of 49 patients with non-Hodgkin lymphoma. Reliance on FNAB for histologic subtyping of lymphoma requires considerable cytologic skill. Often this subtyping is crucial for chemotherapy; therefore, if there is any question regarding the histologic subtype, surgical biopsy is recommended.

AIDS-related Hodgkin disease appears to be significantly less common than non-Hodgkin lymphoma. However, there are distinctive features of this disease in the AIDS population. Patients typically present with advanced stages of Hodgkin disease (clinical stage III or IV) with mixed cellularity or nodular sclerosing histology [28]. In addition, unusual manifestations of Hodgkin disease include involvement of the skin overlying involved lymph nodes [28] and bone marrow involvement without splenic lesions [28]. In our series of 10 patients with AIDS-related Hodgkin disease studied at San Francisco General Hospital, two patients (20%) had bulky mesenteric nodal masses with Hodgkin disease, an uncommon feature in the non-AIDS population [33]. In addition, noncontiguous sites of nodal involvement were identified with pelvic adenopathy without paraaortic involvement.

CT of Abdominal Opportunistic Infections in AIDS

Enteric infections are quite common in the AIDS population, and contribute significantly to its morbidity and mortality [33]. Often they result in a wasting syndrome of chronic diarrhea and marked weight loss. Infections include fungal, viral, and protozoan infestations. Typical gastrointestinal infections in AIDS are esophagitis from *Candida* and small-bowel or colonic infections with *Cryptosporidium*, cytomegalovirus, herpes simplex, or *M. avium-intracellulare.* In general, stool culture, small-bowel aspirates and biopsy, endoscopy, and air-contrast barium studies are the primary methods of diagnosis. The CT findings often demonstrate nonspecific inflammatory changes of the small bowel and colon with focal mural thickening, mucosal irregularity, and thickened small-bowel folds [34] (figs. 8 and 9). On rare occasions we have noted associated viral peritonitis on CT characterized by ascites, thickening of the parietal peritoneal surface, and infiltration of the omentum (fig. 9). This underscores the importances of obtaining routine viral cultures from aspiration specimens.

Disseminated *M. avium-intracellulare* is a systemic infection of increasing importance in the AIDS population. *M. avium-intracellulare* are atypical mycobacteria that are ubiquitous within the environment and are rarely pathogens in immunocompetent individuals. Culturing is necessary to distinguish *M. avium-intracellulare* from *M. tuberculosis*. On intraabdom-

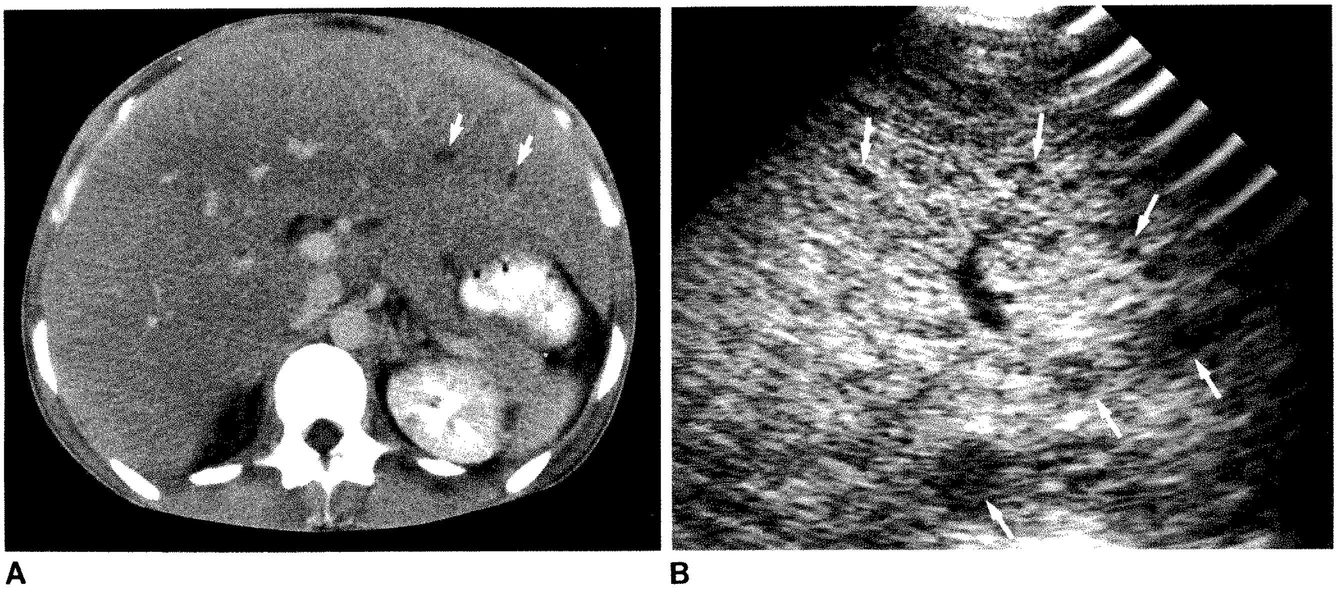

Fig. 7.—Small hepatic lesions in non-Hodgkin lymphoma. **A**, Marked hepatomegaly but only two focal abnormalities on contrast-enhanced CT (*arrows*). **B**, Hepatic sonogram. Diffuse distortion of echogenicity and numerous focal lesions (*arrows*).

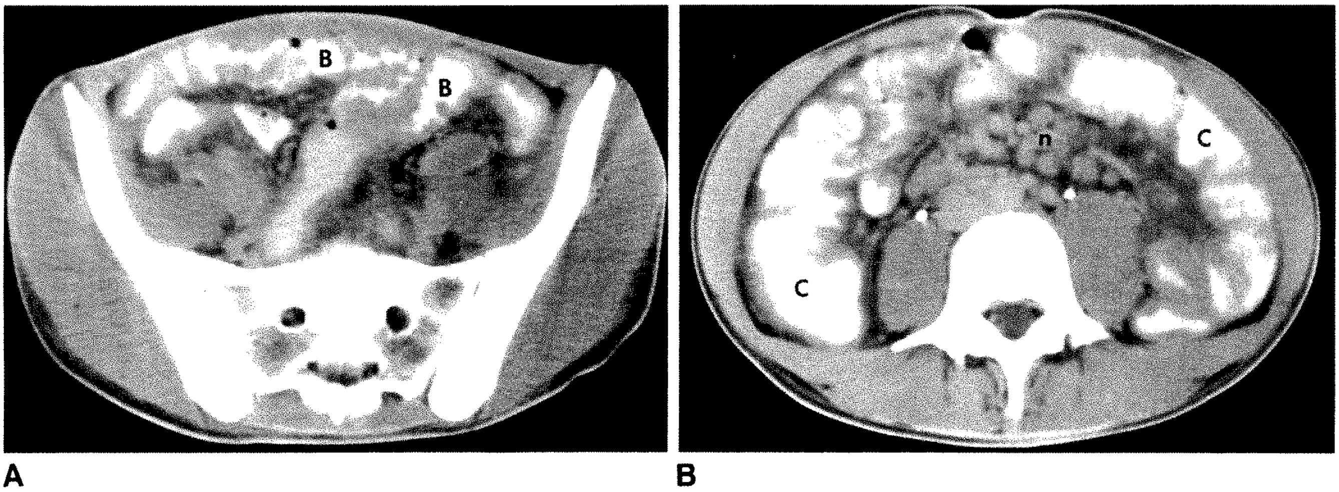

Fig. 8.—Cytomegalovirus enteritis and colitis. **A**, Diffuse small-bowel (B) wall thickening and mucosal irregularity. **B**, Mesenteric adenopathy (n) and pancolitis with focal narrowing of lumen and mural thickening of the colon (C).

inal CT, *M. avium-intracellulare* has a high predilection for retroperitoneal and mesenteric nodal involvement, producing bulky nodal masses that are often indistinguishable from AIDS-related Kaposi sarcoma or lymphoma (fig. 10). In our series of 17 patients with proven abdominal *M. avium-intracellulare*, 14 (82%) had mesenteric or retroperitoneal adenopathy greater than 1.0–1.5 cm on CT [36]. Focal hepatic and splenic lesions were identified by CT or sonography in two patients (fig. 11). We recently encountered a patient with diffuse hepatic *M. avium-intracellulare* on liver biopsy without focal defects on CT. Therefore, AIDS patients with persistent abnormal liver functions and fever may require core liver biopsy to exclude *M. avium-intracellulare*, despite an unremarkable CT scan.

On CT, low-density areas of necrosis may occasionally be identified within abdominal lymph nodes involved with *M. avium-intracellulare* (fig. 12). FNAB in *M. avium-intracellulare* can readily detect macrophages laden with acid-fast bacilli, and thus acid-fast stains should be routinely performed in all FNAB specimens in AIDS. Unfortunately, at present there is no effective medical therapy for *M. avium-intracellulare*.

Rectal and perirectal inflammatory disease are common both in patients with the AIDS-related complex and in those with AIDS. Proctitis is often secondary to venereal infections from gonococci, syphilis, cytomegalovirus, herpes simplex, or lymphogranuloma venereum. In some instances it may be difficult to distinguish rectal Kaposi sarcoma or lymphoma from severe proctitis. CT seems to be of considerable value in distinguishing perirectal cellulitis from abscesses and localizing complex abscesses before surgical drainage (Guillaumin E, unpublished data).

Indications for Abdominal CT in AIDS

Indications for abdominal CT in AIDS include evaluation for suspected visceral or nodal infection with *M. avium-intracellulare*, abdominal or pelvic abscesses, and diagnosis and staging of abdominal neoplasms such as Kaposi sarcoma and lymphoma. In patients with localized symptoms such as right-upper-quadrant pain, sonography is often a useful initial screening method. On occasion, sonography may reveal subtle hepatic lesions difficult to image by CT. Because of the frequency of mesenteric retroperitoneal nodal disease in AIDS, CT remains the primary method for evaluation in most patients. Although chemotherapy for AIDS-related neoplasms is often limited in its effectiveness, repeat abdominal CT is often useful to assess the course of therapy.

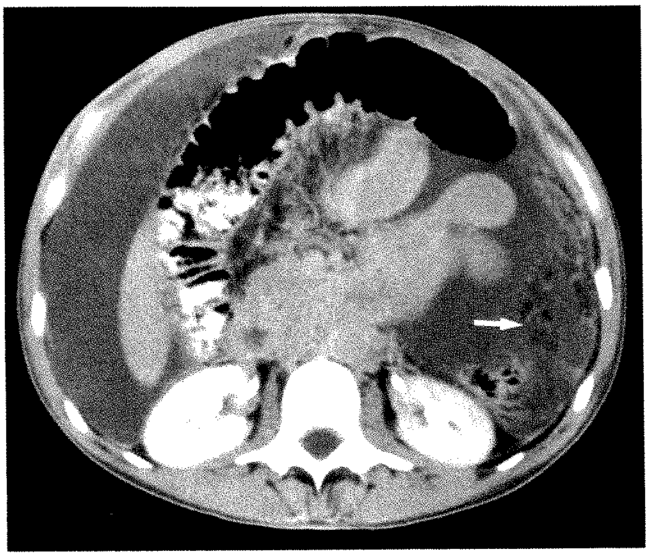

Fig. 9.—Cytomegalovirus peritonitis with marked ascites. Inflammatory infiltration of omentum (*arrow*).

REFERENCES

1. Gottlieb MS, Schroff R, Schanker H, et al. *Pneumocystitis carinii* pneumonia and mucosal candidiasis in previously healthy homosexual men: evidence of a new acquired cellular immunodeficiency. *N Engl J Med* **1981**;305:1425–1431
2. Centers for Disease Control. Kaposi's sarcoma and *pneumocystis* pneumonia among homosexual men—New York City and California. *MMWR* **1981**;30:305–308
3. Masur H, Michelis MA, Greene JB, et al. An outbreak of community-acquired *Pneumocystis carinii* pneumonia: initial manifestation of cellular immune dysfunction. *N Engl J Med* **1981**;305:1431–1438
4. Jaffe HW, Bregman DJ, Selik RM. Acquired immune deficiency syndrome in the United States: the first 1000 cases. *J Infect Dis* **1982**;148:339–345
5. Landesman SH, Ginzburg HM, Weiss SH. Special report: the AIDS epidemic. *N Engl J Med* **1985**;312:521–524
6. Barre-Sinoussi F, Chermann JC, Rey F, et al. Isolation of a T lymphotropic retrovirus from a patient at risk for acquired immune deficiency syndrome (AIDS). *Science* **1983**;220:868–871
7. Gallo RC, Salahuddin SZ, Popovic M, et al. Frequent detection and isolation of cytopathic retroviruses (HTLV-III) from patients with AIDS and pre-AIDS. *Science* **1984**;224:500–503
8. Laurence J, Brun-Vezinet F, Schutzer S, et al. Lymphadenopa-

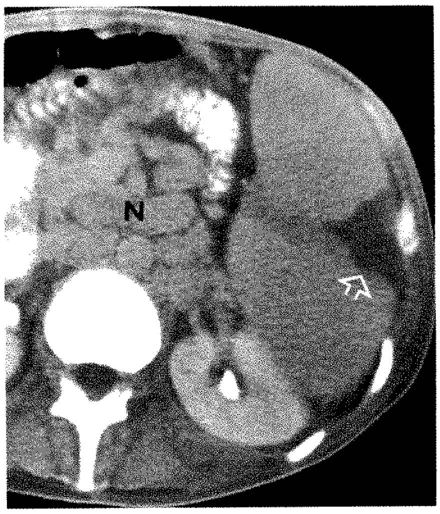

10

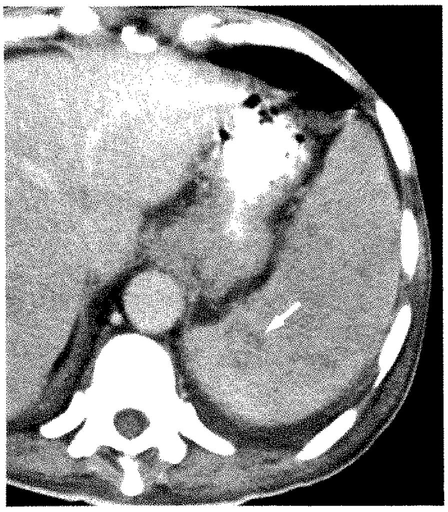

11

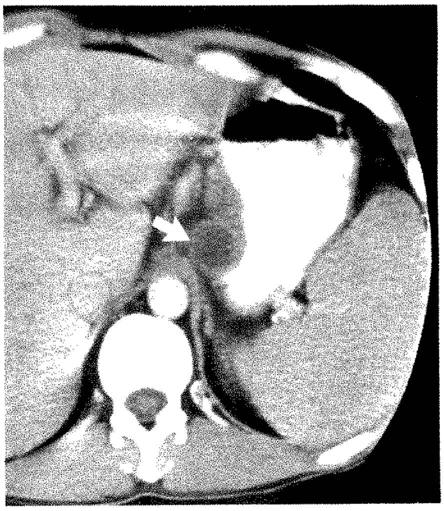

12

Fig. 10.—*Mycobacterium avium-intracellulare* infection producing bulky retroperitoneal adenopathy (N). Large wedgeshaped splenic infarct (*arrow*).

Fig. 11.—Focal splenic lesion (*arrow*) in *Mycobacterium avium-intracellulare*.

Fig. 12.—Necrotic lymph node from *Mycobacterium avium-intracellulare* along gastrohepatic ligament (*arrow*).

thy-associated viral antbody in AIDS. *N Engl J Med* **1984**;311:1269-1273

9. Centers for Disease Control. Update: acquired immunodeficiency syndrome—United States. *MMWR* **1985**;34:245-248
10. Seligmann M, Chess L, Fahey JL, et al. AIDS—an immunologic evaluation. *N Engl J Med* **1984**;1286-1292
11. Landesman SH, Ginzburg HM, Weiss SH. Special report: the AIDS epidemic. *N Engl J Med* **1985**;312:521-524
12. Abrams DI, Lewis BJ, Beckstead JH, Casavant CA, Drew WL. Persistent diffuse lymphadenopathy in homosexual men: endpoint or prodrome? *Ann Intern Med* **1984**;100:801-808
13. Centers for Disease Control. Update: acquired immunodeficiency syndrome (AIDS)—United States. *MMWR* **1984**;32:688-691
14. Selik RM, Haverkos HW, Curran JW. Acquired immune deficiency syndrome (AIDS) trends in the United States, 1978-1982. *Am J Med* **1984**;76:493-500
15. Abrams DI. Lymphadenopathy syndrome in male homosexuals. In: Gallen JI, Fauci AS, eds. *Advances in host defense mechanisms.* New York: Raven, **1985**:75-97
16. Centers for Disease Control. Persistent, generalized lymphadenopathy among homosexual males. *MMWR* **1983**;31:249-251
17. Moon KL, Federle MP, Abrams DI, Volberding P, Lewis BJ. Kaposi sarcoma and lymphadenopathy syndrome: limitations of abdominal CT in acquired immunodeficiency syndrome. *Radiology* **1984**;150:479-483
18. Kaposi M. Idiopathisches multiples Pigmentsarkom der Haut. *Arch Dermatol Syphilis* **1872**;4:265-273
19. Taylor JP, Templeton AC, Vogel CL, Ziegler JL, Kyalwazi SK. Kaposi's sarcoma in Uganda: a clinico-pathologic study. *Int J Cancer* **1971**;8:125-135
20. Rose HS, Balthazar EJ, Megebow AJ. Alimentary tract involvement in Kaposi sarcoma: radiographic and endoscopic findings in 25 homosexual men. *AJR* **1982**;139:661-666
21. Finkbeiner WE, Egbert BM, Groundwater JR, Sageobiel RW. Kaposi's sarcoma in young homosexual men. *Arch Pathol Lab Med* **1982**;106:261-264
22. Abrams DI. Lymphadenopathy syndrome in male homosexuals. In: Gallen JI, Fauci AS, eds. *Advances in host defense mechanisms.* New York: Raven, **1985**:75-97
23. Beckstead JH, Wood GS, Fletcher V. Evidence for the origin of Kaposi's sarcoma from lymphatic endothelium. *Am J Pathol* (in press)
24. Bottles K, Cohen MB, Brodie H, Jeffrey RB, Nyberg DA, Abrams DI. Fine needle aspiration cytology and the differential diagnosis of lymphadenopathy in homosexual males. *Diagn Cytopathol* (in press)
25. Centers for Disease Control. Diffuse, undifferentiated non-Hodgkin's lymphoma among homosexual males—United States. *MMWR* **1982**;31:277-279
26. Ziegler JL, Drew WL, Miner RC, et al. Outbreak of Burkitt's-like lymphoma in homosexual men. *Lancet* **1982**;2:631-633
27. Ziegler JL, Beckstead JA, Volberding PA, et al. Non-Hodgkin's lymphoma in 90 homosexual men: relation to generalized lymphadenopathy and the acquired immunodeficiency syndrome. *N Engl J Med* **1984**;311:565-570
28. Schoeppel SL, Hoppe RT, Dorfman RF, et al. Hodgkin's disease in homosexual men with generalized lymphadenopathy. *Ann Intern Med* **1985**;102:68-70
29. Burgener FA, Hamlin DJ. Histiocytic lymphoma of the abdomen: radiographic spectrum. *AJR* **1981**;137:337-342
30. Oliver TW, Bernardino ME, Sones PJ. Monitoring the response of lymphoma patients to therapy: correlation of abdominal CT findings with clinical course and histologic cell type. *Radiology* **1983**;149:219-224
31. Zanorza J, Ginaldi S. Computed tomography in hepatic lymphoma. *Radiology* **1981**;138:405-410
32. Orell SR, Skinner JM. The typing of non-Hodgkin's lymphoma using fine needle aspiration cytology. *Pathology* **1982**;14:389-394
33. Gottlieb MS, Groopman JE, Weinstein WM, Fahey JL, Detels R. The acquired immunodeficiency syndrome. *Ann Intern Med* **1983**;99:208-220
34. Balthazar EJ, Megebow AJ, Fazzini E, Opulencia JF, Engel I. Cytomegalavirus colitis in AIDS: radiographic findings in 11 patients. *Radiology* **1985**;155:585-590
35. Nyberg DA, Federle MP, Jeffrey RB, Bottles K, Wofsy CB. Abdominal CT findings of disseminated *Mycobacterium avium-intracellulare* infection in AIDS. *AJR* **1985**;145:297-299

Book Reviews

Diagnosis and Treatment of Pineal Region Tumors. Edited by Edward A. Neuwelt. Baltimore: Williams & Wilkins, 393 pp., 1984. $79.95

This book is an up-to-date compendium on pineal region tumors that makes a case for exploratory surgery for these tumors and outlines the controversies about this approach. The work has 21 chapters by 30 contributing authors. There is a complete alphabetical reference listing at the end plus chapter references. The illustrations are excellent and many are in color.

There are excellent sections on pineal gland function, types of tumor cells, clinical management, diagnostic studies, histopathology, surgical management and approaches, stereotaxic radiotherapy, chemotherapy, natural history, ophthalmologic consequences, diagnostic radiology, the Japanese experience, the Mayo Clinic approach, management of brain metastases, and microsurgery of the region. Of more interest to radiologists are the sections on diagnostic radiology, radiotherapy, and anatomy of the pineal region. There are illustrations of the arterial, venous, and ventricular structures. An imaging protocol is outlined for the diagnosis of pineal tumors and radiotherapy is reviewed.

The work is a fine reference for those interested in or who deal with pineal region tumors such as radiologists, neurologists, and neurosurgeons. It brings one up-to-date on what is known of the pineal gland function, reviews intracranial germ cell tumors, and stresses the importance of histologic diagnosis. Early surgical approaches are outlined and recent modifications are discussed. The emphasis is on diagnosis, management, and function. This book will be valuable to all interested in controversies of pineal region tumors and should be helpful to those who diagnose, treat, or do research in this area.

A. Basil Harris
Department of Neurological Surgery
University of Washington
Seattle, WA 98195

Determination of Dose Equivalents Resulting from External Radiation Sources. ICRU Report 39. Bethesda, MD: International Commission on Radiation Units and Measurements, 10 pp., 1985; soft cover. $10

This brief report discusses the dosimetric implications of current recommendations by the International Commission on Radiological Protection for radiation protection purposes. It defines terms that will be useful in the determination of the dose equivalents recommended and also describes the desirable characteristics and current capabilities of instruments for measuring the defined dose equivalents in individuals or in the environment. Thus, adequate estimates of the effective dose equivalent and the dose equivalent to organs near the body's surface can be obtained for effective radiation protection and for demonstrating compliance with regulatory limits and with authorized levels.

Juri Eenmaa
Medical Radiation Physics
University of Washington
Seattle, WA 98195

Velopharyngeal Insufficiency on Videofluoroscopy:

Comparison of Projections

David A. Stringer[1]
Mary Anne Witzel[2]

A prospective study of multiview videofluoroscopy was performed on 50 patients with clinically suspected velopharyngeal insufficiency to determine which views are helpful, so that radiation dosage might be reduced. The lateral view alone was insufficient: In 11 patients, velopharyngeal insufficiency was demonstrated on the basal or Towne view when the lateral view appeared normal. The Towne view demonstrated the velopharyngeal portal better than the basal projection when the adenoids were large. The basal view should be reserved for the few cases in which the Towne and lateral projections give insufficient information.

The lateral, frontal, and basal views have long been used in assessing speech disorders [1–5]. Relatively recently, the Towne projection has been introduced [6, 7] because the basal view is sometimes unsatisfactory. Since the sphincteric velopharyngeal mechanism can be studied on either the Towne or basal view, we report on a prospective study of 50 patients to assess which view is the more satisfactory, especially with reference to the size of the adenoids. We also describe the method of fluoroscopic examination we use and hope this will help others using these procedures.

Subjects and Methods

Using multiview videofluoroscopy, we prospectively examined 50 consecutive patients seen at the Hospital for Sick Children, Toronto, with clinically suspected velopharyngeal insufficiency. The patients (24 boys, 26 girls) were aged 4–18 years (mean, 8.8). There were various clinical diagnoses: cleft lip and palate (16 cases), status post tonsillectomy and adenoidectomy (10), idiopathic hypernasality (eight), submucous cleft palate (six), velocardiofacial syndrome (two), and one case each of Apert syndrome, Cornelia de Lange syndrome, facial asymmetry, generalized hypotonia of uncertain cause, hemifacial microsomia, Moebius syndrome, Pierre Robin syndrome, and Treacher Collins syndrome.

For the examination, 1–2 ml of high-density barium (Polibar 56% wt/wt) was instilled into each nostril and sniffed back into the nasopharynx with the patient supine. The patient was sitting for the lateral view, lying supine for the Towne view, and lying prone for the basal view (figs. 1A, 2A, and 3A). A series of phrases was repeated by the patient in each projection to assess velopharyngeal closure in a variety of speech tasks, and the entire examination was recorded on videotape with sound recording. Each patient repeated the sentences: "Put the baby in the buggy; Give Gary the chocolate cake; Susie sees the sun in the sky; My name is ____________," as well as making the sounds "s," "sh," and "ooh," and counting from one to 10. These phrases were adapted from those used at the Cleft Palate Center, University of Pittsburgh, Pennsylvania.

A detailed assessment of the anatomy and function on each view was performed at the end of every examination, including an assessment of the size of adenoids and consistency of movement. Drawings of the portal, open and closed, were made in each projection. The results of the three projections were compared. Findings were also assessed in terms of presence and size of adenoids.

Received May 20, 1985; accepted after revision September 11, 1985.

Presented at the Congress of the European Society of Paediatric Radiology, Florence, Italy, April 1984.

[1] Department of Radiology, Hospital for Sick Children, 555 University Ave., Toronto, Ontario, Canada M5G 1X8. Address reprint requests to D. A. Stringer.

[2] Department of Speech Pathology, Hospital for Sick Children, Toronto, Ontario, Canada, M5G 1X8.

AJR 146:15–19, January 1986
0361-803X/86/1461-0015
© American Roentgen Ray Society

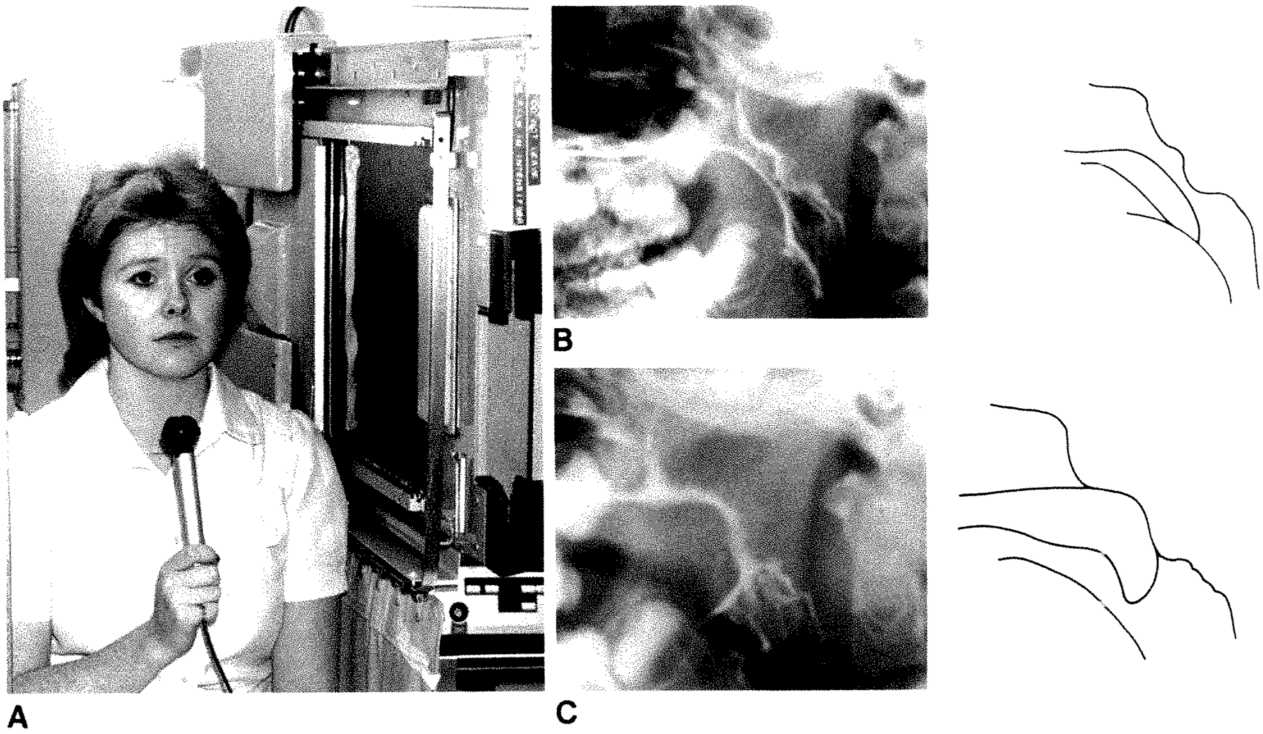

Fig. 1.—Lateral projection. **A**, Position of patient, sitting. **B**, Fluoroscopy of velopharyngeal portal during quiet respiration. **C**, Fluoroscopy of velopharyngeal portal during phonation. Patient has large adenoids.

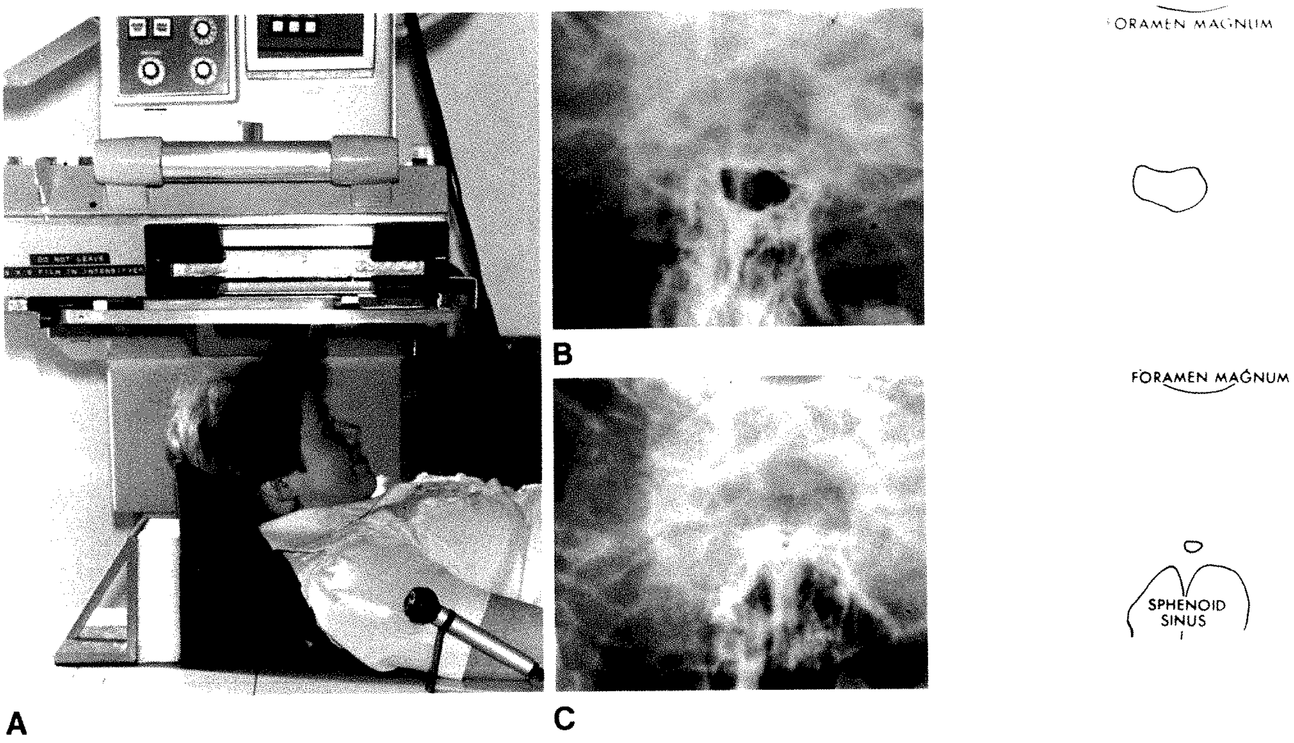

Fig. 2.—Towne projection. **A**, Patient lies supine with head resting on foam cushion. **B**, Fluoroscopy of velopharyngeal portal during quiet respiration. **C**, Fluoroscopy of velopharyngeal portal during phonation. Tiny defect indicates incompetent sphincter that was not visible in basal or lateral view.

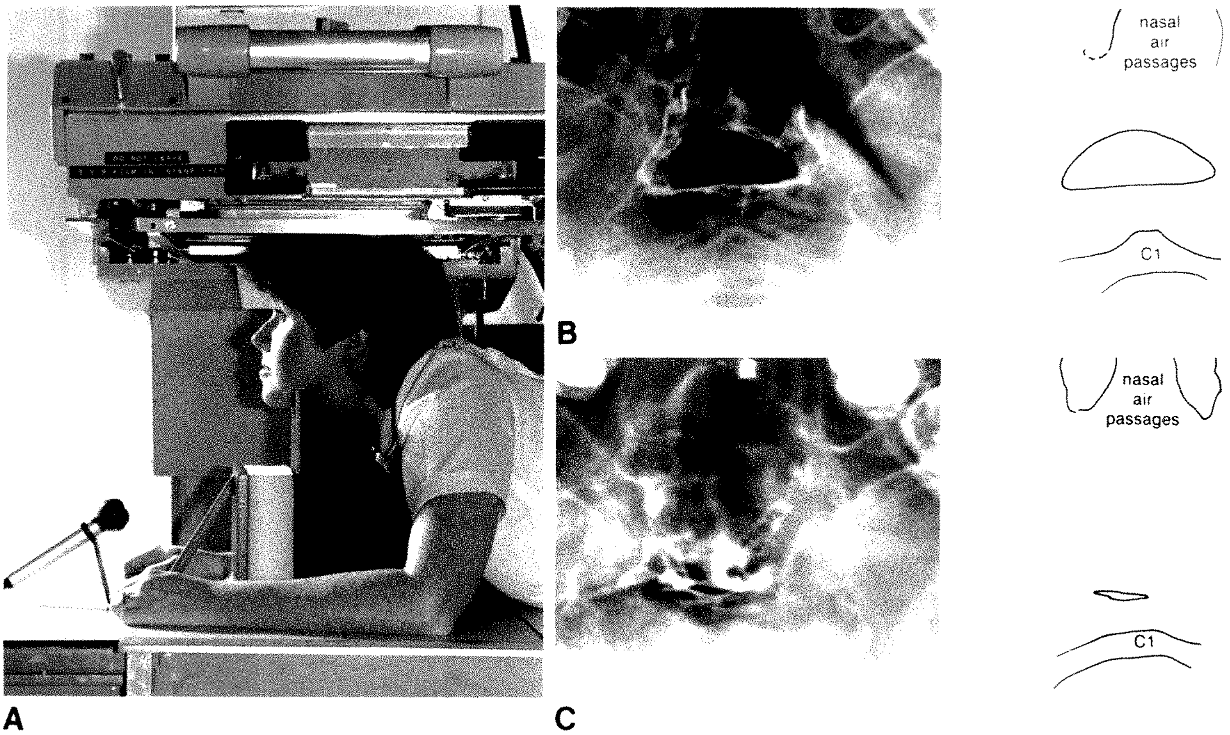

Fig. 3.—Basal projection. **A**, Patient lies prone, resting chin on foam pad. **B**, Fluoroscopy of velopharyngeal portal during quiet respiration. **C**, Fluoroscopy of velopharyngeal portal during phonation. Moderate-sized defect indicates incompetent sphincter. Defect was also seen on Towne view but not on lateral projection.

TABLE 1: **Comparison of Videofluoroscopy using Three Projections in 50 Patients**

Projection	Normal	Abnormal	Equivocal
Lateral	18	31	1
Basal	3	27	20
Towne	7	35	8

Results

The radiologic appearances in each projection during quiet respiration are shown in figures 1B, 2B, and 3B and during phonation in figures 1C, 2C, and 3C. The types of small defects visible on phonation in velopharyngeal insufficiency using the Towne and basal views are demonstrated in figures 2C and 3C, respectively.

The results of our comparison are shown in table 1. For each view, the examination was considered normal when consistent closure of the velopharynx occurred during correctly articulated speech, except for the nasal phonemes ("m," "n," and "ng" sounds), when closure does not normally occur. The examination was abnormal if there was clear failure of closure during consonant speech except for the nasal phonemes. The outcome was considered equivocal if it was difficult to demonstrate definitely normal or abnormal closure. An equivocal result occurred most often when multiple overlying levels gave confusing information about whether closure actually occurred.

Of the 18 patients believed to be normal from lateral views, only seven were confirmed as normal on the Towne and/or basal views.

Three groups were created according to the size of the adenoids (figs. 1B, 1C, 4, and 5), and the findings in each group were analyzed to determine which view was more helpful (table 2).

Discussion

The assessment of speech disorders related to velopharyngeal function depends on clinical, investigative, and endoscopic evaluation as well as fluoroscopic examination. Therefore, an interdisciplinary study team, including a speech pathologist, is essential in the radiologic study of speech disorders [8]. Since radiation dosage must be minimized, video rather than cine recording is used [9].

The lateral view shows the anatomy of the soft palate and provides information on the movement of the tongue, palate, and posterior pharyngeal wall as well as demonstrating any Passavant ridge (fig. 5B). This ridge, originally described in the 19th century in cleft palate patients, is not uncommon in patients with hypernasality and may also be seen in normal subjects. It seems to help complete closure of the velopharyngeal portal. Unfortunately, the lateral view may miss some essential information. Small defects are difficult to see if there is too little barium in the portal to demonstrate bubbling or if the adenoids are irregular, giving multiple lines of barium.

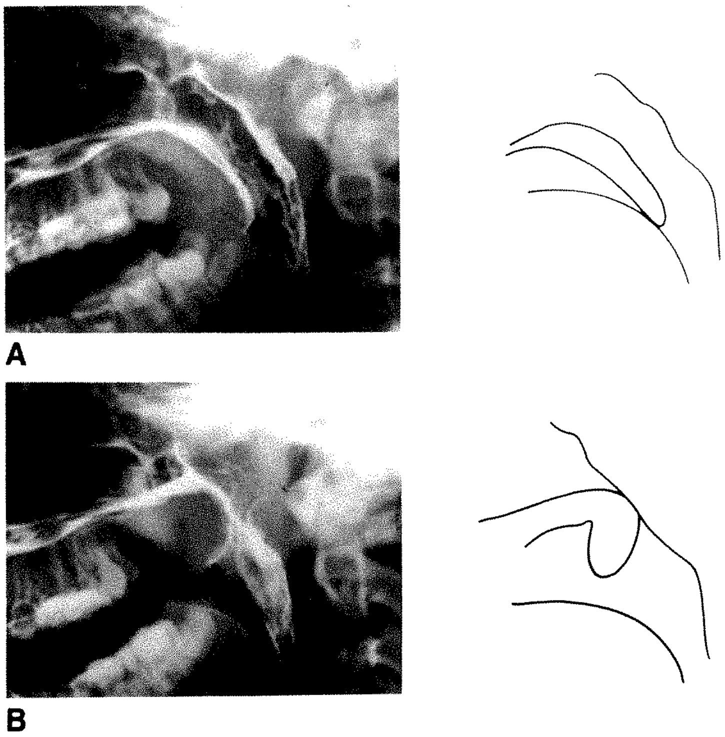

Fig. 4.—Medium-sized adenoids in lateral projection. **A**, Normal soft palate at rest. **B**, Complete velopharyngeal closure during phonation.

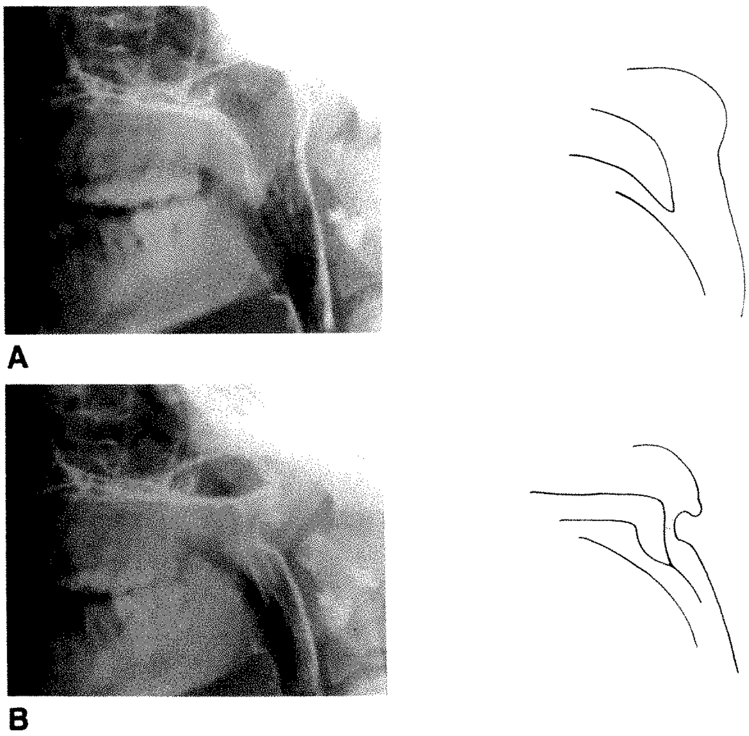

Fig. 5.—Absent adenoids in lateral projection. **A**, Short palate at rest after cleft palate repair. **B**, Failure of velopharyngeal closure during phonation. Passavant ridge, which may aid closure, projects from posterior aspect of pharynx. This ridge, originally described by Passavant in cleft palate patients, is not uncommon in patients with hypernasality and may occasionally be seen in normal subjects.

The lateral view cannot demonstrate movement of the lateral pharyngeal walls or the sphincteric movement of the velopharynx. Lateral pharyngeal walls can move incongruously with respect to the velum [10]. Further, some authors believe the extent of their movement is a reliable predictor of surgical success in velopharyngeal insufficiency [11]. Others think that the site and shape of the velopharyngeal portal defect are important, since central defects do well

TABLE 2: **The Value of the View in Relation to Presence and Size of Adenoids**

View	Adenoid Size		
	Large	Medium	Small or Absent
Towne	19	5	6
Basal	2	3	4
Both	3	4	1
Neither	0	0	3
Total	24	12	14

surgically but lateral defects may not [6].

Lateral wall movement can be assessed by a variety of views. The frontal view was the first to be described and in many patients gives adequate information, even though the data may be difficult to assess because of overlapping structures. However, the frontal view, even when supplemented by oblique views, does not give full information about the sphincteric closure of the velopharyngeal portal, which some surgeons and speech pathologists argue is important in full speech assessment [12]. For this, another view such as the basal or Towne projection is necessary.

Neither the basal nor the Towne view can be performed on standard fluoroscopic equipment without neck extension or flexion. The basal view, which is more widely used, requires marked hyperextension of the neck (fig. 3A), which may exaggerate the degree of incompetence seen during speech [13, 14]. Conversely, the Towne view is performed with the neck well flexed (fig. 2A), which may decrease the degree of incompetence seen during speech [13]. However, in our series the Towne view was more effective at detecting incompetence than the basal or lateral projection, and it never missed a defect seen on the other views. The Towne view was especially helpful when the adenoids were large, whereas a satisfactory basal view has been difficult to obtain in patients with large adenoids [5]. We also found that the Towne position was easier for children to maintain than the basal view. In addition, the Towne view has the advantage of avoiding primary beam irradiation of the thyroid gland. Although the eyes may be irradiated, they can often be excluded from the primary beam by careful coning. Radiation dosage is minimized during the procedure by careful coning, keeping the fluoroscopy to the shortest time necessary for the study, and using video recording rather than cine radiography.

Nasopharyngoscopy is used by some clinicians to investigate suspected velopharyngeal incompetence. The shape and movement of the velopharynx seen with flexible nasopharyngoscopes compares better with that seen on the Towne view than the basal view [15].

In summary, the lateral view alone is insufficient to assess the velopharyngeal portal. The Towne view gives the best visibility, especially if there are large adenoids. It is performed with the patient in a comfortable position that is easily maintained, and the view of the portal is most similar to that shown by a flexible nasopharyngoscope. The basal view can be reserved for the few cases where the Towne view has not given sufficient diagnostic information.

ACKNOWLEDGMENTS

We thank K. Detz, C. G. Salvador, and the Medical Publications Department of the Hospital for Sick Children for help in preparing this paper.

REFERENCES

1. Calnan JS. Movements of the soft palate. *Br J Plast Surg* **1953**;5:286–296
2. Astley R. The movements of the lateral walls of the nasopharynx: a cine-radiographic study. *J Laryngol Otol* **1958**;72:325–328
3. Griffith BH, Monroe CW, Hill BJ, Waldrop WF, White H. Motion of the lateral pharyngeal walls during velo-pharyngeal closure. *Plast Reconstr Surg* **1968**;41:338–342
4. Skolnick ML. Videofluoroscopic examination of the velopharyngeal portal during phonation in lateral and base projections—a new technique for studying the mechanics of closure. *Cleft Palate J* **1970**;7:803–816.
5. Skolnick ML, McCall GN, Barnes M. The sphincteric mechanism of velopharyngeal closure. *Cleft Palate J* **1973**;10:286–305
6. Cotton RT, Quattromani F. Lateral defects in velopharyngeal insufficiency. *Arch Otolaryngol* **1977**;103:90–93
7. Quattromani FL, Benton C, Cotton RT. The Towne projection for evaluation of the velopharyngeal sphincter. *Radiology* **1977**;125:540–542
8. Skolnick ML. A plea of an interdisciplinary approach to the radiological study of the velopharyngeal portal. *Cleft Palate J* **1977**;14:329–330
9. Skolnick ML. Video velopharyngography in patients with nasal speech, with emphasis on lateral pharyngeal motion in velopharyngeal closure. *Radiology* **1969**;93:747–755
10. Shprintzen RJ, Rakoff SJ, Skolnick ML, Lavorato AS. Incongruous movements of the velum and lateral pharyngeal walls. *Cleft Palate J* **1977**;14:148–157
11. Kelsey CA, Ewanowski SJ, Crummy AB, Bless DM. Lateral pharyngeal-wall motion as a predictor of surgical success in velopharyngeal insufficiency. *N Engl J Med* **1972**;287:64–68
12. La Rossa D, Brown A, Cohen H, Spackman T. Video-radiography of the velopharyngeal portal using the Towne's view. *J Maxillofac Surg* **1980**;8:203–205
13. McWilliams BJ, Musgrave RH, Crozier PA. The influence of head position upon velopharyngeal closure. *Cleft Palate J* **1968**;5:117–124
14. Williams WN, Eisenbach CR. Assessing VP function: The lateral still technique vs. cinefluorography. *Cleft Palate J* **1981**;18:45–50
15. Stringer DA, Witzel MA. A comparison of nasopharyngoscopy and multiview videofluoroscopy. In: *Proceedings of the first meeting of the North American Working Group on Cleft Palate and Craniofacial Anomalies*, New York, July **1984** (in press)

Book Reviews

Fuch's Principles of Radiographic Exposure, Processing and Quality Control, 3d ed. By Quinn B. Carroll. Springfield, IL: Thomas, 374 pp., 1985. $29.75

This text addresses the practical aspects of quality image production. The approach is one of a brief scientific discussion with detailed technical guidance for each step toward forming the radiograph.

There are five sections. The first, Producing the Radiographic Image, has information on characteristics and properties of x-rays, methods of recording the radiographic image, and other necessary qualities of the image. Section two, Visability Factors, contains subsections regarding mAs, kVP, quality control, contrast media, grids, screens, and film types. The third section, Geometrical Factors, discusses focal spots, targets, motion, and special techniques such as tomography. Section four, Comprehensive Technique, addresses quality control and automated exposure controls. There is also a chapter with technique problems to solve. The fifth section is Processing the Radiograph and offers information on processing chemicals, manual and automatic processing, duplication and subtraction, and sensitometry. The material is subsequently divided into small explanatory chapters, each summarizing highlights at its conclusion.

The text is generously illustrated with line diagrams, graphs, and well-duplicated radiographs.

In comparison to the second edition, this edition contains a greater number of illustrations. There are added chapters with emphasis on quality control, technique problems, and the construction of technique charts.

Although their brevity makes them more approachable, I believe the chapters on developing technique charts and working through technique problems would benefit from a greater variety and number of sample clinical problems. It is unusual for a well established and functional text to have so improved over a previous edition.

Shauna R. Roberts
Surgical and Medical Education
St. Lukes Hospital
Kansas City, MO 64111

Iatrogenic Disorders of the Fetus, Infant, and Child, vol. II. (Series: Radiology of Iatrogenic Disorders.) Edited by E. George Kassner. New York: Springer-Verlag, 500 pp., 1985. $165

George Kassner has edited this volume and served as the author of multiple chapters along with nine distinguished contributors. The second volume of a series, it deals exclusively with those pediatric disorders related to surgery. Largely, discussion deals with the typical preoperative findings indicating surgery as necessary, anatomic details of common surgical techniques, early or late complications of the surgery, and the expected postoperative appearance. All this is from the viewpoint of the radiologist.

The volume is organized into chapters dealing with surgery of the airways, lungs, thorax, heart, and gastrointestinal tract, also urologic diagnosis and surgery, urinary diversion procedures, and orthopedic and neurologic surgery.

The book accomplishes its mission in superb style. It is liberally illustrated with radiographs showing the abnormalities under discussion, the surgical results, and complications. There are drawings, diagrams, and photographs of the operative procedures, pertinent equipment, and anatomic specimens. Great attention has been paid to detail with good reproduction of the radiographs and excellent organization. At the same time, the authors have managed to avoid too many or inappropriate details. Despite multiple authors and opinions, the book reads smoothly.

Compilation of such material in one book is extremely useful. It is a handy reference and a good discussion of surgery and complications as they ought to be understood by the radiologist. Thus, the text is useful for those persons in hospitals dealing with children undergoing corrective surgical procedures and also for radiologists who may see these patients many years after the original operative procedure. The book is a wise investment for any radiologist—resident, hospital located, or in community practice. All of us should be conversant with the diagnoses, techniques, and complications described.

Beverly P. Wood
University of Rochester Medical Center
Rochester, NY 14642

Radiologic Amyl Nitrite Test for Distinguishing Pseudoachalasia from Idiopathic Achalasia

Wylie J. Dodds[1,2]
Edward T. Stewart[1]
Soad M. Kishk[1]
Peter J. Kahrilas[2]
Walter J. Hogan[2]

In a simple radiologic test, amyl nitrite inhalation seems to distinguish patients with pseudoachalasia from those with idiopathic achalasia. In three pseudoachalasia patients with tumor infiltration of the distal esophagus, the narrow lower esophageal sphincter segment was unaffected by the smooth-muscle relaxant effect of amyl nitrite. In contrast, amyl nitrite caused a measurable increase of 2 mm or more in sphincter diameter in nine patients with idiopathic achalasia. The amyl nitrite test may be a useful method for distinguishing patients with pseudoachalasia from those with idiopathic achalasia.

P24442

Pseudoachalasia of the esophagus, caused by tumor infiltration of the distal esophagus, may closely simulate the esophageal motor and morphologic abnormalities of idiopathic achalasia. [1, 2]. In some instances, the simulation is so perfect that the distinction cannot be made by standard radiographic and manometric examinations or by endoscopy. In achalasia patients, resting tone of the lower esophageal sphincter (LES) is generally increased, and impairment exists in sphincter relaxation [3]. However, the sphincter is not rigid, because in achalasia the LES generally allows passage of an endoscope across the sphincter into the stomach. In addition, on manometry LES pressure decreases substantially in response to amyl nitrite, a smooth-muscle relaxant [4]. In contrast, amyl nitrite generally does not relax the LES segment in pseudoachalasia [5]. We report a simple radiologic test using amyl nitrite that distinguishes patients with pseudoachalasia from those with the more common idiopathic achalasia.

Subjects and Methods

During the 8 years from 1977 through 1984, we did provocative amyl nitrite testing during esophagography in three patients with pseudoachalasia secondary to infiltrating gastric adenocarcinoma and nine unselected patients with idiopathic achalasia. The patients with idiopathic achalasia were aged 40–70 years (mean, 48 years); the pseudoachalasia patients were 67, 71, and 72 years. In the three pseudoachalasia patients, tissue for diagnosis was obtained at laparotomy in two and by endoscopic biopsy in one. All patients complained of dysphagia for liquids and solids. The three pseudoachalasia patients each experienced symptoms for less than 1 year, whereas most of the achalasia patients had esophageal symptoms for more than 1 year, some for more than 10 years.

On radiologic examination all the patients exhibited (1) abnormal opening of the LES segment, (2) absent peristalsis in the thoracic esophagus, and (3) moderate to severe esophageal dilatation. Esophageal-body motor activity was evaluated with the patient recumbent, while LES opening was examined with the patient tilted 60°–90° upright. For evaluation of LES opening, the patient drank 30–120 ml of liquid barium (specific gravity, 1.5) until the barium column was above the aortic arch level. Multiple spot films were obtained of the LES segment when the transverse diameter of the narrow sphincter segment became maximal during esophageal emptying. Films were obtained before and immediately after the patient took four deep inhalations from a freshly broken ampule of amyl nitrite. Measurement of LES diameter was taken as the maximal diameter of the narrowest part of the LES segment. In

Received July 1, 1985; accepted after revision August 28, 1985.

This work was supported in part by U. S. Public Health Service grant AM 25731.

[1] Department of Radiology, Medical College of Wisconsin, Milwaukee County Medical Complex, 8700 W. Wisconsin Ave., Milwaukee, WI 53226. Address reprint requests to W. J. Dodds.

[2] Department of Medicine, Medical College of Wisconsin, Milwaukee County Medical Complex, Milwaukee, WI 53226.

AJR 146:21-23, January 1986
0361-803X/86/1461-0021
© American Roentgen Ray Society

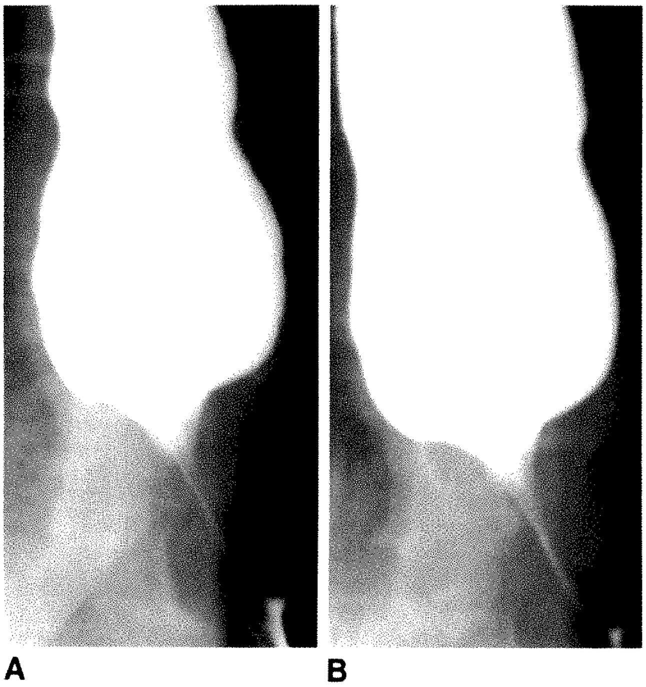

Fig. 1.—Amyl nitrite test in patient with pseudoachalasia. **A**, Before amyl nitrite, LES has fixed narrowed configuration, and some feeble nonperistaltic contractions are seen in dilated esophageal body. **B**, After amyl nitrite, narrowed LES segment remained unchanged in appearance.

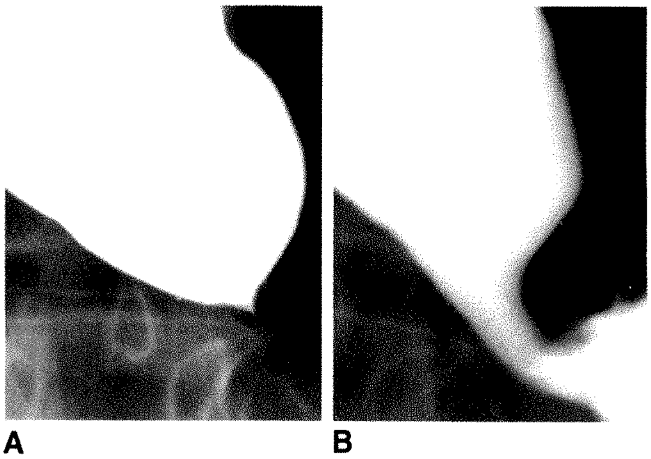

Fig. 2.—Amyl nitrite test in patient with idiopathic achalasia. **A**, Before amyl nitrite, LES segment has bird-beaked configuration. Maximal diameter of LES segment was 2 mm during transient sequences of barium flow. **B**, After amyl nitrite, LES diameter increased to 9 mm and barium flowed freely into stomach.

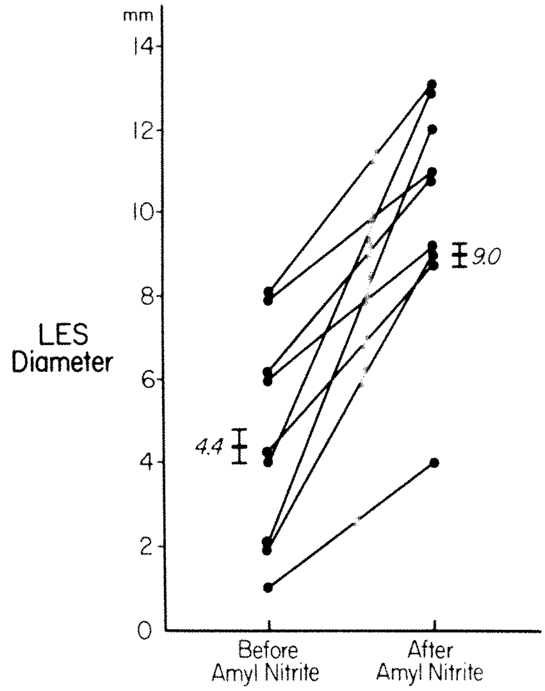

Fig. 3.—Diameter of LES segment before and after amyl nitrite inhalation in nine patients with idiopathic achalasia. In each patient, maximal LES diameter increased by 3 mm or more after amyl nitrite.

most cases, the measurement was obtained from the middle of the sphincter segment.

Results

On esophagography, the largest diameter (uncorrected for magnification) of the LES segment in any of the 12 patients studied was 8 mm or less during the maximal hydrostatic flow of barium into the stomach. This narrow caliber contrasts with that of the normal LES segment, which opens to a caliber of 15 mm or more during the interval of maximal transsphincter flow.

In each subject, four inhalations of amyl nitrite caused the pulse rate to increase by more than 20/min, often accompanied by palpitations and flushing. These effects ended within 2 min. During this interval, the patient was supported at the knees and watched closely for impending syncope. Although several patients experienced mild dizziness, syncope did not occur in any of the individuals studied. For the three patients with pseudoachalasia, the amyl nitrite inhalation did not cause any change in the maximal caliber of the LES segment (fig. 1). In contrast, amyl nitrite inhalation caused a measurable increase in maximal LES diameter of 3 mm or more in each of the patients with idiopathic achalasia (fig. 2). This increase in LES diameter in the achalasia patients averaged 4.6 mm (fig. 3) and was accompanied by enhanced esophageal emptying. When corrected for magnification (about 30%–35%), the real increase in LES diameter after amyl nitrite was at least 2 mm. When spontaneous, nonperistaltic contractions were present in the distal half of the esophageal body, these contractions were transiently abolished by amyl nitrite.

Discussion

Although pseudoachalasia, or secondary achalasia, is an uncommon disorder, occasional patients with pseudoachalasia are likely to be encountered at clinical units that have a large referral of patients with esophageal disease. During the past 15 years, we have seen five patients with pseudoachalasia at our institution, compared with about 175 patients with verified idiopathic achalasia, a ratio of about 35:1. Because all but one of the patients with pseudoachalasia was thought to have achalasia initially, our experience suggests that about 3% of patients believed to have achalasia may prove to have a pseudoachalasia syndrome.

As was the case in our three pseudoachalasia patients, the pseudoachalasia patients reported previously generally had complained of dysphagia for less than 1 year [2]. The dysphagia is often accompanied by significant weight loss of 7 kg or more. In contrast, patients with idiopathic primary achalasia typically have experienced dysphagia for more than 1 year, often for many years, and generally have not had significant weight loss. However, some overlap in these clinical features may occur [6].

The most common cause of pseudoachalasia is gastric adenocarcinoma that invades across the esophagogastric junction [1, 2]. Other causes include squamous carcinoma, metastatic disease, or lymphoma that involves the region of the gastric cardia and distal esophagus [7, 8]. The precise mechanism whereby these conditions simulate idiopathic achalasia is not clear, but three major possibilities have been suggested [1]. First, high-grade obstruction of the esophagogastric region may cause esophageal decompensation that simulates the findings of primary achalasia. Second, in some patients, submucosal tumor may invade the esophageal myenteric plexus. Finally, a circulating tumor product may alter esophageal motor function and thereby elicit an achalasialike syndrome. None of these proposed mechanisms, however, accounts for the pseudoachalasia syndrome in all of the afflicted patients. Undoubtedly several different factors contribute to the genesis of the pseudoachalasia syndrome.

On conventional radiologic, manometric, and endoscopic examination, pseudoachalasia may mimic idiopathic achalasia so closely as to escape detection [1]. Even multiple biopsies or CT examination may fail to detect tumors adjacent to the cardia. This difficulty may, on occasion, lead to a mistaken diagnosis of idiopathic achalasia and ill-advised treatment consisting of pneumatic dilatation of the LES segment. Such treatment has a high risk of causing esophageal perforation. For this reason, a simple radiologic test would be useful to discriminate pseudoachalasia from true idiopathic achalasia. Such a test using amyl nitrite is validated here.

Three provisos require consideration when using the radiologic amyl nitrite test. First, hypertension, hypotension and cardiac disease are contraindications for the test. Second, the subject must inhale sufficient amyl nitrite to achieve a true effect. When the pulse rate does not increase by at least 20/min, we repeat the test. Finally, amyl nitrite is a nonspecific smooth-muscle relaxant that causes relaxation of vascular as well as gastrointestinal smooth muscle. Therefore, the subject must be carefully watched for evidence of impending hypotensive syncope, and the x-ray table is lowered to the horizontal position whenever necessary. In our series, several patients experienced dizziness, but none had syncope.

In our series of patients studied by the radiologic amyl nitrite test, false-positive or false-negative findings were not encountered. Therefore, the findings were encouraging and the test seems to be reliable. However, a false-negative finding might be expected in some pseudoachalasia patients in whom tumor infiltration does not surround the LES completely, or a false-positive finding might occur in occasional patients with idiopathic achalasia, particularly if amyl nitrite inhalation is suboptimal. Therefore, although the radiologic amyl nitrite test is promising, additional data are needed to substantiate the sensitivity, specificity, and accuracy of the test in distinguishing patients with pseudoachalasia from those with achalasia.

REFERENCES

1. Lawson TL, Dodds WJ. Infiltrating carcinoma simulating achalasia. *Gastrointest Radiol* **1976**;1:245–248
2. Tucker HJ, Snape WJ, Cohen S. Achalasia secondary to carcinoma: manometric and clinical features. *Ann Intern Med* **1978**;89:315–318
3. Cohen S, Lipshutz W. Lower esophageal sphincter dysfunction in achalasia. *Gastroenterology* **1971**;61:814–820
4. Dodds WJ, Helm JF, Hogan WJ, Dent J, Arndorfer RC. Cholinergic innervation of the LES in esophageal achalasia (abstr). *Gastroenterology* **1980**;78:1157
5. Helm JF, Dodds WJ, Hogan WJ, Arndorfer RC. Carcinoma of the cardia masquerading as idiopathic achalasia (abstr). *Gastroenterology* **1982**;82:1082
6. Sandler RS, Bozymski EM, Orlando RC. Failure of clinical criteria to distinguish between primary achalasia and achalasia secondary to tumor. *Dig Dis Sci* **1982**;27:209–213
7. Davis JA, Kantrowitz PA, Chandler HL, Schatzki SC. Reversible achalasia due to reticulum-cell sarcoma. *N Engl J Med* **1975**;3:130–132
8. Eaves R, Lambert J, Rees J, King RWF. Achalasia secondary to carcinoma of prostate. *Dig Dis Sci* **1983**;28:278–284

Book Review

Progress in Medical Radiation Physics, vol. 2. Edited by Colin G. Orton. New York: Plenum, 254 pp., 1985. $45

Summarizing the editor's preface, each chapter in this series is designed to provide the reader with just sufficient information to fully understand the development described and to apply the technique or concept. In this way, it is hoped that the series will be a catalyst, encouraging the medical physicist to apply new techniques and developments in daily practice.

The first chapter of this, the second number of the series, is concerned with conformation, or dynamic therapy. The subject is approached through an in-depth discussion of the Tracking Cobalt Project (Royal Northern Hospital, London, 1945–1970, and Royal Free Hospital, London, 1970 to date), with references to parallel approaches employed elsewhere. The chapter is divided into three parts: part I, the origins and clinical rationale for conformation therapy, design of successive machines to achieve the tracking approach, their control, and associated treatment planning. Part II deals with the physical aspects of conformation therapy in more detail, and part III, with computer systems used to control the tracking units to generate the desired dose distribution. The chapter is well written, the illustrations adequate, and the authors avoid being judgmental regarding the value of different approaches. Each part has its own bibliography; these are brief but adequate, though slightly repetitious.

The second chapter is concerned with the measurement of human body composition in vivo. Again, the subject is approached through in-depth examination of experience in one facility, the General Infirmary, Leeds, with references to allied work. Determination of the elementary composition of the body by analysis of tissues (as a reference standard), isotope dilution, and measurements of natural or induced radioactivity are described; also the estimation of specific body tissue from body density, anthropometry, total body water, total body potassium, dilution, total body carbon, nitrogen and calcium, and urine analysis. Instrumentation ranges from a pair of calipers to 14 MeV neutron beam for whole body activation and neutron scattering measurements. Apart from the technology, the chapter is notable for careful differentiation between precision and accuracy, drawing attention to the role of analysis of uncertainty in evaluating an analytical method, and the role of factor analysis in comparing methods.

The third chapter is concerned with medical applications of x-ray fluorescence elemental analysis. The chapter opens with a discussion of the physical basis of the method. The methods of exciting and detecting the x-ray fluorescence, target preparation, and medical applications are discussed. This chapter is in the more classic review format. There are 94 references, half of which are more than 10 years old; the latest is 1981.

Chapter four, entitled Basic Imaging Properties of Radiographic Systems and Their Measurement, is based heavily on the work of the Kurt Rossmann Laboratories of the University of Chicago. The chapter discusses x-ray sensitometry, methods, handling of data, resolution properties of radiographic imaging systems, methods of measurement, factors affecting the results. Methods of measuring the characteristics of x-ray tube focal spots are described and compared to computer simulation of their significance in radiographic images, particularly angiography. The chapter concludes with a discussion of radiographic noise, methods of measuring the Wiener spectra, and typical results.

The volume is well produced; the illustrations appropriate in nature and location in text.

The chapters that approach the subject through an in-depth discussion of the author's own or group's work are easier to read, as the work has its own internal logic and "hands on" details flow naturally. Some inspire thoughts of application elsewhere. The classic review paper chapter may have the greater long term utility as a broad reference source. This is an enjoyable volume with a good mix of subjects.

Peter Wootton
Medical Radiation Physics
University of Washington
Seattle, WA 98195

The Esophagus after Endoscopic Pneumatic Balloon Dilatation for Achalasia

Farooq P. Agha[1]
Horchang H. Lee[2]

The changes seen on contrast esophagrams after endoscopic pneumatic balloon dilation for the treatment of achalasia are described and illustrated. Sixteen patients had esophagrams within 24 hr after dilation and follow-up esophagrams were obtained 6–24 months later. The radiographic features evaluated in the early postdilation period included detection of esophageal perforation, diameter of the esophagogastric channel, proximal esophageal dilatation, mucosal integrity, and emptying dynamics of the esophagus. Fourteen patients (88%) had immediate symptomatic improvement of dysphagia. The mean increase in diameter of the esophagogastric channel was 6.5 mm (range, 4.8–9 mm) relative to a pretreatment esophagram. Emptying dynamics of the esophagus improved significantly in 12 patients (75%). One patient developed esophageal perforation requiring surgery. On the follow-up esophagrams obtained 6–24 months later, the evaluation was for sustained dilatation of esophagogastric channel, decrease in esophageal dilatation, and improved emptying dynamics of the esophagus. The effective esophagogastric channel diameter of 8–10 mm correlated well with improved clinical response in 88% of the patients.

Due to the widespread application of endoscopy, there has been renewed interest in the endoscopic treatment of achalasia by the pneumatic balloon dilation method. Recently 16 patients with achalasia have been treated with this dilation method using the Witzel pneumatic dilator at our institution [1]. We discuss the radiographic evaluation of esophageal achalasia after pneumatic balloon dilation treatment and emphasize its value in assessment of this procedure and its complications.

Subjects and Methods

Between July 1983 and January 1985, we evaluated 16 patients with achalasia by serial esophagrams after pneumatic balloon dilation treatment at the University of Michigan Hospitals. There were nine women and seven men aged 39–80 years (mean, 54). All pneumatic balloon dilations were performed in the endoscopy suite using the Witzel pneumatic dilator (Wimed Med Technik, West Berlin) attached to a forward-viewing gastroscope. The clinical symptoms consisted of dysphagia in all 16 patients, regurgitation in eight, weight loss in four, substernal discomfort and pain in five, and recurrent aspiration in two. Two patients had had a Heller myotomy with recurrence of dysphagia, and one patient had had dilation several years earlier by the hydrostatic method.

Esophageal manometry was performed in all patients before pneumatic balloon dilation. Typical achalasia changes, found in all patients, were aperistalsis to ineffecutal peristalsis in the body of the esophagus and a hypertensive lower esophageal sphincter. The lower esophageal sphincter pressure was 12–70 mm Hg (mean, 33 mm Hg). Relaxation of the lower esophageal sphincter was absent or incomplete in 13 patients and could not be measured in the other three. Endoscopic examination after adequate lavage of the esophagus excluded neoplastic processes of the esophagogastric region. Predilatation esophagrams were performed in all patients 1–7 days before dilation as baseline studies.

The Witzel pneumatic dilator used in this study consists of a 20-cm-long polyvinyl tube with an internal diameter of 10 mm and an external diameter of 11 mm, which is surrounded

Received May 6, 1985; accepted after revision September 9, 1985.

[1] Department of Radiology, University of Michigan Hospitals, Box 013, 1405 E. Ann St., Ann Arbor, MI 48109. Address reprint requests to F. P. Agha.

[2] Department of Internal Medicine, Division of Gastroenterology, University of Michigan Hospitals, Ann Arbor, MI 48109.

AJR **146:25–29, January 1986**
0361–803X/86/1461–0025
© American Roentgen Ray Society

by a 15-cm-long polyurethane balloon (fig. 1). The dilator is fitted over a regular small-caliber forward-viewing fiberoptic gastroscope (OES Gastroscope, model GIF-PIO) with an external diameter of 9 mm and secured by rubber bands at both ends of the dilator. The polyurethane balloon does not expand beyond 40 mm in diameter when inflated to a pressure of 300 mm Hg because of the high coefficient of elasticity of the material. Adequate dilation pressures can be attained in the narrow segment of the esophagus without undue expansion into the adjacent esophagus and stomach.

All patients fasted overnight. Before the procedure, surface anaesthesia of the oropharynx and light sedation by diazepam intravenously were accomplished. Deep sedation was avoided lest it suppress the pain sensation, which could warn of a complication. The dilator was introduced with the endoscope. The tip of the endoscope was angulated 180° in the stomach for direct view of the cardia, and the middle of the balloon was positioned across the narrowed segment of the esophagus under visual control. With the dilator still in view the balloon was dilated to 300 mm Hg for 2 min. The cuff was deflated if pain occured. The procedure was repeated until it was possible to maintain the 300 mm Hg pressure for 2 min. After the dilation, the patients were observed for potential signs and symptoms of esophageal perforation and were hospitalized for 1 day.

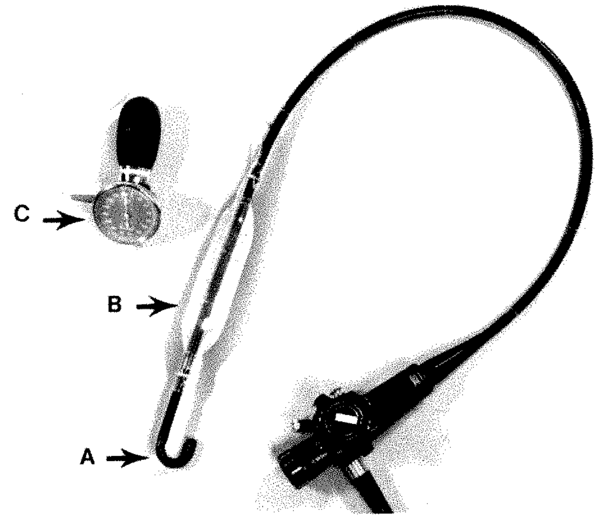

Fig. 1.—Witzel pneumatic dilator: tip of gastroscope (A); pneumatic polyurethane balloon (B, retouched); sphygmomanometer (C).

The contrast esophagrams were obtained within 24 hr after the dilation treatment. Our technique of radiographic examination of the esophagus for potential perforation has been described previously [2-4]. We examined patients in the semiupright position using Gastrografin (Mallinckrodt) initially. If no esophageal perforation was identified, the examination was repeated with a low-density barium sulphate mixture (Sol-O-Pake, E-Z-EM). Films in left posterior oblique, right anterior oblique, and lateral projections were obtained. A 15–20 min delayed film in the upright position to assess emptying status of the esophagus was also obtained. Elective follow-up esophagrams 6–24 months after dilation treatment were obtained using single-contrast technique and low-density barium sulphate mixture. The film sequence and projections were similar to the immediate postdilation examination.

The radiographic features evaluated included the diameter of the esophagogastric channel and proximal esophageal lumen, the intactness of the mucosal contour, and emptying dynamics of the esophagus.

Results

Symptomatic improvement in dysphagia occurred in 14 of the 16 patients immediately after pneumatic balloon dilation

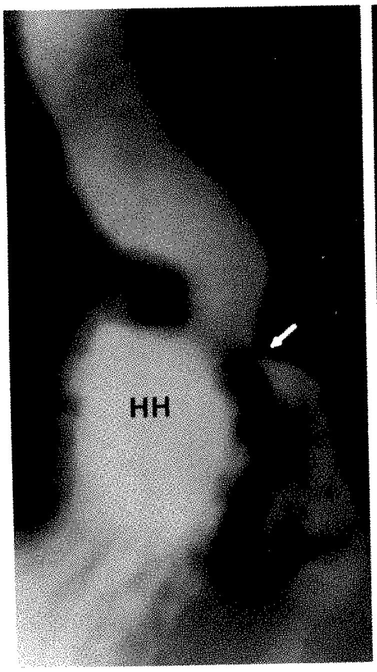

2

Fig. 2.—Esophagram with Gastrografin 2 hr after pneumatic dilation shows free esophageal perforation (*arrow*) immediately adjacent to hiatal hernia (HH) in this patient with achalasia.

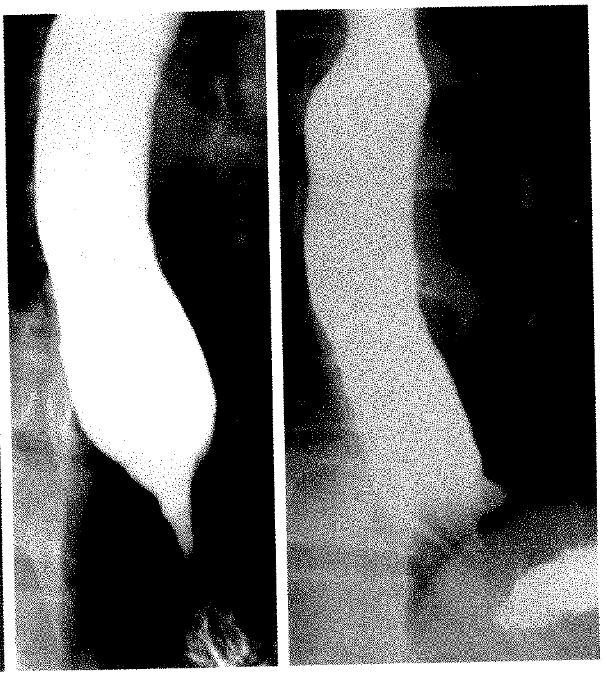

3A 3B

Fig. 3.—**A**, Predilation esophagram. **B**, Post-pneumatic balloon dilation esophagram shows significant widening of esophagastric channel and decrease in esophageal dilatation.

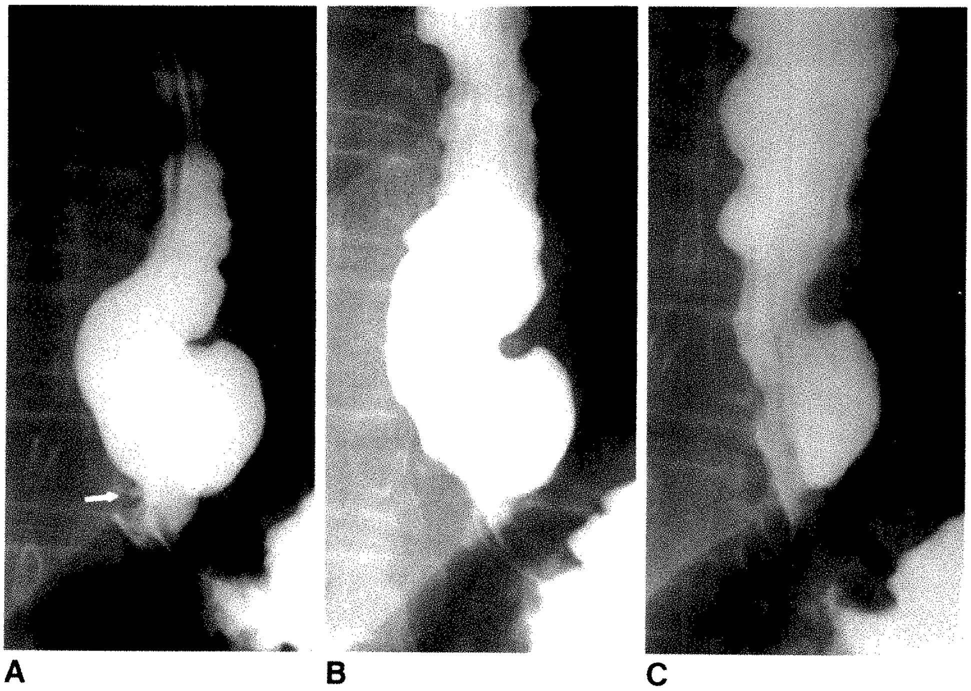

Fig. 4.—**A**, Esophagram after pneumatic balloon dilation shows irregular mucosal contour in distal esophagus with small ulceration and surrounding submucosal edema (*arrow*). Note long area of contraction. **B** and **C**, Dilatation of esophageal lumen and irregular contractions in body of esophagus.

treatment. One patient with a hiatal hernia and achalasia developed esophageal perforation and required surgical management (fig. 2). The caliber of the esophagogastric channel changed from a mean of 3.5 mm (range, 2.5–7 mm) before dilation to a mean of 10 mm (range, 7–12 mm) after dilation, increasing in 14 of the 16 patients (fig. 3). One patient showed minor change, and one patient showed no change in the esophagogastric channel diameter.

The mucosal contour of the distal esophagus was smooth in 12 patients (75%) and irregular in four (25%). One patient with irregular mucosal contour and a mucosal tear (fig. 4) had guaiac-positive stools for 2 days after pneumatic balloon dilation. A localized uncomplicated intramural hematoma with associated mucosal tear of the esophagus occurred in one patient with advanced "sigmoid-shaped" achalasic esophagus (fig. 5). There was improvement in the dysphagia after dilation treatment and the clinical course was unremarkable.

Emptying of the esophagus was rapid in the upright position (under 15 min) in 14 patients and slow (over 15 min) in two patients. In two patients, although the esophagogastric channel was widely patent and emptying of the contrast material was rapid, severe irregular nonpropulsive contractions and flow artifacts due to dysmotility were seen in the body of the esophagus with slow emptying [5] (fig. 6). In patients with marked tortuosity of the esophagus (sigmoid esophagus) some barium stagnated in the redundant tortuous segment, but could be evacuated eventually by change in the position of the patient. None of the patients demonstrated radiographic evidence of gastroesophageal reflux.

The esophageal dilatation was evaluated by measuring the diameter of the body of the esophagus on pre- and postdilation esophagrams. Reduction in the dilatation of the esophagus was seen in 13 of the 16 patients. In three patients with mild dilatation (<5 cm), the esophagus returned to normal caliber (<3 cm) on the esophagram obtained 6 months after dilation. In 10 patients with moderate dilatation (5–8 cm), a definite decrease in caliber was seen on esophagram obtained 6–24 months after dilation (<4 cm internal diameter). Three patients with marked tortuosity and dilatation (>8 cm) did not show any change in the caliber on postdilation esophagrams. All patients on subsequent follow-up at 6–24 months underwent at least one esophageal function test including 24-hr pH monitoring for the detection of gastroesophageal reflux. Only two patients demonstrated nonsymptomatic gastroesophageal reflux.

The clinical results of pneumatic balloon dilation were assessed for a period ranging from 4 to 24 months (mean 12). Eleven patients have remained asymptomatic (excellent response), three had mild symptoms (good response), and two had severe symptoms of dysphagia (poor response). The overall satisfactory clinical response was observed in 14 patients (88%). This correlated well with radiographic improvement in esophagogastric channel diameter in 14, decrease in esophageal dilatation in 13, and improvement in esophageal emptying dynamics in 12 patients on follow-up esophagrams obtained 6–24 months after dilation treatment.

Discussion

The treatment of achalasia is directed at achieving a reduction in lower esophageal sphincter tone without disrupting the sphincter enough to result in gastroesophageal reflux. Two

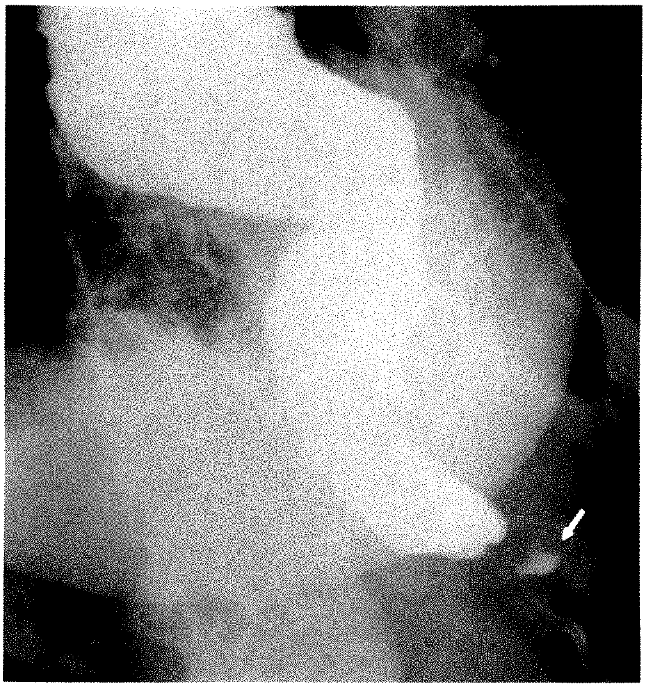

Fig. 5.—Esophagram shows localized intramural hematoma with mucosal disruption (*arrow*) in advanced "sigmoid-shaped achalasic" esophagus. Dysphagia improved after dilation and clinical course was unremarkable.

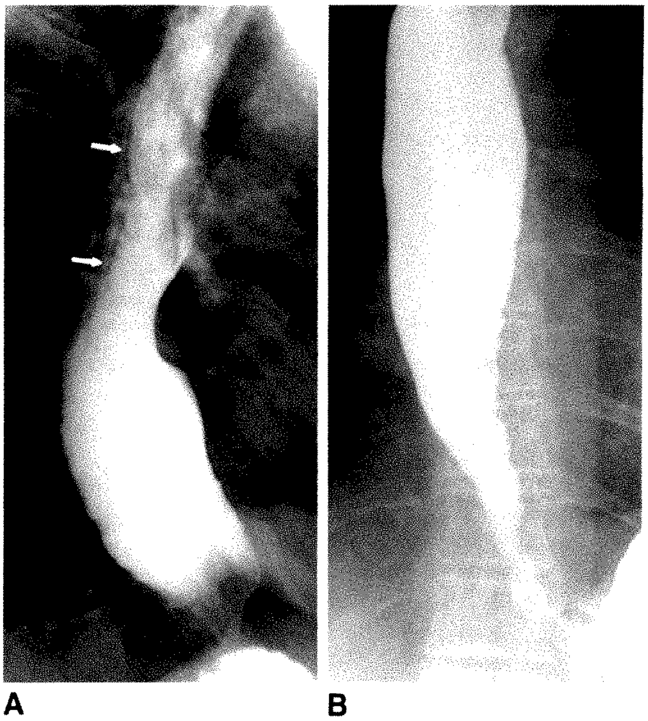

Fig. 6.—**A**, Esophagram 1 year after dilation shows widely patent esophagogastric channel and moderate dilatation of esophagus. Note transient flow artifact (*arrows*) resembling intraluminal diverticulum, indicating esophageal dysmotility. **B**, Another view from same examination shows that artifact is gone, but there are tertiary contractions distally.

modes of therapy, endoscopic mechanical dilation and esophagomyotomy, have gained widespread acceptance. Good to excellent results have been reported from both procedures by various authors [6–14].

Pneumatic dilation is a simple, nonoperative procedure, generally accomplished in one or two dilation sessions. If necessary, further dilation can be performed or the patient may be referred for esophagomyotomy. Although literature regarding esophageal dilation for achalasia indicates that it is an effective form of treatment, differences in techniques and criteria of follow-up make meaningful comparison difficult. Critical analysis of published literature concerning dilation by Wong and Johnson [11] showed a spectrum of 40%–95% of patients having no further dysphagia after the first dilation. Olsen et al. [15] reported that of patients who failed to improve after the first dilation, 38% and 19% improved after second and third dilations, respectively. In their series, the efficacy of pneumatic dilation was not related to the size and tortuosity of the esophagus. Vantrappen and Hellemans [7] noted that young patients did not respond to pneumatic dilation as well as older patients and that patients with a long history of dysphagia before the dilation (mean duration, 8.2 years) did better than patients with a shorter history (mean duration, 2.5 years). Although significant decrease in lower esophageal sphincter pressure occurs immediately after dilation, it tends to increase slightly over a period of time. Neither relaxation of the lower esophageal sphincter with deglutition nor coordinated esophageal peristalsis returns after pneumatic balloon dilation [7].

Vantrappen and Hellemans [7] reported no evidence of reflux after pneumatic dilation evaluated by modified reflux test. Csendes and Strauszer [10] and Bennett and Hendrix [8] reported 7% and 17% incidence of reflux, respectively, but found no evidence of peptic strictures. Vantrappen and Hellemans [7], in a review of 1045 cases collected from 16 published papers on achalasia treated with pneumatic dilations, found a 10% incidence of reflux esophagitis, 3.4% incidence of peptic strictures, and 1.6%–9.4% incidence of esophageal perforation. Ellis et al. [12] and Okike et al. [13], who published the largest surgical series with long-term follow-up, reported a 3% incidence of complications related to gastroesophageal reflux. Since disabling postoperative reflux esophagitis and even Barrett esophagus [16, 17] have been recognized after esophagomyotomy for achalasia, some investigators advocate combining an antireflux operation with esophagomyotomy to counteract this complication [18, 19].

The main emphasis of radiographic examination after dilation therapy had been to detect potential esophageal perforation [20, 21]. Ott et al. [22] recently compared radiographic appearance and clinical response and concluded that the appearance immediately after dilation was a poor predictor of patient response to treatment. Our results differ from theirs and show a radiographic appearance that correlated well with clinical response in 14 (88%) of 16 patients. The diameter of the esophagogastric channel in the 14 patients with improved symptomatology was over 10 mm in seven patients and 8–

10 mm in the other seven patients. Two patients with significant residual dysphagia had esophagogastric channel diameters of 4 and 6 mm, respectively. Therefore, it seems that the minimal effective diameter of the esophagogastric channel for improvement in symptomatology was 8–10 mm in our patients.

ACKNOWLEDGMENT

We thank Barbara Smith for secretarial assistance.

REFERENCES

1. Witzel L. Treatment of achalasia with a pneumatic dilator attached to a gastroscope. *Endoscopy* **1981**;13:176–177
2. Agha FP. The esophagus after endoscopic injection sclerotherapy: acute and chronic changes. *Radiology* **1984**;153:37–42
3. Agha FP, Orringer MB. Colonic interposition: radiographic evaluation. *AJR* **1984**;142:703–708
4. Agha FP, Orringer MB, Amendola MA. Gastric interposition following transhiatal esophagectomy: radiographic evaluation. *Gastrointest Radiol* **1985**;10:17–24
5. Agha FP. Transient intraluminal diverticulum of the esophagus: a significant flow artifact. *Gastrointest Radiol* **1984**;9:99–103
6. Vantrappen G, Hellemans J, Deloof W, Valembois P, Vandenbroucke J. Treatment of achalasia with pneumatic dilatations. *Gut* **1971**;12:268–275
7. Vantrappen G, Hellemans J. Treatment of achalasia and related motor disorder. *Gastroenterology* **1980**;79:144–154
8. Bennett JR, Hendrix TR. Treatment of achalasia with pneumatic dilatation. *Mod Treat* **1970**;7:1217–1228
9. Sanderson DR, Ellis FH Jr, Olsen HM. Achalasia of the esophagus: results of therapy by dilation (1950–1967). *Chest* **1970**;58:116–121
10. Csendes A, Strauszer T. Long term clinical, radiological and manometric follow-up period of patients with achalasia treated with pneumatic dilatation. *Digestion* **1974**;11:124–128
11. Wong RKH, Johnson LF. Achalasia. In: Castell DO, Johnson LF, eds. *Esophageal function in health and disease.* New York: Elsevier Biomedical **1983**:99–123
12. Ellis FH Jr, Gibbs SP, Crozier RE. Esophagomyotomy for achalasia of the eosphagus. *Ann Surg* **1980**;192:157–161
13. Okike N, Payne WS, Neufeld DM, Bernatz PE, Pairolero PC, Sanderson DR. Esophagomyotomy versus forceful dilation for achalasia of the esophagus: results in 899 patients. *Ann Thorac Surg* **1979**;28:119–125
14. Csendes A, Velasco N, Braghetto I, Hendriques A. A prospective randomized study comparing forceful dilatation and esophagomyotomy in patients with achalasia of the esophagus. *Gastroenterology* **1981**;80:789–795
15. Olsen AM, Harrington SW, Moersch HJ, Anderson HA. The treatment of cardiospasm: analysis of a twelve years experience. *J Thorac Cardiovasc Surg* **1951**;22:164–167
16. Kortan P, Warren PE, Gardner J, Ginsberg RJ, Diamant E. Barrett's esophagus in a patient with surgically treated achalasia. *J Clin Gastroenterol* **1981**;3:357–360
17. Feczko PJ, Chan KM, Halpert RD, Batra SK. Barrett's metaplasia and dysphasia in post myotomy achalasia patients. *Am J Gastroenterol* **1983**;78:265–268
18. Tomlinson P, Grant AF. A review of 74 patients with oesophageal achalasia: the results of Hellers cardiomyotomy, with and without Nissen fundoplication. *Aust NZ J Surg* **1981**;51:48–51
19. Pinotti HW, Sakai P, Ishioka S. Cardiomyotomy and fundoplication for esophageal achalasia. *Jpn J Surg* **1983**;13:399–403
20. Stewart ET, Miller WN, Hogan WJ, Dodds WJ. Desirability of roentgen esophageal examination immediately after pneumatic dilation for achalasia. *Radiology* **1979**;130:589–591
21. Zegel HG, Kressel HY, Levine GM, Rosato EF. Delayed esophageal perforation after pneumatic dilatation for the treatment of achalasia. *Gastrointest Radiol* **1979**;4:219–221
22. Ott DJ, Wu WE, Gelfand DW, Richter JE. Radiographic evaluation of the achalasic esophagus immediately following pneumatic dilatation. *Gastrointest Radiol* **1984**;9:185–191

Book Reviews

Noninvasive Diagnostic Techniques in Vascular Disease, 3d ed. Edited by Eugene F. Bernstein. St. Louis: Mosby, 919 pp., 1985.

This is the third edition of this text. The second edition was published in 1982. Because of the expansion in technology and changes in philosophy, this new edition includes 50 chapters that are new or radically revised. The editor is a vascular surgeon and his associate editors are also primarily surgeons with the exception of George R. Leopold. Thus, the emphasis is primarily geared to the vascular surgeon. However, radiologists, cardiologists, and internists interested in the noninvasive evaluation of vascular disease can also learn a great deal from the text.

This new edition has 75 contributors, 10 are from radiology departments. The text is divided into three divisions. Part I deals with the fundamentals of measurement and current instrumentation. Part II addresses areas of application, detection, quantification, and prediction. It is subdivided into extracranial occlusive disease, peripheral arterial disease, and peripheral venous disease. Part III includes the final two chapters and is the most pragmatic part of the text. This deals with the practical aspects of organizing a vascular laboratory and evaluating the data obtained.

The new edition is an excellent reference text for any vascular laboratory or for anyone about to set up such a laboratory, because it deals not only with philosophy but with practical aspects of setting up such a laboratory as well. New areas mentioned in this edition include digital subtraction angiography, positron emission tomography, and magnetic resonance imaging. Each of these methods is described in detail by an expert in the field. Chapter 69 is especially interesting because it discusses the controversies in noninvasive studies of peripheral arterial disease.

However, for a radiologist not primarily involved in a vascular laboratory or in performing Doppler sonography, this text is much too detailed and overwhelming. I do not recommend it for a resident about to take his boards in radiology for these same reasons.

Patricia Ann Randall
Upstate Medical Center
Syracuse, NY 13210

Myelofibrosis. Pathophysiology and Clinical Management. Edited by S. M. Lewis. New York: Dekker, 207 pp., 1985. $65

An international group of experts has collaborated to produce a first-class monograph on this complex disease. The chapters on historical perspectives of the disease and clinical and hematological aspects and treatment will be of interest to all radiologists both diagnostic and therapeutic. The chapter on ferrokinetics and erythrokinetic studies will have a specialized appeal to those practicing nuclear medicine. Most of the book is devoted to cytologic and hematologic matters, unlikely to be of interest to most radiologists.

There is a succinct account of the radiographic appearance of bones in myelofibrosis. Mention is made of the less common osteolytic variety plus the more common osteosclerotic and normal appearances. For most diagnostic radiologists, the value of this monograph will not be in the short radiographic section, but in the superb clinical description of the natural history of this disease. The patient with myelofibrosis may enter the x-ray department with presenting symptoms and signs of anemia, portal hypertension, splenomegaly, or bone pain, and a knowledge of these signs and symptoms will be of value to radiologists.

I particularly enjoyed reading the chapter on clinical hematologic aspects of myelofibrosis by C. G. Geary from University Department of Hematology, Royal Infirmary, Manchester, England, because my first civilian job on demobilization after World War II was bottle washer and "cleaner upper" in this lab.

Leslie Preger
Highland General Hospital
Oakland, CA 94602

Serpiginous Gastric Erosions Caused by Aspirin and Other Nonsteroidal Antiinflammatory Drugs

Marc S. Levine[1]
Anthony Verstandig
Igor Laufer

Erosive gastritis is a common disease, but no etiologic significance has been attributed to the size or shape of these gastric erosions. However, in 12 cases of erosive gastritis caused by aspirin (nine) and other nonsteroidal antiinflammatory drugs (NSAIDs) (indomethacin, two; naproxen, one) double-contrast upper gastrointestinal studies revealed incomplete linear and/or serpiginous erosions in the stomach. In nine cases, these distinctive erosions were clustered focally in the body of the stomach, on or near the greater curvature. All but one patient were symptomatic (epigastric pain, eight; upper gastrointestinal bleeding, two; nausea and vomiting, one), and marked clinical improvement occurred within several days after withdrawal of the offending agent. This experience suggests that incomplete linear or serpiginous erosions, particularly along the greater curvature of the stomach, should be strongly suggestive of aspirin- or other NSAID-induced gastritis. If recent ingestion of these drugs is confirmed, withdrawal of the offending agent should lead to a rapid clinical response in these patients.

Erosive gastritis has become a relatively frequent finding on double-contrast upper gastrointestinal (GI) studies; an overall incidence of 0.5%–20% is reported in the radiologic literature [1–6]. Most patients have complete or "varioliform" erosions in which a punctate or slitlike collection of barium is surrounded by a radiolucent halo of edematous mucosa [3, 5, 7, 8]. In contrast, incomplete or "flat" erosions appear as dots or linear streaks of barium without an edematous halo [6–8]. Because the surrounding mucosa is normal, incomplete erosions have been extremely difficult to detect radiographically, accounting for less than 5% of all erosions seen on double-contrast studies [6].

In about 50% of patients with erosive gastritis, there are no apparent predisposing factors [7]. However, known causes include alcohol, aspirin, other nonsteroidal antiinflammatory drugs (NSAIDs), steroids, stress, trauma, burns, Crohn disease, and viral or fungal infection [7, 9–15]. To our knowledge, no etiologic significance has yet been attributed to the size or shape of these gastric erosions. However, we have observed unusual serpiginous erosions in the stomach on double-contrast upper GI studies performed on several patients who were known to be taking aspirin at the time of the study. We subsequently collected 12 cases of aspirin- and other NSAID-induced gastritis with these distinctive serpiginous erosions.

Materials and Methods

Between 1981 and 1984, 15 cases collected at our hospital had double-contrast upper GI studies that revealed multiple linear and/or serpiginous gastric erosions. A drug history was obtained either by questioning the patient at the time of the examination or by subsequent review of patient records. No recent drug ingestion could be documented in three patients: two had an unknown drug history and one denied taking any drugs. The other 12 patients were found to have taken aspirin or other NSAIDs within 2 days of the radiologic study. The radiographs of all 12 patients were reviewed retrospectively to determine the appearance,

Received June 18, 1985; accepted after revision August 15, 1985.

Presented at the annual meeting of the American Roentgen Ray Society, Boston, April 1985.

[1] All authors: Department of Radiology, Hospital of the University of Pennsylvania, 3400 Spruce St., Philadelphia, PA 19104. Address reprint requests to M. S. Levine.

***AJR* 146:31–34, January 1986**
0361-803X/86/1461-0031
© American Roentgen Ray Society

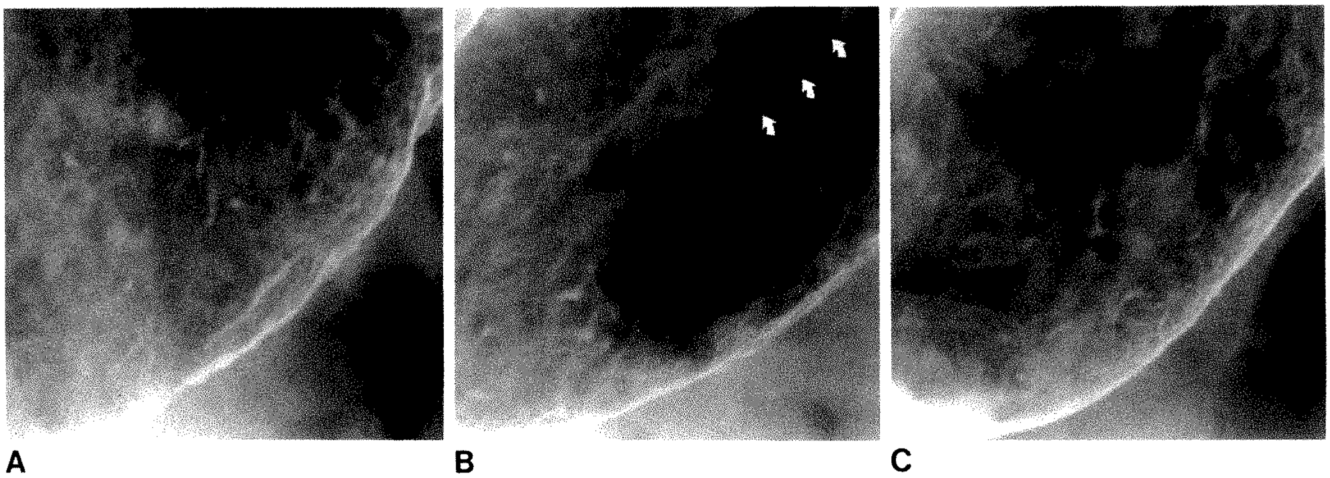

Fig. 1.—Examples of serpiginous erosions in body of stomach caused by aspirin (**A** and **B**) and indomethacin (**C**). In all cases, incomplete linear and serpiginous erosions are predominantly located near greater curvature. In **B**, typical varioliform erosions can also be seen more proximally in stomach, aligned on rugal fold (*arrows*).

number, size, and location of these gastric erosions and to document other associated abnormalities in the stomach or duodenum. Medical records were also reviewed to determine the presenting clinical findings, treatment, and subsequent patient course.

Results

Drug History

Nine patients had histories of recent aspirin ingestion; the dose was 2–8 tablets per day for 2 days to 6 months before the upper GI study. Two patients had taken about three indomethacin capsules per day for 2 weeks, and one had taken three naproxen tablets per day for 3 days before the radiologic study. The major reasons for aspirin or other NSAID use included headaches, muscular pain, temporomandibular joint pain, and arthritis.

Clinical Findings

The major presenting findings were epigastric pain (eight cases), nausea and vomiting (one), and upper GI bleeding (melena, one; guaiac-positive stool, one). One patient was asymptomatic. Follow-up clinical data were available in five cases in which marked clinical improvement occurred within several days after withdrawal of the offending agent and treatment with antacids and/or histamine H_2 blockers.

Radiographic Findings

All 12 patients had distinctive linear and/or serpiginous erosions in the stomach on double-contrast upper GI examinations (figs. 1–3). Because these lesions generally were not associated with a surrounding halo of edematous mucosa, they could be classified radiographically as incomplete erosions. The number of linear or serpiginous erosions seen radiographically was between six and 10 in six patients and more than 10 in six patients. The maximal length of these erosions was generally 2–6 mm, although they were occasionally as long as 1 cm.

In nine cases, these incomplete linear or serpiginous erosions were clustered focally in the body of the stomach, on or near the greater curvature (fig. 1). Two of those patients also had serpiginous erosions in the antrum. In two other cases, these distinctive erosions were confined to the gastric antrum (fig. 2). In the remaining case, the erosions were located near the lesser curvature of the body of the stomach.

Eight patients had other associated radiographic abnormalities in the stomach or duodenum. Four had scattered varioliform erosions in the antrum or body of the stomach (fig. 1B). Three patients on aspirin had antral ulcers (greater curve, one; lesser curve, two) (fig. 3). Finally, one patient had radiographic evidence of duodenitis with thickened, nodular folds in the proximal duodenum.

Endoscopic Findings

Because these patients responded so rapidly to medical treatment, endoscopy was rarely performed. However, an endoscopic examination 1 day after the upper GI study in a patient with a lesser-curvature antral ulcer confirmed the presence of multiple linear erosions in the antrum and body of the stomach and a benign-appearing antral ulcer.

Discussion

Both clinical and laboratory investigations have shown that aspirin and other NSAIDs are capable of disrupting the mucosal barrier in the stomach, causing erosive gastritis and gastric ulcers [10, 11, 16–25]. In one study, 40% of patients on chronic aspirin therapy for 3 months or longer had endoscopic evidence of erosive gastritis and 17% had gastric ulcers [22]. Other studies on healthy volunteers have shown

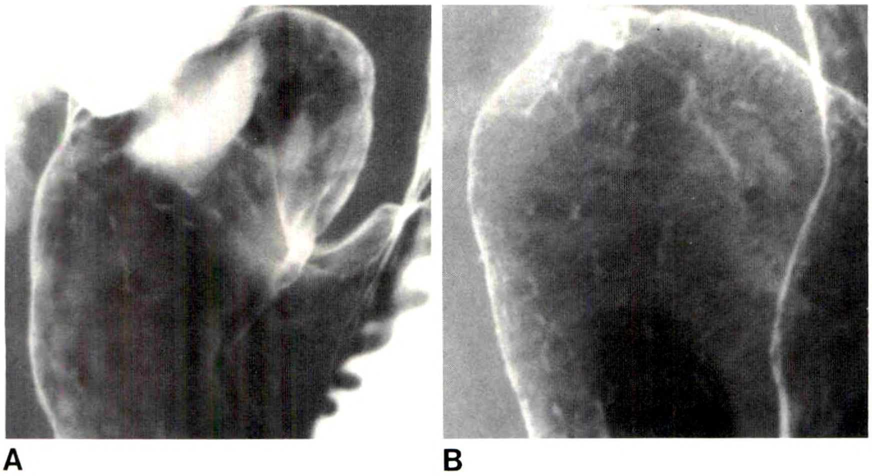

Fig. 2.—Examples of incomplete linear and serpiginous erosions in gastric antrum caused by aspirin (**A**) and naproxen (**B**).

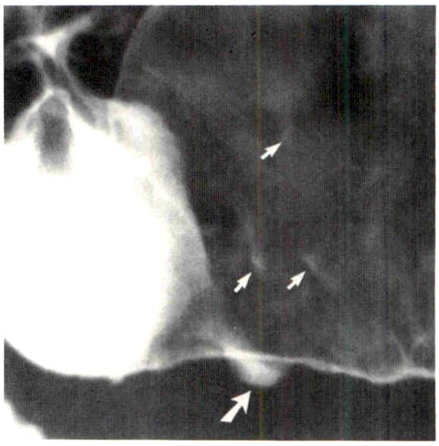

Fig. 3.—Linear erosions in gastric antrum (*small arrows*) with associated ulcer on greater curvature (*large arrow*) caused by recent aspirin ingestion. Additional radiographs showed other serpiginous erosions in body of stomach near greater curvature.

that two or more aspirin tablets may cause an acute erosive gastritis that can be recognized endoscopically within 24 hr after ingesting the drug [23–25]. Maximal damage usually occurs by 1–3 days, and evidence of healing may be documented endoscopically by 1 week [25]. Thus, gastric erosions may form rapidly after aspirin ingestion and may heal rapidly when the drug is withdrawn.

Our experience suggests that aspirin- or other NSAID-induced gastritis may be manifested by distinctive linear and/or serpiginous erosions in the stomach that are readily apparent on double-contrast upper GI examinations (figs. 1–3). In our study, 12 patients with these serpiginous erosions who had a known drug history had taken two or more aspirin, indomethacin, or naproxen tablets within 2 days of the radiologic examination. All but one patient were symptomatic, and follow-up data revealed marked clinical improvement within several days after withdrawal of the medication. Thus, it seems reasonable to conclude that these erosions were drug induced.

The serpiginous erosions observed in these patients should be distinguished radiographically from the more common varioliform erosions that are typically found in the antrum of the stomach, often aligned on rugal folds [3, 5, 14]. In contrast, these incomplete linear or serpiginous erosions were usually clustered on or near the greater curvature of the gastric body and were rarely aligned on rugal folds (fig. 1). As a result, the distinctive appearance of these lesions should be strongly suggestive of aspirin- or other NSAID-induced gastritis. Nevertheless, these patients may also have typical varioliform erosions (fig. 1B) or ulcers (fig. 3) caused by ingestion of these drugs.

The exact pathogenesis of these serpiginous erosions is uncertain. However, it has been shown that gastric mucosal damage after oral doses of aspirin is a topical rather than a systemic effect of the drug [26]. Further, aspirin-induced ulcers are often located on the greater curvature of the body or antrum of the stomach [19, 20, 27]. As a result, it has been postulated that these ulcers result from localized mucosal injury as the dissolving aspirin tablets collect by gravity in the most dependent part of the stomach [27]. Because of their typical location, these benign greater curvature gastric ulcers have been described as "sump ulcers" [27]. Similarly, this phenomenon may account for the frequent location of these serpiginous aspirin-induced erosions in the body of the stomach on or near the greater curvature.

In summary, the presence of incomplete linear and/or serpiginous erosions in the stomach, particularly along the greater curvature, should be strongly suggestive of aspirin- or other NSAID-induced gastritis. Because a drug history may not have been volunteered at the time of the examination, this finding should lead to further questioning of the patient about aspirin or other NSAID use. If recent ingestion of these drugs is confirmed, withdrawal of the offending agent should lead to a rapid clinical response in these patients.

REFERENCES

1. Poplack W, Paul RE, Goldsmith M, Matsue H, Moore JP, Norton R. Demonstration of erosive gastritis by the double-contrast technique. *Radiology* **1975**;117:519–521
2. Laufer I. An assessment of the accuracy of double contrast gastroduodenal radiology. *Gastroenterology* **1976**;71:874–878
3. Op den Orth JO, Dekker W. Gastric erosions: radiological and endoscopic aspects. *Radiol Clin* (Belg) **1976**;45:88–99
4. Op den Orth JO, Dekker W. Gastric polyps or erosions. *AJR* **1977**;129:357–358
5. Tragardh B, Wehlin L, Ohashi K. Radiologic appearance of complete gastric erosions. *Acta Radiol [Diagn]* (Stockh) **1978**;19:634–642
6. Catalano D, Pagliari U. Gastroduodenal erosions: radiological findings. *Gastrointest Radiol* **1982**;7:235–240
7. Laufer I, Hamilton J, Mullens JE. Demonstration of superficial gastric erosions by double contrast radiography. *Gastroenterology* **1975**;68:387–391

8. Laufer I. *Double contrast gastrointestinal radiology with endoscopic correlation*. Philadelphia: Saunders, **1979**:166–173
9. Roberts DM. Chronic gastritis, alcohol, and non-ulcer dyspepsia. *Gut* **1972**;13:768–774
10. Thorsen WB, Western D, Tanaka Y, Morrissey JF. Aspirin injury to the gastric mucosa: gastrocamera observations on the effect of pH. *Arch Intern Med* **1968**;121:499–506
11. Lanza F, Royer G, Nelson R. An endoscopic evaluation of the effects of non-steroidal anti-inflammatory drugs on the gastric mucosa. *Gastrointest Endosc* **1975**;21:103–105
12. Laufer I, Trueman T. Multiple superficial gastric erosions due to Crohn's disease of the stomach. Radiologic and endoscopic diagnosis. *Br J Radiol* **1976**;49:726–728
13. Cronan J, Burrell M, Trepeta R. Aphthoid ulcerations in gastric candidiasis. *Radiology* **1980**;134:607–611
14. McLean AM, Paul RE, Philipps E, et al. Chronic erosive gastritis—clinical and radiological features. *J Can Assoc Radiol* **1982**;33:158–162
15. Kressel HY. Peptic disease of the stomach and duodenum. In: Margulis AR, Burhenne JH, eds. *Alimentary tract radiology*, 3d ed. St. Louis: Mosby, **1983**:794–796
16. Davenport HW. Salicylate damage to the gastric mucosal barrier. *N Engl J Med* **1967**;276:1307–1312
17. Chapman BL, Duggan JM. Aspirin and uncomplicated peptic ulcer. *Gut* **1969**;10:443–450
18. Edmar D. Effects of salicylates on the gastric mucosa as revealed by roentgen examination and the gastrocamera. *Acta Radiol [Diagn]* (Stockh) **1971**;11:57–64
19. Emmanuel JH, Montgomery RD. Gastric ulcer and the anti-arthritic drugs. *Postgrad Med J* **1971**;47:227–232
20. MacDonald WC. Correlation of mucosal histology and aspirin intake in chronic gastric ulcer. *Gastroenterology* **1973**;65:381–389
21. Cameron AJ. Aspirin and gastric ulcer. *Mayo Clin Proc* **1975**;50:565–570
22. Silvoso GR, Ivey KJ, Butt JH, et al. Incidence of gastric lesions in patients with rheumatic disease on chronic aspirin therapy. *Ann Intern Med* **1979**;91:517–520
23. O'Laughlin JC, Hoftiezer JW, Ivey KJ. Effect of aspirin on the human stomach in normals: endoscopic comparison of damage produced one hour, 24 hours, and 2 weeks after administration. *Scand J Gastroenterol* **1981**;16:211–214
24. Lanza FL, Nelson RS, Rack MF. A controlled endoscopic study comparing the toxic effects of sulindac, naproxen, aspirin, and placebo on the gastric mucosa of healthy volunteers. *J Clin Pharmacol* **1984**;24:89–95
25. Graham DY, Smith JL, Dobbs SM. Gastric adaptation occurs with aspirin administration in man. *Dig Dis Sci* **1983**;28:1–6
26. Ivey KJ, Paone DB, Krause WJ. Acute effect of systemic aspirin on gastric mucosa in man. *Dig Dis Sci* **1980**;25:97–99
27. Kottler RE, Tuft RJ. Benign greater curve gastric ulcer: the "sump-ulcer." *Br J Radiol* **1981**;54:651–654

The Effect of Barium Suspension Viscosity on the Delineation of Areae Gastricae

Stephen E. Rubesin[1, 2]
Hans Herlinger[1]

The viscosity of a barium suspension is an important and controllable variable that influences the quality of mucosal detail demonstrated by double-contrast upper gastrointestinal examination. High-density barium suspensions show a notable viscosity response to seemingly trivial changes in the amount of water added. A double-blind trial involving 600 patients used E-Z-HD of the same batch number suspended with 65–70 ml water. Overall, areae gastricae covering at least 25% of the stomach surface were seen in 68.3%; no or minimal areae gastricae were seen in 31.7%. The corresponding figures for the suspension of optimal viscosity were 80% and 20%, respectively.

Double-contrast studies of stomach or colon rely primarily on exquisite mucosal surface detail and secondarily on examination of the lumen and its contour [1, 2]. The ability to outline the areae gastricae is of value in the demonstration of gastric erosions, intestinal metaplasia, ulcer scars, and early malignancy [2–4]. Visibility of areae gastricae is also indicative of good technique [5, 6].

By in vitro studies of five barium products, Virkunnen and Retulainen [4] showed that the density/viscosity interrelation influenced the visibility of the areae gastricae. They were able to measure the thickness of the barium coating on pig gastric mucosa and relate areae gastricae demonstration to an "index of visibility," the ratio of the height of the barium layer on the grooves over that on the areae themselves. An optimum index of visibility could be established for each barium product, with decreased areae gastricae visibility at lesser and at greater viscosity levels.

In pilot experiments, we discovered that the viscosity of barium suspensions changed dramatically and disproportionately to small changes in density. In a clinical trial of 600 patients, we set out to establish the optimum viscosity for precise radiographic diagnosis with E-Z-HD barium.

Materials and Methods

A pilot study was undertaken of some of the variables that alter barium suspension viscosity. Varying amounts of water were carefully added to a single batch of E-Z-HD cups containing 340 g of barium. At constant room temperature, the viscosity of each suspension was measured three times by using a stainless-steel Ford cup viscometer (100-ml volume, 4-mm diameter hole), a technique similar to that used by others [2, 4, 6]. This was repeated with virtually identical results at the start of the clinical study. The effect on the viscosity of altering the temperature of a barium suspension made with 65 ml of water was also investigated.

In the clinical study involving 600 double-contrast upper gastrointestinal (GI) examinations, E-Z-HD barium of the same batch of manufacture was carefully suspended with 65–70 ml of water to provide for six groups of 100 patients each. The viscosity of the suspensions was changed daily without informing the examining radiologists. Routine double-contrast upper GI studies were performed by radiologists of varying experience, using standard projections [1]. The technique included use of E-Z-Gas swallowed with 10 ml of water for gaseous

Received April 25, 1985; accepted after revision August 13, 1985.

[1] Department of Radiology, Hospital of the University of Pennsylvania, 3400 Spruce St., Philadelphia, PA 19104. Address reprint requests to H. Herlinger.

[2] Present address: Russell H. Morgan Department of Radiology and Radiological Sciences, Johns Hopkins Medical Institutions Baltimore, MD 21205.

AJR 146:35–38, January 1986
0361–803X/86/1461–0035
© American Roentgen Ray Society

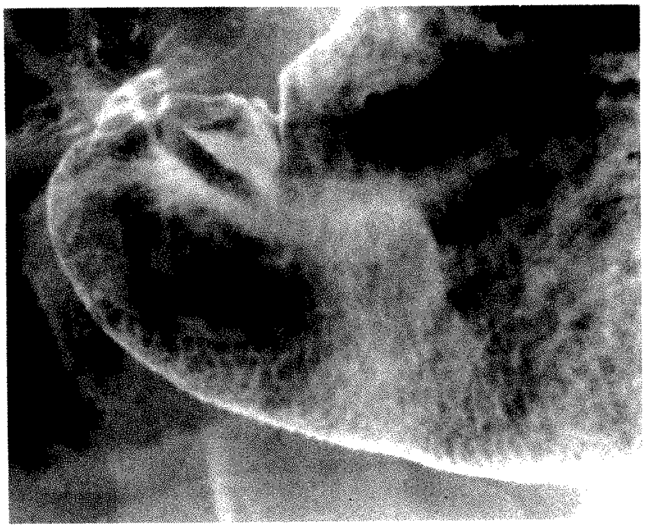

Fig. 1.—Spot film from double-contrast upper GI study. Incomplete mosaic groove pattern outlines areae gastricae.

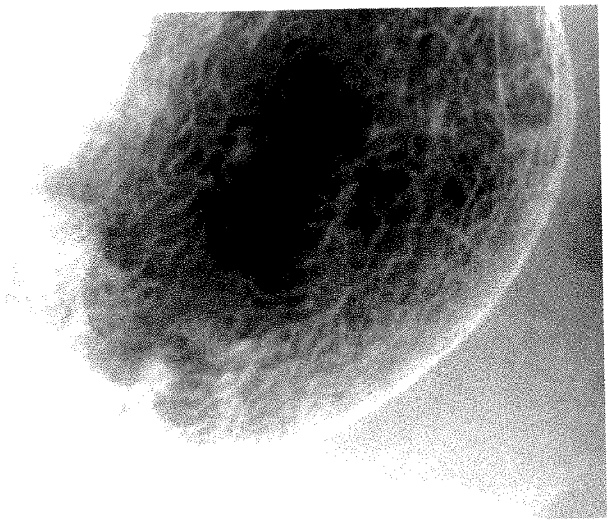

Fig. 2.—Spot film from double-contrast upper GI study. Complete mosaic groove pattern defines areae gastricae.

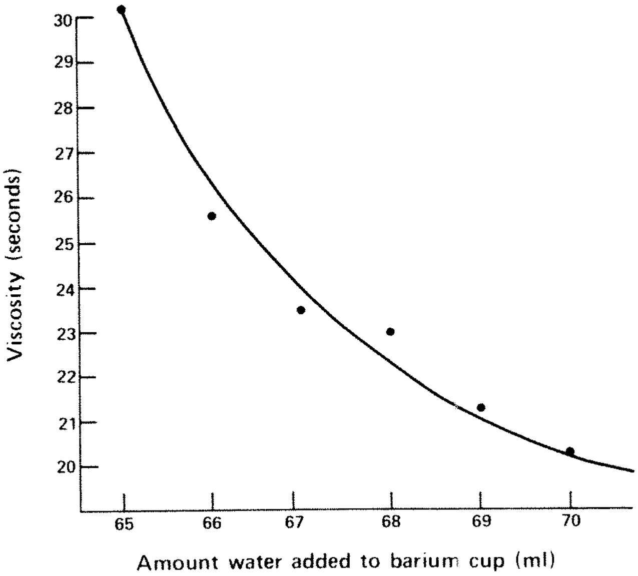

Fig. 3.—Slight (1-ml) variation in amount of water added to 340-g cup of E-Z-HD barium causes significant variation in barium suspension viscosity. Viscosity is expressed as amount of time (sec) for 100 ml of barium suspension to pass continuously through Ford cup viscometer with 4-mm hole.

TABLE 1: **Viscosity Changes in Barium Suspension with Addition of Water**

Amount of Water (ml) Added to Cup of E-Z-HD	Areae Gastricae Visibility in 600 Patients (%)		In vitro Viscosity (Ford cup sec)	In vitro Density (g/ml)
	<25%	25%–100%		
65	34	66	30.2	2.97
66	32	68	25.6	2.96
67	20	80	23.5	2.95
68	36	64	22.9	2.94
69	36	64	21.1	2.92
70	32	68	20.3	2.91

distension and 0.1 ml of glucagon given intravenously for hypotonia. Postoperative patients were excluded. Right lateral, supine, and occasionally left posterior oblique films of each examination were retained by the senior technologist and were tagged by random lettering to record the type of barium used. One of us (S. R.), who had not performed any of the studies, later evaluated the films by an agreed protocol. The quality and quantity of the areae gastricae were subjectively assessed. The amount of areae gastricae shown was expressed as a percentage of the stomach surface free of the barium pool (0–25%, >25%, >50%, >75%, 100%).

With regard to their quality, areae gastricae were assessed as merely "being present" if the mosaic groove pattern was incomplete, partly replaced by interrupted lines (fig. 1). "Good-quality" areae gastricae were surrounded by grooves well delineated with barium (fig. 2). The quality of the mucosal contour line was deemed "poor" if patchy or faint and "satisfactory" if it presented a uniform white line. The amounts of gas bubbles, excess fluid, and gaseous distension were also noted.

The radiographic diagnosis of each patient was recorded after their films were evaluated. Patients with radiographic evidence of peptic disease were divided into four groups: gastric ulcer, erosive gastritis, duodenal ulcer, or duodenal erosions.

Results

In vitro Studies

The viscosity response of barium suspensions at room temperature to the gradual alteration of the amount of added water is shown in figure 3 and table 1. With small (1-ml) amounts of added water, barium suspensions rapidly become less viscous, although their densities changed much less proportionately. With addition of 5–65 ml of water, viscosity diminished by 50%, although density decreased by only 2%. With increasing temperature, the barium suspension viscosity also decreased (fig. 4).

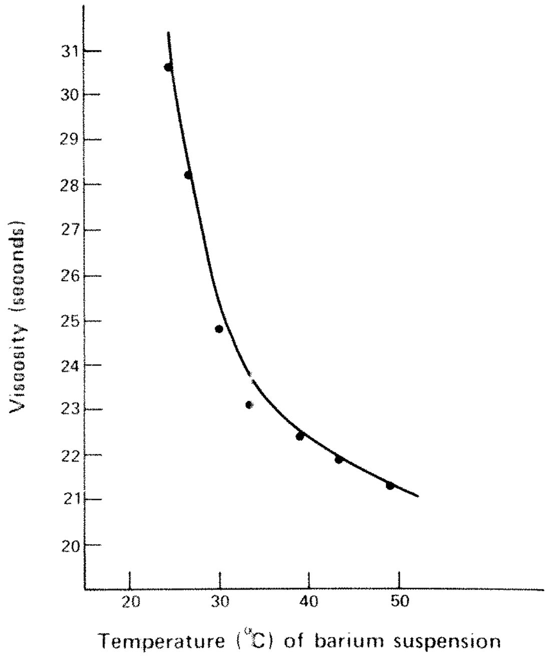

Fig. 4.—Barium suspension viscosity changes dramatically with changes in temperature. Barium suspension was 65 ml of water added to 340-g cup of E-Z-HD barium.

Clinical Trial

The average age of the 600 patients was 51.1 years; 60% were female, 40% male. Twenty percent had radiographic evidence of peptic ulcer disease: gastric or duodenal ulcers and/or erosions.

Extent of areae gastricae visibility expressed as percentage of the mucosal surface free of pooled barium is listed in table 1. Overall, areae gastricae covering more than 25% of the stomach surface were identified in 68.3% of patients, while none or only few areae were identified in 31.7%. With barium of optimum viscosity, areae gastricae extending over more than 25% of the stomach surface were seen in 80% of patients. The image quality of the areae gastricae did not vary to any significant extent within the range of viscosities used. The uniformity and quality of the contour line was also unaffected by the changes in viscosity.

Areae gastricae were seen with greater frequency and quality in patients with radiographic evidence of peptic disease involving the stomach or duodenum (table 2). Areae gastricae covering more than 25% of the stomach surface area were seen in 65% of patients without radiographic evidence of peptic disease and in 80% of patients with peptic disease. There was no difference in areae gastricae visibility between patients with duodenal ulcer and those with gastric ulcer. The image quality of the areae gastricae was shown to be improved in patients with either duodenal or gastric ulcer.

Discussion

Understanding barium suspensions is a prerequisite for precise gastrointestinal radiology. Barium is a strong adsorber of water and salts. When sequential increments of water are added to barium powder, the mixture remains a thick paste until the binding sites on the barium particles not already occupied by salts have been filled by the water. When the binding sites are occupied, excessive water becomes available for slippage between particles and the suspension liquefies. In this range, even small increments of water significantly alter the viscosity.

TABLE 2: **Correlation of Disease with Visibility of Areae Gastricae**

	Areae Gastricae Visibility (%)		Areae Gastricae Quality (%)	
	<25%	25%-100%	Fair	Good
No peptic disease	35	65	42	23
Peptic disease (overall)	20	80	44	36
Duodenal ulcer	19	81	36	45
Gastric ulcer	19	81	35	46
Erosive gastritis	23	77	57	20

The water requirements for fluidity of a suspension depend not only on the amount of salt already adsorbed by the particles, but also on the total surface area of all particles constituting a unit weight of barium powder [7]. The distribution of particle sizes greatly affects the total surface area. The milling process of quarried barium cannot produce a consistently identical heterogeneous pattern of particle sizes. Suspensions prepared from different batches of manufacture of the same brand of barium may, therefore, show a nonuniform range of viscosities [8].

The density (opaqueness) of the barium suspension, although related to viscosity, is a separate quality largely dependent on particle size [7]. In our study, there was a 50% decrease in the viscosity with only a 2% decrease in density of the barium suspension.

Areae gastricae are tufts of gastric mucosa separated by a mosaic of grooves 1-5 mm apart [4, 9]. The mosaic pattern is unchanged with contraction of either muscularis mucosae or muscularis propria or with stretching of the stomach wall [9].

The barium lies on top of and does not penetrate the mucus layer secreted by the gastric mucosa [9]. Demonstration of the groove pattern is primarily affected by the ratio of barium thickness in the grooves vs. that over the tufts [4], a relatively higher proportion of contrast material over the grooves being required. Some investigators believe that rapid sedimentation of larger particles into the grooves contributes to radiographic contrast [7, 10].

A thick, viscous layer of barium may obscure the micromucosal pattern [2] because of an excessive amount of barium over the tufts. Increasing barium viscosity also gives uneven coating and increased bubble retention [6]. Thus, lower viscosities are preferred. However, barium of unduly low viscosity will coat grooves and elevations with an even, thin layer, providing an unfavorable "index of visibility" [4].

Areae gastricae have been shown to be more visible [11] and larger [9] in patients with duodenal ulcer disease, although there is considerable overlap with normal patients.

The enlarged areae gastricae may reflect an increased parietal cell mass [9]. Our study confirms that areae gastricae are seen with greater frequency in patients with duodenal ulcer (table 2) and are seen with greater frequency and prominence in patients with gastric ulcer. It has been shown that the thickness of the native mucus layer in the antrum of duodenal ulcer patients is significantly reduced compared to that in normals (Allen A, personal communication). This presumably allows better barium filling of grooves between tufts of gastric mucosa with better visibility of the mucosal groove pattern.

In vitro testing of barium suspensions in a controlled environment can indicate only the basis beyond which, in the in vivo situation, the presence of intragastric fluids and higher temperatures will alter barium qualities. It is impossible to predict the in vivo barium suspension viscosity in an individual patient. However, the use of in vitro determination as a predictor of barium suspension performance is of value in a large patient sample, as an optimum viscosity for the demonstration of areae gastricae could be established. Overall, areae gastricae covering more than 25% of the stomach surface were demonstrated in 68.3% of patients. This figure correlates with the demonstration rate of about 70% reported by Gelfand [2]. However, with barium of optimum viscosity, 80% of patients had areae gastricae covering more than 25% of the surface.

Our study indicates that the meticulous preparation of barium suspensions is a necessary requirement for optimal mucosal detail. The plastic measuring cup supplied by E-Z-EM for barium suspension is inadequate for accurate measuring of water. E-Z-EM recommend that "approximately 65 ml" be added to their barium container. We recommend the addition of 67 ml of water measured from a graduated cylinder, pipette stand, or syringe with 1-ml incremental markings.

REFERENCES

1. Laufer I. *Double contrast gastrointestinal radiology with endoscopic correlation.* Philadelphia: Saunders, **1978**
2. Gelfand DW. High density, low viscosity barium for fine mucosal detail on double contrast upper gastrointestinal examinations. *AJR* **1978**;130:831-833
3. Miller RE. The areae gastricae: epilogue. *AJR* **1979**;132:1023-1024
4. Virkunnen P, Retulainen M. Visualization of the areae gastricae in double contrast examination. *Gastrointest Radiol* **1980**;5:325-329
5. Seaman WB. The areae gastricae. *AJR* **1978**;131:554
6. Cumberland DC. Optimum viscosity of barium suspension for use in the double-contrast barium meal. *Gastrointest Radiol* **1977**;2:169-174
7. Miller RE, Skucas J. *Radiographic contrast agents.* Baltimore: University Park, **1977**
8. Virkkunen P. Variations in the quality of barium sulfate contrast media. *Radiology* **1981**;140:833-834
9. MacIntosh CE, Kreel L. Anatomy and radiology of the areae gastricae. *Gut* **1977**;18:855-864
10. Anderson W, Harthill JE, James WB, Montgomery D. Areae gastricae. *AJR* **1980**;134:210-211
11. Rose C, Stevenson GW. Correlation between visualization and size of the areae gastricae and duodenal ulcer. *Radiology* **1981**;139:371-374

Radiologic Manifestations of Small-Bowel Toxicity Due to Floxuridine Therapy

Frederick M. Kelvin[1]
Herbert F. Gramm[2]
W. Larry Gluck[3]
Jacob J. Lokich[4]

Floxuridine (5-FUDR) is an antipyrimidine used in the treatment of metastatic colorectal carcinoma. Bowel toxicity, manifested predominantly by diarrhea and abdominal pain, is one of the main complications of 5-FUDR therapy. Six patients who had received 5-FUDR infusion either by hepatic arterial or systemic intravenous routes subsequently developed severe diarrhea and were evaluated by small-bowel series. Radiographic changes were largely confined to the ileum. In four of six patients, the entire ileum or its more distal part was markedly narrowed. In the other two patients, changes consisted of thickening or effacement of the mucosal folds in the distal ileum. The symptoms of all six patients resolved after discontinuation of 5-FUDR therapy. This was accompanied by improvement in the radiographic appearance of the ileum in three patients who underwent a subsequent small-bowel series. The finding of reversible ileal changes, particularly extensive or segmental narrowing, seems to be a characteristic radiographic feature of bowel toxicity due to infusional 5-FUDR delivered by either the intraarterial or the systemic route.

The life expectancy of patients with metastatic colorectal carcinoma averages less than a year. Chemotherapeutic agents administered by either the intravenous or hepatic artery route are sometimes used in an attempt to palliate such patients. The antimetabolites most commonly used are fluorouracil (5-FU) and floxuridine (5-FUDR) [1–3]. In the last few years, a resurgence of interest in hepatic artery chemotherapy with 5-FUDR has resulted from development of a totally implantable infusion pump [3–7].

While stomatitis is the major dose-limiting symptom with 5-FU therapy, diarrhea is the most common toxic manifestation of 5-FUDR infusion [1, 2, 8]. We are unaware of any reports in the radiologic literature that document the radiographic manifestations of small-bowel toxicity of 5-FUDR. We describe the radiographic changes in the small bowel seen in three patients undergoing hepatic arterial infusion, including two cases of arterial infusion already reported by Gluck et al. [9], and three patients with intravenous infusion chemotherapy with 5-FUDR.

Case Reports

Hepatic Arterial Infusion of 5-FUDR

Twenty-four patients with colorectal carcinoma metastatic to the liver were treated with hepatic artery infusion of 5-FUDR at Duke University Medical Center between January 1983 and January 1985. Two of these 24 patients developed diarrhea and fever during chemotherapy and were subsequently evaluated by a small-bowel series. These two patients constitute cases 1 and 2. A third patient with similar findings was treated at the New England Deaconess Hospital and is reported as case 3.

Case 1.—A 47-year-old man with hepatic metastases due to colorectal carcinoma underwent surgical implantation of a hepatic artery infusion pump (Infusaid). Infusion with 5-FUDR via the hepatic artery (0.3 mg/kg/day for 14 days every 4 weeks) was subsequently started. Four months later the patient had fever and diarrhea as well as signs of small-bowel

Received May 23, 1985; accepted after revision September 11, 1985.

[1] Department of Radiology, Duke University Medical Center, Durham, NC 27710. Present address: Department of Radiology, Methodist Hospital of Indiana, P.O. Box 1367, Indianapolis, IN 46202. Address reprint requests to F. M. Kelvin.

[2] Department of Radiology, Harvard Medical School, New England Deaconess Hospital, Boston, MA 02215.

[3] Department of Medicine, Duke University Medical Center, Durham, NC 27710.

[4] Department of Medicine, Harvard Medical School, New England Deaconess Hospital, Boston, MA 02215.

***AJR* 146:39–43, January 1986**
0361–803X/86/1461–0039
© American Roentgen Ray Society

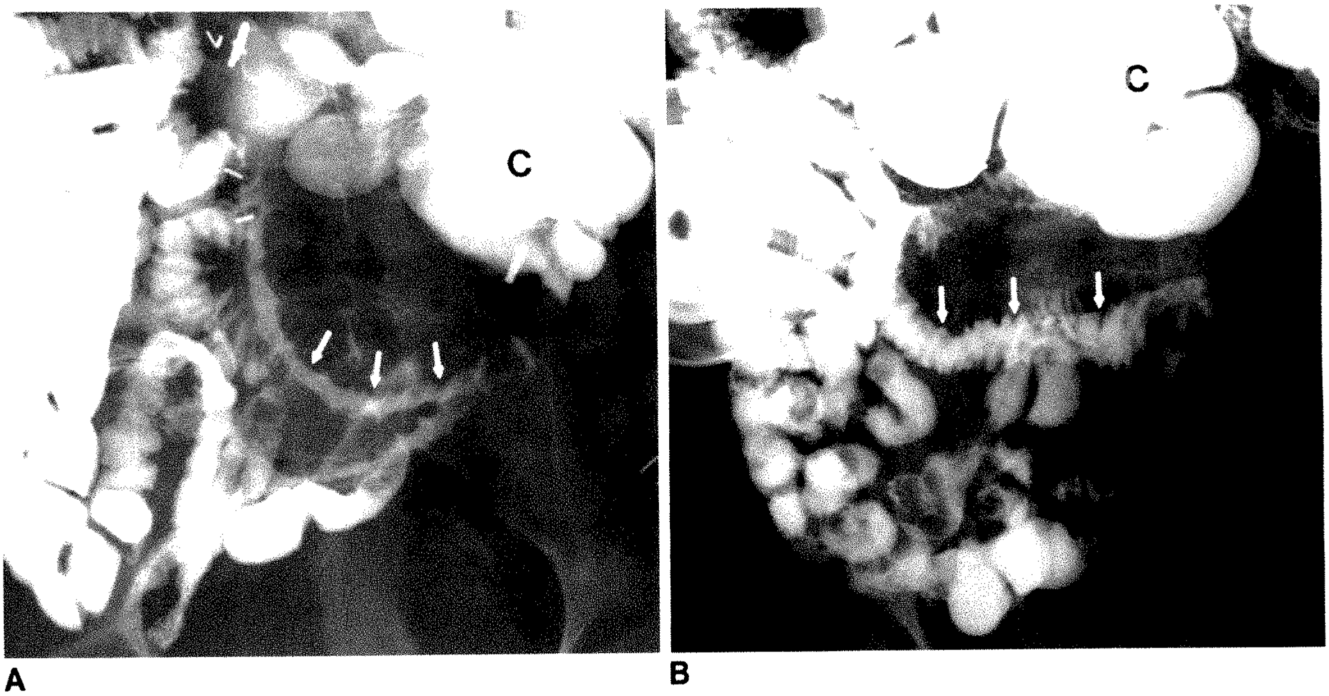

Fig. 1.—Case 1: reversible ileal narrowing. **A**, Marked narrowing of multiple ileal loops with areas of fold thickening and scalloping of bowel margin (*arrows*). **B**, Small-bowel series 2 weeks later. Caliber of ileum appears normal. Only residual abnormality is fold thickening in terminal ileum (*arrows*). C = proximal colon in left side of abdomen secondary to resection of hepatic flexure.

obstruction. A small-bowel series showed marked narrowing of the distal ileum (fig. 1A). After treatment with multiple antibiotics, bowel decompression, and rehydration, the symptoms resolved completely. A repeat small-bowel series showed considerable improvement in the appearance of the distal ileum (fig. 1B). Chemotherapy using a lower dose of 5-FUDR was resumed without recurrence of the patient's symptoms. Three months later, the patient developed pulmonary metastases and subsequently died.

Case 2.—A 73-year-old man underwent sigmoid colectomy for colorectal carcinoma and subsequently developed liver metastases. An infusion pump was implanted surgically with the catheter in the left hepatic artery. A replaced right hepatic artery was ligated at the same time. The regimen for hepatic artery infusion of 5-FUDR was 0.3 mg/kg/day for 14 days every 4 weeks. Three months after starting chemotherapy, the patient had profuse watery diarrhea, fever, and occult blood in the stools. A small-bowel series demonstrated marked narrowing of the entire ileum (fig. 2). After treatment by rehydration and cholestyramine, the patient's symptoms regressed, and a subsequent small-bowel enema demonstrated markedly improved appearances. Chemotherapy with 5-FUDR was subsequently continued at a lower dose rate without return of symptoms. The patient died 10 months later due to extrahepatic metastases.

Case 3.—A 48-year-old woman had undergone resection of carcinoma of the transverse colon complicated by the development of liver metastases. Two courses of continuous intravenous infusion of 5-FU were administered. Because of inadequate tumor response, common hepatic arterial infusion of 5-FUDR (0.4 mg/kg/day for 16 days) was initiated. During this course of therapy, the patient developed crampy abdominal pain, diarrhea, and vomiting. Abdominal films showed moderate small-bowel and colonic distension. A small-bowel series showed dilatation of loops of ileum and areas of narrowing in the distal ileum (fig. 3). The symptoms abated after treatment with antidiarrheal agents, and a subsequent small-bowel series showed a normal appearance. Progression of liver metastases was shown by CT, and the patient died 4 months later.

Intravenous Infusion of 5-FUDR

Twenty patients with colorectal carcinoma metastatic to the liver were treated with subclavian vein infusions of 5-FUDR at New England Deaconess Hospital between January 1982 and January 1985. Three of these patients developed abdominal symptoms severe enough to warrant radiographic evaluation of the small bowel. These three patients constitute cases 4–6.

Case 4.—A 56-year-old woman underwent right hepatic lobectomy for metastatic colon carcinoma. One month later, further hepatic metastases were treated by continuous intravenous infusion of 5-FUDR (0.2 mg/kg/day). This therapy was discontinued after 9 days due to stomatitis, nausea, and vomiting; two courses of the drug at reduced dosage were then given over the next 2 months. One week after completing the second course, the patient was hospitalized with abdominal cramps, nausea, vomiting, and diarrhea. Abdominal films revealed marked distension of multiple loops of small bowel and one or two segments of relatively narrowed distal ileum (fig. 4A). A small-bowel series 1 week later demonstrated narrowing and fold thickening in the distal ileum (fig. 4B). The patient's symptoms resolved after discontinuation of the 5-FUDR infusion. Eleven months later, the patient died as a result of liver metastases.

Case 5.—A 67-year-old man with carcinoma of the transverse colon with extension to the stomach was treated by palliative resection. In view of the residual tumor, two courses of intravenous 5-FUDR infusion (0.2 mg/kg/day for 8 days) separated by a 2-week interval were administered. Both of these courses were complicated only by diarrhea, but a third course of intravenous 5-FUDR (0.15 mg/

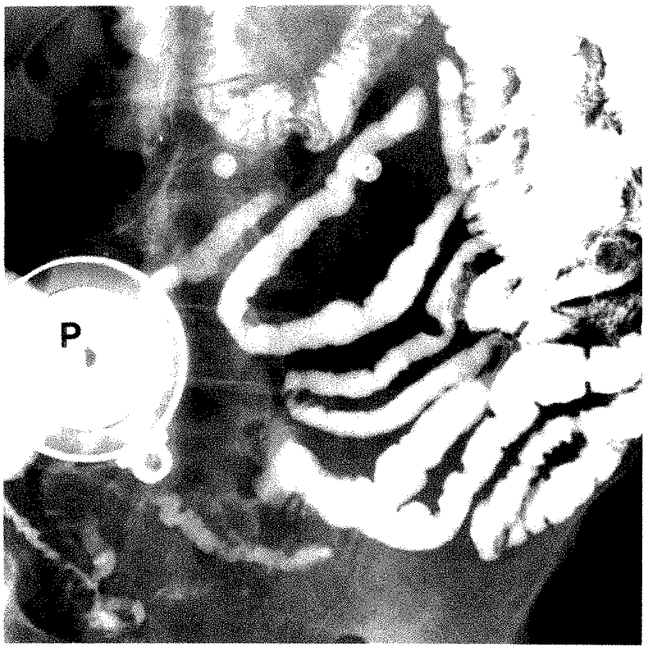

Fig. 2.—Case 2: extensive ileal involvement. Entire ileum is narrowed with widespread loss of mucosal fold pattern. P = pump for hepatic artery infusion. (Reprinted from [6].)

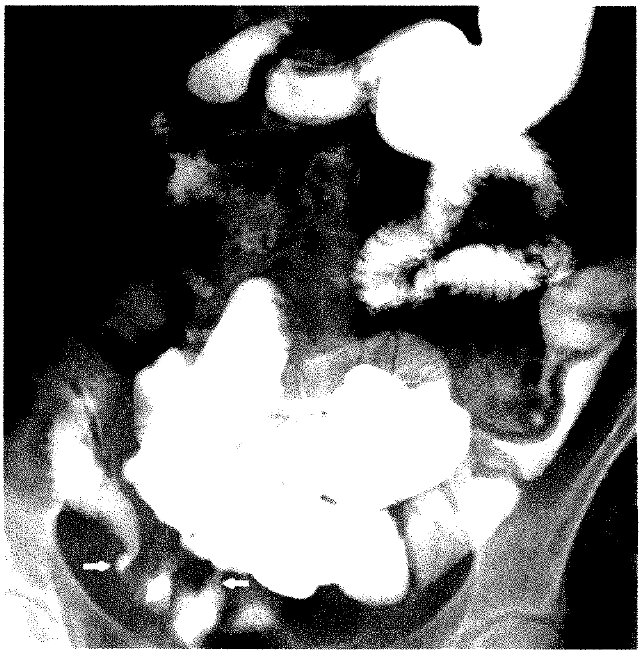

Fig. 3.—Case 3: segmental narrowing of distal ileum. Areas of narrowing in distal ileum (*arrows*), together with dilated loops of more proximal ileum.

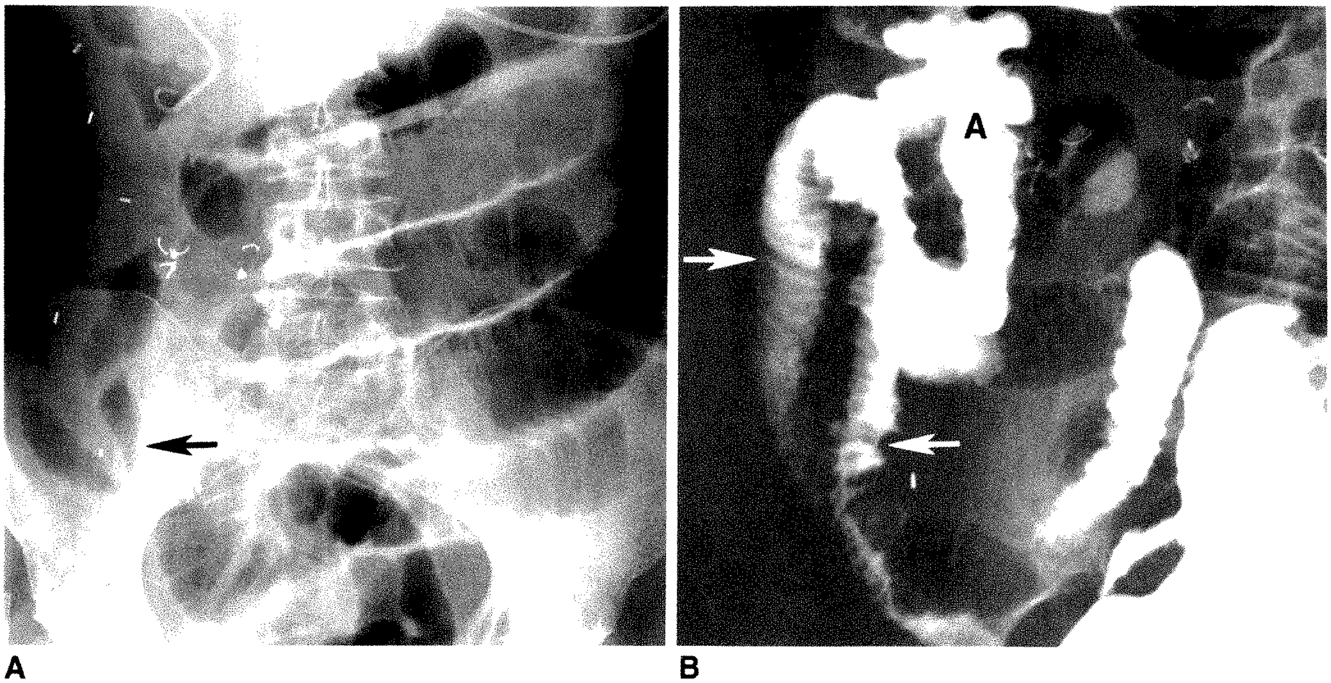

Fig. 4.—Case 4: partial small-bowel obstruction. **A**, Plain abdominal film shows marked dilatation of most of small bowel together with narrowing of one or two loops of distal ileum (*arrow*). **B**, Subsequent small-bowel series. Varying degree of narrowing of distal ileal loops is associated with nonuniform thickening of mucosal folds (*arrows*). A = ileocolic anastomosis following right hemicolectomy.

kg/day) 2 months later also resulted in nausea, vomiting, and abdominal cramps. A small-bowel series demonstrated dilatation of the proximal three-quarters of small bowel. The distal ileum appeared normal in caliber with some evidence of fold effacement. The symptoms abated with antidiarrheal medication and did not recur when 5-FU was used as the infusing agent. The patient remains alive and well 3 years later.

Case 6.—A 73-year-old man underwent right hemicolectomy for carcinoma of the colon with extensive local spread. Over the ensuing 4 months, the patient received several 2-week courses of intravenous infusion of 5-FUDR. A further course of intravenous 5-FUDR (0.1 mg/kg/day for 7 days followed by 0.075 mg/kg/day for 5 days) was stopped because the patient developed severe diarrhea and crampy abdominal pain sufficient to necessitate hospitalization. A small-bowel series showed dilatation of multiple loops of small bowel and marked fold thickening in the terminal ileum. The patient's symptoms showed a gradual improvement off all therapy. Six months later, the patient remains alive and relatively asymptomatic.

Discussion

Both fluorouracil (5-FU) and floxuridine (5-FUDR) are antipyrimidines that have been used as chemotherapeutic agents for more than 20 years. The drugs may be given intravenously (by infusion or, more commonly, by bolus injection) or intraarterially by hepatic artery infusion. Hepatic artery infusion of the antipyrimidines permits a higher concentration of chemotherapeutic agent to be delivered to the target organ compared to intravenous delivery. The agent of choice is 5-FUDR for practical reasons related to solubility and to the fact that unlike 5-FU, almost all 5-FUDR is extracted by the liver after hepatic artery infusion. This decreases the host toxicity and in part explains the current preference of 5-FUDR for the treatment of liver metastases.

Intestinal toxic effects of 5-FUDR are seen with both the intravenous and hepatic arterial routes of chemotherapy in these patients. Systemic toxicity predominantly involves the gastrointestinal tract and is manifested by stomatitis or nausea, vomiting, and diarrhea. Hepatic arterial infusion of 5-FUDR, particularly delivered via the implanted pump, is often associated with biochemical evidence of hepatotoxicity. Elevated liver enzymes that usually return to pretreatment levels after temporary discontinuation of the drug are seen in about 70%–75% of cases [7, 10]. Symptoms of peptic ulcer disease are common; radiologic or endoscopic examination of hepatic artery infusion patients may disclose gastroduodenal ulceration or gastritis [11, 12]. For reasons that are poorly understood, these upper gastrointestinal complications may follow chemotherapy via a surgically implanted hepatic artery infusion pump despite ligation of the right gastric and distal gastroduodenal arteries [7].

All of our patients developed severe diarrhea and/or crampy abdominal pain during or shortly after a course of 5-FUDR administered either by continuous hepatic artery infusion (cases 1–3) or continuous intravenous infusion (cases 4–6). The subsidence of symptoms in all of our patients after discontinuation of the chemotherapy strongly suggests that the symptoms were due to 5-FUDR toxicity. Symptoms of bowel toxicity related to 5-FUDR are well recognized in the oncologic literature [4, 9, 10, 13]. When 5-FUDR is given by continuous intravenous infusion, diarrhea is the main dose-limiting symptom [12]. Related to this, it is of interest that histopathologic changes in the small-bowel mucosa have been attributed to 5-FU therapy [14].

The radiographic changes observed on barium examination of the small bowel predominantly involved the ileum. The most striking abnormality was a lengthy area of narrowing either of virtually the entire ileum (figs. 1A and 2) or of its more distal part (fig. 4B). The appearance of the mucosa within the involved segments was subject to considerable variation, ranging from effacement of the fold pattern (fig. 2) to nonuniform thickening of the folds (fig. 4B). Two of the six cases had less striking barium findings, consisting of either fold thickening or effacement of folds in the distal ileum without any associated narrowing. In three of the six cases, two of whom experienced severe crampy abdominal pain, plain films of the abdomen demonstrated marked gaseous distension of multiple loops of small bowel (fig. 4A); it is probable that the symptoms and radiographic changes in these patients were the result of a partial obstruction induced by the distal ileal involvement (fig. 4). Repeat small-bowel series in cases 1–3 showed considerable or complete regression of the radiographic abnormalities, concomitant with improvement in the clinical status of the patients; the remaining patients had no symptomatic exacerbation on alternative chemotherapy including the "other" antipyrimidine, 5-FU.

Our findings suggest that the radiographic appearances of severe small-bowel toxicity due to 5-FUDR therapy are characterized by reversible ileal abnormalities, most commonly seen as segmental or more extensive narrowing. The possibility that the changes were caused by intestinal infection was considered in cases 1 and 2, but vigorous investigation failed to reveal any evidence of bacterial or toxin-induced enterocolitis. Similar radiographic findings to those seen in our patients may occur in small-bowel ischemia. The absence of gastrointestinal bleeding and the reversibility of the radiographic abnormalities make this an unlikely etiologic consideration. Other conditions that may resemble the small-bowel appearances associated with 5-FUDR toxicity include Crohn disease, chronic radiation enteritis, lymphoma, graft-vs.-host disease, and strongyloidiasis.

The mechanism by which 5-FUDR causes an enteropathy has not been elucidated. In those patients who received intravenous 5-FUDR (cases 4–6), however, it is likely that the enteropathy was a direct consequence of systemic toxicity. The development of small-bowel changes after treatment with hepatic arterial infusion of 5-FUDR is more difficult to explain. In cases 1–3, the hepatic artery catheters were confirmed to be in good position by either technetium-99m macroaggregated albumin (^{99m}Tc-MAA) scans or arteriography. However, ^{99m}Tc-MAA scans in cases 1 and 2 showed increased shunting to the lungs compared to the pretreatment scans, suggesting the possibility of arteriovenous shunting through the tumor bed into the systemic circulation. The finding of arteriovenous shunting on ^{99m}Tc-MAA studies after hepatic artery infusion of 5-FUDR has been previously noted [4].

Whatever the mechanism involved, 5-FUDR therapy may result in small-bowel toxicity that may be manifested radiographically either by a nonspecific pattern of bowel distension or a more characteristic appearance of extensive or segmental ileal narrowing, both of which regress on withdrawal of the therapy. Radiologists should be aware of these radiographic features so that they can suggest their causes in patients with the appropriate clinical background.

REFERENCES

1. Grage TB, Vassilopoulos PP, Shingleton WW, et al. Results of prospective randomized study of hepatic artery infusion with 5-fluorouracil versus intravenous 5-fluorouracil in patients with hepatic metastases from colorectal cancer: a Central Oncology Group Study. *Surgery* **1979**;86:550–555
2. Ansfield F, Flotz J, Nealon T, et al. A phase III study comparing the clinical utility of four regimens of 5-fluorouracil: a preliminary report. *Cancer* **1977**;39:34–40
3. Oberfield RA. Intra-arterial hepatic infusion chemotherapy in metastatic liver cancer. *Semin Oncol* **1983**;10:206–214
4. Barone RM, Byfield JE, Goldfarb PB, Frankel S, Ginn C, Greer S. Intra-arterial chemotherapy using an implantable infusion pump and liver irradiation for the treatment of hepatic metastases. *Cancer* **1982**;50:850–862
5. Balch CM, Urist MM, McGregor ML. Continuous regional chemotherapy for metastatic colorectal cancer using a totally implantable infusion pump. *Am J Surg* **1983**;145:285–290
6. Niederhuber JE, Ehsminger W, Gyves J, Thrall J, Walker S, Cozzi E. Regional chemotherapy of colorectal cancer metastatic to the liver. *Cancer* **1984**;53:1336–1343
7. Kemeny N, Daly J, Oderman P, et al. Hepatic artery pump infusion: toxicity and results in patients with metastatic colorectal carcinoma. *J Clin Oncol* **1984**;2:595–600
8. Lokich JJ, Bothe A, Faie N, Perri J. Phase I study of protracted venous infusion of 5-fluorouracil. *Cancer* **1981**;48:2565–2568
9. Gluck WL, Akwari OE, Kelvin FM, Goodwin BJ. A reversible enteropathy complicating continuous hepatic artery infusion chemotherapy with 5-fluoro-2-deoxyuridine. *Cancer* (in press)
10. Weiss GR, Garrick MB, Osteen RT, et al. Long-term hepatic arterial infusion of 5-fluorodeoxyuridine for liver metastases using an implantable infusion pump. *J Clin Oncol* **1983**;1:337–344
11. Hall DA, Clouse ME, Gramm HF. Gastroduodenal ulceration after hepatic arterial infusion chemotherapy. *AJR* **1981**;136:1216–1218
12. Chuang VP, Wallace S, Stroehlein J, Yap HY, Patt YZ. Hepatic artery infusion chemotherapy: gastroduodenal complications. *AJR* **1981**;137:347–350
13. Lokich JJ, Sonneborn H, Paul S, Zipoli T. Phase I study of continuous venous infusion of floxuridine (5-FUDR) chemotherapy. *Cancer Treat Rep* **1983**;67:791–793
14. White RS, Fuqua WB, Barrett D. The effect of 5-fluorouracil on small bowel mucosa. *J Surg Oncol* **1971**;3:501–506

Book Review

Diagnostic Cardiology. Noninvasive Imaging Techniques. Edited by Patricia Challender Come. Philadelphia: Lippincott, 586 pp., 1985. $67.50

Recent growth in the field of diagnostic cardiology has paralleled major technologic advancements. While the clinical examination, chest radiography, and electrocardiogram continue to be the foundation for evaluation of the patient with heart disease, noninvasive diagnostic imaging techniques have now assumed a major role alongside of the more traditional invasive technique of cardiac catheterization.

The subject of noninvasive cardiology usually has been covered in scattered chapters from multiple different reference books. In contrast, this review conveniently incorporates discussions of a variety of useful diagnostic imaging disciplines to create a single comprehensive reference source. In general, this text is very well organized and easy to read. Discussions about techniques, findings, and cardiac pathophysiology are well written and extensively illustrated with images, diagrams, and graphs. Each chapter includes comprehensive reference lists.

The book is divided into four major sections. "Roentgenographic Examination of the Heart, Great Vessels, and Pulmonary Vasculature" reviews the chest x-ray and cardiac series, cardiac computed tomography (CT), and digital subtraction angiography. There is a good discussion of the radiographic correlates of common cardiac disorders and an excellent illustrative review of cardiac chamber anatomy as visualized by chest radiographs. The discussions of cardiac CT scanning and digital subtraction angiography are at an introductory level, but provide a good basic review. "Magnetic Resonance" includes a thorough illustrated discussion of physics principles and an overview of clinical cardiac applications. The section on "Nuclear Imaging" has a comprehensive review of radiation physics and instrumentation, and devotes a separate chapter each to the assessment of myocardial perfusion, cardiac function, infarct-avid myocardial scintigraphy, and pediatric nuclear cardiology.

The major part of the text (about 440 pages) is devoted to "Echocardiography." The individual chapters are by numerous leading investigators, and the usual basic categories of cardiac pathophysiology are discussed. Separate chapters on prosthetic heart valves, contrast echocardiography, and Doppler echocardiography are also included. There is an extensive discussion of physics/instrumentation, recording techniques, and normal findings (including the current American Society of Echocardiography standards for nomenclature, for both M-mode and 2-D echocardiography). These chapters provide practical self-instruction for the beginning student, and a valuable review for the experienced echocardiographer. The section on 2-D echocardiographic examination shows each standard freeze-frame 2-D view with an accompanying cutaway view illustrating its corresponding gross anatomic features, and is a valuable learning tool and reference aid. Each chapter adequately discusses basic cardiac physiology/pathophysiology as background before reviewing the pertinent echocardiographic findings. The chapter on Doppler echocardiography provides a good, concise introductory review of the basic principles and instrumentation, along with practical tips on recording techniques. The basic clinical applications are well represented, but the illustrative examples in this brief single chapter are limited and there is more emphasis placed on pediatric than adult Doppler echocardiography. While the content is somewhat less detailed than other standard echocardiography texts, most topics are at least briefly introduced, and when indicated the reader is directed to more detailed reference sources.

The strengths of this text are its organization, illustrations/images, reference lists, and its unique treatment of noninvasive diagnostic cardiology as a unified discipline. In addition to its obvious appeal to the academic and clinical cardiologist, this book would be a valuable asset and reference for the cardiovascular radiologist, the nuclear cardiologist, and the various imaging technologists.

Lee C. Amsler
Division of Cardiology
Alan S. Pearlman
Medicine and Bioengineering
University of Washington
Seattle, WA 98195

Coiled-Spring Sign of the Cecum in Acute Appendicitis

Terrence C. Demos[1]
Michael E. Flisak[1]

A concentric ring appearance of the cecal mucosa on a barium enema is a distinctive but nonspecific radiographic finding that has been termed the vortical, whirlwind, or coiled-spring sign. It can be caused by inversion of a postappendectomy stump and transient intussusception of the intact appendix in asymptomatic patients. The sign has also been reported with mucoceles, carcinoma, and endometriosis of the appendix, but there has been little mention of it in connection with acute appendicitis. The records of 18 patients with a coiled-spring sign and nonfilling of the appendix were reviewed. Acute appendicitis was proven in 14 of 18. In five of these 14, this sign was the only finding accompanying nonfilling of the appendix. On review of 53 cases of pathologically proven acute appendicitis studied by preoperative barium enema, 14 had a coiled-spring sign. The coiled-spring sign is nonspecific but can be produced by acute appendicitis, where it may be the only positive sign accompanying nonfilling of the appendix.

In 1929, Artner [1] described concentric ring shadows in the barium-filled cecum in combination with a central filling defect. These ring shadows were demonstrated during barium enema examinations in up to one-third of his patients with prior appendectomies. Using postmortem studies, he proved that these findings were produced by inverted appendiceal stumps. Since then, a similar "vortical," "whirlwind," or "coiled-spring" appearance of the cecal mucosal folds in the location of the appendix has been described in several other pathologic processes involving the appendix [2–5]. A recent study [4] described this sign in patients with intussusception of the appendix. In these studies, there is little or no mention of this distinctive cecal defect occurring in patients with acute appendicitis. We have seen a coiled-spring sign in 18 patients undergoing single- or double-contrast barium enema examinations between 1976 and 1984. In our experience, it was most commonly seen with acute appendicitis.

Materials and Methods

During 9 years from 1976 through 1984, a coiled-spring defect of the cecum associated with nonfilling of the appendix was seen on barium enema examinations in 18 patients. Fourteen were examined because of suspected appendicitis and one because of chronic abdominal pain. Three patients without abdominal symptoms were examined before elective surgery. Twelve patients had single-contrast barium enemas without preparation, and six had double-contrast examinations using the technique described by Laufer [6]. These six patients received 1 mg of intravenous glucagon.

Barium enema examinations were reviewed to determine the radiographic features of the coiled-spring sign, including the presence or absence of appendiceal filling, mass effect on the cecum, and visibility of the lesion on spot, compression spot, overhead, and postevacuation radiographs. Surgical and pathologic diagnoses were available in 16 of 18 patients. Clinical follow-up was available in the other two patients.

Finally, all cases of pathologically proven appendicitis studied by preoperative barium enema from 1976 through 1984 were reviewed in order to determine the frequency of the coiled-spring sign.

Received July 2, 1985; accepted after revision August 15, 1985.

[1] Department of Radiology, Loyola University Medical Center, 2160 S. First Ave., Maywood, IL 60153. Address reprint requests to T. C. Demos.

AJR 146:45–48, January 1986
0361–803X/86/1461-0045
© American Roentgen Ray Society

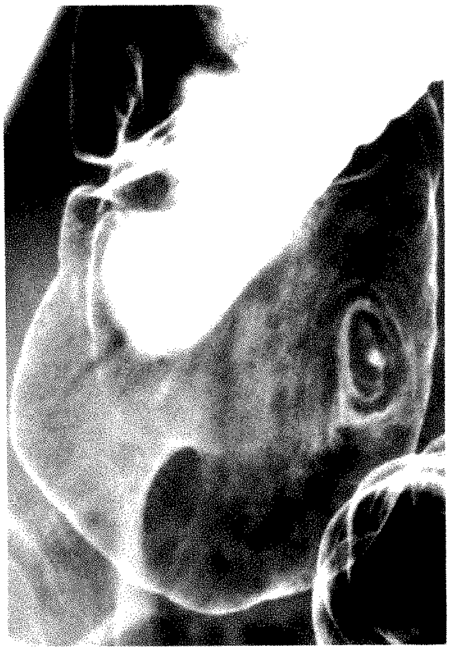

1

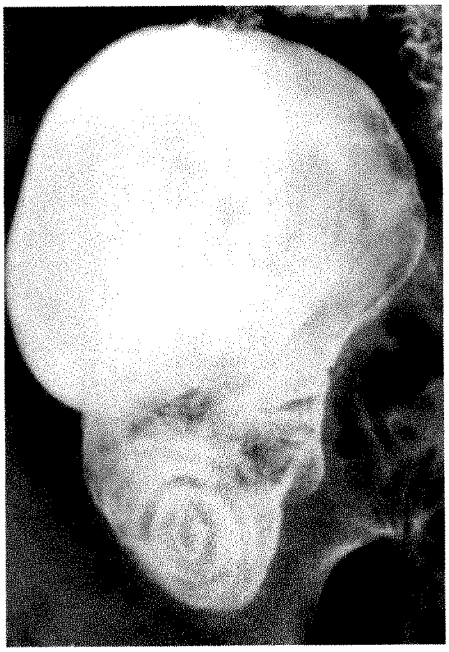

2

Fig. 1.—Acute appendicitis without perforation. Compression spot film shows ring shadows arranged concentrically around central barium collection, producing coiled-spring defect.

Fig. 2.—Acute appendicitis with pericecal abscess. Postevacuation radiograph was only film showing coiled-spring appearance and shallow contour defect of medial cecal wall.

Results

There were 10 male and 8 female patients aged 14–81 years (average, 47.7).

Diagnoses

All 14 patients with coiled-spring defects examined because of suspected appendicitis had surgery within 12 hr of the barium enema examinations. Twelve had acute appendicitis with abscess; two had acute appendicitis without perforation. The patient with chronic pain had surgery and was found to have a mucocele of the appendix.

The three patients without abdominal symptoms did not have pathologic proof. Two of them had had appendectomies. In one, an inverted appendiceal stump was found at surgery, and the other was assumed to have had an inverted appendiceal stump [1]. The third patient had a normal follow-up barium enema examination 2 months later with filling of the appendix and was assumed to have had asymptomatic intussusception of the appendix [4]. All three patients remain asymptomatic.

Radiology

Barium enema examinations showed a coiled-spring sign of the cecum and nonfilling of the appendix in all patients. The defect appeared as concentric ring shadows surrounding either a central barium collection (fig. 1) or a central filling defect. The diameter of the largest ring was 1.5–6 cm. The rings were best demonstrated by en face spot films with or without compression. In 13 of 18 patients, the finding could be seen only on en face spot films of the cecum. In two cases, however, the defect was seen only on the postevacuation radiograph (fig. 2).

The coiled-spring sign was the only abnormality accompanying nonfilling of the appendix in eight of 18 patients. Five of those patients proved to have acute appendicitis. The other three patients had no abdominal symptoms and were examined before elective surgery.

In 10 of 18 patients, the coiled-spring sign and appendiceal nonfilling were associated with additional radiographic findings. A mobile pericecal soft-tissue mass in one patient proved to be an appendiceal mucocele. A fixed pericecal mass or cecal contour defect was present in the other nine patients [7, 8]. It was usually best demonstrated by views approximately at right angles to those best demonstrating the coiled-spring defect (fig. 3). All nine patients had acute appendicitis.

Review of proven cases of acute appendicitis between 1976 and 1984 yielded 53 with preoperative barium enemas. Nonfilling of the appendix and the presence of a coiled-spring sign in at least one view were present in 14 patients.

Discussion

Angulation, spiculation, and distortion of mucosal folds in conjunction with mass effect, intact mucosal surface, and fixation of bowel loops are key findings that indicate an extrinsic process involving the bowel wall [9]. The coiled-spring sign in the cecum can be produced by intussusception of the appendix or appendiceal stump, but may also be produced by disease extrinsic to the cecum.

The inverted appendiceal stump is a well known pseudoneoplasm of the cecum [10]. Typically, these lesions are small and do not cause symptoms. When viewed en face, a coiled-spring sign may be present. Rare cases of late postappen-

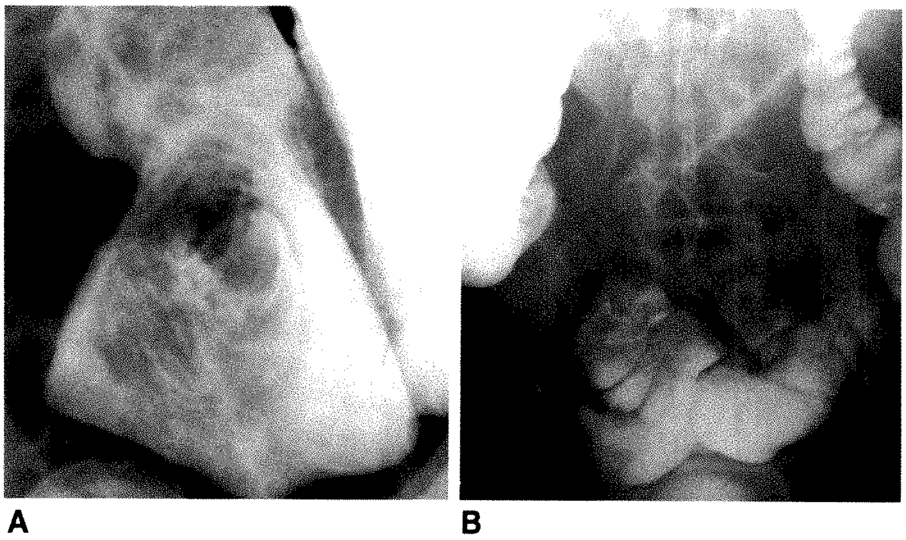

Fig. 3.—Acute appendicitis with pericecal abscess. **A**, Compression spot film with patient in steep right posterior oblique position during single-contrast barium enema shows coiled-spring appearance. **B**, Anteroposterior radiograph shows defect on medial side of cecum.

dectomy sequelae, including abscess formation [11] and cecocecal intussusception [12], have also been reported and should be kept in mind in the symptomatic patient.

Intussusception of the intact appendix can also produce a coiled-spring sign. Levine et al. [4] reported 11 cases with this sign and nonfilling of the appendix on double-contrast barium enemas. There was a history of appendectomy in two cases. A mucocele of the appendix and appendiceal endometriosis leading to intussusception were found at surgery in two other cases. The remaining seven asymptomatic patients were considered to have intussusception of the intact appendix. Filling of the appendix and a normal cecum on delayed films or subsequent examinations indicated the transient nature of the phenomenon in five of seven.

The coiled-spring appearance of the cecal mucosa associated with a mucocele was first described by Jutras [2]. Gelfand et al. [5] also reported a mucocele producing the coiled-spring sign, and considered the finding characteristic of an extrinsic abnormality. The pathologic specimen showed protrusion of the mucocele into the cecal lumen with crowding of the adjacent cecal folds corresponding to the coiled-spring defect. Stiehm and Seaman [3] reported four cases of primary adenocarcinoma of the appendix, and in one case, a coiled-spring appearance was demonstrated.

We have found the coiled-spring defect to be an important sign of acute appendicitis. The barium enema examination is an established means of evaluating patients with atypical abdominal pain and equivocal laboratory and clinical findings in whom acute appendicitis is entertained as a diagnostic possibility [7, 8, 13–15]. Complete filling of a normal-appearing appendix virtually eliminates the diagnosis of acute appendicitis, but nonfilling is nonspecific and is reported in up to 12.5% of normal appendices [16]. Absence of filling in association with other findings in the pericecal area, however, is highly suggestive of acute appendicitis. These findings include flattening of the medial wall of the cecum, a cecal filling defect in the expected location of the appendiceal base, a bilobed cecal filling defect, and inflammatory changes in the terminal ileum [7, 8]. The cecal deformity is caused by inflammation and edema at the base of the appendix with extension to the cecal wall or pressure effect on the cecum by adjacent inflamed tissue [13, 15]. When viewed tangentially, this is seen as a lesion protruding into the cecal lumen to a variable degree. Often, distortion of the adjacent folds is seen in this projection. When viewed en face, this abnormality may have a coiled-spring appearance. In fact, this was demonstrated fluoroscopically in several of our patients.

The coiled-spring sign was present in 14 of 53 preoperative barium enema examinations of symptomatic patients who proved to have acute appendicitis. It is emphasized that the coiled-spring sign due to intussusception of the normal appendix is often transient, and patients are asymptomatic [4].

The coiled-spring sign, seen in association with nonfilling of the appendix, is not a specific finding but was most often (14 of 18 patients) caused by acute appendicitis in our series. In five patients it was the only radiographic finding in addition to nonfilling of the appendix.

ACKNOWLEDGMENT

We thank Barbara Medley for manuscript preparation.

REFERENCES

1. Artner H. Der status post appendectomiam im rontgenbilde. *ROFO* **1929**;39:609–615
2. Jutras A. Les signes radiologiques du mucocele appendiculaire. *Union Med Canada* **1938**;67:251–252
3. Stiehm WD, Seaman WB. Roentgenographic aspects of primary carcinoma of the appendix. *Radiology* **1973**;108:275–278
4. Levine MS, Trenker SW, Herlinger H, Mishkin JD, Reynolds JC. Coiled spring sign of appendiceal intussusception. *Radiology* **1985**;155:41–44
5. Gelfand GJ, Robb PL, Theros EG. An exercise in radiologic–pathologic correlation. *Radiology* **1967**;89:1107–1112

6. Laufer I. *Double-contrast gastrointestinal radiology*. Philadelphia: Saunders, **1979**
7. Schey WL. Use of barium in the diagnosis of appendicitis in children. *AJR* **1973**;118:95–103
8. Shimkin PM. Commentary: radiology of acute appendicitis. *AJR* **1978**;130:1001–1004
9. Kidd R, Freeny PC. Radiographic manifestations of extrinsic processes involving the bowel. *Gastrointest Radiol* **1982**;7:21–28
10. Malbin M. Pseudoneoplasm as a post-appendectomy finding. *Radiology* **1947**;57:751–754
11. Schrager VL. Pathology of appendiceal stump with suggestions for prophylaxis. *Am J Surg* **1941**;54:629–633
12. Weber HM, Good CA. Invaginated appendiceal stumps roentgenologically simulating polypoid neoplasms. *Radiology* **1940**;34:440–443
13. Figiel LS, Figiel SJ. Barium examination of the cecum in appendicitis. *Acta Radiol* **1962**;57:469–480
14. Rajagopalan AE, Mason JH, Kennedy M, Pawlikowski J. The value of the barium enema in the diagnosis of acute appendicitis. *Arch Surg* **1977**;112:531–533
15. Soter CS. The use of barium in the diagnosis of acute appendiceal disease: a new radiological sign. *Clin Radiol* **1968**;19:410–415
16. Sakover RP, Del Fava RL. Frequency of visualization of the normal appendix with the barium enema examination. *AJR* **1974**;121:312–317

Floating Gallstones in Bile without Added Contrast Material

Hsu-Chong Yeh[1]
Joan Goodman
Jack G. Rabinowitz

Floating gallstones can occur without the administration of contrast material to increase the specific gravity of bile. This was observed in three patients in 17 months. After a long fast, a large stone was noticed to float because of the high specific gravity of inspissated bile. This stone sank after the patient resumed food intake. In another patient, some stones floated while others sank due to their difference in specific gravity. Sonographic demonstration of a floating stone, however, requires certain strict criteria.

It is well known that floating gallstones can be observed on oral cholecystography. There have been many discussions about floating stones in the literature [1–6]. Akerlund [1] first suggested in 1938 that gallstones float only during oral cholecystography when the specific gravity of the bile is raised by the presence of contrast material in the bile. Other authors [2, 3] seemed to favor this theory. Scheske et al. [5] further supported it by showing on sonography that nonfloating stones float after intake of Telepaque. Although Carroll and Sommer [6] expressed the opposite opinion by demonstrating three cases, their illustrations did not substantiate it. The apparent "floating stones" in that article were actually due to either obscuration of the posterior part of the stones by acoustic shadows or "piled up" (not truly floating) stones. We present three cases that definitely depict floating stones in native bile without intake of any contrast material into the gallbladder.

Materials and Methods

Sonography was performed during a 17-month period on about 3000 patients who were suspected of having gallbladder disease or upper abdominal pathology. The patients fasted overnight. Examinations were done in 2- to 3-mm intervals with a commercially available manual scanner in supine and semidecubitis or decubitus position, right-side up, in longitudinal, transverse, and oblique planes. Sector or linear-array real-time scanning was also done in some patients.

Results

Floating stones were found in three patients who did not ingest any contrast material for cholecystography before sonography. The size of the floating stones was 0.6–2.0 cm. In one patient who had been fasting for several days due to anorexia, the floating stone was associated with biliary sludge (fig. 1). Ten days later, after the patient resumed food intake, sonography showed that the stones had sunk to the most dependent part of the gallbladder; the gallbladder was smaller and no longer contained biliary sludge.

Another patient had a single floating stone (fig. 2) that was proven at surgery. In the third patient, the gallbladder was dilated due to obstruction of the common bile duct by metastatic colon cancer. There were multiple small floating stones and a few larger ones that sank in the dependent part of the gallbladder (fig. 3). The

Received April 22, 1985; accepted after revision September 6, 1985.

[1] All authors: Department of Radiology, School of Medicine of the City University of New York, Mount Sinai Hospital, One Gustave Levy Pl., New York, NY 10029. Address reprint requests to H.-C. Yeh.

AJR 146:49–50, January 1986
0361–803X/86/1461–0049
© American Roentgen Ray Society

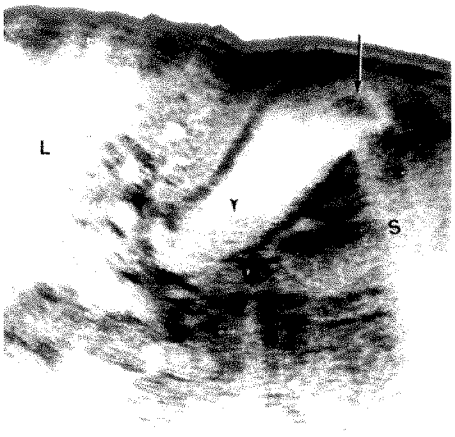

1

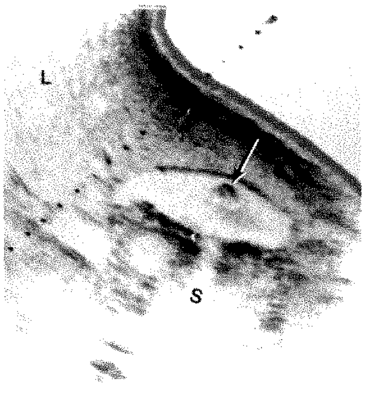

2

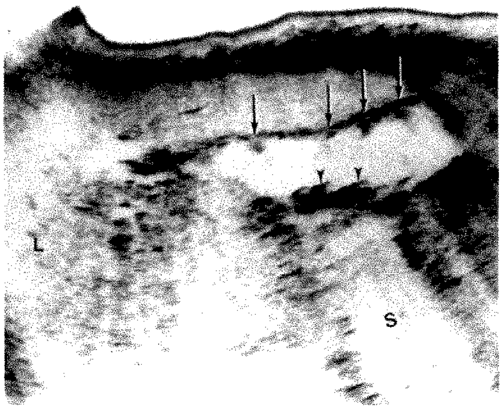

3

Fig. 1.—Large floating gallstone (*arrow*) in patient with prolonged fasting. Gallbladder is dilated with biliary sludge (*arrowhead*) in dependent part. L = liver; S = acoustic shadow. Stone sank after patient resumed food intake (not shown).

Fig. 2.—Floating stone (*arrow*) in patient who had not taken contrast material. L = liver; S = acoustic shadow.

Fig. 3.—Multiple small floating (*arrows*) and nonfloating (*arrowheads*) stones in gallbladder dilated due to obstruction of common bile duct by metastatic colon carcinoma. L = liver; S = acoustic shadow.

larger stones had ring calcifications, as seen on plain radiographs of the abdomen.

Discussion

It has previously been postulated that gallstones will float only when contrast material is present, except those stones containing gas. Since noncalcified stones are usually not seen on radiographs without intake of contrast material, the theory of floating gallstones was difficult to prove in vivo before the invention of sonography. The theory is based on the data that the specific gravity of native bile is always less than that of a stone; that is, that of native bile usually ranges from 1.010 to 1.040 and that of a stone is 1.040–1.056 [1]. In fact, the specific gravity of bile can be higher than 1.040. Elton [7] found in six of 30 cases that the specific gravity of bile ranged from 1.042 to 1.059. Tera [8] proved that all chemical substances (e.g., calcium, bilirubin, cholesterol) and physical properties (specific gravity and relative viscosity) are stratified within the gallbladder. On this basis, we should expect to find some gallstones to float at a level where the specific gravity of the bile and the stones are equal. Since the specific gravity and viscosity of the bile vary from time to time, depending on the food intake and the function of the gallbladder, one may expect certain stones to be floating or not floating in different situations in the same patient and floating at different levels at different times. This is illustrated by our first case. The gallstone first floated in a thick bile caused by prolonged fasting. After the patient resumed food intake, the gallbladder went through many cycles of emptying old thick bile and refilling with new thin bile. The specific gravity of the bile decreased and the stone sank.

To determine by sonography if a gallstone floats or not, some important factors should be considered: (1) The direction of gravity must be determined. This is clear in manual scanning, but may not be perfectly clear on real-time scanning even though the transducer appears to be parallel to the direction of gravity during scanning. (2) When the posterior part of a stone is obscured by its own acoustic shadow, the stone may appear to be floating. The anterior stones in a pile of stones may appear to be floating for the same reason. (3) A small stone may adhere to the anterior wall of the gallbladder [9], or a large stone may be wedged into a small gallbladder fundus and appear to be floating. A stone that is adherent to the gallbladder wall will not move as the patient changes position; in contrast, a floating stone will move.

REFERENCES

1. Akerlund A. Die Verfeinerung der Roentgenologischen Gallenstein-diagnostik der Sedimentierungs—und schichtungs Verhaltnisse in der Gallenblase. *Acta Radiol* (Stockh) **1938**;19:23–43
2. Elsey ED, Jacob DL. Floating gallbladder stones. *Radiology* **1951**;65:73–76
3. Ettinger A. The value of the upright position in gallbladder examinations. *Radiology* **1940**;34:481–488
4. Spillman R. The value of radiography of the gallbladder in the upright position. *Radiology* **1939**;33:77–78
5. Scheske GA, Cooperberg PL, Cohen MM, Burhenne HJ. Floating gallstones: the role of contrast material. *JCU* **1980**;8:227–231
6. Caroll B, Sommer FG. Floating gallstone (letter). *JCU* **1981**;9:A30
7. Elton NW. Bilirubin concentration in the human gallbladder. *Am J Clin Pathol* **1936**;6:81–90
8. Tera H. Stratification of human gallbladder bile in vivo. *Acta Chir Scand* [*Suppl*] **1960**;256:9–85
9. Yeh HC. Update on gallbladder. *In*: Sanders RC, ed. *Ultrasound annual*. New York: Raven, **1982**:135–172

MRI of the Kidneys in Paroxysmal Nocturnal Hemoglobinuria

George P. Mulopulos,[1] David A. Turner,[1] Melvin M. Schwartz,[2] Marcia E. Murakami,[1] and John W. Clark[1]

Paroxysmal nocturnal hemoglobinuria (PNH), a myelodysplastic, hematopoietic stem-cell disorder, is characterized by an increased sensitivity to complement-mediated erythrocyte lysis [1]. Reported radiologic findings include enlarged kidneys, cortical thinning, and evidence of cortical infarcts and papillary necrosis [2]. Histologic examination of the kidneys typically shows deposition of hemosiderin [3, 4]. We report a case of PNH with distinctive magnetic resonance imaging (MRI) findings in the kidneys that we attribute primarily to heavy deposits of hemosiderin in the renal cortex.

Case Report

A 60-year-old woman with a 15-year history of PNH was admitted with a fever of unknown origin. Presenting complaints included malaise, nonproductive cough, headaches, photophobia, and reddish-brown urine. Her admitting urinalysis showed a specific gravity of 1.007, 50–60 leukocytes, 2–3 erythrocytes, 3+ occult blood, 30 mg/dl protein, 5–10 epithelial cells, and trace bacteria. During the patient's hospital stay, blood urea nitrogen was 25–30 mg/dl and creatinine was 2.5–3.0 mg/dl. A ^{99m}Tc-DTPA study demonstrated symmetrically decreased perfusion of both kidneys; a renal radiohippuran study showed slightly decreased tubular function. The estimated total glomerular filtration rate was decreased at 55 ml/min. Respiratory-gated MRI of the abdomen was performed with a commercial MRI system (Teslacon, Technicare), with a superconductive magnet operating at 0.5 T. A spin-echo (SE) pulse sequence was used with TR and TE varied to achieve relative T1 (SE 530/30) and T2 contrast weighting (SE 2120/60 and SE 2120/120). Noted were a reversal of the normal ratio of the renal cortical and medullary intensities on T1-weighted images and a very low cortical signal intensity on T2-weighted images (fig. 1). An open biopsy of the cortex of the left kidney revealed heavy hemosiderin deposition in the proximal tubular epithelial cells, scattered interstitial iron deposits, and a nonspecific chronic interstitial nephritis (fig. 2).

Discussion

Clinical features of PNH include hemoglobinuria, chronic hemolysis, iron deficiency, bleeding, and thromboses. Hemolysis may be precipitated by infections, surgery, transfusions, or reactions to drugs, immunizations, exercise, or radiographic contrast material [2]. Venous thrombosis, especially that involving hepatic veins, is the leading cause of death. The most convenient screening tests for PNH are the sucrose hemolysis test and examination of urine for hemosiderin. The diagnosis should be confirmed using the complete acidified serum (Ham) test. The clinical course of PNH is highly variable. Treatment is mainly supportive with transfusions, antibiotics, and anticoagulants.

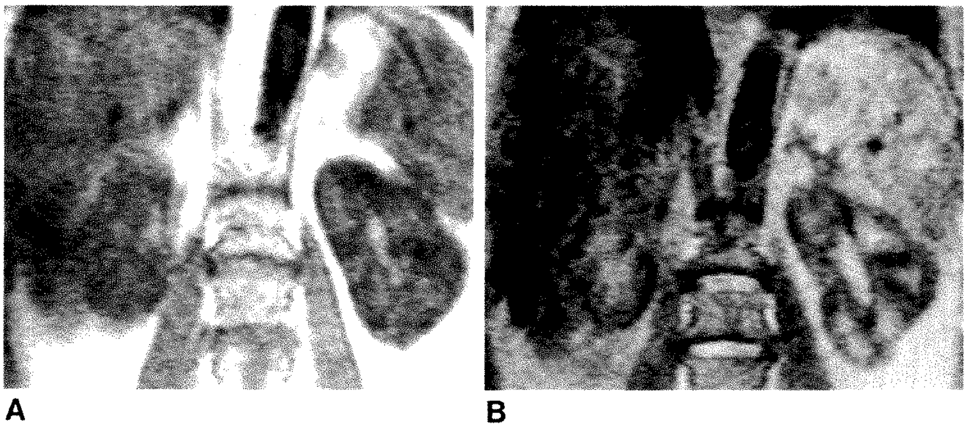

Fig. 1.—Patient with PNH. **A**, Coronal T1-weighted image (SE 530/30) of abdomen. Signal intensity from renal cortices is slightly less than signal intensity from medullary regions. **B**, Coronal T2-weighted image (SE 2120/60). Very low signal intensity from renal cortical tissue and normal high signal intensity from the medulla.

Received May 28, 1985; accepted after revision August 15, 1985.
This work was supported in part by a grant from the Robert R. McCormick Charitable Trust.

[1] Department of Diagnostic Radiology and Nuclear Medicine, Rush-Presbyterian-St. Luke's Medical Center, 1753 W. Congress Pkwy, Chicago, IL 60612. Address reprint requests to D. A. Turner.

[2] Department of Pathology, Rush-Presbyterian-St. Luke's Medical Center, Chicago, IL 60612.

AJR 146:51–52, January 1986 0361-803X/86/1461–0051 © American Roentgen Ray Society

Renal abnormalities in PNH include hyposthenuria, abnormal tubular function, and declining creatinine clearance. Most patients have episodes of hematuria and proteinuria. However, hemosiderinuria is one of the most constant features and has considerable diagnostic importance. Intravascular hemolysis typically results in large deposits of hemosiderin in the tubular epithelium [2] (fig. 2). The concentration of iron in the kidney can be over 80 times normal [4]. Hemoglobinuric crises may precipitate acute renal insufficiency, which usually is short lived and may leave very little apparent residual functional damage [2, 3].

In normal, well hydrated individuals, the renal cortex has a shorter T1 than the medulla and therefore appears more intense than the medulla on T1-weighted MR images [5] (fig. 3A). This normal corticomedullary differentiation is lost in a variety of renal disorders in which the cortex and medulla appear isointense [6]. However, reversal of the normal cortical-to-medullary intensity ratio on T1-weighted images (figs. 1A and 3A) and low cortical intensity on T2-weighted images (figs. 1B and 3B) have not been described previously.

We attribute the unusual MRI findings in this case to the paramagnetic effects of iron, large quantities of which were shown by biopsy to be present in the renal cortex (fig. 2). Paramagnetic agents shorten both the T1 and T2 relaxation times [7]. At relatively low concentrations of these agents, proton signal intensity tends to be enhanced because of the decrease in T1 [7, 8]. However, at very high concentrations, signal intensity will be very low because of a marked decrease in T2. This is the basis of the observation by Stark et al. [8] that the liver emits a signal of very low intensity in patients with hepatic iron overload.

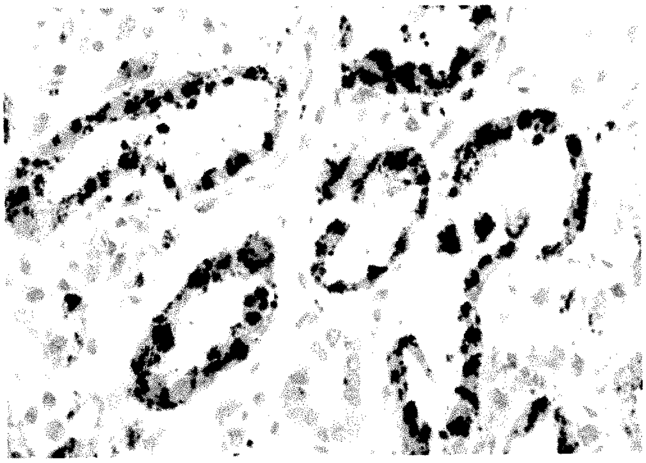

Fig. 2.—Renal cortex with interstitial fibrosis and atrophic tubules containing coarse intracellular granules of iron. Occasional granules are present in interstitium. Prussian blue stain, ×250 (original magnification).

Medullary tissue was not included in the biopsy specimen in this case. Although iron deposits may have been present in the medulla as well as in the cortex, the lower signal intensity of the cortex in both the T1- and T2-weighted images implies that the concentration of iron in the cortex was greater. This is consistent with reports that renal hemosiderin deposition in PNH occurs mainly in the proximal tubular epithelial cells of the cortex [2].

In conclusion, the unique MRI appearance of this patient's kidneys is readily explained by heavy deposits of iron found in her renal cortex. Since cortical hemosiderin deposition is common in PNH, the MRI pattern we have observed may be characteristic of the disease.

REFERENCES

1. Beutler E. Paroxysmal nocturnal hemoglobinuria. In: Williams WJ, Beutler E, Erslev AJ, Lichtman MA, eds. *Hematology*. New York: McGraw-Hill, **1983**:171–175
2. Clark DA, Butler SA, Braren V, Hartmann RC, Jenkins DE Jr. The kidneys in paroxysmal nocturnal hemoglobinuria. *Blood* **1981**;57:83–89
3. Rubin H. Paroxysmal nocturnal hemoglobinuria with renal failure. *JAMA* **1971**;215:433–436
4. Heitzman EJ, Campbell JS, Stefanini M. Paroxysmal nocturnal hemoglobinuria with hemosiderin nephrosis. *Am J Clin Pathol* **1953**;231:975–986
5. Hricak H, Crooks L, Sheldon P, Kaufman L. Nuclear magnetic resonance imaging of the kidney. *Radiology* **1983**;146:425–432
6. Leung AWL, Bydder GM, Steiner RE, Bryant DJ, Young IR. Magnetic resonance imaging of the kidneys. *AJR* **1984**;143:1215–1227
7. Runge VM, Clanton JA, Lukehart CM, Partain CL, James AE. Paramagnetic agents for contrast-enhanced NMR imaging: a review. *AJR* **1983**;141:1209–1215
8. Stark DD, Moseley ME, Bacon BR, et al. Magnetic resonance imaging and spectroscopy of hepatic iron overload. *Radiology* **1985**;154:137–142

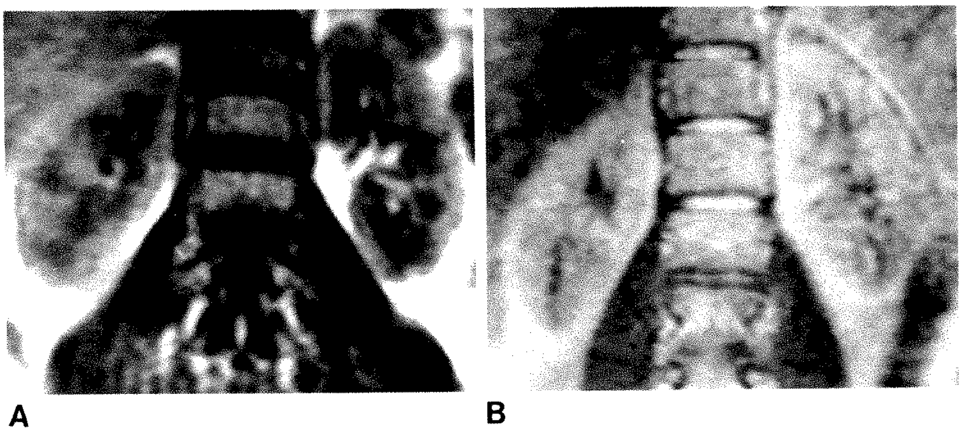

Fig. 3.—**A**, T1-weighted image (SE 530/30) of normal patient shows usual corticomedullary differentiation (cortex emits greater signal intensity than medulla). **B**, T2-weighted image (SE 2120/60) of another normal patient showing homogeneous, high signal intensity of entire kidney.

Sonography of the Hypertrophied Column of Bertin

Michel Lafortune[1]
Andre Constantin
Guy Breton
Claude Vallee

A prospective sonographic analysis of kidneys in 136 adults without clinical or radiologic evidence of renal disease revealed 22 cases of large columns of Bertin. Most were located in the middle third of the kidney, more frequently on the left side. They were bilateral in 18%. Water bath sonograms of normal cadaver kidneys and subsequent anatomic correlation revealed hypertrophied columns and confirmed the sonographic findings seen in vivo. The following are characteristic of a hypertrophied column of Bertin: It is a projection of cortex into the renal sinus (and therefore is isoechogenic with it). The sinus may engulf it in a clawlike fashion. The renal contour is smooth. Sonography is characteristic and obviates further investigation.

In 1744, the French anatomist Exupère Joseph Bertin gave a lecture before the Académie Royale des Sciences on the morphologic structure of the kidney [1]. He stated that "cortical substance not only envelops the external part of the kidney, but also runs in between papillae, separates them and gives rise to 'cloisons' which cross the whole thickness of the kidney." Since then, these intrusions of cortical substance between the pyramids have been called septa or columns of Bertin (translated from the word *colonne* commonly used by French anatomists).

While Bertin's original studies called attention to the fact that some columns are bigger than others and protrude deeply into the renal medulla, it was not until the late 1960s that radiologists became aware of their existence and concerned with their differentiation from renal tumors [2–7]. A number of nephrectomies were done until the radiologic characteristics of the column of Bertin were fully described [8].

During sonography of patients without known renal disease, we found what seemed to be unusual numbers of large or hypertrophied columns of Bertin. We therefore started a prospective study to determine their frequency as seen by clinical sonography and their frequency in normal cadaver kidneys.

Subjects and Methods

The kidneys of 136 adult patients (aged 18–76 years, 84 women, 52 men) without clinical evidence of renal disease were prospectively studied using commercially available real-time sonographic equipment (Philips model SDU 3000, ATL MK-100, 3.5 or 5 MHz transducers). Multiple cuts were obtained in sagittal and coronal planes from an anterior and axillary approach. Thirty-six patients were excluded because of abnormalities of the renal sonograms or because of technically suboptimal sonographic studies. Thirty-nine cadaver kidneys without gross pathology were scanned in a water bath with a static B-scanner (Philips, Sonodiagnost-B). Longitudinal sonograms were compared to corresponding gross sections.

A hypertrophied column of Bertin was defined as an isoechogenic cortical mass projecting into and indenting the hyperechogenic renal sinus. The longitudinal diameter of any such mass was measured as shown in figure 1 and graded on a scale from 1 to 3, where grade 1 was 0.5–1 cm, grade 2 was 1–2 cm, and grade 3 was over 2 cm. All observations and measurements were performed independently by two observers.

Received April 12, 1985; accepted after revision September 11, 1985.

Presented at the annual meeting of the Canadian Association of Radiologists, Vancouver, June 1984.

[1] All authors: Department of Radiology, Saint-Luc Hospital, 1058 St-Denis St., Montreal, Quebec, Canada H2X 3J4. Address reprint requests to M. Lafortune.

***AJR* 146:53–56, January 1986**
0361–803X/86/1461–0053
© American Roentgen Ray Society

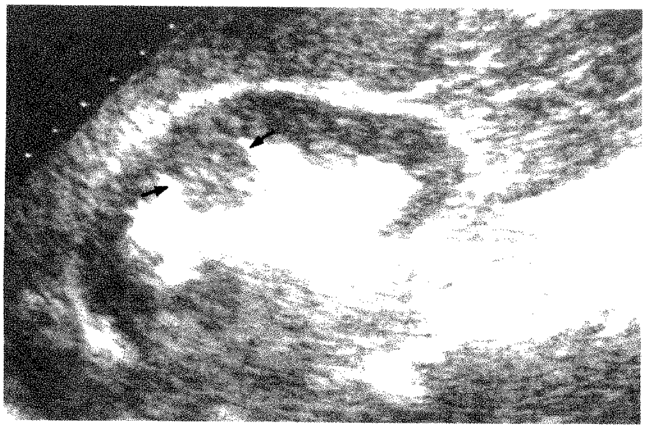

Fig. 1.—Longitudinal sonogram of right kidney. Typical hypertrophied column of Bertin. Mass is at junction of upper and middle third of kidney and projects into renal sinus, which engulfs it in clawlike fashion. It is isoechogenic with renal cortex. Renal contour is smooth. (*Arrows* show site of measurement of longitudinal diameter used in this study.)

Results

In vitro

A comparison of the sonographic studies of cadaver kidneys with their anatomic cuts showed an excellent correlation. The masses indenting the renal sinus in this group of cadaver kidneys were, in fact, hypertrophied columns of Bertin (fig. 2).

In vivo

The incidence and size of masses indenting the sinus echoes are summarized in table 1. Almost one-half of the kidneys examined (47% in vivo, 51% in cadavers) had at least one such mass. Of these, almost half were grade 2 or 3 (more than 1 cm). The most frequent site was the junction of the upper and middle third of the kidney. The left kidney was more frequently involved than the right kidney at a ratio of 2:1. Bilateral masses were more frequent in cadaver kidneys (left:right, 3:2) than in vivo. A few kidneys (18%) had two

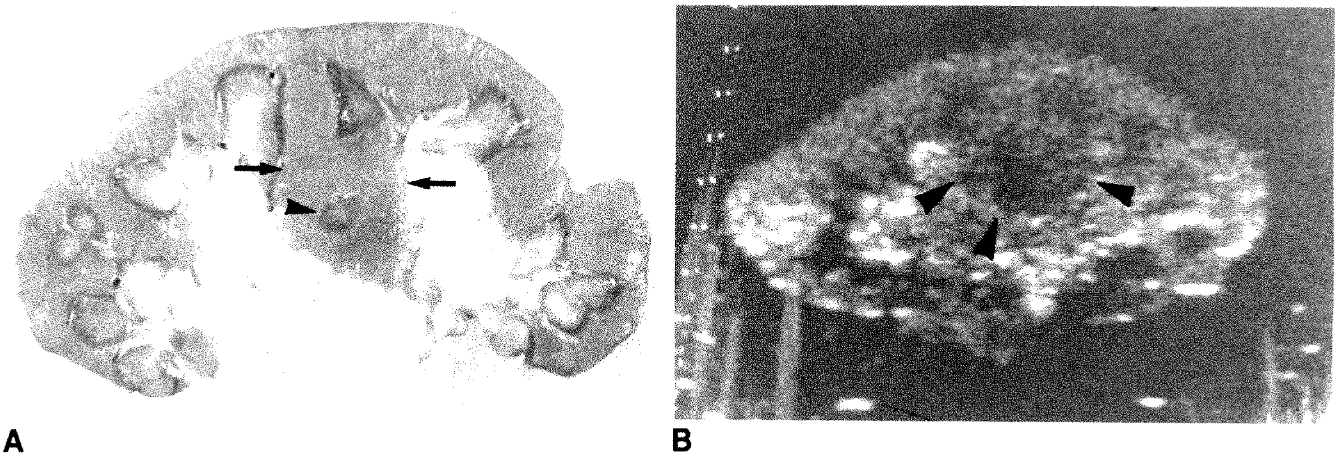

Fig. 2.—Anatomic-sonographic correlation of hypertrophied column of Bertin. **A**, Longitudinal cut of normal cadaver kidney shows large column of Bertin (*arrows*) indenting renal sinus and containing small "imprisoned" papilla (*arrowhead*). **B**, Sonogram of same kidney in water bath. Although visual detail is not as good as in vivo, hypertrophied column is outlined (*arrowheads*).

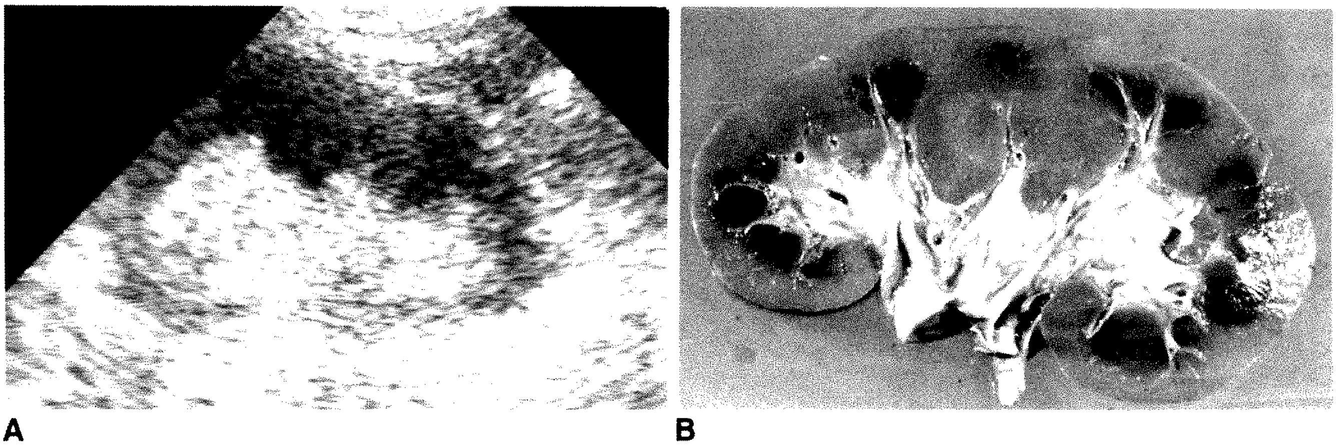

Fig. 3.—Two large columns of Bertin in middle third of kidney. **A**, Longitudinal sonogram in 68-year-old man. **B**, Longitudinal cut of normal cadaver kidney.

TABLE 1: **Incidence and Site of Hypertrophied Column of Bertin**

	Patients (n = 100), no. (%)	Cadaver Kidneys (n = 39), no. (%)
One column	47 (47)	29 (74)
Two columns	4 (4)	2 (5)
Left to right ratio	2:1	3:2
Diameter over 1 cm (grade 2 and 3)	22 (47)	16 (55)
Bilateral	18 (18)	13 (33)

masses (fig. 3). Some columns of Bertin (17%) were the site of a complete split of the sinus echoes, creating a bifid intrarenal collecting system.

The columns of Bertin were isoechogenic with the cortex. They were usually perpendicular or rarely oblique to the renal capsule (fig. 4). The renal contour was always smooth. There was no acoustic enhancement behind a large column of Bertin.

In 22% of patients, the sinus echoes embraced the column of Bertin in a clawlike fashion (fig. 1). In two patients and in one cadaver kidney, the hypertrophied column of Bertin was pierced by a small hypoechogenic focus (fig. 5). On anatomic cut, this focus represented a small engulfed papilla (fig. 2).

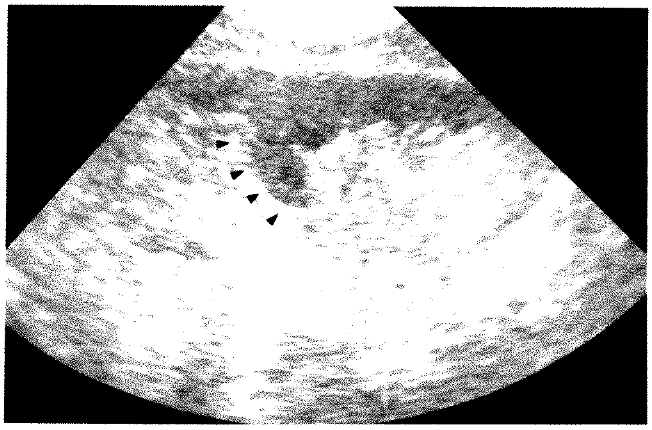

Fig. 4.—Longitudinal cut of kidney. Obliquely directed column of Bertin (*arrowheads*) engulfed by renal sinus fat.

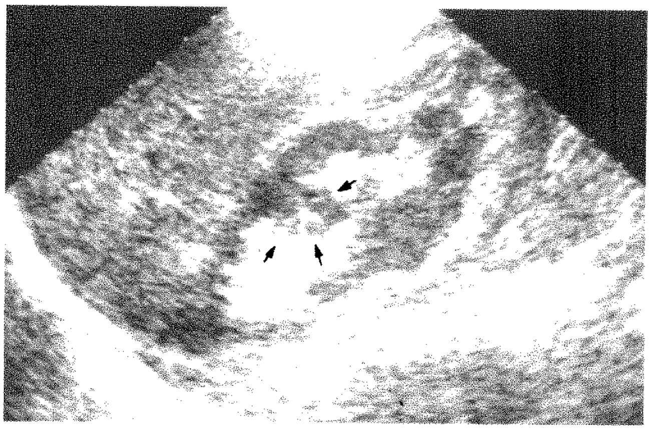

Fig. 5.—Longitudinal sonogram of right kidney. "Imprisoned" papilla (*arrows*) in center of hypertrophied column in 59-year-old woman.

Discussion

Hypertrophied columns of Bertin have been a diagnostic challenge to radiologists, especially since the routine use of nephrotomography as part of the excretory urogram. Because it simulated a solid mass, it resulted in instances of needless nephrectomies before the detailed angiographic signs of an enlarged column of Bertin were described [2–7]. The radiologic descriptions of the hypertrophied column of Bertin are numerous and many synonyms have come into use: renal pseudotumor [3, 6], focal nodular hyperplasia [5], cortical invagination with prominent column of Bertin [6], lobar dysmorphism [7], benign cortical rest [8], cortical nodule [9], and recently, large cloisons [10].

Hodson and Mariani [10], in calling them "large cloisons," returned to the original term used by Bertin in 1744. In his description of the hypertrophied column of Bertin, Hodson [11] traces the formation of such columns through renal development in several animals in which kidneys are formed by the fusion of multiple small kidneys. Each renal lobe is composed of a central mass of medullary tissue enveloped by a cortical layer. In the human, the "cloison" of Bertin is thought to be formed by the fusion of two layers of septal cortex of two adjacent lobes. In the adult, the grooves on the outer surface of the kidney (or fetal lobulation) become less visible than in a child and disappear altogether.

Hodson's classic description of the hypertrophied "cloison" of Bertin shows an increase both in incidence and size of the cloison in the middle third of the kidney. The septa or cloisons seem to be smaller and less intrusive in the polar regions of the kidney.

It is possible that sonography displays large columns of Bertin better than the classic excretory urography and nephrotomography. The kidney is viewed in several planes and from several directions on sonography. We found the axillary view especially revealing in our search for large columns of Bertin. This view is rarely available by excretory urography. In addition, details of parenchymal and sinus architecture are better appreciated by sonography than by excretory urography.

Both in Hodson's description and in our cadaver population, large septa of Bertin were often present bilaterally. Among our patients, hypertrophied columns of Bertin were seen less frequently on the right, possibly because the sonographic axillary view of the right kidney is more cumbersome to perform than the left and is rarely needed.

The sonographic signs of hypertrophied columns of Bertin are characteristic. The only possible pitfall is the parapelvic cyst. Careful analysis of the echogenicity of such a cyst and its acoustic enhancement will help to differentiate it from hypertrophied columns of Bertin. The small hypoechogenic focus that represents an engulfed papilla has already been described at urography [12]. It may be connected to a small or abortive calix [10, 13, 14].

A review of 48 consecutive hypernephromas seen at sonography in our institution did not show one tumor that did not distort the contour of the kidney. The normal renal contour seen with a hypertrophied column of Bertin is thus an important feature distinguishing it from hypernephroma. Similarly, adenomas can be distinguished from hypertrophied columns of Bertin by their cortical rather than parapelvic position and by their mass effect on the outer surface of the kidney. When small, even if they are isoechogenic with the cortex, adenomas are well demarcated [15].

There have been no reports of nephrectomy performed for a hypertrophied column of Bertin since 1976. However, the literature abounds with complex investigative algorithms to establish the diagnosis of hypertrophied columns of Bertin. These usually include selective renal angiography, radionuclide studies, and CT [10, 16-19].

Our study shows that the hypertrophied column of Bertin is a frequent anatomic variant and that it has sonographic features that reliably distinguish it from pathologic renal masses.

ACKNOWLEDGMENTS

We thank Gilles Gariepy, Jean Marchi, and Sylvie Boulanger for their contribution to this article.

REFERENCES

1. Bertin EJ. Mémoire pour servir à l'histoire des reins. In: *Histoire de l'Académie Royale des Sciences*. Paris: Académie Royale des Sciences, **1744**:77-111
2. King MC, Friedenberg RM, Tena LB. Normal renal parenchyma simulating tumor. *Radiology* **1968**;91:217-222
3. Felson B, Moskowitz M. Renal pseudotumors: the regenerated nodule and other lumps, bumps, and dromedary humps. *AJR* **1969**;107:720-729
4. Meaney TF. Errors in angiographic diagnosis of renal masses. *Radiology* **1969**;93:361-366
5. Popky GL, Bogash M, Pollack H, Longacre AM. Focal nodular hyperplasia. *J Urol* **1969**;102:657-660
6. Lopez FA. Renal pseudotumors. *AJR* **1970**;109:172-184
7. Charghi A, Dessureault P, Drouin G, et al. Malposition of a renal lobe (lobar dysmorphism): a condition simulating renal tumor. *J Urol* **1971**;105:326-329
8. Flynn VJ, Gilles RF. Bening cortical rest: a "pseudotumor" of the kidney. *J Urol* **1972**;108:54-57
9. Thornbury JR, McCormick TL, Silver TM. Anatomic/radiologic classification of renal cortical nodules. *AJR* **1980**;134:1-7
10. Hodson CJ, Mariani S. Large cloisons. *AJR* **1982**;139:327-332
11. Hodson CJ. The lobar structure of the kidney. *Br J Radiol* **1972**;44:246-261
12. Dacie JE. The "central lucency" sign of lobar dysmorphism (pseudotumour of the kidney). *Br J Radiol* **1976**;49:39-42
13. Webb JR, Fry K, Charlton CA. An anomalous calix in the kidney: an anatomical variant. *Br J Radiol* **1975**;48:674-677
14. Kunin M. The abortive calix: variations in appearance and differential diagnosis. *AJR* **1982**;139:931-934
15. Goiney RG, Goldenberg L, Cooperberg PL, et al. Renal oncocytoma: sonographic analysis of 14 cases. *AJR* **1984**;143:1001-1004
16. Lams P, Gerlock AJ, Rusu J. Arteriography: aid to urography in determining etiology and diagnosis of renal pseudotumors. *AJR* **1979**;133:149-151
17. Pollack HM, Edell S, Morales JO. Radionuclide imaging in renal pseudotumors. *Radiology* **1974**;111:639-644
18. Older RA, Korobkin M, Workman J, et al. Accuracy of radionuclide imaging in distinguishing renal masses from normal variants. *Radiology* **1980**;136:443-448
19. Mahony BS, Jeffrey RB, Laing FC. Septa of Bertin: a sonographic pseudotumor. *JCU* **1983**;11:317-319

Retroperitoneal Fibrosis: Use of CT in Distinguishing among Possible Causes

Gintaras E. Degesys[1, 2]
N. Reed Dunnick[1]
Paul M. Silverman[1]
Richard H. Cohan[1]
Fernando F. Illescas[1]
Arthur Castagno[1]

Retroperitoneal fibrosis (RF) often presents with characteristic clinical and urographic findings that suggest the diagnosis. However, malignant adenopathy may mimic this appearance. CT examinations of 10 patients with medial deviation of the ureters suggesting retroperitoneal fibrosis were reviewed. Six had idiopathic RF, two had perianeurysmal fibrosis, and two had malignant retroperitoneal adenopathy. The CT findings in idiopathic RF included a homogeneous mass enveloping the ureters, aorta, and inferior vena cava. The aortic aneurysm was easily seen in both patients with perianeurysmal fibrosis. In one of the two patients with malignant retroperitoneal adenopathy, the CT findings mimicked idiopathic RF. In the other patient, the nodes involved with metastatic melanoma caused significant anterior displacement of the aorta and inferior vena cava. This marked anterior displacement of the great vessels is not seen in idiopathic RF, and may be useful in differentiating these entities.

Retroperitoneal fibrosis (RF) is a fibrotic process involving the retroperitoneum. It can be idiopathic or can be provoked by methysergide ingestion, perianeurysmal inflammation, leaking aneurysms, urinomas, or irradiation. The classic findings during excretory urography include medial deviation and narrowing of the ureters near the lower lumbar spine [1, 2]. Mild proximal hydronephrosis is usually present, but with disproportionately elevated creatinine levels. This may result from an interference with ureteral peristaltic activity rather than mechanical obstruction of the ureter by the fibrosis [3]. Treatment consists of either corticosteroid therapy or surgical ureterolysis.

RF typically envelops the midureters, drawing them medially. The diagnosis of RF is often suggested by the characteristic appearance on excretory urography or retrograde pyelography. This urographic appearance can be mimicked, however, by malignant retroperitoneal adenopathy [4]. Previous reports have described the appearance of RF on CT [5–8]. In some cases, the cause of RF can be determined by a history of methysergide use or irradiation. CT can assist in demonstrating other causes, such as an abdominal aortic aneurysm [9, 10] or an adjacent inflammatory process [8]. However, previous attempts to distinguish idiopathic RF from malignant adenopathy have not been successful [6, 7]. We reviewed the CT examinations of 10 patients with typical urographic features of RF to look for features that allow this distinction.

Subjects and Methods

Ten patients with urographic findings suggesting RF underwent a total of 16 CT examinations on GE 8800, GE 9800, or Siemens Somatom II scanners. In these patients, an excretory urogram or retrograde pyelogram demonstrated medial deviation of the midureter with proximal ureteral dilatation. Patients were aged 33–73 years; seven were men and three women. In each patient, contiguous scans were performed using 1-cm collimation at 2- or 1-cm intervals. All patients received dilute oral contrast medium. Intravenous contrast medium was withheld in five patients because of azotemia. Of the remaining patients, one had a

Received June 3, 1985; accepted after revision August 28, 1985

[1] Department of Radiology, Box 3808, Duke University Medical Center, Durham, NC 27710. Address reprint requests to N. R. Dunnick.

[2] Present address: Beachwood, OH 44122.

AJR 146:57–60, January 1986
0361–803X/86/1461–0057
© American Roentgen Ray Society

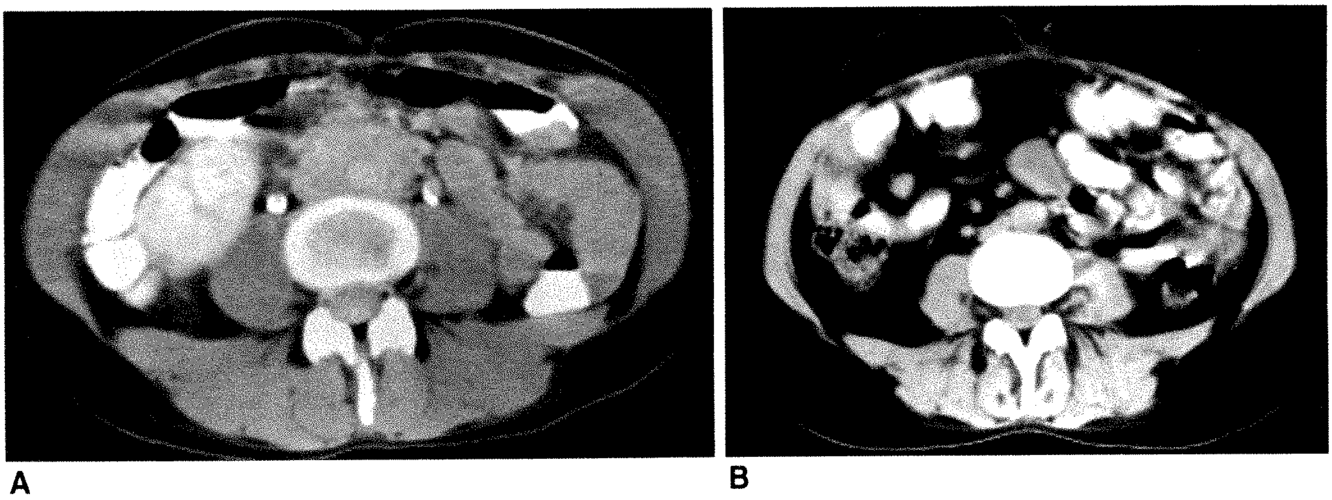

Fig. 1.—CT scans of 45-year-old woman with renal failure. **A**, Paraaortic soft-tissue mass envelops but does not displace aorta. RF was diagnosed. **B**, After 3 months of steroid therapy, there is appropriate resolution with virtually complete disappearance of RF. Also note increase in both retroperitoneal and subcutaneous fat secondary to steroid usage.

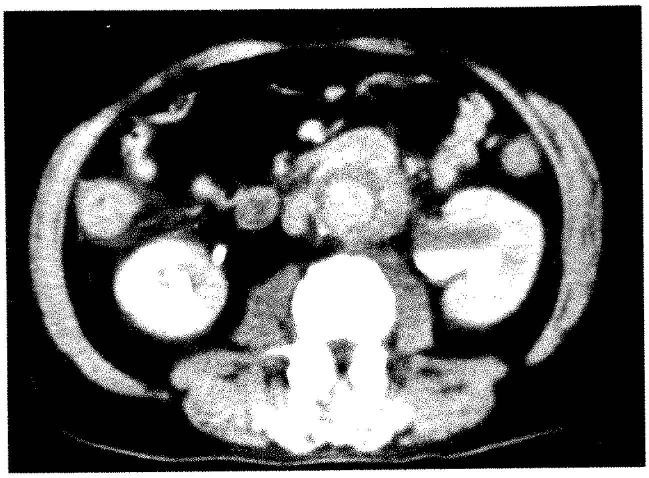

Fig. 2.—Postcontrast CT scan. Paraaortic soft-tissue mass close to intraluminal thrombus within dilated abdominal aorta, diagnostic of perianeurysmal fibrosis.

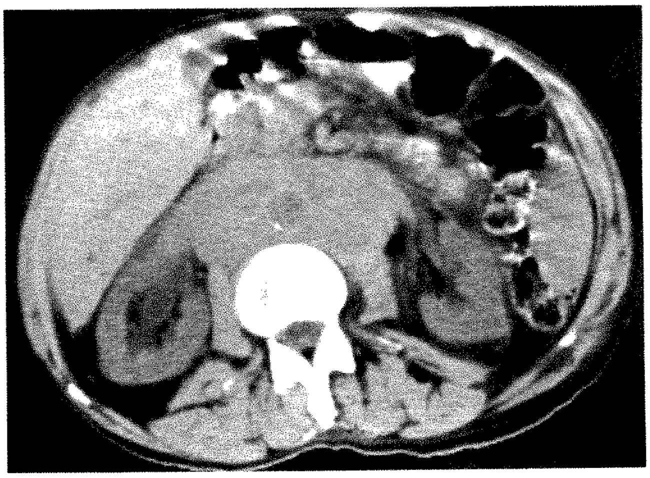

Fig. 3.—CT scan of patient with known melanoma, metastatic to paraaortic lymph nodes, causing anterior displacement of aorta.

noncontrast scan before surgical ureterolysis and a contrast scan after therapy. Two other patients had CT scans both before and after steroid therapy; one of these was obtained after lymphangiography was also performed. The remaining two patients had enhanced scans only.

Results

Seven patients underwent exploratory laparotomy with biopsy of their retroperitoneal masses; six had retroperitoneal fibrosis (five idiopathic and one perianeurysmal), and one had a malignant lymphoma. Of the remaining three patients, one was clinically considered to have idiopathic RF and responded to corticosteroid therapy. Another patient demonstrated an aortic aneurysm in conjunction with RF and was classified as having perianeurysmal fibrosis. The third remaining patient had known melanoma and the retroperitoneal mass, although not biopsy proven, was assumed to represent metastatic disease.

The CT examination in the six patients with idiopathic RF demonstrated homogeneous masses that began above the renal hilum and extended into the pelvis in four patients and were limited to the lower lumbar level in two patients. In all these patients, the fibrotic mass enveloped, but did not displace, the inferior vena cava and aorta. Specifically, the aorta retained its normal relation to the spine with no significant elevation by the retroperitoneal mass. One of these cases demonstrated lobulation; five did not. The anterior margin was sharply delineated in four and poorly defined in two patients. Three patients also had CT with contrast medium infusion obtained after specific therapy (either ureterolysis or steroid therapy). In one patient, the CT scan after 3 months

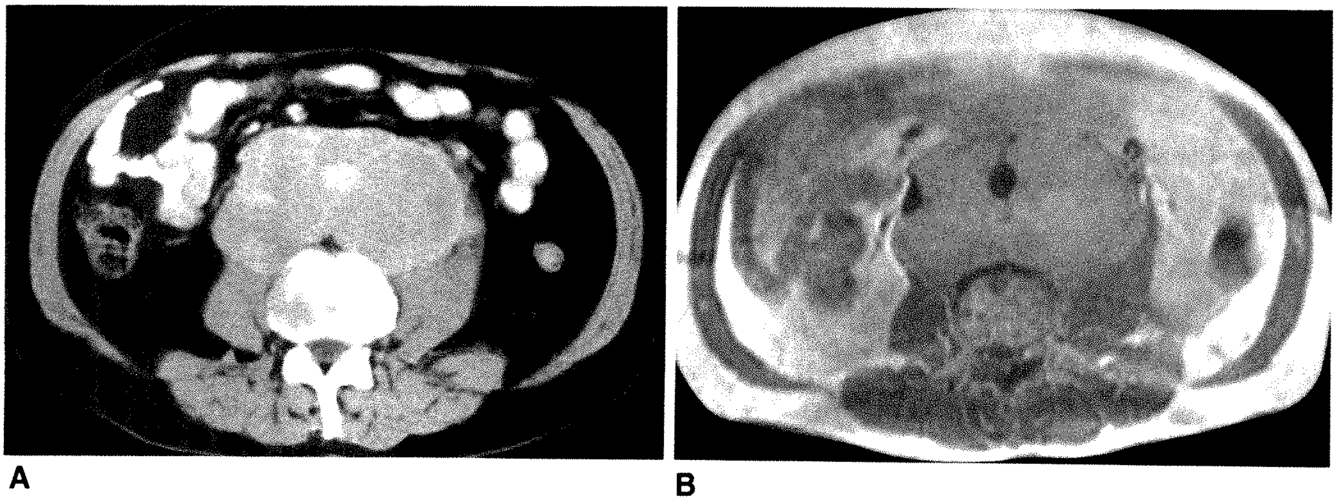

Fig. 4.—Patient with known prostatic carcinoma and metastatic disease involving paraaortic nodes. **A**, Postcontrast CT scan. Marked anterior displacement of aorta. **B**, Subsequent MRI scan better shows not only aorta but also inferior vena cava, both displaced by paraaortic adenopathy.

of steroid therapy showed a dramatic resolution with virtual disappearance of RF (fig. 1).

Two patients demonstrated aneurysmal dilatation of the abdominal aorta in conjunction with a paraaortic soft-tissue mass (fig. 2). One patient had both pre- and postinfusion scans, while the other had only a postcontrast scan. Clot was present in the aneurysm of both patients, but there was no evidence of contrast extravasation. These cases were most consistent with RF secondary to perianeurysmal inflammation, or so-called perianeurysmal fibrosis.

The remaining two patients had paraaortic soft-tissue masses with medial ureteral deviation that mimicked RF. These patients were diagnosed as having malignant involvement of the paraaortic nodes, one by malignant lymphoma and the other by metastatic melanoma. In the latter case, there was anterior displacement of the abdominal aorta by the enlarged lymph nodes (fig. 3).

Discussion

The diagnosis of RF is often suggested on excretory urography or retrograde pyelography by the characteristic medial deviation of the midureter and mild hydronephrosis. The CT findings correlate well with the classic urographic manifestations, including a soft-tissue mass anterior to the lumbar spine that is adjacent to the great vessels and envelops the ureters [5–8].

Several authors have attempted to define characteristic CT features of RF that would differentiate it from paraaortic adenopathy, but with little success. Brun et al. [7] proposed using the extent of the mass as a distinguishing feature. In their experience, lymphoma was more often cephalad in location, while RF was caudal to the renal hilum. Of our cases with RF, only two were in the latter location, while four were both cephalad and caudad. Our single case of lymphoma with medial ureteral entrapment was also caudal to the renal hilum. It is unlikely that position alone will allow confident discrimination between the two entities.

Dalla-Palma et al. [8] noted enhancement of the fibrotic mass in RF. They suggested that the variation in enhancement reflected the degree of inflammation, which was more marked in the periphery. Enhancement was not useful in distinguishing RF from lymphoma in our series, since often only precontrast scans were obtained because of preexisting azotemia. Furthermore, RF secondary to perianeurysmal fibrosis may demonstrate enhancement [9, 10].

Other authors have examined the characteristics of the morphology of retroperitoneal fibrosis, especially shape and margin. Fagan et al. [5] concluded that while the anterior margin of retroperitoneal fibrosis is clearly delineated, it is poorly defined posteriorly. Feinstein et al. [6] attempted to differentiate RF from lymphoma or metastatic disease, which presented a nodular appearance; RF was manifested as a plaquelike or infiltrating pattern. In our experience, distinction based on these characteristics of either the margin or shape is difficult to make. Only one of six patients with idiopathic RF was considered to have nodular masses. The anterior margin was sharply delineated in four, but poorly defined in two.

Fagan et al. [5] noted the tendency of RF to envelop but not displace the aorta or ureters. However, this characteristic was not emphasized, nor was there an attempt to apply it in differentiating RF from malignant processes. There was no significant anterior displacement of the aorta in any of our cases of idiopathic RF. Lymphoma and other malignant processes often elevate the aorta from the spine. The difference in this vascular displacement is presumably due to the position of lymph nodes that lie posterior to the aorta and inferior vena cava. The effect on the vessels depends on which nodes are involved with metastatic tumor. If more posterior nodes are involved with bulky adenopathy, anterior displacement will be marked. This was not seen in idiopathic RF in our series or other series in the literature. Recently, we have had the opportunity to examine a patient with prostatic carcinoma and metastatic involvement of the paraaortic lymph nodes. Both CT and MRI were performed, elegantly demonstrating anterior displacement not only of the aorta, but also of the inferior vena cava (fig. 4).

Biopsy specimens of RF demonstrate densely fibrotic areas of collagen with cellular inflammation [11]. This chronic inflammation and repair are retractile processes, such as that seen with mediastinal fibrosis or retractile mesenteritis. The absence of mass effect by RF is expected, given the retractile nature of the fibrotic process. Although pathologically RF represents fibrosis, it takes on the appearance of a mass. Yet, in relation to its surrounding structures, RF does not cause displacement of adjacent organs or vessels, but rather envelops them. Malignancies such as lymphoma or sarcoma often cause displacement of surrounding structures, since they are more solid in character.

Histologic examination of perianeurysmal RF suggests that it occurs without aneurysm leakage, since hemosiderin-laden macrophages are not present [12]. This finding suggests that perianeurysmal RF may represent an autoimmune reaction to the intraluminal thrombus, with extension of the reaction through the aortic wall. In such cases, the presence of an abdominal aneurysm with clot simplifies the identification of this retroperitoneal mass, as was evident in our two cases (fig. 2).

The characteristic appearance on urography of bilateral medial deviation of both ureters at the L4–L5 level suggests RF. Some causes, such as irradiation or drug use, can be excluded by history, while others, such as aneurysmal fibrosis, are readily detected by CT. The contour, extent, and pattern of contrast enhancement do not allow distinction between idiopathic RF and malignant adenopathy. The presence of significant anterior displacement of the great vessels, however, indicates a malignant cause, as this has not been demonstrated with idiopathic RF.

ACKNOWLEDGMENT

We thank Beverly Johnson for help in manuscript preparation.

REFERENCES

1. Ormond JK. Bilateral ureteral obstruction due to envelopment and compression by an inflammatory retroperitoneal process. *J Urol* **1948**;59:1072–1079
2. Kaude J. Retroperitoneal fibrosis. *Acta Radiol [Diagn]* (Stockh) **1966**;4:331–343
3. Lalli AF. Retroperitoneal fibrosis and inapparent obstructive uropathy. *Radiology* **1977**;122:339–342
4. Arger PH, Stolz JL, Miller WT. Retroperitoneal fibrosis: an analysis of the clinical spectrum and roentgenographic signs. *AJR* **1973**;119:812–821
5. Fagan CJ, Larrieu AJ, Amparo EG. Retroperitoneal fibrosis: ultrasound and CT features. *AJR* **1979**;133:239–243
6. Feinstein RS, Gatewood OMB, Goldman SM, Copeland B, Walsh PC, Siegelman SS. Computerized tomography in the diagnosis of retroperitoneal fibrosis. *J Urol* **1981**;126:255–259
7. Brun B, Laursen K, Sorensen IN, Lorentzen JE, Kristensen JK. CT in retroperitoneal fibrosis. *AJR* **1981**;137:535–538
8. Dalla-Palma L, Rocca-Rossetti S, Pozzi-Mucelli RS, Rizzatto G. Computed tomography in the diagnosis of retroperitoneal fibrosis. *Urol Radiol* **1981**;3:77–83
9. Vint VC, Usselman JA, Warmath MA, Dilley RB. Aortic perianeurysmal fibrosis: CT density enhancement and ureteral obstruction. *AJR* **1980**;134:577–580
10. Aiello MR, Cohen WN. Inflammatory aneurysm of the abdominal aorta. *J Comput Assist Tomogr* **1980**;4:265–267
11. Lepor H, Walsh PC. Idiopathic retroperitoneal fibrosis. *J Urol* **1979**;122:1–6
12. Megibow AJ, Ambos MA, Bosniak MA. Computed tomographic diagnosis of ureteral obstruction secondary to aneurysmal disease. *Urol Radiol* **1980**;1:211–215

Retrograde Ureteral Catheterization via the Ileal Conduit

Yaakov N. Applbaum,[1,2] Arthur B. Diamond,[1] and Arnold S. Rappoport[1]

The complications of ileal conduit urinary diversion, once treated exclusively by surgery, are now often amenable to correction by less invasive uroradiologic means [1–3]. Heretofore, access to the urinary tract has been via percutaneous nephrostomy [1, 2, 4]. We report our experience in 10 patients with ileal (or jejunal) conduits in whom we were able to place ureteral catheters, using a strictly retrograde approach through the ileal conduit. We conclude that such an approach should be attempted in all suitable patients; in our experience, the price for failure has merely been the need to perform a percutaneous nephrostomy for antegrade access, a procedure that otherwise would have been necessary.

Materials and Methods

The study group consisted of 10 patients, six men and four women, aged 44–88 years. All patients had undergone cystectomy with urinary diversion: nine via an ileal conduit and one, whose ileum had undergone radiation necrosis, by a jejunal conduit. Nine of the patients had been operated on for carcinoma of pelvic organs, including the bladder (four), rectosigmoid (two), cervix (two), and prostate (one); one patient had had a neurogenic bladder related to transverse myelitis many years earlier. Intervention was necessary because of leaking at a ureteroileal anastomosis (five patients), stricture or obstruction at the anastomosis or proximal to it (five), fistulae (e.g., rectal conduit, nephrocutaneous) (two patients), and renal calculi (one). Retrograde ureteral catheterization was attempted on all 10 patients. Four patients required multiple procedures for the replacement of clogged stents or for further treatment of calculi.

Procedure

With aseptic precautions and the patient supine, a Foley- or Robinson-type catheter was placed through the stoma into the distal part of the conduit and gently injected by hand with 60% water-soluble contrast material until the entire anatomy of the conduit was delineated. After the ureteral orifice was identified, an angiographic catheter (usually a 5-French Hanafee catheter [Cook]) was used to cannulate the orifice, and a Benson or Lunderquist-Ring torque guide wire (Cook) was advanced into the ureter and renal pelvis (fig. 1). If the catheter and guide wire became caught on the valvulae conniventes, the loop was distended with dilute (30%) contrast material or saline, flattening out the valvulae and allowing easier passage of the catheter. Excess contrast medium and urine constantly drained from the ileal stoma and did not interfere with visibility of the ureteral orifice or of the guide wire or catheter. Alternatively, the blunt-ended Robinson catheter could serve as a "sleeve device" to deliver the guide wire or catheter to the ureteral orifice.

If the initial injection of contrast material did not delineate the ureteral orifices, the wire and catheter were advanced to the presumed site of anastomosis, and blind cannulation was carefully attempted. Prior knowledge of the site and type of anastomosis was helpful in this situation. Careful, controlled manipulation under fluoroscopy using soft catheters and guide wires reduced the risk of anastomotic disruption. Nevertheless, we were not persistent with blind manipulation in recently (<1 month) postoperative patients.

Once the wire was in the renal pelvis, a stent could be positioned. Originally (first two patients), a double pigtail stent was placed with its distal part in the ileal conduit. A suture was tied through a side hole in the distal end and passed out the stoma for future retrieval. Although this positioning of the stent was most acceptable to the patient, we found that these catheters tended to get clogged with inspissated mucus from the ileal conduit. In the last eight patients, we used 7- or 8-French, 35-cm, polyethylene nephrostomy-type catheters, leaving the pigtail in the renal pelvis, while the distal end of the catheter exited the stoma to drain directly into the bag. No side holes were present within the ileal conduit itself (fig. 2).

Results

Retrograde passage through 17 ureters in 10 patients was attempted; 14 ureters were successfully catheterized in a retrograde fashion at least once. In one patient, the right ureter was cannulated via a retrograde approach four different times; in two other patients, the left ureter was catheterized on two separate occasions, each time retrograde. Altogether, 19 (76%) of 25 retrograde passes were successful, although one was only a partial success. In that patient, catheterization was successful, but the patient's midureteral stricture could not be dilated.

There were no intra- or postprocedural complications. At least temporary clinical improvement was noted in all cases. In two early patients in whom double pigtail stents were used, the catheters tended to become clogged with mucus and debris after 1–2 months and were replaced as necessary, over a guide wire if possible or de novo. This problem was later avoided by the use of nephrostomy-type catheters, as described earlier.

Received March 4, 1985; accepted after revision August 29, 1985.

[1] Department of Radiology, Memorial Hospital Medical Center, 2801 Atlantic Ave., Long Beach, CA 90801-1428. Address reprint requests to A. B. Diamond.

[2] Present address: Department of Radiological Sciences, University of Califorina, Irvine Medical Center, Orange, CA 92668.

AJR 146:61–63, January 1986 0361–803X/86/1461–0061 © American Roentgen Ray Society

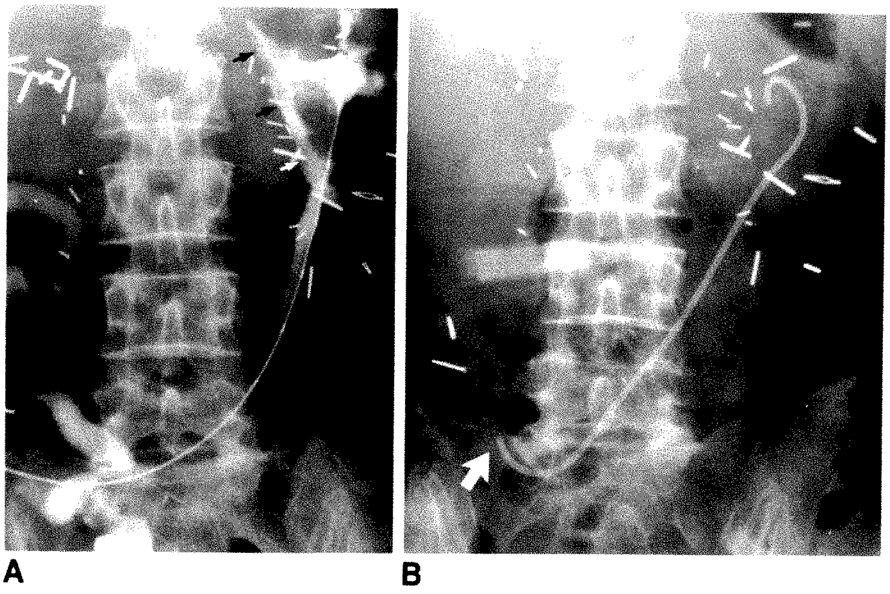

Fig. 1.—Nephrocutaneous fistula from previous nephrolithotomy. **A**, Lunderquist-Ring guide wire introduced into ileal conduit and placed in left renal pelvis. Prior injection of contrast through 5-French catheter shows fistula draining from renal pelvis into perirenal space (*arrows*). **B**, 16-cm-long, 7-French, double-J catheter placed with proximal end in renal pelvis and distal end in ileal conduit (*arrow*).

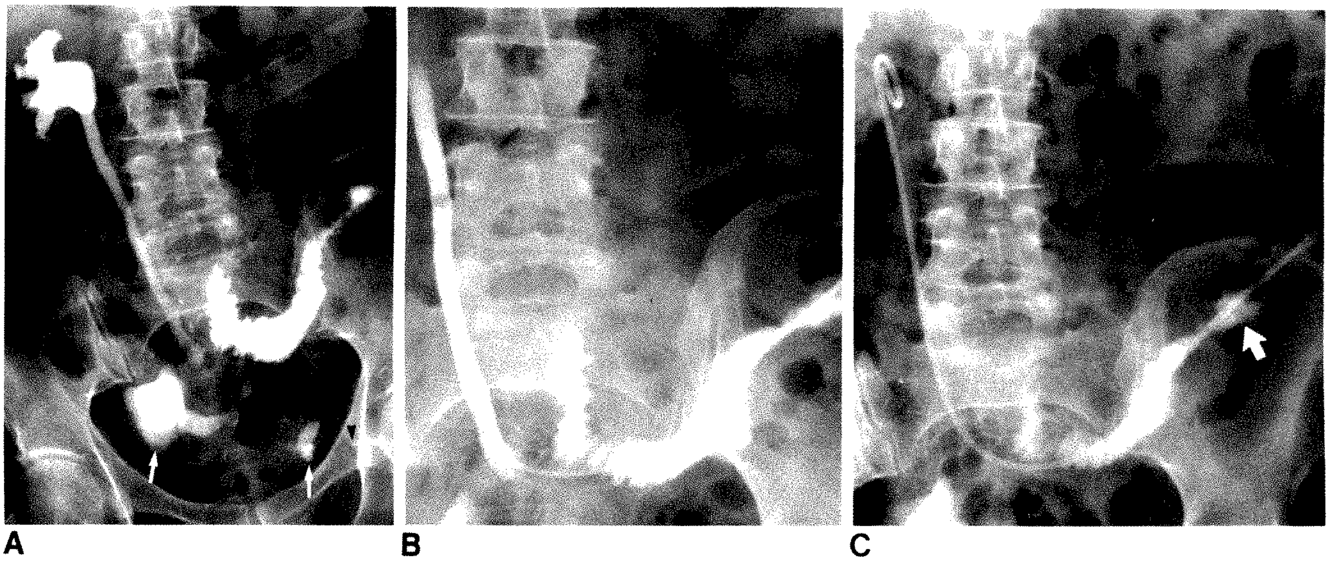

Fig. 2.—Leak at ureteroileal anastomosis. **A**, Loopogram shows reflux into right ureter and renal pelvis, with contrast extravasation into pelvis from leak at right ureteroileal anastomosis (*arrows*), which ultimately drains to skin at site of previous drain placement in left lower abdomen at location of catheter tip (*arrowhead*). **B**, 5-French left-vertebral type catheter advanced through ileal conduit into right ureter. **C**, 5-French nephrostomy catheter placed with pigtail in renal pelvis, draining externally through stoma (*arrow*). Similar attempt to catheterize left ureter was unsuccessful.

One patient was seen in our department over 4 years for recurrent bilateral renal calculi. In a series of manipulations performed through the ileal conduit, part of a fragmented staghorn calculus was removed from the right renal pelvis with a stone-removal basket, after which infusion and drainage catheters were placed adjacent to the remaining fragments in the upper and lower poles, and stone dissolution with Renacidin infusion was successfully achieved. Similar infusion on the left side for a left-upper-pole calculus was not as successful, and this stone was eventually removed percutaneously.

Discussion

A significant percentage of patients undergoing urinary diversion into an ileal conduit have one or more complications directly or indirectly associated with this procedure, the most frequent and important among them being urinary leak at the ureteroileal anastomosis (in the immediate postoperative period), ureteral stricture, and calculi [5].

In recent times, these complications have been treated with methods of stent placement, stricture dilatation by catheter or balloon, and stone removal or lysis, using a percutaneous approach first developed for patients with intact bladders [1–3]. Most groups apparently never even attempted a retrograde approach, while others believed that retrograde catheterization via an ileal conduit is difficult or impossible because of tortuosity, large caliber, distensibility, and length of the conduit [1, 3, 4]. By contrast, we have been successful in most cases in our attempts to gain access to the urinary tract via an ileal conduit. Although a number of urologists have used rigid, and more recently, flexible endoscopy to facilitate retrograde catheterization in patients with ileal conduits [6–8], such an approach by a radiologist without the aid of an endoscope has been reported in only one case [4], and the group that did so does not believe it is a generally feasible procedure.

Our motivation in attempting retrograde catheterization is that percutaneous nephrostomy is associated with morbidity as well as discomfort. Most series report the incidence of major complications to be 4%, including hemorrhage, infection and septicemia, urine leak, and puncture of other organs [9]. Access may be difficult in a nondilated system [10], and in fact those patients presenting with a leak at the ureteroileal anastomosis may not have dilated pelvocaliceal systems. A retrograde approach via an ileal conduit is essentially risk free in most circumstances; it is painless, as evidenced by the lack of need for local anesthesia, and there is little to lose, because if it is unsuccessful, an antegrade percutaneous approach can then be attempted. Finally, irrigation of the nephrostomy catheter by the patient is far easier when it is exiting the anterior abdominal wall than when it is located in the flank.

There is a risk of disruption of the ureteroileal anastomosis in a patient with a postoperative leak. However, as the ureters (and fistulae) are usually demonstrated on loopography in such cases, manipulation from below with fluoroscopic control is not significantly different from such manipulation under endoscopic visualization or similar stent placement techniques using an antegrade approach. Complications have not been described in studies using the last two methods, nor did we experience any complications, such as anastomotic disruption, in our 25 attempts, of which seven were done to treat fistulae in postoperative patients.

In our experience, if the ureter is seen on loopography, then it can generally be catheterized without significant difficulty. Factors that are advantageous include the presence of a short loop of ileum and a relatively wide stoma. Such a stoma allows us to use a finger to manipulate the conduit in a manner that helps position the ureteral orifice to our advantage. While nonvisibility of the ureteral orifices on loopography does make catheterization more difficult, knowledge of the type and position of the anastomosis has been beneficial in some cases. We have found, as anticipated by others [1], that a long, wide, redundant loop of ileum makes wire and catheter manipulation difficult, although not impossible. In long-term cases, ileal loop shortening and narrowing are not unusual [6] and aid in catheter manipulation, although a tight stricture in the loop has been an obstacle when present.

Cannulation of the ureteral orifice has not always ensured successful intervention. In one of our cases, although a guide wire could be advanced through an area of stricture, the balloon catheter would not follow, presumably because the pliable bowel absorbed the forward thrust of the catheter. To advance the balloon catheter through the stenotic segment, it was necessary to anchor the wire at both ends, thus requiring a percutaneous nephrostomy.

In conclusion, in patients with ileal conduits in whom access to the urinary tract is necessary, retrograde catheterization is a safe and painless alternative that should be attempted before resorting to a percutaneous nephrostomy.

REFERENCES

1. Bettman MA, Murray PD, Perlmutt LM, Whitmore WF III, Richie JP. Ureteroilial anastomotic leaks: percutaneous treatment. *Radiology* **1983**;148:95–100
2. Banner MP, Pollack HM, Ring EJ, Wein AJ. Catheter dilatation of benign ureteral strictures. *Radiology* **1983**;147:427–433
3. Smith AD, Lange PH, Reinke DB, Miller RP. Extraction of ureteral calculi from patients with ileal loops: a new technique. *J Urol* **1978**;120:623-625
4. Rosen RJ, McLean GK, Freiman DB, Oleaga JA, Wein AJ, Ring EJ. Obstructed ureteroileal conduits: antegrade catheter drainage. *AJR* **1980**;135:1201–1204
5. Sullivan JW, Grabstald H, Whitmore WJ Jr. Complications of ureteroileal conduit with radical cystectomy: review of 336 cases. *J Urol* **1980**;124:797–801
6. Banner MP, Pollack HM, Bonavita JA, Ellis PS. The radiology of urinary diversions. *Radiographics* **1984**;4:885–913
7. Falkenstein DB, Reich CB, Golimbo MN, Warner RS, Morales PA, Zimmon DS. Endoscopy of ureterointestinal conduits and retrograde pyelography. *Gastrointest Endosc* **1975**;22:24–26
8. Fritzsche P, Moorhead JD, Axford PD, Torrey RR. Urologic applications of angiographic guide wire and catheter techniques. *J Urol* **1981**;125:774–780
9. Barbaric ZL. Percutaneous nephrostomy for urinary tract obstruction. *AJR* **1984**;143:803–809
10. Hawkins IF Jr, Hunter P, Leal G, et al. Retrograde nephrostomy for stone removal: combined cystoscopic/percutaneous technique. *AJR* **1984**;143:299–304

Diagnostic Oncology Case Study

Clear Cell Sarcoma of the Kidney: A Renal Tumor of Childhood that Metastasizes To Bone

A 3-year-old boy presented with painless gross hematuria and was found to have hypertension. A right abdominal mass was palpated on initial examination, and a subsequent sonogram revealed a solid 6-cm mass at the upper pole of the right kidney (fig. 1A). An excretory urogram confirmed the right renal mass and demonstrated a normally functioning left kidney (fig. 1B). An inferior vena cavogram failed to show tumor extension into the cava or a tumor thrombus (fig. 1C). Chest radiographs, chest CT scans, and a bone survey were all within normal limits; a radionuclide bone scan was not performed.

Subsequently, a right radical nephrectomy with retroperitoneal lymph node dissection was accomplished without complication. A 7-cm irregular mass was found in the upper pole of the right kidney, and a histologic diagnosis of clear cell sarcoma of the kidney was established. The resected lymph nodes showed hyperplasia without evidence of tumor. The indentation seen on the inferior vena cavogram (fig. 1C) was caused by the primary tumor, and no tumor was found in the cava or right renal vein. The patient's blood pressure returned to normal after surgery.

The child was then entered into the National Wilms' Tumor Study-3 Protocol (see below) and was treated according to the unfavorable histology division; he received 2200 rad (22 Gy) in 14 treatments to the right renal bed postoperatively, and he is currently receiving a chemotherapy regimen consisting of actinomycin-D, vincristine, Cytoxan, and Adriamycin. He is now 24 months after diagnosis and 6 months after completion of chemotherapy, with no evidence of disease.

Discussion

Only 450 cases of Wilms tumor are recognized annually in the United States. The rarity of this tumor led to the development of a multicenter investigational approach in 1969, with the establishment of the (first) National Wilms' Tumor Study. National Wilms' Tumor Study Groups 2 and 3 were subsequently launched, and National Wilms' Tumor Study 4 is beginning in 1985. The total number of cases on study in National Wilms' Study Groups 1–3 is 895. Quality control with respect to pathology review and treatment has been excellent.

As recently as the 1940s, the diagnosis of Wilms tumor carried a uniformly grave prognosis, with a long-term survival of only 20%. With the advent of effective chemotherapy in the early 1960s, the outlook for these children improved substantially, with an overall survival now of about 80%. Wilms tumors have been classified into favorable and unfavorable histologies, with survivals of 90% and 20%–30%, respectively. Among the unfavorable group are tumors with anaplasia and those with sarcomatous histology. Subsequently, Beckwith [1, 2] has renamed the two sarcomatous subtypes clear cell sarcoma of the kidney and malignant rhabdoid tumor of the kidney (fig. 2). These sarcomatous subtypes are no longer considered as variants of Wilms tumor, but as distinct entities. Over 80% of the deaths in the National Wilms' Tumor Study have been in patients with clear cell sarcoma, rhabdoid sarcoma, or Wilms tumor with anaplasia. The clear cell and the rhabdoid variants have a tendency to recur locally and to metastasize to bone and to brain, respectively. The survival in clear cell sarcoma is under 50%, and survival is common only in the *early* stages (I and II). Overall survival in patients with classic Wilms tumor (without anaplasia) is 70%–75%, which includes all stages (I–IV). The observations that distinguish the classic Wilms tumor from

---

This is another in a series of case reports edited by A. Robert Kagan (Southern California Permanente Medical Group, 1510 N. Edgemont, Los Angeles, CA 90027) and Richard J. Steckel (Jonsson Comprehensive Cancer Center at UCLA, Los Angeles, CA 90024) to present and discuss contemporary problems and procedures in the identification and staging of neoplasms. Case contributed by George Sleight and Michael M. Lock, Department of Radiation Therapy, Southern California Permanente Medical Group, Los Angeles, CA 90027. Address reprint requests to A. R. Kagan.

AJR 146:64-66, January 1986 0361-803X/86/1461-0064 © American Roentgen Ray Society

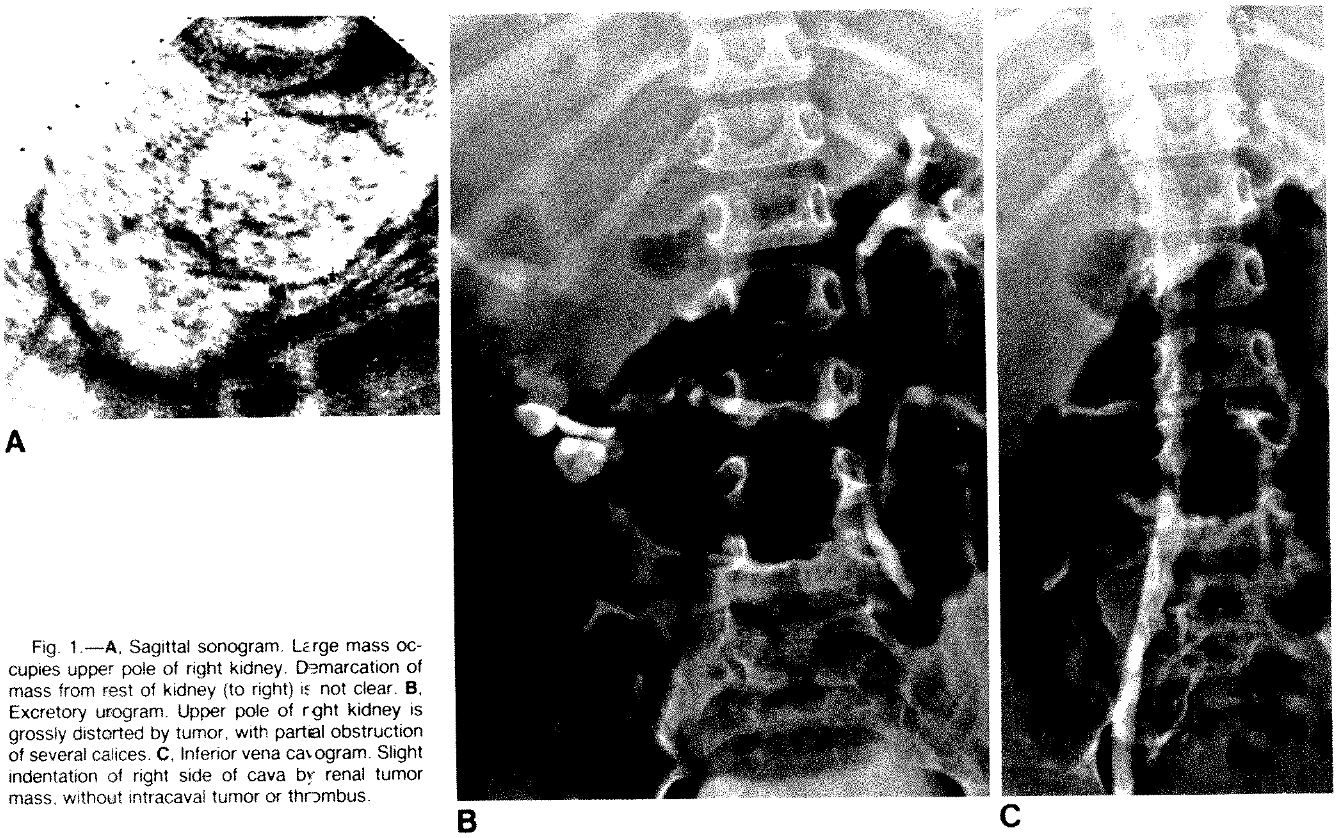

Fig. 1.—**A**, Sagittal sonogram. Large mass occupies upper pole of right kidney. Demarcation of mass from rest of kidney (to right) is not clear. **B**, Excretory urogram. Upper pole of right kidney is grossly distorted by tumor, with partial obstruction of several calices. **C**, Inferior vena cavogram. Slight indentation of right side of cava by renal tumor mass, without intracaval tumor or thrombus.

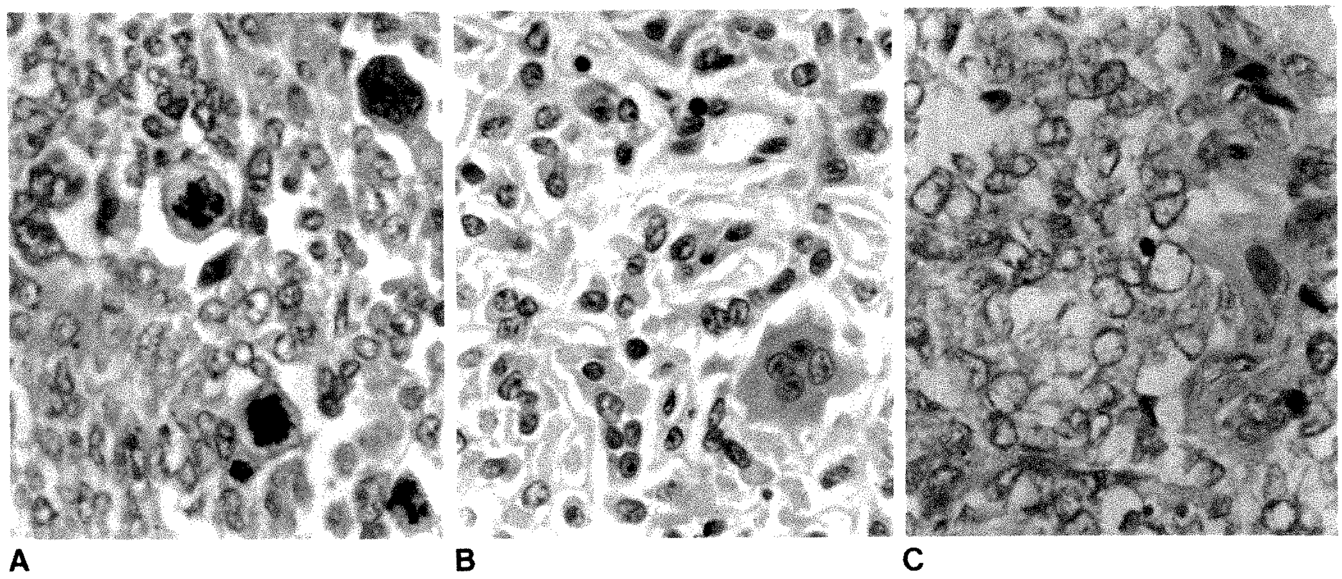

Fig. 2.—Three malignant renal tumors. **A**, Anaplastic cells are distributed between poorly defined tubules in Wilms tumor, suggesting relatively poor prognosis (×40, original magnification). **B**, Rhabdoid sarcoma variant, showing elongated or "tadpolelike" cells. **C**, Clear cell sarcoma of kidney, exhibiting large cells with clear cytoplasm and no tubule formation.

the clear cell and rhabdoid sarcoma variants have now been reproduced and are accepted in all major cancer centers throughout the world.

While rare (about 4% of all childhood renal tumors), clear cell sarcoma of the kidney is highly malignant [1–8]. Histologically, it is monophasic and contains only sarcomatous elements. This is in contrast to classic Wilms tumor (the predominant childhood renal tumor), which is triphasic and contains blastemal, stromal, and epithelial cell types. Clear cell sarcoma also infiltrates the renal parenchyma, instead of forming a well defined pseudocapsule like the common Wilms tumor (fig. 1A). According to Dehner et al. [6] of the Armed Forces Institute of Pathology, the "absence of a fibrous pseudocapsule is the most ominous anatomic feature of renal cell carcinoma in children." While associated congenital anomalies, including aniridia, hemihypertrophy, hypospadias, and cryptorchism, occur in classic Wilms tumor, there has been no such association with clear cell sarcoma of the kidney. A 3:2 male/female ratio has been reported in clear cell sarcoma [2]. As stated, clear cell sarcoma of the kidney has a poor prognosis, with National Wilms' Tumor Studies 1 and 2 reporting a relapse rate of 65% (20 of 31) and a mortality rate of 48% even with aggressive treatment [2]. Furthermore, 50% of the deaths occurred within the first 2 years [1]. The rate of recurrence in the Morgan and Kidd series [9] was equally high (seven of nine), and long-term disease-free survival was only 33% (three of nine), with a follow-up period of 13 months to 9 years. The poor prognosis for this tumor has persisted despite the advent of combined treatment methods of radiation, aggressive surgery, and combination chemotherapy (including actinomycin-D, vincristine, Cytoxan, and Adriamycin).

A salient characteristic of clear cell sarcoma is its predilection to form bone metastases, with a reported incidence of 42% [2] to 76% [6]. In fact, Marsden et al. [7] called this particular entity "bone metastasizing renal tumor of childhood." They reported an incidence of bone metastases of 76% (29 of 38 cases). Furthermore, in 16 of their cases, bone metastases were multiple and extensive. Of the 13 patients in their series with a solitary bone involved, seven had skull lesions. Of the 31 cases entered in National Wilms' Tumor Studies 1 and 2, 42% had metastases to bone [1]. Morgan and Kidd [9], calling the same entity "undifferentiated sarcoma of the kidney," also cited its high tendency for bone involvement. They reported that seven of seven patients with recurrences had skeletal involvement vs. one of 50 patients with classic Wilms tumor. The bone lesions are osteolytic and favor the flat bones (skull and ribs) and the proximal limbs (femur and humerus). Metastases to the tubular bones also tend to involve the proximal one-third of the bones. Bond [4] reported an overall incidence of bone metastases of only 3.5% with Wilms tumors in his analysis of 1267 patients. In the same analysis, he reported a low incidence of *pulmonary* metastasis for clear cell sarcoma of the kidney (one of nine, or 11%). On the other hand, the lung is the predominant initial site of metastasis in Wilms tumor, with an overall incidence of as high as 80% when metastases occur.

While there has been no uniformity in naming clear cell sarcoma of the kidney, there is general consensus that it is a distinct entity based on its clinically aggressive behavior, its histologic characteristics, and its unusual propensity to form bone metastases. An important role of the diagnostic radiologist in childhood tumors of the retroperitoneum must still be to distinguish a renal mass from a tumor of adrenal origin, or from the rare juxtarenal mass that is not adrenal in origin. Intrarenal masses must in turn be distinguished from hydronephrosis or cysts, and the radiologist must be able to document the normal function and appearance of the contralateral kidney before surgery. The lungs must also be examined carefully before operation. Whereas careful initial evaluation of the bones has not been emphasized in Wilms tumor as it has been in neuroblastoma, a preoperative bone scan seems particularly indicated with clear cell sarcoma (a scan was not done in the case reported here, however). On the other hand, if the diagnosis of clear cell sarcoma is first established *after* nephrectomy, the diagnostic radiologist should recommend a complete "bone workup" at that time (a radionuclide scan and radiographs of symptomatic and/or scan-positive areas). The presence of bone involvement will adversely affect prognosis, and more aggressive combination chemotherapy should then be considered.

REFERENCES

1. Beckwith JB. Wilms' tumor and other renal tumors of childhood: a selective review from the National Wilms' Tumor Study Pathology Center. *Hum Pathol* **1983**;14:481–492
2. Beckwith JB, Palmer NF. Histopathology and prognosis of Wilms' tumor: results from the First National Wilms' Tumor Study. *Cancer* **1978**;41:1937–1948
3. Belasco J, D'Angio G. Wilms' tumor. *CA* **1981**;31:258–270
4. Bond JV. Prognosis and treatment of Wilms' tumor at Great Ormond Street Hospital for Sick Children 1960–1972. *Cancer* **1975**;36:1202–1207
5. Caracassone M, Raybaud C, Lebreuil G. Clear cell sarcoma of the kidney in children: a distinct entity. *J Pediatr Surg* **1981**;16:645-648
6. Dehner LP, Leestma JE, Price EB. Renal cell carcinoma in children: a clinicopathologic study of 15 cases and review of the literature. *J Pediatr* **1970**;76:358–360
7. Marsden HB, Fowler W, Kumar PM. Bone metastasizing renal tumor of childhood: morphological and clinical features, and differences from Wilms' tumor. *Cancer* **1978**;42:1922–1928
8. Marsden HB, Fowler W. Bone metastasizing renal tumor of childhood. *Virchows Arch [A]* **1980**;387:341–351
9. Morgan G, Kidd JM. Undifferentiated sarcoma of the kidney: a tumor of childhood with histopathologic and clinical characteristics distinct from Wilms' tumor. *Cancer* **1978**;42:1916–1921

Radiologic-Pathologic Correlation Conference:
SUNY Upstate Medical Center

Flank Mass and Hypertension

Howard Pollack,[1] Philip J. Kenney,[2] John G. McAfee,[2] Gunnar H. Anderson, Jr.,[3] David Jones,[4]
E. Mark Levinsohn,[2] and Bedros Markarian[4]

This is the sixth in a series of Radiologic-Pathologic Correlation Conferences from the State University of New York (SUNY) Upstate Medical Center at Syracuse. Dr. Howard Pollack, Professor of Radiology and Director of the Uroradiology Section from the University of Pennsylvania, was the radiologic consultant. The conference was moderated by Dr. Philip J. Kenney, Chief of the Urologic Radiology Section at Upstate Medical Center, who prepared the clinical resumé.

Dr. Philip J. Kenney.—A 72-year-old woman was admitted for evaluation of hypertension that was first detected 53 years earlier. The hypertension was poorly controlled despite recent trials with numerous antihypertensive regimens which included Hydrodiuril (hydrochlorothiazide), Aldomet (methyldopa), Serpasil (reserpine), Apresoline (hydralazine hydrochloride), Inderal (propranolol hydrochloride), and Catapres (clonidine hydrochloride). Her hypertension had been persistent with no episode of hypertensive crisis. She complained of occasional headaches, mild nervousness, and easy fatigability. She denied chest, abdominal, or flank pain, pallor, flushing, palpitation, hematuria, weight loss, or orthostatic hypotension. The patient did have a mildly elevated glucose tolerance test but did not have glucosuria. Family history was positive for hypertension. There was no history of adrenal, thyroid, or parathyroid disease nor history of von Recklinghausen or von Hipple-Lindau disease.

Physical examination demonstrated a supine blood pressure of 256/138 mm Hg with a pulse rate of 124/min and an erect blood pressure of 232/144 mm Hg with a pulse rate of 144/min. The following laboratory data were determined: hemoglobin 13.2, hematocrit 38.1, sodium 133 mmol/L, potassium 3.4 mmol/L, chloride 94 mmol/L, CO_2 28 mmol/L, glucose 146 mg/dl, blood urea nitrogen 12 mg/dl, creatinine 1.0 mg/dl, urine VMA 26.4 mg/day (normal, $\leq$ 6.8), urine catecholamines 388 μg/day (normal, $<$ 135), urine metanephrines 4.3 mg/day (normal, 0.3–0.9), sitting plasma catecholamines; norepinephrine 2880 pg/ml (normal, 55–320), epinephrine 78 pg/ml (normal, 0–55), and dopamine 0. Dr. Pollack will discuss the radiologic studies.

Dr. Howard Pollack.—An excretory urogram (fig. 1A) shows flattening of the upper pole of the right kidney, suggesting a suprarenal mass. There is also subtle bulging of the right renal margin and caliceal displacement, indicating a mass within the middle part of the kidney. A CT examination (fig. 1B) shows a large heterogenous suprarenal mass. At a lower level (fig. 1C) we see a second mass, which is intrarenal and contains some calcification. A right renal sonogram (fig. 2) shows a well circumscribed complex lesion containing solid and cystic elements. A second mass above the kidney demonstrates an echogenic center and a somewhat less echogenic periphery, suggesting a capsule or a pseudocapsule. An arteriogram (fig. 3A) shows a hypervascular mass within the middle third of the right kidney. There is neovascularity suggestive of tumor. An additional finding is hypertrophy of the inferior adrenal artery supplying a large, well vascularized mass, most likely representing an adrenal neoplasm. The angiographic characteristics of the two right-sided lesions differ considerably. Although both masses are hypervascular, the adrenal lesion has a much more orderly, structured arterial

---

Received May 24, 1985; accepted after revision August 26, 1985.

[1] Department of Radiology, Hospital of the University of Pennsylvania, Philadelphia, PA 19104.

[2] Department of Radiology, State University of New York Upstate Medical Center, 750 E. Adams St., Syracuse, NY 13210. Address reprint requests to E. M. Levinsohn.

[3] Department of Medicine, SUNY Upstate Medical Center, Syracuse, NY 13210.

[4] Department of Pathology, SUNY Upstate Medical Center, Syracuse, NY 13210.

AJR 146:67-72, January 1986 0361-803X/86/1461-0067 © American Roentgen Ray Society

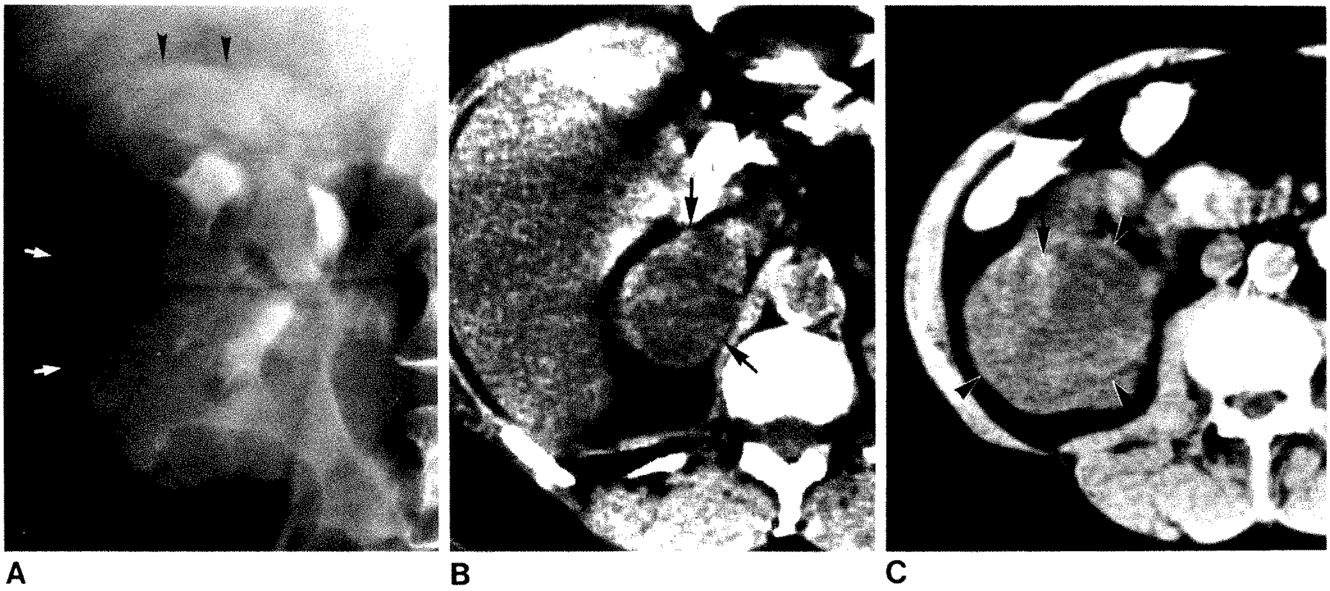

Fig. 1.—**A**, Excretory urogram: flattening of upper pole of right kidney (*arrowheads*) and subtle bulge of right renal margin (*arrows*). Medial displacement of collecting system. **B**, CT scan: right suprarenal mass (*arrows*). **C**, CT scan at lower level: right renal mass (*arrowheads*) with calcification (*arrow*).

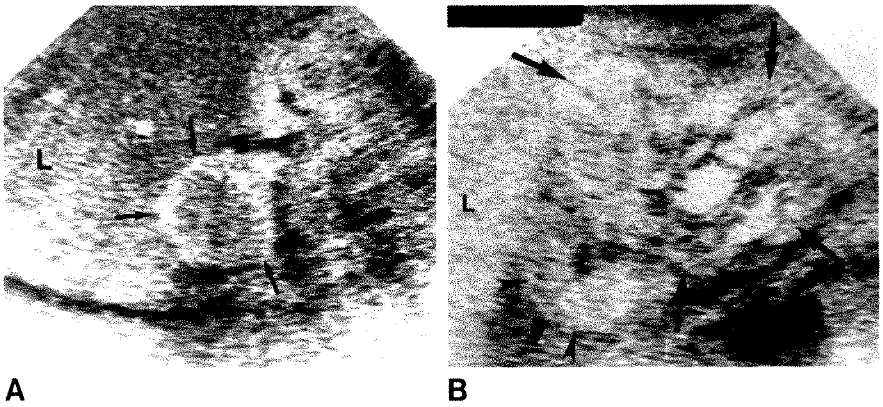

Fig. 2.—**A**, Sagittal sonogram of right flank: right suprarenal solid mass with suggestion of capsule (*arrows*). L = liver. **B**, More lateral sagittal sonogram: complex right renal mass (*arrows*) with cystic areas. *Arrowheads* = right suprarenal mass.

appearance. The renal lesion, on the other hand, shows a disorganized pattern consistent with a renal cell carcinoma.

Dr. John G. McAfee, Professor of Radiology, will now discuss the radionuclide studies performed on this patient.

Dr. John G. McAfee.—A ^{99m}Tc-glucoheptonate renal scan (fig. 3B) shows good concentration of the radionuclide in the normal upper part of the right kidney, with a gradual fading in its abnormal middle part. This most likely represents a renal mass. Another study, using ^{131}I-labeled meta-iodobenzylguanidine (MIBG), was then performed. This agent is specific for catecholamine-secreting tumors (pheochromocytomas, either benign or malignant, and neuroblastomas in childhood). Only the adrenal mass concentrated this agent. The large mass in the middle part of the right kidney did not show any concentration. In order to facilitate localization, a combined ^{131}I-MIBG/^{99m}Tc-glucoheptonate scan was performed to image the kidneys and adrenal glands simultaneously (fig. 3C).

Dr. Kenney.—Preoperative evaluation revealed no evidence of metastatic disease. Embolization of the right renal artery was done to decrease blood loss during surgery. While the procedure was directed at infarcting the renal tumor, some of the blood supplied to the adrenal tumor was affected. Probably as a result, after embolization the patient experienced labile hypertension. A right radical nephrectomy and adrenalectomy were performed. Subsequently the patient had hypertension that was controlled with Hygroton (chlorthalidone). Serum catecholamine levels were normal for 18 months after surgery, and no evidence for metastatic disease developed during the period of follow-up.

Dr. Pollack.—A subtraction arteriogram (not illustrated) obtained immediately after embolization of the renal artery with two detachable balloons shows the balloons have lodged just beyond the point of takeoff of the inferior adrenal artery. Although there remains some perfusion of the adrenal tumor, the right kidney has been infarcted. Dr. David Jones will now discuss the histopathology.

Dr. David Jones.—The tumor removed from the adrenal gland and dissected free from the kidney is seen to be a

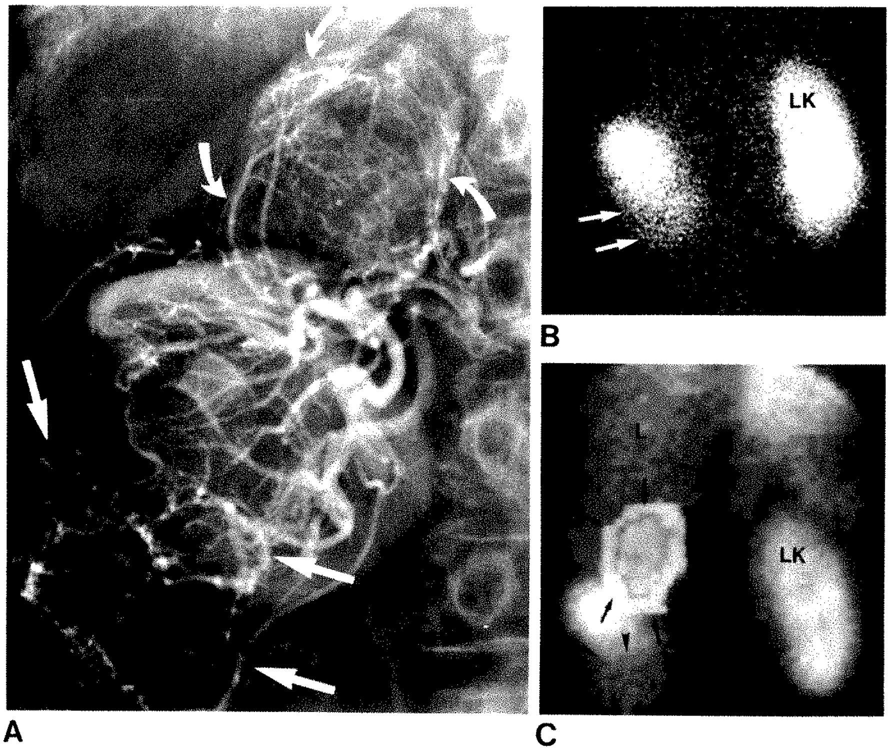

Fig. 3.—**A**, Right selective renal arteriogram: hypervascular renal mass (*straight arrows*) and hypervascular right adrenal mass (*curved arrows*). Arterial appearance of two lesions is dissimilar. **B**, Anteroposterior ^{99m}Tc-glucoheptonate renal scan: flattening of right upper pole and diminished radionuclide concentration in inferior part of right kidney (*arrows*). Right kidney is displaced laterally. LK = left kidney. **C**, Combined image of ^{131}I-MIBG and ^{99m}Tc-glucoheptonate scans: MIBG uptake in right adrenal mass (*arrows*); no MIBG uptake in photopenic region of right kidney (*arrowheads*).

vascular fleshy mass adjacent to normal renal cortex. Microscopically we see an alveolar pattern containing nests of large pleomorphic tumor cells (fig. 4A). This represents the typical appearance of pheochromocytoma. The kidney contains a large tumor showing hemorrhagic degeneration. There are purplish cystic changes apparent on the external surface of the tumor. Although infarction from embolization contributes to some of the hemorrhage that is present in this tumor, hemorrhagic degeneration is very common in renal cell tumors. Histologically, we see sheets of tumor cells with clear cytoplasm interspersed between hemorrhagic and cystic spaces (fig. 4B). This represents a well differentiated, clear cell carcinoma of proximal convoluted tubule origin.

Pheochromocytoma occurs with a prevalence of about one per million per year. Ten percent are bilateral, 10% are extraadrenal in origin, and 5% are malignant. When they occur with other endocrine tumors, as in multiple endocrine neoplasia or Sipple syndrome, they are much more likely to be bilateral. It is not possible to differentiate benign from malignant pheochromocytoma histopathologically. Mitoses, pleomorphism, and invasion are all seen in the clinically benign pheochromocytomas. The only real criterion is the presence of metastases. The histologic diagnosis of pheochromocytoma depends on the classic chromafin reaction caused when catecholamines reduce potassium dichromate. Pheochromocytomas arise from neurocrest cells, which occur in many sites including the spleen, adrenals, paraaortic tissues, organ of Zuckerkandl, and gonads. Electron microscopic analysis of pheochromocytomas shows neurosecretory granules within the cytoplasm. In those cells that produce epinephrine, the granules are round and regular. By contrast, the cells that make norepinephrine tend to have eccentric dark granules within the cytoplasm. Commonly, mixtures of both cell types are present.

Dr. Kenney.—Dr. Gunnar Anderson from the Division of Endocrinology, Department of Medicine, will now discuss the clinical evaluation of adrenal hypertension.

Dr. Gunnar Anderson.—There are four major diagnostic considerations when one evaluates a patient who has both an adrenal mass and hypertension: primary aldosteronism, adrenal adenoma with Cushing syndrome, pheochromocytoma, and an incidental nonfunctioning adrenal mass in a patient with essential hypertension.

Primary aldosteronism is, by definition, caused by excess production of aldosterone. In our experience, 1.5%–2% of all hypertensive patients have primary aldosteronism [1, 2]. The presenting findings are hypertension, hypokalemia, and a low stimulated plasma renin activity. The hypokalemia can cause muscular weakness and also a partial nephrogenic diabetes insipidus. When one looks at the serum potassium level in patients with an aldosterone secreting adenoma, virtually all have a value below 3.6 mEq/L [1]. With bilateral adrenal hyperplasia, the serum potassium value tends to be higher, with many registering in the normal range. In our laboratory, we use the "saline infusion test" to screen for primary aldosteronism [3]. Saline, when rapidly infused over a short period of time (0.9% normal saline over 4 hr), suppresses aldosterone levels. After this saline infusion, a recumbent plasma aldosterone level above 8.5 with a low stimulated plasma renin activity strongly suggests primary aldosteronism. Two major types of primary aldosteronism exist: 60% are caused by an adrenal adenoma and the rest by bilateral adrenal hyperplasia. With unilateral disease, CT evaluation [4] and

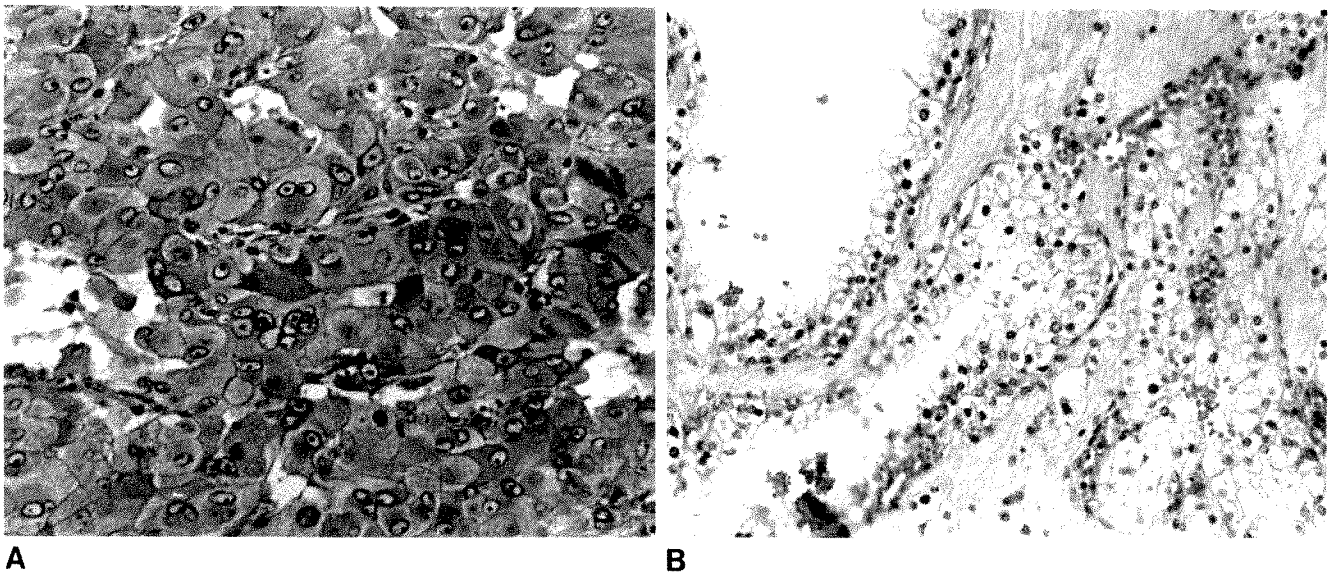

Fig. 4.—**A**, Photomicrograph of pheochromocytoma demonstrating large cells arranged in irregular nests with fine vascular network. Nucleus is large and has prominent nucleolus. Cytoplasm is abundant with granular appearance. H and E, ×500 (original magnification). **B**, Renal cell adenocarcinoma of clear cell type with solid cellular areas and tubuloalveolar pattern. Nuclei are small and uniform in size with pale, abundant cytoplasm. H and E, ×400 (original magnification).

adrenal vein sampling [5] for aldosterone and epinephrine show asymmetric aldosterone findings. The definitive test in diagnosing primary aldosteronism is the "DOCA" test. DOCA (deoxycorticosterone acetate) is a salt-retaining hormone. Patients are admitted to the hospital and are given DOCA (10 mg intramuscularly every 12 hr for 3 days) and a high sodium (200 mEq/day) diet. Those patients with primary aldosteronism show an elevated plasma and urine aldosterone, not suppressible for the salt loading test. Unilateral adrenalectomy is the treatment of choice for an adenoma and spironolactone (an aldosterone antagonist) for hyperplasia.

A second diagnostic consideration is Cushing syndrome caused by an adrenal adenoma [6]. About 10%–15% of patients with Cushing syndrome will have an adrenal adenoma. Many of these patients are hypertensive. Clinically, they can have centripetal obesity, plethora, hirsutism, weakness, acne, striae, osteoporosis, and diabetes mellitus. Screening tests include 24-hr urine for 17-hydroxysteroids (17-OH) and creatinine or an overnight 1 mg dexamethasone test [6, 7]. Diagnostic tests typically show nonsuppressible urinary 17-OH on a high-dose dexamethasone test (2 mg every 6 hr for 2 days). Further diagnostic tests include a low serum ACTH, CT scan showing a unilateral adrenal mass, and adrenal vein catheterization showing high plasma cortisol from the enlarged adrenal gland with contralateral suppression [6]. Rarely an adrenal lesion could be an adrenal carcinoma, which is associated with a high urinary 17-ketosteroid. After removing the adenoma, the reversion of the clinical signs to normal can be striking.

A third consideration in diagnosing the association of an adrenal mass and hypertension is pheochromocytoma. Pheochromocytomas are tumors that produce, store, and secrete catecholamines. They occur in less than 0.1% of the hypertensive population, but if diagnosed are often successfully treated surgically. Clinical features come primarily from release of catecholamines. Hypertension, either intermittent or continuous, is the most common presenting clinical feature, but patients can also have profuse sweating, mild weight loss, orthostatic hypotension, tachycardia, and an impaired glucose tolerance test.

Eight percent of pheochromocytomas are located in one adrenal gland, 10% are bilateral (in both adrenal glands), and 10% are extraadrenal, usually in retroperitoneal areas [8, 9]. They can be associated in a familial manner with other conditions, which include Sipple syndrome (multiple endocrine adenomatosis type II), von Recklinghausen disease (neurofibromatosis), and von Hippel-Lindau disease (retinal cerebellar hemangioretinoblastomas) [10, 11]. Pheochromocytomas are more commonly bilateral in Sipple syndrome and in children.

The diagnosis of pheochromocytoma initially should include a 24-hr urine test for VMA, catecholamines, and metanephrines. Medications such as Aldomet, which can increase urine free catecholamines, should be omitted for at least 2 weeks before measurement of the urine levels. Several groups believe that plasma catecholamines are even a better test in diagnosing pheochromocytomas [12]. The plasma catecholamines should be drawn with a needle in place and the patient recumbent for at least ½ hr. Clonidine, a centrally acting alpha-2 antagonist, has been shown to lower elevated plasma norepinephrine levels in "neurogenic" central hypertension but not in patients with pheochromocytoma, an important differentiating point. CT scans are very helpful in diagnosing pheochromocytomas, and a promising new technique, although not widely available, is the use of metaiodobenzylguanidine [13].

Autopsy series have shown that 1.4%–7% of individuals have nonfunctioning benign adrenal masses; malignant adrenal lesions are very rare [14–17]. Essential hypertension is known to occur in 15%–20% of the population. The identification of an adrenal mass in a patient with hypertension could be a chance finding. Studies should be done to rule out Cushing syndrome, primary aldosteronism, adrenal carcinoma, and pheochromocytoma. If these tests are normal, we recommend surgery for adrenal lesions larger than 6 cm and follow-up CT scans for those that are smaller [18]. Dr. McAfee will now discuss the use of meta-iodobenzylguanidine in evaluating adrenal neoplasms.

Dr. McAfee.—Meta-iodobenzylguanidine (MIBG) is a new agent developed at the University of Michigan [19] for adrenal imaging. It is chemically related to norepinephrine but is much less potent pharmacologically. Adrenergic tissue has granules for storage of norepinephrine and vesicles capable of absorbing norepinephrine from the circulation. It seems that MIBG becomes stored in these adrenergic storage vesicles, presumably a physiologic mechanism for retaining norepinephrine. For localization, one generally follows adrenal imaging with a renal imaging agent such as glucoheptonate. Although the University of Michigan reports visualizing the normal adrenal gland in man only 8% of the time, in our experience we show the normal adrenals more regularly. This becomes a problem in patients who might possibly have bilateral adrenomedullary hyperplasia, neurofibromatosis [20], or multiple endocrine neoplasia [21]. The adrenal concentration is very faint on conventional camera images and is really shown well only by computer enhancement. Pheochromocytomas seem to accumulate this agent much better than normal adrenal tissue [13]. We give 0.5 mCi (18.5 MBq) of MIBG intravenously and imaging is done 1, 2, and 3 days after administration. In our experience, images obtained at 3 days allow better adrenal visualization with less overlap by the liver and spleen. This is because the biologic half-life in the liver is shorter than that in an adrenal tumor. Since one normally sees free radioiodide in the bladder, it is advisable, before injection, to give perchlorate orally to block the thyroid gland. The typical adult dose of 0.5 mCi (18.5 MBq) gives a total body radiation dose of 0.1 rad (1 mGy) and 17 rad (170 mGy) to the adrenal medulla [22]. Of the first 250 patients studied at the University of Michigan, there were 60 pheochromocytomas and only six were false negatives, a sensitivity of 90%. One of the drawbacks of this agent is that in addition to its normal localization in the liver and spleen, it occasionally localizes in myocardium. The ganglionic chain and the sympathetic chain in the posterior mediastinum are uncommon sites for pheochromocytoma. The Michigan group believes that MIBG is particularly valuable for small pheochromocytomas that are not found by CT [22]. They claim that 10% of the lesions they show by MIBG imaging are too small to be found by CT. It is also helpful in multiple pheochromocytomas, some of which may be extraadrenal. MIBG helps to localize metastatic pheochromocytomas and concentrates also in some primary and metastatic neuroblastomas [23]. At the University of Michigan, several inoperable malignant pheochromocytomas have been treated with therapeutic doses of MIBG.

There are some important drugs that interfere with localization of MIBG in the adrenal gland. These include reserpine, imipramine and other tricyclic antidepressants, and amphetaminelike drugs including phenyl-propanolamine (Dexatrim) or pseudoephedrine (Sudafed). Fortunately phenoxybenzamine (Dibenyline), benzothiadiazide diuretics, and propranolol do not interfere with localization.

Dr. Kenney.—Our current practice in screening for pheochromocytoma consists of a CT scan confined to the adrenal gland which, if normal, is followed by an MIBG radionuclide scan to screen the rest of the body. If a mass is found in the adrenal gland, an MIBG scan is then done to confirm the lesion before surgery. This obviates arteriography or venous sampling. Dr. Pollack, would you comment on the value of angiography in today's case?

Dr. Pollack.—In this case a diagnosis of pheochromocytoma was made biochemically and was confirmed with radionuclide imaging. There was also a solid right-kidney mass that did not concentrate MIBG and was therefore not of chromafin cell origin. Its CT and angiographic characteristics were strongly suggestive of renal cell carcinoma. Because renal cell carcinoma is a relatively common tumor, it is not surprising to see one coexisting with a pheochromocytoma. The diagnostic tool most specific for renal cell carcinoma is angiography. About 75% of these neoplasms demonstrate classic findings consisting of a florid circulation, large vascular lakes within the tumor, and in many cases venous shunting [24]. However, absence of these findings does not rule out renal cell carcinoma. The CT findings are less specific but reasonably suggestive in most cases, so that angiography is used much less often than previously.

Patients with pheochromocytoma are at risk to be thrown into a hypertensive crisis with only slight provocation. A rough physical examination, induction of anesthesia, or contrast material administered either intravenously or intraarterially may lead to crisis. We have seen two patients with this tumor in the wall of the bladder. Both patients experienced hypertensive crisis during micturition. The use of adrenergic blockers either prophylactically or therapeutically has substantially reduced this risk, but nonetheless, attempts to diagnose the existence of a pheochromocytoma noninvasively are to be strongly encouraged. As exemplified in this case, this is almost always possible.

Angiography was interesting in this case because the discrepant vascular characteristics of the two masses suggested that they were of different origins. Before the advent of MIBG scanning, angiography would have been the only study with a reasonably good chance of disclosing this disparity. With regard to embolization, although some urologists believe that preoperative infarction facilitates removing a renal cell carcinoma and use it almost routinely, most reserve embolization for the extremely large and well vascularized tumors.

Dr. E. Mark Levinsohn.—Dr. Pollack, could you comment on the association of a renal mass and hypertension?

Dr. Pollack.—There are several renal neoplasms that may be associated with hypertension. One of them is renal cell carcinoma, which may cause hypertension by any of several means including hyperreninism, arteriovenous fistulae, and arterial encasement [25]. Among medical findings associated with renal cell carcinoma are hypercalcemia, polycythemia, and fever. Other renal tumors that are sometimes associated with hypertension are Wilms tumor, renin-producing juxtaglomerular cell tumor, and metastatic pheochromocytoma to the kidney.

The incidence of renal cell carcinoma is relatively high. It is estimated that we will likely see 14,000–15,000 new cases in the U.S. this year [26]. Since the advent of CT has allowed adrenal masses to be seen more frequently than ever, there is a fair chance that any combination of a renal and adrenal mass is coincidental, as in the present case. Obviously, however, one would want to exclude the more ominous possibility of a renal neoplasm metastasizing to or invading the adrenal gland, and, along the same lines, the obverse but less likely association of a primary adrenal neoplasm with renal metastases must also be ruled out. Of interest is the observation that adrenal adenomas are five times more common in patients with renal cell carcinoma than in those without it [27]. Finally, there is the consideration of metastases to both the kidney and the adrenal from a distant primary neoplasm, such as carcinoma of the lung or malignant melanoma. These multiple possibilities mandate a thorough, well reasoned approach to the evaluation of patients with concurrent renal and adrenal neoplasms. The introduction of hypertension into the clinical scenario alters the approach only slightly, but if a pheochromocytoma is identified in conjunction with renal cell carcinoma, von Hippel–Lindau disease should be considered. In most instances of this disease, multiple renal cell carcinomas in association with multiple renal cysts will be present [28]. In the present case, the patient lacked these findings, and this observation, together with the lack of clinical stigmata of the syndrome, suggests that the patient did not have von Hippel–Lindau disease.

In summary, we have a patient with coincidental concurrent pheochromocytoma and ipsilateral renal cell carcinoma. With present imaging techniques, a precise diagnosis of both lesions is a reasonable expectation.

REFERENCES

1. Streeten DHP, Tomycz N, Anderson GH Jr. Reliability of screening methods for the diagnosis of primary adosteronism. *Am J Med* **1979;**67:403–413
2. Streeten DHP, Anderson GH Jr, Springer JM. Outpatient screening procedures for primary aldosteronism. *Clin Sci Mol Med* **1982**;63:125S–127S
3. Kem DC, Weinberger MH, Mayes DM, Nugent CA. Saline suppression of plasma aldosterone in hypertension. *Arch Intern Med* **1971**;128:380–386
4. White EA, Schambelan M, Rost CR, Biglieri EG, Moss AA, Korobkin M. Use of computed tomography in diagnosing the cause of primary aldosteronism. *N Engl J Med* **1980**;303:1503–1507
5. Melby JC. Identifying the adrenal lesion in primary aldosteronism. *Ann Intern Med* **1972**;76:1039–1041
6. Gold EM. The Cushing syndromes: changing views of diagnosis and treatment. *Ann Intern Med* **1979**;90:829–844
7. Streeten DHP, Anderson GH Jr, Dalakos TG, et al. Normal and abnormal function of the hypothalamic-pituitary-adrenocortical system in man. *Endocr Rev* **1984**;5:371–394
8. Moorhead EL, Caldwell JR, Kelly AR, Morales AR. The diagnosis of pheochromocytoma. *JAMA* **1966**;196:91–97
9. Manger WM, Gifford RW Jr. *Pheochromocytoma.* New York: Springer-Verlag **1977**
10. Lips KJM, van der Sluys Veer J, Struyvenberg A, et al. Bilateral occurrence of pheochromocytoma in patients with the multiple endocrine neoplasia syndrome type 2A (Sipple's syndrome). *Am J Med* **1981**;70:1051–1060
11. Horton WA, Wong V, Eldridge R. Von Hippel–Lindau disease: clinical and pathological manifestations in nine families with 50 affected members. *Arch Intern Med* **1976**:136:769–777
12. Bravo EL, Tarazi RC, Fouad FM, Vidt DG, Gifford RW Jr. Clonidine-suppression test: a useful aid in the diagnosis of pheochromocytoma. *N Engl J Med* **1981**;305:623–636
13. Sisson JC, Frager MS, Valk TW, et al. Scintigraphic localization of pheochromocytoma. *N Engl J Med* **1981**;305:12–17
14. Shamma AH, Goddard JW, Sommers SC. A study of the adrenal status in hypertension. *J Chronic Dis* **1958**;8:587–595
15. Russi S, Blumenthal HG, Gray SH. Small adenomas of the adrenal cortex in hypertension and diabetes. *Arch Intern Med* **1945**;76:284–291
16. Kokko JP, Brown TC, Berman MM. Adrenal adenoma and hypertension. *Lancet* **1967**;1:468–470
17. Hedeland H, Ostberg G, Hokfelt B. On the prevalence of adrenal cortical adenomas in an autopsy material in relation to hypertension and diabetes. *Acta Med Scand* **1968**;184:211–214
18. Copeland PM. The incidentally discovered adrenal mass. *Ann Intern Med* **1983**;98:940–945
19. Wieland DM, Wu JI, Brown LE, Mangner TJ, Swanson DP, Beierwaltes WH. Radiolabeled adrenergic neuro-blocking agents: adrenomedullary imaging with (^{131}I) iodobenzylguanidine. *J Nucl Med* **1980**;21:349–353
20. Kalff V, Shapiro B, Lloyd R, et al. The spectrum of pheochromocytoma in hypertensive patients with neurofibromatosis. *Arch Intern Med* **1982**;142:2092–2098
21. Valk TW, Frager MS, Gross MD, et al. Spectrum of pheochromocytoma in multiple endocrine neoplasia: a scintigraphic portrayal using ^{131}I-metaiodobenzylguanidine. *Ann Intern Med* **1981**:94:762–767
22. Sisson JC, Shapiro B, Beierwaltes WH. Locating pheochromocytomas by scintigraphy using ^{131}I-metaiodobenzylguanidine. *CA* **1984**;34:86–92
23. Truener J, Feine W, Niethammer D, et al. Scintigraphic imaging of neuroblastoma with (^{131}I) iodobenzylguanidine. *Lancet* **1984**;1:333–334
24. Watson RC, Flemming RJ, Evans JA. Arteriography in the diagnosis of renal cancer. *Radiology* **1968**;91:888–897
25. Richie JP, Garnick MB. Primary renal and ureteral cancer. In: Rieselbach RE, Garnick MB, eds. *Cancer and the kidney.* Philadelphia: Lea & Febiger, **1982**:p. 611
26. Silverberg E. Cancer statistics 1985. *CA* **1985**;35:19–35
27. Ambos MA, Bosniak MA, LeFleur RS, Mitty HA. Adrenal adenoma associated with renal cell carcinoma. *AJR* **1981**;136:81–84
28. Levine E, Collins DL, Horton WA, Schimke RN. CT screening of the abdomen in von Hippel–Lindau disease. *AJR* **1982**;139:505–510

“Solid” Mediastinal Bronchogenic Cyst: Mineralogic Analysis

Jean-Claude Yernault,[1] Gabriele Kuhn,[2] Pascal Dumortier,[1] Pierre Rocmans,[1] Paulette Ketelbant,[3] and Paul De Vuyst[1]

Mediastinal bronchogenic cysts are ovoid masses in the posterior or middle mediastinum that usually contain serous or white mucoid material [1]. Evaluation of their content by computed tomography (CT) would be expected to yield low CT numbers [2–4]; however several cases have now been reported that simulated solid masses [4, 5]. The reason for this is unclear. We report a case in which large amounts of calcium oxalate were found within the mucoid material.

Case Report

A 41-year-old asthmatic woman was referred to the Chest Department for evaluation of persistent cough despite adequate control of asthmatic attacks by inhaled bronchodilators. Lung auscultation was normal and lung function tests disclosed no sign of airway obstruction. A chest radiograph showed a left mediastinal mass (fig. 1A), which was further evaluated by CT (fig. 1B). Density measurements of the mass varied from 38 to 98 H. The mass was excised, and needle aspiration yielded brownish mucoid material. Pathologic examination revealed a typical bronchogenic cyst.

Further studies of the mucoid material were performed. The possibility of an error in the CT evaluation of the mass density was considered but excluded because CT evaluation of the density of the mucoid material within the syringe gave high numbers (97–113 H).

Examination of a smear of the cyst content by light microscopy revealed the presence of numerous crystallites. Therefore, a detailed mineralogic analysis was performed using the method routinely ap-

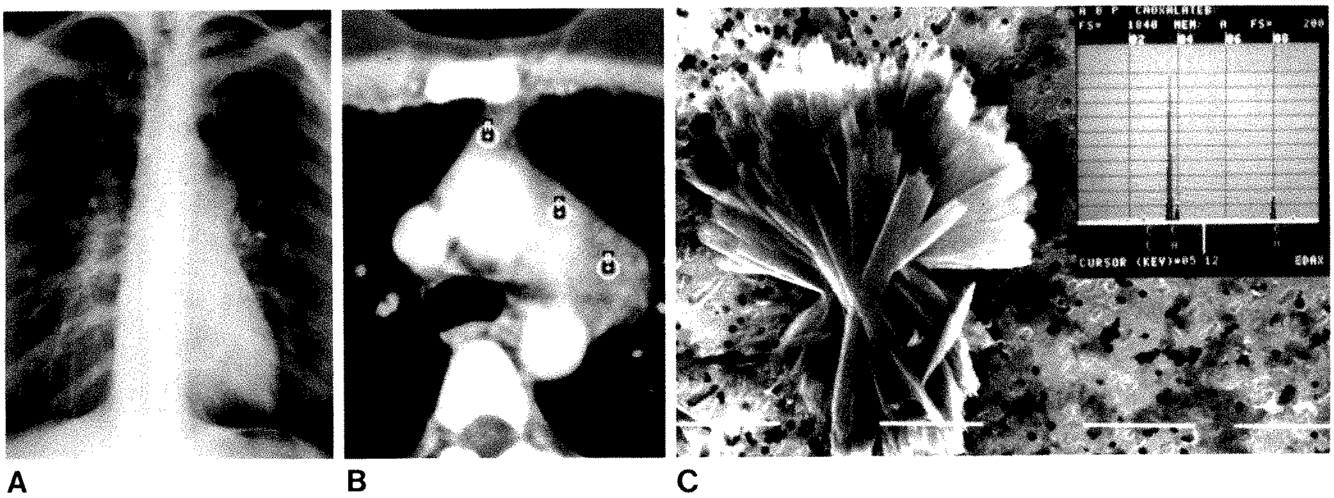

Fig. 1.—**A**, Posteroanterior chest radiograph. Left mediastinal mass. **B**, CT evaluation of density of mediastinal mass, which appears heterogeneous, yielding an average of 45 H. **C**, Radially aggregated calcium oxalate crystals as seen on scanning electron microscopy. Aggregate is about 20 μm wide (one scale bar = 5 μm). Spectrum in upper right corner shows chemical composition of this particle obtained by energy dispersive x-ray spectrometry (EDS). All elements with atomic number >11 could be detected by this method. In this spectrum chlorine (CL) is residue from preparation technique, copper (CU) peak is produced by specimen-supporting grid, and calcium (CA) peak is coming from particle itself.

Received April 3, 1985; accepted after revision September 9, 1985.
This work was supported by contract no. 3.4517.82 from the Fonds de la Recherche Scientifique Medicale.

[1] Chest Department, Cliniques Universitaires de Bruxelles, Hôpital Erasme, Route de Lennik 808, B-1070 Bruxelles, Belgium. Address reprint requests to J. C. Yernault.
[2] Radiology Department, Cliniques Universitaires de Bruxelles, Hôpital Erasme, B-1070 Bruxelles, Belgium.
[3] Pathology Department, Cliniques Universitaires de Bruxelles, Hôpital Erasme, B-1070 Bruxelles, Belgium.

AJR 146:73–74, January 1986 0361–803X/86/1461–0073 © American Roentgen Ray Society

plied for the detection of asbestos bodies and other mineral particles within bronchoalveolar lavage fluids [6]. Briefly, an aliquot of the mucoid material was digested by sodium hypochloride (commercial bleach) and then filtered on a 0.45-μm pore size membrane filter, which was mounted on glass slides for observation under the light microscope (Leitz Ortholux II Pol). Spindle-shaped, transparent, colorless, birefringent crystals, isolated or radially aggregated, were seen. Isolated crystals showed two refractive indices, the first one a little lower and the second one much higher than the index of the immersion oil ($n = 1.518$). Elongation was positive.

The crystallites were examined under a combined transmission and scanning electron microscope (Philips EM 400 T) fitted with an x-ray energy dispersive spectrometer (EDAX PV 9100/45). X-ray spectrometry disclosed only the presence of calcium (fig. 1C). Since no phosphorus could be detected, the crystallites were not calcium phosphates.

Chemical microtests showed that the crystals were soluble in hydrochloric acid but not in dilute acetic acid. This excluded calcium carbonate. On the basis of these combined observations, it was concluded that calcium oxalate monohydrate (whewellite, whose two refractive indices are 1.49 and 1.62) was the main constituent of the material analyzed.

Discussion

On the basis of our observations, we can explain the high attenuation coefficients of this bronchogenic cyst by the presence of large amounts of calcium oxalate crystals. This was not entirely unexpected, since there had been previous observations of material of increased radiographic density layering at the bottom of bronchogenic cysts [7, 8]. However to the best of our knowledge, the exact nature of the radiographically dense intracystic material had not been previously established. However, whether the presence of some amount of calcium oxalates within a bronchogenic cyst is the rule or not remains to be established. Similarly, the mechanism of formation of oxalate within a cyst remains unknown. In any case, our findings help to explain why some bronchogenic cysts appear as "solid" tumors.

REFERENCES

1. Rogers LF, Osmer JC. Bronchogenic cyst: a review of 46 cases. *AJR* **1964**;91:273–283
2. Jost RG, Sagel SS, Stanley RF, Levitt RJ. Computed tomography of the thorax. *Radiology* **1978**;126:125–136
3. Pugatch RD, Faling LJ, Robbins AH, Spira R. CT diagnosis of benign mediastinal abnormalities. *AJR* **1980**;134:685–694
4. Nakata H, Nakayama C, Kimoto T, et al. Computed tomography of mediastinal bronchogenic cysts. *J Comput Assist Tomogr* **1982**;6:733–738
5. Mendelson DS, Rose JS, Efremidis SC, Kirschner PA, Cohen BA. Bronchogenic cysts with high CT numbers. *AJR* **1983**;140:463–465
6. De Vuyst P, Jedwab J, Dumortier P, Vandermoten G, Vande Weyer R, Yernault JC. Asbestos bodies in bronchoalveolar lavage. *Am Rev Respir Dis* **1982**;126:972–976
7. Cornell SH. Calcium in the fluid of mediastinal bronchogenic cyst: a new roentgenographic finding. *Radiology* **1965**;85:825–828
8. Bergstrom JF, Yost RV, Ford KT, List RM. Unusual roentgen manifestations of bronchogenic cysts. *Radiology* **1973**;107:49–54

Measurement of Normal Left Heart Dimensions Using Optimally Oriented MR Images

Sanjiv Kaul[1, 2]
Gary L. Wismer[3]
Thomas J. Brady[3]
Donald L. Johnston[1]
Arthur E. Weyman[1]
Robert D. Okada[1]
Robert E. Dinsmore[3]

In order to establish normal values for left heart dimensions by magnetic resonance imaging (MRI), electrocardiographically gated MRI was performed in 16 normal asymptomatic subjects using a whole-body 0.6-T superconducting magnet with a spin-echo pulse sequence and an echo delay (TE) of 30 msec. Images were oriented along the long and short axes of the left ventricle in planes similar to two-dimensional echocardiograms (2DE). Comparable 2DE images were obtained for validation of the MRI measurements. The following measurements of the left heart were made at end diastole and end systole in both long- and short-axis views using both techniques: left ventricular cavity diameters, interventricular septum and posterior wall thicknesses at chordal and mid-papillary-muscle levels, and anteroposterior mid-left-atrial diameter. There was good correlation between the two techniques in a total of 141 measurements (MRI = 0.94 2DE + 1.42, $p < 0.0001$, $r = 0.97$) and in the individual measurements considered separately ($p < 0.001$). There was no significant difference in the mean values. MRI measurements obtained with the image planes oriented to the intrinsic axes of the heart are similar to those obtained by 2DE. These data provide normal values for measurements of the left heart using a standardized MRI technique.

Magnetic resonance imaging (MRI) is a relatively new noninvasive technique that has been shown to provide high-quality images of cardiovascular structures [1–4]. Contrast between flowing blood and the myocardium is excellent without the need for contrast agents. Images can be acquired at any time in the cardiac cycle with the use of electrocardiographic (ECG) gating [4]. In comparison to two-dimensional echocardiography (2DE), resolution is uniformly good over a large field, without problems of bone or air transmission. Because of these attributes, MRI is a potentially valuable method for study of cardiac dimensions and function.

Previous reports have described the use of transverse, sagittal, and coronal MRI planes [1–4]. However, conventional imaging planes orthogonal to the chest are oblique to the intrinsic axes of the heart, which vary from patient to patient. Thus images in conventional planes are not optimal for cardiac measurements. We have recently described a technique for obtaining image planes oriented to the long and short axes of the left ventricle [5, 6]. The purpose of the present study is to establish normal values for left heart dimensions on standardized MR images. Accordingly, we obtained systolic and diastolic MR images of 16 normal subjects and compared cardiac dimensions with measurements from 2DE in the same subjects using comparable imaging planes. Echocardiography has previously been well validated for measurement of cardiac structures and function [7, 8].

Subjects and Methods

Sixteen asymptomatic normal volunteers (eight men and eight women aged 18–44 years [mean, 38 ± 8]) with no history of any cardiac disorder and normal physical examination comprised the study group. Informed consent as approved by the hospital Subcommittee on Human Studies was obtained from each subject before MRI. MRI and 2DE were performed within 1 week of each other.

Received April 1, 1985; accepted after revision August 6, 1985.

This work was supported in part by the Technicare Corp., Solon, OH. S. Kaul is the recipient of U.S. Public Health Service grant HL 07416. T. J. Brady is the recipient of U.S. Public Health Service grant 5KO4 CA-00848-02 from the National Cancer Institute.

[1] Department of Medicine, Cardiac Unit, Harvard Medical School, Massachusetts General Hospital, Boston, MA 02114.

[2] Present address: Division of Cardiology, University of Virginia, Charlottesville, VA 22908.

[3] Department of Radiology, Harvard Medical School, Massachusetts General Hospital, Boston, MA 02114. Address reprint requests to R. E. Dinsmore.

AJR 146:75–79, January 1986
0361–803X/86/1461–0075
© American Roentgen Ray Society

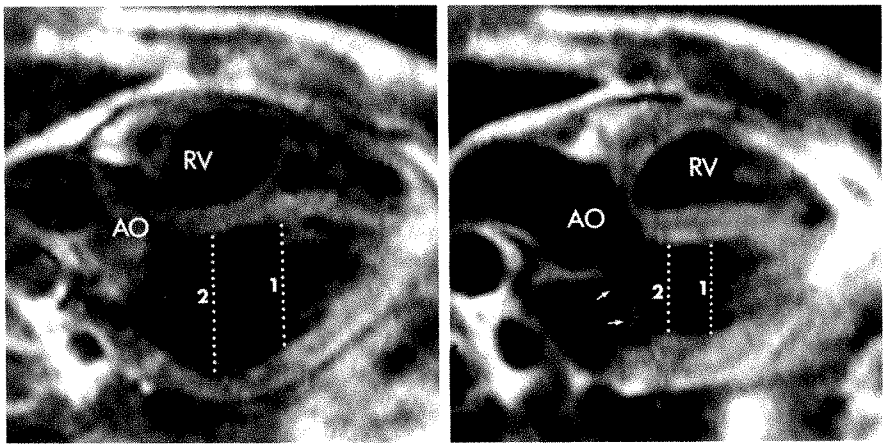

1A

1B

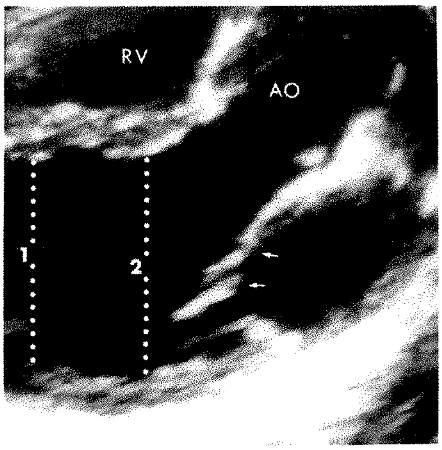

1C

Fig. 1.—Long-axis images of left ventricle in plane through aortic valve and apex, perpendicular to septum. **A**, MRI, diastole. **B**, MRI, systole. **C**, Parasternal long-axis 2DE, diastole. AO = aortic sinuses; RV = right ventricle; *double arrows* = mitral valve plane. Left ventricular diameters were measured at mid-papillary-muscle level (1) and chordal level (2).

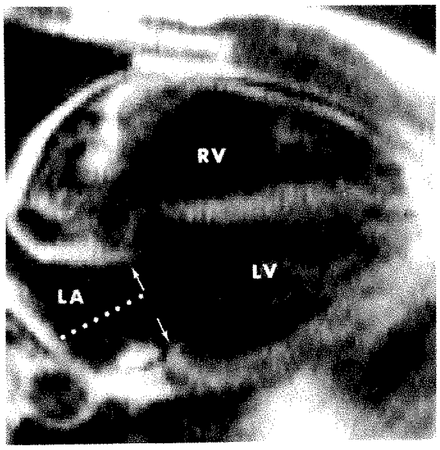

2

Fig. 2.—Diastolic MRI through long axis of left ventricle at mitral valve and left atrial level. Anteroposterior mid-left-atrial diameter, from posterior left atrial wall to plane of mitral anulus, is indicated. LA = left atrium; LV = left ventricle; RV = right ventricle; *arrows* = mitral anulus.

Magnetic Resonance Imaging

A whole-body superconducting magnet (Technicare) with a field strength of 0.6 T corresponding to a proton resonance frequency of 25.4 MHz was used. Data were acquired using a single-slice technique in the early studies (seven cases) and with multislice imaging after this became available. Image slice thickness was 1.5 cm and in-plane resolution 1.6 mm. A spin-echo pulse sequence with an echo delay (TE) of 30 msec was used. The interpulse interval was equivalent to the R-R interval on the ECG. ECG gating was accomplished with the use of nonmagnetic patient leads on both ankles and the left wrist, which were connected to a telemetry device (Hewlett-Packard). This system allows images to be acquired at any part of the cardiac cycle by selection of an appropriate gate delay after the R wave. End-diastolic images were acquired using a 10-msec gate delay and end-systolic images at the downslope of the T wave.

The method for obtaining images oriented to the long and short axes of the heart has been described [5, 6]. For this study, images oriented to the long axis of the left ventricle perpendicular to the interventricular septum and oriented to the short axis of the left ventricle were used. For each image plane, an initial series of contiguous images was obtained with either single- or multislice technique for selection of the appropriate levels for sets of single images at end systole and end diastole. The long-axis images of the left ventricle were obtained in a plane through the aortic valve and the left ventricular apex (fig. 1). The mid-left-atrial dimension was best obtained from a contiguous image offset to the right (fig. 2). The image plane was then rotated 90° to obtain short-axis images of the heart at the chordal level (midway between the aortic valve and the papillary muscle) and mid-papillary-muscle level (the level where the papillary muscle appeared thickest) (fig. 3).

Each acquisition time varied from 3 to 5 min, depending on the heart rate. Studies with single-slice technique took 1–2 hr; the multislice method, about 1 hr. Images were displayed in a matrix of 256 × 256 pixels using 256 shades of gray. Hard copies of images were obtained on x-ray film, and all MRI measurements were made from these hard copies.

Two-Dimensional Echocardiography

2DE was performed using a mechanical sector scanner (ATL Mark III) with a 3.5-MHz transducer. Subjects were positioned in the left lateral decubitus position, and images of parasternal long- and short-axis views were recorded on a videocassette recorder (Panasonic 8950). Optimal cycles were then selected for analysis and transferred to a video disk (Sony SVM 1010). Measurements were made on an off-line analysis system (Microsonics Easyview II). All measurements were made from the inner edge of the echoes [9].

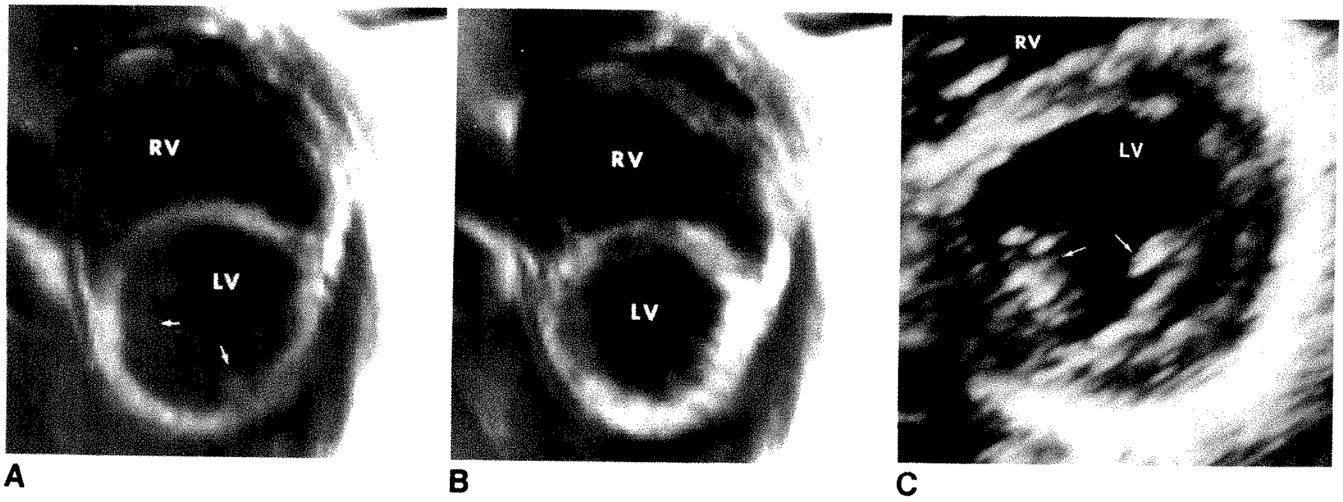

Fig. 3.—Short-axis images of left ventricle at mid-papillary-muscle level. **A**, MRI, diastole. **B**, MRI, systole. **C**, Parasternal short-axis 2DE, diastole. RV = right ventricle; LV = left ventricle; *arrows* = papillary muscles.

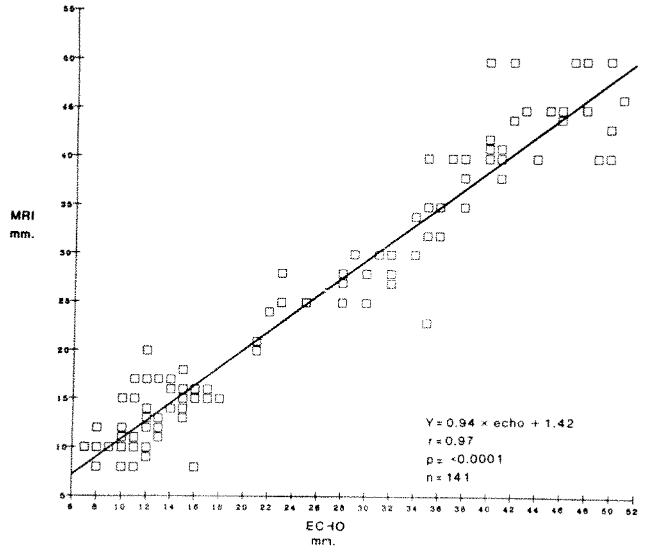

Fig. 4.—Comparison of 141 left heart measurements from MRI and 2DE.

Data Analysis

The MRI and 2DE data were analyzed separately by two independent observers (R. E. D., S. K.) The following dimensions were measured in end diastole and end systole (figs. 1–3): Left ventricular cavity diameters and posterior wall and interventricular septal thicknesses at chordal and mid-papillary-muscle levels were measured on long- and short-axis views; the diastolic anteroposterior mid-left-atrial diameter was measured on long-axis images.

Because of time constraints, not all of the measurements could be obtained in every case, particularly in the earlier studies done before the multislice imaging technique became available. In addition, three subjects experienced claustrophobia during the procedure precluding a complete examination. This occurred early in the study before examinations were expedited by the use of the multislice technique.

TABLE 1: **Comparison of MRI vs. 2D Echocardiographic Measurements**

	n	Regression Equation	*r*	*p*
Left ventricular cavity diameter	45	Y = 0.89 X + 3.7 mm	0.81	<0.001
Left ventricular wall thickness	81	Y = 0.69 X + 4.2 mm	0.66	<0.001
Left atrial cavity diameter	15	Y = 0.67 X + 9.7 mm	0.74	<0.001

Note.—Y = MRI measurements; X = 2D echocardiographic measurements.

All data were expressed as mean +1 SD, and differences in means were considered significant at $p < 0.05$ using analysis of variance (COMPARE, RS1, Bolt, Baraneck, and Newman, Cambridge, MA). For statistical reasons, comparisons were made only where the set of observations was six or more. Linear regression analysis (RS1) was performed to compare MRI and 2DE data in the following groups: (1) all measurements, (2) measurements of the left ventricular cavity diameters, (3) measurement of left ventricular wall thickness, and (4) measurements of the left atrial diameter.

Results

We were able to compare 141 left heart measurements in the 16 subjects using MRI and 2DE (fig. 4, table 1). The correlation between MRI and 2DE was significant when all the data were compared ($p < 0.0001$) and when individual measurements were considered separately ($p < 0.001$). Table 2 compares the mean ± 1 SD values of left heart dimensions from MRI and 2DE at each site and in each image plane. There was no significant difference between MRI and 2DE values, indicating that the image planes and measurement sites were similar. Table 3 shows the MRI measurements for each anatomic site in the 16 normal volunteers.

Discussion

Angiocardiography and echocardiography have both been well validated for measurement of left ventricular dimensions

TABLE 2: **Comparison of Mean Values for Individual Measurements from MRI and 2D Echocardiography (2DE)**

	n	2DE (mm)	MRI (mm)
Long axis, diastole:			
Left atrium	7	23.7 ± 3.4	25.6 ± 4.2
Left ventricle (C)	10	45.0 ± 4.1	44.1 ± 5.1
Left ventricle (PM)	9	42.1 ± 3.7	43.0 ± 3.6
Septum (C)	6	10.6 ± 1.1	9.9 ± 1.0
Posterior wall (C)	6	9.2 ± 1.7	9.7 ± 0.8
Long axis, systole:			
Left ventricle (C)	6	37.0 ± 4.6	34.8 ± 3.6
Left ventricle (PM)	6	30.7 ± 3.0	30.8 ± 3.4
Septum (C)	6	15.0 ± 2.0	14.0 ± 1.3
Septum (PM)	8	15.4 ± 1.5	13.6 ± 3.8
Posterior wall (C)	9	12.0 ± 1.8	14.8 ± 1.5
Short axis, diastole:			
Left ventricle (PM)	8	46.1 ± 4.5	44.8 ± 5.7
Septum (C)	6	9.8 ± 1.7	9.7 ± 1.5
Short axis, systole:			
Left ventricle (PM)	6	34.0 ± 4.1	32.2 ± 5.5
Septum (C)	6	14.8 ± 1.9	16.0 ± 2.9
Septum (PM)	7	15.5 ± 1.2	15.7 ± 0.8
Posterior wall (C)	8	13.8 ± 2.7	15.8 ± 1.0

Note.—Differences between the two sets of data (2DE, MRI) were not significant. C = chordal level; PM = papillary muscle level.

TABLE 3: **Normal Left Ventricular Dimensions in 16 Subjects**

Dimension: Location	Diastole	Systole
Left ventricular cavity diameter (mm):		
Chordal level	46.4 ± 5.5	33.6 ± 3.8
Papillary muscle level	43.4 ± 4.4	29.9 ± 4.8
Septum thickness (mm):		
Chordal level	10.3 ± 0.5	15.5 ± 1.4
Papillary muscle level	10.4 ± 1.8	15.6 ± 2.5
Posterior wall thickness (mm):		
Chordal level	10.2 ± 0.5	15.7 ± 1.0
Papillary muscle level	10.3 ± 1.2	15.4 ± 1.4
Left atrial diameter (mm):		
Anteroposterior	25.6 ± 4.2	. . .

Note.—Left ventricular measurements were made at mid papillary muscle level and midway between the aortic valve and papillary muscle (chordal level). Measurements of the same structure from different planes are consolidated in this table.

[7–9]. For this study, correlation with 2DE was done because it is noninvasive and anatomic display with standard image planes can be closely matched to axially oriented MRI. There was no systematic error when multiple measurements over a large range were made, and separate comparisons of measurements of the left ventricular cavity, left atrium, interventricular septum, and posterior wall were significant to the $p < 0.001$ level in each case.

Previous studies have compared measurements of the heart from MRI in planes transverse to the thorax with 2DE [10, 11]. However MR images in planes orthogonal to the chest wall are oblique to the intrinsic axes of the heart [5, 6]. As a result, any given left ventricular cavity dimension obtained from such images is somewhere between a long and short axis (fig. 5). Since these image planes tend not to be perpendicular to the myocardium, measured wall thickness may theoretically be falsely increased (figs. 5 and 6). For these reasons, Fisher et al. [11], in a study of left ventricular contraction using transaxial MRI, emphasized the assessment of systolic change in left ventricular wall thickness rather than absolute measurement of thickness. An additional problem with the use of imaging planes orthogonal to the chest is that their degree of obliquity with the intrinsic axes of the heart varies, depending on such factors as body habitus and the level of the diaphragm. It is therefore difficult to standardize measurements of the heart using conventional orthogonal views. These potential errors are minimized by the use of images oriented to the left ventricular axes. Axial images are directly comparable from patient to patient and to 2DE and angiocardiography.

Nevertheless, Friedman et al. [10], in comparing cardiac dimensions in normal subjects from transaxial MRI with 2DE, found a good correlation, although correlation coefficients for left ventricular wall thickness were low presumably because of the narrow range of normal values. Thus it appears that in a group of normal volunteers the errors in measurement from transaxial views are small. This may be due to relatively vertical hearts in healthy volunteers, so that a transaxial image plane approaches the true left ventricular short axis. In the present series, the mean angle between the long axis of the left ventricle and the long axis of the body (fig. 5) was 45° ± 8°. In contrast, we previously found this angle to be 57° ± 9° in a group of patients [6], suggesting that errors in measurements from transaxial MRI would be magnified in clinical use because of greater variability in heart size and position.

Potential sources of error in this study include the possibility that the two sets of measurements may not have been made in precisely the same location. As measurements were made independently, interpretation of either the chordal or mid-papillary-muscle level may have varied slightly between the two observers. End-diastolic and end-systolic MR images were triggered by the ECG R wave, with gate delays calculated from the ECG, whereas these end points were selected directly from the 2DE motion display. Thus there may have been slight differences between end points determined electrically as compared to mechanically. The possible effect of respiratory motion on edge definition on MR images, and hence on measurements in this study, is not known as respiratory gating was not used. Inter- and intraobserver error were not established and may also have influenced the results. Higgins et al. [12] have shown that signal may arise within the left ventricular cavity in areas of blood flow stasis resulting from regional akinesis or dyskinesis after myocardial infarction. This occurred on images generated from a second spin-echo with a longer echo delay (TE = 56 msec) than used in our series. However, we have seen signal adjacent to an akinetic area, after infarction, in diastole on first spin-echo, 30-msec-TE images [6]. While this phenomenon did not occur in the present series of normal volunteers, it could present a potential problem in identification of the endocardium in some patients.

Further studies including the evaluation of inter- and intraobserver error are needed. However, we conclude that MRI with images oriented to the intrinsic cardiac axes can be used for the study of cardiac size and function. Our study provides normal values for the left heart using this technique.

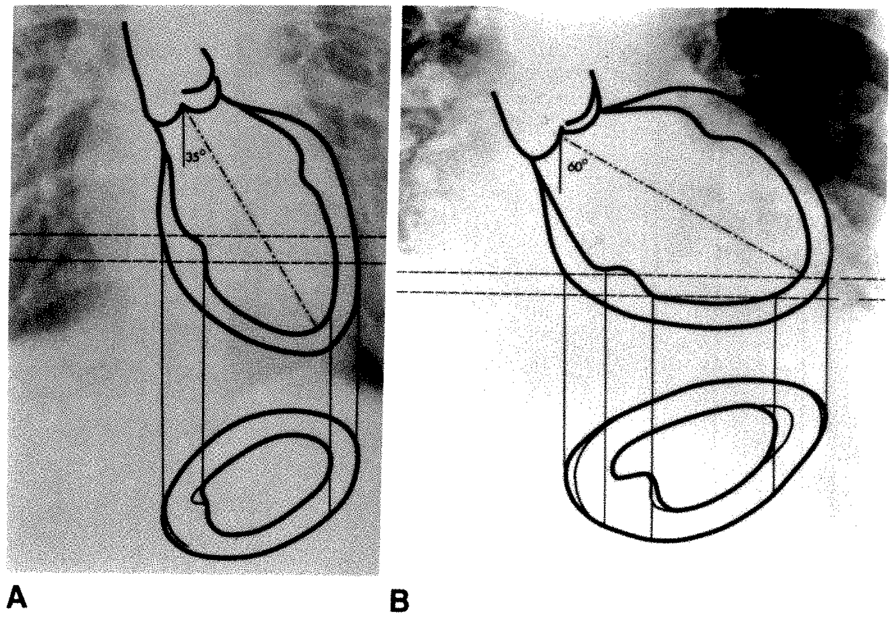

Fig. 5.—Variation in projected transverse thoracic image of left ventricle with varying position of heart in chest. Both images are at level of posterior papillary muscle. **A**, Relatively vertical heart. **B**, More horizontal position. Note falsely increased thickness of projected myocardial wall and difficulty in comparing measurements from one patient with those from another with these image planes. (Reprinted from [6].)

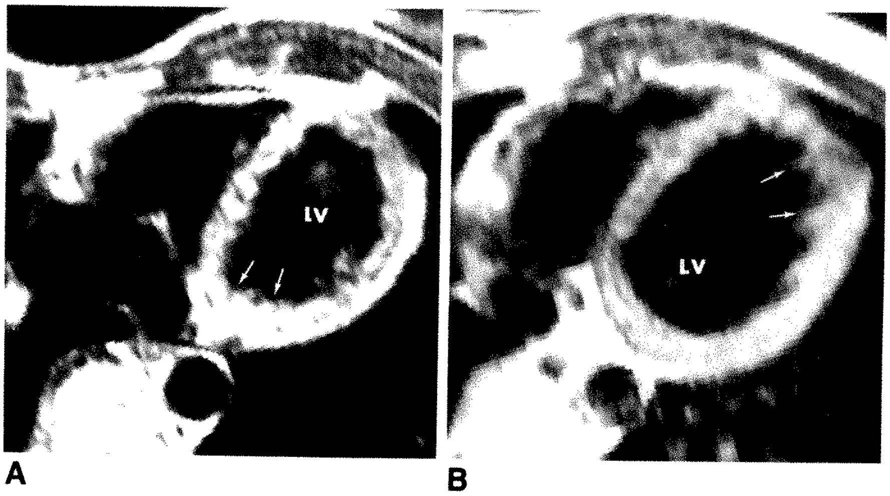

Fig. 6.—Diastolic MRI in plane transverse to thorax in two normal subjects. Apparent relative increase in left ventricular myocardial thickness (*arrows*) posteriorly in **A** and in anterolateral area in **B**. LV = left ventricle.

REFERENCES

1. Higgins CB, Stark D, McNamara M, Lanzer P, Crooks LE, Kaufman L. Multiple magnetic resonance imaging of the heart and major vessels: studies in normal volunteers. *AJR* **1984**;142:661–667
2. Fletcher BD, Jacobstein MD, Nelson AD, Riemenschneider TA, Alfidi RJ. Gated magnetic resonance imaging of congenital cardiac malformations. *Radiology* **1984**;150:137–140
3. Hawkes RC, Holland GN, Moore WS, Roebuck EJ, Worthington BS. Nuclear magnetic resonance (NMR) tomography of the normal heart. *J Comput Assist Tomogr* **1981**;5:605–612
4. Crooks LE, Barker B, Chang H, et al. Magnetic resonance imaging strategies for heart studies. *Radiology* **1984**;153:459–465
5. Dinsmore RE, Wismer GL, Levine RA, Okada RD, Brady TJ. Magnetic resonance imaging of the heart: positioning and gradient angle selection for optimal imaging plane. *AJR* **1984**;143:1135–1142
6. Dinsmore RE, Wismer GL, Miller SW, et al. Magnetic resonance imaging of the heart using image planes oriented to cardiac axes: experience with 100 cases. *AJR* **1985**;145:1177–1183
7. Feigenbaum H, Popp E, Wolfe S. Ultrasound measurements of the left ventricle: correlative study with angiocardiography. *Arch Intern Med* **1972**;129:461–467
8. Weyman AE. *Cross sectional echocardiography*. Philadelphia: Lea & Febiger, **1982**
9. Dodge HT, Baxley WA. Left ventricular volume and mass and their significance in heart disease. *Am J Cardiol* **1969**;23:528–537
10. Friedman BJ, Waters J, Kwan OL, DiMaria AN. Comparison of nuclear magnetic resonance imaging and echocardiography in determination of cardiac dimensions in normal subjects. *J Am Coll Cardiol* **1985**;5:1369–1376
11. Fisher MR, von Schulthess GK, Higgins CB. Multiphasic cardiac magnetic resonance imaging: normal regional left ventricular wall thickening. *AJR* **1985**;145:27–30
12. Higgins CB, Lanzer PA, Stark D, et al. Imaging by nuclear magnetic resonance in patients with chronic ischemic heart disease. *Circulation* **1984**;69:523–531

Book Reviews

Diagnostic Imaging in Hemophilia: Musculoskeletal and Other Hemorrhagic Complications.

By Holger Pettersson and Marvin Gilbert. Berlin: Springer-Verlag, 147 pp., 1985. $49.50

This brief monograph is a compendium of the radiographic aspects of hemophilia. It was written by a radiologist and an orthopedic surgeon and has contributions from four other authors in the fields of internal medicine, nuclear and pediatric radiology, surgery, and hematology. There are 10 chapters. The first discusses hemophilia itself and reviews current concepts, treatment methods, demography, and recent advances. There is even a short section on hephophilia and AIDS.

The second chapter reviews the various imaging techniques available for diagnosis. The remaining chapters discuss the imaging aspects of the various complications of the disease with chapters on Hemophiliac Arthopathy (the longest chapter), Hemophiliac Synovitis, Soft-Tissue Bleeding, Hemophiliac Pseudotumor, Fractures, Central Nervous System Complications, Neck and Chest, and Abdomen and Urinary Tract. Each is well organized and discusses the clinical aspects of the disease, pathology, and diagnostic imaging.

The radiographs and other images are excellent. The chapter on soft-tissue bleeding has sonograms, CT scans, and magnetic resonance images. Each chapter is followed by a reference list that contains both classic and current papers. There are no serious flaws in this book aside from the fact that several illustrations could be larger. The text is kept to a minimum but is complete. The book will be of interest to any radiologist, pediatrician, hematologist, internist, or orthopedic surgeon involved in the treatment of hemophiliacs and will make a useful addition to departmental libraries.

Richard H. Daffner
Allegheny General Hospital
Pittsburgh, PA 15212

World Health Organization Basic Radiological System. Manual of Radiographic Interpretation for General Practitioners.

By P. E. S. Palmer, W. P. Cockshott, V. Hegedüs, and E. Samuel. Geneva: World Health Organization, 216 pp., 1985; soft cover. Sw. fr. 23. Arabic, Spanish, and French editions in preparation. Available in U.S.: WHO Publications Centre, 49 Sheridan Ave., Albany, NY 12210.

This small paperback book is an interesting contribution, which may be more valuable for the information it gives us regarding its origin and its intent rather than for its actual scientific contents. It is designed as a manual to be used by physicians, primarily in developing countries, who have access to basic radiologic equipment but do not have ready access to a radiologist. The World Health Organization has already developed a radiologic system identifying a suitable x-ray installation for various parts of the world and this manual serves to supplement that system.

The book covers basic radiology with over 400 radiographs and line drawings that are well done and of fairly satisfactory reproduction quality. In addition to covering basic radiologic concepts, there is an excellent text that clearly summarizes indications for the use of radiographs, quality control, appropriate positioning, and, even more importantly, discusses problems that might be encountered with contrast reactions. The latter may be the most valuable part of the book.

The radiologic coverage is also very good. The two principle areas of chest and skeletal radiology are outstanding and would even be of use to a medical student or nurse who wished to learn more about basic diagnostic radiology.

The concern one might have about this type of book does not relate to the content itself, but rather to the use of it by some physician who may not realize that this is not a general, all-inclusive text. The authors attempt to emphasize this point and it is hoped this point comes across. If the practitioner realizes this book is only to help make a quick decision, it will be properly used, but should this information be substituted for consult with a properly trained radiologist, the whole project will be counterproductive.

The book cannot be recommended as an addition to a radiologic library and is certainly too elementary for a radiology resident. It might be of use for nurses in radiology or even trainees in other specialties who wish to know more about basic radiology. If one keeps in mind the original intent of this publication and if it is properly used by medical practitioners in isolated areas, it will stand as an outstanding contribution.

Raymond A. Gagliardi
St. Joseph Mercy Hospital
Pontiac, MI 48053

Critical Evaluation of the Radial Head–Capitellum View in Elbow Trauma

Andrew C. Page[1]

The radial head–capitellum view, a radiographic projection of the elbow to show the lateral components, has been advocated for routine use in the investigation of acute elbow trauma. Retrospective and prospective studies in an Accident and Emergency Department were conducted to determine objective benefits in primary diagnostic rate and treatment. None were found, and thus it is suggested the view be for specialized use only when indicated.

The radial head–capitellum view, an oblique lateral projection introduced by Greenspan and Norman [1] has been advocated for standard use in the investigation of acute and chronic elbow trauma [1, 2]. To assess the utility of this view in the investigation of elbow trauma, retrospective and prospective studies of patients with elbow injury seen in the Accident and Emergency Department in Plymouth were undertaken. The retrospective study involved anteroposterior and lateral views only; the prospective study included the supplementary radial head–capitellum view. Factors investigated were the initial diagnosis by the emergency room house officer, final radiologic diagnosis by consultant radiologists and the senior registrar, primary treatment, and follow-up.

Subjects and Methods

The time period for each study was 1 month. During the retrospective study, 4396 patients were seen, 107 with elbow injury. There were 3973 patients in the prospective study, 71 of whom had elbow injury.

The radiology staff involved were unchanged during the studies; although the emergency room house officers changed during the 2 months, their levels of experience were equivalent. In Plymouth, casualty radiographs are reported "cold," usually 12–24 hr later, unless specifically indicated. In patients in whom fractures are missed, immediate recall occurs after radiologic reporting. The radial head–capitellum view was obtained using the technique advocated by Greenspan and Norman [1].

Results

Twenty-one radial head fractures were diagnosed in the retrospective study and 17 in the prospective (table 1). Six fractures were missed initially in each study (table 2). All cases of radial head or other intracapsular fractures had demonstrable effusions. Of patients with extracapsular fractures, 22% and 62.5%, in retrospective and prospective studies, respectively, had joint effusions.

In five adult patients (three prospective, two retrospective), effusions were present without demonstrable fractures. In four of these, however, there was radiologic evidence of osteoarthritis. No effusions were seen in the absence of a fracture in children.

The radial head–capitellum view permitted subsequent diagnosis in two of the

Received May 14, 1985; accepted after revision September 4, 1985.

[1] Department of Radiology, Freedom Fields Hospital, Plymouth, Devon, England PL4 8NL.

AJR 146:81–82, January 1986
0361–803X/86/1461–0081
© American Roentgen Ray Society

TABLE 1: **Elbow Injuries during Each Month of Study**

	Retrospective Study (AP & Lat Views)		Prospective Study (AP, Lat, & RHC Views)	
	Adults	Children	Adults	Children
Total number	60	47	46	25
Radial head and neck fracture	18	3	16	1
Coronoid fracture	1	0	0	1
Other elbow fracture (i.e., supracondylar, olecranon, epicondylar)	7	11	4	4
Distant fracture (e.g., radial, ulnar shaft)	2	3	5	2

Note.—AP = anteroposterior; Lat = lateral; RHC = radial head–capitellum. Children are under 18 years of age.

TABLE 2: **Comparison of Primary Diagnostic Rate with Subsequent Radiologic Assessment of Fractures Involving the Elbow Joint**

Type of Diagnosis	Radial Head and Neck Fracture		Other Elbow Fractures	
	Retrospective	Prospective	Retrospective	Prospective
Number	21	17	18	8
Positive primary	12	8*	13	6
Equivocal primary	3	3	2	0
Missed primary	6	6	3	2
Positive radiologic	19	16*	18	8
Equivocal radiologic	2	1	...	...

* Positive benefit in two patients from radial head–capitellum view.

three prospective cases, as assessed by the radiology staff, but in only one case at the time of injury. There were no recorded instances of return to emergency or orthopedic clinic by patients diagnosed as having no evidence of fracture by both casualty and radiology staff.

Discussion

The claim that the radial head–capitellum view should be incorporated as routine in investigating elbow trauma [1, 2] has been challenged previously [3–5], and the results of our study support this challenge. The view did disclose an occult radial head injury in two cases in the prospective study; however, suspicion of fracture had already been raised by the presence of an elevated fat pad, indicating joint effusion. In normal practice, this would certainly have led to further views. Thus, our study suggests that the radial head–capitellum view should be considered an adjunct rather than a standard view.

The excellent correlation of intracapsular fractures and detectable joint effusion endorses the observations of Bledsoe and Ezenstark [6], as only one case in our study with an effusion did not have a radiologically apparent ascribable cause; the results also correlated well with data presented by Murphy and Siegel [7]. It is concluded that teaching emergency room physicians to recognize this sign would be more beneficial than adding a new view to the routine elbow trauma radiography.

ACKNOWLEDGMENTS

I thank R. R. Cox, Department of Radiology, and I. Stewart, Department of Accident and Emergency, for support and advice, and R. Smee and K. Roberts for secretarial assistance.

REFERENCES

1. Greenspan A, Norman A. Radial head, capitellum view: useful technique in elbow trauma. *AJR* **1982**;138:1186–1188
2. Greenspan A, Norman A, Rosen H. Radial head-capitellum view in elbow trauma: clinical application and radiographic-anatomic correlation. *AJR* **1984**;143:355–359
3. Hall FM. Radiologic assessment of injuries about the elbow (letter). *AJR* **1982**;139:1239–1240
4. Bohrer SP. Another view on the radial head–capitellum issue: useful technique or routine view? (letter). *AJR* **1982**;139:1240
5. Hall-Craggs MA, Shorvon PJ. Radial head–capitellum view (letter). *AJR* **1985**;144:650
6. Bledsoe R, Ezenstark J. Displacement of fat pads in disease and injury of the elbow: a new radiologic sign. *Radiology* **1959**;73:717–721
7. Murphy WA, Siegal MJ. Elbow fat pads with new signs and extended differential diagnosis. *Radiology* **1977**;124:659–665

Trampoline Fracture of the Proximal Tibia in Children

Richard S. Boyer[1, 2]
Richard B. Jaffe[1]
George W. Nixon[1]
Virgil R. Condon[1]

Seven children (aged 2–5 years) sustained fractures of the proximal tibial metaphysis while jumping on a trampoline with a heavier child or adult. Most impaction fractures were transverse and neither angulated nor displaced. None of the children developed permanent disability or impairment. Parents and physicians should be aware of the possible danger to small children while tandem jumping on a trampoline with a heavier partner.

New types of injuries peculiar to specific recreational activities are recognized with increasing frequency in our society, which devotes considerable time and resources to recreation. It is often helpful to associate a typical injury with a particular activity and attempt to elucidate its underlying mechanism to aid in recognizing and preventing injury to persons engaged in that activity. We have recently observed fractures of the proximal tibia in several children who were jumping on a trampoline with another person (usually older and/or heavier). We report our findings and propose the underlying mechanism of injury.

Subjects and Methods

During 1981 through 1984, we observed similar tibial fractures in seven children that were sustained while jumping on a trampoline. Original radiographs of the fracture site were examined by one of us (R. B.). Referring physicians and/or parents were contacted at intervals from 2 months to 3 years after the injury to confirm the circumstances of the injury and assess subsequent impairment.

Results

Seven children, aged 2–5 years (mean, 3.9), sustained fractures of the proximal tibia while jumping on a trampoline with another person. In five of seven cases, the child was jumping with an older child or an adult. The seven children weighed 11.7–25 kg (mean, 17.9) compared to their jumping partners who weighed 22.7–100 kg (mean, 52.3). One child was jumping with several children of the same age, and another with a child of the same age who was 5 kg heavier.

The typical fracture that was observed, a linear transverse fracture of the proximal tibia metaphysis (fig. 1), was seen in five children. In one child, the fracture was comminuted but nondisplaced (fig. 2). In another child, the radiographs showed a cortical buckle (torus) fracture without a visible fracture line (fig. 3). The fracture in one child was mildly angulated and displaced (fig. 4). None of the fractures extended to the articular surface.

After a follow-up period of 2 months to 3 years, parents and/or referring physicians indicated that each child had recovered without apparent deformity or limitation. No follow-up radiographs are available for confirmation.

Received June 24, 1985; accepted after revision August 28, 1985.

[1] All authors: Department of Radiology, University of Utah Medical Center, and Primary Children's Medical Center, 320 Twelfth Ave., Salt Lake City, UT 84103. Address reprint requests to R. B. Jaffe.

[2] Present address: Department of Radiology, Hospital for Sick Children, Toronto, Ontario, Canada M5G 1X8.

AJR **146:83–85, January 1986**
0361-803X/86/1461-0083
© American Roentgen Ray Society

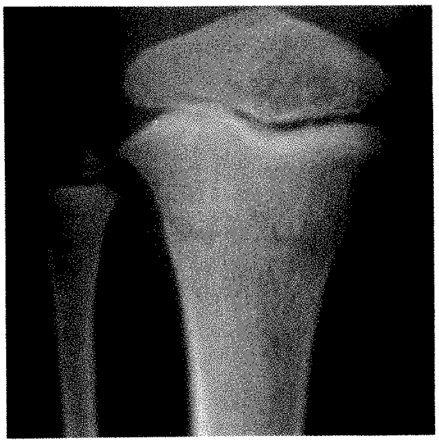
1

Fig. 1.—Anteroposterior view. Linear transverse fracture of proximal tibial metaphysis.

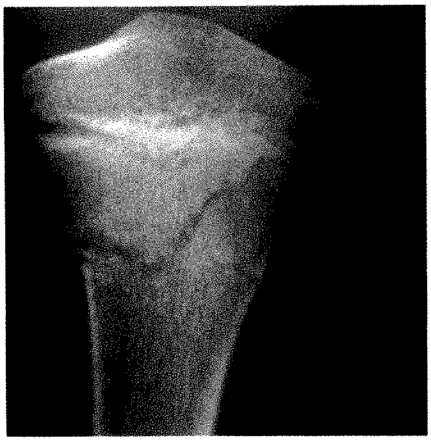
2

Fig. 2.—Anteroposterior view. Comminuted fracture of proximal tibia.

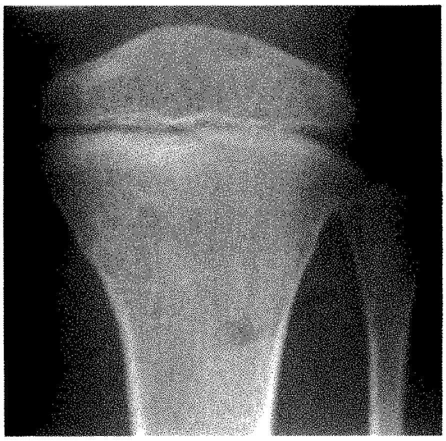
3

Fig. 3.—Anteroposterior view. Cortical buckle (torus) fracture of proximal tibia.

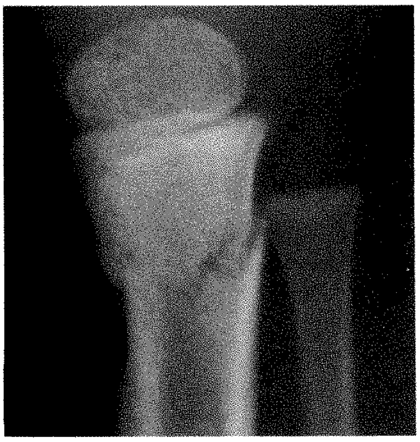
4

Fig. 4.—Lateral view. Mild displacement and angulation at fracture site.

Discussion

We propose that a fracture of the proximal tibia is an understandable occurrence in young children (aged 2–5 years in our patients) who jump on a trampoline with another person if the second person is heavier. As the heavier person jumps (fig. 5), the trampoline mat recoils upward from its stretched downward position. If the smaller child lands on the upward-moving mat at the time when its elasticity is reversed by recoil and the springs are shortening to their unstretched length, there is significant upward impaction force applied to the descending child's legs. The force applied at just the right time and angle of impact may be sufficient to cause the tibial fractures we have observed.

We recently observed a similar injury in a child who was jumping on the top mattress of a bunk bed. The fracture occurred when another child lying on the bottom bunk pushed upward with his feet on the upper mattress as the child above landed on it. We propose a similar effect to that of the recoiling trampoline mat in causing an identical tibial fracture to that seen in the trampoline injuries.

It should be emphasized that the tibial fracture we are reporting is not a stress fracture [1–4]. There is no history of repetitive stress to the proximal tibia, nor is there the typical history of pain relieved by rest and exacerbated by activity as seen with stress fractures. Furthermore, in none of the children who sustained fractures was there radiographic evidence of underlying bone abnormality or history of metabolic bone disease.

The outcome of fractures in the children we report was uniformly good. No child developed deformity or disability after treatment with routine immobilization. Genu valgum did not develop as a complication of these tibial fractures, as has been reported in some children with tibial metaphyseal fractures [4, 5].

We suggest that radiologists, pediatricians, and orthopedists who are aware of the possibility of a "trampoline fracture" of the proximal tibia may be in a better position to recognize this injury and correctly identify its mechanism of injury. Parents and other adults should discourage tandem jumping, especially by children of different sizes, to avoid the

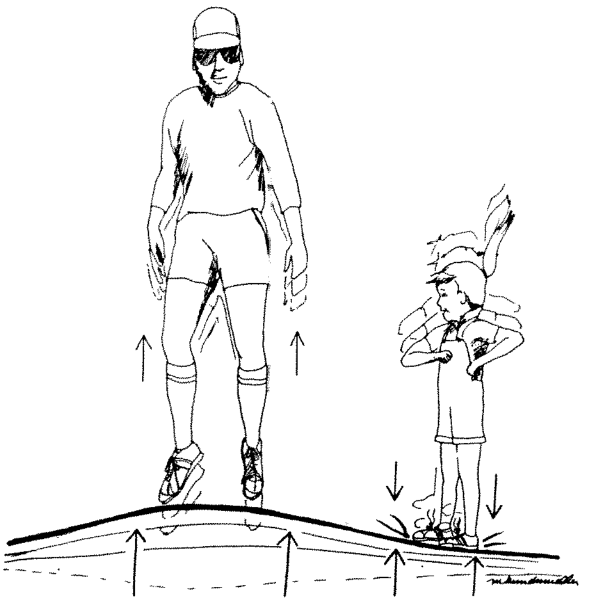

Fig. 5.—Mechanism of injury in "trampoline fracture." As mat recoils, propelling heavier person upward, it strikes descending smaller person (child) with sufficient force to cause fracture of proximal tibia.

potential of this injury with its associated pain and inconvenience.

ACKNOWLEDGMENTS

We thank Valorie Kemp and Deborah Villeneuve for secretarial assistance. Figure 5 was drawn by Marilou Kundmueller, Primary Children's Medical Center.

REFERENCES

1. Salter RB. *Textbook of disorders and injuries of the musculoskeletal system* 2d ed. Baltimore: Williams & Wilkins, **1985**
2. Grusel R. Pseudofractures and stress fractures. *Semin Roentgenol* **1978**;13:81–82
3. Belkin SC. Stress fractures in athletes. *Orthop Clin North Am* **1980**;11:735–742
4. Rogers LF. *Radiology of skeletal trauma.* New York: Churchill-Livingstone, **1982**
5. Currarino G, Pinckney LE. Genu valgum after proximal tibial fractures in children. *AJR* **1980**;136:915–918

Addendum

Since submission of this manuscript, we have seen eight additional cases of similar "trampoline fractures" of the proximal tibia. We thank Richard Keller of Cottonwood Hospital, Salt Lake City, UT, for providing four of these cases for review.

Book Review

***The Radiologic Clinics of North America.* Symposium on Digital Radiography.** Guest Editors: Bruce J. Hillman and John D. Newell II. Philadelphia: Saunders, June 1985;23:175–378. By subscription, 4 issues annually, $52

This volume is an excellent depiction of the scope of development of digital imaging and also summarizes existing knowledge and expectations. Since its development, the use of digital radiography has changed considerably. This volume represents the latest thinking regarding the application and place of digital radiography in the imaging field.

The book is well organized. Topics include digital subtraction angiography (DSA); technology, equipment, and techniques; newer subtraction and filtration techniques; DSA of the arteries of the head and neck; digital radiology of the kidney; peripheral, abdominal, and interventional applications of DSA; pulmonary DSA; digital cardiac radiology; contrast administration and techniques of DSA performance; intraarterial DSA; parametric imaging; processing alternatives for digital chest imaging; use of psychophysical principles in the design of a total digital department; the digital radiology department of the future; teleradiology: part of a comprehensive telehealth system; and DSA in the community hospital.

The thoughtful choice of topics is particularly good. Many applications, unique uses, projections for the future, and the needs of the practicing radiologist are addressed. The material is expertly and clearly presented.

The volume is an excellent handbook for current use of digital radiography. The illustrations and index are excellent. It is strongly recommended for all general radiologists, angiographers, neuroradiologists, and radiology residents.

Jack I. Eisenman
King/Drew Medical Center
Los Angeles, CA 90059

Negative Bone Scans of Joints after Aspiration or Arthrography: Experimental Studies

Paul D. Traughber[1]
B. J. Manaster[1]
Kevin Murphy[2]
Naomi P. Alazraki[2]

It has long been suspected anecdotally that needle aspiration or contrast arthrogram before bone scan may cause a false-positive bone scan. This dictum often directs the sequence of events in the clinical workup of joint disease, yet data to support or refute this are lacking. This study was undertaken to generate such data. Fifty-six joints in mature dogs were examined, including hips, knees, elbows, and shoulders. The joints were examined in pairs; one joint was injected with Conray 60 for an arthrogram, and the contralateral joint was injected with an equal volume of normal saline to simulate a joint aspiration. Confirmation of needle placement and injection into the joints was made with fluoroscopic and digital subtraction imaging. Numbers of attempts required for aspiration and quantity of contrast material extravasated were noted for each joint. Baseline ^{99m}Tc-HDP or ^{99m}Tc-MDP bone scans were done before the experimental joint aspirations, with follow-up scans at 24 and 96 hr. The scans showed no significant change from baseline after either needle aspiration or arthrogram. When the diagnostic workup suggests the need for such a procedure, it should be performed. In contradiction to popular belief, joint aspiration and/or arthrogram did not affect a subsequent bone scan.

Definitive diagnosis of a septic joint is made by aspiration of joint fluid and culture of organisms. In difficult aspirations where only a small amount of fluid is in the joint, it is common to perform the procedure under fluoroscopic control. Nonbacteriostatic normal saline may be injected for aspiration, followed by administration of a small amount of radiographic contrast material to prove that the needle is correctly placed within the joint capsule rather than in the surrounding soft tissues. In evaluating prosthetic joints, aspiration and contrast arthrography are routinely used when infection and/or loosening of the prosthesis is suspected.

Plain radiographs are often normal in early septic joints. Radionuclide bone scans have been demonstrated to be very sensitive for evaluating a variety of joint diseases [1, 2], but it has long been suggested anecdotally that either needle aspiration or contrast arthrogram before bone scan may cause a false-positive bone scan. In the case of needle aspiration alone, it is suggested that a positive bone scan may reflect local trauma from several needle punctures. In the case of an arthrogram, the contrast material itself as an irritating substance may cause a local hyperemia and inflammatory response, leading to a false-positive bone scan.

This concern of inciting an iatrogenic bone scan artifact may affect the course of clinical workup for septic arthritis. Clinicians not infrequently postpone joint aspiration or arthrography until the bone scan has been performed. This delay can be critical, since there is a direct correlation of prognosis with early diagnosis and appropriate treatment [3].

Our review of the literature suggests that although this dictum may direct the sequence of events in the clinical workup of septic arthritis, no careful evaluation of the subject had been published. This experimental animal study was undertaken to gather data to either support or refute the hypotheses that needle aspiration and/or contrast arthrography affect bone scans.

Received May 30, 1985; accepted after revision September 9, 1985.

This work was supported by research funds from the Veterans Administration.

[1] Department of Radiology, Diagnostic Radiology Imaging Laboratory, University of Utah Medical Center, 50 N. Medical Dr., Salt Lake City, UT 84132. Address reprint requests to B. J. Manaster.

[2] Nuclear Medicine Service, Veterans Administration Medical Center, Salt Lake City, UT 84132.

AJR 146:87-91, January 1986
0361-803X/86/1461-0087
© American Roentgen Ray Society

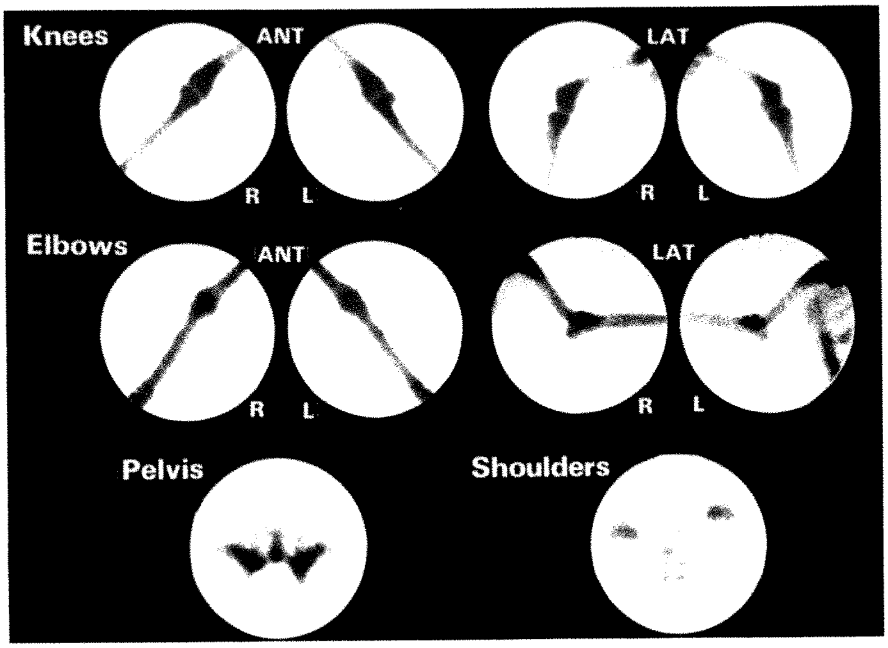

Fig. 1.—Baseline ^{99m}Tc-MDP bone scan illustrating frontal and lateral views of joints.

Subjects and Methods

Fifty-six joints in nine mature mongrel dogs were examined. Normal baseline bone scans were obtained before interventions (fig. 1). Hip, knee, shoulder, and elbow joints were entered and aspirated under sterile conditions and fluoroscopic control. We used 22-gauge spinal needles in hip and elbow joints; this is the size and type of needle customarily used in clinical aspirations of these joints because of the small, rather tight joint capsule in hips and the small potential joint space in elbows. In knees and shoulders, 20-gauge needles were used; this needle is routinely used clinically because of more capacious, easily accessible joint capsule of knees and shoulders. Joints on one side of the body were injected with Conray 60. Volumes of 2 ml in hips and elbows and 4 ml in shoulders and knees were experimentally determined to distend the individual joint spaces, thus reproducing the situation in human prosthetic joint aspiration/arthrograms where maximal joint distension achieves dissection of contrast material around the prosthetic components. Confirmation of injection into joints was made with fluoroscopic and digital subtraction imaging. Contralateral joints were injected with sterile normal saline to further simulate a needle aspiration. Number of attempts required to enter the joint and estimates of volume of inadvertently extravasated contrast material were recorded.

After these interventions, bone scans were performed at 24 and 96 hr. Imaging was performed 2 hr after intravenous administration of 5 mCi (185 MBq) of ^{99m}Tc-HDP (hydroxymethylene diphosphonate) or ^{99m}Tc-MDP (methylene disphosphonate). A 37-photomultiplier-tube scintillation camera set with a 15% window centered on the 140-KeV photopeak of ^{99m}Tc, with general-purpose low-energy collimator, acquired images of each joint for 100,000 counts in frontal and lateral positions. The bone scans were reviewed by a single experienced observer (N. A.), who was unaware of the procedure performed on each joint.

Results

The 24- and 96-hr bone scans were normal and unchanged from the baseline study in 54 of 56 joints. One joint had an equivocally positive postintervention scan at 24 hr that was normal at 96 hr. A second joint had a questionably positive 96-hr postintervention scan (fig. 2). No joints had unequivocally positive postintervention scans.

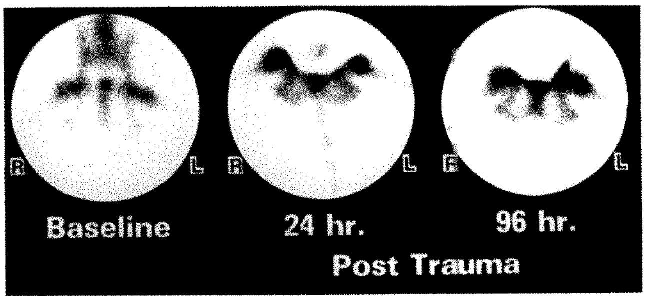

Fig. 2.—Radionuclide (^{99m}Tc-HDP) uptake in left hip was termed equivocally increased in 96-hr postintervention scan. This may be related to commonly encountered artifact (e.g., positioning). It was termed equivocal because our observer believed that in normal practice, it might well be discounted and read as normal.

The two equivocally positive joints had been injected with contrast material, and each had less than 0.5 ml of contrast extravasation. Both were difficult joints to enter and both required multiple needle punctures.

Of the 11 joints requiring multiple needle punctures, nine had normal postintervention scans. All of the 28 joints with saline injection had normal scans even though five required multiple needle punctures for proper positioning. All five joints with 1 ml or more of contrast extravasation had normal postintervention scans. Two joints had small amounts of contrast extravasation; these were the two equivocally positive studies mentioned earlier.

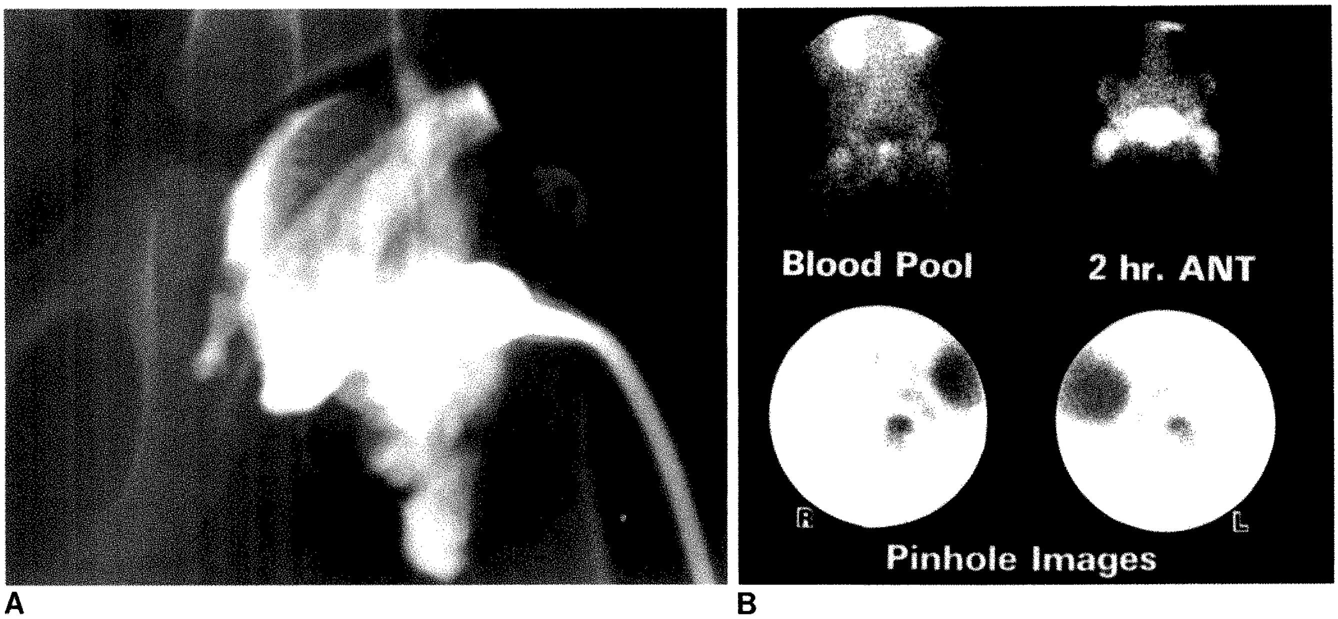

Fig. 3.—**A**, Normal arthrogram in child with suspected septic hip. **B**, ^{99m}Tc-MDP bone scan 24 hr after arthrogram is normal.

Discussion

This study explores two areas related to bone scanning that have not been carefully evaluated before. There are few data in the literature that can be directly compared, but a review of related literature is useful in evaluating our results.

The first issue is whether needle aspiration with saline injection alters subsequent bone scans on the basis of limited local trauma. Our carefully controlled data of 28 of 28 normal 24- and 96-hr scans after aspiration and saline injection of joints suggest that needle aspiration of joints alone will not alter subsequent bone scans. Other reported studies, consisting of retrospective observations only, generally support this observation. Fordham and Ramachandran [4] anecdotally suggested that bone marrow biopsy leads to increased bone scan activity but offered no supporting data. In contrast, McKillop et al. [5] described 45 patients scanned after bone biopsy with needles 1.2–8 mm in diameter. Biopsy sites from 1.2- and 3.5-mm needles were not detected on subsequent bone scans, although there was a wide range of elapsed time from biopsy to scan (1–45 days). In another retrospective study, McCoy et al. [6] described six patients with procedures varying from joint aspiration to bone aspiration, all with normal bone scans obtained 1–7 days later. Tyler and Powers [7] reported 24 patients with no increased scan activity at the site of bone marrow biopsy 1–10 days after biopsy. They postulated that the lack of activity after needle aspiration of bone may be related to the size of the lesion or bone disturbance produced. The low resolution of standard bone scans may not allow detection of bone lesions several millimeters in size. In an experimental animal study of bone needle penetration and drill holes into metaphyseal bone in immature rabbits, Alazraki et al. [8] reported no effect on subsequent bone scans.

A key concept seems to be that lack of uptake on bone scans may be related to severity, size, and position of bony trauma. This is supported by the fact that fractures are routinely detectable on bone scans [9]. In the retrospective study by McKillop et al. [5], 8-mm iatrogenic lesions were detected on subsequent bone scans. This trauma is much more severe than that experienced with routine joint aspiration and/or arthrography.

The second issue involves the use of contrast arthrography in conjunction with needle aspiration. The hypothesis is that an inflammatory and hyperemic response to the contrast medium itself may alter a subsequent bone scan. Our review of the literature reveals neither laboratory nor clinical data addressing this question. Our results of 26 of 28 normal scans after contrast arthrography, with two equivocally abnormal scans, refutes the hypothesis that contrast injection significantly alters subsequent bone scans. Of the 26 clearly normal cases, five had significant contrast extravasation during arthrography; thus, even a poorly performed arthrogram does not seem to alter bone scan results.

In addition to the experimental animal data reported here, we have collected five pertinent patient cases at this institution. In each case, a contrast arthrogram was followed 24 hr later by a bone scan. One child with a suspected septic hip had both a normal arthrogram and a normal bone scan (fig. 3). A second child with a suspected septic hip had a normal arthrogram; the bone scan was normal in the joint but abnormal in the ilium, a site of osteomyelitis (fig. 4). One prosthetic hip had both a normal arthrogram and bone scan. A second prosthetic hip showed typical signs of loosening both arthro-

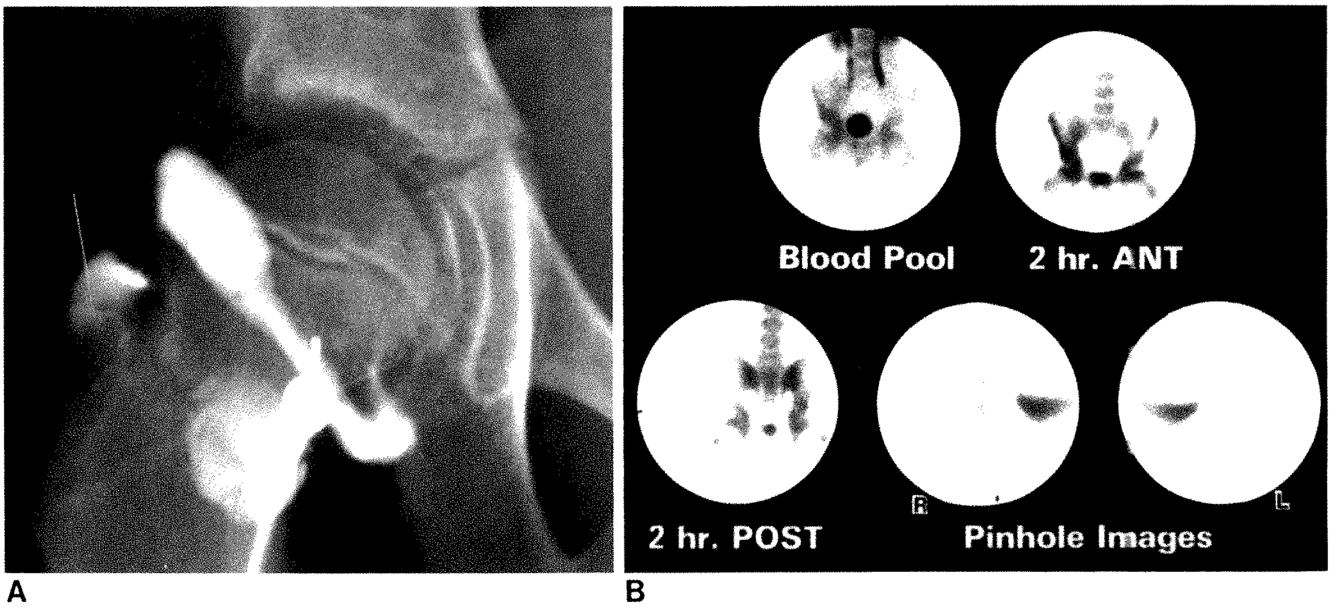

Fig. 4.—**A**, Normal arthrogram in child with suspected septic hip. **B**, ^{99m}Tc-MDP bone scan 24 hr later was normal in joint, as illustrated by equal and symmetric appearance of femoral joints. However, abnormal uptake in iliac bone was later found by biopsy to represent osteomyelitis.

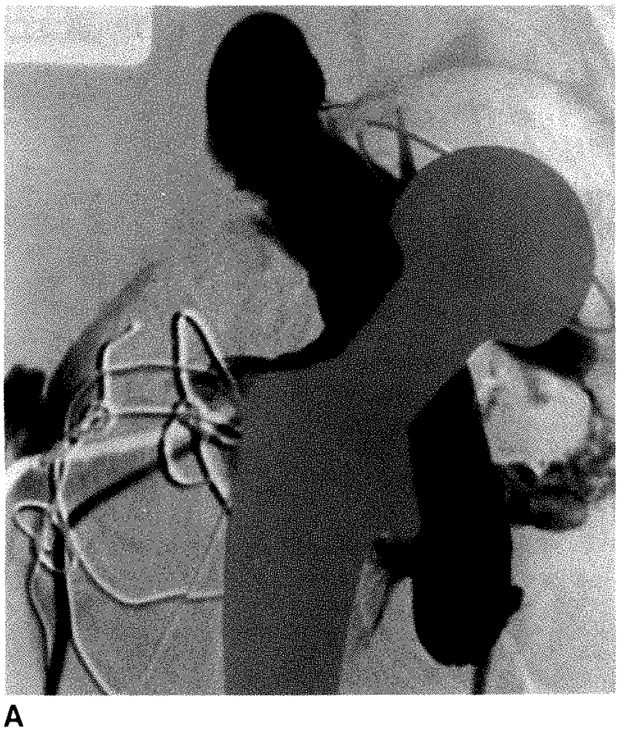

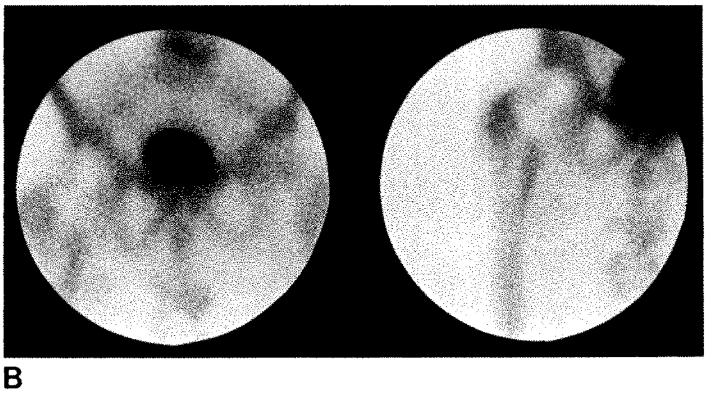

Fig. 5.—**A**, No evidence on arthrography that hip arthroplasty has loosened. However, 40 ml of contrast material entered a huge pseudocapsule that filled bursa in far lateral soft tissues. **B**, ^{99m}Tc-MDP bone scan. No abnormal uptake corresponding to either joint or bursa.

graphically and by bone scan. A third prosthetic hip showed no loosening but a huge pseudocapsule and bursa that filled with 40 ml of contrast material arthrographically; the bone scan showed no abnormal uptake corresponding to either the joint or bursa (fig. 5). Our clinical experience so far corroborates the laboratory findings that neither needle aspiration nor contrast arthrography significantly alters subsequent bone scans. These interventions should be done promptly for early diagnosis and better patient prognosis.

REFERENCES

1. Thomas RH, Resnick D, Alazraki N, Daniel D, Greenfield R. Compartmental evaluation of osteoarthritis of the knee. *Radiol-*

ogy **1975**;116:585-594

2. Weissberg DL, Resnick D, Taylor A, Becker M, Alazraki N. Rheumatoid arthritis and its variants: analysis of scintiphotographic, radiographic and clinical evaluations. *AJR* **1978**; 131:665-673
3. Resnick D, Niwayama G. Osteomyelitis, septic arthritis, and soft tissue infection. In: Resnick D, Niwayama G, eds. *Mechanisms and situations in diagnosis of bone and joint disorders*. Philadelphia: Saunders, **1981**:2044-2129
4. Fordham EW, Ramachandran PC. Radionuclide imaging of osseous trauma. *Semin Nucl Med* **1974**;4:411-429
5. McKillop JH, Maharaj D, Boyce BF, Fogelman I. Bone scan appearances following biopsy of bone and bone marrow. *Radiology* **1984**;153:241-242
6. McCoy JR, Morrissy RT, Seibert J. Clinical experience with the technetium-99 scan in children. *Clin Orthop* **1981**;154:175-180
7. Tyler JL, Powers TA. Bone scanning after marrow biopsy: concise communication. *J Nucl Med* **1982**;23:1085-1087
8. Alazraki N, Moitoza J, Heaphy J, Taylor A. The effect of iatrogenic trauma on the bone scintigram: an animal study. *J Nucl Med* **1984**;25:978-981
9. Matin P. The appearance of bone scans following fractures, including immediate and long-term studies. *J Nucl Med* **1979**;20:1227-1231

Books Received

Receipt of books is acknowledged as a courtesy to the sender. Books that appear of sufficient interest will be reviewed as space permits.

Science and Public Policy III. Annals of the New York Academy of Sciences, vol. 403. Edited by Frances S. Sterrett. New York: New York Academy of Sciences, 120 pp., 1983. $24; soft cover

X-Ray Imaging Equipment. An Introduction. By Euclid Seeram. Springfield, IL: Thomas, 588 pp., 1985. $44.50

Recent Developments in Digital Imaging. Medical Physics Monograph No. 12. Edited by Kunio Doi, Lawrence Lanzl, and Pei-Jan Paul Lin. New York: American Institute of Physics, 576 pp., 1985. $60 ($40 for institute members)

Carbon-14 in the Environment. NCRP Report No. 81. Recommendations of the National Council on Radiation Protection and Measurements. Bethesda, MD: NCRP, 108 pp., 1985. $12; soft cover

Protection of the Patient in Radiation Therapy. ICRP Publication 44. A report of Committee 3 of the International Commission on Radiological Protection. Oxford: Pergamon, 51 pp., 1985; soft cover. $22

X-Rays: Health Effects of Common Exams. By John W. Gofman and Egan O'Connor. San Francisco: Sierra Club, 440 pp., 1985. $25

Introduction to Radiographic Cephalometry. By Alex Jacobson and Page W. Caufield. Philadelphia: Lea & Febiger, 137 pp., 1985. $45

Radiology Today 3. Edited by M. W. Donner and F. H. W. Heuck. Berlin: Springer-Verlag, 203 pp., 1985. $55

Computed Tomography and Magnetic Resonance Imaging of the Head and Neck, 2d ed. By Anthony A. Mancuso and William N. Hanafee. Baltimore: Williams & Wilkins, 503 pp., 1985. $84.75

Radiological Physicists. By Juan A. del Regato. New York: American Institute of Physics, 188 pp., 1985. $25

Practice Enhancement. The Physician's Guide to Success in Private Practice. By Greg N. Korneluk. New York: Macmillan, 284 pp., 1985.

Medical Effects of Ionizing Radiation. By Fred A. Mettler, Jr. and Robert D. Moseley, Jr. Orlando: Grune & Stratton, 288 pp., 1985.

Digital Cardiac Imaging. Edited by Andrew J. Buda and Edward J. Delp. Boston: Nijhoff, 307 pp., 1985. $60

Bone Marrow Disorders. The Biological Basis of Clinical Problems. By M. Y. Gordon and A. J. Barrett. Oxford: Blackwell (U.S. distributor: Mosby/Blackwell), 422 pp., 1985.

Computer Assisted Radiology. *Computergestützte Radiologie.* Proceedings of the International Symposium CAR'85 Computer Assisted Radiology. In English and German. Edited by Herausgegeben von H. U. Lemke, M. L. Rhodes, C. C. Jaffee, and R. Felix. Berlin: Springer-Verlag, 724 pp., 1985. $39

Radiodiagnosis of the Skull. 103 Radiological Exercises for Students and Practitioners. (Series: Exercises in Radiological Diagnosis.) By Jean-Louis Dietemann. Berlin: Springer-Verlag, 168 pp., 1985; soft cover. $19.50

Radiotherapy Treatment Planning, 2d ed. (Series: Medical Physics Handbooks 14.) By Richard F. Mould. Bristol: Hilger (U.S. distributor, International Publishers), 256 pp., 1985. $29

The Selection and Performance of Radiologic Equipment. Edited by William R. Hendee. Baltimore: Williams & Wilkins, 263 pp., 1985.

Sensitivity and Specificity of Common Scintigraphic Procedures. A Review of Clinical Efficacy. By Michael L. Goris. Chicago: Year Book Medical, 127 pp., 1985.

Modern Imaging and Endoscopic Biopsy Techniques in Egyptian Mummies

Derek N. H. Notman[1]
Joseph Tashjian[2]
Arthur C. Aufderheide[3]
Oliver W. Cass[4]
Orrin C. Shane, III[5]
Thomas H. Berquist[6]
Joel E. Gray[6]
Eugene Gedgaudas[1]

Egyptian mummies have been popular subjects of radiographic investigation since 1896. Computed tomography (CT) and magnetic resonance imaging (MRI) have recently been added to the growing list of modern techniques used to study these relics. The Minnesota Mummy Project was organized to examine four well preserved Egyptian mummies dating from the XVIIIth (1575–1308 B.C.) and XXVth (715–663 B.C.) Dynasties. Plain radiographs and CT scans were obtained on all specimens. One individual was selected for additional endoscopic and microscopic correlation with CT findings in the thoracic cavity. The collapsed heart was identified by CT. A percutaneous biopsy of the heart was then performed with a flexible fiberoptic endoscope, passed through a small hole drilled into the chest wall. Microscopy of prepared ventricular specimens revealed striated muscle fibers consistent with myocardium. These results emphasize the utility of CT as a noninvasive paleoradiologic tool. Another mummy was examined by MRI to search for minute quantities of residual moisture possibly trapped within the desiccated tissues. Only a free-induction-decay signal could be obtained, but this was insufficient to generate an image. Thus, it appears that present MRI is not suitable for the paleopathologic investigation of dehydrated structures.

The mummies of ancient Egypt have long been fascinating subjects of scientific research and debate. The first radiograph of mummified Egyptian remains was taken by König in March 1896, only 3 months after Roentgen's historic discovery [1]. Since then, conventional radiography has contributed greatly to the paleopathologic record [2–10]. With the emergence of CT and MRI during the last decade, new imaging techniques have become available for paleoradiologic research. CT has proved to be exceptionally well suited for studying the fragile, wrapped figures of Egyptian mummies, especially those still contained within their decorated plasterlike shells, or cartonnages [11–13]. MRI, on the other hand, was only recently performed on dehydrated specimens, without success.

Egyptian embalmers practiced the elaborate art of mummification for more than three millennia. During the dynasties of the New Kingdom (1600–1085 B.C.) and later periods, it was common for embalmers to remove, cleanse, and dry the internal organs (except the heart) and to return them in individual linen bundles into the abdominal cavity, which was then sealed with a thick coating of molten resin. Such bundles are often encountered on plain radiographs and tend to obscure skeletal details, a problem which was finally solved by CT's cross-sectional imaging. The heart was considered to be the sacred residence of the soul and had to be presented at death to the gods for judgment (the "Weighing of the Heart" ceremony) before the individual would be allowed to enter the afterlife. Therefore, the heart was left in the chest cavity [14–21].

Materials and Methods

The Minnesota Mummy Project was established in 1983 to examine the four Egyptian mummies on display in the Twin Cities. All mummies were radiographed in anteroposterior

Received May 6, 1985; accepted after revision September 9, 1985.

[1] Department of Radiology, University of Minnesota Medical School, Box 382 Mayo Building, 420 Delaware St. S.E., Minneapolis, MN 55455. Address reprint requests to D. N. H. Notman.

[2] Department of Radiology, St. Paul-Ramsey Medical Center, St. Paul, MN 55101

[3] Department of Pathology and Laboratory Sciences, University of Minnesota Medical School, Duluth, MN 55812.

[4] Department of Gastroenterology, Hennepin County Medical Center, Minneapolis MN 55415.

[5] Curator for Archaeology, Science Museum of Minnesota, St. Paul, MN 55101.

[6] Department of Diagnostic Radiology, Mayo Clinic, Rochester, MN 55905.

***AJR* 146:93-96, January 1986**
0361-803X/86/1461-0093
© American Roentgen Ray Society

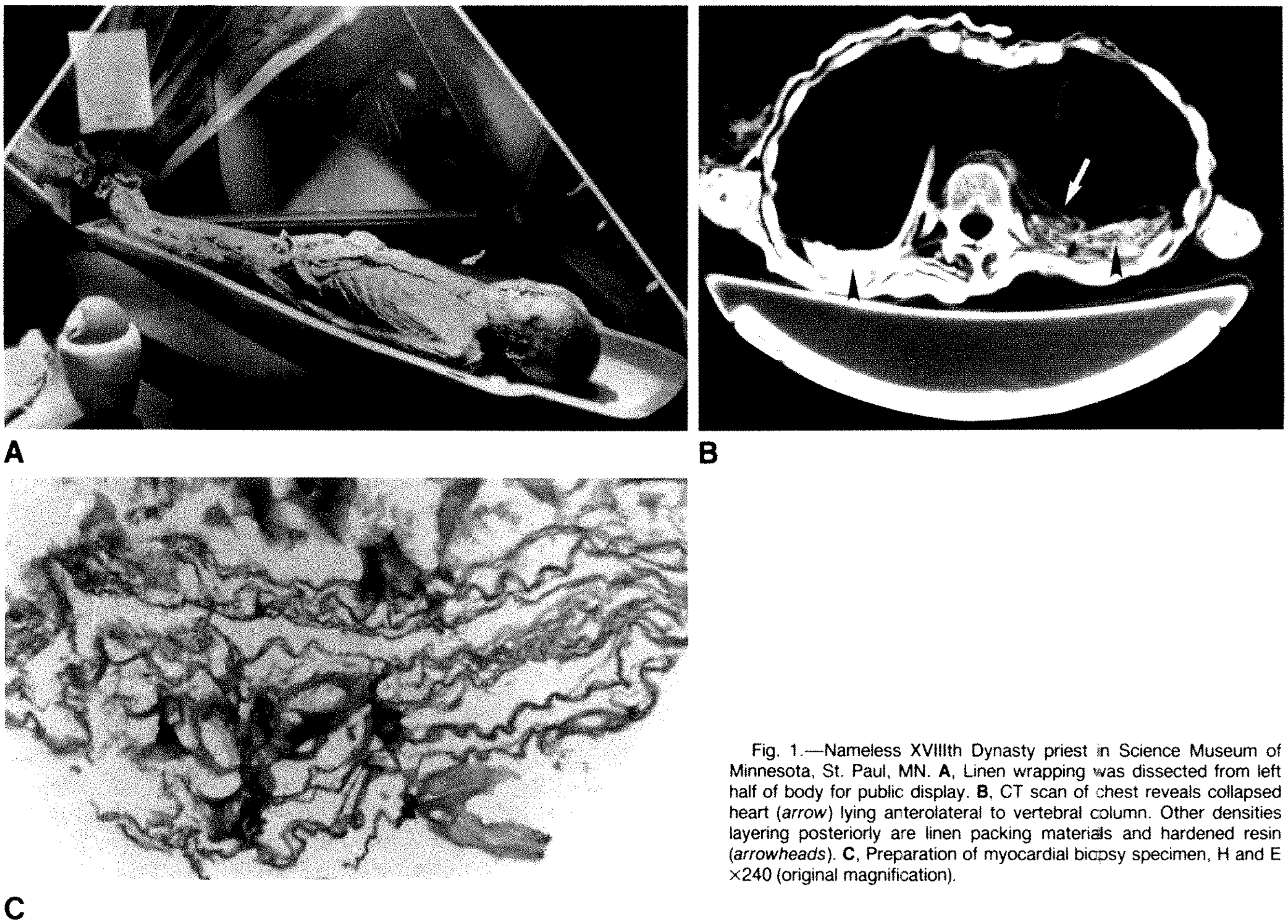

Fig. 1.—Nameless XVIIIth Dynasty priest in Science Museum of Minnesota, St. Paul, MN. **A**, Linen wrapping was dissected from left half of body for public display. **B**, CT scan of chest reveals collapsed heart (*arrow*) lying anterolateral to vertebral column. Other densities layering posteriorly are linen packing materials and hardened resin (*arrowheads*). **C**, Preparation of myocardial biopsy specimen, H and E ×240 (original magnification).

and lateral projections and had total body CT scans. Of these, a nameless XVIIIth Dynasty (1575–1308 B.C.) priest (fig. 1A) at the Science Museum of Minnesota was selected for endoscopic evaluation after CT, in an attempt to correlate CT findings in the chest with direct endoscopic visualization and microscopic analysis of biopsy samples.

An oblong structure resembling a collapsed heart was located in the left chest cavity by CT scanning (fig. 1B). To examine this region by formal autopsy would have caused unacceptable damage to a popular museum display. Endoscopy was considered to be an attractive alternative, because only a small portal was needed to introduce the flexible fiberoptic tubing into the chest. A similar endoscopic procedure was performed on three pharaonic mummies in Cairo in 1975, but in each case the endoscope entered through an existing crack in the body [21].

The well preserved mummy was placed supine on a table, and a Stryker rotary power saw was used to cut out a 3 × 2 cm section of rib in the left midaxillary line (this plug was replaced at the end of the study with barely perceptible alteration to the chest wall). The resulting cloud of dust within the mummy was cleared by blowing into the chest opening, forcing dust out the mummy's nostrils, an intriguing demonstration of tracheal patency.

An Olympus pediatric GIF-XP endoscope (7.8-mm diameter) was then advanced into the left thoracic cavity. Several brownish-black membranes were encountered as the endoscope was directed medially and posteriorly to the pericardial region. Biopsies of these parchmentlike structures showed that they corresponded to mediastinal layers on the CT scans, possibly representing pleura and pericardium. No discernible lung tissue was seen. A deeper posterior chamber was finally entered through a thicker wall, presumed to be that of the left ventricle.

Another mummy, that of Lady Tashat at the Minneapolis Institute of Arts, was examined by MRI to see if residual moisture might still be contained within dehydrated structures. This XXVth Dynasty (715–633 B.C.) mummy was flown by private jet from Minneapolis to Rochester, MN, and was transported to St. Mary's Hospital, where she became the first Egyptian mummy to undergo MRI. Her mummy, contained within a beautifully painted cartonnage (fig. 2), was placed into the Picker International 1100 resistive MR scanner. Because of the size of the cartonnage, the body coil was used for all scans, which consists of two saddle coils, one for radiofrequency transmission, and one for radiofrequency reception. Several scanning sequences were attempted, including spin echo, inversion recovery, and free induction decay (saturation recovery).

Results

XVIIIth Dynasty Priest

Of the 23 specimens obtained for microscopic analysis, only one did not dissolve completely in Ruffer's solution, an alcoholic reconstituting agent (95% ethanol, 1% aqueous

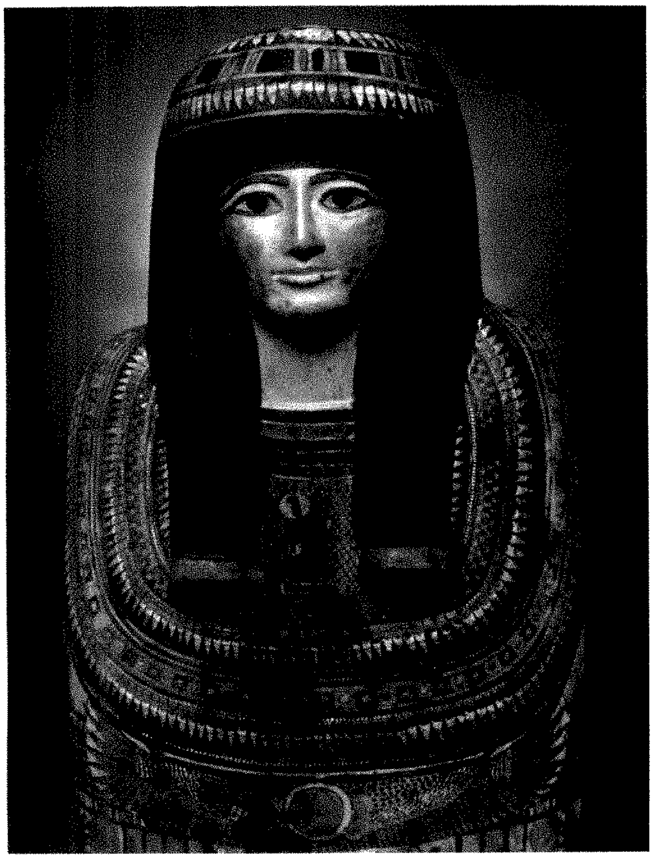

Fig. 2.—Lady Tashat, XXVth Dynasty (715–633 B.C.), Minneapolis Institute of Arts.

formalin, 4% sodium carbonate). Most of the structures sampled contain soluble organic material, probably resins. The single insoluble specimen was sectioned and then stained with hematoxylin and eosin. Microscopic examination revealed syncytial fibers in a pattern quite characteristic of myocardium, although no cross-striations were demonstrated (fig. 1C).

Intrathoracic endoscopic biopsy confirmed the presence of myocardial tissue as localized by CT. Membranelike structures resembling pleura or pericardium on the CT scans did not contain any tissue. These may represent resinous casts of the original membranes, formed during the application of molten resins within the body cavity. The lungs were not identified and were probably removed through an incision in the diaphragm during the preliminary stages of mummification.

Lady Tashat

No MR images could be produced, even with receiver attenuators set at minimum values and amplifiers operating at maximum levels. It was possible, however, to detect a free-induction-decay signal when the mummy was scanned without using a slice select gradient, that is, the entire volume of the mummy in the coil was used to produce the signal. This signal was still too weak for processing into an image, because the MRI system is designed for clinical applications, in which large volumes of protons generate high signal strength. The signal could have resulted from condensed moisture on the smooth external surface of the cartonnage or on the inner linen bandages, exposed to ambient humidity through cracks in the shell.

Discussion

CT has become an invaluable paleoradiologic instrument in the study of Egyptian mummies. Most organs were removed during embalming, but the heart was carefully avoided and is often recognizable on CT scans. This study demonstrates a multidisciplinary approach to the identification of the collapsed heart, with minimal disturbance of the mummy's desiccated exterior. Endoscopy and microscopy provide useful correlation for the CT scans and facilitate their interpretation.

Present MRI, however, does not seem to be applicable to the investigation of desiccated human remains. It is possible that weak free-induction-decay signals will prove useful in assessing the integrity of cartonnage surfaces for purposes of dating or restoration.

REFERENCES

1. König W. 14 Photographien mit Röntgen-Strahlen, aufgenommen im *Physikalischen Verein, Frankfurt A.M.* Leipzig: JA Barth, **1896**
2. Petrie WMF. *Deshasheh, 1897. Egypt Exploration Fund Mem.* London: Egypt Exploration Fund, **1897**:15
3. Smith GE. *The royal mummies.* In: *Catalogue general des antiquités egyptiennes du Musée du Caire.* Cairo: **1912**:61051–61100
4. Ruffer MA. *Studies in the paleopathology of Egypt.* Chicago: University of Chicago Press, **1921**
5. Moodie RL. Roentgenologic studies of Egyptian and Peruvian mummies. In: *Field Museum of Natural History Anthropological Memoires.* Chicago: Field Museum, **1931**
6. Gray PHK. Radiography of ancient Egyptian mummies. *Med Radiogr Photogr* **1967**;4:34–44
7. Dawson WR, Gray PHK. *Catalogue of Egyptian antiquities in the British Museum.* London: Trustees of the British Museum, **1968**
8. Harris JE, Weeks KR. *X-raying the pharaohs.* New York: Scribner's, **1973**
9. Harris JE, Wente EF. *An x-ray atlas of the royal mummies.* Chicago: University of Chicago Press, **1980**
10. Cockburn A, Cockburn E. *Mummies, disease, and ancient cultures.* Cambridge: Cambridge University Press, **1983**
11. Harwood-Nash D. Computed tomography of Egyptian mummies. *J Comput Assist Tomogr* **1979**;3:768–773
12. David AR. *The Manchester Museum mummy project.* Manchester: Manchester University Press, **1979**
13. Castor WR, Baker CG. CT of an Egyptian mummy. *General Electric CT Clinical Symposium* **1982**;5:10
13. Herodotus, translated by de Selincourt A. *Histories.* New York: Penguin, **1954**
15. Diodurus Siculus. In: Smith GE, Dawson WR. *Egyptian mummies.* New York: Dial Press, **1923**:62–63
16. Pettigrew TJ. *History of Egyptian mummies.* London: Longman, **1834**

Cranial Computed Tomography in the Abused Child with Head Injury

Ronald A. Cohen[1, 2]
Robert A. Kaufman[1, 3]
Patricia A. Myers[3]
Richard B. Towbin[1, 3]

Cranial computed tomographic (CT) findings are described in 37 children with head injuries resulting from physical abuse. CT findings included subarachnoid hemorrhage (27 patients), cerebral edema (24), cerebral hemorrhage (11), and subdural hematoma (nine). Intravenous contrast material was administered in 10 children in whom there were neurologic symptoms or signs but no history or physical signs of trauma or abuse. In five of these children, increased vascularity was seen in areas that later showed infarction. Eight children were studied by both CT and sonography. Sonography detected 50% fewer abnormalities than did CT. It was found that children with skull fracture had the same range of injuries as children without fracture, and they had a higher incidence of subarachnoid hemorrhage. In acutely traumatized children, cranial CT should be the method of choice to provide the most accurate diagnosis and documentation of injury. Skull radiographs should also be obtained because they sometimes show fractures not recognized by CT.

Since the early descriptions by Caffey [1] and Silverman [2], the medical community has become increasingly aware of the manifestations of child abuse. Before the availability of computed tomography (CT), the diagnosis and documentation of intracranial injury depended on arteriography, surgery, and autopsy studies. In the past decade CT has become the primary diagnostic method for the evaluation of serious craniocerebral trauma. Previous reports of cranial CT of abused children have demonstrated a wide spectrum of abnormalities, but the examinations were performed primarily on early-generation scanners [3–5]. We have studied 37 abused children by cranial CT. In this selected group of patients we found a 95% incidence of intracranial abnormalities on scans obtained shortly after injury.

Materials and Methods

In the 6 year period from March 1978 through February 1984 there were 1439 reported cases of physical abuse in infants and children seen at CHMC. Ninety (6%) of these had serious clinical head injury. Cranial CT was performed in 40 of these 90 children. One CT scan was nondiagnostic because of motion artifact and two patients had only follow-up scans. The other 37 patients who were scanned at the time of presentation are the subject of this study. The scans were obtained for clinical indications and not for the purpose of retrospective review.

Nine patients were examined on an EMI 5005 and 28 scans were obtained on a GE 8800. CT scans, plain radiographs, other imaging studies, and hospital records were reviewed.

Results

The age range in the 37 children was 1 month to 8 years. Most patients (95%) were less than 1 year of age. Only two patients were older than 2 years. The mean age was 9 months. Twenty-two (59%) were boys and 15 (41%) were girls. Thirty-

This article appears in the November/December 1985 issue of *AJNR* and the January 1986 issue of *AJR*.

Received October 18, 1984; accepted after revision April 1, 1985.

Presented at the annual meeting of the Society for Pediatric Radiology, Las Vegas, April 1984.

[1] Department of Radiology, University of Cincinnati College of Medicine, Children's Hospital Medical Center, Cincinnati, OH 45229. Address reprint requests to R. B. Towbin.

[2] Present address: Department of Radiology, Children's Hospital Medical Center of Northern California, Oakland, CA 94609.

[3] Department of Pediatrics, University of Cincinnati College of Medicine, Children's Hospital Medical Center, Cincinnati, OH 45229.

***AJR* 146:97–102, January 1986**
0361-803X/86/1461-0097
© American Roentgen Ray Society

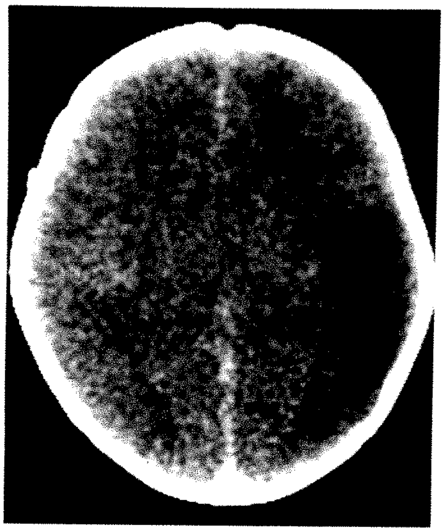

Fig. 1.—1-month-old boy. Unenhanced CT scan. Left parietooccipital low attenuation from brain edema and increased attenuation along anterior and posterior falx cerebri from SAH.

five patients demonstrated intracranial abnormalities. Only two were normal. All patients under 2 years had abnormal scans.

Subarachnoid Hemorrhage (SAH)

SAH occurred in 27 patients (73%). Eight of these patients had lumbar punctures and all had bloody cerebrospinal fluid consistent with SAH (fig. 1).

Cerebral Edema

Cerebral edema occurred in 24 patients (65%). Eighteen patients had focal areas of edema or unilateral hemispheric edema (fig. 1). Six patients had a generalized pattern of edema. In three of these patients the gray matter had lower attenuation than the white matter, a pattern we term the "reversal sign." In these patients the thalamus, brainstem, and cerebellum were relatively spared, maintaining nearly normal density [figs. 2A and 2B).

Cerebral Hemorrhage

Eleven patients (30%) had cerebral hemorrhage, including three with brain lacerations. Five patients had frontal hemorrhage, three parietal, one temporal, one occipital, and one had multifocal areas of hemorrhage. All three patients with brain lacerations had fractures of the overlying calvaria. In two of the three patients, hemorrhage extended into the ventricles; these were the only two patients with intraventricular hemorrhage (fig. 3).

Subdural Hematoma

Nine patients (24%) had subdural hematomas. Five were acute, three were low-attenuation chronic collections, and one was both acute and chronic.

Hypervascularity

Ten patients received intravenous contrast medium on initial scans. Although not routine, contrast-enhanced scans were sometimes obtained when there were neurologic symptoms or signs but no history or physical signs of trauma or abuse. Five of these patients had increased vascularity in areas that later showed infarction (fig. 4).

Follow-up Examinations

Twenty-four patients had follow-up CT examinations 2 weeks to several years after head injury. Six patients developed mild to moderate generalized atrophy. Seventeen patients developed focal unilateral or asymmetric areas of cerebral atrophy (fig. 5). Only one patient, a 17-month-old with an acute anterior interhemisphere subdural hematoma, had a normal follow-up scan. Three patients developed chronic subdural collections. None of our patients developed obstructive hydrocephalus.

Cranial Sonography

Eight patients had cranial sonographic examinations within 5 days of the initial CT scan. Sonography detected 50% fewer (10/20) abnormalities than did CT (table 1). Follow-up sonography was useful in five cases in assessing ventricular dilatation and atrophy.

Skull Fractures

Eleven patients (30%) had skull fractures, none of which were depressed. Except for epidural hematoma and brain laceration, patients without fracture suffered the same gamut of injury as those with fracture, and they actually had a higher incidence of SAH (85% vs. 45%) (table 2).

Associated Skeletal Injuries

Radiographic skeletal surveys showed a variety of fractures in addition to the 11 skull fractures. Fractures of the ribs occurred in six patients, clavicle in four, femur in three, tibia in two, radius and ulna in two, humerus in two, and classical multiple metaphyseal corner fractures in only two.

Outcome

Four patients died. Autopsy examinations were performed by the coroner in all four. Eleven patients had severe impairments, some living in vegetative states in institutions. Nine had minor impairments including mild weakness, visual problems, and seizure disorders. To date, seven patients have no detectable abnormality. Insufficient data are available in six patients.

Discussion

Child abuse is an important cause of morbidity and mortality. About 1.3 million cases of child abuse are reported each

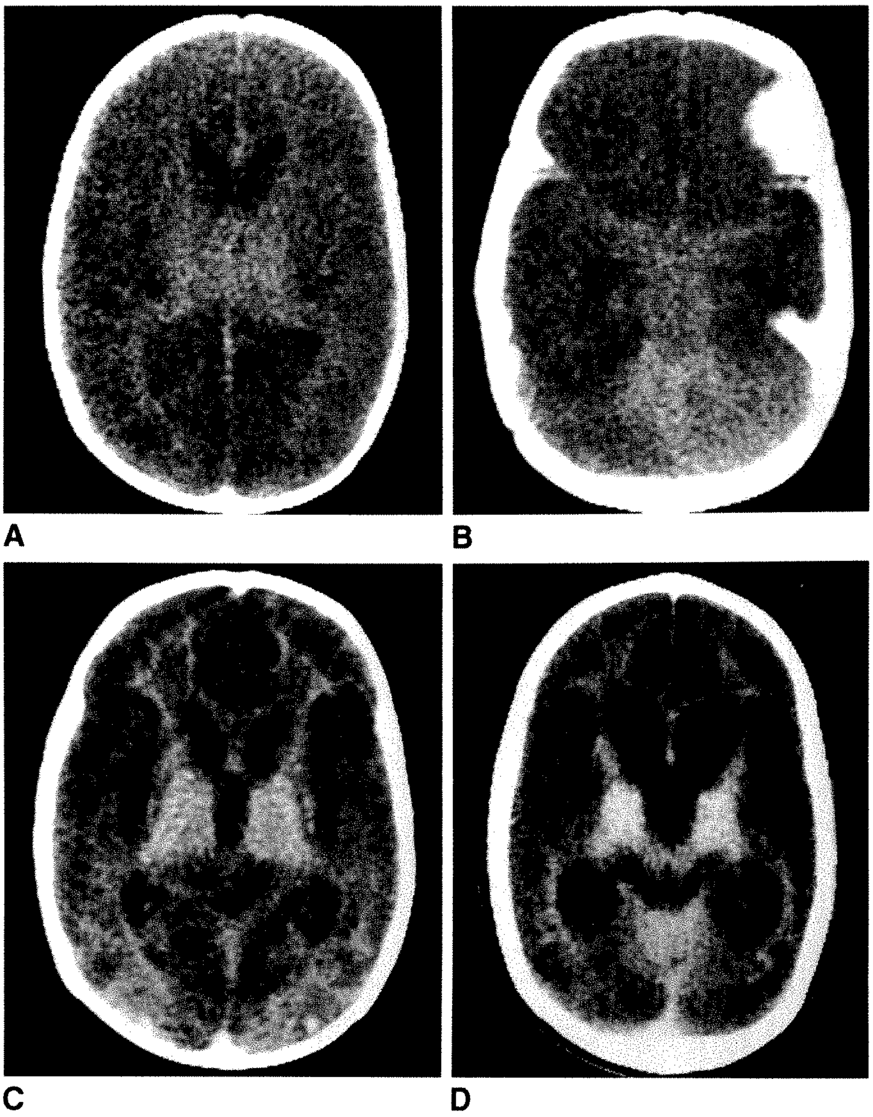

Fig. 2.—4-month-old boy. Reversal sign. Generalized low attenuation but relative sparing of thalami (**A**) and brainstem and cerebellum (**B**). Follow-up examinations at 2 weeks (**C**) and 1 year (**D**) after injury. Progressive ventricular dilatation from severe generalized cortical injury. Brain damage from abuse is irreversible.

year in the United States [6]. Of these, 45% (585,000) are cases of physical abuse. Most victims of child abuse with head injury are under 2 years of age. It is also a well known cause of mental retardation and neurologic impairment.

All of our patients under 2 years of age had abnormal cranial CT scans. The incidence of intracranial abnormalities by CT ranges from 7% of a large unselected group to 96% of a selected group of abused children [3, 7]. In our patients we found a very high incidence of intracranial abnormalities on both initial scans (95%) and follow-up scans (96%). The disparity in previous reports reflects differences in patient selection and referral patterns. Our patient group was also highly selected in that it consisted primarily of young infants who presented with neurologic signs or symptoms. Also, we included only officially reported cases of abuse and excluded suspected cases. The high incidence of intracranial abnormalities in child abuse is also attributed to the increased susceptibility of the infant brain to injury resulting from head trauma [8]. In addition, the higher resolution of current-generation scanners allows for improved detection of intracranial

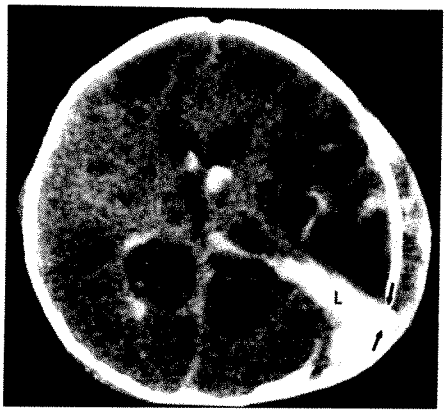

Fig. 3.—2-month-old boy 2 days after injury. Left parietal brain laceration (L) with both SAH and intraventricular hemorrhage, as well as herniation of brain through diastatic fracture (*arrows*). Diffuse brain edema.

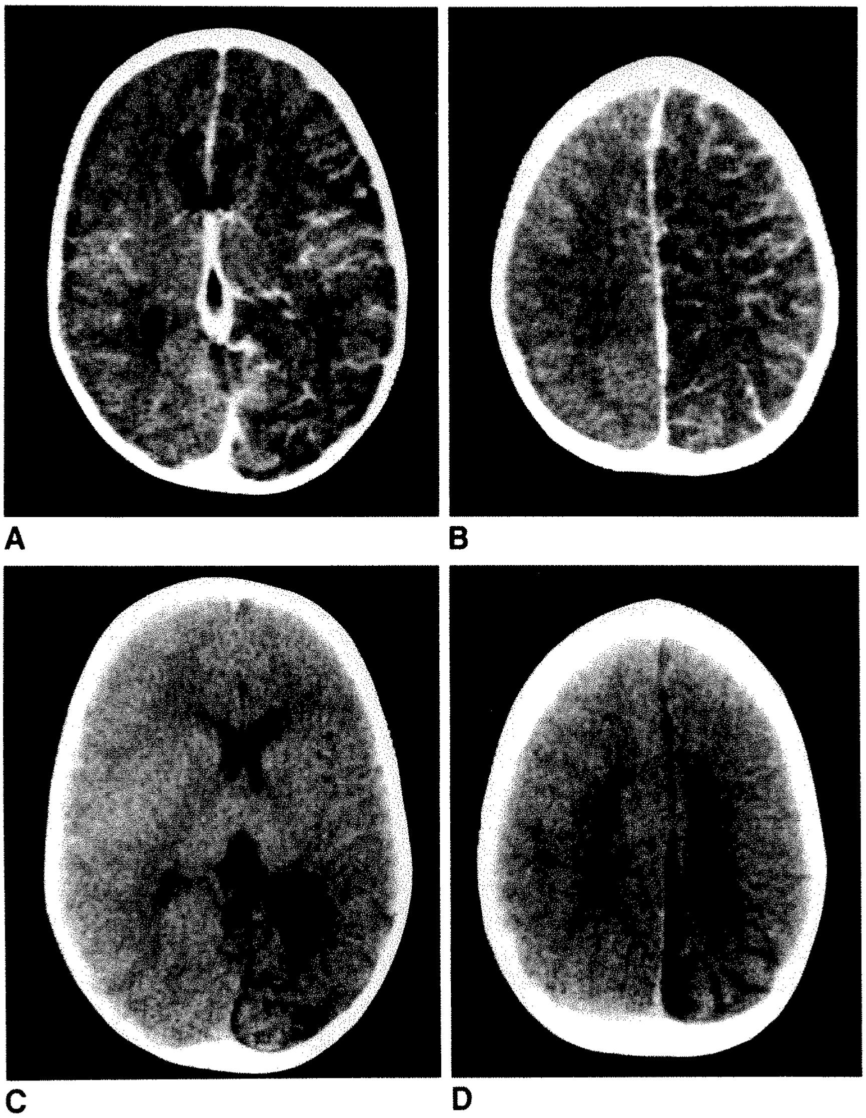

Fig. 4.—10-month-old boy 5 days after injury. **A** and **B**, Contrast-enhanced scans at two levels. Increased vascularity in **A** and swollen left cerebral hemisphere with slight midline shift. **C** and **D**, Follow-up scans 5 months later. Left cerebral hemiatrophy corresponding to area of edema and increased vascularity shortly after injury. Midline shift is now in opposite direction, toward atrophic side.

abnormalities.

The pathophysiology of brain injury in infants differs from that in adults. The softer calvaria, open sutures, and the degree of myelinization are some of the factors that influence the type of injuries that occur with craniocerebral trauma. The mechanism of injury in child abuse varies. Children with fractures or obvious scalp bruises have received impact injuries. Nonimpact injuries resulting from severe "shaking" or "whiplash" also occur, especially when there are no external signs of injury [9, 10]. Both impact and nonimpact trauma may cause intracranial injury.

After SAH (73%), cerebral edema (65%) was the most common abnormality found in our patients. The extent and severity of the cerebral edema depends on the interval from the traumatic event. If scanned early, the findings may be minimal or even absent. Scans obtained days later often show edema and increased mass effect (fig. 6). Patients with a generalized pattern of edema may have suffered diffuse brain damage secondary to hypoxia and/or hypotension. The vascular control mechanisms and blood-brain barrier may be altered by acute brain trauma, which then contributes to the development of edema, either focal or generalized [8, 11].

Three of our patients had what we termed the "reversal sign" where the gray matter had lower attenuation than the white matter. In these patients the thalamus, brainstem, and cerebellum were relatively spared. These findings have also been seen in infants with asphyxia or head trauma not resulting from abuse [12–14]. In our experience all patients with the reversal sign have demonstrated severe brain damage on follow-up scans (figs. 2C and 2D). We have not encountered an instance in which a patient manifesting the reversal sign did not have irreversible brain damage.

Among the 11 patients with cerebral hemorrhage were three who suffered lacerations of the brain. All three had associated fractures of the overlying calvaria. Such linear hemorrhages may represent severe forms of what pathologists term contusional tears, which are seen in young infants with impact injuries with or without skull fracture [15]. Often these tears are microscopic and are located in the white matter near the gray-white junction. However, occasionally

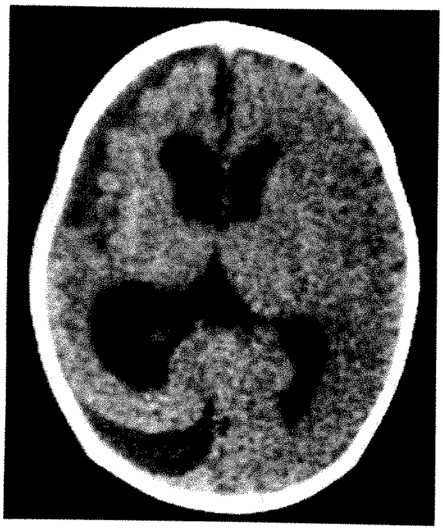

Fig. 5.—2-month-old girl 1 month after injury. Follow-up scan. Brain atrophy and lateral ventricle dilatation, predominantly on right. Enlarged right-sided extraaxial spaces.

they extend through the cortex and ventricular wall, as in two of our cases. One of these patients had a dural tear with associated herniation of brain parenchyma (fig. 3).

Interhemispheric hyperdensity in children may have several causes including normal falx, SAH, interhemispheric subdural hematomas, and diffuse cerebral edema. Zimmerman et al. [3] found a 58% incidence of posterior acute interhemispheric subdural hematomas (AIHSH) in 26 abused children studied by CT. The diagnosis was based on finding a thick, asymmetric area of increased attenuation about the posterior falx cerebri. In another article, Zimmerman et al. [16] noted that AIHSHs are often subtle and more difficult to diagnose in children. Useful criteria for diagnosing AIHSH are a flat medial border and a convex lateral border and/or extension over one tentorial surface. Some asymmetry of the posterior falx cerebri may be normal and, by itself, does not necessarily represent AIHSH.

The falx cerebri appears prominent when there is diffuse cerebral edema. Therefore, in the presence of severe edema, interhemispheric hyperdensity alone is not a reliable sign of SAH. Also, familiarity with normal variations in the appearance of the falx cerebri and the interhemispheric fissure in children is useful in the diagnosis of SAH.

We found it difficult to differentiate AIHSH from SAH and/or intrafalcine hemorrhage We had one patient with a definite AIHSH. Three others had asymmetric blood collections along the posterior falx, and one of these patients died 2 days after injury (fig. 7). An autopsy revealed both subarachnoid and subdural blood but no localized interhemispheric subdural hematoma. In all four patients who died, autopsies demonstrated thin layers of subarachnoid blood and cerebral necrosis. All four had subdural blood as well, but only one had a subdural clot (5 mm thick) located over the convexity.

There is no doubt that AIHSH occurs in child abuse, but we did not find it as often as previously stated. We believe it is likely that increased subdural interhemispheric density may represent a combination of SAH and subdural hemorrhage and is often accentuated by adjacent brain edema.

TABLE 1: **Comparison of CT and Sonographic Findings in Eight Abused Children with Head Injury**

Abnormality	No. Detected	
	CT	Sonography
Ventricular dilatation (mild)	3	3
Intraventricular hemorrhage	1	1
Cerebral hemorrhage	3	1
Subarachnoid hemorrhage	7	4*
Subdural hematoma	1	0
Cerebral edema	5	1
Total	20	10

* Widened interhemispheric fissure.

TABLE 2: **Comparison of Cerebral CT Findings in Abused Children with and without Fracture**

Finding	No. (%)	
	With Fracture ($n = 11$)	Without Fracture ($n = 26$)
Epidural hematoma	1 (9)	0
Acute subdural hematoma	1 (9)	5 (19)
Chronic subdural hematoma	2 (18)	1 (4)
Subarachnoid hemorrhage	5 (45)	22 (85)
Cerebral edema	8 (73)	16 (62)
Cerebral hemorrhage	5 (45)	7 (27)
Brain laceration	3 (27)	0

All but one of 24 patients who had follow-up scans showed persistent abnormalities by CT. In general, the degree of brain damage demonstrated on CT correlates with the severity of neurologic impairment. Most patients had definite signs of parenchymal brain damage. Six had mild to moderate generalized atrophy without evidence of focal brain damage.

It must also be remembered that acute brain injury may be superimposed on abnormalities that have occurred from previous episodes of abuse that were unrecognized. This was evident in one of our patients with concurrent chronic and acute subdural hematomas.

Sonography detected only one-half of the abnormalities seen on CT and was less specific in diagnosis. Sonography is limited by the size of the fontanelle and, therefore, in many cases is impractical or ineffectual in the second year of life. Also peripheral lesions are more difficult to detect by sonography. Therefore, we believe that CT should be the method of choice in acutely traumatized children to provide the most accurate diagnosis and documentation of cranial injury. As long as the anterior fontanelle remains open, sonography may be used for follow-up examinations to assess ventricular dilatation and brain atrophy.

As noted in several previous studies, serious brain injury often occurs in the absence of a skull fracture, particularly in the "whiplash-shaken infant syndrome" [9]. Obviously, serious brain injury also occurs in the presence of skull fractures. Skull radiographs should be included in the skeletal survey for child abuse, because they sometimes show fractures not recognized on CT scans and because skull fracture may be the only clue to the diagnosis of abuse [17].

In many cases of child abuse there is no doubt that injury has been inflicted. In some cases the diagnosis is not clear

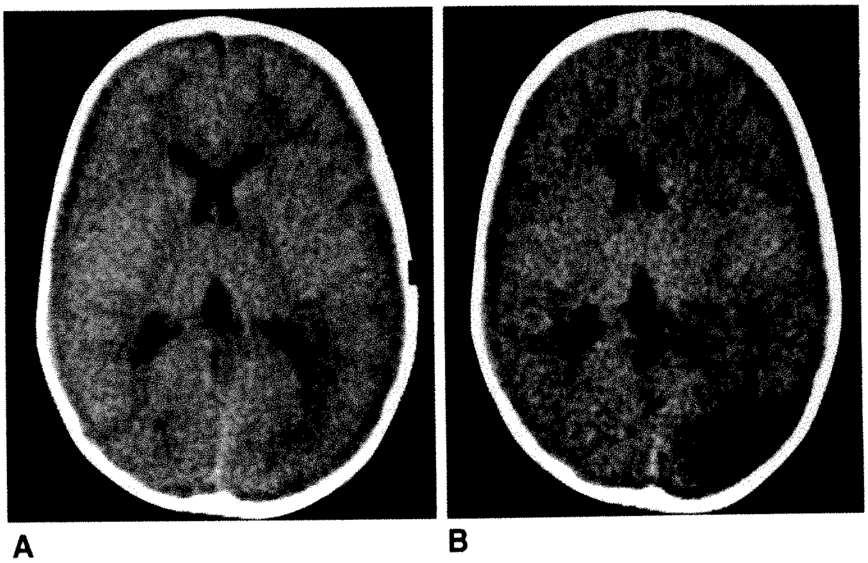

Fig. 6.—10-month-old boy. **A**, Shortly after injury. Low attenuation effacing left occipital horn. **B**, 5 days later. Pronounced left hemispheric edema with occipital predominance.

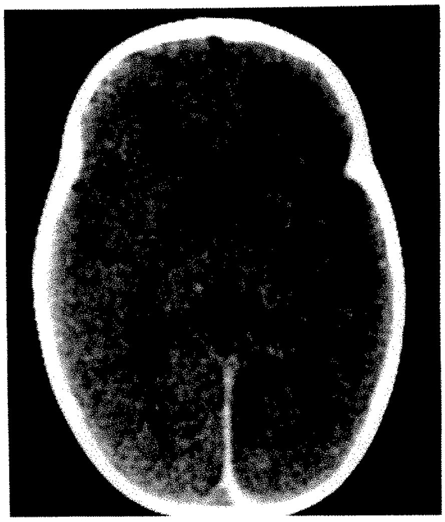

Fig. 7.—4-month-old boy shortly after injury. Increased attenuation along posterior falx cerebri proven at autopsy 2 days later to represent subarachnoid and subdural blood surrounding brain, but no localized interhemispheric subdural clot. Generalized low attenuation of brain substance is worse on left.

and the radiologist may be the first physician to suggest the diagnosis. Although a wide spectrum of injury occurs, the most common abnormalities we encountered were SAH and cerebral edema. Though not specific this constellation of findings in a young infant should suggest the possibility of child abuse even if there are no other signs of trauma.

ACKNOWLEDGMENTS

We thank Richard Isham for photography and Sherrie Henslee for manuscript preparation.

REFERENCES

1. Caffey J. Multiple fractures in the long bones of infants suffering from chronic subdural hematoma. *AJR* **1946**;56:163–173
2. Silverman FN. The roentgen manifestations of unrecognized skeletal trauma in infants. *AJR* **1953**;69:413–427
3. Zimmerman RA, Bilaniuk LT, Bruce D, Schut L, Uzzell B, Goldberg HI. Computed tomography of craniocerebral injury in the abused child. *Neuroradiology* **1979**;130:687–690
4. Ellison PH, Tsai FY, Largent JA. Computed tomography in child abuse and cerebral contusion. *Pediatrics* **1978**;62:151–154
5. Tsai FY, Zee CE, Apthrop JS, Dixon GH. Computed tomography in child abuse head trauma. *CT* **1980**;4:277–286
6. The American Humane Association, Child Protection Division. *National analysis of official child neglect and abuse reporting 1982*. Denver: American Humane Association, **1982**
7. Merten DF, Osborne DRS. Craniocerebral trauma in the child abuse syndrome. *Pediatr Ann* **1983**;12:882–887
8. McLaurin RL, Towbin R. Head injuries in newborns and infants. In: Raimondi AJ, Choux M, DiRicco C, eds. *Principles of pediatric neurosurgery*, vol. I. Baltimore: Williams & Wilkins (in press)
9. Caffey J. The whiplash shaken infant syndrome: manual shaking by the extremities with whiplash-induced intracranial and intraocular bleedings, linked with residual permanent brain damage and mental retardation. *Pediatrics* **1974**;54:396–403
10. Ludwig S, Warman M. Shaken baby syndrome: a review of 20 cases. *Ann Emerg Med* **1984**;12:104–107
11. Bruce DA, Alavi A, Bilaniuk L, Dolinskas C, Obrist W, Uzzell B. Diffuse cerebral swelling following head injuries in children: the syndrome of "malignant brain edema." *J Neurosurg* **1981**;54:170–178
12. Kjos BO, Brant-Zawadzki M, Young RG. Early CT findings of global central nervous system hypoperfusion. *AJNR* **1983**;4:1043–1048, *AJR* **1983**;141:1227–1232
13. Babcock DS, Ball W Jr. Postasphyxial encephalopathy in full-term infants: ultrasound diagnosis. *Radiology* **1983**;148:417–423
14. Fiebach BJO, Dabir K, Hermie P, Grimrath U, Schremmer CN. Cerebral CT in fatal courses of resuscitated sudden infant death. *AJNR* **1983**;4:689–691
15. Lindenburg R, Freytag E. Morphology of brain lesions from blunt trauma in early infancy. *Arch Pathol Lab Med* **1969**;87:298–305
16. Zimmerman RD, Russell EJ, Yurberg E, Leeds NE. Falx and interhemispheric fissure on axial CT: II. Recognition and differentiation of interhemispheric subarachnoid and subdural hemorrhage. *AJNR* **1982**;3:635–642
17. Saulsbury FT, Alford BA. Intracranial bleeding from child abuse: the value of skull radiographs. *Pediatr Radiol* **1982**;12:175–178

Value of Intravenous Contrast Enhancement in the CT Evaluation of Intraspinal Tumors

J. S. Lapointe[1]
D. A. Graeb
R. A. Nugent
W. D. Robertson

The usefulness of intravenous contrast-enhanced CT in delineating intraspinal cord tumors has not been well documented. To determine if intradural spinal tumors enhance, if the location and type of tumor can be determined, and if a double dose of contrast material provides more information than a single dose, a retrospective study of 23 patients with proven intradural extramedullary or intramedullary tumors was performed. All the tumors studied with CT after intravenous contrast enhancement showed that most lesions (18/23) enhanced, contrary to published reports. Contrast-enhanced studies delineated the extent of the tumor, helping to separate solid and cystic components. The enhancement pattern of ependymomas and astrocytomas was similar, while schwannomas had a characteristic appearance. A double dose of intravenous contrast material had no apparent advantage over a single dose.

Intravenous iodinated contrast material has been used to enhance intracranial lesions since the early days of CT scanning. Isolated reports of contrast enhancement of intraspinal lesions were published when body scanning first became available [1, 2]. Subsequently, little attention has been paid to delineation of intramedullary spinal cord lesions with intravenous contrast material, because it is believed that little or no enhancement occurs in these lesions, although enhancement of intradural extramedullary lesions has been documented [3, 4]. The aims of our retrospective study were threefold: (1) to determine how often intradural spinal tumors enhance; (2) to determine if an intravenously enhanced CT scan adds useful information concerning the location of the tumor and the type of tumor; and (3) to determine if a double dose of intravenous contrast material provides more information than a single dose.

Materials and Methods

The myelograms, metrizamide-enhanced CT scans, and the intravenously enhanced CT scans of 23 patients with proven spinal intradural mass lesions, either intramedullary or extramedullary, were reviewed retrospectively. Nineteen myelograms and 18 metrizamide CT scans were available. In all patients, CT was performed after intravenous administration of contrast material, and in two patients this was the only examination.

Eleven of the 23 patients had noncontrast studies. Eight patients received a single dose of contrast material (42 g I as 300 ml of iothalamate meglumine 30%) by drip infusion, while 15 patients received a double dose (84 g I as 300 ml of iothalamate meglumine 60%). Contrast material was dripped as rapidly as possible, usually over a 15 min period, and scanning was initiated toward the end of the infusion or immediately after it was completed.

All CT scans were obtained with a General Electric 8800 or 9800 scanner. Slice thickness was 5 mm, and, while slices were contiguous in most cases, slices were spaced every 10–30 mm in patients with intramedullary lesions, extending from the cervical to the lumbar region.

The location and length of the intraspinal mass was determined on the myelogram or metrizamide CT scan. The height of one vertebral body was taken to correspond to one involved segment of spinal cord. The number of segments involved on the myelogram or

This article appears in the November/December 1985 issue of *AJNR* and the January 1985 issue of *AJR*.

Received December 28, 1984; accepted after revision April 9, 1985.

[1] All authors: Department of Radiology, University of British Columbia, and Vancouver General Hospital, 855 W. 12th Ave., Vancouver, British Columbia, Canada V5Z 1M9. Address reprint requests to J. S. Lapointe.

AJR 146:103–107, January 1986
0361-803X/86/1461-0103
© American Roentgen Ray Society

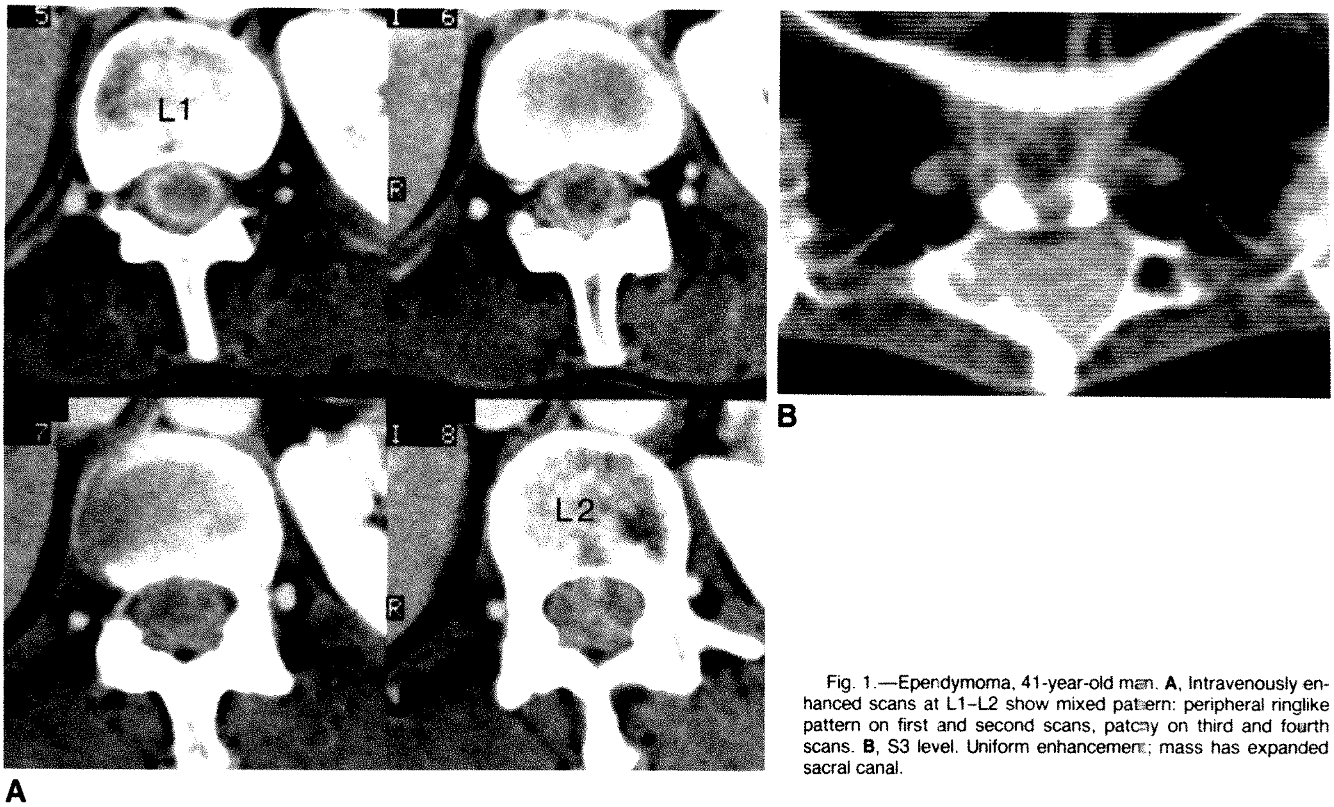

Fig. 1.—Ependymoma, 41-year-old man. **A**, Intravenously enhanced scans at L1–L2 show mixed pattern: peripheral ringlike pattern on first and second scans, patchy on third and fourth scans. **B**, S3 level. Uniform enhancement; mass has expanded sacral canal.

metrizamide-enhanced CT scan was compared with the number of enhancing segments seen on the intravenously enhanced scan.

The patterns of enhancement of the intramedullary and extramedullary lesions were evaluated separately to see if certain features could help in predicting histology. A search for areas of decreased attenuation, definite cerebrospinal fluid (CSF) density, and solid enhancing nodules was made. Cysts were diagnosed radiologically if the lesion was of CSF density or if it filled with metrizamide. Areas of low attenuation were considered cystic when a fluid-filled cavity was encountered at surgery or autopsy. Isodense lesions were similar to spinal cord density on unenhanced or intravenously enhanced scans.

Enhancement of the lesions was classified as mild, moderate, or marked, as Hounsfield measurements were not available in all cases. Correlation with the amount of contrast material administered was then made.

The histology of the lesions was confirmed at surgery or autopsy in all cases, except for a cervicomedullary junction intramedullary mass that was explored but not biopsied.

Results

Lesions were found in 16 males and seven females between the ages of 10 months and 68 years. Fifteen patients (13 males and two females) were young adults between the ages of 16 and 36. Fourteen intramedullary lesions and nine intradural extramedullary lesions were diagnosed. Lesions affecting all parts of the spinal cord were demonstrated, but they predominated in the cervical region (eight cervical, three cervicomedullary, four thoracic, four thoracolumbar, three lumbosacral, one cervical to lumbar). The results in the intra- and extramedullary lesions are tabulated separately.

Intramedullary Lesions

Eleven gliomas, one metastasis, one ependymal cyst of the conus, and one intramedullary lipoma were found. Eight of 11 gliomas and the intramedullary metastasis enhanced moderately to markedly (fig. 1). Two gliomas enhanced mildly and one did not enhance (fig. 2). The intramedullary lipoma was of fat density and the ependymal cyst of the conus was of CSF density; neither enhanced. Unenhanced scans were available in seven of 14 intramedullary tumors, with a variety of densities found within tumors of similar histologies. Only one of four ependymomas was hypodense before enhancement. All ependymomas and astrocytomas were of low grade, histologically.

Intravenously enhanced CT scans helped to localize the solid component of the intramedullary mass in 11 of 14 cases. Of the 11 enhancing lesions, five tumors were of the same length on the myelogram and on the intravenously enhanced CT scan, and five lesions were shorter on CT than on the myelogram. Four of these five lesions had a cyst or area of low density adjacent to the enhancing part of the tumor. In one case, the intravenously enhanced CT scan demonstrated extension of the mass (an ependymoma) into the sacral canal to the level of S3 (fig. 1). This had not been seen on the

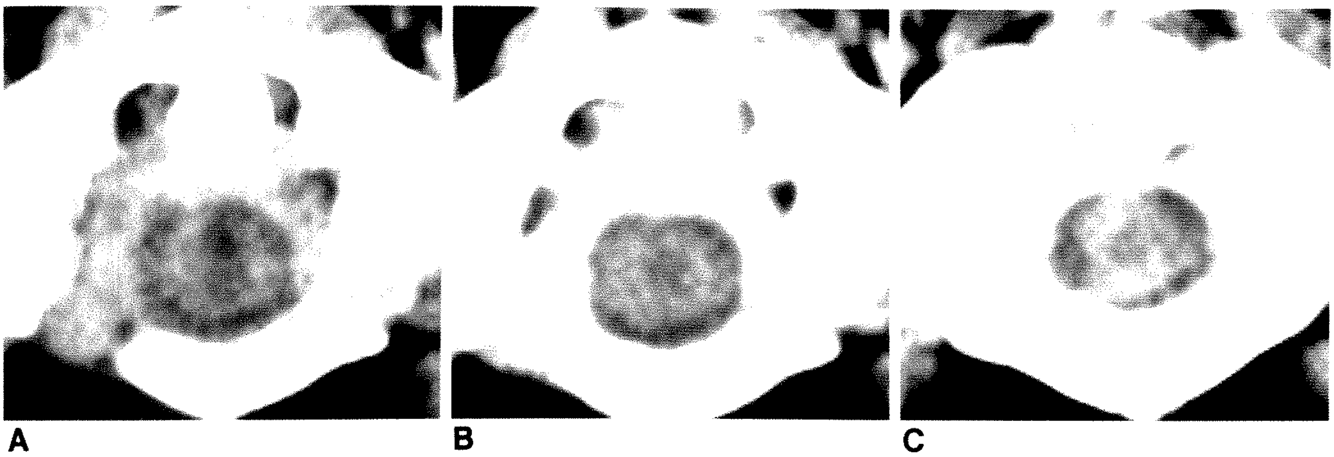

Fig. 2.—Astrocytoma, 47-year-old man. **A**, Unenhanced scan at C1–C2 level. Slightly hyperdense cord with central cyst (narrow window and level settings). Contrast-enhanced scans at C1 (**B**) and C2 (**C**) show cyst to better advantage and mild enhancement of tumor (same settings).

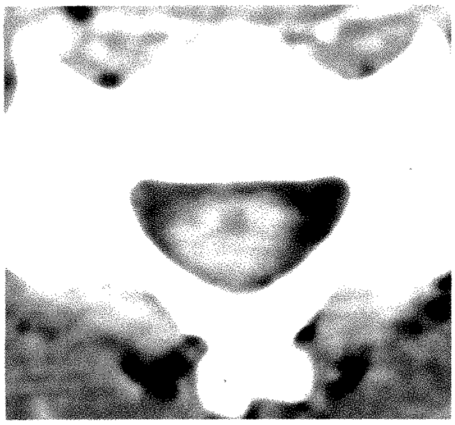

Fig. 3.—Astrocytoma, 26-year-old man. Dense enhancement of cord at C5 level with small midline lucency, which probably represents part of cyst, above and below solid nodule. Cyst contained clear oily fluid, and parts of cyst above and below solid nodule were not demonstrated on delayed metrizamide or intravenously enhanced scans.

myelogram because the dural sac ended at the L5–S1 disk space.

The average length of enhancing cord was three vertebral segments, with two patients having enhancing lesions over eight and 11 segments, respectively. Two other patients had a widened cord from C2 to T11 and T2 to L3, respectively. Both had extensive cysts associated with a short enhancing portion. The first patient's solid nodule was at the C4–C6 level with the cyst proximal and distal to it. The cyst, which contained clear oily fluid, was not seen on metrizamide- or intravenously enhanced CT scans, but was demonstrated at surgery using sonography and was shunted at the T8 level (fig. 3). In the second patient, metrizamide had filled the cyst between T2 and T9, with no cyst evident between T10 and L3. With intravenous contrast material administered at the same time, moderate enhancement at the L1 and L2 levels was found. At surgery, this tumor extended from T10 to L3–L4 (fig. 4).

The histology, the amount of contrast material, and the degree of enhancement of the 14 intramedullary mass lesions are summarized in table 1. Predicting tumor histology by its appearance was not rewarding. Both ependymomas and astrocytomas demonstrated solid, patchy, or ringlike enhancement with cysts or areas of low attenuation (figs. 1–3).

Intradural, Extramedullary Lesions

The results of the nine intradural extramedullary masses are also summarized in table 1. Four schwannomas and one each of meningioma, hemangioblastoma, hemangiendothelioma, lymphosarcoma, and tonsillar cyst were discovered. Five masses enhanced markedly, two only mildly, and two did not enhance. The nonenhancing lesions were the tonsillar cyst (of CSF density) and one small (1 cm) schwannoma.

Only four unenhanced scans were obtained. The meningioma contained punctate calcifications, a large isodense schwannoma had areas of decreased attenuation, and the hemangioblastoma and the hemangioendothelioma (in patients with von Hippel-Lindau disease) were isodense.

In all cases, the area of enhancement corresponded with the location of the mass on myelography. The meningioma, the hemangioblastoma, and one schwannoma enhanced in a dense uniform fashion. Two schwannomas and the lymphosarcoma had patchy, irregular enhancement with areas of low density, and mild uniform enhancement of the hemangioendothelioma was seen.

The degree of extraspinal extension was better appreciated on the intravenously enhanced scan than on the myelogram in two schwannomas (fig. 5). The other lesions had no extradural extension.

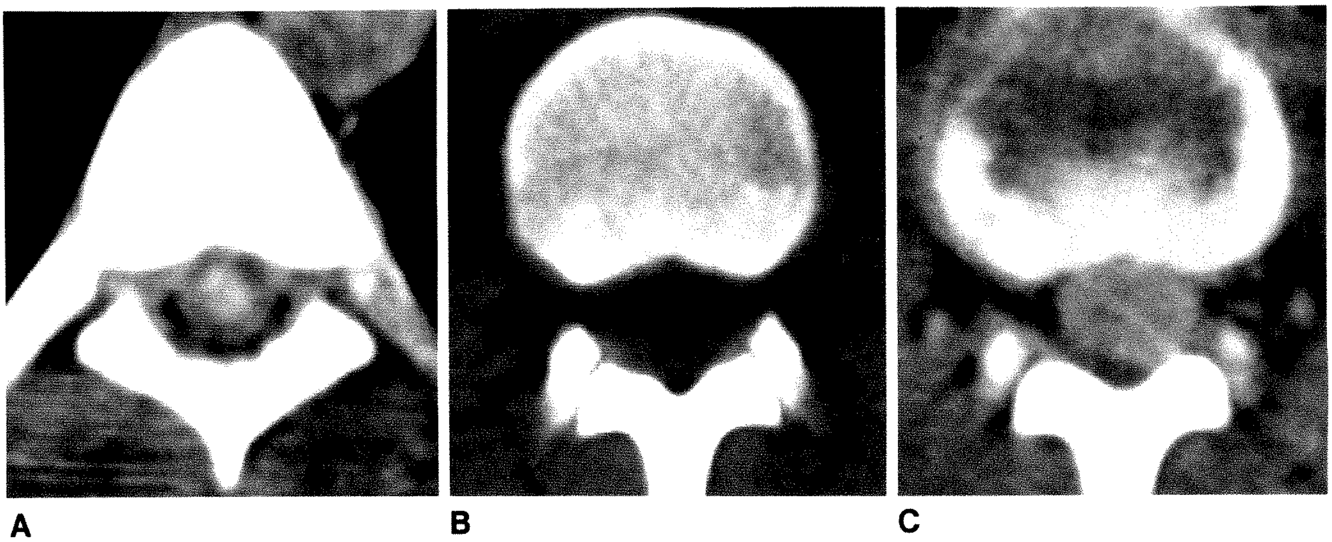

Fig. 4.—Ependymoma, 16-year-old boy. **A**, Unenhanced scan 20 hr after metrizamide myelogram. Dense collection of metrizamide in tumor cyst at T6 level. **B**, L1–L2 level. No cyst is seen. **C**, Same level immediately after **B** and administration of intravenous contrast material. Moderate enhancement of solid tumor nodule, which occupies cord at this level.

TABLE 1: **CT Characteristics of Intradural Masses**

Histology	No. of Tumors				
	Total	Isodense	Enhancing	Degree of Enhancement	Cystic
Intramedullary:					
Ependymoma	6	2	6	Moderate to marked: 2 SD, 3 DD; mild: 1 SD	4
Astrocytoma	4	1	3	Marked: 1 SD, 1 DD; mild: 1 SD; none: 1 DD	2
Glioma (unknown type)	1	. . .	1	Marked: DD	1
Metastasis (lung)	1	1	1	Marked: SD	0
Lipoma	1	. . .	0	None: DD	FD
Ependymal cyst of conus	1	. . .	0	None: DD	1
Extramedullary:					
Schwannoma	4	1	3	Marked: 2 DD; mild: 1 DD; none: 1 DD	1
Hemangioblastoma	1	1	1	Marked: SD	0
Hemangioendothelioma	1	1	1	Mild: DD	0
Meningioma*	1	0	1	Marked: DD	0
Lymphosarcoma	1	. . .	1	Marked: SD	0
Tonsillar cyst	1	. . .	0	None: DD	1

Note.—Isodensity was evaluated on unenhanced scans only, which were not obtained in all cases. Cystic findings were evaluated on either unenhanced or enhanced scans. SD = single dose; DD = double dose; FD = fat density.

* Calcification present.

Single versus Double Doses of Contrast Material

Enhancement ranging from mild to marked was present in 18 of 23 lesions. The two cysts and the lipoma were not expected to enhance. However, one astrocytoma and one schwannoma did not enhance. Both patients had received a double dose of contrast material. Of the four lesions that enhanced mildly (see table 1), two patients had received a single dose and two patients a double dose of contrast material. Fourteen masses enhanced moderately to markedly. Six of these patients had received a single dose and eight a double dose.

Discussion

The spinal cord is difficult to image without the use of intrathecal contrast material [1]. While absorption of metrizamide by the cord may increase attenuation values by about 30 H, intravenous administration of contrast material results in an increase of about 10 H [5].

Previous reports of intravenous contrast enhancement of intramedullary tumors showed disappointing results, with only one of six ependymomas and one of five astrocytomas actually enhancing [1, 3, 6]. Cystic degeneration, known to occur in almost one-half of ependymomas and in more than

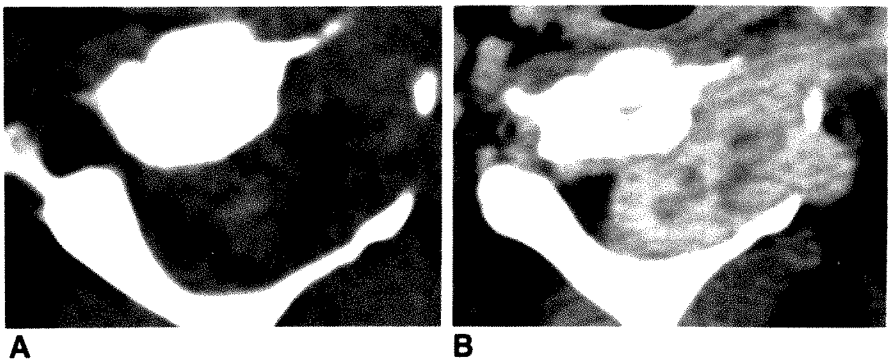

Fig. 5.—Schwannoma, 30-year-old woman. **A**, Unenhanced scan at C2 level. Large mass of mixed density within spinal canal, expanding left intervertebral foramen and extending into paravertebral soft tissues. **B**, Contrast-enhanced scan at same level. Marked tumor enhancement with central lucent defects. Extension of tumor outside foramen and canal and marked displacement of spinal cord to right are better appreciated.

one-third of spinal cord astrocytomas, appeared as hypodense areas in one astrocytoma and in two ependymomas [3, 6–8]. Fifteen of 17 schwannomas enhanced [1, 2, 6], while six intramedullary lipomas were of fat density and did not enhance [1, 6].

Only intramedullary hemangioblastomas have shown consistent enhancement, presumably because of their very vascular nature. One hemangioblastoma was hyperdense and two of three hemangioblastomas enhanced densely. Our two patients with von Hippel-Lindau disease had small extramedullary lesions measuring about 1 cm; one of them enhanced mildly and the other markedly. Four of five meningiomas also enhanced [1, 6].

Table 1 summarizes the CT characteristics of the tumors in this series. The findings on unenhanced scans are similar to published reports. However, our study shows that intramedullary lesions are likely to enhance, contrary to the findings in the literature. This is probably because of the better scanning technique now available with thinner cuts, better resolution, and better localization with scout views.

Predicting the histology of the intramedullary tumors was not rewarding, as the characteristics of ependymoma and astrocytoma were similar. Better imaging techniques and a larger series may prove useful in the future.

Most important is the ability of intravenously enhanced CT to localize intramedullary tumors, as surgical removal is now feasible. Differentiating the solid from the cystic component of the tumor may help to limit the length of the laminectomy. Intraoperative sonography can also be used to localize the mass lesion.

Response to treatment and the presence of residual or recurrent tumors can also be assessed by intravenously enhanced scans, obviating repeat myelography.

A double dose of contrast material did not enhance tumors more densely than did a single dose (table 1).

As predicted by Pettersson and Harwood-Nash [5] in 1982, contrast enhancement of spinal cord tumors has proved valuable. Eighteen of 23 intradural tumors enhanced; enhancement of three of the other five lesions would not be expected. The contrast-enhanced study was useful in delineating the extent of the tumor, especially when a cyst was present, and in helping the surgeon localize the solid tumor before removal. The histology of intramedullary tumors could not be predicted accurately by the enhancement pattern. No advantage of a double dose of contrast material over a single dose was demonstrated in our series, but the study design precludes definite conclusions.

REFERENCES

1. Nakagama H, Huang YP, Malis LI, Wolf BS. Computed tomography of intraspinal and paraspinal neoplasms. *J Comput Assist Tomogr* **1977**;1:377–389
2. Balériaux-Waha D, Terwinghe G, Jeanmart L. The value of computed tomography for the diagnosis of hourglass tumors of the spine. *Neuroradiology* **1977**;14:31–32
3. Lee BCP, Kazam E, Newman AD. Computed tomography of the spine and spinal cord. *Radiology* **1978**;128:95–102
4. Haughton VM, Williams AL. *Computed tomography of the spine*. St. Louis: Mosby, **1982**
5. Pettersson H, Harwood-Nash DCF. *CT and myelography of the spine and cord—techniques, anatomy and pathology in children*. New York: Springer-Verlag, **1982**
6. Aubin ML, Jardin C, Bar D, Vignaud J. Computerized tomography of 32 cases of intraspinal tumor. *J Neuroradiol* **1979**;6:81–92
7. Handel S, Grossman R, Sarwar M. Computed tomography in the diagnosis of spinal cord astrocytoma. Case report. *J Comput Assist Tomogr* **1978**;2:226–228
8. Dorwart RH, LaMasters DL, Watanabe TJ. Tumors. In: Newton TH, Potts DG, eds. *Modern neuroradiology*, vol 1. *Computed tomography of the spine and spinal cord*. San Anselmo, CA: Clavadel, 1983:115–130

AJR Editorial Office Address Change

In January 1986, Robert N. Berk, M.D., will assume the editorship of the *AJR* from Melvin M. Figley, M.D., who will retire. Thus, on Jan. 1, the *AJR* Editorial Office will open in La Jolla, CA. The *AJR* Editorial Office in Seattle will be staffed through Feb. 28.

Please note the addresses of the two offices and the effective dates for the transfer of various editorial operations.

La Jolla Office

AJR Editorial Office
2223 Avenida de la Playa (Suite 306)
La Jolla, CA 92037
(619) 459-2229

Seattle Office

AJR Editorial Office
909 N.E. 43rd Street (Suite 306)
Seattle, WA 98105
(206) 633-2754

Manuscripts and Correspondence

Effective Jan. 1, 1986, send all new and revised manuscripts to the La Jolla office.

Galley Proof

Galley proof for all articles through the March 1986 issue should be returned to the Seattle office. Galleys for the April 1986 and subsequent issues must be mailed to the La Jolla office.

News Items

The Seattle office will compile the news columns through the April 1986 issue of the *AJR*. Mail announcements to the Seattle office until Jan. 15 and to the La Jolla office thereafter.

Classified Advertisements

Send classified advertising copy to the Seattle office through Feb. 1.

	Date La Jolla Address Is Effective
New and revised manuscripts and letters	Jan. 1
Galley proof	Jan. 15
News items	Jan. 15
Classified advertising copy	Feb. 1

Sonographic Appearance of the Torcular Herophili

Sharon R. Segal[1]
Henrietta Kotlus Rosenberg[1]

The sonograms of 12 infants aged 2 days to 7 months were evaluated to determine if the torcular Herophili could be demonstrated routinely on cranial sonography. Sonography, which was performed for a variety of indications (prematurity, seizures, hydrocephalus, sepsis, congenital anomalies, and subarachnoid hemorrhage) demonstrated the torcular Herophili in all cases. It appeared as a variable-sized, anechoic, and triangular or elongated structure inferior to the occipital lobes, posterior to the cerebellum, and just inside the cranial vault. Correlation with computed tomographic scans was available in four patients. A detailed description of the normal anatomy of the torcular Herophili is provided. Knowledge of the variable sonographic appearance of the torcular Herophili is important to distinguish it from a pathologic entity.

Unless the torcular Herophili and dural sinuses are usually prominent, they may not be routinely demonstrated on cranial sonograms. These structures and their variable appearances have been well documented with computed tomography (CT) [1, 2] but not previously with sonography. We wish to review the anatomy of the confluence of the sinuses and present the spectrum of sonographic findings of this important venous structure.

Our initial attention to the torcular Herophili sonographically was established when we examined a 5-day-old 38 week gestation boy with hypoglycemia and seizures. We noted a 3.0 × 3.4 × 0.8 cm anechoic area inferior to the occipital lobes in the midline, suggesting a subdural collection or a prominent torcular Herophili. The examination was otherwise unremarkable (figs. 1A and 1B). A CT scan the same day demonstrated no evidence of abnormal dural collection or hemorrhage (fig. 1C). The final conclusion of the sonographic examination was that the findings did indeed represent the dural sinuses.

Normal Anatomy

The cerebral veins, which do not accompany the arteries, arise from the cortical substance, forming a pial plexus. After a variable distance these veins pass through the subarachnoid space into larger intercommunicating channels, the dural sinuses. These sinuses, located between the meningeal and periosteal layers of the dura, are lined with endothelium, with walls that are composed of the tough fibrous tissue of the dura [3].

The superior sagittal sinus courses within the superior margin of the falx cerebri until it approaches the torcular Herophili at the occipital protuberance. The sinus caliber progressively enlarges as it travels caudally [3].

The inferior sagittal sinus extends caudally along the free border of the falx. At the anterior border of the tentorium, it is joined by the great vein of Galen, which drains the deep structures of the brain; the two veins join to form the straight sinus. This sinus runs backward and downward along the line of attachment of the falx and tentorium to join the superior sagittal sinus near the internal occipital

This article appears in the November/December 1985 issue of *AJNR* and the January 1986 issue of *AJR*.

Received August 29, 1984; accepted after revision April 11, 1985.

[1] Department of Radiology, Subdivision of Ultrasound, Children's Hospital of Philadelphia, 1 Children's Center, Philadelphia, PA 19104. Address reprint requests to H. K. Rosenberg.

AJR 146:109-112, January 1986
0361-803X/86/1461-0109

© American Roentgen Ray Society

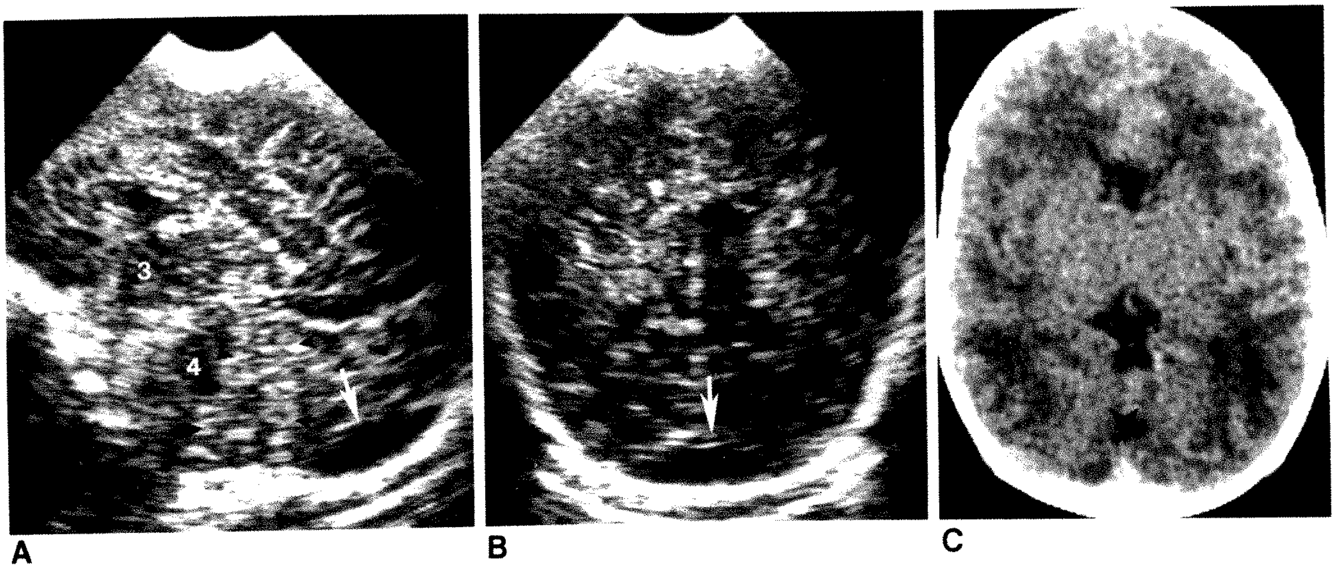

Fig. 1.—**A**, Midsagittal section of brain demonstrating torcular Herophili. Anechoic structure (*arrow*) posterior to cerebellum (*arrowheads*) and inferior to (occipital lobes) cerebral hemispheres consistent with confluence of sinuses. 3 = third ventricle; 4 = fourth ventricle. **B**, Posterior coronal view. Torcular Herophili (*arrow*). **C**, Contrast-enhanced axial CT scan. Torcular Herophili (*arrowhead*).

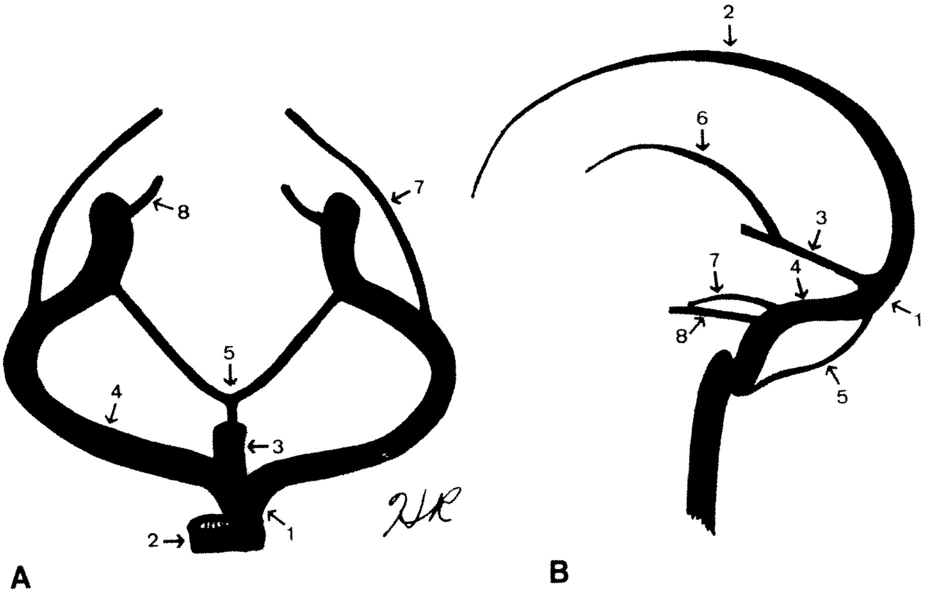

Fig. 2.—Venous anatomy in coronal (**A**) and sagittal (**B**) planes. 1 = torcular Herophili; 2 = superior sagittal sinus; 3 = straight sinus; 4 = transverse sinus; 5 = occipital sinus; 6 = inferior sagittal sinus; 7 = superior petrosal sinus; 8 = inferior petrosal sinus.

protuberance [3].

The transverse sinuses continue from the occipital protuberance. Usually these channels slope downward along the groove on either side of the occipital bone, then anteriorly along the mastoid portion of the parietal and temporal bones, ending at the jugular foramen. The anteroinferior continuation of these channels are the sigmoid sinuses [4].

The torcular Herophili is formed by the joining of the superior sagittal sinus, the transverse sinuses, and the straight sinus (fig. 2). On angiography the torcular Herophili and transverse sinuses usually form an inverted T with the superior sagittal sinus. Venous drainage often is asymmetric [5]. A small unpaired occipital sinus from the area of the foramen magnum rises in the falx cerebelli to join the torcular Herophili [3].

Wide variation is demonstrated by this confluence. Rarely is there actual union of these sinuses. Often the superior sagittal sinus turns to the right to become continuous with the transverse sinus while the straight sinus bends to the left as the left transverse sinus [3]. The torcular Herophili may be displaced from the midline by a superior extension of a large cisterna magna. The confluence may lie as much as 1 cm anterior to the occipital bone or to one side of the midline [2].

Subjects and Methods

A prospective evaluation was done to establish whether or not the torcular Herophili could be demonstrated routinely on cranial sonograms. We performed real-time cranial sonographic examinations in

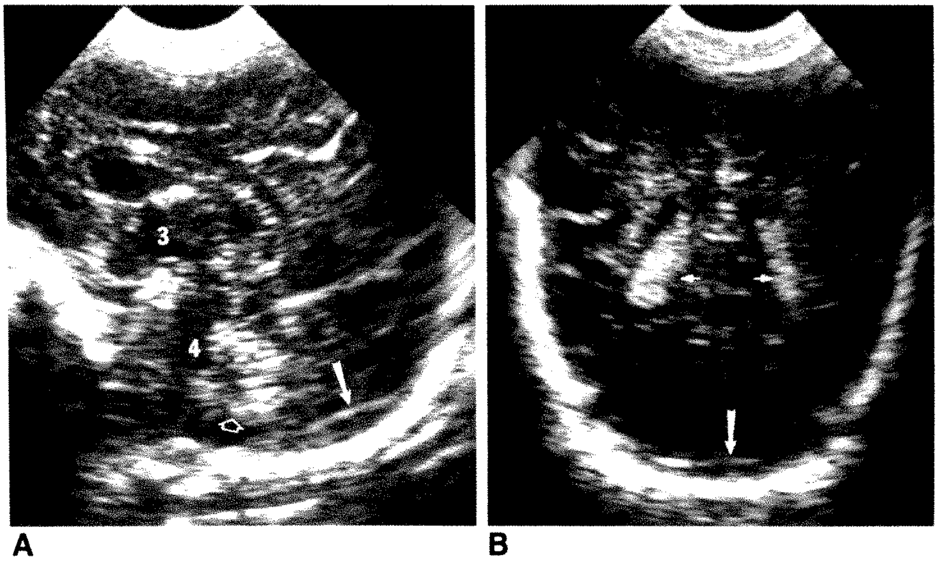

Fig. 3.—**A**, Midsagittal section of brain. Routine appearance of torcular Herophili (*solid arrow*) posterior to cerebellum (*open arrow*) and inferior to occipital lobes. 3 = third ventricle; 4 = fourth ventricle. **B**, Posterior coronal view. Torcular Herophili (*long arrow*). Choroid plexuses (*short arrows*).

12 infants referred for miscellaneous indications (prematurity, six; hydrocephalus, one; seizures, two; sepsis, one; multiple congenital anomalies, one; and subarachnoid hemorrhage on CT, one). The age of the patients ranged from 2 days to 7 months. Gestational ages ranged from 28 to 42 weeks. Four patients had CT scans within 8 days of sonography and the areas of interest were compared.

The sonograms were obtained with the ATL Mark 100 real-time unit (3.0, 5.0, and 7.5 MHz transducer). Coronal and sagittal views were obtained in all the patients. The CT scans were obtained with the GE 8800 scanner and the axial views were reviewed.

Results

The torcular Herophili was identified on all images. It appeared similar on sonograms and on CT scans in all but two cases. One patient demonstrated prominent dural sinuses on sonography and not on CT, while a second patient demonstrated prominent confluence of sinuses on CT and not on sonography.

Best demonstration of the torcular Herophili was made with careful examination of the posterior fossa, with steep angling posterior to the cerebellum. The torcular Herophili was imaged as an anechoic, triangular, or elongated structure just inside the cranial vault, inferior to the occipital lobes, posterior to the cerebellum. The size of the structure was variable (fig. 3).

Discussion

The normal anatomy of the brain has been well demonstrated sonographically [6–12]. Recently, Monsaingeon et al. [13] reported the normal arterial vascular anatomy of the brain. The arterial supply, including branches of the internal carotid artery and the vertebral artery distribution, were demonstrated. The venous anatomy has not been described. However, with careful examination of the area posterior to the cerebellar hemispheres and inferior to the occipital lobes, one can see the torcular Herophili. Attenuation by the echogenic cerebellar hemispheres may impede satisfactory imaging unless appropriate posterior angling is done.

In conclusion, demonstration of the torcular Herophili and dural sinus drainage of the neonatal brain can be performed routinely. The torcular Herophili may vary in size and configuration as an anechoic, triangular, elongated structure inferior to the occipital lobes just behind the cerebellum. This anatomic structure should be recognized sonographically to obviate pathologic study by other methods.

REFERENCES

1. Naidich TP, Pudlowski RM, Leeds NE, Naidich JB, Curisolm AJ, Rifkin MD. The normal contrast-enhanced computed axial tomogram of the brain. *J Comput Assist Tomogr* **1977**;1:16–29
2. Lee SH, Rao KCVG. *Cranial computed tomography*. New York: McGraw Hill, **1983**;48:690
3. Carpenter M, Sutin J. *Human neuroanatomy*. Baltimore: Williams & Wilkins, **1981**:712, 732–737
4. Netter F. *The Ciba collection of medical illustrations*. Summit, NJ: Ciba. **1972**:34
5. Osborn AG. *Introduction to cerebral angiography*. Hagerstown, MD: Harper & Row, **1980**:340–341
6. Pigadas A, Thompson JR, Grube G. Normal infant brain anatomy: correlated real-time sonograms and brain specimens. *AJNR* **1981**;2:339–344, *AJR* **1981**;137:815–820
7. Shuman WP, Rogers JV, Mack LA, Ellsworth CA, Christie DP. Real-time sonographic sector scanning of the neonatal cranium: technique and normal anatomy. *AJNR* **1981**;2:349–356, *AJR* **1981**;137:821–828
8. Slovis TL, Kuhns LR. Real-time sonography of the brain through the anterior fontanelle. *AJR* **1981**;136:277–286
9. Grant EG, Schellinger D, Borts FT, et al. Real-time sonography of the neonatal and infant head. *AJR* **1980**;1:487–492, *AJR* **1981**;136:265–270
10. Edwards MK, Brown DL, Muller J, Grossman CB, Chua GT. Cribside neurosonography: real-time sonography for intracranial

Cystic Neuroblastoma in Infants: Radiographic and Pathologic Features

George O. Atkinson, Jr.[1]
Ghazi S. Zaatari[2]
Robert L. Lorenzo[3]
Brit B. Gay, Jr.[1]
A. Julian Garvin[4]

Cystic neuroblastoma is a rare form of neuroblastoma. Three cases of cystic neuroblastoma in the infant are reported with emphasis on the sonographic findings. In two cases, the tumor was demonstrated in the fetus. The pathologic features of the tumors are described. Development of cysts may be related to a prominent microcystic arrangement of tumor nests.

Neuroblastoma is the most common malignant tumor in the infant [1]. In the neonate, an adrenal origin of neuroblastoma occurs in about 70% of cases [2]. Hemorrhage and necrosis are often seen in neuroblastoma, but cyst formation is uncommon. Three cases in which the tumor was primarily cystic on pathologic examination are presented with emphasis on the sonographic findings. In two of the cases, the mass lesion was demonstrated sonographically in the fetus. The pathologic features of these tumors are described, and the differential diagnosis and possible pathogenesis of the cysts are discussed.

Case Reports

Case 1

A 9-week-old girl was the product of a pregnancy complicated by premature rupture of the membranes 6 weeks before delivery. A sonographic examination at that time revealed a complex mass in the fetal right upper quadrant interpreted as representing a renal mass (fig. 1A). Delivery was uncomplicated, and the infant was referred to Henrietta Egleston Hospital for evaluation. Repeat sonography demonstrated a persistent, complex suprarenal mass compressing the upper pole of the right kidney (fig. 1B). An excretory urogram with total body opacification demonstrated a radiolucent mass displacing the kidney inferiorly. A computed tomographic (CT) scan revealed a predominantly cystic lesion with septations in the area of the upper pole of the right kidney. Laboratory values were unremarkable. No urine vanilylmandelic acid (VMA) analysis was done.

Surgical exploration revealed a 3.5 × 3.5 × 2.5 cm cystic adrenal mass. On sectioning, the mass was primarily cystic and hemorrhagic. The wall of the cyst was fibrotic, 2 mm thick, and lined by fibrinous exudate and blood. On the outer aspect of the cyst wall, there were nests of neuroblasts in a prominent microcystic arrangement (fig. 1C). The adrenal cortex was compressed against the adrenal capsule and was focally infiltrated by the neuroblasts. Pathologic diagnosis was neuroblastoma in situ with hemorrhagic cyst formation. The patient did well after surgery and had no evidence of metastasis or recurrent tumor at 2-year follow-up. (This case has previously been published [3].)

Case 2

A 2-day-old girl, product of a term pregnancy and uncomplicated delivery, was admitted to Henrietta Egleston Hospital for Children for evaluation of a left abdominal mass. Because of a sibling with a neural tube defect, the mother had had serial sonograms throughout her pregnancy. The first study was done at 16 weeks of gestation with no abnormality identified.

Received March 7, 1985; accepted after revision September 9, 1985.

[1] Department of Radiology, Emory University School of Medicine, Henrietta Egleston Hospital for Children, 1405 Clifton Rd., N.E., Atlanta, GA 30322. Address reprint requests to G. O. Atkinson, Jr.

[2] Department of Pathology and Clinical Laboratory Medicine, Emory University School of Medicine, Atlanta, GA 30322.

[3] Department of Radiology, Emory University School of Medicine, Scottish Rite Hospital, Atlanta, GA 30327.

[4] Department of Pathology, Medical University of South Carolina, Charleston, SC 29425.

AJR 146:113-117, January 1986
0361-803X/86/1461-0113
© American Roentgen Ray Society

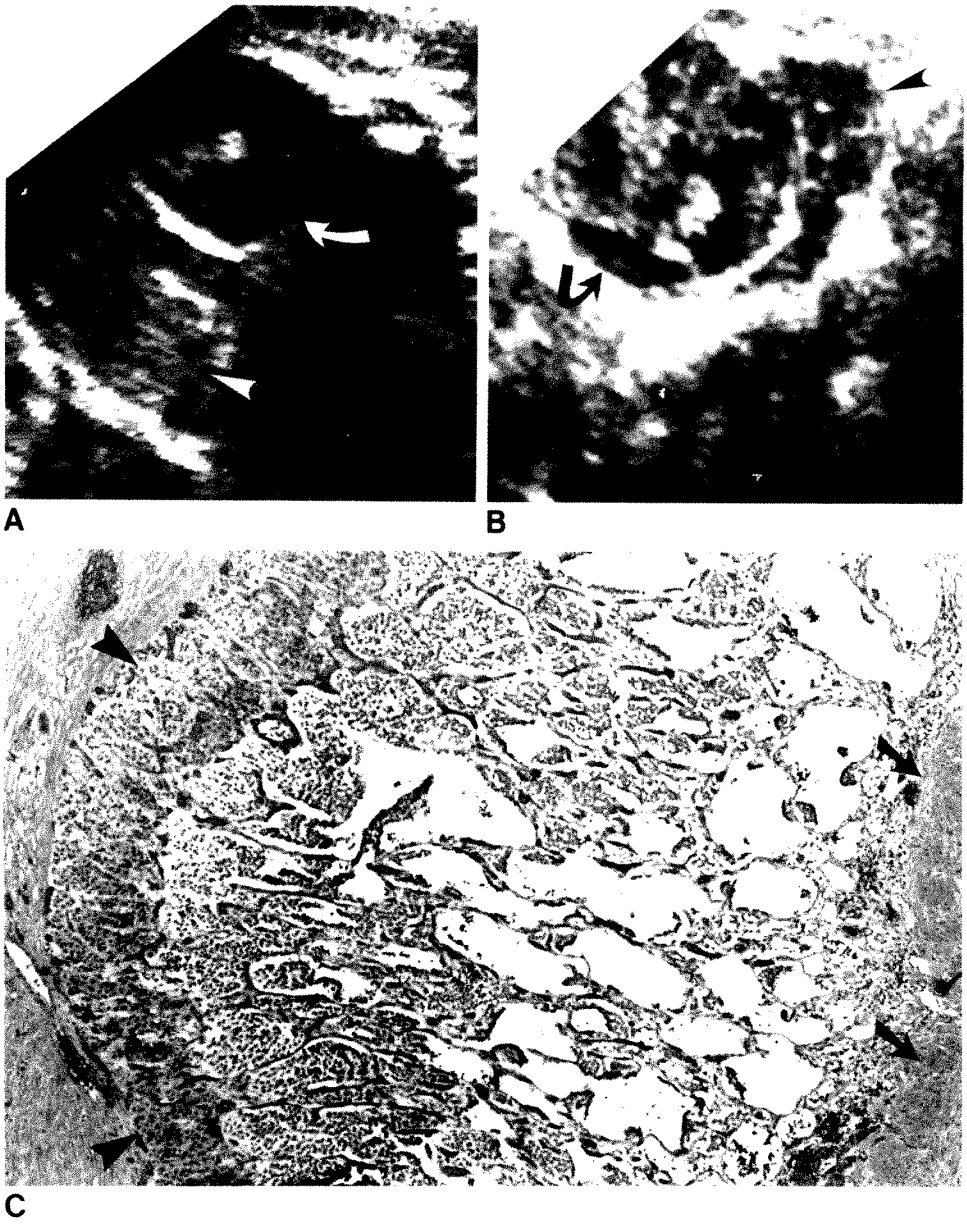

Fig. 1.—Case 1: neuroblastoma in situ with hemorrhagic cyst. **A**, Transverse sonogram of fetal right upper quadrant. Complex mass (*arrow*) posterior to liver (*arrowhead*). **B**, Coronal sonogram at age 10 weeks. Complex mass (*arrow*) at upper pole of right kidney (*arrowhead*). (Reprinted from [3].) **C**, Tumor shows prominent microcyst arrangement adjacent to fibrous wall (*arrows*) of gross cyst. Adrenal cortex (*arrowheads*) is compressed.

At 32 weeks, the sonogram revealed a complex mass in the left upper abdomen of the fetus interpreted as showing hydronephrosis of the left kidney (fig. 2A). A sonogram at 36 weeks was interpreted as normal. After delivery, a left-upper-quadrant abdominal mass was palpated, and the patient was transferred to our hospital. Sonographic examination revealed a multiloculated, complex, echogenic mass superior and medial to the left kidney (fig. 2B). The kidney was displaced inferiorly and laterally. A voiding cystourethrogram was normal. An excretory urogram, with total body opacification, revealed an anechoic mass at the superior aspect of the left kidney that displaced the kidney inferiorly and laterally without distortion of the collecting system. A 24-hr urinanalysis for VMA and homovanillic acid was normal.

At surgery, a 5 × 4 × 3 cm left adrenal mass was removed (fig. 2C). On sectioning, the tumor appeared multiloculated with solid and cystic components. A few cysts contained clear serous fluid, while others were hemorrhagic and contained bloody fibrinous exudate. The solid part of the tumor demonstrated the typical appearance of neuroblastoma with small tumor cells arranged in nests separated by fibrovascular septa. A rich neurophil matrix and calcifications were present (fig. 2D). In the cystic part of the tumor, similar tumor cells were seen, but their nests had a prominent microcystic arrangement in addition to the large cysts. The patient did well after surgery. Radionuclide bone and liver scans and a bone marrow aspiration were normal. The patient received no further therapy, and at 1-year follow-up had no evidence of metastasis or recurrent tumor.

Case 3

An 11-week-old boy was admitted for evaluation of abdominal distension. Physical examination revealed a massively enlarged liver.

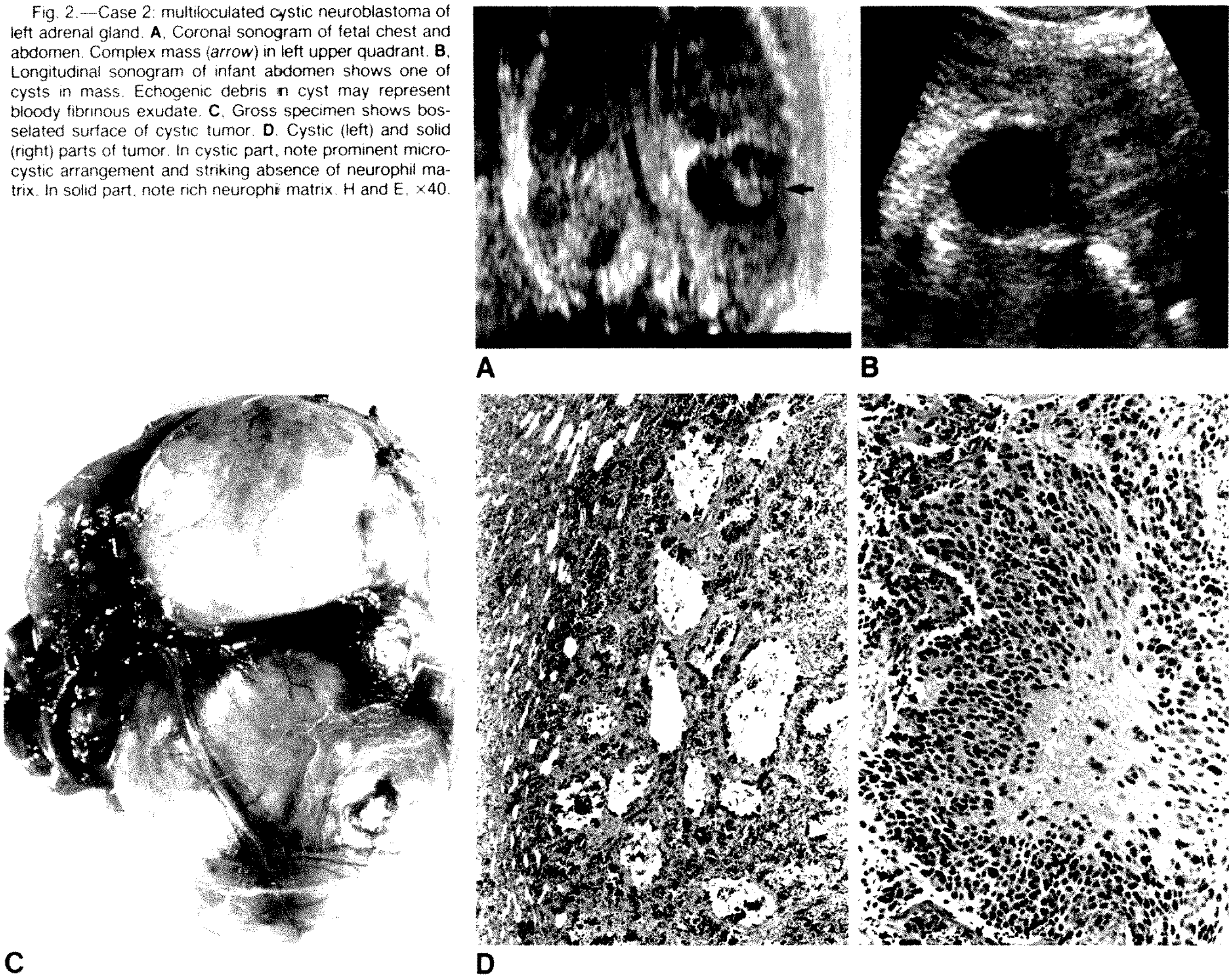

Fig. 2.—Case 2: multiloculated cystic neuroblastoma of left adrenal gland. **A**, Coronal sonogram of fetal chest and abdomen. Complex mass (*arrow*) in left upper quadrant. **B**, Longitudinal sonogram of infant abdomen shows one of cysts in mass. Echogenic debris in cyst may represent bloody fibrinous exudate. **C**, Gross specimen shows bosselated surface of cystic tumor. **D**, Cystic (left) and solid (right) parts of tumor. In cystic part, note prominent microcystic arrangement and striking absence of neurophil matrix. In solid part, note rich neurophil matrix. H and E, ×40.

Urinanalysis for VMA was negative. An excretory urogram showed the left kidney displaced inferiorly and laterally without distortion of the calices. The stomach was displaced anteriorly. A sulfur colloid liver-spleen scan demonstrated multiple filling defects in the enlarged liver. A sonographic examination demonstrated a large cystic mass above the left kidney (fig. 3A) and multiple cystic lesions in the liver (fig. 3B). A bone marrow examination was normal. At surgery, a 10 × 8 × 8 cm cystic hemorrhagic left adrenal mass was resected. Multiple cystic masses of 0.5–2 cm were noted in the liver, and multiple biopsies were obtained of these lesions. The pathologic diagnosis, based on both light and electron microscopy, was neuroblastoma with cystic change in the left adrenal and the metastatic lesions to the liver (fig. 3C).

The infant was classified as stage 4S neuroblastoma and no further therapy was administered. The patient was readmitted at age 6 months for follow-up evaluation. Physical examination revealed hepatomegaly. Sonography now demonstrated a cystic right-adrenal mass (fig. 3D). An excretory urogram showed a 3.5-cm radiolucent area above the right kidney. A radiographic bone survey was negative for metastasis. Repeat surgical exploration showed resolution of the previous liver metastasis and no recurrence of the mass in the left adrenal area. The cystic mass involving the right adrenal was confirmed, but was not resected due to the previous left adrenalectomy. It was believed the lesion represented a metastasis, although a second primary could not be excluded. The patient was discharged after recovery from surgery. No further follow-up is available.

Discussion

Neuroblastoma is the most common malignant tumor in infancy, originating most often in the adrenal gland [1, 2]. Neuroblastoma of the adrenal gland may be a microscopic in situ tumor or a grossly recognizable neoplasm, with or without metastasis. When present, metastases are usually to the liver and retroperitoneal nodes. Our three cases demonstrate these various findings in this medullary tumor; however, all three cases had cystic change as a prominent feature in their clinical presentation.

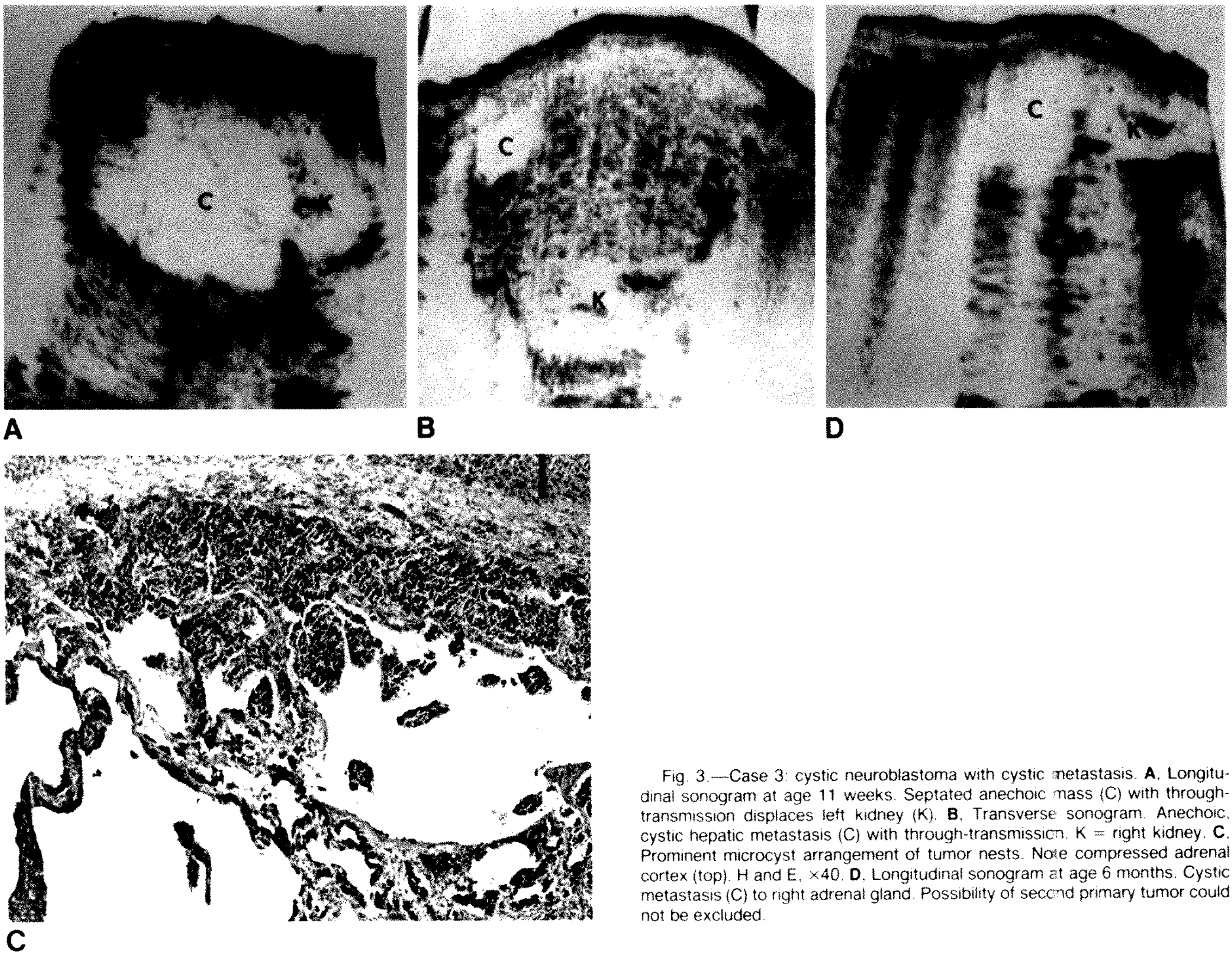

Fig. 3.—Case 3: cystic neuroblastoma with cystic metastasis. **A**, Longitudinal sonogram at age 11 weeks. Septated anechoic mass (C) with through-transmission displaces left kidney (K). **B**, Transverse sonogram. Anechoic, cystic hepatic metastasis (C) with through-transmission. K = right kidney. **C**, Prominent microcyst arrangement of tumor nests. Note compressed adrenal cortex (top). H and E, ×40. **D**, Longitudinal sonogram at age 6 months. Cystic metastasis (C) to right adrenal gland. Possibility of second primary tumor could not be excluded.

Sonography has become the primary method for the investigation of abdominal masses in children of all ages, particularly in the infant. The usual sonographic appearance of an adrenal neuroblastoma is that of an echogenic or complex extrarenal mass compressing or displacing the kidney inferiorly and laterally. Most abdominal neuroblastomas have a variable echogenicity with irregular hyperechoic areas intermixed with less echogenic areas, apparently corresponding to the frequent foci of hemorrhage, necrosis, and microcalcification in these tumors. Large focal calcifications may produce very intense echoes and occasional shadowing [4]. A review of the literature revealed only one sonographic description of a cystic neuroblastoma [5].

Case 1 represents an in situ neuroblastoma associated with a hemorrhagic cyst presenting as an adrenal mass. In situ neuroblastoma is cytologically identical to the appearance of typical neuroblastoma but is microscopic and without metastasis [6]. These microscopic lesions have been reported in 1.5% of infants younger than 3 months who died of unrelated causes. Most of these tumors are clinically insignificant, and presumably either regress or mature into benign neurogenic tissue [6, 7]. Cyst formation in these in situ tumors is rare. Only three additional cases of an in situ neuroblastoma with an associated cyst have been reported [5, 8, 9]. One of these cases presented with features similar to those of our case, with an in situ tumor found in the wall of a suspected adrenal hematoma [9]. Although it is reported that this entity represents adrenal hemorrhage with incidental in situ neuroblastoma in the wall of the hemorrhage, our case questions this hypothesis and suggests a causal relationship. A sonogram during pregnancy in our case demonstrated the presence of the lesion, while adrenal hemorrhage in the newborn is usually associated with birth trauma. In addition, two of the three reported cases of neuroblastoma in situ associated with cyst contained cyst without hemorrhage [5, 8].

Sonography in case 1 demonstrated a complex echogenic mass in both the 34-week fetus and the infant (fig. 1). The internal echoes are presumably related to the hemorrhage and fibrinous exudate demonstrated pathologically within the cyst. Sonographic examination was performed in only one of the previously reported in situ tumors and demonstrated a totally anechoic adrenal mass [5]. Pathologic examination of the mass revealed a 4 × 5 cm cyst filled with a jellylike material with adrenal tissue containing areas of neuroblastoma draped around the cyst.

Case 2 represents a grossly recognizable tumor that had expanded the adrenal gland but was without metastasis. The sonographic pattern depicted the gross pathology of a multiloculated, partly cystic, partly solid tumor divided by fibrous septa (fig. 2). This tumor was also demonstrated in the fetus as a complex mass. Our earlier experience of neuroblastoma in situ associated with a hemorrhagic cyst was a major reason for early surgery in this infant.

The sonographic findings of a cystic neuroblastoma with cystic metastasis are demonstrated in case 3 (fig. 3). The lesions were cystic by sonography, appearing anechoic with posterior enhancement. This case suggests that, although extremely rare, the demonstration of cystic masses in the infant liver or retroperitoneal nodes should dictate scanning the adrenal gland for a possible primary cystic neuroblastoma.

Necrosis and hemorrhage are frequent morphologic characteristics of neuroblastoma. Therefore, it is not surprising to find cyst formation in association with these tumors. These cysts are usually small and have been considered to represent degenerative change within the tumor. In all three cases, we did observe a prominent microcystic arrangement of the tumor nests in areas adjacent to and remote from areas of hemorrhage and the grossly recognized cysts (figs. 1C, 2D, and 3C). Beckwith et al. [6] and Guin et al. [7] included microscopic description and figures of similar microcysts in their cases of in situ neuroblastoma, but they reported no grossly recognizable cyst. Therefore, it is possible that a large clinically detectable cyst formation, as seen in our cases, may be related to this microscopic architecture of the tumor cells. The hypothesis of microcyst leading to larger cyst cannot be proven by these few cases, but search for this association seems warranted in future cases.

In cases 1 and 2, the abnormal fetal adrenal gland was demonstrated by sonography but was interpreted as renal pathology. Identification of the normal adrenal gland in the fetus is emphasized by these cases. The sonographic technique for examination of the fetal adrenal gland has been described [10-12]. In these studies, the fetal adrenal gland could be demonstrated with some regularity at gestational ages varying from as early as 20-32 weeks, with an appearance similar to that of the normal infant adrenal gland.

Adrenal hematoma represents the most common cause of a suprarenal mass lesion in the neonate, and during its natural history may be sonographically entirely echogenic, of complex echogenicity, or anechoic. The presence of a complex mass in the fetal adrenal gland in our two cases made simple adrenal hemorrhage a less likely diagnosis. Other lesions of differential concern include duplication anomaly of the kidney with obstructed upper-pole collecting system, obstructed upper-pole hydrocalix, and cystic Wilms tumor. Adrenal cyst in the infant is extremely rare. It should be noted that the urine VMA levels were normal in our two cases (cases 2 and 3) of cystic neuroblastoma. VMA levels have not been reported elevated in cases of neuroblastoma in situ associated with an adrenal cyst or hemorrhagic cyst.

Although cystic neuroblastoma is a rare form of neuroblastoma in the infant, it should be considered in the differential diagnosis of a cystic adrenal mass. It may appear as a complex echogenic mass or an anechoic mass by sonographic examination. Failure of a cystic suprarenal mass to resolve on follow-up examination is an indication for surgery. Demonstration of anechoic hepatic masses should raise a suspicion of cystic metastasis and mandate careful evaluation of the adrenal glands.

REFERENCES

1. Gross S, Shurin SB, Gordon EM. Congenital malignant disorders. In: Avery ME, Taeusch HW, eds. *Schaffer's diseases of the newborn*. Philadelphia: Saunders, **1984**:933-938
2. Schwartz AD. The blood and hematopoietic system. In: Favaroff AA, Martin RJ, eds. *Behrman's neonatal-perinatal medicine diseases of the fetus and infant*. St. Louis: Mosby, **1983**:747-748
3. Sones PJ. Sonography case of the day. *AJR* **1983**; 140:1025-1026
4. Hartman DS, Sanders RC. Wilms tumor versus neuroblastoma: usefulness of ultrasound in differentiation. *J Ultrasound Med* **1982**;1:117-122
5. Hendry GMA. Cystic neuroblastoma of the adrenal gland—a potential source of error in ultrasonic diagnosis. *Pediatr Radiol* **1982**;12:204-206
6. Beckwith JB, Perrin EV. In situ neuroblastoma: a contribution to the natural history of neural crest tumors. *Am J Pathol* **1963**;43:1089-1099
7. Guin GH, Gilbert EF, Jones B. Incidental neuroblastoma in infants. *Am J Clin Pathol* **1969**;51:126-136
8. Tubergen KDG, Heyn RM. In situ neuroblastoma associated with an adrenal cyst. *J Pediatr* **1970**;76:451-453
9. Sober I, Hirsh M. Unilateral massive adrenal hemorrhage in newborn infant. *J Urol* **1965**;93:430-434
10. Jeanty P, Chervenak F, Grannum P, Hobbins JC. Normal ultrasonic size and characteristics of the fetal adrenal glands. *Prenat Diagn* **1984**;4:21-28
11. Rosenberg ER, Bowie JD, Andreotti RF, Fields SI. Sonographic evaluation of fetal adrenal glands. *AJR* **1982**;139:1145-1147
12. Lewis E, Kurtz AB, Dubbins PA, Wapner RJ, Goldberg BB. Realtime ultrasonographic evaluation of normal fetal adrenal glands. *J Ultrasound Med* **1982**;1:265-270

Memorial

Andreas Roland Gruentzig, 1939–1985

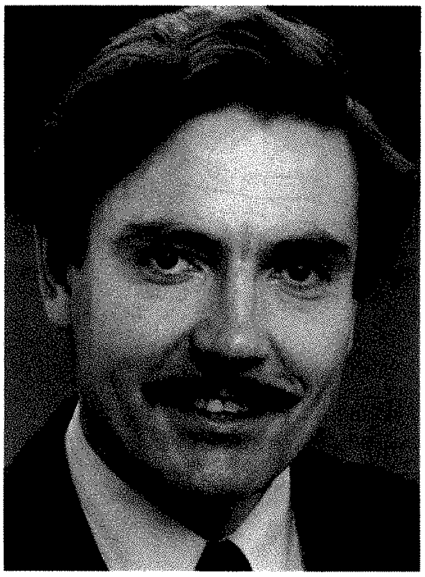

On October 27, 1985, Dr. Andreas Roland Gruentzig and his wife, Dr. Margaret Anne Thorton, were killed when their private airplane crashed in bad weather in a wooded area near Forsyth, GA. Dr. Gruentzig was internationally recognized for introducing percutaneous transluminal coronary angioplasty and related angioplasty techniques to the medical profession. He taught more than 1000 physicians the technique of angioplasty and established the technique as a valuable treatment method in cardiovascular disease. His work changed, forever, the practice of cardiovascular radiology.

Andreas Gruentzig was born in Dresden, Germany, in 1939. During the dreadful war years he and his family barely escaped death during the fire bombing of Dresden by Allied bombers. His father was killed in Berlin in 1945 just before the end of the war. Subsequently, his mother moved Andreas and his brother to West Germany to thwart the communist East German government's plan to train Andreas as a bricklayer.

He eventually graduated from the University of Heidelberg Medical School in 1964. During the next 10 years he received training in physiology, epidemiology, internal medicine, angiology, radiology, and cardiology at University Hospital in Zurich, Switzerland, and from 1979–1980 served as the physician in chief, Department of Cardiology, Medical Policlinic, in Zurich.

In 1980 he came to Emory University as professor of medicine and radiology and director of interventional cardiovascular medicine at Emory University Hospital. He published more than 200 scientific articles.

Margaret Anne Thorton was a 1982 graduate of the Emory University School of Medicine. She had been a resident in the Department of Radiology for 2 years and had planned a career in academic medicine.

Remarks at Memorial Service, Nov. 3

Ten years ago in cardiovascular laboratories all over the world, the possibility of repairing vascular obstructions with the catheters we had in our hands was not seriously considered. A few maverick investigators had made probing preliminary attempts, but the problem remained unsolved with a few exceptions in focal lesions of the femoral artery. Demonstration and recording of vascular disease with safety and precision was enough for most of us. Treatment was for other people with other skills.

Eight years ago in Zurich, Switzerland, I visited a young colleague who had a dream. The dream was to take a new catheter that he had just invented for treating arterial obstructions in the legs and to develop it for use throughout the body. This concept was not the dream of a starry-eyed young idealist, but rather the carefully thought out plan of a young physician who, I was to discover later in Atlanta, GA, combined the dedicated clinical talents of a William Osler with the personal charisma of a Rhett Butler.

Dr. Andreas Gruentzig had planned the development of angioplasty from its beginnings in the peripheral arteries to its central progression to the coronary circulation with scheduled stops in the iliac, renal, subclavian, and other arteries along the way. During the past decade, Dr. Gruentzig and many of his colleagues, who were in reality his students, progressed along the course that led to the success of angioplasty. Technical obstacles that at one time appeared even unapproachable were overcome. Other physicians' healthy skepticism was converted to enthusiastic support. People in other fields began to apply balloon angioplasty techniques to virtually all tubular structures that were heir to strictures or obstructions. Patient reluctance became overwhelming acceptance. Much of this success was due to Dr. Gruentzig's honesty, perseverance, and sensitivity. What we remember most fondly about him was that he not only provided inspiration for future achievement by those who followed but also brought glory to those men who preceded him. The work of Charles Dotter, Melvin Judkins, and Mason Sones—all of whom also died in 1985—was glorified and further recognized by Andreas' work and by Andreas himself. He had the unique capacity to honor the past, light up the present, and inspire the future.

Ten days ago in Atlanta, I was visiting Dr. Gruentzig in the cardiovascular laboratory when a critically ill patient was brought in for an emergency procedure. He was pale and sweating, complaining of chest pain with a somewhat diminished blood pressure, and signs of ischemia on his electrocardiogram. Andreas said, "Come and do this procedure with us." In a compressed period of a very few minutes, the product of years of technical and philosophic evolution that had begun a decade ago in Zurich was graphically relived on the fourth floor of Emory University Hospital. It was now second nature to use all of the guiding catheters, steerable platinum guide wires, low-profile high-tensile-strength balloons, vasodilating drugs, and manual dexterity required to direct the appropriate instrument to the focal lesion in the right coronary artery that was producing the patient's clinical syndrome. There was a 99% narrowing of the right coronary artery with markedly diminished perfusion distally and decreased flow of blood to the oxygen-starved myocardium in the inferior wall of the left ventricle. The guide wire was deftly steered across the lesion, followed by the appropriately sized balloon tailored to this patient's lesion, and successful dilatation performed. Almost immediately, the patient's pain disappeared, the newly perfused myocardium improved its contractility, the blood pressure rose, the T waves on the electrocardiogram returned to normal, and the patient said "Now I feel much better." Afterwards, Andreas put his arm on my shoulder and said, "That's what we were dreaming about 10 years ago in Zurich."

So what was a dream 10 years ago is now a clinical reality not only in Atlanta, but all over the world. The dream became a reality due to the hard work of many people, but that work was inspired, planned, and led largely by one seminal individual.

Ten years from now we will be living with the legacy of these individuals who had more dreams of future successes. Those dreams included new approaches to the diagnosis and treatment of cardiovascular disease and to new procedures as yet undeveloped and untried. It will be our challenge to make these dreams also become reality.

William J. Casarella
Emory University Hospital
Atlanta, GA 30322

Magnetic Resonance Imaging in the Diagnosis of Breast Disease

Nilima Dash[1]
Anthony R. Lupetin
Richard H. Daffner
Ziad L. Deeb
Robert J. Sefczek
Rolf L. Schapiro

Magnetic resonance imaging (MRI) of the breast was performed in 10 volunteers and 102 women with suspected breast disease, using a 0.35-T superconducting magnet. All patients had prior x-ray mammography. MRI was superior to mammography in differentiating solid from cystic lesions and equivalent to mammography in providing information regarding different parenchymal patterns. Of 21 surgically proven carcinomas of the breast, MRI correctly identified 18 and mammography identified 19. The major disadvantage of MRI is its inability to show calcifications, benign or malignant. Future studies will be needed to show the relative values of sonography and MRI in detecting small cysts. In addition, MRI in future should be able to demonstrate small, noncalcified masses in mammographically dense, fibrocystic breasts.

Magnetic resonance imaging (MRI) has gained popularity within the past year [1–4], and early reports of MRI of the breast are very enthusiastic [5–9]. The high incidence of carcinoma of the breast has made both physicians and the general public anxious to explore the possibilities for earlier diagnosis. Mammography remains the diagnostic method of choice; however, our initial experience suggests that MRI will offer an important adjuvant method in breast disease diagnosis.

Subjects and Methods

One hundred and two women with suspected breast disease were prospectively studied with MRI of the breast using a 0.5-T superconducting magnet (Siemens Magnetom) with an operating field strength of 0.35 T and radiofrequency pulse of 15 MHz. All patients had prior mammography within 4 weeks and all patients had physical examinations. The person reading the MR images had prior knowledge of the findings on mammography. All masses detected by physical examination or imaging were biopsied. In addition, 10 normal volunteers were also studied.

The first 22 patients were studied using the body coil as the receiving antenna. The rest were examined with a surface coil designed for the breast. In all but two, the patient's images were obtained in the axial plane with a slice thickness of 10 mm in the body coil and 5 mm in the breast coil. Interdigitated images were obtained in selected cases, thereby acquiring contiguous slices.

The body-coil images were done in the supine position, allowing simultaneous data acquisition on both breasts. Patients studied by surface coil were prone with the breast suspended within the coil. Only two patients who could not remain in the prone position were studied supine with the surface coil placed directly over the breast. A spin-echo (SE) pulsing sequence was used. Four different sets of SE images were obtained by varying the echo delay time (TE) and/or repetition time (TR). This equipment has simultaneous multisilice, multiecho imaging capability. TEs of 35 and 70 msec were used with a TR of 700 msec (SE 700/35 and SE 700/70). TEs of 35 and 120 msec were used with a TR of 1600 msec (SE 1600/35 and SE 1600/120). Images providing the most information were SE 700/35 and SE 1600/120. These will be referred to as T1- and T2-weighted images, respectively. These are not pure T1 and T2 images and are only relative MR parameters of the actual T1 and T2 of the tissue studied at that particular value of TE and TR.

Received February 19, 1985; accepted after revision September 9, 1985.

[1] All authors: Department of Diagnostic Radiology, Allegheny General Hospital, 320 E. North Ave., Pittsburgh, PA 15212. Address reprint requests to N. Dash.

AJR 146:119–125, January 1986
0361–803X/86/1461–0119
© American Roentgen Ray Society

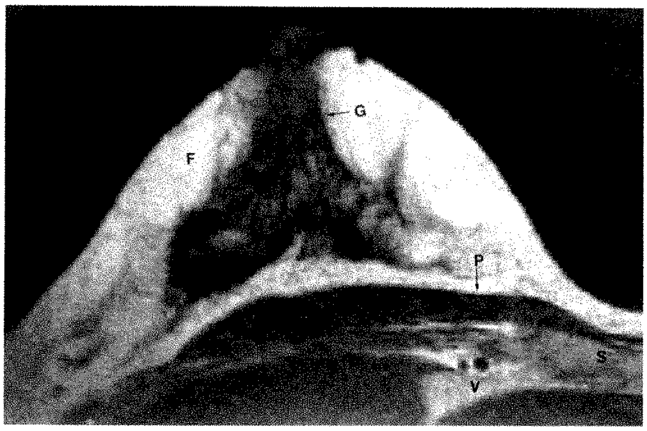

Fig. 1.—SE 700/35: normal breast image of 18-year-old woman obtained with breast coil. G = glandular tissue; F = fat; P = pectoral muscles; S = sternum; V = internal mammary vessels.

Results

Most breast images had two basic signal intensities, high-intensity signal from fat and low-intensity signal from a combination of ductal elements, glandular tissue, and vascular structures. Diseased tissue, either benign or malignant, was identified by comparing its intensity to the two basic signals.

Normal Breast and Different Parenchymal Patterns

Twenty-two patients had normal breasts. As in mammography, the appearance of a normal breast varied with the patient's age. A large amount of glandular tissue seen in young women appeared as areas of low signal intensity, slightly higher than that of chest wall muscles, in a triangular configuration converging toward the nipple (fig. 1). A predominately fatty breast demonstrated increased signals on all SE images. Normal, easily recognized structures were skin, nipple, ductal elements, chest wall muscles, sternum, and internal mammary vessels. Axillary regions were better identified on body-coil images.

The different parenchymal patterns in mammography and their risk to develop carcinoma of the breast have been well described [10], and we believe that MRI can identify these patterns. Although we did not obtain histopathologic proof, in all of these patients there was excellent correlation between mammography and MRI. An N1 pattern shows the entire breast to be of high signal intensity due to fat on all T1-weighted images (SE 700/35) (fig. 2A). Lactiferous ducts are identified as tubular structures emanating from the nipple and are best identified in a section taken at the level of the nipple. P1 and P2 breasts are differentiated according to whether the ductal tissue occupied less than (P1) or more than (P2) 25% of the entire breast (figs. 2B and 2C). We were not able to differentiate actual ductal ectasia from periductal fibrosis. The so-called dysplastic (DY) pattern is recognized by its decreased intensity in a disorganized pattern (fig. 2D). This will be discussed in further detail below.

Fibrocystic Disease

In our series, 46 patients had fibrocystic disease, yielding distinctive MRI appearances. On all SE images, the fibrous variety appears as areas of low-intensity signal identical to that of normal ductal elements. Adenosis, relating to lobular and often ductal hyperplasia, appears as innumerable small nodules of low-intensity signal on all four pulse sequences, giving the typical "snowstorm" appearance similar to that seen on mammography.

The cystic variety of fibrocystic disease shows well defined foci of low signal intensity, lower than that of normal ductal tissue on T1-weighted images (SE 700/35). The cysts change to high signal intensity on T2-weighted images (SE 1600/120) due to the long T2 relaxation time of fluid (fig. 3) [7].

Fibroadenomas

All eight cases of fibroadenomas appeared as well defined masses of low signal intensity in T1-weighted images and did not change with T2-weighted parameters (fig. 4). Calcification in a fibroadenoma, easily demonstrated by mammography, could not be directly identified on MRI. It was clear that the calcified fibroadenomas were inhomogeneous in appearance as compared to the noncalcified variety (fig. 5).

Solitary Cyst

Two patients with a solitary nonpalpable mammographic nodule showed a focus of low signal intensity on T1-weighted images (SE 700/35), which changed to high-intensity signal in T2-weighted images (SE 1600/120). These were, therefore, diagnosed as solitary cysts, proven by biopsy after needle localization.

Carcinoma

Twenty-one patients had carcinoma of the breast. In 17 patients, the carcinomas were identified on SE 700/35 images as a mass of lower intensity than ductal elements, in regions corresponding to the suspicious area in mammography. Intraductal and infiltrating ductal carcinomas were identified by their low signal intensity, as well as their irregular borders with or without radiating spicules. Secondary signs of carcinoma such as skin thickening, skin retraction, and nipple retraction were easily appreciated (fig. 6). All but three masses were of low signal intensity on all four SE images. One of these showed a low-intensity mass on a T1-weighted image, which did have a slight increase in signal intensity on T2-weighted images, but remained lower in signal than fat or fluid. In that case, differential diagnosis was circumscribed carcinoma vs. fibroadenoma and the final pathology showed infiltrating ductal carcinoma. In the other two patients, the carcinomas were cystic on T2-weighted images; however, the presence of thick irregular walls suggested the correct diagnosis.

In four of the 21 carcinoma patients, a discrete mass was not identified on MRI. One patient had inflammatory carci-

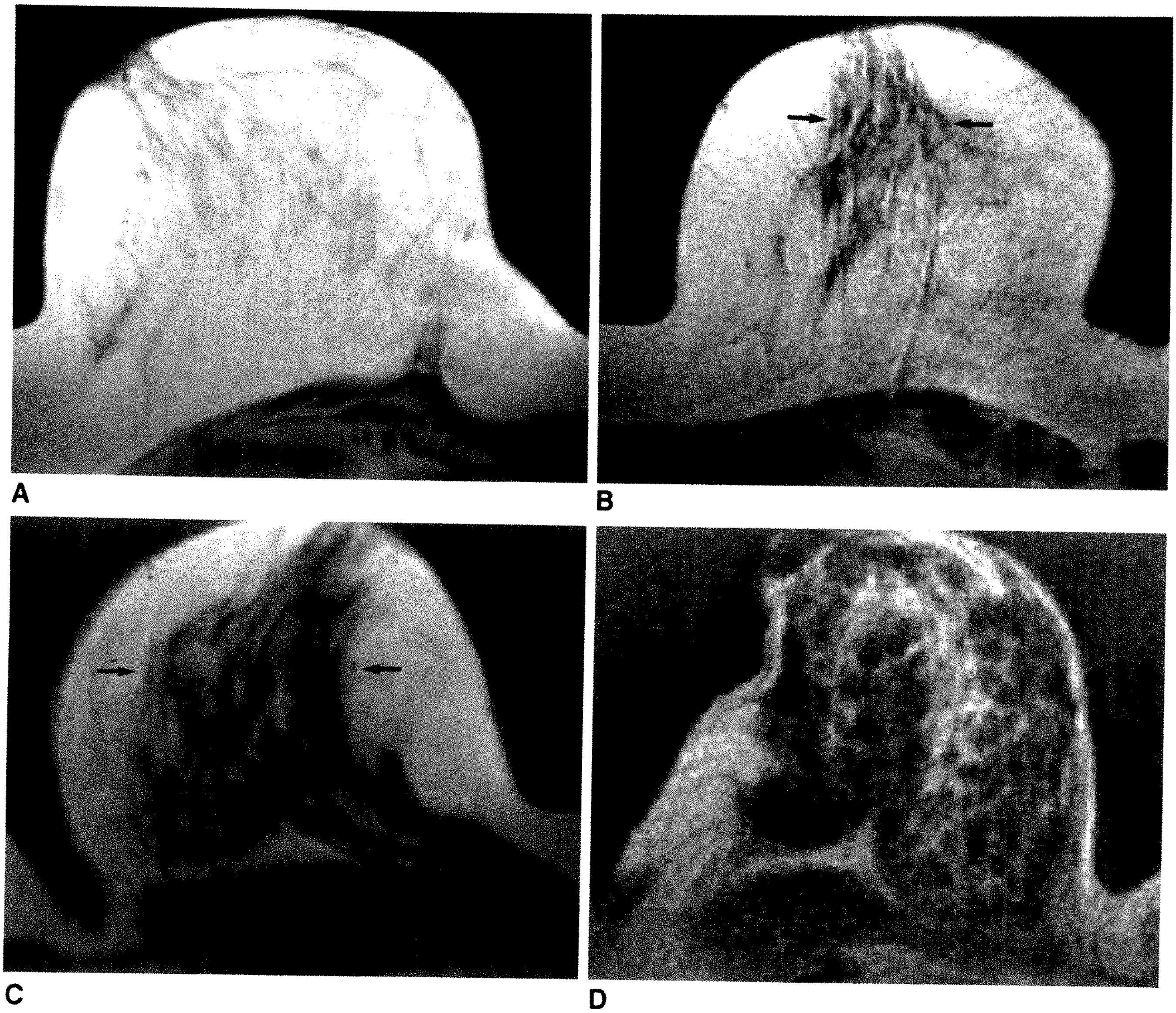

Fig. 2.—SE 700/35: breast parenchymal pattern. **A**, Normal fatty breast in 64-year-old woman. **B**, P1 parenchymal pattern. Ductal tissue (*arrows*) occupies less than 25% of breast. **C**, P2 parenchymal pattern. Ductal tissue (*arrows*) occupies at least 50% of breast. **D**, DY parenchymal pattern.

noma with findings of generalized skin thickening and a generalized decrease in intensity of the entire breast on T1-weighted images (SE 700/35). In addition, there was axillary adenopathy. In the other three patients, neither a mass nor any other sign of malignancy could be identified, even in retrospect. There was diffuse, low signal intensity in all three cases, findings compatible with diffuse mammary dysplasia. Mammographic findings were also that of mammary dysplasia in two of those patients, but in the third, a few clusters of suspicious microcalcifications were noted. Thus, there were three false-negative MRI cases in our series. There were no false positives, and we did not diagnose any occult carcinoma that was not seen by mammography.

Microcalcification was not identified on MRI, but the mass associated with the calcification was seen.

Axillary adenopathy was observed in five patients; internal mammary node involvement, sternal invasion, and cross metastasis to opposite breast in one patient (fig. 7) and recurrence of carcinoma in another patient (fig. 8) were correctly identified. The data are summarized in table 1.

Discussion

The spectrum of breast parenchymal patterns can be easily recognized by MRI. Malignant masses were differentiated from benign solid lesions predominately by their irregular borders, with or without radiating spicules, as in mammography. Differentiation of solid from cystic masses was made

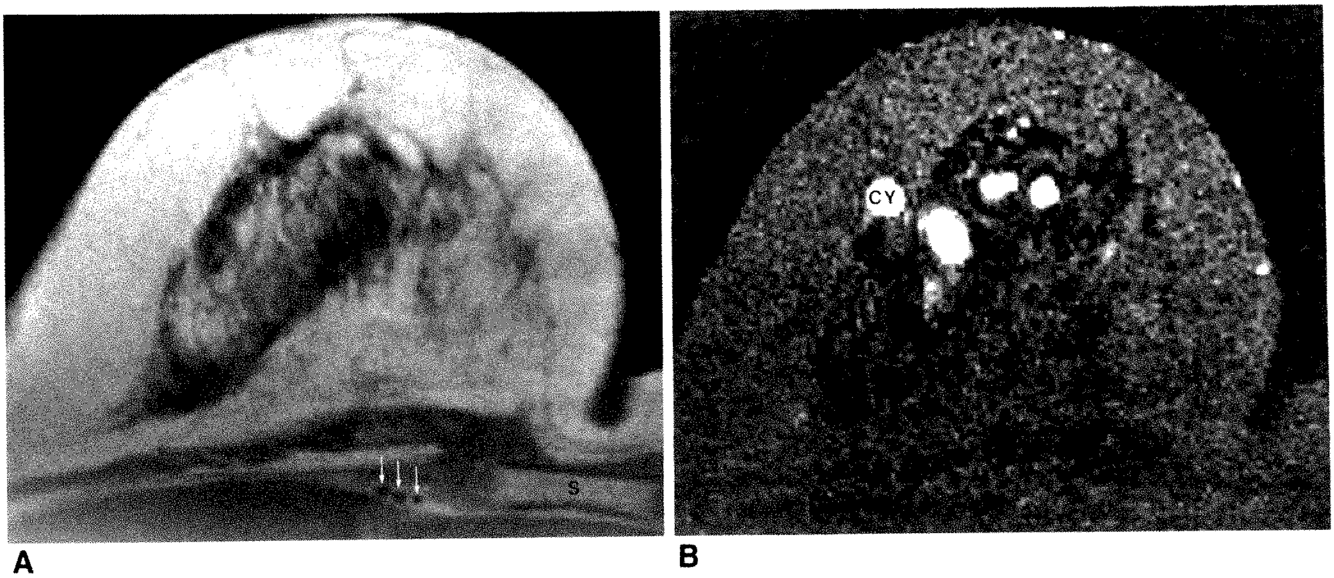

Fig. 3.—Fibrocystic disease. **A**, SE 700/35 (T1-weighted) image shows fibrocystic areas; sternum (S); internal mammary vessels (*arrows*). **B**, SE 1600/120 (T2-weighted) image shows areas of high signal intensity, indicating presence of multiple cysts (CY).

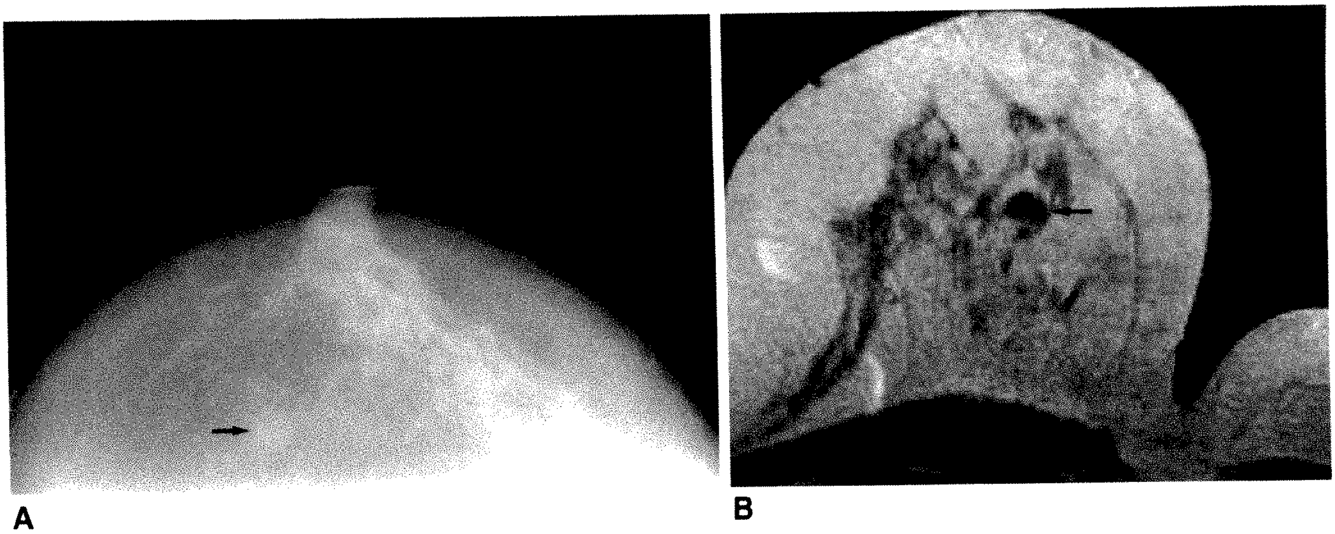

Fig. 4.—Fibroadenoma in 60-year-old woman. **A**, Craniocaudal mammogram shows ductal prominence and 1-cm, well defined nodule (*arrow*) in upper inner quadrant. **B**, SE 1600/120 (T2-weighted) image shows nodule (*arrow*) is of low signal intensity, indicating solid nature. Biopsy after localization revealed this to be fibroadenoma. Ductal prominence was seen in section taken through nipple (not shown).

correctly in every instance by the different signal intensities on T2-weighted images (solid masses were of low signal intensity and cystic lesions were of high signal intensity on SE 1600/120 images). Furthermore, all the solid as well as the solitary cystic lesions were confirmed by excisional biopsy. Since large cysts are often palpable and aspirated in a surgeon's office, the small lesions are the important ones. Thus, patients with nonpalpable mammographic lesions could benefit by this method, since MRI was accurate in distinguishing solid from cystic masses. Sonography is an established imaging method in this regard. Further studies regarding relative spatial resolution of MRI and sonography in a variety of breast sizes and parenchymal architecture will be needed to determine whether MRI offers any advantage over sonography in differentiating cysts.

Identification of a noncalcified solid mass within a fibrocystic breast (fig. 9) may also be easier with MRI than mammography, since the former uses cross-sectional imaging. This is certainly true on a theoretical basis; however, our own case material does not document this.

According to previous authors [6, 7, 9], primary and secondary signs of carcinoma are well seen on MRI. In our series,

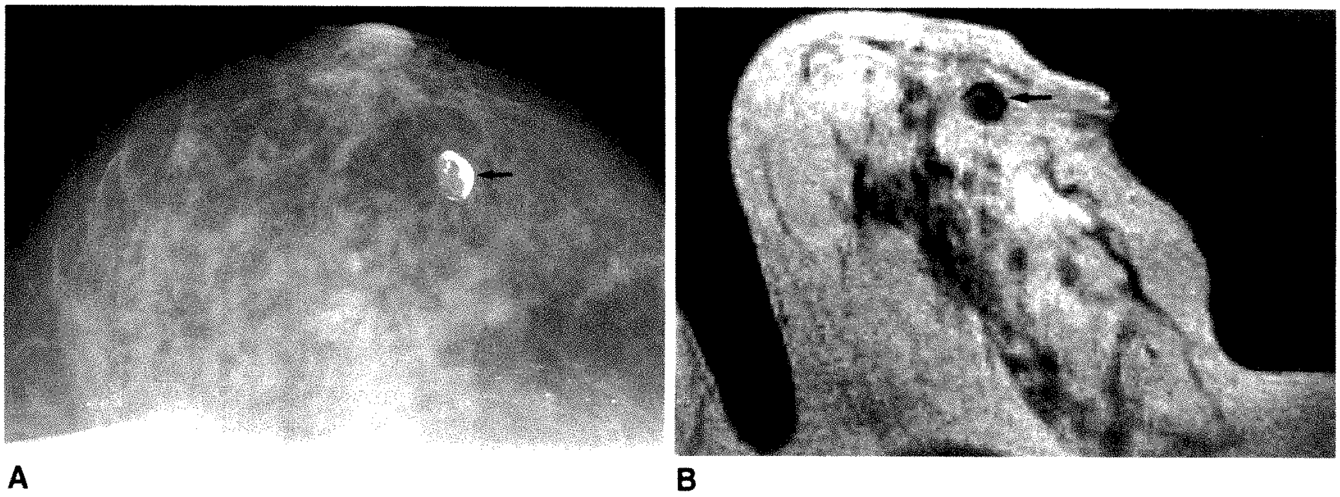

Fig. 5.—61-year-old woman with previous mastectomy had follow-up mammogram (**A**) and SE 1600/120 image (**B**) of remaining breast. Incidental calcified fibroadenoma (*arrows*) was seen. Note inhomogeneous nature of calcified fibroadenoma as opposed to noncalcified type.

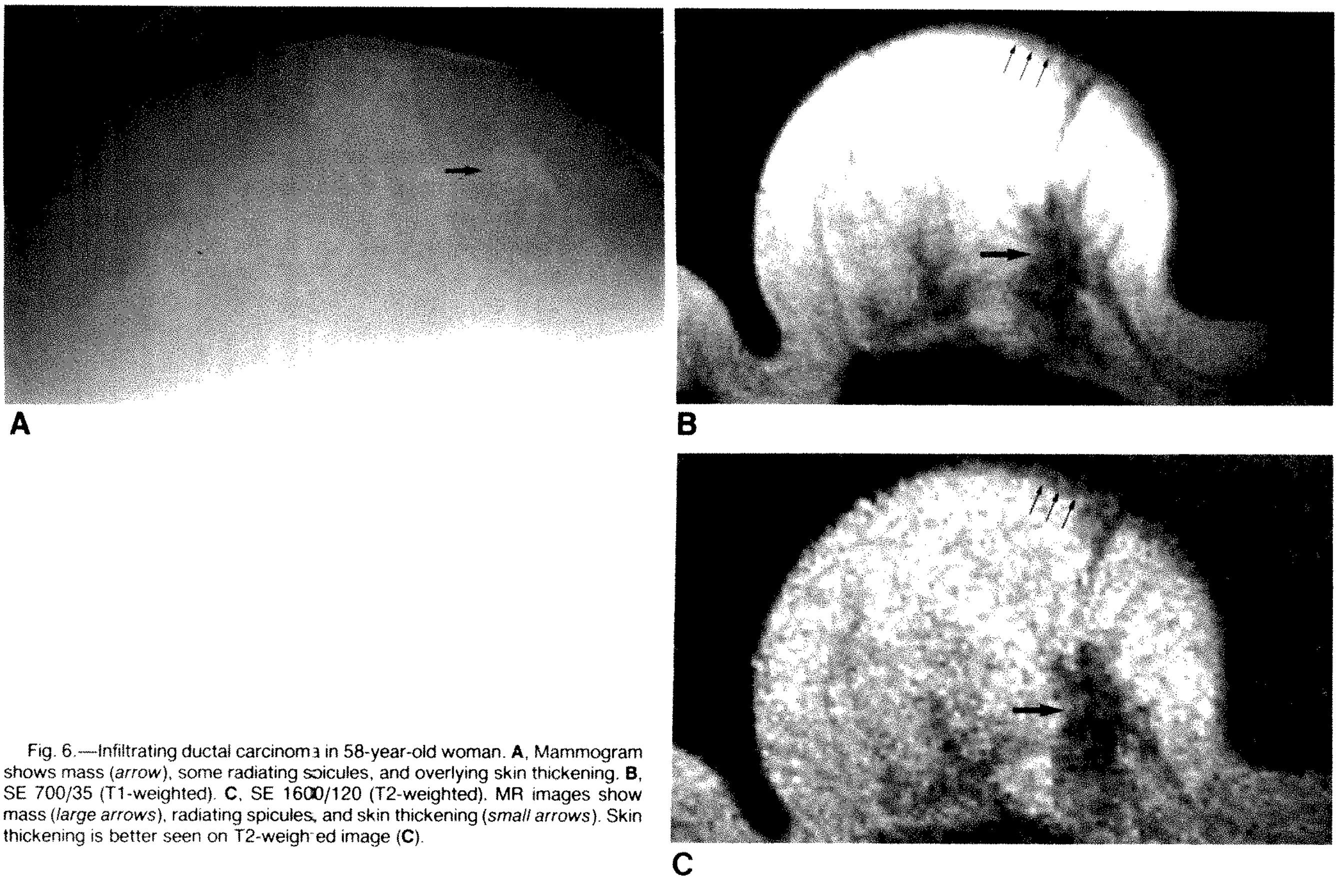

Fig. 6.—Infiltrating ductal carcinoma in 58-year-old woman. **A**, Mammogram shows mass (*arrow*), some radiating spicules, and overlying skin thickening. **B**, SE 700/35 (T1-weighted). **C**, SE 1600/120 (T2-weighted). MR images show mass (*large arrows*), radiating spicules, and skin thickening (*small arrows*). Skin thickening is better seen on T2-weighted image (**C**).

with the exception of malignant microcalcifications, primary and secondary signs of carcinoma were well identified with equal reliability on MRI and mammography. Differentiation between a noncalcified fibroadenoma and a circumscribed carcinoma is still not possible using either method. Axillary adenopathy, internal mammary adenopathy, bony involvement, and cross metastases can also be identified; thus, MRI can provide additional information about advanced lesions. Comparison studies with CT will be needed.

Three of 21 carcinomas were missed by MRI and two of

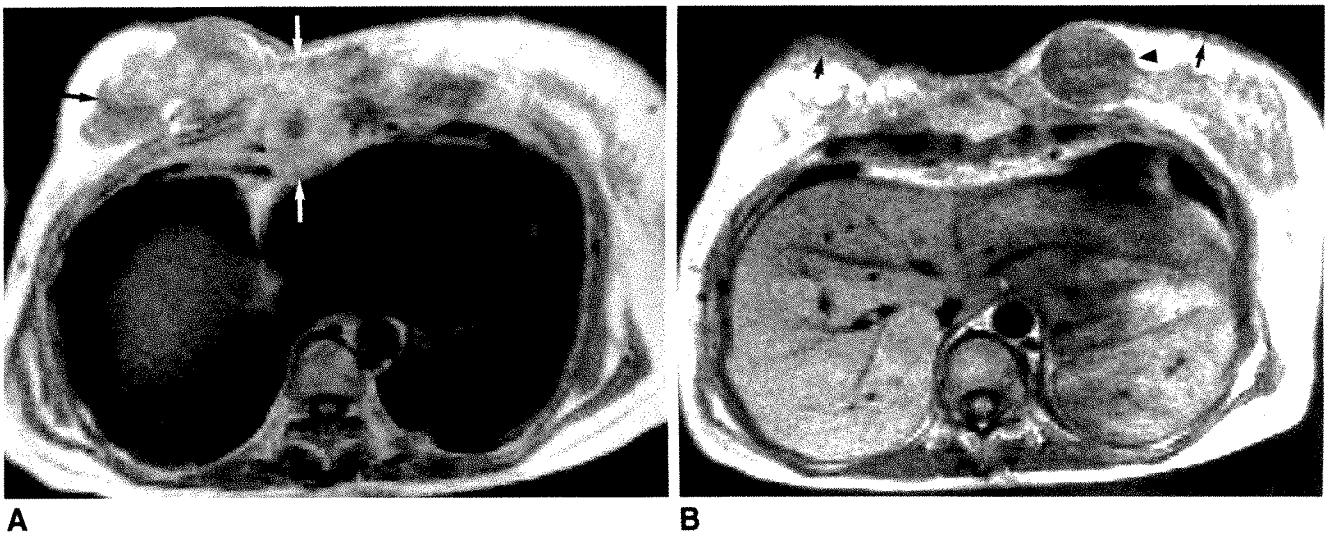

Fig. 7.—Recurrence of tumor, cross metastasis, and sternal invasion in patient with previous right-breast lumpectomy. **A**, SE 700/35 (T1-weighted) image shows multilobulated mass (*black arrow*) in right breast. Also note involvement of chest wall and sternum (*white arrows*). **B**, SE 700/35 (T1-weighted) image at lower level. Significant bilateral skin thickening (*arrows*) and left breast mass (*arrowhead*) due to cross metastasis.

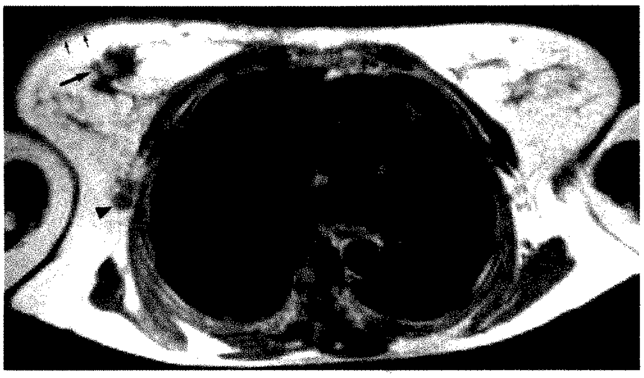

Fig. 8.—Recurrent tumor with axillary adenopathy in woman who had prior right-breast lumpectomy. SE 700/35 (T1-weighted) image shows mass with several radiating spicules (*large arrow*), diffuse skin thickening (*small arrows*), and right axillary adenopathy (*arrowhead*).

TABLE 1: **Correlation of Findings in 102 Patients Studied by MRI and Mammography**

Final Diagnosis	No. of Patients	No. Diagnosed by Mammography	No. Diagnosed by MRI
Carcinoma	21	19	18
Fibroadenoma	8	8	8
Solitary cyst	2	2	2
Intramammary lymph node	1	1	1
Hematoma	1	1	1
Prosthesis	1	1	1
Fibrocystic disease*	46	46	46
Normal*	22	22	22

* Not surgically proven; final diagnosis based on physical examination, mammography, and 1-year follow-up.

these were also missed by mammography. The third showed microcalcifications on mammography. There were no false-positive cases in our series and we did not diagnose any occult carcinoma by MRI that was not seen on mammography.

The limiting factors of MRI as compared to mammography are:

1. Long scanning time, since only one breast can only be examined at a time with the use of a surface coil at present with our equipment. In our institution, at least 45 min to 1 hr of total time is required per patient for both breasts.
2. Higher costs. Currently, we are not billing our MRI patients; however, in the future, the cost of MRI will probably be at least five times that of mammography.
3. Volume averaging is of some concern, but with 5-mm contiguous scanning, we were able to see solid lesions as small as 8 mm and cystic lesions as small as 5 mm.
4. Inability to identify microcalcifications.

We believe that MRI shows promise as an adjuvant method in breast disease diagnosis, particularly for its potential to detect noncalcified tumors in mammographically dense breasts. Additional comparative studies will be needed to assess its role in cyst detection compared to sonography and its value in local staging compared to CT. High costs will preclude its consideration as a screening method.

REFERENCES

1. Kaufman L, Crooks LE, Margulis AR, eds. *Nuclear magnetic resonance imaging in medicine.* New York: Igaku-Shoin, **1981**
2. Gadian DG. *Nuclear magnetic resonance and its applications to living systems.* New York: Clarendon, **1982**

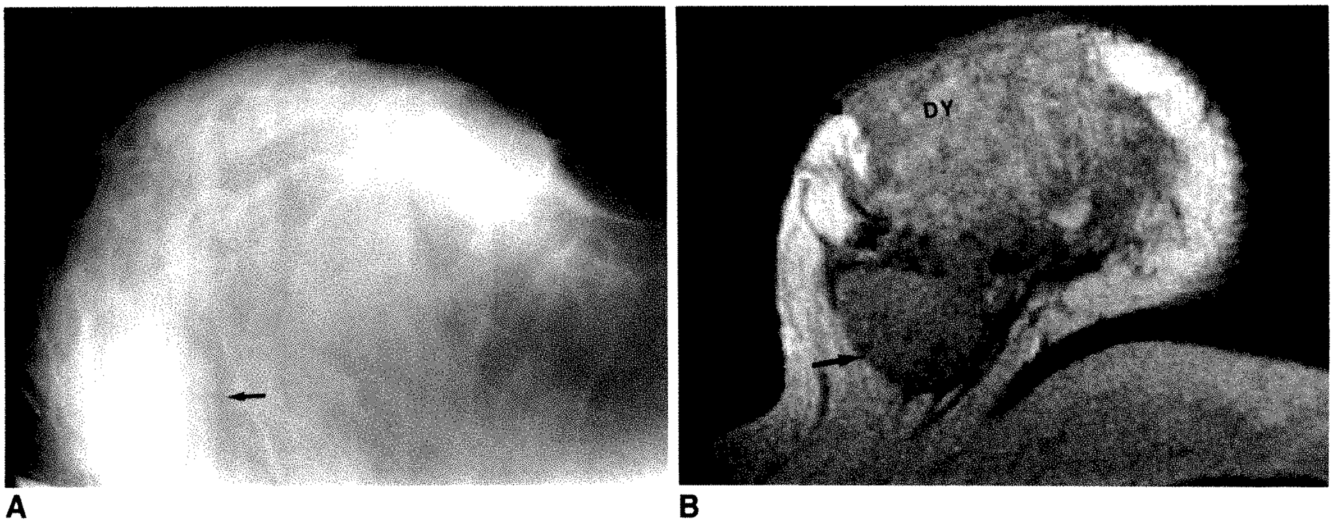

Fig. 9.—46-year-old woman with fibrocystic disease and carcinoma of breast. **A**, Mammogram reveals severe fibrocystic disease and large, well defined mass (*arrow*). **B**, SE 700/35 (T1-weighted) image shows dysplastic changes (DY) and mass (*arrow*) of low signal intensity. On T2-weighted image (SE 1600/120, not shown), mass was believed to be solid; thus diagnosis of fibroadenoma vs. circumscribed carcinoma was made. At surgery, this was infiltrating ductal carcinoma.

3. Partain CL, James AE, Rollo FD, Price RR, eds. *Nuclear magnetic resonance imaging*. Philadelphia: Saunders, **1983**
4. Pykett IL, Newhouse JH, Buonanno FS, et al. Principles of nuclear magnetic resonance imaging. *Radiology* **1982**;143:157-168
5. El Yousef SJ, Alfidi RJ, Duchesneau RH, et al. Initial experience with nuclear magnetic resonance (NMR) imaging of the human breast. *J Comput Assist Tomogr* **1983**;7:215-218
6. El Yousef SJ, Duchesneau RH, Alfidi RJ, Haaga JR, Bryan PJ, LiPuma JP. Magnetic resonance imaging of the breast. *Radiology* **1984**;150:761-766
7. El Yousef SJ, Duchesneau RH. Magnetic resonance imaging of the human breast: a phase 1 trial. *Radiol Clin North Am* **1984**;22:859-877
8. McSweeney MB, Small WC, Cerny V, Sewell W, Powell RW, Goldstein JH. Magnetic resonance imaging in the diagnosis of breast disease: use of transverse relaxation times. *Radiology* **1984**;153:741-744
9. Stelling CB, Wang PC, Lieber A, Mattingly SS, Griffen WO, Powell DE. Prototype coil for magnetic resonance imaging of the female breast. *Radiology* **1985**;154:457-462
10. Wolfe JN, Albert S, Belle S, Salane M. Breast parenchymal patterns and their relationship to risk for having or developing carcinoma. *Radiol Clin North Am* **1983**;21:127-136

Male Mammography

D. David Dershaw[1]

Over a 7-year period, 94 mammograms were performed for male breast disease. Indications included breast enlargement, tenderness, mass, and previous mastectomy. Fatty enlargement was easily diagnosed. Gynecomastia was unilateral in 28 of 40 cases and easily differentiated from malignancy in all but one patient in whom nipple retraction was present. In cases of bilateral gynecomastia, eight showed asymmetric involvement. Three carcinomas were studied, two of which were clinically obvious. One asymptomatic cancer was detected on routine follow-up in a man with previous mastectomy.

Mammography of the male breast is an unusual examination, constituting well under 1% of all mammograms performed at this institution in the past 7 years. The diagnoses were limited to fatty enlargement of the breasts, which is not a pathologic phenomenon, gynecomastia, and carcinoma. Less than 1% of all breast cancers occur in men and this constitutes 0.2% of malignancies in men. Gynecomastia, however, is a common entity, especially in adolescent boys and in men over 50. In adolescents some series cite its frequency at 50% [1]. Experience with mammography in men over a 7-year period is reviewed here.

Materials and Methods

Between 1978 and January 1985, 15,967 mammograms were performed at this hospital. Of these, 94 (0.56%) were performed on 89 men. Follow-up data were available on 49 of these patients and are the basis for this report.

Examinations were performed on dedicated mammography equipment, a CGR Senograph with a nominal 0.6-mm focal spot, molybdenum target, beryllium window, and a 0.03-mm molybdenum filter. Both mediolateral and craniocaudal views of each breast were routinely done. In two patients, a previous mastectomy had been performed and unilateral mammography was performed on three occasions in each of these patients. One patient with gynecomastia had two studies.

Clinical and pathologic data were obtained by review of patient charts. Patients were excluded from this series when charts were not available, surgery was performed outside this institution, or there was inadequate clinical follow-up to confirm a diagnosis. Fifteen patients had biopsies.

Results

Of the 49 patients studied, 40 had gynecomastia, five had fatty breasts without true gynecomastia, three had infiltrating ductal carcinoma, and one patient was status post mastectomy and was being followed with mammography of the clinically normal opposite breast. Patients with gynecomastia were aged 21–81 years (mean, 56). Men with cancer were aged 62, 74, and 82 (mean, 73).

Fatty breasts (fig. 1), which were often associated with clinical obesity, had an absence of retroareolar density, and except for increased volume their pattern was that of a normal male breast. The breasts were radiolucent without any mass or

Received June 21, 1985; accepted after revision September 11, 1985.

[1] Department of Diagnostic Radiology, Memorial Sloan-Kettering Cancer Center, 1275 York Ave., New York, NY 10021.

AJR 146:127–131, January 1986
0361–803X/86/1461–0127
© American Roentgen Ray Society

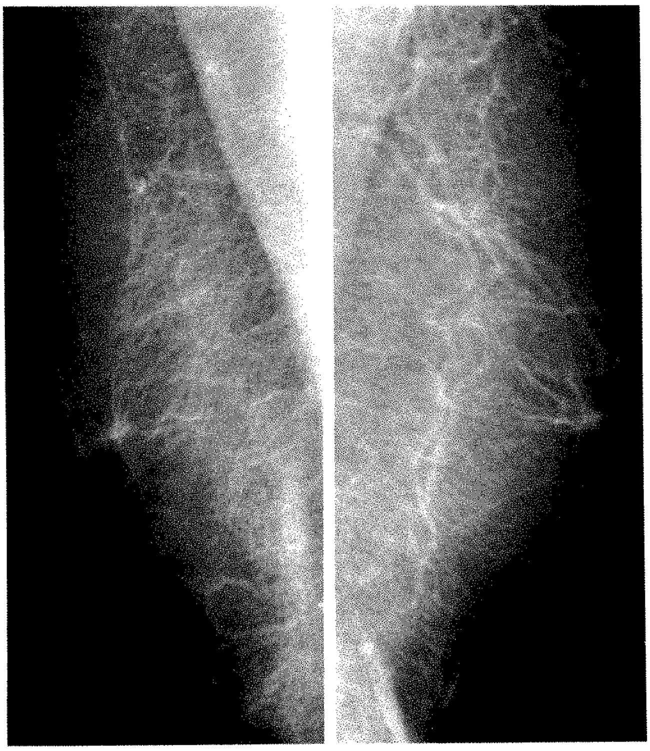

Fig. 1.—Bilateral mediolateral mammograms. Fatty breasts. No retroareolar density is present. Fatty density of breasts is interrupted only by supporting stroma and vasculature.

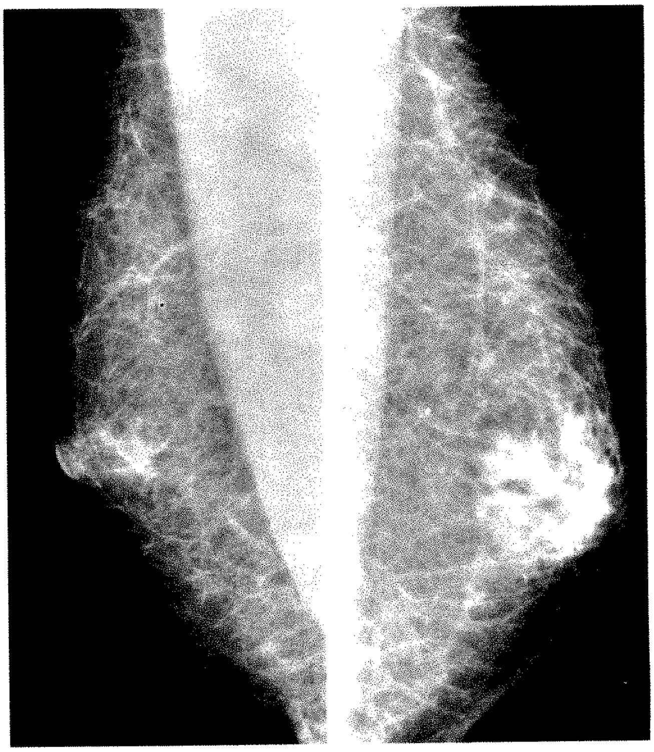

Fig. 2.—Bilateral mediolateral mammograms. Bilateral gynecomastia, left greater than right, in 51-year-old man. Cause is indeterminate. Flame-shaped, glandular proliferation is symmetrically positioned behind nipple.

calcifications. Three of these five patients underwent biopsy for palpable masses. Histology of the specimens revealed fatty or fibrofatty tissue.

In patients with gynecomastia, 28 had unilateral and 12 had bilateral disease. In those affected unilaterally, the left breast was involved in 15 patients and the right in 13. Of those 12 men with bilateral disease, eight had one breast more severely involved than the other. The left breast was more prominently involved in five and the right in three.

All men with gynecomastia showed a pattern of glandular proliferation extending from the nipple into the fatty tissue of the breast. This glandular density was triangular or flame-shaped. In 27 men, this density was symmetrically positioned behind the nipple (fig. 2). Some asymmetry in the pattern was seen in 13 patients. In no patients with gynecomastia was a coexistent malignancy found nor did one develop in these men during the period they were clinically observed.

One patient with gynecomastia had two mammograms done 1 year apart (fig. 3). These showed progressive development of a ductal and glandular pattern.

In patients with unilateral gynecomastia of determinable causes, all were drug-induced. These included digitalis preparations in five patients and thiazides in four. In addition, there were single instances due to spironolactone, diazepam, cyclophosphamide, heroin-methadone abuse, and marijuana-LSD abuse. Two patients had bilateral disease secondary to exogenous estrogen given as part of therapy for prostate carcinoma. Vincristine- and prednisone-induced bilateral disease was seen in another patient. Three other men had systemic diseases resulting in bilateral gynecomastia. These included cirrhosis, chronic renal failure on dialysis, and unspecified chronic liver disease with methadone abuse.

Two men with prostate carcinoma who were receiving exogenous estrogen had a mammographic pattern that differed from that in all other patients. They showed a more diffuse proliferation of ductal and glandular elements and their mammograms resembled those of female breasts (fig. 4). In one of these patients, multiple nodules mimicked a fibrocystic pattern (fig. 5). No further evaluation of this patient was performed.

Nine patients with mammographic findings of gynecomastia had biopsies at this center. In five the specimen was read as gynecomastia. In the other four patients, histologies were interpreted as focal mastitis, papillomatosis, fibrosis and duct hyperplasia, and duct stasis with periductal mastitis and chronic inflammation.

One patient with gynecomastia had nipple retraction associated with a triangular pattern of retroareolar density. No calcifications were present. The pattern was difficult clinically and mammographically to differentiate from breast cancer, and biopsy was required to exclude this diagnosis. Only fibrofatty tissue was found at biopsy.

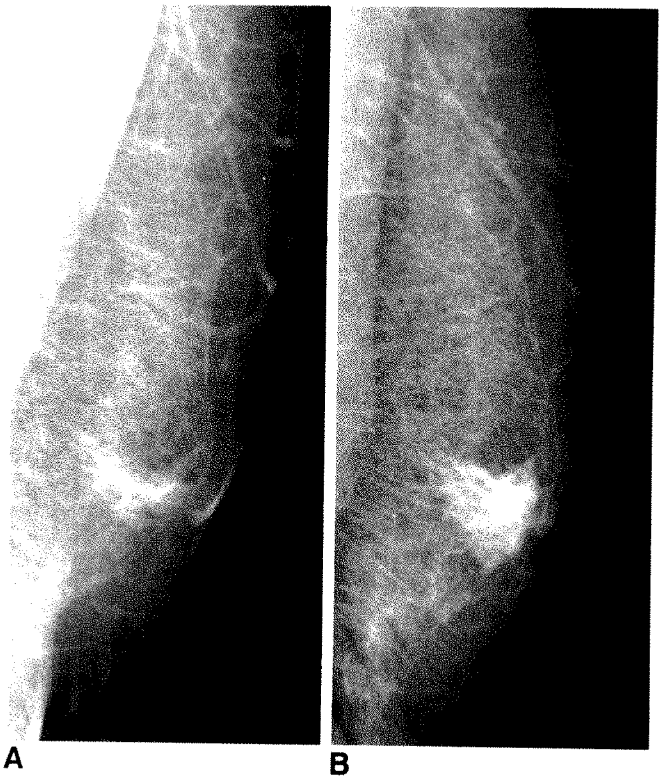

Fig. 3.—Left mediolateral mammograms, 1 year apart in 70-year-old man followed for pronounced, right gynecomastia. Minimal, left subareolar density on original study (**A**) was increased 1 year later (**B**).

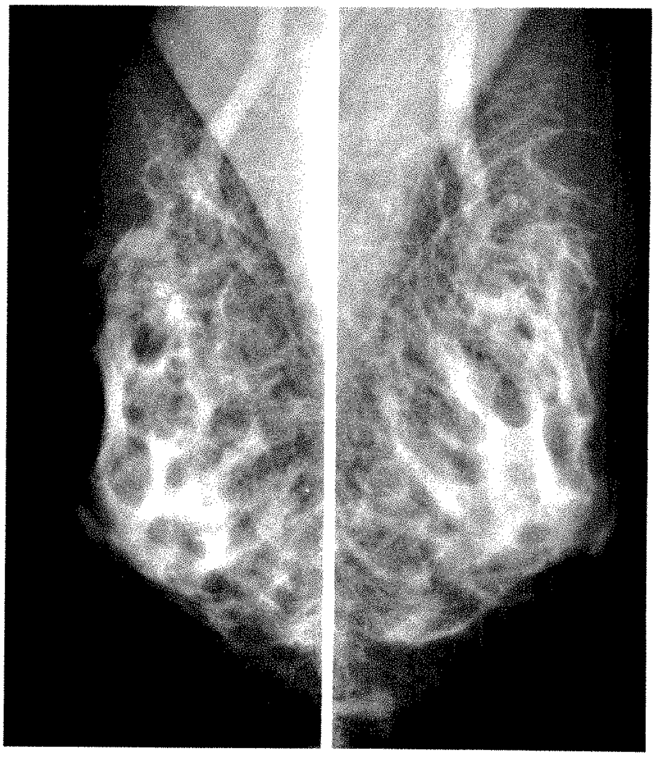

Fig. 4.—Bilateral mediolateral mammograms. Diffuse, markedly increased, glandular density bilaterally in man with carcinoma of prostate treated with estrogen. Bilateral, prominent, draining veins are present.

Infiltrating ductal carcinoma was found in three men. In two the lesion was clinically apparent (fig. 6). Routine, follow-up mammography revealed a nonpalpable nodule in one patient, who had had a mastectomy 7 years earlier (fig. 7). Biopsy of the mass identified a new carcinoma, and a modified radical mastectomy was performed. In this patient and in one of the other two men, the axillary nodes were free of disease. The third patient had positive nodes at level 1.

The two cancers that were clinically evident were central retroareolar lesions. Nipple deformity and skin thickening were present in both men. Scattered, fine calcifications were present in one breast, but were not associated with the tumor mass. They did not have the pattern of malignant microcalcifications. Their significance was undetermined. No increase in vascularity was associated with either lesion.

The nonpalpable malignancy was eccentric in the lower, inner quadrant. This 1-cm nodule had incomplete marginal definition and was new since the mammogram performed 3 years earlier. No microcalcifications or secondary signs of tumor were present.

Discussion

The normal male breast is composed predominantly of fat with few secretory elements. Radiographically it appears lucent with a few strands coursing through its volume.

The most common indication for mammography in men is gynecomastia. The condition has two peak periods: one in adolescence, where it is reported in greater than 50% of normal boys aged 12–15, and again with advancing age, largely in men over 65 [1]. The earlier condition is believed to be due to elevated serum estradiol. The latter condition may reflect testicular failure with diminishing levels of total and free serum testosterone, increasing serum luteinizing hormone, and unchanged serum estradiol [1]. In addition, a large number of drugs and disease states can induce gynecomastia. Drug-induced gynecomastia was seen in many patients in the present series. Digitalis preparations and thiazides were most often responsible, but spironolactone, diazepam, exogenous estrogen, cyclophosphamide, heroin-methadone combination, and marijuana-LSD combination were also causative agents. Gynecomastia also has been associated with the administration of androgens, human chorionic gonadotropin, methyl-dopa, cimetidine, isoniazid, amphetamines, reserpine, and tricyclic antidepressants [1]. A long list of disease states may also produce gynecomastia. Along with the chronic renal and hepatic diseases seen in this series, these include resolving malnutrition, disordered thyroid function, adrenal insufficiency and tumors, Klinefelter syndrome, testicular tumors, and several other tumors and disease states [2]. Of all these causes, only Klinefelter syndrome seems to have an increased incidence of breast cancer associated with gynecomastia [3].

On physical examination in gynecomastia, a subareolar,

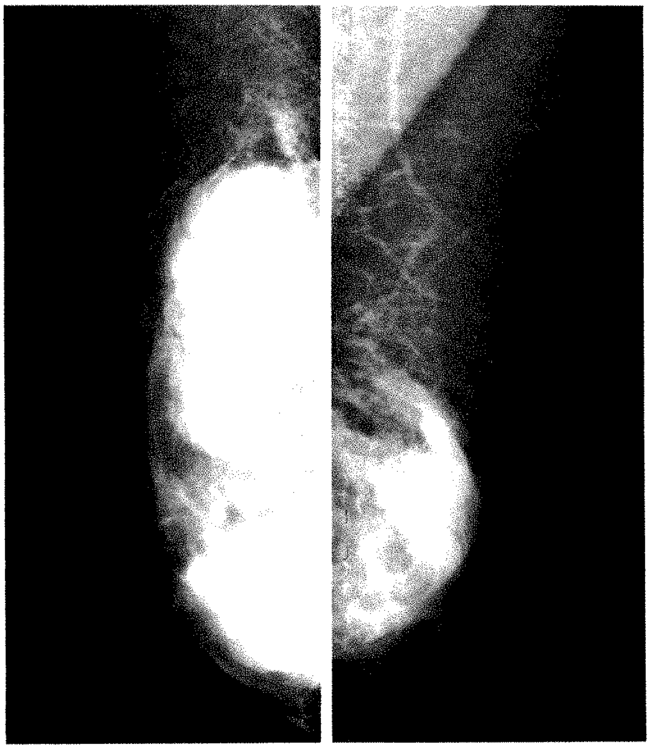

Fig. 5.—Bilateral mediolateral mammograms. Man treated with estrogen for prostatic carcinoma. Dense, nodular pattern in both breasts resembles female fibrocystic disease.

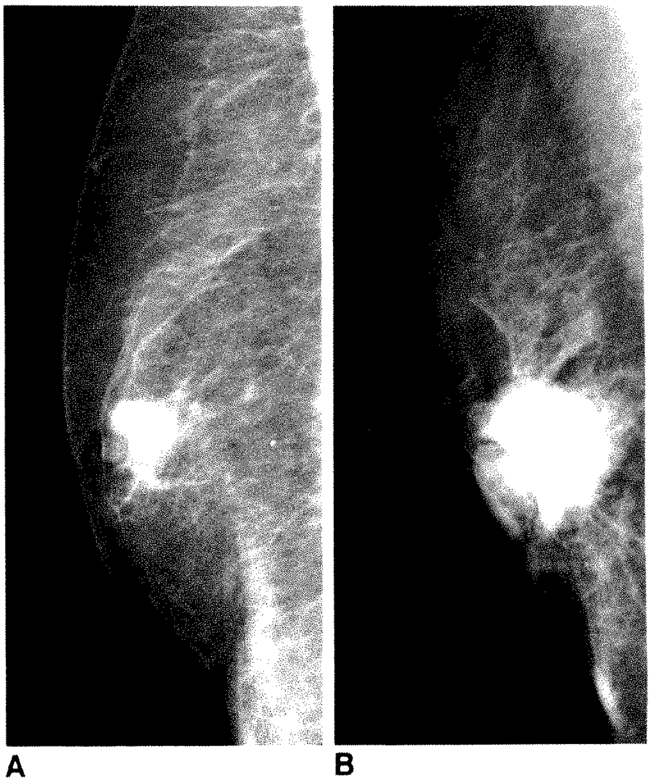

Fig. 6.—Right mediolateral mammograms in two patients with infiltrating ductal carcinoma. **A**, 74-year-old man: eccentric, subareolar mass and nipple retraction. Left breast was normal. **B**, 82-year-old man: stellate, subareolar mass with nipple and skin retraction.

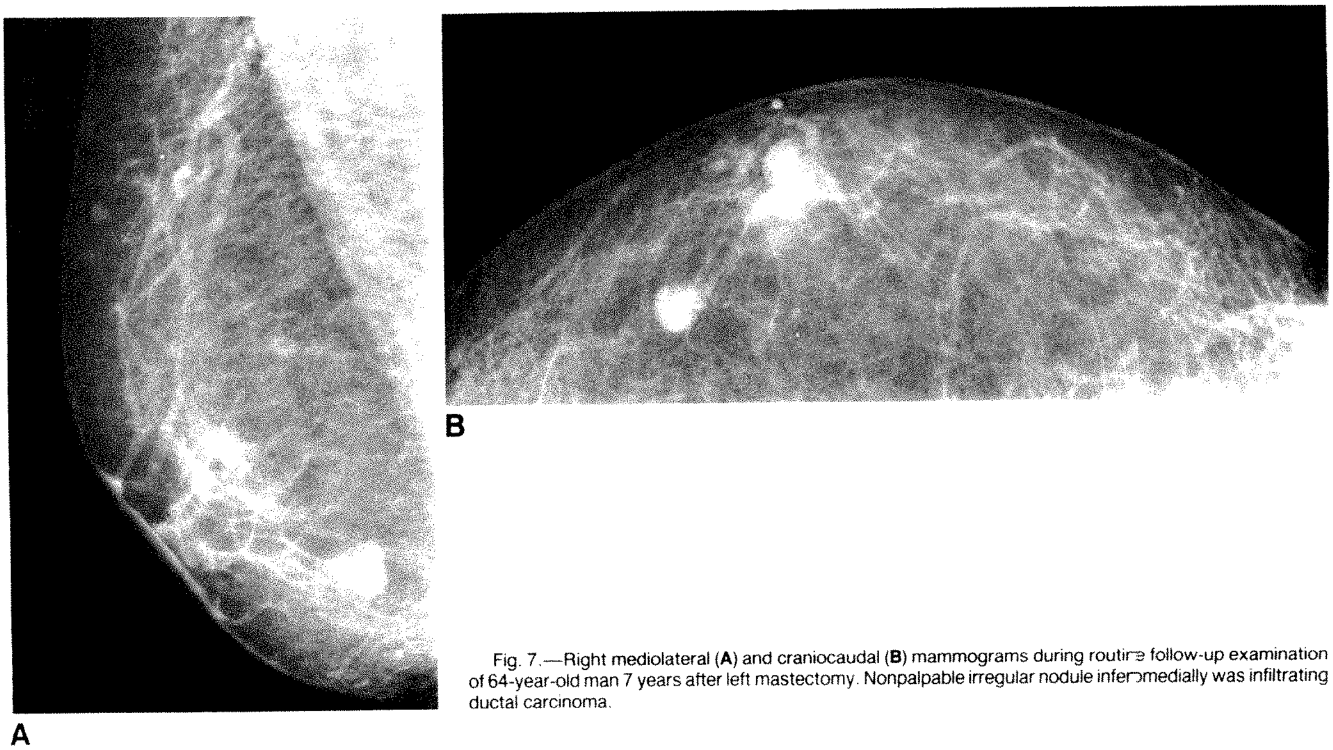

Fig. 7.—Right mediolateral (**A**) and craniocaudal (**B**) mammograms during routine follow-up examination of 64-year-old man 7 years after left mastectomy. Nonpalpable irregular nodule inferomedially was infiltrating ductal carcinoma.

palpable mass, which may be well defined or more diffuse, is present. A localized nodule may be palpable; tenderness may be present. This condition is usually reported as predominantly unilateral. However, at least one recent series reports a predominance of bilateral gynecomastia [4]. In our 40 patients, 28 had unilateral disease, and eight of the 12 bilateral disease cases had asymmetry of involvement.

Histologically, a pattern of dense, fibrous connective tissue is present. Marked proliferation of ducts and stroma is seen. Formation of acini and lobules has never been identified [2, 5]. Some inflammatory reaction may be present.

The prognosis in this condition depends, as would be expected, on the cause. In adolescent gynecomastia, one series demonstrated resolution in all but 8% of 52 boys at the end of 3 years [6]. A series of 115 adult patients with adequate follow-up showed 44% with spontaneous regression of their gynecomastia [2]. In only five patients in the current series was a clinical description of resolution or diminution of symptomatology found.

Carcinoma of the male breast is an unusual lesion with a frequency equaling only about 0.9% of the occurrence of female breast cancer [7] and 0.2% of all malignancies in men [1]. Peak age of the disease is 60 with the peak incidence in the fifth and sixth decades [4, 7]. A case of a 6-year-old boy with breast cancer has been reported; thymic irradiation had been given at birth to this child [8]. The lesion may be central or peripheral. The central position is frequent, and nipple involvement and ulceration of the overlying skin are common [9]. When correlated with lesions of similar stage in women, the overall prognosis is the same [10].

Radiographically, microcalcifications are an unusual finding. Although one report claims they are never present [11], another series of 20 male breast cancers had a 30% frequency of microcalcifications within the tumor mass [12]. One of our patients had small calcifications within fatty tissue adjacent to the tumor mass, but these did not have an appearance of malignant microcalcifications and the significance of their association was undetermined. I have been unable to find a report of a male breast cancer presenting radiographically as microcalcifications without an associated mass.

The malignant mass may be relatively well delineated or may have a stellate appearance like that of scirrhous carcinoma in the female. As well defined breast nodules in men are likely to represent cancer, biopsy of these lesions is indicated [12]. The presence of axillary adenopathy is an important prognostic sign in men as well as in women. No adenopathy was seen in our three patients. On axillary dissection, axillary nodal metastases were found in one of these patients, and this was limited to level 1 nodes.

No reports of mammography in postmastectomy men are available. The single case in this series of diagnosis of a nonpalpable carcinoma in a postmastectomy man suggests that mammography may be indicated on an annual basis in these patients as it is in the postmastectomy woman. These patients remain at risk for disease in the contralateral breast.

Gynecomastia may not always be readily differentiated from carcinoma. Some degree of eccentricity may be present in gynecomastia, although this is more pronounced in carcinoma. Nipple retraction may be associated with gynecomastia [13] as it was in one case in this series, and in this situation biopsy may be needed to exclude the diagnosis of malignancy.

Sonography has been used to evaluate gynecomastia. Patterns of retroareolar hypoechogenicity or a more diffuse pattern of increased echoes is described as characteristic of this condition [14, 15]. A reported case of sonography of male breast cancer indicated only subtle sonographic findings, although obvious malignant mammographic changes were present [16].

REFERENCES

1. Carlson HE. Gynecomastia. *N Engl J Med* **1980**;303:795–799
2. Treves N. Gynecomastia. *Cancer* **1958**;11:1082–1102
3. Scheike O, Visfeldt J, Peterson B. Male breast cancer. 3. Breast carcinoma in association with the Klinefelter syndrome. *Acta Pathol Microbiol Scand* [*A*] **1973**;81:352–358
4. Kapdi C, Parekh NJ. The male breast. *Radiol Clin North Am* **1983**;21:137–148
5. Lewis D, Geschickter CF. Gynecomastia, virginal hypertrophy and fibroadenomas of the breast. *Ann Surg* **1934**;100:779–795
6. Nuttall F. Gynecomastia as a physical finding in normal men. *J Clin Endocrinol Metab* 48:338–340, 1979
7. Yap H, Tashima C, Blumenschein G, Eckles N. Male breast cancer, a natural history study. *Cancer* **1979**;44:748–754
8. Simpson J, Barson A. Breast tumors in infants and children: a 40-year review of cases at a children's hospital. *Can Med Assoc J* **1969**;101:100–102
9. Crichlow R. Breast cancer in men. *Semin Oncol* **1974**;1:145–152
10. Holleb A, Freeman H, Farrow J. Cancer of the male breast. *NY State J Med* **1968**;68:544–553
11. Kalisher L, Peyster R. Xerographic manifestations of male breast disease. *AJR* **1975**;125:656–661
12. Onimet-Oliva D, Hebert G, LaDouceur J. Radiographic characteristics of male breast cancer. *Radiology* **1978**;129:37–40
13. Michaels L, Gold R. Arndt R. Radiography of gynecomastia and other diseases of the male breast. *Radiology* **1977**;122:117–122
14. Wigley K, Thomas J, Bernardino M, Rosenbaum J. Sonography of gynecomastia. *AJR* **1981**;136:927–930
15. Cole-Beuglet C, Schwartz G, Kurtz A, Patchefsky A, Goldberg B. Ultrasound mammography for male breast enlargement. *J Ultrasound Med* **1982**;1:301–305
16. Jackson V, Gilmor R. Male breast carcinoma and gynecomastia: comparison of mammography with sonography. *Radiology* **1983**;149:533–536

Breast Cancer Metastasis to Intramammary Lymph Nodes

Karen K. Lindfors[1, 2]
Daniel B. Kopans[1]
Kathleen A. McCarthy[1]
Frederick C. Koerner[3]
Jack E. Meyer[1, 4]

Metastatic disease to the intramammary lymph nodes from breast cancer may be seen mammographically. In the four cases reviewed, the affected intramammary lymph nodes were enlarged (1 cm or greater in diameter), homogeneous, and well circumscribed. All lacked the lucent center or hilar notch characteristic of benign intramammary nodes. Differentiation of malignant from benign causes of intramammary lymph node enlargement, such as inflammation or hyperplasia, is impossible by mammography. Biopsy is recommended for all intramammary lymph nodes of 1 cm or greater that are not fat infiltrated unless the patient clearly has an associated dermatitis or mastitis. Metastatic disease to the intramammary lymph nodes may be the first clinical and/or mammographic sign of breast cancer and may significantly affect prognosis.

Smoothly marginated masses in the breast are often seen mammographically. In most cases, the histology of such masses is indeterminate. Normal intramammary lymph nodes, however, have a characteristic appearance and position in the breast that allows their identification. Alterations in the typical mammographic appearance of these lymph nodes may signify infiltration with metastatic disease and herald carcinoma elsewhere in the breast. Metastatic disease from breast cancer to intramammary lymph nodes seems to be significant prognostically and may influence therapeutic decisions.

Materials and Methods

From March 1, 1981 to March 1, 1985, about 16,000 mammographic examinations were performed at Massachusetts General Hospital. Among these studies were three cases in which metastasis to intramammary lymph nodes was visible mammographically. A fourth case of metastasis to an intramammary lymph node was referred from another institution for adjunctive therapy after mastectomy.

These patients were aged 56–67 years. Three had palpable upper-outer-quadrant masses. The fourth woman was asymptomatic, and the lesion was detected during a routine screening study.

The involved lymph nodes were all well circumscribed, homogeneous, round or oval masses in the upper-outer quadrants of the breast, and all were larger than 1 cm (range, 1.2–2 cm). Two patients had previous mammograms demonstrating benign-appearing intramammary lymph nodes smaller than 1 cm in the location where the enlarged nodes were later seen (fig. 1).

In three of the women, the node was palpable. In the first, the primary breast cancer was visible by mammography and was also palpable (fig. 2). The second patient had a clinically occult primary lesion that was visible as a poorly defined mass by mammography (fig. 1). In the third patient, the clinically occult intraductal primary cancer was indicated by microcalcifications found by radiography of the mastectomy specimen (fig. 3). In the fourth patient, a routine screening mammogram detected the nonpalpable enlarged intramammary lymph node.

Each of these four women had a modified radical mastectomy. In the three who had their surgery at our institution, the intramammary lymph nodes containing metastatic breast

Received June 24, 1985; accepted after revision September 4, 1985.

[1] Department of Radiology, Massachusetts General Hospital, and Massachusetts General Hospital Cancer Center, Boston, MA 02114. Address reprint requests to D. B. Kopans.

[2] Present address: Department of Radiology, University of California, Davis Medical Center, Sacramento, CA 95817.

[3] Department of Pathology, Massachusetts General Hospital, and Massachusetts General Hospital Cancer Center, Boston, MA 02114.

[4] Present address: Department of Radiology, University of Louisville School of Medicine, Humana Hospital University, Louisville, KY 40202.

AJR 146:133–136, January 1986
0361–803X/86/1461–0133
© American Roentgen Ray Society

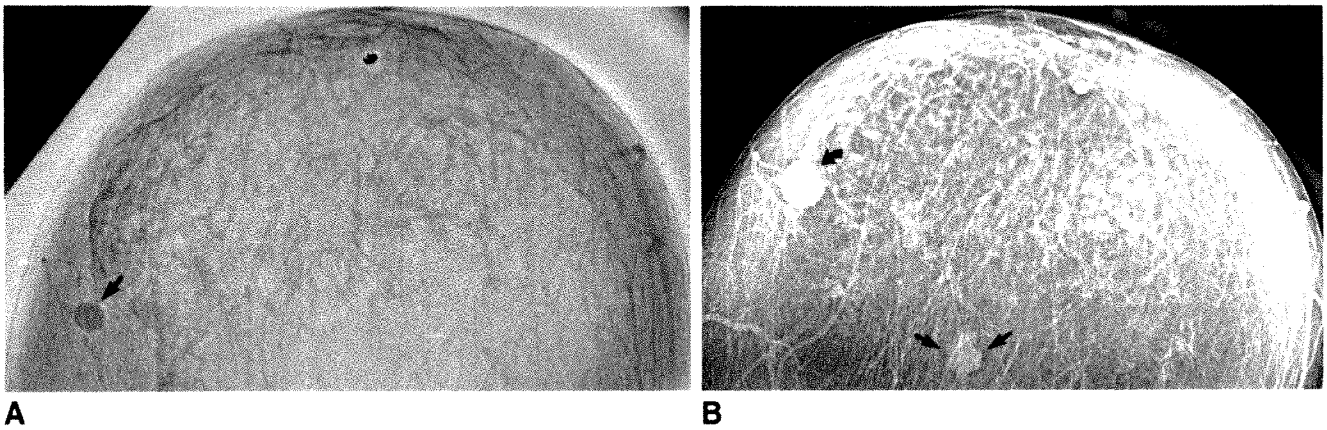

Fig. 1.—**A**, Positive-mode craniocaudal xeromammogram. Sharply defined 0.9-cm density laterally (*arrow*) is intramammary lymph node. **B**, Negative-mode examination 3 years later. Node has enlarged to 2 cm (*curved arrow*); new 1.8-cm mass (*arrows*). Deep mass was infiltrating ductal carcinoma, and node contained metastasis.

Fig. 2.—**A**, Craniocaudal radiograph. Poorly defined 2.5-cm mass with architectural distortion (*arrows*); well defined 1.5-cm intramammary lymph node (*curved arrow*). **B**, Primary intraductal carcinoma (*arrow*) with tumor infiltrating adjacent fat. H and E, ×125 (original magnification). **C**, Node almost totally replaced by metastatic carcinoma with rim of residual lymphoid tissue (*arrow*). H and E, ×10 (original magnification). **D**, Follicle (*arrow*) is surrounded by metastatic carcinoma. H and E, ×125 (original magnification).

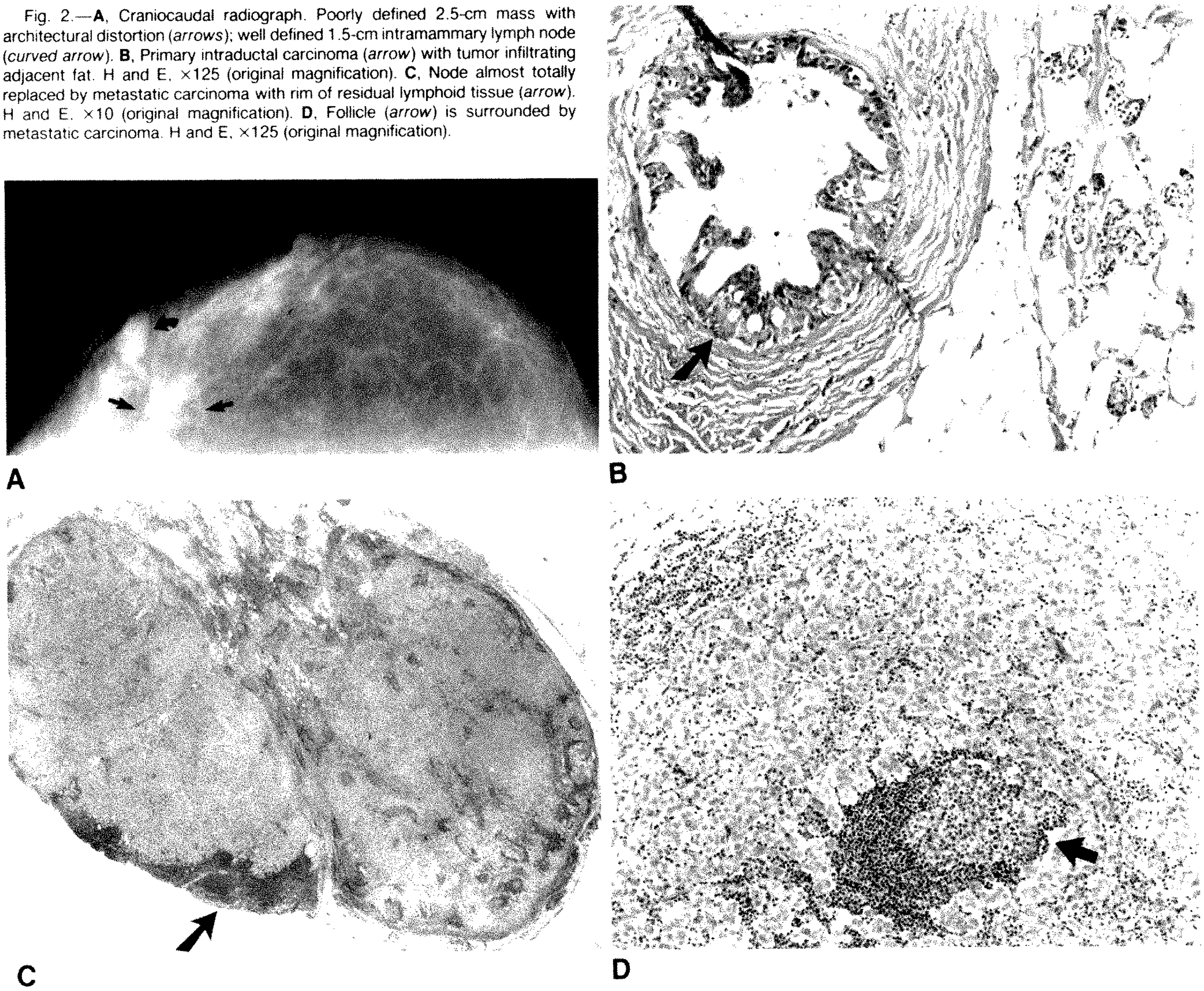

carcinoma appeared grossly as well circumscribed nodules. Two were firm, white, and homogeneous; the third appeared red and soft with a tan necrotic center. On microscopic examination, each had an intact true fibrous tissue capsule and pericapsular fibrosis. In one, there was extranodal extension of tumor. All three nodes were over 80% replaced by malignant epithelial cells.

Pathologic examination of the breast in each of these three cases demonstrated a focus of poorly differentiated carcinoma of ductal origin. Two cases contained macroscopically evident intraductal and invasive carcinoma, while the third had only microscopic foci of intraductal carcinoma. The cytologic features of the breast tumor and the lymph node metastasis were identical in each case. Two cases had no axillary lymph node metastasis, and one had a single positive axillary lymph node.

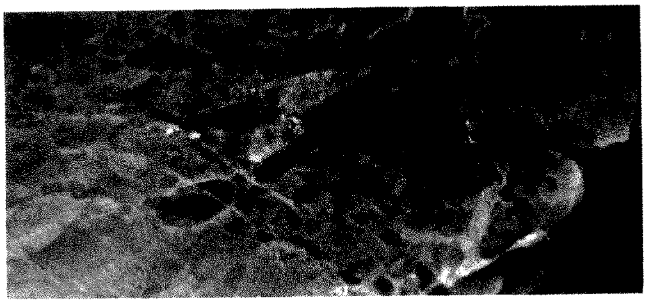

Fig. 3.—Microcalcifications found by xeromammographic study of mastectomy specimen located foci of intraductal carcinoma.

The fourth case of intramammary lymph node metastasis from breast carcinoma was a referred case first diagnosed as medullary carcinoma (fig. 4). The mass had a capsule, and on close inspection showed a subcapsular sinus and residual lymph node architecture with follicles. A poorly differentiated epithelial malignancy growing in loose sheets occupied 80% of the lymph node. Lymphocytes and plasma cells were focally mixed with tumor, creating a histologic appearance simulating medullary carcinoma. The primary focus of breast cancer was neither visible on the mammogram nor found in the mastectomy specimen, and no other cancer was evident in the other breast or elsewhere. On the basis of the histologic assessment of the tumor in the node, however, it came from an occult breast primary.

Discussion

Benign lymph nodes have been found within the mammary parenchyma in up to 28% of breast specimens examined

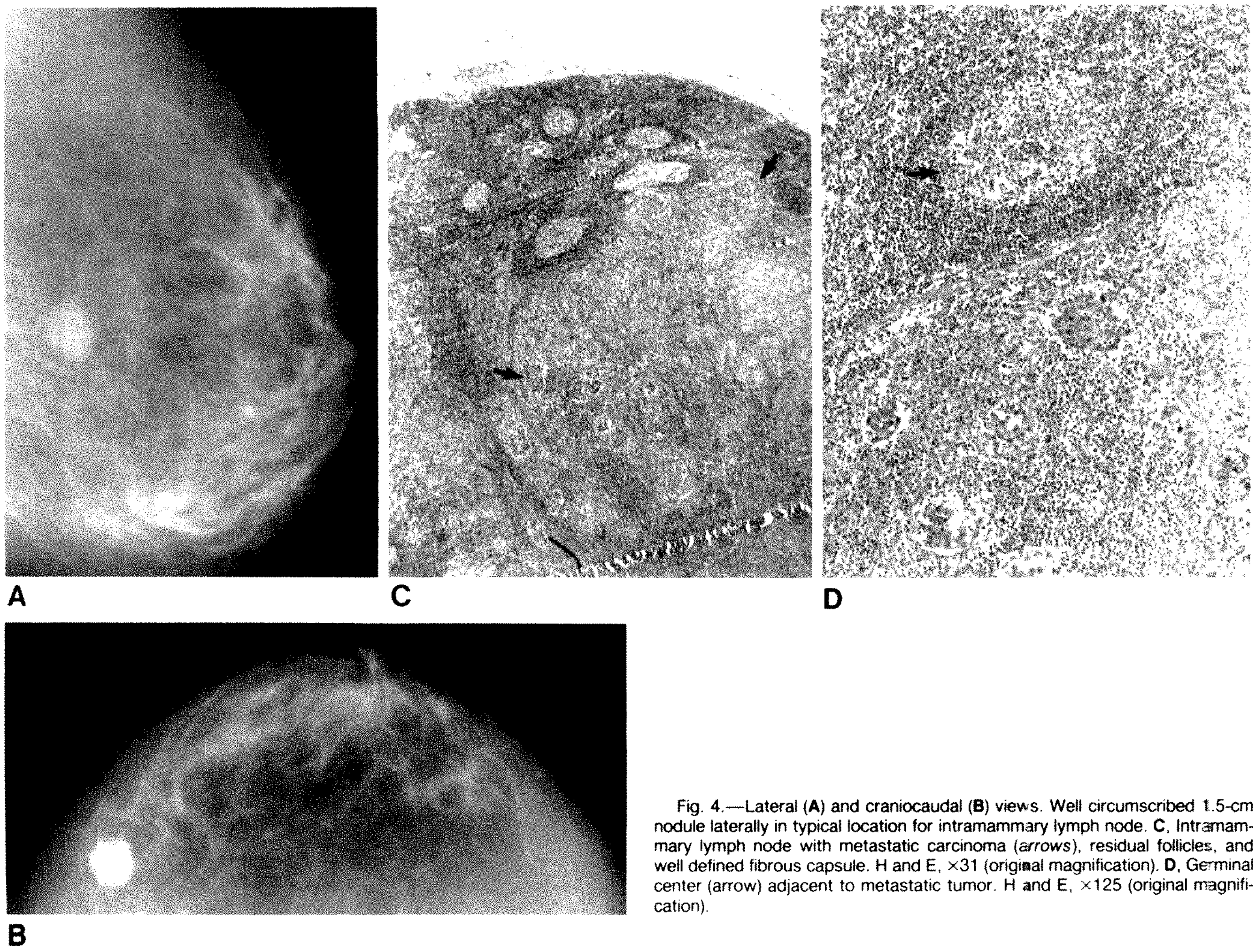

Fig. 4.—Lateral (**A**) and craniocaudal (**B**) views. Well circumscribed 1.5-cm nodule laterally in typical location for intramammary lymph node. **C**, Intramammary lymph node with metastatic carcinoma (*arrows*), residual follicles, and well defined fibrous capsule. H and E, ×31 (original magnification). **D**, Germinal center (arrow) adjacent to metastatic tumor. H and E, ×125 (original magnification).

histopathologically after mastectomy [1]. Intramammary nodes are often seen on routine mammographic examinations [2]. They are normally well circumscribed, lobulated densities smaller than 1 cm that typically have hilar notches and lucent centers if fatty replaced [3]. Although intramammary lymph nodes have been found on histologic evaluation in all quadrants of the breast [1], we are unaware of any proven intramammary nodes visible by mammography in any location other than the lateral half of the breast above the midplane in the posterior three-fourths of the parenchyma.

Enlargement of intramammary lymph nodes can occur as a result of a variety of processes including inflammation, hyperplasia, primary lymphoma [4], or metastases. Regardless of the cause, an enlarged intramammary lymph node has a uniform density with loss of the characteristic central lucency and hilar notch. The node can appear to remain well circumscribed with sharp margins, however, even if involved with malignant disease, and may remain clinically occult. It is impossible to distinguish benign, hyperplastic enlargement of intramammary lymph nodes from malignant causes by mammography. Thus, it has become our policy to recommend biopsy of all intramammary lymph nodes of 1 cm or more that are not fat infiltrated, unless the patient clearly has an associated dermatitis [5] or mastitis. Any intramammary node that has grown in comparison with previous examinations must also be considered suspicious and should be biopsied if no clear cause can be established.

In three of the four cases with metastasis to the intramammary lymph nodes reported here, the primary tumor was visible on the mammograms. An enlarged intramammary lymph node should mandate very careful review of the mammogram, since even microscopic disease can metastasize. There should be a high index of suspicion for subtle mammographic findings including clustered microcalcifications to clarify the cause of intramammary node enlargement.

When metastasis to an intramammary lymph node is suspected, the surgeon and pathologist should be alerted. Proper gross examination including location and relation of the nodule to surrounding structures should be made. Histologic examination should first confirm the anatomy of the nodule as that of a lymph node and then determine the cause for its enlargement. Confusion with medullary carcinoma of the breast can be avoided by the demonstration of an underlying lymph node architecture. Reactive hyperplasia, inflammatory disease, metastatic disease, dermatopathic lymphadenopathy, lymphoma, or certain systemic disease may be excluded on histologic grounds. Careful scrutiny by gross and microscopic examination should prevent misinterpretation of intramammary lymph node pathology.

A poorer prognosis has been suggested for patients who otherwise have stage I breast carcinoma but have metastatic disease to an intramammary lymph node. There seems to be no difference in survival of patients with stage II disease and those with metastasis to intramammary nodes [1, 6]. Consequently, in our institution, patients with intramammary nodal metastasis are considered to have stage II disease even if no axillary nodal metastases are found.

REFERENCES

1. Egan RL, McSweeney MB. Intramammary lymph nodes. *Cancer* **1983**;51:1838–1842
2. Kalisher L. Xeroradiography of axillary lymph node disease. *Radiology* **1975**;114:67–71
3. Meyer JE, Kopans DB, Lawrence WD. Normal intramammary lymph nodes presenting as occult breast masses. *Breast* **1982**;40:30–32
4. Meyer JE, Kopans DB, Long JC. Mammographic appearance of malignant lymphoma of the breast. *Radiology* **1980**;135:623–626
5. Kopans DB, Meyer JE, Murphy GF. Benign lymph nodes associated with dermatitis presenting as breast masses. *Radiology* **1980**;137:15–19
6. McSweeney MB, Egan RL. Prognosis of breast cancer related to intramammary lymph nodes. *Recent Results Cancer Res* **1984**;90:166–172

Hepatic Artery Thrombosis after Liver Transplantation:

Radiologic Evaluation

Mark C. Segel[1]
Albert B. Zajko[1]
A'Delbert Bowen[2]
Klaus M. Bron[1]
M. Leon Skolnick[1]
Ronald J. Penkrot[1]
Thomas E. Starzl[3]

Hepatic artery thrombosis after liver transplantation is a devastating event requiring emergency retransplantation in most patients. Early clinical signs are often nonspecific. Before duplex sonography (combined real-time and pulsed Doppler) capability was acquired in October 1984, 76% of all transplants in this institution referred for angiography with a clinical suspicion of hepatic artery thrombosis had patent arteries. In an effort to reduce the number of negative angiograms, CT, real-time sonography, and pulsed Doppler have been evaluated as screening examinations to determine which patients need angiography. Of 14 patients with focal inhomogeneity of the liver architecture detected by CT and/or real-time sonography, 12 (86%) had hepatic artery thrombosis, one had slow arterial flow with hepatic necrosis, and one had a biloma with a patent hepatic artery. In 29 patients undergoing duplex sonography of the hepatic artery, six (21%) had absence of a Doppler arterial pulse. All six had abnormal angiograms: Four had thrombosis, one had a significant stenosis, and one had slow flow with biopsy-proven ischemia. Of 23 patients with a Doppler pulse, two had hepatic artery thrombosis at surgery. However, real-time sonography demonstrated focal inhomogeneity in the liver in both cases. Our data demonstrate that pulsed Doppler of the hepatic artery combined with real-time sonography of the liver parenchyma currently is the optimal screening test for selecting patients who require hepatic angiography after liver transplantation. A diagnostic algorithm is provided.

Hepatic artery thrombosis after liver transplantation is a devastating event that requires immediate therapeutic intervention in most patients. The typical course is hepatic infarction followed by septic hepatic gangrene and septicemia. Emergency hepatic retransplantation is these patients' only hope for survival [1].

In 1969, Starzl [2] described two cases of fatal hepatic artery thrombosis that were not initially recognized on the basis of clinical findings or laboratory studies. He concluded, "It is likely that aortography will prove to be the only really decisive way of consistently establishing the diagnosis while there is still time to attempt repair, providing the procedure is done at the first suspicion of a vascular accident." Since then, angiography has been the definitive procedure for evaluation of the hepatic artery after liver transplantation.

From January 1981 to October 1984, before availability of duplex sonography (combined real-time and pulsed Doppler), 33 angiographic studies (18 children and 15 adults) were performed at the University Health Center of Pittsburgh for the clinical suspicion of hepatic artery thrombosis after liver transplantation. Of these, 11 (61%) of 18 children and 14 (93%) of 15 adults had patent hepatic arteries. It is clear that clinical criteria alone led us to perform an undesirably large number of normal arteriograms.

We now use three noninvasive imaging techniques to evaluate the liver after transplantation: computed tomography (CT), real-time sonography, and Doppler. We have undertaken a review to determine if these imaging methods can be used to select patients with suspected hepatic artery thrombosis who require angiography.

Received May 7, 1985; accepted after revision August 21, 1985.

Presented in part at the annual meeting of the American Roentgen Ray Society, Boston, April 1985.

[1] Department of Radiology, Presbyterian-University Hospital, DeSoto at O'Hara Sts., Pittsburgh, PA 15123. Address reprint requests to A. B. Zajko.

[2] Department of Radiology, Children's Hospital of Pittsburgh, Pittsburgh, PA 15123.

[3] Department of Surgery, University Health Center of Pittsburgh, Pittsburgh, PA 15261.

***AJR* 146:137-141, January 1986**
0361-803X/86/1461-0137
© American Roentgen Ray Society

Subjects and Methods

During 51 months from January 1981 to April 1985, 330 patients (147 children, 183 adults) received 435 orthotopic liver transplants at the University Health Center of Pittsburgh. Seventy-seven patients received two transplants each and 14 received three transplants each. There were 150 male and 180 female patients aged 4 months to 57 years.

TABLE 1: **Comparison of Angiography (Pre-Doppler) with Results of Computed Tomography and Real-Time Sonography**

Hepatic Artery at Angiography	Computed Tomography		Real-Time Sonography	
	Abnormal*	Normal	Abnormal*	Normal
Patent (*n* = 12)	1/7†	6/7	1/8†	7/8
Occluded (*n* = 7)	5/5	...	4/5	1/5‡
Slow Flow (*n* = 1)§	1	...	...	1

* Focal area of inhomogeneity in liver (see figs. 1 and 2).

† Same patient with biloma in liver.

‡ One study performed 3 days before angiogram, ?interval occlusion.

§ Decreased perfusion confirmed by radionuclide hepatic flow study; patient required retransplantation because of hepatic necrosis.

During this time, 42 angiographic studies (25 children and 17 adults) were performed for evaluation of hepatic artery patency. This includes the initial 33 patients evaluated up to October 1984 (pre-Doppler) and nine additional patients studied since duplex sonography became available. In all cases, angiography was done in the first 2 months after liver transplantation.

Pre-Doppler

Of 15 adult transplant patients with angiograms, five had CT only, one had real-time sonography only, and two had both CT and sonography within a few days of the angiogram. Of 18 pediatric transplant patients with angiograms, one had CT only, six had real-time sonography only, and five had both examinations within a few days of the angiogram. All CT scans were obtained on either a GE 8800 or 9800 scanner at 120 kVp and 4.8-sec (8800) or 3.0-sec (9800) scan times. The entire liver was scanned at 10- or 15-mm intervals at a slice thickness of 10 mm; when clinically permissible, a rapid intravenous drip of iodinated contrast medium was used; in children, the amount was adjusted to weight (maximum, 3 ml/kg). Real-time sonographic evaluation was performed on an Advanced

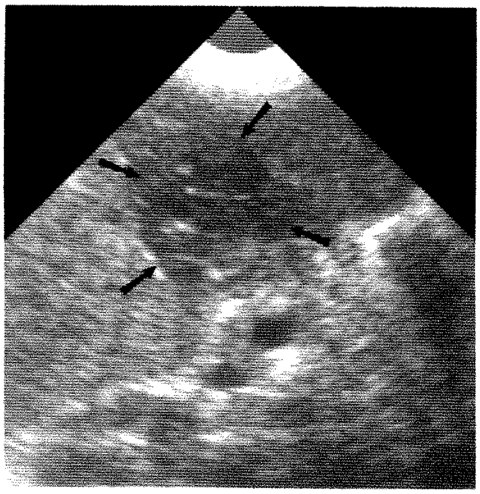
1

Fig. 1.—Focal area of hepatic parenchymal inhomogeneity (*arrows*) on sonogram of 3-year-old girl with hepatic artery thrombosis. At retransplantation, pathology revealed infected infarct.

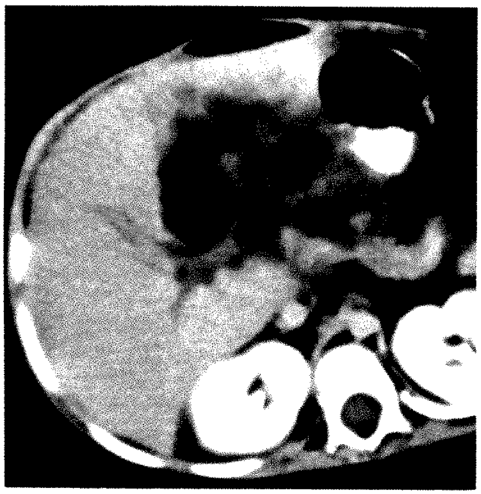
2

Fig. 2.—Large area of abnormal liver parenchyma on CT scan of 2-year-old girl with hepatic artery thrombosis. At retransplantation, pathology revealed infected infarct.

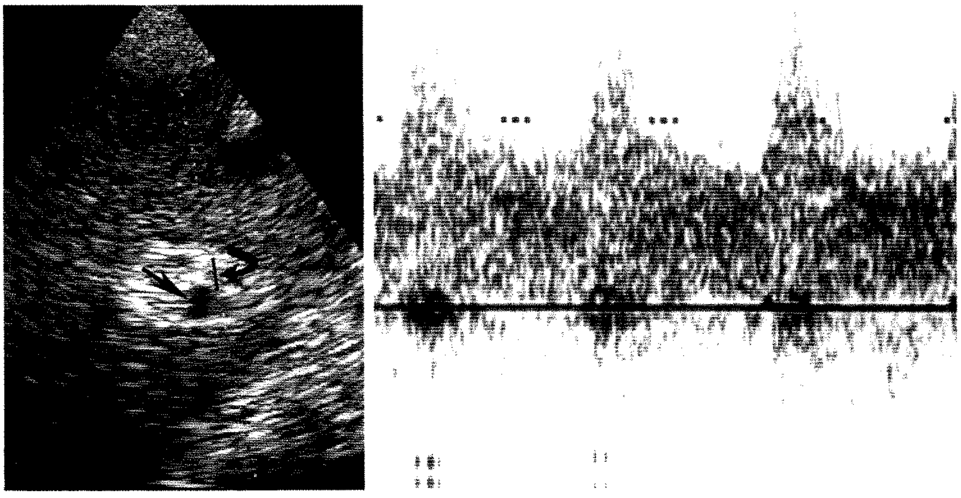
A B

Fig. 3.—Normal Doppler. **A**, Position of cursor line through hepatic artery (*curved arrow*) on sagittal view for Doppler waveform shown in **B**. Portal vein (*straight arrow*). **B**, Normal Doppler artery waveform.

TABLE 2: **Comparison of Pulsed Doppler and Real-Time Sonography as Individual Imaging Tests and as a Combined Test to Screen for Hepatic Artery Abnormalities after Liver Transplantation**

	Pulsed Doppler Sonography of Hepatic Artery Alone	Real-Time Sonography of Liver Parenchyma Alone	Pulsed Doppler & Real-time Sonography Combined
No. of patients	29	29	29
True positive	6*	5†	8‡
True negative	21§	21‖	21¶
False positive	0	0	0
False negative	2	3	0
Sensitivity (%)	75	62.5	100
Significance (*p*)**			<0.00001

* No flow in hepatic artery.
† Focal inhomogeneity in liver.
‡ Either no flow in hepatic artery or focal inhomogeneity in liver.
§ Normal hepatic artery flow.
‖ Normal liver parenchyma.
¶ Normal hepatic artery flow and normal liver parenchyma.
** Computed by Fisher exact test.

Technology Laboratories MK 300 scanner and Hewlett Packard mechanical and phased-array scanners.

Post-Doppler

Since October 1984, pulsed Doppler study of the hepatic artery combined with real-time sonography of the liver parenchyma has been performed on 29 liver transplant patients. Eighteen have been followed clinically without angiography. Nine transplant patients underwent angiography, and two had emergency surgery without angiography. Duplex examinations were performed on Hewlett Packard mechanical and phased-array scanners incorporating pulsed Doppler capabilities.

Results

CT and Real-Time Sonography (Pre-Doppler)

The combined results for adults and children, comparing angiography with CT and real-time sonography, are shown in table 1. Of the five adult transplant patients having only CT, two had focal low-density lesions in the liver. One had hepatic artery thrombosis by angiography. A donor liver was not available for retransplantation. The patient died, and hepatic infarction was present at autopsy. The second had a patent hepatic artery; however, the intrahepatic arteries were narrowed and there was decreased perfusion by angiography. Decreased perfusion was also noted by a radionuclide hepatic flow study. Retransplantation was performed, and pathologic evaluation revealed diffuse coagulation necrosis.

In all six adult transplant patients with normal CT and/or sonography of the liver, the hepatic artery was patent by angiography. One patient had a mild anastomotic stenosis.

Of the 12 children with CT and/or sonography, seven had focal hepatic masses (figs. 1 and 2), and one of the seven had a thrombosed arterial graft detected by real-time sonography. Six of the seven had hepatic artery occlusion by angiography. In one transplant patient with a CT scan showing a focal mass, the hepatic artery was patent. The fluid collection was a biloma that was successfully drained percutaneously. In each of the five children with normal CT and/or sonography of the liver, the hepatic artery was patent by angiography.

In an 11-month-old transplant patient with an occluded hepatic artery, sonography demonstrated a focal area of inhomogeneity in the liver. A donor liver was not available for retransplantation. However, liver function gradually improved. Follow-up angiography 6 weeks later showed arterial collaterals that reconstituted the intrahepatic arterial tree. CT of the liver was normal. Ensuing bile duct stricture was treated by percutaneous balloon dilatation; liver function was normal at 20 months after thrombosis of the hepatic artery.

Pulsed Doppler and Real-Time Sonography

Pulsed Doppler of the hepatic artery combined with real-time sonography of the liver parenchyma was performed on 29 transplanted livers. Of 21 cases with both normal Doppler and real-time sonographic studies, there were no cases of hepatic artery thrombosis. The value of using both tests to screen for hepatic artery abnormalities after liver transplantation is shown in table 2.

In 23 transplant patients, duplex sonography demonstrated arterial flow to the liver (fig. 3). Three had angiography, which demonstrated patent hepatic arteries in each case. In 20, angiography was not performed because of the normal Doppler study. In two of these 20, a focal abscess was identified in the liver by real-time sonography. Because of clinical deterioration, both patients required emergency retransplantation. Both had hepatic artery thrombosis. Of the remaining 18, none has developed hepatic artery thrombosis. Four have required retransplantation for reasons other than hepatic artery thrombosis. Two patients died, one from graft failure and one from cardiac arrest.

In six transplant patients, no evidence of hepatic arterial flow was identified in the liver hilum by pulsed Doppler. Angiography was abnormal in all six cases. Four had hepatic artery thrombosis. In one of the four, angiography also revealed arterial collaterals to the transplanted liver (fig. 4), but a small infarct was seen on sonography. In the fifth case, a severe stenosis was found at the hepatic artery anastomosis. In the sixth, the hepatic arterial tree was narrowed with markedly reduced washout of contrast material within the liver, suggesting slow flow. Liver biopsy showed changes consistent with ischemia.

Discussion

Crucial Role of Hepatic Artery

Hepatic artery thrombosis, a complication that usually occurs within 2 months after liver transplantation, is a major cause for retransplantation [1, 3]. This catastrophic event may result in hepatic gangrene and death unless prompt retransplantation is performed.

The consequences of hepatic arterial thrombosis in liver transplant patients are much more severe than in non-liver-

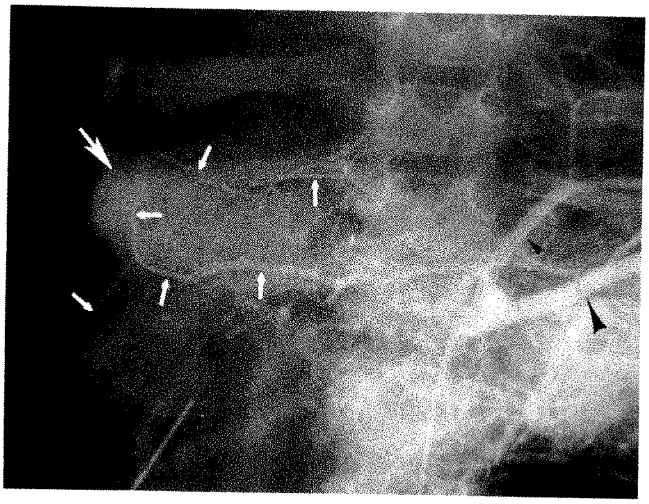

Fig. 4.—Collateral development after hepatic artery thrombosis. Late arterial film from celiac arteriogram 3 weeks after liver transplantation shows occlusion of common hepatic artery at its origin and reconstitution of intrahepatic branch arteries (*small white arrows*). Splenic artery (*large arrowhead*); left gastric artery (*small arrowhead*); portal vein (*large white arrow*).

transplant patients because, with proximal hepatic artery occlusion in a nontransplant liver, collateral arterial supply develops rapidly and prevents hepatic ischemia and infarction [4–10]. Because of the rapidity with which collateral circulation develops, liver survival probably is not solely attributable to a patent portal venous system [11, 12].

When complete dearterialization of a nontransplant liver is accomplished by embolization, septic hepatic infarction will occur [12]. In orthotopic liver transplantation, all potential collaterals have been severed. Hepatic artery occlusion after transplantation completely dearterializes the liver, and hepatic infarction is expected. A massively necrotic liver often becomes infected with Gram-negative enteric organisms in an immunosuppressed patient [13]. After hepatic artery thrombosis is diagnosed, emergency retransplantation is performed as soon as a donor liver is available.

Most transplant patients with hepatic artery thrombosis for whom a donor liver was not immediately available have died. However, four patients did survive with angiographically documented hepatic artery occlusion after transplantation. Massive hepatic infarction did not occur. Two of the four have angiographic documentation of extrahepatic arterial collaterals supplying the transplanted liver (fig. 4). Presumably the other two patients have developed collaterals. How such arterial collaterals develop communications to the transplanted liver remains unclear.

Imaging Approach

Ideally, noninvasive imaging should be able to suggest hepatic artery occlusion before the stage of hepatic gangrene. CT and real-time sonography may document focal hepatic infarction, prompting emergency angiography. Of patients with focal alterations in the liver by CT or real-time sonography, 86% (12 of 14) will have hepatic artery thrombosis. However, at this stage the patient often already has clinical toxic septicemia with marked elevations in serum transaminases.

Consequently, noninvasive evaluation of hepatic artery blood flow is needed to detect occlusion of the hepatic artery before infarction occurs. Early in our experience (1981–1983), radionuclide hepatic flow studies were occasionally done. Unfortunately, because of the difficulty in unequivocally distinguishing the hepatic artery phase from the portal vein phase, this test was not considered reliable to screen for hepatic artery occlusion. Future advances in radionuclide imaging may surmount this problem.

Intravenous digital subtraction angiography (DSA) has been used on occasion when the femoral artery could not be catheterized. As a screening test, it is too costly and lengthy; it also requires suspension of body motion, which is impossible for many sick patients. The test is also invasive, since a catheter should be placed into the right atrium for an optimal study [14]. As a definitive test, it lacks the absolute conclusiveness needed in transplants with suspected hepatic artery abnormalities. Overlying mesenteric and renal vessels could be mistaken for the vascular homografts occasionally used in transplantation. Furthermore, in patients with direct hepatic artery-hepatic artery reconstruction, the vascular anastomosis may be difficult to adequately demonstrate, occasionally requiring several views. If intravenous DSA is nondiagnostic, conventional angiography would be required for a definitive diagnosis. Contrast medium limitations could easily be exceeded, especially in children.

Dynamic intravenous CT scanning of the hepatic artery is not used as a screening test in our institution. CT is costly and motion dependent; emergency scheduling is difficult. Also, we doubt that an intravenous bolus of contrast material from a peripheral vein could adequately demonstrate the hepatic artery in most patients. Failure to image the hepatic artery on CT would necessitate angiographic evaluation, which could result in contrast medium limitations being exceeded.

Visual detection of hepatic artery pulsation with real-time sonography is feasible in children but generally not in adults. In small children, a 5-MHz transducer penetrates adequately, but in adults a lower-resolution 3-MHz transducer often is needed. Using the higher-resolution transducer, our experience in children has shown that unequivocal intrinsic pulsation of the hepatic artery equates with patency. There are two important cautions: (1) Inexperienced examiners may mistake transmitted pulsation from the aorta for intrinsic pulsation, and (2) the surgeon must inform the radiologist of unusual anastomoses, such as those involving iliac and aortic grafts, and the locations of such grafts [15], as they are exceedingly difficult to see with real-time sonography.

In our opinion, pulsed Doppler of the hepatic artery is very useful for detecting hepatic artery thrombosis before infarction occurs. In one patient, 1 day of fever prompted a Doppler study that detected no evidence of arterial flow. Angiography revealed hepatic artery occlusion, and the patient underwent retransplantation the same day. Pathology of the liver revealed no evidence of hepatic infarction, although hepatic artery thrombosis was present.

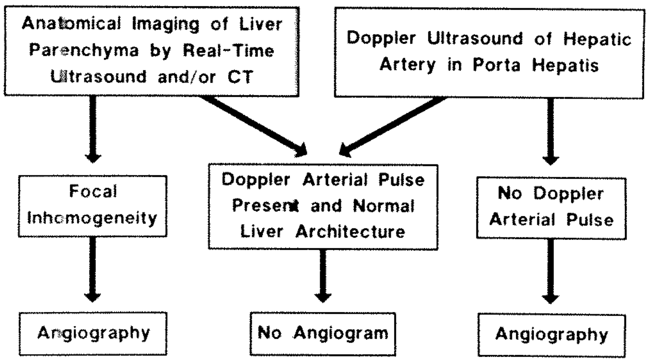
Anatomical Imaging of Liver Parenchyma by Real-Time Ultrasound and/or CT
Doppler Ultrasound of Hepatic Artery in Porta Hepatis
Focal Inhomogeneity
Doppler Arterial Pulse Present and Normal Liver Architecture
No Doppler Arterial Pulse
Angiography
No Angiogram
Angiography

Fig. 5.—Diagnostic algorithm for radiologic evaluation of patient with suspected hepatic artery thrombosis after liver transplantation.

In two patients, the Doppler study was interpreted as demonstrating patent hepatic arteries when occlusions existed. In one, a technical error was made. In the second case, the examiner was inexperienced; Doppler skills require a significant learning period. We believe that a postoperative baseline Doppler study, combined with detailed examination of the liver architecture using real-time sonography, would be useful.

Failure to detect hepatic artery blood flow with Doppler is reliable evidence of a hepatic artery abnormality and warrants angiographic evaluation. In all six patients in whom the sonographer was confident of the absence of Doppler blood flow from a discrete hepatic artery within the porta hepatis, angiograms also were abnormal. Four had hepatic artery thrombosis; three also had focal areas of inhomogeneity in the liver by sonography. One patient with hepatic artery thrombosis had arterial collaterals keeping the liver alive (fig. 4). Of the two transplant patients without Doppler arterial flow who had angiographically patent hepatic arteries, one had a severe stenosis at the hepatic artery anastomosis and the other had markedly reduced washout of contrast material suggesting slow flow. Liver biopsy showed evidence of ischemic damage.

In summary, we believe that pulsed Doppler of the hepatic artery combined with real-time sonography of the liver parenchyma should be the initial imaging test in patients suspected of hepatic artery thrombosis after liver transplantation. CT may give complementary information in difficult or equivocal cases. In experienced hands, Doppler confirmation of hepatic arterial flow with normal liver architecture on real-time sonography obviates angiography. Absence of hepatic artery flow in the porta hepatis by Doppler or the presence of a focal area of hepatic inhomogeneity by real-time sonography or CT warrants immediate angiography (fig. 5).

ACKNOWLEDGMENT

We thank Donna Scahill for manuscript preparation.

REFERENCES

1. Shaw BW Jr, Gordon RD, Iwatsuki S, Starzl TE. Hepatic retransplantation. *Transplant Proc* **1985**;17:264–271
2. Starzl TE (with assistance of Putman CW). Intra- and postoperative complications and care. In: *Experience in hepatic transplantation*. Philadelphia: Saunders, **1969**:144–158
3. Demetris AJ, Lasky S, Van Thiel DH, Starzl TE, Dekker A. Pathology of hepatic transplantation: a review of 62 adult allograft recipients immunosuppressed with a cyclosporine/steroid regimen. *Am J Pathol* **1985**;118:151–160
4. Kim DK, Kinne DW, Fortner JG. Occlusion of the hepatic artery in man. *Surg Gynecol Obstet* **1973**;136:966–968
5. Brittain RS, Marchioro TL, Hermann G, Waddell WR, Starzl TE. Accidental hepatic artery ligation in humans. *Am J Surg* **1964**;107:822–832
6. Chuang VP, Wallace S. Hepatic artery embolization in the treatment of hepatic neoplasms. *Radiology* **1981**;140:51–58
7. Chuang VP, Wallace S, Soo CS, Charmsangauej C, Bowers T. Therapeutic ivalon embolization of hepatic tumors. *AJR* **1982**;138:289–294
8. Mays ET, Wheeler CS. Demonstration of collateral arterial flow after interruption of hepatic arteries in man. *N Engl J Med* **1974**;290:993–996
9. Bengmark S, Rosengren K. Angiographic study of the collateral circulation to the liver after ligation of the hepatic artery in man. *Am J Surg* **1970**;119:620–624
10. Redman HC, Reuter SR. Arterial collaterals in the liver hilus. *Radiology* **1970**;94:575–579
11. Carroll R. Infarction of the human liver. *J Clin Pathol* **1963**;16:133–136
12. Doppman JL, Guton M, Kahn ER. Proximal versus peripheral hepatic artery embolization: experimental study in monkeys. *Radiology* **1978**;128:577–588
13. Starzl TE (with assistance of Putman CW). Acute rejection and hepatic gangrene. In: *Experience in hepatic transplantation*. Philadelphia: Saunders, **1969**:308–328
14. Saddekni S, Sos TA, Sniderman KW, et al. Optimal injection technique for intravenous digital subtraction angiography. *Radiology* **1984**;150:655–659
15. Zajko AB, Bron KM, Starzl TE, et al. Angiography of liver transplantation patients. *Radiology* **1985**;157:305–311

Angiographic and Interventional Radiologic Considerations in Liver Transplantation

John F. Cardella[1]
Wilfrido R. Castaneda-Zuniga
David Hunter
Antony Young
Kurt Amplatz

Of 46 liver transplantations performed, 15 patients are alive at follow-up intervals from 2 to 50 months. The most common indications for liver transplantation were biliary atresia, cirrhosis, and neoplasia. About 50% of the patients had pre- and/or postoperative angiograms. Additional material was available from pretransplant workups in patients subsequently shown to be unsuitable for transplantation. Of 13 preoperative angiographic studies, portal vein patency was confirmed in two, inferior vena caval (IVC) patency was confirmed in two, and diffuse neoplasm was identified in three. These patients subsequently had transplants. Conditions precluding liver transplantation in six patients were inadequate portal vein size (<5 mm) in two, occluded IVC or portal vein in one each, nonvisualized portal vein in one, and neoplasm localized to one lobe in one. Postoperatively 18 vascular studies identified hepatic arterial compromise in nine, postbiopsy arteriovenous fistula in two, and bleeding from a right adrenal artery in one. Postoperative venography showed thrombosis or occlusion of the IVC in five, portal vein thrombosis in one, and splenic vein thrombosis in one. Of the 18 postoperative angiograms, 12 demonstrated findings considered threatening to the transplants' survival. Six of 18 studies demonstrated findings considered compromising to the transplant. Of the nine postoperative cholangiographic studies, six diagnoses were considered threatening to transplant survival: obstruction of the biliary-enteric anastomosis in four, leakage from the biliary-enteric anastomosis in one, and an abscess from biliary leakage in one.

The first attempt to transplant a human liver was made at the University of Colorado on March 1, 1963 by Starzl et al. [1]. During the next 7 months, that patient and eight others died after transplant attempts. On July 23, 1967, the first extended survivor had a transplant. The patient, a 1½ year-old girl, lived 13 months before dying of metastatic hepatoma for which she had initially been treated.

Since these early and somewhat frustrating attempts, about 500 liver transplantations have been performed worldwide. About one-half of these have been performed by Starzl and colleagues. In England, Calne and Williams [2] have reported another 125 cases.

The first human liver transplantation at the University of Minnesota was performed on July 2, 1968. Since then, many patients have been evaluated for possible transplantation and 46 patients have had transplants. Angiographic and interventional procedures have played an important role in the evaluation and care of these patients. We review our experience with the findings and techniques needed to evaluate this complex surgical procedure.

Subjects and Methods

The 46 transplant recipients in this series ranged in age from 7 months to 65 years, and the population consisted of 31 female and 15 male patients. The indications for liver transplantation in this series were extrahepatic biliary atresia (19 patients), alpha-1-antitrypsin deficiency (seven), chronic biliary cirrhosis (six), chronic active hepatitis (six), neoplasia (six),

Received March 11, 1985; accepted after revision August 21, 1985.

[1] All authors: Department of Diagnostic Radiology, Cardiovascular and Interventional Radiology Section, University of Minnesota, Box 701 Mayo Building, 420 Delaware St. S.E., Minneapolis, MN 55455. Address reprint requests to K. Amplatz.

AJR 146:143–153, January 1986
0361-803X/86/1461-0143
© American Roentgen Ray Society

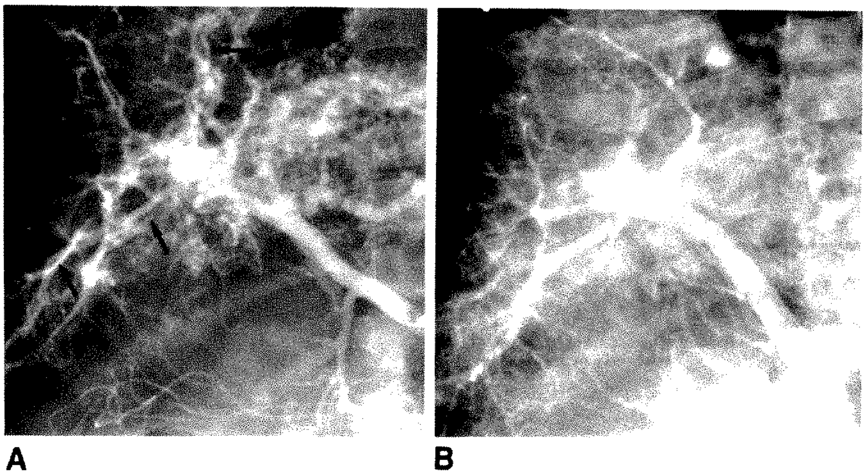

Fig. 1.—4-year-old patient with hereditary tyrosinemia and pathologically proven hepatocellular carcinoma. **A**, Selective hepatic artery injection. Abnormal vessels in right and left lobes. Note simultaneous filling of hepatic artery branches alongside portal vein branches due to sinusoidal shunting (*arrows*) ("railroad tracking"). **B**, Late venous phase of hepatic arteriogram. Nonhomogeneous liver blush; portal venous filling. Findings due to hepatofugal flow from portal venous hypertension secondary to tumor involvement and/or cirrhosis.

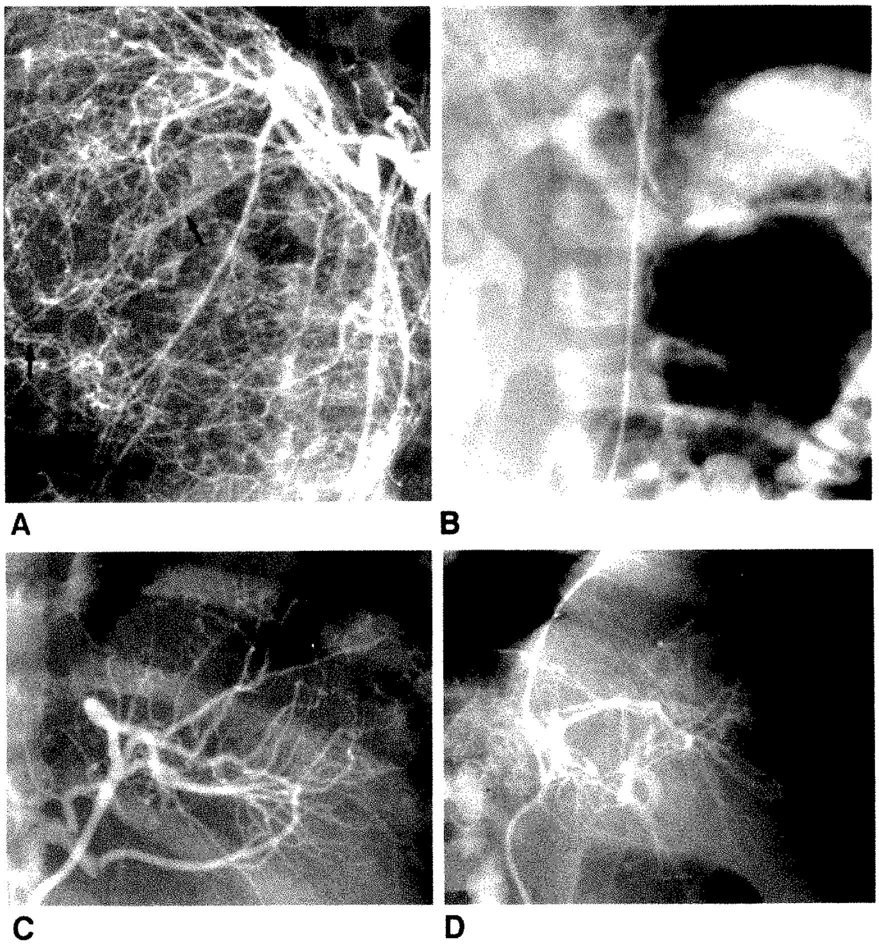

Fig. 2.—Preoperative evaluation of 23-month-old boy with huge hepatoblastoma confined to right hepatic lobe. **A**, Celiac axis injection. Huge tumor with abnormal vessels in right lobe, "railroad tracking" (*arrows*), and vessel draping. **B**, Late venous phase of celiac axis study. Normal-sized patent portal vein is displaced leftward by tumor. **C**, AP view of selective left gastric artery injection. Superimposed gastric and left hepatic branches. **D**, Lateral view clearly distinguishes anteriorly located hepatic branches from posteriorly located gastric branches. Left lobe was angiographically and pathologically tumor-free. Patient subsequently underwent subtotal hepatectomy without transplantation.

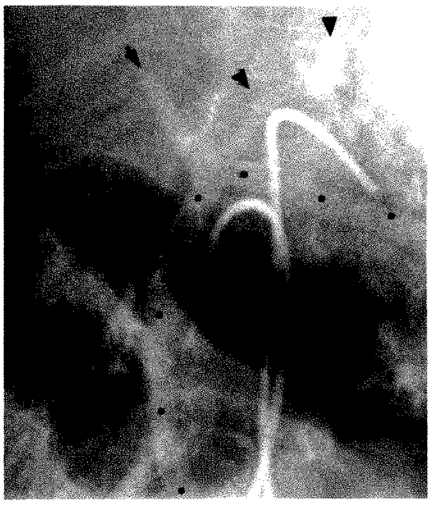

Fig. 3.—Dual-catheter arterial portogram recorded with 30 frame/sec cineradiography. Total injection of 4 ml/kg using Y-adaptor from injector. Late venous phase shows splenic and superior mesenteric veins (*dots*). Portal vein (*arrow*) was small, ended in abrupt tapered fashion, and demonstrated hepatofugal flow. Note large coronary vein and esophageal varices (*arrowheads*). Blood flow direction was appreciated far better on cineradiography than on still frame.

Fig. 4.—Transplenic splenoportogram for evaluation of portal vein size after unsuccessful sonography. **A** and **B**, Normal study. **A**, Power injection of 2 ml/kg opacifies splenic pulp and vein. **B**, Portal venous system well opacified. Superior mesenteric vein origin also seen (*arrow*). Rapid sequence of events best filmed with cineradiography at 30 frames/sec. Normal-sized portal vein with hepatopetal flow. Liver disease clinically not severe enough for transplantation at this time. **C**, Abnormal transplenic splenoportogram in another patient, for comparison. Main portal vein (1) is small (3 mm) with chaotic intrahepatic branching. Hepatofugal flow into superior mesenteric vein (2) and large colic collateral (3) is evident. Large coronary vein (4) and esophageal varices (5) serve as collateral pathways for decompression of portal venous system.

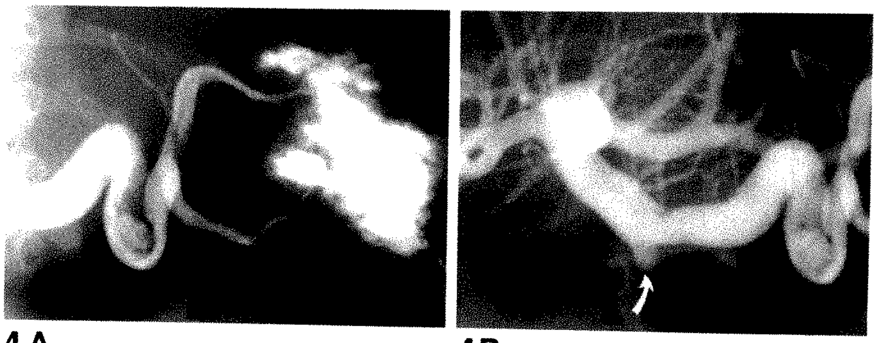

4A **4B**

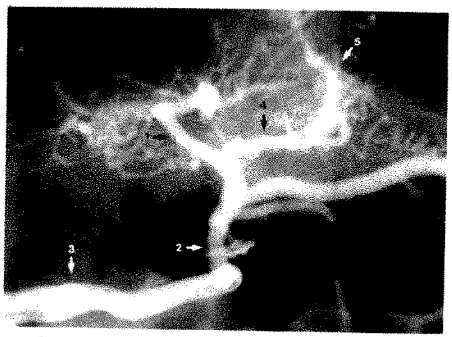

4C

Fig. 5.—Transhepatic portal venogram shows torrential hepatofugal flow with visualization of portal vein (1), superior mesenteric vein (2), splenic vein (3), and large right colic collateral (4).

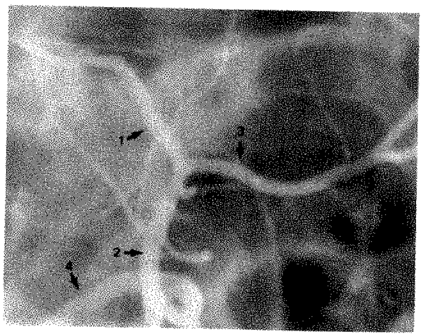

5

cryptogenic cirrhosis (one), and erythropoietic protoporphyria (one). Of the 46 transplants, 45 were orthotopic and one was a heterotopic auxiliary transplant.

Of the 46 patients, 15 are alive with follow-ups ranging from 2 to 50 months. Of the 31 patients who died, the mean survival was 29 days (range, 0–210 days); the median survival time was 22.5 days. The longest survivor of liver transplantation in the world is 12.5 years.

Pretransplant Evaluation

The pretransplant workup is managed by the gastroenterology service. Liver function is assessed biochemically and with radionuclide studies. Preoperative anatomic evaluation is performed with CT and sonography. Factors that must be accurately assessed include portal vein patency and size, inferior vena cava (IVC) size and patency, hepatic involvement by cirrhotic or neoplastic processes, and the presence of ascites or other abdominal abnormalities associated with the liver disease. If CT and sonography fail to unequivocably answer these questions or if there is a further question concerning vascular anatomy, pretransplant angiographic evaluation is indicated.

Seven transplant patients underwent preoperative angiographic studies. Angiographic materia from six additional patients (candidates ultimately not having transplants) was also reviewed. The 13 patients had six arteriograms, four transplenic splenoportograms, three inferior vena cavograms, and one transhepatic portal venogram. The six arteriograms comprised four celiac studies and two aortograms.

Hepatic arteriography has been performed to preoperatively determine the extent of liver disease in cases of neoplasia when sonography and/or CT have been equivocal (fig. 1). A selective common hepatic artery injection is initially performed. If the entire liver vasculature is not identified, selective superior mesenteric and left gastric artery injections are made to identify arteries supplying normal liver (fig. 2).

The portal vein can be visualized in three ways. First, two arterial catheters can be used to simultaneously inject the splenic and superior mesenteric arteries. Delayed filming demonstrates the splenic vein, superior mesenteric vein, and portal vein (fig. 3). This technique requires simultaneous catheterization of both femoral arteries. The single most important piece of information regarding the portal vein is its size. Surgeons at our institution require a minimum portal vein diameter of 5 mm for anastomosis to be technically feasible. Accurate measurements must include correction for radiographic magnification. We use either the size of the catheter or a 1-cm grid placed half-way between the anterior and posterior body wall to correct for magnification. If there is pronounced portal venous hypertension and associated hepatofugal flow, the portal vein may not opacify with arterial injection. In these situations, direct splenoportography will often visualize the portal vein (fig. 4). Injections are made through a 20-gauge Teflon sheath in children and an 18-gauge sheath in adults. The track into the spleen is tamponaded with compressed Gelfoam plugs after the sheath is withdrawn to minimize the risk of bleeding [3].

In one case, hepatofugal flow was so brisk that simultaneous splenic/superior mesenteric artery (SMA) arteriography and transplenic splenoportography both failed to opacify the portal vein. Direct transhepatic portal venography was required (fig. 5). The study can be performed through a 22-gauge needle using the standard right-lateral midaxillary line approach similar to that for transhepatic cholangiography. Aspiration of blood is sought, and then portal vein branch entry is confirmed by injection of contrast material. Transhepatic portal venography is used as the imaging method of last resort, as in many of the extrahepatic biliary atresia patients, the bile is infected (since most have had previous Kasai procedures) and these patients can become septic after transhepatic portal venography. In patients with hepatic scarring secondary to hepatitis or cirrhosis, transhepatic portal venography is difficult technically.

To angiographically evaluate the infra- and suprahepatic segments of the IVC, a puncture is made into one femoral vein, and a small sheath or a short 4- or 5-French catheter is inserted. The abdominal

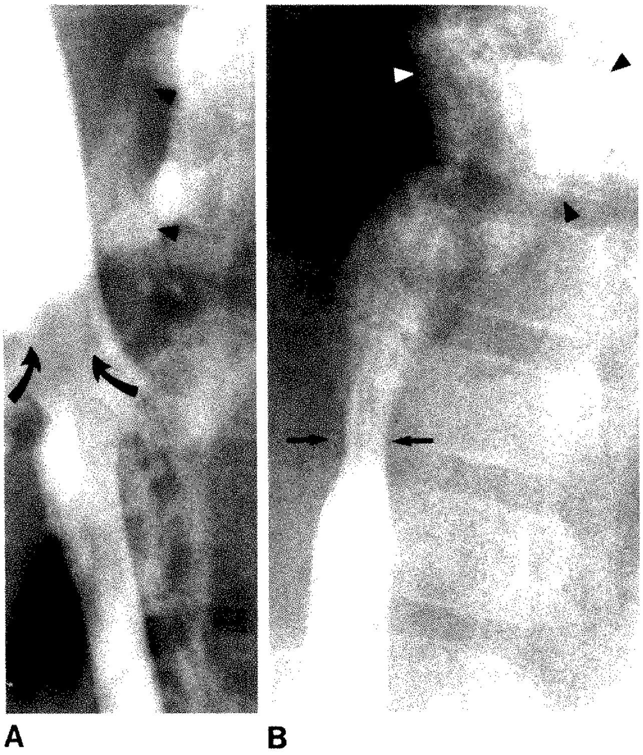

Fig. 6.—Inferior vena cavogram showing evidence of intrahepatic caval stenosis. **A**, Abdominal part of IVC is widely patent with excellent renal vein inflow (*arrows*). Early collateral filling into azygos venous system can be seen projected over spine (*arrowheads*). **B**, Frame at level of right hemidiaphragm shows discretely narrowed segment of intrahepatic vena cava (*arrows*). Contrast material identifiable in right atrium (*arrowheads*).

IVC, intrahepatic vena cava, suprahepatic vena cava, and right atrium must be visualized on the study (fig. 6).

Postoperative Evaluation

Postoperative studies were done to evaluate vascular anastomotic integrity and patency, hepatic arterial inflow, and biliary-enteric outflow. Eighteen postoperative angiographic studies were performed: five celiac and/or hepatic arteriograms, five inferior vena cavograms, three aortograms, three donor arterial conduit aortograms, one splenic arteriogram, and one wedged hepatic venogram. Balloon angioplasty of a suprahepatic caval stenosis was performed on a 4-week-old anastomotic stenosis. The dilatation was successful as judged by an immediate postangioplasty venogram and reduction of a preangioplasty gradient of 60 mm Hg to 15 mm Hg after angioplasty.

Nine cholangiographic studies were performed: six percutaneous transhepatic and three T-tube cholangiograms. Transhepatic cholangiograms were performed using the standard right-lateral midaxillary line approach. Biliary drainage catheters were necessary in six patients and were inserted using the epigastric approach [4]. One internal jugular transvenous liver biopsy was performed. We have found cineradiography very useful in capturing the subtle and frequently rapid blood-flow patterns present in these patients. Rates of 30 frames/sec are used routinely and the panning with the cine unit is performed by the radiologist. A familiarity with abnormal vascular anatomy is needed to successfully perform the studies with cineradiography.

TABLE 1: **Angiographic Findings**

Findings	No. of Patients
Transplant patients ($n = 7$):	
Patent IVC	2
Patent portal vein	2
Diffuse neoplasm:	
Hepatoma	2
Cholangiocarcinoma	1
Nontransplant patients ($n = 6$):	
Small (<5 mm) portal vein (with hepatofugal flow)	2
Occluded IVC	1
Occluded portal vein	1
Nonvisualization of portal vein	1
Neoplasm localized within one hepatic lobe (hepatoblastoma)	1

Note.—IVC = inferior vena cava.

Results

Preoperative

A summary of preoperative angiographic findings for the transplant and nontransplant groups is given in table 1. In six patients, previous sonographic and CT studies were unable to adequately visualize the portal vein. Of these, the portal vein was visualized successfully in five (two with patent normal-sized portal veins, two with patent but small [<5 mm] portal veins, and one with an occluded portal vein). The latter three patients did not have transplants. The patient with nonvisualization of the portal vein also did not have a transplant. This one case, which occurred early in our experience, represents the only failure to answer the pertinent question(s) posed to the angiographer. The portal vein was not identified by either simultaneous SMA/splenic injection or direct transplenic splenoportography. This patient's portal vein also had not been identified sonographically; it was believed to be absent or thrombosed. On the basis of our recent experience, transhepatic portal venography would have been helpful in visualizing this portal vein.

In three patients the patency of the IVC could not be established with certainty by CT or sonography. All three cavae were demonstrated angiographically. Two were shown to be patent and one to be occluded. The latter patient did not receive a transplant.

Three patients studied had diffuse hepatic tumor (two hepatomas and one cholangiocarcinoma) defined as receiving blood supply from both the right and left hepatic arteries. One patient had hepatoblastoma confined to the right hepatic lobe and underwent subtotal hepatectomy rather than transplantation.

Overall, six of 13 patients evaluated by pretransplant angiography were shown to have anatomic or pathologic contraindications to transplantation.

Postoperative

In the 18 postoperative angiographic studies, 19 significant abnormalities were found, 12 of which threatened the transplant and six of which compromised the transplant (table 2).

TABLE 2: **Postoperative Findings in 18 Vascular Studies and 9 Cholangiographic Studies**

Findings	No. of Patients
Arterial:	
Diffuse hepatic arterial branch stenoses	3*
Hepatic artery occlusion	2*
Hepatic arterial anastomotic stenoses	2†
Hepatic arterial thrombosis	2*
Large arteriovenous fistula at biopsy site	2†
Bleeding from right adrenal artery	1
Venous:	
Occluded SHVC (with hepatic venous thrombus)	2*
Stenotic SHVC	1†
Occluded IHVC (with suprarenal caval thrombus)	1*
Stenotic IHVC	1*
Portal vein thrombosis	1*
Splenic vein occlusion	1†
Biliary:	
Obstructed cholecystojejunostomy	2*
Obstructed cystic duct (patients with cholecystojejunostomy)	2*
Extravasation from choledochocholedochostomy	1*
Abscess from biliary leak (fistula to donor aortic conduit)	1*

Note.—SHVC = suprahepatic vena cava; IVCH = infrahepatic vena cava.
* Threatening to transplanted liver survival.
† Compromising to transplanted liver.

Postoperative arterial angiographic findings involved primarily the hepatic artery anastomosis and consisted of occlusion in two cases, thrombosis in two, and anastomotic stenoses in two. Three patients had relatively normal anastomoses but showed diffuse stenoses in the intrahepatic branch arteries.

In one patient, bleeding from the right adrenal artery was identified and subsequently embolized. Although the hemorrhage was not directly threatening to the transplant, its identification and treatment contributed significantly to patient survival. Two additional patients were shown to have arteriovenous fistulae at sites of previous liver biopsies.

Postoperative venous abnormalities involved stenoses or occlusions of the supra- and infrahepatic vena cava. Half of the patients with stenoses or occlusions had thrombus behind the obstructed segment of IVC. One case of portal vein thrombosis and one case of splenic vein occlusion without thrombosis were identified.

In the nine cholangiographic studies, five abnormalities were identified that were threatening to the transplant liver. Four cases were obstructions, all of which occurred in children and involved either the cystic duct of the donor or the gallbladder-jejunal anastomosis. The fifth abnormal finding was a leaking choledochocholedochostomy anastomosis in an adult (figs. 7C and 7D). An abscess around a leaking cholecystojejunostomy was discovered when it filled via a fistula to the donor aortic conduit during a donor aortic injection (fig. 8).

In caring for these 46 transplant patients, several interventional procedures have been performed. Twelve percutaneous transhepatic cholangiograms have been safely performed. One internal jugular transvenous liver biopsy was performed in a postoperative patient with coagulopathy severe enough to preclude transperitoneal biopsy; sufficient tissue was obtained to diagnose rejection. One patient underwent balloon angioplasty of a suprahepatic vena caval anastomotic stenosis 4 weeks after transplantation. A predilatation gradient of 60 mm Hg was reduced to 15 mm Hg after dilatation. One biloma was drained percutaneously via a transperitoneal route; the biloma formed around a leaking choledochocholedochostomy (figs. 7C and 7D).

There have been no procedural complications in any of the pre- or postoperative angiograms nor from the cholangiographic studies. Although splenoportography is not without risk in patients with coagulopathy, we have had no significant bleeding problems.

Discussion

Liver transplantation is a long and technically difficult operation [1, 2, 5–12]. During liver transplantation, the native liver is mobilized and isolated by cross-clamping and ligating the suprahepatic IVC, infrahepatic IVC, hepatic artery, portal vein, and common bile duct. During insertion of the donor liver, the suprahepatic vena cava is anastomosed first, followed by the portal vein, hepatic artery, infrahepatic vena cava, and finally the biliary tree [8]. The biliary anastomosis, of which there are four types (fig. 9), has been the "Achilles heel" of the procedure, with anastomotic obstruction and/or leakage causing major problems. Bouts of cholangitis leading to septicemia have been relatively frequent, especially since these patients are immunosuppressed [13, 14].

The supra- and infrahepatic caval anastomoses are made in an end-to-end fashion and their angiographic identification and patency determination are relatively straightforward. It is important to identify not only contrast material entering the right atrium but also the suprahepatic IVC segment, since contrast material can enter the right atrium via collateral pathways in vena cava thrombosis, especially via the azygos vein (fig. 6). The extensive collateral venous network that develops in response to vena caval obstruction has been described elsewhere [15, 16].

The portal venous anastomosis is made in an end-to-end fashion. Its pre- and postoperative evaluation is more difficult, requiring either high-volume simultaneous splenic/SMA injections, transplenic splenoportography, or transhepatic portal venography. All three of these examinations must be carefully undertaken in these critically ill patients, since high volumes of contrast material can damage already stressed kidneys. Intravenous fluid flushes augmented with diuretics can be used to minimize contrast-induced acute tubular necrosis. We attempt to correct coagulopathies or platelet deficiencies before transplenic splenoportography or transhepatic portal venography, but are willing to accept less than normal values in view of the importance of the results.

Some liver transplant candidates have such torrential hepatofugal flow in the portal vein that it cannot be imaged by simultaneous superior mesenteric and splenic artery injec-

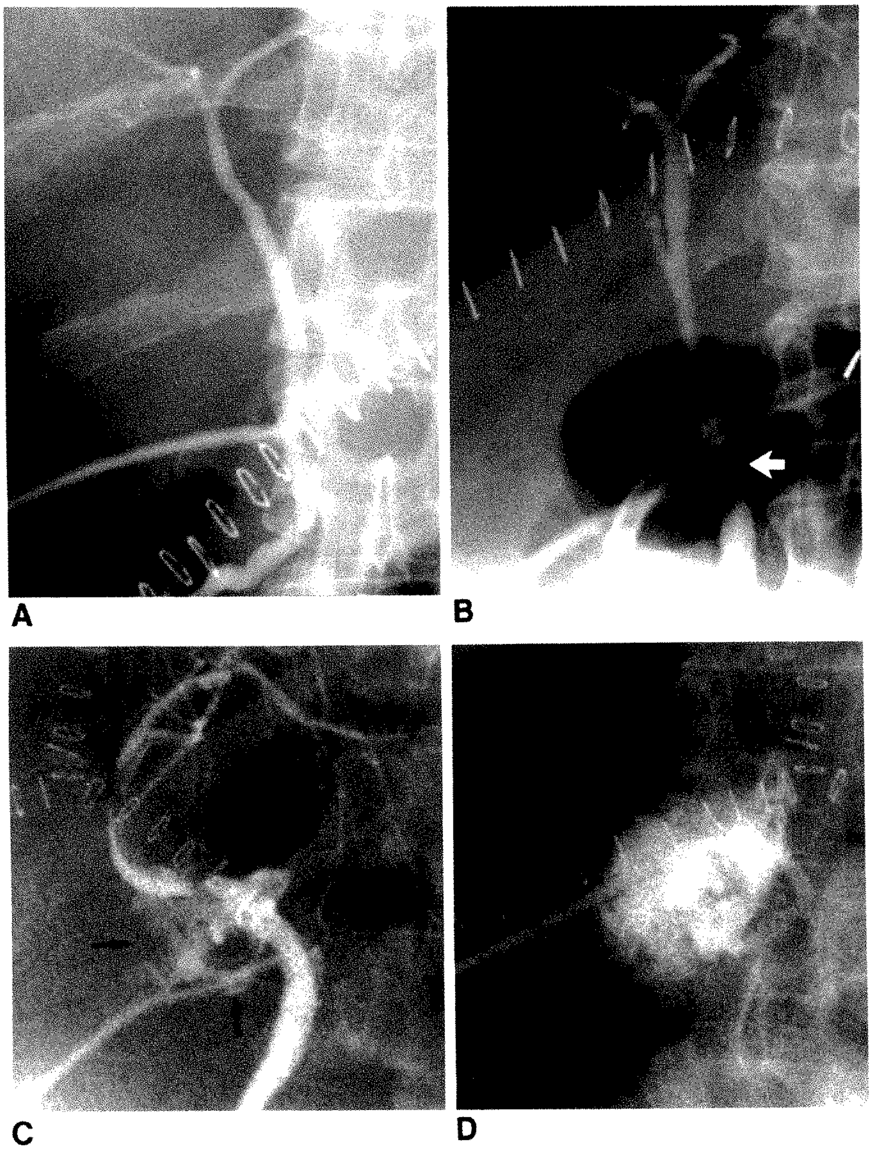

Fig. 7.—Four patients with choledochocholedochostomy. **A**, Normal adult postoperative T-tube cholangiogram. Site of anastomosis is totally inapparent. **B**, By contrast, this choledochocholedochostomy is narrowed just above long arm of T-tube (*arrow*). **C**, Extravasation from choledochocholedochostomy in adult demonstrated by T-tube cholangiography (*arrows*). **D**, Biloma cavity demonstrated by test injection through percutaneously placed drainage catheter.

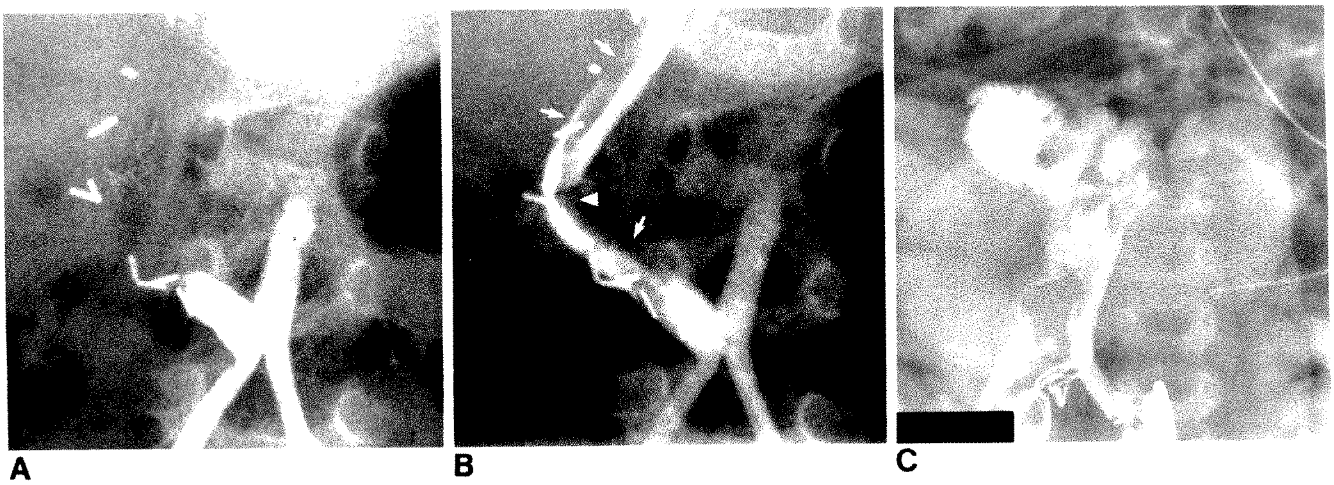

Fig. 8.—**A**, Film 4 weeks after transplant. Distal aortic injection shows complete occlusion of donor aortic conduit 1.5 cm distal to anastomosis to recipient aorta–common iliac artery junction. **B**, Catheter was carefully passed into donor aortic conduit, and injection shows thrombus (*arrows*) proximal and distal to tight stenosis (*arrowhead*) in conduit. **C**, 2 hr later, patient underwent laparotomy and intraoperative repeat arteriography, which shows arterial fistula into large abscess cavity resulting from leak at cholecystojejunostomy site. Patient died 24 hr later.

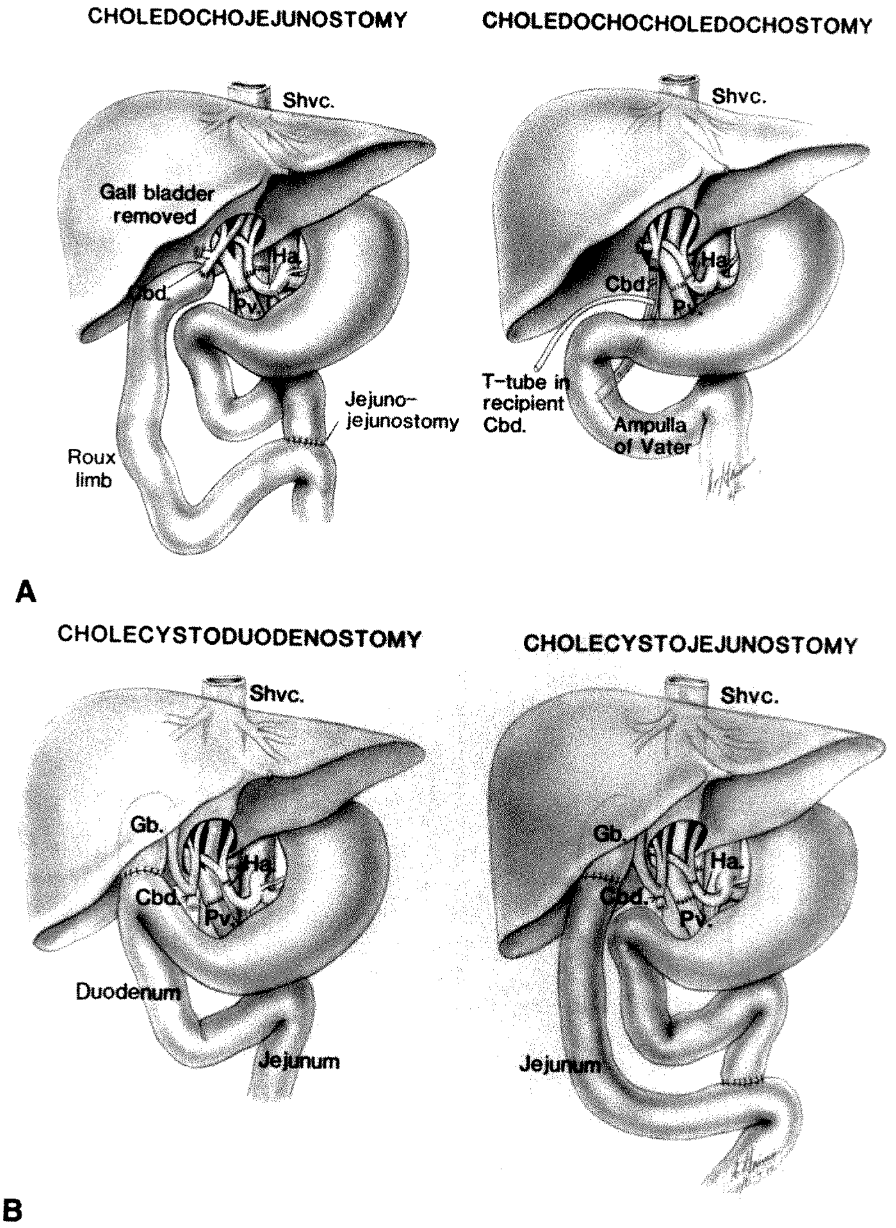

Fig. 9.—Types of biliary-to-enteric anastomoses. **A**, Adult. Note T-tube stenting used in choledochocholedochostomy. **B**, Pediatric. Common bile duct (Cbd.) ligation performed in both. For illustrative purposes, adult-type hepatic arterial (Ha.) anastomosis is shown (see text). Larger size of gallbladder (Gb.) facilitates anastomosis to duodenum or jejunum. Importance of donor cystic duct patency can be readily appreciated. Shvc. = suprahepatic vena cava; Pv. = portal vein.

tions or by transplenic splenoportography. We have had recent experience with an extrahepatic biliary atresia patient rejected for transplant at another institution because of portal vein occlusion and splenic vein thrombosis, based on nonsimultaneous celiac, splenic, and SMA injections. On evaluation here, transplenic splenoportography demonstrated rapid passage of contrast material through the patent splenic vein to a patent superior mesenteric vein, but no portal vein was seen. The wash-in of unopacified blood into the superior mesenteric vein seen on cineradiography prompted us to pursue the portal vein further. Transhepatic portal venography demonstrated a 3.5-mm portal vein with torrential hepatofugal flow (fig. 5). It is probable that the one case of nonvisualization of the portal vein that we had in our early experience was also due to brisk hepatofugal flow.

On the basis of this experience and the importance of the portal vein size determination, our routine pretransplant evaluation of the portal vein includes at least dual-catheter simultaneous SMA/splenic artery injections with high volumes and prolonged filming. If the portal vein is adequately visualized, we stop. If not visualized, we proceed to transplenic splenoportography, and if need be, to transhepatic portal venography. We routinely use magnification cineradiography at 30 frames/sec to film these cases. This enables typically rapid and subtle patterns of blood flow to be detected. The rate of blood flow in these children is amazingly rapid, even in the portal venous system, and the benefits of high-speed magnification filming have been amply proven by our experience in the pediatric heart catheterization laboratory. A centimeter grid placed at the midplane of the body is filmed at identical

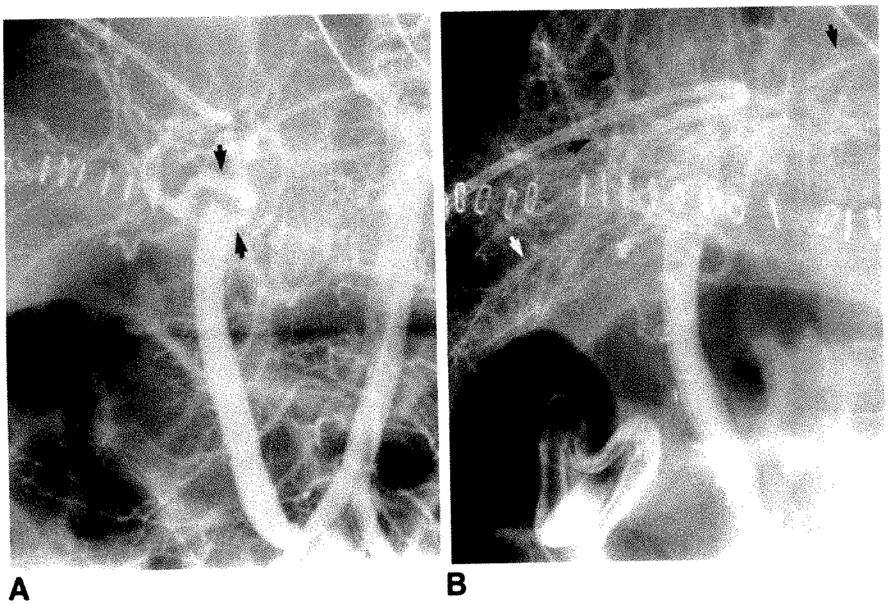

Fig. 10.—Typical pediatric hepatic arterial anastomosis in patient being evaluated for rising liver function tests and suspected rejection. **A**, End-to-side anastomosis of donor aortic conduit to right common iliac artery. Hemostasis clips along donor aorta occlude branch arteries. Redundancy of hepatic artery in porta hepatis due to extra length of common hepatic artery and celiac trunk (*arrows*). Excellent hepatic arterial flow and anastomotic patency. **B**, Hepatogram phase shows symmetric flow throughout liver but evidence of diffuse "railroad tracking" (*arrows*). Patient died 5 days later; postmortem examination showed hepatic necrosis despite excellent arterial inflow, consistent with rejection.

magnification setting, enabling very accurate measurement of the vessels. Portal vein absence or occlusion should not be diagnosed unless the vein fails to visualize on transhepatic portal venography. Absence or occlusion of the portal vein precludes liver transplantation. Our transplant surgeons use 5 mm as the minimum portal vein diameter acceptable for transplantation. Patients with a small but patent portal vein (usually infants with biliary atresia) are carried medically as long as possible to give the portal vein time to grow.

Liver transplantation for primary liver malignancy is controversial since recurrence is always possible because of the limitations of preoperatively excluding occult metastases. The gravity of the operation may not be justifiable in patients with malignancy because even if they survive surgery, recurrence of the malignancy has been reported [8]. At our institution subtotal hepatectomy is performed in preference to liver transplantation when tumor can be localized to one lobe or when one segment can be shown to be free of tumor [17–20].

The hepatic arterial anastomosis varies depending on the size of the recipient artery. In adults, the hepatic artery is large enough for end-to-end anastomosis of the donor and recipient hepatic arteries. However, the small caliber of the hepatic artery in children makes end-to-end anastomosis difficult and long-term patency unlikely. In this series, the pediatric hepatic arterial anastomoses were performed by attaching a conduit of donor aorta, taken with the celiac trunk, to the recipient aorta or right common iliac artery in an end-to-side manner (fig. 10). Therefore, in children we do an abdominal aortogram to determine the site and status of the arterial anastomosis. Depending on the aortographic findings, the decision to selectively catheterize the donor aortic conduit can be made. Generally a 5-French 45°-angled cerebral catheter will selectively catheterize the donor aortic conduit when it originates from the right common iliac artery. When the donor aortic conduit is anastomosed directly to the recipient aorta, a more right-angled wall-seeking catheter such as a 5-French Cobra catheter should be used. Selective catheterization of the donor aortic conduit appears safe; no complications have occurred.

The vascular anastomoses of transplant patients develop four basic angiographically detectable problems: occlusion, stenosis, thrombosis, and diffuse arterial narrowing. Careful review of our cases revealed that complete occlusion (without identifiable thrombus) was the result of trauma to vessels by vascular clamps, either during the harvesting and transport of the liver or during actual transplantation. Occlusions occurred early after transplantation, usually within 7–10 days. The typical occlusion is abrupt and no contrast material passes beyond.

Vascular stenoses occurred at anastomotic sites, especially those between vessels of different sizes, those that required additional buttressing with pledget sutures, and those that were taken down and redone during the initial transplant operation (fig. 11). These stenoses occurred 2–4 weeks after transplantation and were probably the result of fibrosis, reactive edema, or organized thrombus at the anastomotic site. Stenoses occurred at hepatic arterial, suprahepatic vena caval, and infrahepatic vena caval anastomoses. Extrinsic compression of the donor aortic conduit at the point of the mesenteric tunnel was also a common site of arterial stenosis (fig. 11B).

Thrombosis was more common in venous structures, undoubtedly secondary to slower flow in these vessels, but did occur in arteries as well. Thrombosis is defined as the presence of thrombus in a vessel that is not occluded. Thrombosis occurred proximal to venous anastomoses and distal to arterial anastomoses. Despite the greater prevalence of thrombosis in venous structures, we have seen thrombosis of the donor aortic conduit on two occasions. In both cases, the thrombosis was associated with an angiographically significant stenosis of the donor aortic conduit (figs. 8 and 11B).

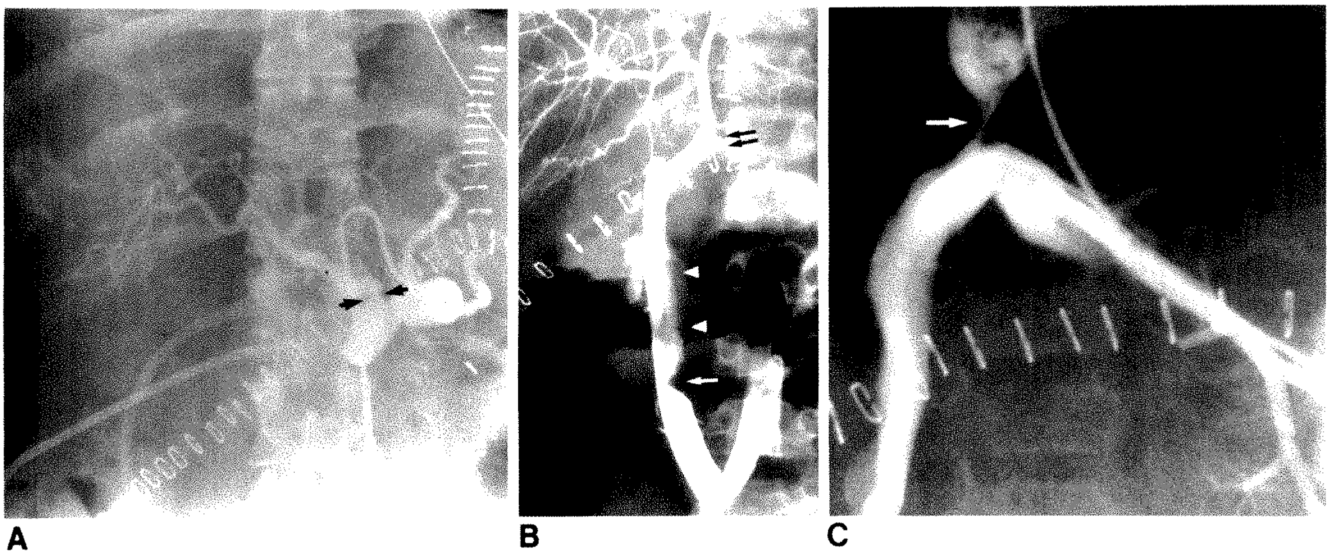

Fig. 11.—Three patients. **A**, Adult with postoperative stenosis of end-to-end hepatic-artery-to-hepatic-artery anastomosis. Study of celiac axis 8 days after transplantation. Marked stenosis at anastomotic site (*arrows*) with redundancy of native celiac axis and proximal hepatic artery. Poor arterial inflow into liver. **B**, Pediatric donor aortic conduit with stenosis 3 cm beyond anastomosis (*white arrow*) possibly at mesenteric tunnel site. Thrombus along left wall of conduit (*arrowheads*). Ligated donor splenic artery can be seen (*black arrows*). **C**, 7-month-old girl with tight venous stenosis of suprahepatic vena cava (*arrow*) just below right atrium on selective left hepatic venogram. Surgical anastomosis of suprahepatic vena cava was complicated by bleeding, necessitating primary revision during initial transplant. Stenosis underwent successfull angioplasty 4 weeks after transplantation.

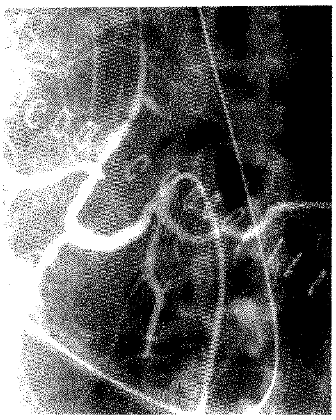

12

Fig. 12.—Selective celiac axis injection shows donor hepatic artery with multiple widespread arterial narrowings in proximal branches typical of rejection. Biopsies on two occasions showed rejection. Patient died next day. Postmortem examination was consistent with rejection.

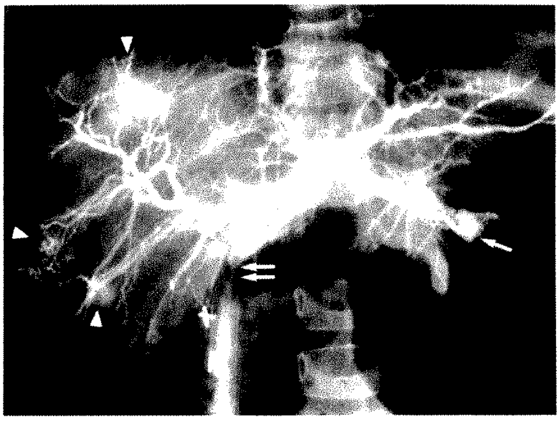

13

Fig. 13.—Subcostal left-lobe biopsy was performed to exclude rejection because of rising SGOT. Arteriovenous fistula (*single arrow*) can be seen filling on midarterial film with shunting into portal vein. Unfortunately, three vascular metastases also visualized in right hepatic lobe (*arrowheads*) in this patient who had transplant because of hepatoma (same patient as fig. 1). Conduit stenosis near distal end (*double arrows*).

Diffuse narrowing (with or without vessel occlusions) of the intrahepatic arterial branches indicates either rejection or hepatic necrosis (fig. 12). The angiographic differentiation of rejection from hepatic necrosis is difficult if not impossible. Rejection is an immunologic phenomenon [21], whereas necrosis can be due to arterial inflow occlusion or high-grade stenosis, prolonged warm ischemia time (during transport or insertion), and hypoperfusion from poor systemic hemodynamics. Acute rejection is reported to be uncommon in the liver because of a poorly understood immunologically privileged status [21]. Therefore, problems in the first week are more likely to be the result of necrosis. However, most transplant patients who develop complications get in trouble during the second to fourth postoperative weeks. Since chronic rejection does occur, the differentiation between rejection and necrosis becomes more difficult, even for the pathologist. On the basis of current interpretation of percutaneous liver biopsies, two angiographic features emerge as correlating with rejection. The first feature is widespread stenoses (or spasm) in the major hepatic arterial branches (fig. 12). The second feature is diffuse "railroad tracking" of vessels in the portal triad, that is, simultaneous filling of hepatic artery and portal vein branches. Previously this feature was described in livers containing neoplasm and has been attributed to sinusoidal shunting. Although it is not entirely understood, perhaps the inflammatory response associated with rejection or immunologic mediators causes similar sinusoidal shunting during rejection (fig. 10B).

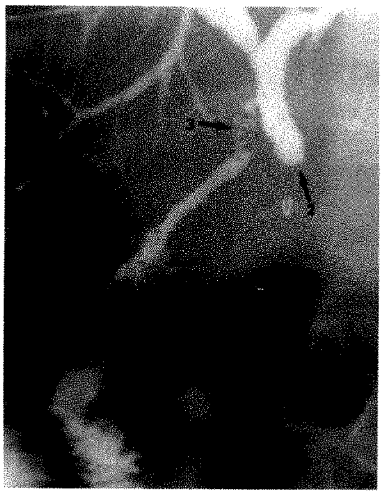

14

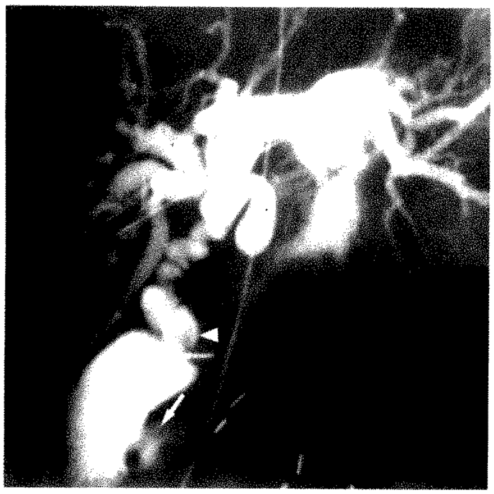

15

Fig. 14.—Close-up of normally functioning cholecystojejunostomy (1) demonstrated on percutaneous transhepatic cholangiogram. Blind-ending common bile duct due to surgical ligation (2). Importance of cystic duct (3) can be appreciated.

Fig. 15.—Pediatric transplant patient with persistent postoperative jaundice had percutaneous transhepatic cholangiogram for evaluation of cholecystojejunostomy. Anastomosis between gallbladder and jejunum was widely patent (*arrow*), but persistent defeat (*arrowhead*) in donor cystic duct caused partial obstruction with moderate dilatation of cystic duct and intrahepatic ducts.

Little has been written about the angiographic signs of rejection in liver transplant patients, but renal artery aneurysm has been described as a sign of renal transplant rejection as has prolonged arterial-phase opacification [22]. Edema in the renal transplant parenchyma is proposed as the mechanism of sluggish arterial perfusion during rejection. A similar mechanism could be postulated for hepatic rejection, although we saw no examples of this in our series.

Percutaneous liver biopsy is often used to evaluate rejection. Three complications of biopsy are prolonged oozing from the site secondary to coagulopathy, hemotobilia, and creation of an arteriovenous fistula. Intraperitoneal extravasation of contrast material, indicating oozing from a biopsy site, was never identified angiographically in this series. There were two cases of documented arteriovenous fistulae in our series (fig. 13).

Bleeding was another important postoperative problem. In our experience, intraperitoneal bleeding is almost always related to oozing from raw liver surfaces or diffuse oozing from other intraperitoneal structures due to the patient's concomitant coagulopathy. In these situations, it is unusual to identify a site of actual extravasation of contrast material; however, we did identify one case of bleeding from a right adrenal artery that was injured in the course of transplantation. This was successfully embolized with Ivalon particles. No intraperitoneal bleeding from leaking vascular anastomoses was identified; presumably these can be seen and corrected before closing the abdomen during the initial surgery. Reoperation for bleeding does occasionally occur, and in cases of massive bleeding with hypotension, surgery is begun without angiography, which is another reason why no leaking anastomoses were identified.

Postoperative patients are routinely followed with Disofenin radionuclide liver-spleen scans to evaluate biliary tract patency. In certain situations, the Disofenin study identifies biliary obstruction but is not anatomically specific enough to define the level of obstruction. In these situations, cholangiography is performed either through a surgically placed T tube (in patients with a choledochocholedochostomy [figs. 7A and 7B]), or by a percutaneous transhepatic approach in patients with a cholecystojejunostomy, cholecystoduodenostomy, or choledochojejunostomy. The latter three anastomoses require no T-tube stenting, and the only access to the biliary tree is percutaneous (fig. 14). Endoscopic retrograde cholangiopancreatography has limited application because the biliary-enteric anastomotic sites are difficult to locate. Postoperative biliary obstruction has primarily been a problem in children because of the technical difficulties associated with small ducts and the abnormal friable ductal tissue present in biliary atresia. In one patient, the cholecystojejunostomy was widely patent but obstruction resulted from a filling defect, believed to be a polyp, stone, or piece of debris, in the donor cystic duct (fig. 15).

In summary, preoperative determination of portal vein size and patency required dual-catheter arterial studies, splenoportography, or transhepatic portal venography. Caval patency can be assessed by a simple inferior vena cavogram. Localization of liver neoplasms should in most cases be done with CT and sonography; an occasional case required angiography to map the vascular supply to decide if subtotal hepatectomy was adequate therapy.

Postoperative studies of the arterial and venous anastomoses are necessary to differentiate transplant failure due to vascular inflow or outflow problems from rejection. Occlusions, stenoses, thromboses, and diffuse arterial narrowings are the primary significant angiographic findings. Postoperative cholangiographic studies have identified both obstruction and leakage at biliary anastomoses.

Interventional radiologic procedures are beginning to be used in the post-liver-transplant patient and undoubtedly will see increasing use. On the basis of our experience with 46 liver transplant patients, we believe there is very definitely a place for both pre- and postoperative angiographic and interventional radiologic evaluation of these patients. Although these procedures involve risks, especially bleeding, that are not a problem with less invasive imaging methods, they provide information critical to clinical decision making, which in many cases is not available by any other means.

REFERENCES

1. Starzl TE, Koep LJ, Halgrimson CG, et al. Fifteen years of clinical liver transplantation. *Gastroenterology* **1979**;77:375–388
2. Calne RY, Williams RW. Liver transplantation. *Curr Probl Surg* **1979**;16:3–44
3. Probst P, Rysavy JA, Amplatz K. Improved safety of splenoportography by plugging of the needle tract. *AJR* **1978**;131:445–449
4. Castaneda-Zuniga WR, Tadavarthy SM, Laerum F. Anterior approach for biliary duct drainage—a useful technique. *Radiology* **1981**;139:746–747
5. Starzl TE. Liver homotransplantation. In: Sabaston DC, ed. *Textbook of surgery*. Philadelphia: Saunders, **1977**:526–539
6. Starzl TE. Liver transplantation. *Johns Hopkins Med J* **1979**;143:73–83
7. Terblanche J, Koep LJ, Starzl TE. Liver transplantation. *Med Clin North Am* **1979**;63:507–521
8. Simmons RL, Finch ME, Ascher NL, Najarian JS. *Manual of vascular access, organ donation, and transplantation.* New York: Springer-Verlag, **1984**:255–284
9. Starzl TE, Iwatsuki S, Van Thiel DH, et al. Evolution of liver transplantation. *Hepatology* **1982**;2:614–636
10. Calne RY. Recent advances in clinical transplantation of the liver and pancreas. *Transplant Proc* **1983**;15:1263–1268
11. Van Thiel DH, Schade RR, Starzl TE. Liver transplantation in adults. *Hepatology* **1982**;2:637–640
12. Krom RAF, Gips DH, Newton D, et al. A successful start of a liver transplantation program. *Transplant Proc* **1983**;15:1276–1278
13. Iwatsuki S, Shaw BW, Starzl TE. Biliary tract complications in liver transplantation under cyclosporine-steroid therapy. *Transplant Proc* **1983**;15:1288–1291
14. Touraine JL. Bone marrow and fetal liver transplantation in immunodeficiencies in inborn errors of metabolism: lack of significant restriction of "T" cell function in long-term chimeras despite HLA-mismatch. *Immunol Rev* **1983**;71:103–118
15. Solomonowitz E, Castaneda-Zuniga WR, Bass JL. Transhepatic collateral pathway due to vena caval obstruction. *AJR* **1984**;142:1210–1212
16. Seltman HJ, Dekker A, Van Thiel DH, Boggs DR, Starzl TE. Budd-Chiari syndrome recurring in a transplanted liver. *Gastroenterology* **1983**;84:640–643
17. Chuang VP, Soo CS, Carrasco CH, Wallace S. Superselective catheterization technique in hepatic angiography. *AJR* **1983**;141:803–811
18. Freeny PC, Marks WM. Computed tomographic arteriography of the liver. *Radiology* **1983**;148:193–197
19. Pagani JJ. Intrahepatic vascular territory shown by computed tomography. *Radiology* **1983**;147:173–178
20. Sexton CC, Zeman RK. Correlation of computed tomography, sonography and gross anatomy of the liver. *AJR* **1983**;141:711–718
21. Pichlmayr R, Brolsch C, Neuhaus P, et al. Report on 68 human orthotopic liver transplantations with special reference to rejection phenomena. *Transplant Proc* **1983**;15:1279–1283
22. Castaneda-Zuniga WR, Sibley R, Zollikofer C. Renal artery aneurysm: an angiographic sign of transplant rejection. *Radiology* **1980**;136:333–335

Abdominal Pseudoaneurysm Arising from a True Aneurysm: Presentation as a Pulmonary Mass

Myung S. Shin,[1] Kang-Jey Ho,[2] John W. Kirklin,[3] John M. Forman,[3] and Lincoln L. Berland[1]

Atherosclerotic aneurysm of the abdominal aorta often produces no symptoms unless it ruptures into the pleural, peritoneal, or retroperitoneal space or compresses adjacent structures [1-4]. The most common symptom is pain, but an asymptomatic, nontender, pulsatile mass is often palpable above the umbilicus. We describe a case of a ruptured atherosclerotic aneurysm of the abdominal aorta with minimal symptomatology that simulated a lower lung mass on conventional chest radiography. The correct diagnosis was made by CT and was confirmed at surgery.

Case Report

A 61-year-old man was admitted with a 3-month history of cough, hemoptysis, and weight loss. He was hypertensive and had a history of seizure disorder probably associated with alcohol abuse and withdrawal. He also had smoked two packs of cigarettes per day for more than 30 years and had only recently reduced to one-half pack per day. His cough was productive of white sputum and occasionally fresh blood and was associated with low back pain and a 17-kg weight loss. The pertinent findings on admission included a blood pressure of 140/100 mm Hg, pulse of 96/min, greatly diminished dorsalis pedis and posterior tibial pulses bilaterally, epigastric tenderness without palpable mass, a packed cell volume of 32%, and hemoglobin of 11 g/dl. A chest radiograph showed a fairly smooth, well demarcated mass at the right lung base (fig. 1A) that had not been present 6 months earlier. The initial clinical impression was bronchogenic carcinoma.

Bronchoscopy revealed a small amount of blood in the anterior basal segment of the right lower lobe but no visible endobronchial lesion. The cytologic studies of the bronchial washing and brushing specimens and the sputums were all negative for malignancy. A CT scan then showed that the mass at the right lung base was the upper part of a 9 × 13.5 cm mass located in the retroperitoneal space between the diaphragm and the renal hila (figs. 1B-1D). The mass had a smooth outline, irregular shape, and homogeneous density with an attenuation value of 40-45 H, similar to that of the blood. The lumen of the abdominal aorta was irregularly dilated with a less dense area between the lumen and calcified wall suggestive of mural thrombus (fig. 1D). These CT findings were compatible with a giant pseudoaneurysm arising from a ruptured atherosclerotic aneurysm of the abdominal aorta and associated with a diaphragmatic eventration.

The patient refused surgical intervention and was discharged; 1 month later he developed massive hemoptysis. When brought to the emergency room, he was in shock followed by apnea and cardiac arrest requiring cardiopulmonary resuscitation. Chest radiography revealed irregular opacification of the right lower lung base with pleural effusion. CT showed marked enlargement of the original false aneurysm, irregular border of the mass of diaphragmatic eventration, and right posterior pleural effusion. At this time the patient agreed to surgery.

At surgery, the giant retroperitoneal false aneurysm was confirmed. After a huge amount of blood clot was evacuated, a large opening measuring 4 × 6 cm became evident on the right side of the abdominal aorta just superior to the origin of the celiac artery. The hematoma also extended through the right hemidiaphragm to the chest cavity, eroding into the lung parenchyma. Although the aortic aneurysm was successfully repaired by patch graft, the patient developed wound dehiscence and aspiration and died 10 days after surgery. No autopsy was performed.

Discussion

Most patients who develop aortic aneurysms are men older than 60; more than half have associated hypertension and many are cigarette smokers [1, 4]. Our patient fits such a profile. However, there are several unique aspects of this case, such as the unusual location of the aneurysm and the long survival with minimal symptoms after the rupture of the aneurysm [5]. The suspicion of lung cancer was unavoidable in a patient with a newly developed chest mass associated with cough, hemoptysis, weight loss, and a long history of heavy cigarette smoking. After a futile clinical search for lung cancer, CT proved extremely useful, as has been the experience of others in identifying aortic aneurysms [6, 7]. CT clearly delineated the extent of the false aneurysm and its relation to the aorta (figs. 1C and 1D). The CT findings of a smoothly outlined, irregularly shaped mass with a density identical to that of blood, lying in direct continuity with a dilated segment of aorta, are quite diagnostic of a false aneurysm secondary to rupture of a true aneurysm.

It has been shown that when the diameter of an aneurysm is greater than 6 cm, the possibility of rupture in a 10-year

---

Received May 21, 1985; accepted after revision September 11, 1985.

[1] Department of Radiology, University of Alabama School of Medicine, Veterans Administration Hospital, and University of Alabama Hospitals, 619 S. 19th St., Birmingham, AL 35233. Address reprint requests to M. S. Shin.

[2] Department of Pathology, University of Alabama School of Medicine and Veterans Administration Hospital, Birmingham, AL 35233.

[3] Department of Cardiovascular Surgery, University of Alabama School of Medicine and Veterans Administration Hospital, Birmingham, AL 35233.

AJR 146:155-156, January 1986 0361-803X/86/1461-0155 © American Roentgen Ray Society

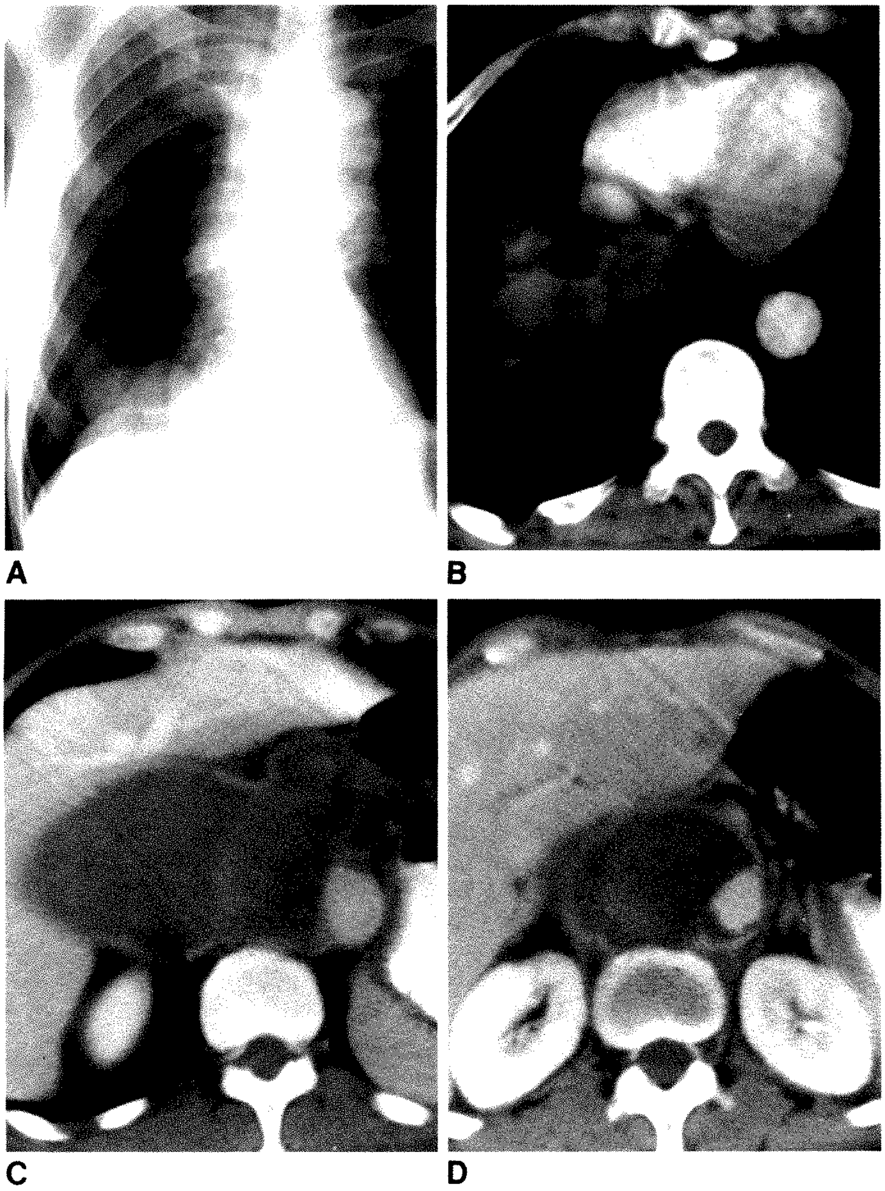

Fig. 1.—**A**, Posteroanterior film on admission. Well demarcated mass lesion at right lung base. Contrast-enhanced CT scans at levels above (**B**) and below (**C**) diaphragm and at renal hila (**D**). Note lobulated demarcated mass adjacent to aorta with diaphragmatic eventration.

period is 45%–50%, whereas it is only 15%–20% when the diameter is less than 6 cm [3, 8]. The actual size of the aneurysm before rupture in this case was unknown. Nevertheless, it did rupture into the retroperitoneal space. It is most likely that the unusually high position of the aneurysm resulted in a massive but contained retroperitoneal hematoma instead of intraperitoneal rupture and rapid demise. The high position of the aneurysm also allowed the false aneurysm to eventrate the diaphragm and present as an intrathoracic mass.

REFERENCES

1. Gore I, Hirst AE Jr. Arteriosclerotic aneurysms of the abdominal aorta. *Prog Cardiovasc Dis* **1973**;16:113–150
2. Bergan JJ, Yao JST. Modern management of abdominal aortic aneurysms. *Surg Clin North Am* **1974**;54:175–193
3. Szilagyi DE, Smith RF, DeRusso EJ, Elliott JP, Sherrin FW. Contribution of abdominal aortic aneurysmectomy to prolongation of life. *Ann Surg* **1966**;164:678–699
4. Melton LJ III, Bickerstaff LK, Hollier LH, et al. Changing incidence of abdominal aortic aneurysms: a population-based study. *Am J Epidemiol* **1984**;120:379–386
5. Makin GS. Some factors influencing hospital mortality in ruptured abdominal aortic aneurysm. *J Cardiovasc Surg* (Torino) **1983**;24:646–648
6. Iliceto S, Ettorre G, Francioso G, Antonelli G, Biasco G, Rizzon P. Diagnosis of aneurysm of the thoracic aorta. Comparison between two noninvasive techniques: two-dimensional echocardiography and computed tomography. *Eur Heart J* **1984**;5:545–555
7. Miller GA Jr, Heaston DK, Moore AV Jr, Korobkin M, Braun SD, Dunnick NR. CT differentiation of thoracic aortic aneurysms from pulmonary masses adjacent to the mediastinum. *J Comput Assist Tomogr* **1984**;8:437–442
8. Darling RC. Ruptured arteriosclerotic abdominal aortic aneurysms: a pathologic and clinical study. *Am J Surg* **1970**;199:397–401

Complications of Intraarterial Urokinase-Lys-Plasminogen Infusion Therapy in Arterial Ischemia of Lower Limbs

Jean-Noel Fiessinger[1]
Jean-François Vitoux[1]
Jean-Marc Pernes[2]
Martine Roncato[3]
Martine Aiach[3]
Jean-Claude Gaux[2]

Thirty five patients with peripheral arterial occlusions were treated by intraarterial infusion of low-dose urokinase associated with bolus of lys-plasminogen. Thrombolysis was achieved in 26 cases (74%), but only 10 patients (28.5%) experienced sustained improvement. Complications of thrombolysis occurred in 11 patients: Five patients developed groin hematoma, five had distal emboli, and one experienced macroscopic hematuria. Catheter-related thrombosis was observed in 14 patients (40%) despite intravenous heparin. Nine patients suffered from recurrent thrombosis and three from proximal emboli. A patient died from catheter-related infection. Limited fibrinolysis could increase pericatheter thrombosis, and further work will be necessary to assess the local risk of intraarterial thrombolysis.

In an attempt to avoid systemic fibrinolytic effect and to reduce hemorrhagic and embolic complications, intraarterial thrombolysis has been proposed [1–3]. The benefit of arterial infusion is unclear. At infusion rates as low as 5000 U/hr of streptokinase, systemic fibrinolytic effects are often encountered [4, 5] and catheter-related thrombosis, a previously unreported complication of thrombolytic therapy, has been disturbingly frequent [6, 7]. We have previously reported that with low-dose intraarterial urokinase (1000 U/kg/hr) systemic fibrinolysis was unusual and that intraarterial infusion of plasminogen increased the efficiency of urokinase [7–9]. In order to assess the incidence of complications related to local thrombolytic therapy, we report a retrospective analysis of our results with intraarterial infusion of urokinase-lys-plasminogen.

Materials and Methods

From September 1983 to October 1984, 35 patients were treated with intraarterial urokinase infusion. There were 23 male and 12 female patients with a median age of 69 years (range, 21–89 years). Twenty-six patients had atherosclerotic occlusions with severe claudication and rest pain (two patients) or critical ischemia (24 patients). Two patients with Buerger disease were treated for distal gangrene. Seven patients had postoperative occlusions: Thrombosis occurred in polytetrafluorethylene grafts in six patients (four aortofemoral grafts, one femorofemoral, one femoropopliteal) and in a saphenous vein graft in femorotibial position in the remaining patient. In all patients the occlusion was less than 30 days old. The decision to use fibrinolytic therapy was based on the severity of ischemia, the accessibility of the thrombus, and the absence of contraindications to thrombolytic therapy.

Urokinase was administered via the catheter using an electric pump at the rate of 1000 U/kg/hr. Every 30 min, the infusion was interrupted and a bolus of 7.5 mg of lys-plasminogen was given through the catheter [8, 9]. All patients received concomitant intravenous heparin in doses sufficient to maintain heparinemia, measured by a chromogenic substrate technique, between 0.15 and 0.4. Urokinase infusion was stopped when complete lysis was achieved, when significant complications occurred, when indication for surgery superseded, or when there was no evidence of thrombolysis during the previous 12 hr. Assays of fibrinogen, alpha-2 antiplasmin, plasminogen, and fibrin degradation products and heparin monitoring tests were carried out before initiating therapy and every 4 hr during the treatment period.

Received April 24, 1985; accepted after revision August 21, 1985.

[1] Chaire de Clinique Medicale et de Pathologie Vasculaire, Hôpital Broussais, 96 rue Didot, 75674 Paris Cedex 14, France. Address reprint requests to J.-N. Fiessinger.

[2] Service de Radiologie Vasculaire, Hôpital Broussais, 75674 Paris Cedex 14, France.

[3] Laboratoire d'Hemostase, Hôpita Broussais, 75674 Paris Cedex 14, France.

***AJR* 146:157–159, January 1986**
0361-803X/86/1461-0157
© American Roentgen Ray Society

Arteriography, using the intraarterial catheter, was repeated at least every 6 hr until the end of the arterial infusion, with a mean of three arteriograms per patient. Arteriograms were retrospectively evaluated for thrombolysis, distal emboli, and proximal thrombosis.

The 35 patients were considered eligible for 37 treatments. A 4-French or more often a 5-French polyethylene catheter was placed at the occlusion site; it was introduced through the homolateral femoral artery in 24 patients and through the contralateral artery in nine patients. In four patients with aortic thrombosis, an axillary approach was used. Thrombus catheterization was not possible in two patients; thus 33 patients received 35 infusions of urokinase-lys-plasminogen. Total infusion time varied from 4 to 20 hr (average, 9.5 hr). Treatment was suspended by hour 4 in four patients: in three cases because of mobilization of the catheter and in one case because of successful treatment.

Results

Thrombolysis was considered to be successful, as judged by arteriography, in 26 of the 35 treatments (74%), but only 10 patients (28.5%) experienced sustained radiologic and clinical improvement. The systemic fibrinolytic effect was moderate; no patient had a fibrinogen level lower than 100 mg/dl or a decrease in serum plasminogen greater than 50%. Two patients had fibrinogen levels between 200 and 100 mg/dl after 8 hr of treatment.

Complications

Hemorrhage.—Bleeding from the catheter entry site occurred in five patients (14%), necessitating institution of blood transfusion in one patient. In a sixth patient, transient macroscopic hematuria developed during the infusion, necessitating discontinuation of urokinase.

Emboli.—Embolic complications were observed in eight patients (23%). Five patients had angiographically documented distal emboli. In two of those cases thrombus resolved with further thrombolytic therapy. Of the other three, two had a brief increase of ischemia, but the third required leg amputation. Three other patients had embolic complications: A 76-year-old woman who was being treated with an axillary catheter experienced cerebellar embolus simultaneously with the withdrawing of the catheter. She died 2 days later and pathologic examination confirmed the diagnosis. The second patient, being treated with a homolateral catheter, had multiple proximal emboli of profunda femoris artery. In the third patient, a contralateral catheterization was unsuccessful and embolic occlusion of popliteal artery developed distal to the puncture site.

Catheter-related thrombosis.—Thrombus surrounding the catheter was observed on arteriograms of 14 patients (40%). In four cases, the thrombosis was serious enough to require immediate surgery.

Recurrent thrombosis.—Early rethrombosis occurred after nine (25.5%) of the successful 26 treatments. Eight patients had poor distal runoff, and one had residual femoral stenosis accessible to percutaneous angioplasty, but groin hematoma contraindicated this procedure.

Infection.—Infection at the catheter entry site occurred in two patients; one of them died from septicemia.

Amputation.—Six patients (17%) required leg amputations. In one patient ischemia was aggravated by distal emboli. The other five patients would have come to amputation in any case.

Deaths.—Four patients (12%) died. An 84-year-old woman was treated for acute ischemia with irreparably damaged tissue. Thrombolysis was unsuccessful and she died the next day. One patient with mesenteric ischemia and leg occlusion developed renal failure during the intraarterial infusion and died. The two remaining patients died of complications related to the treatment: cerebellar emboli in one and septicemia in the other.

Discussion

We have previously reported that low-dose intraarterial urokinase is of limited value in the treatment of arterial thromboembolism [2] and that intraarterial infusion of lysyl plasminogen, a partially degraded form developed from the placenta, increases the efficiency of urokinase [8–10]. Thrombolysis was achieved in 74% of cases. These results are similar to those reported with low-dose streptokinase, which has an average patency rate of 71% [5, 6, 11–13]. However several of our patients experienced complications and only 10 had durable success. Hemorrhagic complications in our series were less frequent than with intraarterial streptokinase [1, 4, 13, 14]: Bleeding from the catheter entry site occurred in five patients, one case requiring a blood transfusion but no discontinuation of urokinase. Systemic bleeding occurred in only one patient, who suffered from transient hematuria, necessitating discontinuation of treatment. This low frequency of systemic hemorrhage could be related to the limited proteolysis induced by our treatment.

The possibility of distal embolization of partially lysed clots is a continuing concern. Five patients in this series experienced distal emboli; in three cases a significant aggravation of ischemia occurred.

Percutaneous catheters pose a risk of infection. Two of our patients developed infection of the catheter entry site and one died from septicemia. We have not used prophylactic antibiotics in our patients. However, since the catheters are in place for several hours and are advanced as clots lysis progresses, the use of antibiotic coverage could minimize the risk of infection [4].

Eskridge et al. [7], in a retrospective study, observed thrombus on the surface of 26% of infusion catheters. Analysis of arteriograms showed clots fixed on the catheter in 14 of our patients (40%) despite concomitant intravenous heparin. This high rate could be related to the limited systemic proteolysis induced by the treatment. The durability of initially successful thrombolysis is related to the presence of underlying atherosclerotic lesions and the achievement of a good runoff: One of our patients underwent a successful femoral angioplasty, but in nine cases (25.5%) recurrent thrombosis occurred. This high percentage of reocclusion could be related to the development of pericatheter thrombi. Pericatheter thrombosis could have been the cause of proximal emboli observed in three patients. In one patient, homolateral puncture was complicated by emboli in the profunda femoris artery; in a second patient, contralateral emboli occurred during an unsuccessful contralateral catheterization; and the third patient experienced cerebellar emboli simultaneously with the withdrawal of an axillary catheter. To our knowledge, this is the first report of emboli complicating catheter-related thrombosis. In our opinion, the risk of cerebral emboli contraindicates the use of axillary punctures for intraarterial thrombolytic treatment.

A patient with mesenteric ischemia and a patient with irreversible peripheral ischemia were treated. Both patients died from a combination of renal failure and electrolyte imbalance. In the first case, successful thrombolysis could have increased myoglobinuria [15]. In accord with Lang [15], we suggest that nonviable tissues are a contraindication to thrombolytic therapy, which increases the risk of "crush syndrome." In the two remaining patients who died, death was directly related to intraarterial therapy; one was the patient with cerebellar infarction, the other was the patient with septicemia.

REFERENCES

1. Dotter CT, Rösch J, Seaman AJ. Selective clot lysis with low-dose streptokinase. *Radiology* **1974**;111:31–37
2. Fiessinger JN, Aiach M, Capron L, Devanlay M, Vayssairat M, Juillet Y. Effect of local urokinase on arterial occlusion of lower limbs. *Thromb Haemost* **1981**;45:230–232
3. Becker GJ. Local thrombolytic therapy: bridging the "generation gap." *AJR* **1983**;140:403–405
4. Graor RA, Risius B, Young JR, et al. Low-dose streptokinase for selective thrombolysis: systemic effects and complications. *Radiology* **1984**;152:35–39
5. Rubenfire M, Blevins RD, Cascade PN, Maltzman JB, Goldberg MJ. The systemic fibrinolytic effect of low-dose intraarterial streptokinase: observations in 12 patients. Work in progress. *Radiology* **1984**;152:41–43
6. Becker GJ, Rabe FE, Richmond BD, et al. Low-dose fibrinolytic therapy. *Radiology* **1983**;148:663–670
7. Eskridge JM, Becker GJ, Rabe FE, et al. Catheter-related thrombosis and fibrinolytic therapy. *Radiology* **1984**;149:429–432
8. Vitoux JF, Pernes JM, Roncato M, et al. Thrombolyse intra-artérielle par l'association urokinase-lysyl-plasminogene: 27 cas d'oblitérations artérielles aigues des membres inférieurs. *Rev Med Intern* **1984**;5:255–261
9. Fiessinger JN, Roncato M, Gaux JC, Vitoux JF, Aiach M, Vandenbroek MD. Intra-arterial infusion of urokinase (UK)-lys-plasminogen (Plg) in arterial ischemia of lower limbs. In: Davidson JF, Donati MB, Coccheri S, eds. *Progress in fibrinolysis VII.* Edinburgh: Churchill Livingstone, **1985**:63–65
10. Iga Y, Greenwald SR, Chandler AB. Uptake of 125I-lys-plasminogen by in vitro thrombi. *Haemostasis* **1983**;13:25–35
11. Wolfson RH, Kumpe DA, Rutherford RB. Role of intra-arterial streptokinase in treatment of arterial thromboembolism. *Arch Surg* **1984**;119:697–702
12. Totty WG, Gilula LA, McClennan BL, Ahmed P, Sherman L. Low-dose intravascular fibrinolytic therapy. *Radiology* **1982**;143:59–69
13. Hargrove WC, Barker CF, Berkowitz HD, et al. Treatment of acute peripheral arterial and graft thromboses with low dose streptokinase. *Surgery* **1982**;92:981–993
14. Sicard GA, Schier JJ, Totty WG, et al. Thrombolytic therapy for acute arterial occlusion. *Vasc Surg* **1985**;2:65–78
15. Lang EK. Streptokinase therapy: complications of intra-arterial use. *Radiology* **1985**;154:75–77

Suture Anchor for Visceral Drainage

Constantin Cope[1]

Recently, interest has increased in devising percutaneous techniques for inserting tubes into the stomach [1] and drains into the gallbladder [2] and other hollow viscera [3]. Because there is an inherent risk of spillage of gastric juices, bile, or infected fluids into the abdominal cavity because of invagination [4] of the visceral wall during tract dilatation or malinsertion of drains due to intraperitoneal coiling of guide wires [5], safer methods have been devised, including percutaneous endoscopic gastrostomy [1], the Hawkins accordion system [6], and air or balloon distension of the stomach [7]. None of these techniques, however, prevents harmful leakage during early drain exchanges or intravisceral catheter manipulations. A new simple removable retention device is described which serves to firmly anchor the visceral wall against the parietal wall for safer drain insertion.

Materials and Methods

The device consists of a stainless-steel cannula or rod 6–10 mm long that is jacketed in a plastic or helical spring sheath (OD, 0.87 mm) and fitted with a center and an end suture. The part of the suture that arises from the center of the anchoring device is armed with a curved cutting needle. The purpose of the sheath is to provide atraumatic floppy ends to the stiff crossbar (fig. 1).

A 15-cm, 22-gauge fine needle over which is telescoped a 5-cm, 16-gauge plastic-sheathed needle is used for puncture. Once the distended viscus lumen is localized with the protruding fine needle, the sheathed needle is advanced over it, and the sheath left in place. The anchor device is aligned with the end suture trailing and pushed through the plastic sheath with a 0.038-inch (0.96-mm) J guide wire into the cavity of the hollow viscus (fig. 2A). When the center suture is pulled back with the sheath, the retention bar will align itself perpendicularly to the needle tract. On further traction the crossbar will engage the visceral wall and eventually bring it into close approximation to the body wall (fig. 2B). With the visceral wall firmly retracted against the parietal wall, there is little chance of intraperitoneal leakage.

The tension of the center thread is maintained by suturing it to the skin, thus preventing retraction of the viscus. The wire guide, which had previously been inserted into the cavity, can now be used to further dilate the tract and insert a drain with impunity (fig. 2C). The loose end suture is taped to the drain. A few days later, when the drain tract has been established and the anchor device may no longer be necessary, it may easily be removed: The center suture is cut to release the retention device within the visceral lumen and a 5-French plastic sheath is threaded over the untaped end suture back into the viscus (fig. 2D); when gentle traction is exerted on the end suture, the crossbar will realign itself along the axis of the sheath lumen and can then be easily withdrawn along with the sheath (fig. 2E).

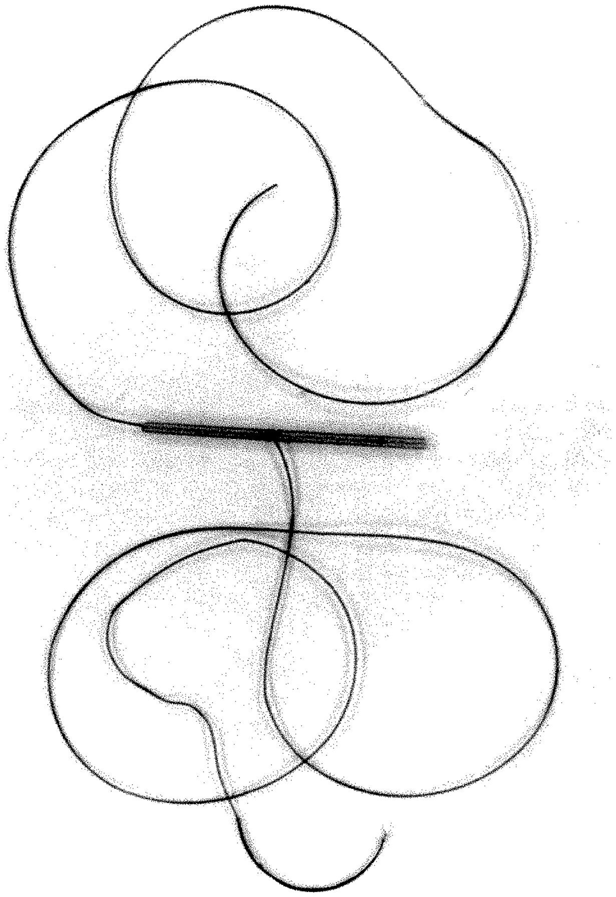

Fig. 1.—Floppy-tip spring-sheathed suture anchor. Center suture with needle is for retraction and fixation; end suture is for removal.

Received December 14, 1984; accepted after revision August 28, 1985.

[1] Department of Radiology, Temple University School of Medicine, Albert Einstein Medical Center, Northern Division, York and Tabor Rds., Philadelphia, PA 19141.

AJR 146:160–161, January 1986 0361–803X/85/1461–0160 © American Roentgen Ray Society

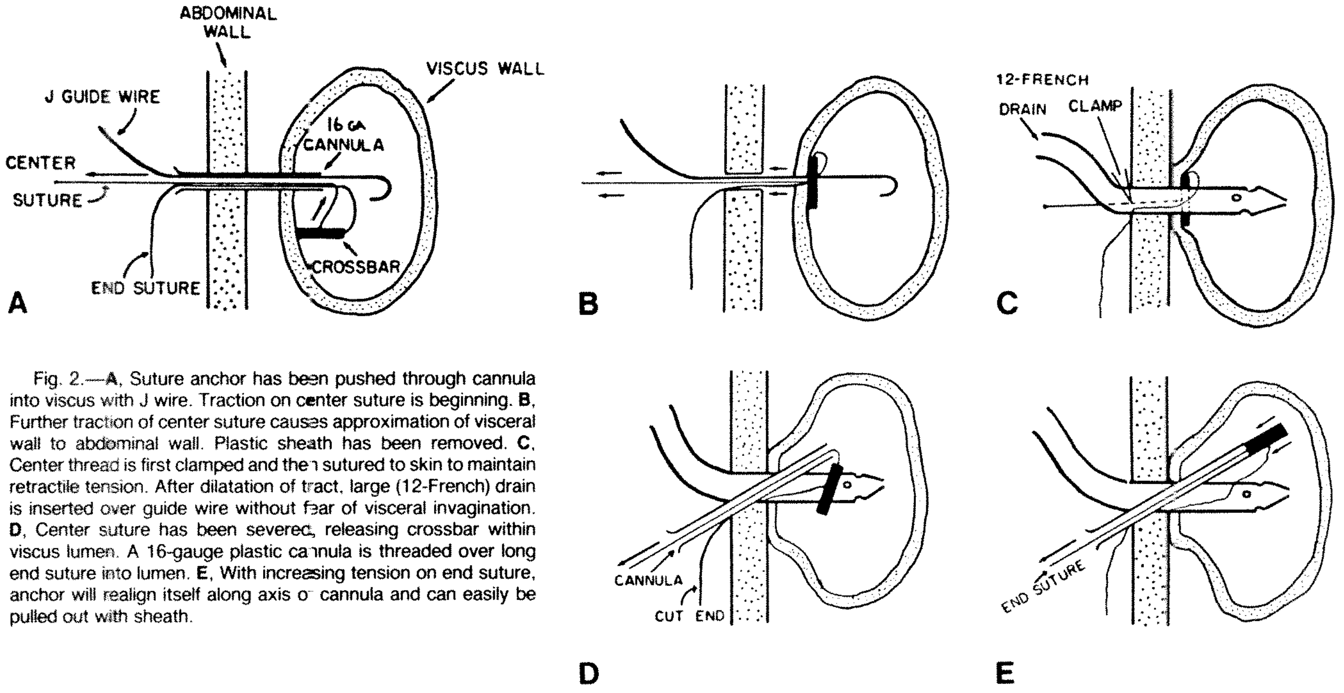

Fig. 2.—**A**, Suture anchor has been pushed through cannula into viscus with J wire. Traction on center suture is beginning. **B**, Further traction of center suture causes approximation of visceral wall to abdominal wall. Plastic sheath has been removed. **C**, Center thread is first clamped and then sutured to skin to maintain retractile tension. After dilatation of tract, large (12-French) drain is inserted over guide wire without fear of visceral invagination. **D**, Center suture has been severed, releasing crossbar within viscus lumen. A 16-gauge plastic cannula is threaded over long end suture into lumen. **E**, With increasing tension on end suture, anchor will realign itself along axis of cannula and can easily be pulled out with sheath.

I have safely used the suture anchor (provided by J. Roberts of Cook) as a preliminary step before inserting a 12-French loop drain [8] in three percutaneous gastrostomies and two cholecystostomies in five patients. Apposition of the anterior wall of the viscus to the parietal peritoneum secured by the suture anchor was further reinforced by gently pulling on the loop retention drain and maintaining that tension by attaching a Molnar disk to the drain at skin level. There were no symptoms of peritonitis or infection. The suture anchors were easily removed 1 week after positioning, and endoscopic inspection with the Needlescope (Dyonics) of the visceral lumen showed no residual inflammatory mucosal changes caused by the device. Although this technique takes advantage of using the same tract for both the suture anchor and the drain, it is also possible to insert additional anchors for better organ fixation through separate punctures, but so far this has not been necessary. Loop gastroduodenostomy feeding tubes (Cook) were exchanged at 3-month intervals, and cholecystostomy loop drains were removed before surgery a few weeks later.

Discussion

The purpose of the suture anchor is to mobilize atraumatically and tamponade internally the wall of the stomach, gallbladder, bowel, and superficial abscesses against the abdominal and chest wall, so that catheter exchanges and manipulations may be performed without intraperitoneal leakage before and while inserting a larger retention drain. Although percutaneous intubation of the gallbladder and stomach have been performed with little morbidity so far in several series [1, 5, 6, 9], I believe that initial percutaneous mobilization and fixation of a hollow viscus by suture anchoring represents a good surgical principle that should result in fewer instances of peritonitis, especially in accidental tube withdrawal [2, 10] before the drain tract is well established, drainage of a tense obstructed viscus [11], catheter manipulation [12], endoscopy of gallbladder, or chemical dissolution of gallbladder stones [13].

In my preliminary experience with the use of the suture-anchoring device, I have found it perfectly safe to selectively intubate the duodenum immediately after the percutaneous gastrostomy in order to place a feeding loop gastroduodenostomy tube without waiting 1–2 weeks for a firm gastrostomy tract to form. Likewise, in one patient with a percutaneous cholecystostomy drain and a common-duct stone, it was possible to temporarily remove the drain 2 days later and catheterize the cystic duct in an attempt to entrap the stone in a basket and push it into the duodenum, without incurring any biliary peritonitis. Further experience is needed to further explore the potential wide usefulness of the suture anchor.

REFERENCES

1. Ponsky JL, Gauderer MWL, Stellato TA. Percutaneous endoscopic gastrostomy: review of 150 cases. *Arch Surg* **1983**;118:913–914
2. Shaver RW, Hawkins IF Jr, Soong J. Percutaneous cholecystostomy. *AJR* **1982**;138:1133–1136
3. Bezreh JS. Percutaneous catheter drainage of closed-loop small-bowel obstruction. *AJR* **1983**;141:797–798
4. Preshaw RM. A percutaneous method for inserting a feeding gastrostomy tube. *Surg Gynecol Obstet* **1981**;152:659–661
5. Wills JS, Ogleby JR. Percutaneous gastrostomy: further experience. *Radiology* **1985**;154:71–74
6. Pearse DM, Hawkins IF Jr, Shaver R, Vogel S. Percutaneous cholecystostomy in acute cholecystitis and common duct obstruction. *Radiology* **1984**;152:365–367
7. vanSonnenberg E, Cubberley DA, Brown LK, Wittich GR, Lyon JW, Stanffer AE. Percutaneous gastrostomy: use of intragastric

balloon support. *Radiology* **1984**;152:531-532

8. Cope C. Improved anchoring of nephrostomy catheters: loop technique. *AJR* **1980**;135:402-403
9. McGahan JP, Walter JP. Diagnostic percutaneous aspiration of the gallbladder. *Radiology* **1985**;155:619-622
10. Strodel WE, Eckhauser FE, Lemmer JH, Knol JA, Dent TL. Endoscopic percutaneous gastrostomy. *Contemp Surg* **1983**;23:17-23
11. Phillips G, Bank S, Kumari-Subaiya S, Kurtz LM. Percutaneous ultrasound-guided puncture of the gallbladder (PUPG). *Radiology* **1982**;145:769-772
12. Mazzariello RM. Residual biliary tract stones: non-operative treatment of 570 patients. *Ann Surg* **1976**;8:130-133
13. Allen MJ, Borody TJ, Bugliosi TF, May GR, et al. Rapid dissolution of gallstones by methyl tert-butyl ether. *N Engl J Med* **1985**;312:217-220

CT Body Stereotaxis: An Aid for CT-Guided Biopsies

Gary Onik[1]
Philip Costello[1]
Eric Cosman[2]
Tren Wells, Jr.[3]
Henry Goldberg[4]
Albert Moss[5]
Robert Kane[1]
Melvin E. Clouse[1]
William Hoddick[4]
Sheila Moore[4]
Barbara Demas[4]

A new body stereotaxic system used to facilitate CT-guided biopsies is described. By scanning through a triangle placed on the patient's skin, the method defines an entry point for the biopsy. An articulating arm is then used to aim the needle at the entry point and hold the needle at the correct angle. The arm can be angled so that complex approaches from one scan plane to another can be made in order to take biopsies of lesions beneath the diaphragm. Using the system, 23 of 25 lesions were hit on the first needle manipulation; two manipulations were needed for each of the other two lesions. In comparison with previous experience, procedure time was decreased and the numbers of needle manipulations and localization scans were decreased 75% and 90%, respectively.

Largely because of the new cross-sectional imaging methods, percutaneous procedures have revolutionized both the diagnosis and treatment of disease. The ability of CT to depict pathology in cross section has allowed guidance of needle biopsies and abscess drainages, obviating exploratory surgery for thoracic and intraabdominal pathology.

Neurologic investigators immediately took advantage of CT localization capability to guide various neurosurgical procedures. Accurate stereotaxic guidance systems have been developed [1] that have made brain biopsy safe and minimally invasive. CT stereotaxic guidance has allowed the development of new treatment methods such as the delivery of interstitial radiation therapy and hyperthermia to brain tumors [2]. The rapid development of CT stereotaxic guidance for neurosurgery is due to the delicate nature of brain surgery and the critical need for exact placement of needles, as well as neurosurgery's long history of stereotaxis guided by plain films.

Because CT-guided procedures for the body use a freehand method of guidance, aspiration of even relatively large lesions can require multiple needle manipulations to localize a needle within the pathology. The use of this method, which is inaccurate and time consuming, has been tolerable because of the inherent safety of fine-needle aspiration techniques.

We have developed a body stereotaxic system with capabilities similar to those of brain stereotaxic systems. We previously reported our phantom studies showing the system's accuracy to within 2 mm of a target point [3]. Our system differs from other reported body stereotaxic systems [4, 5] in that it uses trajectory calculations similar to the hand-guidance method while allowing an approach to targets that are outside an axial scan plane. We report here our initial experience of 25 stereotaxically guided aspirations.

Materials and Methods

Twenty-five consecutive CT-guided aspirations were performed using a stereotaxic system

Received April 1, 1985; accepted after revision September 9, 1985.

G. Onik was supported by the Damon Runyon–Walter Winchell Cancer Fund, DRG-034; E. Cosman was supported by the Whitaker Health Sciences Fund, M.I.T.

[1] Department of Radiology, New England Deaconess Hospital, 185 Pilgrim Rd. Boston, MA 02215. Address reprint requests to G. Onik.

[2] Department of Physics, Massachusetts Institute of Technology, Cambridge, MA 02139.

[3] Treat Wells, Inc., South Gate, CA 90280.

[4] Department of Radiology, University of California School of Medicine, San Francisco, CA 94143.

[5] Department of Radiology, University of Washington School of Medicine, Seattle, WA 98195.

AJR 146:163–168, January 1986
0361–803X/86/1461–0163
© American Roentgen Ray Society

for the body (Radionics) that includes: (1) a localization triangle placed on the patient's body from which a reference point is obtained; (2) a stereotaxic guide that guides the needles along the calculated path; and (3) a method of calculation for approaches that do not fall within the axial scan.

In most patients only one sample was obtained, using 19- or 21-gauge Franseen needles (Cook) or cut biopsy needles (E-Z-EM) to obtain the specimens.

Localization Triangle

In brain stereotaxis, reference coordinates are taken from a rigid frame bolted to the patient's head. The body has no structure to which such a frame can be attached. We therefore use a radiopaque localization triangle placed on the patient's skin as a means of defining a fiducial point. Before the procedure, the patient's diagnostic CT scan is reviewed to determine the optimal position of placement of the triangle. We try to place the triangle so that the entry point is defined by one of the triangle edges. The scout view is obtained and the area is sterilely prepared. A sterile plexiglass right triangle 10 cm long and 10 cm wide is placed on the patient. The base of the triangle is aligned to the CT scan plane using the laser localization lights (fig. 1). The triangle has adhesive along its back to fix it to the skin.

The cross-sectional width of the triangle varies with each of the displayed axial CT images. On the scan slice of interest, the width of the triangle cross section is measured and correlated to the width of the triangle on the patient. The triangle has a scale along its length (fig. 1). A triangle width measured on the CT scan can be found on the triangle itself simply by measuring that distance from the tip of the triangle along its scale, because the width of the triangle equals its height. The lateral margins of the triangle at that width define two points on the scan that can be exactly correlated to two points on the patient. To save time, we use the lateral margin of the triangle as an entry point whenever possible; however, if this is not possible due to an intervening rib or vital structure, we calculate on the CT scan displacements in the x and y directions from the lateral edge of the triangle to a new entry point. To decrease the partial-volume effect on the triangle, we use 1.5-mm-thick sections at 1-cm intervals for our localization scans. A similar method of localization has previously been described [6].

Stereotaxic Guide

After calculating the correct trajectory for the needle and identifying the entry point on the patient's skin, we use a stereotaxic guide to hold the needle at the correct angle (fig. 2A). The frame, made of stainless steel, is free standing beside the CT scanner. It can therefore be placed anywhere in relation to the scanner table and be used with any model scanner. We use the laser localization lights to align the frame to the plane of the CT scan. The whole upper structure of the instrument rests on a large ball bearing, and by loosening and tightening four fixation screws, the upper structure of the instrument can be tilted to ensure that the instrument is level and independent of the incline of the floor (fig. 2B). To save time, we have made marks on the floor beside the scanner table so that the instrument is placed exactly in the same position each time. This allows us to roll the frame up to the scanner and set it down in the correct position without realigning and zeroing the instrument to gravity. We can therefore set up for the biopsy in the time it takes to transfer patients.

The needle is placed in the needle holder and the correct angulation is set on the arc, which is aligned in the plane of the scan (fig. 2C). If a compound angulation is needed, the azimuth is set on the plate through which the 61-cm y travel bar inserts. After the y travel bar is set at an appropriate level in relation to the patient, the x and z travel bars are moved until the needle is aimed at the previously determined entry point. When the guide is properly aimed, the skin is anesthetized and a nick is made in it. The patient is told to hold his breath, and the needle is inserted to the correct depth by hand. A quick-release needle holder permits the release of the needle before the patient resumes respiration, ensuring free movement of the needle with the patient's respiration. The patient is then rescanned with a single 1-cm-thick slice at the level of the needle placement to confirm its placement.

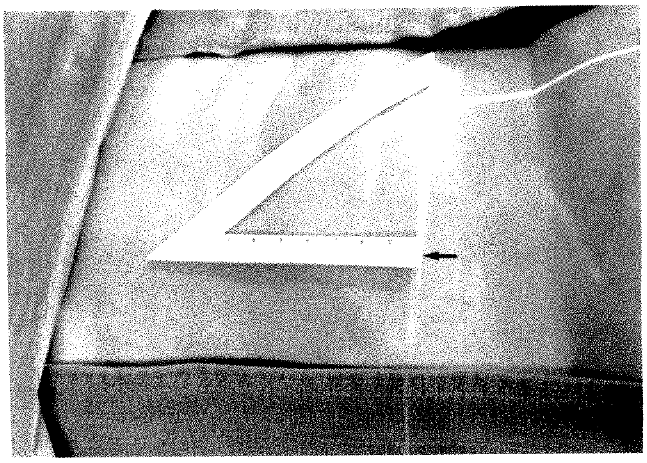

Fig. 1.—Reference triangle on patient. Triangle 10 cm high and 10 cm wide is shown with base aligned to CT scanner laser lights (*arrow*) with scale in centimeters along length. Since height of triangle is equal to width, any width of triangle in axial scan plane can be found by measuring that distance from tip of triangle down to appropriate level on scale.

Calculations for Out-of-Plane Approaches

When the target and entry points are on different scan slices, additional calculations are needed to define the angles and path length needed to reach the target. By knowing the distance along the z axis between the entry slice and target slice (calculated by subtracting the reference distance of one slice from the other) and the x and y coordinates of the entry point and target point, the angle of declination, azimuth, and needle path length can be calculated using simple trigonometry (fig. 3). Once those are known, the coordinates that the needle will pass through on all the intervening slices can also be calculated. This information is useful because it allows one to predict whether a vital structure will be traversed by the intended path. A cursor can then be placed on the CT scan slice of interest at the calculated coordinates using the software available with the CT scanner. We have placed these calculations for complex approaches into an HP-41 CV calculator because they are time consuming to make, although simple in concept.

Results

The location of the 25 aspirations were as follows: chest, 13; liver, four; pancreas, three; renal, one; miscellaneous abdominal, four. Two lesions were less than 1 cm in diameter, two lesions were 1–2 cm, seven 2–3 cm, five 3–4 cm, and the rest were greater than 4 cm in diameter. The average lesion size was 3.4 × 3.3 cm, and the average path length

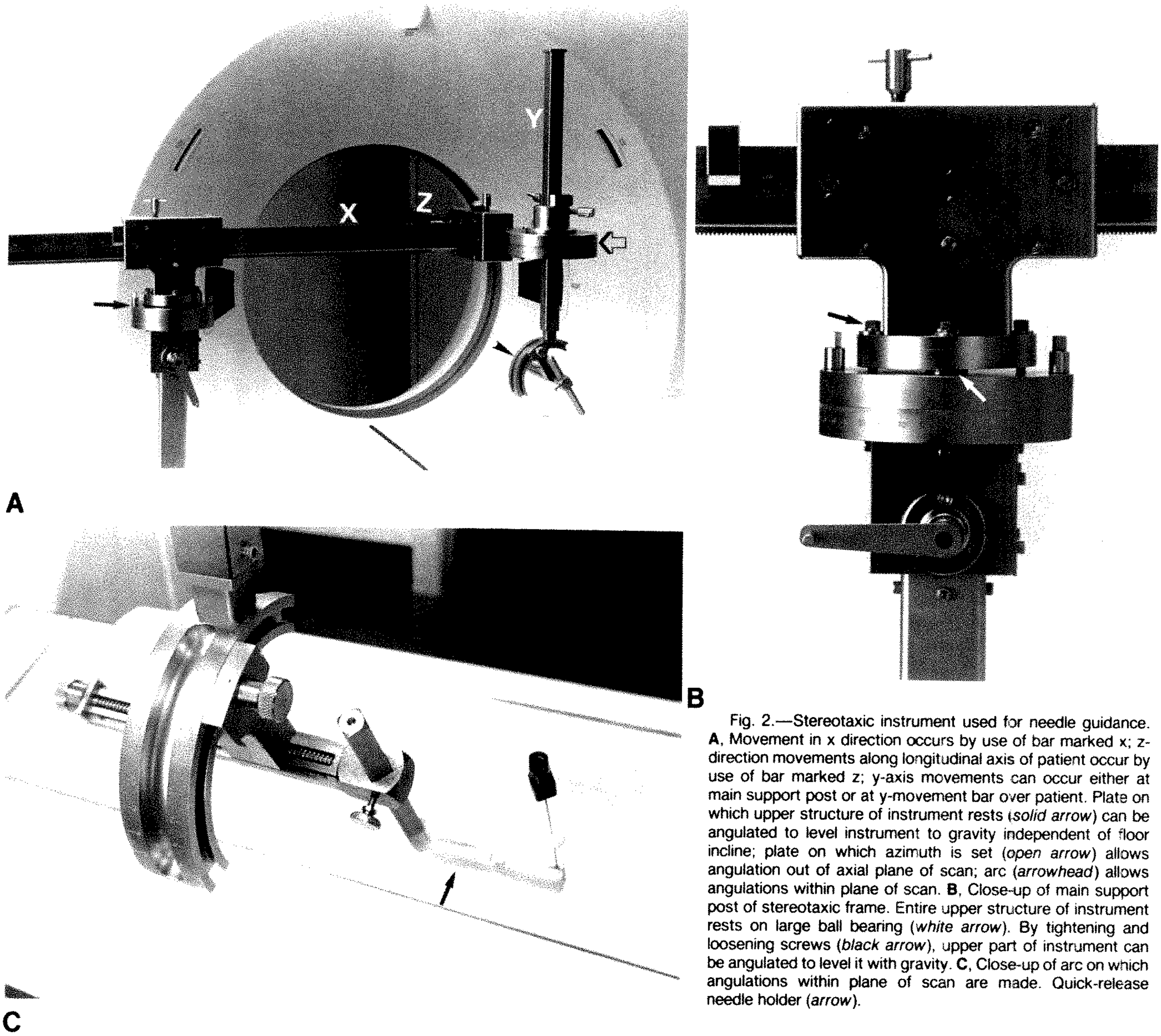

Fig. 2.—Stereotaxic instrument used for needle guidance. **A**, Movement in x direction occurs by use of bar marked x; z-direction movements along longitudinal axis of patient occur by use of bar marked z; y-axis movements can occur either at main support post or at y-movement bar over patient. Plate on which upper structure of instrument rests (*solid arrow*) can be angulated to level instrument to gravity independent of floor incline; plate on which azimuth is set (*open arrow*) allows angulation out of axial plane of scan; arc (*arrowhead*) allows angulations within plane of scan. **B**, Close-up of main support post of stereotaxic frame. Entire upper structure of instrument rests on large ball bearing (*white arrow*). By tightening and loosening screws (*black arrow*), upper part of instrument can be angulated to level it with gravity. **C**, Close-up of arc on which angulations within plane of scan are made. Quick-release needle holder (*arrow*).

was 8 cm. In addition, eight of the 13 chest cases in our series were patients with presumed primary lung carcinoma who because of severe emphysema were not candidates for open lung biopsy and resection; this subgroup of patients was less able to cooperate with breathing instructions. Of 25 lesions, 23 were hit on the first attempt with the stereotaxic method; the other two aspirations required two attempts each to place a needle in the lesion. This represented a decrease of 75% in needle manipulations from our previous experience with hand-guided biopsies. In the first of the missed attempts, the needle was deviated by deflection off a rib. In the second, the triangle as placed on the patient was poorly aligned to the scanner laser, giving an inaccurate scan plane.

The decrease in the number of needle manipulations needed to hit the lesions using the stereotaxic method resulted in decreasing the procedure time by about 30%. With the stereotaxic method, we decreased the number of scans needed for needle localization by 90%, because only one scan slice was generally needed to find needles placed stereotaxically; three are usually needed for the hand-guided method because of the uncertainty of the needle tip location.

Of the eight patients in the subgroup with severe emphysema, four developed pneumothoraces; two of these required short-term chest tube drainage. Of the remaining five chest biopsies, one patient developed a 5%–10% pneumothorax that required no intervention, and one patient had minimal hemoptysis. In our stereotaxic series, abnormal pathologic tissue was obtained in 23 of 25 cases. There were three false-negative biopsies, subsequently proven by repeat biopsy.

Discussion

Any radiologist who has attempted a number of CT-guided biopsies understands the frustration of having difficulty trying to enter a relatively large target. We have found that with the hand-guidance method, lesions as large as 3 cm can require multiple needle manipulations to place the needle anywhere within the lesion. A 3-cm lesion, although appearing large on the screen, does not leave much room for error in attempting a biopsy. Consider that when aiming at the center of a 3-cm lesion, one has 1.5-cm leeway on either side of the target point. If the path is 10 cm long, only a 5° error in the angulation of the needle places the needle tip about 1 cm from the target point. If one angles the needle 5° out of the axial plane of the scan as well, the cross-sectional diameter of the spherical lesion has markedly decreased in the plane where the needle tip finally comes to rest. Therefore, two small errors can result in missing the lesion. If the few millimeters of error in choosing the skin entry point is taken into account as well as the patient's respiratory variation, the difficulty in hitting large lesions becomes understandable.

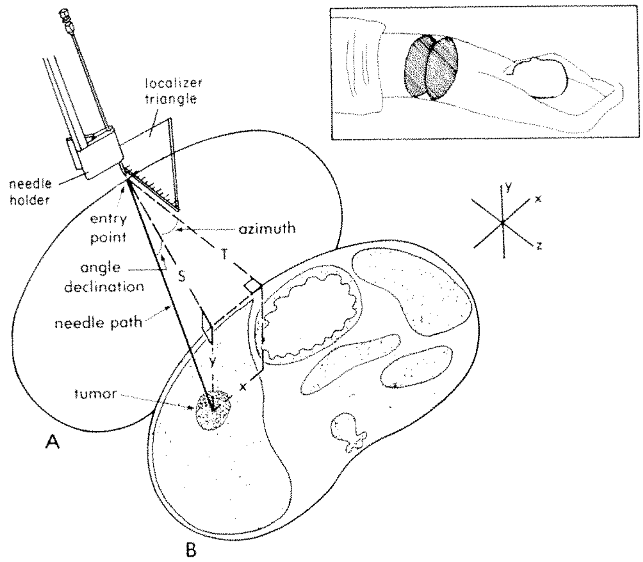

Fig. 3.—Calculation of complex biopsy approach from one scan slice to another. Entry point defined by lateral margin of localization triangle is shown on slice A. By knowing distance T between two slices and distance x (calculated from coordinates of entry and target points), distance S can be calculated using Pythagorean theorem. Azimuth can then be calculated using any trigonometric function. Once distance S is known, same method can be used to calculate angle of declination and needle path length.

Our stereotaxic system has addressed this problem and has made the CT-guided placement of needles more exact. Although the data are still preliminary, we have decreased the number of needle manipulations needed to hit lesions by 75% and as a result have saved an average of 20 min per biopsy and decreased the number of localization scans by 90%. In our experience, there is no savings in time and needle manipulations when the lesions are large; however, as the lesions biopsied become smaller, the benefits of stereotaxis increase dramatically. We may approach the point, however, where our confidence with large lesions will be great enough to eliminate the final confirmation scan, thus saving time even with large lesions. Since we are able to set up the instrument in the time it takes to transfer patients, we do not lose time with the method even with large lesions.

CT body stereotaxis has also increased our ability to biopsy smaller lesions than we would have attempted previously. Three of our biopsies were on lesions 1 cm or smaller (fig. 4). Although our phantom studies indicate that the method can be accurate consistently to within 2 mm, this accuracy has

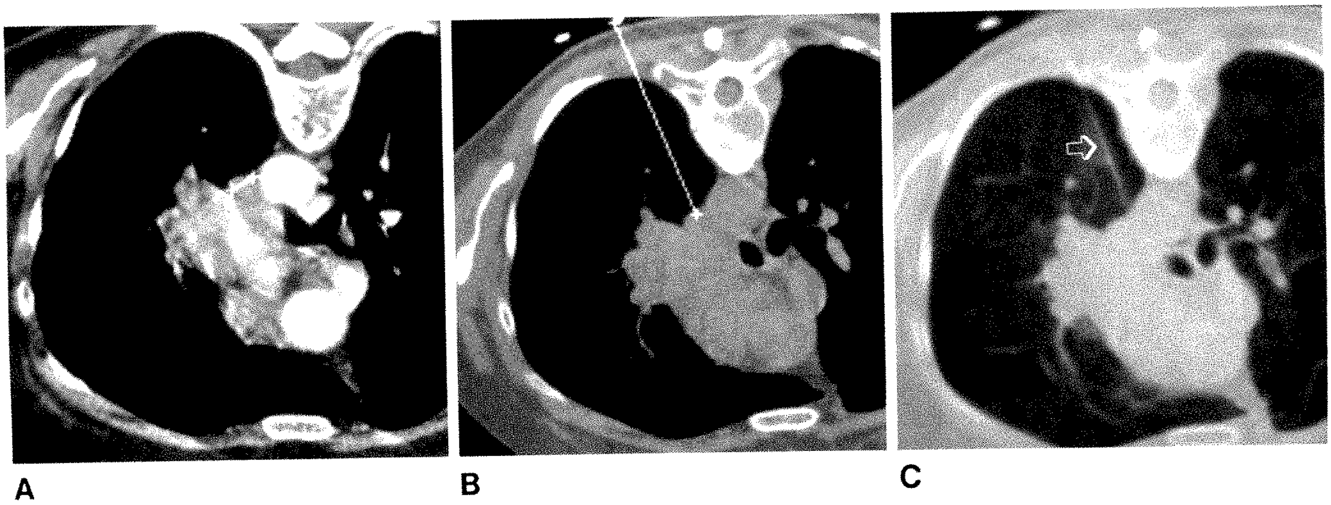

Fig. 4.—Mediastinal biopsy procedure in prone position. **A**, Abnormal tissue between left pulmonary artery and descending aorta. Computer-generated line between aorta and pulmonary artery indicates window to this soft tissue is 1 cm wide. **B**, Calculated path for biopsy. **C**, 22-gauge needle (*arrow*) follows projected path and enters area of abnormal soft tissue. Positive biopsy of metastatic carcinoma was obtained with this one needle placement. This biopsy shows utility of accurate stereotaxic needle placement in patient in whom biopsy would not have been attempted otherwise.

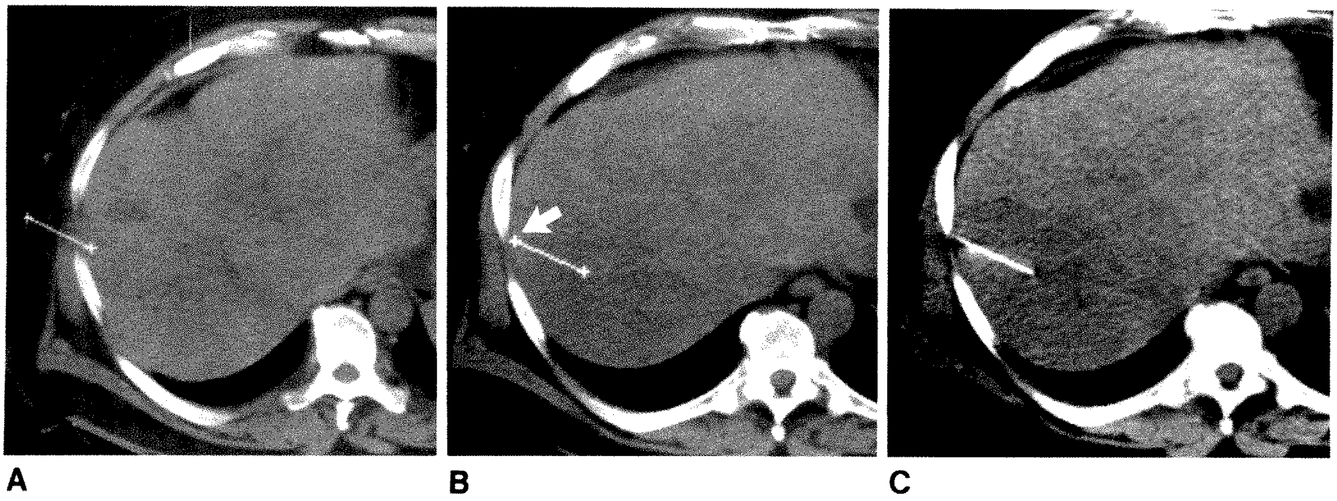

Fig. 5.—Hepatic biopsy procedure in supine position. Slices show projected path of needle going from one slice (**A**) to another (**B**) on projected course superiorly. Projected path will just miss overlying rib (*arrow*). **C**, Needle follows projected course exactly, entering hypodense liver lesion. Rib was just missed, as predicted by computer simulation.

not been consistently achievable in patients due to respiratory variation and tissue inhomogeneities that tend to deviate needles from their intended path. It is clear, however, that when the major variables of finding the exact entry point and holding the needle at the correct angle are controlled, a major improvement in accuracy over the hand guidance method is achieved.

In certain situations, such as a lesion in the dome of the liver, it is important to be able to angle out of the axial plane of the scan in order to avoid pleura. One article [7] has described a triangulation method in which a cephalad path is calculated parallel to the long axis of the patient in order to miss the lung in the posterior sulcus. The method we have described has the flexibility to allow us to choose *any* point on the patient's skin and then reach any point within the body. We are also able to calculate the points that the needle will pass through on intervening scans, confirming whether the needle will hit any obstruction or pass through a vital structure (fig. 5). We have used these capabilities three times in our series to approach lesions surrounded by pleura. This ability to angle out of the scan plane has been particularly crucial in at least one liver abscess drainage in which our entry and target point were separated by six scan slices (fig. 6). An added benefit of the stereotaxic method was noted when this patient's tube was pulled out the day after the procedure. We were able to place him on the CT table and, without relocalizing, replace the catheter using the angle settings of the previous day. Our accuracy has also given us the confidence to place the catheter during drainages in one step, using a trocar instead of the Seldinger technique.

Improvements still need to be made in our technique in order to achieve the best possible results. Both of our misses were due to errors in finding the exact scan level in the z direction. In one biopsy, the base of the triangle was misaligned to the laser light that indicates the axial scan plane; this gave an erroneous measurement of the triangle cross section, resulting in placement 1 cm below the correct level. In the other, we grazed a rib, deviating the needle superior to the lesion. To improve accuracy, we have gone from a 10 × 5 cm to a 10 × 10 cm triangle, and we are making the triangle out of a denser material in order to decrease the effect that partial-volume averaging has on our measurements. The stereotaxic guide itself is being made to a tighter tolerance, and we are currently developing a respiratory gating device similar to that described by Jones [8] to minimize the effect of respiratory variation in our biopsies.

It was our hope that with the ability to hit lesions with a minimum of needle manipulations that fewer patients would have complications. So far this has not been true in the 12 chest biopsies we have attempted, in which five patients had pneumothoraces. Four of the pneumothoraces occurred in our subgroup of eight patients who were nonsurgical candidates due to severe chronic obstructive pulmonary disease, a group with an expected higher frequency of pneumothorax. We believe that the risk of biopsy was justified in this high-risk group of patients, in which pathologic confirmation is essential due to the high morbidity of any therapeutic intervention, including radiation. In two patients, a pneumothorax was visible on the first localization scan with the needle within the lesion. Had the lesion not been hit on the first attempt, the procedure would have been cancelled without a specimen being obtained.

Now that we have the ability to place a needle very exactly, the investigation of various new therapeutic methods becomes a possibility. Brain stereotaxic systems have allowed multiple catheters to be placed exactly in parallel through a tumor volume to deliver interstitial radiation and hyperthermia. Being rectilinear, our system is perfectly suited to placing multiple needles exactly in parallel. After the first needle placement, the instrument is translated the desired distance for the next needle placement; the process of placing an array requires only one path calculation. We are currently investi-

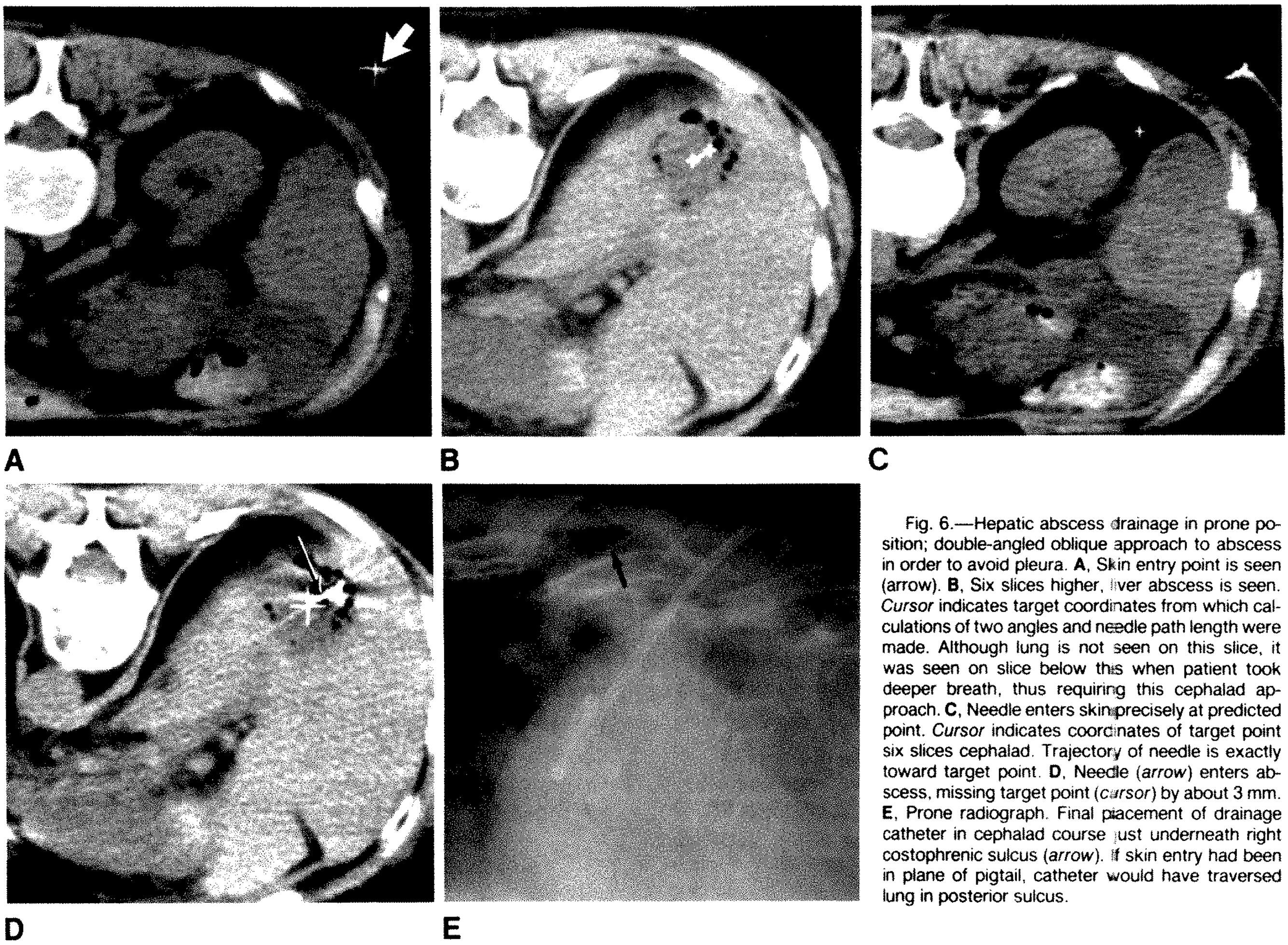

Fig. 6.—Hepatic abscess drainage in prone position; double-angled oblique approach to abscess in order to avoid pleura. **A**, Skin entry point is seen (arrow). **B**, Six slices higher, liver abscess is seen. *Cursor* indicates target coordinates from which calculations of two angles and needle path length were made. Although lung is not seen on this slice, it was seen on slice below this when patient took deeper breath, thus requiring this cephalad approach. **C**, Needle enters skin precisely at predicted point. *Cursor* indicates coordinates of target point six slices cephalad. Trajectory of needle is exactly toward target point. **D**, Needle (*arrow*) enters abscess, missing target point (*cursor*) by about 3 mm. **E**, Prone radiograph. Final placement of drainage catheter in cephalad course just underneath right costophrenic sulcus (*arrow*). If skin entry had been in plane of pigtail, catheter would have traversed lung in posterior sulcus.

gating the application of these techniques to the treatment of visceral tumors.

REFERENCES

1. Brown RA. A stereotaxic head frame for the use with CT body scanners. *Invest Radiol* **1979**;14:300
2. Lyons BE, Brit RH, Strohbehn JW. Localized hyperthermia in the treatment of malignant brain tumors using interstitial microwave antenna array. *IEEE Trans Biomed Eng* **1984**;31
3. Onik GM, Cosman E, Wells T, Moss A, Goldberg HI. CT body stereotaxic instrument for percutaneous biopsy and other interventive procedures: phantom studies. Presented at the annual meeting of the Association of University Radiologists, Newport Beach, CA, May **1984**
4. Wunschik F, George IM, Pastyr O. Stereotaxic biopsy using computed tomography. *J Comput Assist Tomogr* **1984**;8:32–37
5. Fredrick R, Brown TH, Miller MH, et al. Light guidance system to be used for CT guided biopsy. *Radiology* **1985**;154:535–536
6. Ferrucci JT, Wittenberg J. CT guided biopsy of abdominal tumors: aids for localization. *Radiology* **1979**;129:739–744
7. vanSonnenberg E, Wittenberg J, Ferrucci JT, Mueller P, Simeone J. Triangulation method for percutaneous needle guidance: the angled approach to upper abdominal masses. *AJR* **1981**;137:757–761
8. Jones KR. A respiratory monitor for the use with CT body scanning and other imaging techniques. *Br J Radiol* **1982**;55:530–533

Modification of the Cope Drainage Catheter to Facilitate Placement

Howard L. Berman,[1] Curtis W. Bakal, and Stuart G. Katz

Self retention catheters for percutaneous drainage procedures have gained great popularity with the introduction of the Cope Loop [1] and the trillium type nephrostomy, biliary, and abscess drainage catheters (Medi-Tech). However, the Cope-style catheter in its commercial configuration by Cook may occasionally be difficult to advance far enough for adequate positioning. The Cope-type drain is an 8.2- or 10-French polyurethane catheter supplied with a two-part metal intro-

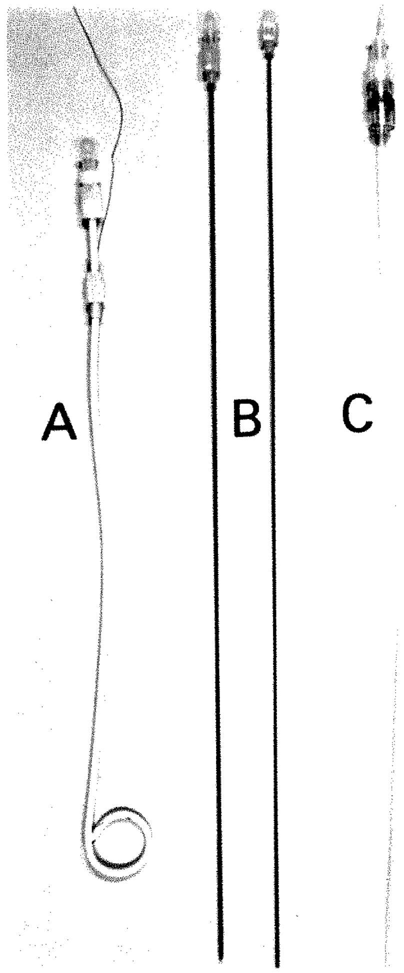

1

Fig. 1.—**A**, Cope-type loop 8.2-French nephrostomy catheter. **B**, Two-part metal stylette. **C**, Nylon flexible stiffening cannula.

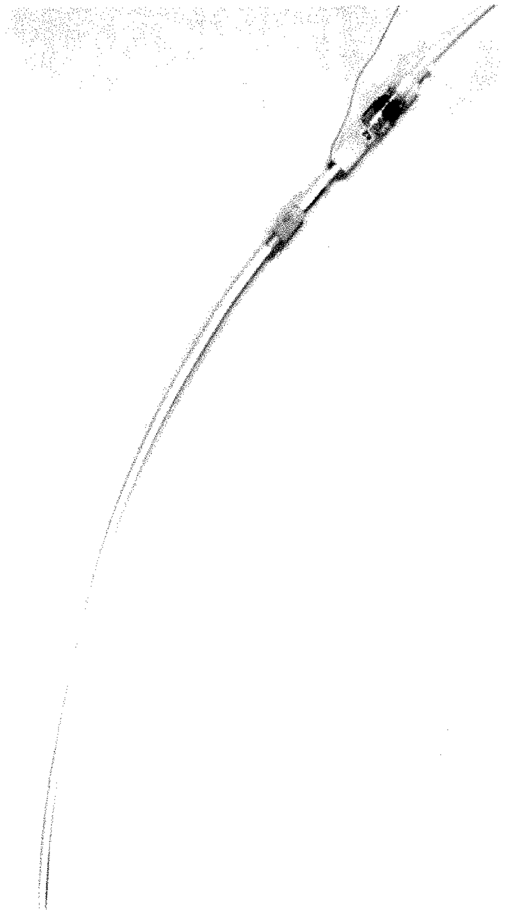

2

Fig. 2.—8.2-French Cope-type loop nephrostomy catheter with flexible nylon stiffening cannula inserted.

Received April 25, 1985; accepted after revision August 29, 1985.

[1] All authors: Department of Radiology, New York Medical College, Valhalla, NY 10595. Address reprint requests to H. L. Berman.

AJR 146:169–170, January 1986 0361–803X/86/1461–0169 © American Roentgen Ray Society

ducing system (fig. 1). The introducer consists of a hollow metal stiffener and an inner stylette. With both pieces of the introducer in place, the catheter can be introduced as a trochar via a single puncture. Removing the solid obturator allows the catheter and metal stiffener to be advanced over a previously positioned 0.038-inch (0.97-mm) guide wire. The catheter-stiffener combination can only pass as far as the first sharp turn; the rigid metal stiffener must then be held fixed as the catheter is advanced off the metal stiffener and forward over the guide wire. This maneuver enables the catheter to navigate this turn and any subsequent tortuosity for final placement. However, if the leading edge of the soft polyurethane catheter meets any significant resistance, the catheter tip may fail to advance and the drain will simply foreshorten in an accordionlike fashion.

Overdilation of the tract by at least two French sizes and lubrication with sterile oil or gel have been advocated as potential remedies (Cope C, personal communication), but these measures are often inadequate. To solve this problem, we have recruited the commercially available flexible stiffener from the Medi-Tech family of trillium catheters. This 55-cm, nylon, semirigid stiffening cannula (no. FSC-38-55) is specifically designed to straighten the spring-loaded Malecot-type retention segment of the trillium catheter. It accepts a 0.038-inch (0.97-mm) guide wire. The stiffener can be used with all 10.0-French Cope drains. With effort, it may even be placed in the smaller 8.2-French nephrostomy drain (fig. 2), but not the 8.2-French biliary drainage catheter, as the longer length of this catheter binds the stiffener. To prevent kinking the stiffener, it should be loaded over a 0.038-inch (0.97-mm) guide wire. The stiffener will stop at the distal end of the drain, as it is too large to pass through the catheter's tapered end hole. Furthermore, the stiffener has a movable compression-ring Luer lock fitting that can be adjusted to attach to the hub end of the Cope catheter, producing a taut drainage catheter, which is fixed both proximally and distally over the stiffener. Any applied force is therefore directly transmitted to the leading edge of the drain, overcoming tract resistance without foreshortening or crimping. The catheter-nylon stiffener combination is semirigid, yet flexible enough to follow a guide wire and to negotiate turns. The use of the nylon stiffener has enabled us to routinely achieve optimum positioning of the Cope catheter when other techniques have failed.

REFERENCE

1. Cope C. Improved anchoring of nephrostomy catheters: loop techniques. *AJR* **1980**;135:402–403

Editorials

Changing of the Guard

This issue marks the end of the distinguished career of Dr. Melvin M. Figley as editor of the *AJR*. None of the editors who preceded him since the Journal was founded in 1906 (table 1) equalled his accomplishments. Under his direction the quality of the *AJR* soared. Its value to readers and its stature in the medical community burgeoned.

Melvin M. Figley.

In an editorial entitled "Changing of the Guard," published in 1976 at the outset of his editorship, Dr. Figley pledged that the Journal's content would be carefully selected by peer review to assure the readers truth and significance to the fullest extent possible [1]. He promised the Journal would strive to become more contemporary, segregation of subjects to selected issues would be terminated to speed publication, and the editorial office would be constantly alert for means to shorten the periods between receipt of a communication, decision as to its acceptability, and its final appearance in print. Dr. Figley was true to his word and achieved all this and more. Indeed, he inspired an astonishing renaissance.

Under Dr. Figley's direction, the *AJR* underwent major cosmetic changes to make the contents easier to locate, read, index, and file. He gave special attention to improving the quality of the illustrations, which are now nonpareil in the medical literature. Comparison of a recent issue with one from 10 years ago makes it obvious just how successful Dr. Figley has been.

His strict policy of anonymous peer review, revisions whenever necessary, and meticulous copy editing resulted in articles with greater clarity, more documentation, and a general abbreviation of expression. The Journal has grown (about

TABLE 1: **Editors of the *American Journal of Roentgenology***

	Period of Tenure
Preston M. Hickey	1906–1916
James T. Case	1916–1918
H. M. Imboden	1918–1924
Arthur C. Christie	1924–1930
Lawrence Reynolds	1930–1947
Merrill C. Sosman	1947–1949
Lawrence Reynolds	1949–1961
Traian Leucutia	1961–1974
E. Frederick Lang (interim)	1974–1975
Melvin M. Figley	1976–1985

500 manuscripts are now published annually), yet Dr. Figley resisted the temptation to enlarge the Journal to the point where readers are presented each month with an encyclopedia so ponderous that none have the diligence to read it thoroughly. His major thrust has consistently been to emphasize quality. The reader's approval has been enthusiastic. The Journal's circulation rate has reached an all time high of nearly 20,000, one-quarter of which are foreign subscribers.

Improvements in the *AJR* have been due in large measure to Dr. Figley's unstinting personal dedication. Another major factor has been his reliance on a large number of highly qualified peer reviewers to evaluate all submitted manuscripts. These dedicated people work with little recognition and no remuneration. The rest of Dr. Figley's team, consisting of dedicated associate editors (Rosalind Troupin, John Harley, and Charles Rohrmann), a superb managing editor (Kathleen Murray), and talented manuscript editors (Marie Leonard and Janine Anderson), guaranteed the Journal's success.

Now after a decade of Dr. Figley's extraordinary leadership, the "guard" is changing once more. This is an appropriate metaphor to describe the transition between editors, because it is the intention of the American Roentgen Ray Society, specifically the Publications Committee, chaired by Dr. M. Paul Capp, to guard those qualities that brought the *AJR* to preeminence under Dr. Figley's direction.

As the weighty responsibilities of editorship fall to me, I undertake the task with a sense of gratitude to the Society's Executive Council for believing that I can carry on in Dr. Figley's footsteps. With Dr. Figley as my inspiration and with the help of the Publications Committee, authors, reviewers, and many more, I am confident the Journal will maintain its reputation for excellence, continue to raise its standards, and successfully respond to the challenges of the future.

Robert N. Berk
Editor

REFERENCE

1. Figley MM. Changing of the guard. *AJR* **1976**;126:188–190

Radiology Manpower: Where Are We?

In the previous issue of the *American Journal of Roentgenology*, Petersdorf [1] has provided a timely perspective of some of the consequences of the rapid increase in numbers of physicians in the United States and the projected excess of 145,000 doctors by the year 2000. The American College of Radiology has been concerned about the number of radiologists and in the early 1970s created a Committee on Manpower. The charge to that Committee was to compile accurate information on the supply of radiologists and to assess and predict forces acting to alter the need for such personnel. This has been done through annual reports at the annual meeting of the College and through the publication of four major reports [2–5]. It was hoped that the timely dispersion of such information would result in adjustments by those responsible for training on a voluntary and regular basis.

In the early 1970s, it was obvious that the rapid expansion in the scope of diagnostic radiology was creating a significant shortage and that the movement toward total separation between diagnostic radiology and radiation oncology required a major effort toward recruitment for programs in therapeutic radiology. In the intervening 15 years, those shortages have in large part disappeared and the specialty now faces a significant surplus beginning about 1990. These days most new radiologists join an established practice group on completion of their training. The costly training of personnel unable to locate a practice opportunity poses a major moral question and certainly does not represent a legitimate expenditure of even more limited funds. Therefore, it becomes especially important to attempt to titrate numbers of trainees to perceived need.

The first half of the 1970s showed a steady increase in numbers of positions offered in both diagnostic and therapeutic radiology training programs. However, in the last 10 years, despite a steady increase in numbers of medical school graduates, the number of newly certified individuals in diagnostic radiology and radiation therapy has remained almost constant at an annual level of about 800 in diagnostic radiology and 100 in therapeutic radiology. The work of the Committee may have played a part in this stability during a time when many other specialties have shown continued steady increases.

Although the number of trainees is stable, overall numbers of radiologists continue to increase. The 800 new diagnostic radiologists certified annually are partially offset by an attrition of about 350, leaving a net increase of 450. Similarly the 100 annual output in radiation therapy is partially balanced by a loss of about 40, resulting in an increase of about 60. These attrition rates are increasing slightly each year as the average age of radiologists increases and will level off at about 3% annually. Within the past 2 years, radiation therapy has rather suddenly attracted more trainees, and it would appear that beginning in 1986, the annual output of radiation therapists may reach as high as 150.

Need is a much more difficult factor to assess than supply. It is a constantly changing level as new and conflicting forces tend to alter it. On the basis of analysis of the slowly decreasing job market, it would seem that the GMENAC calculations of need for radiologists by 1990 are not too far off the mark [6]. These suggest an optimum number of 20,165 diagnostic radiologists and 2513 radiation therapists by that time. The GMENAC predictions of a massive oversupply by 1990, however, seem to have significantly overestimated production and the best estimates of the Committee on Manpower are that at present rates of increase, these figures will be reached by 1991.

There do not seem to be factors in the near future that will require a continued increase in supply beyond that point, and it seems likely that need will either level off or increase only very slowly. If there is no change in the size of training programs, the number of radiologists will stabilize at about 25,000 diagnostic radiologists and 3500–4000 radiation therapists by the year 2010.

There is some preliminary evidence that numbers of positions offered have already been reduced perhaps in the range of 6%–7% [7]. While it would be necessary to cut entry level positions by about 25%–30% to bring things into balance, this seems to represent a beginning in that direction. The Committee on Manpower is at present collecting information to make an accurate assessment of this trend. Currently such changes are voluntary and must be made related to local needs and program resources. As training programs are currently being increased in length from 3 to 4 years, there is a unique opportunity to consider decreasing numbers of positions offered in each year of training without altering significantly the total number of residents in training.

Training residents who are unable to find a place to practice is irrational and a profligate waste of human and economic resources. By keeping the radiologic community informed of the manpower situation, the Committee hopes to assist training program directors in responding to the changing manpower scene as prudence and local needs dictate.

Paul A. Riemenschneider
Department of Radiology
Santa Barbara Cottage Hospital
Santa Barbara, CA 93102

REFERENCES

1. Petersdorf RG. How to cope with the doctor glut in the United States. *AJR* **1985**;145:1128–1130
2. Report of the ACR Task Force on Manpower and Facilities. Chevy Chase: American College of Radiology, **1975**
3. Manpower II, a report of the ACR Committee on Manpower. Chevy Chase: American College of Radiology, **1977**
4. Manpower III, a report of the ACR Committee on Manpower. Chevy Chase: American College of Radiology, **1982**
5. Manpower IV, a report of the ACR Committee on Manpower. Chevy Chase: American College of Radiology, **1985**
6. Garrison LP, Wills J, Perrin EB, Peterson ML. Physician requirements 1990: for five hospital based specialties. Seattle: Batelle Human Affairs Center, **1982**
7. Crowley LE. 85th annual report on medical education in the United States, 1984–1985. *JAMA* **1985**;234:1585–1593

Letters

Cost-Effectiveness vs. Accuracy of Diagnostic Procedures

This is in response to the recent letter by Dr. Koehler [1], commenting on our article in the May 1985 issue of *AJR* [2].

We appreciate Dr. Koehler's desire to save money. However, we maintain that wherever possible, the least expensive—and least invasive—studies should be performed. Even if a certain percentage of patients have to have a CT scan after an inadequate sonogram, it is still cheaper than requiring all patients to undergo CT first. Since most sonography departments can handle extra patients far more easily than most CT scanning facilities, it usually is no problem to schedule the patient for a sonogram and then cancel a scheduled CT scan. Therefore, the argument about keeping the patient in hospital extra days does not hold water. Furthermore, as is happening with most imaging procedures, the workup should be done at outpatient facilities, be they in the hospital or in private offices, so as to avoid the use of hospital beds for investigation and staging.

However, the "bottom line" is that the clinician has to order the examination he trusts. If he can't trust sonography, then CT or magnetic resonance imaging or some other diagnostic procedure will be necessary. Cost and radiation dose are secondary to the degree of confidence that can be transmitted to the referring physician.

Peter L. Cooperberg
Ken Poskitt
Lorne Sullivan
Vancouver General Hospital
Vancouver, B.C.
Canada V5Z 1M9

REFERENCES

1. Koehler PR. Cost of diagnosis vs. hospitalization (letter). *AJR* **1985**;145:1100
2. Poskitt KJ, Cooperberg PL, Sullivan LD. Sonography and CT in staging nonseminomatous testicular tumors. *AJR* **1985**; 144:939–944

Need for Precision in Experimental Design

In the September 1985 issue of *AJR*, Shuman et al. [1] describe the functioning of CORRELATE, a computer program they developed. This program allows the operator to transfer information about tumor margins from cross-sectional CT images onto longitudinal digital radiographs for planning radiation therapy.

The authors compared the results of radiation therapy planning before and after the use of the CORRELATE program and found that a significant change in the original therapy plan occurred in 77% of cases. They further state that "in *no* case did CORRELATE result in confusing or incorrect information" [1].

While it is intuitively attractive to believe that an automated method for transposing information about tumor margins is more accurate than conventional methods, this was not proven by the study. The authors' results indicate only that a discrepancy between the original plan and the program-generated data occurred in 77% of the cases studied. In designing their study, the authors used the CORRELATE program as its own "gold standard." The fallacy of this type of reasoning was explained in a recent article by Gelfand and Ott [2]. One could as easily conclude that the original plans were correct and that the information provided by the computer program was in error.

These comments are not meant to demean the authors' efforts to develop an objective method of providing information for therapy planning. Rather, they are intended to reemphasize the need for properly designed studies to validate the usefulness of new techniques.

Charles G. Jacoby
University of Iowa Hospitals and Clinics
Iowa City, IA 52242

REFERENCES

1. Shuman WP, Griffin BR, Yoshy CS, et al. The impact of CT CORRELATE ScoutView images on radiation therapy planning. *AJR* **1985**;145:633–638
2. Gelfand DW, Ott DJ. Methodologic considerations in comparing imaging methods. *AJR* **1985**;144:1117–1121

Reply

Our article addressed two separate issues. The first issue concerned the accuracy with which the CORRELATE program drew tumor outlines on the ScoutView using operator-generated information from the cross-sectional images. The "gold standard" for this issue was the phantom work reported in this and a previous article [1].

The second issue concerned the frequency with which incremental information provided by the CORRELATE program (when *added to* existing information from all other methods) resulted in changes in therapy. We were not attempting to assess the program's impact on diagnostic "correctness" or on the outcome of the disease process (cure rates, local recurrence rates, etc.). To measure impact on diagnosis or outcome, one would need to know whether CT detected all the diseased tissue; whether all the diseased tissue was included in the marking process; whether the therapy plans were correctly drawn up; and whether the radiation was properly administered. Assessment of impact on diagnosis or outcome would indeed require very rigorous gold standards such as multiple biopsies around the edges of tumors; very thorough surgery or autopsy; and detailed long-term follow-up. Because of the preliminary nature of our investigation and the difficulty in obtaining thorough histologic information before and after therapy, we knew we would be unable to report impact on diagnosis or outcome. Thus, we limited our report to impact on therapy.

I accept Dr. Jacoby's criticism of the statement, "In *no* case did CORRELATE result in confusing or incorrect information;" we should have written, "In no case was CORRELATE information believed by the radiation therapists to be confusing or incorrect in their scoring of impact on therapy." I also endorse [2] Dr. Jacoby's call for greater precision in experimental design and reporting.

William P. Shuman
University of Washington Hospital
Seattle, WA 98195

REFERENCES

1. Shuman WP, Griffin BW, Luk KH, Mack LA, Hanson JA. CT and radiation therapy planning: the impact of LOCATE ScoutView images. *AJR* **1982**;139:985-989
2. Shuman WP. Incidence and prevalence: proper use. *AJR* **1985**;145:649-650

Method for Determining Arterial Entry Site for Catheter

Percutaneous transluminal angioplasty has rapidly become a popular, safe, and cost-effective method for dilating arterial strictures. Occasionally, patients present with arterial stenoses that are amenable to angioplasty but are located close to the site of arterial puncture. If angioplasty is attempted, it is essential that the exact site of the arterial puncture be known lest the angioplasty balloon be inflated inadvertently across the arterial entry point. Inflation of the balloon under these circumstances could produce serious complications such as hemorrhage or major arterial damage. At times, the exact entrance site of the catheter is obvious. However, when the catheter overlies the artery for much of its subcutaneous extraarterial course, the exact location of the catheter's arterial entrance may be obscured.

We suggest a simple method for locating the catheter entry site. After retrograde catheterization of the artery, an injection is made above the stenosis (fig. 1). The site of the arterial puncture is identified at a point just distal to where the radiolucent catheter is seen. The lucent wall is visible because it is outlined on both sides by contrast material. Where the catheter is intramural or subcutaneous, there is no contrast material outside the catheter to outline its wall. This is the key principle for identifying the exact puncture site.

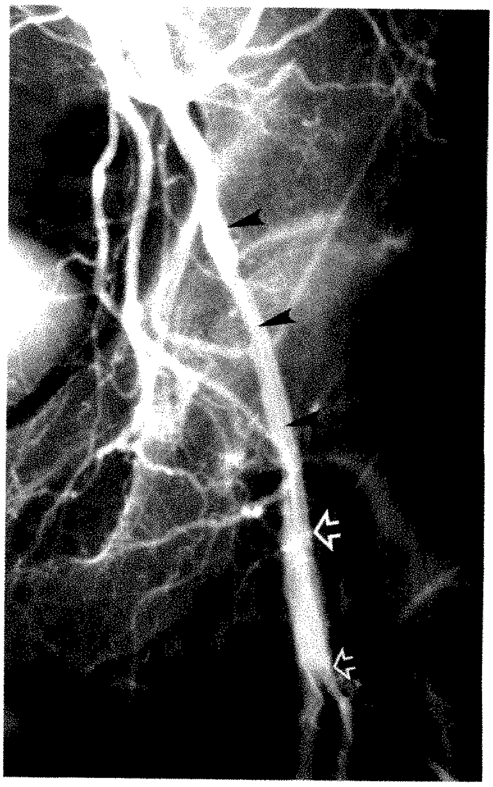

Fig. 1.—External iliac angioplasty in 67-year-old man. Intraarterial balloon catheter (*arrowheads*) placed with tip proximal to stenosis. Catheter entrance at skin (*small arrow*); arterial entrance site (*large arrow*).

Howard L. Dorne
University Hospitals
Ann Arbor, MI 48109
Richard Satin
Max J. Palayew
Sir Mortimer B. Davis Jewish General Hospital
McGill University
Montreal, Quebec
Canada H3T 1E2

Abstracts

Chest

Round atelectasis: report of two cases. Martinez LO, Kim YY, Sheldon J (Mount Sinai Center, Miami Beach, FL). *Rev Interam Radiol* 9:133–136, July 1984

Rounded atelectasis in two patients is described. The first, a 75-year-old woman who previously had both breasts removed for carcinoma, was found to have a nodular opacity on routine chest radiography. A fine-needle aspiration biopsy of the lung lesion was performed and was negative for atypical or malignant cells. However, because of the persistence of the abnormality, the patient had a resection of the lesion, which proved to be rounded atelectasis. The second patient was a 73-year-old woman with a 10-year history of rheumatoid arthritis and three previous admissions for pneumonia. Chest radiographs showed a somewhat nodular lesion in the posterior segment of the left lower lobe with associated pleural thickening; vessels of the left lower lobe converged toward the nodular lesion. Linear tomography and computed tomography were used to further delineate the nodularity, the converging blood vessels, and the pleural changes. The first case is interesting because it showed a more central type of location than has usually been described. The second case is unusual because the vessels arch from above rather than from below the lesion.

Charles M. Nice, Jr.

Heart

Noninvasive pulsed Doppler echocardiographic detection of the direction of shunt flow in patients with atrial septal defect: usefulness of the right parasternal approach. Minagoe S, Tei C, Kisanuki A, Arikawa K, Nakazono Y, Yoshimura H, Kashima T, Tanaka H (University of Southern California School of Medicine, Los Angeles, CA 90033). *Circulation* 71:745–753, April 1985 (by permission American Heart Association)

Noninvasive pulsed Doppler echocardiography combined with two-dimensional echocardiography by the right parasternal approach was performed to detect the shunt flow through the defect in 31 patients with suspected secundum atrial septal defect (ASD). A defect of the interatrial septum was seen on the two-dimensional echocardiograms of 30 of 31 patients. In all 30 patients, Doppler signals of shunt flow could be recorded by placing the sample volume in the center of the defect on the two-dimensional echocardiogram. Neither a defect nor Doppler signal indicating shunt flow were demonstrated in any of 15 normal control subjects. Cardiac catheterization indicated significant shunt flow in all 31 patients with suspected ASD. Doppler signals obtained from the center of the defect showed left-to-right and/or right-to-left shunt flow patterns. The direction of the shunt flow was mainly left to right, with its peak in late systole and atrial systole in 28 of 30 patients; mainly right-to-left flow was present in the remaining two patients, who had Eisenmenger syndrome. The direction of flow as predicted by the Doppler signal was confirmed by the coincidence of direction of flow as seen on the contrast two-dimensional echocardiogram. In 22 patients for whom the measurement of the pulmonary-to-systemic flow ratio by oximetry was believed to be reasonably accurate, the ratio was fairly well corrected with Doppler-determined left-to-right shunt flow velocity ($r = 0.71$, SEE = 7.7 cm/sec). In 13 patients with ASD who underwent surgical repair of the defect, postoperatively the defect on the two-dimensional echocardiogram and the Doppler signals indicating shunt flow disappeared. In conclusion, noninvasive pulsed Doppler echocardiography by the right parasternal approach is useful in the assessment of the direction of shunt flow in patients with ASD.

Author Abstract

Gastrointestinal System

The biphasic enteroclysis. Maglinte DDT, Lappas JC, Miller RE, Ng AC, Burney BT (Methodist Hospital of Indiana, P. O. Box 1367, Indianapolis, IN 46202). *Appl Radiol* 14:39–44, 1984

A simple and flexible method in performing enteroclysis is described. A predetermined amount (450 ml) and precise density (50% w/v) of barium is infused through a 13F small bowel tube with the tip positioned in the duodenojejunal junction. This is followed by infusion of a 0.5% solution of methylcellulose when barium has filled the pelvic segments of ileum or when all the 450 ml of barium has been infused. The amount of methyl cellulose given depends on the appropriate double-contrast appearance desired. This method makes full use of the value of fluoroscopy and compression radiography of the entire small bowel during the single-contrast phase possible because of the appropriate barium density and the hypotonia and true depiction of luminal surface pattern afforded by the double contrast effect of methylcellulose. The fluoroscopic and biphasic radiographic examination is usually completed in about 15 min from the start of infusion.

Author Abstract

Simulation of colonic carcinoma by ischemia. Brandt LJ, Katz HJ, Wolf EL, Mitsudo S, Boley SJ (Division of Gastroenterology, Montefiore Medical Center, Bronx, NY 10467). *Gastroenterology* 88:1137–1142, 1985

In nine cases, initial radiographic, endoscopic, or intraoperative appearances suggested colonic carcinoma. These findings were ultimately determined to be due to colonic ischemia. In seven patients, a barium enema was interpreted as consistent with carcinoma. In three of these, colonoscopy also suggested malignancy. Three patients were considered to have carcinoma from the gross appearance of the lesion at laparotomy. The radiographic features of the cases included irregular, annular, fungating lesions of the sigmoid colon (three cases), splenic flexure (one), ascending colon (one), and cecum (two). The authors suggest that both barium enema and colonoscopy should be used in all patients suspected of having colonic neoplasm by one of the methods described, as the combination of studies will identify the ischemic nature of lesions incorrectly diagnosed by one technique or the other alone.

Charles A. Rohrmann, Jr.

Is ultrasonography useful in the assessment of diffuse parenchymal liver disease? Sandford NL, Walsh P, Matis C, Baddeley H, Powell LW (Rancho Los Amigos Hospital, Liver Unit, 7601E Imperial Highway, Downey, CA 90242). *Gastroenterology* 89:186–191, 1985

Hepatic sonography and liver biopsy were compared in 125 patients. The sonographic features evaluated were loss of detail, echogenicity, and attenuation. Histologic features of fat, fibrosis, and inflammation were scored. Strong correlations were found between fat content and each of the three sonographic features and between the histologic finding of hepatic fibrosis and loss of detail and echogenicity. Hepatic inflammation did not correlate with any of the sonographic features. Although ultrasound had a positive predictive value of 98% in the diagnosis of diffuse parenchymal abnormality, it did not distinguish fat from fibrosis nor reliably diagnose cirrhosis. It gave false-positive results in only two patients but in 17 patients there were false-negative sonograms. The authors conclude that sonography is not a useful screening investigation for parenchymal liver disease nor is it useful for gauging hepatic pathology.

Charles A. Rohrmann, Jr.

Progress article: diagnosis of chronic pancreatitis. Niederau C, Grendall JH (Medical Service, 5-122, Gastroenterology, San Francisco General Hospital, San Francisco, CA 94110). *Gastroenterology* 88:1973–1995, 1985

This review article summarizes the classification and causes of chronic pancreatitis, the methods of diagnosis, and compares the different tests of pancreatic function. It also summarizes imaging techniques and methods for differentiating inflammatory from neoplastic disease. The authors propose an approach to the diagnosis of chronic pancreatitis that is based on an initial imaging evaluation of sonography and/or computed tomography followed by endoscopic pancreatography. Cytology, biopsy, and laparotomy are used to exclude pancreatic carcinoma. The authors provide a cost analysis table of the suggested diagnostic tests. There is a complete reference list with 247 citations.

Charles A. Rohrmann, Jr.

Recurrence after surgery in Crohn's disease. Relationship to location of disease (clinical pattern) and surgical indication. Whelan G, Farmer RG, Fazio VW, Goormastic M (R. Farmer, Dept. of Gastroenterology, Cleveland Clinic Foundation, Cleveland, OH 44106). *Gastroenterology* 88:1826–1833, 1985

The authors followed 592 patients with Crohn disease from 1966, a mean of 13 years. Of these, 438 had undergone operation for resection. The patients with ileocolic disease had the highest recurrence (53%). The patients with colonic disease had 45% recurrence and those with small intestinal disease, 44%. Second recurrences were ileocolic (35%), colonic (34%), and small intestinal (38%). The median time of recurrence was similar among the three groups. The presence of internal fistula or perianal disease indicated a higher likelihood of recurrence and a shortened median time to recurrence. The study supports the concept of conservatism with regard to management of the complications of internal fistula and perianal disease for patients with Crohn disease.

Charles A. Rohrmann, Jr.

In vivo hepatic volume determination using sonography and computed tomography. Validation and a comparison of the two techniques. Van Thiel DH, Hagler NG, Schade RR, Skolnick ML, Heyl AP, Rosenblum E, Gavaler JS, Penkrot RJ (1000J Scaife Hall, University of Pittsburgh, School of Medicine, Pittsburgh, PA 15261). *Gastroenterology* 88:1812–1817, 1985

A total of 99 patients referred for liver transplantation were evaluated by sonography and abdominal computed tomography (CT). Hepatic volume was determined by summing the volumes of 1 cm thick sections. The data obtained were compared with the weight and volume of the same livers after surgical removal at the time of transplantation. CT was less accurate than sonography. Of the hepatic volumes determined sonographically, 34 were greater or less by 10%. Of the calculated CT volumes, 63 were greater or less by 10%. Additionally, CT was less accurate for livers of large volumes than for smaller organs. Sonographic sagittal scanning was superior to transverse scanning by either sonography or CT. The results may be useful in determining size compatibility of the recipient patient and the donated organ.

Charles A. Rohrmann, Jr.

Genitourinary System

Leydig-cell tumors of the adult: value of ultrasonography. Marsot-Dupuch K, Martin-Lalardrie B, Conte J, Tubiana JM, Lelloucheazan M (Service de Radiologie de l'hopital St. Antoine, 27, rue du Faubourg St. Antoine, F 75012 Paris, France). *J Radiol* 66:91–97, Feb 1985

The authors report seven cases of Leydig-cell or interstitial cell tumors in adults aged 25–79 years. These tumors arise from the gonadal stroma and represent 2%–3% of all testicular tumors. In contrast to germ cell tumors, they can occur at any age. Clinical findings of endocrinopathy are present in about 30% of cases. Gynecomastia often is the only symptom of feminization. Impotence or sterility are less common clinical symptoms. Elevated serum estradiol and decreased levels of testosterone are characteristic of such cases. In children, precocious puberty can occur due to the lack of a tumoral enzyme (aromatase) which transforms testosterone into estradiol. Some 10% of Leydig-cell tumors are malignant. Even at pathology, it is somewhat difficult to differentiate a benign tumor from a malignant tumor. Frequently, the long term follow-up is the best distinguishing criterion. Bilaterality can only suggest malignancy, but few cases are bilateral. On sonography, most of these tumors are uniformly hypoechoic and well marginated. Whereas these sonographic characteristics are not specific, their association with the feminizing syndrome should suggest the diagnosis.

Joseph Fakhry

Muscles and Skeleton

Lymphographic documentation of a vertebral lymphangioma (in German). Wenz W, Reichelt A, Rau WS, Adler CP (Abteilung Roentgendiagnostik, Universitatsklinik, Hugstetterstrasse 55, D-7800, Freiburg, West Germany). *Radiologe* 24:381–388, 1984

A case of lymphangioma of the 11th and 12th vertebral body, which posed considerable diagnostic difficulties over a 6-year period, was diagnosed by pedal lymphangiography. The patient complained of chronic back pain and was evaluated by serial radiographs of the spine that showed osteolytic changes involving the 11th and 12th vertebral body, with progressing wedge deformity and gibbus formation. When the patient developed a chylothorax, a lymphangiogram was performed. Droplets of the lymphangiographic contrast medium accumulated in the sponsiosa of the diseased vertebral bodies, indicating an osseous lymphangioma. The presence of an osseous lymphangioma was confirmed by histology.

Peter F. Winter

Angiography

Transluminal angioplasty of aortic narrowing. Castañeda-Zuniga WR, Weens C, Ketchum D, Castaneda F, Amplatz K (University of Minnesota Hospitals, Minneapolis, MN 55455). *Rev Interam Radiol* 9:137–140, July 1984

Five patients are described who were treated by transluminal angioplasty of aortic narrowing. Retroperitoneal fibrosis, Takayasu arteritis, and neurofibromatosis occurred in one patient each; two others had atherosclerotic vascular disease. In general the results of treatment with transluminal angioplasty are better with atheroclerotic aortic changes. Transluminal dilatation in patients with retroperitoneal fibrosis may be difficult. The patient described in this paper has remained asymptomatic for 15 months without differences in pressure between the upper and lower extremities. In the patient with Takayasu arteritis, dilatation with one 9 mm balloon caused no significant relief of the pressure gradient. It is thought that dilatation will have to be performed more than once to obtain a more permanent effect. In patients with neurofibromatosis, dilatation has been successfully accomplished, but residual gradients are more common than after dilatation of atherosclerotic arteritis.

Charles M. Nice, Jr.

Benefit of transcatheter arterial embolization for ruptured hepatocellular carcinoma complicating liver cirrhosis. Sato Y, Fujiwara K, Furui S, Ogata I, Oka Y, Hayashi S, Ohta Y, Iio M, Oka (K. Fujiwara, First Department of Internal Medicine, Faculty of Medicine, University of Tokyo, 7-3-1- Hongo, Bunkyo-ku, Tokyo 113, Japan). *Gastroenterology* 89:157–159, 1985

Transcatheter arterial embolization was performed within 7 days of rupture of hepatocellular carcinoma in six patients with this malignancy complicating liver cirrhosis. All six were thought to be inoperable because of shock or severe hepatic dysfunction. Progressive decrease in the hematocrit ceased in all patients soon after embolization. Five patients survived 31–168 days after embolization. One patient developed septicemia and died 10 days after embolization. All patients were determined to have no occlusion of the main portal trunk and the authors conclude that transcatheter arterial embolization is beneficial as a procedure of first choice for ruptured hepatocellular carcinoma if the portal blood flow is maintained.

Charles A. Rohrmann, Jr.

Surface coil magnetic resonance imaging. Axel L (Hospital of University of Pennsylvania, Philadelphia, PA 19104). *J Comput Assist Tomogr* 8:381–384, June 1984

A surface coil is used as a receiver in a crossed-coil arrangement with a conventional circumferential transmitter coil in a magnetic resonance (MR) imaging system. The improved signal-to-noise ratio for objects near the coil, compared with conventional circumferential saddle-shaped receiver coil, permits higher resolution imaging of relatively superficial structures such as the orbit, neck, chest wall, and lumbar spine. Although simple, the surface coil provides good quality images of superficial structures. Surface coil imaging may provide a useful alternative to the more conventional circumferential coil imaging when higher resolution images are needed of relatively superficial structures that will not fit into a head coil. The nonuniform response pattern of the surface coil is both an advantage and disadvantage. The advantage of the strong coupling to adjacent region is that it permits higher resolution imaging of nearby structures. The decreased response to distant structures reduces potential problems with aliasing of such structures into the imaging region when stronger imaging gradient magnetic fields are used to produce higher resolution images. The disadvantage of the inhomogeneous response is the variation of intensity of the resulting images.

K. Jack Momose

Cerebral NMR and CT imaging in dementia. Erkinjuntti T, Sipponen JT, Iivanainen M, Ketonen L, Sulkava R, Sepponen RE (University Central Hospital, Helsinki, Finland). *J Comput Assist Tomogr* 8:614–618, Aug 1984

The authors studied 13 typical cases of different types of dementia by computed tomography (CT) and magnetic resonance (MR) imaging. Four of the cases had primary degenerative dementia (Alzheimer and Pick disease) and nine had vascular dementia (multiple strokes of the lacunar and Binswanger types). In all 13 cases, there was good overall correlation between CT and MR findings. Hypointense areas in the white matter, seen in vascular dementia, may be overlooked in CT. In vascular dementia caused by multiple strokes the white matter changes were especially prominent around the frontal and occipital horns, corresponding to the so-called watershed areas. In the angiopathic type of vascular dementia, the white matter involvement extended to the corona radiata. These white matter changes were clearly seen by MR when T2 weighted images were used. In contrast, the patients with primary degenerative dementia did not show white matter hypointensity. On the basis of MR and CT findings, the authors found it difficult to distinguish between lacunar and Binswanger types of vascular dementia.

K. Jack Momose

Ultrasound-guided periventricular stereotaxis. Brown FD, Rachlin JR, Rubin JM, Fessler RG, Smith LJ, Schaible KL (University of Chicago Medical Center, Chicago, IL 60637). *Neurosurgery* 15:162–164, Aug 1984

Intraoperative sonography can aid in the biopsy of deep intracranial lesions. The authors used five mongrel dogs to investigate the periventricular gray (PVG) target. All scans were performed in the coronal plane with an ATL NeuroSector real-time ultrasound scanner. The scanning was carried out until the iter of the Sylvian aqueduct and the posterior third ventricle could be visualized. Normal anatomy showed a diamond-shaped third ventricle and a pinpoint aqueduct. The authors evaluated the placement of an electrode in the PVG. Autopsies showed the placement of these electrodes with less than 1 mm error in four of five brains and only a 1.5 mm error in the fifth brain. The potential advantages of this technique over conventional stereotaxis include the avoidance of ventricular catheterization, injection of contrast agent into the ventricles, need for stereotactic frame and multiple x-ray exposures. Also with real-time scanning the surgeon has instant visual confirmation of electrode placement and can observe quickly any significant hematoma formation.

K. Jack Momose

Cervical spondylotic radiculo-myelopathy in patients with athetoid-dystonic cerebral palsy: clinical evaluation and surgical treatment. Hirose G, Kadoya S (Kanazawa Medical School, Uchinadamachi, Kahoku-gun, Ishikawa Prefecture, Japan 920-02). *J Neurol Neurosurg Psychiatry* 47:775–780, Aug 1984

Only a few reports mention the relationship between cervical spondylosis and dyskinesia. The authors describe four patients with athetoid-dystonic cerebral palsy who developed acute symptoms of severe cervical radiculomyelopathy. Ages were 27–41 years. The neurologic and radiologic examination showed that the spondylotic changes of the cervical spine were responsible for new neurologic deficits that lead to the patients being bedridden. Dystonic-athetoid neck movements may cause excessive axial neck rotation and flexion and extension movements of the spine. These repetitive exaggerated movements may result in early degenerative changes of the vertebrae that may enhance the radiculomyelopathy. Myelography showed degenerative disk disease and narrowed spinal canals. All four patients were bedridden before anterior discectomy with interbody fusion. Postoperatively all became ambulatory; some required a cane.

K. Jack Momose

Miscellaneous

Examination of the temporomandibular joint by direct sagittal computed tomography. Raustia AM, Pyhtinen J, Virtanen K (Institute of Dentistry, University of Oulu, Aapistie 3, SF-90220 Oulu 22, Finland). *Clin Radiol* 36:291–296, May 1985

Direct sagittal computed tomography (CT) of 17 temporomandibular joints in 10 patients was performed using a modified accessory stretcher placed lateral to the gantry at an angle of 30°–55° to the scanner trolley. The authors found that all patients were able to tolerate this supine scanning position in contrast to some previously described scanning methods for the temporomandibular joint. The temporomandibular joints were scanned from medial to lateral aspects using 2 mm thick contiguous sections. The optimal scan to demonstrate articular details was then chosen and performed with the mouth in closed, semiopen, and maximally opened positions and before and after clicking. Normal CT appearances and findings in two patients are illustrated from this series. These authors recommend direct sagittal CT as the primary investigation, particularly because of the ability of CT to demonstrate bony structures and soft tissues including the disk in a noninvasive manner in all phases of mouth opening. They reserve arthrography for the investigation of patients with negative CT findings or where disk perforation is suspected.

Noel K. Allan

Pediatric Radiology

Retinoblastoma CT diagnosis. Char DH, Hedges TR, Norman D (Ocular Oncology Unit, Science 315, University of California, San Francisco, CA 94143). *Ophthalmology* 91:1347–1350, Nov 1984

Thirty-three children with retinoblastoma seen between 1977 and 1982 were studied by high-resolution computed tomography (CT) before being treated. Of these patients, 20 had unilateral involvement and 13 had bilateral tumors. Ages were 2 months–4½ years; mean age was 19 months. Twenty-four children presented with leukocoria. Of the 33 patients, 31 had CT evidence of intraocular calcification in at least one eye. The degree of calcification appeared to depend upon tumor size; only small tumors were devoid of calcification. The amount and distribution of calcification was similar on both histologic and CT review. All retinoblastoma-containing eyes that did not demonstrate calcification on CT were subsequently confirmed by the authors. Calcification was demonstrable in all retinoblastoma-containing eyes that presented with leukocoria. In these, there were two patterns of calcification on CT scans: a regular, nonhomogeneous pattern was in most eyes containing large tumors while eyes with smaller tumors showed a homogeneous pattern. All eyes with large tumors were enucleated and had microscopic evidence of tumor spread past the lamina cribrosa of the optic nerve. This was not detected by CT. Four patients with Coats syndrome were also studied. None of these patients had demonstrable calcification on CT.

Harvey I. Wilner

Magnetic resonance imaging of lesions of the posterior fossa and upper cervical cord in childhood. Packer RJ, Zimmerman RA, Bilanuik LT, Leurssen TG, Sutton LN, Bruce DA, Schut L (Children's Hospital of Philadelphia, Philadelphia, PA 10104). *Pediatrics* 76:84–90, July 1985

Forty-six children, aged 2 months–18 years, with diseases of the posterior fossa and cervical spinal cord were evaluated with a 0.12 T resistive proton magnetic resonance imaging (MRI) unit. Concurrently, computed tomography (CT) was performed. MRI demonstrated malignancy in all affected children and best demonstrated the extent of infiltrating lesions in 50% of cases. MRI was also a sensitive measure of response to treatment and treatment failure in these children. In patients with congenital anomalies, MRI showed more extensive disease and better anatomic detail. This study confirms the utility of MRI in visualizing anatomic abnormalities in the posterior fossa and distinguishing between normal and abnormal central nervous system structures. MRI was superior to CT in demonstrating anatomic relationships, evaluating posterior fossa and cervical spinal cord anatomy, and in determining response to treatment in patients with infiltrating tumors. The disadvantages of MRI included: difficulty in separating cerebrospinal fluid cysts from adjacent neoplasia, inability to distinguish calcification from other low-signal intensity areas, and decreased spatial resolution. The authors conclude that MRI is sensitive in the evaluation of posterior fossa and cervical spinal cord diseases in childhood.

Richard Towbin

Sinus histiocytosis with massive lymphadenopathy: skeletal involvement. Puczynski MS, Demos TC, Suarez CR (Pediatrics, Loyola University Medical Center, Maywood, IL 60153). *Pediatr Radiol* 15:259–261, May 1985

Sinus histiocytosis with massive lymphadenopathy is a benign pseudolymphomatous entity with bilateral cervical adenopathy, leukocytosis, elevated erythrocyte sedimentation rate, hypergammaglobulinemia, anemia, and elevated Epstein-Barr virus antibody titers. It is most common in black patients during the first two decades of life, and spontaneous resolution in months to years is expected. While extranodal involvement, including skin, orbit, and nasopharynx, is found in nearly one-third of cases, bone involvement has been well documented in only eight of over 130 reported cases. A 9-year-old black girl developed joint pain and swelling at age 6, with multiple scattered blastic and lytic lesions appearing in epiphyses, metaphyses, and diaphyses of the extremities and remaining for 3 years. Biopsy showed the typical histology of bony trabeculae surrounded by sheets and clusters of leukocytes. The multiple sharp to poorly defined cortical or medullary mostly lytic lesions with variable surrounding sclerosis may be caused by a number of other generalized disorders; biopsy of a bone lesion will then confirm or reveal the diagnosis.

Alan E. Oestreich

CT findings following diphenylhydantoin intoxication. Baier WK, Beck U, Hirsch W (Dept. of Neuropediatrics, University of Kiel, Schwanenweg 20, D2300 Kiel, West Germany). *Pediatr Radiol* 15:220–221, May 1985

The computed tomography (CT) findings of epileptic patients with irreversible ataxia after toxic doses of diphenylhydantoin include cerebellar atrophy, with distinct visualization of cerebellar sulci, and dilated 4th ventricle, basal cisterns, and subarachnoid space.

Alan E. Oestreich

Coxsackievirus group B antibodies in the ventricular fluids of infants with severe anatomic defects in the central nervous system. Gauntt CJ, Gudvangen RJ, Brans YW, Marlin AE (University of Texas Health Science Center, San Antonio, TX 78284). *Pediatrics* 76:64–68, July 1985

The authors sought to determine if there was an association between forebrain defects and infection with Coxsackie group B viruses. Ventricular fluid from four of 28 neonates with severe central nervous system anatomic defects contained neutralizing antibodies to Coxsackie group B viruses. Three of four infants had been infected with Coxsackievirus. Of 11 mother-infant pairs that had neutralizing antibodies to Coxsackieviruses group B in both sera, almost one-half had antibodies against more than one serotype. These data suggest a possible relationship between Coxsackievirus group B infections and central nervous system defects.

Richard Towbin

Narrow trachea in mucopolysaccharidoses. Peters ME, Arya S, Langer LO, Gilbert EF, Carlson R, Adkins W (University Clinical Science Center, 600 Highland Ave., Madison, WI 53792). *Pediatr Radiol* 15:225–228, May 1985

Nine of 56 patients with a mucopolysaccharidosis showed small tracheal diameters on frontal chest radiography (using standards of two standard deviations below the mean of 5 mm at age 4 and 6 mm at age 7). Autopsy of one Hurler patient (age 9) indicated the narrowing was due to mucopolysaccharide deposition. Respiratory difficulty is common in mucopolysaccharidosis and related disorders. Anesthetic catastrophe may occur when intubation of such a child is attempted.

Alan E. Oestreich

ARRS Meeting Section

Invitation to the 1986 American Roentgen Ray Society Meeting in Washington, DC, April 13–18

The American Roentgen Ray Society (ARRS) extends a warm invitation to all interested physicians, health professionals, and others in radiologic health care to attend its 86th annual meeting in Washington, DC. Our headquarters will be the Sheraton Washington, a beautiful hotel in an outstanding and convenient location with the Metro right at your door. This makes participating in the many activities in Washington even more pleasurable.

Scientific Program

A total of 189 papers have been selected from the nearly 500 submitted. These will be presented in parallel sessions, Monday–Thursday, enabling registrants to see works in areas of greatest interest to each. Unfortunately, space and time restraints do not permit presentation of a greater number, but the difficult decisions mean that the quality will be outstanding. The general session on Wednesday morning will feature award papers from the Society of Gastrointestinal Radiology and from the Society for Pediatric Radiology plus the three award papers sponsored by the ARRS Executive Council and the society president.

The Caldwell Lecturer this year will be Benjamin Felson of the University of Cincinnati.

A new addition to this year's meeting will be a daily luncheon discussion designed to bring all of us up-to-date on the changing patterns in health care delivery and how they affect the radiologist. Individuals with special knowledge of this aspect of the practice of radiology will lead the discussions.

Instructional Courses

The instructional courses this year will again *not* conflict with other aspects of the scientific program. Glen Hartman has put together an excellent faculty and the 48 courses will cover a wide variety of topics. The Categorical Course in the Chest is under the direction of Anthony Proto and Reginald Greene, who have done an outstanding job planning this course.

Because of the very positive response to the symposium on the chest last year, we will again have a symposium on Friday morning. The 1986 symposium is Skeletal Radiology '86, and was developed by Jack Edeiken and Lee Rogers.

Exhibits

John Madewell has selected the scientific exhibits from the largest number ever submitted. The available space this year is larger than many times in the past, thus more exhibits have been selected and there will be more room to view them comfortably.

The Case of the Day presentations under the direction of Joe Sackett and Marvin Hinke of the University of Wisconsin will be previewed in the March issue of the *AJR*. They have some new and exciting ideas for this challenging and educational part of our meeting.

Commercial distributors will again display a variety of new developments in radiology and related fields and are anxious to meet you.

Social Events

Charley Bickham, Chairman of the Local Arrangements Committee, and his wife, Melba, have planned an exciting program to take advantage of the many opportunities for sightseeing and shopping within the Washington area.

The golf and tennis tournaments are set for those seeking a challenge. The good fellowship resulting from these tournaments is a real plus for those attending our meeting.

Of course, the reception on Tuesday, which is open to all registrants, is another part of the program that enhances the sense of involvement of all who attend the ARRS meeting.

Please join us in Washington. I look forward to seeing you there.

Jerome F. Wiot
President Elect

Summary of 1986 American Roentgen Ray Society Meeting

Sunday, April 13	Monday, April 14	Tuesday, April 15	Wednesday, April 16	Thursday, April 17	Friday, April 18
	8–9:30. Instructional courses	**8–9:30.** Instructional courses	**8–9:30.** Instructional courses	**8–9:30.** Instructional courses	**8–1.** Symposium: skeletal radiology
10–noon. Categorical course: chest radiology	**10–10:30.** Opening ceremony **10:30–12:30.** Scientific program —GI imaging I —Uroradiology I —Pediatric radiology	**10–12:30.** Scientific program —GI imaging II —Mammography/general radiology —Skeletal radiology I	**10–12:30.** Awards session/Caldwell lecture	**10–12:30.** Scientific program —GI imaging III —Interventional radiology —Chest radiology	
	12:30. Box lunch session	**12:30.** Box lunch session	**12:30.** Box lunch session	**12:30.** Box lunch session	
1:30–5:30. Categorical course: chest radiology	**1:30–5:30.** Categorical course: chest radiology	**1:30–3:30.** Scientific program —Cardiovascular radiology I —Neuroradiology I —Magnetic resonance I	**1:30–3:30.** Scientific program —Uroradiology II —Skeletal radiology I —Magnetic resonance II	**1:30–3:30.** Scientific program —Cardiovascular radiology II —Neuroradiology II —Magnetic resonance III	
		4–5:30. Categorical course: chest radiology	**4–5:30.** Categorical course: chest radiology	**4–5:30.** Categorical course: chest radiology	

American Roentgen Ray Society 1986 Scientific Program

To provide registrants with scientific topics related to their interests, the scientific sessions are divided into parallel sessions. A total of 189 papers will be presented Monday–Thursday, April 14–17. In addition, on Wednesday morning, April 16, a special session will be devoted to award-winning papers and the Caldwell Lecture, which will be delivered by Benjamin Felson of the University of Cincinnati. On Friday, April 18, there will be a special symposium, Orthopedic Radiology 1986.

Monday, April 14, 10:30 a.m.–12:30 p.m.

I. Gastrointestinal Imaging: I

10:30. 1. **The injured spleen—sonographic and clinical evidence to support its nonoperative management.** Fink-Bennett DM, Pernicone JP, Lynch JP, Gibson P, Bree RL, Reed LL (Royal Oak, MI)

10:42. 2. **Endoscopy or barium meal for dyspepsia: a study on patient preference.** Frost RA, Lamping DL, Somers S, Stevenson GW (McMaster University)

10:54. 3. **The anatomy of eee.** Rubesin SE, Jones B (Johns Hopkins Hospital)

11:06. 4. **Caroli Disease: a radiologic perspective.** Sadler LR, Scheid ER, Fuhrman CR (Presbyterian-University Hospital)

11:18. 5. **Gallbladder perforation: a correlative imaging assessment.** Siskind BN, Hawkins HB, Cinti DC, Zeman RK, Burrell MI (Yale University)

11:30. 6. **The role of computed tomography and endoscopic cholangiopancreatography in imaging of pancreatic and biliary disease.** Tobin RS, Vogelzang RL, Gore RM, Keigley B (Northwestern Memorial Hospital)

11:42. 7. **Scout film and patient self-evaluation in the barium enema—is either useful?** Vydareny KH, Trenkner SW (University Hospital, Ann Arbor, MI)

11:54. 8. **Computed tomography of nonpalpable incisional hernias.** Ghahremani GG, Rosenfeld M, Jimenez MA, Rochester D (Evanston Hospital)

12:06. 9. **Vascular complications after liver transplantation: a 5-year angiographic experience.** Wozney P, Zajko AB, Bron KM, Starzl TE (Presbyterian-University Hospital)

II. Uroradiology Imaging: I

10:30. 10. **Factitious retroperitoneal air associated with epidural anesthesia for extracorporeal shock wave lithotripsy.** Roberts MC, Pollack HM, Banner MP, Castro AD, VanArsdalen KN (Hospital of the University of Pennsylvania)

10:42. 11. **Radiation exposure to patient and personnel during ESWL.** Bush WH, Jones D, Gibbons RP (Mason Clinic)

10:54. 12. **Nature of the echogenic focus in prostatic ultrasound.** Dahnert EF, Hamper UM, Eggleston JC, Walsh PC, Sanders RC (Johns Hopkins Hospital)

11:06. 13. **CT evaluation of primary adrenocortical carcinoma with clinical correlation.** Deutch BM, Fishman EK, Hartman DS, Siegelman SS (Johns Hopkins Hospital)

11:18. 14. **Magnetic resonance imaging of hemorrhagic renal cysts in polycystic kidney disease.** Hilpert PL, Friedman AC, Radecki PD, Caroline DS (Temple University)

11:30. 15. **Renal cell carcinoma: current generation CT staging.** Johnson CD, Dunnick NR, Cohan RH, Illescas FF (Duke University)

11:42. 16. **Ultrasound vs. intravenous urography in the preoperative evaluation of patients with benign prostatic hypertrophy.** Saigh JA, Cascione CJ, Imray TJ, Hanson GL (University of Nebraska)

11:54. 17. **The spectrum of sonographic findings in renal dysplasia.** Sanders RC, Nussbaum AR, Solez K (Johns Hopkins Hospital)

12:06. 18. **Staging of renal cell carcinoma: remember dynamic CT!** Zeman RK, Cronan JJ, Rosenfield AT, Choyke PL, Jaffe MH, Clark LR (Georgetown University)

Pediatric Radiology

10:30. 19. **MRI of the head and neck in the pediatric patient.** Dietrich RB, Lufkin R, Kangarloo H, Hanafee WN, Wilson G (UCLA Hospital)

10:42. 20. **Perforation in necrotizing enterocolitis: a review of 19 cases.** Frey EE, Smith WL, Franken EA Jr, Wintermeyer K (University of Iowa)

10:54. 21. **Role of computed tomography in the diagnosis and management of tracheobroncheal anomalies in infants and children.** Mahboubi S (Children's Hospital, Philadelphia)

11:06. 22. **MR imaging of the neonatal head.** McArdle CB, Richardson CJ, Nicholas DA, Amparo EG, Hayden CK (University of Texas Medical Branch)

11:18. 23. **Neurosonographic appearances of congenital CMV infections.** Montana MA, Mack LA, Newman DE, Blumhagen J, Presto ME (University of Washington)

11:30. 24. **Imaging of the immunoblastic disorders in children.** Law B, Miller JH, De Clerck Y (Childrens Hospital, Los Angeles)

11:42. 25. **Radiographic appearance of the postoperative gastroesophageal junction in children.** Robinson AE, Adams AF, Austin AR, Mason WG (University of South Alabama)

11:54. 26. **The extraperitoneal fat sign: a new plain film sign of childhood appendicitis.** Yutaka S, Shunsuke N, Noriaki I, Yakushiji Y, Fujii M (St. Marianna University School of Medicine)

12:06. 27. **Transplant renal artery stenosis in children.** Stanley P, Malekzadeh M, Diament MJ (Childrens Hospital, Los Angeles)

Tuesday, April 15, 10 a.m.–12:30 p.m.

IV. Gastrointestinal Imaging: II

10:00. 28. Nodular transformation "nodular regenerative hyperplasia" of the liver: a mimic of hepatic adenoma. Dachman AH, Ros PR, Goodman ZD, Olmsted WW, Ishak KG (Walter Reed Army Medical Center)

10:12. 29. Computed tomography of periampullary neoplasms. Darweesh RMA, Thorsen MK, Dodds WJ, Lawson TL, Stewart ET, Kishk SMA (MCMC-Milwaukee, WI)

10:24. 30. CT patterns of hepatic hemangioma. Freeny PC, Marks WM (Mason Clinic)

10:36. 31. Preoperative and intraoperative sonography of benign pancreatic insulinoma—a review of 23 patients. Gorman B, Charboneau JW, James EM, Reading CC, Grant C, Van Heerden J, Telander R (Mayo Clinic)

10:48. 32. CT of the pathologic greater omentum. Holley HC, Anderson SD, Van Dyke JA, Berland LL (University Hospital, Birmingham, AL)

11:00. 33. Computed tomography of postoperative intraabdominal abscesses. Mehta S, Raval B, Jaramillo D, St. Ville E (University of Texas)

11:12. 34. Tumors of the small intestine with little or no malignant predisposition. Olmsted WW, Ros PR, Sobin LH, Dachman AH (Armed Forces Institute of Pathology)

11:24. 35. Expandable intrahepatic portocaval shunt stent in dogs with chronic portal hypertension. Palmaz JC, Windeler AS, Sibbitt RR, Garcia F, Schesinger W, Tio FO, Chang P, Reuter SR (UT Health Science Center)

11:36. 36. Fluoroscopically-guided extraction of esophageal foreign bodies. Shaffer HA Jr, Alford BA, Meyer GA, deLange EE (University of Virginia)

11:48. 37. Hepatic fungal infection: CT and pathologic correlation before and after treatment with liposomal amphotericin-B. Shirkhoda A, Lopez-Berestein G, Holbert M, Luna M (Houston, TX)

12:00. 38. Fatty liver metamorphosis: periportal sparing as a cause of hepatic pseudomass. White ME, Simeone JF, Mueller PR, Grant EG (Georgetown University)

12:12. 39. SPECT and Tc-RBC imaging of cavernous hemangioma. Friedman AC, Brodsky RI, Maurer AH, Vitti RA, Radecki PR, Caroline DF, Grumbach K, Malmud LS (Temple University)

V. Mammography/General Radiology

10:00. 40. Minimal breast cancer: radiology and outcomes. Frankl G, Ackerman M (Los Angeles, CA)

10:12. 41. Mammographic decision analysis: sensitivity in a screening population. Schmitt EL, Threatt BA (Detroit, MI)

10:24. 42. Initial screening mammography examination: one vs. two views per breast. Sickles EA (University of California, San Francisco)

10:36. 43. Results of a clinical trial with a new xeroradiographic mammography system. Wolfe JN, Parekh NJ (Hutzel Hospital)

10:48. 44. Radionuclide thyroid angiography—review of 8-year study. Chako AK, Kolina JS, Akau B (Letterman Army Medical Center)

11:00. 45. Inhomogeneities in benign schwannomas: the pathologic basis for the CT appearance. Cohen LM, Rockoff SD, Schwartz AM (George Washington University Medical Center)

11:12. 46. Digital tomosynthesis: advantages and limitations in clinical practice. Friedenberg RM, Nalcioglu O, Roeck W (UCI Medical Center)

11:24. 47. Pixel and matrix requirements for telephone transmission of radiologic images to personal computers. Haskin ME, Haskin PH, Teplick JG, Laffey P, Ehmann M, Teplick SK, Auger A, Kohn M (Philadelphia, PA)

11:36. 48. Paroxysmal nocturnal hemoglobinuria: spectrum of radiographic and clinical findings. Morton KA, Miller FJ (University of Utah)

11:48. 49. Cholescintigraphy of "cystic" intrahepatic and perihepatic pathologic processes. Rao BK, Polcyn RE, Lieberman LM, Weir JG (University of Wisconsin)

12:00. 50. Malignant melanoma: the impact of body computed tomography. Shuman WP, Teefey SA, Greiner WE, Mack LA, Moss AA (University of Washington)

12:12. 51. CT for parotid neoplasia: a new look. Swartz JD, Nunnelly JF, Lansman GV, Marlowe FI, Berger AS, Ardito JM, Popky GL (Medical College of Pennsylvania)

VI. Skeletal Radiology: I

10:00. 52. The costovertebral and costotransverse articulations: radiographic pathologic correlation. Bjorkengren AG, Sartoris DJ, Resnick D, Pate D (Veterans Administration Medical Center, San Diego)

10:12. 53. Radiographic evaluation of joints resurfaced with alogeneic osteochondral grafts. Kusnick C, Sartoris DJ, Meyers MH, Akeson W, Resnick D (University of California, San Diego)

10:24. 54. Potential pitfalls in rotator cuff sonography. Crass JR, Craig EV, Feinberg SB (University Hospitals, Minneapolis)

10:36. 55. High-speed ejection injuries from motor vehicles—radiologic patterns. Daffner RH, Deeb ZL, Lupetin AR, Rothfus WE (Allegheny General Hospital)

10:48. 56. Comparison of dual photon ^{153}Gd bone densitometry (DPBD) and single photon transmission computerized transaxial tomography (SPCT) in normal volunteers—a pilot study. Feiglin DHI, O'Donnell JK, Freeman KL, Mattson RA, Williams LJ, Wholahan CM, Go RT, Belhobek GH, MacIntyre WJ (Cleveland Clinic)

11:00. 57. Adult onset Still disease—a disorder with characteristic radiologic abnormalities. Bjorkengren AG, Sartoris DJ, Resnick D, Terkeltaub R, Esdaile JM, Weisman M, Klofkorn R (VAMC-San Diego)

11:12. 58. The role of the AP radiograph in the evaluation of sagittally oriented fractures of the lateral mass and body of the cervical spine. Lee C, Woodring JH, Goldstein SJ (University of Kentucky)

11:24. 59. Inferior joint space arthrography of normal temporomandibular joints: a reassessment of diagnostic criteria. Kablan PA, Tu HK, Sleder PR, Lydiatt DD (University of Nebraska)

11:36. 60. Incomplete carpal coalition. Resnik CS, Grizzard JD, Simmons BP, Yaghmai I (Richmond, VA)

11:48. 61. Stress examination of the lateral ligaments of the ankle—a follow-up 1 year posttrauma. Rijke AM, Jones B, Vierhout PA (University of Virginia Medical Center)

12:00. 62. Localized transient osteoporosis of the knee. Schneider R, Goldman AB, Vigorita V (Hospital for Special Surgery)

12:12. 63. CT of the shoulder girdle. Shuman WP, Schoenecker SA, Mack LA, Montana MA, Weinberger E, Kilcoyne RE (University of Washington)

Tuesday, April 15, 1:30–3:30 p.m.

VII. Cardiovascular Radiology: I

1:30. 64. **Free fibular graft for femoral osteonecrosis: pre- and postoperative angiographic assessment.** Braun SD, Newman GE, Oke EJ, Perlmutt LM, Dunnick NR (Duke University)

1:42. 65. **Diagnosis and evaluation of hypertrophic obstructive cardiomyopathy in adolescents and young adults using cine computed tomography.** Eldredge WJ, Rees MR, Flicker S, Naidech H (Deborah Heart and Lung Center)

1:54. 66. **Selective three-dimensional magnetic resonance imaging of the heart.** Gallimore GW Jr, Harms SE (Baylor University)

2:06. 67. **Outpatient angiography: initial experience in 500 patients.** Katzen BT, van Breda A, Steinberg DL (Alexandria Hospital)

2:18. 68. **Transluminal angioplasty for intestinal ischemia.** Koch PJ, Wholey MH (Pittsburgh, PA)

2:30. 69. **Significance of anatomic variations and deep venous thrombosis of the lower extremity.** Liu GC, Ferris EJ, Reifsteck JR, Baker ML (University of Arkansas)

2:42. 70. **512 and 1024 digital densitometry for the evaluation of percutaneous transluminal angioplasty (PTA).** Lois JF, Mankovich NJ, Gomes AS (UCLA School of Medicine)

2:54. 71. **MRI evaluation of the IVC—comparison to CT.** Lupetin AR, Beckman I, Dash N, Schapiro RL, Daffner RH, Deeb ZL, Rothfus WE, Contractor FM (Allegheny General Hospital)

3:06. 72. **Intraarterial DSA and the importance of catheter and contrast material selection: an in vitro study.** Rees CR, Merchun G, Becker GJ, Mail JT, Klatte EC (Indiana University)

3:18. 73. **Determination of aortocoronary bypass graft patency by cine computed tomography.** Rees MR, MacMillan RM, Reiter S, Feiring AJ, Rumberger JA, Eldredge WJ, Flicker S, Naidech H, Maranhao V, Clark DL (Killingbeck Hospital)

VIII. Neuroradiology: I

1:30. 74. **Normal faces of the fourth ventricle in children.** Abramson CL, Gado M, Harwood-Nash DC (St. Louis, MO)

1:42. 75. **Characterization of CNS masses by sonography in correlation with CT.** Madrazo BL, Sanders WP, Mehta B, Chason D, Dujovny M (Henry Ford Hospital)

1:54. 76. **MRI and paramagnetic contrast agents in the measurement of CSF flow in experimental hydrocephalus.** Gomez DG, Knowles RJR, Markisz JA, Manzo RP, Whalen JP, Deck M, Cahill PT (Cornell University)

2:06. 77. **Comparison of CT myelography and MRI in acquired spinal cord lesions.** Karnaze MG, Gado MH, Sartor KJ, Hodges FJ III (Mallinckrodt Institute of Radiology)

2:18. 78. **Spinal cord injury—MRI findings.** Knoedler M, Lund G, Roche B, Heitsch G, Cameron J (University of Minnesota)

2:30. 70. **Xenon-CT blood flow imaging in patients with subarachnoid hemorrhage.** Laster RE Bell LW, Bahktian B (Methodist Hospitals)

2:42. 80. **Intraarterial digital subtraction angiography of the carotid artery system.** Madayag MA, Cavallino RP, Nadimpalli SR (Illinois Masonic Medical Center)

2:54. 81. **Surface coil MR imaging of spinal trauma: preliminary experience.** McArdle CB, Calhoun JH, Crofford MJ, Ampara EG (University of Texas Medical Branch)

3:06. 82. **MRI vs. CT in head trauma.** Mulopulos GP, Han JS, Modic MT (University Hospitals, Cleveland)

3:18. 83. **Radiation effects on cerebral white matter: MRI evaluation.** Tsuruda JS, Grossman I, Wheeler D, Von Dalsem W, Bradley TP, Bradley WG (Huntington Medical Research Institutes)

IX. Magnetic Resonance: I

1:30. 84. **Magnetic resonance imaging (MRI) in the clinicopathologic correlation of minor and moderate head injury.** Amparo EG, Levin HS, Mirfakhraee M, McArdle CB, Williams D, Eisenburg H (MRI Division, Galveston, TX)

1:42. 85. **MR imaging of liver cancer with magnetite: a reticuloendothelial contrast agent.** Saini S, Stark DD, Wittenberg J, Ferrucci JT Jr (Massachusetts General Hospital)

1:54. 86. **Magnetic resonance imaging of the trachea.** Edelman RR, McLoud TC, Brady TJ, Grillo HC, Spizarny DL (Massachusetts General Hospital)

2:06. 87. **High-resolution MRI of the supraclavicular region.** Kellman GM, Kneeland JB, Middleton WD, Cates JD, Lawson TL, Foley WD, Jesmanowicz A, Froncisz W, Hyde JS (Milwaukee County Medical Complex)

2:18. 88. **High-resolution MRI of the wrist.** Middleton WD, Kneeland JB, Cates JD, Kellman GM, Foley WD, Lawson TL, Jesmanowicz A, Froncisz W, Hyde JS, Carrera G (Milwaukee County Medical Complex)

2:30. 89. **MRI of renal transplantation: initial observations at 1.5 T using surface coils.** Mitchell DG, Rosa A, Spritzer CE, Perloff LJ, Jorkasky D, Pollack H, Arger PH, Barker CR, Naji A, Grossman RA, Velchik MG, Alavi A, Axel L, Gefter WB, Kressel HY (Hospital of the University of Pennsylvania)

2:42. 90. **Quantitative phase flow imaging by MRI using standard sequences: comparison with flow meter measurements.** Pettigrew R, Dannels W, Pearson T, Millikan W, Henderson JM, Bernardino ME (Emory University)

2:54. 91. **Evolution of splenic hematoma: MR and biochemical features.** Saini S, Stark DD, Hahn P, Greif WSL, Guerrero L, Brady TJ, Ferrucci JT Jr (Massachusetts General Hospital)

3:06. 92. **High-resolution surface coil imaging of the knee at 1.5 T.** Burk DL Jr, Kanal E, Brunberg JA, Johnstone GF, Wolf GL (Pittsburgh NMR Institute)

3:18. 93. **MRI of liver metastases: T1-weighted pulse sequences.** Stark DD, Wittenberg J, Edelman RR, Middleton MS, Saini S, Butch RJ, Brade TJ, Simeone JF, Mueller PR, Ferrucci JT Jr (Massachusetts General Hospital)

Wednesday, April 16, 10–noon (no parallel session)

10:00. **Scientific exhibit awards.** Madewell J

10:15. **Award paper: Society for Pediatric Radiology**

10:30. **Award paper: Society of Gastrointestinal Radiologists**

10:45. **Executive Council Resident Award Paper 1**

11:00. **Executive Council Resident Award Paper 2**

11:15. **The President's Resident Award Paper**

11:30. **The Caldwell Lecture.** Benjamin Felson, University of Cincinnati

Wednesday, April 16, 1:30–3:30 p.m.

X. Uroradiology Imaging: II

1:30. 94. **Sonography of CT indeterminate high-density renal masses.** Castagno AA, Foster WL Jr, Reed DN, Halvorsen RA Jr, (VA Medical Center, Durham, NC)

1:42. 95. **Correlation of radionuclide and ultrasound examinations with biopsy findings for the early diagnosis of renal transplant rejection.** Hall JT, Kim EE, Sandler CM, Pjura GA, Verani R (University of Texas Medical School, Houston)

1:54. 96. **New short 22-gauge needle guide for drainage and biopsy procedures.** Hawkins IF Jr, Hawkins J, Davis JC, Legrande E, Coryell L (University of Florida)

2:06. 97. **Calcified adrenal masses.** Kenney PJ, Van Dyke JA, Stanley RJ (University of Alabama)

2:18. 98. **Prostate cancer—diagnosis by transrectal ultrasound: new ultrasound criteria with histopathologic correlations.** Lee F, Gray JM, McLeary RD, Kumasaka GH, Straub WH, McHugh TA (Ann Arbor, MI)

2:30. 99. **Epidural anesthesia for uroradiologic interventional procedures.** Papanicolaou N, Pfister RC, Roberts J, Yoder IC (Massachusetts General Hospital)

2:42. 100. **The accuracy of CT in the staging of carcinoma of the prostate.** Platt JF, Bree RL, Schwab RE (William Beaumont Hospital)

2:54. 101. **Ultrasound and CT of urinary tract tuberculosis.** Premkumar A, Newhouse JH, Lattimer JK (Presbyterian Hospital, New York City)

3:06. 102. **Progression in medullary sponge kidney: clinical and radiological management.** Spickler EM, Lutz MD, Sandler MA, Kochkodan EJ, Farah R (Henry Ford Hospital)

3:18. 103. **Utility of CT in patients with penile carcinoma.** Thomas AJ, Lewis E (M.D. Anderson Hospital & Tumor Institute)

XI. Skeletal Radiology: II

1:30. 104. **Evaluation of painful total hip replacements.** Aliabadi P, Tumeh SS, Weissman BN, McNeil BJ (Harvard Medical School)

1:42. 105. **The spectrum of paravertebral ossification: from sabretooth cat to modern man.** Bjorkengren AG, Sartoris DJ, Shermis S, Resnick D, Rothchild B (VA Medical Center, San Diego)

1:54. 106. **Hyperflexion sprain: easy to underread and overread.** Bohrer SP (Bowman Gray School of Medicine)

2:06. 107. **3D CT of fractures of the lower extremities.** Burk DL Jr, Mears DC, Cooperstein LA, Ward WT, Swink C (Pittsburgh NMR Institute)

2:18. 108. **Spine fractures in diffuse idiopathic skeletal hyperostosis: a comparison with ankylosing.** Hendrix RW, Urban M, Rogers LF (Chicago, IL)

2:30. 109. **The osseous pelvis: the utility of an innovative algorithm for computed tomographic reformation.** Howie JL (University Hospital, Saskatoon, Saskatchewan)

2:42. 110. **Quantitative CT measurements of bone mineral content: accuracy and precision of the data.** Nickoloff EL, Feldman F (Columbia-Presbyterian Medical Center)

2:54. 111. **Diagnostic approach and radiologic pathologic correlation of parosteal osteosarcoma.** Raymond KA, Shirkhoda A, Lindell ML, Benjamin R, Murray J (M. D. Anderson Hospital)

3:06. 112. **Radionuclide study in skeletal metastases of malignant melanoma.** Ruppert D, Ali S, Marvin C, Thomas H (M. D. Anderson Hospital)

3:18. 113. **Double acetabular line: an unusual roentgenographic finding associated with paraplegia and quadriplegia.** Yagan R, Radivoyevitch M, Khan MA (Cleveland Metropolitan General/Highland View Hospital, Case Western Reserve University)

XII. Magnetic Resonance: II

1:30. 114. **Clinical evaluation of pulmonary sarcoidosis: comparison of magnetic resonance imaging with gallium scanning.** Markisz JA, Romano P, Schultz DA, Henschke C, Bottger BA, Knowles RJR, Whalen JP, Cahill PT, Kazam E (New York Hospital)

1:42. 115. **Alterations in the hepatic and portal venous system in cirrhosis: MRI findings.** Williams D, Cho K, Aisen A (Ann Arbor, MI)

1:54. 116. **Gated cardiac magnetic resonance imaging (MRI)—evaluation of anatomy using 1.5 T and 0.6 T field strengths.** Feiglin DHI, O'Donnell JK, Go RT, MacIntyre WJ (Cleveland Clinic)

2:06. 117. **Quality assurance for MRI.** Knowles RJR, Markisz JA, Whalen JP, Cahill PT (New York Hospital)

2:18. 118. **Magnetic resonance imaging of the spleen.** Adler DD, Glazer GM, Aisen AM (University of Michigan)

2:30. 119. **A comparison of real-time ultrasound and magnetic resonance imaging for the evaluation of fetal anomalies.** Weinreb JC, Brown CEL, Cohen JM (University of Texas Health Science Center, Dallas)

2:42. 120. **Mechanism of syringohydromyelia formation: MRI in an animal model.** Mirfakhraee M, Crofford MJ, Amparo EG, McArdle C, Guinto FC Jr, Benzel E (UTMB)

2:54. 121. **The role of MRI in the evaluation of surgical resectability and extent of hepatic neoplasms.** Mukai JK, Stack CM, Gould RJ, Turner DA, Petasnick JP, Doolas A, Doolas M, Marcia E (Rush-Presbyterian-St. Luke's Medical Center)

3:06. 122. **Evaluation of focal liver lesions by magnetic resonance imaging.** Markisz JA, Auh YH, Rubinstein WA, Zirinski K, Knowles RJR, Whalen JP, Cahill PT, Kazam E (New York Hospital)

3:18. 123. **Evaluation of congenital heart disease by cine magnetic resonance imaging (MRI).** Feiglin DHI, Moodie DS, Gill CC, Sterba R, O'Donnell JK, Go RT, MacIntyre WJ (Cleveland Clinic)

Thursday, April 17, 1986, 10–12:30 p.m.

XIII. Gastrointestinal Imaging: III

10:00. 124. **Pancreas divisum: incidence, detection, and clinical significance.** Agha FP, Williams KD, Trenkner SW, Nostrant TT (University Hospital, Ann Arbor, MI)

10:12. 125. **Radiologic efficacy in the diagnosis of Barrett esophagus: a prospective, blinded, randomized study.** Amberg JR, Chernin MM, Kogan FJ, Morgan TR, Sampliner RE (VA Medical Center, San Diego)

10:24. 126. **Natural history of the obstructed appendix: an experimental model for appendicitis and appendicial mucocele with sonography and CT correlation.** Dachman A, Nichols JB, Patrick

DH, Lichtenstein JE (Walter Reed Army Medical Center)

10:36. 127. Kaposi sarcoma of the pharynx—radiographic manifestations. Emery C, Wall SD, Sooy D, Federle M, Shea W (VAMC, San Francisco)

10:48. 128. Reevaluating the role of radiology in hemoccult screening programs. Feczko PJ, Halpert RD (Henry Ford Hospital)

11:00. 129. The radiographic and colonoscopic detection of dysplasia and cancer in patients with chronic ulcerative colitis. Hooyman JR, MacCarty RL, Carpenter HA, Schroeder KW, Carlson HC (Mayo Clinic)

11:12. 130. Colonic diverticulitis: contrast enema vs. CT comparison. Johnson CD, Baker ME, Rice RP, Thompson WM, Silverman PM (Duke University)

11:24. 131. The role of conventional angiography and radionuclide scanning for evaluation of patients with gastrointestinal hemorrhage: an update. Larkin BT, Sheedy PF, Stephens DH, Brown ML, Stanson AW, Welch TJ, Johnson CM, Miller WE (Mayo Clinic)

11:36. 132. Early esophageal cancer. Levine MC, Dillon EC, Saul SH, Laufer I (Hospital of University of Pennsylvania)

11:48. 133. Sensitivity of single- and double-contrast barium enema for detection of colonic polyps relative to polyp size. Ott DJ, Chen YM, Gelfand DW, Wu WC, Munitz HA (Bowman Gray School of Medicine)

12:00. 134. Limitations of endoscopy in detection of lower esophageal mucosal ring (LEMR). Ott DJ, Chen YM, Wu WC, Gelfand DW, Munitz HA (Bowman Gray School of Medicine)

12:12. 135. Hidden lesions of the right colon: methods for improved accuracy. Spickler EM, Halpert RD, Feczko PJ (Henry Ford Hospital)

XIV. Interventional Radiology

10:00. 136. Successful thrombolysis and angioplasty in treatment of iliac artery occlusions. van Breda A, Katzen BT (Alexandria Hospital)

10:12. 137. Monooctanoin infusion and biliary stone removal via the transparenchymal liver tract in 11 patients. Haskin PH, Teplick SK, Sammon J (Hahnemann University)

10:24. 138. Radiologic and surgical biliary drainage in advanced sclerosing cholangitis: a combined approach. Halden WJ, Kaufman SL, Kadir S, Mitchell SE, Kinnison ML, White RI Jr (Johns Hopkins Hospital)

10:36. 139. The carcinoid syndrome: palliation by hepatic artery embolization. Carrasco CH, Wallace S, Charnsangavej C, Richli W, Ajani JA (M. D. Anderson Hospital)

10:48. 140. Results of fine-needle aspiration biopsy in hepatocellular carcinoma. Bret PM, Labadie M, Bretagnolle M, Paliard P, Fond A, Valette PJ (Montreal General Hospital)

11:00. 141. Pancreatic abscess and necrosis: limitations of percutaneous drainage. Mueller PR, Ferrucci JT Jr, Butch RJ, Simeone JF, Stafford SA, Chafey J, Wittenberg J, White M, Brown AS (Massachusetts General Hospital)

11:12. 142. Intercostal space nephrostomy for percutaneous stone removal. Picus D, Weyman PJ, Clayman RV, McClennan BL (St. Louis, MO)

11:24. 143. Splenic embolization. Spigos D, Mozes M, Abejo R, Jonasson O (University of Illinois)

11:36. 144. Percutaneous pancreaticobiliary biopsies. Teplick SK, Haskin PH, Kline TS (Hahnemann University)

11:48. 145. Percutaneous renal artery revascularization in acute renal failure. van Breda A, Katzen BT, Schwarten D, Scales FE, Bernstein RM (Alexandria Hospital)

12:00. 146. Percutaneous reanastomosis of the common bile duct. Haskin PH, Teplick SK, Schwab F, Pavlides CA (Hahnemann University)

12:12. 147. Percutaneous drainage of diverticular abscess: upstaging surgical therapy. Mueller PR, Wittenberg J, Ferrucci JT Jr, Butch RJ, Saini S, Simeone JF, Stark DD, Rodkey GV (Massachusetts General Hospital)

XV. Chest Radiology

10:00. 148. CT evaluation of pulmonary hila using thin section. Auh YH, Berkmen YM, Rubenstein WA, Zirinsky K, Kazam E (New York Hospital/Cornell Medical Center)

10:12. 149. Radiographic manifestations of bronchiolitis obliterans with organizing pneumonia vs. usual interstitial pneumonia. Chandler PW, Shin MS, Friedman SE, Katzenstein AA, Duncan-Myers JL (University of Alabama Hospitals)

10:24. 150. Thymic rebound in young patients following chemotherapy. Choyke PL, Zeman RK, Clark LR, Hoffer F, Jaffe MH (Georgetown University)

10:36. 151. Aberrant right subclavian artery: further observations. Cuthbert NW, Proto AV, Raider L (Medical College of Virginia)

10:48. 152. Traumatic aortic rupture: associated etiologic factors and related injuries. Dorfman GS, Cronan JJ, Caldarelli JR, Gann DS (Rhode Island Hospital)

11:00. 153. The high diagnostic and management efficacy of thoracic CT. Herman PG, Khan A, Chasen D, Cruz V, Huber D, Vernace F, Ashtari M (Long Island Jewish Medical Center)

11:12. 154. Dual-energy digital chest radiography: study of calcium content of simulated nodules. Hickey NM, Niklason LT, Fraser RG (University of Alabama, Birmingham)

11:24. 155. Pathology of the thymus. Minuk TG, Loewy J (Henderson General Hospital)

11:36. 156. Upper lobe volume loss: the hilar divergence sign. Moser ES Jr, Scheer CE, Proto AV (Medical College of Virginia)

11:48. 157. Computed tomographic evaluation of primary adenocarcinoma of the lung. Roberts L Jr, Putman CE, Ravin CE, Godwin DJ, Chen JJ (Duke University)

12:00. 158. Cystic changes and pneumothorax in pneumocystis carinii pneumonia in AIDS patients: an analysis of its occurrence and natural history. Stroud R, Rockoff SD (Washington, DC)

12:12. 159. Lobectomy vs. pneumonectomy: CT prediction in patients with lung carcinoma. Quint LE, Glazer GM, Orringer MB (University of Michigan)

Thursday, April 17, 1:30–3:30 p.m.

XVI. Cardiovascular Radiology: II

1:30. 160. The effects of coronary revascularization on left ventricular function in patients with unstable angina. Newman GE, Rankin JS, Putman CE (Duke University)

1:42. 161. An improved film technique for peripheral arteriography. Bartol DT, Barth KH, Mertens MA, Hayden L, Lindisch D (Georgetown University)

1:54. 162. Angiographic alterations during thrombolytic therapy of pulmonary vascular obstruction associated with severe adult respiratory distress syndrome. Greene R, Lind S, Jantsch H, Wilson

R, Jones R, Carvalho A, Reid L, Zapol W (Massachusetts General Hospital)

2:06. 163. **Incidence of unsuspected renovascular hypertension in patients undergoing angiographic evaluation.** Katzen BT, van Breda A (Alexandria Hospital)

2:18. 164. **Cardiac imaging by cine computed tomography—analysis of the clinical application in 200 adult patients.** MacMillan RM, Rees MR, Maranhao V, Flicker S, Naidech H, Clark DL (Deborah Heart and Lung Center)

2:30. 165. **CT detection of splanchnic venous thrombosis.** Anschuetz SL, Vogelzang RL, Gore RM (Northwestern Memorial Hospital)

2:42. 166. **Angiographic diagnosis and treatment of massive postoperative bleeding.** Tisnado J, Cho SR (Medical College of Virginia)

2:54. 167. **Cine CT in the evaluation of thoracic aortic aneurysms and dissection.** Stanford W, Renfrew DL (University of Iowa Hospitals)

3:06. 168. **Digital indirect portography.** Sussman SK, Braun SD, Perlmutt LM, Newman GE, Dunnick NR (Duke University)

3:18. 169. **Digital subtraction left ventriculography: a technique with gated contrast injection in patients.** Newman GE, Rankin JS, Putman CE (Duke University)

XVII. Neuroradiology: II

1:30. 170. **Intraoperative cranial neurosonography—correlative imaging with CT and MRI.** Beckman I, Lupetin AR, Dash N, Deeb ZL, Rothfus WE, Sefczek RJ, Maroon JC, Baghai P, Wilberger JE, Prostko ER, Sherman R, Kessler LA, Abla A, Doty PM (Allegheny Central Hospital)

1:42. 171. **The aqueductal flow void phenomenon in the MR diagnosis of normal pressure hydrocephalus.** Bradley WG, Kortman KE, Burgoyne B (Huntington Medical Research Institutes)

1:54. 172. **Residual recurrent disk vs. postoperative scar in the lumbar spine: assessment by MR.** Bundschuh CV, Modic MT, Alfidi RJ, Han JS, Bohlman H, Kaufman B (University Hospitals, Cleveland)

2:06. 173. **Abnormal and "normal" brainstem displacement and deformity from extrinsic masses.** Cohn FS, Simon JH, Holtas SL, Stears JC (University of Rochester)

2:18. 174. **MRI of colloid cysts.** Kortman KE, Bucon KA, Bradley WG (Huntington Medical Research Institutes)

2:30. 175. **MRI of the facial nerve using surface coils.** Lufkin R, Flannigan B, Teresi L, Bentson J, Wilson G, Hanafee WN (UCLA Hospital)

2:42. 176. **Optimizing surface coil imaging of the cervical spine.** Modic MT, Mulopulos GP, Han JS, Kaufman B, Bundschuh CV, Bohlman H, Starewicz P (University Hospitals, Cleveland)

2:54. 177. **MRI of craniopharyngiomas.** Kortman KE, Pusey E, Bradley WG, Flannigan B, Tsuruda J (Huntington Medical Research Institutes)

3:06. 178. **Intravenous contrast enhanced computed tomography of the spine: the study of choice for early diagnosis of diskitis-osteomyelitis (with or without epidural extension).** Shapiro M, Teplick JG, Kier EL, Reed D, Haskin ME, Virapongse C, Spencer D, Piepmeier J (Yale University)

3:18. 179. **CT evaluation of myelographically complete spinal blocks.** Thaete FL, Vijayamohan G (University of Pittsburgh)

XVIII. Magnetic Resonance: III

1:30. 180. **Magnetic resonance imaging of the thorax: a comparison of axial, coronal, and sagittal images.** Batra P, Brown K, Aberle D, Ovenfors C, Collins J, Steckel R (UCLA)

1:42. 181. **Renal cell carcinoma: MRI and CT staging.** Fein AB, Lee JKT, Balfe DM, Glazer HS, Heiken JP, Ling D, McClennan BL (St. Louis, MO)

1:54. 182. **Evaluation of magnetic resonance for the detection and staging of head and neck pathology.** Fisher MR, Gore RM, Vogelzang R, Sider L, Atiyah R, Sisson G (Northwestern Memorial Hospital)

2:06. 183. **High-resolution magnetic resonance imaging (MRI) of the knee. Part I: traumatic injuries.** Reicher MA, Hartzman S, Gold RH, Duckwiler GR, Bassett LW (UCLA)

2:18. 184. **Ewing sarcoma on MRI.** Horvath-Pushkas KA, Pastakia B, Miser J, Doppmann JI, Kinsella T, Trisch T (NIH, Bethesda, MD)

2:30. 185. **Problems and pitfalls in MRI relaxation time measurements.** Morin RL, Lund GB, Koukkari M (University of Minnesota)

2:42. 186. **MRI of the normal and ischemic hips at 1.5 T: observations utilizing T2 contrast.** Mitchell DG, Rao VM, Dalinka M, Spritzer CE, Gefter W, Axel L, Steinberg ME, Kressel HY (Hospital of the University of Pennsylvania)

2:54. 187. **High-resolution magnetic resonance imaging (MRI) of the knee. Part II: nontraumatic disorders.** Hartzman S, Reicher MA, Duckwiler GR, Gold RH, Bassett LW (UCLA)

3:06. 188. **Three years clinical experience with 0.5 T MRI.** Whalen JP, Knowles RJR, Markisz JA, Cahill PT (New York Hospital)

3:18. 189. **Portal vein thrombosis: diagnosis with CT, MR, and sonography.** Zirinsky K, Markisz JA, Auh YH, Rubenstein WA, Morrison H, Kazam E (New York Hospital/Cornell Medical Center)

1986 American Roentgen Ray Society Section on Instruction: Courses and Symposium

Glen W. Hartman, director, and Richard A. McLeod, associate director

Forty-eight instructional courses will be presented during the 86th annual meeting of the American Roentgen Ray Society (ARRS) beginning on Monday, April 14, and continuing through Thursday, April 17. In addition, there will be a series of courses on chest radiology and a symposium on skeletal radiology. The courses are arranged so that there is no overlap. Each of the 48 courses will be 90 min long; no other activities are scheduled simultaneously.

The Categorical Course in Chest Radiology will have 14 hr of instruction and will begin on Sunday, April 13, and conclude on Thursday, April 17. The Symposium on Skeletal Radiology will be on Friday, April 18, from 8 a.m. to 1 p.m. All courses carry Category I credit on an hour for hour basis.

Registration Information

To register for courses, complete the meeting registration form in this section and mail promptly. Tickets will be available at the Instruction Course Registration Desk, Sheraton Washington Hotel, for courses that have not sold out. All courses will take place in the headquarters hotel.

After reviewing the course abstracts, select three for each day. List the course number and first instructor's name on the registration form.

All who register for the Categorical Course in Chest Radiology must pay a fee of $75 (including ARRS members) and must take the entire series of classes. The categorical course totals 14 hr instruction and includes a syllabus.

Course Schedule

Sunday, April 13, through Thursday, April 17

The Categorical Course in Chest Radiology will have 14 hr instruction over 5 days. Table 1 lists topics and instructors.

Monday, April 14, through Friday, April 18

A total of 48 courses will be offered (table 2) plus a Symposium on Skeletal Radiology. Course abstracts follow and a list of faculty.

Monday, April 14

101. CT of the upper gastrointestinal tract. Halvorsen RA, Thompson WM. The mucosa of the upper gastrointestinal (GI) tract is best evaluated by endoscopy and the upper gastrointestinal series. Computed tomography (CT) can provide significant important information about upper gastrointestinal tract abnormalities and complement the endoscopic and upper GI information. CT has been used primarily to

Table 1: Categorical Course in Chest Radiology, April 13–17

Day/Time	Topic/Presenter
Sunday, April 13:	
10	Technical considerations in chest radiography. *Ravin*
10:30	Chest radiograph: perception, detection, digital imaging. *Armstrong*
11:15	Thoracic trauma. *Henry*
1	Congenital anomalies of thorax. *Felson*
1:30	Radiology of diaphragm. *Dietrich*
2	Cystic fibrosis in adolescents and young adults. *Kirkpatrick*
2:30	Radiology of tuberculosis. *Stark*
3:30	Pneumoconioses. *Wiot*
4	Anatomic and physiologic correlations in ICU patients. *Tocino*
4:30	Ultrasound and the chest: update 1986. *Sanders*
5	MRI of thorax: review of uses and comparison with CT. *Webb*
Monday, April 14:	
1:30	Alveolar wall and radiologic interpretation. *Heitzman*
2:15	Pattern recognition in diffuse lung disease. *Genereux*
3	Evaluation of pulmonary function with radionuclides, emission tomography, etc.: clinical applications. *Alderson*
4	Pulmonary drug toxicity. *Kiser*
4:30	Pulmonary infection in immunocompromised host. *McLoud*
5	Radiation changes in lung—conventional studies and CT. *Libshitz*
Tuesday, April 15:	
4	Radiology of extrathoracic airways. *Weber*
4:30	CT of intrathoracic airways. *Shepard*
5	Early diagnosis of COPD: value of plain film vs. CT. *Milne*
Wednesday, April 16:	
4	CT of mediastinum in patients with bronchogenic carcinoma. *Pugatch*
4:45	CT of chest wall and pleura. *Gross*
Thursday, April 17:	
4	Interventional procedures in chest. *Westcott*
4:30	Practical conventional tomography of chest. *Chasen*
5	Optimal strategy for diagnosis of pulmonary embolism. *McNeil*

Table 2: American Roentgen Ray Society Instructional Courses: April 14–18, 1986

Topic	Monday	Tuesday	Wednesday	Thursday
Gastrointestinal radiology	**101.** CT of upper GI tract. *Halvorsen, Thompson*	**201.** Immunology and radiology of small intestine. *Olmsted*	**301.** Acute gastrointestinal hemorrhage. *Staab, Mauro, Jaques*	**401.** Principles of double-contrast diagnosis. *Laufer*
Abdominal imaging	**102.** Hepatic and biliary nuclear imaging: strengths, weaknesses, interrelationships. *Weissmann*	**202.** MRI and CT of liver. *Ferrucci, Stark*	**302.** CT of abdominal trauma. *Churchill*	**402.** Modern pancreatic imaging. *Silver, Glazer*
Uroradiology/ lymphoma	**103.** Integrated approach to imaging GU tract. *Lee*	**203.** Uroradiologic techniques—update 1986. *McClennan*	**303.** Practical overview of CT in renal mass evaluation. *Hartman*	**403.** Imaging and staging lymphomas. *Gedgaudas-McClees, Torres*
Obstetric/pelvic imaging	**104.** OB ultrasound. *Lyons*	**204.** Fetal anomalies and intervention. *Manco-Johnson*	**304.** CT-ultrasound-MRI of pelvis in gynecologic disease. *Kazam*	**404.** CT of pelvis. *Walsh*
Neuroradiology	**105.** Intracranial neoplasms, part I. *Sackett, Naidich*	**205.** Intracranial neoplasms, part II. *Sackett, Naidich*	**305.** Diagnostic evaluation of patients with arteriosclerotic extracranial disease. *Carroll, Strother*	**405.** MR: cerebrovascular and demyelinating disease. *Drayer*
Head and spine imaging	**106.** Neuroradiology for general radiologist: trauma to head and spine. *Rogers, Weinberg*	**206.** Use of high-resolution CT in degenerative disk disease of lumbar and cervical spine—1986 update. *Lukin*	**306.** MRI of spinal cord and vertebral column. *Ramsey*	**406.** Orbital and petrous bone radiology. *Forbes*
Pediatric radiology	**107.** Neonatal chest: full term and premature. *Williams*	**207.** Sonography in pediatric radiology: overview and recent advances. *Swischuk, Hayden*	**307.** Disorders of pelvis and hips in children. *Poznanski*	**407.** Pediatric emergencies—plain film observations and diagnostic methods. *Wood*
Thoracic imaging	**108.** Roentgenologic approach and teaching tips to major forms of heart disease. *Elliott*	**208.** Environmental diseases of lungs. *Theros, Choplin*	**308.** Mediastinal anatomy: overview. *Proto*	**408.** Comparison of MRI with CT in thoracic disease. *Putman*
Interventional radiology	**109.** Vascular interventional radiology. *Clark, Gallant*	**209.** Guided needle biopsy. *Bernardino*	**309.** Interventional radiology of abdomen. *Mueller, vanSonnenberg*	**409.** Interventional uroradiology. *Banner*
Cardiovascular/ mammography	**110.** Film-screen mammography. *Gisvold*	**210.** Cardiovascular MRI. *O'Donnell, Moodie, MacIntyre, Go, Feiglin*	**310.** Coordinated breast imaging. *Kopans*	**410.** Nuclear cardiology in clinical practice. *Thrall*
Selected topics	**111.** Diagnosis of battered child syndrome and conditions with which it might be confused. *Graham*	**211.** AIDS—radiology, epidemiology, pathology. *Federle*	**311.** MR: basic principles (sans mathematics) and practical consequences. *Gray, Morin*	**411.** How to get your manuscript accepted and published without a hassle. *Berk, Figley, Davidson, Hilton, Braude*
Economics/ legal	**112.** Forensic radiology. *Brogdon, Messmer*	**212.** Economic issues for radiology in "new world" of medical practice. *Evens, Drew*	**312.** What the chief didn't tell the braves about the economics of radiology. *James*	**412.** Special legal problems in radiologic malpractice suits. *Reuter*

Note.—On Friday, there will be a symposium: Skeletal Radiology—1986 (table 3).

stage upper gastrointestinal malignancies and most of the presentation will focus on staging esophageal and gastric cancer. The role of CT in staging other upper gastrointestinal malignancies and in evaluating benign conditions will also be presented. Emphasis will be on CT technique and the value of CT in evaluating the upper gastrointestinal tract.

102. Hepatic and biliary nuclear imaging: strengths, weaknesses, and interrelationships. Weissmann HS. Nuclear medicine advances have made available numerous nuclear imaging techniques capable of assessing hepatobiliary morphology, perfusion, and function, e.g., Tc-99m sulfur colloid, Tc-99m red cells, Ga-67 citrate, Tc-99m IDA, infusion techniques, and SPECT. To use these procedures appropriately and to their fullest potential, it is essential that the radiologist be familiar with the unique diagnostic information these nuclear methods can provide. The clinical indications of these techniques, overall accuracy, strengths and weaknesses, and interrelationships with other imaging methods, will be discussed. The current role of nuclear medicine in the evaluation of space-occupying diseases of the liver (e.g., metastases, hemangiomas, abscesses), diffuse hepatic parenchymal disorders, vascular abnormalities, and response to therapy will be critically evaluated. The increasing role of Tc-99m IDA cholescintigraphy in the evaluation of a variety of biliary disorders will be emphasized, e.g., acute cholecystitis, gallbladder perforation, bile leak detection, postoperative complications. Real and imagined cholescintigraphic pitfalls, e.g., fasting, pancreatitis, alcoholism, hyperalimentation, chronic cholecystitis, and acalculous disease will also be explored.

103. An integrated approach to the imaging of genitourinary tract. Lee JKT. The radiologic evaluation of the genitourinary (GU) tract has undergone drastic changes in the last decade. While excretory urography remains the screening procedure in a large percentage of patients, noninvasive techniques such as gray scale sonography and computed tomography (CT) have assumed an ever-increasing role in the evaluation of GU tract. Sonography is highly accurate in detecting renal obstruction and in differentiating cystic from solid lesions. Because of its excellent spatial resolution and contrast sensitivity, CT has become the primary imaging test for staging renal neoplasms. Renal angiography, once considered an integral part of preoperative evaluation of renal neoplasms, is now reserved for problem cases. The advent of sonography and CT has also enhanced our ability to detect and stage bladder and prostatic abnormalities. CT is now routinely used in many institutions for staging bladder and prostatic carcinomas. More recently, the application of magnetic resonance (MR) to the imaging of the body has generated much interest and enthusiasm among the radiologic community. Because of its superior contrast sensitivity, multiplanar imaging capability, and the ability to delineate blood vessels without the use of intravenous contrast media, MR is expected to add a new dimension to the imaging of GU tract. In this presentation, the advantages and disadvantages of each imaging method will be analyzed. An integrated approach to the evaluation of a variety of GU problems will be outlined.

104. Obstetrical ultrasound. Lyons EA. A 90-min refresher course is proposed on one or various aspects of obstetrical ultrasound. An area of significant importance that needs continued emphasis to the radiologic audience is the first trimester of pregnancy, both normal and abnormal, including ectopic gestations. *First trimester normal and abnormal*: The normal features of the early first-trimester gestation up to 12 weeks will be discussed. There are many normal variations, especially using high-resolution real-time equipment, that must be recognized and dealt with appropriately. The early first trimester is a time when the sonologist can make the greatest contribution but also can wreak great havoc in an otherwise normal situation. There will be a discussion of the second sac, the double sac sign, ectopic gestation, molar pregnancy, and multiple gestation. In addition, conditions that coexist with normal intrauterine gestation, such as the presence of an intrauterine contraceptive device and fibroids, will also be discussed. *Ectopic gestation*: With the increased use and awareness of the capabilities of ultrasound, and with the advent of the ultrasensitive beta-HCG analysis, the sonographic diagnosis of ectopic pregnancy has become very difficult and confusing. The importance of clinical data, laboratory data, the sonographic study and, where indicated, the pelvic examination will all be stressed. *Placenta previa*: The diagnosis of placenta previa has been hitherto the domain of ultrasound, but how successful have we been? What are the criteria for the diagnosis of previa? Why is the false-positive rate so high (up to 50%)? A decision of criteria and the appearance of placenta previa will be given.

105. Intracranial neoplasms: parts I and II. Sackett JF, Naidich TP. Neuroradiologic workup of intracranial neoplasms has been modified because of the increased sensitivity of magnetic resonance imaging (MRI) and new methods of neurosurgical management. MRI appears to be more sensitive, but less specific, than computed tomography (CT). Biopsy still is required for proper selecton of therapeutic regimen of all tumors except those in which biopsy itself poses unacceptable morbidity and mortality. Angiography is now used to plan surgery or interventional vascular tumor modification. Sonography has an increasing role in surgical localization, biopsy, or drainage of cystic neoplasm and shunt placement. CT scanning for stereotactic biopsy assists the neurosurgeon in finding a small or deep neoplasm. Special techniques to improve sensitivity include air cisternography and nonionic water soluble contrast cisternography. An approach tailored to the neuroradiologic evaluation of intracranial neoplasms provides the proper basis for therapy of intraaxial and extraaxial neoplasms in adult and pediatric patients. Pathologic and correlations of neuroimages and cost effective management of tumors will be stressed.

106. Neuroradiology for the general radiologist: trauma to the head and spine. Rogers LF, Weinberg PE. This course will acquaint the general radiologist with present neuroradiologic techniques in the evaluation of injuries of the central nervous system, spine, and skull. The CT findings in intra- and extracerebral hemorrhage, fractures of the base of the skull, sinuses, and temporal bone will be presented. The proper plain film evaluation of spinal trauma will be discussed and the indications for standard tomography, myelography, and computed tomography in the evaluation of spinal injury will be reviewed.

107. The neonatal chest—full term and premature. Williams HJ. This course will emphasize the practical aspects of problems encountered in interpretation of the neonatal chest. It will largely reflect experience garnered by the presenter from a close relationship with the dedicated pediatricians and neonatologists of the Children's Hospital of St. Paul, MN, over a 25-year period. The first segment will deal with the radiographic chest examination of the full term infant, including technique, normal structures, and selected congenital anomalies. The second segment will discuss the various medical and surgical causes of respiratory distress in the premature infant. Artifacts that frequently cause confusion will also be presented. The final segment will consider the more common iatrogenic complications that result from employment of various life-saving measures in the premature infant. This will include the respirator, endotracheal tube, umbilical catheters, nasogastric tube, and hyperalimentation tube.

108. Roentgenologic approach and teaching tips to the major forms of heart disease. Elliott LP. Myocardial ischemia, systemic hypertension, aortic valve stenosis, rheumatic valve disease, and their attendant complications and associations comprise over 90% of the cardiac entities in adults. This course will develop a systematic approach for the radiologist to enable recognition of these problems with a high degree of confidence. Emphasis will be on approach, use of physiology via the pulmonary vascularity followed by logical use of cardiac anatomy. Areas of learning strictures traditionally experienced by residents will be discussed.

109. Vascular interventional radiology. Clark RA, Gallant TE. Vascular therapeutic interventions via the angiographic catheter are an integral part of vascular radiology and direct patient management. This course will provide the practicing radiologist an overview of current approaches to vascular interventions. Interventional vascular radiology deals with regional manipulations, either mechanical or pharmacologic, to increase or decrease blood flow. This session will address the uses of transcatheter embolization or occlusive therapy, vasoconstrictive and vasodilatory pharmacotherapy, regional arterial thrombolysis, and percutaneous transcatheter angioplasty. The principles and goals of management, techniques, and equipment will be stressed. There will be clinical examples in the chest, abdomen, and extremities.

110. Film-screen mammography. Gisvold JJ. Several techniques have potential roles in breast evaluation. The cornerstone of breast imaging procedures has been, and remains, mammography. This course will deal strictly with film-screen mammography. Because of a resurgence of interest in film mammography, a review of this subject is considered important. Radiographic technique is critical if films of diagnostic quality are to be obtained. Thus, technique will be covered. Knowledge of basic breast pathology is important and a brief review of pertinent pathology will be presented. Interpretation of mammograms will be the main topic. The importance of calcifications and the wide variety of soft-tissue changes will be reviewed in detail, and the use of special views and techniques, including magnification, will be covered. The wording of interpretations is very important and some clues for most effectively reporting mammograms will be offered. Many clinically occult breast lesions are being discovered and these must be localized preoperatively. The important features of this technique will be reviewed.

111. Diagnosis of the battered child syndrome and conditions with which it might be confused. Graham CB. When suspicions of this potentially lethal situation are raised, indicated imaging studies must be obtained. Musculoskeletal abnormalities are so common that a complete bone survey is most useful. Radiographic findings of fractures and displacements include: unexplained old bone and joint deformities, soft-tissue swelling, subperiosteal hemorrhage, metaphyseal corner fractures ("bucket handle"), other avulsions, cartilage separations, long bone spiral and transverse fractures, multiple rib fractures, periosteal new bone and callus (dating the injuries), and complex skull fractures with spread sutures. The following should be considered in the skeletal differential diagnosis: normal periosteal new bone formation, innocent trauma, neuromuscular abnormality, pain insensitivity, nutritional deficiency (prematurity, scurvy), metabolic bone disease (rickets), leukemia, neuroblastoma, infection (syphilis), infantile cortical hyperostosis (Caffey), kinky-hair syndrome (Menkes), osteogenesis imperfecta, hypophosphatasia, osteopetrosis, mucolipidosis, vitamin A toxicity, and drug effects.

112. Forensic radiology. Brogdon BG, Messmer JM. This course is designed to comfort the radiologist who (usually unexpectedly) occasionally ventures, or is led, into the practice of forensic radiology. An interesting and informative overview will cover the definition, scope and background history, of the subject. Cases from the authors' files will illustrate such areas of forensic activity as: investigation of missile injury, identification of bodies, accident investigation and research, mass casualty problems, identification of abuse victims, and the use of age determination for legal purposes. A section on "witnessing" will conclude the presentation. (Warning: Some of the material to be presented is unsuitable for those with weak stomachs.)

Tuesday, April 15

201. Immunology and the radiology of the small intestine. Olmsted WW. Immunology, a rapidly expanding and very complex field, seems to play a major role in health and disease states of the small intestine. The basic concepts of cellular and humoral immunity will be fully explained in the first portion of this course. Basic immunologic concepts will then be discussed in relation to diseases of the small intestine including gluten-sensitive enteropathy, inflammatory bowel disease, hypo- and dysgammaglobulinemic states (including nodular lymphoid hyperplasia, lymphoma, and Waldenstrom macroglobulinemia), and Whipple disease. Additionally, opportunistic diseases and infections affecting the small bowel and associated with the acquired immune deficiency syndrome (AIDS) will be mentioned. Radiologic-immunologic-pathologic correlation will be stressed throughout. The participant should expect to gain an understanding of the basic concepts of immunity and learn an updated approach to diseases of the small bowel.

202. MRI and CT of the liver. Stark DD, Ferrucci JT Jr. Despite high expectations, the clinical utility of magnetic resonance (MR) scanning of the liver, especially vis a vis CT, remains to be established. Given the fundamental importance of accurate liver imaging to the applications of abdominal MR imaging, we have intensively investigated technical, interpretive, and clinical-pathologic aspects of liver MR imaging in over 300 clinical cases with a 0.6 T superconducting magnet and fourth generation CT equipment. Using the detection of liver metastases as the benchmark for comparison, our main conclusions are: (1) MR surpasses CT in sensitivity and specificity and (2) T1-weighted pulse sequences are preferable for detection while T2-weighted sequences are more suitable for tissue characterization. Screening for focal liver lesions is best achieved using a T1-weighted spin echo (SE) sequence with TR = 260 msec and TE = 15 msec, or less. Averaging of 18 data acquisitions results in a total scan time of 10 min. This degree of signal averaging eliminates respiratory artifacts and, by avoiding respiratory gating, no data are lost. Use of thick slices (1.5 cm) and multislice technique (12 slices with the SE 260/15 sequence) can encompass the entire liver in a 9 min examination. Using T2-weighted images (SE 2000/60, 120, 180), the most common benign lesions, cavernous hemangiomas and cysts, can be distinguished from cancer with 90% accuracy. Experience with in vivo proton chemical shift imaging and experimental development of liver specific paramagnetic contrast agents will also be discussed. Special advantages of MR imaging in medical liver diseases including hemosiderosis, fatty liver, cirrhosis, and the Budd-Chiari syndrome will be considered, time permitting.

203. Uroradiologic techniques—update 1986. McClennan BL. This course will address some of the basic uroradiologic procedures stressing both practical and technical aspects involved in their performance. A major emphasis will be on the intravenous urogram including discussion of dose and method of administration of contrast media. The advantages and disadvantages of the new low osmolality contrast materials will be highlighted as will the optimal approach to patient selection, patient preparation, film sequencing, radiographic technique, abdominal compression, and routine tomography. The future portends major changes in the acquisition and display of uroradiographic images; thus the future role of digital radiography and digital subtraction angiography in uroradiologic practice will be discussed. The evaluation of the patient with supravesical urinary diversion will be explained with special attention to the technique of "loopography" using stomal occluding disks, and vacuum suction. Tips, techniques, and indications for this procedure will be illustrated. Additionally, the many varied uses of the vacuum suction cannula (VUC) in genitourinary radiologic practice will be outlined. This apparatus is the ideal tool for performing retrograde urethrography. Its use allows adequate examination of the patient with hypospadius, perineal urethrotomy, and fistulae. It is equally useful in both males and females. The VUC cannula also has proven to be the most useful and least painful device for performing hysterosalpingography and vaginography in both adults and children. The overall tenor of this course will be practical, focusing on optimization of commonly performed uroradiologic procedures.

204. Fetal anomalies and intervention. Manco-Johnson ML. Careful examination of a pregnancy suspect for significant congenital anomalies can be performed before the 20th week with great confidence. Defects such as anencephaly, omphalocele, gastroschisis, renal agenesis, hydronephrosis, and certain forms of dwarfism can be accurately diagnosed and termination considered. Unfortunately, most fetal anomalies are unsuspected and not detected until later in pregnancy, usually fortuitously. As such, obstetric sonography must be meticulous and thorough. Personal skill with real-time sonography is needed to assure completeness of the study. Fetal edema, cystic hygromas, hydroceles, and meningomyeloceles can routinely be detected. Hydrocephalus is accurately diagnosed before enlargement of the fetal skull. Both structural and rhythm disturbances of the fetal heart can be diagnosed. Certain fetal anomalies and abnormalities can be treated in utero and the results of fetal treatment will be reviewed. Fetal sonography is extremely exciting and will continue to yield further knowledge in the field of fetal medicine.

205. See 105.

206. The use of high-resolution CT in degenerative disk disease of the lumbar and cervical spine—1986 update. Lukin RR. High-resolution computed tomography (CT) of the spine has dramatically altered the diagnostic evaluation of patients with degenerative disk disease. This course will begin with a short review of normal anatomic findings in lumbar spine CT. Various technical approaches to performing this type of CT will also be reviewed. A major segment of this course will be devoted to so-called bulging and herniated lumbar disks and their differentiation. Differential diagnostic considerations and potential traps will be emphasized. The problem of the diagnostic evaluation of the postoperative back will also be reviewed. A second major segment of the discussion will be devoted to the analysis of so-called "spinal stenosis." A lesser amount of time will be devoted to degenerative disk disease in the cervical area. The emphasis here will be on whether high-resolution CT can be justified in the environment of cost containment for the evaluation of cervical herniated disks and cervical spondylosis. The roles of plain cervical CT and water-soluble contrast CT will be reviewed. Different approaches for the clinical presentation of a pure radiculopathy and myelopathy will be emphasized.

207. Sonography in pediatric radiology: overview and recent advances. Hayden CK Jr, Swischuk LE. Sonography has created a great impact on the investigation of pediatric diseases and this course will review its current status. There will be a resume of its use in abdominal masses, but there will be more detail on its newer uses in pediatric neurosonography and urinary tract disease, where in essence, it has replaced the excretory urogram. In addition, newer, and previously unsuspected uses in the gastrointestinal tract will be presented in detail (i.e., pyloric stenosis, gastric ulcer disease in infants, intussusception, volvulus, inperforate anus, etc.). Finally, the place of sonography in the evaluation of the acute abdomen, soft-tissue extremity problems, thoracic abnormalities, and miscellaneous abnormalities in other parts of the body, will be reviewed.

208. Environmental diseases of the lungs. Theros EG, Choplin RH. This discussion will range over three broad categories of inhalants: inorganic dust, organic dust, and toxic chemicals. The responses of the lung to these injurious inhalation agents are so varied that an attempt will be made to organize them in terms of classic tissue reactions and the resultant radiologic patterns. Among the inorganic dust diseases, silicosis and its varied manifestations will dominate the discussion because of its enormous importance. Asbestosis will also be featured because of its growing significance. The organic dusts are probably best represented by so-called "farmer's lung." There are a host of organic dusts that can lead to the same pathogenesis, and a good knowledge of farmer's lung, both radiologically and pathologically, will provide a general grasp of the principles of any organic dust inhalation disease. The various phases of hypersensitivity reactions as they are exemplified radiologically and pathologically, and the more chronic changes, will be discussed in detail. Often, the same organic dust may be the source of granulomatous infection as well, and this too can be verified by the study of farmer's lung. Many toxic chemicals such as beryllium oxides and salts, and irritant gases like nitrogen dioxide, are of great industrial importance. These will be discussed and some of their effects, similar in many ways to those noted in both organic and inorganic dust exposure, will be covered here.

209. The guided needle biopsy. Bernardino ME. Before performing a needle biopsy, the radiologist must determine which imaging method is appropriate. A logical and simplified selection process will be demonstrated. This selection process meets certain criteria and takes into account the imaging resources at most institutions. There will be a discussion of the various types of needles that may be used for percutaneous biopsy. The controversy of needle size will be addressed and the most appropriate needle for specific organs or masses. Proper biopsy technique will be demonstrated: a rotary, coring motion during the biopsy procedure. Selection of access routes is dependent upon the mass to be biopsied and its relationship to surrounding organs or critical anatomic structures such as the aorta, inferior vena cava, or gallbladder. In any discussion of percutaneous biopsy, probable complications should be known before the procedure. Knowledge of possible complications should facilitate certain techniques that would diminish their possibility. Accuracy rates will be discussed. These vary with the organ to be biopsied, needle size, technical expertise of the individual performing the procedure, and the pathologist.

210. Cardiovascular MRI. Feiglin DHI, Go RT, O'Donnell JK, MacIntyre WJ, Moodie DS. The course will cover several aspects of cardiovascular magnetic resonance imaging (MRI). (1) Principles of physiological gating. The possible mechanisms of gating beyond the electrocardiogram will be explored and difficulties relating to type and positioning of leads will be evaluated and differences due to varying magnetic field strength will be described. (2) Techniques of gated imaging. The procedure for obtaining cardiac axis orientation and cine display will be reviewed plus approaches to true T1 and T2 relaxation time images and proton chemical shift imaging. The effects of varying TE and multiplicity of echoes will be shown as they relate to spin-echo sequences. The use of other pulse sequences will be alluded to. (3) Clinical uses. The application of MRI in the clinical setting will be shown along with its particular advantages in congenital heart disease, myopathies, and great vessel anatomic imaging. The current application in coronary artery disease at the CCF will be described. (4) Intermodality comparison. The relative advantages and disadvantages of echocardiography, digital subtraction angiography, nuclear imaging, and contrast interventional studies will be demonstrated as they relate to current MRI in cardiovascular diseases.

211. AIDS—radiology, epidemiology, and pathology. Federle MP. Acquired-immune-deficiency syndrome (AIDS) and the AIDS-related complex (ARC) represent the major public health problem in the United States. As of mid-1985, there were nearly 13,000 diagnosed cases of AIDS, 100,000 cases of ARC and 500,000–1,000,000 patients infected or exposed to HTLV-III, the AIDS virus. These patients are prone to several neoplasms and a multitude of infectious processes including bacterial, fungal, and protozoan. Many of these pathologic processes have distinctive clinical and radiographic manifestations that may be unfamiliar to most physicians. This course will consist of a review of the epidemiology, clinical spectrum, and radiographic manifestations of AIDS and ARC, including plain radiography, computed tomography, and magnetic resonance imaging.

212. Economic issues for radiology in the "new world" of medical practice. Evens RG, Drew PG. Everyone will agree that medical practice in the United States is changing. Changes are driven by economic issues and other issues. This 90 min presentation will focus on three items of interest to radiologists: (a) the economics and utilization of magnetic resonance imaging, (b) radiology practice in health maintenance organizations and independent practice centers, and (c) imaging centers.

Wednesday, April 16

301. Acute gastrointestinal hemorrhage. Staab EV, Mauro M, Jaques PF. The course is divided into three sections. (1) Noninvasive imaging will address the problems associated with triage of patients with gastrointestinal (GI) bleeding and attempt to identify the appropriate role for noninvasive imaging methods. The advantages and limitations of widely available radionuclide techniques and their role with respect to subsequent invasive studies will be stressed. (2) Angiography and intervention in upper GI hemorrhage will provide the attendee with a balanced overview of the diagnostic role of angiography in acute upper GI hemorrhage. The angiographic features of the more frequently encountered causes of upper GI tract bleeding will be presented together with certain diagnostic pitfalls. Technical advice on achieving satisfactory subselective catheter position and the role of embolo- or pharmacotherapy in particular clinical contexts will be presented. (3) Angiography and intervention in lower GI hemorrhage will cover the role of invasive radiology in acute lower GI hemorrhage, including angiographic diagnosis of tumors, angiodysplasia, diverticulosis, and less common etiologies. The value of provocative angiography and therapeutic approaches will be discussed. A selected, annotated bibliography will be made available.

302. CT of abdominal trauma. Churchill RJ. Trauma is a major cause of mortality and morbidity in the U.S. Methods of evaluating the injured patient have changed over the past few years. CT scanning plays a major role in many medical centers not only in diagnosing major organ injury, but also in providing follow-up monitoring of the injury. Hemorrhage with subsequent hematoma formation is a dynamic process and the appearance on CT changes over time. The major changes are related to the formation and retraction of clot and its subsequent lysis. Other variables such as location, anticoagulants, hemoglobin content, etc., also affect the appearance of a hematoma and will be discussed and illustrated. Scanning techniques that maximize the diagnosis of solid organ injury will be presented. Examples of injuries of the liver, spleen, bowel, pancreas, kidneys, and retroperitoneum will be illustrated. Surgical management will be discussed. Many patients with major organ injury are now treated conservatively. Serial scans of several such patients will be shown to demonstrate the outcome of various types of abdominal trauma.

303. A practical overview of CT in renal mass evaluation. Hartman DS. CT is extremely useful in all three phases of renal mass evaluation: detection, characterization, and determination of the extent of disease. This course will emphasize the basic clinical, pathologic, and CT principles that are helpful in renal mass evaluation. When confronted with a renal mass, the radiologist should decide whether the mass is: (1) a simple cyst, (2) a cystic mass not fulfilling the criteria of a simple cyst, or (3) a solid mass. If the mass is cystic, is it unilocular or multiloculated? If the mass is solid, is its growth expansile or infiltrative? Examples of each CT pattern with corresponding differential gamuts will be presented. The varied appearances of benign and malignant neoplasms will be stressed. Whenever a malignant renal neoplasm is suspected, careful CT evaluation to determine the extent of disease should be performed. Examples of the value and limitations of CT staging will be presented.

304. CT-ultrasound-MRI of the pelvis in gynecologic diseases. Kazam E. Normal sectional anatomy of the female pelvis will be illustrated with CT, sonographic, magnetic resonance imaging (MRI), and cadaver sections. Pathologic sectional anatomy will then be discussed with emphasis on correlations amongst the three imaging procedures. Illustrative cases will include abnormalities of the uterus, ovaries, Fallopian tubes, and hollow viscera. The peritoneal and extraperitoneal pelvic compartments will also be discussed.

305. Diagnostic evaluation of the patient with arteriosclerotic extracranial vascular disease. Strother CM, Carroll BA. Over the past seven decades, a relationship between thromboembolic stroke and arteriosclerotic changes of the carotid and vertebral arteries has been established. Simultaneously, extensive efforts have been directed toward development of safe and accurate techniques for assessment of the extracranial vasculature. The optimal management of patients with arteriosclerotic extracranial vascular disease often depends upon the proper use of these methods. This course will review the capabilities and limitations of currently available methods for evaluating the vasculature incriminated in the genesis of thromboembolic stroke and summarize our opinion of a logical method for use of these methods in specific clinical situations. After a brief review of some of the important clinical considerations of arteriosclerotic extracranial vascular disease, evaluation of the patient with anterior circulation transient ischemic attacks, a completed stroke with good neurologic recovery, vertebrobasilar territory transient ischemic attacks, and the asymptomatic bruit will be considered.

306. Magnetic resonance imaging of the spinal cord and vertebral column. Ramsey RG. Magnetic resonance (MR) is an excellent method for evaluation of both the spinal cord and the bony vertebral column. MR allows direct, multiplanar visualization of the spinal cord without interference by the bony structures of the spinal canal. And, as opposed to CT, does not require the use of contrast material for evaluation. MR is accurate for evaluation of the cervicomedullary junction, the presence or absence of syringohydromyelia, the extent and nature of cord tumors, and whether cord tumors are intramedullary, extramedullary, or intradural. MR can also be used to evaluate the presence of degenerated disks; the use of surface coils will soon allow MR to compete with and possibly replace CT for the evaluation of herniated disks. Magnetic resonance is an excellent method to evaluate the presence or absence of metastatic disease to the vertebral column. With metastatic disease, the normal high-signal intensity of the fatty bone marrow becomes decreased in signal intensity when replaced by tumor cells. This alteration in signal intensity is easy to appreciate and, therefore, the presence or absence of metastatic disease is easy to evaluate. The MR studies should be compared to plain film examination. The presence of a paraspinal mass is easy to appreciate and one can determine if there is or is not encroachment on the spinal cord. It appears that MR will replace myelography for the evaluation of cord compression. Examples of these entities, techniques, methods, tips, and pitfalls will be illustrated and discussed and a brief description of the workings of the scanner will be included.

307. Disorders of the pelvis and hips in children. Poznanski AK. This course will describe the various congenital and acquired disorders of the hips and pelvis in children using plain films and the newer techniques. Radiologic evaluation plays an important part in decisions on diagnosis and management of these problems. One of the difficulties in evaluating the hip in childhood has been that a large part of the proximal part of the femur is composed largely of cartilage. The new radiologic methods have made a major impact on our ability to diagnose disorders of the hip by allowing us to evaluate this cartilaginous unossified head. Computed tomography (CT) has been invaluable in the diagnosis and management of children with complex congenital dislocation of the hips, particularly before and after surgical treatment. CT has also been very useful in Perthes disease. Sonography has given us a new window to look at the hip and is becoming more useful in the evaluation of congenital dislocation, hip effusion, and other disorders. Magnetic resonance imaging allows us to see the unossified head clearly and is very sensitive in showing abnormalities. Dislocation, aseptic necrosis, and discongruity can be easily seen. Nuclear medicine, of course, remains an important tool in the evaluation of hip disorders.

308. Mediastinal anatomy: an overview. Proto AV. Cross-sectional imaging has made clear the importance of understanding normal anatomy to adequate diagnostic interpretation. This importance applies equally as well to conventional images. In this refresher course we will review, as time limitations allow, the many reflections formed by contact of the lung with the mediastinum. To promote understanding and retention of this information, the material will be organized in a fashion to show: (a) how a reflection may compare or contrast with another, (b) how a reflection on one side of the mediastinum may have a counterpart on the other side of the mediastinum, and (c) how a reflection relates to a specific coronal plane or structure of the mediastinum. Conventional images will be emphasized, with computed tomography being used as needed for clarification of the conventional images.

309. Interventional radiology of the abdomen. Mueller PR, vanSonnenberg E. This course will stress the advances that have been made in interventional radiology of the abdomen, specifically needle biopsy, percutaneous abscess drainage, and several newer topics including percutaneous cholecystostomy, percutaneous gastrostomy, balloon dilatation of stenotic enteric lesions, and celiac ganglion blocks. The biopsy section will include discussion of large vs. small needle, biopsy of usual and unusual lesions, and specific selection of appropriate guidance systems (i.e., CT vs. sonography). The abscess portion will discuss the full continuum from problems of abscess detection to selection of safe access routes and approach to difficult abscesses (infected hematoma, thick pus, pancreatic phlegmons). Abscesses with fistulous communication, and pancreatic pseudocysts will specifically be discussed. The final section will deal with newer topics and advances in abdominal intervention including various techniques for percutaneous gastrostomy and celiac ganglion block.

310. Coordinated breast imaging. Kopans DB. This course will detail the use of mammography (film/screen and xeroradiography), sonography, and computed tomography (CT) for breast evaluation. These methods plus the efficacy of transillumination, thermography, and magnetic resonance imaging will be discussed along with the future potential of immunoimaging and digital mammography. The differences between detection and diagnosis will be stressed. An approach to breast lesion analysis will be presented plus a detailed discussion of the uses of mammography, sonography, and CT to localize clinically occult lesions.

311. MR: basic principles (sans mathematics) and practical consequences. Gray JE, Morin RL. This nonmathematical refresher course is an introduction to magnetic resonance (MR) principles and practical aspects of MR imaging. The course is designed for radiologists with little or no MR experience. Basic principles to be covered include: definitions, historical background, the MR experiment, the MR signal, relaxation times, MR pulse sequences, MR imaging systems, contrast in MR imaging, biological effects, and future applications. Practical aspects of MR imaging include: site planning, staffing requirements, problems encountered in bringing an imager on-line, details of a typical MR study, patient exclusion, site security and safety, problems and pitfalls of MR imaging, facts and fallacies of MR imaging, and MR spectroscopy. The attendee should gain a "big picture" understanding of MR and an appreciation of some of the practical problems involved in MR imaging.

312. What the chief didn't tell the braves about the economics of radiology. James LR. Residents and wives are encouraged to participate in this informal session on practical economics. Professional contracts and corporate planning will be included along with family financial planning. Financial success is a systematic process that should commence early in one's career. Guidelines will be included for a methodic approach for managing assets and liabilities in this professional era of cost containment, prospective pricing, and capitation reimbursement. Wives are not only invited but encouraged to attend and participate in this family financial planning session. Residents and their wives will be given preference for this refresher course in preparation for radiology 2000.

Thursday, April 17

401. Principles of double-contrast diagnosis. Laufer I. This course covers the principles involved in the performance and interpretation of double-contrast studies of the gastrointestinal tract. Considerations will include the influence of mucosal coating, distention, projection, and compression on the diagnostic content of the radiograph. In addition, the principles of interpretation will be reviewed since these differ considerably from interpretation of conventional single-contrast studies. Emphasis will be on the appearances of protruded and depressed lesions. The appearance of these lesions depends on whether they are on the dependent or nondependent surface. The effect of the morphology of the lesion on its radiographic appearance will also be discussed and the value and hazards of the barium pool will be illustrated.

402. Modern pancreatic imaging. Glazer GM, Silver TM. The goal of this refresher course is to present the current state-of-the-art in pancreatic imaging using computed tomography (CT), sonography, and magnetic resonance. After a brief introduction and review of normal anatomy and imaging principles, the roles of these techniques in neoplastic, inflammatory, and metabolic disease states will be discussed. The techniques, indications, and limitations of each will be stressed and our recommendations concerning appropriate use presented. Newer applications, such as the role of intraoperative sonography and dynamic CT in the evaluation of pancreatic endocrine tumors will be presented. Also, the use of these methods to guide interventional procedures such as biopsy or abscess drainage will be considered.

403. Imaging and staging of lymphoma. Gedgaudas-McClees K, Torres WE. In patients with Hodgkin and non-Hodgkin lymphoma, precise staging is crucial in determining therapy and prognosis. In the past, staging laparotomy and lymphangiography were the methods used in the initial workup. With the advent of CT, the lymphoma patient can be staged using a noninvasive method with accuracy rates in the 72%–90% range. Most cases can now be staged without the use of lymphangiography. CT can accurately assess disease that was clinically or radiographically unsuspected both above and below the hemidiaphragm. It can further image nodal regions not opacified by the lymphangiogram and demonstrate lymphomatous involvement of the liver, spleen, kidneys, and thorax. Some organ systems, such as the gastrointestinal tract, are not well suited for evaluation by CT. Routine fluoroscopic methods and examples of lymphomatous disease in the gastrointestinal tract will be shown.

404. CT of the pelvis. Walsh JW. CT has become a primary pelvic imaging technique, often superseding other examinations such as excretory urography, the barium enema, and sonography. This course will present state-of-the-art images and review the current status of pelvic CT relative to other imaging methods. A practical approach to basic CT anatomy and pathology and clinical problem solving will be stressed. Several purposes of this presentation are: (1) to discuss the indications, technique, anatomy, and routes of disease spread relative to pelvic CT; (2) to illustrate CT staging of genitourinary cancers; and (3) to characterize pelvic masses such as abscess and other fluid collections, soft tissue and musculoskeletal tumors, iliac artery aneurysms, pelvic lipomatosis, and lymphadenopathy. CT findings in patients with femoral neuropathy and sciatica will be presented and percutaneous access routes to pelvic mass biopsy and abscess drainage will be shown.

405. Magnetic resonance: cerebrovascular and demyelinating disease. Drayer BP. Ischemic infarction presents as an area of prolonged T1 and T2 relaxation time in a vascular distribution. The prolonged T2 is more prominent in the acute and subacute stage due to associated ischemic edema. Hemorrhagic infarction presents acutely as prolonged T1 and T2, but in the subacute and chronic phase, the T1 is decreased. Intracranial hematoma also presents with prolongation of T1 and a mixture of increased and decreased T2. The T1 is decreased in subacute and chronic hematoma. Unfortunately, magnetic resonance (MR) is limited in the evaluation of the more uncooperative patient. In addition, early experience suggests that CT may be superior to MR for the most important function of imaging in acute stroke—the distinction of hematoma from infarction. MR is exquisitely sensitive for the detection of lacunar and multiple white matter infarctions. MR has already become the procedure of choice for the detection of multiple sclerosis (MS) and other demyelinating disorders. Prolongation of T2 is far more prominent than prolonged T1. The two major problems in MS diagnosis are the nonspecificity of the MR abnormality (e.g. vascular vs. MS) and the normal presence of punctate areas of increased T2. This distinction may be facilitated using paramagnetic contrast enhancement (e.g. Gd-DTPA) to analyze blood-brain barrier integrity.

406. Orbital and petrous bone radiology. Forbes GS. An overview of orbital and petrous bone imaging will be presented that is directed toward the needs of the general radiologist. Discussion will follow a practical clinical approach so that categories of clinical problems will be related to choice of imaging method and technique. Anatomy and pathology review will lead into discussion of the radiologic appearance. Scanning techniques are emphasized although other methods such as magnetic resonance, plain film tomography, and angiography are included. The course is intended to review the common orbital and petrous lesions and the current radiologic methods used in their diagnostic evaluation.

407. Pediatric emergencies—plain film observations and diagnostic methods. Wood BP. Emergency presentations of infants and children require accurate observation and interpretation of plain films accompanied by appropriate decisions concerning the most expeditious diagnostic procedures. The life-threatening nature and unexpected arrival of emergencies requires that all radiologists maintain facility in their proper handling. Frequently the urgent nature of the patient's affliction is more grave than is clinically suspected, thus, the pathogenesis and clinical implications of the diagnosis should also be understood. Airway obstructions, some complications of pulmonary infection, acute pulmonary edema, and effects of thoracic trauma constitute respiratory emergencies. Gastrointestinal obstruction, identification of its cause, and appropriate contrast studies will be discussed. The diagnostic workup of abdominal trauma, the effect on bowel, the intraperitoneal viscera, and the urinary system, includes the wise use of CT, sonography, scintigraphy, and occasionally angiography. Because unexpected complications may occur with a routine birth, identification of a potential problem causing respiratory distress, a neonatal abdominal emergency, or other relevant diagnosis is important. The radiographic findings that alert the physician to a battered child and unexpected associated injuries of this malady will be illustrated. Plain film findings in most emergency conditions are characteristic and easily recognizable; the related role of contrast studies and additional imaging techniques will be included.

408. Comparison of MRI with CT in thoracic disease. Putman CE. The use and efficacy of CT in the evaluation of the mediastinum, pleura, and lung has been well documented. The impact of magnetic resonance imaging (MRI) in the thorax remains in its infancy, but the importance of comparing this new method to a known entity is extremely important to overall health care. This presentation will focus on all aspects of intrathoracic pathology including cardiovascular disease, malignancy, inflammatory disease, and distinguishing characteristics of CT and MRI for tissue differentiation. The unique and differing roles of each of these technologies for evaluating the thorax will be emphasized.

409. Interventional uroradiology. Banner MP. This course will address those nonvascular interventional genitourinary procedures that are usually performed in percutaneous fashion by radiologists. These include nephrostomy, ureteral stenting, dilatation of ureteral strictures, stone manipulation and pyeloureteral biopsy. Fluoroscopically controlled retrograde pyeloureteral manipulative procedures performed in conjunction with urologists will also be considered. Although indications and contraindications for each procedure will be reviewed, emphasis will be on the techniques involved and the potential complications of each procedure. The current status of upper urinary tract stone management (percutaneous and ureteroscopic extraction and disintegration, chemolysis, extracorporeal shock wave lithotripsy) will be presented, and the role of the radiologist in each of these technologies discussed.

410. Nuclear cardiology in clinical practice. Thrall JH. Nuclear cardiology embraces multiple imaging procedures aimed at diagnosing cardiac diseases and monitoring heart function. In current practice three major procedures encompass most clinical applications. These are the technetium 99m-pyrophosphate infarct avid scan, the thallium-201 myocardial perfusion scan, and the radionuclide ventriculogram or radioangiocardiogram. In this session, the rationale, basic technique, clinical application, and accuracy of the respective procedures will be presented. Applications in the evaluation of patients with coronary heart disease will be emphasized. A strategy for patient selection for each of the respective procedures will be presented within the framework of an analysis of the efficacy of the procedures. In addition to the clinically well established techniques, a number of newer methods of imaging the heart will be briefly presented with emphasis on rationale information available and potential for clinical use in the near future.

411. How to get your manuscript accepted and published without a hassle. Berk RN, Figley MM, Davidson AJ, Hilton SVW, Braude G. The disposition of manuscripts in an editorial office is often looked on as mysterious, capricious, autocratic, and unnecessarily prolonged by authors who are unfamiliar with the editorial process. This course will explain how manuscripts are handled when they arrive in the editorial office. It will show authors how to reduce their chance of rejection and how to avoid the frustration of multiple revisions. Understanding the process helps to expedite the flow of manuscripts as they proceed from reviewers, scientific editors, copy editors, and the publisher. The *AJR* editors will discuss the content that is required in papers, describe the logical manner in which the information should be organized, and review the guidelines for preparing manuscripts recommended by both the *AJR* and *Radiology*. Those who follow these regulations should find their manuscripts have a better chance to be accepted and, when accepted, are more likely to be published expeditiously.

412. Special legal problems in radiological malpractice suits. Reuter SR. As the number of malpractice suits filed and the size of judgments continue to increase, radiologists will inevitably be involved to a greater degree in the legal process. This refresher course is oriented primarily toward special problems that radiologists have in areas of the law that are in transition, including: (1) the duty of care of the radiologist and the missed diagnosis. Does a missed diagnosis, per se, constitute medical negligence? (2) Problems of informed consent. Should consent be obtained for intravenous injection of contrast agents? Who can give consent for radiologic procedures performed on incompetent patients? Do consent forms offer protection against an allegation of lack of informed consent? (3) The participation of the radiologists in the most rapidly expanding area of major damage litigation, prenatal torts. What can be done to potentially diminish liability exposure in this area? (4) Radiologists' liability for the torts of employees and partners. To what exent are radiologists liable for the acts of their office employees and their radiologic partners? Under what circumstances can hospitals escape liability for the acts of their technicians by transferring the liability to the radiologists? These subjects will be discussed, as time allows, along with other problems of radiologic malpractice as the interest of the course participants directs.

Friday, April 18

Symposium on Skeletal Radiology. See table 3 for topics and instructors. Register on registration form for this complimentary program.

Table 3: Skeletal Radiology—1986

Moderator/Time	Topic/Presenter
Lee Rogers:	
8	Localization of arthritis of hand. *Resnick*
8:20	Radiology of ligamentous instability of wrist. *Gilula*
8:40	Diagnostic imaging approach to diabetic foot disorders. *Sartoris*
9	Nuclear imaging in metastatic disease. *Thrall*
9:20	Bone biopsy—why, where, how? *Staple*
9:40	Sonography of rotator cuff. *Crass*
10	MR of femoral ischemic necrosis. *Feldman*
Jack Edeiken:	
10:40	Benign bone lesions simulating malignancy. *Edeiken*
11	Some new bone variants that simulate disease. *Keats*
11:20	A new look at some interesting lesions of the skeleton *Jacobson*
11:40	MR of knee. *Bassett*
noon	Osteoporosis. *Rogers*
12:20	Present status of bone mineral analysis, CT, and nuclear imaging. *Genant*
12:40	Radiographic analysis of spinal stenosis. *Holder*

Note.—There is no fee for this symposium. However, to facilitate planning, please register on the meeting registration form.

ACR Luncheon Presentations on Socioeconomics of Radiology

New at the 1986 ARRS meeting will be a series of luncheon presentations on the socioeconomics of radiology arranged by the American College of Radiology (ACR). A box lunch will be provided. The presentations do not conflict with other elements of the program. Advance registration is required. Cost per session: $10.

Date, Topic, Speaker

Monday, April 14, Federal Programs Affecting Radiology, Otha W. Linton, associate executive director, ACR

Tuesday, April 15, Changes in Federal Tax Legislation Affecting Pensions, Tax Shelters, etc., spokesman from Internal Revenue Service

Wednesday, April 16, Contracts, Governance, and Antitrust, Paul G. Gebhard, legal counsel, ACR

Thursday, April 17, Radiologists, Doctors, and Hospitals , Roy R. Deffenbach, president, ACR

Faculty List

Alderson, Philip O., Columbia-Presbyterian Medical Center
Armstrong, John D., II, Mercy Hospital, Des Moines, IA
Banner, Marc P., Hospital of the University of Pennsylvania
Bassett, Lawrence W., UCLA School of Medicine
Berk, Robert N., University of California, San Diego; *American Journal of Roentgenology*
Bernardino, Michael E., Emory University
Braude, G., *American Journal of Roentgenology*, La Jolla, CA
Brogdon, B. G., University of South Alabama, Mobile
Carroll, Barbara A., Duke University
Chasen, Marvin H., M. D. Anderson Hospital
Choplin, Robert H., Bowman Gray School of Medicine
Churchill, Robert J., Loyola University
Clark, Robert A., University of Cincinnati
Crass, Jeffrey R., University of Minnesota
Davidson, Alan A., Armed Forces Institute of Pathology; *American Journal of Roentgenology*
Deffenbach, Roy R., American College of Radiology
Dietrich, Peter A., Medical Center Hospital of Vermont
Drayer, Burton P., Duke University
Drew, Philip G., Drew Consultants, Carlisle, MA
Edeikin, Jack, Thomas Jefferson University
Elliott, Larry P., Georgetown University
Evens, Ronald M., Mallinckrodt Institute of Radiology
Federle, Michael P., San Francisco General Hospital
Feiglin, David H. I., Cleveland Clinic
Feldman, Frieda, Columbia-Presbyterian Medical Center
Felson, Benjamin, Cincinnati General Hospital
Ferrucci, Joseph T., Jr., Massachusetts General Hospital
Figley, Melvin M., University of Washington
Forbes, Glenn S., Mayo Clinic
Gallant, Thomas E., University of Cincinnati
Gebhard, Paul G., American College of Radiology
Gedgaudas-McClees, R. Kristina, Emory University
Genant, Harry K., University of California, San Francisco
Genereux, George P., University of Saskatchewan
Gilula, Louis A., Mallinckrodt Institute of Radiology
Gisvold, John J., Mayo Clinic
Glazer, Gary M., University of Michigan
Go, Raymundo T., Cleveland Clinic
Graham, C. Benjamin, Children's Orthopedic Hospital, Seattle
Gray, Joel E., Mayo Clinic
Gross, Barry H., University of Michigan
Halvorsen, Robert A., Duke University
Hartman, David S., Armed Forces Institute of Pathology
Hayden, C. Keith, Jr., University of Texas, Galveston
Heitzman, E. Robert, Jr., Upstate Medical Center, Syracuse
Henry, Daniel A., Medical College of Virginia
Hilton, S. V. W., University of California, San Diego; *American Journal of Roentgenology*
Holder, John C., University of Arkansas
Jacobson, Harold G., Montefiore Medical Center
James, Lawrence R., Midwest Medical Imaging Center, Omaha
Jaques, Paul, North Carolina Memorial Hospital, Chapel Hill
Kazam, Elias, New York Hospital-Cornell Medical Center
Keats, Theodore E., University of Virginia
Kirkpatrick, John A., Jr., Children's Hospital, Boston
Kiser, Pamela E., McGuire Veterans Administration Hospital, Richmond, VA
Kopans, Daniel B., Massachusetts General Hospital
Laufer, Igor, Hospital of the University of Pennsylvania
Lee, Joseph K. T., Mallinckrodt Institute of Radiology
Libshitz, Herman I., M.D. Anderson Hospital
Linton, Otha W., American College of Radiology
Lukin, Robert, University of Cincinnati
Lyons, Edward A., Health Sciences Centre, Winnipeg
MacIntyre, William J., Cleveland Clinic
Manco-Johnson, Michael L., University of Colorado
Mauro, Matthew, North Carolina Memorial Hospital, Chapel Hill
McClennan, Bruce L., Mallinckrodt Institute of Radiology

McLoud, Theresa C., Massachusetts General Hospital
McNeil, Barbara J., Brigham and Women's Hospital
Messmer, James M., Medical College of Virginia
Milne, Eric N. C., University of California, Irvine
Moodie, Douglas S., Cleveland Clinic
Morin, Richard L., University of Minnesota
Mueller, Peter R., Massachusetts General Hospital
Naidich, Thomas P., Children's Memorial Hospital, Chicago
O'Donnell, James K., Cleveland Clinic
Olmsted, William W., Armed Forces Institute of Pathology
Poznanski, Andrew K., Children's Memorial Hospital, Chicago
Proto, Anthony V., Medical College of Virginia
Pugatch, Robert D., Brigham and Women's Hospital
Putman, Charles E., Duke University
Ramsey, Ruth G., Rush-Presbyterian-St. Luke's Medical Center
Ravin, Carl E., Duke University
Resnick, Donald L., VA Medical Center, San Diego
Reuter, Stewart R., University of Texas, San Antonio
Rogers, Lee F., Northwestern University
Sackett, Joseph F., University of Wisconsin
Sanders, Roger C., Johns Hopkins Hospital
Sartoris, David J., University of California, San Diego
Shepard, Jo-Anne O., Massachusetts General Hospital
Silver, Terry M., University of Michigan
Staab, Edward V., North Carolina Memorial Hospital, Chapel Hill
Staple, Tom W., Memorial Hospital, Long Beach, CA
Stark, David D., Massachusetts General Hospital
Stark, Paul, University of Texas, Houston
Strother, Charles M., University of Wisconsin
Swischuk, Leonard E., University of Texas, Galveston
Theros, Elias G., Bowman Gray School of Medicine
Thompson, William M., Duke University
Thrall, James H., Henry Ford Hospital, Detroit
Tocino, Irena, University of Utah
Torres, William E., Emory University
vanSonnenberg, Eric, University of California, San Diego
Walsh, James W., Medical College of Virginia
Webb, W. Richard, University of California, San Francisco
Weber, Alfred L., Massachusetts Eye & Ear Infirmary
Weinberg, Peter E., Northwestern Memorial Hospital, Chicago
Weissmann, Heidi S., Montefiore Hospital
Westcott, Jack L., Hospital of Saint Raphael, New Haven, CT
Williams, Hugh J., Children's Hospital of St. Paul, MN
Wiot, Jerome F., University of Cincinnati
Wood, Beverly P., University of Rochester, NY

1986 ARRS Meeting: Local Activities and Tennis and Golf Tournaments

The 86th annual meeting of the American Roentgen Ray Society (ARRS) in Washington, DC, April 13–18, 1986, will feature activities for members, guests, spouses, and friends. Charles E. Bickham, Jr., heads the Local Arrangements Committee. The tennis tournament will be arranged and supervised by Richard D. Newman; the golf tournament by Albert J. Miele. Melba S. Bickham has planned the local programs. To register for these events, please complete the meeting registration form in this issue.

Golf Tournament

The annual golf tournament will be at the Kenwood Golf and Country Club in Bethesda, MD, on Monday, April 14. Buses will leave the Washington Sheraton Hotel at 11 a.m. and will return to the hotel in the early evening at the completion of play. There will be a buffet lunch from 11:45 a.m. to 12:45 p.m. and a shotgun start at 1 p.m. Participants must bring golf clubs. **No rental equipment will be available.**

Fee for the golf tournament is $65 including transportation, luncheon, greens fee, cart, and prizes. Play will be by U. S. Golf Association rules. ARRS members will compete for the Willis F. Manges Trophy at individual net scores and the Exhibitors Trophy at low gross scores. Both members and nonmembers will compete for additional prizes.

Men's and Women's Tennis Tournaments

The annual Men's and Women's Tennis Tournaments will be at the Kenwood Golf and Country Club in Bethesda, MD, on Monday, April 14. Buses will leave the Washington Sheraton Hotel at 11 a.m. and will return to the hotel in the early evening at the completion of play. There will be a buffet lunch from 11:45 a.m. to 12:45 p.m. Matches will begin at 1 p.m. Register early so that arrangements can be made to accommodate all who wish to play. Court space may be limited. Appropriate dress is required. Fee: $50 including transportation, luncheon, court fees, and prizes.

Local Program

Preregistration for these tours is recommended. All events have minimum enrollments and will be cancelled if there is insufficient demand.

Sunday, April 13

Introduction to Washington Champagne Tour, 7–9 p.m. An experienced Washington guide will narrate a leisurely bus tour of historic Washington monuments and government buildings, lighted for nighttime viewing. The group will pass the capitol building, White House, Washington Monument, galleries, museums, and the Watergate complex. There will be stops at the Lincoln, Iwo Jima, Viet Nam, and Jefferson memorials. Along the way, champagne and hors d'oeuvres will be served. Fee: $30.

After the tour, guests will be dropped at prearranged restaurants for dinner. Each restaurant will have a preset menu with several choices of appetizers and main courses. Cocktails and wine will be a la carte. Participants pay their own restaurant bills and return to the hotel on their own.

Restaurants, cuisine, and price ranges are: (1) The Broker, housed in a building constructed in 1847 as a meat brokerage warehouse, a unique architectural and gastronomic delight, moderate–expensive; (2) La Colline, French cuisine, popular bistro for the "Hill," expensive; (3) Four Ways, nouvelle cuisine in restored turn-of-the-century mansion; very expensive; (4) Germaine's, Asian cuisine in atrium, expensive; (5) Jockey Club in Ritz Carlton Hotel along Embassy Row, continental cuisine; expensive; (6) Windows, creative California cuisine in a beautiful setting, expensive.

Monday, April 14

National Gallery of Art and Hirshhorn Museum and Sculpture Garden, 9:30 a.m.–3:30 p.m. Chartered motor coaches will take participants to the National Gallery of Art for a conducted tour of the museum's treasures including America's only painting by Leonardo da Vinci, Rembrandt's self-portrait, Fra Angelico's Adoration of the Magi, and Raphael's Alba Madonna. The museum's first building was donated as a gift to the nation by Andrew W. Mellon and opened in 1941. The East Building is a recent addition of rose-white Tennessee marble designed by I. M. Pei that houses a superb collection of contemporary art. Highlights to be viewed include the largest mobile created by Calder, a tapestry by Miro, and a Henry Moore sculpture. Luncheon will be in the cafe concourse of the underground link connecting the two buildings.

After lunch, the group will visit the Hirshhorn Museum and Sculpture Garden. This unusual circular building houses a large and unique collection of sculpture and paintings that were done during the past 125 years. Fee: $30.

Tuesday, April 15

Georgetown Homes/Georgetown Park, 9:30 a.m.–3:30 p.m. A chartered bus will take participants on a tour of the Georgetown section of Washington, an area that has maintained its individuality since its days as a tobacco port in the late 18th century. Today, row houses of Georgian and federal architectural styles stand side by side with huge Victorian mansions. The group will visit three private homes that represent the special qualities of this historic area. Each has unique characteristics such as traditional federal decor combined with fine contemporary paintings and handsome boxwood gardens. Cooke's Row, built for the first governor of the District of Columbia, has Italian villa style homes with double parlors and bay windows that were much favored by Victorians. Lunch will be in Pisces, a chic, private club in the heart of Georgetown.

After lunch, the tour will visit either Georgetown Park, a shopping mall with more than 100 merchants and restaurants, or the gardens of Dumbarton Oaks. Georgetown Park spans the historic and picturesque C & O Canal, and combines the elegance of the Victorian era with the charm of its original federal architecture. Dumbarton Oaks, a museum containing pre-Columbian art from Central and South America, is sited on 16 acres of formal gardens. Fee: $45.

Wednesday, April 16

Best of Baltimore, 9 a.m.–4 p.m. The group will stop at Fort McHenry, the National Aquarium, and Harborplace before returning to Washington. Fort McHenry was the site of a famous American victory over the British in the War of 1812. It was here that Francis Scott Key was inspired to write the Star Spangled Banner. The National Aquarium, the largest aquarium in the world and just recently opened, is housed in a contemporary building on the Baltimore waterfront. Harborplace, in Baltimore's inner harbor, is the city's newest attraction—an eating and shopping extravaganza. In this European-style marketplace, there are 140 boutiques and restaurants. If time permits, tour participants may visit the U.S. Frigate Constellation, the oldest American warship afloat, moored in Harborplace. Launched in 1797, the Constellation was used against pirates in Tripoli in 1802, the British in1812, and saw action in the Civil War. It was the auxiliary flagship of the Atlantic Fleet in World War II. Fee: $25, excluding lunch.

Thursday, April 17

Annapolis Tour, 9 a.m.–4 p.m. Annapolis, the capital of Maryland, has been called "the most perfect example of a colonial city extant in America today." Experienced guides will conduct a walking tour of the narrow, shaded streets of the colonial area with its exquisitely designed buildings, many of which predate 1800. The group will visit the United States Naval Academy, built on the site of Fort Severn in 1845. Weather permitting, participants will view the noon formation of midshipmen marching into Bancroft Hall. Next stop will be the State House, the oldest capitol building still in use in America today. The group will also visit St. John's College, founded in1695 as King William's School. Here one finds the "Liberty Tree," a tulip poplar said to be the tree under which a peace treaty was signed with Indians in July 1652. The tour will continue past Government House, Hammond-Harwood House, and the Chase House. Lunch will be at a famous inn. Later, the group will browse through some of the shops along picturesque streets and stroll down Maine Avenue to the waterfront. Fee: $40, inclusive.

Friday, April 18

Americana Tour, 9 a.m.–noon. Chartered bus will take the group to the U.S. State Department to visit the Diplomatic Reception Rooms and to see "Project America," initiated in 1961 to furnish the rooms. This great collection of Americana is the finest in the Washington area and the fifth largest collection in the country. The Thomas Jefferson room, furnished in 18th century palladian style, is one of the most beautiful rooms in the United States. Other primary rooms are the John Quincy Adams Room, furnished with Philadelphia Chippendale, the James Monroe Room, furnished in the federal period; and the Benjamin Franklin state dining room.

Next the tour will visit Continental Hall, a neoclassic building housing the museum and archives of the Daughters of the American Revolution. The decorative arts museum has 29 "state rooms" with paintings, furniture, and art objects representing American regional styles and craftsmanship from during the country's formative years including John Hancock's bedroom on the night of Paul Revere's ride, a tea chest from the Boston Tea Party, a victorian parlor, and a New Hampshire attic stocked with dolls, games, and toys. Fee: $15.

May Be Photocopied

Deadline: March 28

Meeting and Local Activities Registration Form: ARRS 86th Annual Meeting, April 13–18, Washington, DC

If you plan to attend, please complete this form. Official badges and program booklets will be available at the ARRS Registration Desk, Sheraton Washington Hotel. **There will be no confirmations before the meeting.** Preregistration by mail will be accepted until March 28. On site registration will be available.

Make all checks payable to: American Roentgen Ray Society

Mail to: American Roentgen Ray Society
1891 Preston White Drive
Reston, VA 2209

Please type or print:

Last Name ______ First Name or Initials ______

Street ______

City ______ State ______ ZIP Code ______

☐ Check here if you wish a program of events for accompanying persons. Indicate the address to which this is to be sent.

Name ______ (Accompanying person's name to be printed on badge)

Street ______

City ______ State ______ ZIP Code ______

Check one:	Registration fee:
☐ Member ARRS	None
☐ Guest	$100
☐ Physician in training (please fill where indicated below)	$25
☐ Course faculty, scientific paper author, scientific exhibitor	None
☐ ACR luncheon course, Monday, April 14	$10
☐ ACR luncheon course, Tuesday, April 15	$10
☐ ACR luncheon course, Wednesday, April 16	$10
☐ ACR luncheon course, Thursday, April 17	$10

Section on Instruction

Please register early for Instruction Courses. Attendance is limited. List first, second, and third choices for each period by course number. Ticket orders are filled according to postmark. ARRS members, nonmembers, and those in radiology training may take all courses without charge except the Categorical Course on Chest Radiology. **For the categorical course, all must pay $75. All who wish to attend courses must complete this section. Residents and nonmembers must pay the meeting registration fee.**

Course tickets will be available at the ARRS Registration Desk of the Section on Instruction at the Sheraton Washington Hotel on and after Saturday, April 12, at 1 p.m.

☐ I wish to take the Categorical Course on Chest Radiology. Fee: $75. Categorical Course registrants may also register for other instructional courses.

Complete section at right for courses other than the categorical course. Be sure to fill out second and third choices for each period.

	First Choice	Second Choice	Third Choice
Monday			
Tuesday			
Wednesday			
Thursday			

Friday ______ Check if you wish to attend the Orthopedic Radiology Symposium (only course offered this day)

For Physicians in Training:

______ is in training in my department

Department Chief ______

Institution ______ Date ______

(OVER)

No refunds after April 1

Local Activities

Sunday, April 13, 7–9 p.m., Introduction to Washington Champagne Tour	____tickets @ $30	$ ____
Monday, April 14, 9:30 a.m.–3:30 p.m., National Gallery of Art and Hirshhorn Sculpture Garden	____tickets @ $30	$ ____
Tuesday, April 15, 9:30 a.m.–3:30 p.m., Georgetown Homes/Georgetown Park	____tickets @ $45	$ ____
Wednesday, April 16, 9 a.m.–4 p.m., Best of Baltimore	____tickets @ $25	$ ____
Thursday, April 17, 9 a.m.–4 p.m., Annapolis Tour . .	____tickets @ $40	$ ____
Friday, April 18, 9 a.m.–noon, Americana Tour	____tickets @ $15	$ ____

Annual ARRS Golf Tournament, Monday, April 14, 11 a.m.

The tournament will be at the Kenwood Golf and Country Club, Bethesda, MD. Transportation, luncheon, greens fee, cart, and prizes are included in the $65 fee. Preregistration is important.

Name: ____________________ Telephone: ____________________

Address: ____

Hotel: ____________________ Handicap (if any) ____________________

My foursome includes (list handicaps): ____

____________________ ____tickets @ $65 $ ____

Men's and Women's Tennis Tournaments, Monday, April 14, 11 a.m.

The tournaments will be at the Kenwood Golf and Country Club, Bethesda, MD. Tennis attire is required. Fee of $50 includes transportation, luncheon, court fees, and prizes.

Name: ____________________ Telephone ____________________

Address: ____

____tickets @ $50 $ ____

May be photocopied **Deadline: March 15**

Hotel Registration Form: ARRS 86th Annual Meeting, April 13–18, Sheraton Washington Hotel

Mail to:

ARRS Housing Bureau
Sheraton Washington Hotel
2660 Woodley at Connecticut Ave., N.W.
Washington, DC 20006

(PLEASE MAKE CHECKS PAYABLE TO HOTEL—*NOT TO THE ARRS*)

Individual guest name ______________________________

Address ______________________________

City & State ______________________________ ZIP ____________

Arrival date ____________________ Departure date ____________________

Individual requesting reservation ______________________________

Address ______________________________

City & State ______________________________ ZIP ____________

Deposit amount: ____________________

One night's deposit is needed to guarantee accommodations. Deposit is refundable with advance notice of cancellation. Deposit guarantees room until 12 midnight on requested arrival date. Make check payable to the Sheraton Washington Hotel.

Check accommodations desired

Room Category	Rate
Single	______ $98, 110, 120
Double	______ $120, 132, 142
1-bedroom suite	______ $200–525
2-bedroom suite	______ $400–625

Important Information:

1. Reservations must be received by the Sheraton/ARRS Housing Bureau no later than March 15 to be assured of written confirmed accommodation.
2. Written confirmation of your reservation will be sent to you by the hotel. Please allow 2–3 weeks for confirmation.
3. All changes such as arrival date, departure date, type room, and name changes must be made directly with the hotel after confirmation is received.
4. If you plan to share a room, please send in only one housing form. Be sure to list all names of occupants of rooms. Assignment is delayed until complete information is received
5. Room assignments will be made in order received.

Delta and United Airlines Offer Fare Discounts to 1986 ARRS Meeting

Again in 1986, Delta and United airlines will be official carriers to the American Roentgen Ray Society (ARRS) meeting and will provide discounted fares to those who use the lines to reach the Washington, DC, event.

Delta Air Lines

Delta will discount fares 35% for those who travel round trip on Delta. The discount applies to day coach fares in the continental U.S. and San Juan, Puerto Rico, that have not been previously discounted. Tickets must be purchased a minimum of 7 days before departure and travel to Washington, DC, must be from April 9 through 15. A maximum stay of 15 days is permitted. The airline invites you or your travel agent to telephone toll-free to learn the lowest rate available. Please identify yourself as an ARRS meeting registrant and give the ARRS account, F-0347. Telephone (800) 241-6760 in the continental U.S., 8:30 a.m.–8 p.m. eastern time daily.

United Airlines

United offers a 40% discount off the normal coach fare with no minimum stay or advance purchase restrictions. For those staying over a Saturday night, there is an additional 5% discount (45% total). To receive United's ARRS convention rate, attendees must travel between April 10 and 22. To take advantage of this special rate, telephone (800) 521-4041 from 8:30 a.m.–8 p.m. eastern time daily. Provide the ARRS account number 602-K. Seats are limited. United's special ARRS convention fare is available to all three Washington-area airports: Dulles, National, and Baltimore-Washington.

1986 ARRS Meeting, April 13–18, Washington, DC

A comprehensive description of the meeting, including the scientific program, Categorical Course in Chest Radiology, and instructional courses, appears in the January 1986 issue of the *AJR*. A special loose insert on the meeting also accompanies the January issue. Meeting and registration forms will be found in the January and February issues. These may be photocopied.

Accreditation

All courses and scientific sessions carry AMA Category I credit on an hour-for-hour basis.

Meeting Format

Scientific Program. Sessions will be grouped in parallel sessions, Monday–Thursday. A total of 189 scientific papers will be presented in 18 sessions. In addition, on Wednesday, April 16, the morning session will feature award papers and the Caldwell Lecture, which will be delivered by Benjamin Felson of the University of Cincinnati. On Friday, there will be a special symposium on orthopedic radiology.

Categorical Course in Chest Radiology. This 14 hr course will be Sunday–Thursday. Registrants may enroll in other courses as well.

Luncheon Sessions. For the first time, registrants may enroll in special luncheon sessions, Monday–Thursday. A box lunch will be provided.

Exhibits

Scientific Exhibits and Case of the Day Presentations will be Monday–Thursday, April 14–17.

Commercial Exhibits will be open daily, Monday–Thursday.

Local Activities

General Reception. Tuesday evening, April 15, for all registrants.

Golf Tournament. Monday, April 14, Kenwood Golf and Country Club, Bethesda, MD. Transportation leaves the hotel at 11 a.m.; shotgun start at 1 p.m.

Men's and Women's Tennis Tournaments. Monday, April 14, Kenwood Golf and Country Club, Bethesda, MD. Transportation leaves the hotel at 11 a.m.

Local Tours. Sunday, April 13, 7–9 p.m., Introduction to Washington Champagne Tour; Monday, April 14, 9:30 a.m.–3:30 p.m., National Gallery of Art and Hirshhorn Museum and Sculpture Garden; Tuesday, April 15, 9:30 a.m.–3:30 p.m., Georgetown Homes/Georgetown Park; Wednesday, April 16, 9 a.m.–4 p.m., Best of Baltimore; Thursday, April 17, 9 a.m.–4 p.m., Annapolis; Friday, April 18, 9 a.m.–noon, Americana Tour.

Meeting Registration

Preregistration will be accepted until March 28. There will be on-site registration. Official badges and program books will be available at the registration desk, Sheraton Washington Hotel. No confirmations will be mailed.

Course Registration

Register early—enrollment is limited. List first, second, and third choices for each period. Also, indicate whether you wish to take the categorical course. Deadline for mail registration is March 28. All ticket orders will be filled by postmark. Course tickets *will not* be mailed. Tickets will be available on and after Saturday, April 12 (after 1 p.m.), at the ARRS registration desk in the Sheraton Washington Hotel. There will be on-site registration for courses not already filled.

Hotel Registration

Reservations are handled by the ARRS Housing Bureau, Sheraton Washington Hotel, 2660 Woodley at Connecticut Ave., N.W., Washington, DC 20006. These must be received by March 15. Make check payable to Sheraton Washington Hotel.

Fees

Meeting:	
ARRS members and resident members	No fee
Nonmembers	$100
Nonmember physicians in training (with verification)	25
Categorical course (all who attend)	75
Luncheon sessions/each	10
Golf tournament	65
Tennis tournaments	50
Local tours	15–45

Cancellations and Fee Refunds

Fees will be refunded only if cancellation is received by April 7. Send to American Roentgen Ray Society, 1891 Preston White Drive, Reston, VA 22091.

Air Transportation

Two airlines, United and Delta, are official meeting air carriers and are offering discounted fares.

Delta Air Lines will discount fares 35%. Tickets must be purchased a minimum of 7 days before departure. Travel to Washington must be from April 9 through 15. A maximum stay of 15 days is permitted. Information: (800) 241-6760 in the continental U S., 8:30 a.m.–8 p.m. eastern time daily. Mention ARRS number F-0347.

United Airlines offers a 40% discount off normal coach fares with no minimum stay or advance purchase restrictions. There is an additional 5% discount (45% total) for those staying over a Saturday night. Travel must be between April 10 and 22. Information: (800) 521-4041, 8:30 a.m.–8 p.m. eastern time daily. Mention ARRS number 602-K. Seats are limited.

Associated Meetings

The *Society for Pediatric Radiology* will meet April 10–13 in the Shoreham Hotel, Washington, DC. The program will appear in the March issue of the *AJR*. For information contact: Donald R. Kirks, M.D., Secretary, Society for Pediatric Radiology, c/o Dept. of Radiology, Duke University Medical Center, Box 3834, Durham, NC 27710; telephone (919) 681-2711, ext. 287.

The *American Association of Women Radiologists* (AAWR) will have a luncheon meeting on Monday, April 14, in the Sheraton Washington Hotel.

News

Interventional Radiology Seminar

The Medical University of South Carolina and the Institute of Radiology and Oncology, University Medical Center, Sarajevo, Yugoslavia, will present a 1-week seminar, Jan. 26–Feb. 1, in Sarajevo. Topics will include magnetic resonance imaging, transluminal angioplasty, laser technology, fibrinolytic therapy, digital subtraction angiography, computed tomography, nonangiographic interventional procedures, and interventional sonography in obstetrics and gynecology. Guest faculty: W. R. Castaneda-Zuniga, I. Enge, A. Kurjak, I. Obrez, J. Struyven, M. H. Wholey, and G. L. Wolf. Program directors: I. Vujic and A. Lovrincevic. Category I credit: 23 hr. Fee: $350. Information: Dept. of Radiology, Medical University of South Carolina, 171 Ashley Ave., Charleston, SC 29425; (803) 792-5071.

Computers for Practicing Physician

Boston University will sponsor a course, Computers for the Practicing Physician: Update 1986, Feb. 5–7, in Lake Buena Vista, FL. Course director: B. M. Manuel. Category I credit: 12 hr. Fee: $300. Information: Dept. of Continuing Medical Education, Boston University College of Medicine, 80 E. Concord St., Boston, MA 02118; (617) 638-4605.

International Education Series

Boston University will sponsor a series of courses in Europe and the Caribbean. Topics, locations, and dates are: Controversies in Medicine, Barbados, Feb. 28–March 6, March 7–14, March 14–21, March 21–28; Controversies in Medicine, Paris/Versailles, April 30–May 8, May 7–15; Update on Laser Therapy, Heidelberg, June 25–July 3, July 2–10; Controversies in Medicine, London, Aug. 14–22, and Aug. 21–29. Category I credit: 20 hr. Fee: $350. Information: Dept. of CME, Boston University School of Medicine, 80 E. Concord St., Boston, MA 02118.

Symposium on Dysphagia

A Symposium on Dysphagia will be Feb. 27–March 1 in Baltimore. Sponsor is the Johns Hopkins University School of Medicine. The conference will offer state-of-the-art evaluation of patients with dysphagia using a sequence of related presentations and panel discussions conducted by recognized leaders in the field. It will communicate new insights into the basic sciences, including neurophysiology, fluid dynamics, the viscosity and elasticity of food, and clinical evaluation methods. Category I credit: 17 hr. Fee: $300, physicians; $150, allied health professionals. Information: Jeanne Ryan, program coordinator, Office of Continuing Education, Johns Hopkins University School of Medicine, 720 Rutland Ave., Turner 22, Baltimore, MD 21205; (301) 955-6046.

Conference on Monoclonal Antibodies

An International Conference on Monoclonal Antibody Immunoconjugates for Cancer will be March 6–8 in San Diego. Sponsor is the University of California, San Diego. Category I credit: 19 hr. Fee: $350. Information: Office of Continuing Medical Education, UC San Diego School of Medicine, M-017, La Jolla, CA 92093; (619) 452-3940.

Winter Conference in Utah

The Radiology Department of Cobb Memorial Hospital will hold its annual winter conference in Park City, UT, March 9–14. Topics will include radiology and sonography, with emphasis on computed tomography. There will be film reading sessions. Speakers: R. L. Wesenberg and J. Van Dyke. Category I credit: 20 hr. Fee: $290. Information: Vincent M. Currier, M.D., program director, P. O. Box 1203, Phenix City, AL 36867; (205) 297-7550.

Functional and Stereotactic Neurosurgery

A symposium, Functional and Stereotactic Neurosurgery, will be March 9–16 in Garmisch-Partenkirchen, West Germany. The symposium will provide an update on selected topics by a distinguished faculty from European universities and the University of California, San Francisco. Topics will include: spinal cord stimulation for peripheral vascular disease; implanted drug delivery system for the control of pain and spasticity; trigeminal ganglionic stimulation for the control of atypical facial pain; brain stimulation for the control of chronic pain; CT-guided stereotactic tumor biopsy and demonstration of BRW system; technique and results of stereotactic brain tumor irradiation by permanent radioactive nuclide implants and intracystic therapy; technique and results of stereotactic brain tumor irradiation by removable radioactive nuclide implants; and effect of focal irradiation on normal brain. Guest faculty: L. E. Augustinsson, University of

Goteborg; G. Broggi, Neurological Institute, Milan; J. Broseta, University of Salamanca; Y. Lazorthes, C. H. U. Toulouse; M. Meglio, Catholic University, Rome; C. B. Ostertag, Neurosurgical University Clinic, Hamburg; A. Struppler, Munich Technical University; and V. Sturm, University of Heidelberg. Program Director: Y. Hosobuchi, University of California, San Francisco. Category I credit: 20 hr. Information: Extended Programs in Medical Education, University of California School of Medicine, Room 569-U, San Francisco, CA 94143; (415) 666-4251.

Trauma Management

The University of California, San Diego, will host a course, Trauma Management 1986, Feb. 3–5 in San Diego. Course director: S. R. Shackford. Category I credit: 18 hr. Information: Continuing Medical Education, M-017, UC San Diego School of Medicine, La Jolla, CA 92093; (619) 452-3940.

Concepts in Diagnostic Radiology

Letterman Army Medical Center, San Francisco, will host a postgraduate course, May 20–23, at the medical center. Title is Present Concepts in Diagnostic Radiology. Topics will include: magnetic resonance imaging; neuroradiology; computed tomography; sonography; chest, skeletal, interventional, genitourinary, and military radiology; also pediatrics and mammography. Faculty: A. R. Margulis, C. B. Higgins, W. Hanafee, H. Hricak, D. Norman, M. P. Federle, R. A. Filly, H. K. Genant, C. A. Helms, E. J. Ring, and E. A. Sickles, all University of California, San Francisco; R. A. Zimmerman, University of Pennsylvania; R. F. Thoeni, Straub Clinic, Hawaii; A. Shkolnik, Children's Memorial Hospital, Chicago; E. K. Lang, Louisiana State University; E. Dolev, retired surgeon general of the Israeli Defense Forces; B. Felson, University of Cincinnati; M. Viamonte, Jr., University of Miami; L. E. Swischuk, University of Texas, Galveston; and A. J. Davidon, Armed Forces Institute of Pathology. Category I credit: 26 hr. Information: Frank L. Quattromani, M.D., Dept. of Radiology, Letterman Army Medical Center, San Francisco, CA 94129-6700; (415) 561-3764.

Magnetic Resonance Imaging Course

Massachusetts General Hospital and Harvard University will present the fourth annual MRI Postgraduate Course, May 21–23, in Boston. This symposium will present magnetic resonance (MR) principles and clinical applications in lectures and workshop format. The course is directed toward new or potential uses of MR. Also, new techniques such as surface coil imaging will be discussed. Category I credit: 16 hr. Fee: $400, $300 for residents and fellows. Information: Thomas J. Brady, M.D., Director of MRI, Massachusetts General Hospital, Boston, MA 02114.

Emergency Radiology

The annual Harvard Medical School Postgraduate Course on Emergency Radiology will be May 28–30 in Boston. Emphasis will be on new imaging techniques. Fee: $350. Information: Dept. of Continuing Education, Harvard Medical School, Boston, MA 02115; (617) 732-1525.

Radiology Update in Scotland

A course, 1986 Radiology Update, will be July 10–21 in Edinburgh and Turnberry, Scotland, preceding the British Open Golf Championship. Sponsors are: Emory University, the University of Miami, and the University of Edinburgh. Faculty will be from the three universities: M. E. Bernardino, W. J. Casarella, and J. C. Hoffman, Jr., Emory; C. A. Poole and R. M. Quencer, University of Miami; and J. Best and M. Buist, University of Edinburgh. Topics: neuroradiology, abdominal imaging, interventional and pediatric radiology with emphasis on use of magnetic resonance imaging and computed tomography. Category I credit: 20 hr. Fee: $400. Information: Joanna Graves, CME Coordinator, Emory University School of Medicine, 1440 Clifton Road, N.E., Atlanta, GA 30322; (404) 727-5695.

Nominations Sought for Kaplan Award

The International Association for Radiation Research has announced the establishment of the Henry S. Kaplan Distinguished Scientist Award. The award, to be presented every 4 years at the International Congress of Radiation Research, consists of a medal, a certificate, and a cash prize. A 1 hr plenary session is designated for the award ceremony, including a lecture by the awardee. The award will honor outstanding contributions to radiation research. Any scientist who has made superior contributions to the field through investigations in biology, chemistry, medicine, or physics is eligible. Nominations may be submitted by any individual, group, or society. Each nomination should include a current curriculum vitae, bibliography, and brief (e.g., three page) narrative describing the accomplishments of the nominee. Supporting letters are not mandatory but will be accepted. Submit nominations for the 1987 award by May 1, 1986, to Dr. Johan J. Broerse, secretary-treasurer, International Association for Radiation Research, c/o Radiobiological Institute TNO, 151 Lange Kleiweg, P.O. Box 5815, 2280 HV Rijswijk, The Netherlands.

Meeting and Course Review

For reader convenience, a summary of upcoming meetings and courses is provided. Detailed listings appear in the *AJR* issues noted in parentheses.

Midwinter Radiological Conference, Los Angeles, Jan. 31–Feb. 2; postconference seminar, Feb. 3–9, Maui (Nov)
Skeletal Symposium, Feb. 1–8, Snomass, CO (Dec)
Seminar in Aspen (CO), Feb. 2–7 (Dec)
MRI Meeting in Rome, Feb. 2–7 (June)
Winter Conference in High Sierras, Feb. 2–7, Lake Tahoe (Oct)
San Diego Courses: Radiologic Imaging and Intervention, Feb. 3–7; **Neuroradiology Update**, March 3–4; **Magnetic Resonance Imaging Update**, March 5–7; **Residents' Review**, April 28–May 2; **Biology and Physics of Radiology**, Sept. 1–5; **Postgraduate Course**, Oct. 13–17; **Imaging of Lumbar Spine and Pelvis**, Oct. 18, all San Diego (Oct)
Uroradiology Course, Feb. 5–6, Bethesda, MD (Dec)
Radiologic-Pathologic Correlation, course, Feb. 6–9, Lake Buena Vista, FL (Dec)
Course in Puerto Rico, Feb. 9–14 (Nov)
New England Roentgen Ray Society Meetings, Feb. 14, March 21, April 11; annual meeting, May 16, all Boston (Nov)
Vail Winter Seminar, Feb. 15–22 (Oct)
MRI Update, course, Feb. 16–19, West Palm Beach, FL (Nov)

Masters Radiology Conference, Feb. 16–21, Kauai (Nov)
Body Imaging Course, Feb. 16–21, Acapulco (Oct)
Neuroimaging Update 1986, course, Feb. 16–21, Paradise Island, Bahamas (Dec)
Angiography and Interventional Radiology, course, Feb. 17–20, Fort Lauderdale, FL (Oct)
Thoracic Imaging Course, Feb. 17–20, Newport Beach, CA (Aug)
Emergency Medicine Course, Feb. 19–21, San Diego (Oct)
UCSF Courses. Diagnostic Imaging: Update 1986, Feb. 22–29, Park City, UT; **Diagnostic Imaging 1986: CT, Ultrasound, MRI, and Emergency Room Radiology,** March 9–14, Kauai, HI; **Advances in Uroradiology,** March 22–23, San Francisco; **Thoracic Imaging Update: 1986**, April 17–19, Monterey, CA (Nov)
Intermountain Imaging Conference, Feb. 22–March 1, Snomass, CO; program extension, March 2–9, Snowbird, UT (Nov)
Practical Radiology Course, Feb. 23–28, Whistler Mountain, BC (Dec)
CT Course, Feb. 27–March 2, Bal Harbour, FL (Nov)
Fleischner Society Symposium, Feb. 28–March 3, Maui (Nov)
Magnetic Resonance Imaging Meeting, March 1–5, Philadelphia (Aug)
Neuroradiology Course, March 3–6, Bal Harbour, FL (Dec)
Radiation and Radiotherapy Courses. Nonionizing Radiation, March 3–7; **Radiation Safety Officer's Course,** May 19–23; **Advanced Radiological Health**, May 12–16, all San Antonio (Sept)
Computer and MRI Meetings: Computers in Medicine, workshop, March 10–11; **MRI meeting**, March 12–15, both Monte Carlo (Nov)
Breast Disease Update, course, March 12–16, Lake Buena Vista, FL (Oct)
South African Ultrasound Congress, March 14–17, Johannesburg (Sept)
Skeletal Radiology Course, March 15–20, Phoenix (Dec)
Ultrasound at Vail, course, March 15–22 (Oct)
Chest Course in Switzerland, March 16–23, Davos (Sept)
Computed Body Tomography Course, March 17–21, Hilton Head Island, SC (Nov)
San Francisco Courses. Postgraduate Course in Diagnostic Radiology, March 24–28; **Ob/Gyn and Abdominal Sonography: Update 1986**, both San Francisco (Dec)
Counseling Strategies for Physicians, course, March 24–29, Oahu (Aug)
Florida Courses. 1986 Update on Diseases and Imaging of the Spine, March 31–April 2; **Interventional Radiology Seminar**, April 3–5, both Lake Buena Vista (Dec)
NCRP Annual Meeting, April 2–3, Washington, DC (Oct)
Hepatobiliary and Pancreatic Imaging, course, April 2–5, Miami (Nov)
Review Course for Residents, April 4–6, Ann Arbor (Dec)
American Radium Society Meeting, April 6–10, San Francisco (Sept)
AAMI Annual Meeting, April 12–16, Chicago (Dec)
American Roentgen Ray Society, annual meeting, April 13–18, Washington, DC (see elsewhere this issue)
Radiation Therapy Research Seminar, April 17–19, Gainesville (Dec)
Neuroreceptors Course, April 18–19, Baltimore (Dec)
Interventional Radiology and DSA, course, April 28–30, Baltimore (Nov)
Interventional Neuroradiology Course, April 28–May 2, New York City (Dec)
Echocardiography Symposium, May 1–3, Boston (Dec)
Radionuclides in Nephrourology, symposium, May 5–7, Lausanne, Switzerland (Aug)
Uroradiology Postgraduate Course, May 5–9, the Netherlands (Aug)
American Thoracic Society Annual Meeting, May 11–14, Kansas City, MO (Dec)
Radiology Course in Hong Kong, May 11–16 (Dec)
Vanderbilt Courses. Sonography Symposium, May 23–24, Nashville; **Advances in Medical Imaging**, June 5–9, Kiawah Island, SC; **Breast Imaging Symposium**, July 25–26, Nashville (Dec)
Pediatric Imaging Course, Aug. 3–6, Colorado Springs (Nov)
Congress of Asean Association of Radiology, Aug. 7–9, Singapore (Dec)
Top of the World Radiology, course, Aug. 9–16, Great Bear Lake, Canada (Dec)
Ultrasound Congress in Denmark, Aug. 19–22, Copenhagen (Oct)
Blood Flow in the Brain, meeting, Sept. 23–25, Glasgow, Scotland (Dec)
Call for Biomedical Engineering Papers, Southern Biomedical Engineering Conference, Oct. 20–21; abstract deadline, March 1 (Dec)
Physics Conference in Bombay, India, Dec. 8–12 (Oct)
1987 Radiology Congress in Lisbon, May 31–June 6 (Oct)

AJR carries announcements of courses, symposia, and meetings of interest to its readers if received a minimum of 4 months before the event. There is no charge; receipt of items by the *AJR* Editorial Office is not acknowledged. Submit items for publication typed double spaced. Provide title, date, location, brief description, sponsor, course directors, fees, category I credit, and address and telephone number for additional information. Faculty from the host institution will not be listed. Guest faculty names will appear **only** if initials are provided. Mail news items to *AJR* Editorial Office, 2223 Avenida de la Playa, Suite 306, La Jolla, CA 92037.

Classified Advertising

Positions Available

ABDOMINAL IMAGING RADIOLOGIST: Applications are being solicited by the American Registry of Pathology for an academically oriented abdominal imaging radiologist. Major responsibility is teaching in the educational program of the Dept. of Radiologic Pathology, Armed Forces Institute of Pathology. Address inquiries and curriculum vitae to: Richard P. Moser, M.D. acting chairman and registrar, Dept. of Radiologic Pathology, Armed Forces Institute of Pathology, Washington DC 20306-6000. 1a

DIAGNOSTIC RADIOLOGIST: Immediate vacancy, well-established hospital-based group in Southwest metropolitan area, seeks associate well-trained or experienced in general diagnostic radiology, including ultrasound, to service 2 small satellite hospitals and a clinic. Few interventional procedures at this time. Rapidly-growing area with superior climate and outdoor recreational activities. Seeking a motivated physician to develop this segment of already established, quality practice. Send curriculum vitae to Diana Welch, Radiology Associate, P.A., 215 Central, NW, Albuquerque, NM 87102. 1a

PHILADELPHIA VA MEDICAL Center has an opening for a staff radiologist, board certified, with expertise in angiography and an interest in teaching at our 524-bed facility dually affiliated with the University of Pennsylvania and Medical College of Pennsylvania. Excellent benefits and salary package. Phone or send CV and reference to Personnel Officer, VAMC Philadelphia, PA 19104; (215) 823-5832. The VA is an EEO/AAP employer. 1a

DIAGNOSTIC RADIOLOGY PHYSICIAN. The University of Minnesota Dept. of Radiology has a full-time probationary tenure track position in the Abdominal and Thoracic Imaging Section available at the rank of assistant professor beginning July 1, 1986. Minimum requirements include board certification in radiology plus 1 year related fellowship or clinical experience in radiology postresidency. Responsibilities will include all facets of abdominal and thoracic imaging, including gastrointestinal/genitourinary (GI/GU) radiology and tomography, requiring expertise in abdominal imaging, CT, and pulmonary radiology, along with interventional radiography of the thorax and abdomen (guided biopsies and abscess drainages). Responsibilities will also include graduate and undergraduate medical instruction in abdominal and thoracic imaging, as well as conducting research on an inter- and intradepartmental basis. Duties will also include both inpatient and outpatient clinical service. Salary is negotiable and is dependent upon past scholarly productivity and post-M.D. experience. Applicants must be licensed or able to obtain a license to practice medicine in the State of Minnesota prior to appointment date. Applications for this position will be accepted through March 31, 1986. Send letters and resumes to: Eugene Gedgaudas, M.D., professor and head, Dept. of Radiology, Box 292 Mayo, University of Minnesota Medical School, 420 Delaware St. S.E., Minneapolis, MN 55455. The University of Minnesota is an equal opportunity educator and employer and specifically invites and encourages applications from women and minorities. 1a

BOARD-CERTIFIED radiologist with expertise in interventional radiology and/or angiography wanted to join medical center based group with 800 beds. For more information send curriculum vitae or contact P.O. Box 67043, Baton Rouge, LA 70896. 1-2a

CHAIRMAN, DEPARTMENT OF RADIOLOGY. The University of Florida College of Medicine seeks a distinguished individual to serve as professor and chairman of the Dept. of Radiology. Applicants should have an M.D. degree, a record of significant accomplishments in research, clinical skills in radiology, and a clear commitment to medical student and postgraduate education. Applications, including curriculum vitae, bibliography, and the names and addresses of at least 3 references should be sent before March 15, 1986 to: Dr. Jerome H. Modell, Chairman, Radiology Search Committee, College of Medicine, University of Florida, Box J-254 JHMHC, Gainesville, FL 32610. Equal Opportunity/Affirmative Action Employer. 1a

RADIOLOGIST, DIAGNOSTIC: Diagnose diseases of human body, using x-rays and radioactive substance; examine internal structures and functions of organ systems, making diagnoses after correlation of x-ray findings with other examinations and tests. Administer radiopaque by injection, orally, or as enemas to render internal structures and organs visible on x-ray films or fluoroscopic screens. Requirements: M.D. degree; 3 years training in diagnostic radiology; 3 years experience as radiologist, diagnostic; knowledge of diagnostic radiology; knowledge of neuromuscular thermography. 40 hr/wk, $70,000/year. Apply at the LA. Office of Employment Security, 617 St. Charles Ave., New Orleans, LA 70130. Refer to job order number 581592. 1a

RADIOLOGY INSTRUCTOR to assist candidate in preparation for Oral Boards. Candidate needs practice in formally discussing cases and answering board-type questions in all exam sections. Would like to meet on a weekly basis beginning early 1986. East coast (esp. Philadelphia/Middle Atlantic states) preferred. Fee negotiable. Reply Box W4 *AJR* (see address this page) or call (215) 342-4110. 11-1a

CHIEF, RADIOLOGY SERVICE. Full-time position immediately available for board certified radiologist in university affiliated VA Medical Center. Faculty appointment assured. Excellent salary and fringe benefits. Send CV to Chief, Personnel Service, VA Medical Center, 4100 W. Third St., Dayton, OH 45428, or call (513) 268-6511, ext. 2506. An Equal Opportunity Employer. 11-1a

CHAIRMAN OF DIAGNOSTIC RADIOLOGY: Position entails administrative ability and expertise in all aspects of diagnostic radiology. Academic and research opportunities. Competitive salary and fringe benefits. Board certification required. Contact Dr. Hewitt McElroy, Radiology Search Committee, Ellis Fischel Cancer Center, 115 Business 70 West, Columbia, MO 65203. An Equal Opportunity Employer. 11-1a

DIAGNOSTIC RADIOLOGIST: Board-certified diagnostic radiologist seeks partner in expanding solo hospital-based practice. Upstate New York. All modalities available. CV to Phillip Berman, M.D., HC61 Box 454, Massena, NY 13662. 9-4a

RADIOLOGIST with special proficiency in ultrasound and mammography. Board certified, board eligible radiologist wanted for outpatient radiology. Free standing clinic in excellent medical community in Midwest. Position will include all aspects of outpatient radiology with special emhasis on obstetrical ultrasound and mammography. Partnership in facility available to qualified individual. Send CV to Box X3 AJR (see address this section). 12-2a

EXCELLENT POSITION available with radiology practice for board certified radiologist with an interest in all areas of radiology. Opportunity for partnership in expanding practice in the Greater New Orleans area serving 3 hospitals. 80,000 inpatient, 24,000 outpatient examinations/year. Send CV to Dr. Harold R. Neitzchman or Dr. Martin A. Belanger, 4400 General Meyer Ave., Suite 221, New Orleans, LA 70114. 12-2a

ABDOMINAL IMAGING—Faculty appointment in abdominal imaging section for a board certified radiologist interested in abdominal diagnostic (fluoro, CT, ultrasound) and interventional procedures at the medical school of the University of Texas at San Antonio. Send curriculum vitae to Robert L. Siegel, M.D., Chief, Diagnostic Radiology, Dept. of Radiology, The University of Texas Health Science Center at San Antonio. 7703 Floyd Curl Dr., San Antonio, TX 78284. 11-1a

Positions Desired

DIAGNOSTIC RADIOLOGY PGY-2 urgently needed for July 1, 1986. Fifth pathway graduate with ECFMG, FLEX, N.Y. license, (currently PGY-1 Internal Medicine), is willing to relocate anywhere for accredited program in U.S. or Canada. Please reply Box H2 AJR (see address this section). 1bp

UNIVERSITY TRAINED, board eligible radiologist, 34, with imaging fellowship seeks permanent association with group practice. Available immediately. Prefer Florida. Reply Box W6 *AJR* (see address this page). 11-1b

Fellowships and Residencies

DIAGNOSTIC IMAGING FELLOWSHIP—ultrasound, CT, and MRI. Emphasizing hands-on scanning and active participation in interventional procedures. Excellent clinical material in obstetric, gynecologic, and general adult and pediatric populations. Available 1 July 1986. Contact Harris Finberg, M.D., Dept. of Diagnostic Radiology, Good Samaritan Medical Center, 1111 E. McDowell Road, Phoenix, AZ 85006; (602) 239-4600. 1c

ADVANCED IMAGING FELLOWSHIP. Jan. 1, 1987, a position will be available for a board certified or board eligible radiologist in a University of Rochester teaching hospital complex, Rochester, NY. This is a 1-year program emphasizing in-depth exposure to CT/ultrasound integrated with invasive procedures and digital vascular imaging. Please respond to Steven G. Herbert, M.D., director, Fellowship Program, Diagnostic Radiology Dept., The Genesee Hospital, 224 Alexander St., Rochester, NY 14607. 12-1c

AJR 146:209, January 1986

ABDOMINAL/THORACIC IMAGING fellowship: The University of Minnesota Dept. of Radiology has a 1-year full-time temporary, nontenured, position in the Section of Abdominal and Thoracic Imaging available at the rank of instructor beginning July 1, 1986. Minimum requirements include board certification in radiology. Responsibilities will include all facets of abdominal and thoracic imaging, including gastrointestinal/genitourinary (GI/GU) radiology and tomography, requiring expertise in abdominal imaging, CT, and pulmonary radiology, along with interventional radiography of the thorax and abdomen (guided biopsies and abscess drainages). Responsibilities will also include graduate and undergraduate medical instruction in abdominal and thoracic imaging, as well as assisting with related department research projects. Duties to include both inpatient and outpatient clinical services. Salary is negotiable and competitive and is dependent upon past scholarly productivity and post-M.D. experience. Applicants must be licensed or able to obtain a license to practice medicine in the State of Minnesota prior to appointment date. Applications for this position will be accepted through May 15, 1986. Send letters and resumes to: Marvin Goldberg, M.D., Dept. of Radiology, Box 292 Mayo, University of Minnesota, 420 Delaware St. S.E., Minneapolis, MN 55455. The University of Minnesota is an equal opportunity educator and employer and specifically invites and encourages applications from women and minorities. 1c

WILLIAM BEAUMONT HOSPITAL'S Dept. of Diagnostic Radiology is accepting applications for 1 year fellowships in diagnostic imaging, including ultrasound, CT, and MRI beginning July 1, 1986. Three positions available. Emphasis is on correlating the imaging modalities and interventional procedures utilizing CT and ultrasound. William Beaumont Hospital is an acute care 929-bed teaching hospital in a suburb of Detroit. Applicants must be board certified or eligible. Fellowship stipend is highly competitive and fringe benefits are generous. For further information and application write: J. Farah, M.D., 3601 W. 13 Mile Road, Royal Oak, MI 48072; (313) 288-7045. 10-1c

NMR VISITING FELLOWSHIPS in northern California. Intensive, structured 1-4 week courses with live instruction, teaching file, and video tape library. For further information contact: Murray A. Solomon, M.D., San Jose MRI Center, 361 S. Monroe St., San Jose, CA 95128. 10-3c

Tutorials/Courses

ALASKA '86—Cruise the Inland Passage, July 5-12, 1986. CME I credit. Topics in ultrasound with Barry B. Goldberg, M.D. Registration U.S. $385 until April 12, after U.S. $425. For additional information write or call ALASKA '86—Medical Seminars International, 21915 Roscoe Blvd., #222, Canoga Park, CA 91304; (800) MED-TOUR or (818) 701-5143. 1-6d

JERUSALEM, ISRAEL—Ultrasound Symposium, June 20-29, 1986. Category I CME program presented in cooperation with the Israeli Ultrasound Society by an International faculty. Fee to April 1986: U.S. $425, thereafter U.S. $460. Information: Medical Seminars International, 21915 Roscoe Blvd., #222, Canoga Park, CA 91304; (800) MED-TOUR or (818) 340-0580, ext. 280. 1-6d

LONDON, ENGLAND—ROME, ITALY, May 10-18, 1986. Attend one or both Spring Seminars. Renowned international faculty. Topics: CT, MRI, DSA. Category I accreditation. Fees: to March 7, U.S. $385, thereafter U.S. $425 each seminar. Combined fee: U.S. $450 and $495, respectively. Information: Medical Seminars, Dept. of Radiology, West Park Hospital, 22141 Roscoe Blvd., Canoga Park, CA 91304; (818) 340-0580 ext. 280 or (818) 701-1624. 11-4d

ZERMATT, SWITZERLAND, Jan 31-Feb. 8, 1986. Winter Congress. Renowned international faculty presents topics in CT, US, MRI, DSA. Category I accreditation. Fees: To Nov. 11, U.S. $395, thereafter U.S. $435 (with London seminar, U.S. $450 and $495 respectively). Contact: Medical Seminars, Dept. of Radiology, West Park Hospital, 22141 Roscoe Blvd., Canoga Park, CA 91304; (818) 340-0580 ext. 280. 9-1d

LONDON, ENGLAND, Feb. 8-12, 1986. Winter Seminar. Renowned international faculty presents topics in CT, US, MRI, DSA. Category I accreditation. Fees: To Nov. 11, U.S. $350, thereafter U.S. $385 (with Zermatt Congress, U.S. $450 and $495 respectively). Contact: Medical Seminars, Dept. of Radiology, West Park Hospital, 22141 Roscoe Blvd., Canoga Park, CA 91304; (818) 340-0580 ext. 280. 9-1d

AJR Indexes

AJR CONSOLIDATED INDICES available in limited quantities. Complete your journal collection. Order by index number. Indices available, years covered and prices: 2, 1938-1942, $10; 3, 1943-1947, $22.50; 4, 1948-1952, $23.50; 5, 1953-1957, $25; 6, 1958-1962, $23.50; 7, 1963-1967, $30; 8, 1968-1972, $40; 9, 1973-1977, $34. Order from: Subscription Dept., Williams & Wilkins, 428 E. Preston St., Baltimore, MD 21202; (301) 528-4000.

AJR Classified Advertising Information

Box Responses and Address for Ad Placement

Write Box ______, AJR, Suite 306, 909 N.E. 43rd St., Seattle, WA 98105 **until Jan. 31, 1986;** (206) 633-2754.

After Jan. 31, 1986: Write Box ______, AJR, Suite 306, Avienda de la Playa, La Jolla, CA 92037; (619) 459-2229.

How to Place an Ad

AJR accepts classified advertising for Positions Available, Positions Desired, Fellowships and Residencies, and Tutorials/Courses. Ads are accepted by mail or telephone. Institutions should supply purchase orders.

Rates. $6.00/line with a $30 minimum charge. Box service is $10 additional for each month the ad appears. There are discounts for multiple insertions: 10% for 2-3 insertions; 20% for 4 or more. To estimate lines, count all words and divide by 5.5.

Billing: Ads may be prepaid or invoices will be sent after the ad appears.

Deadlines. About 3 weeks before the issue mails. *AJR* issues mail in the middle of the month preceding the cover date (e.g., July mails June 17). For specific deadlines, write or telephone the AJR editorial office.

Estimating Ad Charges

Line charge: divide total words by 5.5 and multiply by $6.00 ..... $ ______

Multiple insertions? If so, multiply by number .... × ______

Subtotal .... $

Box response requested? If so, multiply number of months by $10.00 .... + ______

Subtotal .... $

Discount applies to two or more insertions. Subtract 10% if ad appears 2-3 months, 20% if 4 months or more .... − ______

Approximate advertising charge .... $

INDEX TO ADVERTISERS

Delta Airlines A8
Eastman Kodak A4, A5
Elema Schonander Inc. A9
E-Z-EM Company . . . . Cover 2
Manatee Memorial Hospital A23
Picker International A10, A11
Porta Ray A19
Precise Optics/PME, Inc A13
Purdue Frederick Company A22
Pyne Corporation . . . . Cover 3
Radiology Clinics A23
Siemens Corporation A14, A15
S & S X-Ray A17
Tobias Associates A19
Toshiba Medical Systems A6, A7, A20, A21
United Airlines A16

We try to present an accurate index. Occasionally this may not be possible because of a last-minute change or an omission.

CHIEF DEPARTMENT OF RADIOLOGY:

512 bed acute care hospital on West Florida Coast seeks Chief of Radiology to fill pending vacancy. Major responsibilities include Medical Director of Radiology Department and formation and management of Radiology Group.

Department carries out 60,000 x-ray examinations yearly and has facilities for Ultrasound, CT, Angiography, Digital and Nuclear Medicine. Department is involved in teaching x-ray technologists with various programs for physician-staff development. Future plans include addition of MRI, Cardiac Catheterization, free standing imaging center and possible construction of 2nd hospital.

Send complete curriculum vitae with initial letter of inquiry to Gerald Johnson, Radiology Services, Manatee Memorial Hospital, 206 2nd St. E., Bradenton, FL 33508

DIAGNOSTIC RADIOLOGISTS
CENTRAL CONNECTICUT

Small group: includes hospital and diversified practices. Superior abilities in all areas of radiology.

Physician should have completed one year of fellowship after residency and/or equivalent.

Position open from present time to July 1st.

Board certification necessary.

Send C.V. to
P.O. Box 333,
Durham, Connecticut 06422

Increase your expertise in evaluating CNS lesions

AJNR

American Journal of Neuroradiology

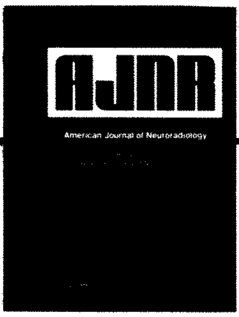

Editor: **Juan M. Taveras, MD**, Harvard Medical School; MGH

Outstanding clinical papers on every aspect of CNS imaging, including spinal diagnosis...informed coverage of head and neck radiology...clear, readable CTs, angiographs, MR imaging and ultrasound studies. These are the features you demand of a quality professional journal. You'll find them in every issue of **AJNR: American Journal of Neuroradiology**.

As you are called upon to perform and interpret more and more sophisticated diagnostic tests — from myelography to CT to newborn ultrasound studies — you need a comprehensive, reliable journal that can keep you abreast of all the latest developments. Each bimonthly issue of **AJNR** brings you timely, clinically pertinent information, as well as important clinical research presented with an eye toward immediate practical application.

Here are just a few of the many excellent articles from the November/December 1985 issue:

Contrast-Enhanced MR Imaging of Malignant Brain Tumors *by Moshe Graif, et al.*

MR Imaging of Cerebral Vascular Malformations *by Benjamin C. P. Lee, et al.*

Cranial Computed Tomography in the Abused Child with Head Injury *by Ronald A. Cohen, et al.*

Cavernous Sinus Invasion by Pituitary Adenomas *by Jamshid Ahmadi, et al.*

Sonography of the Internal Capsule and Basal Ganglia in Infants: 1. Coronal Sections *by Thomas P Naidich, et al.*

Iohexol vs. Metrizamide: Study of Efficacy and Morbidity in Cervical Myelography *by Richard E. Latchaw, et al.*

Superselective Injection of Polyvinyl Alcohol Microemboli for the Treatment of Cerebral Arteriovenous Malformations *by Giuseppe Scialfa and Giuseppe Scott.*

If you can benefit from articles like these, then you should be a regular reader of **AJNR**. Use the attached coupon to subscribe today.

Bimonthly
Personal $95/yr **Institutions** $115/yr **In-training** $65/yr
(add $15.00 outside the US)

☎ ORDER FREE BY PHONE. Just call 1-800-638-6423 from anywhere in the US except AK and HI. MD residents, call 528-4105 *collect.*

Williams & Wilkins
P.O. Box 1496 Baltimore, Maryland 21203
266 Fulham Road London SW10 9EL England

Subscribe to AJNR for 3 years and SAVE

Avoid future rate increases and ensure uninterrupted service by placing a multi-year subscription at current rates.

☐ New subscription ☐ Renewal
☐ 3 yrs ☐ 2 yrs ☐ 1 yr
☐ **Personal** $95 ☐ **Institutions** $115 ☐ **In-training** $65
(add $15.00 outside the US)

☐ Also send me the **1986 Bound Volume** at $45.00 ($50.00 outside the US). $2.00 discount for orders placed before October 1, 1985, and for prepaid orders. I understand that the bound volume is *in addition to* my regular subscription and is available only to subscribers. (To be shipped in early 1987. Sorry, bound volumes for years prior to 1986 are not available.) *All bound volume orders must be received by December 31, 1986.*

☐ Check enclosed ☐ Bill me
☐ VISA ☐ MasterCard ☐ American Express

card # exp.

signature/P.O. #

printed in USA

Name

Address

City/State/Zip

MD residents, please add 5% sales tax. Subscription orders from outside the US must be prepaid in US dollars only.

Residents, Fellows, Interns, and Students: when applying for the in-training rate, available for 3 years, please specify name of institution and training status. Rates valid through October 31, 1986.

Please allow 8 weeks for order processing and delivery of your first issue. Surface mail delivery to countries outside the US may take up to 16 weeks. Airmail rates available upon request.

Williams & Wilkins
P.O. Box 1496
Baltimore, Maryland 21203

266 Fulham Road
London SW10 9EL
England

AJNRAD 94625 86

All the benefits without all the bulk—Williams & Wilkins journals in MICROEDITIONS

AAC: Augmentative and Alternative Communication (*Vol. 1-current*)
Advances in Orthopaedic Surgery (*Vol. 1-current*)
Alcoholism: Clinical and Experimental Research (*Vol. 5-current*)
AJNR: American Journal of Neuroradiology (*Vol. 1-current*)
AJR: American Journal of Roentgenology (*Vol. 132-current*)
The American Journal of Gastroenterology (*Vol. 77-current*)
American Journal of Optometry and Physiological Optics (*Vol. 53-current*)
American Journal of Physical Medicine (*Vol. 1-current*)
The American Journal of Sports Medicine (*Vol. 1-current*)
Critical Care Medicine (*Vol. 1-current*)
Drug Metabolism and Disposition (*Vol. 1-current*)
Ear and Hearing (*Vol. 1-current*)
as Journal of the American Auditory Society (*Vol. 1-5*)
Endocrine Reviews (*Vol. 1-current*)
Endocrinology (*Vol. 102-current*)
Foot & Ankle (*Vol. 1-current*)
Gastrointestinal Endoscopy (*Vol. 1-current*)
Hepatology (*Vol. 1-current*)
Journal of the American Academy of Child Psychiatry (*Vol. 10-current*)
The Journal of Clinical Endocrinology & Metabolism (*Vol. 46-current*)
Journal of Clinical Psychopharmacology (*Vol. 1-current*)
Journal of Developmental and Behavioral Pediatrics (*Vol. 1-current*)
Journal of Endodontics (*Vol. 9-current*)
Journal of Foot Surgery (*Vol. 7-current*)
The Journal of Investigative Dermatology (*Vol. 1-current*)
Journal of Medical Practice Management (*Vol. 1-current*)
The Journal of Nervous and Mental Disease (*Vol. 1-current*)
The Journal of Neuroscience (*Vol. 1-current*)
The Journal of Orthopaedic and Sports Physical Therapy (*Vol. 1-current*)
The Journal of Pharmacology and Experimental Therapeutics (*Vol. 1-current*)
The Journal of Trauma (*Vol. 1-current*)
The Journal of Urology (*Vol. 1-current*)
JPEN: Journal of Parenteral and Enteral Nutrition (*Vol. 1-current*)
Laboratory Investigation (*Vol. 1-current*)
Medicine (*Vol. 1-current*)
Medicine and Science in Sports and Exercise (*Vol. 17-current*)
Molecular Pharmacology (*Vol. 19-current*)
Neurosurgery (*Vol. 1-current*)
Nutrition Today (*Vol. 20-current*)
Obstetrical & Gynecological Survey (*Vol. 1-current*)
Pediatric Emergency Care (*Vol. 1-current*)
Pediatric Infectious Disease (*Vol. 1-current*)
Pediatric Research (*Vol. 1-current*)
Pharmacological Reviews (*Vol. 1-current*)
Plastic and Reconstructive Surgery (*Vol. 1-current*)
SGA Journal (*Vol. 7, #3-current*)
Soil Science (*Vol. 1-current*)
Stain Technology (*Vol. 1-current*)
Survey of Anesthesiology (*Vol. 1-current*)
Transplantation (*Vol. 1-current*)

These journals are available in microfilm only—no longer published by Williams & Wilkins (call for availability)

Acta Cytologica • Behavioral Medicine Abstracts • Cytometry • Gastroenterology • Investigative Urology • Journal of Criminal Law and Criminology • Journal of Histochemistry and Cytochemistry • The Journal of Immunology • Urological Survey

MICROFILM FORMATS:

16 mm reel	35mm reel
16 mm cartridges (3M or KODAK)	positive or negative film

$55/reel (price subject to change without notice)

MICROFICHE:
contact KRAUSE MICROFORM

ORDERING INFORMATION

MICROFICHE
KRAUSE MICROFORM
Route 100, Millwood, NJ 10546
MICROFILM
WILLIAMS & WILKINS
Microfilm Sales
attn: Yvonne Hahn
428 East Preston Street
Baltimore, MD 21202
(301) 528-4144

SANS TACHE Williams & Wilkins

printed in USA JRNLAD 94627 85

If Finding Medical Art is a Chronic Problem . . .

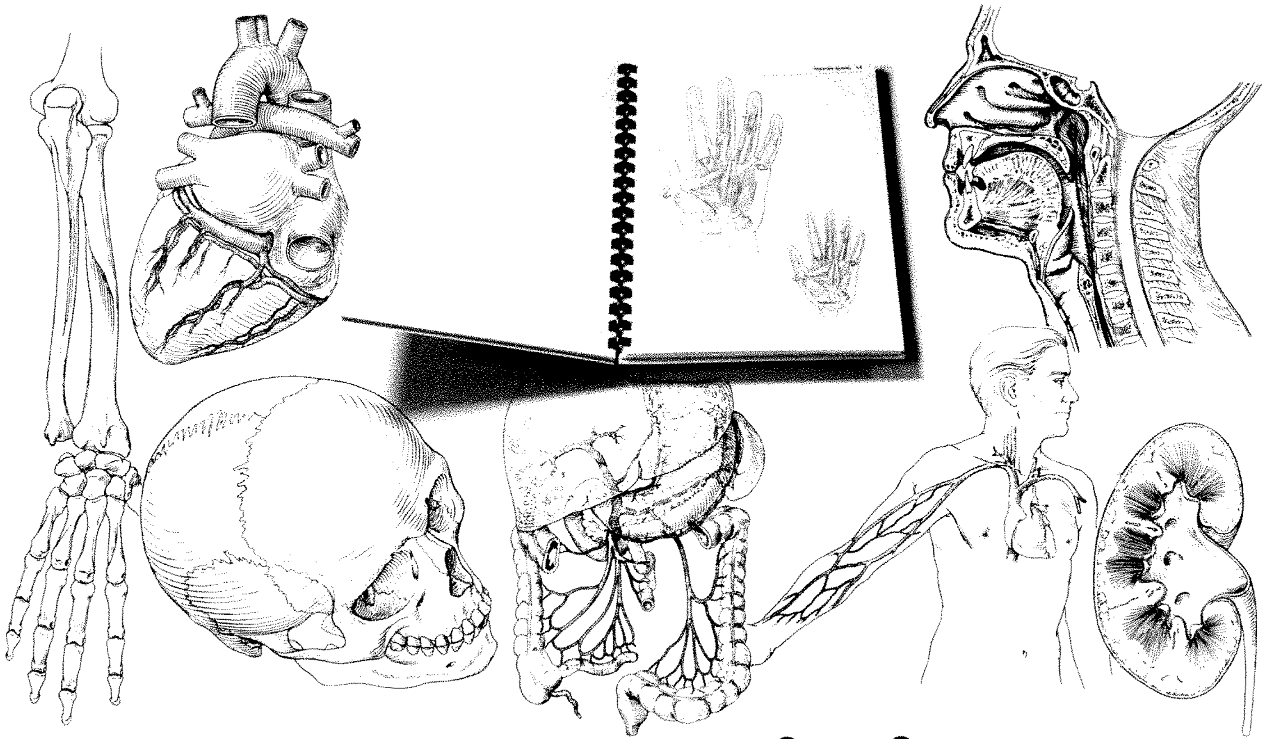

See a Specialist

MEDICAL ART
Graphics for Use
Diane L. Abeloff, MA, AMI

Professional medical illustrator Diane Abeloff has produced a book of high quality anatomical drawings that you can use without reproduction fees. There are 250 clear and anatomically correct line drawings covering all systems of adult human anatomy.

The pages have been printed on one side only to make it easy to clip the figures. And each figure is large enough for you to modify to fit your individual needs. Both ink and felt-tip pens work well on the paper.

The figures may be used as originals or reproduced for slides, for overhead projectors, or as dittos. They're perfect for illustrating papers or any published material . . . creating teaching aids that bring medical terms to life . . . or any project that calls for anatomically correct drawings.

So order your copy today—the next time you need medical illustrations, you won't have to look any farther than your bookshelf.

Williams & Wilkins
Dept. M6, Box 1496, Baltimore, MD 21203

Examine this outstanding collection of medical illustrations free for 20 days.

Please send me

______ copy(ies) of Diane Abeloff's **Medical Art: Graphics for Use** (0033-0) at $68.00 per copy (*$79.00 outside the U.S.*)

☐ Bill me. ☐ VISA
☐ Payment enclosed. ☐ MasterCard

card # ______ exp. date ______

Residents of California, Maryland and Virginia, please add state sales tax. Prices subject to change without notice.

☎ **ORDER TOLL-FREE** . . . from anywhere in the US except Alaska and Hawaii by calling 1-800-638-0672. From area code 301, call 528-4221 collect.

name ______

address ______

city/state/zip ______

Williams & Wilkins
Dept. M6, Box 1496, Baltimore, MD 21203

Printed in U.S.A. ABELAD 77777 82

THE ALTERNATIVE

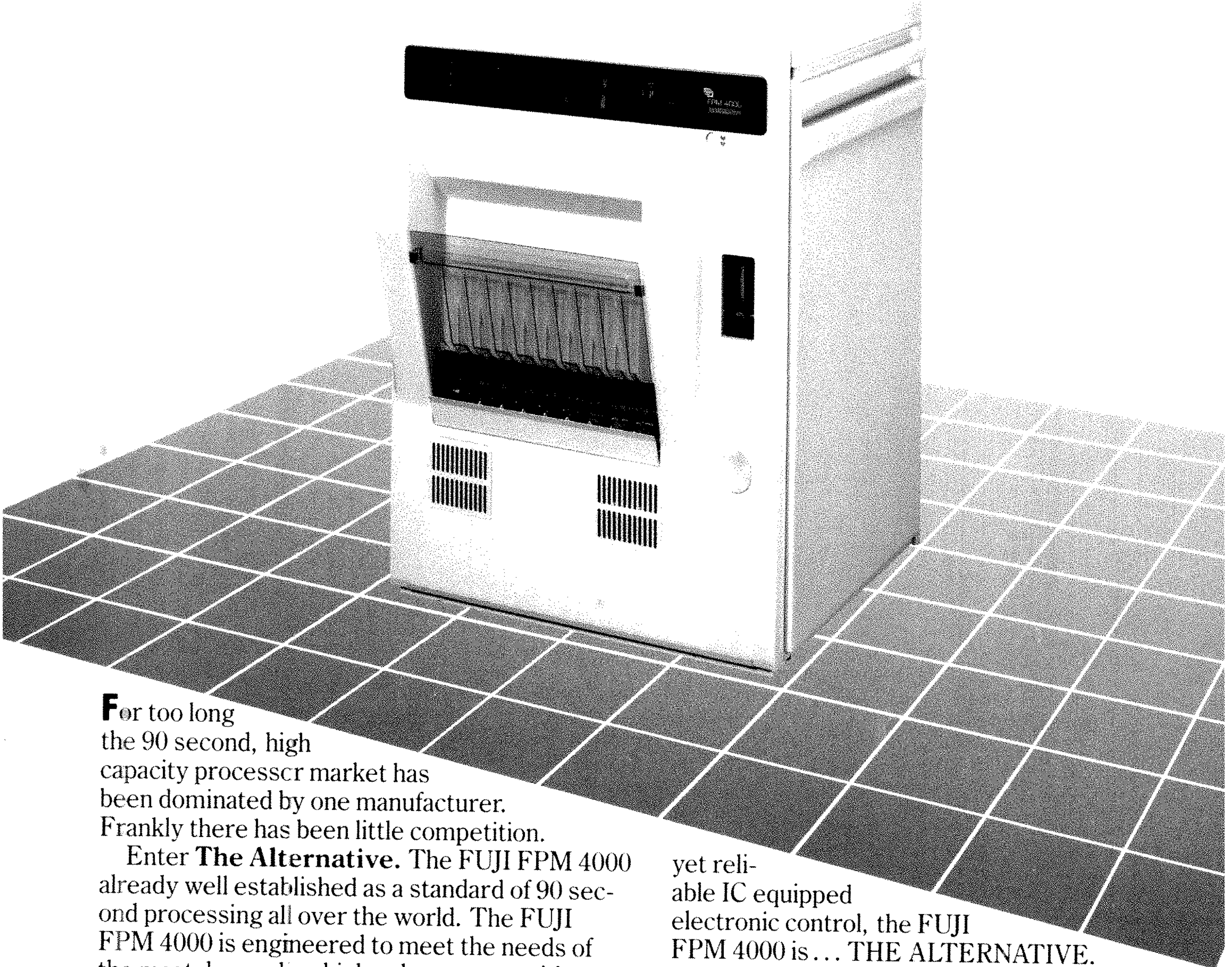

For too long the 90 second, high capacity processor market has been dominated by one manufacturer. Frankly there has been little competition.

Enter **The Alternative.** The FUJI FPM 4000 already well established as a standard of 90 second processing all over the world. The FUJI FPM 4000 is engineered to meet the needs of the most demanding high volume user, with accent on **reliability** and **ease of operation.** With features like cold water operation, built-in standby, waist high film delivery, high capacity (229 14 x 17 sheets per hour) and sophisticated yet reliable IC equipped electronic control, the FUJI FPM 4000 is... THE ALTERNATIVE.

Isn't it nice to finally have a choice?

THE FUJI FPM 4000— A Reason for Change!

For more information call your local Pyne representative,
or call toll free (800) 431-1850
(in New York 914-834-4567)

PYNE CORPORATION
20 North Avenue, Larchmont, NY 10538

Volume 146 **American Journal of Roentgenology** January 1986

GASTROINTESTINAL RADIOLOGY

1 **Multifocal abnormalities of the gastrointestinal tract in AIDS.** *Wall SD, Ominsky S, Altman DF, et al.*
7 **Review. Abdominal CT in acquired immunodeficiency syndrome.** *Jeffrey RB Jr, Nyberg DA, Bottles K, et al.*
15 **Velopharyngeal insufficiency on videofluoroscopy: comparison of projections.** *Stringer DA, Witzel MA*
21 **Radiologic amyl nitrite test for distinguishing pseudoachalasia from idiopathic achalasia.** *Dodds WJ, Stewart ET, Kishk SM, Kahrilas PJ, Hogan WJ*
25 **The esophagus after endoscopic pneumatic balloon dilatation for achalasia.** *Agha FP, Lee HH*
31 **Serpiginous gastric erosions caused by aspirin and other nonsteroidal antiinflammatory drugs.** *Levine MS, Verstandig A, Laufer I*
35 **The effect of barium suspension viscosity on the delineation of areae gastricae.** *Rubesin SE, Herlinger H*
39 **Radiologic manifestations of small-bowel toxicity due to floxuridine therapy.** *Kelvin FM, Gramm HF, Gluck WL, Lokich JJ*
45 **Coiled-spring sign of the cecum in acute appendicitis.** *Demos TC, Flisak ME*
49 **Floating gallstones in bile without added contrast material.** *Yeh HC, Goodman J, Rabinowitz JG*

GENITOURINARY RADIOLOGY

51 **MRI of the kidneys in paroxysmal nocturnal hemoglobinuria.** *Mulopulos GP, Turner DA, Schwartz MM, Murakami ME, Clark JW*
53 **Sonography of the hypertrophied column of Bertin.** *Lafortune M, Constantin A, Breton G, Vallee C*
57 **Retroperitoneal fibrosis: use of CT in distinguishing among possible causes.** *Degesys GE, Dunnick NR, Silverman PM, Cohan RH, Illescas FF, Castagno A*
61 **Retrograde ureteral catheterization via the ileal conduit.** *Applbaum YN, Diamond AB, Rappoport AS*
64 **Diagnostic oncology case study. Clear cell sarcoma of the kidney: a renal tumor of childhood that metastasizes to bone.** *Sleight G, Lock MM, Kagan AR, Steckel RJ*
67 **Radiologic-pathologic correlation conference: SUNY Upstate Medical Center. Flank mass and hypertension.** *Pollack H, Kenney PJ, McAfee JG, et al.*

THORACIC RADIOLOGY

73 **"Solid" mediastinal bronchogenic cyst: mineralogic analysis.** *Yernault JC, Kuhn G, Dumortier P, Rocmans P, Ketelbant P, De Vuyst P*
75 **Measurement of normal left heart dimensions using optimally oriented MR images.** *Kaul S, Wismer GL, Brady TJ, et al.*

SKELETAL RADIOLOGY

81 **Critical evaluation of the radial head–capitellum view in elbow trauma.** *Page AC*
83 **Trampoline fracture of the proximal tibia in children.** *Boyer RS, Jaffe RB, Nixon GW, Condon VR*
87 **Negative bone scans of joints after aspiration or arthrography: experimental studies.** *Traughber PD, Manaster BJ, Murphy K, Alazraki NP*

PALEORADIOLOGY

93 **Modern imaging and endoscopic biopsy techniques in Egyptian mummies.** *Notman DNH, Tashjian J, Aufderheide AC, et al.*

NEURORADIOLOGY

97 **Cranial computed tomography in the abused child with head injury.** *Cohen RA, Kaufman RA, Myers PA, Towbin RB*
103 **Value of intravenous contrast enhancement in the CT evaluation of intraspinal tumors.** *Lapointe JS, Graeb DA, Nugent RA, Robertson WD*
109 **Sonographic appearance of the torcular herophili.** *Segal SR, Rosenberg HK*
113 **Cystic neuroblastoma in infants: radiographic and pathologic features.** *Atkinson GO Jr, Zaatari GS, Lorenzo RL, Gay BB Jr, Garvin AJ*

BREAST IMAGING

119 **Magnetic resonance imaging in the diagnosis of breast disease.** *Dash N, Lupetin AR, Daffner RH, Deeb ZL, Sefczek RJ, Schapiro RL*
127 **Male mammography.** *Dershaw DD*
133 **Breast cancer metastasis to intramammary lymph nodes.** *Lindfors KK, Kopans DB, McCarthy KA, Koerner FC, Meyer JE*

ANGIOGRAPHY AND INTERVENTIONAL RADIOLOGY

137 **Hepatic artery thrombosis after liver transplantation: radiologic evaluation.** *Segel MC, Zajko AB, Bowen AD, et al.*
143 **Angiographic and interventional radiologic considerations in liver transplantation.** *Cardella JF, Castaneda-Zuniga WR, Hunter D, Young A, Amplatz K*
155 **Abdominal pseudoaneurysm arising from a true aneurysm: presentation as a pulmonary mass.** *Shin MS, Ho KJ, Kirklin JW, Forman JM, Berland LL*
157 **Complications of intraarterial urokinase-lys-plasminogen therapy in arterial ischemia of lower limbs.** *Fiessinger JN, Vitoux JF, Pernes JM, Roncato M, Aiach M, Gaux JC*
160 **Suture anchor for visceral drainage.** *Cope C*
163 **CT body stereotaxis: an aid for CT-guided biopsies.** *Onik G, Costello P, Cosman E, et al.*
169 **Modification of the Cope drainage catheter to facilitate placement.** *Berman HL, Bakal CW, Katz SG*

OTHER CONTENT

171 **Editorials. Changing of the guard.** *Berk RN;* **Radiology manpower: where are we?** *Riemenschneider PA*
174 **Letters**
176 **Abstracts**
181 **ARRS 1986 meeting invitation**
183 **ARRS scientific program**
189 **ARRS section on instruction**
199 **ARRS local activities**
201 **ARRS registration forms**
205 **ARRS meeting summary**
206 **News**
209 **Classified ads**
Editorial office address change 6, 108
Book reviews 14, 20, 24, 30, 44, 80, 86
118 **Memorial**
A2 **Guidelines for authors**
S1 **ARRS meeting packet (insert)**

1986 ARRS Meeting: April 13–18, Sheraton Washington (DC)

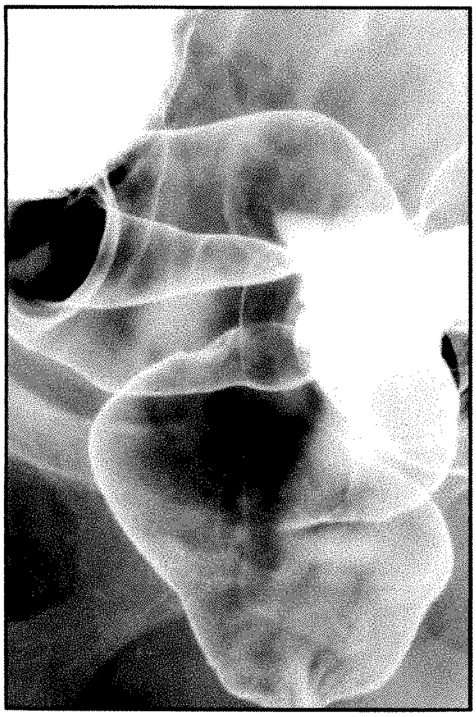

LIQUID POLIBAR™
X-Ray courtesy of Dr. Alec J. Megibow
N.Y.U. Medical Center University Hospital
New York, NY 10016

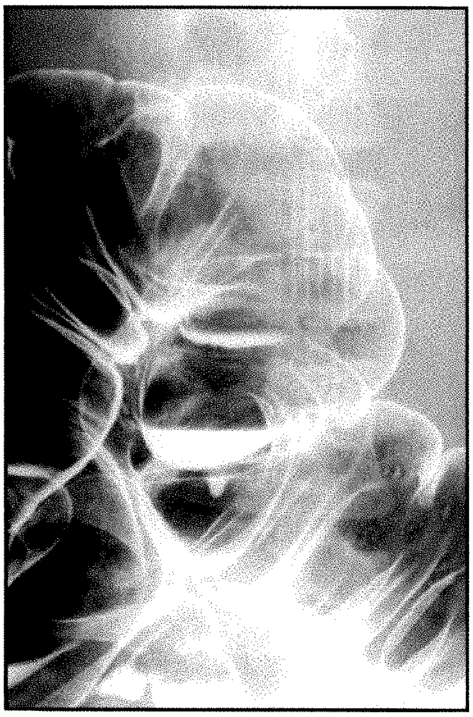

E-Z-AC™
X-Ray courtesy of Dr. Igor Laufer
Hospital of the University of Pennsylvania
Philadelphia, PA 19104

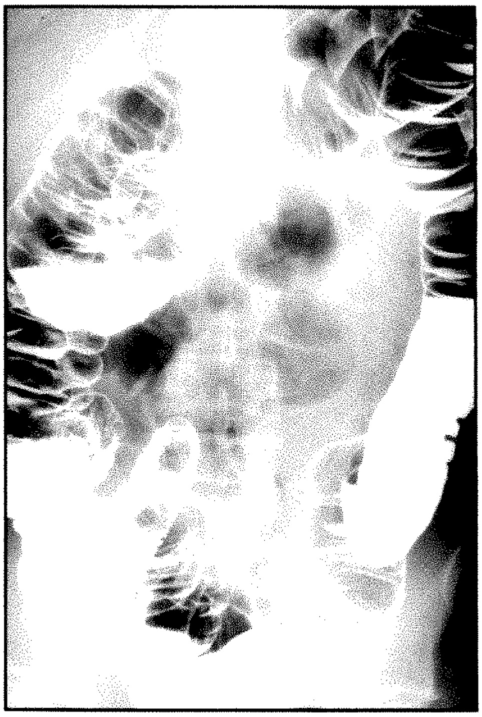

LIQUID POLIBAR™ PLUS
X-Ray courtesy of Dr. David W. Gelfand
Bowman Gray School of Medicine, Wake Forest University
Winston-Salem, NC 27102

Three bariums for superior air-contrast results.

Air Contrast Colon: The procedure of choice with the systems of your choice.

Liquid Polibar™

The original air contrast colon barium with superb coating characteristics. Optimum viscosity assures consistent even coating throughout. Truly the bench mark formulation for air contrast studies.

E-Z-AC™

This fast flowing liquid barium reaches the splenic flexure in only 20 to 30 seconds. Specifically formulated for air contrast procedures where a cleansing enema has not been administered that morning.

Introducing: Liquid Polibar™ Plus

The classic Liquid Polibar formulation modified to achieve a faster flow rate. It has the excellent coating characteristics that you expect from a Polibar formula but is more attuned to the speed necessary in the modern radiology department. Polibar Plus—increased speed and diagnostic consistency.

For samples and additional information, please contact your local E-Z-EM distributor or call E-Z-EM directly.

E-Z-EM

E-Z-EM, Inc. 7 Portland Avenue, Westbury, NY 11590 516-333-8230 800-645-3052

© E-Z-EM, Inc. 1985

Official Journal
American Roentgen Ray Society

AJR

Diagnostic Imaging and Related Sciences

Editor Robert N. Berk

Associate Editors Alan J. Davidson
Saskia vonWaldenburg Hilton

Associate Editor, Neuroradiology Juan M. Taveras

Consulting Editorial Board Christos A. Athanasoulis
Edward Buonocore • Peter L. Cooperberg • John L. Doppman
Kent Ellis • Robert H. Freiberger • Reginald Greene
N. Thorne Griscom • William R. Hendee • Eugene C. Klatte
John G. McAfee • William B. Seaman • Michel M. Ter-Pogossian
Joseph P. Whalen • David M. Witten

Editorial Staff Gita Braude • Elizabeth Whalen
Barbara Rose • Linda Wood

All business correspondence, including display (not classified) advertising, subscriptions, address changes, reprints, and permission requests should be addressed to Williams & Wilkins, 428 East Preston Street, Baltimore, MD 21202. Correspondence regarding editorial matters and classified advertising should be addressed to the editorial office, AJR, 2223 Avenida de la Playa, Suite 306, La Jolla, CA 92037. For manuscript submission, see Guidelines for Authors, next page. Undelivered or damaged copies replaced within 60 days of publication; 90 days for foreign subscribers. Allow 90 days for address changes.

AJR AMERICAN JOURNAL OF ROENTGENOLOGY (ISSN 0361 803X) is published monthly by American Roentgen Ray Society, 428 E. Preston Street, Baltimore, MD 21202. Annual dues include $50 for journal subscription. Second class postage paid at Baltimore, MD and at additional mailing offices. Postmaster send address changes (Form 3579) to Williams & Wilkins, 428 East Preston St., Baltimore, MD 21202. Subscription rates $90 ($115 foreign); institutions $100 ($125 foreign); in training $25; single copy $16 ($19). Japanese Yen price is available from our sole agent USACO Corporation, 13-12, Shimbashi 1-Chome, Minato-Ku, Tokyo 105, Japan, telephone 03-502-6471. Airmail rates furnished on request. Indexed by *Current Contents* and *Index Medicus*. Copyright © 1986 by American Roentgen Ray Society.

0361-803X/86 $2.00

AJR Guidelines for Authors

Address new and revised manuscripts, correspondence, and classified ads to:

AJR Editorial Office
2223 Avenida de la Playa, Suite 306
La Jolla, CA 92037
telephone: (619) 459-2229

Make inquiries regarding subscriptions, display advertising, reprints, or permission to republish *AJR* material to the publisher:

The Williams & Wilkins Co.
428 E. Preston St.
Baltimore, MD 21202
telephone: (301) 528-4133

Publication Policy

The *AJR* publishes original and timely contributions to the advancement of medical diagnosis and treatment with radiologic methods. Although content is predominantly clinical, laboratory investigations are accepted when their relevance to clinical practice is demonstrable. In prospective clinical investigations, authors should document that informed consent was obtained from patients. The material submitted **must** not have been previously published nor be currently submitted for publication elsewhere (prior publication of simple abstracts without illustrations or tables will not prejudice publication of the complete study). Papers dealing with **neuroradiology** should be addressed to: Editorial Office, American Journal of Neuroradiology, Dept. of Radiology, Massachusetts General Hospital, Boston, MA 02114; telephone: (617) 726-8342. At the discretion of the Editor of *AJR*, *AJNR* articles may be republished in *AJR*.

Decisions on manuscripts are based on peer review. Reviewers receive manuscripts without title pages to protect the identity of authors and to ensure an unbiased review; names of reviewers, in turn, are not revealed to the authors. Accepted manuscripts are subject to editing. Statements within an article, including changes made by the Editor or copy editor, are the responsibility of the author and not *AJR* or its publisher. Authors will receive the edited manuscript, galley proof, and proofs of illustrations usually 6–8 weeks after acceptance. If the corresponding author will not be available, arrangements should be made for a coauthor or colleague to read and return the proof.

Copyright Information

In accordance with *AJR* implementation of the U.S. Copyright Law, authors must release first and subsidiary rights to their manuscript at submission (unless the study was performed as part of their duties as an employee of a U.S. government agency). A dated letter with the signatures of all authors should state: "We, the authors, assign first and subsidiary rights to the American Roentgen Ray Society in the event that our manuscript [insert title] is published by *AJR*. We guarantee that this manuscript contains no matter libelous or otherwise unlawful or which invades individual privacy or which infringes any proprietary right. *AJR*, in turn, grants us the right of republication, subject only to crediting the original source of publication and receiving written permission from the publisher. We understand we will receive no royalty or other compensation from *AJR*. We guarantee that this article and illustrations have not been previously published elsewhere or, if previously published in part or in whole, that permission has been obtained for republication. Copies of these permissions are included and previously published text or illustrations have been identified in the manuscript." (Delete the last sentence if it does not apply.) The covering letter also should state that the manuscript has been seen and approved by all the authors.

Manuscript Form

AJR complies with the Uniform Requirements for Manuscripts Submitted to Biomedical Journals (*Ann Intern Med* 1979;90:95–99). Manuscripts must be ***typed double-space throughout***, including references, tables, and figure legends. Each table, the footnotes, and the figure legend section should begin on separate sheets; a separate title page should be provided. Send the original typescript, one copy, and two sets of illustrations (not photocopies). Authors' names should be on the title page **only** so that author anonymity can be maintained during the review process. Permission to reprint previously published material should accompany the manuscript.

Organization of Major Articles

Title Page

Titles should be brief yet precise, accurately conveying the content of the paper. Limit authors to those who made substantial contributions to the work. Include an address for *each* author, and ZIP or postal code; acknowledgment of grant or other financial support when appropriate; name of meeting, location, and date if the paper was presented; a running head (shortened title); and the name, address, and telephone number of the author to whom correspondence and requests for reprints should be addressed.

Abstract

A description of the purpose, methods, results, and conclusions of the study is required. The factual highlights of each section should be recapitulated.

Introduction

Clearly state the purpose of the investigation, including necessary background facts that indicate its current relevance.

Materials [or Subjects] and Methods

Describe the research plan, the materials or subjects, and the methods, in that order. Proof of disease and control of subjectivity in observations should be detailed. Metric measurements should be used throughout. Put measurements in the International System of Units (SI) in parentheses when appropriate; for example, 400 rad (4 Gy).

Results

Present results in logical sequence. If tables are used, do not duplicate tabular data but do describe important points and trends.

Case Reports

Individual cases can be described if there are only a few; one or more cases from a large series can be described individually as Representative Case Reports. Each report should concentrate on the radiologic information and its usefulness.

Discussion

Offer appropriate limitations about the research plan, materials or subjects, and methods to give perspective to their adequacy for the purpose of the study. Interpret the results to lend meaning and importance to the observations. Hypotheses and speculation based

on the results are encouraged. When results differ from those of previous investigations, an attempt should be made to explain the discrepancy. Conclude with a brief statement regarding clinical significance.

Acknowledgments

Acknowledge only persons who have made *substantive* contributions to the study. Mention grant support on the title page.

References

References should be offered to document major assertions of fact and any opposing evidence and concepts. Discretion in number is requested. References should be cited in the text by number (e.g., [3, 4]). The reference list should be arranged in the numeric order that references are cited in the text and ***typed double-spaced throughout***. References cited *first* or *only* in tables or figure legends should be numbered by the sequence in which the table or figure is first identified in the text. Data for each reference should be arranged according to the style adopted by the U.S. National Library of Medicine and used in *Index Medicus*. ***Accuracy of reference data is the responsibility of the author.*** Provide all authors' (or editors') names when fewer than seven; when seven or more, list the first three and add et al. Provide inclusive page numbers; if an article is only one page, please indicate. Abbreviations for titles of medical periodicals should conform to those published in *Index Medicus*. Articles that appear in both *AJR* and *AJNR* should be a single reference that cites both journals (example 3). Examples:

1. Kirks DR, Fram EK, Vock P, Effmann EL. Tracheal compression by mediastinal masses in children: CT evaluation. AJR 1983;141:647–651
2. Khansur T, Yam LT, Tavassoli M. Serum monitors of bone metastasis. In: Stoll BA, Parbhoo S, eds. Bone metastases: monitoring and treatment. New York: Raven, 1983:165–180
3. Sage MR. Review. Kinetics of water-soluble contrast media in the central nervous system. AJNR 1983;4:897–906, AJR 1983; 141:815–824

Unpublished data and personal communications should not be numbered references but should be put in parentheses in the text (e.g., Smith JD, personal communication).

Tables

Tables should be concise and organized to show trends, not merely compilations of raw data. (The Editor may request that tables of backup data too extensive to be published be deposited with the National Auxiliary Publications Service or made available by the author.) Include only data pertinent to the subject. Long itemized case histories are better presented in the text as case reports or summaries. Do not repeat in tabular form material presented in the text. Tables should have titles and headings, but no vertical or horizontal rules.

Illustrations

Figures should be submitted as 13 × 18 cm (5 × 7 inch) glossy, black-and-white prints, ***untrimmed and unmounted***. Labels and arrows must be of professional quality and removable. Number each figure to correspond with the figure legends and indicate the top. Avoid writing directly on the back of the print. Special permission for publication of facial photographs of patients or for previously published pictures is required. Line illustrations or graphs must be professionally drawn in black ink on white background. please send photographic prints (not photocopies), not originals, to avoid damage in handling. Color illustrations will be used at the discretion of the Editor; send color prints. Firm estimates of cost will be sent to the author(s) for approval before publication. Identical anatomic structures in color prints should be the same size to facilitate reproduction and reduce cost.

Legends

Figure legends should carry a title identifying the message of the illustration and the case number if individual cases are described in the text. Legends should be as brief as possible for the informed reader to understand the figure. Detailed clinical data should be avoided. Legends for previously published illustrations should cite the reference number of the source (e.g., Reprinted from [8]).

Organization of Case Reports

Concise case reports will be considered for publication if they present unusual experiences that are medically important and instructive. Clarity and brevity are essential. After preliminary screening by an editor to determine whether the requirement of medical significance has been met, qualifying papers will undergo the same peer review as major papers. To facilitate planning the order and layout of each issue, case reports are limited in length to two journal pages. The introduction should be one short paragraph that gives some general background of the disorder and the specific interest and message of the case presented. Only one case should be described in detail. The case report should concentrate on the radiologic information and its usefulness. The discussion should focus on the specific message of this report and the relevance of radiology in this instance. If the author has encountered other cases, they may be briefly mentioned, and possibly illustrated, but not described in detail. There should be no more than eight references. The figures should be limited to the minimum required to document the case findings, probably not more than four pictures, each a column wide (or the equivalent). Excess illustrations would require severely shortening the text. Figure legends should be as short as possible and should not repeat the text. There can be no tables and no acknowledgments. See previous sections for detailed instructions regarding references and illustrations.

Other Contributions

Technical Notes

Brief descriptions of new techniques or significant modifications of older ones that are directly applicable to the clinical practice will be accepted if review is favorable. Technical notes do not carry abstracts or acknowledgments.

Letters to the Editor

Letters are subject to editing and condensation. Criticism of published articles should be objective and constructive. Letters also may discuss matters of general interest to radiologists.

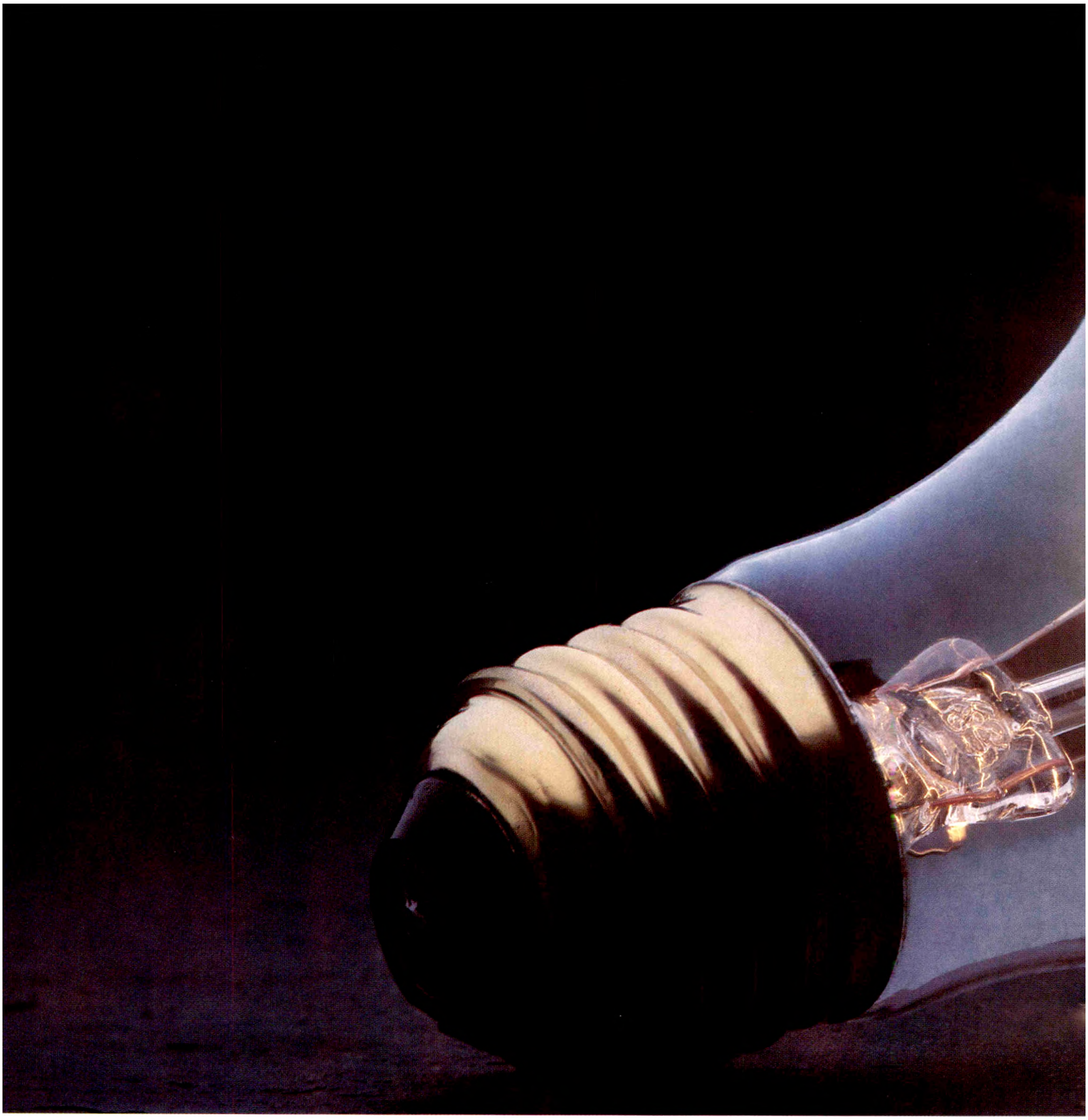

Roomlight film handling.
Light makes it efficient. Kodak makes it reliable.

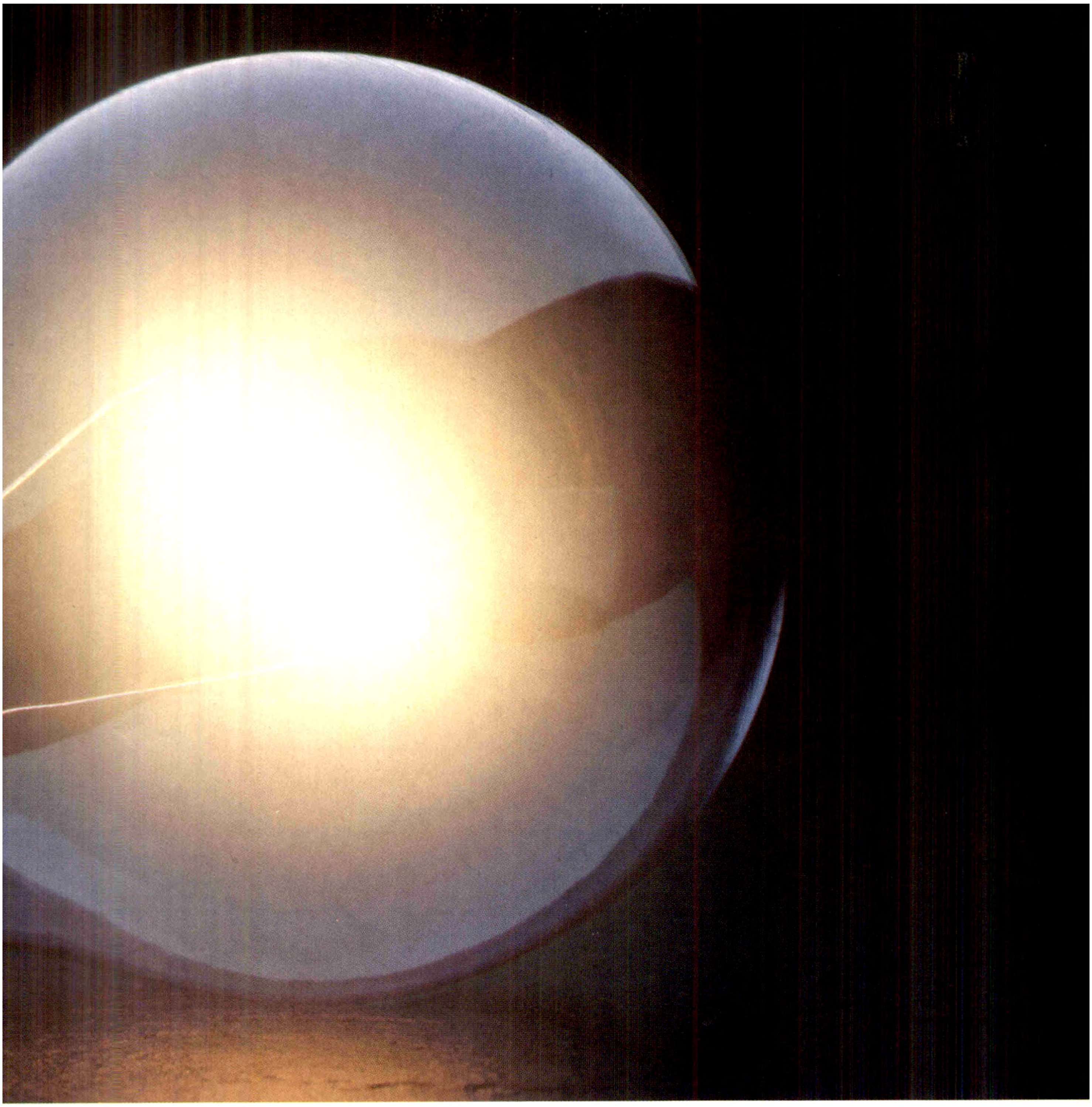

An ordinary light bulb, bright and unfiltered, does wonders for the film-handling efficiency when you combine it with a reliable Kodak roomlight film-handling system. There are two Kodak systems now: centralized and dispersed. One or the other, or some of each, can increase efficiency in any radiology department, whatever the layout.

Kodaflex products.
A flexible, dispersed roomlight system, with versions for both radiographic and video imaging. So flexible it's equally ideal for the main radiology facility or in satellites and emergency rooms. And so reliable, you'll know it's from Kodak. Part of a larger system that includes your favorite Kodak films, screens, and processors.

Kodak multiloader II.
Centralized roomlight equipment that expands your department's capacity without expanding its size. The Kodak multiloader II for Kodak X-Omatic cassettes unloads the film, sends it to a Kodak X-Omat processor, reloads the cassette, and returns it—all in about 15 seconds!

The multiloader II fits into almost any existing layout and, best of all, lets you take advantage of the excellent screen/film contact of your own Kodak X-Omatic cassettes, with no need to invest in new cassettes. Talk to your Kodak representative, or write Eastman Kodak Company, Department 412-LRI, 343 State St., Rochester, NY 14650.

Can you afford anything less?

Kodak

BREAK THROUGH
TO THE NEW STANDARD
IN ANGIOGRAPHIC IMAGING

5605
50 ml
STERILE SOLUTION
HEXABRIX®
(Ioxaglate Meglumine 39.3% and
Ioxaglate Sodium 19.6% Injection)
Each milliliter of solution provides
320 mg of organically bound iodine
FOR INTRAVASCULAR USE
CAUTION: Federal (U.S.A.) law prohibits
dispensing without prescription.
Store Below 30°C (86°F) Do Not Freeze
Mallinckrodt®
Diagnostic Products Division
Mallinckrodt, Inc.
St. Louis MO 63134 USA

HEXABRIX®

(Ioxaglate Meglumine 39.3% and
Ioxaglate Sodium 19.6% Injection)

Another first from Mallinckrodt

CLINICAL EXPERIENCE
WITH OVER 3 MILLION
PROCEDURES WORLDWIDE

A True "Ratio 3" Agent with a unique chemical structure

The osmolality of contrast media is determined by the number of particles in solution the more particles per kilogram of water, the higher the osmolality. Conventional contrast media (ratio 1.5 agents) have a ratio of 3 iodine atoms for every 2 particles in solution and an osmotic activity of 5 to 8 times that of human plasma, depending on their iodine concentration.

Hexabrix: Low Osmolality (600 mOsm/Kg H_2O)
Hexabrix achieves lower osmolality by decreasing the number of particles in solution while maintaining the concentration of iodine for radiographic quality. It is a true "ratio 3" agent as it provides double the number of iodine atoms (6) for every 2 osmotically active particles in solution (6:2 or 3:1). Theoretically, the osmolality of Hexabrix should be ½ that of a conventional (ratio 1.5) agent at the same iodine concentration. In actuality, however, the osmolality of Hexabrix is less than ½ that of such conventional ionic contrast media. This further reduction in osmolality is attributed to submicroscopic aggregation of particles in solution.

The Hexabrix Structure
Hexabrix, an ionic monoacid dimeric contrast medium, accomplishes a reduction in osmolality through a unique chemical structure; it provides 6 iodine atoms per 2 particles in solution (6:2 or 3:1), and an iodine content of 32% or 320 mg/ml.

New low osmolality contrast agent specifically for intravascular procedures

- CEREBRAL ANGIOGRAPHY
- SELECTIVE CORONARY ARTERIOGRAPHY (with or without left ventriculography)
- PERIPHERAL ARTERIOGRAPHY
- SELECTIVE VISCERAL ARTERIOGRAPHY

Hexabrix: Responding to physician concerns

REDUCED PAIN

> "Ioxaglate fulfilled our requirements as a contrast medium for use in femoral angiography in severely arteriosclerotic patients as it significantly reduced the pain and discomfort felt by the patients and enabled them to stay calm during the examination."[1]

REDUCED HEAT

> In a study involving carotid arteriography in 33 patients, "30 patients preferred the ioxaglate solution [Hexabrix] which caused significantly less sensation of heat."[2]

HIGH OSMOLALITY
All conventional contrast agents

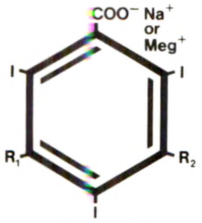

3:2
3 iodine atoms:
2 ionized particles
"Ratio 1.5"

LOW OSMOLALITY
Hexabrix

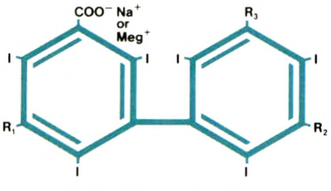

6:2=3:1
6 iodine atoms:
2 ionized particles
"Ratio 3"

STERILE SOLUTION
HEXABRIX
Ioxaglate Meglumine 39.3% and Ioxaglate Sodium 19.6% Injection
FOR INTRAVASCULAR USE

THE MALLINCKRODT COMMITMENT to Angiography

Mallinckrodt®

Diagnostic Products Division
Mallinckrodt, Inc.
Post Office Box 5840
St. Louis, MO 63134

For orders call:
800-354-7442 Toll-Free
(In Kentucky, 606-987-7000 collect)
For medical and/or technical information
800-543-3000, ext. 9009 Toll-Free
(In Ohio, 800-582-1364, ext. 9009 Toll-Free)

HEXABRIX*®

(Ioxaglate Meglumine 39.3% and Ioxaglate Sodium 19.6% Injection)

HEXABRIX®

(Ioxaglate Meglumine 39.3% and Ioxaglate Sodium 19.6% Injection)

Each milliliter of HEXABRIX contains 393 mg of ioxaglate meglumine, 196 mg of ioxaglate sodium and 0.10 mg edetate calcium disodium as a stabilizer. The solution contains 3.48 mg (0.15 mEq) sodium in each milliliter and provides 32% (320 mg/ml) organically bound iodine.

CONTRAINDICATIONS

HEXABRIX is contraindicated for use in myelography.

Refer to PRECAUTIONS, General, concerning hypersensitivity.

WARNINGS

Serious or fatal reactions have been associated with the administration of iodine containing radiopaque media. It is of utmost importance to be completely prepared to treat any contrast medium reaction.

As with any contrast medium, serious neurologic sequelae, including permanent paralysis, can occur following cerebral arteriography, selective spinal arteriography and arteriography of vessels supplying the spinal cord. The injection of a contrast medium should never be made following the administration of vasopressors since they strongly potentiate neurologic effects.

A definite risk exists in the use of intravascular contrast agents in patients who are known to have multiple myeloma. In such instances anuria has developed resulting in progressive uremia, renal failure and eventually death. Although neither the contrast agent nor dehydration has separately proved to be the cause of anuria in myeloma, it has been speculated that the combination of both may be causative factors. The risk in myelomatous patients is not a contraindication to the procedure; however, partial dehydration in the preparation of these patients for the examination is not recommended since this may predispose to precipitation of myeloma protein in the renal tubules. No form of therapy, including dialysis, has been successful in reversing the effect. Myeloma, which occurs most commonly in persons over 40, should be considered before instituting intravascular administration of contrast agents.

Administration of radiopaque materials to patients known or suspected to have pheochromocytoma should be performed with extreme caution. If, in the opinion of the physician, the possible benefits of such procedures outweigh the considered risks, the procedures may be performed; however, the amount of radiopaque medium injected should be kept to an absolute minimum. The blood pressure should be assessed throughout the procedure, and measures for treatment of a hypertensive crisis should be available.

Since intravascular administration of contrast media may promote sickling in individuals who are homozygous for sickle cell disease, fluid restriction is not advised.

In patients with advanced renal disease, iodinated contrast media should be used with caution and only when the need for the examination dictates, since excretion of the medium may be impaired. Patients with combined renal and hepatic disease, those with severe hypertension or congestive heart failure and recent renal transplant recipients present an additional risk.

Renal failure has been reported in patients with liver dysfunction who were given an oral cholecystographic agent followed by an intravascular iodinated radiopaque agent and also in patients with occult renal disease, notably diabetics and hypertensives. In these classes of patients there should be no fluid restriction and every attempt made to maintain normal hydration, prior to contrast medium administration, since dehydration is the single most important factor influencing further renal impairment.

Caution should be exercised in performing contrast medium studies in patients with endotoxemia and/or those with elevated body temperatures.

Reports of thyroid storm occurring following the intravascular use of iodinated radiopaque agents in patients with hyperthyroidism or with an autonomously functioning thyroid nodule, suggest that this additional risk be evaluated in such patients before use of this drug. Iodine-containing contrast agents may alter the results of thyroid function tests which depend on iodine estimation, e.g., PBI, and may also affect results of radioactive iodine uptake studies. Such tests, if indicated, should be performed prior to the administration of this preparation.

PRECAUTIONS

Diagnostic procedures which involve the use of iodinated intravascular contrast agents should be carried out under the direction of personnel skilled and experienced in the particular procedure to be performed. All procedures utilizing contrast media carry a definite risk of producing adverse reactions. While most reactions are minor, life-threatening and fatal reactions may occur without warning, and this risk must be weighed against the benefit of the procedure. A fully equipped emergency cart, or equivalent supplies and equipment, and personnel competent in recognizing and treating adverse reactions of all types should always be available. If a serious reaction should occur, immediately discontinue administration. Since severe delayed reactions have been known to occur, emergency facilities and competent personnel should be available for at least 30 to 60 minutes after administration (See ADVERSE REACTIONS).

Preparatory dehydration is dangerous and may contribute to acute renal failure in the elderly, patients with pre-existing renal insufficiency, patients with multiple myeloma, patients with advanced vascular disease and diabetic patients.

Acute renal failure has been reported in diabetic patients with diabetic nephropathy and in susceptible non-diabetic patients (often elderly with pre-existing renal disease) following the administration of iodinated contrast agents. Therefore, careful consideration of the potential risks should be given before performing this radiographic procedure in these patients.

Severe reactions to contrast media often resemble allergic responses. This has prompted the use of several provocative pretesting methods, none of which can be relied on to predict severe reactions. No conclusive relationship between severe reactions and antigen-antibody reactions or other manifestations of allergy has been established. The possibility of an idiosyncratic reaction in patients who have previously received a contrast medium without ill effect should always be considered. Prior to the injection of any contrast medium, the patient should be questioned to obtain a medical history with emphasis on allergy and hypersensitivity. A positive history of bronchial asthma or allergy (including food), a family history of allergy, or a previous reaction or hypersensitivity to a contrast agent may imply a greater than usual risk. Such a history may be more accurate than pre-testing in predicting the potential for reaction, although not necessarily the severity or type of reaction in the individual case. A positive history of this type does not arbitrarily contraindicate the use of a contrast agent when a diagnostic procedure is thought essential, but does call for caution (See ADVERSE REACTIONS).

Prophylactic therapy including corticosteroids and antihistamines should be considered for patients who present with a strong allergic history, a previous reaction to a contrast medium, or a positive pre-test since in these patients the incidence of reaction is two to three times that of the general population. Adequate doses of corticosteroids should be started early enough prior to contrast medium injection to be effective and should continue through the time of injection and for 24 hours after injection. Antihistamines should be administered within 30 minutes of the contrast medium injection. Recent reports indicate that such pretreatment does not prevent serious life-threatening reactions, but may reduce both their incidence and severity. A separate syringe should be used for these injections.

General anesthesia may be indicated in the performance of some procedures in selected patients; however, a higher incidence of adverse reactions has been reported in these patients, and may be attributable to the inability of the patient to identify untoward symptoms or to the hypotensive effect of anesthesia which can prolong the circulation time and increase the duration of contact of the contrast agent.

Cerebral angiography should be performed with special caution in patients with advanced arteriosclerosis, severe hypertension, cardiac decompensation, senility, recent cerebral thrombosis or embolism, and migraine.

Moderate decreases in blood pressure occur frequently with intra-arterial (brachial) injections. This change is usually transient and requires no treatment; however, the blood pressure should be monitored for approximately ten minutes following injection. During peripheral arteriography, extreme caution during injection of the contrast agent is necessary to avoid extravasation and fluoroscopy is recommended. This is especially important in patients with severe arterial disease.

Selective coronary arteriography with or without left ventriculography should not be performed for approximately two weeks following the diagnosis of myocardial infarction. Mandatory prerequisites to the procedure are experienced personnel, ECG monitoring apparatus and adequate facilities for immediate resuscitation and cardioversion. Patients should be monitored continuously by ECG and vital signs throughout the procedure.

Angiography should be avoided whenever possible in patients with homocystinuria because of the risk of inducing thrombosis and embolism.

Carcinogenesis, Mutagenesis, Impairment of Fertility: No long-term animal studies have been performed to evaluate carcinogenic potential. However, animal studies suggest that this drug is not mutagenic and does not affect fertility in males or females.

Pregnancy Category B: Reproduction studies have been performed in rats and rabbits at doses up to two times the maximum adult human dose, and have revealed no evidence of impaired fertility or harm to the fetus due to HEXABRIX. There are, however, no adequate and well-controlled studies in pregnant women. Because animal reproduction studies are not always predictive of human response, this drug should be used during pregnancy only if clearly needed.

Nursing Mothers: Ioxaglate salts are excreted unchanged in human milk. Because of the potential for adverse effects in nursing infants, bottle feedings should be substituted for breast feedings for 24 hours following the administration of this drug.

Pediatric Use: Safety and effectiveness in children have not been established.

ADVERSE REACTIONS

Adverse reactions to injectable contrast media fall into two categories: chemotoxic reactions and idiosyncratic reactions.

Chemotoxic reactions result from the physio-chemical properties of the contrast media, the dose and the speed of injection. All hemodynamic disturbances and injuries to organs or vessels perfused by the contrast medium are included in this category.

Idiosyncratic reactions include all other reactions. They occur more frequently in patients 20 to 40 years old. Idiosyncratic reactions may or may not be dependent on the dose injected, the speed of injection, the mode of injection and the radiographic procedure. Idiosyncratic reactions are subdivided into minor, intermediate and severe. The minor reactions are self-limited and of short duration; the severe reactions are life-threatening and treatment is urgent and mandatory.

NOTE: Not all of the following adverse reactions have been reported with HEXABRIX. Because HEXABRIX is an iodinated intravascular contrast agent, all of the side effects and toxicity associated with agents of this class are theoretically possible, and this should be borne in mind when HEXABRIX is administered.

Fatalities have been reported following the administration of HEXABRIX as well as other iodine-containing contrast agents. Based upon clinical literature, the incidence of death for iodine-containing contrast agents is reported to range from one in 10,000 (0.01 percent) to less than one in 100,000 (0.001 percent). Experience with HEXABRIX is limited, but mortality rates from foreign experience do not suggest a higher risk.

The most frequent adverse reactions are nausea, vomiting, facial flush and a feeling of body warmth. These are usually of brief duration. In double-blind clinical trials, HEXABRIX produced less discomfort upon injection (pain and heat) when compared to various other contrast agents. Other reactions include the following:

Hypersensitivity reactions: Dermal manifestations of urticaria with or without pruritus, erythema and maculopapular rash. Dry mouth. Sweating. Conjunctival symptoms. Facial, peripheral and angioneurotic edema. Symptoms related to the respiratory system include sneezing, nasal stuffiness, coughing, choking, dyspnea, chest tightness and wheezing, which may be initial manifestations of more severe and infrequent reactions including asthmatic attack, laryngospasm and bronchospasm with or without edema, pulmonary edema, apnea and cyanosis. Rarely, these allergic-type reactions can progress into anaphylaxis with loss of consciousness, coma, severe cardiovascular disturbances, and death.

Cardiovascular reactions: Generalized vasodilation, flushing and venospasm. Occasionally, thrombosis or, rarely, thrombophlebitis. Extremely rare cases of disseminated intravascular coagulation resulting in death have been reported. Severe cardiovascular responses include rare cases of hypotensive shock, coronary insufficiency, cardiac arrhythmia, fibrillation and arrest. These severe reactions are usually reversible with prompt and appropriate management; however, fatalities have occurred.

Technique reactions: Extravasation with burning pain, hematomas, ecchymosis and tissue necrosis, vascular constriction due to injection rate, thrombosis and thrombophlebitis.

Neurological reactions: Spasm, convulsions, aphasia, syncope, paresis, paralysis resulting from spinal cord injury and pathology associated with the syndrome of transverse myelitis, visual field losses which are usually transient but may be permanent, coma and death.

Other reactions: Headache, trembling, shaking, chills without fever, hyperthermia and lightheadedness. Temporary renal shutdown or other nephropathy.

The major causes of cerebral arteriographic adverse reactions appear to be repeated injections of the contrast material, administration of doses higher than those recommended, the presence of occlusive atherosclerotic vascular disease and the method and technique of injection. Adverse reactions are normally mild and transient. A feeling of warmth in the face and neck is frequently experienced. Infrequently, a more severe burning discomfort is observed. Transient visual hallucinations have been reported. Serious neurological reactions that have been associated with cerebral angiography and not listed under Adverse Reactions, Neurological, include stroke, amnesia and respiratory difficulties. Visual field defects with anopsia and reversible neurological deficit lasting from 24 hours to 48 hours have been reported. Confusion, disorientation with hallucination, and absence of vision sometimes lasting for one week have also been reported. Cardiovascular reactions that may occur with some frequency are bradycardia and either an increase or decrease in systemic blood pressure. The blood pressure change is transient and usually requires no treatment.

Following peripheral arteriography, hemorrhage and thrombosis have occurred at the puncture site of the percutaneous injection. Brachial plexus injury has been reported following axillary artery injection.

During selective coronary arteriography, patients may have clinically insignificant ECG changes during the procedure. The following adverse effects have occurred in conjunction with the administration of iodinated intravascular contrast agents for this procedure: hypotension, shock, anginal pain, myocardial infarction, cardiac arrhythmias (bradycardia, ventricular tachycardia, ventricular fibrillation) and cardiac arrest. Fatalities have been reported. Complications to the procedure include dissection of coronary arteries, dislodgement of atheromatous plaques, perforation, hemorrhage and thrombosis.

OVERDOSAGE

Overdosage may occur. The adverse effects of overdosage are life-threatening and affect mainly the pulmonary and cardiovascular systems. The symptoms may include cyanosis, bradycardia, acidosis, pulmonary hemorrhage, convulsions, coma and cardiac arrest. Treatment of an overdose is directed toward the support of all vital functions and prompt institution of symptomatic therapy.

Ioxaglate salts are dialyzable.

The intravenous LD_{50} values of HEXABRIX (in grams of iodine/kilogram body weight) were 11.2 g/kg in mice, >8 g/kg in rats, >6.4 g/kg in rabbits and >10.2 g/kg in dogs.

DOSAGE AND ADMINISTRATION

Details on dosage are provided in the package insert. *CONSULT FULL PACKAGE INSERT BEFORE USE.*

REFERENCES

1. Holm M, Praestholm J: Ioxaglate: a new low osmolar contrast medium used in femoral angiography. *Br J Rad* 52:169-172, 1979.
2. Grainger RG: A clinical trial of a new low osmolality contrast medium; sodium and meglumine ioxaglate (Hexabrix) compared with meglumine iothalamate (Conray) for carotid arteriography. *Br J Rad* 52:781-786, 1979.

*Licensed by Guerbet, S.A. Registered U.S. Patent and Trademark Office

© Mallinckrodt, Inc. 1985

Mallinckrodt®

Diagnostic Products Division
Mallinckrodt, Inc.
Post Office Box 5840
St. Louis, MO 63134

How to reduce the costs of bowel preparation before and after the X-ray

Before

Evac-Q-Kwik® helps keep hospital costs down by eliminating the staff time and labor involved in giving enemas. And everything needed for effective bowel evacuation is contained in one cost-effective kit.

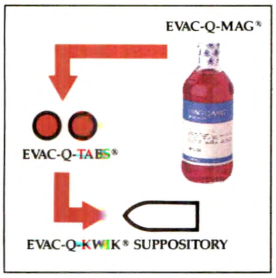

Nurses appreciate Evac-Q-Kwik because it can be administered during a single shift and completed during one 6-hour period. Patients prefer the simple, comfortable Evac-Q-Kwik procedure, too. Evac-Q-Kwik contains no sugar, no alcohol, and is low in sodium.

After

Evac-Q-Kwik is the ideal bowel prep for today's cost-conscious climate. It effectively cleans the colon for clear X-rays *the first time*, to reduce the need for expensive, time-consuming retakes that escalate hospital costs.

Evac-Q-Kwik®

Adria®

Adria Laboratories
Columbus, OH 43215

SIEMENS

The bottom line...

THEIRS...

More output in your CT clinically and financially

In CT, accuracy is essential, quality images are a must... but *productivity* is the measure by which system efficiency is judged.

SOMATOM CT gives you the highest productivity in the business.

It effectively reduces overall exam time. You can actually scan, reconstruct, image, and archive in less time than it takes other systems just to reconstruct. That's nearly 40% more productivity to measurably improve the overall economics of your CT operation.

SOMATOM productivity increases efficiency.

You can routinely process 30 patients in just 8 hours. The result: more efficient use of resources and, in many cases, the end of second shift staffing. SOMATOM's output enables you to shrink a 12 hour workday to 8 hours and save the reserve capacity for future growth.

SOMATOM productivity improves patient management.

With instant reconstruction, you can verify each scan without the customary wait. Bottlenecks are eliminated and so is batch reconstruction.

Department,

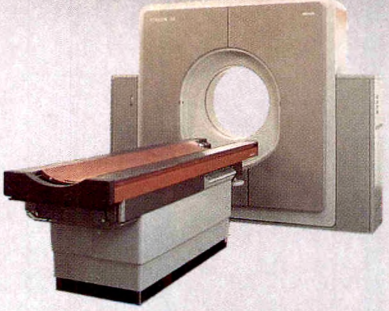

You set your caseload and proceed. Images are ready and accessible while the patient is still on the table. Inconvenient retakes are eliminated, too, because you're not forced to scan "blind". And with exam results available sooner, there's no delay in getting the diagnosis to referring physicians.

SOMATOM productivity includes superior image quality.

It's a fact that the SOMATOM is the fastest reconstructing CT scanner, and that its speed costs you *nothing*. No compromising image quality and no costly add-on array processors. You have the best of both worlds – image quality *and* speed.

SOMATOM improves more than the bottom line.

SOMATOM quality and dependability are assured by the Siemens name. No quality has been sacrificed to offer you speed. No corners cut to offer you efficiency. Contact your Siemens CT representative today. Get the facts that can improve your figures from the company that continues to invest in CT R&D.

Siemens Medical Systems, Inc.
186 Wood Ave. South, Iselin, N.J. 08830 (201) 321-4500

In Canada: Siemens Electric Ltd.
1180 Courtney Park Dr., Mississauga, Ont. L5T 1P1

©1986 THOMSON CGR Medical Corporation

"This is one part I couldn't turn down.

Because the issue is so important. One in eleven women will develop breast cancer during her life. But with early detection, nine out of ten cases are curable. The best way to detect it that early is mammography. Safe, low-dose breast x-rays that can see cancer up to three years before you can feel it. If you're over 35, ask your doctor about a mammogram. We can't change the statistics for getting breast cancer. We can change them for curing it."

Diahann Carroll, Actress

For more information about mammography, write THOMSON-CGR, 10150 Old Columbia Rd., Columbia, Maryland 21046. We're THOMSON-CGR. We want you to know.

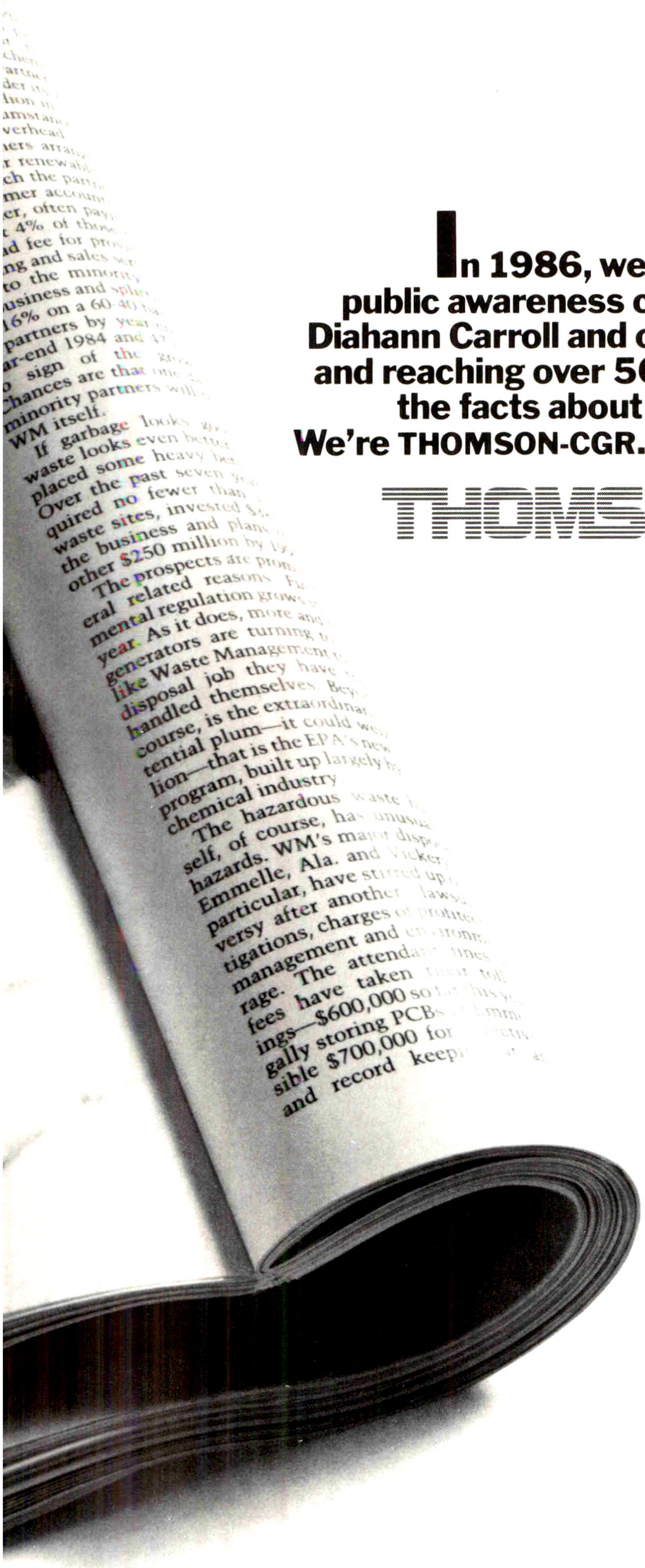

cher
artne
der its
lion in
umstan
verhead
ners arra
r renewab
ch the partn
mer accoun
er, often pay
t 4% of those
ad fee for pro
ng and sales se
to the minority
usiness and split
16% on a 60-40 ba
partners by year-e
ar-end 1984 and 4
o sign of the gro
Chances are that one
minority partners will
WM itself.
If garbage looks go
waste looks even better
placed some heavy bet
Over the past seven yea
quired no fewer than
waste sites, invested $
the business and plans
other $250 million by 19
The prospects are prom
eral related reasons. F
mental regulation grows
year. As it does, more and
generators are turning t
like Waste Management
disposal job they have
handled themselves. Bey
course, is the extraordinar
tential plum—it could we
lion—that is the EPA's new
program, built up largely b
chemical industry
The hazardous waste
self, of course, has unusu
hazards. WM's major disp
Emmelle, Ala. and Vicker
particular, have stirred up
versy after another lawsu
tigations, charges of profite
management and environm
rage. The attendant fines
fees have taken their toll
ings—$600,000 so far this y
gally storing PCBs at Emm
sible $700,000 for
and record keep

In 1986, we'll sponsor a public awareness campaign featuring Diahann Carroll and other notable women, and reaching over 50 million people with the facts about mammography. We're THOMSON-CGR. We want you to know.

THOMSON CGR

PORTA RAY IS PROUD TO INTRODUCE

pixie II

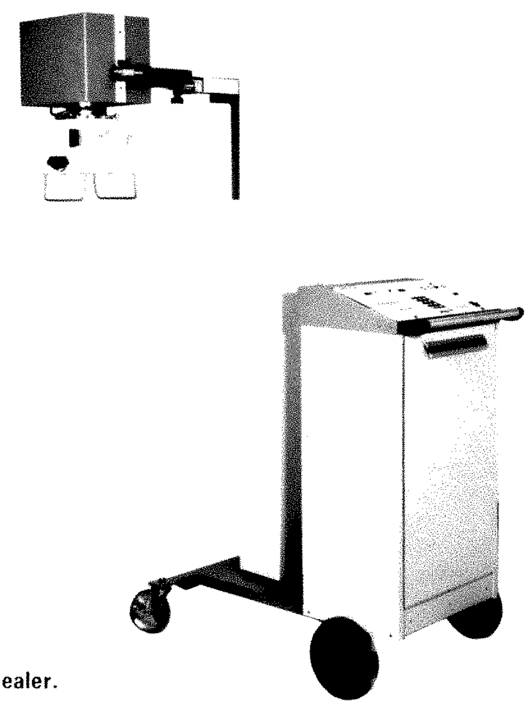

THE BEST OF PIXIE - PLUS

- MICROPROCESSOR CONTROLLED
- SOLID STATE - DIGITALLY PROGRAMMED
- AUTOMATIC EXPOSURE CONTROL - BUILT IN
  Any Size Cassette, Any Examination
- 50mA - 100kVp - 200mas
- AUTOMATIC LINE VOLTAGE REGULATOR
- NO BATTERIES TO CHARGE - AVAILABLE FOR USE 24 HRS. A DAY
- MANUFACTURED IN U.S.A.
- CERTIFIED TO BE IN COMPLIANCE WITH ALL GOVERNMENT REGULATIONS

For more information contact Porta Ray or your local X-Ray dealer.

porta ray inc. 19 Jefryn Blvd. West, Deer Park, N.Y. 11729 U.S.A. (516) 242-0022

Two step film control

Minimize X-ray exposure. Optimize image quality. Stabilize film processor performance, film speed and contrast. Quickly. Easily.

1. The Tobias Model RF Wejex Sensitometer

Produces a precise 11-step wedge exposure on *your* X-ray film. Exposure made just before processing eliminates latent image fade problem.* Features: Precise shutter exposure control. Variable lamp intensity. Provisions for 2″×2″ ANSI blue, green or other filters, double sided exposures, 8″×10″ and 35mm test film alignment. And more.

*Lawrence, D.J.: **A Simple Method of Processor Control,** Med. Rad. and Photog. 49, 2-6, 28, 1973 (Reprints available on request)

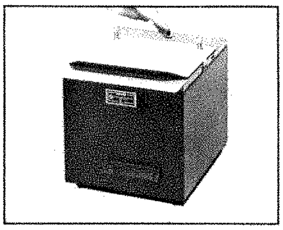

Wejex Universal Model RF
Also available: Wejex Standard Model R

For a demonstration, call your Tobias dealer.
Or write for our brochure. Ask about our 30 day free trial.

2. The Tobias Model TBX Digital Densitometer

Measures optical transmission density of the Wejex-exposed step wedge over a density range of 0 to 4.50. Accuracy ±0.02. Repeatability ±0.01. State-of-the-art electronics. Lighted digital display. 5 second warm up. Easily portable. Virtually no zero drift.

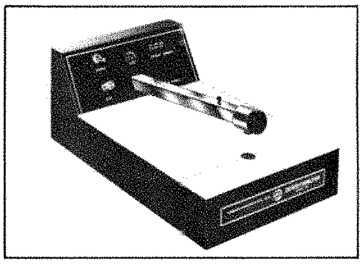

TOBIAS ASSOCIATES, INC.
50 Industrial Drive, P.O. Box 2699, Ivyland, PA 18974, (215) 322-1500

☐ Send literature on the Wejex Sensitometer and TBX Densitometer.

☐ Please send me a copy of D.J. Lawrence's "A Simple Method of Processor Control."

☐ Tell me more about your 30 day free trial policy.

Name ____________
Title/Organization ____________
____
Address ____________
City ____________ State ____________
Zip ____________ Tel. ____________

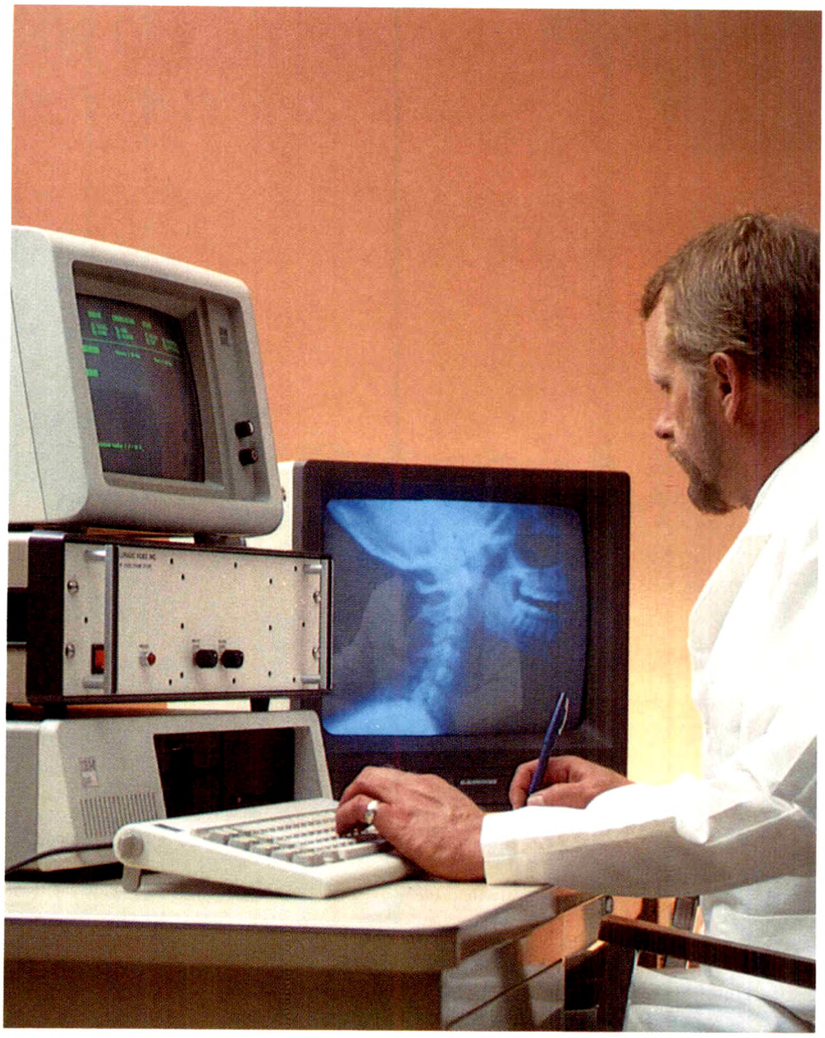

COMPUTERIZED TELERADIOLOGY SYSTEM

Colorado Video's new 950 Digital Image Communications System combines the functions of high quality image transmission by telephone with a convenient image storage system. Controlled by an IBM PC/XT®, this teleradiology system uses standard CCTV cameras and video monitors to capture and display detailed pictures with a resolution of 512 x 480 picture elements and 256 shades of gray.

The 950 system can simultaneously display up to three images for side-by-side comparison. Either a 30- or 200-picture storage unit may be selected for retention of X-rays, nuclear, CT, MRI or ultrasound scans. Stored images may be captioned or annotated and are easy to access, add or remove.

The 950 joins the Colorado Video family of diversified analog and digital teleradiology products which are sold to imaging professionals worldwide. For information please call or write:

COLORADO VIDEO

P.O. Box 928, Boulder, CO 80306 USA
303/444-3972 · TWX 910-940-3248 (COLO VIDEO BDR)

American Roentgen Ray Society:
Officers, Committees, and Meeting Information

Officers

President: Eugene Gedgaudas
President-elect: Jerome F. Wiot
1st Vice-president: Lee F. Rogers
2d Vice-president: Thomas C. Beneventano
Secretary: Raymond A. Gagliardi
Treasurer: Ronald G. Evens

Executive Council: E. Gedgaudas, J. F. Wiot, L. F. Rogers, T. C. Beneventano, R. A. Gagliardi, R. G. Evens, M. M. Figley, R. N. Berk, F. L. Angell, J. E. Madewell, M. P. Capp, G. W. Hartman, B. G. Brogdon, G. A. Kling, H. C. Carlson, A. K. Poznanski, A. E. James, Jr., J. A. Kirkpatrick, Jr., R. H. Troupin, S. S. Siegelman, chairman

Committees 1984–1985

Editorial Policy: S. S. Sagel, W. J. Casarella, J. T. Ferrucci, Jr., N. C. Whitley, S. Hilton, A. J. Davidson, J. M. Taveras, M. M. Figley, R. N. Berk, M. P. Capp, chairman

Education and Research: C. E. Putman, A. R. Margulis, J. R. Thornbury, R. A. McLeod, G. W. Hartman, ex officio, B. G. Brogdon, chairman

Finance and Budget: B. P. Wood, L. R. James, J. A. Kirkpatrick, Jr., R. H. Troupin F. L. Angell, chairman

Instruction Courses: R. A. McLeod, associate chairman, G. W. Hartman, chairman

Program: H. C. Carlson, R. A. Gagliardi, R. H. Troupin, S. S. Siegelman, M. P. Capp, J. E. Madewell, B. G. Brogdon, G. W. Hartman, G. A. Kling, A. V. Proto, C. E. Bickham, J. F. Wiot, chairman.

Publications: W. J. Casarella, J. T. Ferrucci, Jr., S. S. Sagel, N. C. Whitley, M. P. Capp, chairman

Scientific Exhibits: S. G. Kirchner, E. R. Heitzman, Jr., S. M. Goldman, J. E. Madewell, chairman

Nominating: J. P. Tampas, G. M. Stevens, J. A. Kirkpatrick, chairman

Representatives to Other Organizations

American Board of Radiology: E. C. Klatte, R. W. McConnell, L. F. Rogers

American College of Radiology: J. L. Gwinn, G. A. Kling, G. W. Hartman, J. M. Dennis, E. J. Ferris

American Medical Association House of Delegates: S. F. Ochsner, K. C. Krabbenhoft, alternate

American National Standards Institute: M. Haskin

National Council on Radiation Protection and Measurements: E. L. Saenger, H. L. Friedell

Meetings, Membership, Business Information

Annual Meetings: April 13–18, 1986, Sheraton Washington (DC); April 26–May 2, 1987, Fontainebleau-Hilton, Miami Beach; May 1–6, 1988, Westin Bonaventure, Los Angeles

Scientific Program 1985 Meeting: Jerome F. Wiot, president-elect, Dept. of Radiology, University of Cincinnati Hospital, 234 Goodman St., Cincinnati, OH 45267-0742

Director Annual Meeting: George A. Kling, Harper Hospital, Detroit, MI 48201

ARRS Membership: Stanley S. Siegelman, Dept. of Radiology and Radiological Science, Johns Hopkins Hospital, 601 N. Broadway, Baltimore, MD 21205. The ARRS has two membership categories: active and in-training. For active membership, applicants must practice radiology in the U.S. or Canada. Each must have graduated in good standing from an approved medical school or hold an advanced degree in a physical, chemical, or biological science and be certified by the American Board of Radiology, the Royal College of Physicians and Surgeons of Canada, or otherwise adequately document training and credentials. A member-in-training must be in a radiology residency, a postresidency fellowship program, or a postgraduate student in an allied science. Status must be verified by the program director. For consideration during the 1986 ARRS meeting, completed applications must be received by Dr. Siegelman no later than Feb. 1, 1986.

Business Office: George J. O'Hop, controller, American College of Radiology, Suite 1660, 20 N. Wacker Dr., Chicago, IL 60606

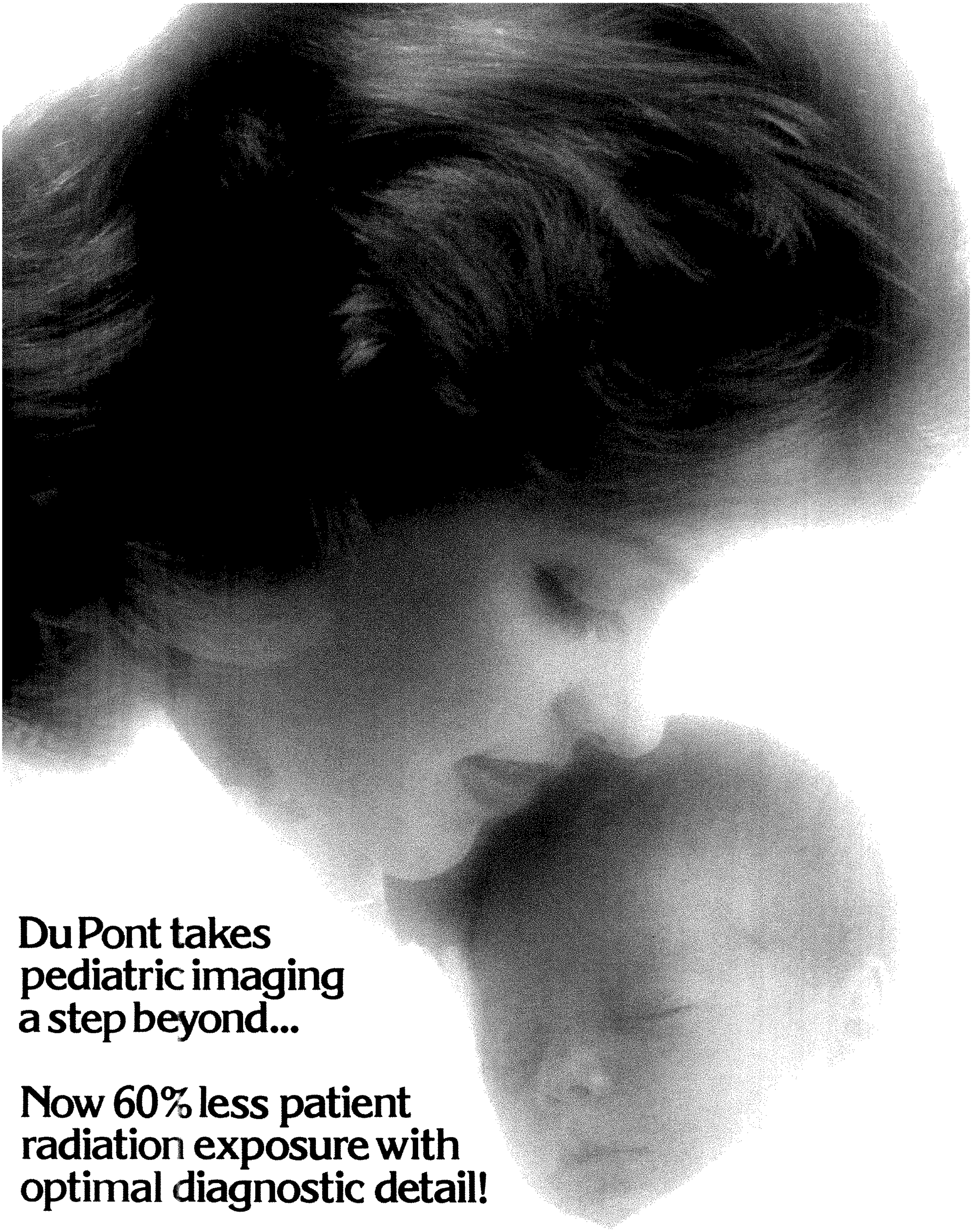

Du Pont takes
pediatric imaging
a step beyond...

Now 60% less patient
radiation exposure with
optimal diagnostic detail!

Introducing the Du Po
OPTIMATCH film/scree

Reduce radiation exposure more than 60%

OPTIMATCH film/screen combinations permit a 25% reduction in patient radiation exposure at 50 kVp with no loss of diagnostic information. Conventional Rare Earth screens undergo a marked falloff in light output below 70 kVp. But not QUANTA Detail and Fast Detail screens. Their patented, high-density yttrium tantalate phosphor emits 25% more light at low kVp levels. And this light is in the UV spectrum that optimally matches the sensitivity of CRONEX® films—providing higher detail imaging. That's why we call it OPTIMATCH.

Cassettes of KEVLAR® aramid fiber shorten exposures another 37%. Conventional cassettes actually "steal" radiation at low kVp levels (absorbing over a third of the rays so they never reach the film) while the Du Pont cassettes of KEVLAR are so radiation "transparent" that they allow 87% of the rays through, permitting much shorter exposures.

ediatric Radiography System:
lus new cassettes of KEVLAR®

Arrange for a demonstration of this extraordinary reduced-radiation system today...Call (800) 527-2601 or send in the coupon now.

Result: more than twice the motion-stopping speed with highest diagnostic detail. Even compared to 400-speed systems, the Du Pont Pediatric Radiography System allows 35% shorter exposures, while producing measurably sharper diagnostic images. Because you can use less than half the exposure time of competitive 250-speed film/screen systems, you reduce repeats due to patient motion. Fewer "blurrographs!"

Du Pont Company
Room X50133
Wilmington, DE 19801

Please contact me to arrange a demonstration of the new Du Pont Pediatric Radiography System...

NAME
TITLE
HOSPITAL
ADDRESS
CITY STATE ZIP
PHONE

The Du Pont Pediatric Radiography System

OPTIMATCH film/screens plus cassettes of KEVLAR®

The combination that supercedes anything in pediatric radiography.

Half the radiation exposure of conventional Rare Earth systems

☐ Twice the motion-stopping speed

☐ Highest diagnostic detail

DU PONT

REG U.S. PAT & TM OFF

Printed in U.S.A.

The Raytheon RMS-90/15 Table gives you the best moves in the profession.

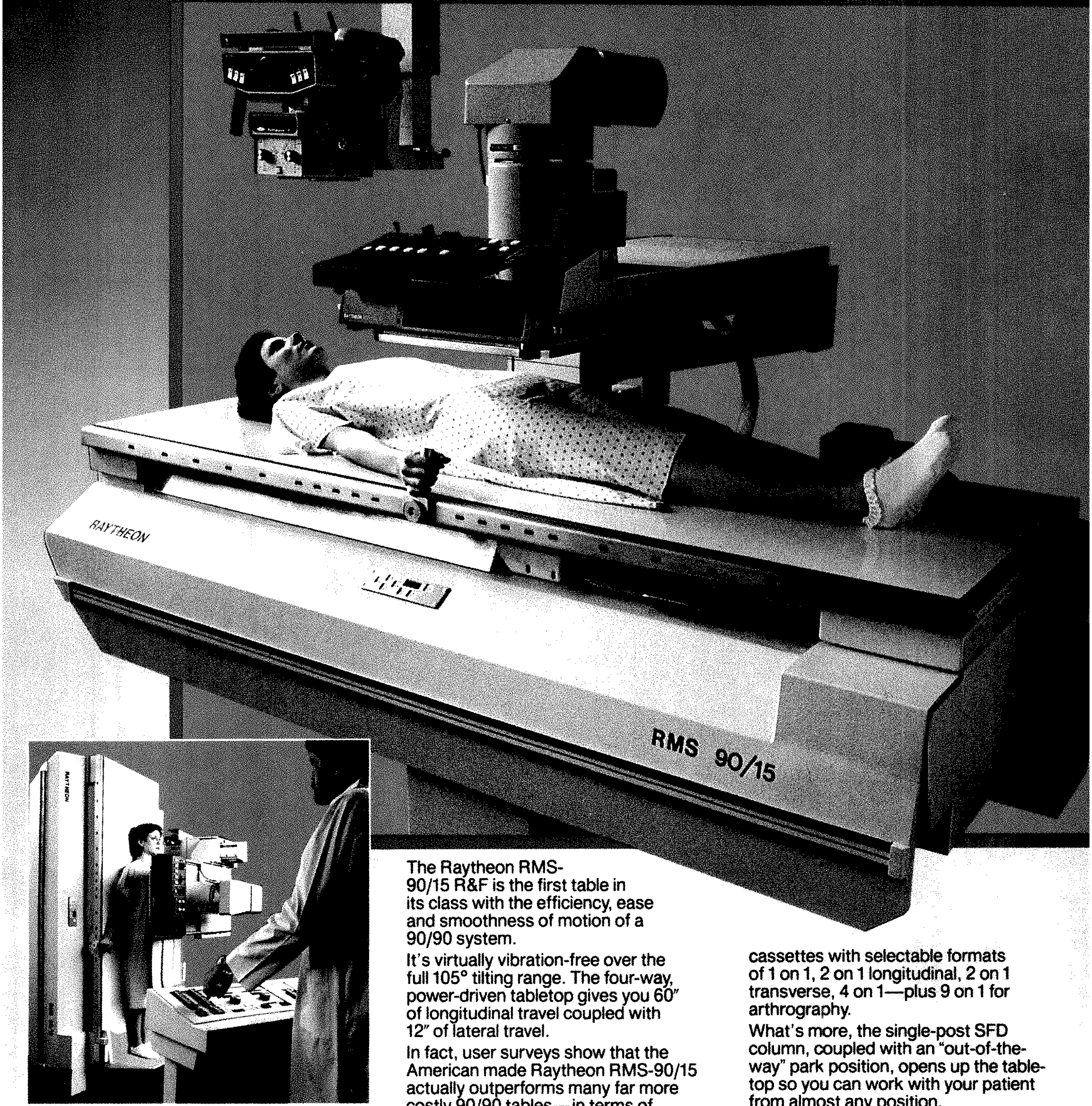

The Raytheon RMS-90/15 R&F is the first table in its class with the efficiency, ease and smoothness of motion of a 90/90 system.

It's virtually vibration-free over the full 105° tilting range. The four-way, power-driven tabletop gives you 60" of longitudinal travel coupled with 12" of lateral travel.

In fact, user surveys show that the American made Raytheon RMS-90/15 actually outperforms many far more costly 90/90 tables—in terms of smooth operation and total power assist.

The RMS-90/15 R&F Table also features the SFD-099 spotfilmer device with full power assist. It's microprocessor-controlled for easy and repeatable programming. It accepts 9.5" x 9.5" cassettes with selectable formats of 1 on 1, 2 on 1 longitudinal, 2 on 1 transverse, 4 on 1—plus 9 on 1 for arthrography.

What's more, the single-post SFD column, coupled with an "out-of-the-way" park position, opens up the tabletop so you can work with your patient from almost any position.

And, the fluoro carriage supports even a three-port 9" image system with 100mm or 105mm camera without additional ceiling support.

Learn more about the RMS-90/15. Contact your dealer. Or call us toll-free at 1-800-323-2213 (in IL, 1-312-865-2600).

Raytheon
MEDICAL EQUIPMENT DIVISION

©1985 The Raytheon Company

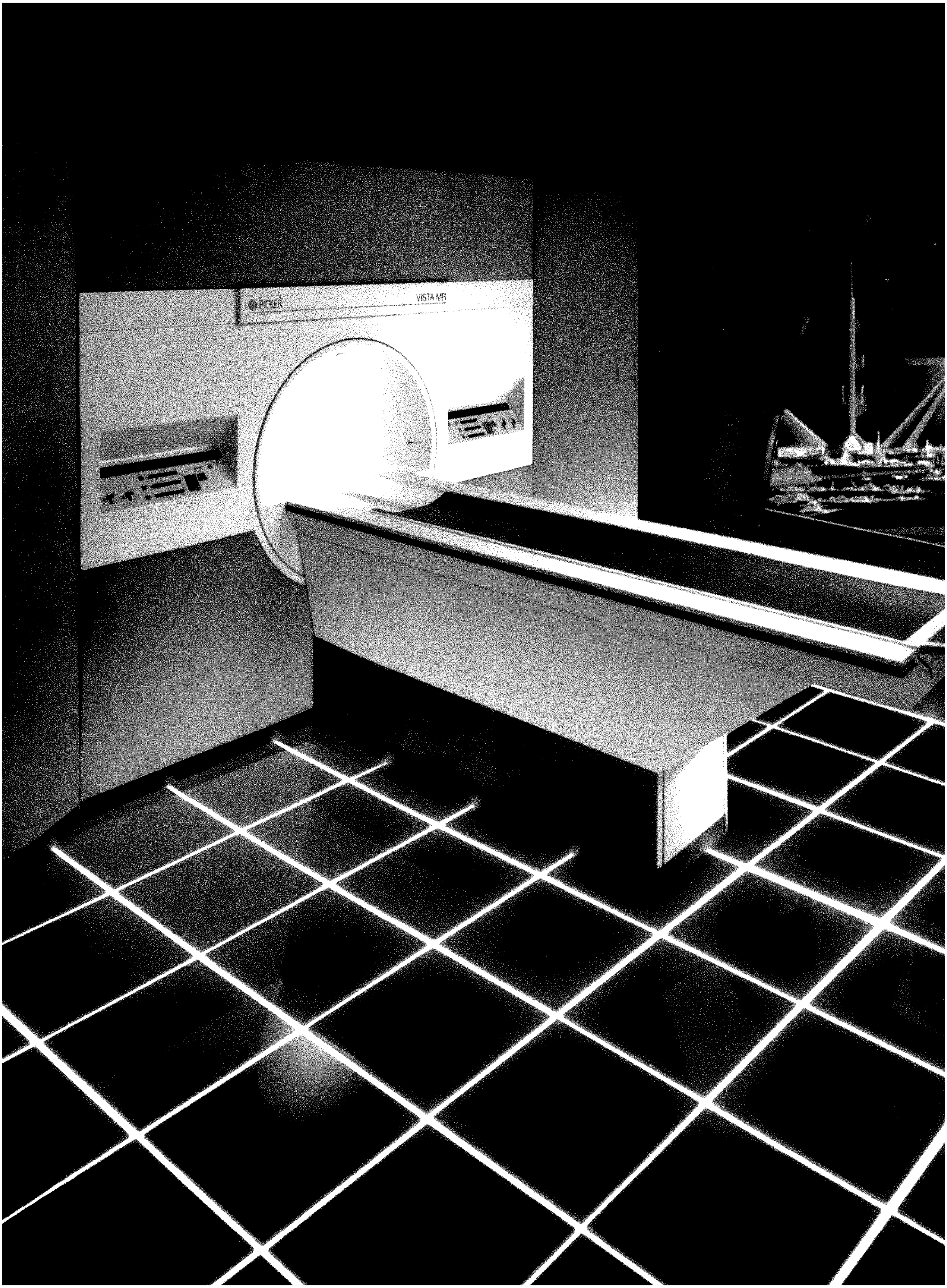
PICKER
VISTA MR

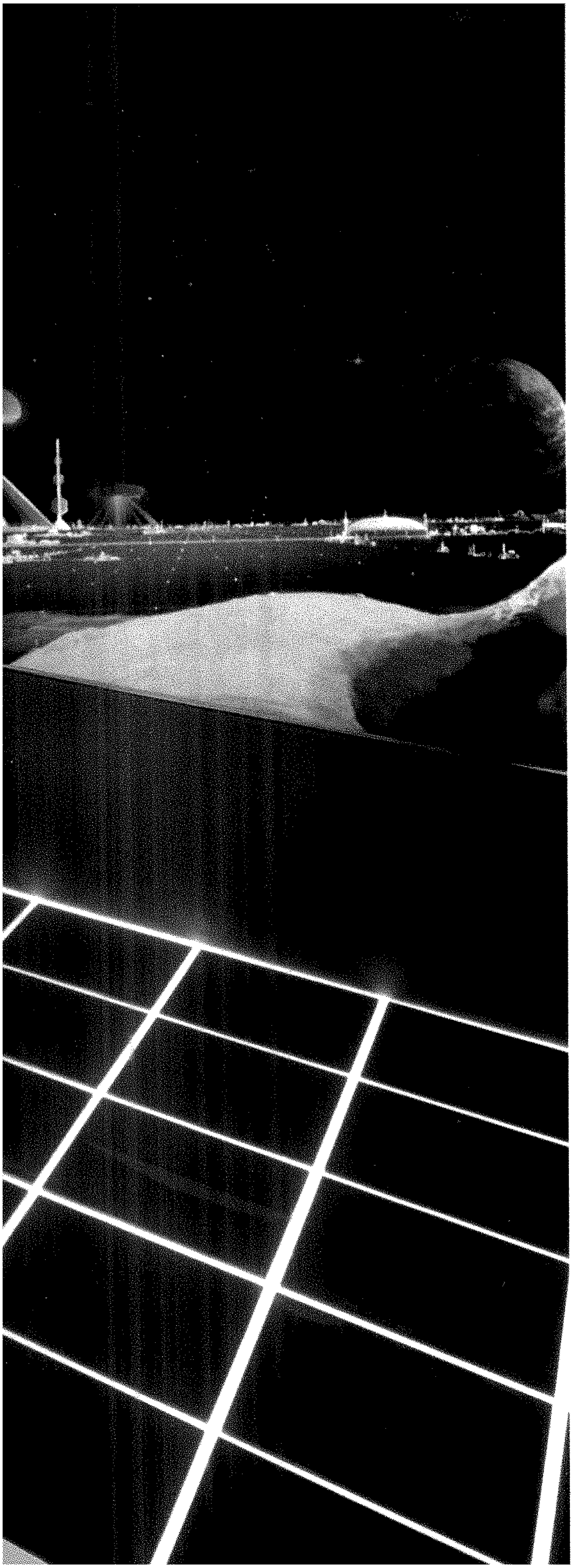

GUARANTEE YOUR MR FUTURE.

Dynamic Blood Flow Analysis, Quantified Cardiac Functions, Time Efficient Volume Studies, Multi-Nuclear Imaging, High Resolution 512^2 Acquisition, 3-D Displays, Ultra-thin Slice Scanning, Real Time Chemical Shift Correction, Variable Field Operation, In Vivo Spectral Analysis, Tumor Differentiation, Thermal Contouring, Therapeutic Application, Stereotaxic Localization, Satellite Data Transmission...

Isn't this your vision of MR tomorrow? Our "vista" of MR includes providing for these capabilities in today's product family.

When selecting your high image quality, high throughput system today, make sure you include basic specifications that accommodate tomorrow's applications. The Vista MR 2055 family has been developed with High Performance (HP) architecture including:

- 10-90 MHz Broadband RF Electronics
- 15 kW RF Power
  12 mT/m Maximum Gradient Power
- HYBRID Imaging
- Direct Angle Oblique Acquisition
- 32 bit Array Processor with 18×10^6 Floating Point Operations per Second.
- User Selectable — TE Range: 10-240 msec.
  TI Range: 100-900 msec.
- 64 Contiguous Slices Maximum for Total Organ Coverage in a single 4 Echo Multiple Slice Study.

There are many serious questions when considering the right MR system. With Picker, it is easier to be confident in meeting your future MR needs because you know that your system has the intrinsic specifications to get you there.

PICKER

NOTE: NMR systems are classified as investigational devices in the United States under the Medical Device Amendments to the Food, Drug and Cosmetic Act. These devices will become commercially available in the U.S.A.

Conventional wisdom: Fly United to Washington, D.C.

The American Roentgen Ray Society and United Airlines have joined to provide savings on air fares when you fly to Washington, D.C. for the 1986 Annual Meeting, April 14–18, 1986.

United offers you at least 40% off normal Coach fares with no minimum stay restrictions. Or, if you are staying over a Saturday night, a 45% discount can be obtained.

To take advantage of this offer, you or your Travel Agent should call United's toll-free number, 800-521-4041 between 8:00 a.m. and 8:00 p.m. E.S.T. 7 days a week. Just give the Society account number: **602K.**

United's Convention Specialists will provide all information on these fares and any special promotional fares that may be offered from your city. Seats are limited, so call early for the best selection.

You're not just flying, you're flying the friendly skies.

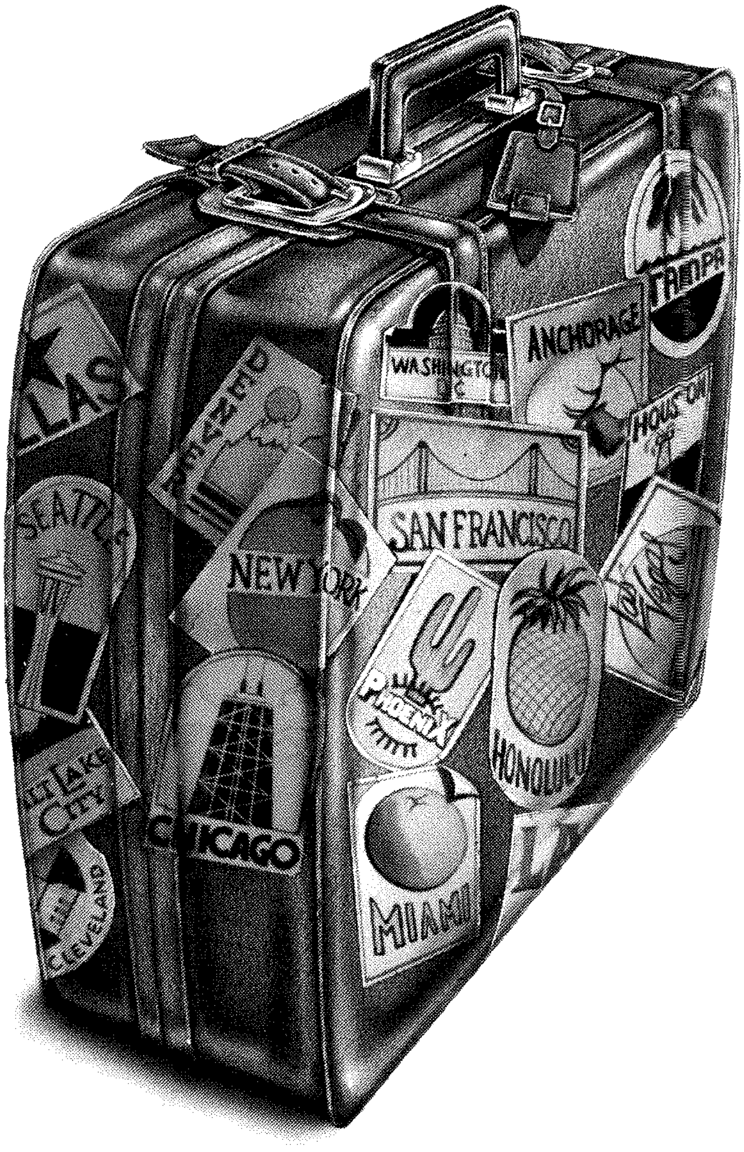

fly the friendly skies®

United

illumination
EXCELLENCE

S&S X-Ray medical film reading illumination excellence has provided radiologists with unequalled quality and reliability for over 30 years.

The S&S commitment to quality and R&D has earned the reputation for excellence we enjoy, and has made S&S the world's largest manufacturer of Motorized Viewers.

Models' film capacity range from 48 14″x17″ radiographs to 400 (4 over 4).

Whether stationary or motorized, S&S viewers together with our complete line of x-ray accessories are designed and engineered to fit every need, every budget.

Catalog available upon request.

Modular Mobile Illuminator

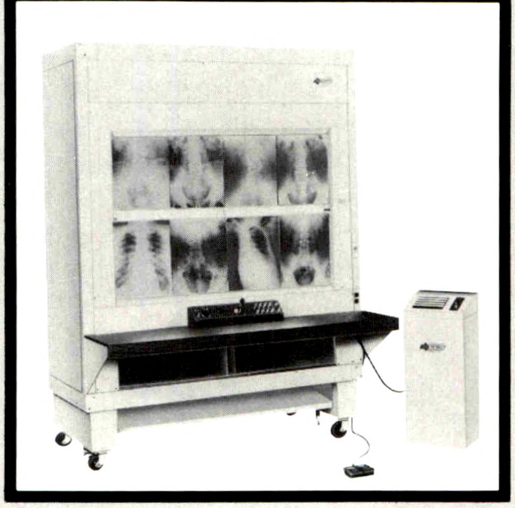

Model MV200A with optional MV 200C and MV200T

Engineered and produced by the world's leading manufacturer of X-Ray Accessories

S&S X-RAY PRODUCTS, INC.

87-93 Jay Street, Brooklyn, NY 11201
Telex: 219262 TLX UR
Tel: In NY State: (718) 852-6900
Toll Free: (800) 221-6634

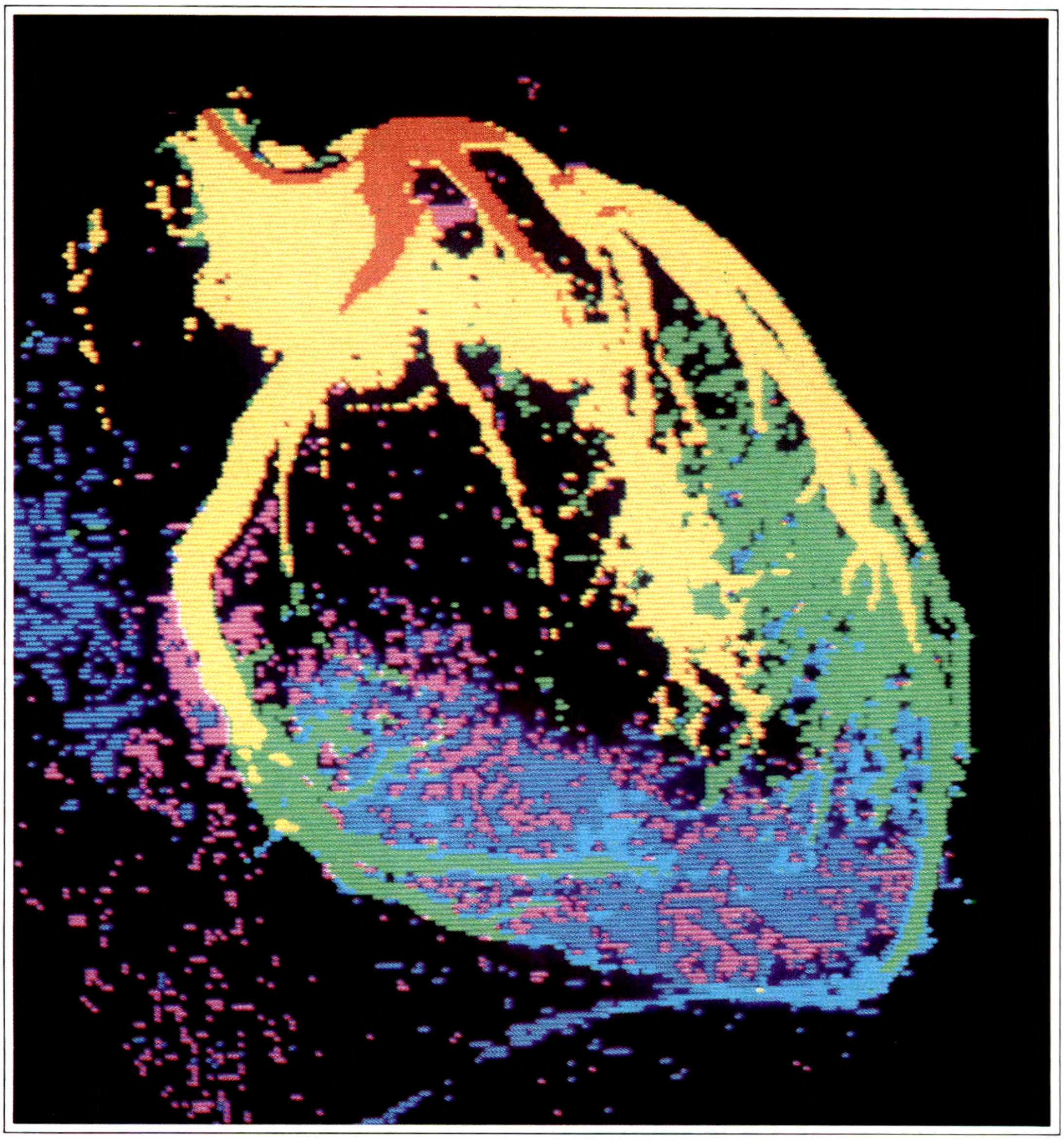

An analytical computation of a myocardial perfusion radiograph from the Philips APU. It shows blood flowing through the heart during a single cardiac cycle.

"A DANGER FORESEEN IS HALF AVOIDED."

Thomas Fuller. M.D. 1732.

To further advance the art of seeing into the body, Philips, a leader in diagnostic imaging, continues to provide superior new products. We took a pioneering step in 1980 with the first system for digital subtraction angiography. Our TOMOSCAN 60/TX has put refined CT scanning technology within the reach of medical institutions of all sizes. And our thirteen years of international research have produced an integrated system for magnetic resonance imaging that sets new performance standards for both clinical applications and high magnetic field research. Philips Medical Systems, Inc. Shelton, Connecticut 06484.

PHILIPS

PHILIPS

CURIX® Film Handling Center...

“So simple to use, it revolutionizes film handling, and it’s cost effective”

Roland McGraner
Administrative Director of Radiology Services
Methodist Hospitals of Memphis, Tennessee

“Now we can unload, reload and process our x-ray films in normal roomlight… automatically in One Step!”

“All we have to do is insert the CURIX® (or SCOPIX®) Cassette. Just one step…everything else is automatic.

“The CURIX Film Handling Center opens the cassette, extracts the exposed film and feeds it into the processor. Then, it selects a film from one of the Center’s film magazines, reloads the cassette and ejects it…all in about 10 seconds.”

“Increased efficiency and cost reduction are its real benefits.”

“We have improved our department operating efficiency from 85% to 95% based upon relative workload units…techs spend more time with patients … less with tedious darkroom chores.

“Our largest fixed costs … staff and overhead have been reduced. The result is, we’ve expanded our department capacity without adding darkroom techs or additional facilities.

“We also expect that gentle handling of cassettes and film will double the life of our intensifying screens.”

“Microprocessors are the heart of its operating systems … it actually communicates with us.”

“Displayed user instructions prevent operating errors and simplify servicing. It also maintains a log of film usage by size and type plus other operating data in its electronic memory.

“Its microprocessor-controlled operation also reduces chemical consumption, film waste, and film repeats due to use of unloaded film cassettes, light fog caused by careless darkroom loading, and handling artifacts.

“Its interchangeable, easy to load film magazines hold up to 125 sheets of CURIX or SCOPIX films.

“For consistently superior results, our department utilizes the complete CURIX System, including CURIX Films, Rare Earth Screens, Cassettes, and Automatic Patient I.D. Camera.

“The CURIX Film Handling Center helps everyone … technical personnel, Department Administrative Directors, and Hospital Administrators … what more can I say?”

For additional information, call or write:

AGFA-GEVAERT REX, INC.
925 Westchester Avenue,
White Plains, NY 10604
(914) 682-5650

In Canada contact:
Photo Importing Agencies, Ltd.
Concord, Ontario L4K1E7

CURIX® Capacity System

The new generation in roomlight x-ray film processing

AGFA-GEVAERT Agfa

CURIX and SCOPIX are registered trademarks of Agfa-Gevaert, Leverkeusen/Antwerp.

DELTA the Official Airline of the American Roentgen Ray Society

In cooperation with the American Roentgen Ray Society, Delta Air Line's is offering a 35% discount on your round trip Delta Day Coach fare to Washington, D.C.

If you are traveling to Washington, D.C., between April 10-17, 1986, you are eligible for a 35% discount off the regular round-trip, non-discounted Day Coach fares in the Continental U.S. or, if other fares offering greater savings are available, Delta will confirm your reservations at that rate. Either way, special fares have restrictions and/or limited seats, so make your reservations early.

If you normally use the services of a travel agent, have them place your reservations through our toll-free number to obtain the same advantages.

Call 1-800-241-6760 for reservations from 8:30 a.m. to 8:00 p.m. Eastern Time—Daily. **REFER TO FILE NUMBER F0347.** This discount is available only through this number.

We are the State OF THE IMAGE

Precise Optics is the World's Largest Manufacturer *specializing only* in the production of Image Intensifier Systems and Components.

With *over thirty years of experience,* Precise has achieved an unsurpassed capability in the design and manufacture of Imaging Systems, suppling major equipment manufacturers throughout the world with our complete Systems and components.

With budgetary constraints and DRGs a current fact of life, Precise Systems offer a *viable high-quality alternative* to more expensively priced equipment.

Precise produces many hundreds of Imaging Systems every year, at an obvious volume cost savings and with *superior tube selection advantage,* while tailoring systems and components to meet your individual, specialized needs.

Our application and production expertise assures that any System requirement can and will be met without compromise, with the performance, reliability and service expected from an industry leader.

All Systems are compatible with new or existing equipment, while satisfying DHHS standards.

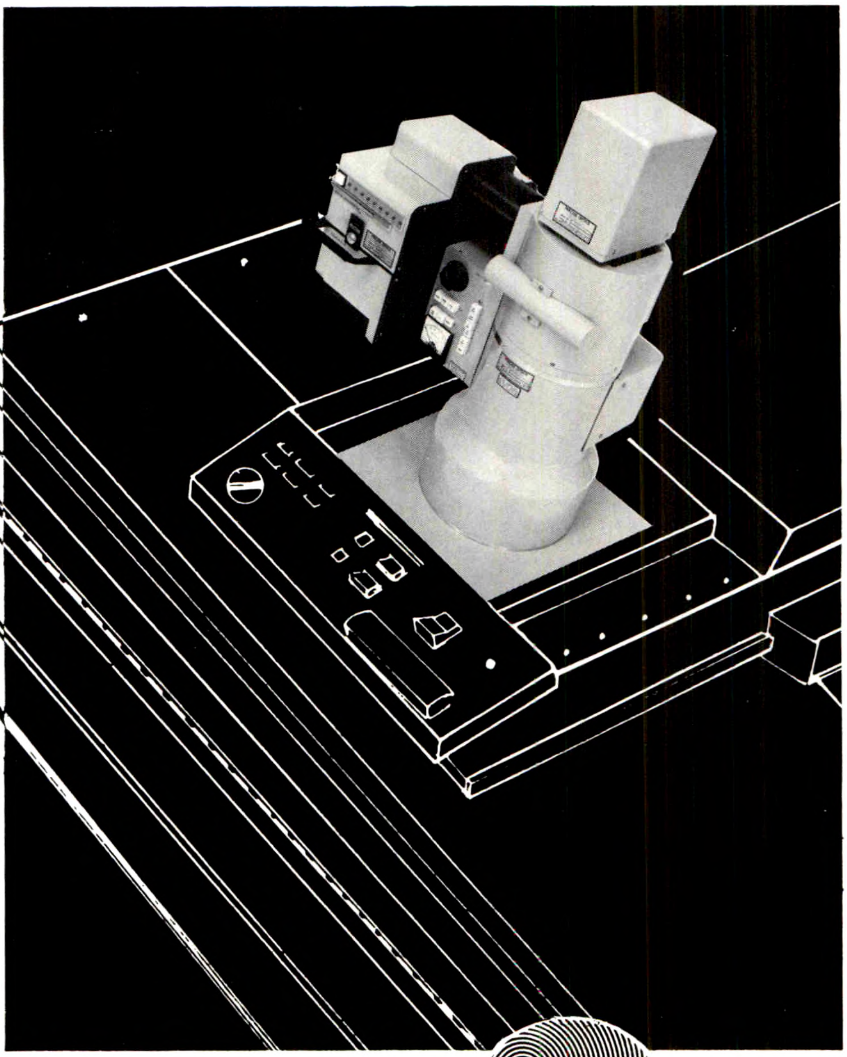

For more information on our line of 6, 9, 12 & 16 inch, Single & Multi-mode Image Intensifier Systems. Write or call . . .

precise optics ®

PHOTO MEDIC
EQUIPMENT, INC.

Efficient bowel evacuants for diagnostic procedures

Take one

X-Prep®
for a cleaner, clearer film

Excellent visualization...fewer retakes

- ■ 95% efficacy proven with X-PREP® Liquid in 749 patients prepared for diagnostic procedures such as barium enemas and IVPs*
- ■ Effective for colonoscopy and sigmoidoscopy*

X-PREP® Liquid
2½ fl. oz. (74 ml) (standardized extract of senna fruit)

*Data on file, Medical Department, The Purdue Frederick Company.

Gray Pharmaceutical Co., Affiliate
The Purdue Frederick Company
Norwalk, CT 06856

X-PREP® Bowel Evacuant Kit-1
Contains two SENOKOT-S® Tablets (standardized senna concentrate and docusate sodium), one bottle of X-PREP Liquid 2½ fl. oz. (74 ml), one RECTOLAX® Suppository (bisacodyl 10 mg), plus easy-to-follow instructions.

X-PREP® Bowel Evacuant Kit-2
Contains one pack CITRALAX® Granules 1.06 oz. (effervescent citrate/sulfate of magnesia), one bottle of X-PREP Liquid 2½ fl. oz. (74 ml), one RECTOLAX Suppository, plus easy-to-follow instructions.

X-Prep Bowel Evacuant Kit-2
X-Prep Bowel Evacuant Kit-2
with CITRALAX™ Granules and RECTOLAX® Suppository
X-Prep Bowel Evacuant Kit-1
X-Prep Bowel Evacuant Kit-1
X-Prep LIQUID

© 1984, Gray Pharmaceutical Co. PFR-081/84

"Horseshoe" Lung: Report of Five New Cases

Robert M. Freedom[1]
Patricia E. Burrows[2]
C. A. F. Moes[2]

A "horseshoe" lung is a rare congenital anomaly in which the posterobasal segments of the right and left lungs are fused behind the pericardial reflection at the cardiac apex. Most patients with such pulmonary fusion share many of those cardiovascular anomalies typical of the "scimitar" or hypogenetic right lung syndrome. The clinical diagnosis of horseshoe lung can be made by pulmonary angiography, which shows a branch of the right pulmonary artery originating from its proximal but inferior aspect and coursing into the left hemithorax. Thus, there are two conditions in which an artery from the right lung supplies part or all of the left lung: errant right pulmonary artery in the horseshoe lung deformity and so-called left pulmonary artery sling.

The so-called "horseshoe" lung is an uncommon congenital anomaly in which partial fusion of the right and left lungs occurs posterior to the cardiac apex [1-6]. As pointed out by Dische and others [2-7], the cardiovascular anomalies associated with a horseshoe lung tend to embrace the spectrum of malformations seen in the "scimitar" syndrome [8-12]. To the present time, there are about seven well described cases of horseshoe lung. We review the spectrum of cardiovascular anomalies in five new cases of horseshoe lung and describe the radiographic and angiographic findings in these and the other well documented cases.

Case Material

We identified five patients at the Hospital for Sick Children in Toronto with the horseshoe lung anomaly and reviewed their chest radiographs, angiographic studies in four patients, and pathologic material in four patients, including a postmortem bronchogram in one patient. The diagnosis of horseshoe lung anomaly was made from pulmonary angiography in four patients and confirmed at autopsy in three of these, from pulmonary angiography alone in one patient, and from autopsy findings alone in one patient.

Four of the five patients became symptomatic in the neonatal period. One of these had complex congenital heart disease with hypoplastic left heart syndrome, severe coarctation of the descending aorta, and double-outlet right ventricle and died in the neonatal period. The four other patients had features of scimitar syndrome. Three of these presented in early infancy with respiratory distress, believed to be at least partly secondary to congestive heart failure, and died in the first few months of life. The fifth patient, who also had features of the scimitar spectrum, was asymptomatic and was investigated angiographically after a chest radiograph showed dextrocardia, small right lung, and abnormal pulmonary vascular markings. She has subsequently remained asymptomatic.

Seven additional patients with horseshoe lung anomaly have been reported in the world literature [1-6].

Results

Description of Lung Anatomy

From the four present cases subjected to autopsy examination and from the

Received May 1, 1985; accepted after revision August 26, 1985.

[1] Division of Cardiology and Department of Pathology, University of Toronto, Faculty of Medicine, and Hospital for Sick Children, 555 University Ave., Toronto, Ontario, Canada M5G 1X8. Address reprint requests to R. M. Freedom (Division of Cardiology, room 1503).

[2] Departments of Pediatrics and Radiology, University of Toronto, Faculty of Medicine, and Hospital for Sick Children, Toronto, Ontario, Canada M5G 1X8.

AJR 146:211-215, February 1986
0361-803X/86/1462-0211
© American Roentgen Ray Society

available information in the literature [1–6], the horseshoe lung deformity derives its name from the observation that parts of the right and left lungs are fused together by a tongue of parenchyma posteroinferior to the pericardial reflection at the cardiac apex. This implies some sharing of a common parietal pleural reflection as well, although from the literature there is scant mention of the pleural anatomy [2].

Among the four patients who underwent postmortem examination at the Hospital for Sick Children, two had fusion of the right and left lung parenchyma within the isthmus; in the other two patients, the right and left lungs were separated by a fissurelike layer of visceral pleura. In three patients described in detail by Orzan et al. [5], Cipriano et al. [3], and Dische et al. [2], the lungs were confluent within the isthmus in two patients and separated by a fissure in one. The postmortem bronchogram in one of our patients demonstrated right and left bronchi of equal length (bilateral hyparterial bronchi). The left bronchial tree had a relatively normal branching pattern, while the right bronchus trifurcated into a short upper bronchus lobe, an inferior bronchus with fewer than the normal number of lower-lobe segmental bronchi, and an elongated bronchus that crossed the thoracic midline, within the isthmus. There also appeared to be mild focal stenoses involving the origins of segmental bronchi, although these were not confirmed by cross-sectional examination.

Focal stenoses in the trachea and bronchi and abnormal bronchial bifurcation with absence of the right eparterial bronchus and bilateral hyparterial bronchi have been described in other patients with horseshoe anomaly [2, 3] and were believed by Halasz et al. [8] to be a frequent component of the scimitar syndrome.

The right lung is often hypoplastic (four of our five cases), lacking normal identifiable fissures and lobes, while the left lung is more normal in appearance. The right lung may lack the normal eparterial bronchus, and bilateral hyparterial bronchi may be evident [2]. A branch of the right bronchus courses posteroinferiorly to provide airway supply to the fused segment of the lung (fig. 1).

Arterial supply to the right lung is provided both by the mediastinal right pulmonary artery and by anomalous arterial supply originating from the descending aorta. The so-called horseshoe part is supplied by a branch of the right pulmonary artery and from contributions from the left pulmonary artery.

Spectrum of Cardiovascular Anomalies

While the horseshoe deformity may occur in relative isolation, most patients (11 of 12) exhibit the spectrum of anomalies observed in the scimitar or hypogenetic right lung syndrome [1–6, 8–12] (four of our five cases). These anomalies include a small right lung and right hemithorax (11 of 12), hypoplastic right pulmonary artery, anomalous connections of some or all of the right pulmonary veins to the inferior vena cava–right atrial junction (10 of 12), abnormal systemic arterial supply from the descending thoracic or abdominal aorta to the right lung (eight of 12), and a variable degree of bronchial sequestration. Two of the patients from our institution had total anomalous pulmonary venous return, and one of these two patients had a complex form of double-outlet right ventricle, a hypoplastic left ventricle, and coarctation of the aorta. Pulmonary venous stenosis was observed in three of our patients. In our most recently studied patient, the right pulmonary veins were extremely hypoplastic and common ostium in the inferior vena cava was only 1.0 mm in diameter. This same patient demonstrated severe stenosis of a common left pulmonary vein at its left atrial ostium.

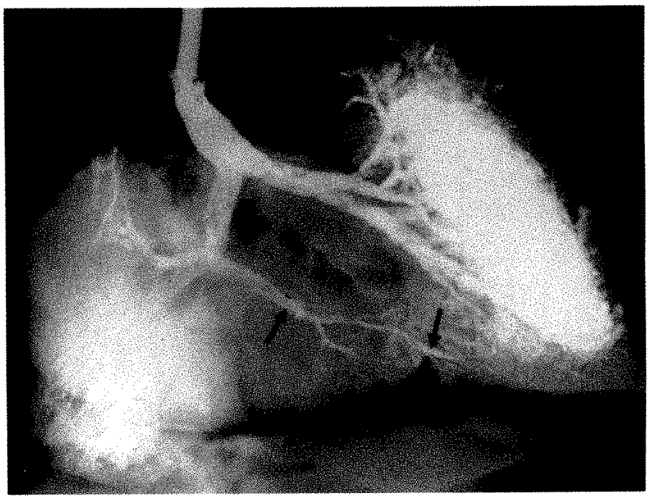

Fig. 1.—Postmortem bronchogram in infant where horseshoe deformity was not recognized clinically. Note elongated bronchus (*arrows*), which crosses thoracic midline within pulmonary isthmus.

Chest Radiographic Findings

There are no plain chest film findings that seem pathognomonic of a horseshoe lung deformity [2–13]. In those patients with associated right-lung hypoplasia and the scimitar constellation, the frontal chest radiograph demonstrates dextrocardia, a variable degree of right hemithorax hypoplasia, and a large left lung (fig. 2). These findings are typical of the scimitar syndrome, with or without posterior fusion of the basal segments of the right and left lungs. In the rare patient with a horseshoe deformity of the lungs but without significant hypoplasia of the right lung (and thus with a left-sided heart), we do not think one would even entertain the diagnosis from the plain chest radiograph.

In each of our five patients with horseshoe lung anomaly and dextrocardia, the vascular markings were diminished in the right lung and increased in the left lung. Abnormal densities caused by anomalous pulmonary veins were present in the lower right lung. Although none of our patients had focal pulmonary consolidation to indicate bronchopulmonary sequestration, this finding was present in the patient with multiple airway stenoses reported by Cipriano et al. [3].

Scintigraphic lung perfusion imaging, performed in three patients with horseshoe lung anomaly, showed persistent

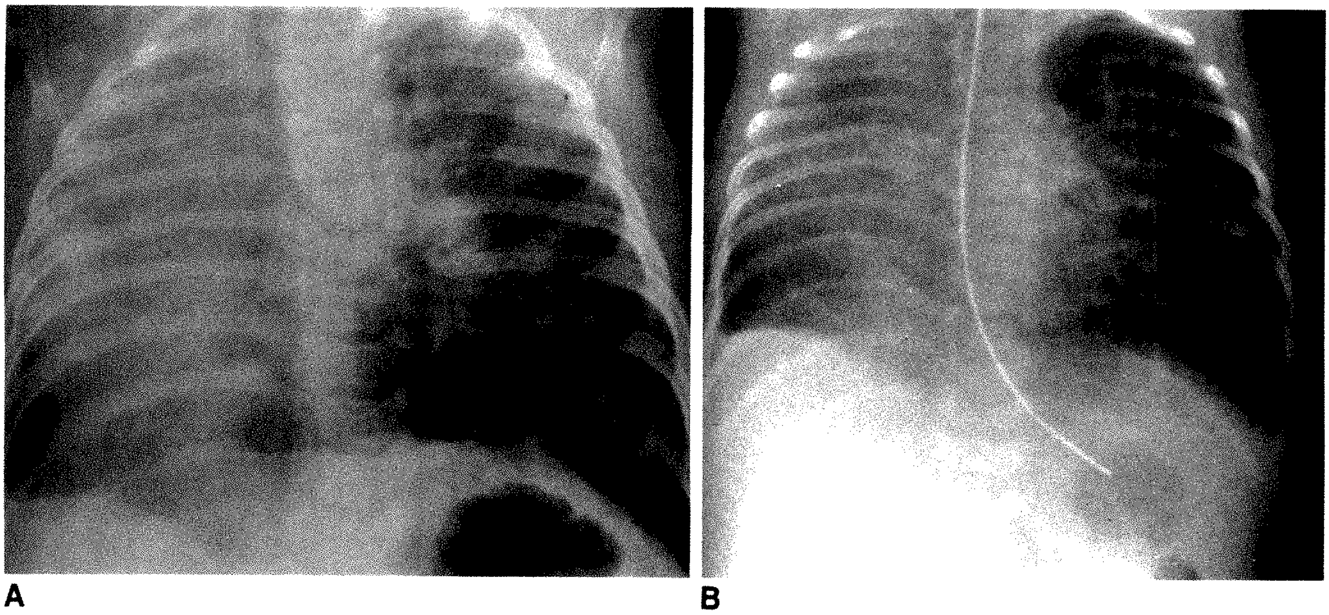

Fig. 2.—Frontal chest radiographs of two children show opacified right chest, dextrocardia, and enlarged left hemithorax. So-called "scimitar" venous anomaly is not visible in these instances. (Figs. 1 and 2B are same patient.)

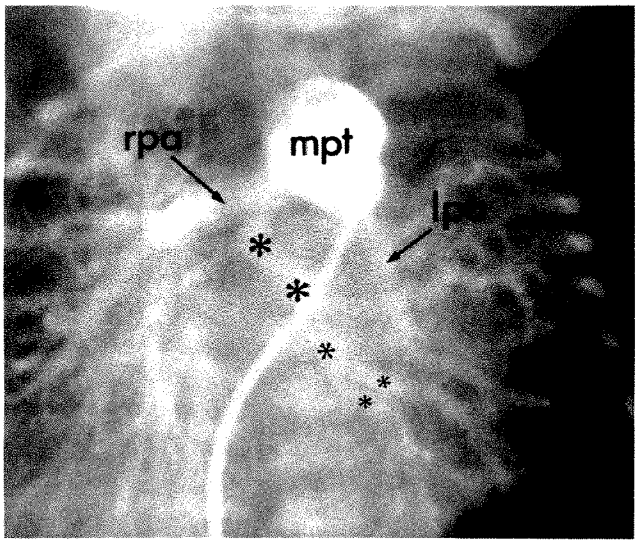

Fig. 3.—Pulmonary arteriogram in necropsy-proven case of horseshoe lung deformity. Main pulmonary trunk (mpt) has right (rpa) and left (lpa) pulmonary branches. From proximal and inferior aspect of right pulmonary artery, branch (*asterisks*) courses across midline to enter left lower lobe. This child also had complex form of double-outlet right ventricle, small left ventricle, coarctation of aorta, and total anomalous pulmonary venous connections.

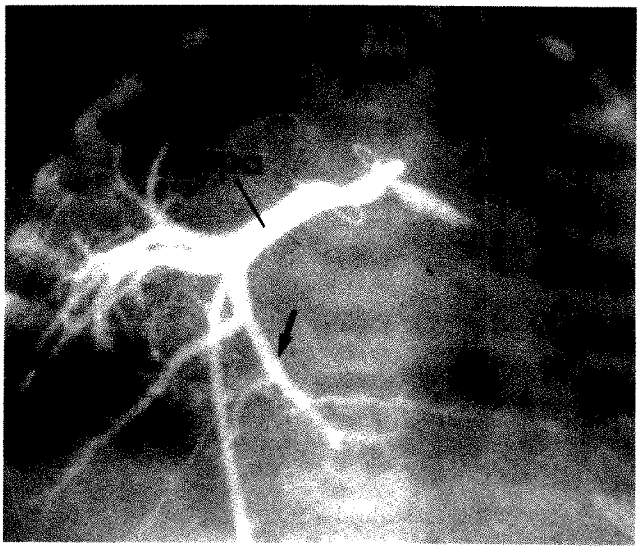

Fig. 4.—Selective injection in right pulmonary artery (rpa) shows errant branch originating from right pulmonary artery and coursing (*arrow*) into left chest. This neonate also had dextrocardia, small right lung, and total anomalous pulmonary venous connections to right atrium with pulmonary venous ostial stenosis.

perfusion defects throughout the right lung [3, 5, 6], most likely due to the presence of systemic arterial perfusion of these areas.

Axial computed tomographic imaging of the chest in one patient has shown the aerated isthmus between the posterior pericardium and the spine [6].

Pertinent Angiographic Findings

The diagnosis of the horseshoe lung deformity is made by pulmonary arteriography performed in the frontal projection (figs. 3–6). The right pulmonary artery exhibits variable degrees of hypoplasia with decreased number and abnormal distribution of the segmental branches. The abnormal course

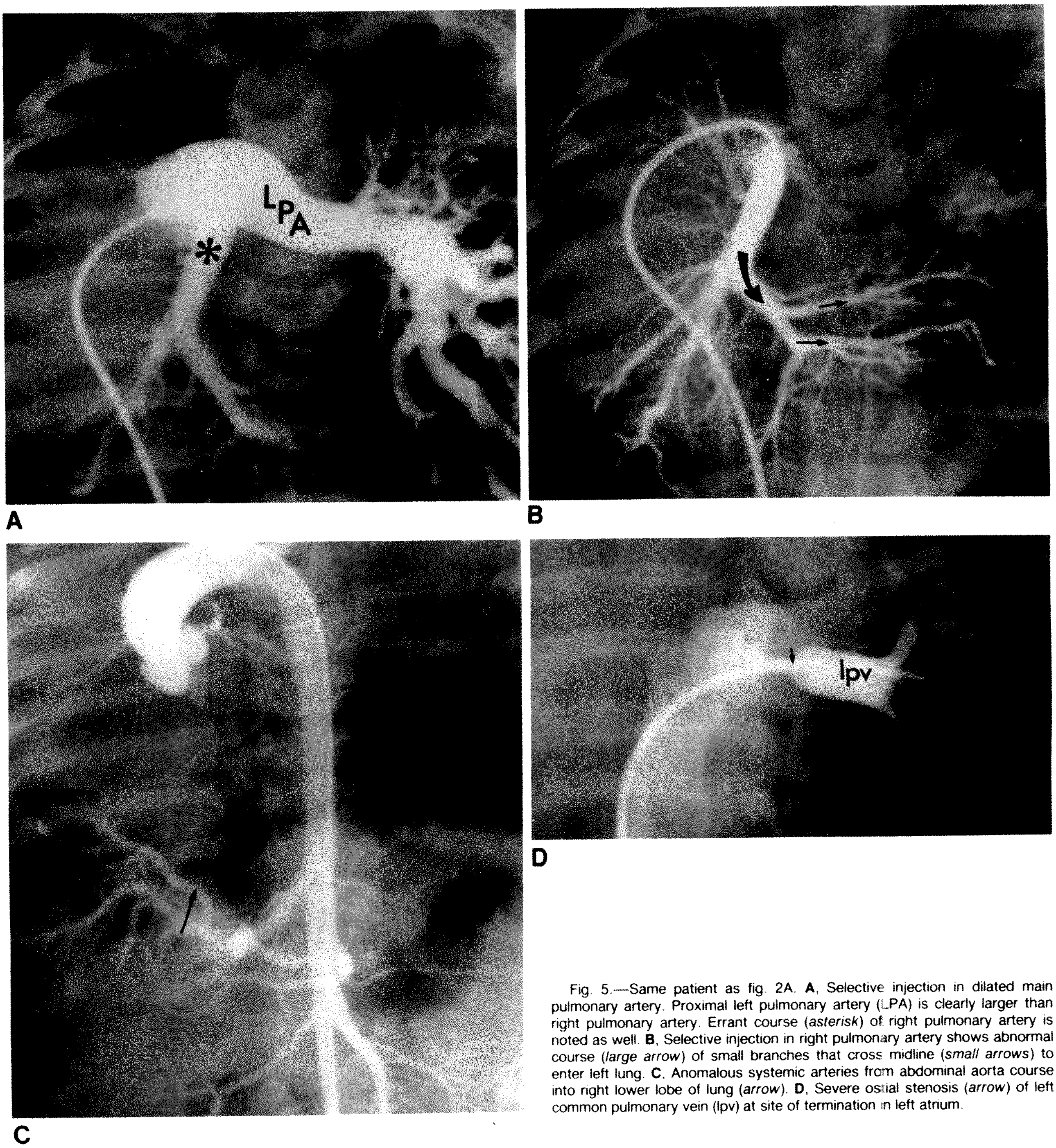

Fig. 5.—Same patient as fig. 2A. **A**, Selective injection in dilated main pulmonary artery. Proximal left pulmonary artery (LPA) is clearly larger than right pulmonary artery. Errant course (*asterisk*) of right pulmonary artery is noted as well. **B**, Selective injection in right pulmonary artery shows abnormal course (*large arrow*) of small branches that cross midline (*small arrows*) to enter left lung. **C**, Anomalous systemic arteries from abdominal aorta course into right lower lobe of lung (*arrow*). **D**, Severe ostial stenosis (*arrow*) of left common pulmonary vein (lpv) at site of termination in left atrium.

of branches originating from the right pulmonary artery and coursing to the lower medial part of the left hemithorax has been identified only in those patients with pleural-parenchymal fusion of the basal segments of the right and left lungs [4–7]. Patients with this horseshoe deformity may also exhibit anomalous connection of the right pulmonary veins, anomalous systemic arterial supply, or pulmonary vein stenosis (figs. 5C and 5D).

Discussion

Horseshoe lung is rare, and most of the reported cases share the same spectrum of cardiovascular anomalies identified in the scimitar syndrome [1–6, 14]. A small right hemithorax with secondary dextrocardia, some degree of hypoplasia of the right pulmonary artery, anomalous connections of the right pulmonary veins to the right atrium or inferior vena

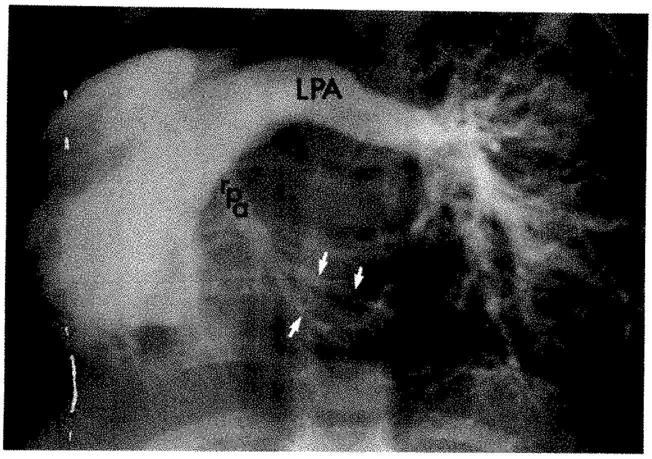

Fig. 6.—Branches (*arrows*) of right pulmonary artery (rpa) pursue errant course in isthmic parenchyma. Note disparity in size between left pulmonary artery (LPA) and hypoplastic right pulmonary artery (rpa).

caval–right atrial junction, and anomalous systemic arterial supply: One or more of these features is observed in most patients with horseshoe lung deformity. The diagnosis of horseshoe deformity should be suspected in any patient with features of the scimitar syndrome, and it can be confirmed by conventional pulmonary arteriography performed in frontal and lateral projections. Bronchography and/or axial CT of the chest may also be diagnostic of the horseshoe deformity.

Thus, there are two conditions, both quite uncommon, in which a branch from the right pulmonary artery courses into the left hemithorax and supplies all or part of the left lung: errant right pulmonary artery in the horseshoe deformity and so-called pulmonary sling [15–19]. In the latter condition, usually occurring in isolation, the left pulmonary artery originates from the superior aspect of the right pulmonary artery and courses between the trachea and esophagus to supply the *entire* left lung. In the horseshoe lung deformity, a branch of the right pulmonary artery originates inferiorly from the proximal right trunk to supply only part of the left lung.

REFERENCES

1. Spencer H. *Pathology of the lung*, 2d ed. Oxford: Pergamon, **1968**:73
2. Dische MR, Teixeira ML, Winchester PH, Engle MA. Horseshoe lung associated with a varient of the "scimitar" syndrome. *Br Heart J* **1974**;36:617–620
3. Cipriano P, Sweeney LJ, Hutchins GM, Rosenquist GC. Horseshoe lung in an infant with recurrent pulmonary infections. *Am J Dis Child* **1975**;129:1343–1345
4. Purcaro A, Caruso L, Ciampani N, Inglese L. Polmone a ferro di cavallo malposizione cardiaca, Ed. Anomalie vascolari polmonari: una sindrome caratteristica. *G Ital Cardiol* **1976**;6:312–316
5. Orzan F, Angelini P, Oglietti J, Leachman RD, Cooley DA. Horseshoe lung: report of two cases. *Am Heart J* **1977**;93:501–505
6. Beitzke A. Scimitar syndrome with horseshoe lung. *ROFO* **1982**;136:265–269
7. Freedom RM, Culham JAG, Moes CAF. *Angiocardiography of congenital heart disease*. New York: Macmillan, **1984**:258–260
8. Halasz NA, Halloran KH, Liebow AA. Bronchial and arterial anomalies with drainage of the right lung into the inferior vena cava. *Circulation* **1956**;14:826–845
9. Neill CA, Ferencz C, Sabiston DC, Sheldon H. The familial occurrence of hypoplastic right lung with systemic arterial supply and venous drainage: "scimitar syndrome." *Bull Johns Hopkins Hosp* **1960**;107:1–21
10. Kulper-Oosterwal EH, Moulaert A. The scimitar syndrome in infancy and childhood. *Eur J Cardiol* **1973**;1:55–61
11. Haworth SG, Sauer U, Buhlmeyer R. Pulmonary hypertension in scimitar syndrome in infancy. *Br Heart J* **1983**;50:182–189
12. Thilenius OG, Ruschhaupt DG, Replogle RL, Bharati S, Herman T, Arcilla RA. Spectrum of pulmonary sequestration: association with anomalous pulmonary venous drainage in infants. *Pediatr Cardiol* **1983**;4:97–103
13. Roehm JOF, Jue KL, Amplatz K. Radiographic features of the scimitar syndrome. *Radiology* **1966**;86:856–859
14. Heithoff KB, Sane SM, Williams HJ, et al. Bronchopulmonary forecut malformations: a unifying etiological concept. *AJR* **1976**;126:46–55
15. Jue KL, Raghib G, Amplatz K, Adams P. Jr, Edwards JE. Anomalous origin of the left pulmonary artery from the right pulmonary artery: report of two cases and review of the literature. *AJR* **1965**;95:598–610
16. Tesler U, Balsara RH, Niguidula FN. Aberrant left pulmonary artery (vascular sling): report of five cases. *Chest* **1974**;66:402–407
17. Lubbers WJ, Tegelaers WHH, Losekoot TG, Becker AE. Aberrant origin of left pulmonary artery (vascular sling): report of the clinical and anatomic features in three patients. *Eur J Cardiol* **1975**;2:477–483
18. Lenox CC, Crisler C, Zuberbuhler JR, et al. Anomalous left pulmonary artery: successful management. *Thorac Cardiovasc Surg* **1979**;77:748–752
19. Gumbiner CH, Mullins CE, McNamara DG. Pulmonary artery sling. *Am J Cardiol* **1980**;45:311–315

Book Review

Diagnostic Imaging in Clinical Medicine, 3d ed. By Rosalind H. Troupin. Chicago: Year Book Medical, 210 pp., 1985. $19.95; soft cover

This small 200-page paperback was sheer delight to read. Clearly, since its origin in handouts to medical students more than 10 years ago, it has been revised, rewritten, reevaluated, and rewritten again and again to achieve such a fine end product where every sentence seems to be important. Input into the revisions to produce this third edition included "field-testing" on medical students and critical advice from Lucy Frank Squire, the "mother" of radiological teaching to medical students. The book is intended to teach the fundamentals of all aspects of radiology to students. This updated edition was produced because of the rapid changes in the specialty of imaging and image interpretation.

An introductory chapter briefly discusses expected subjects such as the nature of the radiographic image and some topics not often included in radiology texts for medical students such as x-ray requests and reports, the imaging consultant, imaging charges, radiation exposures, and genetic effects of radiation.

The second chapter explains imaging techniques including emission computed tomography and magnetic resonance imaging. There is liberal use of many types of images throughout the book: angiograms, nuclear scans, magnetic resonance images, sonograms, etc. They are not just added as an afterthought to update an older edition as one sees in some new editions. They are an integral part of the book as they are in any modern radiology department. In the author's words, the new techniques are integrated with the traditional.

The remaining eight chapters are organ-system oriented including chest, abdomen, liver/pancreas, gastrointestinal, urinary, reproductive/endocrine, skeletal, and head and neck. Almost half of the content is on chest and skeletal.

The author clearly has had considerable experience teaching medical students (something we might expect the author of such a book to have, but not all do.) She not only has a radiologist's perspective of what they should know but the student's perspective of what they want to know. Using this as background, chapters vary in format and approach. There is even an introductory section explaining this deliberate variation because in "real life" clinicians are involved in imaging problems of different organ systems in different ways. For example, the chest and bone sections include more on image analysis than others. The gastrointestinal chapter has more on indications, costs, and alternatives because image analysis is less important for the nonradiologist. Some chapters are mainly problem oriented, some use case studies, others are disease oriented. The entire book reflects a sensitivity and concern for the patient and his/her pocketbook.

The reproductions, many of which are rather small, are of superb quality throughout and clearly show what is intended with appropriate arrows when required. There are also helpful line drawings.

I read this little paperback more thoroughly than usual, not only because it was easy and enjoyable to read and informative, but every reviewer tries to find at least one (little, if necessary) thing to criticize in any book reviewed. Here, there is virtually nothing to fault. I was inconvenienced several times when I had to turn the book sideways to look at figures and captions oriented that way. The worst I could find was a stress view of an ankle (fig. 9-20B) which shows part of an ungloved hand providing the stress. Perhaps it should be stated for the nonradiologist that this is not good technique.

In summary, this little gem is highly recommended to medical students and others wanting to know about our specialty, such as physician assistants and nurses. It is also appropriate for nonradiologist physicians seeking to learn a little radiology.

Stanley P. Bohrer
Bowman Gray School of Medicine
Winston-Salem, NC 27103

Horseshoe Lung: Clinical, Pathologic, and Radiologic Features and a New Plain Film Finding

Jane L. Frank[1]
Catherine A. Poole[1]
Gilberto Rosas[1, 2]

Horseshoe lung is a rare congenital malformation in which an isthmus of pulmonary parenchyma extends from the right lung base across the midline behind the pericardium and fuses with the base of the left lung. Six cases are presented and eight previously published case reports are reviewed. Eleven of these 14 cases occur in conjunction with scimitar syndrome, the complex of anomalies including hypoplasia of the right lung, anomalous right pulmonary venous return, and anomalous arterial supply to the right lung. Differentiation of scimitar syndrome from horseshoe lung can be made on the plain chest film, if, in addition to the typical radiographic findings of scimitar syndrome, there is evidence of a fine linear density in the medial aspect of the left base representing the lateral extent of the pulmonary isthmus. Recognition of horseshoe lung is important because children present in the first few years of life with significant respiratory symptoms, whereas the scimitar syndrome alone is usually discovered fortuitously after the first decade of life.

The term "horseshoe lung" was first used by Spencer [1] in 1962 to describe a malformation in which the base of the right and left lungs were joined by a narrow isthmus posterior to the heart. There was mention of a similar malformation in the French literature at the end of the 19th century [2] but without a detailed description of the entity. We have been able to locate eight additional cases [3–9] in the world literature, five of which also have the classic features of scimitar syndrome [3, 6, 7, 9], a complex of anomalies including hypoplasia of the right lung, anomalous right pulmonary venous return, and anomalous arterial supply to the right lung. One of these was reported as scimitar syndrome without mention of typical angiographic features of horseshoe lung, which were clearly evident [9].

We describe our experience with six additional cases of horseshoe lung, all of which occurred in conjunction with scimitar syndrome. The clinical and radiographic spectra of both anomalies are described, and we report for the first time a plain film finding that appears to be specific for horseshoe lung when it occurs with scimitar syndrome.

Materials and Methods

The diagnosis of horseshoe lung was first made following cardiac catheterization and angiography in a patient with scimitar syndrome. A retrospective review of all cases of suspected scimitar syndrome at this medical center in the preceding 23 years revealed three additional cases. Two cases were subsequently diagnosed prospectively by plain chest film findings. All six were studied angiographically and three also had bronchography.

A review of the literature revealed eight cases of horseshoe lung, five associated with scimitar syndrome. Insufficient information was available to include the first two examples of horseshoe lung mentioned in the literature [1, 2]. Two examples of "bridging bronchus" have been reported [10, 11], which may represent a variant of horseshoe lung, although no bridging isthmus of pulmonary tissue was present in either case.

Received August 19, 1985; accepted after revision November 8, 1985.

Presented in part at the annual meeting of the Society for Pediatric Radiology, San Francisco, March 1981.

[1] Department of Radiology, Pediatric Radiology Section, University of Miami School of Medicine, P.O. Box 016960, Miami, FL 33101. Address reprint requests to J. L. Frank.

[2] Present address: Clinica Soma Radiol QF 311, Medellin-Antioquia, Colombia.

AJR **146:217–226, February 1986**
0361-803X/86/1462-0217
© American Roentgen Ray Society

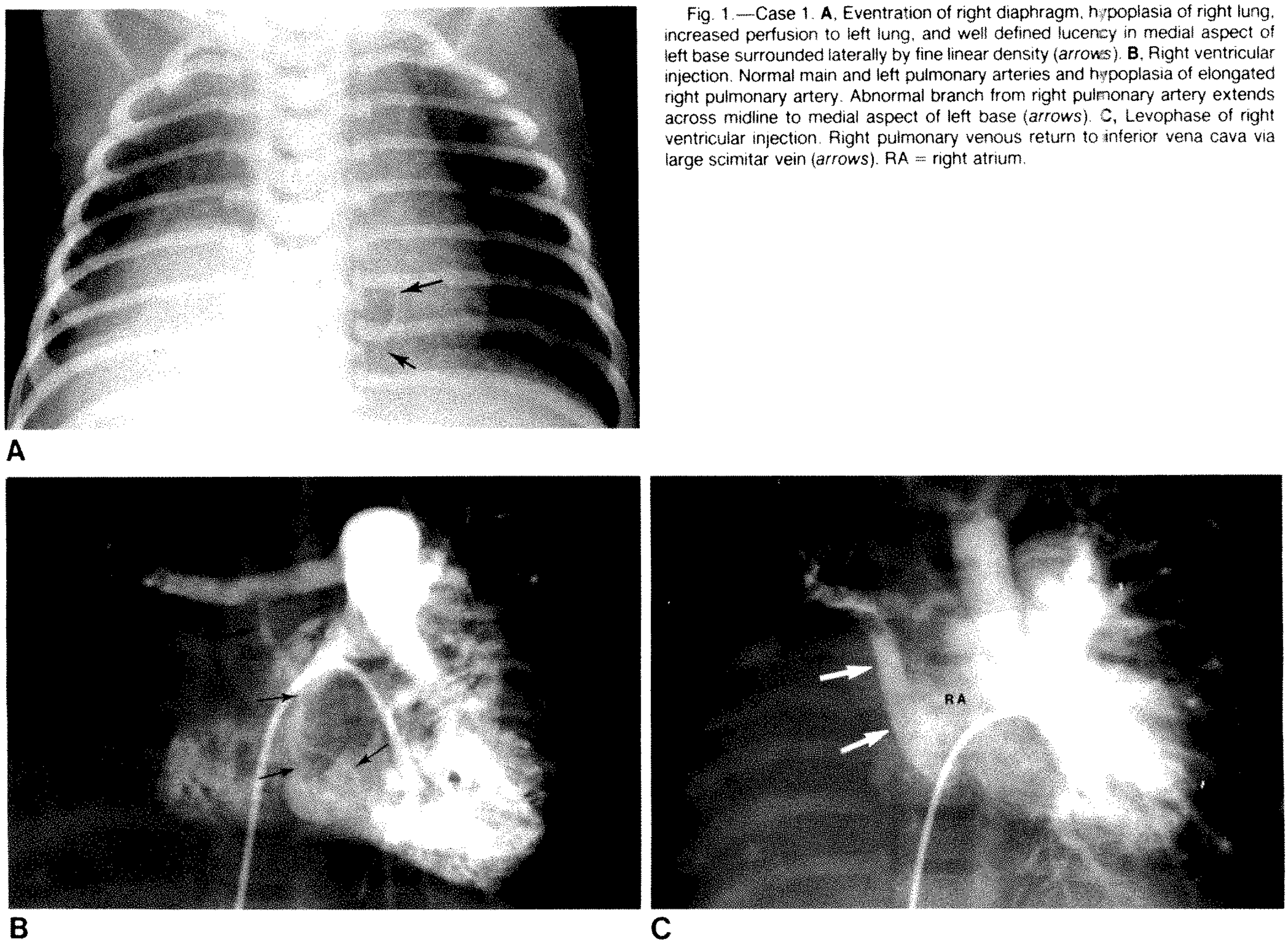

Fig. 1.—Case 1. **A**, Eventration of right diaphragm, hypoplasia of right lung, increased perfusion to left lung, and well defined lucency in medial aspect of left base surrounded laterally by fine linear density (*arrows*). **B**, Right ventricular injection. Normal main and left pulmonary arteries and hypoplasia of elongated right pulmonary artery. Abnormal branch from right pulmonary artery extends across midline to medial aspect of left base (*arrows*). **C**, Levophase of right ventricular injection. Right pulmonary venous return to inferior vena cava via large scimitar vein (*arrows*). RA = right atrium.

Case Reports

Case 1

A full-term female infant presented at birth with mild dyspnea and again at 10 months of age with pneumonia. Chest films showed eventration of the right diaphragm, hypoplasia of the right lung, midline position of the heart, increased perfusion to the left lung, and a lucency in the medial aspect of the left base subtended laterally by a curvilinear density (fig. 1A). Because of cyanosis and increasing respiratory distress, cardiac catheterization and angiography were performed. The right pulmonary artery was hypoplastic, and from its proximal aspect a branch arose which extended to and supplied the medial aspect of the left lung base (fig. 1B). The right pulmonary venous return was by way of a large anomalous vein into the inferior vena cava (scimitar sign) (Fig. 1C). A small systemic vessel from the abdominal aorta supplied the base of the hypoplastic right lung. A small atrial septal defect was identified with minimal shunting. Pulmonary artery pressure was normal.

Recurrent pulmonary problems requiring intubation and assisted ventilation prompted pulmonary resection at 14 months of age. At surgery the base of the right lung, the diaphragm, and the liver were virtually fused. The right lung was dissected with difficulty but no retrocardiac exploration was performed. Gross examination of the specimen revealed marked pulmonary hypoplasia with complete absence of fissures. The patient had a stormy postoperative course and died 1 month after surgery from cardiorespiratory arrest, having never been weaned from the respirator.

Case 2

A full-term female infant was admitted at 9 months and 16 months of age for episodes of respiratory tract infection. Chest films showed hypoplasia of the right lung with cardiac dextroposition, a density at the right base suggesting a scimitar vein, and increased perfusion to a relatively large left lung. A triangular area demarcated laterally by a thin linear density was present in the medial aspect of the left base (fig. 2A). Bronchography revealed incomplete filling of a hypoplastic, seemingly bilobed right lung, with branches from the lower bronchus extending to the left base. Angiography demonstrated a hypoplastic right pulmonary artery, branches of which coursed to the medial aspect of the left base. Right pulmonary veins drained anomalously into the right atrium, either directly or by way of the inferior vena cava. Large systemic vessels from the abdominal aorta supplied the lower half of the right lung (fig. 2C).

At 18 months of age, a right pneumonectomy was performed. After dissection of the right lung, a residual empty serous-lined cavity separate from and posterior to the pericardium was described, which was left open to the right pleural space. The surgical specimen was

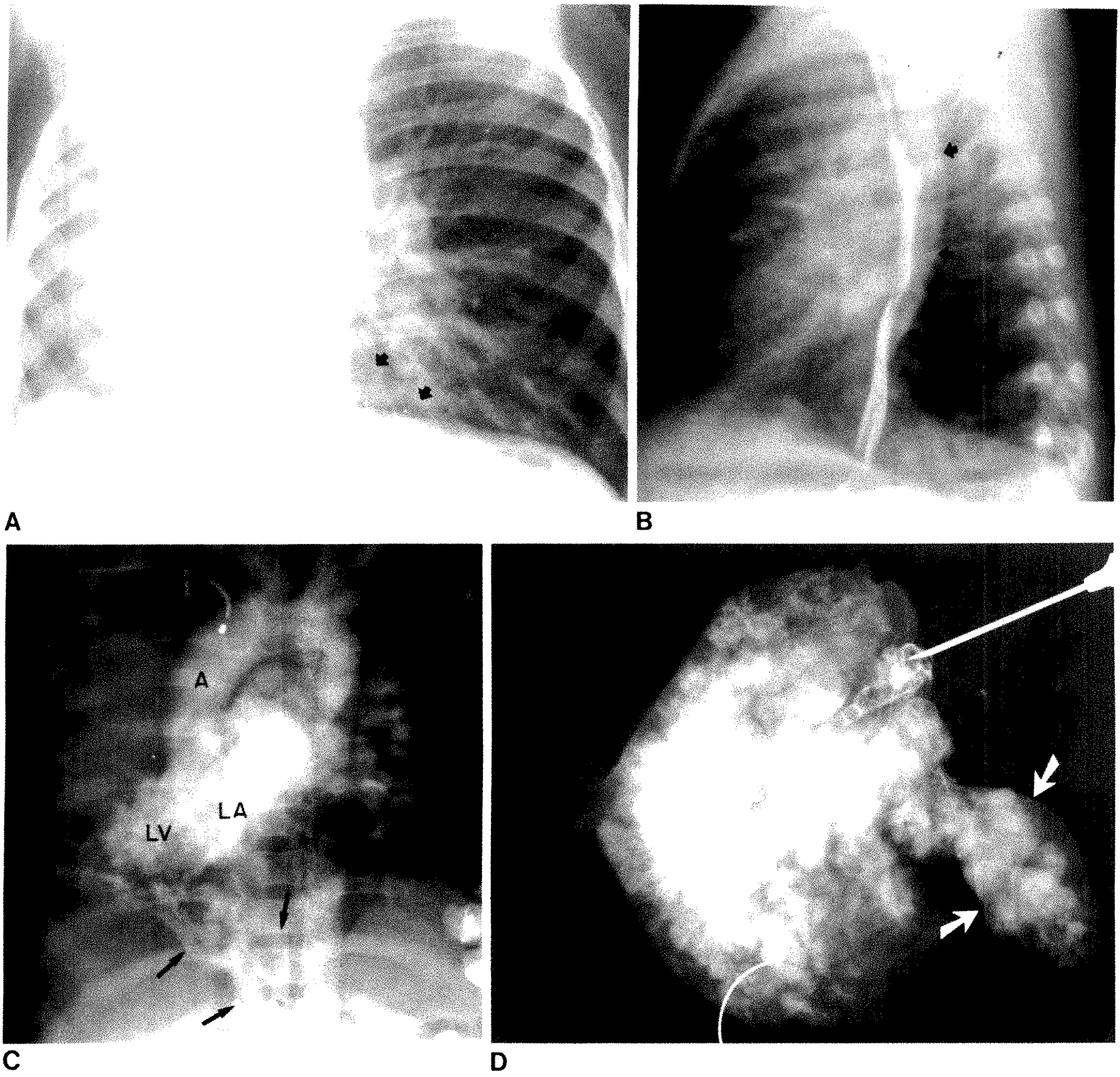

Fig. 2.—Case 2. **A**, Hypoplasia of right lung, cardiac dextroposition, and linear density subtending triangular area in medial aspect of left base (*arrows*). Vague abnormal density at right base suggests scimitar vein. **B**, Lateral chest film. *Arrows* identify curvilinear posterior margin of soft-tissue density representing extrapleural areolar connective tissue. Hypoplastic right lung located posteriorly. **C**, Levophase of angiogram. Filling of large systemic vessels to right base from abdominal aorta (*arrows*). LA = left atrium; LV = left ventricle; A = aorta. **D**, Surgical specimen with alveolarized contrast. Well demonstrated isthmus (*arrows*) arises from base of right lung.

described as a totally anomalous hypoplastic lung with one major subdivision of the main bronchus yielding two small segments, the medial one having the configuration of an isthmus (fig. 2D). A small bronchial diverticulum was also present. The patient was discharged in satisfactory condition after an uneventful postoperative course and was subsequently lost to follow-up.

Case 3

A full-term female infant was admitted at 10 months and again at 2½ years of age with recurrent pulmonary infection accompanied by febrile seizures. Chest films showed hypoplasia of the right lung with cardiac dextroposition, an anomalous vessel at the right base (scim-

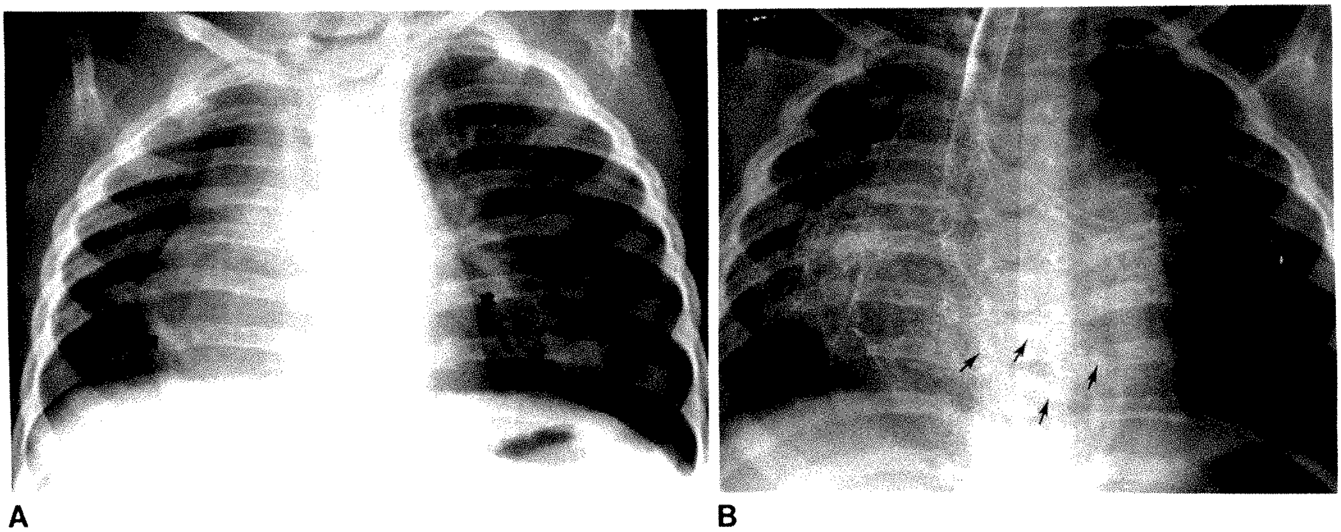

Fig. 3.—Case 3. **A**, Hypoplasia of right lung, cardiac dextroposition, scimitar vein at right base (*single arrow*), and linear density bordering triangular lucency in medial aspect of left base (*arrows*). **B**, Bronchogram. Abnormal bronchial pattern on right side with faintly opacified branches from main bronchus crossing midline to left base (*arrows*).

itar sign), and a lucent area in the medial aspect of the left base demarcated laterally by a fine linear density (fig. 3A). Increased perfusion to the left lung was evident. Bronchography revealed disorganized branching of the right bronchial tree with a large branch from the right main bronchus crossing the midline to the left base (fig. 3B). Angiography revealed a hypoplastic right pulmonary artery, small branches of which coursed inferiorly toward the medial aspect of the left base. The right pulmonary veins were entered from the inferior vena cava at catheterization. A large systemic vessel from the abdominal aorta supplied the right lung base. Because of recurrent infections and respiratory difficulty, a right pneumonectomy was recommended but refused by the parents. The patient was discharged and subsequently lost to follow-up.

Case 4

A full-term female infant was referred to the medical center at 4 months of age with a diagnosis of pneumonia with empyema. Examination of the chest revealed changes consistent with scimitar syndrome. She was discharged without further intervention. The patient experienced frequent respiratory symptoms, and repeat films at 8 months and 3½ years of age showed no interim change except for the eventual appearance of a triangular lucent area in the left base demarcated laterally by a thin linear density. In retrospect, this latter finding was present on the initial chest film, although it was very subtle (fig. 4A). Angiography at 3½ years of age showed a relatively normal-sized right pulmonary artery from which small branches arose coursing to the left base (fig. 4C). The right pulmonary veins drained anomalously into the inferior vena cava (fig. 4D), and a small systemic vessel from the abdominal aorta supplied the right lung base. Pulmonary artery pressures were normal.

It is of historical interest in this case that the child's mother had a history of asthma since birth. She was diagnosed at 16 years of age as having scimitar syndrome. Review of her workup, which included pulmonary angiography and bronchography, revealed no evidence of a coexisting horseshoe lung.

Case 5

A full-term female infant in respiratory distress had a chest film at 12 hr of age demonstrating opacification of the right thorax, cardiac dextroposition, elevation of the right diaphragm, and a triangular lucent area in the medial aspect of the left base. This area was subtended by a thin linear density resembling a fissure (fig. 5). A prospective diagnosis of horseshoe lung was made. Cardiac catheterization and angiography demonstrated cardiac dextroposition, a large atrial septal defect, a small ventricular septal defect, a persistent left superior vena cava, hypoplasia of the right pulmonary artery with anomalous pulmonary venous return to the inferior vena cava, and systemic arterial supply to the lower half of the right lung from the abdominal aorta. Bronchography showed a hypoplastic right lung with abnormal branching of the bronchial tree. The isthmus was supplied by branches of the right pulmonary artery and right-lower-lobe bronchus. The patient clinically deteriorated, and surgical resection of the hypoplastic, consolidated right lung was performed. The retrocardiac isthmus of lung tissue was contained within a pleural-lined space and was simultaneously removed. There was also a small central diaphragmatic defect, with liver adherent to the right lung base. After a prolonged postoperative course with assisted ventilation, the patient was discharged in good condition at the age of 21 months.

Case 6

A 26-day-old boy was admitted with difficulty breathing, cough, and fever. Chest films demonstrated opacification of the right thorax with cardiac dextroposition and increased vascularity of the left lung. Additional observations included a density at the right base consistent with an anomalous draining vein and a triangular area in the medial aspect of the left base bordered on its lateral margin by a diagonal linear density (fig. 6A). On the basis of these findings, the diagnosis of scimitar syndrome with horseshoe lung was prospectively made. Angiography revealed an approximately normal-sized right pulmonary artery with inferior branches extending to the left lung base (fig. 6B).

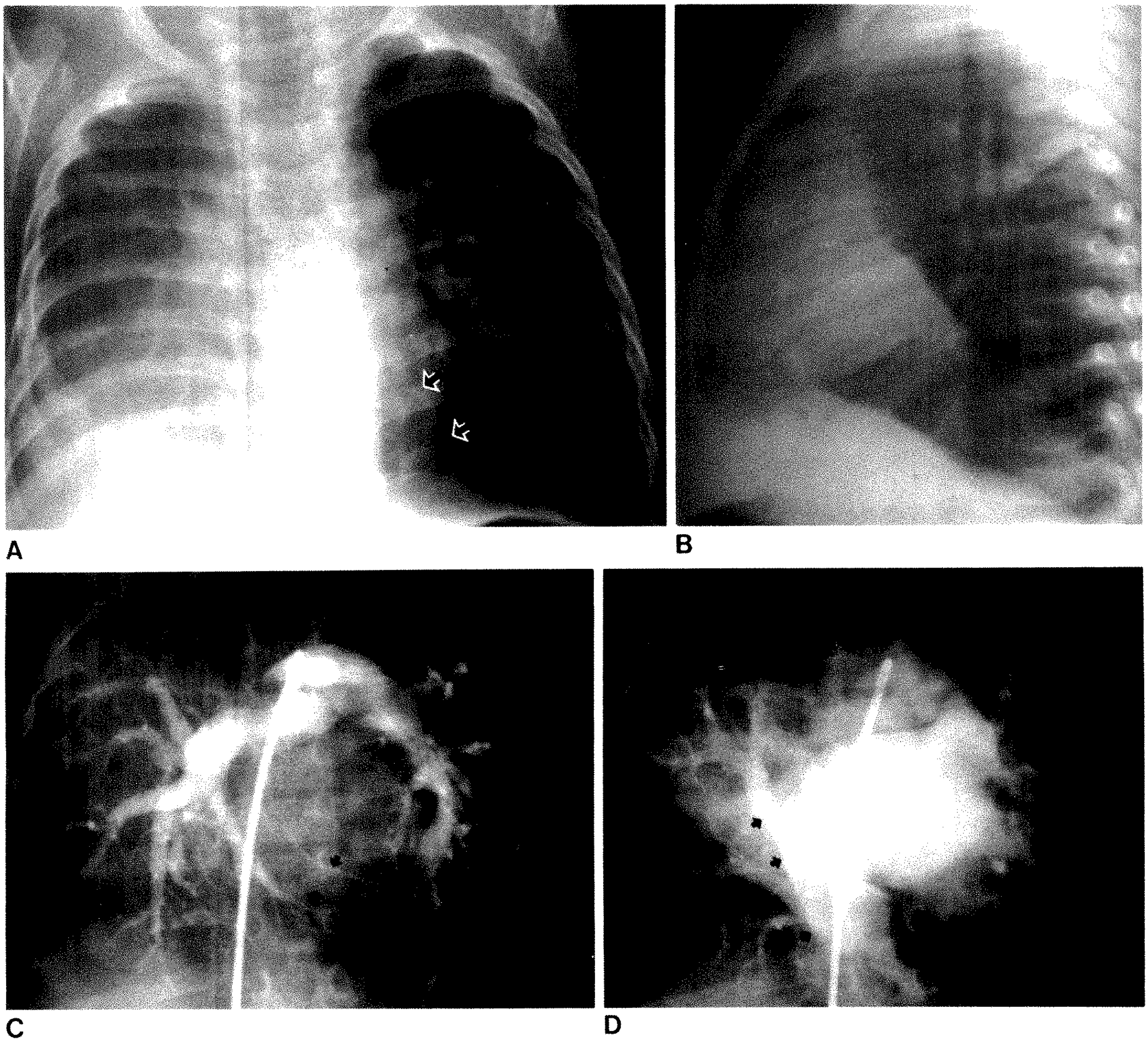

Fig. 4.—Case 4. **A**, Right lung hypoplasia, cardiac dextroposition, and faintly visualized linear density in medial aspect of left base (*arrows*). **B**, Lateral chest film. Soft-tissue density representing extrapleural connective tissue anteriorly, with lucent hypoplastic lung posteriorly. **C**, Pulmonary artery injection. Normal-sized right pulmonary artery with inferior branches crossing midline to left base (*arrows*). **D**, Levophase. Right pulmonary veins draining into anomalous scimitar vein entering inferior vena cava (*arrows*). Opacification of left atrium from normal drainage of left pulmonary veins.

The right pulmonary veins drained anomalously into the inferior vena cava. An anomalous systemic artery from the abdominal aorta supplied the lower half of the right lung. A secundum-type atrial septal defect was found. The pulmonary artery pressure was normal. One day after cardiac catheterization and angiography, the patient was discharged in satisfactory condition to be followed as an outpatient.

Results

Eleven cases of horseshoe lung in association with scimitar syndrome, six reported here and five from the literature, have striking clinical and radiographic similarities (table 1). All presented with respiratory symptoms under 1 year of age with the exception of a single child first seen at age 4 years. Plain films of the chest show characteristic features of hypoplasia of the right lung in all 11 cases, with a scimitar vein being evident in eight. A well demarcated area resembling an "inferior accessory lobe and fissure" in the medial aspect of the left lung base is present in all six of our cases and at least one [6] and possibly two additional [3, 7] reports in the literature.

Angiography in 10 cases and autopsy in the 11th case revealed typical features of scimitar syndrome in each instance, with anomalous pulmonary venous return from the right lung to the inferior vena cava (directly to the right atrium in one case) and systemic arterial supply from the abdominal aorta to the right lung base. The right pulmonary artery was hypoplastic in seven cases and relatively normal sized in four, and in all cases branches of the right pulmonary artery extended medially and inferiorly supplying the isthmus of pulmonary tissue bridging the right lung to the left lung posteriorly behind the heart. Atrial septal defects were present in five cases (our cases 1, 5, and 6; cases 1 and 2 of Orzan et al. [6]), two of which had additional anomalies (one ventricular septal defect with left superior vena cava (our case 5) and one patent ductus arteriosis (case 2 of Orzan et al. [6]). A sixth case had only a small patent ductus arteriosus [9]. Pulmonary artery pressures were measured in seven cases: Four were normal and three were elevated with no apparent relation to pulmonary/systemic flow ratios (Qp/Qs), which were calculated in six cases and ranged from 1.2 to 6.

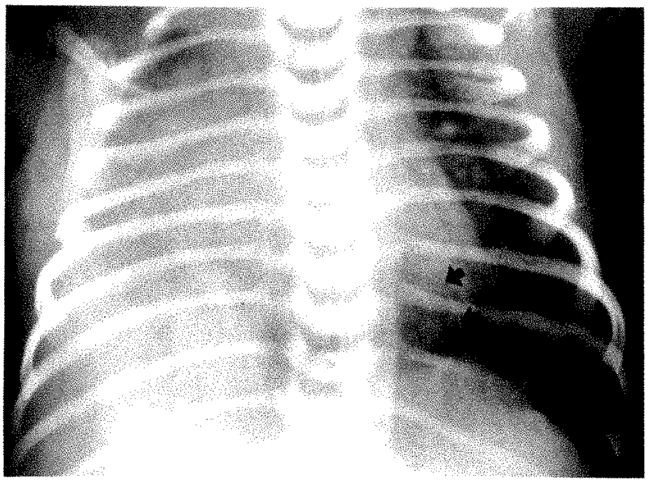

Fig. 5.—Case 5. Opaque appearance of right thorax, cardiac dextroposition, and linear density defining triangular lucency in medial aspect of left base (*arrows*).

The right bronchial tree was evaluated by bronchography in three cases and at autopsy in one case. In each case an abnormal branching pattern was noted, with branches from the right bronchus extending to the isthmus of pulmonary tissue joining the right and left lung bases.

The right lung was examined surgically in six cases and at autopsy in another case. Description of the gross specimen revealed a hypoplastic lung devoid of fissures in each instance.

One patient died before surgical intervention [3]. Of six patients undergoing pneumonectomy, two died postoperatively (our case 1 and the case of Haworth et al. [9]) and four were discharged clinically well (our cases 2 and 5; cases 1 and 2 of Orzan et al. [6]), one subsequently having been lost to follow-up. Four had no surgical intervention (our cases 3, 4, and 6; the case of Beitzke et al. [7]); two are clinically doing well and two have been lost to follow-up.

Discussion

The common denominator in all cases of horseshoe lung is the coexistence of unilateral pulmonary hypoplasia occurring in 100% of our cases (6/6) as well as those previously reported in the literature (8/8). Congenital unilateral pulmonary hypoplasia can occur secondary to mechanical interference with growth of the fetal lung (i.e., congenital diaphragmatic

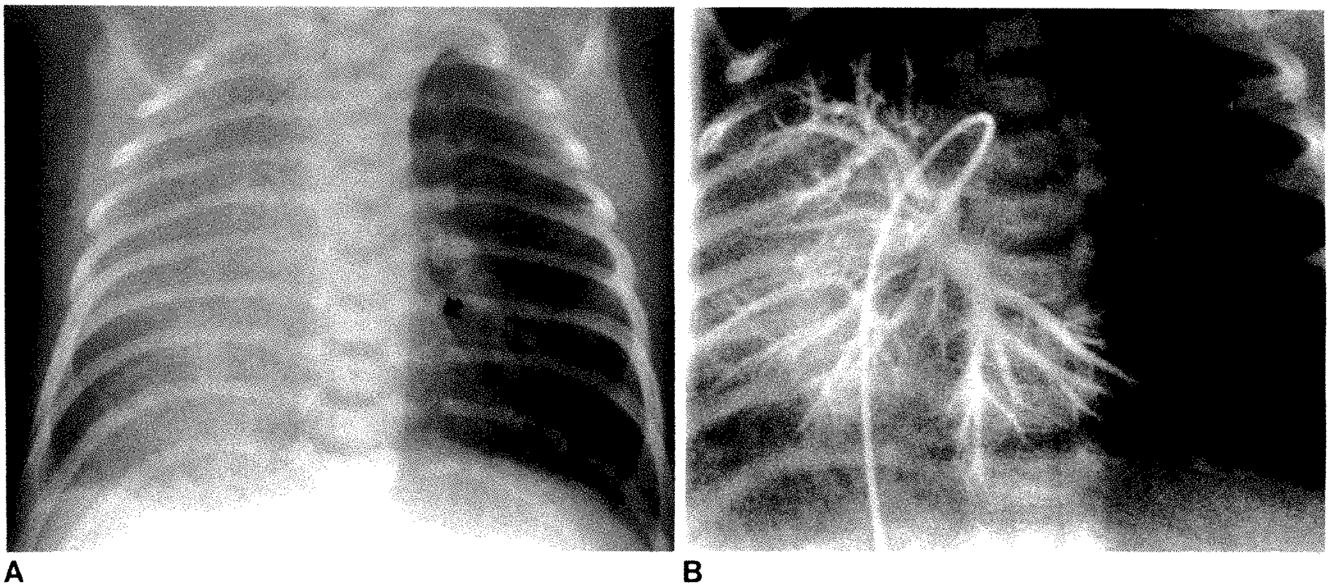

Fig. 6.—Case 6. **A**, Opacification of right thorax, cardiac dextroposition, abnormal density at right base (scimitar vein), and linear density defining lateral margin of triangular area at left base (*arrows*). **B**, Selective right pulmonary artery injection. Large inferior branches cross to medial aspect of left base.

hernia) or as a primary embryologic defect. Primary hypoplasia of one lung can occur as an isolated anomaly (simple hypoplasia) or in association with absence of a pulmonary artery, anomalous venous return to the inferior vena cava or right atrium, accessory diaphragm, or pulmonary sequestration with diaphragmatic defects [8]. Overlapping features of these conditions suggest a common embryogenesis, which has not, however, been established. There is a definite propensity for the coexistence of horseshoe lung with one specific type of pulmonary hypoplasia, the "scimitar syndrome," as occurred in 11 (79%) of 14 cases (all six of ours and five of eight previously reported) (table 1). Three previously published cases of horseshoe lung were associated with pulmonary hypoplasia without additional features of scimitar syndrome (table 2). These will be discussed separately.

Horseshoe Lung with Scimitar Syndrome

Also known as congenital pulmonary venolobar syndrome [12], hypogenetic lung syndrome [13], mirror-image lung syndrome [14], epibronchial right pulmonary artery syndrome [15], and vena cava bronchovascular syndrome [16], the scimitar syndrome as originally coined by Neill et al. [17] is the most common term used to describe a spectrum of anomalies involving, with rare exceptions, the right lung. Several excellent reviews on scimitar syndrome have appeared in the literature [18–21] and reference is made to the anomaly involving the left lung on only three occasions [12, 22].

The right lung in scimitar syndrome is abnormal in terms of its size, lobation, and bronchial tree. The lung is hypoplastic, varying from extreme to indiscernible, 10% falling into either category with the majority somewhere in between [21]. The hypoplasia is recognized in the frontal projection by diminution in volume of the right thorax with mediastinal shift to the right and a hazy appearance of the right cardiac border. In the lateral projection, a linear oblique line that parallels the posterior margin of the sternum with increased density anterior to the line can be identified [23]. This density is due to extrapleural areolar connective tissue filling space normally occupied by absent lobe(s) [8, 13, 22]. The most common abnormality of lobation is absence of one lobe. Total absence of lobation is less common, and only rarely are three lobes present [21]. Abnormalities of the bronchial tree are invariably present, including abnormal bronchial distribution, areas of stenosis, or areas of atresia with cystic dilatation or diverticulum formation. In no instance of scimitar syndrome has the involved lung been completely normal [18, 21].

The pulmonary artery to the right lung is usually hypoplastic with an abnormal branching pattern. In rare cases it is totally absent, but in 40% of cases it is of approximately normal size [20]. Depending on the degree of pulmonary artery hypoplasia, perfusion to the left lung is correspondingly increased. Pulmonary drainage of some or all of the right lung is anomalous, usually entering the inferior vena cava between the hepatic veins and the right atrium. The anomalous pulmonary veins typically join to form a single large trunk that curves inferiorly, parallel to the right heart border. The anomalous channel is evident on the plain chest film in most cases and has been likened to a Turkish sword (scimitar) whence the syndrome derives its name. Rarely the anomalous vein drains normally into the left atrium [24]. The left-to-right shunt from the anomalous pulmonary venous return is rarely of clinical significance. However, pulmonary perfusion to the left lung will be increased in direct proportion to the diminished flow to the hypoplastic right lung.

Systemic arterial supply to the right lung is usually present, with one or more vessels from the abdominal aorta piercing the right diaphragm to supply the base of the lung. Anomalous vessels occasionally arise from the thoracic aorta, or bronchial arterial supply may predominate [18, 20, 21].

Dextroposition and rotation of the heart is present as a result of and in direct proportion to the degree of hypoplasia of the right lung. Congenital heart disease is present in about 25% of cases, and in at least half the lesion is an atrial septal defect. Other lesions reported include ventricular septal defect, patent ductus arteriosus, tetralogy of Fallot, and coarctation [18, 21].

The unique anatomic feature of horseshoe lung is an isthmus of pulmonary parenchymal tissue arising from the right lung base, bridging the right and left lungs posterior to the pericardial sac and anterior to the aorta and esophagus. Pulmonary arterial and bronchial extensions to the isthmus are derived from the right pulmonary artery and right bronchus, respectively. In those cases undergoing complete surgical exploration or autopsy, the isthmus has been described to be sheathed in its own pleural covering behind the pericardium.

Despite the similarities in scimitar syndrome with and without horseshoe lung, the clinical presentations of the two are strikingly different. Both occur predominantly in females [18] and are rarely familial [17, 27, 28], but most scimitar syndromes are relatively asymptomatic and seldom require surgical treatment [12, 19]. The diagnosis is uncommonly made before the second decade of life [18], whereas all cases with a coexistent horseshoe lung were diagnosed in young children with pulmonary problems. Precisely why patients with horseshoe lung tend to present earlier is not clear. The degree of pulmonary hypoplasia is not greater as a rule, nor is the incidence or severity of associated congenital heart disease increased. Pulmonary arterial hypertension has been implicated as the cause of early onset of symptoms in scimitar syndrome [9, 19], but it occurred in only three of seven patients with horseshoe lung in whom pulmonary arterial pressures were recorded at catheterization. In neither situation is the shunt due to the anomalous pulmonary vein of significant magnitude, Q_p/Q_s rarely being greater than 2 [18, 21].

Horseshoe Lung without Scimitar Syndrome

Table 2 lists three cases of horseshoe lung occurring without all components of the scimitar syndrome but in association with a hypoplastic lung. One case was a 4-year-old boy with hypoplasia of the right lung and an isthmus of pulmonary tissue supplied by small branches from the left

TABLE 1: **Horseshoe Lung with Scimitar Syndrome**

		Plain Chest Film			Angiography					
Cases	Age, Gender	Hypoplastic Right Lung	Scimitar Vein	Pleural Line Left Base	RPA	Site of RPVR	Source of SAS to RL	Isthmus Supply	PAP	Q_p/Q_s
Current case no.:										
1	N, F	+	–	+	Hypoplastic	IVC	Abd Ao	RPA	30/11	1.2
2	9 mo, F	+	+	+	Hypoplastic	IVC or RA	Abd Ao	RPA	. . .	. . .
3	10 mo, F	+	+	+	Hypoplastic	IVC	Abd Ao	RPA	. . .	. . .
4	4 mo, F	+	+	+	Normal size	IVC	Abd Ao	RPA	31/11	1.5
5	N, F	+	+	+	Hypoplastic	IVC	Abd Ao	RPA	. . .	. . .
6	1 mo, F	+	+	+	Normal size	IVC	Abd Ao	RPA	22/7	2.9
Case from reference:										
[3]	N, M	+	+	?	Hypoplastic	RA*	. . .	RPA*	. . .	. . .
[6] case 1	3 mo, F	+	+	–	Normal size	IVC	Abd Ao	RPA	50/18	6
[6] case 2	2 mo, F	+	–	+	Hypoplastic	IVC	Abd Ao and bronchial	RPA	72/20	2.5
[7]	4 yr, M	+	+	?	Normal size	IVC	Abd Ao	RPA	"Normal"	. . .
[9]	2 mo	+	–	–	Hypoplastic	IVC	Abd Ao	RPA	85/45	2.4

Note.—N = newborn; + = present; – = not evident; RPA = right pulmonary artery; RPVR = right pulmonary venous return; SAS to RL = systemic arterial supply to right lung; PAP = pulmonary artery pressure; Q_p/Q_s = pulmonary to systemic flow ratio; IVC = inferior vena cava; RA = right atrium; Abd Ao = abdominal aorta.

TABLE 2: **Horseshoe Lung without Scimitar Syndrome**

	Case from Reference:		
	[4]	[5]	[8]
Age and gender	Neonate, M	Neonate, F	4 years, M
Hypoplastic lung	Right	Left	Right
Isthmus from	Right lung	Right lung	Left lung
Pathology	Hypoplastic unilobed lung with intervening pleura	Hypoplastic lung with no intervening pleura	None

TABLE 3: **Bridging Bronchus**

	Case from Reference:	
	[10]	[11]
Age and gender	Neonate, F	Neonate, F
Hypoplastic lung	Right	Right*
Isthmus	None	None
Pathology	Hypoplastic right lung; fusion of upper and middle lobes; right-lower-lobe bronchus from left	Hypoplastic right lung; fusion of upper and middle lobes; right-lower-lobe bronchus from left

* With lucency in base.

pulmonary artery and left main-stem bronchus [8]. Clinical course and pathologic confirmation of that case were not available. The other two cases both presented with recurrent pneumonias and died in the first year of life. One male infant [4] had hypoplasia of the right lung, right pulmonary artery, and right bronchial tree, but had normal pulmonary venous return to the left atrium and no systemic vascular supply to the right lung. Arterial and bronchial supply to the isthmus was not described. The final case was a female infant with hypoplasia of the left lung and agenesis of the left pulmonary artery [5]. Each lung received its own bronchus but supply to the isthmus was not described. The single right pulmonary artery supplied the entire right lung, the isthmus, and the hypoplastic left lung. Venous return from the right lung and isthmus was anomalous into the right atrium, but was normal from the hypoplastic left lung. An atrial septal defect, ventricular septal defect, and pulmonic valvular stenosis were also present. Pulmonary arterial pressures were normal.

Bridging Bronchus

Two cases of "bridging bronchus" reported in the literature [10, 11] (table 3) have certain anatomic and clinical features suggesting a possible embryologic relation with horseshoe lung. Though there was no isthmus of pulmonary tissue connecting the right and left lung, in both cases a branch from the left main-stem bronchus crossed the mediastinum and entered the right lower lobe. The right lung in both cases was bilobed, and areas of stenosis in the tracheobronchial tree were present. Both were female infants who died from recurrent pulmonary problems in the first 2 months of life.

The unique radiologic finding in horseshoe lung with scimitar syndrome is a well demarcated faint linear or curvilinear density at the medial aspect of the left base, which can be appreciated on the frontal chest film and corresponds to the left lateral margin of the pulmonary isthmus as it extends beyond the left side of the spine. The plain chest film finding was present in each of our cases, although it might easily have been missed because of its subtlety. Reproductions are such that with one notable exception [6], it is difficult to determine if this finding is present in the case reports in the literature. Since none of our cases occurred without scimitar

TABLE 1 continued

Bronchography		
Right Lung	Isthmus Supply from	Pathology
Not done	. . .	Hypoplastic unilobed lung
Hypoplasia with disorganized branching and diverticulum	Right bronchus	Hypoplastic unilobed lung with isthmus
Hypoplasia with disorganized branching	Right bronchus	None
Not done	. . .	None
Hypoplasia with disorganized branching and stenosis	Right bronchus	Hypoplastic unilobed lung with isthmus
Not done	. . .	None
Hypoplasia with disorganized branching*	Right bronchus*	Hypoplastic unilobed lung with isthmus, no intervening pleura*
Not done	. . .	Hypoplastic unilobed lung, no intervening pleura
Not done	. . .	"Consolidated right lung," no other description
Not done	. . .	None
Not done	. . .	Hypoplastic unilobed lung

* Autopsy findings.

syndrome, we cannot be certain if the plain film finding applies to that group. Previous reports have stated that diagnosis of horseshoe lung may be difficult if not impossible to make preoperatively or ante mortem [4] and may even be overlooked at necropsy [3]. A more recent report mentioned that the diagnosis is not apparent in routine studies and can only be made by angiography or bronchography [6]. However, we believe that the finding of a linear density subtending a triangular (or less commonly circular) area in the medial aspect of the left base in a case of scimitar syndrome is indeed specific for the coexistence of horseshoe lung. Noninvasive confirmation of the diagnosis can be established by computed tomography, as illustrated in a recent report [7].

The isthmus of pulmonary tissue seen at the left base is often lucent, presumably because it is hypovascular compared to the adjacent left lower lobe, which is normally or hyperperfused. The isthmus may be fused to the left lung parenchyma either without intervening pleura or with intervening pleura that resembles an interlobular fissure [4]. The presumption is made that intervening pleura is the linear density identifiable on plain films demarcating the lateral extent of the isthmus. Histologically the parenchyma of the isthmus is relatively normal [3, 4, 9].

The appropriate management of horseshoe lung and/or scimitar syndrome is surgical in the presence of recurrent infection [6], a left-to-right shunt in excess of 50% [7], or progressive pulmonary hypertension [9, 19]. Resection of the hypoplastic lung and isthmus is carried out if functional impairment and chronic infection exist. Anastomosis of the right "scimitar" vein to the left atrium can be performed if a significant shunt is present and if resection is not indicated [18–21]. As in most scimitar syndromes, treatment is conservative in horseshoe lung if the pulmonary-to-systemic flow ratio is calculated to be 2 or less and if recurrent pulmonary infection is not a problem.

ACKNOWLEDGMENTS

We thank C.P. Fliegel, Department of Radiology, and M. Rutishauser, Department of Pediatric Pulmonology of the Children's Hospital of Basel, Switzerland, for contributing case 5, and Louise Rhodes for assistance in manuscript preparation.

REFERENCES

1. Spencer H. *Pathology of the lung*, 3d ed. Oxford: Pergamon, **1977**:75–76
2. Morestin J, Porregaux G. Ectopie du poumon. *Bull Soc Anat Paris* **1894**;69:968–983
3. Dische MR, Teixeira ML, Winchester PH, Engle MA. Horseshoe lung associated with a variant of the "scimitar" syndrome. *Br Heart J* **1974**;36:617–620
4. Cipriano P, Sweeney LJ, Hutchins GM, Rosenquist GC. Horseshoe lung in an infant with recurrent pulmonary infections. *Am J Dis Child* **1975**;129:1343–1345
5. Purcaro A, Caruso L, Ciampani N, Inglese L. Polmone a ferro di cavallo, malposizione cardiaca ed anomalie vascolari polmonari: una sindrome caratteristica. *G Ital Cardiol* **1976**;6:312–316
6. Orzan F, Angelini P, Oglietti J, Leachman RD, Cooley DA. Horseshoe lung: report of two cases. *Am Heart J* **1977**;93:501–505
7. Beitzke A, Gypser G, Sager WD. Scimitarsyndrom mit Hufeisenlunge. *ROFO* **1982**;136:265–269
8. Currarino G, Williams B. Causes of congenital unilateral pulmonary hypoplasia: a study of 33 cases. *Pediatr Radiol* **1985**;15:15–24
9. Haworth SG, Sauer U, Buhlmeyer K. Pulmonary hypertension in scimitar syndrome in infancy. *Br Heart J* **1983**;50:182–189
10. Gonzales-Crussi F, Padilla L, Miller JK, Grosfeld JL. "Bridging bronchus": a previously undescribed airway anomaly. *Am J Dis Child* **1976**;130:1015–1018
11. Starshak RJ, Sty JR, Woods G, Kreitzer FV. Bridging bronchus: a rare airway anomaly. *Radiology* **1981**;140:95–96
12. Felson B. *Chest roentgenology*. Philadelphia: Saunders, **1973**:87–92
13. Felson B. Pulmonary agenesis and related anomalies. *Semin Roentgen* **1972**;7:17–30
14. Dalith F, Neufeld H. Radiological diagnosis of anomalous pulmonary venous connection: a tomographic study. *Radiology* **1960**;74:1–18
15. Richter K, Böck G. Die Anomalie der epibronchialen rechten Pulmonalarterie als Leitsymptom eines pulmo-kardiovaskulären

Syndroms. *ROFO* **1967**;107:31-38

16. Kittle CF, Crockett JE. Vena cava bronchovascular syndrome: a triad of anomalies involving the right lung. *Ann Surg* **1962**;156:222-223
17. Neill CA, Frencz C, Sabiston DS, Sheldon H. The familial occurrence of hypoplastic right lung with systemic arterial supply and venous drainage: "scimitar syndrome." *Bull Johns Hopkins Hosp* **1960**;107:1-21
18. Kiely B, Filler J, Stone S, Doyle EF. Syndrome of anomalous venous drainage of the right lung to the inferior vena cava: a review of 67 reported cases and three new cases in children. *Am J Cardiol* **1967**;20:102-116
19. Mathey J, Galey JJ, Logeais Y, et al. Anomalous pulmonary venous return into inferior vena cava and associated bronchovascular anomalies (the scimitar syndrome). *Thorax* **1968**;23:398-407
20. Farnsworth AE, Ankeney JL. The spectrum of the scimitar syndrome. *J Thorac Cardiovasc Surg* **1974**;68:37-42
21. Folger GM Jr. The scimitar syndrome. Anatomic, physiologic. developmental and therapeutic considerations. *Angiology* **1976**;27:373-407
22. D'Cruz IA, Arcilla RA. Anomalous venous drainage of the left lung into the inferior vena cava. *Am Heart J* **1964**;67:539-544
23. Cremin BJ, Bass EM. Retrosternal density: a sign of pulmonary hypoplasia. *Pediatr Radiol* **1975**;3:145-148
24. Morgan JR, Forker AD. Syndrome of hypoplasia of the right lung and dextroposition of the heart: "scimitar sign" with normal pulmonary venous drainage. *Circulation* **1971**;43:27-30
25. Davis WS, Allen RP. Accessory diaphragm: duplication of the diaphragm. *Radiol Clin North Am* **1968**;6:253-263
26. Wille L, Holthusen W, Willich E. Accessory diaphragm: report of 6 cases and a review of the literature. *Pediatr Radiol* **1975**;4:14-20
27. Gwinn JL, Barnes GR. Radiological case of the month. *Am J Dis Child* **1967**;114:585-586
28. Tomsick TA, Moesner SE, Smith WL Jr. The congenital pulmonary venolobar syndrome in three successive generations. *J Can Assoc Radiol* **1976**;27:196-199
29. Freedom RM, Burrows PE, Moes CAF. "Horseshoe" lung: report of five new cases. *AJR* **1986**;146:211-215

Addendum

We have had the opportunity to preview the article by Freedom et al. [29] in this issue of the *AJR*. The previously published cases of horseshoe lung discussed by them are identical to the ones that we have included with a few exceptions. Of the seven cases included by Freedom et al., the example mentioned by Spencer [1] has been referred to in our article but was omitted from our list of eight cases since little anatomic or clinical information was available. We made reference to another case described in a 19th-century French pathology text by Morestin and Porregaux [2] and have included two additional cases [8, 9]. Thus, the total number of previously published examples of horseshoe lung is 10, and the total number of cases to date is 21.

“Communicating” Bronchopulmonary Foregut Malformations

Richard E. Leithiser, Jr.[1]
Marie A. Capitanio[2]
Roderick I. Macpherson[1]
Beverly P. Wood[3]

The clinical, radiologic, and pathologic features of four children with uncommon variations of congenital bronchopulmonary foregut malformations are presented. In each case, the malformation included a persistent communication between lung tissue and the gastrointestinal tract. One case, in which an esophageal bronchus was associated with esophageal atresia and tracheoesophageal fistula, is considered extremely unusual. The embryogenesis of these communicating bronchopulmonary foregut malformations is outlined, and the key radiologic features are discussed.

Congenital bronchopulmonary foregut malformations are tracheobronchial anomalies that occur in combination with anomalies of the upper gastrointestinal tract, the diaphragm, and the pulmonary and systemic arterial and venous systems [1]. Included is the rare anomaly in which a main stem, lobar, or accessory bronchus arises from the esophagus or stomach [2]; fewer than 40 such malformations containing lung tissue have been reported previously [3, 4]. The association of an esophageal bronchus with esophageal atresia and a tracheoesophageal fistula is extremely rare and has been described only once previously [5].

We present one new case of an infant with esophageal atresia, tracheoesophageal fistula, and esophageal bronchus; show the radiologic features of three additional previously unreported cases of esophageal and gastric bronchi; review the embryogenesis of congenital bronchopulmonary foregut malformations with particular emphasis on the malformations associated with a persistent pulmonary and esophagogastric communication; and present the radiologic features fundamental to the diagnosis of such persistent communications.

Case Reports

Case 1

The initial chest radiograph (fig. 1A) of a full-term infant revealed a dilated proximal esophageal pouch consistent with esophageal atresia, air in the intestinal tract below the diaphragm indicative of a lower tracheoesophageal fistula, a small hypoaerated right lung, and rib anomalies. After an uneventful primary repair of esophageal atresia and insertion of a feeding gastrostomy, atelectasis of the right lung recurred and persisted. An esophagram at age 13 days (fig. 1B) revealed a patent and intact primary anastomosis, as well as a branching tubular structure filled with barium extending from the distal third of the esophagus to the right lung parenchyma: an esophageal bronchus. A tracheobronchogram (fig. 1C) showed the absence of the right main bronchus. Pulmonary angiography demonstrated a small right pulmonary artery with only two branches to the right lung instead of the normal three, and venous drainage to the left atrium. At age 1 month, a right pneumonectomy was done because of continued infection; the child recovered uneventfully.

Cases 2–4

The highlights of our second, third, and fourth cases are included in the following discussion.

Received May 20, 1985; accepted after revision September 6, 1985.

[1] Department of Radiology, Division of Pediatric Radiology, Medical University of South Carolina, 171 Ashley Ave., Charleston, SC 29425. Address reprint requests to R. Leithiser.

[2] Department of Radiology, Temple University School of Medicine, Medical College of Pennsylvania, St. Christopher's Hospital for Children, Philadelphia, PA 19133.

[3] Department of Radiology, University of Rochester, Strong Memorial Hospital, Rochester, NY 14642.

AJR 146:227–231, February 1986
0361-803X/86/1462-0227
© American Roentgen Ray Society

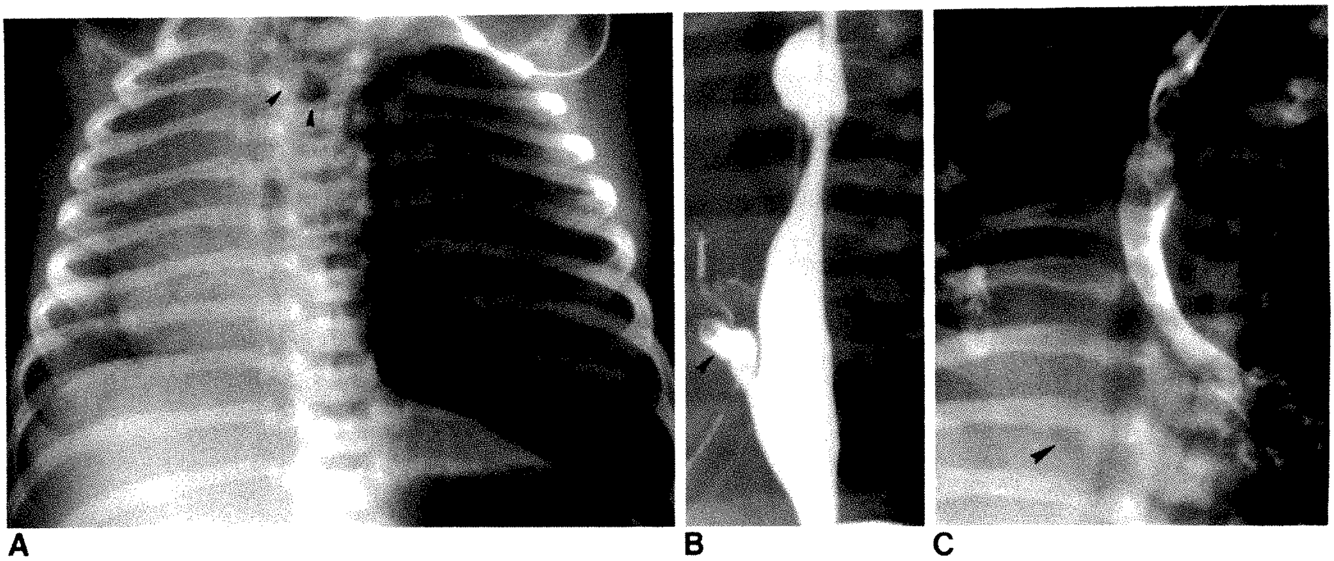

Fig. 1.—Case 1. **A**, Plain film, day 1. Air-filled proximal esophageal pouch (*arrowheads*) with volume loss in right lung and left rib anomalies. **B**, Postoperative esophagram, day 13. Esophageal bronchus (*arrowhead*). Right lung was completely collapsed. **C**, Tracheobronchogram. Absence of tracheal origin of right main bronchus, which can be seen filled with air (*arrowhead*) arising from esophagus. Residual barium in periphery of right lung.

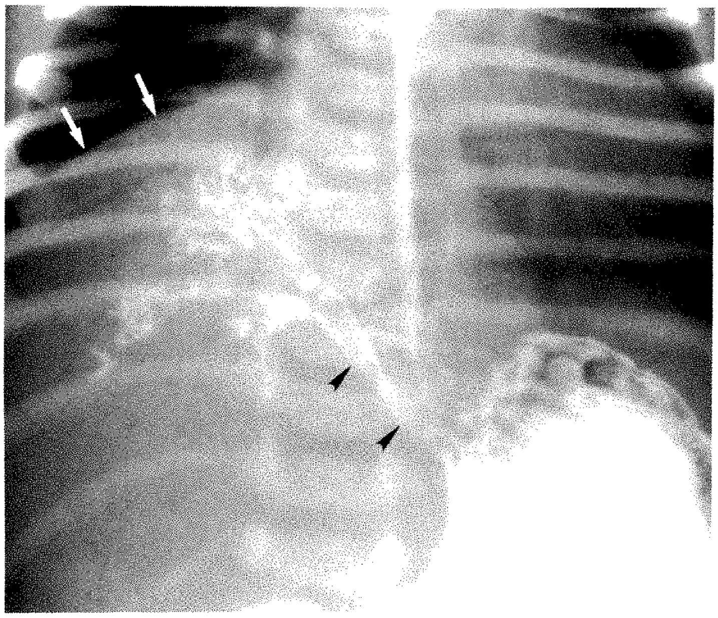

Fig. 2.—Case 2. Esophagram shows aberrant bronchus arising from gastric fundus (*arrowheads*) and extending into mass (*arrows*) in lower right hemithorax. (Case courtesy of Dr. Armando R. Amoedo, Brazil.)

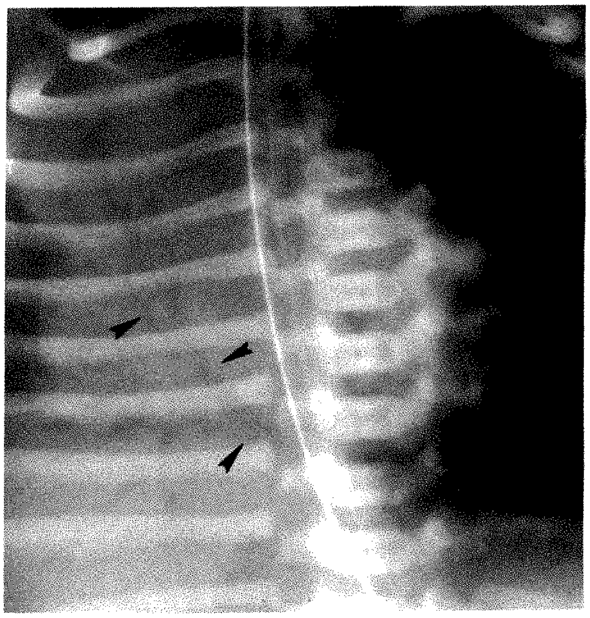

Fig. 3.—Case 3. Chest film, day 1. Atelectatic right lung with branching tubular air-filled bronchi (*arrowheads*) arising from lower chest medially.

Case 2 demonstrates a gastric-to-pulmonary communication (fig. 2), and cases 3 and 4 show the more common esophageal-to-pulmonary communications (figs. 3 and 4) and several associated organ system anomalies.

Embryogenesis of Bronchopulmonary Foregut Malformations

The evolution of our understanding of the embryogenesis of bronchopulmonary foregut malformations began in 1874 when a communication between accessory lung tissue and the gastrointestinal tract was first described [1]. It was not until 1928 that accessory lung was defined by Muller as "an organ-like formation, consisting of pulmonary tissue and separated from the rest of the lung" [1]. Smith [6] and most authors before 1960 divided accessory lung tissue into two distinctly different entities: intra- and extralobar sequestrations. In 1962, Halasz et al. [7] proposed that intra- and extralobar sequestrations have a common origin.

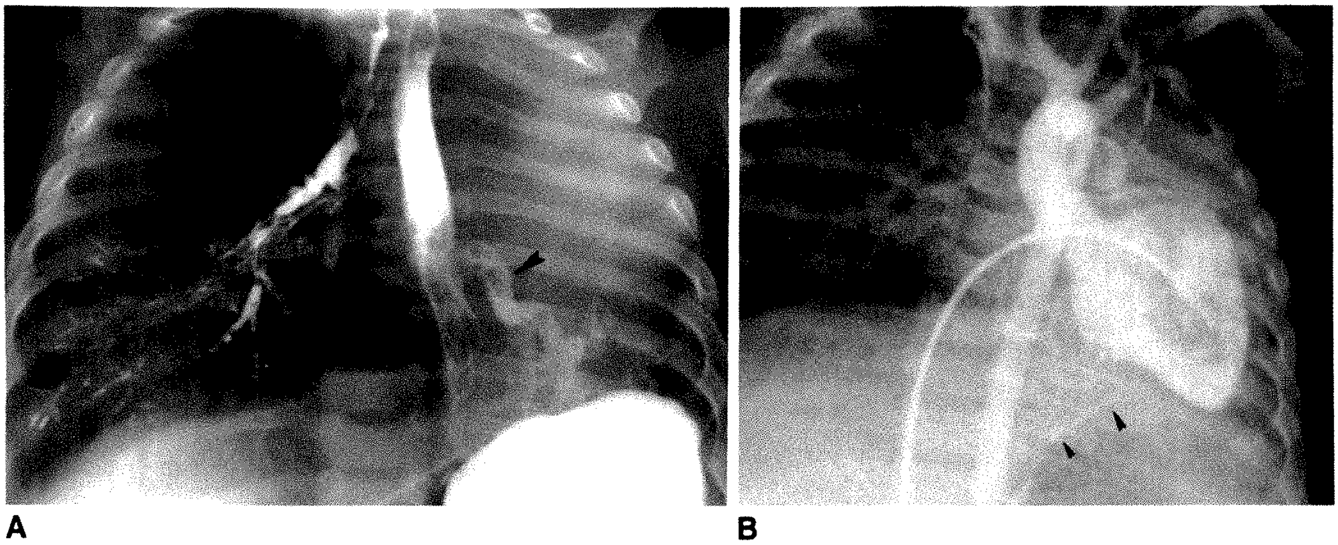

Fig. 4.—Case 4. **A**, Simultaneous esophagram and bronchogram. Left main bronchus (*arrowhead*) arises from esophagus and not from trachea. **B**, Left ventriculogram. Aberrant artery arises from aorta (*arrowheads*) to supply "left lung."

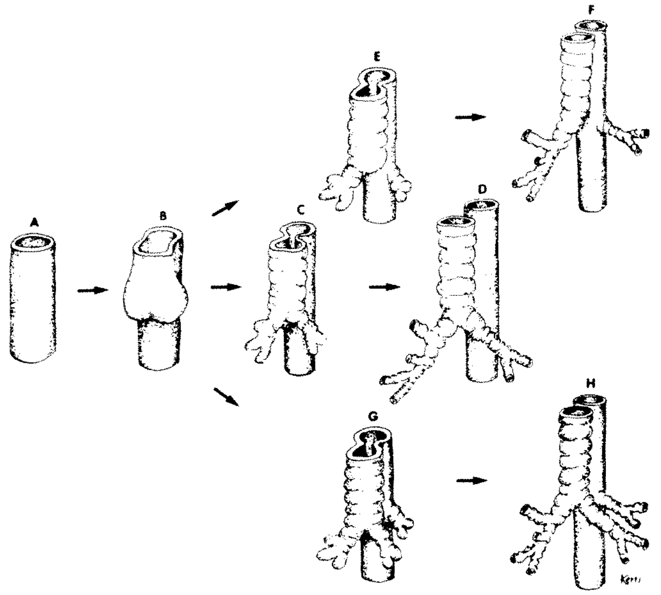

Fig. 5.—Pathogenesis of esophageal bronchus. Normal development of laryngotracheal tube and esophagus from primitive foregut is sequence ABCD; mechanisms of formation of communicating bronchopulmonary foregut malformation (esophageal bronchus) are sequences ABEF and ABGH.

The term "bronchopulmonary foregut malformation" was introduced by Gerle et al. [1] in 1968. It collectively identifies many anomalies previously considered entirely separate entities, such as pulmonary sequestrations, esophageal atresia, duplication cysts of pulmonary and gastrointestinal origin, diverticula of the gastrointestinal or pulmonary tree, and accessory pulmonary tissue with a foregut communication (either patent or nonpatent). The type of malformation observed depends on the embryologic stage during which it developed. This unifying concept was refined in 1976 by Heithoff et al. [2] into the currently accepted theory presented here.

During the fourth to fifth week of embryogenesis, a primitive diverticulum arises from the ventral aspect of the pharynx and grows caudad. Two lateral ridges form between the diverticulum and the dorsal foregut and fuse to become the tracheoesophageal septum, dividing the ventral respiratory laryngotracheal tube from the dorsal esophagus [2]. A primitive lung bud develops at the caudal end of the laryngotracheal tube; by 7 weeks, it divides into two bronchopulmonary buds, which become the right and left lungs (fig. 5) [8].

Bronchopulmonary foregut malformations occur when independent collections of cells with respiratory potential arise from the primitive esophagus caudal to the normal lung bud or when part of the lung bud originates from the dorsal esophagus instead of the ventral laryngotracheal tube (fig. 5). These collections of cells evaginate into adjacent normally developed pulmonary tissue, but often are connected to the parent viscus by a pedicle. As the pedicle outgrows its blood supply, it involutes and a simple bronchopulmonary foregut malformation or sequestration forms. Occasionally fibrous remnants of this pedicle are found between the anomalous pulmonary tissue and the esophagus. The remnants of the pedicle frequently consist of both pulmonary and gastrointestinal tissue [2, 9].

If the pedicle fails to involute, the accessory lung is in free communication with the gastrointestinal tract, and a *communicating* bronchopulmonary foregut malformation occurs, usually between the distal esophagus and the lung (fig. 1B). A gastric-to-pulmonary communication occurs when the pedicle arises late in embryologic development from that part of the distal esophagus that is eventually incorporated into the body of the stomach (case 2, fig. 2).

Location, pleural investment, and blood supply are not consistent among bronchopulmonary foregut malformations. About one-third of the communicating malformations arise from evagination of pulmonary tissue into the right hemithorax and are associated with agenesis or hypoplasia of the right lung (cases 1–3; figs. 1–3). Another third of the malformations are formed by aberrant pulmonary tissue evaginating into the left lower lobe. Bronchopulmonary foregut malformations have been observed in other parts of the lung; however, the upper lobes are the least frequently involved. If the evagination of pulmonary tissue occurs early in embryologic development, it is invested in the normal pulmonary pleura (intralobar sequestration). Evaginated pulmonary tissue arising later forms within its own separate pleura (extralobar sequestration) [2]. The arterial supply to the bronchopulmonary foregut malformations is variable and independent of the type of pleural investment present. Arterial supply may be from the pulmonary artery or the aorta and its branches (case 4; fig. 4); venous drainage is frequently to the left atrium, but may also be systemic [2, 9, 10, 11].

Discussion

The cases presented here are unusual variants in the spectrum of bronchopulmonary foregut malformations. The common factor in the development of all forms of bronchopulmonary foregut malformations is the presence of lung tissue arising from the primitive gastrointestinal tube. The type of bronchopulmonary foregut malformation that develops depends on (1) the stage of embryologic development when the accessory lung tissue arises; (2) the direction in which the aberrant pulmonary tissue grows; and (3) the retention or involution of the communication between the accessory lung tissue and the parent viscus [10].

The clinical presentation in most infants with a communicating bronchopulmonary foregut malformation is respiratory distress, which is exacerbated during feedings. If there is significant arteriovenous shunting within the malformation, the infant may present with congestive heart failure [10, 11]. Associated clinical findings include oculoauriculovertebral dysplasia (Goldenhar anomalad) [3] and congenital heart disease [12]. In the older child or adult, chronic and recurrent pneumonia with bronchiectasis, hemoptysis, gastrointestinal bleeding, and dysphagia have also been reported [2]. The plain chest film findings include persistent alveolar densities, usually in the lower lobes [10]; pulmonary hypoplasia; and varying degrees of atelectasis [12]. Another plain film finding is a "soap-bubble" pattern of cystic or tubular lucencies within the lung density (fig. 3). These lucencies represent air in the persistent communicating structure between the gastrointestinal tract and the aberrant pulmonary tissue [11].

In 20%–40% of children with a communicating bronchopulmonary foregut malformation, there are associated anomalies of the ribs and vertebrae [3]. Case 1, in addition to illustrating the very rare combination of an esophageal bronchus, esophageal atresia, and a tracheoesophageal fistula (only one similar case was previously reported) [5], also shows associated left rib anomalies (fig. 1A). Our second case, the uncommon gastric-to-pulmonary communication, has associated lumbar vertebral anomalies. Case 3, one of the esophageal-to-pulmonary communications, has associated multicystic dysplastic kidneys, imperforate anus, and gastric duplication cysts. Additional reported anomalies include congenital diaphragmatic hernia, duodenal stenosis or atresia, and other gastrointestinal and genitourinary anomalies [2, 13, 14].

A contrast study of the esophagus and stomach using barium or bronchographic contrast medium is essential if a bronchopulmonary foregut malformation is suspected [2]. To facilitate the filling of an aberrant bronchus, the contrast study may be carried out with the abnormal lung in a dependent position. The contrast material is injected through a feeding tube into the distal one-third of the esophagus, where an aberrant bronchus is most likely to arise. Passing a feeding tube across a recent esophageal atresia repair may be contraindicated, but contrast material can be introduced into the stomach via gastrostomy in these patients and the distal esophagus and stomach evaluated by gastroesophageal reflux.

Additional evaluation may include tracheobronchography, to delineate other abnormalities of the laryngotracheal tube, and angiography. In case 4, a simultaneous esophagram and bronchogram showed a communicating bronchus arising from the esophagus and the absence of the normal left main bronchus (fig. 4A). Angiocardiography demonstrated the absence of a left pulmonary artery and the presence of a systemic artery arising from the abdominal aorta to supply the left lung (fig. 4B). In general, the arterial supply to the bronchopulmonary foregut malformations may be pulmonary or systemic; the venous drainage is usually normal and to the left atrium [9–11]. The mapping of the vascular supply and drainage of these malformations can aid the surgeon in planning his approach to the lesion.

Four new cases illustrating a variety of communicating bronchopulmonary foregut malformations have been presented. All cases were suspected from plain films and confirmed by simple contrast studies. It is important to remember that communicating bronchopulmonary foregut malformations may be part of a complex association of multiple organ system anomalies, and in addition to simple contrast studies, bronchography and especially angiography may be helpful before surgery [15].

REFERENCES

1. Gerle RD, Jaretzki A, Ashley CA, Berne AS. Congenital bronchopulmonary-foregut malformation: pulmonary sequestration communicating with the gastrointestinal tract. *N Engl J Med* **1968**;278:1413–1419
2. Heithoff KB, Sane SM, Williams HJ, et al. Bronchopulmonary foregut malformations: a unifying etiological concept. *AJR* **1976**;126:46–55
3. Bowen AD, Parry WH. Bronchopulmonary foregut malformation in the Goldenhar anomalad. *AJR* **1980**;134:186–188
4. Reilly BJ, Macdonald P, Cummings WA, Simpson JS. Three cases of congenital bronchopulmonary foregut malformation. *Ann Radiol* (Paris) **1973**;16:281–285
5. Keeley JL, Schairer AE. The anomalous origin of the right main bronchus from the esophagus. *Ann Surg* **1960**;152:871–874
6. Smith AR. Theory of origin of intralobar sequestration of lung. *Thorax* **1956**;11:10–24
7. Halasz NA, Lindskog GE, Liebow AA. Esophagobronchial fistula and bronchopulmonary sequestration. *Ann Surg* **1962**;155:215–220

8. Hanna EA. Broncho-esophageal fistula with total sequestration of the right lung. *Ann Surg* **1964**;159:599–603
9. Telander RL, Lennox C, Sieber W. Sequestration of the lung in children. *Mayo Clin Proc* **1976**;51:578–584
10. O'Connell DJ, Kelleher J. Congenital intrathoracic bronchopulmonary foregut malformations in childhood. *J Can Assoc Radiol* **1979**;30:103–108
11. Crawford DB, Cole S, Danielson KS, Henken EM, Maenza RM, Westcott JL. Malformation of bronchopulmonary foregut with systemic and pulmonary arterial blood supply. *Chest* **1978**;73:421–423
12. Lacina S, Townley R, Radecki L, Stockinger F, Wyngaarden M. Esophageal lung with cardiac abnormalities. *Chest* **1981**;79:468–470
13. Ashcraft KW, Holder TM. Esophageal atresia and tracheo-esophageal fistula malformations. *Surg Clin North Am* **1976**;56:299–315
14. St. Raymond AH, Hardy JD, Robbins SG. Lower accessory lung communicating with the esophagus and associated with congenital diaphragmatic hernia. *J Thorac Surg* **1956**;31:354–358
15. Stanley P, Vachon L, Gilsanz V. Pulmonary sequestration with congenital gastroesophageal communication: report of two cases. *Pediatr Radiol* **1985**;15:343–345

Book Review

X-Ray Imaging Equipment. An Introduction. By Euclid Seeram. Springfield, IL: Thomas, 588 pp., 1985. $44.50

This text is intended for introductory courses in x-ray imaging instrumentation for programs in radiologic technology, as a reference for the professional technologist, and as a supplemental text for applied fields such as biomedical technology. It should be used concurrently with a course in radiologic physics; elements of basic radiation physics and mathematical formulas are not included.

The book is divided into four parts. Ten chapters cover conventional x-ray imaging equipment; there are four chapters on fluoroscopy, x-ray television imaging and recording schemes, digital image processing and computers, and computed tomography and digital radiography; and finally, a chapter on quality assurance concepts. Because the book is directed primarily at student technologists, the format is oriented toward a question and answer approach with an appendix at the end that contains 222 questions related to each of the chapters. This material would have been easier to use if the questions had followed each chapter rather than being grouped together at the end of the text. The answers are provided in the final section.

The description of the basic radiographic equipment is similar to that in many standard physics textbooks. However, the author includes much more detail about the various available commercial units and discusses practical aspects of the functioning of the equipment.

The author supplements his discussion of the various topics in several places by including extensive quotations from the literature under "Opinion." There are also brief descriptions of research studies that have been carried out with imaging equipment. These items are included to stimulate the student to read further on the subjects.

The text is very complete. The chapters on image intensifiers, image transfer mechanisms (television, cameras, monitors, and image transmission), digital imaging, and quality control are especially well done.

It is difficult to find fault with this text, which contains an immense amount of information for the student radiographer. Radiology residents in training could find valuable information, especially in the sections mentioned in the preceding paragraph. There are only a few minor errors. The author describes penumbra in the context of scattered radiation without stating clearly that it relates to the size of the focal spot and the tube film distance. The word "penumbra" is not in the index, which is otherwise complete. The description of tomography includes the statement that it produces a greater degree of contrast and detail than conventional techniques. Of course, for a given technique, there is less contrast on a tomogram than there is on a conventional radiograph.

There is no discussion of magnetic resonance imaging, although the dust cover states that it is covered in the appendix. The illustrations are a combination of well done line drawings and photographs from radiographic manufacturers. Finally, the price may seem high to the student in training, but there is a great deal of information in this large text. Thus, I would recommend it highly to its intended audience. If there is too much material for the average technology program, certain sections could be selected for classroom use.

R. F. Kilcoyne
University of Washington
Seattle, WA 98195

Dimensions of the Growing Trachea Related to Age and Gender

N. Thorne Griscom[1]
Mary Ellen B. Wohl[1]

Computed tomography measured the lengths, anteroposterior (AP) diameters, transverse diameters, cross-sectional areas, and contained volumes of the tracheas of 130 subjects in their first two decades. Patients below age 6 were scanned at low lung volumes. The others were scanned at or near total lung capacity. The results are shown by age and gender. There were no differences between boys and girls until age 14, when girls' tracheas stopped growing. The data suggest that male tracheas continue to enlarge (but not lengthen) for a time after growth in height ceases. Mean transverse diameters tended to be greater than mean AP diameters to the age of 6; the diameters were then nearly identical until age 18, when the AP diameters usually became slightly larger. The tracheas were nearly round in cross section, especially at high lung volumes. In individual tracheas, changes from level to level were small. These measurements should be useful in the detection of tracheal abnormalities, in problems in respiratory physiology, and in endotracheal intubation, endoscopy, and tracheostomy.

Computed tomography (CT) is an excellent method of displaying the cross-sectional anatomy of the growing trachea. Unlike autopsy and bronchoscopy, CT [1, 2] causes little or no disturbance of tracheal anatomy. This report therefore presents the lengths, mean anteroposterior (AP) and transverse diameters, mean cross-sectional areas, and contained volumes of the growing trachea, as derived from the CT examination of 130 children and adolescents. The measurements are related to age and gender. The measurements of most of the subjects above age 4 have been analyzed in relation to body height and reported previously [3].

Subjects and Methods

The tracheas of 130 children and adolescents were examined by CT, usually as part of a search for pulmonary metastases. The distribution by age and gender is shown in table 1. Patients with nearby tumors or with other local processes likely to affect the trachea were excluded. Malignant disease elsewhere and its therapy had no effect on the dimensions of the trachea [3].

The details of the system of measurement are given elsewhere [1, 3, 5]. All patients were supine. Twenty-eight of the youngest patients were asleep. Slightly older subjects either were sedated and were breathing quietly during the examination or were awake and stopped breathing for each CT image. All of these children presumably were scanned somewhere near functional residual capacity. At age 6 and older, however, the patients were scanned at or near total lung capacity (full inspiration).

Tracheal length (from vocal cords to carina) was determined from the AP ScoutView (digital radiograph). Diameters and cross-sectional areas were determined from each section and averaged. Intratracheal volume was calculated by multiplying length by mean cross-sectional area. The five measurements were plotted against age (figs. 1–7).

The system was tested by measuring diameters and areas of air-containing holes, 0.400–2.000 cm in diameter, milled in two plastic phantoms (CT number −35 to −40). The system gave an average error of 0.01 cm in diameter and 0.01 cm^2 in area. The errors were fairly well distributed on each side of zero and showed no tendency to increase or decrease with

Received August 6, 1985; accepted October 10, 1985.

This work was supported in part by grant HL27372 from the National Institutes of Health.

[1] Departments of Radiology and Pediatrics, Harvard Medical School; Departments of Radiology and Medicine, Children's Hospital, 300 Longwood Ave., Boston, MA 02115. Address reprint requests to N. T. Griscom.

AJR 146:233-237, February 1986
0361-803X/86/1462-0233
© American Roentgen Ray Society

TABLE 1: **Tracheal Dimensions to the 20th Birthday: Males and Females Shown Separately at Age 14 and Older**

	Age, years													
	0–2	2–4	4–6	6–8	8–10	10–12	12–14	14–16	16–18	18–20	14–16	16–18	18–20	Overall
No. of girls	5	6	4	6	4	4	7	6	13	4	. . .	. . .	. . .	59
No. of boys	8	9	4	5	7	4	8	. . .	. . .	. . .	6	13	7	71
Average age, years	1.0	3.2	4.9	6.5	9.2	11.2	13.2	15.1	16.7	18.6	15.0	16.8	19.2	
Average height percentile [4]	40	47	57	54	54	49	58	67	47	60	53	47	62	51.7
Tracheal length, cm, mean (±1 SD)	5.4	6.4	7.2	8.2	8.8	10.0	10.8	11.2	12.2	11.8	12.4	12.4	13.1	
	(0.7)	(0.5)	(0.8)	(0.7)	(0.9)	(1.0)	(1.5)	(1.2)	(1.1)	(1.0)	(0.6)	(1.3)	(0.9)	
Average of mean AP diameters, cm (±1 SD)	0.53	0.74	0.80	0.92	1.05	1.16	1.30	1.39	1.37	1.42	1.45	1.57	1.75	
	(0.10)	(0.08)	(0.06)	(0.11)	(0.05)	(0.10)	(0.18)	(0.07)	(0.17)	(0.18)	(0.08)	(0.14)	(0.17)	
Average of mean transverse diameters, cm (+1 SD)	0.64	0.81	0.90	0.93	1.07	1.18	1.33	1.46	1.40	1.39	1.43	1.59	1.66	
	(0.12)	(0.07)	(0.09)	(0.08)	(0.06)	(0.09)	(0.16)	(0.07)	(0.12)	(0.11)	(0.06)	(0.16)	(0.16)	
Average of mean cross-sectional areas, cm^2 (±1 SD)	0.28	0.48	0.58	0.69	0.89	1.10	1.39	1.62	1.54	1.59	1.62	2.01	2.30	
	(0.09)	(0.08)	(0.10)	(0.11)	(0.09)	(0.18)	(0.36)	(0.14)	(0.29)	(0.29)	(0.13)	(0.30)	(0.39)	
Volume, cm^3, mean (±1 SD)	1.57	3.11	4.16	5.67	7.87	11.1	15.4	18.2	18.8	18.9	20.2	25.1	30.3	
	(0.67)	(0.61)	(0.86)	(1.20)	(1.45)	(2.3)	(6.0)	(2.2)	(4.3)	(4.2)	(2.4)	(5.2)	(5.9)	

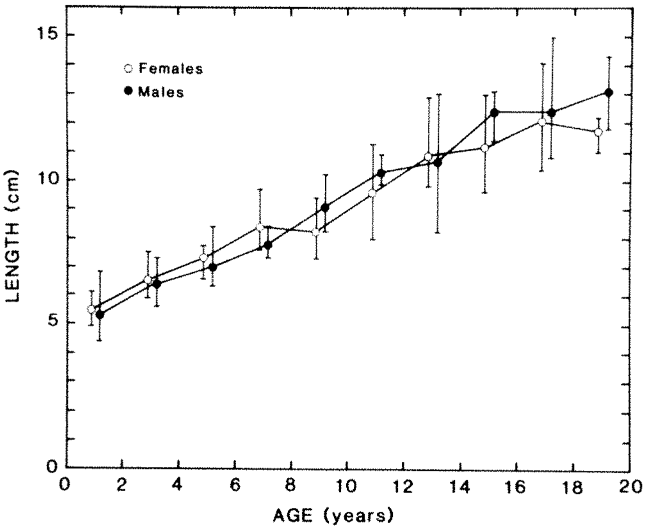

Fig. 1.—Lengths of trachea from birth to 20th birthday. Values for each 2-year period were averaged; these averages and ranges are shown.

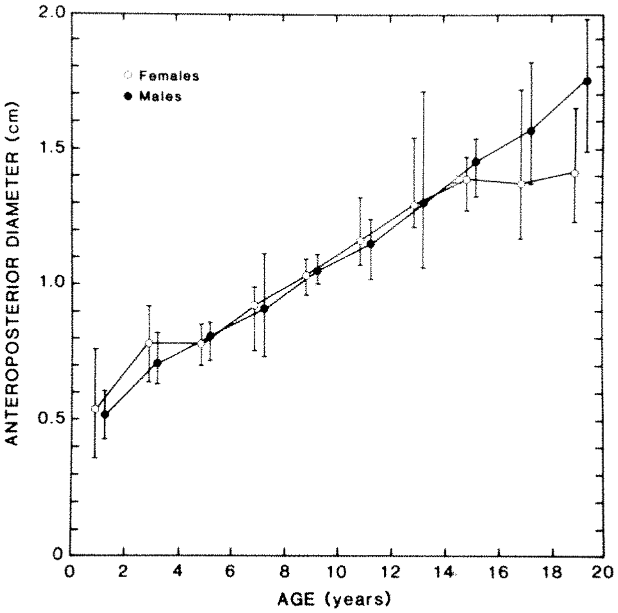

Fig. 2.—Mean anteroposterior diameters of trachea according to age.

size of hole.

To quantitate section-to-section change in diameter and area, the coefficients of variation with tracheal level were derived.

Results

Lengths and mean AP and transverse diameters of the trachea are plotted in figures 1–3. Figure 4 pools the girls' AP and transverse diameters and contrasts them with the boys' pooled diameters. Figure 5, the converse of figure 4, pools all the AP diameters, male and female, and contrasts them with the transverse diameters, pooled from both genders. Mean cross-sectional areas and intratracheal volumes are shown by figures 6 and 7. The numerical results are given in table 1. No significant male-female differences were found until late in adolescence. Table 1 therefore shows boys and girls together until age 14.

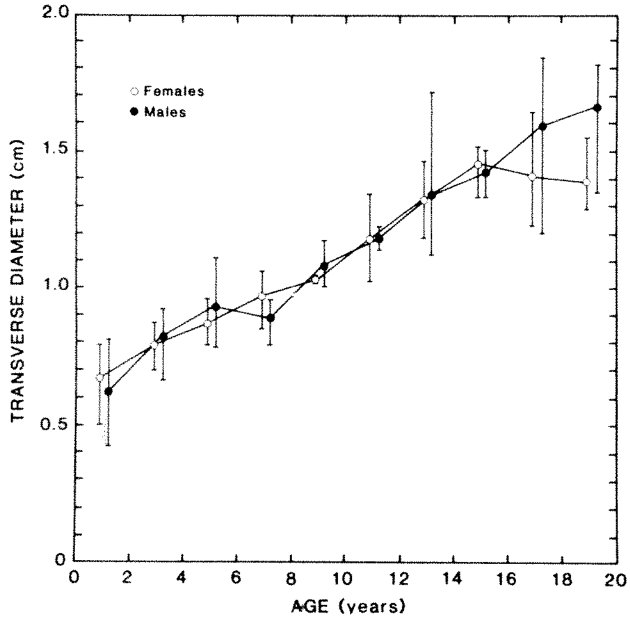

Fig. 3.—Mean transverse diameters of trachea according to age.

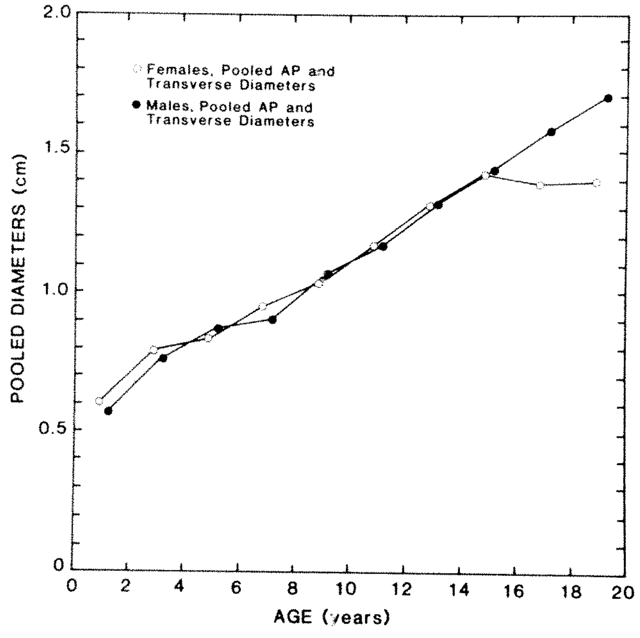

Fig. 4.—Pooled mean anteroposterior (AP) and transverse diameters according to age.

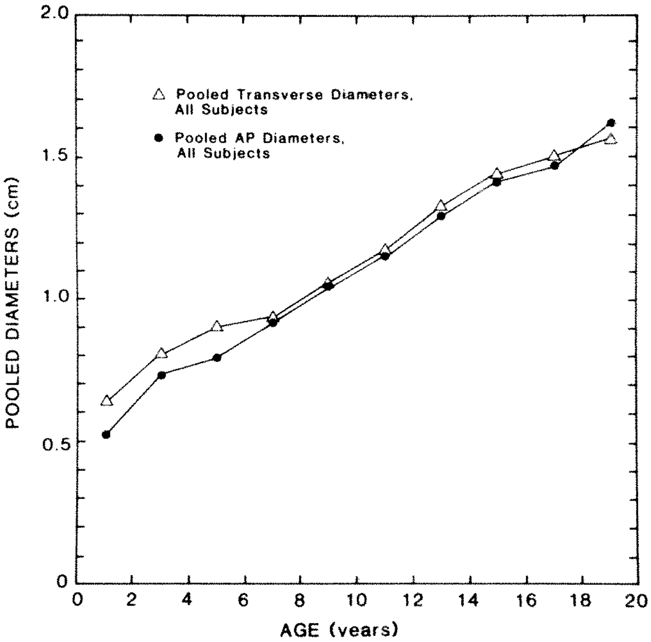

Fig. 5.—Diameters pooled from both genders, showing AP and transverse diameters separately according to age.

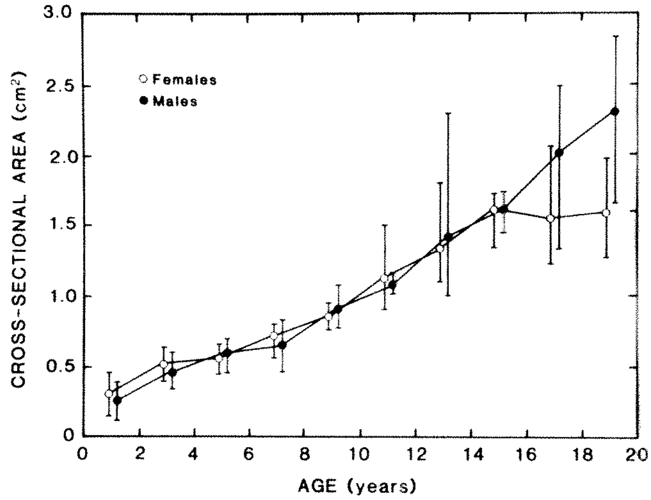

Fig. 6.—Mean cross-sectional areas of trachea according to age.

The 20 males in the two oldest groups (ages 16–18 and 18–20) and the 23 females in the three oldest groups (age 14 to the 20th birthday), on average were 0.5% above and 0.7% below the final 50th percentile heights for American males and females [6]; in other words, they were as tall as young adults. Young adult men in the general population are, on average, 7% taller than young adult women [4]. Correspondingly, the tracheas of these 20 oldest males were 7% longer than those of the 23 oldest females. Gender differences in the other four measurements, however, were substantially greater: 18% for AP diameter, 14% for transverse diameter, 28% for cross-sectional area, and 44% for volume. Furthermore, these measurements in the males failed to show (figs. 2–4, 6, and 7) the plateaus expected at maturity; their tracheas were apparently still growing.

In individual tracheas, discrepancies between the mean AP diameter and the mean transverse diameter were seldom large; few tracheas were far from round under the circum-

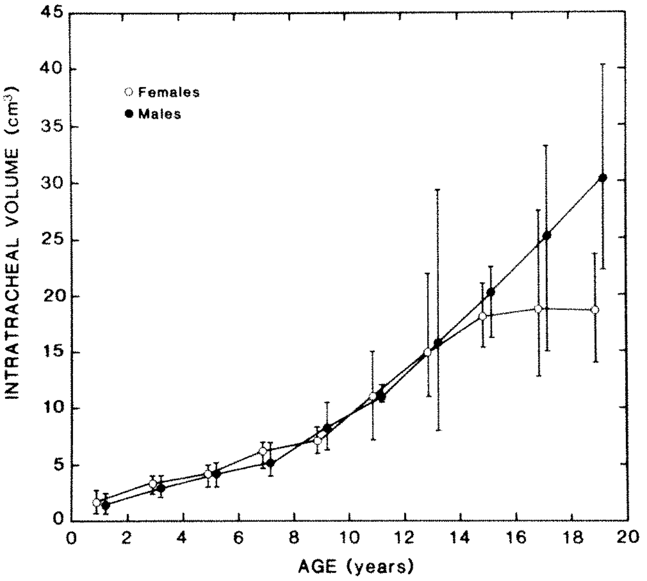

Fig. 7.—Intratracheal volumes according to age.

TABLE 2: **Mean Coefficients of Variation from Section to Section along Trachea**

	Coefficient of Variation (%)		
	Anteroposterior Diameter	Transverse Diameter	Cross-Sectional Area
All 130 subjects	7.6	5.8	8.9
71 males	7.7	5.3	9.0
59 females	7.3	6.4	8.7
72 subjects at age 10 and older	6.1	4.9	6.8
58 subjects under age 10	9.3	7.0	11.4
102 waking subjects	6.9	5.4	7.9
28 sleeping subjects	9.8	7.2	12.3

stances of this study. In 93% of the females and in 83% of the males, the difference between the means of the two diameters was less than 15%. The seven largest discrepancies (21% to 37%, based on the transverse diameters) all occurred in sleeping patients below age 4; their tracheas were flattened from front to back.

Mean transverse diameters were significantly greater than mean anteroposterior diameters up to the age of 6 ($p < 0.001$) (fig. 5). Then through age 17 the two diameters were virtually identical. Only in the oldest group, adolescents 18 and 19 years old, did the AP diameter tend to be greater than the transverse ($p < 0.05$).

Analysis of the coefficients of variation (standard deviations expressed as percentages of the mean) in diameters and area with location in the trachea showed that, after the section depicting the supracarinal widening and any section showing subglottic narrowing were eliminated, changes from section to section were quite small (table 2). On average, there was less variation in the transverse diameter than in the AP diameter, less in either diameter than in the cross-sectional area, less in the adolescents than in the younger children, and less in the 102 waking subjects than in the 28 sleeping infants and young children.

Discussion

Tracheal dimensions undergo considerable change from moment to moment. Intraluminal pressure [5] and respiratory phase [7, 8] are known to change tracheal size and shape substantially. Position (erect, supine, prone, in flexion or extension or rotation) probably does so also. The data presented here must be taken, therefore, as representing the trachea only for the circumstances of the examinations: supine, at relatively low lung volumes up to age 6 and holding the breath near total lung capacity thereafter.

There is more variability in the data from the younger patients (table 1) for several reasons. Below the age of 6, scans were usually obtained during breathing; at age 6 and older, the children were scanned during breath-holding near total lung capacity. Position in the scanner was better standardized in later childhood and adolescence. The infants' tracheas were less likely to be straight. In the taller subjects, more sections were available for analysis and averaging. The unchanging size of the pixel and the diminution of perimeter-to-area ratio with growth also led to greater precision and accuracy in the older subjects.

Although many of these children had malignancies (none close to the trachea), the presence of malignant disease elsewhere and its therapy had no detectable effect on the dimensions of the trachea [3].

Figures 1–7 show no gender difference throughout childhood (which disagrees with one prior report [9]) but appreciable differences with the approach of maturity. This immediately brings into question whether the male-female differences in tracheal dimensions at age 16–19 are entirely explainable by stature. On this point the data are incomplete. Multiple regression analyses using gender as a covariate showed no differences in tracheal dimensions between the two genders after the effect of height was eliminated [3]. However, figures 1–7 show that female dimensions reach a plateau as expected, but those of males (especially AP diameter, area, and volume) do not. This lack of a postadolescent plateau cannot be explained by aberrations in age distribution within the male age groups or by unusual tallness of the oldest boys.

There is thus the possibility that when boys stop growing taller, their tracheas stop growing in length but do not immediately do so in diameter, cross-sectional area, and volume. This supposition is supported by measurements of tracheal diameters [10, 11] and cross-sectional areas [10] from radiographs of adults and by CT measurements at functional residual capacity of an adult woman and an adult man of the same height and age [5]. Two parallels are the clavicles, in which late enchondral growth makes men's shoulders relatively broad for height, and the larynx, the cartilages of which are about 25% larger in linear dimensions in men than in women [12]. Apparently, late in male adolescence, the clavicles, larynx, and trachea continue to grow for some years after the spine, bones of the legs, and other components of height have stopped.

The measurements reported here are generally larger than those found at autopsy [13-15]. The lengths we found, however, are substantially less than those found by two endoscopic studies [16, 17] presumably because of tracheal stretching caused by the rigid bronchoscope and by hyperextension of the neck during the procedure. Our diameters correspond reasonably well to those obtained from radiographs of the chest [11, 18-20] in children and adolescents, although the diameters we found in males at age 18 and 19 are less than those reported [10] from radiographs of a group of males aged 19-23, perhaps because of continued growth of male tracheas in early adulthood. Our measurements of area (fig. 6) correspond well to the areas reported by others from the CT scans of 30 children [2].

CT allows considerable precision of measurement. Its errors and distortions are not major, and it is possible to correct for them. We submit that the data presented here accurately represent children's tracheas under the circumstances of the study.

ACKNOWLEDGMENTS

We thank Michael Feldstein, Morris Gold, and Harriet Peterson of the Biostatistics Consulting Laboratory, Harvard School of Public Health for statistical assistance; Jere Mead, John Kirkpatrick, and Clifton Harris for helpful comments; Judith Cohen for scretarial help; and Daniel Griscom for calculating the coefficients of variation.

REFERENCES

1. Griscom NT. Computed tomographic determination of tracheal dimensions in children and adolescents. *Radiology* **1982**; 145:361-364
2. Effmann EL, Fram EK, Vock P, Kirks DR. Tracheal cross-sectional area in children: CT determination. *Radiology* **1983**; 149:137-140
3. Griscom NT, Wohl MEB. Dimensions of the growing trachea related to body height. *Am Rev Respir Dis* **1985**;131:840-844
4. Hamill PV, Drizd TA, Johnson CL, Reed RB, Roche AF, Moore WM. Physical growth: National Center for Health Statistics percentiles. *Am J Clin Nutr* **1979**;32:607-629
5. Griscom NT, Wohl MEB. Tracheal size and shape: effects of change in intraluminal pressure. *Radiology* **1983**;149:27-30
6. Vaughan VC III. Growth and development. In: Behrman RE, Vaughan VC III, eds. *Nelson textbook of pediatrics*, 12th ed. Philadelphia: Saunders, **1983**:30-31
7. Macklin CJ. X-ray studies on bronchial movements. *Am J Anat* **1925**;35:303-329
8. Wittenborg MH, Gyepes MT, Crocker D. Tracheal dynamics in infants with respiratory distress, stridor, and collapsing trachea. *Radiology* **1967**;88:653-662
9. Pagtakhan RD, Bjelland JC, Landau LI, et al. Sex differences in growth patterns of the airways and lung parenchyma in children. *J Appl Physiol* **1984**;56:1204-1210
10. Osmanliev D, Bowley N, Hunter DM, Pride NB. Relation between tracheal size and forced expiratory volume in one second in young men. *Am Rev Respir Dis* **1982**;126:179-182
11. Breatnach E, Abbott GC, Fraser RG. Dimensions of the normal human trachea. *AJR* **1984**;142:903-906
12. Kahane JC. A morphological study of the human pre-pubertal and pubertal larynx. *Am J Anat* **1978**;151:11-20
13. Engel S. *Lung structure: the child's lung.* Springfield, IL: Thomas, **1962**:6-9
14. Butz RO. Length and cross-section growth patterns in the human trachea. *Pediatrics* **1968**;42:336-341
15. Bebeke G, Endres O, Becker H, Nitschke H. Wachstum und altersäbhangige Strukturveränderungen der menschlichen Trachea. *Virchows Arch [A]* **1966**;341:353-364
16. Fearon B, Whalen JS. Tracheal dimensions in the living infant. *Ann Otol Rhinol Laryngol* **1967**;76:964-974
17. Morgan GAR, Steward DJ. Linear airway dimensions in children: including those with cleft palate. *Can Anaesth Soc J* **1982**;29:1-8
18. Menu Y, Lallemand D. Détermination du diamètre transversal normal de la trachée chez l'enfant. *Ann Radiol* **1981**;24:73-75
19. Griscom NT. Tracheal dimensions (letter). *AJR* **1984**;143:1352
20. Breatnach E, Abbott G, Fraser RG. Tracheal dimensions (reply). *AJR* **1984**;143:1352-1353

Book Review

Roentgen Signs in Diagnostic Imaging, 2d ed. Volume 2: Appendicular Skeleton. By Isadore Meschan. Philadelphia: Saunders, 560 pp., 1985. $70

This book is an extensive revision of the skeletal section of *Analysis of Roentgen Signs in General Radiology*, volume I, 1973. An additional 124 pages of text have been added including 32 pages on computed tomography (CT) with a contribution by Barbara Carter. Other contributors include James Johnston and Alan Klein.

The book is profuse with charts, tables and diagrams, and many new radiographs. The quality of the reproductions is generally good considering the difficulty in demonstrating osteosclerotic and osteoblastic lesions, but figure 6-55 fails to show the "sunburst" it was intended to. While the sections on fractures and fracture healing are good, the Smith-Petersen nail should be supplanted by the compression nail and the theory of the compression nail and plate should be mentioned.

While the chapter on CT shows its importance in delineating acetabular fractures, the chapter on fractures has not expanded its scope to anterior and posterior column fractures. The chapter on congenital and hereditary abnormalities is much more complete than the previous edition, but some of its categorization is rather confusing, i.e., abnormal extremities, thorax, pelvis, and skull; occasionally minimal involvement of the spine. I am unsure why trisomy 13–15 and trisomy 17–18 are listed as not being detectable at birth. The chapter on Bone Diseases of the Extremities Characterized by Increased Density or Expansion claims adamantinoma where I would have preferred to find it under Radiolucent Disease Confined to a Single Extremity. Some entities are difficult to categorize by this system, such as an osteomyelitis that might be epiphyseal, metaphyseal, or diaphyseal and might be either acute, subacute, or chronic with resultant repetition and duplication. There is no mention of DISH (Diffuse Idiopathic Skeletal Hyperostosis). The references have been expanded and, while including many recent ones, are weighted towards the older literature. Many of these, however, are of a classic nature and are of great value.

In a larger sense the book has been expanded into a substantial and useful text with enough new illustrations to serve as an atlas and, with some limitations, a reference book. The book is still, as was originally intended, designed for residents with an orientation to organization and teaching. Bone maturation, normal cross-sectional anatomy, the differentiation of benign and malignant bone lesions, and different forms of periosteal reaction are all used for teaching.

Thus, this is a much improved book, primarily designed for the radiology resident, although many practicing general radiologists will find it of value.

David H. Carlson
Newton-Wellesley Hospital
Newton, MA 02162

Microcolon of Prematurity:
A Form of Functional Obstruction

John Amodio[1]
Walter Berdon[1]
Sara Abramson[1]
Charles Stolar[2]

Six premature infants (birth weights 920–1320 g) developed marked abdominal distension after birth, and contrast enema examination showed a microcolon. Four of the six were born to mothers with toxemia who received magnesium sulfate. Bilious emesis was absent in all six, despite marked distension and failure to pass meconium. None of the patients had aganglionosis or cystic fibrosis; five of six were followed without surgery and recovered spontaneously. The sixth had perforation 8 hr after contrast enema and required bowel diversion; this infant also survived. This appears to be an equivalent form in small premature infants of the "small-left-colon syndrome" seen in term infants. Surgery should be reserved for complications; it is not necessarily indicated by the finding of a microcolon in such patients.

A microcolon may be defined as a colon of abnormally small caliber. However, there are no absolute standards for this measurement [1]. The finding of a microcolon on contrast enema study in distended newborns usually suggests distal ileal obstruction, with ileal atresia, meconium ileus, or occasionally total colonic aganglionosis being found as a cause of the problem [1]. Such conditions require immediate treatment, either surgically or by a hyperosmolar contrast enema examination.

We report six cases of microcolon in very premature infants (birthweight <1370 g) that were detected because of abdominal distension and failure to pass meconium immediately after birth. All six infants had contrast enema examinations showing a total microcolon; four of the six had a history of maternal magnesium sulfate ingestion for toxemia.

The microcolon appears to be the result of a functional abnormality with failure of the small-bowel contents to pass into the colon in utero. The condition appears to parallel the degree of prematurity and may, in addition, reflect a depressive effect of transplacental magnesium sulfate on bowel function. "Microcolon of prematurity" appears to be the presentation, in the least mature newborns, of the functional intestinal obstruction well known in larger infants as "small-left-colon syndrome" [2, 3]; it has the same relation to maternal factors, including toxemia and the use of magnesium sulfate in the mother. We demonstrate that a microcolon in very premature infants may be the result of a functional obstruction and not necessarily an organic one.

Materials and Methods

The records of six premature infants who had nonorganic intestinal obstruction and were born at Babies Hospital from 1980 through 1984 were reviewed. All were 29–32 weeks of gestation and had birth weights of 920–1370 g. All six babies had plain film and contrast enema studies, using either barium or diluted water-soluble contrast material. In no instance was full-strength Gastrografin used. Follow-up plain films and/or clinical records were available in all cases.

Received June 10, 1985; accepted after revision September 20, 1985.

Presented at the annual meeting of the Society for Pediatric Radiology, Boston, April 1985.

[1] Department of Pediatric Radiology, Babies Hospital, Columbia-Presbyterian Medical Center, 622 W. 168th St., New York, NY 10032. Address reprint requests to J. Amodio.

[2] Department of Pediatric Surgery Babies Hospital, Columbia-Presbyterian Medical Center, New York, NY 10032.

***AJR* 146:239–244, February 1986**
0361-803X/86/1462-0239
© American Roentgen Ray Society

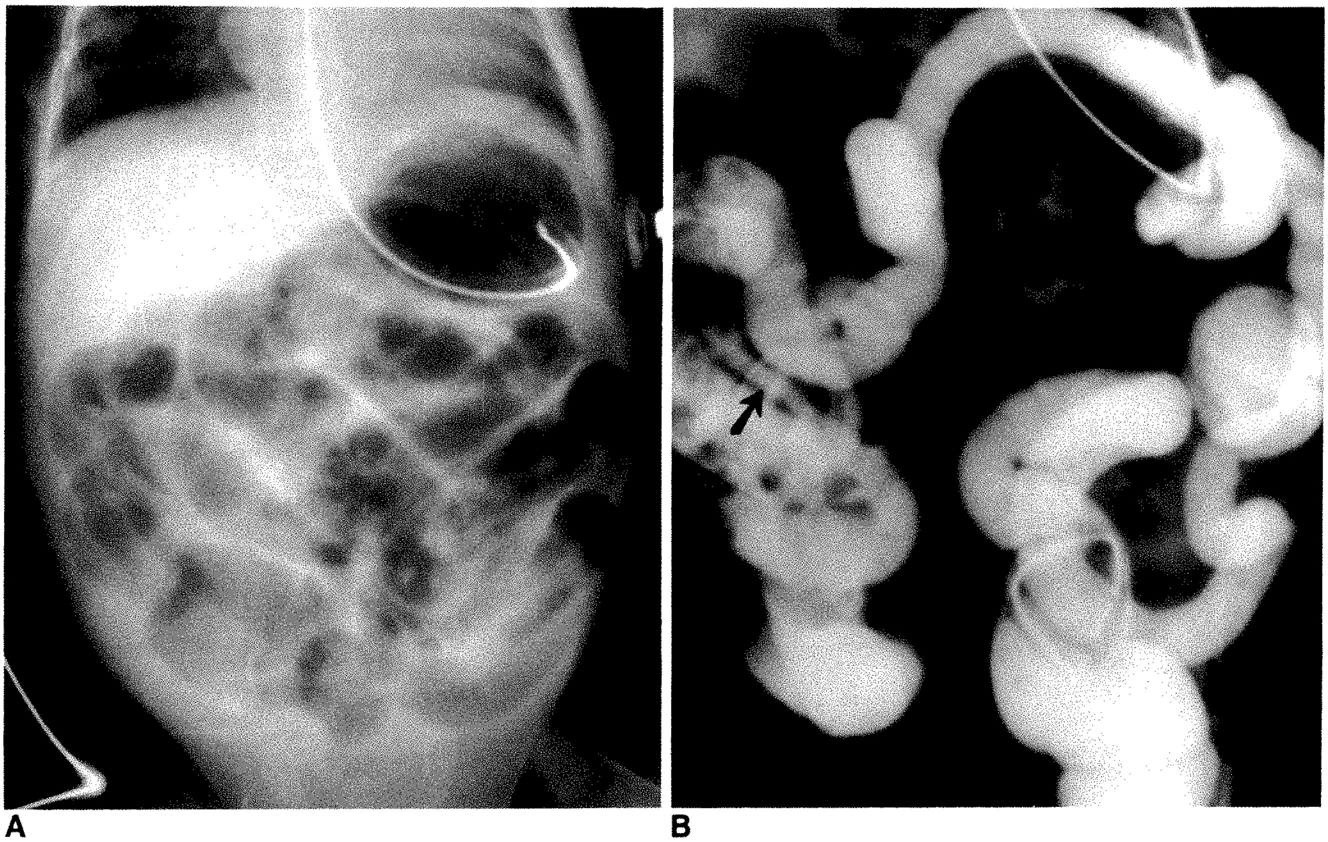

Fig. 1.—32-week-gestation, 980-g boy, smallest of quadruplets. **A**, Supine abdominal film at 24 hr: multiple distended loops of bowel. **B**, Contrast enema at same time: redundant microcolon. Appendix is filled (*arrow*) with reflux into dilated small bowel.

Results

The clinical signs and symptoms were identical in each case, that is, failure to pass meconium within the first 24 hr with progressive abdominal distension. All infants had radiographically demonstrated progressive bowel distension (figs. 1A, 2A, and 3A). *None* of the infants had a history of bilious or nonbilious vomiting. All infants underwent contrast enema examination, which demonstrated total microcolon in all cases (figs. 1B, 2B, 3B, 4, and 5B). Several days after the initial contrast enema, a repeat contrast enema study in one infant demonstrated return of the colon to normal caliber (fig. 5).

Only one patient had surgical intervention for delayed perforation of the right colon 8 hr after contrast enema (fig. 2C). This infant later had a second perforation of the terminal ileum. These were believed to be due to ischemia. Both perforations were surgically corrected. The other five cases were followed clinically. Suction rectal biopsy and trichloracetic acid tests (for cystic fibrosis) were performed in all cases, but in no case was the diagnosis of aganglionosis or cystic fibrosis made. In addition, long-term clinical follow-up failed to demonstrate any signs of those diseases. Bowel function returned to normal within 2 weeks after the initial studies. Four of the six infants had a history of maternal magnesium sulfate ingestion for toxemia of pregnancy.

Discussion

Functional intestinal obstruction in premature infants has been the subject of several prior publications. Sieber and Girdany [4] reported five premature infants in a study of seven infants with functional intestinal obstruction but morphologically normal intestinal tracts. All seven were explored with a preoperative diagnosis of aganglionosis. All had dilated small-bowel loops at surgery, with the dilatation extending to the upper jejunum in one, the ileum in two, and the terminal ileum in four. No contrast enema studies were performed, but the colons were described as packed with firm fecal or meconium masses.

Cremin [5] reported two sets of premature twins with functional obstruction in the smaller of each pair. Small-bowel dilatation was present, but the contrast enema studies were reported as normal (with meconium plugs in the colon); after the enema, bowel function returned and the patients did well.

Lequesne and Reilly [6] studied 12 premature infants with functional intestinal obstruction; the largest babies had contrast enemas showing a dilated colon to the splenic flexure (small-left-colon syndrome), but three very small infants in their series had transition sites on contrast enemas proximal to the splenic flexure. One had a transition at the hepatic flexure, while two had a microcolon, as in our cases. They

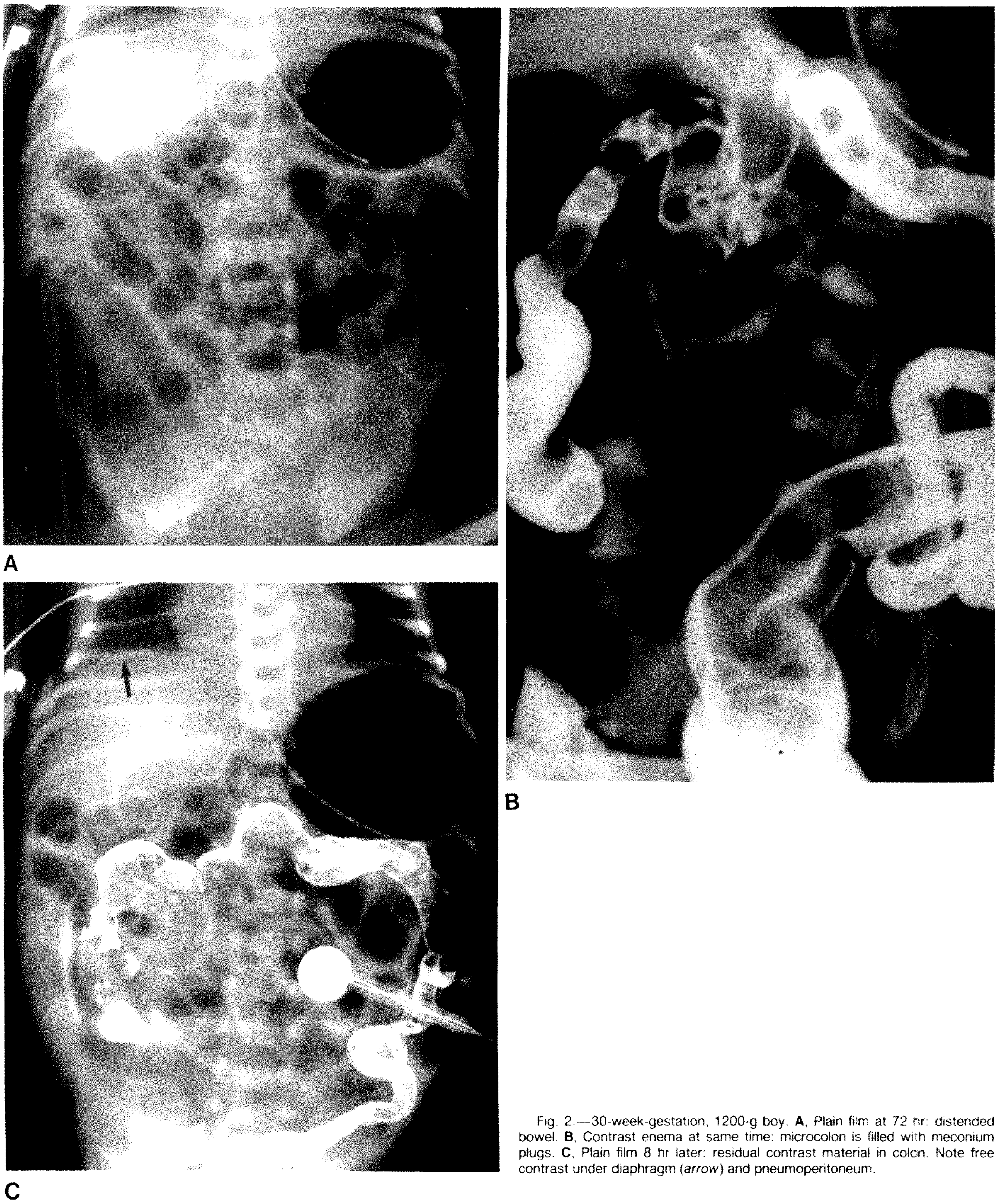

Fig. 2.—30-week-gestation, 1200-g boy. **A**, Plain film at 72 hr: distended bowel. **B**, Contrast enema at same time: microcolon is filled with meconium plugs. **C**, Plain film 8 hr later: residual contrast material in colon. Note free contrast under diaphragm (*arrow*) and pneumoperitoneum.

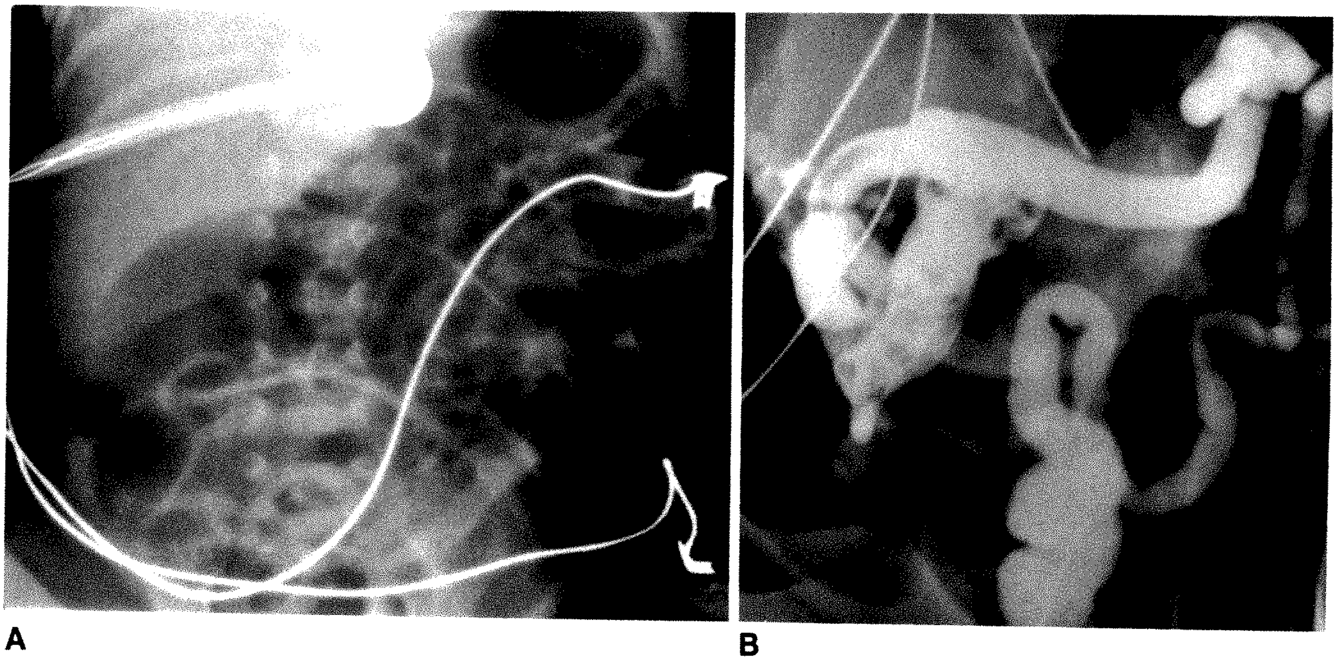

Fig. 3.—32-week-gestation, 1000-g boy. **A**, abdominal plain film at 48 hr: distended loops of bowel. **B**, Contrast enema at same time: microcolon with meconium plug in hepatic flexure.

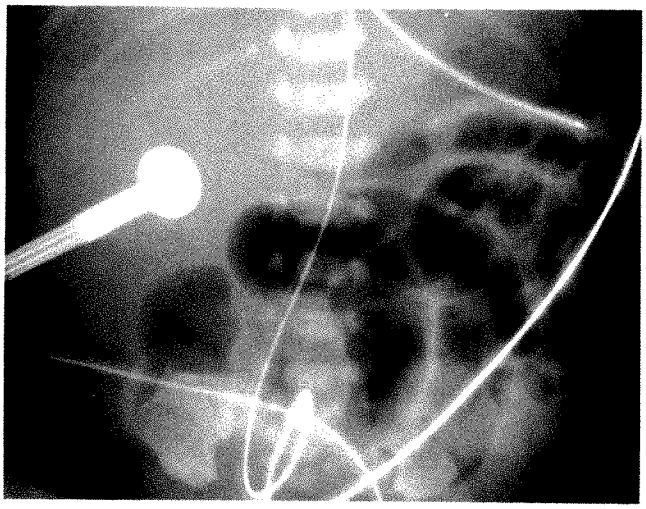

Fig. 4.—29-week-gestation, 1370-g boy. Contrast enema at 24 hr: microcolon with absence of meconium plugs.

noted that the level of transition seemed to correlate with maturation and age; the younger the infant, the more proximal the transition zone.

An earlier pathologic study by Smith [7] showed that ganglion cell morphologic maturation proceeds in a craniocaudal direction and continues after birth. The distal bowel (especially the rectum) may have immature-appearing ganglion cells on biopsy in the newborn, and this must not be mistaken for aganglionosis. Van Houtte and Katzman [8] reported an ileus or dysfunctional pattern in premature newborns, which they related to immaturity of the neural plexus. They suggested that premature interruption of pregnancy may lead to an infant whose gastrointestinal tract is too immature to allow evacuation of meconium.

The small-left-colon syndrome reported previously [9] has a special predilection for infants of diabetic mothers. These infants may be large but immature, and this may account for their presence in neonatal intensive care units, with respiratory distress and cardiac problems in addition to varying degrees of intestinal functional obstruction.

The history of maternal magnesium sulfate administration in four of the six infants adds another factor that can affect bowel function in the newborn. Hutchinson et al. [10] reported the direct depressive effect of magnesium on smooth muscle cells: del Castillo and Engbaek [11] earlier suggested a decrease in neurotransmitter liberated at the nerve ends under the influence of magnesium. This would diminish the action of acetycholine and depress the excitability of muscle nerve fibers, affecting subsequent muscle actions. Sokal et al. [12] reported two larger (although immature) infants whose mothers had received magnesium sulfate and in whom a picture of small-left-colon syndrome had developed. They also had a benign course without later problems attributable to either aganglionosis or cystic fibrosis.

Sieber and Girdany [4] also referred to earlier reports of functional obstruction occurring in infants whose mothers had taken ganglion-blocking agents (although their own cases had no such history). In recent years, infants born to addicted mothers (both heroin and methadone) have been noted to have functional intestinal obstruction [13].

Microcolon as such is a nonspecific result of failure of small-bowel contents to be propelled into the colon in utero; it can occur in meconium ileus and ileal atresia and can be seen in

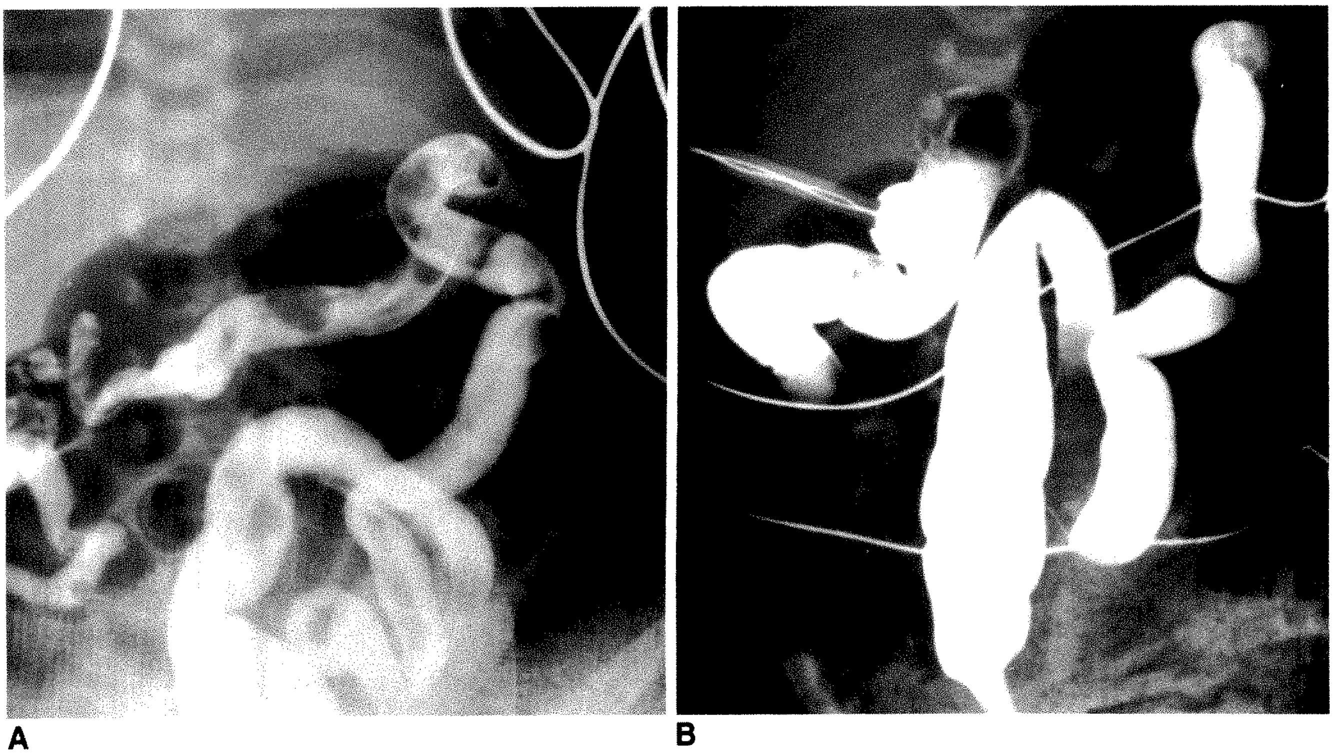

Fig. 5.—30-week-gestation, 1000-g boy, smaller of twins. **A**, Contrast enema: microcolon with meconium plugs. **B**, Contrast enema 2 weeks later: normal-caliber colon. Infant was clinically well.

some cases of aganglionosis of the entire colon, as noted by Sane and Girdany [14] and, more recently, by DeCampo et al. [15]. We have resorted to rectal suction biopsy in our premature infants with functional obstruction and microcolon, although all to date have had normal ganglion cells on biopsy. (During this period, one premature infant found with aganglionosis showed a typical rectosigmoid transition zone both on barium enema and on pathologic examination.)

The finding of microcolon has been reported by Berdon et al. [16] in a group of female infants who also had giant bladders (megacystis) and nonrelenting intestinal hypoperistalsis leading to death, although some survived months to years on hyperalimentation.

In summary, the microcolon seen in our very premature infants seems secondary to functional obstruction on the basis of ganglion cell dysfunction and depressive effects of magnesium sulfate. All except one of the infants did well with conservative management. It was because of the extreme immaturity of these nonvomiting infants and previous reports of magnesium sulfate effects on intestinal motility that our surgical consultants were willing to adopt a "watch and wait" attitude. Moreover, the enemas were helpful in initiating evacuation of meconium and stool. We, therefore, recommend close observation of premature infants showing progressive abdominal distension in whom no vomiting is demonstrated. The presence of microcolon per se should not lead to surgical intervention.

REFERENCES

1. Girdany B. The abdomen and gastrointestinal tract. In: Silverman F, ed. *Caffey's pediatric x-ray diagnosis,* vol 2. Chicago: Year Book Medical, **1985**:1401–1570
2. Davis WS, Campbell JB. Neonatal small left colon syndrome. *Am J Dis Child* **1975**;29:1024–1029
3. Davis WS, Allen RP, Favara BE, Slovis TL. Neonatal small left colon syndrome. *AJR* **1974**;120:322–329
4. Sieber WK, Girdany BR. Functional intestinal obstruction in newborn infants with morphologically normal gastrointestinal tracts. *J Pediatr Surg* **1963**;11:357–361
5. Cremin BJ. Functional intestinal obstruction in premature infants. *Pediatr Radiol* **1973**;1:109–112
6. LeQuesne G, Reilly B. Functional immaturity of the large bowel in the newborn infant. *Radiol Clin North Am* **1975**;13:331–342
7. Smith B. Pre- and postnatal development of the ganglion cells of the rectum and its surgical implications. *J Pediatr Surg* **1966**;3:386–391
8. Van Houtte J, Katzman D. Roentgenographic manifestations of immaturity of the intestinal neural plexus in premature infants. *Radiology* **1973**;106:363–367
9. Berdon WE, Slovis TL, Campbell JB, Baker DH, Haller JO. Neonatal small left colon syndrome. Its relationship to aganglionosis and meconium plug syndrome. *Radiology* **1977**;125:457–462
10. Hutchinson HT, Nichols MM, Kuhn CR. Effects of magnesium sulfate on uterine contraction, intrauterine fetus and infant. *Am J Obstet Gynecol* **1984**;88:747–758

11. del Castillo J, Engbaek L. The nature of neuromuscular block produced by magnesium. *J Physiol* **1954**;124:370-384
12. Sokal M, Koenigsberger R, Rose J, Berdon WE. Neonatal hypermagnesemia and the meconium plug syndrome. *N Engl J Med* **1972**:823-825
13. Berdon WE, Baker DH, Santulli TV, Amoury R, Blanc W. Microcolon in newborn infants with intestinal obstruction. *Radiology* **1968**;90:878-885
14. Sane S, Girdany B. Total aganglionosis coli. *Radiology* **1973**;107:397-399
15. DeCampo JF, Wayne V, Boldt DW, DeCampo M. Radiological findings in total aganglionosis coli. *Pediatr Radiol* **1984**;14:205-209
16. Berdon WE, Baker DH, Blanc WA, Gay B, Santulli TV, Donovan C. Megacystic microcolon intestinal hypoperistalsis syndrome: a new cause of intestinal obstruction in the newborn. Report of radiologic findings in five newborn girls. *AJR* **1976**;126:957-964

The Radiologic “Lead Band” Revisited

Johan G. Blickman[1]
Robert H. Wilkinson[1]
John W. Graef[2]

After prolonged heavy metal exposure (e.g., lead) “lead bands” develop at the metaphyseal ends of growing bones. These “lead bands,” while a constant finding, are used as additional laboratory evidence to diagnose plumbism. In this study, the role of the proximal fibula in distinguishing physiologic sclerosis from pathologic thickening of the zone of provisional calcification is assessed. In addition, laboratory values are compared to radiographic findings in a controlled fashion to establish levels at which “lead bands” appear. The former is a useful adjunct in the radiographic diagnosis of plumbism, while the minimum blood levels at which “lead bands” are seen is much lower than previously described.

The radiologic diagnosis of chronic lead poisoning has been described [1], and consists of radiologic examination of the abdomen for evidence of recent ingestion and examination of fast-growing areas of bone formation (traditionally, knees, wrists, and occasionally the iliac crests) to evaluate the effects of lead on the radiographic appearance. The Lead Clinic at the Children's Hospital sees children with elevated lead levels. They have either been screened for plumbism in the Massachusetts Lead Screening Program or had other clinical indications, such as a history of ingestion of paint chips.

As part of the evaluation, an anterioposterior (AP) film of both knees and one of the abdomen are obtained to look for “lead bands” in bones and metallic densities in the bowel. While there is general agreement that radiologic density of the zones of provisional calcification is sensitive to the effect of lead on calcium resorption [1, 2], no controlled studies have been done to establish whether certain anatomic areas are more specific for this effect or at what level of lead in the blood radiographic changes are evident.

In addition, anecdotal reports mention the usefulness of the proximal fibula in establishing the radiographic diagnosis of plumbism (Neuhauser EBD, personal communication). While additional reports state that “lead bands” do not occur until lead levels reach 70 μg/dl whole blood [3], our experience has suggested that this effect may be observed at blood lead concentrations well below this figure.

The objects of this report are therefore (1) to evaluate the role of the proximal fibula in distinguishing between physiologic sclerosis and pathologic thickening of the zone of provisional calcification, and (2) to evaluate the minimum blood lead concentration at which a radiographic “lead band” is visible.

Materials and Methods

Two radiologists independently reviewed 104 cases of documented lead poisoning from the Children's Hospital Lead Clinic interspersed with 18 age-matched controls. Age range was 2–10 years. The controls consisted of films of the knee obtained from patients who were referred for trauma. These had no evidence of plumbism, as established by ascertaining that screening tests for lead were negative. (Initial screening includes erythrocyte protoporphyrin

Received May 6, 1985; accepted after revision September 20, 1985.

[1] Department of Radiology, Harvard Medical School, Children's Hospital, 300 Longwood Ave., Boston, MA 02115. Address reprint requests to R. H. Wilkinson.

[2] Department of Medicine, Harvard Medical School, Children's Hospital, Boston, MA 02115.

AJR 146:245–247, February 1986
0361-803X/86/1462-0245
© American Roentgen Ray Society

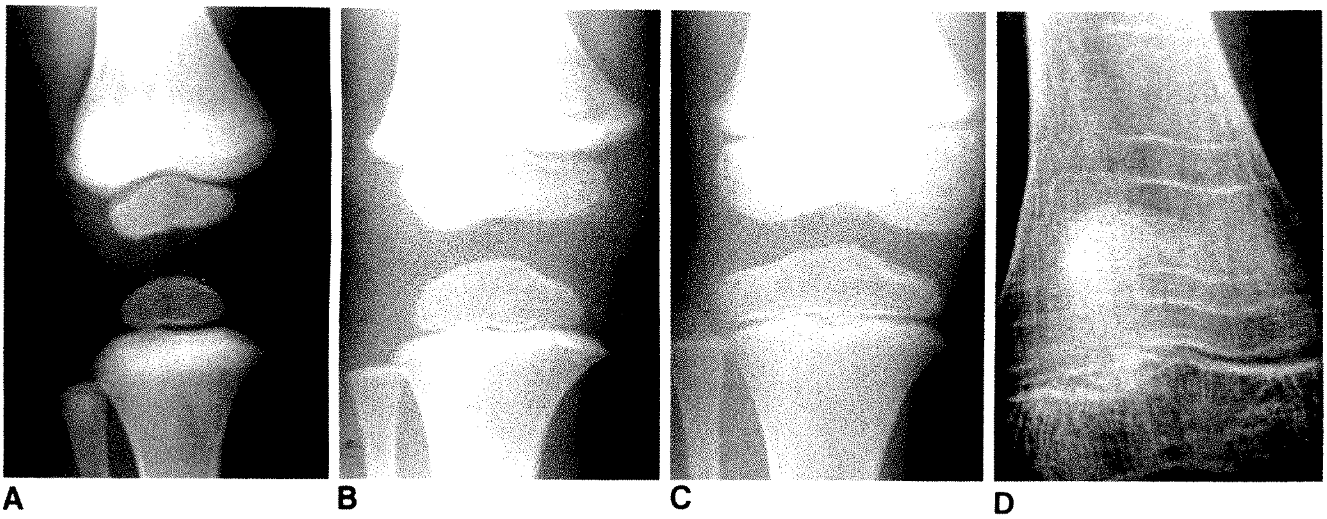

Fig. 1.—Four patients. **A**, Classic bone changes of plumbism; increased bone density and broadening of provisional zones of calcification, additional "lead bands," and remodeling changes of distal femoral metaphysis. **B**, 4-year-old boy with elevated EP and blood lead levels. Increased density and broadening of provisional zone of calcification of distal femur, proximal tibia, *and* fibula. **C**, 4.5-year-old girl with diffuse knee pain and no history or laboratory evidence for plumbism. "Normal" physiologic density of provisional zone of calcification of distal femur and proximal tibia; less evident in proximal fibula and not as broad. **D**, Classic "post-growth-arrest" lines in American Indian child with multiple major infections. The more remote the episode, the less complete the line, due to differential remodeling changes. (Courtesy of E. Stuart Houston, Saskatoon.)

[EP] levels, and the EP levels of this control group were less than 49 μg/dl. Levels below 49 μg/dl are believed to reflect blood lead levels below 30 μg/dl in more than 95% of patients [4].)

Diagnostic radiologic criteria included increased density and broadening of provisional zones of calcification, additional "lead bands," and remodeling changes (fig. 1A). In addition, the density of the proximal fibular metaphysis was examined, and its density was compared to that of the distal femur and proximal tibia to decide whether it influenced the decision that radiographic evidence of lead poisoning was present (fig. 1B). In a subset of 10 cases (seven with documented lead poisoning), a *lateral* view of the proximal fibular metaphysis was also assessed as to whether increased density at that site influenced the final impression.

Results

In 95% of cases (115 of 122), the two radiologists agreed concerning the presence or absence of lead poisoning; 81.6% were considered to be positive by both. All the controls were considered negative by both (0 positive radiographs), while the radiographs were interpreted differently by both examiners in seven cases of the study group. In addition, when comparing the proximal fibular zone of provisional calcification to the zones of provisional calcification of the tibia and femur, no false-positive or false-negative reports were obtained. The lateral film of the fibula, taken as an adjunct in the subset of these patients, did not alter the false-positive or false-negative interpretations.

The *mean* blood lead level in the group who had positive radiographs was 49 ± 17.3 μg/dl; it was 18 ± 5.4 μg/dl in the control group of those with negative radiographs ($p < 0.01$ by Student's two-tailed t-test).

Discussion

The value of the radiograph in a diagnosis of lead poisoning is based on the relatively rapid growth of bone between the second and sixth years of life, not so coincidentally the same time span when most lead ingestion occurs [5]. The knee is an ideal area to examine for evidence of metabolic bone disease because the distal femur and proximal tibia and fibula grow rapidly. They are also at some distance from the gonadal region, and thus radiation exposure to the gonads is less, probably insignificant. The "lead band" is thought to be due to failure of remodeling of calcified cartilage in the zone of provisional calcification and primary trabeculae of bone. The increased density is thus not due to the radiopaque properties of metallic lead, and becomes more prominent with time [6].

Occasionally the normal provisional zone of calcification is more dense than usual. This has been termed normal "physiologic sclerosis" [1] and is often found in healthy children with no apparent history of lead exposure (fig. 1C). However, specific differentiation of these lines from the "lead band" has been described using several criteria [3]:

1. *Age*. Generally, normal physiologic sclerosis is seen in patients older than 3 years. Our age range, however, was 2–10 years, making differentiation on the basis of age difficult.
2. *Absence of migration* of the physiologic dense band. Events other than lead exposure may alter bone density intermittently, causing other "growth-arrest" bands (fig. 1D) [6].
3. *Blood lead levels*. If these were normal, "physiologic sclerosis" was assumed. However, "lead bands" are noted at *mean* blood lead levels of 49 μg/dl in this study, significantly below the previously described 70 μg/dl.

It had further been observed (Neuhauser EBD, personal communication) for some time that the difference in density of the zone of provisional calcification of the proximal fibula and proximal tibia is different. In normal patients, the proximal zone or provisional calcification of the tibia could appear dense, while the proximal fibula did not show a band of similar density and width; in patients with lead poisoning, however, the dense line would appear in *both* proximal tibial and proximal fibular metaphyses. Although an absolute measurement of this phenomenon is not possible, the density and width of the zone of provisional calcification of the proximal fibula is shown to be useful as an *adjunct* to establish the presence or absence of "lead bands," if these need to be differentiated from physiologic sclerosis in the face of normal or near-normal laboratory results and the absence of clinical symptoms. The value of this approach lies in helping to avoid false positives caused by apparently normal variations in rates of bone growth, particularly in those 1–3 years of age.

In conclusion, the radiographic diagnosis of plumbism may be helped by evaluation of the proximal fibula; also, laboratory values at which these findings become evident are lower than previously reported.

REFERENCES

1. Caffey J. *Pediatric x-ray diagnosis*, 8th ed. Silverman FN, ed. Chicago: Year Book Medical, **1985**:486–493
2. Leone AJ. On lead lines. *AJR* **1968**;103:165–167
3. Sachs HK. The evolution of the radiologic lead line. *Radiology* **1981**;139:81–85
4. Department of Health, Education and Welfare. Preventing lead poisoning in young children. Rockville, MD: DHEW, **1978**:6
5. Maresh MM. Linear growth of long bones of extremities from infancy through adolescence. *Am J Dis Child* **1955**;89:725–742
6. Park EA. The imprinting of nutritional disturbances on the growing bone. *Pediatrics* (suppl) **1964**;33:815–862

Book Reviews

Recent Developments in Digital Imaging. Medical Physics Monograph No. 12. Edited by Kunio Doi, Lawrence Lanzl, and Pei-Jan Paul Lin. New York: American Institute of Physics, 576 pp., 1985. $60 ($40 for institute members)

This book is a collection of papers originally presented at the 1984 Summer School of the American Association of Physicists in Medicine (AAPM). The papers provide information in three major categories: (1) basic imaging theory; (2) digital fluorographic systems; and (3) digital radiographic systems. The authors are physicists and engineers who work in digital radiography in hospitals, universities, and industry.

The topics covered include imaging theory: basic theory, noise analysis and signal detection, image assessment, modulation transfer functions, and contrast-detail analysis. Alternative approaches to digital imaging systems are presented including methods of digital fluoroscopy, scanned projection radiography, electrostatic imaging, digitized x-ray film conversion, stimulated photoluminescence, and proximity focus digital radiography. Under digital subtraction angiography (DSA) are found papers on system theory, design, and operation; temporal, matched filtering, and hybrid subtraction; quantitative analysis; DSA performance specifications, acceptance testing, and use of phantoms.

This book provides a convenient reference to the current status of research and implementation of digital radiographic imaging systems. Despite editing, the stylistic format of the book is nonuniform and hence the book is more a collection of individual chapters than an integrated summary of the field. Encyclopedic in character, each chapter provides considerable detail of the subject matter treated. While the information is up-to-date, a few topics in digital imaging are notably absent, such as image archiving, display, and transmission.

The material is highly mathematical and technical. Thus the book will likely have no appeal to clinicians. Further, I found it lacking in sufficient general introductory information to make it suitable for students of medical imaging systems as a didactic textbook. However, this book will be of considerable interest to physicists and engineers who work in digital radiography in industry and/or academic research laboratories. In addition, it is recommended to hospital physicists concerned with the installation, maintenance, acceptance testing, and performance assessment of digital fluoroscopy equipment used for DSA. While much of the material in individual chapters is repeated in the literature, this book provides a convenient and relatively comprehensive summary. To engineers and physicists working in the field, this book will prove to be a worthy reference.

William R. Brody
Stanford University
Stanford, CA 94305

Proceedings of the Eighth Conference on Computer Applications in Radiology. American College of Radiology. Chevy Chase, MD: ACR Publications, 703 pp., 1984. $75 ($50 for ACR members)

The American College of Radiology sponsors a biannual conference on Computer Applications in Radiology. The eighth conference took place in St. Louis, MO, in May 1984. The *Proceedings* from that conference contains most of the papers presented there. Because these biannual meetings provide the most comprehensive forum in radiology for the presentation and dissemination of new, practical applications of computer technology, the proceedings are a valuable source of reference material and provide an overview of the current status of computers and radiology.

The present proceedings from the eighth conference contains 700 pages with 56 papers and review articles. The papers cover a wide range of topics including data base management systems, telecommunications, digital image processing, picture archiving and storage (PACS), and professional applications for personal computers. The wealth of material is extensive, but the articles vary greatly in their readability, information, and usefulness. Thus, the book should be considered mainly a reference source. While some papers provide sufficient information for implementation of practical new techniques at one's own institution, most papers merely introduce a topic and lack sufficient enough detail to directly help the reader. However, the reader does gain a familiarity with the range of computer applications in radiology and is free to write or call authors of interesting papers for more information.

The price of the proceedings is reasonable considering its large size and content. Purchase is recommended for radiology libraries and for both the novice and the expert with particular interest in computers and radiology.

Tim B. Hunter
John D. Newell
University of Arizona
Tucson, AZ 85724

Sonographic Recognition of Idiopathic Arterial Calcification of Infancy

David M. Rosenbaum[1] and Joel D. Blumhagen[1]

Idiopathic arterial calcification of infancy is a rare disease of unknown cause. It is characterized by patchy destruction and disruption of the internal elastic membrane, with deposition of calcium hydroxyapatite in this layer [1]. In most cases there is also patchy intimal proliferation and fibrosis, which narrows the lumen of the vessel, leading to ischemia. The process affects both systemic and pulmonary arteries of all sizes, but it is myocardial ischemia due to coronary artery involvement that usually leads to death before 1 year of age.

Although most of the approximately 80 reported cases were diagnosed at autopsy, the arterial calcifications could usually be perceived retrospectively on radiographs done during life. Among the 13 reported cases in which the findings were recognized ante mortem, there have been four survivors [1-4]. The radiographic findings can be very subtle [5, 6], but we recently encountered an infant in whom sonography revealed striking echogenicity of the arterial walls, which suggested the diagnosis.

Case Report

A 2180-g boy, estimated 32-week gestation, was delivered by cesarian section because of progressive nonimmune hydrops diagnosed by prenatal sonography. Endotracheal intubation and treatment for congestive heart failure were initiated at birth. Systolic blood pressure was elevated, ranging from 120 to 170 mm Hg, but diastolic pressure was normal or only mildly raised. Plasma renin level was 30 times the upper limit of normal, and hypertension was successfully controlled with captopril. Microscopic hematuria appeared, and abdominal sonography was done on the sixth day of life to evaluate the possibility of renal vein thrombosis. Sonography revealed intense echogenicity of the aorta and its branches, with striking acoustic shadowing from the vessel walls (fig. 1A). Although the kidneys were not enlarged, renal parenchyma was diffusely hyperechoic (fig. 1B). The arterial echogenicity prompted a review of the patient's radiographs, whereupon faint but extensive arterial calcification was identified on all radiographs (fig. 1C). Progressive congestive heart failure led to death at 1 month of age. At autopsy, intimal hyperplasia and extensive medial calcification of the aorta and its branches,

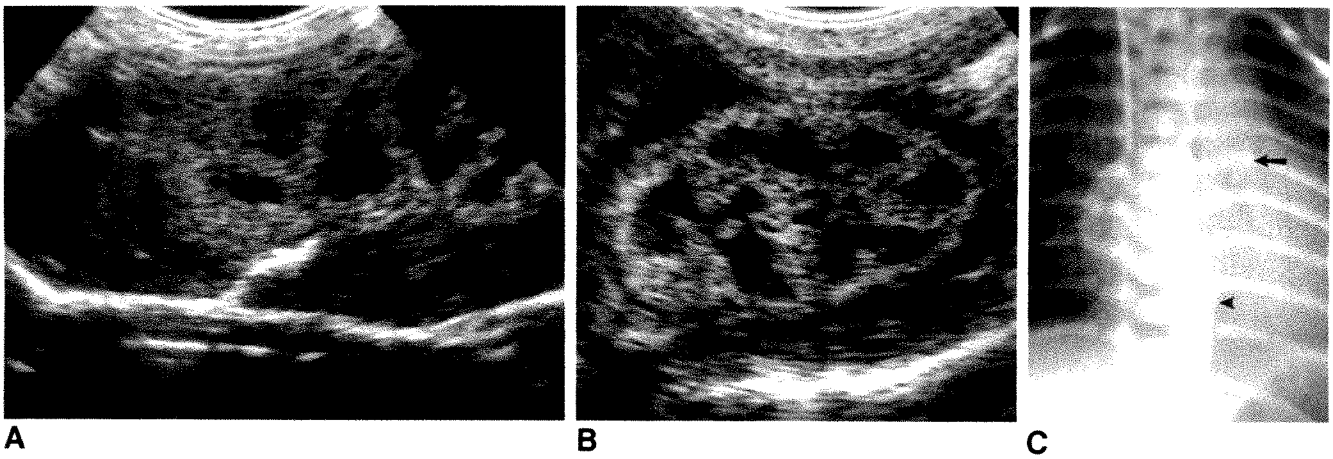

Fig. 1.—**A**, Left coronal sonogram of abdomen. Aortic walls and left renal artery are intensely echogenic. Acoustic shadowing to right of aorta. Umbilical arterial catheter is faintly visible within aortic lumen. **B**, Parasagittal sonogram shows striking diffuse hyperechogenicity of right kidney. **C**, AP chest radiograph. Faint calcification is present in descending aorta (*arrowhead*) and pulmonary artery (*arrow*.)

Received July 9, 1985; accepted after revision September 11, 1985.

[1] Department of Radiology, University of Washington School of Medicine, and Children's Orthopedic Hospital and Medical Center, P.O. Box C-5371, Seattle, WA 98105. Address reprint requests to D. M. Rosenbaum.

***AJR* 146:249-250, February 1986** 0361-803X/86/1462-0249 © American Roentgen Ray Society

including coronary arteries, were found. There was also microscopic calcification of the renal tubules and glomeruli.

Discussion

Generalized arterial calcification in infants can be caused by hypervitaminosis D and primary or secondary hyperparathyroidism, which result in abnormalities of calcium metabolism; when laboratory investigation suggests normal calcium metabolism, however, the condition is assigned to the idiopathic group. Recognizing the diagnosis of idiopathic arterial calcification is difficult because (1) the symptoms are nonspecific (e.g., poor feeding, respiratory distress, and lethargy), (2) there is a rapid, downhill clinical course, and (3) the radiographic findings are often subtle. We believe that the striking hyperechogenicity and acoustic shadowing of arterial walls seen on sonography should allow earlier suspicion of the diagnosis in some cases, prompting confirmation with radiographs. These patients often will be referred for abdominal or cardiac sonography to evaluate nonimmune hydrops, hematuria, hypertension, and/or congestive heart failure.

The primary clinical problem in these patients is often hypertension [7], which results from two major mechanisms: (1) increased vascular resistance from widespread luminal narrowing and stiff arterial walls, which cause a wide pulse pressure, and (2) renal artery stenosis with elevation of renin levels. The relation of widespread microscopic calcification of renal structures to hypertension in our patient is uncertain, but it probably contributed to the diffuse increase we observed in renal parenchymal echogenicity. Ischemic damage to the kidney can also cause it to appear hyperechoic, and is much more common in neonates than is nephrocalcinosis. Sonography can be very useful in this clinical setting to show aortic thrombosis, which is common in sick neonates who have umbilical arterial catheters, but arterial calcification might masquerade as calcified intraluminal thrombus in some cases if the anatomic definition is inadequately detailed.

Whether ante mortem diagnosis will affect survival is not known, but three of the four reported survivors received treatment that may have influenced their outcome: thyroid extract, estrogens, and steroids [2]; diphosphonate [1]; and Didronel (editronate) [3]. Although the arterial calcifications resolved by the age of 5 in one survivor, the long-term prognosis is unknown [4].

REFERENCES

1. Meradji M, de Villeneuve VH, Huber J, de Bruijn WC, Pearse RG. Idiopathic infantile arterial calcification in siblings: radiologic diagnosis and successful treatment. *J Pediatr* **1978**;92:401–405
2. Lussier-Lazaroff J, Fletcher BD. Idiopathic infantile arterial calcification: roentgen diagnosis of a rare cause coronary artery occlusion. *Pediatr Radiol* **1973**;1:224–228
3. Jaffe RB. Idiopathic infantile arterial calcification. Presented at the annual meeting of the Society for Pediatric Radiology, Las Vegas, April **1984**
4. Sholler GF, Yu JS, Bale PM, Hawker RE, Celermajer JM, Kozlowski K. Generalized arterial calcification of infancy: three case reports, including spontaneous regression with long-term survival. *J. Pediatr* **1984**;105:257–260
5. Weems HS, Marin CA. Infantile arteriosclerosis. *Radiology* **1956**;67:168–174
6. Kirchner SG, Heller RM, Kasselberg AG. Idiopathic arterial calcification of infancy. *South Med J* **1979**;72:1328–1330
7. Milner LS, Heitner R, Thompson PD, et al. Hypertension as the major problem of idiopathic arterial calcification of infancy. *J Pediatr* **1984**;105:934–938

Diagnostic Oncology Case Study

Retroperitoneal Mass with Intradural Extension: Value of Magnetic Resonance Imaging in Neuroblastoma

Neuroblastoma is one of the most common childhood malignancies [1, 2]. Knowledge of local tumor extent as well as accurate staging of the disease are essential for proper treatment [3]. In resectable stage I (confined to the site of origin) and stage II (extending beyond the site of origin but not crossing the midline), surgery alone is usually sufficient without the need for chemotherapy or radiotherapy. By contrast, in stage III (tumor extending beyond the midline) and stage IV (remote metastases to bones or lymph nodes), chemotherapy and/or radiotherapy are generally required.

Multiple radiologic studies, many of which are invasive and/or require the administration of intravenous contrast material, are often performed to evaluate a child with known or suspected neuroblastoma [4]. When spinal involvement by tumor is known to be present or is suspected, an intrathecal contrast injection may also be required. On the other hand, magnetic resonance imaging (MRI) is a noninvasive procedure that appears to have unique clinical advantages in evaluating childhood neoplasms [5]. It provides excellent differentiation of soft-tissue planes without the need for ionizing radiation or contrast injection. The availability of multiple imaging planes allows careful evaluation of the adrenal glands, kidneys, liver, major vessels, and spinal canal [6–10]. This report concerns an infant with stage III neuroblastoma in whom the following imaging procedures were performed: abdominal sonography, excretory urography, computed tomography, myelography, MRI, and radionuclide bone scans. MRI proved more useful than any single study and, in retrospect, could have obviated excretory urography, CT, and myelography.

Case Report

A 5-month-old girl was the product of an uncomplicated term gestation and was well until quite recently, when her mother noted periodic episodes of irritability and the development of a mass on her back just to the right of midline. Her pediatrician diagnosed a urinary tract infection, and she was started on a course of Bactrim. Anteroposterior and lateral radiographs of the abdomen were reported to be negative. Ten days later the urinary infection had cleared, but a weight loss of 187 g was noted. The mass was unchanged in size, and sonography demonstrated a solid retroperitoneal mass. An oncologist was consulted, and exploratory surgery with biopsy of the mass was performed at another hospital. The retroperitoneal tumor was found to be more extensive than previously thought, and while no neurologic signs were evident, intraspinal involvement was thought to be a strong possibility because of the size and location of the lesion. Surgical biopsy (without excision of the tumor) revealed neuroblastoma, and the child was transferred to the UCLA Medical Center.

A repeat abdominal sonogram on arrival at UCLA demonstrated a large echogenic mass in the right retroperitoneum displacing the right kidney superiorly and laterally. The mass also displaced the inferior vena cava and aorta to the left, but the great vessels did not seem to be involved intrinsically by tumor. The left kidney and adrenal gland appeared normal. Scout radiographs obtained for an excretory urogram demonstrated calcifications within the right paravertebral mass. Scalloping of the posterolateral aspects of the lumbar vertebrae and erosion of the right pedicles were also noted. Postinjection radiographs (fig. 1) demonstrated mild hydronephrosis and displacement of the right kidney. In order to evaluate intraspinal involvement, a metrizamide myelogram (fig. 2) and a metrizamide CT scan (fig. 3) were obtained, both of which demonstrated the presence of intraspinal tumor.

This is another in a series of case reports edited by A. Robert Kagan (Southern California Permanente Medical Group, Los Angeles, CA 90027) and Richard J. Steckel (Jonsson Comprehensive Cancer Center at UCLA, Los Angeles, CA 90024) to present and discuss contemporary problems and procedures in the identification and staging of neoplasms. Case contributed by Rosalind B. Dietrich and Hooshang Kangarloo, Department of Radiological Sciences, Section of Pediatric Radiology, UCLA School of Medicine, Los Angeles, CA 90024. Address reprint requests to R. B. Dietrich.

AJR 146:251–254, February 1986 0361–803X/86/1462–0251 © American Roentgen Ray Society

MRI was then performed as part of an ongoing investigation to evaluate the role of MRI in staging childhood neoplasms. A Fonar 0.3-T imaging system with a permanent magnet was used. Sections were 6–9 mm thick, with 3–4 mm between adjacent sections. Multiplane T1-weighted images requiring 8½ min scanning time and T2-weighted images requiring 17 min were obtained with a spin-echo (SE) pulse sequence. A combination of Demerol (2 mg/kg), Phenergan (1 mg/kg), and Thorazine (1 mg/kg) was administered intramuscularly 30 min before scanning, and a physician and the patient's mother remained in the scanning room during the procedure.

A 5-cm soft-tissue mass was confirmed in the right paravertebral region extending from T11 to L4 (fig. 4). The right kidney was again shown to be displaced and mildly hydronephrotic, and extension of the retroperitoneal mass into the spinal canal was clearly demonstrated. On T1-weighted images (500 msec TR, 28 msec TE), the signal intensity from the tumor was less than that from the liver; on T2-

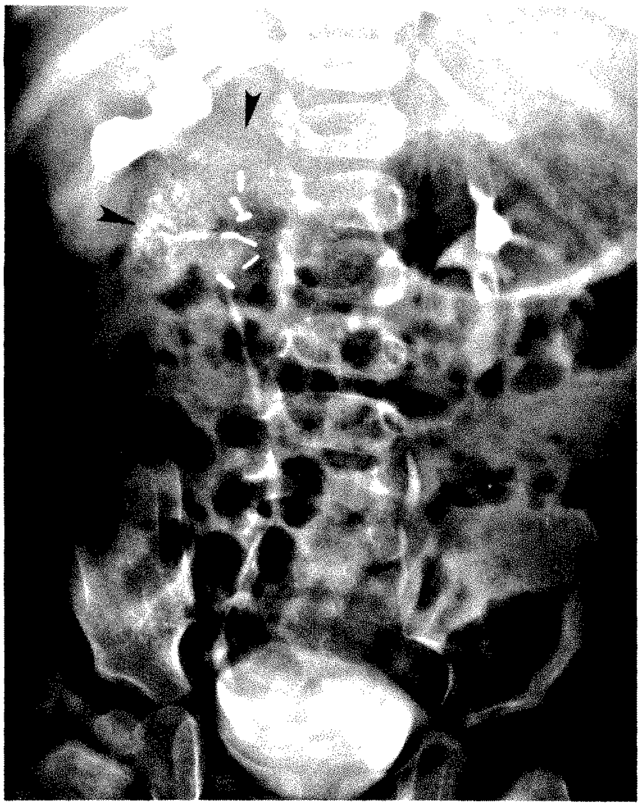

Fig. 1.—Excretory urogram. Calcified paravertebral soft-tissue mass (*arrowheads*) displaces lower pole of right kidney and obstructs proximal ureter.

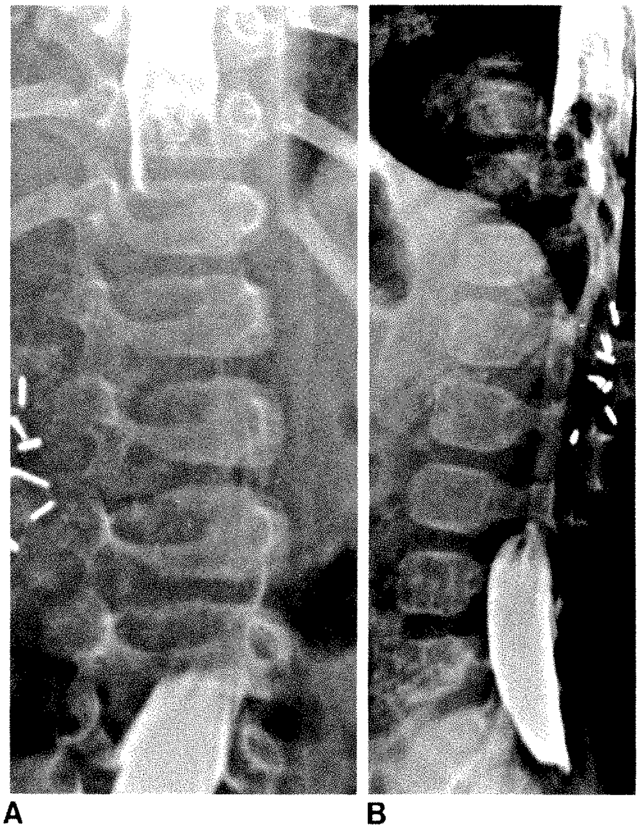

Fig. 2.—Metrizamide myelogram, oblique (**A**) and lateral (**B**) views. Extradural and intramedullary extension of soft-tissue mass, which extends within spinal canal from T11 to L2.

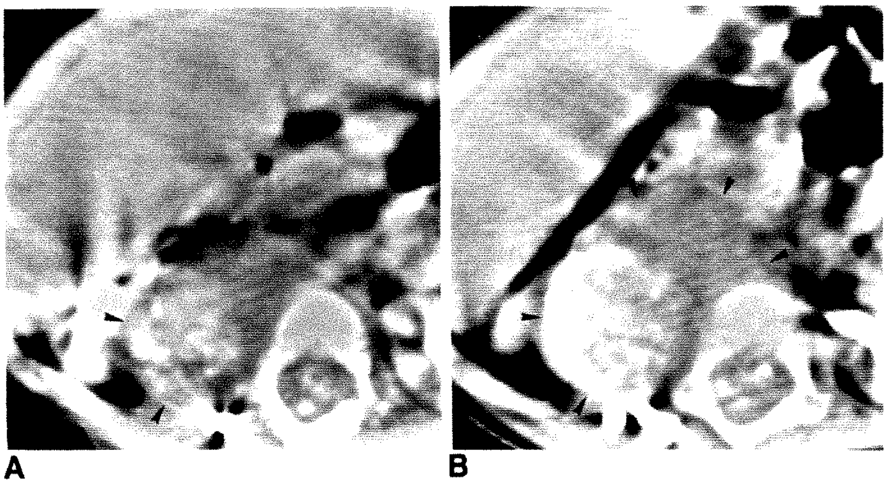

Fig. 3.—Axial CT scans after intravenous contrast and intrathecal metrizamide administration. **A**, Right paravertebral mass (*arrowheads*) displaces right kidney and extends into spinal canal. **B**, Calcified mass (*arrowheads*) is again shown in slightly more caudal plane of section

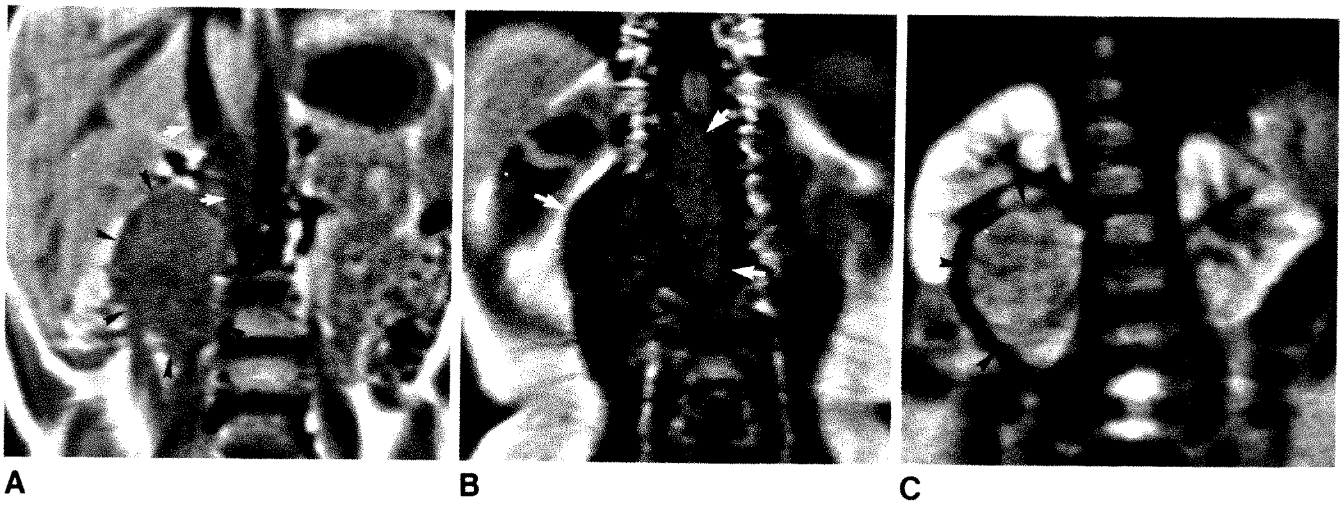

Fig. 4.—Coronal MRI. **A**, SE 500/28 (TR/TE). Paravertebral soft-tissue mass (*arrowheads*) displaces inferior vena cava (*arrows*) leftward. **B**, More posterior T1-weighted image. Intraspinal extension of mass (*arrows*). **C**, T2-weighted image (SE 2000/112). Mass (*arrowheads*) has higher intensity signal than it had on T1-weighted images, but lower intensity than adjacent kidney.

weighted images (2000 msec TR, 112 msec TE), it was significantly greater than that of the liver. Although there was less difference between the signal intensities of the tumor and the adjacent kidney, it was possible to demonstrate a tissue cleavage plane between the tumor and the kidney. The child was started on a treatment regimen consisting of cyclophosphamide and Adriamycin. Repeat MRI studies (2 weeks, 1½ months, and 4 months after therapy) have demonstrated a good response to therapy. Four months after completion of chemotherapy, the imaging studies show almost complete disappearance of the tumor without residual intraspinal involvement.

Comments on Patient Preparation for MRI.—In infants, chloral hydrate (40 mg/kg) given orally is usually sufficient for sedation. However, in our patient chloral hydrate was tried during a prior CT examination and was found to be ineffective. Sedation of a child may be one of the most difficult parts of an MRI study. The examination time is usually long in comparison with CT, and it is necessary for a physician or nurse to monitor the child (visually and by using a plastic stethoscope) during the actual scanning procedure. When we are not able to sedate a child with chloral hydrate or with Demerol, Phenergan, and Thorazine, or if a child is intubated, we ask for assistance from the Department of Anesthesiology to sedate and monitor the patient.

Discussion

Neuroblastoma usually presents as an asymptomatic abdominal mass in a child [2, 5]. In addition to chest and plain abdominal radiographs, multiple imaging studies are often performed in the course of preoperative diagnosis and staging [3], with sonography and excretory urography being the studies most frequently used. CT and radionuclide scans are also used to assist in staging the disease, and in particular to evaluate the patient for spread of tumor across the midline and to rule out possible involvement of the liver, regional lymph nodes, and bones If intraspinal involvement is suspected, myelography or a metrizamide CT scan is often performed [4].

Several sequential imaging studies were performed in our patient, and each did in fact provide additional information. In retrospect, however, one preoperative study (MRI in the coronal plane), if performed alone, would have given most of the information that was obtained with the other studies without the need for ionizing radiation or an invasive procedure using contrast material. Coronal MRI clearly defined the size and extent of the primary tumor mass, the displacement (but lack of intrinsic involvement) of the inferior vena cava, the presence and extent of intraspinal involvement, and the absence of metastatic involvement of the liver and the visualized parts of the bone marrow.

MRI in the *coronal* plane demonstrated the origin of the patient's mass in relation to the kidney, as well as the relation of the tumor to the inferior vena cava and aorta and the extent of spinal involvement better than axial MRI could have done. However, visualization of certain aortic branch vessels (in particular the origins of the celiac and superior mesenteric arteries) can be obtained better with axial and/or sagittal MRI. While the CT images (after intravenous contrast injection and intrathecal administration of metrizamide) gave similar information with respect to intraspinal involvement and displacement of the great vessels and right kidney, these features are in fact better delineated in the coronal plane by MRI.

The diagnostic workup of a child with suspected neuroblastoma is similar to that for any other abdominal mass. Imaging evaluation should begin with a plain film of the abdomen and a sonogram. While the performance of sonography may be difficult in young children and is "operator dependent," it is possible with sonography to differentiate between cystic and solid abdominal masses. If the mass is solid, one should subsequently try to define its origin and extent and, depending on the initial sonographic findings, further imaging methods may be indicated. Many institutions follow a specific diagnostic protocol for solid childhood neoplasms including excretory urography, CT, and radionuclide bone scans. However, not all of these procedures may be necessary in some children with abdominal masses. It is essential to tailor the planned imaging procedures to each clinical situation and to gauge the potential effects these procedures might have upon patient management. For example, if neuroblastoma is suspected after clinical evaluation and sonography, it is essential to delineate the location and local extent of the lesion and to rule out distant disease. Neuroblastomas that appear to be localized to the adrenal gland and that are situated relatively anteriorly are not likely to have spinal canal involvement [4]; as a result, there may be no indication for metrizamide myelography and/or metrizamide CT in such patients. After an initial sonogram in these patients, confirmation of exact size and local extent of the lesion may be accomplished with a CT scan of good quality (using oral and intravenous contrast) *or* an MRI scan [5].

On the other hand, if the tumor appears to be paraspinal in location and/or the child has neurologic signs suggesting intraspinal extension, it is essential to evaluate the spinal canal and cord [4]. This can be accomplished by metrizamide myelography or metrizamide CT, but MRI may play a significant alternative role. Not only can the origin and size of the primary tumor be easily defined by MRI, MRI in the coronal plane also appears to be an excellent noninvasive method for evaluating intraspinal tumor extension and for determining the relation of the mass to the great vessels, without the use of contrast material.

Finally, some general comments can be made with respect to the current management of neuroblastoma [11]. Survival rates for early (stage I and II) disease are the same for surgery alone as for combinations of surgery with chemotherapy or radiotherapy. Hence, in patients with established early-stage disease, simple resection of the primary lesion is indicated. In more advanced stages, when the tumor is not completely resectable, chemo- and/or radiotherapy should be considered. Neuroblastoma is responsive to a variety of chemotherapeutic agents, and vincristine and cyclophosphamide are among the most effective. As with other childhood tumors, combination chemotherapy appears to be more effective than any single agent. Because of the varied therapeutic regimens that are now available, defining the extent of the tumor is particularly important and imaging techniques should also be used to assess the response to therapy. If the lesion in this patient had not responded to chemotherapy, radiotherapy could have been used. Alternatively, if the primary lesion had responded incompletely to therapy but had become smaller, a delayed surgical resection could have been considered.

REFERENCES

1. Miller RW. Fifty-two forms of childhood cancer: United States mortality experience, 1960–1966. *J Pediatr* **1969**;75:685–689
2. MacManus M. The diagnosis and staging of neuroblastoma. *Clin Radiol* **1983**;34:523–527
3. Stark DD, Moss AA, Brasch RC, et al. Neuroblastoma: diagnostic imaging and staging. *Radiology* **1983**;148:101–105
4. Armstrong EA, Harwood-Nash DCF, Ritz CR, Chuang SH, Pettersson H, Martin DJ. CT of neuroblastomas and ganglioneuromas in children. *AJR* **1982**;139:571–576
5. Fletcher BD, Kopiwoda ST, Strandjord SE, Nelson D, Pickering SP. Abdominal neuroblastoma: magnetic resonance imaging and tissue characterization. *Radiology* **1985**;155:699–703
6. Hricak H, Crooks L, Sheldon P, Kaufman L. Nuclear magnetic resonance imaging of the kidney. *Radiology* **1983**;146:425–432
7. Hricak H, Williams RD, Moon KL, et al. Nuclear magnetic resonance imaging of the kidney: renal masses. *Radiology* **1983**;147:765–772
8. Moon KL, Hricak H, Crooks LE, et al. Nuclear magnetic resonance imaging of the adrenal gland: a preliminary report. *Radiology* **1983**;147:155–160
9. Schultz CL, Haaga JR, Fletcher BD, Alfidi RJ, Schultz MA. Magnetic resonance imaging of the adrenal glands: a comparison with computed tomography. *AJR* **1984**;143:1234–1240
10. Cohen MD, Weetman R, Provisor A, et al. Magnetic resonance imaging of neuroblastoma with a 0.15-T magnet. *AJR* **1984**;143:1241–1248
11. Levine AS. *Cancer in the young*. New York: Masson, **1982**

Indium-111 Leukocyte Scanning Localization for Detecting Early Myocarditis in Kawasaki Disease

Michael R. Williamson,[1] Susan L. Williamson,[2] and Joanna J. Seibert[2]

Mucocutaneous lymph node syndrome is a multi-organ-system inflammatory disease of unknown cause. It is predominantly seen in children under age 5. Cardiac involvement is a prominent feature of the disease. Because Kawasaki disease initially presents as a fever of unknown origin, the diagnosis may be difficult and delayed while other entities are excluded. We have had the opportunity to perform indium-labeled leukocyte scans on four patients who were later diagnosed as having Kawasaki disease. All four patients showed diffuse cardiac activity. One representative case is presented.

Case Report

A 2-year-old boy had a 9-day history of fever to 40°C that was unresponsive to antibiotics, irritability, and tender hands. Physical examination showed edema of hands and feet and axillary adenopathy. Laboratory values revealed an erythrocyte sedimentation rate of 64/mm^3 and a platelet count of 507,000/mm^3. Admission electrocardiogram was normal. The next day, an ^{111}In leukocyte scan was performed using autologous white blood cells at a dose of 240 mCi (8880 MBq), based on a dosage range of 8–10 mCi/kg (296–370 MBq/kg). Diffuse uptake in the heart was noted at 3, 24, and 48 hr after injection (fig. 1). Myocarditis was suspected. An echocardiogram showed a prominent right coronary artery. The patient was discharged after 8 days with a diagnosis of Kawasaki disease.

Discussion

The clinical course of Kawasaki disease consists of three phases [1, 2]. The first lasts about 1–2 weeks and consists of lymphadenopathy, rash, fevers, and intense leukocytosis. The second phase lasts about 2–5 weeks and is usually identified by desquamation of the rash and joint involvement. The convalescent (third) phase lasts until the sedimentation rate is normal and all clinical signs have disappeared.

The diagnosis of Kawasaki disease is usually difficult and one of exclusion. We believe that diffuse cardiac activity on a labeled leukocyte scan in a febrile patient under age 5 should suggest the diagnosis of Kawasaki disease. There are no other laboratory or imaging tests that suggest the diagnosis in the early stages. Echocardiograms may detect coronary artery aneurysms only in the second stage of the disease [2].

Our four patients (aged 7–30 months) were all in the first or early subacute phases of the disease. In performing these studies, we acquired anterior images of the chest for 100,000 counts, which usually required about 6 min.

At autopsy, myocarditis has been a prominent finding [3]. The basic lesion at cardiac biopsy has been a round cell myocarditis with the severity of the myocarditis worse when the biopsy was performed within 5 months of onset of illness [4]. Since subclinical myocarditis is a basic pathologic feature

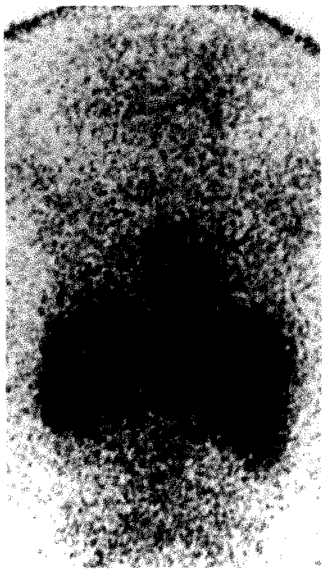

Fig. 1.—AP image over chest at 48 hr shows intense cardiac uptake.

Received July 22, 1985; accepted after revision October 16, 1985.

[1] Department of Radiology, University of Arkansas for Medical Sciences, 4301 W. Markham St., Little Rock, AR 72205. Address reprint requests to M. R. Williamson.

[2] Department of Radiology, Arkansas Children's Hospital, Little Rock, AR 72202.

AJR 146:255–256, February 1986 0361-803X/86/1462-0255 © American Roentgen Ray Society

of the early disease, an ^{111}In-labeled leukocyte scan may be the most sensitive way to diagnose the condition. (The electrocardiogram and echocardiogram are usually normal during the acute myocarditis.) Other diseases may also produce diffuse cardiac uptake on indium scanning, such as viral myocarditis [5], acute myocardial infarcts [6], or uremic pericarditis [7, 8]. Blood pool activity can also be a cause of diffuse uptake, but this can be excluded by obtaining a 48-hr scan. In none of our cases was this a factor. However, cardiac activity on a labeled leukocyte scan in the febrile child with other clinical criteria of Kawasaki disease will lead to the proper diagnosis.

Most deaths occur in the second stage of the illness and are secondary to coronary artery aneurysms with occlusion or invasion of the conduction system [4]. It may be possible to predict the severity of the cardiovascular manifestations on the basis of the intensity of the cardiac uptake.

In summary, we believe that ^{111}In leukocyte scans are very useful in diagnosing Kawasaki disease and may even have some prognostic significance.

REFERENCES

1. Baker A, Maggiolino R, Rothenberg R, et al. Kawasaki syndrome—United States. *MMWR* **1983**;32:98–100
2. Melish ME. Kawasaki syndrome: a new infectious disease? *J Infect Dis* **1981**;143:317–324
3. Fujiwara H, Hamashima Y. Pathology of the heart in Kawasaki disease. *Pediatrics* **1978**;61:100–107
4. Yutani C, Go S, Kaniya T, et al. Cardiac biopsy of Kawasaki disease. *Arch Pathol Lab Med* **1981**;105:470–473
5. McDougall IR, Baumert JE, Launtier RL. Evaluation of In-111 leukocyte whole body scanning. *AJR* **1979**;133:849–854
6. Thakur ML, Gottschalk A, Zaret BL. Imaging experimental myocardial infarction with indium-111-labeled autologous leukocytes: effects of infarct age and residual regional myocardial blood flow. *Circulation* **1979**;60:297–305
7. Goodgold HM, Gentilcore RC, Hendershott LR, Fletcher JW, Samuels LD. Significance of diffuse cardiac activity on indium-111 leukocyte scans. Presented at the annual meeting of the Radiological Society of North America, Washington, DC, November **1976**
8. McAfee JG, Samin A. In-111 labeled leukocytes: a review of problems in image interpretation. *Radiology* **1985**;155:221–229

Cavernous Sinus Invasion by Pituitary Adenomas

Jamshid Ahmadi[1]
Charles M. North[1]
Hervey D. Segall[1]
Chi-Shing Zee[1]
Martin H. Weiss[2]

One hundred ninety-eight surgically explored pituitary adenomas were evaluated preoperatively by high-resolution computed tomography (CT). At surgery, evidence of direct cavernous sinus invasion was demonstrated in 19. CT findings in these cases included cavernous sinus expansion (17 patients) and visible encasement of the internal carotid artery (14 patients). The invasive tumor often enhanced to a lesser degree than the cavernous sinuses and ipsilateral internal carotid artery. Intracavernous cranial nerve compression, obliteration, or displacement (14 patients), invasion of the lateral wall of the cavernous sinus (seven patients), and diffuse bone destruction (seven cases) were other findings. Magnetic resonance imaging in three patients provided excellent demonstration of intracavernous internal carotid artery encasement, but displacement and obliteration of intracavernous cranial nerves was not shown as well as it was with CT. Histologically, only three patients showed anaplastic features and only one of them had distant metastases. There was no correlation between histologic features, hormone assays, and invasiveness. This experience indicates any type of pituitary adenoma, regardless of its endocrinologic activity, can invade the cavernous sinus. Cavernous sinus involvement makes complete surgical removal difficult. Preoperative recognition of invasive behavior of these tumors has prognostic value and aids in designing appropriate management. CT is the most useful technique generally available for evaluation and follow-up.

Although invasive pituitary adenomas are known to exist, only rarely has the diagnosis of cavernous sinus invasion been made preoperatively [1–4]. Generally adenomas that penetrate into the cavernous sinus are difficult to resect completely, and they are associated with a greater risk of morbidity and mortality [4, 5]. Therefore, preoperative demonstration of cavernous sinus invasion may aid the neurosurgeon and endocrinologist in planning appropriate medical and surgical management. The purpose of this study was to determine the computed tomographic (CT) (and, more recently, magnetic resonance [MR] imaging) signs of cavernous sinus invasion. Such invasion was further correlated with tumor histopathology and hormone assays. We performed a retrospective review of high-resolution CT studies in 19 surgically documented cases of cavernous sinus invasion by pituitary tumor. Patients having bone invasion without cavernous sinus involvement were not included in this study.

Materials and Methods

Of 198 surgically explored pituitary adenomas evaluated by high-resolution CT, direct cavernous sinus involvement was demonstrated in 19. Six of these patients had had previous pituitary surgery. There were 14 men and five women (age range, 16–85 years). The CT studies were performed at three separate institutions affiliated with the University of Southern California School of Medicine and, hence, techniques differed. Fifteen patients were evaluated with a General Electric CT/T 8800 scanner using overlapping 5 mm collimation and 3 mm spacing. Two patients were scanned with a Picker 1200 SX scanner using 3 mm slice

This article appears in the November/December 1985 issue of *AJNR* and the February 1985 issue of *AJR*.

Received December 12, 1984; accepted after revision May 14, 1985.

[1] Department of Radiology, Section of Neuroradiology, University of Southern California School of Medicine, Los Angeles, CA 90033. Address reprint requests to J. Ahmadi, LAC/USC Medical Center, Box 2, 1200 N. State St., Los Angeles, CA 90033.

[2] Department of Neurological Surgery, University of Southern California School of Medicine, Los Angeles, CA 90033.

***AJR* 146:257–262, February 1986**
0361-803X/86/1462-0257
© American Roentgen Ray Society

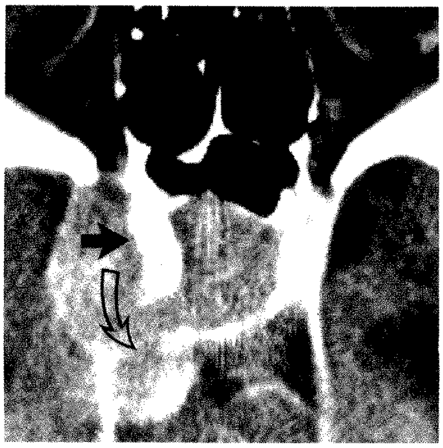

Fig. 1.—Pituitary adenocarcinoma extending into right cavernous sinus in 84-year-old patient. The intracavernous part of partly calcified internal carotid artery is engulfed and slightly displaced medially (*solid arrow*). Tumor had penetrated dural barrier a second time and extended into posterior fossa (*open arrow*).

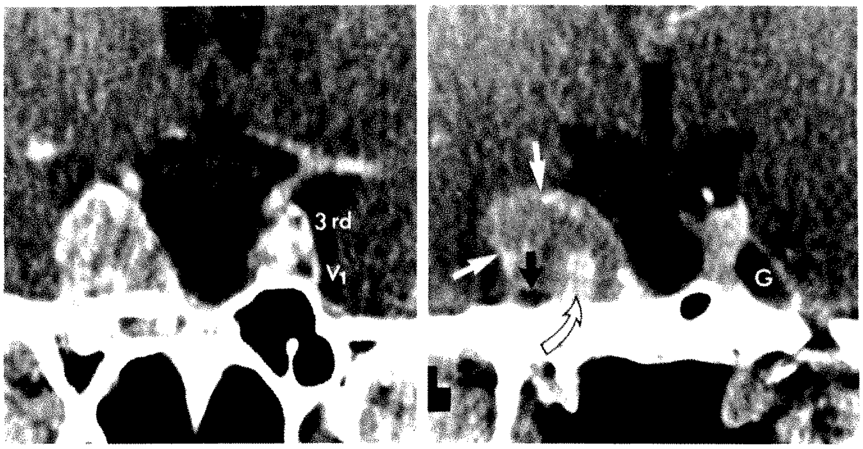

Fig. 2.—Null-cell adenoma. Intra- and suprasellar part of tumor was resected 2 months earlier. Obvious compression and partial obliteration of right gasserian ganglion (*black arrow*) and nerves V_1 and III (cf. normal appearances of these nerves on opposite side). Engulfment of intracavernous right internal carotid artery is also seen as it exits from carotid canal (*open arrow*). *White arrows* show where enhancing dura mater, which forms lateral margins of cavernous sinus, is interrupted with tumor bulging locally through and beyond this area. G = gasserian ganglion.

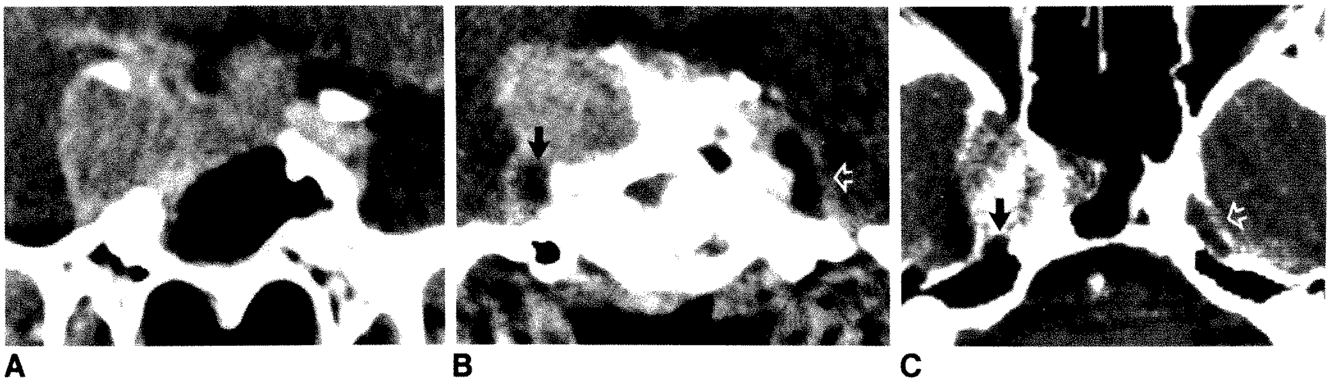

Fig. 3.—Prolactin-cell adenoma. Displacement and compression of right gasserian ganglion/V_1–V_2 complex (*solid arrows*) on both coronal (**A** and **B**) and axial (**C**) views. (Cf. opposite side [*open arrows*].)

thickness and 2 mm spacing. The other two patients were examined with a Philips Tomoscan 310 scanner using 3 mm collimation and 1.5 mm spacing. Nine patients were scanned in the axial plane only (with coronal and sagittal reformation), three in the direct coronal plane only, and the other seven in both coronal and axial planes. Most CT scans were obtained after rapid drip infusion of iodinated contrast material (Reno-M-DIP, 42.3 g I/300 ml solution). Four patients had an intravenous bolus plus a drip infusion of contrast material (71.3 g I). Three patients also had MR scanning. Medical records, including operative notes, of all these patients were reviewed. The results of pituitary hormone assays, histologic features of the surgical specimens, and CT were correlated. Surgical specimens in nine patients were also examined by immunohistologic staining techniques and electron microscopy.

Results

CT revealed unilateral involvement of the cavernous sinus in 14 patients, with bilateral invasion in the other five cases. Tumor size was variable. There was a suprasellar component (ranging from 1 to 6 cm above the diaphragma sellae) in 16 patients; three patients had no suprasellar extension. In 17 patients, invasion of the cavernous sinus through the lateral dural envelope of the sella resulted in varying degrees of cavernous sinus expansion with bulging of the lateral margin of the sinus. In seven of these patients, the tumors had grown outside of the cavernous sinus (having penetrated the dural barrier a second time) into the middle or posterior cranial fossa (figs. 1 and 2). Invasive tumor often enhanced to a lesser degree than did the cavernous sinuses and internal carotid artery. The intracavernous internal carotid artery was clearly demonstrated in 14 patients because it enhanced to a greater degree than did the surrounding tumor. In the other five patients, however, carotid artery engulfment was difficult to distinguish from adjacent tumor because of an almost equal degree of enhancement. A larger bolus of contrast material or dynamic scanning might have enabled demonstra-

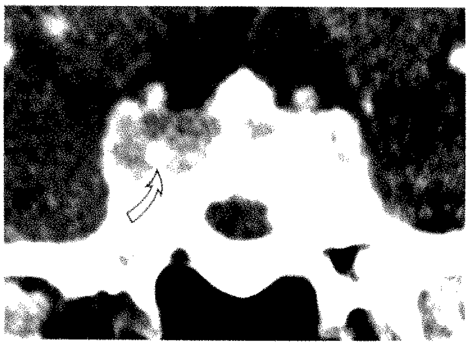

4

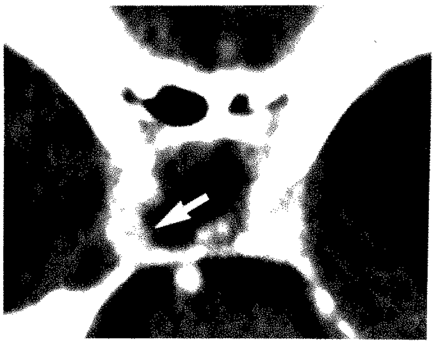

5

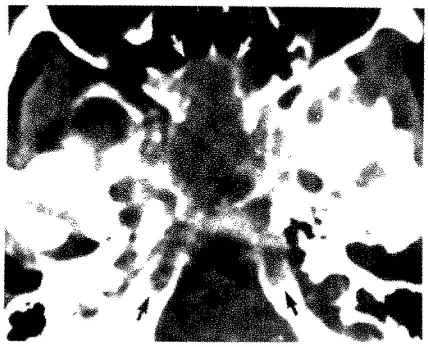

6

Fig. 4.—Corticotrophic cell adenoma. Rapid invasion of right cavernous sinus developed after bilateral adrenalectomy for control of hypercortisolism (Nelson syndrome). Displacement and engulfment of intracavernous right internal carotid artery (*arrow*) is readily visible because it enhances to a greater degree than surrounding tumor.

Fig. 5.—Corticotrophic cell microadenoma with recent pituitary apoplexy and infarction. Minimal extension into right cavernous sinus (*arrow*) without clearly evident increase in width of cavernous sinus. At this stage, it would be somewhat difficult to distinguish invasion from focal displacement of cavernous sinus.

Fig. 6.—Null-cell adenoma. Axial CT scan of base of skull reveals extensive destruction of sphenoid body, greater sphenoid wings, pterygoid plates, vomer, petrous apices, clivus, and basiocciput (*black arrows*). Tumor extends into sphenoid and posterior ethmoid sinuses (*white arrows*). Histologically, it had benign microscopic appearance.

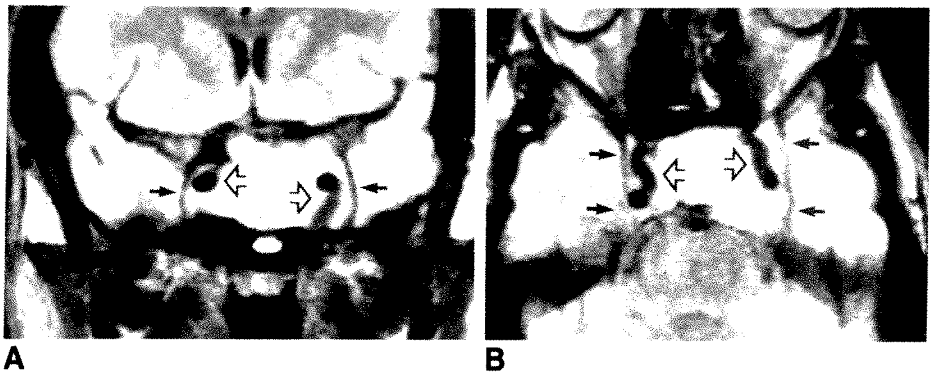

Fig. 7.—Null-cell adenoma. MR images. Coronal (**A**) and axial (**B**) spin-echo scans, 2 sec TR, 40 msec TE. Bilateral extension of pituitary tumor into cavernous sinuses, left greater than right (*solid arrows*), and engulfment of intracavernous internal carotid arteries (*open arrows*).

tion of the internal carotid artery in more of these cases had the study been performed prospectively.

Extension of the tumor into the cavernous sinus resulted in displacement, compression, or obliteration of the intracavernous cranial nerves in 14 patients (figs. 2 and 3). In 10 patients, both carotid artery engulfment and cranial nerve compression were present (fig. 2). In four patients, carotid artery engulfment could not be seen. However, compression of the intracavernous cranial nerves was present (fig. 3). In four patients, the carotid artery was visibly engulfed, but we were unable to detect compression of the cranial nerves (fig. 4). In only one patient was there neither expansion of the cavernous sinus nor engulfment or compression. In this case, invasion was exhibited by very subtle bulging into the cavernous sinus (fig. 5). This case presented the greatest difficulty in distinguishing extrinsic compression from invasion of the cavernous sinus. Direct coronal scans might have been more helpful in demonstrating subtle invasion. Nevertheless, invasion into the cavernous sinus was proven at surgery.

In six patients, the significance of osseous abnormalities could not be assessed easily because of previous transsphenoidal surgery. In seven of the other 13 patients, there were varying degrees of destruction of the sella and adjacent bones (fig. 6). The CT findings in these 19 patients were cavernous sinus expansion (17 patients), compression of the gasserian ganglion V_1 complex (14), visibly engulfed internal carotid artery (14), invasion of the lateral wall of the cavernous sinus (seven), and diffuse bone destruction (seven). (Diffuse bone destruction was evaluated in only 13 of the 19 patients because of difficulties involved in differentiating surgical changes from tumor invasion.) MR imaging in three patients clearly showed engulfment of the internal carotid artery by an invasive pituitary tumor. The low signal intensity of flowing blood in the carotid artery provided excellent contrast to the high signal intensity of the surrounding tumor (fig. 7).

The serum prolactin level was substantially elevated (ranging from 105 to 50,000 ng/ml) in only eight patients (table 1). Hypopituitarism was present before surgery in four patients. Histologic examination of surgical specimens showed benign pituitary adenoma in 16 patients. Histologically, marked cellular pleomorphism, multinuclear cells, and mitotic features were present in three patients, and only one of them had distant metastases (positive cerebrospinal fluid cytology and liver lesions).

TABLE 1: **Functional Classification of Invasive Pituitary Tumors**

Cell Types	No. of Cases ($n = 19$)	Level of Prolactin in ng/ml (Other Hormones)
Prolactin-cell adenoma	7	195–50,000
Corticotropic (ACTH) cell adenoma	2	11, 16 (ACTH: 4325, 342)
Growth-hormone- (GH) cell adenoma	1	12 (GH: 0.7)*
Mixed prolactin- and GH-cell adenoma	1	105 (GH: 45)
Null-cell adenoma	7	14–47
Adenocarcinoma	1	19

Note.—Normal values: prolactin, <20 ng/ml; ACTH, 10–100 ng/ml; GH, <1 ng/ml.

* In this patient, serum GH hormone was normal. However, GH granules were identified in the tumor by electron microscopy and immunocytologic staining. Similar cases have been well documented [6].

These patients have been followed for periods of 2 months to 5 years. Two patients with a small amount of cavernous sinus invasion had a total resection of their tumors with no recurrence (they have been followed 1½ and 3 years, respectively). Five patients were treated with bromocriptine and partial resection (the size of the residual tumor was reduced in three patients and remained unchanged in two other patients). Nine patients had partial resection followed by radiation therapy. There was a dramatic response to radiation therapy in two of the nine patients. Both of these patients had anaplastic features histopathologically. There was a minimal response to radiation therapy in another two. The residual tumor was unchanged in three patients and was actually larger in the other two. Two patients had partial resection and bromocriptine and radiation therapy. One of these had a mild response and the other had no response. One patient with cerebrospinal fluid and liver metastases died 2 months after the diagnosis of pituitary adenocarcinoma was documented.

Discussion

On the basis of their biologic behavior, tumors that originate in the adenohypophysis may be divided into expanding adenomas, invasive adenomas, and carcinomas [1–5, 7]. Most pituitary adenomas are slow-growing and tend to grow in an upward direction into the suprasellar cistern. Intrasellar expansion of these adenomas may erode the sella turcica and compress the cavernous sinuses laterally. The dura matter forming the medial walls of the cavernous sinus remains intact but is displaced somewhat because of pressure from the expanding pituitary adenoma. Most pituitary adenomas demonstrate a globular configuration regardless of their size. The diaphragma sellae, however, may impose a waistline indentation between the intrasellar and suprasellar components of large adenomas [5]. Occasionally, more rapid growth of one part of an adenoma results in an asymmetric configuration. Nodular outgrowths may burst (focally) through the thin mesodermal envelope (pituitary adenomas do not have a capsule) encasing the adenoma. This has been likened to a bud perforating the skin of a potato [5]. In some cases this nodular outgrowth may destroy adjacent structures by invading them.

Those tumors that invade directly into adjacent soft tissue and osseous structures are often referred to as "invasive pituitary adenomas" [1–5, 7]. Most of the invasive pituitary tumors in our series had a benign microscopic appearance, which demonstrates the poor correlation between biologically aggressive behavior and histopathologic features. A review of the literature revealed a diversity of opinion with regard to nomenclature in connection with pituitary adenomas. Several authors have indicated that features such as increased cellularity, cellular pleomorphism, and the presence of mitotic features are not necessarily proof of malignancy [2, 7–12]. They believe that the diagnosis of pituitary carcinoma can be considered conclusively only when distant metastases occur. Others consider anaplastic histopathologic features to be sufficient for the diagnosis of carcinoma [13–15].

Hardy [16] proposed a classification of pituitary tumors based on biologic behavior. Grade I is localized to the sella, grade II extends into the suprasellar cisterns, grade III refers to localized invasion of the floor of the sella, and grade IV indicates diffuse invasion. Grade V was added to indicate distant metastases [5]. Using this grading system our report basically consists of grade IV tumors, although one patient had progressed to grade V. Invasion of the sella turcica and adjacent bones may result in extensive destruction of the base of the skull. The tumor may extend into the nasopharynx or sphenoid and/or ethmoid sinuses. Posterior extension may lead to destruction of the clivus and petrous apices (fig. 6); occasionally it may be difficult to distinguish an invasive pituitary adenoma having such a destructive pattern from other neoplasms, such as metastases, chordomas, and nasopharyngeal carcinomas [17, 18]. Furthermore we have also seen meningiomas, as well as one glomangioma and one dysgerminoma, that invaded the cavernous sinus.

Although the abnormal serum levels of hormones produced by functional pituitary tumors generally correlate with the size of the tumor, there are occasions when a small tumor may be related to marked elevations of serum prolactin. Very high serum prolactin values (over 1000 ng/ml) have been implicated as strong evidence of invasion of pituitary adenomas into the cavernous sinuses [3, 19]. Nonetheless, a normal serum prolactin level may be seen with invasive pituitary tumors. In 11 of 19 cases of invasive pituitary tumors in our report, there was no significant elevation of serum prolactin values (table 1).

There is no rule that facilitates predicting when invasion of the surrounding structures will begin. In three of our patients as well as in a few other reports [16, 19], invasion of the cavernous sinus began when the tumor was small and was limited to the sellar region. Furthermore, one of our patients had cavernous sinus invasion only a few months after clinical onset of galactorrhea and amenorrhea. On the other hand, another patient had a 27 year history of pituitary adenoma before a diagnosis of cavernous sinus invasion was made. In our series and in others [2–4, 19] males predominated; more men than women appeared to have larger and more aggressive tumors. Symptoms such as decreased libido, impotence, and perhaps sterility tended to be either ignored by patients or undiagnosed. Therefore, in men the diagnosis of pituitary tumor is more likely to be made later, and consequently, the

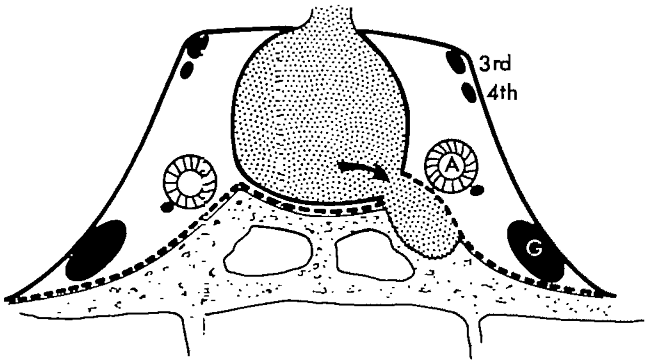

Fig. 8.—Coronal cross section of sellar region. Extradural subcavernous extension of pituitary tumor without invasion into cavernous sinus (*arrow*). Dura mater forming medial and lateral walls of cavernous sinus (*thick, solid line*); periosteal layer of dura (*broken line*). A = intracavernous internal carotid artery; G = gasserian ganglion.

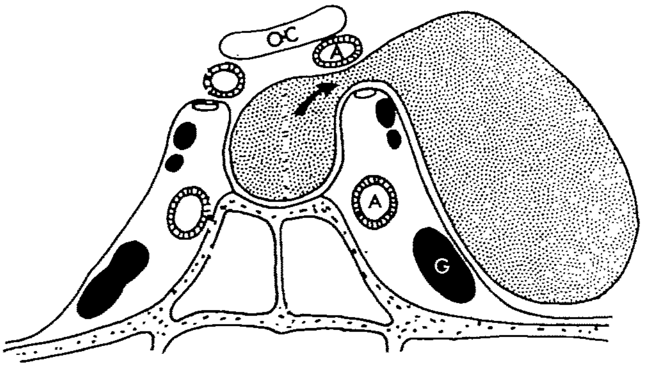

Fig. 9.—Intradural parasellar extension of pituitary tumor without invasion into cavernous sinus. Intracavernous cranial nerves and carotid artery (A) are not involved. OC = optic chiasm; G = gasserian ganglion.

tumor is usually considerably larger at presentation.

In evaluating pituitary tumors, careful attention should be paid to certain intracavernous structures. Appreciation of involvement of the intracavernous cranial nerves and/or carotid artery by tumor enabled a CT diagnosis of cavernous sinus invasion in 18 of the 19 cases in this series. Normally, the gasserian ganglion/V_1–V_2 complex is consistently demonstrated on CT as a relatively symmetric, oblong, intracavernous structure [20, 21]. Although in 14 of our patients there was partial obliteration or compression of the cranial nerves traversing the cavernous sinus, only six of our patients exhibited opthalmoplegia, trigeminal anesthesia, or pain.

The infrequency of cranial nerve signs and symptoms suggests that these tumors do not invade but rather displace or encircle the nerves. In addition, CT demonstration of visible engulfment of the intracavernous carotid artery, obliteration of the gasserian/V_1–V_2 complex, and direct penetration of the dura of the cavernous sinus aids in differentiating tumor invasion of the cavernous sinus from two other types of extension. On occasion, pituitary adenomas may displace the cavernous sinus laterally after perforating the dura at the junction of the floor of the sella and the cavernous sinus. Subcavernous extension of tumor, growing in an extradural location between the cavernous sinus and sphenoid bone, may develop without invasion into the cavernous sinus [4, 5] (fig. 8). Another possibility is upward expansion of a pituitary adenoma into the suprasellar cistern. The tumor may then extend laterally above the cavernous sinus. It may pass between either the supraclinoid carotid artery and the upper margin of the cavernous sinus or between the carotid artery and the optic chiasm. The adenoma then can extend into the middle cranial fossa intradurally and between the cavernous sinus on its medial aspect and the temporal lobe on its lateral aspect [7] (fig. 9). In either situation, intracavernous structures such as the carotid artery and the gasserian ganglion are neither engulfed nor compressed by tumor. This will help to differentiate cavernous sinus invasion from these two possible routes of tumor growth.

Cavernous sinus invasion by a pituitary tumor has been related to a relatively low surgical cure rate because of the complexities of surgical exploration when carried into the cavernous sinus [1–5, 7]. With preoperative recognition of cavernous sinus invasion by a pituitary tumor, particularly the commonly occurring prolactin-secreting tumor, one would attempt to reduce the size of the tumor by medical means in an effort to make surgical excision less difficult [22, 23]. When a good CT study has been obtained documenting a small amount of cavernous sinus invasion, an experienced neurosurgeon may be able to resect the tumor completely. Thus, CT is very helpful in surgical planning. In the case of larger tumors, where total resection has not been possible, CT enables recognition of persistent tumor and will be helpful in judging the response resulting from chemical manipulation or radiation therapy. CT is particularly valuable in the case of secretory-inactive adenomas where hormone markers are not present to enable evaluation for persistence of tumor in the cavernous sinus.

ACKNOWLEDGMENTS

We thank Vivian Chandrasoma, Department of Pathology, USC School of Medicine, who reviewed the histology of these patients; Richard Yadley, Robert Wycoff, and William Bradley, Department of Radiology, Huntington Memorial Hospital, who performed some of the CT and MR studies; and Andrea Kovacs and associates, who performed electron microscopy and immunocytochemistry in some of our cases.

REFERENCES

1. Jefferson G. The invasive adenomas of the anterior pituitary. *In: The Sherrington lectures*, vol. 3. Liverpool: University of Liverpool, 1955
2. Martins AN, Hayes GJ, Kempe LG. Invasive pituitary adenomas. *J Neurosurg* 1965;22:268–276
3. Lundberg PO, Drettner B, Hemmingsson A, Stenkvist B, Wide L. The invasive pituitary adenoma. A prolactin-producing tumor. *Arch Neurol* 1977;34:742–749
4. Symon L, Jakubowski J, Kendall B. Surgical treatment of giant

pituitary adenomas. *J Neurol Neurosurg Psychiatry* **1979**; 42:973–982

5. Wilson CB. Neurosurgical management of large and invasive pituitary tumors. In: Tindall GT, Collins WF, eds. *Clinical management of pituitary disorders*. New York: Raven, **1979**:335–342
6. Zimmerman EA, Defendini R, Frantz AG. Prolactin and growth hormone in patients with pituitary adenomas: a correlative study of hormone in tumor and plasma by immunoperoxidase technique and radioimmunoassay. *J Clin Endocrinol Metab* **1974**;38:577–585
7. Landolt AM, Wilson CB. Tumors of the sella and parasellar area in adults. In: Youmans JR, ed. *Neurological surgery*. Philadelphia: Saunders, **1982**:3107–3162
8. Epstein JA, Epstein BS, Molho L, Zimmerman HM. Carcinoma of the pituitary gland with metastases to the spinal cord and roots of the cauda equina. *J Neurosurg* **1964**;21:846–853
9. Madonick MJ, Rubinstein LJ, Dasco MR, et al. Chromophobe adenoma of pituitary gland with subarachnoid metastases. *Neurology* (NY) **1963**;13:836–840
10. Rubinstein LJ. Tumors of the central nervous system. In: *Atlas of tumor pathology*, 2d series, fasc 6. Washington, DC: Armed Forces Institute of Pathology, **1972**:313–314
11. Ogilvy KM, Jakubowski J. Intracranial dissemination of pituitary adenomas. *J Neurol Neurosurg Psychiatry* **1973**;36:199–205
12. Martin NA, Hales M, Wilson CB. Cerebellar metastases from a prolactinoma during treatment with bromocriptine. Case report. *J Neurosurg* **1981**;55:615–619
13. Wise BL, Brown HA, Naffziger HC, et al. Pituitary adenomas, carcinomas and craniopharyngiomas. *Surg Gynecol Obstet* **1955**;101:185–193
14. Newton TH, Burhenne HJ, Palubinskas AJ. Primary carcinoma of the pituitary. *AJR* **1962**;87:110–119
15. D'Abrera VStE, Burke WJ, Bleasel KF, Bader L. Carcinoma of the pituitary gland. *J Pathol* **1973**;109:335–343
16. Hardy J. Transsphenoidal microsurgical treatment of pituitary tumors. In: Linfoot JA, ed. *Recent advances in the diagnosis and treatment of pituitary tumors*. New York: Raven, **1979**:375–388
17. Virapongse C, Bhimani S, Sarwar M, Greenberg A, Kim J. Prolactin-secreting pituitary adenomas: CT appearance in diffuse invasion. *Radiology* **1984**;154:447–451
18. Kendall BE, Lee BCP. Cranial chordomas. *Br J Radiol* **1977**;50:687–698
19. Shucart WA. Implications of very high serum prolactin levels associated with pituitary tumors. *J Neurosurg* **1980**;52:226–228
20. Kline LB, Acker JD, Post MJD, Vitek JJ. The cavernous sinus: a computed tomographic study. *AJNR* **1981**;2:299–305
21. Hasso AN, Pop PM, Thompson JR, et al. High resolution thin section computed tomography of the cavernous sinus. *Radiographics* **1982**;2:83–100
22. Weiss MH. Medical and surgical management of functional pituitary tumors. *Clin Neurosurg* **1981**;28:374–383
23. Vassilouthis J, Richardson AE. Prolactin levels in aggressive pituitary tumors. *J Neurosurg* **1980**;53:131–132

Computed Tomographic Demonstration of the Posterior Pituitary

Jean-François Bonneville[1]
Françoise Cattin
Claudine Portha
Evelyne Cuenin
Philippe Clere
Brigitte Bartholomot

From a series of 700 thin, axial, contrast-enhanced CT scans of the sellar region, the posterior lobe of the pituitary was studied. Empty sellae and pituitary lesions larger than 8 mm in diameter were excluded from the study. Of the 320 remaining axial contrast-enhanced CT scans, the posterior lobe of the pituitary was apparent in 124 (39%) as an oval lucency 3–4 mm thick, located medially or paramedially just in front of the dorsum sellae. Normally, the anterior limit of the posterior lobe is always regularly convex forward, but in the presence of a microadenoma of the anterior lobe it may be compressed. The lesser enhancement of the posterior lobe probably correlates with the different volumes of the interstitial spaces in the anterior and in the posterior lobes. The normal picture of the posterior lobe of the pituitary must not be confused with a posteriorly located microadenoma.

The development, histology, blood supply, and function of the posterior lobe of the pituitary gland are very different from those of the anterior lobe. While the anterior lobe is derived from the ectoderm of the stomodeum, the neurohypophysis is derived from the neural ectoderm of the floor of the forebrain. The neurohypophysis is composed of the posterior lobe, the neural part of the stalk, and the expanded upper end of the stalk, which is the median eminence [1]. The object of this report is to describe our computed tomographic (CT) observations of the posterior lobe of the hypophysis.

Materials and Methods

We reviewed 1600 thin coronal and/or axial CT examinations of the pituitary gland, including 700 thin axial CT examinations. In our department, CT of the pituitary gland is performed with a GE CT/8 8800 or 9800 scanner, mainly using 1.5 mm, thin, coronal sections; for the past 2 years CT has been performed in the dynamic mode after intravenous injection of 60 ml of a 32% iodinated contrast medium [2, 3]. Axial sections are only obtained in special conditions. If they are needed, a perfusion of 100 ml of contrast material is given intravenously after the bolus injection to maintain the plasma iodine level during the procedure. The head of the patient is positioned so that the petrous bones are not included in the sections (−10° to −20° to the orbitomeatal line). The gantry is generally not angulated. All images were targeted. Of the 700 cases, 320 constitute the material of this study of posterior pituitary gland.

Results

From a series of 700 thin, axial, contrast-enhanced CT studies of the pituitary gland, we eliminated all patients whose scans showed an empty sella or a pituitary adenoma more than 8 mm in diameter; as a result, 320 patients were analyzed in this study of the posterior lobe of the pituitary. The posterior lobe was clearly identified as a well defined oval lucency in 124 patients (39%). This area of low attenuation is located in the posterior part of the sella, just in front of the dorsum.

This article appears in the November/December 1985 issue of *AJNR* and the February 1986 issue of *AJR*.

Received October 3, 1984; accepted after revision March 20, 1985.

Presented at the annual meeting of the American Society of Neuroradiology, Boston, June 1984.

---

[1] All authors: Department of Neuroradiology, University Hospital of Besançon, 25030 Besançon, France. Address reprint requests to J-F Bonneville.

***AJR* 146:263–266, February 1986**
0361–803X/86/1462–0263

© American Roentgen Ray Society

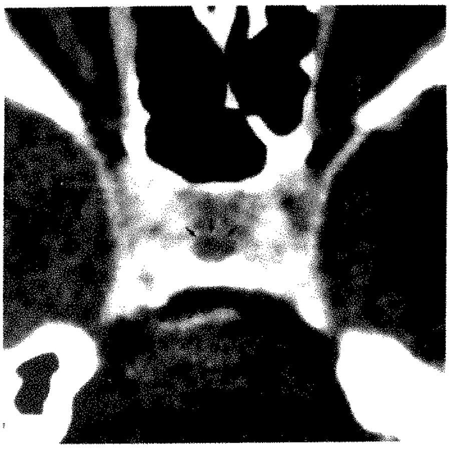

Fig. 1.—Contrast-enhanced 1.5-mm-thick axial CT scan through pituitary. Posterior lobe is oval lucency at posterior part of sella (*arrows*).

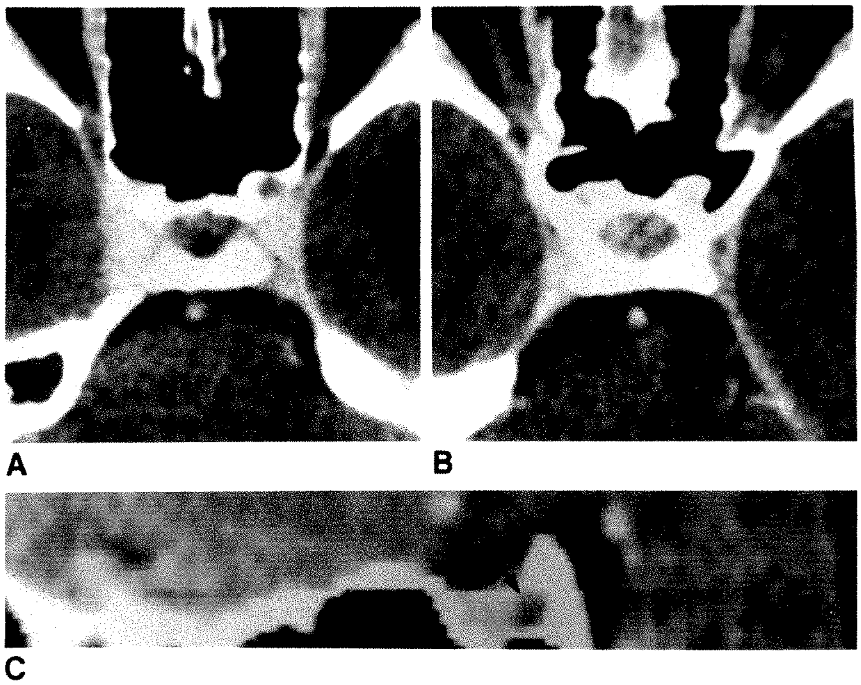

Fig. 2.—**A** and **B**, 1.5-mm-thick contiguous axial scans through pituitary. Posterior lobe is apparent only in **A** and is not visible on upper cut through pituitary (**B**). **C**, Sagittal reconstruction of sellar region. Posterior lobe appears as low-density area just in front of dorsum (*arrow*).

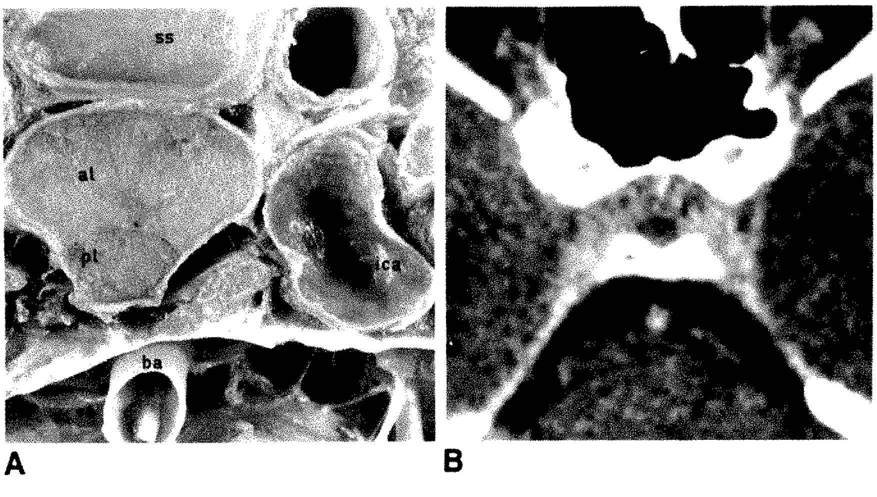

Fig. 3.—**A**, Anatomic specimen, axial section. Posterior lobe (pl) is invested on each side by dorsal extension of anterior lobe (al). ss = sphenoid sinus; ica = internal carotid artery; ba = basilar artery. **B**, CT scan of posterior lobe, axial section. Regular convexity of anterior border

When clearly identified (124 cases), the posterior lobe measured 5–6 mm by 3–4 mm (fig. 1) in all cases. In 26% of the selected procedures, the posterior lobe of the pituitary was poorly seen so that its size could not be measured accurately. In 34% of the procedures the posterior lobe was not identified at all. When demonstrated the posterior pituitary was generally apparent on only one or two 1.5-mm-thick contiguous sections. We were never able to identify the posterior lobe on the uppermost cut through the pituitary (figs. 2A and 2B). This may be explained in part by the fact that the top of the posterior lobe is covered by some tissue of the pars anterior [1] and by partial-volume averaging of the posterior lobe at the sellar diaphragm level. Sagittally reformatted images (fig. 2C) may also show the posterior lobe well.

The anterior limit of the posterior lobe of the pituitary is always regularly convex forward in normal cases (fig. 3) and is invested by dorsal extension of the anterior lobe on each side. In the presence of a microadenoma of the anterior lobe, the anterior limit of the posterior lobe may or may not be compressed (figs. 4 and 5). The posterior lobe border is often

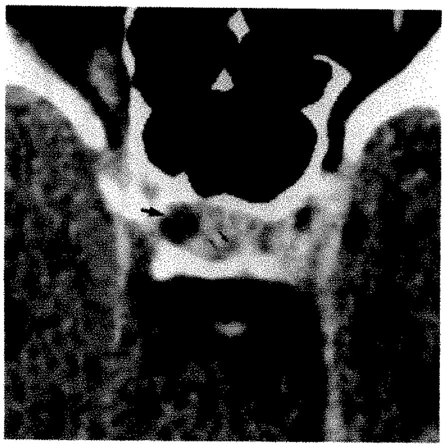

4

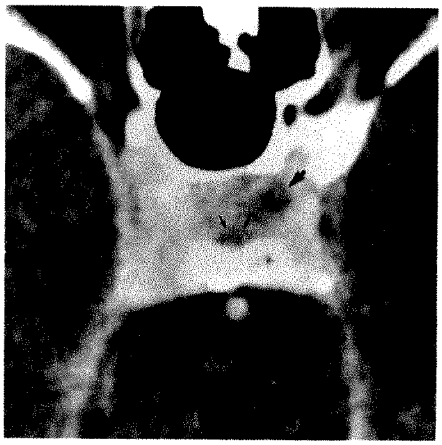

5

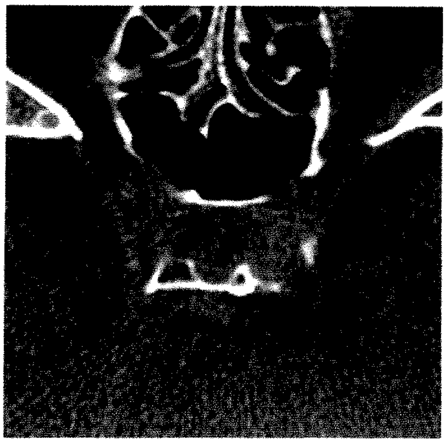

6

Fig. 4.—Flattening of right side of posterior lobe (*small arrows*) by right intrasellar prolactinoma (*large arrow*).

Fig. 5.—Left intrasellar microadenoma (*large arrow*) without any change of posterior lobe (*small arrows*).

Fig. 6.—Axial CT section through dorsum sellae (bone window). Imprint of posterior lobe on anterior aspect of dorsum.

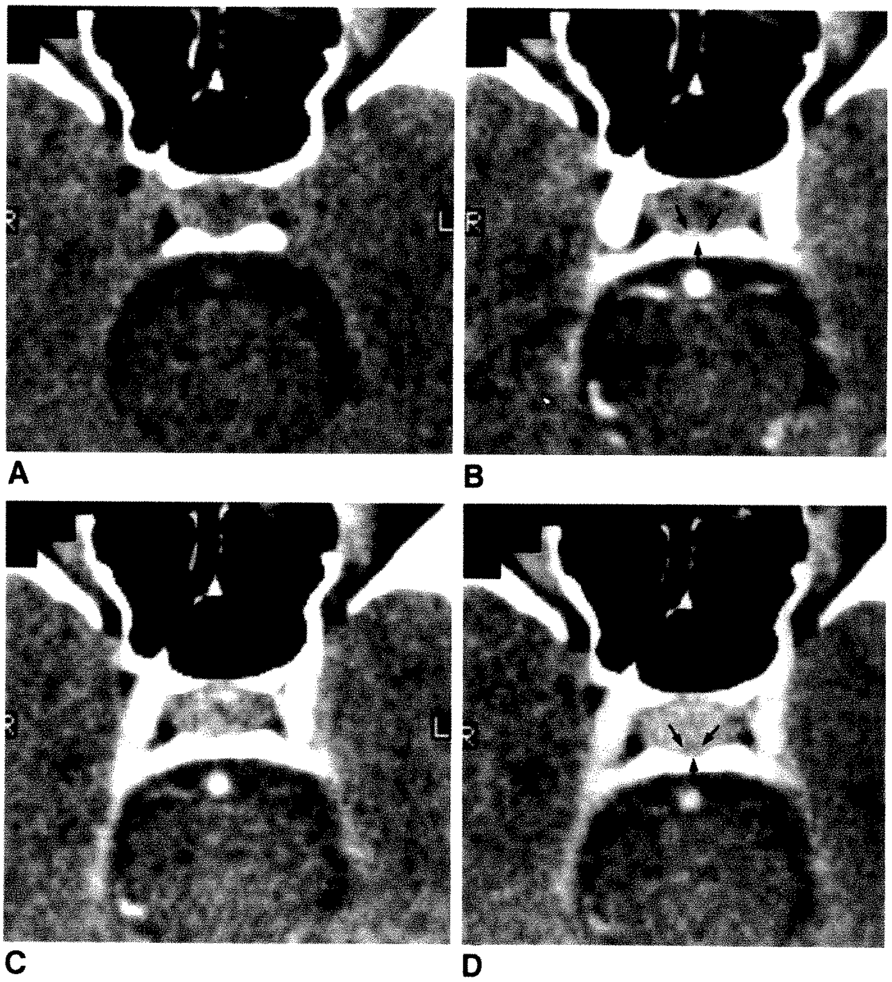

Fig. 7.—Axial dynamic CT scans of pituitary. **A**, Before bolus injection. **B**, 10 sec after bolus injection. Opacification of intracavernous carotid arteries and enhancement of intravascular compartment of posterior lobe (*arrows*). **C**, 20 sec after bolus injection. Enhancement of anterior pituitary. Posterior lobe is not seen clearly. **D**, 50 sec after bolus injection. Maximal enhancement of anterior lobe. Posterior lobe appears as low-density area (*arrows*).

located just in front of a concave imprint of the dorsum (fig. 6). This imprint is midline in only 50% of the cases [4]. In the other cases, the center of the imprint of the dorsum and the center of the posterior lobe can be situated as far as 3 mm from the midline. The findings using dynamic axial CT (figs. 7 and 8), although not part of our 320 cases, are included to

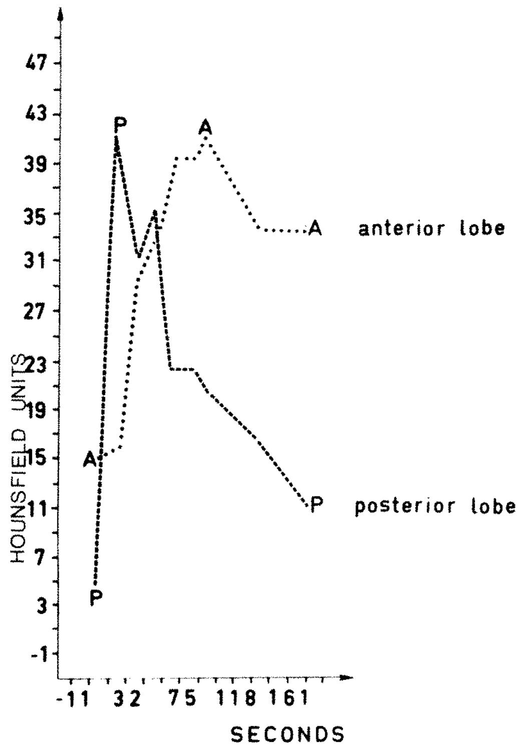

Fig. 8.—Time-density curves for anterior lobe and posterior lobe of pituitary gland. *Y* axis is labeled in Hounsfield units.

explain the appearance of the posterior part of the pituitary. Figures 7 and 8 are from a series of 20 dynamic axial CT scans obtained in normal patients.

Discussion

Our investigation indicates that in nearly 40% of cases the posterior pituitary will appear on thin, axial, contrast-enhanced CT scans as a low-density area in the posterior part of the sella (figs. 1–4). This area of low attenuation must not be confused with a posteriorly located pituitary microadenoma. In addition, we have noted that the position of the posterior pituitary corresponds in location to the indentation on the dorsum (fig. 6). We have found that the posterior lobe is best demonstrated when it is prominent in size and when there is a wide superior bony aperture of the sella. Low-density areas reported in the literature as probable incidental microadenomas [5] are, in our opinion, more likely to represent large but normal neurohypophyses. A normal posterior lobe should therefore be added to the list of regions of low density on contrast-enhanced CT scans of the pituitary gland.

The whole pituitary gland resides outside the blood-brain barrier [6]. After a bolus injection of contrast medium, as shown by axial dynamic CT (figs. 7 and 8), the intravascular compartment of the posterior lobe is opacified first, because of its direct arterial blood supply through the meningohypophyseal trunk [7]. This agrees with the observations of Wislocki [8]. But, at some time after the injection, when the contrast medium equilibrates between the intravascular and extravascular interstitial spaces, less enhancement of the posterior lobe is present (figs. 7 and 8), which may correlate with the lesser volume of the interstitial spaces of the posterior lobe [9]. We believe that these data explain our observations that the posterior lobe of the pituitary gland appears less enhanced than the anterior lobe after routine injection of contrast material.

ACKNOWLEDGMENTS

We thank the technical staff of the Department of Neuororadiology for their contributions and Michel Gaudron for photographic work.

REFERENCES

1. Williams PL, Warwick R, eds. *Gray's anatomy*, 36th ed. New York: Churchill Livingstone, **1980**:1439–1442
2. Bonneville JF, Poulignot D, Cattin F, Couturier M, Mollet E, Dietemann JL. Computed tomographic demonstration of the effects of bromocriptine on pituitary microadenoma size. *Radiology* **1982**;143:451–455
3. Bonneville JF, Cattin F, Moussa-Bacha K, Portha C. Dynamic computed tomography of the pituitary gland: the "tuft sign." *Radiology* **1984**;147:145–148
4. Wortzman G, Rewcastle NB. Tomographic abnormalities simulating pituitary microadenomas. *AJNR* **1982**;3:505–512
5. Chambers EF, Turski PA, LaMasters D, Newton TH. Regions of low density in the contrast-enhanced pituitary gland: normal and pathologic processes. *Radiology* **1982**;144:109–113
6. Sage MR. Review. Kinetics of water-soluble contrast media in the central nervous system. *AJNR* **1983**;4:897–906, *AJR* **1983**;141:815–824
7. Xuereb GP, Prichard MML, Daniel PM. The hypophysial portal system of vessels in man. *Q J Exp Physiol* **1954**;39:219–230
8. Wislocki GB. The vascular supply of the hypophysis cerebri of the rhesus monkey and man. *Res Publ Assoc Nerv Ment Dis* **1938**;17:48–68
9. Roppolo HMN, Latchaw RE. Normal pituitary gland: 2. Microscopic anatomy—CT correlation. *AJNR* **1983**;4:937–944

Intracranial Calcification in Adults with Chronic Lead Exposure

Patricio F. Reyes[1, 2]
Carlos F. Gonzalez[3]
Malgorzata K. Zalewska[1]
Anatole Besarab[4]

Computed tomographic (CT) findings of cerebral and cerebellar calcification are described in three American adults with raised serum lead levels and known exposure to lead for 30 or more years. Calcification patterns were punctiform, curvilinear, speck-like, and diffuse and were found in the subcortical area, basal ganglia, vermis, and cerebellum. Admission serum lead levels ranged from 54 to 72 μg/dl (normal, 0–30 μg/dl). Nonspecific neurologic manifestations consisted of dementia, diminished visual acuity, peripheral neuropathy, syncope, dizziness, nystagmus, easy fatigue, and back pain. Two patients developed chronic renal disease and hypertension; in both cases, serum parathormone was elevated. Blood, calcium, and phosphorus were normal in all three. No other structural abnormalities were observed with CT. Although the pathophysiologic mechanism of these findings remains poorly understood, it is suggested that chronic lead exposure should be included in the differential diagnosis of unexplained intracranial calcifications in adults.

Clinical and experimental data have convincingly shown that repeated exposure to excessive amounts of inorganic lead can result in dose-related dysfunction of the central nervous system (CNS), kidneys, bone marrow, peripheral nerves, muscles, endocrine glands, and joints [1–4]. Exposure usually occurs through inhalation, although more recently, human respiratory absorption has been confirmed [1]. It has also been suggested that ingestion may become a more important route in heavy metal intoxication as air lead levels are better controlled [5]. Other possible sources of poisoning could come from retained bullets in the body, inadequately fired ceramics, indoor firing ranges, cosmetics, and herbal medicinals [6–9]. Several studies have demonstrated significantly higher incidences of neuropsychiatric manifestations in patients with known chronic lead exposure and elevated serum lead levels [1, 2, 10]. These symptoms include headache, dizziness, fatigue, depression, irritability, insomnia, and diminished libido. The nonspecificity of these complaints does not commonly alert clinicians that lead is the offending agent unless occupational risks are previously known. In our review of the literature, we found a single pathologic study that reported increased cerebellar calcification using autopsy material from patients with increased blood lead levels [11]. All of them were from Queensland, Australia, and in three patients cerebellar calcium deposits were verified by computed tomography (CT) [12]. In this report we describe three American adults who worked in a lead smelting plant for several years, had elevated serum lead levels, and were found to have subcortical, basal ganglionic, and cerebellar calcifications.

Case Reports

Case 1

A 56-year-old man had worked in a lead smelting plant for 31 years. Several serum lead levels were elevated, and on admission his level was 72 μg/dl (normal, 0–30 μg/dl). BUN,

This article appears in the November/December 1985 issue of *AJNR* and the February 1986 issue of *AJR*.

Received October 24, 1984; accepted April 26, 1985.

[1] Departments of Neurology and Pathology, Thomas Jefferson University, 1025 Walnut St., Room 503, Philadelphia, PA 19107. Address reprint requests to P. F. Reyes.

[2] Department of Neurology, Coatesville Veterans Administration Medical Center, Coatesville, PA 19320.

[3] Department of Radiology, Thomas Jefferson University, Philadelphia, PA 19107.

[4] Department of Medicine, Thomas Jefferson University, Philadelphia, PA 19107.

AJR 146:267–270, February 1986
0361–803X/86/1462–0267
© American Roentgen Ray Society

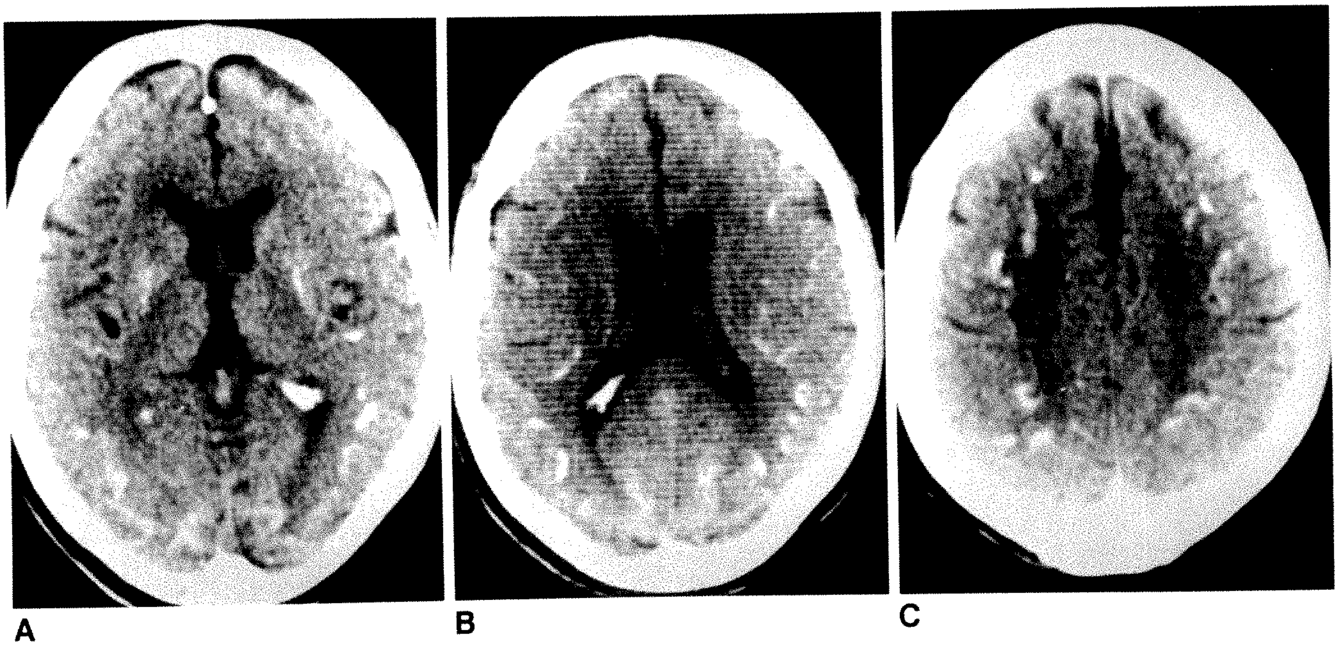

Fig. 1.—Case 1. **A**, Axial CT scan at lower level. Specklike calcifications in both thalamic regions; punctiform calcification in occipital cortex. **B**, Level of midventricular region. Multiple specklike and curvilinear calcifications involving subcortical area in both occipital lobes. Ventricular size is slightly enlarged; there is minimal degree of cortical brain atrophy. **C**, Centrum semiovale. Similar subcortical calcifications involving both cerebral hemispheres.

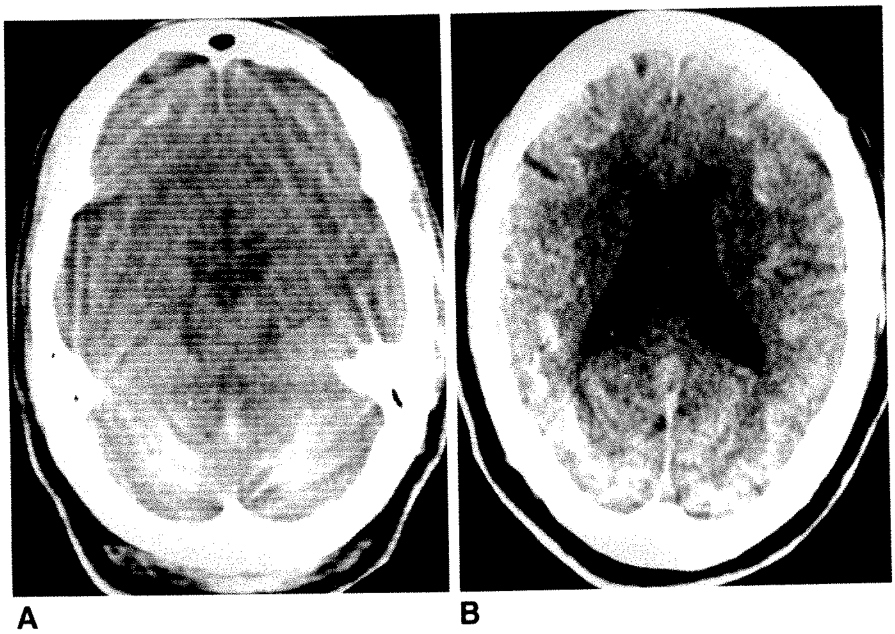

Fig. 2.—Case 2. **A**, Lower axial scan of posterior fossa. Multiple calcifications in vermis and in both cerebellar hemispheres. **B**, Higher section at midventricular level. Multiple subcortical calcifications involving both cerebral hemispheres are more prominent in occipital region.

creatinine, serum calcium, phosphorus, and parathormone values were normal. His neurologic examination revealed evidence of dementia and peripheral neuropathy. CT showed multiple punctiform and curvilinear calcifications in the subcortical area and basal ganglia (fig. 1).

Case 2

A 57-year-old man had worked in a lead smelting plant for 34 years. At one point he had a serum level of 102 μg/dl. He was advised to retire in 1979, after he developed renal disease and hypertension. On admission, he had elevated serum lead level, 66 μg/dl; BUN, 31.0 mg/dl (normal, 12–27 mg/dl); creatinine, 3.2 mg/dl (normal, 0.7–1.4 mg/dl); and parathormone, 546 pg/dl (normal, 80–375 pg/dl). Serum calcium and phosphorus were normal. Neurologic evaluation showed recent memory loss, decreased visual acuity in one eye, and diminished vibration and proprioception distally in the arms. He also complained of intermittent dizziness. CT revealed curvilinear calcifications in the subcortical region, vermis, and cerebellar hemispheres (fig. 2).

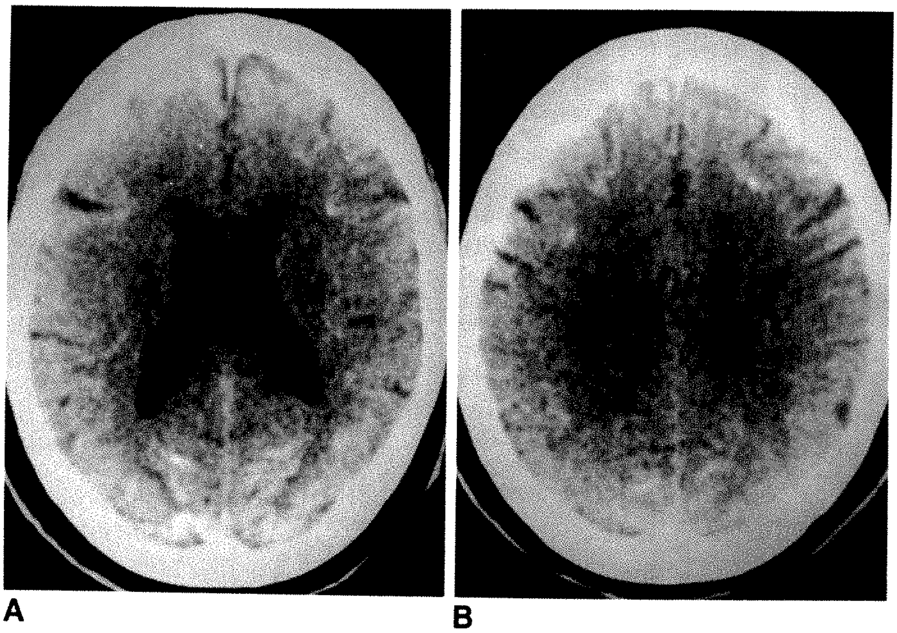

Fig. 3.—Case 3. **A**, Axial scan at midventricular level. Multiple calcifications in subcortical white matter of both cerebral hemispheres. **B**, Higher section. Few specklike punctiform calcifications in subcortical area in both cerebral hemispheres, predominantly in frontoparietal region.

Case 3

A 54-year-old man had worked in a lead smelting plant for 30 years. He had had elevated serum lead levels since 1974. He retired in 1979 because of renal disease and hypertension. He later developed gouty arthritis. His laboratory studies revealed blood glucose, 160 mg/dl (normal, 60–110 mg/dl); uric acid, 10.6 mg/dl (normal, 3.5–8.0 mg/dl); creatinine, 3.2 mg/dl (normal, 0.7–1.4 mg/dl); serum lead level, 54 μg/dl; and parathormone, 638 pg/dl. Serum calcium and phosphorus were within normal limits. On neurologic examination he had memory loss for recent and remote events, diminished comprehension, horizontal nystagmus, bilateral decreased visual acuity, and signs of peripheral neuropathy. He also gave a history of syncopal episodes, easy fatigue, and back pains. CT demonstrated multiple specklike calcifications in the subcortical region and diffuse calcification in the cerebellum (fig. 3).

Discussion

Intracranial calcification occurs in physiologic and pathologic conditions. Some structures or parts of the brain normally calcify after a certain age, and these include the pineal gland, choroid plexus, dura habenula, and blood vessels [13]. In abnormal states, calcium deposition is often categorized into dystrophic and metastatic types [14]. By definition, dystrophic calcification develops in damaged CNS tissues that are bathed by extracellular fluid containing normal levels of calcium and phosphate. This can be seen in ischemic infarction and degenerative disorders wherein the plasma membrane of cells has been rendered more permeable to calcium. In contrast, the metastatic variety is accompanied by hypercalcemia, which predisposes the normal brain parenchyma to deposition of calcium salts. The calcium equilibrium across the membrane is presumably altered so that more calcium enters the cell. In both processes, the final result is the formation of an insoluble calcium phosphate mineral in the form of hydroxyapatite [14]. When these calcium deposits reach a certain size, they can be imaged by neuroradiologic methods such as CT. In many instances, the size, distribution, and pattern of calcification observed on a brain CT scan help clinicians identify neuroanatomic landmarks and confirm their suspicion of pathologic processes.

Calcification of the cerebellum in patients with chronic lead exposure was recently demonstrated in Queensland, Australia, by postmortem studies [11]. These findings were subsequently confirmed by cerebral CT in similar patients who came from the same area [12]. Most recently, in North America, Swartz et al. [15] described cortical calcific deposits in the cerebrum in a patient who had chronic renal disease and occupational history of lead exposure. In their patient, serum lead levels were persistently within normal limits and parathormone levels were markedly elevated. They implied that chronic renal disease, increased serum calcium, and increased circulating parathormone may have led to deposition of calcium salts within the brain parenchyma. The clinical and radiographic features of our cases were different. All our patients had documented exposure to lead at work for several years and toxic lead levels in the serum. Chronic renal disease in two cases was believed to be related to chronic lead toxicity, and both patients had hypertension. In one patient neither hypertension nor renal disease was reported. Signs and symptoms of cerebrovascular disease were absent. We were the first to show basal ganglionic and curvilinear cerebral subcortical calcification in such groups of patients. We also found similar cerebellar lesions as described by Graham et al. [12].

Although CNS lesions in acute lead poisoning are well known, the mechanism of toxicity in subacute and chronic human cases is poorly understood. This is largely because the brain abnormalities seen after prolonged exposure to lead are frequently accompanied by pathologic changes in the kidneys, blood vessels, and other visceral organs. In the series of Henderson [10], 60% of lead-intoxicated children followed longitudinally died of either renal or vascular disease. The studies of Tonge et al. [11] that showed calcium deposits around cerebellar arteries and arterioles along the horizontal fissures correlate well with the CT pattern of cerebellar calcification we described in our patients. Using histochemical techniques, they further suggested that transudation of polysaccharides across blood vessels occurs in acute lead toxicity, and the deposition of calcium salts ensues at a later stage [16]. This mechanism would also explain the cerebral subcortical and basal ganglionic calcifications in our cases. However, it is important to remember that, in certain instances, calcium deposits can be verified only by microscopy and, therefore, may not be seen by the usual radiographic technique.

It is not possible for us to relate our CT findings to any particular biochemical or local structural abnormality. Parathormone level was increased in only two cases, while the serum calcium and phosphorus values were normal in all three. The latter measurements, however, do not exclude the possibility that hypercalcemia and metastatic calcification occurred in the past. It is also difficult to suggest that calcium deposition developed in previously damaged brain parenchyma. The CT studies did not reveal other focal lesions, and neurologic deficits referable to the calcified areas were absent. To clarify these important issues, we need to follow patients with known acute and chronic lead exposure longitudinally using various neurodiagnostic methods and collect postmortem tissue for histologic and biochemical studies. However, despite the absence of an acceptable pathophysiologic mechanism, we suggest that chronic lead exposure should be considered one of the etiologic factors of intracranial calcification.

REFERENCES

1. Cullen MR, Robins JM, Eskenazi B. Adult inorganic lead intoxication: presentation of 31 new cases and a review of recent advances in the literature. *Medicine* (Baltimore) **1983**;62:221–247
2. Whitfield CL, Ch'ien LT, Whitehead JD. Lead encephenlopathy in adults. *Am J Med* **1972**;52:289–298
3. Hanninen H. Behavioral effect of occupational exposure to mercury and lead. *Acta Neurol Scand [Suppl]* **1982**;66:167–175
4. Seppalainen AM. Lead poisoning: neurophysiological aspects. *Acta Neurol [Suppl]* **1982**;66:177–184
5. Roels H, Buchet JP, True J, Croquet F, Lauwreys R. The possible role of direct ingestion on the overall absorption of cadmium and arsenic in workers exposed to CdO or As 203 dust. *Am J Ind Med* **1982**;3:53–65
6. Linden MA, Manton WI, Stewart RM, Thal ER, Feit H. Lead poisoning from retained bullets. *Ann Surg* **1982**;195:305–313
7. Brearley RL, Forsythe AM. Lead poisoning from aphrodisiacs: potential hazards in immigrants. *Br Med J* **1978**;2:1748–1749
8. Fischbein A, Rice C, Sarkozi L, Kon SH, Petrocci M, Selikoff IJ. Exposure to lead in firing ranges. *JAMA* **1979**;241:1141–1144
9. Graziano JH, Leong JK, Friedheim E. 2, 3-dimercaptosuccinic acid: a new agent for the treatment of lead poisoning. *J Pharmacol Exp Ther* **1978**;206:696–700
10. Henderson DA. A follow-up of cases of plumbism in children. *Aust Nz J Med* **1954**;3:219–234
11. Tonge JI, Burry AF, Saal JR. Cerebellar calcification: a possible marker of lead poisoning. *Pathology* **1977**;9:289–300
12. Graham J, Jayasinghe L, Baddeley H. Cerebellar calcifications. *Diagn Imag Clin Med* **1981**;50:99–106
13. Taveras JM, Wood FH. The skull. In: Taveras JM, Wood EH, eds. *Diagnostic neuroradiology.* Baltimore: Williams & Wilkins, **1976**:205–230
14. Anderson HC. Calcific disease. *Arch Pathol Lab Med* **1983**;107:341–348
15. Swartz JD, Faerber EN, Singh N, Polinsky MS. CT demonstration of cerebral cortical calcifications. *J Comput Assist Tomogr* **1983**;7:476–479
16. Saal JR, Coombe IF, Thomas BW, Tonge JI, Burry AF. Cerebellar calcification ultrastructure and histochemistry. *Pathology* **1978**;10:351–363

Radiographic Findings in 32 Cases of Primary CNS Lymphoma

Clifford R. Jack, Jr.[1]
David F. Reese[1]
Bernd W. Scheithauer[2]

Computed tomographic (CT) or angiographic (or both) findings were analyzed in 32 cases of pathologically proved primary non-Hodgkin lymphoma of the central nervous system. CT scans were available in 28 of the 32 cases. Thirty lesions were found in the 28 cases. In comparison with previous literature, the frequency of involvement of deep central structures (30%), multiple lesions (11%), and subependymal lesions (4%) was lower and that of lesions in the periphery of the supratentorial compartment was higher (46%). In agreement with previous literature, most of the lesions were of increased density (63%), enhanced (100%), and enhanced homogeneously (71%). Twenty-nine of the 32 patients underwent cerebral angiography. In 12 patients, a homogeneous vascular stain was found that appeared in the late arterial or early venous phase and had a meningiomalike pattern. This staining pattern has not been emphasized sufficiently in previous literature. It was believed that such an angiographic pattern in a dense, homogeneously enhancing parenchymal lesion is suggestive of a primary lymphoma of the central nervous system. Magnetic resonance imaging was performed in one patient with two lesions, and both lesions demonstrated prolonged T2 relaxation times.

Primary lymphoma of the central nervous system (CNS) is a rare tumor, representing 0.2%–2% of all primary CNS malignancies [1, 2]. Various pathologic terms have been applied to this entity, including histiocytic sarcoma, reticulum cell sarcoma, microglioma, perivascular sarcoma, and perithelial sarcoma [1, 3]; such terms have been abandoned for more modern functional classifications of lymphoid neoplasia. Ninety-three percent of all CNS lymphomas are primary [4]. We analyzed the computed tomographic (CT) and angiographic findings in 32 cases of pathologically proved primary CNS lymphoma. The findings on magnetic resonance (MR) imaging, which was performed in one case, are also presented.

Materials and Methods

The clinical records and radiographic findings of 32 patients with pathologically proved primary CNS lymphoma were studied retrospectively. Examinations were performed between 1972 and 1984. Microscopic slides were reviewed by one of us (B. W. S.), and the tumors were verified to represent non-Hodgkin lymphoma. Of the 32 patients, 28 had preoperative CT scans, with or without (or both) contrast medium (25 of the 28 also underwent cerebral angiography). Seventeen of the CT scans were obtained with early-generation scanners and 11 with late-generation scanners. The CT scans were evaluated for lesion location, density, enhancement, homogeneity of enhancement, mass effect, edema, and definition of lesion margin. For each lesion, these parameters were graded and assigned to one of three groups—none, minimum to moderate, and marked—by two of us (D. F. R. and C. R. J.). The first choice recorded at the time of initial scan interpretation was noted for each case.

Preoperative cerebral angiograms were obtained in 29 of the 32 cases (in five of these 32 cases, preoperative CT scans were not available). Each angiogram was evaluated and graded for mass effect. Medullary veins, arterial encasement, arteriovenous shunting, tumor stain, and tumor neovascularity were graded as either positive or negative. One patient underwent MR scanning on a 0.15-T scanner (Picker).

This article appears in the November/December 1985 issue of *AJNR* and the February 1985 issue of *AJR*.

Received October 24, 1984; accepted after revision April 22, 1985.

Presented at the annual meeting of the American Society of Neuroradiology, New Orleans, February 1985.

[1] Department of Diagnostic Radiology, Mayo Clinic and Mayo Foundation, Rochester, MN 55905. Address reprint requests to D. F. Reese.

[2] Section of Surgical Pathology, Mayo Clinic and Mayo Foundation, Rochester, MN 55905.

***AJR* 146:271–276, February 1986**
0361-803X/86/1462-0271
© American Roentgen Ray Society

Results

The ages of the 32 patients (21 males and 11 females) were 9–79 years (average, 58.8). The group showed the usual proportions of histopathologic subtypes reported in the recent literature. The first radiographic examination was done between 1972 and 1976 in nine of these patients, between 1976 and 1980 in 12 patients, and between 1980 and 1984 in 11 patients, demonstrating a fairly constant incidence over the three time periods. Three patients could be classified as being immunosuppressed: one had undergone a renal transplant, one had rheumatoid arthritis with steroid treatment, and one had multiple myeloma. The interval from pathologic diagnosis to death was documented in 16 cases. The average was 21.8 months (range, 4 days to 57 months). Seven patients were still alive at the time of this study. Follow-up was not available on the other nine patients.

Of the 32 patients, 28 had preoperative CT scans. These 28 patients had 30 lesions. Twenty-five patients had a single nodular lesion, two had two lesions, and one had diffuse subependymal spread involving the third and lateral ventricles. The 30 lesions were grouped into one of five categories according to location: (1) deep central (including basal ganglia, thalamus, third ventricle, and corpus callosum; (2) white matter; (3) cortical; (4) corticomedullary junction; and (5) posterior fossa. Although large lesions often involved more than one of the above zones, each lesion was assigned to only one of the above locations on the basis of the best estimate (by D. F. R. and C. R. J.) of the epicenter of the lesion. In three patients, the lesions could not be localized precisely by CT. In two of the three patients, the lesions were of the same density as the surrounding edema, and in the third patient, the CT scan revealed only intraparenchymal hemorrhage. These three cases are listed as "cannot verify" in the lesion location column of table 1, because the tumor could not be demarcated from adjacent edema or hemorrhage. However, all three lesions were in the frontal lobes. Three patients did not have contrast-enhanced CT scans and one had only a contrast-enhanced study. Tumor size could not be evaluated in the three patients with no margin definition or in the one patient with diffuse subependymal spread.

Twenty-nine of the 32 patients underwent preoperative cerebral angiography; there were 31 lesions in this group. In each of the two patients with two lesions, the angiogram failed to demonstrate any abnormality at the site of one of the two tumor nodules. Aside from mass effect (25 of 31 lesions), the only abnormality present in a significant number of cases was tumor stain. This was seen in 12 (39%) of 31 lesions. In each case, the tumor stain appeared during the late arterial or capillary phase and had a diffuse homogeneous appearance. This stain is similar to that commonly seen with meningiomas (fig. 1). Of the 31 lesions, five displayed prominent medullary veins; two, arterial encasement; none, dural arterial supply or arteriovenous shunting; and three, tumor neovascularity.

MR imaging was performed in one patient. Axial sections were obtained using a spin-echo pulse sequence (30 msec echo time, 4000 repetition time). This patient had lesions adjacent to both the third and fourth ventricles. Both lesions demonstrated a prolonged T2 relaxation time, which was equal to that of cerebrospinal fluid (CSF). This made distinction between the lesion and ventricular fluid difficult in both instances (fig. 2).

TABLE 1: **Summary of CT Findings in 28 Cases of Primary Lymphoma of the Central Nervous System**

Finding	No. of Lesions ($n = 30$)
Lesion location:	
Deep	9
White matter	9
Corticomedullary	2
Cortical	2
Posterior fossa	4
Cannot verify	3
Precontrast density:	
Markedly increased	5
Moderately increased	14
Isodense	7
Decreased	2
Cannot verify	2
Edema:	
Marked	10
Moderate	16
None	4
Degree of enhancement:	
Marked	13
Moderate	10
Cannot evaluate	7
Homogeneity of enhancement:	
Marked	11
Moderate	6
Mottled	3
Ringlike	4
Cannot evaluate	6
Definition of tumor nodule margin:	
Marked	10
Moderate	13
Poor	4
Cannot evaluate	3

Note.—Average tumor size was 3.9 cm (range, 1–8 cm). The main diagnostic choices were "tumor," eight cases; glioma, six; meningioma and lymphoma, three each; abscess and infarct, two each; colloid cyst, germinoma, hemorrhage, and metastases, one each.

Discussion

Our epidemiologic data are in agreement with previous studies [1, 5]. The average age for our group was 58.8 years (range, 9–79). The average age in the Spillane et al. [1] series was 55.6 ± 13.6 years (range, 25–80), while in the Enzmann et al. [5] series, the average was 44 years (range, 14–68). The nearly 2:1 male-to-female ratio in our series is also in agreement with the male predominance in the Spillane et al. [1] series. The mean survival time of 21.6 months in our series is somewhat longer than that cited in the series of Spillane et al. [1] or Mendenhall et al. [6], who cited 15.2 months with radiation therapy. Three patients (9%) in our series were immunosuppressed. The increased incidence of primary CNS lymphoma in immunosuppressed patients (especially renal transplant recipients) is well documented in the literature [2, 4–8]. Mendenhall et al. [6] stated that the incidence of primary CNS lymphoma in immunosuppressed patients is 350 times that in the general population. Patients with acquired immunodeficiency syndrome also have been shown to have a higher incidence of primary CNS lymphoma [8]. Our data do not, however, support claims that the incidence of primary

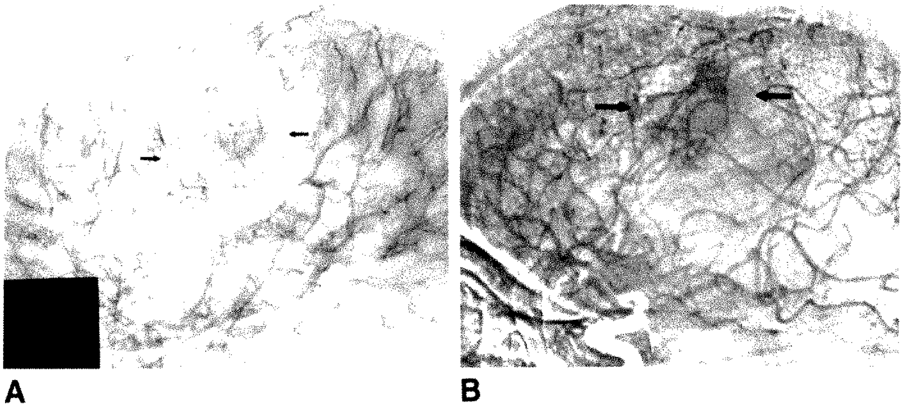

Fig. 1.—Diffuse meningiomalike vascular staining in two patients with primary CNS lymphoma. A 50-year-old (**A**) and 76-year-old (**B**) man, each with tumor in white matter of right frontoparietal lobe (*arrows*).

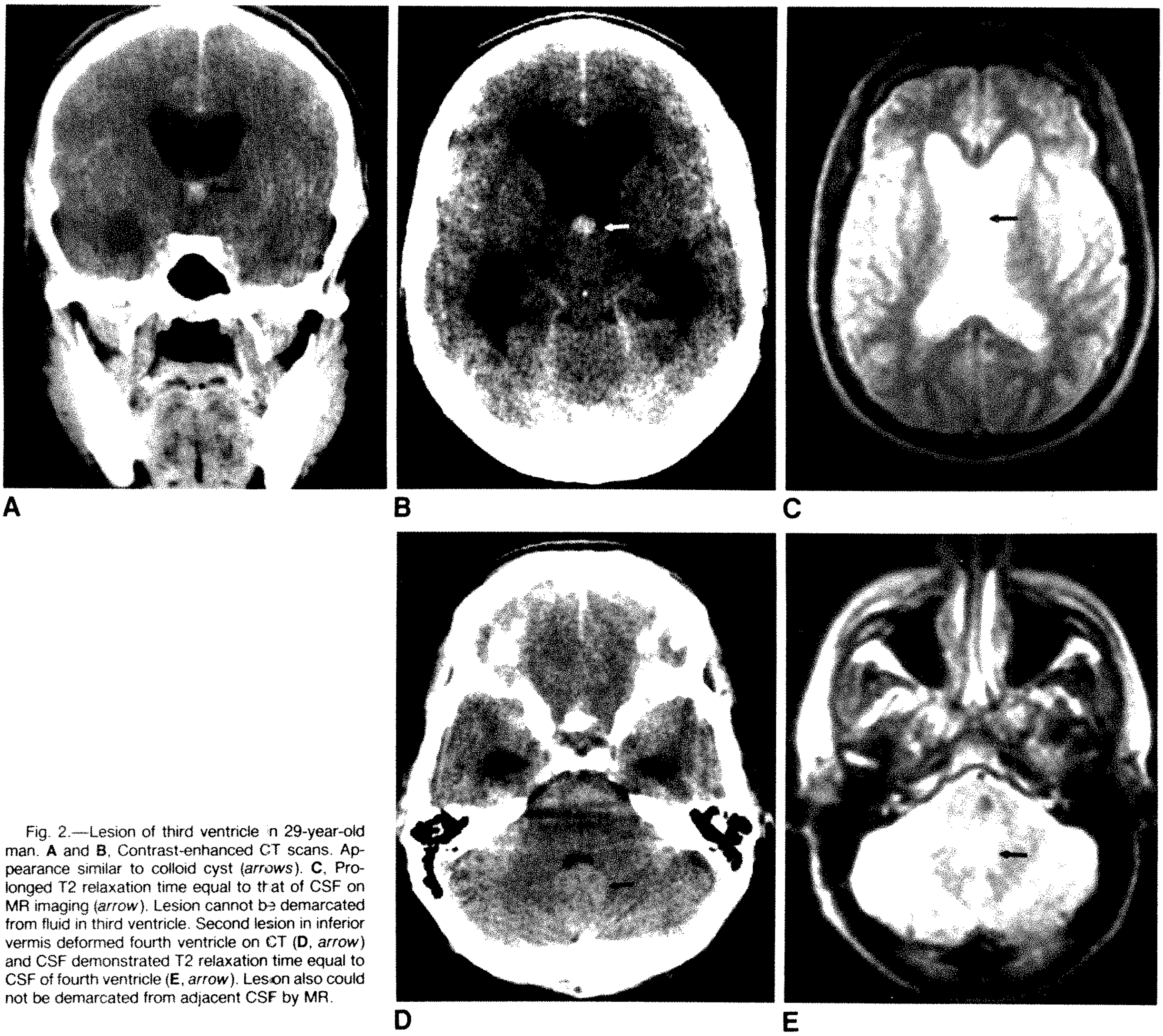

Fig. 2.—Lesion of third ventricle in 29-year-old man. **A** and **B**, Contrast-enhanced CT scans. Appearance similar to colloid cyst (*arrows*). **C**, Prolonged T2 relaxation time equal to that of CSF on MR imaging (*arrow*). Lesion cannot be demarcated from fluid in third ventricle. Second lesion in inferior vermis deformed fourth ventricle on CT (**D**, *arrow*) and CSF demonstrated T2 relaxation time equal to CSF of fourth ventricle (**E**, *arrow*). Lesion also could not be demarcated from adjacent CSF by MR.

CNS lymphoma has been increasing in recent years [1]. A possible explanation for this observation may rest with the nature of the clinical practice at our institution. The increase in transplant surgery and associated primary CNS lymphoma at select centers in recent years may not be reflected in the neurosurgical practice at our institution. The incidence of primary CNS lymphoma, when grouped into 4-year periods dating back to 1972, has been fairly constant. No correlation

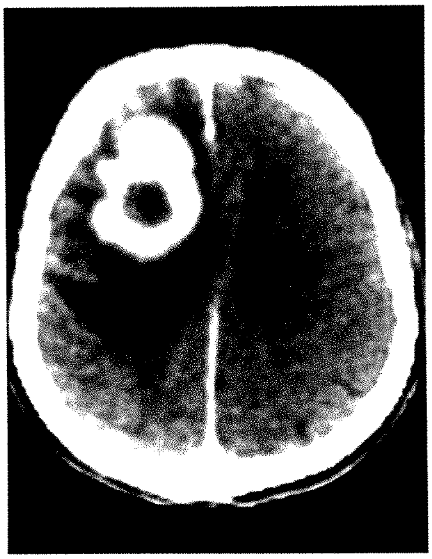

Fig. 3.—CT scan of 69-year-old man. Intensely enhancing tumor nodule in right frontal white matter has low-density center. Enhancing wall is characteristically thick, being 1.0–2.0 cm.

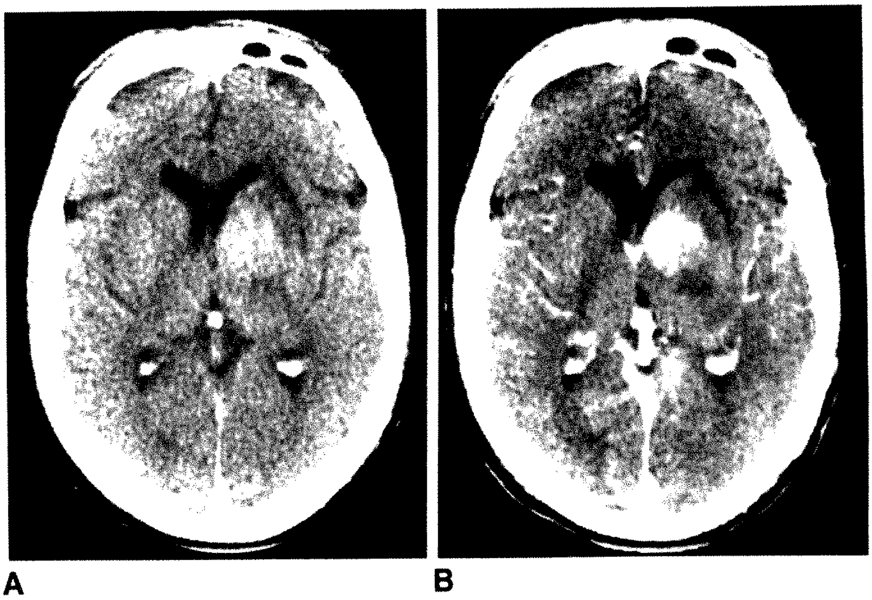

Fig. 4.—Pre- (**A**) and post- (**B**) contrast CT scans of 64-year-old man. Characteristic location and appearance of deep central lesion. Tumor nodule, in left basal ganglia, is of increased density, and enhances intensely and homogeneously.

between radiographic findings and pathologic subtype was found.

The CT data in our series with regard to tumor density, enhancement, edema, and size are in agreement with most previous series [1–3, 5, 9, 10]. Nineteen of 28 lesions in our series were of increased density. Similar results are cited by Valavanis et al. [11], Spillane et al. [1], Kazner et al. [9], and Radvany and Levine [10]. All lesions that could be evaluated for contrast enhancement showed enhancement, and 17 of 24 enhanced homogeneously. All referenced series cited similar results [1–3, 5, 9, 10]. We did have a higher incidence (four of 24) of ringlike enhancement than has been described previously [5]. The enhancing wall of the tumor nodule was quite thick in all four of our cases. This is in sharp contrast to the thin wall commonly seen with abscess [12]. This may be a helpful differential point in immunosuppressed patients who have an increased incidence of both primary CNS lymphoma and abscess [5] (fig. 3).

A prominent peritumoral edema zone was common in our series (26 of 30). This was also seen in the series of Enzmann et al. [5], Tallroth et al. [3], and Tadmor et al. [2]. All four lesions that did not have an associated edema zone were small and were deep or located in the posterior fossa. The tumor nodules in our series were generally large (average size, 3.9 cm), which also agrees with previous literature [5]. Tumor nodule margins in our series were well defined in 23 of 27 lesions. Previous literature, conversely, has emphasized blurred tumor margins [9, 11]. We found that the prominent edema zone around the tumor nodule in most cases provides a well defined margin. All four tumors with poor margin demarcation were lesions with only a moderate zone of edema.

Our CT data with regard to lesion location, multiplicity, and the incidence of subependymal spread differ from previous literature [1, 2, 5, 11]. In our series, 30% of lesions were located in deep central structures, 46% peripherally, and 13% in the posterior fossa. Although the division of supratentorial lesions into deep central and peripheral locations may be somewhat artificial, we believe that the lack of central involvement in our study was in striking contrast to the rate of involvement cited in previous large series. We sought to emphasize this finding by grouping supratentorial lesions in this manner. Tadmor et al. [2] stated that more than 50% of lesions were in the basal ganglia, whereas Spillane et al. [1] cited a 60% involvement rate of deep structures. Enzmann et al. [5] found the basal ganglia were involved in 50% of the cases of single lesions and in 100% of the cases of multiple lesions (fig. 4). Conversely, our data do not support a central location as a hallmark of primary CNS lymphoma (figs. 5 and 6).

In our series, the finding of 13% of the lesions in the posterior fossa is slightly higher than the overall average of 8% noted by Valavanis et al. [11].

Our data also differ from the existing CT literature with regard to lesion multiplicity [1, 5, 6]. Eleven percent of our patients had more than one lesion (including one with multiple subependymal nodules). Spillane et al. [1], however, cited a multiplicity rate of 30%; Enzmann et al. [5], 43%; and Mendenhall et al. [6], 50%. Our data suggest a need to deemphasize multiplicity as characteristic of primary CNS lymphoma. Spillane et al. [1] found subependymal spread in three of 20 cases, whereas this finding was only present in one of 28 in our series.

The correct diagnosis appeared as the diagnosis of choice on the CT report in only three (11%) of 28 patients in our series. The efficacy of CT in correctly predicting this diagnosis is therefore quite poor. This has also been noted in previous series [1]. Spillane et al. [1] suggested that, if the lesions are multiple on CT, the scan most often is labeled (incorrectly) metastases. In our series, of the two patients with multiple

Fig. 5.—Pre- (**A**) and post- (**B**) contrast CT scans of 70-year-old woman. Characteristic location and appearance of peripheral lesion. Tumor nodule is in left temporal white matter, is isodense, and enhances intensely and homogeneously.

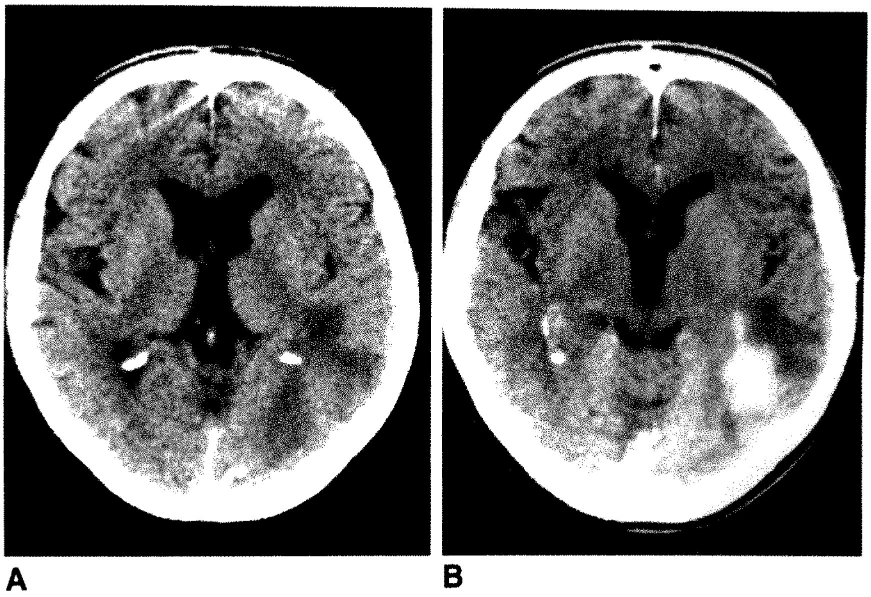

Fig. 6.—Contrast-enhanced CT scans. Intensely and homogeneously enhancing peripheral lesions.

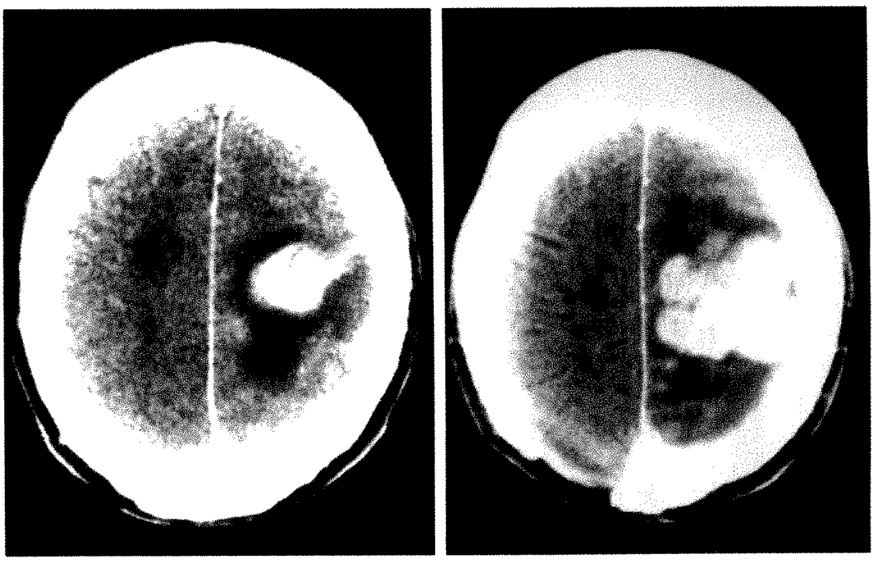

lesions, one was diagnosed as having metastases and the other as having lymphoma. The patient with diffuse subependymal spread of tumor was misdiagnosed as having a germinoma. Spillane et al. [1] also suggested that the most common misdiagnosis for a solitary lesion is meningioma, whereas in our series these lesions were most often labeled tumor. Enzmann et al. [5] stated that primary CNS lymphoma in immunosuppressed patients is most often misdiagnosed by CT as abscess. In our series, two of the three immunosuppressed patients were diagnosed as having glioma and one as having meningioma. The two patients in our series with noncortical lesions who were misdiagnosed as having meningioma were studied on early-generation CT scanners. Presumably, the lesions were believed to be intraventricular meningiomas at the time of preoperative CT interpretation. Based on the operative report, the two lesions were subsequently assigned to the deep and white matter locations when reviewed for this study. The third tumor misdiagnosed as a meningioma was cortical in location and presumably was believed to be extraaxial at the time of preoperative interpretation.

Twenty-five (81%) of our 31 cases displayed a mass effect angiographically. This compares with 100% (14 of 14) in the Kishikawa et al. [13] series. Prominent medullary veins were found in five of 31 lesions in our series, in one of 10 in the series of Spillane et al. [1], and in five of 14 in the series of Kishikawa et al. Arterial encasement was described as a hallmark of primary CNS lymphoma by Leeds et al. [14] and has been mentioned in other series: Spillane et al. [1], one of 10; Enzmann et al. [5], one of seven; and Kishikawa et al. [13], four of 14. This finding was rare in our series, being present in only two of 31 lesions. Dural arterial supply was described in one of 10 cases by Spillane et al. [1]; none of our cases demonstrated this finding. Arteriovenous shunting was not seen in any of our cases. Tumor neovascularity was seen in three of 31 cases in our series and in two of 14 cases in the Kishikawa et al. [13] series. The only characteristic angiographic finiding of primary CNS lymphoma in our series

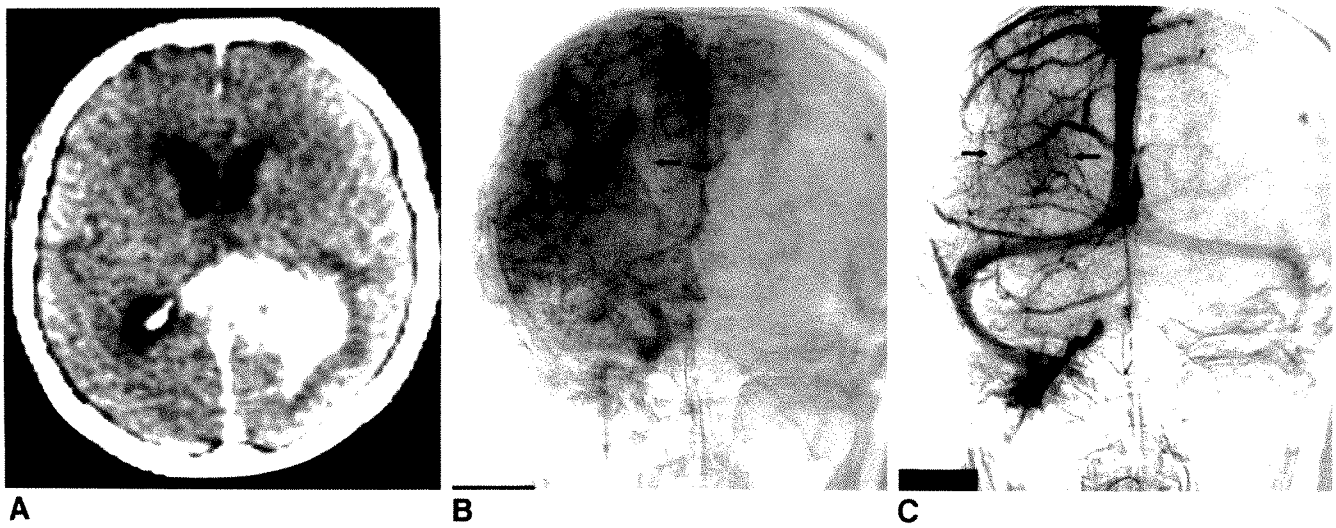

Fig. 7.—CT and angiographic findings characteristic of primary lymphoma of central nervous system in 72-year-old woman. **A**, CT scan. Large, enhancing right temporal lesion involves splenium of corpus callosum. Angiographically, lesion demonstrates diffuse homogeneous cloudlike stain (**B**, *arrows*) that persists into venous phase (**C**, *arrows*).

was a diffuse, homogeneous, cloudlike tumor stain that appeared in the late arterial or capillary phase and persisted through the venous phase. This blush had the same appearance commonly associated with meningiomas, except that the vascular supply was intraaxial in all cases (fig. 1). This was demonstrated in 12 (39%) of 31 cases in our series and required film-subtraction technique for demonstration in most cases. This finding has been described previously, but generally at a lower incidence: Spillane et al. [1], 30%; Enzmann et al. [5], 14%; Kishikawa et al. [13], 21%; Schaumburg et al. [15], 7%; and Gunderson et al. [16], 100%.

Our CT and angiographic studies indicate that neither method alone will consistently demonstrate findings that are specific for primary CNS lymphoma. However, our data suggest that a combination of CT and angiographic findings may be characteristic of this entity. Angiographically, the lesion should demonstrate the diffuse vascular staining pattern described above. The lesion on CT should be unifocal, large, well defined, dense, homogeneously enhancing, and surrounded by a prominent zone of edema (fig. 7).

Both Tallroth et al. [3] and Radvany and Levine [10] stated that a combination of CT and angiographic findings is characteristic of primary CNS lymphoma, whereas Spillane et al. [1] and Enzmann et al. [5] cited characteristic CT findings and found that angiography was not useful.

The one MR examination of a primary CNS lymphoma in our series did not demonstrate any specific findings. Prolongation of T2 relaxation time in and around most CNS tumors and other lesions has been well documented in the literature [17, 18].

REFERENCES

1. Spillane JA, Kendall BE, Moseley IF. Cerebral lymphoma: clinical radiological correlation. *J Neurol Neurosurg Psychiatry* **1982**;45:199–208
2. Tadmor R, Davis KR, Roberson GH, Kleinman GM. Computed tomography in primary malignant lymphoma of the brain. *J Comput Assist Tomogr* **1978**;2:135–140
3. Tallroth K, Katevuo K, Holsti L, Andersson U. Angiography and computed tomography in the diagnosis of primary lymphoma of the brain. *Clin Radiol* **1981**;32:383–388
4. Henry JM, Heffner RR Jr, Dillard SH, Earle KM, Davis RL. Primary malignant lymphomas of the central nervous system. *Cancer* **1974**;34:1293–1302
5. Enzmann DR, Krikorian J, Norman D, Kramer R, Pollock J, Faer M. Computed tomography in primary reticulum cell sarcoma of the brain. *Radiology* **1979**;130:165–170
6. Mendenhall NP, Thar TL, Agee OF, Harty-Golder B, Ballinger WE Jr, Million RR. Primary lymphoma of the central nervous system: computerized tomography scan characteristics and treatment results for 12 cases. *Cancer* **1983**;52:1993–2000
7. Schneck SA, Penn I. Cerebral neoplasms associated with renal transplantation. *Arch Neurol* **1970**;22:226–233
8. Kelly WM, Brant-Zawadzki M. Acquired immunodeficiency syndrome: neuroradiologic findings. *Radiology* **1983**;149:485–491
9. Kazner E, Wilske J, Steinhoff H, Stochdorph O. Computer assisted tomography in primary malignant lymphomas of the brain. *J Comput Assist Tumogr* **1978**; 2:125–134
10. Radvany J, Levine H. Computed tomography in the diagnosis of primary lymphoma of the central nervous system. *J Comput Assist Tomogr* **1978**;2:215–217
11. Valavanis A, Imhof HG, Klaiber R, Dabir K. The diagnosis of solitary primary reticulum cell sarcoma of the posterior fossa with computed tomography. *Neuroradiology* **1981**;21:213–217
12. Lee SH, Rao KCVG. *Cranial computed tomography.* New York: McGraw-Hill, **1983**;518
13. Kishikawa T, Numaguchi Y, Fukui M, et al. Primary intracranial sarcomas: radiological diagnosis with emphasis on arteriography. *Neuroradiology* **1981**;21:25–31
14. Leeds NE, Rosenblatt R, Zimmerman HM. Focal angiographic changes of cerebral lymphoma with pathologic correlation: a report of two cases. *Radiology* **1971**;99:595–599
15. Schaumburg HH, Plank CR, Adams RD. The reticulum cell sarcoma—microglioma group of brain tumours: a consideration of their clinical features and therapy. *Brain* **1972**;95:199–212
16. Gunderson CH, Henry J, Malamud N. Plasma globulin determinations in patients with microglioma: report of five cases. *J Neurosurg* **1971**;35:406–415
17. Randell CP, Collins AG, Young IR, et al. Nuclear magnetic resonance imaging of posterior fossa tumors. *AJNR* **1983**;4:1027–1034, *AJR* **1983**;141:489–496
18. Hawkes RC, Holland GN, Moore WS, Kean DM, Worthington BS. NMR tissue characterization in intracranial tumors: preliminary results. *AJNR* **1983**; 4:830–832

Cervical Spinal Cord Injuries in Patients with Cervical Spondylosis

Victor S. Regenbogen[1]
Lee F. Rogers[1]
Scott W. Atlas[1,2]
Kwang S. Kim[1]

Eighty-eight patients over age 40 with traumatic cervical spinal cord injuries were clinically and radiographically evaluated, and comparison was made with 35 spinal cord injury patients under age 36. While most older patients sustained obvious bony and/or ligamentous damage commensurate with their neurologic findings, 25 (28%) of the 88 patients had no demonstrable bony abnormalities and 17 (20%) of the 88 patients had only minimal evidence of bony injury. Of particular interest are the patients with severe cord injuries, yet no bony abnormalities, who seem to form a distinct subgroup of the cervical spinal cord injury patient on the basis of radiographic and clinical features. Of these 25 patients, 24 (96%) had severe cervical spondylosis. Fourteen (56%) of the 25 patients were injured in falls, five (36%) of these 14 being of a seemingly trivial nature. Of the 42 patients with minimal or no demonstrable bony abnormalities, 33 (79%) were evaluated with plain tomography and no occult fractures or other significant pathology was demonstrated. Pantopaque myelography in 27 (64%) of the 42 cases revealed no extruded disk or other surgical lesion in any patient. In large measure, these injuries can be attributed to cervical spondylosis, which narrows the canal and makes the cord more susceptible to compression by the bulging ligamenta flava during hyperextension.

Of all traumatic cervical spinal cord injuires, 27% -39% occur in people over 40 [1-3]. There is a distinct subpopulation within this group of older people who demonstrate little or no radiographic abnormality, despite the presence of a profound neurologic deficit. Individuals within this subgroup will often incur spinal cord injury as a result of a relatively minor traumatic event (in contrast to major trauma, such as motor vehicle or diving accidents that commonly causes neurologic injury in young adults). In large measure, these differences in susceptibility can be attributed to spondylosis of the cervical spine.

In order to further characterize patients in whom there appears to be a disparity between the severity of the neurologic and bony injury, we reviewed 104 cervical spinal cord injuries in individuals over age 40 with particular attention to their clinical presentation and radiographic findings. The pathomechanics of injury and the role of spondylosis in the creation of neurologic deficits in older individuals are explained.

Materials and Methods

All cases of traumatic cervical spinal cord injuries in patients over age 40 were evaluated during the 5-year period from 1979 to 1984 (104 cases). Gunshot and stabbing injuries were excluded (10 cases), as were pathologic fractures (one case). Also excluded were patients whose radiographs or medical records could not be located or were incomplete (five cases). The remaining 88 patients were evaluated.

Medical records were reviewed to determine the circumstances of injury (e.g., fall, motor vehicle accident, dive into shallow water). The neurologic level and pattern of spinal cord injuries were noted. All levels of injury were classified according to the lowest level of preserved function. The pattern of spinal cord injury refers to assessment of the completeness of the lesion as well as the clinical syndrome where applicable (e.g., central cord syndrome).

Received May 1, 1985; accepted after revision October 10, 1985.

Presented at the annual meeting of the Radiological Society of North America, Washington, DC, November 1984.

[1] Department of Radiology, Northwestern University Medical School, 303 E. Chicago Ave., Chicago, IL 60611. Address reprint requests to L. F. Rogers.

[2] Present address: Department of Neuroradiology, Hospital of the University of Pennsylvania, Philadelphia, PA 19104.

AJR 146:277-284, February 1986
0361-803X/86/1462-0277
© American Roentgen Ray Society

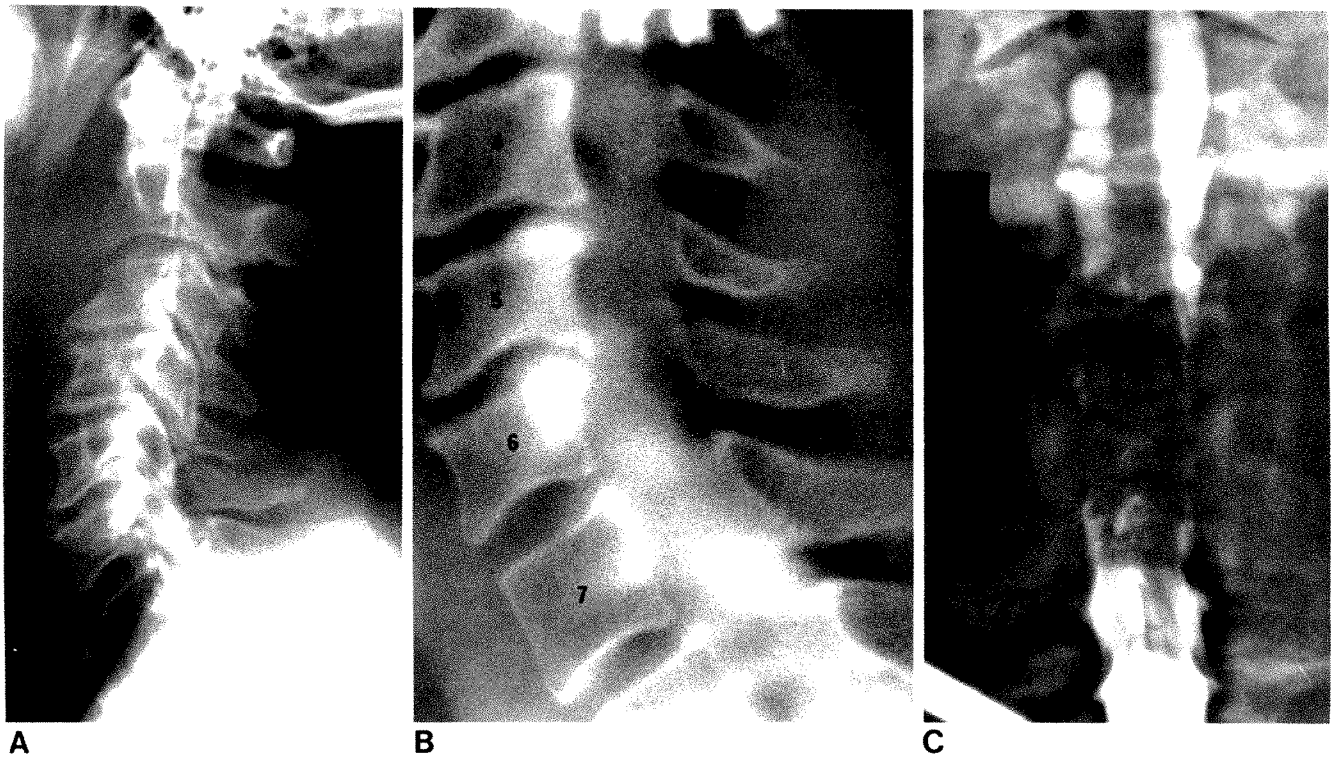

Fig. 1.—50-year-old woman who was injured in fall down stairs suffered incomplete C5 quadriplegia. **A**, Initial lateral film. Prevertebral soft-tissue swelling and degenerative changes of cervical spine but no evidence of fracture or dislocation. **B**, Tomogram through middle of spinal canal. Posterior spur formation at C4–C5 and C5–C6 with associated disk-space narrowing at these levels. **C**, AP film from myelogram. Widening of spinal cord with associated narrowing of subarachnoid space from C4 to C6. Lateral view (not shown) confirmed intramedullary process, and widening was believed to represent cord edema.

The admission physical examination was reviewed to search for clues to the mechanism of injury (e.g., forehead contusion, which would be consistent with a hyperextension injury). Plain radiographs, tomograms, and myelograms were reviewed. The presence or absence of cervical spondylosis was determined on the basis of the presence of anterior or posterior osteophytes and intervertebral disk-space narrowing. The sagittal canal diameter was measured from the posterior aspect of the C5 vertebral body to the spinolaminar line at the same level [4, 5]. Values less than 12 mm were considered abnormal.

The presence of prevertebral soft-tissue swelling was determined using criteria proposed by Penning [6].

For purposes of comparison, 35 young adults aged 15- 36 were similarly analyzed.

Results

Definition of Series

The 88 patients over age 40 with cervical spinal cord injury were placed into one of three groups: 46 patients (52%) had obvious bony and/or ligamentous disruption entirely consistent with their neurologic injuries; 25 (28%) had no evidence radiographically of fracture or dislocation; and 17 (20%) had only subtle radiographic evidence of injury. It is the latter two groups, with severe neurologic injuries and little or no radiographic evidence of bony injury, that are the subject of this report. These 42 patients ranged in age from 40 to 88 years (mean, 61.0); there were 33 male and nine female patients.

Causes of Injury

The most common cause of injury was a fall, accounting for 26 (62%) of the 42 cases, often occurring at home. Motor vehicle accidents were responsible for 14 cases (33%). Of the remaining two patients, one was a construction worker who was struck in the head with a wrecking ball, and the other was injured while surfing.

Pattern and Level of Cervical Spinal Cord Injury

In 20 (48%) of the 42 patients, the C5 level was affected. C4 was involved in 12 cases (28%), and levels C6 and C7 were each affected in five patients (12% each).

Of the 42 patients, 31 (74%) had incomplete lesions and 11 (26%) had complete lesions. Of the 31 incomplete lesions, 17 (55%) demonstrated the acute cervical central cord syndrome.

Radiographic Manifestations of Injury

Of the 42 patients, 25 (59%) demonstrated prevertebral soft-tissue swelling. Bony injury was not seen in 25 (28%) of 88 patients at the time of admission (fig. 1). Of these 25 patients, 21 (84%) underwent plain tomography of the cervical spine, which confirmed the absence of bony fracture.

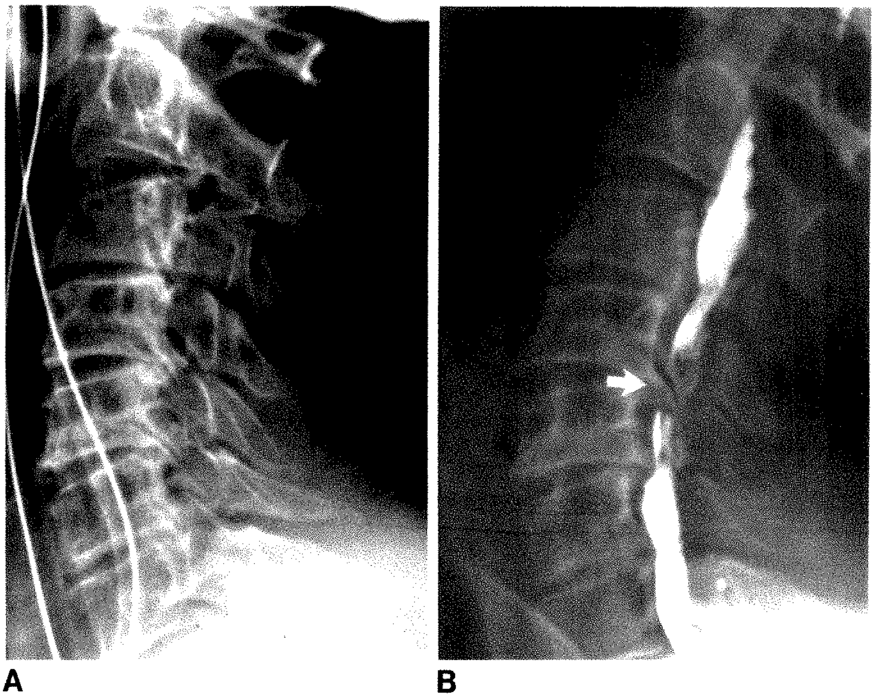

Fig. 2.—59-year-old man in motor vehicle accident suffered incomplete C5 quadriplegia. Large forehead contusion was consistent with hyperextension trauma. **A**, Lateral view reveals no evidence of fracture or dislocation. There is marked cervical spondylosis with anterior and posterior osteophyte formation and multilevel disk-space narrowing. Note absence of swelling. **B**, Lateral view from myelogram. Prominent ventral bar defect at C4–C5 (*arrow*) with lesser ventral bar defects at C3–C4, C5–C6, and C6–C7. Shallow ventral extradural defect from C3 to C5 may reflect shallow epidural hematoma.

Pantopaque myelography, performed in 16 (64%) of these 25 patients, revealed moderate to severe cervical spondylosis in all cases (fig. 2). Epidural hematoma was seen as a shallow ventral extradural defect in two (13%) of 16 patients (fig. 2B). Three patients (19%) demonstrated widening of the cord shadow on anteroposterior (AP) and lateral projection, consistent with cord edema (fig. 1C). Three (19%) of the 16 patients studied with myelography revealed disk-space disruption when their heads were extended, which had not been suspected previously.

Of 88 spinal cord injury patients, 17 were placed in the category of relatively minor radiographic abnormalities (figs. 3–5). Of those 17 patients, eight (47%) had small avulsion fractures from the anteroinferior aspect of a vertebral body (figs. 3, 4, 6A, and 7A). Avulsion occurred at C4 in four cases, C3 in three cases, and C5 once. Two (12%) of the 17 patients had chip fractures from the anterosuperior aspect of the C4 vertebral body.

Six (35%) of the 17 patients had an obviously disrupted disk space on initial examination (fig. 5). The disruption was manifested by widening of the anterior aspect of an intervertebral disk space without bony malalignment. Disk-space disruption was clearly evident after these patients were placed in tongs and traction, and in one case (fig. 6) was not suspected before traction.

One (6%) of the 17 patients suffered an isolated spinous process fracture as his only radiographic abnormality.

Plain tomography was performed in 12 (71%) of these 17 patients to look for associated fractures, but none were identified. In one patient with a small avulsion fracture at C6, obvious disk-space disruption was identified at tomography (fig. 7).

Pantopaque myelography, performed in 11 (65%) of these 17 patients, revealed mild to severe spur formation in all cases. Cord edema was seen in two (18%) of 11 patients who were studied emergently.

Presence of Cervical Spondylosis

Of the 42 patients, 38 (90%) had evidence of moderate to severe cervical spondylosis and 36 (86%) of these 42 patients demonstrated anterior osteophytic changes at multiple levels. Of the 42 patients, 22 (52%) demonstrated posterior spurring, most commonly arising from C3 to C6. Of the 25 patients with no fractures, 17 (68%) had posterior spur formation. Narrowing of the intervertebral disk space was identified at multiple levels in 32 (76%) of 42 patients. Narrowing of the spinal canal was seen in only seven (17%) of 42 cases.

Control Group

In our comparison group of 35 young adults with cervical spinal cord injury, the age range was 16–36 years (mean, 24). There were 30 male and five female subjects.

In contrast with the group of older patients only four (11%) of the 35 young patients were injured in falls and none of these was any less severe than a 4.5-m fall. Of the 35 subjects, 22 (63%) were injured in motor vehicle accidents, seven (20%) by diving into shallow water, and two (6%) during athletic activities.

The level of injury was similar to our older patients with 40% affected at the C5 level, 23% at C6, 14% at C4, 11% at C7, 6% at C8, and 6% at C3. Eighteen (51%) of 35 suffered

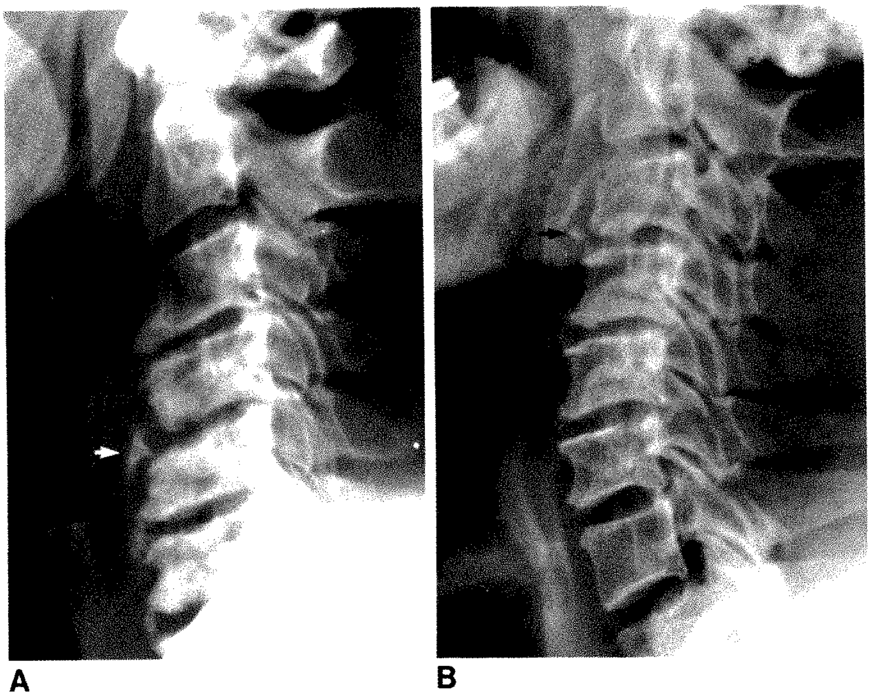

Fig. 3.—Two patients with small anterior chip fractures. **A**, 48-year-old man who fell developed C5 central cord syndrome. Severe degenerative changes, soft-tissue swelling, and avulsion fracture at C4 (*arrow*). **B**, 55-year-old man with C4 central cord syndrome injured in fall down stairs. Only minimal prevertebral soft-tissue swelling and small fleck of bone at anteroinferior surface of C3 (*arrow*). Moderate degenerative changes are also present.

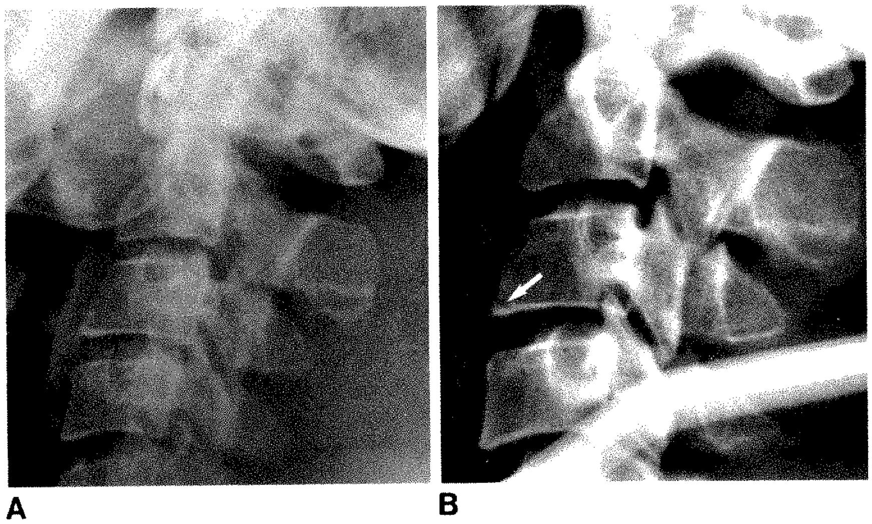

Fig. 4.—41-year-old man in motor vehicle accident suffered C5 cervical central cord injury. **A**, Initial radiograph reveals no obvious fracture or dislocation. Soft tissues are normal. **B**, Film 3 weeks later demonstrates fracture (*arrow*). In retrospect, this fracture was faintly visible on initial film, demonstrating subtle nature of many of these fractures.

complete cord injuries, compared to only 26% of our older population. The central cervical cord syndrome was present in only one (6%) of 17 cases of the patients with incomplete cord lesions, also a much lower percentage than in the older population.

In marked contrast to our older spinal cord injury patients, only two (6%) of the young adults had little or no radiographic evidence of bony injury. One of these patients, a 36-year-old man, had no evidence of fracture or dislocation, despite an incomplete C5 quadriplegia. However, he was found to have a narrowed sagittal diameter of the spinal canal (11 mm) at C5. The other patient, a 26-year-old man with a C7 central cord syndrome, had suffered a hyperextension injury and was found to have a chip fracture of the anteroinferior body of C6. The remaining 94% of young adults all demonstrated obvious fractures and/or fracture dislocations on initial radiographs.

Discussion

It is often confusing to the clinician when confronted with a trauma patient suffering a severe neurologic deficit with little or no radiographic abnormality to explain that deficit. Our results indicate that this is a relatively common situation in the cervical spinal cord injury patient over age 40. Of 88 patients in our series, 42 (48%) fit into this category, with

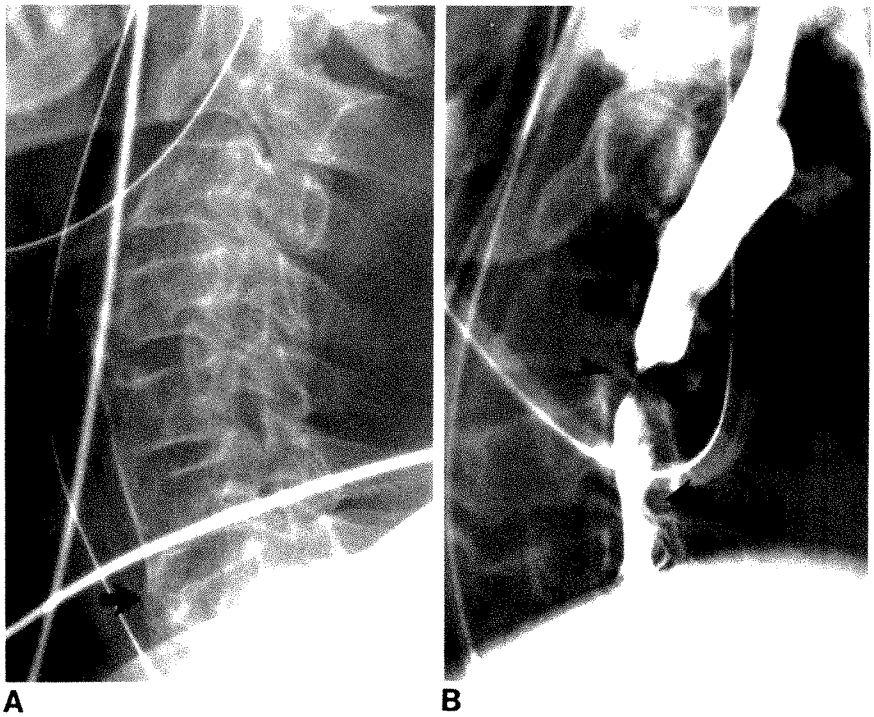

Fig. 5.—76-year-old man suffered C4 incomplete spinal cord injury in fall. **A**, Initial lateral radiograph in neutral position shows changes of diffuse idiopathic skeletal hyperostosis in lower cervical spine with disruption of hyperostotic spur at C6–C7 (*arrow*). Note minimal widening of anterior intervertebral disk space at C3–C4. **B**, Myelogram shows ventral extradural defect at C3–C4 due to retrolisthesis of C3 and C4 (*arrowhead*). Posterior aspect of thecal sac is compressed at multiple levels by infolded ligamentum flavum (*arrows*). Again, widened intervertebral disk space at C3–C4 is noted.

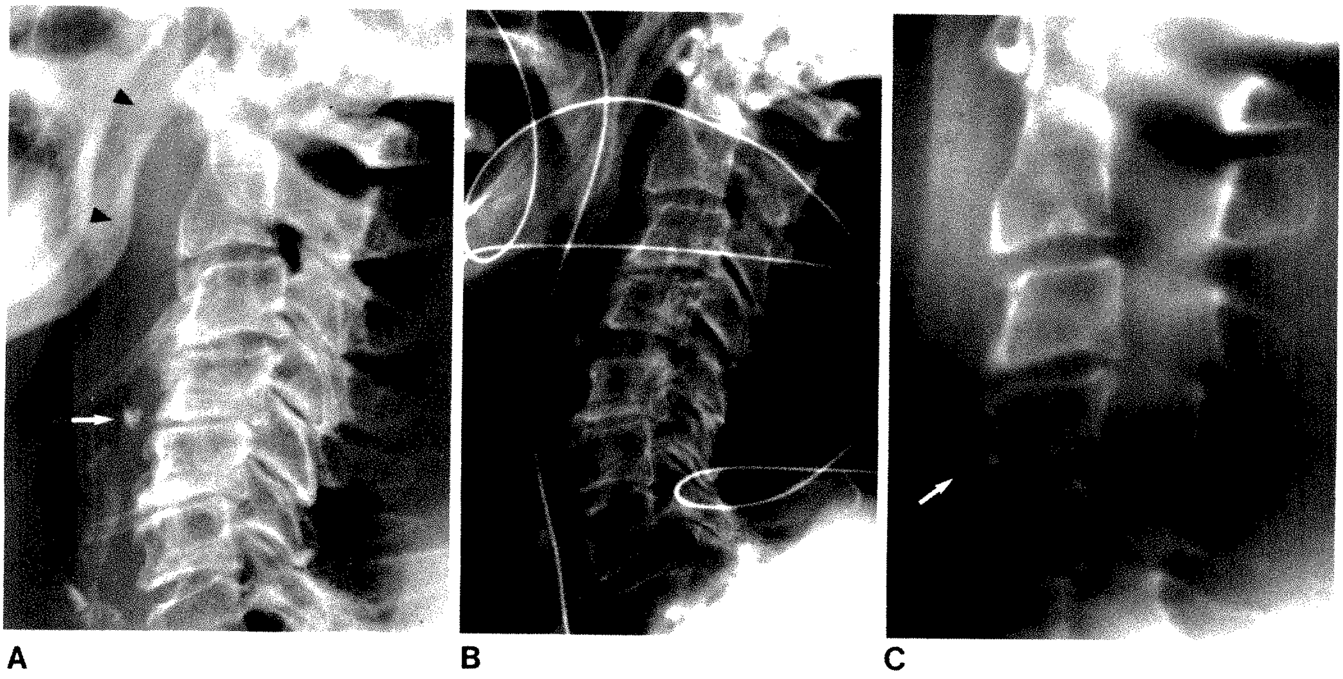

Fig. 6.—88-year-old woman with C5 quadriplegia was injured in fall down stairs. **A**, Initial lateral radiograph demonstrates severe degenerative joint disease manifested by joint-space narrowing, retrolisthesis, and spur formation. Bony fleck is noted at anteroinferior aspect of C4 (*arrow*) and there is prevertebral soft-tissue swelling (*arrowheads*). **B**, Traction view demonstrates widening of disk space at C4–C5 level. **C**, Midline tomogram reveals minimal retrolisthesis at C4–C5 and C5–C6 secondary to degenerative disease. Small posterior spurs are present at C4 and C5 levels. Smallest sagittal canal diameter is 13 mm from posterior spur at C4 to subjacent lamina. Since two vertebral bodies are involved in this latter measurement, actual diameter may be 2 mm less in extension. Small fracture fragment at anteroinferior aspect of C4 (*arrow*) is again seen.

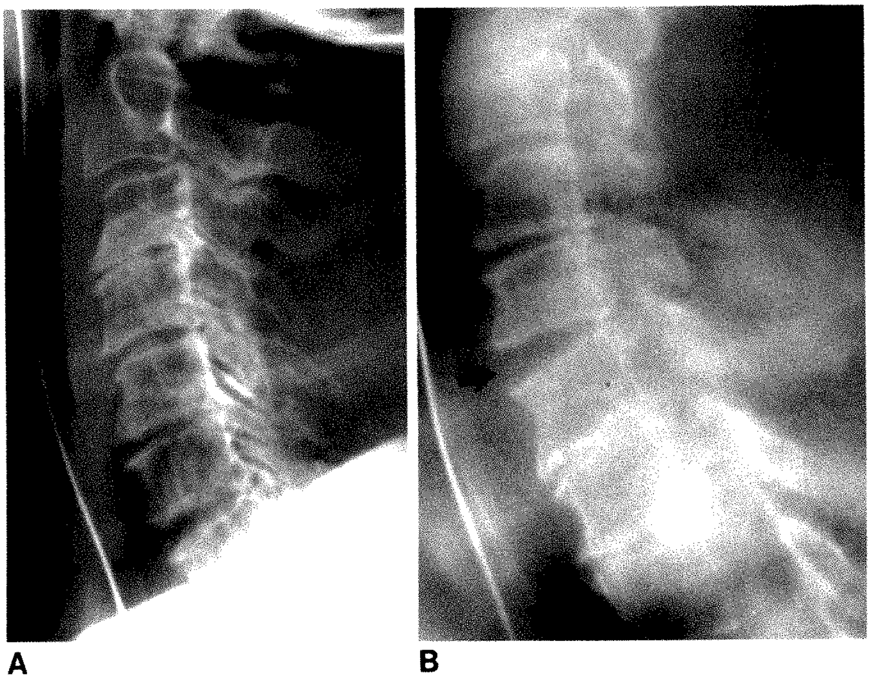

Fig. 7.—77-year-old man suffered C6 central cord injury in fall down stairs. **A**, Lateral film reveals severe degenerative changes but no definite evidence of fracture or dislocation. There is minimal increase in width of prevertebral soft tissue, slight widening of anterior aspect of C6–C7 disk space (*arrow*), and small bony fleck in widened disk space. **B**, Tomogram during extension stress reveals definite widening of anterior aspect of C6–C7 intervertebral disk space (*arrow*).

28% having no bony radiographic abnormality at all. Similar findings have been described by other investigators [2, 3].

Fundamental to an understanding of this group of patients is an understanding of the mechanism by which they are injured. In extension of the cervical spine, the posteriorly located ligamentum flavum bulges anteriorly into the spinal canal. The spinal cord can then be pinched between the vertebral body, spurs, or disk in front and the bulging ligamentum flavum behind [7–9] (figs. 5B and 8). Normally, at the level of the cervical enlargement, the spinal cord occupies most of the spinal canal; in extension, when the ligamentum flavum folds in and the cross-sectional diameter of the spinal cord increases [10], there is just enough room for the spinal cord, dura, and nerve roots [11]. Encroachment on the spinal canal by posteriorly directed osteophytes or narrowing of the sagittal diameter of the spinal canal will obviously increase the risk of incurring spinal cord damage in hyperextension. Extending anteriorly, posterior spurs will act as counterpoints to the pressure of the forward-bulging ligamentum flavum. Since no locking occurs in hyperextension, on recoil of the neck the radiograph can be entirely normal, despite the presence of a profound neurologic deficit.

Roaf [12] has shown that the intervertebral disks, joints, and ligaments are very resistant to pure hyperextension strain and that rupture of the anterior longitudinal ligament by a pure hyperextension force does not occur. The addition of a component of rotation, however, makes the ligaments and disks very susceptible to rupture. As the vertebral column above the ruptured disk moves posteriorly, the spinal cord is pinched between the posteroinferior margin of the dislocated vertebral body above and the leading edge of the subjacent lamina [13] (fig. 9). Since no locking occurs, muscle action allows elastic recoil of the neck and spontaneous reduction of the momentary dislocation. Reflex muscle spasm will maintain the reduction, and no evidence of dislocation need be present on the initial radiographs.

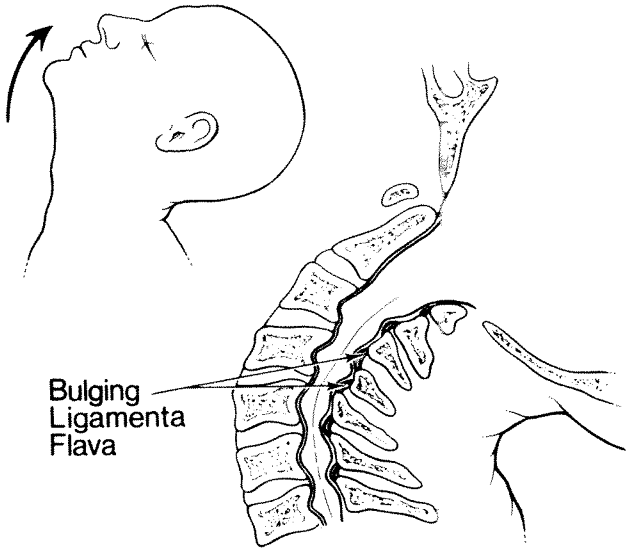

Fig. 8.—Illustration of pinching of spinal cord, during extension, between bulging ligamentum flavum and posterior osteophytes.

Although the paucity of bony injury is the most obvious characteristic shared by these patients, there are a number of additional clinical and radiographic features that help to sort out this subgroup of cervical spinal cord injuries. Since the likelihood of cord compression is increased in patients with cervical spondylosis, a process that narrows the spinal

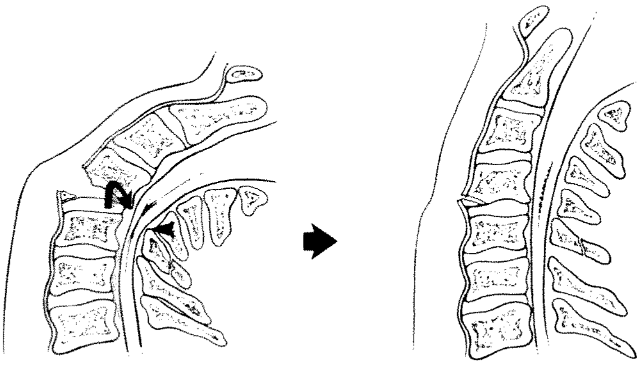

Fig. 9.—In hyperextension injury with disruption of anterior longitudinal ligament and intervertebral disk, cord is pinched between posteroinferior margin of dislocated vertebral body above (*curved arrow*) and leading edge of subjacent lamina (*arrowhead*). Since this momentary dislocation will be immediately reduced by elastic recoil of neck, initial radiographs may appear deceptively normal. Note characteristic fracture at anteroinferior aspect of vertebral body.

canal, it is not unexpected that all of our 25 patients with no bony injury had severe spondylotic changes of the cervical spine. Posterior osteophyte formation, seen in 17 (68%) of those 25 patients, appears to be the one feature common to most of these cases [14]. As would be anticipated, these patients were elderly, with a mean age of 66 years. In contrast, neurologic injury in the absence of fracture or dislocation was rare in our young adult population. Only one (2.8%) of the 35 young patients suffered such an injury in our series, and he was found to have four critical cervical spinal stenoses. Thus, when neurologic injury in a young patient is not associated with fractures or dislocation, spinal canal narrowing or encroachment must be excluded. In the older patient, however, this is not the case, as narrowing of the canal was seen in only seven (17%) of our 42 patients.

Since hyperextension trauma is the mechanism of injury in these patients, physical or radiographic evidence to support this can often be found. In cases where classic hyperextension injuries are visible on the radiograph, such as a chip fracture of the inferior aspect of a vertebral body [15], the mechanism of injury is clear. In the patient with no bony injury, however, the only hard evidence of extension trauma may be the presence of a forehead or facial bruise. This physical finding was seen in 10 (40%) of our 25 patients with no bony injuries and is often the only clue to the forces that were operative at the time of injury.

A striking and frightening feature of these older patients is their propensity to suffer major cord injury from seemingly minor trauma. Nine (21%) of our 42 patients were injured in this manner. This group included six patients injured when they fell from a standing height, two who fell and hit their heads on a table, and one who fell off a toilet seat. In contrast, none of our younger patients incurred cord injury after such minor injury.

One additional clinical feature of this group that deserves mention is the pattern of neurologic injury. Of the 42 older patients with incomplete cord injury in our series, 17 (40%) suffered from the acute central cervical cord syndrome. This syndrome is characterized by disproportionally greater motor impairment of the upper than the lower extremities, bladder dysfunction, and variable degrees of sensory loss below the lesion. Schneider et al. [16] described a full spectrum of spinal cord damage in hyperextension injury, ranging from a transient central cord syndrome due to cord concussion to complete transverse cord necrosis. This syndrome is consistent with a lesion in the central part of the cervical cord, since the motor innervation to the upper extremities is located most centrally in the lateral corticospinal tract with the thoracic and lumbar fibers located more laterally. The occurrence of this syndrome following hyperextension injury is well known and undoubtedly accounts for its frequency in our older patients.

Our radiographic workup in the neurologically compromised patient with little or no radiographic abnormality included tomograms in 33 (78%) of 42 cases and myelography in 27 (64%). Although some abnormalities were identified with tomography and myelography, no discovery changed the treatment plan for the patient, which was conservative in all cases. Cord edema was seen in five of 42 patients (12%), epidural hematoma in two patients (5%), and previously subtle or unsuspected disk-space widening in four cases (9%). Importantly, no extruded disk or other surgical lesion was identified at myelography, although the extent of spondylotic change was clearly demonstrated. Similarly, plain film tomography revealed no cases of occult fracture.

An appreciation of the existence of this distinct subgroup of cervical spinal cord injuries without bony abnormalities is vitally important for any physician charged with their care. An awareness of the high frequency of occurrence in the elderly population should allow the clinician to feel comfortable when faced with a patient in whom the radiographs do not seem to correlate with the severity of the neurologic findings. Our results indicate that the approach to these patients, in the acute setting, need not focus on a search for an occult fracture, since one is usually not found. Not only are tomography and myelography usually unnecessary, but inadvertent neck extension during these studies may exacerbate cord injuries that have occurred in extension. We believe that in the appropriate clinical setting, high quality AP and lateral radiographs are all that is required for the evaluation of these patients in the acute setting.

REFERENCES

1. Kurtzke JF. Epidemiology of spinal cord injury. *Exp Neurol* **1975**;48:163–236
2. Rowed DW, Tator CH. Cervical spondylosis in acute cervical cord injuries. In: Tator C, ed. *Early management of acute spinal cord injury*. New York: Raven, **1982**:335–345
3. Hardy AG, Cervical spinal cord injury without bony injury. *Paraplegia* **1977**;14:296–305
4. Wolf BS, Khilnani M, Malis L. The sagittal diameter of the bony cervical spinal canal and its significance in cervical spondylosis. *J Mt Sinai Hosp* **1956**;23:283–292
5. Murone I. The importance of the sagittal diameters of the cervical spinal canal in relation to spondylosis and myelopathy. *J Bone Jt Surg [Br]* **1974**;56:30–36
6. Penning L. Prevertebral hematoma in cervical spine injury: inci-

dence and etiological significance. *AJNR* **1980**;1:557–565, *AJR* **1981**;136:553–561

7. Taylor AR, Blackwood W. Paraplegia in hyperextension cervical injuries with normal radiographic appearances. *J Bone Jt Surg [Br]* **1948**;30:245–248
8. Taylor AR. The mechanism of injury to the spinal cord in the neck without damage to the vertebral column. *J Bone Jt Surg [Br]* **1951**;33:543–547
9. Schneider RC, Thompson JM, Bebin J. The syndrome of acute central cervical spinal cord injury. *J Neurol Neurosurg Psychiatry* **1958**;21:216–227
10. Breig A, Turnbull I, Hassler O. Effects of mechanical stresses on the spinal cord in cervical spondylosis: a study on fresh cadaver material. *J Neurosurg* **1966**;25:45–56
11. Stoltmann HF, Blackwood W. The role of the ligamenta flava in the pathogenesis of myelopathy in cervical spondylosis. *Brain* **1962**;137:45–49
12. Roaf R. A study of the mechanics of spinal injuries. *J Bone Jt Surg [Br]* **1960**;42:810–823
13. Forsyth HF. Extension injuries of the cervical spine. *J Bone Jt Surg [Am]* **1964**;46:1792–1797
14. Scher AT. Cervical spinal cord injury without evidence of fracture or dislocation: an assessment of the radiological features. *S Afr Med J* **1976**;50:962–965
15. Cintron E, Gilula LA, Murphy WA, Gehweiler JA. The widened disk space: a sign of hyperextension injury. *Radiology* **1981**;141:636–644
16. Schneider RC, Cherry G, Patek H. The syndrome of acute central cervical spinal cord injury with special reference to the mechanisms involved in hyperextension injuries of the cervical spine. *J Neurosurg* **1954**;11:546–577

The Role of CT in Staging Radiographic $T_1N_0M_0$ Lung Cancer

Laurence R. Heavey[1]
Gary M. Glazer[1]
Barry H. Gross[1]
Isaac R. Francis[1]
Mark B. Orringer[2]

Thirty-one patients with non-small-cell bronchogenic carcinoma and standard chest radiographs showing $T_1N_0M_0$ tumors underwent preoperative chest and upper abdominal computed tomography (CT) with subsequent thorough surgical-pathologic correlation of their disease status. Eight patients (25.8%) had tissue-proven mediastinal or distant metastasis at presentation. In five (62.5%) of these eight patients the presence of unresectable disease was detected by CT and an unnecessary thoracotomy was avoided. These five patients comprised three with mediastinal lymph-node metastasis, one with adrenal metastasis, and one with a coexistent contralateral, proximal endobronchial tumor. Three patients with unresectable disease not detected by CT (CT false negatives) had metastasis to normal-sized mediastinal lymph nodes. There were two CT false-positive diagnoses of adrenal metastasis in patients proven by CT-guided aspiration to have benign adrenal masses, and these patients subsequently underwent curative lung resection. Although the data base is relatively small, the authors conclude that preoperative CT may be useful in evaluating patients with radiographic $T_1N_0M_0$ lung cancer.

Many studies have tried to clarify the role of computed tomography (CT) in the preoperative staging of non-small-cell bronchogenic carcinoma [1-13]. The results are mixed and the conclusions often contradictory. Since surgical resection offers the only realistic chance for cure, the usefulness of CT depends on its ability to provide an accurate preoperative evaluation of resectability (e.g., detection of disease in sites that would preclude resection), thereby sparing some patients the unnecessary risks and costs of a thoracotomy. The efficacy of preoperative CT may be affected by the presurgically determined TNM clinical stage of disease. Several authors have questioned the value of CT in the subset of patients with $T_1N_0M_0$ disease on standard chest radiographs [2, 3, 8, 14] because of the presumed low prevalence of mediastinal or distant metastatic disease with these neoplasms. Pearlberg et al. [2] recently addressed this issue in a study of 23 patients with conventional radiographic $T_1N_0M_0$ disease, demonstrating CT evidence of unresectability in only one patient (4%). They concluded that CT is not likely to provide information that would alter the treatment of radiographically determined $T_1N_0M_0$ lung cancer. We report 31 patients with radiographic $T_1N_0M_0$ non-small-cell bronchogenic carcinoma who underwent preoperative chest and upper abdominal CT with subsequent thorough surgical-pathologic correlation of their disease status.

Materials and Methods

The records of all patients with bronchogenic carcinoma treated at our institution from January 1981 to January 1985 were reviewed retrospectively. Within this group were 31 patients with non-small-cell lung cancer and plain chest radiographs showing $T_1N_0M_0$ tumors. In accordance with the American Joint Committee for Cancer Staging TNM Criteria for Bronchogenic Carcinoma, a $T_1N_0M_0$ lesion on standard posteroanterior and lateral chest

Received May 20, 1985; accepted after revision September 20, 1985.

This work was supported in part by a Robert A. Sullivan memorial grant for cancer research (no. PDT-242) from the American Cancer Society.

[1] Department of Radiology, University of Michigan Medical Center, Ann Arbor, MI 48109-0010. Address reprint requests to G. M. Glazer (Box 13).

[2] Department of Surgery, Section of Thoracic Surgery, University of Michigan Medical Center, Ann Arbor, MI 48109-0010.

AJR 146:285-290, February 1986
0361-803X/86/1462-0285
© American Roentgen Ray Society

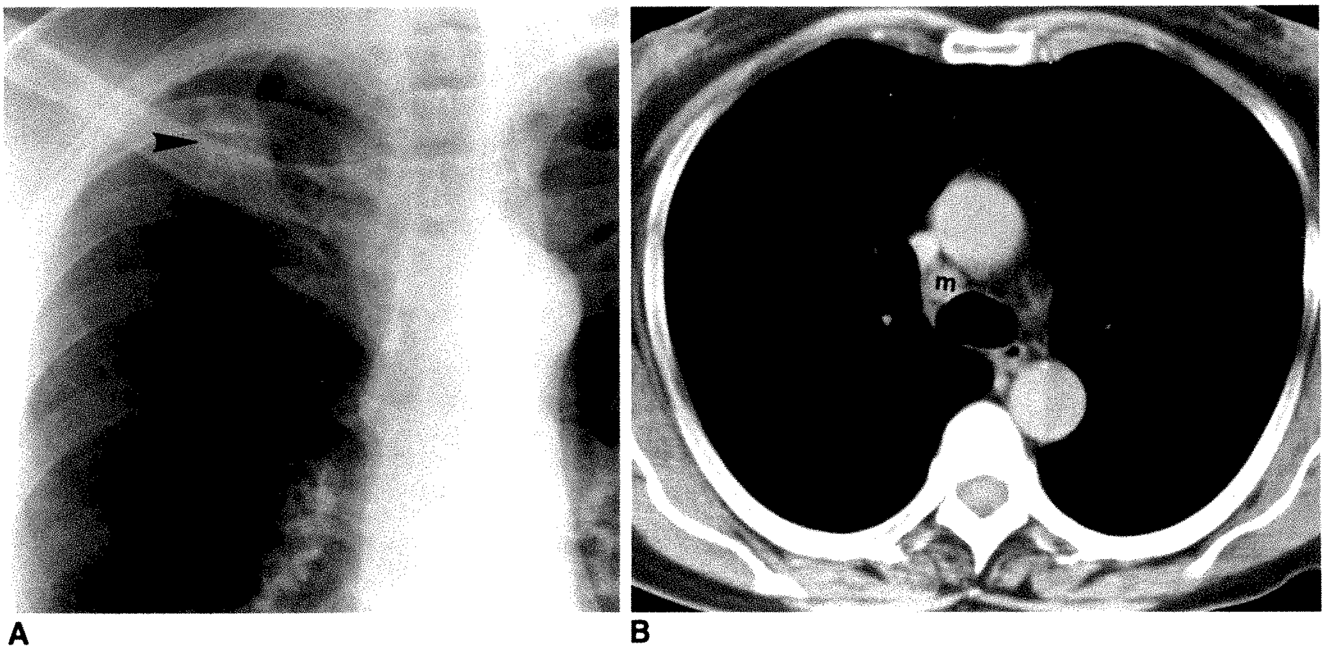

Fig. 1.—**A**, Posteroanterior chest radiograph shows 1.5-cm adenocarcinoma in right upper lobe (*arrowhead*). **B**, CT scan in same patient at level of azygos arch demonstrates 11-mm right tracheobronchial lymph node metastasis (m) in region 10R.

radiographs was defined as a solitary pulmonary nodule of 3 cm or less in diameter, completely surrounded by lung parenchyma, with a normal appearance of the pulmonary hila and mediastinum. The nodules were further categorized as central (within 3 cm of the hilum) or peripheral. The conventional radiographic studies were reviewed independently by two experienced radiologists (L. R. H. and B. H. G.) in order to ensure that the primary tumors were T1 lesions.

There were 17 men (age range, 50–82 years; mean, 64) and 14 women (age range, 47–71 years; mean, 59). On the standard chest radiographs, nodule size ranged from 1.4 to 3.0 cm (mean, of 2.3). Of the 31 nodules, 12 were in the right upper lobe, 11 in the left upper lobe, four in the right lower lobe, three in the left lower lobe, and one in the right middle lobe. Seven nodules were classified as central in location and 24 were peripheral. Histologic type was adenocarcinoma in 16 patients (including two with alveolar cell carcinoma), squamous-cell carcinoma in 12, large-cell carcinoma in one, poorly differentiated carcinoma in one, and carcinoid in one.

All 31 patients had preoperative chest and upper abdominal CT scans performed on either a General Electric 8800 or 9800 CT/T scanner. Contiguous 1-cm-thick sections were obtained from the lung apices through the adrenal glands. Rapid intravenous drip infusion of 30% meglumine iothalamate (Conray-30) was given in every case. At the level of the pulmonary hila, dynamic incremental scanning was performed during and after bolus intravenous injection of 50–75 ml of 60% meglumine iothalamate [15]. Scans were reviewed for evidence of metastatic tumor involving the mediastinal and/or hilar lymph nodes, chest wall, pulmonary parenchyma, adrenal glands, and visualized parts of the bones, liver, and upper abdomen. Mediastinal lymph nodes were identified using commonly accepted criteria and classified according to region using the American Thoracic Society scheme [16]. Mediastinal nodes were considered abnormal if they exceeded 10 mm in short axis [1, 17]. Nonenhancing hilar soft tissue greater than 10 mm in short axis was considered abnormal [18]. Adrenal masses were diagnosed in the presence of adrenal nodularity. CT examinations were reviewed independently by three of us (L. R. H., G. M. G., and I. R. F.) who are experienced in CT. In equivocal cases (either CT or conventional radiographs) a consensus was reached by the entire group.

If at CT the mediastinum and adrenal glands were normal, with no evidence of spread to other visualized distant organs, the patient underwent thoracotomy, pulmonary resection, and mediastinal lymph-node dissection. The dissection included systematic excision of all identifiable subcarinal and ipsilateral paratracheal, superior mediastinal, and inferior pulmonary ligament lymph nodes. If CT demonstrated enlarged mediastinal lymph nodes, local biopsy of these abnormal nodes was performed by mediastinoscopy or mediastinotomy. Patients undergoing mediastinoscopy had routine sampling of high and low right paratracheal, anterior subcarinal, and left paratracheal nodes, if present. A positive biopsy precluded thoracotomy (except in patients with ipsilateral low paratracheal nodes). Negative biopsies in patients with enlarged mediastinal nodes were followed by pulmonary resection with mediastinal node dissection. CT-guided fine-needle aspiration was performed for suspected metastases in the adrenals or other distant organs, and thoracotomy was not undertaken if metastatic disease was confirmed.

Final histologic diagnosis was obtained at thoracotomy and mediastinal exploration in 26 patients, at mediastinoscopy in three, by CT-guided fine-needle aspiration in one, and at bronchoscopy in one.

Results

CT detected metastatic disease and significantly altered therapy in five patients (16.1%). Three patients were found to have abnormally enlarged mediastinal lymph nodes at CT examination. The first of these patients had a peripheral 1.5-cm adenocarcinoma in the right upper lobe and an 11-mm right tracheobronchial lymph node (region 10R, fig. 1). The

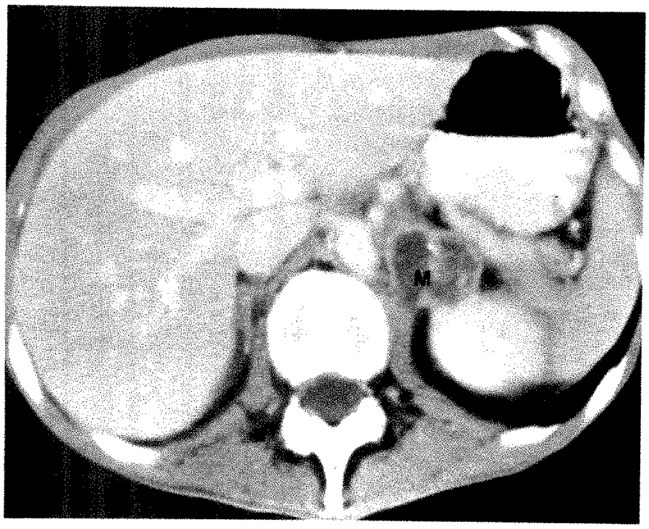

Fig. 2.—3-cm low-attenuation left adrenal metastasis (M).

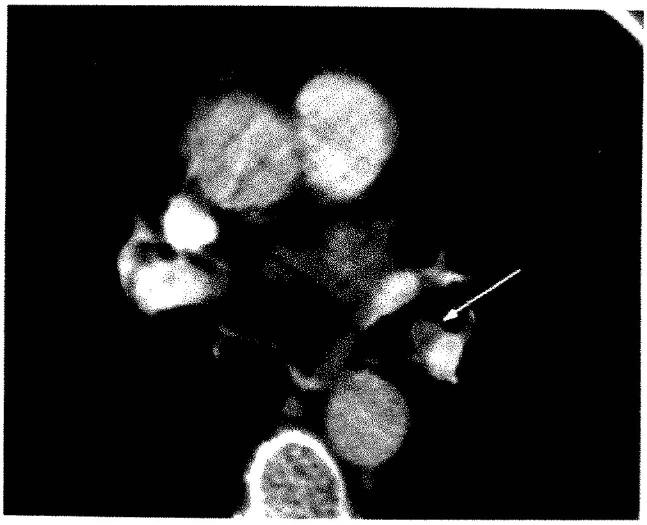

Fig. 3.—1.2-cm endobronchial primary tumor near junction of left main and left-upper-lobe bronchi (*arrow*).

second patient had a peripheral 2-cm squamous-cell carcinoma in the right upper lobe and a 20-mm right tracheobronchial lymph node (region 10R). The third patient had a peripheral 1.5-cm adenocarcinoma in the left lower lobe and enlarged nodes in the left upper paratracheal (11 mm; region 2L), right upper paratracheal (14 mm; region 2R), and right tracheobronchial (10 mm; region 10R) regions. In all three patients mediastinal metastasis was subsequently confirmed at mediastinoscopy. One patient with a 3-cm adenocarcinoma in the right upper lobe had a 3-cm left adrenal metastasis (fig. 2) detected by CT and confirmed by CT-guided fine-needle aspiration. One patient with a 1.5-cm peripheral nodule in the right upper lobe had a 1.2-cm endobronchial mass at the junction of the left main and left-upper-lobe bronchi (fig. 3). Bronchoscopy with biopsy confirmed the presence of endobronchial squamous-cell carcinoma. Subsequent fluoroscopically guided fine-needle aspiration of the right-upper-lobe nodule yielded metastatic squamous-cell carcinoma. In these five patients thoracotomy was averted and palliative therapy begun.

Three additional patients, two with adenocarcinoma (both peripheral) and one with squamous-cell carcinoma (central), were discovered at thoracotomy (but not at CT) to have mediastinal lymph nodes containing tumor. In all three patients the positive nodes were 10 mm or less in shortest axis and thus, according to our size criteria, would not have been considered abnormally enlarged. There were thus three false-negative CT scans in this study. Overall, of our 31 patients judged clinically to have $T_1N_0M_0$ disease, eight (25.8%) had metastatic disease at presentation.

Three patients had tumor spread to ipsilateral hilar lymph nodes, necessitating postsurgical classification as $T_1N_1M_0$. This does not preclude attempted curative surgery, and thoracotomy with lobectomy was performed in each of these patients. There were two false-positive CT scans for hilar adenopathy. In one of these patients a small endobronchial squamous-cell tumor in the superior segmental bronchus of the right lower lobe was mistakenly interpreted as an enlarged hilar node. In the other patient an enlarged hilar node was present but was histologically benign.

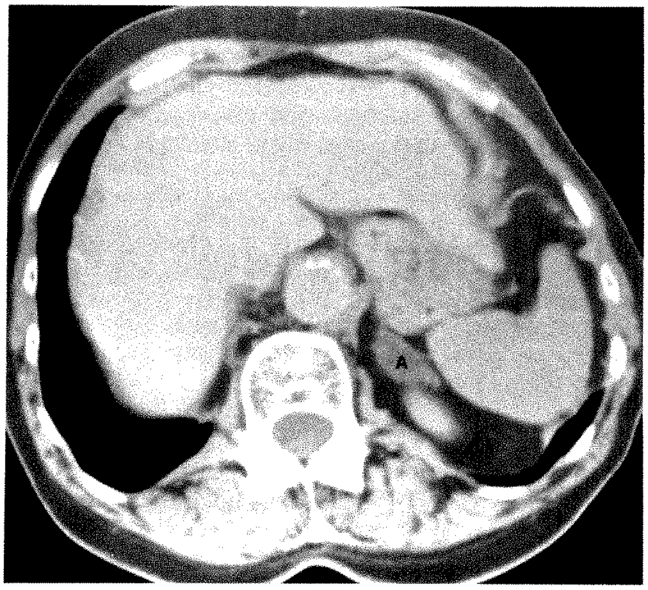

Fig. 4.—False-positive CT scan for adrenal metastasis: 1.8-cm, homogeneous, low-attenuation left adrenal adenoma (A). (Cf. fig. 2.)

Two patients had left adrenal masses measuring 1.8 cm (fig. 4) and 3.0 cm, respectively, that yielded benign histology at CT-guided fine-needle aspiration (representing either adenoma or nodular hyperplasia). Thoracotomy with lobectomy was subsequently performed in both patients. These were the only CT false positives in this study.

The remaining 16 patients had normal CT of the mediastinum, hila, and adrenal glands. All 16 underwent thoracotomy with lobectomy and mediastinal exploration, and no mediastinal or hilar lymph node metastasis was found at surgery.

Discussion

Whether preoperative CT is warranted in patients with radiographically determined $T_1N_0M_0$ non-small-cell lung cancer depends on such factors as the prevalence of metastatic spread of disease to the mediastinum or distant sites, the likelihood of detection of nodal or distant tumor by CT, the frequency of false-positive CT scans, and the cost of normal CT scans as compared to the cost of unnecessary thoracotomies that would otherwise be performed. In our study, eight (25.8%) of 31 patients with $T_1N_0M_0$ lung cancer on standard chest radiographs were discovered to have metastatic disease. Six patients (19.3%) had mediastinal metastasis, one (3.2%) had an adrenal metastasis, and one had a peripheral nodule and a contralateral proximal endobronchial lesion. CT detected disease occult to conventional radiography in five (62.5%) of these eight patients, thereby preventing unnecessary thoracotomy.

The true prevalence of occult distant tumor spread in radiographic $T_1N_0M_0$ disease is difficult to ascertain from the literature because of variability in the patient populations studied (not all studies have used the standard TNM classification) and in the methods of evaluating various sites for spread of disease (e.g., the mediastinum). There are several studies in the surgical literature [19–24] that report the results of preoperative staging mediastinoscopy and/or mediastinotomy in lung cancer patients. Baker et al. [19] studied a group of 80 patients with $T_1N_0M_0$ lesions on standard chest radiographs, 40 of whom had preoperative mediastinoscopy and 40 of whom went directly to thoracotomy. Both groups received "mediastinal palpation" at thoracotomy for evidence of lymphadenopathy. In neither group was the mediastinal pleura routinely opened, nor were mediastinal lymph nodes routinely sampled. The prevalence of mediastinal metastasis was 7.5% in the group undergoing preoperative mediastinoscopy and 5% in the combined groups. Baggs and Braun [20] reported a 4.8% prevalence of mediastinal lymph-node metastasis in 42 patients with peripheral $T_1N_0M_0$ lesions. All patients received preoperative mediastinoscopy, but the method of mediastinal exploration at thoracotomy was not stated. Of 32 patients with peripheral lesions of 4 cm or less in diameter, Hutchinson and Mills [21] found mediastinal metastases in 10 (31%). In that study only two (10%) of 20 patients with squamous-cell carcinoma or adenocarcinoma had mediastinal metastases, while eight (67%) of 12 patients with small-cell, large-cell, and undifferentiated carcinoma had positive mediastinal nodes. Not all of these patients underwent preoperative mediastinoscopy. The authors did not describe their method of mediastinal exploration at thoracotomy, nor did they specify how often mediastinal tumor was evident on chest radiographs. In 11 patients with peripheral non-small-cell lesions (size not specified), Stanford et al. [22] found one patient (9%) with mediastinal tumor at mediastinoscopy. These results were not correlated with results of thoracotomy. Smith et al. [23] found a 6.6% (4/61) prevalence of mediastinal metastasis in patients with "peripheral" ($\leq$ 4 cm in diameter; outer two-thirds of lung) non-small-cell lung cancers. Preoperative mediastinoscopy was not performed in these patients, and details of mediastinal evaluation at surgery were not disclosed. Whitcomb et al. [24] reported that of 33 patients with peripheral squamous-cell carcinoma or adenocarcinoma of 4 cm or less in diameter, only one (3%) had mediastinal metastasis. Twenty-one of these patients did not undergo preoperative mediastinoscopy, and details of mediastinal node exploration at surgery were not given.

The prevalence of mediastinal metastases in patients with lung cancer has been addressed also in the radiologic literature [1–13]. Only Pearlberg et al. [2] specifically studied a population with radiographic $T_1N_0M_0$ tumors. They found an 8.7% (2/23) prevalence of mediastinal metastases. Two other studies have reported patients with $T_1N_0M_0$ lesions. Libshitz et al. [3] found mediastinal metastases in two (15.3%) of 13 whereas Glazer et al. [1] found mediastinal metastases in four (26.7%) of 15. The prevalence of mediastinal disease in our current study is six (19.3%) of 31 patients. Since this study includes the 15 patients from our earlier report as well as 16 new patients, we believe the prevalence of 19.3% is a more accurate reflection of the experience at our institution. One important difference between the studies is that in both our study and the study of Libshitz et al. [3], excision of all identifiable subcarinal and ipsilateral mediastinal nodes was carried out, whereas in the study of Pearlberg et al. [2] all mediastinal nodal groups were not routinely sampled.

It is quite clear from these data that there is considerable difference of opinion in the surgical and radiologic literature about the true prevalence of mediastinal metastasis in radiographic $T_1N_0M_0$ disease. Studies from the surgical literature indicate that about 3%–10% of patients with small, peripheral lung cancers will have mediastinal metastasis. This is probably not completely accurate for $T_1N_0M_0$ tumors nor directly comparable to our study for several reasons. In several investigations, lesions greater than 3 cm (and thus not T1 tumors) were included in the analysis. Also, a major problem in the surgical studies was the use of undirected mediastinoscopy in mediastinal nodal sampling along with incomplete surgical exploration of the mediastinum. Although the first problem might lead to an overestimation of the true prevalence of mediastinal metastasis, the latter two would result in underestimation. As noted above, routine mediastinal nodal sampling was not performed in the study of Pearlberg et al. [2]. This may explain in part the differences in results between their study and ours. The prevalence of mediastinal metastasis revealed in our study, in which CT was used to direct mediastinoscopy and where systematic, comprehensive mediastinal nodal dissection was done in all patients, may more closely approximate the true prevalence of mediastinal disease. There is a suggestion that the increased prevalence of mediastinal metastasis in T1 lesions that we report shows a trend of being significantly different from that of comparable studies ($p = 0.06$ between our study and references 2, 3, 19, and 20 using the Fisher exact test). Clearly, additional studies of many more $T_1N_0M_0$ lesions are needed to accumulate statistically meaningful results.

The efficacy of CT in detecting mediastinal metastasis is another controversial issue that has been reviewed recently [1, 14]. Although the actual accuracy of CT in this regard has not yet been definitively determined, many would agree with us that CT serves a useful role in directing surgical biopsy of abnormally enlarged mediastinal lymph nodes and that a normal mediastinum at CT eliminates the need for additional staging procedures before thoracotomy. In the current study, which represents a highly selected population that is not at all representative of the usual patient with lung cancer, we found a 50% (3/6) false-negative rate for CT detection of mediastinal metastasis. This is a much higher false-negative rate than in our previous report, which studied a more representative patient population. All of our CT false negatives in the current study were metastases in normal-sized nodes. In this regard it is noteworthy that a recent study suggests a far more favorable prognosis for patients with non-small-cell lung cancer and mediastinal metastasis discovered only at thoracotomy (and not at mediastinoscopy), as compared to the prognosis for patients with mediastinal metastasis discovered at mediastinoscopy [25]. We believe that mediastinal metastases missed by mediastinoscopy probably occur in normal-sized nodes whereas most metastases identified at mediastinoscopy occur in enlarged nodes.

Three (9.7%) of our patients had adrenal masses, one of which (3.2%) proved to be a metastasis. This is similar to the results of Oliver et al. [26], who found a 2.4% (8/330) prevalence of adrenal metastases in patients with non-small-cell bronchogenic carcinoma. As in our series, about two-thirds of their patients with adrenal masses had benign lesions. However, since they did not detail the TNM classification of their patients, the two studies are not strictly comparable.

Is CT of radiographic $T_1N_0M_0$ tumors cost-effective? At our institution the cost of an uncomplicated thoracotomy with lobectomy is about $16,000. This includes immediate preoperative mediastinoscopy and rigid bronchoscopy under general anesthesia. In comparison, current fees are about $550 for outpatient CT, $950 for diagnostic mediastinoscopy, $560 for CT-guided fine-needle aspiration, $250 for fluoroscopically guided fine-needle aspiration, and $500 for bronchoscopy with biopsy. In this study the five thoracotomies not performed because of metastatic disease detected by CT would have cost at least $80,000. The cost of CT examinations for all 31 patients plus the diagnostic tests resulting from CT evidence of potential metastatic disease in seven patients (five true-positive unresectable masses and two false-positive adrenal masses) was about $22,500. Thus, preoperative staging CT resulted in net savings of $57,500, or about $1855 per patient.

In conclusion, we believe our results support a role for CT in the preoperative staging of standard radiographic $T_1N_0M_0$ non-small-cell lung cancer. We found a higher prevalence of distant tumor spread at presentation in this subset of lung cancer patients than has been reported. CT correctly identified more than half of the patients with unresectable disease, thereby preventing unnecessary thoracotomies and resulting in major cost savings. However, since our results and conclusions differ significantly from those of other studies and because the total number of patients with radiographic $T_1N_0M_0$ disease in all of the studies is small, further investigation of the role of CT in this subset of lung cancer patients is warranted.

REFERENCES

1. Glazer GM, Orringer MB, Gross BH, Quint LE. The mediastinum in non-small cell lung cancer: CT-surgical correlation. *AJR* **1984**;142:1101–1105
2. Pearlberg JL, Sandler MA, Beute GH, Madrazo BL. $T_1N_0M_0$ bronchogenic carcinoma: assessment by CT. *Radiology* **1985**;157:187–190
3. Libshitz HI, McKenna RJ Jr, Haynie TP, McMurtrey MJ, Mountain CT. Mediastinal evaluation in lung cancer. *Radiology* **1984**;151:295–299
4. Baron RL, Levitt RG, Sagel SS, White MJ, Roper CL, Marbarger JP. Computed tomography in the preoperative evaluation of bronchogenic carcinoma. *Radiology* **1982**;145:727–732
5. Osborne DR, Korobkin M, Ravin CE, et al. Comparison of plain radiography, conventional tomography, and computed tomography in detecting intrathoracic lymph node metastases from lung carcinoma. *Radiology* **1982**;142:157–161
6. Lewis JW Jr, Madrazo BL, Gross SC, et al. The value of radiographic and computed tomography in the staging of lung carcinoma. *Ann Thorac Surg* **1982**;34:553–558
7. Richey HM, Matthews JI, Helsel RA, Cable H. Thoracic CT scanning in the staging of bronchogenic carcinoma. *Chest* **1984**;85:218–221
8. Faling LJ, Pugatch RD, Jung-Legg Y, et al. Computed tomographic scanning of the mediastinum in the staging of bronchogenic carcinoma. *Am Rev Respir Dis* **1981**;124:690–695
9. Hirleman MT, Yiu-Chiu VS, Chiu LC, Shapiro RL. The resectability of primary lung carcinoma: a diagnostic staging review. *CT* **1980**;4:146–163
10. Yee ES, Raper SE, Thomas AN, Ebert PA. Technical accuracy and clinical efficacy of thoracic computed tomography. *Am J Surg* **1982**;144:35–43
11. Rea HH, Shevland JE, House AJS. Accuracy of computed tomographic scanning in assessment of the mediastinum in bronchial carcinoma. *J Thorac Cardiovasc Surg* **1981**;81:825–829
12. Moak GD, Cockerill EM, Farber MO, Yaw PB, Manfred F. Computed tomography vs. standard radiology in the evaluation of mediastinal adenopathy. *Chest* **1982**;82:69–75
13. Underwood GH Jr, Hooper RG, Axelbaum SP, Goodwin DW. Computed tomography scanning of the thorax in the staging of bronchogenic carcinoma. *N Engl J Med* **1979**;300:777–778
14. Libshitz HI. CT of mediastinal lymph nodes in lung cancer: Is there a "state of the art"? *AJR* **1983**;141:1081–1085
15. Glazer GM, Francis IR, Gebarski K, Samuels BI, Sorenson KW. Dynamic incremental computed tomography in evaluation of the pulmonary hila. *J Comput Assist Tomogr* **1983**;7:59–64
16. Clinical staging of primary lung cancer. American Thoracic Society node mapping scheme. *Am Rev Respir Dis* **1983**;127:659–669
17. Glazer GM, Gross BH, Quint LE, Francis IR, Bookstein FL, Orringer MB. Normal mediastinal lymph nodes: number and size according to American Thoracic Society mapping. *AJR* **1985**;144:261–265
18. Glazer GM, Gross BH, Aisen AM, Quint LE, Francis IR, Orringer

MB. Imaging of the pulmonary hilum: a prospective comparative study in patients with lung cancer. *AJR* **1985**;145:245–248

19. Baker RR, Lillemoe KD, Tockman MS. The indications for transcervical mediastinoscopy in patients with small peripheral bronchial carcinoma. *Surg Gynecol Obstet* **1979**;148:860–862
20. Baggs KJ, Braun RA. An evaluation of mediastinoscopy as a guide to diagnosis and therapy. *Arch Surg* **1976**;111:703–706
21. Hutchinson CM, Mills NL. The selection of patients with bronchogenic carcinoma for mediastinoscopy. *J Thorac Cardiovasc Surg* **1976**;71:768–773
22. Stanford W, Steele S, Armstrong RG, Larsen GL. Mediastinoscopy. *Ann Thorac Surg* **1975**;19:121–126
23. Smith SR, Hooper RG, Beechler CR, Whitcomb MF. Indications for mediastinal lymph node evaluation. *Chest* **1982**;81:599–604
24. Whitcomb ME, Barham E, Goldman AL, Green DC. Indications for mediastinoscopy in bronchogenic carcinoma. *Am Rev Resp Dis* **1976**;113:189–195
25. Pearson FG, DeLarue NC, Ilves R, Todd TRJ, Cooper JD. Significance of positive mediastinal nodes identified at mediastinoscopy in patients with resectable cancer of the lung. *J Thorac Cardiovasc Surg* **1982**;83:1–11
26. Oliver TW Jr, Bernardino ME, Miller JI, Mansour K, Greene D, Davis WA. Isolated adrenal masses in nonsmall-cell bronchogenic carcinoma. *Radiology* **1984**;153:217–218

Low-Attenuation Thoracic Metastases in Testicular Malignancy

David M. Yousem[1]
John C. Scatarige
Elliot K. Fishman
Stanley S. Siegelman

Low-density abdominal and pelvic lymph nodes are seen in nearly half of patients with testicular cancers. Thoracic low-attenuation metastases are much less common. Three cases of low-density metastases to lung parenchyma and mediastinal nodes are presented. In a man of appropriate age, a low-attenuation pulmonary or mediastinal mass should prompt a search for a primary testicular neoplasm.

Representing less than 1% of all fatal cancer in males, testicular malignancy is nevertheless a leading cause of cancer-related death in men 25–34 years of age [1]. The value of computed tomography (CT) in the staging, treatment planning, and follow-up of patients with testicular cancer has been established in the radiologic and urologic literature [2–13]. A pattern of low-attenuation (<30 H) nodal metastasis has been described in 43%–46% of patients with testicular cancer and a positive CT study [10, 13]; with one exception [13], all such metastases have been confined to abdominal and pelvic lymph nodes.

We present three additional patients with testicular malignancy whose thoracic CT examinations using a Siemans Somatom DR-3 scanner disclosed low-density metastases to lung parenchyma and mediastinal nodes.

Case Reports

Case 1

A 32-year-old man had a painless left testicular mass and extensive cervical lymph-node enlargement. Radiologic studies revealed mediastinal and retroperitoneal adenopathy. Left orchiectomy disclosed embryonal cell carcinoma, and a course of vinblastine, bleomycin, and cisplatin chemotherapy was instituted. The patient's human chorionic gonadotropin and alpha-fetoprotein tumor markers fell precipitously, but a contrast-enhanced CT scan 13 months after cessation of chemotherapy revealed multiple bilateral lung nodules up to 2.5 cm in diameter, mediastinal and hilar lymphadenopathy, and subcrural and paraaortic abdominal nodes. CT attenuation values ranged from −8 to 8 H (fig. 1). The patient elected to be followed with biannual CT scans since he was asymptomatic and had tolerated chemotherapy poorly.

Case 2

A 19-year-old white man with painless right testicular swelling had a nonproductive cough, dyspnea, and lethargy. A CT scan after admission chest radiograph revealed right-lower-lobe consolidation with low-density parenchymal masses and mediastinal adenopathy (fig. 2). Orchiectomy revealed teratocarcinoma as did bronchoscopic sampling of subcarinal and right hilar lymph nodes. After four courses of vinblastine, bleomycin, and cisplatin therapy, his abdominal nodes had resolved; thoracotomy specimens of residual enlarged nodes demonstrated only benign teratoma with no evidence of active malignancy. Despite histologic maturation of the tumor, the CT attenuation of the thoracic nodes remained the same on serial examinations. The patient was doing well at 10 months after cessation of therapy.

Received June 3, 1985; accepted after revision September 9, 1985.

[1] All authors: Russell H. Morgan Department of Radiology and Radiological Sciences, The Johns Hopkins Hospital, 600 N. Wolfe St., Baltimore, MD 21205. Address reprint requests to D. M. Yousem.

AJR 146:291–293, February 1986
0361–803X/86/1462–0291
© American Roentgen Ray Society

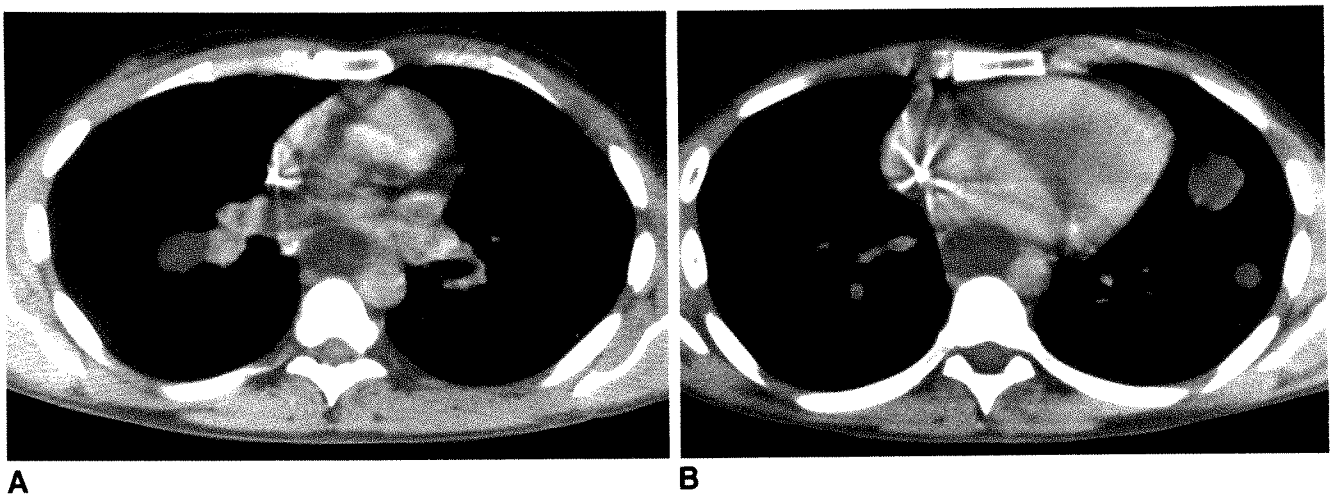

Fig. 1.—Case 1. Axial CT scans at level of right hilum (**A**) and heart (**B**) reveal low-density mass lateral to right hilum; paraesophageal lymph nodes; and low-density masses in left lung, largest of which has attenuation value of −8 H.

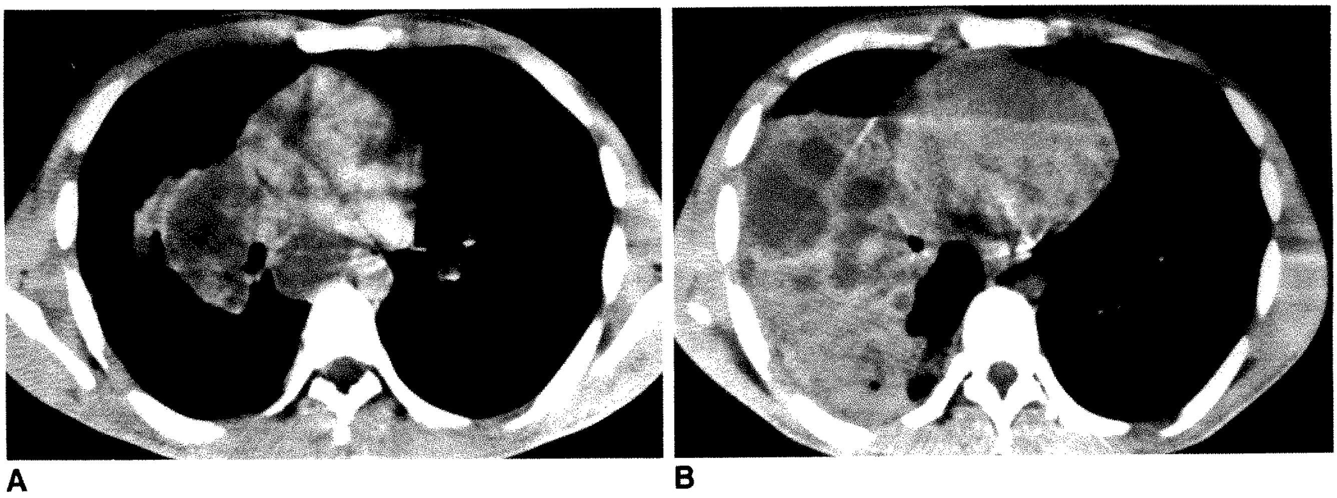

Fig. 2.—Case 2. Contrast-enhanced CT scans at level of right hilum (**A**) and right lower lobe (**B**) demonstrate low-density right hilar, subcarinal lymph nodes and multiple low-density areas within consolidated right lung. Subsequent orchiectomy and bronchoscopic biopsy of right mediastinal lymph nodes revealed teratocarcinoma.

Case 3

A 19-year-old white man had a painless right testicular mass. Orchiectomy disclosed an immature teratoma with elements of choriocarcinoma. The patient underwent retroperitoneal lymph-node dissection and subsequent vinblastine, bleomycin, and cisplatin chemotherapy. After four courses of therapy, thoracic CT revealed a large paraspinal lymph node with an attenuation value of 15.5 H, extending into the posterior mediastinum (fig. 3). The patient is continuing chemotherapy and will be followed with serial CT scans.

Discussion

Although testicular cancer typically spreads to retroperitoneal and supradiaphragmatic nodes before hematogenous dissemination occurs [2, 14], thoracic metastasis is not uncommon. Up to 81% of patients with testicular choriocarcinoma, 19% with seminoma, and 18% with nonseminomatous testicular tumors will develop pulmonary metastases during the course of their disease [2, 5, 9, 15]. Even with retroperitoneal nodes free of tumor, 10%–13% of patients with nonchoriocarcinomatous testicular cancer develop thoracic metastases [16]. Burney and Klatte [2] reported that 19% of patients with a normal chest radiograph at the time of clinical presentation eventually developed thoracic metastasis.

CT has been compared to lymphangiography, sonography, and magnetic resonance imaging in the staging of testicular cancer in recent studies. In all cases, CT has been as accurate as or more accurate than the other imaging methods [2, 4, 5, 12, 17]. Specific low-attenuation nodes or metastases on CT scanning have shown no characteristic magnetic resonance

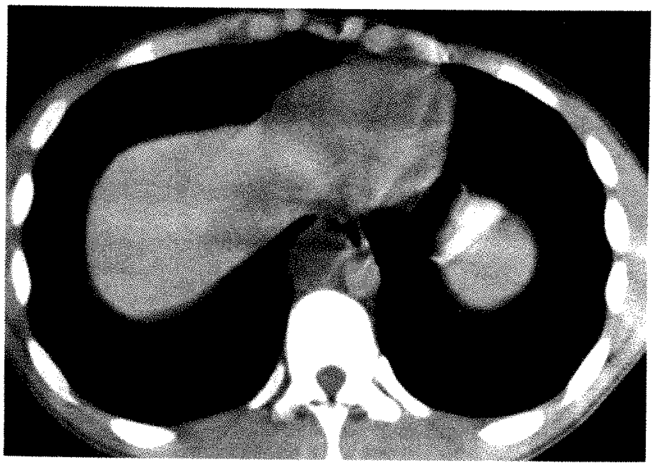

Fig. 3.—Case 3. CT scan through lower chest demonstrates oval paraesophageal low-density mass with attenuation value of 15.5 H. Patient had undergone retroperitoneal lymph-node dissection and chemotherapy for immature teratoma.

or sonographic features that would serve to distinguish these testicular metastases from other malignant deposits. CT therefore remains the examination of choice for the staging of testicular neoplasms.

The low-attenuation metastases reported in testicular malignancy have been ascribed to necrosis or cystic degeneration of tumor masses; lipid-laden macrophages with cholesterol clefts within necrotic cancer; or intrinsic properties of the malignancy [2, 6, 8, 9, 11, 13]. Husband et al. [11] proposed that a reduction in the mean CT number during treatment indicated that the residual mass did not contain viable malignant tissue. Other studies have failed to corroborate this finding [7, 13]. Indeed, patients may present with low-attenuation metastases before treatment is initiated [2, 6, 7, 11, 13], as in two of the three cases reported here. Zingas et al. [18] noted that in their series, all the "cystic" and "semicystic" metastases from testicular neoplasms contained teratomatous components, with the more cystic masses generally containing more mature teratomatous elements. They also observed that solid metastases were more likely to derive from seminomas or pure embryonal cell carcinomas [18].

The differential diagnosis of a low-attenuation intrathoracic mass includes abscess, bronchogenic and neurenteric cyst, resolving hematoma, treated lymphoma, lipoma, neurofibroma, tuberculous lymph nodes, cystic metastases from ovarian or gastric cancer, and hydatid disease. Clinical history, mass location, and laboratory data often provide critical information in narrowing the differential or in arriving at a specific diagnosis. We suggest that, in a man of appropriate age, CT discovery of an unexplained low-density pulmonary or mediastinal mass should prompt a search for a primary testicular neoplasm.

REFERENCES

1. MacKay EN, Sellers AH. A statistical review of malignant testicular tumours based on the experience of the Ontario Cancer Foundation Clinics, 1938–1961. *Canad Med Assoc J* **1966**;94:889–899
2. Burney BT, Klatte EC. Ultrasound and computed tomography of the abdomen in the staging and management of testicular carcinoma. *Radiology* **1979**;132:415–419
3. Lee JKT, McClennan BL, Stanley RJ, Sagel SS. Computed tomography in the staging of testicular neoplasms. *Radiology* **1979**;130:387–390
4. Dunnick NR, Javadpour N. Value of CT and lymphography: distinguishing retroperitoneal metastases from nonseminomatous testicular tumors. *AJR* **1981**;136:1093–1099
5. Thomas JL, Bernardino ME, Bracken RB. Staging of testicular carcinoma: comparison of CT and lymphangiography. *AJR* **1981**;137:991–996
6. Pillari G, Rubenstein WA, Siess J. Seminoma: improved imaging and tumor characterization with computed tomography. *J Urol* **1980**;123:41–43
7. Soo CS, Bernardino ME, Chuang VP. Ordonez N. Pitfalls of CT findings in post-therapy testicular carcinoma. *J Comput Assist Tomogr* **1981**;5:39–41
8. Javadpour N, Anderson T, Doppman JL. Computed tomography in evolution of testicular cancer during intensive chemotherapy. *J Urol* **1979**;122:565–567
9. Husband JE, Peckham MJ, MacDonald JS, Hendry WF. The role of computed tomography in the management of testicular teratoma. *Clin Radiol* **1979**;30:243–252
10. Husband JE, Peckham MJ, MacDonald JS. The role of abdominal computed tomography in the management of testicular tumours. *CT* **1980**;4:1–16
11. Husband JE, Hawkes DJ, Peckham MJ. CT estimations of mean attenuation values and volume in testicular tumors: a comparison with surgical and histologic findings. *Radiology* **1982**;144:553–558
12. Lien HH, Kolbenstvedt A, Talle K, Fossa SD, Klepp O, Ous S. Comparison of computed tomography, lymphography, and phlebography in 200 consecutive patients with regard to retroperitoneal metastases from testicular tumor. *Radiology* **1983**;146:129–132
13. Scatarige JC, Fishman EK, Kuhajda FP, Taylor GA, Siegelman SS. Low attenuation nodal metastases in testicular carcinoma. *J Comput Assist Tomogr* **1983**;7:682–687
14. Fraley EE, Lange PH, Williams RD, Ortlip SA. Staging of early non-seminomatous germ-cell testicular cancer. *Cancer* **1980**;45:1762–1767
15. Schwartz SI, Shires GT, Spencer FC, Storer EH. *Principles of surgery*, 3d ed. New York: McGraw-Hill, **1979**
16. Staubitz WJ, Early KS, Magoss IV, Murphy GP. Surgical management of testis tumor. *J Urol* **1974**;111:205–209
17. Ellis JH, Bies JR, Kopecky KK, Klatte EC, Rowland RG, Donohue JP. Comparison of NMR and CT imaging in the evaluation of metastatic retroperitoneal lymphadenopathy from testicular carcinoma. *J Comput Assist Tomogr* **1984**;8:709–719
18. Zingas AP, Jain AB, Loredo RD, Kling GA. The spectrum of computed tomographic appearance of metastatic masses from testicular neoplasms. *CT* **1984**;8:53–60

Book Reviews

Bockus Gastroenterology, 4th ed. Edited by J. Edward Berk, William S. Haubrich, Martin H. Kalser, James L. A. Roth, and Fenton Schaffner. Philadelphia: Saunders, 5408 pp. in seven volumes (including 106 pp. index in each volume), 1985. Vol. I: Clinical Approach to the Patient, Diagnostic Procedures, 665 pp. Vol. II: Esophagus, Stomach, and Duodenum, 772 pp. Vol. III: Intestine, Part One. Small Intestine; Vascular Disorders; Specific Infectious Diseases, 654 pp. Vol. IV: Intestine, Part Two. Chronic Inflammatory Bowel Disease; Colon, 532 pp. Vol. V: Liver, 824 pp. Vol. VI: Biliary Tract and Pancreas, 728 pp. Vol. VII: Peritoneum; Parasites; Nutrition; Relationships with Other Systems; Cancer, 554 pp. $495 set or $80/volume

It would be presumptuous of me to say that I had more than sipped of the heady draught that is the fourth edition of *Bockus Gastroenterology*, some 5408 pages in seven volumes. The list of contributors is a "Who's who" of international gastroenterology and hepatology. What I did was to record my impressions of my browsing during a month when I was trying to keep abreast of a very good fellow and student on the gastrointestinal consultative service. Here are some of my impressions:

Acute pancreatitis: a good adequate description.

Cystadenoma of the pancreas: reproduction of the radiographs were poor, and the photomicrograph was nearly useless.

Anal incontinence: this was a short section of little help. Left out was a description of operant conditioning.

Sclerosing cholangitis: a good succinct description.

Whipple disease: a very good section; references up to 1982.

Zinc metabolism: no information on how it is absorbed.

Thus, a specialist will probably find these volumes uneven in quality. Published in April of 1985, the references go up to 1983, so ambitious textbooks, such as Bockus, become outdated in this era of information overload. However, a library, such as in a Division of Radiology, might want to have a single source of conventional wisdom for gastroenterology and liver disease. Bockus would be a good tome to open before pursuing a subject further in the current literature. At the price of $495 for the set of seven volumes, libraries will be the main buyers.

David R. Saunders
Division of Gastroenterology
University of Washington
Seattle, Washington 98195

Nuclear Medicine Annual 1985. Edited by Leonard M. Freeman and Heidi S. Weissmann. New York: Raven, 352 pp., 1985. $59.50

Nuclear Medicine Annual 1985 is a collection of review articles on nuclear medicine topics. In no sense is it a substitute for the *Yearbook of Nuclear Medicine*, which abstracts and comments on the prior year's nuclear medicine research. The annual also is not a substitute for *Seminars in Nuclear Medicine*, which like the annual is another Freeman project. The seminars usually deal with one topic per issue or set of issues. The annual can best be thought of as a supplement to Dr. Freeman's textbook of nuclear medicine, now in its third edition and considered the standard in the field.

Each of the individual review articles in the annual is good. There is a certain symmetry in Dr. Merle K. Loken's walk through nuclear medicine, the first chapter, which begins with the early use of P^{32}. The last chapter is by Drs. Douglas Van Norstrand and Edward B. Silberstein and reviews the therapeutic uses of P^{32}. In between there are chapters on Inflammatory Diseases, Blood Pool Imaging, Cholecystagogues, Pediatric Nuclear Gastroenterology, Pulmonary Nuclear Medicine, and Bone Scanning in Dental and Maxillofacial Disorders. This last chapter explores a neglected topic.

In addition there are two cardiac tomography chapters, one on Thallium Tomography, and the other Cardiac Magnetic Resonance Imaging (MRI). It seems every nuclear medicine periodical editor feels compelled to include at least one MRI topic. Both cardiac tomography chapters are from groups at the Cleveland Clinic.

Dr. D. Fink-Bennett's article on CCK, Sincalide, and Ceruletide diethylamine represents a fine compendium on the details of using these cholecystagogues.

Those readers liking the concept of a collection of review articles on various topics will find this collection diverting.

Marvin Guter
Richmond Memorial Hospital
Richmond, Va 23227

Talc: Understanding Its Manifestations in the Chest

David S. Feigin[1]

Four distinct forms of pulmonary disease caused by talc have been defined. The first form, *talcosilicosis*, is caused by talc mined with high-silica-content mineral. Findings in this form are identical with those of silicosis. *Talcoasbestosis* closely resembles asbestosis and is produced by crystalline talc, generally inhaled with asbestos fibers. Pathologic and radiographic abnormalities are virtually identical with those of asbestosis, including calcifications and malignant tumor formation. The third form, *talcosis*, caused by inhalation of pure talc, may include acute or chronic bronchitis as well as interstitial inflammation; radiographically, it appears as interstitial reticulations or small, irregular nodules, typical of small-airway obstruction. The fourth form, due to *intravenous administration* of talc, is usually associated with abuse of oral medications and production of vascular granulomas manifested by consolidations, large nodules, and masses. Radiographic abnormalities associated with talc can be predicted when there is sufficient history of the nature of exposure, including the region of origin of the talc in cases of inhalation. Radiographic changes, such as diaphragmatic plaques, often attributed to both talc and asbestos have not been documented to be caused by talc alone. The author provides review of 18 well-documented cases.

The term *talc* is applied both to a pure silicate of magnesium and to a mixture of minerals containing the pure substance and many other constituents [1]. Talc may be only a minor component of such a mixture. The clinical, pathologic, and radiographic manifestations that have been attributed to talc thus are often associated with the inhalation of other minerals. The specific minerals and classes of minerals inhaled with talc differ markedly, primarily on the basis of regional differences in the type of minerals found with talc deposits.

Wegman et al. [2] have suggested that inhalation of pure talc in nonsmokers causes bronchial and pulmonary disease but not the clinical and radiologic abnormalities usually attributed to its inhalation. Although this view is now widely accepted by specialists in diseases of inhalation [3], radiographic manifestations of talc in the lungs have not previously been analyzed with regard to the specific nature of other minerals inhaled with the talc. By knowing the nature of the mineral deposits in the region in which the patient was exposed, one can anticipate the possible contributions of minerals other than talc. Corroboration may be obtained by pathologic examination of the lung with identification of the foreign materials found. Such analysis leads to a conception of the manifestations of talc that is becoming well accepted by pathologists and other specialists in occupational diseases. As outlined in 1981 by Lockey [3], findings related to talc exposure can be divided into four principal categories, three forms by inhalation and one by intravenous administration. The four forms display marked differences in the nature of disease and radiographic changes that result.

I reviewed 18 cases of talc exposure documented both by pathology and by specific histories of exposure to either inhalational or intravenous administration. The findings demonstrate which manifestations of talc are clearly attributable to that mineral alone and which are attributable to other minerals. It is clear that many

Received April 15, 1985; accepted after revision September 16, 1985.

Presented at the annual meeting of the American Roentgen Ray Society, Boston, April 1985.

The opinions and assertions contained herein are solely those of the author and in no way represent those of the Department of the Army, Department of Defense, or Veterans Administration.

[1] Department of Radiology (V-114), University of California, San Diego Medical Center, La Jolla, CA 92093, and Veterans Administration Medical Center, San Diego, CA 92161.

AJR 146:295-301, February 1986
0361-803X/86/1462-0295

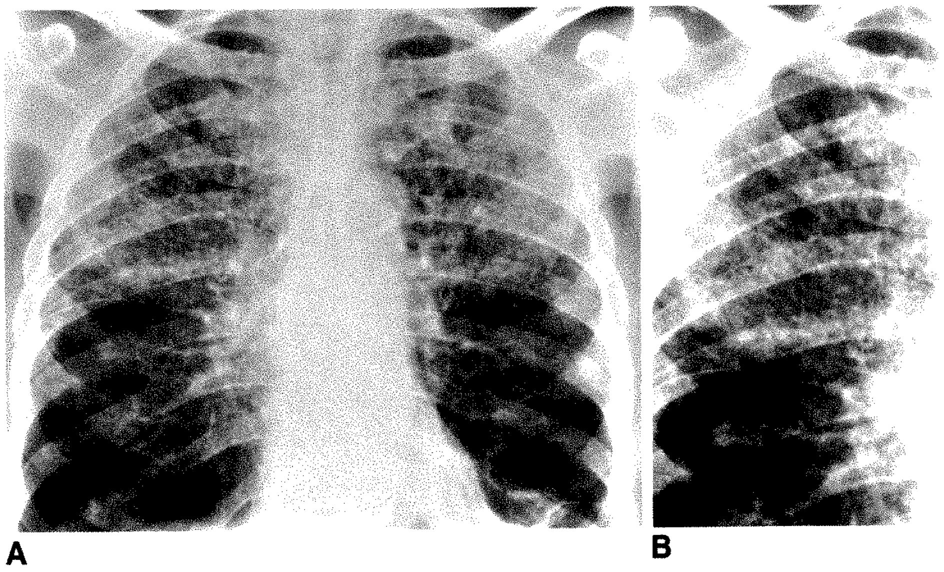

Fig. 1.—Talcosilicosis in California talc miner. **A**, Frontal chest film. Numerous small nodules in both upper lung fields, with hilar enlargement by large lymph nodes. Findings resemble those of simple silicosis. **B**, Closeup view of right upper lung field. (AFIP negative no. 81-604.)

of the roentgenographic manifestations previously attributed to talc inhalation are seen only in association with inhalation of other minerals. Differences between inhalation and intravenous exposures are clarified.

Materials and Methods

Eighteen cases of pulmonary disease with talc in the lungs were studied. The case material was obtained principally from the archives of the department of radiologic pathology of the Armed Forces Institute of Pathology (AFIP) in Washington, DC. One case was obtained from the George Washington University Hospital, Washington, DC, and two came from the University of California, San Diego, including one from the collection of the late Dr. Averill Liebow. All cases of talc exposure from each of these sources with sufficient documentation available were included. All patients were adults (15 men and three women).

Cases were documented by the findings of talc in the lungs in biopsy (11 cases) or autopsy (seven) specimens. Chest radiographs had been obtained within a few months before the pathologic specimens were obtained. Exposure histories were available in sufficient detail to document the nature of the exposure and, in cases of inhalation, the regional origin of the inhaled talc. Smoking histories generally were not available in sufficient detail to be useful for correlation with other findings. Cases were excluded in which the amount of talc found in the pathologic material was considered minimal in comparison with the presence of other minerals.

Identification of the minerals and estimation of the relative prevalence of each was performed using light and polarized microscopy in all cases. New techniques, permitting more accurate identification and quantitation, are scanning electron microscopy and x-ray microanalytic techniques [4, 5]; these were used in the four most recent cases from the AFIP.

Results

The 18 cases were classified into four distinct forms of talc disease on the basis of the pathologic analysis of the mineral within the lung. In all cases, the mineral content was correlated with histories of exposure. The four forms that were distinguished were talcosilicosis (three cases); talcoasbestosis (four cases); inhalation of pure talc, termed talcosis (four cases); and intravenous administration of talc (seven cases). Clinical, pathologic, and radiographic findings for each form are described separately.

Talcosilicosis

Talcosilicosis is inhalation of talc associated with free silica and other nonasbestiform minerals [3]. It was documented, by microscopic identification of both talc and silica particles in profusion and producing significant pathologic reaction in lung, in three of the 18 cases. The cases all showed clinical, pathologic, and radiographic findings typical of exposure to silica alone. The only difference between silicosis and talcosilicosis was the presence of talc in these specimens of lung; the talc was visible in quantities that were judged substantial in comparison with the amount of silica.

Radiographic abnormalities in one case from mining in California (fig. 1) were typical of simple silicosis, in which multiple fine nodules are present diffusely throughout the lung fields; lymph nodes in both hila and the mediastinum were moderately enlarged. No calcifications or other abnormalities were present. The International Union against Cancer (UICC) code was 2/1 in principal category p and secondary category q.

Radiographic abnormalities typical of complicated silicosis were seen in the two other cases, one from mining in Italy and one from California. Peripheral conglomerate masses were present in the upper lung fields bilaterally, typical of UICC A and B masses. Small, irregular nodules and linear reticulations were present in the lungs of both patients (UICC categories p, q, s, and t), and moderate lymph-node enlargement was also evident. One case showed calcification of lymph nodes without an "eggshell" appearance.

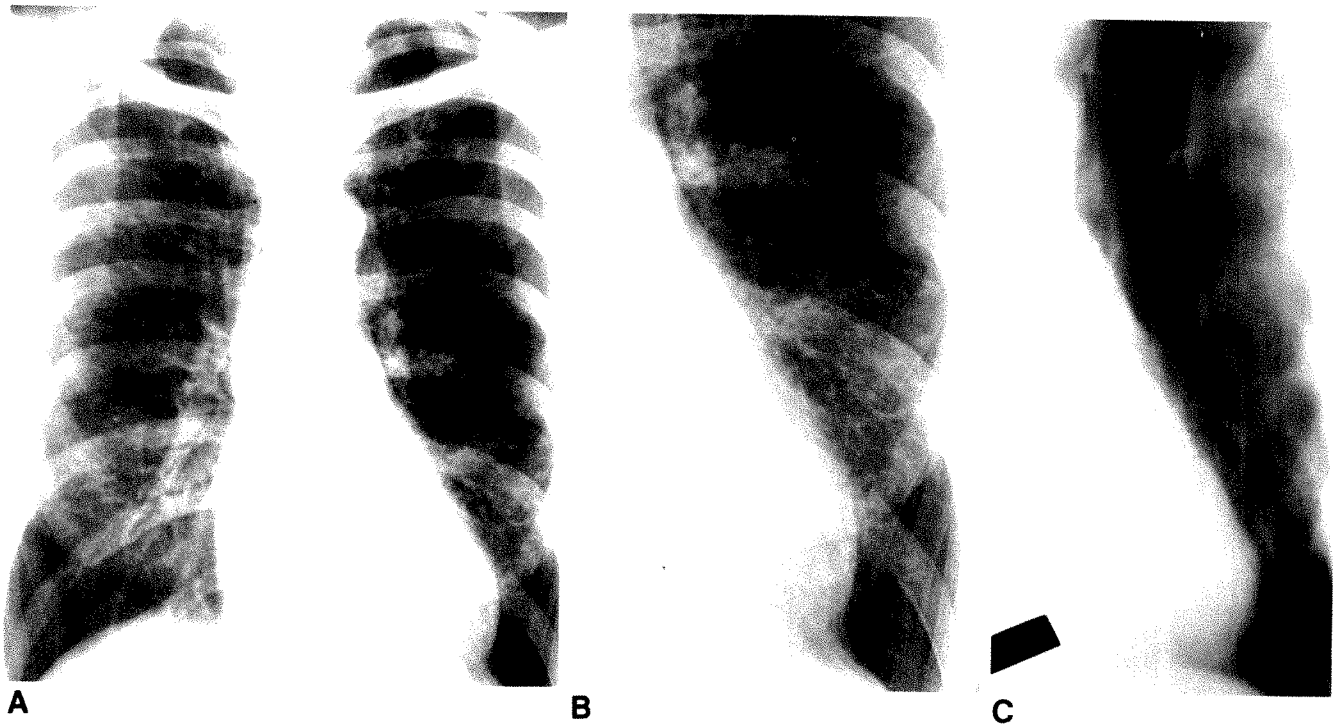

Fig. 2.—Talcoasbestosis in long-term talc worker, using talc from a region of Quebec adjacent to upper New York State. **A**, Frontal chest film. Diffuse reticulations throughout both lung fields. **B**, Closeup view of left lower lung field shows pleural plaques as well as pulmonary reticulations. **C**, Tomogram shows bilateral pleural plaques in periphery of both lower lung fields. (AFIP negative no. 60-5439. Courtesy of Notre Dame Hospital, Montreal, Quebec, Canada.)

Talcoasbestosis

This form was represented by four cases, all of which showed radiographic and pathologic abnormalities typical of asbestos-related disease (fig. 2). Bilateral pleural plaques in the lateral parts of the lower lung fields were seen in radiographs of all four patients, and true asbestosis with pulmonary parenchymal reticulations (UICC s and t densities) was definitely present in two cases and questionably present in one additional case. Diaphragmatic plaques with calcification, often considered pathognomonic of asbestos exposure, were clearly seen in two of the four patients' films. Lymph-node enlargement was not seen in any case, nor was there evidence of pleural effusions.

All patients had histologic evidence of both talc and asbestos particles producing lung disease and had historical documentation of exposure to talc mined in or near New York State, where talc is found with large quantities of asbestos. Two of the four were known to have worked in the Gouveneur region, an area of particularly high asbestos concentration (see Discussion). Clinical complaints of dyspnea and chronic cough were present in all patients with parenchymal asbestosis as diagnosed pathologically.

Pure Talcosis

Inhalation of talc in the absence of other minerals was documented histologically in four of the 18 patients. Radiographic abnormalities in all four cases consisted of small nodules and reticulations (UICC categories p, q, s, and t), which were diffuse in two cases and predominantly in the lower lung fields in the other two cases (figs. 3 and 4). Lymph-node enlargement was moderate in one case, mild in one case, and questionable in a third case. No calcifications were present. Minimal pleural thickening in the lower part of the left lower lung field was present in one case. Distinct pleural plaques and pleural effusions were absent. Pathologic findings were inflammation of alveolar walls and septa with diffuse talc deposition. Small-airway inflammation was also present.

Exposure histories were from Vermont in two cases and California in two cases. Talc deposits in these regions contain only trace quantities of silica and asbestiform minerals and are thus considered virtually pure talc [5]. All patients were involved in mining or processing of talc for cosmetic use.

Intravenous Talc

Seven of the 18 cases showed pathologic evidence of intravenous administration of talc. Vascular and perivascular granulomas with particles of talc were found in all cases. Such granulomas and particles were also found in other organs whenever specimens of other organs were available. Talc particles identified pathologically in the lungs were significantly larger in size than those seen in patients with inhaled talc (particle diameter always exceeded 10 μm). Smaller particles were found in other organs in some patients.

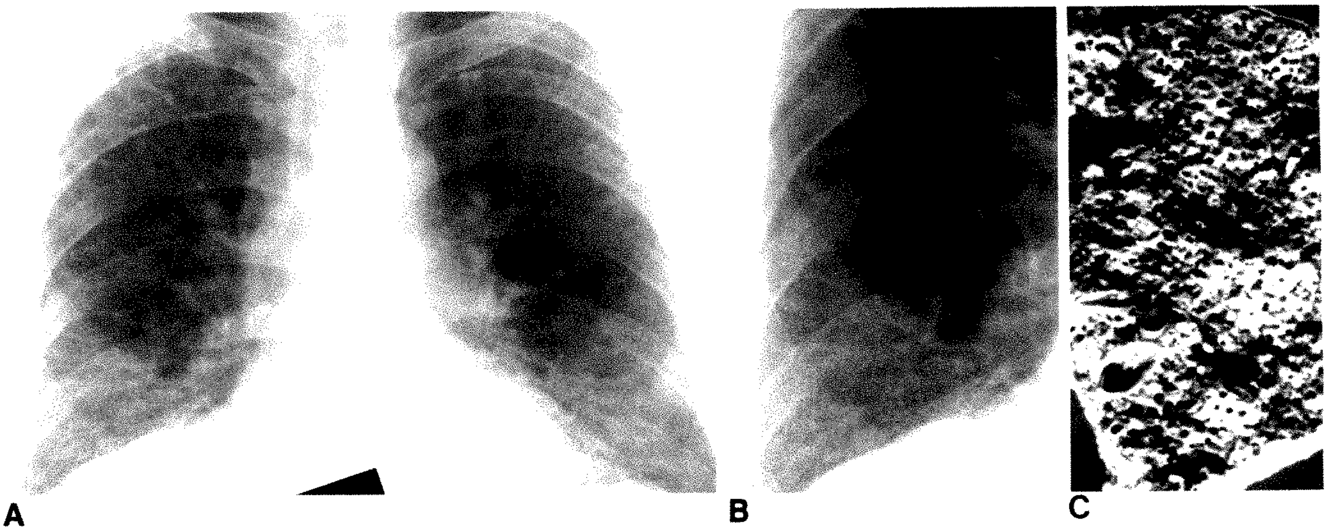

Fig. 3.—Pure talcosis in soapstone worker from California. **A**, Frontal chest film. Diffuse reticular densities and tiny irregular nodules, most marked in lower and peripheral lung fields. **B**, Closeup view of right lower lung field better shows reticular pattern punctuated by nodules. **C**, Photograph of gross specimen from lung of same patient. Diffuse thickening of pulmonary interstitium by deposition of talc. Histology also showed diffuse inflammation. (AFIP negative nos. 69-2216 [**A** and **B**] and 71-12728 [**C**].)

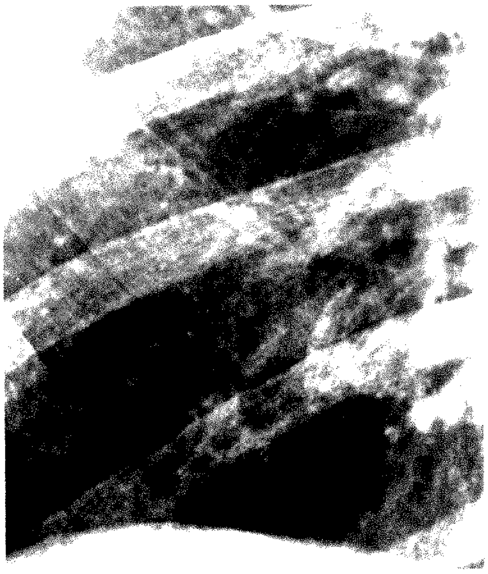

Fig. 4.—Pure talcosis in cosmetic product worker exposed to Vermont talc. Closeup view of right lower lobe of lung. Fine nodular and reticular densities (UICC p and s categories). (AFIP negative no. 68-7265.)

Radiographic abnormalities were far more variable than in the three forms of talc inhalation. Consolidative infiltrates were seen in four patients, most commonly involving the upper parts of the lungs and periphery of the midlung fields (fig. 5). Irregular nodules of various sizes (UICC categories q and r) were visible in three cases. Massive lymph-node enlargement was present in four of the seven cases and enlarged lymph nodes were visible in all the others. Pleural effusions were bilateral in two patients and on the left only in one other patient. Diffuse, reticular densities (t and s categories) were seen in two patients. Calcifications were not seen.

Intravenous abuse of oral medications was established by history in all seven patients. All histories documented a variety of abused medications, generally including pentazocine or methadone or both. The oral medications had been ground to a powder and injected into many different sites, principally in the arms or legs and including the axilla and groin regions. No attempt was made to document the origin of the talc used in the oral medications. No other minerals were found in the lungs pathologically, although other pathologic abnormalities were visible, especially inflammation (possibly secondary to infection) in three of the seven cases.

Discussion

Talc in its pure mineral form as crystalline magnesium silicates occurs as microscopic plates or sheets (fig. 6); this shape is responsible for its lubricating quality [3]. Talc is not only used as a cosmetic and lubricant of consumer goods, such as rubber gloves, but is also important as an industrial lubricant in the form of soapstone and similar products.

Among the soluble salts of silica (silicates), those that are fibrous are often considered more likely to cause clinical disease than nonfibrous silicates [6]. Fibrous silicates are those that are found or used as fibers, defined as having a length at least three times their width [7]. Talc is not a fibrous silicate by this definition, but it is often confused with fibers that are, especially with those fibrous silicates that are classified as asbestiform fibers because they meet specific physical criteria of tensile strength and separation into filamentous strands [3]. Many deposits of talc also contain such fibrous silicates.

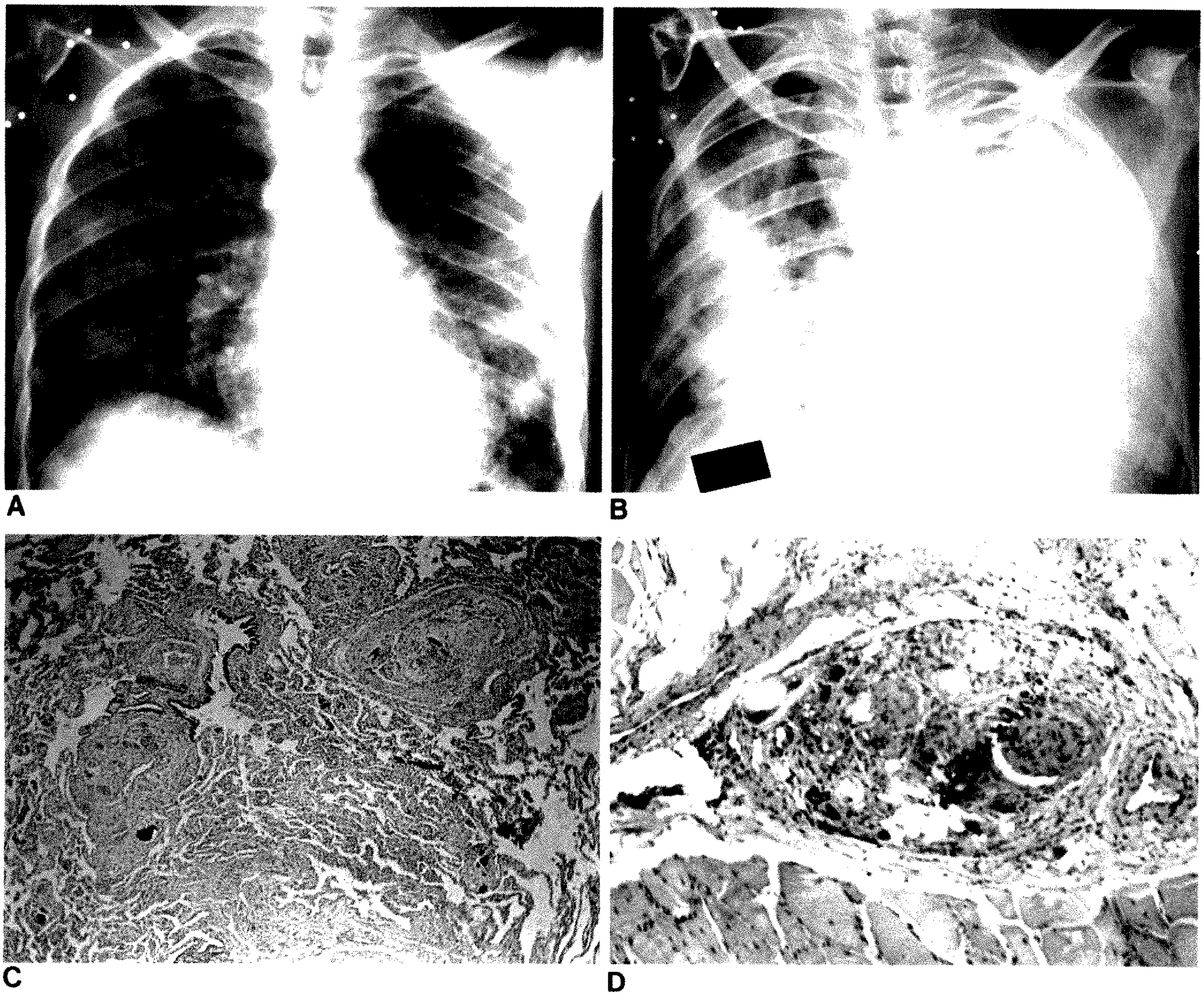

Fig. 5.—Intravenous talc disease secondary to self-administration of oral medications. **A**, Initial chest film. Minimal consolidation of left lower lobe and interstitial infiltration elsewhere, especially on left. A left pleural effusion is also present. **B**, 7 months later. Severe bilateral consolidation with diffuse hypoventilation. **C**, Photomicrograph of histologic specimen of lung (×2). Granulomas and diffuse interstitial thickening by inflammation. **D**, Photomicrograph of histologic specimen of intravenous granuloma within muscle (×8). Granuloma contains numerous talc granules and inflammation. (AFIP negative no. 73-10492. Courtesy of Department of Radiology, Emory University, Atlanta, GA.)

Confusion about the clinical, pathologic, and radiographic manifestations of talc has been caused principally by its association with asbestiform fibers, especially tremolite and anthophyllite [8, 9]. Thus, early descriptions of radiographic abnormalities from talc have attributed findings associated with asbestos exposure to talc exposure [10]. Mining or use of pure talc, or talc associated only with nonasbestiform silicates, has not been shown to produce the radiographic changes usually attributed to asbestos; thus, there is no evidence to support the contention that pleural or diaphragmatic plaques or calcification may be caused by talc alone [1, 2, 11].

Talcosilicosis, the disease produced by talc inhaled with silica, is indistinguishable from silicosis, produced by silica inhalation alone [7]. This form of talc disease has not been studied extensively, and most of the reports come from Italy where the free silica content of dust in talc mining operations may be as high as 18% [12]. Similar talc is also found in coastal regions of California. The specific contribution of talc to the production of disease is uncertain whenever the silica content of the inhaled dust exceeds levels generally sufficient to produce silicosis.

Talcoasbestosis has radiographic, clinical, and pathologic abnormalities identical to those that have been documented from exposure to asbestos free of talc. Most reported cases are of patients exposed to talc from New York State, especially the upstate Gouveneur region [10]. Bilateral lower-lung-field linear and reticular densities typical of asbestosis are

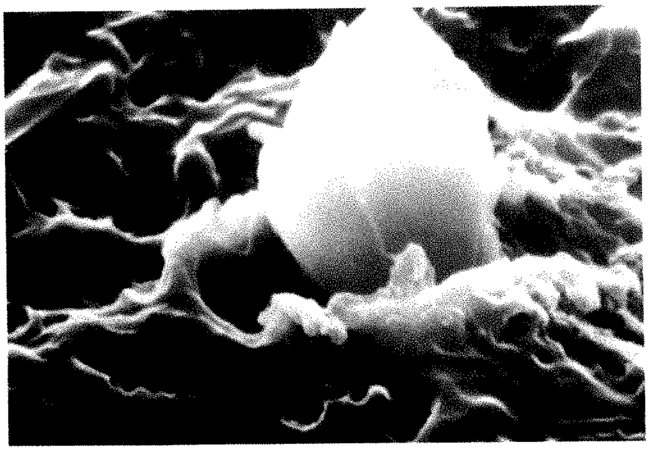

Fig. 6.—Scanning electron micrograph (×5000) shows sheetlike shape of talc particles in lung specimen. (AFIP negative no. 55-3780.)

seen, as is bilateral pleural thickening, principally involving the lower parts of the lateral lung fields. Pleural and diaphragmatic calcifications are identical with those produced by asbestos alone. It is significant that linear diaphragmatic calcification is often regarded as pathognomonic for asbestos exposure, with the exception that it also is believed to occur in talc exposure. In fact, diaphragmatic calcification in talc exposure has been described in talcoasbestosis but not in the other forms of talc-related pulmonary disease.

Talcoasbestosis seems to be associated with malignancies, including bronchogenic carcinoma and malignant mesothelioma [7]. It is not yet clear whether the incidence of malignancies is as high as in asbestos exposure, and incidence may vary with the type of asbestos inhaled with the talc [13].

Pure talcosis from inhalation is well documented in individuals exposed both occupationally and nonoccupationally to talc free of silica and asbestiform mineral as mined in Vermont, Montana, and inland areas of California. The talc may be found in admixture with other minerals, such as carbon in Texas, in which the impurities are not in themselves commonly productive of disease. Pure talc produces restrictive pulmonary disease by parenchymal inflammation, resulting in the radiographic reticular pattern of diffuse interstitial thickening. Pure talc may also cause airway obstruction [11]. Clinical disease has been documented most often in miners and workers producing cosmetics and glove powders, but only when the exposures have been very heavy and prolonged [14, 15]. Typical radiographic findings of small-airway obstructions, especially irregular, hazy, nodular densities scattered through the lung fields, are seen in such patients in addition to diffuse reticular densities.

Pure talc may also cause acute onset of pulmonary symptoms when very large quantities are aspirated. Such exposure may be accidental and has been documented most often in infants who inhale cosmetic talc [7, 16]. Pleural instillation of pure talc may result in pleural thickening and fibrosis [7, 17, 18] and may cause significant pulmonary disease if the talc enters the lung.

Pure talc causes granuloma formation, as documented by Tukiainen et al. [14], as well as interstitial inflammation and fibrosis [19] when inhaled. The granulomas are probably responsible in part for the nodularity of the radiologic appearance of both inhaled talc and talc administered intravenously. By studying clinical evaluations and histories of 116 miners and millers of talc ore in Vermont, Wegman et al. [2] demonstrated that pure talc produces pulmonary disease with both decreased diffusion capacity and small-airway obstruction, and parenchymal radiographic changes consisting of both nodules and reticulations.

Intravenous administration of talc is especially common as a result of intravenous abuse of oral medications. Talc is used as a lubricating and diluting substance in many oral medications that are subject to abuse, usually by being crushed and injected [20]. Such abused medications include pentazocine, methadone, and many other related medications. Severe vascular occlusive disease results from the formation of vascular and perivascular granulomas in the lung.

Numerous recent reports of the radiographic manifestations of intravenous talc are available [21–23]. Four of the cases here corroborate these reports of large, irregular, nodular densities or consolidations in the upper parts of the midlung fields, which may rapidly progress into large masses or massive consolidations. Widespread irregular nodules may also occur, and loss of pulmonary volume may be permanent. The large mass densities resemble those of massive pulmonary fibrosis in silicosis and anthracosis; they may, however, appear far closer to the hilum than in the latter diseases [21]. Lymph-node enlargement is common and may be massive [22]. The radiologic findings thus also resemble the findings of sarcoid, although lymph-node enlargement, which may be marked, is less frequent in intravenous talc disease than in sarcoid.

In three of the seven cases of intravenous talc studied here, as well as in many previously reported cases [22–24], including a recent report by Lewis et al. [24] in a patient with disseminated talc granulomatosis who probably had acquired immunodeficiency syndrome, some of the radiographic abnormalities undoubtedly are related to other causes besides talc granuloma formation, especially infection. Further, manifestations of thromboembolic disease are uniformly present as a result of the granuloma formation in perivascular tissues, and infarction can occur. Thus, it is not possible to attribute all the described radiologic findings definitively to the presence of talc. Paré et al. [22], however, did note increased profusion and size of opacities in their cases with the greatest quantities of injected pills. Three of my cases, like others reported previously [21, 23], showed no pathologic evidence of inflammation and were radiologically indistinguishable from the four with inflammation.

Use of the newest techniques for identifying minerals in the lungs [4, 5] may lead to further observations concerning the division of talc manifestations by associated mineral exposures, but these techniques have become widely used only in the last few years. Scanning electron microscopy has greatly improved the ability to detect and identify minerals, but quantification of mineral content from tissue samples remains difficult and is subject to marked imprecision by sampling errors, especially when only small biopsy samples are available. Analysis of homogenates of very large specimens by x-ray spectrometry is the most precise quantification method now in use, but this technique was not available for application to any case in this study.

It is important for radiologists to be aware of the differences among the forms of talc disease since findings of asbestos and silica inhalation apparently have been attributed to talc. Most significant is the fact that talc alone has not been documented to produce either the radiographic abnormalities nor the malignancies that are well documented in asbestos inhalation.

ACKNOWLEDGMENTS

I thank David S. Hartman and Frank B. Johnson, both of the AFIP, Washington, DC, for advice and assistance; the photographic branch of the AFIP for processing the illustrations; and Joyce Sly for secretarial and administrative support

REFERENCES

1. Gamble JF, Fellner W, Dimeo MJ. An epidemiologic study of a group of talc workers. *Am Rev Respir Dis* **1979**;119:741-752
2. Wegman DH, Peters JM, Boundy MG, Smith TJ. Evaluation of respiratory effects in miners and millers exposed to talc free of asbestos and silica. *Br J Ind Med* **1982**;39:233-238
3. Lockey JE. Nonasbestos fibrous minerals. *Clin Chest Med* **1981**;2:203-218
4. Abraham JL. Recent advances in pneumoconiosis: the pathologist's role in etiologic diagnosis. In: Thurlbeck WT, Abell MR, eds. *The lung*, IAP monograph 19. Baltimore: Williams & Wilkins, **1978**:96-137
5. Vallyathan NV, Green FHY, Craighead JE. Recent advances in the study of mineral pneumoconiosis. In: Sommers SC, Rosen PP, eds. *Pathol Annu* **1980**;15:77-104
6. Lapp NL. Lung disease secondary to inhalation of nonfibrous minerals. *Clin Chest Med* **1981**;2:219-233
7. Morgan WKC, Seaton A. *Occupational lung diseases*, 2d ed. Philadelphia: Saunders, **1984**
8. Porro FW, Patton JR, Hobbs AA Jr. Pneumoconiosis in the talc industry. *AJR* **1942**;47:507-524
9. Siegal W, Smith AR, Greenburg L. The dust hazard in tremolite talc mining, including roentgenological findings in talc workers. *AJR* **1943**;49:11-29
10. Smith AR. Pleural calcification resulting from exposure to certain dusts. *AJR* **1952**;67:375-382
11. Scully RE, Mark EJ, McNeely BU. Case records of the Massachusetts General Hospital: case 35-1982. *N Engl J Med* **1982**;307:605-614
12. Rubino GF, Scansetti G, Piolatto G, et al. Mortality and morbidity among talc miners and millers in Italy. In: Lemon RA, Dement JM, eds. *Dusts and disease*. Park Forest South, IL: Pathotox, **1979**:357-363
13. Ng TK. Talc and mesothelioma. *Med J Aust* **1984**;140:452-453
14. Tukiainen P, Nickels J, Taskinen E, Nyberg M. Pulmonary granulomatous reactions: talc pneumoconiosis or chronic sarcoidosis? *Br J Ind Med* **1984**;41:84-87
15. Wells IP, Dubbins PA, Whimster WF. Pulmonary disease caused by the inhalation of cosmetic talcum powder. *Br J Radiol* **1979**;52:586-588
16. Moffenson HC, Greensher J, DiTomasso A, Ojun S. Baby powder—a hazard! *Pediatrics* **1981**;68:265-266
17. Bouchama A, Chastre J, Gaudichet A, et al. Acute pneumonitis with bilateral pleural effusion after talc pleurodesis. *Chest* **1984**;86:795-797
18. Rinaldo JE, Owens GR, Rogers RM. Adult respiratory distress syndrome following intrapleural instillation of talc. *Thorac Cardiovasc Surg* **1983**;85:523-526
19. Vallyathan NV, Craighead JE. Pulmonary pathology in workers exposed to nonasbestiform talc. *Hum Pathol* **1981**;12:28-35
20. Farber H, Fairman RP, Glauser FL. Talc granulomatosis: laboratory findings similar to sarcoidosis. *Am Rev Respir Dis* **1984**;125:258-261
21. Crouch E, Churg A. Progressive massive fibrosis of the lung secondary to injection of talc. A pathologic and mineralogic analysis. *Am J Clin Pathol* **1983**;80:520-526
22. Paré JAP, Fraser RG, Hogg JC, Howlett JG, Murphy SB. Pulmonary "mainline" granulomatosis: talcosis of intravenous methadone abuse. *Medicine* **1979**;58:229-239
23. Sieniewicz DJ, Nidecker AC. Conglomerate pulmonary disease: a form of talcosis in intravenous methadone abusers. *AJR* **1980**;135:697-702
24. Lewis JH, Sundeen JT, Simon GL, et al. Disseminated talc granulomatosis: an unusual finding in a patient with acquired immunodeficiency syndrome and fatal cytomegalovirus infection. *Arch Pathol Lab Med* **1985**;109:147-150

Attention *AJR* Contributors

Effective January 1, 1986, Dr. Robert N. Berk assumed the editorship of the *AJR*, and the editorial office moved from Seattle to La Jolla, California. The new address and telephone number are:

AJR Editorial Office
2223 Avenida de la Playa
La Jolla, CA 92037
(619) 459-2229

Chronic Posttraumatic Aneurysm of the Thoracic Aorta: Surgically Correctable Occult Threat

Frans M. Heystraten[1]
Gerd Rosenbusch[1]
Lucas M. Kingma[2]
Leon K. Lacquet[3]

The clinical and radiographic findings of 11 patients with a chronic traumatic aneurysm were reviewed. Each patient had been under medical care at the time of injury but acute aortic rupture was not recognized in any, although several signs of mediastinal hemorrhage were present on the immediate posttraumatic radiographs. The average time between the initial trauma and the detection of the aneurysm was 5.3 years. Seven patients showed no or minimal specific complaints. Four patients showed more or less severe complaints of dysphagia, severe thoracic pain, hoarseness, and dyspnea. In all patients the chest radiograph was abnormal: Four patients showed a mass lesion at the level of the aortic knob. The other seven patients showed contour deformities of the descending aorta, sometimes subtle, with (five) or without (two) calcification. Esophagography and CT were useful in several patients. In the light of the unpredictable course of a chronic traumatic aneurysm and the low operative mortality, early operation after detection is recommended. Preoperative angiography is usually desirable.

Acute traumatic rupture of the aorta is usually promptly fatal, but about 2.5% of patients survive without recognition and treatment and develop a chronic posttraumatic aneurysm [1–3]. For survival and the formation of an aneurysm, either the adventitial wall must be preserved or the surrounding tissues must be able to contain the pulsating hematoma that is formed after the layers of the aortic wall are torn. Many patients with a posttraumatic aneurysm have a symptom-free period varying from months to years, but in most patients symptoms eventually occur [1–4].

Progressive enlargement and the risk of rupture increase the longer the aneurysm is present [4, 5]. Because of the low operative mortality and the unpredictable course of such aneurysms, elective operation is recommended by most surgeons [6, 7]. Although there are many reports regarding the radiological findings in patients with acute aortic rupture [8–10] reports of the radiological appearance of chronic aneurysms are scarce [11–13]. We present the clinical radiological and surgical findings of 11 patients.

Subjects and Methods

The University Clinics of Nijmegen and Groningen are cardiac-thoracic referral centers. Between 1971 and 1983, we saw 11 patients with a posttraumatic aneurysm. In the same period, we treated 57 patients with an acute aortic rupture. Four patients were female, seven male. The age at the time of the primary trauma and admission ranged from 16 to 39 years (average, 25.2). At the time the aneurysm was recognized, the age ranged from 21 to 40 years (average, 29.5). The time between the injury and recognition of the aneurysm averaged 5.3 years (range, 3 months to 12 years). All patients but one were hospitalized at the time of the initial trauma. All patients were involved in motor vehicle accidents (one was a motorcycle) as drivers or passengers.

The patients' records were reviewed for the clinical symptoms. In three patients the aneurysms were detected during mass screening, in two on a preoperative chest film, and in

Received April 15, 1985; accepted after revision August 23, 1985.

[1] Department of Radiology, Catholic University of Nijmegen, Geert Grooteplein Zuid 18, 6525 GA Nijmegen, The Netherlands. Address reprint requests to F. M. Heystraten.

[2] Department of Radiology, University of Groningen, Groningen, The Netherlands.

[3] Department of Thoracic, Cardiac, and Vascular Surgery, Catholic University of Nijmegen, Nijmegen, The Netherlands.

***AJR* 146:303-308, February 1986**
0361-803X/86/1462-0303
© American Roentgen Ray Society

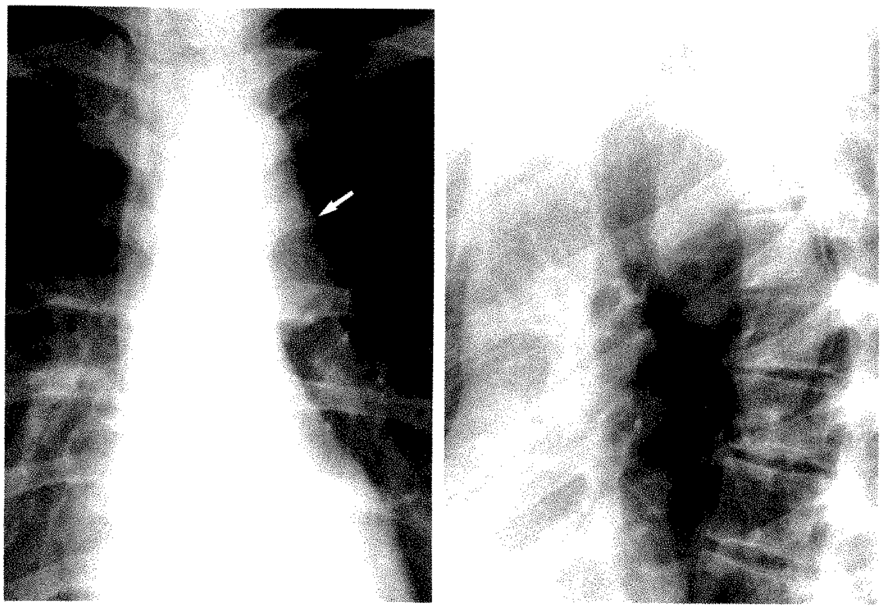
1A
1B

Fig. 1.—Case 4: traumatic aneurysm in 23-year-old woman. **A**, Chest film at time of detection, 6 years after trauma: abnormal contour at level of aortic knob (*arrow*). **B**, Left anterior oblique: impression by aneurysm on dorsal tracheal wall. **C**, Angiogram: large false aneurysm at isthmus.

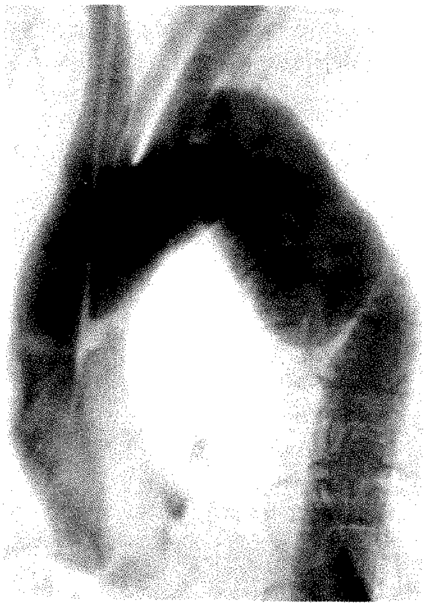
1C

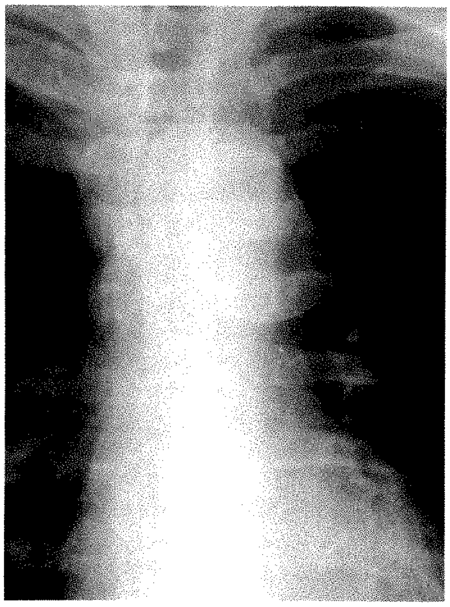
2

Fig. 2.—Case 5: traumatic aneurysm in 24-year-old man. Chest film at time of detection, 6 years after trauma: mass lesion with calcified rim at level of aortic knob.

one on a chest film taken for unrelated reason; in five patients, complaints were the reason for a chest radiograph.

The chest radiographs of the 11 patients at the time of detection of the aneurysm were reviewed. Other radiographic investigations were performed in four patients including esophagography (two), bronchography (one), and computed tomography (CT) of the thorax (one). Angiography of the thoracic aorta was performed in all patients: in 10 patients by the femoral artery and in one patient by femoral and axillary approach because the catheter could not pass the aneurysm from below. In another patient, a contrast injection in the central pulmonary artery was performed for visualization of the aortic arch.

In five of the 11 patients, the chest films obtained immediately after the initial trauma could be reevaluated for signs of hemomediastinum and acute aortic rupture. Nine of the 11 patients were operated on within weeks after the detection of the chronic aneurysm and one after 2 years; the other died before operation.

Results

Clinical Symptoms

Four patients had no complaints at all at the time of detection of the aneurysm. Three patients had mimimal non-thoracic pain; four patients had more severe complaints of dysphagia, severe thoracic pain, hoarseness, and dyspnea, suggesting acute dissection of the thoracic aorta. In only two patients, a systolic murmer at the back could be heard.

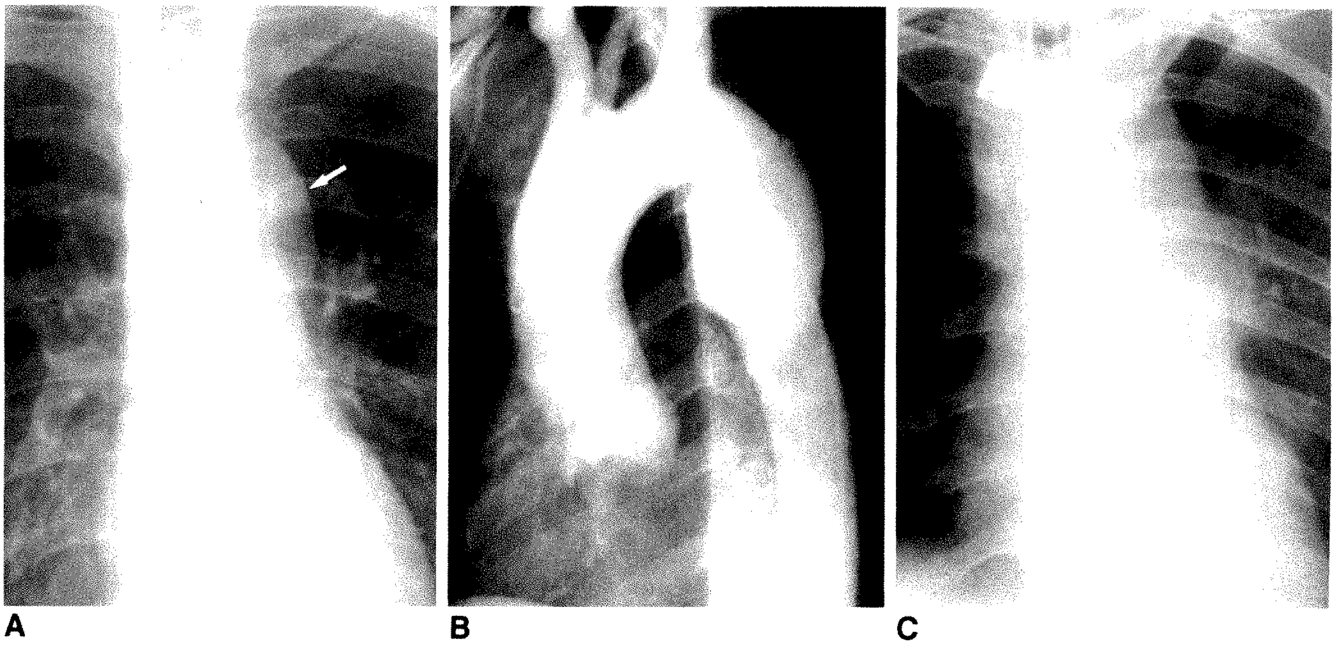

Fig. 3.—Case 7: traumatic aneurysm in 26-year-old woman. **A**, Chest film at time of detection, 5 years after trauma: abnormal contour of aortic knob (*arrow*). **B**, Angiogram. **C**, Chest film at time of trauma: discrete widening of mediastinum (7.5 cm); normal position of trachea and nasogastric tube; aortic knob not visible; widened paratracheal stripe. Diagnosis was missed.

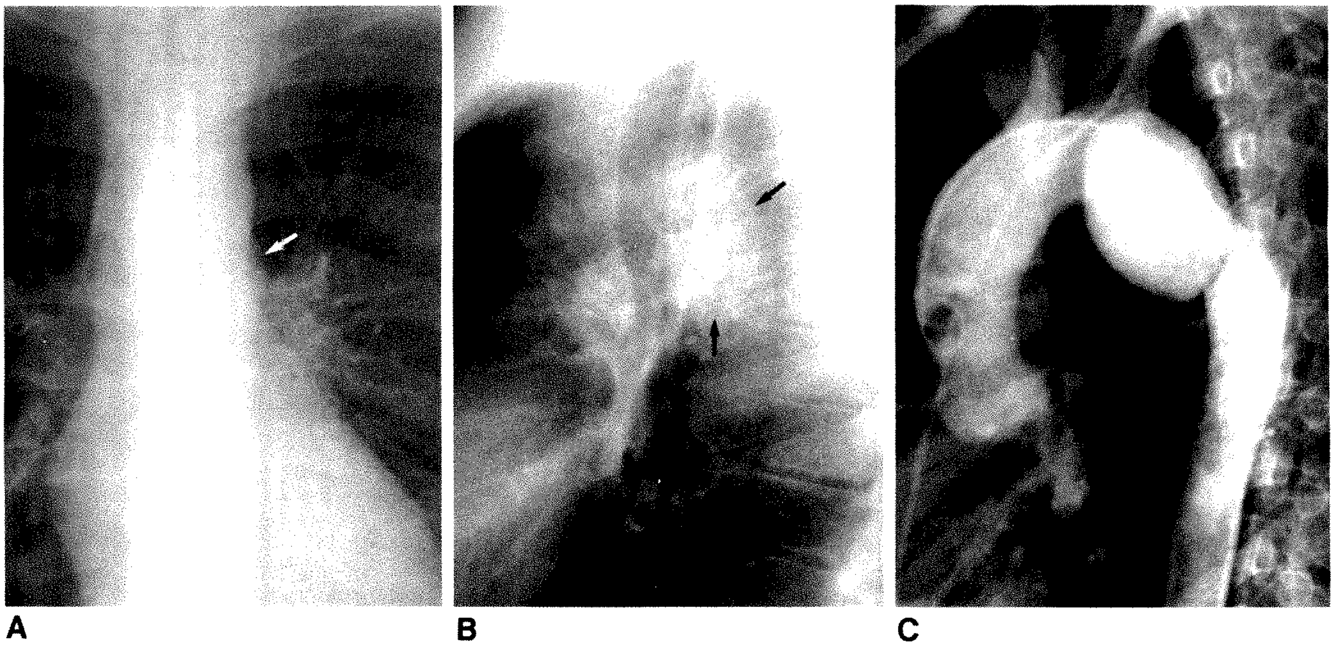

Fig. 4.—Case 8: traumatic aneurysm in 18-year-old man. Frontal (**A**) and lateral (**B**) chest films at time of detection, 10 years after trauma: tracheal displacement to right; abnormal configuration below aortic knob (*white arrow*); calcified mass lesion on lateral film (*black arrows*). **C**, Angiogram: note absence of clot.

Radiographic Findings

On films diagnostic of the aneurysms, four patients showed a mass density contiguous to the aortic knob. In six patients, a more or less subtle contour deformity of the aortic knob or of the proximal descending aorta was present. A rim of calcification was detected in the periphery of the mass in five patients (often best seen in the lateral projection), and old rib fractures were seen in three patients. In several patients, combinations of the above findings were present (figs. 1–6).

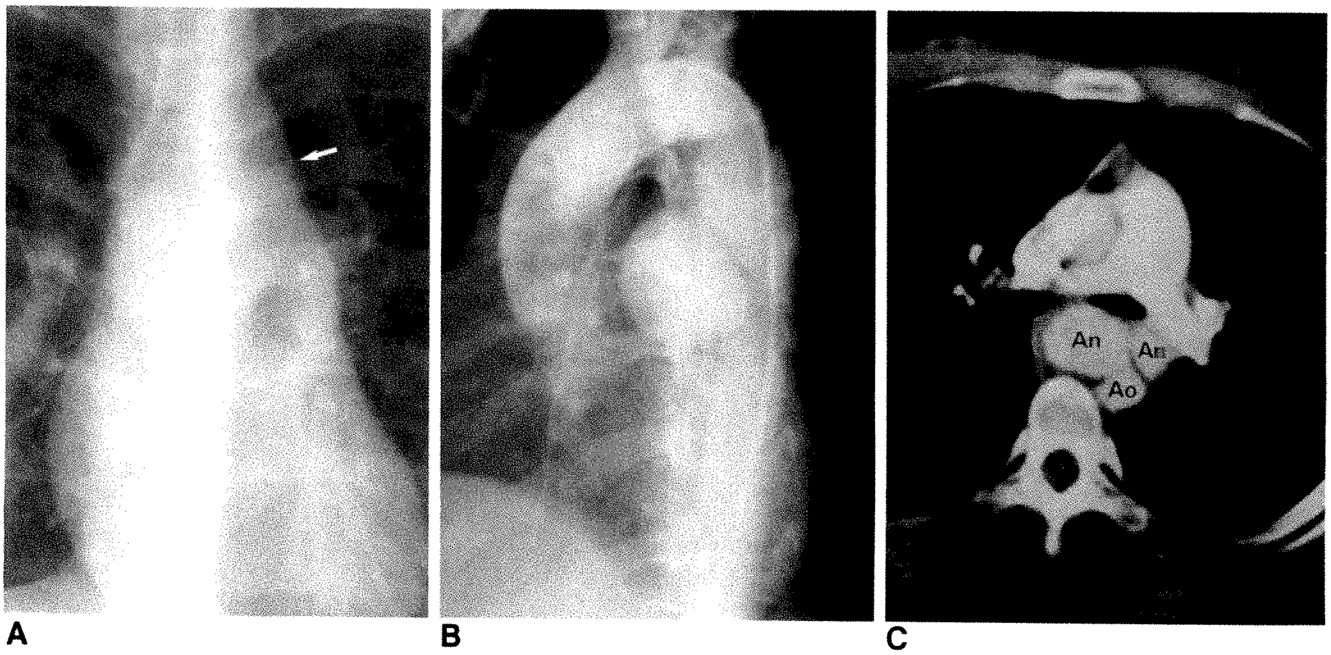

Fig. 5.—Case 10: traumatic aneurysm in 21-year-old woman. **A**, Chest film at time of detection, 4 months after trauma: abnormal contour of aortic knob (*arrow*) and subcarinal mass. **B**, Angiogram: aneurysm is more saccular than most. **C**, Contrast-enhanced CT scan: "two-chambered" false aneurysm (An) at level of aortic isthmus. Ao = aortic lumen.

In one patient, enlargement of the aneurysm was documented over a period of 6 months.

The available admission chest films obtained immediately after trauma were evaluated retrospectively. In five patients, signs indicating a hemomediastinum [8–10] were present (table 1). Examples of the chest films of the initial trauma are shown in figures 3C and 6C.

On angiography, all 11 patients showed a false aneurysm with varying diameter at the isthmus. In all patients the aneurysm was filled with contrast material without detectable clotting. Most aneurysms were located at the inner face of the aortic arch with ventral extension. No aneurysms of the brachiocephalic vessels were discovered. No complications due to angiography were encountered. In one patient (case 4), it was not possible to pass the false aneurysm from below and an angiography via the axillary approach had to be performed to obtain information on the brachiocephalic vessels and the aortic arch.

Esophagography of two patients showed impression (slight in one and large in the other) on the esophagus caused by the false aneurysm. In another patient, bronchography showed a stenosis of the left main bronchus due to external compression. On a CT examination, an aneurysm of the proximal descending aorta could be seen after intravenous administration of contrast material (fig. 5C).

Surgery

Nine patients were operated on within weeks after the detection of the aneurysm. In one patient there was a delay of 2 years (for unknown reasons) before an angiogram of the thoracic aorta was obtained. Another patient died unexpectedly of rupture of the aneurysm 36 hr after angiography.

At surgery, varying degrees of transection of the aorta were found. In three patients, the tear circumference was one-third of the aortic wall, in two patients half the circumference, in one two-thirds, and in two patients the aortic wall was completely transected. In one patient the aneurysm was technically irresectable, and in another patient the extent of the circumferential tear was not mentioned in the surgical report. Five patients' operations included a pulsatile left heart bypass, and in four patients no shunt was used. In eight patients a graft was interposed in the proximal descending aorta; in one patient the defect in the aortic wall was corrected with a patch. There were no cases of postoperative paraplegia. One woman (case 3) suffered from a severe pulmonary embolus on the 11th postoperative day, requiring exploration of the pulmonary artery during extracorporeal circulation.

Outcome

One patient (case 6) died during surgery from rupture of the false aneurysm into the mediastinum and pericardium, as cross-clamping of the aorta was not possible. Another patient died unexpectedly 36 hr after angiography and before operation due to acute rupture with perforation of the aneurysm into the left main bronchus. The other nine patients had uneventful recoveries without postoperative complications, except one patient with a postoperative pulmonary embolism.

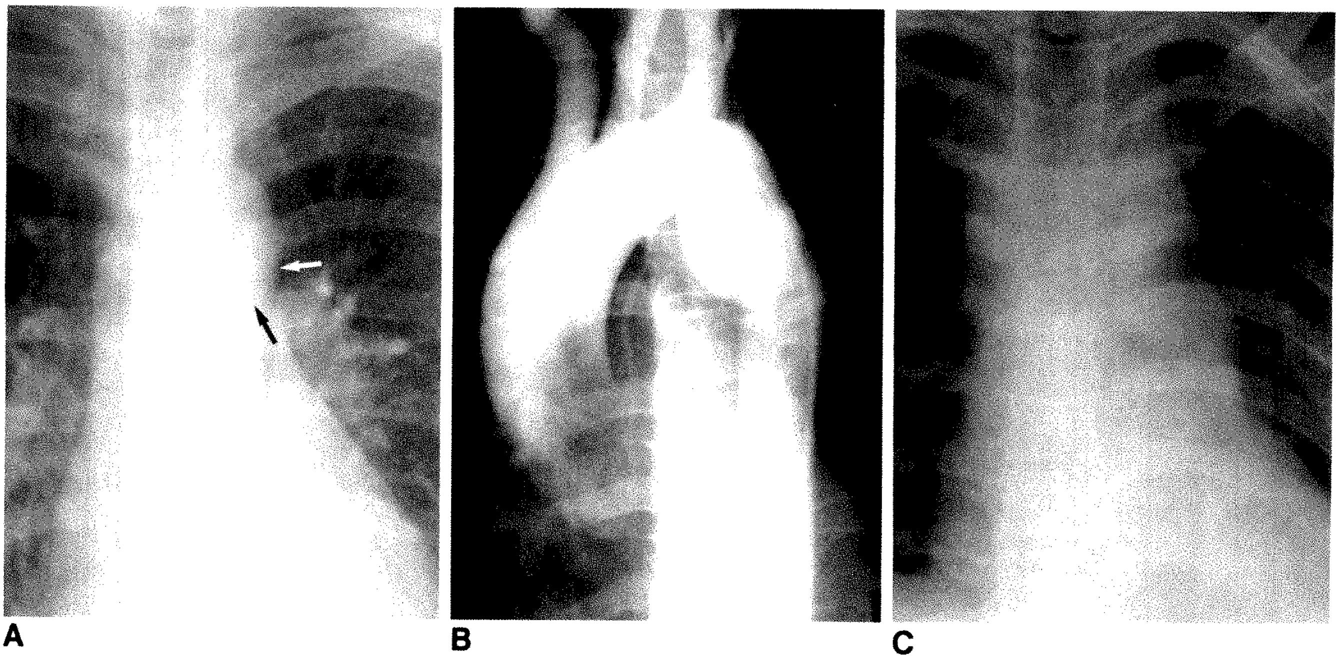

Fig. 6.—Case 3: traumatic aneurysm in 19-year-old woman. **A**, Chest film at time of detection, 5 years after trauma: abnormal aortic contour with rim of calcification (*arrows*). **B**, Angiogram. **C**, Chest film at time of trauma: discrete widening of mediastinal shadow (7 cm); unsharp outline; normal tracheal position. Diagnosis was missed.

TABLE 1: **Signs on the Immediate Posttrauma Chest Film in Five Patients with Subsequent Aortic Aneurysms**

Chest Radiographic Signs	Case No.				
	3*	7†	8	10	11
Mediastinal width 6–8 cm	+	+	+		
Mediastinal width 8–10 cm				+	+
Tracheal displacement to right	−	−	−	+	+
Downward displacement of left main bronchus	−	−	−	+	+
Displacement of nasogastric tube	−	−	−	+	−
Unsharp aortic outline	+	+	+	+	+
Broadening of paratracheal stripe	+	+	+	+	+
Displacement of right paraspinal line	−	−	−	−	−
Displacement of left paraspinal line	−	−	−	+	−
Fracture of first or second rib	−	−	−	−	−
Other rib fractures	+	−	+	−	+
Hemothorax	+	−	+	−	+
Apical cap	+	+	?	+	−
Displacement of superior vena cava	−	−	±	−	−
Opacified pulmonary window	+	+	±	−	−

* See fig. 6C.
† See fig. 3C.

To date, no late complications have occurred in the operated patients.

Discussion

Although there were many, sometimes subtle, signs on the chest films of the patients with traumatic aortic rupture at their initial admission (table 1), the diagnosis was missed in all patients. One major reason is that a careful evaluation of the mediastinal configuration on chest films of patients with blunt chest trauma was not usual in the early 1970s, and the radiographic findings of aortic rupture were less well known. In addition, orthopedic or neurosurgical problems may so dominate the clinical picture that the chest film is not carefully evaluated [7]. Furthermore, vascular injury may escape diagnosis because rupture at the isthmus is associated with little external evidence of chest trauma in one-third of the cases [13].

Clinical Presentation of Aneurysms

Severe symptoms, such as dysphagia, severe thoracic pain, hoarseness, and dyspnea, were present in only four of 11 patients despite the relative short interval (5.3 years) between the primary trauma and the detection of the aneurysm. Because most traumatic aneurysms are located at the isthmus in proximity to the left main bronchus, recurrent laryngeal nerve, and esophagus, symptoms such as dyspnea, cough, hoarseness, and dysphagia are easily explained. Symptoms were present in 50% of the patients in the series of Bennett and Cherry [1] and in 65% of those reported by Finkelmeyer et al. [4]. Pain was the leading symptom in one-third of their patients, presumably due to compression or stretching of the viscera and nerves in the vicinity of the aneurysm. The onset of symptoms is indicative of the expansion of the aneurysmal sac [13]. In two of our 11 patients, a systolic murmur at the back could be heard; murmurs have been described in 40% of chronic posttraumatic aneurysms [11]. The fact that symptoms develop and increase in severity with time and that additional ones appear is further evidence for the progressive enlargement of the aneurysms that so frequently occurs [1, 4, 11].

Radiography

The chest radiograph plays an essential role in the detection of these aneurysms. The most important findings are contour deformities of the mediastinum at the level of or below the aortic knob, sometimes with discrete calcification. This was present in five of our 11 patients. Enlargement of the aneurysm may be seen on serial films. Contrast examination of the esophagus can show a local impression by the aneurysm, depending on the location and the size.

A chronic traumatic aneurysm must be differentiated from other aneurysms (syphilitic, arteriosclerotic, congenital, mycotic) in the proximal descending aorta. The syphilitic type is usually associated with aortitis; an irregular, dilated, calcified ascending aorta often accompanies a syphilitic aneurysm. A positive serologic test for syphilis is confirmatory [2]. In atherosclerotic aneurysms, there are often other signs of atherosclerosis. A history of a deceleration trauma and the age of the patient are other differentiating factors. Tumors of the mediastinum are readily differentiated by other radiologic methods (tomography, angiography, CT). Not infrequently, chronic traumatic aneurysms are detected by chest films taken for unrelated reasons.

Natural History and Prognosis

McClenathan and Brettschneider [5] believe that traumatic aneurysms have a natural history similar to that of syphilitic or arteriosclerotic aneurysms. In a 5-year follow-up study of 97 unclassified thoracic aorta aneurysms, DeBakey et al. [6] reported that 31 patients had died, most from rupture of the aneurysm.

Of 60 patients with traumatic aneurysms, not subjected to operative treatment compiled by Finkelmeyer et al. [4], 20 (30%) died from aortic rupture during the period in which they were followed. In light of the unpredictable course, elective surgery is recommended by most authors [6, 7].

Surgical Therapy

Flemming and Green [11] reported a mortality rate of 3.5% in 33 patients operated on for chronic traumatic aneurysms, and in a review Finkelmyer et al. [4] reported deaths of 4.6% of 332 patients undergoing operation for these aneurysms. The fact that these chronic aneurysms are usually found in young and otherwise healthy persons, free of degenerative vascular disease, explains the low surgical mortality rate. Because of these low mortality rates, there has been increasing endorsement of elective surgery for all cases of chronic traumatic aneurysms, even the calcified, asymptomatic lesions of many years' duration [7, 14].

Surgical repair consists of incision of the aneurysm and patching or resection and grafting [6, 15]. Distal ischemia during surgery is prevented by left-atrial-to-left-femoral pulsatile bypass with an interposed pump or pharmacologic control of blood pressure during simple cross-clamping of the aorta below the left subclavian artery [6, 14]. Once a posttraumatic aneurysm is detected, immediate repair seems advisable because of the unpredictable course and the low operative mortality.

REFERENCES

1. Bennett DE, Cherry JK. The natural history of traumatic aneurysms of the aorta. *Surgery* **1967**;61:516–524
2. McBurney RP, Vaughan RH. Rupture of the thoracic aorta due to nonpenetrating trauma. *Ann Surg* **1961**;153:670–680
3. Parmley LF, Mattingly TW, Manion WC, Jahnke EJ Jr. Nonpenetrating traumatic injury of the aorta. *Circulation* **1958**;17:1086–1102
4. Finkelmeyer BA, Mentzer RM, Kaiser DL, Tegtmeyer CJ, Nolan SP. Chronic traumatic thoracic aneurysm. *J Thorac Cardiovasc Surg* **1982**;84:257–266
5. McClenathan JE, Brettschneider L. Traumatic thoracic aortic aneurysm. *J Thorac Cardiovasc Surg* **1965**;50:74–78
6. DeBakey ME, Cooley DA, Crawford ES, Morris GC. Aneurysms of the thoracic aorta. *J Thorac Surg* **1958**;36:393–421
7. Schonholtz GJ, Janhnke EJ Jr. Occult injury of the thoracic aorta associated with orthopaedic trauma. *J Bone Joint Surg* [*Am*] **1964**;46:1421–1432
8. Barcia TC, Livoni JP. Indications for angiography in blunt thoracic trauma. *Radiology* **1983**;147:15–19
9. Fisher RG, Hadlock F, Ben-Manachem Y. Laceration of the thoracic aorta and brachiocephalic arteries by blunt trauma. *Radiol Clin North Am* **1981**;19:91–111
10. Gundry SR, Williams S, Burney RE, Mackenzie JR, Cho KJ. Indications for aortography, Radiography after blunt chest trauma: a reassessment of the radiographic findings associated with traumatic rupture of the aorta. *Invest Radiol* **1983**;18:230–238
11. Fleming AW, Green DC. Traumatic aneurysms of the thoracic aorta. *Ann Thorac Surg* **1974**;18:91–102
12. Fishbone G, Robbins DI, Osborn DJ, Grnja V. Trauma to the thoracic aorta and great vessels. *Radiol Clin North Am* **1973**;11:543–555
13. Steinberg I. Chronic traumatic aneurysm of the thoracic aorta. *N Engl J Med* **1957**;257:913–918
14. Crawford ES, Rubio PA. Reappraisal of adjuncts to avoid ischemia in the treatment of aneurysms of the descending thoracic aorta. *J Thorac Cardiovasc Surg* **1973**;66:693–705
15. Dubost C, Blondeau P, Piwnica A, Cachera JP. Traitment chirurgical des anévrysmes d'aorte thoracique à propos de 25 cas explorés chirurgicalement. *J Chir* (Paris) **1962**;83:331–360

Magnetic Resonance Imaging of Thoracic Aortic Aneurysms: Comparison with Other Imaging Methods

Robert E. Dinsmore[1]
Richard R. Liberthson[2]
Gary L. Wismer[1]
Stephen W. Miller[1]
Peter Liu[2]
Randall Thompson[2]
Theresa C. McLoud[1]
Jane Marshall[2]
Sanjay Saini[1]
Edna J. Stratemeier[1]
Robert D. Okada[2]
Thomas J. Brady[1]

Fifteen patients with thoracic aortic aneurysms had magnetic resonance images (MRI) and at least one additional diagnostic image study: thoracic aortography, computed tomography (CT), or two-dimensional echocardiography. Twenty aneurysms were demonstrated by MRI, 19 by the other studies. One small saccular aneurysm was missed by CT. There was complete agreement between MRI and other studies regarding aneurysm morphology, and good correlation in diameter measurements of the aneurysms and at multiple additional aortic levels.

Electrocardiographically (ECG)-gated magnetic resonance images (MRI) in transverse, sagittal, and coronal planes have been reported to provide high quality examinations of the normal aorta [1] and a variety of abnormalities including dissecting hematoma [2, 3], posttraumatic false aneurysm [4], and coarctation [5]. MRI has a number of characteristics that are particularly well suited to study of the aorta. These include excellent contrast between flowing blood and cardiovascular structures without introduction of contrast medium, images in any desired plane with uniformly high quality throughout a large field, and absence of biologic effect allowing serial examination without risk to the patient. As a result, MRI is potentially the imaging method of choice for study of aortic pathology.

We report a prospective study of MRI of patients with saccular and fusiform aneurysms of the thoracic aorta. Aneurysms were assessed for morphology, location, and size by MRI and other imaging techniques. Images were acquired in both the conventional short-axis (transverse) plane and a true long-axis plane obtained by altering either patient position or magnetic gradient angle [6, 7].

Subjects and Methods

Fifteen patients aged 7–84 years were studied. Ten had clinical signs of Marfan syndrome. Informed consent as approved by the Subcommittee on Human Studies was obtained from each subject. Each patient had previous demonstration of at least one thoracic aortic aneurysm by other imaging methods: four had CT, six had selective aortography, and seven had two-dimensional echocardiography.

Imaging Techniques

MR images were acquired with a whole-body superconducting magnet system (Technicare) with a magnetic field strength of 0.6-T corresponding to a proton resonance frequency of 25 MHz. The body coil has a diameter of 55 cm. Spin-echo (SE) pulse sequences with echo delays (TE) of 30 msec were used for data acquisition. Spatial encoding was achieved using a two-dimensional Fourier transform technique with 128 Y phase encoding gradients. Plane selection was accomplished by a 90° selective pulse (4 msec). Single or multiple 1.0-cm-thick images were acquired. The pulse repetition time (TR) was equivalent to the R-R interval of the ECG, which ranged from 600 to 1000 msec corresponding to heart rates from 60 to 100 beats/min. Images were acquired in a matrix of 256 vertical (interpolated from 128) by 256

Received April 8, 1985; accepted after revision September 20, 1985.

Presented at the annual meeting of the American Roentgen Ray Society, Boston, April 1985.

This work was supported in part by Public Health Service grant 5 K04 CA-00848-02 from the National Cancer Institute and in part by the Technicare Corp., Solon, OH.

[1] Department of Radiology, Massachusetts General Hospital, Boston, MA 02114. Address reprint requests to R. E. Dinsmore.

[2] Cardiac Unit, Massachusetts General Hospital, Boston, MA 02114.

AJR 146:309–314, February 1986
0361–803X/86/1462–0309
© American Roentgen Ray Society

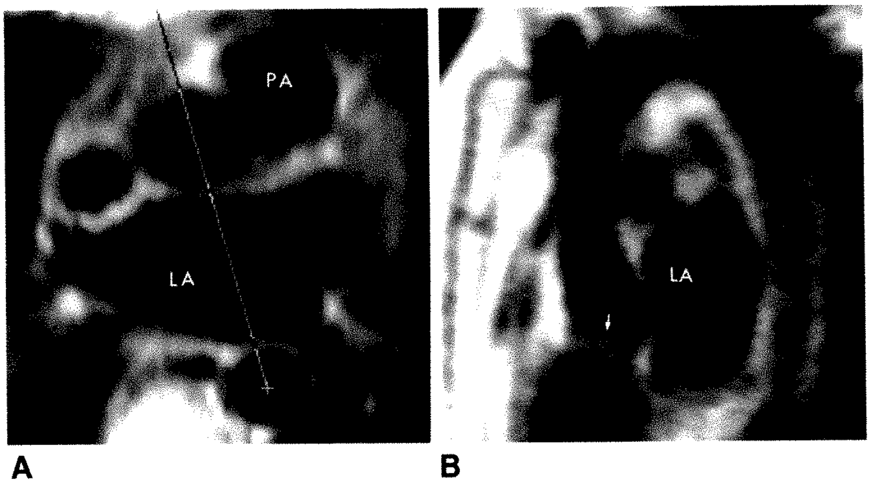

Fig. 1.—MR images of normal aorta in short axis (**A**) and long axis (**B**). In **A**, cross has been placed over descending aorta and cursor passes through ascending aorta in order to measure projected angle formed with sagittal plane. *Arrow* = aortic valve; LA = left atrium, PA = pulmonary artery.

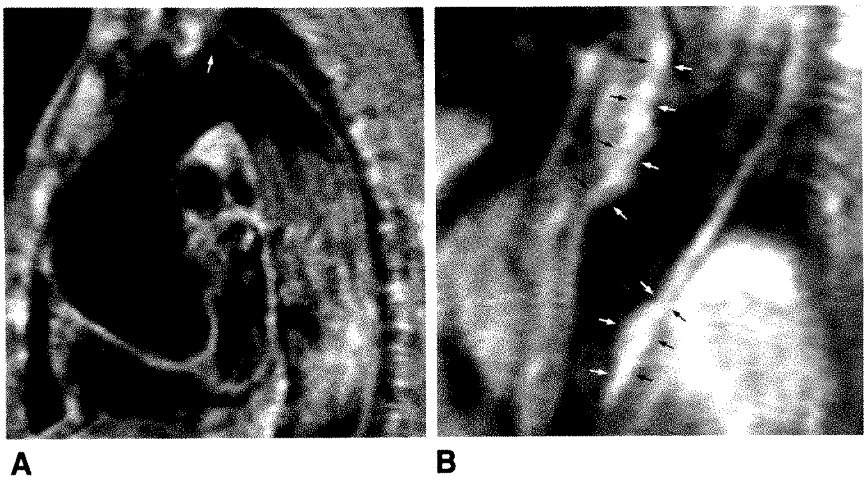

Fig. 2.—MR images of 28-year-old man with giant cell aortitis and fusiform aneurysm involving ascending and descending thoracic aorta. **A**, Thoracic aorta in long axis. *Arrow* indicates occluded left subclavian artery. **B**, Thoracoabdominal aorta in long axis. *Arrows* indicate thickened aortic wall. Note that thickening extends into nonaneurysmal part of aorta.

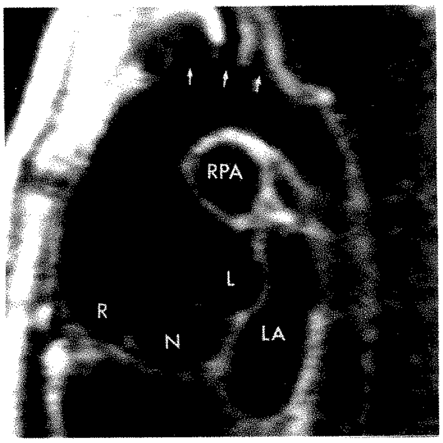

Fig. 3.—MR image of aorta, in long axis, of 29-year-old woman with Marfan syndrome. Note origins of brachiocephalic branches (*arrows*) and normal thickness of aortic wall in comparison with patient in fig. 2. RPA = right pulmonary artery; LA = left atrium; L, R, and N = left, right, and noncoronary sinuses of Valsalva.

horizontal picture elements and displayed using 256 shades of gray. ECG gating was accomplished by using a telemetry system (Hewlett Packard) with three standard electrodes on the extremities with nonmagnetic lead wires. The imaging system permits image acquisition in any plane by adjusting a set of gradient angles that may be varied to define any vector through the subject [6].

MR images of the aorta were obtained using a technique previously described [6, 7]. First, a series of short-axis images of the aorta are obtained in a conventional image plane transverse to the thorax cage. An additional long-axis image, designed to display the sweep of the aortic arch on a single image, is then obtained as follows: A transverse image at or immediately below the middle arch is selected, and a line is projected through the center of the ascending and descending parts of the aorta. The angle subtended by this line and a vertical line is measured (fig. 1A). Long-axis images may then be obtained by either of two methods. In the first, the patient's right shoulder is rotated anteriad by the measured number of degrees, so that the line passing through both ascending and descending aorta is vertical. Then, images in a vertical image plane longitudinal to the core of the magnet (i.e., using the magnet's coordinate axes for a conventional sagittal plane) will show the true long axis of the aortic arch (fig. 1B). In practice, this can be expedited by obtaining the initial transverse images with the patient's right shoulder rotated anteriad about 25°, and making any minor position adjustment needed after measurement of the precise angle from these images. In the second method, the patient is left in the supine position and the long-axis images are obtained by appropriate rotation of gradient angle about the magnet's Z axis (Euler angle phi) [6–8]. Since rotation of gradient angle is more precise than rotation of the patient, the second method is slightly more efficient than the first, although the results appear to be equivalent. Correction for magnification was established by the use of a phantom with known dimensions.

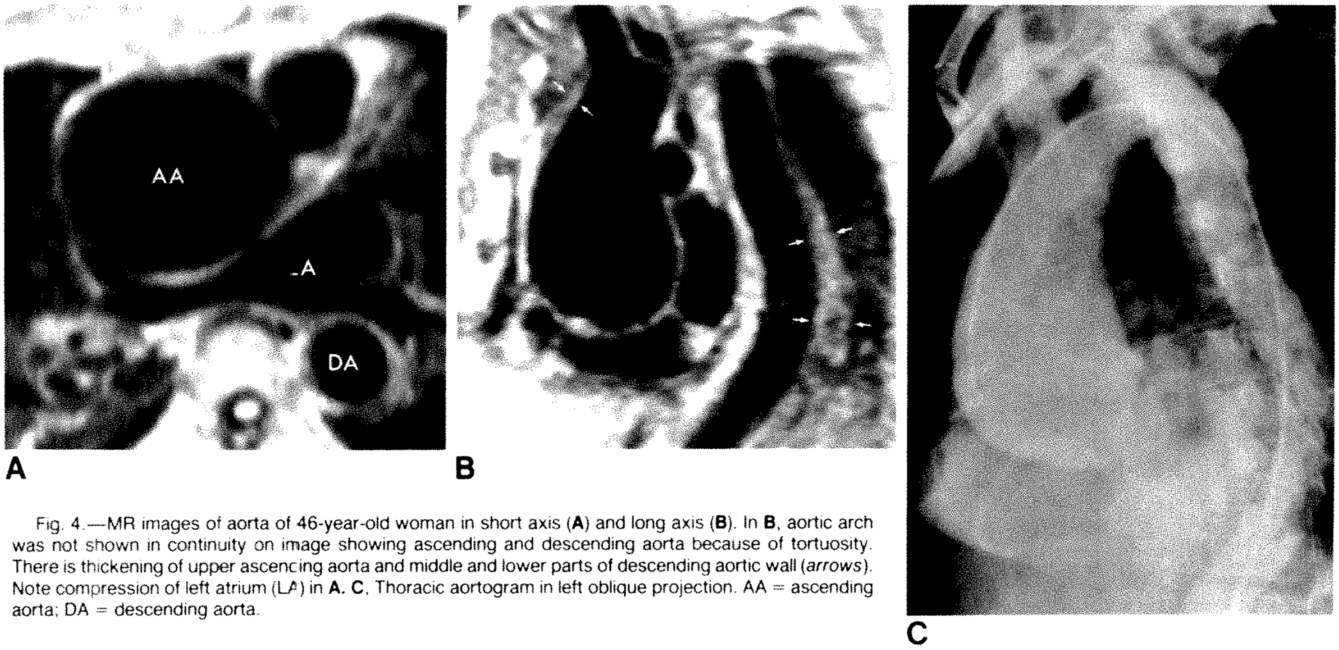

Fig. 4.—MR images of aorta of 46-year-old woman in short axis (**A**) and long axis (**B**). In **B**, aortic arch was not shown in continuity on image showing ascending and descending aorta because of tortuosity. There is thickening of upper ascending aorta and middle and lower parts of descending aortic wall (*arrows*). Note compression of left atrium (LA) in **A**. **C**, Thoracic aortogram in left oblique projection. AA = ascending aorta; DA = descending aorta.

CT scans were obtained with 3-sec acquisition time, using 10-mm slice thicknesses at 10-mm intervals, with either an Omni 7070 or Technicare 2060 scanner. A bolus of 50 ml of Renografin-76 was injected into an antecubital vein, and dynamic scanning initiated after injection of about 25 ml.

Two-dimensional sonography was done with either a Hewlett-Packard 7702 or an ATL Mark III sector scanner with 2.5-, 3.0-, or 3.5-MHz transducer. Standard parasternal long- and short-axis imaging planes and suprasternal images of the arch were used.

Selective thoracic aortography was done with an Elema-Schonander rapid film changer, at three frames/sec. The magnification factor was established by measurement of the projected external catheter diameter divided by the true external diameter.

Evaluation of Images

MR images were obtained without knowledge of the details of other diagnostic studies, although the general diagnosis was known at the time of referral. Aneurysms were defined as fusiform if the entire circumference was involved and saccular if only part of the circumference was affected. Saccular dilation of any degree was considered to be an aneurysm. Since fusiform dilation may occur in a number of conditions, such as systemic hypertension or aortic valve incompetence, without abnormality of the aortic wall or development of pathologic or clinical aneurysm sequelae, fusiform aneurysm was defined for purposes of this study as dilation greater than 1.5 times normal. The normal limits used for adults were adapted from reported pathologic [9], angiocardiographic [10], CT [11], and echocardiographic [12] measurements as follows: aortic sinuses of Valsalva, 3.5 cm; ascending aorta, 3.0 cm arch, 2.5 cm; and mid descending aorta, 2.3 cm. Normal values used for children were those given by Williams and Tucker [13]. Measurements were made of maximum aneurysm diameter on MR images and correlated with measurements by the other imaging methods. In each case, the diameter used was the largest found on any of the available images. In the case of fusiform aneurysms, the largest transverse dimension was recorded. In addition, in order to assess the accuracy of MRI in evaluation of the entire thoracic aorta and to define the limits of abnormality, additional measurements of the aorta were made in each case at the following levels: (1) the aortic sinuses of Valsalva; (2) the mid ascending aorta; (3) the middle arch, between innominate and left subclavian origins; and (4) the descending aorta at the level of the carina.

Results

Detection of Aneurysms

Twenty aneurysms were detected by MRI in the 15 patients in this series. Only 19 were detected by other imaging techniques; one small saccular aneurysm was missed by CT examination. Two patients each had three aneurysms, one had two aneurysms, and 12 patients each had one aneurysm.

Morphology, Location, and Extent of Aneurysms

Among the 20 aneurysms detected by MRI, five were classified as saccular and 15 fusiform. There was no disagreement in assessment of morphology of the 19 aneurysms detected by other imaging techniques. Three of the fusiform aneurysms were limited to the aortic sinuses of Valsalva, five involved the sinuses of Valsalva and ascending aorta, one extended from the sinuses into the middle arch, three extended from the sinuses to the descending thoracic aorta, two affected the ascending aorta alone, and one involved the descending aorta (figs. 2–4). There was agreement in the assessment of extent of aneurysms between MRI and the other imaging methods. One patient with a fusiform aneurysm had associated long plaquelike areas of thickening of the aortic wall to 11 mm (fig. 2) and occlusion of the left subclavian artery near its origin. These findings were also shown by aortography, along with stenosis of an intercostal artery. At

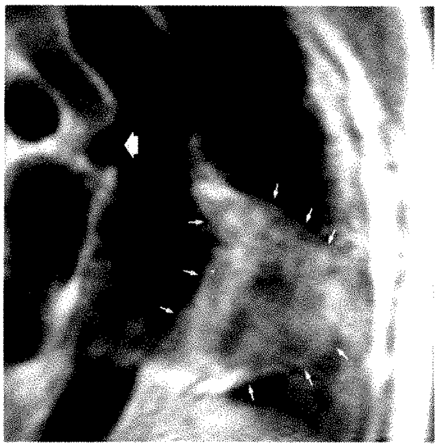

Fig. 5.—Detail of an MR image of descending thoracic aorta, in long axis, of 84-year-old man with two saccular aneurysms. *Large arrow* indicates small aneurysm that was not detected by CT. *Arrows* outline area of bright signal due to thrombus in large aneurysm.

surgery, the patient was found to have giant cell aortitis. Another patient had similar areas of thickening of the aortic wall up to 15 mm, but has not had surgery (fig. 4).

Ten patients had clinical findings of Marfan syndrome, with thin-walled fusiform aneurysms typically involving the aortic sinuses and proximal aorta.

Two of the saccular aneurysms were in the upper and two in the lower descending thoracic aorta, and one was at the junction of the ascending aorta with the innominate artery. These were considered to be atherosclerotic in origin. One saccular aneurysm 1 cm in diameter was detected by long-axis MRI but missed by CT and by short-axis MRI (fig. 5). Thrombus was believed to be present in three saccular aneurysms by both MRI and CT. In these cases systolic long- and short-axis MR images showed little or no signal arising from the moving blood in the central part of the aneurysm; however, the periphery showed a bright nonhomogeneous signal that persisted through the cardiac cycle, thought to be due to thrombus (fig. 5). Aortography in two and CT images in the third showed lack of contrast enhancement of the perimeter of the aneurysms with a comparable appearance, confirming the presence of thrombus.

Measurements of Aortic Diameter

As shown in figure 6A, measurements of maximum aortic diameter from MRI correlated very well with similar measurements from the other imaging techniques ($r = 0.95$). There was also excellent correlation of aortic diameter measurements at multiple levels (aortic sinuses, mid ascending aorta, middle arch, and descending aorta) from MRI compared with each of the other imaging techniques: echocardiography ($r = 0.97$), CT ($r = 0.90$), and aortography ($r = 0.97$) (figs. 6B–6D).

Discussion

Aneurysms of the thoracic aorta enlarge progressively and are often clinically silent until life threatening. Early management consists of serial observation for either development of symptoms or of signs that may indicate the need for surgery, such as change in size or morphology. An ideal diagnostic image method should be sensitive, accurate, complete, and noninvasive, allowing safe, frequent follow-up examination. Each of the established methods of aortic imaging has limitations and advantages. Angiography involves the introduction of catheters and contrast medium and the use of radiation. However, it provides excellent spatial resolution and a large image field. While major brachiocephalic branches can be shown by MRI or CT, angiography shows detail of smaller branches. Selective aortography remains the standard method of analysis of aortic regurgitation, which may complicate aneurysms of the ascending aorta.

Among noninvasive tests, CT has good spatial and excellent contrast resolution, and cross-sectional imaging essentially eliminates the problem of overlap of structures. However, display is limited to the transverse plane and the technique involves ionizing radiation as well as intravenous administration of contrast medium. Two-dimensional echocardiography is completely noninvasive and flexible in display. High-frequency acquisition permits study of aortic valve leaflets, which may be useful in some cases, and the presence of aortic regurgitation can be assessed by Doppler shift studies. However, problems of bone and air transmission reduce image quality in many older children and adults, particularly of the arch and descending aorta. MRI has good spatial resolution and excellent contrast between flowing blood and cardiovascular structures. Images may be obtained in any desired plane and are of uniformly high quality throughout a large field. The examination is completely noninvasive and well suited to serial follow-up examination. For these reasons, MRI is potentially the imaging method of choice for study of aortic pathology.

In most cases, morphology, location, and size of aneurysms could be adequately evaluated on either long- or short-axis images. However, the smaller saccular aneurysm shown on the long-axis image in figure 5 was missed on CT and also was not detected on short-axis MR images.* It would presumably have been equally well shown on conventional sagittal images. The potential advantages of long-axis over sagittal or coronal images are not objectively established by this series, since the latter planes were not used. However, display of the extent of aortic arch abnormality in continuity on a single long-axis image (fig. 2) appeared subjectively, at least, to be superior to piecing together the same information from multiple short-axis, sagittal, or coronal images. While it was not possible to display the entire aorta from aortic valve to diaphragm on a single image in the presence of aortic tortuosity, in such cases a single image of the arch from the

---

* Since completion of this series, we have seen an additional example of a small saccular descending aortic aneurysm shown only on the long-axis image.

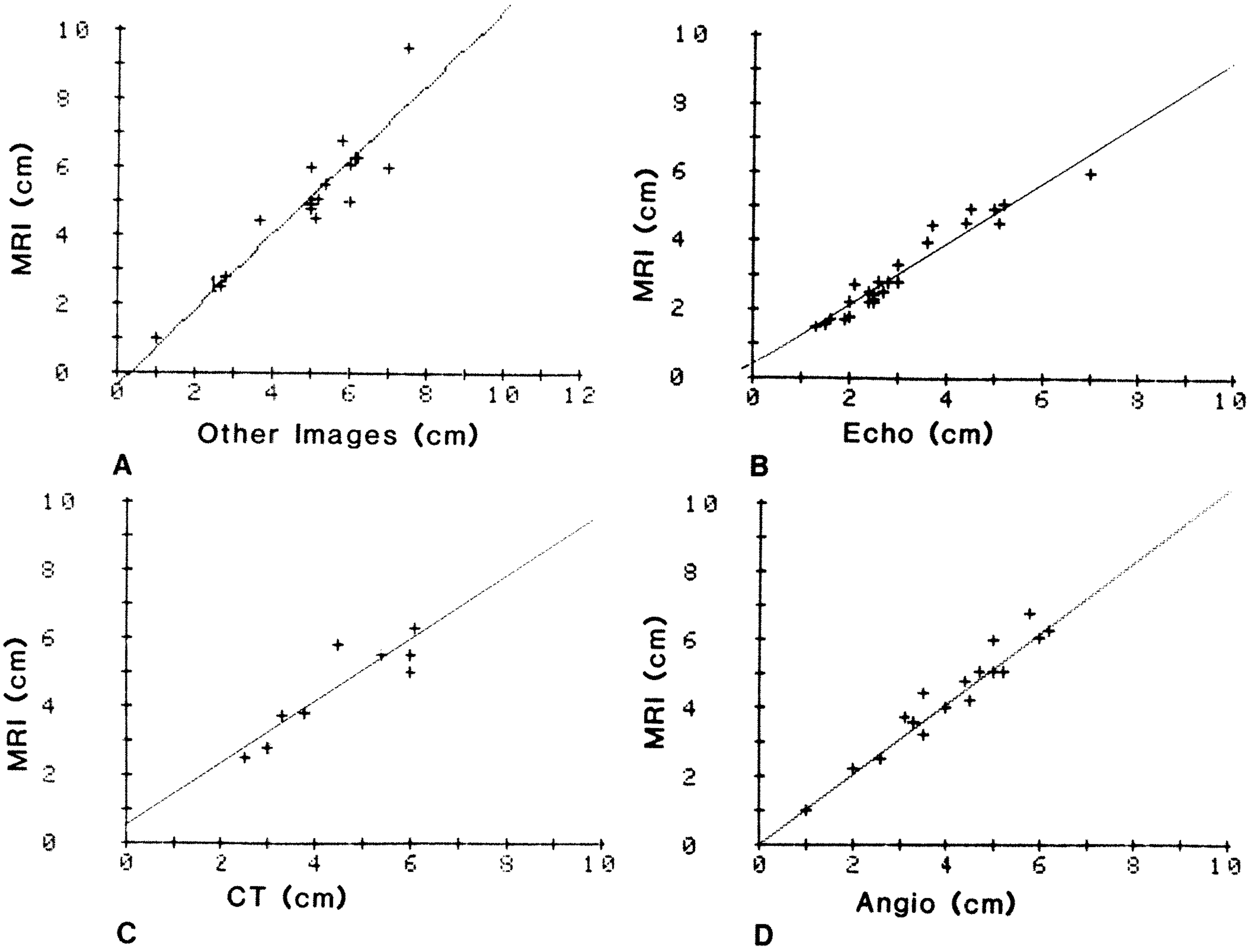

Fig. 6.—Comparison of measurements of aorta by MRI with those from other imaging methods. **A**, Measurements of maximum aneurysm diameter by MRI compared with maximum diameters from all other imaging techniques. Relation is described by regression equation: Y (MRI diameters) = 1.1 X (diameters, other imaging techniques) − 0.38, r = 0.95. Measurements of aorta at multiple levels by MRI are compared in **B** with echocardiography [Y (MRI measurements) = 0.96 X (echo measurements) + 0.32, r = 0.97], in **C** with computed tomography [Y (MRI measurements) = 0.87 X (CT measurements) + 0.6, r = 0.90], and in **D** with aortography [Y (MRI measurements) = 1.05 X (angio measurements) + 0.38, r = 0.97].

upper ascending aorta through the isthmus could usually be obtained by the long-axis technique.

In the present study, MRI compared favorably with other imaging techniques in the detection and assessment of aortic aneurysms, and the excellent correlation in measurements of aortic diameter at multiple levels attests to the ability of MRI to evaluate the entire thoracic aorta. Aortic wall thickness was well shown with possible pathologic implications. Most fusiform aneurysms were thin-walled and occurred in patients with Marfan syndrome due to cystic medial necrosis (fig. 3). Two patients in this series with fusiform aneurysms had plaquelike areas of wall thickening, one subsequently proven due to giant cell aortitis. In both cases, the thickening spared the areas of maximum aortic dilation (figs. 2 and 4). Three of the saccular aneurysms had thickening typical of thrombus. Although recent studies suggest that MRI can provide information about flow volume and direction [14], at present patients needing evaluation for aortic regurgitation would also require other studies, usually aortography and left heart catheterization.

REFERENCES

1. O'Donovan PB, Ross JS, Sivak ED, O'Donnell JK, Meaney TF. Magnetic resonance imaging of the thorax: the advantages of coronal and sagittal planes. *AJR* **1984**;143:1183–1188
2. Herfkens RJ, Higgins CB, Hricak H, et al. Nuclear magnetic resonance imaging of the cardiovascular system: normal and pathologic findings. *Radiology* **1983**;147:749–759
3. Amparo EG, Higgins CB, Hoddick W, et al. Magnetic resonance

imaging of aortic disease: preliminary results. *AJR* **1984**;143:1203-1209

4. Moore EH, Webb WR, Verrier ED, et al. MRI of chronic posttraumatic false aneurysms of the thoracic aorta. *AJR* **1984**;143:1195-1196
5. Amparo EG, Higgins CB, Shafton EP. Demonstration of coarctation of the aorta by magnetic resonance imaging. *AJR* **1984**;143:1192-1194
6. Dinsmore RE, Wismer GL, Levine RA, Okada RD, Brady TJ. Magnetic resonance imaging of the heart: positioning and gradient angle selection for optimal imaging planes. *AJR* **1984**;143:1135-1142
7. Dinsmore RE, Wismer GL, Miller SW, et al. Magnetic resonance imaging of the heart using image planes oriented to cardiac axes: experience with 100 cases. *AJR* **1985**;145:1177-1183
8. Newman WM, Sproull RF. *Principles of interactive computer graphics*, 2d ed. New York: McGraw-Hill, **1979**
9. Morse DE. Embryology, anatomy and histology of the aorta. In: Lindsay J Jr, Hurst JW, eds. *The aorta.* New York: Grune & Stratton, **1979**
10. Dotter CT, Steinberg I. The angiocardiographic measurement of the normal great vessels. *Radiology* **1949**;52:353-357
11. Guthaner DF, Wexler L, Harell G. CT demonstration of cardiac structures. *AJR* **1979**;133:75-81
12. Weyman AE. *Cross-sectional echocardiography*. Philadelphia: Lea & Febiger, **1982**
13. Williams RG, Tucker CR. *Echocardiographic diagnosis of congenital heart disease.* Boston: Little, Brown, **1977**
14. Wedeen V, Rosen B, Chesler D, Brady TJ. MR velocity imaging by phase display. *J Comput Assist Tomogr* **1985**;9:530-536

Magnetic Resonance Imaging of Chronic Myocardial Infarcts in Man

Michael T. McNamara[1]
Charles B. Higgins[1]

To evaluate the magnetic resonance imaging (MRI) features of chronic myocardial infarction (MI), 22 patients and several normal volunteers were studied with a 0.35-T cryogenic imaging system. The MIs were 9 months to 16 years old. The patients also had either left ventriculography (17 patients) or two-dimensional echocardiography (17 patients). At least one abnormality indicative of prior infarction was demonstrated on MRI in 20 of the 22 patients. Wall thinning was seen in 20 patients; in six of these, the thinning resulted in aneurysm formation. The other 14 patients had sufficient residual wall thickness to permit measurement of T2 relaxation times and MR signal intensity in the infarcted region. Ten of these 14 patients demonstrated low intensity and shortened T2 of the thinned segments (mean T2 = 28.7 msec) compared to adjacent normal myocardium (mean T2 = 45.4 msec) and to the myocardium of volunteers (mean T2 = 41.3 msec). The percentage of difference in intensity between thinned and normal myocardium was greater on 56-msec-TE images (98.2%) than on 28-msec-TE images (46.1%). In the other four patients, no difference in intensity of the myocardium was perceptible in the thinned region of the myocardial wall. Thus MRI shows regional wall thinning at the site of prior MI. In some patients, the chronic infarct is characterized as decreased spin-echo signal intensity and shortened T2 consistent with replacement of myocardium by fibrous scar.

As a leading cause of mortality and morbidity in industrialized society, occlusive coronary heart disease has been the subject of widespread investigation. The contribution that magnetic resonance imaging (MRI) may make is under active study [1-6]. It has already produced images of the heart with excellent anatomic resolution and has the capability to achieve differential characterization of myocardial tissue [2].

Initial experience with MRI in patients with ischemic heart disease has demonstrated focal myocardial wall thinning after previous myocardial infarction [7]. Additional findings in these patients include abnormal flow signal due to myocardial dysfunction and mural thrombus adherent to the ventricular wall. Tissue characterization of fully evolved myocardial infarctions has not yet been performed, and this was a major objective of this study.

We evaluated additional patients with chronic ischemic heart disease using electrocardiographically (ECG)-gated MRI to assess the appearance of previously infarcted, and presumably scarred, myocardium and related sequelae and characterized the spin-echo (SE) signal intensity and T2 relaxation time of evolved myocardial infarctions relative to normal myocardium. If MRI can reliably detect and estimate the extent of evolved myocardial infarctions, it would be useful for defining residual myocardium in patients in whom myocardial revascularization is being considered.

Received March 25, 1985; accepted after revision October 7, 1985.

[1] Department of Radiology, University of California Medical Center, San Francisco, CA 94143. Address reprint requests to C. B. Higgins.

AJR **146:315-320, February 1986**
0361-803X/86/1462-0315
© American Roentgen Ray Society

Subjects and Methods

Subject Selection

Twenty-nine adults were studied by ECG-gated proton MRI after giving informed consent. Seven of these individuals were asymptomatic normal volunteers with no known cardiovascular abnormalities. Their age range was 26–34 years; five subjects were men. The 22 patients had documented myocardial infarction (MI) within 9 months to 16 years before MRI. The age range of these patients was 39–78 years; 17 were men. Seven patients were included in a previous study [7]. The purpose of that study was to identify the morphologic characteristics of chronic ischemic heart disease. The MRI characteristics of infarcted segments were not assessed. Criteria for inclusion in this study were the diagnosis of transmural MI confirmed by ECG abnormalities and diagnostic elevation of serum myocardial creatinine phosphokinase (CPK) isoenzyme level. Patients were not selected on the basis of patient age, infarct size, or infarct age. Isoenzymes were not obtained in one patient with a 16-year-old infarct. One patient had an abnormal elevation of the MB fraction of CPK (12%) but no demonstrable ECG abnormalities. All 22 patients had either two-dimensional echocardiography (17 patients) and/or left ventriculography (17 patients). Wall motion abnormality was documented by one of these studies in 20 of 22 patients.

MR Imager and Imaging Techniques

MRI was performed with a superconducting system operating at 0.35 T (Diasonics MT/S). The corresponding hydrogen resonant frequency was 15 MHz. This system has been previously described in detail [8].

Nonferromagnetic ECG leads were placed on the right subclavian and right and left upper abdominal regions. A specially designed gating device for use in high electromagnetic fields and rapidly switched field gradients was used to obtain the gating signal [6]. The gating signal was initiated by the R-wave of the ECG signal complex. Initiation of the multislice pulse sequence started at 2 msec after inscription of the R-wave. The dual SE signal sequence required 60 msec at each of the five levels in the multislice technique. A multislice technique was used to acquire five contiguous 7-mm-thick sections from the base to the apex of the heart with a delay of 100 msec between the initiation of pulse sequences at each adjacent section. The fifth section was 400 msec later in time than the first section in the multislice sequence. The adjacent sections were therefore 100 msec out of phase with the previous section, and succeeding images of each section were acquired further into the cardiac cycle. The radiofrequency (RF) and gradient magnetic pulse sequences were applied in 512 cardiac cycles to obtain images. This required two averages with a 256 × 256 matrix and four averages with a 256 × 128 matrix.

An SE technique was used to obtain images with echo delay times (TE) of 28 msec and 56 msec between application of the initial RF pulse and receipt of the corresponding SE signal. Since a gating technique was used, the pulse repetition time (TR) was determined by the subject's heart rate and thus varied from about 0.6 to 0.9 sec (70–100 beats/min). With the multislice technique, the data for the most cephalic slice were acquired at end diastole while each slice progressing caudally corresponded to 100 msec later in the cardiac cycle. Consequently, the data for the most caudal of the five slices were acquired 400 msec after the QRS complex.

The SE signal intensity was determined by the following equation:

$$I = N(H)f(v)\exp(-TE/T2)[1 - \exp - (TR/T1)]$$

where I = MRI signal intensity; N(H) = mobile hydrogen spin density; f(v) = velocity function, which relates the effects of flow and the percentage of protons that are moving; TE = time to reception of the SE signal (28 msec or 56 msec after 90° RF pulse); T2 = spin-spin or transverse relaxation time; TR = RF pulse sequence repetition time (heart-rate-dependent in this study); and T1 = spin-lattice or longitudinal relaxation time. It is apparent that SE signal intensity is increased with either shortening of T1, prolongation of T2, or increase in spin density.

Data Analysis

Two-Dimensional Echocardiography and Left Ventriculography

Studies were assessed for wall motion abnormalities and aneurysms. The angiographic definition for aneurysm in our study was based on the criteria established by Gorlin et al. [9]. They defined an aneurysm as a motion disturbance in which part of the left ventricular cavity exhibited either localized akinesia or dyskinesia during systole. The 2D echocardiographic definition of an aneurysm was a bulging diastolic deformity of the ventricle. This was valid only if the ventricular outline was seen during diastole.

Magnetic Resonance Images

For each of the five adjacent MRI sections of the normal volunteers, a computer-generated region of interest was constructed in the anterior wall of the left ventricle (LV) where signal intensity (arbitrary units) and T2 relaxation time were measured. Most studies were gated only to every heart beat and therefore a T1 could not be obtained because only one TR was used. A similar region of interest was constructed in the posterior wall of the left ventricle to calculate both the signal intensity and T2 relaxation time. For the 22 patients, each series of images was visually inspected to assess the uniformity of wall thickness of the left ventricular myocardium. Wall thinning was defined as greater than 50% wall thinning compared to adjacent myocardium with a well defined zone of transition between normal and thinned myocardium. For each patient, focal segments of wall thinning were correlated with the site of the prior infarction as documented by ECG, echocardiographic, and angiographic data. For patients with anterior wall thinning, the posterior myocardial LV was considered the normal myocardium; for patients with posterior wall thinning, the anterior LV wall was considered the normal myocardium. There were no clinical or laboratory findings to suggest previous infarction within the region considered to be normal myocardium. The criteria for aneurysms on MR images have not yet been established. Our criteria for aneurysms included severe LV wall thinning such that the remaining myocardium measured 1–3 mm with or without a focal bulge.

Region-of-interest analysis was performed within the focal segment of wall thinning to obtain the SE signal intensity and a T2 relaxation time for each patient with an abnormal MR study who had sufficiently thick myocardium to permit analysis (14 patients). The percent difference in MRI signal intensity between anterior and posterior regions of interest for the normal volunteers was calculated as follows:

$$\%\ \text{difference}\ I = \frac{I\ (\text{anterior}) - I\ (\text{posterior})}{I\ (\text{posterior})} \times 100\%$$

where I = SE signal intensity; I (anterior) = intensity of anterior wall of the left ventricle; and I (posterior) = intensity of the posterior wall of the left ventricle.

The percentage of difference in signal intensity between thinned and normal-thickness myocardium for the chronic MI patients was calculated as follows:

$$\%\ \text{difference}\ I = \frac{I\ (\text{normal}) - I\ (\text{MI})}{I\ (\text{MI})} \times 100\%$$

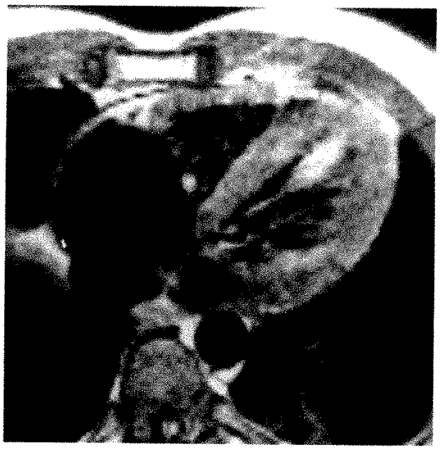

1

Fig. 1.—Normal subject (subject 3, table 1). ECG-gated, 28-msec-TE image: Myocardium is of uniform signal intensity and wall thickness without evidence of abnormalities.

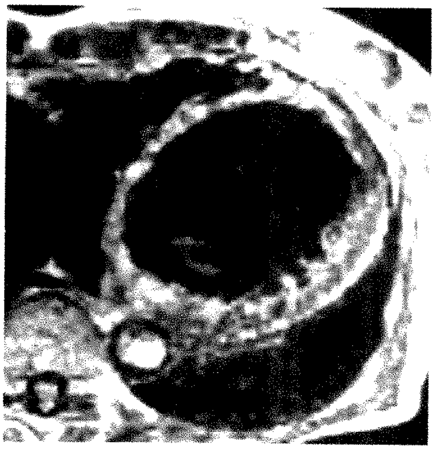

2

Fig. 2.—Old anteroseptal infarct. ECG-gated, 28-msec-TE image at level of mid left ventricle: moderate thinning of anterior and septal wall.

where I (MI) = MRI signal intensity of previously infarcted myocardium and I (normal) = signal intensity of normal left ventricular myocardium.

Subjects were divided into three groups for statistical analysis. Group 1 consisted of the seven normal volunteers. The 10 group 2 MI patients had visible and measurable low intensity of thinned myocardium. The four patients in group 3 had wall thinning but did not have low intensity of the thinned myocardium. Two MI patients had normal MRI studies and thus were not included in either of these groups. The remaining six MI patients had LV aneurysms and such severe wall thinning that analysis of regional myocardial relaxation times was not feasible.

Statistical Analysis

For the 14 patients who had sufficient residual tissue for region-of-interest analysis at the site of previous infarction, statistical significance of the difference between the thinned myocardium and normal myocardium for signal intensity and T2 was calculated using Student's two-tailed t-test. A p value of less than 0.05 was considered statistically significant.

Results

Normal Volunteers (Group 1)

The series of gated MR images of each of the normal volunteers demonstrated good resolution of the cardiac structures. In these subjects, wall thickness was uniform throughout the various regions of the LV (fig. 1). There was 17.5 ± 11.4% difference in signal intensity between the anterior wall and posterolateral wall of the LV on 28-msec-TE images (table 1). This difference decreased or remained similar on the second-echo image. Figure 1 shows a gated first-echo (28 msec TE) image of the heart of a normal volunteer at the level of the LV. No significant regional differences in signal intensity or T2 times were noted in the volunteers (table 1).

Wall Thinning

Focal thinning of a segment of the LV relative to adjacent myocardium was noted in 20 of the 22 patients with chronic infarcts. The two patients with normal MR studies had either a normal 2D echocardiogram (one patient) or a normal left ventriculogram (one patient). Anteroseptal, posterior wall, and anterior infarcts are illustrated in figures 2–4. Isolated involvement of the septum was not seen in any patients.

TABLE 1: **T2 Times and Percentage Intensity Difference* between Anterior and Posterior Myocardium: Normal Volunteers—Group 1**

Subject No.	T2 (msec)		Intensity Difference (%)	
	Anterior Wall	Posterior Wall	28 msec	56 msec
1	39	47	21.2	7.3
2	42	41	26.3	27.5
3	41	48	0.7†	9.6†
4	38	47	18.3	2.4
5	40	41	3.7†	6.8†
6	39	43	20.8	12.8
7	35	35	31.7	30.4
Mean	39.1	43.1	17.5	13.8
SD	2.3	4.3	11.4	10.8

Note.—SD = standard deviation.

* Defined as (posterior wall intensity minus anterior wall intensity) divided by posterior intensity × 100%.

† Anterior wall intensity greater than posterior wall intensity.

In six patients the degree of wall thinning was so severe that only a 1- to 3-mm-thick segment of myocardium was seen on MRI. All of these had LV aneurysms documented by echocardiography (six patients) and angiography (one patient). Figures 5 and 6 demonstrate the extreme degree of wall thinning with LV aneurysms involving the anteroseptal and posterolateral regions of the LV, respectively. Two patients had LV aneurysms that were diagnosed by 2D echocardiography but were not recognized by MRI. One patient had an LV aneurysm on angiography that was not diagnosed by MRI.

Low-Intensity Segments

Region-of-interest analysis demonstrated significantly greater MRI signal intensity of normal myocardium versus thinned myocardium ($p < 0.05$) for 10 (group 2) of the 14 patients who had sufficient myocardial thickness for region-

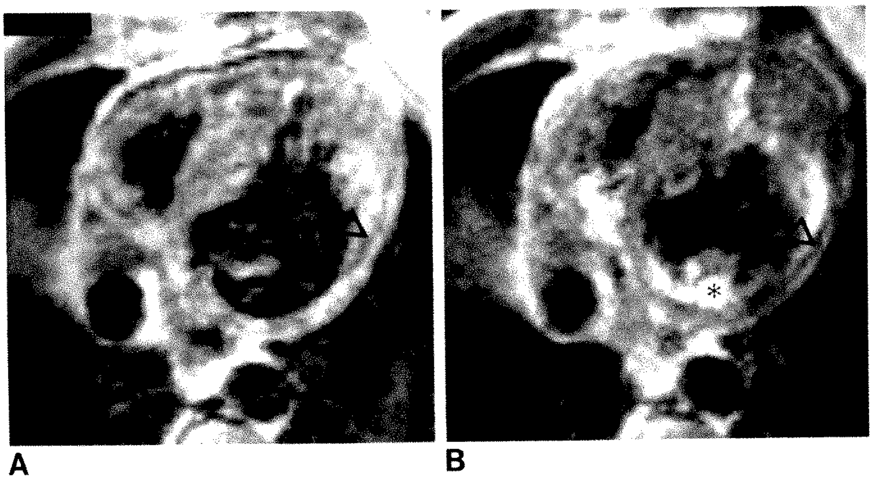

Fig. 3.—Old posterior infarct (3 years old). ECG-gated SE images at 28 msec TE (**A**) and 56 msec TE (**B**): marked thinning of posterior wall of left ventricle. Note low signal intensity (*arrows*) of thinned myocardium, which is better seen on second-echo image (**B**). High-intensity flow signal adjacent to myocardial walls also best seen on second-echo image (*asterisk*).

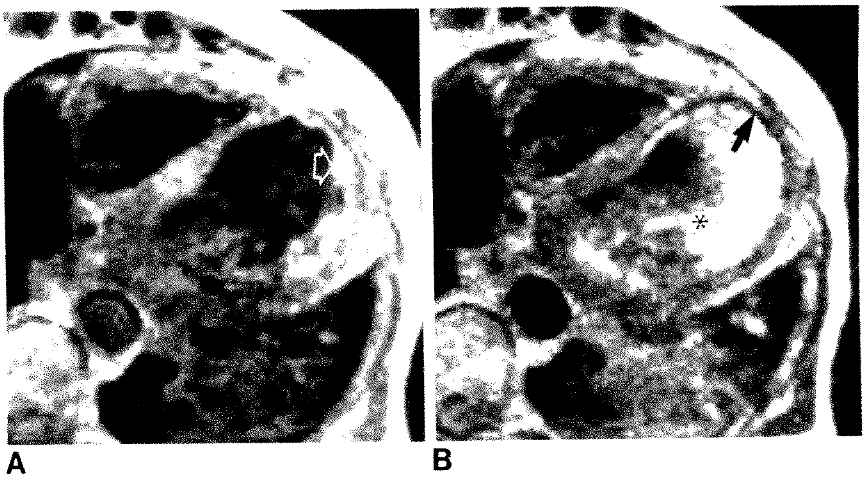

Fig. 4.—Old anteroseptal myocardial infarction. ECG-gated SE images at 28 msec TE (**A**) and 56 msec TE (**B**): anterior wall thinning and adherent mural thrombus within left ventricle (*open arrow*). Thinned myocardium (*solid arrow*) is characterized by relatively low signal intensity. Intracavitary flow signal (*asterisk*) appears on second-echo image.

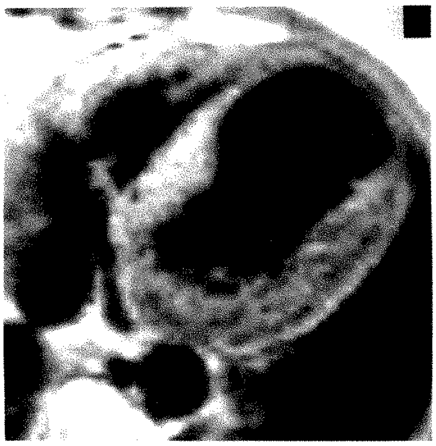

Fig. 5.—Aneurysm of ventricular apex. ECG-gated, 28-msec-TE image: severe anteroseptal wall thinning of left ventricle. Patient had anteroseptal wall myocardial infarction 3 years before imaging.

of-interest analysis (table 2). The percentage of difference in intensity between normal and thinned myocardium was greater on 56-msec-TE images (98.2 ± 62.0%) than on 28-msec-TE images (46.1 ± 50.0%). The signal intensity of the previously infarcted myocardial wall was less than that of normal myocardium in eight of these patients on both 28-msec-TE and the 56-msec-TE images; two patients (cases 9 and 10, table 2) had slightly greater intensity (measurable but not visible) of MI versus normal myocardium on the 28-msec-TE images (5.5% and 16.5%, respectively) but on the 56-msec-TE images had less intensity of thinned areas compared to normal myocardium (20.9% and 64.7%, respectively). Examples of the low intensity of the thinned segment and the greater contrast between the thinned segment and normal myocardium on the 56-msec-TE image compared to the 28-msec-TE image are shown in figures 3 and 4.

Four patients with sufficient wall thickness to evaluate the infarct region had no visible or only small measurable difference of signal intensity relative to normal myocardium (group 3). The mean percentage of difference between thinned and normal myocardium was 19.6 ± 11.0% and 8.2 ± 4.5% on 28-msec-TE and 56-msec-TE images, respectively (table 3).

T2 of Normal Myocardium and Chronic Infarct

The 10 group 2 patients who had a visible segment of low intensity had a shorter T2 relaxation time of the infarcted region (mean $T2 = 28.7 \pm 9.9$ msec) compared to normal myocardium (mean $T2 = 45.4 \pm 9.9$ msec) (table 2). The difference in T2 between normal and infarcted myocardium was statistically significant ($p < 0.05$). The mean T2 of thinned myocardium was also significantly ($p < 0.05$) shorter than the mean T2 value for myocardium of the normal volunteers

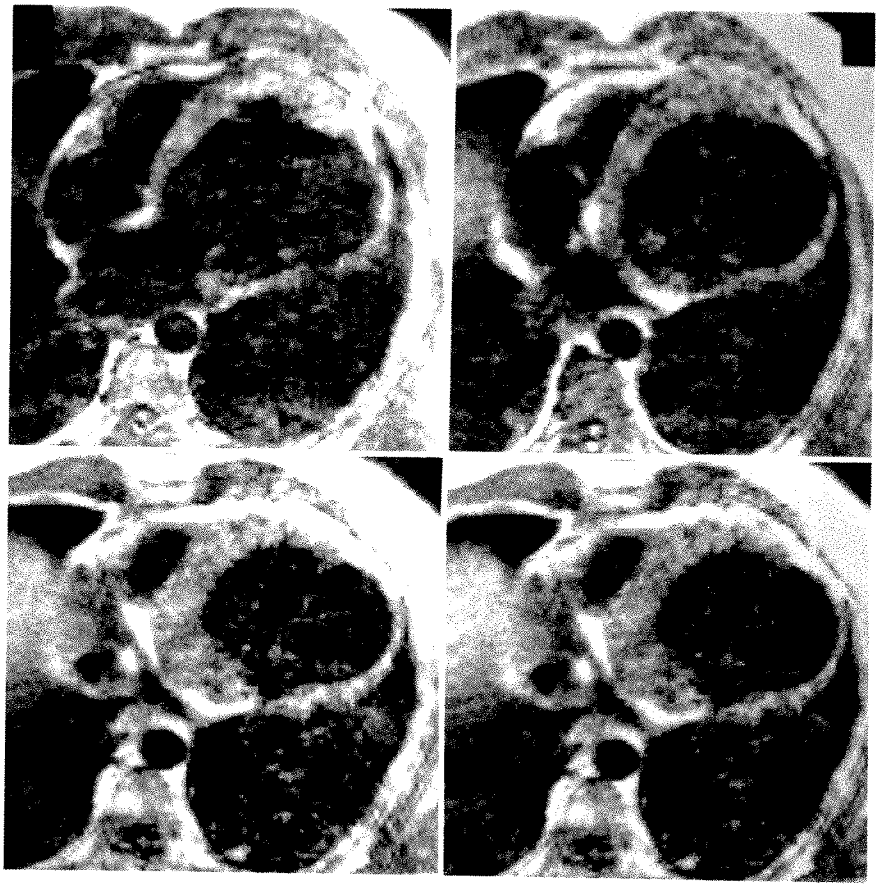

Fig. 6.—Old myocardial infarction (7 years old). Adjacent images: severe aneurysmal posterolateral wall thinning of left ventricle.

TABLE 2: **T2 Times and Percentage Intensity Difference* between Normal and Thinned Myocardium: MI Patients—Group 2**

Case No.	T2 (msec)		Intensity Difference (%)	
	Thin	Normal	28 msec	56 msec
1	31	48	32.7	88.0
2	29	42	29.6	72.4
3	39	53	133.2	154.5
4	32	42	7.7	30.2
5	28	36	136.0	202.2
6	30	37	23.8	48.1
7	22	65	8.3	159.2
8	23	34	67.8	142.2
9	30	41	5.5†	20.9
10	23	56	16.5†	64.7
Mean	28.7	45.4	46.1	98.2
SD	5.1	9.9	50.0	62.0

Note.—SD = standard deviation.

* Defined as (normal myocardial intensity minus thinned myocardial intensity) divided by thinned myocardial intensity × 100%.

† Intensity of thinned myocardium greater than intensity of normal myocardium.

TABLE 3: **T2 Times and Percentage Intensity Difference* between Normal and Thinned Myocardium: MI Patients—Group 3**

Case No.	T2 (msec)		Intensity Difference (%)	
	Thinned	Normal	28 msec	56 msec
1	38	37	35.0	14.2
2	48	45	19.7	8.4
3	42	40	14.1	3.6
4	47	44	9.7	6.6
Mean	43.8	41.8	19.6	8.2
SD	4.6	3.9	11.0	4.5

Note.—SD = standard deviation.

* Defined as (normal myocardial intensity minus thinned myocardial intensity) divided by thinned intensity × 100%.

(mean T2 = 39.1 ± 2.3 msec [anterior wall] and 43.1 ± 4.3 msec [posterior wall]).

The four patients in group 3 had no difference in mean T2 between normal and thinned myocardium (41.8 ± 3.9 msec vs. 43.8 ± 4.6 msec, respectively) (table 3). In addition, there was no significant T2 difference between the mean values in the group 3 patients and the normal group 1 subjects.

Discussion

The current study evaluated the MRI signal intensity and T2 relaxation time characteristics of evolved (chronic) myocardial infarctions. It demonstrated in a larger population of patients similar morphologic findings previously reported in patients with chronic ischemic heart disease [7]. However, the signal intensity and T2 relaxation characteristics of thinned, and presumably scarred, myocardium have not been previously reported.

The two MI patients who had normal MR images also had no regional contraction abnormality on corroborative studies. One patient had an abnormal elevation of the MB fraction of CPK but had no ECG abnormalities. Thus, MRI demonstrated excellent sensitivity for the detection of morphologic abnormalities due to previous MI.

The measurement of tissue characteristics in patients with old myocardial infarctions was possible in only 14 patients because the thickness of the infarcted myocardium had been reduced to only a few millimeters in six of the patients. In the 10 of these 14 patients with prior MI and residual sufficient wall thickness for analysis of relaxation times, measurements confirmed the visual findings of lower signal intensity within the thin region relative to adjacent normal myocardium (table 2). The mean signal intensity of noninfarcted myocardium was 98.2% greater than the thinned myocardium in these patients on the 56-msec-TE images. Although a direct comparison of signal intensity differences cannot be made with the control subjects due to the arbitrary nature of the units of signal intensity, it was noteworthy that the mean percentages of difference in signal intensity between the anterior and posterior LV walls in the control subjects were only 17.5% and 13.8% on 28-msec-TE and 56-msec-TE images, respectively. In addition, the four group 3 patients with wall thinning but no decrease in signal intensity had mean percentage differences of intensity between normal and thinned myocardium of 19.6% and 8.2% on 28-msec-TE and 56-msec-TE images, respectively.

The regional determination of T2 relaxation times within the previously infarcted myocardium gives insight into the nature of decreased signal intensity. SE signal intensity is determined by T1 and T2 such that a decrease in T1 or an increase in T2 results in an increase in signal intensity. A previous investigation has demonstrated increased signal intensity of acute myocardial infarctions in humans due to T2 prolongation [10]. Conversely, an increase in T1 or a decrease in T2 will result in decreased SE signal intensity. The mean T2 of thinned, and presumably scarred, myocardium averaged 16.7 msec less than that of normal myocardium in the 10 group 2 patients with low-signal-intensity MI. The decrease in T2 therefore produces the observed decrease in MRI signal intensity. No significant difference between T2 of anterior LV wall versus posterior LV wall was found in the seven control subjects.

Although this finding of contrast between normal and thinned myocardium was, in general, observed on both first- and second-echo images, the percentage of difference or contrast was greater on second-echo images (98.2%) versus first-echo images (46.1%). The longer T2 of normal myocardium compared to thinned myocardium results in relatively greater signal intensity of normal myocardium on the 56-msec-TE images, thereby producing the visibly increased contrast. SE signal intensity is also affected by mobile proton spin density. The fibrotic nature of scarred tissue does, in fact, have less spin density than other types of soft tissue and organs. An in vivo example of the relation between fibrotic tissue and SE signal intensity is seen in patients with chronic pericarditis, in whom the fibrotic scarred myocardium has low signal intensity relative to adjacent fat and myocardium [11].

MRI demonstrated utility for the diagnosis of LV aneurysms in this study. All six of the patients who had aneurysms diagnosed on MRI had corroborative findings on either 2D echocardiography or left ventriculography. These six patients had immeasurably thin LV myocardium with a variable degree of focal bulging. Three patients had LV aneurysms diagnosed by other studies that were not seen on MRI. The two patients who had an LV aneurysm on the 2D echocardiogram and the patient who had an apical LV aneurysm on the left ventriculogram that were not diagnosed by MRI did have focal LV wall thinning in these regions on the MR images.

From this study of selected patients with previous myocardial infarction, we found MRI has the capability for identifying wall thinning, aneurysms, and alterations of intensity and T2 caused by previous MI. The infarcted segments showing low intensity and decreased T2 in some patients may represent substantial replacement of the myocardium by fibrous scar. On the other hand, the thinned myocardial segment with normal intensity and T2 may represent infarcted sites at which considerable residual myocardium exists. This supposition requires confirmation with pathologic findings and further studies should be done to determine the clinical significance of this variable appearance of evolved myocardial infarctions.

REFERENCES

1. Herfkens RJ, Higgins CB, Hricak H, et al. Nuclear magnetic resonance imaging of the cardiovascular system: normal and pathologic findings. *Radiology* **1983**;147:747–759
2. Wesbey G, Higgins CB, Lanzer P, Botvinick E, Lipton MJ. In vivo and characterization of acute myocardial infarction using gated nuclear magnetic resonance. *Circulation* **1984**;69:125–130
3. Dinsmore RE, Wisner GL, Levine RA, Okada RD, Brady TJ. Magnetic resonance imaging of the heart: positioning and gradient angle selection for optimal imaging planes. *AJR* **1984**;143:1135–1142
4. Choyke PL, Kressel HY, Reichek N. Nongated cardiac magnetic resonance imaging: preliminary experience at 0.12 T. *AJR* **1984**;143:1143–1150
5. Higgins CB, Stark D, McNamara MT, Lanzer P, Crooks LE, Kaufman L. Multiple magnetic resonance imaging of the heart and major vessels: studies in normal volunteers. *AJR* **1984**;142:556–561
6. Lanzer P, Botvinick EH, Schiller NB, et al. Cardiac imaging using gated magnetic resonance. *Radiology* **1984**;150:121–127
7. Higgins CB, Lanzer P, Stark D, et al. Imaging by nuclear magnetic resonance in patients with chronic ischemic heart disease. *Circulation* **1984**;69:523–531
8. Crooks LE, Arakawa M, Hoenninger J, et al. Nuclear magnetic resonance whole-body imager operating at 3.5 KGauss. *Radiology* **1982**;143:169–174
9. Gorlin R, Klein MD, Sullivan JM. Prospective correlative study of ventricular aneurysm. *Am J Med* **1967**;42:512–531
10. McNamara MT, Higgins CB, Schechtmann N, Botvinick E, Amparo EG, Chatterjee K. Detection and characterization of acute myocardial infarctions in man using gated magnetic resonance imaging. *Circulation* **1985**;71:717–724
11. Stark DD, Higgins CB, Lanzer P, et al. Magnetic resonance imaging of the pericardium: normal and pathologic findings. *Radiology* **1984**;150:469–474

Strangulated Diaphragmatic Hernia with Pneumothorax due to Colopleural Fistula

D. Randall Radin,[1] Marilyn J. Ray, and James M. Halls

The diagnosis of traumatic diaphragmatic hernia, both in the acute phase and in the delayed obstructive phase, is often missed and requires a high index of suspicion [1]. Recently we saw a patient who presented with a diaphragmatic hernia 5 years after being stabbed in the chest. The diagnosis was not made until he developed a pneumothorax due to perforation of strangulated colon. To our knowledge, pneumothorax has not yet been reported in the radiologic literature as a complication of strangulated diaphragmatic hernia. Radiographic features that may aid in establishing the diagnosis are discussed.

Case Report

A 38-year-old man was admitted with a 1-day history of intermittent midepigastric pain. Five years earlier, he had been stabbed in the left neck and chest. On physical examination no breath sounds were heard over the left lower chest, which was also dull to percussion.

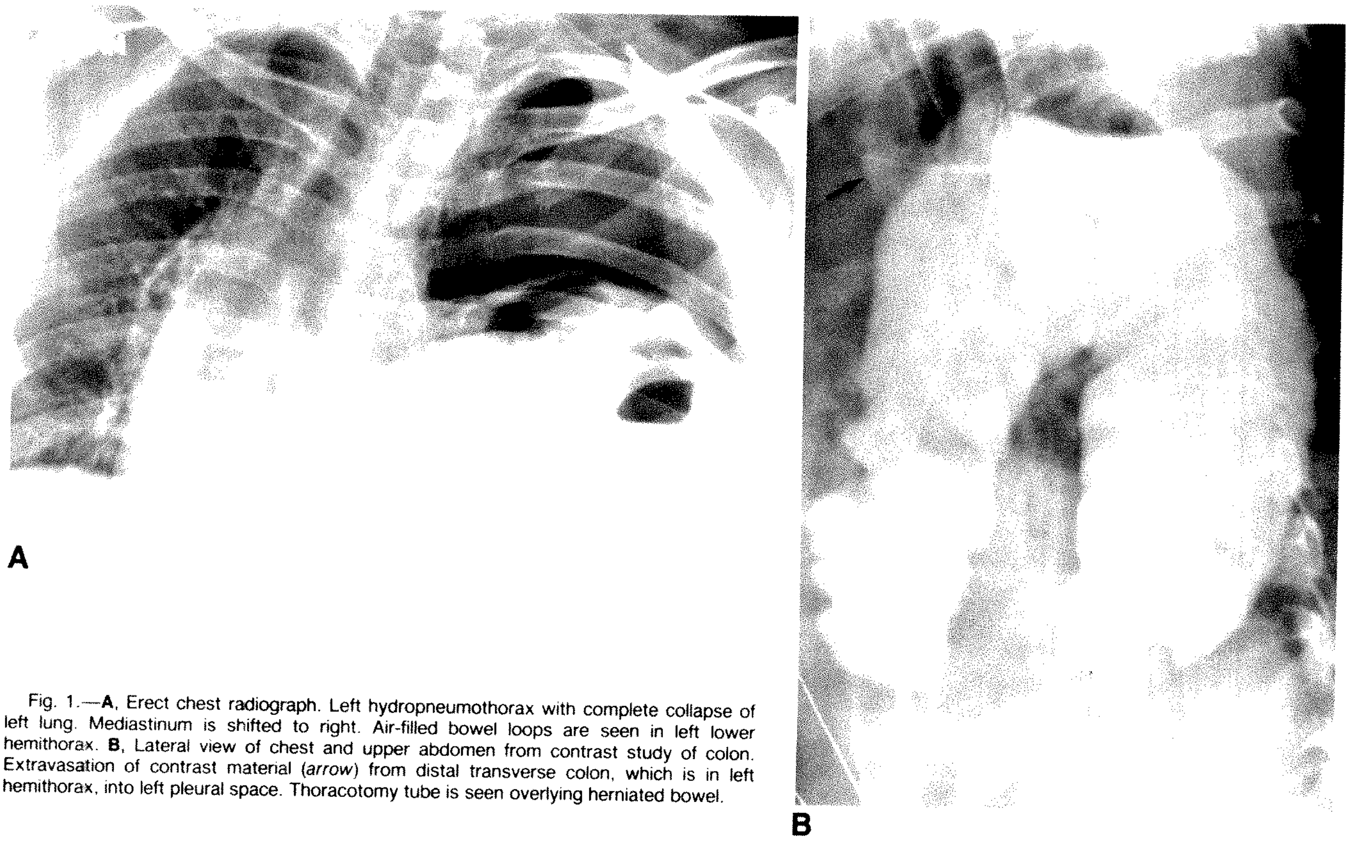

Fig. 1.—**A**, Erect chest radiograph. Left hydropneumothorax with complete collapse of left lung. Mediastinum is shifted to right. Air-filled bowel loops are seen in left lower hemithorax. **B**, Lateral view of chest and upper abdomen from contrast study of colon. Extravasation of contrast material (*arrow*) from distal transverse colon, which is in left hemithorax, into left pleural space. Thoracotomy tube is seen overlying herniated bowel.

Received June 24, 1985; accepted after revision September 12, 1985.

[1] All authors: Department of Radiology, University of Southern California School of Medicine, Los Angeles County-USC Medical Center, 1200 N. State St., Los Angeles,CA 90033. Address reprint requests to D. R. Radin.

AJR 146:321-322, February 1986 0361-803X/86/1462-0321 © American Roentgen Ray Society

There was auscultatory evidence of paralysis of the left hemidiaphragm. The midepigastrium was tender on palpation. Occult blood was detected in the stool. Chest radiography showed marked elevation of the left hemidiaphragm. Radiography of the abdomen was normal.

On the fifth hospital day the patient's epigastric pain began to radiate to his left chest, and he became tachypneic. A chest film revealed a large left hydropneumothorax with total collapse of the left lung; there was a marked shift of the mediastinum to the right, and bowel loops were present in the left lower hemithorax (fig. 1A). A thoracotomy tube was placed in the left pleural space, and serosanguinous fluid was obtained. Over the next several hours, 1200 ml of yellow-green material with a pH of 7.0 was drained from the left pleural space. The patient's temperature rose to 38.7°C, his bowel sounds decreased, and persistent respiratory distress and hypoxemia required intubation.

Retrograde study of the colon with water-soluble contrast material showed herniation of the distal transverse colon into the left hemithorax with extravasation from the apex of the herniated loop into the pleural space (fig. 1B). The patient was then taken to the operating room, where a segment of necrotic transverse colon was found herniated into the left hemithorax through a 7-cm tear in the anterior aspect of the left hemidiaphragm. The diaphragmatic defect was believed to be due to the prior knife wound.

Discussion

In our reivew of the literature, we found only two other cases of pneumothorax due to strangulated diaphragmatic hernia. Both patients were children who developed gastropleural fistula following incarceration of the stomach in a Bochdalek hernia [2, 3]. Thus our patient is the first reported with pneumothorax due to *colo*pleural fistula or to strangulated *traumatic* diaphragmatic hernia.

A distinctive radiographic feature of the pneumothorax in our patient was complete collapse of the lung with contralateral shift of the mediastinum but without depression of the ipsilateral hemidiaphragm. An identical combination of findings was seen in each of the two patients with gastropleural fistula due to strangulated Bochdalek hernia [2, 3]. The total pulmonary collapse and contralateral mediastinal shift can be explained by the steep gradient between the high intraluminal pressure in the incarcerated bowel and the negative intrathoracic pressure. Of course, concomitant depression of the ipsilateral hemidiaphragm, as would be expected in so-called tension pneumothorax, is not seen because the diaphragm is not intact and the lower hemithorax is occupied by incarcerated bowel.

Strangulated diaphragmatic hernia with perforation of incarcerated stomach or colon has not been listed as a cause of pneumothorax [4, 5]. However, this rare entity should be included in the differential diagnosis, especially when there is contralateral shift of the mediastinum without depression of the ipsilateral hemidiaphragm. The diagnosis can be confirmed immediately by performing contrast studies of the stomach and colon. If the pH of pleural fluid aspirate is less than 6.0, indicating the presence of gastric acid [2], passage of a nasogastric tube and radiographic demonstration of its characteristic abnormal course may suffice [6].

REFERENCES

1. Ball T, McCrory R, Smith JO, Clements JL Jr. Traumatic diaphragmatic hernia: errors in diagnosis. *AJR* **1982**;138:633–637
2. Spinola SM, Ingram DL, Cerwin RA, Denny FW. Pyopneumothorax in a 14-year-old boy. *J Pediatr* **1981**;98:328–332
3. Hermann RE, Barber DH. Congenital diaphragmatic hernia in the child beyond infancy. *Cleve Clin Q* **1963**;30:73–80
4. Felson B. Pneumothorax. In: *Chest roentgenology*. Philadelphia: Saunders, **1973**:366–371
5. Fraser RG, Paré JAP. Pneumothorax. In: *Diagnosis of diseases of the chest*. Philadelphia: Saunders, **1979**:1770–1776
6. Perlman SJ, Rogers LF, Mintzer RA, Mueller CF. Abnormal course of nasogastric tube in traumatic rupture of left hemidiaphragm. *AJR* **1984**;142:85–88

Plasma Electrolyte Status after Small-Bowel Enteroclysis

Thomas J. Barloon[1]
E. A. Franken[1]

Plasma electrolyte values were measured in 10 consecutive patients before and after small-bowel enteroclysis. All patients had normal electrolyte values before enteroclysis. No clinically significant change in electrolyte status was observed after enteroclysis, although some dilution occurred. Small-bowel enteroclysis can be safely performed in patients with normal plasma electrolyte values.

Examination of the small bowel by enteroclysis provides a detailed small-bowel evaluation by rapid infusion of large quantities of barium, allowing adequate distension and separation of small-bowel loops. The rapid introduction of large quantities of fluid into patients undergoing this examination has caused us to question if electrolyte status may be affected. This study was undertaken to determine if electrolyte balance is affected by small-bowel enteroclysis.

Subjects and Methods

Ten consecutive adult patients undergoing small-bowel enteroclysis formed the study group. Six patients had normal small-bowel enteroclysis examinations. In two patients, Crohn disease was present but confined to the terminal ileum. One patient had an enterocutaneous fistula, and one patient had radiation enteritis confined to several loops of the distal jejunum. Enteroclysis was performed according to standard methods with a small-bowel catheter introduced to the level of the ligament of Trietz [1]. Barium suspension consisted of 400 ml HD85 (Lafayette Pharmacal) plus 1200 ml of water for a total volume of 1600 ml of fluid at 25 wt/vol. The enteroclysis catheter was connected to a dialysis infusion pump (Redy Pump CCT Life Systems) and was infused at a delivery rate of 240 ml/min. The infusion continued for 4–5 min, until the terminal ileum and cecum were filled. An average volume of 1200 ml of barium suspension was given.

Blood samples for hematocrit, blood urea nitrogen (BUN), serum osmolarity, sodium, potassium, and creatinine were measured in each patient immediately before the procedure, immediately after complete filling of the small bowel, and 1 hr after the procedure was completed.

Results

All participants had normal laboratory values on the blood samples before the examination. The serial samples showed no consistent changes in hematocrit, potassium, BUN, creatinine, or carbon dioxide. Metabolic changes associated with the enteroclysis examination are shown in figures 1–3. Mean sodium concentration fell from 142 to 139 mEq/L immediately after the procedure and remained at that level 1 hr later. There were similar small but definite decreases in serum chloride levels and measured osmolarity, indicating some dilution effect. In all three variables, the mean value of samples obtained after the examination was significantly different than the baseline ($p < 0.5$). However, at no time did any of the values fall outside the normal range. Although the changes were measurably different, we judged them to be of no clinical significance.

Received July 22, 1985; accepted after revision September 20, 1985.

[1] All authors: Department of Radiology, University of Iowa Hospitals and Clinics; Radiology Service, Veterans Administration Medical Center, Iowa City, IA 52240. Address reprint requests to T. J. Barloon.

AJR **146:323–325, February 1986**
0361-803X/86/1462-0323
© American Roentgen Ray Society

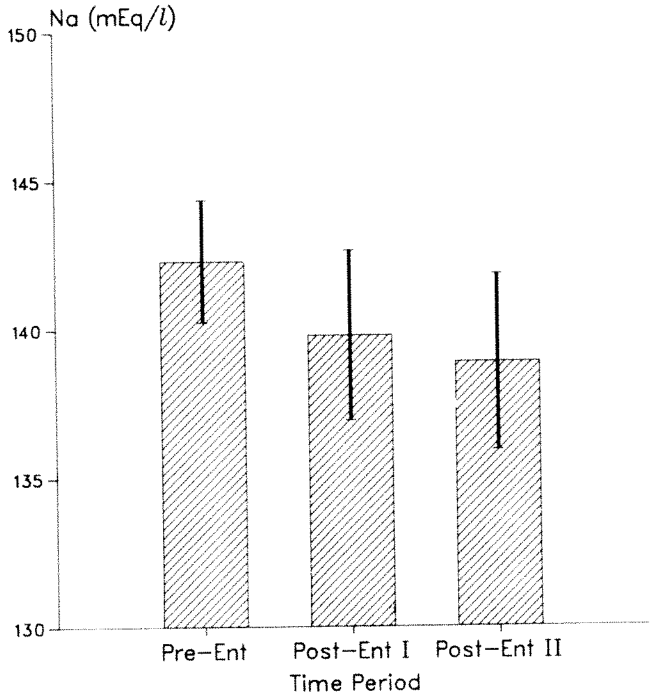

Fig. 1.—Serum sodium before (Pre-Ent), at completion of (Post-Ent I), and 1 hr after enteroclysis (Post-Ent II). Bar graphs indicate mean value for all samples; range markers indicate distribution of all samples.

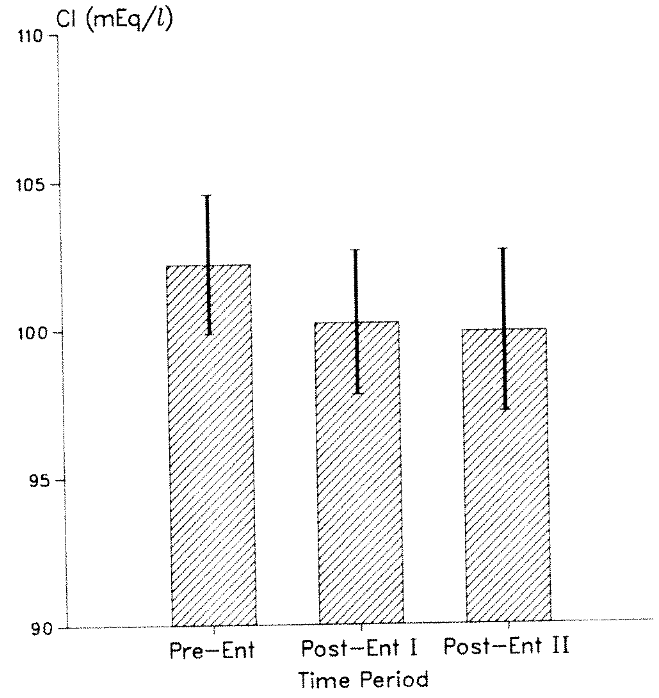

Fig. 2.—Serum chloride before (Pre-Ent), at completion of (Post-Ent I), and 1 hr after enteroclysis (Post-Ent II). Bar graphs indicate mean value for all samples; range markers indicate distribution of all samples.

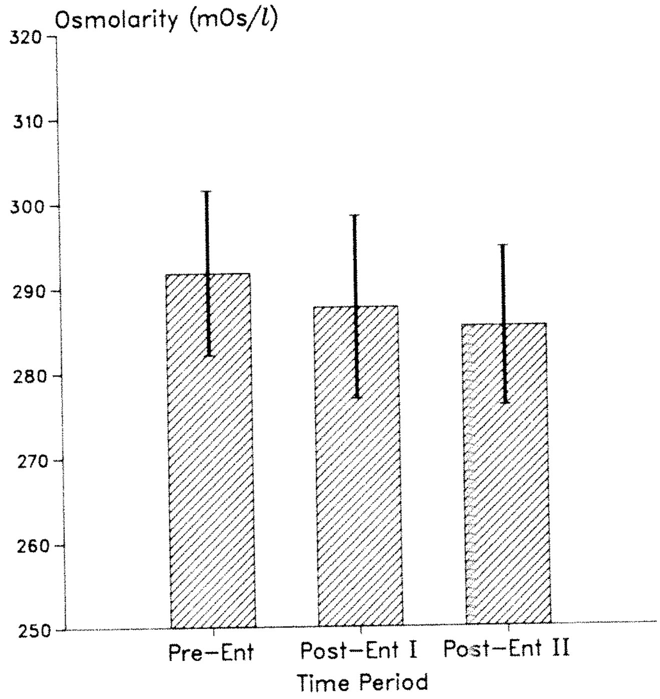

Fig. 3.—Serum osmolarity before (Pre-Ent), at completion of (Post-Ent I), and 1 hr after enteroclysis (Post-Ent II). Bar graphs indicate mean value for all samples; range markers indicate distribution of all samples.

Discussion

Toxicity from absorption of intestinal water has been described in infants associated with water enemas and in subsequent barium examinations in patients with Hirschsprung disease [2]. Conversely, dehydration can occur in infants receiving hyperosmolar contrast material via contrast enemas due to shifts of body water into the gut [3]. Enteroclysis differs from more traditional barium examinations in that a large amount of fluid is introduced directly into the small bowel, bypassing the stomach, over a short period of time. Water absorption from the small bowel is affected by a number of factors, including volume and osmolarity of the intraluminal fluid. The maximum rate of absorption by a normal individual is 35 ml/min/cm of small bowel [4].

It had been our concern that the rapid addition of large amounts of fluid of low osmolarity to the small bowel might produce toxicity by rapid absorption with expansion of the circulating blood volume or extracellular fluid. The small but significant drop in serum sodium, chloride, and osmolarity indicate that significant water absorption, with dilution of circulating blood volume, does occur with enteroclysis. However, the minimal changes measured were judged clinically insignificant, not indicating toxicity. We plan to assess the significance of water absorption during enteroclysis in patients with small-bowel disease and in those patients with fluid balance disorders, such as renal failure.

ACKNOWLEDGMENT

We thank Patricia Donovan for secretarial assistance.

REFERENCES

1. Miller RE, Sellink JL. Enteroclysis: the small bowel enema—how to succeed and how to fail. *Gastrointest Radiol* **1979**;4:269-283
2. Steinbach HL, Rosenberg RH, Grossman M, Nelson TL. Potential hazard of enemas in patients with Hirschsprung disease. *Radiology* **1955**;64:45-50
3. Waggert J, Bishop HC, Koop CE. Experience with Gastrografin enema in the treatment of meconium ileus. *J Pediatr Surg* **1970**;5:649-654
4. Palma R, Vidon N, Bernier JJ. Maximum capacity for fluid absorption in human bowel. *Dig Dis Sci* **1981**;10:929-934

George Andrew Miller, Sr., 1920–1985

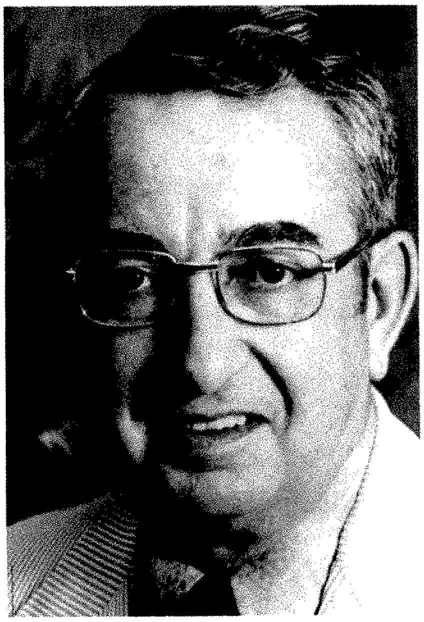

Dr. George Andrew Miller, Sr., died September 30, 1985, of cancer after a short but active 9 months of retirement.

He was born September 4, 1920, in Madison, WI, and spent most of his youth in Iowa. He earned both his Bachelor of Science and Doctor of Medicine degrees from the University of Iowa, served his internship and radiology residency at Harper Hospital in Detroit, and completed postgraduate studies at the University of Vienna, Austria, while a captain of the U.S. Army Medical Corps during World War II.

Dr. Miller was a general radiologist with special expertise in gastrointestinal disease and sonography. For 35 years he was at the Carle Clinic in Urbana, IL, where he served as radiology department head from 1963 to 1971 and then as a Carle Foundation board member.

Throughout his career, Dr. Miller was active in organized medicine including the American Medical Association, the Radiology Society of North America (RSNA), the American Roentgen Ray Society, and the American College of Radiology of which he was a fellow. He served as president of the Illinois Radiology Society and Champaign County Medical Society, secretary of the Central Illinois Radiologic Society, and councilor and alternate councilor of the American College of Radiology for many years.

Dr. Miller was the author and coauthor of scientific articles and presented refresher courses in gastrointestinal diseases at the RSNA for many years. He operated the Carle Foundation School of X-ray Technology and was a clinical associate professor at the University of Illinois.

He was a man with strong opinions that he backed up with hard work and personal example. His demand for high standards stemmed from a desire for excellent patient care, not on a rigid personality. Patients, friends, and family will miss his gentle touch.

Dr. Miller is survived by his wife, Ruth, a daughter, Barbara Hoppe, a son, G. Andrew, and many noisy grandchildren.

G. Andrew Miller, Jr.
1919 E. Crescent Drive
Seattle, WA 98112

Oriental Cholangiohepatitis:

Diagnostic Imaging and Interventional Management

Eric vanSonnenberg[1]
Giovanna Casola[1]
Don A. Cubberley[1]
Nicholas A. Halasz[2]
Octaviano A. Cabrera[1]
Gerhard R. Wittich[1]
Robert F. Mattrey[1]
F. William Scheible[1]

Diagnostic and therapeutic radiologic experience with six patients who had oriental cholangiohepatitis is described. These patients combined had 10 prior operations. Postoperatively each had recurrent cholangitis, numerous stones, concretions, and/or bile duct strictures. Diagnostically, sonography was valuable in the detection of intra- and extrahepatic stones and extrahepatic dilatation of ducts. An important pitfall in sonography was poor visualization of intrahepatic ductal dilatation (due to echogenic sludge filling the ducts) in most patients. CT was helpful diagnostically in all respects. Interventional procedures used postoperatively included percutaneous transhepatic cholangiography and biliary drainage, dilatation of strictures, Fogarty-type removal of intrahepatic stones, and flushing techniques. Most patients were treated during multiple sessions as outpatients. Cholangitis was the only complication from the procedures. Sectional imaging and interventional radiology perform valuable diagnostic and therapeutic roles in the pre- and postoperative management of patients with oriental cholangiohepatitis.

Changing demographic patterns have introduced the disease oriental cholangiohepatitis (OCH) (also known as recurrent pyogenic hepatitis) into the United States. OCH is characterized by a constellation of findings: recurrent abdominal pain (often for years), episodic cholangitis and jaundice, and dilatation of intra- and extrahepatic bile ducts which are packed with pigmented bilirubinate stones. These stones have a claylike consistency and often fill the ducts with casts [1-6]. Biliary strictures are common (35% of cases) with a predilection for the left ducts [1, 7, 8]; gallbladder stones are relatively uncommon (20%-40%) in comparison with Western-type biliary disease [9-11].

The acute infectious phase of OCH, characterized by cholangitis and sepsis, may be fatal; in this emergent situation, a 28% mortality even with operation has been reported [1]. Surgical problems are formidable in OCH, due to diagnostic difficulties and the chronicity and extent of the disease. The syndrome may not be recognized at initial surgery, resulting in a suboptimal operation [11]. Significant postoperative complications have been reported in up to 45% of patients [12]. Recurrent disease is common postoperatively [6, 9, 11-13]; a recent report described 31 operations in 21 patients [12]. Aggressive operations including partial hepatectomy have been necessary in some patients [1, 12-15].

Most cases and publications on OCH have come from the Far East, especially Hong Kong and Southeast Asia. The location of the University of California (UC) on the west coast provides a referral center for immigrants from the Far East. A recent paper from UC San Francisco related benefits of interventional radiology in OCH [16]. In an 18-month period, we have had the opportunity to participate in the management of six patients with OCH. We describe our diagnostic and therapeutic radiologic experience and the assistance these techniques provided in the care of these patients.

Received April 11, 1985; accepted after revision September 20, 1985.

[1] Department of Radiology and Medicine, University of California San Diego Medical Center, 225 Dickinson St., San Diego, CA 92103. Address reprint requests to E. vanSonnenberg, Dept. of Radiology (H-755).

[2] Department of Surgery, University of California San Diego Medical Center, San Diego, CA 92103.

AJR 146:327-331, February 1986
0361-803X/86/1462-0327
© American Roentgen Ray Society

TABLE 1: **Clinical Characteristics of Patients with Oriental Cholangiohepatitis**

Case No. (age, gender)	Geographic Background	Symptoms	Duration of Symptoms (years)	Alkaline Phosphatase (ng/ml)	Bilirubin (mg/dl)
1 (44, F)	Laotian	Abdominal pain, vomiting, jaundice	15	626	6.1
2 (43, F)	Vietnamese	Pain, nausea, vomiting, jaundice	3	387	6.3
3 (29, F)	Filipino	Recurrent cholangitis (initially during pregnancy)	2	223	0.4
4 (28, M)	Cuban/Mexican; lived in Philippines	Recurrent cholangitis	3	220	0.9
5 (41, F)	Laotian	Cholangitis, recurrent pain, nausea, vomiting	¼	227	4.6
6 (46, F)	Laotian	Recurrent pain	1	585	0.8

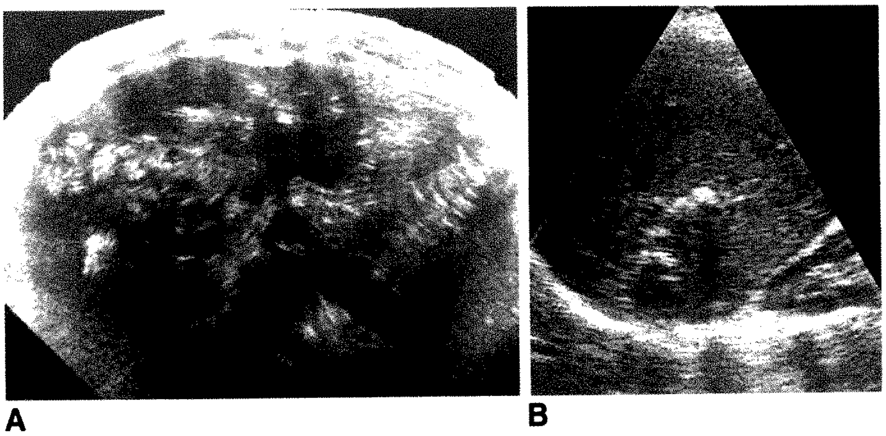

Fig. 1.—Characteristic sonograms in OCH show typical findings and pitfalls. **A**, Case 3. Transverse scan. Multiple echogenic areas in liver represent intrahepatic stones and casts. No shadowing or dilated intrahepatic ducts are seen. **B**, Case 5. Sector scan. Echogenic foci (intrahepatic stones) do shadow; dilated ducts are not seen.

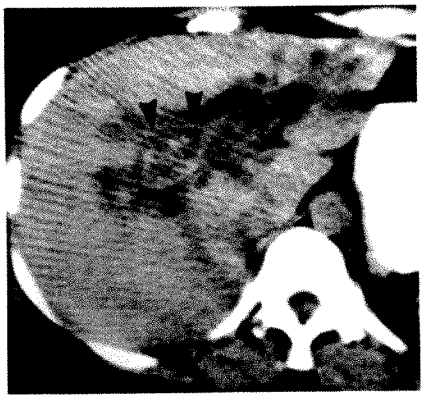

Fig. 2.—Case 1. CT adds further information to sonographic findings in OCH. CT scan shows dilated intrahepatic ducts and various densities representing casts and sludge in ducts (*arrowheads*).

Materials and Methods

The five women and one man were aged 28–44 years. Their geographic backgrounds are summarized in table 1, as are other clinical data. Each patient had the clinical features of the disease, although none had parasites in the stool or bile.

All patients underwent previous surgery for OCH, totaling 10 operations in the six patients (cholecystectomy, common duct exploration, choledochoduodenostomy, choledochojejunostomy, and anastomotic revisions). Postoperatively, all patients had residual symptoms, with intra- and extrahepatic stones, and three patients had a total of five ductal strictures (common duct, 2; left hepatic duct, 2; right hepatic duct, 1).

Sonography was performed on all patients, and computed tomography (CT) was done in two patients. Two patients underwent percutaneous transhepatic cholangiography (PTC) and percutaneous biliary drainage (PBD). The bulk of radiologic management consisted in removal of retained stones. Several techniques were used, including basketing, flushing, crushing, occlusion balloon or Fogarty catheter dislodgement, and attempted chemical dissolution. Biliary strictures were dilated with balloon catheters and insertion of catheters through the strictures. Endoscopic retrograde cholangiopancreatography with papillotomy was performed in one patient.

Most work was done on an outpatient basis (1, 2, 3, 5, 6, and 9 sessions); admission was dictated by clinical circumstances. Antibiotics were administered to all patients before and for at least 1 day after manipulation.

Results

Cross-Sectional Studies

Sonography was highly accurate in the detection of intrahepatic stones (6/6), extrahepatic dilatation of bile ducts (6/6), and of gallstones (3/3). However, sonography was less sensitive for intrahepatic ductal dilatation (3/6 prospectively, 4/6 retrospectively) and extrahepatic stones (3/5). Echogenic material was seen in the ducts in all cases, although the intrahepatic dilated ducts themselves were not always evident. Shadowing was variable with both intra- and extrahepatic stones (fig. 1). Biliary strictures were not detected (0/5).

CT accurately visualized intra- and extrahepatic ductal dilatation in two patients. Stones and variable densities of biliary mud and pigment were visible with CT (fig. 2).

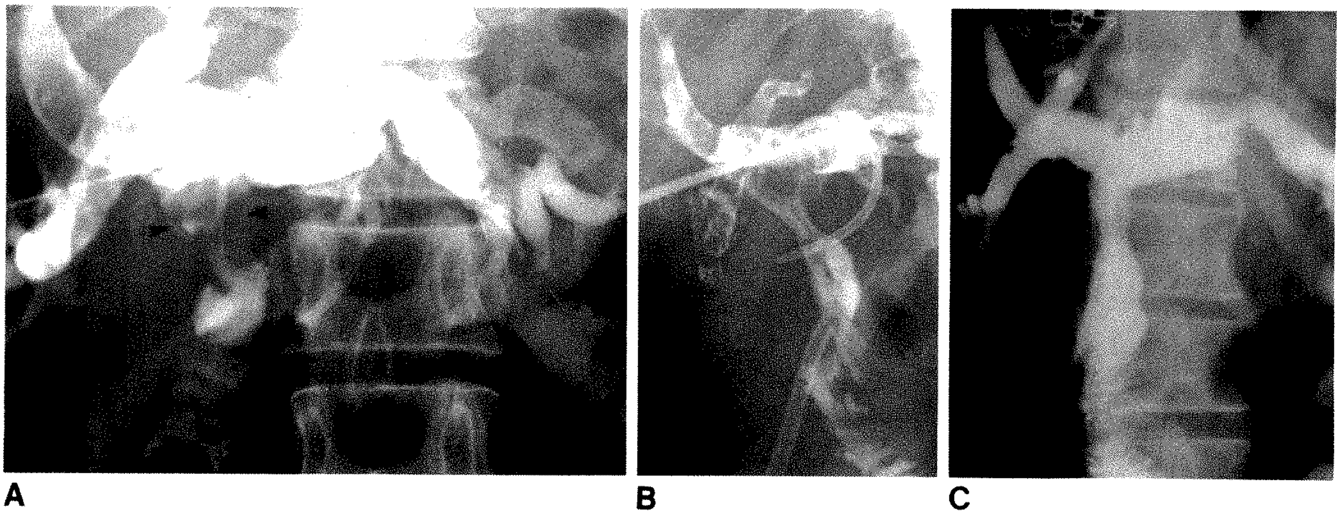

Fig. 3.—Case 2: acute cholangitis. **A**, Percutaneous transhepatic cholangiogram shows dilated intrahepatic ducts with numerous large stones. Stone is impacted at choledochojejunostomy (*arrowheads*). Percutaneous biliary drainage was performed to decompress and treat acute cholangitis. **B**, After second operation (revision of anastomosis, removal of several stones, T-tube insertion), injection of drainage catheter shows many casts and stones. The two catheters provide excellent ante- and retrograde access. **C**, After basketing, flushing, and Fogarty removal of intra- and extrahepatic stone, ducts are clear.

Interventional Procedures

In two patients, all intra- and extrahepatic stones were removed (fig. 3). Two patients had all stones removed, but intrahepatic casts remained (fig. 4). One patient had all intrahepatic stones removed and strictures dilated, but two extrahepatic stones remained (he had a high choledochoenterostomy for drainage) (fig. 5). In the sixth patient, a few stones were removed, but the patient was lost to follow-up.

PTC and PBD (after antibiotic coverage) were technically straightforward. Each patient was cannulated within five passes. No complications were encountered; previously, concern for the feasibility and safety of these procedures in OCH patients had been emphasized due to the frequency of ductal infection [17]. One PTC demonstrated an enterobiliary anastomosis, which had not been appreciated previously due to the language problem. PBD acutely decompressed a febrile patient and provided antegrade access to the biliary tract.

Two admissions were related to the procedures: one patient was admitted due to cholangitis from our manipulations; another patient was admitted for observation after a difficult session. These patients were discharged on the following day. A third patient was admitted electively for solvent infusion.

Numerous organisms were cultured from the bile: These included *E. coli*, *Streptococcus faecalis*, *Bacteroides fragilis*, *Fusobacterium nucleatum*, *Veillonella parvula*, *Klebsiella pneumoniae*, *Proteus vulgaris*, *P. mirabilus*, and *Clostridium perfringens*. Solvent therapy was attempted in vivo in one patient and in vitro in another. Composition of the stones was unknown at the time of these infusions. In neither case did the stones respond to monooctanoin.

Long-term follow-up is available in five patients. One has intermittent symptoms 2 years after manipulations; four patients have been symptom free for 1.5–2.5 years. One patient has been lost to follow-up.

Discussion

Prior reports on OCH have emphasized the importance of surgery and the need for multiple operations [2, 9, 12, 13, 15]. Operation, particularly an internal biliary drainage procedure, is indeed essential therapeutically [11], and was so in our patients. Our series confirms the postoperative chronicity of the disease and the value of alternative means to manage these problems after surgical drainage techniques. Despite 10 operations in our six patients, stones, casts, and strictures resulted in continued morbidity. One large series had only a 13.3% ultimate cure rate by surgery [15], and several episodes of postoperative cholangitis prolonged hospital stay or necessitated repeat hospitalization. Chang and Passaro [2], in a surgical review of OCH, pointed out that "no effective surgical procedure for OCH has been found."

Stone removal by basketing through a steerable catheter during multiple outpatient sessions constituted most of our postoperative work. PTC and PBD were helpful diagnostically and therapeutically. Access to the biliary tree by surgical T-tubes was our major working conduit. As has been emphasized by Burhenne [18], suboptimal tracts result in unnecessary technical difficulty; large, laterally placed tracts with large-bore tubes are preferred. Access to intrahepatic ducts through a standard T-tube may be difficult. PBD catheters or surgical U-tubes are helpful to reach intrahepatic stones [16]. Use of Fogarty and occlusion balloons to disimpact stones, balloon and straight catheters to dilate strictures, endoscopic papillotomy, and flushing and infusion via percutaneously placed catheters constitute the array of techniques

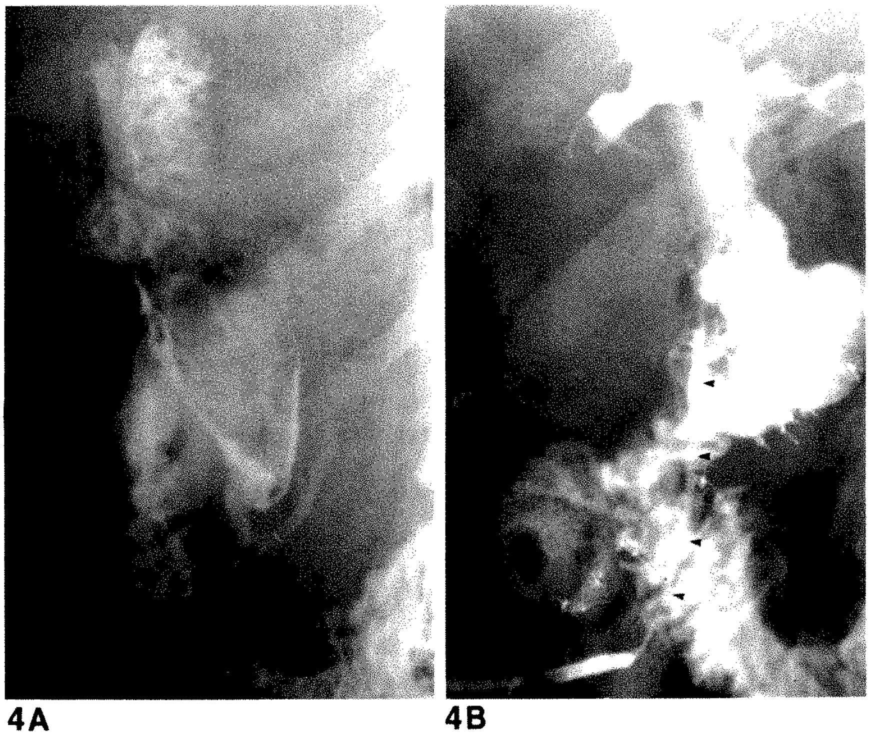

4A

4B

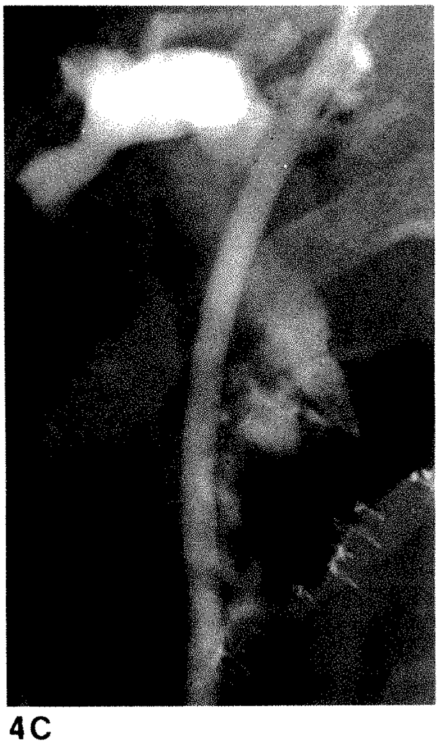

4C

Fig. 4.—Case 1: problems associated with percutaneous management of OCH. **A**, Intraoperative cholangiogram shows enormous extrahepatic stones and casts filling extrahepatic system. **B**, Choledochojejunostomy was performed; through postoperative T-tube tract, numerous stones were removed. However, patient experienced pain along tract due to multiple passes. Injection reveals marked narrowing of tract (*arrowheads*) indicating inflammation from repeated manipulations. Tract was recatheterized with difficulty, and session was terminated. **C**, Worst complication occurred when gentle contrast injection into left hepatic ducts, which are filled with casts, caused acute cholangitis with shaking chills (although patient had received antibiotics), necessitating admission. Patient recovered and further work was done in later sessions.

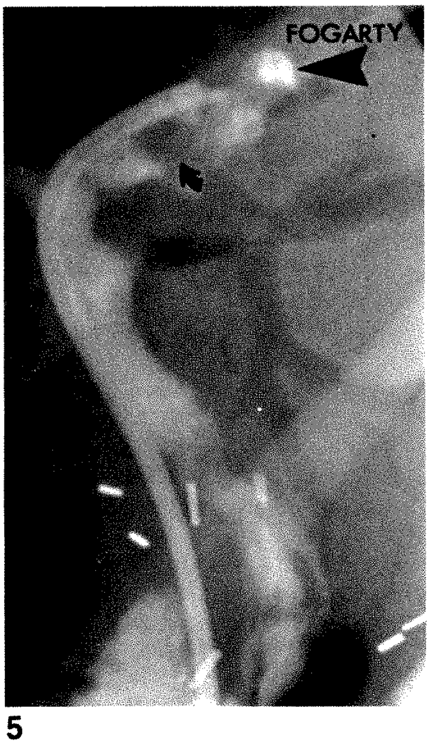

5

Fig. 5.—Case 4: use of Fogarty (or occlusion balloon) catheter to remove intrahepatic stones. Catheter with contrast-filled balloon (*arrowhead*) is passed peripheral to stone (*arrow*) and withdrawn, dragging this stone and others into main duct, where they can be extracted more easily and safely.

that are useful for the multiple complications of OCH. Intrabiliary sonographic lithotripsy was planned in one patient; however, she moved and was lost to follow-up.

Our patients were treated mainly as outpatients, and antibiotics were administered for all procedures. Cholangitis and observation after difficult manipulation prompted the two postprocedure admissions. Both of these were related to intrahepatic injections and manipulation. The degree and extension of intrahepatic stones and casts, in addition to the multiple bacterial organisms in the bile, make intrahepatic work precarious despite attempts to be gentle. Antibiotic coverage, low-pressure injections of contrast material, and time-limited sessions due to patient fatigue probably prevent more frequent cholangitis.

Our results were not uniformly successful, although all patients benefited. The surgically created anastomoses provided an easy avenue for antegrade crushing and flushing of stones, rather than having to remove them. Monooctanoin (in vitro and in vivo) was unsuccessful, as was an attempt at endoscopic stone removal in one patient. Poor or no response to monooctanoin is predictable, since these stones are largely bilirubinate.

A major sonographic pitfall in diagnosis was poor recognition of intrahepatic ductal dilatation. In most patients dilatation is reliably detected by sonography. However, our experience has confirmed earlier reports [17, 19, 20] that sludge impaction obscures the dilated ducts themselves. Bright echogenic, intrahepatic reflectors are characteristic of the ductal debris. Postoperative air in the biliary tree may be a source of sonographic confusion in these patients [11, 17]. In one of our patients, the echogenic material was mistaken for tumor. CT accurately displayed intra- and extrahepatic dilatation in two patients; in addition, various densities of sludge and stones could be differentiated in both the intra- and extrahepatic systems. CT may well be the preferred imaging method for intrahepatic extent and characterization of disease [12].

In conclusion, radiologic techniques are quite helpful in the de novo diagnosis and postoperative management problems of OCH, and offer an important alternative for postoperative care. Sonography and CT provide excellent and at times unique intrahepatic information. Preoperative diagnosis of OCH is important to ensure that the correct operation is performed, lest there be suboptimal operations that lead to reoperation once the diagnosis is established. Surgery is indeed mandatory when the patients become quite ill; plans for postoperative radiologic management, including optimally placed large T-tubes (or U-tubes), should be important considerations at the time of operation. Surgery may become more limited, realizing the facility with which stones and strictures can be managed percutaneously. One approach recently advocated has been surgical creation of a Roux-en-Y loop connected to the subcutaneous tissues for endoscopic or catheter access percutaneously [16]. With correct preoperative diagnosis, and with surgical and radiologic cooperative planning, morbidity, repeat operations, and radical surgery such as hepatic resection may be avoided [11, 14]. PTC and PBD with precautions (antibiotics, gentle manipulation) are helpful diagnostically, may treat the acute biliary septic episode, and are a conduit for stone removal to inaccessible areas by the T-tube [13, 15, 16]. Writing on the problem of recurrence in OCH, Cook et al. [3] in 1954 stated that "laparotomy is indicated in all cases of recurrence." This concept probably can be modified in many cases.

While surgical and radiologic techniques are jointly beneficial, the ultimate panacea for the disease may be medical control of biliary lithogenic factors. The cause of OCH continues to be controversial [1–14]; several authors favor *Clonorchis sinensis*. However many patients with OCH have no evidence of *C. sinensis* (none of ours did). Alternative hypotheses for the cause include other helminths (*Ascaris*), bacteria (*E. coli*), biliary obstruction, drugs (opiates), socioeconomic factors, or a combination [3–6, 13–15].

ACKNOWLEDGMENTS

We thank Deborah Lynn, Peggy Clark, and Ed Keenen for assistance.

REFERENCES

1. Ong GB. A study of recurrent pyogenic cholangitis. *Arch Surg* **1962**;84:199–225
2. Chang TM, Passaro E. Intrahepatic stones: the Taiwan experience. *Am J Surg* **1983**;146:241–244
3. Cook J, Hou PC, Ho HC, McFadzean AJS. Recurrent pyogenic cholangitis. *Br J Surg* **1954**;42:188–203
4. Digby KH. Common-duct stones of liver origin. *Br J Surg* **1930**;17:578–591
5. Ho CS, Wesson DE. Recurrent pyogenic cholangitis in Chinese immigrants. *AJR* **1974**;122:368–374
6. Stock FE, Fung JHY. Oriental cholangiohepatitis. *Arch Surg* **1961**;84:409–412
7. Lam SK, Wong KP, Chan PKW, Ngan H, Ong GB. Recurrent pyogenic cholangitis: a study by endoscopic retrograde cholangiography. *Gastroenterology* **1978**;64:1196–1203
8. Wastie ML, Cunningham IGE. Roentgenologic findings in recurrent pyogenic cholangitis. *AJR* **1973**;119:71–77
9. Fung J. Liver fluke infestation and cholangio-hepatitis. *Br J Surg* **1964**;48:404–415
10. Harrison-Levy A. The biliary obstruction syndrome of the Chinese. *Br J Surg* **1962**;49:674–685
11. Stock FE, Tinckler LF. Choledochoduodenostomy in the treatment of cholangiohepatitis. *Surg Gynecol Obstet* **1955**;101:599–606
12. Carmona RH, Crass RA, Lim RC Jr, Trunkey DD. Oriental cholangitis. *Am J Surg* (in press)
13. Yellin AE, Donovan AJ. Biliary lithiasis and helminthiasis. *Am J Surg* **1981**;142:128–136
14. Turner WW, Cramer CR. Recurrent oriental cholangiohepatitis. *Surgery* **1983**;93:397–401
15. Wen CC, Lee HC. Intrahepatic stones: a clinical study. *Ann Surg* **1972**;175:166–176
16. Kerlan RK, Pogany AC, Goldberg HI, Ring EJ. Radiologic intervention in oriental cholangiohepatitis. *AJR* **1985**;145:809–813
17. Federle MP, Cello JP, Laing FC, Jeffrey RB Jr. Recurrent pyogenic cholangitis in Asian immigrants: use of ultrasonography, computed tomography, and cholangiography. *Radiology* **1982**;143:151–156
18. Burhenne HJ. Percutaneous extraction of retained biliary tract stones: 661 patients. *AJR* **1980**;134:888–898
19. Ralls PW, Colletti PM, Quinn MF, Lapin SA, Morris UL, Halls J. Sonography in recurrent oriental pyogenic cholangitis. *AJR* **1981**;136:1010–1012
20. Scheible FW, Davis GB. Oriental cholangiohepatitis: preoperative radiographic and ultrasonographic diagnosis. *Gastrointest Radiol* **1981**;6:269–271

Errata

In the November 1985 issue of the *AJR*, there is an error in the article, "Caldwell Lecture. Magnetic Resonance Imaging: Its Impact on Diagnostic Radiology," by Steiner (*AJR* 1985;145:883–893). For figure 18, the photographs do not match the legend; parts A and B should be transposed (i.e., the picture labeled A is described in the legend as B and vice versa).

Also in the November 1985 issue, in the article by White et al., "Percutaneous Drainage of Postoperative Abdominal and Pelvic Lymphoceles" (*AJR* 1985;145:1065–1069), there is an error in the Results section. In the last paragraph of that section, "50 ml of tetracycline solution (1 mg/ml)" should read "500 ml of tetracycline solution (10 mg/ml)."

Localization of ^{99m}Tc-HMDP in Hepatic Metastases from Colonic Carcinoma

Wei-Jen Shih[1]
Peggy A. Domstad[1]
Arthur Lieber[2]
Frank H. DeLand[1]
John J. Coupal[1]

To evaluate the significance and frequency of skeletal imaging agent localization in hepatic metastases from colonic carcinoma, scintigrams from 54 patients were retrospectively studied. Of 54 patients, 22 had hepatic metastases, and skeletal metastases were present in seven of 54. Six of the seven patients with skeletal metastases had concurrent hepatic deposits. Two patterns of bone agent localization in liver metastases occurred: diffuse and mild (10 patients) and ringlike in appearance (two patients). Twelve of the 22 patients had localization of skeletal imaging agent in hepatic metastases and extensive or large liver lesions. Concurrent serum calcium values for nine of 12 patients were reviewed; none had a high level of serum calcium. Among available plain films and/or CT scans of the abdomen for 21 of the 22 patients, only one patient with extensive colonic metastases had multiple calcifications shown on CT but not seen in plain films. The data indicate a high frequency of hepatic metastases in colon carcinoma (22/54, 40%) and a high frequency of skeletal imaging agent localization in the hepatic colonic metastases (12/22, 54.5%). Once skeletal metastases are observed, there are almost always hepatic metastases present (6/7). There was no relation between elevated serum calcium values and bone agent localization in hepatic deposits. The relation between skeletal imaging agent localization or radiographic calcifications and histopathology of colonic carcinoma was inconclusive. The presence of bone agent localization in a ^{99m}Tc hydroxymethylene diphosphonate (HMDP) bone study indicates colonic hepatic metastases that are substantially widespread and/or bulky.

Colon carcinoma has one of the highest incidences of malignant neoplasms and often metastasizes to the liver. Bone scintigraphy using ^{99m}Tc hydroxymethylene diphosphonate (HMDP) has been widely used for the detection of skeletal metastases, and extraosseous localization of the bone-imaging agent has been observed in various malignant tumors [1–9]. Extraosseous localization is especially common in hepatic metastases from colon carcinoma [7–9], but not all colonic carcinoma metastases in the liver localize the bone agent. We evaluated retrospectively the frequency and significance of bone agent localization in hepatic metastases from colon carcinoma.

Materials and Methods

We selected 54 patients wtih colonic carcinoma by these criteria: (1) patients who proved to have colonic carcinoma by histopathology; and (2) patients who had ^{99m}Tc-HMDP bone scintigraphy and ^{99m}Tc sulfur colloid (SC) liver scintigraphy or abdominal CT studies within 2 weeks. Those patients whose ^{99m}Tc-SC studies were done within 24 hr preceding a bone study were excluded from the study. Thin-layer chromatography of the ^{99m}Tc-HMDP radiopharmaceutical was performed by the method of Majewski et al. [10], modified by predrying the chromatogram strip for assay of hydrolyzed reduced ^{99m}Tc (^{99m}Tc "colloid") [11].

The role of the serum calcium level in bone-imaging agent localization in liver metastases was evaluated by review of the serum calcium values during 1 week before or after bone scintigraphy. To evaluate the possible relations among calcifications in hepatic metastases, skeletal agent localization, and the histopathology of colonic carcinoma, we reviewed abdom-

Received June 18, 1985; accepted after revision October 1, 1985.

[1] Nuclear Medicine Service, Veterans Administration Medical Center, and Division of Nuclear Medicine, University of Kentucky Medical Center, Lexington, KY 40536. Address reprint requests to W.-J. Shih at University of Kentucky Medical Center.

[2] Department of Diagnostic Radiology, University of Kentucky Medical Center, Lexington, KY 40536.

AJR 146:333–336, February 1986
0361–803X/86/1462–0333
© American Roentgen Ray Society

inal plain films and/or CT scans, available for 21 of 22 patients and taken as close to the time of bone scintigraphy as possible. A nonenhanced CT scan was preferred when available. Histopathologic classification of colonic carcinoma was available for 18 of 22 patients.

Results

Of the 54 patients with colonic carcinoma, 22 had hepatic metastases demonstrated by a ^{99m}Tc-SC study and/or abdominal CT; seven of the 54 patients had skeletal metastases demonstrated by scintigraphy. Six of the seven patients with skeletal metastases also had hepatic metastases. The bone scintigrams of 12 of the 22 patients with hepatic metastases showed accumulation of the skeletal agent in the hepatic metastatic lesions, and all 12 patients had extensive or large hepatic metastases demonstrated by ^{99m}Tc-SC or abdominal CT studies. In 10 of the 12 patients, ^{99m}Tc-HMDP scintigrams showed mild and diffuse radioactivity in the hepatic metastases, with an intensity less than that of the sternum or ribs (fig. 1). Two of the 12 patients had a ringlike pattern of radioactivity in the hepatic lesions on the ^{99m}Tc-HMDP scan (figs. 2A and 2B); the concurrent abdominal CT showed two large metastatic lesions (fig. 2C). In contrast, the 10 patients without uptake of bone agent in the hepatic metastases had small lesions in the liver shown by ^{99m}Tc-SC and/or CT studies. The concurrent serum calcium values of 16 patients were within normal limits; values were not available for the other six patients.

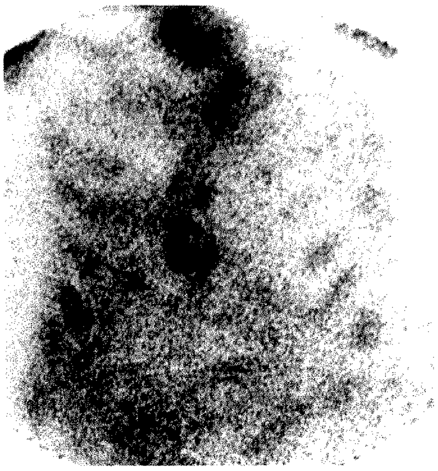

Fig. 1.—Anterior ^{99m}Tc-HMDP bone scan of 65-year-old woman with colon carcinoma. Diffuse uptake in region of right lower thorax and upper abdomen.

The degree of cellular differentiation of the colonic carcinomas in the 18 cases with available histopathology data was classified as follows: three well differentiated, nine moderately differentiated, three poorly differentiated, and three of mucinous type. The histopathologic classification of the four unclassified adenocarcinomas was not available because the surgical/biopsy procedures were not performed in our institution. None of the three patients with mucinous type had calcification either on CT scans of the abdomen or abdominal plain films. Among the abdominal CT scans and/or plain films for 21 patients, only one patient with extensive hepatic colonic metastases had multiple calcifications seen on CT (fig. 3) but not on abdominal plain films. The specific histologic type of the colonic adenocarcinoma of this particular patient was unknown because the surgical procedure was not performed in our hospital.

Discussion

Our data indicate a high frequency of hepatic metastases (22/54) in colon carcinoma, a high frequency of bone-imaging agent localization in hepatic colonic metastases (12/22), and

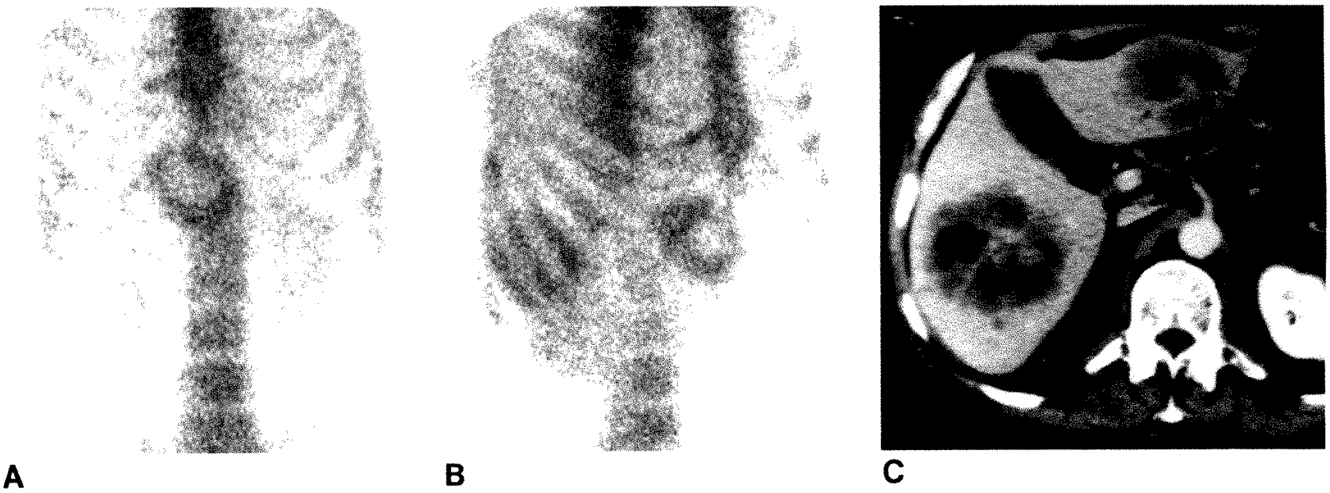

Fig. 2.—66-year-old man with colon carcinoma. **A**, Anterior ^{99m}Tc-HMDP bone scan: ringlike appearance of radioactivity in upper abdomen corresponds to left hepatic lobe. **B**, Right anterior oblique ^{99m}Tc-HMDP scan: rounded, diffuse increase in radioactivity in region corresponding to right lobe of liver posteriorly. **C**, Enhanced CT scan of abdomen: two large metastatic lesions in liver, one in left lobe and one in right lobe posteriorly.

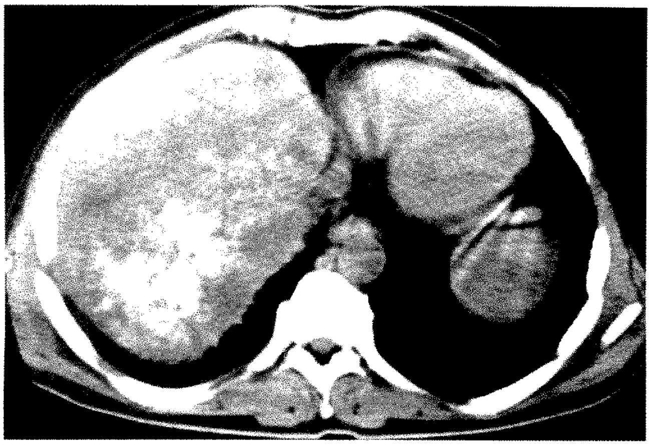

Fig. 3.—Unenhanced CT scan of abdomen: multiple areas of amorphous calcifications in low-density metastatic lesions in liver.

the frequent coexistence of hepatic metastases in patients found to have skeletal metastases (6/7). There was no relation between elevated serum calcium levels and localization of the bone agent in the hepatic lesion(s).

Two patterns of localization of the bone-imaging agent were observed: a diffuse and mild uptake in 10 of 12 patients and a ringlike appearance in two patients. To our knowledge, the ringlike appearance in hepatic metastases has not previously been documented. The intensity of the ring activity was high, at least equal to that of the ribs, suggesting an active calcification process in the peripheral zone of the tumor. A lack of blood supply in the center of a tumor has been described in a hepatoma with a central necrosis that exhibited absent or poor perfusion in the central zone on a radioindium chloride blood pool study [12]; this resulted in a ringlike appearance. The ring or "doughnut" sign seen in cerebral tumors is presumably due to the same mechanism [13]. A ringlike pattern of tracer uptake in hepatic colonic metastases therefore may be presumed due to a bulky tumor mass with insufficient blood supply.

Diffuse hepatic radioactivity in a bone scan may result from faulty radiopharmaceutical preparation, a ^{99m}Tc-SC study done within 24 hr before a bone study, massive hepatic necrosis, or hepatic amyloidosis. In hepatic amyloidosis [14, 15] or massive hepatic necrosis [16, 17], the intensity of uptake is high, usually higher than that in the sternum or ribs. Clinically, ^{99m}Tc "colloid" would localize in the liver and spleen. In patients without liver disease, colloid ^{99m}Tc content up to 1.73% in the skeletal radiopharmaceutical did not result in hepatic radioactivity. On one occasion, three patients without liver disease receiving ^{99m}Tc-HMDP containing 4.92% colloid ^{99m}Tc per dose did show liver activity in their images. Awareness of a prior ^{99m}Tc-SC study done within 24 hr and the performance of appropriate quality control in radiopharmaceutical preparation should eliminate those causes of false-positive results. Right pleural effusion may mimic diffuse uptake in the liver; this situation can be ruled out by correlation with the concurrent chest radiograph.

Calcified hepatic metastases are usually, but not exclusively, of colonic cancer origin [18, 19]; mucinous colonic carcinoma is the most common metastatic tumor to the liver containing calcified deposits [18].

Our three patients with mucinous carcinoma had no evidence of calcifications either on CT scans or plain radiographs. CT scans and/or ^{99m}Tc-SC scintigrams showed extensive metastases. We found no relation between bone-imaging agent localization or radiographic calcification and the histopathology of the colon carcinoma. Extensive calcifications in the hepatic metastases in the one patient were shown only on CT; this higher sensitivity of CT in the detection of calcification as compared to plain radiographs concurs with the previous report [19].

Whether the serum calcium level influenced the bone-seeking agent localization is unknown. Stone and Sisson [5] reported a case of hepatic localization of a bone-imaging agent in a lymphoma patient who had hypercalcemia. Presumably, the bone-imaging agent localized in a tumor that was secreting a calcium-mobilizing factor. While the exact mechanism is unknown, there is a high frequency of skeletal imaging agent localization in colonic hepatic metastases, and the uptake pattern is either mild and diffuse or ringlike. Once bone-imaging agent localization in the liver occurs, either diffuse or ringlike in appearance on the ^{99m}Tc-HMDP bone study, the colonic hepatic metastases are likely to be substantially widespread or bulky.

ACKNOWLEDGMENT

We thank Sara Brandenburg for help in manuscript preparation and Aleene Miller for typing.

REFERENCES

1. Que L, Wiseman J, Hales B. Small cell carcinoma of the lung: primary site and hepatic metastases both detected on Tc-99m pyrophosphate bone scan. *Clin Nucl Med* **1980**;6:260–262
2. Lowenthal IS, Tow DE, Chang YC. Accumulation of Tc-99m polyphosphate in two squamous cell carcinomas of the lung. *J Nucl Med* **1975**;16:1021–1032
3. Poulose KD, Reba RC, Eckelman WC, Goodyear M. Extraosseous localization of Tc-99m Sn pyrophosphate. *Br J Radiol* **1975**;48:724–726
4. Heisel AM, Miller JH, Reid BS, Siegel SE. Radionuclide bone scan in neuroblastoma. *Pediatrics* **1983**;71:206–209
5. Stone CK, Sisson JC. What causes uptake of Tc-99m methylene diphosphonate by tumors? A case where the tumor appeared to secrete a hypercalcemia-causing substance. *J Nucl Med* **1985**;26:250–253
6. Baumert JE, Lanteri RL, Horning S, et al. Liver metastases of breast carcinoma detected on ^{99m}Tc-methylene diphosphonate. *AJR* **1980**;134:389–391
7. Balachandran S. Localization of Tc-99m-Sn-pyrophosphate in liver metastasis from carcinoma of colon. *Clin Nucl Med* **1976**;1:165–166
8. Garcia AC, Yeh SDJ, Benau RS. Accumulation of bone seeking radionuclides in the liver metastasis from colon carcinoma. *Clin Nucl Med* **1977**;2:265–269
9. Stevens JS, Clark EE. Liver metastasis of colon adenocarcinoma demonstrated on Tc-99m pyrophosphate bone scan. *Clin Nucl Med* **1977**;2:270–271
10. Majewski W, Zimmer MA, Spies SM. Radiopharmaceutical evaluation of Tc-99m hydroxymethylene diphosphonate. *J Nucl Med*

Technol **1983**;11:23–25

11. Robbins PJ. *Chromatography of technetium-99m radiopharmaceuticals—a practical guide.* New York: Society of Nuclear Medicine, **1984**:17
12. Yeh SH, Shih WJ, Liang JC. Intravenous radionuclide hepatography in the differential diagnosis of intrahepatic mass lesion. *J Nucl Med* **1973**;14:565–567
13. Kim EE. Ring sign in radionuclide cerebral images. *Semin Nucl Med* **1981**;11:168–169
14. Vanek JA, Cook SA, Bukowski RM. Hepatic uptake of Tc-99m labeled diphosphonate in amyloidosis: case report. *J Nucl Med* **1977**;18:1086–1088
15. Janssen S, van Rijsnijk MH, Piers DA, et al. Soft tissue uptake of Tc-99m diphosphate in systemic amyloidosis. *Eur J Nucl Med* **1984**;9:538–541
16. Lyons KP, Kuperus J, Green HW. Localization of Tc-99m pyrophosphate in the liver due to massive necrosis: case report. *J Nucl Med* **1977**;18:550–552
17. Hansen S, Stadalnik RC. Liver uptake of Tc-99m pyrophosphate. *Semin Nucl Med* **1981**;12:89–91
18. Moss AA, Gamsu G, Genant HK. *Computed tomography of the body.* Philadelphia: Saunders, **1983**:666
19. Bernardino ME. Computed tomography of calcified liver metastasis. *J Comput Assist Tomogr* **1979**;3:32–35

Value of Sonographic Screening for Gallstones in Patients with Chest Pain and Normal Coronary Arteries

Alan B. Fein[1, 2]
Robert F. Rauch, II[1]
James D. Bowie[1]
David B. Pryor[3]
Seymour Grufferman[3, 4]

The prevalence of sonographically detectable gallstones in patients with chest pain and normal coronary arteries was compared with the prevalence of gallstones in patients referred to sonography for nonbiliary disease. Among 545 patients with chest pain and normal coronary arteriograms, 101 (18.5%) were referred for sonographic examination of the gallbladder. This test group was compared to a matched control group ($n = 101$) undergoing abdominal sonography for nonbiliary disease. Six patients (5.9%) in the test group and eight patients (7.9%) in the control group were found to have gallstones by accepted sonographic criteria. Studies based on oral cholecystogram screening of healthy populations have claimed a prevalence of cholelithiasis of 2.3%–6.2% for males and 2.3%–12% for females. The authors were unable to demonstrate a higher prevalence of sonographically identified gallstones in patients with chest pain and normal coronary arteries than in patients examined for nonbiliary disease. The frequency of gallstones in this test group is comparable to that reported for a screened population of healthy men and women.

Gallbladder disease can mimic, and at times be clinically indistinguishable from, the pain of ischemic heart disease [1–3]. A substantial number of patients with chest pain but without significant lesions at coronary arteriography are referred for sonographic examination of the gallbladder to exclude cholelithiasis as the cause of their pain. Review of the literature has failed to reveal any studies of the utility of sonographic examination of the gallbladder in this group of patients. We report a retrospective study of the prevalence of sonographically detectable gallstones in patients with chest pain and normal coronary arteries, with comparison to the prevalence of gallstones in a matched group of patients referred to sonography for nonbiliary disease.

Materials and Methods

Among 3488 consecutive patients with chest pain catheterized for suspected coronary artery disease at the Duke University Medical Center between January 1979 and March 1983, 545 patients had normal coronary angiograms (defined as $<25\%$ luminal diameter narrowing in any vessel). This figure excludes patients with valvular disease, pericardial disease, cardiomyopathies including idiopathic hypertrophic subaortic stenosis, or other cardiovascular diseases noted at catheterization such as mitral valve prolapse, coronary artery anomalies, and coronary vasopasm. Patients with clinical evidence of hepatobiliary disease or a history of cholecystectomy, or with documented supraventricular or ventricular tachycardia, were also excluded on the basis of information obtained from each patient's problem list, discharge summary, and laboratory results. Of these 545 "normal" patients, the 101 who had undergone sonographic examination of the gallbladder within 30 days of cardiac catheterization for the clinical indication of "chest pain, unknown etiology" were included in the test group.

A control group was then assembled using the following approach:

Step 1: 202 potentially eligible controls were generated by identifying the two adult patients examined for nonbiliary disease listed closest in the consecutive sonography log book to

Received June 6, 1985; accepted after revision September 12, 1985.

This work was supported in part by grant HS04873 from the National Center for Health Services Research (OASH), grant HL-17670 from the National Heart, Lung and Blood Institute, and grants from the Kaiser Family Foundation and Andrew W. Mellon Foundation. S. Grufferman is the recipient of a Public Health Service Preventive Oncology Academic Award K07CA00726 from the National Cancer Institute.

[1] Department of Radiology, Duke University Medical Center, Durham, NC 27710.

[2] Present address: Mallinckrodt Institute of Radiology, Washington University School of Medicine, 510 S. Kingshighway Blvd., St. Louis, MO 63110. Address reprint requests to A. E. Fein.

[3] Department of Medicine, Duke University Medical Center, Durham, NC 27710.

[4] Department of Pediatrics, Duke University Medical Center, Durham, NC 27710.

AJR 146:337–339, February 1986
0361–803X/86/1462–0337
© American Roentgen Ray Society

each patient in the test group. Patients being examined for chest pain or epigastric pain, patients with known gallbladder or biliary disease, and patients whose examinations were inadequate for evaluation of the gallbladder were excluded; the next eligible patient in the log book was used in this circumstance. Patients examined on the same day and by the same examiner were used whenever possible, and constituted 85% of those selected.

Step 2: The 202 potentially eligible control patients generated in step 1 were then matched for age (±5 years), gender, and race to an alphabetized list of test patients. If more than one potentially eligible control patient could be matched to a test patient, the eligible control closest in age to the test patient was used.

The final control group therefore consisted of 101 patients matched for age, gender, and race with the test group. Specifically, the test group and control group each consisted of 57 men (56%) and 44 women (44%) with a mean age of 52 years (range, 29–73 years) in the test group and 53 years (range, 25–78 years) in the control group. Ninety percent of the patients in both groups were Caucasians.

Data were obtained using the following sources: (1) a computerized data bank containing catheterization results, clinical information, and pertinent demographic information for all patients who had undergone coronary arteriography at our institution; (2) a computerized radiology file containing pertinent demographic information and the dates of all radiographic examinations performed on each patient within the radiology department; (3) a sequential, continuous sonography log book containing the names, reasons for referral, and examination results for all patients who had undergone sonographic examination in our department during the period of the study; and (4) the patient's medical record and radiographic film jacket.

All patients referred for sonography received a complete "abdominal search" including examination of the liver, gallbladder, and biliary system (with the patient in the supine, right and left anterior oblique, and upright/sitting positions) [4], the pancreas, spleen, kidneys, and abdominal vasculature. When possible, a limited examination of the pelvis was also performed. An examination was considered positive for gallstones if accepted sonographic criteria of an echogenic focus or foci demonstrating acoustic shadowing and movement could be identified within the gallbladder or biliary ducts [5]. If an echogenic focus with shadowing but without definite movement was identified (one patient, test group), the examination was considered to be positive. No patients with abnormalities of the gallbladder wall, sludge in the gallbladder without definite stones, or with dilated ducts were identified. All examinations were performed with either an ATL Mk 3500 or Diasonics RA-1 real-time sector scanner using a 3.0-, 3.5-, or 5-MHz transducer. The prevalence of sonographically demonstrated gallstones was calculated for each group.

Results

From January 1979 through March 1983, 545 patients with chest pain referred for cardiac catheterization at the Duke University Medical Center had normal cardiac catheterizations. Of these patients, 101 (18.5%) were referred for sonography of the gallbladder within 30 days of arteriography (mean, 2.3 days; range, 0–20 days) and were included in the test group. The control group consisted of 101 patients matched for age, gender, and race who received abdominal sonography during the same period as the test group.

Six patients in the test group (5.9%) were found to have gallstones by accepted sonographic criteria. Ninety-five (94%) were negative for gallstones. Gallstones were identified in eight patients in the control group (7.9%). Ninety-three examinations in the control group (92%) revealed a normal gallbladder without cholelithiasis. According to the patients' medical records, none of the patients in the test group underwent hepatobiliary radionuclide testing of cholecystectomy during the period of the study.

Discussion

Although the pain of gallbladder disease may mimic the pain of cardiac ischemia, no role for sonography of the gallbladder in the patient with chest pain and normal coronary arteries has been established. Given recent estimates that 20%–37% of the approximately 300,000 coronary angiograms performed annually in the United States will be normal or show insignificant disease [6–8], the need for an explanation of their pain becomes significant. From our experience, about 20% of patients with normal cardiac catheterizations will undergo sonographic examination of the gallbladder in an effort to determine the cause of their pain. The cost of performing sonographic examinations on this group of patients accounts for a substantial expenditure of funds in a health care system concerned with cost efficiency and in which a limited number of health care dollars is allocated for each diagnosis-related group (DRG).

Studies based on oral cholecystographic screening of healthy Caucasian populations claim a prevalence of cholelithiasis of 2.3%–6.2% for males and 2.3%–12% for females [9–11]. In our study, we were unable to demonstrate a higher prevalence of sonographically identified gallstones in patients with chest pain and normal coronary arteries than in a control group of patients without chest pain examined for nonbiliary disease. The frequency of gallstones in our test group is comparable to that reported for a screened outpatient population of healthy men and women.

Although we urge caution in extrapolating the findings of our study due to the relatively small sample size, the inclusion of retrospective data, and the lack of historical controls based on sonography and radionuclide hepatobiliary imaging, our results do suggest that cholelithiasis is an infrequent cause of isolated chest pain in patients with normal coronary arteries.

Since the importance of identifying cholelithiasis in the nondiabetic, asymptomatic patient has been questioned [9–11] and the long-term prognosis of patients with chest pain and normal coronary arteries is excellent even when the cause of their chest pain remains obscure [3, 12–23], the value of gallbladder investigation in this group needs to be reassessed. In the absence of a prospective study, our findings suggest that screening for cholelithiasis in patients with isolated chest pain and normal coronaries is of minimal benefit.

REFERENCES

1. Gunn A, Keddie N. Some clinical observations on patients with gallstones. *Lancet* **1972**;2:239–241
2. Schneider RR, Seckler SG. Evaluation of acute chest pain. *Med Clin North Am* **1981**;65:53–66
3. DeMaria AN, Lee G, Amsterdam EA, Low R, Mason DT. The

angina syndrome with normal coronary arteries: etiologic and prognostic considerations. *JAMA* **1980**;244:826-828

4. Rosenberg ER, Bowie JD, Clair MR, Hidalgo H, Ram PC. The routine use of real time ultrasound in abdominal examinations. *Med Ultrasound* **1983**;7:1-5
5. Crade M, Taylor KJW, Rosenfeld AT, et al. Surgical and pathologic correlations of cholecystosonography and cholecystography. *AJR* **1978**;131:227-229
6. Coronary artery bypass surgery—National Center for Health Care Technology Assessment Forum. *JAMA* **1981**;246:1645-1649
7. Proudfit WL, Shirey EK, Sones FM. Selective cine coronary arteriography: correlation with clinical findings in 1,000 patients. *Circulation* **1966**;33:901-910
8. Kemp HG Jr, Vokonos PS, Cohn PF, Gorlin R. The anginal syndrome associated with normal coronary arteriograms: report of a six-year experience. *Am J Med* **1973**;54:735-742
9. Gracie WA, Ransohoff DF. The natural history of silent gallstones: the innocent gallstone is not a myth. *N Engl J Med* **1982**;307:798-800
10. Wilbur RS, Bolt RJ. Incidence of gallbladder disease in "normal" men. *Gastroenterology* **1959**;36:251-255
11. Bainton RM, Davies GT, Evans KT, Gravelle IH. Gallbladder disease: prevalence in a South Wales industrial town. *N Engl J Med* **1976**;294:1147-1149
12. Waxler EB, Kimbris D, Dreifus LS. The fate of women with normal coronary angiograms and chest pain resembling angina pectoria. *Am J Cardiol* **1971**;28:25-32
13. Bruschke AV, Proudfit WL, Sonos TM Jr. Clinical course of patients with normal and slightly or moderately abnormal coronary arteriograms: a follow-up study on 500 patients. *Circulation* **1973**;47:936-945
14. Bemiller CR, Pepine CJ, Rogers AK. Long-term observations in patients with angina and normal coronary arteriogram. *Circulation* **1973**;47:36-43
15. Proudfit WL, Bruschke AVG, Sones FR Jr. Clinical course of patients with normal or slightly or moderately abnormal coronary arteriograms: 10 year follow-up of 521 patients. *Circulation* **1980**;62:712-717
16. Day LJ, Sowton E. Clinical features and follow-up of patients with angina and normal coronary arteries. *Lancet* **1976**;2:334-337
17. Marchandise B, Bourassa MG, Chaitman BR, Lesperance J. Angiographic evaluation of the natural history of normal coronary arteries and mild coronary artherosclerosis. *Am J Cardiol* **1975**;41:216-220
18. Levey EM, Winkel RA. Continuing disability of patients with chest pain and normal coronary arteriograms. *J Chronic Dis* **1979**;32:191-196
19. Pasternak RC, Thibault GE, Savoia M, DeSanctis RW, Hutter AM. Chest pain with angiographically insignificant coronary arterial obstruction. *Am J Med* **1980**;68:813-817
20. Ockene JS, Shay MJ, Alpert JS, Weiner BH, Delen JE. Unexplained chest pain in patients with normal coronary arteriograms. *N Engl J Med* **1980**;303:1249-1252
21. Isner JM, Salem DN, Banas JS, Levine HT. Long-term clinical course of patients with normal coronary arteriography: follow-up study of 121 patients with normal or nearly normal coronary arteriograms. *Am Heart J* **1981**;102:645-653
22. Faxon DP, McCabe CH, Kreigel DE, Ryan TJ. Therapeutic and economic value of a normal coronary angiogram. *Am J Med* **1982**;73:500-505
23. Califf RM, Lee KL, Harrell FE Jr, Kim SYS, Grufferman S, Rosati RA. Assessment of the use of the age and sex specific United States population as a control group for analysis of survival in coronary artery disease. *Am J Cardiol* **1982**;50:1279-1282

1986 ARRS Meeting, April 13–18, Washington, DC

A comprehensive description of the meeting, including the scientific program, Categorical Course in Chest Radiology, and instructional courses, appears in the January 1986 issue of the *AJR*. A special loose insert on the meeting also accompanies the January issue. Meeting and registration forms will be found in the January and February issues. These may be photocopied.

Accreditation

All courses and scientific sessions carry AMA Category I credit on an hour-for-hour basis.

Meeting Format

Scientific Program. Sessions will be grouped in parallel sessions, Monday–Thursday. A total of 189 scientific papers will be presented in 18 sessions. In addition, on Wednesday, April 16, the morning session will feature award papers and the Caldwell Lecture, which will be delivered by Benjamin Felson of the University of Cincinnati. On Friday, there will be a special symposium on orthopedic radiology.

Categorical Course in Chest Radiology. This 14 hr course will be Sunday–Thursday. Registrants may enroll in other courses as well.

Luncheon Sessions. For the first time, registrants may enroll in special luncheon sessions, Monday–Thursday. A box lunch will be provided.

Exhibits

Scientific Exhibits and Case of the Day Presentations will be Monday–Thursday, April 14–17.

Commercial Exhibits will be open daily, Monday–Thursday.

Local Activities

General Reception. Tuesday evening, April 15, for all registrants.

Golf Tournament. Monday, April 14, Kenwood Golf and Country Club, Bethesda, MD. Transportation leaves the hotel at 11 a.m.; shotgun start at 1 p.m.

Men's and Women's Tennis Tournaments. Monday, April 14, Kenwood Golf and Country Club, Bethesda, MD. Transportation leaves the hotel at 11 a.m.

Local Tours. Sunday, April 13, 7–9 p.m., Introduction to Washington Champagne Tour; Monday, April 14, 9:30 a.m.–3:30 p.m., National Gallery of Art and Hirshhorn Museum and Sculpture Garden; Tuesday, April 15, 9:30 a.m.–3:30 p.m., Georgetown Homes/Georgetown Park; Wednesday, April 16, 9 a.m.–4 p.m., Best of Baltimore; Thursday, April 17, 9 a.m.–4 p.m., Annapolis; Friday, April 18, 9 a.m.–noon, Americana Tour.

Meeting Registration

Preregistration will be accepted until March 28. There will be on-site registration. Official badges and program books will be available at the registration desk, Sheraton Washington Hotel. No confirmations will be mailed.

Course Registration

Register early—enrollment is limited. List first, second, and third choices for each period. Also, indicate whether you wish to take the categorical course. Deadline for mail registration is March 28. All ticket orders will be filled by postmark. Course tickets *will not* be mailed. Tickets will be available on and after Saturday, April 12 (after 1 p.m.), at the ARRS registration desk in the Sheraton Washington Hotel. There will be on-site registration for courses not already filled.

Hotel Registration

Reservations are handled by the ARRS Housing Bureau, Sheraton Washington Hotel, 2660 Woodley at Connecticut Ave., N.W., Washington, DC 20006. These must be received by March 15. Make check payable to Sheraton Washington Hotel.

Fees

Meeting:	
ARRS members and resident members	No fee
Nonmembers	$100
Nonmember physicians in training (with verification)	25
Categorical course (all who attend)	75
Luncheon sessions/each	10
Golf tournament	65
Tennis tournaments	50
Local tours	15–45

Cancellations and Fee Refunds

Fees will be refunded only if cancellation is received by April 7. Send to American Roentgen Ray Society, 1891 Preston White Drive, Reston, VA 22091.

Air Transportation

Two airlines, United and Delta, are official meeting air carriers and are offering discounted fares.

Delta Air Lines will discount fares 35%. Tickets must be purchased a minimum of 7 days before departure. Travel to Washington must be from April 9 through 15. A maximum stay of 15 days is permitted. Information: (800) 241-6760 in the continental U.S., 8:30 a.m.–8 p.m. eastern time daily. Mention ARRS number F-0347.

United Airlines offers a 40% discount off normal coach fares with no minimum stay or advance purchase restrictions. There is an additional 5% discount (45% total) for those staying over a Saturday night. Travel must be between April 10 and 22. Information: (800) 521-4041, 8:30 a.m.–8 p.m. eastern time daily. Mention ARRS number 602-K. Seats are limited.

Associated Meetings

The *Society for Pediatric Radiology* will meet April 9–13 in the Westin Hotel, Washington, DC. The program will appear in the March issue of the *AJR*. For information contact: Donald R. Kirks, M.D., Secretary, Society for Pediatric Radiology, c/o Dept. of Radiology, Duke University Medical Center, Box 3834, Durham, NC 27710; telephone (919) 681-2711, ext. 287.

The *American Association of Women Radiologists* (AAWR) will have a luncheon meeting on Monday, April 14, in the Sheraton Washington Hotel.

Pancreatic Sonography:

Enhancement by Metoclopramide

Rene P. duCret[1]
Valerie P. Jackson
Chester Rees
Richard Lowe
Nancy E. Davison

Abdominal sonograms were obtained before and after intravenous metoclopramide administration in 25 patients with a wide variety of abdominal complaints. Visualization of the pancreas was improved by this pharmacologic treatment in 44% of those patients in whom gas obscured the pancreatic bed. There was no improvement when fat was the primary prevention of visualization of the pancreas. There were no significant side effects of metoclopramide administration.

Gas in the stomach and duodenum commonly obscures sonographic visualization of the pancreas. Metoclopramide hydrochloride (Reglan, A. H. Robins) is known to stimulate gastric and duodenal contractions and has been frequently and successfully used for treatment of diabetic gastroparesis. Other accepted uses include short-term treatment of gastroesophageal reflux, prevention of nausea and vomiting secondary to cancer chemotherapy, facilitation of small-bowel intubation, and enhancement of barium transit during radiologic examination. We studied the possible benefits of metoclopramide administration for reduction of gastric and duodenal gas artifact during sonographic examination of the pancreas.

Materials and Methods

Twenty-five patients with a wide variety of abdominal complaints in whom fat and/or gas obscured the pancreatic bed were examined in the supine position with sonography before and immediately after metoclopramide administration. Ten milligrams (2 ml) of Reglan was injected intravenously over 2–3 min. All patients had been fasting for at least 8 hr before the sonographic examination. Sonograms were performed by one technologist, using a Phillips SDR 2000 real-time unit with either a 3.5- or 5.0-MHz transducer. Efforts were made to produce sonograms of similar level and orientation before and after metoclopramide administration. The patients were monitored for complaints at all times by a physician. Pre- and postmetoclopramide sonograms were then mounted in random order on a film rotator and read in blind fashion by four radiologists at different times. Each observer recorded whether diagnostic images of the pancreatic head, body, and tail were present on each study, and which one of each of the paired pre- and postmetoclopramide studies was of overall greater diagnostic value. When at least three of the four readers agreed on a change in visualization of specific parts of the pancreas, this was recorded as a significant improvement or degradation of image quality by metoclopramide administration.

Results

Gas was judged to obscure the pancreas in 18 of 25 patients. Fat alone obscured the pancreas in four patients, and a combination of fat and gas caused poor visualization of the pancreas in the remaining three patients. As shown in table 1, for the 18 patients in whom gas alone obscured the pancreatic bed, metoclopramide improved visualization of the pancreatic head in three, the pancreatic body in five, and the pancreatic tail in five patients (fig. 1). When fat alone was judged to degrade

---

Received July 15, 1985; accepted after revision September 20, 1985.

[1] All authors: Department of Radiology, Indiana University School of Medicine, 926 W. Michigan St., Indianapolis, IN 46223. Address reprint requests to V. P. Jackson.

AJR 146:341–343, February 1986
0361–803X/86/1462–0341
© American Roentgen Ray Society

the sonogram, there was no benefit from metoclopramide injection. Of the three patients in whom both fat and gas caused significant artifact, only one benefited from metoclopramide administration. In two of 25 patients, the overall quality of the postmetoclopramide study was judged to be poorer than the pre-Reglan study.

Minimal side effects were noted in two patients in whom transient drowsiness developed after rapid injection of the metoclopramide. No complaints were elicited when the pharmaceutical was injected more slowly, over a 2–3 min period. There were no major side effects from the drug in any of the patients in this study.

Discussion

Many maneuvers have been used in attempts to improve the diagnostic quality of pancreatic sonography. An early method was the use of oral simethicone to produce coalescence of small air bubbles into larger ones with subsequent expulsion from the upper gastrointestinal tract [1]. This technique met with some success, but as it required 1–2 days of patient preparation, it was applicable to a limited patient population. Dietary restrictions and laxatives [2] have also been tried, but without discernible effect on decreasing subjective amounts of abdominal gas. Water distension of the stomach [3] requires ingestion of large volumes (300 ml) of water by straw, and multiple patient positions for benefit. The erect gastric window technique was reported as beneficial in a high percentage of patients, but requires a combination of water ingestion (540 ml), oral Lipomul, and occasionally intravenous or subcutaneous glucagon to delay gastric emptying [4]. Various other fluid combinations have been tried, including 1% methylcellulose, pith suspended in orange juice, and 2% barium [5]. All these techniques require the patient to ingest and tolerate relatively large volumes of fluid, and some materials are not readily available. A simpler technique is the upright scanning position to move the liver caudally and induce movement of gas from the antrum to the fundus, thus creating a sonic window to the pancreas [4, 6].

TABLE 1: **Sonographic Visibility of the Pancreas before and after Metoclopramide Administration in 25 Patients**

Premetoclopramide-Obscuring Factor: Part of Pancreas	Postmetoclopramide Improvement (no.)
Gas ($n = 18$):	
Head	3
Body	5
Tail	5
Total patients	8
Fat ($n = 4$):	
Head, body, and tail	0
Fat and gas ($n = 3$):	
Head	1
Body and tail	0

The benefits of intravenous secretin administration were reported by Bolondi et al. [7]. This hormone dilates the pancreatic ducts by stimulation of water and bicarbonate secretion from the pancreas, with resultant filling of the duodenum to give a "fluid cap" around the pancreatic head. Disadvantages of this technique include high cost, relative lack of availability, and applicability to only a very select patient population.

Metoclopramide sensitizes tissues to acetylcholine, producing increased tone and amplitude of gastric contractions, increased peristalsis of the duodenum and jejunum, and relaxation of the pylorus and duodenal bulb. These changes lead to accelerated gastric emptying and intestinal transit. There is no effect on motility of the colon or gallbladder, and no stimulation of pancreatic, gastric, or biliary secretions. Onset of action is rapid, generally within 1–3 min of intravenous injection.

The advantages of the use of metoclopramide include its low cost, ready availability in most radiology departments, ease of administration, and proven safety with widespread

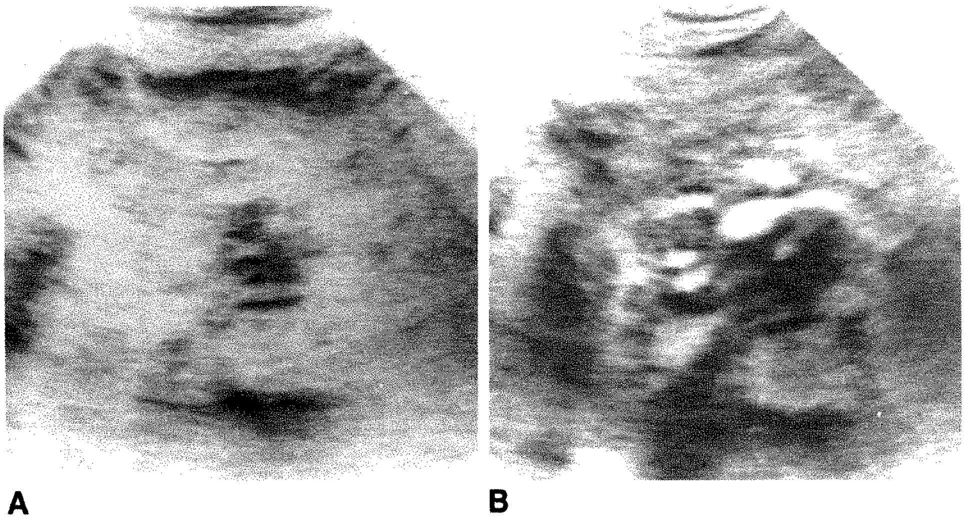

Fig. 1.—**A**, Before metoclopramide. Transverse scan of pancreatic bed in 50-year-old man with severe abdominal pain and history of alcoholism. Suggestion of diffuse pancreatic enlargement, but most of pancreas is obscured by overlying gas. **B**, After metoclopramide. Transverse sonogram 5 min after intravenous metoclopramide administration. Excellent visualization of enlarged pancreatic head and body; tail was visible in other planes. Cystic spaces in pancreas are segments of dilated, tortuous pancreatic duct.

use. The only deterrent to its use may be the intravenous route used in this study. An oral form of the drug is now available, and this may in the future benefit pancreatic sonography while maximizing patient comfort. Because there was net improvement or no change in the image quality in 92% of our patients, it is possible that routine premedication with oral metoclopramide might be beneficial.

There are several contraindications to the use of metoclopramide. These include situations in which stimulation of gastrointestinal motility might be dangerous, as in gastrointestinal tract obstruction, hemorrhage, or perforation. The drug should be used cautiously, if at all, in patients with pheochromocytoma (possible catecholamine release) and in epileptics or patients receiving medications that may cause extrapyramidal symptoms (rare exacerbation of extrapyramidal symptoms).

In our series, there were two patients in whom the sonographic visualization of the pancreas was degraded by metoclopramide administration. In both patients, there was moderate visualization of the pancreatic head and body and nonvisualization of the tail before metoclopramide. After Reglan injection, a large amount of gas accumulated in the duodenum, obscuring the pancreatic head.

In summary, we believe that metoclopramide administration can, at low cost and risk, improve the diagnostic quality of pancreatic sonography in a significant number of patients in whom gas artifact is present and in whom standard positional maneuvers fail to improve image quality. Of patients with suboptimal pancreatic visualization because of gas, 44% had significant improvement after metoclopramide administration, and only 8% of the entire group of study patients had image degradation, indicating the overall benefit of the use of this pharmaceutical in selected pancreatic sonograms.

REFERENCES

1. Sommer G, Filly RA, Laing FC. Use of simethicone as a patient preparation for abdominal sonography. *Radiology* **1977**;125:219–221
2. Meire HB, Farrant P. Preparation of the patient for abdominal ultrasound imaging. *Br J Radiol* **1978**;51:387–388
3. Crade M, Taylor KJW, Rosenfield AT. Water distension of the gut in the evaluation of the pancreas by ultrasound. *AJR* **1978**;131:348–349
4. MacMahon H, Bowie JD, Beezhold C. Erect scanning of pancreas using a gastric window. *AJR* **1979**;132:587–591
5. Picker RH, Kossoff G, Warren P. Comparison of fluids for use in the fluid-filled stomach as an ultrasonic window. In: *Abstracts of the Fourth World Congress on Ultrasonics in Medicine* (July 22–27, 1979, Miyazaki, Japan). Tokyo: Scimed, **1979**:93
6. Crade M, Jacobson P, Taylor KJW. The upright position while giving water for evaluation of the pancreas. *JCU* **1978**;6:353–354
7. Bolondi L, Gaiani S, Casanova P, Testa S, Priori P, Labo G. Improvement of pancreatic ultrasound imaging after secretin administration. *Ultrasound Med Biol* **1983**;9:497–501

The Anechoic Crescent in Abdominal Aortic Aneurysms: Not a Sign of Dissection

Patricia S. King[1]
Peter L. Cooperberg
Stephen M. Madigan

In six cases, abdominal aortic aneurysms simulated dissections because an anechoic crescent was seen peripheral to the echogenic intraluminal thrombus. Thrombus can easily be identified by sonography, but the layered echogenic and anechoic appearance has not been described. Three of these cases are presented to illustrate this sonographic pattern of thrombus so that it will not be misinterpreted as a dissection. CT scans were performed on all three patients and an arteriogram and surgery in one, all of which confirmed that these were not dissections but two layers of thrombus with the intima peripheral to the anechoic layer. At surgery, the anechoic layer medial to the intima in one case proved to be serosanguinous fluid and, therefore, likely liquefaction of the clot.

Sonography has been established as the procedure of choice in the initial evaluation of abdominal aortic aneurysms [1–4]. The advantages of sonography are numerous and include its noninvasive nature, ease of performance, and lack of ionizing radiation. It can accurately define the presence of thrombus [5], aneurysm size, and the complications of dissection [6–8] and leak [9].

In the past 4 months, we have seen six abdominal aortic aneurysms that contained an anechoic crescent peripheral to the echogenic intraluminal thrombus. Three cases are presented to illustrate the representative findings. In all three cases, sonography was performed initially, followed by contrast-enhanced CT scans. One case had an aortogram, followed by surgery.

Case Reports

Case 1

An 82-year-old man was admitted to the hospital because of congestive heart failure and chronic obstructive pulmonary disease. On physical examination, he had a nontender, midline, pulsatile mass. Static and real-time sonograms confirmed an abdominal aortic aneurysm. There was an eccentric lumen surrounded by echogenic thrombus with an anechoic crescent more peripherally (figs. 1A–1C). CT, performed to determine what was in the anechoic crescent, showed that the peripheral crescent was of lower density than both nonopacified and contrast-opacified blood and was even lower than the more solid thrombus. This suggests that the peripheral crescent was either serous or serosanguinous. Furthermore, the calcified intima was noted to be peripheral to the anechoic layer, confirming that this was not an aortic dissection (fig. 1D). Because of the patient's multiple medical problems and the asymptomatic nature of the aneurysm, surgery was not performed.

Case 2

A 55-year-old asymptomatic woman was admitted with the diagnosis of abdominal aortic aneurysm. Real-time sonography revealed an abdominal aortic aneurysm that contained a lumen surrounded by an inner echogenic layer of thrombus and peripheral anechoic crescentic layer (fig. 2A). CT showed that the anechoic crescent was of low density with no contrast

Received March 19, 1985; accepted after revision August 28, 1985.

[1] All authors: Department of Radiology, University of British Columbia, Vancouver General Hospital, 855 W. 12th Ave., Vancouver, BC, Canada V5Z 1M9. Address reprint requests to P. L. Cooperberg.

AJR 146:345–348, February 1986
0361–803X/86/1462–0345
© American Roentgen Ray Society

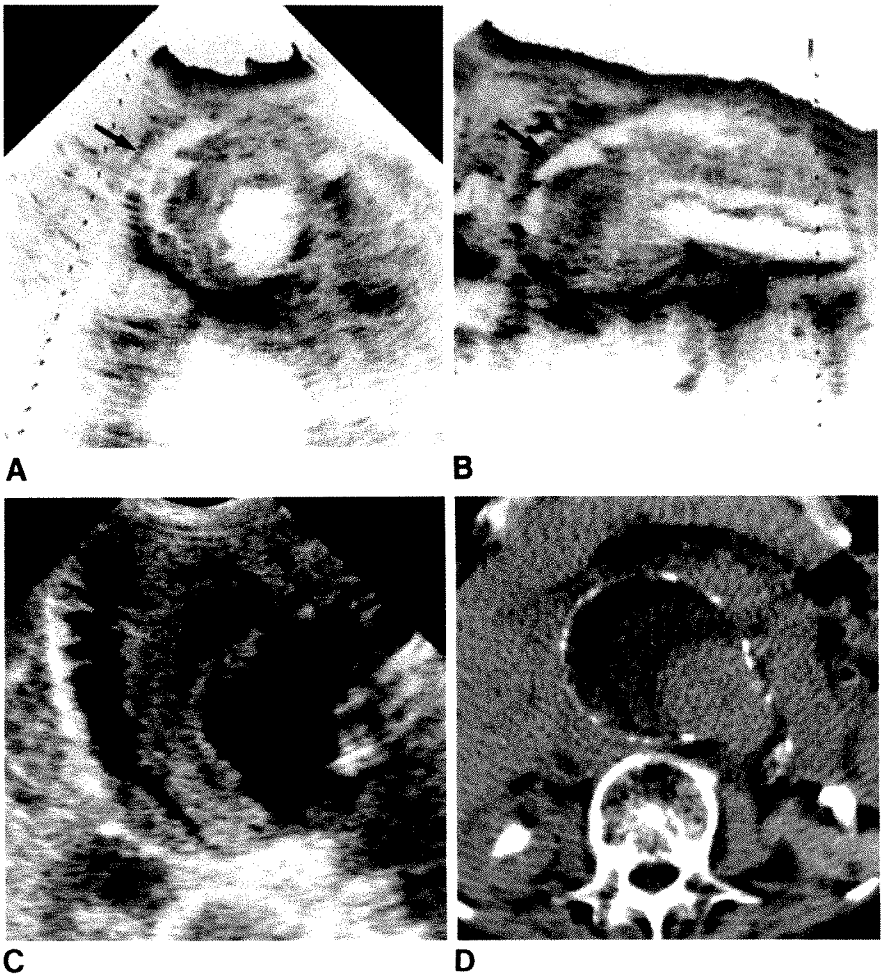

Fig. 1.—Case 1. Transverse (**A**) and longitudinal (**B**) static scans show aortic aneurysm with lumen posteriorly, echogenic thrombus, and anechoic crescent peripherally, anterior and to right (*arrows*). **C**, Real-time sector scan shows clear-cut fluid peripheral to thrombus in aneurysm. **D**, CT scan after bolus contrast injection shows low-density crescent superficial to medium-density thrombus around contrast-enhanced lumen. Calcified intima is peripheral to fluid and solid parts of thrombus.

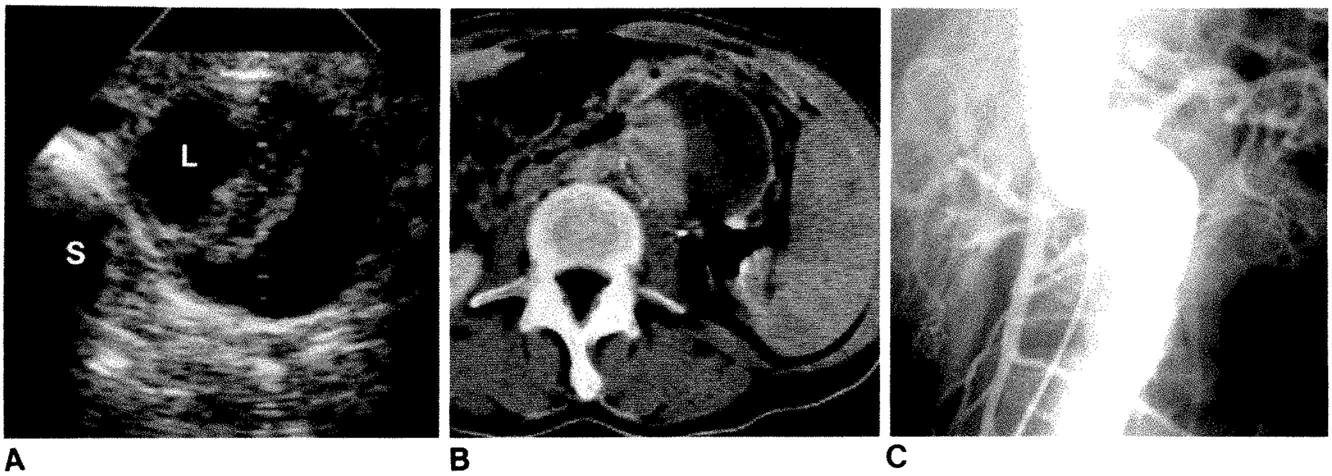

Fig. 2.—Case 2. **A**, Transverse real-time sector scan shows abdominal aortic aneurysm tortuous to left side of spine (S) with lumen (L) separated by echogenic solid thrombus from large crescentic fluid collection laterally. **B**, Contrast-enhanced CT scan shows lumen medially and relatively low-density fluid crescent laterally. **C**, Aortogram shows lumen of distal abdominal aorta deviated leftward. Note there is no contrast opacification of lateral part of aneurysm, confirming that this is not a dissection.

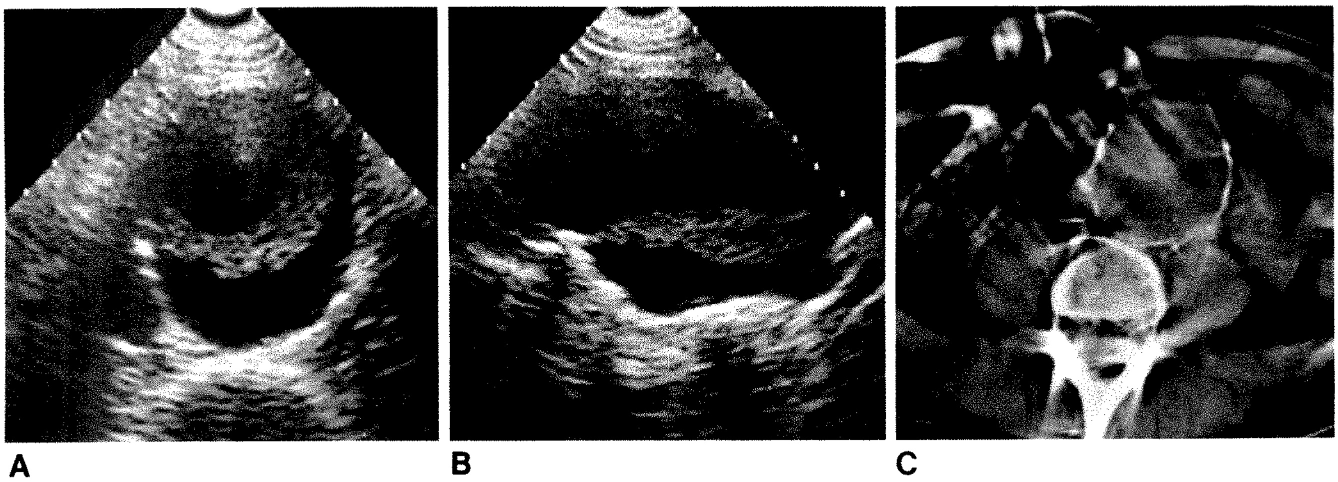

Fig. 3.—Case 3. Transverse (**A**) and longitudinal (**B**) real-time sonograms through abdominal aortic aneurysm show lumen anteriorly separated by solid thrombus from anechoic crescent posteriorly. **C**, Contrast-enhanced CT scan is suboptimal but clearly shows calcified intima surrounding fluid-filled crescent posteriorly.

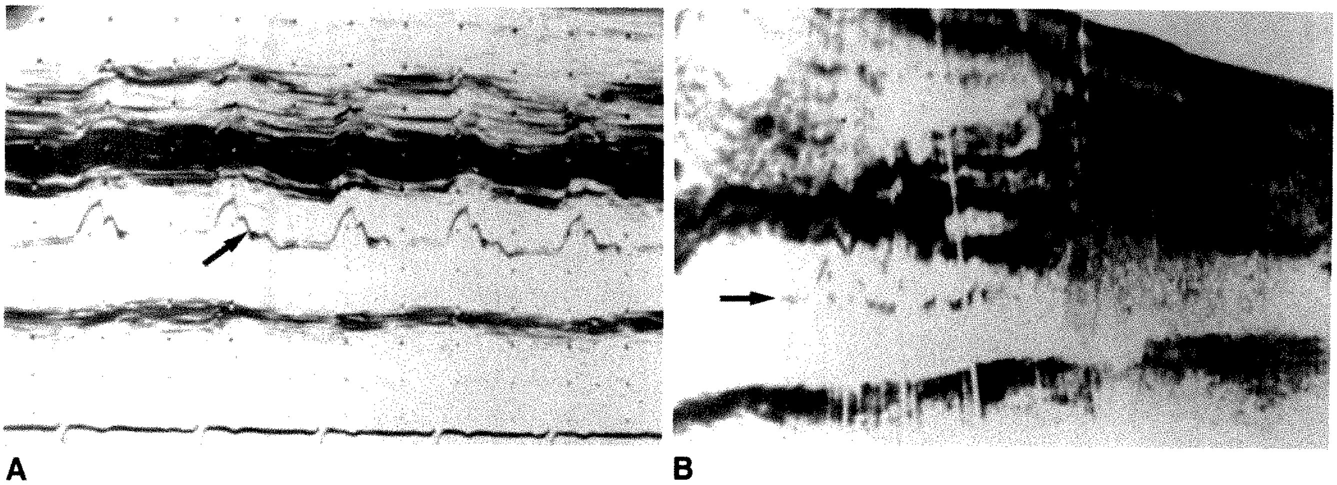

Fig. 4.—M-mode (**A**) and longitudinal static (**B**) scans through aortic dissection show pulsatile intimal flap (*arrow*) moving toward and away from transducer with each cardiac cycle.

enhancement and that the calcification was peripheral, ruling out a dissection (fig. 2B). An aortogram (fig. 2C) showed no dissection. Surgical repair of the aneurysm was performed and confirmed that there was serosanguinous fluid peripheral to the solid thrombus within the aortic lumen.

Case 3

A 61-year-old man was admitted for replacement of a degenerated porcine aortic valve. On abdominal examination, a large nontender, asymptomatic, pulsatile mass was discovered. Real-time sonography revealed an abdominal aortic aneurysm containing a central lumen with echogenic and anechoic layers of thrombus peripheral to it (figs. 3A and 3B). CT showed the calcified intima peripheral to the thrombus (fig. 3C). Because of the patient's unstable cardiac status and postoperative valve replacement complications, the aneurysm was not repaired.

Discussion

Thrombus may or may not be present in an aortic aneurysm. There is a tendency for thrombus to fill in around the periphery, leaving a lumen of more normal size. We have also noted that the residual lumen tends to be in line with the proximal normal part of the aorta. This explains why the residual lumen is often eccentric and may be on either side, posteriorly, or even occasionally anteriorly situated. It is because of the peripheral thrombus that sonography and CT give a much clearer image of the actual size of the aortic aneurysm than is apparent on the aortogram.

Normally the peripherally situated thrombus is entirely homogeneous from the wall of the aorta through to the lumen. Occasionally, there is an anechoic crescent peripheral to the more solid-looking thrombus. At first, we questioned whether this was in fact a dissection or even a leak with hemorrhage outside the aortic wall. The latter possibility seemed unlikely, especially since the patients were relatively asymptomatic with respect to their aneurysms. The sonographic and CT appearances of dissections are well established [6, 8, 10–12]. On real-time sonography, the intimal flap can usually be seen undulating back and forth with the cardiac cycle. This is particularly easy to identify on real-time scanning but can be documented using M-mode (fig. 4A) or a slow static scan (fig. 4B). On CT with a bolus injection, contrast enhancement should be noted first on one side of the flap and then very shortly thereafter on the other side of the flap. Occasionally, if there is thrombosis within the false or true lumen, there will be no contrast enhancement; then the CT density should be the same as that of the thrombus. In our cases, the peripheral crescent had a lower density. Furthermore, CT clearly shows that the calcification (which is in the intima) is peripheral to the thrombus.

In a dissection, the intimal flap with calcification will be displaced centrally. At surgery in one case, serosanguinous fluid was found between the solid thrombus and the intima. Discussion with the surgeons revealed that this is not an infrequent finding. Since the position and CT density of the peripheral crescent correspond exactly to the position where the serosanguinous fluid is found, we propose that this is due to reliquefaction of part of the clot. This certainly occurs elsewhere in the body following hemorrhage and thrombosis, and one could expect a similar change in thrombus within an aortic aneurysm.

Dissecting aortic aneurysms are relatively uncommon, symptomatic, and often lead to catastrophic events [13]. The appearance of liquefaction around solid thrombus in asymptomatic abdominal aortic aneurysms is not uncommon. We have seen six of these cases in a 4-month period. The frequency of occurrence and the asymptomatic nature of these aneurysms make it important to clearly differentiate them from dissecting aortic aneurysms.

REFERENCES

1. Winsberg F, Cole CM. Continuous ultrasound visualization of the pulsating abdominal aorta. *Radiology* **1972**;103:455–457
2. Wheeler WE, Beachley MC, Ranniger K. Angiography and ultrasonography: a comparative study of abdominal aortic aneurysms. *AJR* **1976**;126:95–100
3. Leopold GR, Goldberger LE, Bernstein EF. Ultrasonic detection and evaluation of abdominal aortic aneurysms. *Surgery* **1972**;72:939–945
4. Dauber E, Rankin R. The role of abdominal aortic ultrasound. *Australas Radiol* **1980**;24:67–71
5. Harter LP, Gross BH, Callen PW, Barth RA. Ultrasonic evaluation of abdominal aortic thrombus. *J Ultrasound Med* **1982**;8:315–318
6. Bresnihan ER, Keates PG. Ultrasound in dissection of the abdominal aorta. *Clin Radiol* **1980**;31:105–108
7. Goodman A, Lipinski JK. Occult thoracic-abdominal dissecting aneurysm in a patient with Marfan's syndrome: diagnosis by real-time ultrasound. *JCU* **1984**;12:115–119
8. Conrad MR, Davis GM, Green CE, Curry TS. Real-time ultrasound in the diagnosis of acute dissecting aneurysms of the abdominal aorta. *AJR* **1979**;132:115–116.
9. Clayton MJ, Walsh WW, Brewer WH. Contained rupture of abdominal aortic aneurysms: sonographic and CT diagnosis. *AJR* **1982**;138:154–156
10. Thorsen MK, SanDretto MA, Lawson TL, Foley WD, Smith DF, Berland LL. Dissecting aortic aneurysms: accuracy of computed tomographic diagnosis. *Radiology* **1983**;148:773–777
11. Godwin JD, Herfkens RL, Skiöldebrand CG, Federle MP, Lipton MJ. Evaluation of dissections and aneurysms of the thoracic aorta by conventional and dynamic CT scanning. *Radiology* **1980**;136:125–133
12. Kumari SS, Pillari G, Mandon V, Bank S. Case reports: occult aortic dissection—diagnosis by ultrasound. *Br J Radiol* **1980**;53:1093–1095
13. Hume DM, Porter RR. Acute dissecting aortic aneurysms. *Surgery* **1963**;53:122–154

Incidental Detection of Impalpable Testicular Neoplasm by Sonography

S. Stoll,[1] M. Goldfinger,[1] R. Rothberg,[1] M. B. Buckspan,[2] B. J. Fernandes,[3] and J. Bain[4]

High-resolution sonography is an effective technique for demonstrating clinically nonpalpable testicular tumors. However, the patients reported to date in the literature all presented initially with large mediastinal, retroperitoneal, and/or supraclavicular nodal metastases, in the case of primary germ cell tumors [1–3], or with gynecomastia, in the case of interstitial cell tumor of the testis [4, 5]. Their testicular tumors were found in a directed search for the primary tumor. This report documents a case of clinically unsuspected and nonpalpable testicular neoplasm discovered during routine scrotal sonography and its surgical management.

Case Report

A 29-year-old man was referred for scrotal sonography as part of a workup for infertility. Semen analysis demonstrated oligospermia and abnormal forms. Serum hormonal levels were normal, as was the physical examination. Sonographic examination using a 7.5-MHz real-time small-parts transducer (Diasonics) showed a small left-sided varicocele, but in addition revealed a 4-mm hypoechoic solid nodule in the right testis. (fig. 1A). The testes were otherwise normal. No retroperitoneal adenopathy or other evidence of metastatic neoplasm was found. Although the differential diagnosis included small granuloma or benign tumor, testicular exploration was performed to exclude early malignancy.

In order to facilitate intraoperative localization of the lesion, intraoperative sonography was used. The 7.5-MHz transducer was liberally covered with gel and then wrapped in sterile gloves. The intratesticular lesion was easily seen when the sterile transducer was applied to the surgically exposed testis. Using sonography as a guide, the surgeon excised the nodule. Quick section revealed an interstitial cell tumor, and an orchidectomy was not performed. Biopsy of uninvolved testicular tissue showed normal spermatogenesis.

On pathologic examination, the nodule was tan colored. Microscopic examination revealed sheets of polygonal cells with abundant eosinophilic cytoplasm and well defined cell borders. Nuclei were round to oval and contained occasional nucleoli. Intracellular lipid and Reinke crystalloids were identified. The diagnosis was Leydig cell tumor of the testis (fig. 1C).

Discussion

About 95% of primary testicular tumors arise from germ cells. They are generally malignant, and often cause pain and testicular enlargement. Nongerminal tumors arise either from stromal (Leydig cell) or sex-cord (Sertoli and granulosa cell tumors) derivatives. These neoplasms are usually smaller and generally benign. Only about 10% show malignant behavior [6].

Leydig cell tumors constitute about 2% of testicular tumors. They occur in all age groups, may be bilateral, and may elaborate androgens, estrogens, or even corticosteroids. In children, these tumors have been known to cause precocious masculinization or feminization. Adults can present with gynecomastia and impotence [6]. Leydig cell tumors may also be associated with absence or arrest of spermatogenesis [7]. If, as in our case, the neoplasm occurs in an infertile patient, biopsy of uninvolved testicular tissue must be done to assess spermatogenesis.

In addition to the described case, we have seen two additional cases of completely asymptomatic and impalpable Leydig cell tumor that presented in the same manner, as a 3–5 mm hypoechoic nodule in a testis (fig. 1B). In both these cases, the lesion was also localized by sonography in the operating room, and a testicular-sparing lumpectomy was performed.

As remarked previously, all the "occult" testicular neoplasms reported in the literature to date presented initially with signs of disease elsewhere. Our experience shows that the incidental discovery of nonpalpable and unsuspected 3–4 mm testicular neoplasms without evidence of disease elsewhere is possible, and that high-resolution sonography is an excellent method for localizing these lesions at surgery, so that an intraoperative diagnosis may be reached; if benign, a testicular-sparing resection can then be achieved.

Is the sonographic appearance of a small, well defined, hypoechoic solid nodule in a testis typical for an interstitial tumor, or can an early, asymptomatic germ-cell tumor also

---

Received May 24, 1985; accepted after revision September 20, 1985.

[1] Department of Radiological Sciences, Mount Sinai Hospital, 600 University Ave., Toronto, Ontario, Canada M5G 1X5. Address reprint requests to S. Stoll.
[2] Department of Urology, Mount Sinai Hospital, Toronto, Ontario, Canada.
[3] Department of Pathology, Mount Sinai Hospital, Toronto, Ontario, Canada.
[4] Department of Endocrinology, Mount Sinai Hospital, Toronto, Ontario, Canada.

AJR 146:349–350, February 1986 0361–803X/86/1462–0349 © American Roentgen Ray Society

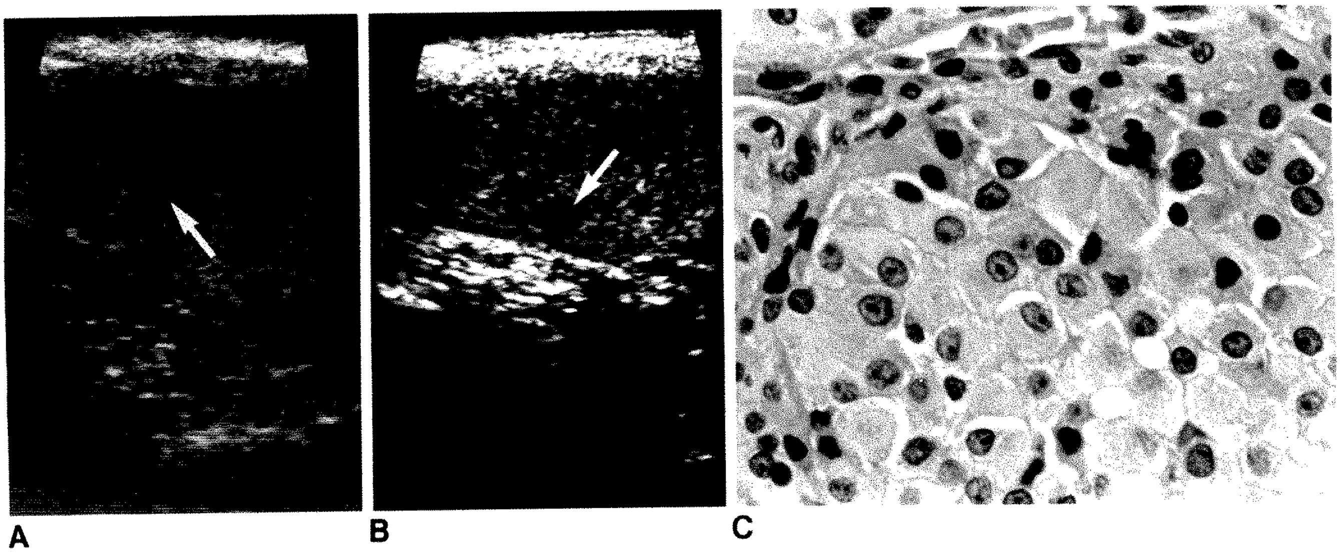

Fig. 1.—**A**, 4-mm Leydig cell tumor (*arrow*) in upper-pole right testis in asymptomatic 29-year-old man. **B**, 4-mm Leydig cell tumor (*arrow*) in posterior aspect of right testis in asymptomatic 31-year-old man. **C**, Leydig cell tumor. Sheets of polygonal cells with abundant cytoplasm, well defined cytoplasmic borders, and regular nuclei with occasional nucleoli. H and E ×500.

present in this manner before metastatic spread occurs? Experience with further cases will shed more light on the nature of these testicular nodules.

REFERENCES

1. Bockrath JM, Schaeffer AJ, Kies MS, Neiman HL. Ultrasound identification of impalpable testicle tumor. *J Urol* **1983**;130:355–356
2. Leopold GR, Woo VL, Scheible FW, Machtsheim D, Gosink BB. High-resolution ultrasonography of scrotal pathology. *Radiology* **1979**;131:719–722
3. Glazer HS, Lee JKT, Melson GL, McClennan BL. Sonographic detection of occult testicular neoplasms. *AJR* **1982**;138:673–675
4. Emory TH, Charboneau JW, Randall RV, Scheithauer BW, Grantham JG. Occult testicular interstitial-cell tumour in a patient with gynecomastia: ultrasonic detection. *Radiology* **1984**;151:474
5. Hendry WS, Garvie HH, Ah-See AK, Bayliss AP. Ultrasonic detection of occult testicular neoplasms in patients with gynecomastia. *Br J Radiol* **1984**;57:571–572
6. Robbins SL, Cotran RS, Kumar V. Male genital system. In: *Pathologic basis of disease*, 3d ed. Philadelphia: Saunders, **1984**:1081–1108
7. Symington T, Cameron KM. Endocrine and genetic lesions. In: Pugh RCB, ed. *Pathology of the testis*. London: Blackwell Scientific, **1976**:265–303

Incidental Prostatic Carcinoma Detected by MRI and Diagnosed by MRI/CT-Guided Biopsy

Steven D. Herman,[1] Arnold C. Friedman, Paul D. Radecki, and Dina F. Caroline

The clinical applications of magnetic resonance imaging (MRI) are just beginning to be evaluated. We have discovered another possibility to add to the list. We report a clinically occult prostatic carcinoma discovered by MRI and not demonstrated on computed tomography (CT). MRI localization was used to direct the CT-guided fine-needle aspiration for cytology.

Case Report

An 84-year-old man, who had had a colostomy and abdominoperineal resection for rectal carcinoma 3 years earlier, was being evaluated for possible recurrent tumor in the presacral space. The CT scan showed an irregular soft-tissue mass in the operative bed suspicious for recurrent tumor (fig. 1A). MRI using a Fonar 0.3-T nonsuperconductive magnet was performed with a slice thickness of 9 mm and slice interval of 12 mm. Transverse scans were obtained using the spin-echo (SE) pulse sequence with a repetition time (TR) of 2000 msec and echo times (TE) of 28 and 56 msec. Sagittal views were obtained using SE 2000/28, SE 2000/56, and inversion recovery (IR) with 1500 msec TR, 310 msec TI (inversion time), and 28 msec TE. A discrete nodule 2.0 cm in diameter, which was hypointense in comparison with the surrounding parenchyma, was seen in the left lateral lobe of the prostate on the SE 2000/28 scan only (fig. 1B). The nodule could not be identified retrospectively on the CT scan at comparable transverse levels. The patient was already scheduled for CT-guided fine-needle aspiration for cytology of his suspected recurrent tumor mass, so we decided to do a biopsy of the prostatic nodule at the same time, even though we could not see it on CT. Using the bony and soft-tissue landmarks from the transverse MR scan at the level of the nodule, we placed the needle into the expected location of the mass using CT guidance (fig. 1A). Cytology on the aspirates were conclusive for malignancy from both locations. The recurrent tumor mass was well differentiated adenocarcinoma, and the prostatic nodule was moderate to poorly differentiated adenocarcinoma.

Discussion

Although this is the first case, to our knowledge, of a clinically occult, incidentally discovered prostatic carcinoma on MRI, several other authors have described MRI findings in known cases of prostatic cancer. The findings show great variability depending on the pulse sequence used. Whereas all authors described the normal prostate as having a homogeneous signal pattern on all pulse sequences [1–4], most found a heterogeneous pattern in cases of carcinoma [1–3]. Poon et al. [1] were unable to find statistically significant differences among the MRI appearances of normal prostates, those with benign prostatic hypertrophy, and those with carcinoma. They also were unable to detect either benign or malignant nodules, and could not identify intraprostatic structures. Hricak et al. [2] described inhomogeneous areas of higher intensity signals than the surrounding benign gland with SE 1000/28 images. Bryan et al. [3] described a very inhomogeneous signal pattern in prostatic carcinoma, and were able to identify nodules with a weaker signal than the adjacent benign gland using SE 500/30 and IR pulse sequences. Buonocore et al. [4] described a heterogeneous pattern in prostatic cancer, especially on T2-weighted images, but found the same appearance in both acute and chronic prostatitis and also demonstrated that MRI is not helpful in demonstrating microscopic lymph node metastases. Smith et al. [5] were able to detect prostatic carcinoma as regions of prolonged T1 on a resistive unit operating at 0.04 T.

All authors agreed that MRI is better than CT at demonstrating invasion of periprostatic tissues, such as the periprostatic venous plexus and gland capsule. Our case demonstrated a hypointense, well circumscribed nodule within an otherwise homogeneous gland on one pulse sequence. Multiple other pulse sequences showed no prostatic abnormality. We have seen similar findings on MR scans from our machine in some patients with known prostatic carcinoma. We would expect these malignant foci to give an increased signal on the second-echo (56 msec TE) sequences, and are investigating why this has not occurred.

The question occurred to us that the malignancy in the prostate could conceivably represent not a primary prostatic tumor, but rather a metastasis from the known primary and locally recurrent rectal cancer. Except for lymphomas, the prostate is a very uncommon site of metastatic tumor involvement. The tumors that most commonly do give rise to prostatic metastases are melanomas and lung cancers [6]. Also, a standard textbook of surgical pathology makes no mention of rectal cancer metastasizing to the prostate [7]. We conclude that because the prostatic nodule was clearly separate

---

Received July 15, 1985; accepted after revision September 18, 1985.

[1] All authors: Department of Diagnostic Imaging, Temple University Hospital, 3401 N. Broad St., Philadelphia, PA 19140. Address reprint requests to A. C. Friedman.

AJR 146:351-352, February 1986 0361-803X/86/1462-0351 © American Roentgen Ray Society

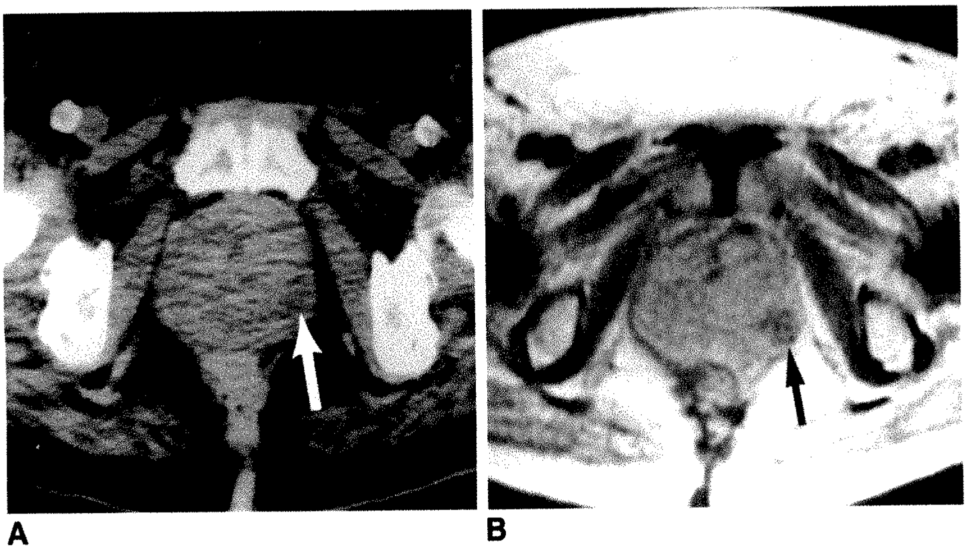

Fig. 1.—**A**, Axial CT scan of pelvis; *arrow* indicates direction of needle placement into nonvisualized prostatic nodule. Recurrent rectal carcinoma is seen just posterior to prostate in midline. **B**, Axial SE 2000/28 at comparable anatomic level to CT: well demarcated hypointense nodule (*arrow*) within otherwise homogeneous prostate gland.

from any adjacent masses, the cytologies of the two tumors were different, and because rectal carcinoma metastases to prostate are extremely rare, it is almost certain that the prostatic nodule could represent nothing other than a primary adenocarcinoma of the prostate.

By carefully correlating the anatomic landmarks present on MRI with those on CT, it is possible to successfully localize and do percutaneous biopsies of lesions visible on MRI but not detectable by other modes. Major technologic changes in bore size, scan speed, and needle design are needed before MRI can directly guide percutaneous biopsies.

REFERENCES

1. Poon PY, McCallum RW, Henkelman MM, et al. Magnetic resonance imaging of the prostate. *Radiology* **1985**;154:143–149
2. Hricak H, Williams RD, Spring DB, et al. Anatomy and pathology of the male pelvis by magnetic resonance imaging. *AJR* **1983**;141:1101–1110
3. Bryan PJ, Butler HE, Lipuma JP, et al. NMR scanning of the pelvis: initial experience with a 0.3 T system. *AJR* **1983**;141:1111–1118
4. Buonocore E, Hesemann C, Pavlicek W, Montie JE. Clinical and in vitro magnetic resonance imaging of prostatic carcinoma. *AJR* **1984**;143:1267–1272
5. Smith FW, Cherryman GR, Steyn JH. Higher sensitivity of T1 measurement at low field strength in the diagnosis of prostatic carcinoma. Presented at the annual meeting of the Society of Magnetic Resonance in Medicine, New York, August **1984**
6. Harrison JH, Gittes RF, Perlmutter AD, Stamey TA, Walsh PC. *Campbell's urology*, 4th ed. Philadelphia: Saunders, **1979**:1092
7. Rosai J. *Ackerman's surgical pathology*, 6th ed. St. Louis: Mosby, **1981**:531–541, 856–865

MRI in the Detection of Malignant Infiltration of Bone Marrow

Richard H. Daffner[1]
Anthony R. Lupetin
Nilima Dash
Ziad L. Deeb
Robert J. Sefczek
Rolf L. Schapiro

Magnetic resonance imaging (MRI) at 0.35 T with a superconductive magnet was performed on 80 patients with known or suspected malignant disease of the bone marrow. The group comprised 50 patients with known primary malignancy and 30 with known multiple myeloma. The MRI scan was correlated with plain films and radionuclide bone scans. In 40 patients with suspected metastatic disease, areas of decreased signal intensity on T1-weighted spin-echo images were observed. Ten patients had no MRI evidence of metastasis, and the abnormalities suspected on bone scanning were shown to be due to other causes. All the myeloma patients had abnormalities demonstrated by MRI. This was significant, since most had normal bone scans. All diagnoses were confirmed by needle biopsy. MRI was shown to be a sensitive method of detecting areas of malignancy within the bone marrow toward which biopsy could be directed.

Diseases affecting the bone marrow include osteomyelitis, myeloma, metastases, myeloproliferative diseases, and hemochromatosis. The traditional radiographic evaluation of these diseases has been with plain films, computed tomography (CT), and radionuclide scanning. With the development of magnetic resonance imaging (MRI), it soon became apparent that while cortical bone had very low signal intensity, the marrow space was usually of high intensity for most spin-echo sequences. Presumably, this signal intensity should change when the normal fatty marrow space is replaced by other tissue. The changes produced in osteomyelitis have been previously described [1]. Because metastases and myeloma constitute the largest group of patients with bone marrow disease, a prospective study was designed to determine the sensitivity of MRI in detecting malignant infiltrations. Further, we sought to compare MRI with other imaging methods in detecting malignant infiltrations of bone marrow in a highly selective group of patients with known malignancies.

Subjects and Methods

Eighty patients were studied. There were 50 with known malignancy who were suspected of having skeletal metastases; 30 had known multiple myeloma. All patients were studied by plain films and radionuclide bone scan as well as by MRI. Fifteen patients from each group were studied by CT. In addition, studies of 100 patients examined for suspected lumbar disk disease (80) or suspected aseptic necrosis of the hip (20) were reviewed for comparison of their marrow spaces.

All patients were examined on a Siemens Magnetom, 0.5-T superconductive machine operated at 0.35 T. Several pulse sequences were initially tried, with dual-echo images obtained at echo times (TE) of 35–120 msec and repetition times (TR) of 600–2100 msec with two to eight repetitions. We selected TE of 35 msec and TR of 700 msec with four repetitions (T1 weighting) on the basis of our observations that these parameters consistently delineated normal marrow from abnormal marrow within the shortest time period. The time of examination became important because of patient comfort as well as for patient "throughput." Our selection of these scan parameters parallels that of other investigators [2–4]. We

Received January 25, 1985; accepted after revision October 10, 1985.

[1] All authors: Department of Diagnostic Radiology, Allegheny General Hospital, 320 E. North Ave., Pittsburgh, PA 15212. Address reprint requests to R. H. Daffner.

***AJR* 146:353–358, February 1986**
0361–803X/86/1462–0353
© American Roentgen Ray Society

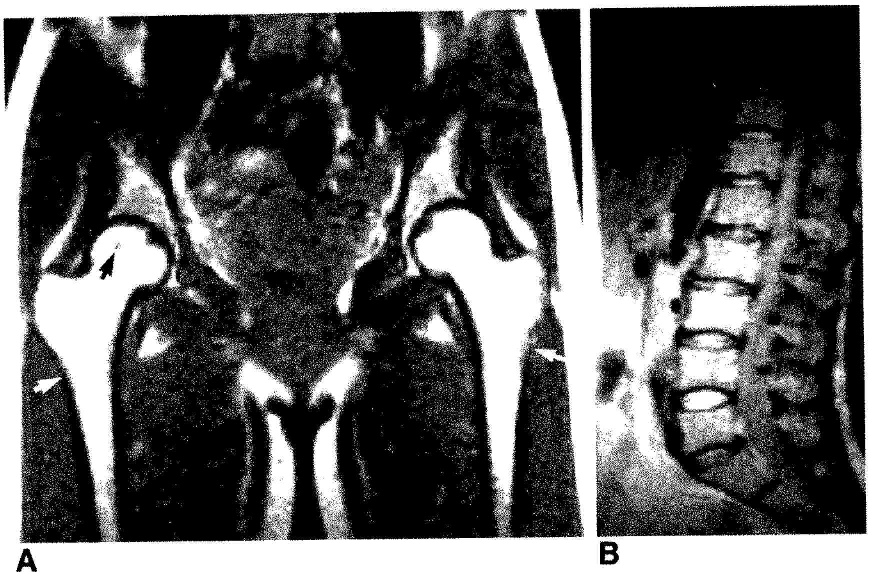

Fig. 1.—MRI appearance of normal bone marrow, which has high signal intensity. **A**, Coronal section of hips. Symmetric bands (*white arrows*) of low signal may represent large amounts of red marrow. Low-signal area in right hip (*black arrow*) is bone island. **B**, Sagittal section of lumbar vertebral column. Trail-off of brightness at ends of section is normal appearance caused by field inhomogeneity.

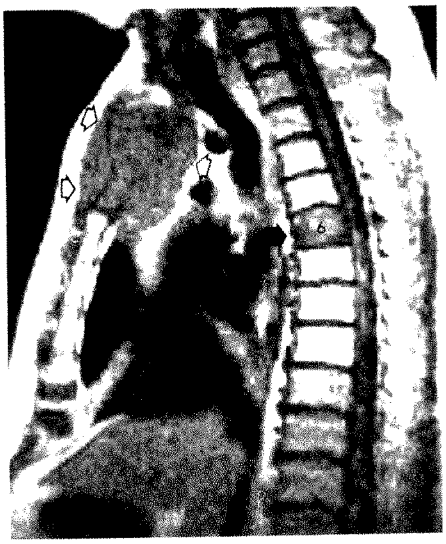

Fig. 2.—Sagittal MRI section shows abnormal marrow in patient with lymphoma. Note mass in manubrium with extraosseous extension (*open arrows*). Area of low signal in T6 (*solid arrow*) appeared as "ivory vertebra" on plain film. Note trail-off of signal in cervical and lumbar regions. Additional scans at those levels were normal.

made no attempt to differentiate abnormalities using MRI at T2 weighting because of the extremely variable appearance of different lesions at T2 levels.

Areas of abnormal signal intensity were initially determined by visual inspection and then confirmed by reading of pixel values of a region of interest within a space of 25 pixels. In most instances, measurements were not necessary because of the striking appearances of areas of abnormality. This may be related to the highly selective nature of the group studied.

The areas studied were either directed or nondirected. A directed study was one in which there was an area of suspected abnormality by clinical symptoms, bone scan, or plain film. In these patients, only the suspected bone or bones were scanned. In a nondirected study in which both the radionuclide scan and plain films were normal, the lumbar vertebral column, pelvis, and hips, which represent areas of high marrow content, were examined. All diagnoses were confirmed by needle biopsy of marrow from the affected bones.

Results

Normal bone marrow has high signal intensity on T1-weighted scans (fig. 1) because of its high fat content. Abnormal bone marrow was diagnosed when there was either focal or diffuse decrease in signal from the marrow areas studied. This decrease in signal was constant at T1 but varied at T2 sequences. None of the control group of patients had abnormal signal from their marrow areas. Of 50 patients with suspected metastases, the radionuclide bone scans were abnormal in all. Plain films, however, showed evidence of osteolytic or osteoblastic metastatic disease in 33. MRI detected areas of abnormal marrow in these 33 and in seven additional patients (figs. 2 and 3). All 15 patients studied by CT had abnormal studies. Ten patients with known primary malignancy and an abnormal bone scan had plain film evidence of other abnormalities (arthritis, seven; old fractures, three) to account for the abnormal scan. In each of these 10 patients, the MRI study showed normal marrow. There were no false-positive or false-negative MRI studies in this group. Needle biopsies were not performed on these patients, who were believed to represent true negatives. Follow-up studies for as long as 18 months showed no change in their radiographs.* Seven patients with proven metastases had repeat examinations, and these showed progression of the metastatic disease.

In 30 patients with myeloma, radionuclide bone scans were positive in six. Plain films showed abnormalities in these six and in an additional 14 patients. Eleven of these patients had abnormal CT studies. The remaining four had studies that were indistinguishable from osteoporosis. MRI, however, detected abnormalities in all 30 patients (figs. 4 and 5), which were confirmed by needle aspiration of marrow. Once again, an abnormal study was one in which there was decreased signal from the marrow-containing areas. There were no false-negatives in this group. In five patients, repeat examination showed progression of the disease. Tables 1 and 2 summarize the findings.

---

* At the time of this writing, the MRI unit had been in operation for less than 2 years. Follow-up studies continue on these patients.

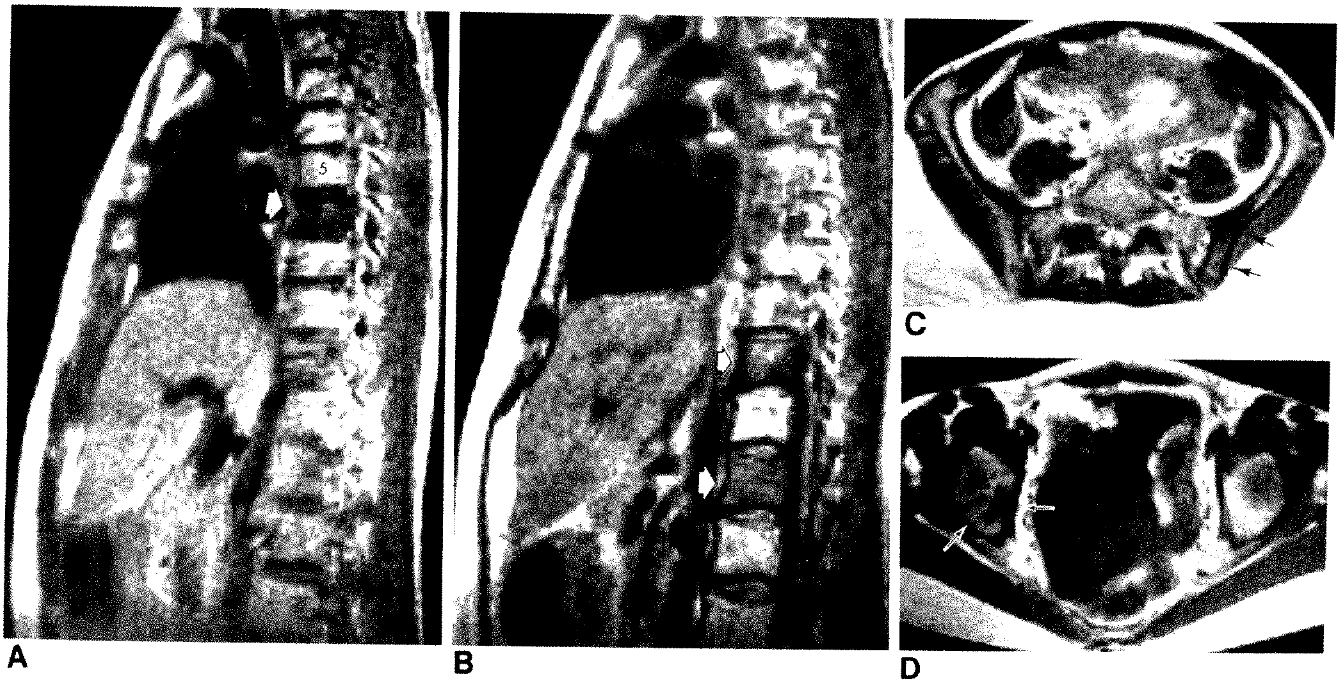

Fig. 3.—MRI of metastases from breast carcinoma. **A** and **B**, Sagittal sections of thoracic vertebral column. Multiple vertebrae with low signal (*arrows*). There was radiographic evidence of bone destruction at T6 only. **C** and **D**, Transverse sections of pelvis. Multiple areas of decreased signal (*arrows*) were apparent on plain films.

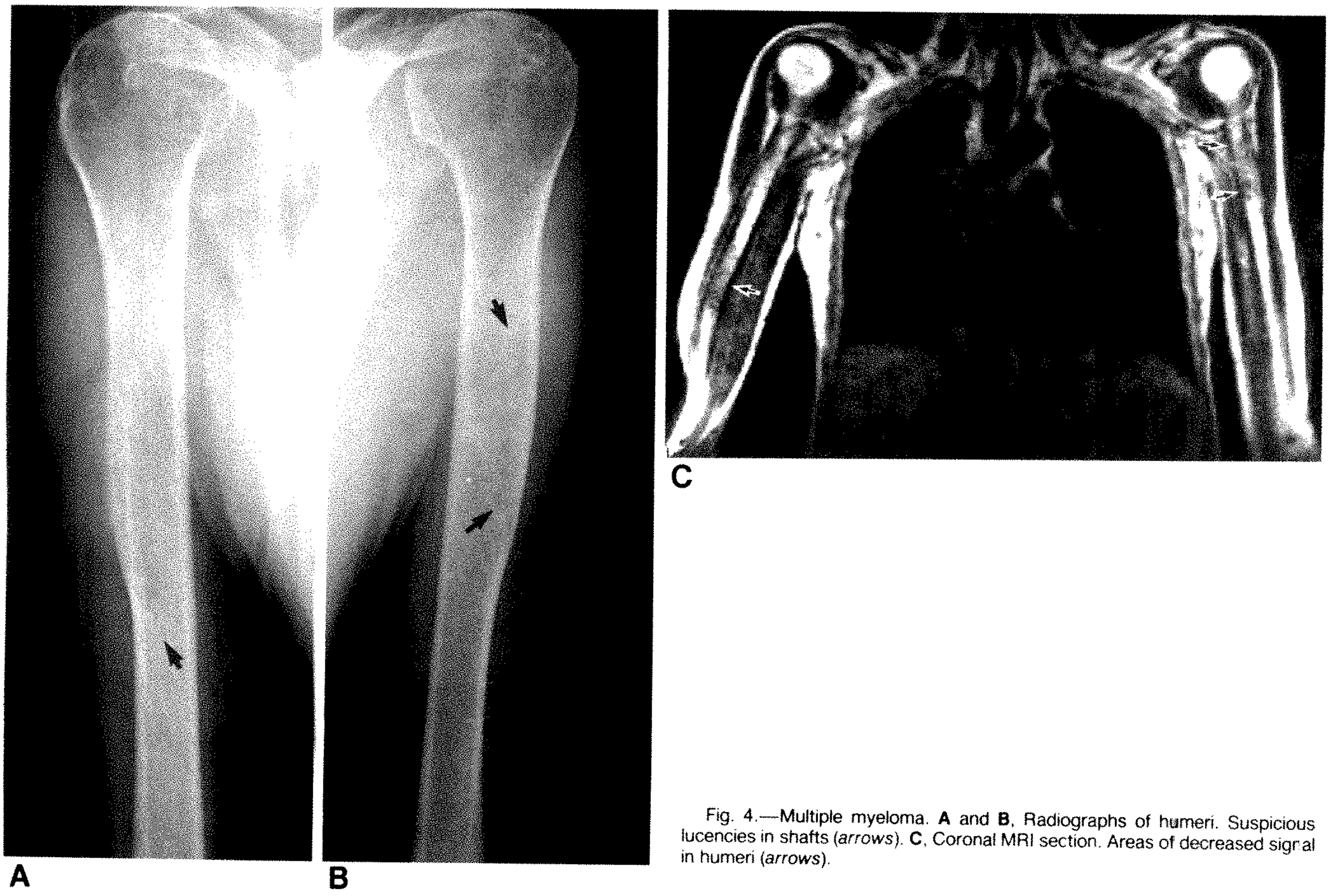

Fig. 4.—Multiple myeloma. **A** and **B**, Radiographs of humeri. Suspicious lucencies in shafts (*arrows*). **C**, Coronal MRI section. Areas of decreased signal in humeri (*arrows*).

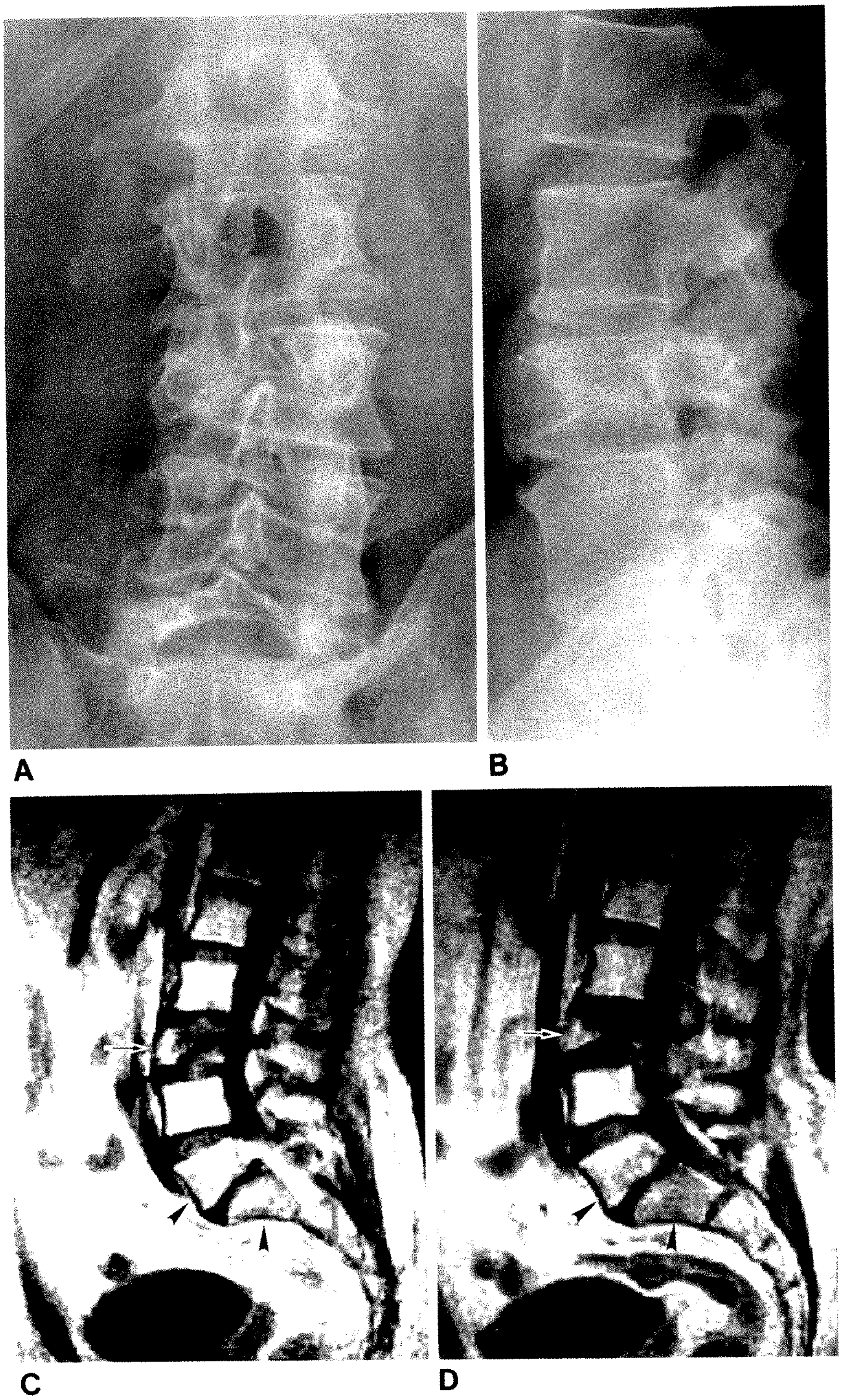

Fig. 5.—Multiple myeloma. Frontal (**A**) and lateral (**B**) views of lumbar vertebral column show partial collapse of L3. **C** and **D**, Sagittal MRI sections. Collapse of L3 has marked low signal (*arrow*). Biopsy showed no tumor. Low-signal areas in L5 and S1 (*arrowheads*) were considered normal radiographically. Needle aspirate showed abnormal plasma cells.

Discussion

The musculoskeletal applications of MRI have previously been directed toward the detection of abnormalities affecting the spine, ligamentous structures of the knee, bone ischemia, and primary bone and soft-tissue neoplasms [3–9]. The first two reports of MRI application to bone marrow disease dealt with children [1, 10]. Fletcher et al. [1] did MRI studies of five patients with osteomyelitis and reported that areas of abnormal marrow showed low signal intensity.

Cohen et al. [10] reported their findings in seven children with a variety of neoplastic processes involving the bone marrow. Their findings also showed that abnormal marrow areas produced decreased signal. Boyko et al. [3] and Mc-

TABLE 1: **Accuracy of Imaging Studies in the Detection of Bone Marrow Metastases in 50 Patients**

	Radionuclide Bone Scans	Radiographis	MRI	CT*
True positive	40	33	40	15
True negative	0	10	10	0
False positive	10	0	0	0
False negative	0	7	0	0

* Only 15 patients studied.

TABLE 2: **Accuracy of Imaging Studies in the Detection of Myeloma in 30 Patients**

	Radionuclide Bone Scans	Radiographs	MRI	CT*
True positive	6	20	30	11
True negative	0	0	0	0
False positive	0	0	0	0
False negative	24	10	0	4

* Only 15 patients studied.

Millin et al. [4] reported similar results. Our results parallel theirs and thus affirmatively answer the question whether MRI could detect bone marrow disease.

The abnormal appearance of MRI in bone marrow disease appears to be related to the change that occurs in marrow once it has become infiltrated. Cohen et al. [10] emphasized the fact that images obtained are mainly those of fat located within the marrow space. Normal bone marrow has high signal intensity at both T1 and T2 scan sequences due to its fat content. Any process that alters or replaces marrow fat will decrease the T1 signal. The T2 signal strength will depend on the type of tissue that replaces the normal marrow. Necrotic tissue, hematoma, and inflammatory debris will have higher T2 signals than neoplastic tissue [9]. Fibrotic or sclerotic tissue has low signal on both T1- and T2-weighted sequences.

MRI was shown to be useful in demonstrating areas of unsuspected neoplastic involvement (figs. 3 and 5). In a similar fashion, MRI was useful in the following patients, and, as mentioned above, showed progression of disease in seven patients with metastases and five with myeloma.

Our study of this highly selective group of patients indicates that MRI is a sensitive method for detecting areas of malignant marrow infiltration. When correlated with other imaging studies, we had no false-positive or false-negative cases. It has been long known that the radionuclide bone scan, while sensitive to areas of increased skeletal metabolic activity, is notoriously negative in patients with myeloma. It is in these patients that MRI may have its greatest impact in diagnosing marrow disease. We were unable to compare the accuracy of CT with MRI because of the small numbers in this series. Zimmer et al. [9] believe that MRI is clearly superior to CT. However, in myeloma, MRI may prove to be the better study, particularly in the earlier stages when CT cannot differentiate tumor from osteoporosis. We are currently conducting a prospective study comparing MRI and CT in patients with myeloma and bone marrow metastases.

Although MRI is extremely sensitive in detecting areas of abnormal marrow, its specificity has yet to be assessed. Our study was undertaken to determine the efficacy of MRI in detecting malignant marrow infiltration only. Unlike CT technology, in which differences in tissue density may be used to characterize various structures, we were unable to confidently differentiate among the various conditions. By using extended scanning times and different sequences, it may be possible to differentiate among these lesions. The changes seen at T1 and T2 sequences in osteomyelitis have been described [9, 10]. The extreme variability in tumor biology, behavior, and histology may make confident differentiation by MRI alone difficult. Furthermore, Dooms et al. [2] have shown variability in T1 and T2 relaxation times depending on patient age. We believe, however, that MRI can identify abnormal marrow areas at T1 parameters for needle aspiration.

Several pitfalls inherent in this technique that could cause diagnostic difficulties including averaging effect, old fractures, degenerative changes, and background density effect. The averaging effect relates to changes in perceived density on the final image due to sampling within the section. This is similar to radiographic density changes that occur on CT examinations. We have observed a peculiar phenomenon in MRI examinations at the ends of the images where there is a trailing-off of brightness due to field inhomogeneity (figs. 1B and 2). Again, careful correlation with plain films and radionuclide studies should be performed. Rescanning by centering on the area of question also should resolve this difficulty.

Old fractures and degenerative changes produce hypertrophic bone, which usually has extremely low signal on MRI (fig. 5). Correlation between bone scan and plain films is necessary to differentiate these areas. It may be necessary, however, to perform a needle biopsy of the area in question if this is the only abnormality in the symptomatic patient. Background density effect may cause a problem in interpretation. This was previously reported as a Mach band type of abnormality, which could affect CT scans [11]. In this phenomenon, the perceived density on the final image is directly influenced by the background density of the adjacent structures. This is most likely to occur where there is close proximity of structures of different signal intensity.

Areas of large amounts of red marrow in younger individuals may also slightly decrease the signal on MRI. We have encountered these on several occasions within the hips of young individuals, and have observed them to be symmetrical changes (fig. 1A) [12]. Careful correlation with plain films and isotope studies should help to eliminate this pitfall. A further aid is that most individuals with metastatic disease or myeloma are in an age group in which an abundance of red marrow does not present a diagnostic problem.

In conclusion, we believe that MRI is valuable in detecting abnormalities of the bone marrow. It compares favorably with more conventional imaging methods. It is extremely useful, in particular, in examining patients with suspected multiple myeloma in whom the radionuclide bone scan is negative and is most useful for identifying areas of abnormal marrow from which aspiration of tissue may be accomplished.

ACKNOWLEDGMENTS

We thank William Murphy for review of the manuscript and Maggie Cauley for manuscript preparation.

REFERENCES

1. Fletcher BD, Scoles PV, Nelson AD. Osteomyelitis in children: detection by magnetic resonance. *Radiology* **1984**;150:57–60
2. Dooms GC, Fisher MR, Hricak H, Richardson M, Crooks LE, Genant HK. Bone marrow imaging: magnetic resonance studies related to age and sex. *Radiology* **1985**;155:429–432
3. Boyko OB, Cory DA, Cohen MD, Mirkin D, Provisor AJ, DeRosa GP. Magnetic resonance imaging of osteogenic and Ewing's sarcoma. Presented at the annual meeting of the American Roentgen Ray Society, Boston, April **1985**
4. McMillin KI, Pennes DR, Aisen A, Braunstein E, Martel W. MRI and CT evaluation of primary bone and soft tissue tumors. Presented at the annual meeting of the American Roentgen Ray Society, Boston, April **1985**
5. Modic MT, Weinstein MA, Pavlicek W, et al. Nuclear magnetic resonance imaging of the spine. *Radiology* **1983**;148:757–762
6. Moon KL Jr, Genant HK, Helms CA, Chafetz NI, Crooks LE, Kaufman L. Musculoskeletal applications of nuclear magnetic resonance. *Radiology* **1983**;147:161–171
7. Totty WG, Murphy WA, Ganz WY, Kumar B, Daum WJ, Siegel BA. Magnetic resonance imaging of the normal and ischemic femoral head. *AJR* **1984**;143:1273–1280
8. Han JS, Kaufman B, El Yousef SJ, et al. NMR imaging of the spine. *AJR* **1983**;141:1137–1145
9. Zimmer WD, Bergquist TH, McLeod RA, et al. Bone tumors: magnetic resonance imaging versus computed tomography. *Radiology* **1985**;155:709–718
10. Cohen MD, Klatte EC, Baehner R, et al. Magnetic resonance imaging of bone marrow disease in children. *Radiology* **1984**;151:715–718
11. Daffner RH. Visual illusions and computed tomography: phenomena related to Mach effect. *AJR* **1980**;134:261–264
12. Kricun ME. Red-yellow marrow conversion: its effect on the location of some solitary bone lesions. *Skeletal Radiol* **1985**;14:10–19

Magnetic Resonance Imaging of Arachnoid Cysts Destroying the Sacrum

Murali Sundaram[1] and Eric E. Awwad[1]

Arachnoid cysts are known to cause focal lysis in adjacent bony sacral segments. We present a case in which the arachnoid cysts caused an expanded, destructive-appearing lesion of the sacrum, which on initial computed tomographic (CT) examination suggested an aggressive process. Magnetic resonance imaging (MRI) strongly indicated that arachnoid cysts were the probable cause of the destructive lesion, and this was confirmed by metrizamide CT.

Case Report

A 74-year-old woman with abdominal and pelvic discomfort was referred for a CT scan of the abdomen and pelvis. An expansile

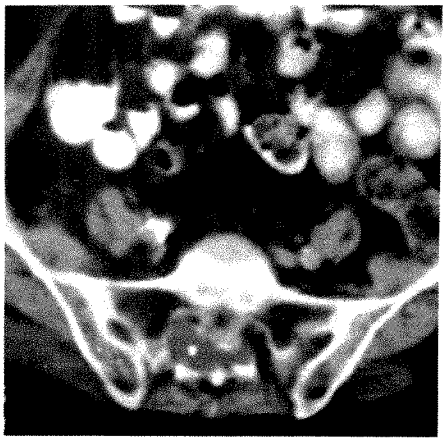

Fig. 1.—CT scan of abdomen and pelvis. Expansile destructive lesion of sacrum measures 5–20 H.

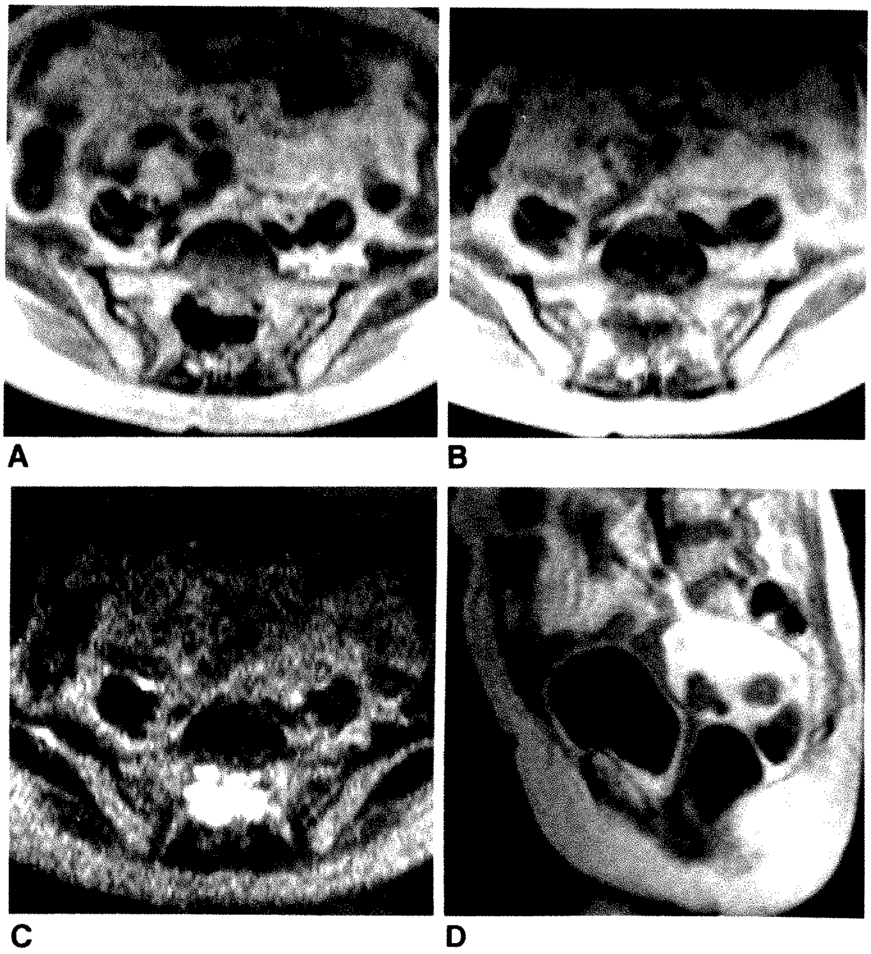

Fig. 2.—**A**, Axial SE (spin-echo) 530/30 (TR/TE), T1 weighted. Low signal intensity at site of sacral abnormality. Lesion crosses midline but is more pronounced on right side. **B**, SE 2240/30, T2 weighted. Increase in signal intensity. **C**, SE 2240/240, more heavily T2 weighted. Further increase in signal intensity. Lesion now has higher signal intensity than any of surrounding structures. **D**, Sagittal SE 530/30. Low signal intensity, similar to **A**, in neural canal, suggestive of CSF in dilated arachnoid cysts

---

Received June 13, 1985; accepted after revision September 18, 1985.

[1] Department of Radiology, St. Louis University Hospital, 1325 S. Grand Blvd., St. Louis, MO 63104. Address reprint requests to M. Sundaram.

***AJR* 146:359–360, February 1986** 0361–803X/86/1462–0359 © American Roentgen Ray Society

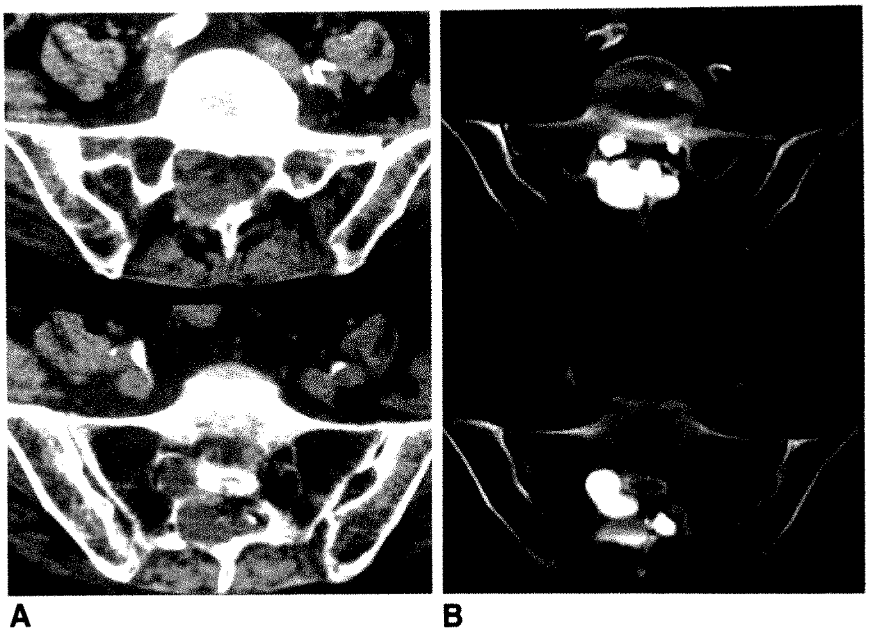

Fig. 3.—Pre- (**A**) and postmetrizamide (**B**) CT scans confirm sacral destruction by dilated arachnoid cysts.

destructive lesion of the right second sacral segment that measured 5–25 H was identified (fig. 1). Although the CT number was low, the possibility of this being either a metastatic lesion or a plasmacytoma could not be excluded. As part of an ongoing prospective evaluation of all primary lesions of bone, MRI was carried out. This showed that the lesion had a long T1 and T2 (fig. 2). The sagittal scan showed dilated cerebrospinal fluid (CSF)-containing structures in the region of the cauda equina. The signal intensity of the lesion of the T1-weighted axial images was identical to that demonstrated on the sagittal views. The possibility that this entire lesion was filled with CSF and that the destruction of the sacrum was caused by dilated arachnoid cysts was considered. Instead of a biopsy, a CT scan limited to the sacrum with and without metrizamide was carried out, confirming the diagnosis (fig. 3). The patient was discharged to be followed as an outpatient. The only history of note in this patient was a partial thyroidectomy.

Discussion

The type of lesion shown in this patient was first described by Enderle [1] as an occult intrasacral meningocoele, but it has also been described as an intrasacral intradural communicating arachnoid cyst [2] and an intrasacral cyst [3]. Since the original description, there have been about 50 cases reported in the world literature [2]. Moon et al. [4] demonstrated a sagittal SE 1500/28 image of an intrasacral cyst with low-intensity signals indicating a long T1. T2-weighted images of this lesion were not shown or discussed.

A recent publication characterizing intracranial cystic lesions showed CSF and arachnoid cysts to have a long T1 and long T2 [5]. An ongoing prospective MRI evaluation of lesions of bone at this institution suggests MRI is sensitive in depicting extent of disease. However, our understanding of the significance of appearances of T1- and T2-weighted images of bone has not permitted a high degree of specificity. The case presented here shows the characteristic features of fluid with a long T1 and long T2, which in conjunction with the anatomic information from axial and sagittal images permitted diagnostic specificity. In view of the patient's age and lack of neurologic signs and symptoms, it was elected to observe her as an outpatient.

REFERENCES

1. Enderle C. Meningocele intrasacrale occulto. *Riv Neurol* **1932**;5:418–423
2. Rengachary SS, Boynick PO, Karlin CA, Batnitzky S, Price H. Intrasacral extradural communicating arachnoid cyst: case report. *Neurosurgery* **1981**;3:236–240
3. Mink JH. Intrasacral "occult-intrasacral meningocoele." *Skeletal Radiol* **1985**;13:314–317
4. Moon KL, Genant HK, Helms CA, Chafetz NJ, Crooks LE, Kaufman L. Musculoskeletal applications of nuclear magnetic resonance. *Radiology* **1983**;147:161–171
5. Kjos BO, Brant-Zawadski M, Kucharczyk W, Kelly WM, Norman D, Newton TH. Cystic intracranial lesions: magnetic resonance imaging. *Radiology* **1985**;155:363–369

CT Arthrography of Capsular Structures of the Shoulder

Mahvash Rafii[1]
Hossein Firooznia[1]
Cornelia Golimbu[1]
Jeffrey Minkoff[2]
John Bonamo[2]

The capsular mechanism of the shoulder joint consists of the joint capsule, which is strengthened by the glenohumeral ligaments and the rotator cuff, the glenoid labrum, and a variable number of synovial recesses. Although the fibrous capsule is a lax structure, the normal function of the capsular mechanism makes it an effective barrier against anterior dislocation, particularly in external rotation. There has been a tendency in the past to overestimate the role of the glenoid labrum in stability of the shoulder joint. In patients with instability, the significance of the capsular attachment or its anomalous insertions to the glenoid has not been adequately recognized. Labral tears may develop as secondary lesions due to repeated dislocations and subluxations rather than representing the primary lesion responsible for instability. Operative visualization of capsular defects or detachments is often difficult. Prior knowledge of these lesions can effectively help the choice of an appropriate surgical procedure and reduce operating time. The results of computed tomographic (CT) arthrography of the shoulder joint in 45 patients are reported and the normal and pathologic variations of the joint capsule and particularly the capsular insertions are described. Configuration of the joint recesses and the glenoid labrum are also evaluated. These CT findings were correlated and verified by surgery or arthroscopy in 26 cases.

In 1938, Bankart [1] described a highly successful surgical repair procedure in a group of patients with recurrent anterior dislocation of the shoulder in whom he had observed a common anatomic abnormality. The so-called essential lesion of recurrent dislocation consisted of a torn or detached "glenoid labrum" with or without fracture of the glenoid margin. A similar lesion was subsequently noted in most patients with transient subluxations [2, 3]. Numerous reports since have presented the significance of various pathologic findings in shoulder instability and their specific surgical repair [4–8]. A number of investigators have disputed the concept of the glenoid labrum as an important stabilizing factor, attributing the success of Bankart's procedure to reattaching of the fibrous capsule to the glenoid rim [4, 6]. In this view, stability is mainly dependent on the capsular mechanism, that is, the ability of the capsule to become an effective barrier against projection of the humeral head in external rotation [5, 6]. The function of the labrum in this regard as a stabilizer is considered minimal if any, and the labral lesions, although commonly observed, are believed to be the result, rather than the cause, of recurrent instability [6].

Nevertheless, the frequent association of labral lesions with shoulder instability has caused it to be sought as a reliable sign of instability by the newly developed techniques of arthrotomography and CT arthrography [9–12]. Both techniques offer remarkable improvement in the visualization of the glenoid labrum; CT arthrography has proven to be more comprehensive, easier to perform, and slightly more accurate than conventional arthrotomography [13]. However, the capsular anatomy and its pathologic changes have received only slight attention [12]. We used CT arthrography in 45 patients with various abnormalities of the shoulder joint. In this prospective study, we assessed the abnormalities of the glenoid

Received July 15, 1985; accepted after revision October 17, 1985.

Presented in part at the annual meeting of the American Roentgen Ray Society, Boston, April 1985.

[1] Department of Radiology, NYU Medical Center, 560 First Ave., New York, NY 10016. Address reprint requests to M. Rafii.

[2] Department of Orthopedic Surgery, NYU Medical Center, New York, NY 10016.

AJR 146:361–367, February 1986
0361–803X/86/1462–0361
© American Roentgen Ray Society

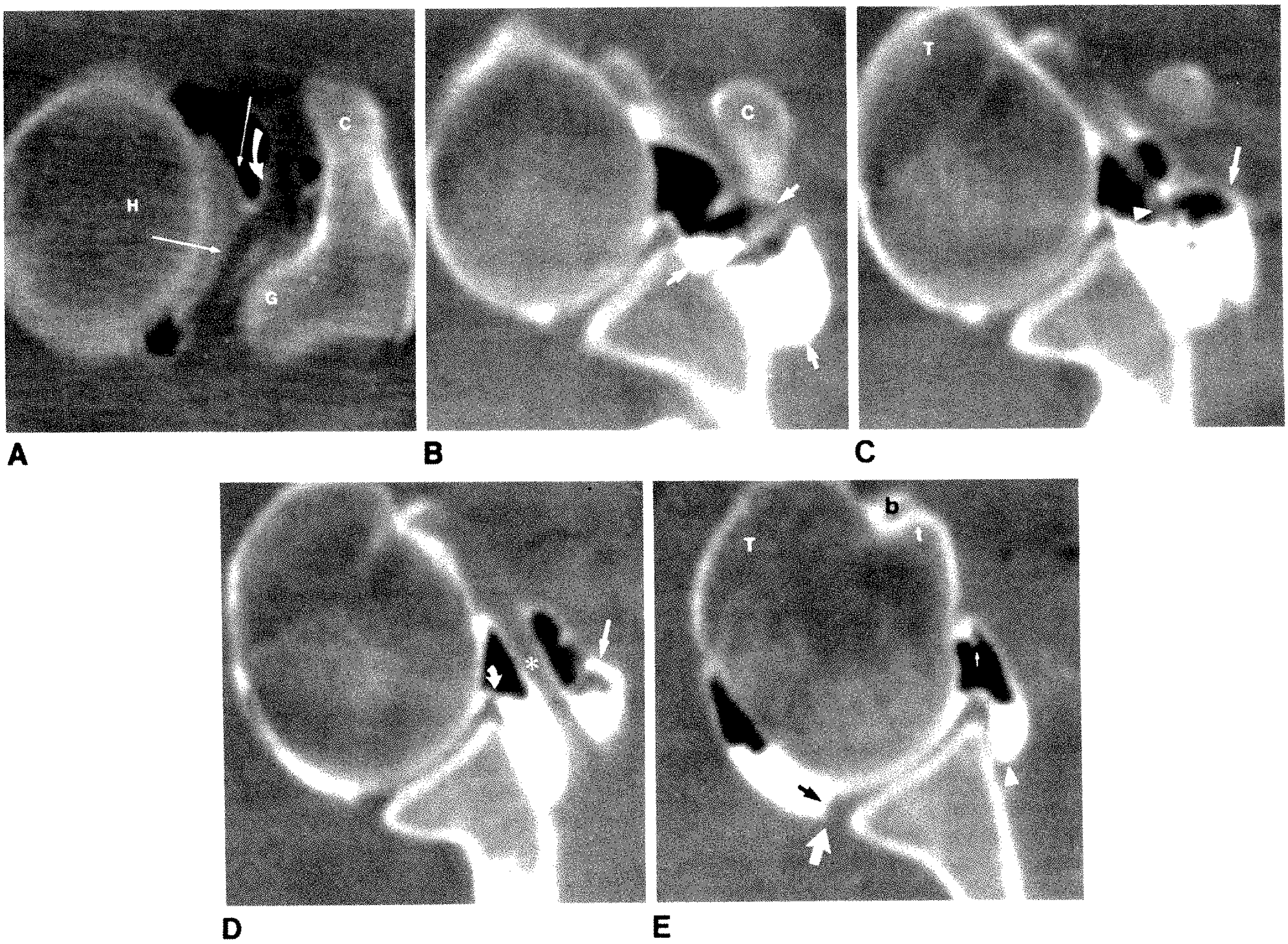

Fig. 1.—Normal capsular anatomy on consecutive sections of right shoulder beginning at superior glenoid margin (**A**) and extending below subscapular bursa. **A**, Anterior capsule and superior glenohumeral ligament (*curved arrow*) insert onto glenoid (G) immediately adjacent to common insertion of bicipital tendon and superior labrum (*straight arrows*). **B**, At level below base of coracoid process. Subscapular bursa (*arrows*) forms below superior glenohumeral ligament and coracoid process (C). Ridge(s) of capsular tissue may normally be present. **C** and **D**, Consecutive sections below **B**. Subscapular bursa overrides subscapular tendon (*asterisk*), forming separate compartment over ventral-superior margin of this tendon (*straight arrows*). Deep capsular lamina forms synovial ridge over free margin of tendon (*arrowhead*). Note triangular contour of anterior labrum (*curved arrow*). **E**, At level below subscapular bursa. Anteriorly, at its scapular insertion, capsule reflects smoothly over scapula, extending toward and blending with glenoid labrum; it forms narrow furrow between subscapularis muscle and glenoid margin (*arrowhead*). In this individual, capsular insertion is near labrum (type I). Posterior capsular insertion is always labral, and peripheral surface of labrum may not be coated with contrast material (*large white arrow*). Visualization of surface can be accomplished by external rotation of humerus, resulting in formation of capsular fold (not shown). Rounded contour of posterior labrum (*black arrow*). Mid-glenohumeral ligament only partially seen (*small white arrow*). H = humeral head; T = greater tuberosity; t = lesser tuberosity; b = bicipital tendon sheath and tendon in bicipital groove.

labrum, the joint capsule, and the synovial bursae in each group and correlated them with the clinical manifestations and surgical findings.

Anatomy

The anatomic structures of the anterior capsular mechanism of the shoulder joint include the fibrous capsule and the anterior glenohumeral ligaments, the synovial membrane and its recesses, the glenoid labrum, the subscapularis muscle and tendon, and the scapular periosteum. The posterior capsular mechanism consists of the posterior capsule, the synovial membrane, the glenoid labrum and periosteum, and the posterosuperior tendinous cuff and associated muscles (supraspinatus, infraspinatus, and teres minor). The tendon of the long head of the biceps and its insertion to the supraglenoid tubercle constitute the superior, and the triceps insertion to the infraglenoid tubercle the inferior, aspects of this division [5]. Variations may exist in the anatomic development of these structures, especially that of the glenohumeral ligaments and the synovial bursae, contributing to inherent instability of this joint.

The fibrous capsule is usually a lax and redundant structure [14]. The glenohumeral ligaments, which are thickened fibrous bands formed within the capsule, act as reinforcing structures. These ligaments extend from their attachment to the humeral head adjacent to the lesser tuberosity to the anterior glenoid rim. Their function is limitation of lateral rotation of the humeral

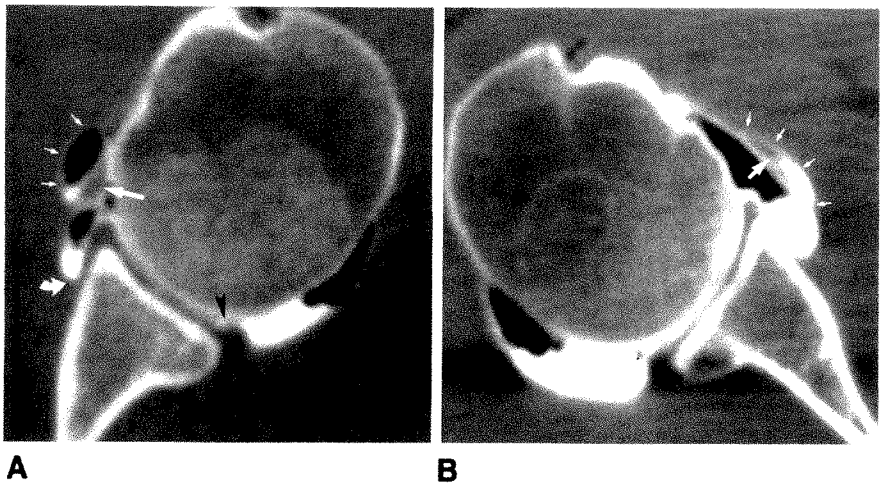

Fig. 2.—Two variations of mid-glenohumeral ligament. **A**, Axial section of left shoulder at mid-glenoid level. Well developed mid-glenohumeral ligament (*large straight arrow*) forms small synovial recess, limited by deep capsular lamina (*small arrows*). Note sharp reflection of anterior capsule (*curved arrow*). Notched appearance of posterior labrum is normal (*arrowhead*). **B**, Axial section of right shoulder at mid-glenoid level. In this individual, ligament (*large arrow*) is thinner and larger recess is seen (*small arrows*). In both individuals, capsular insertion is classified as type I.

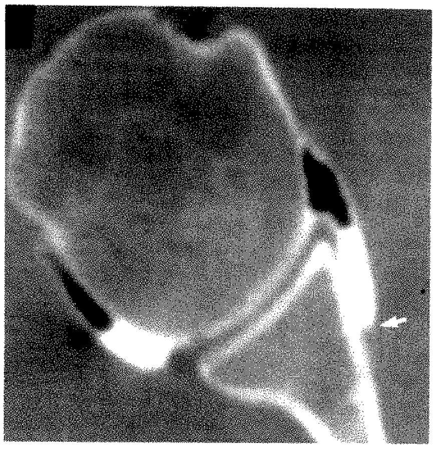

Fig. 3.—Anatomic variation of anterior capsular insertion. Axial image of right shoulder at mid-glenoid level. Capsule approaches scapular neck (type III), creating large recess (*arrow*). Middle and inferior glenohumeral ligaments were not seen.

head [5]. However, their presence is not constant and their attachment to the glenoid may vary. The capsule and the superior glenohumeral ligament extend medially to the base of the coracoid process and include the tendinous origin of the long head of biceps [4, 5] (fig. 1A). The mid-glenohumeral ligament, which is the most variable, inserts onto the glenoid below the superior glenohumeral ligament. The capsular opening for the subscapularis synovial bursae is found between these two ligaments adjacent to their glenoid insertion [5–15] (fig. 1B). These ligaments are not totally independent of the capsule. However, formation of one or more synovial recesses in their vicinity permits their identification by CT (fig. 2). The inferior glenohumeral ligament inserts onto the inferior one-third of the glenoid margin immediately adjacent to the labrum [16]. It is often seen on CT as a partial or complete capsular ridge attached to the immediate periphery of the labrum.

The synovial bursa most often encountered is the superior subscapular (80%–89%). This synovial pouch protrudes from the anterior opening of the fibrous capsule between the superior and middle glenohumeral ligaments, extends medially toward the inferior surface of the coracoid process, and along the superior tendinous border of the subscapularis muscle [5] (figs. 1B–1D). It may extend over the subscapularis tendon, thus providing a gliding mechanism for this tendon and the coracoid process. The size of this bursa varies. In patients with chronic anterior instability, it is usually large and may extend as far as 8 cm medially from the capsule [5].

The subacromion-subdeltoid bursa is separated from the joint by the superior aspect of the tendinous cuff, to which it is adherent [15]. Two other noncommunicating bursae, one on the ventral aspect of the subscapularis tendon and one between the infraspinatous tendon and the joint capsule, may also be present.

Unless interrupted by formation of the synovial bursae (figs. 1B–1D) and recesses, the capsular insertion onto the anterior glenoid is seen on CT arthrography as a smooth reflection of the contrast-coated synovium that blends with the lateral surface of the labrum (fig. 1E). It is distinguished from the cortical bone by a thin band of soft tissue that includes the periosteum of the glenoid. The posterior insertion of the capsule along the glenoid rim is more constant, and formation of a synovial recess in this region is rare (fig. 1). Laterally, the capsule is inserted on the anatomic neck superiorly, and extends inferiorly and medially along the surgical neck of humerus.

Variations exist in insertion of the anterior fibrous capsule onto the glenoid [17]. In type 1, the fibrous capsule, including the middle glenohumeral ligaments, inserts on the glenoid rim in close proximity to the glenoid labrum (figs. 1E and 2). In types II and III, the capsular insertion is further away from the glenoid rim and may reach the scapular neck (fig. 3). These latter variations, which may also be associated with an underdeveloped middle or inferior glenohumeral ligament, often create a large subscapularis recess with no passive restraint to anterior dislocation [15–17].

The glenoid labrum, which usually has a triangular contour in cross section, is a rim of soft tissue that is attached to the bony glenoid, blending with the tendon of the long head of biceps superiorly [5–14] (fig. 1A). This structure is composed of dense fibrous tissue and is believed to be a fold of the articular capsule [5]. It is contiguous with the capsule along its lateral surface, except anteriorly where the synovial bursae are found [5] (fig. 1). This surface may also be covered by a layer of synovial tissue [15]. Another surface is contiguous with the hyaline articular cartilage of the glenoid fossa. The triangular contour of the anterior glenoid labrum is constant. However, in our experience, posteriorly the labrum may normally appear rounded or slightly notched in contour (figs. 1 and 2). Occasional separation of the labrum from the hyaline articular cartilage of the glenoid, observed on anatomic sections and on CT, is considered a normal anatomic finding

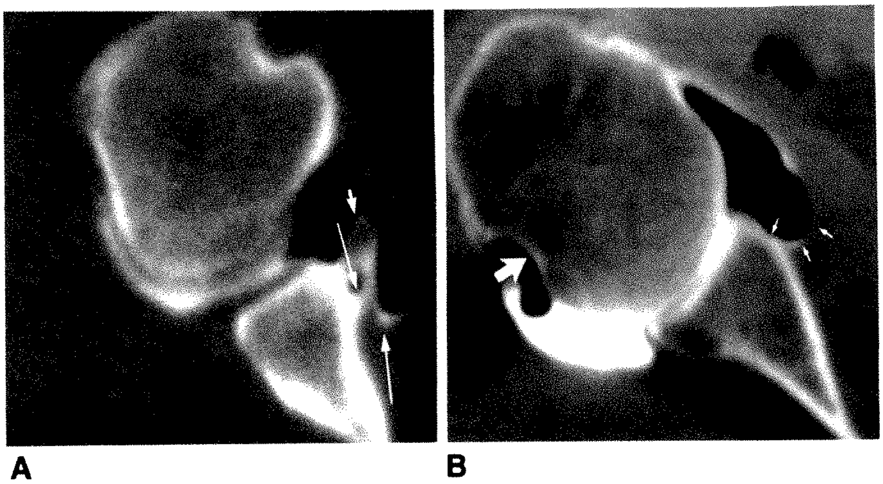

Fig. 4.—Anterior instability. **A**, Patient with recurrent subluxation of right shoulder. Axial section at inferior glenoid level. Typical Bankart lesion is present with detached labrum (*short arrow*), capsule, and periosteal new bone formation from scapula (*long arrows*). **B**, Recurrent dislocation of right shoulder in another patient. Axial section at mid-glenoid level. Widening of capsular reflection (larger furrow) over glenoid, with no intervening soft tissues remaining over glenoid (*small arrows*). Anterior labrum is also entirely disintegrated. Well defined Hill-Sachs deformity (*large arrow*) and degenerative attenuation of posterior labrum.

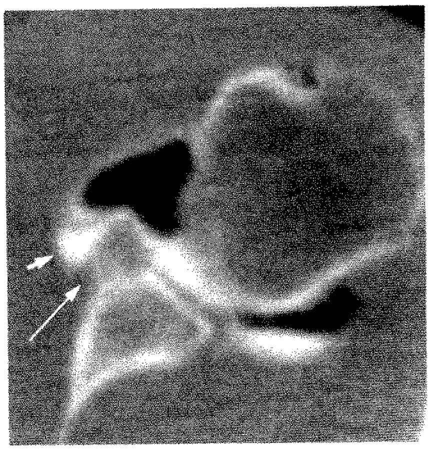

Fig. 5.—Anteroinferior instability of left shoulder. Axial section at mid-glenoid level. Widening of capsular reflection (*short arrow*). Intervening soft tissues are thickened and include periosteal new bone formation (*long arrow*). Labrum is intact.

[13]. The glenoid labrum is believed to add slightly more depth to the shallow glenoid fossa and increase its articulating surface against the much larger humeral head.

Subjects and Methods

Our 45 patients, 39 men and six women, were aged 15–58 years. They were divided into two groups on the basis of their clinical presentation. The first group (nine patients) had documented manifestations of shoulder instability (three dislocations, six subluxations). The second group (36 patients) had less specific symptoms, with varied clinical diagnoses of suspected instability, labral tear, and rotator cuff tear; 34 patients had a history of trauma that had resulted in tuberosity fracture in three patients.

All patients had a conventional double-contrast arthrogram before CT. Three milliliters of positive contrast medium (Renografin-60) and 0.3 ml of 1:1000 epinephrin were used when there were no clinical contraindications, and 10–12 ml of room air was also injected. After removal of the needle and mild exercise, supine axillary and upright frontal radiographs were obtained for evaluation of the rotator cuff as previously described [18]. This was immediately followed by CT examination. With the patient supine and the arm in neutral position, 3-mm-thick (on a GE-9800) or 5-mm-thick (on a GE-8800 CT/T) contiguous sections were obtained covering the region of the glenohumeral joint. A large body field of reconstruction was used, and target review magnification of the region of interest was obtained using standard algorithm. Images were recorded both with a wide window setting of 2000 H/200 (GE extended scale) for optimal visualization of contrast-coated soft tissue as well as bony structures and a narrow window setting (1000 H/150) for evaluation of periarticular soft tissues.

CT examinations were reported with attention to the abnormalities of the joint capsule, the glenoid labrum, the joint bursae, and the tendinous cuff. These findings were correlated with clinical manifestations and surgical (18 patients) or arthroscopic (eight patients) results. Five patients were lost to follow-up.

Results

Nine patients had clinically documented instability of the shoulder: three had recurrent anterior dislocations, and four had anterior subluxations; in two, the direction of instability was uncertain and multidirectional instability was suspected. There were no major differences in the capsular and labral abnormalities detected by CT in patients with recurrent dislocation or subluxation. One or more capsular abnormalities were present in each patient. The most constant abnormality, which was detected in all, involved the region of capsular insertion onto the glenoid. This determination was based on the distorted appearance of the capsular reflection with either loss or thickening of the intervening soft-tissue layer over the scapular margin. In four patients, this was associated with periosteal new bone formation arising from the glenoid (fig. 4). In seven patients, the subscapularis bursa was enlarged. Labral abnormalities (tear, detachment, attenuation) were present in all but one patient (fig. 4). In this patient with anteroinferior instability, the labrum was slightly deformed but there was no tear present (fig. 5). One of two patients with suspected multidirectional instability had confirmatory CT findings with major changes involving the posterior aspect of the joint (fig. 6). Eight patients in this group had surgical correlation of the CT findings, with the direction of instability verified in all under anesthesia.

Thirty-six patients had no clinically documented instability. Their complaints included pain (all) and limited range of motion (15 patients). Other findings included clicking, crepitation, and tenderness. Six patients had a completely normal CT examination. CT detected an isolated labral tear in one patient. Under anesthesia, the joint was stable and the torn labrum was subsequently removed. Significant abnormalities suggestive of instability were present in five patients, in an anterior

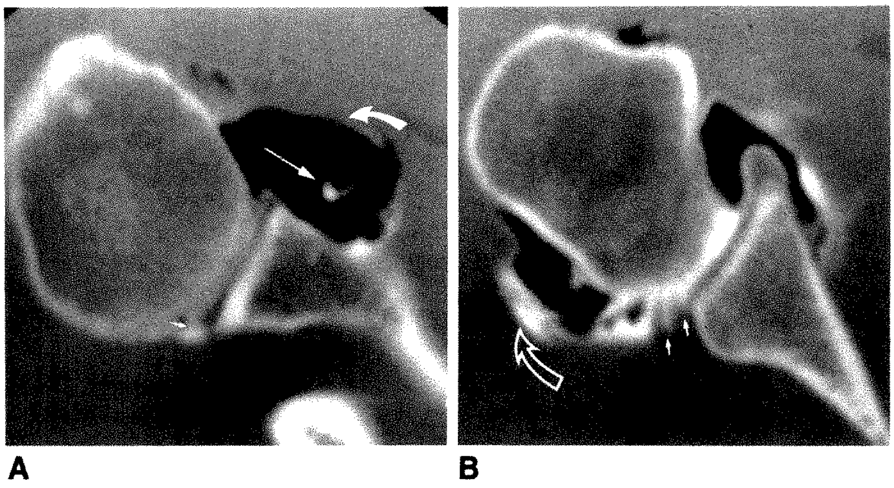

Fig. 6.—Multidirectional instability of right shoulder. Axial sections at level of subscapularis bursa (**A**) and mid-glenoid (**B**). Large subscapular bursa (*solid curved arrow*). Posteriorly, labral tears are noted (*small arrows*) as well as wide capsular tear that includes infraspinatous tendon (*open curved arrow*). Mid-glenohumeral ligament is not seen; free ridge probably is remnant of torn ligament (*long straight arrow*).

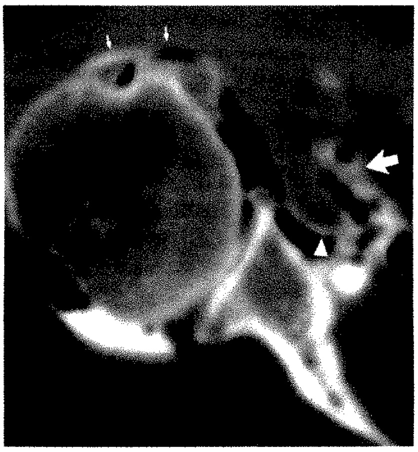

Fig. 7.—Patient with rotator cuff tear and anterior instability of right shoulder. Image at level immediately below coracoid process. Only distal and anterior end of subdeltoid bursa is seen (*small arrows*). Anterior capsule is detached from glenoid (*arrowhead*). Spilled contrast medium is under belly of subscapular muscle, and small amount is spreading under its superficial fascia (*large arrow*). Anterior labrum is severely attenuated.

Fig. 8.—Labral manifestations of degenerative disease in two patients. Axial sections of right shoulder. **A**, At inferior glenoid level. Near-total separation of glenoid labrum (*black arrows*); sclerosis of glenoid; subchondral cyst (*white arrows*). **B**, At mid-glenoid level. Anterior glenoid labrum is hypertrophied and has irregular outline (*arrow*).

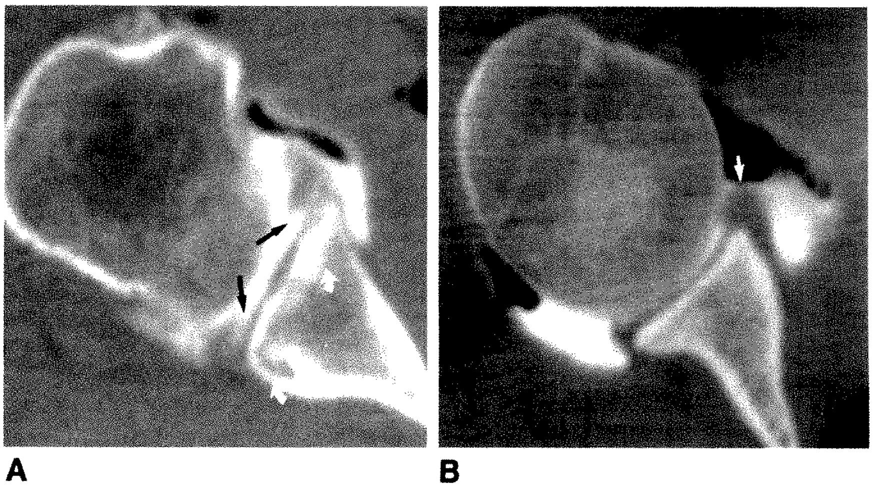

direction in four and posteriorly in one. These changes, which were associated with rotator cuff tear in one patient (fig. 7), included prominent subscapular opening and bursa (three), abnormal insertion of the capsule (four), and torn or disintegrated labrum (three). Two patients in this group underwent reconstructive surgery of the joint with good results (9 and 14 months follow-up); in two patients, CT findings were confirmed by arthroscopy. The remaining two patients did not consent to surgery; one remains symptomatic and the other has since been lost to follow-up.

Other significant findings in this group (excluding patients with rotator cuff tear) that were considered to be degenerative included an isolated labral tear and a hypertrophied labrum (fig. 8). Ten additional patients had various degrees of degenerative process including irregularity and attenuation of labrum and synovial hypertrophy. Arthroscopic examination in six patients confirmed the CT findings. In only one patient did arthroscopy detect a superficial tear of the rotator cuff (1–2 mm deep) that was not seen on arthrographic or CT examination.

Thirteen patients had a complete rotator cuff tear on the basis of conventional arthrographic findings, including two with a tuberosity fracture. There was optimal visualization on CT of the extent of supraspinatous tendon tear and fibrillation in three patients. Cuff tear extended to involve the infraspinatous tendon in two patients. In four cases a large subdeltoid bursa was opacified, and in two patients it extended to reach the anterior surface of the subscapularis muscle, presumably due to communication with subcoracoid bursa. Abnormalities of the capsular and articular structures in these patients included osteochondral fracture of the glenoid in one, stripped posterior capsule in two, enlarged subscapularis bursa in four, anterior labral tear in two, and various degrees of irregularity and attenuation of the labrum in all. Surgical correlation was available in eight patients.

Discussion

The shoulder joint is the most mobile joint in the body. This wide range of motion is based on articular components that are considerably different in size [14]. The round surface of the humeral head is about twice the size of the oval and relatively flat glenoid fossa. The fibrous capsule and the strong tendinous cuff help provide stability for this inherently unstable structure [5–14]. The function of the glenoid labrum, which has been compared with that of the menisci, has been closely related to joint stability [9–17]. Nevertheless, in the course of capsular repair procedure in patients with unstable shoulders, torn or detached glenoid labra are often removed with no ill effects on the surgical outcome. Also, experimental removal of the glenoid labrum, leaving the capsule intact, has been carried out without resultant instability [6].

Contrary to Bankart's opinion [1], recurrent dislocation is not exclusively due to dislocation following a blow to the posterior aspect of the joint. Indeed it is most often the result of a fall on an outstretched hand or abducted arm [6]. In this type of anterior dislocation, the humeral head is almost always in extreme external rotation. In this position the lax capsule wraps around the humeral head and becomes increasingly taut, thus providing resistance against the projecting force of the head by limiting the degree of external rotation. Continuing forceful external rotation is possible only if the anterior capsule gives way; this is accomplished either by rupture or detachment of the anterior glenohumeral ligaments from their insertion onto the glenoid [6]. In this position, there is virtually no contact between the humeral head and the anterior glenoid labrum; however, the labrum may detach from the glenoid along with the capsule. More often, the labrum is damaged secondarily during the outward motion of the head [6]. An isolated labral detachment is not likely unless other developmental capsular abnormalities, resulting in a lax anterior capsule, are present. Also, an unusually large opening for the subscapular bursa and a second opening of the anterior capsule further laterally have been described in association with anterior recurrent dislocation. Isolated tears of the glenoid labrum in athletes have only been recently described, and are considered to cause the syndrome of functional instability, which is due to catching of the torn labral fragment [19].

Experimental and arthrographic studies following shoulder dislocation have revealed various types of capsular injuries that both are age related and have different clinical outcomes [20–21]. Capsular detachment from the glenoid is prevalent in the young and it shows no tendency to heal; capsular rents or ruptures are most often encountered in the elderly, and unless there is also splitting of the glenohumeral ligaments, usually heal [21]. This concept explains the prevalence of the recurrent state in the young despite higher incidence of dislocation in the aged.

The most appropriate method of surgical repair of an unstable shoulder is aimed at correction of the specific problem [3]. Therefore, a detailed intraoperative evaluation of the joint has been strongly recommended. The site of the capsular insertion onto the glenoid is specifically noted to be an important but more difficult site of inspection [1–6].

In our experience, CT arthrography proved to be an accurate and relatively noninvasive method for evaluation of the capsular mechanism of the shoulder joint in patients with suspected internal joint derangement. The accuracy of this technique for the evaluation of labral lesions has been previously suggested [12, 13]. Our data are in accord with these reports with no false positives or false negatives among those who underwent surgical repair or arthroscopy. Observing the capsular changes further improved our results, with accurate diagnosis suggested in two patients who had instability in whom there was no labral tear. This concept is well established in the surgical literature [15]. Capsular pathology has been the most common abnormality found in several large series of operated unstable shoulders [4, 5], and this underscores the value of capsular evaluation in addition to the detection of other intraarticular abnormalities such as labral tears by CT arthrography.

Anatomic variations of the shoulder joint capsule may be a potential source of error in interpretation of CT findings [13]. However, some of these anatomic variations, such as formation of large recesses, may in fact be predisposing or major contributing factors to the instability of the joint [5–16]. In these patients, especially early in the course of the disorder, labral damage may be nonexistent or very minimal, and the detection of capsular anomalies may be the only clue to an accurate diagnosis. The CT arthrographic appearance of these capsular variations can easily be mastered. Also, in our experience, the small but unavoidable variation of air and positive contrast material injected has not been a problem in proper evaluation of capsular abnormalities. This is mainly because an abnormally lax capsule encompasses a larger surface whether or not it is distended. Further, the site of insertion of the capsule is usually optimally visualized independent of the degree of joint distension or the amount of contrast medium injected.

Various manifestations of the degenerative process either due to athletic activities or secondary to aging can be recognized by CT. These include various degrees of labral attenuation, thinning of the hyaline articular cartilage, and synovial hypertrophy. While these changes may not be amenable to surgical or arthroscopic treatment, two other degenerative changes that could be detected by CT, hypertrophy of the labrum and advanced separation of this structure from the glenoid articular cartilage, may have therapeutic implications. Labral hypertrophy as a manifestation of degenerative arthritis has been previously discussed in detail, and is due to proliferation of the synovium, which creeps over the glenoid labrum resulting in irregularity of the outline and an apparent enlargement of this structure [15]. Pronounced separation of the labrum from the hyaline articular cartilage of the glenoid in our patient was observed in association with other degenerative changes (fig. 8). This CT appearance is reminiscent of the nonpathologic labral separation that is mostly seen in the young adult, and may indicate this seemingly innocuous finding has the potential of becoming a progressive process. Both phenomena could cause "catching," and the abnormal labra could be removed by arthroscopic surgery.

The diagnosis of the rotator cuff tear in our patients was made on the basis of conventional arthrography. The necessity of CT examination in this group is debatable. However, the posterior extent of the tendinous tear or presence of associated capsular and labral lesions can be accurately determined by CT. The tendinous cuff tear may occasionally coexist with other pathologic changes in patients with shoulder instability [20]. Therefore the recognition and appropriate repair of capsular and labral lesions may help improve the surgical results. Our patients also had generalized laxity of their capsule and exhibited advanced degenerative changes. These changes were thought in some patients to be related to the long duration of the disorder and the lack of protective function of the tendinous cuff.

Accurate diagnosis of shoulder joint disorders can be difficult. Many articular and periarticular disorders, as well as disease processes of cervical spine, the sternoclavicular joint, and the brachial plexus, may cause similar symptoms [2]. A thorough clinical evaluation is a prerequisite in localizing the site and the cause of the disability. While conventional arthrography remains the method of choice for evaluation of rotator cuff tears, its value in evaluation of internal joint structures is limited.

CT arthrography provides excellent visualization of internal joint structures and the joint capsule, and may be a valuable tool in investigating two groups of patients. In patients with documented instability, it can determine the site and extent of labral and capsular pathology and aid in selection of the appropriate surgical procedure. A significant contribution in this regard would be in patients with transient subluxations in whom the direction of instability might not be totally clear and multidirectional instability might exist. The recognition of this latter disorder is a particularly important factor in selection of an appropriate surgical approach. Otherwise, surgical failure is likely. In this regard, patients with rotator cuff tear may also benefit from this procedure. In patients with suspected instability who may present with persistent but nonspecific symptoms such as pain, the clinical manifestations may resemble those of other intraarticular disorders such as isolated labral tear and degenerative disease. It is clear that the treatment approach for these patients varies. While unstable joints require surgical repair, others may benefit from the less invasive procedure of arthroscopic surgery.

REFERENCES

1. Bankart ASB. The pathology and treatment of recurrent dislocation of the shoulder joint. *Br J Surg* **1938**;26:23–29
2. Rowe CR, Zarins B. Recurrent transient subluxation of the shoulder. *J Bone Joint Surg [Am]* **1981**;63:863–871
3. Protzman RR. Anterior instability of shoulder. *J Bone Joint Surg [Am]* **1980**;62:909–918
4. Rowe CR, Patal D. The Bankart procedure. A long-term end-result study. *J Bone Joint Surg [Am]* **1978**;60:1–16
5. Moseley HF, Overgaard B. The anterior capsular mechanism in recurrent anterior dislocation of shoulder Morphological and clinical studies with special reference to the glenoid labrum and the gleno-humeral ligaments. *J Bone Joint Surg [Br]* **1962**;44:913–927
6. Townley CO. The capsular mechanism in recurrent dislocation of the shoulder. *J Bone Joint Surg [Am]* **1950**;32:370–380
7. DuToit GT, Roux D. Recurrent dislocation of the shoulder. A twenty-four year study of the Johannesburg stapling operation. *J Bone Joint Surg [Am]* **1956**;38:1–12
8. Neer CS II, Foster CR. Inferior capsular shift for involuntary inferior and multidirectional instability of the shoulder. A preliminary report. *J Bone Joint Surg [Am]* **1980**;62:897–908
9. El-Khoury GY, Albright JP, Abu-Yousef MM, Montgomery WJ, Tuck SL. Arthrotomography of the glenoid labrum. *Radiology* **1979**;131:333–337
10. Braunstein EM, O'Connor G. Double contrast arthro-tomography of the shoulder. *J Bone Joint Surg [Am]* **1982**;64:192–195
11. Kleinman PK, Kanzaria PK, Goss TP, Pappas AM. Axillary arthrotomography of the glenoid labrum. *AJR* **1984**;141:993–999
12. Shuman WP, Kilcoyne RF, Matsen FA, Rogers JV, Mack LA. Double-contrast computed tomography of the glenoid labrum. *AJR* **1983**;141:581–584
13. Deutch AL, Resnick D, Mink J, et al. Computed and conventional arthrotomography of the glenohumeral joint: normal anatomy and clinical experience. *Radiology* **1984**;153:603–609
14. Williams PL, Warwick R. In: *Gray's anatomy*, 36th ed. Philadelphia: Saunders, **1980**:456
15. DePalma AF. *Surgery of the shoulder*, 3d ed. Philadelphia: Lippincott, **1983**:51–63, 211–241
16. Turkel SJ, Panio MW, Marshal JL, Girgis FG. Stabilizing mechanisms preventing anterior dislocation of the gleno-humeral joint. *J Bone Joint Surg [Am]* **1981**;63:1208–1217
17. Rothman RH, Marvel JP, Heppenstall RB. Anatomic consideration in glenohumeral joint. *Orthop Clin North Am* **1975**;6:341–352
18. Goldman AB, Ghelman B. The double contrast shoulder arthrogram. A review of 158 studies. *Radiology* **1978**;127:655–663
19. Pappas AM, Goss TP, Kleinman PK. Symptomatic shoulder instability due to lesions of the glenoid labrum. *Am J Sports Med* **1983**;11:279–288
20. Reeves B. Arthrography of the shoulder. *J Bone Joint Surg [Br]* **1966**;48:424–435
21. Reeves B. Experiments on the tensile strength of the anterior capsular structures of the shoulder in man. *J Bone Joint Surg [Br]* **1968**;50:858–865

Percutaneous Transluminal Angioplasty of the Lower Abdominal Aorta

Normand Charlebois[1]
Guy Saint-Georges[1]
Gilles Hudon[2]

Percutaneous transluminal angioplasty (PTA) of the lower abdominal aorta was performed in 14 patients aged 29-66 years (mean, 50). The disease was largely isolated to the distal aorta in this group. There were 13 women and 1 man; all were heavy smokers. Initial success, defined as improved or subsided clinical symptoms, improved ankle/arm indices, and improved angiogram, was achieved in all but one patient who thrombosed at the puncture site. At a mean follow-up period of 16 months (range, 1-58), a persistent beneficial effect was maintained in all patients. These results suggest that PTA is a safe alternative to surgery in patients with signs and symptoms of aortoiliac disease secondary to a significant but short stenotic segment of the lower abdominal aorta.

In 1980, Grollman et al. [1] and Velasquez et al. [2] each reported a successful percutaneous transluminal angioplasty (PTA) of the lower abdominal aorta in one patient. Subsequently, Heeney et al. [3] successfully dilated localized stenoses of the lower abdominal aorta in six women. However, these series are small, and no long-term follow-up of patients with lower abdominal aortic dilatation by PTA exists. We retrospectively analyzed the results of 14 consecutive patients who underwent PTA for discrete stenoses of the lower abdominal aorta since 1980.

Materials and Methods

Patient Population

Over 5 years (1980–1985), angiographic evaluation for peripheral vascular disease revealed discrete and significant lower abdominal aortic stenosis in 14 patients aged 29–66 years (mean, 50). There were 13 women and one man (the youngest). All patients were heavy smokers (>25 cigarettes/day), had bilateral intermittent claudication involving primarily the buttocks and the thighs, and were acceptable surgical candidates. The 29-year-old man had a family history of hyperlipidemia (type II-A) and smoked over 90 cigarettes per day. A 45-year-old diabetic woman with severe small-vessel disease had sustained a stroke a few years earlier.

Initial Noninvasive and Angiographic Evaluation

Baseline ankle/arm index determination or Doppler sonography (velocity curve waveform analysis) were done in all but two patients. All patients had a baseline abdominal aortogram and lower limb arteriography.

Most stenotic segments were severe (≥80%) and very short, mean length being only 8 mm (range, 5–13 mm). Three were situated within 10 mm and three others within 20 mm of the bifurcation. All other lesions were infrarenal and within 42 mm of the aortoiliac bifurcation. The dimension of the contrast-filled lumen of the aorta 10 mm above the stenosis appeared small with a mean value of 12 mm (range, 10–18 mm). The highest value, 18 mm, was found in the only male of this series. Eleven patients had normal runoff arteriograms, two patients had mild peripheral arterial disease, and one patient had severe small-vessel disease.

Received May 21, 1985; accepted after revision September 18, 1985.

[1] Department of Radiology, Université de Montreal and Hôpital du Sacré-Coeur, 5400, Blvd. Gouin West, Montreal, P.Q., Canada, H4J 1C5. Address reprint requests to N. Charlebois.

[2] Department of Radiology, Université de Montreal and Institut de Cardiologie, Montreal, P. Q., Canada.

AJR 146:369–371, February 1986
0361-803X/86/1462-0369
© American Roentgen Ray Society

TABLE 1: **Systolic Pressure Gradient and Ankle/Arm Indices before and after PTA at End of Follow-up**

Case No.	Systolic Gradient		Ankle/Arm Indices		Follow-up (months)
	Before PTA	After PTA	Before PTA	After PTA	
1	31	11	0.30/0.25	0.92/1.0	45
2	27	0	0.37/0.41	0.71/0.64	3
3	30	0	0.80/0.80	0.95/1.0	20
4	...	...	...	0.91/0.83	8
5	64	0	0.79/0.79	1.0/0.91	7
6	74	0	0.56/0.53	0.56/0.86	3
7	45	0	0.46/0.46	0.91/0.91	1
8	...	12	...	...	6
9	...	12	0.57/0.56	0.45/0.9	3
10	60	0	...	...	6
11	65	25	Doppler*	1.0/1.0	42
12	41	10	0.84/0.78	0.96/0.96	22
13	25	10	0.71/0.64	1.0/0.86	1
14	72	12	Doppler*	1/0/1.0	58

* Patient had Doppler sonography only.

Technique

PTA was performed by the femoral route in all cases. The morning of the procedure, each patient received 650 mg of acetylsalicylic acid. Once the lesion was crossed, 5000 IU of heparin was given intraarterially.

Balloon size was selected by taking the measurement of the aorta above the stenosis on the angiogram. A single 8-mm balloon was used in two patients, 9-mm in four, 10 mm in two, and 12-mm in five patients. In one patient, two side-by-side 7- and 9-mm balloons were used simultaneously. The end-point of the PTA was reached when the balloon was easily inflated without any residual deformation. Pressure gradients were obtained before and after PTA in all but one patient. The procedure was ended if the pressure gradient was lower than 50% of its initial value. Postinterventional antiplatelet therapy consisted of 50 mg of dipyridamole (Persantin) twice a day for 3 months and 650 mg/day of coated acetylsalicylic acid for life.

Follow-up Examinations

Ankle/arm index determination and/or Doppler sonography were done within 2 days of PTA and were repeated every 3–6 months for the first year, every 6 months for the second year, and as necessary thereafter.

Results

Immediate Results (table 1)

Before PTA, the systolic gradients ranged between 25 and 74 mm Hg (mean, 47 mm Hg). After PTA, the pressure gradients were reduced to 0–25 mm Hg (mean, 13 mm Hg). An immediate postprocedure angiogram was done in all cases, but we relied more on measurement of postangioplasty pressure gradient for assessing success or failure of the angioplasty than on the morphologic result, which sometimes was inconclusive.

Complications

There were only two complications. One patient (case 9) developed a right iliofemoral thrombosis 3 hr after completion on an initially successful aortic PTA. An uneventful local thrombectomy was subsequently performed, and she was discharged well a few days later. Three months after PTA this patient remains asymptomatic, although her ankle/arm index is abnormal (0.45) on the side of the thrombectomy. A second patient (case 14) had a rupture of the PTA balloon. The ruptured balloon was removed without problems.

Late Results (table 1)

Thirteen of the 14 patients remain asymptomatic. Two patients asymptomatic after 6 months did not have noninvasive tests. Eleven patients are asymptomatic with normal tests at a mean of 16 months (range, 1–58) after PTA. One patient developed intermittent claudication within 3 months of PTA and has an abnormal ankle/arm index at rest and after exercise. No follow-up angiogram is available.

Discussion

PTA has gained acceptance within the medical community, but most published studies still concern coronary, renal, or peripheral vessels. PTA of the abdominal aorta has been reported only sporadically [1–7]. Our study identifies a subset in the large population of atherosclerotic patients presenting with aortoiliac disease that is characterized by a relatively young age at clinical presentation, an almost exclusive female distribution, and a universal smoking habit. The only male was hyperlipidemic and the youngest member and heaviest smoker of the group.

These patients all had a discrete aortic stenosis located slightly above the aortoiliac bifurcation, with a normal or near-normal distal runoff. All but one had a small aorta which, however, could not be considered to be hypoplastic, as defined by Cronenwett and Garrett [8]. These patients were all succesfully treated by PTA, with good short- and long-term results (fig. 1). The mean duration of the follow-up is 16 months, during which time 93% of the patients are symptom free. Fourteen percent (two patients) had abnormal noninva-

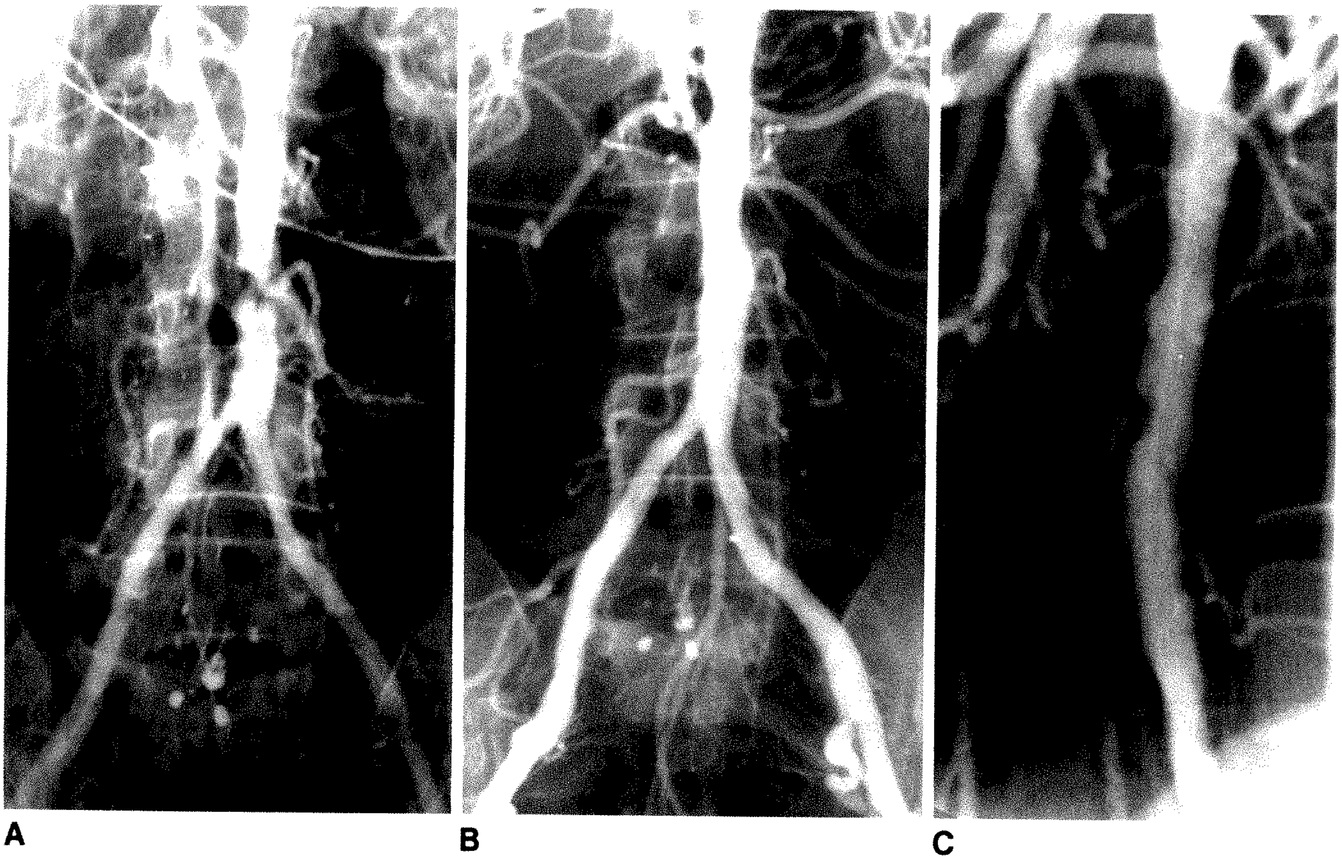

Fig. 1.—**A**, Abdominal aortogram before percutaneous transluminal angioplasty (PTA). Stenosis (≥90%) immediately below origin of inferior mesenteric artery. **B**, Abdominal aortogram 12 months after PTA. No residual stenosis; aortic coronal diameter at site of previous arterial dilatation is 17 mm compared with 12 mm for above infrarenal segment, due to incorporation into arterial lumen of long left lateral wall dissection seen on immediate postdilatation angiogram. **C**, After PTA. Slight narrowing (≤25%) at site of dilatation; inferior mesenteric artery stenotic (50% at origin) but patent.

sive vascular tests at the end of the follow-up period; only one of these is symptomatic.

Before the advent of PTA, such patients underwent surgery. Aortic PTA seems an acceptable alternative to bypass surgery, especially if the absence of mortality, the minimal morbidity, a low complication rate, a lack of anesthetic risk, a lack of impotence risk in men, a reduced cost of treatment, and a very good patient acceptance are considered. Further, failure of angioplasty, either early or late, does not prevent subsequent surgical bypass. Our results demonstrate that in patients with a short stenosis in a nonaneurysmal abdominal aorta, dilatation by PTA is probably the treatment of choice.

ACKNOWLEDGMENTS

We thank Martial Bourrassa and Jean-Lucien Rouleau for reviewing the manuscript.

REFERENCES

1. Grollman JH, Delvicario M, Mittal AK. Percutaneous transluminal abdominal aortic angioplasty. *AJR* **1980**;134:1053–1054
2. Velasquez G, Castaneda-Zuniga W, Formanek A, et al. Nonsurgical aortoplasty in Leriche syndrome. *Radiology* **1980**;134:359–360
3. Heeney D, Bookstein J, Daniels E, Warmath M, Horn J, Rowley W. Transluminal angioplasty of the abdominal aorta. *Radiology* **1983**;148:81–83
4. Hudon G, Bonan R, Hébert Y. Abdominal aortic angioplasty: a case report with angiographic follow-up. *J Can Assoc Radiol* **1982**;33:262–264
5. Saint-Georges G, Mercier C. Sténose de l'aorte abdominale: dilatation percutanée par cathéter de Gruntzig. *Union Med Can* **1983**;112:73–76
6. Kumpe DA. Percutaneous dilatation of an abdominal aortic stenosis: three-balloon-catheter technique. *Radiology* **1981**;141:536–538
7. Ingrisch H, Stiegler H, Rath M. Non-operative treatment of infrarenal aortic stenoses by catheter dilatation. *Rontgenpraxis* **1983**;36:363–367
8. Cronenwett JL, Garrett HE. Arteriographic measurement of the abdominal aorta, iliac, and femoral arteries in women with atherosclerotic occlusive disease. *Radiology* **1983**;148:389–392

Aortic Rupture: A Complication of Transluminal Angioplasty

Thomas Berger,[1] Reingard Sörensen,[1] and Jochen Konrad[2]

Focal, concentric, hemodynamically significant stenoses of the infrarenal abdominal aorta are reported to be successfully treated by percutaneous transluminal angioplasty (PTA) [1–5]. In dilating a large-diameter vessel such as the aorta, however, there is a risk of overstretching the arterial wall at a lower pressure than expected [1, 6]. As yet, no case of an aortic rupture by PTA has been described in the literature. We report a case of late aortic rupture after an initially successful treatment of an infrarenal aortic stenosis.

Case Report

A 59-year-old woman with diabetes mellitus and a 12-year history of bronchial asthma had claudication in both legs 8 weeks before admission. Her walking distance was limited to about 200 m. Angiography revealed a concentric calcified plaque causing a stenosis of the abdominal aorta 4 cm above the aortic bifurcation (fig. 1A). There also was a stenotic segment involving the right common iliac artery, an occlusion of the right superficial femoral artery, and an occluded right anterior tibial artery.

PTA of the aorta and the right common iliac artery was performed with two 9-French Medi-Tech catheters with 8 mm × 4 cm balloons. The balloons were placed side by side in the stenotic segment (kissing balloon technique). Dilatation was performed by simultaneous manual inflation with two 10-cm^3 syringes. The pressure was slowly increased, and the balloons were inflated three times until the patient reported mild abdominal discomfort. The procedure was terminated at that point. Angiography showed the dilated aortic lumen and the flow into both legs was improved (fig. 1B). There was no visible dissection of the vascular wall and no contrast extravasation.

Eight hours after the procedure, the patient complained of increasing abdominal pain and developed signs of hypovolemic shock. The lower extremities showed no sign of ischemia. Immediate surgical

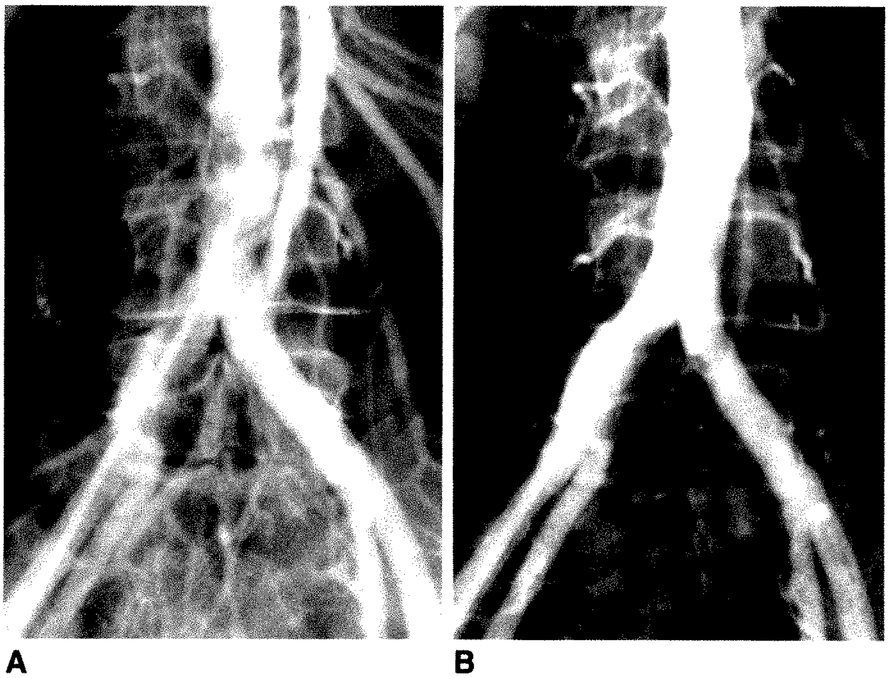

Fig. 1.—A, Calcified plaques and concentric stenosis of distal abdominal aorta. B, Dilated lumen of distal abdominal aorta after angioplasty.

Received July 15, 1985; accepted after revision October 10, 1985.

[1] Department of Diagnostic Radiology, Free University of Berlin, Klinikum Steglitz, Hindenburgdamm 31, 1000 Berlin 45, FRG Germany. Address reprint requests to R. Sörensen.

[2] Department of Surgery, Free University of Berlin, Klinikum Steglitz, 1000 Berlin 45, FRG Germany.

AJR 146:373–374, February 1986 0361–803X/86/1462–0373 © American Roentgen Ray Society

exploration revealed a major retroperitoneal hemorrhage. There was a 3-cm tear of the aortic wall at the area of the segment treated by PTA. The laceration was covered by the adventitial layer, which was partially disrupted posteriorly and had allowed hemorrhage into the retroperitoneal space. Two rocklike spiculated calcified arteriosclerotic plaques could be identified within the wall of the aorta. They had been partially forced through the vessel wall by the balloon catheters. Thrombectomy and removal of the plaques was followed by a repair of the aortic wall with a venous patch graft. The patient recovered and was discharged after 8 days.

Discussion

Concentric, focal, hemodynamically significant stenosis of the infrarenal abdominal aorta is believed to be treated best by PTA, whereas diffuse atheromatous and long obstructive abdominal aortic lesions are thought to be surgically treated lesions [1, 3]. The law of Laplace indicates that the danger of overstretching and rupturing the arterial wall increases with the diameter of the vessel treated. Pain during dilatation is considered to be an indicator for overstretching the vascular wall [6]. Some investigators consider calcified plaques of the aortic wall an absolute contraindication for PTA [7], whereas others do treat them by PTA [3, 5, 8]. Accurate characterization of an atheromatous lesion seems to remain the most important factor in performing PTA successfully [8, 9]. Experience of the operator and appropriate instrumentation are further prerequisites for safe and successful intervention. In the reported case, an eccentric calcified aortic stenosis was treated by PTA and showed an immediate radiographic success, even though rupture had already taken place. We conclude that eccentric and calcified lesions of large-diameter vessels should be treated with extreme caution and should definitely not be overdilated.

REFERENCES

1. Heeney D, Bookstein J, Daniels E, Warmath M, Horn J, Rowley W. Transluminal angioplasty of the abdominal aorta. *Radiology* **1983**;148:81–83
2. Haynes IG, Simon J, West RJ, Hamer JD. Idiopathic retroperitoneal fibrosis with occlusion of the abdominal aorta treated by transluminal angioplasty. *Br J Surg* **1982**;69:432–433
3. Hudon G, Bonan G, Hébert Y. Abdominal aortic angioplasty: a case report with angiographic follow-up. *J Can Assoc Radiol* **1983**;33:262–264
4. Velasquez G, Castaneda-Zuniga WR, Formanek AG, et al. Nonsurgical aortoplasty in Leriche syndrome. *Radiology* **1980**;134:359–360
5. Grollman JH Jr, Del Vicario M, Mittal AK. Percutaneous transluminal abdominal aortic angioplasty. *AJR* **1980**;134:1053–1054
6. Colapinto RF, Harries-Jones EP, Johnston KW. Percutaneous transluminal dilatation and recanalization in the treatment of peripheral vascular disease. *Radiology* **1980**;135:583–587
7. Motarjeme A, Keifer JW, Zuska AJ. Percutaneous transluminal angioplasty of the iliac arteries: 66 experiences. *AJR* **1980**; 135:937–944
8. Simonetti G. Iliac artery rupture during transluminal angioplasty. *AJR* **1984**;142:1295
9. Simonetti G, Rossi, P, Passariello R, et al. Iliac artery rupture: a complication of transluminal angioplasty. *AJR* **1983**;140:989–990

Experimental Enhancement of Drug Uptake Using Short-Term Flow Occlusion: A Comparison of Balloon and Tourniquet Techniques

David M. Woods[1, 2]
Kenneth C. Wright[1]
C. Humberto Carrasco[1]
Sidney Wallace[1]

Three groups of dogs, four per group, were used to examine the safety of short-term arterial flow occlusion and potential benefits of balloon and/or tourniquet occlusion-infusion techniques. In part 1, local plasma gases and pH were monitored during a 1-hr period of vascular occlusion. Tourniquet occlusion was found to significantly ($p = 0.01$) lower pO_2. In part 2, local muscle and venous blood samples were obtained during and after a 30-min intraarterial infusion of floxuridine (FUDR). A tourniquet was added to try to eliminate collateral circulation. Local FUDR concentration was increased by 1.3 times in muscle and 19.6 times ($p < 0.01$) in ipsilateral femoral vein serum when a tourniquet was added to arterial balloon occlusion-infusion. In addition, the combination of the two occlusion techniques produced a 4.1-fold reduction ($p < 0.05$) in systemic venous FUDR levels during infusion when compared to balloon occlusion.

Intraarterial chemotherapy was introduced to obtain higher drug concentrations with the hope of producing greater tumoricidal effects in a limited anatomic area. Since its initial application to liver tumors in 1950 [1, 2], the clinical results have been encouraging but remain controversial. In addition to drug concentration, the other variables that affect drug uptake by the tumor are the drug-tissue contact time and the changes in tumor permeability to the chemotherapeutic agent, perhaps produced by hypoxia [3].

Drug-tissue contact time can be increased if the arterial flow is decreased through peripheral embolization before infusion, through chemoembolization (combining embolic material with the drug), or through proximal occlusion by either surgical ligation or balloon catheter occlusion. Although Anderson et al. [4] found that tissue drug levels dramatically increased when balloon occlusion was added to intraarterial infusion, collateral circulation can reduce or eliminate this benefit in certain situations. The use of a tourniquet, however, may eliminate this problem in the extremities. Since this procedure is associated with additional risks such as limb ischemia, both safety and efficacy must be shown before clinical application.

This experimental study was designed to examine the metabolic consequences of several occlusive techniques and to check for significant enhancement of drug uptake. Dogs were used to compare the risks and benefits of balloon occlusion, of tourniquet occlusion, and of combined balloon and tourniquet occlusion. Floxuridine (FUDR, Roche) was the agent selected for infusion because of its availability, relatively low cost, and ease of assay.

Subjects and Methods

There were two major parts in this study. Part 1 evaluated the flow and possible ischemic changes produced by balloon occlusion, by tourniquet occlusion, and by a combination of the two methods. Part 2 compared local venous, systemic venous, and local tissue FUDR levels achieved by the three occlusion techniques.

Twelve dogs were used, four dogs in each group. One hind limb of each animal was used for part 1 and the other for part 2. All dogs were fasted for 18 hr before each procedure.

Received June 3, 1985; accepted after revision October 10, 1985.

This work was supported in part by the John S. Dunn Research Foundation and the George Alfred Cook Memorial Fund.

[1] Department of Diagnostic Radiology, University of Texas M. D. Anderson Hospital and Tumor Institute, 6723 Bertner Ave., Houston, TX 77030. Address reprint requests to K. C. Wright.

[2] Present address: Department of Radiology, St. Joseph's Hospital, Hamilton, Ontario, Canada L8N 1Y4.

AJR 146:375-380, February 1986
0361-803X/86/1462-0375
© American Roentgen Ray Society

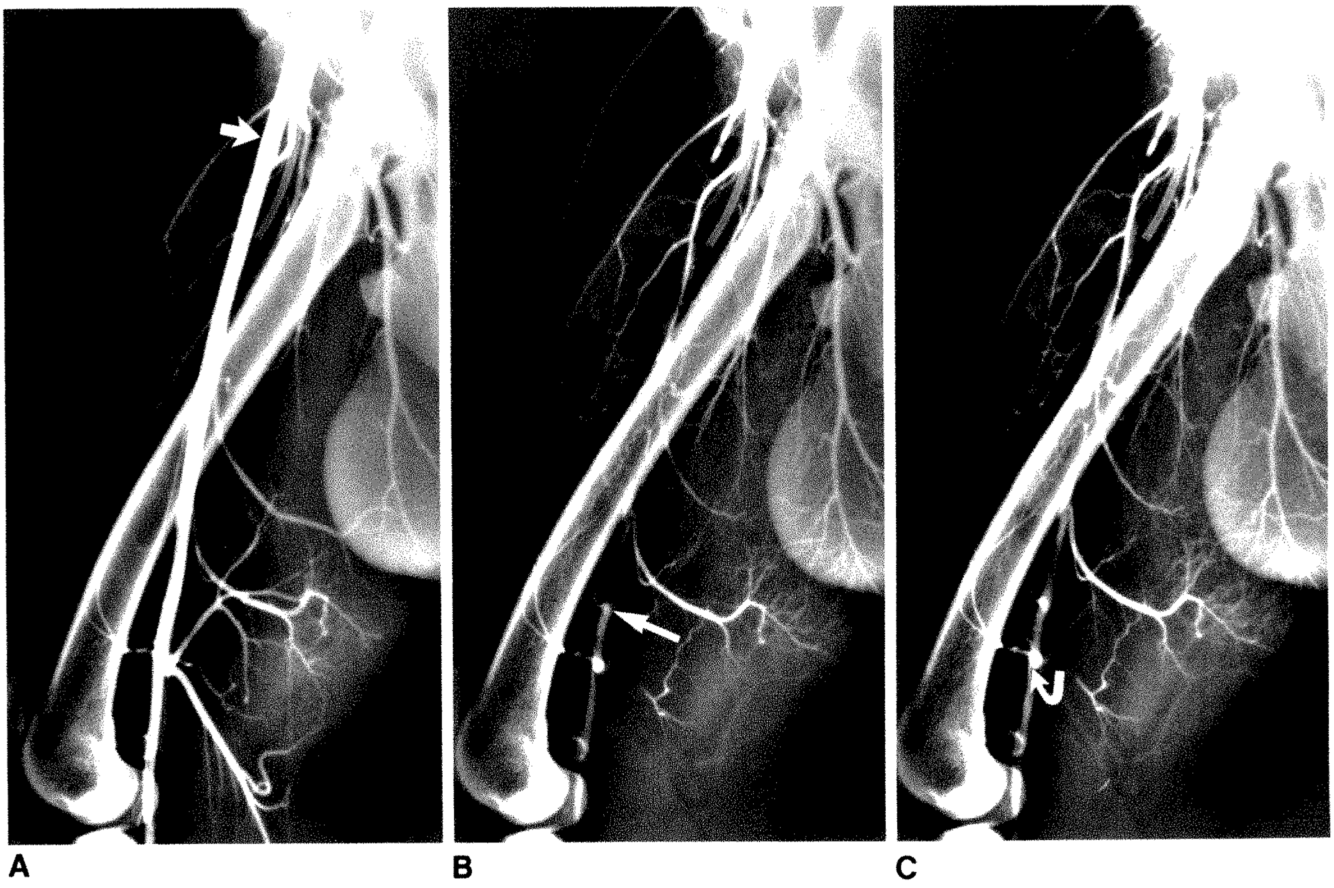

Fig. 1.—Balloon occlusion. **A**, Angiogram shows position of noninflated balloon (*arrow*) and femoral venous catheter. **B** and **C**, Arteriograms show immediate postinflation collateral circulation and reconstitution of distal superficial femoral artery (*arrows*).

Anesthesia was induced with sodium pentobarbital (Nembutal, 30 mg/kg) and maintained with a mixture of halothane, oxygen, and nitrous oxide. Under fluoroscopic monitoring, a 5-French polyethylene catheter (Cook) was placed in a superficial femoral artery (SFA), and a second 5-French catheter was positioned in the ipsilateral external iliac artery via the carotid approach. A third 5-French catheter was placed via a jugular vein into the superficial femoral vein of the same limb 2 cm beyond the site of tourniquet or balloon occlusion to collect venous blood samples. A 5-French Swan-Ganz balloon catheter (Edwards) was placed in the femoral artery to provide the balloon occlusion-infusion. A pneumatic tourniquet (Kidde OR pediatric tourniquet, Walter Kidde) attached to a sphygomomanometer produced tourniquet occlusion pressures of 240–280 mm Hg.

Part 1

After anesthesia and catheter positioning were achieved, baseline arterial and venous blood samples were drawn for analysis of plasma gases (pO_2, pCO_2, pH, and $pHCO_3$) and creatine phosphokinase (pCPK). A preocclusion arteriogram was performed. Each dog then underwent a 1-hr period of balloon occlusion, tourniquet occlusion, or both. During this interval, femoral venous samples were obtained at 1, 3, 5, 15, 30, and 60 min for blood gas determinations. After the 1-hr period, arteriograms were made both above and below the site of obstruction. Systemic venous blood samples were drawn from a jugular vein at 24 and 48 hr to monitor for changes in pCPK levels. In three dogs, an electromagnetic flow probe (Narco Scientific) was placed around the superficial femoral artery 2 cm below the site of obstruction so that the flow rates produced by each of the occlusion techniques could be examined.

Part 2

At least 10 weeks after the flow study, the same dogs were anesthetized and the catheters placed in the same manner as before except in the opposite limbs. After balloon or tourniquet occlusion was applied, either separately or in combination, a 30-min infusion of FUDR (5 mg/kg) was administered using a Harvard syringe pump at a rate of 2 ml/min. At the end of the infusion the occlusion was released. Drug levels in the femoral venous blood of the occluded limbs were checked at 0, 1, 3, 5, 10, 15, 30, and 60 min. Drug levels were also checked in hamstring muscles by wedge biopsy (1 g/sample) at 30 and 60 min. To check for drug spillover, systemic (jugular vein) FUDR determinations were made at 15, 30, and 60 min. Because constant occlusion time, total drug dose, drug concentration, and infusion time were maintained, the results of the three occlusion-infusion techniques could be compared.

Drug analysis was carried out using a Waters Associates Model 204 liquid chromatograph equipped with a variable-wave-length ultraviolet detector operating at 268 nm. Separation was done with a Waters Associates μBondapak/C_{18} column (30 cm × 3.0 mm I.D.) with a mobile phase of filter-deionized water flowing at a rate of 2 ml/min.

The standard curve (peak area vs. drug concentration) was prepared from FUDR obtained from the Drug Development Branch of the National Cancer Institute. The curve was linear over a concentration range of 0.1–1000 μg/ml.

Muscle specimens were homogenized in saline and centrifuged: The supernatant was then treated as was the plasma. Samples were ultrafiltered through CF-25 membrane cones (Amicon) for 1 hr at 120× gravity in a Sorvall RC2-B centrifuge and then applied to the column. Peak areas were determined by a Varian CDS 111 integrator and a model 9176 recorder. Results were compared statistically using Student's *t*-test.

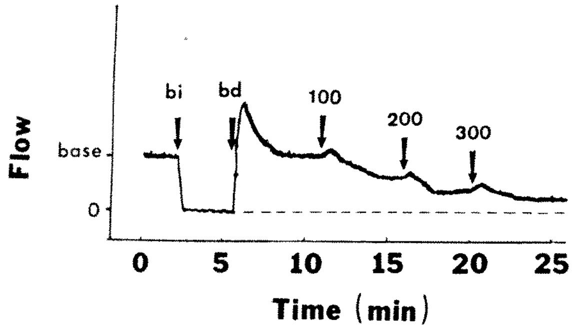

Fig. 2.—Femoral artery blood flow vs. time. After balloon inflation (bi), flow rate immediately below balloon drops to zero. After balloon deflation (bd), there is return to baseline. Successive tourniquet pressures of 100, 200, and 300 mm Hg fail to eliminate flow in superficial femoral artery.

Results

Part 1

Arteriograms showed that collateral circulation instantaneously developed around the balloon-occluded SFA (fig. 1). In addition, blood flow in the SFA persisted despite a tourniquet inflation pressure of more than 320 mm Hg, even though a palpable pulse was obliterated at 160 mm Hg; blood flow reached zero only with balloon obstruction (fig. 2).

After the 1-hr occlusion had been achieved by each of the three different methods, only one dog developed mild leg swelling, which lasted for 3–4 days. This animal had undergone tourniquet occlusion. All dogs had elevated pCPK levels throughout the 48 hr after occlusion; the highest level was 10 times the preocclusion measurement. Except for the one case of transient leg swelling, no change in appearance or function of the dogs' limbs was observed in the 10-week follow-up period. Three of the 12 dogs had arteriograms made of the limb after this interval, and no arteriographic sequelae were found.

Figure 3 shows the changes of the plasma gas levels in the superficial femoral vein (SFV) of the occluded limb. SFV oxygenation dropped by 27% with balloon occlusion, 47% with tourniquet occlusion, and 45% with combination occlusion (fig. 3A). Both tourniquet-occlusion groups exhibited a significantly larger drop in the pO_2 ($p = 0.01$) than did the balloon-only group. There was no significant difference among the three groups in venous carbon dioxide level (pCO_2), hydrogen ion level (pH), or bicarbonate level ($pHCO_3$) (fig. 3B).

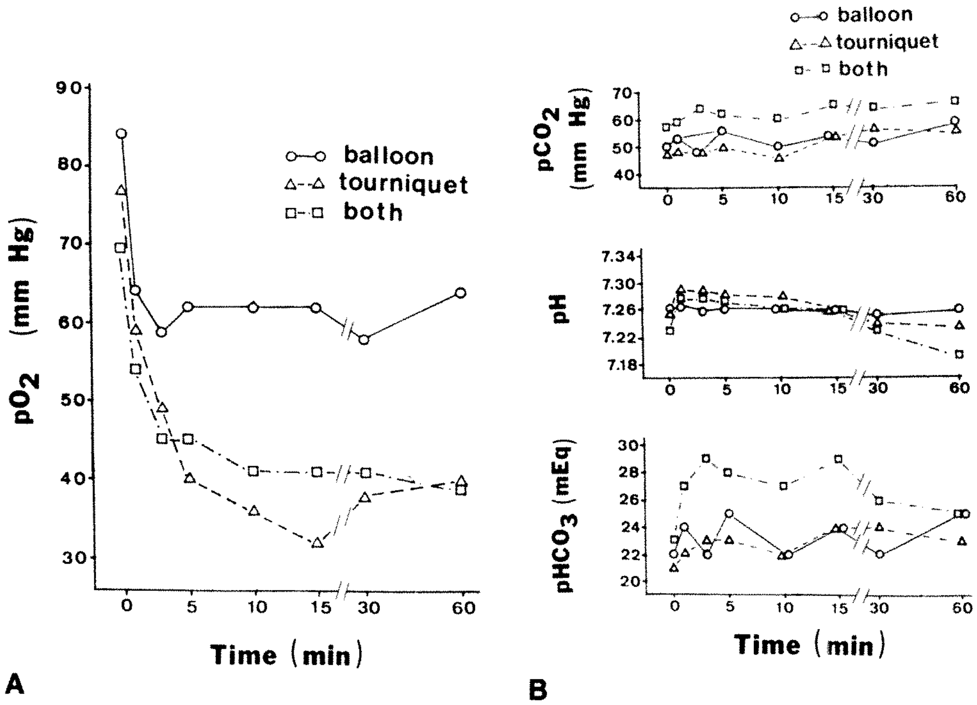

Fig. 3.—**A**, Local femoral vein oxygenation during 1-hr occlusion. **B**, Local femoral vein pCO_2, pH, and $pHCO_3$ changes during 1-hr occlusion.

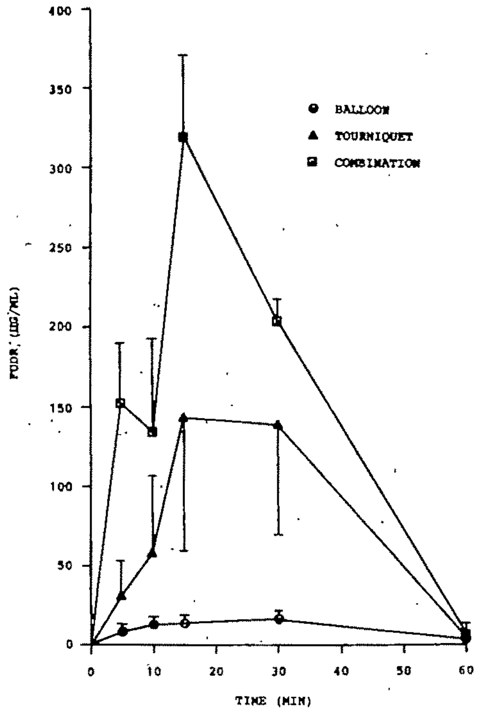

Fig. 4.—Local femoral vein drug levels during and after 30-min arterial infusion with concurrent balloon, tourniquet, or combination occlusion. Each point represents mean ± SE of four dogs.

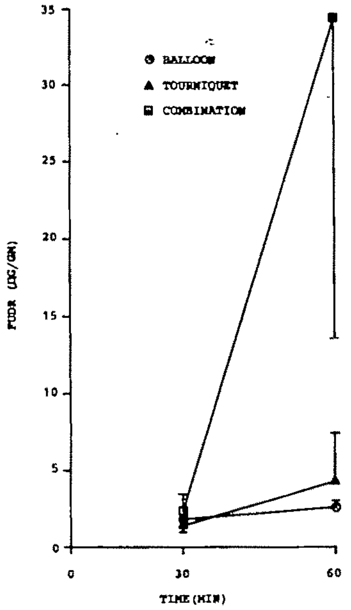

Fig. 5.—Local tissue (skeletal muscle) FUDR levels after 30-min arterial infusion with simultaneous balloon, tourniquet, or combination occlusion. Each point represents mean ± SE of four dogs.

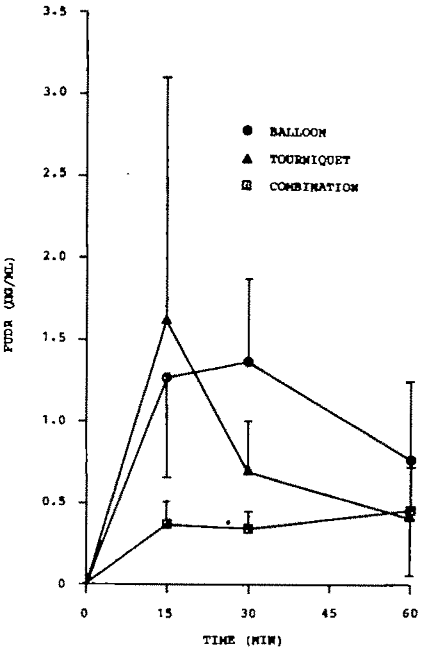

Fig. 6.—Systemic FUDR levels during and after 30-min arterial infusion with concurrent balloon, tourniquet, or combination occlusion. Each point represents mean ± SE of four dogs.

The levels of pCO_2 and $pHCO_3$ appeared to increase gradually in all groups during the occlusion.

Part 2

The femoral vein FUDR levels in all three groups peaked between 15 and 30 min and, by 1 hr (30 min after the completion of the infusion), had returned to almost zero (fig. 4). The combination occlusion produced local venous drug levels that were 2.2 times greater than those produced by the balloon. Statistically, local femoral vein FUDR levels achieved during balloon-occlusion were significantly lower ($p < 0.05$) than those produced using tourniquet alone, and drug levels produced by infusion during combination occlusion were significantly greater than those obtained with the balloon ($p < 0.01$) or tourniquet ($p < 0.05$) techniques.

Muscle FUDR levels are depicted in figure 5. They are similar for all three techniques immediately following administration. However, 30 min after FUDR infusion, local tissue levels produced by the combination occlusion were on the average 9.1 times greater than those produced by the tourniquet occlusion and 13.4 times greater than those produced by the balloon occlusion.

Drug infusion during balloon occlusion resulted in systemic FUDR levels that were similar to those achieved with the tourniquet alone, but significantly greater ($p < 0.05$) than those produced by the combination occlusion technique (fig. 6). Thirty minutes after releasing the arterial occlusion, jugular vein FUDR levels were similar.

Discussion

Several attempts have been made in both experimental [5, 6] and clinical [7–9] situations to enhance the benefits of intraarterial chemotherapy through occlusion. Karakousis et al. [5] showed a 40-fold increase in muscle uptake of drug after tourniquet occlusion. They found no difference between results produced by simple intraarterial infusion and those produced by infusion after femoral artery occlusion. This finding differs from the 7- to 9-fold increased muscle uptake after balloon occlusion that was demonstrated by Anderson et al. [4]. In the experiment of Karakousis et al. [5], however, only one muscle sample was obtained, at 1 hr after the infusion was completed. In the work of Anderson et al. [4], the differences were most pronounced during the infusion; within 30 min after the infusion was completed, these differences were small. Both the balloon [8] and tourniquet [7] infusion methods have been used clinically, but no controlled studies have been reported.

Because of a previous study, which showed that balloon occlusion-infusion is dramatically superior to intraarterial and intravenous infusion [4], simple intraarterial infusion without occlusion was not studied.

There are few guidelines for the clinical application of tourniquets [10, 11]. For provision of a bloodless surgical field in extremities, recommended inflation pressures are 300 mm Hg in the arm and 500 mm Hg in the thigh for periods of less than 1 and 1.5 hr, respectively [11]. Potential complications include ischemia, peripheral nerve injury, and local skin necrosis. Results from part 1 of this study, however, show that all three occlusion techniques can be applied to the canine hind limb without any serious long-term clinical consequences. Despite the use of tourniquet pressures that were at least 50% higher than systolic pressure, neither acidosis nor serious venous hypoxemia developed. Although pCPK levels were elevated in all dogs, this finding may be related to the fact that all animals underwent a surgical procedure for catheter introduction.

As shown in figure 1, collateral circulation can begin immediately after occlusion. Some sites of circulation can be demonstrated angiographically, whereas others such as interosseous vessels are not demonstrated. Soft tissue, muscle, and bone provide enough resistance to externally applied pressure to allow maintenance of some flow in major vessels (fig. 2). Use of a tourniquet resulted in significantly lower femoral vein pO_2 (fig. 3A), indicating there was less collateral circulation to the lower leg. This is supported by the angiograms, but is not surprising since sudden occlusion of the femoral artery has been shown to decrease limb blood flow to 35% of resting flow with rapid recovery to 60% within 1 hr [12]. Therefore, tourniquet occlusion reduces collateral circulation to the infused area producing greater local hypoxemia than balloon occlusion, which may in turn increase vascular and cellular drug permeability [3]. The similarity in femoral vein oxygen content produced by the tourniquet alone and by the tourniquet plus balloon has two possible explanations. One is that the number of dogs in each group (four) was too small to display differences between the two groups. The second is that even the noninflated catheter may provide partial intraluminal occlusion and thus diminish the differences between the two groups.

Unlike other chemotherapeutic agents, a hypoxic environment should not alter the action or metabolism of FUDR, because the drug works intracellularly to block DNA synthesis by inhibiting thymidylate synthetase [13]. Therefore, hypoxia may, if anything, improve the effectiveness of the FUDR by increasing vascular and cellular permeability to the drug.

Femoral vein FUDR levels may reflect drug levels in the capillaries and thus the concentration of drug to which the tissue is exposed. Figures 4 and 5 show that, as expected, the highest FUDR levels occurred when both a tourniquet and a balloon catheter were used; the lowest levels resulted when only the balloon was used. The combination occlusion produced drug levels in the local muscle and venous plasma that on the average were 1.3 and 19.6 times higher, respectively, than the levels achieved by the balloon occlusion. This means that although combination occlusion produced significantly greater FUDR levels in the local vasculature, there was only a slight increase in skeletal muscle drug levels. Although the situation may differ in tumors, this indicates that increasing local drug levels alone may not increase the amount of drug taken up by a tissue over a given period of time. Thirty minutes after release of arterial occlusion, local muscle drug levels were significantly higher after combination occlusion. This suggests that the occlusion produces local changes that progressively increase drug uptake. However, since the initial muscle sampling may have altered local blood flow, these results need to be verified by further research. In addition, comparative studies are necessary to determine whether the techniques would increase drug uptake by neoplastic tissues.

Ideally, enhancement of local drug uptake would make less chemotherapeutic agent available to spill over into the systemic circulation and produce unwanted side effects. The amount of drug entering the systemic circulation was significantly lower during combination occlusion-infusion. This indicates the technique substantially reduced the amount of venous return from the lower limb. However, since no systemic sample was collected soon after release (5 min) of tourniquet occlusion, no conclusions can be drawn regarding systemic drug levels resulting from these techniques.

The addition of tourniquet occlusion decreases local venous pO_2, increases local venous drug levels, and reduces systemic drug leak during infusion of FUDR. However, the risk of vascular thrombosis is increased, even though it was not noted in this study or in the investigation by Karakousis et al. [5]. Although the use of tourniquets for periods up to 1 hr appears to be physiologically safe, two problems will probably be encountered during clinical application. First, the use of a tourniquet for 30 min would probably be unbearably painful or unpleasant in the unanesthetized patient. Second, the high drug levels produced would probably cause drug-related chemical skin reactions. Karakousis et al. [5] noted that Adriamycin and methotrexate administered through tourniquet occlusion-infusion caused erythema, blistering, and darkening of the skin that reversed itself over a 4-week period [7]. In any event, additional studies seem warranted to further evaluate the combination of balloon and tourniquet occlusion-infusion of cytotoxic agents.

ACKNOWLEDGMENTS

We thank Raquel Collins and Irene Szwarc for technical assistance, J. B. Ragland and Jeane Hester for blood-gas determinations, Barry Brown for statistical analysis, and Rosalind Barnaby and Shirley A. Davis for manuscript preparation.

REFERENCES

1. Klopp CT, Alford TC, Bateman J, et al. Fractional regional cancer chemotherapy. *Ann Surg* **1950**;132:811–832
2. Bierman HR, Byron RL Jr, Miller ER, et al. Effects of intraarterial administration of nitrogen mustard. *Am J Med* **1950**;8:535
3. Wallace S, Chuang VP, Carrasco CH, et al. Physioanatomic concepts and radiologic techniques for intraarterial delivery of therapeutic agents. *Cancer Bull* **1984**;36:6–14
4. Anderson JH, Gianturco C, Wallace S. Experimental transcatheter intraarterial infusion-occlusion chemotherapy. *Invest Radiol* **1981**;16:496–500
5. Karakousis CP, Kanter PM, Lopez R, Moore R, Holycke ED. Modes of regional chemotherapy. *J Surg Res* **1979**;26:134–141
6. Wright KC, Charnsangavej C, Wallace S, Chuang VP, Savaraj N.

A Modified Cope Introducing Dilator to Allow Straight Guide Wire Introduction

Robert L. Vogelzang[1]

The Cope introduction set is widely used in interventional radiology [1, 2]. It has significant advantages over the use of a sheathed needle in that it allows less traumatic initiation of percutaneous access via a thin 21-gauge tract. We currently use it as the system of choice for obtaining initial access to both the biliary ductal and renal collecting systems. Some of the problems in the use of the Cope introduction set and draining catheters have been elucidated by Berman et al. [3], as well as Greenwood et al. [4], who also suggested some solutions. The latter group indicated that the 6.3-French introducing dilator for conversion from an 0.018-inch (0.46-mm) to a 0.038-inch (1-mm) guide wire can still cause difficulty with guide wire exit if the tip is bent excessively or completely straightened out. Chuang et al. [5] described similar difficulties and advocated the substitution of an 18-gauge Teflon sheath for the Cope dilator in such cases. They also used the technique during entry of a small lumen.

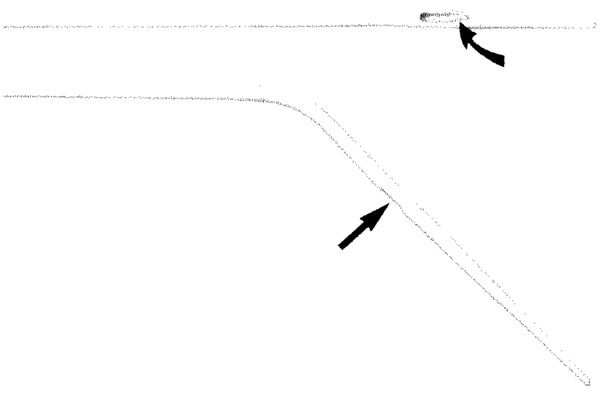

Fig. 1.—Curved Cope introducing dilator with side hole (*straight arrow*) has been straightened in modified form (top). In addition, side hole has been moved closer to tip and grooved (*curved arrow*) to allow passage of straight guide wire.

We have experienced similar difficulties with the system but the most vexing is the problem of entry into nondilated biliary ductal and renal collecting systems when insufficient room exists for the J guide wire to exit unobstructed from the side hole. This may be particularly true in renal calices with a narrow infundibulum and in small peripheral biliary radicles. Diffusely narrowed ductal systems, as in sclerosing cholangitis, may present similar problems. A recent modification of the 6.3-French introducing dilator (OS-2, Medi-Tech) allows the Cope system to be more readily used in all circumstances. The previously curved dilator has been straightened and the side hole moved closer to the tip. The hole has also been grooved to allow passage of a straight guide wire (fig. 1). The closer position of the side hole to the tip allows accurate positioning in smaller, more peripheral biliary radicles and in nondilated renal collecting systems where purchase and clearance may be limited.

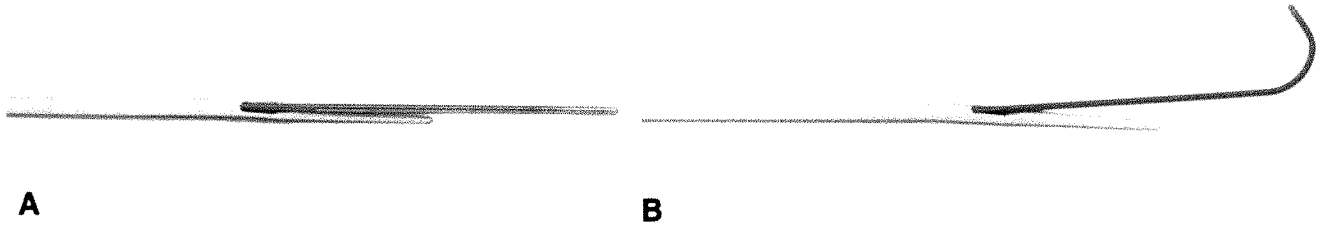

Fig. 2.—**A**, Straight guide wire exits easily from side hole. **B**, J-tip guide wire also may be used.

Received July 10, 1985; accepted after revision October 16, 1985.

[1] Department of Diagnostic Radiology, Northwestern University Medical School, Northwestern Memorial Hospital, Superior St. and Fairbanks Ct., Chicago, IL 60611.

AJR 146:381-382, February 1986 0361-803X/86/1462-0381 © American Roentgen Ray Society

The side hole modification permits a straight wire to emerge directly forward into a small or nondilated system. Other guide wires, including a 15-mm J, may also be used, which allows complete flexibility in guide wire choice (fig. 2). We have used this system in over 30 cases and have had no failures of guide wire emergence. We find it a significant improvement.

REFERENCES

1. Cope C. Conversion from small (0.018 inch) to large (0.39 inch) guide wires in percutaneous drainage procedures. *AJR* **1982**;138:170–171
2. Cope C. Stiff fine-needle guidewire for catheterization and drainage. *Radiology* **1983**;147:264
3. Berman HL, Bakal CW, Katz SG. Modification of the Cope drainage catheter to facilitate placement. *AJR* **1985**;146:169–170
4. Greenwood LH, Yrizarry JM, Brown SB. Observations on the use of the Cope introduction set. *AJR* **1984**;144:257–258
5. Chuang VP, Alspaugh JP, Harris SA Jr, et al. A modified application of the Cope introduction set. *AJR* **1985**;145:1073–1074

Removal of Retained Common Bile Duct Stones with Angiographic Occlusion Balloons

Steven G. Meranze,[1] Eric J. Stein, Dana R. Burke, William H. Hartz, and Gordon K. McLean

Interventional biliary radiology has a well established role in the management of retained common bile duct stones [1–5]. In most cases, a Dormia stone basket is passed through a T-tube track to extract the retained calculi or to pass them into the duodenum. If the stones are large, it may be necessary to fragment them before they can be engaged in the basket and pulled through the T-tube track or pushed through the ampulla of Vater. When the T-tube track forms an acute angle with the common bile duct, it may be impossible to position the basket properly. In difficult cases such as these, we have used angiographic occlusion balloon catheters to extract the stones from peripheral ducts and/or then push them down through the common duct and the ampulla of Vater into the duodenum. We have used this technique in 16 patients with excellent clinical results and no complications.

Materials and Methods

Over the past 12 months, we have used angiographic occlusion balloons to remove common bile duct stones in 16 patients. All patients are placed on parenteral or oral antibiotics before and for at least 1 day after the procedure. Pain is controlled by a narcotic and sedatives as needed. Initially, a thorough cholangiogram is performed with spot films obtained in multiple obliquities to evaluate the size and position of the stone(s) (fig. 1). A suitable balloon occlusion catheter is selected on the basis of the size of the duct containing the stone(s). Generally, a balloon (Medi-Tech Occlusion) diameter of 13 mm is satisfactory, although balloons of up to 2 cm diameter may be used if the duct is particularly capacious. A Lunderquist-Ring torque wire (Cook) is then passed through the access tube and directed down the common bile duct and into the duodenum. The T-tube or drainage catheter is then exchanged for the balloon catheter, and the patient is tilted into a semierect position allowing the stones to fall as far distally as possible into the common duct. By leaving the patient recumbent until this point, contrast material is more likely to remain within the duct, aiding in stone visualization. The balloon is inflated proximal to the stone and advanced over the wire and into the duodenum, pushing the stone ahead of it. It is essential not to overdistend the balloon to avoid traumatizing the duct. At any point the wire can be removed and contrast material injected to opacify the duct. The wire can then be reinserted to help direct the balloon catheter. By controlling the volume of the balloon with the syringe, it is possible to carefully modulate its size in the duct. Minor adjustments in volume will help it pass through the ampulla if this is difficult. The balloon may be inflated with saline, allowing easy visualization in the contrast-filled common bile duct.

When there is question as to whether the stone is too large to pass through the sphincter of Oddi, the balloon is passed distally beyond the stone and then inflated until it is the same size as the stone. If the balloon passes easily through the ampulla, then the stone should pass as well. If there is difficulty in passing the balloon, the ampulla may be dilated with an angioplasty balloon, or endoscopic sphincterotomy may be done. After the stone is extruded, the balloon catheter is deflated and removed, and a new biliary drainage catheter or T-tube is placed. A repeat cholangiogram is performed several days later to confirm a stone-free biliary system.

If the stone(s) is/are located within the intrahepatic biliary tree, a safety wire is first directed through the ampulla to maintain access. After a wire is manipulated beyond the stone, a balloon of appropriate size is inserted, inflated, and gently withdrawn, pulling the stone into the common duct. The stone is then withdrawn through the T-tube track or directed through the ampulla as described above. Care must be taken not to overinflate the occlusion balloon within the intrahepatic ducts, as ductal rupture may result. A major advantage of the angiographic occlusion balloon over the Fogarty embolectomy balloon is that the former's central lumen allows the guide wire to be removed and contrast material to be injected during the procedure to opacify distal ducts.

Results

Access to the biliary tree was afforded by a T-tube track in seven patients, by a transhepatic catheter in five patients, and by a cholecystostomy tube in two patients. Of these 14 patients, three had prior endoscopic sphincterotomy, and four underwent balloon dilatation of the sphincter of Oddi before stone extrusion. One in this group had a sphincterotomy followed by balloon dilatation to enlarge the ampulla. The occlusion balloon technique was also used on two additional patients with oriental cholangiohepatitis and multiple stones.

In all patients, except for one of the two with oriental cholangiohepatitis, we were able to either extrude the stones into the duodenum or withdraw them through the previously established access track. In that one patient, the presence of

---

Received July 9, 1985; accepted after revision September 20, 1985.

[1] All authors: Department of Radiology, Hospital of the University of Pennsylvania, 3400 Spruce St., Philadelphia, PA 19104. Address reprint requests to S. G. Meranze.

AJR 146:383–385, February 1986 0361–803X/86/1426–0383 © American Roentgen Ray Society

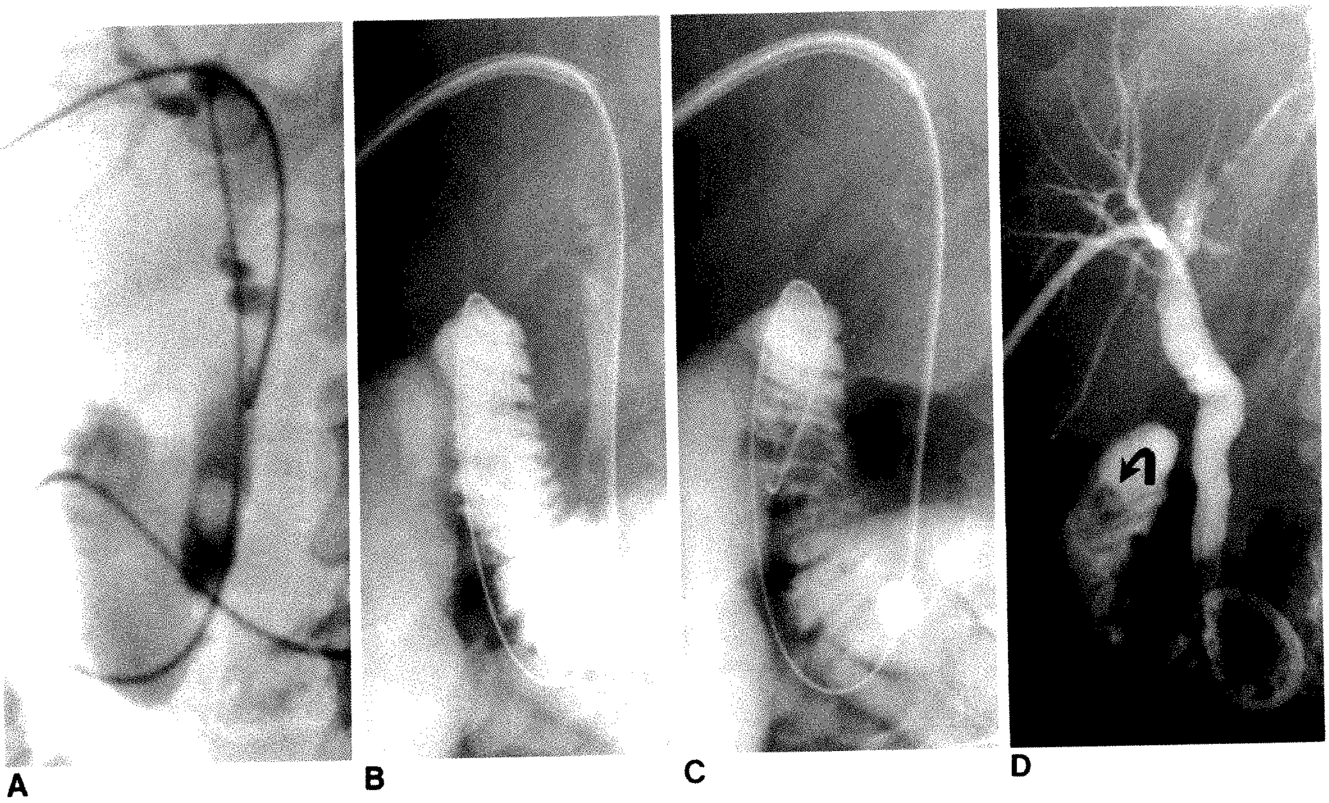

Fig. 1.—**A**, Injection of nasobiliary tube and transhepatic catheter. Large stone within common bile duct. **B**, Sheath stabilizes balloon catheter. **C**, Balloon catheter through ampulla has pushed stone into small bowel. **D**, After insertion of Cope biliary drainage catheter, bile duct was stone free. Note stone in duodenum (*arrow*).

strictures and the fragility of the stones prevented us from rendering her stone free. No patients developed pancreatitis during or after the procedure.

Discussion

Most interventional radiologic procedures for extraction of retained common bile duct or cystic duct calculi are performed through an indwelling T-tube track or via a transhepatic approach. Typically, a Dormia stone basket is used to entrap the stone, and the stone is removed through the track. Small stones can sometimes be removed by irrigation or suction with a large-bore catheter. If the angle of the access track with the distal common bile duct is very acute, it may prevent effective manipulation of the Dormia basket around the stone. It may also be difficult to "twirl" the basket if a relatively straight line cannot be maintained.

When the stone is too large to be removed through the track, it is sometimes possible to push the basketed stone through the ampulla. However, it may be difficult to release the stone from the basket, particularly if it is exceptionally large. A firm stone that cannot be crushed and is too large to be removed through a transhepatic or T-tube track may thus become trapped in the basket, potentially requiring surgical removal. In addition, the rigid tip of the Dormia basket may not easily pass through the ampulla, and can traumatize it. Although a basket has been designed for this particular use (Schwarz basket, Cook), the leading wire of this basket often makes it difficult to "twirl" the basket and engage the stone.

The use of the Fogarty embolectomy balloon in the biliary tree has been described previously [5]. The balloon is placed beyond the stone fragment or impacted stone and withdrawn. This has been demonstrated to be a safe procedure when overdistension of the balloon is prevented and meticulous technique is used [6]. Using similar techniques, we have used angiographic occlusion balloons with excellent results. One advantage of the angiographic occlusion balloon catheter is that, unlike the Fogarty, it has an end hole. Thus, it can be inserted into almost any duct into which a selective guide wire is passed, and the duct can be opacified through the catheter lumen. This permits continuous fluoroscopic observation of the duct while the balloon is inflated, avoiding inadvertent overdistension and possible duct rupture. While others have used angioplasty balloon catheters to extrude biliary calculi [7, 8], we believe that the shorter occlusion balloon is safer, particularly when positioned in the intrahepatic ducts.

Any attempt to push a stone through the distal common duct into the duodenum risks impaction of the stone in the ampulla. Should this occur, the occlusion balloon can be deflated, advanced over the guide wire past the stone, reinflated in the duodenum, and then drawn back, disimpacting the stone. The presence of the guide wire also helps avoid this problem by making it more difficult for the stone to impact. The Fogarty balloon embolectomy catheter is quite thin and, when an attempt is made to push a large stone, it may be difficult to direct without the use of a stiff guiding catheter. The presence of the guide wire within the occlusion balloon is usually effective in supporting the balloon. A Teflon sheath may be used to provide additional stiffness if necessary, as in two of our cases.

Pancreatitis from overdistension of the pancreatic duct or from the lodging of a stone fragment in the duct origin is a theoretical problem that we have not encountered. Again, the presence of the guide wire and the controlled nature of the procedure help prevent this. We believe this technique to be a useful adjunct in the management of retained common bile duct stones.

REFERENCES

1. Ring EJ, Kerlan RK Jr. Interventional biliary radiology. *AJR* **1984**;142:31–34
2. Taylor BR, Ho CS. Nonsurgical treatment of common-bile-duct stones. *Can J Surg* **1984**;27:28–32
3. Burhenne HJ. Nonoperative retained biliary tract stone extraction; a new roentgenologic technique. *AJR* **1973**;117:388–399
4. Burhenne HJ. Percutaneous extraction of retained biliary tract stones: 661 patients. *AJR* **1980**;134:888–898
5. Burhenne HJ. The technique of biliary duct stone extraction. *Radiology* **1974**;113:567–572
6. Viamonte M Jr. Positioning device for cardiac series. *Radiology* **1979**;133:803
7. Fataar S, Bassiony H, Abou-Neema T. The percutaneous "stretch and push" technique for removing retained biliary calculi. *Br J Radiol* **1982**;55:456–459
8. Centola CAP, Jander HP, Stauffer A, Russinovich NAE. Balloon dilatation of the papilla of Vater to allow biliary stone passage. *AJR* **1981**;136:613–614

Attention *AJR* Contributors

Effective January 1, 1986, Dr. Robert N. Berk assumed the editorship of the *AJR*, and the editorial office moved from Seattle to La Jolla, California. The new address and telephone number are:

AJR Editorial Office
2223 Avenida de la Playa
La Jolla, CA 92037
(619) 459-2229

Pictorial Essay

Markers for Implanted Devices: Need for Standardization

William W. Scott, Jr.,[1] Paul S. Wheeler, and Sally E. Mitchell

Some preventable diagnostic problems and risks related to medical devices indicate the need for logical marker standards and for input from radiologists in the design of these devices. The problems range from undetectable items inserted in the body to external equipment that needlessly hides detail on radiographs.

The variety and absolute numbers of such devices used in patient care and monitoring are rapidly increasing. Some voluntary standards for radiologic detectability exist, but there is no organized method for the dissemination of these standards.

A surprising variety of important devices are invisible or poorly opaque, ensuring lack of detection by radiography. These include venous catheters, vascular grafts, heart valve and breast prostheses, feeding tubes, and even ventricular shunts. Abstract markers for surgical sponges and pads can be mistaken for drains, surgical clips, or wire sutures [1, 2]. Single wire markers found in tubes, aortic balloons, and venous catheters are similar to transcutaneous nerve stimulators and electrocardiographic leads. Rarely used specialty prostheses can be confusing without a detailed clinical history.

All devices intentionally placed in patients or left in accidentally pose risks of infection, breakage, and displacement. Tubes and grafts may obstruct or leak. Casts, braces, and other external equipment can hide underlying anatomy and pathology. Dressings and stopcocks may cause confusing radiographic shadows. The following examples from a large hospital illustrate these problems (figs. 1–8).

Discussion

A departmental risk prevention program identified a number of device-related problems. The most important were implanted devices not labeled radiographically and external devices that needlessly obscured potentially important radiographic findings. These problems resulted in missed and delayed diagnosis, wasted time and resources, and needless risk.

Catheters can move from satisfactory to dangerous locations. Such changes in position of poorly opaque catheters may be undetectable until some complication ensues. Such catheters may then only be located by guide-wire placement or injection of contrast material, requiring unnecessary expense and a small added risk.

In general, if a device such as a catheter or drain tube is entirely impregnated with radiodense material, the person observing the radiograph will often be able to identify it by size and shape. A simple wire marker does not provide this assistance. The tips of all tubes should be especially well defined. Optimal marking of devices is especially important in cases in which obesity or bedside filming results in loss of image contrast.

Vascular grafts, heart valves, and breast prostheses can be nonopaque. Problems may also arise if a patient receives medical care from a physician unfamiliar with the patient's previous surgery. The patient may be unable to supply details as to the type of cardiac valve prosthesis or other hardware

---

Received June 5, 1985; accepted after revision September 20, 1985.

[1] All authors: Russell H. Morgan Department of Radiology and Radiological Sciences, Johns Hopkins Medical Institutions, 600 N. Wolfe St., Baltimore, MD 21205. Address reprint requests to P. S. Wheeler.

AJR 146:387–390 February 1986 0361–803X/86/1462–0387 © American Roentgen Ray Society

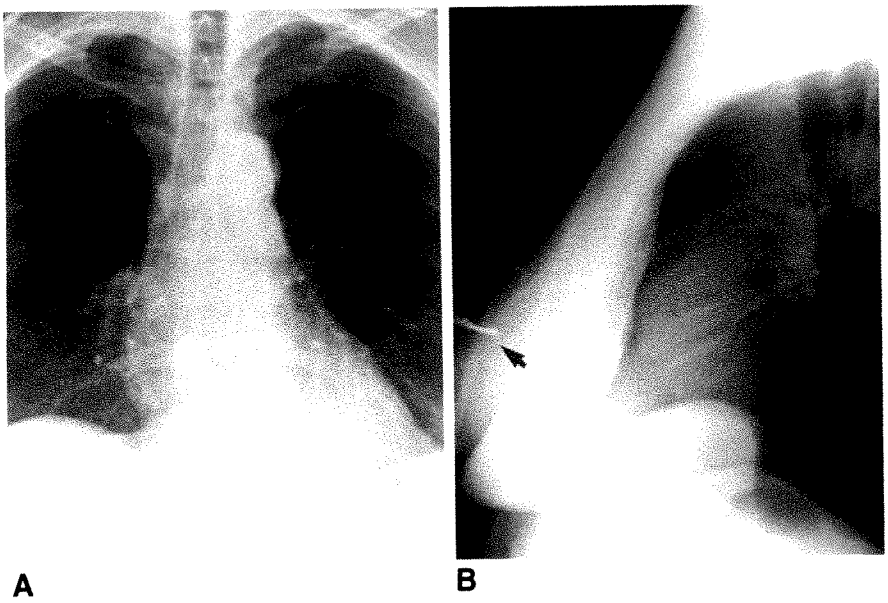

Fig. 1.—40-year-old woman with lymphoproliferative disorder. Metal clamp on anterior chest wall (*arrow*) is only indication of Hickman catheter used for chemotherapy. Catheter is completely nonopaque, and its tip cannot be located.

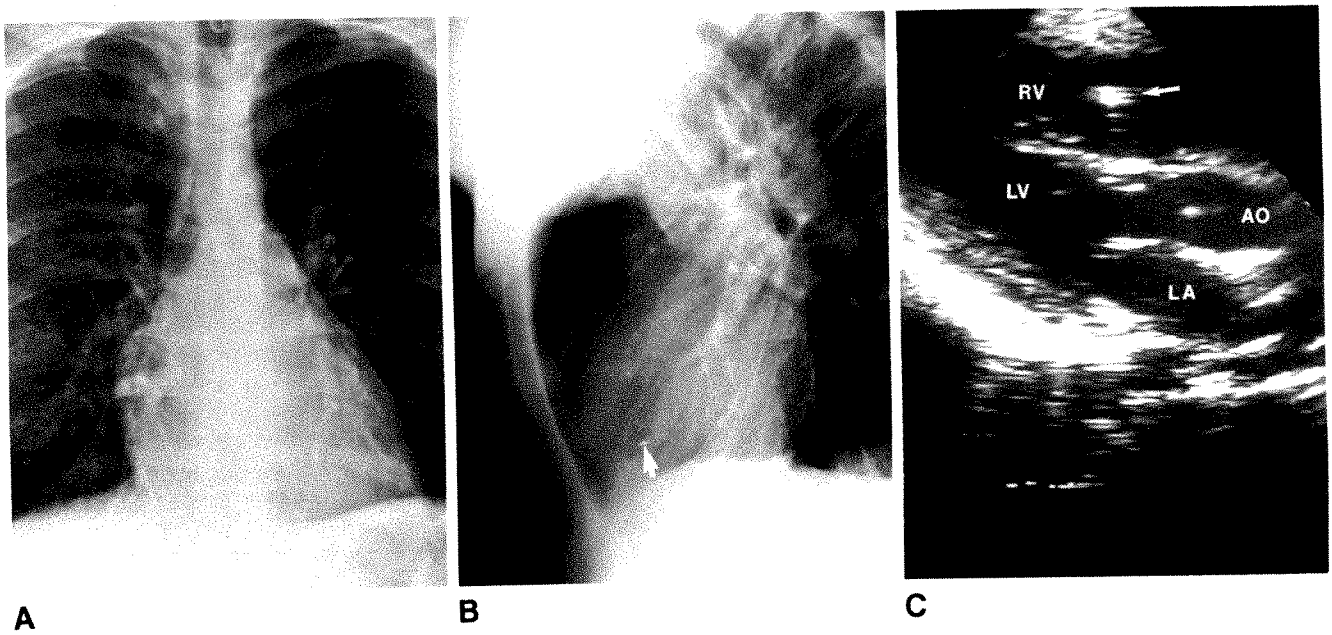

Fig. 2.—27-year-old man developed sepsis and heart murmur years after treatment of brain tumor with ventriculoatrial shunt. Shunt had not functioned for 6 years. Infection of shunt catheter was suspected, but location of shunt was a mystery until sonography. **A**, Posteroanterior chest film. **B**, Lateral chest film shows only a small metallic density in region of right ventricle (*arrow*). **C**, Sonogram. Broken ventriculoatrial shunt coiled in right ventricle (*arrow*). RV = right ventricle; LV = left ventricle; LA = left atrium; AO = aorta. Sonography also showed vegetations on shunt and tricuspid valve, confirming clinical diagnosis of subacute bacterial endocarditis. Catheter was removed transvenously.

used. If standardized, logical marking schemes were used, such important surgical information would be available on the radiograph.

Markers for surgical sponges and pads tend to be confusing, with either a small opaque thread or a barium impregnated tape being used. A plethora of sponges is used without proper radiopaque labels, and markers may simulate broken wire sutures [1]. Neurosurgical sponge markers can simulate surgical clips [2]. Many of these items could be marked with a radiopaque tape clearly identifying their role. The ease with which sponges can be lost even by the most experienced surgeon is well described in the classic work of Crossin and Crossin [3].

All devices that can be placed in patients should be opaque

Fig. 3.—29-year-old woman receiving chemotherapy for malignancy developed ventricular arrhythmias. Moderately opaque Hickman catheter used for chemotherapy can be seen with its tip in right ventricle. Repositioning catheter cured arrhythmias. Had catheter been radiolucent variety as in fig. 1, diagnosis might have been delayed.

Fig. 4.—Elderly woman with heart surgery complicated by several postoperative cardiac arrests. Several days after cardiac surgery, it appears that all tubes but one have been removed. Wire on right side of mediastinum was misinterpreted initially as marker in remaining mediastinal tube. Actually, it was guide wire inadvertently left in inferior vena cava.

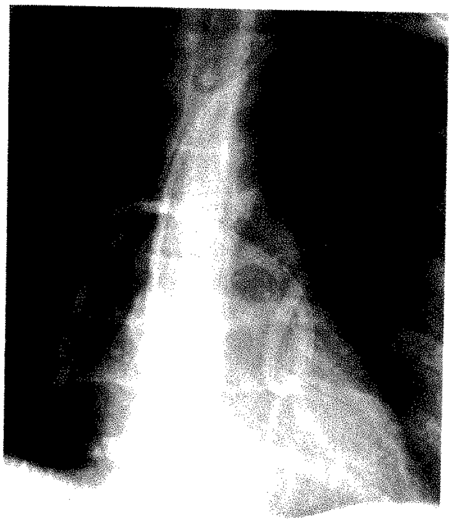

3

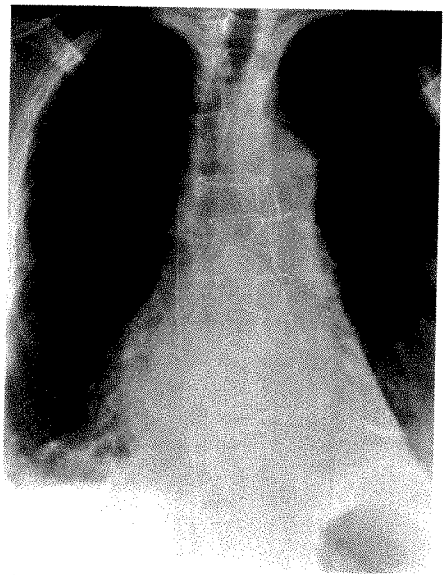

4

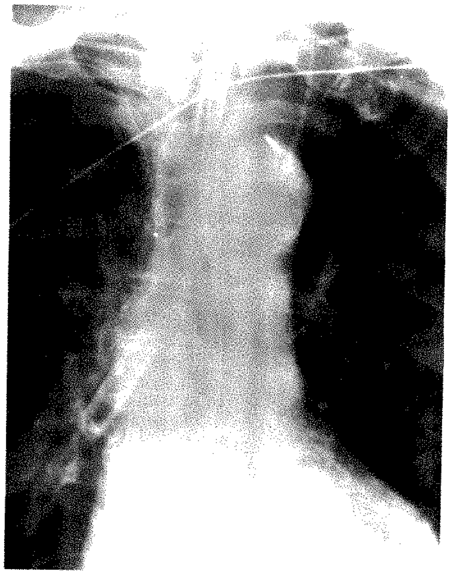

5

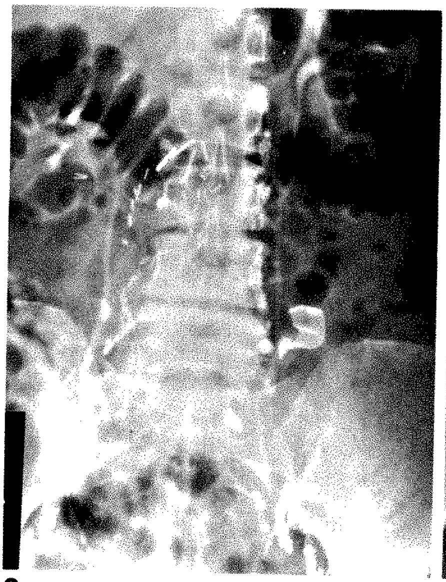

6

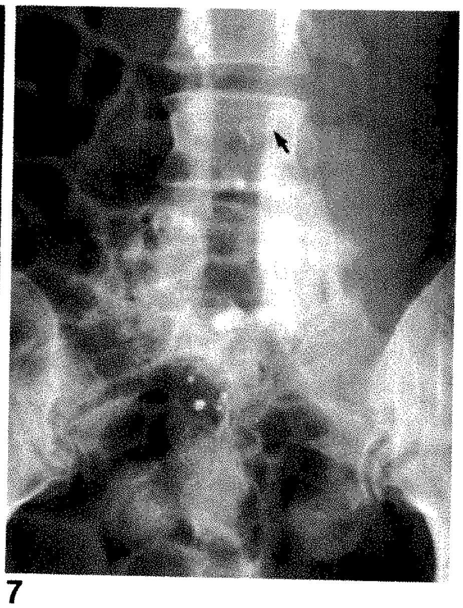

7

Fig. 5.—Elderly man recovering from congestive heart failure. Bilateral venous catheters, tracheostomy tube, and nasogastric tube. Metallic density at upper margin of aortic arch mimics surgical clip but is marker for tip of aortic counter pulsation balloon positioned somewhat high in aorta.

Fig. 6.—Febrile patient after urinary tract surgery. Representative film from excretory urogram. Normal kidneys and ureters and residual lymphangiographic contrast material in pelvic and paraaortic nodes. Radiodensity to left of L5 was interpreted as Penrose drain, which it resembles, but was marker on retained surgical pad.

Fig. 7.—Patient with history of multiple lumbar spine operations; fever developed after last operation. Abdominal film. Extensive lumbar spine laminectomy. Lower lumbar spine posterior fusion. Linear radiodensity over L4, which was overlooked or believed to be broken wire (*arrow*), is sponge marker. At reexploration, abscess was found around this foreign body.

with a rational marker system that, when possible, should be self-explanatory. Marker systems could be standardized at the design stage by voluntary agreement with industry using input from imaging consultants. Information on new and existing devices should be disseminated to radiologists on a regular basis directly from companies, in journals, or through the American College of Radiology, the National Center for Devices, and Radiological Health publications.

This problem involves several medical disciplines as well as industry. Surgeons must communicate to radiologists regard-

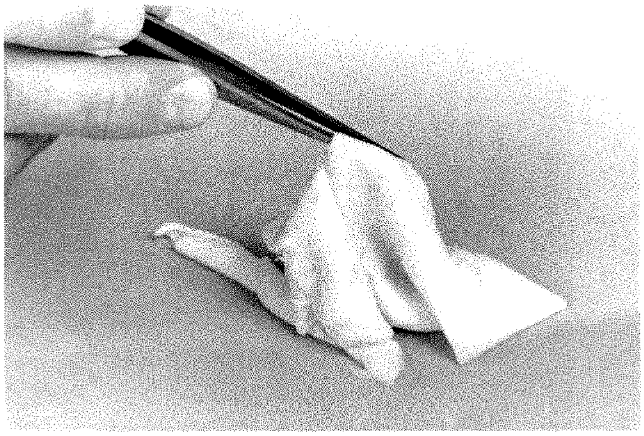

Fig. 1.—Endocyst of ruptured hydatid cyst of lung from patient shown in fig. 3. Endocyst tears easily when lifted by forceps.

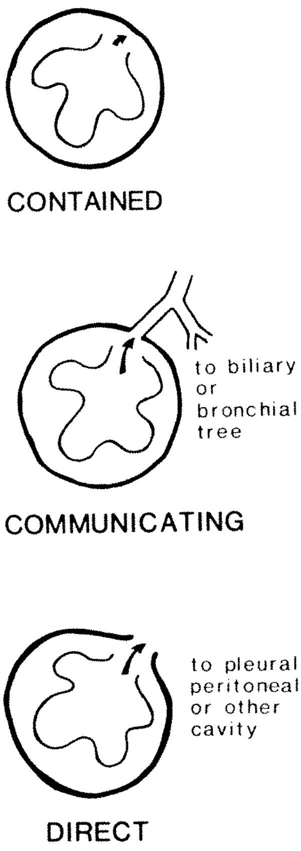
CONTAINED
to biliary or bronchial tree
COMMUNICATING
to pleural, peritoneal or other cavity
DIRECT

Fig. 2.—Classification of echinococcal cysts.

These two structures are usually referred to collectively as the endocyst. The endocyst produces hydatid fluid and scoleces, which are infectious miniature adult tape worms. Intracystic fluid pressures of up to 80 cm of water [10] keep the parasitic membranes tightly applied to the pericyst. The endocyst is fragile [9, 11] with the texture and tensile strength of partly cooked egg white (fig. 1). It is normally protected from rupture by the tougher pericyst.

In reviewing our material on cyst rupture, it became apparent that the mechanisms for various complications such as biliary obstruction have not been satisfactorily explained in the literature. We therefore set out to clarify the mechanisms of cyst rupture and the ensuing complications and to formulate a classification of rupture. We classified rupture into three categories. Contained rupture is when only the endocyst is torn and cyst contents are confined within the surrounding layer of host reactive tissue, the pericyst (fig. 2A). Communicating rupture consists of a tear of the endocyst with escape of cyst contents via bronchioles or biliary radicles that have been incorporated in the pericyst (fig. 2B). A tear of both the pericyst and endocyst allowing cyst contents to spill into the peritoneal or pleural spaces is direct rupture (fig. 2C).

Materials and Methods

Between January 1977 and November 1984, 97 patients were seen at the King Faisal Specialist Hospital with cysts due to *Echinococcus granulosus*. Twenty-four of these patients had proved rupture of a cyst. There were 13 male and 11 female patients with an average age of 33 years. Twelve had rupture of a liver cyst and 12 of a lung cyst. Proof of rupture was based on findings at surgery in 22 of 24 patients. The remaining two patients had percutaneous transthoracic aspiration of a lung cyst, which produced clear fluid containing scoleces and resulted in the waterlily sign on radiographs.

Results

Twenty patients had radiographic, CT, or sonographic evidence of separation of the endocyst from the pericyst and six had a decrease in the size of the cyst between radiologic examinations.

Lung Cysts

Of the 12 lung cysts, the rupture was communicating in four and direct in five. It was both communicating and direct in three, all following fine-needle aspiration biopsy. None were contained. The waterlily sign was present on standard chest radiographs, CT, and/or sonography in nine (75%) of 12 patients with ruptured pulmonary echinococcal cysts. The other three patients had solid mass lesions that appeared similar on chest radiographs to intact echinococcal cysts. One had a pneumothorax and another a pleural effusion, both indicative of communication of the cyst with the pleural space. The third patient had pericyst pneumonitis due to rupture into the lung. The signs in these three patients were suggestive but not diagnostic of cyst rupture.

Liver Cysts

Two of the ruptured cysts were contained, eight were communicating, and two were direct. In eight (66.7%) of 12 patients, the preoperative diagnosis of cyst rupture was based on the CT or sonographic waterlily sign of detachment of the endocyst from the pericyst. Of the four patients in whom cyst rupture was not recognized before operation, two

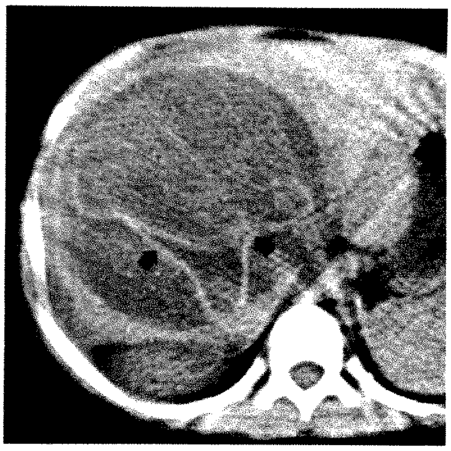

3

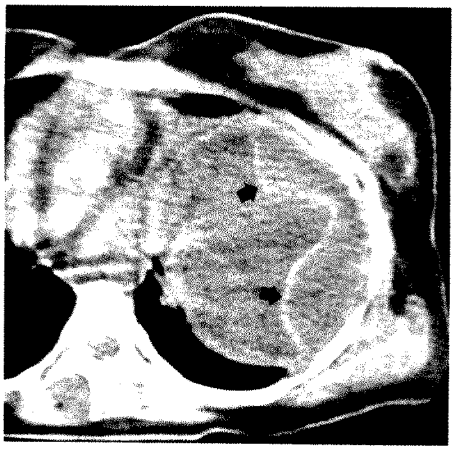

4

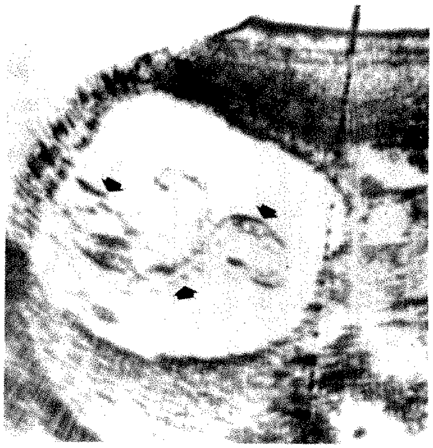

5

Fig. 3.—CT scan of liver cyst after contained rupture. Note separated endocyst (*arrows*). This is CT equivalent of waterlily sign.

Fig. 4.—CT scan of lung cyst after direct rupture. Cyst diminished on successive conventional chest radiographs, and on second examination there was pleural effusion. Detached endocyst is clearly seen (*arrows*).

Fig. 5.—Sonogram of liver cyst after communicating rupture. Detached endocyst (*arrows*) floats in hydatid fluid. Three weeks earlier, cyst was larger and there was no detached membrane. This examination was performed because patient reported that his palpable lesion had become smaller.

cysts were infected and were thought to be abscesses. The third cyst, which had the appearance of a solid mass by CT and sonography, occurred in a woman with a large renal cell carcinoma and was thought to be a hepatic metastasis. The fourth was collapsed after spontaneous rupture through the diaphragm into the right pleural space.

Discussion

Rupture may have several causes. Degeneration of the parasitic membranes due to chemical or host defense mechanisms or due to aging is likely to cause rupture of the contained type. This may in time become communicating, as described below. Trauma may tear only the endocyst or both the endocyst and pericyst to cause direct rupture. The avascularity of the pericyst and the lack of connection of the endocyst with the host blood system suggest that infection of the intact cyst is impossible, despite previous reports to the contrary [12, 13]. We believe that bacteria can enter a hydatid cyst only after the cyst has ruptured.

Contained Rupture

When the endocyst ruptures, hydatid fluid escapes into the potential space between the pericyst and the endocyst, and the endocyst collapses. Both CT and sonography show undulating membranes (fig. 3) without a reduction in cyst size, but conventional radiographs provide no clue that rupture has occurred. Contained rupture is unlikely to have infectious or allergic sequelae.

Communicating Rupture

Because hydatid fluid is at a higher pressure than bile, it may in time convert a contained rupture of a liver cyst to a communicating rupture by forcing fluid, hydatid sand, daughter cysts, or membranes into biliary radicles that have been incorporated in the pericyst. Previous explanations of rupture of liver hydatid cysts into the biliary tree [14, 15] have not been satisfactory, as they have not taken into account the great fragility of the endocyst [9, 11]. In the lung, communication may be established with the bronchial tree by bronchioles incorporated in the pericyst. When either a liver or lung cyst undergoes communicating rupture, the cyst becomes smaller and undulating membranes will be seen by CT or sonography (figs. 4 and 5). If air replaces cyst fluid in a pulmonary lesion, the classic waterlily sign will be seen on plain radiographs (fig. 6). Communicating rupture in the lung will lead to expectoration of fluid and membranes, and it may result in evacuation and cure of the cyst [16]. We presume that communicating rupture of a liver cyst may also lead to evacuation of the cyst. This may be one mechanism of transformation of living liver cysts into the densely calcified, dead structures we have designated type III lesions [17]. Daughter cysts and fragments of membrane may cause biliary obstruction with a mortality as high as 50% [5]. We have not seen evidence that transbiliary or transbronchial dispersion of scoleces causes dissemination of echinococcal disease.

Direct Rupture

When both the pericyst and the endocyst are torn, cyst contents escape by a nonanatomic route into the peritoneal space or through the diaphragm into the pleural cavity. Occasionally rupture may be into a hollow viscus such as the colon. Direct intraperitoneal rupture may be manifest by detached membranes or a reduction in cyst size on CT or sonography or by the development of peritoneal fluid, biliary obstruction, or infection. Unlike the alveolar form of hydatid (*E. multilocularis*), *E. granulosus* does not reproduce by external budding. However, herniation of cyst contents may occur through a weakness in the pericyst, and this may be a prelude to direct rupture (fig. 7). Direct rupture of a lung cyst is usually into the pleural space and rarely into the lung

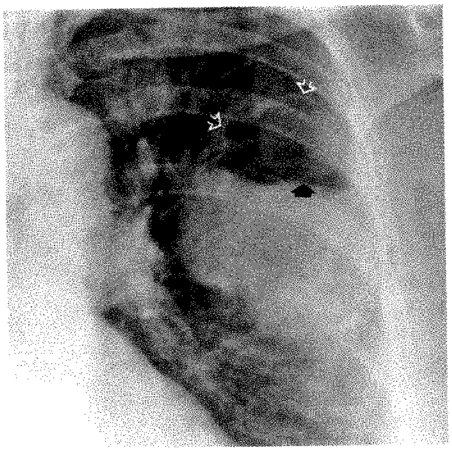

6

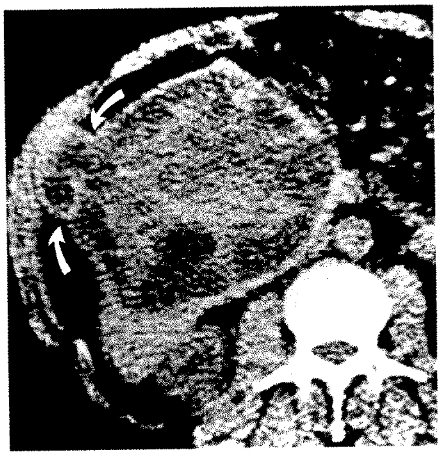

7

Fig. 6.—Waterlily sign after communicating rupture. Pericyst, derived from reactive host tissue, is thin (*open arrows*). Undulating level is due to floating endocyst (*solid arrow*).

Fig. 7.—Liver cyst herniating through weakness in pericyst (*arrows*). Herniated part is not protected by pericyst and is prone to direct rupture.

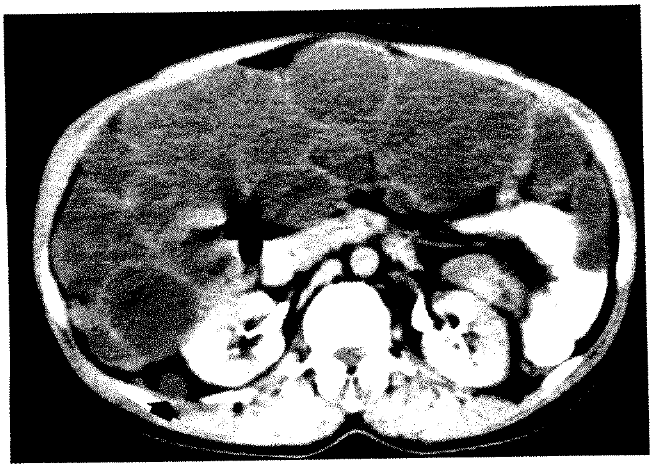

Fig. 8.—Peritoneal hydatidosis after direct rupture into lesser sac. Secondary hydatids are within distended lesser sac, except for one small cyst lateral to right kidney (*arrow*).

parenchyma. It may be manifest by detached membranes, reduction in cyst size, pneumothorax, pleural effusion, or pericyst pneumonitis. Direct rupture may cause an allergic reaction to the hydatid fluid. Allergic reactions are not as common as once thought, although fatal anaphylaxis does occur [18]. Four of our patients (16.7%) had symptoms or history of an allergic episode following cyst rupture, but none had fatal anaphylaxis. The most serious usual complication of rupture is bacterial infection. A long-term sequela of direct rupture into the peritoneal cavity is implantation of scoleces leading to metastatic hydatosis (fig. 8). Both rupture and infection can change the appearance of a hydatid cyst and make diagnosis difficult [4].

It is not possible in every case to distinguish among types of rupture, especially between contained and communicating rupture in the liver, but it is important to attempt to make the distinction. Bile ducts and bronchioles that were incorporated in the pericyst may not be patent initially but may eventually open and convert a contained into a communicating rupture. Patients with direct rupture should be treated with antihelminthic drugs to prevent peritoneal or pleural hydatosis. Most patients, except those with densely calcified dead lesions, will have their echinococcal cysts removed. Those with sonographic or CT evidence of any form of rupture should be considered for surgical treatment at the first opportunity to avoid potentially fatal complications.

ACKNOWLEDGMENT

We thank Pamela Kline for assistance in scanning and data collection.

REFERENCES

1. Oosthuirzen SF, Fainsinger MH. Hydatid disease. *Radiology* **1949**;53:248–254
2. Balikian JP, Mudarris FF. Hydatid disease of the lungs. *AJR* **1974**;122:692–707.
3. Schlanger PM, Schlanger H. Hydatid disease and its roentgen picture. *AJR* **1948**;60:331–347
4. Niron EA, Ozer H. Ultrasound appearances of liver hydatid disease. *Br J Radiol* **1981**;54:335–338
5. McCorkell SJ. Echinococcal cysts in the common bile duct: an uncommon cause of obstruction. *Gastrointest Radiol* (in press)
6. Borrie J, Shaw JFH. Hepatobronchial fistula caused by hydatid disease. *Thorax* **1981**;36:25–28
7. Poole JB, Marcial-Rojas RA. Echinococcosis. In: Marcial-Rojas RA, ed. *Pathology of protozoal and helminthic diseases.* Baltimore: Williams & Wilkins, **1971**:635–657
8. Cameron TWM. Some modern biological conceptions of hydatid. *Proc R Soc Med* **1927**;20:272–283
9. Weirich WL. Hydatid disease of the liver. *Am J Surg* **1979**;138:805–808
10. Harris JD. Rupture of hydatid cysts of the liver into the biliary tracts. *Br J Surg* **1965**;52:210–214
11. Saidi F, Nazarian I. Surgical treatment of hydatid cysts by freezing of cyst wall and instillation of 0.5 percent silver nitrate solution. *N Engl J Med* **1971**;284:1346–1350
12. Lewis JW, Koss N, Kerstein MD. A review of echinococcal disease. *Ann Surg* **1975**;181:390–396
13. Yacoubian HD. Thoracic problems associated with hydatid cyst of the dome of liver. *Surgery* **1976**;79:544–548
14. Macris GT, Galanis NN. Rupture of echinococcus cysts of the liver into the biliary ducts: report of nine cases. *Am Surg* **1966**;32:36–44
15. Subramanyam BR, Balthazar EJ, Naidich DP. Ruptured hydatid cyst with biliary obstruction: diagnosis by sonography and computed tomography. *Gastrointest Radiol* **1983**;8:341–343
16. Latham WJ. Hydatid disease. *J Fac Radiol* **1953**;5:65–81
17. Lewall DB, McCorkell SJ. Hepatic echinococcal cysts: sonographic appearance and classification. *Radiology* **1985**; 155:773–775
18. Beggs I. The radiologic appearances of hydatid disease of the liver. *Clin Radiol* **1983**;34:555–563

Radiological Aspects of Primary Hyperoxaluria

Deborah L. Day[1]
Jon I. Scheinman[2,3]
John Mahan[2,4]

Primary hyperoxaluria is a rare metabolic disorder characterized by excessive synthesis and urinary excretion of oxalate. Nephrocalcinosis with or without calcium oxalate nephrolithiasis leads to renal failure in infancy through young adulthood. Oxalosis is the condition in which the highly insoluble calcium oxalate crystals are deposited in extrarenal tissues including bone, blood vessels, heart, and the male urogenital system. The radiographic abnormalities in 14 patients with primary hyperoxaluria are described. These abnormalities include nephrolithiasis, nephrocalcinosis, dense vascular calcifications, abnormal bone density, and characteristic metaphyseal abnormalities. Changes of renal osteodystrophy and pathologic fractures are common. Radiographic bone abnormalities are dependent on the age of the patient when renal failure occurred and the degree of success of renal transplantation. Characteristic skeletal changes are present in six of seven patients who developed renal failure when less than 7 years of age.

Primary hyperoxaluria is a rare autosomal recessive genetic disorder that results in excessive synthesis and urinary excretion of oxalate [1, 2]. There are two general presentations of primary hyperoxaluria. The "classic" presentation is characterized by recurrent calcium oxalate nephrolithiasis in childhood and nephrocalcinosis leading to progressive renal insufficiency and failure in early adulthood. The infantile presentation is characterized by nephrocalcinosis without calculi, leading to chronic renal failure in infancy or very early childhood [3–6]. Oxalosis is the deposition of calcium oxalate crystals in extrarenal tissues. Major sites of deposition include bone, bone marrow, heart, blood vessels, cartilage, the male urogenital system, the central nervous system, and peripheral nerves [1, 2]. Characteristic radiographic abnormalities include nephrolithiasis, nephrocalcinosis, vascular calcifications, and skeletal abnormalities.

Materials and Methods

Between February 1976 and August 1984, 14 patients with primary hyperoxaluria were treated for chronic renal failure and evaluated for renal transplantation at the University of Minnesota. At presentation, the patients ranged in age from 2 months to 23 years. Seven of the eight patients who had uremia were children, five of whom were younger than 1 year. In these patients, dialysis was instituted within days of presentation. The other six patients with primary hyperoxaluria had the "classic" presentation of recurrent nephrolithiasis. Five of these six patients were 10 years or younger at the time of initial presentation, but did not require dialysis until their late teens or mid-20s. The remaining patient was 23 years old at the time of presentation and was started on dialysis at age 47.

Of the 14 patients, 13 received a total of 18 renal transplants. At time of transplantation, the nine female and five male patients ranged in age from 6 months to 47 years. All patients under 10 years at time of transplantation were female. Of those patients 22 years and older at time of transplantation, five were male and two were female. At the time of this review, five patients had no renal biopsy evidence of calcium oxalate deposition; one patient had minimal evidence. These six patients had relatively good renal transplant function with a 4-

Received June 26, 1985; accepted after revision October 10, 1985.

Presented in part at the annual meeting of the American Roentgen Ray Society, Boston, April 1985.

[1] Department of Radiology, University of Minnesota Hospitals, Box 292 Mayo Memorial Bldg, 420 Delaware St. S.E., Minneapolis, MN 55455. Address reprint requests to D. L. Day.

[2] Department of Pediatrics, University of Minnesota, Minneapolis, MN 55455.

[3] Present address: Department of Pediatrics, Duke University Medical Center, Durham NC 27710.

[4] Present address: Children's Hospital, Columbus, OH 43205.

AJR 146:395–401, February 1986
0361–803X/86/1462–0395
© American Roentgen Ray Society

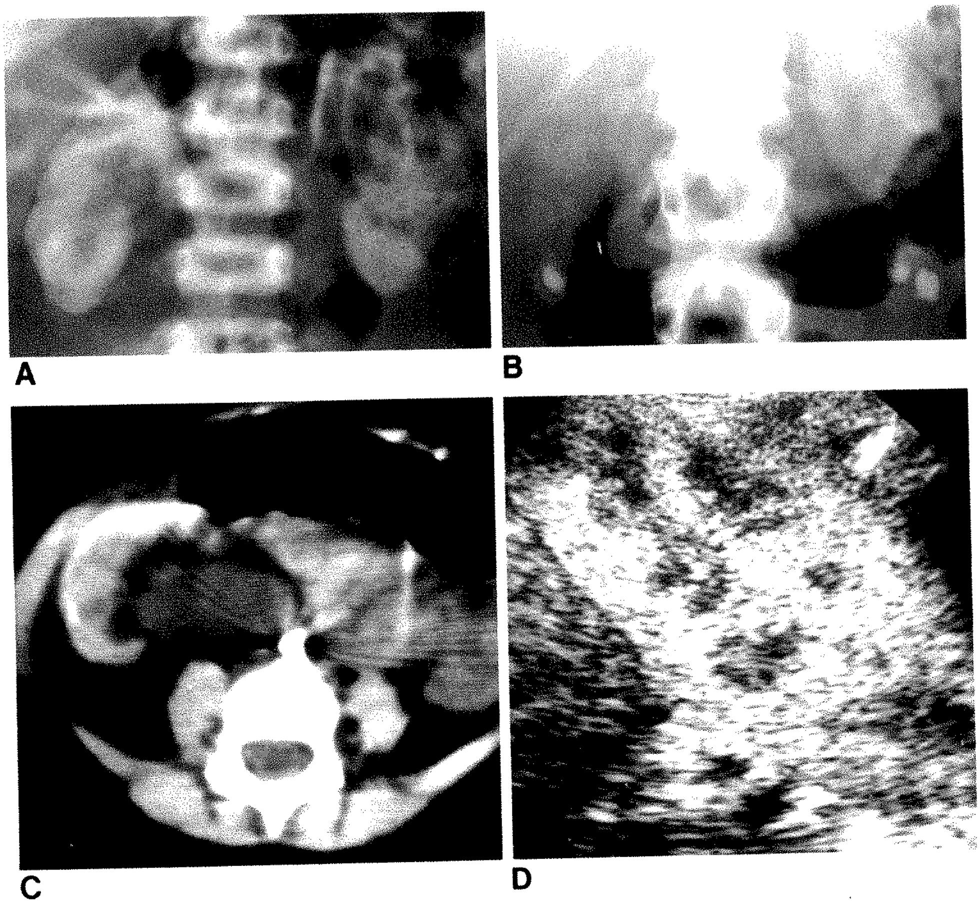

Fig. 1.—Nephrocalcinosis and nephrolithiasis in four patients. **A**, Diffuse nephrocalcinosis and small, scarred kidneys typical of end-stage disease in 10-month-old infant with fulminant hyperoxaluria (no contrast medium). No renal calculi. **B**, Small scarred kidneys (partial right nephrectomy) with inhomogeneous, patchy nephrocalcinosis and bilateral nephrolithiasis typical of end-stage disease in "classic" indolent hyperoxaluria in 24-year-old woman. **C**, Minimal renal deposition of calcium oxalate seen as homogeneous cortical calcification in renal allograft in 2-year-old infant. Calcifications not seen on plain film. **D**, Minimal renal deposition of calcium oxalate produces diffuse increased parenchymal echogenicity in renal allograft in 1-year-old girl. Calcifications not seen on plain film.

month to 8-year follow-up (mean, 3.2 years). The other 12 kidneys had failed, with biopsy evidence of severe calcium oxalate crystal deposition.

Radiographs were available in all 14 patients, including chest films in all 14, abdominal films in 13, and extremity films in 13. Serial extremity radiographs were available in six of the seven children. Time span of follow-up was 3 months to 10 years.

Results

Radiologic abnormalities include nephrolithiasis and/or nephrocalcinosis in the native and/or transplant kidneys (figs. 1A and 1B). All patients had nephrocalcinosis or reported nephrocalcinosis if anephric at time of evaluation. Six of the seven adults and two of the seven children had renal stones or history of stones. In four of the 14 patients, with onset of renal insufficiency serial radiographs demonstrated an increase in density and decrease in size of the kidneys over a 3- to 24-month period. On plain films, nephrocalcinosis is generally diffuse and homogeneous, but may be predominantly cortical or patchy. The kidneys may be normal in size or small and scarred. Cortical calcification was demonstrated on CT in one renal allograft, and diffuse parenchymal nephrocalcinosis was shown by sonography in one allograft when nephrocalcinosis was not evident by plain radiography (figs. 1C and 1D).

Dense vascular calcifications in the soft tissues of the trunk and extremities were present in two of the seven adult patients before transplantation (fig. 2). Another adult patient had faint vascular calcifications probably due to secondary hyperparathyroidism. Nonvascular soft-tissue calcifications were clinically apparent as hard masses in the soft tissues in three patients. The affected areas were not radiographed.

Skeletal abnormalities were present in six of the seven children with oxalosis. Six of the seven patients were osteopenic. Three of the seven children also had a coarse trabecular pattern consistent with renal osteodystrophy. Metaphyseal abnormalities, present in six patients, included dense metaphyseal bands, submarginal metaphyseal lucency, a wide translucent metaphyseal zone with sclerosis of the adjacent diaphysis, and metaphyseal "waisting" or focal narrowing (fig. 3). Other specific bony changes included a radiolucent or dense rim around the epiphyses, carpal, and tarsal bones (six patients) (fig. 4); alternating lucent and dense zones in the flat bones (three patients) (fig. 5); cystic bone changes (four patients) (fig. 6); epiphyseal invagination (two patients) (fig. 7A); drumstick-shaped metacarpals (two patients) (fig. 7B); bulbous growth of rib ends and clavicles (one patient) (fig. 7C); and "woolly" osteosclerosis (one patient) (fig. 8A). Other skeletal abnormalities included rickets (one patient, before treatment), subperiosteal resorption (two patients), rugger-

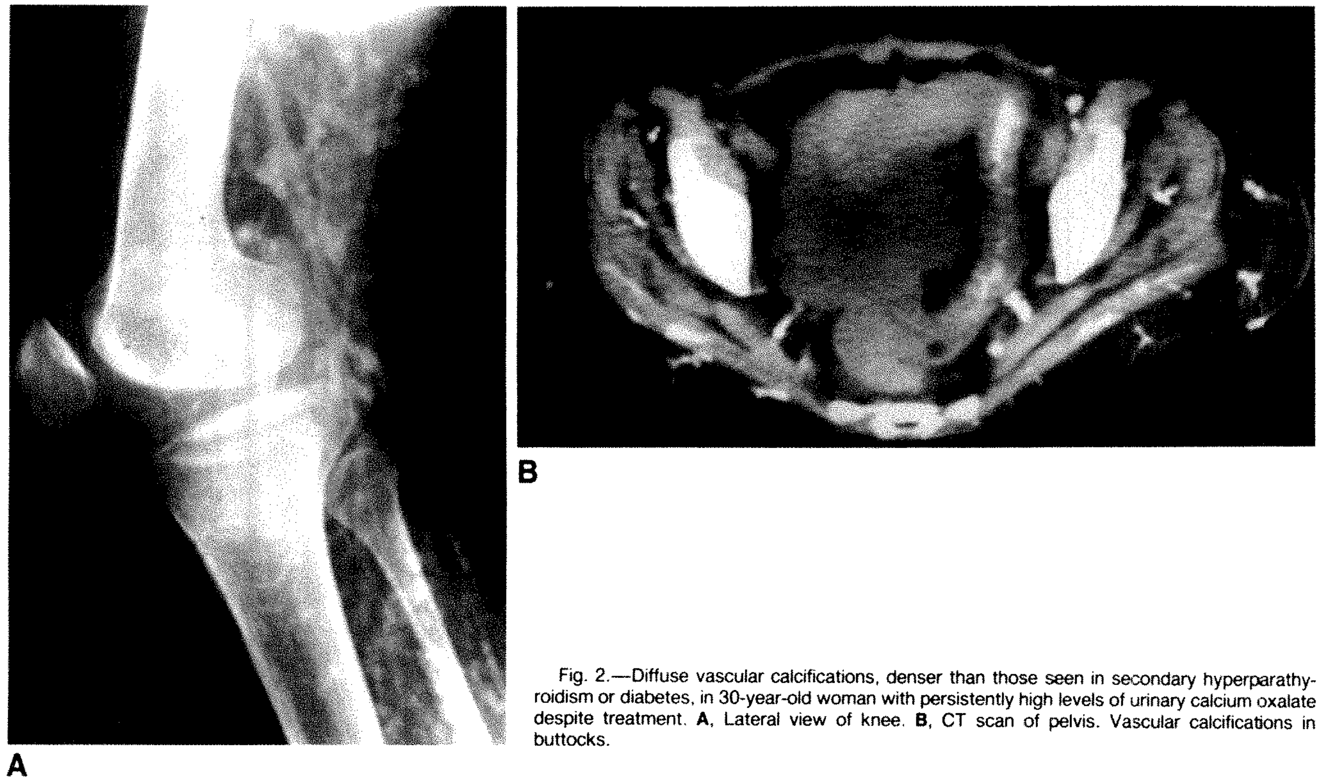

Fig. 2.—Diffuse vascular calcifications, denser than those seen in secondary hyperparathyroidism or diabetes, in 30-year-old woman with persistently high levels of urinary calcium oxalate despite treatment. **A**, Lateral view of knee. **B**, CT scan of pelvis. Vascular calcifications in buttocks.

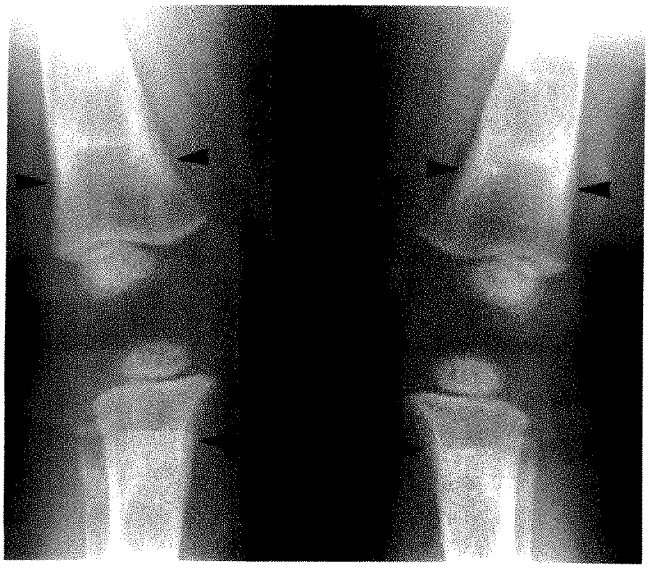

Fig. 3.—Striking wide translucent metaphyseal zone with sclerotic zone adjacent to diaphysis and metaphyseal "waisting" (*arrowheads*) in 18-month-old girl with infantile presentation of hyperoxaluria.

jersey spine (three patients), vertebral bone-within-a-bone appearance (one patient), and multiple pathologic fractures (four patients). The pathologic fractures occurred in the region of the sclerotic zone adjacent to a wide metaphyseal translucent band (fig. 9).

In four of the seven children, sequential extremity films were available, making it possible to correlate the radiographic changes with renal function. All children who presented with uremia had osteopenia and dense metaphyseal bands. With institution of hemodialysis, bone formation resumed at the growth plate. With time, the dense metaphyseal bands "migrated" from the epiphyseal plate toward the diaphysis. With adequate treatment (e.g., renal transplantation), the newly formed bone was relatively normal (fig. 10). The previously uniformly dense metaphyseal bands adjacent to the diaphysis became cystic and then less obvious over time. With inadequate treatment (e.g., anything less than a functioning renal transplant [7]), progressive skeletal abnormalities resulted. Delayed bone maturation and growth dysfunction such as drumstick-shaped metacarpals and epiphyseal invagination occurred. Over time, the trabecular pattern became blurred. The bones gradually developed cystic rarefaction and then eventually "woolly" or "pagetoid" osteosclerosis.

Skeletal abnormalities were absent (three patients) or nonspecific (three patients) in the seven patients who developed renal failure in adulthood. Nonspecific abnormalities included diffuse osteopenia (one patient), osteosclerosis (one patient), and a coarse trabecular pattern (two patients). The other adult patient had "pagetoid" osteosclerosis (fig. 8B). These adults had no other skeletal abnormalities, including changes of secondary hyperparathyroidism.

Bone biopsies in six of the seven children at time of transplantation demonstrated calcium oxalate crystals and no evidence of renal osteodystrophy. One of the six bone biopsies showed normal bone and no calcium oxalate crystals.

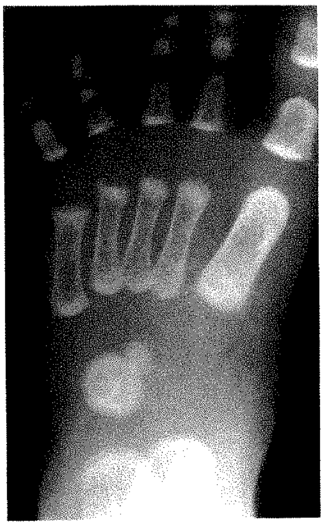

4

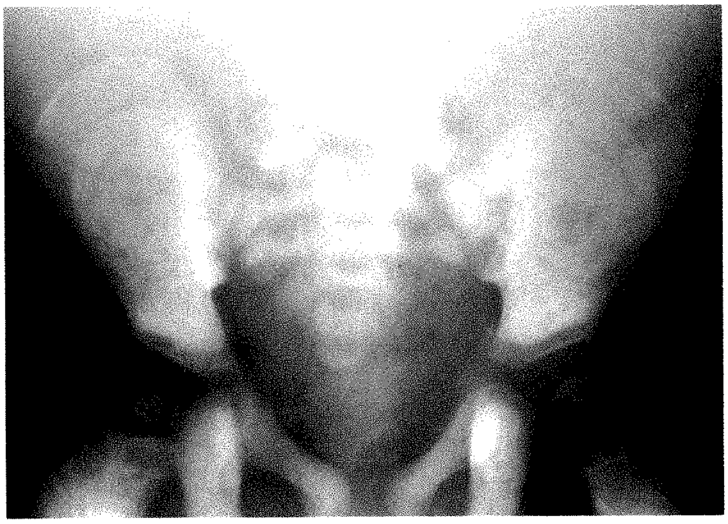

5

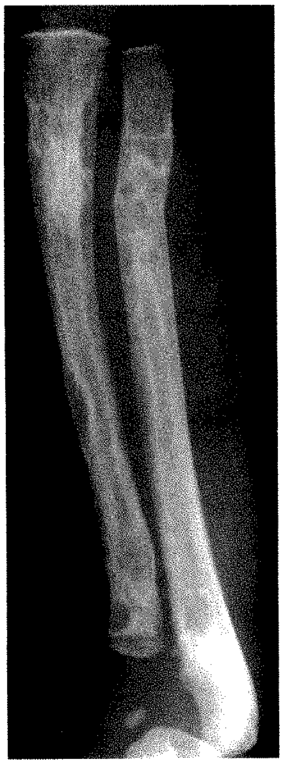

6

Fig. 4.—Dense or lucent peripheral rims may be present in large epiphyses and tarsal and carpal bones as in this 12-month-old girl with hyperoxaluria.

Fig. 5.—Alternating zones of increased density and rarefaction in flat bones of 12-month-old girl with hyperoxaluria several months after successful renal transplantation.

Fig. 6.—Cystic rarefaction in 3-year-old girl with poorly functioning renal transplant. Cystic changes are probably due to combination of histiocytic reaction induced by diffuse calcium oxalate deposition and secondary hyperparathyroidism.

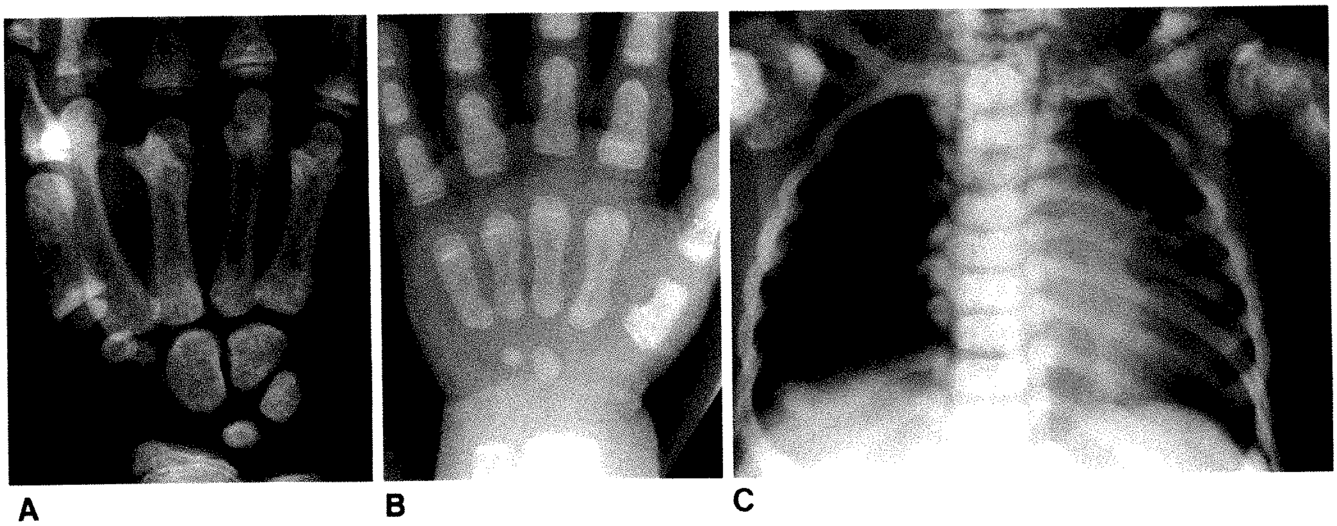

Fig. 7.—Other evidence of growth dysfunction in children on hemodialysis for months to years after failed renal transplants. **A**, Epiphyseal invagination (*arrowheads*) in 7-year-old girl. **B**, Drumstick-shaped metacarpals in 19-month-old girl. **C**, Bulbous growth of clavicles and anterior rib ends in 10-year-old girl.

Discussion

Primary hyperoxaluria is a rare genetic disorder of glyoxylate metabolism. Two specific types have been identified biochemically. Both are transmitted as autosomal recessive traits. In type I hyperoxaluria, there is a deficiency of a alpha-ketoglutarate/glyoxylate carboligase that metabolizes glyoxylate. This results in excessive synthesis of oxalate and

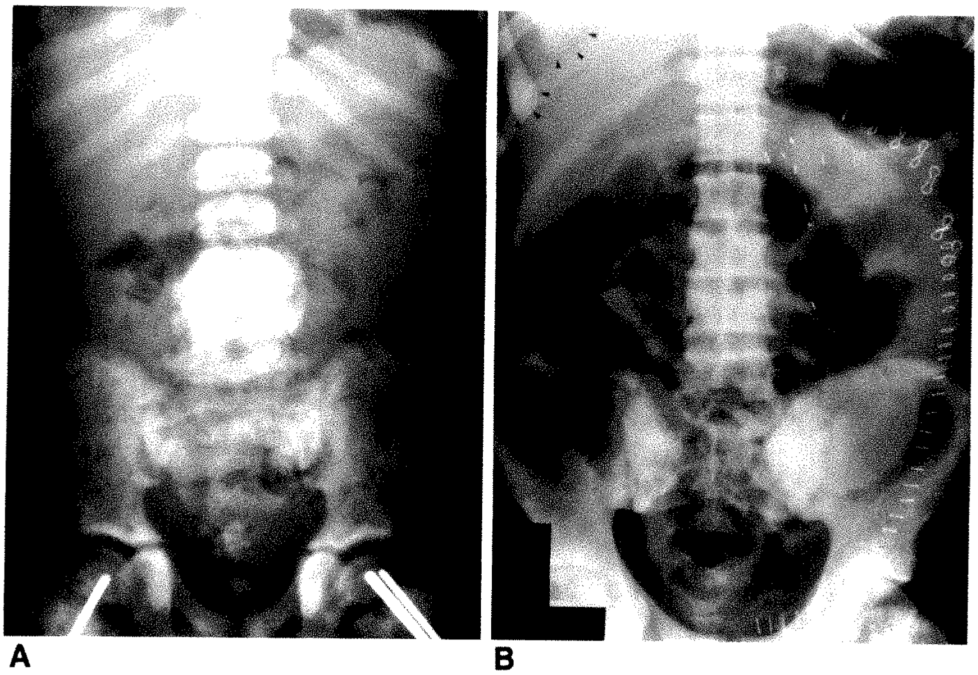

Fig. 8.—Characteristic abnormal bone density in two patients. **A**, "Woolly" pattern in 10-year-old child on long-term hemodialysis. **B**, "Pagetoid" osteosclerosis in 22-year-old adult on long-term hemodialysis. Note bulbous rib ends (*arrowheads*).

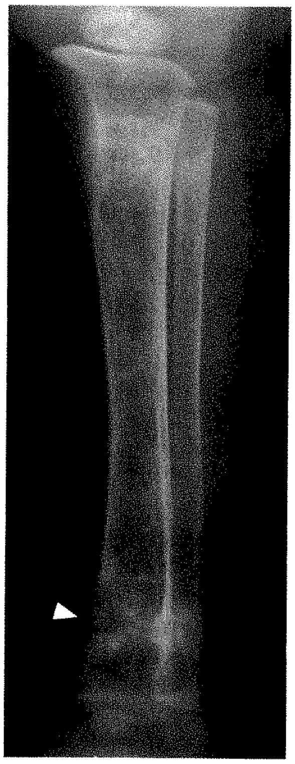

Fig. 9.—Pathologic fractures are common and occur with minor or no trauma. As in this 19-month-old girl on hemodialysis, they typically occur near dense band at metaphyseal-diaphyseal junction (*arrowhead*).

glycolate, which are excreted in the urine. In type II hyperoxaluria, there is a deficiency of leukocyte D-glyceric dehydrogenase activity. The exact cause of excessive oxalate synthesis has not been completely clarified. The second type is exceedingly rare [1].

Clinically, two general presentations of primary hyperoxaluria occur, although a clinical spectrum of disease does exist. The typical patient with primary hyperoxaluria presents in childhood with symptoms of recurrent nephrolithiasis. In 65% of patients, symptoms due to renal calculi begin before age 5 [1]. Recurrent nephrolithiasis leads to recurrent urinary tract infections and chronic pyelonephritis. Renal failure eventually develops as a result of severe interstitial nephritis secondary to oxalate deposits [8]. Death from uremia usually develops before or during the third decade, with an 80% mortality by the 20th year [1]. An adult form of this typical presentation is differentiated only by an older age of onset and a mild severity of disease [1]. An infant or young child may present fulminantly with uremia and chronic renal failure owing to nephrocalcinosis without calculi [3–6]. Although this presentation has been considered rare, it accounted for five of our 14 patients.

Oxalosis is the condition in which the highly insoluble calcium oxalate crystals are deposited in extrarenal tissues. Inflammatory reaction to the crystals causes tissue damage [8]. Calcium oxalate crystals are not actively incorporated into growing tissues (e.g., bone) [9]. The distribution of crystal deposition is probably most closely related to organ vascularity, with precipitation of oxalate crystals when blood concentrations reach a critical level [9]. There also appears to be a predilection for crystal deposition at sites of tissue injury, such as foci of fibrosis or a chronic granulomatous inflammation in lungs or lymph nodes [1, 2]. Major sites of deposition include bone, bone marrow, heart, blood vessels, cartilage, the male urogenital system, the central nervous system, and peripheral nerves [1, 2]. The predilection for crystal deposition in blood vessels probably accounts for reports of deposition in many other organs including thyroid, spleen, liver, thymus, pituitary, adrenal, pancreas, and parathyroids [1, 2, 8]. Arthritis, cardiac conduction defects, localized ischemic lesions of the skin,

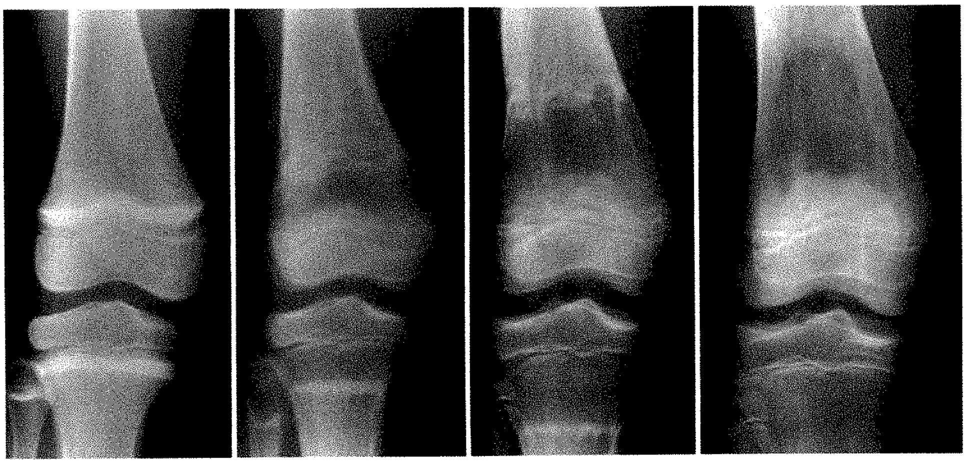

Fig. 10.—Evolution of metaphyseal changes with adequate treatment (e.g., functioning renal transplant). Patient received transplant at age 9 years and is doing well 4 years later. Annual films (left to right). See text for discussion.

and peripheral neuropathy have all been associated with deposition of calcium oxalate crystals in our patients and others [1, 8]. Tissue oxalosis has not been described in the rare type II syndrome.

The kidney is invariably involved in oxalosis [2]. Renal damage results from a combination of nephrolithiasis, nephrocalcinosis, and secondary interstitial fibrosis. Pathologically, there is considerable range in the extent and severity of abnormality. In affected infants and minimally involved renal allografts, the renal tubules, especially the cortical convoluted tubules, contain many pale, doubly refractile crystals arranged in rosettes. Patchy areas of necrosis in the affected tubules are a local consequence of intratubular crystalline deposits. Large crystalline masses are also present in the more heavily scarred areas of interstitial tissue. These crystals probably originally were within tubules, but caused necrosis and disappearance of the tubular cells. Scarring is a result of interstitial inflammatory reaction. The glomeruli are usually normal except for moderate pericapsular fibrosis [1].

Extensive vascular calcifications and other soft-tissue calcifications have been described [10, 11]. The two adult patients in our series with extremely dense vascular calcifications had persistently high urinary oxalate levels and other clinical evidence of diffuse oxalate deposition, including peripheral neuropathy in both and peripheral hard soft-tissue masses in one patient. The vascular calcifications in these cases most likely represent calcium oxalate deposition rather than the thin "tram-track" vascular calcifications characteristic of diabetes or hyperparathyroidism often seen in the typical renal failure patients. Although no other soft-tissue calcifications were radiographically evident in the 14 patients in our series, this is probably because the affected areas were not radiographed, since at least three patients had hard masses in the soft tissues that probably represented calcium oxalate depositions.

Pathologic involvement of bone is common. Crystal depositions occur in the Haversian systems in younger patients and in the marrow at all ages. The crystals lie in sheets on the surface of bone spicules [2]. No or very few crystals are present in the bone matrix, indicating that calcium oxalate deposition is different from the incorporation of hydroxyapatite in the mineralization of bone. The distribution of crystals in bone at the sites of endochondral or intramembranous ossification suggests precipitation at vascular sites when blood levels are high [9]. Bone resorption in severely involved bone is due to a combination of hyperparathyroidism and oxalate crystal-induced histiocytic inflammatory response [9, 10, 12].

The radiographic spectrum of skeletal changes in primary hyperoxaluria and oxalosis is due to many factors that influence bone metabolism in this complex disorder, including high levels of calcium oxalate, secondary hyperparathyroidism, and renal rickets or osteomalacia. Other than tufting of the distal phalanges of the fingers [11], each aspect of the full spectrum of radiographic abnormalities described in the literature [10, 11, 13–16] was present in at least one of our 14 patients.

The metaphyseal abnormalities histologically resemble Harris lines of growth retardation or growth-arrest lines [9]. Very high calcium oxalate levels develop in patients with primary hyperoxaluria and renal failure; therefore, crystal deposition occurs throughout the bones but especially in areas of high vascularity such as the ends of bones. Over time, the inflammatory reaction induced by the very insoluble oxalate crystals causes bone resorption, which can be seen radiographically as cystic rarefaction of the bone; this is especially evident in the previously uniformly dense metaphyseal zones adjacent to the diaphysis. Eventually, the trabecular pattern is blurred and finally destroyed as the bone develops the "woolly" or "pagetoid" pattern characteristic of severe bone disease in primary hyperoxaluria [10, 14]. This pattern is most likely due in part to the diffuse calcium oxalate deposition in bone marrow and the reaction to it (fig. 8).

The treatment of choice in primary hyperoxaluria is renal transplantation [7]. Regular hemodialysis may prolong survival, but does not allow adequate removal of the oxalate. Vigorous medical treatment is necessary in conjunction with transplantation to reduce oxalate synthesis and decrease the tendency of crystallization of calcium oxalate in the urine. The medical treatment consists of pyridoxine to enhance the alternative pathway of glyoxylate metabolism to glycine and therefore reduce the amount of glyoxylate available for conversion to oxalate, oral phosphate to suppress intestinal absorption of calcium with consequent reduction in urinary excretion of calcium, and oral phosphate and magnesium to decrease the tendency of crystallization of calcium oxalate in the urine [17, 18].

REFERENCES

1. Williams HE, Smith LH Jr. Primary hyperoxaluria. In: Stanbury JB, Wyngaarden JB, Fredrickson DS, Goldstein JL, Brown MS, eds. *The metabolic basis of inherited disease*, 5th ed. New York: McGraw-Hill, **1982**:204–228
2. Hockaday TDR, Clayton JE, Frederick EW, Smith LH Jr. Primary hyperoxaluria. *Medicine* **1964**;43:315–345
3. Katzuni E, Sandbank U. Oxalosis. *Arch Dis Child* **1959**;34:60–62
4. Young LW. Radiological case of the month. *Am J Dis Child* **1978**;132:517–518
5. Luers PR, Lester PD, Siegler RL. CT demonstration of cortical nephrocalcinosis in congenital oxalosis. *Pediatr Radiol* **1980**;10:116–118
6. Brennan JN, Diwan RV, Makker SP, Cromer BA, Bellon EM. Ultrasound diagnosis of hyperoxaluria in infancy. *Radiology* **1982**;145:147–148
7. Scheinman JI, Najarian JS, Mauer SM. Successful strategies for renal transplantation in primary oxalosis. *Kidney Int* **1984**;25:804–811
8. Williams HE. Oxalic acid and the hyperoxaluric syndromes. *Kidney Int* **1978**;13:410–417
9. Lagier R, Revell P, Schoenboerner A. Calcium oxalate deposition in growing bone: anatomic and radiologic study in a case of primary oxalosis. *Metab Bone Dis Res Relat* **1982**;4:49–59
10. Brancaccio D, Poggi A, Ciccarelli C, et al. Bone changes in end-stage oxalosis. *AJR* **1981**;136:935–939
11. Breed A, Chesney R, Friedman A, Gilbert E, Langer L, Lattoraca R. Oxalosis-induced bone disease: a complication of transplantation and prolonged survival in primary hyperoxaluria. *J Bone Joint Surg* [*Am*] **1981**;63:310–316
12. Gherardi G, Poggi A, Sisca S, Calderaro V, Bonucci E. Bone oxalosis and renal osteodystrophy. *Arch Pathol Lab Med* **1980**;104:105–111
13. Wiggelinkhuizen J, Fisher RM. Oxalosis of bone. *Pediatr Radiol* **1982**;12:307–309
14. Caffey J. *Pediatric x-ray diagnosis*, 7th ed. Chicago: Year Book Medical, **1978**:1539–1540
15. Carsen GM, Radkowski MA. Calcium oxalosis: a case report. *Radiology* **1974**;113:165–166
16. Kalifa G, Dossans B, Gagnadoux MF, Sauvegrain J. Aspects radiologiques de l'oxalose. *J Radiol* **1979**;60:45–49
17. Dent CE, Stamp TCB. Treatment of primary hyperoxaluria. *Arch Dis Child* **1970**;45:735–745
18. Halverstadt DB, Wenzl JE. Primary hyperoxaluria and renal transplantation. *J Urol* **1974**;111:398–402

MRI of Extracranial Hematomas: Preliminary Observations

Evan C. Unger[1]
Harvey S. Glazer
Joseph K. T. Lee
David Ling

Thirteen patients (16 examinations) with extracranial hematomas (four mediastinum, three pelvis, two calf, two psoas muscle, one liver, one abdominal wall) were examined with magnetic resonance imaging (MRI). With the exception of an acute hematoma (<48 hr), which did not have a distinctive MRI appearance, subacute and chronic hematomas (up to 10 months' duration) had areas of high signal intensity on both T1- (TR 500/TE 30) and T2- (TR 1500/TE 90) weighted pulse sequences. The hematomas in 10 of the patients were also evaluated by computed tomography (CT). The MRI findings complemented those seen on CT. Low-intensity parts of the hematoma on both T1- and T2-weighted images corresponded to areas of high attenuation on CT, whereas high-intensity zones correlated with regions of low attenuation. This observation was more apparent on the T1-weighted images. While older hematomas did not exhibit areas of hyperdensity that would allow a specific diagnosis on CT, MRI did demonstrate regions of high signal intensity indicative of hemorrhage.

The appearance of intracranial hemorrhage on magnetic resonance imaging (MRI) has been described. Initial reports suggested that a hematoma has a high signal intensity on both T1- (short-TR, short-TE) and T2- (long-TR, long-TE) weighted spin-echo (SE) pulse sequences [1–4]. However, subsequent reports have demonstrated that an acute intracranial hematoma may have a low MRI signal intensity and appear isointense or hypointense with surrounding cerebral tissue [5]. More recent studies indicate that the intensity of a hematoma increases with its age [6, 7]. While much work has been done on intracranial hemorrhage, the MRI features of extracranial hematoma have not been thoroughly studied [8]. We undertook this study to evaluate the MRI appearance of extracranial hematomas of varying ages and to compare MRI features with CT findings.

Materials and Methods

From April 1984 to March 1985, 16 MRI examinations were performed on 13 patients with uncomplicated extracranial hematoma. None of these hematomas were associated with tumor, infection, or urine. The subjects were aged 23–65 years (average, 45). Eight were men and five were women. Six of the hematomas were confirmed either by surgery or needle aspiration. In the other seven, the diagnosis was established by a combination of CT findings, strong clinical history (acute onset of localized pain and precipitous drop in hematocrit in an anticoagulated patient), and physical findings (palpable mass). The hematomas were located in the anterior mediastinum (four), pelvis (three), calf (two), psoas (two), liver (one), and anterior abdominal wall (one). They ranged in size from 4 to 25 cm. The age of the hematomas varied from 16 hr to 10 months (average, 61 days). One hematoma was acute (16 hr), 12 were subacute (6 days to 3 months), and three were chronic (4–10 months).

Of 16 MRI examinations, 15 were performed on a Siemens Magnetom, a 0.5-T superconductive magnet. Thirteen of these 15 studies were performed at an operating field strength of 0.35 T and two were carried out at an operating field strength of 0.5 T. One patient was examined with a 2-T (operating at 1.5 T) Siemens Magnetom. With the exception of the two calf hematomas, all studies were obtained with a body coil, which has a useful aperture of

Received July 22, 1985; accepted after revision October 10, 1985.

Presented at the annual meeting of the American Roentgen Ray Society, Boston, April 1985.

[1] All authors: Mallinckrodt Institute of Radiology, Washington University School of Medicine, 510 S. Kingshighway Blvd., St. Louis, MO 63110. Address reprint requests to J. K. T. Lee.

AJR 146:403–407, February 1986
0361–803X/86/1462–0403
© American Roentgen Ray Society

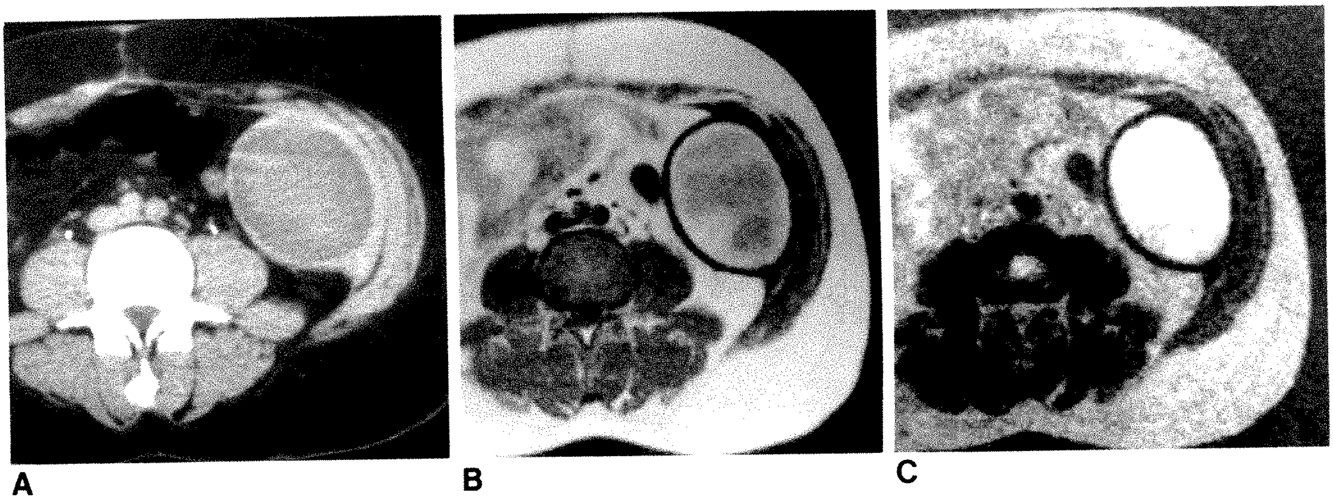

Fig. 1.—3-month-old abdominal wall hematoma after knife wound in 31-year-old man. **A**, On CT, hematoma is hypodense with some central areas of isodense material. Hematoma is surrounded by soft-tissue-density capsule. **B**, T1-weighted (SE 500/30) image shows peripheral areas of high intensity approaching that of fat. Central area of hematoma corresponding to area of relatively higher density on CT has decreased intensity on MRI. Capsule appears as low-intensity rim. **C**, T2-weighted (SE 1500/90) image shows mass with signal intensity greater than that of fat. Heterogeneity of hematoma is less well appreciated but could be seen after adjusting window settings.

59 cm. The two calf hematomas were examined with a 25-cm-diam head coil. Data were acquired and displayed using 256 × 256 matrix elements. The pixel size was 2 × 2 mm for the body coil and 1.2 × 1.2 mm for the head coil. Transaxial views were obtained in all patients; additional sagittal and coronal images were obtained in some patients.

While a variety of pulse sequences were attempted initially, 12 of 13 patients were examined with both a T1- and a T2-weighted SE technique. The most commonly used sequences were 500 msec TR with 30 msec TE (T1 weighting) and 1500 msec TR with 90 msec TE (T2 weighting).

Ten of 13 patients had a CT examination (12 examinations), usually within 1 day of the MRI study. All CT studies were performed on a sub-5-sec scanner (Siemens Somatom DR3). Ten patients had noncontrast scans only; two patients had both pre- and postcontrast scans.

All MRI and CT studies were retrospectively reviewed. MRI features were compared to CT findings. In addition, the signal intensity (pixel brightness) of the hematoma, skeletal muscle, and subcutaneous fat was measured. In cases in which the hematomas had areas of high and low signal intensity, only the high-signal-intensity area was measured and recorded. Measurement of the signal intensity of skeletal muscle and subcutaneous fat was obtained adjacent to the hematoma in an effort to decrease the effect of field inhomogeneity. The signal intensity was obtained in absolute numbers by defining the area of interest with a cursor on a CRT monitor. In order to minimize the effect of technical variability in signal intensity, we elected to calculate signal intensity ratios between hematomas and skeletal muscle/subcutaneous fat rather than absolute intensity values. Signal intensity ratios were obtained from both T1- and T2-weighted images.

Results

MRI Features

On six of the examinations (one acute, two subacute, three chronic) the hematomas appeared homogeneous on both T1- and T2-weighted images. On the other 10 examinations (subacute), the hematomas were inhomogeneous with a central low-intensity area surrounded by a higher-intensity periphery (fig. 1). This appearance was better appreciated on T1-weighted images than on T2-weighted images. On T1-weighted images, the signal intensity of the hematoma appeared equal to that of fat in one and slightly less than that of fat in 14 examinations (figs. 1–4). The signal intensity of the 16-hr hematoma was much lower than that of fat and only slightly higher than that of muscle (Fig. 5). On T2-weighted images, the signal intensity of hematomas was higher than that of subcutaneous fat in all cases.

A peripheral low-intensity capsule was noted in nine examinations (age, 1–10 months; average, 100 days) and not seen in seven (age, 16 hr to 1 month; average, 29 days).

Table 1 lists the mean intensity ratios between the hematoma and muscle or fat on T1- and T2-weighted images. These quantitative data supported our visual impression that the signal intensity of a subacute or chronic hematoma approaches that of fat on T1-weighted images. The mean mass/muscle and mass/fat intensity ratios derived from T1-weighted images of subacute and chronic hematomas were higher than that of the acute hematoma. However, since there was only one acute hematoma, it was not possible to test for statistical significance. Although there was no statistically significant difference between the mean mass/muscle intensity ratio of subacute and chronic hematomas, the mean mass/fat intensity ratio of subacute hematomas was significantly higher than that of chronic hematomas ($p < 0.05$), suggesting that the intensity of these two groups of hematomas decreases over time on T1-weighted images.

The mean mass/muscle and mass/fat intensity ratios derived from T2-weighted images of subacute and chronic hematomas were not statistically different. No T2-weighted images were obtained on the acute hematoma.

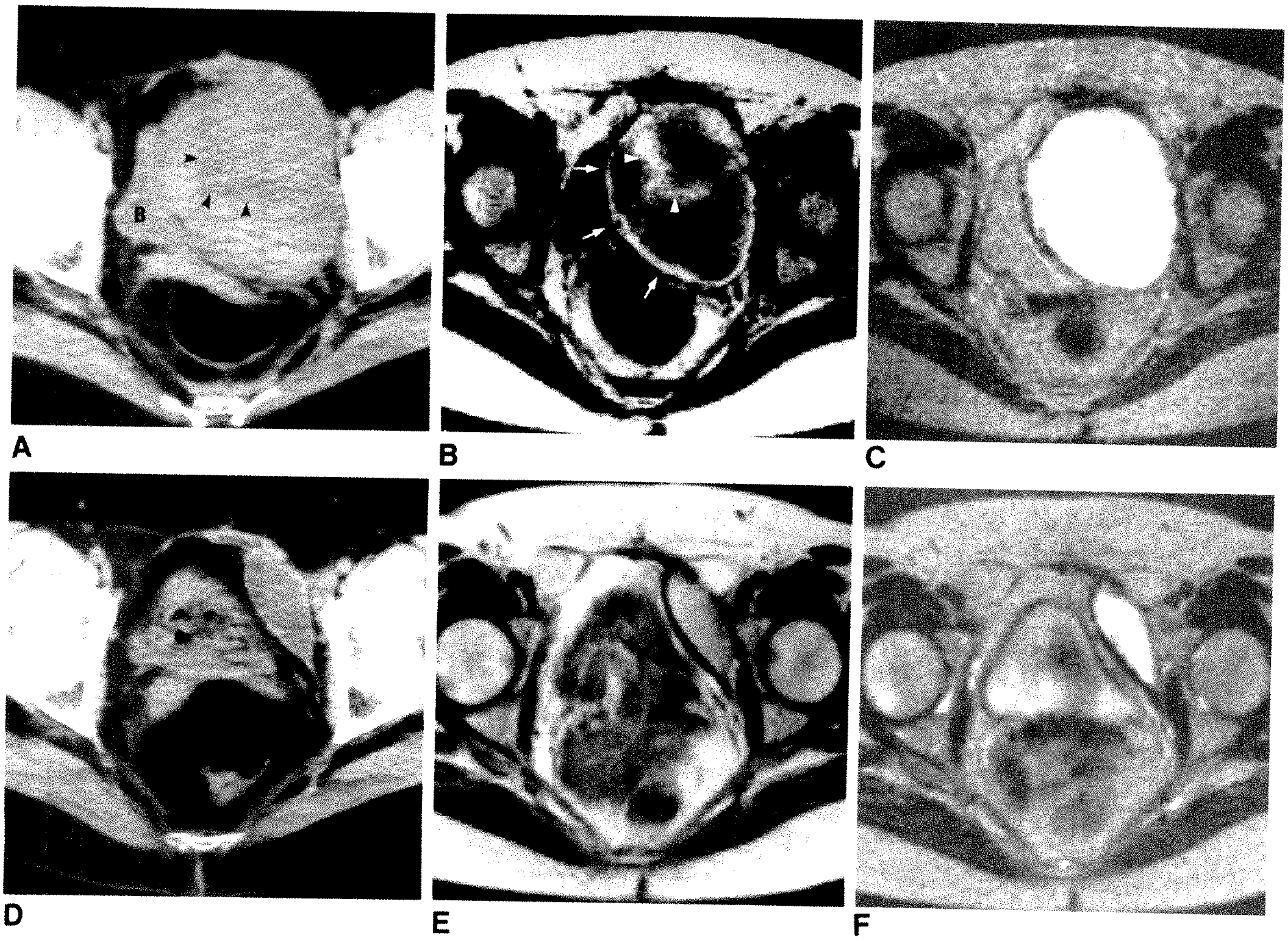

Fig. 2.—33-day-old hematoma in 53-year-old woman who had been on anticoagulant therapy. **A**, CT scan shows large pelvic mass displacing urinary bladder (B) to right. With exception of linear band (*arrowheads*), attenuation value of central part of hematoma is slightly higher than that of pelvic musculature. **B**, T1-weighted (SE 500/30) image at same level shows hyperintense band (*arrowheads*) corresponding to hypodense area on CT. Central part of hematoma, which was hyperdense on CT, is of low intensity on MRI. Peripheral margin of hematoma appears hyperintense on MRI. Surrounding capsule (*arrows*) of low intensity is also seen. **C**, T-2 weighted (SE 1500/90) image shows hematoma as high-intensity mass. Heterogeneous parts of hematoma are less well defined but could be seen after adjusting window settings. **D**, Follow-up CT scan at 300 days shows uniformly hypodense mass surrounded by thin rim of soft-tissue density. **E**, On T1-weighted (SE 500/35) image, 300-day-old hematoma is homogeneous and has signal intensity approaching that of fat. Well defined, low-intensity capsule is present. **F**, On T2-weighted (SE 1500/90) image, signal intensity of hematoma exceeds that of fat. Low-intensity capsule is again noted.

CT Features

Of 12 hematomas studied with CT, eight appeared heterogeneous and four appeared homogeneous. The attenuation of the hematoma appeared greater than that of paraspinal muscles in seven (age, 6–33 days; average, 18 days) and equal to or less than that of paraspinal muscles in five (age, 1–10 months; average, 4 months). A peripheral rim or capsule of soft-tissue density was noted in four hematomas aged 3–10 months.

MRI–CT Comparison

Of the six MRI examinations in which the hematoma had a homogeneous appearance, four had CT examinations. Of these, all appeared homogeneous on CT.

Of 10 MRI examinations in which the hematoma had inhomogeneous appearance, eight had CT examinations. All eight hematomas had an inhomogeneous appearance on CT as well. In this group, the central part of the hematoma had a low MRI signal intensity, whereas the peripheral area had a much higher MRI signal intensity. On CT, the central part of the hematoma was isodense or hyperdense (higher than paraspinal muscle), whereas the peripheral area was hypodense (lower than paraspinal muscle).

Of eight hematomas that had a low-intensity capsule on MR, seven had CT examinations. Four of these seven cases had a soft-tissue density capsule on CT. In no case was a capsule shown by CT and not by MRI.

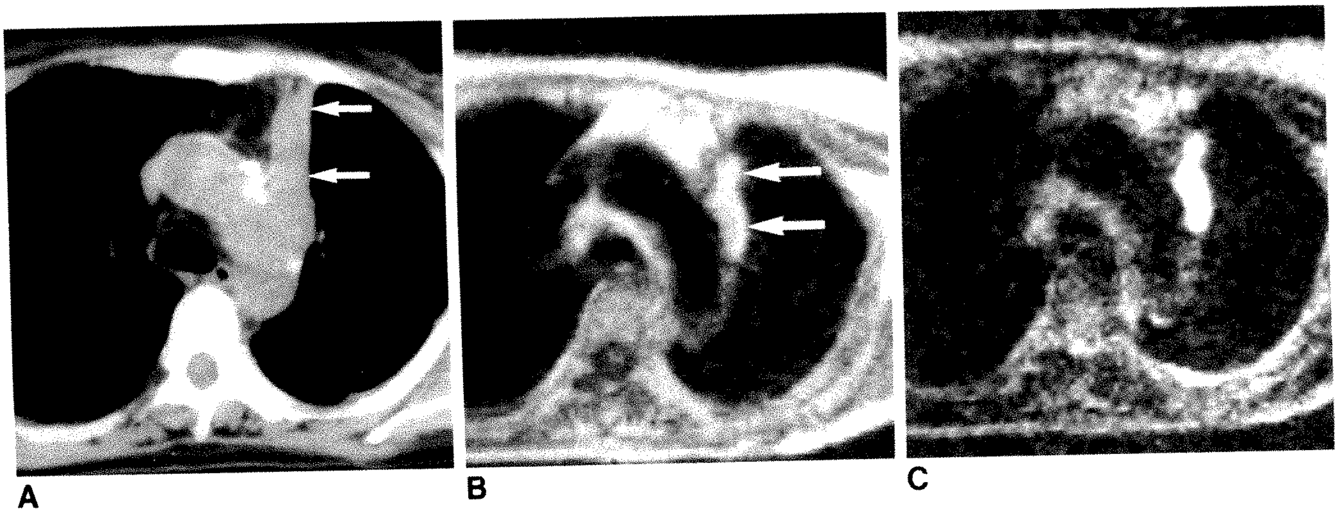

Fig. 3.—1-month-old mediastinal hematoma, after aneurysm repair, in 58-year-old woman. **A**, CT scan shows soft-tissue density mass (*arrows*) in anterior mediastinum. **B**, On T1-weighted (SE 500/30) image, hematoma (*arrows*) is nearly isointense with fat. **C**, On T2-weighted (SE 2100/90) image, signal intensity of hematoma is higher than that of fat.

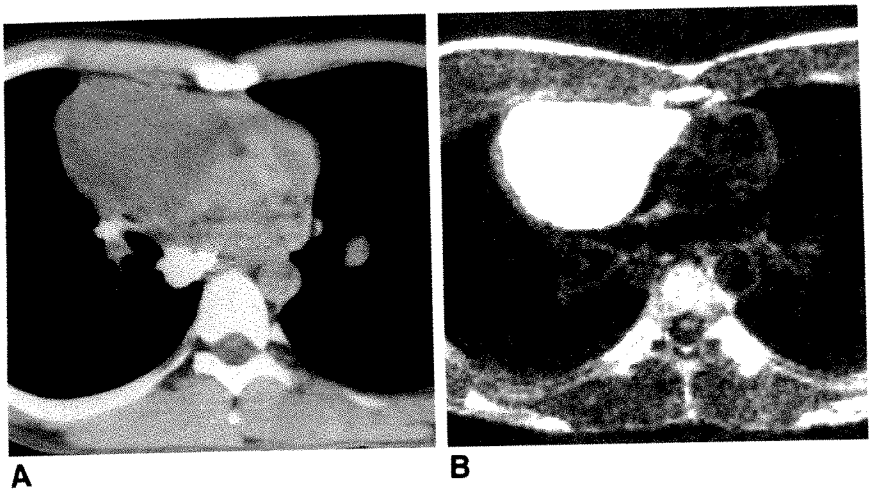

Fig. 4.—2-month-old hemorrhage in thymic cyst in 22-year-old man. **A**, CT scan shows homogeneous, hypodense anterior mediastinal mass. **B**, T1-weighted (SE 300/30) image shows well circumscribed, homogeneous anterior mediastinal mass. Intensity of mass is similar to that of fat.

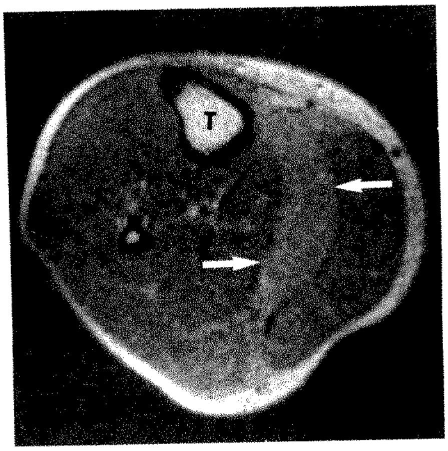

Fig. 5.—16-hr-old posttraumatic hematoma in left calf of 38-year-old man. T1-weighted (SE 300/30) image shows elliptical structure (*arrows*) with intensity slightly greater than that of muscle and much less than that of fat. Patient was examined feet-first, accounting for right-left reversal. T = tibia.

Discussion

Our data show that an extracranial hematoma may appear homogeneous or heterogeneous on MRI. While a hematoma less than 48 hr old had a signal intensity only slightly greater than that of muscle, a subacute or a chronic hematoma (1 week to 10 months) has a signal intensity similar to that of fat on T1-weighted images. The observed increased signal intensity of a hematoma after 48 hr on T1-weighted images is suggestive of a shortening of its T1 value.

The mechanism of T1 shortening in a hematoma is probably very complex. However, recent work by Bradley and Schmidt [9] suggests that methemoglobin at least partially accounts for the observed changes. As a hematoma ages, hemoglobin, which contains ferrous iron, is oxidized to methemoglobin, which contains ferric iron [9]. Bradley and Schmidt [9] have shown that oxyhemoglobin is diamagnetic and that deoxyhemoglobin, although paramagnetic, has little or no effect on the T1 relaxation time of aqueous solution secondary to shielding of the paramagnetic center. Methemoglobin, on the other hand, causes pronounced T1 shortening effects. As in vitro blood stored under hypoxic conditions ages, the concentration of methemoglobin increases, reaching a maximum at 80–90 hr. T1 shortening parallels the formation of methemoglobin [9].

TABLE 1: **Mean Intensity Ratios of Hematomas**

	Acute (16 hr) [$n = 1$]	Subacute (6 days to 3 months) [$n = 7$]	Chronic (4–10 months) [$n = 3$]
Hematoma/muscle:			
T1-weighted image . . .	1.78	3.29 ± 0.96	2.19 ± 0.22
T2-weighted image . . .	. . .	5.36 ± 1.96	6.61 ± 1.66
Hematoma/fat:			
T1-weighted image . . .	0.35	0.84 ± 0.09	0.69 ± 0.06
T2-weighted image . . .	. . .	1.40 ± 0.35	1.79 ± 0.21

Note.—Data on 11 examinations: Digitized floppy disks on only 12 of the 16 examinations were available or technically adequate for measurement of signal intensity. In addition, the one patient examined at 1.5 T was not included for measurement.

Our data show that with the exception of the acute hematoma (<48 hr), subacute and chronic hematomas (up to 10 months' duration) had a high signal intensity on both T1- and T2-weighted images. While most fluid-containing structures and benign and malignant neoplasms also may have a high signal intensity on T2-weighted images, none of these processes has a high signal intensity on T1-weighted images. In our series, the signal intensity ratio between a hematoma and fat was 0.84 ± 0.09 on T1-weighted images for subacute hematomas and 0.69 ± 0.6 for chronic hematomas. In contrast, the tumor/fat intensity ratio was much lower, with a mean of 0.44 ± 0.05 in our previously published series [10]. Inasmuch as subacute and chronic hematomas can be differentiated from neoplasms on the basis of their signal intensity differences on T1-weighted images, it may be difficult to distinguish an uncomplicated hematoma from hemorrhage into a tumor. Whether these two entities can be differentiated by quantitative means (e.g., intensity ratios) remains to be seen.

Our comparison of MRI and CT features of hematoma yielded several interesting observations. Most of the subacute hematomas appeared inhomogeneous with a low-intensity center and a high-intensity periphery on MRI. The low-intensity center corresponded to an area of high attenuation, whereas the peripheral high-intensity zone correlated with an area of low attenuation on CT. This finding was best appreciated on the T1-weighted images but could also be seen on T2-weighted images after adjusting the window settings. Although it is well established that the high density of a hematoma on CT is largely due to its protein content [11, 12], the underlying mechanism accounting for the observed MRI appearance is unclear and may be related to the differential distribution of methemoglobin, protein, and water molecules within a hematoma.

The MRI findings in patients with extracranial hematomas complement those seen on CT. Although acute hematomas do not have a distinctive MRI appearance, they usually can be diagnosed on CT because of their characteristic high attenuation (higher than that of paraspinal muscles). In older hematomas that do not exhibit areas of hyperdensity, it may not be possible to make a specific diagnosis by CT. In contrast, it may be possible to diagnose older hematomas by MRI because of their high signal intensity on both T1- and T2-weighted images. Although the exact role of MRI in the evaluation of hematomas is uncertain, our study suggests that it may provide a more specific diagnosis in less acute cases (i.e., without hyperdensity on CT).

REFERENCES

1. Bailes DR, Young IR, Thomas DJ, Straughan K, Bydder GM, Steiner RE. NMR imaging of the brain using spin-echo sequences. *Clin Radiol* **1982**;33:395–414
2. Bydder GM, Steiner RE, Young IR, et al. Clinical NMR imaging of the brain: 140 cases. *AJR* **1982**;139:215–236
3. Crooks LE, Mills CM, Davis PL, et al. Visualization of cerebral and vascular abnormalities by NMR imaging: the effects of imaging parameters on contrast. *Radiology* **1982**;144:843–852
4. Brant-Zawadzki M, Davis PL, Crooks LE, et al. NMR demonstration of cerebral abnormalities: comparison with CT. *AJNR* **1983**;140:847–854
5. Han JS, Kaufman B, Alfidi RJ, et al. Head trauma evaluated by magnetic resonance and computed tomography: a comparison. *Radiology* **1984**;150:71–77
6. DeLaPaz RL, New PJ, Buonanno FS, et al. NMR imaging of intracranial hemorrhage. *J Comput Assist Tomogr* **1984**;8:599–607
7. Sipponen JT, Sepponen RE, Sivula A. Chronic subdural hematoma: demonstration by magnetic resonance. *Radiology* **1984**;150:79–85
8. Cohen J, Weinreb JC, Maravilla KR. Fluid collections in the intraperitoneal and extraperitoneal spaces: comparison of MR and CT. *Radiology* **1985**;155:705–708
9. Bradley WG Jr, Schmidt PG. Effect of methemoglobin formation on the MR appearance of subarachnoid hemorrhage. *Radiology* **1985**;156:99–103
10. Glazer HS, Lee JKT, Levitt RG, et al. Differentiation of radiation fibrosis from recurrent tumor by MRI. *Radiology* **1985**;156:721–726
11. Wolverson MK, Crepps LF, Sundaram M, Heiberg E, Vas WG, Shields JB. Hyperdensity of recent hemorrhage at body computed tomography: incidence and morphologic variation. *Radiology* **1983**;148:779–784
12. Norman D, Price D, Boyd D, Fishman R, Newton TH. Quantitative aspects of computed tomography of the blood and cerebrospinal fluid. *Radiology* **1977**;123:335–338

Solenoid Surface Coils in Magnetic Resonance Imaging

Robert B. Lufkin[1]
Jan Votruba[2]
Murray Reicher[1]
Lawrence Bassett[1]
S. David Smith[1]
William N. Hanafee[1]

A nonplanar solenoidal surface radiofrequency coil is used as a receiver with a conventional transmitter coil in a magnetic resonance imaging system. The improved signal-to-noise ratio, compared with that of conventional fixed saddle or solenoid receiver coils, permits higher resolution imaging and thinner image sections. In addition, the problem of signal dropoff that occurs in deep structures with planar and other noncircumferential surface coils is eliminated. Solenoid surface coils are particularly useful in imaging deep structures in anatomic regions that do not fit standard head and body coils, such as the neck, knees, and other smaller body parts.

The weak coupling that occurs in magnetic resonance imaging (MRI) when large body or head coils are used to image smaller structures, such as the neck or extremities, results in poor signal-to-noise response and generally poor image quality. Planar surface coils have recently been used in this situation. They were initially used for in vivo phosphorus spectroscopy [1, 2]. When applied to imaging, a dramatic improvement in image quality for small, superficial structures over conventional coil types was possible [3, 4]. Surface coils have a strong coupling and high signal-to-noise response to nearby signals, which drop off rapidly beyond one radius from the center of the coil [5]. They are therefore limited to imaging superficial structures only. The planar surface coil may be modified to a solenoidal configuration that surrounds the patient. This allows excellent signal-to-noise performance without the associated deep signal dropoff of the flat coils.

Materials and Methods

By separating the receiver coil from the transmitter coil, it is possible to optimize each coil for its particular function. The standard body saddle configuration transmitter coil was used for radiofrequency (RF) transmission. This coil was large (55.9 × 32.4 cm), with a relatively low quality factor (Q, see discussion) and had good RF homogeneity in order to produce uniform tip angles.

The receiver coil should be as small as possible relative to the body part being examined and have a high Q. The surface coil was made up of several turns of thin copper foil. The foil is more efficient than solid conductors because of the tendency for flux to concentrate at the surface of the material at the higher frequencies used in MRI. Hollow copper tubing is even more efficient than the foil but was not used because its relative inflexibility limits how the coils are applied. The use of flexible copper foil allowed the coils to be applied directly like a belt around the patient and secured with Velcro fasteners (fig. 1). The number of turns was determined by the eventual decrease in coil Q due to the effects of phase shift and distributed capacitance with increasing conductor length. All the solenoidal coils have lengths less than lambda/10 where lambda = free space wavelength at 12.8 MHz (23 m) [5]. Various sizes (diameters of 3–50 cm) were made for imaging structures of different sizes. Coil leads were made of tinned pure copper and kept to a minimum length to avoid adding unnecessary inductance to the circuit.

The inductive coupling of the surface coils to the transmitter was not a critical factor that allowed greater flexibility in their application. They did not disturb the transmitter field

Received July 8, 1985; accepted after revision October 1, 1985.

This work was supported by Public Health Service grant 1K08 CA 00979-01 awarded by the National Cancer Institute, and by the University of California Cancer Research Coordinating Committee funds.

[1] Department of Radiological Sciences, UCLA School of Medicine, Los Angeles, CA 90024. Address reprint requests to R. B. Lufkin.

[2] Fonar Corp., Melville, NY 11747.

AJR 146:409–412, February 1986
0361–803X/86/1462–0409

© American Roentgen Ray Society

appreciably even if oriented parallel to the transmitter coil. A pair of protection diodes was sufficient to protect the preamplifier during the RF pulse. The vertical orientation of the main magnetic field in our system allowed the RF coils to be placed parallel to the long axis of the patient, which was ideal for imaging the neck and extremities.

Images were obtained on a 0.3-T permanent magnet imaging system (Fonar β-3000) using a two-dimensional Fourier-transform multislice spin-echo (SE) technique with a repetition time (TR) of 500 msec and an echo delay time (TE) of 28 msec. The images were acquired on either a 256 × 256 or 512 × 512 matrix and displayed on a 512 × 512 image matrix. High-resolution image acquisition was possible with pixels as small as 0.375 mm^2. Slice thickness was variable down to 3 mm with an interslice gap of 2 mm. Four signal averages were generally used, resulting in an imaging time of 8.5 min for seven slices with the standard 256 × 256 acquisition matrix. A uniform phantom was filled with 2.5 mM NiCl (T1 = 460 msec at 0.3 T), which produces a consistently high signal using this pulse sequence (SE 500/28). Normal volunteers were also scanned after giving informed consent.

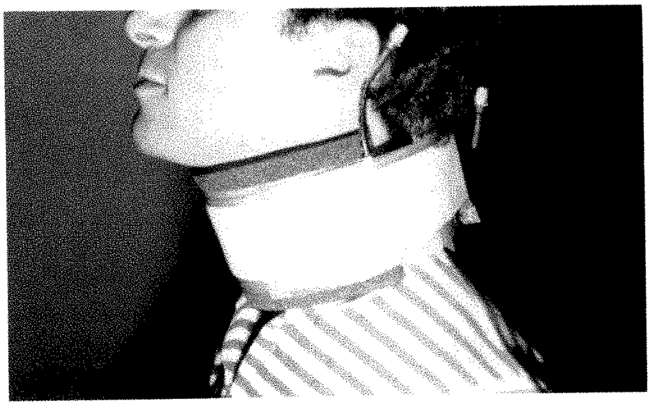

Fig. 1.—Solenoid surface coil is applied like collar for imaging neck.

Results

The strong coupling of the surface coils resulted in improved signal-to-noise ratio over images obtained with the standard body and head coils (figs. 2 and 3). Signal-to-noise ratios recorded from the 9-cm and 14-cm planar (near the coil surface), solenoidal surface, and conventional head and body coils from the phantom were 55, 53, 50, 28, and 9, respectively. The improvement in signal-to-noise ratio allowed the use of steeper magnetic field gradients in order to obtain thinner sections and higher spatial resolution or "zooming" (fig. 4). These higher resolution images were clearly superior to images of the same patient without surface coils [6, 7]. In addition, the problem of rapid dropoff of signal with distance when using planar surface coils did not occur (fig. 3). Even deep structures could be imaged at high resolution. A variety of body parts were studied using appropriately sized coils.

Discussion

Signal-to-noise ratio (S/N) in MR receiver coils is represented by the following relation:

$$S/N \approx \sqrt{Q_L * \eta} \qquad (1)$$

where Q_L is the quality factor of the coil loaded with a patient

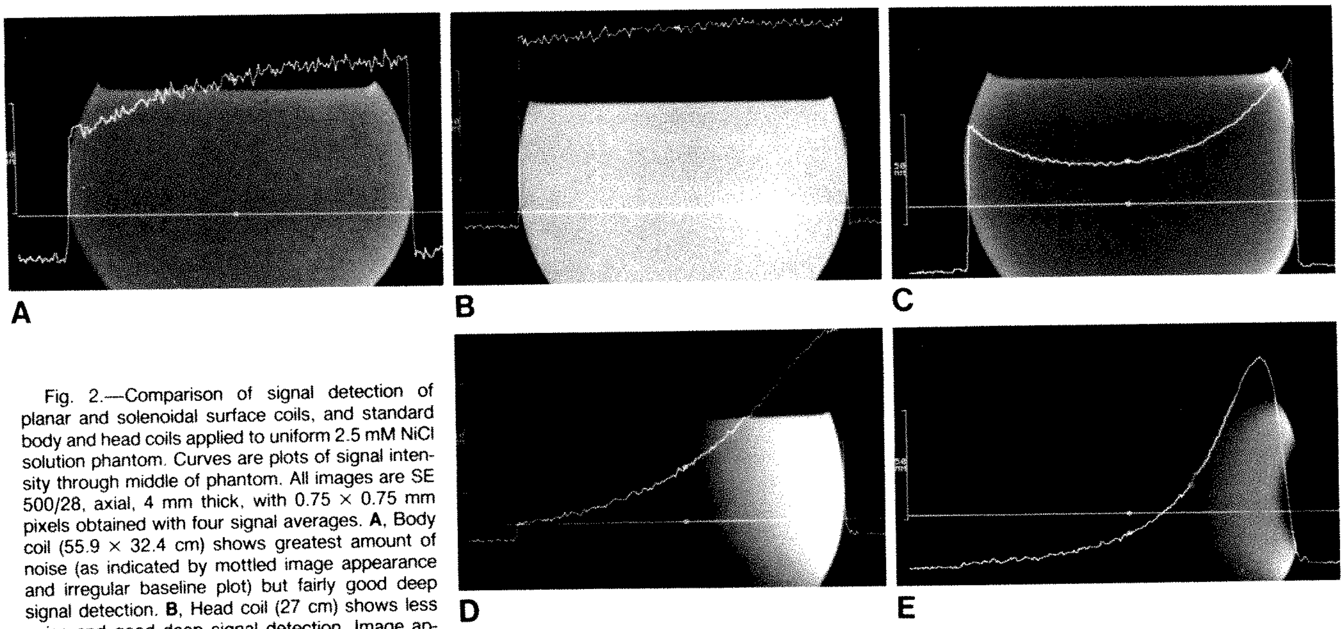

Fig. 2.—Comparison of signal detection of planar and solenoidal surface coils, and standard body and head coils applied to uniform 2.5 mM NiCl solution phantom. Curves are plots of signal intensity through middle of phantom. All images are SE 500/28, axial, 4 mm thick, with 0.75 × 0.75 mm pixels obtained with four signal averages. **A**, Body coil (55.9 × 32.4 cm) shows greatest amount of noise (as indicated by mottled image appearance and irregular baseline plot) but fairly good deep signal detection. **B**, Head coil (27 cm) shows less noise and good deep signal detection. Image appears slightly brighter due to slightly different window setting. **C**, 14.5-cm solenoid surface coil shows slightly less deep signal intensity but markedly less image noise. **D**, 14-cm planar surface coil shows low noise and high superficial signal detection but rapid signal dropoff with increasing distance from the coil surface. **E**, 9-cm planar surface coil shows better superficial signal-to-noise ratio but even more rapid signal dropoff with increasing distance from coil surface.

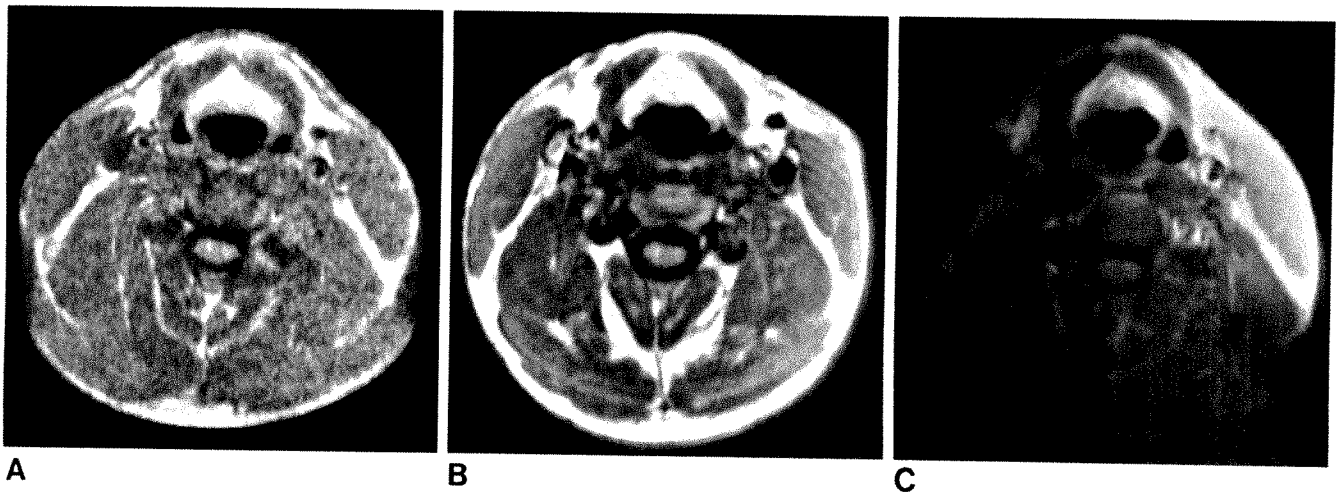

Fig. 3.—Normal neck with body coil, solenoidal surface coil, and planar surface coil; same imaging parameters were used as in fig. 2. **A**, Images obtained using body coil have good signal uniformity but rather poor signal-to-noise ratio, measured to be 9. **B**, Using 14.5-cm solenoid surface coil, signal-to-noise ratio is dramatically improved (50) while reasonable signal uniformity is maintained. **C**, Images produced using 9-cm planar surface coil resulted in even better signal-to-noise ratio near coil surface (55) but marked loss of signal from deep structures.

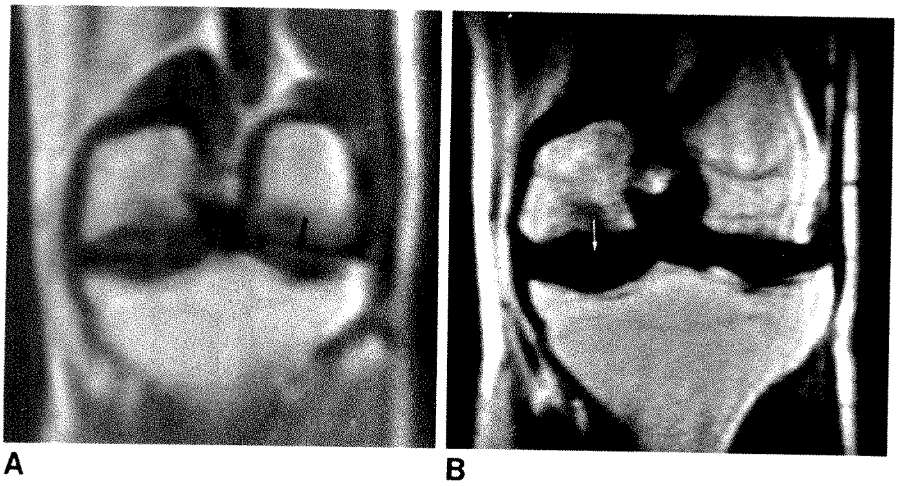

Fig. 4.—27-year-old with history of osteochondritis dissecans involving left medial femoral condyle was studied using standard body coil and solenoid surface coil. Both studies were SE 500/28, coronal, with four signal averages. **A**, With body coil, standard 9-mm-thick slices with 1.33 × 1.33 mm pixels were obtained. Although articular cartilage (*arrow*) can be detected, no definite abnormalities are seen. **B**, When solenoidal surface coil was used, improved signal-to-noise ratio allowed use of steeper gradients and higher resolution images. This section is 4 mm thick with 0.75 × 0.75 mm pixels. Low-signal osteochondral body (*arrow*) is now visible within articular cartilage.

and η is the filling factor of the coil (which also depends on the relation of the patient to the coil). The quality factor of the coil is described by the following equation:

$$Q = (\text{frequency})/(a + b\sqrt{\text{frequency}} + d * \text{frequency}^2) \qquad (2)$$

where a is proportional to the DC resistivity of the coil material (copper), b is proportional to the RF resistivity of the coil material, and d is dependent on coil loading by the patient. At the higher frequencies currently used for imaging of 12.8 MHz (0.3 T) and greater, the frequency squared term (and therefore the effects of coil loading by the patient) dominates in the denominator of formula 2 and consequently determines the signal-to-noise ratio in these coils. This is true for coils whose design has been optimized such that the noise due to coil materials is minimized ($Q_{\text{empty}} \gg Q_{\text{loaded}}$).

There is a significant improvement in coil loading and filling factor with surface coils over standard body coils resulting in improved signal-to-noise ratio and image quality. This allows the production of thin sections and high-resolution images essential for many applications. The solenoid coil configuration also has a theoretical threefold improvement in signal-to-noise ratio over the conventional saddle configuration used for head and body coils in systems with horizontal main magnetic field axes (the majority of superconducting and resistive systems) [8]. In practice, this difference may be less significant because of variation in filling of the coils [9].

Planar and other noncircumferential surface coils have a marked loss of signal beyond one radius from the center of the coil [10–12]. This dropoff in signal intensity limits the effectiveness of this coil when imaging deeper structures. Only superficial structures within roughly one radius of the coil's center may be imaged with satisfactory signal-to-noise performance.

The solenoid surface coil does not have this limitation. By extending the planar coil into a solenoidal design surrounding the patient, any point in the imaging volume lies within one radius from the coil center. The deep signal dropoff therefore is less pronounced, resulting in images of more uniform intensity. This simplifies relaxation time calculations and the use of simulated or interpolated pulse-sequence images.

Solenoid surface coils are easily applied to the patient and are comfortable to wear during scanning. They tend to have greater stability in their attachment to the patient than planar surface coils, which must be placed under the patient or taped in position. This minimizes coil movement and makes it easier to maintain the necessary orientation to minimize inductive coupling and remain orthogonal to the main field. It is possible to use solenoid surface coils to image a variety of different structures that do not fill standard head or body coils. A 15-cm coil works well for imaging the neck and knee; 20-cm coils are used for imaging the temporal bone and tongue base; 40-cm solenoidal surface coils may be applied directly to the chest for mediastinal studies. Because the coils must of course be oriented perpendicular to the main magnetic field, they work best for the above applications in a system with a vertical field. In a system with a horizontal field, the coils would work well on the breast or similarly oriented structures.

The major difference between the work reported here and previous work on surface coil imaging is the use of the solenoid configuration to encircle the patient while still maintaining the coil's proximity to the patient. This preserves strong coupling of the surface coil and the region of interest without the problem of loss of signal intensity from deep structures.

Solenoid surface coil imaging should be very useful in MRI of the neck, joints of the extremities, and breasts, depending on the orientation of the main magnetic field of the imager. The technique allows high-resolution thin-section imaging of both superficial and deep tissues not possible with planar surface coils.

REFERENCES

1. Ackerman JJH, Grove TH, Wong GG, Gadian DG, Radda GK. Mapping of metabolites in whole animals by ^{31}P NMR using surface coils. *Nature* **1980**;283:167–170
2. Gadian DG. *Nuclear magnetic resonance and its applications to living systems*. Oxford: Clarendon, **1982**
3. Bernardo ML, Cohen AJ, Lauterbur PC. Radiofrequency coil designs for nuclear magnetic zeugmatographic imaging. In: *IEEE proceedings of the international workshop on physics and engineering in medical imaging*. March **1982**:277–284
4. Axel L. Surface coil magnetic resonance imaging. *J Comput Assist Tomogr* **1984**;8:381–384
5. Smyth WR. *Static and dynamic electricity*. New York: McGraw-Hill, **1968**
6. Reicher MA, Rauschning W, Gold RH, Bassett LW, Lufkin RB, Glen W Jr. High-resolution magnetic resonance imaging of the knee joint: normal anatomy. *AJR* **1985**;145:895–902
7. Lufkin R, Hanafee W. Application of surface coils to NMR anatomy of the larynx. *AJNR* **1985**;6:491–497
8. Hoult DI, Richards RE. Signal to noise ratio of nuclear magnetic resonance experiment. *J Mag Res* **1976**;24:71–85
9. Arakawa M, Crooks LE, McCarten B, et al. Comparison saddle-shaped and solenoidal coils for magnetic resonance imaging. *Radiology* **1985**;154:227–228
10. Fitzsimmons JR, Thomas RG, Mancuso AA. Proton imaging with surface coils on a 0.15-T resistive system. *J Mag Res Med* **1985**;2:180–185
11. Schenck JF, Foster TH, Henkes JL, et al. High field surface coil MR imaging of localized anatomy. *AJNR* **1985**;6:181–186
12. Schenck JF, Hart HR, Foster TH, et al. Improved MR imaging of the orbit at 1.5 T with surface coils. *AJNR* **1985**;6:193–196

Computer Page

Computer-Generated Examinations for Residents in Radiology

Jeffrey R. Crass[1]

At the University of Minnesota we evaluate residents at the completion of each month's rotation. This evaluation is based on impressions from direct supervision of the resident during the rotation. In order to have a less subjective method of evaluating the residents, I decided to institute a monthly written test. It seemed that a test that would be given monthly would lose validity rapidly as the examinee group learned the questions. Rather than write a new test every month, a series of computer programs was developed that would generate unique monthly examinations from a large question file. I have not seen previous references or advertisements for programs that could perform this function.

The initial step was creation of a question file. A series of 230 questions, similar to those used in the written board examination, were dictated with answers and page references. As the examinations were to be for the chest rotation, the text by Paré and Fraser [1], *Synopsis of Diseases of the Chest*, was used as the basic reference. The programs are not specific for this question file, however. A file of questions on any desired subject matter written in the same format could be used to create examinations for that subject. Either multiple-choice or true-false questions can be used. I used primarily true-false questions, which ranged from easy, basic knowledge questions (the majority) such as:

*True 545 143 The primary roentgenographic signs of emphysema are those of pulmonary overinflation and oligemia.

to questions in greater depth:

*True 383 94 The clinical presentation of nitrofurantoin-induced lung disease is acute with cough, chills, fever, and dyspnea.

(The numbers refer to the page reference and the question number in the master file, respectively. The asterisk allows separation of the questions in later processing.) This was transcribed to a file on a 5.25-inch (13.3-cm) floppy disk using a standard word processing program (Wordstar version 3.24, 1982, Micro Pro International).

Our word processing and programming are done on IBM Personal Computers with dual 320-kbyte floppy disk drives and 256 kbytes of random access memory. Using IBM's Basic Compiler (version 1.00, 1982), a series of three programs were written in Basic and then compiled for processing the question file and test generation. The first removed special characters, which our word processor places in text files. This would not have been necessary with most other word processing programs. The second program created an index on disk of the question file. The third program was the test generation program. Tests of any length up to the length of the question file can be generated. The program selects questions in a random order. In then checks that the question has not been used yet in the test being generated. If the question is a new one, the asterisk, answer, page references, and question number are removed. The question is renumbered in sequence and added to a disk file created by the program for that test. After writing all the questions, the program adds an additional page containing the answers and

---

Received August 26, 1985; accepted August 30, 1985.

[1] Department of Radiology, University of Minnesota Hospitals and Clinics, Box 292 Mayo Memorial Bldg., 420 Delaware St. S.E., Minneapolis, MN 55455.

AJR **146:413–414, February 1986** 0361–803X/86/1462–0413 © American Roentgen Ray Society

page references. This resultant test file is then ready for proofreading and printing using the word processor.

I have been using these programs for 6 months and have found them to be a valuable addition to my resident evaluations. Scores on my 50-question tests have ranged from 6 to 27 wrong (mean, 14.5 wrong). Although it will take a very long time to collect enough data to statistically analyze the test, the results of the tests so far have given an objective measure of resident knowledge that consistently agrees with my subjective impressions. The residents appreciate their objectivity as well as the learning experience when we go over the results together. I would like to make these programs (with source code and instructions) and my question file available to anyone who will send a blank diskette onto which to copy them.

REFERENCE

1. Paré JAP, Fraser RG. *Synopsis of diseases of the chest.* Philadelphia: Saunders, **1984**

Editorials

The Impact of Maternity on Radiologists: The AAWR Position and Its Acceptance by Women

Yolanda T. Adler,[1] Sandra K. Fernbach,[2] L. Anne Hayman,[3] Helen C. Redman,[4] and Carol Rumack[5]

The American Association of Women Radiologists (AAWR) was founded in 1980 to address issues of concern, but not necessarily unique, to women in radiology. A major problem for women is the necessity and difficulty of maintaining professional activities during childbearing years. In response to many requests for guidelines that would ease relations between young women and their colleagues, the AAWR formed a committee (composed of the authors of this article) charged with addressing this issue. The committee's report addressed three principal subjects: the medical aspects of work performance, particularly fluoroscopy; medical maternity leave; and ways of balancing family and work responsibilities. This document, abstracted below, was approved by the Executive Board of the AAWR and published in the newsletter of the association. Three hundred women wrote to us, giving their opinions and comments. Their responses indicated that women's involvement with family responsibilities sometimes curtails the amount of time they devote to their career but not their commitment to the practice of quality radiology.

Highlights of the Report on the Impact of Maternity on Radiologists

Performing Fluoroscopy Procedures during Pregnancy

A radiologist performing routine fluoroscopic procedures in a large metropolitan hospital, using conventional protective measures, would be expected to expose her fetus to no more than a 50-mR (13-μC/kg) dose [1] over a 9-month period. There is a theoretical risk to the fetus from such a small amount of radiation. From estimates of the National Council on Radiation Protection and Measurements (NCRP), the worst possible effect of a 50-mR (13-μC/kg) conceptus dose would be to increase the chance of childhood cancer and malformation only by 0.005% (4.100%–4.105%) [2]. To reduce even this small exposure, a contoured, appropriately reinforced maternity apron has been designed [3].

On the basis of the available data, the elimination of fluoroscopy at any time during pregnancy cannot be justified on scientific grounds. It can, however, be argued that if fluoroscopy is to be curtailed, it should be done when the fetus is most sensitive to radiation, that is, at 2–6 weeks old. This precaution is of course impractical, since most pregnancies are undetected during this time. Lead-lined underwear is available to women who are apprehensive about radiation to the gonads or are contemplating pregnancy. The exclusion of fertile women from fluoroscopy on the basis of radiation risks to the fetus is both unnecessary and undesirable, as it may encourage discrimination. Rationally, women of childbearing age who enter the specialty of radiology should be willing to accept the theoretical risks involved in fluoroscopy. Counseling and information about radiation during pregnancy should be given to all women considering making radiology their career choice.

Received June 6, 1985; accepted after revision August 26, 1985.

[1] Department of Diagnostic Radiology and Nuclear Medicine, Rush-Presbyterian-St. Luke's Medical Center, 1753 W. Congress Parkway, Chicago, IL 60612.
[2] Department of Radiology, Children's Memorial Hospital, Chicago, IL 60614.
[3] Department of Radiology, Baylor College of Medicine, Houston, TX 77030.
[4] Department of Radiology, University of Texas Health Science Center, Southwestern Medical School, Dallas, TX 75235.
[5] Department of Radiology, University of Colorado Health Science Center, Denver, CO 80262.

AJR 146:415–417, February 1986 0361–803X/86/1462–0415 © American Roentgen Ray Society

Medical Maternity Leave

About 95% of pregnancies in women 25–35 years of age will require no prenatal leave time. Women over 35 years will have a slight increase in morbidity due to concomitant medical disease. Minor medical problems commonly encountered during pregnancy generally do not require time off. Postnatal time off will vary. Most professional women return to work 4–8 weeks after delivery, but complications may require a longer leave of absence.

Child Care and Its Effect on Professional Activities

The AAWR recognizes that the decision of how much time should be diverted from professional activities to family responsibilities is complex and personal. However, women are still a minority in radiology, and often class perceptions are based on individual experiences. Radiology is almost always practiced by groups sharing the work load. The loss of one productive member's time will result in an added burden to others in the group. The ability of colleagues to adjust to this loss depends on the complexity and size of the practice. Women who want the rewards of traditional roles in academia or private practice must be willing to make a substantial commitment of time and effort, and can have a responsible but not traditional family life. Women who choose to practice part time or to take extended leaves of absence cannot demand or expect advancements at a rate equal to their full-time colleagues. Part-time practitioners should be given appropriate professional recognition, should not be expected to do only the least desirable jobs, and should be compensated on the same scale as their full-time colleagues.

Stereotyped patterns of practice should be abandoned. Small practices will achieve flexibility of scheduling and increase their range of services by securing the part-time services of women who desire to limit their time commitment. Goodwill must be earned, and concessions made by both male and female colleagues must be recognized and reciprocated. There are many tangible ways to compensate for duties that cannot be performed, such as arranging and paying for suitable locum tenens, covering weekends in addition to the usual assignment, and being available during peak working hours.

Commentary

To achieve a good match between the needs of the established practices or institutions and the women joining them, open communication between senior radiologists and prospective women candidates is necessary. Sometimes a blanket, if covert, avoidance of women candidates is used to elude possibly embarrassing or legally dangerous implications. This restricts the chances of employment for all women. A recommended approach for recruiters is to clearly outline the degree of flexibility possible in their situations. Women will find that if they approach the subject, there will be a decrease in underlying tension and their credibility will be improved. Open discussion will allow both parties to make realistic decisions.

Response to the Report and Commentary

The main purpose of publishing our report in the AAWR newsletter was to disseminate it. To sample the reaction to its contents, we included a questionnaire requesting some personal information; this began:

Which of the following statements describes your reaction to the AAWR report on pregnancy and childcare:

I agree with it totally.
I have some reservations but will support it.
I disagree substantially and cannot support it.

If you cannot support this proposal, indicate the section(s) to which you object.

Since many physicians ignore or dispose of unsolicited mail, we were pleasantly surprised to receive 300 responses within 3 months. Of these, 194 (65%) agreed totally with the proposal, 82 (27%) had reservations but would support it, and 24 (8%) disagreed substantially and could not support it. There were no significant differences in the response to the above questions between the women who had children (211) and those who did not (89). A total 201 respondents added comments ranging from a few words to two pages. The transcription of those notes filled 22 typewritten pages.

The section on performing fluoroscopy during pregnancy caused most of the negative comments. "I did not want to expose my baby even to the theoretical risk of radiation" was a typical statement. The recommendation was based on data published in recognized scientific journals and by the NCRP, but it was questioned. Contradictory evidence was not cited. Even respondents who fully supported the proposal stressed that women should not be pressured to perform fluoroscopy during pregnancy, regardless of the objective evidence. The fear of causing an anomaly by willful exposure of a fetus to radiation is deeply rooted. Since about 2%–3% of live-born children manifest a congenital anomaly at birth without a known exposure to a teratogen [4], inevitably, such misfortune will strike some radiologists. Whether he or she performed fluoroscopy or not, the radiation worker whose child has an anomaly or a tumor will wonder if occupational exposure contributed to the tragic event.

The problem of establishing safety guidelines was well stated by Hulka [5]: "One of the provocative quirks about the scientific method is that we can never prove beyond doubt that there is no association between an exposure factor of interest and a particular disease." The argument "I do not want to take a chance" can be carried to avoidance of fluoroscopy by both genders when trying to conceive or even before. However, if one wishes to practice radiology, the scientific evidence is reassuring. There are misconceptions about the actual amounts of radiation that reach the conceptus during occupational exposure of a woman who keeps a full fluoroscopy schedule, and few people are aware that the doses involved often are less than those from unavoidable environmental sources [6]. Dissemination of the available information should help alleviate the devastating emotional trauma and guilt suffered by all radiation workers with affected children.

Care must be taken that possible curtailment of professional activities is not used as a rationalization for discriminatory practices when hiring women. A woman who is informed about the scientific evidence and feels comfortable with occupational levels of radiation exposure should not be prevented from working as she wishes. In a recent federal court decision, a diagnostic radiation technologist charged her employer-hospital with discrimination [7]. When she announced her pregnancy, the radiation safety director recommended her removal from all areas in which ionizing radiation was being used. The institution claimed that alternative work in the department was not available, and she was dismissed. In this case, the court accepted as authoritative the standards set by the NCRP. It also rejected the argument that avoidance of potential litigation constituted a business necessity and justified curtailing the employee's activities. The 11 pages of opinion and notes in the Federal Registry indicate the complexity of the issue.

The section on medical maternity leave produced few adverse comments. Most women reported mixed reactions from their colleagues. We got the impression that women in staff positions encountered neutral or supportive attitudes from colleagues, but those who became pregnant during residency experienced an alarming degree of hostility. This negative attitude has appeared in the literature, sometimes barely disguised as humor or wit [8]. Since 58% of our respondents with children had at least one pregnancy during residency, we speculate that the difficulty in rearranging schedules year after year may tax people's resourcefulness [9]. The requirement of the American Board of Radiology for residents to have no more than 6 weeks off for any reason in any year accentuates the problem, and more flexibility appears necessary. Training is precious and should not be curtailed, our respondents emphasized, but there were discrepancies concerning ways to compensate for time lost.

While there were few objections to the section on child care and its effect on professional activities, the experience of most respondents in balancing family and professional life caused them to enlarge on the ideas presented. Some stressed how much diplomatic skill was required to negotiate compromises in a department without established policies. Many women felt that they were unfairly penalized when needing time to meet family responsibilities while male colleagues took equal time for personal reasons without stigma. On the positive side, male colleagues were frequently cited as understanding and helpful, especially those who considered their own family time valuable.

Conclusions

Many published works explore attitudes toward women in medicine. The AAWR report was written by women, and the response to its dissemination may be useful in giving some insight on how women view themselves and their commitment to the profession. Our correspondence indicated a high percentage of support for the AAWR position and membership of the AAWR doubled in the 9 months following the publication of the report in the newsletter. Those who disagreed substantially expressed different attitudes but an equally enthusiastic and responsible dedication to their careers.

Social changes often precede the framework necessary to cope with the new situation. Many women are already in radiology and their numbers will increase. There is a need for open discussion and flexible policies dealing with pregnancy, maternity leave, and family responsibilities, and we hope the AAWR report will provide an impetus to discussion and lead to the development of widely accepted reasonable guidelines.

REFERENCES

1. Wagner LS, Hayman LA. Pregnancy and women radiologists. *Radiology* **1982**;145:559–562
2. *Review of NCRP radiation dose limit for embryo and fetus in occupationally-exposed women*, NCRP report no. 53. Washington, DC: National Council on Radiation Protection and Measurements, **1977**
3. Witrak BJ, Sprawls P. Maternity lead apron. *Radiology* **1984**;150:597
4. Shepard TH. *Catalogue of teratogenic agents*, 2d ed. Baltimore: Johns Hopkins University Press, **1976**
5. Hulka BS. When is the evidence for "no association" sufficient? *JAMA* **1984**; 252:81–82
6. Committee on Radiological Units, Standards, and Protection. *Medical radiation: a guide to good practice*. Reston, VA: American College of Radiology, **1985**:24, 31–32
7. *Hayes vs. Shelby Memorial Hospital*, 82-7296 Federal Report, 2d series. **1984**:1543
8. Felson B. Letters to the editor. *Semin Roentgenol* **1985**;21:102
9. AMA Ad Hoc Committee on Women Physicians in Organized Medicine: Formica PE, Brubacher L, Kuffner MG, et al. *Maternity leave for residents*. Chicago: American Medical Association, **1984**

Device Identification: Deficient Marking Systems

Paul S. Wheeler[1]

A departmental risk prevention/quality assurance program that focuses on errors and complications will recognize man-made devices as causes of problems ranging from missed diagnoses to fatalities. Devices that can be inserted in patients intentionally or left in by mistake are a true growth industry. Radiologists encounter these devices everyday and should be aware of several facts. There is no requirement for devices to be radiographically detectable. Manufacturers are not obliged to advise physicians of their marker systems. This failure to engage in useful patient care communication contrasts with the commercial zest for advertising and aggressive marketing.

Several bitter experiences have taught us the importance and difficulty of dealing with device-related problems. The first was the recognition that a certain short, stiff, taper-tipped venous catheter placed from the left subclavian approach tended to penetrate the vena cava, causing massive effusions and several deaths. The brochure stated the catheter could be used for venous pressures and infusion of drugs and fluids. It had become very popular with the house staff because of its ease of insertion. The manufacturer was alerted but assured us that it was a problem unique to our hospital. We later learned that this was not true. The serious complications ended when this catheter was replaced by a softer and longer one. Unfortunately, the new catheters are very poorly opaque and especially hard to identify on bedside films and in obese patients. The excellent detectability of the Swan-Ganz catheter shows that some manufacturers can do things right. The National Center for Devices and Radiological Health informed us that the standards for radiodetectability are optional and compliance is not required.

This information proved useful when we helped defend a young radiologist at another hospital who had mistaken a laparotomy pad marker for a drain on a postoperative excretory urogram. The report was never read by the surgeon, and, when an abscess developed, the patient sued the radiologist, surgeon, and hospital. Our qualification as an expert witness was based on 5 years of experience with an active risk prevention program that dealt with several missed diagnoses caused by sponges and pads. A call to the sponge manufacturer resulted in two bits of advice: Do not leave the product in patients and do not ask the manufacturer to make their markers more logical. We suggested use of tapes with opaque letters but were told this would be a needless expense. The jury was shown the confusing nature of sponge markers and informed that the manufacturers have been remiss in failing to standardize and disseminate systems. Anyone who has never seen a particular sponge or pad marker is at a disadvantage, and in this case the verdict was for acquittal of the radiologist.

Invisible or barely opaque tubes and prostheses create a range of problems. Some feeding and gastrostomy tubes are difficult to detect and localize. Silastic breast prostheses are undetectable on chest films, ensuring a missed diagnosis that generally will be more amusing than significant. However, a nonopaque ventricular shunt is another matter. In one case (illustrated in this issue [1]), a ventricular atrial shunt broke, coiled in the right atrium and tricuspid valve area, and developed infected vegetations. Only a tiny marker dot at the tip was visible on radiography and fluoroscopy, but sonography defined the problem. The patient was in congestive failure from bacterial endocarditis. Risking further damage to the heart valve and chordae, a transvenous extraction was performed, hindered by the shunt being invisible. When the broken tubing was withdrawn, a shower of septic emboli hit the lungs. We were stunned that a neurosurgeon and a manufacturer would join two vital organs with a nondetectable tube. Opaque ventricular shunts have since been introduced in our hospital, but this is only a local "fix."

The tendency of manufacturers to use single thin, wirelike lines to mark a variety of tubes can lead to confusion. The endotracheal tube should have a distinctive tip to distinguish it from a misplaced nasogastric tube. Neck braces should be nonopaque, but many obscure underlying detail. These examples indicate the tunnel vision that results when industry caters to narrow specialty demands.

The American College of Radiology was consulted and several letters and conference calls with the American College of Surgeons confirmed the difficulty of dealing with "boundary" problems, even when simple preventable medical-legal problems are involved. A 2-hr presentation on device-related complications at the National Center for Devices and Radiological Health resulted in requests for samples of devices used in our hospital ranging from intraaortic balloons to venous catheters. Their tests confirmed what we knew already: some devices were poorly opaque. A long list of commercially

---

[1] Russell H. Morgan Department of Radiology and Radiological Sciences, Johns Hopkins Medical Institutions, 600 N. Wolfe St., Baltimore, MD 21205.

AJR 146:418–419, February 1986 0361-803X/86/1462–0418 © American Roentgen Ray Society

available devices was compiled and letters circulated, but our two objectives are still unfulfilled: to see the center's bulletin used to help inform us about devices and marker systems and to have radiologists consulted by industry in the product design stage.

Problem-solving in this area can be unrewarding and time-consuming. Radiologists do not buy or insert most devices and can be considered troublemakers when they complain. No friends are made when an obvious mistake in design is pointed out to the producers and users. Dealing with bureaucratic agencies and professional associations requires patience and political savvy. Suggestions to manufacturers may be accepted, but purchasing better alternative products is faster.

However, the goal of eliminating needless risks to patients (and radiologists) justifies perserverance. We are encouraged by the fact that radiologists were instrumental in bringing the battered child syndrome to public attention. Device-related problems have some regrettable similarities to this syndrome in being widespread and unsavory. The exact incidence of complications is often impossible to determine because of legal consequences, and reporting them is constructive but certainly not endearing. Fortunately, unlike the battered child, the solutions to some of the device problems are simple, at least in theory: logical marker systems to identify all products placed in patients; input from imaging specialists at the design stage; and widespread dissemination of device information to physicians who will encounter them in practice.

REFERENCE

1. Scott WW Jr, Wheeler PS, Mitchell SE. Pictorial essay. Markers for implanted devices: need for standardization. *AJR* **1986**;146:387-390

What Radiologists Say about PACS

John Vanden Brink[1]

If you do not know what PACS means, you are not alone. At least one-third of radiologists do not know either. That is one of the findings of a mail and telephone survey on medical image processing, archiving, and communications conducted early in 1985. Over 500 chiefs of radiology, radiologists, imaging specialists and radiology administrators in institutions with more than 200 beds participated.

PACS, which means picture archiving and communications systems, is variably defined. To some it means a "complete electronically integrated multimodality system that enables high-speed communication and image processing between multiple sites including a high-density digital archiving module." A less encompassing perception is that PACS "consists of any product, system, or component, manual or electronic, which is used in the management of medical images." While these two definitions are somewhat contradictory, the prospects for PACS have been characterized by such contradictions. In the February 1985 issue of the *AJR*, Seeley et al. [1] anticipate the total digital radiology department, another definition for PACS, and take issue with a December 1984 editorial by Gray et al. [2], which questions the feasibility or desirability of a total digital radiology department.

Such contradictions and debates inevitably accompany the emergence of significant new technology and create a challenge for both users and manufacturers to determine schedules and priorities for allocating limited resources to the development and acquisition of the technology. The survey provides an insight into the perceptions of potential users. Following are some of the key findings.

As perceived by physicians, the primary benefit of PACS is to provide fast, simple access to files for multiple users for intradepartmental communication. Secondary benefits are to promote more accurate diagnosis and improved communication with the referring physician.

Respondents believe that by 1995, about half of primary diagnoses will be made directly on a display screen (CRT), the other half being done on film. Few believe that film will ever be completely replaced, but many anticipate that film and archiving will be displaced by electronic archiving and film substitutes. Half of those responding believe that electronic archiving will be adequate for legal purposes, as will destructively compressed data.

Most respondents believe a radiology information management system (RIMS) should be in place before PACS is installed. Minimal information in addition to the image would be patient name, ID number, imaging diagnosis and patient history. While most respondents provide a written diagnosis to the referring physician with review of the image only in the

---

[1] Technology Marketing Group, Ltd., 950 Lee St., Des Plaines, IL 60016.

AJR **146:419-420, February 1986** 0361-803X/86/1462-0419 © American Roentgen Ray Society

radiology department, there is a strong expressed need to communicate directly with the referring physician using a CRT.

Nearly one-fourth of respondents plan to have a PAC system for at least one modality by 1986, and will not wait for installation of a RIMS if they do not already have it. They will focus on digitized radiographs, CT, or point-to-point communication as application sites for initial installation.

The key obstacles to installation of PACS are equipment costs and the comparative costs of present technology. Most believe x-ray images will have to be produced digitally before installation of PACS is cost effective. However, others believe there is a potential for savings that is substantive enough to justify the cost of even the most expensive installation, provided the technology performs to user requirements. The average cost for producing a hard-copy image is currently estimated at $23.00 per procedure, which includes personnel requirements for processing, transporting, and archiving that may constitute as much as two-thirds of total personnel in a department.

When asked at what cost PACS that meet respondent specifications could be cost-justified, the average response was about $425,000 or, based on a 5-year amortization, $85,000 per year. However, estimates of costs by manufacturers and knowledgeable users indicate that a complete multimodality system for a 500-bed hospital will cost at least three to four times this amount. For lack of knowledge of present costs or for other reasons, most respondents evidently do not feel justified at this time in making an investment of this magnitude. This low-level response by potential buyers is currently reflected in the priorities of manufacturers who must evaluate development investment on the basis of return to shareholders.

What does this suggest about the future for potential users? Certainly, the activists by their purchasing intentions indicate that the path to the eventual all-encompassing multimodality system will be through subsets of that system, such as RIMS, point-to-point communications, high-resolution video, and "smart" multiformat imagers. Experimentation can begin with smaller, less expensive subsystems to begin to address the operational and human factor elements.

Enthusiasts anticipate that as systems or subsystems are installed, it is likely that imaging workstations will proliferate both inside and outside the institution and clinic, enhancing the role of diagnostic imaging in the diagnostic process and increasing its use. Thus PACS technology may become a key factor bringing the radiologist and referring physician in closer communication on a more timely, cost-effective basis to enhance the diagnostic process. However, the study also clearly indicates that the majority view is a "wait and see" attitude, not based on apathy but on a concern for cost effectiveness, the state of the technology, and the need to better define requirements before making commitments.

REFERENCES

1. Seeley GW. The total digital radiology department: an alternative view. *AJR* **1985**;144:421–422
2. Gray JE, Karsell PR, Becker GP, Gehring DG. Total digital radiology: is it feasible? or desirable? *AJR* **1984**;143:1345–1349

Editor's Note

Copies of the report of the survey can be obtained at cost from Technology Marketing Group Ltd., 950 Lee St., Des Plaines, IL 60016, telephone (312) 297-1404.

Letters

Erratum

Drs. Shin and Berland [1] are to be congratulated on their pictorial essay in the July 1985 issue of *AJR*. However, we believe the enhancing structure identified in their figure 4B as the thoracic duct (*solid arrow*, fig. 1) is the azygos vein. Our reasons are as follows: (1) The structure enhances equally with the aorta and the vena cava; (2) the thoracic duct contains chyle, which would be expected to have an attenuation coefficient between those of fat and of water; (3) there is no reason to expect the thoracic duct to enhance; and (4) an unenhanced low-density structure (*open arrow*, fig. 1) is present between the arrowed structure and the aorta, in the position of the thoracic duct, as the authors show in an adjacent diagram.

We are sure that this small error is a printer's gremlin; our minor criticism should not detract from the merits of this excellent award-winning essay, but should perhaps serve as a warning that errors do occur, despite the combined expertise of referees and award-making committees.

Harris Jackson
Bharat Raval
University of Texas Medical School
Houston, TX 77030

REFERENCE

1. Shin MS, Berland LL. Computed tomography of the retrocrural spaces: normal, anatomic variants, and pathologic conditions. *AJR* **1985**;145:81-86.

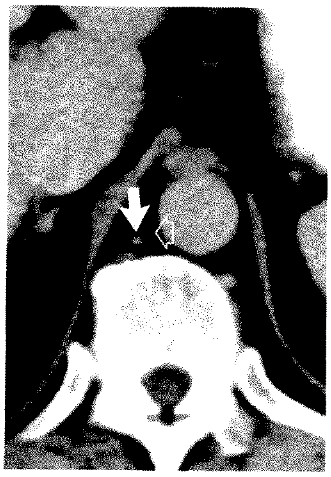

Fig. 1.—Retrocrural space in normal subject. Azygos vein (*solid arrow*), incorrectly identified as thoracic duct (*open arrow*). (Reprinted from [1].)

Reply

We thoroughly agree with the four points made by Drs. Jackson and Raval. The arrow in our figure 4B was inadvertently placed on the azygos vein rather than on the thoracic duct.

We thank Drs. Jackson and Raval for their meticulous observation and careful reading of our article, and we regret any confusion caused by the error.

Myung S. Shin
Lincoln L. Berland
University of Alabama at Birmingham
Birmingham, AL 35294

More Evidence for Aortic Rupture into Retroperitoneum

We noticed the interesting letter from Hopper et al. [1] in the August 1985 issue of *AJR* concerning aortic aneurysm rupture into the retroperitoneum. They refer to the article by Rosen et al. [2] in the August 1984 issue, in which it is postulated that the aorta, as a perirenal structure, ruptures selectively into the perirenal space. Hopper et al., however, believe that of those abdominal aortic aneurysms that rupture, most bleed into the psoas muscle and—with increasing pressure—into the pararenal space.

In their reply, Korobkin and Rosen [3] state that there is no surgical, postmortem or other documentation from the cases mentioned in their article or in the literature that such hematomas really extend into the psoas muscle. They say that even in the cases of Hopper et al. [1], direct proof of hematomas extending into the psoas muscle was not present. We believe the theory of Hopper et al. [1] is correct, as demonstrated by the following case report:

A 65-year-old man was admitted to our hospital with increasing pain in the left groin extending to the upper left leg. Abdominal radiography revealed a left-sided bulging psoas contour. Dynamic CT scanning of the abdomen demonstrated clearly a ruptured aneurysm with bleeding extending into the psoas muscle (fig. 1). A definite thrombus was present at the bleeding site, and a clear interface could be seen between thrombus in the psoas muscle and psoas muscle itself. A transverse slice in a plane through the mid-lower pole of the left kidney demonstrated the most cranial extension of the bleeding in the left psoas muscle. No further extension of the bleeding (as, for example, into the pararenal space) could be demonstrated. A laparotomy was performed, and the operative findings correlated well with the CT findings; the bleeding was indeed restricted to the psoas muscle. The pararenal region was searched carefully, but no further

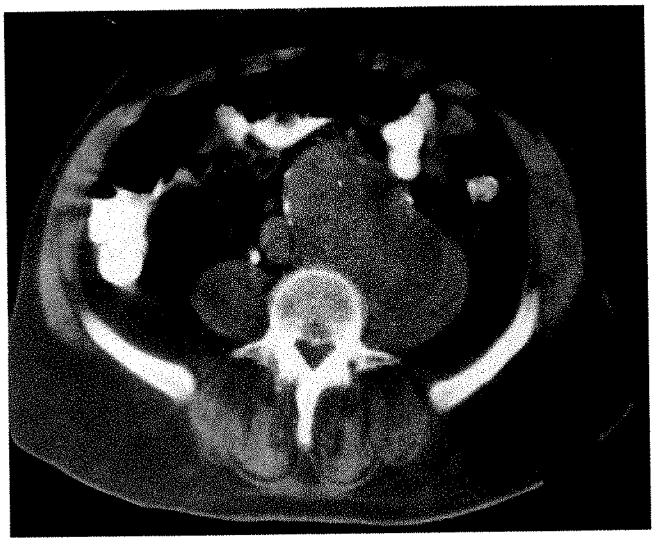

Fig. 1.—Ruptured aortic aneurysm bleeding into psoas muscle. Delineation of thrombosed bleeding and bulging psoas tissue is obvious.

extension of the bleeding was found. An aortic prosthesis was implanted, and the postoperative course was satisfactory.

This case report gives strong support to the theory of Hopper et al. [1] that abdominal aortic aneurysm ruptures will bleed primarily into the psoas muscle and, as pressure builds, secondarily into the pararenal space.

Leo E. H. Lampmann
Hein A. J. M. van Heesch
Thijs E. A. M. de Jong
St. Elisabeth Hospital
5000 LC Tilburg
The Netherlands

REFERENCES

1. Hopper KD, Sherman JL, Ghaed N. Aortic rupture into retroperitoneum (letter). *AJR* **1985**;145:435–437
2. Rosen A, Korobkin M, Silverman P, Moore AJ Jr, Dunnick NR. CT diagnosis of ruptured abdominal aortic aneurysms. *AJR* **1984**;143:262–268
3. Korobkin M, Rosen A. *Reply* to Hopper et al., Aortic rupture into retroperitoneum (letter). *AJR* **1985**;145:437

Ascending Aortic Laceration

In the October 1985 issue of *AJR*, Lundell et al. [1] reported three cases of ascending aortic laceration diagnosed angiographically. In addition, they described four cases from the literature with similar angiographic demonstrated of ascending aortic laceration.

Four additional cases were documented by us in 1981 [2]. One was a case from our institution; the other three were extracted from previous literature. All were diagnosed with aortography. This would bring the total number of cases thus documented to eleven.

Richard G. Fisher
Yoram Ben-Menachem
Frank P. Hadlock
Baylor College of Medicine
Houston, TX 77030

REFERENCES

1. Lundell CJ, Quinn MF, Finck EJ. Traumatic laceration of the ascending aorta: angiographic assessment. *AJR* **1985**;145:715–719
2. Fisher RG, Hadlock F, Ben-Menachem Y. Laceration of the thoracic aorta and brachiocephalic arteries. Report of 54 cases and review of the literature. *Radiol Clin North Am* **1981**;19:91–110

Reply

We appreciate the interest of Dr. Fisher and his colleagues in our recent publication and have reviewed the section entitled "Laceration of the Ascending Aorta" from their article [1] as well as the four cases from the literature that they cited therein [2–5]. In our article, we specifically described patients with acute ascending aortic root tears due to blunt trauma who survived emergent aortography and surgery. In particular, our purpose was to illustrate the difference between the mechanism of injury involving the ascending aorta and that involving the more commonly seen isthmic aortic laceration. We wish to explain why we would not group the patients mentioned by Fisher et al. [1] with our reported cases, although we acknowledge that at least two of the former cases were documented lacerations within the ascending aorta.

Fisher et al. [1] describe two patients, one of whom had a tear within the ascending aorta at the base of the innominate artery. The second patient died before aortography, and the exact site of ascending aortic tear was not stated. The cause of injury was not reported in either case.

Appelbaum et al. [2] described a case of ascending aortic tear 2 cm proximal to the innominate artery and "extensive injury involving the entire aortic arch." Neither an in-depth description nor an illustration of this aortic tear was provided. We cannot determine the distal or proximal extent of the laceration; the ascending aortic component may have been an extension of a tear beginning at either the isthmus or a great vessel.

Bross [3] described two patients with large "aneurysms" of the ascending aorta. In the first case, aortography demonstrated an "aneurysm" involving the ascending aorta in a patient who had fallen downstairs 2 months earlier. The exact site of laceration is neither described nor illustrated. The second patient, admitted for aortic insufficiency, had sustained "blunt trauma"; aortography revealed an "aneurysm of the ascending aorta" [3]. A single view of the aortogram demonstrated opacification of a large pseudoaneurysm just below the level of the innominate artery. However, the aortic root is not opacified, and injury to this region—and particularly to the valve—is not described. At surgery an aortic valve prosthesis and a 4-cm-long Dacron graft were placed. Although there may have been a laceration at the aortic root, this is not explicitly described or illustrated.

Freed and Bosher [4] reported only cases with great-vessel injuries. Matleff and Morton [5] described one patient with multiple tears that included the subclavian artery, posterior wall of the ascending aorta, and an intimal tear of the mid-descending aorta. This patient did not have aortography and died before surgery. The exact level of ascending aortic laceration is not mentioned.

In summary, we would not include these reported patients with our cases because the tears were not definitely located at the aortic root; not all patients presented acutely; and the site of laceration was not documented by aortography in some cases.

Caroline J. Lundell
Michael F. Quinn
Ethel J. Finck
Los Angeles County/University of Southern California
Medical Center
Los Angeles, CA 90033

REFERENCES

1. Fisher RG, Hadlock F, Ben-Menachem Y. Laceration of the thoracic aorta and brachiocephalic arteries by blunt trauma. Report of 54 cases and review of the literature. *Radiol Clin North Am* **1981**;19:91–110
2. Appelbaum A, Karp RB, Kirklin JW. Surgical treatment for closed thoracic aorta injuries. *J Thorac Cardiovasc Surg* **1975**;71:458–460
3. Bross W. Injuries of the thoracic aorta. *J Cardiovasc Surg* **1971**;12:95–107
4. Freed TA, Bosher LH Jr. Arteriographic demonstrated of laceration of great vessels secondary to blunt chest trauma. *Radiology* **1968**;90:88–89
5. Matloff DB, Morton JH. Acute trauma to the subclavian arteries. *Am J Surg* **1968**;115:675–680

Focal Lytic Lesion Associated with Acetabular Loosening in Total Hip Prosthesis

I read with great interest the article by Scott et al. [1] in the May 1985 issue of *AJR*, on focal lytic lesions in the femur associated with loose total hip prostheses. I have seen this phenomenon quite often at my hospital, where large numbers of patients are referred from other institutions for revision of loose hip prostheses.

The authors described lesions associated only with the femoral component. I have seen two cases of an identical lesion associated with a loose acetabular component and suspect that this is a much rarer entity. The following is a report of the more recent of these two cases:

A 58-year-old woman underwent a total hip replacement in 1976. A postoperative radiograph was unremarkable (fig. 1A). Serial films over the next 7 years demonstrated a slowly developing lytic lesion in the ischium just inferior to the acetabular cup, with associated progressive widening of the zone of lucency at the bone-cement interface of the cup and a fracture of the acetabular cement (fig. 1B). An arthrogram obtained in 1983 confirmed the plain-film impression of cup loosening. Interestingly, the lytic lesion did not fill with contrast material (fig. 1C). On curettage at the time of subsequent revision of the prosthesis, the lesion was found to be filled with "synoviallike" tissue. There was no infection.

Thus it seems that the process described by Scott et al. [1] in the femur may occur also in the acetabulum.

Gary S. Silverstein
Hahnemann University
Philadelphia, PA 19102

REFERENCE

1. Scott WW Jr, Riley LH Jr, Dorfman HD. Focal lytic lesions associated with femoral stem loosening in total hip prosthesis. *AJR* **1985**;144:977–982

Reply

We too have noted lytic lesions around the acetabular components of total hip prostheses. We did not intend to imply that such lesions occurred only adjacent to the femoral component of hip prostheses. The greater frequency of femoral-component loosening probably explains the greater frequency with which such histiocytic lesions are seen in the femur rather than the acetabulum.

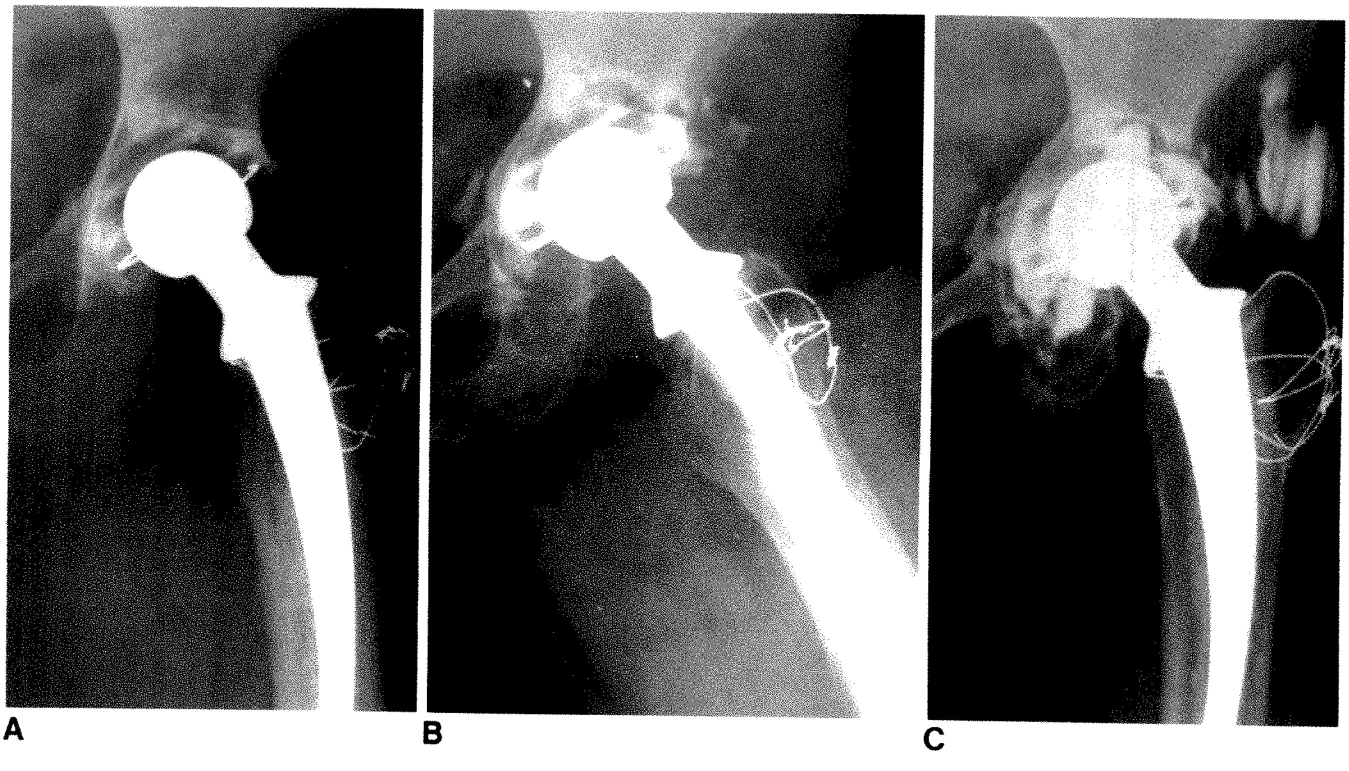

Fig. 1.—**A**, Plain radiograph obtained 1 month after original total hip replacement is unremarkable. **B**, 7 years later. Focal lytic lesion in left ischium associated with wide zone of lucency at bone-cement interface of cup and fracture of acetabular cement suggests loosening of cup. **C**, Arthrogram confirms plain-film impression of cup loosening. Lytic area does not fill with contrast material.

In our study we choose to concentrate on femoral lesions because we had more experience with these lesions and a larger series of patients with histologic confirmation of the diagnosis. Also, loosening of the prosthesis appears to be an important precursor to the formation of such lesions, and loosening is more easily documented radiographically for the femoral component than for the acetabular component.

We thank Dr. Silverstein for clarifying a point that may have confused some readers.

William W. Scott, Jr.
Johns Hopkins University School of Medicine
Baltimore, MD 21205

Radiologic Search for Duodenal Ulcer

The September 1985 issue of *AJR* contains an informative article by Gelfand et al. [1] on the radiologic detection of duodenal ulcer. These authors found the sensitivity of radiologic diagnosis of 91 endoscopically proven duodenal ulcers to be only 61% and to vary from 44% to 80%, the variation depending on the individual examiner and, to a lesser extent, on the size and location of the ulcer and the type of examination (single or double contrast). True sensitivity was presumably higher because radiologically obvious ulcerations are less likely to undergo endoscopic verification. It was concluded that "a biphasic or multiphasic approach to the upper GI series should be used in an effort to maximize diagnostic yield" and that "a 10%–20% improvement in overall sensitivity can be expected" [1]. Gelfand et al. [1] included only patients with endoscopically verified duodenal ulcers in their study, and the reader does not know how increased sensitivity, achieved by whatever means, might relate to an increase in the number of false-positive diagnoses.

The indications for radiologic and endoscopic examination were not stated by Gelfand et al. [1]. I assume that many of the patients in their series, as in other reported series, were examined for abdominal pain rather than gastrointestinal bleeding. I question the need for aggressive radiologic evaluation of the duodenal bulb in such patients. The diagnosis or the exclusion of the duodenal ulcer by radiologic or endoscopic methods very rarely affects long-term treatment or prognosis. Barium examination is performed in most instances of suspected duodenal ulcer in order to exclude more ominous causes of abdominal pain, such as gastric neoplasm. In the United States, young patients with presumed peptic ulcer symptoms have such a low instance of carcinoma that an upper gastrointestinal barium examination, with its attendant radiation and expense, is seldom indicated, particularly if symptoms are relieved with antacid therapy. The same reasoning applies to endoscopy. Most of my clinical colleagues who specialize in gastroenterology concur with this approach.

Fluoroscopists have always been enamored with the duodenal bulb. The number of spot radiographs of the bulb reflect this fascination. I discourage residents from such an aggressive approach, particularly when examining young patients. Given limited radiologic and medical resources, as well as time constraints and radiation concerns, I would choose to direct more attention to the stomach or to a more thorough search for colonic polyps on a subsequent barium enema. More aggressive radiologic evaluation of the duodenal bulb is justified in patients who are being examined for acute gastrointestinal bleeding, but such examinations are rarely indicated [2] and, as emphasized by Gelfand et al. [1], the accuracy of the radiologic diagnosis of duodenal ulcer is mediocre.

Radiology has played a major role in our understanding and diagnosis of peptic ulcer disease. Fortunately, as regards the patient, duodenal ulcers have become less common at the same time that new diagnostic and particularly therapeutic methods have made their radiologic demonstration relatively unimportant.

Ferris M. Hall
Beth Israel Hospital
Boston, MA 02215

REFERENCES

1. Gelfand DW, Dale WJ, Ott DJ, Wu WC, Meschan I. The radiologic detection of duodenal ulcers: effects of examiner variability, ulcer size and location, and technique. *AJR* **1985**;145:551–553
2. Steer ML, Silen W. Diagnostic procedures in gastrointestinal hemorrhage. *N Engl J Med* **1983**;309:646–650

Reply

Dr. Hall's thoughtful letter raises two points on which we wish to comment:

In a subsequent investigation [1], we found that higher sensitivities for detecting duodenal ulcer are indeed accompanied by lower positive predictive values, which are in turn caused by a greater number of false-positive diagnoses.

We agree that diagnosis of a duodenal ulcer rarely affects the outcome of treatment by antacids or H_2 blockers and that the barium examination is most useful in excluding more serious diseases, such as gastric cancer. However, we also believe that the radiologist owes both the patient and the referring physician a report of the highest possible accuracy. In our view, this means devoting sufficient time for a careful examination of the esophagus, the stomach, and the duodenum as well when performing an upper gastrointestinal series.

David W. Gelfand
David J. Ott
Bowman Gray School of Medicine
Winston-Salem, NC 27103

REFERENCE

1. Ott DJ, Chen YM, Gelfand DW, et al. Positive predictive value and examiner variability in diagnosing duodenal ulcer. *AJR* **1985**;145:1207–1210

Possible Complication of Percutaneous Femoral Introduction of Kimray-Greenfield Filter

The percutaneous femoral method of delivering a Kimray-Greenfield filter, described by Denny et al. [1] in the October 1985 issue of *AJR*, will be welcomed by many interventional radiologists. Although there are obvious advantages to a percutaneous femoral approach for umbrella filter insertion, a major disadvantage is the increased danger of initial embolization of the device should the struts fail to open. The guide wire through the center of the umbrella will not prevent cephalad movement as it should when the introducer capsule is superior to the device (as in a jugular approach). I offer the following advice as one who has had the misfortune of strut failure via a jugular cutdown approach:

Raising the patient about 30° head-up (Fowler's position) will cause a free-floating umbrella to sink inferiorly in the inferior vena cava by force of gravity. One can actually titrate the position of the device in the cava by adjusting the angulation of the patient. In my patient, the struts of the filter sprang open one by one after about 15 min of anxious waiting. Strut failure presumably was caused by clot in the capsule from a prolonged manipulation time.

I strongly recommend the use of a fluoroscopic tilting table for the femoral percutaneous umbrella insertion technique. The table should be tilted head-up 30° just before the device is expelled, then lowered under fluoroscopic control to ensure stability and proper position.

Anthony E. Baumstark
Choate Memorial Hospital
Woburn, MA 01801

REFERENCE

1. Denny DF, Cronan JJ, Dorfman GS, Esplin C. Percutaneous Kimray-Greenfield filter placement by femoral vein puncture. *AJR* **1985**;145:827–829

Reply

Dr. Baumstark's suggestion that a tilt table be used for femoral Kimray-Greenfield filter insertion is a good one. This is also useful for the right internal jugular vein route, where placing the patient in the Trendelenburg position will decrease the risk of air embolus. Unfortunately, a tilt table is not a part of many angiographic laboratories, and some type of rapid-sequence filming must be available for performing an inferior vena cavogram.

Failure of the struts to open is caused either by crossing of the filter struts or by formation of thrombus within the carrier. The former is prevented by careful loading technique. The latter is prevented by continuous infusion of heparinized solution through the carrier lumen and by minimizing the time spent in placing the filter once the capsule is within the vein [1]. We believe the percutaneous femoral approach offers the fastest route of placement, especially when the Bell-Thompson rule is used as an aid to localization. The internal jugular vein approach requires passage through the eustachian valve and avoidance of the right renal vein. The time spent in performing these maneuvers can be minimized by using a floppy J-tipped or straight 0.035-inch (0.89-mm) guide wire for tract dilatation, leaving the tip in the inferior vena cava, then advancing the filter carrier through the sheath over the prepositioned wire.

Donald F. Denny, Jr.
John J. Cronan
Gary S. Dorfman
Yale University School of Medicine
New Haven, CT 06510

REFERENCE

1. Greenfield LJ, Stewart JR, Crute S. Improved techniques for Greenfield vena cava filter insertion. *Surg Gynecol Obstet* **1983**;156:217–219

Radiologic Terminology

Clinicians often misuse radiologic terms out of ignorance; radiologists may do so out of habit. This is unfortunate in a specialty that is so dependent on effective intraprofessional communication. Improper or imprecise use of radiologic terminology by radiologists reflects poorly on the specialty as well as on the individual. I offer a personal list of "least favorite" terms:

Dye: Contrast media, other than barium sulfate, have no color.

Intravenous pyelography (IVP); *Pyelo-* refers only to the renal pelvis. *Intravenous urography* (IVU) or *excretory urography* is preferable.

Hip fracture: Joints dislocate and bones fracture. No one refers to a knee fracture.

Shoulder separation: The shoulder consists of two articulations, the glenohumeral and the acromioclavicular. These diarthrodial joints *dislocate* or *subluxate*.

KUB: The kidneys, ureters, and bladder are among those structures least well visualized on this abdominal radiograph. Radiographs of the upper and lower abdomen are not referred to as KU and UB.

Flat plate of abdomen: Most of us would not recognize a glass photographic plate.

Subselective: A misnomer for *super*selective [1]. Proximal pulmonary or aortic arteriograms are the quintessence of subselectivity.

Poor inspiratory effort: This phrase is subjective, possibly disparaging, and often incorrect. High diaphragms generally reflect body build and are usually remarkably similar on chest radiographs obtained at different times under different circumstances.

Aphthous ulcer: An aphtha is a small ulcer or blister on a mucous membrane. This redundant term therefore designates a small ulcerous ulcer.

Epicenter: *Epicenter* means "over the center." There may be some rationale to referring to the epicenter instead of the center of a lesion when viewing a two-dimensional radiograph. However, to paraphrase Gertrude Stein, a center is a center is a center.

Coin lesion: This term is a slight improvement over "spot on the lung." It may be descriptive in the light of the two-dimensionality of the radiograph, but it does not describe a nodule.

Echolucent: This term is derived from *radiolucent* and reflects traditional radiologic imaging terminology. Sonography uses sound waves rather than electromagnetic waves, so *anechoic or hypoechoic* seems preferable. Ultrasonographers should march to their own drummer.

Scan: *Scan* traditionally refers to a nuclear medicine image. However, the term is nonspecific, and products of other imaging methods such as computed tomography, sonography, magnetic resonance imaging, and digital studies are also referred to as scans. *Scintigram* is a more specific term.

Azygos lobe: This mythical lobe is a fissure. There is no anomaly of bronchial branching.

Fibrocystic disease, mastitis, or dysplasia: Use of these terms by mammographers as well as by pathologists reflects a basic misunderstanding of normal breast histology and incorrectly implies an abnormality [2, 3]. More appropriate radiographic terms would be *fibroglandular opacities*, *densities*, or *changes*.

Portable radiographs: All radiographs are portable, but no modern radiographic machine is hand-carried. I prefer the term *bedside* [4].

X-rays: These rays must be distinguished from hard-copy radiographs.

Wet reading: For persons rendering such interpretations, I would recommend a film processor and a new business manager.

Ferris M. Hall
Beth Israel Hospital
Boston, MA 02215

REFERENCES

1. Athanasoulis CA. Selective criticism (letter). *AJR* **1980**;134:211
2. Homer MJ. The mammography report. *AJR* **1984**;142:643–644
3. Love SM, Gelman RS, Silew W. Fibrocystic "disease" of the breast—a nondisease. *N Engl J Med* **1982**;307:1010–1014
4. Shehadi WH. Erroneous terminology? (letter) *AJR* **1984**;143:198

Editor's Note

Dr. Hall has been an incisive observer of radiology in general and of the *AJR* in particular. His letter is of special interest in that he shares the editors' concerns for precision in communication. His commentary makes each of us squirm a little as we recognize our favorite "misspeak."

For the reader who enjoys finesse in construction and expression, references to earlier offerings may be useful. In November 1980 we published a letter by Dr. Shehadi [1] on medical terminology. In 1983 we carried a series of four thoughtful editorials by Dr. Friedman [2–5] on the construction and terminology of radiologic reports, oriented to pulmonary problems. These essays have served me well in instructing incoming trainees on the principles of a good radiologic report; they also inspired several letters to the editor [6–9] and another editorial [10]. The September 1984 issue of *AJR* featured a glossary of terms for thoracic radiology, carefully assembled by members of the Fleischner Society [11]; this has since been updated [12]. Most recently we focused on two words, *incidence* and *prevalence*, with guidance from Dr. Shuman [13] in their proper use.

Although a picture may be worth a thousand words, we often must resort to words about pictures—or words *without* pictures. Dr. Hall reminds us of the need to be precise in our use of words.

MMF

REFERENCES

1. Shehadi WH. More on medical terminology (letter). *AJR* **1980**;135:1118
2. Friedman PJ. Radiologic reporting: structure. *AJR* **1983**; 140:171–172
3. Friedman PJ. Radiologic reporting: the hierarchy of terms. *AJR* **1983**;140:402–403
4. Friedman PJ. Radiologic reporting: describing the lungs and pleura. *AJR* **1983**;140:1030–1031
5. Friedman PJ. Radiologic reporting: the description of alveolar filling. *AJR* **1983**;141:617–618
6. Evens RG. Radiologic reporting (letter). *AJR* **1983**;140:1038
7. Revak CS. Dictation of radiologic reports (letter). *AJR* **1983**;141:210
8. Trapnell DH. Radiologic reporting (letter). *AJR* **1984**;142:233–234
9. Hunter TB. Radiologic reports: structure and review (letter). *AJR* **1984**;142:647–648
10. Orrison WW, Nord TE, Kinard RE, Juhl JH. The language of certainty: proper terminology for the ending of the radiologic report. *AJR* **1985**;145:1093–1095
11. Tuddenham WJ, chairman. Glossary of terms for thoracic radiology: recommendations of the Nomenclature Committee of the Fleischner Society. *AJR* **1984**;143:509–517
12. Austin J, Simon M, Trapnell D, Fraser RG. The Fleischner Society glossary: critique and revisions. *AJR* **1985**;145:1096–1098
13. Shuman WP. Incidence and prevalence: proper use. *AJR* **1985**;145:649–650

Abstracts

Gastrointestinal System

Esophageal infections in immunosuppressed patients after marrow transplantation. McDonald GB, Sharma P, Hackman RC, Meyers JD, Thomas ED (1660 S. Columbian Way, Seattle, WA 98108). *Gastroenterology* 88:1111-1117, 1985

During a 2-year period 21 infections were found in 46 fiberoptic esophagoscopic examinations in 39 patients for an incidence of 46%. Single organisms were responsible for 17 infections: seven cytomegalovirus, six herpes simplex virus, and four *Candida sp.* Multiple organisms were responsible for four infections, three due to cytomegalovirus plus herpes simplex virus and one due to herpes simplex plus *Candida sp.* During the period of this study, autopsies revealed 25 cases of infective esophagitis among 59 patients. Single organisms were responsible for 20 infections, herpes simplex virus and cytomegalovirus, six each; varicella zoster virus, one; and a virus that could not be classified, two. Two were fungal and three were bacterial. In the five remaining cases, two cases had fungus plus bacteria, one each with herpes simplex virus plus bacteria, cytomegalovirus plus bacteria, and cytomegalovirus plus fungus. Endoscopic findings included diffuse shallow erosions in the distal half of the esophagus in most patients. These were often large (1-2 cm) with serpiginous borders and a yellow base. The ulcers often had normal surrounding mucosa and were located at the gastroesophageal junction. Although the authors could predict whether an infection was present, the endoscopic appearance could not accurately predict the organism causing the infection. Because accurate diagnosis is needed for proper treatment, biopsy, brushings, and culture must be obtained.

Charles A. Rohrmann, Jr.

Prognostic factors in colorectal carcinomas arising in adenomas: implications for lesions removed by endoscopic polypectomy. Haggitt RC, Glotzbach RE, Soffer EE, Wruble LD (Division of Hospital Pathology, University Hospital, Seattle, WA 98195). *Gastroenterology* 89:328-336, 1985

A total of 129 colorectal carcinomas arising in adenomas were removed by endoscopic polypectomy or colectomy. Level of invasion (confined to mucosa, invasion into the head, neck, stalk, or submucosa of underlying colonic wall), histology, grade of carcinoma, vascular invasion, and adequacy of excisional margins were compared with patient outcome. Sixty-three patients were treated by polypectomy alone and 66 by colectomy (21 preceded by polypectomy). Mean follow up time was 81 months. None of 65 patients with carcinoma confined to the mucosa died but eight of 64 patients with invasive carcinoma did. Invasion of the submucosa of the underlying colonic wall and rectal location were the only statistically significant adverse prognostic factors. Seven of 28 lesions invading the submucosa and six of 42 rectal lesions had adverse outcome. The authors conclude that the level of invasion is a major factor in determining prognosis for the management of carcinoma arising in an adenoma.

Charles A. Rohrmann, Jr.

Balloon dilatation of benign and malignant esophageal strictures. Graham DY, Smith JL (Digestive Disease Section, VA Medical Center, Houston, TX 77211). *Gastrointest Endosc* 31:171-174, 1985

Balloon dilatation of 22 patients with dysphagia secondary to benign or malignant strictures was undertaken using dilating balloons over an Eder-Puestow spring-tipped guide wire. The guide wire was placed using a fiberendoscope either "blind," with fluoroscopy, or with a combination of both. Attempt was made to achieve esophageal diameter of 15 mm at the initial dilatation and was achieved in most instances. Patient discomfort was used to determine maximum dilatation. The authors do not provide follow up information.

Charles A. Rohrmann, Jr.

Endoscopic ultrasonography: a preliminary report. Thatcher BS, Sivak MV Jr, George C (M. V. Sivak, Jr., Dept. of Gastroenterology, Cleveland Clinic, 9500 Euclid Ave., Cleveland, OH 44106). *Gastrointest Endosc* 31:237-242, 1985

Using a prototype ultrasound fiberoptic endoscope developed by the Olympus Corp. (model GF-UM1) and an endoscopic sonographic observation unit (model EU-M1), the authors obtained endoscopic sonograms in 25 patients. Retroperitoneal structures, pancreatic parenchyma, and pancreatic ductal structures were imaged. The authors propose that differentiation of mucosal from intramural diseases and evaluation of neoplasms are possible.

Charles A. Rohrmann, Jr.

Incidence of portal vein thrombosis in liver cirrhosis. An angiographic study in 708 patients. Okuda K, Ohnishi K, Kimura K, Matsutani S, Simida M, Goto N, Nusha H, Takashi M, Suzuki N, Shinagawa T, Suzuki N, Ohtsuki T, Arakawa M, Nakashima T (Dept. of Medicine, Chiba University Hospital, Chiba, Japan (280). *Gastroenterology* 89:279-286, 1985

The incidence of angiographically demonstrable portal vein thrombosis was studied in 708 consecutive patients with cirrhosis seen over a 10-year period. The patients were studied either by transhepatic portography or superior mesenteric arterial portography and were included only if the main portal venous system was clearly seen. Two cases were excluded due to prior splenectomy. There were four cases of portal vein thrombosis related to cirrhosis, all in a decompensated state. Thus, the incidence of portal vein thrombosis was 0.57% of all cirrhotic patients without splenectomy. These comprised 24% of the 17 cases of extrahepatic portal vein obstruction encountered during the same period. These data, when compared with a statistical survey from the Japan autopsy registry, showed that portal vein thrombosis is not a common complication of cirrhosis in Japan.

Charles A. Rohrmann, Jr.

Oesophageal function tests: are they of value? Channer KS, Virjee JP (Dept. of Cardiology, Bristol Royal Infirmary, Bristol, Great Britain). *Clin Radiol* 36:493–496, Sept 1985

Esophageal function was assessed in 15 unselected control patients, eight patients with systemic sclerosis, 10 diabetics with autonomic neuropathy, and 24 diabetic controls. Water bolus transit time was derived from esophageal scintigraphy, barium swallow, and by timing the transit of a barium sulphate-filled capsule through the esophagus. Water transit times and capsule transit times were significantly prolonged in patients with systemic sclerosis and diabetics with autonomic neuropathy in comparison with controls. Barium swallow was abnormal in seven of eight patients with systemic sclerosis, whereas water transit time was abnormal in all eight and capsule transit time was abnormal in six of seven. Nine of 10 patients with diabetic autonomic neuropathy had abnormal barium swallows and water transit times but all 10 had prolonged capsule transit times. Eleven of 24 diabetic controls had abnormal barium swallows and water transit times, but 21 had abnormally prolonged capsule transit times. Six of 15 controls had abnormal barium swallows, four had abnormal water transit times, and 12 had abnormal capsule transit times. Thus, water and capsule transit times are sensitive tests of esophageal function and are as effective as barium swallow in detecting esophageal motility disorders associated with systemic sclerosis and diabetic autonomic neuropathy. Capsule transit time is less expensive, involves a smaller radiation exposure than esophageal scintigraphy, and may be more sensitive.

Author abstract

Gastric emptying in chronic renal failure. McNamee PT, Moore GW, McGeown MG, Doherty CC, Collins BJ. (B. J. Collins, Dept. of Medicine, Institute of Clinical Science, Royal Victoria Hospital, Belfast BT12 6BJ, Northern Ireland). *Br Med J* 291:310–311, Aug 1985

Gastric emptying was studied in a group of 14 patients with uremia and compared with the findings in 11 healthy volunteers. The uremic patients were all experiencing nausea and vomiting, but these symptoms were less severe in the four patients who were undergoing hemodialysis. Barium meal studies in all patients showed no evidence of peptic ulceration. No patient was taking any medication likely to influence gastric motility. A standard meal to which 11.1 MBq (300 Ci) technetium-99m tin colloid had been added was ingested after a 6 hr fast. Successive 90 sec images obtained over a 90 min period were recorded. The gastric images were then delineated and the total counts within this area were calculated for each of the 60 images. A gastric emptying curve was produced. The patients with uremia showed significantly greater retention of isotope in the stomach as judged by counts at 30, 60, and 90 min. Three of the four patients undergoing hemodialysis had normal gastric emptying times confirming the results of a previous study on patients with renal failure undergoing hemodialysis. The etiology of delayed gastric emptying was not elucidated by this study. Possible mechanisms were discussed. The study suggests a rationale for the use of drugs to accelerate gastric emptying in uremic patients with nausea and vomiting.

Noel K. Allan

Is bile acid malabsorption underdiagnosed? An evaluation of accuracy of diagnosis by measurement of SeHCAT retention. Merrick MV, Eastwood MA, Ford MJ (Dept. of Nuclear Medicine, Western General Hospital, Edinburgh EH4 2XU, Scotland). *Br Med J* 290:665–668, March 1985

A total of 106 individuals, including 63 normal controls, were studied using the retention of SeHCAT as a measure of the presence of bile acid malabsorption. A tracer dose of less than 100 g SeHCAT labelled with 40 kBq (1 Ci) of selenium-75 was administered and the proportion of this synthetic bile salt retained at 7 days after oral administration was measured using a whole body counting technique. These authors have previously shown that in normal subjects, more than 15% of administered selenium radioactivity is retained, with less than 8% retained being definitely abnormal. Three types of malabsorption of bile acid were recognized. Type I follows resection or destruction of the ileal mucosa. Type II, primary idiopathic malabsorption, is thought to be rare. Type III, of uncertain pathogenesis, is associated with cholecystectomy, vagotomy, and certain drugs. Using these criteria, the cause of intractable chronic diarrhea was found to be malabsorption of bile acids in 23 of 26 patients with a history of small bowel resection (type I), six of 29 patients with a history of previous vagotomy or surgery for peptic ulcer disease (type III), and five of 42 patients thought to have the irritable bowel syndrome. Of the 29 patients with persistent diarrhea after vagotomy, 34% showed evidence of bile acid malabsorption. These results suggest that bile acid malabsorption types II and III occur more commonly than previously recognized.

Noel K. Allan

Genitourinary System

Improved diagnostic evaluation of mass occupying lesions of the pancreas by CT—directed fine needle biopsy (in German). Lüning M, Kursuwe R, Lorenz D, Menzel A, Schöpke W, Stargardt A, Hoppe E, Meyer R (Institut für Röntgendiagnostik, Bereich Medizin (CHARITÉ) der Humboldt-Universität zu Berlin, DDR01040 Berlin, Schumanstrasse 20/21, GDR). *Radiol Diagn* 25:701–717, 1984

The authors retrospectively analyzed the diagnostic accuracy of computed tomography (CT), CT-guided fine needle biopsy (CT-FNB), sonography, angiography, and endoscopic retrograde cholangiopancreatography (ERCP) in the diagnosis of mass occupying lesions of the pancreas. Of 141 consecutive pancreatic lesions studied, 44 proved malignant, 74 nonmalignant, and 23 were pancreatic pseudocysts. The diagnostic accuracy for malignant tumor was: CT 52% (23 cases); CT-FNB 73% (32/44); sonography 29% (10/34); angiography 48% (10/21); and ERCP 41% (seven/17). In 74 patients with nonmalignant lesions, the diagnostic accuracy was: CT 27%; CT-FNB 89%; sonography 56%; angiography 38%; ERCP 46%. In the pancreatic pseudocysts the diagnostic accuracy was: CT 83%; CT-FNB 100%; sonography 67%; angiography: diagnosis of no malignancy in two cases and malignancy in three; and ERCP 70%. The total correct evaluation of the processes was: CT 44% (62/141); CT-FNB 86% (121/141); sonography 47% (42/89); angiography 42% (21/50); and ERCP: 49% (27/55). The specificity was respectively: 40%, 92%, 38%, and 53%. The authors recommend that in suspected cases of pancreatic lesions that the diagnostic imaging investigations begin with CT followed by CT-FNB. This would lead to a more directed and correct use of angiography and ERCP and eliminate sonography.

A. F. Govoni

The use of a low-osmolality contrast medium in hysterosalpingography: comparison with a conventional contrast medium. Davies AC, Keightley A, Borthwick-Clarke A, Walters HL (King's College Hospital, London, Great Britain). *Clin Radiol* 36:533–536, Sept 1985

Hexabrix 320 and Conray 280 were compared in a randomized double-blind study of 97 patients undergoing hysterosalpingography. Although the lower osmolality and higher viscosity of Hexabrix should make this a superior contrast agent to Conray for hysterosalpingography, in this study no significant differences between the two contrast media either in the incidence of side effects or in radiographic image quality were detected. Pain was felt maximally at the time of injection of contrast medium; after the examination greatest pain occurred on the evening of the examination with both types of contrast media. The authors conclude that the osmolality of the contrast medium is not the most important determinant of abdominal pain after hysterosalpingography.

Noel K. Allan

Current imaging of renal masses. Ling D, van der Vliet AH, McClennan BL (Mallinckrodt Institute of Radiology, Washington University School of Medicine, St Louis, MO 63110). *Rev Interam Radiol* 10:53–60, April 1985

While the excretory urogram remains the major screening test for detection of the renal mass sonography and computed tomography have, to a large extent, replaced angiography and cyst aspiration in the characterization of the renal mass. Magnetic resonance imaging (MRI) appears to be an imaging means of great promise. The initial experience indicates that MRI can successfully detect and define renal masses and accurately stage renal neoplasms. However, the role of MRI and the evaluation of the renal mass is uncertain and it remains to be determined whether this technique will actually replace or merely complement any of the other currently available imaging methods.

Charles M. Nice, Jr.

Current trends in endourology: transrenal ureteral interventions. Nunez D Jr, Hansen D (University of Miami, Jackson Memorial Medical Center, Miami, FL 33103). *Rev Interam Radiol* 10:47–51, April 1985

Operative correction of ureteral strictures may imply a very extensive surgical procedure and retrograde dilatation is a technically demanding procedure. Thus, the percutaneous transrenal approach is becoming an attractive alternative for ureteral stenting and dilatation. Treatment of ureteral leaks and fistulas should be based on two basic principles: (1) urine flow through the anastomotic breakdown must be suppressed so that the desmoplastic effects of urine extravasation can be minimized; and (2) the continuity and caliber of the anastomosis should be preserved so that stricture formation is prevented. These two goals can be accomplished by percutaneous nephrostomy and transrenal ureteral stenting. Urine is diverted and the stent provides a tubular mold around which prompt epithelialization can occur.

Charles M. Nice, Jr.

Muscles and Skeleton

Sonography of tendinopathies involving the Achilles tendon of athletes (in Italian). Campani R, Pisani A, Benazzo F, Castelli C, Meroni L, Barazzoni G (Istituto di Radiologia dell'Universitá, Policlinico S. Matteo, Piazzale Golgi, I-27100 Pavia PV, Italy). *Radiol Med* 71:44–50, 1985.

Sonography and xeroradiography were performed in 185 athletes who presented with symptoms indicative of a pathologic process involving the Achilles tendon. In 79 cases, the two examinations were negative for abnormalities. In 106 patients the following processes were demonstrated by sonography: peritendinitis, 23; peritendinitis and tendinosis, 38; tendinopathy at the level of the insertion of the tendon, 34; and tendon rupture, 11. In tendinitis, sonography showed a nonuniform thickening and hypoechogenicity of the triangle of Krager. The findings of tendinopathy at the point of insertion of the tendon included swelling of the pretendon bursa, nonhomogeneous tendon echogenicity, and calcifications in the tendon. Tendinosis showed as focal or diffuse irregular thickening of the tendon with ill-defined contours. A rupture of the tendon was demonstrated by hypoechogeneous area at the rupture site, which also showed irregular contours and degenerative nodules. Thirty-nine patients were operated on; in 33 the diagnosis reached at sonography was confirmed.

A. F. Govoni

Ultrasonographic evaluation of pathologic processes involving the Achilles tendon (in Italian). De Nicola T, Calzolaro C, Lombardo S, Bacarini L, La Gioia M, Martinelli B (Servizio di Radiologia Ospitaliero, Ospedale Maggiore, Via Stuparich, 1, I-30125 Trieste TS, Italy). *Radiol Med* 71:51–55, 1985

The authors sonographically examined 54 patients presenting with symptoms suggesting Achilles tendon abnormalities. The results and the findings were similar to those reported by Campani et al. (see preceding abstract).

A. F. Govoni

Disk-space hypodensity in CT: the first radiological sign of postoperative diskitis. Lähde S, Puranen J (Oulu University, SF-90220 Oulu, Finland). *Eur J Radiol* 5:190–192, 1985

From January 1982–December 1983, 320 operations for herniated disk were performed; in six patients a postoperative diskitis developed. The patients presented symptoms of severe back pain and muscle spasms 4–14 days after surgery. The symptoms were associated with mild fever and elevated sedimentation rate. Standard radiographs of the lumbar spine and multidirectional tomography showed narrowing of the disk space and erosions of the involved end plates. Computed tomography showed significant hypodensity of the disk spaces affected and, in three patients, this finding was the first evidence of the diskitis, which appeared 10 days after the first onset of the symptoms.

A. F. Govoni

MR imaging of the intervertebral disc: a quantitative study. Jenkins JPR, Hickey DS, Zhu XP, Machin M, Isherwood I (University of Manchester, Manchester, Great Britain). *Br. J Radiol* 58:705–709, Aug 1985

The T1 and T2 relaxation times and the proton density of the nucleus pulposus have been measured in 107 normal and 18 surgically proven degenerative intervertebral disks. Data from total saturation recovery and spin-echo sequences were utilized in a robust multipoint method and relaxation times and proton density calculated. The results show that both the T1 and T2 values of the normal nucleus pulposus decrease with age. There was no significant correlation between proton density and age in normal disks. At all ages there was a highly significant difference between the T1 values of normal and degenerative disks. With T2 a highly significant difference in the younger age groups reduced to no distinction in the seventh decade. The observed change in the T1 and T2 values of the nucleus is in agreement with the reduction of water content known to occur with age. The results indicate that quantitative magnetic resonance imaging may assist in the diagnosis of intervertebral disk degeneration.

Author abstract

Plasma cell diseases: a review. Casal GL, Bella JD, Viamonte-Ros AM, Inchausti BC, Secton DL (Mount Sinai Medical Center, Miami Beach, FL 33140). *Rev Interam Radiol* 10:1–25, Jan 1985

Clinical, laboratory, and radiographic findings in localized and generalized varieties of plasma cell diseases were reviewed. Although these conditions have a common cellular origin, they may differ in their manifestations. These diseases may be considered as a part of the spectrum of immunoproliferative (B-cell) disorders. The authors provide extensive clinical and laboratory discussion of these conditions. The aggressiveness of multiple myeloma cannot be judged from the presence, number, or type of bone lesions, but only from the progression of the disease and its response to chemotherapy. The degree of malignancy appears to be independent of immunoglobulin produced in multiple myeloma, with the exception of one rare IgD variety that appears more aggressive and Waldenstrom macroglobulinemia that has a more benign course. Bone scintigraphy is of limited value in multiple myeloma and should not be included in the workup. There is occasional increase of radionuclide uptake in patients who have sclerotic changes and also in patients who have fractures. When the plain films are not diagnostic, limited use of computed tomography of the lumbar spine or specific area may provide, in selected cases, an image compatible with the diagnosis of multiple myeloma. Iodinated contrast may be used if absolutely necessary in a patient with multiple myeloma, but only after proper hydration and evaluation of urinary L-Chain and serum levels of calcium and uric acid. The radiologist must be aware of the soft-tissue manifestations of multiple myeloma and the possibility that these are associated with amyloid deposits.

Charles M. Nice, Jr.

Nervous System

Correlation of computed tomography and conventional hypopharyngography findings in hypopharyngeal tumours. Ĉatic Dž, Lovrinčević A (University Medical Center, Sarajevo, Moše Pijade 25, Yugoslavia). *Eur J Radiol* 5:178–180, 1985

Thirty-two patients with carcinoma of the hypopharynx were studied by computed tomography (CT) and hypopharyngography. The findings obtained by both procedures were then compared with those observed at endoscopy. The results showed that in 17 cases both radiologic procedures obtained equivalent findings. However, in 13 cases CT also demonstrated: destruction of the thyroid cartilage (four cases), enlarged regional lymph nodes (four), and infiltration of the surrounding structures (five). These findings were not seen at hypopharyngography. The contrast study, however, showed an abnormal swallowing mechanism in 11 cases, suggesting that the two procedures offer complementary information in the staging of this tumor.

A. F. Govoni

Measurement of blood flow, oxygen utilisation, oxygen extraction ratio, and fractional blood volume in human brain tumours and surrounding oedematous tissue. Lammertsma AA, Wise RJS, Cox TCS, Thomas DGT, Jones T (MRC Cyclotron Unit, Hammersmith Hospital, Ducane Road, London W12 0HS, England). *Br J Radiol* 58:725-734, Aug 1985

The blood flow, oxygen utilization, oxygen extraction ratio, and fractional blood volume were measured in brain tumors and the surrounding cerebral tissues. A total of 21 patients were studied. These included 10 primary tumors, eight secondary, and three with unknown histology. Measurements were performed using the oxygen-15 steady state inhalation technique and positron emission tomography. Within the tumors no relation between blood flow, oxygen utilization, and blood volume was found. In all tumors oxygen supply was in excess of the oxygen demand of the tissues as reflected in oxygen extraction ratios that were lower than those of normal brain tissue. No indication of local ischemia in peritumor edema was found.

Author abstract

Intraarterial digital angiography in the evaluation of transitory cerebral ischemia (In Spanish). Mendez G, Nunez D, Yrizarry JM (University Hospital, Tamarac, FL). *Rev Interam Radiol* 9:201–205, Oct 1984

Intraarterial digital subtraction angiography permits rapid, accurate, and safe evaluation of the patient with cerebral vascular insufficiency. The procedure permits the use of smaller amounts of contrast material, which is safer for the patient. For carotid arteries 2–3 ml/sec for a total of 6 ml is given. For the vertebral artery, 1.5 ml/sec for a total of 5–6 ml is given. In the study of the aortic arch, contrast is given at the rate of 10 ml/sec for a total of 30 ml. The concentration of 200–280 mg of iodine/ml is chosen. Five case studies are presented. Advantages of arterial injection include easy visualization of contrast, reduction of duration of the procedure, reduction in film cost, and sometimes avoidance of a selective catheterization. The procedure has proved most useful in the evaluation of patients with transient ischemic attacks. The authors note that in their institutions, digital subtraction angiography has almost replaced conventional angiography for the evaluation of such patients.

Charles M. Nice, Jr.

Orbital pneumosinus dilatans. Lloyd GAS. (Royal National Throat, Nose, and Ear Hospital, London, Great Britain). *Clin Radiol* 36:381–386, July 1985

Pneumosinus dilatans consists of an abnormal dilatation of the paranasal air sinuses that contain air only and are lined by normal epithelium. The condition is most commonly observed when it affects the sphenoidal sinus as a response to a local meningioma of the tuberculum sellae or planum sphenoidale. Pneumosinus dilatans affecting the walls of the paranasal sinuses that form the boundaries of the orbit is less common; six patients reported here presented with either unilateral or bilateral exophthalmos. The frontal sinus and ethmoid cells were affected unilaterally in four patients with the maxillary antra bilaterally in two. The condition was associated with a meningioma in three patients and with fibroosseous disease in three patients. The importance of recognizing this condition is in alerting the radiologist to the possible presence of an occult meningioma requiring soft-tissue imaging techniques (computed tomography or magnetic resonance). The presence of fibroosseous disease can usually be recognized by plain radiography.

Author abstract

Optic nerve sheath meningiomas. Clinical manifestations. Sibony PA, Krauss HR, Kennerdell JS, Maroon JC, Slamovits TL. (Dept. of Neurology, HSC, SUNY-Stony Brook, Stony Brook NY 11794). *Ophthalmology* 91:1313–1326, Nov 1984

The authors retrospectively studied optic nerve sheath meningiomas in 22 patients, aged 18–66 years (median, 43 years; 82% were 33–59 years). Some 68% were women. All patients except two exhibited unilateral disease. Both patients with bilateral optic nerve sheath meningiomas were women. The presenting symptom in 77% was decreased vision; 23% presented with transient visual obscurations. In 68% there was proptosis of 2–6 mm. Only two patients showed radiographic findings of intracranial involvement. Transfemoral angiography was performed in seven cases and revealed a vascular blush in five. Computed tomography showed three characteristic patterns of optic nerve enlargement. Tubular thickening of all or part of the intraorbital optic nerve was most common (64%). Fusiform enlargement usually involving the middle or posterior part of the nerve was present in 23%. Anterior or posterior globular peroptic masses were found in 23%. The optic nerve could sometimes be identified as a central lucency through the mass. No optic nerve calcification was seen. The posterior apical area of the optic nerve was the most common site of involvement (81%) among all patterns of enlargement. Four of 10 patients studied with tomography of the optic canals had enlargement of the involved canal. Hyperostosis of the canal was seen in one case.

Harvey I. Wilner

Human brain glucose utilization and cognitive function in relation to age. Duara R, Grady C, Haxby J, Ingvar D, Sokoloff L, Margolin RA, Manning RG, Cutler NR, Rapoport SI (S. I. Rapoport, Laboratory of Neurosciences, Section on Brain Aging and Dementia, National Institute on Aging, Clinical Center, National Institutes of Health, Bethesda, MD 20205). *Ann Neurol* 16:702–713, Dec 1984

Brain oxidative metabolism was examined with positron emission tomography and ^{18}F 2-deoxy-D-glucose in 40 healthy men aged 21–83 years under conditions of reduced visual and auditory stimulation. The mean cerebral metabolic rate for glucose (CMR$_{glc}$) equaled 4.6 to 4.7 mg/100 gm^{-1}/min^{-1} and did not correlate significantly with age ($p > 0.05$). Regional cerebral metabolic rates for glucose (rCMR$_{glc}$) and Q ratios (rCMR$_{glc}$/CMR$_{glc}$), which had lower coefficients of variation than did rCMR$_{glc}$, also did not correlate with age. Hyperfrontality of cerebral metabolism was absent at all ages. Age decrements were demonstrated in the error score on the Benton Revised Visual Retention Test and in the performance subtest scaled score of the Wechsler Adult Intelligence Scale (WAIS) but not in the verbal subtest scaled score of the WAIS. The cognitive test scores did not correlate with brain metabolic rates. The results indicate that brain oxidative metabolism, when measured under resting conditions with reduced sensory input, is not reduced in relation to age in healthy men. Further, no significant relations between intelligence and resting cerebral metabolism are evident.

L. Cala

Nuclear magnetic resonance imaging in evaluation of clinical stroke syndromes. DeWitt LD, Buonanno FS, Kistler JP, Brady TJ, Pykett IL, Goldman MR, Davis KR (J. P. Kistler, Behavior-Stroke Laboratory, Burnham 802, Massachusetts General Hospital, Boston, MA 02114). *Ann Neurol* 16:535–545, Nov 1984

Proton magnetic resonance (NMR) imaging was performed on normal volunteers and patients with various types of clinical strokes. True three-dimensional volumetric data were obtained for subsequent reconstruction of images at various orientations, including transverse, coronal, and sagittal, and for specific matching to x-ray computed tomographic planes. Various radiofrequency pulse sequences were used to generate images weighted by the MR parameters spin density and spin-lattice (T1) and spin-spin (T2) relaxation times. Quantitative T1 data and qualitative T2 information were obtained from appropriate sequences. Proton MR images embodying T1 information provided adequate delineation of normal intracranial anatomic structure and a high level of gray matter–white matter contrast. High lesion detection sensitivity in various clinical forms of stroke was seen in images providing both T1 and T2 information. T1 and T2 relaxation times were prolonged in embolic, thrombotic, and watershed infarctions and in lacunae. Hematomas had a shortening of T1 and T2. Arteriovenous malformations can be diagnosed but are reported with variable parameters. Quantitation of ^{1}H MR parameters, or proton chemical shift imaging, may aid in the ability to diagnose stroke disease, evaluate treatment protocols, and possibly to understand better the pathophysiologic mechanisms of ischemia vs. infarction in stroke.

L. Cala

Dural arteriovenous malformations and intracranial hemorrhage. Malik GM, Pearce JE, Ausman JI, Mehta B (Henry Ford Hospital, Detroit, MI 48202). *Neurosurgery* 15:332–339, Sept 1984

Dural arteriovenous malformations are vascular anomalies of the dura mater that are supplied exclusively by branches of the carotid or vertebral arteries before they penetrate the dura. Venous return may remain in the dura or enter the leptomeningeal and cortical veins. Such malformations comprise roughly 6% of the supratentorial and 35% of the infratentorial arteriovenous malformations (AVM). Most dural malformations arise within or adjacent to a major venous sinus and have predominantly dural venous drainage. The authors report six cases of intracranial hemorrhage among their past 10 patients with dural malformations. A literature search provided 27 other cases of intracranial hemorrhage from a total of 213 reported dural AVM. Although hemorrhage was relatively infrequent with dural AVM located primarily within a major venous sinus, bleeding episodes were more common in cases of malformations outside a major sinus. Primary leptomeningeal venous drainage may be associated with large variceal dilation. Dural AVM outside a major sinus are uncommon; they have a propensity for serious intracranial hemorrhage. Of the 213 cases of dural AVM reviewed, 135 involved the transverse-sigmoid sinus and 39 involved the cavernous sinus. Common locations outside a sinus were the tentorium, basifrontal, clival, or convexity dura.

K. Jack Momose

Spinal cord or nerve root compression in patients with malignant disease: CT evaluation. Wang AM, Lewis ML, Rumbaugh CL, Zamani AA, O'Reilly GV (Harvard Medical School, Boston, MA 02115). *J Comput Assist Tomogr* 8:420–428, June 1984

Fifty patients with malignant disease who developed acute spinal cord or nerve root compression were studied by computed tomography (CT). Of these, 48 had positive CT findings, 22 showed involvement of multiple contiguous levels, and five had involvement of noncontiguous levels. All patients who had radiographic evidence of spinal cord or spinal nerve compression received radiation therapy, surgical decompression, or both. Most of the patients showed dramatic clinical improvement. In two of 50 cases spinal CT was inconclusive, but myelography was diagnostic. Cerebrospinal fluid seeding with nerve root involvement was present in one case while conus medullaris involvement was found in the other. Metastases affect the spinal cord or nerve roots in one of two ways, parenchymal invasion (rare) or epidural invasion (more common). In this report, all epidural metastases could be well evaluated on CT. When there are parenchymal metastases, CT may be inconclusive and myelography is the preferred radiologic examination.

K. Jack Momose

Miscellaneous

Internal mammary lymphoscintigraphy in the conservative management of breast carcinoma: an update and recommendations for a new TNM staging. Ege GN, Clark RM (Dept. of Nuclear Medicine, The Princess Margaret Hospital, Toronto, Ontario M4X 1K9, Canada). *Clin Radiol* 36:469–472, Sept 1985

The results of internal mammary lymphoscintigraphy (IML) in 524 patients with breast carcinoma who underwent partial mastectomy, with or without axillary dissection, demonstrate the predictive value of an abnormal lymphoscintigram. There was a significant difference ($P < 0.0005$) in actuarial survival between patients with normal and abnormal IML. In view of the increased mortality associated with metastases to both internal mammary and axillary lymphatics compared with involvement of either site alone, and the most favorable outcome in patients with involvement of neither site, it is proposed that the current TNM staging for breast carcinoma should henceforth include the status of internal mammary lymph nodes determined by radiocolloid lymphoscintigraphy. Further refinement of the N status into Na (axilla) and N1 (internal mammary nodes) is suggested. Stages I, II, and III should designate, respectively, patients with no evidence of involvement of either lymphatic site, patients with involvement of one or the other site, and patients with involvement of both sites. This would constitute a more rational approach to the staging and management of the patient with breast carcinoma and would also provide a more accurate means of evaluating the true efficacy of current strategies in comparable groups of patients. Unrecognized internal mammary lymphatic metastases have probably confounded the results of past prospective trials.

Author abstract

Diaphanography in breast carcinoma: correlation with clinical examination, mammography, cytology, and histology. Wallberg H, Alveryd A, Bergvall U, Nasiell K, Sundelin P, Troell S (Dept. of Surgery, Huddinge University Hospital, S-14186 Huddinge, Sweden). *Acta Radiol [Diagn]* (Stockh) 26:33–42, 1985

From January 1978 to July 1980, 108 breast cancer patients were available for the evaluation of diaphanography in conjunction with results obtained from clinical examination, mammography, cytologic fine-needle biopsy, and histologic examination of surgical specimens. Diaphanography was performed in a darkened room after adequate adaptation of the examiner and the transilluminated image of the breast documented on infrared film. On the basis of the outline of the breast lesion, color of illumination, and absence or presence of vessels, the diaphanographic findings were visibly classified. The mammographic findings were classified using conventional criteria such as the general appearance of the breast, focal tumor characteristics, and calcifications. In 86 cases (78.2%), the findings of both mammography and diaphanography were positive for malignancy. In six cases, the breast carcinomas were not diagnosed by either mammography or diaphanography. Seven breast carcinomas were correctly diagnosed by diaphanography, but not by mammography. Five of these tumors were palpable. The diaphanographic images showed a darkly shaded region in four cases and a lightly shaded area in three cases, with vessels in the tumor region seen in all cases. The mammographic images showed abundant glandular tissue, with no localized abnormalities seen in five cases and a benign appearing lesion in two cases. Eleven breast carcinomas were correctly diagnosed by mammography, but not by diaphanography, which failed to show any focal abnormality. Six of these carcinomas were palpable. The authors conclude that diaphanography can be considered a useful adjunct to clinical examination and mammography.

Peter F. Winter

Pediatric Radiology

Facial port-wine stains and Sturge-Weber syndrome. Enjoiras O, Riche MC, Merland JJ (Hôpital Tarnier [CHU COCHIN], 89 rue d'Assas, 75006 Paris, France). *Pediatrics* 76:48–51, 1985

A retrospective review of 106 patients with facial port wine stain revealed 12 children with Sturge-Weber syndrome. Sturge-Weber syndrome is defined as facial port wine stain associated with ipsilateral leptomeningeal vascular anomalies and inconsistent ipsilateral choroidal vascular malformation with glaucoma. The authors conclude that only children with port wine stains in the ophthalmic (V1) distribution are at risk for neuroocular pathology. On the basis of their patient population, they hypothesize that Sturge-Weber syndrome results from a dysmorphogenesis of cephalic neuroectoderm.

Richard B. Towbin

Nephroblastoma with "egg-shell" calcifications. Chaabane M, Diard F, Calabet A, Laurent F, Tavernier J (Service de Radiologie, Hôpital des Enfants, 168, cours de l'Argonne, F33077 Bordeaux Cedex, France). *J Radiol* 65:657–663, Oct 1984

Three cases of nephroblastoma displaying "egg shell" calcifications are reported in children of 2 and 3 years of age. This pattern of peripheral calcifications is compared to the much better known coarse central calcifications that occur in nephroblastomas. The pathophysiology of these egg shell calcifications is not well understood. They do not seem to carry any specific prognostic significance. In the presence of such calcifications, the workup remains similar to that of other renal masses. Whereas various possible entities that may present with this pattern of calcifications are discussed, the authors stress the importance of renal adenocarcinoma of children as the main differential diagnosis. Although the age of onset can be a distinguishing factor between these two malignant neoplasms, the final diagnosis can only be asserted at pathology.

Joseph Fakhry

Bile duct dilatation and immunodeficiency in children. Report of four cases. Garel L, Brunelle F, Fischer A, Sirinelli D, Sauvegrain J (Service de Radiopediatrie, Hôpital des Enfants Malades, 149 rue de Sevres, 75730 Paris Cedex 15, France). *Ann Radiol* 28:259–263, 1985

Four cases of congenital immunodeficiency syndrome associated with bile duct dilatation are reported. The deficiency was of humoral origin in one case, cellular origin in another, and related to humoral and cellular factors in the remaining two cases. In all patients, firm hepatomegaly was the first sign referring to right upper quadrant pathology. Laboratory results were compatible with cholestasis. Sonography showed mild dilatation of intra- and extrahepatic bile ducts was uniformly present. Transhepatic cholangiography demonstrated a pattern similar to that of sclerosing cholangitis. Biopsy revealed periportal fibrosis in two cases, steatosis in one case, and normal findings in the fourth. Bile duct dilatation was stable on repeat sonography performed after an interval of 1–4 years. While the long term prognosis (particularly with respect to the risk of biliary cirrhosis) is not known, the evidence of hepatic complication represents a contraindication to potential bone marrow transplant.

Joseph Fakhry

Association of septic shock caused by early-onset group B streptococcal sepsis and periventricular leukomalacia in the preterm infant. Faix RG, Donn SM (Box 007, L32023 Women's Hospital, Ann Arbor, MI 48109-0010). *Pediatrics* 76:415–419, Sept 1985

During a 2-year period, 628 infants admitted to the Neonatal Intensive Care unit underwent serial brain sonography. Periventricular leukomalacia (PVL) was diagnosed in eight. The underlying etiology was early-onset group B streptococcal sepsis in four, shock not related to infection in three; one infant developed PVL without shock or hypotension. Early-onset group B streptococcal sepsis was diagnosed in 12 infants: seven developed shock and three died within the first 24 hr. The remaining four all developed PVL. None of the survivors without shock developed PVL. The earliest sonographic changes were noted at 7 days. Three of the four with PVL survived and all have significant neurologic impairment. The authors recommend serial sonography in all preterm infants surviving early-onset group B streptococcal sepsis.

Richard B. Towbin

Increased risk of gastrointestinal perforation in neonates mechanically ventilated with either face mask or nasal prongs. Garland JS, Nelson DB, Rice T, Neu J (Dept. of Pediatrics, Milwaukee Children's Hospital, Milwaukee, WI 53233). *Pediatrics* 76:406–410, Sept 1985

The authors reviewed 20 cases of gastrointestinal perforation not associated with necrotizing enterocolitis or bowel obstruction that occurred over 10 years. Fifteen infants suffered perforations during face mask or nasal prong cycled ventilation. This represented nearly a 30 fold increased risk for development of gastric or intestinal perforation when compared to infants ventilated via endotracheal tube. The authors suggest that routine use of mechanical ventilation either with nasal prongs or face mask appears to be associated with an unacceptable risk of gastrointestinal perforations in sick neonates.

Richard B. Towbin

Antenatal sonographic diagnosis of fetal gastrointestinal malformations. Barss VA, Benacerraf BR, Frigoletto FD Jr (Dept. of Obstetrics and Gynecology, Brigham and Women's Hospital, Boston, MA 02115). *Pediatrics* 76:445–449, Sept 1985

In a 26-month period, 17 fetuses with gastrointestinal anomalies were detected sonographically. Nine had malformations involving organ systems other than the gastrointestinal tract. The remaining eight had only gastrointestinal anomalies. A correct diagnosis was made in 16 of 17 cases. In one fetus with gastroschisis, the anterior wall defect was not seen because of severe oligohydramnios. Of the 17 cases, there were two therapeutic abortions, five still births or immediate perinatal deaths, and 10 survivors.

Richard B. Towbin

Pancreatic lipomatosis in the Shwachman-Diamond syndrome. Identification by sonography and CT-scan. Robberecht E, Nachtegaele P, Van Rattinghe R, Afschrift M, Kunnen M, Verhaaren R (Kliniek voor Kinderziekten C. Hooft, Akademisch Ziekenhuis, De Pintelaan 185, B9000 Ghent, Belgium). *Pediatr Radiol* 15:348–349, July 1985

Shwachman-Diamond syndrome is second to cystic fibrosis as a cause of exocrine pancreatic insufficiency. In a 14-year-old boy with this syndrome, a strongly echogenic pancreas (much more echogenic than the liver) was confirmed by low-attenuation computed tomography to be due to fat. These findings thus represent fatty infiltration.

Alan E. Oestreich

Hypoplasia of the odontoid with atlanto-axial subluxation in Hurler's syndrome. Thomas SL, Childress MH, Quinton B (M. H. Childress, Howard University Hospital, Washington, DC 20060). *Pediatr Radiol* 15:353–354, July 1985

A 3-year-old boy with Hurler syndrome presented with quadriparesis 1 day after falling from his tricycle. On skull film, there was dense hypoplasia and atlanto-axial subluxation (and, incidentally, calcification of the stylohyoid ligament and other signs of Hurler syndrome). This is apparently the third report of atlanto-axial subluxation leading to a cord compression in Hurler syndrome, which is far more frequent in Morquio syndrome. Such patients may benefit from preventive stabilization. This child improved in a collar and then C2 to C2 fusion, but symptoms recurred because of inadequate fusion.

Alan E. Oestreich

Imaging Technology

Angio-computed tomography: exposure timing and subsequent venous washing (in Italian). Schadn, Rohde U, Pastremoli A (A. Pastremoli, Servizio di Radiologia, Ospedale Civile, I-40026 Imola, Italy). *Radiol Med* 70:369–373, 1984

The authors reviewed 168 angiographic computed tomography (CT) studies. In 157 the timing was correct, however, in 11 it was unsuccessful. The examinations are performed with single intravenous injection of 30 to 40 ml of contrast medium at 8–10 ml/sec. Immediately after the introduction of the contrast medium, an injection of 15–30 ml of physiologic solution follows as a "washing." The angiographic-CT studies are done after a predeterminate number of heart cycles, which would allow, therefore, the contrast medium to reach the arterial territory under investigation during its first passage. The purpose of the immediate venous flushing is to obtain a compact bolus of contrast medium. The technique is based on the previous studies by Schad (1977, 1980) and Schad et al. (1981, 1982). Several demonstrative angiographic-CT scans of the central nervous system, heart, and abdomen are reproduced.

A. F. Govoni

Mechanisms of contrast in NMR imaging. Wehrli FW, MacFall JR, Shutts D, Breger R, Herfkens RJ (NMR Applications Laboratory, General Electric Medical Systems, Milwaukee, WI 53201). *J Comput Assist Tomogr* 8:369–380, June 1984

In computed tomography (CT) image brightness is essentially determined by the differential x-ray beam attenuation caused by the interactions of the x-ray photons with orbital electrons. This attenuation increases with increasing atomic number. The equivalent of electron density in magnetic resonance (MR) is nuclear spin density; in proton MR imaging it is the density of body hydrogen. Protons that are part of solid structures such as bone or protons in large biological macromolecules such as proteins are characterized by very short spin-spin relaxation times (T2) and long spin lattice relaxation times (T1). The protons that are usually detected in MR imaging are those of water, fatty acid triglycerides (fat), and low molecular weight metabolites. It is well known that the primary determinants of image contrast are the relaxation times and it has generally been assumed that density plays an insignificant role. The authors confirm the former, but demonstrate at the same time that variations in spin density are important. The ability to predict and compute image contrast between two adjacent tissues is critically dependent on intrinsic parameters T1, T2, and proton density. T1 and T2 are best obtained from nonlinear least square fitting of the pixel values in a series of images obtained with operator-selectable time variables such as interpulse delay (e.g., inversion recovery) or echo delay (e.g., spin echo/Carr-Purcell-Meiboom-Gill). The parameter relevant to image perception is the contrast-to-noise ratio (C/N). The authors computed MR pixel intensity and C/N and show these in graph form for various tissues in the normal central nervous system.

K. Jack Momose

News

Pediatric Emergency Radiology

Boston University School of Medicine will sponsor a course, Pediatric Radiology in the Emergency Room, Feb. 7–9, in Lake Buena Vista, FL. Course director: J. O'Connor. Category I credit: 12 hr. Fee: $275, $200 for residents. Information: Dept. of Continuing Medical Education, Boston University School of Medicine, 80 E. Concord St., Boston, MA 02118; (617) 638-4605.

Winter Seminar and Symposium

The Hospital of the University of Pennsylvania has announced two courses. The **Winter Imaging Seminar: An Appraisal of Developing and Mature Imaging Methods** will be Feb. 17–21 in Cancun, Mexico. This seminar will assess such imaging methods as sonography, computed tomography (CT), and magnetic resonance imaging (MRI). There will be in-depth refresher seminars in renal imaging, chest CT, carotid imaging, obstetrical sonography, and liver and pancreatic imaging, plus briefer looks at pelvic and superficial sonography, spinal CT, and cardiovascular, musculoskeletal, and pelvic MRI. Category I credit: 19 hr. Fee: $450 physicians, $375 residents, $225 technicians.

The ninth annual **Skeletal Symposium** will be March 2–7 in Sun Valley, ID. This will emphasize practical aspects of bone and joint disease including the latest imaging techniques. Newer radiologic approaches for detecting and diagnosing musculoskeletal diseases will be emphasized plus the roles of CT, MRI, and arthrography. Category I credit: 23 hr. Fee: $425 physicians, $325 residents.

Information for both courses: Ms. Janice Ford, CME Coordinator, Dept. of Radiology, Hospital of the University of Pennsylvania, 3400 Spruce St., Philadelphia, PA 19104; (215) 662-6904.

Sierra Radiology Conference

The annual Sierra Radiology Conference, sponsored by the Sacramento Radiology Research and Education Foundation and the Northern California Radiology Society, will be March 4–7 in Incline Village, NV. Emphasis will be on clinical imaging and invasive techniques. Faculty will be from the University of California, Davis; also E. van Sonnenberg, University of California, San Diego, and M. Brant-Zawadzki, University of California, San Francisco. Program directors: J. P. McGahan and J. P. Walter. Category I credit: 20 hr. Fee: $345 physicians; $275 residents or fellows. Information: Sacramento Radiology Research and Education Foundation, P.O. Box 19184, Sacramento, CA 95819.

Planning an MRI Facility

Planning for and Operating a Magnetic Resonance Imaging (MRI) Facility will be presented by George Washington University March 17–19 in San Diego and May 12–14 in Toronto. This course will provide a broad perspective on MRI installations with a focus on the specific problems that must be addressed: safety, personal training, and effects on current clinical procedures. Both clinical and research systems will be covered. Principal speaker: E. Schempp. Fee: $750. Information: Ron Donais, Continuing Engineering Education Program, George Washington University, Washington, DC 20052; (800) 424-9773 in the U.S.; (800) 535-4567 in Canada.

Pediatric Radiology

Children's Hospital of Philadelphia will present a course, Pediatric Radiology 1986, March 20–22, in Philadelphia. This in-depth look at state of the art imaging in infants and children will cover a wide gamut of diseases. Lectures and workshops will discuss the appropriate applications of sonography including Doppler, magnetic resonance imaging, computed tomography, scintigraphy, digital subtraction angiography, contrast agents in sonography, the lithotripter, and interventional techniques. Course director: H. K. Rosenberg. Category I credit will be awarded. Fee: $265 physicians; $175 residents, fellows, technologists. Information: Janet Birkmann, Dept. of Radiology, Children's Hospital of Philadelphia, 34th Street and Civic Center Blvd., Philadelphia, PA 19104; (215) 596-9308.

Weekend Courses

The University of California, Irvine Medical Center, and the Great Teacher Foundation International will present four foreign programs in 1986.

New Diagnostic Imaging Approaches to Chest Diagnosis will be March 24–28 in Paris. Faculty: J. Kirkpatrick, E. N. C. Milne, C. Rabin, and E. Zerhouni.

Abnormal Lung Function—Detection and Diagnosis by Imaging will be July 7–11 in Venice, Italy.

Frontiers in Chest Diagnosis 1986 will be Sept. 22–26 in Edinburgh.

Bone and Genitourinary Imaging—Advanced Diagnostic Approaches is slated for Nov. 3–7 in Marbella, Spain.

Category I credit for each: 24 hr. Information: Dawne Ryals, P.O. Box 610203, DFW Airport, TX 75261; (214) 659-9590.

New York Spring Meeting

The New York Roentgen Society will hold its annual Spring Meeting, April 2-5, in New York City. The program will be an overview of general radiology with emphasis on chest disease. Other topics of interest will include pediatrics, genitourinary radiology, and neuroradiology. A special lecture will be delivered by Rosalyn Yalow, Nobel laureate. Faculty consists of members of the society and guests. Society faculty: F. Feldman, T. Naidich, H. Mitty, H. Jacobson, J. G. Rabinowitz, and S. Rakoff. Guest faculty: J. Kirkpatrick, J. Kleinerman, L. Love, R. Lukin, P. Sheedy, L. Swischuk, and E. Theros. Also, K. Krabbenhoft, American College of Radiology. Fee: $300; $150, residents. Category I credit will be awarded. Information: Seymour Sprayregan, M.D., Montefiore Hospital Medical Center, 111 E. 210th St., Bronx, NY 10467.

Mammography Course

Tufts-New England Medical Center will sponsor a course, Mammography for the General Radiologist, April 14-17, June 2-5, Sept. 8-11, and Oct. 20-23 in Boston. Category I credit: 28 hr. Fee: $600. Information: Dr. M. J. Homer, Box 388, Dept. of Radiology, New England Medical Center Hospital, 171 Harrison Ave., Boston, MA 02111.

Pittsburgh Nuclear Medicine Meeting

The Pittsburgh Chapter of the Society of Nuclear Medicine will meet April 19-20. Topic is Central Nervous System Nuclear Medicine; Cardiac Nuclear Medicine and Clinical Update. Faculty: T. Hill, J. Naddahi, E. G. DePuey, and chapter members. Category I credit: 8 hr. Fee (member fee): physicians $60 ($40); technologists $20 ($10). Information: Jeffrey A. Levy, M.D., Dept. of Radiology, Conemaugh Valley Memorial Hospital, 1086 Franklin St., Johnstown, PA 15905; (814) 536-6671.

Physicists Spring Seminar

The Southern California Chapter of the American Association of Physicists in Medicine will hold its spring seminar May 5-7 in Stateline, NV. Topic is the Physics of Emergent Modalities in Clinical Radiology. The seminar will cover the physics required to support new clinical procedures and will include imaging and radiation oncology. The seminar is expected to be of interest to both physicists and physicians. Information: Dr. Norman A. Baily, Dept. of Radiology, M-010, University of California, San Diego, La Jolla, CA 92093.

London and Rome Seminars

Medical Seminars International will present two consecutive seminars in London and Rome. May 10-14 will be the fourth annual London Spring Seminar in Diagnostic Imaging. The annual Europe Spring Seminar in Diagnostic Imaging will follow in Rome, May 14-18. The seminars may be taken together or separately. Both seminars will cover computed tomography, digital radiography, conventional radiography, and magnetic resonance imaging. Faculty for the London seminar: A. Dixon, Addenbrookes Hospital, Cambridge; R. Dick, Royal Free Hospital, London; J. Husband, Royal Marsden Hospital, Surrey; and A. Moss, University of Washington, Seattle. Faculty in Rome: A. Chiesa, Universita Degli Studi, Brescia; R. Passariello, Universita Degli Studi, L'Aquila; P. Pavone and P. Rossi, both Universita "La Sapienza," Rome; also J. Husband and A. Moss. Category I credit will be awarded.

Fee: (before March 7) $385 for either seminar or $450 for both; thereafter, $425 for either or $495 for both.

Information: Medical Seminars International, 21915 Roscoe Blvd., Suite 222, Canoga Park, CA 91304; (800) 633-8687.

European Pediatric Congress

The 23rd Congress of the European Society of Pediatric Radiology will be May 21-24 in Barcelona, Spain. The congress will be preceded by the 11th International Course of Pediatric Radiology, May 19-20, also in Barcelona. Information: Dr. Javier Lucaya, Clinica Infantil, Ciudad Sanitaria Valle de Hebrón, 08035 Barcelona, Spain; telephone (93) 358-3311.

Cincinnati Refresher Course

The 28th Refresher Course in Diagnostic Roentgenology directed by B. Felson will be May 27-31 at the University of Cincinnati College of Medicine. Topics will include radiation physics and nuclear medicine. Category I credit will be awarded. Fee: $350. Information: Dr. Harold B. Spitz, Dept. of Radiology, University Hospital, 234 Goodman St., Mail Location 742, Cincinnati, OH 45267; (513) 872-7226.

Israel Sonography Symposium

Israel 86—Ultrasound Symposium will be in Jerusalem, June 20-29. This category I-approved program will be sponsored by West Park Hospital, Canoga Park, CA, and the Israel Ultrasound Society. Participants may also attend the Israeli Ultrasound Society meeting and the fourth annual Barry B. Goldberg Lecture without additional charge. Faculty: T. Ben Ami, M. Graif, Y. Itshak, and S. Straus, all Sackler School of Medicine, Tel Aviv; J. Kaftori, Haifa; P. Lebensart, Hadassah University Hospital, Tel Aviv; I. Timor, Rambam Medical Center, Haifa; R. Shilo, Tel Aviv Medical Center; F. Weill, University of Besançon, France; H. Zakut, Tel Aviv; P. Cooperberg, University of British Columbia, Canada; and B. Goldberg, Thomas Jefferson Hospital, Philadelphia. Fee: $425 to April 18, $460 thereafter. Information: Israel Symposium, Dept. of Radiology, West Park Hospital, 22141 Roscoe Blvd., Canoga Park, CA 91304; (800) 633-8687.

Radiation Oncology Physics

The American Association of Physicists in Medicine will hold its summer school July 27-Aug. 1 at Miami University, Oxford, OH. Title is: Radiation Oncology Physics—1986. Information: AAPM Executive Secretary, 335 E. 45th St., New York, NY 10017; (212) 661-9404.

Radiology Congress in Salzburg

The University of Connecticut has announced its eighth International Radiology Congress will be Sept. 7-13 in Salzburg, Austria. Cosponsor is the Landeskrankenstatten Hospital, Salzburg. Topics will include magnetic resonance imaging, computed tomography of the head and body, sonography including Doppler, mammography, and interventional and therapeutic radiology. Guest faculty: W. Bradley, F. Laing, S. Sagel, and C. Tegtmeyer. Category I credit: 35 hr. Fee: $550, $300 for residents and technicians. Information: D. Beatty

Crawford, M.D., program director, Dept. of Radiology, University of Connecticut Health Center, Farmington, CT 06032; (203) 674-3322.

Organ Imaging Review

The University of Toronto will present Organ Imaging Review—1986, Sept. 8-12, in Toronto. The practical aspects of modern radiology will be stressed with emphasis on interaction of conventional and newer techniques in imaging specific organ systems including the chest, heart, head and neck, gastrointestinal and genitourinary systems, and skeletal, pediatric, and neuroradiology. Category I credit: 30 hr. Fee (Canadian): $500, $350 for residents and fellows. Information: E. Kassel, M.D., program chairman, Dept. of Radiology, University of Toronto, Room 139 Fitzgerald Bldg., Faculty of Medicine, Toronto, Ontario, Canada M5S 1A8; (416) 978-6801.

San Diego Courses

The San Diego Imaging Symposium, sponsored by the University of California, San Diego, will be Oct. 30-Nov. 1. Program director: B. Gosink. Category I credit: 20 hr. Fee: $325.

The 11th annual San Diego Postgraduate Radiology course, announced in the September 1985 issue of the *AJR*, has been rescheduled. This course will be in Coronado, CA, on Oct. 6-10 rather than Oct. 13-17.

Information for both: Dawne Ryals, P.O. Box 610203, DFW Airport, TX 75261; (214) 659-9590.

Call for Papers

Papers are requested for the second International Conference on Computer Assisted Radiology, which will be July 1-4, 1987, in Berlin, West Germany. The symposium will focus on fundamental principles and applications of computers in radiology. Topics will include image generation, storage, transmission, viewing, analysis, and interpretive aids for medical images. Four copies of 200-500 word abstracts, including six keywords, must be submitted by May 31, 1986, to AMK Berlin, Messedamm 22, D-1000 Berlin 19, West Germany; telephone (030) 3038-3629.

ACR Moves to Virginia

The American College of Radiology (ACR) has moved from its long-time home in Chicago to a 45,000 square foot structure in Reston, VA. The organization's new address is: American College of Radiology, 1391 Preston White Dr., Reston, VA 22091; (703) 648-8900.

AIUM Officers

The American Institute of Ultrasound in Medicine has elected the following officers for 1985-1986: R. A. Meyer, president; C. R. B. Merritt, president-elect; C. W. Hohler, vice president; B. J. Weinstein, treasurer; R. C. Sanders, secretary; and M. C. Ziskin, past president.

Meeting and Course Review

For reader convenience, a summary of upcoming meetings and courses is provided. Detailed listings appear in the *AJR* issues noted in parentheses.

International Education Series. Controversies in Medicine, Feb. 28–March 6, March 7–14, March 21–28, Barbados; April 30–May 8, May 7–15, Paris; Aug. 14–22, Aug. 21–29, London. **Update on Laser Therapy,** June 25–July 3, July 2–10, Heidelberg (Jan)

Magnetic Resonance Imaging Meeting, March 1–5, Philadelphia (Aug)

San Diego Courses: Neuroradiology Update, March 3–4; **Magnetic Resonance Imaging Update,** March 5–7, **Residents' Review,** April 28–May 2; **Biology and Physics of Radiology,** Sept. 1–5; **Postgraduate Course,** Oct. 13–17, all San Diego (Oct)

Neuroradiology Course, March 3–6, Bal Harbour, FL (Dec)

Radiation and Radiotherapy Courses. Nonionizing Radiation, March 3–7; **Radiation Safety Officer's Course,** May 19–23; **Advanced Radiological Health,** May 12–16, all San Antonio (Sept)

Conference on Monoclonal Antibodies, March 6–8, San Diego (Jan)

Winter Conference in Utah, March 9–14, Park City (Jan)

UCSF Courses. Diagnostic Imaging: CT, Ultrasound, MRI, and Emergency Room Radiology, March 9–14, Kauai; **Advances in Uroradiology,** March 22–23, San Francisco; **Thoracic Imaging Update,** April 17–19, Monterey, CA (Nov)

Functional and Stereotactic Neurosurgery, symposium, March 9–16, Garmisch-Partenkirchen, West Germany (Jan)

Computers in Medicine, workshop, March 10–11; **MRI meeting,** March 12–15, both Monte Carlo (Nov)

Breast Disease Update, course, March 12–16, Lake Buena Vista, FL (Oct)

South African Ultrasound Congress, March 14–17, Johannesburg (Sept)

Skeletal Radiology Course, March 15–20, Phoenix (Dec)

Ultrasound at Vail, course, March 15–22 (Oct)

Chest Course in Switzerland, March 16–23, Davos (Sept)

Computed Body Tomography Course, March 17–21, Hilton Head Island, SC (Nov)

New England Roentgen Ray Society meetings, March 21, April 11; annual meeting, May 16, all Boston (Nov)

San Francisco Courses. Postgraduate Course in Diagnostic Radiology, March 24–28; **Ob/Gyn and Abdominal Sonography: Update 1986,** April 11–13, both San Francisco (Dec)

Counseling Strategies for Physicians, course, March 24–29, Oahu (Aug)

Florida Courses. 1986 Update on Diseases and Imaging of the Spine, March 31–April 2; **Interventional Radiology Seminar,** April 3–5, both Lake Buena Vista (Dec)

NCRP Annual Meeting, April 2–3, Washington, DC (Oct)

Hepatobiliary and Pancreatic Imaging, course, April 2–5, Miami (Nov)

Review Course for Residents, April 4–6, Ann Arbor (Dec)

American Radium Society Meeting, April 6–10, San Francisco (Sept)

AAMI Annual Meeting, April 12–16, Chicago (Dec)

American Roentgen Ray Society, annual meeting, April 13–18, Washington, DC (see elsewhere this issue)

Radiation Therapy Research Seminar, April 17–19, Gainesville (Dec)

Neuroreceptors Course, April 18–19, Baltimore (Dec)

Interventional Radiology and DSA, course, April 28–30, Baltimore (Nov)

Interventional Neuroradiology Course, April 28–May 2, New York City (Dec)

Echocardiography Symposium, May 1–3, Boston (Dec)

Radionuclides in Nephrourology, symposium, May 5–7, Lausanne, Switzerland (Aug)

Uroradiology Postgraduate Course, May 5–9, the Netherlands (Aug)

American Thoracic Society Annual Meeting, May 11–14, Kansas City, MO (Dec)

Radiology Course in Hong Kong, May 11–16 (Dec)
Concepts in Diagnostic Radiology, course, May 20–23, San Francisco (Jan)
Magnetic Resonance Imaging Course, May 21–23, Boston (Jan)
Vanderbilt Courses. Sonography Symposium, May 23–24, Nashville; **Advances in Medical Imaging,** June 5–9, Kiawah Island, SC; **Breast Imaging Symposium,** July 25–26, Nashville (Dec)
Emergency Radiology, course, May 28–30, Boston (Jan)
Radiology Update in Scotland, course, July 10–21, Edinburgh and Turnberry (Jan)
Pediatric Imaging Course, Aug. 3–6, Colorado Springs (Nov)
Congress of Asean Association of Radiology, Aug. 7–9, Singapore (Dec)
Top of the World Radiology, course, Aug. 9–16, Great Bear Lake, Canada (Dec)
Ultrasound Congress in Denmark, Aug. 19–22, Copenhagen (Oct)
Blood Flow in the Brain, meeting, Sept. 23–25, Glasgow, Scotland (Dec)
Call for Biomedical Engineering Papers, Southern Biomedical Engineering Conference, Oct. 20–21; abstract deadline, March 1 (Dec)
Physics Conference in Bombay, India, Dec. 8–12 (Dec)
1987 Radiology Congress in Lisbon, May 31–June 6 (Oct)

AJR carries announcements of courses, symposia, and meetings of interest to its readers if received a minimum of 4 months before the event. There is no charge; receipt of items by the *AJR* Editorial Office is not acknowledged. Submit items for publication typed double spaced. Provide title, date, location, brief description, sponsor, course directors, fees, category I credit, and address and telephone number for additional information. Faculty from the host institution will not be listed. Guest faculty names will appear **only** if initials are provided. Mail news items to *AJR* Editorial Office, 2223 Avenida de la Playa, Suite 306, La Jolla, CA 92037.

May be photocopied

Deadline: March 15

Hotel Registration Form: ARRS 86th Annual Meeting, April 13–18, Sheraton Washington Hotel

Mail to:

ARRS Housing Bureau
Sheraton Washington Hotel
2660 Woodley at Connecticut Ave., N.W.
Washington, DC 20006

(PLEASE MAKE CHECKS PAYABLE TO HOTEL—*NOT TO THE ARRS*)

Individual guest name ____________________

Address ____________________

City & State ____________________ ZIP __________

Arrival date ____________________ Departure date ____________________

Individual requesting reservation ____________________

Address ____________________

City & State ____________________ ZIP __________

Deposit amount: __________

One night's deposit is needed to guarantee accommodations. Deposit is refundable with advance notice of cancellation. Deposit guarantees room until 12 midnight on requested arrival date. Make check payable to the Sheraton Washington Hotel.

Check accommodations desired

Room Category	Rate
Single	______$98, 110, 120
Double	______$120, 132, 142
1-bedroom suite	______$200–525
2-bedroom suite	______$400–625

Important Information:

1. Reservations must be received by the Sheraton/ARRS Housing Bureau no later than March 15 to be assured of written confirmed accommodation.
2. Written confirmation of your reservation will be sent to you by the hotel. Please allow 2–3 weeks for confirmation.
3. All changes such as arrival date, departure date, type room, and name changes must be made directly with the hotel after confirmation is received.
4. If you plan to share a room, please send in only one housing form. Be sure to list all names of occupants of rooms. Assignment is delayed until complete information is received.
5. Room assignments will be made in order received.

May Be Photocopied

Deadline: March 28

Meeting and Local Activities Registration Form: ARRS 86th Annual Meeting, April 13–18, Washington, DC

If you plan to attend, please complete this form. Official badges and program booklets will be available at the ARRS Registration Desk, Sheraton Washington Hotel. **There will be no confirmations before the meeting.** Preregistration by mail will be accepted until March 28. On site registration will be available.

Make all checks payable to: American Roentgen Ray Society

Mail to: American Roentgen Ray Society
1891 Preston White Drive
Reston, VA 22091

Please type or print:

Last Name ______ First Name or Initials

Street

City ______ State ______ ZIP Code

☐ Check here if you wish a program of events for accompanying persons. Indicate the address to which this is to be sent.

Name (Accompanying person's name to be printed on badge)

Street

City ______ State ______ ZIP Code

Check one:	Registration fee:
☐ Member ARRS	None
☐ Guest	$100
☐ Physician in training (please fill where indicated below)	$25
☐ Course faculty, scientific paper author, scientific exhibitor	None
☐ ACR luncheon course, Monday, April 14	$10
☐ ACR luncheon course, Tuesday, April 15	$10
☐ ACR luncheon course, Wednesday, April 16	$10
☐ ACR luncheon course, Thursday, April 17	$10

Section on Instruction

Please register early for Instruction Courses. Attendance is limited. List first, second, and third choices for each period by course number. Ticket orders are filled according to postmark. ARRS members, nonmembers, and those in radiology training may take all courses without charge except the Categorical Course on Chest Radiology. **For the categorical course, all must pay $75. All who wish to attend courses must complete this section. Residents and nonmembers must pay the meeting registration fee.**

Course tickets will be available at the ARRS Registration Desk of the Section on Instruction at the Sheraton Washington Hotel on and after Saturday, April 12, at 1 p.m.

☐ I wish to take the Categorical Course on Chest Radiology. Fee: $75. Categorical Course registrants may also register for other instructional courses.

Complete section at right for courses other than the categorical course. Be sure to fill out second and third choices for each period.

	First Choice	Second Choice	Third Choice
Monday			
Tuesday			
Wednesday			
Thursday			

Friday ______ Check if you wish to attend the Orthopedic Radiology Symposium (only course offered this day)

For Physicians in Training:

______ is in training in my department

Department Chief ______

Institution ______ Date ______

(OVER)

No refunds after April 1

Local Activities

Sunday, April 13, 7–9 p.m., Introduction to Washington Champagne Tour	____tickets @ $30	$ ________
Monday, April 14, 9:30 a.m.–3:30 p.m., National Gallery of Art and Hirshhorn Sculpture Garden	____tickets @ $30	$ ________
Tuesday, April 15, 9:30 a.m.–3:30 p.m., Georgetown Homes/Georgetown Park	____tickets @ $45	$ ________
Wednesday, April 16, 9 a.m.–4 p.m., Best of Baltimore	____tickets @ $25	$ ________
Thursday, April 17, 9 a.m.–4 p.m., Annapolis Tour	____tickets @ $40	$ ________
Friday, April 18, 9 a.m.–noon, Americana Tour	____tickets @ $15	$ ________

Annual ARRS Golf Tournament, Monday, April 14, 11 a.m.

The tournament will be at the Kenwood Golf and Country Club, Bethesda, MD. Transportation, luncheon, greens fee, cart, and prizes are included in the $65 fee. Preregistration is important.

Name: ________________ Telephone: ________________

Address: ________________________________

Hotel: ________________ Handicap (if any) ________________

My foursome includes (list handicaps): ________________________________

________________________________ ______tickets @ $65 $ ________

Men's and Women's Tennis Tournaments, Monday, April 14, 11 a.m.

The tournaments will be at the Kenwood Golf and Country Club, Bethesda, MD. Tennis attire is required. Fee of $50 includes transportation, luncheon, court fees, and prizes.

Name: ________________ Telephone ________________

Address: ________________________________

______tickets @ $50 $ ________

Classified Advertising

Positions Available

ISRAEL, DIAGNOSTIC RADIOLOGY. Opportunities for 3–4 week or longer working vacations in a number of Israeli medical centers, on a volunteer basis. Positions varied, arrangements flexible. For information contact: Jonathan H. Fish, M.D., 1844 San Miguel Dr., #302, Walnut Creek, CA 94596; (415) 947-0560. 2-7a

GENERAL RADIOLOGIST for diagnostic outpatient and emergency radiology, assistant professor level. Prerequisite: American Board of Radiology certification, plus 2 years of experience. Hours 10 a.m.-7 p.m. Send resume to: L. R. Bennett, M.D., acting chairman, Dept. of Radiological Sciences, UCLA Medical Center, Los Angeles, CA 90024. Equal opportunity/ affirmative action employer. 2a

RADIOTHERAPY DIRECTOR. The University of Arkansas for Medical Sciences seeks a director for the Division of Radiotherapy. The director also serves as Medical Director of the Central Arkansas Radiation Therapy Institute. Candidates should be experienced radiotherapists with board certification and academic interest. Submit curriculum vitae to: Glen F. Baker, M.D., Associate Dean for Clinical Affairs/ Medical Director, Chairman, Search Committee, University of Arkansas for Medical Sciences, 4301 W. Markham, Slot 600, Little Rock, AR 72205. We are an equal opportunity employer. 2a

BOARD CERTIFIED RADIOLOGIST—to join a 3-member department in a 204-bed community hospital. Interest in nuclear medicine would be helpful. Salary and partnership terms are negotiable. Reply with CV to D. W. Boyd, M.D., Good Samaritan Hospital, Pottsville, PA 17901. 2-4ap

BOARD CERTIFIED RADIOLOGIST seeks an associate to service a 40-man multispecialty group and 155-bed med-surg hospital, all part of a medical center complex. Excellent opportunity to practice state-of-art imaging with CT, ultrasound, arteriography, and nuclear cardiology (no MRI). Experience in therapeutic radiology optional. The facility is located in a city of 45,000, just 40 miles from a major metropolitan center in the midwest area of the country. Initial guarantee generous and early partnership is anticipated. Send CV. Reply Box J1 AJR, 2223 Avenida de la Playa, Suite 306, La Jolla, CA 92037. 2-5a

SEEKING A THIRD board certified radiologist for partnership in a 40 physician multispecialty clinic. The practice covers 85% of the clinic's radiology using 2 hospitals (325 + 325 beds) and a large outpatient clinic. Need proficiency in general and neuroangiography, Amipaque myelography including cervical puncture, CT (new Seimans DR3 and GE 8800), nuclear medicine, and ultrasound (Accuson), xeromammography and fluoroscopy, and plain film. Some preference given to some MRI experience. North Texas community of 95 000 population; 120 miles from Dallas. Send CV to the Wichita Falls Clinic, Attn. Dr. Dan Miller/Dr. Doug Miner, 501 Midwestern Pkwy. E., Wichita Falls, TX 76302. 2a

RADIOLOGY CHAIRPERSON: The Oregon Health Sciences University School of Medicine is recruiting a chairperson for the Dept. of Diagnostic Radiology. The department serves the University Hospital and has a VAMC Dean's Committee affiliation. Activities include ultrasound, angiography, computed tomography, special procedures, and animal research. General radiology residency and fellowship programs in ultrasound, computed tomography, neuroradiology, and vascular/interventional radiology exist. Curriculum vitae and the names/addresses of 3 references should be submitted to Wendell C. Stevens, M.D., Chairman, Radiology Search Committee, School of Medicine, Oregon Health Sciences University, Portland, OR 97201. Applications/recommendations accepted until position is filled. The Oregon Health Sciences University is an affirmative action/equal opportunity employer. 2-3a

NEURORADIOLOGY—Faculty appointment for a trained neuroradiologist with interest in teaching and research at the medical school of the University of Texas Health Sciences Center at San Antonio. Send curriculum vitae to: Robert L. Siegle, M.D., chief, Diagnostic Radiology, Dept. of Radiology, The University of Texas Health Science Center at San Antonio, 7703 Floyd Curl Dr., San Antonio, TX 78284. Equal employment opportunity/affirmative action employer. 2-4a

DIAGNOSTIC RADIOLOGIST: Board-certified diagnostic radiologist seeks partner in expanding solo hospital-based practice. Upstate New York. All modalities available. CV to Phillip Berman, M.D., HC61 Box 454, Massena, NY 13662. 9-4a

RADIOLOGY INSTRUCTOR to assist candidate in preparation for Oral Boards. Candidate needs practice in formally discussing cases and answering board-type questions in all exam sections. Would like to meet on a weekly basis beginning early 1986. East coast (esp. Philadelphia/Middle Atlantic states) preferred. Fee negotiable. Reply Box W4 *AJR* (see address this page) or call (215) 342-4110. 11-2a

BOARD-CERTIFIED radiologist with expertise in interventional radiology and/or angiography wanted to join medical center based group with 800 beds. For more information send curriculum vitae or contact P.O. Box 67043, Baton Rouge, LA 70896. 1-2a

BOARD CERTIFIED RADIOLOGIST, with proficiency in multimodality breast imaging. Free standing breast center in southeast seeking an associate. Send CV to Box J3, AJR, Suite 306, 2223 Avenida de la Playa, La Jolla, CA 92037. 2a

NUCLEAR MEDICINE PHYSICIAN-Internist needed to join board certified nuclear medicine physician private practice in North Carolina. Board certification in both specialties required. Responsibilities as internist and assisting the director of nuclear medicine at a 460-bed hospital affiliated with Duke University. Please send resume in confidence to: HealthCare Connections, Ltd., 416 Washington St., Duxbury, MA 02332; (617) 934-7125. 2a

DIAGNOSTIC RADIOLOGIST. Immediate opening for a board certified diagnostic radiologist to join the staff of a small, modern, well-equipped acute care community hospital located in historic Gettysburg, PA. Some experience in interventional radiology preferred but not required. For confidential consideration please submit curriculum vitae to: Joseph C. Jones, M.D., director, Radiology Services, The Gettysburg Hospital, 147 Gettys St., Gettysburg, PA 17325. (717) 334-2121, ext. 207. 2-3a

DIRECTOR, DIVISION OF NUCLEAR Medicine, Dept. of Radiology University of Colorado Health Sciences Center, Denver, CO, beginning July 1986. Excellent equipment (Picker SX300 15 inch noncircular SPECT, GE 400 AT 15 inch SPECT, portable Picker, Dynamo 10, all with upgraded computers), complete hot lab facilities and animal research facilities in newly renovated diagnostic imaging center. Department has an excellent radiology residency program along with superb divisions of diagnostic ultrasound, radiology, radiation therapy, and radiological sciences. Departmental equipment acquisitions include a .35 Tesla MRI system and a brand new fast CT scanner. The division chief sits on the department Executive Committee and will have a major role in planning activities of the department. For more information, write to Michael L. Manco-Johnson, M.D., professor and acting chairman, Dept. of Radiology, C277, University of Colorado Health Sciences Center, 4200 E. 9th Ave., Denver, CO 80262, or phone (303) 394-7817. Equal opportunity/AA Employer. 2a

RADIOLOGIST with special proficiency in ultrasound and mammography. Board certified, board eligible radiologist wanted for outpatient radiology. Free standing clinic in excellent medical community in Midwest. Position will include all aspects of outpatient radiology with special emhasis on obstetrical ultrasound and mammography. Partnership in facility available to qualified individual. Send CV to Box X3 AJR (see address this section). 12-2a

EXCELLENT POSITION available with radiology practice for board certified radiologist with an interest in all areas of radiology. Opportunity for partnership in expanding practice in the Greater New Orleans area serving 3 hospitals. 80,000 inpatient, 24,000 outpatient examinations/year. Send CV to Dr. Harold R. Neitzchman or Dr. Martin A. Eelanger, 4400 General Meyer Ave., Suite 221, New Orleans, LA 70114. 12-3a

Fellowships and Residencies

NMR VISITING FELLOWSHIPS in northern California. Intensive, structured 1-4 week courses with live instruction, teaching file, and video tape library. For further information contact: Murray A. Solomon, M.D., San Jose MRI Center, 361 S. Monroe St., San Jose, CA 95128. 10-3c

VANDERBILT FELLOWSHIPS. The Dept. of Radiology and Radiological Sciences at Vanderbilt University is currently offering 1-year fellowships in (1) CT with MRI, (2) chest, (3) bone, (4) pediatrics. Successful applicants will commence duties July 1, 1986. Applicants must be board certified or eligible and be able to obtain a Tennessee license. Applications should be addressed to: M. I. Shaff, M.D., Chairman, Fellowship Committee, Dept. of Radiological Sciences, Vanderbilt University-CCC 1100 Medical Center N., Nashville, TN 37232. 2-4c

Tutorials/Courses

MRI TUTORIAL PROGRAM. Diagnostic Radiological Imaging Medical Group offers 1 week training programs in clinical magnetic resonance imaging (MRI) for physicians with limited or no experience in MRI. The program is individualized to the applicant and the physician may subscribe to 1 or more weeks. Only 2 physicians per week are accepted. The MRI scanner is utilized in an outpatient imaging facility and 8-10 examinations per day are scheduled. Individual tutorials in MRI physics, equipment evaluation, clinical indications for MRI examination, performance of MRI studies, discussion of case material, and review of an extensive teaching file are offered. The faculty are A. B. Dublin and M. H. Reid. The fee is $600 and 40 hrs of Category I credit are available/week. For further information, contact Michael H. Reid, Ph.D., M.D., Diagnostic Radiological Imaging Medical Group, 79 Scripps Dr., Suite 100, Sacramento, CA 95825. Telephone: (916) 921-1300. 2dp

ALASKA '86—Cruise the Inland Passage, July 5-12, 1986. CME I credit. Topics in ultrasound with Barry B. Goldberg, M.D. Registration U.S. $385 until April 12, after U.S. $425. For additional information write or call ALASKA '86—Medical Seminars International, 21915 Roscoe Blvd., #222, Canoga Park, CA 91304; (800) MED-TOUR or (818) 701-5143. 1-6d

JERUSALEM, ISRAEL—Ultrasound Symposium, June 20-29, 1986. Category I CME program presented in cooperation with the Israeli Ultrasound Society by an International faculty. Fee to April 1986: U.S. $425, thereafter U.S. $460. Information: Medical Seminars International, 21915 Roscoe Blvd., #222, Canoga Park, CA 91304; (800) MED-TOUR or (818) 340-0580, ext. 280. 1-6d

LONDON, ENGLAND—ROME, ITALY, May 10-18, 1986. Attend one or both Spring Seminars. Renowned international faculty. Topics: CT, MRI, DSA. Category I accreditation. Fees: to March 7, U.S. $385, thereafter U.S. $425 each seminar. Combined fee: U.S. $450 and $495, respectively. Information: Medical Seminars, Dept. of Radiology, West Park Hospital, 22141 Roscoe Blvd., Canoga Park, CA 91304; (818) 340-0580 ext. 280 or (818) 701-1624. 11-4d

Other

ARE YOU INTERESTED in selling your radiology practice? We serve as representatives for a group of radiologists who are interested in purchasing radiology practices throughout the Midwest, Southeast, and South Central United States. Please call us for a confidental conference. The Lakewood Group, Ltd., 214 N. Henry St., Madison, WI 53703; (608) 255-0177. 2ep

AJR Indexes

AJR CONSOLIDATED INDICES available in limited quantities. Complete your journal collection. Order by index number. Indices available, years covered and prices: 2, 1938-1942, $10; 3, 1943-1947, $22.50; 4, 1948-1952, $23.50; 5, 1953-1957, $25; 6, 1958-1962, $23.50; 7, 1963-1967, $30; 8, 1968-1972, $40; 9, 1973-1977, $34. Order from: Subscription Dept., Williams & Wilkins, 428 E. Preston St., Baltimore, MD 21202; (301) 528-4000.

AJR Classified Advertising Information

Box Responses and Address for Ad Placement

Write Box ______, AJR, Suite 306, 909 N.E. 43rd St., Seattle, WA 98105 **until Jan. 31, 1986;** (206) 633-2754.

After Jan. 31, 1986: Write Box ______, AJR, Suite 306, Avenida de la Playa, La Jolla, CA 92037; (619) 459-2229.

How to Place an Ad

AJR accepts classified advertising for Positions Available, Positions Desired, Fellowships and Residencies, and Tutorials/Courses. Ads are accepted by mail or telephone. Institutions should supply purchase orders.

Rates. $6.00/line with a $30 minimum charge. Box service is $10 additional for each month the ad appears. There are discounts for multiple insertions: 10% for 2-3 insertions; 20% for 4 or more. To estimate lines, count all words and divide by 5.5.

Billing: Ads may be prepaid or invoices will be sent after the ad appears.

Deadlines. About 3 weeks before the issue mails. *AJR* issues mail in the middle of the month preceding the cover date (e.g., July mails June 17). For specific deadlines, write or telephone the AJR editorial office.

Estimating Ad Charges

Line charge: divide total words by 5.5 and multiply by $6.00 ..... $ ______
Multiple insertions? If so, multiply by number .... × ______
Subtotal .... $
Box response requested? If so, multiply number of months by $10.00 .... + ______
Subtotal .... $
Discount applies to two or more insertions. Subtract 10% if ad appears 2-3 months, 20% if 4 months or more .... − ______
Approximate advertising charge .... $

DIAGNOSTIC RADIOLOGISTS
CENTRAL CONNECTICUT

Small group: includes hospital and diversified practices. Superior abilities in all areas of radiology.

Physician should have completed one year of fellowship after residency and/or equivalent.

Position open from present time to July 1st.

Board certification necessary.

Send C.V. to
P.O. Box 333,
Durham, Connecticut 06422

Radiologist

The Hospital for Joint Diseases, Orthopaedic Institute-affiliated with NYU School of Medicine; with a Residency Program affiliated with Beth Israel Medical Center, has an immediate opening for a Board Certified Radiologist to work in our 230 bed orthopaedic/rheumatic institute offering an excellent mix of clinical cases.

Please call 598-6373 to schedule an interview or send curriculum vitae to Alex Norman, MD, Chairman of Radiology,

Hospital for Joint Diseases
Orthopaedic Institute
301 East 17 St., NYC 10003

Equal Opportunity Employer M/F

Help us to serve you better.....

USE YOUR ZIP CODE

Remember, your zip code provides faster, more direct delivery of your journals. Use it on all correspondence, too.

Neuroradiologist

The School of Medicine at SUNY Stony Brook is currently recruiting for the position of Neuroradiologist with academic appointment commensurate with prior experience in a rapidly expanding department. Candidates should be Board Certified or Board eligible. The University Hospital is a tertiary care center on the highly desirable north shore of Long Island, N.Y. Position is available from July 1986.

Send CV to Morton A. Meyers, M.D., Chairman, Department of Radiology, School of Medicine, Health Sciences Center, SUNY Stony Brook, N.Y. 11794.

SUNY Stony Brook is an affirmative action/equal opportunity educator and employer. AK#341-85.

for prompt subscription service...

attach label here

Please use this coupon and attach a *recent* label in the space provided when writing to us about:

- change of address
- renewal
- questions regarding your subscription

Please use the space below to indicate your *new* address.

Name of Journal________________

Name________________

Address________________

City________________

State/Zip________________

The Williams & Wilkins Co.
428 East Preston Street
Baltimore, Maryland 21202

INDEX TO ADVERTISERS

Adria Laboratories	A9
Agfa-Gevaert-Rex	A28, A29
Colorado Video	A15
Delta Airlines	A30
DuPont	A17, A18, A19, A20
Eastman Kodak	A4, A5
E-Z-EM Company	Cover 2
Hospital for Joint Diseases	A33
Mallinckrodt	A6, A7, A8
Philips Medical Systems, Inc.	A26, A27
Picker International	A22, A23
Porta Ray	A14
Precise Optics/PME, Inc.	A31
Purdue Frederick Company	A32
Pyne Corporation	Cover 3
Radiology Clinics, P.C.	A33
Siemens Corporation	A10, A11
S & S X-Ray	A25
SUNY-Stoney Brook	A33
Thompson CGR	A12, A13
Tobias Associates	A14
United Airlines	A24

We try to present an accurate index. Occasionally this may not be possible because of a last-minute change or an omission.

Increase your expertise in evaluating CNS lesions

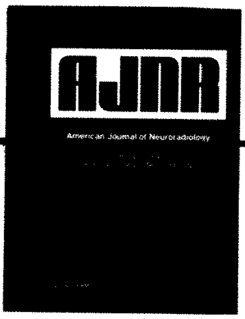

AJNR
American Journal of Neuroradiology

Editor: **Juan M. Taveras, MD,** Harvard Medical School; MGH

Outstanding clinical papers on every aspect of CNS imaging, including spinal diagnosis...informed coverage of head and neck radiology...clear, readable CTs, angiographs, MR imaging and ultrasound studies. These are the features you demand of a quality professional journal. You'll find them in every issue of **AJNR: American Journal of Neuroradiology.**

As you are called upon to perform and interpret more and more sophisticated diagnostic tests — from myelography to CT to newborn ultrasound studies — you need a comprehensive, reliable journal that can keep you abreast of all the latest developments. Each bimonthly issue of **AJNR** brings you timely, clinically pertinent information, as well as important clinical research presented with an eye toward immediate practical application.

Here are just a few of the many excellent articles from the November/December 1985 issue:

Contrast-Enhanced MR Imaging of Malignant Brain Tumors *by Moshe Graif, et al.*

MR Imaging of Cerebral Vascular Malformations *by Benjamin C. P. Lee, et al.*

Cranial Computed Tomography in the Abused Child with Head Injury *by Ronald A. Cohen, et al.*

Cavernous Sinus Invasion by Pituitary Adenomas *by Jamshid Ahmadi, et al.*

Sonography of the Internal Capsule and Basal Ganglia in Infants: 1. Coronal Sections *by Thomas P Naidich, et al.*

Iohexol vs. Metrizamide: Study of Efficacy and Morbidity in Cervical Myelography *by Richard E. Latchaw, et al.*

Superselective Injection of Polyvinyl Alcohol Microemboli for the Treatment of Cerebral Arteriovenous Malformations *by Giuseppe Scialfa and Giuseppe Scott.*

If you can benefit from articles like these, then you should be a regular reader of **AJNR.** Use the attached coupon to subscribe today.

Bimonthly
Personal $95/yr **Institutions** $115/yr **In-training** $65/yr
(add $15.00 outside the US)

☎ ORDER FREE BY PHONE. Just call 1-800-638-6423 from anywhere in the US except AK and HI. MD residents, call 528-4105 *collect.*

Williams & Wilkins
P.O. Box 1496 Baltimore, Maryland 21203
266 Fulham Road London SW10 9EL England

Subscribe to AJNR for 3 years and SAVE

Avoid future rate increases and ensure uninterrupted service by placing a multi-year subscription at current rates.

☐ New subscription ☐ Renewal
☐ 3 yrs ☐ 2 yrs ☐ 1 yr
☐ **Personal** $95 ☐ **Institutions** $115 ☐ **In-training** $65
(add $15.00 outside the US)

☐ Also send me the **1986 Bound Volume** at $45.00 ($50.00 outside the US). $2.00 discount for orders placed before October 1, 1985, and for prepaid orders. I understand that the bound volume is *in addition to* my regular subscription and is available only to subscribers. (To be shipped in early 1987. Sorry, bound volumes for years prior to 1986 are not available.) *All bound volume orders must be received by December 31, 1986.*

☐ Check enclosed ☐ Bill me
☐ VISA ☐ MasterCard ☐ American Express

card # exp.

signature/P.O. #

printed in USA

Name

Address

City/State/Zip

MD residents, please add 5% sales tax. Subscription orders from outside the US must be prepaid in US dollars only.

Residents, Fellows, Interns, and Students: when applying for the in-training rate, available for 3 years, please specify name of institution and training status. Rates valid through October 31, 1986.

Please allow 8 weeks for order processing and delivery of your first issue. Surface mail delivery to countries outside the US may take up to 16 weeks. Airmail rates available upon request.

Williams & Wilkins
P.O. Box 1496
Baltimore, Maryland 21203

266 Fulham Road
London SW10 9EL
England

AJNRAD 94625 86

Control the future of your practice

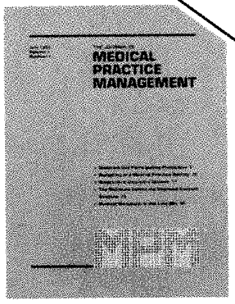

NEW!

The Journal of MEDICAL PRACTICE MANAGEMENT

Editor: **Marcel Frenkel, MD, MBA**

A new journal gives you the management skills you need to pull ahead

Right now you need information on some important topics that weren't covered in medical school. Topics that are having a profound impact on private practice and hospital-based physicians across the country.

Like competition from HMOs. Industrialization of medicine. The sheer number of physicians competing for your patients. Increasing costs.

You know the issues. What you need to know is the best way to face them so your practice will flourish in years to come.

And that's where **The Journal of Medical Practice Management** comes in.

Keep up with the issues that are changing your way of practice forever

The Journal of Medical Practice Management is a new quarterly publication that covers *your* concerns...issues affecting the way you practice now — and the way you'll practice in the future.

Four times a year, an expert editorial board headed by Dr. Marcel Frenkel brings you concise, readable coverage of today's issues and tomorrow's trends.

You'll find departments covering • office procedures and management • malpractice • marketing • manpower • computers • taxation • legal and legislative affairs • and health policy.

You'll also find pertinent features like the **Washington Report,** telling you what's up in the nation's capital and how it affects you...a **Letter from Abroad,** offering perspectives on how physicians are handling health care issues in other countries...and profiles of profit and not-for-profit health care delivery systems.

A multidisciplinary editorial board

Members of the editorial board for **The Journal of Medical Practice Management** have been carefully chosen for their knowledge of the management aspects of practicing medicine. These experts, many with experience in more than one field, give you the perspectives you need from medicine, law, management, government, and education.

You can control the future of your practice

The issues you can't afford to ignore are in **The Journal of Medical Practice Management**. It's a lot of information for a little money. And that's good business for you.

Reserve your charter subscription today!

Just return the attached coupon, or **call our FREE number,** 800-638-6423, from anywhere in the US except Alaska and Hawaii. In Maryland, call 528-4105 collect. **Quarterly**

Williams & Wilkins

428 East Preston Street
Baltimore, Maryland 21202

266 Fulham Road
London SW10 9EL England

YES, I want to control the future of my practice!

Please enter my subscription to **The Journal of Medical Practice Management** (quarterly)

☐ Individuals and Institutions $40

All subscribers: add $10 outside the U.S.

☐ Check enclosed ☐ Bill me
☐ MasterCard ☐ American Express ☐ VISA

Card # Exp. date

Signature

Name

Address

City/State/Zip

Maryland residents add 5% sales tax. Subscriptions outside the US must be prepaid. All subscriptions must be paid in US dollars. Rates valid through April 30, 1987.

Please allow 8 weeks for delivery of your first issue, up to 16 weeks for surface delivery outside the US. Airmail rates available on request.

Williams & Wilkins

P.O. Box 1496
Baltimore, Maryland 21203

266 Fulham Road
London SW10 9EL England

MPMAD 95048 86

FUJI

DRG's and changes in third party reimbursements have dramatically affected health care and specifically your radiology department. We have all had to tighten our belts and Fuji will continue to be cost effective.

But in the "high-tech" environment of today's radiology department, **the poorest economy is the sacrifice of quality.**

That's why, at Fuji, what's in our box will always be more important than what it costs....

Think about it.

Call your local Pyne Representative or toll free 800-431-1850
(in N.Y. call 914-834-4567.)

PYNE CORPORATION
20 North Avenue, Larchmont, NY 10538

Volume 146 **American Journal of Roentgenology** **February 1986**

PEDIATRIC RADIOLOGY

211 **"Horseshoe" lung: report of five new cases.** *Freedom RM, Burrows PE, Moes CAF*
217 **Horseshoe lung: clinical, pathologic, and radiologic features and a new plain film finding.** *Frank JL, Poole CA, Rosas G*
227 **"Communicating" bronchopulmonary foregut malformations.** *Leithiser RE Jr, Capitanio MA, Macpherson RI, Wood BP*
233 **Dimensions of the growing trachea related to age and gender.** *Griscom NT, Wohl MEB*
239 **Microcolon of prematurity: a form of functional obstruction.** *Amodio J, Berdon W, Abramson S, Stolar C*
245 **The radiologic "lead band" revisited.** *Blickman JG, Wilkinson RH, Graef JW*
249 **Sonographic recognition of idiopathic arterial calcification of infancy.** *Rosenbaum DM, Blumhagen JD*
251 **Diagnostic oncology case study. Retroperitoneal mass with intradural extension: value of magnetic resonance imaging in neuroblastoma.** *Dietrich RB, Kangarloo H, Kagan AR, Steckel RJ*
255 **Indium-111 leukocyte scanning localization for detecting early myocarditis in Kawasaki disease.** *Williamson MR, Williamson SL, Seibert JJ*

NEURORADIOLOGY

257 **Cavernous sinus invasion by pituitary adenomas.** *Ahmadi J, North CM, Segall HD, Zee CS, Weiss MH*
263 **Computed tomographic demonstration of the posterior pituitary.** *Bonneville JF, Cattin F, Portha C, Cuenin E, Clere P, Bartholomot B*
267 **Intracranial calcification in adults with chronic lead exposure.** *Reyes PF, Gonzalez CF, Zalewska MK, Besarab A*
271 **Radiographic findings in 32 cases of primary CNS lymphoma.** *Jack CR Jr, Reese DF, Scheithauer BW*
277 **Cervical spinal cord injuries in patients with cervical spondylosis.** *Regenbogen VS, Rogers LF, Atlas SW, Kim KS*

THORACIC RADIOLOGY

285 **The role of CT in staging radiographic $T_1N_0M_0$ lung cancer.** *Heavey LR, Glazer GM, Gross BH, Francis IR, Orringer MB*
291 **Low-attenuation thoracic metastases in testicular malignancy.** *Yousem DM, Scatarige JC, Fishman EK, Siegelman SS*
295 **Talc: understanding its manifestations in the chest.** *Feigin DS*
303 **Chronic posttraumatic aneurysm of the thoracic aorta: surgically correctable occult threat.** *Heystraten FM, Rosenbusch G, Kingma LM, Lacquet LK*
309 **Magnetic resonance imaging of thoracic aortic aneurysms: comparison with other imaging methods.** *Dinsmore RE, Liberthson RR, Wismer GL, et al.*
315 **Magnetic resonance imaging of chronic myocardial infarcts in man.** *McNamara MT, Higgins CB*
321 **Strangulated diaphragmatic hernia with pneumothorax due to colopleural fistula.** *Radin DR, Ray MJ, Halls JM*

ABDOMINAL RADIOLOGY

323 **Plasma electrolyte status after small-bowel enteroclysis.** *Barloon TJ, Franken EA*
327 **Oriental cholangiohepatitis: diagnostic imaging and interventional management.** *vanSonnenberg E, Casola G, Cubberley DA, et al.*
333 **Localization of ^{99m}Tc-HMDP in hepatic metastases from colonic carcinoma.** *Shih WJ, Domstad PA, Lieber A, DeLand FH, Coupal JJ*
337 **Value of sonographic screening for gallstones in patients with chest pain and normal coronary arteries.** *Fein AB, Rauch RF II, Bowie JD, Pryor DB, Grufferman S*
341 **Pancreatic sonography: enhancement by metoclopramide.** *duCret RP, Jackson VP, Rees C, Lowe R, Davison NE*
345 **The anechoic crescent in abdominal aortic aneurysms: not a sign of dissection.** *King PS, Cooperberg PL, Madigan SM*
349 **Incidental detection of impalpable testicular neoplasm by sonography.** *Stoll S, Goldfinger M, Rothberg R, Buckspan MB, Fernandes BJ, Bain J*
351 **Incidental prostatic carcinoma detected by MRI and diagnosed by MRI/CT-guided biopsy.** *Herman SD, Friedman AC, Radecki PD, Caroline DF*

SKELETAL RADIOLOGY

353 **MRI in the detection of malignant infiltration of bone marrow.** *Daffner RH, Lupetin AR, Dash N, Deeb ZL, Sefczek RJ, Schapiro RL*
359 **Magnetic resonance imaging of arachnoid cysts destroying the sacrum.** *Sundaram M, Awwad EE*
361 **CT arthrography of capsular structures of the shoulder.** *Rafii M, Firooznia H, Golimbu C, Minkoff J, Bonamo J*

INTERVENTIONAL RADIOLOGY

369 **Percutaneous transluminal angioplasty of the lower abdominal aorta.** *Charlebois N, Saint-Georges G, Hudon G*
373 **Aortic rupture: a complication of transluminal angioplasty.** *Berger T, Sörensen R, Konrad J*
375 **Experimental enhancement of drug uptake using short-term flow occlusion: a comparison of balloon and tourniquet techniques.** *Woods DM, Wright KC, Carrasco CH, Wallace S*
381 **A modified Cope introducing dilator to allow straight guide wire introduction.** *Vogelzang RL*
383 **Removal of retained common bile duct stones with angiographic occlusion balloons.** *Meranze SG, Stein EJ, Burke DR, Hartz WH, McLean GK*

GENERAL RADIOLOGY

387 **Pictorial essay. Markers for implanted devices: need for standardization.** *Scott WW Jr, Wheeler PS, Mitchell SE*
391 **Rupture of echinococcal cysts: diagnosis, classification, and clinical implications.** *Lewall DB, McCorkell SJ*
395 **Radiological aspects of primary hyperoxaluria.** *Day DL, Scheinman JI, Mahan J*
403 **MRI of extracranial hematomas: preliminary observations.** *Unger EC, Glazer HS, Lee JKT, Ling D*
409 **Solenoid surface coils in magnetic resonance imaging.** *Lufkin RB, Votruba J, Reicher M, Bassett L, Smith SD, Hanafee WN*
413 **Computer page. Computer-generated examinations for residents in radiology.** *Crass JR*

OTHER CONTENT

415 **Editorials. The impact of maternity on radiologists: the AAWR position and its acceptance by women.** *Adler YT, Fernbach SK, Hayman LA, Redman HC, Rumack C*; **Device identification: deficient marking systems.** *Wheeler PS*; **What radiologists say about PACS.** *Vanden Brink J*
421 **Letters**
427 **Abstracts**
434 **News**
438 **ARRS 1986 registration forms**
441 **Classified ads**
Book reviews 216, 232, 238, 248, 294
Editorial office address change 302, 386
326 **Memorial**
332 **Errata**
340 **ARRS 1986 meeting summary**
A2 **Guidelines for authors**

Acc.
18.9.87

AJR

American
Journal of
Roentgenology

March 1986

UNIVERSITY
LIBRARY

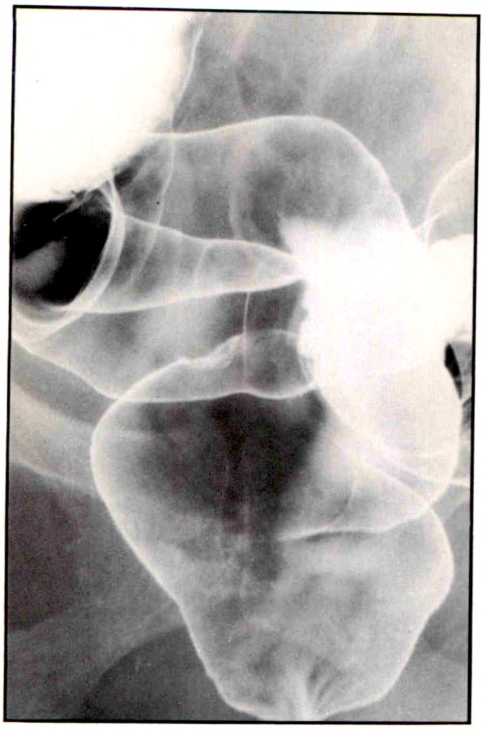

LIQUID POLIBAR™
X-Ray courtesy of Dr. Alec J. Megibow
N.Y.U. Medical Center University Hospital
New York, NY 10016

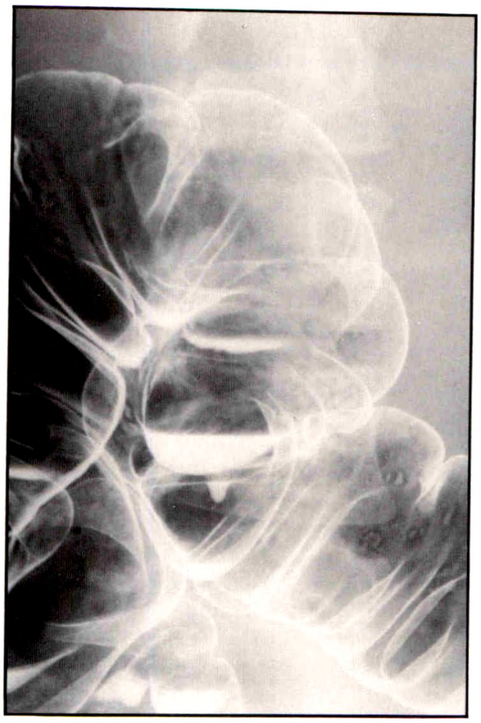

E-Z-AC™
X-Ray courtesy of Dr. Igor Laufer
Hospital of the University of Pennsylvania
Philadelphia, PA 19104

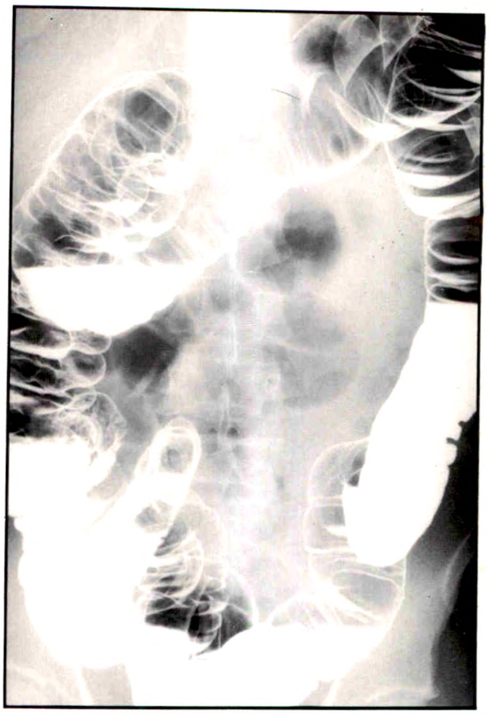

LIQUID POLIBAR™ PLUS
X-Ray courtesy of Dr. David W. Gelfand
Bowman Gray School of Medicine, Wake Forest University
Winston-Salem, NC 27102

Three bariums for superior air-contrast results.

Air Contrast Colon: The procedure of choice with the systems of your choice.

Liquid Polibar™

The original air contrast colon barium with superb coating characteristics. Optimum viscosity assures consistent even coating throughout. Truly the bench mark formulation for air contrast studies.

E-Z-AC™

This fast flowing liquid barium reaches the splenic flexure in only 20 to 30 seconds. Specifically formulated for air contrast procedures where a cleansing enema has not been administered that morning.

Introducing: Liquid Polibar™ Plus

The classic Liquid Polibar formulation modified to achieve a faster flow rate. It has the excellent coating characteristics that you expect from a Polibar formula but is more attuned to the speed necessary in the modern radiology department. Polibar Plus—increased speed and diagnostic consistency.

For samples and additional information, please contact your local E-Z-EM distributor or call E-Z-EM directly.

E-Z-EM®

E-Z-EM, Inc. 7 Portland Avenue, Westbury, NY 11590 516-333-8230 800-645-3052

© E-Z-EM, Inc. 1985

Official Journal
American Roentgen Ray Society

AJR

Diagnostic Imaging and Related Sciences

Editor Robert N. Berk

Associate Editors Alan J. Davidson
Saskia vonWaldenburg Hilton

Associate Editor, Neuroradiology Juan M. Taveras

Consulting Editorial Board Christos A. Athanasoulis
Edward Buonocore • Peter L. Cooperberg • John L. Doppman
Kent Ellis • Robert H. Freiberger • Reginald Greene
N. Thorne Griscom • William R. Hendee • Eugene C. Klatte
John G. McAfee • William B. Seaman • Michel M. Ter-Pogossian
Joseph P. Whalen • David M. Witten

Editorial Staff Gita Braude • Elizabeth Whalen
Barbara Rose • Linda Wood

All business correspondence, including display (not classified) advertising, subscriptions, address changes, reprints, and permission requests should be addressed to Williams & Wilkins, 428 East Preston Street, Baltimore, MD 21202. Correspondence regarding editorial matters and classified advertising should be addressed to the editorial office, AJR, 2223 Avenida de la Playa, Suite 306, La Jolla, CA 92037. For manuscript submission, see Guidelines for Authors, next page. Undelivered or damaged copies replaced within 60 days of publication; 90 days for foreign subscribers. Allow 90 days for address changes.

AJR AMERICAN JOURNAL OF ROENTGENOLOGY (ISSN 0361 803X) is published monthly by American Roentgen Ray Society, 428 E. Preston Street, Baltimore, MD 21202. Annual dues include $50 for journal subscription. Second class postage paid at Baltimore, MD and at additional mailing offices. Postmaster send address changes (Form 3579) to Williams & Wilkins, 428 East Preston St., Baltimore, MD 21202. Subscription rates $90 ($115 foreign); institutions $100 ($125 foreign); in training $25; single copy $16 ($19). Japanese Yen price is available from our sole agent USACO Corporation, 13-12, Shimbashi 1-Chome, Minato-Ku, Tokyo 105, Japan, telephone 03-502-6471. Airmail rates furnished on request. Indexed by *Current Contents* and *Index Medicus*. Copyright © 1986 by American Roentgen Ray Society.

0361-803X/86 $2.00

AJR Guidelines for Authors

Address new and revised manuscripts, correspondence, and classified ads to:

AJR Editorial Office
2223 Avenida de la Playa, Suite 306
La Jolla, CA 92037
telephone: (619) 459-2229

Make inquiries regarding subscriptions, display advertising, reprints, or permission to republish *AJR* material to the publisher:

The Williams & Wilkins Co.
428 E. Preston St.
Baltimore, MD 21202
telephone: (301) 528-4133

Publication Policy

The *AJR* publishes original and timely contributions to the advancement of medical diagnosis and treatment with radiologic methods. Although content is predominantly clinical, laboratory investigations are accepted when their relevance to clinical practice is demonstrable. In prospective clinical investigations, authors should document that informed consent was obtained from patients. The material submitted **must** not have been previously published nor be currently submitted for publication elsewhere (prior publication of simple abstracts without illustrations or tables will not prejudice publication of the complete study). Papers dealing with **neuroradiology** should be addressed to: Editorial Office, American Journal of Neuroradiology, Dept. of Radiology, Massachusetts General Hospital, Boston, MA 02114; telephone: (617) 726-8342. At the discretion of the Editor of *AJR*, *AJNR* articles may be republished in *AJR*.

Decisions on manuscripts are based on peer review. Reviewers receive manuscripts without title pages to protect the identity of authors and to ensure an unbiased review; names of reviewers, in turn, are not revealed to the authors. Accepted manuscripts are subject to editing. Statements within an article, including changes made by the Editor or copy editor, are the responsibility of the author and not *AJR* or its publisher. Authors will receive the edited manuscript, galley proof, and proofs of illustrations usually 6–8 weeks after acceptance. If the corresponding author will not be available, arrangements should be made for a coauthor or colleague to read and return the proof.

Copyright Information

In accordance with *AJR* implementation of the U.S. Copyright Law, authors must release first and subsidiary rights to their manuscript at submission (unless the study was performed as part of their duties as an employee of a U.S. government agency). A dated letter with the signatures of all authors should state: "We, the authors, assign first and subsidiary rights to the American Roentgen Ray Society in the event that our manuscript [insert title] is published by *AJR*. We guarantee that this manuscript contains no matter libelous or otherwise unlawful or which invades individual privacy or which infringes any proprietary right. *AJR*, in turn, grants us the right of republication, subject only to crediting the original source of publication and receiving written permission from the publisher. We understand we will receive no royalty or other compensation from *AJR*. We guarantee that this article and illustrations have not been previously published elsewhere or, if previously published in part or in whole, that permission has been obtained for republication. Copies of these permissions are included and previously published text or illustrations have been identified in the manuscript." (Delete the last sentence if it does not apply.) The covering letter also should state that the manuscript has been seen and approved by all the authors.

Manuscript Form

AJR complies with the Uniform Requirements for Manuscripts Submitted to Biomedical Journals (*Ann Intern Med* 1979;90:95–99). Manuscripts must be ***typed double-space throughout***, including references, tables, and figure legends. Each table, the footnotes, and the figure legend section should begin on separate sheets; a separate title page should be provided. Send the original typescript, one copy, and two sets of illustrations (not photocopies). Authors' names should be on the title page **only** so that author anonymity can be maintained during the review process. Permission to reprint previously published material should accompany the manuscript.

Organization of Major Articles

Title Page

Titles should be brief yet precise, accurately conveying the content of the paper. Limit authors to those who made substantial contributions to the work. Include an address for *each* author, and ZIP or postal code; acknowledgment of grant or other financial support when appropriate; name of meeting, location, and date if the paper was presented; a running head (shortened title); and the name, address, and telephone number of the author to whom correspondence and requests for reprints should be addressed.

Abstract

A description of the purpose, methods, results, and conclusions of the study is required. The factual highlights of each section should be recapitulated.

Introduction

Clearly state the purpose of the investigation, including necessary background facts that indicate its current relevance.

Materials [or Subjects] and Methods

Describe the research plan, the materials or subjects, and the methods, in that order. Proof of disease and control of subjectivity in observations should be detailed. Metric measurements should be used throughout. Put measurements in the International System of Units (SI) in parentheses when appropriate; for example, 400 rad (4 Gy).

Results

Present results in logical sequence. If tables are used, do not duplicate tabular data but do describe important points and trends.

Case Reports

Individual cases can be described if there are only a few; one or more cases from a large series can be described individually as Representative Case Reports. Each report should concentrate on the radiologic information and its usefulness.

Discussion

Offer appropriate limitations about the research plan, materials or subjects, and methods to give perspective to their adequacy for the purpose of the study. Interpret the results to lend meaning and importance to the observations. Hypotheses and speculation based

on the results are encouraged. When results differ from those of previous investigations, an attempt should be made to explain the discrepancy. Conclude with a brief statement regarding clinical significance.

Acknowledgments

Acknowledge only persons who have made *substantive* contributions to the study. Mention grant support on the title page.

References

References should be offered to document major assertions of fact and any opposing evidence and concepts. Discretion in number is requested. References should be cited in the text by number (e.g., [3, 4]). The reference list should be arranged in the numeric order that references are cited in the text and ***typed double-spaced throughout***. References cited *first* or *only* in tables or figure legends should be numbered by the sequence in which the table or figure is first identified in the text. Data for each reference should be arranged according to the style adopted by the U.S. National Library of Medicine and used in *Index Medicus*. ***Accuracy of reference data is the responsibility of the author.*** Provide all authors' (or editors') names when fewer than seven; when seven or more, list the first three and add et al. Provide inclusive page numbers; if an article is only one page, please indicate. Abbreviations for titles of medical periodicals should conform to those published in *Index Medicus*. Articles that appear in both *AJR* and *AJNR* should be a single reference that cites both journals (example 3). Examples:

1. Kirks DR, Fram EK, Vock P, Effmann EL. Tracheal compression by mediastinal masses in children: CT evaluation. AJR 1983;141:647–651
2. Khansur T, Yam LT, Tavassoli M. Serum monitors of bone metastasis. In: Stoll BA, Parbhoo S, eds. Bone metastases: monitoring and treatment. New York: Raven, 1983:165–180
3. Sage MR. Review. Kinetics of water-soluble contrast media in the central nervous system. AJNR 1983;4:897–906, AJR 1983; 141:815–824

Unpublished data and personal communications should not be numbered references but should be put in parentheses in the text (e.g., Smith JD, personal communication).

Tables

Tables should be concise and organized to show trends, not merely compilations of raw data. (The Editor may request that tables of backup data too extensive to be published be deposited with the National Auxiliary Publications Service or made available by the author.) Include only data pertinent to the subject. Long itemized case histories are better presented in the text as case reports or summaries. Do not repeat in tabular form material presented in the text. Tables should have titles and headings, but no vertical or horizontal rules.

Illustrations

Figures should be submitted as 13 × 18 cm (5 × 7 inch) glossy, black-and-white prints, ***untrimmed and unmounted***. Labels and arrows must be of professional quality and removable. Number each figure to correspond with the figure legends and indicate the top. Avoid writing directly on the back of the print. Special permission for publication of facial photographs of patients or for previously published pictures is required. Line illustrations or graphs must be professionally drawn in black ink on white background; please send photographic prints (not photocopies), not originals, to avoid damage in handling. Color illustrations will be used at the discretion of the Editor; send color prints. Firm estimates of cost will be sent to the author(s) for approval before publication. Identical anatomic structures in color prints should be the same size to facilitate reproduction and reduce cost.

Legends

Figure legends should carry a title identifying the message of the illustration and the case number if individual cases are described in the text. Legends should be as brief as possible for the informed reader to understand the figure. Detailed clinical data should be avoided. Legends for previously published illustrations should cite the reference number of the source (e.g., Reprinted from [8]).

Organization of Case Reports

Concise case reports will be considered for publication if they present unusual experiences that are medically important and instructive. Clarity and brevity are essential. After preliminary screening by an editor to determine whether the requirement of medical significance has been met, qualifying papers will undergo the same peer review as major papers. To facilitate planning the order and layout of each issue, case reports are limited in length to two journal pages. The introduction should be one short paragraph that gives some general background of the disorder and the specific interest and message of the case presented. Only one case should be described in detail. The case report should concentrate on the radiologic information and its usefulness. The discussion should focus on the specific message of this report and the relevance of radiology in this instance. If the author has encountered other cases, they may be briefly mentioned, and possibly illustrated, but not described in detail. There should be no more than eight references. The figures should be limited to the minimum required to document the case findings, probably not more than four pictures, each a column wide (or the equivalent). Excess illustrations would require severely shortening the text. Figure legends should be as short as possible and should not repeat the text. There can be no tables and no acknowledgments. See previous sections for detailed instructions regarding references and illustrations.

Other Contributions

Technical Notes

Brief descriptions of new techniques or significant modifications of older ones that are directly applicable to the clinical practice will be accepted if review is favorable. Technical notes do not carry abstracts or acknowledgments.

Letters to the Editor

Letters are subject to editing and condensation. Criticism of published articles should be objective and constructive. Letters also may discuss matters of general interest to radiologists.

When all the figuring is done, you can't afford anything less than the quality of Kodak products and services.

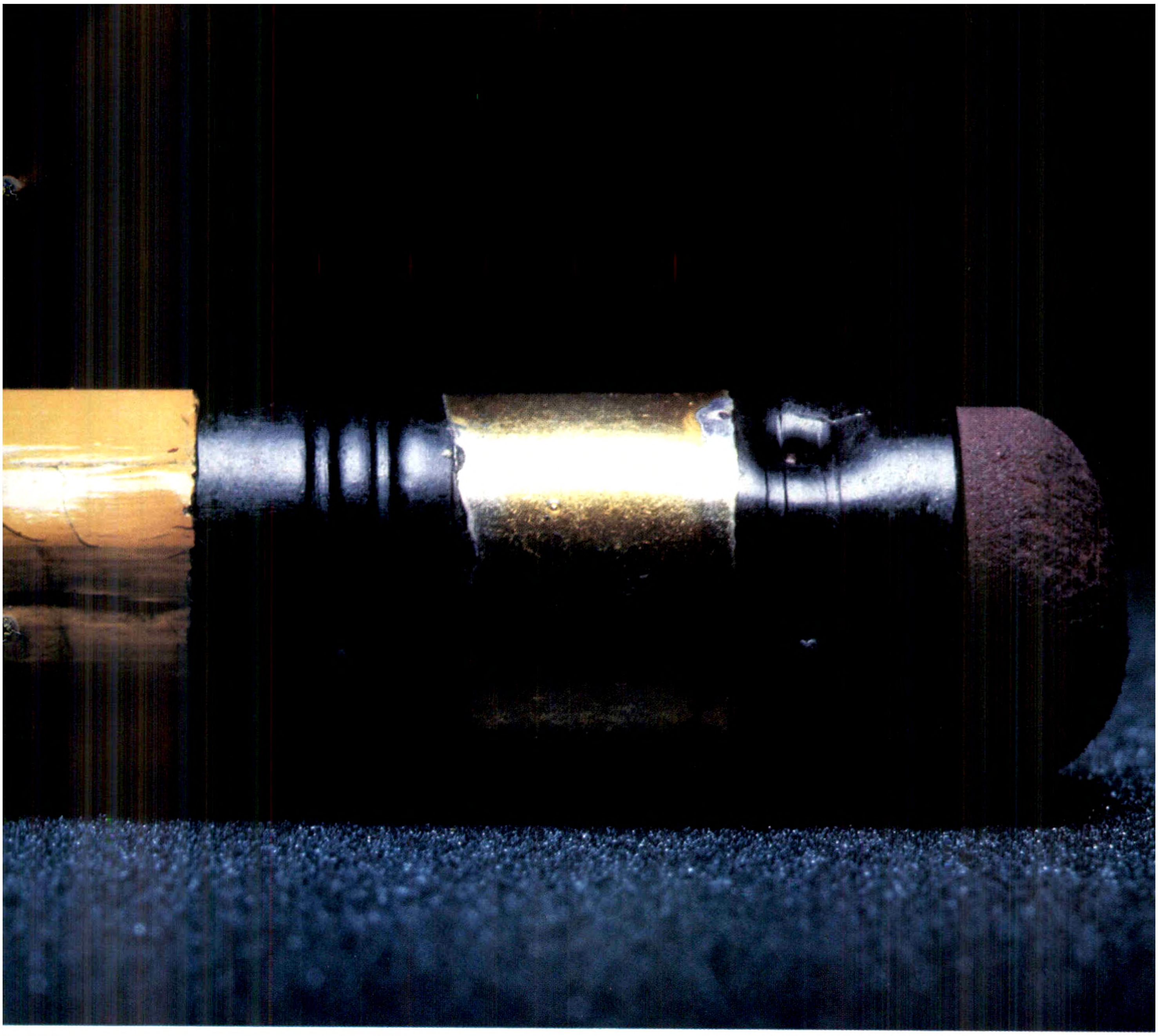

Sharpen your pencils. Warm up your calculators and computers. It's time to look for ways to cut costs in the radiology department. Prediction: When the figures are in, the numbers are crunched, and the conclusions are drawn, the word will be that quality costs less. The quality of Kodak products. Can you afford anything less?

One example: repeat reduction.

Reducing repeats is a great way to cut costs, and Kodak helps. With quality, because that means consistency. And technical innovation. Films with wide dynamic ranges, such as Kodak T-Mat L film, mean fewer repeats due to exposure variations. And high system speeds mean fewer repeats due to patient motion. If a problem elsewhere in the imaging chain is causing repeats, we'll track it down with a computerized program we call "RRA"—Radiographic Repeat Analysis.

BackUp from Kodak.

There's an almost endless list of extras like "RRA," each of which contributes to cost-effectiveness. There are hands-on, nuts-and-bolts programs like processor seminars. There's a superbly practical Custom Computer Technic Service that provides highly precise charts on a room-by-room basis, as well as a video imaging program to give you the video look you like. And there are also BackUp programs for administrators. Things like Procedural Costing, Room Utilization, Financial Planning.

Your TSR brings it all.

Provider of all these services, and your ally in all things radiographic, is your Kodak technical sales representative. A professional consultant, highly trained and technically experienced in imaging technology and administrative challenges. Troubleshooter, answer person, friend. Whether you call for technical assistance or to arrange a long-term educational program, the response will be immediate and enthusiastic. And a big part of the reason why you can't afford anything less than the quality of Kodak products.

Can you afford anything less?

Kodak

©1986 THOMSON-CGR Medical Corporation

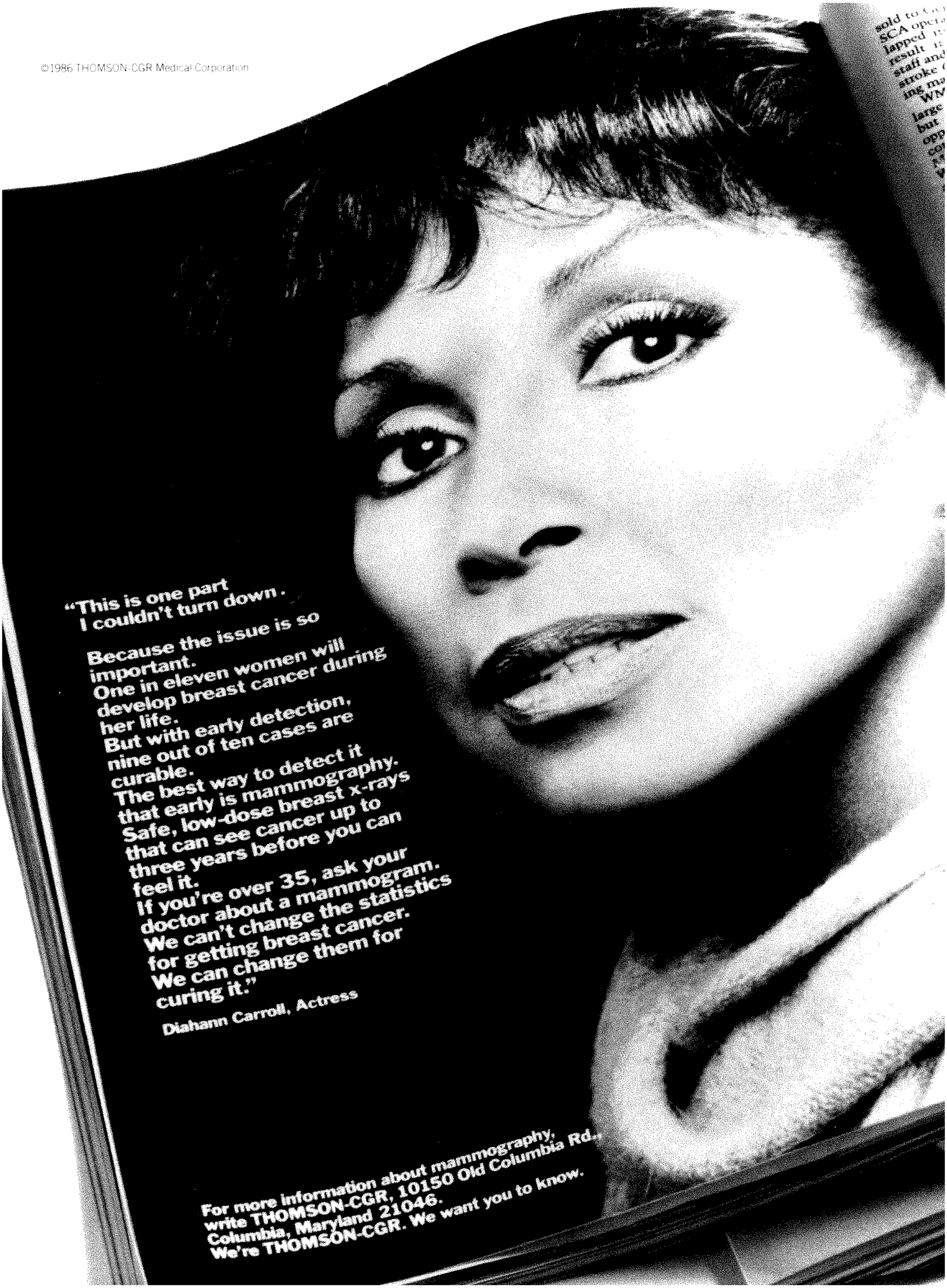

"This is one part I couldn't turn down.

Because the issue is so important.
One in eleven women will develop breast cancer during her life.
But with early detection, nine out of ten cases are curable.
The best way to detect it that early is mammography.
Safe, low-dose breast x-rays that can see cancer up to three years before you can feel it.
If you're over 35, ask your doctor about a mammogram.
We can't change the statistics for getting breast cancer.
We can change them for curing it."

Diahann Carroll, Actress

For more information about mammography, write THOMSON-CGR, 10150 Old Columbia Rd., Columbia, Maryland 21046.
We're THOMSON-CGR. We want you to know.

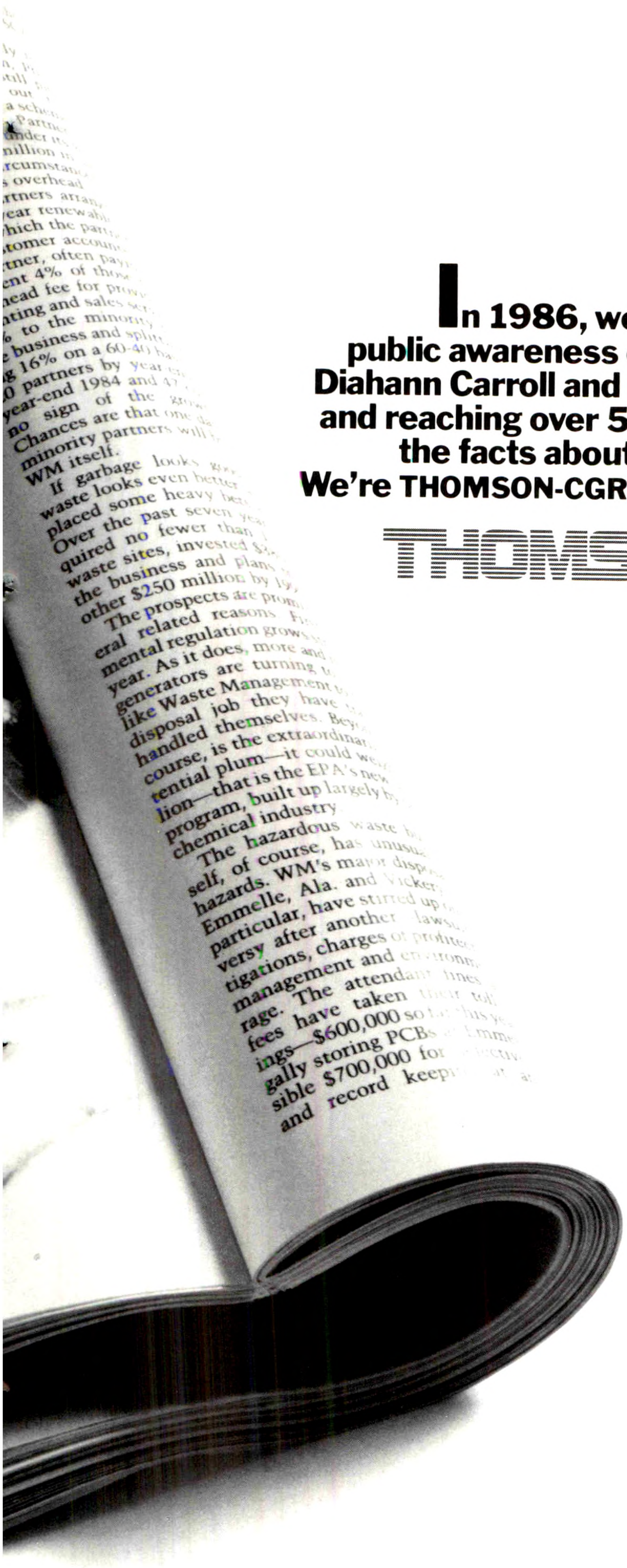

In 1986, we'll sponsor a public awareness campaign featuring Diahann Carroll and other notable women, and reaching over 50 million people with the facts about mammography. We're THOMSON-CGR. We want you to know.

THOMSON CGR

We are the State
OF THE IMAGE

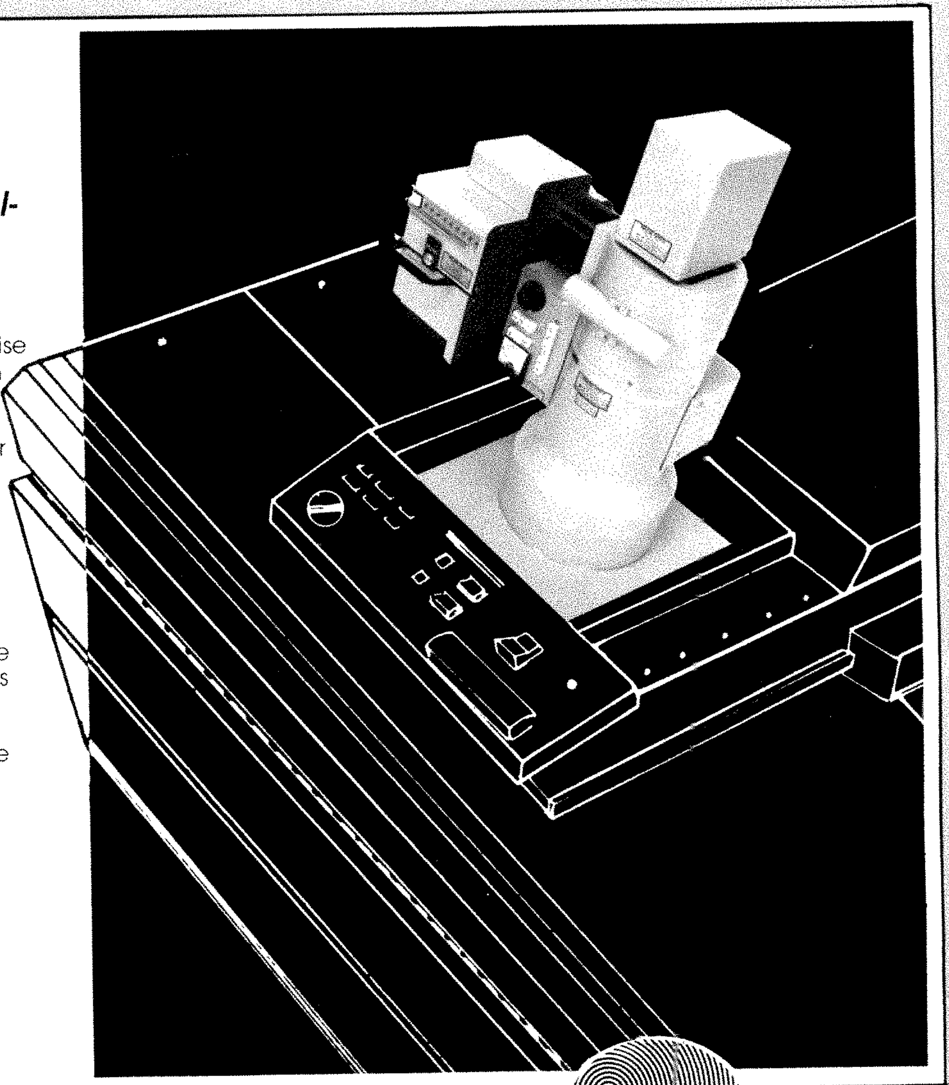

Precise Optics is the World's Largest Manufacturer *specializing only* in the production of Image Intensifier Systems and Components.

With *over thirty years of experience*, Precise has achieved an unsurpassed capability in the design and manufacture of Imaging Systems, suppling major equipment manufacturers throughout the world with our complete Systems and components.

With budgetary constraints and DRGs a current fact of life, Precise Systems offer a *viable high-quality alternative* to more expensively priced equipment.

Precise produces many hundreds of Imaging Systems every year, at an obvious volume cost savings and with *superior tube selection advantage*, while tailoring systems and components to meet your individual, specialized needs.

Our application and production expertise assures that any System requirement can and will be met without compromise, with the performance, reliability and service expected from an industry leader.

All Systems are compatible with new or existing equipment, while satisfying DHHS standards.

For more information on our line of 6, 9, 12 & 16 inch, Single & Multi-mode Image Intensifier Systems. Write or call . . .

precise optics®

PHOTO MEDIC
EQUIPMENT, INC.

the development of nonionic contrast media, introduces...

An important innovation for vascular and subarachnoid imaging.

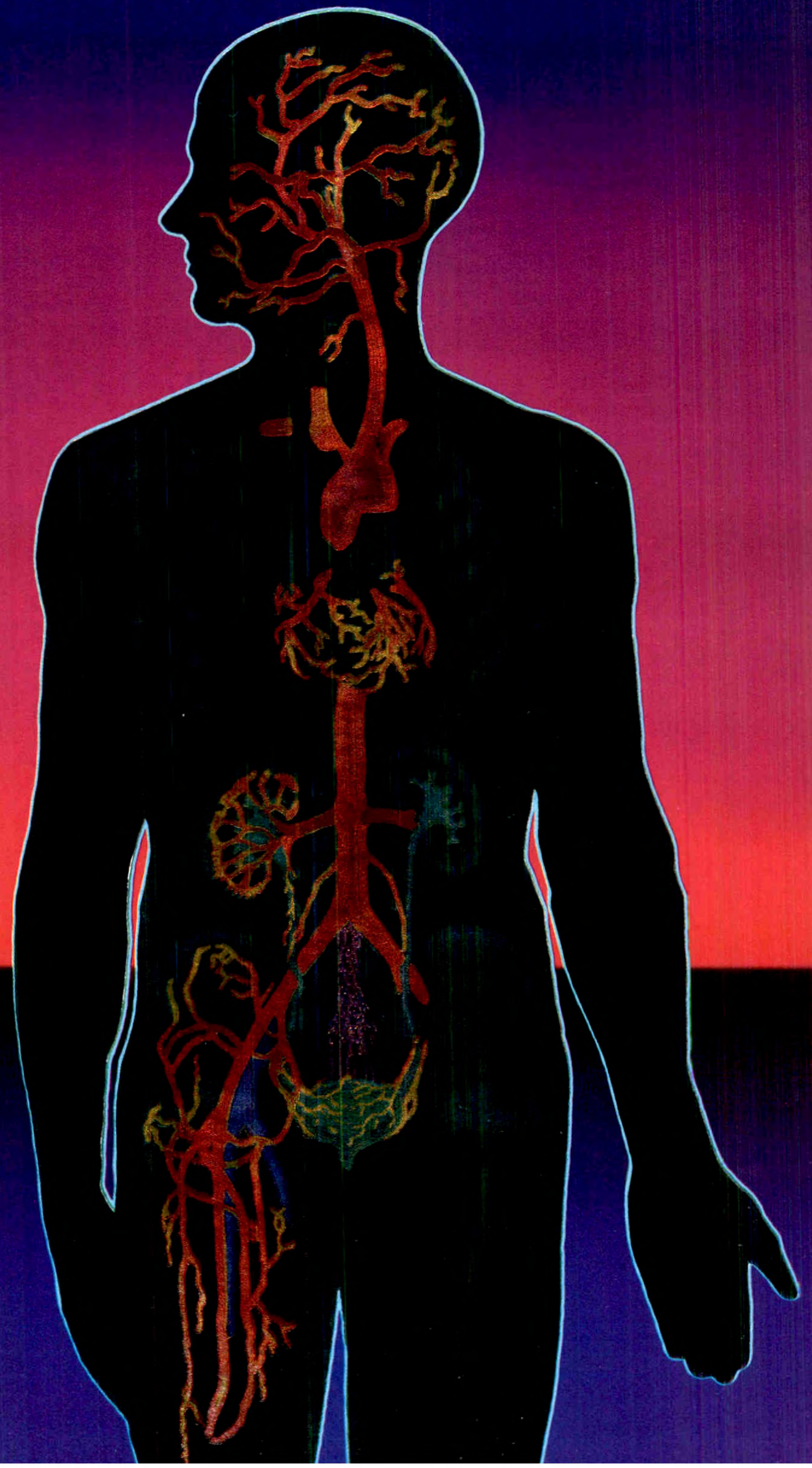

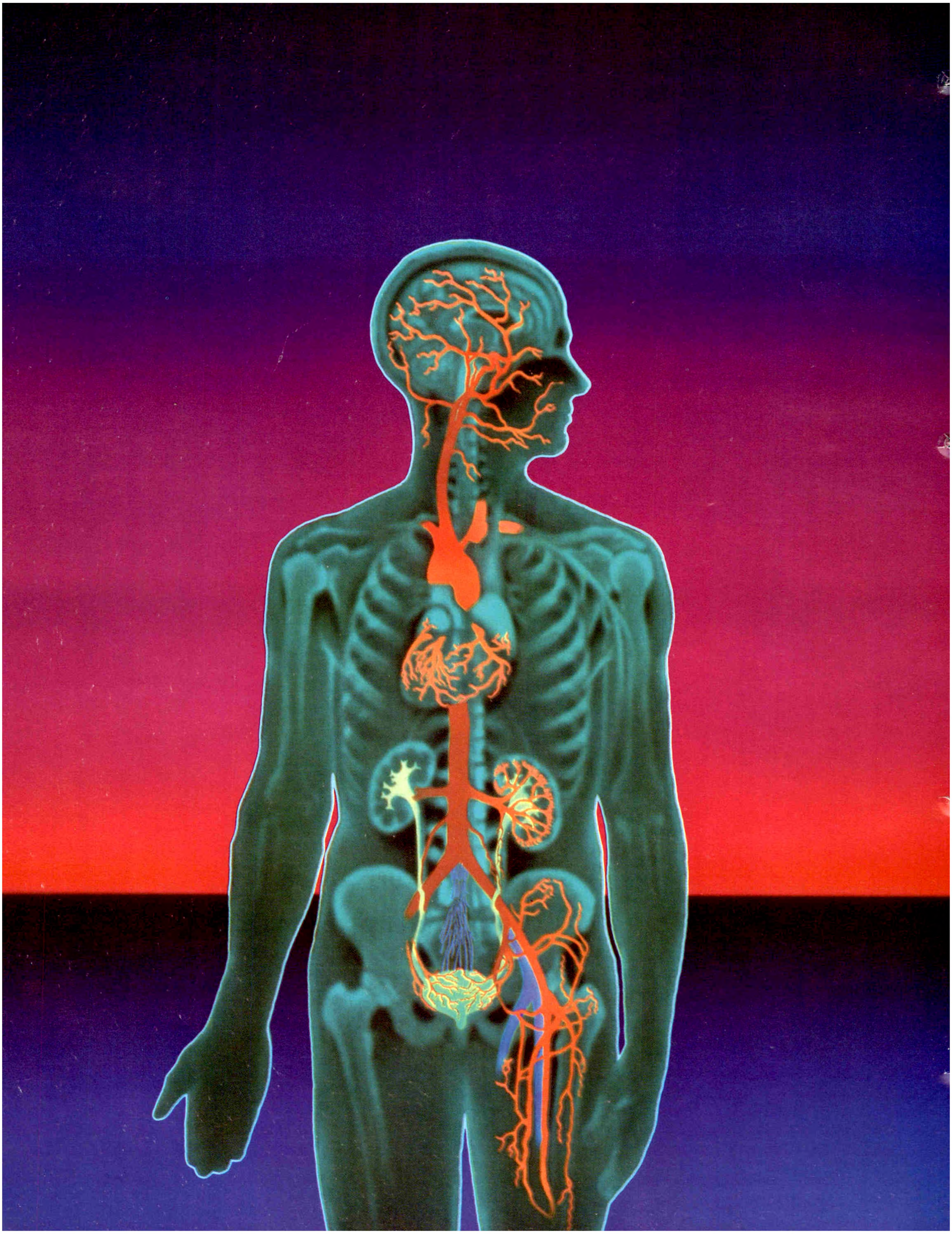

NEW NONIONIC

OMNIPAQUE®

(IOHEXOL)

Improving the safety profile in a broad spectrum of applications.

Indicated for:

- Angiocardiography
- Cerebral Arteriography
- I.V. Digital Subtraction Angiography of Head and Neck
- Peripheral Arteriography
- Peripheral Venography
- Aortography
- Excretory Urography
- Lumbar and Thoracic Myelography
- CT Myelography

See last pages for important product information concerning

NEW NONIONIC

OMNIPAQUE®

(IOHEXOL)

SIGNIFICANT IMPROVEMENT IN PATIENT TOLERANCE

Incidence of Adverse Reactions After Intravenous Injections*

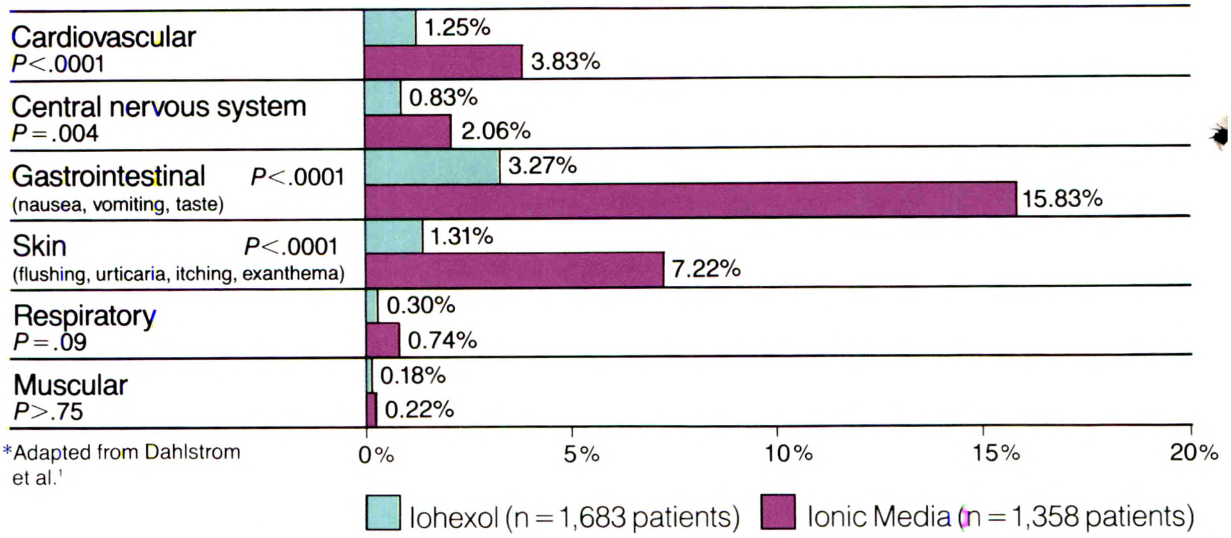

*Adapted from Dahlstrom et al.[1]

NO CONFUSION OR DISORIENTATION AFTER MYELOGRAPHY REPORTED IN CLINICAL STUDIES[2†]

Elderly patients may present a greater risk following myelography. Physicians should remain alert for the occurrence of adverse effects which have occurred with other nonionic water-soluble media.

GREATER PATIENT COMFORT IN VASCULAR APPLICATIONS[3-7]

More comfortable procedures for patients, especially those who have severe stenotic disease or experienced pain during a previous examination.

Improved patient cooperation can result in increased patient throughput.

For myelography: recommended concentrations—
OMNIPAQUE 180 (180 mgI/mL) or OMNIPAQUE 240 (240 mgI/mL).

Improving the safety profile in a broad spectrum of applications

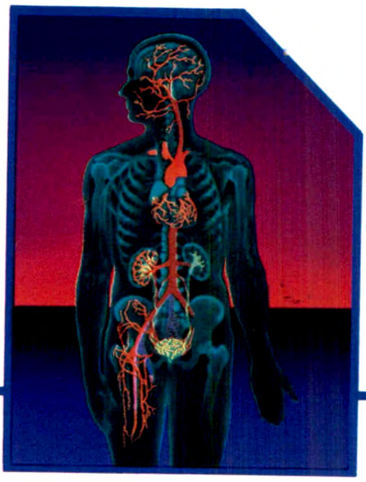

IMPROVING THE PATIENT SAFETY PROFILE

For all patients, including those hypersensitive to ionic media.[8] Since adverse reactions can occur with nonionic media, similar preparations to those recommended for ionic media should be planned to handle severe or potentially fatal reactions.

Improving the nephrotoxicity profile.

- Minimal effect on glomerular filtration rate, permeability, or albumin excretion.[9,10] Not recommended for patients with anuria.

Improved hemodynamic profile.[11,12] Clinical relevance is yet to be determined.

- Less reduction in systolic and diastolic pressures.
- Minimal effect on myocardial conduction or contractility.

Excellent neurotoxicity profile.[2,13-16]

Elderly patients may be at greater risk following contrast media administration.

GREATER CONVENIENCE IN ADMINISTRATION

One ready-to-use agent for most examinations.

No dilution or reconstitution necessary.

Flexible application with the four most used iodine concentrations.

Product	Concentration (mgI/mL)	Color Coding	Indications for Use
OMNIPAQUE® 180	180	🟥	Lumbar, Thoracic, and CT Myelography
OMNIPAQUE® 240	240	🟦	Lumbar and Thoracic Myelography, Peripheral Venography
OMNIPAQUE® 300	300	🟫	Urography, Cerebral Arteriography, Peripheral Arteriography, Peripheral Venography
OMNIPAQUE® 350	350	🟩	Angiocardiography, Urography, Peripheral Arteriography, I.V. Digital Subtraction Angiography

NEW NONIONIC

OMNIPAQUE®

(IOHEXOL)

CONSISTENT DIAGNOSTIC QUALITY

SUBARACHNOID IMAGES EQUAL TO OR BETTER THAN THOSE OBTAINED WITH A FIRST-GENERATION NONIONIC.[17]

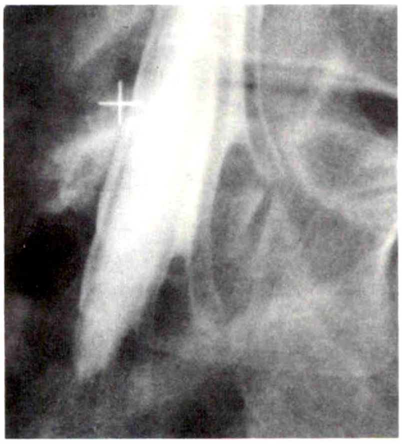

Excellent filling of root sleeves.

Excellent visualization of root and conus medullaris.

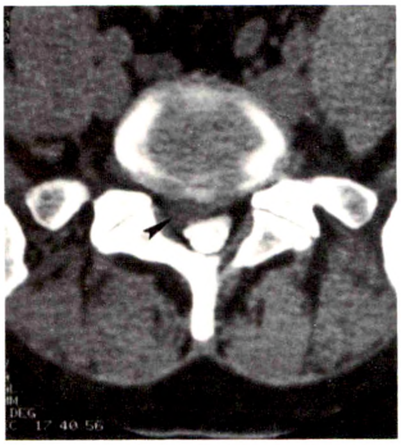

Diagnostic CSF enhancement for CT evaluation.

No aspiration of contrast medium required.

See following pages for important product information concerning

Improving the safety profile in a broad spectrum of applications

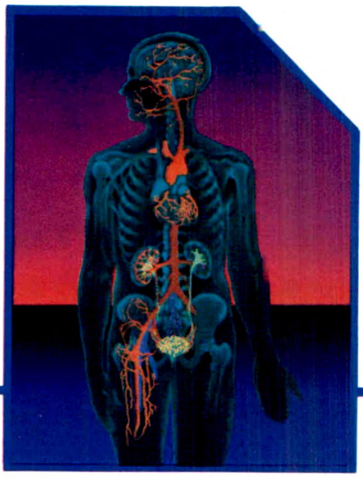

EXCELLENT VASCULAR IMAGING

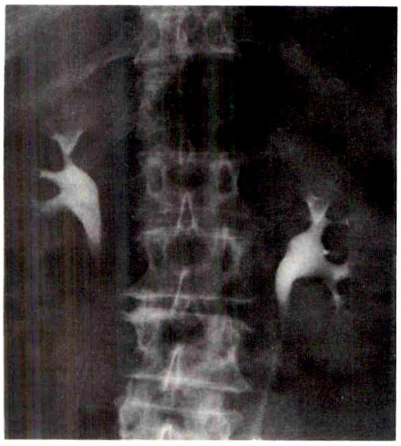

Excellent pyelographic density.[18,19]

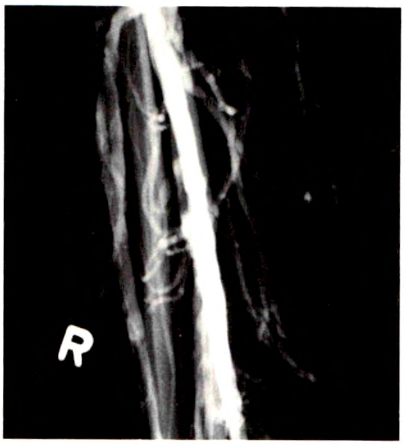

Excellent diagnostic quality in peripheral studies.[6,7]

A preferred medium for lower-limb venography.[5]

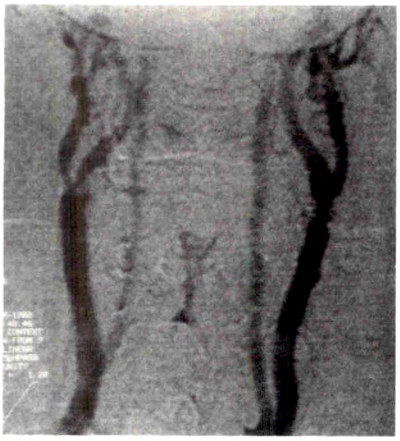

Image degradation due to swallowing, motion, and coughing is less with iohexol than with ionic contrast media.[3,4]

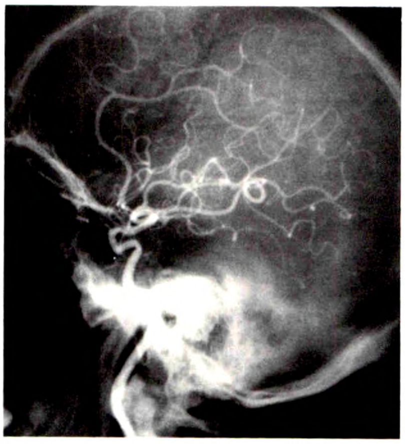

Excellent results in cerebral arteriography.[14,15]

Less movement due to pain.[13]

OMNIPAQUE® 180 240 300 350
INJECTION (IOHEXOL)

PLEASE CONSULT FULL PRODUCT INFORMATION BEFORE USING.
A SUMMARY FOLLOWS:
OMNIPAQUE is a nonionic, water-soluble, radiographic contrast medium.
INDICATIONS AND USAGE: OMNIPAQUE is indicated in adults for angiocardiography (ventriculography, selective coronary arteriography); aortography, including studies of the aortic root, aortic arch, ascending aorta, abdominal aorta, and its branches; cerebral arteriography; digital subtraction angiography; peripheral angiography including arteriography and venography (phlebography); excretory urography; and lumbar and thoracic myelography, by conventional technique and in computerized tomography.

Administration of contrast media should be performed by qualified personnel familiar with the procedure and an appropriate technique should be utilized.
CONTRAINDICATIONS: OMNIPAQUE should not be administered to patients with a known hypersensitivity to iohexol.

Lumbar puncture ordinarily should not be performed in the presence of local or systemic infection where bacteremia is likely.

Intrathecal administration of corticosteroids with OMNIPAQUE is contraindicated.

Because of the possibility of overdosage, immediate repeat myelography in the event of technical failure is contraindicated (see DOSAGE AND ADMINISTRATION).
WARNINGS—General: OMNIPAQUE should be used with extreme care in patients with severe functional disturbances of the liver and kidneys, severe thyrotoxicosis, or myelomatosis. Diabetics with a serum creatinine level above 3 mg/dL should not be examined unless the possible benefits of the examination clearly outweigh the additional risk. OMNIPAQUE is not recommended for use in patients with anuria.

Radiopaque contrast agents are potentially hazardous in patients with multiple myeloma or other paraproteinemia, particularly in those with therapeutically resistant anuria. Although neither the contrast agent nor dehydration has separately proven to be the cause of anuria in myeloma, it has been speculated that the combination of both may be causative factors. The risk in myelomatous patients is not a contraindication; however, special precautions are necessary. Partial dehydration in the preparation of these patients prior to injection is not recommended since this may predispose the patient to precipitation of the myeloma protein in the renal tubules. No form of therapy, including dialysis, has been successful in reversing the effect. Myeloma, which occurs most commonly in persons over age 40, should be considered before instituting intravascular administration of contrast agents.

Ionic contrast media, when injected intravenously or intraarterially, may promote sickling in individuals who are homozygous for sickle cell disease.

Administration of radiopaque materials to patients known or suspected of having pheochromocytoma should be performed with extreme caution. If, in the opinion of the physician, the possible benefits of such procedures outweigh the considered risks, the procedures may be performed; however, the amount of radiopaque medium injected should be kept to an absolute minimum. The patient's blood pressure should be assessed throughout the procedure and measures for the treatment of hypertensive crisis should be readily available.

Reports of thyroid storm following the use of iodinated, ionic radiopaque contrast media in patients with hyperthyroidism or with autonomously functioning thyroid nodule suggest that this additional risk be evaluated in such patients before use of any contrast medium.

Urography should be performed with caution in patients with severely impaired renal function and patients with combined renal and hepatic disease.

Caution is advised in patients with a history of epilepsy, severe cardiovascular disease, chronic alcoholism, or multiple sclerosis.

Elderly patients may present a greater risk following myelography. The need for the procedure in these patients should be evaluated carefully. Special attention must be paid to dose and concentration of the medium, hydration, and technique used.

Patients who are receiving anticonvulsants should be maintained on this therapy. Should a seizure occur, intravenous diazepam or phenobarbital sodium is recommended. In patients with a history of seizure activity who are not on anticonvulsant therapy, premedication with barbiturates should be considered.

Prophylactic anticonvulsant treatment with barbiturates should be considered in patients with evidence of inadvertent intracranial entry of a large or concentrated bolus of the contrast medium since there may be an increased risk of seizure in such cases.

Drugs which lower the seizure threshold, especially phenothiazine derivatives, including those used for their antihistamine properties, should not be used with OMNIPAQUE. Others include MAO inhibitors, tricyclic antidepressants, CNS stimulants, and psychoactive drugs described as analeptics, major tranquilizers, or antipsychotic drugs. Such medication should be discontinued at least 48 hours before myelography, should not be used for the control of nausea and vomiting, and should not be resumed for at least 24 hours postprocedure.

Care is required in patient management to prevent inadvertent intracranial entry of a large dose or concentrated bolus of the medium. Also, effort should be directed to avoid rapid dispersion of the medium causing inadvertent rise to intracranial levels (eg, by active patient movement). Direct intracisternal or ventricular administration for standard radiography (not CT) is not recommended.

In most reported cases of major motor seizures with other nonionic myelographic media, one or more of the following factors were present. Therefore avoid:

- Deviations from recommended procedure or in myelographic management.
- Use in patients with a history of epilepsy.
- Overdosage.
- Intracranial entry of a bolus or premature diffusion of a high concentration of the medium.
- Medication with neuroleptic drugs or phenothiazine antinauseants.
- Failure to maintain elevation of the head during the procedure, on the stretcher, or in bed.
- Excessive and particularly active patient movement or straining.

If grossly bloody CSF is encountered, the possible benefits of a myelographic

PRECAUTIONS—General: Diagnostic procedures which involve the use of radiopaque diagnostic agents should be carried out under the direction of personnel with the prerequisite training and with a thorough knowledge of the particular procedure to be performed. Appropriate facilities should be available for coping with any complication of the procedure, as well as for emergency treatment of severe reactions to the contrast agent itself. After parenteral administration of a radiopaque agent, competent personnel and emergency facilities should be available for at least 30 to 60 minutes since severe delayed reactions have occurred (see ADVERSE REACTIONS).

Preparatory dehydration is dangerous and may contribute to acute renal failure in patients with advanced vascular disease, diabetic patients, and in susceptible nondiabetic patients (often elderly with preexisting renal disease). Dehydration in these patients seems to be enhanced by the osmotic diuretic action of urographic agents. It is believed that overnight fluid restriction prior to excretory urography generally does not provide better visualization in normal patients. *Patients should be well hydrated prior to and following iohexol administration.*

In patients with severe renal insufficiency or failure, compensatory biliary excretion of the drug is anticipated to occur, with a slow clearance into the bile. Patients with hepatorenal insufficiency should not be examined unless the possibility of benefit clearly outweighs the additional risk.

Acute renal failure has been reported in diabetic patients with diabetic nephropathy and in susceptible nondiabetic patients (often elderly with preexisting renal disease) following excretory urography. Therefore, careful consideration of the potential risks should be given before performing this radiographic procedure in these patients.

Immediately following surgery, excretory urography should be used with caution in renal transplant recipients.

The possibility of a reaction, including serious, life-threatening, fatal, anaphylactoid, or cardiovascular reactions should always be considered (see ADVERSE REACTIONS). It is of utmost importance that a course of action be carefully planned in advance for immediate treatment of serious reactions, and that adequate and appropriate personnel be readily available in case a severe reaction should occur.

The possibility of an idiosyncratic reaction in susceptible patients should always be considered (see ADVERSE REACTIONS). The susceptible population includes patients with a previous reaction to contrast media, patients with a known sensitivity to iodine per se, and patients with a known clinical hypersensitivity: bronchial asthma, hay fever, and food allergies.

The occurrence of severe idiosyncratic reactions has prompted the use of several pretesting methods. However, pretesting cannot be relied upon to predict severe reactions and may itself be hazardous for the patient. It is suggested that a thorough medical history with emphasis on allergy and hypersensitivity, prior to the injection of any contrast media, may be more accurate than pretesting in predicting potential adverse reactions.

A positive history of allergies or hypersensitivity does not arbitrarily contraindicate the use of a contrast agent where a diagnostic procedure is thought essential, but caution should be exercised (see ADVERSE REACTIONS). Premedication with antihistamines or corticosteroids to avoid or minimize possible allergic reactions in such patients should be considered. Recent reports indicate that such pretreatment does not prevent serious life-threatening reactions, but may reduce both their incidence and severity.

Even though the osmolality of OMNIPAQUE is low compared to diatrizoate- or iothalamate-based ionic agents of comparable iodine concentration, the potential transitory increase in the circulatory osmotic load in patients with congestive heart failure requires caution during injection. These patients should be observed for several hours following the procedure to detect delayed hemodynamic disturbances.

General anesthesia may be indicated in the performance of some procedures in selected adult patients; however, a higher incidence of adverse reactions has been reported in these patients, and may be attributable to the inability of the patient to identify untoward symptoms, or to the hypotensive effect of anesthesia which can reduce cardiac output and increase the duration of exposure to the contrast agent.

Angiography should be avoided whenever possible in patients with homocystinuria, because of the risk of inducing thrombosis and embolism.

In angiographic procedures, the possibility of dislodging plaques or damaging or perforating the vessel wall should be borne in mind during the catheter manipulations and contrast medium injection. Test injections to ensure proper catheter placement are recommended.

Selective coronary arteriography should be performed only in those patients in whom the expected benefits outweigh the potential risk. The inherent risks of angiocardiography in patients with chronic pulmonary emphysema must be weighed against the necessity for performing this procedure.

Administration of contrast media should be performed by qualified personnel familiar with the procedure and appropriate patient management. Sterile technique must be used with any spinal puncture.

When OMNIPAQUE is to be injected using plastic disposable syringes, the contrast medium should be drawn into the syringe and used immediately.

If nondisposable equipment is used, scrupulous care should be taken to prevent residual contamination with traces of cleansing agents.

Parenteral products should be inspected visually for particulate matter and discoloration prior to administration. If particulate matter or discoloration is present, do not use.

Repeat Procedures: If, in the clinical judgment of the physician, sequential or repeat subarachnoid examinations are required, a suitable interval of time between administrations should be observed to allow for normal clearance of the drug from the body.
Information for Patients: Patients receiving injectable radiopaque diagnostic agents should be instructed to:

1. Inform your physician if you are pregnant.
2. Inform your physician if you are diabetic or if you have multiple myeloma, pheochromocytoma, homozygous sickle cell disease or known thyroid disor-

3. Inform your physician if you are allergic to any drugs, food, or if you had any reactions to previous injections of dyes used for x-ray procedures.
4. Inform your physician about any other medications you are currently taking, including nonprescription drugs, before you are administered this drug.

Drug/Laboratory Test Interaction: If iodine containing isotopes are to be administered for the diagnosis of thyroid disease, the iodine-binding capacity of thyroid tissue may be reduced for up to two weeks after contrast medium administration. Thyroid function tests which do not depend on iodine estimation, eg, T_3 resin uptake or direct thyroxin assays, are not affected.

Drug Interactions: Drugs which lower the seizure threshold—especially phenothiazine derivatives including those used for their antihistaminic or antinauseant properties—should not be used with OMNIPAQUE. Others include monoamine oxidase (MAO) inhibitors, tricyclic antidepressants, CNS stimulants, and psychoactive drugs described as analeptics, major tranquilizers, or antipsychotic drugs. Such medications should be discontinued at least 48 hours before myelography, should not be used for the control of nausea or vomiting during or after myelography, and should not be resumed for at least 24 hours postprocedure. In nonelective procedures in patients on these drugs, consider prophylactic use of anticonvulsants.

Carcinogenesis, Mutagenesis, Impairment of Fertility: No long-term animal studies have been performed to evaluate the potential of iohexol in these areas.

Pregnancy Category B: Reproduction studies have been performed in rats and rabbits with up to 100 times the recommended human dose. No evidence has been established of impaired fertility or harm to the fetus due to OMNIPAQUE; there are, however, no studies in pregnant women. Because animal reproduction studies are not always predictive of human response, this drug should be used during pregnancy only if clearly indicated.

Nursing Mothers: Caution should be exercised when OMNIPAQUE is administered to a nursing woman; it is not known to what extent iohexol is excreted in human milk.

Pediatric Use: Safety and effectiveness in children have not been established.

ADVERSE REACTIONS:

Intrathecal: Adverse reactions to the intrathecal use of OMNIPAQUE in general have been mild to moderate in degree, and of short duration. The incidence of these occurrences, based on clinical trials of 584 patients, is as follows:

Headaches: The most frequently occurring adverse reaction following myelography with OMNIPAQUE has been headache, with an incidence of less than 20%. Headache may be caused either as a direct effect of the contrast medium or by CSF leakage at the dural puncture site. However, in managing the patient, it is considered more important to minimize intracranial entry of contrast medium by postural management than to attempt to control possible CSF leakage.

Pain: Mild pain including backache, stiffness, and neuralgia occurred following injection with an incidence of about 8%.

Nausea and Vomiting: Nausea was reported, with an incidence of about 6%, and vomiting of about 3% (based on clinical trials of 584 patients—see PATIENT MANAGEMENT). Maintaining normal hydration is very important. The use of phenothiazine antinauseants is contraindicated. Reassuring the patient that the nausea will clear is usually all that is required.

Dizziness: Transient dizziness was reported in about 2% of the patients.

Other Reactions: Other reactions, occurring with an individual incidence of less than 0.1%, included feeling of heaviness, hypotension, hypertonia, sensation of heat, sweating, vertigo, and loss of appetite. All were transient and mild, with no clinical sequelae.

General Adverse Reactions to Contrast Media: Physicians should remain alert for the occurrence of adverse effects in addition to those discussed above, particularly those already reported in the literature for other nonionic, water-soluble myelographic contrast media. These have included but are not limited to aseptic and bacterial meningitis, and CNS and other neurologic disturbances.

Intravascular: Adverse reactions to the intravascular use of OMNIPAQUE have usually been of mild to moderate severity. However, serious, life-threatening and fatal reactions, mostly of cardiovascular origin, have been associated with the administration of iodine-containing contrast media, including OMNIPAQUE. The injection of contrast media is frequently associated with the sensation of warmth and pain, especially in peripheral angiography; pain and warmth are less frequent and less severe with OMNIPAQUE than with many ionic media, but lower osmolality media are similar in this respect. The incidence of these occurrences in clinical trials is as follows:

Cardiovascular System: Arrhythmias including PVCs and PACs (3%), angina/chest pain (2%), and hypotension (1%). Others including cardiac failure, asystole, bradycardia, tachycardia, and vasovagal reaction were reported with an individual incidence of less than 0.8%. In controlled clinical studies involving 900 patients, one fatality occurred. In widespread clinical use, the incidence of fatality is estimated at 0.0003%.

Nervous System: Pain (6%), photomas (3%), headache (2%), and metallic taste (0.8%). Others including anxiety, blurred vision, dizziness, fever, motor and speech dysfunction, convulsion, light-headedness, paresthesia, somnolence, vertigo, stiff neck, hemiparesis, and nystagmus were reported, with an individual incidence of less than 0.3%.

Respiratory System: Dyspnea, laryngitis, and throat irritation, with an individual incidence of 0.1%.

Gastrointestinal System: Nausea (2%) and vomiting (0.5%). Others including diarrhea, dyspepsia, and dry mouth were reported, with an individual incidence of 0.1%.

Skin and Appendages: Urticaria (0.3%) and purpura (0.1%).

Individual adverse reactions which occurred to a significantly greater extent or a specific procedure are listed under that indication.

General Adverse Reactions to Contrast Media: Physicians should remain alert for the occurrence of adverse effects in addition to those discussed above. The following reactions have been reported after administration of other intravascular iodinated contrast media. *Reactions due to technique:* hematomas and ecchymoses. *Hemodynamic reactions:* vein cramp and thrombophlebitis following intravenous injection. *Cardiovascular reactions:* rare cases of cardiac arrhythmias, reflex tachycardia, chest pain, cyanosis, hypertension, hypotension, peripheral vasodilatation, shock, and cardiac arrest. *Renal reactions:* occasionally, transient proteinuria, and rarely, oliguria or anuria. *Allergic reactions:* Asthmatic attacks, nasal and conjunctival symptoms, dermal reactions such as urticaria with or without pruritus, as well as pleomorphic rashes, sneezing and lacrimation and, rarely, anaphylactic reactions. Rare fatalities have occurred, due to this or unknown causes. *Signs and symptoms related to the respiratory system:* pulmonary or laryngeal edema, bronchospasm, dyspnea; *or to the nervous system:* restlessness, tremors, convulsions. *Other reactions:* flushing, pain, warmth, metallic taste, nausea, vomiting, anxiety, headache, confusion, pallor, weakness, sweating, localized areas of edema, especially facial cramps, neutropenia, and dizziness. Rarely, immediate or delayed rigors can occur, sometimes accompanied by hyperpyrexia. Infrequently, "iodism" (salivary gland swelling) from organic iodinated compounds appears two days after exposure and subsides by the sixth day.

CONSULT PACKAGE INSERT FOR A MORE DETAILED DISCUSSION OF ADVERSE REACTIONS to both intrathecal and intravascular use of OMNIPAQUE.

DOSAGE AND ADMINISTRATION: CONSULT FULL PACKAGE INSERT BEFORE USE. Details on dose, concentration, and administration are provided for each of the indicated procedures.

References: 1. Dahlstrom K, Shaw DD, Clauss W, et al: Summary of U.S. and European intravascular experience with iohexol based on the clinical trial program. *Invest Radiol* 1985; 20(suppl 1):117-121. **2.** Shaw DD, Bach-Gansmo T, Dahlstrom K: Iohexol: summary of North American and European clinical trials in adult lumbar, thoracic, and cervical myelography with a new nonionic contrast medium. *Invest Radiol* 1985; 20(suppl 1):44-50. **3.** Sackett JF, Bergsjordet B, Seeger JF, et al: Digital subtraction angiography: Comparison of meglumine-Na diatrizoate with iohexol. *Acta Radiol* 1983; suppl 366, pp 81-84. **4.** Cacayorin ED, Bernstein AD, Fruehan CT, et al: Intravenous digital subtraction angiography with iohexol. *AJNR* 1983; 4:329-332. **5.** Enge I: Phlebography: Survey and present state. *Acta Radiol* 1983; suppl 366, pp 50-53. **6.** Wolf GL: Adult peripheral angiography: Results from four North American randomized clinical trials of ionic media versus iohexol. *Acta Radiol* 1983; suppl 366, pp 166-170. **7.** Gordon IJ, Skoblar RS, Chicatelli PD, et al: A comparison of iohexol and Conray-60 in peripheral angiography. *AJR* 1984; 142:563-565. **8.** Holtås S: Iohexol in patients with previous adverse reactions to contrast media. *Invest Radiol* 1984; 19:563-565. **9.** Törnquist C, Holtås S: Renal angiography with iohexol and metrizoate. *Radiology* 1984; 150:331-334. **10.** Zachrisson BE, Jagenburg R: Comparison of iohexol with metrizoate in urography: A single blind parallel investigation. *Acta Radiol* 1983; suppl 366, pp 30-37. **11.** Bettmann MA: Angiographic contrast agents: conventional and new media compared. *AJR* 1982; 139:787-794. **12.** Selin K, Emanuelsson H, Renaa T: Iohexol in coronary angiography: A comparison of ionic and non-ionic contrast media. *Acta Radiol* 1983; suppl 366, pp 115-120. **13.** Bryan RN, Miller SL, Roehm JO, et al: Neuroangiography with iohexol. *AJNR* 1983; 4:344-346. **14.** Kido DK, Morris TW, Ekholm S, et al: Comparison of iohexol and meglumine-Na diatrizoate in cerebral angiography. *Acta Radiol* 1983; suppl 366, pp 142-146. **15.** Ahlgren P: Iohexol compared to urografin meglumine in cerebral angiography: A randomized, double blind cross-over study. *Neuroradiology* 1982; 23:195-198. **16.** Sortland O, Nestvold K, Kloster R, et al: Comparison of iohexol with metrizamide in myelography. *Radiology* 1984; 151:121-122. **17.** Kieffer SA, Binet EF, Davis DO, et al: Lumbar myelography with iohexol and metrizamide: a comparative multicenter prospective study. *Radiology* 1984; 151:665-670. **18.** Ekelund L: Iohexol in urography: Survey and present state. *Acta Radiol* 1983; suppl 366, pp 25-29. **19.** Winfield AC, Dray RJ, Kirchner FK, Jr, et al: Iohexol for excretory urography: A comparative study. *AJR* 1983; 141:571-573.

Winthrop-Breon

An important innovation for vascular and subarachnoid imaging.

NEW NONIONIC

OMNIPAQUE®

(IOHEXOL)

Improving the safety profile in a broad spectrum of applications.

Indicated for:

- Angiocardiography
- Cerebral Arteriography
- I.V. Digital Subtraction Angiography of Head and Neck
- Peripheral Arteriography
- Peripheral Venography
- Aortography
- Excretory Urography
- Lumbar and Thoracic Myelography
- CT Myelography

Winthrop-Breon

Winthrop-Breon Laboratories
Division of Sterling Drug Inc.
New York, NY 10016

41286/3567

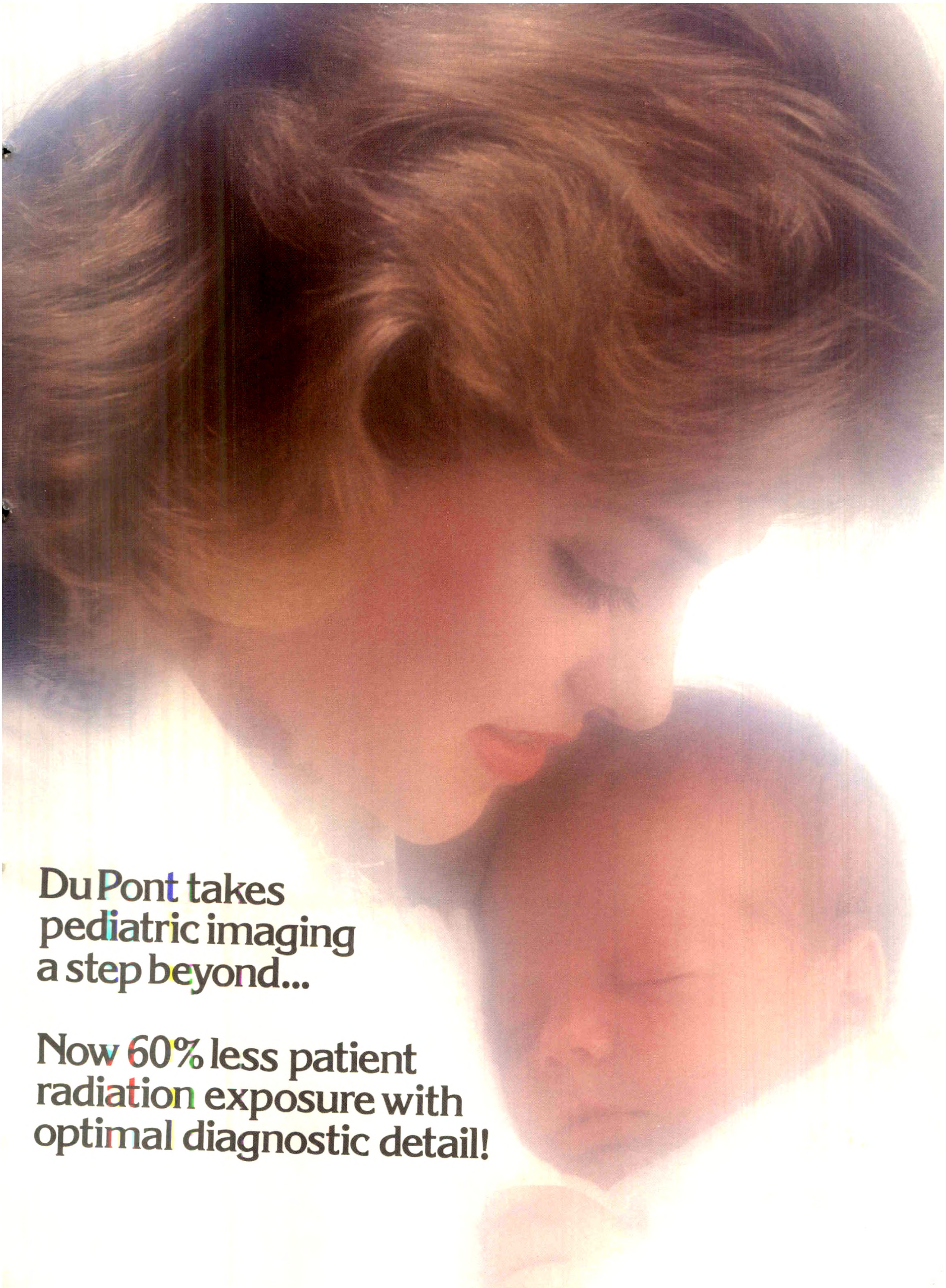

Du Pont takes pediatric imaging a step beyond...
Now 60% less patient radiation exposure with optimal diagnostic detail!

Introducing the Du Pont OPTIMATCH film/screens

Reduce radiation exposure more than 60%

OPTIMATCH film/screen combinations permit a 25% reduction in patient radiation exposure at 50 kVp with no loss of diagnostic information. Conventional Rare Earth screens undergo a marked falloff in light output below 70 kVp. But not QUANTA Detail and Fast Detail screens. Their patented, high-density yttrium tantalate phosphor emits 25% more light at low kVp levels. And this light is in the UV spectrum that optimally matches the sensitivity of CRONEX® films—providing higher detail imaging. That's why we call it OPTIMATCH.

Cassettes of KEVLAR® aramid fiber shorten exposures another 37%. Conventional cassettes actually "steal" radiation at low kVp levels (absorbing over a third of the rays so they never reach the film) while the Du Pont cassettes of KEVLAR are so radiation "transparent" that they allow 87% of the rays through, permitting much shorter exposures.

Pediatric Radiography System:
plus new cassettes of KEVLAR®

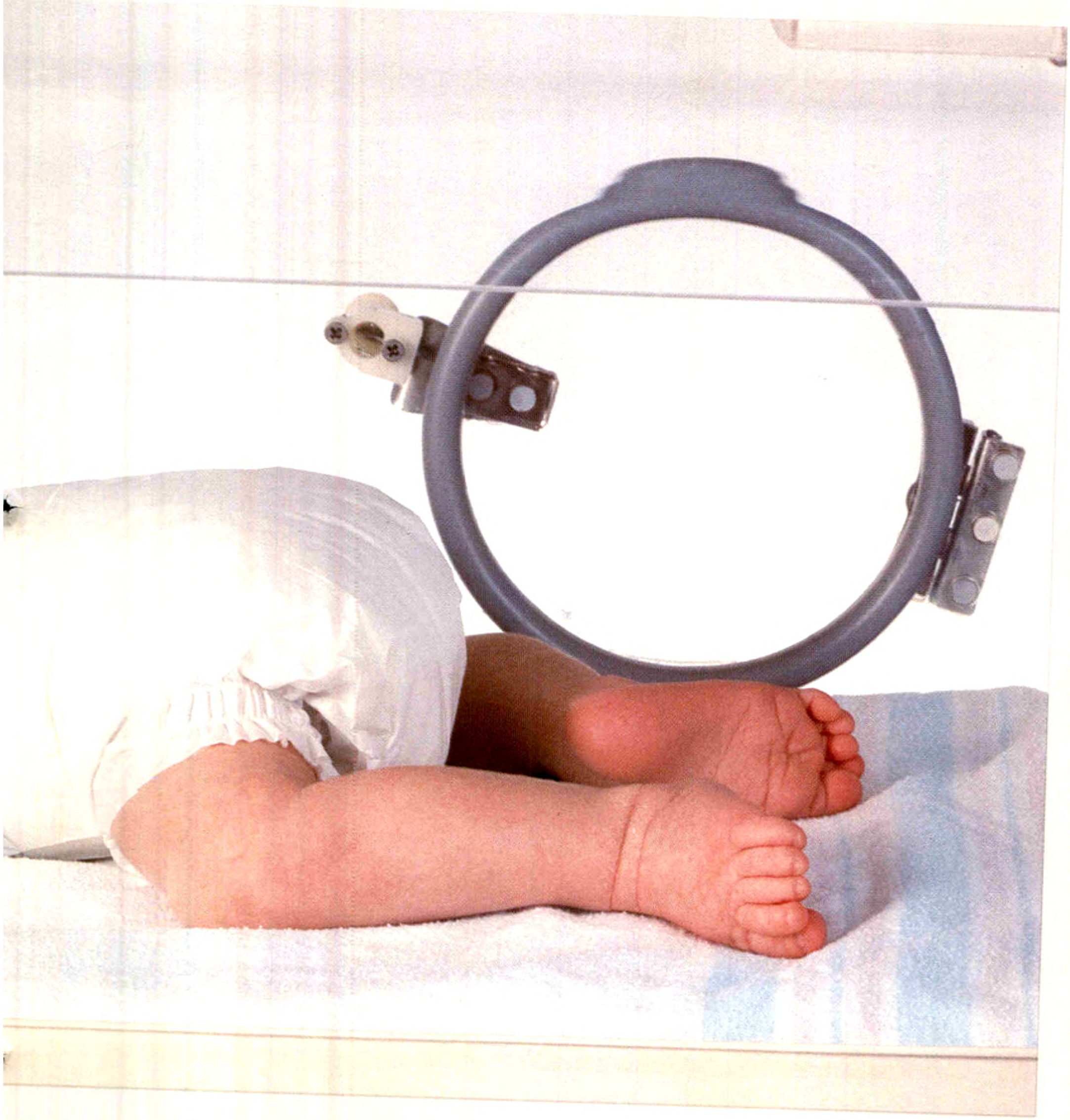

Arrange for a demonstration of this extraordinary reduced-radiation system today...Call (800) 527-2601 or send in the coupon now.

Result: more than twice the motion-stopping speed with highest diagnostic detail. Even compared to 400-speed systems, the Du Pont Pediatric Radiography System allows 35% shorter exposures, while producing measurably sharper diagnostic images. Because you can use less than half the exposure time of competitive 250-speed film/screen systems, you reduce repeats due to patient motion. Fewer "blurrographs!"

Du Pont Company
Room X50133
Wilmington, DE 19801

Please contact me to arrange a demonstration of the new Du Pont Pediatric Radiography System...

NAME
TITLE
HOSPITAL
ADDRESS
CITY STATE ZIP
PHONE

The Du Pont Pediatric Radiography System

OPTIMATCH film/screens plus cassettes of KEVLAR®

The combination that supercedes anything in pediatric radiography.

Half the radiation exposure of conventional Rare Earth systems

☐ Twice the motion-stopping speed

☐ Highest diagnostic detail

DU PONT

REG U.S PAT & TM OFF

Printed in U.S.A.

You get what you pay for

Signa offers essential capabilities other scanners ignore

Beware of magnetic resonance bargains. Others may promise you many things, but only GE is delivering:

☐ Thin slice and multi-slice/multi-echo imaging at minimal acquisition times

☐ Cardiac gating and respiratory motion compensation *at no extra cost*

☐ Echo delay times of 20 msec. or less for superb T1-weighted images

☐ Simultaneous scan, display, filming and archiving *on one console*

☐ Display screen paging modes for cine-like review of up to 32 images in rapid sequence

☐ Mobile scanning tables for fast scan room emergency evacuation and, with a second table, simultaneous prepping and scanning of patients

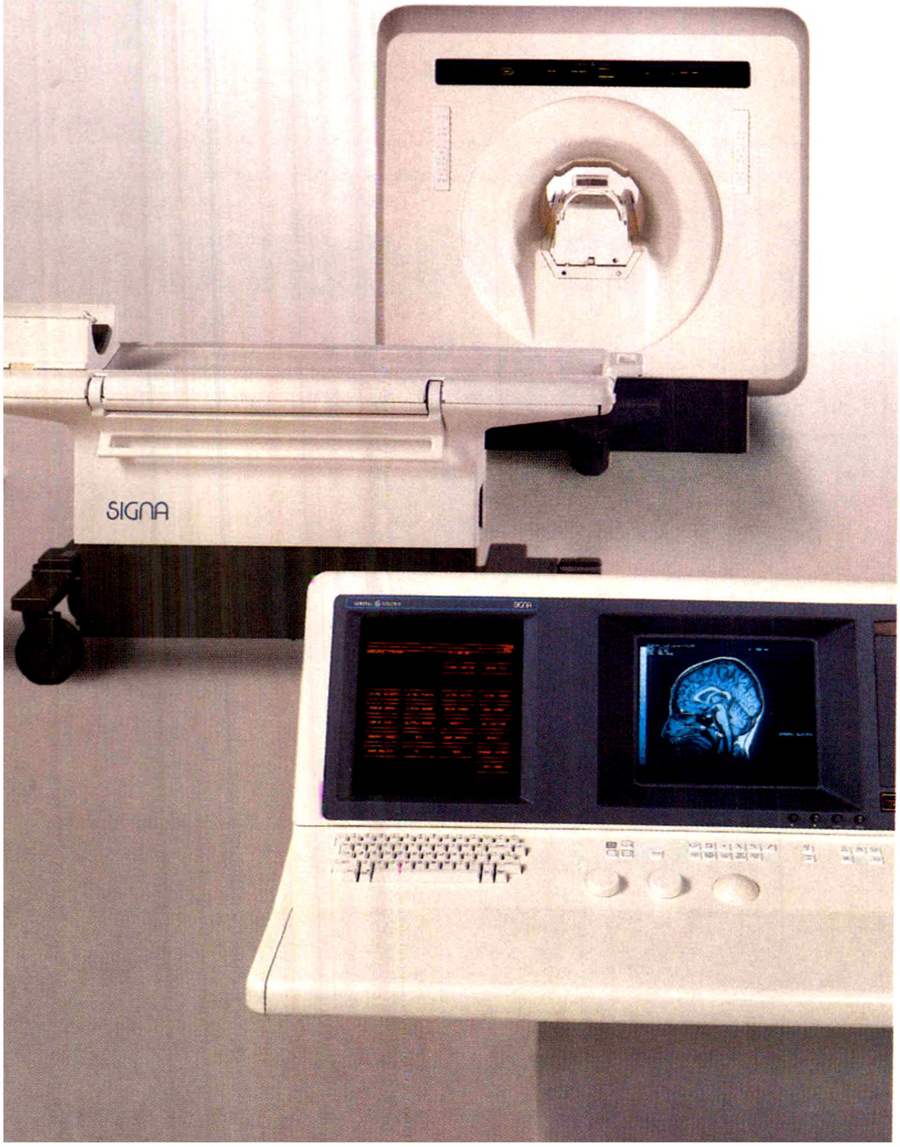

☐ A range of surface coils* that can be positioned outside the scan room

The fact is, only one system offers it all, including financing and site design services to make it affordable: the Signa™ system from GE. Anything less is really no bargain. For details, call us.

800-433-5566 Ext. 5402

GENERAL ELECTRIC

*This feature is currently classified as investigational and is limited by federal law to investigational use. As such, it cannot be made commercially available until necessary government approval is granted.

PORTA RAY IS PROUD TO INTRODUCE

pixie II

THE BEST OF PIXIE - PLUS

- MICROPROCESSOR CONTROLLED
- SOLID STATE - DIGITALLY PROGRAMMED
- AUTOMATIC EXPOSURE CONTROL - BUILT IN
  Any Size Cassette, Any Examination
- 50mA - 100kVp - 200mas
- AUTOMATIC LINE VOLTAGE REGULATOR
- NO BATTERIES TO CHARGE - AVAILABLE FOR USE 24 HRS. A DAY
- MANUFACTURED IN U.S.A.
- CERTIFIED TO BE IN COMPLIANCE WITH ALL GOVERNMENT REGULATIONS

For more information contact Porta Ray or your local X-Ray dealer.

porta ray inc. 19 Jefryn Blvd. West, Deer Park, N.Y. 11729 U.S.A. (516) 242-0022

Two step film control

Minimize X-ray exposure. Optimize image quality. Stabilize film processor performance, film speed and contrast. Quickly. Easily.

1. The Tobias Model RF Wejex Sensitometer

Produces a precise 11-step wedge exposure on *your* X-ray film. Exposure made just before processing eliminates latent image fade problem.* Features: Precise shutter exposure control. Variable lamp intensity. Provisions for 2″×2″ ANSI blue, green or other filters, double sided exposures, 8″×10″ and 35mm test film alignment. And more.

*Lawrence, D.J.: **A Simple Method of Processor Control,** Med. Rad. and Photog. 49, 2-6, 28, 1973 (Reprints available on request)

Wejex Universal
Model RF
Also available:
Wejex Standard
Model R

For a demonstration, call your Tobias dealer.
Or write for our brochure. Ask about our 30 day free trial.

2. The Tobias Model TBX Digital Densitometer

Measures optical transmission density of the Wejex-exposed step wedge over a density range of 0 to 4.50. Accuracy ±0.02. Repeatability ±0.01. State-of-the-art electronics. Lighted digital display. 5 second warm up. Easily portable. Virtually no zero drift.

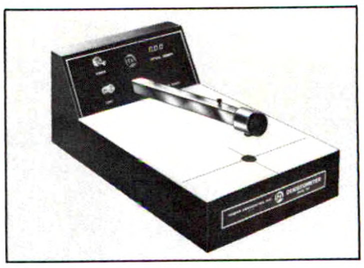

TOBIAS ASSOCIATES, INC.
50 Industrial Drive, P.O. Box 2699, Ivyland, PA 18974, (215) 322-1500

☐ Send literature on the Wejex Sensitometer and TBX Densitometer.

☐ Please send me a copy of D.J. Lawrence's "A Simple Method of Processor Control."

☐ Tell me more about your 30 day free trial policy.

Name ____________
Title/Organization ____________
____
Address ____________
City ____________ State ____________
Zip ____________ Tel. ____________

How to reduce the costs of bowel preparation before and after the X-ray

Before

Evac-Q-Kwik® helps keep hospital costs down by eliminating the staff time and labor involved in giving enemas. And everything needed for effective bowel evacuation is contained in one cost-effective kit.

After

Evac-Q-Kwik is the ideal bowel prep for today's cost-conscious climate. It effectively cleans the colon for clear X-rays *the first time*, to reduce the need for expensive, time-consuming retakes that escalate hospital costs.

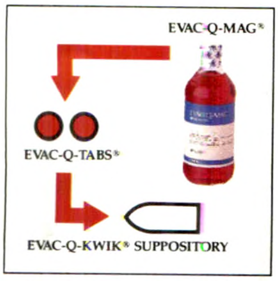

Nurses appreciate Evac-Q-Kwik because it can be administered during a single shift and completed during one 6-hour period. Patients prefer the simple, comfortable Evac-Q-Kwik procedure, too. Evac-Q-Kwik contains no sugar, no alcohol, and is low in sodium.

Evac-Q-Kwik®

Adria®

Adria Laboratories
Columbus, OH 43215

American Roentgen Ray Society:

Officers, Committees, and Meeting Information

Officers

President: Eugene Gedgaudas
President-elect: Jerome F. Wiot
1st Vice-president: Lee F. Rogers
2d Vice-president: Thomas C. Beneventano
Secretary: Raymond A. Gagliardi
Treasurer: Ronald G. Evens

Executive Council: E. Gedgaudas, J. F. Wiot, L. F. Rogers, T. C. Beneventano, R. A. Gagliardi, R. G. Evens, M. M. Figley, R. N. Berk, F. L. Angell, J. E. Madewell, M. P. Capp, G. W. Hartman, B. G. Brogdon, G. A. Kling, H. C. Carlson, A. K. Poznanski, A. E. James, Jr., J. A. Kirkpatrick, Jr., R. H. Troupin, S. S. Siegelman, chairman

Committees 1985–1986

Editorial Policy: S. S. Sagel, W. J. Casarella, J. T. Ferrucci, Jr., N. C. Whitley, S. Hilton, A. J. Davidson, J. M. Taveras, M. M. Figley, R. N. Berk, M. P. Capp, chairman

Education and Research: C. E. Putman, A. R. Margulis, J. R. Thornbury, R. A. McLeod, G. W. Hartman, ex officio, B. G. Brogdon, chairman

Finance and Budget: B. P. Wood, L. R. James, J. A. Kirkpatrick, Jr., R. H. Troupin F. L. Angell, chairman

Instruction Courses: R. A. McLeod, associate chairman, G. W. Hartman, chairman

Program: H. C. Carlson, R. A. Gagliardi, R. H. Troupin, S. S. Siegelman, M. P. Capp, J. E. Madewell, B. G. Brogdon, G. W. Hartman, G. A. Kling, A. V. Proto, C. E. Bickham, J. F. Wiot, chairman.

Publications: W. J. Casarella, J. T. Ferrucci, Jr., S. S. Sagel, N. C. Whitley, M. P. Capp, chairman

Scientific Exhibits: S. G. Kirchner, E. R. Heitzman, Jr., S. M. Goldman, J. E. Madewell, chairman

Nominating: J. P. Tampas, G. M. Stevens, J. A. Kirkpatrick, chairman

Representatives to Other Organizations

American Board of Radiology: E. C. Klatte, R. W. McConnell, L. F. Rogers

American College of Radiology: J. L. Gwinn, G. A. Kling, G. W. Hartman, J. M. Dennis, E. J. Ferris

American Medical Association House of Delegates: S. F. Ochsner, K. C. Krabbenhoft, alternate

American National Standards Institute: M. Haskin

National Council on Radiation Protection and Measurements: E. L. Saenger, H. L. Friedell

Meetings, Membership, Business Information

Annual Meetings: April 13–18, 1986, Sheraton Washington (DC); April 26–May 2, 1987, Fontainebleau-Hilton, Miami Beach; May 1–6, 1988, Westin Bonaventure, Los Angeles

Director Annual Meeting: George A. Kling, Harper Hospital, Detroit, MI 48201

ARRS Membership: Stanley S. Siegelman, Dept. of Radiology and Radiological Science, Johns Hopkins Hospital, 601 N. Broadway, Baltimore, MD 21205. The ARRS has two membership categories: active and in-training. For active membership, applicants must practice radiology in the U.S. or Canada. Each must have graduated in good standing from an approved medical school or hold an advanced degree in a physical, chemical, or biological science and be certified by the American Board of Radiology, the Royal College of Physicians and Surgeons of Canada, or otherwise adequately document training and credentials. A member-in-training must be in a radiology residency, a postresidency fellowship program, or a postgraduate student in an allied science. Status must be verified by the program director. For consideration during the 1986 ARRS meeting, completed applications must be received by Dr. Siegelman no later than Feb. 1, 1986.

Business Office: George J. O'Hop, controller, American College of Radiology, 1891 Preston White Dr., Reston, VA 22091.

ELEMA-SCHONANDER

PUCK Angiographic Filmchanger Systems

Trained, experienced SERVICE network...nationwide

2

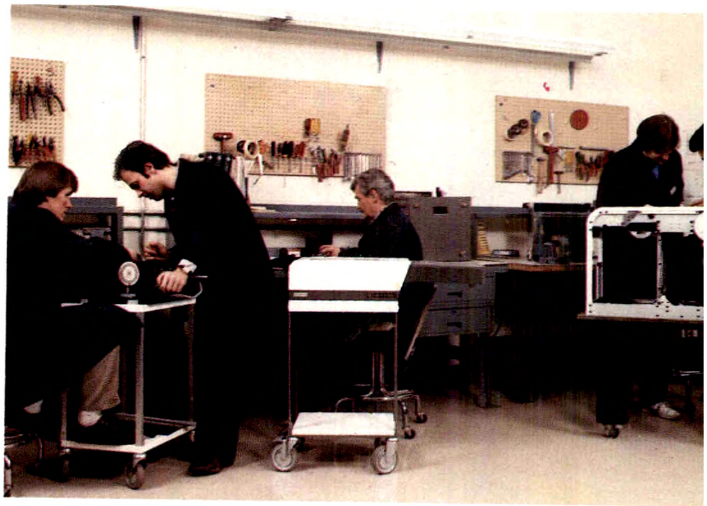

1

1 *Headquarters shop service for major refurbishing.*

2 *On-site hospital field service by trained distributor service engineers, backed by Elema-Schonander's technical staff.*

3 *Headquarters technical training for distributor service organizations.*

3

PUCK Filmchangers have a reputation for reliability. When service is needed, distributor service technicians, trained by Elema-Schonander, are locally available for immediate assistance. They are supported in the field by our own staff of filmchanger specialists, operating out of our Schaumburg, IL (Chicago) headquarters and from several major cities across the country.

A comprehensive inventory of factory spare parts is always on hand and urgent needs can usually be filled within hours.

We operate a year-round training school at our headquarters for distributor service engineers, as well as for the continuing education of our own service force.

85224

elema-schonander

Elema-Schonander, Inc.
2360 North Palmer Drive
P.O. Box 94517
Schaumburg, IL 60195
Telephone (312) 397-5900

There are reasons

S.&S. X-RAY ACCESSORIES

are preferred...

PROVEN the best in X-Ray Departments throughout the world

UNEQUALLED in design, construction and—quality

REPUTATION unmatched for RELIABILITY and PERFORMANCE

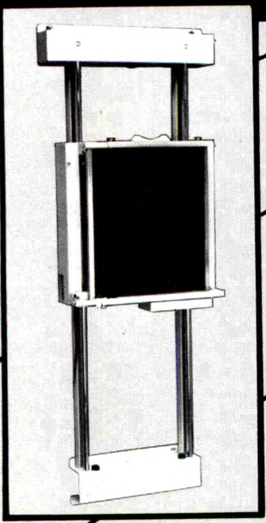

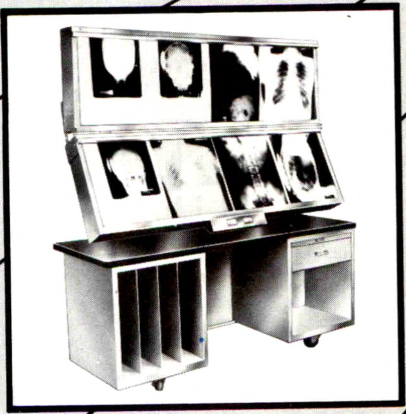

- Motorized Viewers
- Illuminators
- Transfer Cabinets
- File Cabinets
- Protective Panels
- Protective Aprons
- Wall Cassette Holders
- Dryers
- Safelights
- Dark Room Cabinets
- Storage Chests
- Loading Bins
- X-Ray Accessories

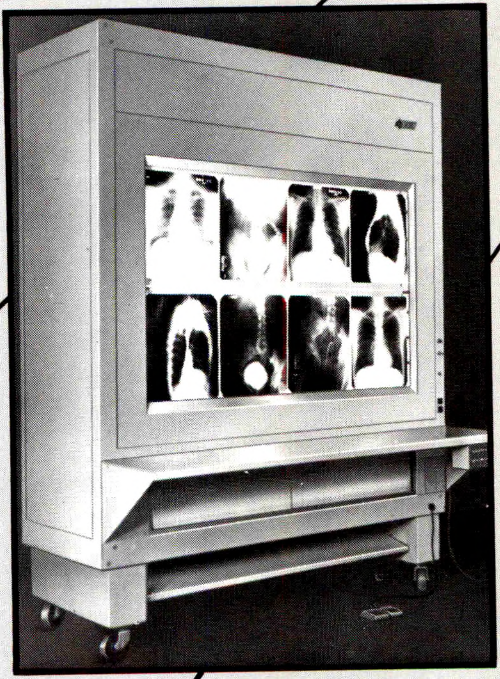

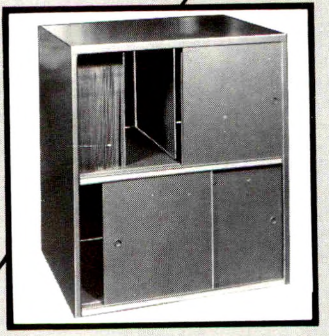

For more than 30 years, S. & S. has been meeting Radiologists' needs with a complete line of illuminators and accessories.

Contact S. & S. or your local x-ray dealer for additional information.

MANUFACTURED BY
S. & S. X-RAY PRODUCTS INC.
The Complete Line of
X-Ray Accessories
(800)221-6634
Telephone: (212) 852-6900
87-93 JAY STREET, BROOKLYN, N.Y. 11201

Now available: a new nonionic agent

**Squibb Diagnostics
has improved contrast media
where the need for
improvement was greatest.**

Patient tolerance.

SQUIBB™
Diagnostics

New for peripheral arteriography

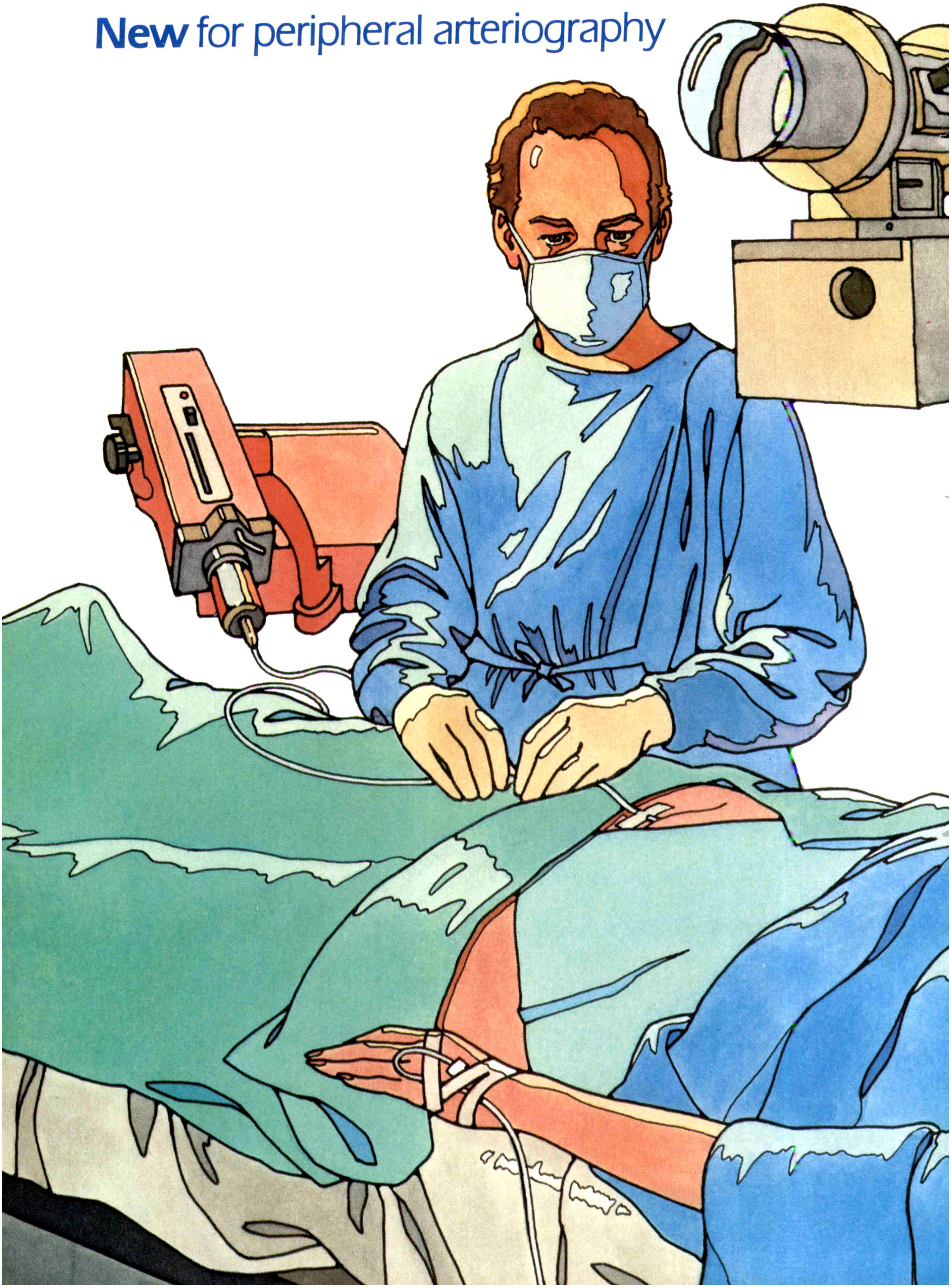

Squibb Diagnostics introduces

ISOVUE®-300

iopamidol injection 61%

Nonionic contrast media that causes less pain than a leading ionic agent.

With Isovue, patients found procedures less painful; physicians saw fewer signs of distress

Isovue-300 is low in osmolality—616 mOsm/kg water.

Using a visual analog scale, patients undergoing peripheral arteriography ranked their pain from "no pain" to "the worst pain I ever had." On a linear scale from zero to 12.4 cm, the mean pain rating for 99 patients given a total of 155 injections of Isovue-300 was 2.3 cm compared with 6.3 cm for 97 patients given a total of 144 injections of the ionic agent diatrizoate meglumine and diatrizoate sodium 52%/8%.

By observing signs of distress, such as movement and/or vocalization, physicians ranked patient distress as being absent, mild, moderate, or severe. When Isovue was compared with diatrizoate meglumine and diatrizoate sodium 52%/8%, the number of injections judged to cause severe distress was 2/299 (1%) compared with 23/293 (8%); moderate distress, 13/299 (4%) compared with 58/293 (20%); mild distress, 59/299 (20%) compared with 94/293 (32%); and no distress, 225/299 (75%) compared with 108/293 (37%), respectively.

As with all injectable contrast agents, the possibility of severe reactions should be borne in mind. (See brief summary of prescribing information on the last pages of this advertisement for a discussion of CONTRAINDICATIONS, WARNINGS, PRECAUTIONS, and ADVERSE REACTIONS.)

ISOVUE®
iopamidol injection

Nonionic. Low in osmolality.
Also for cerebral and
selective visceral arteriography;
aortography; intravenous CECT
head and body imaging.

SQUIBB™
Diagnostics

For brief summary of prescribing information, see last pages of this advertisement.

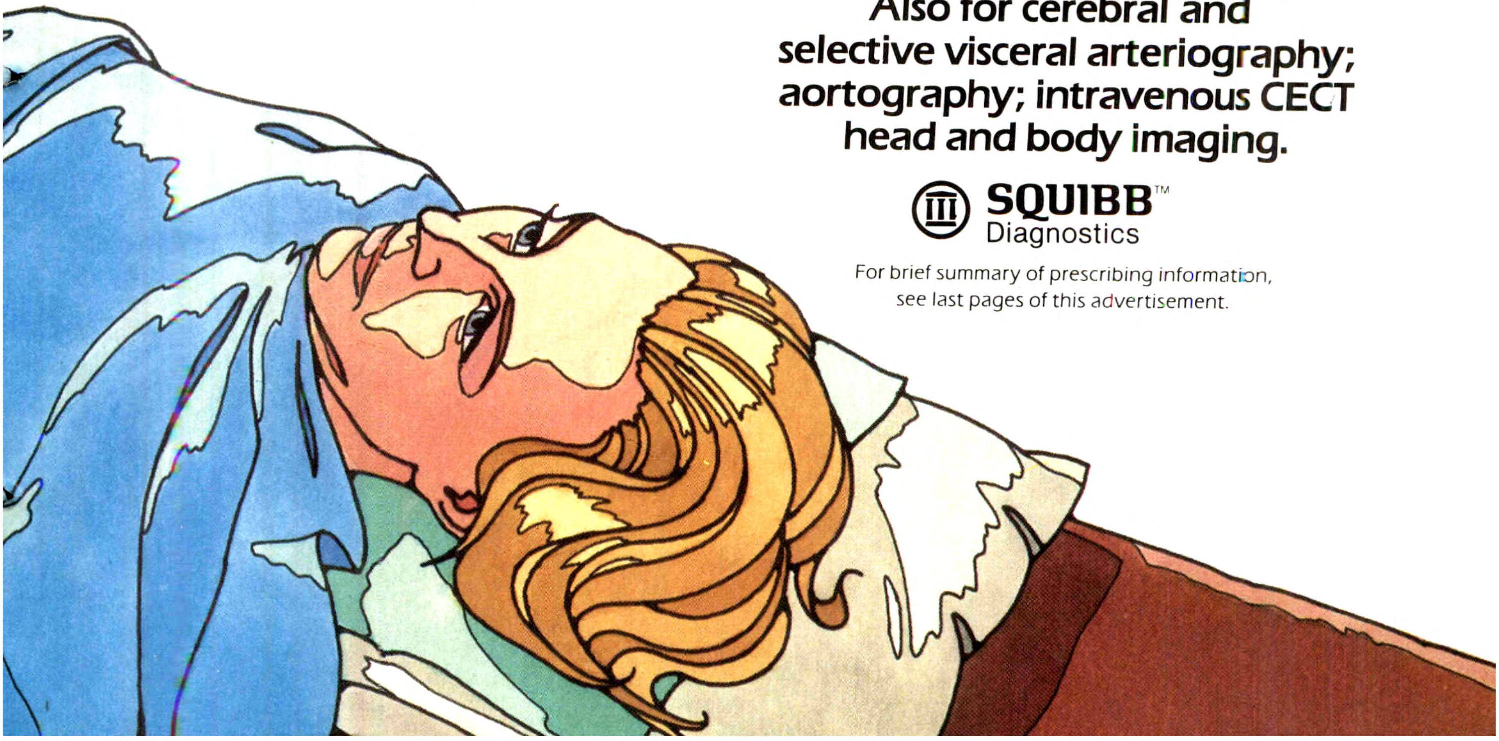

New for myelography

Squibb Diagnostics introduces

ISOVUE-M® 200

iopamidol injection 41%

ISOVUE-M® 300

iopamidol injection 61%

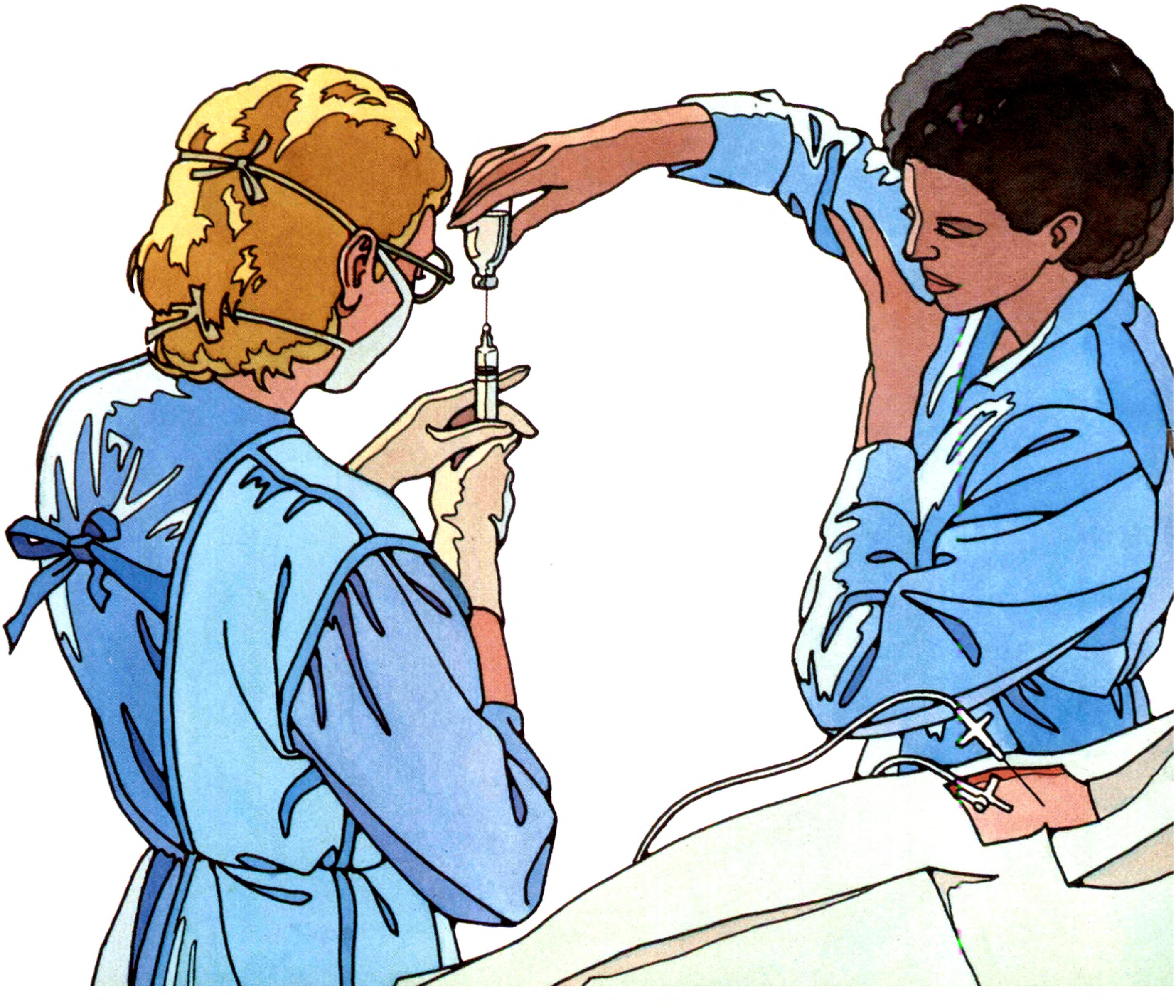

Nonionic contrast media that present a different picture: fewer headaches, and less nausea and vomiting than with metrizamide when compared in a multicenter study

Isovue-M 200 (iopamidol injection 41%) and Isovue-M 300 (iopamidol injection 61%) are low in osmolality — 413 and 616 mOsm/kg water, respectively.

In randomized, double-blind trials, involving 304 patients requiring lumbar, thoracic, cervical, or total columnar myelography or CT cisternography, adverse reactions occurred in 54 of 158 patients (34%) receiving Isovue-M 200 or Isovue-M 300 and in 82 of 146 patients (56%) receiving metrizamide 200 or 300 mgI/ml.

Adverse reactions most commonly reported with both media were headache, nausea, vomiting, and musculoskeletal pain. The incidence of each of these reactions was lower with Isovue than with metrizamide, except for musculoskeletal pain, where the incidence was similar for the two agents.

As with all injectable contrast agents, the possibility of severe reactions should be borne in mind. (See brief summary of prescribing information on the last pages of this advertisement for a discussion of CONTRAINDICATIONS, WARNINGS, PRECAUTIONS, and ADVERSE REACTIONS.)

ISOVUE-M®
iopamidol injection

No reconstitution required. Nonionic. Low in osmolality.
Also for CECT cisternography and ventriculography. Available as ISOVUE®-300 (iopamidol injection 61%) for cerebral arteriography and intravenous CECT head and body imaging.

SQUIBB™
Diagnostics

For brief summary of prescribing information, see last pages of this advertisement.

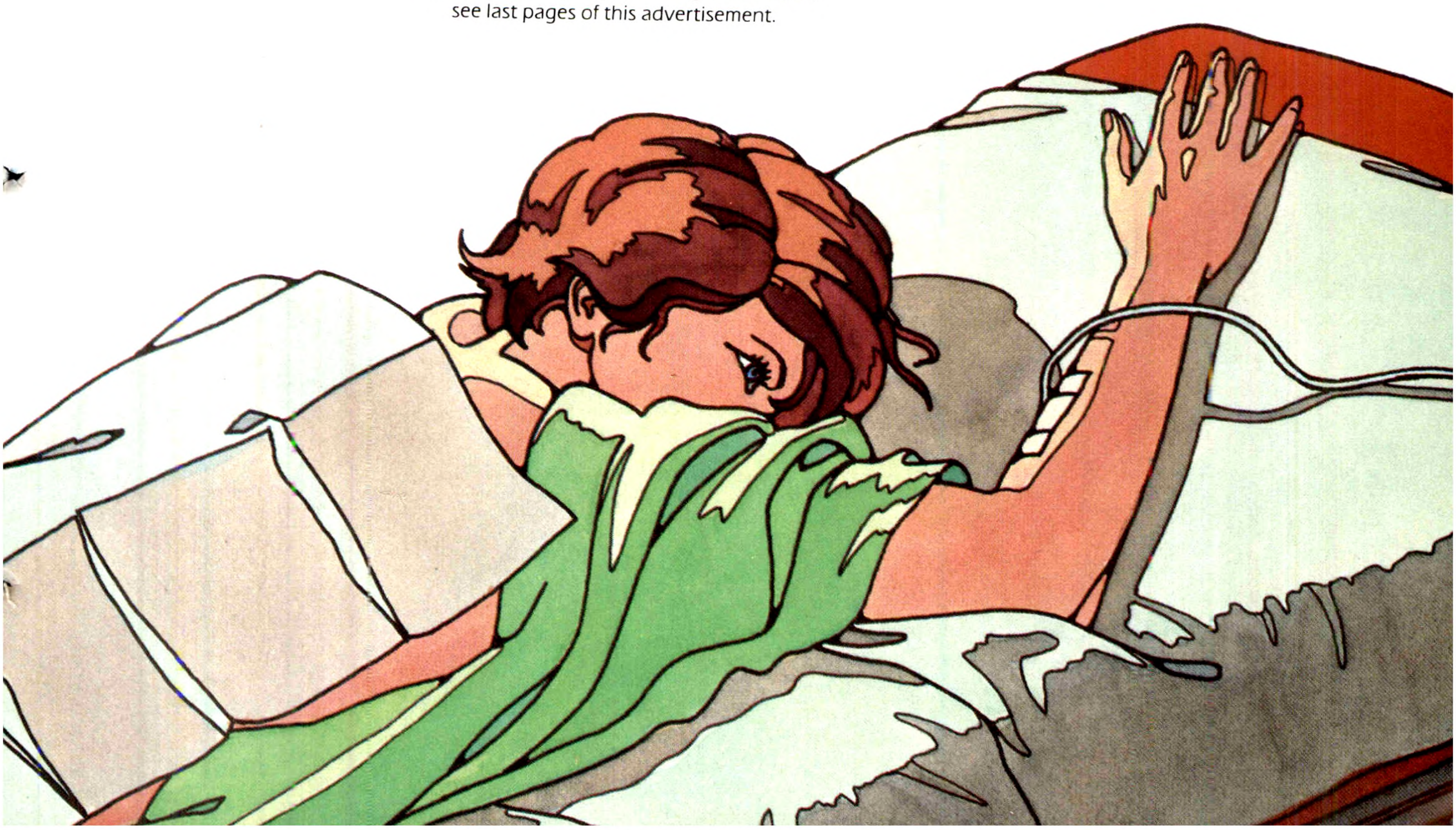

New for coronary arteriography and left ventriculography

Squibb
Diagnostics
introduces
nonionic

ISOVUE®-370
iopamidol injection 76%

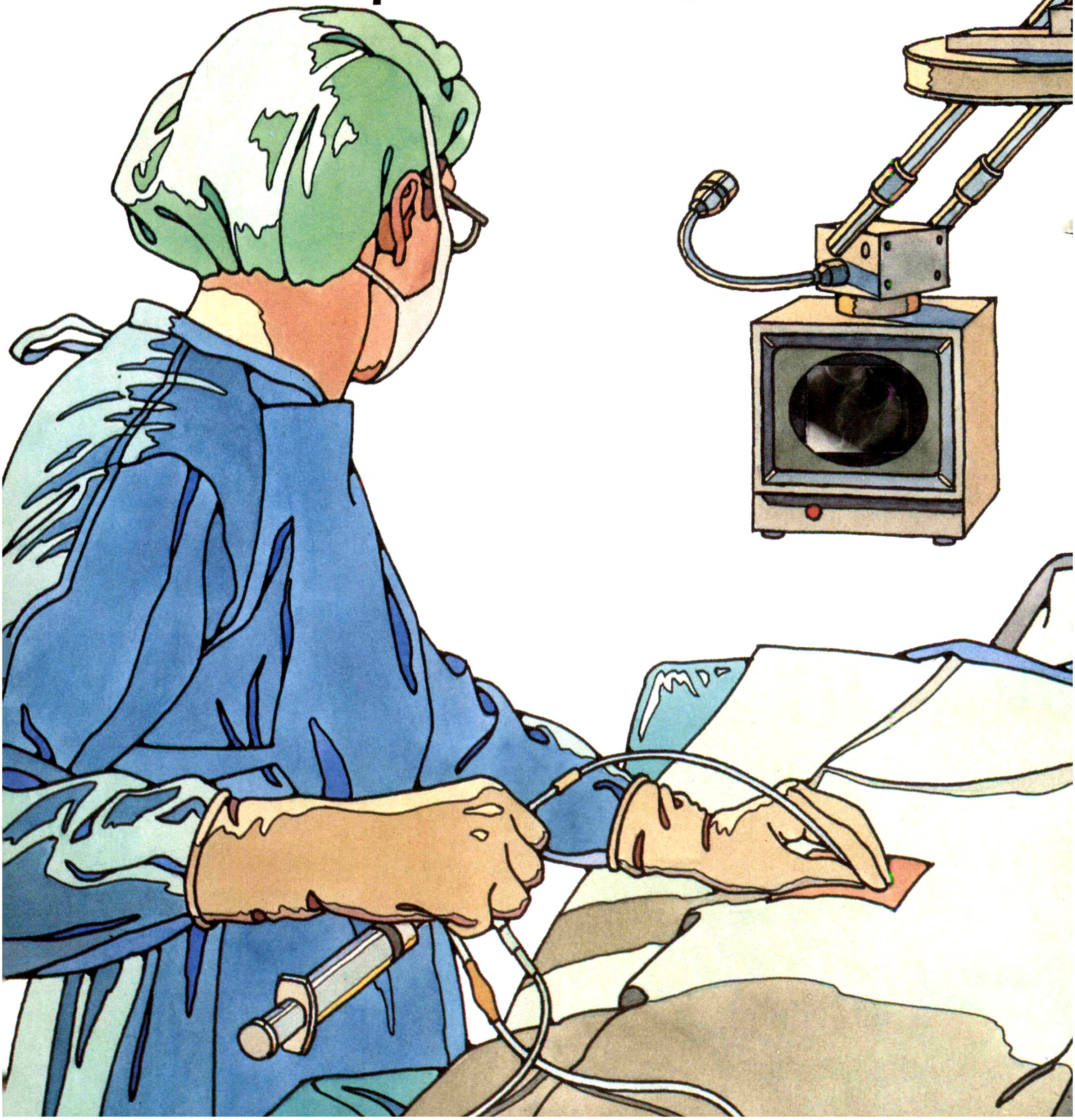

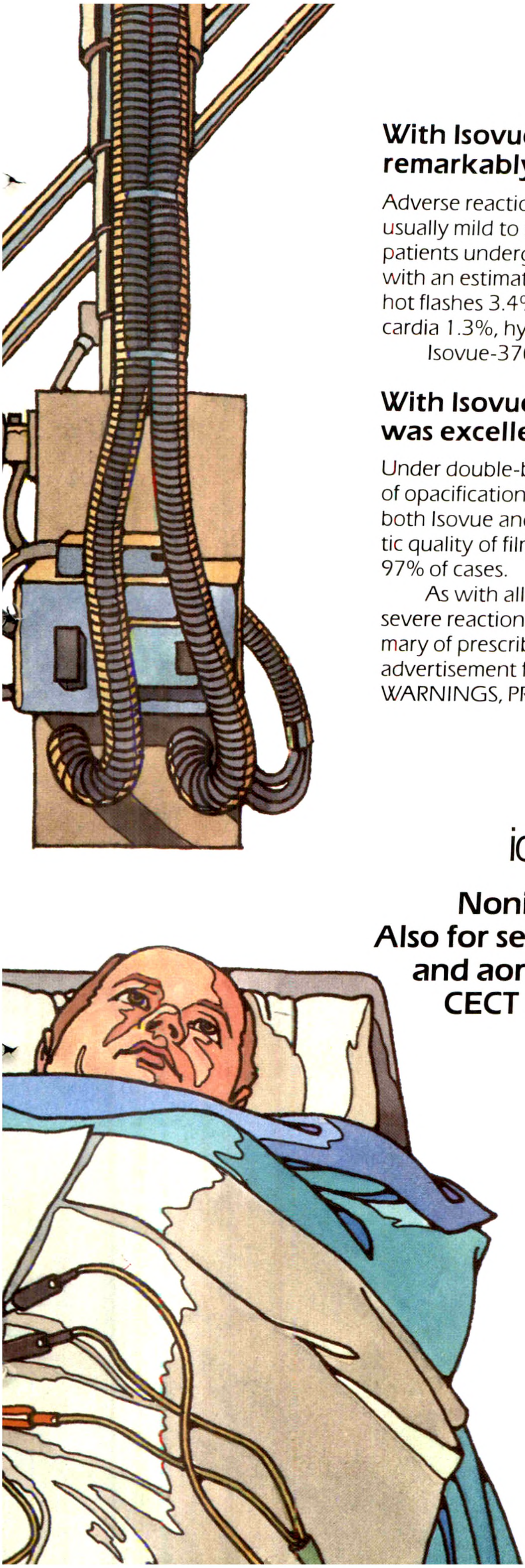

With Isovue, angiocardiography was remarkably well tolerated

Adverse reactions following the use of Isovue-370 are usually mild to moderate, self-limited, and transient. In 597 patients undergoing angiocardiography, adverse reactions with an estimated incidence of one percent or higher were: hot flashes 3.4%, angina pectoris 3.0%, flushing 1.8%, bradycardia 1.3%, hypotension 1.0%, hives 1.0%.

Isovue-370 is low in osmolality — 796 mOsm/kg water.

With Isovue, the technical quality of films was excellent

Under double-blind conditions, radiologists rated the quality of opacification as superior, adequate, faint, or none. For both Isovue and the ionic comparison drug, overall diagnostic quality of films was rated adequate or superior in 97% of cases.

As with all injectable contrast agents, the possibility of severe reactions should be borne in mind. (See brief summary of prescribing information on the last pages of this advertisement for a discussion of CONTRAINDICATIONS, WARNINGS, PRECAUTIONS, and ADVERSE REACTIONS.)

ISOVUE®
iopamidol injection

Nonionic. Low in osmolality.
Also for selective visceral arteriography
and aortography, and intravenous
CECT head and body imaging.

SQUIBB™
Diagnostics

For brief summary of prescribing information, see last pages of this advertisement.

ISOVUE®-300
Iopamidol Injection 61%
ISOVUE®-370
Iopamidol Injection 76%
ISOVUE-M® 200
Iopamidol Injection 41%
ISOVUE-M® 300
Iopamidol Injection 61%

DESCRIPTION—ISOVUE and ISOVUE-M (iopamidol injection) are nonionic radiopaque contrast media for diagnostic use. The formulations are stable, aqueous, sterile, and nonpyrogenic solutions for intravascular and intrathecal administration, respectively. Each mL of ISOVUE-300 (iopamidol injection 61%) provides 612 mg iopamidol with 1 mg tromethamine and 0.39 mg edetate calcium disodium. The solution contains approximately 0.037 mg (0.002 mEq) sodium and 300 mg organically bound iodine per mL. Each mL of ISOVUE-370 (iopamidol injection 76%) provides 755 mg iopamidol with 1 mg tromethamine and 0.48 mg edetate calcium disodium. The solution contains approximately 0.046 mg (0.002 mEq) sodium and 370 mg organically bound iodine per mL. Each mL of ISOVUE-M 200 (iopamidol injection 41%) provides 408 mg iopamidol with 1 mg tromethamine and 0.26 mg edetate calcium disodium. The solution contains approximately 0.025 mg (0.001 mEq) sodium and 200 mg organically bound iodine per mL. Each mL of ISOVUE-M 300 (iopamidol injection 61%) provides 612 mg iopamidol with 1 mg tromethamine and 0.39 mg edetate calcium disodium. The solution contains approximately 0.037 mg (0.002 mEq) sodium and 300 mg organically bound iodine per mL. The pH of each solution has been adjusted to 6.5 to 7.5 with hydrochloric acid.

CONTRAINDICATIONS: ISOVUE (iopamidol injection)—None.

ISOVUE-M (iopamidol injection)—Intrathecal administration of corticosteroids with iopamidol is contraindicated. Because of overdosage considerations, immediate repeat myelography in the event of technical failure is contraindicated (see interval recommendation under DOSAGE AND ADMINISTRATION in the product package insert). Myelography should not be performed in the presence of significant local or systemic infection where bacteremia is likely.

WARNINGS: ISOVUE (iopamidol injection)—Use caution in patients with severely impaired renal function, combined renal and hepatic disease, or anuria, particularly when larger doses are administered. Radiopaque diagnostic contrast agents are potentially hazardous in patients with multiple myeloma or other paraproteinemia, particularly in those with therapeutically resistant anuria. It has been speculated that the combination of the contrast agent and dehydration may be causative of anuria in myelomatous patients. This risk is not a contraindication; however, special precautions are required. Contrast media may promote sickling in individuals who are homozygous for sickle cell disease when injected intravenously or intraarterially. Administration to patients known or suspected of having pheochromocytoma should be performed with extreme caution. If the possible benefits outweigh the considered risks, the procedures may be performed; however, the amount of the medium injected should be kept to an absolute minimum. Assess blood pressure throughout the procedure and measures for treatment of a hypertensive crisis should be available. Monitor such patients very closely. Use caution in patients with hyperthyroidism or with an autonomously functioning thyroid nodule because of risk of thyroid storm.

ISOVUE-M (iopamidol injection)—Carefully evaluate the need for myelographic examination. Administer with caution in patients with increased intracranial pressure or suspicion of intracranial tumor, abscess or hematoma, those with a history of convulsive disorder, severe cardiovascular disease, chronic alcoholism, or multiple sclerosis, and elderly patients. Particular attention must be given to state of hydration, concentration of medium, dose, and technique used in these patients. If frankly bloody cerebrospinal fluid is observed, the possible benefits of the examination should be considered in terms of risk to the patient. Patients on anticonvulsant medication should be maintained on this therapy. Direct intracisternal or ventricular administration for standard radiography (without computerized tomographic enhancement) is not recommended. Inadvertent intracranial entry of a large or concentrated bolus of agent, which increases the risk of neurotoxicity, can be prevented by careful patient management. Avoid rapid dispersion of the medium causing inadvertent rise to intracranial levels. if such entry of the medium occurs, prophylactic anticonvulsant treatment with diazepam or barbiturates orally for 24 to 48 hours should be considered. Use of medications that may lower the seizure threshold should be carefully evaluated. While the contributory role of such medications has not been established, these agents are often discontinued at least 48 hours before and for at least 24 hours following intrathecal use. Motor seizures have been reported after intrathecal use, however higher than recommended doses were employed. Therefore *avoid:* deviations from recommended neuroradiologic procedure or patient management; use in patients with a history of epilepsy; overdosage; intracranial entry of a bolus or premature diffusion of a high concentration of the medium; failure to maintain head elevation during procedure, on stretcher, and in bed; excessive and active patient movement or staining.

PRECAUTIONS: General—Diagnostic procedures should be carried out under the direction of personnel with the prerequisite training and a thorough knowledge of the particular procedure to be performed. Appropriate facilities should be available for coping with any complications for emergency treatment of severe reaction to the agent itself. After parenteral administration, competent personnel and emergency facilities should be available for at least 30 to 60 minutes since severe delayed reactions may occur. Preparatory dehydration is dangerous and may contribute to acute renal failure in susceptible patients. *Patients should be well hydrated prior to and following administration.* Reactions to the medium, including serious, life-threatening, fatal, anaphylactoid or cardiovascular reactions, should always be considered (see ADVERSE REACTIONS in the product package insert). Patients at increased risk include those with a history of a previous reaction to a contrast medium, a known sensitivity to iodine per se, and those with a known clinical hypersensitivity (bronchial asthma, hay fever, and food allergies). Pretesting cannot be relied upon to predict severe reactions and may itself be hazardous for the patient. A thorough medical history with emphasis on allergy and hypersensitivity prior to the injection of any contrast medium may be more predictive and accurate than pretesting. Premedication with antihistamines or corticosteroids to avoid or minimize possible allergic reactions in such patients should be considered (see CONTRAINDICATIONS). If nondisposable equipment is used, scrupulous care should be taken to prevent residual contamination.

ISOVUE (iopamidol injection)—General anesthesia may be indicated in some procedures in selected patients; however, a higher incidence of adverse reactions has been reported in anesthetized patients, which may be attributable to the inability of the patient to identify untoward symptoms, or to the hypotensive effect of anesthesia which can reduce cardiac output and increase the duration of exposure to the agent. Even though the osmolality is low compared to diatrizoate or iothalamate based ionic agents of comparable iodine concentration, the potential transitory increase in the circulatory osmotic load in patients with congestive heart failure requires caution during injection. Observe these patients for several hours following the procedure. In angiographic procedures, be aware of the possibility of dislodging plaques or damaging or perforating the vessel wall during catheter manipulations and contrast medium injection. Test injections to ensure proper catheter placement are suggested. Perform *selective coronary arteriography* only in those in whom the expected benefits outweigh the procedural risk. The inherent risks of *angiocardiography* in patients with chronic pulmonary emphysema must be weighed against the necessity for performing this procedure. *Angiography* should be avoided whenever possible in patients with homocystinuria, because of the risk of inducing thrombosis and embolism.

Drug Interactions: General—Other drugs should not be admixed with iopamidol (see CONTRAINDICATIONS, and DOSAGE AND ADMINISTRATION, Drug Incompatibilities).

ISOVUE (iopamidol injection)—Renal toxicity has been reported in a few patients with liver dysfunction who were given oral cholecystographic agents followed by intravascular contrast agents. Administration of intravascular agents should therefore be postponed in any patient with a known or suspected hepatic or biliary disorder who has recently received a cholecystographic contrast agent.

Drug/Laboratory Test Interactions—PBI and radioactive iodine uptake studies will not accurately reflect thyroid function for up to 16 days following administration, however T3 resin uptake and total or free thyroxine (T4) assays are not affected.

Carcinogenesis, Mutagenesis, Impairment of Fertility—In animal reproduction studies performed on rats, intravenously administered iopamidol did not induce adverse effects on fertility or general reproductive performance. In studies to determine mutagenic activity, iopamidol did not cause any increase in mutation rates.

Pregnancy Category B—No teratogenic effects attributable to iopamidol have been observed in teratology studies performed in animals. There are, however, no adequate and well controlled studies in pregnant women. It is not known whether iopamidol crosses the placental barrier or reaches fetal tissues. Because animal studies are not always predictive of human response, this drug should be used during pregnancy only if clearly needed. Radiologic procedures involve a certain risk related to the exposure of the fetus to ionizing radiation.

Labor and Delivery: ISOVUE (iopamidol injection)—It is not known whether use during labor or delivery has immediate or delayed adverse effects on the labor, the delivery or the newborn.

Nursing Mothers—It is not known whether iopamidol is excreted in human milk. Use caution when contrast media are administered to nursing women because of potential adverse reactions; consideration should be given to temporarily discontinuing nursing.

Pediatric Use—Safety and effectiveness in children have not been established.

ADVERSE REACTIONS: ISOVUE (iopamidol injection)—Usually mild to moderate, self-limited and transient. In angiocardiography (597 patients), the adverse reactions with an estimated incidence of one percent or higher are: hot flashes 3.4%; angina pectoris 3.0%; flushing 1.8%; bradycardia 1.3%; hypotension 1.0%; hives 1.0%. Intravascular injection is frequently associated with the sensation of warmth and pain, especially in peripheral arteriography; pain and warmth are less frequent and less severe with ISOVUE than with diatrizoate meglumine and diatrizoate sodium injection. The following table of incidence of reactions is based on clinical studies with ISOVUE in about 1760 patients:

Adverse Reactions

	Estimated Overall Incidence	
System	>1%	≤1%
Cardiovascular	none	tachycardia hypotension hypertension myocardial ischemia circulatory collapse S-T segment depression bigeminy extrasystoles ventricular fibrillation angina pectoris bradycardia transient ischemic attack thrombophlebitis

Adverse Reactions (continued from previous page)

System	Estimated Overall Incidence	
	>1%	≤1%
Nervous	pain (2.2%) burning sensation (1.4%)	vasovagal reaction tingling in arms grimace faintness
Digestive	nausea (1.2%)	vomiting anorexia
Respiratory	none	throat constriction dyspnea pulmonary edema
Skin and Appendages	none	rash urticaria pruritus flushing
Body as a Whole	hot flashes (1.5%)	headache fever chills excessive sweating back spasm
Special Senses	none	taste alterations warmth in throat/ arms/chest nasal congestion visual disturbances
Urogenital	none	urinary retention

Regardless of the agent employed, overall estimated incidence of serious adverse reactions is higher with *coronary arteriography* than with other procedures. Cardiac decompensation, serious arrhythmias, or myocardial ischemia or infarction may occur during *coronary arteriography and left ventriculography.* Following coronary and ventricular injections, certain electrocardiographic changes (increased QTc, increased R-R, T-wave amplitude) and certain hemodynamic changes (decreased systolic pressure) occurred less frequently with ISOVUE (iopamidol injection) than with diatrizoate meglumine and diatrizoate sodium injection; increased LVEDP occurred less frequently after ventricular iopamidol injections. In *aortography,* the risks of procedures also include injury to the aorta and neighboring organs, pleural puncture, renal damage including infarction and acute tubular necrosis with oliguria and anuria, accidental selective filling of the right renal artery during the translumbar procedure in the presence of preexisting renal disease, retroperitoneal hemorrhage from the translumbar approach, and spinal cord injury and pathology associated with the syndrome of transverse myelitis. Adverse effects reported in literature include arrhythmia, arterial spasms, hematuria, periorbital edema, involuntary leg movement, malaise, and triggering of deglutition; some of these may be procedural. Other reactions due to procedural hazards include hemorrhage or pseudoaneurysms at the puncture site, brachial plexus palsy following axillary artery injections, chest pain, myocardial infarction, and transient changes in hepatorenal chemistry tests; and rarely arterial thrombosis, displacement of arterial plaques, venous thrombosis, dissection of the coronary vessels and transient sinus arrest.

ISOVUE-M (iopamidol injection)—The most frequently reported following intrathecal administration are headache, nausea, vomiting, usually mild to moderate, and musculoskeletal pain. These usually occur 1 to 10 hours after injection, almost all occurring and ending within 24 hours. Backache, neck stiffness, numbness and paresthesias, leg or sciatic-type pain occurred less frequently. Transient alterations in vital signs may occur and should be assessed on an individual basis. The following table of incidence of reactions is based on clinical studies with ISOVUE-M in about 615 patients:

Adverse Reactions

System	Estimated Overall Incidence	
	>1%	≤1%
Body as a Whole	headache (18.1%)	pyrexia muscle weakness hot flashes malaise fatigue weakness
Digestive	nausea (7.3%) vomiting (3.7%)	diarrhea heartburn
Musculoskeletal	back pain (2.3%) leg pain (1.4%) neck pain (1.1%)	leg cramps sciatica cervicobrachial irritation meningeal irritation radicular irritation, lumbosacral other musculoskeletal pain involuntary movement burning sensation
Cardiovascular	hypotension (1.1%)	tachycardia hypertension chest pain
Nervous	none	emotional stress dizziness paresthesia confusion hallucinations lightheadedness syncope numbness cold extremities
Urogenital	none	urinary retention
Respiratory	none	dyspnea
Skin and Appendages	none	rash
Miscellaneous	none	injection site pain

(continued on next column)

Other adverse effects reported in literature include major motor seizures, facial neuralgia, tinnitus, and sweating. Transitory EEG changes occur and usually take the form of slow wave activity. The following adverse reactions may occur because they have been reported with other nonionic contrast agents: cardiovascular (arrhythmias); aseptic meningitis syndrome; allergy or idiosyncrasy (chills, pruritus, nasal congestion, Guillain-Barre syndrome); CNS irritation (psycho-organic syndrome: mild and transitory perceptual aberrations such as depersonalization, anxiety, depression, hyperesthesia, disturbances in speech, sight, or hearing, and disorientation; in addition, hyperreflexia or areflexia, hypertonia or flaccidity, restlessness, tremor, echoacousia, echolalia, asterixis or dysphasia have occurred). Profound mental disturbances have rarely been reported (various forms and degrees of aphasia, mental confusion or disorientation); the onset is usually 8 to 10 hours and lasts for about 24 hours without aftereffects. However, occasionally they have been manifest as apprehension, agitation, or progressive withdrawal to the point of stupor, rarely accompanied by transitory hearing loss or other auditory symptoms and visual disturbances. Also reported: persistent cortical loss of vision in association with convulsions, and ventricular block, transitory weakness in the leg or ocular muscles, *peripheral neuropathies,* including sensory and/or motor or nerve root disturbances, myelitis, persistent leg muscle pain or weakness, or sixth nerve palsy, or cauda equina syndrome, muscle cramps, fasciculation or myoclonia, spinal convulsion, or spasticity.

General Adverse Reactions To Contrast Media—Reactions known to occur (mostly mild—moderate in degree) with parenteral administration of iodinated ionic contrast agents (see the listing below) are possible with any nonionic agent. Life-threatening reactions and fatalities, mostly of cardiovascular origin, have occurred. Reported incidences of death from administration of other iodinated contrast media range from 6.6 per 1 million (0.00066%) to 1 in 10,000 patients (0.01%). Foreign experience in approximately 2.4 million patients receiving iopamidol suggest a lower risk of mortality. Most deaths occur during injection or 5 to 10 minutes later, the main feature being cardiac arrest with cardiovascular disease as the main aggravating factor with isolated reports of hypotensive collapse and shock (est. 0.005%). Experience with iopamidol suggests less discomfort (e.g., pain and/or warmth) with peripheral arteriography. Fever changes are noted in ventricular function after ventriculography and coronary arteriography. During intrathecal use, there is a lower incidence of electroencephalographic changes as well as neurotoxicity by virtue of the intrinsic properties of the iopamidol molecule. The reported incidence of adverse reactions to contrast media in patients with a history of allergy is twice that for the general population; patients with a history of previous reactions to a contrast medium are three times more susceptible. Although most reactions to intravascular contrast agents appear within 1-3 minutes after start of injection, delayed reactions may occur (see PRECAUTIONS, General). Adverse reactions reported with other intravascular contrast agents and therefore theoretically possible with iopamidol include: *Cardiovascular:* vasodilation, cerebral hematomas, petechiae, hemodynamic disturbances, sinus bradycardia, transient electrocardiographic abnormalities, ventricular fibrillation; *Nervous:* paresthesia, dizziness, convulsions, paralysis, coma; *Digestive:* nausea, vomiting, severe unilateral or bilateral swelling of the parotid and subparotid glands; *Respiratory:* increased cough, asthma, laryngeal edema, pulmonary edema, bronchospasm, rhinitis; *Skin and Appendages:* injection site pain usually due to extravasation and/or erythematous swelling, skin necrosis, urticaria; *Urogenital:* osmotic nephrosis of proximal tubular cells, renal failure, pain; *Special Senses:* bilateral ocular irritation; lacrimation; conjunctival chemosis, infection, and conjunctivitis, perversion of taste; *Other:* neutropenia, thrombophlebitis, flushing, pallor, weakness, severe retching and choking, wheezing, cramps, tremors, and sneezing.

OVERDOSAGE—Treatment is directed toward the support of all vital functions, and prompt institution of symptomatic therapy. In myelography, even use of a recommended dose can produce mental aberrations tantamount to overdosage, if incorrect management of the patient during or immediately following the procedure permits inadvertent early intracranial entry of a large portion of the medium. Treatment is directed toward the support of all vital functions, and prompt institution of symptomatic therapy.

HOW SUPPLIED—ISOVUE-300 (iopamidol injection 61%) and ISOVUE-370 (iopamidol injection 76%) are available in cartons of ten single dose vials, and ten 100 mL single dose vials. ISOVUE-370 is also available in cartons of ten 200 mL single dose vials. ISOVUE-M 200 (iopamidol injection 41%) and ISOVUE-M 300 (iopamidol injection 61%) are available in cartons of ten 20 mL single dose vials.

For full prescribing information consult package insert. (J3-652B/653B)

Under license from Bracco Industria Chimica S.p.A. U.S. Patent #4,001,323

© 1986 E.R. Squibb & Sons, Inc., Princeton, NJ 08540 645-503 Issued: February 1986

Efficient bowel evacuants for diagnostic procedures

Take one
X-Prep®
for a cleaner, clearer film

Excellent visualization...fewer retakes

- 95% efficacy proven with X-PREP® Liquid in 749 patients prepared for diagnostic procedures such as barium enemas and IVPs*
- Effective for colonoscopy and sigmoidoscopy*

X-PREP® Liquid
2½ fl. oz. (74 ml) (standardized extract of senna fruit)

*Data on file, Medical Department, The Purdue Frederick Company.

Gray Pharmaceutical Co., Affiliate
The Purdue Frederick Company
Norwalk, CT 06856

X-PREP® Bowel Evacuant Kit-1
Contains two SENOKOT-S® Tablets (standardized senna concentrate and docusate sodium), one bottle of X-PREP Liquid 2½ fl. oz. (74 ml), one RECTOLAX® Suppository (bisacodyl 10 mg), plus easy-to-follow instructions.

X-PREP® Bowel Evacuant Kit-2
Contains one pack CITRALAX® Granules 1.06 oz. (effervescent citrate/sulfate of magnesia), one bottle of X-PREP Liquid 2½ fl. oz. (74 ml), one RECTOLAX Suppository, plus easy-to-follow instructions.

X-Prep Bowel Evacuant Kit-2
2
X-Prep Bowel Evacuant Kit-2
with
CITRALAX™ Granules and
RECTOLAX® Suppository
X-Prep Bowel Evacuant Kit-1
X-Prep Bowel Evacuant Kit-1
X-Prep
LIQUID

© 1984, Gray Pharmaceutical Co. PFR-081/84

Periventricular Hyperintensity as Seen by Magnetic Resonance:

Prevalence and Significance

Robert D. Zimmerman[1]
Cynthia A. Fleming
Benjamin C. P. Lee
Leslie A Saint-Louis
Michael D. F. Deck

Periventricular hyperintensity was identified using long repetition and echo times in spin-echo magnetic resonance imaging of patients with white-matter disease (e.g., multiple sclerosis) caused by local demyelination and in hydrocephalic patients caused by transependymal migration of spinal fluid. A review of 365 consecutives studies revealed that some degree of periventricular hyperintensity is present in most patients (93.5%) regardless of diagnosis. Mild periventricular hyperintensity was seen in patients with no other evidence of intracranial pathology. Periventricular hyperintensity is a normal finding that should not be considered indicative of either demyelinating disease or hydrocephalus. More extensive and severe periventricular hyperintensity is associated with intracerebral pathology, but the finding often is nonspecific. For example, mild periventricular edema from hydrocephalus is impossible to differentiate from the increased periventricular hyperintensity seen in patients with multiple white-matter lesions. Thus, the pattern of periventricular hyperintensity has proven to be of limited value in the clinical assessment of hydrocephalic patients.

One of the earliest and most impressive clinical applications of magnetic resonance imaging (MRI) has been in the evaluation of patients with multiple sclerosis [1–8] and other white-matter diseases [5] including subcortical atherosclerotic encephalopathy [5, 9], radiation necrosis [7], and systemic lupus erythematosus [10]. In these diseases focal and/or diffuse areas of supratentorial white-matter hyperintensity are commonly imaged adjacent to the ventricular lining. In patients with obstructive hydrocephalus MRI scans have demonstrated a smooth, hyperintense halo surrounding the ventricles believed to be indicative of edema from transependymal resorption of cerebrospinal fluid [2, 6, 7, 11]. Because focal and/or diffuse periventricular hyperintensity (PVH) seemed to be present in many patients with a variety of pathologic processes, and even in patients with otherwise normal examinations, a retrospective evaluation of the incidence and possible significance of PVH was undertaken.

Materials and Methods

We retrospectively evaluated MRI studies performed between October 1983 and April 1984 on a 0.5 T superconducting MR imager manufactured by the Technicare Corp. To be included in the study a transversely oriented spin-echo (SE) image with a repetition time (TR) of 1500 msec and echo time (TE) of 90 msec ("T2-weighted") of adequate quality had to be available for review. With this technique intraventricular spinal fluid was approximately isointense to white matter. All scans were obtained with a single-echo multislice technique. Clinical data were correlated with MR findings. A total of 365 cases were evaluated. The patients were 6–84 years of age (mean age, 42). Of the 365 cases, 17 were ≤ 10 years old, 27 were 11–20, 61 were 21–30, 72 were 31–40, 60 were 41–50, 65 were 51–60, 38 were 61–70, and 25 were ≥ 71. The gender distribution was roughly equal.

Five PVH patterns of increasing extent and intensity were delineated: (0) no PVH (fig. 1); (1) discontinuous PVH—rounded hyperintense foci seen at the angles of the frontal horns

This article appears in the January/February 1986 issue of *AJNR* and the March 1986 issue of *AJR*.

Received February 22, 1985; accepted after revision July 30, 1985.

Presented at the annual meeting of the American Society of Neuroradiology, Boston June 1984.

[1] All authors: Department of Radiology, Cornell University Medical College, New York Hospital, 525 E. 68th St., New York, NY 10021. Address reprint requests to R. D. Zimmerman.

***AJR* 146:443-450, March 1986**
0361-803X/86/1463-0443
© American Roentgen Ray Society

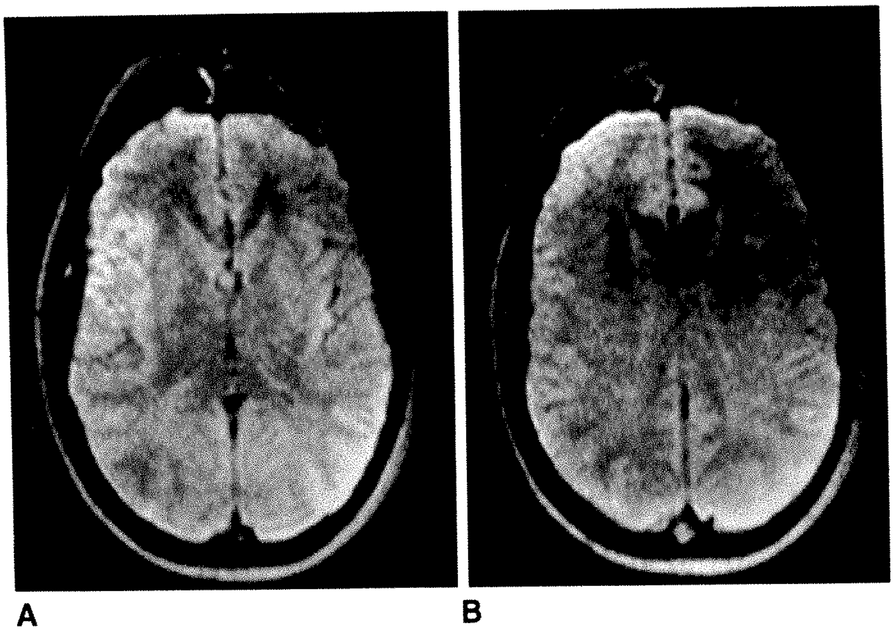

Fig. 1.—Pattern 0 in 17-year-old boy with history of seizures and negative CT scan. Scans to level of foramen of Monro (**A**) and bodies of lateral ventricles (**B**) show no PVH.

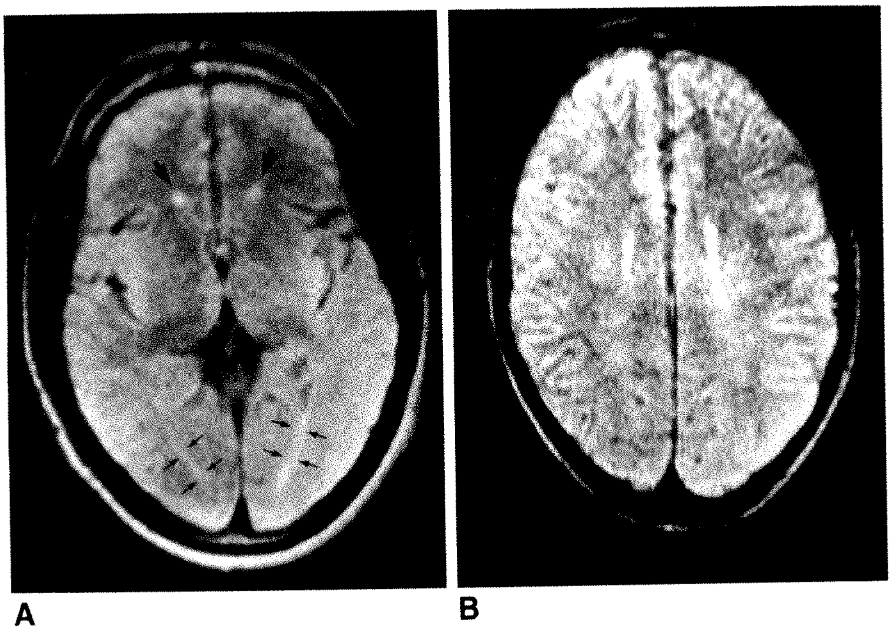

Fig. 2.—Pattern 1 in 32-year-old woman studied to rule out demyelinating disease. **A**, Level of foramen of Monro. Bilateral, symmetric, rounded foci of hyperintensity just anterior to frontal horns (*large arrows*). Thin caps of hyperintensity surround small occipital horns (*small arrows*). **B**, At level of body of lateral ventricles. Streaks of hyperintensity just lateral to atria.

bilaterally (fig. 2A), caps of hyperintensity surrounding the occipital horns medially and laterally (fig. 2A), and streaks of hyperintensity extending along the atria of the lateral ventricles (fig. 2B); (2) continuous PVH—a pencil-thin continuous line of hyperintensity surrounding the ventricles (fig. 3); (3) periventricular halo—a band of hyperintensity of variable thickness with smooth lateral margins surrounding the ventricles (fig. 4) (this pattern has been described as indicative of periventricular edema from hydrocephalus [2, 6, 7, 11]; and (4) diffuse white-matter abnormality—hyperintensity extending from the ventricular lining to the corticomedullary junction involving all or most of the white matter, the lateral margins of the hyperintensity being irregular (fig. 5). This pattern has been described in patients with diffuse demyelinating disease [1, 5, 8]. The studies were also evaluated for the presence and number of focal areas of white-matter hyperintensity independent of the PVH.

The MRI patterns were tabulated (table 1) and correlated with clinical data including CT scans when available. The studies were divided into those cases demonstrating no other evidence of abnormality on MRI ("otherwise normal group"—table 2, fig. 6A). And those cases in which pathology was present ("pathology group"— table 3, fig. 6B). The otherwise normal group was divided into patients under and over 30 years of age, and the pathologic cases were grouped into four broad diagnostic categories: (1) trauma, (2) supratentorial tumors, (3) white-matter diseases, and (4) hydrocephalus.

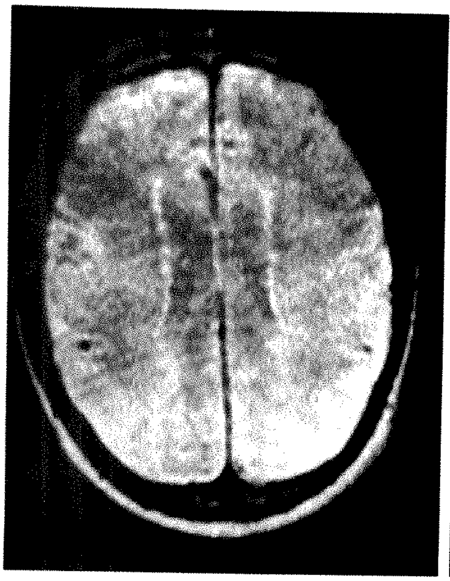

3

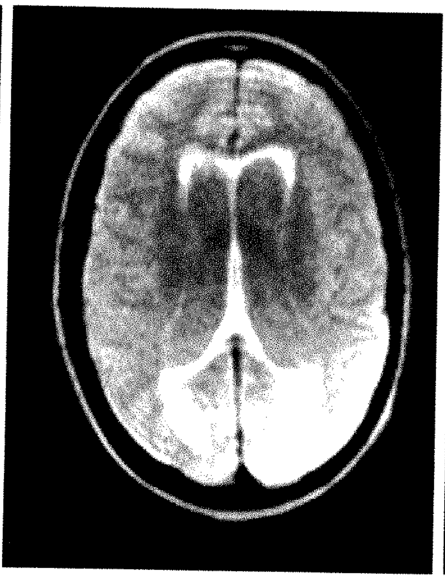

4

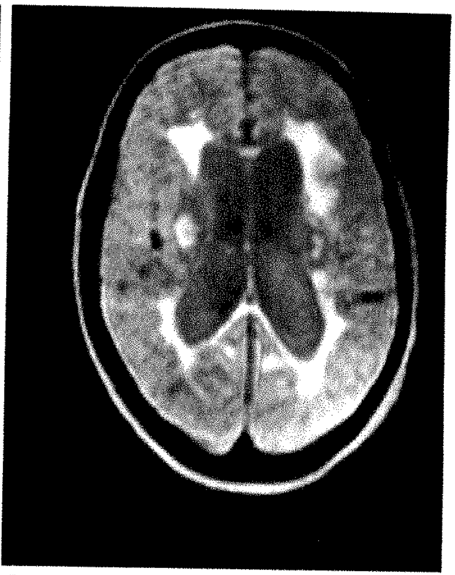

5

Fig. 3.—Pattern 2 in 57-year-old man with seizures and/or transient ischemic attacks. Diffuse continuous pencil-thin line of hyperintensity surrounds ventricles.

Fig. 4.—Pattern 3 in 37-year-old woman with obstructive hydrocephalus secondary to pineal region tumor. Smooth halo of hyperintensity surrounds bodies of lateral ventricles. Findings reflect increase in periventricular water (edema) secondary to transependymal resorption of spinal fluid.

Fig. 5.—Pattern 4 in 47-year-old woman with long-standing history of multiple sclerosis. Diffuse periventricular hyperintensity with irregular lateral margins. In many areas hyperintensity extends to corticomedullary junction.

Results

PVH was seen in 93.4% of patients regardless of age, gender, clinical diagnosis, or other MRI findings (table 1). The PVH patterns most often encountered were 1 (43.3%) and 2 (29.9%). When the patients were divided into those with otherwise normal examinations and those with other evidence of pathology, several trends were noted both between the groups and within each group.

In patients with otherwise normal examinations (table 2, fig. 6A), patterns 0–2 (figs. 1–3) were encountered and pattern 1 (fig. 2) was seen most often (68.3% of cases). Within this group there was a definite increase in PVH with increasing age. Two-thirds of the patients in each subgroup had pattern 1, but in older patients (over 30 years of age), pattern 2 was twice as common as in younger patients (23.9% vs. 12.2%). Conversely, in younger patients (under 30 years of age), there was a higher incidence of pattern 0 (18.2% vs. 9.5%).

There was also a dramatic increase in PVH in patients with other evidence of pathology (table 3, fig. 6B). Thus, patterns 0 and 1 were seen in only 31% of these patients as opposed to 81% of the otherwise normal group. Patterns 3 and 4 were always associated with pathology, while patterns 0 and 1 were more typically seen in patients whose studies were otherwise normal. Pattern 2 was a nonspecific pattern frequently encountered in all groups.

Evaluation of the patients with other evidence of pathology revealed several findings. Patients with trauma (fig. 7) and supratentorial tumors had a greater degree of PVH than did patients with otherwise normal examinations. Fifty percent of trauma patients and 62.7% of supratentorial tumor patients had patterns 2–4 as compared with 19% of the otherwise normal group.

PVH was even more extensive in patients with white-matter diseases (fig. 8). Of these patients, 80% had patterns 2–4. When only several lesions were present, pattern 2 was usually encountered, and, as the number of lesions increased, so did the PVH, which became broader and more intense (pattern 3). When many lesions were present, these foci coalesced with each other and the PVH to produce an appearance that was intermediate between patterns 3 and 4 (fig. 8). In pattern 4 the white matter was diffusely hyperintense and there was no separation of the periventricular region from the rest of the white matter. This pattern was encountered in two patients with radiation change (diffuse necrotizing leukoencephalopathy) (fig. 9) and in several patients with long-standing multiple sclerosis (fig. 5).

The patients with hydrocephalus had the greatest degree of PVH (90.5% had patterns 2–4) (table 4). MRI was more sensitive than CT in detecting periventricular abnormalities in these cases. None of the patients with pattern 2 PVH on MRI had periventricular hypodensity on CT. Of 37 patients with patterns 3 and 4 PVH, 28 also had periventricular hypodensity on CT, but in all cases the degree of PVH on MRI was more extensive than the periventricular lucency on CT (fig. 10). Nine patients had pattern 3 PVH on MRI and no periventricular hypodensity on CT (fig. 11). PVH was more extensive in those patients with CT evidence of periventricular hypodensity than in those patients with no periventricular abnormalities on CT. The extent of the PVH was related to the severity and duration

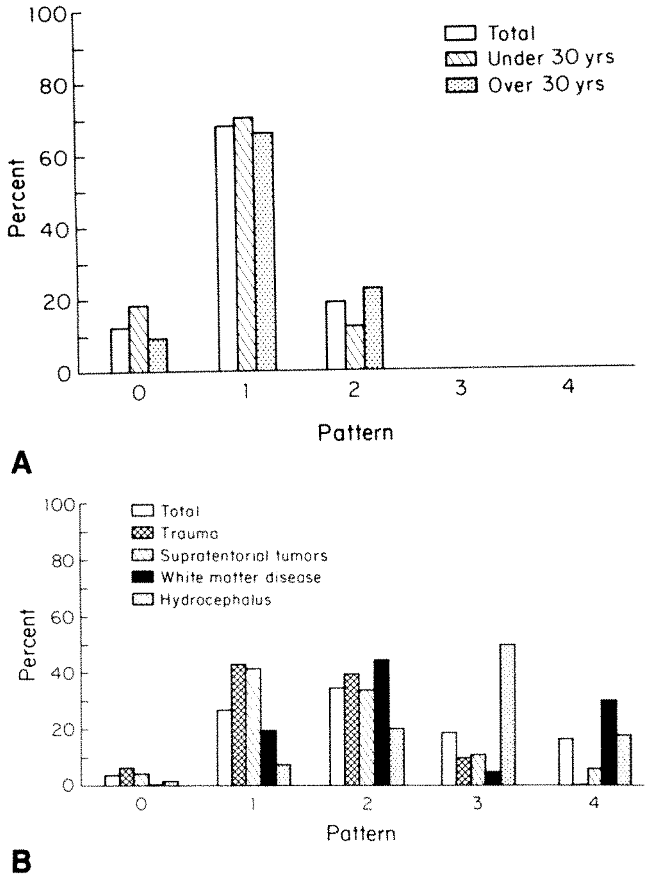

Fig. 6.—Incidence of PVH patterns. **A**, Otherwise normal group. All patients fall into patterns 0–2. Pattern 1 is most common. Pattern 2 is second most common in patients over 30 years of age, while pattern 0 is second most common pattern in patients under 30 years of age. **B**, In Patients with other evidence of pathology, all five patterns are present. Pattern 2 is seen in all groups. Pattern 3 is most typically seen in patients with hydrocephalus. Also, some hydrocephalic patients had patterns 2 and 4. Pattern 4 is commonly seen in patients with demyelinating disease.

TABLE 1: **Distribution of Patients by Pattern of Periventricular Hyperintensity**

Pattern	No. of Cases	(%)
0	24	(6.6)
1	158	(43.3)
2	109	(29.9)
3	41	(11.2)
4	33	(9.0)
Total	365	(100.0)

TABLE 2: **Patterns of Periventricular Hyperintensity in Otherwise Normal Examinations**

Pattern	No. (%)		
	Total	<30 Years	>30 Years
0	13 (12.5)	7 (17.2)	6 (9.5)
1	71 (68.5)	29 (70.6)	42 (66.5)
2	20 (19.0)	5 (12.2)	15 (23.9)
Total	104	41	63

Note.—There were no instances of pattern 3 or 4 in otherwise normal examinations.

of the hydrocephalus (table 4). It was most extensive in patients with obstructive hydrocephalus secondary to mass lesions or basal meningitis. Thirty-one of these 34 patients had pattern 3 or 4 PVH. Two patients with early mild hydrocephalus had pattern 2. Of note was one patient with basal meningitis and 6 months of signs and symptoms of hydrocephalus with progressive ventricular dilatation identified on CT. Only pattern 1 PVH was identified on MRI (fig. 12). Patients with chronic and/or mild hydrocephalus had less severe PVH. Of six patients with normal-pressure hydrocephalus, two had mild, nonspecific PVH (pattern 2). Four had more severe PVH (patterns 3 and 4), but in all cases foci of hyperintensity were present in the white matter. The extent, configuration, and intensity of the PVH in these patients was indistinguishable from that seen in other elderly patients with white-matter infarctions who had no clinical or radiographic evidence of normal-pressure hydrocephalus (cf. figs. 8 and 13). Patients with arrested and adequately shunted hydrocephalus had absent (pattern 0) or mild (pattern 1 or 2) PVH. Two patients with shunt malfunction had more severe PVH (pattern 3).

Discussion

PVH on long TR/long TE (T2-weighted) MRI has been reported in demyelinating diseases [1–10] and hydrocephalus [2, 6, 7, 11]. The hyperintensity is a reflection of a pathologic increase in tissue water resulting in prolongation of T2 relaxation [4–6, 8]. In demyelinating diseases the increased water and its resultant PVH is said to result from destruction of hydrophobic myelin [5] (figs. 5, 8, and 9), while in hydrocephalus periventricular edema from transependymal resorption of spinal fluid produces a halo of hyperintensity [7] (figs. 4 and 11). Our review of a large series of unselected cases confirms that PVH is most common and severe in patients with demyelinating disease and hydrocephalus, but the study also documents that some degree of PVH is present in most patients (93.4%) regardless of diagnosis (table 1).

The pathophysiologic mechanisms invoked to explain PVH in patients with demyelinating diseases and hydrocephalus do not explain the PVH seen in normal patients or in patients with abnormalities that do not directly involve the ependyma or adjacent white matter (tables 2 and 3, fig. 6). These phenomena require a physiologic rather than a pathophysiologic explanation for increased water in the periventricular region. The normal flow of interstitial water into the lateral ventricles from the extracellular space [12, 13] can be invoked to explain the higher concentration of water in the periventricular region than in the rest of the white matter. Water, which normally (or pathologically) escapes from the vascular system into the extracellular space, is reabsorbed across the epen-

TABLE 3: **Pathology Groups in Patients with Patterns of Periventricular Hyperintensity**

Pattern	No. (%)				
	Total	Trauma	Supratentorial Neoplasm	White-Matter Disease	Hydrocephalus
0	7 (3.2)	2 (6.7)	4 (5.6)	0	1 (1.9)
1	59 (27.5)	13 (43.3)	30 (41.7)	12 (20.0)	4 (7.5)
2	75 (34.9)	12 (40.0)	25 (34.7)	27 (45.0)	11 (20.8)
3	41 (19.1)	3 (10.0)	8 (11.1)	3 (5.0)	27 (50.9)
4	33 (15.3)	0	5 (6.9)	18 (30.0)	10 (18.9)
Total	215	30	72	60	53

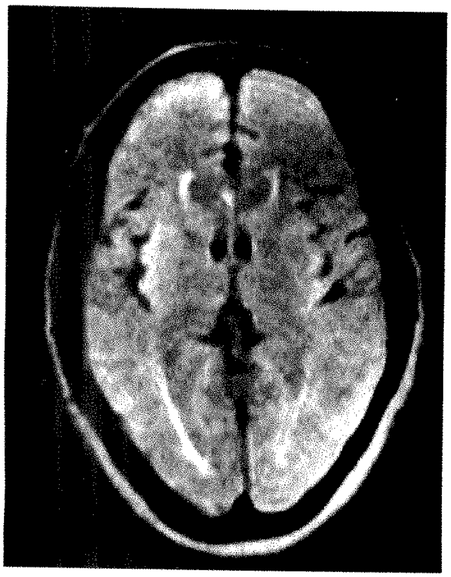

7

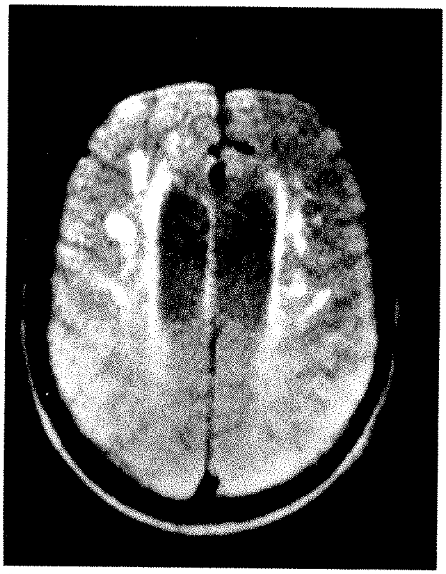

8

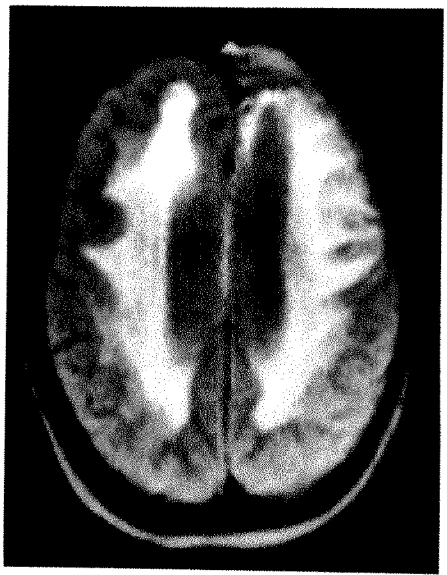

9

Fig. 7.—47-year-old woman with history of head trauma several months after drainage of subdural hematoma. Thin, continuous line of PVH (pattern 2).

Fig. 8.—77-year-old hypertensive patient with dementia. CT scan (not shown) showed atrophy and subtle white-matter hypodensities, considered consistent with infarction. No clinical or CT evidence of hydrocephalus. MR image shows multiple foci of hyperintensity in supratentorial white matter. In addition, halo of PVH around ventricles (pattern 3) is indistinguishable from findings in patients with hydrocephalus. Several of foci in white matter are nearly confluent with each other and with band of PVH. Thus, findings are intermediate between patterns 3 and 4.

Fig. 9.—54-year-old patient with reticulum cell sarcoma treated with radiotherapy about 2 years before. CT scan (not shown) showed no evidence of residual tumor but diffuse hypodensity of supratentorial white matter. MR image shows diffuse, irregular supratentorial white-matter PVH (pattern 4). Discrete periventricular halo of hyperintensity cannot be separated from rest of white-matter hyperintensity. Findings consistent with radiation damage (diffuse necrotizing leukoencephalopathy), but are indistinguishable from those seen in patients with other diffuse demyelinating processes, such as severe multiple sclerosis.

dymal lining into the lateral ventricles [13], accounting for 10%–60% of normal spinal fluid production [14–17]. The PVH seen in normal patients may therefore, be a reflection of the higher concentration of interstitial water at the ventricular lining resulting from concentric bulk flow within the white matter from larger more peripheral sites toward the more confined periventricular region.

If this hypothesis is correct, it would also explain the trends identified in this study. The progressive increase in PVH seen in older patients with otherwise normal examinations might reflect a slight increase in interstitial water caused by vascular damage with leakage of fluid into the extracellular space even when obvious focal abnormalities are not seen. Any pathologic cause of increased interstitial water would produce a secondary increase in PVH as this water flows to the ependymal lining to be reabsorbed into the ventricles. The transependymal resorption of traumatic edema fluid has been documented in animal studies [18, 19], and it is likely that the increased PVH seen in patients with traumatic and neoplastic edema is a reflection of this phenomenon. There is also an increase in interstitial water in patients with demyelinating diseases caused by the destruction of hydrophobic myelin [5] and damage to the blood-brain barrier [20, 21]. Thus, at least some of the PVH in patients with demyelinating diseases may

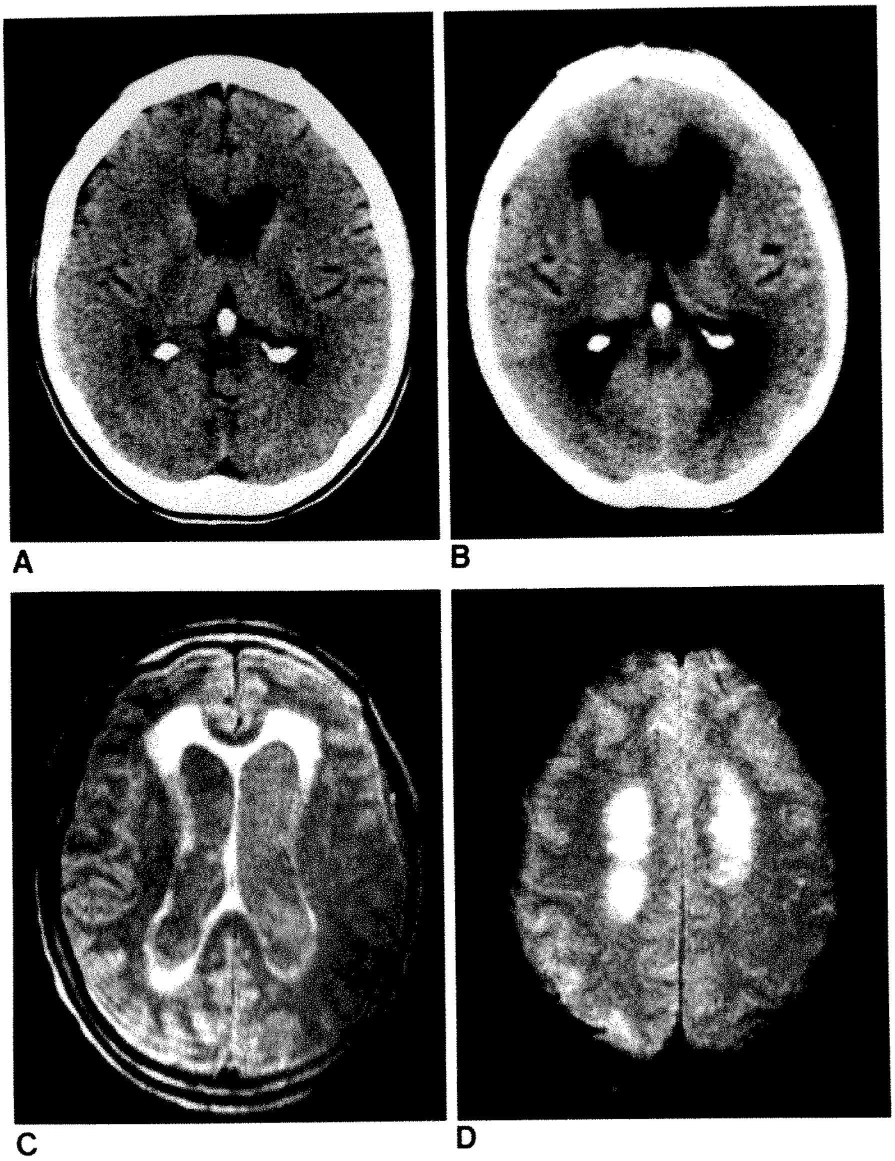

Fig. 10.—61-year-old patient with carcinomatous meningitis and secondary communicating hydrocephalus. **A**, Initial CT scan. Normal-sized ventricles. **B**, Follow-up CT scan 4 months later. Marked ventricular dilatation and bifrontal periventricular hypodensity, classic CT findings of periventricular edema due to transependymal resorption of spinal fluid. **C**, MR image at same time as **B**. Diffuse broad periventricular halo completely surrounds ventricles. Edema in **C** is more extensive than on CT. **D**, Higher level. Superior irregularities in periventricular edema cause superficial resemblance to diffuse demyelination. Irregularities are more lobulated than those seen in diffuse demyelinating disease. In addition, hyperintensity does not extend to corticomedullary junction.

TABLE 4: **Types of Hydrocephalus in Patients with Patterns of Periventricular Hyperintensity**

Pattern	No. of Cases by Type of Hydrocephalus				
	Total	Obstructive	Normal-Pressure	Arrested	Shunted
0	1	0	0	1	0
1	4	1	0	2	1
2	11	2	2	3	4
3	27	22	3	0	2
4	10	9	1	0	0
Total	53	34	6	6	7

be secondary to increased reabsorption of interstitial water rather than a reflection of primary involvement of the periventricular white matter by the demyelinating process itself (fig. 8). This explanation would help explain the observation that as the number of white-matter lesions increased so did the extent of PVH.

In hydrocephalic patients the increased hydrostatic pressure causes a reversal of the direction of transependymal flow. Fluid is forced out of the ventricles into the periventricular white matter. Although the direction of flow is different, the distribution, and, in many cases, the amount of periventricular water is similar in patients with hydrocephalus and in those with increased interstitial water from parenchymal abnormalities; thus, the PVH patterns encountered on MRI in these conditions may be indistinguishable.

Elucidation of the causes (both physiologic and pathophysiologic) of PVH must await experimental verification, but there are several clinical implications of the phenomena observed in this study: (1) Mild PVH (pattern 1 or 2) is normal, and thus rounded hyperintense foci seen adjacent to the frontal horns (fig. 2A) should not be mistaken for areas of demyelination;

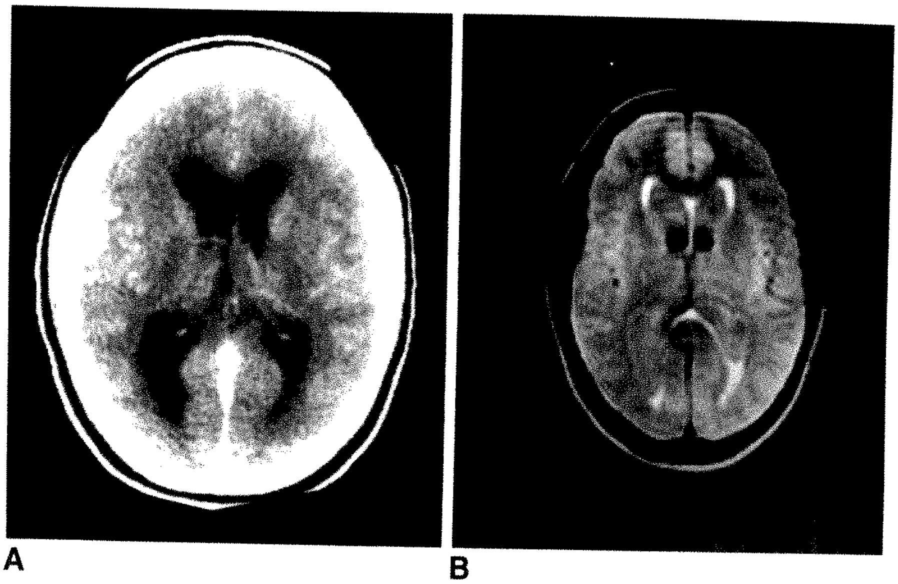

Fig. 11.—42-year-old woman with posterior fossa arachnoid cyst with secondary obstructive hydrocephalus. **A**, CT scan at level of lateral ventricles. Dilated ventricles but no obvious periventricular hypodensity. **B**, MR image at same level. Definite periventricular halo (pattern 3) indicative of edema from transependymal reabsorption of spinal fluid.

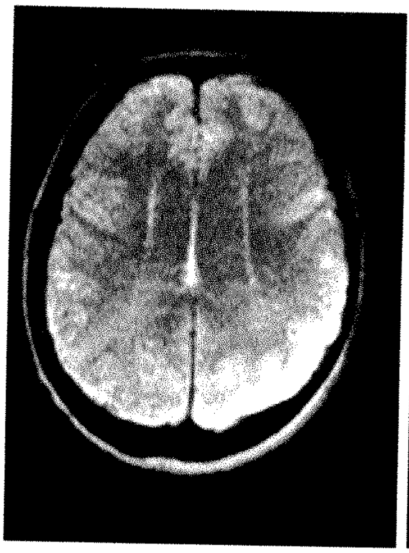

12

Fig. 12.—26-year-old man with communicating hydrocephalus secondary to basal meningitis of about 6 months duration. MR image shows dilated ventricles but only mild discontinuous PVH (pattern 1). Therefore, there is no evidence of transependymal resorption or spinal fluid or edema, despite good clinical evidence of active hydrocephalus.

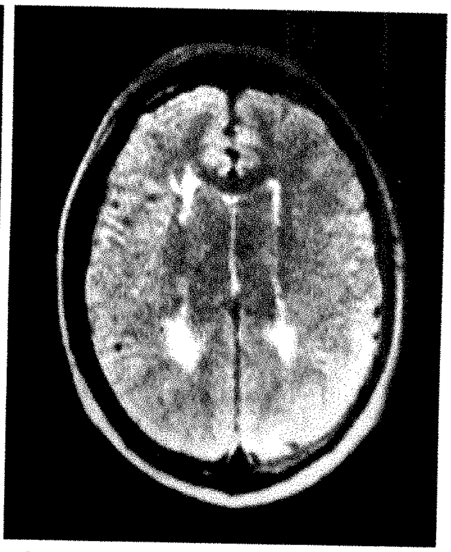

13

Fig. 13.—76-year-old man with progressive dementia and gait disturbances. CT scans (not shown) showed progressive ventricular dilatation over a 2 year period. Clinical and CT findings were consistent with normal-pressure hydrocephalus. Patient responded well to shunting. MR image shows narrow halo of PVH that could represent transependymal resorption of spinal fluid. In addition to halo, there are multiple foci of hyperintensity in white matter confluent with periventricular halo, presumably representing coexistent white-matter infarcts. MRI features in this patient are indistinguishable from those in patient with multiple infarcts alone (cf. fig. 8).

(2) Pattern 2 is nonspecific and may be seen in a wide range of circumstances. Its presence in older patients without other abnormalities may be considered normal (fig. 3), just as atrophy may be normal in elderly patients but in younger patients it may be a nonspecific indicator of cerebral insult (e.g., trauma [fig. 7] or early mild hydrocephalus), even in the absence of other MRI abnormalities; (3) Patterns 3 and 4 are always pathologic and are most typically seen in hydrocephalus (figs. 4 and 10) and extensive demyelination (figs. 5 and 9), respectively. There is, however, overlap between the two patterns; (4) In severe hydrocephalus, the periventricular halo becomes irregular, especially at its superior margins (fig. 10D), thus mimicking the hyperintensity seen in diffuse demyelination (pattern 4). The hyperintensity seen in severely hydrocephalic patients (nine cases) could, however, be distinguished from the hyperintensity seen in patients with diffuse demyelination (18 cases) on the basis of subtle differences in the configuration of the hyperintensity. In severe hydrocephalus, the peripheral margins of the PVH are irregular but blunted, and they do not extend to the corticomedullary junction (fig. 10D). In demyelinating diseases, the PVH is more sharply angled and usually does extend to the corticomedullary junction (figs. 5 and 9); (5) In patients with extensive multifocal demyelination there is a general increase in PVH (pattern 3) indistinguishable from mild to moderate periventricular edema secondary to hydrocephalus (cf. figs. 8 and 13).

These phenomena have a significant impact on the use of MRI in the evaluations of patients for hydrocephalus. The greater sensitivity of MRI relative to CT in the detection of edema [22] had led to the hope that MRI would be more sensitive than CT in detecting mild periventricular edema and that this finding could be used as a criterion for shunting patients in whom a diagnosis of hydrocephalus could not be made by other criteria [23] (e.g., normal-pressure hydrocephalus suspects). This study confirms that MRI is more sensitive than CT in detecting periventricular edema (cf. figs. 10 and 11), but it also indicates that this finding is of limited clinical value. Those hydrocephalic patients with severe PVH on MRI with or without CT evidence of edema were easily diagnosed using standard clinical and radiographic criteria. The diagnoses of mild hydrocephalus and normal-pressure hydrocephalus remain difficult with MRI because its increased sensitivity is accompanied by a decrease in specificity. In mild or early active hydrocephalus only a thin band of PVH (pattern 2) may be seen, and this nonspecific finding cannot be used as a criterion for shunting. Our experience in patients with normal-pressure hydrocephalus, although limited to six cases, has been particularly disappointing. Two patients had mild nonspecific PVH (pattern 2). Four patients had prominent PVH (three patients, pattern 3; one patient, pattern 4), but in all cases multiple white-matter hyperintense foci (presumably representing infarction) were also present (fig. 13). The degree of PVH was similar to that seen in nonhydrocephalic elderly patients with white-matter infarcts alone, and, therefore, the PVH pattern could not be used as a criterion for shunting. Since these infarcts are commonly seen on MRI in elderly patients [24], their concurrent occurrence in patients with normal-pressure hydrocephalus limits the usefulness of the PVH pattern to those few cases where PVH is seen in the absence of focal white-matter lesions.

While most patients with hydrocephalus show relatively extensive PVH, absent or mild PVH (pattern 0 or 1) was also encountered occasionally. In four cases this reflected either arrested hydrocephalus or adequate shunt function, but one patient with active hydrocephalus who subsequently responded to shunting showed only mild PVH (fig. 12). It is unclear why periventricular edema did not develop, and one might speculate that spinal fluid absorption occurred via alternate routes (e.g., perineural or perivascular lymphatics [14]), but it is clear that simple reliance on the degree of PVH cannot be used as a criterion for shunting.

REFERENCES

1. Young IR, Hall AS, Pallis CA, Bydder GM, Legg NJ, Steiner RE. Nuclear magnetic resonance imaging of the brain in multiple sclerosis. *Lancet* **1981**;2:1063–1066
2. Bydder GM, Steiner RE, Young IR, et al. Clinical NMR imaging of the brain: 140 cases. *AJNR* **1982**;3:459–480, *AJR* **1982**;139:215–236
3. Lukes SA, Crooks LE, Aminoff MJ, et al. Nuclear magnetic resonance imaging in multiple sclerosis. *Ann Neurol* **1983**;13:592–601
4. Brant-Zawadzki M, Davis PL, Crooks LE, et al. NMR demonstration of cerebral abnormalities: comparison with CT. *AJNR* **1983**;4:117–124, *AJR* **1983**;140:847–854
5. Young IR, Randell CP, Kaplan PW, James A, Bydder GM, Steiner RE. Nuclear magnetic resonance (NMR) imaging in white-matter diseases of the brain using spin-echo sequences. *J Comput Assist Tomogr* **1983**;7:290–294
6. Brant-Zawadzki M, Norman D, Newton TH, et al. Magnetic resonance of the brain: the optimal screening technique. *Radiology* **1984**;152:71–77
7. Bradley WG, Waluch V, Yadley RA, Wycoff RR. Comparison of CT and MR in 400 patients with disease of the brain and cervical spinal cord. *Radiology* **1984**;152:695–702
8. Runge VM, Price AC, Krishner HS, Allen JH, Partain CL, James AE Jr. Magnetic resonance imaging of multiple sclerosis: a study of pulse-technique efficacy. *AJNR* **1984**;5:691–702
9. Bradley WG Jr, Waluch V, Brant-Zawadzki M, Yadley RA, Wycoff RR. Patchy periventricular white matter lesions in the elderly: a common observation during MRI imaging. *Noninvasive Medical Imaging* **1984**;1:35–41
10. Vermess M, Bernstein RM, Bydder GM, Steiner RE, Young IR, Hughes GRV. Nuclear magnetic resonance (NMR) imaging of the brain in systemic lupus erythematosis. *J Comput Assist Tomogr* **1983**;7:461–467
11. Brant-Zawadzki M, Badami JP, Mills CM, Norman D, Newton TH. Primary intracranial tumor imaging: a comparison of magnetic resonance and CT. *Radiology* **1984**;150:435–440
12. Cserr HF, Ostrach LH. Bulk flow of interstitial fluid after intracranial injection of Blue Dextran 2000. *Exp Neurol* **1974**;45:50–60
13. Rosenberg GA, Kyner WT, Estrada E. Bulk flow of brain interstitial fluid under normal and hyperosmolar conditions. *Am J Physiol* **1980**;238:F42–F49
14. McComb JG. Recent research into the nature of cerebrospinal fluid formation and absorption. *J Neurosurg* **1983**:59:369–383
15. Pollay M, Curl F. Secretion of cerebrospinal fluid by the ventricular ependyma of the rabbit. *Am J Physiol* **1967**;213:1031–1038
16. Milhorat TH, Hammock MK, Fenstemacher JD, Rall DP, Levin VA. Cerebrospinal fluid production by the choroid plexus and brain. *Science* **1971**;173:330–332
17. Potts DG, Gomez DG. Cerebrospinal fluid production, function and absorption. In: Newton TH, Potts DG, eds. *Radiology of the skull and brain*, vol. 3. *Anatomy and pathology*. St. Louis: Mosby, **1977**:2915–2937
18. Reulan JH, Tsuyumu M, Tack A, Fenske AR, Prioleau GR. Clearance of edema fluid into cerebrospinal fluid. A mechanism for resolution of vasogenic brain edema. *J Neurosurg* **1978**;48:754–764
19. Cao M, Lisheng HE, Shouzheng S. Resolution of brain edema and in severe brain injury at controlled high and low intracranial pressures. *J Neurosurg* **1984**;61:707–712
20. Broman T. Blood-brain barrier damage in multiple sclerosis: Supravital test observations. *Acta Neurol Scand* [*Suppl*] **1964**;40:21–24
21. Viñuela FV, Fox AJ, Debrun GM, Feasby TE, Ebers GC. New perspectives in computed tomography of multiple sclerosis. *AJNR* **1982**;3:277–281
22. Brant-Zawadzki M, Bartkowski HM, Pitts LH, et al. NMR imaging of experimental and clinical edema. *Noninvasive Medical Imaging* **1984**;1:43–47
23. George AE, de Leon M, Rosner L, et al. Magnetic resonance and positron emission tomography evaluation of hydrocephalus. Presented at the annual meeting of the American Society of Neuroradiology, Boston, June **1984**
24. Brant-Zawadzki M, Fein G, Van Dyke C. Magnetic resonance imaging (MRI) of the aging brain: patchy white matter lesions and dementia. Presented at the annual meeting of the Society of Magnetic Resonance in Medicine, New York, August **1984**
25. Bradley WG, Waluch V, Wycoff RR, Yadley RA. Differential diagnosis of periventricular abnormalities in MRI of the brain. Presented at the annual meeting of the Society of Magnetic Resonance in Medicine, New York, June **1984**

CT of Pineal Region Tumors

S. Ramaiah Ganti[1]
S. K. Hilal[1]
B. M. Stein[2]
A. John Silver[1]
M. Mawad[1]
P. Sane[1]

The computed tomographic (CT) features of pineal region tumors were analyzed in 60 histologically proven tumors. This is the largest reported series of histologically verified pineal region tumors studied with CT. The tumors were classified as germ-cell tumors, glial tumors, pineal parenchymal tumors, and meningiomas. Preenhancement germinomas revealed characteristically high-density areas with calcification; uniform enhancement was seen after injection of contrast material. When present, pineal calcification was engulfed by the tumor. Teratomas, present only in male patients, revealed areas of mixed densities (e.g., calcification and fatty areas) and did not show significant contrast enhancement. Spontaneous intraventricular rupture was noted in one case. Unlike other tumors, the original pineal calcification could be recognized in two-thirds of glioma cases and was displaced anteriorly and superiorly in most. Gliomas were hypodense to isodense on precontrast scans and enhanced in a nodular and a ring fashion. Benign pineal parenchymal tumors showed iso- to hyperdense areas with nodular enhancement after injection of contrast material. Pineoblastomas were well defined hyperdense masses without calcification on precontrast scans. After injection of contrast material, they showed well defined enhancement with occasional small, central lucencies. Meningiomas were hyperdense in most cases, uniformly enhanced in a homogeneous fashion, and showed a tentorial attachment.

Pineal region tumors constitute 2% of intracranial tumors. Masses in the region of the pineal body form a group whose anatomic location has usually precluded histologic verification before treatment [1]. The pineal body has a close relation to the quadrigeminal plate cistern, posterior part of the thalamus, posterior third ventricle, and vein of Galen. Lesions may infiltrate these adjacent structures by contiguous spread, and sometimes it may be impossible even at necropsy to determine the primary site. This has often resulted in grouping of the tumors in this area as pineal region tumors [1]. In general, documented by surgical and autopsy series, about 25% of the tumors of the pineal region are benign and encapsulated. These lesions are generally considered insensitive to radiotherapy, and because of their defined borders are amenable to surgical removal [2].

In the past, neurologic management of pineal region tumors has been strongly influenced by unfavorable results after direct surgical intervention. Mortality ranged from 29% in one series [3] to 70% in another [4]. In 1960, a representative series was reported of third ventricular tumors at Neurological Institute of New York [5]. Among the pineal tumors there was total removal in five cases, resulting in three deaths. Keeping in mind the above results, a retrospective study of histologically proven pineal tumors studied by computed tomography (CT) was undertaken to correlate CT appearance with various histologic tumor types.

Materials and Methods

CT scans of 60 patients with histologically proven pineal region tumors were studied. There were 44 males and 16 females. CT scans were obtained before and after enhancement

This article appears in the January/February 1986 issue of the *AJNR* and the March 1986 issue of *AJR*.

Received March 19, 1984; accepted after revision June 4, 1985.

Presented at the Symposium Neuroradiologicum, Washington, DC, November 1982, and at the annual meeting of the American Society of Neuroradiology, San Francisco, June 1983.

[1] Department of Radiology, Division of Neuroradiology, Columbia Presbyterian Medical Center, New York City, NY 10032. Address reprint requests to S. R. Ganti, Department of Radiology, Englewood Hospital, 350 Engle St., Englewood, NJ 07631.

[2] Department of Neurosurgery, Neurological Institute of New York, New York City, NY 10032.

***AJR* 146:451–458, March 1986**
0361–803X/86/1463–0451
© American Roentgen Ray Society

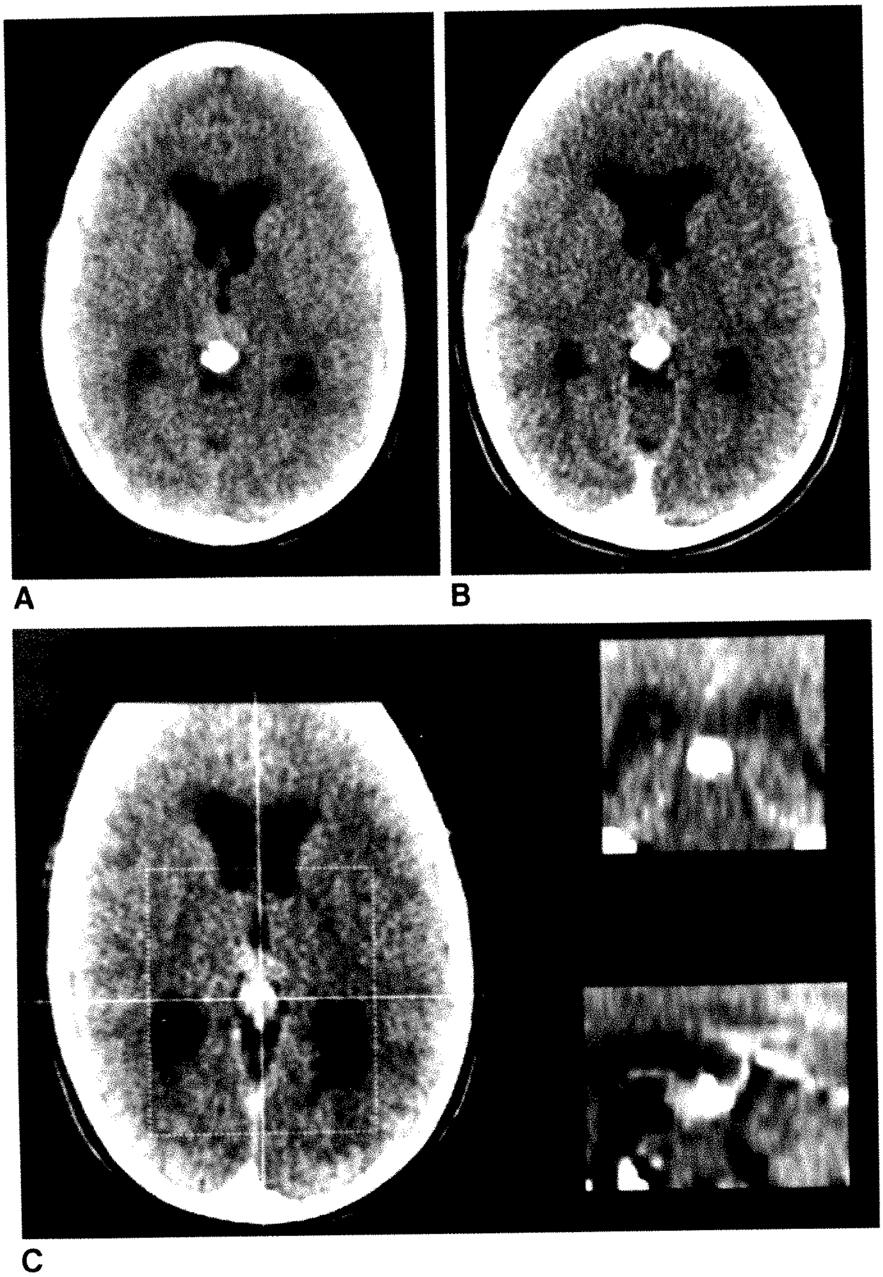

Fig. 1.—Germinoma. **A**, Precontrast scan. Calcified prominent pineal gland is associated with high-density mass anteriorly. Mild hydrocephalus. **B**, Postcontrast scan. Enhancement in high-density region. **C**, Reconstructed coronal and sagittal views. Calcified and enhancing lesion in pineal area.

in almost all patients. Coronal views were obtained whenever possible and were considered necessary (12 of 60). Angiograms were obtained in most patients (53 of 60) to identify vascular supply and venous drainage. It was not our intent to offer specific CT and angiographic correlations, but rather to correlate CT and histology of pineal region tumors. Age and gender were important factors in the differential diagnosis, since certain pineal region tumors, such as teratomas, germinomas, and pineoblastomas, occur either exclusively or predominantly in males.

Results

Pineal region tumors were divided into four broad categories according to the pathologic classification of Rubinstein [6]. They were divided into germ-cell tumors, glial tumors, pineal parenchymal tumors, and meningiomas.

Germ Cell Tumors

Under this category there were four subdivisions: germinomas, teratomas, embryonal cell carcinoma, and choriocarcinoma.

Germinomas. There were 16 cases of pineal germinoma, 13 in males and three in females. In 15 cases the lesion was denser than brain on unenhanced CT scans. The other patient did not have an unenhanced study. Moderate-to-marked enhancement was noted in 14 cases, slight enhancement in one

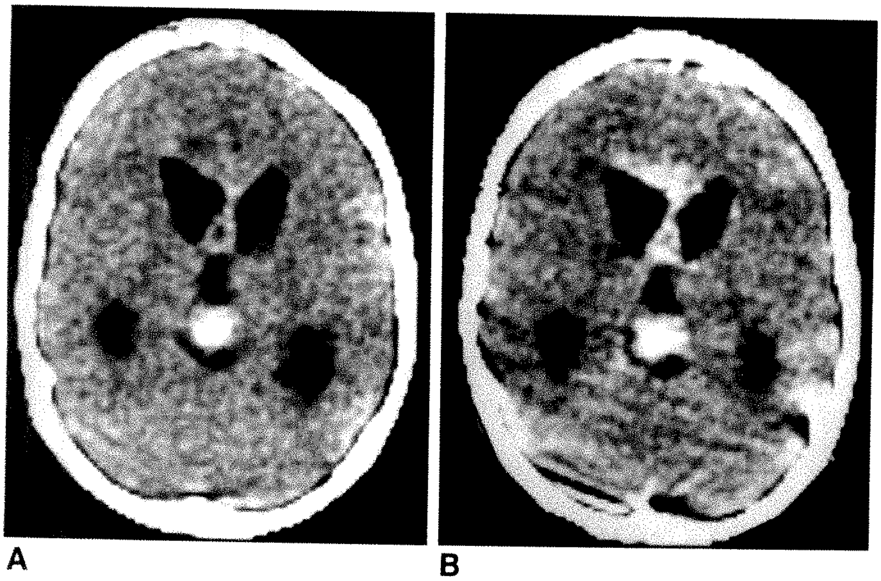

Fig. 2.—Germinoma with seeding. **A**, Precontrast scan. Prominent pineal calcification with hyperdense mass associated with periventricular high density and hydrocephalus. **B**, Postcontrast scan. Enhancing pineal mass with periventricular enhancement consistent with tumor seeding.

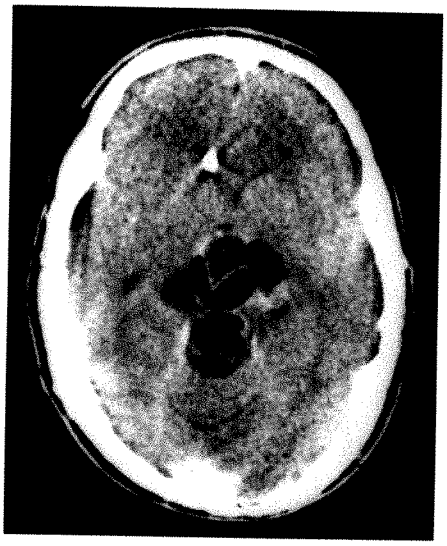

Fig. 3.—Teratoma. Postcontrast axial view. Mixed densities, including fatty areas and cystic areas associated with linear calcifications. No significant enhancement. Shunt tip is in right lateral ventricle.

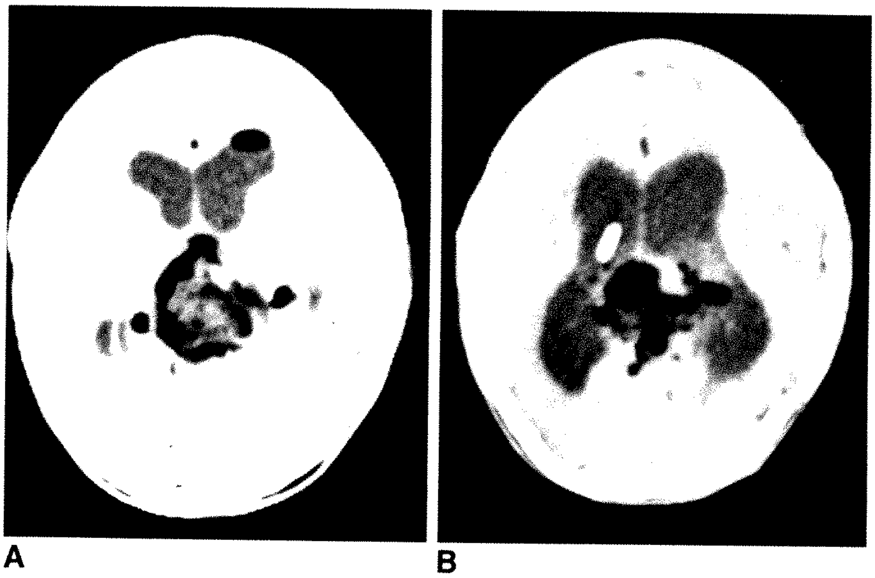

Fig. 4.—Spontaneous rupture of teratoma. **A**, Wide window at frontal horn level. Fatty densities in pineal area, frontal horn, and pericallosal cistern. **B**, Fatty tumor has ruptured into lateral ventricles. Shunt tip in right lateral ventricle.

case, and no enhancement in one case. A prominent and slightly enlarged pineal calcification was noted in six cases and was engulfed by enhancing tumor in all (fig. 1). The prominent pineal gland calcification was recognized by its discrete character and its close-to-midline location. On the other hand, parenchymal calcification of the tumor was recognized by a coarse, nodular pattern on either side of the pineal body. This was observed in 10 cases. Meningeal and ependymal seeding was found in five cases and was demonstrated by CT in the subarachnoid space and the ventricular wall (fig. 2). Spinal seeding was detected by myelography.

Teratomas. There were five cases of teratoma; all were in males. The teratomas were all sharply demarcated from the surrounding brain. Another distinct feature, fatty substances with a low CT attenuation, was identified in all five cases. No other tumor in this series showed these fatty densities. In four of the five cases there was tumor calcification showing a mixture of linear and nodular densities (fig. 3). No significant contrast enhancement was observed. In one case, a small area of malignant transformation was detected histologically. In this case, the initial CT interpretation was of a teratoma. On follow-up, there was subarachnoid seeding in the suprasellar area and periventricular enhancement. Spontaneous intraventricular rupture of a teratoma was seen in one case (fig. 4).

Embryonal cell carcinoma and choriocarcinoma. There was

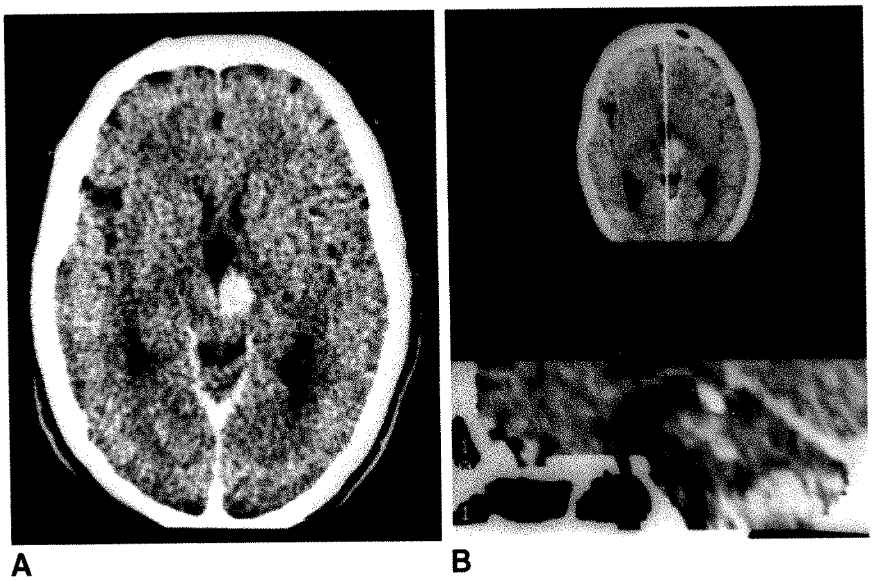

Fig. 5.—Nodular glioma. **A**, Postcontrast axial scan. Nodular enhancement around posterior third ventricle. **B**, Sagittal reconstruction. Nodular enhancement below calcified pineal gland.

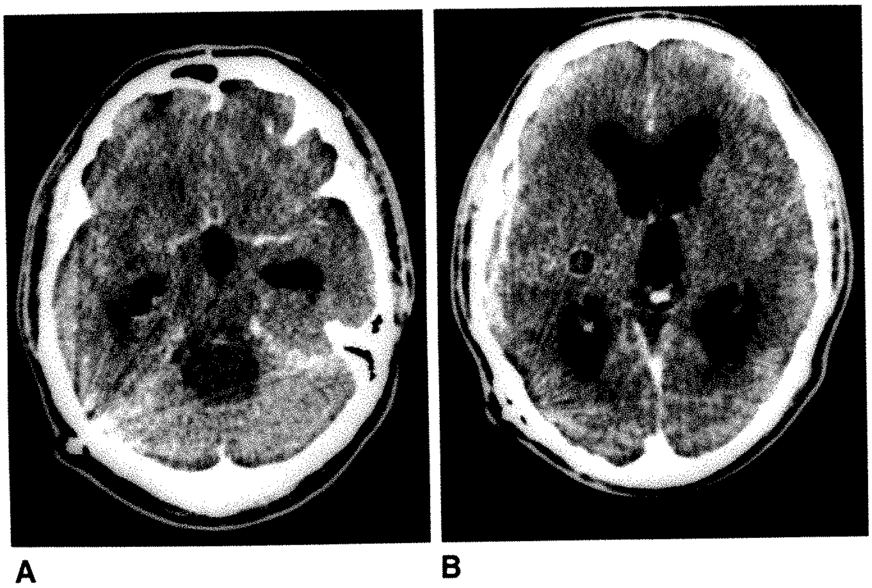

Fig. 6.—Cystic glioma. **A**, Postcontrast scan. Lucent, nonenhancing cystic lesion projecting into posterior fossa, without fat densities. **B**, Higher level. Calcified pineal displaced superiorly by inferiorly located tumor.

one case each of embryonal cell carcinoma and choriocarcinoma; both tumors were hyperdense on unenhanced scans, but enhanced markedly after administration of contrast material. There was no abnormal pineal calcification or parenchymal calcification within the tumor. In this group angiography provided a very useful clue for the diagnosis, showing pronounced vascularity.

Glial Tumors

There were 16 cases of glioma, 10 in males and six in females. Twelve cases revealed hypodense areas, two were isodense, one had mixed density with coarse calcification, and one had hydrocephalus with no detectable mass. Normal pineal calcification was observed in 11 patients in this group. The pineal calcification was displaced upward and forward in 10 cases and posteriorly in one. In the other four cases, no pineal calcification was detected. The pineal calcification appeared to be normal and was identified in the midline as a discrete density. The patient with no detectable mass and hydrocephalus on CT had a magnetic resonance (MR) scan at another institution; it revealed a definite mass in the pineal region. After intravenous injection of contrast material, moderate-to-marked enhancement was noted in 11 cases, mild enhancement in four, and no abnormal enhancement in one (the case in which a lesion was evident on MR). The enhancement pattern was a single nodule in six cases (fig. 5), a "ring" in six cases, and no enhancement pattern in one case. Two cases appeared "cystic" with no enhancing cyst wall (fig. 6).

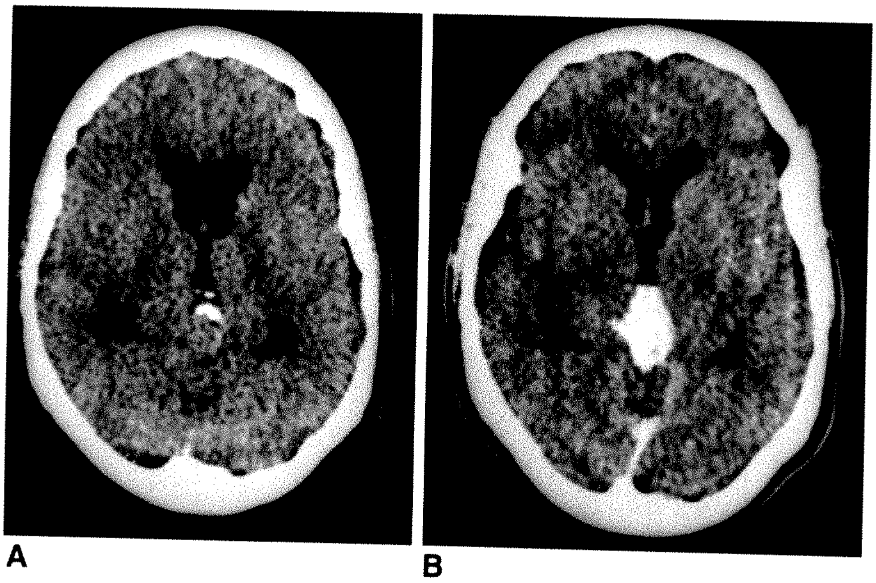

Fig. 7.—Pineocytoma. **A**, Precontrast scan. Partly calcified and isodense mass in pineal area associated with mild hydrocephalus. **B**, Postcontrast scan. Nodular enhancement.

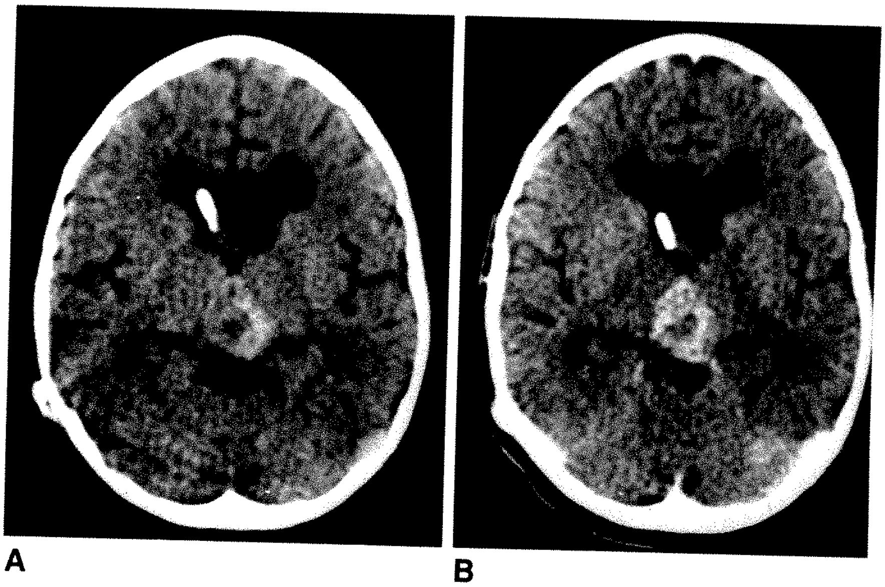

Fig. 8.—Pineoblastoma. **A**, Precontrast CT scan. Hyperdense mass with central lucency in pineal area, mild hydrocephalus, and shunt tip in right frontal horn. **B**, Postcontrast scan. Enhancement with central lucency probably representing necrotic area.

Pineal Parenchymal Tumors

There were 13 cases of pineal parenchymal tumors; they were subdivided into benign-type pineocytomas (eight cases) and malignant-type pineoblastomas (five cases). Of the eight pineocytomas, five were in males and three in females. Pineocytomas were isodense to hyperdense relative to brain on unenhanced CT scans in seven cases; no preenhancement CT scan was obtained in one case. The tumor enhanced as a well defined, homogeneous nodule in seven cases (fig. 7), and no enhancement occurred in one case. One case had an abnormally large pineal calcification, one case had a normal pineal calcification, and six cases showed no pineal calcification.

The five cases of pineoblastomas were all in males. All had a well defined mass without calcification. Four cases showed moderate enhancement with a small central lucency, unlike the benign pineocytomas (fig. 8). Ependymal seeding in the lateral ventricle was seen in one case.

Meningiomas

There were eight cases of meningioma occurring in the pineal region, four in females and four in males. There was a case of meningeal sarcoma in this group. Six cases were hyperdense on precontrast CT and two cases had no precontrast CT scan. All cases showed homogeneous intense enhancement. Three cases had coronal CT, which demonstrated the tentorial attachment (fig. 9).

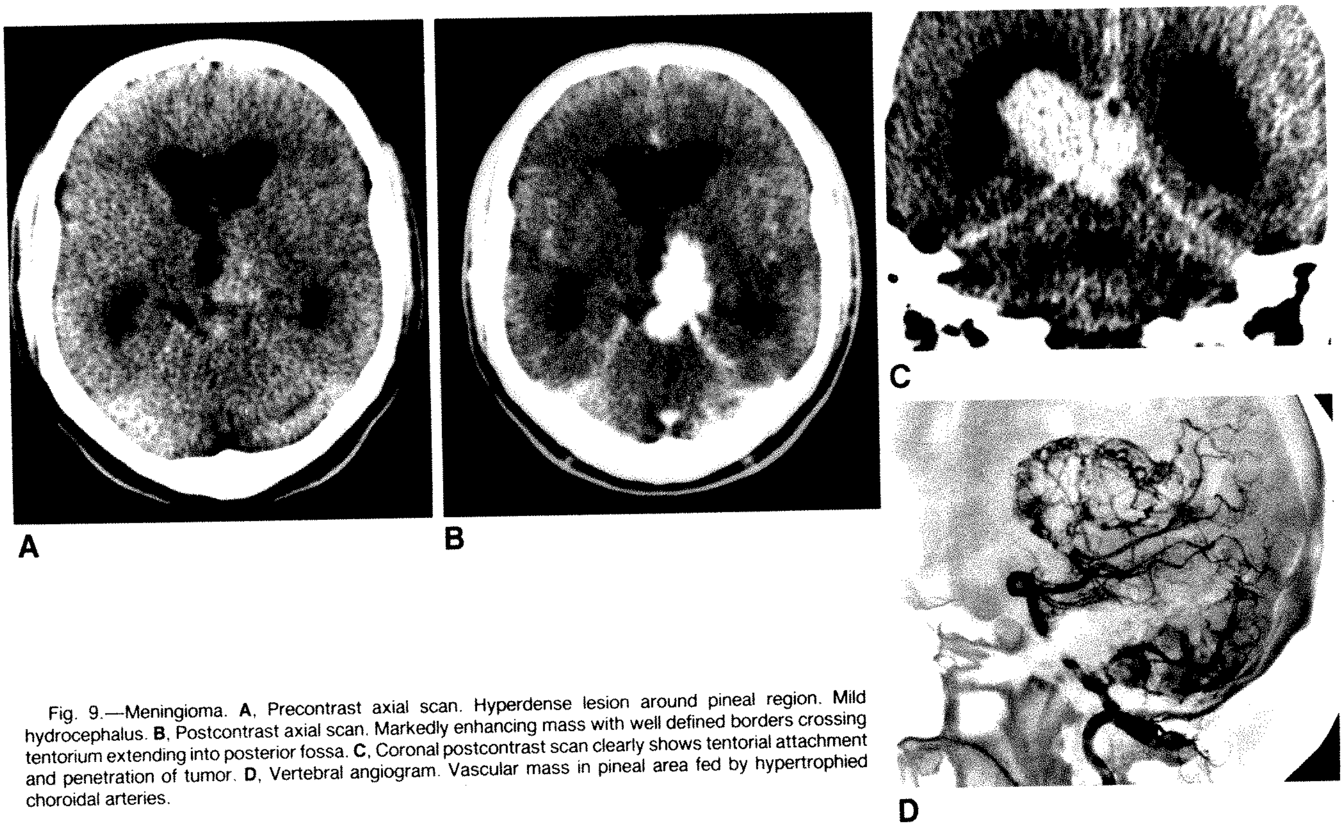

Fig. 9.—Meningioma. **A**, Precontrast axial scan. Hyperdense lesion around pineal region. Mild hydrocephalus. **B**, Postcontrast axial scan. Markedly enhancing mass with well defined borders crossing tentorium extending into posterior fossa. **C**, Coronal postcontrast scan clearly shows tentorial attachment and penetration of tumor. **D**, Vertebral angiogram. Vascular mass in pineal area fed by hypertrophied choroidal arteries.

Discussion

We are reporting the largest series of histologically proven pineal tumors studied by CT. Previous reports [7–10] included a smaller number of histologically documented lesions, specifically 33, 22, nine, and seven cases, respectively.

Germinomas

The cell origin of germinomas is usually ascribed to primitive germ cells that are said to migrate over wide areas of the embryo during early fetal life. The pineal area is the most common site of intracranial germinomas. Many arise in the midline in the hypothalamic region and are frequently called ectopic pinealomas or suprasellar germinomas. Most germinomas are reported to occur in the second and third decades of life, and this was true in our series also. Germinomas of the pineal region show an overwhelming male preponderance. Germinomas of the suprasellar region show a lesser preponderance of males [6]. Germinomas are the most common tumor of the pineal region, accounting for 50% of all neoplasms in this area [6]. In our series, this neoplasm was the most common single type, accounting for 16 of 60 cases. In the series reported by Jooma and Kendall [7], germinoma was the most common tumor, constituting 17 of 33 cases. The incidence of calcification in the germinomas in our series was higher than in the series of Jooma and Kendall, probably because our patients were studied with high-resolution CT.

The characteristic CT features of germinoma are of a well defined, hyperdense, occasionally calcified tumor occurring in a young male, engulfing the pineal gland, and enhancing homogeneously. Pathologically, germinomas are highly cellular neoplasms, usually containing no hemorrhage, necrosis, or cystic degeneration [11]. The hyperdense areas on CT may correlate with the densely cellular nature of these tumors. A prominently calcified pineal gland engulfed by tumor tissue, a characteristic feature of germinomas in our series, was not seen in any other pineal tumors. Germinomas are histologically malignant, and infiltrative spread is likely to occur along the floor and walls of the third ventricle. Seeding along the lateral ventricles and cerebrospinal fluid (CSF) spaces is common. Five of our 16 cases revealed CSF seeding either at the initial or later stages of the tumor.

Teratomas

The pineal is the most common site of intracranial teratomas. In an analysis of 94 reported cases of teratomas involving the brain [12], 39 cases were in the pineal area. The incidence of teratomas is highest in the second and third decades, as was true for germinomas. Teratomas also occur predominantly in males; all our five cases were in males.

Pathologically, teratomas have well defined borders with variegated cut surfaces. Teratomatous elements such as cartilage, bone, and hair are often seen. All five teratomas demonstrated fat densities and four revealed calcification. Unlike the coarse, stippled calcification of germinomas, teratomas possess a mixture of linear and nodular calcifications. Spontaneous rupture of teratomas into ventricles has been reported only once in the CT literature [13]. Our case is the second. Besides teratomas, dermoids and epidermoids are also known to rupture spontaneously. In brief, the CT features of teratomas should include hypodense areas of various fats and linear or nodular calcification, either in the periphery or in the center of the tumor. The calcific nodules are usually larger than those observed in germinomas. The other less frequently occurring germ-cell tumors are choriocarcinomas and chorioepitheliomas. There was one case of each, and no specific CT characterization can be made except that they were hyperdense, enhanced after intravenous administration of contrast material like other germ-cell tumors, and contained no fat densities. They were very vascular angiographically.

Pineal Cell Tumors

Tumors arising from the pineal parenchymal cells are probably less common than germinomas and teratomas [6]. However, in our series, pineal parenchymal cell tumors outnumbered teratomas. The term "pinealoma" would, strictly speaking, be appropriate only for tumors arising from the pineal parenchymal cells. Those arising from the pineal parenchymal cells are divided into more mature pineocytomas and more primitive pineoblastomas. The pineocytoma is usually well circumscribed, noninvasive, slowly growing, may be found at any age, and both genders are equally affected. The CT features of pineocytomas include isodense and hyperdense areas on unenhanced CT. Enhancement was homogeneous without apparent breakdown or necrosis in the tumor. In males pineocytomas cannot be distinguished from noncalcified germinomas. When pineal calcification is seen in a female, the lesion is more likely a pineocytoma.

Pineoblastomas are usually frankly invasive and highly malignant. Histologically, the tumor is densely cellular. Hemorrhage and calcification are not found, but cystic degeneration is observed occasionally. Cystic degeneration was noted in our series as ring enhancement with central low density. Extension of pineoblastomas to involve the cerebellar vermis is not uncommon and often raises the question of medulloblastoma. Histologically, pineoblastomas and medulloblastomas are very similar. On CT scans, pineoblastomas are characterized by a lucent center, which differentiates them from the benign pineocytoma.

Glial Tumors

Since the normal pineal gland includes fibrillary astrocytes, it is possible that it may be the source of glial tumors such as astrocytomas and glioblastomas. However, by the time these tumors are examined pathologically, they are so extensive that the precise origin may be difficult to identify. Many of these tumors probably arise from the quadrigeminal plate or from the wall of the third ventricle [6].

In 22 cases of pineal region tumors studied by Zimmerman et al. [8], there were eight gliomas and seven germinomas. In another series [7], there were three gliomas out of 33 cases. In our series gliomas constituted 16 of 60, the second most common tumor after germ-cell tumors. Most gliomas in our series displaced the pineal gland anteriorly and superiorly, which suggested the tumor was extrapineal in origin. The precontrast CT scan usually helped establish the CT diagnosis of gliomas, since they were hypodense relative to brain. The two cases presenting as nonenhancing cysts were apparently unique; such a morphology has not been reported before. Gliomas occurred in males and females in equal numbers, and age distribution did not provide any help in the diagnosis.

Meningiomas

Meningiomas arising in the pineal area are rare. In the series of Zimmerman et al. [8] and Jooma and Kendall [7], no meningiomas were reported. Sachs et al. [14] reported three cases of meningiomas in the pineal region. At that time, there was a total of 20 cases of meningiomas in this location in the literature, including their own three cases. In one series of 20 pineal region tumors, one tumor was a meningioma [2]. There were eight cases of meningiomas in our series. Both males and females were equally affected, although, in general, meningiomas are more often found in females than in males.

Meningiomas occupying the pineal area may arise from the velum interpositum or from the free edge of tentorium, where it is joined by the inferior margin of the falx. The meningiomas in the pineal area were hyperdense in most cases on unenhanced CT and enhanced in a nodular fashion after intravenous administration of contrast material. The characteristic feature of dural attachment was best seen on the coronal view. Angiography helped in identifying the feeders to the tumor and the characteristic homogeneous blush. One case showed sarcomatous changes and there was also spinal seeding into the lumbar subarachnoid space. No other cases had seeding and none had fat densities.

Clinical Management

Stein [2, 15] used an infratentorial supracerebellar approach, which reaches the tumor below the deep venous system. In his series of over 60 cases, there were three deaths and no significant operative morbidity.

Treatment programs in nonresectable tumors are tailored to the histologic nature of the tumor. In germinomas, CSF is evaluated three times for abnormal cells, and a myelogram is obtained. If there is any evidence of CSF seeding, radiation therapy is applied to the entire brain with a boost to the tumor site as well as radiation to the spinal canal. In astrocytomas, radiation is directed to the site of the tumor only. In pineal cell tumors, radiation is directed primarily to the tumor site. In embryonal cell tumors such as embryonal carcinoma and choriocarcinoma, chemotherapy may be the treatment of first choice. In germinomas that escape the effects of radiotherapy, chemotherapy is considered.

REFERENCES

1. Greitz T. Tumors of the quadrigeminal plate and adjacent structures. *Acta Radiol* (Stockh) **1972**;13:512–538
2. Stein B. Surgical management of pineal tumor. *Clin Neurosurg* **1979**;29:Chapt. 19
3. Dandy WE. An operation for the removal of pineal tumors. *Surg Gynecol Obstet* **1921**;33:113–119
4. Rand RW, Lemmen LJ. Tumors of posterior portion of third ventricle. *J Neurosurg* **1953**;10:1–18
5. Camins MB, Schlesinger EB. Treatment of tumors of posterior part of third ventricle and pineal region—a long term follow up. *Acta Neurochir* (Wien) **1978**;40:121–143
6. Rubenstein I. Tumors of the central nervous system. In: *Atlas of tumor pathology*, 2d series. Washington, DC: Armed Forces Institute of Pathology, **1970**:269–284
7. Jooma R, Kendall G. Diagnosis and management of pineal tumors. *J Neurosurg* **1983**;58:654–665
8. Zimmerman RA, Bilaniuk LT, Wood JH, Bruce DA, Schut L. CT of pineal, parapineal, and histologically related tumor. *Radiology* **1980**;137:669–677
9. Kleefield J, Solis O, Davis K, et al. CT of tumor of pineal region. *Comput Radiol* **1977**;1:257–265
10. Futrell NN, Osborn AG, Cheson BD. Pineal region tumors: computed tomographic-pathologic spectrum. *AJNR* **1981**;2:415–420, *AJR* **1981**;137:951–956
11. DeGirolami U. *Pathology of pineal tumors.* In: Schmidek HH, ed. New York: Masson, **1977**:1–18
12. Hosoi K. Teratoma and teratoid tumors of brain. *Arch Pathol Lab Med* **1930**;9:1207–1297
13. Ghoshhajra K, Baghai-Naiini P, Hahn HS, Pena CE, Hayat S. Spontaneous rupture of pineal teratoma. *Neuroradiology* **1979**;17:215–217
14. Sachs E Jr, Avman N, Fisher RG. Meningiomas of pineal region and posterior part of third ventricle. *J Neurosurg* **1962**;10:325–331
15. Stein B. The intratentorial supracerebellar approach to pineal lesions. *J Neurosurg* **1971**;35:197–202

Exophthalmos Caused by Excessive Fat: CT Volumetric Analysis and Differential Diagnosis

Robert G. Peyster[1]
Ferris Ginsberg[2]
Jeffrey H. Silber[3]
Lee P. Adler[1]

CT has proven to be excellent in identifying orbital pathology responsible for proptosis. Occasionally, no discrete mass or extraocular muscle enlargement to explain the exophthalmos is found, only an appearance suggestive of an abnormal increase in orbital fat volume. Fifteen patients were studied with proptosis apparently resulting from increased orbital fat. Clinical follow-up revealed that four of them had Graves orbitopathy, unilateral in one; two had Cushing disease/syndrome; and nine were obese without endocrinopathy. The orbital volume and percentage orbital fat volume were measured by CT software analysis in these patients and in a control group of 16 patients without proptosis. Measurements of proptosis and thickness of the scalp fat pad at the inion level were also performed. Significantly greater values for orbital fat volume, percentage fat volume, and proptosis were found in the proptosis group compared with the control group. There was excellent correlation between proptosis and percentage fat volume, supporting the contention that increased orbital fat is responsible for the proptosis. The thickness of the scalp fat pad at the inion level was significantly greater in obese and Cushing patients than in control subjects, but the thickness was not significantly greater in Graves patients than in controls. Proptosis and inion fat were well correlated (r = 0.74) in the control and obese patients, which suggests a relation between general body fat and orbital fat volume.

Exophthalmos, unilateral or bilateral, is a frequent indication for orbital CT scanning and medical evaluation. CT has proven to be excellent in identifying orbital pathoogy responsible for proptosis. Occasionally, no discrete mass or extraocular muscle enlargement to explain the proptosis is found, except for an appearance suggestive of an abnormal increase in orbital fat volume [1–8]. There are a few reports of exophthalmos resulting from excessive orbital fat in patients with Graves disease [1–6], Cushing disease or syndrome [1, 7], and obesity [1, 8–10]. No previous report investigates all three etiologies or considers differential diagnoses.

It is the intention of this study to document a greater orbital fat volume in patients with a CT diagnosis of excess orbital fat proptosis compared with a control group of people without proptosis; to correlate orbital fat volume with the amount of proptosis; and to investigate whether a measurement of the thickness of scalp fat at the level of the inion is predictive of obesity and thereby might serve as a CT differential diagnostic sign between Graves disease versus obesity or Cushing disease/syndrome when clinical data are unavailable.

Subjects and Methods

Fifteen patients with exophthalmos determined by CT and clinical criteria in whom CT did not reveal an orbital mass or enlargement of the extraocular muscles represent the proptosis group. Clinical follow-up showed that four had Graves disease, unilateral in one; two had Cushing disease/syndrome (one from chronic steroid administration for sarcoidosis; the other from an ACTH-producing pituitary adenoma); and nine were grossly obese with no endocrine

This article appears in the January/February 1986 issue of *AJNR* and the March 1986 issue of *AJR*.

Presented at the annual meeting of the American Society of Neuroradiology, New Orleans, February 1985.

[1] Department of Diagnostic Radiology, Hahnemann University Hospital, 230 N. Broad St., Philadelphia, PA 19102. Address reprint requests to R. G. Peyster.

[2] Department of Radiology, Monmouth Medical Center, Long Branch, NJ 07740.

[3] Robert Wood Johnson Foundation Clinical Scholars Program, University of Pennsylvania School of Medicine, Philadelphia, PA 19104.

AJR 146:459–464, March 1986
0361-803X/86/1463-0459
© American Roentgen Ray Society

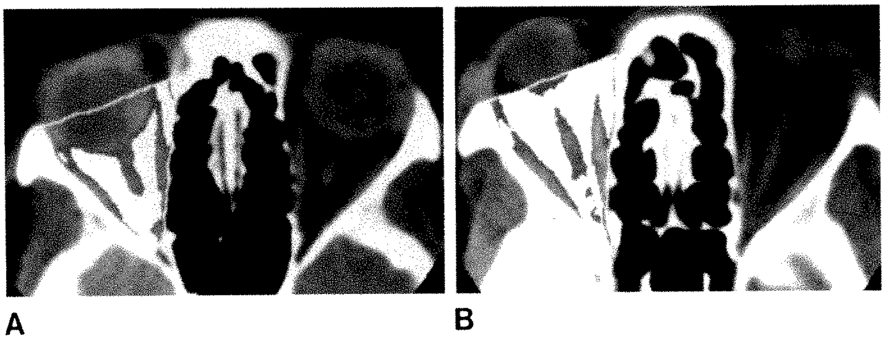

Fig. 1.—Orbital boundaries and volume measurements. **A**, Midorbital axial CT section, control subject. No evidence of proptosis. Volume measurements were performed on right orbit. Anterior orbital boundary is defined by white line passing through globe from zygoma to lacrimal bone. Traced line continues along edge of orbital bony margin. Patches of white within these boundaries represent pixels with density values in range of fat. White areas conform to areas filled with fat in opposite orbit. **B**, Slightly higher section in patient with proptosis caused by excess orbital fat. Considerably more orbital fat compared with control patient.

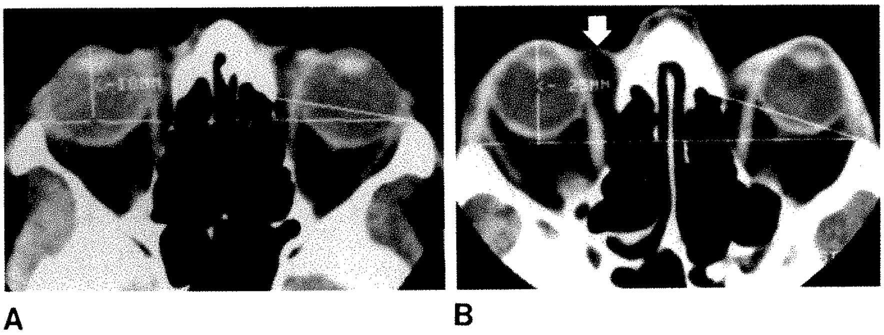

Fig. 2.—CT proptosis measurements and guidelines. **A**, Axial orbital CT section including lenses, control subject. Interzygomatic line is drawn. Length of perpendicular line from anterior margin of globe to this line in millimeters represents proptosis measurement, as illustrated for right orbit. In this case, measurement of 18 mm falls well below upper limit of normal (21 mm). **B**, Patient with excess fat exophthalmos. Proptosis measurement is 25 mm. Anterior bowing of right medial orbital septum (*arrow*) is well seen.

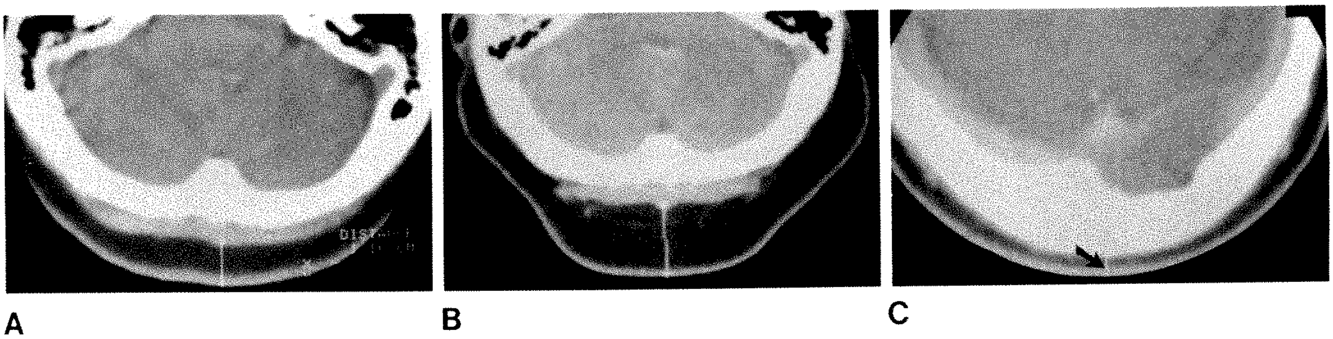

Fig. 3.—Measurement of scalp fat thickness at inion level. **A**, Obese patient with excess fat exophthalmos. Measurement shown by line between cursors, which extends from scalp margin posterior to inion to muscle. Fat thickness (1.16 cm or 11.6 mm) is recorded beneath *DISTANCE* in lower right corner. **B**, Scalp fat measures 24 mm in patient with Cushing syndrome caused by long-term steroid treatment. **C**, Scalp fat measurement (*arrow*) of 3.4 mm in patient with Graves ophthalmopathy was smallest scalp fat measurement in any patient, including control group.

abnormality. A control group of 16 subjects without exophthalmos by either clinical or CT criteria were randomly obtained from 74 patients with untreated unilateral primary choroidal melanoma limited to the globe. These patients all had complete axial CT orbital examinations available for analysis on floppy disks.

All scanning was performed on a GE 8800 CT/T scanner. The orbits were scanned with either contiguous 1.5 or 5-mm-thick slices in the axial plane at 0° to −10° to the orbitomeatal line.

Measurements of orbital volume and orbital fat volume were made for both orbits using the volume measurement function in General Electric Display (GEDIS) experimental software (General Electric, Milwaukee). This program requires the examiner to define on a CT section the boundaries of the area of interest with the trace CT console function and to designate a density range in Hounsfield units for the tissue whose volume is to be determined. The computer sums the voxels within the prescribed density range to derive the partial volume of the tissue of interest. The total volume within the traced boundaries, the density of the tissue of interest, and the percentage of the total volume occupied by the tissue of interest are also calculated. This operation was performed for all CT orbital sections to obtain total orbital volume and orbital fat volume. For this study, the orbital boundaries for orbital volume determination were defined by tracing along the edge of the bony walls of the orbit. On slices where the anterior boundary of the orbit was not defined by bone, the anterior aspects of the medial and lateral orbital bony margins were connected by a straight line to form the anterior boundary (fig. 1). By choosing the anterior boundary in this fashion, in cases of marked proptosis, some of the postseptal orbital fat would be excluded from measurement, but erroneous inclusion of periorbital fat would be avoided and identical boundaries could be used for all patients. A density range of −200 to −3 H was chosen for the measurement of orbital fat volume since no other intraorbital tissue lies within this density range, as shown by initial trials (fig. 1). The percentage of total orbital volume (OV) occupied by fat (FV) was

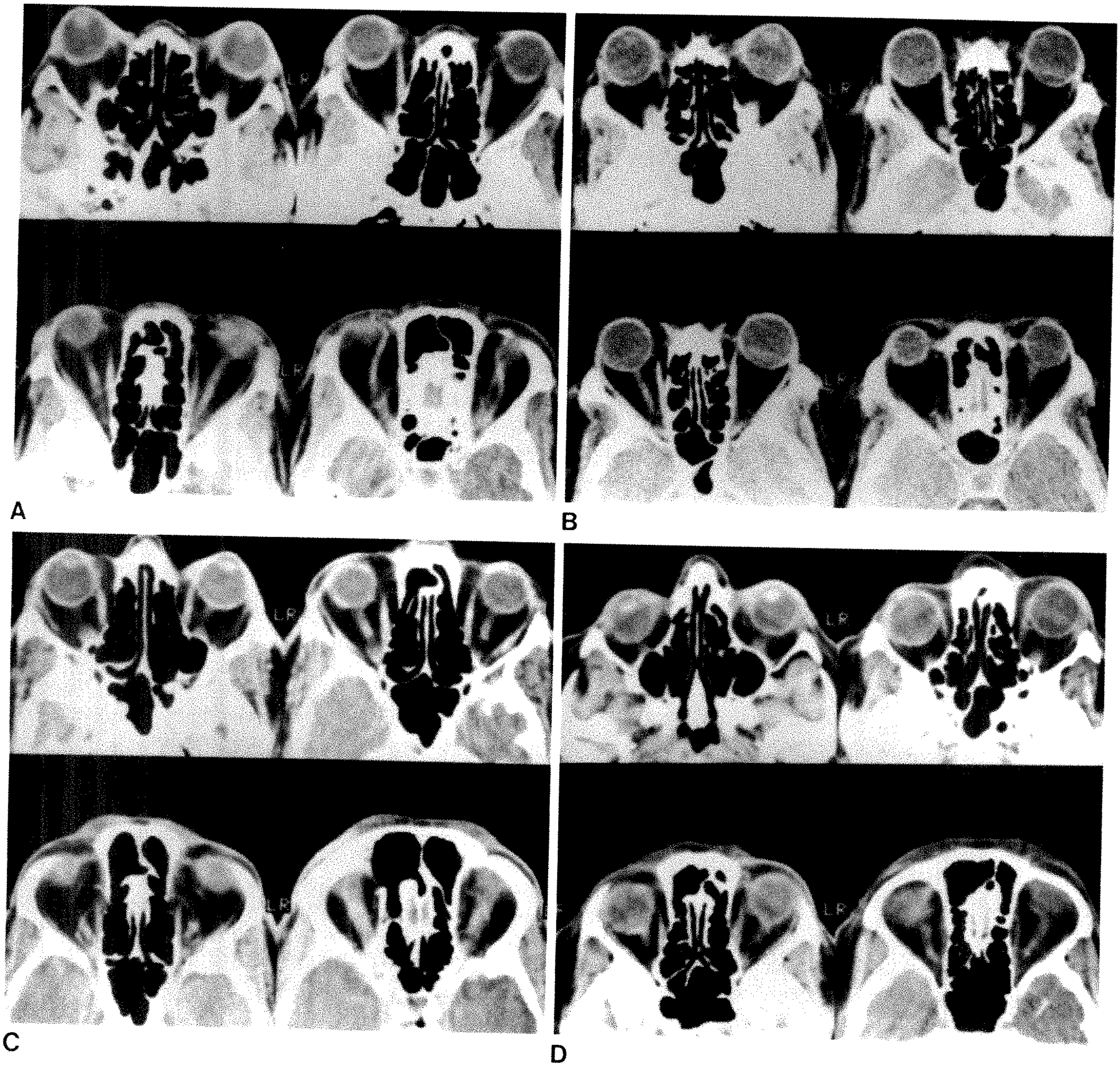

Fig. 4.—CT appearance of excess fat exophthalmos. **A**, Axial orbital CT sections in obese patient. Bilateral proptosis, normal extraocular muscles, and no evidence of discrete orbital mass. Orbital septa bowed anteriorly. Apparent bilateral increase in orbital fat. **B**, Orbital scans in patient with Cushing syndrome show same findings as in **A**. **C**, Graves ophthalmopathy. No detectable enlargement of extraocular muscles, and CT findings are essentially identical to **A** and **B**. **D**, Graves ophthalmopathy. Excess fat exophthalmos only on left.

obtained by %FV = FV/OV × 100.

Proptosis in millimeters was measured by dropping a perpendicular line from the most anterior aspect of the globe on a section including the lens to a line drawn between the anterior tips of the frontal processes of the zygomas (fig. 2).

The thickness of the scalp fat pad in millimeters was measured posterior to the inion on a slice that also included the sella using the CT cursor measure distance function (fig. 3).

Statistical analysis of the data was performed in several ways: Paired Student *t* tests were used for comparing the percentage of fat in the right versus left orbit and in the orbit containing the choroidal melanoma versus the normal orbit of the control group. Independent Student *t* tests were used for comparing measurements of orbital volume, orbital fat, percentage orbital fat, proptosis, and inion fat from the control group with measurements from the proptosis group and its subdivisions. Linear and multiple regression analyses were used for correlation of percentage orbital fat, proptosis, and inion fat for all 31 subjects and a subgroup without endocrinopathy composed

TABLE 1: **Measurements by Patient Group**

Group	Mean ± SD				
	Orbital Fat (cm^3)	Orbital Volume (cm^3)	% Orbital Fat	Proptosis (mm)	Scalp Fat Pad (mm)
Control	8.16 ± 1.68	19.82 ± 3.68	41.51 ± 7.6	15.44 ± 2.52	6.78 ± 1.34
Proptosis	11.04 ± 1.76	18.97 ± 2.00	58.15 ± 6.85	24.77 ± 2.45	10.84 ± 5.39
Obesity	11.34 ± 1.4	18.93 ± 1.93	59.84 ± 4.54	25.03 ± 2.07	10.42 ± 1.95
Graves	9.60 ± 0.63	19.15 ± 1.59	50.20 ± 4.73	23.90 ± 3.85	8.20 ± 3.82
Cushing	12.53 ± 3.64	18.75 ± 4.31	66.15 ± 4.31	25.30 ± 0.99	18.00 ± 14.14

of the control and obese patients. Values of $p > 0.05$ derived from the t tests were interpreted as demonstrating a lack of significant difference between the groups being compared.

Results

The orbital CT findings in excess fat exophthalmos did not vary with etiology (fig. 4). These findings were proptosis, no enlargement of the extraocular muscles nor any other discrete orbital mass to account for the proptosis, and the subjective impression that there is more than the usual amount of fat in the orbit(s). Anterior bowing of the orbital septa is an ancillary finding (fig. 2B).

The control group was examined for possible influence of their melanoma on orbital fat content. The mean volume of fat was 41.4% for eyes with melanoma and 41.7% for eyes without melanoma. A paired t test showed no significant difference between normal and melanoma eyes ($p = 0.687$). The mean fat volumes were 41.8% and 41.2% for the right and left eyes, respectively, in the control group, and again no significant difference was found (paired t test, $p = 0.538$). The values for the right and left orbit for each patient were averaged for orbital fat, percentage orbital fat, proptosis, and orbital volume for further analysis. It is recognized that for the patient with unilateral Graves ophthalmopathy who had an orbital fat volume of 9.7 cm^3 (51.9%) for the abnormal left orbit and 7.8 cm^3 (44.4%) for the right orbit, using the average values for the two orbits would partially obscure this unilateral abnormality.

The means and standard deviations for orbital fat, orbital volume, percentage orbital fat, proptosis, and inion fat are shown in table 1 for the control and proptosis groups and for the etiologic subdivisions of the proptosis group. Comparison by independent t tests of the control and proptosis groups for percentage orbital fat, proptosis, and inion fat showed significantly higher values in the proptosis group for these variables ($p < 0.001$). There was no significant difference between the orbital volume of the proptosis and control groups. Comparison of the control group versus the group of nine obese patients for these same variables yielded essentially the same results, with significantly greater percentage orbital fat, inion fat, and proptosis in the obese group ($p < 0.001$) and no significant difference in orbital volume. For the two patients with Cushing disease/syndrome, orbital and inion fat and proptosis were also significantly greater than in the control group ($p < 0.001$), again with no significant difference in orbital volume. The percentage of orbital fat of the four patients with Graves ophthalmopathy was significantly greater than that of the control group ($p = 0.02$), proptosis for the Graves group was significantly greater than that of the control group ($p < 0.001$), but inion fat and orbital volume were not significantly different for the Graves and control subjects.

TABLE 2: **Multiple Regression Analyses of Proptosis versus Orbital Fat and Scalp Fat Pad**

Group: Variable	Coefficient	Probability
All subjects ($n = 31$):		
%Orbital fat	0.35	0.001
Scalp fat pad	0.09	0.60
Control + obese ($n = 25$):		
%Orbital fat	0.26	0.001
Scalp fat pad	0.91	0.007

Note.—For all subjects, intercept = 1.75; multiple correlation = 0.77; multiple $r^2 = 0.59$ ($F = 19.8$; $p < 0.001$). For control plus obese subjects, intercept = −0.78; multiple correlation = 0.86; multiple $r^2 = 0.73$ ($F = 30.4$; $p < 0.001$).

TABLE 3: **Correlations of Orbital Fat, Scalp Fat, and Proptosis**

Group: Variable	% Orbital Fat	Scalp Fat	Proptosis
All subjects ($n = 31$):			
% Orbital fat	1	0.46	0.76
Scalp fat	...	1	0.41
Proptosis	...	...	1
Control + obese ($n = 25$):			
% Orbital fat	1	0.61	0.79
Scalp fat	...	1	0.74
Proptosis	...	...	1

Table 2 shows the results of multiple regression analysis of proptosis versus percentage orbital fat and inion fat for all 31 patients. The correlation between proptosis and orbital fat was 0.76 ($p < 0.001$), with moderate correlation between proptosis and inion fat at 0.41 and between orbital fat and inion fat at 0.46 (table 3). The multiple regression model shows that 59% of the variance of proptosis can be explained by percentage orbital fat and inion fat together (table 2).

Table 2 also shows the multiple regression analysis for the control group plus the obese group, eliminating the patients with Graves and Cushing. All three correlations are greater than when all patients were included, with 73% of the variance now explained by the multiple regression model. The coefficients for percentage orbital fat and inion fat are highly significant. A scatter diagram with best-fitted line is shown for proptosis versus percentage fat volume for all 31 patients in

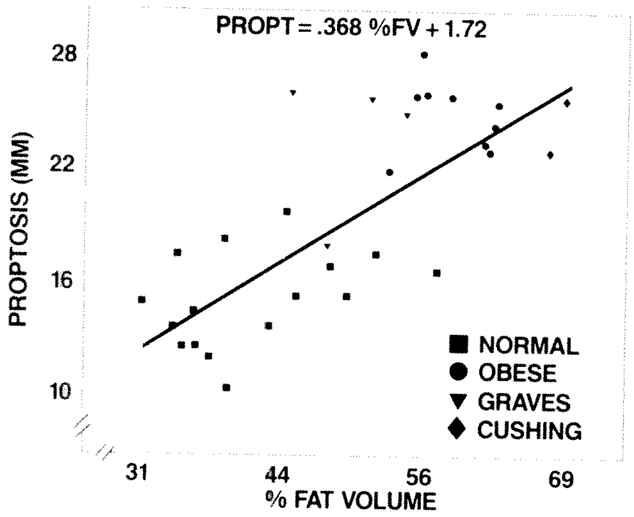

Fig. 5.—Scatter diagram with best-fitted line for proptosis versus percentage fat volume for all 31 patients. As indicated by data and line, proptosis increases with increase in percentage fat volume.

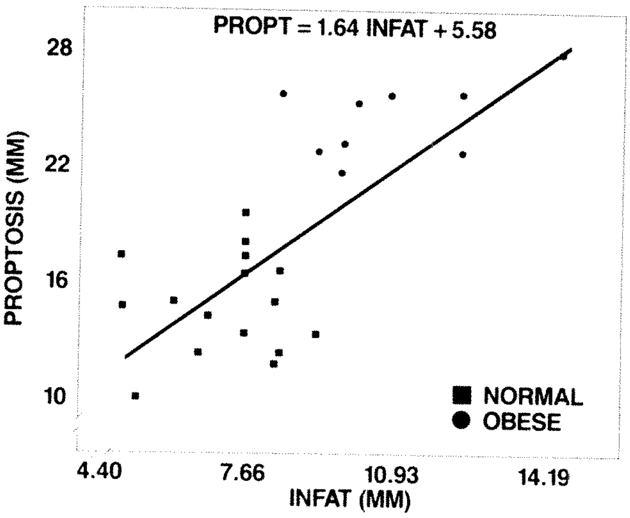

Fig. 6.—Scatter diagram with best-fitted line for proptosis versus thickness of scalp fat pad at inion level (INFAT) for control and obese patients. Proptosis increases with increase in scalp fat. Control patients, all of whom had proptosis measurements less than 21 mm, are grouped in lower left, and obese patients, all of whom had proptosis measurements exceeding 21 mm, are grouped in upper right.

figure 5. It may be seen that the Graves patients had, among the proptosis group, relatively lower values for orbital fat; the Graves subject with unilateral disease showed a mean proptosis measurement of 18 mm because of the influence of averaging in the normal orbit. A scatter diagram for proptosis versus inion fat for the normal plus obese group is shown in figure 6. The density of orbital fat was normal in all 31 subjects.

Discussion

Exopthalmos resulting from an increase in orbital fat volume has been described in Graves ophthalmopathy [1–6], in Cushing disease/syndrome [1, 7], and with obesity [1, 8–10]. No previous report has discussed all etiologies of this condition nor attempted to establish CT criteria to distinguish between them.

The results of our report demonstrate that the 15 patients with CT diagnoses of exophthalmos considered to be caused by an increase in orbital fat have a significantly greater proportion of their orbits occupied by fat than do the 16 control subjects lacking proptosis. The number of cases in each subcategory of the proptosis group, particularly Graves and Cushing diseases, unfortunately, is small. Despite this, statistically significant differences for percentage orbital fat between the proptosis versus the control subjects, and for inion fat between the obese and Cushing versus control subjects, were obtained. We hope to have the opportunity to study more subjects with excess fat exophthalmos to increase our confidence in generalizing our conclusions regarding the populations of patients in each etiologic subcategory of this condition.

Several previous studies have used CT to measure orbital volume and intraorbital soft-tissue volume [2, 11–13]. Forbes et al. [2] measured the volume of orbital fat and muscle in 19 normal subjects and in 19 patients with Graves ophthalmopathy. They found two distinct groups among the patients with Graves ophthalmopathy. Nine patients constituted their type A Graves, in which there was a marked increase in orbital muscle volume and a decrease, compared with their normal group, in orbital fat volume. This group had little or no clinical proptosis. Their type B Graves group consisted of 10 patients, most of whom had increase in both orbital fat volume and extraocular muscle volume, but some of whom had exclusive increase in orbital fat volume. Exophthalmos was clinically evident in this group. Feldon et al. [12] measured extraocular muscle volume in 50 patients with Graves ophthalmopathy and found relatively poor correlation between proptosis and the extent of muscle enlargement. This observation would suggest that increase in nonmuscular orbital soft tissue, namely fat, must influence the degree of proptosis. While the mean orbital fat volume and percentage orbital fat volume were higher in the patients in our study with Graves ophthalmopathy than in the control group, even higher values for these measurements were found among the obese patients and those with Cushing disease/syndrome. Proptosis was well correlated with the quantity of orbital fat in our study, which supports the contention of a cause-and-effect relation between the increase in orbital fat and the proptosis noted in the proptosis group, as was suspected from the CT appearance of their orbits.

There is no satisfactory explanation in the literature regarding the pathogenesis of increased orbital fat volume occurring with Graves ophthalmopathy. It has been proposed that infiltration of the fat by edema and inflammatory cells is responsible for the increase in fat volume [2, 13, 14]. Trokel and Jakobiec [6] reviewed biopsy material including orbital fat in patients with Graves ophthalmopathy and were unable to find evidence for inflammatory infiltration of the fat. They also stated that, in their experience, the CT density of orbital fat in Graves disease is identical to normal orbital fat, which suggests against infiltration of the fat. The density of the orbital fat was normal in our three cases of Graves ophthalmopathy. There is generalized increase in body fat in obesity and Cushing disease/syndrome [7, 8]. An increase in orbital fat in these two conditions presumably reflects this generalized fatty accumulation. The relatively strong correlation between scalp fat thickness, orbital fat volume, and extent of proptosis noted in our study would support this hypothesis. Little is known about the circumstances under which orbital fat pads will participate along with other fat depots in increased fat accumulation; racial, genetic, and developmental factors may be involved. Excess fat exophthalmos is not seen in most patients on steroid therapy who manifest other cushingoid changes [7]. The percentage of obese patients that would exceed normal limits of measurement for proptosis, either by CT or exophthalmometry, is unknown.

In cases of Graves ophthalmopathy with combined increases of extraocular muscle and orbital fat volumes, CT diagnosis is not difficult. In cases with isolated increase in orbital fat volume, differential diagnosis from obesity and Cushing disease/syndrome becomes more challenging. Clinical and laboratory evidence, when available, of Graves disease or Cushing disease/syndrome will establish the diagnosis in these patients. In obese patients with excess fat exophthalmos, one must first exclude endocrinopathy before blaming the obesity for the proptosis. When the radiologist is faced with a CT scan suggestive of excess fat exophthalmos without immediate access to the patient or clinical data, certain information on the scan may aid in differential diagnosis. Unilateral excess fat exophthalmos has not been reported with obesity or Cushing disease/syndrome, nor is it logical that it should occur in these conditions. While unilateral orbital involvement in Graves ophthalmopathy is uncommon, occurring in about 5% of cases [4, 5], it remains the most common cause of unilateral proptosis [8, 14] and should be the favored diagnosis in cases of unilateral excess fat exophthalmos. The thickness of the scalp fat pad at the inion level was significantly greater among the obese patients than in the control group in our study. This finding is perhaps made more significant since no effort was made to exclude overweight subjects from the control group. The patients with Cushing disease/syndrome also had large inion fat measurements, significantly greater than those of the control group. The mean inion fat measurement for the patients with Graves ophthalmopathy was not significantly greater than that of the control group; in fact, one of the patients with Graves disease had the smallest inion fat measurement (3.4 mm) of any patient studied. A large inion fat measurement in a patient with excess fat exophthalmos is not helpful in the differential diagnosis, since patients with Graves ophthalmopathy can also be obese. However, our data suggest that a small inion fat measurement associated with excess fat exophthalmos is unlikely to be found in obesity or Cushing disease/syndrome, and a diagnosis of Graves ophthalmopathy should be suggested under these circumstances.

The density of the orbital fat appeared normal in all of our subjects. There are conditions, however, such as orbital pseudotumor, leukemia, lymphoma, and, in children, metastatic neuroblastoma, that can diffusely infiltrate orbital fat, inhomogeneously raising its density (the "dirty orbit"), and cause proptosis [8, 15–17]. It is important to recognize the alteration of the appearance of the orbital fat in these conditions to distinguish them from those entities described above, which cause proptosis by increasing the volume of normal orbital fat.

In summary, this study has shown that there is an increased amount of orbital fat in patients with Graves orbitopathy, Cushing disease/syndrome, and obesity with proptosis and a CT scan showing no orbital mass other than an appearance suggesting excessive orbital fat to account for exophthalmos. The larger inion fat measurements in the obese and Cushing subjects suggest that the amount of scalp fat may reflect total body fat and that a small scalp fat measurement in a patient with excess fat exophthalmos would favor a diagnosis of Graves orbitopathy over obesity or Cushing disease/syndrome.

REFERENCES

1. Peyster RG, Hoover ED. *Computerized tomography in orbital disease and neuroophthalmology*. Chicago: Yearbook, **1984**:97–99, 110–114
2. Forbes G, Gorman CA, Gehring D, Baker HL Jr. Computer analysis of orbital fat and muscle volumes in Graves ophthalmopathy. *AJNR* **1983**;4:737–740
3. Hodes BL, Frazee L, Szmyd S. Thyroid Orbitopathy: an update. *Ophthalmic Surg* **1979**;10:25–33
4. Trokel SL, Hilal SK. Recognition and differential diagnosis of enlarged extraocular muscles in computed tomography. *Am J Ophthalmol* **1979**;87:503–512
5. Enzmann DR, Donaldson SS, Kriss JP. Appearance of Graves' disease on orbital computed tomography. *J Comput Assist Tomogr* **1979**;3:815–819
6. Trokel SL, Jakobiec FA. Correlation of CT scanning and pathologic features of ophthalmic Graves' disease. *Ophthalmology* **1981**;88:553–564
7. Cohen BA, Som PM, Haffner PH, Friedman AH. Steroid exophthalmos. *J Comput Assist Tomogr* **1981**;5 907–908
8. Carlson RE, Scheribel KW, Hering PJ, Wolin L. Exophthalmos, global luxation, rapid weight gain: differential diagnosis. *Ann Ophthalmol* **1982**;14:724–729
9. Offenbach B. Dislocation (luxation) of the eyeball. *N Engl J Med* **1954**;251:338–339
10. Ruedemann A, Roberts N, Seligson A. Voluntary luxation of globes. *Am J Ophthalmol* **1954**;37:351–354
11. Feldon SE, Weiner JM. Clinical significance of extraocular muscle volumes in Graves' ophthalmopathy: a quantitative computed tomography study. *Arch Ophthalmol* **1982**;100:1266–1269
12. Feldon SE, Muramatsu S, Weiner JM. Clinical classification of Graves' ophthalmopathy: identification of risk factors for optic neuropathy. *Arch Ophthalmol* **1984**;102 1469–1472
13. Hahn FJ, Chu W-K. Ocular volume measured by CT scans. *Neuroradiology* **1984**;26:419–420
14. Grove AS Jr. Evaluation of exophthalmos. *N Engl J Med* **1975**;292:1005–1013
15. Enzmann D, Donaldson SS, Marshall WH, Kriss JP. Computed tomography in orbital pseudotumor (idiopathic orbital inflammation). *Radiology* **1976**;120:597–601
16. Forbes GS, Sheedy PF II, Waller RR. Orbital tumors evaluated by computed tomography. *Radiology* **1980**;136:101–111
17. Forbes GS, Earnest F IV, Waller RR. Computed tomography of orbital tumors, including late-generation scanning techniques. *Radiology* **1982**;142:387–394

Incremental Dynamic Computed Tomography:

Practical Method of Imaging the Carotid Bifurcation

Brian M. Tress[1,2]
Stephen Davis[3]
John Lavain[2]
Andrew Kaye[4]
John Hopper[5]

A simple, practical method of applying incremental dynamic computed tomography (CT) to the imaging of 20 carotid bifurcations is described. The results are compared with those obtained by conventional carotid angiography and intravenous digital subtraction angiography (DSA). Conventional angiography provided additional information about the carotid bifurcation in only one of 14 cases, while incremental dynamic CT provided information not available from intravenous DSA in two of eight cases. Conventional brain CT is being used increasingly in the workup of patients with transient ischemic symptoms, and dynamic CT scanning at 3-mm increments requires only an extra 5 min of scanner time. The addition of incremental dynamic CT through the carotid bifurcation to the conventional brain CT scan procedure may obviate other screening tests before more definitive angiographic procedures.

Embolism from atheromatous disease at the carotid bifurcation in the neck is the most common cause of transient cerebral ischemic attacks (TIAs) [1]. Despite the development of alternative, less invasive techniques, selective carotid angiography remains the definitive technique for demonstrating the anatomy of the carotid bifurcation. However, even in the best hands, carotid angiography has a significant morbidity and mortality [2], particularly when performed in elderly patients with symptomatic cerebrovascular disease and when there are marked stenoses of the internal carotid arteries [3].

Noninvasive techniques for the evaluation of the carotid bifurcation have been described and reviewed [4]. When used in the experienced, noninvasive vascular laboratory as a "battery" of tests, these methods can provide information about the severity and potential hemodynamic consequences of bifurcation disease with a maximum accuracy of about 90% [5]. The main purpose of the noninvasive battery, which monitors physiology as well as morphology, is to better select patients for arteriography.

Intravenous digital subtraction angiography (DSA) is a less invasive rapid procedure that can produce a 97% accuracy in the assessment of disease of the carotid bifurcation with good or excellent demonstration. However, inadequate studies occur in up to 15% of cases, and in these the accuracy is reduced to 64% [6].

Computed tomography (CT) is used increasingly in the evaluation of patients with TIAs to rule out hemorrhage, tumor, arteriovenous malformation, and demyelination, any of which may have clinical features simulating transient ischemia. The ability of CT to detect infarction and to distinguish lacunar from cortical infarction [7] may influence decisions concerning immediate management and further investigation. Methods of imaging the carotid bifurcation by CT have been described [8–11], but these are time-consuming or involve the use of sophisticated computer-based contour programs not readily available. The object of our study was to develop a rapid, practicable method of imaging the carotid bifurcation that could be used as an adjunct to the standard cerebral CT examination in the evaluation of patients with TIAs.

This article appears in the January/February 1986 *AJNR* and the March 1986 *AJR*.

Received January 29, 1985; accepted after revision May 21, 1985.

This work was supported in part by grants from the Higginbotham Neurosciences Foundation and the Victor Hurley Medical Research Fund.

[1] Department of Radiology, University of Melbourne, Victoria, Australia 3050.

[2] Department of Radiology, Royal Melbourne Hospital, Victoria, Australia 3050. Address reprint requests to B. M. Tress.

[3] Department of Neurology, Royal Melbourne Hospital, Victoria, Australia 3050.

[4] Department of Neurosurgery, Royal Melbourne Hospital, Victoria, Australia 3050.

[5] Department of Medicine, Royal Melbourne Hospital, Victoria, Australia 3050.

***AJR* 146:465–470, March 1986**
0361-803X/86/1463-0465
© American Roentgen Ray Society

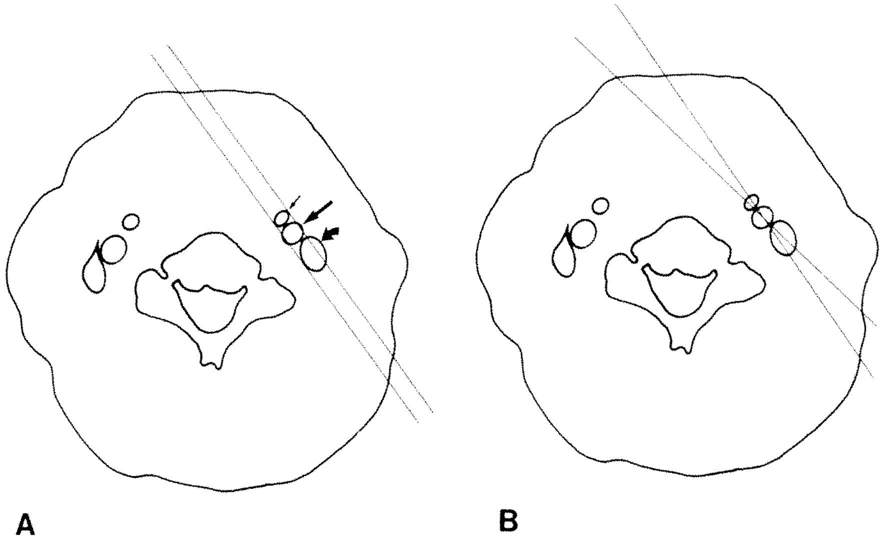

Fig. 1.—Diagrams of axial CT image of neck immediately superior to carotid bifurcation. **A**, Internal jugular vein (*curved arrow*), internal carotid artery (*long straight arrow*), and external carotid artery (*short straight arrow*). *Parallel lines* indicate limits of contiguous paraxial reformations. **B**, Variations in paraxial planes along which reformations are made.

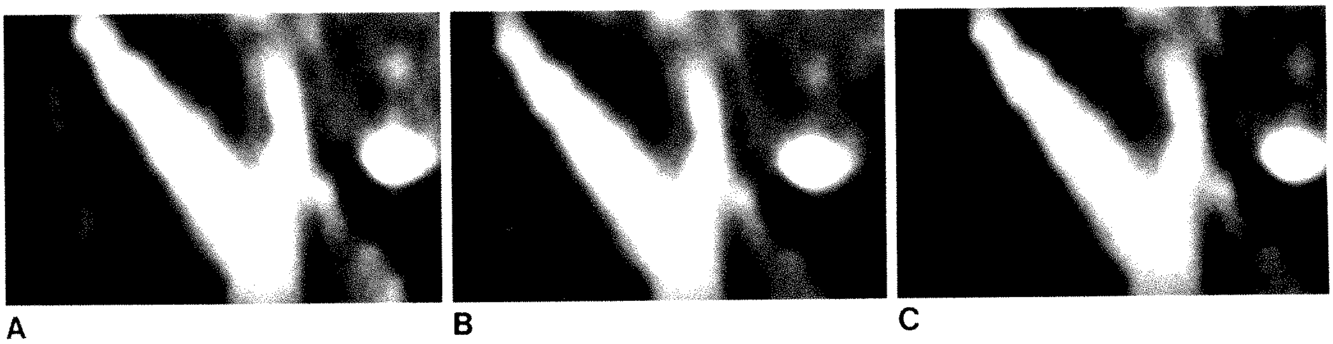

Fig. 2.—Normal carotid bifurcation. Paraxial reformatted images are 1 (**A**), 2 (**B**), and 3 (**C**) pixels thick.

Subjects and Methods

Ten patients presenting with internal carotid territory TIAs had a thorough history and examination performed by a neurologist (S. D.). Seven patients were investigated with bilateral transfemoral carotid angiography and four with intravenous DSA. One patient had both carotid angiography and intravenous DSA. All patients had a CT examination on a GE 9800 scanner within 4 days of angiography. The CT examination consisted of an incremental dynamic CT evaluation of the carotid bifurcation in the neck and a subsequent cerebral scan.

An 18- or 20-gauge intravenous sheath (Jelco IV Catheter Placement Unit, Critikon, Tampa, FL) was introduced into an antecubital vein and connected by plastic tubing to a mechanical pump (Cordis flow rate injector). Fifty to eighty ml of Urografin 76% (10% meglumine diatrizoate and 66% sodium diatrizoate, Schering) was injected at rates of 2–8 ml/sec. A lateral computed radiograph (ScoutView, GE, Milwaukee) of the cervical spine was obtained. Between 12 and 16 contiguous axial scans of 3 mm slice width were obtained from the level of the middle of the fifth cervical vertebra to the upper margin of the third cervical vertebra. The incremental dynamic program was used with increments of 3 mm, 2 sec scan durations, and interscan intervals of 2.3 sec. Preparation delays (the interval from the beginning of contrast-medium injection to commencement of scanning) of 8–14 sec were incorporated. At the completion of the dynamic scan program, a standard, postenhancement head scan series was obtained.

Inspection of the hard-copy axial neck images enabled the sites of the common carotid bifurcation and internal and external carotid arteries to be determined. An image clearly depicting the proximal segments of the internal and external carotid arteries was selected. Using the standard "Arrange" program (GE, Milwaukee), paraxial images were reformatted along the axis of the internal and external carotid arteries at 1, 2, or 3 pixel (0.5 mm, 1 mm, or 1.5 mm) intervals (fig. 1A). The "batch mode" software program (GE, Milwaukee) enabled these multiple reformations to be subsequently computed. Slight variations in the paraxial plane chosen for reformation (fig. 1B) were reviewed so that the plane best depicting the maximum diameter of the internal carotid artery was selected for hard-copy recording. The procedure was repeated for the opposite carotid bifurcation. The images were displayed with window levels of 100–150 H and window widths of 100–250 H. The image was photographed either as a standard negative image or as a positive image by using the "video reverse" command.

The degree of stenosis of the origin of the internal carotid artery as seen on carotid angiography, intravenous DSA, and incremental dynamic CT was graded on a 0–6 scale: 0 = normal, 1 = minimal stenosis (1%–19%), 2 = mild stenosis (20%–39%), 3 = moderate stenosis (40%–49%), 4 = moderate to marked stenosis (60%–79%), 5 = marked stenosis (80%–99%), and 6 = complete occlusion, according to the method described by Chilcote et al. [6]. In comparing

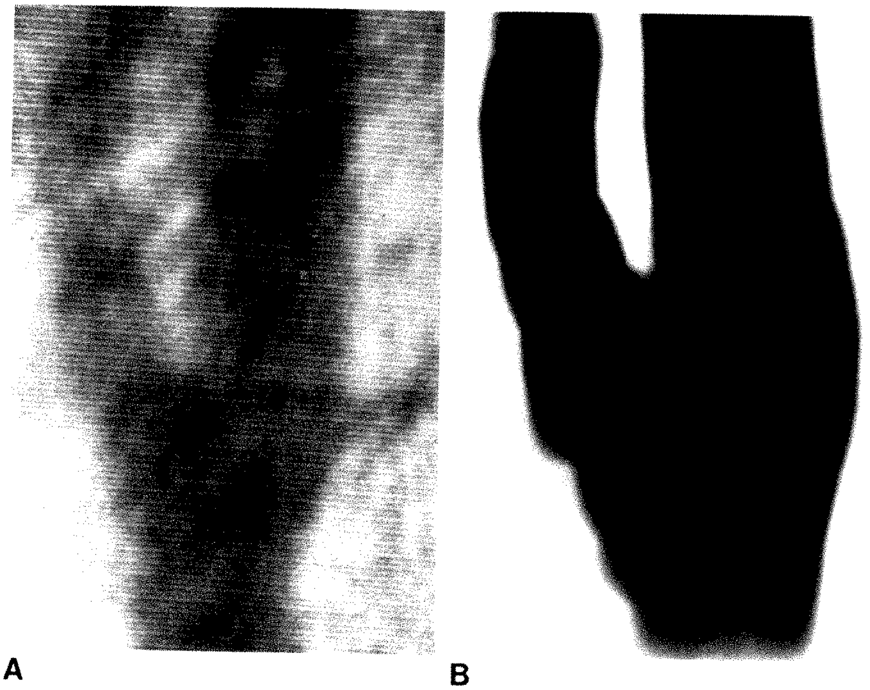

Fig. 3.—Normal common carotid bifurcation. Intravenous DSA (**A**) and incremental dynamic CT (**B**). Internal carotid artery is on reader's right.

the results of incremental dynamic CT with intravenous DSA or carotid angiography, the findings were regarded as concordant if there was no more than one grade difference in the perceived degree of stenosis.

The images obtained by incremental dynamic CT (including axial and reformatted images), DSA, and carotid angiography were graded as poor, acceptable, or excellent. An *excellent* study was one in which the lumen of the terminal part of the common carotid artery and proximal 2 cm of internal carotid artery were clearly seen on axial and reformatted images, without movement-induced artifacts. An *acceptable* image was one on which diagnostic information was considered to be available, although the image was not of optimal quality. A *poor* image did not allow sufficient information for diagnosis. The quality of reformations using 1 pixel width (0.5 mm), 2 pixels (1 mm), and 3 pixels (1.5 mm) was compared, as was that of reformations using "soft-tissue," "standard," and "bone" computer reconstruction algorithms.

Results

The quality of all of the studies was classified as acceptable or excellent. Both standard and soft-tissue computer reconstruction algorithms resulted in reconstruction quality vastly superior to those obtained using the bone algorithms. The quality of the reformatted images obtained by reformations using thicknesses of 1, 2, and 3 pixels was not significantly different (fig. 2).

Of the 20 bifurcations imaged by incremental dynamic CT, five were considered to be normal, 11 showed degrees of stenosis (seven minimal to mild, grades 1 and 2; two moderate to marked, grades 3 and 4; and two marked, grade 5) and four were completely occluded. Examples of each of these categories are illustrated (figs. 3–5). In only one of 14 bifurcations imaged by incremental dynamic CT and carotid angiography were the results of the evaluations discordant. In that case both carotid angiography and incremental dynamic CT showed bilateral internal carotid occlusions, but carotid angiography also showed that the left external carotid artery was occluded. In addition, carotid angiography demonstrated that two patients had moderate to marked middle cerebral artery stenosis.

Eight carotid bifurcations were imaged by both incremental dynamic CT and intravenous DSA. In six of the eight the results were concordant. In one case intravenous DSA failed adequately to demonstrate one of the carotid bifurcations, because of laryngeal artifact and overlap of vessels. In a second case, intravenous DSA was reported to show left internal carotid occlusion (grade 6). Incremental dynamic CT revealed a thin stream of contrast medium in the patent, but severely stenosed, internal carotid artery (grade 5), a finding confirmed by carotid angiography (fig. 6).

A preparation delay of at least 14 sec between injection of contrast medium and scanning was necessary to ensure that the common and internal carotid arteries were satisfactorily opacified on the first scan, as 8 sec delays in some patients with myocardial disease and limited cardiac output did not allow the contrast medium to reach the carotid arteries in time for the first scan. A contrast-medium injection rate as slow as 2 ml/sec adequately opacified all of the neck vessels. Postenhancement scans showed no abnormality in four patients, white-matter ischemia and lacunae in four, a recent cortical infarct in one, and a chronic subdural hematoma in one.

Discussion

Carotid angiography remains the definitive technique for the evaluation of the carotid circulation, including the carotid

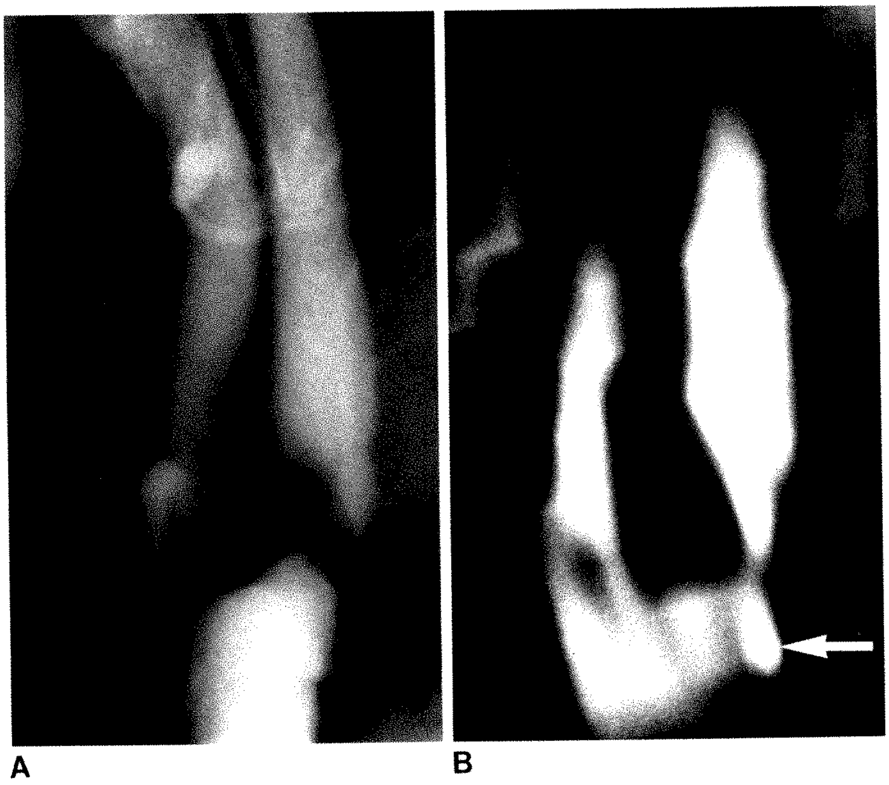

Fig. 4.—Carotid angiogram (**A**) and incremental dynamic CT scan (**B**). Marked stenosis (grade 5) of internal and external carotid arteries. Calcified plaque at origin of internal carotid artery (*arrow*).

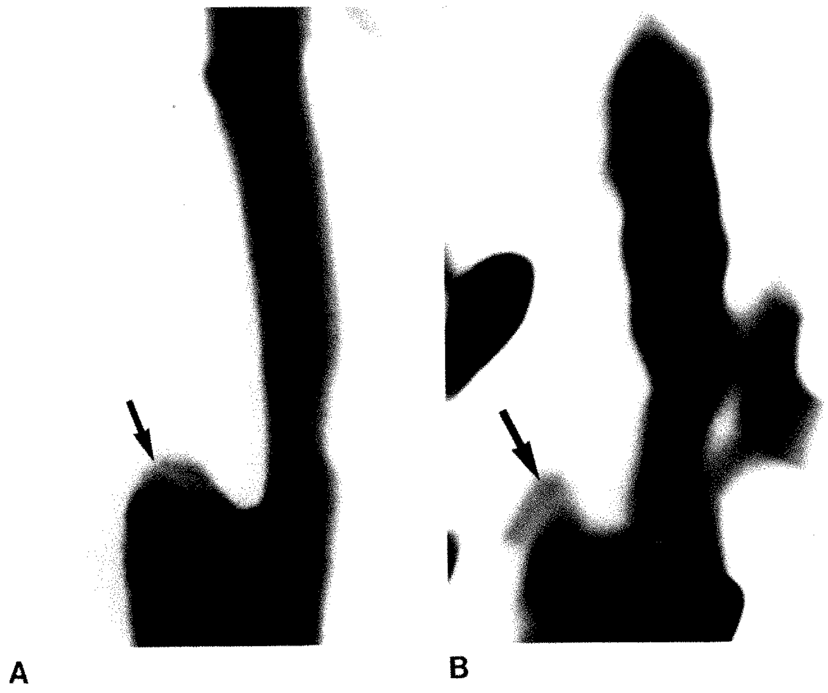

Fig. 5.—Carotid angiogram (**A**) and incremental dynamic CT scan (**B**). Occluded internal carotid artery (*arrows*).

bifurcation. In all 14 carotid bifurcations imaged by both incremental dynamic CT and carotid angiography, the CT-generated images of the bifurcation were considered to be concordant with the angiographic data in estimating the degree of stenosis of the internal carotid artery, although carotid angiography showed occlusion of an external carotid artery not detected by CT in a patient who had bilaterally occluded internal carotid arteries. Management would not have been

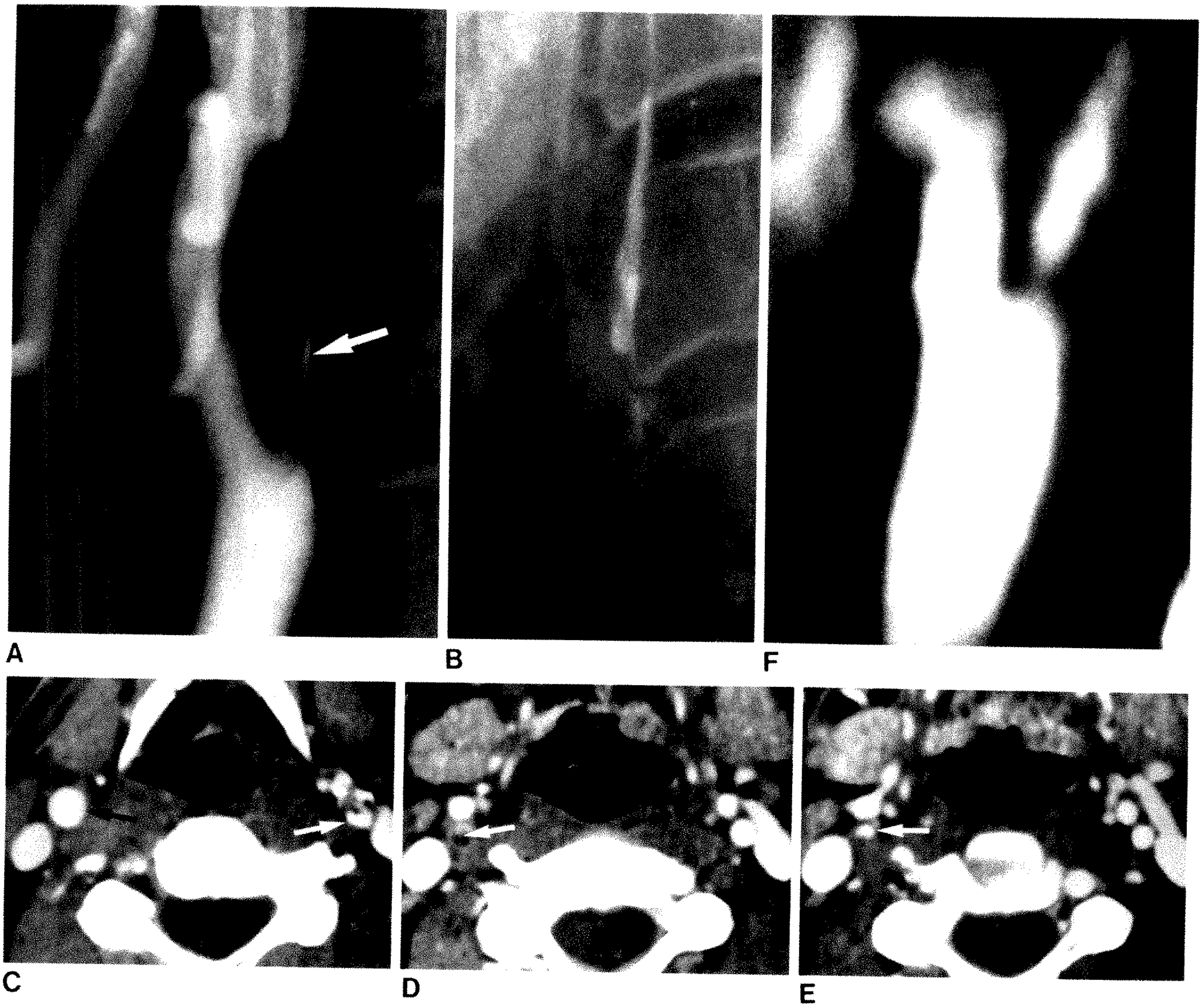

Fig. 6.—**A**, Carotid angiogram, arterial phase. Sliver of contrast medium (*arrow*) in severely stenosed right internal carotid artery. **B**, Carotid angiogram, venous phase. Very slow passage of contrast medium through internal carotid artery. **C**, Axial CT scan through neck 3 mm inferior to termination of right common carotid artery. Right common carotid artery is normal (*black arrow*). Left internal carotid artery is moderately stenosed at its origin (*white arrow*). **D**, Axial CT scan through origin of right internal carotid artery. Right internal carotid artery is almost occluded by atheromatous plaque containing fat-density material. Only a tiny contrast-medium-containing lumen remains (*arrow*). Left internal carotid artery is of normal caliber at this level. **E**, Axial CT scan 3 mm above **D**. Right internal carotid artery now has larger contrast-medium-containing lumen (*arrow*) than in **D**. Rest of true lumen contains relatively isodense thrombus. **F**, Paraxial reformation through right internal carotid artery origin. Severe stenosis and thin distal column of contrast medium.

affected in this patient, as formal angiography was essential as a prelude to extracranial-intracranial bypass surgery.

Incremental dynamic CT and intravenous DSA were discordant in the assessment of two of eight carotid bifurcations. A swallowing-induced misregistration artifact on one projection and an overlap of vessels on the other prevented the demonstration of one carotid bifurcation in the first case. This is a well recognized problem with intravenous DSA [12]. One of the distinct advantages incremental dynamic CT has over intravenous DSA is that each vessel can be clearly distinguished on axial CT images and paraxial reformatted images. The sensitivity of incremental dynamic CT in detecting high degrees of stenosis was graphically demonstrated in a second patient, whose intravenous DSA study had indicated occlusion of an internal carotid artery (fig. 6). The carotid angiogram showed only a very thin column of contrast medium within the proximal segment of the internal carotid artery, due to slow flow of contrast material and consequent layering. However, efficient dispersion of contrast medium throughout the intravascular compartment and the sensitivity of CT to even very dilute iodine concentrations allowed incremental dynamic CT to demonstrate clearly the full extent of the residual lumen of the severely stenosed internal carotid artery (fig. 6). Differentiation between severe stenosis and occlusion is extremely important, as the demonstration of patency allows the possibility of endarterectomy and thrombectomy with successful restoration of a normal internal carotid artery lumen [13].

Two of the patients investigated by CT and carotid angiography were shown by carotid angiography to have significant middle cerebral artery stenoses. Such lesions cannot be detected by the noninvasive carotid tests and are unreliably diagnosed by intravenous DSA [14]. Earnest et al. [14] reported an 8% incidence of "significant" intracranial atheromatous lesions in their comparison of intravenous DSA and conventional angiography in 78 patients and found that these intracranial lesions were often missed by intravenous DSA.

A 3 mm slice width is very practical, allowing the scanning of 4–5 cm of the common carotid artery and its internal and external carotid branches. Slices of 1.5 mm are impractical, because tube heat-loading limits prevent more than a 1.5–2 cm segment being scanned using the incremental dynamic scan program. Five mm slices result in a loss of spatial resolution and unacceptable image degradation on reformatted images.

Incremental dynamic CT is a simple technique and only adds about 5 min to the time taken for a normal contrast-enhanced CT scan. This incorporates the time involved in connecting and securing the intravenous catheter to the mechanical pump and about 1.5 min of scanning time. A conventional head scan can follow immediately. Reformations can be done electively, using the standard Arrange program (GE, Milwaukee), in about 15 min. Operator time can further be reduced by using the "batch mode" option, which allows the reformations to be done after all other computer functions. Patient tolerance is excellent. Instructions other than to keep still are unnecessary with scan durations of 2 sec per scan. Swallowing does not constitute a problem.

At present, the technique is limited to evaluating only the terminal common carotid artery and proximal 2–3 cm of the internal carotid artery. However, most clinically significant atheromatous disease occurs in this segment of the carotid arterial tree [1]. Although incremental dynamic CT cannot reliably detect ulceration, both intravenous DSA and carotid angiography may identify only 50% of surgically confirmed ulcers [14].

Contrast-medium volumes of 140–175 ml are generally used for intravenous DSA studies of the carotid system [15]. In a series of 2488 patients studied with intravenous DSA, four (0.16%) suffered complications related to the total volume of contrast medium [16]. Reducing the volume of contrast medium to a maximum of 80 ml has been recommended for patients with a cardiac history, diabetes, or renal impairment [16]. Incremental CT does not require more than 80 ml of contrast medium.

Cerebral CT scans are increasingly regarded as part of the protocol in the evaluation of patients with TIAs. This preliminary study suggests that the addition of incremental dynamic CT of the carotid bifurcation to the cerebral CT scan can provide valuable and accurate anatomic information, which can help select those patients requiring a more definitive angiographic procedure.

ACKNOWLEDGMENTS

We thank Robyn Fisher and Elizabeth Mobilio for assistance in manuscript preparation.

REFERENCES

1. Millikan CH. Studies in cerebrovascular disease versus the use of anticoagulant drugs in the treatment of intermittent insufficiency of the internal carotid arterial system. *Mayo Clin Proc* **1955**;30:578–586
2. Earnest F IV, Forbes G, Sandok BA, et al. Complications of cerebral angiography: prospective assessment of risk. *AJNR* **1983**;4:1191–1197, *AJR* **1984**;142:247–253
3. Faught E, Trader SD, Hanna GR. Cerebral complications of angiography for transient ischemia and stroke: prediction of risk. *Neurology* **1979**;29:4–15
4. Ackerman RH. Non-invasive carotid evaluation: current concepts of cerebrovascular disease. *Stroke* **1980**;11:675–678
5. Ackerman RH, D'Alton JG, Davis KR, Hesselink JR, Donnan GA, Taveras JM. Complementary roles of non-invasive test battery and DSA in evaluating carotid artery disease. *AJNR* **1983**;4:757–758
6. Chilcote WA, Modic MT, Pavlicek WA, et al. Digital subtraction angiography of the carotid arteries; a comparative study in 100 patients. *Radiology* **1981**;139:287–295
7. Donnan GA, Tress BM, Bladin P. CT in lacunar infarction. *Neurology* **1982**;32:49–56
8. Heinz ER, Dubois P, Drayer B. Intravenous carotid imaging using the third dimension (abstr). *AJNR* **1980**;1:363
9. Brant-Zawadzki M, Jeffrey RB Jr. CT with image reformation for noninvasive screening of the carotid bifurcation: early experience. *AJNR* **1982**;3:395–400
10. Heinz ER, Pizer SM, Fuchs H, et al. Examination of the extracranial carotid bifurcation by thin-section dynamic CT: direct visualization of intimal atheroma in man (part 1). *AJNR* **1984**;5:355–359
11. Heinz ER, Fuchs J, Osborne D, et al. Examination of extracranial carotid bifurcation by thin-section dynamic CT: direct visualization of intimal atheroma in man (part 2). *AJNR* **1984**;5:361–366
12. Hoffman MG, Gomes AS, Pais SO. Limitations in the interpretation of intravenous carotid digital subtraction angiography. *AJNR* **1983**;4:1167–1170, *AJR* **1984**;142:261–264
13. Heros RC, Sekhar LN. Diagnostic and therapeutic alternatives in patients with symptomatic "carotid occlusion" referred for extracranial-intracranial bypass surgery. *J Neurosurg* **1981**;54:790–796
14. Earnest FN, Houser OW, Forbes GS, Kispert DB, Folger WN, Sundt TM Jr. The accuracy and limitations of intravenous digital subtraction angiography in the evaluation of atherosclerotic cerebrovascular disease: angiographic and surgical correlation. *Mayo Clin Proc* **1983**;58:735–746
15. Sheldon JJ, Janowitz W, Leborgne JM, Sivina M, Rojo N. Intravenous DSA of extracranial carotid lesions: comparison with other techniques and specimens. *AJNR* **1984**;5:547–552, *AJR* **1984**;143:1289–1294
16. Pinto RD, Manuell M, Kricheff II. Complications of digital intravenous angiography: experience in 2488 cervicocranial examinations. *AJNR* **1984**;5:553–557, *AJR* **1984**;143:1295–1299

Prevalence of "Compressed" and Asymmetric Lateral Ventricles in Healthy Full-Term Neonates: Sonographic Study

Patricia Winchester[1]
Paula W. Brill[1]
Rebecca Cooper[2]
Alfred N. Krauss[2]
Hart deC Peterson[2, 3]

The premature infant brain has been thoroughly studied by sonography, and normal standards for ventricular size have been established. Whether these apply to normal full-term infants is uncertain. Fifty-three healthy full-term infants were electively examined by real-time sonography through the anterior fontanelle on the first to sixth days of life. Nine had asymmetric lateral ventricles; two of these had unexpected evidence of intracranial hemorrhage, while a third had a ventricular cyst. Forty-four infants had symmetric ventricles, but in 36 the ventricles had little or no cerebrospinal fluid. Vaginal delivery had a statistically significant association with these "compressed' lateral ventricles. This study indicates that seemingly healthy infants may have unsuspected intracranial hemorrhage, that asymmetric ventricular size may be normal, and that shortly after birth most healthy infants have "compressed" lateral ventricles that should not be interpreted as cerebral edema.

The normal appearance of the brain and the changes that occur in intracranial hemorrhage have been well described in sonographic studies of the preterm infant. The full-term infant usually has been examined only when anoxic brain damage, cerebral infection, or a malformation have been suspected. Since routine screening by cranial sonography is generally restricted to the premature infant, normal standards for the full-term infant have not been established. To determine the normal appearance of the lateral ventricles, real-time cranial sonography was performed in a group of healthy full-term infants. The suspicion that standards might differ between the full-term and premature infant was based on the observation in our neonatal intensive care unit that some full-term infants suspected of anoxic brain damage had excellent outcomes despite the sonographic finding of "compressed" lateral ventricles.

Subjects and Methods

Fifty-three healthy infants were selected for the study from the well-baby nursery. Each infant was the product of a full-term, uncomplicated gestation and had an Apgar score of 9 or 10 at 1 and 5 min and a normal physical examination. Both parents gave informed consent. Sonography was performed through the anterior fontanelle with the infant supine. Sonograms were obtained in coronal and sagittal planes using a real-time scanner (Diasonics) with a mechanical sector 6 mHz transducer. The infants ranged in age from 1 to 6 days. The sonograms were assessed for ventricular symmetry and size and the presence of intracranial hemorrhage or other abnormal findings. The lateral ventricles were graded as to size on the basis of qualitative assessment of the amount of cerebrospinal fluid (CSF) seen in the ventricles on both sagittal and coronal views. Asymmetry was recorded if the size of the bodies of the lateral ventricles differed in both craniocaudal and transverse dimensions. There was no attempt to assess asymmetry limited to the occipital horns because of possible errors caused by transducer obliquity when scanning in this region. Complete neurologic examination was performed in those infants in whom asymmetry of the ventricles was noted. Follow-up sonograms were obtained in two of the three infants in whom abnormalities were detected.

This article appears in the January/February 1986 issue of *AJNR* and the March 1986 issue of *AJR*.

Received January 8, 1985; accepted after revision May 29, 1985.

Presented at the annual meeting of the Society for Pediatric Radiology, Las Vegas, April 1984.

[1] Department of Radiology, New York Hospital-Cornell Medical Center, 525 E. 68th St., New York, NY 10021. Address reprint requests to P. Winchester.

[2] Department of Pediatrics (Perinatology Center), New York Hospital-Cornell Medical Center, New York, NY 10021.

[3] Department of Neurology, New York Hospital-Cornell Medical Center, New York, NY 10021.

AJR 146:471-475, March 1986
0361-803X/86/1463-0471
© American Roentgen Ray Society

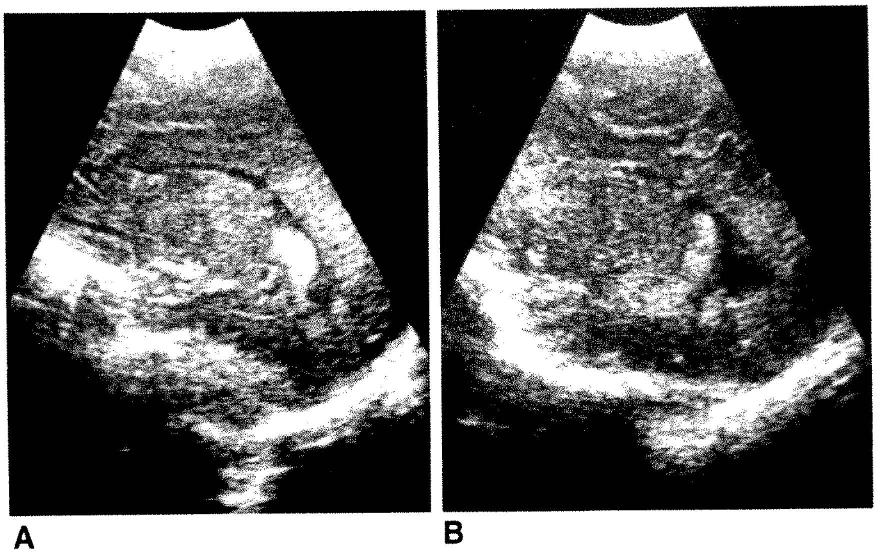

Fig. 1.—Asymmetric ventricles, 3100 g boy, low forceps vaginal delivery. Sonogram on day 2. Sagittal sonogram of right (**A**) and left (**B**) lateral ventricles through trigone. Left lateral ventricle is larger than right.

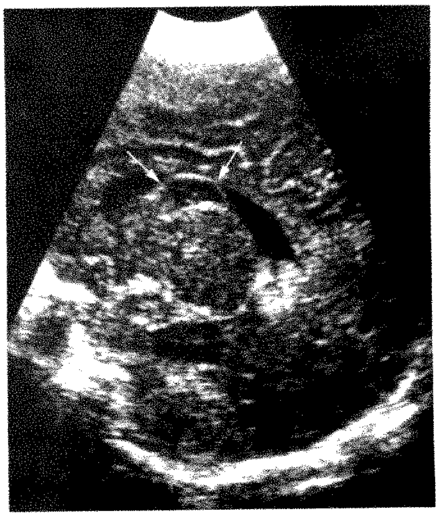

Fig. 2.—Asymmetric ventricles with liquefying subependymal hemorrhage, 4800 g boy delivered by cesarean section to 16-year-old G2, P1 woman. Sonogram on day 3. Sagittal view to left of midline. Anechoic mass (*arrows*) projects into slightly enlarged left lateral ventricle near head of caudate nucleus. Right lateral ventricle was normal.

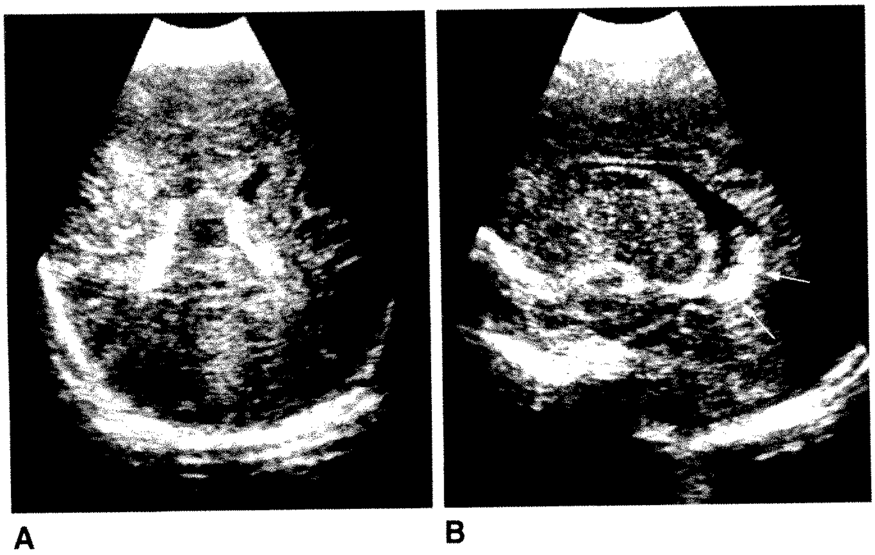

Fig. 3.—Asymmetric ventricles with intraventricular hemorrhage, 4100 g boy born by vaginal delivery. Sonogram on day 2. **A**, Coronal sonogram through bodies of lateral ventricles. Left ventricle is larger than right. **B**, Sagittal sonogram to left of midline. Echogenic material (*arrows*) extends from choroid plexus into left occipital horn.

Results

Of the 53 infants examined, 27 were boys and 26 were girls. The mean weight was 3600 g (range, 2600–4800). The maternal age varied from 15 to 42 years (mean age, 31 years). Twenty of the infants were first-born, 15 were second-born, 11 were third-born, and seven were higher in birth order. Fifteen sonograms were obtained on the first day of life, 11 on the second, 12 on the third, and 15 on days 4–6.

Nine (17%) of the 53 infants has asymmetrical lateral ventricles. The left lateral ventricle was larger than the right in eight infants. The asymmetry was more marked in the posterior body and occipital horn than in the frontal horn and anterior body (fig. 1). Three of the nine infants with asymmetric ventricles had other findings on the cranial sonogram. A liquefying subependymal hemorrhage was present near the head of the caudate nucleus adjacent to the larger left lateral ventricle in one infant (fig. 2). This infant had been born by cesarean section because of a previous section. Follow-up at 2 months continued to show the anechoic hemorrhage; at 4

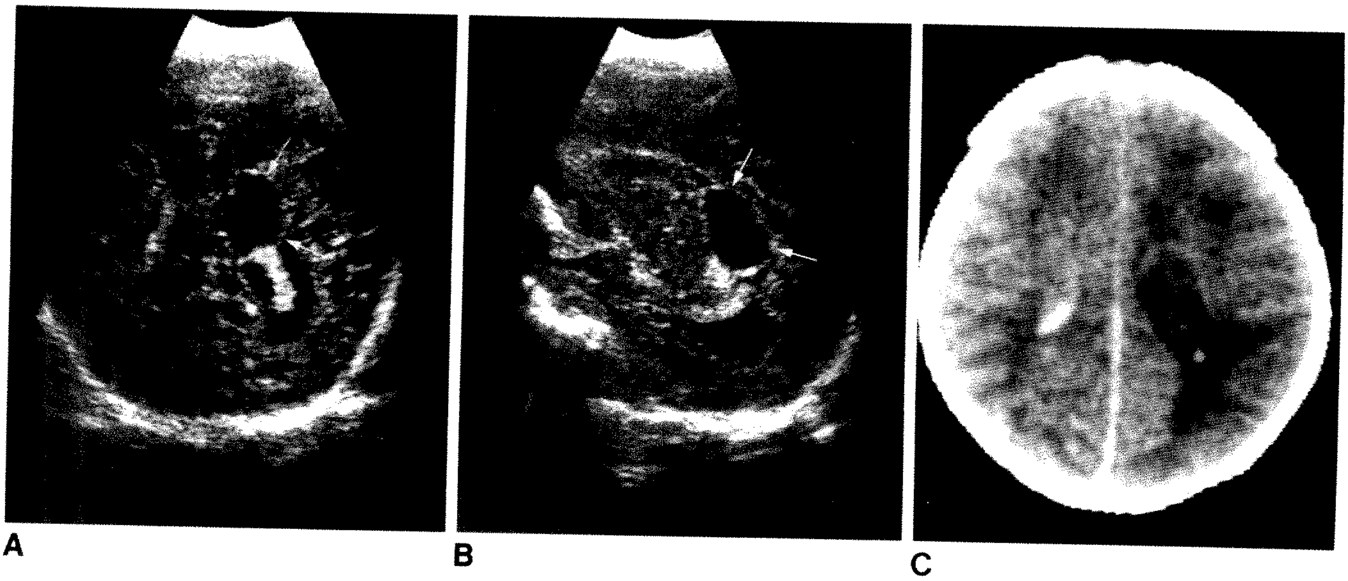

Fig. 4.—Asymmetric ventricles with large cyst in choroid plexus, 3680 g girl born by vaginal delivery. Sonogram on day 2. **A**, Coronal sonogram through bodies of lateral ventricles. Left ventricle is large with its choroid plexus displaced posteriorly. Well defined cystic structure in body of left ventricle (*arrows*). Choroid on right is normal. **B**, Left sagittal sonogram. Frontal horn is normal. Cystic mass measuring 3 × 3 × 2 cm in body of ventricle (*arrows*). Occipital and temporal horns are large. **C**, Postenhancement CT scan. Intraventricular mass does not enhance. It is less dense than brain parenchyma and denser than CSF. Choroid plexus enhancement about mass.

months there was complete resolution. The left lateral ventricle remained larger than the right. Neurologic examination was normal at birth and at 4 and 10 months of age.

Another infant with asymmetric lateral ventricles had irregularity of the margin of the left choroid plexus. Echogenic material extended from the choroid plexus into the left occipital horn (fig. 3). No free blood was noted. The findings suggested intraventricular hemorrhage with clot adherent to the choroid plexus. The study was performed on the first day of life. Birth was by vaginal delivery. Neurologic examination was normal at birth and at 11 months.

In a third infant the body and the occipital and temporal horns of the left lateral ventricles were dilated. A 3 × 3 × 2 cm cystic structure occupied the posterior body of the left lateral ventricle (figs. 4A and 4B). Echogenic strands extended from the choroid plexus to the cyst. The right lateral ventricle and choroid plexus were normal. To rule out the possibility of an intraventricular tumor additional studies were done. A lumbar puncture was normal. Pre- and postenhancement computed tomography (CT) showed a nonenhancing mass in the left lateral ventricle (fig. 4C) corresponding to the cystic lesion demonstrated by sonography. A follow-up sonogram at 2 months of age showed no change in ventricular size or shape or in the appearance of the cyst. The infant's neurologic examination, growth, and development have been normal to 14 months.

The lateral ventricles were symmetric in 44 of the 53 infants examined. Thirty-six of the 44 infants with symmetric ventricles had little or no visible CSF (fig. 5), while in the other eight infants, fluid was easily demonstrable in the bodies and occipital horns of the lateral ventricles (fig. 6). Occasionally the anterior horns were also well seen. No correlation was found between the size of the lateral ventricles and gender of the infant, age or parity of the mother, or the date relative to birth of the sonographic examination. There was, however, a correlation between the type of delivery and the visibility of CSF in the lateral ventricles. Twenty-eight (64%) of the 44 infants with symmetric ventricles were born by vaginal delivery and 16 by cesarean section. Of the eight infants with obvious fluid in symmetric lateral ventricles, six were born by cesarean section. Chi-square and Fisher one-tailed statistical analyses were significant at $p < 0.0189$. The vaginally delivered infants with visible fluid were not examined at an older age than the others. One was studied on day 1 and the other on day 2.

Discussion

In a population of healthy full-term infants selected for normal gestations and Apgar scores of 9 and 10, a 6% incidence of unsuspected abnormalities was noted. All are presumed to be the result of intrauterine intracranial hemorrhage. One hemorrhage occurred in the subependymal region near the head of the caudate nucleus. This hemorrhage showed signs of cystic liquefaction when discovered on the second day of life, suggesting it had occurred during intrauterine life. It resolved in 4 months. Another infant had evidence of intraventricular hemorrhage without apparent involvement of the subependymal germinal matrix. Adherent choroidal clot was present at the trigone extending into the occipital horn on the second day of life. No free ventricular blood was found. The third infant had a large cyst of the left choroid plexus that may have resulted from in utero hemor-

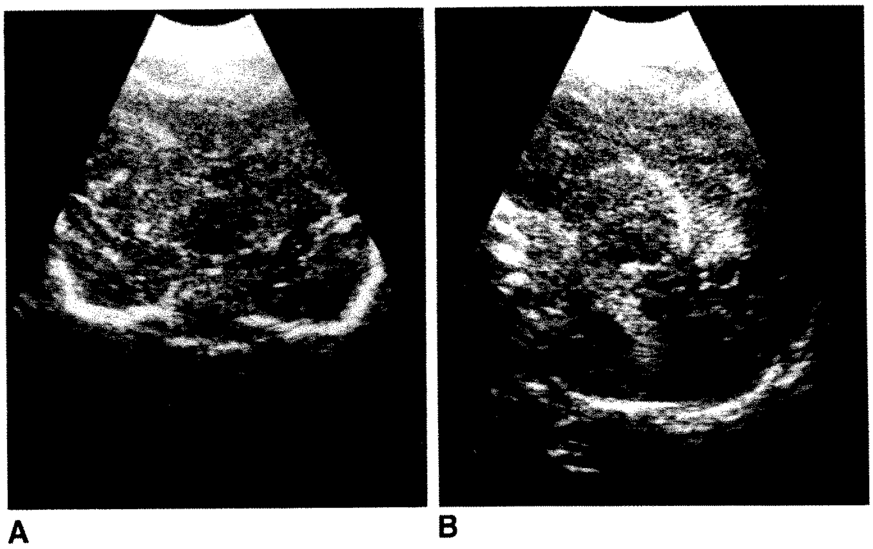

Fig. 5.—Symmetric ventricles with little or no visible CSF, 3060 g boy born by vaginal delivery. Sonogram on day 4. **A**, Coronal sonogram just posterior to foramen of Monro. Little or no visible CSF in lateral ventricles. Brain parenchyma of normal echogenicity. **B**, Sagittal sonogram to right of midline. Normal echogenic choroid plexus in lateral ventricle; no obvious CSF.

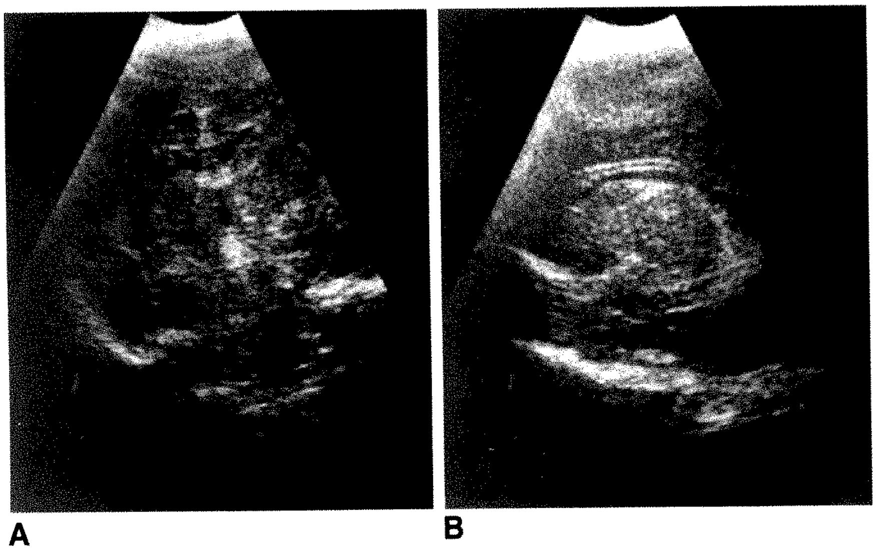

Fig. 6.—Symmetric ventricles with easily seen CSF, 3620 g boy delivered by cesarean section. Sonogram on day 2. **A**, Coronal sonogram through third ventricle. Fluid is easily seen in bodies of lateral ventricles and in third ventricle. **B**, Sagittal sonogram to left of midline. CSF in frontal horn and body of lateral ventricle.

rhage of the choroid plexus. It was unchanged at a 2 month follow-up. Our incidence of intracranial abnormality is similar to the 4.6% incidence found in a large series of full-term infants reported from the University of Texas, Galveston [1]. Subependymal hemorrhage was the only type of intracranial bleeding reported by this group.

Asymmetry of the lateral ventricles has been noted frequently with pneumoencephalography in adults [2] and in older children [3] without abnormalities in the brain. In a recent study of preterm infants with otherwise normal cranial sonograms, Hobar et al. [4] noted that the left lateral ventricle was larger than the right in 32% and that the right lateral ventricle was larger in 6%. Our lower incidence of asymmetry (17%) may reflect the fact that all the infants were studied during the first 6 days of life, a time when the ventricles usually appear "compressed," and subtle differences in size are not apparent. It is interesting that an obvious abnormality was present on the side of the larger ventricle in three of the nine infants with asymmetry. This raises the possibility that intrauterine intracranial hemorrhage may lead to ventricular asymmetry in some cases.

The very small amount of CSF visible in the lateral ventricles of most normal full-term infants indicates that the isolated appearance of "compressed" lateral ventricles is not a reliable sign of cerebral edema in the first few days of life. While the ventricles appear "compressed" in infants with cerebral edema secondary to hypoxia, additional findings such as loss of definition of the interhemispheric fissure and increase in parenchymal echogenicity are necessary for the sonographic diagnosis of cerebral edema [5]. No difference in the overall size of the ventricles was noted in those infants examined on day 1 ($n = 15$) as compared with those studied on days 4–6 ($n = 15$). Sonography was not repeated in this normal population because it did not seem justified to recall healthy infants for sonograms after discharge from the nursery in order to determine the age at which CSF becomes visible in the ventricles.

The high incidence of "compressed" lateral ventricles in healthy infants delivered vaginally invites comparison with the occurrence of retinal hemorrhages in healthy infants. In a study of the fundi of normal newborn infants on the first day of life, Schenker and Gombos [6] found no retinal hemorrhage in infants born by cesarean section and a 19.2% incidence of retinal hemorrhage in those born vaginally. The authors concluded that prolonged labor and various obstetric complications were the main causes of eyeground hemorrhages. In our series, the delivery records of the 16 infants born by cesarean section who had symmetric ventricles (10 "compressed," six "noncompressed") were reviewed to determine whether a trial of labor, the type of anesthesia, or the amount of intravenous fluid the mother received during labor influenced the size of the lateral ventricles. No association was found between these factors and the amount of visible CSF.

We conclude that "compressed" lateral ventricles are the rule not the exception in healthy full-term babies. This appearance of the ventricles cannot be diagnosed as cerebral edema without abnormal periventricular white matter, indistinct sulci and fissures, or decreased cerebral pulsations. Asymptomatic antenatal hemorrhage may be as frequent as 6% in full-term infants. Lateral ventricular asymmetry is usually a normal finding, but if present, a careful search for a resolving or resolved intrauterine intracranial hemorrhage is indicated.

REFERENCES

1. Hayden CK Jr, Shahuck KE, Richardson CJ, Ahrendt DK, House R, Swischuk LE. Subependymal germinal matrix hemorrhage in full-term neonates. *Pediatrics* **1985**;75:714–718
2. McRae DL, Branch CL, Milner B. The occipital horns and cerebral dominance. *Neurology* **1968**;18:95–98
3. Strauss E, Fitz C. Occipital horn asymmetry in children. *Ann Neurol* **1980**;8:437–438
4. Hobar JD, Leahy KA, Lucey JF. Ultrasound identification of lateral ventricular asymmetry in the human neonate. *JCU* **1983**;11:67–69
5. Babcock DS, Ball W Jr. Postasphyxial encephalopathy in full-term infants: ultrasound diagnosis. *Radiology* **1983**;148:417–423
6. Schenker JG, Gombos GM. Retinal hemorrhage in the newborn. *Obstet Gynecol* **1966**;27:521–554

Book Reviews

Radiodiagnosis of the Skull. 103 Radiological Exercises for Students and Practitioners. (Series: Exercises in Radiological Diagnosis.) By Jean-Louis Dietemann. Berlin: Springer-Verlag, 168 pp., 1985; soft cover. $19.50

This little book is one of a series from the Strasbourg School of Radiology. It consists of 103 plain film skull diagnostic cases, each presented with one or two films and no text. A second section follows, consisting of line drawings of the films—each accompanied by a short paragraph discussing the entity. Dr. Dietemann selected an appropriate range of disease entities, included cases that nicely illustrate his points, and arranged the cases to form an effective exercise, especially for review. For the beginning student this book would be an effective way to test knowledge previously gained from a basic textbook having a greater range of discussion.

Springer-Verlag is to be congratulated for producing this paperback book. It has good paper, nice reproduction of the radiographs, and is priced reasonably. The line drawings identify and emphasize the findings in a clear, uncluttered way, and the explanatory paragraphs are concise, clear, and provide a proper amount of detail. The translation is optimal; it does not appear to be a translation.

The author accomplished his purpose with this book. It is recommended for students and as a quick review for practitioners.

Frank W. Farrell, Jr.
Forsyth Memorial Hospital
Winston-Salem, NC 27103

Information Processing in Medical Imaging. Proceedings of the 8th Conference, Brussels, 29 August–2 September 1983. Edited by F. Deconinck. Boston: Nijhoff, 580 pp., 1984.

Information Processing in Medical Imaging is the proceedings of a conference held in August 1983. The book contains 32 papers that are disparate in their content.

Some of the papers, such as the one by Venot et al., "Digital Methods for a Changed Detection in Medical Images," cover a broad topic and are in the nature of a review. Others, such as the paper by Oppenheim and Appledorn, "ART vs. Convolution Algorithms for ECT," are very specific in nature. Some papers, such as that by Bizais et al. on "Coded Aperture Tomography Revisited," discuss topics that have been of interest for a long time, while others, such as "Image Analysis—Topological Methods" by Toet et al., discuss topics that will be novel to most readers.

In addition, some papers, such as "Application of Linear Classifiers to the Recognition of Temporal Behavior of the Heart" by Duvernoy et al., are highly mathematical; while others, such as "Rapid Automatic Functional Imaging of the Heart and the Application of Time Images" by Brown et al., are more descriptive. Most papers have some relation to nuclear imaging methods. Some also include computed tomography, sonography, and magnetic resonance imaging. There are also a small number of papers on the application of statistics to imaging, and several papers on topics such as acoustic-optic deconvolution systems and the visual performance of the human eye.

It is impossible in a short review to discuss these papers in any detail. As a group, they can be characterized as relating more to the fundamentals of imaging science rather than to clinical applications. A positive feature is that they are of reasonable length (average length: about 15 pages), so the authors had adequate opportunity to develop their topic in some detail. This means that papers on topics that will be obscure to most imaging scientists can be read, albeit with some effort. Nevertheless, this book suffers, as do many of its type, because some papers are well written, however, others are poorly organized and presented.

Because it has been a full 2 years since the conference, it is interesting to see that some topics presented at the meeting have developed rapidly but in other areas nothing more has been heard.

Even though the papers in the book are well written and cover a wide variety of interesting topics, it is difficult to discern the intended audience for this book. Researchers in the field would know of the work and that the time elapsed since the conference has made some of the material obsolete. The book's fundamental science and mathematical orientation limits its audience to those doing research in imaging science. People working in this area, especially those who would like to enlarge their horizons, might enjoy browsing through this work.

G. Donald Frey
Medical University of South Carolina
Charleston, SC 29425

CT in Silicosis: Correlation with Plain Films and Pulmonary Function Tests

Colleen J. Bergin[1]
Nestor L. Müller[1]
Sverre Vedal[2]
Moira Chan-Yeung[2]

To investigate the usefulness of computed tomography (CT) in the qualitative and quantitative assessment of silicosis, CT scans, chest radiographs, and pulmonary function tests were obtained in 17 patients with silicosis and six controls. CT scans were graded for extent of silicosis visually and using mean attenuation values. The extent of associated emphysema was also determined. Extent of silicosis as assessed by CT was compared with extent estimated from the chest radiographs using the ILO 1980 classification and pulmonary function tests. Significant correlation was found between both the mean attenuation values ($r > 0.62$, $p < 0.001$) and the visual CT scores ($r > 0.84$, $p < 0.001$) compared with the ILO category of profusion. There was good inter- and intraobserver correlation for the visual CT grades of silicosis ($r > 0.93$, $p < 0.001$). There was poor correlation between the pulmonary function tests and the nodular profusion on the chest radiograph and CT ($r < 0.50$). Correlation was significant, however, between the CT emphysema score and both the FEV_1 % predicted ($r > 0.66$, $p < 0.001$) and the diffusing capacity ($r > 0.71$, $p < 0.001$). Using chest film assessment of the extent of silicosis, visual CT quantitation of silicosis is accurate and reproducible. Attenuation values were less reliable and their use is not recommended as an independent assessment of disease severity. The reduced levels of lung function in these patients correlated with superimposed emphysema rather than the nodular profusion. Emphysema associated with silicosis was easily detected on CT but not on the radiograph.

Estimation of disease severity in silicosis conventionally involves a combination of radiographic and pulmonary function assessment [1]. The chest radiograph is used to detect the characteristic interstitial changes and lymphadenopathy. Pulmonary function tests are the basis for assessing functional limitation.

Description of the CT appearance of silicosis in radiologic literature has been limited [2]. Computed tomography (CT), however, has proven superior to the chest radiograph in the early detection of pulmonary nodules [3] and interstitial changes [4]. The advantage of decreased superimposition of parenchymal structures provided by using thin CT slices in the transaxial plane allows clear visualization of the distribution and severity of parenchymal changes [4, 5]. Recent reports have also suggested that CT is useful in detecting emphysema, which may be associated with any pulmonary disease [6–8].

To describe the range of abnormalities in silicosis visible by CT and to compare disease extent assessed by CT with that estimated from the ILO classification of radiographs and pulmonary function, we performed CT, chest radiography, and pulmonary function tests on 17 patients with silicosis and six patients with no history of exposure to silica dust. We found CT to be informative in quantitating the extent of silicosis and in detecting the presence of associated emphysema.

Subjects and Methods

CT scans were performed on 23 patients, 17 of whom had previously been diagnosed as

Received June 5, 1985; accepted after revision November 20, 1985.

This work was supported by a grant from the British Columbia Lung Association to N. L. Müller and M. Chan-Yeung.

[1] Department of Radiology, University of British Columbia, Vancouver General Hospital, 855 W. 12th Ave., Vancouver, BC, Canada V5Z 1M9. Address reprint requests to N. L. Müller.

[2] Department of Medicine, University of British Columbia, Vancouver General Hospital, Vancouver, BC, Canada, V5Z 1M9.

AJR 146:477–483, March 1986
0361–803X/86/1463–0477
© American Roentgen Ray Society

having silicosis. The diagnosis was based on a history of exposure to silica and radiographic changes consistent with silicosis. Because of their occupational histories, all of which involved either hard rock mining or sandblasting, these patients are evaluated annually with physical examination, chest radiography, and pulmonary function tests. As part of their evaluation during the period from January 1984 to February 1985, 17 patients consented to have a chest CT scan. Six patients with no history of exposure to silica acted as a control group.

The average age of the 17 men with silicosis was 58.6 years (range 40–84) and all but two of them were heavy smokers (mean, 23.8 pack-years). They had an average of 19.1 years exposure to silica (table 1). Their lung function was slightly to moderately impaired. The six controls had no history of exposure to silica or of any respiratory problems. They had normal pulmonary function tests.

The CT scans were performed on either the GE 9800 or GE 8800 scanner at 1-cm intervals using 10-mm collimation from the apex of the lungs to the base of the diaphragm during breath-holding after deep inspiration. Scans were viewed at window levels appropriate for pulmonary parenchyma (window level −500 to −700, window width 1000 to 2000). Visual scoring systems were devised to evaluate the extent of the silicosis and the extent of emphysema using CT. The CT scans were read on two occasions by two observers working independently. Inter- and intraobserver correlations were assessed.

CT Grading System for Silicosis

Grade 0 was given if there were no definite nodules. Grade I was given if a small number of nodules was detected (fig. 1A). With small numbers of nodules, there was no disruption of vascular markings. Grade II indicated the presence of many nodules, but with no confluence (fig. 1B). Normal parenchymal markings were visible. Grade III CT scans demonstrated confluence of nodules, usually associated with disruption of vascular markings (fig. 1C). Grade IV was given for confluence of nodules extending over two or more slices, consistent with the diagnosis of progressive massive fibrosis (PMF) (fig. 1D).

Mean Attenuation Values

Lung density was measured at three levels in the right hemithorax: at the level of the aortic arch, at the carina, taking care to avoid the minor fissure, and immediately above the diaphragm. The region of interest was determined by hand using the cursor to trace the perimeter of the right lung, with the medial border being lateral to the right hilum. Mean attenuation values of the slices and an average of the mean attenuation values of all three slices were calculated.

Standard posteroanterior chest radiographs were read using the ILO 1980 classification of radiographs of pneumoconioses by an independent radiologist. This radiologist routinely interprets the radiographs of patients with pneumoconioses and was not involved with the CT assessments. Correlation coefficients between the visual and numerical CT grades and the ILO category of profusion were calculated.

CT Grading System for Emphysema

The CT scans were scored for the extent of emphysema using a visual scoring system similar to the one described by Goddard et al [6]. We considered areas of abnormally low attenuation, as determined visually, vascular disruption, or obvious bullae to indicate the presence of emphysema [6]. We assessed all slices and graded the CT scans using a 4-point system based on estimating the percentage of the overall area that demonstrated emphysematous or bullous changes: 1 was given if less than 25% of the lung parenchyma was involved, 2 if 25%–50% of the parenchyma demonstrated emphysematous changes, 3 if 50%–75% of the area was abnormal, and 4 if more than 75% of the lung parenchyma was affected by emphysematous changes.

TABLE 1: **Pulmonary Function Tests on the 17 Patients with Silicosis**

Test	% Predicted	
	Mean	SD
FEV_1	80.1	29.5
FEV_1/FVC	93.9	14.1
TLC	93.3	16.9
DCO	87.3	10.3

Note.—FEV_1 = forced expiratory volume in 1 sec; FVC = forced vital capacity; TLC = total lung capacity; DCO = single-breath carbon-monoxide diffusing capacity.

Pulmonary Function Testing

All subjects performed tests of spirometry, diffusing capacity, and lung volumes. Maximum forced vital capacity (FVC) maneuvers were performed as recommended by the American Thoracic Society [9], with the best "sum" curve (largest sum of FVC and forced expiratory volume in 1 sec [FEV_1]) being used for the analysis. Testing was done either on a 10 L Ohio rolling-seal spirometer (16 subjects) or on a 12 L Morgan rolling-seal spirometer (four subjects). There was no systematic difference in measurements made on the two spirometers. Single-breath carbon-monoxide diffusing capacity (DCO) and steady-state helium-dilution lung volumes were also measured. The maximum of two DCOs was used if the DCO divided by the single-breath helium-dilution lung volume was reproducible within 10%. Reference equations of Crapo et al. [10–12] were used to define percentage of predicted value.

Pulmonary function tests were correlated with the visual CT emphysema scores and extent of disease estimated from both the chest radiographic and CT scores using linear regression analysis.

Results

The pulmonary function tests in the patients with silicosis are summarized in table 1. Slight to moderate impairment prevailed.

Qualitative Analysis of Silicosis

The feature most characteristic of silicosis on CT is the presence of nodules. In patients with mild silicosis, these nodules were seen only in the upper lobes. They varied in size but all were less than 1 cm in diameter (fig. 1A). In 13 of the 17 patients with silicosis, a posterior predominance of nodules was seen on the CT scans (fig. 1B). This distribution was not obvious from the chest radiographs. Increased linear densities were not a prominent feature of either the chest radiograph or CT scan in mild silicosis. More severe silicosis was characterized on CT by an increase in the number and size of nodules. Disruption in the normal vascular markings in the pulmonary parenchyma and bullous formation were prominent when the nodules became confluent (fig. 1C). In four patients with PMF, there was gross disruption of the pulmo-

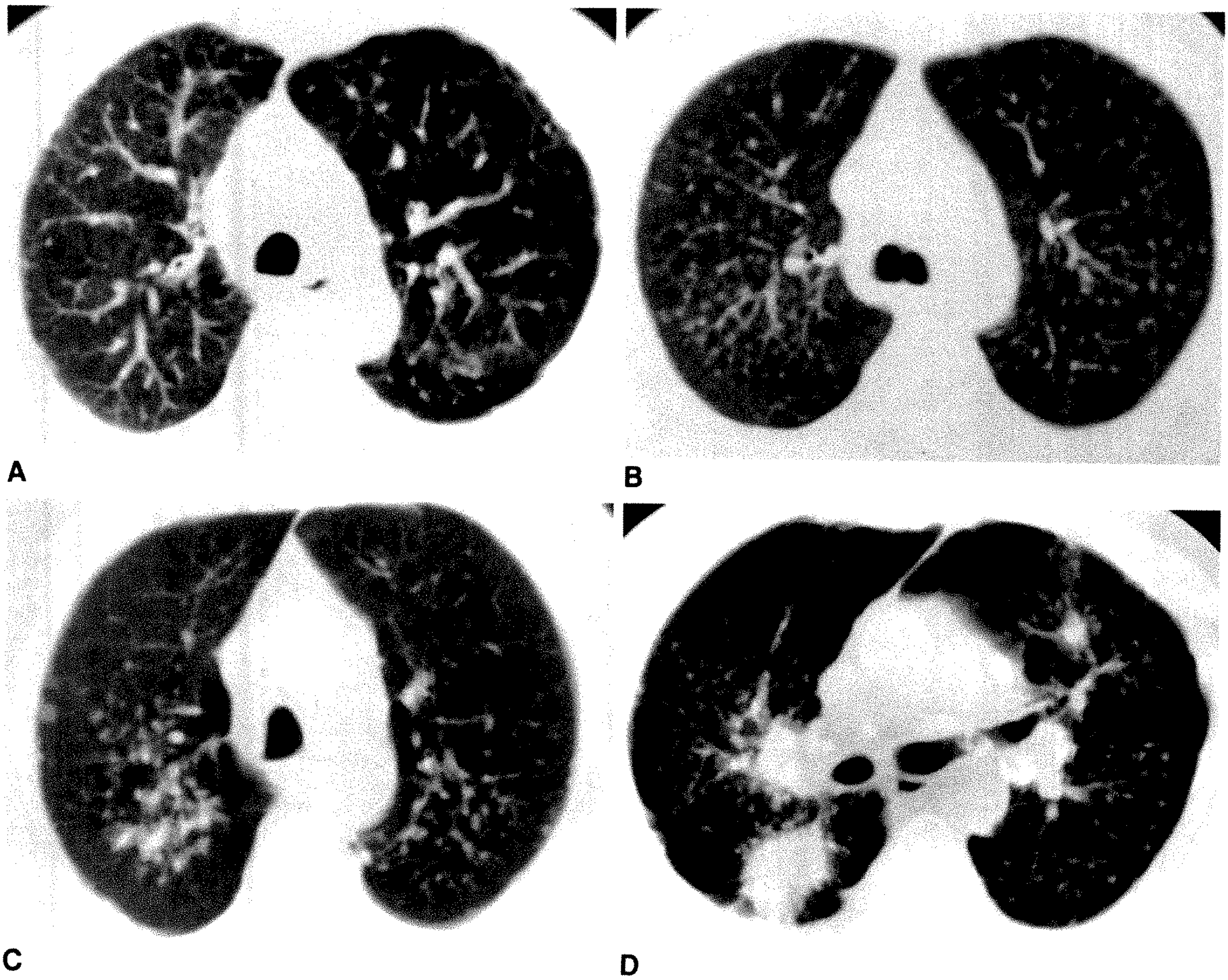

Fig. 1.—Silicosis on CT. **A**, Grade I: scan through carina in patient with mild silicosis. A few nodules are present, with otherwise normal lung parenchyma. **B**, Grade II: Many nodules are present, but without confluence. **C**, Grade III: Confluence of nodules is seen, associated with some disruption of vascular markings on right. Nodules are predominantly posterior in distribution. Paraseptal bullae are present in right lung adjacent to mediastinum. **D**, Grade IV: Dense confluence of nodules extended over four CT slices. This was considered consistent with progressive massive fibrosis. Calcification is also present within hilar nodes.

nary parenchyma in the upper lung zones. This was more readily appreciated on the CT scan than on the chest radiograph (fig. 2). Increased linear densities and some pleural scarring were also seen, but the prominent feature of PMF was the masslike consolidation associated with apical parenchymal scarring and bullous changes.

Diffuse emphysematous changes consisting of small bullae and areas of low attenuation were seen both in patients with few and in those with many nodular densities. These changes suggestive of centrilobular emphysema involved both the apices and the lung bases and were seen to a marked degree in six patients, all but one of whom had been heavy smokers. The ILO reading of the chest radiograph for four of these patients included the term "bu" which indicated detection of some bullous changes; however, there is no effective way of quantitating these changes using the chest radiograph.

Mediastinal and hilar lymph nodes in the patients with silicosis varied from 0.5 to 2.0 cm in diameter. Calcification was commonly seen in the lymph nodes. No calcification of the pleura was seen.

Quantitative Analysis of Silicosis

There was good correlation between the CT assessment of the extent of silicosis by both observers and the ILO category of profusion by one observer ($r > 0.84$, $p < 0.001$) (fig. 3). Significant but lower correlation was also obtained for assessment of silicosis extent using mean attenuation values compared with profusion ($r > 0.64$, $p < 0.001$). The visual assessment of silicosis by CT proved reproducible, with good intra- and interobserver correlation. The intraobserver correlation coefficients for CT silicosis scores were $r = 0.95$ for

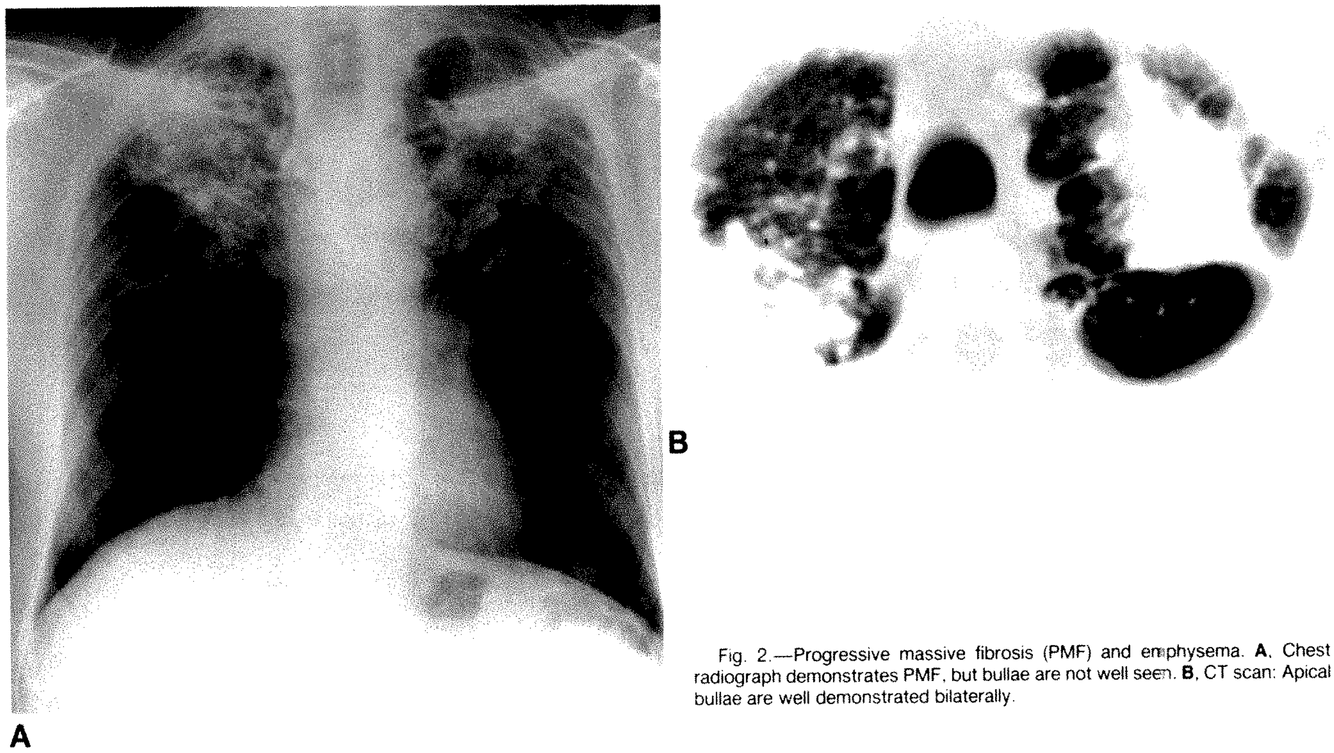

Fig. 2.—Progressive massive fibrosis (PMF) and emphysema. **A**, Chest radiograph demonstrates PMF, but bullae are not well seen. **B**, CT scan: Apical bullae are well demonstrated bilaterally.

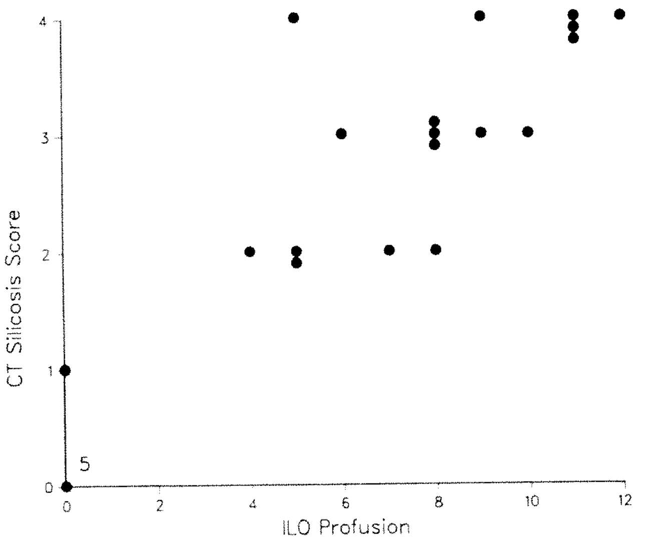

Fig. 3.—Correlation between CT silicosis score (mean of four observers) and ILO category of profusion in 17 patients with history of exposure to silica dust and six control subjects ($r = 0.94$).

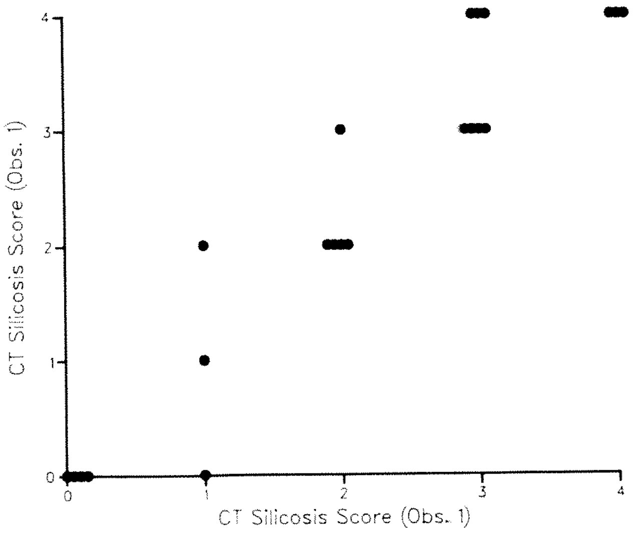

Fig. 4.—Intraobserver correlation for CT silicosis scores in 16 patients with history of silica exposure and six control subjects ($r = 0.95$). (One patient was added to the study after this observer had made this initial analysis of 22 subjects.)

observer 1 (fig. 4) and $r = 0.96$ for observer 2. The lowest interobserver correlation coefficient was $r = 0.94$ (fig. 5). There was also good intra- and interobserver reproducibility of the CT emphysema scores ($r > 0.85$, $p < 0.001$).

Poor correlation was seen between the pulmonary function tests and the extent of silicosis as assessed by chest radiograph and CT scan ($r < 0.50$, $p > 0.05$). Significant correlation was obtained, however, between the visual CT emphysema score and the FEV_1 % predicted ($r > 0.64$, $p < 0.001$) and the DCO % predicted ($r > 0.70$, $p < 0.001$) (figs. 6 and 7). Lower correlation was seen between the CT emphysema

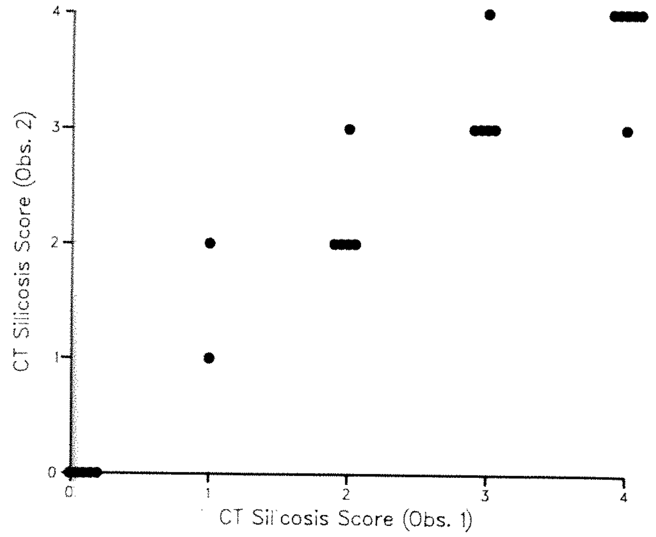

Fig. 5.—Interobserver correlation for CT silicosis scores in 17 patients with history of silica exposure and six control subjects ($r = 0.96$).

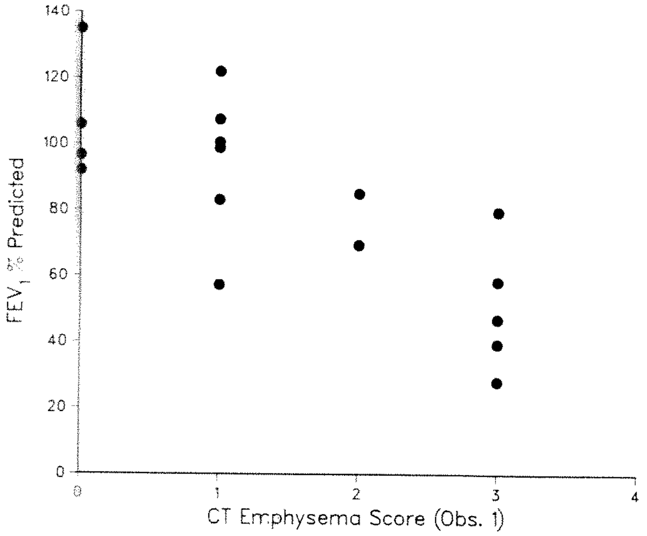

Fig. 6.—Correlation between CT emphysema score and FEV$_1$ % predicted in 17 patients with silicosis ($r = 0.80$).

score and FEV$_1$/FVC ratio ($r > 0.57$, $p < 0.001$), and there was no correlation with total lung capacity (TLC) % predicted.

Discussion

The characteristic radiographic and pathologic picture of silicosis results from exposure of a patient to high concentrations of silica or silicon dioxide. In North America, hard rock mining is the occupation most frequently associated with chronic silicosis, and sandblasting is the most common cause of acute silicosis. The diagnosis of silicosis requires the combination of an appropriate history of silica exposure and the characteristic chest radiograph appearance.

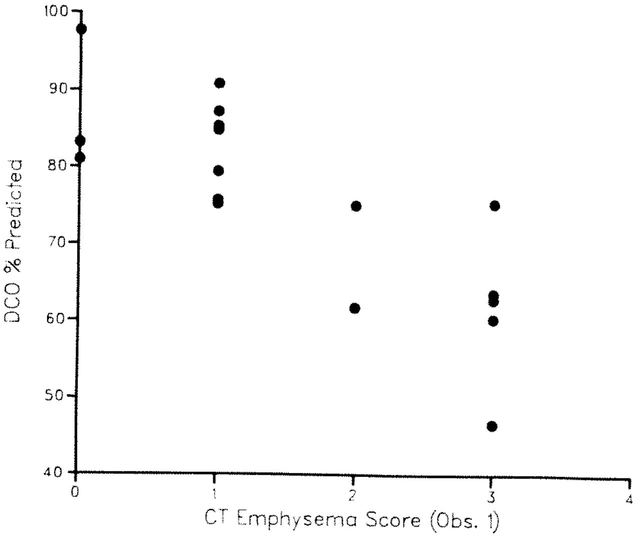

Fig. 7.—Correlation between CT emphysema score and DCO % predicted in 17 patients with silicosis ($r = 0.80$).

By convention, the extent of silicosis is evaluated radiographically according to the ILO 1980 classification of radiographs of pneumoconioses [13]. This system was designed to quantitate radiographic changes of the pneumoconioses in a simple reproducible manner. In the chest radiograph of silicosis, nodular opacities are the predominant finding [1, 14, 15]. In severe disease, aggregation of nodules into masses consistent with PMF are observed.

We have described the CT appearance of patients with increasing extent of silicosis. The chest radiograph ILO category of profusion of nodules was used as the standard of silicosis extent. The transaxial view of the lung provided by CT readily demonstrated the number, size, and distribution of nodules in silicosis. The decreased superimposition of parenchymal structures enables CT to demonstrate nodular densities without the chest radiographic problem of "subtraction of nodules" referred to by Heitzman [15]. In quantitating the extent of silicosis using CT, the number of nodules and the presence of consolidation were the features most readily assessed. Increased interstitial markings were seen in some patients with silicosis, but these were minimal and sufficiently infrequent to be excluded in devising a CT grading system of severity. The ILO 1980 classification of radiographs has a separate category for large nodular opacities, which includes PMF. Our system for grading the extent of silicosis on CT is based on a spectrum of increasing area of the pulmonary parenchyma occupied by nodular opacities from grade I, representing a few nodules, to grade IV, representing areas of consolidation consistent with PMF. This grading system compared closely with the radiographic assessment of extent using the ILO category of profusion of nodular opacities and was consistently reproducible in our group of patients. One of the limitations of our study is that we have compared one radiologic procedure (chest radiograph) with a second radiologic method (CT). The ILO readings of the chest radiographs are the generally used "gold standard" of silicosis extent, but comparison with pathologic specimens would more accurately assess both methods.

Quantitative measurements of pulmonary parenchymal disease using mean attenuation values have stimulated considerable interest recently. Goddard et al. [6] found significant differences in mean attenuation values between patients with normal lungs and those with emphysema, and also patients with interstitial fibrosis. An objective system for quantitating silicosis would be very desirable, but there are technical problems with CT lung densitometry. Mean attenuation values are known to vary in the same patient depending on the phase of respiration [16]. Operator positioning of the region of interest (ROI) is a further source of variation in the mean attenuation value, independent of the disease process [4]. In advanced silicosis, the upper lobes of the lungs are often very dense. This marked difference from normal lung might provide a basis for the useful density measurements in silicosis as in other parenchymal diseases where there is less of a difference between normal and abnormal lung tissue. In our series, there was significant correlation between the mean attenuation values and the ILO profusion category. However, these values underestimated the more advanced grades of silicosis in some patients when compared with both the visual CT silicosis score and the ILO profusion category. There was also variation between values obtained from the two different CT scanners. This problem has been described previously [17]. Obviously, the mean attenuation value in advanced grades of silicosis is influenced by how much of a given slice is affected by PMF, and the slice choice for the ROI is operator dependent. To avoid observer bias, an average density for all of the upper lobe slices would be needed. This is time-consuming but may prove helpful in the future in quantitating silicosis. At present, we do not recommend that CT lung density be used as an independent assessment of disease extent in silicosis.

A major advantage that CT provides, in addition to the chest radiograph assessment in silicosis, is evaluation of parenchymal destruction. The chest radiograph may detect large bullae but is notably insensitive in detecting more diffuse emphysematous changes [18]. In the ILO classification, the presence of bullae is denoted by the symbol "bu," but there is no system for quantitating bullous changes. The CT scan allowed quantitation of emphysematous changes seen in association with the silicotic nodules. The degree of parenchymal destruction seen on CT correlated well with the % predicted DCO and FEV_1 and less so with the FEV_1/FVC. Pulmonary function tests may be normal in early silicosis. More severe disease reflects two pathologic states with opposing effects on pulmonary function: fibrosis causing restrictive changes, and the development of secondary emphysema causing hyperinflation and decreased air flow [19]. Further obstructive changes may result from smoking; five of the six patients in our series with evidence of severe parenchymal destruction had been heavy smokers. Quantitation of the nodular changes both by chest radiograph and CT did not correlate well with pulmonary dysfunction.

Apical bulla formation secondary to scarring of the pulmonary parenchyma in silicosis is well known. Associated centrilobular or panacinar emphysema in the lower lobes is usually attributed to cigarette smoking. The CT scan can identify large apical bullae, but it is yet to be determined whether the pattern of parenchymal destruction seen in the lower lobes of patients with a history of silica exposure who were not smokers is different from patients with emphysema secondary to smoking alone. Further investigation of parenchymal destruction in nonsmoking patients with silicosis is required.

In conclusion, we have described the CT changes seen in silicosis and a method for quantitating these changes. Using this method, we have demonstrated good correlation between the visual CT assessment of silicosis and the ILO category of profusion. Use of a visual scoring system is likely to prove more reproducible than mean attenuation values; however, further evaluation of lung density as a measure of disease severity is warranted. More importantly, however, in this group of patients, CT changes of emphysema effectively predicted pulmonary dysfunction. This information is not obtainable from the chest radiograph.

Because of the cost of CT compared with the chest radiograph, we do not recommend use of CT in the routine assessment of silicosis. In all our patients, the nodules were clearly seen on the chest radiograph. We also do not suggest the use of CT in the diagnosis of emphysema in these patients. The pulmonary function tests are obviously superior in assessing the degree of pulmonary disability. Our study indicates that the deterioration of pulmonary function in patients with silicosis correlates with the extent of associated emphysema and not with the profusion of nodules.

ACKNOWLEDGMENTS

We thank Dr. Charles A. Maclean for help with reading chest radiographs, Joe Comeau for statistical analysis, and Betty Fowler for secretarial assistance.

REFERENCES

1. Fraser RG, Paré JA. *Diagnosis of diseases of the chest.* Philadelphia: Saunders, **1982**:573–582
2. Raithel HJ, Valentin H. Computer-tomographic examination of patients with asbestosis and silicosis. *Prax Klin Pneumol* **1983**;37:1119–1129
3. Coddington R, Mera SL, Goddard PR, Bradfield JWB. Pathological evaluation of computed tomography images of lungs. *J Clin Pathol* **1982**;35:536–540
4. Naidich DP, Zerhouni EA, Siegelman SS. *Computed tomography of the thorax.* New York: Raven, **1984**:201–206
5. Kreel L. Computed tomography of interstitial pulmonary disease. *J Comput Assist Tomogr* **1982**;6:181–199
6. Goddard PR, Nicholson EM, Laszlo G, Watt I. Computed tomography in pulmonary emphysema. *AJR* **1978**;130:429–440
7. Foster WL Jr, Durham NC, Halvorsen RA Jr, Godwin JD, Roggli VL, Pratt PC. CT and pathologic correlation in centrilobular emphysema. Abstract. *Radiology* **1984**;153(P):236
8. Hayhurst MD, MacNee W, Flenley DC, et al. Diagnosis of pulmonary emphysema by computerized tomography. *Lancet* **1984**;2:320–322
9. Gardner RM, Chairman. ATS statement—Snowbird workshop on standardization of spirometry. *Am Rev Respir Dis*

1979;119:831–838

10. Crapo RO, Morris AH, Gardner RM. Reference spirometric values using techniques and equipment that meet ATS recommendations. *Am Rev Respir Dis* **1981**;123:659–664
11. Crapo RO, Morris AH. Standardized single breath normal values for carbon monoxide diffusing capacity. *Am Rev Respir Dis* **1981**;123:185–189
12. Crapo RO, Morris AH, Clayton PD, Nixon CR. Lung volumes in healthy nonsmoking adults. *Bull Europ Physiopathol Respir* **1982**;18:419–425
13. Classification of radiographs of the pneumoconioses. *Med Radiogr Photogr* **1981**;57:1–17
14. McLoud TC, Gaensler EA, Carrington CB. Chronic diffuse infiltrative lung disease: newer approaches. *Clin Chest Med* **1984**;5:332–344
15. Heitzman ER. *The lung: radiologic-pathologic correlations*. Toronto: Mosby, **1984**:92–98
16. Rosenblum LJ, Mauceri RA, Wellenstein DE, et al. Density patterns in the normal lung as determined by computed tomography. *Radiology* **1980**;137:409–416
17. Levi C, Gray JE, McCullough EC, Hattery RR. The unreliability of CT numbers as absolute values. *AJR* **1982**;139:443–447
18. Thurlbeck WM, Simon G. Radiographic appearance of the chest in emphysema. *AJR* **1978**;130:429–440
19. Bates DV, Macklem PT, Christie RV. *Respiratory function in disease*. Philadelphia: Saunders, **1971**:376–379

Book Reviews

Computer Assisted Radiology. Computergestützte Radiologie. Proceedings of the International Symposium, CAR'85 Computer Assisted Radiology (in English and German). Edited by Heinz U. Lemke, Michael L. Rhodes, C. C. Jaffee, and Roland Felix. Berlin: Springer-Verlag, 724 pp: 1985. $39

This tome represents the syllabus of a symposium held in Berlin at some unspecified time in 1985, most likely June, as far as can be gleaned from the preface. Thus, one certainly cannot quibble over outdated material. However, the unindexed text appears to be a direct offset compilation of submitted manuscripts and abstracts, presenting a rather disruptive variety of typefaces, type sizes and intensities, dot matrix printouts, and even a few lines of manuscript. There appears to have been a lack of editing, as witness overstrikes, and the like. The graphics are primarily photographs, graphs, and equations, while the few radiographs suffer from the matte surface of the paper.

Enough said of form. Does the substance come out ahead on balance? This reviewer feels that the need to get rapidly developing and changing original material rushed into print and disseminated justifies the unorthodox, at least to most radiologists, format. After all, I am not certain this book is even directed toward most radiologists.

The text represents six conference sessions and two workshops. Most papers are in English with the balance in easily comprehensible German.

The discussion of digital image generation encompasses computed tomography, magnetic resonance imaging, nuclear medicine, and digital radiography, dealing with the developmental and engineering aspects of techniques and software which, one assumes, lie in the future for the medical consumer. There are few images presented.

The brief section on picture archiving and communication systems (PACS) deals primarily with engineering aspects of data transmission. The papers on applications are directed toward the radiologic and related equivalents of computer assisted design (CAD), as pertinent to radiation therapy and orthopedics, while the sections on computer vision and graphics are concerned with image manipulation and multidimensional presentation respectively. The remainder of the volume deals principally with present and potential computer graphics applications in radiology.

In summary, this book presents current research data on computer directions and use in radiology. Most clinical radiologists very likely will prefer to have these data professionally sifted before encountering them, as in the appropriate specialty periodicals. Departmental physics and engineering personnel may find the book more to their liking, but must realize the contents are as long-lived as those of a monthly journal's "work-in-progress." All readers may find the lack of an index, except to authors, and the raw manuscript appearance a bit trying.

Stephen A. Kanter
282 Wigmore Drive
Pasadena, CA 91105

Digital Cardiac Imaging. Edited by Andrew J. Buda and Edward J. Delp. Boston: Nijhoff, 307 pp., 1985. $60

As the title indicates, this book covers cardiac imaging by different means that employ digital processing. It begins with a short overview; the next five chapters consist of basic considerations and principles related to digital image processing and physical principles. Computer hardware and physiologic concepts are included plus analysis of left ventricular motion in a geometric perspective.

The next 10 chapters discuss clinical applications of different imaging methods. Left ventricular function, coronary flow reserve, and quantitative coronary arteriography as pertaining to digital angiography are described. Cardiac computed tomography, digital two-dimensional echocardiography, and Doppler echocardiography are in successive chapters. Finally, radionuclide imaging, positive emission computed tomography, and magnetic resonance imaging are covered. The final chapter is on future directions and an integrated approach in digital cardiac imaging.

This book is hardbound, relatively easy to read, and is well organized. Many pathologic states are not covered in detail. Likewise, there are few excellent illustrations. This is meant more as a review of current research and the latest in evaluation of cardiac disease as opposed to a thorough comprehensive text. It is intended for the invasive or image oriented cardiologist or cardiovascular radiologist, especially those with digital imaging equipment.

Harris Newmark III
1324 Brinkley Ave.
Los Angeles, CA 90049

The Radiographic Appearance of the Medtronic Hall Valve Prosthesis

Alexander C. Mamourian[1] and Walter E. Pae[2]

The Medtronic Hall prosthetic heart valve, also referred to as the Hall-Kaster valve, was introduced for human use in 1977. Since then its clinical use has been increasing, although its radiographic appearance has not yet been reported. The advantages of this valve configuration are a very low incidence of thromboembolism and a large anulus-to-valve-orifice ratio [1]. The valve has a disk with a central hole, which follows the contour of a single long metal strut (fig. 1). The disk has a two-part motion that permits it to open widely. Three smaller metal struts arrest the disk motion in its open position at a 75° angle with the valve ring. When the valve is in the aortic or mitral position, there is a relatively unobstructed flow of blood allowing low transvalvular gradients. On the lateral view of the chest, the Medtronic Hall valve has a strikingly incomplete appearance (fig. 2). Without previous knowledge of this valve configuration, it might be mistaken for a Björk-Shiley valve with strut fracture. This is particularly important in light of the recent reports of Björk-Shiley valve fractures. Both inlet strut and, in more recent models, outlet strut fracture is possible in Björk-Shiley valves [2, 3] (fig. 3).

In the clinical setting of the patient with dyspnea or hypotension and a prosthetic heart valve, it is important to correctly identify and assess the valve. Since there is a radiopaque marker in the pyrolytic carbon disk in Björk-Shiley valves manufactured after 1975, these valves should be readily identified (fig. 4). Absence of a radiopaque marker, however, is not as helpful. The disks of the older Björk-Shiley valves are nonopaque as are those of the Medtronic Hall valve. In addition, the disk may escape from a fractured Björk-Shiley valve ring [4]. The Medtronic Hall valve can be identified by its characteristic curving central strut, which is best seen on an overpenetrated frontal film of the chest. A strut fracture of the Medtronic Hall valve has not been reported, but mechanical dysfunction may occur in both the mitral and aortic positions. Intermittent aortic regurgitation may occur as well as occlusion of the mitral valve by ruptured papillary muscles

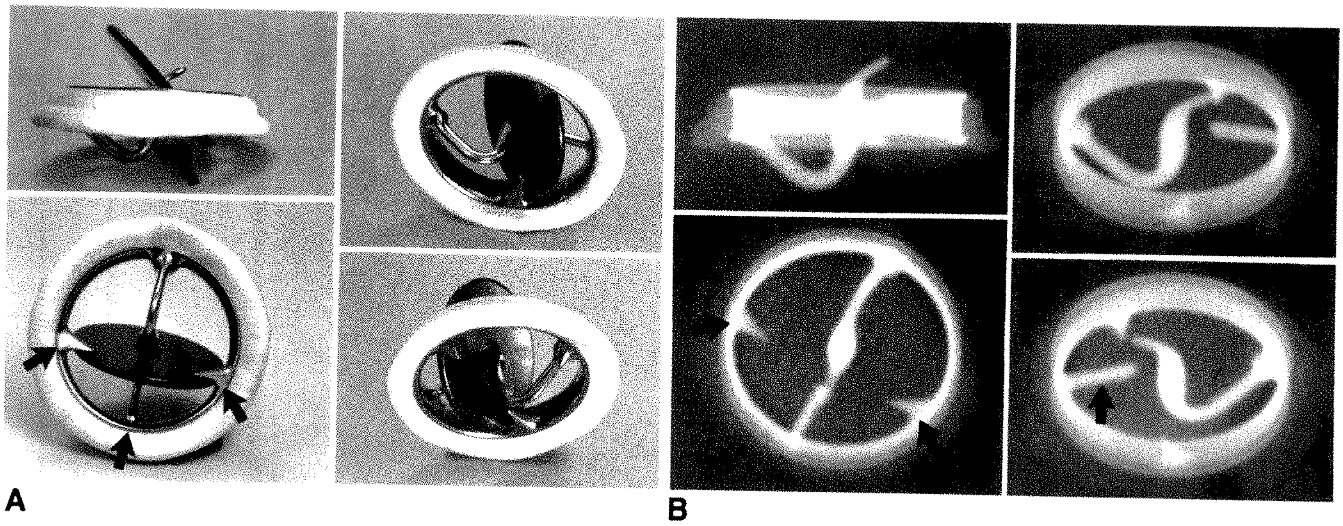

Fig. 1.—Photographs (**A**) and corresponding radiographs (**B**) of four views of Medtronic Hall mitral valve show long central strut (*curved arrows*) and three shorter stop struts (*straight arrows*). Occluder disk is radiolucent.

Received August 12, 1985; accepted after revision November 13, 1985.

[1] Department of Radiology, Milton S. Hershey Medical Center, Pennsylvania State University, Hershey, PA 17033. Address reprint requests to A. C. Mamourian.
[2] Department of Cardiothoracic Surgery, Milton S. Hershey Medical Center, Pennsylvania State University, Hershey, PA 17033.

AJR 146:485–486, March 1986 0361–803X/86/1463–0485 © American Roentgen Ray Society

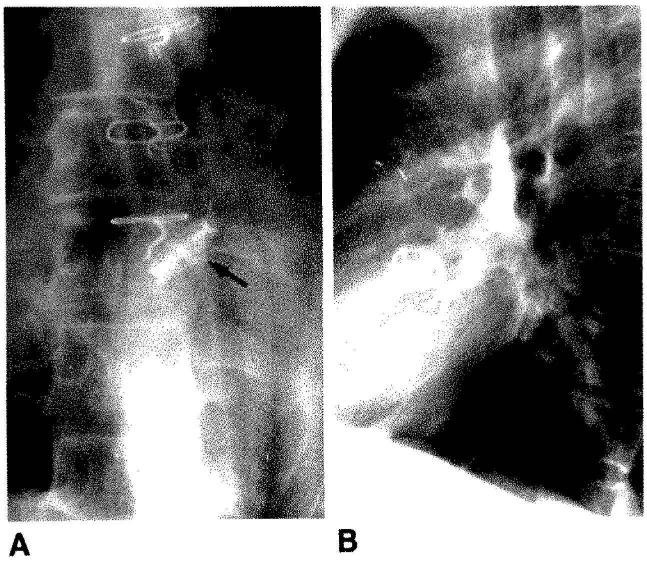

Fig. 2.—Posteroanterior (**A**) and lateral (**B**) radiographs demonstrate in vivo appearance of Medtronic Hall valve. Note characteristic curved strut on frontal radiograph (*arrow*).

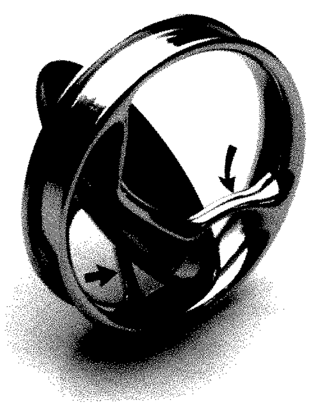

3

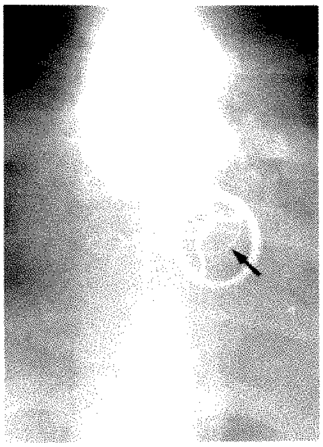

4

Fig. 3.—Björk-Shiley valve: inlet strut (*curved arrow*) and outlet strut (*straight arrow*) are separated by occluder disk.

Fig. 4.—Film of patient with Björk-Shiley aortic valve demonstrates radiopaque ring in disk (*arrow*).

[5, 6]. In these situations, it is important for the radiologist to recognize the Medtronic Hall valve and not mistake its unusual appearance for a fractured Björk-Shiley valve.

REFERENCES

1. Semb BK, Nitter-Hauge S, Hall KV. Hall-Kaster disc valve prosthesis: clinical and hemodynamic observations in patients undergoing aortic valve replacement. *J Cardiovasc Surg* **1980**;21:387-394
2. Guit GL, Van Voorthuisen AE, Steiner RM. Outlet strut fracture of the Björk-Shiley mitral valve prosthesis. *Radiology* **1985**; 154:298
3. Jaumin P, Ponlot R, Schoevaerdts JC, Brasseur L, Chalant CH. Strut fracture of the Björk-Shiley aortic valve. *J Thorac Cardiovasc Surg* **1984**;88:787-791
4. Davis PK, Myers JL, Pennock JL, Thiele BL. Strut fracture and disc embolization in Björk-Shiley mitral valve prostheses: diagnosis and management. *Ann Thorac Surg* **1985**;40:65-68
5. Antines MS, Colsen PR, Kinsley RH. Intermittent aortic regurgitation following aortic valve replacement with the Hall-Kaster prosthesis. *J Thorac Cardiovasc Surg* **1982**;84:751-754
6. Trites PN, Kiser JC, Johnson C, Tycast FJ, Gobel FL. Occlusion of Medtronic Hall mitral valve prosthesis by ruptured papillary muscle and chordae tendineae. *J Thorac Cardiovasc Surg* **1984**;88:301-302

Impending Catheter Perforation of Superior Vena Cava: Radiographic Recognition

Irena M. Tocino[1]
Arthur Watanabe[1]

In six of nine patients with superior vena caval perforation by a central venous catheter, the chest radiograph showed a gentle curve at the tip of the catheter 4 hr to 7 days before clinical or radiographic recognition of perforation. This radiographic sign should prompt catheter repositioning to avoid the morbidity and potential mortality associated with superior vena caval perforation.

Catheterization of central veins has become increasingly common in the management of critically ill patients. Monitoring of central venous pressures, rapid fluid replacement, hyperalimentation, and drug administration are the major indications for central venous catheters. Complications related either to catheter insertion or to the presence of the indwelling catheter within the vessel are correspondingly more frequent.

While some complications occur early, such as pneumothorax [1] and accidental arterial puncture [2], superior vena caval perforation tends to occur hours to days after insertion of the catheter, and iatrogenic injury may not be clinically suspected [3]. Because of the morbidity and potential mortality [4] of superior vena caval perforation, particularly when large pleural effusions or pericardial tamponade result, early signs of superior vena caval perforation need to be recognized so that prompt withdrawal of the catheter may avert these serious complications. We report a peculiar configuration of the tip of the catheter that may precede, by a significant time interval, other clinical or radiographic signs of superior vena caval perforation.

Materials and Methods

During the 19-month period from January 1983 through July 1984, we observed nine cases of superior vena caval perforation by central venous catheters. These cases were collected from the intensive care unit at the University of Utah and the shock-trauma unit at LDS Hospital in Salt Lake City.

Indications for line placement were rapid replacement of fluid in two patients with acute gastrointestinal bleeding and total parenteral nutrition in seven patients. Five catheters were single-lumen Silastic catheters and four were triple-lumen polyurethane catheters (Arrow International). The route chosen for catheter insertion was the left subclavian vein in six patients, the left jugular vein in two, and the right subclavian vein in one. Initial position of the catheter was always documented with a chest radiograph obtained immediately after line placement. This postprocedure radiograph as well as any additional chest radiographs obtained until superior vena caval perforation became clinically apparent were reviewed retrospectively.

All patients who developed perforation of the superior vena cava complained of chest pain and shortness of breath, which prompted radiography. Mediastinal widening and pleural effusions were seen in all patients. Pericardial effusion was present in one patient. The clinical and radiographic findings prompted thoracentesis, which yielded two bloody pleural effusions and seven effusions with a glucose content greater than 400 mg/dl. All catheters were

Received August 6, 1985; accepted after revision November 5, 1985.

[1] Department of Diagnostic Roentgenology and Nuclear Medicine, LDS Hospital, Eighth Ave. and C St., Salt Lake City, UT 84143. Address reprint requests to I. M. Tocino.

AJR 146:487–490, March 1986
0361-803X/86/1463-0487
© American Roentgen Ray Society

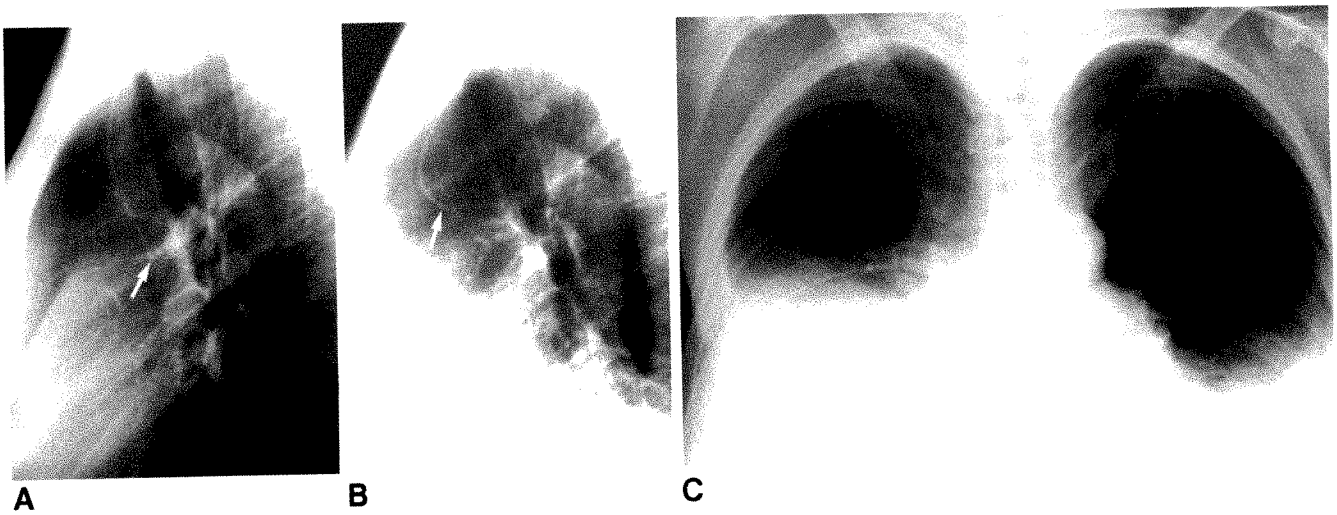

Fig. 1.—Triple-lumen catheter inserted via left subclavian vein for total parenteral nutrition. **A**, Lateral view at time of insertion. Catheter in usual position in superior vena cava (*arrow*). **B**, 4 days later. Gentle curve of catheter tip (*arrow*) is directed toward posterior wall of superior vena cava. **C**, Posteroanterior chest radiograph obtained 18 hr after **B**. Bilateral pleural effusion yielded hyperalimentation solution at thoracentesis.

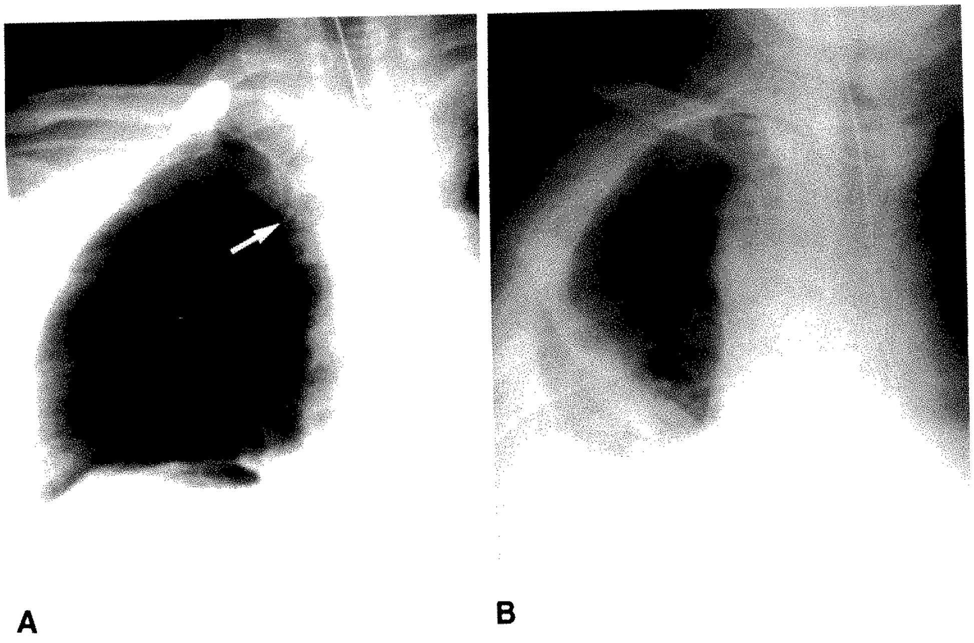

Fig. 2.—Catheter inserted for rapid fluid replacement in acute upper gastrointestinal bleeding. **A**, Supine view after insertion of catheter shows gentle curve of catheter tip (*arrow*) from medial to lateral. **B**, 4 hr later, there is mediastinal widening and pleural effusion. Thoracentesis revealed hemothorax.

removed immediately without further complication, and the patients recovered uneventfully.

Results

Retrospective review of chest radiographs of the nine patients with proven superior vena caval perforation revealed a gentle curve at the tip of the catheter in six cases (fig. 1). The curved catheter tip was observed on the lateral view in four patients, on the supine view in one patient (fig. 2), and on both posteroanterior and lateral chest radiographs of another patient.

Of the six patients with a curved catheter tip, four had single-lumen Silastic catheters and two had the relatively stiffer triple-lumen polyurethane catheters. Of the three patients without the curved-tip sign, two had a triple-lumen catheter and one a single-lumen catheter.

Superior vena caval perforation was recognized 4 hr to 9 days (fig. 3) after catheter insertion. The curved-tip sign was observed immediately after placement of the catheter in one patient 4 hr before clinical evidence of perforation (fig. 2). In the other five cases, the line was in satisfactory position at the time of insertion and on the available radiographs obtained in subsequent days before the smooth curve became appar-

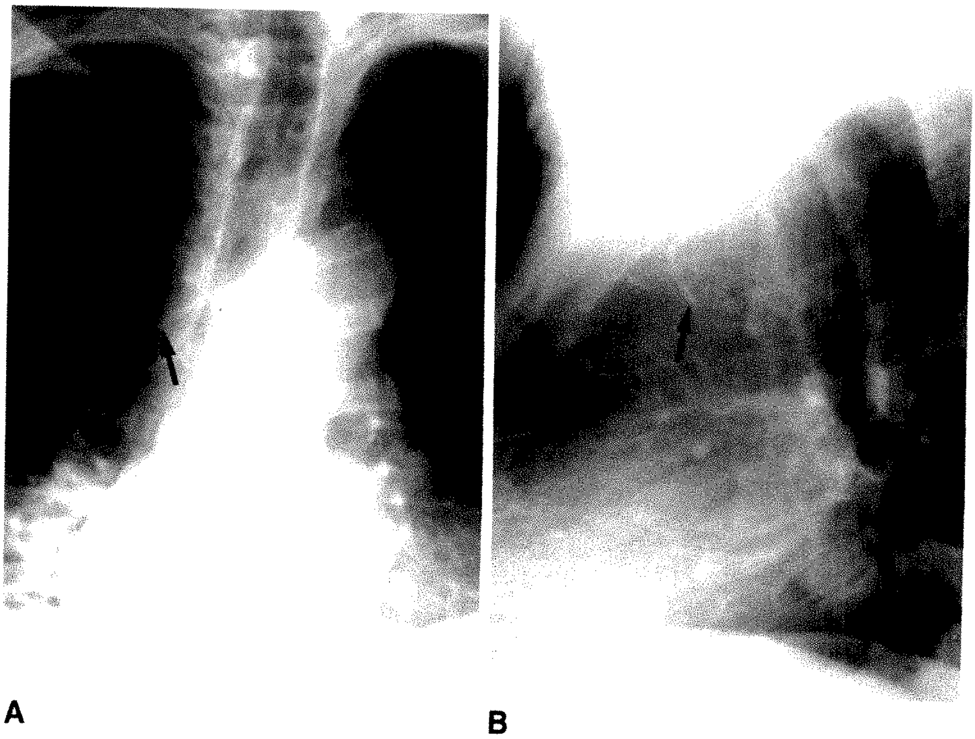

Fig. 3.—Triple-lumen catheter inserted for total parenteral nutrition and antibiotic therapy. Supine view 2 days after catheter insertion (**A**) shows catheter with tip (*arrow*) directed toward right lateral wall of superior vena cava. **B**, Lateral view same day shows gentle curve of catheter tip (*arrow*) from anterior to posterior. CT scan 7 days later, with contrast material injected through catheter, confirmed extravascular position of central line.

ent. This sign preceded superior vena caval perforation by 10 hr to 7 days. In three patients without the curved-tip sign, we observed that the catheter tip was directed toward the right lateral wall of the superior vena cava at a wide angle (fig. 3A) from the time of insertion until the time when perforation became evident.

In a retrospective review, there was no evidence of a curved catheter tip in the radiographs of 50 patients with central venous lines. Twelve of these patients had both anteroposterior and cross-table lateral views.

Discussion

Placement of central venous catheters has become common practice in the intensive care unit. While 28% of all central lines were found by Langston [5] to be in unsatisfactory position, more serious complications such as perforation of the superior vena cava are uncommon. The use of softer catheters with blunt tips and avoidance of brachial routes in favor of subclavian vein catheterization have resulted in a substantially lower frequency of superior vena caval or right cardiac chamber perforation [6, 7].

Two types of catheters were used in our patients: single-lumen Silastic catheters and multilumen polyurethane catheters. The type of catheter used was unrelated to vessel perforation. By contrast, access route was causally related to perforation. Perforation was noted in five of six patients in whom the left subclavian vein was catheterized. Because of the horizontal orientation of the left brachiocephalic vein and its 90° junction with the superior vena cava, catheters introduced via the left brachiocephalic and left jugular vein must turn a right angle to enter the vena cava. The catheter tip may be positioned against the right lateral wall of the superior vena cava at a wide angle. This catheter position was present in three of our cases (fig. 3A) and has been implicated previously in vessel perforation [8].

Catheters that have not been properly secured may slowly advance to an undesirable position against a vessel wall. Barton et al. [9] observed continuous catheter motion at fluoroscopy during respiratory and cardiac cycles, resulting in tenting of the right lateral wall of the superior vena cava even when a smooth curve of catheter from brachiocephalic vein to superior vena cava was seen on chest radiographs. This continuous motion and spontaneous catheter migration could explain the observed endothelial injury and secondary mural thrombi that occur preferentially at the innominate-caval junction demonstrated at autopsy in 19% of patients with central venous catheters [10].

We postulate that the curved catheter tip, seen in six of our nine cases of superior vena caval perforation, may represent the radiographic manifestation of endothelial injury at the time when the catheter tip occupies an intramural position. The distal 2 cm of the catheter could then buckle and acquire a smooth curvilinear configuration. The mural thrombus resulting from endothelial injury provides hemostasis and may explain the gradual nature of perforation. In fact, most instances of superior vena caval perforation occur many hours to days after catheter insertion [3, 4, 11]. Delayed perforation is associated with a higher incidence of hydrothorax, in contrast to hemothorax, which is more commonly found when perforation occurs at the time of catheter insertion.

The curved-tip sign preceded other clinical and radiographic signs of perforation by hours, usually days. Since it occurred substantially after catheter insertion, catheter perforation of the caval wall was not considered to be a likely explanation for the patient's deterioration. The diagnosis may be further delayed by the observation of prompt blood return from the catheter. However, blood return does not exclude an extravascular position of the catheter tip, since most catheters have side holes. All lumina of multilumen catheters must be checked before one can conclude that a catheter is appropriately positioned and functioning.

The central venous catheter should be placed in the superior vena cava distal to the last venous valve in the innominate veins and proximal to the pericardial reflection over the superior vena cava. This corresponds in the chest radiograph to the segment of the superior vena cava between the head of the clavicle and the arch of the azygos vein. The tip of the catheter should be parallel to the wall of the vessel. Catheter position should be checked periodically with chest radiographs in all patients with central venous lines. Since this sign was seen most often on lateral chest radiographs, this view should be included at some point in the follow-up of central lines. Recognition of a gentle curve of the catheter tip should prompt readjustment of its position or replacement to avoid vessel perforation, which may result in hydrothorax and pneumothorax, hydromediastinum, and pericardial effusion, all potentially life-threatening complications.

ACKNOWLEDGMENT

We thank Dr. John D. Armstrong II for manuscript review.

REFERENCES

1. Mitchell SE, Clark RA. Complications of central venous catheterization. *AJR* **1979**;133:467–476
2. Holt S, Kirkham N, Myerscough E. Hemothorax after subclavian vein cannulation. *Thorax* **1977**;32:101–103
3. Edwards H, King TC. Cardiac tamponade from central venous catheters. *Arch Surg* **1982**;117:965–967
4. Maschke SP, Rogove HJ. Cardiac tamponade associated with a multilumen central venous catheter. *Crit Care Med* **1984**;12:611–613
5. Langston CS. The aberrant central venous catheter and its complications. *Radiology* **1971**;100:55–59
6. Krog M, Berggren L, Brodin M, et al. Pericardial tamponade caused by central venous catheters. *World J Surg* **1982**;6:138–142
7. Brandt RL, Foley WJ, Fink GH, Regan WJ. Mechanism of perforation of the heart with production of hydropericardium by a venous catheter and its prevention. *Am J Surg* **1970**;119:311–316
8. Iberti TJ, Katz LB, Reiner MA, et al. Hydrothorax as a late complication of central venous indwelling catheters. *Surgery* **1983**;94:842–846
9. Barton BR, Herman G, Weil R III. Cardiothoracic emergencies associated with subclavian hemodialysis catheters. *JAMA* **1983**;250:2660–2662
10. Ducatman BS, McMichan JC, Edwards WD. Catheter-induced lesions of the right side of the heart: a one-year prospective study of 141 autopsies. *JAMA* **1985**;253:791–795
11. Reilly JJ, Cosimi AB, Russell PS. Delayed perforation of the innominate vein during hyperalimentation. *Arch Surg* **1977**; 112:96

Circumflex Retroesophageal Right Aortic Arch Simulating Mediastinal Tumor or Dissecting Aneurysm

Wade H. Shuford[1]
Robert G. Sybers[1]
Ira J. Gordon[1,2]
Murray G. Baron[1]
Gordon C. Carson[1]

The authors present three cases of circumflex right aortic arch, a retroesophageal arch in which the aorta crosses from right to left behind the esophagus to descend on the left side. The findings on the frontal chest films resembled those of a left arch with mediastinal widening, simulating a mass. Aortography revealed four-vessel branching of the arch vessels, typical of right aortic arch with aberrant left subclavian artery. Computed tomography and barium studies of the esophagus demonstrated the retroesophageal course of the aorta. In two patients, obstruction of the thoracic portion of the left subclavian artery resulted in differences in blood pressure and pulse between the arms, supporting the clinical impression of dissecting aortic aneurysm.

Right aortic arch with aberrant left subclavian artery is a common arch anomaly occurring in about 0.05% of the population. Its usual radiographic manifestations have been well described and are readily recognized [1-6]. There is, however, an anatomic variation of this right aortic arch, the circumflex retroesophageal right arch, which has an unusual and often confusing radiographic appearance. The circumflex retroesophageal right arch resembles a left arch with widening of the mediastinum (fig. 1). It may be mistaken for a mediastinal tumor or aortic aneurysm [7-11], especially in patients with differences in blood pressure and pulse between the upper extremities. We present three patients with this rare anomaly.

Case Reports

Case 1: Retroesophageal Right Aortic Arch with Stenosis of the Left Subclavian Artery Simulating Dissecting Aneurysm

A 42-year-old woman presented to the emergency room with left-sided chest pain. Pertinent physical findings included an elevated blood pressure with moderate side-to-side differential (right arm, 140/110 mm Hg; left arm, 125/108 mm Hg). Carotid and lower-extremity pulses were equal and symmetric, but there was diminution of the left brachial and radial pulses as compared with the right side.

A frontal chest radiograph (fig. 2A) showed a markedly widened superior mediastinum at the level of the aortic arch, supporting the clinical diagnosis of dissecting aortic aneurysm. The aortic arch arteriogram with a catheter in the upper ascending thoracic aorta (fig. 2B) demonstrated absence of the innominate artery and separate origin of the right common carotid and right subclavian arteries. The left subclavian artery was the last branch off the arch. The left common carotid artery was not opacified. Because of the absence of an innominate artery and separate origin of the right subclavian and right common carotid arteries, a right aortic arch was suspected. It was thought that the left common carotid artery was the first branch off the arch but failed to opacify because of the high catheter position with inadequate visualization of the aortic root. The catheter was placed in the immediate supravalvular region, and a repeat aortogram was obtained. This study (figs. 2C and 2D) showed the left common carotid artery to be the first branch off the arch, establishing the presence of a right aortic arch. The right arch impinged on the right lateral and posterior walls of the esophagus. An additional injection in the left posterior oblique projection (fig. 2E)

Received May 2, 1985; accepted after revision September 25, 1985.

[1] Department of Radiology, Emory University School of Medicine and Affiliated Hospitals, Atlanta, GA 30322. Address reprint requests to W. H. Shuford, Department of Radiology, Grady Memorial Hospital, 80 Butler St., S.E., Atlanta, GA 30335.

[2] Present address: Department of Radiology, Akron General Medical Center, Akron, OH 44307.

AJR **146:491-496, March 1986**
0361-803X/86/1463-0491
© American Roentgen Ray Society

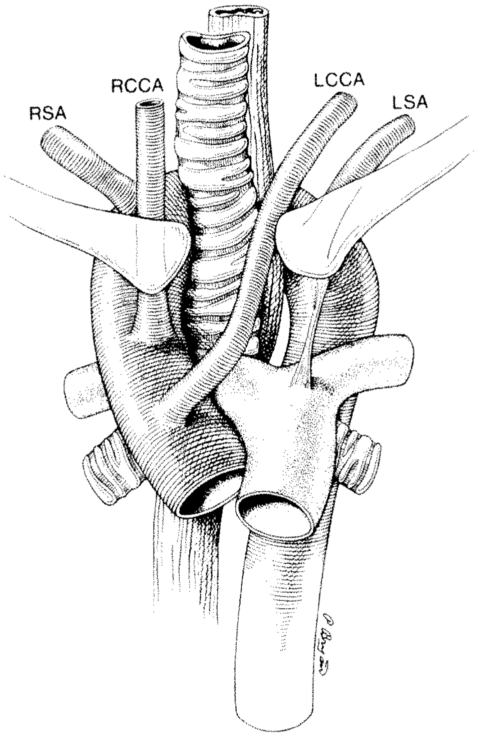

Fig. 1.—Circumflex retroesophageal variation of right aortic arch with aberrant left subclavian artery. LCCA = left common carotid artery; RCCA = right common carotid artery; RSA = right subclavian artery; LSA = left subclavian artery.

demonstrated mild stenosis of the left subclavian artery at its origin, which accounted for the blood pressure differential between the arms. There was no evidence of dissecting aortic aneurysm, and the patient's chest pain resolved spontaneously.

Case 2: Retroesophageal Right Aortic Arch with Obstruction of the Left Subclavian Artery and Subclavian Steal Simulating Dissecting Aneurysm

A 63-year-old man was hospitalized because of acute urinary retention. Physical examination revealed a diminished pulse in the left arm. Blood pressures in the right arm were 182/98 mm Hg (standing) and 150/84 mm Hg (supine); in the left arm, 106/84 mm Hg (standing) and 108/80 mm Hg (supine).

Chest radiographs showed bulging of the mediastinum to the right and left sides at the level of the aortic arch. The trachea was displaced toward the left (fig. 3A). A rounded superior-mediastinal density displaced the trachea anteriorly (fig. 3B) and indented the posterior aspect of the esophagus (fig. 3C). Because of the differences in blood pressure and pulse between the arms and because of mediastinal widening, a chronic dissecting aortic aneurysm was suspected. Aortography (figs. 3D and 3E) showed a markedly redundant aorta that descended on the left side. The first branch off the arch was a left common carotid artery; this was followed by the right common carotid and right subclavian arteries, establishing the presence of a right aortic arch. The proximal left subclavian artery was not visualized. The distal left subclavian artery was subsequently opacified via retrograde flow in the left vertebral artery. There was no evidence of aortic dissection.

The patient was seen again 10 years later, and computed tomography (CT) without contrast enhancement (figs. 3F and 3G) confirmed the presence of a retroesophageal right arch with a left descending aorta.

Case 3: Retroesophageal Right Aortic Arch

A 60-year-old woman gave a 10-year history of diabetes mellitus and hypertension. Physical findings included elevated blood pressures (right arm, 160/118 mm Hg; left arm, 180/110 mm Hg). A frontal chest radiograph (fig. 4A) showed marked bilateral symmetric widening of the superior mediastinum with extension above the level of the clavicles. The trachea was indented on the right side. A lateral esophagogram revealed a deep localized posterior indentation on the esophagus at the level of T2–T3 (fig. 4B). Chest CT with contrast enhancement confirmed the presence of a retroesophageal right arch with a left-sided descending aorta. The first branch off the arch was the left common carotid artery, which traversed horizontally in front of the trachea (figs. 4C and 4D).

Discussion

Right aortic arch has been classified into various types according to the branching of the arch vessels [1, 2, 5]. Of these, right aortic arch with aberrant left subclavian artery is the most common. Ordinarily, this type is not associated with congenital heart disease, and it is the type of right arch found incidentally in adults on routine chest radiographs [1, 2, 5]. In this anomaly the first branch arising from the aortic arch is the left common carotid artery, which is followed by the right carotid, right subclavian, and left subclavian arteries in that order. The right arch passes between the superior vena cava and right side of the trachea and esophagus, crossing over the right main-stem bronchus to join the descending aorta.

There are variations of right arch with aberrant left subclavian artery depending upon the relation of the right arch to the esophagus [5]. In one form the right arch maintains a position to the right of the esophagus and descends on the right side of the spine. In the more common form, the right arch passes behind the esophagus to turn abruptly downward, descending usually on the right side or near the midline. These forms present little difficulty in diagnosis and are readily recognized on the frontal radiograph by the following findings: The trachea is displaced to the left by the right arch; the aortic knob is seen to the right of the trachea, somewhat higher than the position of the normal left aortic knob; and the image produced by the normal aortic arch along the left mediastinal border is absent.

Infrequently, the right arch crosses the midline behind the esophagus to descend on the left side of the spine, resulting in the circumflex retroesophageal right aortic arch (fig. 1) [6, 10–12]. This variation of right arch presents a different radiologic appearance.

The radiologic features of our three cases were striking and remarkably similar. There was bilateral symmetric enlargement of the superior mediastinum, simulating a mass. The descending aorta located to the left of the midline gave

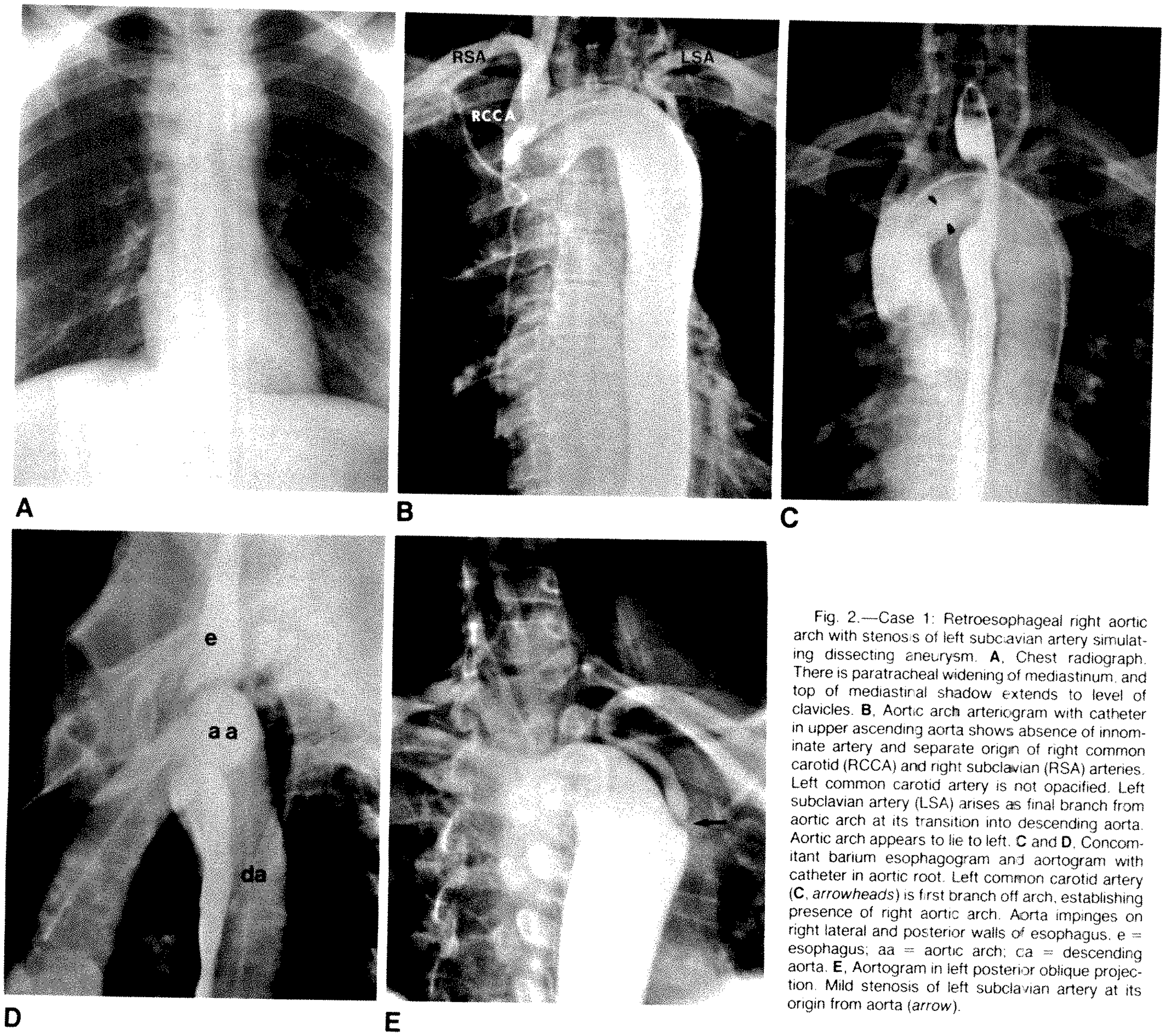

Fig. 2.—Case 1: Retroesophageal right aortic arch with stenosis of left subclavian artery simulating dissecting aneurysm. **A**, Chest radiograph. There is paratracheal widening of mediastinum, and top of mediastinal shadow extends to level of clavicles. **B**, Aortic arch arteriogram with catheter in upper ascending aorta shows absence of innominate artery and separate origin of right common carotid (RCCA) and right subclavian (RSA) arteries. Left common carotid artery is not opacified. Left subclavian artery (LSA) arises as final branch from aortic arch at its transition into descending aorta. Aortic arch appears to lie to left. **C** and **D**, Concomitant barium esophagogram and aortogram with catheter in aortic root. Left common carotid artery (**C**, *arrowheads*) is first branch off arch, establishing presence of right aortic arch. Aorta impinges on right lateral and posterior walls of esophagus. e = esophagus; aa = aortic arch; da = descending aorta. **E**, Aortogram in left posterior oblique projection. Mild stenosis of left subclavian artery at its origin from aorta (*arrow*).

the misleading impression of a normal left arch. The prominent mediastinal border on the right side was due to the ascending aorta and right arch. The left mediastinal border was formed by the upper part of the descending aorta bulging into the left lung. In two patients the superior border of the mediastinal shadow extended upward above the level of the clavicles and represented the high position of the transverse segment of the right arch. The tracheal air column was indented on the right side. Two of our patients were older persons with elongation and tortuosity of the thoracic aorta, which contributed to the mediastinal widening.

Do these cases represent a rare type of right aortic arch? Aortography and CT revealed branching of the arch vessels, typical of right aortic arch with aberrant left subclavian artery. The unusual factor in these cases is not the type of right arch, but the degree of mediastinal widening due to the high position of the circumflex aorta as it passes behind the esophagus to continue as a left-sided descending aorta.

Since most radiologists are unfamiliar with the appearance of a circumflex right aortic arch, this anomaly may not be considered in the differential diagnosis of a widened mediastinal shadow. Often, especially in older individuals, it resembles a mediastinal tumor or aneurysm.

Our observations indicate several radiographic features that are of considerable value in diagnosing circumflex right aortic arch. Bilateral symmetric widening of the superior mediastinum, particularly with upward extension high in the thorax, should suggest this anomaly. However, displacement of the trachea to the left is the most helpful clue. On the lateral projection the retroesophageal aorta may be visible as a large,

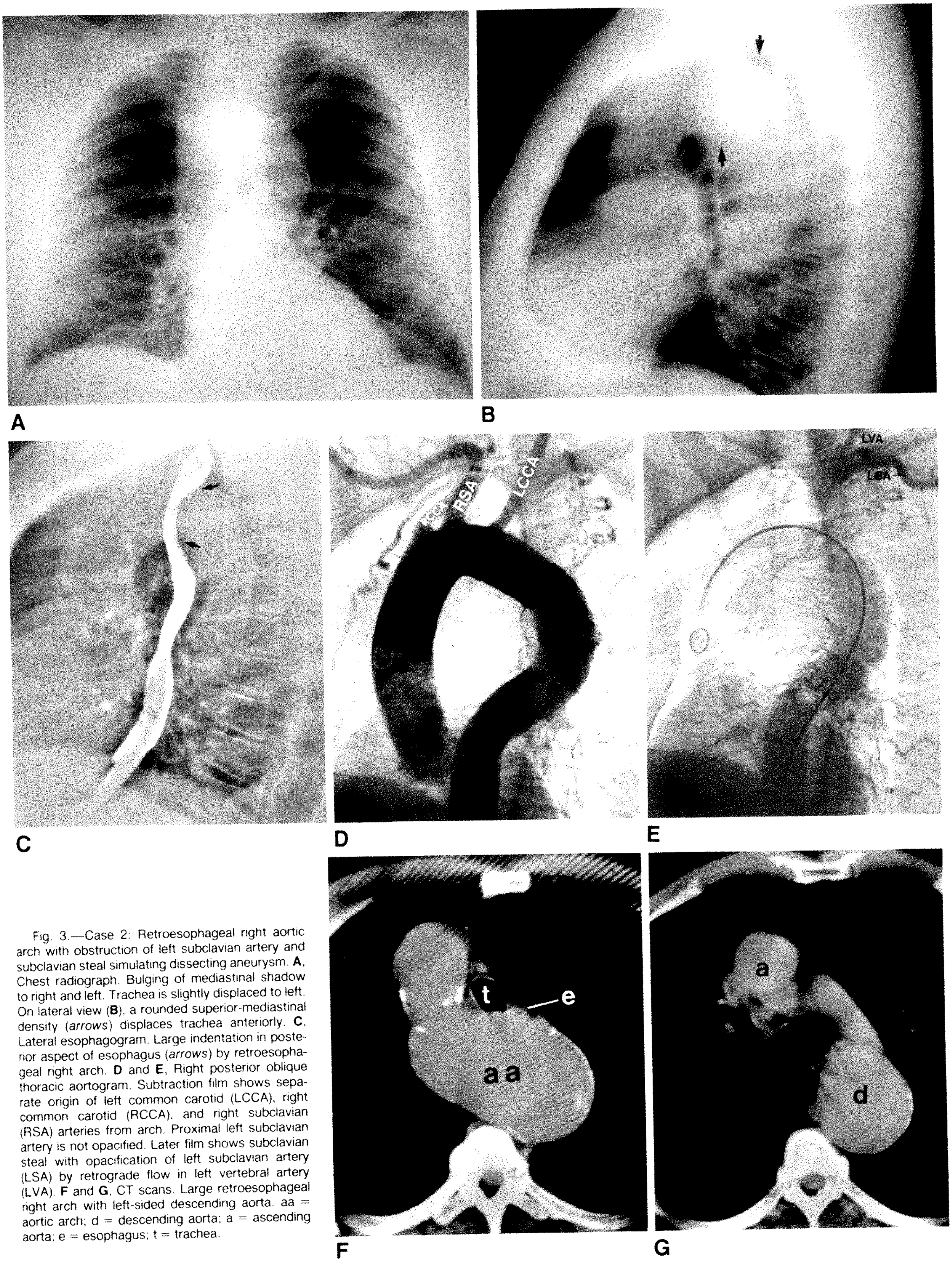

Fig. 3.—Case 2: Retroesophageal right aortic arch with obstruction of left subclavian artery and subclavian steal simulating dissecting aneurysm. **A**, Chest radiograph. Bulging of mediastinal shadow to right and left. Trachea is slightly displaced to left. On lateral view (**B**), a rounded superior-mediastinal density (*arrows*) displaces trachea anteriorly. **C**, Lateral esophagogram. Large indentation in posterior aspect of esophagus (*arrows*) by retroesophageal right arch. **D** and **E**, Right posterior oblique thoracic aortogram. Subtraction film shows separate origin of left common carotid (LCCA), right common carotid (RCCA), and right subclavian (RSA) arteries from arch. Proximal left subclavian artery is not opacified. Later film shows subclavian steal with opacification of left subclavian artery (LSA) by retrograde flow in left vertebral artery (LVA). **F** and **G**, CT scans. Large retroesophageal right arch with left-sided descending aorta. aa = aortic arch; d = descending aorta; a = ascending aorta; e = esophagus; t = trachea.

Fig. 4.—Case 3: Retroesophageal right aortic arch. **A**, Chest radiograph. Bilateral symmetric enlargement of superior mediastinum with upward extension above level of clavicles. Trachea is indented on right. **B**, Lateral esophagogram. Large posterior compression defect on esophagus (*arrowhead*) by retroesophageal right arch. **C** and **D**, CT scans with contrast enhancement. Right aortic arch (aa) crosses midline posterior to trachea (t) and esophagus (e) at level of clavicles. Left common carotid artery (LCCA) arises from ascending aorta (a) as first branch and crosses to left in front of trachea. Descending aorta (d) is on left.

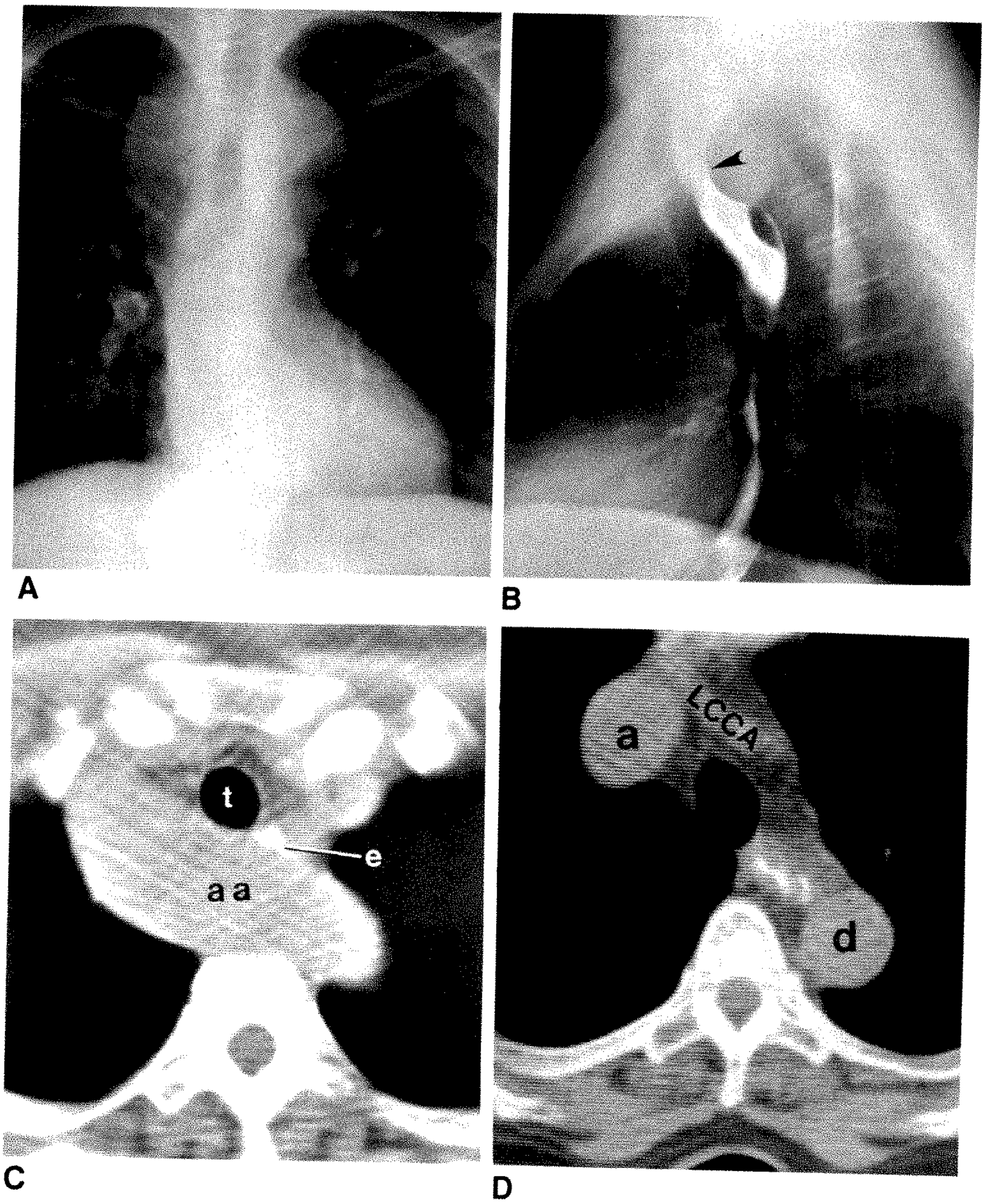

round, superior-mediastinal density displacing the trachea anteriorly.

The barium swallow is the simplest method for diagnosing retroesophageal right aortic arch. In addition to the vascular impression on the right side of the esophagus, the aorta deeply indents the esophagus from behind, producing a large posterior defect on the contrast-filled esophagus. CT is ideally suited for analysis of the widened mediastinum and is capable of specifically diagnosing right aortic arch [11, 13, 14].

Aortography may be misleading in the diagnosis of this variation of right aortic arch, since it is impossible to determine on the frontal aortogram whether the aorta crosses in front of or behind the trachea and esophagus. On the frontal aortogram, a circumflex retroesophageal right arch resembles a normal left arch. The only indication of a right arch in this projection is the branching pattern of the arch vessels. It is important that the root of the aorta be visualized adequately to establish the left common carotid artery as the first branch. We believe that concomitant angiographic visualization of the aorta and barium esophagography yield the most exact morphologic information about an aortic arch malformation [15].

In patients with circumflex right aortic arch there may be clinical and radiologic features that suggest the presence of dissecting aortic aneurysm. In both conditions there may be mediastinal widening. In both there may be differences in blood pressure and pulse between the upper extremities [2]. Rarely in right aortic arch with aberrant left subclavian artery there is congenital stenosis or atresia of the proximal left subclavian artery, which creates the potential for subclavian steal [2, 16–20]. In one of our patients the left subclavian artery was stenotic at its origin from the aorta. In another patient there was complete occlusion of the left subclavian artery, and retrograde vertebral-subclavian flow was demonstrated. While barium studies of the esophagus will diagnose a right aortic arch, angiography or CT may be required to exclude a dissecting aortic aneurysm. However, well-defined mediastinal contours with absence of change; a posterior tracheal mass; and the high position of the mediastinum in the thorax make the diagnosis of aortic dissection unlikely.

REFERENCES

1. Stewart JR, Kincaid OW, Edwards JE. *An atlas of vascular rings and related malformations of the aortic arch system*. Springfield, IL: Thomas, **1964**
2. Shuford WH, Sybers RG. *The aortic arch and its malformations*. Springfield, IL: Thomas, **1974**
3. Baron MG. Right aortic arch. *Circulation* **1971**;44:1137–1145
4. Stewart JR, Kincaid OW, Titus JL. Right aortic arch: plain film diagnosis and significance. *AJR* **1966**;97:377–389
5. Knight L, Edwards JE. Right aortic arch. *Circulation* **1974**;50:1047–1051
6. Klinkhamer AC. *Esophagography in anomalies of the aortic arch*. Amsterdam: Excerpta Medica, **1969**
7. O'Hara J. Right aortic arch simulating a mediastinal tumor. *Dis Chest* **1959**;36:661–664
8. Schwartz E, Kalter HH. Right aortic arch versus mediastinal tumors and densities. *Dis Chest* **1955**;28:91–97
9. Choy DSJ, McPeak CJ. Aberrant aorta presenting as a superior mediastinal tumor. *Amer Rev Respir Dis* **1967**;95:496–498
10. Hastreiter AR, D'Cruz IA, Cantez T. Right-sided aorta: II. Right aortic arch, right descending aorta, and associated anomalies. *Br Heart J* **1966**;28:772–739
11. Taber P, Chang LWM, Campion GM. Diagnosis of retroesophageal right aortic arch by computed tomography. *J Comput Assist Tomogr* **1979**;3:684–685
12. Salomonowitz E, Edwards JE, Hunter DW, et al. The three types of aortic diverticula. *AJR* **1984**;142:673–679
13. Haaga JR, Alfidi RJ. *Computed tomography of the whole body*, vol 1. St. Louis: Mosby, **1983**:441–444
14. Lee JKT, Sagel SS, Stanley RJ. *Computed body tomography*. New York: Raven, **1983**
15. Tonkin IL, Elliot LP, Bargeron LM. Concomitant axial cineangiography and barium esophagography in the evaluation of vascular rings. *Radiology* **1980**;135:69–76
16. Gerber N. Congenital atresia of the subclavian artery. *Am J Dis Child* **1967**;113:709–713
17. Levine S, Serfas LS, Rusinko A. Right aortic arch with subclavian steal syndrome (atresia of left common carotid and left subclavian arteries). *Am J Surg* **1966**;111:632–637
18. Victorica BE, Van Mierop LHS, Elliot LP. Right aortic arch associated with contralateral congenital subclavian steal syndrome. *AJR* **1970**;108:582–590
19. Wychulis AR, Kincaid OW, Danielson GK. Congenital vascular ring. *Mayo Clin Proc* **1971**;46:182–188
20. Antia AU, Ottesen OE. Collateral circulation in subclavian stenosis or atresia: angiographic demonstration of retrograde vertebral-subclavian flow in two cases with right aortic arch. *Am J Cardiol* **1966**;18:599–604

Update: The Radiographic Features of Pulmonary Tuberculosis

John H. Woodring[1]
H. Mac Vandiviere[2]
Andrew M. Fried[1]
Marcus L. Dillon[3]
Terry D. Williams[1]
Irene G. Melvin[2]

Pulmonary tuberculosis produces a broad spectrum of radiographic abnormalities. During the primary phase of the disease these include pulmonary consolidation (50%), which often involves the middle or lower lobes or the anterior segment of an upper lobe; cavitation (29%) or pneumatocele formation (12%); segmental or lobar atelectasis (18%); pleural effusion (24%); hilar and mediastinal lymphadenopathy (35%); disseminated miliary disease (6%); and a normal chest radiograph (15%). During the postprimary phase of the disease, common abnormalities include exudative and/or fibroproductive parenchymal densities (100%), predominantly in the apical and posterior segments of the upper lobes (91%); cavitation (45%) with bronchogenic spread of disease (21%); marked fibrotic response in the lungs (29%); and pleural effusion, empyema, and fibrosis (18%, 4%, and 41%, respectively). Upper-lobe masslike lesions are seen occasionally (7%); spontaneous pneumothorax and intrathoracic lymphadenopathy are rare (5% each). Common causes of a missed diagnosis of tuberculosis are (1) failure to recognize hilar and mediastinal lymphadenopathy as a manifestation of primary disease in adults, (2) exclusion of tuberculosis because disease predominates in or is limited to the anterior segment of an upper lobe or the basilar segment of a lower lobe, (3) overlooking of minimal fibroproductive lesions or reporting them as inactive, (4) failure to recognize that an upper-lobe mass surrounded by satellite fibroproductive lesions might be tuberculous, and (5) failure to consider healed sequelae of primary disease or a positive purified protein derivative skin test as contributory to identifying the patient's pulmonary disease.

During the last decade, various authors have enumerated the "unusual" manifestations of pulmonary tuberculosis in the adult population [1–6]. These unusual manifestations usually have been implicated in the frequent failure of both radiologist and clinician to recognize that tuberculosis could be the cause of an abnormal chest radiograph in patients who are subsequently, and rather surprisingly, proven to have tuberculosis. As Choyke et al. [7] indicate, these so-called unusual manifestations of tuberculosis in adults are actually typical of the disease: What is unusual is that they often represent primary disease occurring in the adult population.

Although physicians are more familiar with the radiographic manifestations of postprimary tuberculosis than with those of primary disease, problems in radiographic diagnosis do occur. Minimal exudative or fibroproductive tuberculosis may be overlooked or, commonly, fibroproductive lesions may be assumed to be inactive even though the patient subsequently proves to be sputum-positive for *Mycobacterium tuberculosis* [1, 5, 8]. Miller and MacGregor [1] reported several cases of advanced postprimary tuberculosis with extensive upper-lobe cavitation in which tuberculosis was not even considered as a diagnostic possibility!

Because of the apparent widespread difficulty in recognizing the radiographic manifestations of pulmonary tuberculosis, we thought it would be beneficial to review the spectrum of radiographic abnormalities attributable to *M. tuberculosis* in a university medical center. We emphasize the radiographic features of primary

Received April 15, 1985; accepted after revision November 4, 1985.

[1] Department of Diagnostic Radiology, Albert B. Chandler Medical Center, University of Kentucky College of Medicine, 800 Rose St., Lexington, KY 40536-0084. Address reprint requests to J. H. Woodring.

[2] Department of Pediatrics, Albert B. Chandler Medical Center, University of Kentucky College of Medicine, Lexington, KY 40536-0084.

[3] Department of Cardiovascular and Thoracic Surgery, Albert B. Chandler Medical Center, University of Kentucky College of Medicine, Lexington, KY 40536-0084.

AJR 146:497–506, March 1986
0361–803X/86/1463–0497
© American Roentgen Ray Society

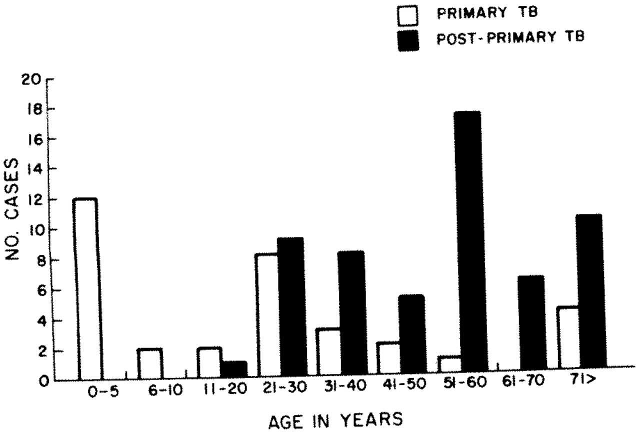

Fig. 1.—Prevalence of primary and postprimary tuberculosis by age in 90 patients.

TABLE 1: **Location of Pulmonary Consolidation in 73 Patients with Pulmonary Tuberculosis**

Site of Consolidation	Type of Pulmonary Tuberculosis	
	Primary ($n = 17$)	Postprimary ($n = 56$)
Right upper lobe:		
Anterior	4	18
Apical	0	41
Posterior	1	31
Right middle lobe	2	10
Right lower lobe:		
Superior	1	13
Basal	3	16
Left upper lobe:		
Anterior	2	16
Apical	1	33
Posterior	2	30
Lingula	2	14
Left lower lobe:		
Superior	2	14
Basal	4	10
Totals	24	246

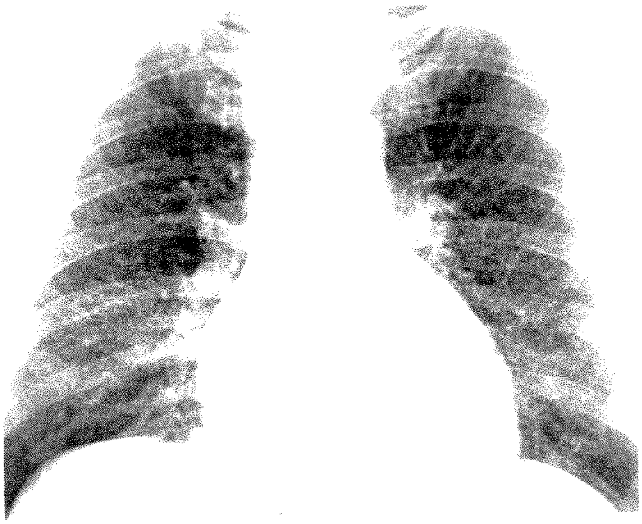

Fig. 2.—Primary lymphohematogenous dissemination with miliary pattern in 43-year-old man.

and postprimary disease, similarities and differences between the two, and the recognition of certain patterns that should lead to suspicion of pulmonary tuberculosis. The pathogenesis of pulmonary tuberculosis is also discussed.

Materials and Methods

The chest radiographs and medical records of patients diagnosed as having clinically active *M. tuberculosis* were reviewed. Between 1974 and 1984, 107 patients with active pulmonary tuberculosis were documented at the University of Kentucky Medical Center. Of these, 17 patients had insufficient information in their medical records to determine whether they had primary or postprimary disease with *M. tuberculosis*. These 17 patients were excluded from the study. The Centers for Disease Control and American Thoracic Society criteria for confirmation of tuberculosis were met in the 90 remaining cases, that is, (1) either bacteriologic confirmation of current disease or both a significant skin reaction to the purified protein derivative (PPD) and clinical and/or radiographic evidence of current disease, and (2) radiographic improvement after administration of two or more antituberculous drugs [9, 10].

Primary tuberculosis was documented in 34 (38%) of the 90 patients on the basis of the following criteria: (1) recently documented conversion of the PPD skin test coupled with a positive culture of *M. tuberculosis* from tissue or body fluids (24 patients); (2) recently documented conversion of the PPD skin test coupled with clinical and radiographic evidence of current disease although subsequent cultures for *M. tuberculosis* were negative (seven patients, all children); and (3) positive culture for *M. tuberculosis* with no prior history of tuberculosis, a previously negative PPD skin test, and a previously normal chest radiograph (three patients). At the time of illness these patients were anergic and the PPD skin test was nonreactive. Of the 34 patients with primary tuberculosis, 19 were female and 15 were male; the patients were between 6 months and 87 years of age (average, 24 years) (fig. 1). Of these 34 patients, 19 (56%) were 18 years of age or older. These 19 adults with primary tuberculosis comprised 25% of the 75 adults with active pulmonary tuberculosis in our total study population of 90 individuals. As shown in figure 1, four of the patients with primary tuberculosis were over 71 years of age. There was no evidence that these four patients had ever had tuberculosis or a positive PPD skin test previously to suggest that the booster effect was the cause of the recent PPD conversion. One of these four elderly patients was quite debilitated with chronic lymphocytic leukemia. Two of the other adults with primary tuberculosis had diabetes mellitus (one case each of juvenile-onset and adult-onset diabetes).

Postprimary tuberculosis was documented in 56 (62%) of the 90 patients on the basis of the following criteria: (1) positive culture for *M. tuberculosis* obtained on one or more admissions to the hospital (all 56 patients), either from the sputum (53 cases), from material obtained from fiberoptic bronchoscopy (two), or from gastric aspirates (one); and (2) evidence of previous primary infection with tuberculosis (all 56 patients) based on a documented positive PPD skin test before the episode of current disease (39 patients), radiographic evidence of the previous primary infection (35), and/or a previously positive culture for *M. tuberculosis* without antituberculous treatment before

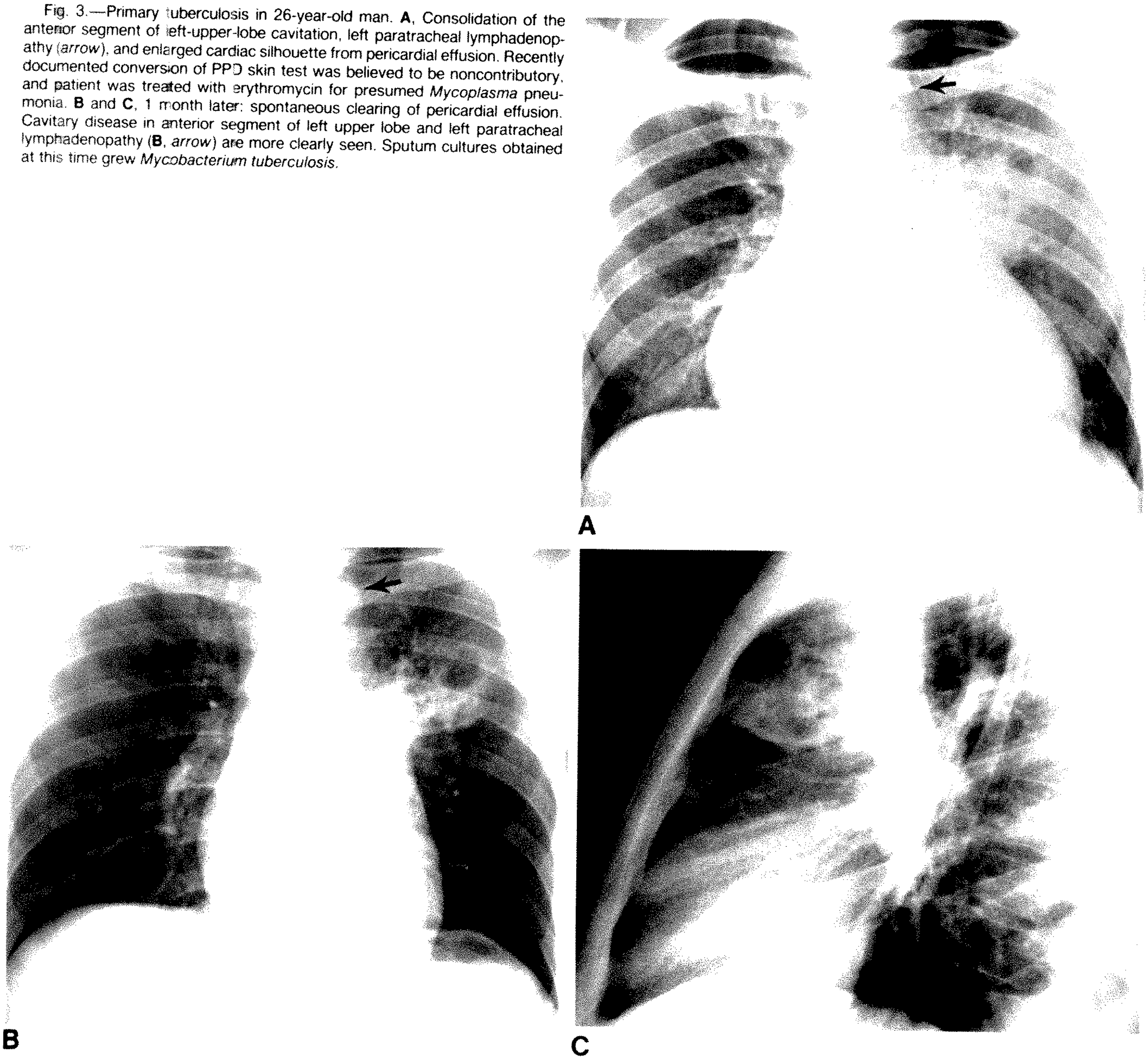

Fig. 3.—Primary tuberculosis in 26-year-old man. **A**, Consolidation of the anterior segment of left-upper-lobe cavitation, left paratracheal lymphadenopathy (*arrow*), and enlarged cardiac silhouette from pericardial effusion. Recently documented conversion of PPD skin test was believed to be noncontributory, and patient was treated with erythromycin for presumed *Mycoplasma* pneumonia. **B** and **C**, 1 month later: spontaneous clearing of pericardial effusion. Cavitary disease in anterior segment of left upper lobe and left paratracheal lymphadenopathy (**B**, *arrow*) are more clearly seen. Sputum cultures obtained at this time grew *Mycobacterium tuberculosis*.

the time of diagnosis (11). Of the 56 patients with postprimary tuberculosis, 36 were men and 20 were women; the patients were between 20 and 87 years of age (average, 51) (fig. 1). Five of these 56 patients had associated conditions that may have contributed to the development of postprimary tuberculosis, including chronic renal failure (two cases) and acute lymphocytic leukemia, chronic alcoholism, and pregnancy (one case each).

The patients in our study were from central and eastern Kentucky. Although these patients are similar in many respects to those seen at other major medical centers, the majority came from small rural communities (less than 10,000 population) rather than urban inner-city areas. In fact, Kentucky is unique in that the case rate of tuberculosis is significantly greater in the nonurban population.

The chest radiographs of the 90 patients were reviewed and evaluated for abnormalities of the lung parenchyma, airways, intrathoracic lymph nodes, and pleura. Finally, the initial radiographic report and clinical diagnosis in each patient's medical record was reviewed with attention directed to the degree of initial suspicion of tuberculous disease. The initial radiographic interpretations were prepared in conjunction by a radiology resident and board-certified diagnostic radiologist in all cases. Specific historical information concerning the status of the PPD skin test or a high degree of clinical suspicion of active tuberculosis was provided to the initial interpreters in less than one-half of cases. Potential causes of a nondiagnosis of tuberculosis were evaluated.

Results

Primary Tuberculosis

A normal chest radiograph coupled with a positive culture for *M. tuberculosis* was found in five (15%) of the 34 patients with primary tuberculosis, who were clinically thought to have endobronchial disease. Two patients presented with a diffuse miliary pattern (fig. 2). The remaining 27 patients had pulmonary parenchymal consolidation, atelectasis, intrathoracic lymphadenopathy, pleural effusion, and pericardial effusion as either isolated or combined findings.

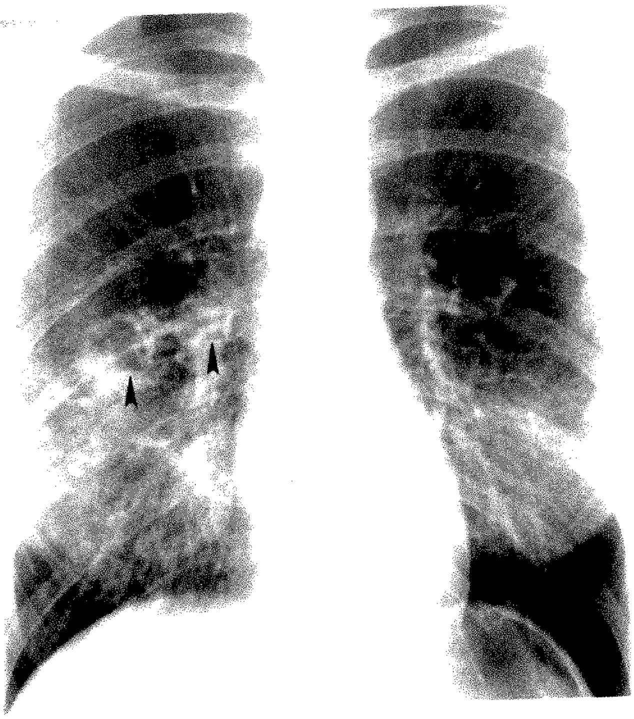

Fig. 4.—Primary tuberculosis in 24-year-old female diabetic with recent conversion of PPD skin test. Multiple cavities with air-fluid levels (*arrowheads*) in superior segment of right lower lobe.

Pulmonary consolidation occurred in 17 patients (50%). In 13 patients a single area of pulmonary consolidation was encountered; in four patients multiple areas of parenchymal consolidation were present. Overall, 24 areas of consolidation were encountered in these 17 patients (table 1). The right and left lungs were equally affected; the mid and lower parts of the lungs were involved slightly more often than the upper lung zones; however, when the upper lobes were involved, anterior segment involvement was more common than involvement of the apical or posterior segments (table 1, fig. 3).

Cavitation had developed in five (29%) of the 17 patients with pulmonary consolidation (figs. 3 and 4); in one case air-fluid levels were noted. In two patients pneumatoceles were present (fig. 5). In seven of these patients pulmonary consolidation was an isolated finding; however, in 10 patients consolidation was associated with other findings including lymphadenopathy, pleural effusion, pericardial effusion, and lobar atelectasis.

Segmental or lobar atelectasis occurred in six patients (18%) (fig. 6). The anterior segment of the right upper lobe was involved in one case, the right middle lobe in two cases, and the right lower lobe in three cases.

Pleural effusion was present in eight (24%) of the 34 patients (fig. 7). Effusion was unilateral in seven cases and bilateral in one. The size of the effusion was judged to be small in two cases, medium in one, and large in six according to the criteria of Roper and Waring [11]. Three patients presented with isolated pleural effusions; however, in five patients effusion was associated with parenchymal consolidation and/or lymphadenopathy. Pericardial effusion was seen in only one case (fig. 3). Echocardiography was not

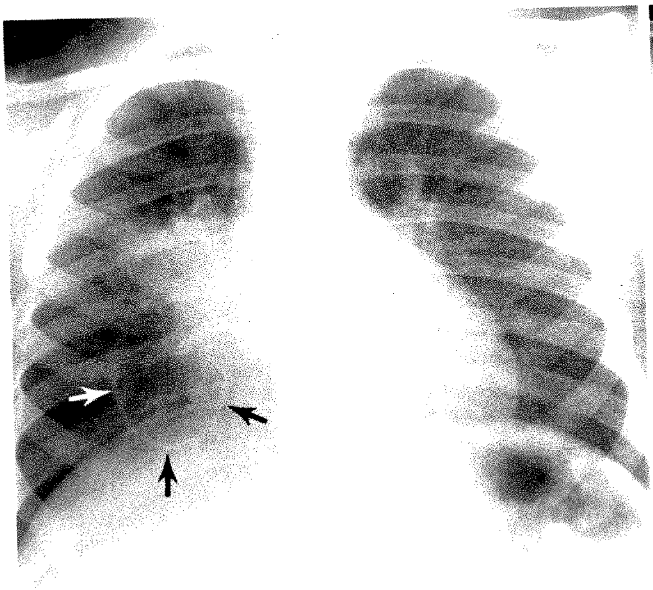

Fig. 5.—Primary tuberculosis in 3-year-old boy. Right hilar lymphadenopathy and thin-walled pneumatocele (*arrows*) in right lower lobe.

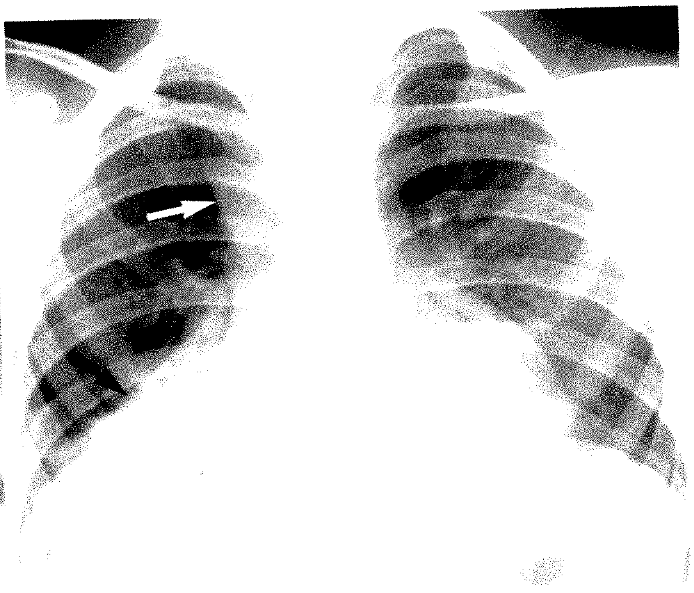

Fig. 6.—Primary tuberculosis in 4-year-old girl. Right lower-lobe collapse (*black arrow*) and shift of upper mediastinum to right (*white arrow*).

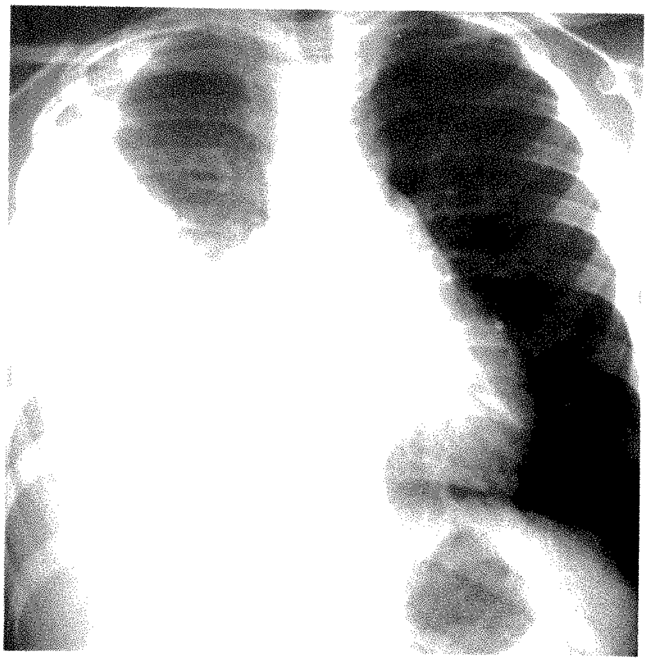

Fig. 7.—Primary tuberculosis in 8-year-old girl. Large pleural effusion on right.

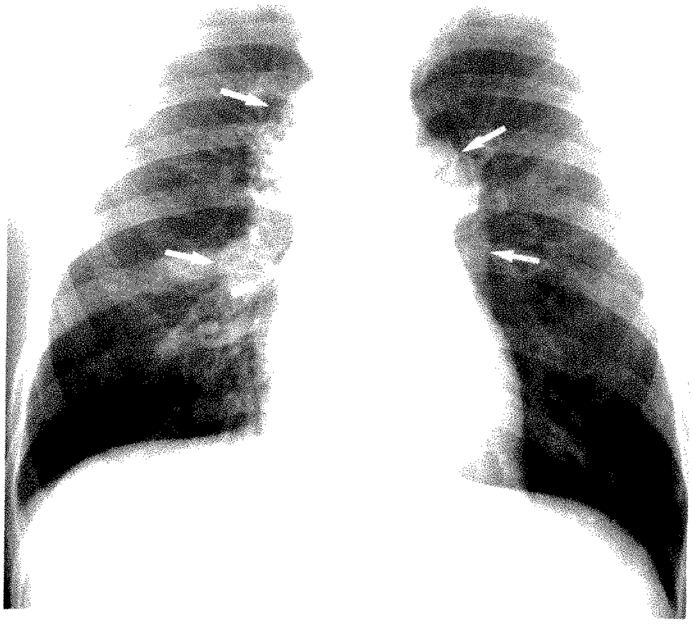

Fig. 8.—Primary tuberculosis in 13-year-old boy. Bilateral hilar, right paratracheal, and aortic-pulmonic window lymphadenopathy (*arrows*) resembles sarcoidosis, lymphoma, or metastatic disease.

performed routinely and therefore was not evaluated in this retrospective study.

Hilar and/or mediastinal lymphadenopathy was present in 12 (35%) of the 34 patients (figs. 3, 5, and 8). Lymphadenopathy was present in six of the 15 children and six of the 19 adults. Lymphadenopathy was limited to the hilum in six cases, involved both hilar and mediastinal nodes in three, and was limited to the mediastinum in three. In two patients lymphadenopathy was an isolated finding; however, in 10 instances lymphadenopathy was associated with pleural effusion, consolidation, and/or atelectasis.

The radiographic diagnosis was initially correct in only 11 (34%) of these patients with primary tuberculosis. Radiographic patterns most often diagnosed as tuberculosis included a miliary pattern, parenchymal consolidation accompanied by lymphadenopathy in a child, and cavitation. Patterns least likely to elicit a diagnosis of tuberculosis included a normal chest radiograph, hilar and mediastinal lymphadenopathy in an adult, and isolated findings of parenchymal consolidation, atelectasis, or pleural effusion.

The clinical diagnosis was initially correct in 29 cases (85%) on the basis of the history and physical examination, chest radiograph report, and knowledge of a recent conversion of the PPD skin test. However, in five patients, all adults, tuberculosis was initially excluded as a possible diagnosis because the chest radiograph was felt to be incompatible with the diagnosis of tuberculosis in an adult. Four of these patients demonstrated hilar and/or mediastinal lymphadenopathy and the fifth had consolidation of the anterior segment of the right upper lobe.

Postprimary Tuberculosis

Pulmonary parenchymal disease was present in all 56 patients with postprimary tuberculosis. In seven patients a single segment of lung was involved; in 49, two or more areas of the lungs were involved. Overall, 246 areas of pulmonary disease were present in these 56 patients (table 1). The apical and posterior segments of the upper lobes were the most commonly involved parts of the lungs (figs. 9 and 10).

Involvement of unusual parts of the lung was common in postprimary tuberculosis (fig. 11). Twenty-four patients had disease involving the anterior segment of an upper lobe; 18 patients had involvement of the basilar segments of the lower lobes. However, in the vast majority of these cases, disease was present in more typical parts of the lung as well, for example, the apical and posterior parts of the upper lobes or superior segment of a lower lobe. In only one case each was postprimary tuberculosis isolated to the anterior segment of an upper lobe or basilar segment of a lower lobe.

The pulmonary parenchymal disease was characterized as being exudative, fibroproductive (fibronodular and/or fibrocalcific), and nodular. The most common finding (79%) was that of a mixture of exudative and fibroproductive lesions. In 18% the pulmonary disease was purely fibroproductive in nature, and in 3% the disease was purely exudative in nature. In 11 patients virtually all parts of both lungs were involved, and the disease was considered to be extensive. Lobar enlargement was noted in one case. Large nodules or masslike densities were seen in four patients. These always occurred in the upper lobes and were always accompanied by other

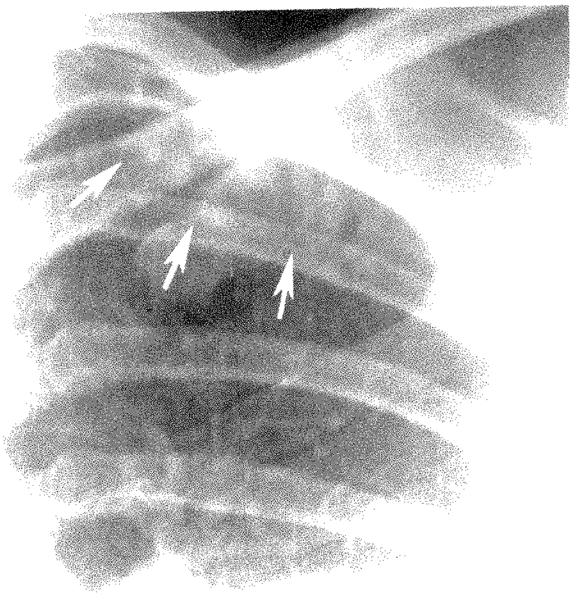

9

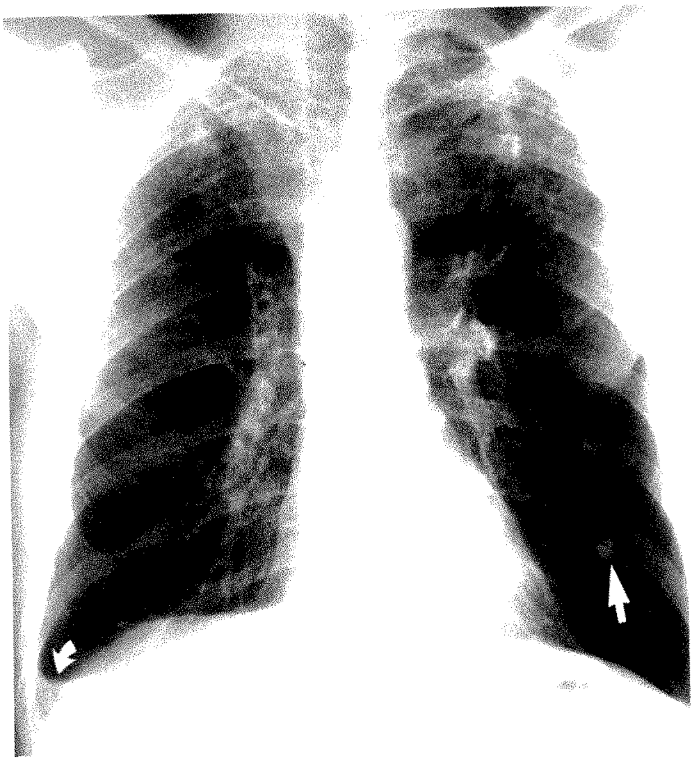

10

Fig. 9.—Postprimary tuberculosis. Fibroproductive (fibronodular) densities in apical segment of left upper lobe (*arrows*), initially interpreted as old, inactive scarring. Sputum culture obtained 1 year later grew *Mycobacterium tuberculosis*.

Fig. 10.—Postprimary tuberculosis in apical and posterior segments of both upper lobes in 36-year-old man. Blunting of right costophrenic angle (*curved arrow*) and calcified Ghon lesion in lingula (*straight arrow*) were residual findings from primary infection.

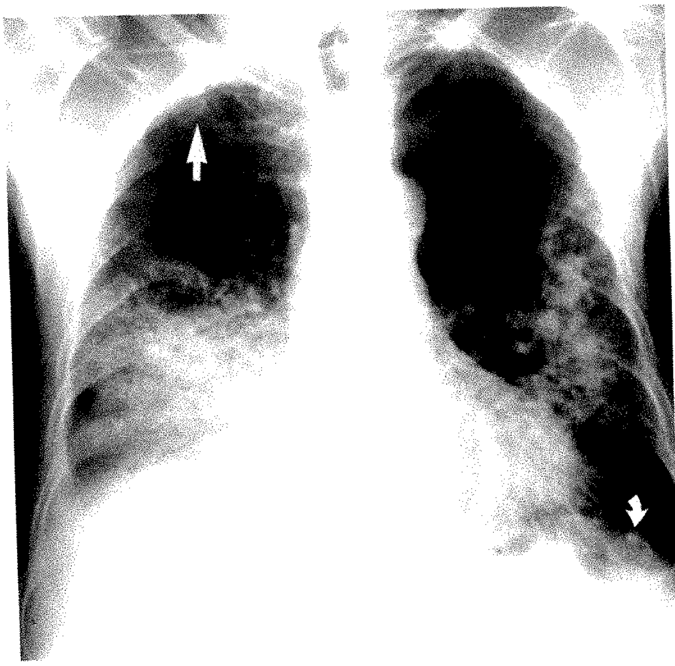

Fig. 11.—Postprimary tuberculosis in 77-year-old man. Homogeneous consolidation of right middle and lower lobes and mottled consolidation of left lower lobe. Subtle fibroproductive lesions in apical segment of right upper lobe (*straight arrow*) and calcified Ghon lesion in left lower lobe (*curved arrow*). Bilateral apical pleural thickening.

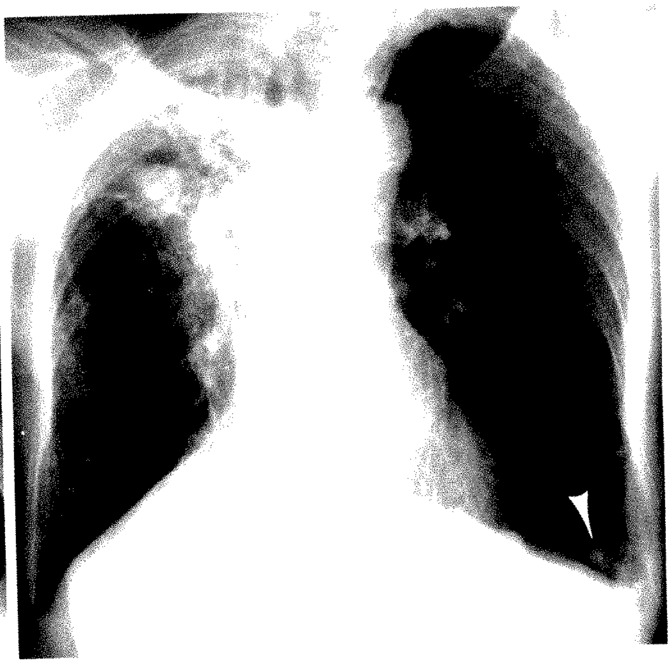

Fig. 12.—Postprimary tuberculosis in 87-year-old woman. A 2-cm nonneoplastic masslike density is seen associated with marked fibrosis of right upper lobe with upward retraction of right hilum and displacement of trachea to right. There is marked right apical pleural thickening. Fibroproductive lesions are present in basilar segments of right lower lobe and apical segment of left upper lobe. Calcified Ghon lesion in left lower lobe (*arrowhead*).

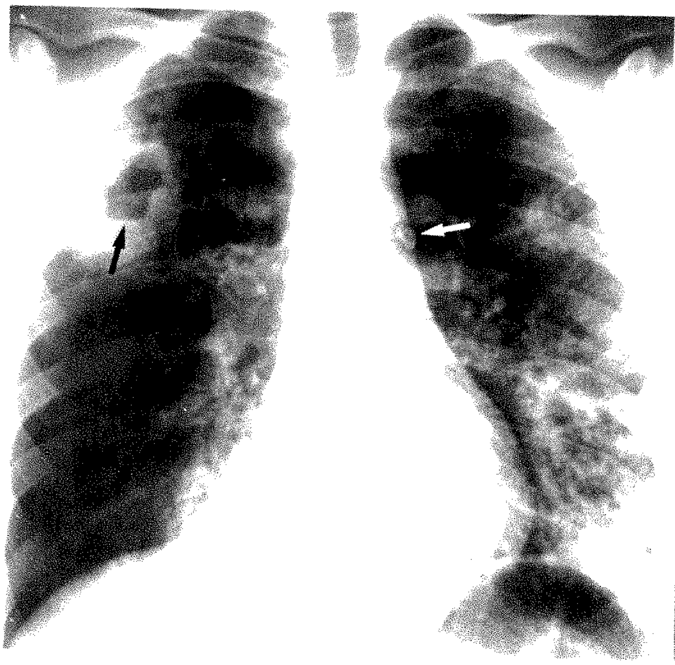

Fig. 13.—Postprimary tuberculosis in 20-year-old man. A 5-cm thick-walled cavity in posterior segment of right upper lobe contains air-fluid level (*black arrow*). Bronchogenic spread with acute tuberculous pneumonia involving basilar segments of right lower lobe, left upper lobe and lingula, and basilar segments of left lower lobe. *White arrow* indicates calcified aortic-pulmonic window node from previous primary infection.

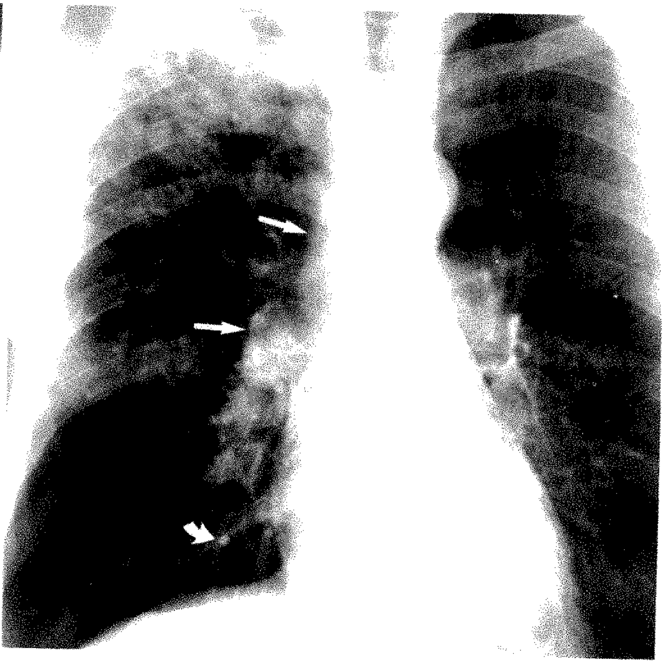

Fig. 14.—Postprimary tuberculosis. Extensive fibroproductive and exudative densities with cavitation in apical and posterior segments of right upper lobe. Right hilar and paratracheal lymphadenopathy (*straight arrows*). *Curved arrow* indicates calcified Ghon lesion in right lower lobe.

areas of fibroproductive or exudative densities (satellite lesions) (fig. 12).

Cavitation was common, being present in 25 (45%) of the 56 patients (fig. 13). In six cases a single cavity was present; in 19 cases there were multiple cavities. The cavity walls ranged from very thin and smooth to very thick and nodular. Air-fluid levels were present in five cases. Pneumatoceles were encountered in only one case. Bronchogenic spread of tuberculous material from upper-lobe cavities to other parts of the ipsilateral and/or contralateral lung was presumed to have occurred in 12 of the 56 patients (fig. 13) and often resulted in extensive abnormalities on the chest radiograph.

A marked fibrotic response was evoked in the lungs of 16 patients (29%) (fig. 12). This was manifested by lobar atelectasis in nine patients, upward hilar retraction in 10, downward hilar retraction in one, tracheal deviation in seven, and acquired tracheomegaly in four.

Pleural effusion occurred in 10 (18%) of the 56 patients with postprimary tuberculosis. Effusion was unilateral in eight cases and bilateral in two. The size of effusion was small in seven cases and medium in three. In two cases air-fluid levels were present in the pleural space, indicating bronchopleural fistula with empyema formation. Apical pleural thickening was present in 23 cases (41%) (figs. 11, 12, and 14); it was unilateral in 14 cases and bilateral in nine. The extent of apical pleural thickening was usually 1 cm or less; in only three cases was the apical pleura over 1 cm in thickness. Spontaneous pneumothorax was noted in three of 56 patients and was usually associated with extensive disease with multiple cavities.

Hilar and/or mediastinal lymphadenopathy was present in three patients (5%) with postprimary tuberculosis (fig. 14). Lymph node groups involved included the right hilar, right paratracheal, and subcarinal nodes. The presence of intrathoracic lymphadenopathy in these three cases accompanied rather extensive parenchymal disease with multiple areas of cavitation. By comparison with the lung disease, lymphadenopathy was not a prominent feature of postprimary tuberculosis in these three cases.

Residual evidence of the original primary infection was apparent in 35 cases (63%). This included calcified or noncalcified Ghon lesions in 24 patients, calcified hilar and/or mediastinal lymph nodes in nine, and blunting of the lateral costophrenic angle in nine (figs. 10–14).

The radiographic diagnosis was initially correct in 33 (59%) of these 56 patients. In 12 patients the radiograph was interpreted as abnormal but tuberculosis was not considered as a diagnosis, and in 11 patients the chest radiograph was interpreted as being normal (six cases) or as showing inactive lung scars (five cases). Common pitfalls in radiographic interpretation included the following: Fibroproductive lesions were either overlooked entirely or interpreted as being inactive; involvement of the anterior segments of the upper lobes or basal parts of the lower lobes was used as evidence against the diagnosis of tuberculosis; and large nodular or masslike densities were interpreted as being neoplastic. The clinical diagnosis was initially correct in only 31 cases (55%). In 12 patients the pulmonary symptoms were mild and nonspecific, and tuberculosis was not thought to be the cause; in addition, in several cases the chest radiographic abnormalities and positive PPD skin test were considered to be noncontributory to the present illness. In 13 patients the pulmonary symptoms were so slight that pulmonary disease was not clinically suspected. In all, there were 17 patients (30%) in which neither the radiologist nor clinician initially suspected tuberculosis, resulting in a delay of 1-3 years in the diagnosis.

Discussion

Primary tuberculosis is an airborne infection. The site of primary tuberculosis in the lungs reflects areas of greatest ventilation; the most common sites are the middle or lower lung zones or the anterior segment of an upper lobe [12]. The regional multiplication of organisms is followed by hilar and/or mediastinal lymphadenopathy and the lymphohematogenous dissemination of organisms diffusely to the lungs and to numerous extrapulmonary sites [12]. During this time, most patients are either asymptomatic or develop mild to moderate systemic symptoms [12]. Tuberculin conversion occurs in 4-8 weeks, at which time the patient will demonstrate a positive PPD skin test [12]. This corresponds to an activation of macrophage responsiveness, when activated macrophages become capable of containing the primary infection [12]. In 2%-6% of cases, the lymphohematogenous dissemination of massive numbers of viable organisms results in clinical and radiographic evidence of miliary tuberculosis [7, 12, 13]. This event is life-threatening and is characterized clinically by fever, weight loss, prostration, and, if untreated, death from respiratory failure and disseminated intravascular coagulation [12]. In about 10% of primary infections, acquired immunity is inadequate to contain the primary infection, and regional multiplication is followed by chronic, progressive parenchymal disease [12]. This phenomenon is distinguishable from postprimary disease only by documentation of a recent conversion of the PPD skin test [14]. In the remainder of cases the primary infection is contained but remains a significant risk for postprimary tuberculosis unless preventive treatment is given [15, 16]; memory lymphocytes become immunologically committed, and patients with primary infection generally retain both tuberculin reactivity and immunity from primary reinfection for life [12].

Primary tuberculosis was once thought to be strictly a disease of childhood. During this century there has been a marked decrease in the incidence of tuberculosis in the United States as a result of careful public health measures and the advent of antituberculous chemotherapy. Because of this, only a small percentage of American adults have a positive PPD skin test, indicating that most adults today are susceptible to the development of primary tuberculosis [1, 7]. We can be reasonably certain that 25% of the adults with pulmonary tuberculosis in our series had the primary form of the disease. Figure 1 shows three age-related peaks of highest prevalence. The highest prevalence of primary tuberculosis was noted in the 0-5-year age group; a second peak was noted in the 21-30-year age group; and a third peak was noted in patients 71 years of age or older. The high prevalence of primary tuberculosis in young adults may be related to mobile, healthy, susceptible individuals living or working in crowded environments or under poor socioeconomic conditions [5]; primary tuberculosis in the elderly may be related to poor or crowded living conditions in addition to chronic or debilitating disease and immunosuppression [5]. Because of the recent increased prevalence of primary tuberculosis in adults, the term "childhood" tuberculosis to describe primary tuberculosis should be abandoned.

Postprimary tuberculosis is the name given to a clinical and radiographic pattern of disease that correlates pathogenetically with acquired hypersensitivity and immunity [13]. The careful observations and retrospective analyses of Stead [14, 17] and others [12] have led to the understanding that in 90% of cases, postprimary tuberculosis results from reactivation of a previously dormant primary infection; a minority of cases represent a continuation of the primary disease [13, 14]. Rarely, postprimary tuberculosis is exogenous superinfection on an inactive or even active original infection—true reinfection [13].

The early parenchymal infiltrate of postprimary tuberculosis results from the intensive inflammatory reaction in the hypersensitive host [18]. This may lead to caseous necrosis, which over time is apt to slough into a bronchus, leaving a cavity [18]. The most commonly involved parts of the lungs in postprimary disease are the apical and posterior segments of an upper lobe [1, 5, 8, 13, 18-20]. Two main factors have been postulated to explain this common location of postprimary tuberculosis. The higher regional oxygen tensions of the apical and subapical parts of the upright lung (114 to 132 mm Hg) have been highly touted as being responsible for apical localization of postprimary disease. It is suggested that the demonstrated higher oxygen tensions in the apex of the upright lung produce increased mycobacterial virulence; the lower parts of lung where alveolar oxygen tension is 108 mm Hg or less are theorized to be quite resistant to the development of postprimary tuberculosis [18]. This concept may best be put to the test by observing populations dwelling at high altitude. Above 10,000 feet (3048 m) of elevation, alveolar oxygen tension is substantially less than 100 mm Hg; above 15,000 feet (4570 m), alveolar oxygen tension is well below 80 mm Hg, even in the extreme apex of the lung [18]. Nevertheless, native permanent residents of the Peruvian highlands (10,300-14,300 feet [3138-4357 m]) seem to be especially disposed to tuberculosis as compared to lowland natives (sea level) [18, 21].

A more likely explanation of the apical localization of postprimary tuberculosis is related to impaired clearance mechanisms from poor lymph flow [18]. Pulmonary lymph flow is related to two factors: microvascular pressure and respiratory motion. In the erect lung, owing to gravitational effect, pulmonary perfusion and microvascular pressure are reduced in the apex relative to the middle and lower lung zones; as a result, apical lymph flow is also relatively deficient compared to the more dependent parts of the lung [18]. In addition, lymph flow in small lymphatic channels is directly related to respiratory excursion. Since the anterior rib cage moves with respiration but the posterior rib cage is relatively fixed, lymph flow is also restricted in the posterior parts of the lung [18]. In primary tuberculosis, lymphohematogenous dissemination results in the seeding of mycobacterial organisms to many or all parts of the lungs; the decreased lymph flow in the apical and posterior parts of the lungs would result in decreased clearance of organisms from these parts of the lung and would favor the development of postprimary tuberculosis in these locations [18].

Our study reveals a broad spectrum of radiographic abnormalities in primary and postprimary tuberculosis not unlike those demonstrated in other reports on this subject. It also provides helpful insights into common causes for a misdiagnosis of tuberculosis.

In children, a clinical diagnosis of primary tuberculosis usually is made when an abnormal chest radiograph is coupled with clinical evidence of pulmonary disease and a documented conversion of the PPD skin test. Certain radiographic patterns, such as parenchymal consolidation associated with hilar and/or mediastinal lymphadenopathy, or isolated hilar and/or mediastinal lymphadenopathy, in children elicit a frequent diagnosis of primary tuberculosis on the basis of the chest radiograph alone.

In adults, these same findings often are viewed as unusual, atypical, or even incompatible with tuberculosis, and tuberculin conversion may be viewed as a coincidental and unrelated phenomenon. Four adults in our 34 cases of primary tuberculosis escaped initial radiographic and clinical diagnosis because hilar and/or mediastinal lymphadenopathy were considered by the clinician and radiologist alike to be incompatible with "adult" tuberculosis. Hilar and mediastinal lymphadenopathy are nonspecific findings that occur in bronchogenic carcinoma, metastatic neoplasm, sarcoidosis, lymphoma, and fungal disease. But if the lymphadenopathy in these adults had been recognized as a possible manifestation of primary tuberculosis, the conversion of the PPD skin test might have been viewed as related to the patient's illness, and a correct diagnosis of primary tuberculosis might have been made. In another adult patient, tuberculosis was excluded as a possibility because parenchymal consolidation was limited to the anterior segment of an upper lobe. While disease limited to the anterior segment of an upper lobe or basilar segment of a lower lobe is rare in postprimary tuberculosis and common in nontuberculous pneumonia, it should be remembered that these findings are rather common in primary tuberculosis.

Postprimary disease in adults is often misdiagnosed also. The clinical symptoms often are minimal and the patient may report only a nonspecific "smoker's cough" or no symptoms at all. In our series, 17 (30%) of 56 cases of active postprimary tuberculosis were missed by both the clinician and the radiologist, resulting in a 1–3-year delay in diagnosis on one or more hospital admissions.

Incorrect appraisal of disease activity was the most common cause of misdiagnosis. In local fibroproductive (fibronodular, fibrocalcific) tuberculosis the exudative lesion is gradually replaced by one or more sharply circumscribed shadows, which are often irregular and angular in contour [13]. Stranding toward the hilum occurs, and calcification in one or more of the nodules often appears [13]. This pattern of pulmonary abnormality is characteristic of granulomatous disease and is seldom, if ever, found in other bacterial infections. However, we found that it was this characteristic pattern fo parenchymal tuberculosis that caused the greatest difficulty in diagnosis. It is this stage of postprimary tuberculosis that is often overlooked entirely or is reported as "old scarring" or "no active disease." This is incorrect, since many of these patients may be sputum-positive. Without films dating back at least 6 months, an accurate statement about the stability of a fibroproductive lesion cannot be made; all of these lesions should be reported as "possible tuberculosis or fungal disease, activity indeterminant" [10, 22]. Even in patients with unchanging tuberculous scars, active tuberculous infection can still be present on sputum culture [1]. Therefore, these patients should be reported as "radiographically stable" rather than "inactive" [10, 22]. The term *fibrotic*, often used to describe this pattern of disease, is not recommended [10] because it implies inactivity.

The second most common cause for a misdiagnosis of postprimary tuberculosis was involvement of an anterior segment of an upper lobe or basilar segment of a lower lobe by parenchymal disease. It is a common misconception that involvement of these areas excludes tuberculosis. This is certainly not true of primary disease; moreover, in postprimary disease we found the anterior segments of the upper lobes to be involved in 46% of cases and the basilar segments of the lower lobes to be involved in 32% of cases. In most of these cases cavitary or fibroproductive disease was present in typical locations; many of these patients also showed residual radiographic evidence of the previous primary disease—subtle but helpful adjunctive findings in arriving at a correct diagnosis.

The third most common cause for misdiagnosis of postprimary disease was the presence of large nodular or masslike densities that were considered to be neoplastic. Typically, these were upper-lobe-predominant, rather than basilar, and were associated with fibroproductive lesions in typical locations.

As Palmer [19] states, "pulmonary tuberculosis continues to keep the physician humble." Since the advent of antituberculous chemotherapy 30 years ago, there has been a dramatic drop in the incidence of tuberculosis in this country. This has created a generation of American physicians who have little experience with it. Although the case rate of tuberculosis is relatively stable in many areas of the country, some areas are experiencing a marked increase in incidence. In addition, the recent increased prevalence of primary tuberculosis in adults has produced a confusing spectrum of disease seldom encountered in adults in the past. Because of the infectious nature of tuberculosis, the morbidity and mortality of the natural course of the disease, and the excellent therapeutic results of antituberculous chemotherapy in most cases, there is good reason for all physicians to be sensitive to the continued existence of this disease. The presence of healed sequelae of primary disease or a positive PPD should suggest that almost any radiographic abnormality could represent active tuberculosis. The recognition of primary disease in the adult and close scrutiny for and proper reporting of fibroproductive lesions could further improve the detection and diagnosis of active tuberculosis.

REFERENCES

1. Miller WT, MacGregor RR. Tuberculosis: frequency of unusual radiographic findings. *AJR* **1978**;130:867–875
2. Lian CF, Robinson AE. Atypical radiographic appearance and clinical presentation of pulmonary tuberculosis. *South Med J* **1976**;69:1317–1322
3. Amorosa JK, Smith PR, Cohen JR, Ramsey C, Lyons HA. Tuberculous mediastinal lymphadenitis in the adult. *Radiology* **1978**;126:365–368
4. Liu C-I, Fields WR, Shaw C-I. Tuberculous mediastinal lymphadenopathy in adults. *Radiology* **1978**;126:369–371
5. Miller WT. Tuberculosis in the adult. *Postgrad Radiol* **1981**; 1:147–167
6. Hadlock FP, Park SK, Awe RJ, Rivera M. Unusual radiographic findings in adult pulmonary tuberculosis. *AJR* **1980**;134:1015–1018
7. Choyke PL, Sostman HD, Curtis AM, et al. Adult-onset pulmonary tuberculosis. *Radiology* **1983**;148:357–362
8. Woodring JH. The radiographic manifestations of pulmonary tuberculosis. *J Ky Med Assoc* **1984**;82:17–23
9. *Guide for completing reports of verified cases of tuberculosis.* Atlanta, GA: Centers for Disease Control, Division of TB Control, **1984**
10. Diagnostic standards and classification of tuberculosis and other mycobacterial diseases, 14th ed. *Am Rev Respir Dis* **1981**; 123[suppl]:343-358
11. Roper WH, Waring JJ. Primary serofibrinous pleural effusion in military personnel. *Am Rev Respir Dis* **1955**;71:616–634
12. Geppert EF, Leff A. The pathogenesis of pulmonary and miliary tuberculosis. *Arch Intern Med* **1979**;139:1381–1383
13. Fraser RG, Paré JAP. *Diagnosis of diseases of the chest*, vol 2, 2d ed. Philadelphia: Saunders, **1978**:731–761
14. Stead WW, Kerby GR, Schlueter DP, Jordahl CW. The clinical spectrum of primary tuberculosis in adults: confusion with reinfection in the pathogenesis of chronic tuberculosis. *Ann Intern Med* **1968**;68:731–745
15. Ferebee SH. Controlled chemoprophylaxis trials in tuberculosis, a general review. *Bibl Tuberc* **1970**;26:28–106
16. Dash LA, Comstock GW, Flynn JPG. Isoniazid preventive therapy: retrospect and prospect. *Am Rev Respir Dis* **1979**; 119[suppl]:398
17. Stead WW. Pathogenesis of the sporadic case of tuberculosis. *N Engl J Med* **1967**;277:1008–1012
18. Goodwin RA, DesPrez RM. Apical localization of pulmonary tuberculosis, chronic pulmonary histoplasmosis, and progressive massive fibrosis of the lung. *Chest* **1983**;83:801–805
19. Palmer PES. Pulmonary tuberculosis—usual and unusual radiographic presentations. *Semin Roentgenol* **1979**;14:204–243
20. Jacobson HG, Shapiro JH. Pulmonary tuberculosis. *Radiol Clin North Am* **1963**;1:411–427
21. Monge C Sr, Monge C Jr. *High altitude diseases*. Springfield, IL: Thomas, **1966**
22. *Diagnostic standards and classification of tuberculosis.* New York: National Tuberculosis and Respiratory Disease Association, **1969**

Early Esophageal Cancer

Marc S. Levine[1]
Edward C. Dillon[1, 2]
Scott H. Saul[3]
Igor Laufer[1]

Early esophageal cancer (EEC) accounted for only seven (4.7%) of 148 cases of esophageal cancer diagnosed at the authors' hospital between 1977 and 1984. Two patients with EEC had squamous cell carcinoma and five had adenocarcinoma arising in Barrett's mucosa. All seven patients had associated clinical findings, including low-grade gastrointestinal bleeding (three cases), odynophagia (one case), and chronic reflux symptoms due to underlying reflux esophagitis and Barrett esophagus (three cases). Since Barrett esophagus is a premalignant condition, the high proportion of adenocarcinomas in this series presumably reflects the more frequent radiologic evaluation of symptomatic patients with Barrett esophagus. On esophagography, four patients had 3–4.5-cm polypoid intraluminal masses that could not be distinguished radiographically from advanced esophageal carcinoma. In the other three patients, esophagrams revealed secondary achalasia, irregular flattening of the esophageal wall, and diffuse nodularity of the mucosa. The authors conclude that "early" esophageal cancers are not necessarily small cancers, since they may undergo considerable intraluminal or intramural growth and still be classified histologically as EEC. Radiologists should be aware of these findings, since EEC has an excellent prognosis with a 5-year survival approaching 90%.

Early esophageal cancer (EEC) is defined histologically as cancer limited to the mucosa or submucosa without lymph-node metastases [1]. Unlike advanced esophageal cancer, which has a dismal prognosis, EEC is a readily curable lesion with reported 5-year survival rates approaching 90% [2–4]. However, most cases of EEC have been detected in China or in other areas where the high incidence of esophageal cancer has led to mass screening of asymptomatic patients to detect these lesions at the earliest possible stage. In contrast, symptomatic patients with esophageal carcinoma usually develop dysphagia only after the tumor has invaded periesophageal lymphatics or other mediastinal structures [5, 6]. Thus, most esophageal cancers diagnosed outside of China have been advanced, unresectable lesions at the time of presentation.

EECs are generally thought to appear radiographically as sessile or plaquelike lesions under 3.5 cm in diameter [7–13]. As a result, some authors have described these lesions as "small" rather than "early" esophageal cancers [7, 10, 11]. However, we recently encountered a case of histologically proven EEC in which the lesion appeared radiographically as a 4.5 cm polypoid mass in the distal esophagus. This led to further investigation to determine the prevalence of EEC at our institution as well as the clinical and radiographic findings in these patients.

Materials and Methods

Pathology records at the Hospital of the University of Pennsylvania revealed 148 cases of proven esophageal cancer during an 8-year period between 1977 and 1984. The tumor was surgically resected in 58 cases. A retrospective review of the 58 resected surgical specimens and/or accompanying pathology reports revealed seven cases that could be classified

Received August 30, 1985; accepted after revision November 14, 1985.

[1] Department of Radiology, Hospital of the University of Pennsylvania, 3400 Spruce St., Philadelphia, PA 19104. Address reprint requests to M. S. Levine.

[2] Present address: Department of Medicine, Pennsylvania Hospital, Philadelphia PA 19107.

[3] Department of Pathology, Hospital of the University of Pennsylvania, Philadelphia, PA 19104.

AJR 146:507–512, March 1986
0361–803X/86/1463–0507
© American Roentgen Ray Society

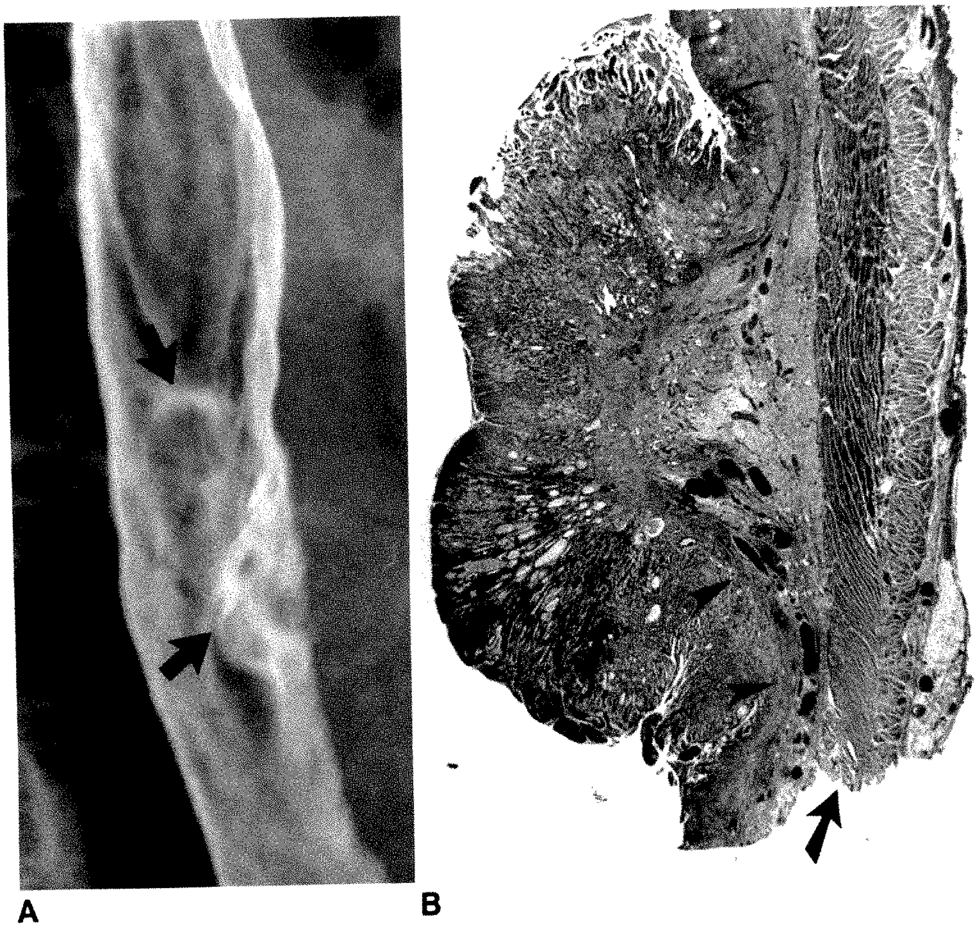

Fig. 1.—EEC with polypoid radiographic appearance. **A**, Double-contrast esophagram. Irregular, polypoid mass (*arrows*) in midesophagus cannot be distinguished radiographically from advanced cancer. This patient had squamous cell carcinoma. **B**, Photograph of whole-mount histologic section in another case shows polypoid adenocarcinoma. Tumor extends through lamina muscularis mucosae (*arrowheads*) into submucosa but does not penetrate lamina propria mucosae (*arrow*) (H and E, × 4). All resected lymph nodes were negative for metastatic adenocarcinoma. Thus, lesion can be classified as EEC despite its gross appearance.

histologically as EEC according to criteria established by the Japanese Society for Esophageal Diseases (i.e., malignant invasion limited to the mucosa or submucosa without lymph-node or other metastases) [1]. The seven cases of EEC were further reviewed to determine the gross and histologic features of these lesions. All seven patients had preoperative esophagrams (five double-contrast esophagrams at our hospital and two unspecified-type esophagrams at outside hospitals), and the radiographs or radiographic reports were reviewed retrospectively to determine the radiologic features of these lesions. Finally, medical records were reviewed to determine the clinical presentation, treatment, and subsequent course of the disease.

Results

Pathologic Findings

Of 58 resected esophageal cancers, 27 were squamous cell carcinomas and 31 were adenocarcinomas arising in Barrett's mucosa. Although adenocarcinoma accounts for only 20% of all esophageal cancers diagnosed at our hospital [14], it comprised over 50% of those that were resected. The high proportion of adenocarcinomas in this group presumably reflects their more frequent location in the distal esophagus, so that they are relatively amenable to esophagogastrectomy [14, 15]. In contrast, squamous cell carcinomas tend to be located more proximally in the esophagus and are more radiosensitive tumors, so that surgery is performed less frequently in these patients.

Seven of the 58 resected cases were classified histologically as EEC and 51 as advanced esophageal carcinoma. In the remaining 90 cases, there were no pathologic records to indicate that surgery had been performed. However, a random sample of medical charts from several patients in this group showed that surgery had been contraindicated because of local or widespread metastatic disease. It therefore seems reasonable to assume that the vast majority of the 90 unoperated cases were advanced lesions. Thus, EEC accounted for at least seven (4.7%) of the 148 cases of esophageal cancer diagnosed at our hospital during this period.

Pathologic examination of the seven resected EECs revealed carcinoma in the mucosa and submucosa in six cases (fig. 1B), while the depth of invasion was limited to the mucosa in one case. Two patients with EEC had squamous cell carcinoma and five had adenocarcinoma arising in Barrett's mucosa. Four patients with adenocarcinoma had esophageal dysplasia directly adjacent to areas of invasive carcinoma, and one had multifocal dysplasia within Barrett's mucosa at sites remote from the primary tumor.

Six of the EECs involved the distal esophagus and one the midesophagus. Four cases appeared grossly as polypoid

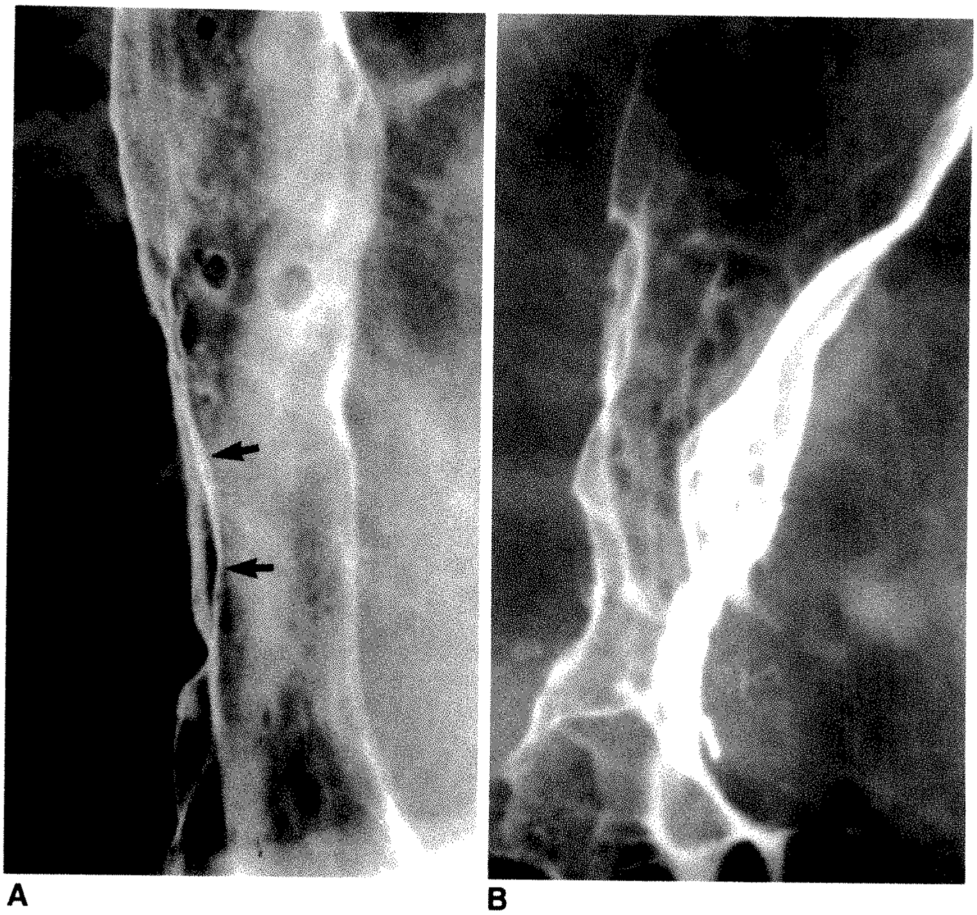

Fig. 2.—**A**, Double-contrast esophagram shows relatively long peptic stricture in distal esophagus with irregular flattening of one wall of stricture (*arrows*). At surgery, patient had early adenocarcinoma in Barrett esophagus with malignant involvement confined to mucosa. **B**, Repeat esophagram 3 years after esophagogastrectomy. Advanced, circumferentially infiltrating lesion above esophagogastric anastomosis due to recurrent carcinoma.

masses, which were 3–4.5 cm in diameter. In one case, areas of ulceration were identified within the mass. Of the remaining three patients, one had irregular flattening of one wall of the esophagus, one had a circumferentially infiltrating but superficial lesion, and one had mucosal erythema and nodularity without a discrete lesion.

Radiographic Findings

In four patients with EEC (three adenocarcinomas and one squamous cell carcinoma), esophagography revealed discrete polypoid lesions in the midesophagus (one case) or distal esophagus (three cases) with the lesions ranging from 3 to 4.5 cm in diameter (fig. 1A). Another patient with adenocarcinoma confined to the mucosa had a mild but relatively long stricture in the distal esophagus with irregular flattening of one wall of the stricture (fig. 2A). In this case, a repeat esophagram three years after esophagogastrectomy revealed an advanced, circumferentially infiltrating lesion above the esophagogastric anastomosis due to recurrent carcinoma (fig. 2B). Another patient with adenocarcinoma had extensive mucosal nodularity and irregularity over an approximately 7-cm-long segment of the distal esophagus without a discrete lesion (fig. 3). Finally, one patient with squamous cell carcinoma had smooth, tapered distal esophageal narrowing with poor primary peristalsis (fig. 4). While the radiographic findings in this case suggested early achalasia, the length of the narrowed segment was somewhat atypical for this disease.

Of the five patients with early adenocarcinomas, four had sliding hiatal hernias and three had spontaneous gastroesophageal reflux observed fluoroscopically. Although none had evidence of esophagitis, one had a mild peptic stricture in the distal esophagus. Neither of the two patients with early squamous cell carcinomas had hiatal hernias or gastroesophageal reflux on the radiologic study.

Clinical Presentation and Course

The seven patients with EEC were 50–72 years of age (mean, 59.6). Five patients were men and two were women. Both patients with squamous cell carcinoma were symptomatic at the time of diagnosis. One had a 3-week history of substernal chest pain and odynophagia. The other had a 1-month history of melena and a presenting hemoglobin of 7.6 g/dl. Of the five patients with adenocarcinoma, three had chronic reflux symptoms and had been treated previously for reflux esophagitis with biopsy-proven Barrett esophagus. In all three patients, EEC was detected fortuitously during radiologic and endoscopic evaluation of their reflux disease. The remaining two patients with adenocarcinoma had clinical evi-

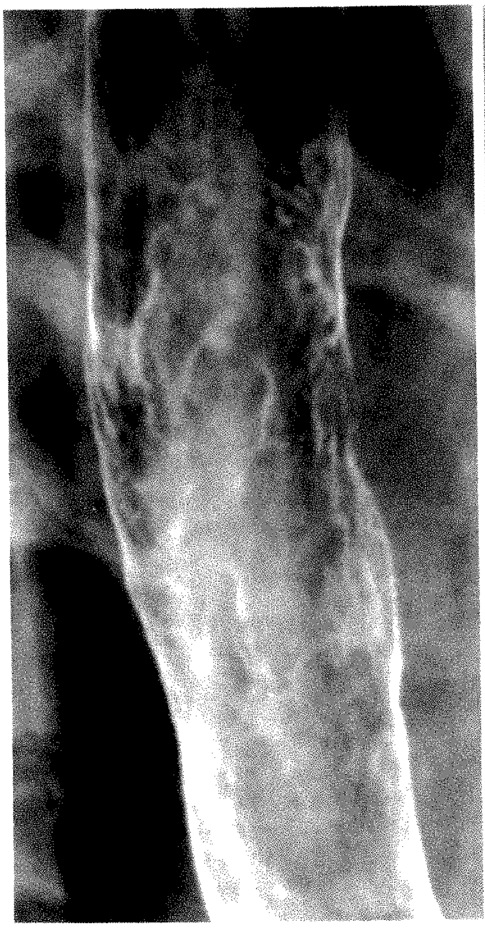

3

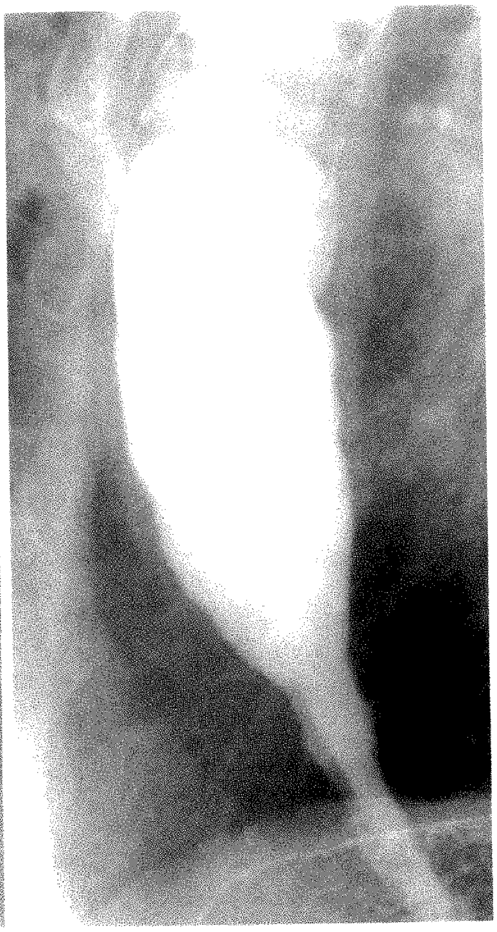

4

Fig. 3.—Early adenocarcinoma in Barrett esophagus. Double-contrast esophagram reveals extensive nodularity and irregularity of distal esophageal mucosa without discrete lesion, representing superficial spreading form of EEC involving mucosa and submucosa.

Fig. 4.—Early squamous cell carcinoma. Single-contrast esophagram reveals smooth, tapered narrowing of distal esophagus, suggesting early achalasia; however, length of stricture is somewhat atypical for achalasia. Examination of resected specimen showed tumor circumferentially infiltrating mucosa and submucosa without invasion of lamina propria mucosae.

dence of low-grade gastrointestinal bleeding with guaiac-positive stool and presenting hemoglobins of 8.6 and 10 g/dl, respectively. In both, however, Barrett esophagus was unsuspected at the time of the radiologic examination.

All seven patients with EEC underwent esophagogastrectomy and gastric pullthrough as a curative surgical procedure. One patient died 1 month after surgery because of postoperative sepsis and renal failure. One patient died 3 years after surgery because of recurrent carcinoma above the esophagogastric anastomosis, and another had significantly deteriorated 3 years later owing to widespread bone metastases. The remaining four patients were alive and well for an average duration of 22.5 months (range, 6–67 months) after surgery.

Discussion

Early esophageal cancer, *superficial esophageal cancer*, and *small esophageal cancer* have been used interchangeably to describe malignant esophageal tumors diagnosed at an "early" stage. However, these lesions should not be considered synonymous, since they have different histopathologic features that may drastically alter the prognosis of this disease. According to the Japanese Society for Esophageal Diseases, EEC and superficial esophageal cancer both are defined as tumors in which malignant invasion is limited to the mucosa or submucosa [1]. However, lymph nodes are always free of tumor in EEC, whereas lymph-node metastases may be present in superficial esophageal cancer [1]. *Small esophageal cancer* is another term used to describe tumors less than 3.5 cm in diameter, regardless of the depth of invasion or the presence or absence of lymph-node metastases [7, 10, 11, 16]. Previous studies have shown that the 5-year survival rate for esophageal cancer decreases dramatically when regional lymph nodes are involved by tumor [5, 17]. Thus, some "superficial" or "small" esophageal cancers may be "early" lesions histologically, but others may have invaded regional lymph nodes with a prognosis comparable to that of advanced esophageal carcinoma [16–18]. For this reason, strict histologic criteria should always be used for the diagnosis of EEC.

Nearly all reported cases of EEC have been squamous cell carcinomas. Most of those cases have been reported in the Chinese or Japanese literature [2–4, 7–9, 12, 13]. In our study, however, five of seven histologically proven EECs were adenocarcinomas. All five adenocarcinomas were found to arise in Barrett's mucosa. Barrett esophagus is a well recognized complication of longstanding reflux esophagitis in which the normal squamous epithelium in the esophagus has been replaced by a columnar epithelial lining [19–21]. There is considerable evidence that it is a premalignant condition associated with a significantly increased incidence of adenocarcinoma [14, 21–24]. Thus, the high proportion of early adenocarcinomas in our series presumably reflects the greater prevalence of reflux esophagitis and Barrett esophagus in Western countries than in the Orient.

Although most esophageal cancers are advanced lesions at the time of clinical presentation, all of our patients with EEC had related clinical findings. Three patients presented with low-grade gastrointestinal bleeding (i.e., melena or guaiac-positive stool) and iron-deficiency anemia. One patient had acute odynophagia. The other three patients had chronic reflux symptoms due to underlying reflux esophagitis and Barrett esophagus. Others have also found that EEC may cause mild esophageal symptoms or low-grade bleeding because of the friability of the tumor [3, 6, 8, 10]. Thus, our experience suggests that EEC usually will be detected in symptomatic patients, especially those with underlying Barrett esophagus.

Radiologic descriptions of EEC have been limited by the small number of cases diagnosed on esophagography. However, these lesions usually have appeared radiographically as small, protruded lesions under 3.5 cm in diameter [7–13]. Most reported cases have been plaquelike lesions (often with central ulceration) or flat sessile polyps with a smooth or slightly lobulated contour [9–13]. Others have been superficial lesions with focal irregularity, nodularity, and/or ulceration of the esophageal wall [12, 13]. While most cases of EEC have been small, localized lesions, the Japanese have reported occasional cases with diffuse granularity or nodularity of the mucosa due to so-called superficial spreading carcinoma [13, 25].

In our study, however, most patients had polypoid lesions ranging from 3 to 4.5 cm in diameter. Unlike the small, protruded lesions described previously, these were relatively bulky intraluminal masses that could not be distinguished radiographically from advanced esophageal carcinoma (fig. 1). One patient had a superficial spreading lesion similar to that described by the Japanese with diffuse nodularity of the mucosa, but no focal lesion [fig. 3]. Another patient had tapered narrowing of the distal esophagus, suggesting primary achalasia (fig. 4). Thus, our experience suggests that "early" esophageal cancers are not necessarily small cancers, since they may undergo considerable intraluminal or intramural growth and still be classified histologically as EEC.

Although EEC accounted for only 4.7% of all esophageal cancers diagnosed at our institution, the Chinese have reported EEC detection rates as high as 70%–80% [2–4, 26]. This discrepancy can be attributed to the unusually high incidence of esophageal cancer in parts of northern China (i.e., 108/100,000/year), which has led to mass screening of asymptomatic patients by exfoliative balloon cytology to detect these lesions at an early stage [2, 4]. As a result, the high proportion of EECs detected in this region has dramatically altered the prognosis of this disease. The reported 5-year survival for these patients has ranged from 85% to 90% [2–4]. Esophageal cancer has therefore become a curable lesion in this part of the world.

On the basis of the Chinese experience with early squamous cell carcinoma, it seems reasonable to assume that early adenocarcinoma arising in Barrett's mucosa should have a better prognosis than advanced lesions. However, the incidence of all types of esophageal carcinoma in the United States is only about 4% of that in northern China (i.e., 4/100,000/year) [27]. As a result, it is difficult to advocate mass screening for esophageal carcinoma in this country, particularly since the major risk factors for developing this disease—namely, smoking and drinking alcohol—are shared by a significant percentage of the population. Nevertheless, many investigators have advocated periodic surveillance of patients known to be at increased risk for developing esophageal cancer due to Barrett esophagus [21–24], head and neck tumors [28, 29], achalasia [30–32], lye strictures [33, 34], or celiac disease [35, 36]. It has not yet been demonstrated whether surveillance of these patients will lead to increased detection of EEC.

In summary, five (71%) of our seven patients with EEC had adenocarcinoma in Barrett's mucosa, although adenocarcinoma accounted for only 20% of all esophageal cancers diagnosed at our hospital. It seems likely that the signs and symptoms of the underlying reflux disease led to the early diagnosis of cancer in these patients. These findings indicate the importance of careful and ongoing radiologic evaluation of the distal esophagus in patients with reflux esophagitis. While some cases of EEC may appear radiographically as subtle lesions, others may present as relatively large polypoid masses in the esophagus. Radiologists therefore should not assume that all large lesions are necessarily advanced, since they may still be classified histologically as EEC, and these patients may have an excellent prognosis despite the radiographic findings.

REFERENCES

1. Japanese Society for Esophageal Diseases. Guidelines for the clinical and pathologic studies on carcinoma of the esophagus. *Jpn J Surg* **1976**;6:69–78
2. Coordinating group for research on esophageal cancer, Linhsien County, Honan. Early diagnosis and surgical treatment of esophageal cancer under rural conditions. *Chin Med J [Engl]* **1976**;2:113–116
3. Guojun H, Lingfang S, Dawei Z, et al. Diagnosis and surgical treatment of early esophageal carcinoma. *Chin Med J [Engl]* **1981**;94:229–232
4. Shu YJ. Cytopathology of the esophagus: an overview of esophageal cytopathology in China. *Acta Cytol* (Baltimore) **1983**;27:7–16
5. Mannell A. Carcinoma of the esophagus. *Curr Probl Surg* **1982**;19:553–647
6. Skinner DB. Surgical treatment for esophageal carcinoma. *Semin Oncol* **1984**;11:136–143
7. Endo M, Kobayashi S, Suzuki H, Takemoto T, Nakayama K. Diagnosis of early esophageal cancer. *Endoscopy* **1971**;2:61–66
8. Suzuki H, Kobayashi S, Endo M, Nakayama K. Diagnosis of early esophageal cancer. *Surgery* **1971**;71:99–103

9. Yamada A, Kobayashi S, Kawai B, Fujimoto A, Nakayama K. Study on x-ray findings of early oesophageal cancer. *Australas Radiol* **1972**;16:238-246
10. Koehler RE, Moss AA, Margulis AR. Early radiographic manifestations of carcinoma of the esophagus. *Radiology* **1976**;119:1-5
11. Moss AA, Koehler RE, Margulis AR. Initial accuracy of esophagograms in detection of small esophageal carcinoma. *AJR* **1976**;127:909-913
12. Zheng-Yan W. Radiological appearances in early oesophageal carcinoma. *J R Soc Med* **1980**;73:849-852
13. Itai Y, Kogure T, Okuyama Y, Akiyama H. Superficial esophageal carcinoma: radiological findings in double-contrast studies. *Radiology* **1978**;126:597-601
14. Levine MS, Caroline D, Thompson JJ, Kressel HY, Laufer I, Herlinger H. Adenocarcinoma of the esophagus: relationship to Barrett mucosa. *Radiology* **1984**;150:305-309
15. Agha FP. Barrett carcinoma of the esophagus: clinical and radiographic analysis of 34 cases. *AJR* **1985**;145:41-46
16. Zornoza J, Lindell MM. Radiologic evaluation of small esophageal carcinoma. *Gastrointest Radiol* **1980**;5:107-111
17. Yamada A. Radiologic assessment of resectability and prognosis in esophageal carcinoma. *Gastrointest Radiol* **1979**;4:213-218
18. Soga J, Tanaka O, Sasaki K, Kawaguchi M, Muto T. Superficial spreading carcinoma of the esophagus. *Cancer* **1982**;50:1641-1645
19. Burgess JN, Payne WS, Andersen HA, Weiland LH, Carlson HC. Barrett esophagus: the columnar-epithelial-lined lower esophagus. *Mayo Clin Proc* **1971**;46:728-734
20. Mangla JC. Barrett's esophagus: an old entity rediscovered. *J Clin Gastroenterol* **1981**;3:347-356
21. Sjogren RW, Johnson LF. Barrett's esophagus: a review. *Am J Med* **1983**;74:313-321
22. Hawe A, Payne WS, Weiland LH, Fontana RS. Adenocarcinoma in the columnar epithelial-lined-lower (Barrett) oesophagus. *Thorax* **1973**;28:511-514
23. Naef AP, Savary M, Ozzello L. Columnar-lined lower esophagus: an acquired lesion with malignant predisposition. *J Thorac Cardiovasc Surg* **1975**;70:826-835
24. Radigan LR, Glover JL, Shipley FE, Shoemaker RE. Barrett esophagus. *Arch Surg* **1977**;112:486-491
25. Itai Y, Kogure T, Okuyama Y, Akiyama H. Diffuse finely nodular lesions of the esophagus. *AJR* **1977**;128:563-566
26. Yang CS. Research on esophageal cancer in China: a review. *Cancer Res* **1980**;40:2633-2644
27. Cancer statistics, 1985. *CA* **1985**;35:19-35
28. Goldstein HM, Zornoza J. Association of squamous cell carcinoma of the head and neck with cancer of the esophagus. *AJR* **1978**;131:791-794
29. Thompson WM, Oddson TA, Kelvin F, Daffner R, Postlethwait RW, Rice RP. Synchronous and metachronous squamous cell carcinomas of the head, neck and esophagus. *Gastrointest Radiol* **1978**;3:123-127
30. Wychulis AR, Woolam GL, Andersen HA, Ellis FH. Achalasia and carcinoma of the esophagus. *JAMA* **1971**;215:1638-1641
31. Seliger G, Lee T, Schwartz S. Carcinoma of the proximal esophagus: a complication of long-standing achalasia. *Am J Gastroenterol* **1972**;57:20-25
32. Hankins JR, McLaughlin JS. The association of carcinoma of the esophagus with achalasia. *J Thorac Cardiovasc Surg* **1975**;69:355-360
33. Appelqvist P, Salmo M. Lye corrosion carcinoma of the esophagus: a review of 63 cases. *Cancer* **1980**;45:2655-2658
34. Hopkins RA, Postlethwait RW. Caustic burns and carcinoma of the esophagus. *Ann Surg* **1981**;194:146-148
35. Harris OD, Cooke WT, Thompson H, Waterhouse JAH. Malignancy in adult celiac disease and idiopathic steatorrhea. *Am J Med* **1967**;42:899-912
36. Collins SM, Hamilton JD, Lewis TD, Laufer I. Small-bowel malabsorption and gastrointestinal malignancy. *Radiology* **1978**;126:603-609

Radiologic Manifestations of Early Gastric Lymphoma

Tadayuki Sato[1]
Yoshiko Sakai[1]
Shingo Ishiguro[2]
Hiroshi Furukawa[3]

The radiologic features of 12 early gastric lymphomas in six patients were analyzed and correlated with the clinicopathologic findings. One 0.7-cm lesion on the anterior wall of the corpus could not be detected radiologically either prospectively or retrospectively. All tumors were smaller than 7.0 cm (mean, 3.5) and located within the stomach. A frequent finding was localized, slight enlargement of folds with a smooth contour, suggesting submucosal tumor infiltration. These folds were more apparent in the radiograph than in the surgical specimen, and were easily deformed by the compression method or became less prominent in the more distended stomach. Ulcer was demonstrated in all lesions, usually appearing as an unicentral, indefinite shallow depression. Deep, well demarcated ulcer was found in three lesions, and a smooth marginal elevation indicated a submucosal tumor growth. These findings were proven to be helpful in differential diagnosis from carcinoma and peptic diseases. All patients are alive and free of recurrence 15–112 months (mean, 53) after surgical resection.

Primary gastric lymphoma has been considered an unusual tumor, accounting for less than 5% of all gastric malignancies. However, of all extranodal lymphomas, primary gastric lymphoma is the most common, and about one-half of all gastrointestinal lymphomas are found in the stomach [1].

Generally, the overall 5-year survival rate for gastric lymphoma is better than that for carcinoma [2, 3]. Yet, when one compares lymphoma patients with carcinoma patients stage by stage, there is no definite difference in the survival rate of these groups [4, 5]. Numerous factors that affect the prognosis of patients with primary gastric lymphoma have been vigorously investigated in recent clinicopathologic reports. Of these, the most significant predictive factors were found to be the depth of invasion and the nodal involvement [1, 6, 7]. In these reports, one encounters a few cases with a submucosal tumor who show a good survival.

Several articles have described the radiologic features of primary gastric lymphoma, and some have established valuable criteria for differentiating lymphoma from other gastric diseases [8–10]. However, all of the reported cases were in the advanced stage, and, to our knowledge, there is little in the radiologic literature concerning early-stage lymphoma. This study describes the radiologic features of early gastric lymphoma and discusses differential diagnosis. We define early gastric lymphoma as a tumor located in the mucosa and the submucosa, according to the Japanese criteria for early gastric cancer. We will later refer to this definition and show why it is preferred.

Materials and Methods

During the period 1975–1983, there were 22 gastric resections performed for primary gastric lymphoma at the Center for Adult Diseases, Osaka. All lymphomas were proven to be tumors originating in the stomach by the initial clinical, laboratory, radiologic, and pathologic examinations and also by follow-up studies. A review of the pathology records revealed that six of these cases showed tumors within the mucosa and the submucosa that did not extend

Received July 29, 1985; accepted after revision October 16, 1985.

[1] Department of Diagnostic Radiology, Center for Adult Diseases, Osaka, 1-3-3 Nakamichi, Higashinari-ku, Osaka, Japan 537. Address reprint requests to T. Sato.

[2] Department of Pathology, Center for Adult Diseases, Osaka, Japan.

[3] Department of Surgery, Center for Adult Diseases, Osaka, Japan.

AJR 146:513–517, March 1986
0361–803X/86/1463–0513
© American Roentgen Ray Society

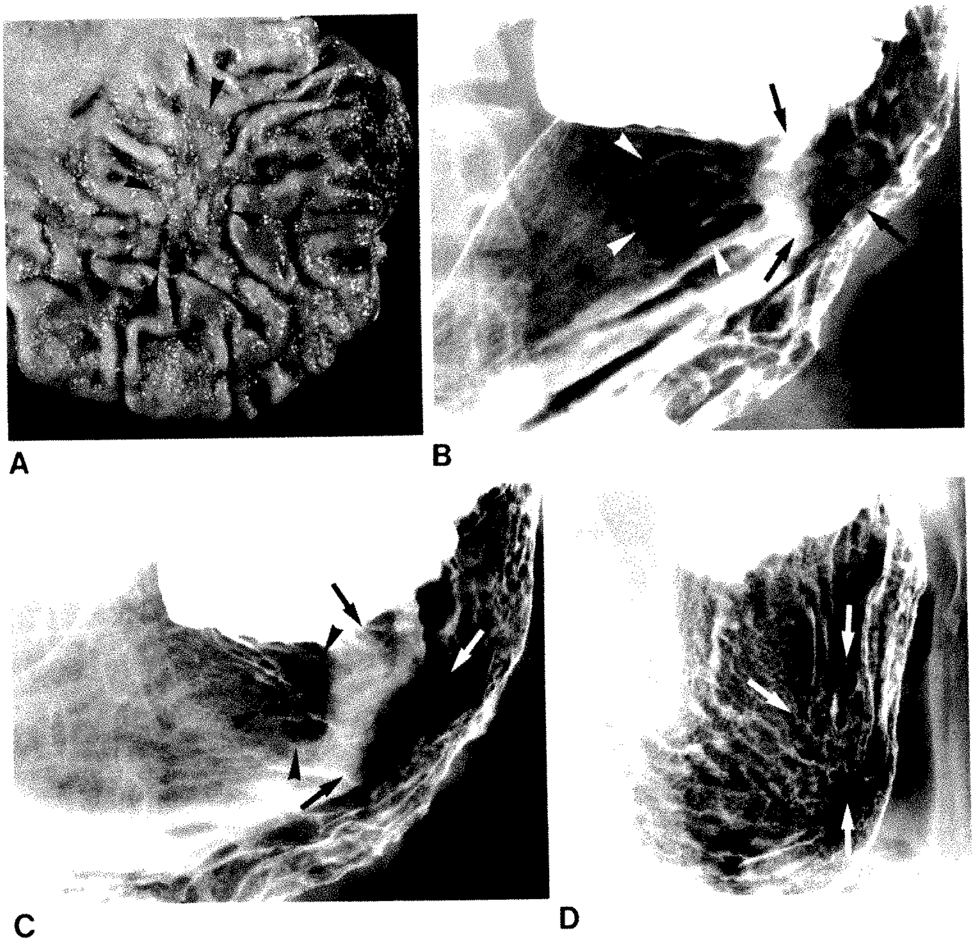

Fig. 1.—Multiple early gastric lymphomas. **A**, Resected specimen shows poorly defined shallow ulcer (*arrowheads*) on posterior wall of corpus surrounded by slightly enlarged smooth folds. **B**, Double-contrast supine film. Rugal folds (*arrowheads*) with contiguity to shallow depression (*arrows*). **C**, Rugal folds (*arrowheads*) are less prominent on more distended double-contrast film. *Arrows* indicate ulceration. **D**, Lesion on anterior wall of corpus. Double-contrast film (prone position, table tilted head-down) shows poorly defined, granular depression (*arrows*) with slightly rugal folds.

into the deeper layer. The entire resected specimen in each case was serially sectioned at intervals of 0.5–1.0 cm in the pathology room, so that the extent and the depth of tumor invasion could be accurately revalued for each lesion.

Radiologic examination was performed on all six cases, primarily with double-contrast technique. After an injection of hypotonic drug, the patient drank 250 ml of 140% wt/vol barium suspension. Air insufflation was achieved by effervescent agents. The fluoroscopic table was lowered to the supine position, and the patient was rotated to obtain favorable mucosal coating of the posterior gastric wall, then returned to the prone position. The table was tilted into a 45°–60° head-down position for double-contrast views of the distal anterior wall, then raised to the semierect position for double-contrast views of the proximal anterior wall. The examination was completed with upright barium-filled views and compression study.

We retrospectively analyzed the clinical, pathologic, and radiologic findings of these six cases with early gastric lymphoma.

Results

Clinicopathologic Findings

Early gastric lymphoma was found in four women and two men aged 27–67 years (mean, 50). All but one patient complained of epigastric pain with a duration of 4–9 months; that one presented with vague abdominal discomfort.

Gastric endoscopy was done on all cases, and 10 lesions were revealed. Their endoscopic diagnosis was carcinoma type IIc in five lesions, lymphoma or suspicion of lymphoma in four, and ulcer scar in one. Biopsy specimens were endoscopically taken in every case. Three cases were reported as diagnostic or suspicious of lymphoma and two as diagnostic of carcinoma. In one case initially reported as negative for malignancy, biopsy was repeated and malignant cells were finally recognized in massive lymphoid cell infiltration.

Half the resected specimens had multiple lesions, displaying two, three, and four lesions, respectively, so that 12 lesions were proven pathologically. The most frequent site of involvement was the body (10 lesions) followed by the antrum (two). In the transverse direction, the largest number, six, were on the anterior wall as opposed to three on the posterior wall. Of the remaining three, two were found on the greater curvature and one on the lesser curvature.

On gross inspection, the resected specimens showed no contraction. All the lesions were localized, and none extended into the duodenum and/or the esophagus. The maximum diameter of the tumors was 0.7–6.8 cm (mean, 3.5). Ulcers were present in all lesions, appearing as poorly defined, shallow depressions (fig. 1A) or as a dimple or a well defined deep crater (fig. 2A). All but three of the ulcers coexisted with rugal folds (fig. 1A). These folds, some of which showed slight convergence, displayed a smooth surface and were easily deformed by manipulation. Three lesions with a deep ulceration were surrounded with a poorly defined, smooth marginal elevation (fig. 2A).

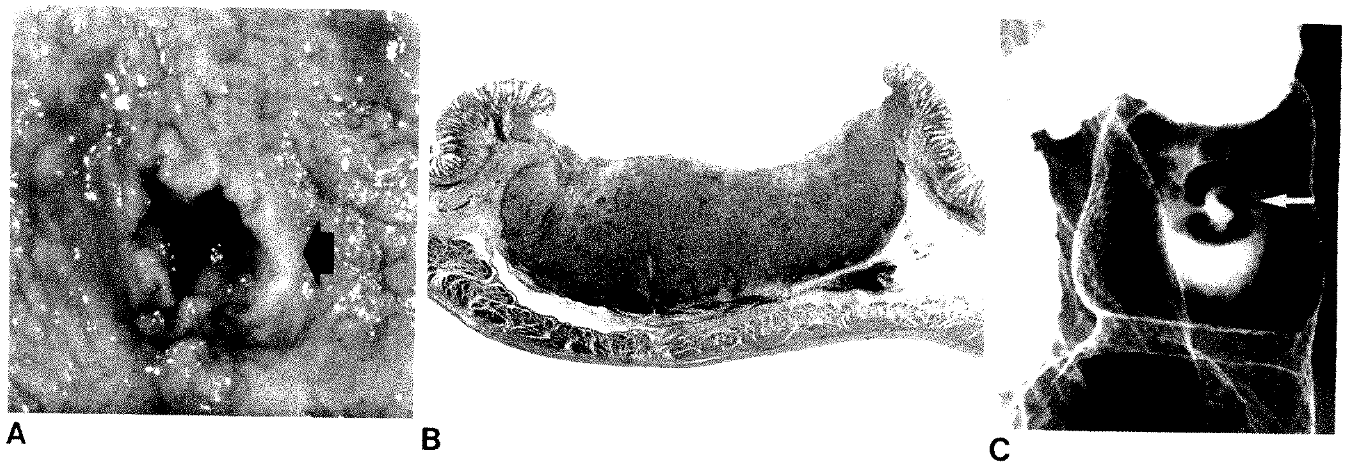

Fig. 2.—Early gastric lymphoma on anterior wall of antrum. **A**, Resected specimen. Irregular deep ulcer crater (*arrow*). Edge, covered with normal mucosa, is raised but gradually sloped. **B**, Low-power photomicrograph of lesion shows well demarcated ulcerated tumor in submucosa. **C**, Double-contrast film in prone, left-anterior-oblique position shows irregular deep crater and smooth marginal elevation (*arrow*).

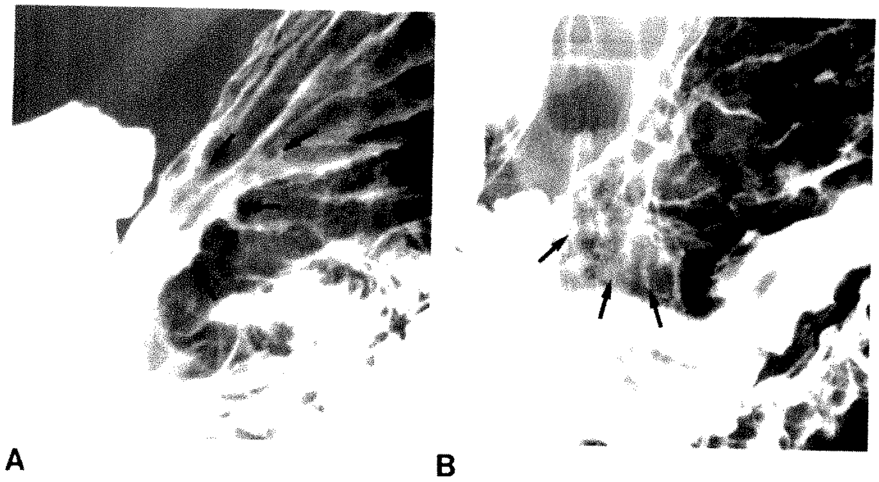

Fig. 3.—Early gastric lymphoma on lesser curvature of corpus. Double-contrast supine film. **A**, Shallow depression (*arrows*) with radiating rugal folds. **B**, Poorly defined uneven ulcer bed in distal part of lesion (*arrows*).

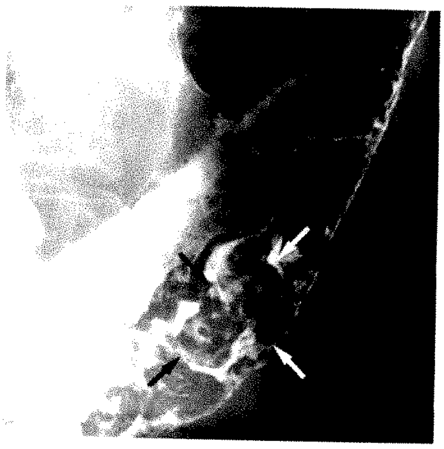

Fig. 4.—Early gastric lymphoma on greater curvature of corpus. Double-contrast prone film shows localized rugal folds (*arrows*) with central shallow ulceration in diffuse, nontumorous rugal folds. Distensibility of gastric wall is well preserved.

As defined by Rappaport's classification [11], both histiocytic and lymphocytic type lesions were found in equal numbers. The depth of tumor involvement was limited to the mucosa and the submucosa (fig. 2B), and no lesion was confined only to the mucosa. There was no case with either regional lymph node involvement or distant metastasis. The length of follow-up was 15–112 months (mean, 53), and all patients are well and free of disease.

Radiologic Findings

Of 12 lymphomas in six patients, only one, a small (0.7 cm) lesion located on the anterior wall of the middle corpus, could not be identified by initial or by retrospective radiologic analysis. The remaining 11 lesions were all detected radiologically.

The predominant finding in this study was localized smooth enlargement of the folds, found in eight lesions (fig. 1B). These folds were easily deformed and became inconspicuous using the compression method or by gastric distension with additional air insufflation (fig. 1C). Of these eight lesions with enlarged folds, seven showed folds radiating to an ulcer (fig. 3). The radiation and enlargement of the folds were usually slight and equivocal. The ulcer was unicentral in all, and was seen most often as an indefinite shallow depression (fig. 1D) with an uneven bed. In one lesion, dimpling was demonstrated with scarcely enlarged, radiating folds.

The lesion that was located on the greater curvature of the corpus demonstrated diffuse prominent hypertrophy of the folds, while gastric distensibility was fairly well preserved (fig. 4). However, pathologic confirmation showed a relatively localized tumor that appeared on the radiograph as a shallow ulceration surrounded by the enlarged folds.

An irregular deep ulcer crater was found in three lesions. In each case the margin was sharply demarcated with a smooth marginal elevation, which suggested tumor formation in the submucosa (fig. 2C). This type of ulceration appeared in the distal part of the stomach, where the mucosal pattern showed coarse area gastricae with the absence of folds.

Consistent with the pathologic findings, no lesion showed radiologic evidence of duodenal and/or esophageal involvement. On initial radiographic interpretation, only four lesions were considered lymphoma or suspicious of lymphoma, and these were all in recent cases. The other initial diagnoses were early carcinoma type IIc in four lesions, advanced carcinoma in one, and ulcer scar in two.

Discussion

Several trends have been determined from clinical findings and histopathologic results concerning the prognosis of primary gastric lymphoma [3–5, 8, 12–14], relating the factors of gender, age, size and location of tumor, histologic type, depth of invasion, nodal status, choice of treatment method, and the like. According to recent major reports [1, 6, 7], the depth of invasion and regional lymph node involvement play a decisive role in the survival of patients with gastric lymphoma.

With the detailed clinicopathologic analysis of 58 cases, Brooks and Enterline [1] concluded that patients with a submucosal lesion showed an 86% 5-year survival rate, compared with 47% for deeper lesions, and that patients without local lymph node involvement had an 86% survival rate compared to 55% for those with involved nodes. They also recognized a close interrelation among tumor size, depth of invasion, the stage of the disease, and the prognosis.

Our durations of follow-up are not enough for final conclusions to be drawn, because 5 years have passed for only half of the cases following surgical resection. However, our results do show a promising correlation between a favorable prognosis and a submucosal tumor without nodal metastasis. Taking into account the fact that gastric lymphoma arises from the lymphoid tissue in the lamina propria and the submucosa [15], our results support the definition of early gastric lymphoma as a tumor limited to the mucosa and submucosa [16].

Preoperative diagnosis of gastric lymphoma by clinical, endoscopic, and cytological examination is difficult, and a correct diagnosis is obtained in less than 20% of cases [13]. Radiologic diagnosis has encountered similar difficulties [7, 8, 12], and some authors [17–19] have concluded that the role of barium study in this disease is limited to the detection of a lesion and to the demonstration of its location and extent.

Several attempts to clarify the characteristic radiologic features of gastric lymphoma were reported with relatively large series [9, 10, 20, 21]. Various combinations of the following features were thought to suggest a diagnosis: multiple masses or ulcerations, diffuse thickening of the folds, extensive submucosal infiltration, extension across the pylorus or the esophagogastric junction, large tumors over 10 cm in diameter, and preservation of pliability of the gastric wall due to a lack of the desmoplastic reaction. However, these findings were for advanced lymphoma, and there is little reference concerning early lymphoma in the English literature.

Sugiyama [22] reported the radiologic findings of 10 cases with early gastric lymphoma, and classified them into four types according to the gross pathologic features: superficial depressed type, polypoid type, ulceropolypoid type, and giant rugae type. In his study, the superficial depressed type was the most common and the giant rugae type was rare.

Our findings also showed that the predominant features were shallow ulceration or uneven mucosa with enlarged radiating folds, corresponding to the superficial depressed type. These enlarged folds, which suggested submucosal tumor infiltration, were more clearly recognized on the radiograph than on the resected specimen. In lesions of this type that we studied, ulceration was single and unicentral, while Sugiyama found a high frequency (50%) of multiple ulcers. Three of our lesions were found to be of the second most frequent type, ulceropolypoid, and their submucosal nature was easily recognized from a smooth marginal elevation.

Although we had one lesion that presented similarly to the giant rugae type, the histologic diagnosis showed a relatively localized lymphoma amid diffuse, nontumorous hyperrugosity. When a lymphoma is found on the rugal greater curvature of the corpus, the extent of actual tumor infiltration should be carefully estimated. The polypoid type, which Culver et al. [8] also considered an early form, is rather rare. In both Sugiyama's series and our own, there was no occurrence of the polypoid type, and as far as we know only two case reports can be found in the literature [23, 24]. This suggests that lymphomas are apt to be ulcerated even in the early stage.

Cases with multiple gastric lymphomas are not unusual. In our study, half of the cases had multiple independent lesions, while other studies have shown slightly lower rates of 14% [22] to 40% [20]. This difference is probably due, in part, to the stage of disease selected in our study, because in an advanced stage tumors are likely to join together to form a single lesion. The distribution of lesions in this study exclusively favored the corpus (83%), which is in accord with the results of Fleming et al. [13], but in contrast with other reports [6, 25].

As with advanced lymphoma, it is necessary to differentiate early lymphoma from carcinoma, peptic disease, and lymphoid hyperplasia. Among them, gastric carcinoma, especially of early type IIc, presents the most frequent diagnostic problem [16, 22]. Absence of narrowing and obliterated peristalsis, sign of extension into the duodenum or the esophagus, and large size of tumors do not suggest a diagnosis of early lymphoma. These same findings can be found in early carcinoma, and only indicate the progress of a tumor. Carcinoma that originates in the mucosa produces mucosal destruction and desmoplastic changes in the submucosa. In type IIc carcinoma, these pathologic changes are radiographically manifested by a usually well defined, irregular shallow depression with the abrupt disruption of the normal mucosa and often by a striking convergence of the relief. In contrast, early lymphoma that arises from the lymphatic tissue in the deeper layer mainly produces submucosal tumor growth, and desmoplastic reaction is rare. Our results indicate that smooth, enlarged folds with slight convergence reflect the submucosal nature of early lymphoma. Also, lymphoma is a more likely possibility when the ulceration is poorly defined, whether wholly or partly.

Peptic ulcer also presents a smooth marginal elevation surrounding an ulcer in the acute stage and smoothly enlarged, radiating folds in the healing stage. However, the difference from lymphoma is that these inflammatory changes are usually restricted to a narrow part symmetrically around the niche and, with an adequate medical therapy, resolve early during the course of healing.

Lymphoid hyperplasia, although a rare condition, presents the most difficult radiologic problem [26, 27], and even microscopic examination by endoscopic biopsy often fails to result in a correct diagnosis [28, 29]. In such a case, a follow-up study with repeated cytologic examinations is recommended, keeping in mind that lymphoid hyperplasia precedes lymphoma on rare occasions [30].

In conclusion, although no decisive, specific feature is present in the radiologic findings of early gastric lymphoma, the radiologist should play two clinically significant roles in this disease. First, all lesions throughout the entire stomach should be displayed to their full extent on the radiograph, because lymphoma in the early stage tends to occur with multiple lesions. This provides important information for the surgical resection. Second, when endoscopically biopsied specimens fail to show malignant cells in a case with the radiologic diagnosis or suspicion of lymphoma, the radiologist can recommend a repeated biopsy from the site of ulceration, where lymphoma is exposed and a chance to yield a positive result is higher.

ACKNOWLEDGMENT

We thank Peter Fincke for help in manuscript preparation.

REFERENCES

1. Brooks JJ, Enterline HT. Primary gastric lymphomas. A clinicopathologic study of 58 cases with long-term follow-up and literature review. *Cancer* **1983**;51:701–711
2. Burgess JN, Dockerty MB, ReMine WH. Sarcomatous lesions of the stomach. *Ann Surg* **1971**;173:758–765
3. Hoerr SO, McCormack LJ, Hertzer NR. Prognosis in gastric lymphoma. *Arch Surg* **1973**;107:155–158
4. Lim FE, Hartman AS, Tan EGC, Cady B, Meissner WA. Factors in the prognosis of gastric lymphoma. *Cancer* **1977**;39:1715–1720
5. Sandler RS. Primary gastric lymphoma: a review. *Am J Gastroenterol* **1984**;79:21–25
6. Shiu MH, Karas M, Nisce L, Lee BJ, Filippa DA, Lieberman PH. Management of primary gastric lymphoma. *Ann Surg* **1982**;195:196–202
7. Dworkin B, Lightdale CJ, Weingrad N, et al. Primary gastric lymphoma: a review of 50 cases. *Dig Dis Sci* **1982**:27:986–992
8. Culver GJ, Bean BC, Berens DL. Gastric lymphoma. *Radiology* **1955**;65:518–529
9. Menuk LS. Gastric lymphoma, a radiologic diagnosis. *Gastrointest Radiol* **1976**;1:157–161
10. Hricak H, Thoeni RF, Margulis AR, Eyler WR, Francis IR. Extension of gastric lymphoma into the esophagus and duodenum. *Radiology* **1980**;135:309–312
11. Nathwani BN, Kim H, Rappaport H, Solomon J, Fox M. Non-Hodgkin's lymphomas. A clinicopathologic study comparing two classifications. *Cancer* **1978**;41:303–325
12. Salmela H. Lymphosarcoma of the stomach: a clinical study of 39 cases. *Acta Chir Scand* **1968**;134:567–579
13. Fleming ID, Mitchell S, Dilawari RA. The role of surgery in the management of gastric lymphoma. *Cancer* **1982**;49:1135–1141
14. Shimm DS, Dosoretz DE, Anderson T, Linggood RM, Harris NL, Wang CC. Primary gastric lymphoma. An analysis with emphasis on prognostic factors and radiation therapy. *Cancer* **1983**;52:2044–2048
15. Morson BC, Dawson IMP. *Gastrointestinal pathology*. Oxford: Blackwell, **1972**:166–168
16. Shirakabe H, Maruyama M. Neoplastic diseases of the stomach. In: Margulis AR, Burhenne HJ, eds. *Alimentary tract radiology*, 3d ed. St. Louis: Mosby, **1983**:721–765
17. Jenkinson EL, Epperson KD, Pfisterer WH. Primary lymphosarcoma of the stomach. *AJR* **1954**;72:34–44
18. Portmann UV, Dunne EF, Hazard JB. Manifestations of Hodgkin's disease of the gastrointestinal tract. *AJR* **1954**;72:772–787
19. Reed BL. Lymphosarcoma of the stomach review and case reports. *AJR* **1959**;82:634–650
20. Sherrick DW, Hodgson JR, Dockerty MB. The roentgenologic diagnosis of primary gastric lymphoma. *Radiology* **1965**;84:925–932
21. Fork FT, Ekberg O, Haglund U. Radiology in primary gastric lymphoma. *Acta Radiol* [*Diagn*] Stockh **1984**;25:481–488
22. Sugiyama N. Radiological diagnosis of malignant lymphoma of the stomach based on its macroscopical classification with special reference to early malignant lymphoma. *Jpn J Gastroenterol* **1974**;71:34–46
23. Akaike Y, Ushio K, Tsubouchi R, et al. A case of primary malignant lymphoma of the stomach. *Stomach Intestine* **1972**;7:925–930
24. Tanehiro K, Yoshii Y, Kasugai T, Morimoto T. Malignant lymphoma of the stomach simulating polypoid carcinoma. *Stomach Intestine* **1980**;15:939–942
25. Mittal B, Wasserman TH, Griffith RC. Non-Hodgkin's lymphoma of the stomach. *Am J Gastroenterol* **1983**;78:780–787
26. Chiles JT, Platz CE. The radiographic manifestations of pseudolymphoma of the stomach. *Radiology* **1975**;116:551–556
27. Martel W, Abell MR, Allan TNK. Lymphoreticular hyperplasia of the stomach (pseudolymphoma). *AJR* **1976**;127:261–265
28. Mattingly S, Cibull ML, Ram MD, Hagihara PF, Griffen WO. Pseudolymphoma of the stomach. *Arch Surg* **1981**;116:25–29
29. Perrillo RP, Tedesco FJ. Gastric pseudolymphoma. A spectrum of presenting features and diagnostic considerations. *Am J Gastroenterol* **1976**;65:226–230
30. Wolf JA, Spjut HJ. Focal lymphoid hyperplasia of the stomach preceding gastric lymphoma: case report and review of the literature. *Cancer* **1981**;48:2518–2523

Book Reviews

Computed Tomography and Magnetic Resonance Imaging of the Head and Neck, 2d ed. By Anthony A. Mancuso and William N. Hanafee. Baltimore: Williams & Wilkins, 503 pp., 1985. $84.75

When Mancuso and Hanafee's first edition of this work, *CT of the Head and Neck*, was published in 1982 it was the only available text on head and neck imaging. The written material in the initial text was an excellent summary of head and neck clinical imaging issues, but the computed tomography (CT) illustrations were disappointing. The second edition blends an updated text with outstanding state-of-the-art CT and magnetic resonance (MR) illustrations.

The book is divided into 11 chapters arranged by major anatomic area. Each chapter is subdivided into a text part and an illustrations section. The text excels in its focus on the specific imaging issues of each anatomic area of the head and neck. With this provided background information, the practicing radiologist can then use the illustrations within the chapter as a problem solving device in everyday practice.

Perhaps the finest aspect of this book can be found in the later chapters where the staging of head and neck squamous cell carcinoma is discussed. Lucid patterns of spread diagrams provide a useful, global perspective on the natural history of tumors of the pharynx and larynx. CT examples in chapters 9–11 graphically depict the CT/MR staging issues.

The clinical-imaging issues in head and neck radiology combined with exquisite illustrations make this textbook an unusually useful reference in the clinical arena. As the use of CT and MR in academic and nonacademic practices increases, the demand for more sophisticated radiographic interpretation pushes the radiologist further into the field of head and neck radiology. Any physician dealing with the areas of otology and head and neck surgery will find a wealth of useful material between the covers of this book.

Ric Harnsberger
Anne G. Osborn
University of Utah
Salt Lake City, UT 84132

Essentials of Radiology Physics. By Charles A. Kelsey. St. Louis: Green, 467 pp., 1985. $47.50

The author states that this is an entry level physics book for technicians, students, and residents. He emphasizes that it is to be used with a competent instructor. Accepting these stipulations, this is an excellent text for its purpose.

It begins with four chapters on very basic mathematics, physics, atomic structure, electricity, and magnetism. It continues with rudimentary discussions of most of the current technologies in medical imaging including sonography, nuclear medicine, computed tomography, and magnetic resonance imaging. The book concludes with two short chapters on risk factors and radiation protection.

The discussions are lucid and clearly illustrated, but very brief and would require considerable amplification by a knowledgeable instructor plus other reading. For example, the discussion on timing the x-ray exposure is a single one sentence paragraph. The instructor would have to supplement such topics extensively or direct students to other textbooks. Each chapter ends with a series of questions; the answers are in a section at the end of the book. Otherwise, there are no appendices. The short index seems adequate.

I recommend *Essentials of Radiology Physics* for the purpose intended by the author: a basic physics book for technician students and residents in a course taught by a competent instructor. Other more detailed texts should be available for the more curious students.

William A. Wilcox
Minneapolis, MN

Radiographic Appearance of the Esophagus and Stomach after Laser Treatment of Obstructing Carcinoma

Ellen L. Wolf[1]
Joseph Frager[2]
Lawrence J. Brandt[2]
David H. Frager[1]
Leslie H. Bernstein[2]
Thomas C. Beneventano[1]

Nd:YAG laser therapy is an attractive palliative treatment for carcinoma of the esophagus and gastric cardia. Twenty-five patients with these tumors underwent laser therapy over a 2-year period, receiving a total of 52 courses of therapy with 189 treatments. Treatments per course averaged 3.6, with a mean of two courses per patient. Luminal diameter is increased with this method; symptomatic improvement in dysphagia occurred in all patients after one course of therapy. Radiographic improvement also is seen. The complication rate in this series was four (2.1%) of 189 procedures, consisting of one perforation, one tracheoesophageal fistula, one pneumopericardium, and one pneumoperitoneum without leak.

The use of high-energy lasers has recently added a new dimension to therapeutic endoscopy. Initially used to control upper gastrointestinal hemorrhage, lasers are now being increasingly used as a palliative technique to treat malignant obstructions of the gastrointestinal tract [1-7]. Carcinoma of the esophagus and gastric cardia is particularly well suited for laser treatment.

Laser is an acronym derived from "light amplification by stimulated emission of radiation." Electrons are released and light is emitted when a substance is excited to a higher energy state and then allowed to return to a lower energy state. The light produced is intense, monochromatic, and readily focused. Of the three types of lasers commonly used for medical purposes—argon, carbon dioxide, and neodymium-yittrium-aluminum-garnet (Nd:YAG)—the last has the greatest depth of penetration and is the usual laser used for tumor ablation.

Laser therapy may be used to destroy neoplastic tissue by tumor ablation. This is a palliative procedure to increase luminal diameter for relief of dysphagia in patients with malignant obstructions of the esophagus and esophagogastric junction. The patients selected for this type of therapy generally are not considered curable and will have advanced disease and/or metastases or are poor surgical risks. Symptomatic improvement usually lasts about 3-6 months and may be repeated whenever necessary as symptoms recur.

In this report, we characterize the radiographic features of these tumors as they are treated by laser energy. In addition, our results and complications of the treatment are discussed.

Subjects and Methods

From 1983 to 1985, 15 patients with squamous carcinoma of the esophagus and 10 with adenocarcinoma of the gastric cardia underwent palliative endoscopic Nd:YAG laser therapy. These patients were 15 men and 10 women aged 48-94 years (mean 73). All 25 patients had endoscopic biopsies of lesions with histologic confirmation of malignancy before laser therapy was initiated. In all patients, barium studies of the esophagus and stomach were performed before laser treatment. In 10 patients, studies were performed after completion of one course of laser therapy, and in three other patients barium studies were done after multiple treatment sessions performed over 6-13 months. Patients were considered for laser

Received July 15, 1985; accepted after revision November 18, 1985.

[1] Department of Radiology, Albert Einstein College of Medicine, Montefiore Medical Center, 111 E. 210th St., Bronx, NY 10467. Address reprint requests to E. L. Wolf.

[2] Department of Medicine, Albert Einstein College of Medicine, Montefiore Medical Center, Bronx, NY 10467.

AJR 146:519-522, March 1986
0361-803X/86/1463-0519
© American Roentgen Ray Society

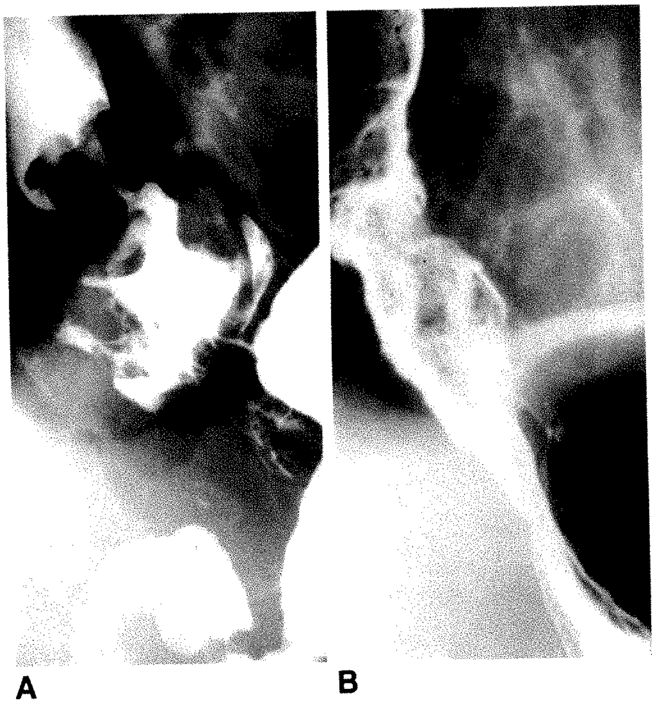

Fig. 1.—**A**, Before Nd:YAG laser therapy. Concentric neoplasm and high-grade stricture from carcinoma extending to esophagogastric junction and hiatus hernia. **B**, 12 days after laser therapy, lumen has been restored and no obstruction is present, but persistent tumor is seen.

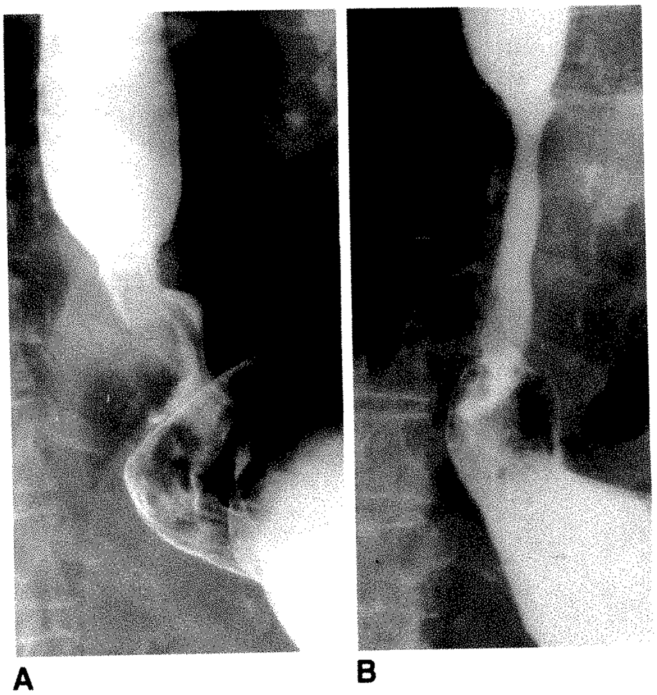

Fig. 2.—**A**, Initial examination shows tumor mass at esophagogastric junction due to gastric carcinoma. **B**, After eight courses of laser therapy over 12-month period, mass is not apparent and radiographic appearance is that of benign-appearing stricture.

therapy if they had a symptomatic lesion and if they were not candidates for surgical therapy either because computed tomography (CT) showed distant metastasis or extension beyond the esophagus and/or there was significant cardiac or pulmonary disease.

Endoscopic laser therapy was performed using a Nd:YAG laser (Cooper Lasersonics). Laser energy was conveyed via a quartz waveguide through the biopsy channel of a conventional two-channel Olympus (GIF-2T) endoscope. Treatments were performed in multiple sessions until the lumen was sufficiently open to permit passage of the endoscope (36 French) into the stomach. In three patients, the endoscope was passed through an existing gastrostomy in order to optimize access to the tumor, and laser therapy was initiated from the lower end of the lesion in a cephalad direction.

Results

Radiographic Findings

Thirteen patients had 14 radiographic studies done before laser therapy that were available for review. Studies were done on an average of 21.3 days before laser therapy (range, 5–52 days). All these patients plus one additional patient had at least one study after laser therapy, with a total of 20 studies available for review; 14 were done after the first course, four after the second, and two after the third course of therapy. The mean number of days between the last course of laser therapy and the examination was 9.4 days (range, 0.5–60 days).

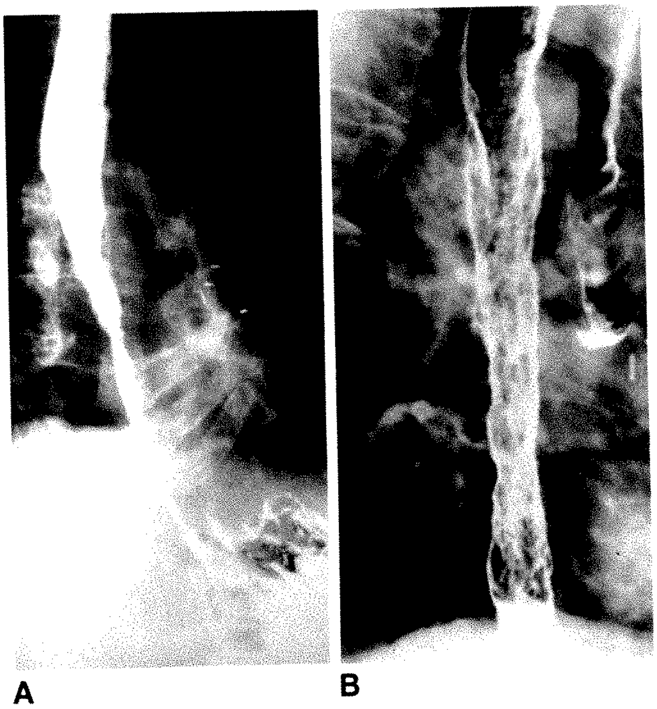

Fig. 3.—**A**, Esophagram 1 month before laser therapy shows long stricturing adenocarcinoma secondary to Barrett esophagus. **B**, 2 days after laser therapy, radiographic appearance simulates esophagitis. Lumen has been restored.

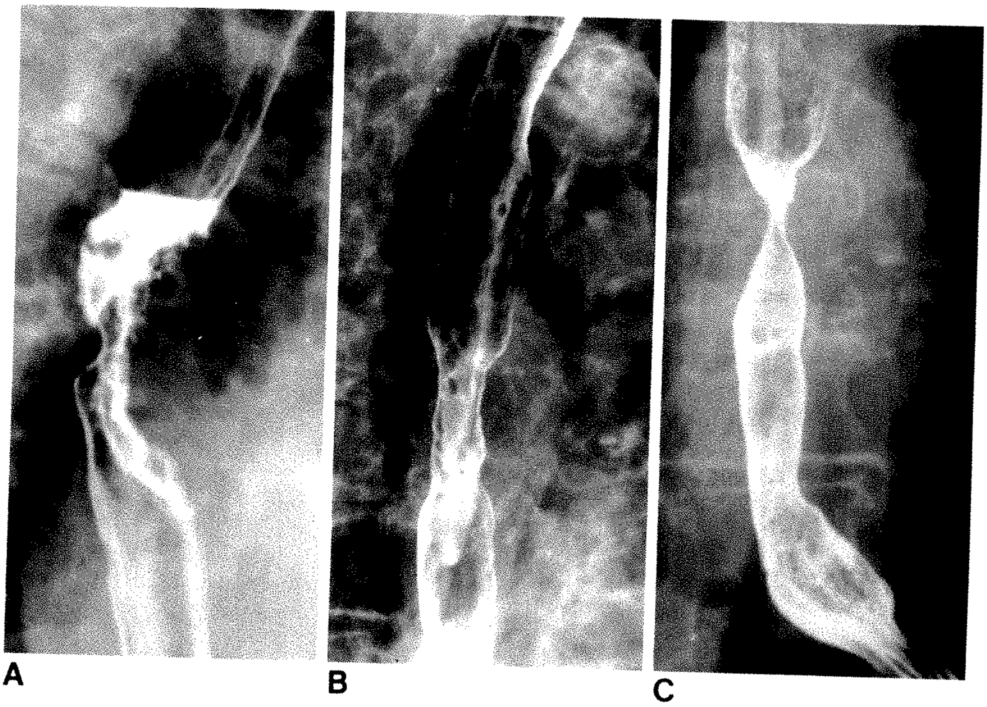

Fig. 4.—Series of esophageal spot films. **A**, Before laser treatment of esophageal carcinoma. **B**, 4 days after laser treatment. **C**, Subsequent regrowth of tumor 4½ months later. Tumor regrowth has more strictured appearance and less bulky neoplastic component than original tumor.

Radiographic improvement was observed after successful tumor ablation. The luminal diameter was seen to increase in all patients studied. Luminal diameter and length of tumor measurements were equivalent both radiographically and endoscopically before and after laser treatment. In six patients, residual tumor with an increase in luminal diameter was observed both radiographically and endoscopically after laser therapy (fig. 1). In three patients, the radiographic appearance after laser treatment simulated a benign structure and no tumor was observed endoscopically (fig. 2). In the remaining five patients, the radiographic features after treatment resembled severe esophagitis (fig. 3), although necrotic tumor was observed endoscopically in all five.

Figure 4 demonstrates successful dilatation of a midesophageal carcinoma, but with subsequent regrowth of tumor 4½ months later. A repeat course of therapy was necessary. One patient with total obstruction of the esophagus due to carcinoma had successful dilatation and was able to eat solids (case not illustrated).

Clinical Correlation

Twenty-five patients were given 52 courses of therapy, with a total of 189 treatments over the 2-year period from June 1983 to June 1985 The average number of treatments per course was 3.6, and the average number of courses per patient was 2.0. Twelve patients underwent a second course of therapy, seven underwent a third course, and four a fourth. One patient, who represents the longest survivor after initiation of laser therapy, underwent eight courses of therapy consisting of 41 treatments over a 16-month period.

The mean length of tumor at the initiation of laser therapy was 8.2 cm (range, 4–15 cm). The mean luminal diameter before laser therapy was 2.4 mm (range, 0–5 mm), and all 25 patients had significant dysphagia for solids. All 25 patients had luminal diameters greater than 12 mm at the end of their first course of therapy. All of these patients were able to tolerate a soft diet.

Of the 12 patients requiring a second course of laser therapy because of tumor regrowth, 10 (83%) achieved a luminal diameter greater than 12 mm and were able to tolerate a soft diet. The remaining two patients required feeding gastrostomy. Of the seven patients undergoing a third course of laser therapy, six achieved a luminal diameter greater than 12 mm; of the four patients undergoing a fourth course of laser therapy, three achieved a luminal diameter greater than 12 mm.

The first course of laser therapy was separated by an average of 46.3 days from the second course. The second course was on average separated by 41 days from the third course, and the third course was separated on average by 60.5 days from the fourth.

Four patients underwent radiation therapy, two before laser therapy, one concomitantly with laser therapy, and one after laser therapy. Three patients received chemotherapy, two before laser therapy and one after. No significant increase in survival was noted in either group of patients compared to the overall group.

One patient had undergone an attempted curative surgical procedure before laser therapy: a total gastrectomy with esophagojejunostomy 1 year before recurrence of tumor and initiation of laser therapy.

The mean survival for the overall group of patients from initiation of laser therapy was 7.5 months (range, 1–16 months). In those patients who have died, the longest survival after initiation of laser therapy was 16 months. In those patients alive as of June 1985, the average survival has been 6.3 months. The mean survival for patients with esophageal carcinoma was 8.6 months, and for patients with gastric cardia carcinoma, 6.5 months.

Of the 25 patients in this series, there was one perforation, one tracheoesophageal fistula, and one benign pneumoperitoneum without perforation or leak, and one pneumopericardium that led to the only death directly related to the laser treatment. This complication rate of four (2.1%) of 189 procedures is quite acceptable in this group of patients with unresectable tumors and/or far-advanced disease.

Discussion

Of the tumors involving the gastrointestinal tract, carcinomas of the esophagus and gastric cardia are particularly well suited to laser palliative therapy because they are easily reached with the endoscope. That the laser is a worthwhile mode of palliation is reasonable in view of the quality of life and very brief survival following other means of treatment. The 5-year survival rate after traditional methods of surgery and/or radiation therapy in esophageal carcinoma is only 5%–6% [1]; it is somewhat higher for carcinoma of the gastric cardia. Chemotherapy has not as yet been shown to alter the outcome in esophageal carcinoma, and is of limited value in gastric carcinoma. Radiation therapy may take weeks to provide improvement of symptoms; it is not ordinarily used for recurrences, since maximal doses have usually already been administered; and it is associated with side effects in a significant number of cases, including nausea, malaise, and potential damage to organs outside the esophagus. In some patients, a feeding gastrostomy is necessary to prevent death by starvation, since these patients are unable to swallow.

Laser therapy for carcinomas of the esophageal and gastric cardia is a useful form of palliation that is used mainly for the relief of dysphagia because of obstruction in patients who have distant metastasis or extension of tumor beyond the esophagus or stomach or who are poor surgical candidates because of advanced age and cardiopulmonary limitations. The advantages of laser therapy over more traditional methods of therapy are as follows: (1) general anesthesia can be avoided; (2) no systemic side effects are produced; (3) treatments are accomplished quickly with minimum discomfort to the patient, sometimes without the need for hospitalization; and (4) treatment can be repeated whenever necessary.

In most cases, improvement generally lasts about 3–6 months [4]. Repeat laser therapy may be performed as necessary whenever the tumor increases enough to diminish luminal diameter and produce symptoms. Most patients experience an overall improved quality of life; dysphagia is usually decreased, and solid foods are again enjoyed.

In one representative study by Fleischer and Sivak [4], 40 patients treated with YAG laser had mean endoscopic luminal diameters improved from 3.3 to 12.1 mm. In our series, mean luminal diameter improved from 2.4 mm to greater than 12 mm. Other workers have reported similar results [5]. Mellow et al. [5] reported a prolonged survival with laser therapy compared with a retrospective control group treated with radiotherapy. Further studies that are controlled and randomized are needed to compare laser to other palliative techniques.

Complications after laser treatment have been reported in about 15% of patients [7]. Perforation and tracheoesophageal fistula are the most common complications. Since these problems are seen with esophageal carcinoma in the absence of treatment and in some patients who have had previous or concomitant radiation, the role of the laser in the development of these complications is sometimes difficult to assess.

In summary, laser therapy for esophageal and gastric cardia carcinoma is an effective and well tolerated palliative treatment. It is most likely that it will be used more often as more centers become familiar with its capabilities.

REFERENCES

1. Fleischer D, Kessler F. Endoscopic Nd:YAG laser therapy for carcinoma of the esophagus: a new form of palliative treatment. *Gastroenterology* **1983**;85:600–606
2. Fleischer D. Endoscopic laser therapy for gastrointestinal disease. *Arch Intern Med* **1984**;144:1225–1230
3. Fleischer D. The current status of gastrointestinal laser activity in the United States. *Gastrointest Endosc* **1982**;28:157–161
4. Fleischer D, Sivak M. Endoscopic Nd:YAG laser therapy as palliative treatment for advanced adenocarcinoma of the gastric cardia. *Gastroenterology* **1984**;87:815–820
5. Mellow M, Pinkus H, Frank J, Waxman M, Avigan M. Endoscopic therapy for esophageal carcinoma with Nd:YAG laser: prospective evaluation of efficacy, complications and survival (abstr). *Gastrointest Endosc* **1983**;29:165
6. Cello JP, Gerstenberger PD, Wright T, Melnick J, Meiselman MS. Endoscopic neodymium—YAG laser palliation of nonresectable esophageal malignancy. *Ann Intern Med* **1985**; 102:610–612
7. Jacobs WH. Endoscopic YAG laser therapy in a community hospital. *Am J Gastroenterol* **1985**;80:270–273

Sonographic Detection of Postsurgical Recurrence of Crohn Disease

G. DiCandio[1]
F. Mosca
A. Campatelli
M. Bianchini
F. D'Elia
C. Dellaçiovampaola

Sonography, contrast radiography, and endoscopy of the small and large intestine were performed in 32 patients, who had already undergone one or more intestinal resections for Crohn disease, with the aim of detecting possible relapses. Eleven patients proved to have had relapses; sonography revealed nine cases, with two false negatives and no false positives. Sensitivity proved to be 82%, specificity 100%, and overall accuracy 93.7%. Sonography enables the operator to distinguish between inflammatory and neoplastic lesions by means of structural study of the thickened bowel wall, paying particular attention to integrity of its layers.

Most artifacts that may be encountered in abdominal sonography are produced by the alimentary tract, with its contents of gas, liquid, and waste products, which obstruct the passage of the ultrasonic beam, sometimes even causing its total reflection. Thus, certain difficulties arise in interpretation with possible errors in diagnosis [1–4]. However, in some cases of inflammation or neoplasm, these difficulties are noticeably reduced because the wall thickening does not permit gaseous distension.

A characteristic picture occurs, formed by an anechoic rim of a thickened bowel wall surrounding the strongly echogenic central area (luminal contents). This has been described in the literature with various terms such as cockade, doughnut, target, and pseudokidney. This aspect, although correlated with bowel disease in 90% of cases [5], is considered nonspecific [6]. In our opinion, however, there are several differential signs, both intrinsic and extrinsic, which can point toward a correct diagnosis of the nature of the reniform mass, at least in the two largest groups: inflammatory bowel disease and tumors. These signs can be noted with high-resolution real-time and linear 5-MHz transducers, which permit a structural study of the intestinal wall and the layers that make it up, already described in detail in an investigation performed with linear or sector ultrasonic endoscope [7–9]. Various authors in the last few years have indicated that sonography is useful in assessing Crohn disease and its progression. Sonography would seem able to identify the affected tract and to assess the extent, the remission or progress of the disease over a period of time, and possible complications.

We assessed the reliability of sonography in diagnosing Crohn disease, with particular reference to postoperative recurrence and to the possibility of the existence of differential features with the neoplastic diseases of the intestine.

Materials and Methods

Between January and July 1983, 32 patients with Crohn disease, who had already undergone one or more intestinal resections, were examined with sonography with the aim of detecting possible relapses. At the time of the sonogram, the operator was unaware of the patient's symptoms and results of other tests performed. All sonographic examinations were performed by the same team (two sonographers), using a real-time linear scanner with

Received April 24, 1985; accepted after revision November 18, 1985.

[1] All authors: Istituto di Clinica Chirurgica Generale, Sezione Ultrasuoni, Universita de Pisa, Via Roma 67, 56100 Pisa, Italy. Address reprint requests to G. DiCandio.

AJR 146:523–526, March 1986
0361–803X/86/1463–0523
© American Roentgen Ray Society

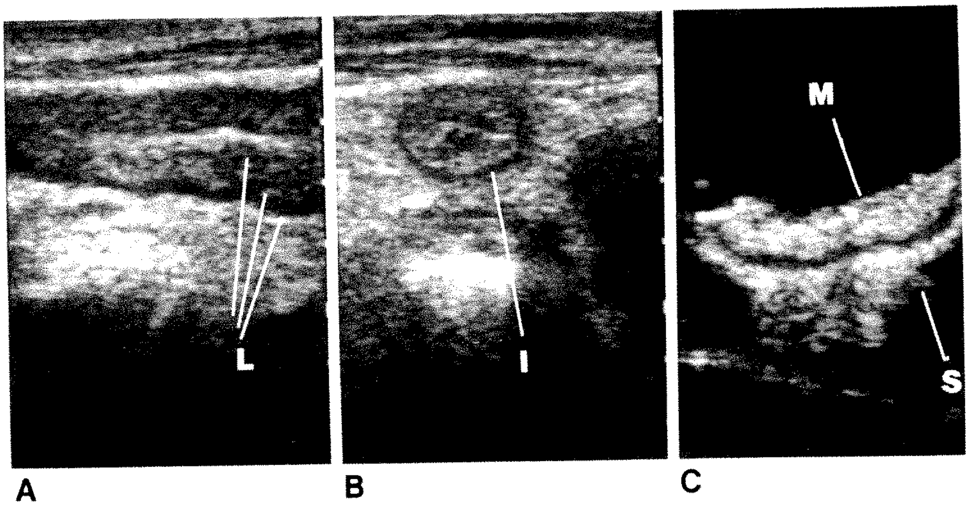

Fig. 1.—Postsurgical Crohn recurrence. **A**, 5-MHz parasagittal scan of right lower quadrant: bowel-wall thickness with regular rim and layers (L). **B**, Transverse sonogram shows inflammatory (I) reniform mass (thickened but undamaged layers). **C**, In vitro scan of surgical specimen (diseased wall) demonstrates integrity of wall layers. M = mucosa; S = serosa.

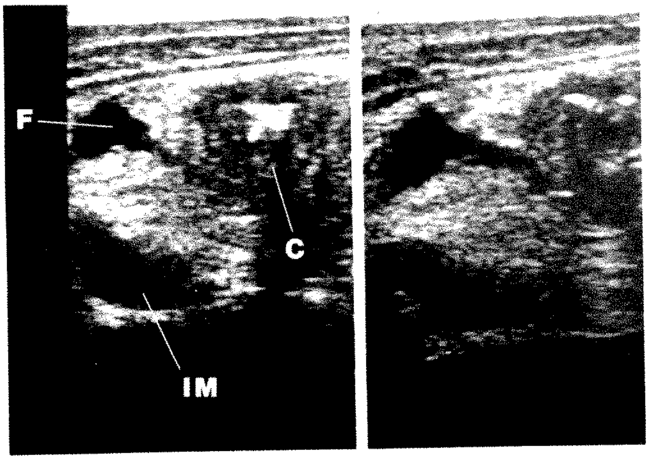

Fig. 2.—5-MHz transverse scan of lower right quadrant reveals thickened small bowel loop (C) with perivisceral fistula (F) confirmed at surgery. IM = right iliac muscle.

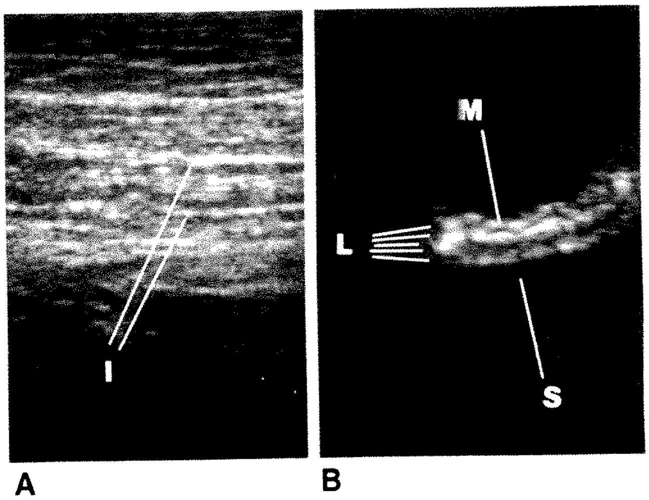

Fig. 3.—5-MHz short-focus linear probe. **A**, Multiple undistended small bowel loops (I) scanned longitudinally. **B**, Water-bath sonogram shows layers (L) that make up bowel wall. M = mucosa, S = serosa.

2.4- to 3.5-MHz transducers (Toshiba SAL 30A). Suspect areas were further scanned with a high-definition, short-focus 5-MHz transducer.

An ileocolonic wall with a thickness of more than 5 mm was considered pathologic. It was measured by transverse scan to avoid artifactual enlargement due to sectioning in an oblique plane. The distance between the serous and lumen was also measured. Longitudinal section was useful in following the loop and measuring the diseased tract. Changes in the degree of bowel loop compressibility, peristalsis and progression of food, luminal narrowing, dilated fluid-filled loops, lymph nodes, fistulas, abscesses, and loop conglomeration were also looked for. Preparation for sonography required only solid and liquid fasting for at least 8 hr.

In the 2 weeks after sonography, the patient underwent upper and lower barium gastrointestinal examination and endoscopy with biopsy sample of the suspected lesions. Also we carried out in vivo and in vitro scans (5-MHz linear probe) on tracts (10 in all: four from the ileum and six from the colon), on intestinal wall affected with Crohn disease (five in all: three from the ileum and two from the colon), and on neoplastic intestinal wall (15 in all: one from the ileum, four from the stomach, and 10 from the colon). In this way, it was possible to assess not only the differences in thickness but also the echostructural differences and especially the modifications to the sequence of the five parietal layers produced by the various kinds of pathology.

Results

Thirty-two patients (24 male and eight female) were studied. The mean age was 41.5 years (range, 22–70). The time interval between the last operation and sonography ranged from 1 to 12 years (mean, 4.5). Twenty-eight patients had ileocolonic anastomoses and four, ileorectal anastomoses (radical resection had been performed in all cases). Five of the 32 patients already had symptoms pointing to a relapse of the disease (diarrhea, malabsorption, abdominal cramps, anal and perianal lesions).

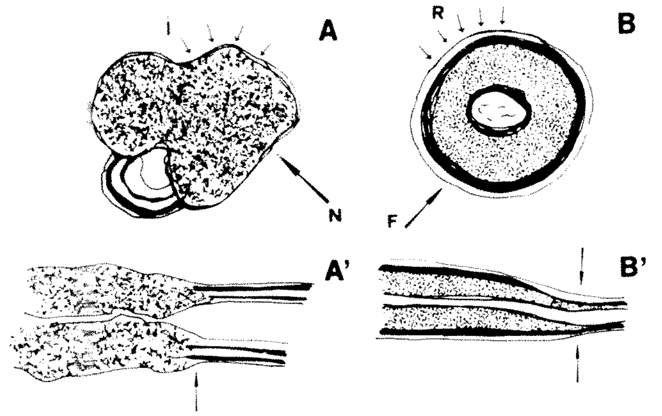

Fig. 4.—Echostructural differences between malignant (**A**, **A′**) and inflammatory (**B**, **B′**) pseudokidney as seen on transverse (**A**, **B**) and longitudinal (**A′**, **B′**) scans. I = irregular rim; R = regular rim; N = neoplasm; F = inflammatory disease.

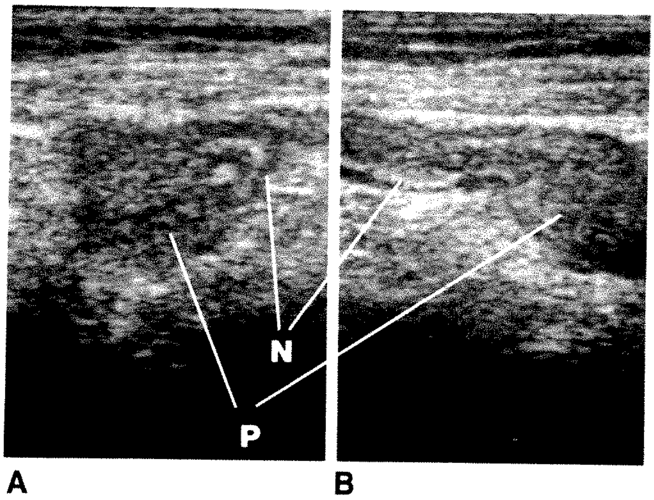

Fig. 5.—Sigmoid carcinoma on transverse (**A**) and longitudinal (**B**) scans. Left lower abdominal scans (5 MHz) reveal irregular and asymmetric thickened large bowel walls and narrowed lumen (confirmed at surgery). N = normal wall; P = diseased tract without layers.

Sonography revealed a pathologic bowel wall (thickness greater than 5 mm) in nine of the 32 cases (five symptomatic and four asymptomatic patients): at the ileocolonic anastomosis in eight of these and in the descending colon in one (fig. 1). The mean thickness of the diseased wall was 7.2 mm (range, 6–10 mm). A relapse of the Crohn disease was confirmed in all cases by radiography and endoscopy/biopsy.

In 23 patients who were asymptomatic and negative on sonography, contrast radiography and endoscopic examination showed a relapse in its initial stages in two patients (two false negatives). In two relapses diagnosed by sonography (symptomatic patients), abscesses were diagnosed and then confirmed at surgery (fig. 2). In four of the 32 cases, the presence of chance pathology was revealed: three patients with multiple gallstones and one with stones in the left kidney complicated by hydronephrosis and hydroureter.

At the end of the study, sonographic accuracy in diagnosing relapse of Crohn disease was found to be 93.7%, sensitivity proved to be 82%, and specificity 100%. However, these values should be critically evaluated in the light of the number of cases and the absence of ileorectal relapse, which would have increased the number of false negatives and false positives due to the existing difficulty in exploring the pelvic area, only partially resolved by a filled urinary bladder.

In vivo and in vitro (water bath) sonography of the intestine shows there is a distinct difference in appearance between inflammatory and neoplastic walls. In the former, the increase in thickness occurs in all the layers of which the wall is composed (fig. 3); these remain whole and there is a gradual transition from the healthy tract to the pathologic tract (fig. 4). In the latter, an interruption is seen in the layers, which is proportional to the parietal infiltration by a lesion that is usually anechoic and that is abruptly adjacent to the healthy tissue (fig. 5).

Discussion

The ability of sonography to demonstrate the thickening of the intestinal wall is extensively described in the literature [5, 10–13]. Some authors actually include sonography in the protocol for diagnosis of Crohn disease, both for monitoring the diseased wall during medical treatment and to demonstrate complications linked to progression of the disease [6, 14–19].

The sonographic picture of the gastrointestinal tract is correlated to the degree of intestinal distension and to the type of endoluminal content (liquid, mixed, or mainly gassy). Studies with endoscopic or transrectal probes have shown that the intestinal wall is echogenically divided into five layers, alternating hyperechoic (three) and hypoechoic (two). The first two are the mucosa, the third the submucosa, the fourth (more evident and less dense) the muscularis propria, and the fifth the serosa. These layers can also be seen on normal transabdominal scans, especially using a 5-MHz transducer and in vitro studies. The mean thickness varies from 5 mm in the stomach to 3 mm in the small intestine and colon [11] and should be measured in transverse section. Differentiation between the small and large intestine is facilitated by the different appearances of the two, by the constant presence of air in the colon and, in distension, by possible recognition of the valvular conniventes of the small intestine, which are thin and dense in contrast to the sparse and wide semilunar valves.

In inflammatory bowel disease or tumors, the affected loop increases in thickness (over 5 mm in the small intestine and colon) and is more evident. This is followed by an appearance defined as pseudokidney or reniform mass, composed of an anechoic ring (wall) which surrounds a strongly hyperreflective area (lumen).

However, this lesion is considered nonspecific. It is, for example, associated with primary and secondary tumors, inflammation, intussusception, parietal hematomas, pyloric hypertrophy, and radiation-induced lesions [5, 10–13, 20–24]. However, there are some characteristics, which when present, suggest a correct diagnosis of the nature of pseudokidney. These characteristics should be sought in ultrastructural study of the walls, with reference to the five layers described. In the case of primary neoplasm or metastases, a rough asymmetric insertion of tumoral tissue in the undamaged wall can often be observed, with the disappearance of normal layers. The profile of the loop is irregular both on the serous and endoluminal sides with, for example, retention of the air, absence of peristalsis, and stasis above. This picture is obvious only in the case of advanced neoplasm with deep infiltration.

The inflammatory reniform mass has a different appearance (e.g., diverticulitis, idiopathic colitis, granulomatous enterocolitis, pseudomembranous colitis). The intestine, although swollen, keeps its symmetry. In transverse section, the profile is regular with a target aspect, the still-preserved parietal layers alternating around the stenotic and hyperdense lumen. This is particularly evident in ileocolonic Crohn disease, where the increase in the wall thickness is uniform, at least initially, involving all the layers and especially the mucosa and submucosa (layers 1–3), which intermingle and become scarcely distinguishable in transabdominal scans. The lumen is reduced to a thin, hyperdense line, and it is possible to observe the slow passage of the intestinal contents. The "matted loops" pattern is typical of advanced stages, especially in subjects who have undergone a simple intestinal bypass operation, in which the diseased tract, left in situ, in time is affected by the disease progression. Measurement of the parietal thickness, on average, reaches values of 10.9 mm, significantly higher than the 8 mm of idiopathic colitis [19]. Our mean value of 7.2 mm is probably correlative with measurements in patients with recent relapses in whom the inflamed loop had not yet reached maximum potential thickness.

Other signs to look for in the intestinal loop are the gradual demarcation with the healthy wall, a rigidity to the pressure exerted with the ultrasonic probe (advanced stages), a sluggish or absent peristalsis, and above, the possibility of dilatation with hyperperistalsis and water and air stasis.

Sonography also permits the study of the perivisceral space (e.g., fistulas, free abscesses between the loops, lymph nodes). Yeh and Rabinowitz [17] demonstrated abscesses in 28 of 51 patients, and Kaftori et al. [18] reported them in four of 18 patients. In our series, two of 11 relapses were abscesses.

In conclusion, sonography demonstrates the presence of pathologic thickenings of the intestinal wall and enables the operator to diagnose the nature of the swelling. However, the diagnosis is confirmed by contrast radiography and endoscopy, with which sonography still plays a complementary role. Moreover, sonography is more frequently becoming the first examination to be performed in the case of abdominal colic and swelling. It is therefore indispensable in recognizing and evaluating the structure of these lesions. In Crohn disease, in particular, it is possible to point out early postoperative relapses, even in the subclinical phase, or to evaluate the response to medical treatment (variations in parietal thickness) and to demonstrate extraparietal complications.

REFERENCES

1. Holm HH, Rasmussen SN, Kristensen JK: Errors and pitfalls in ultrasonic scanning of the abdomen. *Br J Radiol* **1972**;45:835–840.
2. Cunningham JJ. False positive gray-scale ultrasonography for intra-abdominal abscesses. *Arch Surg* **1976**;111:810–811
3. Lawson TL, Albarelli JN. Diagnosis of gynecologic pelvic masses by gray-scale ultrasonography: analysis of specificity and accuracy. *AJR* **1977**;128:1003–1006
4. Fleisher AC, Dowling AD, Weinstein ML, James AE Jr. Sonographic patterns of distended fluid-filled bowel. *Radiology* **1979**;133:677–680
5. Bluth EI, Merrit CRB, Sullivan MA. Ultrasonic evaluation of the stomach, small bowel and colon. *Radiology* **1979**;133:681–685
6. Sonnenberg A, Erckenbrecht J, Peter P, Niederau C. Detection of Crohn's disease by ultrasound. *Gastroenterology* **1983**; 83:430–434
7. Stroh WD, Phillip J, Hagenmuller F, Classen M. Ultrasonic tomography by means of an ultrasonic fiberendoscope. *Endoscopy* **1980**;12:241–244
8. Di Magno EP, Regan PT, Clain JE, James EM, James LB. Human endoscopic ultrasonography. *Gastroenterology* **1982**;83:824–829
9. Yamanaka T. Clinical evaluation of the ultrasonic endoscope. *Toshiba Med Rev* **1983**;11:1–4
10. Scheible W, Goldberger LE. Diagnosis of small bowel obstructions: the contribution of diagnostic ultrasound. *AJR* **1979**; 133:685–688
11. Fleisher AC, Muhletaler CA, James AE Jr. Sonographic assessment of the bowel wall. *AJR* **1981**;136:887–891
12. Morgan C, Trought W, Oddson T, Clark W, Rice R. Ultrasound patterns of disorders affecting the gastrointestinal tract. *Radiology* **1980**;135:129–135
13. Yeh HC, Rabinowitz JG. Ultrasonography and computed tomography of the gastric wall lesions. *Radiology* **1981**;141:147–155
14. Seitz K, Rettenmaier G, Schultz RD. Sonographische Diagnostik bei Morbus Crohn. In: Hinselmann M, Anliker M, Meudt R, eds. *Ultrashalldiagnostik in der Medizin*. Stuttgart: Thieme, **1980**:86–97
15. Wellmann Von W, Gebel M, Freise J, Grote R. Sonographie in der Diagnostik der Ileitis Terminalis Crohn. *ROFO* **1980**; 133:146–148.
16. Holt S, Samuel E: Gray scale ultrasound in Crohn's disease. *Gut* **1979**;20:590–595
17. Yeh HC, Rabinowitz JG. Granulomatous enterocolitis: findings by ultrasonography and computed tomography. *Radiology* **1983**;149:253–259
18. Kaftori JK, Pery M, Kleinhaus U. Ultrasonography in Crohn's disease. *Gastrointest Radiol* **1984**;9:137–142
19. Dubbins PA. Ultrasound demonstration of bowel wall thickness in inflammatory bowel disease. *Clin Radiol* **1984**;35:227–231
20. Schwerk WJ, Braun B, Dombrosky H. Real time ultrasound examination in the diagnosis of gastrointestinal tumours. *JCU* **1979**;7:425–431
21. Bowerman RA, Silver TM, Jaffe MH. Real time ultrasound diagnosis of intussusception in children. *Radiology* **1982**;143:527–529
22. Wilson DA, Vanhoutte JJ. The reliable sonographic diagnosis of hypertrophic pyloric stenosis. *JCU* **1984**;12:201–204
23. Lee TG, Brickman FE, Avecilla LS. Ultrasound diagnosis of intramural intestinal hematoma. *JCU* **1977**;5:423–424
24. Bolondi L, Ferrentino M, Trevisani F, Bernardi M, Gasbarrini G. Sonographic appearance of pseudomembranous colitis. *J Ultrasound Med* **1985**;4:489–492

Review Intussusception in Adults

Farooq P. Agha[1]

A review of 25 adult patients with intussusception is reported. Intussusception in adults constituted 16.6% of 150 intussusception cases observed during 1956–1985. The underlying pathologic processes were identified in 23 patients (92%). Etiologically, adult intussusception could be categorized into four groups: (1) tumor-related (13 cases, 52%); (2) postoperative (nine cases, 36%); (3) miscellaneous—Meckel diverticulum (one case, 4%); and (4) idiopathic (two cases, 8%). The tumor-related intussusceptions were caused by benign tumors in five and malignant tumors in eight patients. Postoperative intussusceptions were related to various factors including suture lines, ostomy closure sites, adhesions, long intestinal tubes, bypassed intestinal segments, submucosal edema, abnormal bowel motility, electrolyte imbalance, and chronic dilatation of the bowel. The sites of involvement of intussusception were jejunogastric (one), jejunojejunal (seven), ileoileal (four), ileocolic (10), and colocolic (three patients). Four patients had synchronous multiple (ileoileal and jejunojejunal), four had compound (ileoileal-colic), and two had recurrent intussusceptions. When an intussusception is encountered in adults, an underlying pathologic process usually can and should be determined for proper management.

Intussusception is defined as telescoping of a segment of the gastrointestinal tract into an adjacent one. It is the leading cause of intestinal obstruction in children and ranks second only to appendicitis as the most common cause of acute abdominal emergency in children [1, 2]. However, in adults intussusception is rare, accounting for 0.1% of all adult hospital admissions [3–5] and 5%–16% of all intussusceptions [3, 6, 7]. About 90% of intussusceptions in adults occur in the small or large bowel; the other 10% involve the stomach or surgically created stomas [8–12]. In contrast to childhood intussusception, which is idiopathic in 90% of cases, adult intussusception has a demonstrable cause in over 90% of cases [1–7].

This report summarizes a review of intussusception in 25 adult patients observed at one institution during the last 30 years. In 23 (92%) of these, causative factor or factors were identified, and two were considered idiopathic.

Materials and Methods

Between 1956 and 1983, 150 patients with the final diagnosis of intussusception were identified by the medical information department at the University of Michigan Hospitals; 25 (16.6%) were adults (18 years or older). The medical records of these 25 adult patients with final diagnosis of intussusception were reviewed and correlated with available radiologic and pathologic studies.

Results

There were 13 men and 12 women aged 18–69 years (mean, 52). The underlying offending factors conducive to the development of intussusception were: tumors

Received August 6, 1985; accepted after revision October 17, 1985.

[1] Department of Radiology, Box 013, University of Michigan Hospitals, 1406 E. Ann St., Ann Arbor, MI 48109.

AJR 146:527–531, March 1986
0361–803X/86/1463–0527
© American Roentgen Ray Society

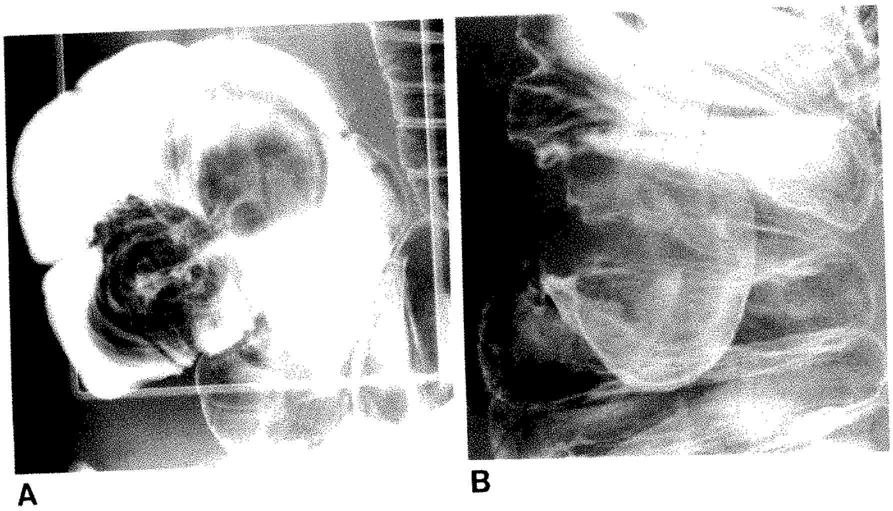

Fig. 1.—Benign condition in 27-year-old woman. **A**, Spot film during barium enema. Colocolic intussusception in transverse colon. **B**, Successful reduction of large polypoid pedunculated mass in ascending colon, which was intussuscepting inflammatory fibrovascular polyp.

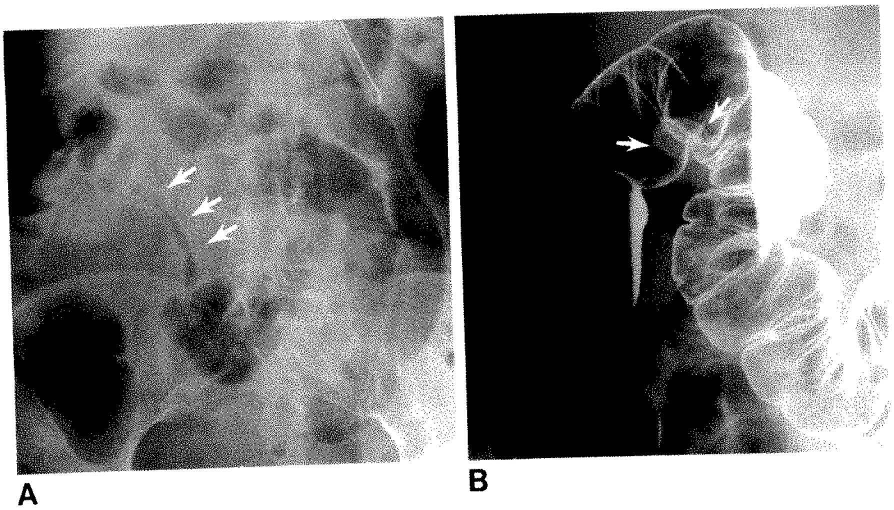

Fig. 2.—Malignant polyp in 69-year-old woman. **A**, Plain abdominal film. Long narrowed segment in proximal transverse colon secondary to colocolic intussusception (*arrows*). **B**, Barium enema 3 days later. Multiple small polyps and large polypoid carcinoma in hepatic flexure (*arrows*) that was intussuscepting at presentation.

in 13 patients (52%) (benign tumors in five and malignant tumors in eight) (figs. 1 and 2); postoperative factors in nine (36%); and a Meckel diverticulum in one patient (4%). In two patients, no underlying cause could be ascertained. The benign tumors were leiomyoma and neurofibromas of the jejunum, lipoma of the ileum and colon, and a solitary large inflammatory fibrovascular polyp of the colon (fig. 1) in one patient each. The malignant tumors were lymphoma of the ileum in three patients, metastatic melanoma of the ileum in two, metastatic carcinoma of the ileum in one, primary adenocarcinoma of the colon in one (fig. 2), and primary reticulum cell sarcoma of the colon in one patient.

The postoperative group comprised patients who had had any abdominal or pelvic surgery during the previous 5 years. The postoperative intussusceptions were related to suture lines in three patients (fig. 3), ostomy closure sites in three (fig. 4), adhesions and abnormal bowel motility in five, long intestinal tubes in three (fig. 5), gastrojejunostomy with jejunogastric intussusception in one, and a bypassed ileal segment after jejunoileal bypass shunting operation for morbid obesity in one patient. Usually several factors were present in patients with postoperative intussusception. For example, dense adhesions were present adjacent to suture lines in all three patients. Submucosal bowel-wall edema, motility disorder, electrolyte imbalance, and chronically dilated bowel loops were important factors that contributed to the postoperative development of intussusception. The various types of intussusception by site were: jejunogastric, one (postoperative); jejunojejunal, seven (four postoperative); ileoileal, four (one postoperative); ileocolic, 10 (one postoperative); and colocolic, three (one cecocolic, one splenic flexure, and one descending colon). Four patients had multiple synchronous intussusceptions (ileoileal and jejunojejunal), four had compound intussusceptions (ileoileocolic), and two had recurrent ileoileal intussusceptions (one postoperative).

Discussion

Intussusception is primarily a disease of infants and children; about 5% of cases occur in adults. Whereas 90% of

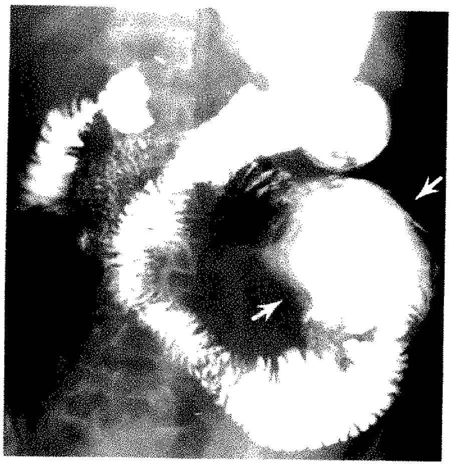

3

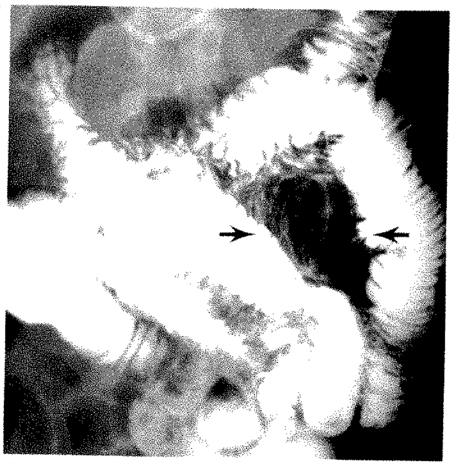

4

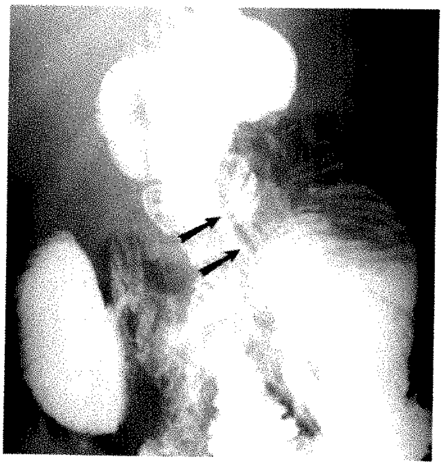

5

Fig. 3.—37-year-old woman had Billroth II partial gastrectomy with gastrojejunostomy in 1980 for peptic ulcer disease, which was revised to Roux-en-Y gastrojejunostomy 1 year later because of bile reflux. After another year, she presented with high intestinal obstructive symptoms. Upper gastrointestinal series shows jejunojejunal intussusception with classic "coiled-spring" appearance (*arrows*) and complete obstruction of jejunum. Suture line of Roux-en-Y anastomosis was lead point of intussusception in this case.

Fig. 4.—39-year-old man had several previous operations, including tube jejunostomy, mesenteric plication, and lysis of adhesions. Recent episode of small-bowel obstruction prompted barium study, which shows jejunojejunal intussusception. Proximal jejunum is dilated; classic "coiled-spring" pattern is present (*arrows*). Intussusception was related to site of previous tube jejunostomy.

Fig. 5.—20-year-old man had long intestinal tube placed postoperatively after total gastrectomy for Zollinger-Ellison syndrome. Recurrent emesis and obstructive symptoms prompted barium study, which shows jejunojejunal intussusception related to intestinal tube (*arrows*).

childhood-type intussusceptions are idiopathic, an underlying pathologic process is usually identifiable in over 90% of adult cases. On the basis of the present study, adult intussusception may be categorized into (1) tumor-related, (2) postoperative, (3) miscellaneous, and (4) idiopathic intussusceptions.

Tumor-Related Intussusceptions

Felix et al. [10], in a review of 1214 reported cases of intussusception in adults from 11 series [1, 3, 4, 6–9, 13–16], estimated that 63% (759/1214) of all intussusceptions in adults were tumor related. Of those, 45% (546/1214) involved the colon and 55% (668/1214) the small bowel. Among the colonic intussusceptions, 48% resulted from malignant tumors and 21% from benign lesions. Of the small-bowel intussusceptions, 17% were due to malignant tumors and 40% to benign tumors. They concluded that intussusceptions in adults involving the colon were more often related to a primary carcinoma of the colon, and that intussusception involving the small bowel was usually related to a benign tumor and less often to a malignant tumor, which was usually a metastatic lesion. Aston and Machleder [11], in their review, arrived at similar conclusions. In the present series, 13 patients (52%) had tumor-related intussusceptions (eight malignant, 61.5%; five benign, 38.5%). In contrast to previous reports, in the present series six patients had malignant tumors in the ileum or jejunum and only two had colonic malignant lesions. There was only one case of primary adenocarcinoma of the colon, presenting as acute small-bowel obstruction (fig. 2), and the second patient had reticulum cell sarcoma of the colon.

Postoperative Intussusception

Although intussusception in infants and children following abdominal operations is a well known cause of bowel obstruction in 10%–15% of cases [17–21], its counterpart in adult patients is rarely considered among causes of postoperative bowel obstruction. Postoperative intussusception in adults has recently been recognized as a distinct entity and been the subject of a few reports [21–24]. The most frequent postoperative intussusceptions are retrograde jejunogastric intussusception after Billroth II partial gastrectomy with gastrojejunostomy [25–28] and intussusception of the excluded intestinal segment after jejunoileal bypass operation for morbid obesity [29–33]. Postoperative intussusception in adults may be related to a variety of predisposing factors, including suture lines (intestinal anastomatic suture lines, e.g., end-to-end, end-to-side, and Roux-en-Y types), oversewn ileum in jejunoileal bypass, previous jejunostomy site, adhesions, submucosal bowel edema, intestinal dysmotility, electrolyte imbalance, long intestinal tubes, and chronic dilatation of the bowel.

One of our patients presented with postoperative jejunojejunal intussusception 1 year after Roux-en-Y gastrojejunostomy (fig. 3). It is speculated that the lead point of this intussusception was the operative suture line. The development of adhesions around the suture lines and discoordinate contractions probably stimulated the initial kink and antegrade invagination. In three other patients, the site of a previous tube jejunostomy performed 2 years earlier, aided by the adjacent dense adhesions, served as a stimulating factor for producing the initial kink and lead point of jejunojejunal intussusception [34] (fig. 4). The long intestinal tubes are known to produce telescoping of bowel [35, 36], and were indeed the causative factor in three patients in the present series (fig. 5). In one patient the clinical diagnosis of postoperative intussusception was not suspected, and it was thought that abdominal distension was related to prolonged abdominal ileus. No long intestinal tube was used. At postmortem examination there was significant submucosal edema of the jejunum and proximal ileum in addition to a jejunojejunal intussusception. Since there were no other abnormalities or predisposing factors, it is speculated that submucosal bowel edema probably initiated this postoperative jejunojejunal intussusception.

Postoperative intussusception in laboratory animals is common following a laparotomy, and is often the cause of death in dogs [37]. In infants and children, at the time of closure of the abdominal wound multiple transient areas of intussusception, which can be easily reduced manually and presumably never produce clinical symptoms, are common. However, it is possible occasionally one of those intussusceptions could persist and produce postoperative bowel obstruction.

The diagnosis of postoperative intussusception can be difficult, and a high index of suspicion is necessary for its early detection. The classic clinical triad of conventional intussusception consisting of abdominal pain, palpable sausage-shaped mass, and "currant-jelly" stools is rarely present. In most postoperative patients, the abdominal pain is attributed to the surgical wound, and the most important symptoms are vomiting and abdominal distension. Bloody stools are unusual, and a palpable abdominal mass rare. Sonography, computed tomography, and oral barium contrast examination of the upper gastrointestinal tract with small-bowel follow-through have been found to be helpful in the diagnosis of postoperative intussusception [30–33].

Miscellaneous Causes

Meckel diverticulum, a common cause of childhood intussusception, is rarely found associated with intussusception in adults [1, 3, 9, 38]. In the present series, only one patient was found to have a Meckel diverticulum definitely causing ileocolic intussusception. In adults with celiac disease or sprue, transient nonobstructive intussusceptions have been recognized. These are probably related to chronic dilatation, flaccid bowel, and the secretions [39, 40]. Frank and O'Connell [41] reported an unusual case of the celiac disease complicated by pneumatosis cystoides intestinalis that developed obstructing intussusception of the bowel due to small gas cysts in the ileum.

Idiopathic Intussusception

In a small percentage of adult intussusceptions, no cause can be found [3, 11, 42–44]. Smith and Gillespie [42] reported a series of 34 patients with adult intussusceptions of whom 50% had no demonstrable organic lesion. Gupta et al. [43] reported 38% of their cases in adults as idiopathic, and Donhauser and Kelly [3] reported 10%–15% of their intussusceptions in adults as primary or idiopathic. A most unusual instance of idiopathic intussusception occurring in father and son has been reported [45]. In my experience, primary intussusception in adults is quite rare. In the present series only two cases (8%) were considered idiopathic intussusceptions. This is in sharp contrast to childhood intussusception, where 80%–90% of the cases are usually idiopathic.

The exact mechanism that precipitates intussusception is still not known. Stimulation of the intestine normally produces an area of constriction above the stimulus and relaxation below. It is generally believed that any lesion in the bowel wall or irritant within the bowel lumen that alters the normal peristaltic pattern is capable of initiating an invagination. Occasionally, a lead point such as a tumor, polyp, Meckel diverticulum, or appendiceal stump [10] can be identified. In those patients with no definable lead point, intussusception may be related to submucosal bowel edema, fibrous adhesions, or dysrhythmic contractions.

The diagnosis of intussusception in adults should stimulate a search for an offending cause such as a neoplasm, and in patients with a history of abdominal surgery, postoperative intussusceptions should be suspected among causes of bowel obstruction.

ACKNOWLEDGMENT

I thank Barbara Smith for assistance in manuscript preparation.

REFERENCES

1. Coran AG. Intussusception in adults. *Am J Surg* **1969**;177:735–738
2. Raffensperger JG, Baker JR. Postoperative intestinal obstruction in children. *Arch Surg* **1967**;94:450–459
3. Donhauser JL, Kelly EC. Intussusception in the adult. *Am J Surg* **1950**;79:673–677
4. Deterling RA Jr, O'Mallery RD, Knox W. Intussusception in the adult with emphasis on retrograde type. *Arch Surg* **1953**;67:854–864
5. Briggs DF, Carpathios J, Zollinger RW. Intussusception in adults. *Am J Surg* **1961**;101:109–113
6. Brayton D, Norris WJ. Intussusception in adults. *Am J Surg* **1954**;88:32–43
7. Coltar AM, Cohen I Jr. Intussusception in adults. *Am J Surg* **1961**;101:114–120
8. Stubenborg WT, Thorbjarnarson B. Intussusception in adults. *Ann Surg* **1970**;172:306–310
9. Burmeister RW. Intussusception in the adult: an elusive case of recurrent abdominal pain. *Am J Dig Dis* **1962**;7:360–374
10. Felix EL, Cohen MH, Bernstein AD, Schwartz JH. Adult intussusception: case report of recurrent intussusception and review of the literature. *Am J Surg* **1976**;131:758–761
11. Aston SJ, Machleder HI. Intussusception in the adult. *Am Surg* **1975**;41:576–580
12. Lou CJ. Intussusception in adults: an analysis of 92 cases. *Clin Med J [Engl]* **1982**;95:297–300
13. Brown CH, Michels AG. Intussusception in adults: report of 15 cases. *Surgery* **1952**;31:538–543
14. Dean DL, Ellis FH Jr, Sauer WG. Intussusception in adults. *Arch Surg* **1956**;73:6–11
15. Weilbaecher D, Bolin JA, Hearn D, Odgen W. Intussusception in adults: review of 160 cases. *Am J Surg* **1971**;121:531–535
16. Roper A. Intussusception in adults. *Surg Gynecol Obstet*

1956;103:267–268
17. McGovern JB, Gross RE. Intussusception as a postoperative complication. *Surgery* **1968**;63:507–513
18. Mollitt DL, Ballantine TVN, Grosfeld JL. Postoperative intussusception in infancy and childhood: analysis of 119 cases. *Surgery* **1979**;86:402–408
19. Holgersen LO, Stanley-Brown EG. Idiopathic postoperative intussusception in infancy and childhood. *Am Surg* **1978**;44:305–308
20. Franken EA Jr, King H. Postoperative intussusception in children. *AJR* **1972**;116:584–586
21. Cox JA, Martin LW. Postoperative intussusception. *Arch Surg* **1973**;106:263–266
22. Sarr MG, Norgorney DM, McIlrath DC. Postoperative intussusception in the adult: a previously unrecognized entity. *Arch Surg* **1981**;116:144–148
23. Hertz I, Train J, Keller R, Slater G, Greenstein A. Adults' postoperative enteroenteric intussusception in Crohn's disease. *Gastrointest Radiol* **1982**;7:583–589
24. Wolfson S, Shachor D, Freund U. Ileocolic intussusception in an adult: a postoperative complication of appendectomy. *Dis Colon Rectum* **1984**;27:265–266
25. Charboneau JW. Case of the fall season: retrograde jejunogastric intussusception. *Semin Roentgenol* **1979**;14:263–265
26. Marx WJ. Reduction jejunogastric intussusception during upper gastrointestinal examination. *AJR* **1978**;131:334–336
27. Waits JO, Beart RW Jr, Charboneau JW. Jejunogastric intussusception. *Arch Surg* **1980** 115:1449–1452
28. Burdrick TJ, Turner MA. Retrograde jejunogastric intussusception. *Rev Interam Radiol* **1981**;6:21–24
29. Starkloff GB, Shively RA, Gregory JG. Jejunal intussusception following small bowel bypass for morbid obesity. *Ann Surg* **1977**;185:386–390
30. Kaude JV, McDowall JD, Neustein CL, Woodward ER, Wright PG. Intussusception after jejunoileal bypass as diagnosed by ultrasound. *Gastrointest Radiol* **1981**;6:135–140
31. Miller DR. Intussusception of the bypassed segment after jejunoileal bypass for obesity: a cryptic problem. *Am J Gastroenterol* **1979**;72:434–440
32. Lo G, Fisch AE, Brodey PA. CT of the intussuscepted excluded loop after intestinal bypass. *AJR* **1981**;137:157–158
33. Billimaria PE, Fabian TM, Schulz EE. Computed tomography of intussusception in the bypassed jejunoileal segment. *J Comput Assist Tomogr* **1982**;6:86–88
34. Reymond RD. A mechanism of the kink formation which precedes intussusception. *Invest Radiol* **1971**;6:61–64
35. Brown EO, Miller JM. Retrograde jejunal intussusception following the use of a cantor intestinal tube. *Am J Proctol Gastroenterol Colon Rectal Surg* **1981**;32:28–33
36. Redmond P, Ambos M, Berliner L, Pachter HL, Megibow A. Iatrogenic intussusception: a complication of long intestinal tubes. *Am J Gastroenterol* **1982**;77:39–42
37. Houck CR, Moore AW, Ellison WB, Gilmer R. Intestinal intussusception in chronic nephrectomized dogs maintained on peritoneal dialysis. *Science* **1954**;119:845–846
38. Williamson RC, Cooper MJ, Thomas WE. Intussusception of invaginated Meckel's diverticulum. *J R Soc Med* **1984**;77:652–655
39. Cohen MD, Lintott DJ. Transient small bowel intussusception in adult celiac disease. *Clin Radiol* **1978**;29:529–534
40. Ruoff M, Lindner AE, Marshak RH. Intussusception in sprue. *AJR* **1968**;104:525–528
41. Frank PH, O'Connell DJ. Pneumatosis intestinalis and obstructing intussusception in celiac disease. *Gastrointest Radiol* **1977**;2:109–111
42. Smith IS, Gillespie G. Adult intussusception in Glasgow. *Br J Surg* **1968**;55:925–928
43. Gupta S, Udupa KN, Gupta S. Intussusception in adults. *Int Surg* **1976**;61:231–233
44. Cambell R, Devereux D, Forrest H. Primary intussusception in the adult. *J R Coll Surg Edinb* **1982**;27:185–186
45. Thomas MP, McKay DG. Idiopathic intussusception occurring in father and son with postoperative intussusception in the son. *Aust Paediatr J* **1979**;15:281–282

Book Review

A Handbook of Radioactivity Measurements Procedures, 2d ed. NCRP Report No. 58. Recommendations of the National Council on Radiation Protection and Measurements. Bethesda: NCRP, 592 pp. 1985. $22

This is a detailed handbook of measurement procedures covering most types of radioactivity counting applications, including sections on measurement statistics and standards for quality assurance. This edition is a substantial revision of the first, which was published in 1978. Each section begins with an introduction that does not assume a prior knowledge of the subject covered. A detailed reference list is provided as an appendix for those who wish to pursue more detailed information. The layout and design of the book make it useful for physicians, technologists, laboratory personnel, and physicists who work with radioactive material. The book will not be useful for diagnostic radiologists unless they have an interest in nuclear medicine applications. The illustrations, figures, and equations are well identified and located near the text where they are discussed. The book is divided into eight sections covering a broad range of topics.

The first section is an introduction to radioactivity and radioactive decay. The various interactions of radiation with matter and methods of radioactivity standardization are discussed. The physics of radiation detection is discussed in detail in the second section including a discussion of corrections for dead time, decay, and background. Fundamental or direct measurements of radioactivity are covered in the third section. This is followed by a section on indirect or comparative measurement techniques including identification of isotopes by energy spectrometry, liquid scintillation counting, and use of ionization chambers. Preparation of standard sources for radioactivity measurements is discussed in section five. The determination of radioactivity in environmental, medical, and industrial applications is described in section six.

The last two sections deal with treatment of counting data, statistics of measurement processes, standards, traceability, and estimates of measurement uncertainty. The book is an excellent practical handbook for reference; it also would be an excellent text for a course on radioactivity measurements.

David L. Williams
Imaging Physicist
Veterans Administration Medical Center
Seattle, WA 98108

Regenerating Nodules in Cirrhosis: Sonographic Appearance with Anatomic Correlation

Mark P. Freeman[1]
C. Whitley Vick[2]
Kenneth J. W. Taylor[3]
Robert L. Carithers[4]
William H. Brewer[1]

A sonographic-anatomic correlation study was undertaken to define the sonographic appearance of regenerating nodules in cirrhotic livers. Three cirrhotic livers with multiple regenerating nodules were obtained from patients undergoing liver transplantation. Sonograms of the resected livers were made and correlated directly with the anatomic specimens. Using a 3-MHz transducer, no discrete alterations in the echo texture of the livers were seen to correspond to the regenerating nodules. With a 7.5-MHz transducer, discrete islands of liver parenchyma were identified corresponding to regenerating nodules anatomically. The nodules were recognized because of visualization of thin, slightly more echogenic borders, which corresponded pathologically to fibrous and fatty connective tissue surrounding and separating the nodules.

The sonographic appearance of regenerating nodules in the cirrhotic liver is not well defined. One report [1] contends that regenerating nodules are seen as focal hypoechoic lesions in the cirrhotic liver, while other authorities [2] believe that regenerating nodules do not produce specific focal alterations in the echo texture of a cirrhotic liver. Precise sonographic-pathologic correlation is not available to support or refute either of these contentions. However, the question is not trivial, because liver malignancies such as hepatoma or metastases are known to produce focal alterations of echo texture in cirrhotic livers. Obviously it is clinically important to differentiate cirrhosis with regenerating nodules from cirrhosis with malignancy.

As an initial step toward defining the sonographic appearance of regenerating nodules, we undertook this study in which sonograms of resected cirrhotic livers with multiple regenerating nodules were correlated directly with gross and microscopic anatomic findings.

Materials and Methods

Three livers with pathologically proven cirrhosis were obtained from patients undergoing liver transplantation at the Medical College of Virginia. The cause of cirrhosis was sclerosing cholangitis in two cases and cryptogenic in one case. The livers were brought directly to the sonographic laboratory from the operating room immediately after surgical resection. Fixed-arm and real-time scans were done using 3-, 5-, and 7.5-MHz transducers. A water bath was used as necessary to place the liver parenchyma in the focal zone of the transducer. Gain settings were adjusted to give the liver parenchyma a homogeneous texture with medium-level echoes, similar to that of "normal-appearing" liver parenchyma in situ. The presence of any focal alteration within or on the surface of the liver was noted.

After scanning, each liver was sliced with a knife in a plane similar to the sonographic sections. The sonographic findings were correlated directly with gross anatomic findings. The livers were then submitted for formalin fixation and histologic evaluation. Preoperative liver sonographic studies were also reviewed in each case.

Received August 26, 1985; accepted after revision November 14, 1985.

[1] Department of Radiology, Medical College of Virginia/Virginia Commonwealth University, Box 615, MCV Station, Richmond, VA 23298. Address reprint requests to M. P. Freeman.

[2] Rome Radiology Group, Rome, GA 30161.

[3] Department of Radiology, Yale University School of Medicine, New Haven, CT 06510.

[4] Department of Internal Medicine, Medical College of Virginia/Virginia Commonwealth University, Richmond, VA 23298.

AJR 146:533-536, March 1986
0361-803X/86/1463-0533
© American Roentgen Ray Society

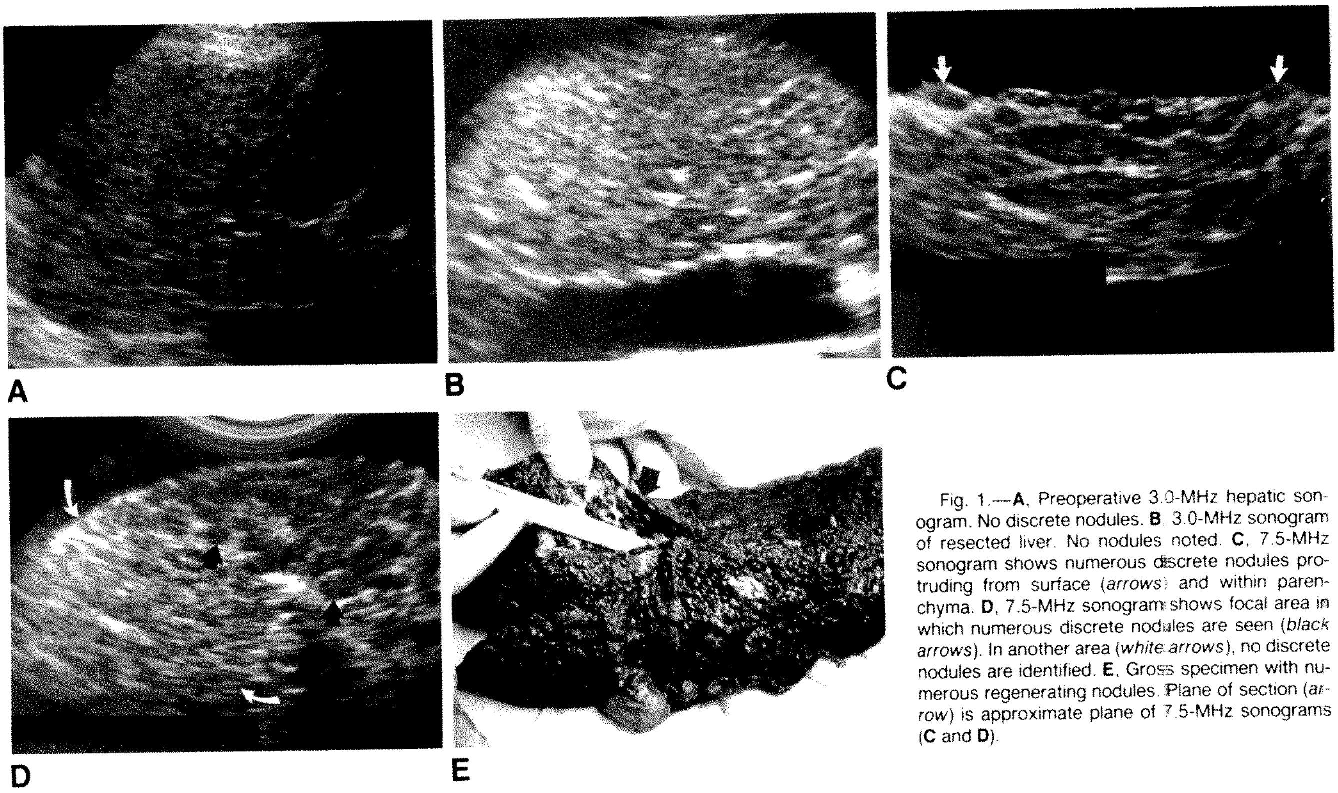

Fig. 1.—**A**, Preoperative 3.0-MHz hepatic sonogram. No discrete nodules. **B**, 3.0-MHz sonogram of resected liver. No nodules noted. **C**, 7.5-MHz sonogram shows numerous discrete nodules protruding from surface (*arrows*) and within parenchyma. **D**, 7.5-MHz sonogram shows focal area in which numerous discrete nodules are seen (*black arrows*). In another area (*white arrows*), no discrete nodules are identified. **E**, Gross specimen with numerous regenerating nodules. Plane of section (*arrow*) is approximate plane of 7.5-MHz sonograms (**C** and **D**).

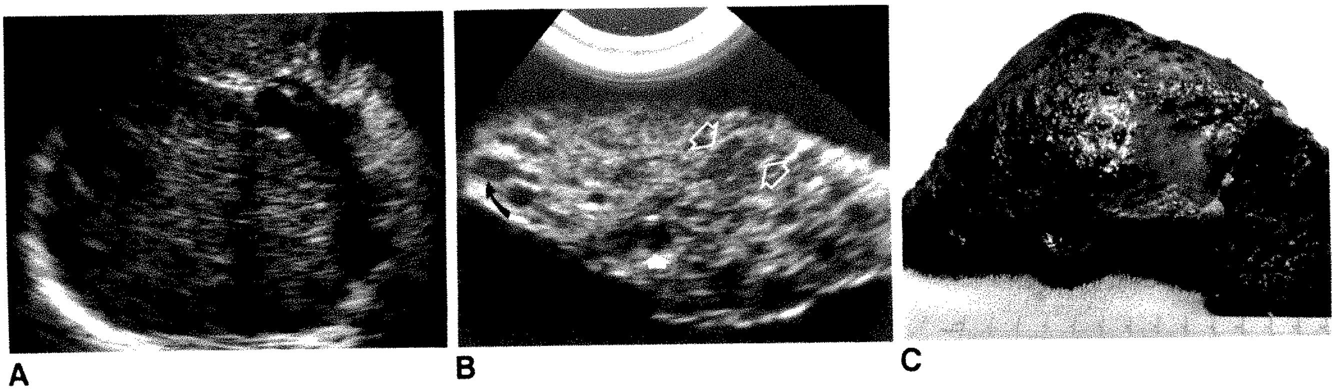

Fig. 2.—**A**, Preoperative 3.0-MHz transverse sonogram shows no discrete nodules. **B**, 7.5-MHz sonogram shows 7-mm nodule (*open arrows*) with internal echoes similar in appearance to normal liver. Other nodules are more hypoechoic, probably due to sound attenuation (*solid white arrow*) or thick surrounding connective tissue (*black arrow*). **C**, Gross specimen. Surface is studded with regenerating nodules.

Results

The gross appearance of each of the resected cirrhotic livers exhibited innumerable regenerating nodules ranging in size from several millimeters to 2 cm (figs. 1 and 2). Most nodules ranged from 0.5 to 1.5 cm in diameter. Histologically, the regenerating nodules were surrounded by fibrous connective tissue about 0.1–1.0 mm thick. The pathologic appearance in each case was that of mixed cirrhosis with macronodular and micronodular components.

The sonographic findings were similar in each case, and varied depending on the frequency of the transducer used to study the liver. With the 3-MHz transducer, no specific focal alterations in the liver parenchyma were identified (fig. 1). Subtle inhomogeneity or coarsening of the parenchymal echo pattern was observed, but this finding was subjective and difficult to quantify. The surface of the livers could be studied using the water bath, and multiple small surface irregularities were observed, giving the liver margin a "knobby" contour (fig. 1). The gross appearance of these surface irregularities corresponded to regenerating nodules protruding from the surface of the liver. The convexity of a surface irregularity seen on sonography corresponded to the actual bulging of a regenerating nodule, and the concavity of a surface irregular-

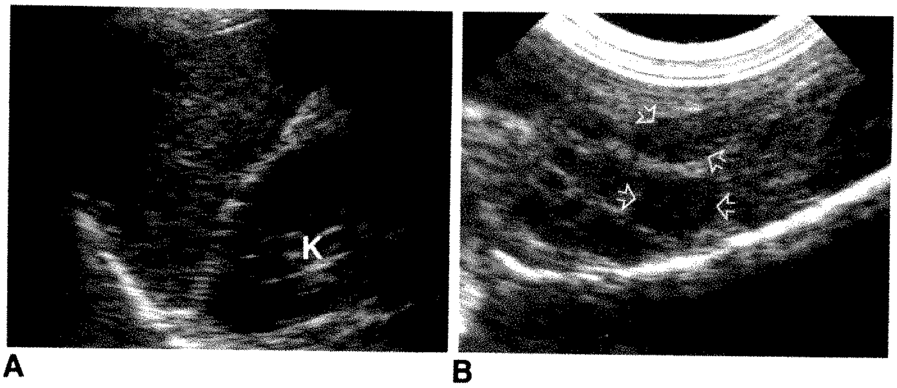

Fig. 3.—**A**, Preoperative 3.0-MHz longitudinal scan through right lobe of liver shows relatively homogeneous echo texture. K = right kidney. **B**, 7.5-MHz sonogram shows discrete nodules (*arrows*) with echogenic borders. Echo texture of nodules is similar to that of normal liver.

ity corresponded to fibrous tissue separating adjacent nodules.

Preoperative sonographic studies on the livers in situ were all done using 3-MHz transducers, and the preoperative sonographic findings were similar to those seen using the 3-MHz transducer to study the resected specimens. In no case were focal parenchymal abnormalities identified on preoperative sonograms. In one case, surface irregularities were seen preoperatively, and in this case the presence of ascites permitted sonographic interpretation of the liver surface. On scans made with the 7.5-MHz transducer, a strikingly different pattern was seen. In many areas, discrete foci or islands of parenchyma were identified, and anatomic correlation showed these areas to correspond precisely with regenerating nodules (figs. 1–3). On closer inspection, the islands of parenchyma could be identified as discrete structures because they were surrounded by slightly more echogenic borders of variable thickness. The borders seen on sonography corresponded anatomically to thin bands of fibrous/fatty connective tissue separating adjacent regenerating nodules.

The multiple, closely spaced nodules and their thin connective tissue borders produced a "cobblestone" appearance both sonographically and anatomically. Echoes within the regenerating nodules were homogeneous in distribution but variable in amplitude depending on gain settings used. For example, echo amplitude within the nodules could be made to look similar to "normal" liver parenchyma or hypoechoic using different gain settings. Lack of a reference organ when studying the resected specimens made it difficult to standardize gain settings. Relative echo amplitude also seemed to depend in part on the thickness of surrounding fibrous/fatty tissue, with nodule echogenicity seemingly more hypoechoic the thicker the surrounding band of connective tissue (fig. 2). In general, if an attempt was made to optimize gain settings as one would in studying a liver in situ, the nodules had a uniform texture with medium-level echoes similar to those of normal liver parenchyma.

In some areas of the cirrhotic livers, discrete nodules were not observed using the 7.5-MHz transducer, although regenerating nodules were present on gross examination. The reason for nonvisibility of the nodules in these areas is not readily apparent. Imaging with the 5-MHz transducer showed a pattern with some features seen with both the 3- and the 7.5-MHz transducers. In general, the 5-MHz-transducer images were closer to those at 3 MHz than those at 7.5 MHz. The liver parenchyma tended to appear coarser and less uniform using the 5-MHz transducer compared to the 3-MHz transducer, but only rarely were apparent discrete islands of parenchyma identified corresponding to regenerating nodules.

Discussion

This study documents that sonography can demonstrate small regenerating nodules in the cirrhotic liver. However, such nodules were identified in our study only using a high-frequency transducer placed directly on resected cirrhotic livers. With the lower frequency transducers that are typically used to study adult livers in situ, discrete nodules were not identified sonographically, despite the presence of myriad regenerating nodules seen anatomically. Presumably the greater resolution provided by the high-frequency transducer permits visualization of the connective tissue strands surrounding and separating the nodules. Visualization of the borders of the nodules is tantamount to identification of the actual nodule as a discrete structure.

Our study corroborates the findings of previous studies, which typically show no focal sonographic alterations in cirrhotic livers, although parenchymal echogenicity may be diffusely increased and coarsened [2]. Presumably, the cirrhotic livers in these previous studies contained numerous regenerating nodules as in our cases, although direct sonographic-pathologic correlation is lacking.

A related issue involves the use of sonography to clarify findings on liver-spleen radionuclide scanning with sulfur colloid. Cold areas seen on radionuclide scans of cirrhotic patients may be due to fibrosis, avascular areas due to shunting of blood, neoplasm, or, rarely, regenerating nodules. If hepatoma superimposed on cirrhosis is suggested on the radionuclide scan, the results of this study indicate that sonographic scanning should show no focal abnormality in the presence of cirrhosis alone. On the other hand, hepatoma characteristically produces gross distortion of the hepatic echo texture [3].

Three anatomic types of cirrhosis are recognized: micronodular, macronodular, or mixed. The livers we studied had mixed cirrhosis, characterized by connective tissue bands of varying thickness, by nodules of variable size, and by normal lobules in the larger nodules [4]. Most commonly, the nodules are 2–3 mm to 1–2 cm in diameter, as in our cases. Very large regenerating nodules (5–15 cm) are rarely encountered, and our pathologic material did not include such a case. Laing et al. [5] described two such cases in which sonography showed the large nodules as focal alterations of the echo texture of the liver mimicking a malignant neoplasm. Fortunately, such large regenerating nodules seem to be quite uncommon, as these were the only two cases found in a population of about 2500 cirrhotic patients studied with sonography.

In conclusion, our study provides sonographic-anatomic correlation supporting the contention that small regenerating nodules are not identified as focal or discrete alterations in the parenchyma of cirrhotic livers on liver sonography as clinically practiced. In the laboratory setting, small regenerating nodules may be identified using a high-frequency transducer placed directly on a resected cirrhotic liver.

REFERENCES

1. Birnholz JC. Ultrasound evaluation of diffuse liver disease. In: Taylor KJW, ed. *Diagnostic ultrasound in gastrointestinal disease, clinics in diagnostic ultrasound*, Vol 1. New York: Churchill Livingstone, **1979**:23–33
2. Taylor KJW. The liver. In: Taylor KJW, ed. *Atlas of ultrasonography*, 2d ed, chap 8. New York: Churchill Livingstone, **1985**:429–540
3. Taylor KJW, Gorelick FS, Rosenfield AT, Riely CA. Ultrasonography of alcoholic liver disease with histological correlation. *Radiology* **1981**;141:157–161
4. Sherlock S. Hepatic cirrhosis. In: *Diseases of the liver and biliary system*, 6th ed, Chap 18. Oxford: Blackwell Scientific, **1981**:323–333
5. Laing FC, Jeffrey RB, Federle MP, Cello JP. Noninvasive imaging of unusual regenerating nodules in the cirrhotic liver. *Gastrointest Radiol* **1982**;7:245–249

Optimal Cholangiographic Technique for Detecting Bile Duct Stones

William M. Thompson[1, 2]
Robert A. Halvorsen[1, 2]
William L. Foster[1, 2]
Leroy Roberts[1, 2]
Rebecca Gibbons[1-3]
Margaret E. Williford[1, 2]
Frederick M. Kelvin[2, 4]
Reed P. Rice[2]

Twenty-eight patients with proven bile duct stones were evaluated during either operative or T-tube cholangiography. Two radiographs were obtained for each patient without changing patient position between films. The first was performed with low peak kilovoltage (75–80 kVp) and 15% iodinated contrast medium and the second with high kVp (110) and 38% iodinated contrast. Seven radiologists evaluated the radiographs individually and in matched pairs for ductal filling, ductal penetration, motion unsharpness, overall quality, and stone detectability. The high-kVp radiographs were rated significantly better overall than the low-kVp studies ($p < 0.001$) for all five criteria. In the second evaluation, which compared the pairs from the same patients, the 28 high-kVp radiographs were considered superior to the 28 low-kVp studies by the radiologists in almost two-thirds of the comparisons (ductal filling, 68%; penetration, 59%; less motion unsharpness, 65%; overall quality, 77%; stone detection, 62%). On the basis of the results of this study, high-kVp technique with full-strength contrast medium for operative and T-tube cholangiography is recommended.

Most retained bile duct stones are missed at surgery because of nondiagnostic cholangiograms rather than nonperformance of operative cholangiography [1, 2]. The variables that determine image quality during operative and T-tube cholangiography include density of contrast medium, motion unsharpness, degree of ductal filling, and patient positioning to avoid superimposition of the biliary system over the spine. A number of authors have evaluated the factors that affect image quality during cholangiography [3–19]. In 1956, Ashmore et al. [3] suggested that diluting the contrast agent for operative cholangiography might improve stone detectability. Later Hur et al. [7] developed a formula to determine the optimum dilution of the contrast agent based on the caliber of the duct. More recently, Machi et al. [16] performed phantom studies and concluded that variable radiographic exposures are necessary to demonstrate both central and peripheral calculi, especially for small calculi in large ducts. On the basis of phantom studies, Lundstrom et al. [17] and Thompson et al. [18] demonstrated that high kilovoltage (kVp) and high contrast-agent concentration produce better quality operative and T-tube cholangiograms than the currently recommended low kVp and low contrast-agent concentration. Thompson et al. [18] also evaluated 56 patients with normal operative and T-tube cholangiograms and six with stones, and showed that the high-kVp with high-contrast-agent-concentration technique was superior.

We are unaware of any other clinical study evaluating the detection of common duct stones using the various factors that determine image quality. The purpose of this study was to determine if high kVp and high contrast-agent concentration in operative and T-tube cholangiography is a better method for detecting common duct stones than the previously recommended technique of low kVp and diluted contrast-agent concentration.

Received July 15, 1985; accepted after revision October 29, 1985.

Presented in part at the annual meeting of the American Roentgen Ray Society, Boston, April 1985.

This work was supported by Veterans Administration grant 525-96-7552.

[1] Department of Radiology, Durham Veterans Administration Hospital, Durham, NC 27710.

[2] Department of Radiology, Duke University Medical Center, Box 3808, Durham, NC 27710. Address reprint requests to W. M. Thompson.

[3] Present address: 1058 Cherryfield Ave., Worthington, OH 43085.

[4] Present address: Department of Radiology, Methodist Hospital, Indianapolis, IN 46206.

AJR 146:537–541, March 1986
0361–803X/86/1463–0537
© American Roentgen Ray Society

Subjects and Methods

Twenty-eight patients with documented bile duct stones were evaluated. In each patient, two radiographs were obtained without change in patient position between the radiographs (13 operative and 15 T-tube cholangiograms). In each patient, the bile ducts were first filled with an adequate amount (10–15 ml) of 15% iodinated contrast material (Renografin 30), and a radiograph was exposed using 75–80 kVp. The bile ducts were then filled with Renografin 76 (38% iodine), and a radiograph was obtained at 110 kVp. All operative and 12 T-tube studies were obtained with an overhead tube. Three T-tube studies were performed with fluoroscopic spot films. The specific ampere-seconds used was based on the patient's body habitus and determined by the technologist performing the study. For the low-kVp film, this varied from 32 to 64 mAs, and for the 110 kVp film, from 2 to 12 mAs. The mean size of the 28 common bile ducts was 12.8 mm (range, 5–18 mm). Eight ducts measured 5–10 mm, 14 were 11–15 mm, and 6 were larger than 15 mm.

Seven radiologists were asked to evaluate the radiographs after all identifying labels had been obscured. Two different analyses of the films were performed with an 8-week interval between the two evaluations.

TABLE 1: **Average Scores for Seven Reviewers: T-Test for Independent Means**

	Low kVp	High kVp
Ductal filling	2.55 ± 0.08	3.24 ± 0.06
Penetration	2.34 ± 0.08	2.75 ± 0.07
Least motion unsharpness	2.23 ± 0.08	2.99 ± 0.06
Quality	2.03 ± 0.08	2.74 ± 0.06
Stone detectability	2.23 ± 0.08	2.80 ± 0.08

Note.—$p < 0.0001$ for all comparisons; $n = 56$, scale 0 to 4, mean ± SEM.

Method 1

The 56 films were randomized, and the seven radiologists independently evaluated each radiograph for ductal filling, degree of ductal penetration, motion unsharpness, overall quality, and stone detectability using a scale of 0 to 4. These results were analyzed with an analysis of variance (ANOVA) and Student's *t*-test for both paired and unpaired means [20, 21]. The individual scores for each of the seven radiologists were evaluated using the *t*-test for paired means at a 95% confidence level [20].

Method 2

After identifying labels had been obscured, each pair of radiographs was labeled A and B. The seven radiologists independently compared the radiographs in each pair ($n = 28$) and rated them as either better or the same in terms of ductal filling, ductal penetration, least motion unsharpness, overall quality, and stone detectability. The results were tabulated and differences between means were tested using Student's *t*-test [20, 21].

Results

Method 1—Individual Radiograph Evaluation

The stones were identifiable on all of the high-kVp studies. In three of 28 low-kVp studies, the stones were not seen because of motion unsharpness. The seven radiologists indicated that in 15 (7.7%) of the 196 total evaluations of the low-kVp films (seven radiologists × 28 films), the stones were not detectable. This occurred in four (2%) of the 196 high-kVp evaluations. In the rest of the low- and high-kVp films, the radiologists were able to detect the stones. While the

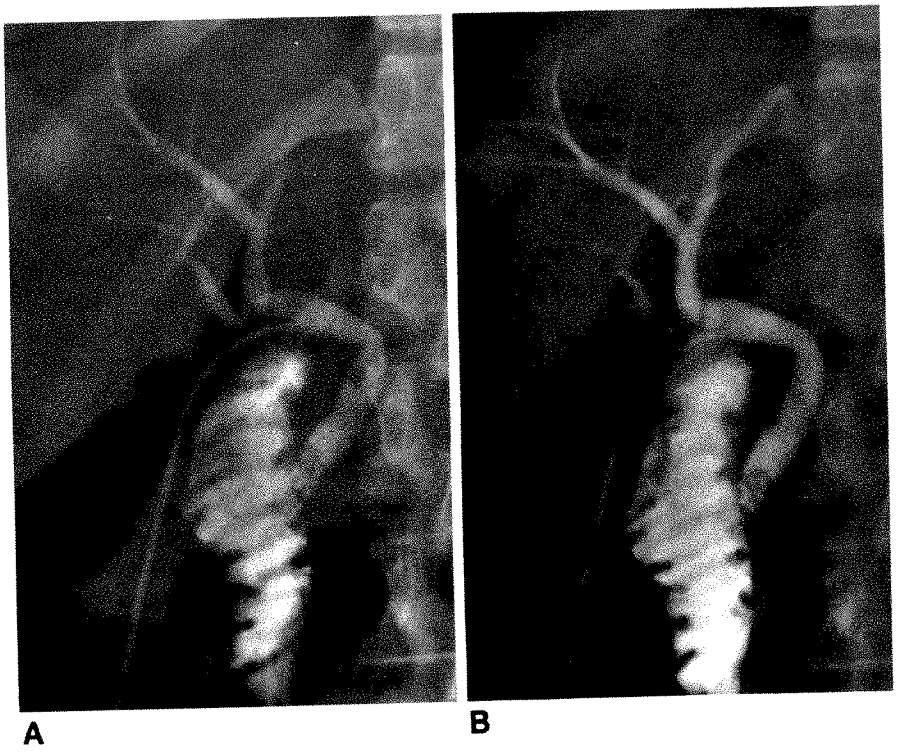

Fig. 1.—Low-kVp operative cholangiogram (**A**) and high-kVp study (**B**) from same patient. High-kVp study was rated higher than low-kVp radiograph.

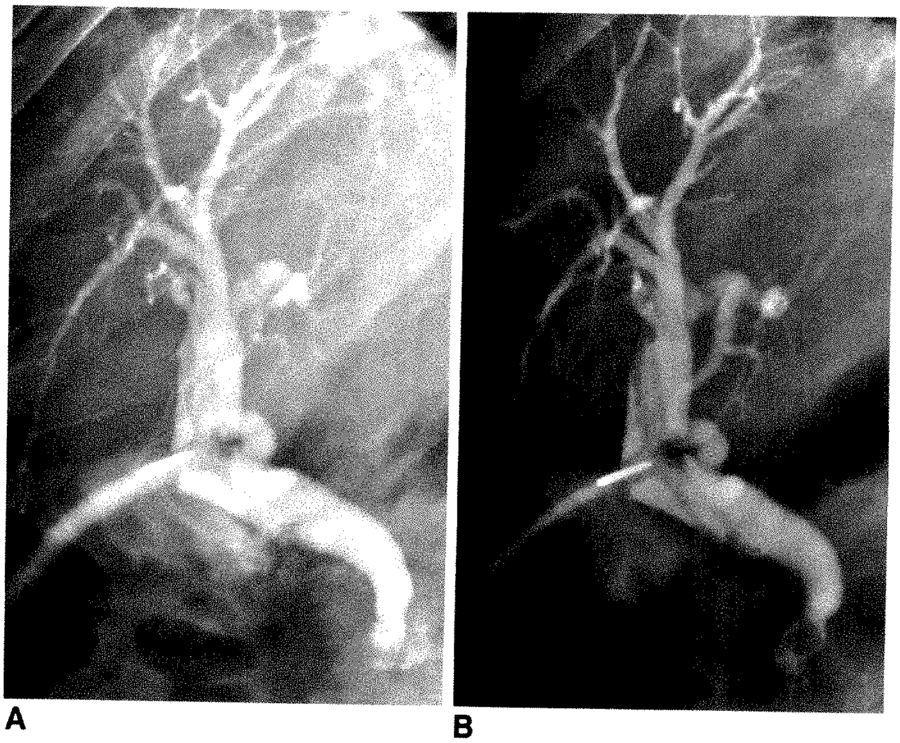

Fig. 2.—Low-kVp T-tube cholangiogram (**A**) and high-kVp study (**B**) from same patient. High-kVp study was rated higher than low-kVp radiograph. Note that tube in bile duct and stone are much better seen on high-kVp study.

TABLE 2: **Scores of Individual Reviewers: T-Test for Paired Means**

Reviewer	Ductal Filling		Penetration		Least Motion Unsharpness		Quality		Stone Detectability	
	Low kVp High kVp	*p*	Low kVp High kVp	*p*	Low kVp High kVp	*p*	Low kVp High kVp	*p*	Low kVp High kVp	*p*
1	2.36 ± 0.23		2.57 ± 0.2		2.04 ± 0.2		2.00 ± 0.2		2.11 ± 0.2	
	2.96 ± 0.17	0.009	2.86 ± 0.2	0.2	2.86 ± 0.12	0.0008	2.46 ± 0.14	0.02	2.29 ± 0.2	0.50
2	2.39 ± 0.20		2.17 ± 0.2		2.12 ± 0.20		2.00 ± 0.18		2.14 ± 0.20	
	3.00 ± 0.15	0.006	2.50 ± 0.2	0.1	3.00 ± 0.15	0.0002	2.54 ± 0.18	0.02	2.57 ± 0.21	0.1
3	2.54 ± 0.24		2.17 ± 0.21		2.11 ± 0.18		2.00 ± 0.17		2.14 ± 0.20	
	3.07 ± 0.20	0.02	2.54 ± 0.17	0.08	2.89 ± 0.13	0.0004	2.82 ± 0.14	0.0001	2.64 ± 0.20	0.055
4	3.32 ± 0.17		3.03 ± 0.22		3.04 ± 0.23		2.86 ± 0.26		3.29 ± 0.16	
	3.82 ± 0.07	0.006	3.57 ± 0.11	0.009	3.68 ± 0.10	0.01	3.39 ± 0.14	0.004	3.64 ± 0.11	0.03
5	2.54 ± 0.17		2.50 ± 0.22		2.64 ± 0.16		2.00 ± 0.22		2.18 ± 0.26	
	3.36 ± 0.15	0.0005	2.61 ± 0.17	0.6	2.92 ± 0.14	0.2	2.75 ± 0.14	0.001	2.68 ± 0.22	0.055
6	2.25 ± 0.19		2.50 ± 0.19		2.42 ± 0.17		2.04 ± 0.19		2.42 ± 0.20	
	2.96 ± 0.20	0.004	2.75 ± 0.18	0.1	2.96 ± 0.11	0.003	2.75 ± 0.15	0.001	3.11 ± 0.17	0.004
7	1.96 ± 0.25		1.93 ± 0.28		1.86 ± 0.26		1.75 ± 0.23		2.00 ± 0.26	
	3.04 ± 0.21	0.0001	2.57 ± 0.20	0.005	2.86 ± 0.22	0.002	2.46 ± 0.20	0.002	2.61 ± 0.26	0.03

Note.—$n = 56$, scale 0 to 4, mean ± SEM.

high-kVp technique detected more stones than the low-kVp technique, this study was not designed to specifically address this point because the stones were demonstrated on 53 of 56 films.

When mean scores for the five criteria were compared, high-kVp radiographs were rated significantly better than low-kVp radiographs using the *t*-test for either independent or paired means (table 1, figs. 1 and 2). Since there was no difference between the *t*-test using independent or paired means, only the independent means are reported (table 1).

Individually the seven radiologists rated the high-kVp radiographs better than the low-kVp studies (figs. 1 and 2, table 2). All seven reviewers rated the high-kVp radiographs significantly better than the low-kVp studies for ductal filling and film quality. Six of the seven reviewers rated the high-kVp radiograph as having significantly less motion unsharpness. In terms of penetration, three of the reviewers' ratings showed the high-kVp studies to be significantly better. The other four reviewers found no difference. Three reviewers rated the high-kVp radiographs significantly better in terms of stone detectability, and two of the reviewers' results were almost significant ($p = 0.055$) (table 2, reviewers 3 and 5).

TABLE 3: **Results of Paired Evaluation of Radiographs**

	Technique Used (n = 28)		
	High kVp (%)	Low kVp (%)	No Difference (%)
Better ductal filling	19.1 ± 1.8 (68)	3.2 ± 0.5 (11)	5.9 ± 2.0 (21)
Better penetration	16.4 ± 1.8 (59)	6.7 ± 0.9 (24)	4.9 ± 2.0 (17)
Less motion unsharpness	18.0 ± 0.9 (65)	4.0 ± 0.8 (15)	5.3 ± 1.3 (20)
Better radiograph	21.4 ± 0.9 (77)	5.7 ± 0.9 (20)	0.9 ± 0.4 (3)
Better stone detection	17.3 ± 0.8 (62)	5.4 ± 0.9 (19)	5.4 ± 1.5 (19)

Note.—Results given as mean ± SEM for seven radiologists.

In every criterion the seven reviewers rated the high-kVp radiographs better, although the differences were not always statistically significant (table 2). Reviewer 4 rated each criterion almost a full point higher than the other six reviewers. This reviewer also rated the high-kVp studies superior in all five criteria (table 2).

The results were consistent for both the 13 operative and 15 T-tube studies (figs. 1 and 2). As expected, the 15 T-tube studies were rated higher in terms of film quality than the 13 operative cholangiograms by all seven reviewers (mean ± SEM; 2.76 ± 0.08 vs. 2.06 ± 0.08, respectively) ($p < 0.001$).

There was no statistically significant difference in the results between the different duct sizes. The stones in the eight normal-sized ducts (<10 mm) were better detected than in the six large ducts (>15 mm). Using the low-kVp technique, stone detectability was 2.74 in the normal ducts as compared to 2.24 in the large ducts. The opposite was true using the high-kVp technique; stone detectability for the large ducts was 3.4 vs. 3.0 in the normal ducts. The groups were too small for adequate statistical comparisons.

Method 2—Paired Film Evaluation

The results for the paired film evaluation are shown in table 3. The high-kVp studies had better ductal filling in 68% of the cases (figs. 1 and 2). In only 11% of cases was there better ductal filling on the low-kVp films. Of the high-kVp studies, 59% had better penetration, compared to 24% of the low-kVp studies (fig. 2). The high-kVp radiographs were selected as having less motion unsharpness four times as often as the low-kVp radiographs (65% vs. 15%) (figs. 1 and 2). The high-kVp radiograph was picked as a better film almost four times more often than the low-kVp radiograph (77% vs. 20%) (figs. 1 and 2). Stones were better detected on the high-kVp radiograph in 62% of the cases vs. 19% for the low-kVp film, and in 19% of the cases no difference was noted (figs. 1 and 2).

Discussion

The goal of most direct cholangiography is to produce maximum contrast difference between intraductal lesions (mainly stones) and the contrast-agent-filled duct. Most authors have recommended the use of a low-kVp technique (70–75 kVp) to produce the maximum difference in attenuation between the iodinated contrast agent and the surrounding tissues. A limitation of this low-kVp technique is that the contrast agent may produce so much attenuation of x-ray photons that intraductal stones are obscured. Besides differential attenuation, adequate ductal penetration is essential during direct cholangiography. In order to allow adequate bile duct penetration, many authors have recommended contrast agent dilution [3, 6, 7]. Our results provide clinical evidence to support the hypothesis that a technique of high kVp and high contrast-agent concentration is an attractive alternative to the recommended low-kVp exposure and diluted contrast-agent concentration.

There was very good agreement among the seven radiologists, even though reviewer 4 rated all categories higher than the other six. However, his evaluations were similar to those of the other reviewers in that he showed the high-kVp studies to be better than the low-kVp radiographs. The lack of variation is remarkable since the seven reviewers were not shown any standard radiographs before their blinded review. They rated the studies on the basis of their prior experience evaluating operative and T-tube cholangiograms.

The high-kVp technique films were always obtained after the low-kVp radiographs. This explains why all seven radiologists rated the ducts better filled on the high-kVp radiographs (tables 1–3, figs. 1 and 2). While there was a significant difference in ductal filling, this was mainly in filling of the left hepatic and small intrahepatic ducts. Equal filling of the major bile ducts was a prerequisite for inclusion in the evaluation.

The seven radiologists rated the amount of penetration produced by high kVp significantly better than that by low kVp (fig. 2, table 1). In the paired comparison, the seven radiologists selected the high-kVp radiograph as having superior penetration over twice as often as the low-kVp radiograph (59% vs. 24%). These results suggest that diluting the contrast agent and using low kVp is not as useful as using full-strength contrast agent and a high-kVp technique.

Since the high-kVp technique required significantly less time for each exposure than low kVp (~8 mAs vs. 48 mAs), it is not surprising that all but one of the radiologists rated the high-kVp studies significantly better in terms of less motion unsharpness (tables 1–3). This is a major benefit of the high-kVp technique.

Film quality in direct cholangiography is based on ductal filling, proper radiographic exposure (i.e., adequate penetration), and image clarity (minimal motion unsharpness). All three criteria were rated significantly better on the high-kVp radiographs. It follows that all seven radiologists rated film quality significantly higher on the high-kVp radiographs (tables 1–3).

In this study stone detectability was evaluated as a separate criterion after the radiologists had evaluated the other criteria and determined overall film quality. The group rated stone detection significantly better on the high-kVp radiographs (table 1), but only three individual radiologists' results showed statistical significance ($p < 0.05$) (table 2). Two others' results were almost significant ($p = 0.055$). Although the high-kVp radiographs were rated better in terms of quality by all seven radiologists, the group felt that there was no difference between the two types of radiographs in the ability to diagnose the stones in about 20% of cases (table 3).

Low kVp has distinct disadvantages for operative cholangiography compared to high kVp. Low kVp requires high mAs, leading to increased motion unsharpness because of the longer exposure time. Using a portable x-ray unit, radiographs exposed at 75 kVp require two to three times more exposure time than those made at 110 kVp.

The radiographs obtained using the low-kVp technique in this study were exposed at five to six times the mAs needed for the high-kVp radiograph. This amounts to twice the radiation dose to the patient using the low-kVp technique [18, 22]. Our prior results indicated that the dose to the surrounding operating room personnel is about 30% less with the high-kVp technique than with the low-kVp technique [18].

The high-kVp technique has four definite advantages over the low-kVp technique: (1) It provides greater exposure latitude ensuring a better radiograph; (2) there is shorter exposure time and thus less motion unsharpness; (3) there is a lower radiation dose to the patient and operating room personnel; and (4) large ducts are more likely to be well penetrated, increasing the chance of detecting stones within dilated ducts.

In summary, the high kVp and high contrast-agent concentration combination has definite advantages over the technique of low kVp and low contrast-agent concentration. On the basis of this study, we recommend using a high-kVp technique (100–110 kVp) with full-strength contrast medium (at least 30% iodine).

REFERENCES

1. Hall RC, Sakiyalak P, Kim SK, Rogers LS, Webb WR. Failure of operative cholangiography to prevent retained common duct stones. *Am J Surg* **1973**;125:51–63
2. Burhenne HJ. Problem areas in the biliary tract. *Curr Probl Radiol* **1975**;5:28–40
3. Ashmore JD, Kane JJ, Pettit HS, Mayo HW Jr. Experimental evaluation of operative cholangiography in relation to calculus size. *Surgery* **1956**;40:191–196
4. Whitaker PH, Parkinson EG, Hughes JH. Television fluoroscopy for operative cholangiography: an analysis of 150 cases. *Clin Radiol* **1968**;19:368–378
5. Grace RH, Peckar VG. The value of operative cholangiography using an image intensifier and a television monitor. *Br J Surg* **1968**;55:933–938
6. Nishizawa R. Experimental evaluation of contrast medium concentration for operative cholangiography. *Hirosaki Med J* **1968**;20:306–310
7. Hur KB, Park YO, Rice RG, Minks. Use of a dye-dilution technic to demonstrate biliary calculi in the operative cholangiogram. *Ann Surg* **1972**;176:663–668
8. Peresleny V, Cimmino C. The oblique view in operating-room cholangiography. *Radiology* **1972**;102:442–443
9. Shipps F, McKirdie M. Operative cholangiography using a 6:1 crisscrossed grid. *AJR* **1973**;119:46–51
10. Sachatello CR, Griffin WO. Operative cholangiography. *Arch Surg* **1974**;109:454–456
11. Rabinov K, MacArthur J. A simple effective technique for performing intraoperative cholangiography. *Arch Surg* **1976**;111:608
12. Marks CG, Kelvin FM. Operative cholangiography: criteria which make exploration of the common bile duct desirable. *Br J Surg* **1976**;63:51–54
13. Borge J. Operative cholangiography. *Arch Surg* **1977**;112:340–342
14. Berci G, Hamlin JA, Morgenstern L, Fisher DL. Modern operative fluorocholangiography: utopia or overlooked entity? *Gastrointest Radiol* **1978**;3:401–406
15. Foster ME, Foster DR. Operative cholangiography—techniques and inadequacies. *J R Soc Med* **1984**;77:645–647
16. Machi J, Sigel B, Spigos DG, Beitler JC, Justin JR. Critical factors in the image clarity of operative cholangiography. *J Surg Res* **1983**;35:480–489
17. Lundstrom B, Rydh A, Wickman G. Experimental evaluation of tube potential and contrast medium concentration for cholangiography. *Acta Radiol* [*Diagn*] (Stockh) **1976**;17:353–360
18. Thompson WM, Halvorsen RA, Gedgaudas RK, et al. High kVp vs. low kVp for T-tube and operative cholangiography. *Radiology* **1983**;146:635–642
19. Foster ME, Foster DR. Glucagon in operative cholangiography. *J R Coll Surg Edinb* **1984**;29:301–302
20. Snedecor GW, Cochran WG. *Statistical methods*, 6th ed. Ames: Iowa State University, **1967**
21. Helwig JT, Council KA. *SAS user's guide*, 1979 ed. Raleigh, NC: SAS Institute, **1979**
22. Linos DA, Gray JE, McIlrath DC. Radiation hazard to operating room personnel during operative cholangiography. *Arch Surg* **1980**;115:1431–1433

Books Received

Receipt of books is acknowledged as a courtesy to the sender. Books that appear of sufficient interest will be reviewed as space permits.

Radionuclide Imaging Techniques. Medical Physics Series. By Peter F. Sharp, Philip P. Dendy, and W. Ian Keyes. London: Academic, 271 pp., 1985. $63.50

Consultation in Diagnostic Imaging. Medical Consultation Series. By William W. Scott, Jr., and Penelope P. Scott. Philadelphia: Decker, 229 pp., 1985; soft cover

General Concepts for the Dosimetry of Internally Deposited Radionuclides. NCRP Report No. 84. Recommendations of the National Council on Radiation Protection and Measurements. Bethesda, MD: NCRP, 109 pp., 1985. $12; soft cover

The Computer in Radiology. Edited by Tim B. Hunter. Rockville, MD: Aspen, 355 pp., 1986. $39.95

Some Issues Important in Developing Basic Radiation Protection Recommendations. Proceedings of the Twentieth Annual Meeting of the National Council on Radiation Protection and Measurements. NCRP Proceedings No. 6. Bethesda, MD: NCRP, 325 pp., 1985. $19; soft cover

SI Units in Radiation Protection and Measurements. NCRP Report No. 82. Bethesda, MD: NCRP, 64 pp., 1985. $10; soft cover

The Experimental Basis for Absorbed-Dose Calculations in Medical Uses of Radionuclides. NCRP Report No. 83. Bethesda, MD: NCRP, 109 pp., 1985. $13; soft cover

Future Use of New Imaging Technologies in Developing Countries. World Health Organization Technical Report Series 723. Report of a WHO Scientific Group. Geneva: World Health Organization, 67 pp., 1985. Sw. fr. 7; soft cover. (Available U.S.: WHO Publications Centre, 49 Sheridan Ave., Albany, NY 12210)

The Fundamentals of X-Ray and Radium Physics, 7th ed. By Joseph Selman. Springfield, IL: Thomas, 632 pp., 1985. $29.75.

Nuclear Imaging in Pediatrics. By Aslam R. Siddiqui. Chicago: Year Book Medical, 306 pp., 1985.

Pocket Atlas of Normal Ultrasound Anatomy. By Matthew D. Rifkin and Larry Waldroup. New York: Raven, 70 pp., 1985. $12.50

Ultrasound Annual 1985. Edited by Roger C. Sanders and Michael C. Hill. New York: Raven, 371 pp., 1985. $69.50

***The Radiologic Clinics of North America.* Symposium on New Imaging Technology: Pitfalls and Controversies.** Edited by Robert K. Zeman. Philadelphia: Saunders, September 1985;23:379–586. By subscription, 4 issues annually, $52

Lymphatic Imaging: Lymphography, Computed Tomography and Scintigraphy, 2d ed. Golden's Diagnostic Radiology. Edited by Melvin E. Clouse and Sidney Wallace. Baltimore: Williams & Wilkins, 526 pp., 1985. $87.50

Radioisotope Studies in Cardiology. Series: Developments in Nuclear Medicine. Edited by H. J. Biersack and P. H. Cox. Dordrecht: Nijhoff, 404 pp., 1985. $59.50

Radiology of Liver Circulation. Series in Radiology. By Claude L'Herminé. Boston: Nijhoff, 174 pp., 1985. $60

Radiation Oncology. A Handbook for Residents and the Allied Health Professionals. By Stewart M. Jackson. St. Louis: Green, 249 pp., 1985.

Double Contrast Examination of the Colon. Principles and Practice. By A. Weissman, M. Clot, and J. Grellet. Berlin: Springer-Verlag, 165 pp., 1985. $39.50.

Functional Mapping of the Brain in Vascular Disorders. Edited by Wolf-Dieter Heiss. Berlin: Springer-Verlag, 126 pp., 1985. $19.50; soft cover

Lung Cancer. Diagnostic Procedures and Therapeutic Management with Special Reference to Radiotherapy. Edited by Charles W. Scarantino. Berlin: Springer-Verlag, 173 pp., 1985. $39.50

Atlas of Positron Emission Tomography of the Brain (in English and German). By W.-D. Heiss, C. Beil, K. Herholz, G. Pawlik, R. Wagner, and K. Wienhard. Berlin: Springer-Verlag, 130 pp., 1985. $52

Radiolabeled Cellular Blood Elements. Pathophysiology, Techniques, and Scintigraphic Applications. NATO Advanced Science Institute Series. Edited by M. L. Thakur, M.D. Ezikowitz, and M. R. Hardeman. New York: Plenum, 434 pp., 1985. $69.50

Magnetic Resonance Imaging of the Prostate

Patrick J. Bryan[1]
Harold E. Butler[1]
A. Dennis Nelson[1]
Joseph P. LiPuma[1]
Susan Y. Kopiwoda[1]
Martin I. Resnick[2]
Alan M. Cohen[1]
John R. Haaga[1]

The prostate was examined by magnetic resonance imaging (MRI) in 33 subjects, including five normal volunteers, 18 with prostatic carcinomas, seven with benign nodular hyperplasias, two cases of acute prostatitis, and one case of chronic prostatitis. Of 18 prostatic carcinomas, 16 produced an inhomogeneous signal intensity, with areas of diminished signal on T1-weighted scans and usually increased signal on T2-weighted images relative to the rest of the prostate. However, a similar appearance was also seen in five cases of benign nodular hyperplasia. It is doubtful at present whether MRI is able to reliably differentiate benign from malignant prostatic disease. Extraprostatic tumor extension and pelvic adenopathy was well shown, and MRI is very promising as a method for the preoperative staging of known prostatic carcinomas.

Carcinoma of the prostate is the second most common malignancy in the male population and also has the second highest death rate [1]. Diagnostic blood tests for prostatic carcinoma are imperfect, and the disease is commonly well advanced by the time it is first diagnosed. The traditional methods of diagnosing carcinoma of the prostate are mainly digital examination per rectum and estimation of serum acid phosphatase levels. The former remains the single most valuable diagnostic tool, as acid phosphatase activity can be normal as long as the tumor is still confined to the gland.

Sonographic examination, particularly transrectal high-resolution sonography, has been reported to have a high diagnostic yield in the detection of carcinoma. However, benign diseases such as benign prostatic hypertrophy and chronic prostatitis can give similar sonographic appearances. Transrectal sonography is capable of showing direct extracapsular spread, but does not show involvement of regional lymph nodes. Computed tomography (CT) is useful in demonstrating both extracapsular spread and nodal involvement. However, CT cannot detect tumor confined within the capsule, and it also fails to detect tumor within lymph nodes that are still of normal size.

Magnetic resonance imaging (MRI) has recently been shown to produce high-quality images of the pelvis [2–10], and we have been evaluating its role in imaging the prostate and in staging prostatic carcinoma.

Materials and Methods

Prostates in 33 subjects were examined. Of these, five were normal volunteers, 18 had prostatic carcinoma, seven had benign nodular hyperplasia, two had acute prostatitis, and one had chronic prostatitis. Twenty-three of the patients with abnormal prostates also had CT scans done on fourth-generation scanners (Technicare 2060). Of the 18 patients with carcinoma, two had stage B disease, six had stage C, and 10 had stage D disease. All patients had histologic confirmation of the diagnosis. Four patients had transurethral prostatectomies. Three additional patients underwent pelvic lymphadenectomy, with radical prostatectomy in two. The third was found to have metastatic adenopathy and prostatectomy was therefore not done. One patient underwent autopsy 3 weeks after the MRI scan. Patients

Received June 25, 1985; accepted after revision October 31, 1985.

[1] Department of Radiology, Case Western Reserve University, University Hospitals of Cleveland, 2074 Abington Rd., Cleveland, OH 44106. Address reprint requests to P. J. Bryan.

[2] Department of Urology, Case Western Reserve University, University Hospitals of Cleveland, Cleveland, OH 44106.

AJR 146:543–548, March 1986
0361–803X/86/1463–0543
© American Roentgen Ray Society

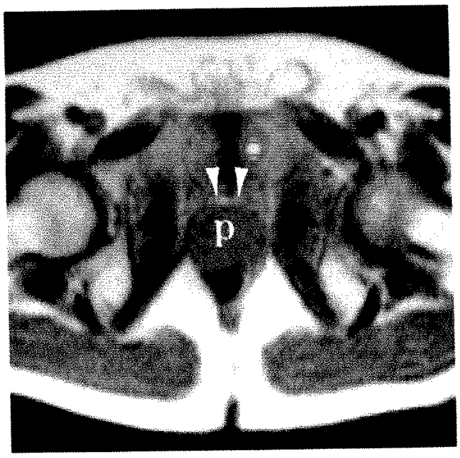

Fig. 1.—Transverse SE 500/30/2 scan through prostate (p). Fat in space of Retzius (*arrowheads*) is seen but not as well as on sagittal scans, as it usually lies in plane oblique to axial scan plane (cf. figs. 2 and 3).

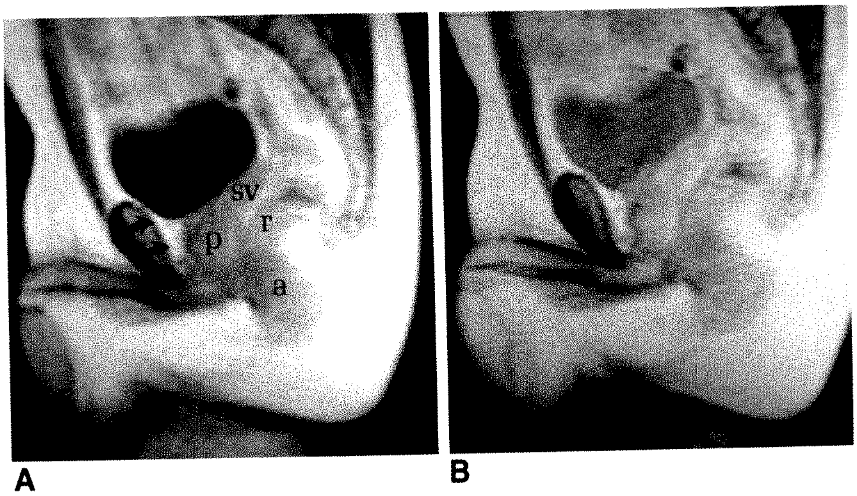

Fig. 2.—**A**, Sagittal SE 1000/30/1 scan. Almost no signal from urine in bladder. p = prostate; sv = seminal vesicles; r = rectum; a = anal sphincter. *Arrows* point to fat in space of Retzius. **B**, SE 2000/30/1 scan. Signal from prostate is closer to that of fat. There is now also signal from urine in bladder. Bladder neck is better defined on this pulse sequence than on shorter-TR scan.

did not have pelvic lymphadenectomy if they had obvious local spread or lymphadenopathy on CT (nine cases), were found to have bladder invasion at cystoscopy (six cases), had a fixed prostate on examination under anesthesia, had an elevated serum acid phosphatase, or were of advanced age or otherwise unsuitable for surgery.

The MRI scanner used a superconducting magnet operating at 0.3 T (Teslacon, Technicare). Pulse sequences used have been previously described [2]. Initial scanning was done using either 3D scanning or multiple planar spin-echo (SE) scans using the pulse sequence SE 500/30/2 (500 msec TR/30 msec TE/2 averages). Of the 33 patients, 31 had SE 500/30/2 scans, which are T1-weighted, and 29 had SE 1000/60/1 scans, which are T2-weighted. Eighteen patients had 3D volume acquisition scans using the pulse sequence SE 250/30/2. In addition, 11 patients had SE 1000/30/1 scans and four patients had SE 2000/60/1 scans. Inversion recovery (IR) scans, which are T1-weighted, were done on most patients, but were usually inferior to the short-TR/TE SE scans because of poor signal-to-noise ratio.

Calculated T1 values were done on three normal prostates and five patients with carcinoma. T1 values were calculated using a 2-point measurement technique based on two simultaneously acquired SE 500/30 and IR 1000/300/30 (TR/TI/TE) images.

The MRI studies were retrospectively read independently by two observers (P. J. B., H. E. B.) without knowledge of the final clinical staging. The MRI studies were evaluated with regard to (1) size of prostate; (2) signal of prostate on T1- and T2-weighted images, that is, whether homogeneous or inhomogeneous; (3) relative signal of prostatic nodules compared to the rest of the prostate; (4) evidence of invasion of periprostatic fat; (5) evidence of invasion of other pelvic organs; and (6) presence or absence of pelvic adenopathy. Interobserver differences occurred in three cases (two regarding spread and one homogeneity). These were resolved by consensus.

MRI scans were read independent of the CT studies in an attempt to eliminate bias, but completely blind reading was not always possible, as the CT scan had sometimes been previously seen by the readers. After evaluation of the MRI studies alone, MRI and CT were read together and compared as to their demonstration of presumed or known extracapsular disease.

Results

Normal Prostate

The prostate appeared homogeneous in four of the five normal volunteers. A central area of slightly diminished signal intensity was seen on short-TE/TR scans in the fifth normal prostate. This may correspond to the central zone of the prostate described in *Gray's Anatomy* [11]. The signal intensity of the prostate, relative to skeletal muscle, varies with the pulse sequence used. The relative signal intensity of the prostate is lowest on IR scans, being about equal to that of skeletal muscle. On SE scans with a TE of 30 msec, the relative signal intensity of the prostate compared to muscle increases as the TR is increased. On 60-msec-TE scans (T2-weighted scans) the relative intensity of the prostate compared to muscle is even greater than on 30-msec-TE scans, since the signal from prostate, which has a longer T2, decays more slowly than that from muscle.

The periprostatic fat is best seen laterally and posteriorly on transverse scans (fig. 1), whereas the anterior fat (in the space of Retzius) is best seen on sagittal scans (figs. 2 and 3). The space of Retzius is usually in an oblique plane and is not clearly seen on the transverse scans due to partial volume averaging. The levator ani muscle, which separates the true pelvis from the perineum, is best shown on coronal scans.

Benign Prostatic Hypertrophy

We examined seven patients with benign nodular hyperplasia. Five of these had prostatectomy for bladder carcinoma, and the other two were confirmed by biopsy. The MRI findings are summarized in table 1. Two of the seven patients with benign nodular hyperplasia had enlarged prostates with homogeneous signal intensities on all pulse sequences, indistin-

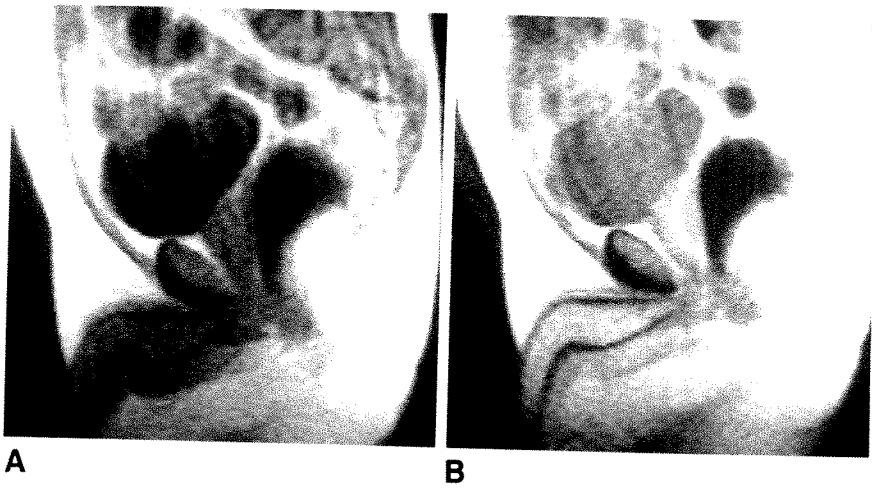

Fig. 3.—Benign nodular hyperplasia. **A**, SE 500/30/2 scan, relatively T1-weighted. Prostate appears homogeneous and is not very large, but elevates bladder slightly. Note oblique plane of space of Retzius. **B**, SE 1000/60/1 scan, T2-weighted. Prostate still appears homogeneous in signal intensity.

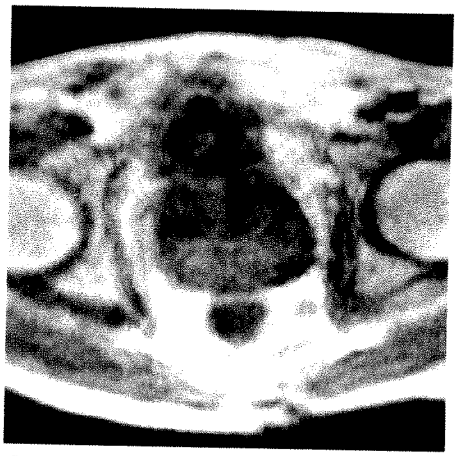

4

Fig. 4.—Benign nodular hyperplasia, 3D SE 250/30/2 scan. Prostate is enlarged, with nodules of diminished signal intensity relative to rest of gland.

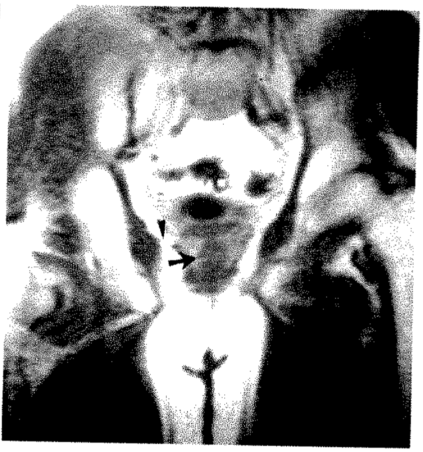

5

Fig. 5.—Prostatic carcinoma, coronal SE 500/30/2 scan. Nodule of diminished signal intensity (*arrow*) in prostate. Periprostatic fat appears clear, indicating no evidence of extracapsular spread. Levator ani muscle (*arrowhead*) is outlined by pelvic and perineal fat.

guishable from the signal of normal prostates (fig. 3). Five had inhomogeneous signal intensity in the prostate with nodules of diminished signal intensity on short TR/TE scans (T1-weighted) (fig. 4). Nodules varied in intensity on long TR/TE scans (T2-weighted) with some of diminished and some of increased signal relative to the rest of the prostate (table 2).

Prostatitis

The only case of chronic prostatitis that we examined also had a slightly inhomogeneous signal intensity, whereas both cases of acute prostatitis appeared homogeneous, with a signal intensity similar to that of normal prostates on both T1- and T2-weighted scans. All three cases of prostatitis were histologically confirmed after prostatectomy for bladder carcinoma.

Prostatic Carcinoma

Of the 18 patients, 16 with prostatic carcinoma had inhomogeneous signal intensities with nodules, some well defined and some poorly defined, of diminished signal intensity relative to the rest of the prostate on T1-weighted scans (figs. 5 and 6), and of mixed relative intensity, though predominantly increased, on T2-weighted scans (table 2). Two malignant prostates had homogeneous signal, indistinguishable from normal prostates.

Extension of tumor beyond the prostatic capsule into the periprostatic fat was seen as areas of diminished signal intensity that contrasted sharply with the strong signal of normal fat (figs. 7 and 8), best seen on the short TR/TE sequences. Lateral and posterior extension was best seen on transverse scans (fig. 7), whereas anterior extension into the space of Retzius was best seen in the sagittal plane (figs. 8 and 9). Internal iliac, obturator, external iliac, and common iliac adenopathy was seen in 10 cases (fig. 6). Enlarged nodes had a signal intensity greater than that of skeletal muscle on both short TR/TE and long TR/TE scans. Adenopathy was more easily identified on the former. Surgically proven pelvic adenopathy was missed in one patient, and in one case an enlarged 2-cm node seen on MRI was considered neoplastic, but was found on histology to be hyperplastic.

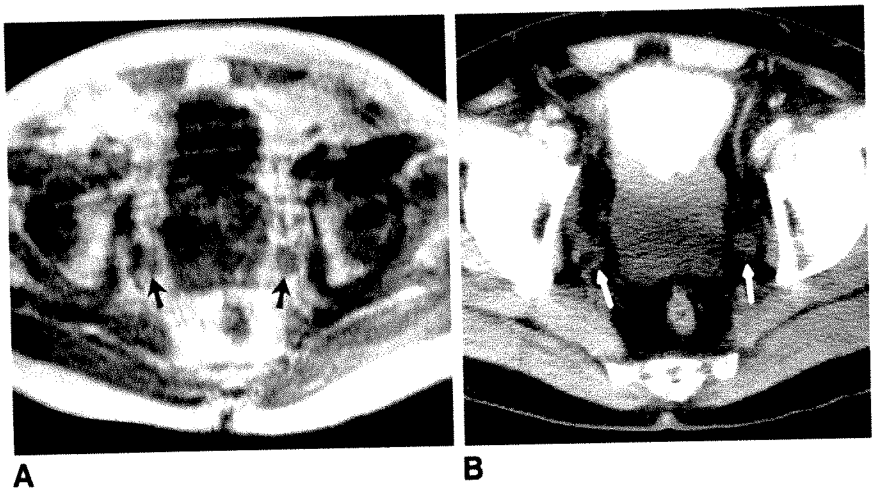

Fig. 6.—Prostatic carcinoma. A, 3D SE 500/30/2 scan. Prostate is enlarged and inhomogeneous, with several nodules of diminished signal intensity. This was one of series of anisotropic 3D scans and contains some semicircular motion artifacts. These artifacts were more frequently seen on 3D than on 2D. Invasion of bladder wall, which was proven at cystoscopy, is somewhat obscured by artifacts. Enlarged obturator nodes are present on both sides (*arrows*). **B**, CT scan at same level. Enlarged prostate is seen, but its inhomogeneous consistency cannot be appreciated. Enlarged obturator nodes (*arrows*) and bladder invasion are quite obvious.

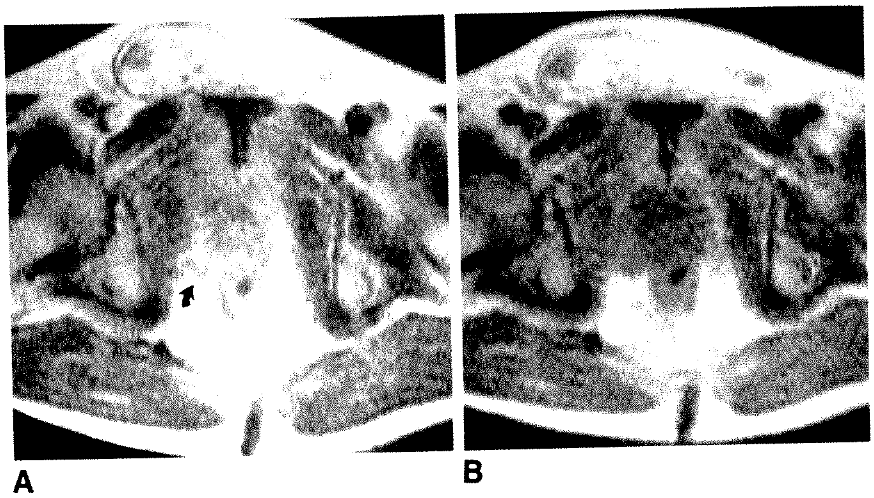

Fig. 7.—Prostatic carcinoma. **A**, SE 1000/60/1 scan. Prostate is inhomogeneous in signal intensity, and there is evidence of tumor extension beyond margin of gland (*arrow*). **B**, SE 500/30/2 scan. Inhomogeneity of prostate is less apparent, but extracapsular spread is seen to be much more extensive on this shorter-TR/TE scan (cf. **A**).

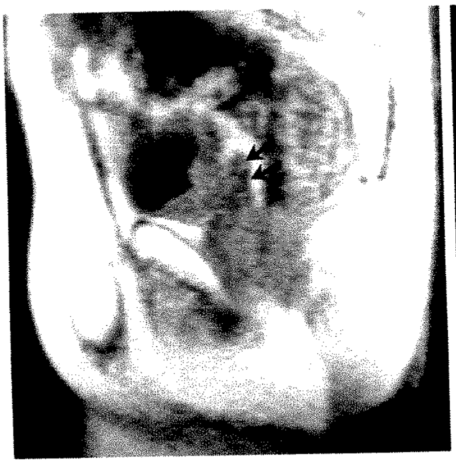

8

Fig. 8.—Prostatic carcinoma, sagittal SE 500/30/2 scan. Extension of carcinoma to involve floor, posterior wall, and posterior dome of bladder is particularly well shown on this view. Inferior part of space of Retzius is obliterated. There is also evidence of extension into seminal vesicle (*arrows*).

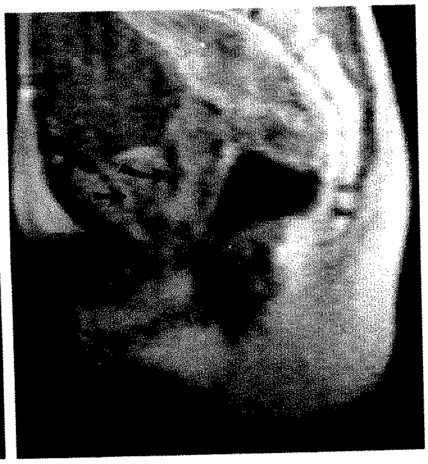

9

Fig. 9.—Sagittal SE 1000/60/1 scan. Dilated prostatic urethra after TURP (*curved arrow*). There is extension of tumor into space of Retzius anteriorly (*straight arrow*).

Invasion of the bladder wall was seen in five of six patients (figs. 6 and 8), all confirmed by cystoscopy and biopsy, but was missed in one. Bladder invasion was most readily identified on T1-weighted scans in two cases and on T2-weighted scans in three. Signal alteration in the seminal vesicles was seen in five patients (fig. 8), which was presumed to represent tumor invasion, but surgical confirmation was available in only one patient. Surgically, seminal vesicle involvement was

TABLE 1: **Summary of MRI Findings**

	Normal	Benign Prostatic Hypertrophy	Prostatitis		Carcinoma
			Acute	Chronic	
Number	5	7	2	1	18
Size	Normal, 5	Enlarged, 7	Normal, 2	Normal, 1	Enlarged, 18
Signal:					
Homogeneous	5	2	2	...	2
Inhomogeneous:					
T1-weighted	...	5	...	1	16
T2-weighted	...	5	...	1	16
Spread:					
Fat (presumed)					8
Bladder (confirmed)					5/6
Seminal vesicles (4 presumed, 1 confirmed)					5
Lymph nodes (presumed)					10

TABLE 2: **Signal Intensity of Nodules Relative to Rest of Prostate**

	T1-weighted	T2-weighted
Benign prostate hypertrophy:		
Increased	...	1
Decreased	5	1
Mixed	...	3
Carcinoma:		
Increased	...	8
Decreased	16	4
Mixed	...	4

missed in one patient in whom the seminal vesicles had not been included on the scans. Urine-filled defects in the prostate following transurethral resection were readily identified (fig. 9).

Various pulse sequences were evaluated in terms of their ability to demonstrate tumor nodules in the prostate. Nodularity was more obvious on the long TR/TE scans in 10 patients, on the short TR/TE scans in two, and they were judged to be equal in six patients. There was no correlation between tumor grade (Gleason scale) and degree of inhomogeneity or nodularity.

Although we did not have operative proof of pelvic fat invasion and of adenopathy in 14 of the 18 patients with carcinoma, it was presumed by invasion of fat planes or enlarged lymph nodes on imaging, in conjunction with clinical factors such as a fixed prostate on examination under anesthesia and increased acid phosphatase indicating extracapsular disease. Of the four patients who underwent surgery or autopsy, MRI staging was confirmed in two, one was found to have been overstaged (an enlarged node was found to be hyperplastic), and one was understaged (adenopathy and seminal vesicle invasion were missed by MRI and CT). On direct comparison of MRI and CT, they were considered to be equivalent in 13 patients, spread into pelvic fat was better seen on three with MRI, and adenopathy and bladder invasion were better shown by CT in one patient each.

Discussion

MRI is an exciting new method for the evaluation of pelvic diseases. Because of the relative lack of respiratory motion of pelvic organs, there is considerably less motion blurring in the pelvis than occurs in the upper abdomen during the prolonged scan times necessary in MRI. Advantages of MRI over CT included the ability to do multidimensional imaging, which was particularly useful in delineating the extent of disease, such as anterior spread into the space of Retzius or invasion of the base of the bladder, which are better shown on sagittal scans.

Because of the high inherent contrast of MRI due to variations in T1, T2, and proton density, it was hoped that tissue-specific diagnoses would be possible. Our early experience, however, suggests that benign and malignant prostatic diseases can have very similar appearances and that tissue-specific diagnoses are not possible at present, when disease is confined to the gland. Since we do not have histologic proof of the nature of all the nodules seen in malignant prostates, it is possible that some of them may represent benign nodular hyperplasia or prostatitis in conjunction with malignant nodules. Poon et al. [10] recently were also unable to differentiate benign from malignant disease. They used a lower field strength (0.15 T) than in our study, and were unable to detect nodularity or inhomogeneity of the prostate in either benign prostatic hypertrophy or carcinoma.

The T1 values that we measured in prostatic carcinoma were slightly prolonged compared to those of normal prostate, but there was considerable overlap between the two groups. Therefore, on the basis of this limited number of cases, we cannot differentiate with certainty malignant from normal prostates on the basis of T1 values alone.

Hricak et al. [4] have found longer TR (1–2 sec) and TE (56 msec) techniques to be more useful in providing tissue differentiation in the pelvis compared to the shorter TR/TE techniques. While we also found the long TE/TR technique to be superior in most cases in demonstrating prostatic inhomogeneity, extension into pelvic fat was better shown on short-TE scans because of increased contrast between tumor and fat (fig. 7).

While we have histologic proof of bladder invasion in all cases, we do not have histologic or operative proof of pelvic fat invasion or adenopathy in 14 of our 18 cases of prostatic carcinoma, as it was not considered justifiable to subject the patients to surgery or CT-guided biopsy when the diagnosis had been established by prostatic biopsy, extension and/or adenopathy was demonstrated cystoscopically or by CT, and the acid phosphatase was elevated. Persistent elevation of acid phosphatase alone is associated with metastatic disease in about 80% of patients and is considered a contraindication to surgery [12]. Because of the absence of surgical proof in so many patients, and the small number of tumors that were confined to the gland, the definitive role of MRI in staging prostatic carcinoma will have to await completion of larger series.

Should MRI prove in the future to be capable of distinguishing prostatic carcinomas from benign disease, it would be ideal for evaluating palpable prostatic nodules. However, because of its high cost, it is unlikely to be used as a screening procedure.

Until now, CT has been the single best staging method for prostatic carcinoma. However, one of its major weaknesses is the inability to detect tumor in regional lymph nodes that are within normal limits of size (about 1.5 cm in diameter). This inability to detect early tumor involvement of nodes accounts for about 20% understaging of pelvic neoplasms by CT [13, 14]. We have not as yet been able to demonstrate such early metastatic involvement of nodes by MRI, and we do not know whether it is possible to do so. In our present study, we found MRI comparable to CT in detecting presumed pelvic adenopathy, which is in agreement with the findings of Lee et al. [8]. MRI does have the advantage that it can differentiate the medium signal of lymph nodes from the signal void of blood vessels on short-TE scans without the use of contrast medium, and this was helpful in two of our cases. There was one enlarged (2 cm) node, which we thought was neoplastic but which proved on histology to be hyperplastic. We do not know whether it will be possible to make that differentiation in the future.

ACKNOWLEDGMENTS

We thank Mark Clampitt for technical assistance in performing the MRI scans, Joseph Molter for photography, and Pamela Edwards for preparation of the manuscript.

REFERENCES

1. Murphy GP, Slack NH, Karr JP. Natural history, staging, and grading of prostatic cancer. In: Javadpour N, ed. *Principles and management of urologic cancer*, 2d ed. Baltimore: Williams & Wilkins, **1983**
2. Bryan PJ, Butler HE, LiPuma JP, et al. NMR scanning of the pelvis: initial experience with a 0.3 T system. *AJR* **1983**; 141:1111–1118
3. Bryan PJ, Alfidi RJ. Clinical nuclear magnetic resonance imaging: central nervous system, spine, and body. In: Moss AA, ed. *NMR, interventional radiology, and diagnostic imaging modalities*. San Francisco: University of California, **1983**:381–400
4. Hricak H, Williams RD, Spring DB, et al. Anatomy and pathology of the male pelvis by magnetic resonance imaging. *AJR* **1983**;141:1101–1110
5. Hricak H, Alper C, Crooks LE, Sheldon PE. Magnetic resonance imaging of the female pelvis: initial experience. *AJR* **1983**;141:1119–1128
6. Alfidi RJ, Haaga JR, El Yousef SJ, et al. Preliminary experimental results in humans and animals with a superconducting whole body nuclear magnetic resonance scanner. *Radiology* **1982**;143:175–181
7. Buonocore E, Hesemann C, Pavlicek W, Montie JE. Clinical and in vitro magnetic resonance imaging of prostatic carcinoma. *AJR* **1984**;143:1267–1272
8. Lee JKT, Heiken JP, Ling D, et al. Magnetic resonance imaging of abdominal and pelvic lymphadenopathy. *Radiology* **1984**;153:181–188
9. Bryan PJ, Butler HE, LiPuma JP. Magnetic resonance imaging of the pelvis. *Radiol Clin North Am* **1984**;22:897–915
10. Poon PY, McCallum RW, Henkelman MM, et al. Magnetic resonance imaging of the prostate. *Radiology* **1985**;154:143–149
11. Warwick R, Williams PL, eds. *Gray's anatomy*. Philadelphia: Saunders, **1973**:1330–1351
12. Whitezel JA, Donohue RE, Mani JH, et al. Acid phosphatase: its influence on the management of carcinoma of the prostate. *J Urol* **1984**;131:70–72
13. Bryan PJ, Cohen WN, Seidelmann FE. The pelvis. In: Haaga JR, Alfidi RJ, eds. *Computed tomography of the whole body*. St. Louis: Mosby, **1983**:786–834
14. Lee JKT, Balfe DM. Pelvis. In: Lee JKT, Stanley S, Sagel S, eds. *Computed body tomography*. New York: Raven, **1983**:393–413

Renal Sonography in American Burkitt Lymphoma

Simon Strauss[1]
Eugene Libson[2]
Eli Schwartz[3]
Nili Peylan-Ramu[4]
Pinchas D. Lebensart[2]
Ronald A. Bloom[2]
Yacov Itzchak[1]

Renal involvement is a common finding at necropsy in patients with American Burkitt lymphoma, but its in vivo sonographic features have received little attention in the literature. Of 29 patients with American Burkitt lymphoma who underwent sonography, 10 were found to have renal involvement. The 10 patients demonstrated a range of abnormalities, notably renomegaly (nine patients), diffuse increase in cortical echogenicity (six), and focal renal masses (three). The focal infiltrations were, unexplicably, hypoechoic in two patients and hyperechoic in one. Hydronephrosis was seen in five patients. One patient had evidence of calcium phosphate renal stones. Response to therapy can be assessed by changes in renal size and cortical echogenicity, as well as disappearance of focal lesions.

American Burkitt lymphoma is a distinct clinical entity differing from the African variety by having a lower incidence of jaw tumors but a higher incidence of abdominal tumors, pleural effusions, and peripheral lymph node involvement [1, 2]. While renal infiltration is commonly found at necropsy in patients with Burkitt lymphoma, its antemortem radiographic demonstration was described in only two (5%) of 40 [1] and three (25%) of 12 [2] patients in two reported series.

There have been only scant reports in the literature on the sonographic features of renal involvement by American Burkitt lymphoma [1, 3–6]. We report the sonographic findings in 10 patients with renal parenchymal infiltration.

Materials and Methods

The sonographic files of 29 patients with biopsy-proven Burkitt lymphoma in the past 6 years in two hospitals were retrospectively reviewed. Ten patients, found to have sonographic evidence of renal infiltration, form the basis of this report. The patients were aged 3–20 years (mean, 9.5); seven were male and three female.

The kidneys were evaluated for length and cortical echogenicity and the presence of focal hypoechoic or hyperechoic masses. Kidney size was assessed by comparing the maximum renal length measured with the growth chart published by Rosenbaum et al. [7] for different age groups. Cortical echogenicity was considered increased if equal to or greater than that of the liver or spleen [8]. Evidence of hydronephrosis and intrarenal stone formation were also noted.

All examinations were performed with commercially available dynamic and static sonographic equipment, using 2.25- and 3.5-MHz focused transducers.

Results

Renal Length

Nine (90%) of 10 patients showed bilateral increase in renal size. In most of the patients, the renomegaly was striking, and in six there was also diffuse increase in the cortical echogenicity. In one patient, the kidneys were normal in size but contained multiple focal hypoechoic masses.

Received August 9, 1985; accepted after revision October 31, 1985.

[1] Division of Diagnostic Ultrasound, Chaim Sheba Medical Center, Sackler School of Medicine, Tel-Aviv University, Tel-Aviv, Israel 52621. Address reprint requests to S. Strauss.

[2] Department of Diagnostic Radiology, Hadassah University Hospital, Jerusalem, Israel 91120.

[3] Department of Internal Medicine "E", Chaim Sheba Medical Center, Sackler School of Medicine, Tel-Aviv University, Tel-Aviv, Israel 52621.

[4] Department of Radiotherapy and Medical Oncology, Hadassah University Hospital, Jerusalem, Israel 91120.

AJR 146:549–552, March 1986
0361–803X/86/1463–0549
© American Roentgen Ray Society

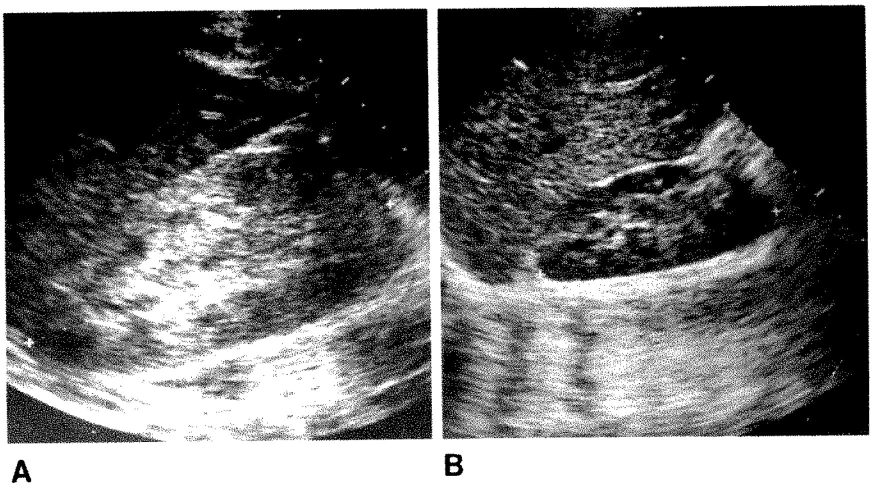

Fig. 1.—4-year-old girl. **A**, Longitudinal sonogram of right kidney before therapy. Renomegaly (kidney length, 12.4 cm) and increased cortical echogenicity. **B**, Longitudinal sonogram after therapy. Normal kidney length (7.8 cm) and normal cortical echogenicity.

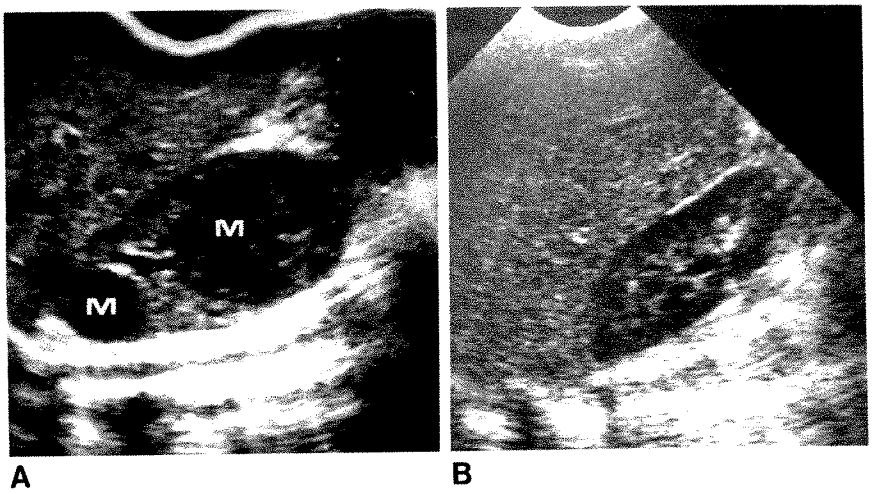

Fig. 2.—4-year-old boy. **A**, Longitudinal sonogram of right kidney before therapy. Two hypoechoic masses (M) in enlarged (9.8 cm length) kidney. **B**, Same kidney, after therapy. Normal appearance and normal length (7.4 cm).

Cortical Echogenicity

In six patients, the renal cortex was more echogenic than the adjacent liver or spleen and was considered abnormal. In three of these six patients, follow-up sonographic studies were available and showed a return to normal in the cortical echogenicity (fig. 1). In four patients, there was no evidence of diffuse increase in cortical echogenicity, although three of these four demonstrated focal infiltrations.

Focal Renal Masses

Focal infiltrations were seen in three patients; in two the masses were hypoechoic in relation to adjacent renal parenchyma, and in one there were multiple bilateral hyperechoic masses. The renal lesions were not well defined, and there was no evidence of encapsulation or of increased posterior sound transmission. Follow-up studies were obtained in two of three patients, showing disappearance of the focal masses within 4 months in one patient and within 2 months in the other (figs. 2 and 3).

Hydronephrosis

Five patients had sonographic evidence of hydronephrosis (unilateral in three patients and bilateral in two). One patient had resolution of hydronephrotic changes on the follow-up sonogram 1 month after institution of therapy, with concomitant disappearance of abdominal masses.

Renal Stones

In one patient, several echogenic foci with acoustic shadowing consistent with renal stones were demonstrated (fig. 4). These findings were noted on an examination following the institution of chemotherapy, and were associated with acute tumor lysis syndrome. At the time of examination there was marked hyperphosphatemia (11 mg/dl) and hypocalcemia (4.6 mg/dl), but serum uric acid was normal (6.8 mg/dl).

Discussion

Burkitt lymphoma is a type of non-Hodgkin lymphoma occurring in African and North American forms. The tumor is

Fig. 3.—5-year-old boy. Hyperechoic masses (M) in left (**A**) and right (**B**) kidneys. **C**, Sonogram of left kidney 4 months after onset of chemotherapy. Normal renal structure.

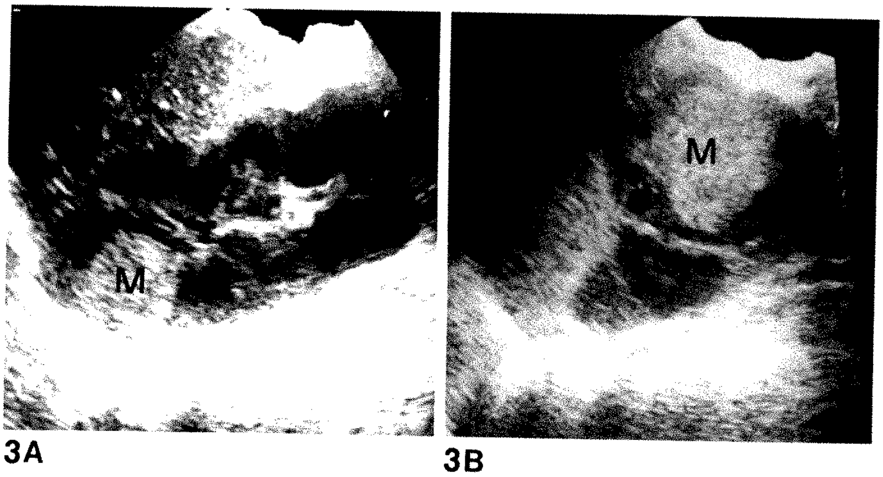

3A

3B

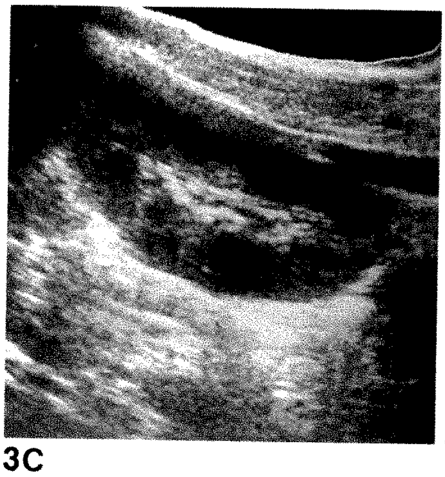

3C

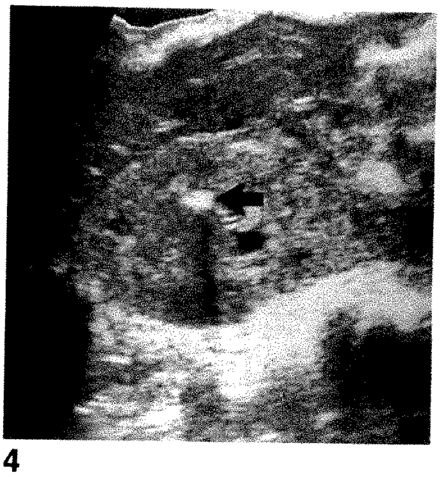

4

Fig. 4.—3-year-old boy. Transverse sonogram of right kidney shows renal stone (*arrow*). Cortical echogenicity is greater than that of adjacent liver.

a very aggressive neoplasm of B-cell origin, and is distinguished from other lymphomas by a "starry sky" appearance histologically [9]. Both North American and African types have a male preponderance, with a mean age of 11 years in the former and 7 or 8 years in the latter [10]. Abdominal masses are more frequent in the American form, while jaw lesions predominate in the African form. Pleural effusions and peripheral lymphadenopathy are more common in American as compared to African Burkitt lymphoma.

Lymphoma of the kidneys and ureters is rare in Hodgkin disease and only slightly more frequent in non-Hodgkin lymphoma [11]. Burkitt lymphoma, however, has a particular affinity for renal involvement. Of the 20 cases reported from the Armed Forces Institute of Pathology, eight of nine that went to autopsy had renal involvement [12]. In a series of 17 autopsy cases from the National Institutes of Health, 16 patients had renal involvement [13]. Despite the high incidence at autopsy of renal infiltration by Burkitt lymphoma, there have been only scant reports in the literature describing the sonographic features of the condition. In most of these reports, the renal involvement has been focal, appearing as discrete hypoechoic or anechoic masses [1, 3, 4, 6]. In one reported case, sonography demonstrated renomegaly with diffusely increased cortical echogenicity [5]. The demonstration of hyperechoic focal masses, as seen in one of our cases, appears to be unique. Furthermore, diffusely increased cortical echogenicity, while reported only once previously [5], was a prominent feature in most of our cases.

Hydronephrosis, as a result of abdominal or pelvic Burkitt lymphoma, has been reported in two of seven patients [14] and in six of 11 patients [3] who underwent excretory urography. In our series, five of 10 patients had sonographic evidence of hydronephrosis.

The differential diagnosis of a focal renal mass is usually not a problem in patients with Burkitt lymphoma because other systemic abnormalities of lymphoma, in particular abdominal and pelvic masses, are usually present. In one patient in this series, however, bilateral enlarged and echogenic kidneys were the sole manifestations of lymphoma seen in sonography of the abdomen. This patient, a 20-year-old woman, had Burkitt leukemia with central nervous system involvement but no abdominal or pelvic masses demonstrated. Although leukemia with Burkitt cells may occur as a terminal manifestation of Burkitt lymphoma, a true leukemic presentation, as in this case, has been reported in isolated cases [15].

In children, conditions with renomegaly and increased cortical echogenicity that should be considered in the differential diagnosis include acute leukemia, acute tubular necrosis, renal vein thrombosis, acute and chronic glomerulonephritis, amyloidosis, myoglobinuric renal failure, congenital nephrosis, primary hyperoxaluria, and hemolytic uremic syndrome [16].

Clinically, Burkitt lymphoma is the most dramatic and rapidly progressive of the lymphomas. It has a cell doubling time as short as 24 hr, and although the initial tumor response to therapy may be very dramatic, the ultimate overall survival rate is quite low [11]. Acute renal failure associated with the acute tumor lysis syndrome in patients treated for lymphoproliferative disorders usually is a consequence of acute uric acid nephropathy. Less frequently hyperphosphatemia has been implicated as a possible cause [17]. Hyperphosphatemia is a result of massive cytolysis after chemotherapy, and is associated with hypocalcemia and precipitation of calcium phosphate salts [18]. In our patient, it seems logical to assume that the renal stones seen on sonography were calcium phosphate deposits and not uric acid stones, since the laboratory findings at the time of sonography included hyperphosphatemia and hypocalcemia, but normal serum uric acid. In the series of Burkitt lymphoma reported by Shawker et al. [3], the sonographic examinations in three patients with hyperuricemia were normal. The kidneys of the patient with stones in our series showed signs of diffuse lymphomatous infiltration as evidenced by increased size and cortical echogenicity.

Our series demonstrates a spectrum of renal sonographic findings in patients with American Burkitt lymphoma. In some patients, diffuse cortical echogenicity and renomegaly were the prominent features; in others, the disease appeared to be focal. We have no explanation for the fact that the focal lesions were hypoechoic in two patients and hyperechoic in one. Response to therapy was rapid in both types of focal infiltration.

Sonography is most useful for establishing the extent of abdominal involvement in patients with Burkitt lymphoma, and can be a sensitive indicator of renal infiltration. Patients undergoing therapy should be followed by sonography so that shifts in cortical echogenicity and changes in renal size and structure can be documented.

REFERENCES

1. Dunnick NR, Reaman GH, Head GL, Shawker TH, Ziegler JL. Radiographic manifestations of Burkitt's lymphoma in American patients. *AJR* **1979**;132:1–6
2. Alford BA, Coccia PF, L'Heureux PR. Roentgenographic features of American Burkitt's lymphoma. *Radiology* **1977**;124:763–770
3. Shawker TH, Dunnick NR, Head GL, Magrath IT. Ultrasound evaluation of American Burkitt's lymphoma. *JCU* **1979**;7:279–283
4. Andre C, Garel L, Sauvegrain J. Ultrasound of kidney lymphoma in children: a report of nine cases. *Ann Radiol* **1982**;25:385–394
5. Charboneau JW, James EM, Reading CC. Sonography case of the day. *AJR* **1984**;142:1077–1078
6. Shirkhoda A, Staab EV, Mittelstaedt CA. Renal lymphoma imaged by ultrasound and gallium-67. *Radiology* **1980**;137:175–180
7. Rosenbaum DM, Korngold E, Teele RL. Sonographic assessment of renal length in normal children. *AJR* **1984**;142:467–469
8. Hricak H, Cruz C, Romanski R, et al. Renal parenchymal disease: sonographic-histologic correlation. *Radiology* **1982**;144:141–147
9. Berard C, O'Conor GT, Thomas LB, Torloni H. Histopathological definition of Burkitt's tumor. *Bull WHO* **1969**;40:601–607
10. Mandell GA, Swacus JR, Rosenstock J, Buck BE. Danger of urography in hyperuricemic children with Burkitt's lymphoma. *J Can Assoc Radiol* **1983**;34:273–277
11. Kushner DC, Weinstein HJ, Kirkpatrick JA. The radiologic diagnosis of leukemia and lymphoma in children. *Semin Roentgenol* **1980**;15:316–334
12. O'Conor GT, Rappaport H, Smith EB. Childhood lymphoma resembling "Burkitt tumor" in the United States. *Cancer* **1965**;18:411–417
13. Banks PM, Arseneau JC, Gralnick HR, Canellos GP, De Vita VT, Berard CW. American Burkitt's lymphoma: a clinicopathologic study of 30 cases. *Am J Med* **1975**;58:322–329
14. Herlitzka AJ, Badruddoja M, Dube VE. Clinical and pathologic features of Burkitt's lymphoma. *Surg Gynecol Obstet* **1973**;136:81–86
15. Minerbrook M, Schulman P, Budman DR, et al. Burkitt's leukemia: a re-evaluation. *Cancer* **1982**;49:1444–1448
16. Graif M, Shohet I, Strauss S, Yahav J, Itzchak Y. Hemolytic uremic syndrome: sonographic–clinical correlation. *J Ultrasound Med* **1984**;3:563–564
17. Monballyu J, Zachee P, Verberckmoes R, Boogaerts MA. Transient acute renal failure due to tumor-lysis-induced severe phosphate load in a patient with Burkitt's lymphoma. *Clin Nephrol* **1984**;22:47–50
18. Cohen LF, Balow JE, Magrath IT, Poplack DG, Ziegler JL. Acute tumor lysis syndrome: a review of 37 patients with Burkitt's lymphoma. *Am J Med* **1980**;68:486–491

Gastric Diverticulum Simulating an Adrenal Mass: CT Appearance and Embryogenesis

Alan N. Schwartz,[1] Robert C. Goiney,[1] and Daniel O. Graney[2]

Diverticula that arise from the gastric cardia are uncommon, with a prevalence of 0.1%–2.6% in autopsy series [1]. These diverticula have a characteristic appearance on upper gastrointestinal (GI) barium studies [2]. We report a patient with a diverticulum of the gastric cardia that simulated a cystic adrenal mass on CT scan. An embryologic mechanism is presented explaining the unusual occurrence of bowel herniating into the retroperitoneum adjacent to Gerota's fascia.

Case Report

A 63-year-old man underwent an abdominal CT scan for preoperative evaluation of an abdominal aortic aneurysm. Transverse scans were obtained on a GE 8800 scanner in 10-mm sections spaced 20 mm from diaphragm to pelvic inlet. Oral and bolus intravenous contrast media were administered in standard fashion.

An incidental 3 × 3 cm, thin-walled cystic mass with an air-fluid level was identified adjacent to the left adrenal gland (fig. 1A). The cystic mass appeared to be located within Gerota's fascia, insinuating itself between the left adrenal gland and the upper pole of the left kidney. A repeat scan in 10-mm sections with additional oral contrast material demonstrated a barium-fluid-air level within the mass, indicating communication with the GI tract. The site of communication between the cystic mass and the posterior gastric wall was identified on the more cephalad images. An upper GI series confirmed the presence of a diverticulum of the gastric cardia (fig. 1B).

Discussion

Diverticula that arise from the posterior gastric cardia have been described as having a characteristic upper GI appearance. It is unknown whether such diverticula are acquired or congenital. Gastric diverticula have been noted in the embryo [3], suggesting a developmental origin in at least some cases. Both true and false diverticula have been described [3–5].

A review of embryogenesis suggests how a gastric diverticulum can be located within the retroperitoneal space, adjacent to Gerota's fascia, and simulate an adrenal mass on CT. Between the 20th and 50th day of gestation, the stomach is transformed from a fusiform swelling of the foregut into its adult form. At this time, there is a 90° rotation of the stomach, which carries with it the duodenal loop, the pancreas, and the mobile dorsal mesentery. The posterior body wall and dorsal

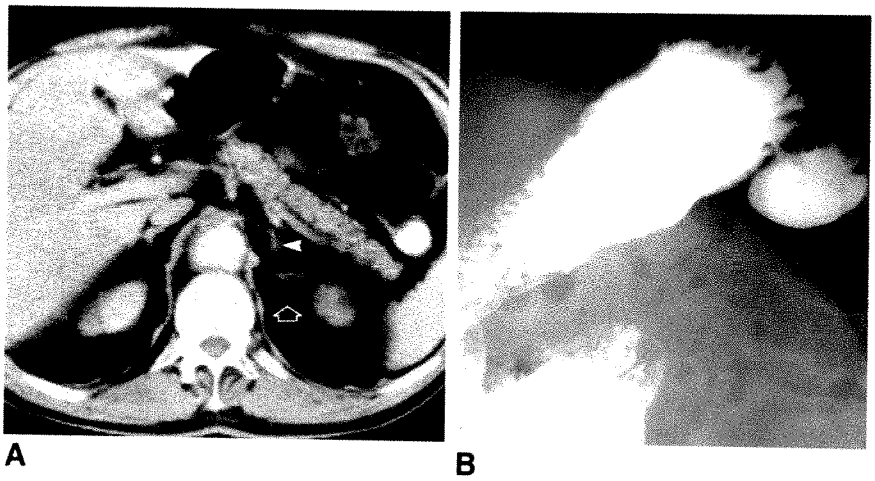

Fig. 1.—**A**, Transverse CT scan of abdomen after oral administration and during intravenous infusion of contrast material. Thin-walled 3 × 3 cm mass (*arrow*) with air-fluid level adjacent to left adrenal gland (*arrowhead*) protrudes within Gerota's fascia, is posterior to pancreas, and is anteromedial to left superior renal pole. **B**, Lateral abdominal film from upper gastrointestinal series. Diverticulum projects posterior from gastric cardiac with appearance typical for gastric diverticulum.

Received August 20, 1985; accepted after revision November 26, 1985.

[1] Department of Radiology, Seattle Veterans Administration Medical Center, Seattle, WA 98108. Address reprint requests to A. N. Schwartz.
[2] Department of Biological Structure, University of Washington School of Medicine, Seattle, WA 98195.

AJR 146:553–554, March 1986 0361–803X/86/1463–0553 © American Roentgen Ray Society

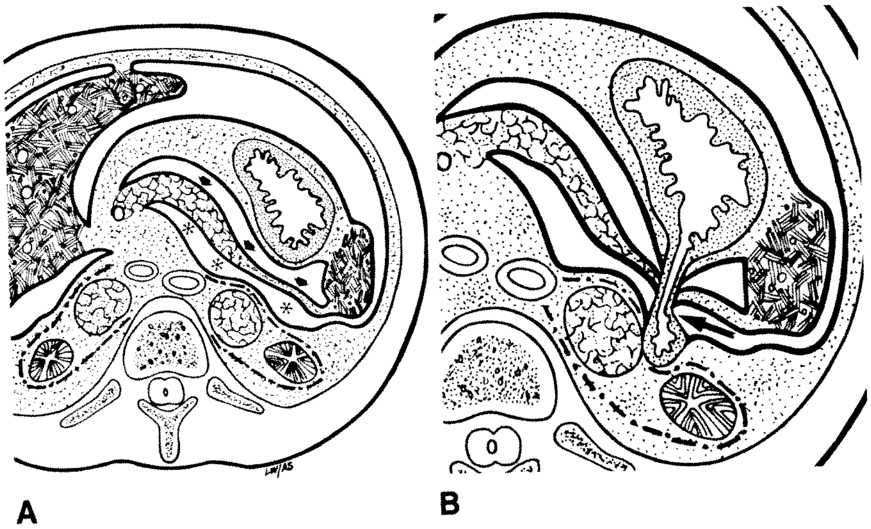

Fig. 2.—**A**, Transverse representation of embryonic abdomen at level of adrenal (day 49). Pancreas and dorsal mesentery (*arrows*) have not yet fused to posterior body wall. Potential retroperitoneal space (*asterisks*) exists at this time. Embryonic adrenals are large and rounded. **B**, Transverse representation demonstrates proposed herniation of diverticulum within potential retroperitoneal space. Diverticulum (*arrow*) projects within Gerota's fascia between kidney and large embryonic adrenal. With fusion of dorsal mesentery and posterior body wall, diverticulum becomes trapped within retroperitoneum.

mesentery then fuse (fig. 2A), encapsulating the pancreas within the retroperitoneum and establishing its adult form [6].

A diverticulum of the posterior wall of the gastric cardia hypothetically could herniate through an area of dorsal mesentery before its fusion with the left posterior body wall. Initially, the diverticulum would lie superior to the pancreas. With further extension, the diverticulum could project posterior to the pancreas. The inferior aspect of the diverticulum would then lie adjacent to Gerota's fascia and the left adrenal gland (fig. 2B).

If migration of the diverticulum occurs before renal ascent, the diverticulum could indent Gerota's fascia and interdigitate itself between the left kidney and the left adrenal gland, as noted in our case. A diverticulum forming after fusion of the dorsal mesentery might be expected to lie within the lesser sac.

The differential diagnosis of a thin-walled cystic mass with an air-fluid level in the region of the left adrenal is limited. Adrenal, pancreatic, and renal cysts, as well as duplication cysts and diverticula of bowel, are possibilities. Gas present in the cystic mass suggests infection, necrotic tumor, or communication with the gastrointestinal tract. Abscess and necrotic neoplasm more commonly have a thick, shaggy wall. A thin-walled cystic retroperitoneal mass may occur with pancreatitis or gastric ulcer disease. In the absence of these disease entities, however, the CT diagnosis of a gastric diverticulum is most plausible. The CT appearance of a gastric cardia diverticulum within the retroperitoneum should be included in the differential diagnosis of a thin-walled cystic mass lesion in the region of the left adrenal gland.

REFERENCES

1. Meeroff M, Gollan JRM, Meeroff JC. Gastric diverticulum. *Am J Gastroenterol* **1967**;47:189–203
2. Akerlund A. Diverticula of the stomach from a roentgenological point of view. *Acta Radiol* (Stockh) **1923**;2:476–485
3. Martin L. Diverticula of the stomach. *Ann Intern Med* **1936**;10:447–465
4. Bell J, Golden R. Diverticula of the stomach. *JAMA* **1930**;94:534–539
5. Palmer ED. Collective review of gastric diverticula. *Int Abstr Surg* **1951**;92:417–428
6. Love L, Meyers MA, Churchill RJ, Reynes CJ, Monceda R, Gibson D. Computed tomography of extraperitoneal spaces. *AJR* **1981**;136:781–789

Pitfalls of Rotator Cuff Sonography

William D. Middleton[1, 2]
William R. Reinus[1]
G. Leland Melson[1]
William G. Totty[1]
William A. Murphy[1]

Experience with rotator cuff sonography in 106 patients was analyzed to identify the causes of scan misinterpretation. Possible interpretive errors may be classified into four categories: those from failure to recognize normal anatomy, those caused by soft-tissue abnormalities, those caused by bony abnormalities, and those caused by technical limitations of the study. Errors in recognition of normal anatomy are easily overcome by experience and comparison to the normal, contralateral rotator cuff. Errors resulting from soft-tissue abnormalities were seen in two patients with calcific tendinitis simulating rotator cuff tears. Problems in interpretation resulting from fractures in two patients and inferior glenohumeral subluxation in two other patients could have been avoided by review of the plain films before performing sonography. The major technical limitation of the study arises from the inability to image the rotator cuff beneath the acromion. Fortunately, rotator cuff tears are rarely isolated in this location, and passive maneuvers often allow otherwise hidden parts of the cuff to be imaged.

Until recently, shoulder joint arthrography was the only reliable radiologic means of detecting rotator cuff tears. Currently, investigators at several institutions are reporting sonographic examination of the shoulder to be a rapid, noninvasive means of diagnosing rotator cuff tears with an accuracy comparable to that of arthrography [1–4]. Increased application of shoulder sonography can be anticipated. While the technique is relatively simple and the anatomy straightforward, several potential sources of interpretive error exist. We believe that a description of these potential pitfalls and the steps necessary to avoid them will improve the accuracy of the technique as it proliferates in the radiologic community.

Subjects and Methods

Between April 1983 and December 1984, bilateral shoulder sonograms were performed on 106 consecutive patients referred for shoulder arthrography. Verbal informed consent was obtained in all cases. The indication for arthrography in the vast majority of patients was to rule out rotator cuff tear. All shoulder sonograms were performed by a radiologist immediately before arthrography. A 10-MHz, real-time mechanical sector scanner (Diasonics Wide View) was used in most cases. When this transducer was not available a 7.5-MHz transducer was used. During the latter part of our study, a 5-MHz electronic phased-linear-array transducer (Acuson) was used.

A familiarity with the normal sonographic anatomy of the shoulder was initially gained by the first author through careful scanning of asymptomatic volunteers. A series of 39 patients was then scanned to determine the feasibility of using sonography as a noninvasive means of detecting rotator cuff tear [1]. The remaining 67 patients were scanned subsequently and during this part of the study, the technique was learned by the other authors as well as several residents and staff in the radiology department. Various errors in interpretation were made throughout the study, and these account for part of the pitfalls that are described. The other pitfalls represent potential errors that were encountered as less experienced examiners learned the technique from more experienced examiners during the second part of the study.

Patients were scanned while seated with the humerus held in a neutral position and the

Received July 15, 1985; accepted after revision November 18, 1985.

[1] Mallinckrodt Institute of Radiology, Washington University School of Medicine, 510 S. Kingshighway Blvd., St. Louis, MO 63110. Address reprint requests to W. R. Reinus.

[2] Present address: Department of Radiology, Milwaukee County Medical Complex, 8700 W. Wisconsin Ave., Milwaukee, WI 53226.

AJR 146:555–560, March 1986
0361–803X/86/1463–0555
© American Roentgen Ray Society

shoulder adducted. In many instances, the patient was instructed to shrug the shoulder so that parts of the rotator cuff otherwise hidden by the acromion might be examined. Each sonogram was interpreted prospectively without knowledge of the results of arthrography. In all cases the arthrogram was used as the "gold standard" except for those patients in whom surgical correlation was available.

Each sonogram was judged as positive, negative, or indeterminate for rotator cuff tear on the basis of previously described criteria [1, 4]. These include (1) focal thinning of the rotator cuff, (2) nonvisualization of the cuff, (3) discontinuity of the normal homogeneous echogenicity of the cuff, and (4) replacement of the cuff by a central echogenic band. Using these criteria, 37 scans were interpreted as positive and 63 were interpreted as negative for rotator cuff tears. Six scans were indeterminate. Focal areas of increased echogenicity, an additional criterion described by other authors [2], was not encountered in our patients.

All arthrograms were performed using standard double-contrast technique [1, 4] and were evaluated for the presence or absence of rotator cuff tears and other soft-tissue abnormalities. In all patients, conventional radiographs were reviewed for evidence of calcific tendinitis, fractures, or arthritic changes.

The three examinations (conventional shoulder radiographs, double-contrast arthrograms, and sonograms) were reviewed and compared in all cases (106) in an effort to document sources of error in sonographic interpretation.

Results

Errors of sonographic interpretation could be classified into one of four categories: normal anatomy mimicking an abnormality, soft-tissue abnormalities confusing the echo pattern, bony abnormalities distorting normal landmarks, and inherent limitations of the technique.

Misinterpretation of Normal Anatomy

The normal sonographic anatomy of the rotator cuff and biceps tendon has been carefully described [2, 5, 6]. The rotator cuff appears as a band of tissue between the deltoid muscle and the humeral head. In most patients, the echogenicity of the rotator cuff is greater than that of the deltoid muscle. Occasionally, however, the echogenicity of the rotator cuff is equal to or less than that of the deltoid muscle. As seen in table 1, this occurs most often in older patients, but is still relatively uncommon. This decreased echogenicity should not be and was not interpreted as evidence for a rotator cuff tear. It was, however, confused with nonvisualization of the cuff by those less experienced with the technique.

As the technique was being mastered, the anterior aspect of the rotator cuff, which contains the intraarticular part of the biceps tendon, was a consistent source of confusion. Two potential pitfalls exist from a lack of familiarity with the normal anatomy of this region. First, on transverse views of the anterior cuff, the intraarticular biceps tendon itself appears as an echogenic focus opposed to the humeral head located between the supraspinatus and subscapularis part of the rotator cuff (fig. 1). Failure to recognize this echogenic focus as the biceps tendon could result in diagnostic error, because rotator cuff tears have been reported to have a similar appearance in other series [2]. In addition, a focal area of decreased echogenicity is often observed immediately posterior to the intraarticular biceps tendon (fig. 2). This appearance most likely results from a void of tissue between the biceps tendon and the anterior aspect of the supraspinatus. It may be confused with areas of rotator cuff discontinuity secondary to rotator cuff tears. Careful scanning of normal volunteers before patient scanning and use of the contralateral shoulder for comparison helped to avoid diagnostic errors secondary to these two potential pitfalls.

TABLE 1: **Rotator Cuff Echogenicity**

Age (years)	Greater Than Deltoid	Less Than or Equal to Deltoid
10–20	7	0
20–30	18	2
30–40	14	1
40–50	10	4
50–60	16	5
60+	21	8

The thickness of the anterior and posterior parts of the normal rotator cuff are different. Bretzke et al. [2] measured the thickness of the normal rotator cuff and found thinning posteriorly. In their study, the anterior cuff averaged 6 mm in thickness, while the posterior cuff averaged 3.6 mm. Our experience is similar. Although this normal posterior thinning was not interpreted as focal thinning secondary to a rotator cuff tear in our patient population, it did represent a frequent site of suspected pathologic thinning to inexperienced examiners (fig. 3).

In some patients with normal arthrograms, the sonogram shows mild inhomogeneities in the rotator cuff. The inhomogeneities most often appear as focal areas of decreased echogenicity, lacking abrupt transition from the rest of the rotator cuff, which are relatively symmetric with the rotator cuff on the opposite side (figs. 4A and 4B). In five patients, these inhomogeneities resulted in false-positive diagnoses of rotator cuff tears. Four of these cases occurred early in the study and are most likely related to inexperience with the technique at that time. Three patients' sonograms demonstrated a marked decrease in echogenicity of the central part of the rotator cuff (fig. 4C). Diagnostic error was avoided in these cases by noting symmetry with the opposite side.

Errors Caused by Soft-Tissue Abnormalities

Sonograms were performed in two patients with calcific tendinitis of the rotator cuff detected on conventional radiographs. In one patient, a small calcification, limited to the supraspinatus tendon, appeared as an echogenic focus within the substance of the rotator cuff and it did not produce acoustic shadowing (fig. 5). Its appearance was indistinguishable from that of focal areas of increased echogenicity secondary to rotator cuff tears [2]. A false-positive interpretation was avoided by careful inspection of plain films before the examination. In the other patient, the calcification was more extensive and caused multiple nonshadowing echogenic foci that distorted the anatomic appearance of the rotator cuff.

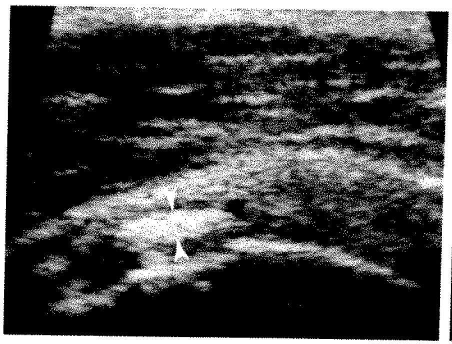

1

Fig. 1.—Normal intraarticular biceps tendon. Transverse scan demonstrates intraarticular biceps tendon in cross section as echogenic focus (*arrowheads*), which should be distinguished from echogenic foci secondary to rotator cuff tears.

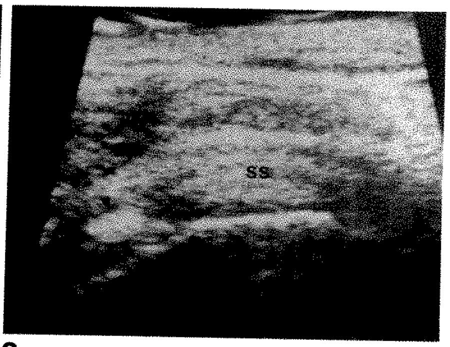

2

Fig. 2.—Normal discontinuity posterior to biceps tendon. Transverse scan shows normal area of decreased echogenicity between biceps tendon (*arrowheads*) and supraspinatus (SS) in normal volunteer. This should not be confused with discontinuity in rotator cuff (as in fig. 7C).

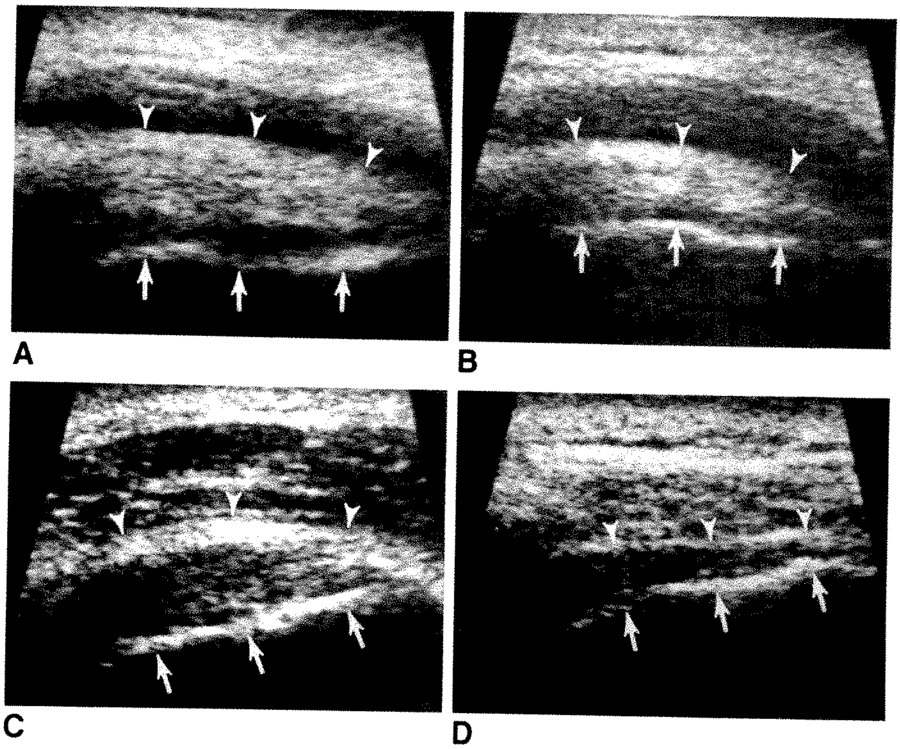

Fig. 3.—Normal posterior thinning. **A**, Longitudinal scan of normal anterior rotator cuff seen between deep surface of deltoid muscle (*arrowheads*) and humeral head (*arrows*). **B**, Longitudinal scan of normal posterior rotator cuff, which is thinned compared to anterior cuff. Deep surface of deltoid muscle (*arrowheads*); humeral head (*arrows*). **C**, Longitudinal scan through normal-appearing anterior part of rotator cuff in patient with rotator cuff tear. Deep surface of deltoid muscle (*arrowheads*); humeral head (*arrows*). **D**, Longitudinal scan of same patient as in **C** through pathologically thinned part of rotator cuff. No normal rotator cuff tissue is seen between deep surface of deltoid muscle (*arrowheads*) and humeral head (*arrows*).

Failure to review the plain films before this examination resulted in an indeterminate examination in this patient; the rotator cuff was intact on arthrography.

Errors Caused by Bony Abnormalities

In four patients, failure to review plain films of the shoulder before the sonographic examination compromised interpretation of their sonograms. In two patients, fractures distorted the anatomy to such an extent that the scans were classified as indeterminate. Inferior glenohumeral subluxation resulted in a false appearance of rotator cuff thickening in two other patients (fig. 6). The cause of this appearance was not appreciated in the first patient, and the scan was interpreted as indeterminate. In the second, the pitfall was recognized.

Errors Due to Technical Limitations

The inability to image the part of the rotator cuff that lies deep to the shadow-inducing acromion process is the major technical limitation of sonography. This limitation resulted in one false-negative interpretation (fig. 7). On a repeat sonogram after the arthrographic diagnosis, with the arm repositioned in extension, the tear was clearly visible as an area of sonographic discontinuity in the rotator cuff. In another patient with marked degenerative changes in the glenohumeral joint, complete shoulder adduction was not possible and the rotator cuff was not visualized. The examination was interpreted as a large rotator cuff tear, when, in fact, the tear was small. In this patient, the normal part of the rotator cuff was hidden from sonographic view by acromial shadowing.

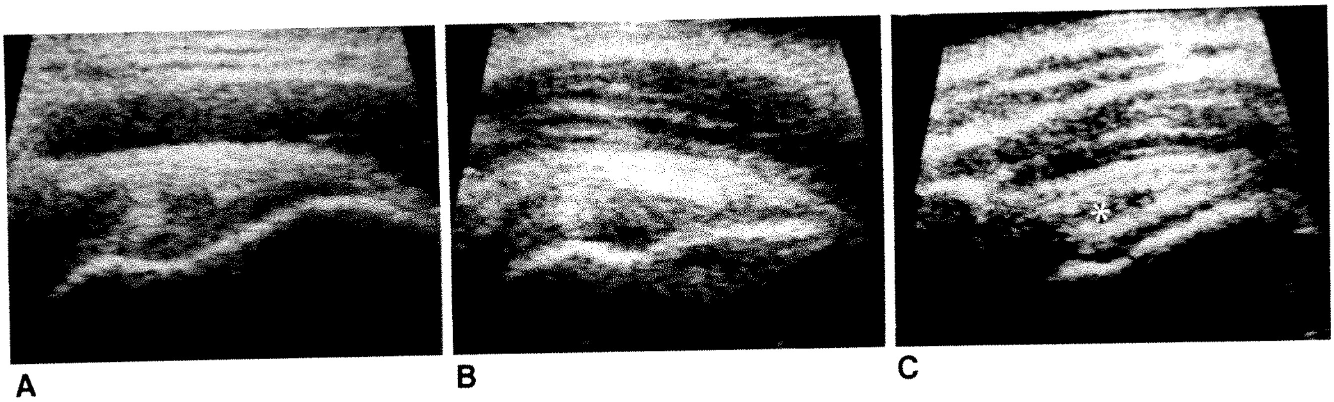

Fig. 4.—Spectrum of normal inhomogeneity in rotator cuff. **A**, Normal rotator cuff inhomogeneity in patient with normal arthrogram. **B**, Normal rotator cuff inhomogeneity in asymptomatic volunteer. **C**, Decreased central rotator cuff echogenicity (*) in patient with normal arthrogram.

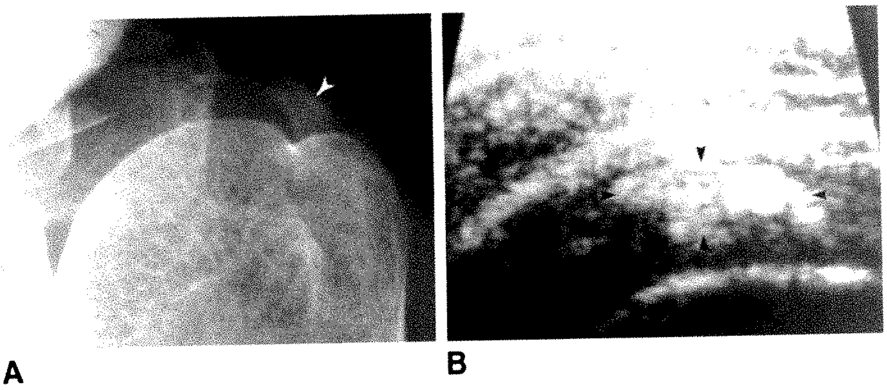

Fig. 5.—Calcific tendinitis of rotator cuff in one patient. **A**, Conventional radiograph demonstrates calcification at insertion of supraspinatus (*arrowhead*). **B**, Transverse sonogram shows echogenic focus (*arrowheads*) at calcium deposit without acoustic shadowing, which must be differentiated from echogenic foci secondary to rotator cuff tears.

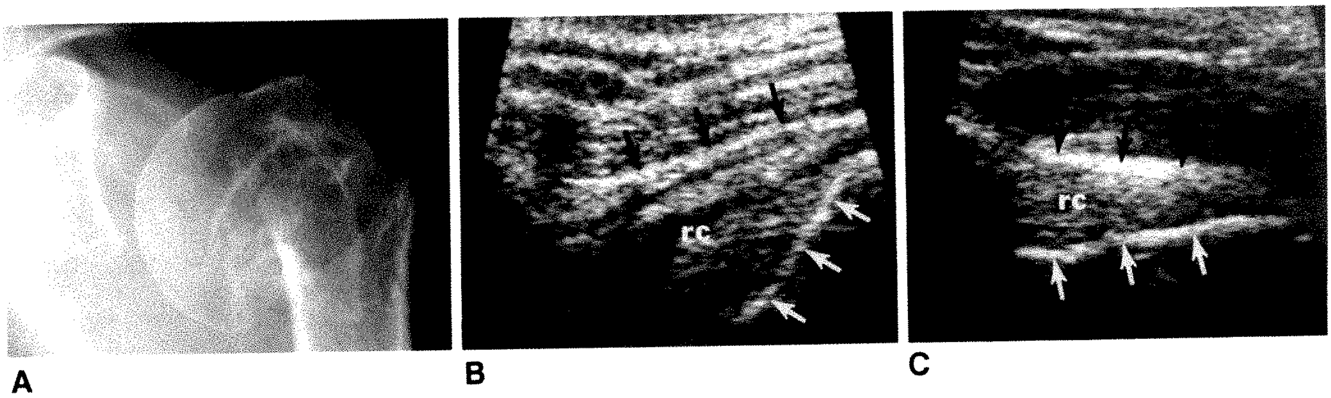

Fig. 6.—Distortion of sonographic anatomy due to bony abnormality in one patient. **A**, Conventional radiograph shows fracture of humeral neck and inferior subluxation of humeral head. **B**, Longitudinal sonogram of symptomatic side shows apparent thickening of rotator cuff (rc), which led to indeterminate interpretation. Deep surface of deltoid muscle (*black arrows*); humeral head (*white arrows*). **C**, Normal opposite shoulder for comparison. Rotator cuff (rc); deep surface of deltoid muscle (*black arrows*); humeral head (*white arrows*).

Discussion

In our experience, focal thinning and nonvisualization of the rotator cuff are the most common sonographic findings in rotator cuff tears. Focal disruptions in the normal homogeneous echogenicity of the rotator cuff or replacement of the rotator cuff by an echogenic band are encountered less frequently [1, 4]. Although we have not encountered hyperechoic foci associated with rotator cuff tears, others have described this sign as a common sonographic manifestation of rotator cuff tears [2].

In our experience, focal thinning of the rotator cuff has a 100% predictive value in diagnosing rotator cuff tears [4]. Confusion caused by the normal posterior thinning of the rotator cuff potentially could result in a false-positive diagnosis of rotator cuff tear. Several features can help to distinguish

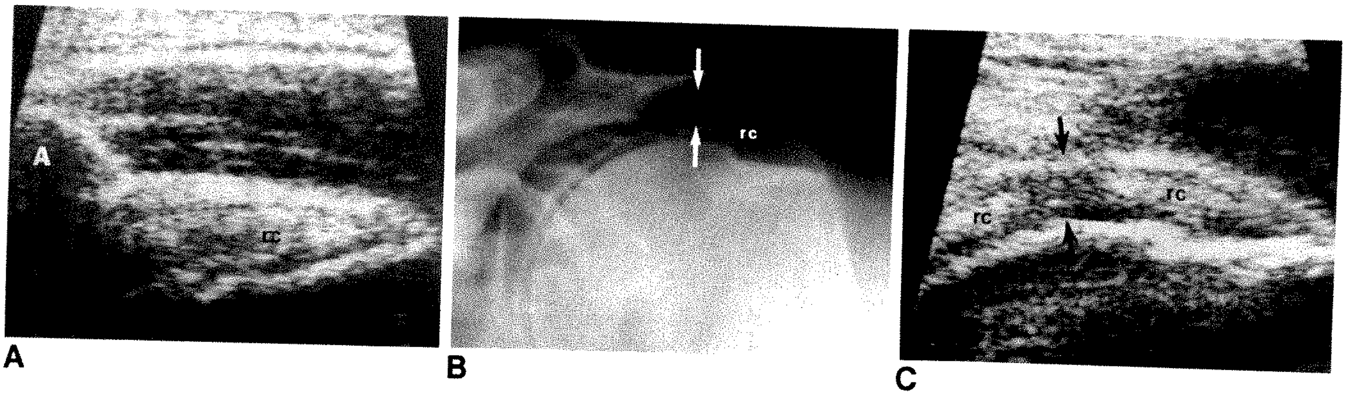

Fig. 7.—False negative sonogram due to subacromial rotator cuff tear in one patient. **A**, Initial longitudinal sonogram shows apparently normal rotator cuff (rc). Acromion process (A). **B**, Anteroposterior arthrogram shows subacromial rotator cuff tear (*arrows*) and normal distal rotator cuff (rc). **C**, Repeat longitudinal sonogram with arm extended shows discontinuity (*arrows*) in rotator cuff (rc).

normal posterior thinning from pathologic thinning. Posterior thinning should be symmetric in both shoulders, whereas tears should be asymmetric. Focal thinning secondary to rotator cuff tear manifests as an abrupt transition between the normal and abnormal rotator cuff, whereas normal posterior thinning has a gradual transition. Pathologic thinning is almost always more pronounced than the normal posterior thinning. Normal rotator cuff tissue cannot be seen in areas of focal pathologic thinning, whereas normal but thinned tissue can be seen posteriorly. Finally, it should be remembered that rotator cuff tears most commonly are anterior in the region of the supraspinatus. Isolated posterior tears in the region of the infraspinatus and teres minor are quite unusual.

Nonvisualization of the rotator cuff also has a 100% predictive value in diagnosing rotator cuff tears [4]. Nonvisualization refers to cases where sonography demonstrates close apposition of the deep surface of the deltoid muscle to the humeral head over the entire humeral head. It results from large tears when the cuff avulses from its insertion and retracts under the acromion process, leaving no rotator cuff tissue between the deltoid muscle and the humeral head. This appearance should be distinguished from the appearance occasionally seen in older patients where the echogenicity of the cuff is less than that of the deltoid muscle, resulting in a relatively "nonvisualized" rotator cuff. In the latter situation, the deep surface of the deltoid is separated from the humeral head by a normal, although hypoechoic rotator cuff. Increased gain settings should be used in these patients to fully evaluate the internal characteristics of the cuff. Symmetry with the contralateral side allows for recognition of this normal variant.

Discontinuity in the normal homogeneous echogenicity of the rotator cuff is another sonographic finding of rotator cuff tear. When the discontinuity is large, well defined, and clearly asymmetric compared with the opposite side, it is a reliable indicator of rotator cuff tear. Unfortunately, slight inhomogeneities in the rotator cuff echogenicity are occasionally encountered in normal patients and can be mistaken for rotator cuff tears. An appreciation of the normal variability in rotator cuff homogeneity can be gained best with experience and comparison to the opposite side. Mack et al. [3] also have emphasized using passive shoulder motion during real-time scanning as an aid in making the differentiation between normal inhomogeneity and pathologic discontinuity. We have less experience with this maneuver.

A normal area of discontinuity is present on transverse scans between the intraarticular part of the biceps tendon and the anterior part of the supraspinatus. This can be differentiated easily from a rotator cuff tear if the intraarticular part of the biceps tendon is confirmed. This is best accomplished by locating the biceps tendon within the biceps tendon groove and following it proximally over the humeral head.

Recognition of the intraarticular part of the biceps tendon is also important because it appears as an echogenic focus on transverse scans through the anterior part of the rotator cuff. Bretzke et al. [2] describe hyperechoic foci as the most frequent sonographic sign of rotator cuff tear and postulate that this is caused by granulation tissue and hypertrophied synovium filling the defect in the rotator cuff. Published images demonstrating this sign document that this appearance may be identical to the appearance of the intraarticular part of the biceps tendon. Therefore, great care must be taken in interpreting hyperechoic foci in the anterior part of the cuff as rotator cuff tears without first clearly identifying the biceps tendon as a separate structure.

Hyperechoic foci secondary to rotator cuff tears can also be confused with hyperechoic foci caused by calcific tendinitis of the rotator cuff. Careful inspection of conventional radiographs before sonographic examination is necessary to avoid false-positive diagnoses of rotator cuff tears from calcific tendinitis. If the radiographs show calcification in the rotator cuff, sonography should rely on criteria other than hyperechoic foci to diagnose rotator cuff tears. If the calcification is extensive on radiographs, then it may be more appropriate to perform arthrography as the initial imaging procedure.

Examination of conventional radiographs is also important to detect bony abnormalities, such as fracture or subluxation, which may alter the anatomy extensively and make sonographic interpretation difficult. If such bony abnormalities are present, arthrography should be done instead of sonography.

Finally, the patient's arm must be positioned carefully to avoid false-negative sonograms secondary to rotator cuff tears hidden beneath the acromion process. We have found that adducting the shoulder as much as possible and scanning with the humerus in neutral position allows for adequate visualization in most cases. Crass et al. [7] have emphasized internally rotating the arm to allow optimal visualization of the lateral and posterior parts of the cuff. In either case, having the patient shrug the shoulder is an easy way of visualizing more proximal parts of the cuff. Extension of the arm, while awkward, may be necessary in rare cases to further visualize the cuff proximally. Fortunately, visualization of the subacromial parts of the cuff is not necessary to detect the vast majority of tears. Most tears occur in a zone of relative hypovascularity near the insertion of the supraspinatus to the greater tuberosity [8]. Since this "critical" part of the rotator cuff is anterior and lateral to the acromion process, it is examined easily by sonography provided the patient's arm is maintained in adduction. If bony abnormalities prevent full adduction, arthrography should be done instead of sonography.

In summary, we believe that sonography represents a reliable, effective, noninvasive means of detecting rotator cuff tears. However, a number of potential pitfalls do exist. In general, these can be avoided by thoroughly understanding the normal anatomy, strictly insisting on proper patient positioning, using the opposite shoulder for comparison, and carefully inspecting conventional shoulder radiographs before sonographic examination.

REFERENCES

1. Middleton WD, Edelstein G, Reinus WR, Melson GL, Totty WG, Murphy WA. Sonographic detection of rotator cuff tears. *AJR* **1985**;144:349–353
2. Bretzke CA, Crass JR, Craig EV, Feinberg SB. Ultrasonography of the rotator cuff: normal and pathologic anatomy. *Invest Radiol* **1985**;20:311–315
3. Mack LA, Matsen FA, Kilcoyne RF, Davies PK, Sickler ME. Ultrasound evaluation of the rotator cuff. *Radiology* **1985**;157:205–209
4. Middleton WD, Reinus WR, Totty WG, Melson GL, Murphy WA. Ultrasonographic evaluation of the rotator cuff and biceps tendon. *J Bone Joint Surg [Am]* (in press)
5. Middleton WD, Edelstein G, Reinus WR, Melson GL, Murphy WA. Ultrasound of the rotator cuff: technique and normal appearance. *J Ultrasound Med* **1984**;3:549–551
6. Middleton WD, Reinus WR, Totty WG, Melson GL, Murphy WA. Ultrasonography of the biceps tendon apparatus. *Radiology* **1985**;157:211–215
7. Crass JR, Craig EV, Thompson RC, Feinberg SB. Ultrasonography of the rotator cuff: surgical correlation. *JCU* **1984**;12:487–492
8. Rathbeun JB, MacNab I. The microvascular pattern of the rotator cuff. *J Bone Joint Surg [Br]* **1970**;52:540–553

Sonography of the Postoperative Rotator Cuff

Jeffrey R. Crass[1]
Edward V. Craig[2]
Samuel B. Feinberg[1]

In experienced hands, high-resolution real-time sonography has been shown to be an accurate noninvasive method for diagnosis of rotator cuff tears. The sonographic appearance of the postoperative rotator cuff has not been previously reported. Forty postoperative patients were studied sonographically 1 week to 6 years after rotator cuff repair. The postoperative rotator cuff is abnormally echogenic and can be very similar in appearance to a small rotator cuff tear in a nonoperated patient. Soft-tissue planes about the tendon are distorted or absent. Criteria for diagnosis of retear must be different from those used in detecting new tears in a nonoperated cuff. Postoperative echogenicity is normal, but the finding of a defect or gap within the rotator cuff tendon is the only accurate sign of a recurrent rotator cuff tear.

Previous work by our group and others [1–4] has shown sonography of the rotator cuff to be a valuable and accurate method of diagnosing rotator cuff tears. The sonographic appearance of the normal rotator cuff and examples of both small and moderate-sized rotator cuff tears are shown in figure 1. The appearance of the postoperative rotator cuff has not been previously described. This study was undertaken to define the normal anatomy of the postoperative rotator cuff and to assess the role of sonography in the diagnosis of new rotator cuff tears in the patient with previous rotator cuff surgery.

Subjects and Methods

This study was undertaken in a prospective manner and comprised 40 patients, each of whom underwent bilateral shoulder sonography. The period since shoulder surgery ranged from 1 week to 6 years. There were 11 asymptomatic patients and 29 patients with recurrent pain or weakness.

Sonographic examinations were done using standard technique with a 10-MHz small-parts real-time transducer. Positioning was in internal rotation with hyperextension as previously described [3, 4]. Thirteen of the symptomatic patients underwent shoulder arthrography using either single- or double-contrast techniques. Ten patients were surgically explored including one who had not undergone arthrography. Both sonography and arthrography were performed without knowledge of the results of the other. On completion of the study the sonograms, arthrograms, and surgical findings were reviewed and analyzed.

Results

The sonographic appearance of the postoperative shoulders was not normal in any case. The appearance in the asymptomatic patients was that of a loss of soft-tissue planes surrounding the rotator cuff tendon and an abnormally increased echogenicity in the tendon (figs. 2A and 2B). In only one patient was the rotator cuff itself not abnormally echogenic. The thickness of the rotator cuff substance was maintained despite the abnormal increased echogenicity. Nineteen patients in the symptomatic group had a similar appearance, with echogenicity and irregularity

Received August 9, 1985; accepted after revision November 27, 1985.

Presented in part at the annual meeting of the American Roentgen Ray Society, Boston, April 1985.

[1] Department of Radiology, University of Minnesota Hospitals and Clinics, Box 292 Mayo Building, 420 Delaware St. S.E., Minneapolis, MN 55455. Address reprint requests to J. R. Crass.

[2] Department of Orthopaedic Surgery, University of Minnesota Hospitals and Clinics, Minneapolis, MN 55455.

AJR 146:561–564, March 1986
0361–803X/86/1463–0561
© American Roentgen Ray Society

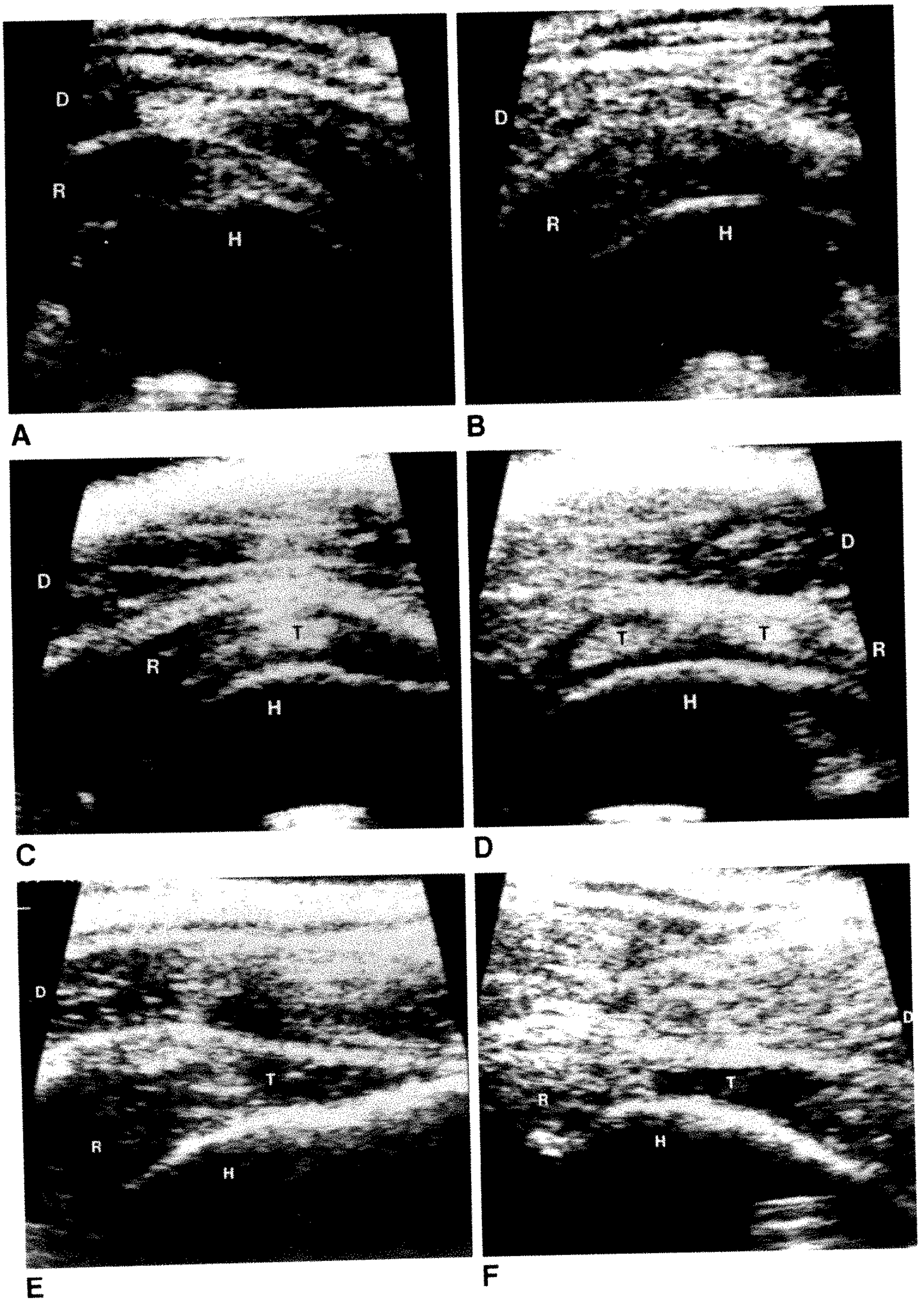

Fig. 1.—Typical sonographic findings in normal (**A**, sagittal; **B**, transverse), small echogenic rotator cuff tear (**C**, sagittal; **D**, transverse), and moderate-sized tear with defect (**E**, sagittal; **F**, transverse). D = deltoid muscle; R = rotator cuff; H = humerus; T = rotator cuff tear.

of the rotator cuff. Four of these underwent surgical exploration because of the degree of their symptomatology. Of these, two had positive arthrograms: One had a subscapularis avulsion, and the other had a normal rotator cuff at surgery. Two others were explored without arthrography and no tear was identified.

An additional finding was noted in the other 10 symptomatic patients. These patients exhibited a gap or defect within the abnormal-appearing rotator cuff tendon (figs. 2C and 2D). Six of these have been explored surgically, with recurrent tears demonstrated in all. Of these, three had positive arthrograms and two had negative arthrograms. Two other patients in this group have not yet undergone surgery but have positive arthrograms.

When the findings of arthrography were reviewed in the patients with symptomatic shoulders, there were four negative and nine positive arthrograms. Of patients with negative arthrograms, two had positive surgical explorations for cuff

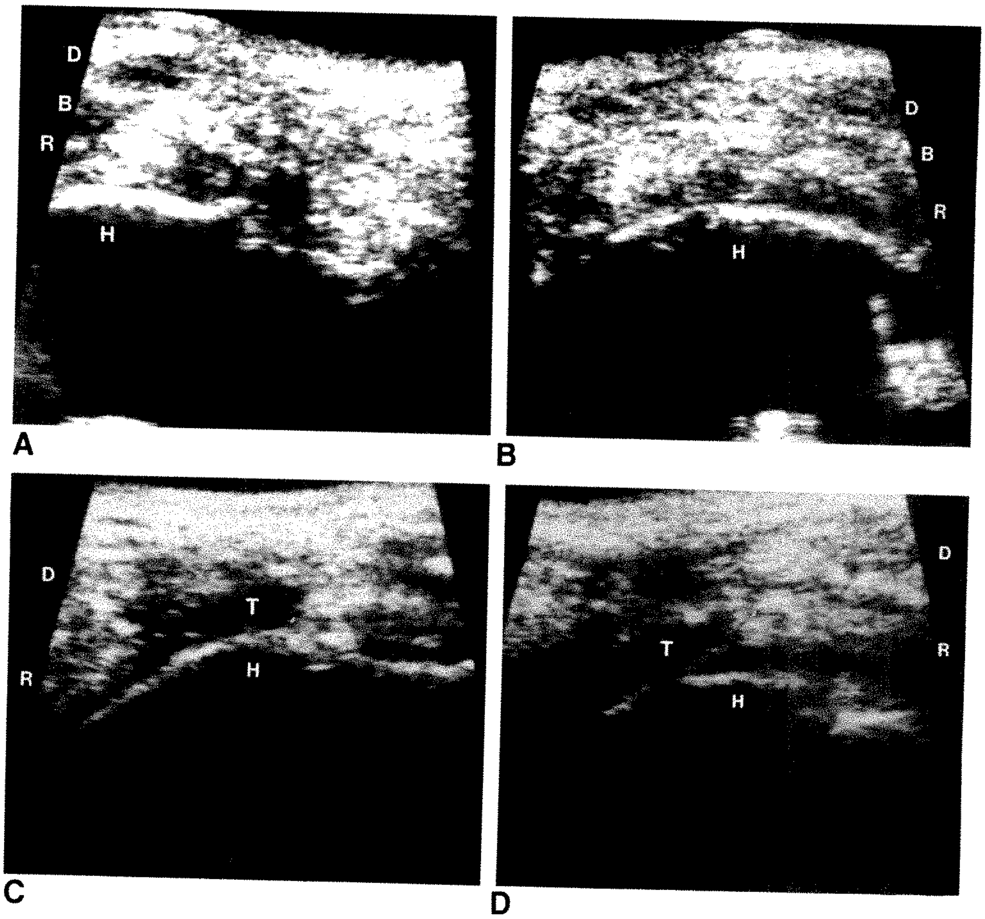

Fig. 2.—Usual postoperative appearance of rotator cuff; note disorganization and loss of soft-tissue planes (**A**, sagittal; **B**, transverse). With recurrent rotator cuff tear, gap is seen within tendon (**C**, sagittal; **D**, transverse). D = deltoid muscle; R = rotator cuff; B = subdeltoid bursa; H = humerus; T = rotator cuff tear.

tears, one had a normal cuff at surgery, and one has not yet been explored. Of the patients with positive arthrograms, four had surgical confirmation of tears, one was normal at surgery, and four have not yet had surgical exploration.

Although the numbers are too small for statistical significance, analysis reveals the following: When arthrography is compared with surgery in the postoperative patients, sensitivity is 66%, specificity 50%, and accuracy 62.5%. When the sonographic finding of a gap or defect within the tendon is compared with surgery, the sensitivity is 85%, the specificity 100%, and the accuracy 90%.

Discussion

In the postoperative shoulder patient with recurrent symptomatology, the primary differential considerations are impingement, rotator cuff tear, and frozen shoulder. The overlap in signs and symptoms among these entities can make their clinical distinction difficult.

Arthrography has been the procedure of choice for evaluation of these patients. Although our numbers are small, they suggest that arthrography has significant problems in evaluating these postoperative patients for new or recurrent rotator cuff tears. These problems are partly caused by a combination of anatomic distortion resulting from the surgical reconstruction and adhesions between the rotator cuff and the deltoid muscle, obliterating the subdeltoid bursa. Obliteration of the bursa will prevent the leakage of contrast material into the bursa—the hallmark of the positive arthrogram.

If the criteria for a positive sonogram were not modified for the postoperative patient, sonography would have great difficulties as well. The echogenic appearance of small rotator cuff tears is mimicked by the postoperative changes. This is likely due to the nature of tendon healing. Although there is a tendency for reorganization of the tendon fibers after repair, significant disorganization and irregular collagen bundles persist [5]. These probably result in the persistent echogenicity. This persistent echogenicity would make it impossible to diagnose a small echogenic-type rotator cuff tear in the postoperative patient. If small echogenic tears did occur postoperatively, they were either not seen in our series or did not have sufficient symptomatology to warrant reexploration. The one tear found in the four patients with echogenic tendons who were reexplored did not involve the echogenic supraspinatus and infraspinatus. The tear was in the subscapularis, a part of the rotator cuff that was not sonographically examined routinely at that time.

As rotator cuff tears enlarge, the sonographic appearance changes from that of an echogenic area to that of a gap or defect within the rotator cuff tendon [4]. Ten of our symptomatic postoperative patients had this appearance. Six of them have undergone surgery, which confirmed rotator cuff tears in all, and two others have had positive arthrograms. This suggests that the presence of a defect within the postoperative rotator cuff is a reliable sign of retear.

Our study has shown that the rotator cuff tendon does not return to a sonographically normal appearance in the 6 postoperative years spanned by our patient population. The usual appearance is that of an echogenic tendon with a loss of tissue planes about the tendon. This echogenicity of the tendon would make the diagnosis of small new or recurrent tears impossible. Finding a defect or gap within the tendon, however, allows confident diagnosis of a retorn rotator cuff. Although the numbers are small, our study suggests that sonography is more accurate than arthrography in evaluating the rotator cuff in the postoperative shoulder.

REFERENCES

1. Crass JR, Craig EV, Thompson RC, Feinberg SB. Ultrasonography of the rotator cuff: surgical correlation. *JCU* **1984**;12:487–492
2. Middleton WD, Edelstein G, Reinus WR, Melson GL, Totty WG, Murphy WA. Sonographic detection of rotator cuff tears. *AJR* **1985**;144:349–354
3. Bretzke CA, Crass JR, Craig EV, Feinberg SB. Ultrasonography of the rotator cuff: normal and pathologic anatomy. *Invest Radiol* **1985**;20:311–315
5. Crass JR, Craig EV, Bretzke CA, Feinberg SB. Ultrasonography of the rotator cuff. *Radiographics* **1985**;5:941–953
5. Steiner M. Biomechanics of tendon healing. *J Biomech* **1982**;12:951–958

MRI of Normal and Pathologic Skeletal Muscle

William A. Murphy[1]
William G. Totty[1]
James E. Carroll[2]

Lower extremity skeletal muscle of 22 individuals (five normal volunteers and 17 patients with muscular or neuromuscular diseases) was studied with magnetic resonance imaging. Axial images generated with spin-echo pulse sequences using short repetition times (500–900 msec TR) and short echo times (30–60 msec TE) provided excellent contrast between fat (high signal intensity) and muscle (intermediate signal intensity). Seventeen patients with clinically verified muscle disorders were evaluated in a manner similar to the normal volunteers. Conditions studied include Duchenne muscular dystrophy (three patients), limb-girdle muscular dystrophy (five), facioscapulohumeral dystrophy (three), and spinal muscular atrophy, amyotrophic lateral sclerosis, hereditary sensorimotor neuropathy, cerebral palsy, poliomyelitis, and Kearn-Sayre mitochondrial muscle disease (one each). General patterns of muscle abnormality were common among the diseases and included decreased or increased muscle size and a spectrum of muscle replacement by fat. Variable patterns were observed within disease groups and for each patient. Much phosphorus-31 spectroscopy has been performed in a blind fashion with no proton map of normal/abnormal muscle distribution to guide the spectroscopist. This study emphasizes the worth of having a muscle proton map of patients with muscle dysfunction to assure that meaningful phosphorus spectroscopic information is obtained from a volume of tissue limited to an appropriate muscle.

Among the many attractive features of human magnetic resonance imaging (MRI) methods is the potential to study energy metabolism using phosphorus-31 (^{31}P) spectroscopic techniques. The potential applications are great, particularly for the study of cardiac physiology. First, however, phosphorus spectroscopic techniques must be validated in a simpler environment (e.g., more readily accessible skeletal muscle). Several laboratories have invested considerable effort in obtaining ^{31}P spectroscopic data from normal and "diseased" skeletal muscle in vivo [1–4]. However, these experiments have been limited to the forearm, where the actual normal or abnormal status of the muscle volume being measured was not known. We undertook the current proton imaging study of lower extremity muscle to verify the capability of MRI to image normal muscle, to detect and map abnormal muscle, and to validate proton muscle imaging as a required adjunct to ^{31}P measurements.

Subjects and Methods

MRI was performed using a 0.5-T Oxford superconducting magnet (Siemens Magnetom) operated at 0.35 T. For thigh muscle, the body coil was both transmitter and receiver; for calf muscle, the head coil served as receiver. Software supported spin-echo (SE) and inversion-recovery (IR) routines with multislice and dual-echo acquisition. Sections 1 cm thick were obtained with 1-cm interspaces.

Normal volunteers for muscle studies were from the University staff. Patient volunteers were chosen from the University's Jerry Lewis Neuromuscular Research Center and Irene Walter Johnson Institute of Rehabilitation. Normal and patient volunteers all gave informed consent according to guidelines and procedures approved by the local human studies committee.

Received August 6, 1985; accepted after revision November 7, 1985.

Presented in part at the annual meeting of the American Roentgen Ray Society, Boston, April 1985.

[1] Mallinckrodt Institute of Radiology, Washington University School of Medicine, 510 S. Kingshighway Blvd., St. Louis, MO 63110. Address reprint requests to W. A. Murphy.

[2] Jerry Lewis Neuromuscular Research Center, Washington University School of Medicine, St. Louis, MO 63110. Present address: Departments of Neurology, Pediatrics, and Cell & Molecular Biology, Medical College of Georgia, Augusta, GA 30912.

***AJR* 146:565–574, March 1986**
0361–803X/86/1463–0565
© American Roentgen Ray Society

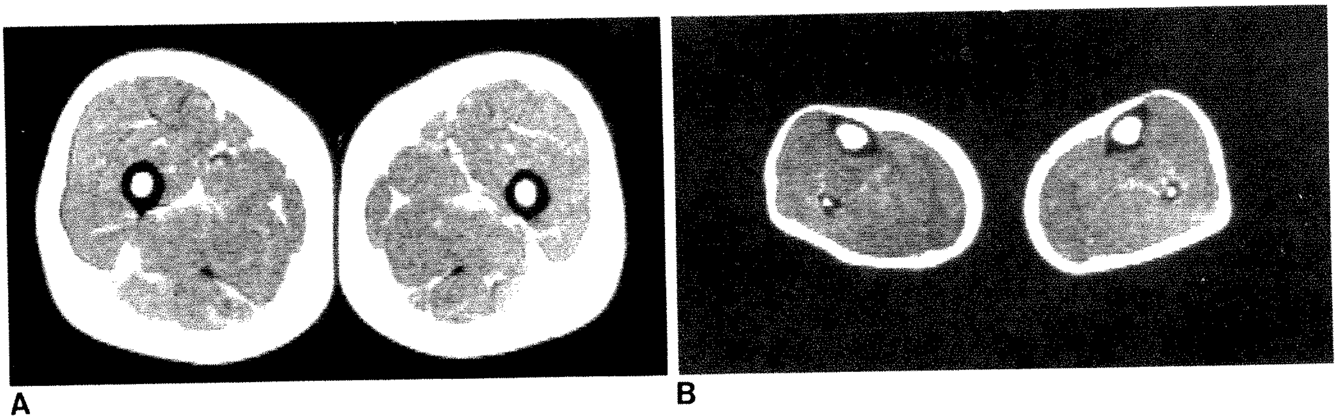

Fig. 1.—Normal muscle in 38-year-old man. **A,** Transaxial SE 1500/30 image through mid thigh shows normal quadriceps, adductor, and hamstring muscle groups. **B,** Transaxial SE 500/30 image through mid calf shows normal anterior, lateral, and posterior muscle groups.

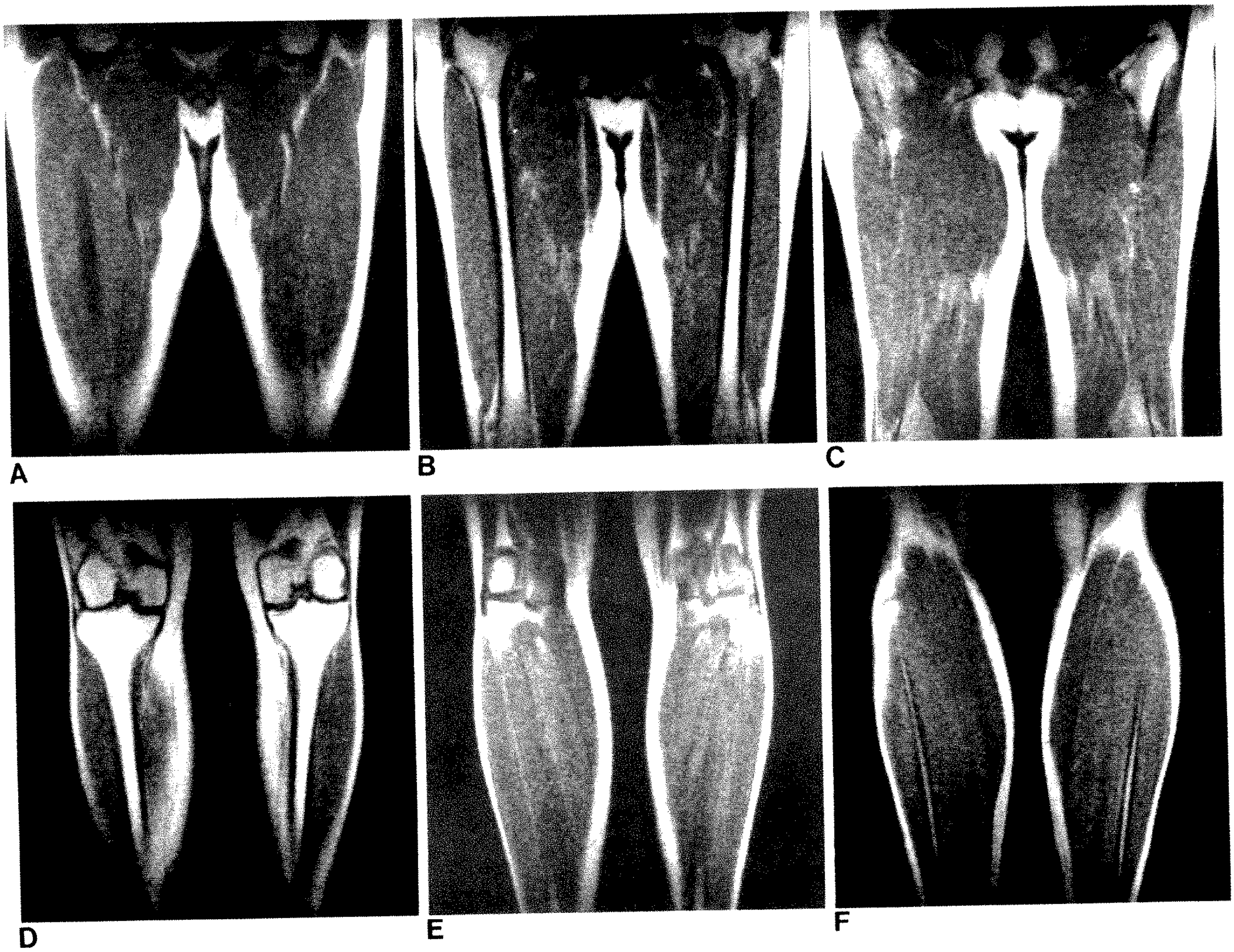

Fig. 2.—Normal muscle in 38-year-old man. **A–C,** Coronal SE 500/30 images through thigh show longitudinal anatomy of quadriceps, adductor, and hamstring muscle groups. **D–F,** Coronal SE 500/30 images through calf show longitudinal anatomy of calf muscles.

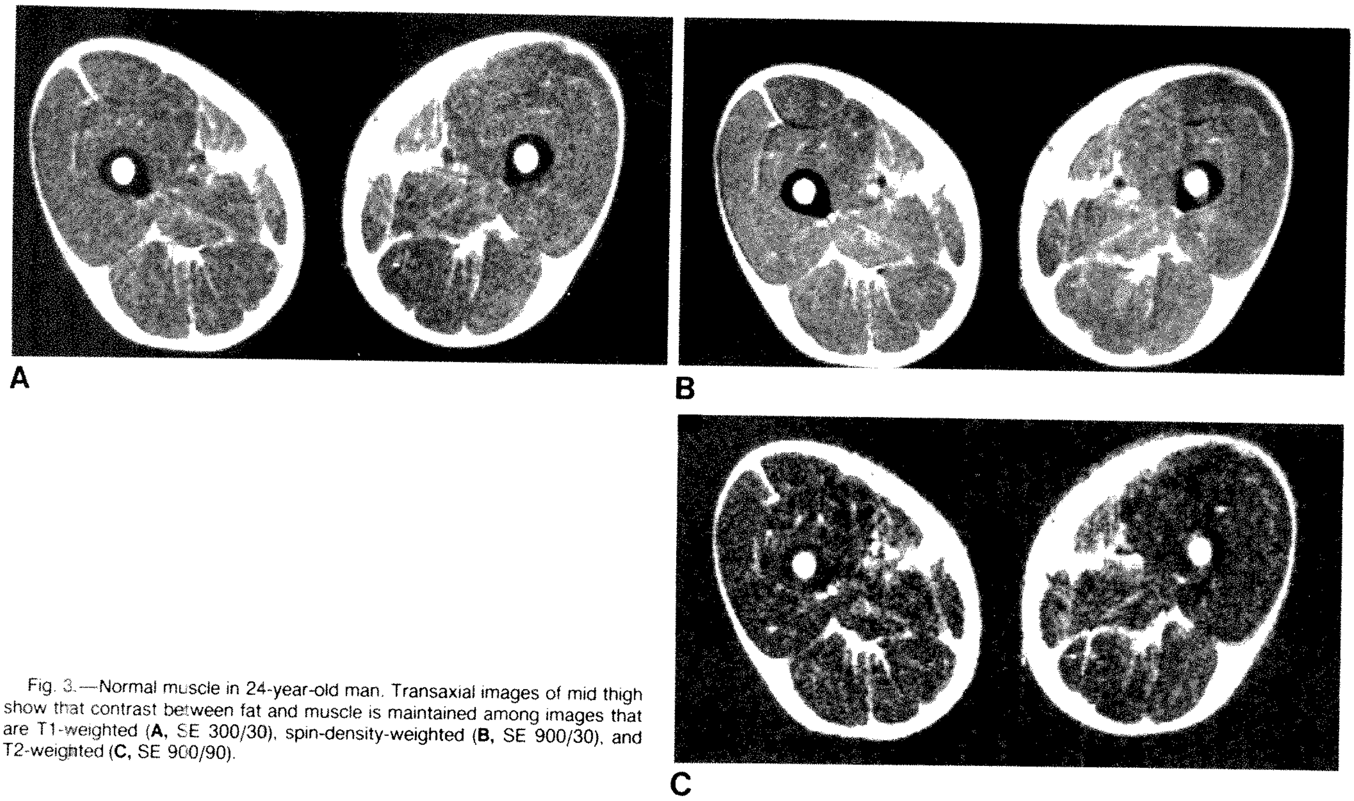

Fig. 3.—Normal muscle in 24-year-old man. Transaxial images of mid thigh show that contrast between fat and muscle is maintained among images that are T1-weighted (**A**, SE 300/30), spin-density-weighted (**B**, SE 900/30), and T2-weighted (**C**, SE 900/90).

IR sequences were performed on four individuals using 1600 msec TR, 400 msec inversion time (TI), and 30 msec TE (IR 1600/400/30). SE sequences were performed on all individuals with TR of 300–1500 msec and TE of 30–120 msec. A typical sequence was 700 msec TR with a dual TE of 30 and 60 msec (SE 700/30, SE 700/60), resulting in 14 images, seven at each TE. Both axial and coronal sections were obtained of thigh and calf muscle in nearly all volunteers. A study of thigh and calf muscle in two planes required about 90 min.

All normal and patient volunteer studies were retrospectively reviewed to determine the best pulse sequence for detection of normal and abnormal muscle. Abnormal muscle was qualitatively described according to pattern and symmetry of distribution. Certain thigh or calf muscles or groups of muscles were individually identified. These were the quadriceps, adductor, hamstring, gracilis, and sartorius muscles of the thigh and the anterior, lateral, and posterior muscle groups of the calf. Each was quantitated on a 5-point scale for the amount of fatty replacement, where 0 was normal and 4 was complete replacement. General and individual qualitative and quantitative patterns were identified.

Results

Normal Volunteers

Five normal individuals with no evidence of muscle disease were evaluated. Three were women and two were men, aged 23–38 years (mean, 29.6). Thigh and calf muscle was studied using IR and SE pulse sequences, with TR of 300–1500 msec and TE of 30–120 msec on SE sequences.

Retrospective review showed that normal thigh and calf muscle could be imaged successfully in transaxial (fig. 1) and coronal planes (fig. 2). Sagittal planes were not evaluated in this protocol. Subcutaneous fat, intermuscular fat, and bone marrow were of high signal intensity. Muscle was intermediate signal intensity and cortical bone very low signal intensity. Transaxial images of the thigh permitted discrimination of individual muscle groups because of interposed fat, resulting in an effective cross-sectional survey. Transaxial images of the calf also displayed the muscle tissue, but because intermuscular fat was sparse, individual muscle groups were difficult to identify. Coronal images of thigh and calf provided longitudinal anatomic definition of muscle groups. The relative signal intensities of fat, muscle, and cortical bone were similar on all pulse sequences tested, including T1-weighted, spin density-weighted, and T2-weighted pulse sequences (fig. 3).

In designating an optimized pulse sequence to study skeletal muscle, several conclusions were reached. In this initial experience, IR pulse sequences were no more effective than a T1-weighted SE pulse sequence, and the SE technique was determined to be preferable because it was more versatile. Because T2-weighted SE sequences required more time to acquire and had less signal strength with longer echos, pulse sequences with shorter TR and TE were chosen. In order to survey a reasonable volume of muscle tissue within a relatively short length of time while preserving overall signal and contrast, an optimized SE pulse sequence was chosen having the following characteristics: 500–900 msec TR, dual 30/60 msec TE, 10-mm section thickness, and 10-mm section gap.

TABLE 1: **MRI of Pathologic Skeletal Muscle**

Case No., Age (years)	Disease Duration (years)	Relative Severity, Thigh/Calf*	Muscle Groups Involved, Thigh, Calf†	Symmetry‡
Duchenne muscular dystrophy:				
1, 15	12	3/4	All Groups	S
2, 14	9	4/4	All Groups	S
3, 13	11	3/3	All Groups	S
Limb-girdle dystrophy:				
4, 41	14	2/0	Q, A, H	A
5, 37	22	3/3	Q, A, H/A, L, P	S
6, 35	24	3/3	Q, A, H/A, L, P	S
7, 22	15	4/3	A, H, G/A, L, P	S
8, 20	6	4/0	Q, A, H/	S
Fascioscapulohumeral dystrophy:				
9, 56	35	2/2	Q, A, H, G/A, P	A
10, 30	15	1/2	/A, L, P	A
11, 22	8	3/1	Q, A, H/A	A
Mitochondrial myopathy:				
12, 55	15	4/4	Q, A, H, G/A, L, P	A
Spinal muscular atrophy:				
13, 26	11	3/–	Q, A, H, S, G/	S
Amyotrophic lateral sclerosis:				
14, 51	1	0/1	/A	A
Hereditary sensorimotor neuropathy:				
15, 37	30	1/0	H/	A
Cerebral palsy:				
16, 14	14	–/0	Decreased volume only	A
Poliomyelitis:				
17, 35	25	–/4	/P	A

* Relative severity of fatty replacement: 0 = normal; 1 = slight; 2 = half replaced; 3 = mostly replaced; 4 = totally replaced; – = not studied.

† Thigh: Q = quadriceps; A = adductors; H = hamstrings; S = sartorius; G = gracilis. Calf: A = anterior compartment; L = lateral compartment; P = posterior compartment.

‡ S = symmetric; A = asymmetric.

Patient Volunteers

Seventeen patients with muscular or neuromuscular diseases were evaluated (table 1). There were 13 male and four female patients, aged 13–56 years (average, 30.8). Thigh and calf muscle was studied using IR (three patients) and SE (all patients) pulse sequences, with 300–900 msec TR and 30–120 msec TE on SE sequences.

Retrospective review showed that abnormal muscle could be successfully imaged using IR and SE pulse sequences. These diseases are clinically characterized by volume changes such as "pseudohypertrophy" and atrophy accompanied by weakness. Among the many histologic changes, fatty replacement predominates. MRI detected volume changes and/or fatty replacement in all 17 patients. Using a simple 5-point scale, it was possible to roughly quantitate the severity of muscle involvement. Comparison of left and right sides determined the symmetry of the condition.

Three patients with severe X-linked Duchenne muscular dystrophy were studied. All showed advanced fatty replacement of muscle (fig. 4). The outlines of the individual muscles were retained, presumably because fibrous intermuscular septae persisted and are shown as low-signal curvilinear lines. One of the patients showed the increased volume in the calf clinically termed "pseudohypertrophy" (fig. 4); the other two showed decreased volume of calf muscle. All three had decreased volume of thigh muscle. All three showed relative sparing of the sartorius and gracilis muscles.

In the patients with Duchenne muscular dystrophy, various pulse sequences were reviewed to determine an optimal sequence for display of abnormal muscle and for detection of any feature unique to a particular pulse sequence. Those sequences reviewed included IR (two patients), T1-weighted SE 300/30 (all patients), T2-weighted SE 900/90 (two patients), and several other intermediate SE sequences. As in the normal volunteers, an SE sequence using a fairly short TR (500–900 msec) and short TE (30–60 msec) was optimal (fig. 5). No unique feature was identified.

Five patients with limb-girdle muscular dystrophy were scanned. All showed fatty replacement of thigh muscle, but only three showed replacement of calf muscle. In four of the five, the distribution of muscle involvement was symmetric. The severity of the disease varied from severe and symmetric (fig. 6) to moderate and asymmetric (fig. 7). Disease duration did not directly correlate with disease distribution or severity as displayed by MRI.

Three patients with facioscapulohumeral muscular dystrophy, a more mild adult disease, were studied. These patients also showed fatty replacement of muscle, but of a severity less than that documented in the Duchenne and limb-girdle dystrophy groups. Fewer muscles were involved to a lesser degree, and the distribution was always asymmetric. Severity varied from total replacement of a substantial number of muscles (fig. 8) to partial or patchy replacement of a limited number of muscles (fig. 9). Again, disease severity did not seem directly related to disease duration.

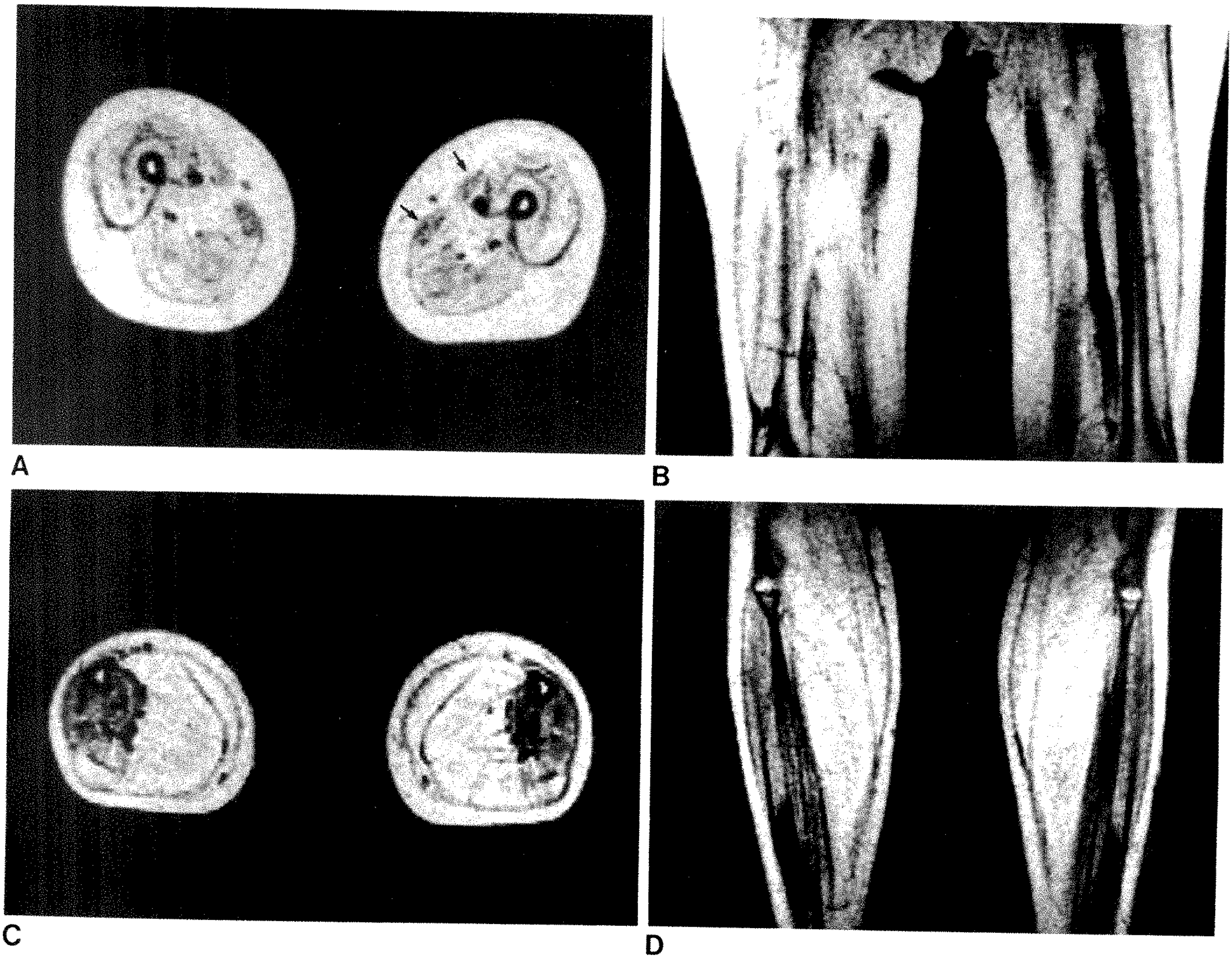

Fig. 4.—Duchenne muscular dystrophy in 14-year-old boy. **A**, Transaxial IR 1600/400/30 image through mid thigh shows nearly complete fatty replacement of all muscle groups with some sparing of sartorius and gracilis muscles (*arrows*). **B**, Coronal SE 500/30 image shows similar features. **C**, Transaxial SE 500/30 image through mid calf shows complete replacement of gastrocnemius and soleus muscles with apparent preservation of intermuscular fibrous septa. Large size of these muscles is MRI correlation for clinical "pseudohypertrophy." **D**, Coronal SE 500/30 image shows similar features in longitudinal display.

Six other patients with a spectrum of muscle or neuromuscular disease were studied. They too showed patterns of muscle replacement or atrophy. The amount of fatty replacement varied from severe in the mitochondrial myopathy and spinal muscular atrophy patients (figs. 10 and 11) to very slight in the amyotrophic lateral sclerosis and hereditary sensorimotor neuropathy patients. Five of the six patients had asymmetric involvement, which was most pronounced in the cerebral palsy and poliomyelitis patients. It is of interest that the cerebral palsy patient showed only calf-muscle atrophy (fig. 12), while the poliomyelitis patient with a similar-sized calf showed extensive fatty replacement (fig. 13).

Discussion

This study has shown that MRI can display both normal and pathologic skeletal muscle. The signal intensity of normal muscle is intermediate between those of fat and cortical bone. Because the signal intensity difference between fat and muscle is so great, the thin intermuscular fat planes are readily imaged, thereby separating the muscle mass into individual muscles or groups of muscles. Likewise, because many muscle disorders result in fatty replacement of normal muscle, diseased muscle is easily detected.

MRI can characterize muscle diseases in terms of the size of the involved muscle, the number and distribution of diseased muscles, and the pattern of fatty replacement. Involved muscles can be of normal, decreased, or increased size and of variable fatty replacement. While the severity of involvement does not seem directly related to disease duration, it does seem to parallel the clinical severity of the condition. In general, the patients with greater clinical severity showed a greater number of involved muscles, with more complete muscle replacement by fat and greater symmetry of involvement. However, distribution of muscle involvement and patterns of fatty replacement did not permit specific identification

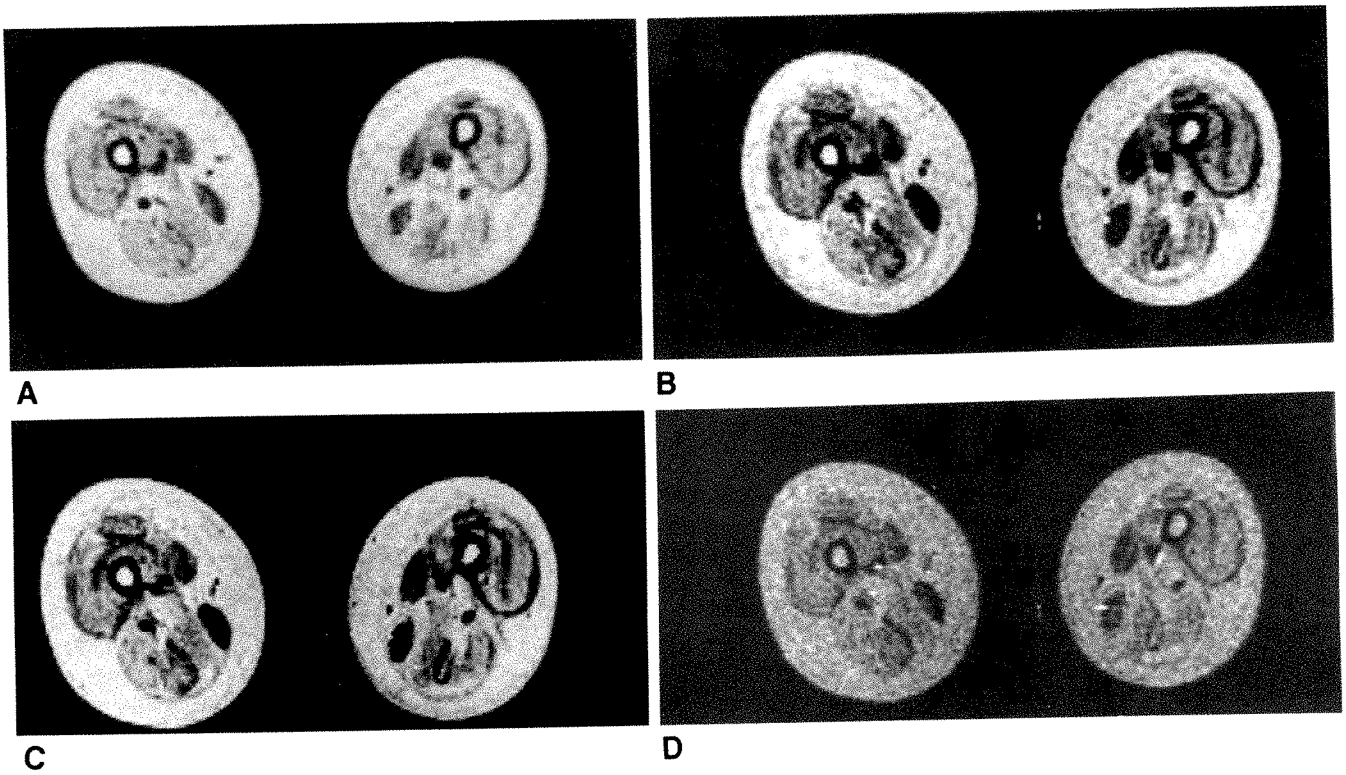

Fig. 5.—Duchenne muscular dystrophy in 15-year-old boy. Transaxial images through mid thigh show that MRI display of muscle size and fatty replacement is similar for spectrum of pulse sequences: **A,** IR 1600/400/30. **B,** SE 300/30. **C,** SE 900/30. **D,** SE 300/90. Note that sartorius and gracilis muscles are relatively spared.

of a given patient's condition. These MRI findings are similar to the experience with computed tomography (CT) of normal and pathologic skeletal muscle [5, 6].

Our MRI experience with these 22 normal and patient volunteers indicates that an SE pulse sequence with a relatively short TR (500–1000 msec) and short TE (30–60 msec) optimizes both the contrast among fat, muscle, and bone and the overall signal intensity from the extremity. No advantage of spin-density- or T2-weighted sequences was identified. A multislice routine that yields 5- to 10-mm-thick sections seems adequate to survey a region of interest in transaxial or coronal views. For most purposes, the transaxial plane appears adequate; coronal sections can be added when longitudinal spatial localization is desired.

CT and MRI are both effective for surveying skeletal muscle diseases. MRI has the advantage of having no associated ionizing radiation and no known adverse biological effects, in addition to the ability to obtain direct multiplanar sections. These features make MRI more attractive for imaging muscle diseases than CT, especially when sequential studies are anticipated in children and young adults.

Finally, MRI offers the potential to study energy metabolism through ^{31}P spectroscopy. This has already been studied in laboratory animals and human beings [1–3]. The basic reasons to perform ^{31}P spectroscopy on skeletal muscle are to study normal energy metabolism, to describe diseased energy metabolism, to better understand and diagnose muscle diseases, and to provide a new method to help design and monitor new therapies.

The usual ^{31}P experiment is to obtain spectra from resting muscle, from muscle during defined dynamic exercise, and from muscle during recovery after exercise. The spectra for normal muscle have been well described and are similar among individuals and at all ages [4]. Spectra have been generated from forearm muscles of patients with a variety of muscle diseases, and patterns have now been recognized for several of these diseases [1–3].

There are specificity problems with these early ^{31}P experiments in patients with muscle diseases. Many of the problems stem from the fact that the volume of tissue from which the spectra originate is not adequately defined. Although the physical characteristics of the surface coils used in these experiments are known, the actual anatomic distribution of muscle involvement in the patient undergoing examination has not been known. For ^{31}P spectroscopy of skeletal muscle to continue to develop, it will be necessary to know precisely the volume of tissue generating the phosphorus signals and the condition of the muscle within that volume.

Proton MR images map the location and severity of skeletal muscle disease. These proton maps can be used to assure correct positioning of surface coils for MR ^{31}P spectroscopy. By combining proton maps of skeletal muscle diseases and ^{31}P spectroscopy, altered skeletal muscle energy metabolism will be better studied. Perhaps through the application of MRI technology, a new understanding of muscle diseases, their therapy and management may develop.

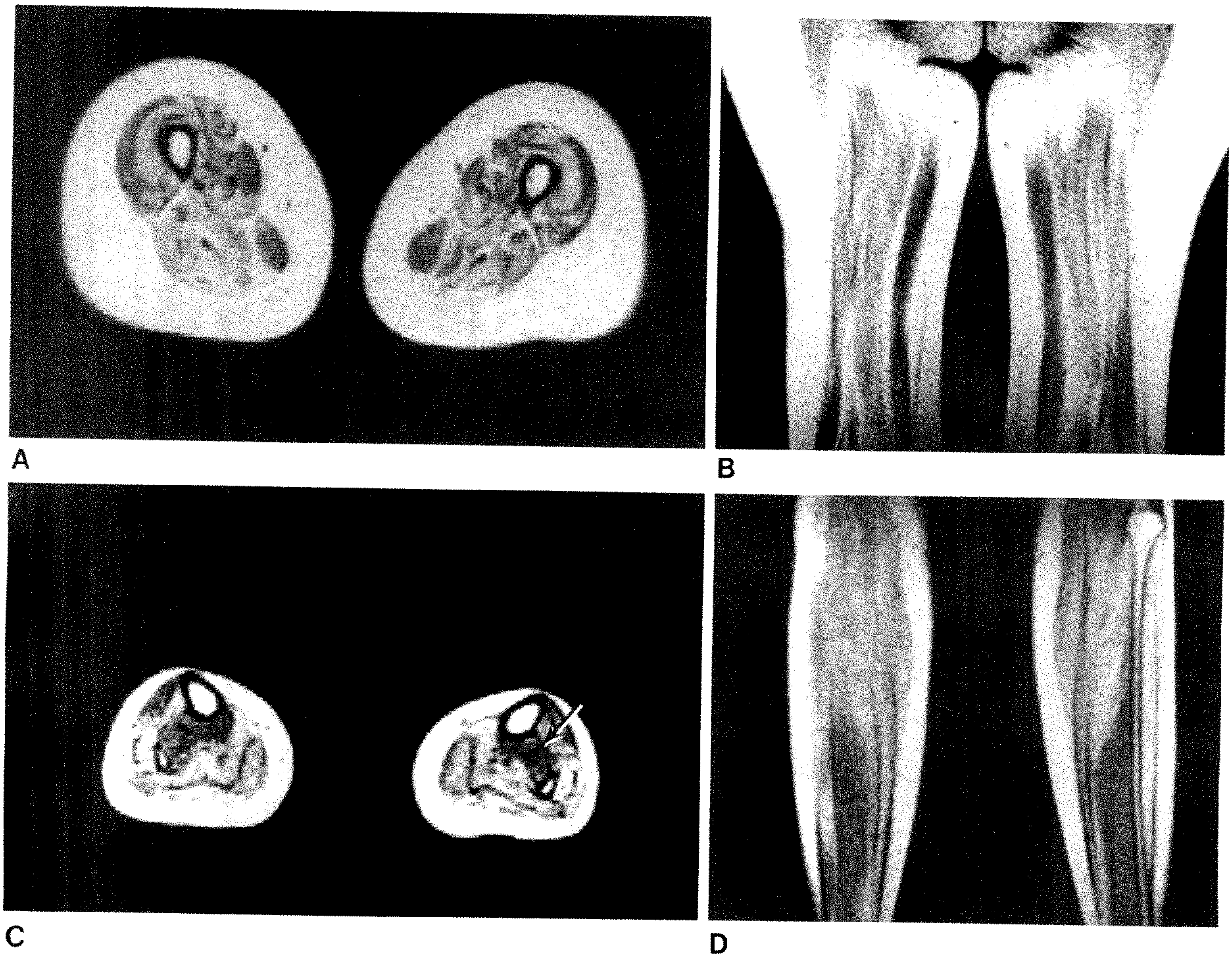

Fig. 6.—Limb-girdle dystrophy in 37-year-old woman. **A,** Transaxial SE 700/30 image through mid thigh shows decreased muscle volume and moderately severe fatty replacement, similar to but not as severe as in patients with Duchenne muscular dystrophy. Note relative sparing of sartorius and gracilis muscles. **B,** Coronal SE 700/30 image through posterior thigh shows similar findings with sparing of gracilis muscles. **C,** Transaxial SE 700/30 image through mid calf shows fatty replacement of posterior compartment and parts of anterior and lateral compartments. Tibialis posterior muscle (*arrow*) is relatively spared. **D,** Coronal SE 500/30 image through mid calf confirms sparing of tibialis posterior muscle.

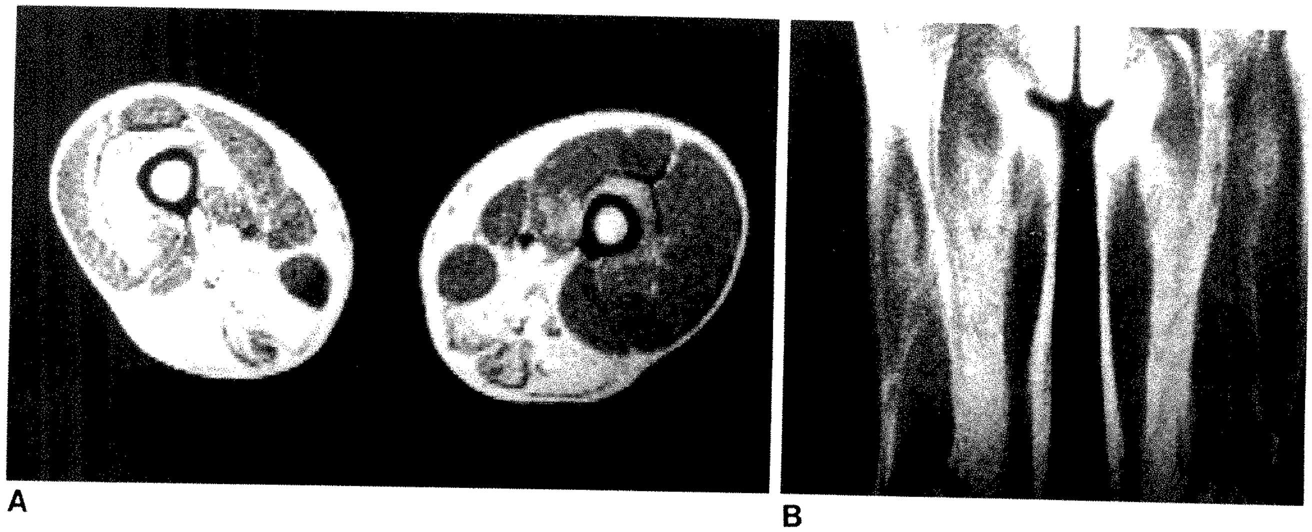

Fig. 7.—Limb-girdle dystrophy in 41-year-old man. **A,** Transaxial SE 700/30 image through mid thigh shows symmetric replacement of hamstring muscles, but asymmetric replacement of quadriceps muscles. **B,** Coronal SE 500/30 image just posterior to femora confirms asymmetric quadriceps involvement.

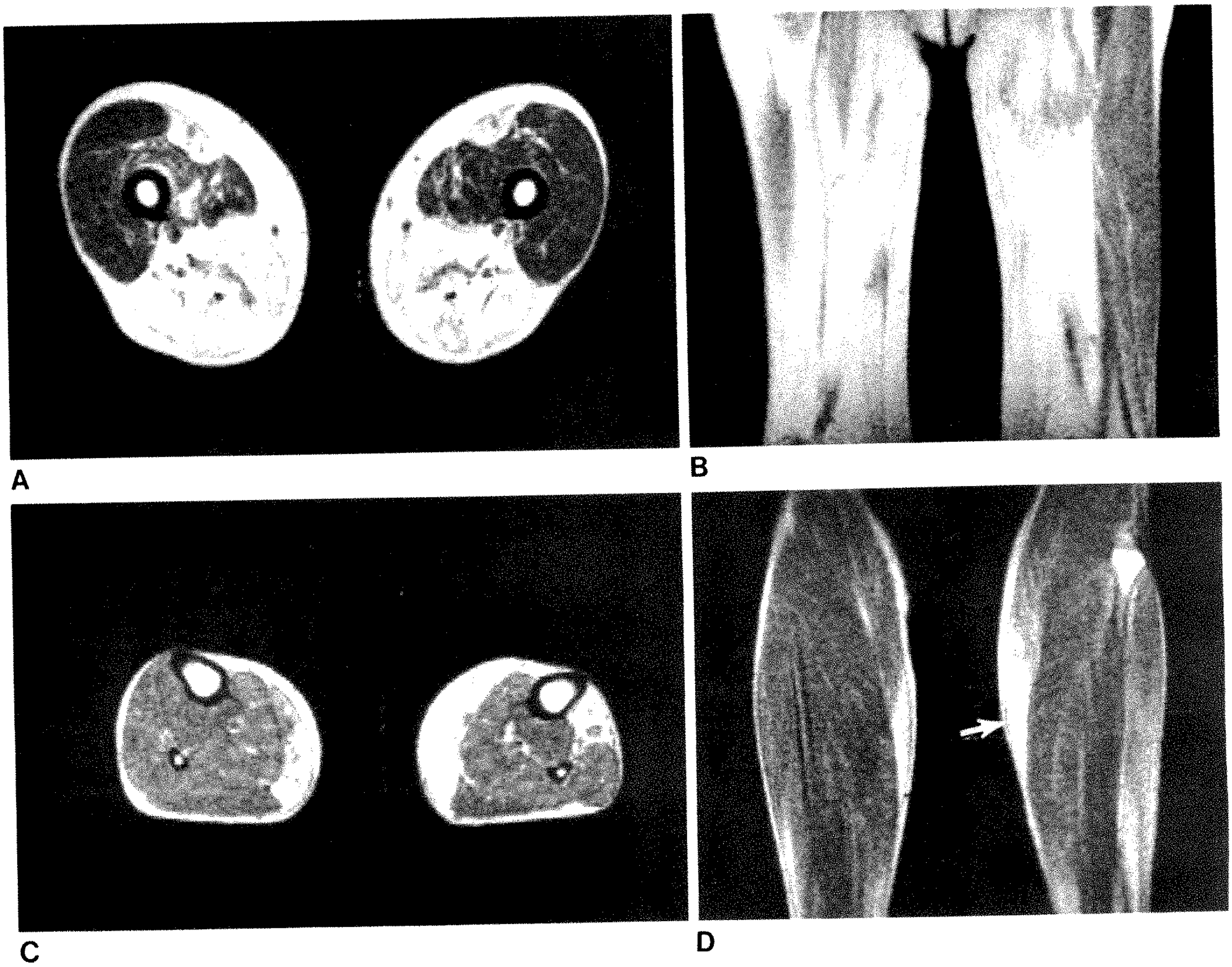

Fig. 8.—Facioscapulohumeral dystrophy in 56-year-old man. **A,** Transaxial SE 300/30 image through mid thigh shows symmetric fatty replacement of hamstring and rectus femoris muscles but asymmetric involvement of vastus intermedius and adductor muscles. **B,** Coronal SE 900/30 image through posterior thigh confirms complete fatty replacement of hamstring group. **C,** Transaxial SE 700/30 image through mid calf shows asymmetric fatty replacement of gastrocnemius muscle. **D,** Coronal SE 500/30 image through mid calf confirms preservation of soleus muscle and fatty replacement of gastrocnemius (*arrow*).

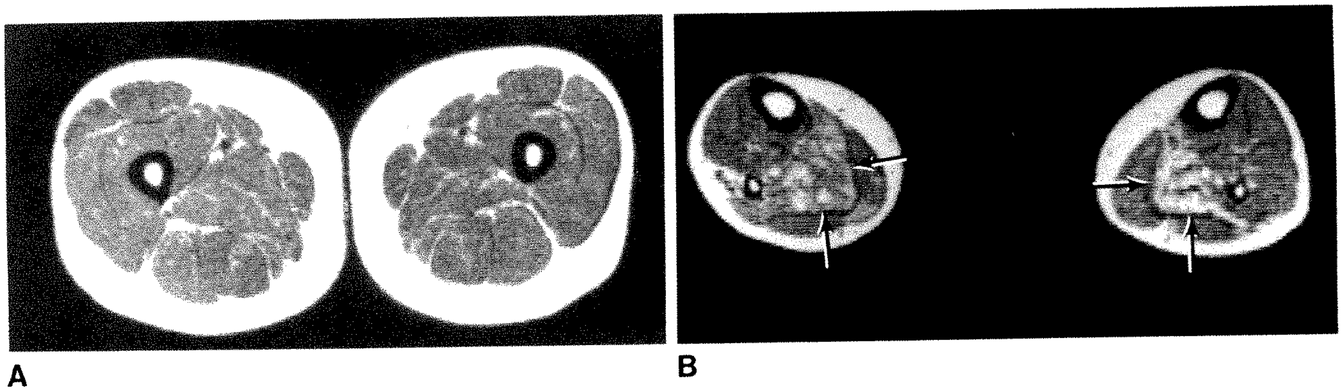

Fig. 9.—Facioscapulohumeral dystrophy in 30-year-old man. **A,** Transaxial SE 900/30 image through mid thigh shows no abnormality. **B,** Transaxial SE 700/30 image through mid calf shows focal patchy fatty replacement of soleus muscles (*arrows*), more on left side than on right.

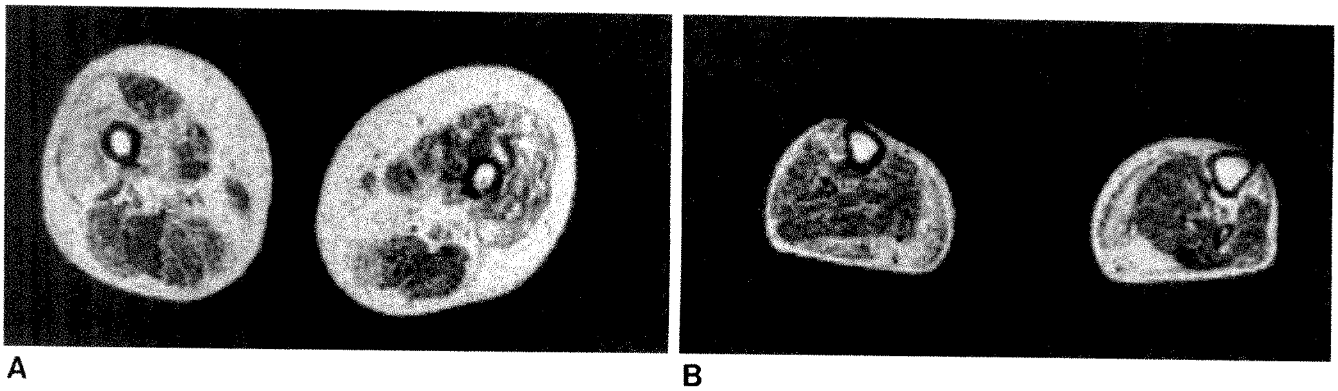

Fig. 10.—Kearn-Sayre mitochondrial muscular dystrophy in 55-year-old man. Transaxial SE 500/60 images of thigh (**A**) and calf (**B**) show asymmetric atrophy and fatty replacement.

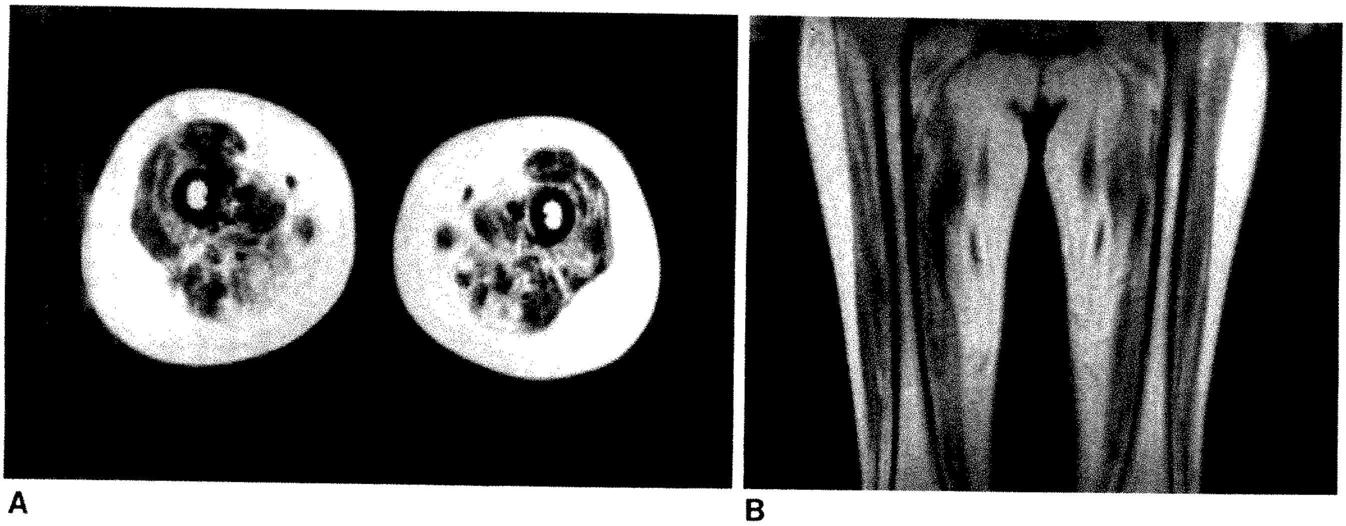

Fig. 11.—Spinomuscular atrophy in 26-year-old man. Transaxial (**A**) and coronal (**B**) SE 900/30 images show advanced atrophy and fatty replacement of thigh muscles.

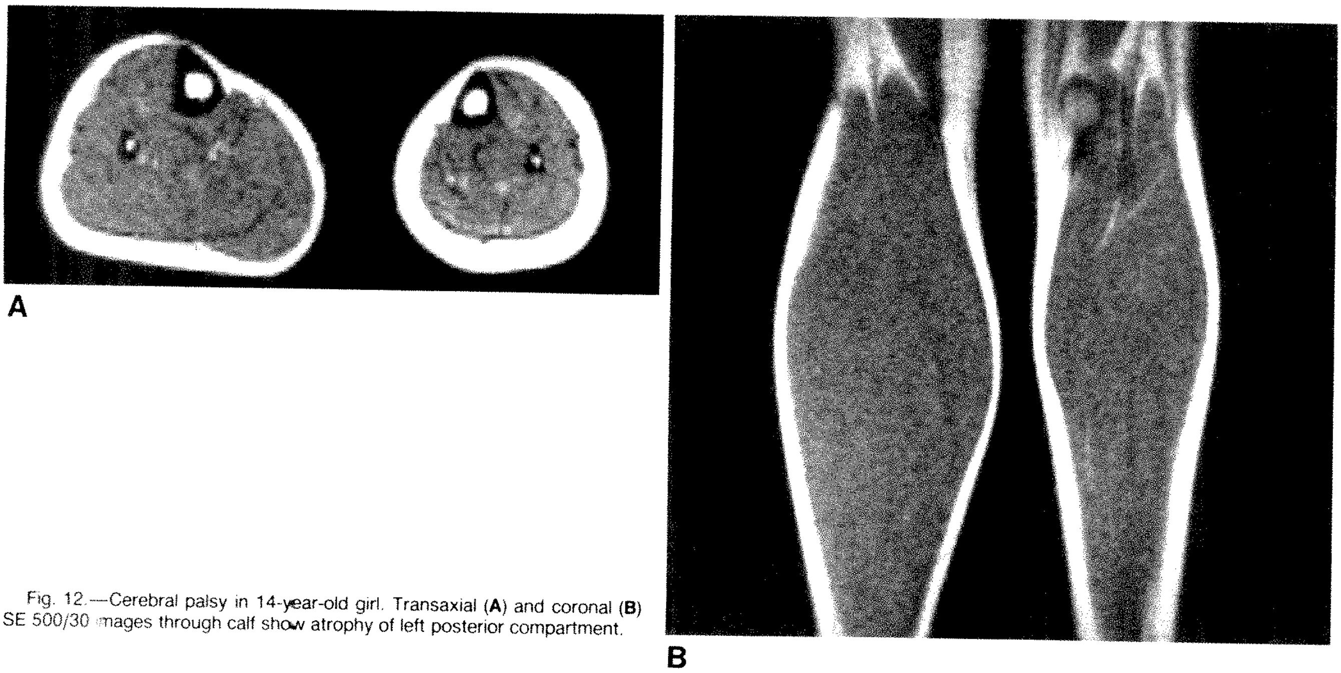

Fig. 12.—Cerebral palsy in 14-year-old girl. Transaxial (**A**) and coronal (**B**) SE 500/30 images through calf show atrophy of left posterior compartment.

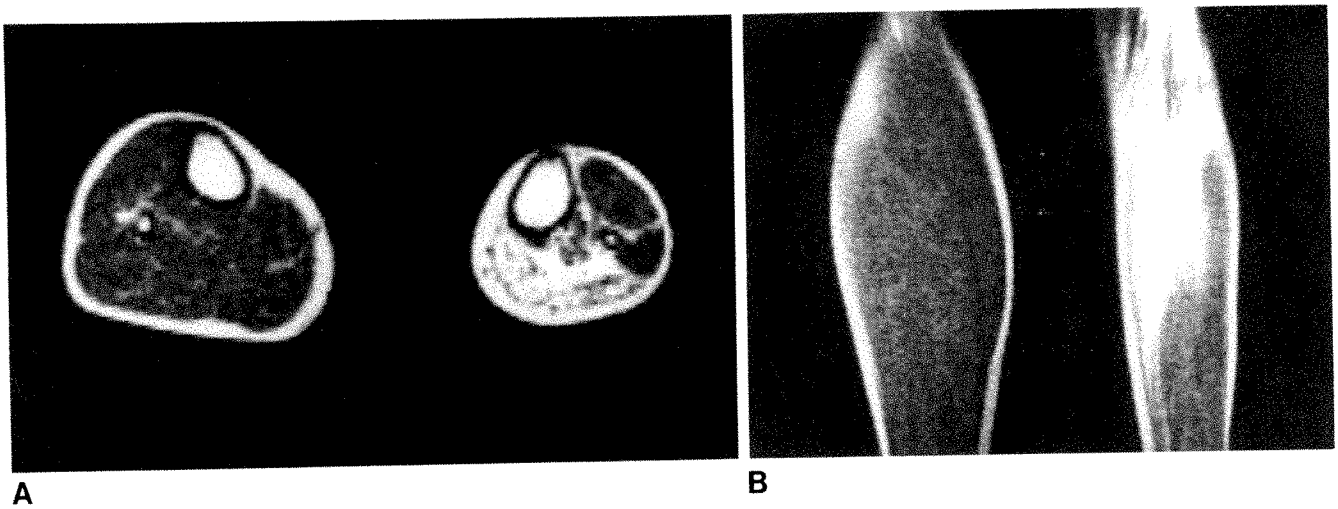

Fig. 13.—Poliomyelitis in 35-year-old man. Transaxial SE 300/30 (**A**) and coronal SE 500/30 (**B**) images through calf show fatty replacement of left posterior compartment.

REFERENCES

1. Chance B. Applications of ^{31}P NMR to clinical biochemistry. *Ann NY Acad Sci* **1984**;428:318–332
2. Newman RJ. Clinical applications of nuclear magnetic resonance spectroscopy: a review. *J R Soc Med* **1984**;77:774–779
3. Radda GK, Bore PJ, Rajagopalan B. Clinical aspects of ^{31}P NMR spectroscopy. *Br Med Bull* **1983**;40:155–159
4. Taylor DJ, Crowe M, Bore PJ, Styles P, Arnold DL, Radda GK. Examination of the energetics of aging skeletal muscle using nuclear magnetic resonance. *Gerontology* **1984**;30:2–7
5. Termote JL, Baert A, Crolla D, Palmers Y, Bulcke JA. Computed tomography of the normal and pathologic muscular system. *Radiology* **1980**;137:439–444
6. Hawley RJ Jr, Schellinger D, O'Doherty DS. Computed tomographic patterns of muscles in neuromuscular diseases. *Arch Neurol* **1984**;41:383–387

Locking and Unlocking of the Knee: Arthrographic Demonstration

Jorge E. Salazar,[1] Robert A. Duke, and Helen T. Winer-Muram

Locking of the knee joint is a common complaint in patients referred for knee arthrography. We recently observed a patient in whom locking and unlocking of the knee joint occurred during performance of arthrography. To the best of our knowledge, demonstration of arthrographic correlation with the clinical occurrence of locking and unlocking of the knee joint has not been reported before.

Case Report

A 58-year-old man sustained a sudden twist of the right knee associated with pain in the joint, causing him to fall to the ground. On arising he was unable to extend the joint. Subsequently, after painful manipulation, "locking" was reduced and full extension of the knee was accomplished. He has had several episodes of locking and unlocking of the knee since the initial injury and pain on the medial side of the knee. The patient was referred for arthrography.

About 40 ml of hemorrhagic fluid was aspirated from the joint. Renografin 60 (5 ml)(Squibb) mixed with 0.3 ml of 1:1000 epinephrine and 40 ml of room air was injected, followed by passive exercise of the knee by the examiner. While in the prone position and during distraction of the joint, the patient indicated that locking of the knee had taken place. During filming, amputation of the medial meniscus throughout its entire length was seen (fig. 1A). Since the nature of the injury could not be properly assessed during fluoroscopy, we opted for additional supine filming of the medial meniscus. On distraction in the supine position, the patient said, "You have just unlocked my knee." Subsequent filming showed a bucket-handle tear of the medial meniscus with no displacement of the torn fragment (fig. 1B). The lateral meniscus was normal.

Discussion

Locking of the knee joint usually means that the knee is held in a flexed position; while further flexion is possible, the patient is unable to extend the knee completely. Locking of the knee is most commonly associated with meniscal tears. A displaced fragment interposes between the tibia and the femur, preventing full extension of the joint. Locking can also occur in the presence of loose bodies, abundant fat pad, synovial fringes [1], or plicae. Conversely, during unlocking the tissue interposed between the tibia and the femur moves away from the joint space, allowing full extension of the knee joint with disentanglement and relief of symptoms.

Double-contrast knee arthrography has proven to be a safe and accurate technique in evaluating internal derangements of the knee, particularly those related to the menisci [2–6]. In

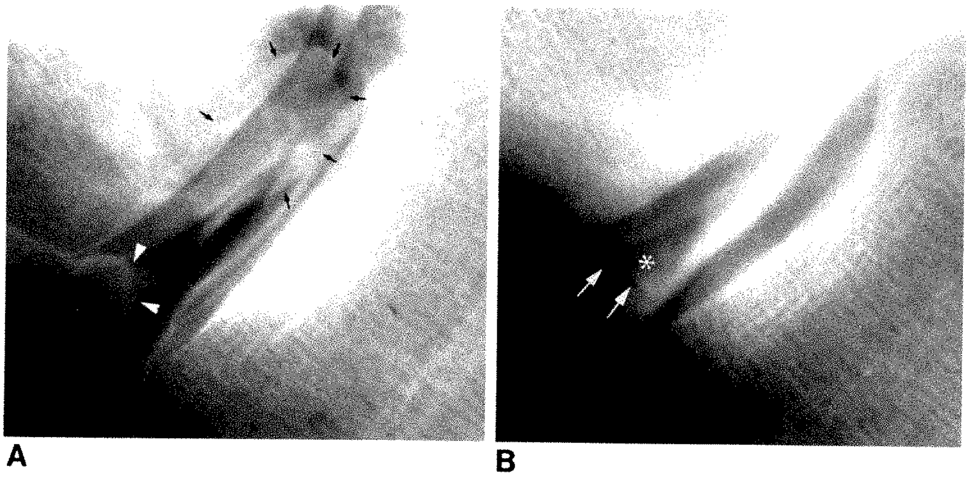

Fig. 1.—**A**, During locking, amputation of meniscus (*arrowheads*) occurs. *Arrows* denote fragment displaced toward intercondylar notch. **B**, Unlocking: meniscal tear is seen (*arrows*). Displaced fragment has returned to usual location (*asterisk*).

Received August 19, 1985; accepted October 10, 1985.

[1] All authors: Department of Radiology, University of Tennessee Center for the Health Sciences, and the Veterans Administration Medical Center, 865 Jefferson Ave., Memphis, TN 38163. Address reprint requests to J. E. Salazar.

AJR 146:575–576, March 1986 0361–803X/86/1463–0575 © American Roentgen Ray Society

this case, the additional supine filming clarified the abnormalities demonstrated during fluoroscopy, consequently allowing observation of what actually occurs during locking and unlocking of the knee joint in the presence of a torn meniscus.

REFERENCES

1. Lewin P. *The knee and related structures*. Philadelphia: Lea & Febiger, **1952**:200–201
2. Butt WP, McIntyre CB. Double contrast arthrography of the knee. *Radiology* **1969**;92:487–499
3. Kaye JJ, Nance EP. Meniscal abnormalities in knee arthrography. *Radiol Clin North Am* **1981**;19:277–286
4. Thijn CP. Accuracy of double contrast arthrography and arthroscopy of the knee joint. *Skeletal Radiol* **1982**;8:187–192
5. Freiberger RH, Killoran PJ, Cardone G. Arthrography of the knee by double contrast method. *AJR* **1966**;97:736–747
6. Dalinka MK, Coren GS, Wershba M. Knee arthrography. *CRC Crit Rev Diagn Imaging* **1973**;4:1–59

Percutaneous Gastrostomy and Gastroenterostomy:

1. Techniques Derived from Laboratory Evaluation

Eric vanSonnenberg[1,2]
Gerhard R. Wittich[1]
Linda K. Brown[1,3]
Lawrence B. Tanenbaum[1]
John B. Campbell[4]
Don A. Cubberley[1]
John F. Gibbs[1]

Various techniques, guidance systems, instruments, and the postmortem effects of percutaneous gastrostomy (PG) and percutaneous gastroenterostomy (PGE) were evaluated in 30 laboratory animals and five human cadavers. Methods to distend the stomach included air, fluid, intragastric balloon, and percutaneous needle inflation; a variety of trocar systems and catheters inserted by Seldinger technique (including those adapted from other uses and several designed specifically) were assessed. Fluoroscopy was the preferred guidance system, though sonography proved valuable (liver position, depth calculation to the stomach, localization of vessels to avoid), and the entire PG procedure was performed under sonographic guidance in four animals. Although the procedure was safe in most cases, several major complications did occur: laceration of a low-lying liver with exsanguination, malpositioned catheters in the lesser sac and adjacent to the spleen, and violation of the backwall of the stomach with laceration of celiac and splenic vessels. The animals and cadavers underwent autopsy. Autopsy revealed that firm gastrocutaneous tracts were formed by 7 days. There were few instances of wound infection, intraperitoneal fluid leakage, or evidence of trauma to the stomach when the catheters were well seated. Injury to the inferior epigastric artery is a potential hazard, and in cadaver dissections was located between the middle third and outer margin of the rectus abdominis muscle. Laboratory experience has been, and continues to be, an important means to improve and use new techniques for PG and PGE.

Nonoperative gastrostomy and jejunostomy appear promising as alternatives for enteric alimentation. One report in animals [1] and clinical articles [2–8] describe various techniques and equipment. Our study in dogs and human cadavers details experimental evaluation of these variables and several new methods. The trials included assessment of gastric distension (type and degree), techniques for catheter introduction, guidance systems, catheter types, and postmortem observations. On the basis of our experience in animals and cadavers, preferred techniques and equipment were used in our initial series of patients. The clinical material is described in the second article on our study [9].

Subjects and Methods

The laboratory studies were largely empirical, prompted by practical laboratory problems and clinical situations, rather than rigorous randomized comparisons. In the animal experiments, the procedure was initially performed on 22 dogs that had undergone cardiac experiments and had been sacrificed. Eight live dogs were used in the second phase of the study; these animals were maintained on antibiotics after gastrostomy. After sacrifice, autopsy and histologic evaluation were performed. In the third phase of the study, evaluation of percutaneous gastrostomy (PG) and gastroenterostomy (PGE) techniques and instrumentation was done on human cadavers. In three human cadavers, the inferior epigastric artery in the anterior abdominal wall was dissected to ascertain the exact position of the artery and thereby facilitate avoidance during puncture.

The aspects of PG and PGE that were evaluated included method and degree of gastric

---

Received April 29, 1985; accepted after revision November 5, 1985.

Presented at the annual meetings of the Society of Gastrointestinal Radiology, Napa, CA, September 1984 and the American Roentgen Ray Society, Boston, April 1985 (as the SGR Award Paper).

[1] Department of Radiology, University of California Medical Center (H-755), 225 Dickinson St., San Diego, CA 92103. Address reprint requests to E. vanSonnenberg.

[2] Department of Medicine, University of California Medical Center, San Diego, CA 92103.

[3] Present address: Department of Radiology, Duke University Medical Center, Durham, NC 27710.

[4] Department of Pathology, University of California Medical Center, San Diego, CA 92103.

AJR 146:577–580, March 1986
0361–803X/86/1463–0577
© American Roentgen Ray Society

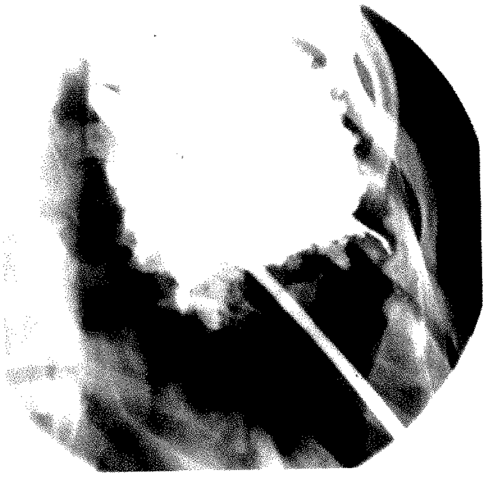

Fig. 1.—Trocar puncture for PG with intragastric balloon assistance: 12-French Stamey catheter is well seated in stomach of laboratory animal. Contrast has been injected for confirmation of position. This catheter was left in place for 5 weeks.

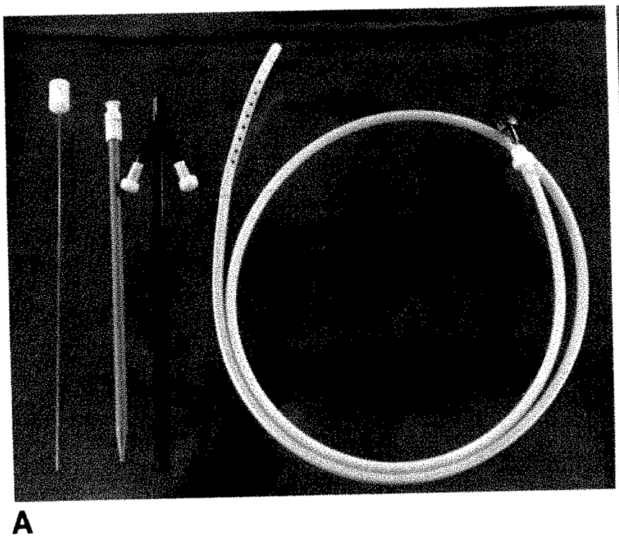

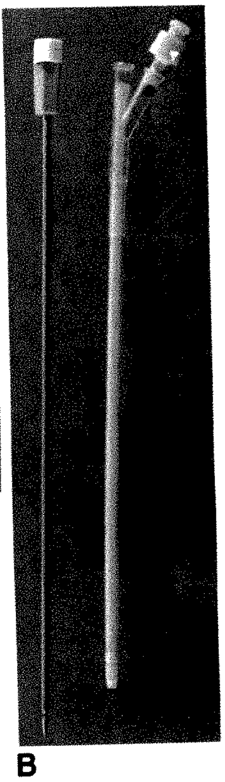

Fig. 2.—Prototype catheters for PG and PGE. **A**, This system may be inserted by Seldinger or trocar technique. It uses dilator with coaxial peel-away sheath. This enables 9- or 12-French, soft, multihole feeding tube to be placed into stomach or small bowel at initial procedure. This has become our preferred system (Cook). **B**, Another trocar catheter (12 French), which has two lumina, permitting balloon anchoring within stomach (Medi-Tech).

distension, Seldinger and trocar techniques for insertion, fluoroscopic and sonographic guidance, types of catheters, assessment of leakage, tract formation, and complications.

Gastric distension was achieved with air or fluid (water or contrast material) through nasogastric tubes or introduced into a balloon affixed to the end of a nasogastric tube. Gastric inflation with air also was performed by direct needle puncture into the stomach in two cadavers. Glucagon was used in several live animals to decrease gastric peristalsis.

Seldinger and trocar insertion methods were attempted, as was puncture with 18-gauge needles, 19-gauge needle/18-gauge sheath, and various size trocar catheters (fig. 1). The punctures were made after localization of the stomach, transverse colon, liver, and aorta and splenic vessels. After skin nick and soft-tissue dissection, the insertion instrument (needle or trocar) was inserted into the peritoneal cavity, then into the stomach by a short but firm thrust. Guide wires were placed, and either catheters were inserted directly (trocar technique) or tract dilatation preceded catheter insertion (Seldinger technique). Catheter sizes ranged from 6 to 14 French (F). Some catheters had intragastric anchor devices (pigtail, balloon, mushroom tip, Cope loop), and catheters without anchors were tried as well. Two specifically designed prototypes also were tested (Cook, Medi-Tech) (fig. 2).

Sonography (real-time) and fluoroscopy provided guidance for PG and PGE. Localization, puncture, and catheter insertion were attempted by fluoroscopy alone and sonography alone, and in combination. Complications were assessed by autopsy of all animals and examination of the cadavers after the procedures. Possible leakage of gastric contents was determined by follow-up sonograms, tube injections, and autopsies of animals at various stages after gastrostomy. Finally, gastrostomy tracts were removed en bloc, sectioned, and studied microscopically to evaluate tract maturation.

Results

Many of the results are qualitative impressions rather than quantitative. The ease of gastric access depended on the type and volume of gastric distension and the instrument used for puncture. Direct percutaneous puncture of the nondistended stomach was difficult (particularly with a paucity of gastric air to aim at) and even potentially deleterious. In cadavers, perigastric veins were entered and accidentally jected with air (fig. 3). Infusion of more than 500 ml of air or fluid via a nasogastric tube facilitated puncture; distension of more than 1 L was better, as it provided added firmness to the gastric wall. The position of the nasogastric tube was important: Too distal positioning of the tip of the tube allowed air to escape into the duodenum, and gastric distension was not maintained. Air distension of the stomach required the largest volumes (compared to fluid or intragastric balloon) to optimize puncture. The intragastric balloon provided the best support of the gastric wall to assist puncture.

Puncture was influenced significantly by the type of puncture assembly. An 18-gauge needle was the simplest instrument with which to pierce the stomach. Well tapered trocar-catheter systems could be passed into a well distended stomach, especially with intragastric balloon support. Thus, Sacks, Cook prototype, Medi-Tech prototype, and Stamey catheters were feasible; on the other hand, blunt-tipped catheters (Medi-Tech and Cook abscess and fluid drainage catheters) backed the gastric wall away and were unsuccessful.

Complications were more frequent with poor gastric disten-

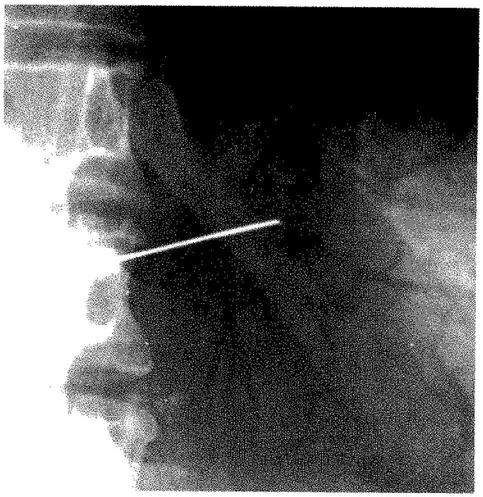

3

Fig. 3.—Direct needle puncture of cadaver stomach without distension simulates high-grade pharyngeal or esophageal obstruction and inability to pass nasogastric tube. Potential hazard is demonstrated as air was introduced inadvertently into perigastric veins in cadaver. Without gastric distension, puncture might best be done with CT guidance and by injecting sterile fluid.

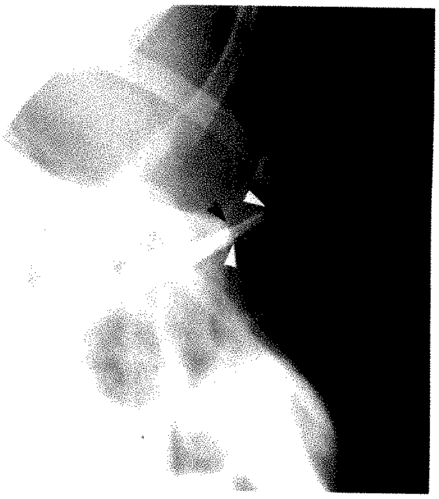

4

Fig. 4.—Complication of PG due to perforation of backwall of stomach: This needle-catheter assembly (*arrowheads*) transgressed posterolateral wall of stomach and caused retrogastric hematoma and vascular injury. There is free contrast material and air. Prior measurement of backwall depth of stomach and marking on instrument should avoid this problem.

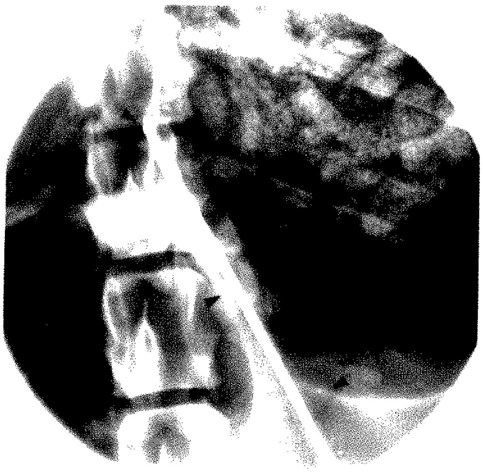

5

Fig. 5.—Problem of compliant stomach wall being displaced, rather than punctured, during PG. 12-French trocar catheter pushes greater curvature of air-distended stomach inward (*arrowheads*) rather than piercing it. Gastric displacement may occur during puncture or with dilators or catheters over guide wires as well.

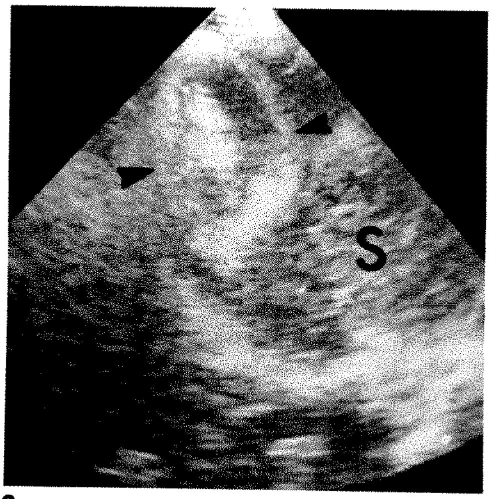

6

Fig. 6.—Sonographic guidance for PG uses intragastric balloon distension of stomach (S) as target. Parasagittal sonogram in left upper quadrant of dog demonstrates partially inflated intragastric balloon (*arrowheads*) with 50 ml of water. Another 500 ml of fluid provides good distension and support of gastric wall. This method is particularly helpful for trocar puncture and when sonography is the sole guidance system.

sion and suboptimal instruments, since the entry thrust needed to be greater and, hence, more hazardous. Excessively hard thrusts against the stomach increased the chance of backwall perforation of the stomach (fig. 4). Inward displacement rather than puncture of the gastric wall occurred with underdistension of the stomach or with blunt catheters, and with fascial dilators which occasionally pushed the wall away (fig. 5). On occasion, this resulted in buckling of guide wires in the peritoneal cavity and loss of gastric access in several animals.

Fluoroscopy was most useful for actual puncture and catheter positioning. However, the depth of puncture (to the anterior and posterior gastric wall) and localization of the left lobe of the liver were better determined by sonography. The entire procedure was performed with fluoroscopy alone and with sonography alone. With sonography, distension of the stomach or intragastric balloon with fluid rather than air was necessary for gastric target localization (fig. 6). With sonography, PG was performed, rather than PGE.

Anchoring was achieved by catheters with balloons, Cope loops, pigtail catheters, mushroom-tipped designs, and distal placement in small bowel (fig. 6). Balloons (Ingram and Argyll catheters) were most reliable, as the other systems dislodged in some animals. Cope loops anchored Sacks catheters, which dislodged too easily without the loops.

Animals underwent autopsy up to 5 weeks after the procedure. Postmortem examinations demonstrated mature gastrocutaneous tracts after 7 days in four animals. Before this 7 days, tracts were immature and in danger of being lost with catheter manipulations. No free intraperitoneal fluid was seen at autopsy in animals whose catheters were correctly positioned in the stomach.

Autopsy dissection in cadavers revealed the inferior epigastric artery to course medially as it ascends cephalad. At the site of puncture for PG, the artery lies at the junction of the medial two-thirds and lateral one-third of the rectus muscle.

Complications in animals included exsanguination due to hepatic laceration, two lesser sac hematomas due to splenic and great vessel puncture, and perisplenic fluid due to catheter malposition. Intraperitoneal fluid was not seen in any animal in whom the catheter was well positioned. Potential leakage was assessed in vivo by sonography of the subphrenic, subhepatic, pelvic, and lesser sac spaces in the live animals.

Discussion

Laboratory experience has demonstrated that PG and PGE are feasible by radiologic methods, that both instrumentation and technique affect the success, and that if done improperly, significant complications may occur. We modified several of our early concepts on the basis of the laboratory trials. For example, the combination of fluoroscopic and sonographic guidance has advantages (although either may be used alone), gastric wall puncture is more difficult than initially suspected and requires proper distension and well designed instruments, and that anchoring of the stomach to the abdominal wall may not be necessary. Although PG and PGE generally are safe procedures, a few major problems in the animals underscore the need for careful planning, meticulous technique, and continued refinement of materials. Albeit infrequent, prior reports have documented death, peritonitis, and major bleeding with PG [7-9].

Ease of catheter insertion depends on the method of gastric distension and the design of the needle-catheter system. The stomach is a compliant, muscular structure, and puncture of it differs from puncture of pathologic fluid collections, such as cysts or abscess cavities. It has a tendency to back away from incoming needles and catheters. Volume of distension is important to aid puncture, and greater than 500 ml is advisable (1 L or greater is even better) with air insufflation. Position of the nasogastric tube is important, as too-distal positioning of it permits air to escape into the duodenum. Glucagon may be beneficial to assist gastric distension. Trocar puncture is facilitated by the intragastric balloon assistance method with air (preferable) or fluid for support [6]. Puncture should be as smooth as possible and preferably with one or not more than two attempts. When access is not readily achieved and multiple punctures are made, there obviously is greater risk of leakage [3, 5, 9].

Fluoroscopy is the optimal method for puncture, catheter and guide wire maneuvering, and final catheter positioning. Sonography offers further advantages in the performance of PG and PGE. The depth to the anterior and posterior walls of the stomach, hepatic-gastric relationship, and anteroposterior position of the catheter within the stomach (when sonography is the sole guidance system) are information provided by sonography. Several complications might have been avoided had we used sonography: The death of one animal from inadvertent hepatic puncture and knowledge of the depth of puncture may have prevented both a large lesser sac collection and injury to the celiac and splenic vessels due to backwall transgression of the stomach. Perhaps most intriguing as a guidance possibility is that the entire procedure may be accomplished with portable real-time sonographic guidance. This may be appropriate for bedside gastrostomy. (The palpable intragastric balloon also is particularly suited for this use.) PG was accomplished successfully four times using sonographic guidance alone in animals.

Postmortem studies demonstrated several useful concepts. First, tracts matured by a week, and then catheter exchange could be performed without the risk of losing access to the stomach. Prior to that, we had instances where continuity to the stomach was lost as the guide wire became dislodged. Second, with catheters in correct position, leakage of fluid did not occur, despite not juxtaposing the anterior stomach wall to the abdominal wall. Finally, dissection of the inferior epigastric artery in the cadavers demonstrated its position (along the mid to outer third of the rectus muscle); avoidance of the vessel should remove this potential hazard for PG and PGE puncture.

Several problems remain unanswered and await further laboratory evaluation and clinical trials: final design of the optimal catheter, the choice of trocar or Seldinger technique, and whether or not to appose the anterior gastric wall to the abdominal wall. Many aspects of PG and PGE probably will be individualized, as is the case with other interventional techniques. Laboratory experience has demonstrated the procedure to be effective and safe when done correctly, and that it may be performed entirely by radiologic techniques. Major complications may be avoided with the proper precautions and with appropriately designed tools.

ACKNOWLEDGMENTS

We thank Deborah Lynn and Peggy Clark for manuscript preparation.

REFERENCES

1. Sacks BA, Vine HS, Palestrant AM, Ellison HP, Shropshire D, Lowe R. A nonoperative technique for establishment of a gastrostomy in the dog. *Invest Radiol* **1983**;18:485-487
2. Ho CS. Percutaneous gastrostomy for jejunal feeding. *Radiology* **1983**;149:595-596
3. Wills JS, Oglesby JT. Percutaneous gastrostomy. *Radiology* **1983**;149:449-453
4. McLean GK, Rombeau JL, Caldwell MD, Ring EJ, Freiman DB. Percutaneous gastrostomy. *AJR* **1982**;139:1129-1133
5. Preshaw RM. A percutaneous method for inserting a feeding gastrostomy tube. *Surg Gynecol Obstet* **1981**;152:659-660
6. vanSonnenberg E, Cubberley DA, Brown LK, Wittich GR, Lyon JW, Stauffer AE. Percutaneous gastrostomy: use of intragastric balloon support. *Radiology* **1984**;152:531-532
7. Bretagnolle M, Bret PM, Fond A, Ponchon T, Lambert R, Bret P. Percutaneous insertion of a feeding gastrostomy tube. Presented at the annual meeting of the Radiological Society of North America, Washington, DC, November **1984**
8. Willis JS, Oglesby JT. Percutaneous gastrostomy: further experience. *Radiology* **1985**;154:71-74
9. vanSonnenberg E, Wittich GR, Cabrera OA, et al. Percutaneous gastrostomy and gastroenterostomy: 2. Clinical experience. *AJR* **1986**;146:581-586

Percutaneous Gastrostomy and Gastroenterostomy:

2. Clinical Experience

Eric vanSonnenberg[1,2]
Gerhard R. Wittich[1]
Octaniano A. Cabrera[1]
Stephen F. Quinn[1]
Giovanna Casola[1]
Arthur A. Lee[1]
Robert A. Princenthal[1]
James W. Lyons[1,3]

This report describes the authors' initial experience with percutaneous gastrostomy (PG) and gastroenterostomy (PGE) in 40 patients. Indications for PG and PGE included alimentation (35 patients) and small bowel decompression (five). Seldinger technique with air distension of the stomach via a nasogastric tube (20 patients) is a simple method to insert small (7–9 French) and firm catheters; tube exchanges for larger and softer catheters often are necessary by this method (23 procedures in 17 patients). Coaxial trocar technique (19 patients) permits initial insertion of softer and often larger catheters (9–14 French feeding tubes), which are less likely to clog or require exchange; the intragastric balloon support method facilitates trocar insertion. Now preferred is a system that uses 18-gauge needle puncture and allows coaxial insertion of a final soft feeding tube at the initial procedure. Small bowel catheter positioning (PGE) (31 patients) was more common than gastrostomy alone (8 patients); "downhill puncture" toward the gastric antrum assists direct guide-wire cannulation of the duodenum via the gastric puncture (12 patients). Five complications occurred; two were major and included catheter dislodgement in one patient. Another patient, who had a pharyngeal tumor, suffered profound respiratory difficulty from premedication and nasogastric tube malposition; patients with head and neck tumors present particular problems with nasogastric tube passage and airway monitoring. Inability to pass a nasogastric tube does not preclude PG and PGE, as direct puncture of the stomach is feasible.

Nutritional support by gastrostomy feeding is an important treatment adjunct when there is major swallowing difficulty or with debilitating diseases. Surgical creation of a gastrostomy, while generally effective, requires general anesthesia in up to 25% of cases [1], has complications in 3%–35% [1–6], a mortality of 1%–6% [1–6], and is costly. Thus, alternative percutaneous [7–13] and endoscopic [14–16] methods for placement of gastrostomy tubes have begun to be developed.

We describe our initial clinical experience with 40 patients. A variety of techniques was used, based in part on experience and safety developed during animal and cadaveric studies [11]. Our study varies in several respects from prior reports [7, 8, 10]—we emphasize tailoring the procedure (e.g., method of gastric distension, puncture instrument, catheter type) to the particular clinical situation, the uses of sonography, the technical utility of the "downhill puncture," PG and PGE for enteric decompression as well as nutrition, and the advantages of coaxial duodenal and jejunal tubes, which, among other things, permit feeding to be done immediately [9].

Subjects and Methods

Radiologic PG and PGE have been performed in 40 patients over a 2-year period. There were 24 men and 16 women aged 43–76 years. Indications for PG and PGE were dysphagia and cachexia from malignancy (head and neck, nine; gynecologic, six; esophageal, two; brain, one) and neurologic disorders (stroke, 18; Alzheimer disease, one; organic brain syndrome, one; psychiatric disorder, one; and Kuf disease, one). Two patients had prior surgical

Received April 29, 1985; accepted after revision November 5, 1985.

Presented at the annual meetings of the Society of Gastrointestinal Radiology, Napa, CA, September 1984 and the American Roentgen Ray Society, Boston, April 1985 (as the SGR Award Paper).

[1] Department of Radiology, University of California Medical Center (H-755), 225 Dickinson St., San Diego, CA 92103. Address reprint requests to E. vanSonnenberg.

[2] Department of Medicine, University of California Medical Center, San Diego, CA 92103.

[3] Community Hospital of Chula Vista, Chula Vista, CA 92010.

AJR 146:581–586, March 1986
0361–803X/86/1463–0581
© American Roentgen Ray Society

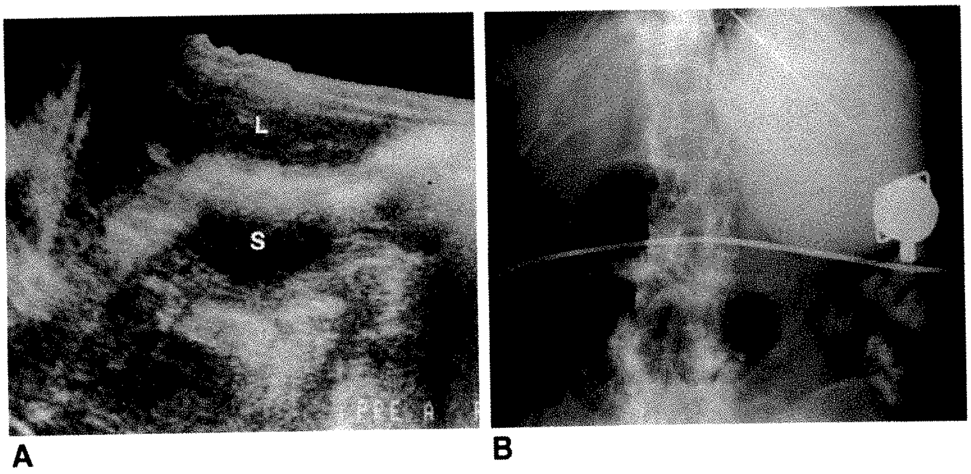

Fig. 1.—Preprocedure localization of liver and transverse colon for safe PG and PGE. **A**, Parasagittal sonogram demonstrates thin overhanging left lobe of liver (L), which is draped over stomach (S). **B**, Overhead abdominal radiograph with distended intragastric balloon. Caudal extent of liver (as determined by sonography) is marked by catheter placed at inferior aspect of the liver. Potential hazard of hepatic puncture is apparent. Note contrast in large bowel and narrow access to stomach in this patient.

gastrostomies that became dislodged accidently with loss of the tracts; de novo radiologic gastrostomies were inserted.

All procedures were performed in the Radiology Department under fluoroscopic control. In 35 patients, portable real-time sonography was used to localize the liver (fig. 1) and to determine the depth of puncture. Sterile tape was applied to the trocar or needle for the appropriate puncture depth. The transverse colon was identified by visible gas on plain film or when water-soluble contrast medium was instilled per rectum (six patients). Gastric distension was achieved through a nasogastric tube in all cases except one (direct puncture of the stomach). The distending agent was either air (14 patients) or water-contrast mixture (five patients) in the stomach itself, or air (12 patients) or fluid (eight patients) into an intragastric balloon [12]. Glucagon (1 or 2 mg intravenously) was used routinely in the last 26 patients to help augment gastric distension. Both Seldinger (20 patients) and trocar (19 patients) methods were used for puncture and catheter insertion. A variety of catheters (6.2 to 14 French [F]) was placed at the initial procedure. These included Stamey (two), Ingram (one), long pigtail catheters (10 patients), and new, specifically designed soft or standard feeding tubes (9–12 F) (26 patients) (Cook, Medi-Tech). Catheter exchanges were performed in 23 cases. Coaxial 7 to 12 F catheters eventually were placed in the duodenum or jejunum in 31 patients.

Insertion technique involved sterilization of the skin and local anesthesia at the puncture site. The puncture site was chosen to avoid the inferior epigastric artery (mid to outer third of rectus abdominis muscle); thus punctures were made lateral to the rectus muscle, or in the midline in five patients. A skin nick was made with a no. 11 scalpel blade, and the soft tissues were dissected bluntly and deeply. Trocars or needles were inserted either by direct puncture into the stomach or by initial insertion into the peritoneal cavity (sometimes up to the gastric wall, which could be pushed), and then into the stomach. With trocar catheters or the new combined set (18-gauge needle puncture, coaxial sheath permitting insertion of soft feeding tube), inner coaxial long feeding tubes were advanced into the duodenum or jejunum over a guide wire that had been placed through the peel-away sheath (Cook) (fig. 2).

After catheter insertion, the nasogastric tubes were used to aspirate intragastric fluid or air after balloon puncture, and were left within the stomach for 1–5 days for decompression. Removal of the nasogastric tubes was without problem in all cases (with or without an attached balloon). In one patient, no nasogastric tube was passed due to large cervical osteophytes obstructing the esophagus; the 22-gauge removable hub needle set with the coaxial single large guide wire technique was used for direct puncture of the stomach and placement of a 7.6 F catheter in the jejunum [17]. Catheters were affixed to the skin by a Molnar disk or by adhesive tape flagged on the catheter and sutured to the skin.

Results

PG and PGE catheters were inserted successfully in all 39 patients in whom puncture was attempted. Puncture was not made in one patient who suffered respiratory distress due to preprocedure sedation (Demerol 75 mg intramuscularly, Phenergan 25 mg intramuscularly, Valium 10 mg orally) and difficulty in nasogastric tube passage.

Preprocedure sonographic localization was particularly valuable in four patients in whom thin, low-lying left lobes of the liver shielded the stomach. Minor difficulties were encountered in initial access in six patients. In one of these patients, two prior surgical gastrostomies resulted in firm fibrous tissue which prevented easy puncture. In two other patients, the intragastric balloon was ruptured but the tip of the incoming instrument could not be confirmed to be within the stomach. In two patients, large trocars (14 F) were unable to puncture an air-filled stomach by reasonable thrusts. Subsequent punctures with 18-gauge needles were successful in these patients. In two patients with procedures done by Seldinger technique and another by trocar, dilators and an improperly fitting catheter backed the anterior stomach wall away. The guide wires dislodged from the stomach and access was lost. Repuncture was necessary in each case and no untoward effects occurred. No free fluid was observed by follow-up sonographic examination or catheter sinogram in the patients where these technical problems occurred.

Small bowel feeding tubes were used in 31 patients. These consisted of a variety of 7 to 14 F catheters (with and without pigtail tips). Feeding was begun between days 1 to 5 after tube insertion and was tolerated well. Gastrostomy catheters were exchanged for Foley catheters in two patients and for Ingram catheters in two patients (fig. 3). The balloon on the Foley catheter spontaneously burst after 10 days in one patient, which necessitated tube exchange (table 1).

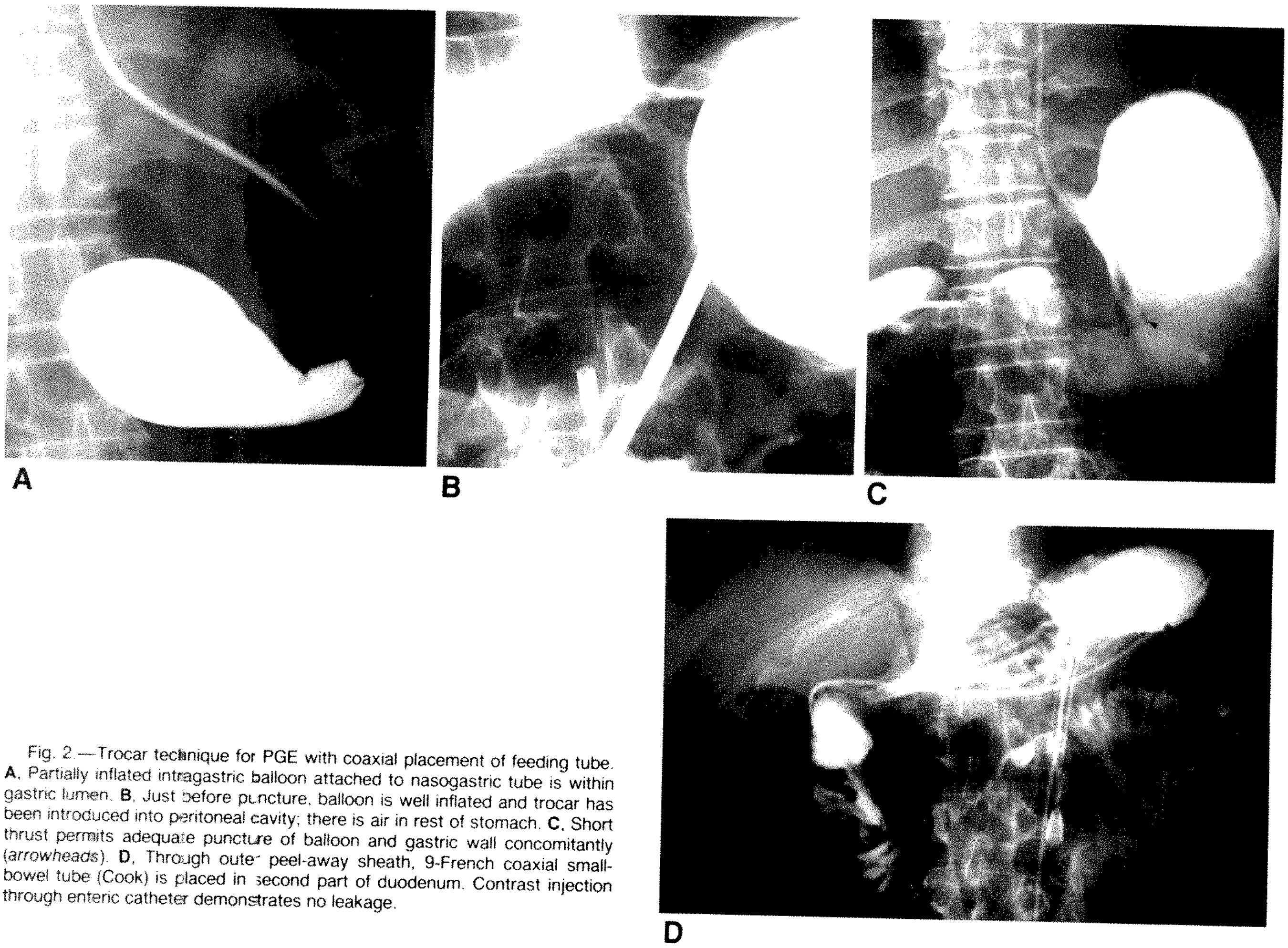

Fig. 2.—Trocar technique for PGE with coaxial placement of feeding tube. **A**, Partially inflated intragastric balloon attached to nasogastric tube is within gastric lumen. **B**, Just before puncture, balloon is well inflated and trocar has been introduced into peritoneal cavity; there is air in rest of stomach. **C**, Short thrust permits adequate puncture of balloon and gastric wall concomitantly (*arrowheads*). **D**, Through outer peel-away sheath, 9-French coaxial small-bowel tube (Cook) is placed in second part of duodenum. Contrast injection through enteric catheter demonstrates no leakage.

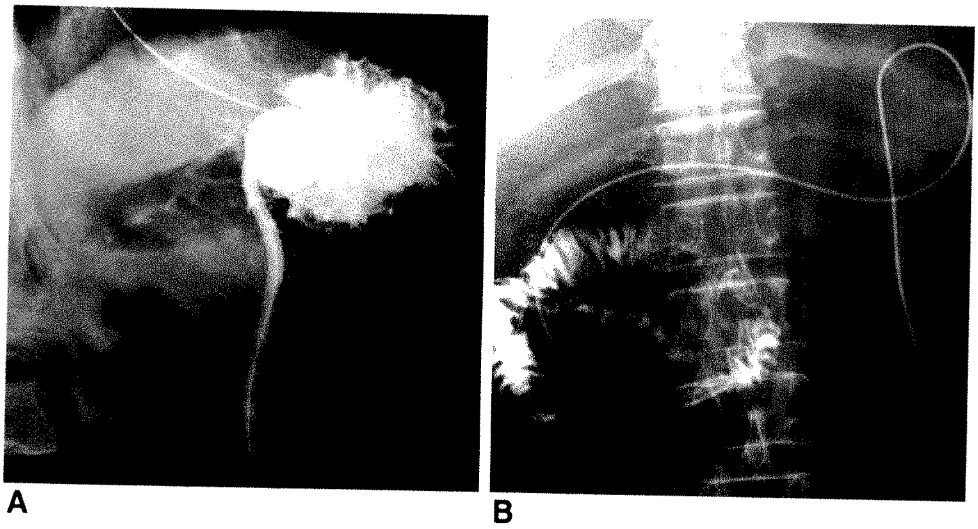

Fig. 3.—Optimal final positions for gastric vs. small bowel feeding. **A**, 14-French Foley catheter with inflated balloon tip is well seated in stomach. **B**, Coaxial placement of 10-French catheter in distal duodenum. Nasogastric tube has been removed and feeding was begun on first postprocedure day. Note that contrast flows antegrade, eliminating chance of gastroesophageal reflux.

TABLE 1: **Summary of Techniques Used for PG and PGE**

Technique	No. of Patients ($n = 40$)
Method of gastric distension:	
Intragastric balloon:	
Air	14
Fluid	6
Via nasogastric tube:	
Air	16
Contrast-water mixture	3
Direct puncture of stomach	1
Insertion technique and initial catheters:	
Trocar:	
Stamey	2
Ingram	1
Cook gastroenterostomy	12
Medi-Tech gastrostomy	4
Seldinger:	
18-gauge needle	19
Coaxial (17)	1
Site and type of final feeding catheters:	
Stomach:	
Foley (12 French)	2
Ingram (12 French)	1
Fluid drainage (Cook 9 French)	1
Duodenum:	
Coaxial Cook feeding tube (11 French)	13
Coaxial Medi-Tech (9 French)	3
Jejunum	
Pigtail (7–9 French)	9
Cook feeding tube	4
Argyle nasogastric tube	9

Complications occurred in five patients: Two were considered major and three minor. The minor complications included one patient who had chronic gastroesophageal reflux, who actually refluxed the inner coaxial enteric feeding tube. On the postprocedure radiograph, the malpositioned tube was noted (fig. 4) and withdrawn to the correct position. Another patient had about 10 ml of sanguinous material aspirated from the nasogastric tube after the procedure. One patient had skin irritation due to leakage of gastric contents back along the tube tract; he had no intraperitoneal fluid by sonography. The major complications included one patient in whom a pigtail 7 F catheter became dislodged from the stomach and lay free within the peritoneal cavity 5 days after the procedure. The mechanism of dislodgement was unclear; however, the patient suffered no residua, and follow-up radionuclide and sonographic studies revealed no leak (fig. 5). The other major complication was described previously (respiratory distress). No complications required surgery. There were no procedure-related deaths.

Discussion

Our early experience indicates that PG and PGE are feasible and may be accomplished safely by a variety of techniques, each of which has advantages and disadvantages. Our methods and instruments changed as clinical problems arose or when new materials or ideas needed testing in the laboratory [11]. Thus instrument design has been refined, specific indications for the various techniques have become more apparent, further uses for PGE have evolved (enteric decompression, small bowel feeding), and complications have been minimized.

Several preparatory steps are necessary for safe performance of PG and PGE. Identification of the transverse colon by fluoroscopy (or contrast per rectum) avoids the reported complication of colonic fistula formation, which has occurred using radiographic, endoscopic, and surgical techniques [13, 14, 18]. Inadvertent and dangerous puncture of the left lobe of the liver is avoided by sonographic localization [8, 9, 11]; a low-lying left lobe of the liver may not be appreciated by fluoroscopy alone. Depth measurement to the wall of the stomach or to the intragastric balloon is an added benefit of sonography. The posterior measurement is valuable to avoid puncture of the splenic and great vessels, the pancreas, and the spleen; however, it can only be assessed accurately if fluid is used to distend the stomach (air distension shadows the posterior wall). A fluoroscopic C-arm or cross-table lateral radiograph also may be helpful for depth determination.

The several methods of gastric distension each have advantages and disadvantages. The intragastric balloon offers added support for the compliant gastric wall and is valuable for trocar insertion. Most candidates for PG and PGE are thin, allowing the intragastric balloon to protrude visibly on the abdominal wall and to be palpable, which provides an excellent target. This method is applicable in patients with neurologic disorders or for bowel decompression, when a well fitting nasogastric tube–balloon assembly can be passed without difficulty. The drawback is the patient with a head and neck or esophageal tumor, where a nasogastric tube alone must suffice due to the partial obstruction. Patients in whom nasogastric tube passage is impeded due to high-grade obstruction present a special problem. Direct puncture at fluoroscopy aimed toward intragastric air is feasible and was successful in one patient.

We came to prefer air for either direct gastric distension or the balloon method. The rationale is to reduce the chance for aspiration into the lungs or for fluid spillage into the peritoneum. A caveat with air distension is that the stomach wall may be pushed rather than punctured, particularly by trocar technique. Preshaw [10] described unsuccessful catheter insertion in three of 11 cases with air as a distending agent. The 9 F trocar puncture device (Cook) is simple and safe, especially with balloon support, and is expeditious since the final catheter may be placed at the initial procedure.

Trocar and Seldinger techniques each have benefits and disadvantages. Trocar technique offers the simplicity of fewer guide wire and dilator exchanges and fewer materials. Also larger, soft tubes may be inserted primarily, obviating further procedures. Seldinger technique with air distension does not require balloon assistance. The puncture is easy, although the final large, soft catheters are more difficult to insert at the initial sitting. A problem inherent to puncture of viscuses (stomach, gallbladder) is that needles, dilators, and catheters may push the wall, rather than enter it. In our series, gastric access was even lost in a few patients. Wills and Oglesby

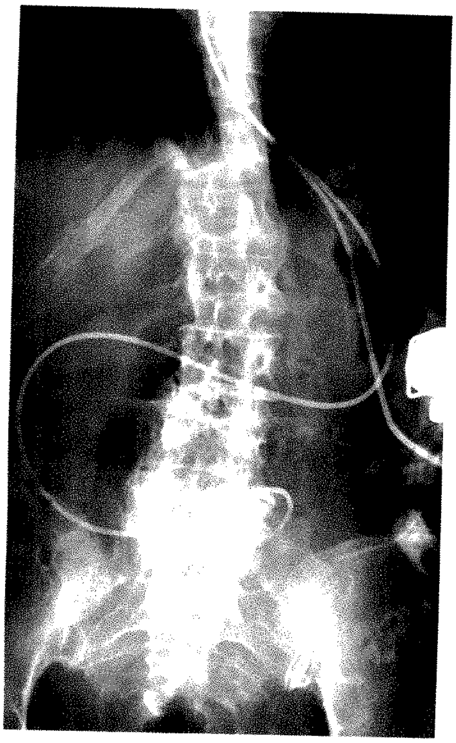

Fig. 4.—Complication of PGE: 62-year-old woman with ovarian carcinoma had trocar placement of gastroenterostomy tube; 9-French feeding tube was placed coaxially in jejunum. Overhead radiograph taken at end of procedure showed that part of feeding tube had been refluxed into esophagus. Tube was pulled back and repositioned in jejunum; feeding began next day.

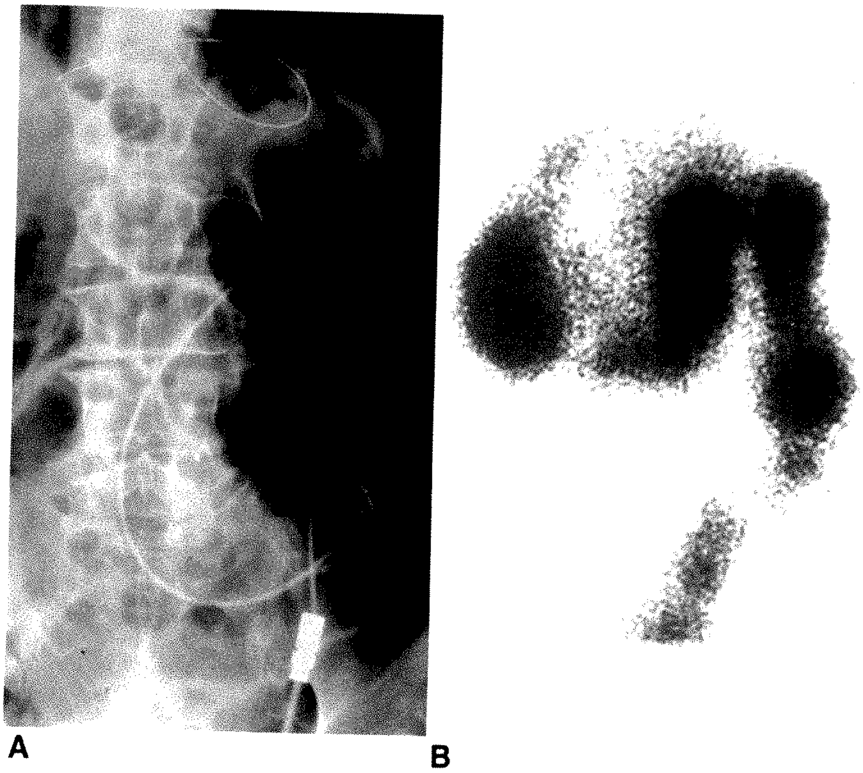

Fig. 5.—Complication of PGE—tube dislodgement. **A**, 5 days after uneventful jejunal positioning of PGE tube, follow-up overhead film demonstrated malpositioned catheter in peritoneum. **B**, Radionuclide examination with technetium sulfur colloid through nasogastric tube demonstrates no leak of contents from gastrointestinal tract (all radionuclide contained within small bowel loops). Patient remained well, and procedure was redone.

[13] and Ho et al. [19] report similar problems of gastric wall displacement and guide wire buckling. We have progressed to a system that combines benefits of several techniques: 18-gauge needle puncture may be converted to a sheath system (similar to trocar technique), which then allows placement of large soft catheters, while still using a relatively small needle.

Through gastrostomy access, feeding may be accomplished into the stomach, duodenum, or the jejunum. We now prefer small bowel position of the catheters for three reasons: Alimentation can be initiated sooner (less chance of gastric leak with distal feeding), the possibility of gastroesophageal reflux is minimized (a particular hazard in many patients with neurologic and pharyngeal disorders), and there is an extra measure of anchoring and safety with the more distally seated catheter. Gastroenterostomy tubes also may be used for enteric decompression in patients with chronic partial small bowel obstruction, in addition to the usual alimentation indication; this eliminates long-term use of nasogastric tubes and has been especially appreciated by these patients.

Although a few complications occurred, none prompted operation and no catheter-related complication caused significant clinical deterioration. Minor complications included partial gastroesophageal reflux of a small bowel feeding tube, leakage along the gastrostomy tract with local inflammation, and postprocedure blood-tinged fluid; all were treated conservatively and without problem. One complication necessitated redo of the procedure (dislodgement of the tube into the peritoneal cavity on the fifth postprocedure day). The patient had mild abdominal pain for a day but no other sequela or evidence of gastric leak. Clearly the worst complication was respiratory distress due to sedation and nasogastric tube malposition in a patient with a head and neck tumor. Standard preprocedure preparation that was used for other patients was deleterious for him. This group of patients with potential airway problems (usually head and neck tumors) requires assistance from their surgeons and anesthesiologists for safe passage of nasogastric tubes, for intraprocedural airway and cardiac monitoring, and for sedation due to their tenuous airways. This clearly is a higher risk group. However, this is an indication for radiologic PG and PGE, since endoscopic gastrostomy is unfeasible and surgery usually is undesirable.

Follow-up plain radiographs to ascertain catheter position may be helpful. In one patient, information from the radiograph averted a problem: Appreciation of rupture of the Foley balloon in the stomach prompted replacement before the tube could become dislodged. In three other patients, retrograde movement of catheters from the jejunum to the proximal duodenum was noted and corrected easily.

Potential leakage from the stomach may be assessed by contrast sinography, sonography of the peritoneal compartments, and by radionuclide dynamics after injection into the catheter. Ho [9] has pointed out that coaxial small bowel feeding tubes may obviate apposing the stomach to the anterior abdominal wall. Our experience so far supports this—no leaks were documented in our patients, even in patients in whom puncture was difficult or in the patient whose catheter became dislodged. In our series, we used two types of catheters with balloons at their tips (Ingram, Medi-Tech prototype); however, no definite advantage was demonstrated. Several patients had sonographic studies after PGE and one had CT. In no patient was peritoneal fluid seen.

In summary, as with most interventional radiology procedures, a variety of methods is workable for PG and PGE. Currently, our preferences include the 18-gauge needle puncture and peel-away coaxial sheath for initial insertion of large soft catheters when possible. Trocar technique (with or without balloon assistance) is applicable in neurologic patients or those with small bowel obstruction. In patients with head and neck or esophageal tumors, distension with a nasogastric tube alone or of the stomach itself and Seldinger puncture is preferable. Inability to pass a nasogastric tube does not contraindicate PG or PGE. Combined sonographic-fluoroscopic localization is advantageous, and we almost always place catheters into the small bowel to improve anchoring and start feeding earlier. We believe PG alone rarely is indicated or preferred [19], and PGE is easily accomplished by standard radiologic techniques, even if a second sitting is required.

ACKNOWLEDGMENTS

We thank Deborah Lynn, Peggy Clark, Brian Bates, and Joe Roberts for assistance.

REFERENCES

1. Wasiljew BK, Ujiki GT, Beal JM. Feeding gastrostomy: complications and mortality. *Am J Surg* **1982**;143:194–195
2. Gallagher MW, Tyson KRT, Ashcraft KW. Gastrostomy in pediatric patients: an analysis of complications and techniques. *Surgery* **1973**;74:536–539
3. Haws EB, Sieber WKl, Kiesewetter WB. Complications of tube gastrostomy in infants and children: 15-year review of 240 cases. *Ann Surg* **1966**;164:284–290
4. Connar RG, Sealy WC. Gastrostomy and its complications. *Ann Surg* **1956**;143:245–250
5. Campbell JR, Sasaik TM. Gastrostomy in infants and children: an analysis of complications and techniques. *Am Surg* **1974**; 40:505–508
6. Holder TM, Leape LL, Ashcraft KW. Gastrostomy: its use and dangers in pediatric patients. *N Engl J Med* **1972**;286:1345–1347
7. Sacks BA, Vine HS, Palestrant AM, Ellison HP, Shropshire D, Lowe R. A nonoperative technique for establishment of a gastrostomy in the dog. *Invest Radiol* **1983**;18:485–487
8. Wills JS, Oglesby JT. Percutaneous gastrostomy. *Radiology* **1983**;149:449–453
9. Ho CS. Percutaneous gastrostomy for jejunal feeding. *Radiology* **1983**;149:595–596
10. Preshaw RM. A percutaneous method for inserting a feeding gastrostomy tube. *Surg Gynecol Obstet* **1981**;152:659–660
11. vanSonnenberg E, Wittich GR, Brown LK, et al. Percutaneous gastrostomy and gastroenterostomy: 1. Techniques derived from laboratory evaluation. *AJR* **1986**;146:577-580
12. vanSonnenberg E, Cubberley DA, Brown LK, Wittich GR, Lyon JW, Stauffer AE. Percutaneous gastrostomy: use of intragastric balloon support. *Radiology* **1984**;152:531–532
13. Wills JS, Oglesby JT. Percutaneous gastrostomy: further experience. *Radiology* **1985**;154:71–74
14. Larson DE, Fleming CR, Ott BJ, Schroeder KW. Percutaneous endoscopic gastrostomy—simplified access for enteral nutrition. *Mayo Clin Proc* **1983**;58:103–107
15. Ponsky JL, Gauderer MWL, Stellato TA. Percutaneous endoscopic gastrostomy: review of 150 cases. *Arch Surg* **1983**; 118:913–914
16. Gauderer MWL, Ponsky JL, Izant RJ Jr. Gastrostomy without laparotomy: a percutaneous endoscopic technique. *J Pediatr Surg* **1980**;15:872–875
17. vanSonnenberg E, Wittich GR, Stauffer AE, et al. Modified coaxial technique to simplify nephrostomy, biliary drainage, and biopsies. *Radiology* (in press)
18. Cook RCM. Gastrocolic fistula: a complication of gastrostomy in infancy. *J Pediatr Surg* **1969**;4:346–349
19. Ho C, Gray RR, Goldfinger M, Rosen IE, McPherson R. Percutaneous gastrostomy for enteral feeding. *Radiology* **1985**; 156:349–351

Nonsurgical Drainage of Appendiceal Abscesses

Diego Nunez, Jr.[1]
Jonathan S. Huber
Jose M. Yrizarry
Gaston Mendez
Edward Russell

Five patients with abdominal abscesses complicating appendicitis were successfully treated by catheter drainage. In two patients, the percutaneous procedure was performed after incomplete surgical drainage; in three patients it was used as the only means of initial drainage. No interval appendectomy was required and no complications were associated with the procedure. Percutaneous management of appendiceal abscesses can be proposed as an alternative to surgical drainage.

While appendectomy is accepted as the treatment of choice for presumed uncomplicated appendicitis, the management of perforative appendicitis with abscess formation remains controversial. Both conservative and aggressive surgical treatments have been proposed [1–4]. Most agree, however, that initial treatment of appendiceal abscess must include surgical drainage [4, 5], while the necessity for interval appendectomy is controversial.

The management of intraabdominal abscesses by means of radiologically-guided catheter drainage has been established. We describe our initial experience with percutaneous drainage of appendiceal abscesses as an alternative to surgical drainage.

Subjects and Methods

Three male and two female patients, aged 10–75 years, with appendiceal abscesses were treated by percutaneous catheter drainage. The clinical diagnosis of appendicitis was entertained on admission, and the subsequent complaints and physical findings were related to the site of abscess formation. Symptoms had been present for an average of 6 days before the procedure was undertaken. The presumptive diagnosis of appendiceal abscess was established by CT (all cases) and sonography (three cases). Fluid collections in various locations were demonstrated within the abdomen: one each in the right subhepatic and subphrenic spaces, one intrahepatic, one posterior pararenal, and two in the right lower quadrant.

Of the five abscesses drained, three were suspected as appendiceal in origin. In these cases, high surgical risk and surgical failure to completely evacuate the abscess were the indications for percutaneous drainage. The other two cases were unsuspected appendiceal abscesses, and percutaneous drainage was considered a better alternative than surgery.

Diagnostic needle aspiration was performed with a 22-gauge Chiba needle using combined sonographic and fluoroscopic guidance. The selection of the entry site and the preferred access route were established by CT (fig. 1A). After initial puncture by the Chiba needle, either the Cope one-stick introducer system or tandem insertion of an 18-gauge Teflon-sheath needle was used to facilitate guide wire placement. Subsequently, depending on abscess size, either an 8-French Cope nephrostomy or 12-French vanSonnenberg sump catheter was left for drainage [6].

An angled posterior subcostal route and a lateral intercostal approach were used, respectively, for each of the two collections in the right upper quadrant. A midlumbar penetration with the patient in the prone position was used for the pararenal abscess, and an anterior perpendicular approach was used for the pelvic collections.

Received July 8, 1985; accepted after revision November 13, 1985.

[1] All authors: Department of Radiology, University of Miami/Jackson Memorial Medical Center, P.O. Box 016960, Miami, FL 33101. Address reprint requests to D. Nunez.

AJR 146:587–589, March 1986
0361–803X/86/1463–0587
© American Roentgen Ray Society

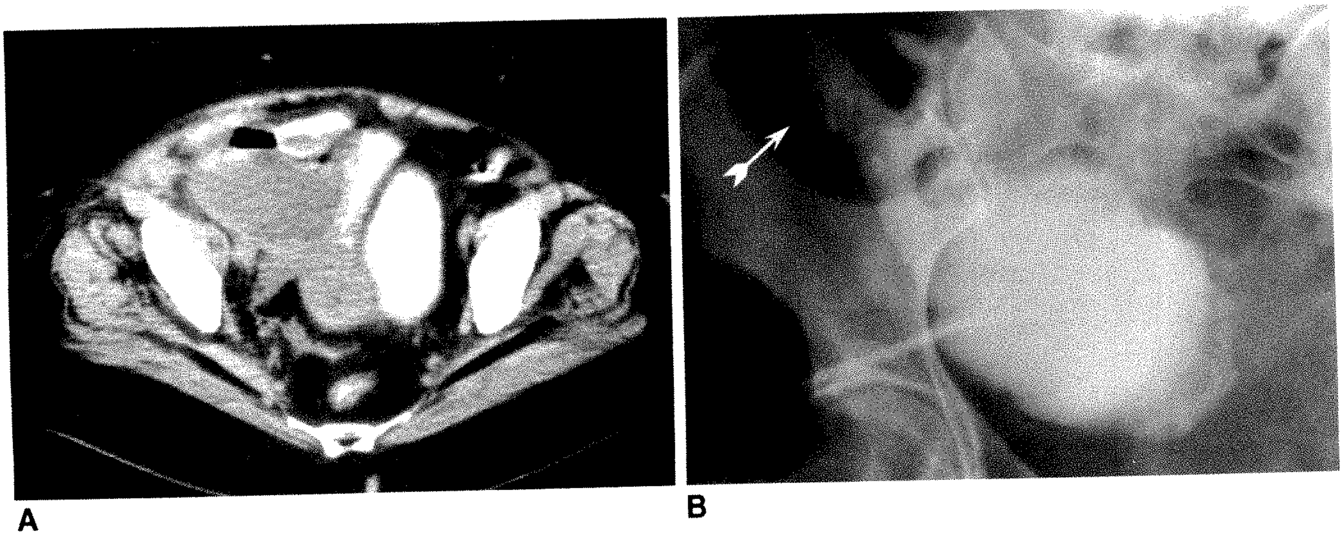

Fig. 1.—**A**, CT scan shows periappendiceal abscess. Entry site for drainage is established after assessing its relation with bowel loops. **B**, Injection of contrast into cavity. Cephalad extension (*arrow*) to retrocecal area is demonstrated.

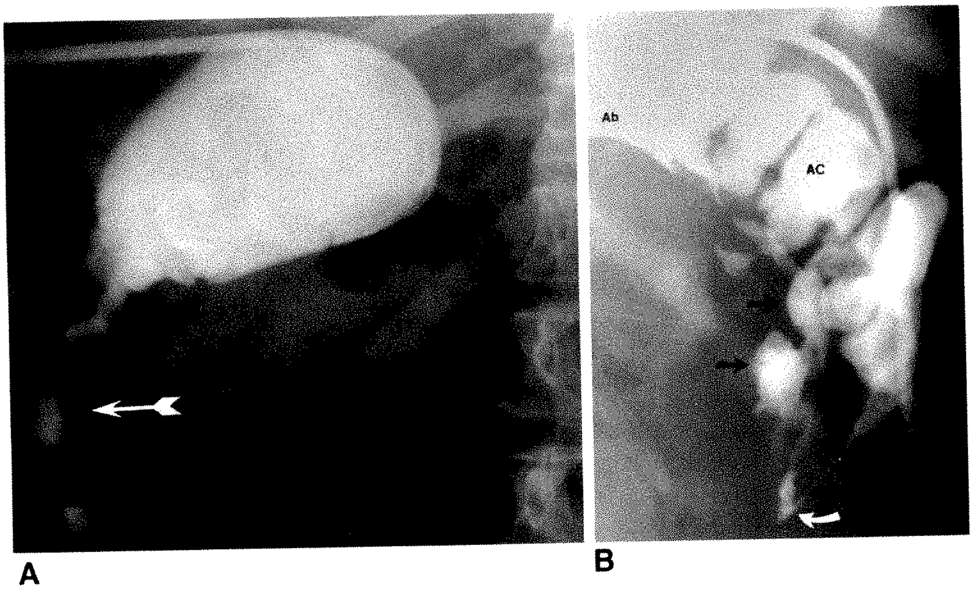

Fig. 2.—**A**, Contrast injection into intrahepatic abscess demonstrates sinus tract extending inferiorly (*arrow*). **B**, Lateral film of abdomen after injection of cavity (Ab) shows sinus (*black arrows*) and communication with ascending colon (AC) through perforated appendix (*white arrow*).

Two abscesses (one pelvic and one subphrenic) were percutaneously drained several days after incomplete surgical drainage, as evidenced by a follow-up CT scan. In three patients, the percutaneous procedure was used as the primary method of treatment. Contrast injection through the catheter, both initially and on subsequent abscessograms, was used to define the extent of the cavity (fig. 1B) and to establish the presence of sinus tracts. Follow-up abscessograms were performed about every 3 days to assess progressive resolution and to determine the need for catheter exchange or withdrawal. CT or sonography was also performed before discharge.

Long-term clinical and radiologic follow-ups have been obtained from 2 months to 3 years.

Results

Five intraabdominal abscesses complicating acute appendicitis were successfully drained percutaneously in five patients. The amount of purulent aspirate was 15–300 ml. Cultures revealed *E. coli* and *Bacteroides* as the prevalent microorganisms. Four patients defervesced within 72 hr and one patient 6 days after drainage. The length of catheter drainage varied from 2 to 17 days. In two patients, a sinus tract communicating with the appendix was demonstrated by contrast injection of the cavity (fig. 2) at the initial catheter placement. This communication was eventually shown to close in the repeated follow-up abscessograms before catheter withdrawal.

All patients have remained asymptomatic, and interval appendectomy has not been performed. No patient has had clinical evidence of recurrent appendicitis. No complications resulted from the drainage procedure.

Discussion

Complicating abscesses have been reported to occur in 2.3% of all cases of acute appendicitis [2] and in 20% of those that evolve to the perforative form of the disease [5]. The management of appendiceal abscess is controversial. Hoffmann et al. [1] supported the practice of conservative treatment, consisting of antibiotics and observation. If these patients failed to respond, surgical drainage without interval appendectomy was performed. Operative management with interval appendectomy is recommended in other series [2], and Foran et al. [3] pointed out that similar results can be obtained with either approach. Controversies aside, simple surgical drainage is the most widely accepted treatment for appendiceal abscesses [5]. This is supported by the experience of Paull and Bloom [4], showing that significant added morbidity is encountered when appendectomy is performed at the time of drainage. On the other hand, conservative medical treatment has been reported to have a failure rate of 22% [2]. In addition, if the patient's clinical condition deteriorates during conservative therapy, the surgeon may be forced to perform a higher risk operation.

The dynamics of fluid flow in the different abdominal compartments has been well demonstrated in Myers' studies [7]. Infected material moves from the pelvis to the right subhepatic space, and from there the exudate can reach the right subdiaphragmatic space. Also, infected material in the right pararenal space can spread superiorly to the bare area of the liver, explaining the occasional development of liver abscesses in patients with extraperitoneal appendicitis. Abscesses in these locations were present in two of our patients. In one, surgery had to be limited to partially draining the subhepatic space, and the percutaneous approach was used to completely drain the subphrenic extension of the collection.

Extension of abscess to the posterior pararenal space (one case) is less frequent but certainly predictable from an extraperitoneal appendix rupture. An undescended subhepatic cecum was recognized in the three cases where the periappendiceal abscess was distant to the right lower quadrant.

It is well recognized that other lesions, such as perforated carcinoma, perforated right-sided diverticuli, and abscesses of pelvic origin, can mimic an appendiceal abscess. Therefore, the value of aggressive radiologic workup and follow-up cannot be overemphasized in suspected appendiceal abscess. This is especially true in those abscesses presenting in locations remote from the appendix.

Open surgical drainage of appendiceal abscesses carries a morbidity of 16% [4], mainly incomplete drainage requiring reexploration, complicating infections, or fistula formation. We believe that surgical morbidity can be reduced by imaging-guided percutaneous drainage, especially when the abscesses are in locations remote from the appendix where surgical intervention carries a higher risk. The percutaneous procedure does not in itself preclude or alter further management. Whether interval appendectomy or expectant therapy is chosen, percutaneous drainage can be offered as the initial approach for drainage of appendiceal abscesses.

REFERENCES

1. Hoffman J, Lindhard A, Hans-Eric J. Appendix mass: conservative management without interval appendectomy. *Am J Surg* **1984**;148:379–382
2. Arnbjornsson E. Current concepts: management of appendiceal abscess. *Curr Surg* **1984**;41:4–9
3. Foran B, Berne TV, Rosoff L. Management of the appendiceal mass. *Arch Surg* **1978**;113:1144–1145
4. Paull DL, Bloom GP. Appendiceal abscess. *Arch Surg* **1982**;117:1017–1019
5. Condon RE. Appendicitis. In: Sabiston D, ed. *Davis-Christopher textbook of surgery*, 12th ed, vol 1. Philadelphia: Saunders, **1981**:1048–1063
6. vanSonnenberg E, Ferrucci JT Jr, Mueller PR, Wittenberg J, Simeone JF. Percutaneous drainage of abscesses and fluid collections: technique, results, and applications. *Radiology* **1982**;142:1–10
7. Myers MA. *Dynamic radiology of the abdomen*, 2d ed. New York: Springer-Verlag, **1982**

Replacing the Broken Suture in the Cope-Style Loop Retention Catheter

Howard L. Berman,[1] Stuart G. Katz, and Curtis W. Bakal

The Cope self-retention loop catheter has gained wide acceptance for percutaneous drainage procedures [1]. The commercially available Cope-style catheters may occasionally require additional side holes for effective use. Such modification may be necessary when draining high biliary duct obstruction, using the biliary drainage catheter as a ureteral stent, or when draining a very large abscess. During such changes, the thread used to form the distal loop may be broken. We recommend a simple, inexpensive technique for replacement of the broken string. The repair requires a nylon surgical suture mounted on a straight skin needle. To be more specific, we use a 3-0 Ethilon surgical suture on a cutting KS needle with 76-cm-long black monofilament nylon. The monofilament nylon suture is preferable to other suture material such as silk, as it is stronger and less likely to compromise the catheter lumen.

The initial step in repairing the loop self-retention catheter is the removal of all of the original broken suture material. In the Cook version of the Cope drain, this will require unscrewing the Luer lock hub and pulling out the loose thread through the proximal side hole. The new nylon suture is then introduced through the same side hole from which the original suture was removed. This will require forcing the cutting needle through the catheter wall and enlarging of the side hole. Using the catheter's metal stylette, the needle is advanced distad. Either through a side hole at the appropriate level or by simply pushing the cutting needle through the wall, the suture is then delivered to the surface. After passing the needle through two distal side holes, the end of the suture is tied securely in place. The excess thread and needle is then cut off. The two distal side holes used should be about 1 cm apart to ensure adequate wall strength to hold the suture. In our experience, the new suture has held securely and has not damaged or pulled through the catheter wall. It does not interfere with the catheter's passage over guide wires or insertion of the metal stylette. However, we have found that the side hole through which the needle was initially introduced may leak; this can be remedied with a drop of "super glue" once the suture has been pulled back to form the retention loop and tied in place.

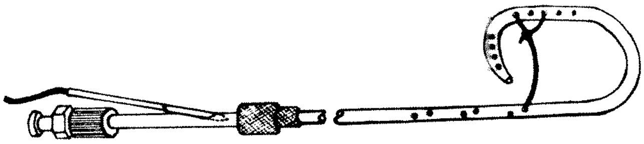

Fig. 1.—Diagram of Cope catheter repair emphasizing introduction of new suture through existing side hole near catheter hub and final fixation of suture distally.

This simple technique using a readily available surgical suture will safely repair an otherwise unusable expensive catheter and eliminate the fear of damaging the retention thread while cutting side holes. The repair can also be used to convert other commercially available large-bore pigtail drainage catheters into self retention devices.

REFERENCE

1. Cope C. Improved anchoring of nephrostomy catheters: loop techniques. *AJR* **1980**;135:402–403

Received July 16, 1985; accepted after revision October 31, 1985.

[1] All authors: Department of Radiology, New York Medical College, Valhalla, NY 10595. Address reprint requests to H. L. Berman.

AJR 146:590, March 1986 0361-803X/86/1463-0590 © American Roentgen Ray Society

Radiopaque Suspension of Polyvinyl Alcohol Foam for Embolization

Irene A. Szwarc,[1] C. Humberto Carrasco, Sidney Wallace, and William Richli

Polyvinyl alcohol (PVA) foam has been our primary embolic material since 1978. It is available as particles measuring 149–1000 μm in diameter (Unipoint Labs.), but the tendency of the PVA to aggregate makes the effective size of the emboli considerably larger than that of the individual particles. Ultrasonic vibration usually results in clumping of the PVA after about 1 week and the particles do not resuspend on agitation. Kerber et al. [1] suggested passing the suspension between two syringes through a partially closed stopcock to break up the aggregates, but performing this maneuver at the time of the procedure is relatively time-consuming and not very effective. Berenstein and Graeb [2] achieved a better dispersion of the particles by washing, blending, and filtering the PVA, sterilizing it, and then storing it in jars filled with sterile water. However, some preparation prior to use is still required because the water needs to be decanted and the particles resuspended in iodinated contrast medium at the time of embolization. We have modified the latter method to prepare a suspension of the PVA particles in contrast medium that can be stored and ready for use without additional preparation.

Materials and Methods

One gram of nonradiopaque PVA particles measuring 149–250 μm is placed in a filter funnel lined with a Whatman #1 qualitative filter. Barium-impregnated particles are not used because they do not remain dispersed as long as the standard material, and the barium tends to separate from the PVA. Low to medium suction is applied to the filtering apparatus while the PVA is washed for at least 20 min with more than 300 ml of sterile water. The washed particles are then blended with 100 ml of Conray 60 in a standard kitchen blender for 15 min at low speed. The PVA particles that adhere to the sides of the blender are mixed into the suspension and blended for an additional 5 min at high speed. Again the particles adhering to the sides of the blender are mixed into the suspension, which is then divided between two 60-ml bottles. The bottles are allowed to cool for 30 min at room temperature before being capped with rubber stoppers and metal ring seals. The following day, the bottles are heat-sterilized at 120°C for 30 min. The bottles must be agitated immediately after sterilization and periodically during the cooling period to prevent PVA clumping. This suspension of PVA at a concentration of 10 mg/ml can be stored for prolonged periods. It remains sterile for up to 12 months without aggregation of the particles. The amount of PVA needed for an embolization can then be drawn out from the bottle into a syringe with an 18-gauge needle.

The PVA particles prepared by this method were compared to those of the embolic material obtained by passing the soaked PVA through a stopcock between two syringes [1] by measuring them with a microscope eyepiece micrometer. Three canine kidneys were also embolized using the two different preparations of PVA, and the degree of arterial occlusion was determined histologically in each kidney.

Results

The particles subjected to blending and autoclaving ranged in size from 150 to 400 μm in comparison to soaked particles passed between two syringes [1], which measured between 300 and 700 μm. However, measurement of the particles prepared by the latter method was very difficult because of their tendency to clump together making the actual size of the particles considerably larger. Bacterial cultures obtained from samples of one of the vials of the PVA preparation described failed to demonstrate bacterial growth up to 13 months. The preparation used to embolize the canine kidneys had been in storage 2–6 weeks.

Histologic examination of the kidneys embolized with the preparation obtained by passing the particles between two syringes demonstrated occlusion of several, but not all, of the large arteries at the corticomedullary junction by the PVA particles. These particles contained fissures which were partially lined by endothelium. No PVA particles were observed in the smaller vessels beyond the corticomedullary junction.

The kidneys embolized with the PVA particles prepared by the currently described method demonstrated occlusion of a greater number of the arteries at the corticomedullary junction. The embolic particles were also observed in the smaller arteries beyond the corticomedullary junction, including some afferent arterioles and glomerular capillaries.

Received July 19, 1985; accepted after revision November 5, 1985.

This work was supported in part by the John S. Dunn Research Foundation, the George A. Cook Memorial Fund, and research grant CA-16672 from the National Cancer Institute

[1] All authors: Department of Diagnostic Radiology, University of Texas M. D. Anderson Hospital and Tumor Institute, 6723 Bertner Ave., Houston, TX 77030. Address reprint requests to I. A. Szwarc.

AJR 146:591–592, March 1986 0361–803X/86/1463–0591 © American Roentgen Ray Society

Discussion

PVA particles tend to clump, and their passage between two syringes through a partially closed stopcock does not result in their complete dispersion. Thus, therapeutic embolization using this embolic material results in a relatively more proximal occlusion, which may predispose to earlier reconstitution of the embolized arterial territory by collateral vessels. A more thorough dispersion of the PVA particles is achieved using the preparation described above, which provides for a more peripheral arterial occlusion. Therapeutic embolization using this latter preparation is probably more effective in delaying collateral reconstitution of the occluded vascular territory. In addition, preparation of the embolic material in contrast medium and the ability to store it for prolonged periods of time facilitates its use considerably.

REFERENCES

1. Kerber CW, Bank WO, Horton JA. Polyvinyl alcohol foam: prepackaged emboli for therapeutic embolization. *AJR* **1978**;130:1193–1194
2. Berenstein A, Graeb DA. Convenient preparation of ready-to-use particles in polyvinyl alcohol foam suspension for embolization. *Radiology* **1982**;145:846

Fatal Outcome after Ethanol Renal Ablation in Child with End-Stage Kidneys

L. Garel,[1,2] J. L. Mareschal,[1] M. F. Gagnadoux,[3] D. Pariente,[1] M. Guilbert,[4] and J. Sauvegrain[1]

At our institution, until the end of 1983 children with terminal uremia and severe hypertension underwent surgical nephrectomy to prevent persistent hypertension after successful renal transplantation. According to that protocol, the left nephrectomy was performed first; the right kidney was removed later, at the time of transplantation of the donor kidney into the right iliac fossa.

As an alternative to surgery, we started a program of left renal ethanol ablation in 1984. Twelve ablations of left end-stage kidneys were done without significant complications. The occurrence of a lethal complication in the 13th patient urged us to report the case in detail.

Case Report

A 3-month-old boy was seen for familial nephrosis. Periodic hemodialysis was initiated at 9 years of age because of terminal renal failure. Severe hypertension was present. The patient was scheduled for kidney transplantation, and left renal ablation was accordingly planned. After 8 months of hemodialysis, the renal ablation procedure

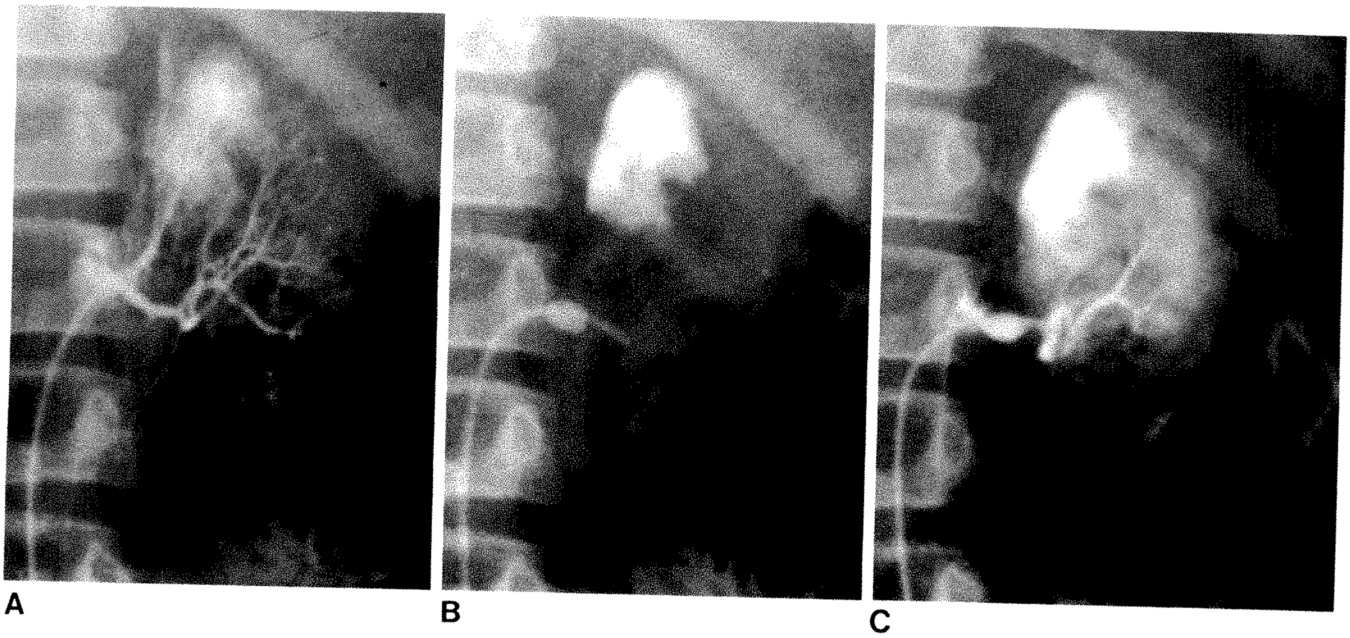

Fig. 1.—A, Contrast injection in superior polar branch of left renal artery with backflow in main renal trunk (balloon not inflated). Extravasation of contrast material at upper pole. Adrenal gland is well demonstrated. B, Catheter has been repositioned in main inferior trunk; after inflation of balloon, 3 ml of ethanol was injected. C, Follow-up opacification (balloon deflated) shows localized arterial dilatation at balloon site, very reduced renal flow with some reflux in aorta, and irregular nephrogram. Persistent visibility of small branches in middle third of kidney prompted second ethanol injection (1.5 ml) after balloon reinflation.

Received May 8, 1985; accepted after revision November 1, 1985.

[1] Service de Radiologie Pédiatrique, Hôpital des Enfants-Malades, 75730 Paris cedex 15, France.
[2] Present address: Département de Radiologie, Hôpital Sainte-Justine, 3175 Chemin Sainte-Catherine, Montreal, Quebec, Canada H3T 1C5. Address reprint requests to L. Garel.
[3] Département de Néphrologie Pédiatrique, Hôpital des Enfants-Malades, 75730 Paris cedex 15, France.
[4] Département d'Anesthésiologie, Hôpital des Enfants-Malades, 75730 Paris cedex 15, France.

AJR 146:593–594, March 1986 0361–803X/86/1463–0593 © American Roentgen Ray Society

was performed during general anesthesia with cardiac and respiratory monitoring. Through a left femoral artery approach, a 5-French, 5-mm occluding balloon catheter was positioned in the left renal artery.

On the first set of films, before ethanol injection, the tip of the catheter was located in the superior polar artery (fig. 1A). The renal artery and its branches were extremely small and the circulatory speed was reduced. Interstitial extravasation of contrast medium could be seen at the upper pole of the kidney. The adrenal gland was partially opacified, with an inferior adrenal artery arising from the superior polar branch of the renal artery and the left renal vein clearly visible on late films. A transient rise in blood pressure level was noted after this opacification. No injection of ethanol was made at that time.

The catheter was then repositioned in the main inferior trunk of the left renal artery and the balloon was inflated (fig. 1B). After a test injection of contrast material, the entire kidney was opacified; the adrenal gland showed no further opacification. Absolute ethanol (3 ml) was then injected, the balloon remaining inflated for 20 min. A control injection of contrast material after balloon deflation showed the reflux of contrast material into the aorta and the absence of venous return (fig. 1C). Because of persistent opacification of several small distal intrarenal branches, a second injection of ethanol (1.5 ml) was made in the same location after balloon reinflation. After 20 sec, a cardiac arrest supervened, which could not be reversed despite immediate resuscitation. Autopsy was refused by the patient's family.

Discussion

Without pathologic data, only questions and speculations can be raised regarding the mechanism of death. Hypokalemia had been documented several times in this patient, but the serum level of potassium was normal the day of the procedure; cardiac monitoring showed no disturbances of rate and rhythm. Contrast medium toxicity or allergy appeared unlikely in a patient who had undergone multiple previous contrast studies without complication.

A sudden reflex vagal stimulation with decreased cardiac output is uncommon in a patient under general anesthesia. Acute hypertension associated with cardiac arrhythmia has been noted after ethanol injection in the adrenal artery [1]; in our patient, a 20-mm increase in systolic and diastolic blood pressure was recorded after the first injection of ethanol. However, the adrenal artery was spared by the alcohol injection in the main renal artery trunk (fig. 1B). Therefore, there is no evidence that adrenal toxicity was the cause of death. Reflux of ethanol into the aorta seems very unlikely because of the use of a balloon catheter.

Finally, one may question whether the renal artery may have ruptured, noting the disparity in size between the balloon and the artery (Figs. 1A and 1B) and the residual arterial dilatation at the site of balloon inflation (fig. 1C). However, all patients in our series had similar end-stage kidneys with extremely small renal arteries and in all cases balloon catheters were used without complications. Moreover, Nanni et al. [2] also reported use of occluding balloon catheters; no specific problems were noted in the children of their series, including the two cases of bilateral ablation of end-stage kidneys.

Although we cannot explain the cause of death, the reported case emphasizes the hazards of the technique. These hazards must be weighed against the 10% and 2% operative fatality rate quoted in diabetic and nondiabetic hemodialyzed patients, respectively, who undergo bilateral nephrectomy [3].

REFERENCES

1. Fink IJ, Girton M, Doppman JL. Absolute ethanol injection of the adrenal artery: hypertensive reaction. *Radiology* **1985**;154:357–358
2. Nanni GS, Hawkins IF Jr, Orak JK. Control of hypertension by ethanol renal ablation. *Radiology* **1983**;148:51–54
3. Matas AJ, Simmons RL, Buselmeier TJ, Najarian JS, Kjellstrand CM. Lethal complications of bilateral nephrectomy and splenectomy in hemodialyzed patients. *Am J Surg* **1975**;129:616–620

Pain Control after Percutaneous Biliary Drainage: Local Infiltration with Bupivacaine and Epinephrine

Robert P. Lieberman[1] and Pauline R. Sleder[1]

All patients who undergo percutaneous biliary drainage experience pain for several days thereafter. Most patients require parenteral narcotics and some get little relief from these otherwise potent drugs. Besides distressing the patient, pain at the catheter site may cause splinting and atelectasis and may make the patient unwilling to endure a second biliary procedure.

We discovered the ability of local anesthetics to control this pain by chance. A patient complained that narcotics made her dysphoric but did not actually relieve the pain. She asked if a local anesthetic would help. We infiltrated the catheter site and achieved complete pain relief.

Technique

The agent used for the block is 0.5% bupivacaine (Marcaine, Breon Labs.) containing 1/200,000 epinephrine. About 10 ml is infiltrated around the biliary catheter through a 25-gauge, 1.5-inch (3.8 cm) needle. If the skin is not already numb, the drug is injected slowly over 2–4 min, since rapid injection of any local anesthetic is painful. Special care is taken to insert the needle through broken skin directly adjacent to the catheter. Needle insertion in this fashion is almost painless, whereas insertion through intact skin is as painful as any routine needle puncture. The needle is advanced along the track on all sides of the catheter down to the ribs and peritoneum. Aspiration for blood during infiltration is unnecessary.

Results

The block has been used 12 times in nine patients. Nine infiltrations were performed at the bedside for significant pain. Complete or nearly complete pain relief was achieved in each case. Three other infiltrations were performed prophylactically just after biliary catheter insertion. Duration of anesthesia has ranged from 6 to 10 hr. No complications have been encountered.

Discussion

Pain felt during biliary drainage procedures has two components. A somatic part arises from the body wall and is mediated through the intercostal nerves. A visceral part arises from the bile ducts and is probably mediated through the celiac plexus. During routine procedures the body wall becomes fully anesthetized by infiltration with local anesthetic. Hence pain encountered during procedures is largely if not completely visceral.

A casual observer would assume that pain felt hours to days after catheter placement is also largely visceral. The present study shows this assumption to be false. The surprising effectiveness of local anesthetic in relieving postoperative pain indicates that this pain is largely somatic. Visceral pain is produced only during catheter manipulation and abates soon after manipulation is stopped.

Bupivacaine, a widely used local anesthetic agent, was first synthesized in 1957 and has been extensively studied. It has been mentioned recently in the radiology literature [1]. Bupivacaine has a good safety margin, with a maximum single dose of 200–250 mg in the presence of epinephrine [2, 3]. An amide-type agent, it probably does not cause allergic reactions. Bupivacaine has the longest duration of action of all local anesthetics, ranging from 3 to 12 hr under various conditions. Its prolonged activity suggested bupivacaine as the most appropriate agent for pain control after biliary procedures.

A literature review was conducted to determine which commercially available bupivacaine preparation was longest acting. There is evidence that increasing drug concentration from 0.25% through 0.5% to 0.75% lengthens the duration of action [4–7], although the actual differences were sometimes small and individual variations marked. We chose 0.5% bupivacaine because it was readily available and because the stronger 0.75% preparation is not recommended for infiltration anesthesia.

The literature is conflicting on the value of adding epinephrine to bupivacaine. Some authors found epinephrine to prolong anesthetic effect [4, 7], while others did not [5, 8]. We prefer to use epinephrine for reasons other than its possible effect on duration of action. Epinephrine retards systemic absorption of bupivacaine, making the block safer. Epinephrine also reduces local bleeding and staining of the bandage after the block.

Received June 21, 1985; accepted after revision November 5, 1985.

[1] Department of Radiology, University of Nebraska Medical Center, Omaha, NB 68105. Address reprint requests to R. P. Lieberman.

AJR 146:595–596, March 1986 0361-803X/86/1463-0595 © American Roentgen Ray Society

Given our preference for bupivacaine in this context, one may ask whether bupivacaine should replace lidocaine in all local anesthetic applications. Lidocaine has two distinct advantages. Its onset of action is faster than bupivacaine [2] and it costs only one-fourth as much. Lidocaine has a single disadvantage, shorter duration of action. The anesthetic effect of 1% lidocaine without epinephrine lasts only 60–90 min, while that of 0.5% bupivacaine lasts 3–7 hr [2, 3]. Adding epinephrine extends the action of 1% lidocaine to 4–6 hr, more than enough for long angiographic and interventional cases. The radiologist who is afraid of epinephrine will find bupivacaine advantageous. We, however, continue to prefer 1% lidocaine with epinephrine as a general purpose anesthetic agent and reserve the use of bupivacaine to the block described here.

Infiltration of bupivacaine has now become our routine after biliary catheter insertion just before dressings are applied. A second infiltration is performed at the patient's bedside in the evening or the next day. One or two bedside infiltrations usually suffice to carry the patient over the painful early period. Oral analgesics are effective thereafter. Close observation of these patients has convinced us that bupivacaine block is an effective and humane way to manage pain after biliary catheter insertion.

REFERENCES

1. Clayman RV, Castaneda-Zuniga W. Nephrolithotony: percutaneous removal of renal calculi. *Urol Radiol* **1984**;6:95–112
2. *AMA drug evaluations*, 5th ed. Philadelphia: Saunders, **1983**:382, 389
3. Cousins MJ, Bridenbaugh PO. *Neural blockade in clinical anesthesia and management of pain.* Philadelphia: Lippincott, **1980**:91, 97
4. Trieger NT, Gillen GH. Bupivacaine anesthesia and post-operative analgesia in oral surgery. *Anesth Progr* **1979**;26:20–23
5. Laskin JL, Wallace WR, DeLeo B. Use of bupivacaine hydrochloride in oral surgery: a clinical study. *J Oral Surg* **1977**;35:25–29
6. Nespeca JA. Clinical trials with bupivacaine in oral surgery. *Oral Surg* **1976**;42:301–307
7. Swerdlow M, Jones R. The duration of action of bupivacaine, prilocaine and lignocaine. *Br J Anaesth* **1970**;42:335–339
8. Nesheim BI. Which local anesthetic is best suited for paracervical blocks? *Acta Obstet Gynecol Scand* **1983**;62:261–264

Postoperative Assessment of Splenorenal Shunts with MRI: Preliminary Investigation

Jesse M. Cohen[1]
Jeffrey C. Weinreb
Helen C. Redman

Magnetic resonance imaging (MRI) was performed on nine patients with hepatic cirrhosis and portal hypertension after selective distal splenorenal shunt for decompression of bleeding esophageal varices. MRI demonstrated the splenorenal anastomosis and patency of the shunt, splenic vein, and left renal vein in each case. Imaging in the transverse plane provided optimal visualization of the shunts. The authors conclude that MRI is a safe, noninvasive technique for the postoperative evaluation of selective distal splenorenal shunts.

Selective distal splenorenal (SDSR) shunt surgery is a well established method of effectively decompressing esophageal varices while maintaining anterograde portal venous flow [1–5]. This is accomplished by converting the esophageal-gastric-splenic venous complex into a low-pressure system by isolating it from the main portal vein with an end-splenic-vein–side-left-renal-vein shunt and by ligating the left gastric and gastroepiploic veins. Although massive variceal bleeding is a common complication of occluded splenorenal shunts, hemorrhage from esophageal varices is unusual in the presence of a documented patent shunt [2]. Angiography is currently the most reliable method of determining postoperative shunt patency, but it is not without limitation and risk. We report the use of magnetic resonance imaging (MRI) in the postoperative assessment of SDSR shunts.

Materials and Methods

Nine patients with biopsy-proven cirrhosis of the liver were studied. The patients were 17–59 years of age; seven were male. Five patients had postnecrotic cirrhosis (four with serology positive for HBsAg, one cryptogenic); the other four had alcoholic (Laennec) cirrhosis. All had undergone SDSR shunt for control of bleeding esophageal varices secondary to portal hypertension. At the time of surgery, seven of the patients were classified as Childs A and two as Childs B cirrhotics.

MRI was performed between 1 week and 42 months after surgery (mean, 61 weeks). All of the shunts were believed to be patent on clinical grounds, since there was no recurrent variceal bleeding. Computed tomographic (CT) confirmation of shunt patency was available in one case, and angiography confirmed another.

A 0.35 T superconducting imaging system (Diasonics MT/S) was used with spin-echo pulse sequences. Multislice, multiecho images were obtained with echo delay times (TE) of 28 and 56 msec at each level. The first patient was studied in the transverse (repetition time [TR] = 1.5 sec) and coronal (TR = 2.0 sec) planes. The other eight patients were scanned using a protocol consisting of one coronal (TR = 1.0 sec; 10 sections, 7 mm thick with a 3-mm gap between contiguous sections) and one transverse (TR = 1.0 sec; 20 sections, 5 mm thick) acquisition. Respiratory gating was not used. Each examination was completed in 1 hr.

Each MRI study was reviewed retrospectively by two radiologists (J. M. C., J. C. W.) to determine the ability of MRI to demonstrate a patent splenorenal anastomosis and to demonstrate patency of the splenic and left renal veins. The appearance of the superior mesenteric vein and portosystemic collaterals was noted.

Received August 9, 1985; accepted after revision November 27, 1985.

[1] All authors: Department of Radiology, University of Texas Health Science Center at Dallas, Dallas, TX 75235. Address reprint requests to J. C. Weinreb, NMR Imaging Center, 1311 Record Crossing, Dallas, TX 52235.

AJR 146:597–600, March 1986
0361–803X/86/1463-0597
© American Roentgen Ray Society

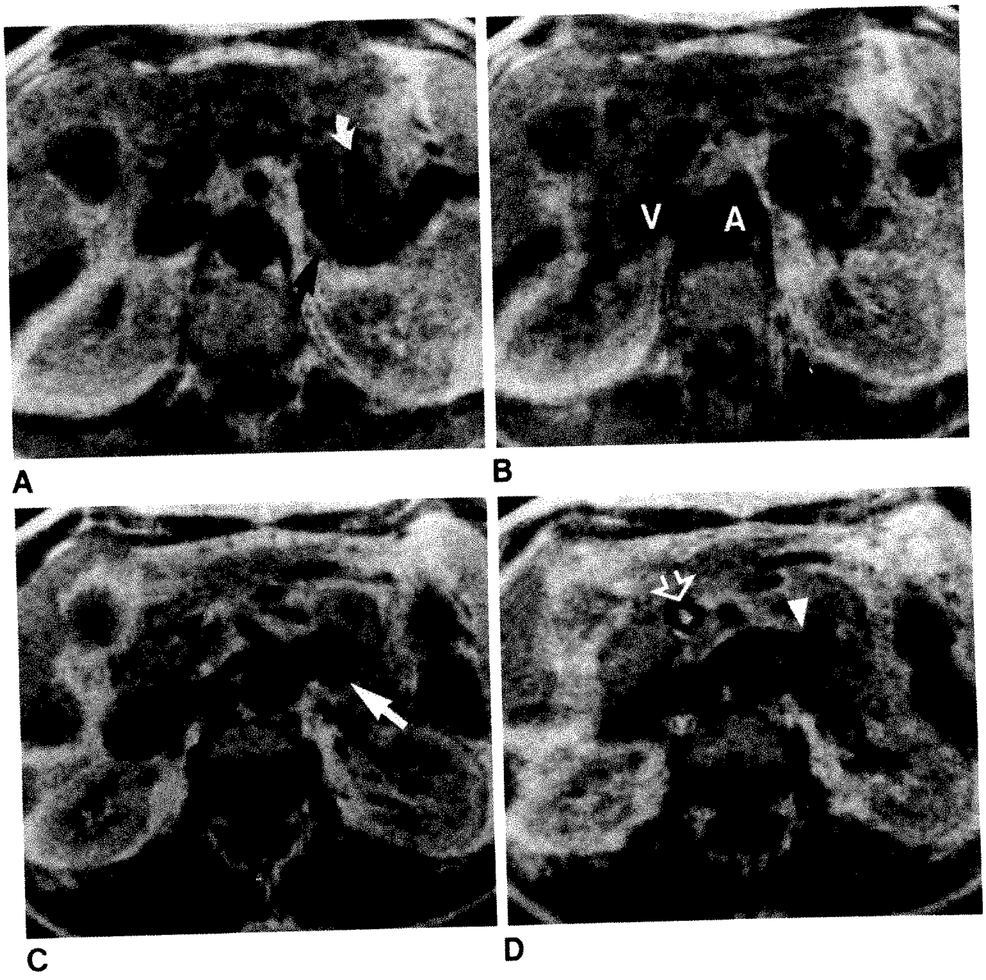

Fig. 1.—Spin-echo scans (TR = 1.0 sec; TE = 28 msec). **A–D**, Sequential transverse images demonstrate course of splenic vein (*straight, solid arrows*) to its anastomosis with left renal vein (*arrowhead*). Signal voids are seen within these two veins and at anastomosis, indicating rapidly flowing blood through patent shunt. High-intensity signal within lumen of superior mesenteric vein (*open arrow*) is due to flow phenomenon rather than thrombus (see text). Varices (*curved arrow*) are seen in splenic hilum. A = aorta; V = inferior vena cava.

Results

By following the course of the splenic vein from the splenic hilum to its junction with the left renal vein, the surgical anastomosis was identified in all nine patients (figs. 1 and 2). The anastomosis was seen on transverse images in all nine patients and on coronal images in four. Intraluminal low signal due to the "flow void" phenomenon of rapidly flowing blood was observed at the anastomosis and in the splenic and left renal veins in each case.

In eight patients, high-intensity signal was seen within the lumen of the superior mesenteric vein on each first-echo image of the transverse multislice acquisition in which this vein was included. The signal demonstrated an absolute increase in intensity on second-echo images (i.e., even-echo rephasing), indicating the presence of flowing blood (as opposed to thrombus) [6, 7]. The superior mesenteric vein could not be identified on the transaxial image in one patient. In the three cases in which this vein was unequivocally demonstrated on coronal images, similar findings were observed.

Enlarged portosystemic collaterals were seen in the perigastric region in all nine patients, in the peripancreatic region in four patients, and in the juxtarenal area in two patients. One patient had a dilated patent umbilical (paraumbilical) vein.

Discussion

The SDSR shunt, popularized by Warren et al. [1], is an effective means of reducing the incidence of esophageal varix hemorrhage associated with portal hypertension. Since recurrent hemorrhage from esophageal varices seems to be a function of shunt occlusion [2], evaluation of shunt patency is recommended in patients with recurrent gastrointestinal bleeding after SDSR shunt. Furthermore, since shunt occlusion usually occurs within 2 weeks after surgery and requires immediate revision, some advocate that all patients be evaluated for shunt patency before discharge from the hospital [2].

A variety of techniques has been used to assess shunt patency, including angiography, CT, sonography, radionuclide angiography, scintisplenoportography, and D-xylose clearance [8–12]. Selective celiac or splenic arteriography is the most widely accepted method of documentation [13–15]. Angiography, however, is invasive and exposes patients to the potential hazards of iodinated contrast media. Avoidance of risks associated with vessel puncture and catheterization may be particularly important in patients with diminished clotting factors secondary to liver disease. For this reason, SDSR shunts are seldom evaluated routinely in the immediate

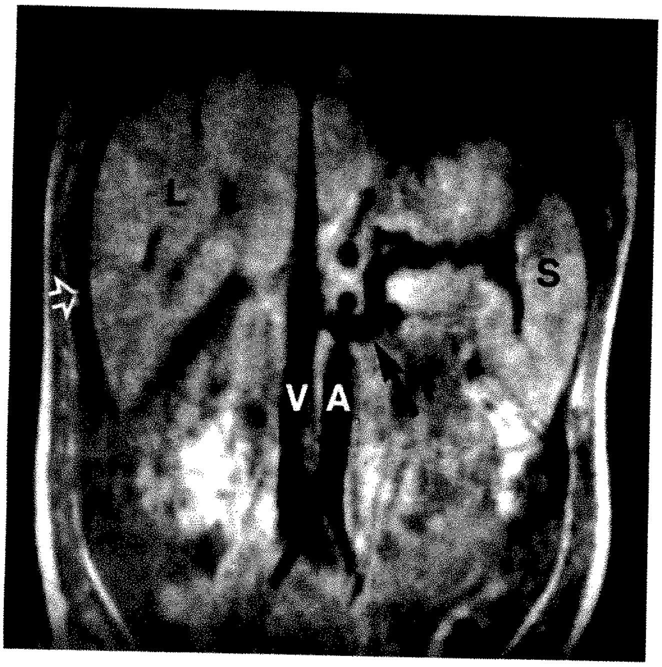

Fig. 2—Spin-echo scan (TR = 1.0 sec; TE = 28 msec). Coronal image demonstrates splenorenal anastomosis (*solid arrow*) and patency of splenic and left renal veins. Hepatosplenomegaly and ascites (*open arrow*) are present. A = aorta; V = inferior vena cava; L = liver; S = spleen.

postoperative period. Arterial aberrations may prevent catheterization of the appropriate artery to obtain sufficient venous opacification. Selective renal venography may be useful in such cases; however, retrograde shunt opacification may be extremely difficult. Dynamic CT is an alternative diagnostic tool that requires the simultaneous or sequential enhancement of the splenic and left renal veins to document shunt patency [9, 16]. The presence of metallic surgical clips and the large volume of contrast material often required may serve to contraindicate CT. In addition, the sensitivity and specificity of CT have not been firmly established. A safe, reliable, noninvasive method of determining shunt patency would be preferable to either angiography or CT.

Because rapidly flowing blood produces no discernible MRI signal, patent blood vessels can be depicted without intravascular contrast media [6, 7]. In this study, the splenic and left renal veins were easily traced to their junction at the end-to-side surgical anastomosis. The demonstration of an actual communication between the two vessels and a flow-void effect in both limbs of the anastomosis probably reflects a patent shunt. Definitive proof of patency would have required angiography. Now that we have demonstrated to our surgical colleagues the ability to depict the shunts noninvasively, the next stage of our investigation will include a comparison of angiography and MRI for the evaluation of shunt patency.

Our imaging protocol allowed good visualization of the mid and upper abdominal viscera and blood vessels. Initial imaging in the coronal plane identified the approximate level of the shunt. This facilitated positioning of the patient for transverse imaging. Theoretically, the examination could have been terminated after the first pulse sequence in the four instances in which a patent shunt was depicted on coronal images. Although segments of the splenic and left renal veins were seen on coronal images in the remaining five cases, the anastomosis itself was not demonstrated. This may be attributable to the gap between contiguous coronal images or to the vessels' coursing obliquely to the imaging plane.

Our primary objective in studying these patients was to demonstrate the shunt and determine whether it was patent. This was more consistently and graphically accomplished with transverse images. If imaging had been performed solely in the transverse plane, localizing the level of the shunt may have been difficult. In such cases, a "localizer" or "scout" view (which has recently become available to us) could have provided this information.

It is not surprising that patent portosystemic collaterals were demonstrated after shunting. Superior mesenteric venous hypertension provides a continued stimulus for portosystemic collateralization. Varices may, therefore, persist or reappear even after successful decompression [4, 13, 17].

Bidirectional blood flow occurs in branches of the portal venous system before and after shunting [15]; thus, unusual blood flow patterns might be expected on MRI. A review of our 75 most recent normal abdominal MRI scans failed to reveal a case where high signal was detected within the lumen of the superior mesenteric vein on the first echo of each image in a transverse multislice acquisition. The presence of such signal in all of our postshunt patients in whom this vein was identified may indicate a disturbance of normal mesenteric venous blood flow (e.g., bidirectional or impeded flow).

Because MRI depicts vascular structures without catheterization, this imaging method may also find a role in the preoperative splenorenal shunt workup by providing information similar to that provided by angiography concerning suitability of size and position of the splenic and left renal veins. This is the subject of current investigation at our institution and has already been used successfully in two cases.

In summary, our preliminary experience indicates that MRI is a useful technique for demonstrating patent splenorenal shunts. Further experience is necessary to determine the appearance of occluded shunts and the potential role of MRI in the preoperative assessment of SDSR shunt candidates.

REFERENCES

1. Galambos JT, Warren WD, Rudman D, Smith RB, Salam AA. Selective and total shunts in the treatment of bleeding varices. *N Engl J Med* **1976**;295:1089–1095
2. Nordlinger BM, Nordlinger DF, Fulenwider JT, et al. Angiography in portal hypertension: clinical significance in surgery. *Am J Surg* **1980**;139:132–141
3. Warren WD, Salam AA, Faraldo A, Hutson D, Smith RB. End-renal vein-to-splenic-vein shunts for total or selective portal decompression. *Surgery* **1972**;72:995–1006
4. Rikkers LF, Rudman D, Galambos JT, et al. A randomized, controlled trial of the distal splenorenal shunt. *Ann Surg* **1978**;188:271–282
5. Warren WD, Salam AA, Hutson D, Zeppa R. Selective distal

splenorenal shunt. *Arch Surg* **1974**;108:306–314

6. Mills CM, Brant-Zawadzki M, Crooks LE, et al. Nuclear magnetic resonance: principles of blood flow imaging. *AJR* **1984**;142:165–170
7. Bradley WJ Jr, Waluch V, Lai K-S, Fernandez EJ, Spalter C. The appearance of rapidly flowing blood on magnetic resonance images. *AJR* **1984**;143:1167–1174
8. Teres J, Herranz R, Visa J, Lomena F, Pera C, Rodes J. Scintisplenoportography in assessing patency of distal splenorenal shunts. *Am J Surg* **1983**;145:780–783
9. Foley WD, Gleysteen JJ, Lawson TL, et al. Dynamic computed tomography and pulsed Doppler ultrasonography in the evaluation of splenorenal shunt patency. *J Comput Assist Tomogr* **1983**;7:106–112
10. Rypins EB, Fajman W, Sarper R, et al. Radionuclide angiography of the liver and spleen. Noninvasive method for assessing the ratio of portal venous to total hepatic blood flow and portosystemic shunt patency. *Am J Surg* **1981**;142:574–579
11. Goldberg BB, Patel J. Ultrasonic evaluation of portacaval shunts. *JCU* **1977**;5:304–306
12. Smith RC, Macpherson AIS. Assessment of portosystemic shunt patency by estimation of D-xylose excretion. *Br J Surg* **1976**;63:435–437
13. Nabseth DC, Johnson WC, Widrich WC, O'Hara ET, Vollman RW. Spleno-renal shunts in portal hypertension. *J Cardiovasc Surg* **1979**;20:201–207
14. Widrich WC, Robbins AH, Nabseth DC, O'Hara ET, Johnson WC, Loughlin KV. Portal hypertension changes following selective splenorenal shunt surgery. *Radiology* **1976**;121:295–302
15. Nabseth DC, Widrich WC, O'Hara ET, Johnson WC. Flow and pressure characteristics of the portal system before and after splenorenal shunts. *Surgery* **1975**;78:739–748
16. Gleysteen JJ, Foley WD, Lawson TL, Unger GF. Patency evaluation of distal splenorenal shunt with dynamic computed tomography. *Surg Gynecol Obstet* **1982**;154:689–694
17. Widrich WC, Robbins AH, Johnson WC, Nabseth DC. Long-term follow-up of distal splenorenal shunts. *Radiology* **1980**;134:341–345

Detection of the Intimal Flap of Aortic Dissection on Unenhanced CT Images

Terrence C. Demos,[1] Harold V. Posniak, and Robert J. Churchill

Computed tomography (CT) has been established as an accurate method for diagnosing aortic dissection [1, 2]. The diagnosis is made by identifying two aortic lumens or an intimal flap after intravenous injection of contrast material. The diagnosis may be suggested on unenhanced images, however, when calcified atheromatous plaques are displaced within the aortic silhouette or when the false lumen contains a high-attenuation blood clot [1, 2, 5]. We present three patients with aortic dissection who had an intimal flap that was visible on unenhanced CT scans. This finding, which has not been previously reported to our knowledge, allowed diagnosis before contrast enhancement.

Case Report

A 65-year-old woman was transferred to our hospital with progressively worsening substernal chest pain radiating to her back. Four months earlier she had undergone aortic valve replacement and single aortocoronary bypass graft. Blood pressure was 112/90 mm Hg, and an electrocardiogram showed no changes suggestive of a recent infarct. There were small bilateral pleural effusions and questionable widening of the mediastinum on a chest radiograph. A CT study was done because aortic dissection was suspected. The hemoglobin at the time of the scan was 9.1 g/dl. The unenhanced images demonstrated a dilated ascending aorta with a linear density traversing the lumen, which was thought to represent an intimal flap. This was confirmed after an intravenous bolus injection of contrast material (fig. 1). At surgery, an aortic dissection extended from the left coronary sinus to just proximal to the origin of the brachiocephalic artery. This was repaired by Dacron graft interposition with reanastomosis of the coronary artery bypass graft. The patient was discharged 18 days later.

Discussion

Aortic dilation, pleural effusion, and pericardial effusion are nonspecific findings of aortic dissection on unenhanced CT

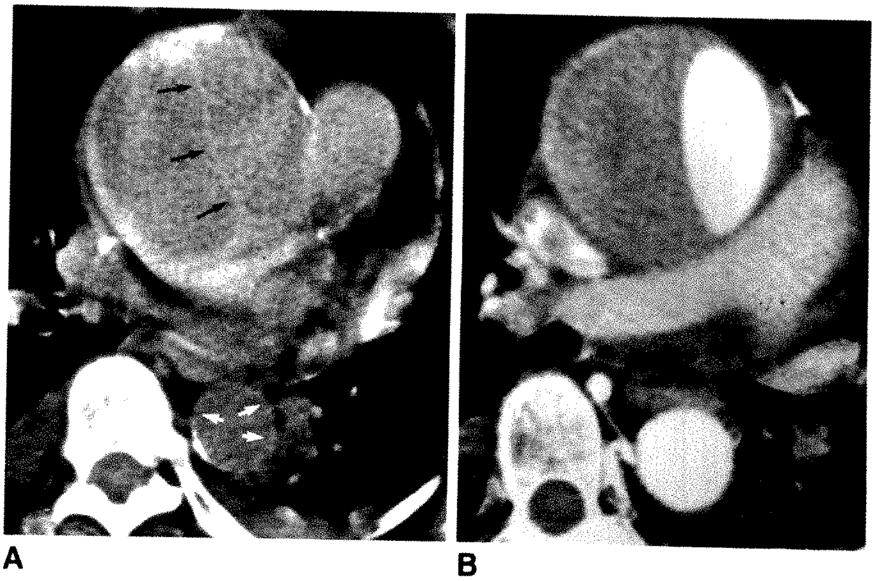

Fig. 1.—Case 1. **A**, Unenhanced CT scan. Intimal flap (*black arrows*) and walls of ascending and descending aorta (*white arrows*) are visible. **B**, After bolus enhancement, true lumen of dissection is densely opacified.

Received July 8, 1985; accepted after revision October 18, 1985.

[1] All authors: Department of Radiology, Loyola University Medical Center, 2160 S. First Ave., Maywood, Illinois 60153. Address reprint requests to T. C. Demos.

AJR 146:601–603, March 1986 0361-803X/86/1463-0601 © American Roentgen Ray Society

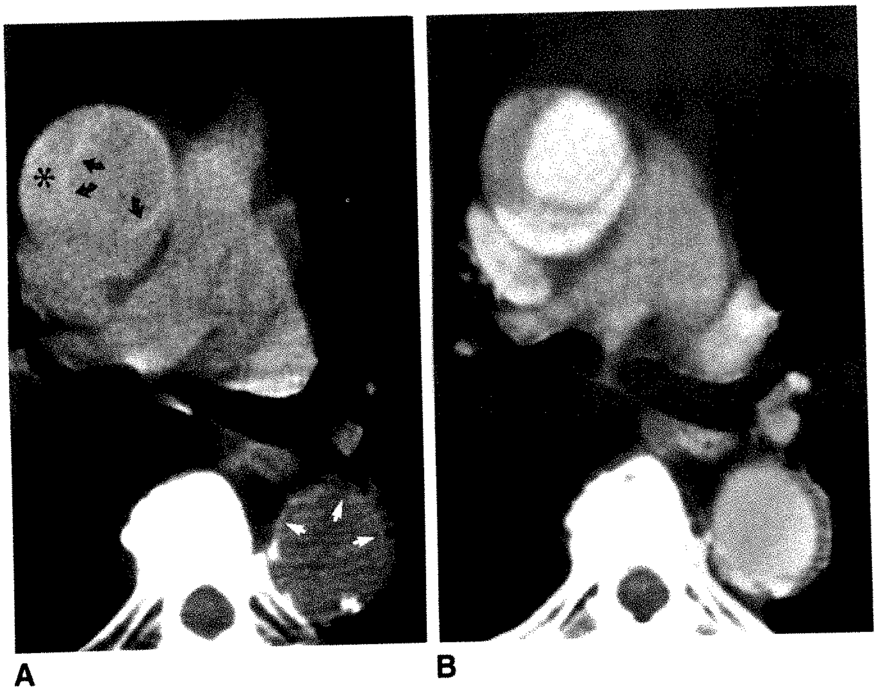

Fig. 2.—Case 2. **A**, Unenhanced CT scan. Curvilinear intimal flap (*black arrows*) and superolateral wall of ascending and wall of descending aorta (*white arrows*) are visible. Note clot (*asterisk*) in false lumen. **B**, After bolus enhancement, true and false lumens are densely opacified. Laterally located false lumen contains clot.

images. More specific findings are inwardly displaced calcified atheromatous plaques and high attenuation of a clotted false lumen [1, 2].

Some patients with aortic dissection will not demonstrate enhancement of the false lumen because there is no intimal tear [3] or because the false lumen is filled with clotted blood [1, 2, 4]. It may be extremely difficult on the basis of CT or angiographic criteria to differentiate these patients from patients with a clot containing fusiform aneurysms. It has been found, however, that high attenuation on at least two contiguous unenhanced images is reliable evidence of clotted blood in a false lumen and thus allows the diagnosis of aortic dissection [5].

Most aortic dissections begin with an intimal tear that allows the bloodstream direct access to the aortic wall. The subsequent dissection usually occurs between the middle and outer layers of the media. If there are calcified atheromatous plaques of the intima, they will be carried inward with the displaced intima-media flap. The finding of displaced calcification is suggestive of aortic dissection but does not allow a definitive diagnosis [4]. Displacement may be simulated because of volume averaging, which commonly occurs at the superior and inferior aspects of the aortic arch and at sharp bends in the aorta. In addition, nonvascular pathologic processes such as fibrotic tissue or neoplasm contiguous with the aortic wall can also simulate inward displacement of calcified plaques. Finally, the surface of blood clot in an arteriosclerotic aneurysm may calcify and simulate a displaced intimal plaque. Intravenous enhancement is thus required to confirm aortic dissection.

The identification of two or more aortic lumens and intimal flaps are the definitive signs of aortic dissection. The intimal flap may be demonstrated by echocardiography [6] and magnetic resonance imaging [7] without the use of any type of enhancement, but demonstration of the flap by CT without intravenous contrast material enhancement has not before been described. It is generally stated that demonstration of the flap by CT requires contrast medium injection [7].

In the past year we have identified an intimal flap on unenhanced CT images in three patients. The first patient is reported as case 1. The second case was a 70-year-old woman with an acute proximal aortic dissection (fig. 2). Her hematocrit was 9.8 g/dl. The third case, a 42-year-old woman with Marfan syndrome, had a known residual false lumen (fig. 3) distal to a Dacron graft of the ascending aorta. The graft had been used to treat an acute aortic dissection 8 years earlier. Her hemoglobin was 11.5 g/dl.

In all these patients the wall of the aorta could also be identified on unenhanced images, so that visibility of the flap was most likely due to contrast provided by the diminished density of the blood. Two patients had a hemoglobin of less than 10 g/dl, and the third had a hemoglobin of 11.5 g/dl. The ability to discriminate the wall of the aorta in anemic patients is well known. A 1981 study [8] stated that the interventricular septum of the heart could be seen when the hemoglobin was 10 g/dl or less and that the aortic wall became visible with a hemoglobin below 8 g/dl. The ability to see the aortic wall in a patient with a hemoglobin higher than this threshold could be in part due to improvement in CT hardware and software currently in use.

The intimal flap of an aortic dissection may be visible on unenhanced images obtained with sub 5-sec scanners. These

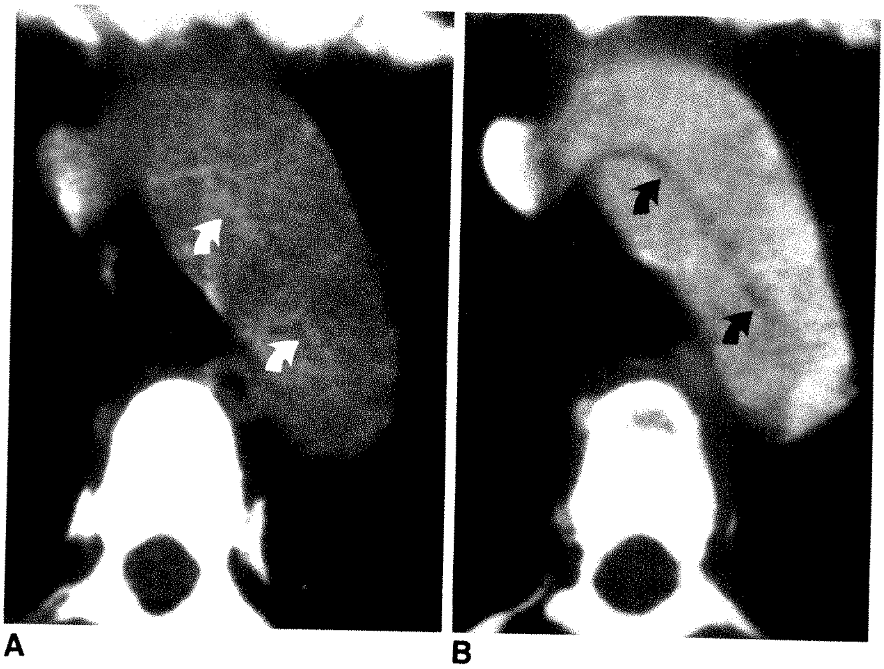

Fig. 3—Case 3. **A**, Unenhanced CT scan. Curvilinear intimal flap (*arrows*) of aortic arch is visible. **B**, Bolus enhancement confirms presence of intimal flap (*arrows*).

images should be examined for an intimal flap. A narrow window may be needed in order to identify a subtle linear or curvilinear density within the aortic lumen.

Addendum

Since this paper was accepted for publication, we have encountered two more patients with type I dissections of the thoracic aorta who had intimal flaps seen on unenhanced CT images.

REFERENCES

1. Thorsen MK, San Drett MA, Lawson TL, Foley WD, Smith DF, Berland LL. Dissecting aortic aneurysms: accuracy of computed tomographic diagnosis. *Radiology* **1983**;148:773–777
2. Oudkerk M, Overbosch E, Dee P. CT recognition of acute aortic dissection. *AJR* **1983**;141:671–676
3. Hirst AC, Jones VJ, Kime SW. Dissecting aneurysm of the aorta; review of 505 cases. *Medicine* **1958**;37:217–279
4. Godwin JD, Breiman RS, Speckman JM. Problems and pitfalls in the evaluation of thoracic dissection by computed tomography. *J Comput Assist Tomogr* **1982**;6:750–756
5. Heiberg E, Wolverson MK, Sundram M, Shields JB. CT characteristics of aortic artherosclerotic aneurysm versus aortic dissection. *J Comput Assist Tomogr* **1985**;9:78–84
6. Victor MF, Mintz GS, Kotler AR, Wilson R, Segal BL. Two dimensional echocardiographic diagnosis of aortic dissection. *Am J Cardiol* **1981**;48:1155–1159
7. Geisinger MA, Risius B, O'Donnell SA, et al. Thoracic aortic dissections: magnetic resonance imaging. *Radiology* **1985**; 155:407–412
8. Doppman JJ, Rienmuller R, Lissner J. The visualized interventricular septum on cardiac computed tomography: a clue to the presence of severe anemia. *J Comput Assist Tomogr* **1981**;5:157–160

Memorial

Harold A. Baltaxe, 1931–1985

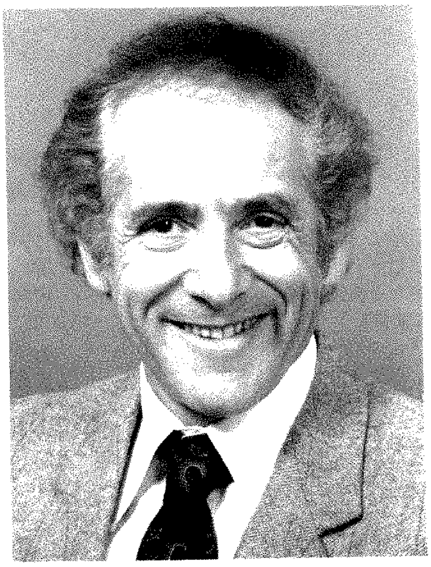

Dr. Harold A. Baltaxe died unexpectedly of a myocardial infarction on August 24, 1985. The death of a friend is always sad, but never moreso than when it deprives us of one who was at the peak of an active and productive career. Harry received his M.D. from the University of Lausanne, Switzerland, having graduated first in his class, then did his internship and radiology residency at the State University of New York in Buffalo. After 2 years on the staff at SUNY in Syracuse, he took a cardiovascular radiology fellowship with Dr. Kurt Amplatz at the University of Minnesota Hospital during 1968–1969. He then became head of the cardiovascular radiology section at New York Hospital—Cornell Medical Center from 1969 to 1976, during which time he established himself as a leader in that field and progressed rapidly to the rank of Professor of Radiology. In 1976 he accepted the post of Professor and Chairman of the Department of Radiology at the University of Nebraska Medical Center. He remained there for 5 years, then became Professor and Chairman of Radiology at the University of California, Davis in 1981.

In spite of the demands on his time as a department head, he continued his active participation in both clinical and experimental research. Harry was an author of 113 published articles or book chapters and one of the early textbooks on coronary angiography. He was a tireless and effective worker for cardiovascular radiology and, at one time or another, occupied leadership positions in virtually every major organization in the field. He served as President of the North American Society for Cardiac Radiology and the Society for Cardiac Angiography and was President-Elect of the Society of Throacic Radiology at the time of his death.

These essential facts say little about the man himself. He was energetic, vibrant, intelligent, and curious. Although widely known as a friendly and outgoing person, he never shrank from confronting those with whom he disagreed. He had a fine sense of humor and fair play. He was an active sportsman who participated regularly in skiing, tennis, and running. He was also an accomplished linguist with fluency in English, French, German, and Spanish, and a working knowledge of several other languages.

Harry will be greatly missed by his many friends and colleagues throughout the worldwide radiology community. His death is a special loss to his wife Claire and their three children, Debbie, David, and Bernie. At least they had the good fortune to grow up with their father and to be able to remember him as a loving and accomplished person.

Thomas A. Sos
New York Hospital-Cornell Medical Center
New York, NY 10021
David C. Levin
Brigham and Women's Hospital
Boston, MA 02115

The In Situ Saphenous Vein Bypass Graft: Radiologic Aspects

Warren Schwarz[1]
Jerome Nozick[2]
David Richmand[2]
Brian Rodgers[3]
Alec Simpson[2]
Charles Argila[2]
Steven Honickman[1]

The use of the in situ saphenous vein for bypassing arterial occlusions in the lower extremities appears to have a higher patency rate than other bypass procedures but presents unique technical problems, such as lysing valves and occluding venous tributaries. Forty-four patients undergoing in situ bypasses had preoperative arteriograms. Special attention was paid to the small runoff vessels around the ankle, which are not suitable for reversed bypass procedures but may be adequate for in situ bypasses. Eight patients also had preoperative saphenous venograms, which revealed surgically important abnormalities in six cases. Postoperative arteriograms obtained within 2 weeks in 10 patients and within 2–12 months in 15 patients revealed persistent arteriovenous fistulas in four patients, stenoses in nine, occlusions in five, and progressive disease in the nonbypassed arteries in five patients. Early recognition of these problems led to 11 surgical repairs; nine repairs used the interventional radiologic procedures of balloon angioplasty, transcatheter embolization, and catheter thrombolysis. In this group of 44 patients, five patients died with patent bypasses and three patients required amputation despite functioning bypasses. Only four amputations were attributed to bypass failure. This low figure may be due to the close cooperation of the vascular surgeons and the vascular radiologists in dealing with these complicated cases.

Until recently, most bypass operations for arterial occlusive disease in the lower extremities involved the interposition of either a prosthetic conduit or a length of saphenous vein surgically removed from the leg and reversed. The in situ vein bypass also uses the saphenous vein, but only the proximal and distal ends are mobilized; most of the vein is left in its vascular bed. This seems to afford a higher patency and vein use rate then when the vein is reversed [1–3]. However, this procedure creates special technical problems that require the attention of not only the surgeon but the vascular radiologist.

In the reversed vein graft, the valves are reversed and do not obstruct flow, but the valve leaflets must be individually incised when the in situ vein is used. Venous tributaries must also be ligated, because while small arteriovenous communication may actually improve the patency rate of in situ bypasses, patent large tributaries will steal blood from the foot [4].

We present here the first 44 in situ saphenous vein bypasses done in 41 patients by one surgical group at our hospital. While this series is not yet large enough or old enough to evaluate the long-term utility of this operation, the radiologist's contribution is already apparent.

Subjects and Methods

Patients were aged 28–85 years (except for one woman with juvenile-onset diabetes, all subjects were over 60), 26 men and 15 women. Twenty patients were diagnosed previously as having diabetes mellitus. Twenty-three bypasses were done on the left leg and 21 on the right. Of 44 bypasses, two were done for claudication, 20 for treatment of rest pain, 19 for

Received July 8, 1985; accepted after revision October 22, 1985.

Presented at the annual meeting of the American Roentgen Ray Society, Boston, April 1985.

[1] Department of Radiology, Muhlenberg Hospital, Randolph Rd. and Park Ave., Plainfield, NJ 07060. Address reprint requests to W. Schwarz.

[2] Department of Surgery, Muhlenberg Hospital, Plainfield, NJ 07060.

[3] Rutgers University Medical School, New Brunswick, NJ 08903.

AJR 146:605–608, March 1986
0361–803X/86/1463–0605
© American Roentgen Ray Society

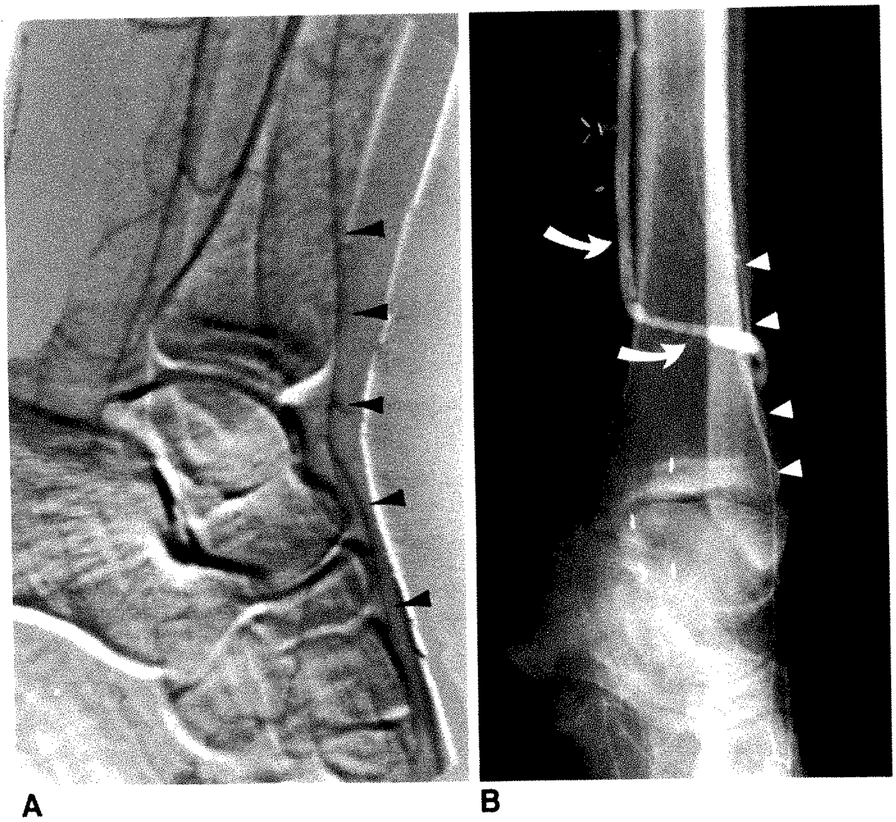

Fig. 1.—Routine runoff arteriogram in 28-year-old juvenile diabetic showed no opacified major vessels below midthigh. **A**, Intraarterial digital subtraction angiogram of lateral foot shows small but patent distal anterior tibial artery and dorsalis pedis artery (*arrowheads*). **B**, Arteriogram after in situ bypass shows vein bypass (*arrows*) anastomosing to very small (1.5-mm) distal anterior tibial artery (*arrowheads*).

limb salvage, and three for popliteal aneurysms. Eight patients required amputations of toes or transmetatarsal amputation for gangrene at the time of bypass surgery.

In all cases, the proximal anastomosis was made to the common femoral artery or to the proximal superficial femoral artery. The distal anastomosis was made to the distal popliteal artery in eight cases, a proximal tibial artery in 15, a peroneal artery in four, and a distal tibial artery in 17. Therefore, all bypasses crossed the knee joint.

Arteriograms were obtained using standard techniques. Surgical techniques have been previously described [5]. Saphenous valve lysis was done with a "hockey stick" instrument, inserted through a tributary. This device has a small cutting blade at the angle, which incises a valve leaflet when it is drawn downward. Intraoperatively, venous tributaries were identified under direct vision and with the use of operative Doppler.

Results

Of 44 in situ bypasses done in 41 patients, 29 are still functioning with follow-up of up to 24 months. Five patients died (two of whom had bilateral in situ bypasses). In two cases, death was directly related to bypass surgery. Five in situ bypasses occluded at intervals of 2 weeks, 1 month, 3 months, 5 months, and 7 months after surgery, resulting in four amputations. Three patients required amputations for ongoing infection despite functioning bypasses.

For discussion, we divided the radiologic management of in situ bypasses into five areas: preoperative arteriogram, saphenous venogram, early postoperative arteriogram, late postoperative arteriogram, and radiologic intervention.

Preoperative Arteriogram

All patients had preoperative arteriograms to evaluate the status of the vasculature to the lower extremities. These studies were the same as routine runoff arteriograms, except special attention was paid to the vessels around the ankle since in situ bypasses offer the possibility of successfully grafting to these small arteries.

In six cases, the tibial arteries could not be seen below the knee on the routine runoff films. An intraarterial contrast medium injection with digital subtraction imaging of the lateral ankle showed the posterior tibial artery or dorsalis pedis artery in these cases [6], allowing the surgeons to perform the bypass operation in these patients (fig. 1).

Saphenous Venogram

Nine preoperative saphenous venograms were done in eight patients in whom there was a history of venous thrombosis or of previous surgery using the saphenous vein, or in whom the surgeon was unable to adequately evaluate the vein clinically. Since the intent of the in situ bypass procedure is to cause the minimum amount of trauma to the vein, and since contrast material is known to damage endothelium [7], careful attention to technique is essential. We used Conray 60 diluted to 30% with an equal amount of 50% normal saline injected directly into the saphenous vein at the ankle via a 23-gauge butterfly needle. Camera spot films were obtained

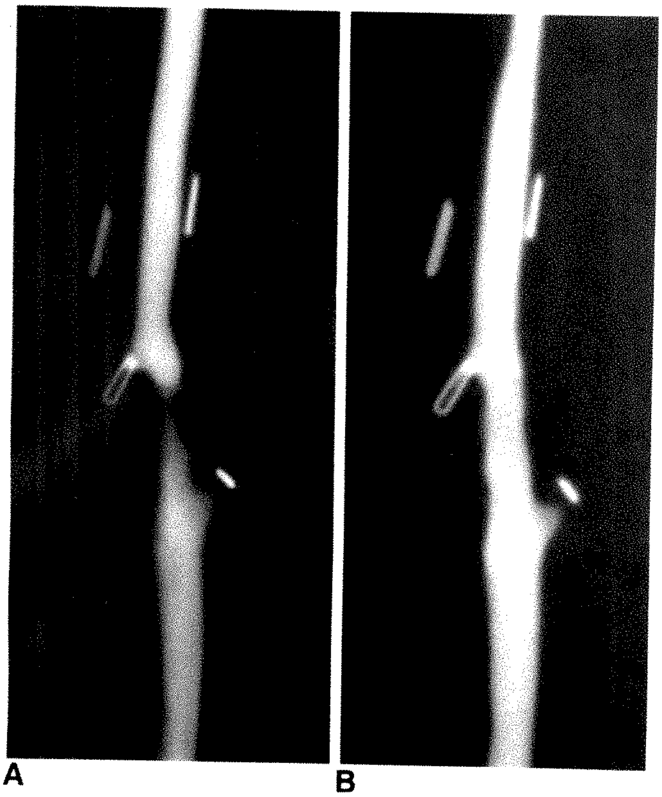

Fig. 2.—A, Tight stenosis in in situ vein bypass at site of valve lysis 6 months after surgery was discovered on routine noninvasive follow-up examination. B, After percutaneous balloon angioplasty, luminal diameter of bypass was restored. In situ bypass continues to function 12 months after dilation.

with the patient horizontal as the contrast material went up the vein. Immediately afterward, the vein was flushed with normal saline solution while contrast material was gently milked out under fluoroscopic control. If nonionic contrast material had been available to us, it would have been used [8].

Saphenous venography revealed three patients with veins inadequate for bypasses. One patient had a narrowed irregular but usable vein. One patient was missing the distal part of the vein due to a previous coronary bypass, but enough length of saphenous vein remained for a successful femoropopliteal bypass. In two cases, the saphenous vein was seen to be duplicated in part. This is important because in these two patients and two other patients with unsuspected duplicated systems, there were postoperative problems requiring ligation of arteriovenous communications. In the remaining two cases, the saphenous veins were normal.

Early Postoperative Arteriogram

Ten patients needed arteriograms within 2 weeks after surgery to evaluate persistent ischemia. One patient was found to have a satisfactorily functioning bypass but poor outflow due to underlying disease. Three patients had bypasses containing early stenoses in the vein. Four patients had large arteriovenous connections due to unligated collateral veins. The bypass graft failed to appear on arteriography in only two patients. One had a graft occlusion. In the other, a pulsating graft could be palpated, and direct puncture revealed an outflow problem due to kinking of the vein near the distal anastomosis [9].

In these 10 patients, early detection of flow problems resulted in six surgical repairs and three interventional angiographic repairs (see below). Amputation was required for early complications in one case.

Late Postoperative Arteriogram

Fifteen arteriograms were obtained in 13 patients within 2–12 months after surgery (one patient required three follow-up arteriograms). Arteriography was performed when decreased blood flow was detected by noninvasive studies or when patients became symptomatic.

Arteriography showed occluded bypasses in four patients. Six graft stenoses were discovered in four patients (one patient had three follow-up arteriograms for a recurrent stenosis). In four patients, the bypass was normal but arterial disease had progressed either proximally or distally to the bypassed area. In one case no problem was found.

Late complications resulted in three amputations in this group. Surgical repair was accomplished in five patients and interventional radiologic repair in four (see below).

Radiologic Intervention

Nine interventional radiologic procedures were done in eight patients. In three patients, percutaneous balloon angioplasties were performed for stenoses that developed within the bypass. This has been previously described for the reversed saphenous vein grafts [10] and is the same for the in situ bypasses (fig. 2). In two patients, the balloon angioplasty had a good long-term result. One patient had two attempts at balloon angioplasty that seemed to be successful initially, but each time a restenosis developed at the same site within 2 months. He went on to have a successful surgical repair of this segment of vein.

Three patients had percutaneous transcatheter embolizations of arteriovenous communications discovered in the early postoperative period. This was done by antegrade catheterization of the in situ bypass from a femoral approach. The tip of the catheter was selectively placed into each major communicating vein, and stainless-steel coils were discharged [11]. In each case, there was an immediate and dramatic result, with the foot becoming noticeably warmer and pedal pulses improving (fig. 3).

One patient required transcatheter thrombolysis with streptokinase followed by balloon angioplasty of a distal anastomotic stenosis, which salvaged the graft. In one patient, percutaneous balloon angioplasty was performed on a native iliac artery that became stenotic after a bypass was placed in the same leg. Although there was minimal flow through the in situ bypass, it had remained open and the iliac angioplasty restored pedal pulses.

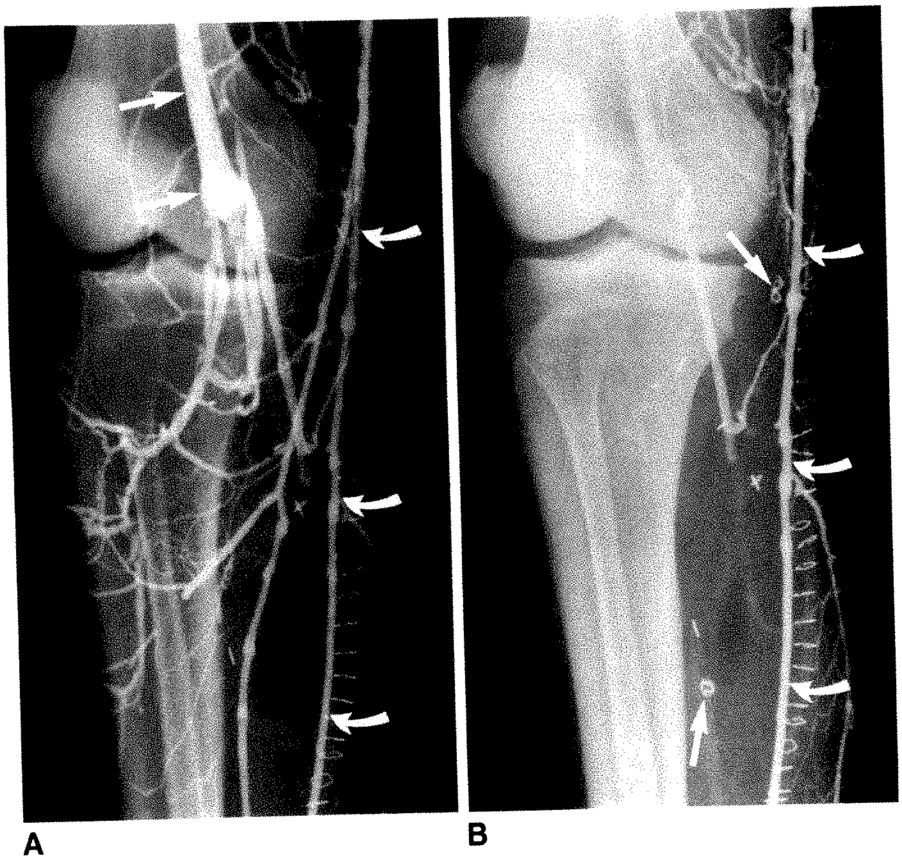

Fig. 3.—**A**, Arteriogram 1 week after operation. In situ saphenous vein bypass is well opacified (*curved arrows*). Almost simultaneous visualization of deep veins of leg (*straight arrows*) indicates large arteriovenous communication. **B**, After placement of two Gianturco coils (*straight arrows*), bypass graft is seen (*curved arrows*) but opacification of deep venous system is greatly reduced.

Discussion

In situ saphenous vein bypasses seem to offer the potential of grafting to smaller, more distal runoff vessels than was possible with conventional reversed vein grafts [12]. While our series of 44 in situ bypasses is not large enough or old enough to evaluate the long-term results in these patients, the radiologic aspects of this surgical procedure are already clear.

Close cooperation between the vascular surgeon and the vascular radiologist is essential, not only to the proper preoperative evaluation of bypass candidates but to the postoperative management. In our series, 23 in situ vein bypasses were studied after surgery. This resulted in the prompt treatment of problems either by surgery or interventional techniques. We believe that without this cooperation, the number of amputations would have exceeded the four that occurred from graft occlusion.

REFERENCES

1. Leather RP, Powers SR, Karmody AM. A reappraisal of the "in-situ" saphenous vein arterial bypass: its use in limb salvage. *Surgery* **1979**;86:453–460
2. Leather RP, Shah DM, Karmody AM. Infrapopliteal arterial bypass for limb salvage: increased patency and utilization of the saphenous vein used "in-situ." *Surgery* **1981**;90:1000–1007
3. Buchbinder D, Singh JK, Karmody AM, Leather RP, Shah DM. Comparison of patency rate and structural changes of in-situ and reversed vein arterial bypass. *J Surg Res* **1981**;30:213–222
4. Leather RP, Corson JD, Naraynsingh V, Young HL, Shah DM, Karmody AM. The use of the long saphenous vein for lower limb salvage: technique and results of in situ saphenous vein bypass. *Contemp Surg* **1984**;24:31–39
5. Leather RP, Shah DM, Buchbinder D, Annest SJ, Karmody AM. Further experience with the saphenous vein used in situ for arterial bypass. *Am J Surg* **1981**;142:506–510
6. Crummy AB, Stieghorst MF, Turski PA, et al. Digital subtraction angiography: current status and use of intraarterial injection. *Radiology* **1982**;145:303–307.
7. Zinner G, Gottlob R. Morphologic changes in vessel endothelium caused by contrast media. *Angiology* **1959**;10:207–213
8. Thomas ML, Posniak HV. Saphenography. *AJR* **1983**;141:812–814
9. Schwarz W, McLean GK, Ring EJ, Barker CF. The nonvisualized, nonoccluded graft. *AJR* **1983**;140:979–982
10. Alpert JR, Ring EJ, Berkowitz HD, et al. Treatment of vein graft stenosis by balloon catheter dilation. *JAMA* **1979**;242:2769–2771
11. Chuang VP, Wallace S, Gianturco C. A new improved coil for tapered-tip catheter for arterial occlusions. *Radiology* **1980**;135:507–509
12. Connolly JE, Kwaan JHM. In situ saphenous vein bypass. *Arch Surg* **1982**;117:1551–1557

Sonography of Neck Masses in Children

Richard Kraus[1, 2]
Bokyung K. Han[1]
Diane S. Babcock[1]
Alan E. Oestreich[1]

The sonograms and medical records of 49 patients were reviewed to determine if there is a characteristic sonographic appearance for certain neck masses. Neck masses included: inflammatory masses (12), noninflammatory masses (23), and thyroid masses (14). Four entities including thyroglossal duct cyst, fibromatosis colli, cystic hygroma, and multiple lymphadenopathy showed characteristic sonographic appearance. Thyroglossal duct cysts were seen as midline or slightly off midline cystic masses. A sinus tract extending superiorly was nicely demonstrated in one patient. The mass in fibromatosis colli (neonatal torticollis) appeared as a well defined mass clearly within the sternocleidomastoid muscle, uniformly echogenic, but less echogenic than the normal surrounding muscle, without good through-transmission. A cystic or primarily cystic mass with linear septations was the characteristic finding of the cystic hygroma. Multiple lymphadenopathy demonstrated multiple discrete, oval, relatively hypoechoic masses along the cervical lymphatic chain. The sonographic appearance of inflammatory masses was variable, being either inhomogeneously echogenic or of mixed echogenicity. Hemangiomas were either echogenic with cystic vascular spaces or linear septations or relatively homogeneously echogenic. Intrinsic thyroid masses could be distinguished from extrinsic masses in most cases. The demonstration of calcification in a mass was useful in narrowing the differential diagnosis. Although it is not a specific finding, the presence of calcification highly suggests a neoplastic lesion, particularly neuroblastoma or teratoma. Not only can the location, extent, and internal characteristics of a mass be determined, but in certain entities, the sonographic appearance is characteristic and an accurate diagnosis can be made.

Sonographic evaluation of neck masses in children is useful in demonstrating the location, extent, and internal characteristics of a mass [1, 2]. The purpose of our study was to determine if, in addition, any masses had a characteristic appearance which would lead to an accurate sonographic diagnosis.

Materials and Methods

The sonograms of 49 patients referred for neck masses between 1978 and 1985 were reviewed. The patients ranged in age from 3 weeks to 18 years. The sonograms were performed with sector real-time (ATL MK300, MARK 3) and static articulated equipment (Picker 80-L) using 5- and/or 7.5-MHz transducers. In many cases, a water bath was used, which was helpful in imaging superficial lesions. The medical records were reviewed to correlate the diagnosis and clinical course with our sonographic findings. In many cases there was pathologic verification.

Results

Table 1 is a summary of our cases. The masses were divided into inflammatory and noninflammatory. The noninflammatory masses were further subdivided into benign and malignant. The thyroid masses were categorized separately.

Received June 27, 1985; accepted after revision October 1, 1985.

Presented in part at the annual meeting of the Society for Pediatric Radiology, Boston, April 1985.

[1] Departments of Radiology and Pediatrics, University of Cincinnati College of Medicine, Children's Hospital Medical Center, Elland and Bethesda Aves., Cincinnati, OH 45229. Address reprint requests to B. K. Han.

[2] Present address: Montreal Children's Hospital, Montreal, Quebec, Canada H3H 1P3.

AJR 146:609–613, March 1986
0361–803X/86/1463–0609
© American Roentgen Ray Society

Inflammatory Masses

These 12 cases were clinically diagnosed as lymphadenitis and/or abscess. The sonographic characteristics of inflammatory masses varied, being either inhomogeneously echogenic (fig. 1) or of mixed echogenicity (fig. 2A). All had relatively good through-transmission, with abscesses demonstrating the best through-transmission. Four patients had, in the vicinity of the mass, multiple, discrete, smaller anechoic masses compatible with associated lymphadenopathy (fig. 2B). All patients were treated with intravenous antibiotics and clinically improved. Those with abscesses had surgical drainage.

Benign Noninflammatory Masses

Thyroglossal duct cysts.—Four of these six patients had masses located in the midline; two had masses to the left of the midline. The position of the thyroglossal duct cyst varied from the submental region to the level of the manubrium. In one patient, the cyst was seen in the suprasternal region and was associated with a thin sinus tract extending to the submandibular region (fig. 3). Four of the masses were typically cystic, demonstrating an anechoic, well marginated structure with good through-transmission. In two cases, the cyst was infected. One showed a primarily anechoic mass with a thick echogenic wall (fig. 4); the other was a solid-appearing inhomogeneously echogenic mass. The latter was seen in a patient who had had six episodes of neck cellulitis. Pathologic examination showed chronic granulation tissue and squamous metaplasia, which accounted for the atypical sonographic appearance.

TABLE 1: **Neck Masses**

Type of Mass	No. of Cases
Inflammatory masses (nonthyroid)	12
Noninflammatory masses:	
Benign:	
Thyroglossal duct cyst	6
Sternocleidomastoid mass	4
Cystic hygroma/lymphangioma	5
Hemangioma/vascular malformation	4
Malignant:	
Neuroblastoma	1
Teratoma	1
Leukemia/lymphoma	2
Thyroid masses:	
Thyroid abscess	3
Hashimoto thyroiditis/goiter	5
Cyst	3
Adenoma	2
Ectopic thyroid	1

Sternocleidomastoid masses.—In these four patients, fibromatosis colli (neonatal torticollis) was seen in three. It appeared as a well defined mass within the sternocleidomastoid muscle, uniformly echogenic, without good through-transmission. These masses were of mild to moderate echogenicity and in each case, of less echogenicity than the normal surrounding muscle (fig. 5). With real-time examination, the mass moved synchronously with the sternocleidomastoid muscle. The fourth patient was a hemophiliac who had a sternocleidomastoid muscle hematoma. The involved muscle was diffusely enlarged with relatively decreased echogenicity compared to normal muscle. There was minimal through-transmission of sound.

Cystic hygroma/lymphangioma.—Three of these five patients showed masses with both echogenic and anechoic areas. The anechoic regions contained septations (fig. 6). Another patient demonstrated a cystic mass that had multiple fine septations. The fifth patient had a sclerosing lymphangioma (extensive reactive inflammatory and cicatricial change). It appeared as a primarily echogenic ovoid mass with a few small cystic areas.

Hemangioma/vascular malformation.—The three hemangiomas were superficial in location. Sonographically, they had variable features. They were mild to moderately echogenic. One showed several, small, anechoic areas suggesting vascular spaces. Another showed echogenic linear septations. The third mass was relatively homogeneous. One patient had a venous malformation, showing an anechoic ovoid mass with a central echogenic area that produced acoustic shadowing. The appearance suggested a calcified thrombosis. Direct percutaneous injection of contrast material into the mass confirmed the sonographic findings.

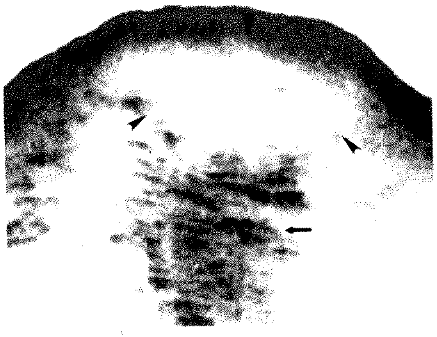

Fig. 1.—Abscess. Diffusely echogenic mass (*arrowheads*) with good through-transmission (*arrow*). Surgically drained.

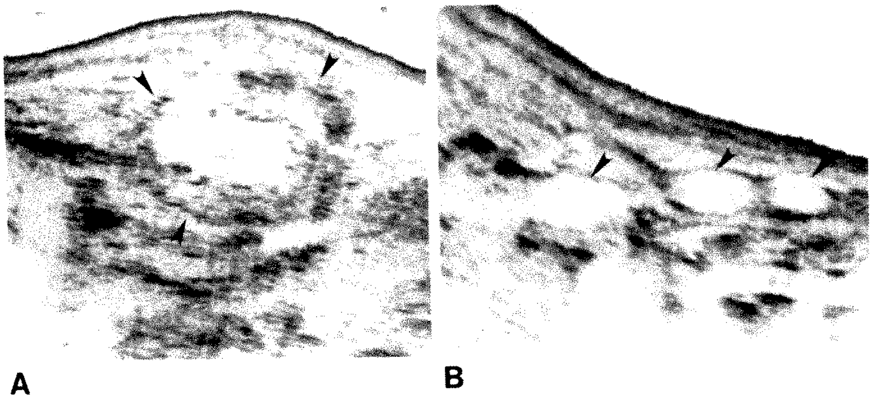

Fig. 2.—Inflammatory mass with associated lymphadenopathy. **A**, Longitudinal scan shows poorly marginated mass of mixed echogenicity (*arrowheads*). **B**, Multiple smaller anechoic masses (*arrowheads*) compatible with lymphadenopathy.

Fig. 3.—Thyroglossal duct cyst. Midline longitudinal scan shows cystic mass (C) above sternal notch associated with sinus tract extending cephalad (*arrowheads*).

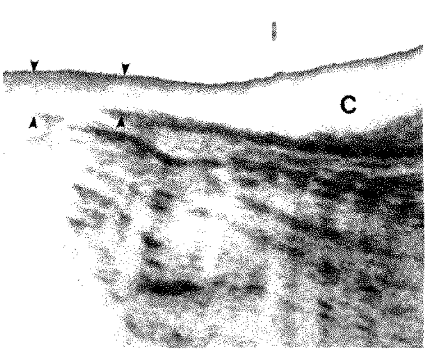

3

Fig. 4.—Infected thyroglossal duct cyst. Midline longitudinal scan demonstrates primarily anechoic mass in submandibular region with thick echogenic wall (*arrowheads*).

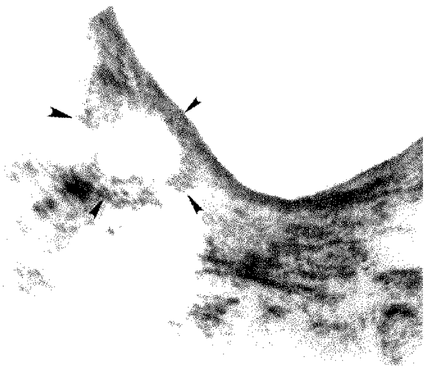

4

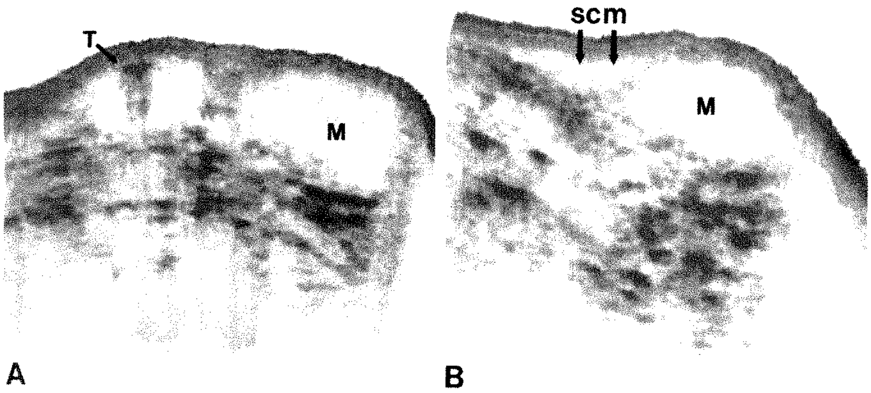

Fig. 5.—Fibromatosis colli. **A**, Transverse scan demonstrates fairly well marginated, diffusely echogenic superficial mass (M) left of midline. T = trachea. **B**, Longitudinal scan shows mass (M) surrounded by normal sternocleidomastoid muscle (SCM). Echogenicity of mass is less than that of normal surrounding muscle.

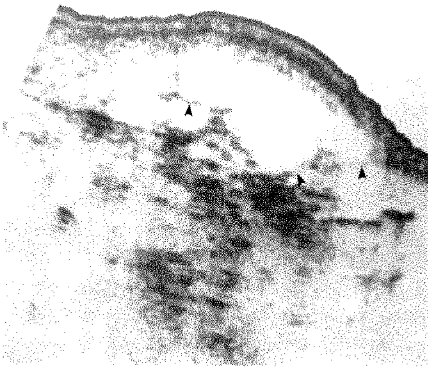

Fig. 6.—Cystic hygroma. Longitudinal scan demonstrates mass of mixed echogenicity. Within anechoic regions are thin linear septations (*arrowheads*).

Malignant Masses

Neuroblastoma.—The one cervical neuroblastoma was a markedly echogenic, inhomogeneous, solid mass with calcifications (fig. 7).

Teratoma.—This mass was moderately echogenic with discrete cystic areas and calcifications (fig. 8).

Leukemia and lymphoma.—Both patients had multiple, bilateral, discrete oval masses that were situated along the cervical lymphatic chain. The sonographic appearance was compatible with lymphadenopathy. Some of the enlarged lymph nodes had fine echoes with good through-transmission (fig. 9).

Thyroid Masses

Thyroid abscesses.—These three masses had a variable sonographic appearance. Two cases showed mild to moderate echogenicity, but the intensity of the echoes was less than that of the adjacent normal thyroid. The third abscess was moderately echogenic and had a primarily anechoic center containing a few scattered echoes. All three abscesses had mass effect, displacing the trachea.

Hashimoto thyroiditis/goiter.—Four patients (three with thyroiditis, one with goiter) showed a diffusely enlarged thyroid gland with a homogeneous echo pattern but without a localized mass. One patient with multinodular goiter had a mass of mixed echogenicity in the right lobe with a smaller hypoechoic, solid-appearing mass in the left lobe.

Cysts.—In two of these three patients, the mass was clearly cystic; that is, anechoic with well marginated borders and very good through-transmission (fig. 10). One of these masses had fine echoes in the dependent part, which moved freely on changing the position of the patient. The third patient had an infected cyst. It was inhomogeneously echogenic, but showed good through-transmission, indicating the primarily fluid nature of the mass.

Adenomas.—In both patients, the mass was primarily echogenic with small anechoic areas. The degree of echogenicity was greater than that of surrounding normal thyroid tissue.

In all patients with thyroid cysts and adenomas, the intrinsic location of the mass was clearly demonstrated on sonography.

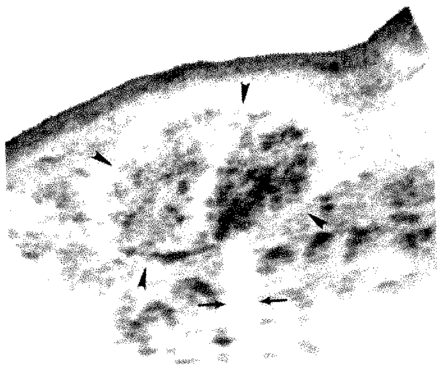

7

Fig. 7.—Neuroblastoma. Poorly marginated inhomogeneously echogenic mass (*arrowheads*). Highly echogenic area with shadowing (*arrows*) represents calcification.

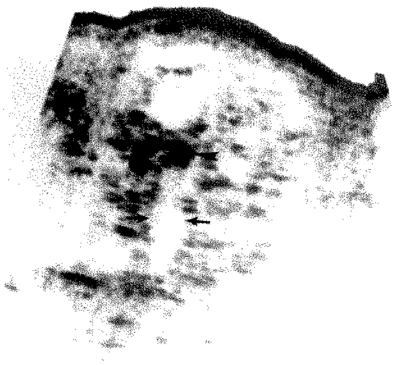

8

Fig. 8.—Teratoma. Mass of mixed echogenicity with discrete cystic areas and calcifications (*arrowhead*) with shadowing (*arrows*).

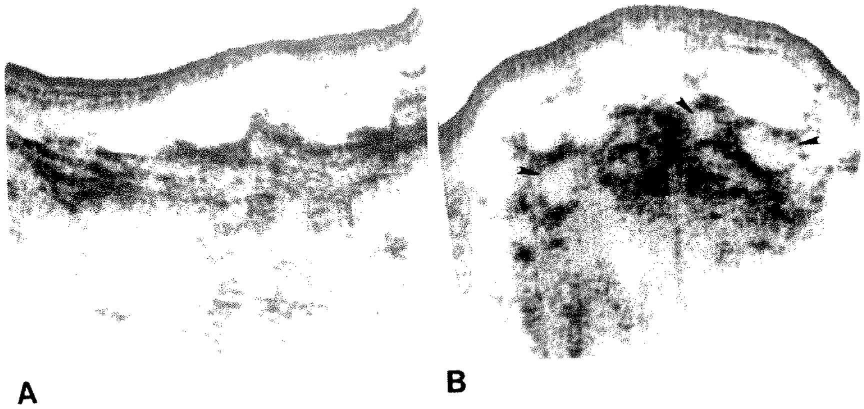

Fig. 9.—Lymphoma. **A**, Longitudinal scan shows multiple superficial anechoic masses situated along cervical lymphatic chain. **B**, Transverse scan reveals discrete, separate masses; some show low-level echoes (*arrowheads*) and relatively good through-transmission.

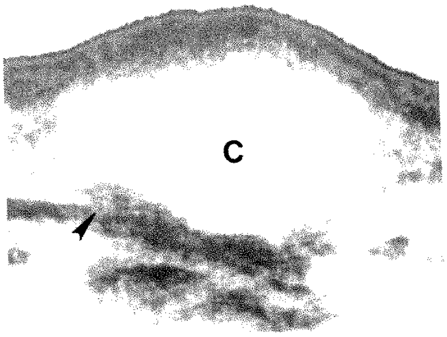

Fig. 10.—Thyroid cyst. Longitudinal scan shows beaklike extension (*arrowhead*) of normal thyroid tissue around cystic mass (C), confirming intrinsic location of mass.

Ectopic thyroid.—In one patient sonography showed a homogeneously echogenic mass similar to normal thyroid in echogenicity. It was anterior to the left carotid artery and inferior to, but inseparable from, the left lobe of the thyroid. Thyroid tissue in an ectopic location was proved by surgery.

Discussion

Sonography has proved useful in imaging neck masses [1–4], but its use in children has not been extensively reported [1, 2]. Friedman et al. [1] reviewed their cases of noninflammatory masses and concluded that sonography was nonspecific but did identify the location, extent, and internal characteristics of a mass. Sherman et al. [2] published their experience and found sonography valuable for localizing a mass and demonstrating its relation to other structures within the neck. Our review confirmed their results and, in addition, we found that certain entities have a characteristic appearance that can lead to an accurate sonographic diagnosis. These are thyroglossal duct cysts, fibromatosis colli, cystic hygroma, and multiple lymphadenopathy.

The most common midline lesion of the neck in a child is a thyroglossal remnant [5]. Thyroglossal duct cysts, which present as midline or slightly lateral to midline cystic masses, have a characteristic sonographic appearance. They can be found at any level from the base of the tongue to the thyroid isthmus. If the sinus tract can be demonstrated (fig. 3), the diagnosis is further assured. The ability to diagnose confidently is lost when the cyst becomes infected. A complex mass evolves, which is indistinguishable from other complex masses (fig. 4).

Fibromatosis colli or neonatal torticollis presents as a neck mass in infancy. It is believed to be the result of perinatal injury causing pressure necrosis and secondary fibrosis of the sternocleidomastoid muscle [6]. The sonographic appearance is characteristic. Within the sternocleidomastoid muscle is a homogeneously echogenic, well marginated mass of less echogenicity than the surrounding normal muscle. Sonographic recognition of this entity is important since surgery can be avoided. Initial treatment involves stretching exercises [5]. Surgery is reserved for failure of this exercise regimen.

The sonographic appearance of cystic hygroma in the neck is similar to that at other sites in the body. A cystic or primarily cystic mass with linear septations is the characteristic finding.

Multiple lymph nodes, whether from inflammatory or malignant disease, have a typical appearance. The presence of multiple discrete, oval, relatively hypoechoic masses along the cervical lymphatic chain suggests the diagnosis.

Inflammatory masses have a variable sonographic appearance, reflecting their changing nature. Our cases were of mixed echogenicity or were inhomogeneously echogenic. In most cases they demonstrated good through-transmission, even in masses that were solid in appearance. In one-third of the cases, adjacent lymphadenopathy was seen.

Hemangiomas were superficial in location and variable in appearance.

The demonstration of calcification within a mass is an important differential diagnostic finding but is not specific. Calcifications may be seen in hemangiomas, hematomas, neuroblastomas, teratomas, and with chronic inflammation. The case of cervical neuroblastoma showed a strongly echogenic mass with calcifications. The sonographic appearance is similar to another example published by Sherman et al. [2]. Therefore, the demonstration of a strongly echogenic mass with calcifications should suggest neuroblastoma. Teratomas, which may also contain calcification, characteristically show discrete solid and cystic areas. The appearance of teratomas in the neck is similar sonographically to their appearance at other sites in the body.

The sonographic appearance of thyroid masses has been well documented [7–10]. Our study was concerned with the ability to distinguish intrinsic from extrinsic thyroid masses. In all but one case, we could distinguish intra- from extrathyroid location. The exception was a large poorly defined mass which proved to be a thyroid abscess. Intrinsic masses such as cysts and adenomas showed normal thyroid tissue completely or partially surrounding the mass. Often a beaklike extension of normal thyroid tissue was seen partially encompassing the mass (fig. 10). This configuration was reminiscent of normal renal tissue surrounding an intrarenal mass. Diffuse glandular enlargement without a discrete mass is seen in Hashimoto thyroiditis. It is difficult to determine whether the echogenicity in this entity is increased or decreased relative to normal thyroid tissue, since there is no standard structure with which to compare.

In summary, sonography is a useful imaging method in the evaluation of neck masses in children. Although some entities, most notably inflammatory masses, have a variable appearance, certain masses have a characteristic appearance, and an accurate sonographic diagnosis can be made.

REFERENCES

1. Friedman AP, Haller JO, Goodman JD, Nagar H. Sonographic evaluation of non-inflammatory neck masses in children. *Radiology* **1983**;147:693–697
2. Sherman NH, Rosenberg HK, Heyman S, Templeton J. Ultrasound evaluation of neck masses in children. *J Ultrasound Med* **1985**;4:127–134
3. Gooding GAW, Herzog KA, Laing FC, McDonald EJ Jr. Ultrasonographic assessment of neck masses. *JCU* **1977**;5:248–252
4. McCurdy JA, Nadalo LA, Yim DWS. Evaluation of extrathyroid masses of the head and neck with gray scale ultrasound. *Arch Otolaryngol* **1980**;106:83–87
5. Solomon JR, Rangecroft L. Thyroglossal-duct lesions in childhood. *J Pediatr Surg* **1984**;19:555–561
6. Holder TM, Ashcraft MD. *Pediatric Surgery*. Philadelphia: Saunders, **1980**:1072–1074
7. Scheible W, Leopold GR, Woo VL, Gosink BB. High-resolution real-time ultrasonography of thyroid nodules. *Radiology* **1979**;133:413–417
8. Sackler JP, Passalaqua AM, Blum M, Amorocho L. A spectrum of diseases of the thyroid gland as imaged by gray scale water bath sonography. *Radiology* **1977**;125:467–472
9. Simeone JF, Daniels GH, Mueller PR, et al. High-resolution real-time sonography of the thyroid. *Radiology* **1982**;145:431–435
10. Bachrach LK, Daneman D, Daneman A, Martin DJ. Use of ultrasound in childhood thyroid disorders. *J Pediatr* **1983**;130:547–552

Erratum

In the January issue of the *AJR*, Dr. Paul B. Googe's name was mistakenly omitted from the list of authors of the article "Breast Cancer Metastasis to Intramammary Lymph Nodes" (*AJR* 1986;146:133–136). Dr. Googe, of the Department of Pathology, Massachusetts General Hospital, Boston, MA 02114, should be the third author listed.

Normal Renal Growth in Children with Myelodysplasia

George W. Gross[1]
Alan J. Thornburg[2]
Mark F. Bellinger[3]

Optimum urologic management of children with myelodysplasia includes periodic assessment of upper tract anatomy and renal growth. To investigate the perception that many children with spina bifida but without a history of intrinsic renal disease have small kidneys when compared with age-matched standard renal growth charts, 212 children with spina bifida were studied retrospectively, measuring renal length on excretory urograms. Patients with known vesicoureteric reflux of grade 2 or greater, congenital renal anomalies, hydronephrosis, renal scarring, or urinary diversion were excluded. For 95 patients aged 2 days to 19 days, 249 urograms were available for evaluation. Renal lengths were measured on the supine 5-min urogram. Mean values and standard deviations were calculated for each age group. Mean renal length for each age group fell below the mean of the standard curves devised by Hodson and Currarino, with increasing deviation from the mean with age.

Children with neuropathic vesical dysfunction are at risk for renal damage from hydronephrosis, vesicoureteric reflux, and infection. Optimal urologic management of these children includes periodic assessment of both upper tract anatomy and renal growth. Although renal sonography is rapidly replacing excretory urography as the preferred method for imaging the urinary tracts of children with spina bifida, considerable knowledge has accumulated regarding excretory urography in this group, and renal growth is commonly monitored by comparison with standard renal growth charts derived from measurement of renal size on excretory urograms [1–3].

Our perception has been that many children with spina bifida but without a history of pyelonephritis, vesicoureteric reflux, hydronephrosis, or structural abnormality of the upper urinary tract have renal length measurements based on excretory urography that are below mean values for standard renal growth charts. We therefore undertook a study of renal growth in spina bifida children to confirm our perception and determine if existing renal growth curves should be modified to better conform to the pattern of renal growth in the spina bifida population.

Materials and Methods

The clinical records and radiographic files of 212 patients seen at the Spina Bifida Clinic at the Elizabethtown Hospital and Rehabilitation Center of Pennsylvania State University were reviewed. Those patients included for study had normal-appearing kidneys on all urograms reviewed. Patients were excluded from the study if, by clinical history or radiologic examination, gross renal disease or morphologic abnormality was evident; this included documented vesicoureteric reflux of grade 2 or greater, congenital renal anomalies (e.g., solitary kidney, horseshoe or fused kidney, duplex kidney), chronic pyelonephritis by history or radiographic evaluation, hydronephrosis, and previous urinary tract diversion. Ninety-five patients qualified for inclusion in the study. Fifty-one patients (53%) were male; 44 (46.3%) were female; age range was 4 days to 19 years. Thirty-nine patients (38%) had had at least one voiding cystourethrogram (VCUG), while 56 (59%) had no documented VCUG.

Received July 15, 1985; accepted after revision November 14, 1985.

[1] Department of Radiology, Pennsylvania State University, Milton S. Hershey Medical Center, P.O. Box 850, Hershey, PA 17033. Address reprint requests to G. W. Gross.

[2] Pennsylvania State University College of Medicine, Hershey, PA 17033.

[3] Department of Surgery, Pennsylvania State University, Milton S. Hershey Medical Center, Hershey, PA 17033.

AJR 146:615–617, March 1986
0361–803X/86/1463–0615
© American Roentgen Ray Society

TABLE 1: **Number of Renal Length Measurements, Mean Renal Length, and Standard Deviation for Each Spina Bifida Age Group**

Age	No. of Kidneys	Mean (cm)	SD (cm)
Months:			
0–1	34	4.94	0.72
1–4	29	5.31	0.69
4–8	20	6.11	0.61
8–12	16	6.31	0.53
Years:			
1–2	47	6.92	0.70
2–3	36	7.36	0.71
3–4	37	7.66	0.65
4–5	37	8.01	0.75
5–6	32	8.60	0.78
6–7	22	8.42	0.56
7–8	19	9.04	0.86
8–9	20	8.84	0.76
9–10	28	9.13	0.67
10–11	27	9.80	1.16
11–12	13	9.75	0.65
12–13	15	10.56	1.18
13–14	13	9.85	0.68
14–15	11	10.68	1.22
15–16	4	9.97	0.78
16–17	4	9.72	0.51
17–18	5	10.58	0.41
18–19	6	11.60	1.03
19–20	3	12.67	1.66
Total	478		

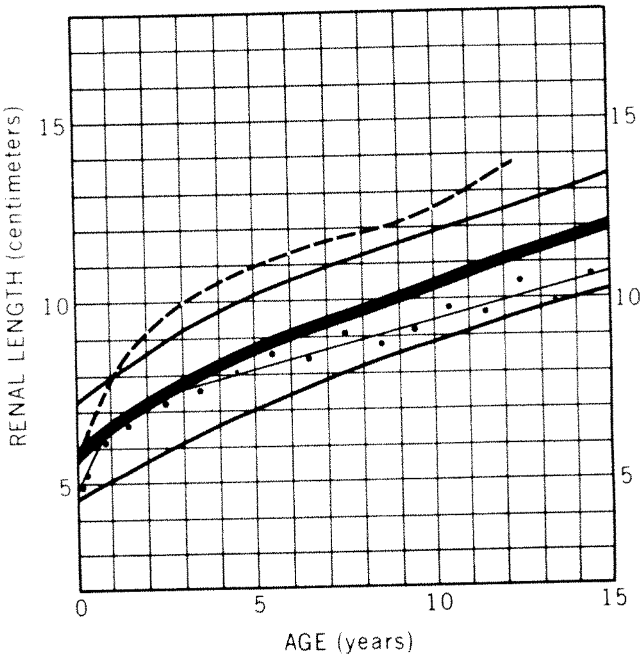

Fig. 1.—Mean renal length measurements for spina bifida patients, for each age group, shown by dots. Thin solid lines represent regression lines calculated for two age groups. Data are superimposed on standard renal growth and hypertrophy curves based on non-spina-bifida children, where thick and medium solid lines represent mean renal length and 2 SD, respectively, and dashed line represents renal growth hypertrophy for solitary kidney.

We reviewed 249 urograms; 227 (91.2%) were performed at either the Elizabethtown Hospital and Rehabilitation Center or the Milton S. Hershey Medical Center, while 22 (8.8%) were performed at outside hospitals. Many patients had more than one urogram available for review. However, 34 patients (36%) had a single urogram, 27 patients (28%) had two urograms, and the maximum number of urograms per patient was seven. In almost all cases, the 5-min postinjection supine radiograph was used to measure renal length to the nearest millimeter; in a few cases, usually due to lack of renal definition on the earlier radiograph or absence of a 5-min film, a 10-min film was used for renal length measurement. No film later than 10 min after contrast injection or with the patient in other than the supine position was used. Four patients had a unilateral duplex collecting system and only the contralateral nonduplex kidney was included in the data base. In 20 studies, only one kidney could be accurately measured. In total, 478 kidney length measurements were obtained. The distribution of kidneys measured at each age is shown in table 1.

Additional data collected included the most cephalad level of the myelodysplasia defect (cervical, one patient; thoracic, 19; high lumbar [L1–L3], 20; low lumbar [L4–L5], 50; sacral, five); body weight and height; L1–L3 and L1–L4 vertebral body lengths; presence, pattern, and curvature measurements of associated scoliosis; and history of urinary tract infection. All patients in the study were under the supervision of a urologist. Bladder regimens included spontaneous voiding, intermittent catheterization, and/or pharmacologic manipulation.

Results

The left kidney was larger than the right at each age group, with an approximate average difference of 0.3 cm, consistent with previous observations [1, 4, 5]. In the analysis of our data, no distinction was made between right and left kidneys, or between male and female patients (no significant renal length difference by gender has been reported in children) [1, 5, 6].

Mean values and standard deviations (SD) for renal length were calculated for each age group (table 1); the age groups chosen are similar to those analyzed by others [4, 6]. Figure 1 shows mean renal length vs. age for spina bifida patients superimposed on the standard renal growth and hypertrophy curves as developed by previous investigators [1–3, 5, 7].

Regression analysis was performed on the data after division of the population into two groups: less than 1 year of age, and 1 year or older. This partition is the same as that used by Rosenbaum et al. [4] and reflects the proportionately greater change in renal size in infancy. For the patient population under 1 year of age, the formula length (cm) = 4.95 + 0.147 (age in months) was obtained, with a correlation coefficient of 0.848 and an SD of 0.67 for renal length. For the patients over 1 year of age, the formula length (cm) = 6.82 + 0.258 (age in years) was obtained, with a correlation coefficient of 0.877 and an SD of 1.33 for renal length. These correlation coefficients compare favorably with those obtained by Hodson et al. [1] for renal growth vs. age (some of the correlation may be attributed to the serial nature of part of our data).

Discussion

Measurement of renal growth in children has practical value both in normal children and in those with a variety of congenital and acquired disorders. This is particularly true in spina bifida patients who are at increased risk of developing renal disease secondary to complications of neurovesical dysfunction. Factors used to measure renal size have included length, width, area, and volume although renal length on excretory urography is the most practical and accurate method for estimating renal size [8, 9]. Hodson et al. [1] has stated that radiographic measurement of kidney length "is a fair indication of its total size in the absence of any nephrological abnormality," a conclusion supported by a postmortem study of renal size by Griffiths et al. [10].

Renal length in children as determined by excretory urography has been correlated with patient age [1-6], patient length/height [1, 9], and length of segments of the lumbar spine [5, 6, 8]. Although there is disagreement as to whether renal growth in children correlates most closely with patient height [1] or lumbar vertebral segmental height [8], the most convenient and widely used chart of renal growth compares renal length with chronologic age. In our patient population with spina bifida, correlation with lumbar segmental length is inappropriate due to variable location and severity of spinal malformation, and patient height/length is difficult to determine with accuracy and consistency. Therefore, we have chosen to compare renal length and patient age in this group of patients.

Our data demonstrate that mean renal length in spina bifida falls below the mean of the standard renal growth curve determined by Hodson et al. [1] for normal children in all age groups. In addition, divergence from the standard curve increases with patient age. Using the revised SD of Currarino et al. [3], mean renal length values in spina bifida become greater than 1 SD below normal mean renal length values at about age 8 (fig. 1) and approach 2 SD below normal means in older children. The reason for this reduced renal size in spina bifida children with normal kidneys is not clear, but it may in part reflect diminished body weight due to lower-extremity dysfunction and lack of normal musculoskeletal development.

We believe that the standard renal growth curve based on normal children requires modification when applied to spina bifida patients who have normal kidneys and no intrinsic renal disease, to reflect their reduced rate of renal growth. The data in table 1 provide normal renal growth standards for spina bifida children, with direct clinical applicability.

ACKNOWLEDGMENTS

We thank Judy Perry for manuscript preparation and Mary Bartholomew for statistical analysis.

REFERENCES

1. Hodson CJ, Drewe JA, Karn MO, King A. Renal size in normal children: radiographic study during life. *Arch Dis Child* **1962**;37:616-622
2. Lebowitz RL, Hopkins T, Colodny AH. Measuring the kidneys—practical applications using a growth and hypertrophy chart. *Pediatr Radiol* **1975**;4:37-42
3. Currarino GC, Williams B, Dana K. Kidney length correlated with age: normal values in children. *Radiology* **1984**;150:703-704
4. Rosenbaum DM, Korngold E, Teele RL. Sonographic assessment of renal length in normal children. *AJR* **1984**;142:467-469
5. Currarino GC. Roentgenographic estimation of kidney size in normal individuals with emphasis on children. *AJR* **1965**;93:464-466
6. Gatewood OMB, Glasser RJ, Vanhoutte JJ. Roentgen evaluation of renal size in pediatric age groups. *Am J Dis Child* **1965**;110:162-165
7. Laufer I, Griscom NT. Compensatory renal hypertrophy: absence in utero and development in early life. *AJR* **1971**;113:464-467
8. Eklof O, Ringertz H. Kidney size in children. *Acta Radiol [Diagn]* (Stockh) **1976**;17:617-625
9. Effmann EL, Ablow RC, Siegel NJ. Renal growth. *Radiol Clin North Am* **1977**;15:3-17
10. Griffiths GJ, Cartwright G, McLachlan MSF. Estimation of renal size from radiographs: is the effort worthwhile? *Clin Radiol* **1974**;26:249

1986 ARRS Meeting, April 13–18, Washington, DC

A comprehensive description of the meeting, including the scientific program, Categorical Course in Chest Radiology, and instructional courses, appears in the January 1986 issue of the *AJR*. A special loose insert on the meeting also accompanies the January issue. Meeting and registration forms will be found in the January and February issues. These may be photocopied.

Accreditation

All courses and scientific sessions carry AMA Category I credit on an hour-for-hour basis.

Meeting Format

Scientific Program. Sessions will be grouped in parallel sessions, Monday–Thursday. A total of 189 scientific papers will be presented in 18 sessions. In addition, on Wednesday, April 16, the morning session will feature award papers and the Caldwell Lecture, which will be delivered by Benjamin Felson of the University of Cincinnati. On Friday, there will be a special symposium on orthopedic radiology.

Categorical Course in Chest Radiology. This 14 hr course will be Sunday–Thursday. Registrants may enroll in other courses as well.

Luncheon Sessions. For the first time, registrants may enroll in special luncheon sessions, Monday–Thursday. A box lunch will be provided.

Exhibits

Scientific Exhibits and Case of the Day Presentations will be Monday–Thursday, April 14–17.

Commercial Exhibits will be open daily, Monday–Thursday.

Local Activities

General Reception. Tuesday evening, April 15, for all registrants.

Golf Tournament. Monday, April 14, Kenwood Golf and Country Club, Bethesda, MD. Transportation leaves the hotel at 11 a.m.; shotgun start at 1 p.m.

Men's and Women's Tennis Tournaments. Monday, April 14, Kenwood Golf and Country Club, Bethesda, MD. Transportation leaves the hotel at 11 a.m.

Local Tours. Sunday, April 13, 7–9 p.m., Introduction to Washington Champagne Tour; Monday, April 14, 9:30 a.m.–3:30 p.m., National Gallery of Art and Hirshhorn Museum and Sculpture Garden; Tuesday, April 15, 9:30 a.m.–3:30 p.m., Georgetown Homes/Georgetown Park; Wednesday, April 16, 9 a.m.–4 p.m., Best of Baltimore; Thursday, April 17, 9 a.m.–4 p.m., Annapolis; Friday, April 18, 9 a.m.–noon, Americana Tour.

Meeting Registration

Preregistration will be accepted until March 28. There will be on-site registration. Official badges and program books will be available at the registration desk, Sheraton Washington Hotel. No confirmations will be mailed.

Course Registration

Register early—enrollment is limited. List first, second, and third choices for each period. Also, indicate whether you wish to take the categorical course. Deadline for mail registration is March 28. All ticket orders will be filled by postmark. Course tickets *will not* be mailed. Tickets will be available on and after Saturday, April 12 (after 1 p.m.), at the ARRS registration desk in the Sheraton Washington Hotel. There will be on-site registration for courses not already filled.

Hotel Registration

Reservations are handled by the ARRS Housing Bureau, Sheraton Washington Hotel, 2660 Woodley at Connecticut Ave., N.W., Washington, DC 20006. These must be received by March 15. Make check payable to Sheraton Washington Hotel.

Fees

Meeting:	
ARRS members and resident members	No fee
Nonmembers	$100
Nonmember physicians in training (with verification)	25
Categorical course (all who attend)	75
Luncheon sessions/each	10
Golf tournament	65
Tennis tournaments	50
Local tours	15–45

Cancellations and Fee Refunds

Fees will be refunded only if cancellation is received by April 7. Send to American Roentgen Ray Society, 1891 Preston White Drive, Reston, VA 22091.

Air Transportation

Two airlines, United and Delta, are official meeting air carriers and are offering discounted fares.

Delta Air Lines will discount fares 35%. Tickets must be purchased a minimum of 7 days before departure. Travel to Washington must be from April 9 through 15. A maximum stay of 15 days is permitted. Information: (800) 241-6760 in the continental U.S., 8:30 a.m.–8 p.m. eastern time daily. Mention ARRS number F-0347.

United Airlines offers a 40% discount off normal coach fares with no minimum stay or advance purchase restrictions. There is an additional 5% discount (45% total) for those staying over a Saturday night. Travel must be between April 10 and 22. Information: (800) 521-4041, 8:30 a.m.–8 p.m. eastern time daily. Mention ARRS number 602-K. Seats are limited.

Associated Meetings

The *Society for Pediatric Radiology* will meet April 9–13 in the Westin Hotel, Washington, DC. The program will appear in the March issue of the *AJR*. For information contact: Donald R. Kirks, M.D., Secretary, Society for Pediatric Radiology, c/o Dept. of Radiology, Duke University Medical Center, Box 3834, Durham, NC 27710; telephone (919) 681-2711, ext. 287.

The *American Association of Women Radiologists* (AAWR) will have a luncheon meeting on Monday, April 14, in the Sheraton Washington Hotel.

Noninvasive Evaluation of Neonatal Aortic Thrombosis Secondary to Umbilical Artery Catheterization

Brian D. Fellmeth,[1] Martin P. Sandler,[1] Gary A. Thieme,[1] Arthur C. Fleischer,[1] and Wallace W. Neblett[2]

Neonatal aortic thrombosis, once a rare entity, is now seen with increasing frequency as a complication of umbilical artery catheterization (UAC). Two studies used contrast aortography to demonstrate that the incidence of thrombosis in asymptomatic infants with indwelling UACs is greater than 90% [1, 2]. Although these studies show that varying amounts of thrombus formation are usually present after catheterization, most of these thromboses apparently resolve spontaneously without clinical sequelae. Occasionally, the aortic thrombosis progresses to occlusion, with a very high nonoperative mortality rate [3]. Recent advances in vascular surgery have made thrombectomy feasible in affected infants, and most can now be successfully managed by prompt emergency aortotomy [3, 4]. Sensitive, specific, and minimally invasive diagnostic methods are needed to help identify those neonates who require surgical intervention. This case report illustrates the relative roles of real-time sonography, duplex pulsed Doppler sonography, and radioisotope angiography in evaluating this problem.

Case Report

A term, 3000-g infant with poor Apgar scores was delivered vaginally from a diabetic primigravida. Perinatal asphyxia was diagnosed, and early intubation was required. A UAC was present on days 1–3 and used to deliver hypertonic glucose and antibiotics.

On day 10, the respiratory status had improved, but the lower extremities were noted to be pulseless. Real-time sonography showed echogenic material in the infrarenal aorta. A duplex pulsed Doppler study showed arterial flow in the proximal aorta above the intraluminal echogenic material (fig. 1A) but no flow in the distal aorta (fig. 1B). On day 11, the sonographic findings were confirmed by a technetium-99m (^{99m}Tc) DTPA flow study. Dynamic and static images demonstrated an abrupt cutoff of perfusion to the lower half of the body. Normal bilateral renal blood flow was noted (fig. 1C).

At aortotomy on day 12, extensive infrarenal aortic clot was removed. A follow-up ^{99m}Tc-DTPA study on day 16 (fig. 1D) revealed normal perfusion to the pelvis and lower limbs. A repeat duplex pulsed Doppler examination also confirmed the reestablishment of aortic flow. Six-month follow-up demonstrated normal lower extremity blood flow, renal function, and blood pressure.

Discussion

Since 1980, five patients with UAC-related aortic occlusion have been evaluated at our institution; each has been managed successfully with thrombectomy. In four of these cases, the level of obstruction and presence or absence of renal artery involvement was correctly predicted preoperatively with noninvasive imaging, and aortography was not needed (the fifth case went directly to cardiac catheterization for evaluation of a presumed coarctation, and unexpected aortic thrombosis was found).

Contrast aortography has been used to evaluate suspected aortic thrombosis [1, 5]. This approach requires either an arterial puncture into an already compromised arterial tree or a delay in the withdrawal of the thrombogenic UAC. In addition, a contrast load is delivered in the setting of hemodynamic instability and acute renal failure that often accompanies cases of suspected aortic thrombosis.

The ideal method would spare the patient a contrast load and allow for rapid portable study on the ward. Real-time sonography has proved quite sensitive for the detection of thrombosis. A prospective study of 71 serial UACs with sonography found excellent correlation between clinical evidence of thrombosis and echogenic material in the aorta and/or iliac arteries [6]. Those infants found to have sonographic evidence of thrombosis were followed, and anechoic aortas and iliac arteries were noted 2–8 days after catheter removal. None of these thromboses progressed to occlusion, and even bulky thromboses were noted to resolve spontaneously.

Sonography was part of the preoperative evaluation in three of our cases, and the location of the intraluminal echoes correlated well with the operative findings. An anterior parasagittal approach using the left lobe of the liver as an acoustic window was best for viewing the upper abdominal aorta, and a coronal view from a left flank approach was best for imaging the middle and lower abdominal aorta.

Received April 1, 1985; accepted after revision November 1, 1985.

[1] Department of Radiology, Vanderbilt University Medical Center, Nashville, TN 37232. Address reprint requests to M. Sandler.
[2] Departments of Surgery and Pediatrics, Vanderbilt University Medical Center, Nashville, TN 37232.

AJR 146:619–620, March 1986 0361–803X/86/1463–0619 © American Roentgen Ray Society

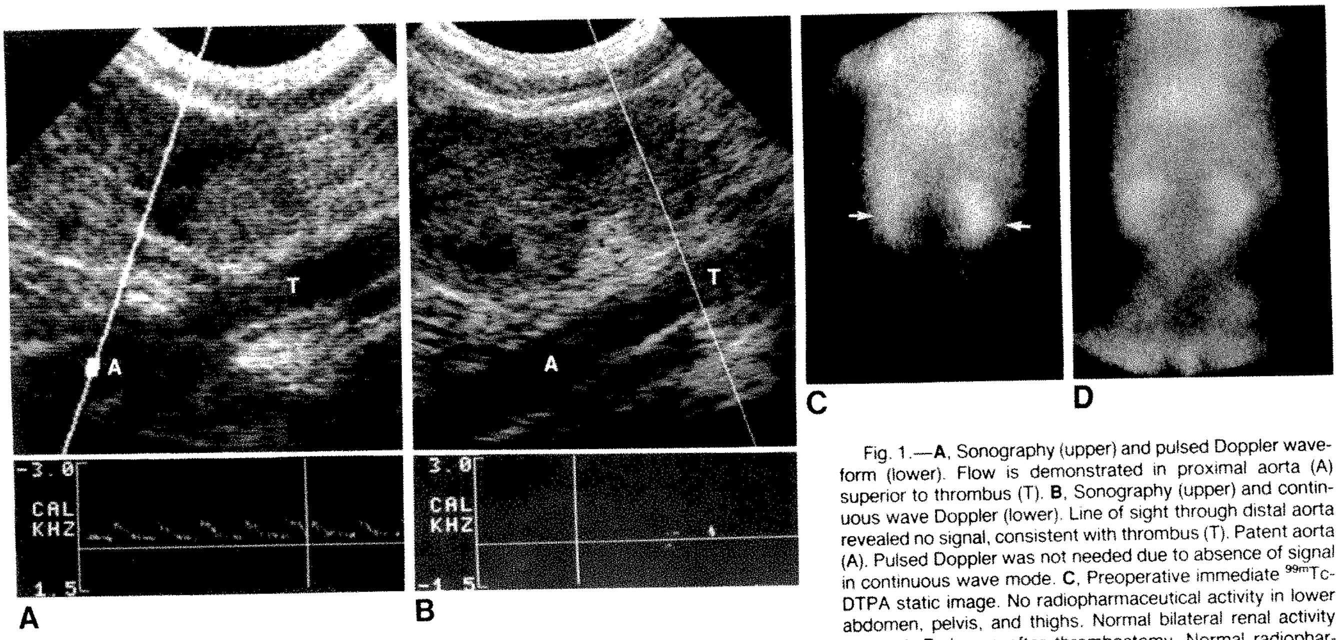

Fig. 1.—**A**, Sonography (upper) and pulsed Doppler waveform (lower). Flow is demonstrated in proximal aorta (A) superior to thrombus (T). **B**, Sonography (upper) and continuous wave Doppler (lower). Line of sight through distal aorta revealed no signal, consistent with thrombus (T). Patent aorta (A). Pulsed Doppler was not needed due to absence of signal in continuous wave mode. **C**, Preoperative immediate ^{99m}Tc-DTPA static image. No radiopharmaceutical activity in lower abdomen, pelvis, and thighs. Normal bilateral renal activity (*arrows*). **D**, Image after thrombectomy. Normal radiophar-

Real-time sonography alone cannot distinguish bulky but nonocclusive, reversible thrombosis from a frank aortic occlusion that may require thrombectomy. A duplex pulsed Doppler study can help make this distinction by supplying flow data (figs. 1A and 1B).

In four of our cases, a preoperative radionuclide aortogram correctly predicted the level of occlusion and showed whether the renal arteries were involved. The scintiflow scan is also useful for postoperative follow-up, especially when persistent renal artery stenosis is present [7]. We have found that poor intravenous access can degrade the flow study. A central venous injection is best, but a scalp or upper extremity vein usually produces a satisfactory study. Injection into a lower extremity vein will spread the bolus, particularly in these infants with poor lower extremity blood flow. Immediate static images may be helpful (figs. 1C and 1D), particularly in the presence of a poor bolus.

We recommend sonography as the initial study in infants with suspected UAC-related aortic occlusion because of its sensitivity, speed, and portability. A negative sonogram, particularly if augmented by a negative duplex pulsed Doppler, would virtually exclude occlusive thrombosis. Neonates with sonograms positive for aortic thrombosis need to have aortic occlusion excluded by either duplex pulsed Doppler or radionuclide flow study or both. If either of these is positive for occlusion, emergency thrombectomy should be considered [3, 4]. If both are negative, the patient has nonocclusive thrombosis and should be followed with sonography until the aorta is anechoic.

REFERENCES

1. Williams HJ, Jarvis CW, Neal WA, Reynolds JW. Vascular thromboembolism complicating umbilical artery catheterization. *AJR* **1972**;116:475–485
2. Mokronisky ST, Levine RL, Blumhagen JD, Wesenberg RL, Simmons MA. Low positioning of umbilical-artery catheters increases associated complications in newborn infants. *N Engl J Med* **1978**;299:561–564
3. Flanigan DP, Stolar CJ, Pringle KC, Schuler JJ, Fisher E, Vidyasager D. Aortic thrombosis after umbilical artery catheterization. *Arch Surg* **1982**;117:371–374
4. O'Neill JA, Neblett WW, Born ML. Management of major thromboembolic complications of umbilical artery catheters. *J Pediatr Surg* **1981**;16:972–977
5. Goetzman BW, Stadalnik RC, Bogren HG, Blankenship WJ, Ikeda RM, Thayer J. Thrombotic complications of umbilical artery catheters: a clinical and radiographic study. *Pediatrics* **1975**;56:374–379
6. Oppenheimer DA, Carroll BA, Garth KE. Ultrasonic detection of complications following umbilical artery catheterization in the neonate. *Radiology* **1982**;145:667–672
7. Merten DF, Vogel JM, Adelman RD, Goetzman BW, Bogren HG. Renovascular hypertension as a complication of umbilical artery catheterization. *Radiology* **1978**;126:751–757

Uptake of ^{111}In-Labeled Leukocytes by Tumor

Alexandra Fortner[1]
Frederick L. Datz
Andrew Taylor, Jr.
Naomi Alazraki

The ^{111}In-labeled leukocyte scan is a sensitive and specific technique for the detection and localization of abscesses. However, in reviewing an unselected series of 249 scans, six (2.3%) were false-positive cases in which leukocyte uptake by tumor mimicked an abscess. This represented 12% (6/51) with known tumor at the time of imaging. Five of the cases were primary or metastatic tumors to the soft tissues; the sixth was a skeletal metastasis. The intensity of tumor activity has been characterized as mild in the few cases of leukocyte uptake reported in the literature, suggesting that the degree of uptake is helpful in distinguishing tumor from abscess. In this study, however, variable degrees of tumor-associated activity were seen ranging from mild to very intense. These findings indicate that tumor accumulates labeled leukocytes more frequently than has been previously appreciated, that primary and metastatic neoplasms involving both the soft tissues and skeleton are involved, and that the intensity of uptake is not a reliable criterion to distinguish tumor from abscess.

Indium-111-labeled leukocyte imaging is a highly sensitive and specific method for the detection and localization of abscesses [1-6]. The accuracy of the leukocyte scan in cancer patients has been shown to be similar to that reported in patients without malignancies [5]. Sporadic cases of tumor uptake mimicking abscess have been cited [5-13], with neoplasms involving bone implicated more frequently than primary or metastatic disease outside the skeleton [9]. In these previously reported cases, tumor uptake has been mild in contrast to the more intense activity characteristic of abscesses, allowing the two to be differentiated on the basis of the degree of leukocyte uptake.

We undertook a retrospective study to determine the frequency of false-positive leukocyte scans due to tumor uptake, to see how often tumors outside the skeleton are involved, and to see if the intensity of uptake was helpful in differentiating tumor from abscess.

Materials and Methods

All leukocyte scans performed over a 2-year period were retrospectively reviewed for tumor uptake by two independent observers. The patients' charts were then reviewed. Tumor was verified by biopsy in all patients. Among patients who showed uptake of leukocytes by biopsy, infection was excluded as the cause of uptake on the basis of surgical findings; blood, urine, sputum, and biopsy specimen cultures; CT and sonographic findings; the lack of antibiotic therapy; and the lack of evidence of infection on follow-up over 4 months.

All scans were performed with autologous leukocytes, which were labeled with ^{111}In oxine according to a modification of Thakur [14, 15]. Specifically, the labeling was performed as follows:

1. Venous blood (30-50 ml) was obtained in a syringe containing 1-2 ml of heparin. The cells were allowed to settle for 60 min in the inverted syringe.
2. The leukocyte-rich supernatant was then removed from the syringe using a butterfly catheter and was placed in a centrifuge tube.

Received August 19, 1985; accepted after revision November 7, 1985.

[1] All authors: Department of Radiology, University of Utah Health Sciences Center, 50 N. Medical Dr., Salt Lake City, UT 84132. Address reprint requests to F. L. Datz.

AJR 146:621-625, March 1986
0361-803X/86/1463-0621
© American Roentgen Ray Society

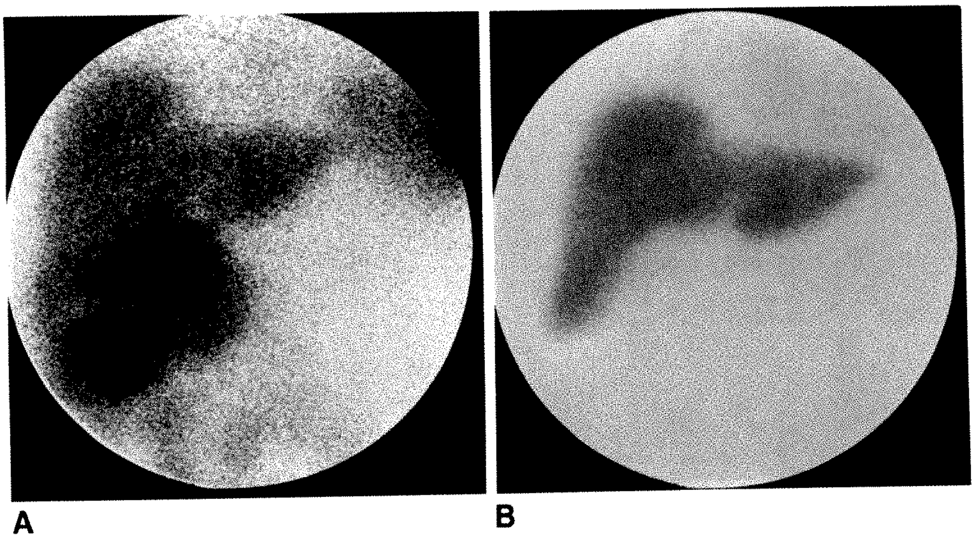

Fig. 1.—Case 1: 74-year-old man with anaplastic sarcoma. **A**, Intense subhepatic uptake of ^{111}In-labeled leukocytes. **B**, Comparison with sulfur colloid images delineates margin of abnormal uptake, which correlated with tumor seen at laparotomy.

3. To obtain a white-cell button, the supernate was centrifuged at 300–350 g for 5 min.
4. Leukocyte-poor plasma supernate was removed and stored in an identical sterile centrifuge tube.
5. The white-cell button was resuspended in 5 ml of sterile saline.
6. ^{111}In oxine (1 mCi [37MBq]) was added to the concentrated cell suspension and incubated for 30–40 min. During the incubation, the suspension was gently agitated every 10 min.
7. Leukocyte-poor plasma (5–8 ml) was added to the suspension of leukocytes, and the mixture was centrifuged for 5 min at 450 g. This removed unbound indium.
8. The supernatant was removed and saved for evaluation of labeling efficiency. The previously obtained leukocyte-poor plasma (5–8 ml) was gently added to the labeled white-cell button and agitated to resuspend the labeled cells. These cells were assayed in a dose calibrator.
9. The ^{111}In-labeled leukocytes were then drawn into a syringe and reinjected into the patient. The activity in the final product was limited to a maximum of 500 μCi (18.5 MBq) (range, 397–500 μCi [14.7–18.5 MBq]). The maximum time for blood drawing to reinjection was about 2 hr.

Patients received about 500 μCi (18.5 MBq) of labeled cells. Imaging was done at 24 hr after injection using a large-field-of-view gamma camera equipped with a medium-energy parallel-hole collimator using 20% windows set on the 173- and 247-KeV photopeaks of ^{111}In.

Tumor uptake was graded as follows: Mild uptake was greater than that of the background but less than that of the liver; moderate uptake was equal to that of the liver; intense uptake was greater than that of the liver.

Results

Of 249 scans reviewed, six (2.3%) were false-positive cases in which leukocyte uptake by tumor mimicked an abscess. This represented 12% (6/51) with known tumor. Five cases (two carcinomas, two lymphomas, and a sarcoma) involved soft tissues outside the skeleton; the sixth case was due to carcinoma metastatic to the spine. The degree of tumor uptake covered a spectrum of intensities ranging from mild to very intense, including a case with activity greater than that of the spleen. Specifically, two cases showed intense uptake: an anaplastic sarcoma in the subhepatic space and a gastric carcinoma of the antrum. Two cases showed moderate uptake: a histiocytic lymphoma of the cecum and hepatic carcinoma metastatic to the lumbar spine. Mild uptake was present in a case of breast carcinoma metastatic to the lungs and in a case of Hodgkin disease in cervical, axillary, and inguinal lymph nodes.

Case Reports

Case 1

A 74-year-old man with 6 weeks of abdominal bloating and melena was noted to have a right-upper-quadrant abdominal mass. A barium enema revealed tumor at the hepatic flexure. At exploratory laparotomy, at which time the patient was afebrile without signs of infection, a massive tumor was demonstrated and the biopsy showed anaplastic sarcoma containing large numbers of inflammatory and pleomorphic malignant cells. Two weeks after surgery, the patient developed an intermittent low-grade fever and mild leukocytosis. An ^{111}In leukocyte scan showed intense uptake in the right-upper-quadrant mass (fig. 1). However, subsequent sonographic and CT scanning indicated that the right-upper-quadrant mass was solid without evidence of an abscess. Sputum, blood, and urine cultures were negative. Repeat abdominal sonography again failed to identify an abscess in the tumor. Over several weeks without antibiotic treatment, the patient's fever subsided. The patient remained free of any evidence of infection on follow-up. The final diagnosis was fever secondary to malignancy without infection.

Case 2

A 53-year-old man with chronic low back pain presented with exacerbation of his pain and 18-kg weight loss. Hepatomegaly and left hip flexor weakness were noted on physical examination. Lumbar spine films showed absence of the right L3 pedicle, and there was blockage at this level on a myelogram. Multiple large cold hepatic defects were demonstrated on a liver-spleen scan, and a bone scan

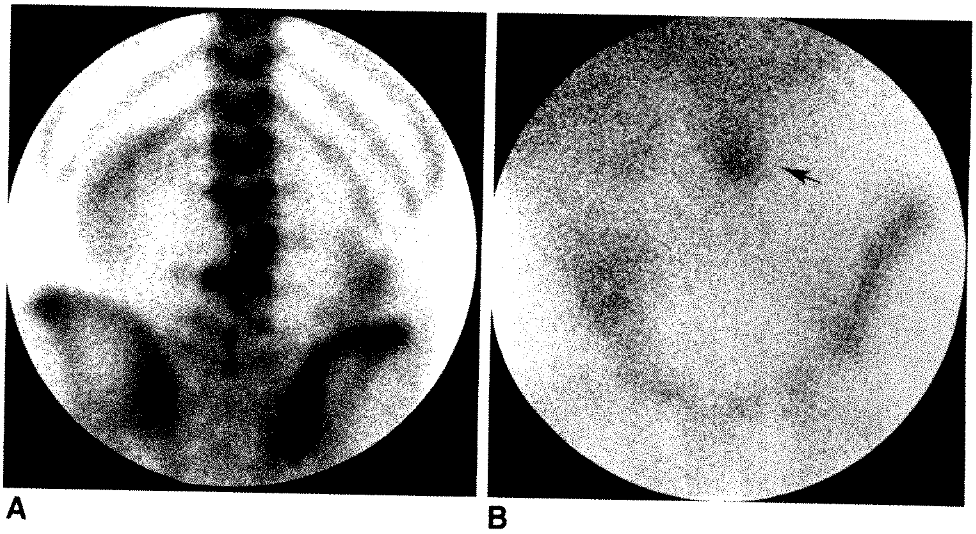

Fig. 2.—Case 2: 53-year-old man with clear cell variant of hepatocellular carcinoma. A, Posterior bone scan shows cold defect in same region as absent pedicle was seen on lumbar spine radiographs. B, Anterior ^{111}In leukocyte scan shows uptake in L3 area (*arrow*).

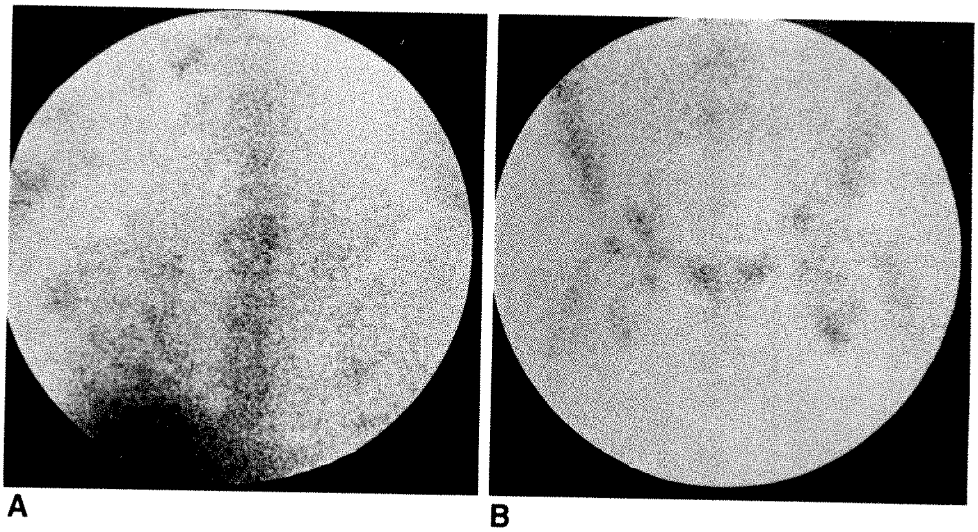

Fig. 3.—Case 3: 30-year-old man with Hodgkin lymphoma. Anterior chest (**A**) and pelvis (**B**) images show mild uptake of ^{111}In-labeled leukocytes in region of clinically involved cervical, right axillary and inguinal lymph nodes.

confirmed the presence of metastases to the lumbar spine. The liver biopsy indicated a clear cell variant of hepatocellular carcinoma. After the liver biopsy, the patient developed leukocytosis with a shift to the left. For this reason, an ^{111}In leukocyte scan was done, which showed uptake in the midabdomen corresponding to the location of the bone metastasis (fig. 2). Sonography did not identify a fluid collection in the area of the abnormal leukocyte activity, and blood and spinal fluid cultures were negative. The patient was not treated with antibiotics. Over the course of several months of follow-up, the patient showed no evidence of an abscess.

Case 3

A 30-year-old man with stage IVB nodular sclerosing Hodgkin lymphoma diagnosed 4 years earlier presented with shaking chills and fever after a course of chemotherapy. Physical examination showed right axillary, left inguinal, and cervical adenopathy secondary to his lymphoma. An ^{111}In leukocyte scan was normal except for mild uptake in right axillary, inguinal, and cervical nodes (fig. 3). Gram-negative sepsis, found on blood cultures, responded to appropriate antibiotic therapy. Biopsy and culture of the lymph nodes showed Hodgkin disease but no infection. No focal source for his gram-negative sepsis was ever demonstrated.

Discussion

Many large clinical series have demonstrated that the ^{111}In-labeled leukocyte scan is a very sensitive and highly specific method for detecting and localizing infection [1–6]. The accuracy of the leukocyte scan in cancer patients has been shown to be similar to that reported in clinical series of patients without malignancies [5]. Among agranulocytic cancer patients, the use of homologous donor leukocytes gives comparable results [16].

Previous reports have indicated that leukocyte uptake in tumors is a relatively rare occurrence. Carroll et al. [1] found no tumor associated ^{111}In leukocyte activity among 25 patients with primary and metastatic malignancies. Schell-Frederick et al. [5] studied 117 patients with cancers and found only one patient, with breast carcinoma, who had abnormal leukocyte activity in a bone metastasis. Similarly, most cancer patients studied by other groups had no uptake of indium-labeled leukocytes [2, 3, 9, 10, 16, 17].

Sporadic cases of tumor uptake mimicking abscesses have been reported [5–13]. In our study, we found that although only 2.3% of our cases showed tumor uptake, this represented 12% of patients with known malignancies at the time of imaging. This could lead to a significant number of false-positive studies.

We are not certain why our results differ from those previously reported by Schell-Frederick et al. [5]. Our labeling technique, like that of Schell-Frederick et al., is based on Thakur's original method. We have made only minor modifications of this technique. Evidence of the effectiveness of our ^{111}In leukocyte preparation is found in the 95% sensitivity for infection we have previously reported [15]. The technique of Schell-Frederick et al. [5] also differs somewhat from Thakur's technique, but there is no evidence their changes affected leukocyte function.

The mechanism underlying the uptake of leukocytes by tumor has been speculated on but is not completely understood. Increased blood-pool activity may contribute to tumor-associated activity, especially in highly vascular neoplasms. However, significant cardiac blood-pool activity or femoral vessel activity was not seen in any of the patients in our study, indicating that blood pooling was not a significant contributing factor.

Some tumor uptake may be related to free indium in the plasma. When released from the cell, ionic indium binds immediately to transferrin. The ^{111}In transferrin complex was previously proposed as a possible tumor imaging agent by Goodwin et al. [18] who noted accumulation of the labeled complex in patients with head and neck cancers. However, only a small fraction of free indium is found in the plasma of patients who have received ^{111}In-labeled leukocytes, 7%–12% in most cases [3, 14]. Studies previously reported from our institution indicate that 11.9% of ^{111}In activity is associated with the plasma with our labeling technique [14].

Although neutrophils can be obtained as a pure population, most institutions, including ours, use a mixed population of cells containing lymphocytes, monocytes, and platelets as well as neutrophils. After cell labeling, Thakur [19] showed that about 15% of indium is labeled to lymphocytes. Studies of ^{111}In-labeled lymphocytes in patients with Hodgkin lymphoma have shown accumulation of the labeled lymphocytes in lymph nodes involved with Hodgkin disease [20, 21]. However, in the study of Schell-Frederick et al. [5], 14 patients with lymphomas were studied with ^{111}In labeled to mixed leukocyte populations, and no uptake was noted in the lymph nodes of these patients. In our study, which used mixed cells, activity was seen in the lymph nodes of a patient with Hodgkin disease, while another patient had uptake in a histiocytic lymphoma. McDougall's group [10] also noted uptake of labeled leukocytes in a histiocytic lymphoma, and McAfee and Samin [9] reported uptake in a bone metastasis in a patient with Hodgkin lymphoma.

Macrophages are involved in the host's immune surveillance against tumors and generally constitute a greater percentage of tumor-associated inflammatory cells than lymphocytes. Svennevig et al. [22] found that 1%–28% of the cells in a series of human tumors were monocytes, while the tumors studied by Wood's group [23] contained 2%–56%. Morantz et al. [24] noted that neurologic tumors are composed of even greater numbers of macrophages. Thus, tumor uptake of indium-labeled leukocytes may be attributed, at least in part, to the presence of variable numbers of inflammatory cells in certain tumors. One of the patients in our series had activity at the site of an anaplastic sarcoma, which contained a large number of inflammatory cells in the biopsy specimen. Although this patient's tumor was fairly large, no necrosis was associated with it, in contrast to a false-positive reported by Sfakianakis et al. [13] of a mucoepidermoid carcinoma metastatic to the foot.

On the basis of previous isolated reports, it appeared that primary and secondary tumors involving the soft tissues had less propensity for leukocyte uptake than neoplasms involving the skeleton [9]. However, we did not find this to be true. In our study, five of the six positive cases were in tumors outside the skeleton; only one case was due to a skeletal metastasis.

Some authors have suggested that the intensity of leukocyte uptake may be used to distinguish false-positive tumor uptake from that due to abscess [3, 7, 8, 13]. These groups noted that abscesses were usually associated with intense activity, greater than that of the liver, while nonsuppurative processes such as tumor were associated with lesser degrees of uptake. Among the six patients reported here, however, there was a spectrum of intensities related to tumor-associated indium leukocyte activity. Mild activity, categorized as less than that of the liver, was seen in only two patients. The cecal histiocytic lymphoma and bone metastasis of hepatocellular carcinoma were associated with uptake that was about equal to that of the liver, while the gastric carcinoma took up labeled leukocytes with an intensity greater than that of the liver but less than that of the spleen. Finally, the anaplastic sarcoma was associated with very intense activity, greater than that of the spleen. These cases demonstrate that the degree of tumor uptake of indium-labeled leukocytes can be variable and cannot reliably be used to distinguish abscess from tumor.

In summary, although tumor uptake of ^{111}In is uncommon, its frequency is higher than has been previously appreciated. Primary and metastatic neoplasms involving the soft tissues as well as the skeleton are involved. The intensity of leukocyte uptake is not a reliable technique for distinguishing tumor from an abscess.

REFERENCES

1. Carroll B, Silverman PM, Goodwin DA, McDougall IR. Ultrasonography and indium 111 white blood cell scanning for the detection of intraabdominal abscesses. *Radiology* **1981**;140:155–160
2. Coleman RE, Welch DM, Baker WJ, Beightol RW. Clinical experience using indium-111-labeled leukocytes. In: Thakur ML, ed. *Proceedings of Yale symposium on radiolabeled cellular elements.* New York: Trivirium, **1979**:103–118

3. Goodwin DA, Doherty PW, McDougall IR. Clinical use of indium-111-labeled white cells: an analysis of 312 cases. In: Thakur ML, ed. *Proceedings of Yale symposium on radiolabeled cellular elements.* New York: Trivirium, **1979**:131–145
4. Datz FL, Bedont RA, Baker WJ, Alazraki NP, Taylor A Jr. No difference in sensitivity for occult infection between tropolone- and oxine-labeled indium-111 leukocytes. *J Nucl Med* **1985**;26:469–473
5. Schell-Frederick E, Fruhling J, Vander Auwera P, VanLaethem Y, Klastersky J. ^{111}Indium-oxine labeled leukocytes in the diagnosis of localized infection in patients with neoplastic disease. *Cancer* **1984**;54:817–824
6. Seabold JE, Wilson DG, Lieberman LM, Boyd CM. Unsuspected extra-abdominal sites of infection: scintigraphic detection with indium-111-labeled leukocytes. *Radiology* **1984**;151:213–217
7. Fawcett HD, Goodwin DA Lantieri RL. In^{111} leukocyte scanning in inflammatory renal disease. *Clin Nucl Med* **1981**;6:237–241
8. Kipper MS, Basarab K Kipper SA, Witztum K. Positive In-111 white cell scan in a patient with multiple metastases. *Clin Nucl Med* **1985**;10:86–89
9. McAfee JG, Samin A. In-111 labeled leukocytes: a review of problems in image interpretation. *Radiology* **1985**;155:221–229
10. McDougall IR, Baumert JE, Lantieri RL. Evaluation of ^{111}In leukocyte whole body scanning. *AJR* **1979**;133:849–854
11. Rovecamp MH, Van Royen EA, Reinders Folmer SCC. Diagnosis of upper abdominal infection by In^{111} labeled leukocytes with Tc-99m colloid subtraction technique. *J Nucl Med* **1983**;24:212–216
12. Schauwecker DS, Park HM, Mock BH, et al. Evaluation of complicating osteomyelitis with Tc-99m MDP, In-111 granulocytes and Ga-67 citrate. *J Nucl Med* **1984**;25:849–853
13. Sfakianakis GN, Mnaymreh W, Ghanduc-Mnaymneh L, Al-Sheikh W, Hourani M, Heal A. Positive ^{111}In leukocyte scintigraphy in a skeletal metastasis. *AJR* **1982**;139:601–603
14. Beightol RW, Baker WJ. Labeling autologous leukocytes with indium 111 oxine. *Am J Hosp Pharm* **1980**;37:847–850
15. Datz FL, Jacobs J, Baker W, et al. Decreased sensitivity of early imaging with In-111 oxine-labeled leukocytes in detection of occult infection: concise communication. *J Nucl Med* **1984**;25:303–306
16. Dutcher JP, Schifter CA, Johnston GS. Rapid migration of ^{111}indium labeled granulocytes to sites of infection. *N Engl J Med* **1981**;304:586–589
17. Gordon I, Vivian G. Radiolabelled leucocytes: a new diagnostic tool in occult infection/inflammation. *Arch Dis Childhood* **1984**;59:62–66
18. Goodwin DA, Good R, Brown L, Imbornone CJ. ^{111}In-labeled transferrin for the detection of tumor. *Radiology* **1971**;100:175–179
19. Thakur ML, Lavender JP, Arnot RN, Silvester DJ, Segal AW. Indium-111-labeled autologous leukocytes in man. *J Nucl Med* **1977**;18:1012–1019
20. Lavender JP, Goldman JM, Arnot RN. Kinetics of indium-111 labeled lymphocytes in normal subjects and in patients with Hodgkin's disease. *Br Med J* **1977**;2:797–799
21. Wagstaff J, Gibson C, Thatcher N. Human lymphocyte traffic assessed by indium-111 oxine labelling: clinical observation. *Clin Exp Immunol* **1981**;43:443–449
22. Svennevig JL, Lovik M, Svaar H. Isolation and characterization of lymphocytes and macrophages from solid malignant human tumors. *Int J Cancer* **1979**;23:626–631
23. Wood GW, Gollahon KA. Detection and quantitation of macrophage infiltration into primary human tumors with the use of cell surface markers. *J Natl Cancer Inst* **1977**;59:1081–1087
24. Morantz RA, Wood GW, Foster M, Clark M, Gollahon K. Macrophages in experimental and human brain tumors. Part 2. Studies of the macrophage content of human brain tumors. *J Neurosurg* **1979**;50:305–311

ARRS Case of the Day

The Case of the Day presentation is always one of the most popular of the scientific exhibits at the annual meeting of the American Roentgen Ray Society. The throng of radiologists clustered around the daily cases often makes it difficult for all to adequately analyze these interesting films. Thus ARRS and *AJR* offer the Case of the Day selections before the April meeting. This will give the attendees and the readers of *AJR* an opportunity to study them more conveniently and deliberately. Explanation of the features and brief descriptions of the entities will follow in the May issue of *AJR*.

This year the Case of the Day is organized differently from previous years. Instead of three cases to identify each day (Monday through Thursday), there will be four. Also the cases will be grouped by discipline, that is, chest, musculoskeletal, abdominal, and neuroradiology, rather than as adult, pediatric, or sonographic. The pediatric cases (case 1 of each discipline) will be presented on Monday of the ARRS meeting for the convenience of those attending the Society for Pediatric Radiology meeting.

We are grateful to the contributors from the University of Wisconsin for their Case of the Day selections. It is hoped that a large number of participants will correctly diagnose the cases. These "winners" will be acknowledged at the meeting in Washington, DC.

Chest Case of the Day

June M. Unger,[1] Mary Ellen Peters, and Marvin L. Hinke

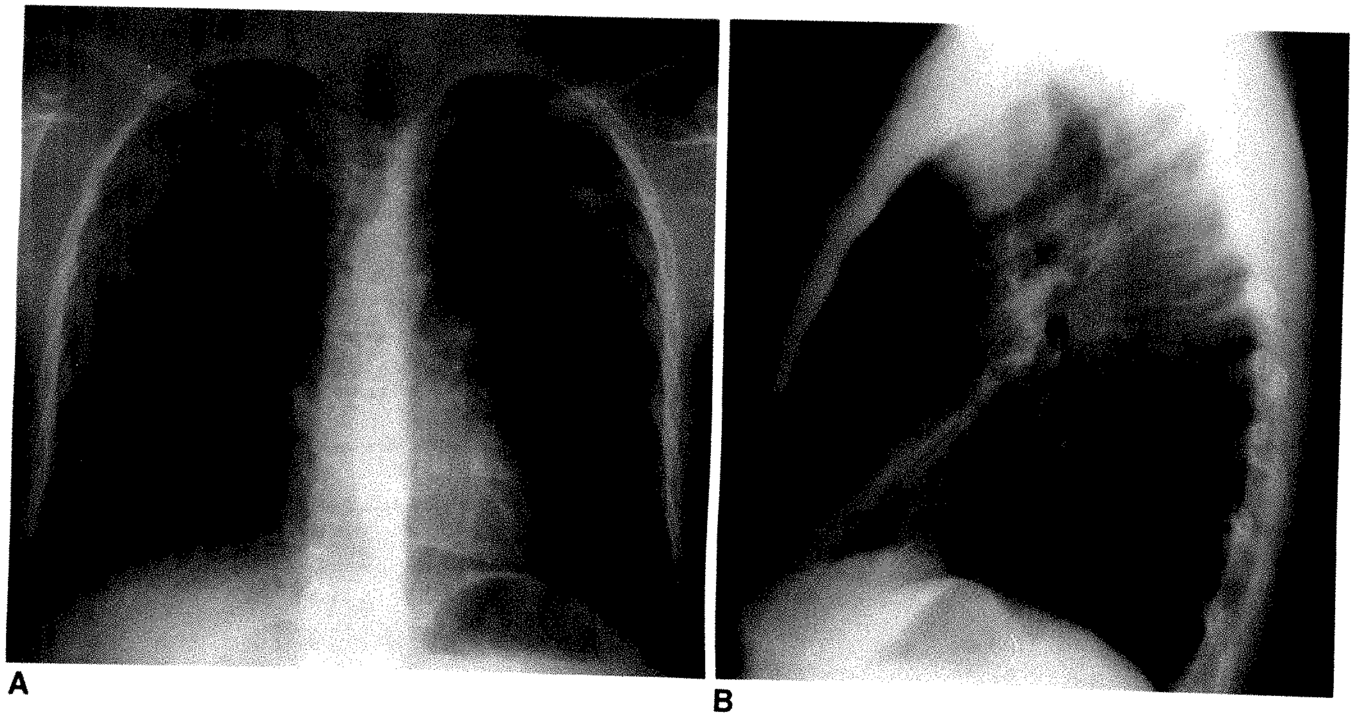

Fig. 1.—Case 1: 10-year-old boy had preoperative chest radiograph for acute appendicitis. He was referred 15 days later for further evaluation of abnormal chest film; physical examination and laboratory studies were normal. Posteroanterior (**A**) and lateral (**B**) chest radiographs.

---

[1] All authors: Department of Radiology, University of Wisconsin Clinical Science Center, 600 Highland Ave., Madison, WI 53792. Individual cases were prepared by M. E. Peters (case 1), J. M. Unger (case 2), J. M. Unger and M. E. Peters (case 3), and J. M. Unger (case 4). M. L. Hinke is the coordinator of the Case of the Day series.

AJR 146:627–630, March 1986 0361–803X/86/1463–0627 © American Roentgen Ray Society

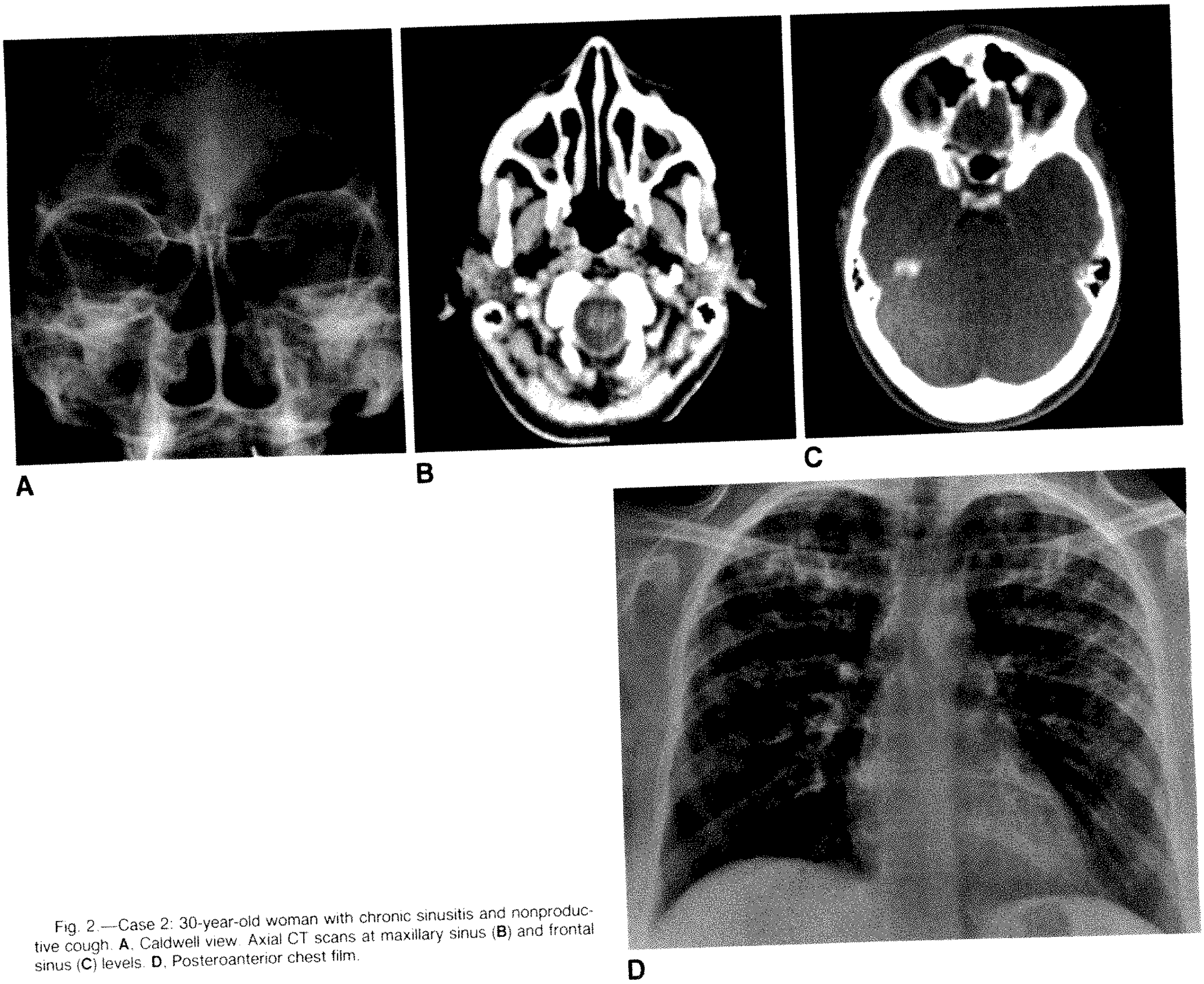

Fig. 2.—Case 2: 30-year-old woman with chronic sinusitis and nonproductive cough. **A**, Caldwell view. Axial CT scans at maxillary sinus (**B**) and frontal sinus (**C**) levels. **D**, Posteroanterior chest film.

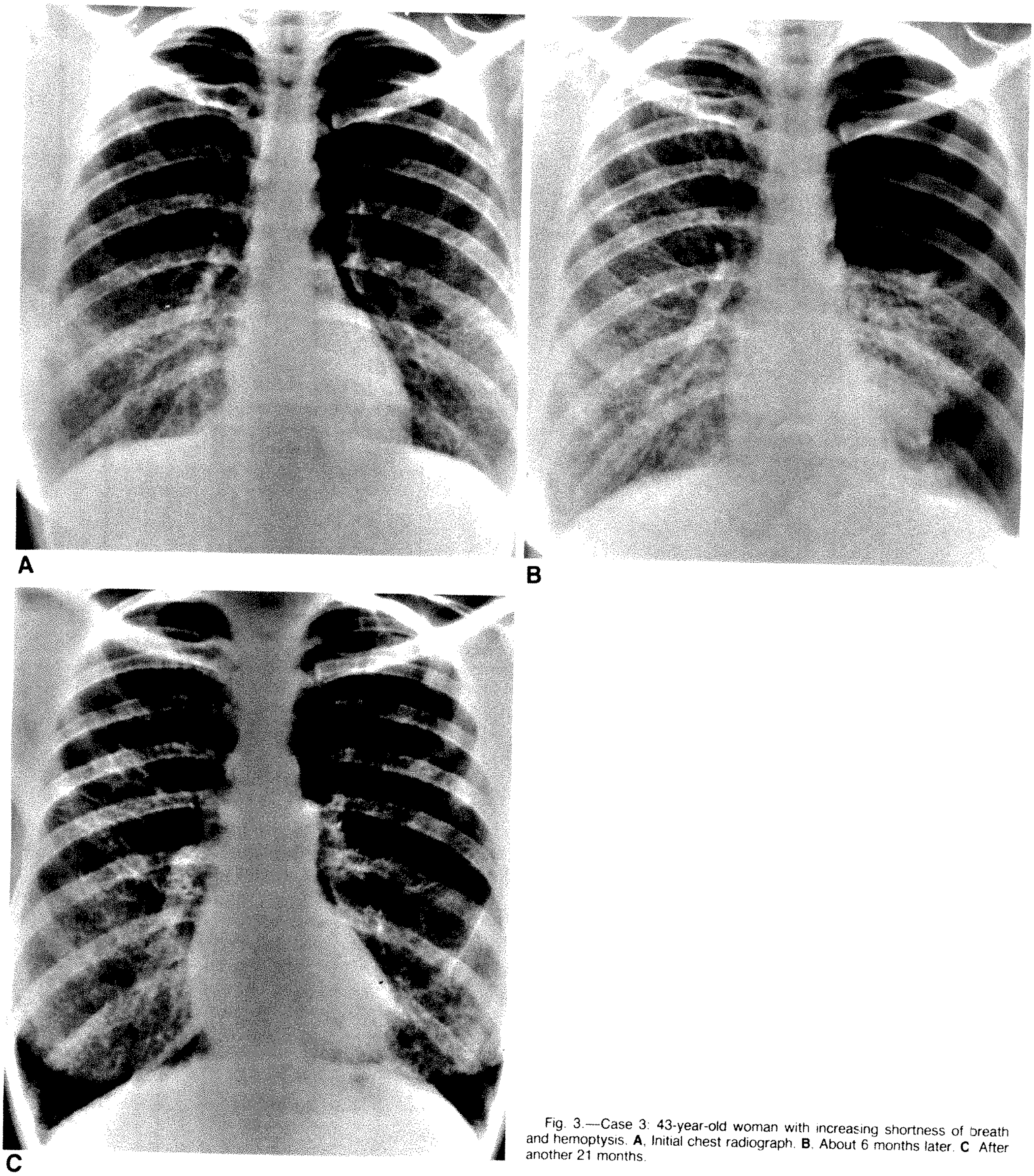

Fig. 3.—Case 3: 43-year-old woman with increasing shortness of breath and hemoptysis. **A**, Initial chest radiograph. **B**, About 6 months later. **C**, After another 21 months.

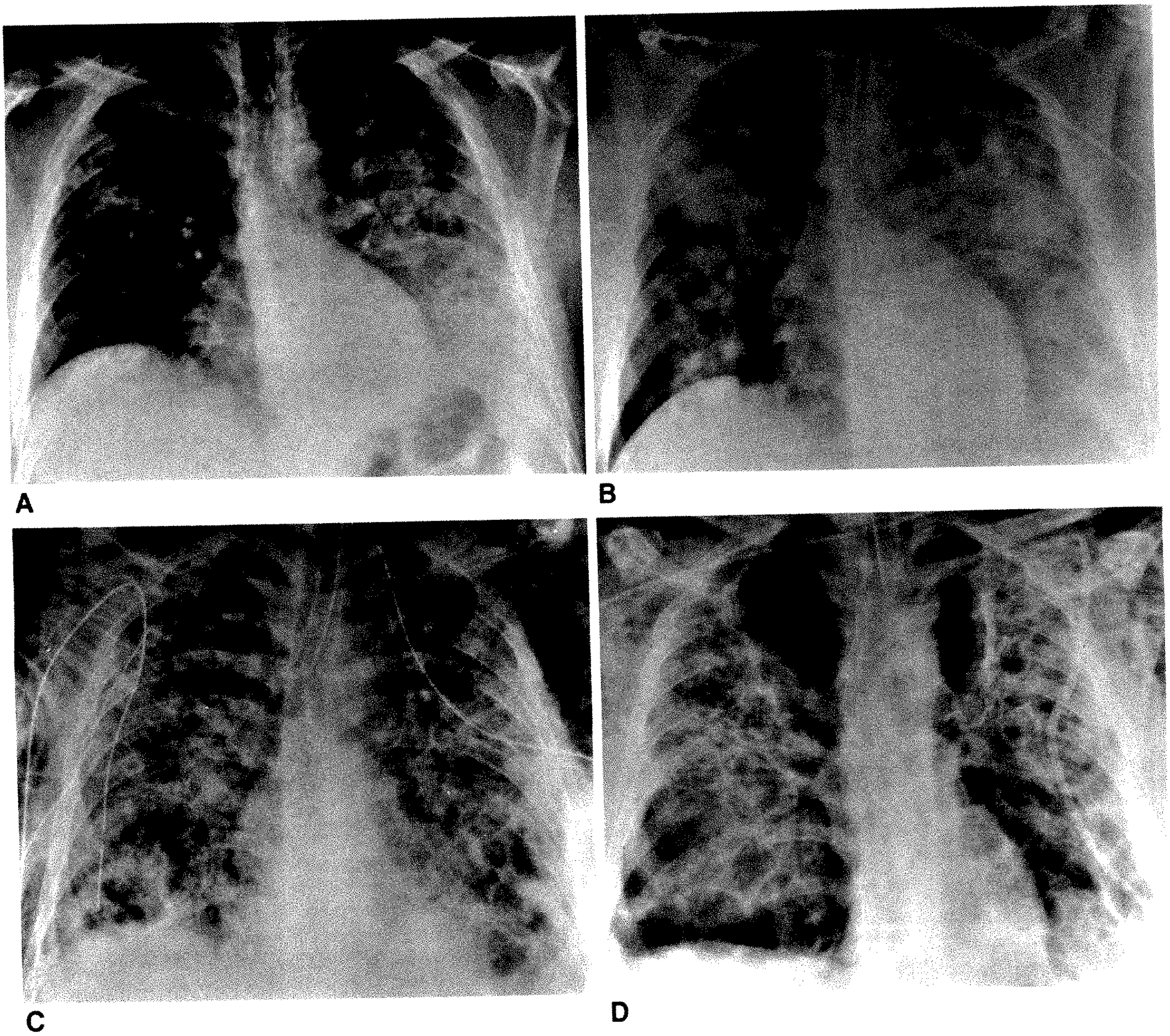

Fig. 4.—Case 4: 38-year-old man from northern Wisconsin admitted because of cough, low-grade fever, and bloody sputum. **A**, Admission chest film. Films in intensive care unit: **B**, 5 days after **A**. **C**, About 1 month later. **D**, After another month.

Abdominal Case of the Day

Bhaskara K. Rao,[1] Kathleen A. Scanlan, and Marvin L. Hinke

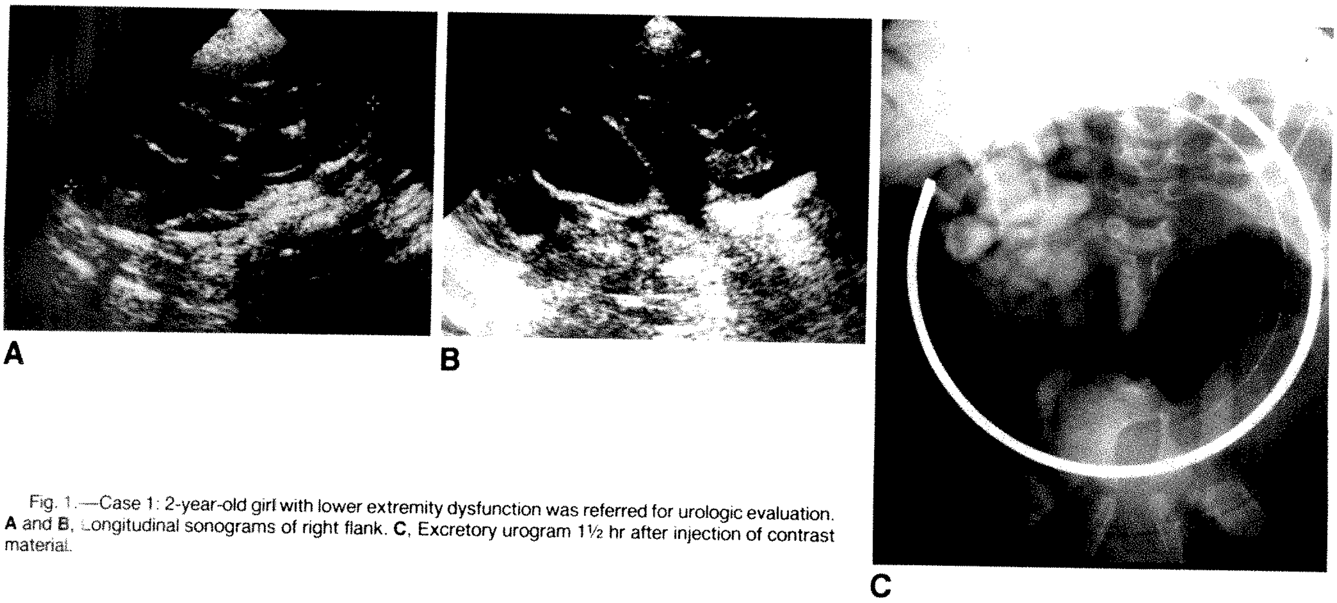

Fig. 1.—Case 1: 2-year-old girl with lower extremity dysfunction was referred for urologic evaluation. **A** and **B**, Longitudinal sonograms of right flank. **C**, Excretory urogram 1½ hr after injection of contrast material.

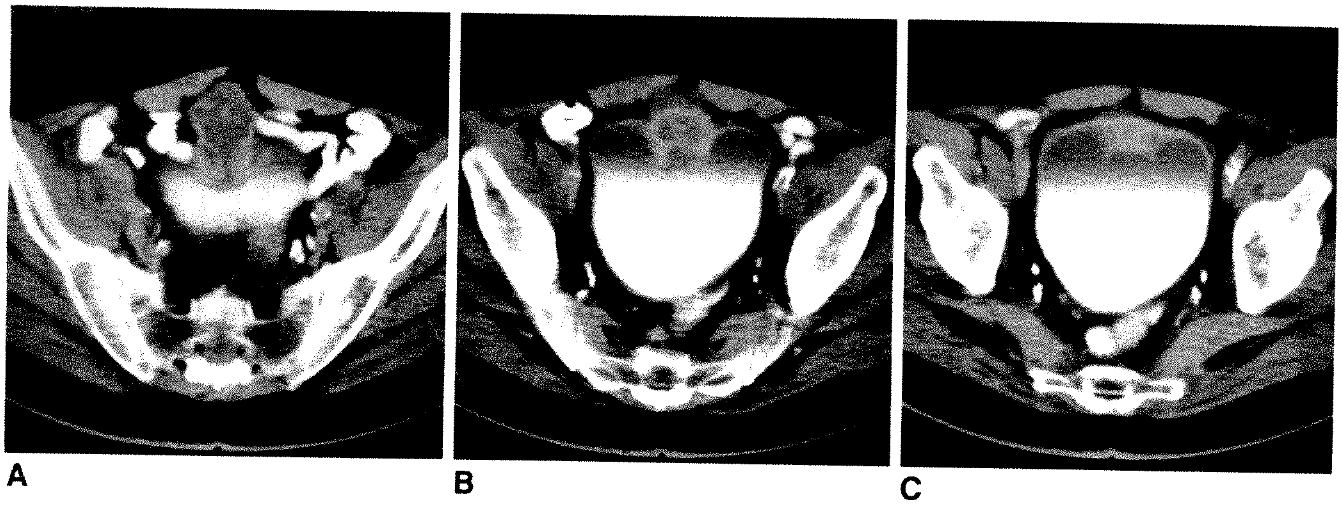

Fig. 2.—Case 2: 39-year-old man was found to have microscopic hematuria during routine physical and laboratory examination. **A–C**, 10-mm-thick slices through pelvis 2.6 cm apart after oral and intravenous drip administration of contrast material.

---

[1] All authors: Department of Radiology, University of Wisconsin Clinical Science Center, 600 Highland Ave., Madison, WI 53792. Individual cases prepared by K. A. Scanlan (case 1) and B. K. Rao (cases 2–4). M. L. Hinke is the coordinator of the Case of the Day series.

AJR 146:631–633, March 1986 0361–803X/86/1463–0631 © American Roentgen Ray Society

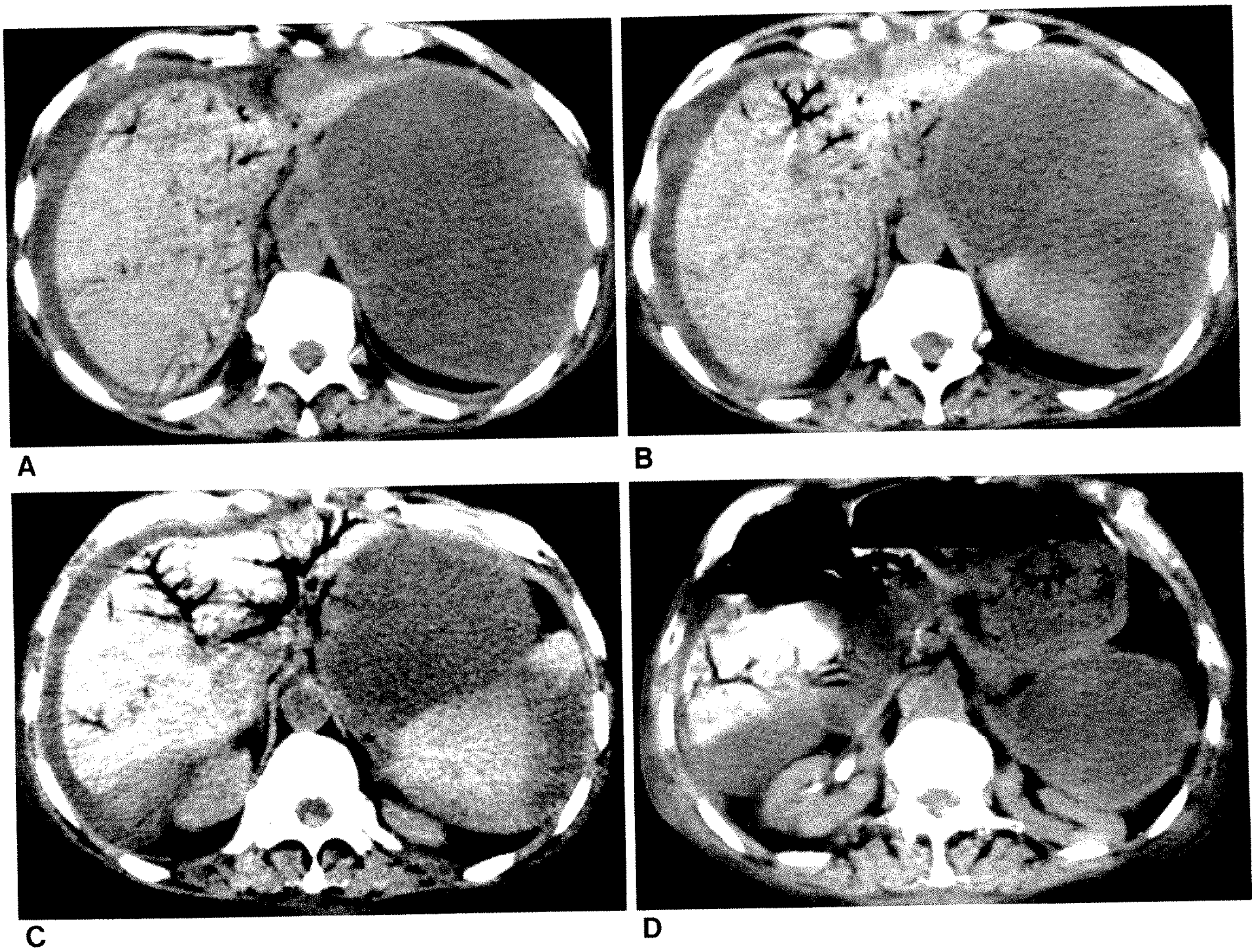

Fig. 3.—Case 3: 27-year-old man, a chronic alcohol abuser, was brought to emergency room in shock; he had sustained blunt trauma to abdomen 2 weeks earlier and was managed conservatively. **A** and **B**, Noncontrast images 3 cm apart above umbilicus level. **C** and **D**, Contrast-enhanced images 5 cm apart.

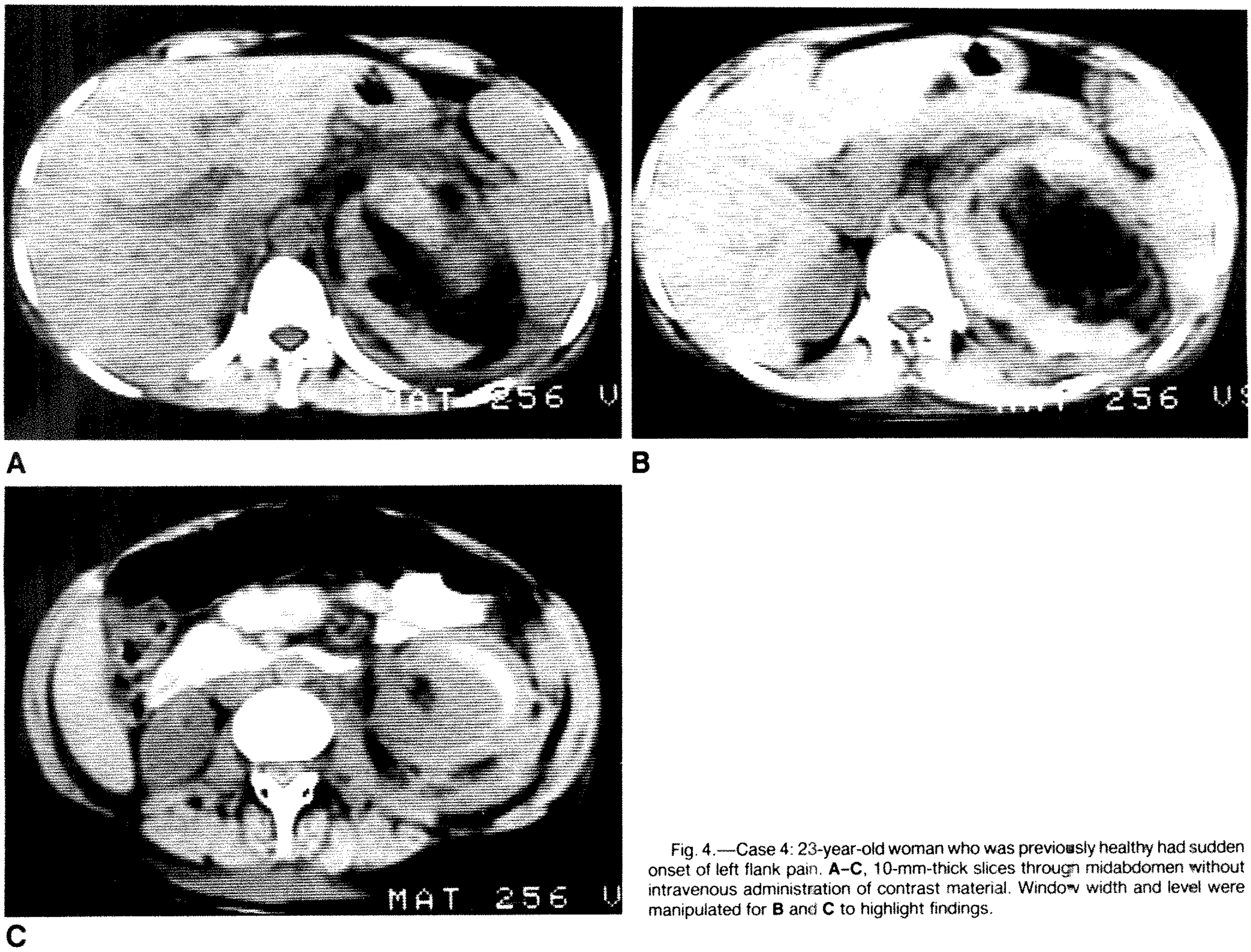

Fig. 4.—Case 4: 23-year-old woman who was previously healthy had sudden onset of left flank pain. **A–C**, 10-mm-thick slices through midabdomen without intravenous administration of contrast material. Window width and level were manipulated for **B** and **C** to highlight findings.

Musculoskeletal Case of the Day

David R. Fisher[1] and Marvin L. Hinke[1]

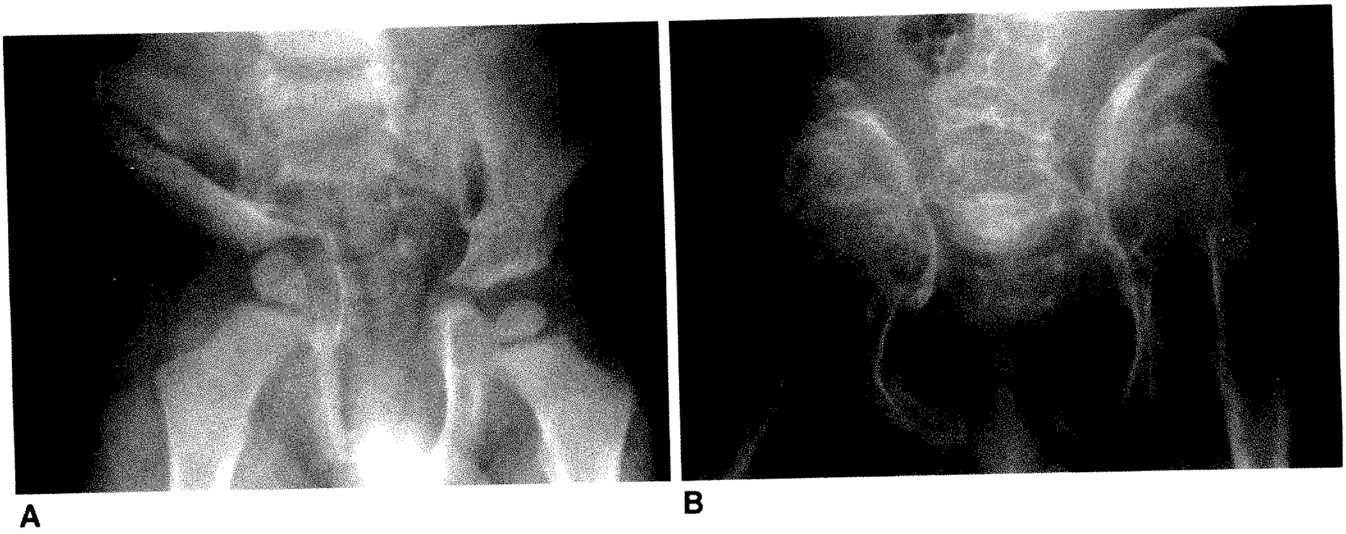

Fig. 1.—Case 1: Boy with limp and right upper thigh mass. Anteroposterior radiographs of pelvis at age 2 (**A**) and age 10 years, 5 months (**B**).

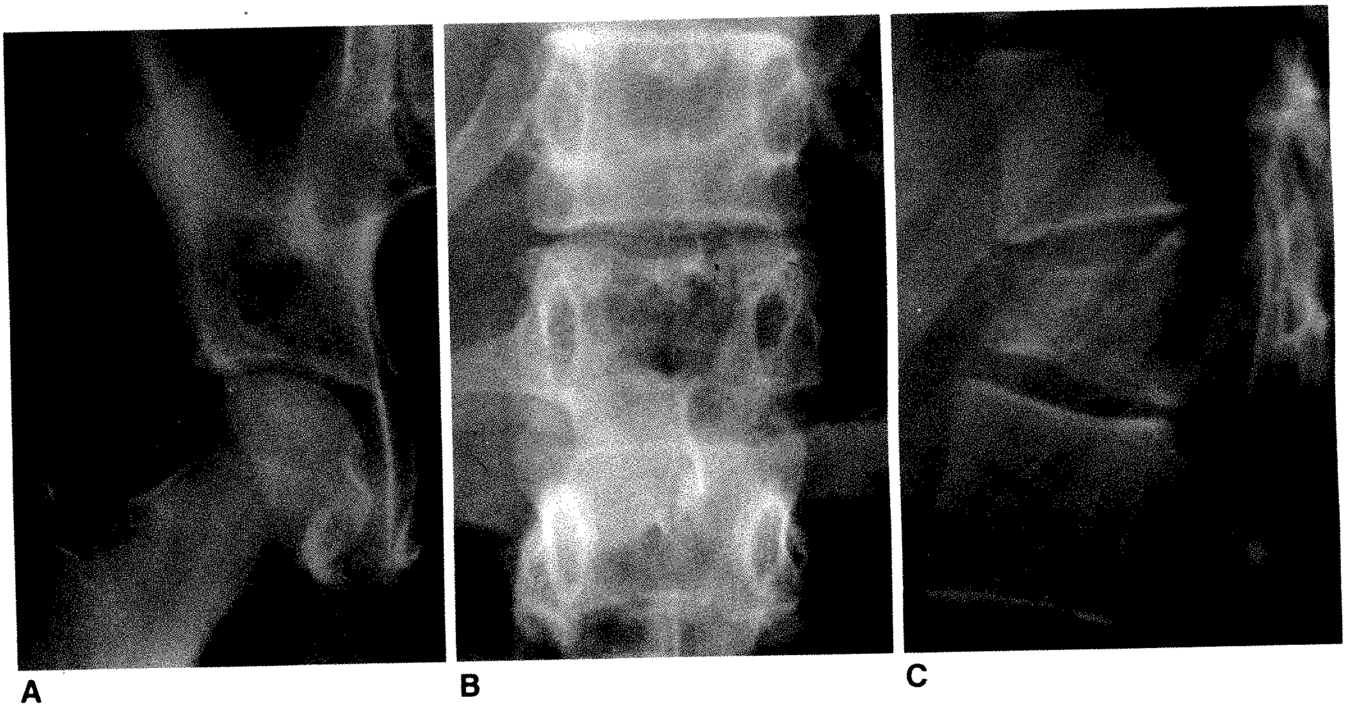

Fig. 2.—Case 2: 16-year-old girl with right hip pain. Skeletal survey; chest, spine, and pelvic CT scans; and radionuclide scans were all negative except in locations as illustrated: **A**, Anteroposterior radiograph of right hip. Anteroposterior (**B**) and lateral (**C**) radiographs of spine at thoracolumbar junction.

---

[1] Department of Radiology, University of Wisconsin Clinical Science Center, 600 Highland Ave., Madison, WI 53792. Cases 1–4 prepared by D. R. Fisher. M. L. Hinke is the coordinator of the Case of the Day series.

***AJR* 146:634–636, March 1986** 0361–803X/86/1463–0634 © American Roentgen Ray Society

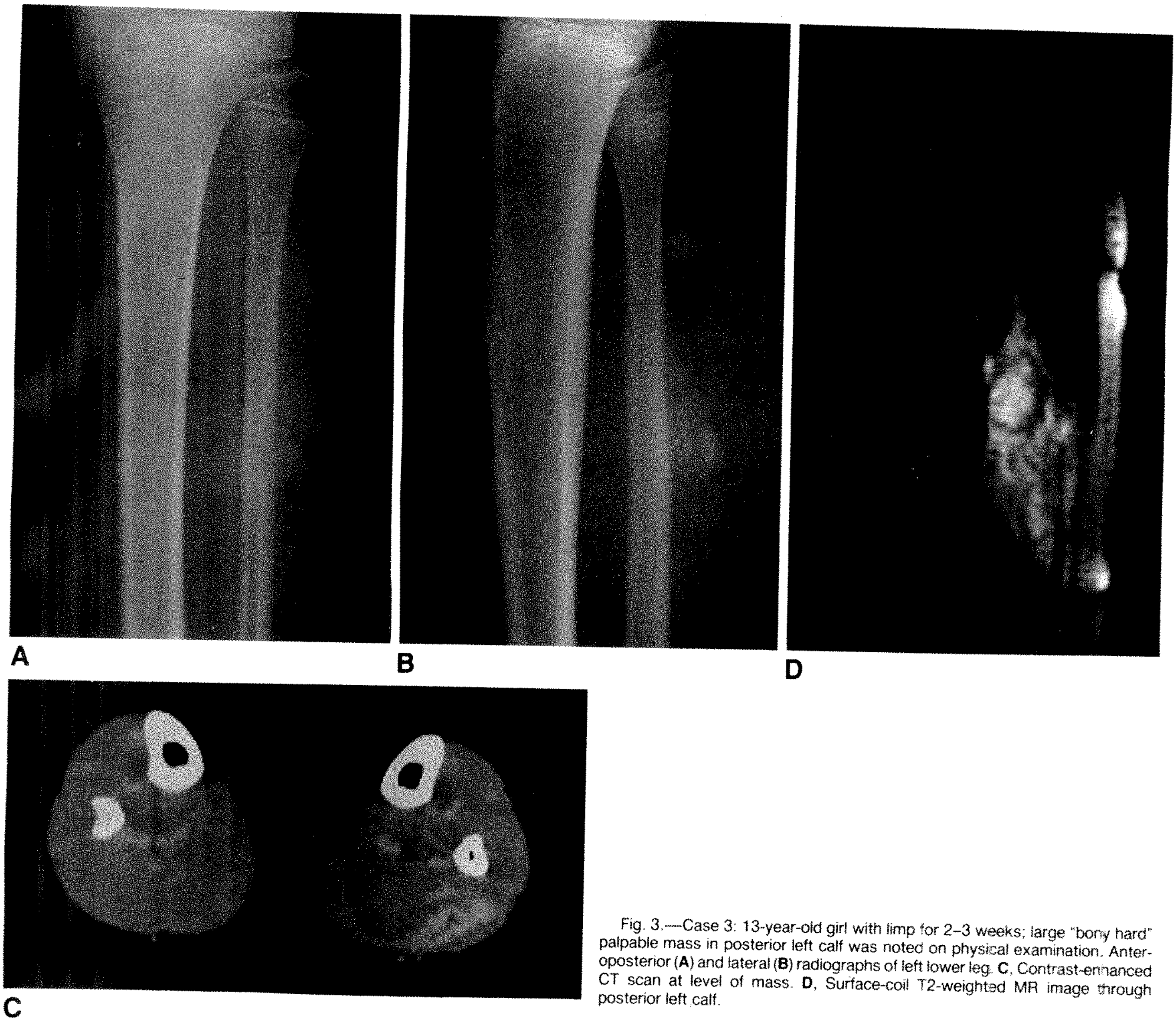

Fig. 3.—Case 3: 13-year-old girl with limp for 2–3 weeks; large "bony hard" palpable mass in posterior left calf was noted on physical examination. Anteroposterior (**A**) and lateral (**B**) radiographs of left lower leg. **C**, Contrast-enhanced CT scan at level of mass. **D**, Surface-coil T2-weighted MR image through posterior left calf.

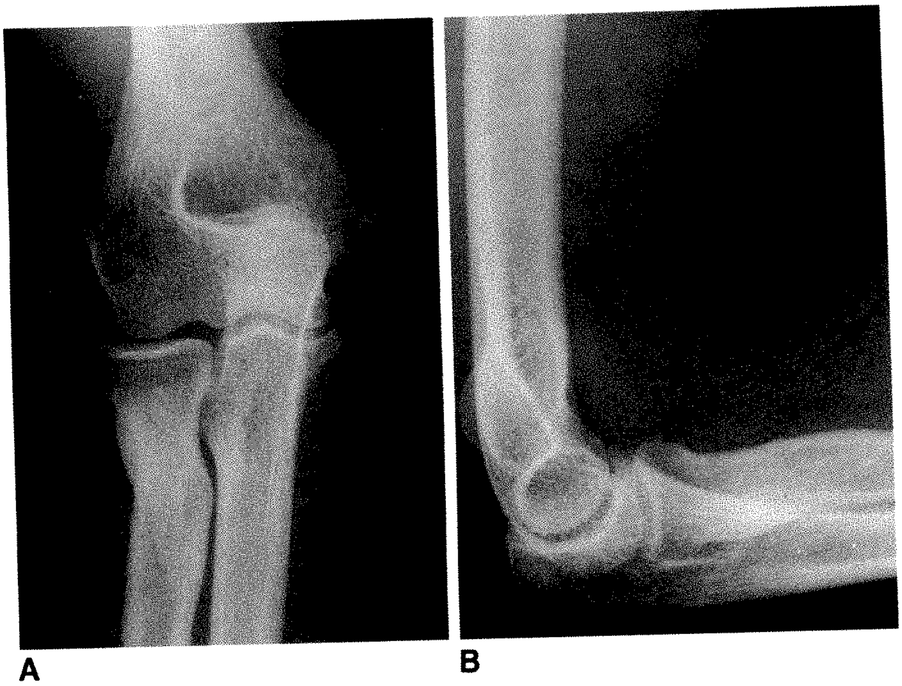

Fig. 4.—Case 4: 37-year-old right-handed woman with right elbow pain for 18 months, first noted after packing and unpacking in change of residence; laboratory data, including erythrocyte sedimentation rate, were within normal limits. Anteroposterior (**A**) and lateral (**B**) radiographs of right elbow.

Neuroradiology Case of the Day

Lanning W. Houston[1] and Marvin L. Hinke[1]

Fig. 1.—Case 1: 18-year-old girl with headache. Coronal magnetic resonance images. **A**, Partial saturation, 300 msec TR. **B**, Multiple spin-echo 2000/128 (TR/TE).

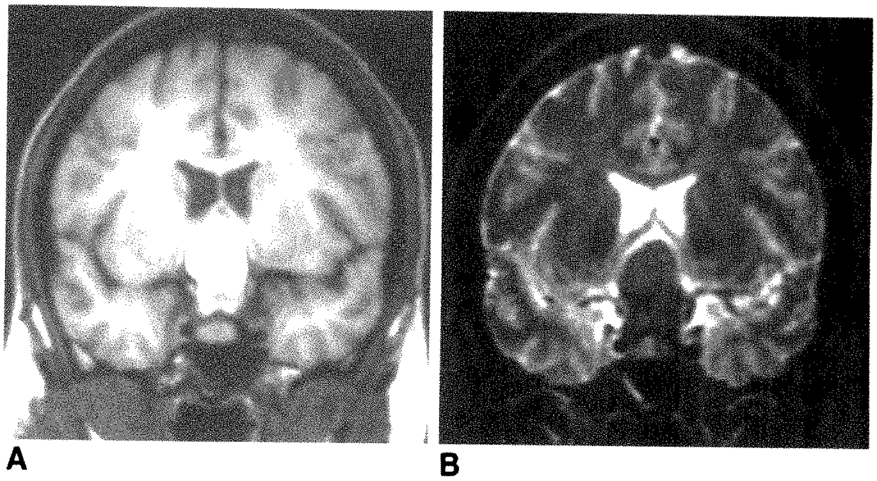

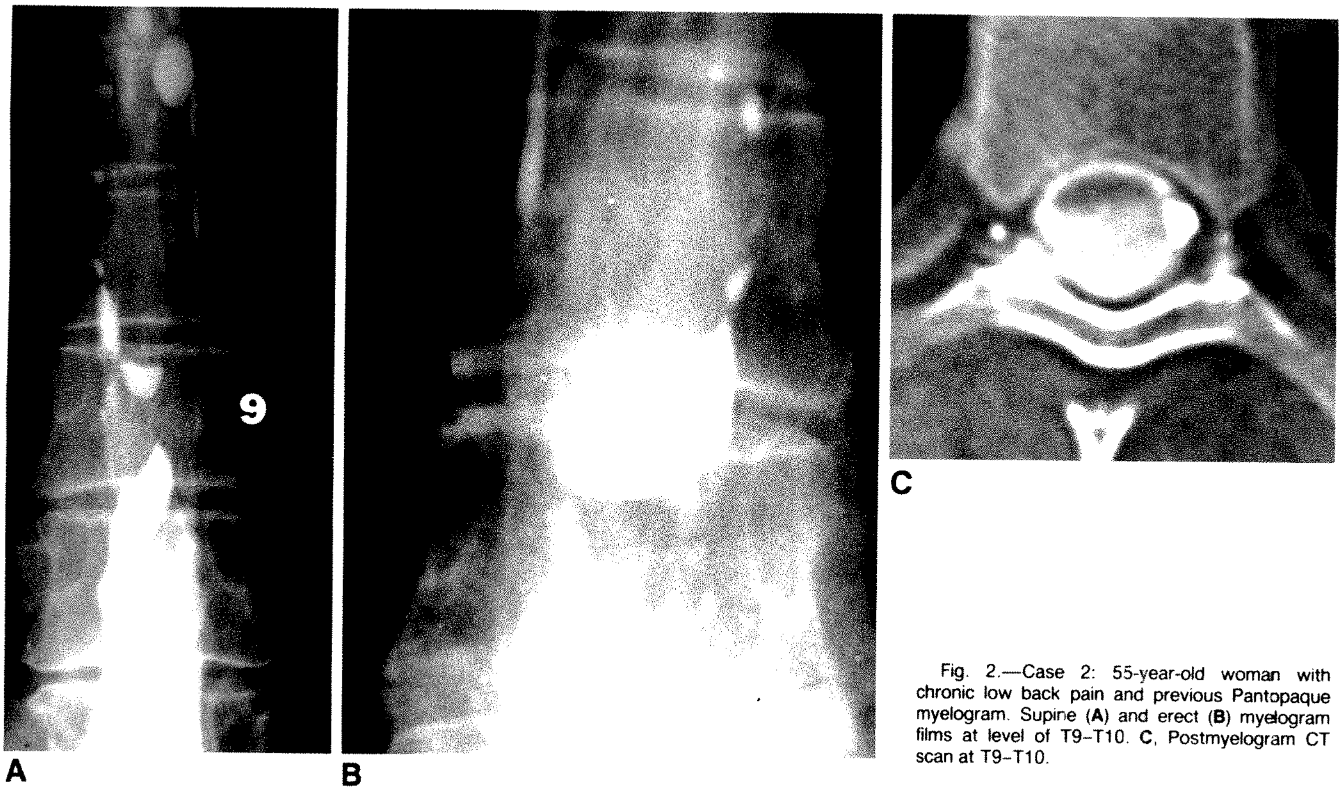

Fig. 2.—Case 2: 55-year-old woman with chronic low back pain and previous Pantopaque myelogram. Supine (**A**) and erect (**B**) myelogram films at level of T9–T10. **C**, Postmyelogram CT scan at T9–T10.

---

[1] Department of Radiology, University of Wisconsin Clinical Science Center, 600 Highland Ave., Madison, WI 53792. Cases 1–4 prepared by L. W. Houston. M. L. Hinke is the coordinator of the Case of the Day series.

AJR 146:637–638, March 1986 0361-803X/86/1463-0637 © American Roentgen Ray Society

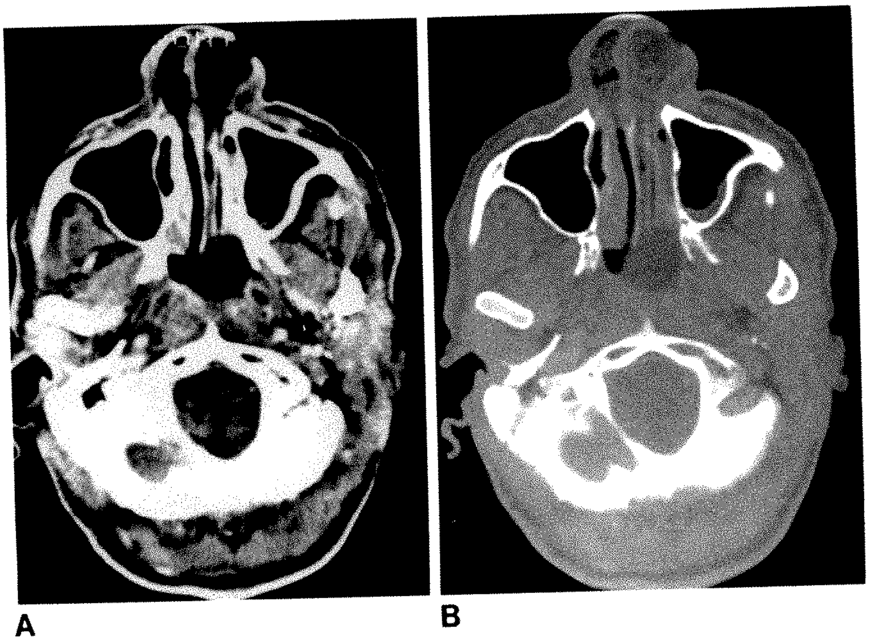

Fig. 3.—Case 3: 43-year-old man with epistaxis. CT scans displayed at soft-tissue (**A**) and bone (**B**) window settings.

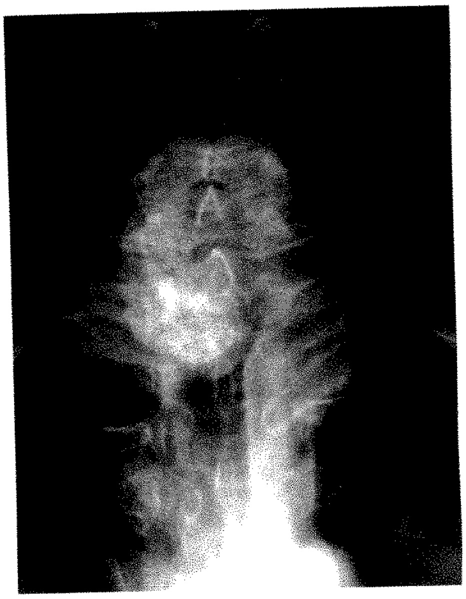

Fig. 4.—Case 4: 55-year-old man with difficulty breathing. Anteroposterior plain film of neck.

Editorial

The Presence of Parents with their Children during Imaging Procedures

Mervyn D. Cohen,[1] Beverly P. Wood,[2] and Christopher H. Hodgman[3]

"Having an x-ray" may be a frightening experience for a young child. Unfamiliar faces and strange machinery are often intimidating. Not many years ago, most children's hospitals had severe restrictions limiting parental entry into the hospital building. There was a great fear that liberal visiting hours would interfere with patient care. Quite the contrary has proved to be the truth. Unrestricted parental visiting has proven to be a definite asset in patient care, resulting in more cooperation and approval from patient families and happier children.

Are parents a help or a hindrance when they accompany their children into the imaging room in the radiology department? Two independent questionnaire surveys were recently carried out to ascertain the current status of parents accompanying their children in pediatric radiology departments throughout North America. In addition to answering the questions, the respondents were invited to make any general comments they wished. A third survey was performed to ascertain parental attitudes.

The departments surveyed included university and private groups, large children's hospitals, and independently functioning pediatric sections of large departments. The questionnaires were fully completed by the chief radiologist in 62 of 66 departments replying to the first survey and by 112 or 118 pediatric radiologists responding to the second survey. The answers reflected current departmental policies.

Parents are permitted into the imaging rooms of departments frequently (40%), sometimes (18%), occasionally (35%), and never (7%). Of the departments surveyed, only 23% routinely invited parents to accompany their children into the imaging room.

Parents are much more likely to be granted access for the noninvasive procedures such as sonography (72%–81%), nuclear medicine (45%), plain film radiography (35%–46%), and barium studies (40%–43%) (two percentages represent the results of the two surveys), than for invasive procedures such as myelography and angiography, where they are almost never allowed. For CT, parents are regularly present during only 24% of studies. An equal number of radiologists felt uncomfortable without the parents present as with them.

There is a wide range of current attitudes. Some institutions positively deter parents from accompanying their children, whereas others go out of their way to invite parents to do so. The reason for this diversity of opinions may reflect local prejudices and traditions, different pressures from hospital administrators and pediatricians, local hospital policies and state regulations, and the environment in which the various radiologists and technicians were trained. It is possible that many were taught that parents and observers should be excluded from the radiographic room and have never seriously considered experimenting with alternatives.

The size of the institution did not seem to be a factor in determining its attitudes and policies. Eighteen states including New York and Indiana have state regulations that, depending on their interpretation, would inhibit parental access into imaging rooms. In all the states with such regulations, the requirements are very similar. In Indiana, the State Board of Health regulations states that "only the staff and ancillary personnel required for the medical procedure or training shall be in the room during radiographic exposure." In New York, only "essential" or "required" persons and not trainees can be in the room.

---

[1] Department of Radiology, Indiana University School of Medicine, Riley Hospital for Children, 702 Barnhill Dr., Indianapolis, IN 46223. Address reprint requests to M. D. Cohen.

[2] Department of Radiology, University of Rochester Medical Center, Rochester, NY 14642.

[3] Department of Psychiatry, University of Rochester Medical Center, Rochester, NY 14642.

AJR 146:639–641, March 1986 0361–803X/86/1463–0639 © American Roentgen Ray Society

The state bureaus of health have believed that changing this practice would expose others to unnecessary radiation. Since parental involvement during other nonradiologic procedures has worked so well, one questions whether it would not be equally advantageous to the patient and to the radiologist to have a parent present during radiographic procedures, if desired. Furthermore, radiation exposure from scatter to a shielded person in the fluoroscopic room is negligible [1].

The potential disadvantages of permitting parents into the imaging room with their children may be summarized:

- The radiology staff may be inhibited by the parents' presence from performing a procedure as they believe optimal.
- Parents may be used to immobilize the child, thus increasing radiation exposure.
- Social interactions between workers may be restricted.
- Resident and technician teaching may be inhibited.
- Discussion about a differential diagnosis may be reduced.
- Parents may interfere with patient cooperation, making the children more difficult to handle and lengthening the procedure.
- Radiation exposure of a potentially pregnant mother is a possibility. If a baby is subsequently born with an abnormality, could the mother blame the radiology department for the baby's deformities?
- Time is needed to explain to the parents what is required of them in the imaging room: Injections, catheterizations, and the use of restraining straps need to be explained, and parents need to be told that under certain circumstances they could be asked to leave the room.

Thirty-six percent of the respondents believe that parents can hinder the procedure and prove to be a nuisance in the imaging room; 32% reported having experienced specific problems. Most of these problems were relatively minor, such as a parent feeling faint and having to leave the room. A few radiologists reported more serious problems of parents strongly objecting to the manner in which a study was done and complaining to the hospital administrator.

Although this list of disadvantages is lengthy, institutions that routinely permit parents to accompany their children find that in practice most of the fears prove to be unfounded.

There are many potential advantages to parents being with their children in the imaging room:

- Parents have a feeling of participating in the care of their child.
- Friction, resulting from denial of access to imaging rooms, is avoided.
- Closer liaison between the parent and radiologist promotes goodwill and increases the confidence of the parent.
- Parental presence is effective in calming and quieting children and keeping them from being upset.

Sixty-four percent of the radiologists surveyed believe parents are of help. Various studies have demonstrated the advantages of involving the parent in the child's care. Preparation of parents and children for head CT scanning greatly decreases the anxiety of both and helps the child to settle quickly in the scanner [2]. Rehearsing cardiac catheterization procedures with both parents and children also decreased the anxiety of the child, permitted the child to remain quieter during the study, and resulted in less regression and aggression afterward [3]. Twelve institutions that routinely permit parents into the radiographic rooms reported that the parents' presence facilitated positioning of the child [4].

In order to evaluate the opinion of parents concerning their attendance during radiographic procedures, the parents of 107 children aged 7 weeks to 7 years were sent a questionnaire. All were parents of children who had undergone fluoroscopic examinations at the University of Rochester Medical Center within the previous 18 months. In none of these instances had the parents accompanied their child in the radiographic room. Almost all the parents would have preferred to be present. Forty-seven percent of respondents would *very much* have preferred to be present in the room during the procedure and 43%, while willing to wait outside the room, would have liked to be present. Fifty-seven percent of the parents believed that their presence would have made the procedure easier for the child, and 41% believed that their presence would have made the procedure easier for the radiologist and technician. More than half of the parents believed that their child would have preferred them to be in the room.

The parents believed that they had an adequate understanding of the purpose and the mechanics of the radiologic procedure (88%). Although the parents had not been present in the room during the procedure, 50% believed that their child's treatment had been excellent and 33% reported good treatment. Thirty-nine percent of the parents rated their children's experience as negative, 31% as neutral, and 15% as positive.

The reasons the parents gave for wishing to be included in the room during the procedure were to comfort and calm their child and make him or her feel more comfortable in a strange situation. Overall, the parents wished for the option of deciding whether to be present in the room. Most parents recognized that it was not always appropriate to have a parent present. Many thought that the physician or technician should maintain the right to exclude a parent or ask them to leave if they believed it would be advantageous to the performance of the examination.

Two extreme views are often quoted for and against permitting parents into the imaging room. One states that "the child, deprived of the parents' presence, will receive irrevocable psychological damage." There is little scientific proof for this view. The opposite view holds that removing the child from the parent is part of the process of building the child's character and preparing him for life's experiences. Again there is little scientific evidence for this view, and many would hold that there are other, more controlled methods of preparing the child to achieve social independence.

While many pediatric radiologists believe that technicians and residents would in general be opposed to the presence of parents, experience has shown that those departments that permit parental access to the imaging rooms find this to be a positive experience and none wishes to revert back to complete parental exclusion.

Seventy percent of the departments surveyed believe that parents have a right to demand to accompany their child for the imaging procedure and 76% believe the radiologist has a right to say no. This is a difficult situation involving conflicting ethical rights of the doctor, parent, and child. The law is required to respect important ethical values and to monitor and reform itself as needed [5]. Parents enjoy legal powers over their children, but children enjoy independent legal rights over which the courts are guardians. Therefore, there may be situations in which the courts could require an imaging procedure to be done even if the parent refused consent because he was not permitted to accompany his child into the imaging room [5].

To function successfully, a policy of permitting parents to accompany their children must retain a balance. The radiology staff must retain the right to exclude a parent while attempting to respect parental views whenever possible. Parents too must have the opportunity of declining an invitation to accompany their chlid.

Some parents and some pediatric radiologists hold strong feelings on the issue of parents being with their child during imaging procedures. That it is controversial is indicated by the wide range of attitudes and practices. The fact that some institutions do operate effectively and without problems by permitting parental access to the imaging rooms indicates that this mode of operation is feasible. It may be a good time for radiologists to carefully consider their policies concerning the involvement of family members during radiographic procedures. Parental inclusion during radiographic procedures should be seen as the optimal approach. For many, this will be a change from the past and its introduction may be resisted. It acknowledges the greater permissiveness in modern society, while encouraging greater parental participation and responsibility. Both have their merits.

ACKNOWLEDGMENTS

We thank the members of the Society for Pediatric Radiology who participated in this study. A copy of the questionnaire and an analysis of all the replies is available on request from the authors.

REFERENCES

1. National Council on Radiation Protection and Measurements. *Radiation protection in pediatric radiology*, report no. 68. Washington, DC: NCRP, **1981**
2. Mills GC. Preparing children and parents for cerebral computerized tomography. *Matern Child Nurs J* **1980**;5:403–407
3. Naylor D, Coates TJ, Kan J. Reducing distress in pediatric cardiac catheterization. *Am J Dis Child* **1984**;138:726–729
4. Gyll C. Investigations into and a comparative study of techniques for basic radiography in children's hospitals. *Radiography* **1982**; 48:175–196
5. Dickens BM. Interests of parents in pediatric laboratory medicine—ethical and legal. *Clin Biochem* **1984**;17:60–63

Scientific Program: 29th Annual Meeting of the Society for Pediatric Radiology, Washington, DC, April 9–13

The 29th annual meeting of the Society for Pediatric Radiology will be at the Westin Hotel in Washington, DC, and symposia and general scientific sessions will be in the Westin Ballroom. Additional registration information can be obtained from Donald R. Kirks, M.D., secretary, Society for Pediatric Radiology, Department of Radiology, P.O. Box 3834, Duke University Medical Center, Durham, NC 27710; (919) 681-4678.

Titles of presentations and scientific papers and authors are as follows:

SPR Symposia

Wednesday, April 9, 1 p.m., Imaging in Urinary Tract Infection

1. Opening remarks. Leonidas JC
2. UTI: a pediatrician's view. Hellerstein S
3. Pathology of UTI and sequelae. Bernstein J
4. Sonography in UTI. Slovis T
5. CT of urinary tract anomalies. Kuhn J
6. Nuclear medicine in UTI. Sty J
7. MRI in UTI: how useful is it? Kangarloo H
8. Conventional and interventional radiology in UTI. Lebowitz RL
9. What does it all mean for the clinician? A urologist's view. Perlmutter A
10. Discussion and comments. Berdon WE

Thursday, April 10, 7:30 a.m., Magnetic Resonance: Update 1986

11. Opening remarks. Leonidas JC
12. Practical physical principles of MRI. Wolf G
13. MRI in CNS disease: comparison to CT. Latchaw R
14. MRI in oncology. Gooding CA
15. Cardiopulmonary MRI. Fletcher B
16. MRI in abdominal and musculoskeletal disease: new frontiers. Cohen M
17. MRI of GU tract. Kangarloo H

Scientific Papers

Thursday, April 10, 1 p.m., GU; Skeletal

1. The renal cortex and medulla in the neonatal kidney: sonographic evaluation of pathologic states. Slovis TL, Haller JO
2. Sonographic assessment of the bladder wall in the pediatric age group. Jequier S, Rousseau O
3. MRI of the pelvis and perineum in children. Dietrich RB, Kangarloo H, Boechat MI
4. Patterns of calcium deposition in the kidneys of children: in vivo demonstration of the Anderson Carr progression. Patriquin H, Robitaille P
5. Segmental function in duplex kidneys: assessment from the Tc-99m DTPA renogram. Shore RM, Koff SA
6. The duplex collecting system in female children with urinary tract infection. Bisset GS III, Strife JL, Dunbar JS
7. The pseudohorseshoe deformity in children with congenital gibbus. Fernbach SK, Davis TM
8. Radiologic and histopathologic correlates of posterior rib fractures in abused infants: an alternate mechanism of injury. Kleinman PK
9. Late radiological patterns of the hip in JRA. Blane CE, Ragsdale CG, Hensinger RN
10. Osteochondrodysplasias: prenatal sonographic diagnosis. Diagnostic criteria and differential diagnosis. Filiatrault D, Perrault G, Grignon A, Paille N
11. Acute compression injuries of bone: or, the toddler's fracture revised. Conway JJ, Poznanski AP
12. Changes in skeletal scintigraphy secondary to bone aspiration in the young. Jones BE, Davis RT, Treves ST
13. Bone density changes in normal children. Gilsanz V, Senac M, Roe T, Wells T, Landing B, Libaneti C, Schultz E, Cann C
14. The use of CT scan in unstable hip reconstruction. Mahboubi S, Horstmann H

Friday, April 11, 9 a.m., GI; Cardiovascular-Chest

15. The position and mobility of the normal ligament of Treitz and cecum. Katz ME, Siegel MJ, Shackelford GD, McAlister WH
16. Contrast imaging to improve specificity in the diagnosis of necrotizing enterocolitis. Uken P, Smith W, Franken E Jr, Ellerbroek C
17. Massive esophageal dilatation in postoperative chest films of patients with diaphragmatic hernia supported by extracorporeal membrane oxygenation (ECMO). Stolar C, Berdon W, Dillon P, Abramson S, Amodio J
18. Patterns of liver injury in childhood: CT analysis. Stalker HP, Kaufman RA, Towbin RB
19. Doppler investigation of children with portal hypertension. Patriquin H, Garel L, Weber A, Blanchard H
20. Cholelithiasis or sludge in infancy and in utero: a spectrum. Daneman A, Davies C, Roberts E, Stringer DA, Wilson S
21. Significance of umbilical artery catheter (UAC) related aortic thrombosis (AT) in neonates. Seibert JJ, Taylor BJ, Williamson SL, Williams BJ, Szabo JS
22. Contribution of MR imaging to the anatomic evaluation of right AV valve atresia. Fletcher BD, Jacobstein MD, Abramowsky CR, Anderson RH
23. Role of CT in the evaluation of the pulmonary arteries in children with right ventricular outflow obstructive lesions. Hernandez RJ, Bank ER, Shaffer EM, Snider AR, Rosenthal A
24. Evaluation of chronic pediatric airway obstruction with cine-CT. Frey E, Smith W, Wagener J, Grandgeorge S, Franken E Jr, McCrae P

25. The detection of sites of pulmonary hemorrhage in patients with cystic fibrosis utilizing technetium-99m red blood cells. Miller JH, Wong C, Osher A
26. Myocardial scintigraphy in complete transposition of the great arteries (TGA) after arterial switch repair. Nancarrow P, Hougen T, Potter C, Colan S, Hernanz-Schulman M, Castaneda A, Treves S

Saturday, April 12, 8 a.m., Neuroradiology; Miscellaneous

27. Normal ultrasonic anatomy of the neonatal spine. Gusnard DA, Yousefzadeh DK, Naidich TP
28. Magnetic resonance imaging of the spinal neuraxis in childhood. Barnes PD, Lester PD
29. The hippocampal formation. Naidich TP, Yousefzadeh DK, Haughton VM
30. Magnetic resonance imaging of spinal dysraphism. Altman NR, Altman DH
31. Neurosonographic and Doppler studies in full-term asphyxia. Daneman A, Hellman J, Barks J, Soto G
32. Computed tomography of the orbital mass in children. Ball WS, Towbin RB, Han BK
33. Computed evaluation of orbital lesions—computed sonography (CS) and computed tomography (CT). Slovis TL, Watts FB Jr, Baker J
34. Prevalence of incidental sinus opacification in children and adolescents: a study based on computed tomography. Diament MJ, Senac M, Gilsanz V, Baker S, Gillespie T, Larsson S
35. Reliability of retropharyngeal soft-tissue measurements in infants and children: new standards based on 586 normals. Rivero HJ, Young LW, Flom L
36. Nembutal sedation for pediatric CT. Strain JS, Harvey LA, Foley LC, Campbell JB
37. Gastroschisis and omphalocele: prenatal sonographic diagnosis and postnatal evolution. Grignon A, Filiatrault D, Yazbeck S
38. Detection of neuroblastoma with ^{131}I-meta-iodobenzylguanidine. Conway JJ, Weiss S, Cohn S, Karesh S, Gaynon P
39. Kevlar cassettes: further reduction in radiation exposure during routine pediatric radiography. Wesenberg RL, Amundson GM, Mueller DL
40. Digital teleradiology in a pediatric practice. Kuhn JP, Seidel FG
41. Magnetic resonance appearance of blood and blood products. Cohen MD, Smith JA, Cory DA
42. Urgent and emergent embolization of lesions of the head and neck in children: indications and results. Burrows PE, Lasjaunias P, Terbrugge K, Flodmark O

Saturday, April 12, 1:30 p.m., Members' Miscellany; Neuhauser Lecture

1:30 p.m., Members' Miscellany I

4:00 p.m., **Neuhauser Lecture: Genetics and Prenatal Diagnosis.** Kurt Hirschhorn, Mt. Sinai School of Medicine, New York, NY

Sunday, April 13, 8 a.m., Members' Miscellany; Special Interest Sessions

8:00. Members' Miscellany II

10:00. Research by pediatric radiologists: past accomplishments and future opportunities. Effmann EL

10:45. Water-soluble contrast media: new vs. old. Harwood-Nash DC, McAlister WH, Tonkin ILD

12:30. Contrast media in intussusception. Leonidas JC, Campbell JB, Dunbar JS

1:15. Role of ultrasound in the infant with vomiting. Kirks DR, Swischuck LE, Berdon WE

2:00. Members' Miscellany III

Letters

Errata

In the article by Glass et al. [1] in the October 1985 issue of *AJR*, I noticed two errors in figure 3B (fig. 1 below). First, mention is made of a low-attenuation lesion related to the left quadratus muscle. This lesion is not related to the quadratus muscle but rather to the interspinalis and multifidus muscles and possibly the longissimus muscle.

The second—and less grave—error is the authors' statement that the right psoas mass extends into the spinal canal and displaces the spinal cord. It appears that the CT scan is below the level of the spinal cord and at the level of the cauda equina.

Russ M. Savit
Hospital of the Medical College
of Pennsylvania
Philadelphia, PA 19129

REFERENCE

1. Glass RBJ, Fernbach SK, Conway JJ, Shkolnik A. Gallium scintigraphy in American Burkitt lymphoma: accurate assessment of tumor load and prognosis. *AJR* **1985**;145:671-676

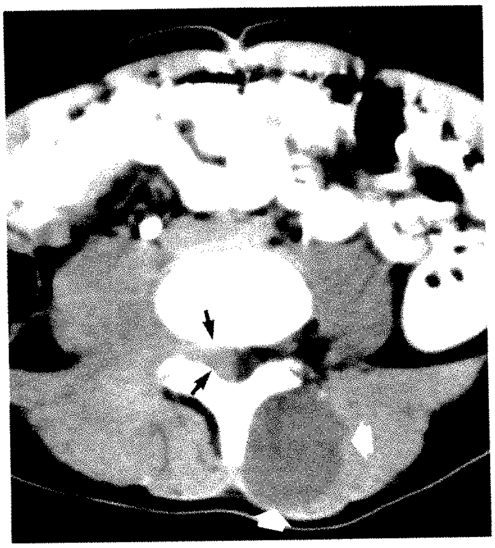

Fig. 1.—CT scan after 7 months of chemotherapy. Two paraspinal masses: One, in right psoas region, displaces cauda equina (*black arrows*); other, of low attenuation, involves deep muscles of back. (Reprinted from [1].)

Reply

Dr. Savit has correctly pointed out errors in the labeling of figure 3B in our article. The low-attenuation tumor deposit is posteromedial to the quadratus lumborum. The lesion involves the deep muscles of the back, namely, the multifidus and the erector spinae (which comprises the iliocostalis, longissimus, and spinalis muscles).

The superior extent of the psoas mass displaced the spinal cord but, as pointed out by Dr. Savit, indeed displaces only the cauda equina at the level of the section shown in the figure.

I thank Dr. Savit for the correction and apologize to the editor and *AJR* readers for these inaccuracies.

Ronald B. J. Glass
The Children's Memorial Hospital
Chicago, IL 60614

CT of Calcaneal Fractures

In the July 1985 issue of *AJR*, Heger et al. [1] described the computed tomographic (CT) characteristics of calcaneal fractures. They referred to the shortening and broadening of the calcaneus, the bony medial spike, and involvement of the anterior process. However, they erroneously concluded that the sustentaculum is displaced.

My colleagues and I reviewed 32 acute intraarticular calcaneus fractures with coronal CT and found that the sustentaculum was never displaced [2, 3]. We agree with Heger et al. [1] that the principal deformities are widening and shortening of the calcaneus with lateral calcaneofibular impingement. The tuberosity fragment typically is displaced laterally and superiorly. The sustentacular fragment, however, remains anatomically aligned with the talus. There is a very definite anatomic reason for the maintenance of this relationship. The sustentaculum is rigidly connected to the talus by the two strongest ligaments in the foot: the deltoid ligament and talocalcaneal interosseous ligament. Our studies indicated that the major fracture line is lateral to the interosseous ligament and that the articular surface of the sustentaculum is not disturbed.

This is not merely an argument of semantics. The concept of an anatomically aligned sustentacular fragment is the key to understanding the pathomechanics of calcaneus fractures. More important, it is the key to open reduction of these fractures [4]. The sustentaculum must be considered as the stable fragment on which the displaced tuberosity fragment can be reconstructed. This is accomplished surgically by placing a transverse Steinman pin in the displaced tuberosity fragment and pulling it caudad and mediad to reach proper orientation with the undisplaced, stable sustentaculum.

In summary, although we agree in large part with the data shown by Heger et al. [1], they have misinterpreted their findings by mistakenly referring to the sustentaculum fragment as displaced. Only the tuberosity and posterior facet fragments are displaced.

John E. Herzenberg
The Hospital for Sick Children
Toronto, Canada M5G 1X8

REFERENCES

1. Heger L, Wulff K, Seddigi MSA. Computed tomography of calcaneal fractures. *AJR* **1985**;145:131–137
2. Gilmer PW, Herzenberg JE, Frank JL, Goldner JL. Calcaneal fractures—diagnosis and treatment improved by use of computerized tomography (Abstr). *Orthop Trans* **1985**;9:57
3. Gilmer PW, Herzenberg JE, Frank JL, Silverman PM, Martinez S, Goldner JL. Computerized tomographic analysis of acute calcaneal fractures. *Foot Ankle* (in press)
4. Burdeaux BD. Reduction of calcaneal fractures by the McReynolds medial approach technique and its experimental basis. *Clin Orthop* **1983**;177:87–103

Reply

I agree that there is generally no dislocation of the sustentacular fragment in relation to the talus and that it is probably more correct to describe this very characteristic fracture displacement as dislocation of the tuberosity fragment. We chose to call it *sustentacular* displacement in order to distinguish this very common type from the various types of extraarticular displacement and other less common types of displacement of the tuberosity fragment that we described in the article.

In our experience this typical intraarticular fracture displacement between the sustentaculum and the tuberosity fragment is best demonstrated in the described tuberosity plane of section (30° to a plantar plane) and significantly less well in the coronal sectional plane mentioned. From the surgical point of view I agree that it is very important to understand the mechanics of this type of fracture displacement, which is demonstrated so beautifully by CT. It is perhaps less important whether it is called a sustentacular or a tuberosity displacement.

Krister Wulff
Ystad Hospital
271 00 Ystad, Sweden

Sonographic “Parallel Channel” Sign in Obstructive Jaundice

In the July 1985 issue of *AJR*, Wing et al. [1] cited an article describing the “parallel channel” sign in obstructive jaundice [2]. As author of that article, I wish to reply to their implication that a positive parallel channel sign is not reliable in the diagnosis of obstructive jaundice. Although Wing et al. [1] cited our sign freely, they did not adhere to our stipulated criteria and ignored our guidelines in distinguishing “normal” parallel tubular structures from truly dilated bile ducts.

The authors departed from our criteria by considering the mere presence of two adjacent tubular structures (i.e., “parallel tubes”) in the liver parenchyma or central porta hepatis as constituting a positive parallel channel sign and by using segmental branches of the portal vein in their assessment. We used only the right or left *main* portal vein branches and their *confluence* in establishing the presence of a positive sign. A suspected tubular structure was diagnosed as an enlarged bile duct only if it met the following criteria: (1) an enlarged tubular structure approximating the diameter of the adjacent, posterior portal vein; (2) a length of about 2.0 cm; and (3) tortuosity [2].

Imaging of “normal” parallel tubular structures was also addressed specifically in our article, though not emphasized by Wing et al. [1]. Normal parallel tubular structures were distinguished from dilated ducts by their (1) relatively straight course and rapid tapering over a distance of 1.0–1.5 cm; (2) small diameter (≤ one-third the size of the adjacent portal vein); and (3) lack of tortuosity [2]. Figures 7 and 8 in our article illustrated normal tubular parallel structures, and figure 9 demonstrated a normal prominent left main hepatic artery segment.

Modern high-resolution real-time imaging allows the careful and dynamic assessment of the right and left main portal vein branches and their confluence in the transverse plane, which was essential in our approach. A prominent or ectatic hepatic artery that simulates a parallel channel sign is generally easy to recognize by documentation of its origin from the celiac axis and not from the hepatic duct confluence; by the pulsatile quality that may on occasion be recognized with improved real-time imaging; and by exaggerated tortuosity.

I appreciate the contribution of Wing et al. [1]; however, in my opinion, the parallel channel sign remains a valid and reliable criterion if used according to the guidelines set forth by my colleagues and myself [2]. Quite simply, normal tubular structures usually are “skinny” complements to the right and left main portal vein and their confluence, and they are not a problem in the vast majority of cases.

Melvyn R. Conrad
203 Nacogdoches
Jacksonville, TX 75766

REFERENCES

1. Wing WV, Laing FC, Jeffrey RB, Guyon J. Sonographic differentiation of enlarged hepatic arteries from dilated intrahepatic bile ducts. *AJR* **1985**;145:57–61
2. Conrad MR, Landay MJ, Janes JO. Sonographic “parallel channel” sign of biliary tree enlargement in mild to moderate obstructive jaundice. *AJR* **1978**;130:279–286

Midcarpal Wrist Arthrography

The article by Tirman et al. [1] in the January 1985 issue of *AJR* demonstrates how midcarpal wrist arthrography can be used to outline the distal surfaces and tears of the scapholunate and lunotriquetral ligaments. In our experience of over 200 wrist arthrograms, we find confirmation of many of their observations but also questions that we hope they can answer.

“Partial” and “small and partially healed” intercarpal ligament tears are described; what are the criteria for recognizing such tears, and have any of these partial tears been proved at surgery? It would be helpful if the authors could illustrate these abnormalities.

Our more general concern is the practical value of midcarpal wrist arthrography as the *primary* procedure to evaluate wrist abnormalities. If the midcarpal injection fails to demonstrate an abnormality, radiocarpal arthrography is often needed. This is especially important with ulnar-sided symptoms, when one is concerned about the triangular fibrocartilage, a lunotriquetral ligament tear, or other abnormalities on the ulnar side of the wrist; and with radial-sided pathology such as radial capsular or ligament tears with radial-sided symptoms. We believe two injections are unnecessary, since the information desired can be obtained from a primary *radiocarpal* injection if one follows the technique that we described earlier [2].

Radiocarpal injection has the advantage of demonstrating capsular tears. The authors state that they have not seen capsular ligament tears. We have identified a number of capsular tears, and we surmise that tears of the radial and ulnar capsules are not routinely demonstrated with the midcarpal injections.

As a point of technique, if there is a problem in delineating surfaces of the lunotriquetral and scapholunate ligaments, a simple fluoroscopic profile of the ligaments (to be described in a forthcoming article) can clarify the problem. This technique is valuable in any situation where there is a possible abnormality of the scapholunate and/or lunotriquetral ligaments, including the problems mentioned by Tirman et al. [1], namely "overinjecting the radiocarpal joint, failure to continuously monitor the injection with careful observation of the interosseous ligaments, and losing fluoroscopy due to technical fault at the crucial moment when leakage into the midcarpal joint is occurring."

We commend the authors for their excellent patient selection criteria, which resulted in a high rate of arthrographic abnormalities and a high frequency of radiocarpal joint filling. Indeed, they state that normal midcarpal arthrograms can be kept to a minimum by careful preliminary clinical screening to ensure a high probability of arthrographically demonstrable scapholunate or lunotriquetral ligament tears [1]. Since Tirman et al. [1] have a high abnormality rate, it would be useful if they would indicate what features of their physical examination allowed them to predict specific ligament abnormalities with such a high degree of accuracy.

We have found two rare indications where we feel there is a place for midcarpal arthrography with a normal radiocarpal arthrogram: (1) to show the entire width and the appearance of the distal surface of a ligament (e.g., the presence of an intercarpal ganglion [enlargement of the soft tissues in the areas of the scapholunate or lunotriquetral ligaments]; and (2) to evaluate the possibility of localized synovitis in an area of the midcarpal joint (e.g., at the scaphotrapezial joint area), suggested by a normal radiocarpal arthrogram associated with focal radionuclide uptake and bone scintigraphy.

We thank the authors for their fine article demonstrating the technique for midcarpal arthrography, but suggest that this approach should play a limited role if primary radiocarpal injection is used for evaluation of soft-tissue abnormalities about the wrist.

Louis A. Gilula
William R. Reinus
William G. Totty
Mallinckrodt Institute of Radiology
St. Louis, MO 63110

REFERENCES

1. Tirman RM, Weber ER, Snyder LL, Koonce TW. Midcarpal wrist arthrography for detection of tears of the scapholunate lunotriquetral ligaments. *AJR* **1985**;144:107–108
2. Gilula LA, Totty WG, Weeks PM. Wrist arthrography. *Radiology* **1983**;146:555–556

Reply

Dr. Gilula and his associates raise some valid and interesting points for discussion.

With regard to their first question, in reference to the criteria for recognition of incomplete (partial) tears and small and partly healed tears of the intercarpal ligaments of the proximal carpal row, this was based on two cases (fig. 1). Under fluoroscopy, contrast medium was seen leaking from the intercarpal ligament and appeared to be extending into the radiocarpal joint space. However, in each of these two cases, the contrast medium remained as a single thin streak adjacent to the carpal bone and did not spread into the radiocarpal joint space in subsequent filming. At surgery, the orthopedist found a fissure that admitted a probe and led into the articular cartilage of the triquetrum in one case and the lunate in the other. Since that time our hand surgeon, Dr. Weber, has entered private practice and obtained 70 additional arthrograms, in which he states that he encountered three more such cases with subsequent operative proof. Without midcarpal arthrography these would not have been detected.

The next point of concern is that of midcarpal arthrography as the primary procedure for evaluation of wrist abnormalities. The authors point out the necessity of performing a second injection (radiocarpal) if the first-injection (midcarpal) arthrogram is normal, so as not to overlook pathology in the radiocarpal joint (e.g., a tear in the triangular fibrocartilage) that could be causing the patient's symptoms. We recognize that radiocarpal arthrography has been the procedure of radiologists for years and that most would probably prefer this as the primary choice, particularly since it requires only one injection. However, as we pointed out in our article, the number of *normal* midcarpal arthrograms can be kept to a minimum or possibly even eliminated by careful preliminary clinical screening to ensure a high probability of arthrographically demonstrating a scapholunate or lunotriquetral tear. When the midcarpal arthrogram is abnormal, showing intercarpal

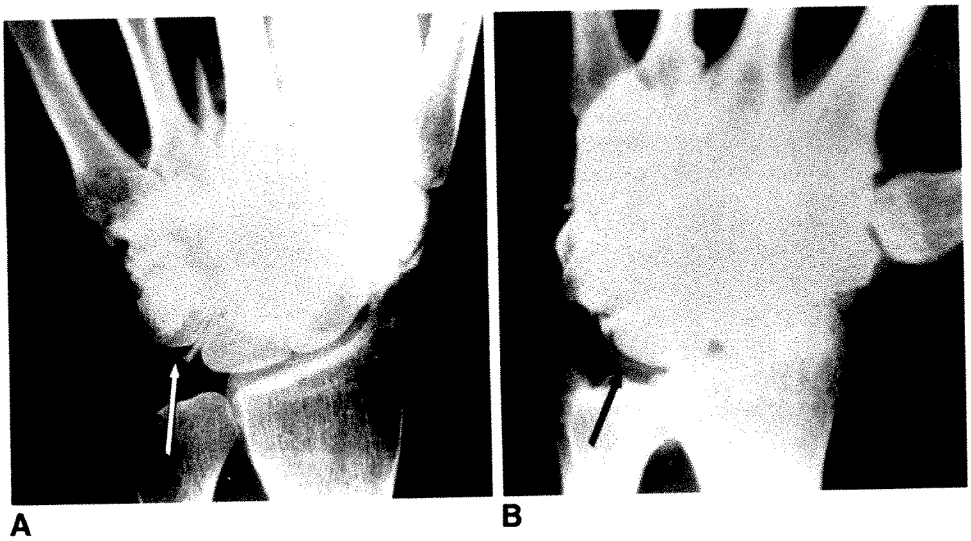

Fig. 1.—Two cases showing leakage of contrast medium (**A**, into cartilage fissure over triquetrum (*arrow*); **B**, into cartilage fissure over lunate (*arrow*)) from incomplete or partly healed tears in lunotriquetral ligament. Damage to ligament was confirmed at surgery.

tear of proximal carpal row ligament, no further injection is needed; this has been borne out by most of our arthrograms to date because of careful prearthrogram clinical screening.

The next question is in regard to the features of the physical examination that allow an accurate prediction of specific ligament abnormalities. Dr. Weber gives this response: "Radiocarpal injection is good for diagnosing tears of the triangular fibrocartilage but gives only inexact data about lesions of the proximal carpal row. One can tell precisely where the leakage occurs only if it can be demonstrated on a videotape replay. This is difficult with the proximal row injection because the dorsal bursa often fills before leakage of dye from the proximal row into the midcarpal row. Because of this dorsal bursa effect, it is more difficult to diagnose capsular tears from the proximal carpal row injection. Capsular tears are easily seen, however, on midcarpal row injections, since communication with the normal dorsal bursa does not take place. The selection criteria for our patients were wrist symptoms, usually consisting of a generalized synovitis for a period of at least 6 months. Eight views of the wrist were obtained preoperatively to rule out the presence of any osseous abnormality and to demonstrate the kinematics of the intercarpal motion. We found these studies useful but not nearly as precise in their diagnostic ability as the midcarpal arthrogram. Since the time of our original paper, I have operated on over 30 wrists on the basis of the diagnosis suggested by the midcarpal arthrogram and found the diagnosed pathology in each case. In two cases, pathology was present that was not delineated by the midcarpal arthrogram. In both cases, both the interosseous ligaments between the lunate and the scaphoid and the lunate and triquetrum were torn. It is possible, of course, to delineate only that ligament which leaks first, since when the proximal row is filled, the three-dimensional overlay of contrast material can be deceiving. This fact makes the possibility of two ligament lesions difficult to assess."

We thank Dr. Gilula and colleagues for their comments and for pointing out further indications for midcarpal arthrography. We agree that a second injection—when necessary for completeness of wrist evaluation for abnormalities—is a disadvantage, but we believe this is offset to a significant degree by the advantages brought out in the original article and elaborated on by Dr. Weber.

Robert M. Tirman
University of Arkansas for Medical Sciences
Little Rock, AR 72205
Edward R. Weber
Hand Surgery Consultants
Little Rock, AR 72204
Thomas W. Koonce
University of Arkansas for Medical Sciences
Little Rock, AR 72205
Linda L. Snyder
Radiology Consultants
Little Rock, AR 72205

Detection of Vesicoureteral Reflux in Children

In the September 1985 issue of *AJR*, Ginalski et al. [1] point out that renal growth retardation may be the only sign of significant vesicoureteral reflux in children. In 141 children undergoing surgery for vesicoureteral reflux shown by voiding cystourethrography, 154 (67.5%) of 228 refluxing ureters had signs by excretory urography. In 48 (21%) of the 228, renal growth retardation was the only sign. The authors emphasize the clinical value of using the Hodson method [2] of assessing renal growth in all children, especially those suspected of urinary tract infection. They note that their patients, all requiring surgery, had moderate to severe reflux.

My coworkers and I studied the value of excretory urography in urinary tract infection in children [3]. Of 389 consecutive children with infection, only 22.5% had signs by excretory urography. When reflux was equal to or greater than grade II of V, only 26.7% had signs. We did not apply Hodson's index; the experience of Ginalski et al. [1] suggests that had we done so, another 5%–7% would have shown renal growth retardation. Even so, the overall prevalence of urographic abnormalities in urinary tract infections in children is low when all grades of reflux are considered. We conclude that excretory urography is an insensitive method for detecting vesicoureteral reflux and recommend that voiding cystourethrography be the first radiologic investigation of urinary tract infections in children.

George A. Taylor
Children's Hospital
National Medical Center
Washington, DC 20010

REFERENCES

1. Ginalski J-M, Michaud A, Genton N. Renal growth retardation in children: sign suggestive of vesicoureteral reflux? *AJR* **1985**;145:617–619
2. Hodson CJ, Davies Z, Prescod A. Renal parenchymal radiographic measurement in infants and children. *Pediatr Radiol* **1985**;3:16–19
3. Blickman JG, Taylor GA, Lebowitz RL. Voiding cystourethrography: the initial radiologic study in children with urinary tract infection. *Radiology* **1985**;156:659–662

Reply

We agree that voiding cystourethrography should be the first radiologic investigation of vesicoureteral reflux and that among *all* children suffering from vesicoureteral reflux, the percentage of signs suggesting this diagnosis on excretory urography is low. The high percentage (67.5%) found in our study can be explained by our study population: It consisted entirely of children undergoing surgery for their reflux. The indications for surgery were (1) severe vesicoureteral reflux or (2) a less severe vesicoureteral reflux (affecting the pyelocaliceal system without dilating it) accompanied on cystoscopy by a severe anomaly of the ureteric orifice and/or accompanied on excretory urography by a severe nephropathy.

We wished to emphasize that when renal growth retardation is found on a child's excretory urogram (obtained for *any* reason), such retardation could be the only sign of a possible vesicoureteral reflux. Voiding cystourethrography is then mandatory to confirm or invalidate this diagnosis.

Jean-M. Ginalski
Centre Hospitalier Universitaire Vaudois
1011 Lausanne, Switzerland

Hypertrophied Fold or Torus Hypertrophy?

In the September 1985 issue fo *AJR*, Glick et al. [1] described a submucosal-appearing filling defect between the gastric antrum and the duodenal bulb. From endoscopic observations they concluded that this represented a prominent fold that was the result of gastric inflammation, but they did not have resected specimens to examine directly. We also have noticed this finding (fig. 1) and likewise have not obtained surgical proof of what it represents.

An alternative explanation for a filling defect in this region was presented by Dr. William Seaman [2] in 1966. In 12 cases with a similar radiographic appearance—eight from the literature and four his own—surgical or autopsy findings were available. Focal smooth-muscle hypertrophy at the lesser curvature aspect of the pylorus was the common finding. Associated gastritis and duodenal ulcer were

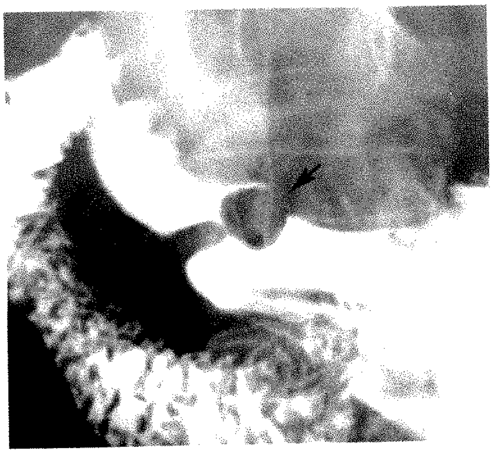

1

Fig. 1.—Filling defect (*arrow*) between gastric antrum and base of duodenal bulb, believed to represent either hypertrophied antral-pyloric fold or localized pyloric muscle hypertrophy.

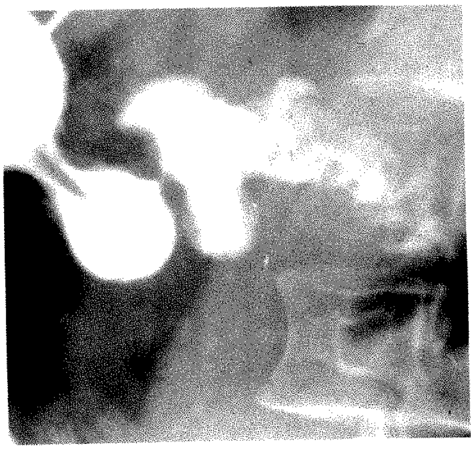

2

Fig. 2.—Surgically proved focal pyloric hypertrophy presenting as widening of space between lesser curvature of antrum and base of duodenal bulb. (Reprinted from [2].)

described less often (fig. 2).

The pyloric muscle consists of two circular muscle bundles that converge on the lesser curvature. This accounts for a prominence on the lesser curvature known as the torus [2]. Localized torus hypertrophy is a plausible alternative explanation for the radiographic findings described by Glick et al. [1], but why it develops is less clear. The filling defect is generally along the lesser curvature in the area of the torus. Localized pyloric hypertrophy has been reported also along the greater curvature side of the antrum but is distinctly less frequent [3].

Stephen W. Trenkner
University Hospitals
Ann Arbor, MI 48109

REFERENCES

1. Glick SN, Cavanaugh B, Teplick SK. The hypertrophied antral-pyloric fold. *AJR* **1985**;145:547–549
2. Seaman WB. Focal hypertrophy of the pyloric muscle—torus hyperplasia. *AJR* **1966**;96:388–392
3. Knight CD. Hypertrophic pyloric stenosis in the adult. *Ann Surg* **1961**;153:899–910

Reply

Dr. Trenkner suggests that the radiographic finding we described represents focal hypertrophy of the pyloric muscle. This alternative is based on an analysis of a previously published article [1] rather than personal experience with radiographic-pathologic correlation. We do not doubt that pyloric muscular hypertrophy can indent the contour of the antral-pyloric region when viewed in tangent. However, in several of our cases the hypertrophied fold could be identified on air-contrast views as a discrete structure traversing the antral-duodenal region with preservation of the normal tangential contour of the antrum and pylorus. We speculate that focal enlargement of the circular muscle of the pylorus by its geometry and anatomic location would distort the gross anatomic configuration. The radiographs in Dr. Seaman's article [1], although single-contrast studies, demonstrated such a contour defect in the distal antrum. Such a defect can occur with the hypertrophied fold, but distended air-contrast views usually permit precise identification. In addition, the nodular contour of the fold in some cases indicates the presence of a mucosal-submucosal process.

Although we do not have resected specimens to confirm our observations, we believe our endoscopic correlation was sufficient to justify our conclusions as to the anatomic, if not the pathophysiologic, etiology of this radiographic finding. Thus, while local hypertrophy of the pyloric muscle should be included in the radiographic differential diagnosis of filling defects in this location, the hypertrophied antral-pyloric fold does exist as a discrete entity with a characteristic radiographic appearance. The clinical distinction between these two processes is probably academic, since both are benign conditions not warranting further investigation or therapy.

Seth N. Glick
Hahnemann University
Philadelphia, PA 19102

REFERENCE

1. Seaman WB. Focal hypertrophy of the pyloric muscle—torus hyperplasia. *AJR* **1966**;96:388–392

Sacral Foraminal Lines

Sacral foraminal lines are the subject of an article by Amorosa et al. [1] in the October 1985 issue of *AJR*. These authors state that "the best projection for depicting the sacral lines is the tilted view of the sacrum. Tube angulation is 15° craniad. . . ." [1].

The standard projection described by Amorosa et al. [1] may offer the best overall view of the sacrum but, in my experience, it is not the best view for visualization of the sacral foraminal lines. This opinion is shared by others. In an article on this subject that was cited by Amorosa et al. [1], Jackson et al. [2] state that "the sacral arcs are consistently well seen on adequately exposed anteroposterior pelvic or abdominal radiographs. The latter are sometimes better, because they bring the surfaces of the costal elements into profile, accentuating the arcuate lines. The same effect can be achieved in an anteroposterior pelvic radiograph with slight caudad tilt. . . . The standard anteroposterior view of the sacrum with craniad tilt tends to obliterate the arcs and is therefore more difficult to interpret than an anteroposterior radiograph of the pelvis."

Ferris M. Hall
Beth Israel Hospital
Boston, MA 02215

REFERENCES

1. Amorosa JK, Weintraub S, Amorosa LF, Safer JN, Mahvash R. Sacral destruction: foraminal lines revisited. *AJR* **1985**;145:773–775
2. Jackson H, Kam J, Harris JH Jr, Harle TS. The sacral arcuate lines in upper sacral fractures. *Radiology* **1982**;145:35–39

Reply

Both Dr. Hall and I can substantiate our views. According to Meschan [1], cephalad tube angulation is useful for obtaining a view of the sacrum: "In the straight anteroposterior projection of the pelvis, the lower segments of the sacrum and coccyx are seen to underlie the pubic symphysis and thus are partially obscured. By tilting the tube about 15° toward the head and flexing the thighs so that the sacrum is against the table, a somewhat distorted view of the sacrum is obtained, but the sacrum is completely visualized."

It seems that in the absence of a well controlled study on sacral views with attention to the sacral lines, the choice of projection for obtaining the best sacral view will remain controversial. This interesting technical detail should not overshadow our aim in the article, which was to call attention to careful examination and comparison of the sacral arcuate lines—whether on a straight anteroposterior sacral view, a distorted sacral view, or a plain abdominal or pelvic film.

Judith K. Amorosa
Rutgers Medical School
New Brunswick, NJ 08903

REFERENCE

1. Meschan I. *An atlas of anatomy basic to radiology*. Philadelphia: Saunders, **1975**:131

Outpatient DSA Using Transbrachial Approach

I read with interest the article by McCreary et al. [1] in the November 1985 issue of *AJR*, in which the authors point out that intravenous digital subtraction angiography (DSA) has proven disappointing in the outpatient evaluation of cerebral vascular disease. This is well known. The authors go on to extol the virtues of the transbrachial approach.

I must take issue with the routine transbrachial approach on several points. I have been doing outpatient arteriography using the transfemoral approach and—after over 250 examinations of all types—have experienced no complications. The authors describe a complication rate of 3.4% (which is about double the usual acceptable complication rate) and seem to believe that this "testifies to the safety of our brachial approach" [1]. My question is, Why use a potentially dangerous procedure when we already have a time-tested, safe, and flexible method in the transfemoral approach? The brachial artery is notorious for developing severe spasm, which can lead to thrombosis and potential loss of limb. This spasm often is unrelated to catheter size, needle size, or period of catheterization. Catheter exchange also can induce spasm even when the initial entry has been uneventful.

Another point of contention is the lack of flexibility of the examination. Philosophically I regard the DSA imaging mode as an alternative method of recording an image using standard angiographic techniques. In our hands, the patient gets a definitive angiographic evaluation whether he/she is an inpatient or an outpatient. This includes selective injections of the cerebral vessels when needed. The transbrachial method precludes the easy selective catheterization that is afforded by the transfemoral approach.

I think outpatient arteriography, when properly performed, is a viable and increasingly popular procedure. However, the method described by McCreary et al. [1] is, in my opinion, unnecessarily dangerous and limited in its scope.

Robert S. Francis
West Side Hospital
Nashville, TN 37203

REFERENCE

1. McCreary JA, Schellhas KP, Brant-Zawadzki M, Norman D, Newton TH. Outpatient DSA in cerebrovascular disease using transbrachial arch injections. *AJR* **1985**;145:941–947, *AJNR* **1985**;6:795–801

Reply

Dr. Francis inferred from our article that we suggested outpatient arteriography should not be performed using the transfemoral approach. This was not the implication of our article. We, too, perform transfemoral outpatient studies when selective catheterization of the cervicocranial vasculature is needed. However, at the time of our study, a great deal of enthusiasm still surrounded the technique of intravenous DSA; therefore, patients who were being referred for the study expected a needle puncture in the forearm and refused groin puncture. The transbrachial approach offered a compromise, and it was exceedingly well accepted by the patients and the referring clinicians. A routine evaluation of the cervicocranial vasculature for atherosclerotic disease is easily done with this method; moreover, the quality of the images has improved greatly with experience.

Both the brachial and the femoral routes are "potentially dangerous," in the words of Dr. Francis. The complication rate mentioned in our series included only transient complications, with self-limited spasm representing the most serious one. Such a complication is no more potentially serious than femoral artery dissection, which is not a rare occurrence with the femoral technique (and may even go unrecognized). The notoriety of the brachial artery approach for producing spasm and thrombosis comes from the cardiology experience, where large catheters were used for selective studies and multiple catheter exchanges were made during the performance of those studies. Finally, it should be noted that our quoted complication rate occurred in the initial experience of the angiographers with a limited series of patients. We have subsequently performed these studies in over 200 patients without any major complications. We still feel that this route offers the advantages mentioned in the article, namely, obviation of axillary puncture in patients with limited femoral access, in those who refuse femoral puncture, and in those who wish early ambulation.

Finally, there are as many approaches to angiography as there are persons experienced with it. Our article did not imply superiority of one approach versus the others. Each individual case must be approached in its own clinical context and with due consideration of the preferences of the patient and his or her referring physician.

Michael Brant-Zawadzki
University of California
San Francisco, CA 94143

Abstracts

Heart

A Doppler-two-dimensional echocardiographic method for quantitation of mitral regurgitation. Ascah KJ, Stewart WJ, Jiang L, Guerrero JL, Newell JB, Gillam LD, Weyman AE (Massachusetts General Hospital, Boston, MA 02114). *Circulation* 72:377–383, Aug 1985

This open chest investigation in animals attempts to quantitate the severity of mitral insufficiency by Doppler-two-dimensional echocardiography. Regurgitant mitral flow should represent the difference between forward mitral flow and the aortic blood flow. The authors determined transvalvular mitral and aortic flow by Doppler examination during variable mitral regurgitation and compared regurgitant flow and regurgitant fraction calculated by Doppler-two-dimensional echocardiography with those measured by flow meter. The Doppler derived estimates of forward flow through the aortic valve correlated well with flow measured by flow meter ($r = 0.92$) and regurgitant flow and regurgitant fraction calculated by Doppler-two-dimensional echocardiography compared well with those measured by flow meter ($r = 0.84$ and 0.83, respectively). The authors conclude that an acceptable measure of mitral regurgitant flow and regurgitant fraction can be calculated by Doppler-two-dimensional echocardiography in the experimental setting.

Richard B. Jaffe

Continuous-wave Doppler echocardiographic assessment of severity of calcific aortic stenosis: a simultaneous Doppler-catheter correlative study in 100 adult patients. Currie PH, Seward JB, Reeder GS, Vlietstra RE, Bresnahan DR, Bresnahan JF, Smith HC, Hagler DJ, Tajik AJ (Mayo Clinic, Rochester, MN 55905). *Circulation* 71:1162–1169, June 1985 (by permission American Heart Association)

Studies of the correlation of aortic valve gradient determined by continuous-wave Doppler echocardiography and that determined at catheterization have, to date, involved young patients and nonsimultaneous measurements. We therefore obtained simultaneous Doppler echocardiographic and catheter measurements of pressure gradient in 100 consecutive adults (mean age 69, range 50 to 89 years). In 63 patients pressure measurements were obtained with dual-catheter techniques and in 37 they were obtained by withdrawal of the catheter from the left ventricle to the ascending aorta. Forty-six of these patients also underwent an outpatient Doppler study 7 days or less before catheterization. The simultaneous pressure waveforms and Doppler spectral velocity profiles were digitized at 10 msec intervals and maximum, mean, and instantaneous gradients (mm Hg) were derived for each. The correlation between the Doppler-determined gradient and the simultaneously measured maximum catheter gradient was $r = 0.92$ (SEE = 15 mm Hg), that between the Doppler-determined and mean catheter gradient was $r = 0.93$ (SEE = 10 mm Hg), and that between Doppler and peak-to-peak catheter gradient was $r = 0.91$ (SEE = 14). The correlation between the nonsimultaneously Doppler-determined gradient and the maximum gradient measured by catheter was not as strong ($r = 0.79$, SEE = 24). The continuous-wave Doppler echocardiographic velocity profile represents the instantaneous transaortic pressure gradient throughout the cardiac cycle. The best correlation with continuous-wave Doppler-determined gradient was obtained with maximum and mean gradients measured by catheter. Continuous-wave Doppler echocardiography can be used to reliably predict the pressure gradient in adults with calcific aortic stenosis.

Author Abstract

Gastrointestinal System

The pathogenesis of post-irradiation chronic diarrhoea: measurement of SeHCAT and B_{12} absorption for differential diagnosis determines treatment. Ludgate SM, Merrick MV (Dept. of Radiation Oncology, Western General Hospital, Edinburgh, Scotland). *Clin Radiol* 36:275–278, May 1985

The absorption of vitamin B_{12} and a synthetic bile acid analogue 75SeHCAT was measured simultaneously in 26 patients who presented with persistent diarrhea after pelvic irradiation for carcinoma of the cervix. Also, conventional medication had not proved effective. Four patient groups were identified. Thirteen patients showed isolated bile acid malabsorption with retention of 75SeHCAT at 7 days of less than 8% as compared to initial values and the standards. Twelve of these 13 patients obtained full symptomatic relief after oral administration of cholestyramine. Eight patients had normal retention of both vitamin B_{12} and 75SeHCAT and were subsequently shown to have a variety of disease processes including large bowel strictures, colonic diverticular disease, peritoneal metastases, and a pelvic abscess. Two patients had normal bile acid absorption but impaired B_{12} absorption and also demonstrated a raised breath hydrogen concentration after oral administration of 50 g of glucose, indicative of small bowel colonization. These two patients did not respond to cholestyramine, but obtained symptomatic relief after treatment with a broad spectrum antibiotic. Three patients had impaired absorption of both 75SeHCAT and B_{12} and responded symptomatically to cholestyramine administration. This technique permits patients with chronic postirradiation diarrhea to be separated into four groups: those with ileal mucosal damage, those with large bowel damage, those with colonization, and those with other causes. Each group requires different therapy.

Noel K. Allan

Significance of diffuse granularity and nodularity of the esophageal mucosa at double-contrast radiography. Graziani L, Bearzi I, Romagnoli A, Pesaresi A, Montesi A (Dr. A. Montesi, Dipartimento di Radiologia, Universita-Ospedale, Piazza Cappelli, 60100 Ancona, Italy). *Gastrointest Radiol* 10:1-6, 1985

Of 5000 consecutive double-contrast esophagrams, 50 cases were found to have a diffuse finely granular or nodular mucosa. Endoscopy and biopsy established the diagnosis in 38 cases: 23 were due to reflux esophagitis. Of the remaining 15, the diagnoses were candidiasis (four), leukoplakia (two), glycogenic acanthosis (one), diffuse leiomyomatosis (one), and normal mucosa in seven cases. The authors conclude that although reflux esophagitis is the cause of most cases of nodular esophageal mucosa, less commonly it is due to other lesions.

Charles A. Rohrmann, Jr.

Gastric interposition following transhiatal esophagectomy: radiographic evaluation. Agha FP, Orringer MB, Amendola MA (University of Michigan Hospitals, Ann Arbor, MI 48109). *Gastrointest Radiol* 10:17-24, 1985

Barium esophagrams were obtained in 138 patients who had transhiatal esophagectomy with gastric interposition. The procedure was done for 33 benign conditions and 105 malignant lesions. All patients were evaluated on the 10th postoperative day with barium esophagram and earlier with water soluble contrast medium if anastomotic leak was suspected. Early postoperative complications included anastomotic leaks (15), cricopharyngeal incoordination with aspiration (six), and gastric perforation (2). Late postoperative complications included anastomotic strictures (12), pyloric stenosis (four), recurrence of tumor (three), and transhiatal visceral herniation (two). The authors present numerous radiographs defining the expected and complicated manifestations of this procedure.

Charles A. Rohrmann, Jr.

Assessment of gallbladder function using ceruletide in oral cholecystography. Morewood DJW, Whitehouse GH (G. H. Whitehouse, Royal Liverpool Hospital, Liverpool, L7 8XP, England). *Gastrointest Radiol* 10:97-105, 1985

Fifty patients received 0.3 μg/kg body weight of ceruletide to assess gallbladder contractility and bile duct delineation after oral cholecystography. The mean percent reduction in gallbladder area at 5 min was 27%, at 10 min, 41%, and at 20 and 40 min, 49%. Nausea (24%), abdominal pain (24%), and flatulence (22%) were the most common side effects. Other side effects included vomiting, dizziness, headache, and sweating. Adenomyomatosis was detected in one case after ceruletide and was not apparent on the initial films. All other cholecystograms were regarded as normal. No relationship was found after ceruletide administration between the radiographic appearances of the biliary tract and reproduction of patients' biliary type symptoms. The authors conclude that ceruletide cholecystography is inaccurate in the investigation of biliary tract function.

Charles A. Rohrmann, Jr.

Cholecystokinetic cholecystography. Ritsema GH (Zuiderziekenhuis, Groene Hilledijk 315, 3075 EA Rotterdam, The Netherlands). *Gastrointest Radiol* 10:107-109, 1985

In a prospective clinical trial of 100 patients receiving either intramuscular ceruletide or a fatty meal, gallbladder contraction was similar in both groups. Ceruletide caused significantly more adverse reactions and is of doubtful diagnostic worth since, in only one patient was the diagnosis changed after administration of the agent.

Charles A. Rohrmann, Jr.

Towards a radiologic definition of idiopathic megacolon. Preston DM, Lennard-Jones JE, Thomas BM (J. E. Lennard-Jones, St. Mark's Hospital, London ECIV 2PS, England). *Gastrointest Radiol* 10:167-169, 1985

Using 50 barium enemas from patients studied for rectal bleeding, but in whom the examination and follow-up evaluation were considered normal, the authors found the mean rectal width at the pelvic brim to be 4.2 cm. The mean maximal colonic width in centimeters was sigmoid (4.4), descending colon (4.8), transverse colon (6.2), and ascending colon (6.7). Eighteen women who had prolonged whole gut transit time shown by prolonged retention of ingested radiopaque markers had measurements similar to the normal controls. Twenty patients were diagnosed as having idiopathic megacolon based on exclusion of other disease processes and enlarged colonic calibers by measurement. Mean maximal colonic widths in these patients were rectum (10), sigmoid (10), descending colon (7.2), transverse colon (7.8), and ascending colon (8.2). The study provides measured normal colonic widths and concludes that if known causes of colonic enlargement such as Hirschsprung disease or recurrent obstruction are excluded, a group of patients with idiopathic megacolon can be defined.

Charles A. Rohrmann, Jr.

Genitourinary System

Current imaging in renal failure. Willson SA, Talner SB (University of California, San Diego, CA 92103). *Rev Interam Radiol* 10:61-68, April 1985

Ultrasound has become the primary investigation for patients with renal failure. It safely and accurately demonstrates renal size and the presence or absence of hydronephrosis. High-dose urography and retrograde pyelography, once commonly used to image kidneys of azotemic patients, are rarely needed today. Sonograms may be unsatisfactory in obese patients or when the kidneys are small and scarred. In general, the ureters and retroperitoneum cannot be sufficiently well visualized to show the site or cause of obstruction in patients with obstructive hydronephrosis. However, the pelvis should be scanned to examine the bladder and to search for pelvic masses causing ureteral obstruction. In settings where good quality sonography is unavailable, high-dose urography can still be used to answer important questions in patients with azotemia of unknown cause. The patient should not be dehydrated. Approximately 600 mg/kg of iodine is injected as a bolus to provide an optimal nephrogram phase. Immediate tomograms are taken of the kidneys followed by a plain abdominal film at 10 min. If opacification is poor, delayed tomograms of the kidney are especially useful. Computed tomography (CT) is the best method for imaging small, endstage kidneys that are difficult to demonstrate by urography or sonography. Recently CT has been shown to be sensitive at detecting hydronephrosis even without intravenous contrast material. It also can show the site and cause of ureteric obstruction. Because radionuclide studies are dependent on renal function, isotope studies cannot play a primary role in investigation of patients with renal failure, especially if azotemia is advanced. However, there are a few situations in which radioisotope studies can be helpful despite the presence of mild renal failure. These include quantitating individual renal functions and serial studies for renal transplant patients. To quantitate individual renal function, split function studies using ^{99m}Tc DTPA can measure the relative glomerular filtration rate for each kidney. Effective renal plasma flow can be measured with hippuran (131). Serial studies with radionuclides can be used to follow renal function in transplants, in patients with neuropathic bladders, and in the follow-up of patients with relieved obstruction. Radionuclide cystography is the preferred method of following children with vesicoureteric reflux already proven by voiding cystourethrography. Sonography is the most effective method for evaluating surgical complications in the transplanted kidney. Hydronephrosis and fluid collections are easily shown. Excellent images can be produced using higher frequency and better resolution transducers because of the superficial location of the transplant kidney and the absence of overlying bowel gas. In acute rejection, enlargement of the kidney, focal or generalized lucencies in the renal parenchyma, and an indistinct corticomedullary junction seem to be the most common findings. These are thought to represent edema, hemorrhage, and infarction.

Charles M. Nice, Jr.

Percutaneous management of staghorn and large pelvic stones. Nuñez D, Marti AJ, Lynne CM, Russell E, Guerra JJ (University of Miami/Jackson Memorial Medical Center, Miami, FL 33101). *Rev Interam Radiol* 9:187–191, Oct 1984

Thirty patients with large renal pelvic stones and staghorn calculi were treated with ultrasonic nephrostolithotomy. Eighty percent of the patients had successful removal in the initial setting with an overall incidence of complications of 6.6%. Complications can be largely avoided by very carefully selecting the site and by careful planning of the procedure with the urologist.

Charles M. Nice, Jr.

Muscles and Skeleton

Spondylarthrography: the demonstration of spondylolysis by apophyseal joint arthrography. Park WM, McCall IW, Benson D, Seal PV, O'Brien JP (Robert Jones and Agnes Hunt Orthopaedic Hospital, Oswestry, Shropshire, Great Britian). *Clin Radiol* 36:427–430, July 1985

Twenty selected patients with spondylolysis were studied after apophyseal joint arthrography. These patients were all sufficiently symptomatic for surgical treatment to be considered. All had low central back pain. Ten patients also had radiation of pain down one leg and eight patients had radiation of pain to the buttock region. All lesions involved the lower two lumbar levels; 13 affecting the lumbosacral junction. Ten patients showed grade I intervertebral displacement and 10 had grade II displacement. In each instance a communication with the defect of the pars interarticularis was demonstrated by the extension of contrast medium from injection into the adjacent facet joint; in 17 patients contrast medium also delineated a communication with the distal apophyseal joint. In three patients, contrast medium also passed without further injection into the epidural space from the false capsule surrounding the spondylolytic defect. Radiculography was performed on six patients where associated root entrapment was clinically suspected with the demonstration of extradural deformity of the theca and attenuation of the emergent nerve roots in three cases. Of the patients, 65% experienced significant relief of pain symptoms when long acting local anesthetic was introduced into the facet joint. Barium paste arthrography of the L4–L5 and L5–S1 articulation in a cadaveric specimen with spondylolysis demonstrated the anatomic basis for some of the findings seen in apophyseal joint arthrography in this group of patients. The true incidence of communication of the pars interarticularis and its surrounding pseudocapsule with adjacent apophyseal joints is not known. The authors discuss the causes of pain in patients with spondylolysis and the therapeutic implications of their arthrographic findings.

Noel K. Allan

The asterisk sign and adult ischemic necrosis of the femoral head (in German). Dihlmann W, Heller M (Allgemeines Krankenhaus Hamburg-Barmbek, Ruebenkamp 148, D-2000 Hamburg 60, West Germany). ROEFO 142:430–435, 1985

The asterisk sign describes a stellate density normally seen in the femoral head on computed tomography that represents the trabeculae in the femoral head. Its appearance depends on the collodiaphyseal angle and it becomes more prominent with age. In adult ischemic necrosis of the femoral head, the asterisk sign changes at a stage before collapse of the head is evident. These changes include partial or total fragmentation of the asterisk, central or peripheral aggregation of sclerotic densities, and centrifugal sclerotic pseudopod formation.

Peter F. Winter

Chondroblastoma: a review of seventy cases. Springfield DS, Capanna R, Gherlinzoni F, Picci P, Capanacci M (Dept. of Orthopaedics, University of Florida, Gainesville, FL 32610). *J Bone Joint Surg [Am]* 67:748–755, June 1985

The authors reviewed 70 patients with chondroblastoma, 63 of whom were between 11 and 30 years of age. Of the lesions, 18 involved the proximal end of the humerus and 15 each were found in the proximal and distal ends of the femur. The lesions were usually in the epiphysis, but patients with closing epiphyseal plates tended to have involvement of the plate or the metaphysis. Calcification was found in the lesion in 20 patients, however, no lesions were studied by computed tomography so the actual incidence of calcification may be higher. After treatment seven patients had local recurrence. No tumors were considered malignant and no metastases were detected. Surgical treatment with curettage is recommended.

R. F. Kilcoyne

Complications following Harrington instrumentation for fractures of the thoracolumbar spine. McAfee PC, Bohlman HH (Dept. of Orthopaedics, Johns Hopkins Hospital, Baltimore, MD 21205). *J Bone and Joint Surg [Am]* 67:672–686, June 1985

The authors studied 40 patients who had significant complications after Harrington instrumentation for the treatment of thoracolumbar fractures. The goals of this internal fixation are to reduce the fracture, decompress the spinal canal, create stability of the fracture site, and shorten the hospitalization. The complications included five patients who had neurologic deterioration, nine with inadequate reduction of translational displacement of a vertebral fracture, 16 with dislodgement or disengagement of the Harrington components with resultant loss of fixation, six with deep wound infections, three with complete wound dehiscence with exposure of metal, and 16 with persistent unrecognized neural compression. Factors associated with these failures included: flexion rotation injuries of the osteoligamentous middle column; failure to obtain postoperative myelograms, computed tomograms, or both; failure to identify persistent neural compression; wound dehiscence; the use of distraction rods for high thoracic kyphosis; and instrumentation across the lumbosacral joint.

R. F. Kilcoyne

Nervous System

Cerebral torulosis: clinical features and correlation with computed tomography. Daunt N, Jayasinghe LS (Royal Brisbane Hospital, Brisbane, Queensland, Australia). *Clin Radiol* 36:485–490, Sept 1985

Cryptococcus neoformans is found worldwide but is particularly common in Queensland, Australia. Although infection tends to be opportunistic, infection has been reported in previously healthy patients. The only known habitat of this organism is bird manure. In this series 15 patients, average age 37 years, with *C. neoformans* involving the central nervous system were reviewed. Eleven were Caucasian and four were aboriginal; one was pregnant at the time of diagnosis and two had a history of pulmonary sarcoidosis. On computed tomography (CT) four patients showed no abnormality, five showed ventricular dilatation only, and six had intracranial masses. Two of this last group also had associated hydrocephalus. Overall

12 patients (80%) had lung changes, five requiring lobectomies. The major findings were the disproportionate severity of clinical signs and symptoms when compared with CT findings, which often were either normal or demonstrated only small granulomas without significant mass effect. Of note was the absence of enhancement of the granulomas in two patients and the observation of calcification during treatment in one patient. These authors suggest the diagnosis of torulosis should be considered in patients with headaches and papilledema, especially in endemic areas when the CT examination is normal or shows only a small mass lesion without mass effect; in immunosuppressed patients, especially during pregnancy; and in susceptible racial groups, particularly the aboriginals.

Noel K. Allan

Progressive spasticity and scoliosis in children with myelomeningocele. Park TS, Cail WS, Maggio WM, Mitchell DC (Dept. of Neurosurgery, University of Virginia School of Medicine, Charlottesville, VA). *J Neurosurg* 62:367–375, March 1985

Seventeen myelodysplastic patients who underwent surgical treatment for progressive scoliosis and spasticity were retrospectively reviewed. Metrizamide myelography was performed in 12 patients, ventriculography in two, and a hydromyelic cavity was injected in three patients. Hydromyelia was demonstrated in nine patients, while compression of the brain stem was seen in five. Of 12 patients who underwent obex plugging procedures, eight demonstrated partial or complete resolution of spasticity and an increase in motor strength with no significant postoperative complications. In five patients, posterior fossa decompression and/or ventriculoperitoneal shunting procedures alone did not lead to a favorable neurologic outcome. The authors conclude that hydromyelia may occur more commonly among the myelodysplastic patients than previously recognized, and may be treated most effectively by obex plugging procedures.

Arthur B. Dublin

The natural history of aneurysms and arteriovenous malformations. Jane JA, Kassell NF, Torner JC, Winn HR (Dept. of Neurosurgery, University of Virginia, Charlottesville, VA). *J Neurosurg* 62:321–323, March 1985

Experiences relating to the natural history of aneurysms and arteriovenous malformations (AVM) were reviewed. The data were collected from the Atkinson Morley's Hospital, Wimbledon, England, the Cooperative Aneurysm Study, the International Cooperative Study on the Timing of Aneurysm Surgery, and an analysis of incidental aneurysms in Charlottesville, VA. There is no peak at 7 days in rebleeding from previously ruptured aneurysms as was originally thought. Ruptured aneurysms have their highest rate of rebleeding on day 1, and at least 50% rebleed during the 6 months after the first hemorrhage. Thereafter, the rate dropped to about 3%/year. Patients with unruptured incidental and unruptured multiple aneurysms rebleed at a rate of 1%/year, as do patients with subarachnoid hemorrhage of unknown etiology. The risk of rebleeding for AVM is 3%/year.

Arthur B. Dublin

NMR imaging in temporal lobe epilepsy due to gliomas. Aaron J, New PFJ, Strand R, Beaulieu P, Elmden K, Brady TJ (Massachusetts General Hospital, Boston MA 02114). *J Comput Assist Tomogr* 8:608–613, Aug 1985

The superiority of magnetic resonance (MR) imaging over x-ray computed tomography (CT) in detecting a broad spectrum of intracranial lesions has been well documented. This paper presents three cases in which temporal lesions were better shown by MR than CT. The first case was a temporal lobe glioma that was obscured in the CT scan due to bone artifact while coronal CT showed the lesion poorly. This lesion proved to be an oligodendroglioma and was well shown by MR images. The second case, a 21-year-old man who had seizures since age 1 year, showed a small calcification in the righ temporal fossa on CT. MR showed a well circumscribed 1 × 1.5 cm mass in the right lateral temporal lobe. The last case, a 45-year-old man, demonstrated a large lesion in the left temporal lobe on both CT and MR images. However, MR showed the lesion as a single tumor while two lesions were suspected on CT. The authors conclude that MR will significantly contribute to evaluation of lesions in the temporal lobes, especially where CT is negative, shows minima abnormalities, or is of poor quality due to bone artifacts.

K. Jack Momose

Supraophthalmic carotid infusion for brain chemotherapy. Experience with a new single-lumen catheter and maneuverable tip. Kapp JP, Parker JL, Tucker EM. (Dept. of Neurosurgery, University of Mississippi Medical Center, Jackson, MI 39216). *J Neurosurg* 62:823–825, June 1985

Thirty-one patients underwent 50 consecutive supraophthalmic intracarotid infusions of chemotherapeutic agents for central nervous system neoplasms. The authors describe a single lumen catheter with a maneuverable tip that does not incorporate a balloon for delivery of the chemotherapeutic agents. Surgical exposure of the carotid artery was necessary for introduction of the catheter. None of the 31 patients who underwent these procedures developed optic neuropathy or loss of vision. However, 10 patients developed Marcus-Gunn pupils (ipsilateral to the infused carotid artery in two, contralateral to the infused carotid artery in eight). Thrombosis of the carotid artery occurred after infusion in one patient. The authors suggest that this infusion technique protects the eye from the high concentration first pass of chemotherapeutic agents administered via the carotid artery.

Arthur B. Dublin

Prediction of survival in glioma patients by means of positron emission tomography. Patronas NJ, Di Chiro G, Kufta C, Bairamian D, Kornblith PL, Simon R, Larson SM, (Neuroimaging Section, Clinical Center, Bldg. 10, Room 1C453, National Institutes of Health, Bethesda, MD 20205). *J Neurosurg* 62:816–822, June 1985

Forty-five consecutive patients with proven high-grade astrocytomas (grade III and IV) were evaluated by positron emission tomography (PET) with fluorine-18-2-deoxyglucose (FDG). There were 33 men and 12 women, mean age about 42 years. Forty-two patients had undergone partial resection of the tumor, two had a needle biopsy only, and one had a diagnosis of malignancy made from cytologic study of the cerebrospinal fluid. All patients had received radiation therapy, and, in addition, 32 patients had completed or were receiving a course of chemotherapy during their hospitalization. CT demonstrated residual tumor or recurrence of a previously treated tumor in all patients. In those patients exhibiting high glucose utilization as determined by PET-FDG, the mean survival time was 5 months. However, in patients with gliomas showing lower glucose use, the mean survival period was 19 months. Thus, the authors suggest that PET-FDG prognostic techniques are superior to CT or angiography. In addition, PET-FDG scans may be used to monitor the short-term tumor response to a given treatment

Arthur B. Dublin

Comparison of CT and MR in 400 patients with suspected disease of the brain and cervical spinal cord. Bradley WG Jr, Walunch V, Yadley RA, Wycoff RR (Huntington Medical Research Institutes, Pasadena, CA 91105). *Radiology* 152:695–702, Sept 1984

Over a 5-month period, 416 consecutive patients with suspected disease of the brain and cervical spinal cord were evaluated with magnetic resonance (MR) and computed tomography (CT). Patient ages were 3 months–91 years. MR was performed with a Diasonics 0.35 T superconducting whole body imager; sequence times were selected that were thought to optimize discrimination of suspected disease. The spin-echo sequence (90°-180°-80°) generated two images at echo times (TE) of 28 and 56 msec. Repetition times (TR) of 0.5, 1.0, 1.5, and 2.0 seconds were used depending on the suspected pathology. A two-dimensional Fourier transform was employed. The routine MR evaluation was performed with a TR of 2.0 sec and TE of 28 and 56 msec. Most CT scans were performed on a GE 8800 CT/T or on a GE 9800 CT/T. Of 325 positive diagnoses, MR detected abnormality while CT was normal in 93, however, MR was more specific in 68 and MR and CT gave equivalent information in 129. CT was the more specific in 32 and CT was positive while MR was normal in three. MR was superior to CT in detection of multiple sclerosis, subcortical arteriosclerotic encephalopathy, posterior fossa infarcts and tumors, small extraaxial fluid collections, and cervical syringomyelia. CT was preferable in evaluating meningiomas and separation of tumor from edema. Using available sequence parameters, MR missed three 1 cm calcified meningiomas that were clearly seen on CT. CT takes less time and may be preferable in patients with acute trauma and in the very young or elderly. These two studies should be considered complementary.

K. Jack Momose

Traumatic dural tear: CT diagnosis using metrizamide. Morris RE, Hasso AN, Thompson JR, Hinshaw DB Jr, Vu LH (Loma Linda University School of Medicine, Loma Linda, CA 92350). *Radiology* 152:443–446, Aug 1984

Computed tomography (CT) with intrathecal metrizamide has proved useful in spinal trauma. Six patients aged 5–26 years were studied. All had significant neurologic deficits such as sensory loss, paralysis or paresis. Dural tears with contrast material escaping outside the subarachnoid space were documented in five cases. In one case, the thecal laceration had healed and the contrast material was confined in a posttraumatic meningocele. The characteristics of dural tears are demonstrable by metrizamide CT, either in conjunction with myelography or as a separate procedure. Neurologic deficits after spinal trauma may be aggravated by dural tears with entrapment of the spinal nerve roots. Metrizamide-enhanced spinal CT may be favored over conventional myelography in the diagnosis of dural tears for several reasons. Myelography can miss small tears that may be apparent on CT. With large tears, contrast material dilution can compromise the quality of metrizamide myelography, but CT may still be effective. Intraspinal posttraumatic meningoceles may be missed on myelography, but can accurately be delineated with CT.

K. Jack Momose

CT scan in severe diffuse head injury: physiology and clinical correlations. Teasdale E, Cardoso E, Galbraith, Teasdale G (Institute of Neurological Science, Glasgow G51 4TF, United Kingdom). *J Neurol Neurosurg Psychiatry* 47:600–603, June 1984

Computed tomography (CT) is accurate in diagnosing cerebral compression caused by intracranial clot or other focal traumatic space occupying lesions. Severe diffuse brain damage, in the absence of a clot, can also cause increased intracranial pressure (ICP), but this affects only a minority of patients, even of those in coma. Thirty-seven patients who had diffuse severe head injury were studied. All were in coma at the time of the scan and none had a lucid interval between injury and investigation. Most (90%) were scanned within 12 hr of injury. After the scan an intraventricular catheter was inserted and the ICP was monitored for 24 hr. CT identified three groups of patients: (1) 18 in whom both the third ventricle and basal cistern were normal; (2) nine in whom these spaces were obliterated (the third ventricle in two of eight; also in two the basal cisterns were seen only because they contained blood); and (3) 10 in whom neither the third ventricle nor the basal cisterns could be detected. Compression of the third ventricle and basal cisterns closely correlated with an intracranial pressure greater than 20 mm Hg, with clinical signs of midbrain dysfunction, and a worse prognosis. These CT findings can indicate whether intracranial monitoring is appropriate.

K. Jack Momose

Solitary eosinophilic granuloma of the skull. Rawling CE III, Wilkins RH (Duke University Medical Center, Durham, NC 27710). *Neurosurgery* 15:155–161, Aug 1984

Solitary eosinophilic granuloma of the skull is a rare lesion. The course and ultimate outcome of the disease are not well known. The authors studied 26 cases of solitary eosinophilic granuloma of the skull collected over a 40-year period at Duke University. There were 16 males and 10 females; age ranged from 18 months to 49 years, average 16 years. The radiographic appearance of the solitary eosinophilic granuloma was similar. The parietal bone was the most frequently involved followed by the frontal bone. The lesion ranged from a 1 × 1 cm to a 5 × 6 cm rounded lytic bony defect, with sharp edges and no sclerosis. Three cases were studied by computed tomography; two were read as normal. The third case showed bone erosion with a soft-tissue mass intracranially contiguous to the bone. The enhancing margins extended epidurally and extracranially. All cases were treated surgically for diagnosis and management. Fifteen were treated by radiation. Follow-up was 1 month–25 years; average, 8.1 years. The lesions in the skull showed sclerosis in 6 months to 2 years; in younger patients they healed completely. In cases that did not heal, there was no progression for a 4–24 year period. Eight patients had recurrence or lesions in other bones or in the brain. Five cases developed recurrent disease at multiple sites, three others had single lesions in the hypothalamus, cerebellum, and femur, respectively. The time of first relapse was 6 months–12 years after the primary lesion was treated. One patient developed multiple lesions 17 years after the diagnosis of a primary cranial eosinophilic granuloma.

K. Jack Momose

Pediatric Radiology

Rib osteomyelitis in children. Early radiologic and ultrasonic findings. Bar-Ziv J, Barki Y, Maroko A, Mares AJ (Dept. of Pediatric Radiology, Soroka University Hospital, Beer-Sheva, Israel). *Pediatr Radiol* 15:315–318, July 1985

Before osteomyelitis is evident by bone changes on radiography, deep-seated edema is present. As nicely demonstrated in this article, not only may pericostal edema from osteomyelitis be manifest as inward displacement of the pleural line on chest radiographs within a few days of onset of symptoms, but pericostal edema can be directly seen sonographically, together with inward displacement of lung echoes. Although pericostal edema is not specific to osteomyelitis, it is a strong warning sign within the overall clinical picture of osteomyelitis. Sonography affords a quick, easy, and reliable method to diagnose pericostal edema.

Alan E. Oestreich

Dystrophic calcification in obliterated umbilical artery. Currarino G, Weinberg A (Children's Medical Center, 1935 Amelia St., Dallas, TX 75235). *Pediatr Radiol* 15:346–347, July 1985

A characteristic calcification near the pelvic triradiate cartilage was identified in three 2–3-year-old children, bilaterally in one and shown to represent calcification in the horizontal pelvic portion of the obliterated umbilical artery. It is also visible in the appropriate location on the lateral film.

Alan E. Oestreich

Ultrasonic demonstration of porto-caval anastomosis in portal hypertension in children. Boucher D, Brunelle F, Bernard O, Forel F, Autrel D, Hadchouel P, Chaumont P (F. Brunelle, Service de Radiopédiatrie, Centre Hospitalier de Bicêtre, 78 rue de Général Leclerc, F94270 Le Kremlin Bicêtre, France). *Pediatr Radiol* 15:307–310, July 1985

Seventy-one children who had received a surgical portocaval anastomosis after gastrointestinal hemorrhage secondary to portal hypertension were studied by sonography. Preoperative studies were also available. Most of the anastomoses were jugular vein grafts between the superior mesenteric vein and the inferior vena cava; the second most common type were splenorenal. The patency of shunt was directly demonstrated in 70%: superior mesenteric to cava shunts were best seen through the right kidney from posteriorly; splenorenal shunts were seen through the spleen or left kidney; direct portocaval shunts were seen through the liver as were mesenteroatrial shunts. Indirect sonographic signs of patency were decreased thickness of lesser omentum, decreased gastroesophageal collaterals, decreased portal vein size, and increased diameter of inferior vena cava. One of five thrombosed shunts was directly demonstrated; none of the indirect signs was found in the other four. At least one indirect sign was present in all 68 patent shunts.

Alan E. Oestreich

Aseptic meningitis secondary to metrizamide lumbar myelography in a 4½-month-old infant. DiMario FJ (University Pediatrics, University Health Center, Burlington, VT 05401). *Pediatrics* 76:259–262, Aug 1985

A 4½-month-old girl underwent metrizamide myelography for evaluation of lower extremity asymmetry. Under general anesthesia a lumbar puncture was performed at the L4–L5 disk space and 5 ml of 170 mgI/ml was injected. At 12–18 hr after myelography the child became febrile to 40.2° C and had three episodes of vomiting. Approximately 30 hr after myelography she became increasingly lethargic, continued vomiting, and had a stiff neck. Lumbar puncture revealed cerebrospinal fluid with a red blood cell count of 200/ml, white blood cells of 50,000/ml with 95% PML and 2% lymphocytes, glucose of 100 mg/dl, and protein of 294 mg/dl. Gram stain and counterimmunoelectrophoresis for *Hemophilus influenzae* and *Neisseria meningitidis* A and C were negative. About 60 hr after myelography, the symptoms subsided. Aseptic meningitis has rarely been reported in adults after metrizamide myelography. This is thought to be the first case reported in children.

Richard B. Towbin

Healing rates of treated and untreated bone lesions in histiocytosis X. Womer RB, Raney RB, D'Angio GJ (Children's Cancer Research Center, Philadelphia, PA 19104). *Pediatrics* 76:286–288, Aug 1985

Twelve boys and nine girls with histiocytosis X of bone, ages 4 months–14 years, were retrospectively studied. They were treated with various combinations of surgery, radiotherapy, chemotherapy, and local steroid injection. Median times to a given degree of healing were similar across treatment groups and in untreated lesions. The authors conclude that the type of therapy does not strongly influence the healing rate of bone lesions. However, within 4 months after initiation of therapy the lesions should be 25%–75% smaller and have well established sclerosis and sharp margins. The authors believe that treatment is indicated only if the bone lesions are causing intense pain, are producing unacceptable deformity, or are in a weight-bearing area and pose a risk of pathologic fracture.

Richard B. Towbin

Complications resulting from use of arterial catheters: retrograde flow and rapid elevation in blood pressure. Butt WW, Gow R, Whyte H, Smallhorn J, Koren G (Division of Neonatology, Hospital of Sick Children, Toronto, Ontario, Canada M5G 1X8). *Pediatrics* 76:250–254, Aug 1985

Fourteen neonates with peripheral arterial catheters were studied. The infants ranged in gestational age from 24 to 41 weeks, and had a mean weight of 1836 g (range 680–4180 g). There were five radial artery catheters, two posterior tibial artery catheters, and seven umbilical artery catheters. The umbilical artery catheters were positioned between the third and fourth lumbar vertebrae. Catheters were flushed with 0.5 ml of 1.0 ml of normal saline over 1 or 5 sec and monitored sonographically. The effect of flushing on blood pressure was also evaluated. Flushing of the radial artery catheters produced retrograde flow into the aortic arch and left common carotid artery, while flushing the posterior tibial or umbilical artery catheters resulted in retrograde flow into the descending aorta and superior mesenteric artery. Both 0.5 ml and 1.0 ml of flush caused retrograde flow only when injected over a 1 sec period. No retrograde flow occurred when a 5 sec flush was performed. Retrograde flow was also associated with a brief but significant blood pressure elevation. Arterial catheters have been associated with serious complications. The authors suggest that these phenomena can be prevented by flushing with 0.5 ml of solution over a 5 sec period.

Richard B. Towbin

Giant cell reparative granuloma of the cranial vault: exceptional bone lesion. Garza-Mercado R, Cavazos E, Hernandez-Batres F (Col. V. Hermosa, Aleutignas 396, Monterrey, Nuevo Léon, Mexico). *Neurosurgery* 15:228–231, Aug 1984

Giant cell reparative granuloma (GCRG) is an uncommon nonneoplastic lesion of bone. Originally considered to be peculiar to the jawbone, GCRG has been described in other locations, such as the short tubular bones of hand and foot and the facial (paranasal) bones. The authors describe a GCRG arising in the cranial vault in a 31-month-old boy. The lesion presented as a nonpainful, slow growing, right frontal swelling, apparently related to trauma that occurred 21 months earlier. Plain skull films showed an irregular circular osteolytic lesion with scalloped edges and faint trabeculation on the right frontal bone. The internal table of the skull seemed intact, whereas the external table appeared expanded. Computed tomography revealed normal intracranial contents and a bone lesion of mixed densities in the frontal bone. At surgery the lesion was a friable grayish, nodular tissue occupying the diploic space. Histologically, the outstanding feature was the presence of groups of multinucleated osteoclastic-like giant cells irregularly distributed throughout the lesion. The etiology of GCRG is unknown, however, it is thought to result from traumatic intraosseous hemorrhage or periosteal reaction.

K. Jack Momose

Focal cerebral hypoperfusion in children with dysphasia and/or attention deficit disorder. Lou HC, Henriksen L, Bruhn P, Psych C (Kennedy Instituttet, Gamel Landeve, 7-9, 2600 Glostrup, Denmark). *Arch Neurol* 41:825–829, Aug 1984

Developmental cognitive disorders are common. At least 5% of all children suffer from some degree of developmental dysphasia and/or attention deficit disorder and the neural mechanisms involved in learning disorders are largely unknown. The authors studied three-dimensional regional cerebral blood flow (rCBF) in 13 children with dysphasia and/or attention deficit disorder using xenon-133 inhalation and emission computed tomography. The rCBF distribution was abnormal in both hemispheres in all patients, as compared with the mean CBF distribution of nine normal children. Regions of hypoperfusion and, by inference, low metabolic activity were predominantly seen in the periventricular white matter and in border zones between major arterial territories. In patients with dysphasia, parts of both perisylvian regions were hypoperfused, and object-naming tasks failed to produce an increased flow in relevant cortical regions. All 11 patients with attention deficit disorders had hypoperfusion in the white matter of the frontal lobes and seven also had hypoperfusion in the caudate nuclei. Methylphenidate hydrochloride increased perfusion in the central region, including the mesencephalon and the basal ganglia, and decreased perfusion of motor and primary sensory cortical areas. The location of hypoperfused structures in cognitive disorders of childhood is consistent with an early hypoxic-ischemic event in their origin.

K. Jack Momose

News

Nuclear Medicine Meetings

The annual meeting of the Southwestern Chapter, Society of Nuclear Medicine, will be March 14–16, in Dallas. A 1-day symposium will precede the annual scientific meeting on March 13. Information: Society of Nuclear Medicine, Jean Parker, P.O. Box 40279, San Francisco, CA 94140; telephone (415) 647-1668.

Doppler for Radiologists

Yale University will present a course, Doppler for Radiologists, in New Haven on two dates: March 17–19 and June 2–4. Emphasis will be on recent progress in application of Doppler techniques to carotid, abdominal, and pelvic imaging including obstetrics. Course director: K. J. W. Taylor. Category I credit: 21 hr. Fee: $375 for physicians; $300 for sonographers and residents. Information: Janice Gore, Office of Graduate and Continuing Education, 333 Cedar St., New Haven, CT 06510; (203) 785-4578.

Neuroradiology at Snowmass

The Department of Radiology, Hospital of the University of Pennsylvania, will present a program, Neuroradiology at Snowmass (CO), March 24–28. Basic principles of interpretation of computed tomograms of the head and spine will be presented with emphasis on radiologic-anatomic-pathologic correlations. The roles of new techniques will also be discussed including magnetic resonance imaging. Category I credit: 23 hr. Fee: $475 physicians; $350 residents. Information: Ms. Janice Ford, Dept. of Radiology, Hospital of the University of Pennsylvania, 3400 Spruce St., Philadelphia, PA 19104; (215) 662-6904.

Fundamentals of MRI

The fifth annual Fundamentals of MRI will be March 26–29 in San Antonio. Sponsor: Dept. of Radiology, University of Texas Health Science Center at San Antonio. Category I credit: 28 hr. Fee: $395; $250 for residents. Information: Continuing Medical Education Services, University of Texas Health Science Center at San Antonio, 7703 Floyd Curl Dr., San Antonio, TX 78284-7980; (512) 691-6295.

Harvard Courses

The Department of Radiology, Harvard Medical School, has announced three courses.

Ultrasound 1986, offered by Harvard and Brigham and Women's Hospital, will be April 1–4. Basics of ultrasound will be discussed during a special session on April 1. Program director: P. M. Doubilet. Category I credit: 32 hr. Fee: $450, $325 for residents, fellows, and technologists. The basics course is $100.

Clinical Nuclear Medicine 1986 will be April 7–10. Sponsors are the joint program in nuclear medicine at Beth Israel, Brigham and Women's, and Children's hospitals and the Dana-Farber Cancer Institute. Program director: W. D. Kaplan. Category I credit: 25 hr. Fee: $425; $300 for residents, fellows, and technologists.

Coronary Angiography 1986: Imaging Techniques, PTCA, Thrombolysis, and Bypass Surgery will be June 9–12. This is offered by Harvard, Brigham and Women's Hospital, and is cosponsored by the Council on Cardiovascular Radiology of the American Heart Association. Program director: D. C. Levin. Category I credit: 29 hr. Fee: $450; $300 for residents, fellows, and technologists.

Information for all: Dept. of Continuing Education, Harvard Medical School, 25 Shattuck St., Boston, MA 02115; (617) 732-1525.

Radiology and MR Course

Sacred Heart Medical Center, Spokane, will present its 15th annual Refresher Course in Diagnostic Radiology, April 3–5, at the medical center. The course is for the practicing radiologist and will review current diagnostic challenges and update new procedures and techniques. The third day will be a symposium on magnetic resonance imaging. Category I credit: 22 hr. Fee: $300. Information: Marvin J. Gottschall, M.D., director of radiology, Sacred Heart Medical Center, W. 101 Eighth Ave., TAF-C9, Spokane, WA 99220; (509) 455-3131.

Medical Ultrasound Course

Bowman Gray School of Medicine will present an 8-week course on medical ultrasound, April 14–June 6. Topics will include physics, neurosonology, peripheral vascular, cardiology I, cardiology II, abdomen, abdomen and urology, and obstetrics. Participants may take segments of 1–8 weeks in length. Category I credit: 30 hr/week. Fee: $525/week; $4000 for 8 weeks. Information: Dr. Frederick W. Kremkau, director, Center for Medical Ultrasound, Bowman Gray School of Medicine, 300 S. Hawthorne Road, Winston-Salem, NC 27103; (919) 748-4505.

Interventional Radiology Conference

The Department of Radiology, Alexandria Hospital, is sponsoring the Sixth Annual Washington Imaging Conference, May 5–9, in

Washington, DC. Title: Interventional Radiology 1986. The course will be a practical review of current interventional techniques including angioplasty, thrombolysis, embolization, genitourinary interventions, and biopsy techniques. Course directors: B. T. Katzen and A. van Breda. Other faculty: K. H. Barth, Georgetown University; W. R. Castaneda-Zuniga, University of Minnesota; E. M. Druy, George Washington University; E. Martin, Columbia-Presbyterian Medical Center; G. McLean, Hospital of the University of Pennsylvania; P. Mueller and A. Waltman, Massachusetts General Hospital; E. J. Ring, University of California, San Francisco; R. J. Rosen, New York University; D. Schwarten, St. Vincent's Hospital, Indianapolis; T. A. Sos, New York Hospital-Cornell Medical Center; and C. J. Tegtmeyer, University of Virginia. Category I credit: 25 hr. Fee: $450. Information: Mrs. Pam Donais, Dept. of Radiology, Alexandria Hospital, 4320 Seminary Road, Alexandria, VA 22304; (703) 379-3102.

Breast Cancer Conference

The American College of Radiology has announced its 22nd National Conference on Breast Cancer will be May 12–16 in Boston. This multidisciplinary conference is designed to attempt to meet the needs of physicians who deal with the problems of breast cancer in daily practice. It will provide up-to-date information on the diagnosis, epidemiology, pathology, psychology, and clinical management of women with breast malignancies. Cosponsors are: American Cancer Society, American Society for Therapeutic Radiology and Oncology, College of American Pathologists, and the Plastic Surgery Educational Foundation. There will be plenary sessions, workshops, panel discussions, and proffered papers.

Faculty: R. J. Bartrum, Jr., Dartmouth-Hitchcock Medical Center; S. K. Carter, Bristol Myers Laboratories; C. M. Cole-Beuglet, University of California, Irvine; R. Costlow, P Greenwald, D. E. Henson, I. J. Masnyk, and R. Yancik, all National Cancer Institute; E. De Sombre, Ben May Laboratories for Cancer Research, Chicago; W. D. DeWys, Kaiser Permanente, Springfield, VA; C. J. D'Orsi, University of Massachusetts; S. A. Feig, Thomas Jefferson University; R. S. Foster, Vermont Regional Cancer Center; P. G. Gebhard, Veder, Price, Kaufman & Kammholz, Chicago; D. E. Haagensen, New England Deaconess Hospital; J. R. Harris, Harvard Medical School; W. H. Hartmann, Vanderbilt University; I. C. Henderson, Dana-Farber Cancer Institute; J. C. B. Holland, Memorial Sloan Kettering Center; A. I. Holleb, American Cancer Society; M. Homer, Tufts New England Medical Center; R. V. P. Hutter, St. Barnabas Medical Center, Livingston, NJ; Tilde S. Kline, Lankenau Hospital, Philadelphia; D. Kopans, Massachusetts General Hospital; S. Levy, University of Pittsburgh; W. W. Logan, consultant, Roswell Park Memorial Institute; R. Love, University Hospital, Madison, WI; R. G. Margolese, Jewish General Hospital, Montreal; K. McCarty, Jr., Duke University; R. McLelland, University of North Carolina; A. B. Miller, University of Toronto; M. Moskowitz, University of Cincinnati; B-P Robra, Zentralinstitut fur die Kassenarztliche, Haedenkampstr, West Germany; N. L. Sadowsky, Faulkner Hospital, Jamaica Plain, MA; W. S. Schain, private practice, Bethesda, MD; E. A. Sickles, University of California, San Francisco; R. K. Snyderman, private practice, Princeton, NJ; M. L. S. Vachon, Clarke Institute of Psychiatry, Toronto; J. N. Wolfe, Hutzel Hospital; W. C. Wood, Massachusetts General Hospital; and R. Zamenhof, New England Deaconess Hospital.

Category I credit: 31 hr. Fee: $475. Information: Breast Cancer Conference, American College of Radiology, 1891 Preston White Dr., Reston, VA 22091; (703) 648-8900.

Radiology in Otolaryngology

The 17th Annual Conference on Radiology in Otolaryngology and Ophthalmology, sponsored by the American Society of Head and Neck Radiology, will be May 15–17 in Seattle. Category I credit: 20 hr. Information: Dexter W. Johnson, M.D., course chairman, Swedish Hospital Medical Center, Dept. of Radiology, 747 Summit Ave., Seattle, WA 98104.

Imaging Courses

The Medical University of South Carolina has announced two imaging courses. The first, **Imaging at Spoleto**, will be May 26–30 in Charleston, SC. This seminar will emphasize computed tomography (CT), diagnostic radiology, neuroradiology, and nuclear medicine. Guest faculty: J. Campbell, B. Felson, and H. Jacobson. Program director: P. Ross. Fee: $350. Information: Mrs. Susan Jones, meeting coordinator, Dept. of Radiology, Medical University of South Carolina, 171 Ashley Ave., Charleston, SC 29425; (803) 792-5071.

The second course, *Imaging at Wimbledon*, will be June 21–28 in London. This will emphasize magnetic resonance imaging, CT, diagnostic radiology, nuclear medicine, and neuroradiology. Guest faculty: G. Bydder, G. Lloyd, J. Orr, and a representative from Picker International. Program director: P. Ross. Fee: $475. Information: Imaging at Wimbledon, 490 Old Dock Road, Kiawah Island, SC 29455; (803) 768-1033.

Radiology and Nuclear Medicine

The Department of Radiology, Bowman Gray School of Medicine, will present its third annual summer continuing education meeting June 16–20 in Charleston, SC. Category I credit: 20 hr. Fee: $425. Information: Carolyn Shaver, Dept. of Radiology, Bowman Gray School of Medicine, Winston-Salem, NC 27103; (919) 748-2470.

Cavernous Sinus Symposium

The International Symposium on Cavernous Sinus will be in Ljubljana, Yugoslavia, June 29–July 3. Information: Vinko V. Dolenc, M.D., Dept. of Neurosurgery, University Medical Centre, Zaloška 7, 61105 Ljubljana, Yugoslavia.

Sonography Cruise

Topics in ultrasound will be presented during a cruise, July 5–12, titled Alaska 86—Cruise the Inland Passage. B. B. Goldberg, Thomas Jefferson University, will lead the course. Fee: $385 before April 12, $425 thereafter. Information: Medical Seminars/Alaska 86, 21915 Roscoe Blvd., Suite 222, Canoga Park, CA 91304; (800) MED-TOUR.

Roentgen Revisited Course

The University of California, San Francisco, Medical Center will present its sixth annual course, Roentgen Revisited, July 13–18, in Garmisch-Partenkirchen, West Germany. Information: University of California, San Francisco, Radiology Postgraduate Education—Room C324, San Francisco, CA 94143.

Hyperthermia Institute

Physics and Technology of Hyperthermia, a NATO Advanced Study Institute, will be July 26–Aug. 9 in Urbino, Italy. Deadline for application for participation is March 31. The number admitted will be limited to 80 and those selected will assure an interdisciplinary character. A limited number of grants is available. Goal is to present to physicists and engineers the basic physics and technology of hyperthermia with sufficient clinical and biological background of hyperthermia oncology to enable competent design and development of methods and systems for experimental research and clinical studies. Lecturers: J. B. Andersen and J. Overgaard, Denmark; C. K. Chou, C. Durney, T. C. Cetas, J. Oleson, R. B. Roemer, and J. W. Strohbehn, all United States; C. Franconi, G. Arcangeli, R. Cavaliere, and F. Mauro, all Italy: J. Hand and S. B. Field, United Kingdom; J. Hunt, Canada; J. W. Langendjik and H. Reinhold, The Netherlands; and M. Gautherie, France. Information: S. B. Field, MRC Cyclotron Unit, Hammersmith Hospital, Ducane Road, London W12, United Kingdom; telephone 44-1-743-4594. Information also from: C. Franconi, Medical Physics Institute, 11 University of Rome, Via O. Raimondo, 00173 Rome, Italy; telephone 39-6-613-1200.

Computers for Physicians

Computers for the Practicing Physician: Update 1986, will be presented July 27–30 in New Seabury, Cape Cod, MA. Sponsor: Boston University School of Medicine. Course director: B. M. Manuel. Category I credit: 12 hr. Fee: $275. Information: Dept. of Continuing Medical Education, Boston University School of Medicine, 80 E. Concord St., Boston, MA 02118; (617) 638-4605.

Sonography Seminars

The Center for Medical Ultrasound, Bowman Gray School of Medicine, has announced two seminars. An **Advanced Neurosonology Seminar** will be July 28–30 and the **Advanced Applied Ultrasound in Obstetrics Seminar** will be July 31–Aug. 2. Both will be in Snowmass, CO.

The first program will explore advanced vascular evaluation of the extracranial and intracranial vessels in normal and pathologic conditions. It will focus on interpretation of vascular studies and introduce intracranial Doppler. Program director: W. M. McKinney. Category I credit will be awarded. Fee: $350.

The seminar on application of ultrasound in obstetrics will focus on advanced problems in application of diagnostic sonography and correlation with surgical and clinical management. Guest faculty: F. P. Hadlock, Baylor College of Medicine; C. W. Hohler, St. Joseph's Hospital; and D. J. Sahn, San Diego Medical Center. Program director: L. H. Nelson. Category I credit: 10 hr. Fee: $350.

Information for both: Dr. Frederick W. Kremkau, director, Center for Medical Ultrasound, Bowman Gray School of Medicine, 300 S. Hawthorne Road, Winston-Salem, NC 27103; (919) 748-4505.

Diagnostic Imaging Symposium

The seventh annual Symposium on Diagnostic Imaging, sponsored by Rhode Island Hospital and Brown University, will be Aug. 11–14 in Newport, RI. Category I credit: 16 hr. Fee: $400. Information: Sandra Moran, Radiology Dept., Rhode Island Hospital, 593 Eddy St., Providence, RI 02902; (401) 277-4707.

Australasian Meeting

The 37th annual scientific meeting of the Royal Australasian College of Radiologists will be in Singapore, Sept. 13–19. Faculty and speakers include members of the Royal Australasian College of Radiologists and guests. Information: Dr. Angus Robertson, 2 Heathcote Crescent, Millswood S.A. 5034, Australia.

European Symposium

The 1986 symposium of the European Association of Radiology will be Oct. 1–4 in Vienna. Topics will include tumors and imaging of the colon, mamma, and bronchus. Official languages (with simultaneous translation) are: English, French, and German. Information: Prof. Dr. H. Pokieser, president, c/o Wiener Medizinische Akademie, Alser Strasse 4, A-1090 Vienna, Austria.

ARRS Luncheon Speaker Changes

The 1986 American Roentgen Ray Society (ARRS) meeting in Washington, DC, will have four luncheon sessions. Topics and speakers have been altered from the listing that appeared in the ARRS meeting section of the January issue of the *AJR*. There is a $10 charge for each, a box lunch will be provided, and advance registration is required (see forms in January and February issues).

Dates, topics, and speakers:

Monday, April 14: Difficulties, Confusions, and Other Federal Initiatives, Otha W. Linton, Associate Executive Director, American College of Radiology.

Tuesday, April 15: New Forms of Insurance Programs (HMOs, TPOs, etc.)—Their Impact on Radiology, Ronald G. Evens, Mallinckrodt Institute of Radiology.

Wednesday, April 16: The Radiology Interface Alternate Delivery Systems, Thomas Dehn, Good Samaritan Medical Center, Milwaukee.

Thursday, April 17: The Radiologist's Economic and Ethical Position in Freestanding Imaging Centers, Steven Hirschtick, attorney, Los Angeles.

AJR carries announcements of courses, symposia, and meetings of interest to its readers if received a minimum of 4 months before the event. There is no charge; receipt of items by the *AJR* Editorial Office is not acknowledged. Submit items for publication typed double spaced. Provide title, date, location, brief description, sponsor, course directors, fees, category I credit, and address and telephone number for additional information. Faculty from the host institution will not be listed. Guest faculty names will appear **only** if initials are provided. Mail news items to *AJR* Editorial Office, 2223 Avenida de la Playa, Suite 306, La Jolla, CA 92037.

Classified Advertising

Positions Available

AMERICAN-TRAINED RADIOLOGIST to work in salaried position in 6-member, multispecialty group radiology practice in office and hospital setting in metropolitan New York area. Reply Box K10 AJR (see address this section). 3a

GROUP OF RADIOLOGISTS want to purchase a contract with hospital or clinic. Terms negotiable. All areas considered. Reply Box K8 AJR (see address this section). 3ap

ABDOMINAL IMAGER: The University of Washington's Dept. of Radiology has an opening for an academically oriented radiologist in the area of abdominal imaging, including gastrointestinal and genitourinary radiology with expertise in CT and ultrasound. This position will also involve interventional radiology of the abdomen including biopsies and abscess drainage. Responsibilities include instructing medical students and residents and conducting research. Applicant must possess board certification in radiology plus 1 year related fellowship or clinical experience in radiology postresidency. Send letter and resume to Albert A. Moss, M.D., Dept. of Radiology SB-05, University of Washington, Seattle, WA 98195. The University of Washington is an equal opportunity employer. 3a

RADIOLOGISTS—sought by quality-oriented, nationwide referral service for medical-legal consultation. Highly rewarding opportunity. Send inquiries to ExpertNet, 2020 W. State St., Suite 164, Milwaukee, WI 53233. 3ap

DIAGNOSTIC RADIOLOGIST—with skills in general radiology, nuclear medicine, ultrasound, and angiography to be the Chief of Service at this 342-bed GM&S medical center located in Roseburg, OR. Competitive salary together with generous U.S. government fringe benefits including malpractice liability protection, 30 days paid vacation etc. Roseburg is a family-oriented community with unlimited recreational opportunities. The position is immediately available. Interested individuals should contact Dr. Paul Nichol, chief of staff, Veterans Administration Medical Ctr., Roseburg, OR 97470; (503) 672-4411. An Equal Opportunity Employer. 3a

ISRAEL, DIAGNOSTIC RADIOLOGY. Opportunities for 3-4 week or longer working vacations in a number of Israeli medical centers, on a volunteer basis. Positions varied, arrangements flexible. For information contact: Jonathan H. Fish, M.D., 1844 San Miguel Dr., #302, Walnut Creek, CA 94596; (415) 947-0560. 2-7a

BOARD CERTIFIED RADIOLOGIST seeks an associate to service a 40-man multispecialty group and 155-bed med-surg hospital, all part of a medical center complex. Excellent opportunity to practice state-of-art imaging with CT, ultrasound, arteriography, and nuclear cardiology (no MRI). Experience in therapeutic radiology optional. The facility is located in a city of 45,000, just 40 miles from a major metropolitan center in the midwest area of the country. Initial guarantee generous and early partnership is anticipated. Send CV. Reply Box J1 AJR, 2223 Avenida de la Playa, Suite 306, La Jolla, CA 92037. 2-5a

BOARD CERTIFIED RADIOLOGIST—to join a 3-member department in a 204-bed community hospital. Interest in nuclear medicine would be helpful. Salary and partnership terms are negotiable. Reply with CV to D. W. Boyd, M.D., Good Samaritan Hospital, Pottsville, PA 17901. 2-4ap

DIAGNOSTIC RADIOLOGIST. Immediate opening for a board certified diagnostic radiologist to join the staff of a small, modern, well-equipped acute care community hospital located in historic Gettysburg, PA. Some experience in interventional radiology preferred but not required. For confidential consideration please submit curriculum vitae to: Joseph C. Jones, M.D., director, Radiology Services, The Gettysburg Hospital, 147 Gettys St., Gettysburg, PA 17325. (717) 334-2121, ext. 207. 2-3a

RADIOLOGY CHAIRPERSON: The Oregon Health Sciences University School of Medicine is recruiting a chairperson for the Dept. of Diagnostic Radiology. The department serves the University Hospital and has a VAMC Dean's Committee affiliation. Activities include ultrasound, angiography, computed tomography, special procedures, and animal research. General radiology residency and fellowship programs in ultrasound, computed tomography, neuroradiology, and vascular/interventional radiology exist. Curriculum vitae and the names/addresses of 3 references should be submitted to Wendell C. Stevens, M.D., Chairman, Radiology Search Committee, School of Medicine, Oregon Health Sciences University, Portland, OR 97201. Applications/recommendations accepted until position is filled. The Oregon Health Sciences University is an affirmative action/equal opportunity employer. 2-3a

NEURORADIOLOGY—Faculty appointment for a trained neuroradiologist with interest in teaching and research at the medical school of the University of Texas Health Sciences Center at San Antonio. Send curriculum vitae to: Robert L. Siegle, M.D., chief, Diagnostic Radiology, Dept. of Radiology, The University of Texas Health Science Center at San Antonio, 7703 Floyd Curl Dr., San Antonio, TX 78284. Equal employment opportunity/affirmative action employer. 2-4a

RADIOLOGY INSTRUCTOR to assist candidate in preparation for Oral Boards. Candidate needs practice in formally discussing cases and answering board-type questions in all exam sections. Would like to meet on a weekly basis beginning early 1986. East coast (esp. Philadelphia/Middle Atlantic states) preferred. Fee negotiable. Reply Box W4 *AJR* (see address this page) or call (215) 342-4110. 11-3a

EXCELLENT POSITION available with radiology practice for board certified radiologist with an interest in all areas of radiology. Opportunity for partnership in expanding practice in the Greater New Orleans area serving 3 hospitals. 80,000 inpatient, 24,000 outpatient examinations/year. Send CV to Dr. Harold R. Neitzchman or Dr. Martin A. Belanger, 4400 General Meyer Ave., Suite 221, New Orleans, LA 70114. 12-3a

DIAGNOSTIC RADIOLOGIST: Board-certified diagnostic radiologist seeks partner in expanding solo hospital-based practice. Upstate New York. All modalities available. CV to Phillip Berman, M.D., HC61 Box 454, Massena, NY 13662. 9-4a

Positions Desired

BOARD CERTIFIED DIAGNOSTIC radiologist. Have completed 3 formal postgraduate fellowships in nuclear medicine, CT/US, and neuroradiology/MR. Extensive practical angiography experience. Flexible starting date. Reply Box K4 AJR (see address this section). 3-6b

NEURORADIOLOGIST with MRI experience. University trained. Board certified. Adept all phases diagnostic radiology. Seeks position leading to partnership; private or academic with MRI or plans for. (518) 489-8732 or write Box K6 AJR (see address this section). 3bp

Fellowships and Residencies

NMR VISITING FELLOWSHIPS in northern California. Intensive, structured 1-4 week courses with live instruction, teaching file, and video tape library. For further information contact: Murray A. Solomon, M.D., San Jose MRI Center, 361 S. Monroe St., San Jose, CA 95128. 10-3c

VANDERBILT FELLOWSHIPS. The Dept. of Radiology and Radiological Sciences at Vanderbilt University is currently offering 1-year fellowships in (1) CT with MRI (2) chest, (3) bone, (4) pediatrics. Successful applicants will commence duties July 1, 1986. Applicants must be board certified or eligible and be able to obtain a Tennessee license. Applications should be addressed to: M. I. Shaff, M.D., Chairman, Fellowship Committee, Dept. of Radiological Sciences, Vanderbilt University-CCC 1100 Medical Center N., Nashville, TN 37232. 2-4c

Tutorials/Courses

KNOXVILLE, TN, April 4, 1986, Controversies in Diagnosis and Medical Management of Minimal Breast Cancer: Facts and Recommendations—1986. Location: University of Tennessee Hospital, Wood Aud. No fee. Contact: CME, D-116, 1924 Aloca Hwy, Knoxville, TN 37920; (615) 544-9190. 3d

ALASKA '86—Cruise the Inland Passage, July 5-12, 1986. CME I credit. Topics in ultrasound with Barry B. Goldberg, M.D. Registration U.S. $385 until April 12, after U.S. $425. For additional information write or call ALASKA '86—Medical Seminars International, 21915 Roscoe Blvd., #222, Canoga Park CA 91304; (800) MED-TOUR or (818) 701-5143. 1-6d

JERUSALEM, ISRAEL—Ultrasound Symposium, June 20-29, 1986. Category I CME program presented in cooperation with the Israeli Ultrasound Society by an International faculty. Fee to April 1986: U.S. $425, thereafter U.S. $460. Information: Medical Seminars International, 21915 Roscoe Blvd., #222, Canoga Park, CA 91304; (800) MED-TOUR or (818) 340-0580, ext. 280. 1-6d

LONDON, ENGLAND—ROME, ITALY, May 10-18, 1986. Attend one or both Spring Seminars. Renowned international faculty. Topics: CT, MRI, DSA. Category I accreditation. Fees: to March 7, U.S. $385, thereafter U.S. $425 each seminar. Combined fee: U.S. $450 and $495, respectively. Information: Medical Seminars, Dept. of Radiology, West Park Hospital, 22141 Roscoe Blvd., Canoga Park, CA 91304; (818) 340-0580 ext. 280 or (818) 701-1624. 11-4d

Other

ARE YOU INTERESTED in selling your radiology practice? We serve as representatives for a group of radiologists who are interested in purchasing radiology practices throughout the Midwest, Southeast, and South Central United States. Please call us for a confidental conference. The Lakewood Group, Ltd., 214 N. Henry St., Madison, WI 53703; (608) 255-0177. 2ep

AJR Indexes

AJR CONSOLIDATED INDICES available in limited quantities. Complete your journal collection. Order by index number. Indices available, years covered and prices: 2, 1938-1942, $10; 3, 1943-1947, $22.50; 4, 1948-1952, $23.50; 5, 1953-1957, $25; 6, 1958-1962, $23.50; 7, 1963-1967, $30; 8, 1968-1972, $40; 9, 1973-1977, $34. Order from: Subscription Dept., Williams & Wilkins, 428 E. Preston St., Baltimore, MD 21202; (301) 528-4000.

AJR Classified Advertising Information

Box Responses and Address for Ad Placement

Write Box ______, AJR, Suite 306, Avenida de la Playa, La Jolla, CA 92037; (619) 459-2229.

How to Place an Ad

AJR accepts classified advertising for Positions Available, Positions Desired, Fellowships and Residencies, and Tutorials/Courses. Ads are accepted by mail or telephone. Institutions should supply purchase orders.

Rates. $6.00/line with a $30 minimum charge. Box service is $10 additional for each month the ad appears. There are discounts for multiple insertions: 10% for 2-3 insertions; 20% for 4 or more. To estimate lines, count all words and divide by 5.5.

Billing: Ads may be prepaid or invoices will be sent after the ad appears.

Deadlines. About 3 weeks before the issue mails. *AJR* issues mail in the middle of the month preceding the cover date (e.g., July mails June 17). For specific deadlines, write or telephone the AJR editorial office.

Estimating Ad Charges

Line charge: divide total words by 5.5 and multiply by $6.00 ..... $ ______
Multiple insertions? If so, multiply by number .... × ______
Subtotal .... $
Box response requested? If so, multiply number of months by $10.00 .... + ______
Subtotal .... $
Discount applies to two or more insertions. Subtract 10% if ad appears 2-3 months, 20% if 4 months or more .... − ______
Approximate advertising charge .... $

This announcement appears as a matter of record only.

We are pleased to announce the formation of

Medical Imaging Partners L.P.

A Limited Partnership formed to develop, invest in, and own
Diagnostic Imaging Centers.

Total Equity Capital

$25,000,000

General Partner

Imaging Sciences, Inc.
A subsidiary of Merrill Lynch & Co., Inc.

The undersigned organized Medical Imaging Partners L.P.
and arranged the distribution of the Limited Partnership Units.

Project & Lease Financing

Merrill Lynch Capital Markets

December 18, 1985

Head, Division of Neurosurgery

Required for 698 (rated) bed paediatric teaching hospital with cross-appointment to the Division of Neurosurgery at the University of Toronto. The Division provides neurosurgery services for approximately 1,000 surgical procedures each year.

Applicants must have academic standing and interest in research as well as aptitude for paediatric service and departmental management. Full-time appointment and academic rank are to be commensurate with qualifications and experience.

Apply to:
Mr. W.M. Davis
Administrative Assistant and Secretary, Neurosurgery Search Committee
The Hospital for Sick Children
555 University Avenue
Toronto, Ontario, Canada
M5G 1X8

*This advertisement is directed to persons who are eligible to work in Canada.

HSC

THE HOSPITAL FOR SICK CHILDREN

DIAGNOSTIC RADIOLOGISTS
CENTRAL CONNECTICUT

Small group: includes hospital and diversified practices. Superior abilities in all areas of radiology.

Physician should have completed one year of fellowship after residency and/or equivalent.

Position open from present time to July 1st.

Board certification necessary.

Send C.V. to
P.O. Box 333,
Durham, Connecticut 06422

Help us to serve you better.....

If your mailing label does not contain your zip code, note it on the label and return it to us for correction.

Remember, your Zip Code provides faster, more direct delivery of your journals. Use it on all correspondence, too.

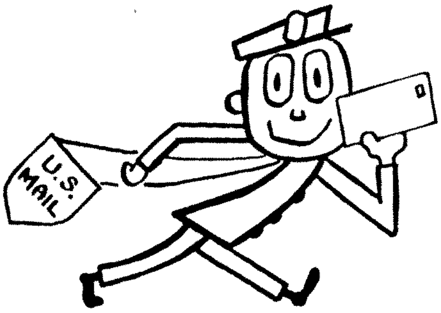

INDEX TO ADVERTISERS

Adria Laboratories . . . A25

DuPont . . . A19, A20, A21, A22

Eastman Kodak . . . A4, A5

Elema Schonander Inc. . . . A27

E-Z-EM Company . . . Cover 2

General Electric . . . A23

Hospital For Sick Children . . . A39

Merrill Lynch & Co., Inc. . . . A39

Porta Ray . . . A24

Precise Optics/PME, Inc. . . . A8

Purdue Frederick Company . . . A38

Pyne Corporation . . . Cover 3

Radiology Clinics . . . A39

E.R. Squibb & Sons . . . A29, A30, A31, A32, A33, A34, A35, A36, A37

S & S X-Ray . . . A28

Thompson CGR . . . A6, A7

Tobias Associates . . . A24

Winthrop Laboratories . . . A9, A10, A11, A12, A13, A14, A15, A16, A17, A18

We try to present an accurate index. Occasionally this may not be possible because of a last-minute change or an omission.

THE ALTERNATIVE

For too long the 90 second, high capacity processor market has been dominated by one manufacturer. Frankly there has been little competition.

Enter **The Alternative.** The FUJI FPM 4000 already well established as a standard of 90 second processing all over the world. The FUJI FPM 4000 is engineered to meet the needs of the most demanding high volume user, with accent on **reliability** and **ease of operation.** With features like cold water operation, built-in standby, waist high film delivery, high capacity (229 14 x 17 sheets per hour) and sophisticated yet reliable IC equipped electronic control, the FUJI FPM 4000 is . . . THE ALTERNATIVE.

Isn't it nice to finally have a choice?

THE FUJI FPM 4000—
A Reason for Change!

For more information call your local Pyne representative,
or call toll free (800) 431-1850
(in New York 914-834-4567)

PYNE CORPORATION
20 North Avenue, Larchmont, NY 10538

Volume 146 **American Journal of Roentgenology** **March 1986**

NEURORADIOLOGY

443 **Periventricular hyperintensity as seen by magnetic resonance: prevalence and significance.** *Zimmerman RD, Fleming CA, Lee BCP, Saint-Louis LA, Deck MDF*
451 **CT of pineal region tumors.** *Ganti SR, Hilal SK, Stein BM, Silver AJ, Mawad M, Sane P*
459 **Exophthalmos caused by excessive fat: CT volumetric analysis and differential diagnosis.** *Peyster RG, Ginsberg F, Silber JH, Adler LP*
465 **Incremental dynamic computed tomography: practical method of imaging the carotid bifurcation.** *Tress BM, Davis S, Lavain J, Kaye A, Hopper J*
471 **Prevalence of "compressed" and asymmetric lateral ventricles in healthy full-term neonates: sonographic study.** *Winchester P, Brill PW, Cooper R, Krauss AN, Peterson HDC*

THORACIC RADIOLOGY

477 **CT in silicosis: correlation with plain films and pulmonary function tests.** *Bergin CJ, Müller NL, Vedal S, Chan-Yeung M*
485 **The radiographic appearance of the Medtronic Hall valve prosthesis.** Mamourian AC, Pae WE
487 **Impending catheter perforation of superior vena cava: radiographic recognition.** *Tocino IM, Watanabe A*
491 **Circumflex retroesophageal right aortic arch simulating mediastinal tumor or dissecting aneurysm.** *Shuford WH, Sybers RG, Gordon IJ, Baron MG, Carson GC*
497 **Update: the radiographic features of pulmonary tuberculosis.** *Woodring JH, Vandiviere HM, Fried AM, Dillon ML, Williams TD, Melvin IG*

GASTROINTESTINAL RADIOLOGY

507 **Early esophageal cancer.** *Levine MS, Dillon EC, Saul SH, Laufer I*
513 **Radiologic manifestations of early gastric lymphoma.** *Sato T, Sakai Y, Ishiguro S, Furukawa H*
519 **Radiographic appearance of the esophagus and stomach after laser treatment of obstructing carcinoma.** *Wolf EL, Frager J, Brandt LJ, Frager DH, Bernstein LH, Beneventano TC*
523 **Sonographic detection of postsurgical recurrence of Crohn disease.** *DiCandio G, Mosca F, Campatelli A, Bianchini M, D'Elia F, Dellagiovampaola C*
527 **Review. Intussusception in adults.** *Agha FP*
533 **Regenerating nodules in cirrhosis: sonographic appearance with anatomic correlation.** *Freeman MP, Vick CW, Taylor KJW, Carithers RL, Brewer WH*
537 **Optimal cholangiographic technique for detecting bile duct stones.** *Thompson WM, Halvorsen RA, Foster WL, et al.*

GENITOURINARY RADIOLOGY

543 **Magnetic resonance imaging of the prostate.** *Bryan PJ, Butler HE, Nelson AD, et al.*
549 **Renal sonography in American Burkitt lymphoma.** *Strauss S, Libson E, Schwartz E, et al.*
553 **Gastric diverticulum simulating an adrenal mass: CT appearance and embryogenesis.** *Schwartz AN, Goiney RC, Graney DO*

MUSCULOSKELETAL RADIOLOGY

555 **Pitfalls of rotator cuff sonography.** *Middleton WD, Reinus WR, Melson GL, Totty WG, Murphy WA*
561 **Sonography of the postoperative rotator cuff.** *Crass JR, Craig EV, Feinberg SB*
565 **MRI of normal and pathologic skeletal muscle.** *Murphy WA, Totty WG, Carroll JE*
575 **Locking and unlocking of the knee: arthrographic demonstration.** *Salazar JE, Duke RA, Winer-Muram HT*

INTERVENTIONAL RADIOLOGY

577 **Percutaneous gastrostomy and gastroenterostomy: 1. Techniques derived from laboratory evaluation.** *vanSonnenberg E, Wittich GR, Brown LK, et al.*
581 **Percutaneous gastrostomy and gastroenterostomy: 2. Clinical experience.** *vanSonnenberg E, Wittich GR, Cabrera OA, et al.*
587 **Nonsurgical drainage of appendiceal abscesses.** *Nunez D Jr, Huber JS, Yrizarry JM, Mendez G, Russell E*
590 **Replacing the broken suture in the Cope-style loop retention catheter.** *Berman HL, Katz SG, Bakal CW*
591 **Radiopaque suspension of polyvinyl alcohol foam for embolization.** *Szwarc IA, Carrasco CH, Wallace S, Richli W*
593 **Fatal outcome after ethanol renal ablation in child with end-stage kidneys.** *Garel L, Mareschal JL, Gagnadoux MF, Pariente D, Guilbert M, Sauvegrain J*
595 **Pain control after percutaneous biliary drainage: local infiltration with bupivacaine and epinephrine.** *Lieberman RP, Sleder PR*

VASCULAR RADIOLOGY

597 **Postoperative assessment of splenorenal shunts with MRI: preliminary investigation.** *Cohen JM, Weinreb JC, Redman HC*
601 **Detection of the intimal flap of aortic dissection on unenhanced CT images.** *Demos TC, Posniak HV, Churchill RJ*
605 **The in situ saphenous vein bypass graft: radiologic aspects.** *Schwarz W, Nozick J, Richmand D, et al.*

PEDIATRIC RADIOLOGY

609 **Sonography of neck masses in children.** *Kraus R, Han BK, Babcock DS, Oestreich AE*
615 **Normal renal growth in children with myelodysplasia.** *Gross GW, Thornburg AJ, Bellinger MF*
619 **Noninvasive evaluation of neonatal aortic thrombosis secondary to umbilical artery catheterization.** *Follmeth BD, Sandler MP, Thieme GA, Fleischer AC, Neblett WW*

NUCLEAR MEDICINE

621 **Uptake of ^{111}In-labeled leukocytes by tumor.** *Fortner A, Datz FL, Taylor A Jr, Alazraki N*

AMERICAN ROENTGEN RAY SOCIETY

627 **Chest case of the day.** *Unger JM, Peters ME, Hinke ML*
631 **Abdominal case of the day.** *Rao BK, Scanlan KA, Hinke ML*
634 **Musculoskeletal case of the day.** *Fisher DR, Hinke ML*
637 **Neuroradiology case of the day.** *Houston LW, Hinke ML*

OTHER CONTENT

639 **Editorial. The presence of parents with their children during imaging procedures.** *Cohen MD, Wood BP, Hodgman CH*
642 **Society for Pediatric Radiology 1986 program**
644 **Letters**
650 **Abstracts**
656 **News**
659 **Classified ads**
Book reviews 476, 484, 518, 532
604 **Memorial**
614 **Erratum**
618 **ARRS 1986 meeting summary**
A2 **Guidelines for authors**

1986 ARRS Meeting: April 13–18, Sheraton Washington (DC)